Micro Total Analysis Systems 2004
Volume 1

Proceedings of μTAS 2004
8th International Conference on Miniaturized Systems for Chemistry and Life Sciences

Malmö, Sweden
September 26-30, 2004

edited by

Thomas Laurell
Lund Institute of Technology, Sweden

Johan Nilsson
Lund Institute of Technology, Sweden

Klavs Jensen
Massachusetts Institute of Technology, USA

D. Jed Harrison
University of Alberta, Canada

Jörg P. Kutter
Technical University of Denmark, Denmark

RS•C
advancing the chemical sciences

Special Publication No. 296

ISBN 0-85404-643-7

A catalogue record for this book is available from the British Library

Published by The Royal Society of Chemistry,
Thomas Graham House, Science Park, Milton Road,
Cambridge CB4 0WF, UK

Registered Charity Number 207890

For further information see our web site at www.rsc.org

Printed by Athenaeum Press Ltd, Gateshead, Tyne and Wear, UK

PREFACE

The 8th International Conference on Miniaturisation in Chemistry and Life Sciences, MicroTAS (Micro Total Analysis Systems) is celebrating its 10th anniversary year. The conference developed from a small gathering of researchers active in the field of MicroTAS in Enschede, The Netherlands, in 1994 with 160 participants. The success of this first meeting was followed by an equally appreciated μTAS workshop in Basel, Switzerland, in 1996 with a remarkable increase in the number of participants to 275. Optimism in the research field continued and the subsequent event was the truly unforgettable conference organised in Banff, Canada in 1998, with a record-breaking 420 conference delegates and about 130 papers submitted. At the following meeting in 2000, the conference returned to its birth place in Europe (at the University of Twente, Enschede, The Netherlands) again breaking new records for the MicroTAS conference with close to 500 attendees and about 140 scientific papers accepted (230 submissions). Due to the increasing interest that the MicroTAS/Lab-On-A-Chip field was generating, the subsequent meeting in 2001, in Monterey, CA, USA, forced the conference format into two parallel oral sessions in order to meet the pressure from the scientific community. In spite of the 9-11 terrorist attack and subsequent restrictions in international travelling, the conference attracted about 790 delegates and 276 accepted scientific contributions. The meeting was also characterised by an impressive commercial exhibition, demonstrating the transition of several of the earlier μTAS developments into the industrial sector. The subsequent conference (2002) in Japan is forever etched into our minds both with respect to the excellent organisation and scientific programme as well as the wonderful setting in ancient Nara. Although difficulties were developing in the industrial and financial sectors, following the IT-crash, the Nara meeting attracted 710 delegates with 316 accepted scientific contributions. The next μTAS conference was organised in another glorious location, Squaw Valley, CA, USA, in October 2003 and despite the setback in the global economy which clearly also affected academic budgets the conference attracted over 650 delegates with 325 accepted scientific presentations.

This year's conference confirms the continuing increase in interest in the μTAS-research field. More papers were submitted than ever before, 657, giving the Technical Programme Committee a difficult task in the abstract evaluation procedure. Again the scientific programme expanded, now to encompass a total of 422 accepted scientific contributions. We also see a continuing strong presence from the industrial area with some new players, indicating a recovery in the financial sector.

These two volumes contain the proceedings of the MicroTAS 2004 conference in Malmö, Sweden, September 26-30. Every paper presented will also be made available from the Royal Society of Chemistry, Lab on a Chip web-site at www.rsc.org/loc. The proceedings from the μTAS 2003 conference can also be accessed from this site.

The content of this year's MicroTAS conference clearly shows that the efforts in developing cell-based microsystems are increasing. Not only is work quite frequently focused on cell manipulation, and on-chip culturing but also on complete microsystems

for cell transport, culturing, analysis and monitoring including feed-back systems are now presented. The transition to polymer-based technologies continues and the now widely used SU-8/PDMS platform has opened up the μTAS-field to all those who do not necessarily have access to high performance clean-rooms, which vastly broadens the number of players that can now access and work in the field. A clear trend is also the increase in microfluidic two-phase systems, which seems to have come to a point where the two-phase fluid handling is well controlled and, *e.g.,* applications with compartmentalised chemistry in oil-immersed aqueous droplets in streaming microsystems are seen. The more mature areas of chip-based separation science are still very strong moving towards applications in genomics, proteomics and diagnostics. An exciting development is the continued progress in nanotechnology and the study of microfluidic transport, and molecular interaction and separation in nanoscale channels, this year displaying a representation equal to those in cell-based microsystems.

Looking back at μTAS conferences over the last ten years I can conclude that the field has matured and broadened from the original very strong focus on chip-based capillary electrophoresis systems to encompass a new science field of an extremely interdisciplinary nature with materials physicists and analytical chemists at one end and cell & molecular biologists and clinicians at the other. The field of microfluidics with all its aspects in combination with micro- and nanotechnology and life science research is accelerating, finding new areas where the miniaturised scale really makes a difference, and this is, of course, what research in this area is all about! We can confidently look forward to another ten years of exciting developments in this scientific field.

Finally, I would like to express my thanks to all of those who helped in organising this conference. The local organising committee for their broad network to industrial supporters and exhibitors and for all the work that is not seen but is yet so necessary. The Technical Programme Committee for the seemingly endless work reading and evaluating the 650 submitted abstracts in a medieval castle in southern Sweden. This is a task on which the whole foundation of the MicroTAS conference rests. Malmö Conference Agency is greatly acknowledged and I would especially like to thank, Lars Nilsson, Anna Martinsson and Niklas Swedenborg for their excellent and hard work in making all the necessary practical arrangements come to fruition. I would like to express my deepest gratitude to Johan Nilsson and Jörg Kutter, without whom, the administration would have been a total disaster, and for their expedient and fluent processing of all protocols and endless abstract and proceedings databases.

Last but not least, I thank all of you in the μTAS-science community for compiling and contributing your cutting-edge research for these two proceeding volumes. Without you there would be no meeting!

Thomas Laurell
μTAS 2004 Chairman
July 14, 2004

Programme Committee

Thomas Laurell
(Conference Chairman)
Lund University

Jörg P. Kutter
(Conference Co-chairman)
Technical University of Denmark

Yoshinobu Baba
University of Tokushima

David Beebe
University of Wisconsin - Madison

D. Jed Harrison
University of Alberta

Klavs Jensen
Massachusetts Institute of Technology

Takehiko Kitamori
University of Tokyo

Johan Nilsson
Lund University

M. Allen Northrup
Microfluidic Systems Inc.

Shuichi Shoji
Waseda University

J. Michael Ramsey
University of North Carolina

Sabeth Verpoorte
University of Groningen

Jean Louis Viovy
Curie Institute

The Programme Committee and The Local Organising Committee kindly acknowledge the support from the following:

Gold sponsors

VINNOVA

The Crafoord Foundation

SCIENCE • TECHNOLOGY • MEDICINE

Swedish Foundation for Strategic Research

MCPT

micralyne

Silver sponsors

SAMSUNG

microplastab®
www.microplast.se

GYROS

LUND
UNIVERSITY

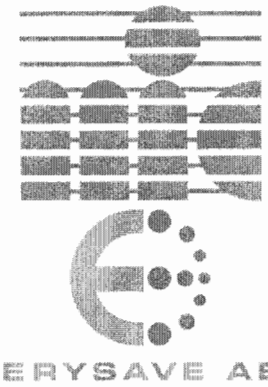

ATS MEDICAL

Bronze sponsors

silex MICROSYSTEMS

Johnson & Johnson

Caliper LifeSciences

MFSI MICROFLUIDIC SYSTEMS, INC.

Other support

analytical chemistry

Science AAAS

LAB ON A CHIP

www.rsc.org/loc

JOURNAL OF SEPARATION SCIENCE

Table of Contents
Volume 1

Day 1 – Monday, September 27, 2004

Plenary I

Monday Session A – Particle Sorting

Monday Session B – Motormolecules

Monday Session A – Cell Positioning

Monday Session B – MEMS

Monday Plenary II

Monday Poster Sessions – Applications I

Monday Poster Session – Microfluidics I

Monday Poster Session – Nanotechnology

Monday Poster Session – Others

Monday Session A – Fluid Pumping

Monday Session B – Proteomics

Day 2 – Tuesday, September 28, 2004

Tuesday Session A– Cell Culture I

Tuesday Session B – Nanochannels

Tuesday Session A – Particles

Tuesday Session B – Optical Detection

Tuesday Plenary IV

Tuesday Poster Session – Applications II

Tuesday Poster Session – Microfluidics II

SINGLE MOLECULE NANO-BIOSCIENCE

Toshio Yanagida

Graduate School of Frontier Bioscience and Graduate School of Medicine, Osaka University, 1-3, Yamadaoka, Suita, Osaka, 565-0871, Japan

1. Introduction

Biomolecules assemble to form molecular machines such as molecular motors, cell signal processors, DNA transcription processors and protein synthesizers to fulfill their functions. Their collaboration allows the activity of biological systems. The reactions and behaviors of molecular machines vary flexibly while responding to their surroundings. This flexibility is essential for biological organisms. The underlying mechanism of molecular machines is not as simple as that expected from analogy with man-made machines. Since molecular machines are only nanometers in size and has a flexible structure, it is very prone to thermal agitation. Furthermore, the input energy level is not much difference from average thermal energy, k_BT. Molecular machines can thus operate under the strong influence of this thermal noise, with a high efficiency of energy conversion. They would not overcome thermal noise but effectively use it for their functions. This is in sharp contrast to man-made machines that operate at energies much higher than the thermal noise. In recent years, the single molecule detection (SMD) and nano-technologies have rapidly been expanding to include a wide range of life science. The dynamic properties of biomolecules and the unique operations of molecular machines, which were previously hidden in averaged ensemble measurements, have now been unveiled. The aim of our research is to approach the engineering principle of adaptive biological system by uncovering the unique operation of biological molecular machines. I survey our SMD experiments designed to investigate molecular motors, enzyme reactions, protein dynamics and cell signaling, and discuss the mechanism of biological molecular machines.

2. Single-molecule detection (SMD) techniques

How advantageous is SMD for investigations? Observing and manipulating biomolecules allows their dynamic behaviors to be directly revealed, as has been demonstrated for motor proteins. Reactions of biological molecules are generally stochastic. Therefore, even if the reactions of molecules are initiated at the same time, they cannot be synchronized, so the dynamic behaviors of individual molecules are averaged and hidden in ensemble-averaged measurements. *In vivo*, biomolecules work in dynamic and complicated heterogeneous systems, involving different kinds of molecules such as cell-signaling proteins. It is difficult to quantitatively detect dynamic behaviors of target molecules in such systems by ensemble-averaged measurements. The SMD techniques are expected to overcome these difficulties and have already been successfully applied to study the dynamic properties of biological molecules such as motor proteins, enzymes, RNA polymerase and cell-signaling proteins [1, 2].

The SMD techniques are based on two key technologies for single-molecule imaging and single-molecule nanomanipulation. First, the imaging technique will be explained. The size of biomolecules and even their assemblies are in the order of nanometers, so they are too small to observe by optical microscopy. To overcome this problem, biomolecules can be fluorescently labeled and visualized using fluorescence microscopy. Single fluorophores in aqueous solution were first observed in 1995 by using total internal reflection fluorescence microscopy (TIRFM) and conventional inverted fluorescence microscopy [3]. The major problem to overcome when visualizing single fluorophores in aqueous solution is the huge background noise, which can be

caused by Raman scattering from water molecules, incident light breaking through filters, luminescence arising from the objective lens, immersion oil and dust. In this system, the evanescent field was formed when the laser beam was totally reflected by the interface between the solution and the glass. The evanescent field was not restricted to the diffraction limit of light, thus it could be localized close to the glass surface, which resulted in the penetration depth (~150 nm) being several-fold shorter than the wavelength of light. Therefore, the illumination was restricted to fluorophores either bound to the glass surface or located close by, thereby reducing the background light. Furthermore, by careful selection of optical elements, the background noise could be reduced by 2000-fold compared with that of conventional fluorescence microscopy. This made it possible to clearly observe single fluorophores in aqueous solution. Fluorescence measurements from fluorophores attached to biomolecules and ligands allow the detection of, for example, the movements, conformational changes, enzymatic reactions and cell-signal processes of biomolecules at the single molecule level.

The second key technology is single-molecule nanomanipulation. Biomolecules and even single molecules can be captured by a glass needl[e] [5-7] or by beads trapped by optical tweezers. The optical tweezers are the tool to trap and manipulate particles of 25 nm to 25 μm in diameter by the force of laser radiation pressure. The particle is trapped near the focus of laser light when focused by a microscope objective with a high numerical aperture. The optical tweezers produce forces in the piconewton range on the particles. Biomolecules are too small to be directly trapped by the optical tweezers, so they are generally attached to an optically-trapped bead. Microneedles or a bead trapped by a laser act as a spring that expands in proportion to the applied force. Thus, the force and the displacement caused by the biomolecules can be measured. The displacement of a microneedle and a bead has been determined with a subnanometer accuracy, much less than the diffraction limit of an optical measurement. This accuracy of displacement corresponds to the sub-piconewton accuracy in the force measurements. Thus, the mechanical property of biomolecules can be determined directly at the single-molecule level. Furthermore, combined with the single-molecule imaging technique, simultaneous measurements of mechanical and chemical reactions of single biomolecules are possible.

3. Movement and ATPase turnovers of biological molecular motors

The SDM techniques were first used to study molecular motors. The example discussed here is that of a microtubule-based kinesin motor, which transports organelles along a microtubule in cells. Kinesin is composed of two heavy chains, each consisting of a force-generating globular domain (head), a long α-helical coiled-coil and a small globular C-terminal domain (tail). Microtubules are cylinders comprising parallel protofilaments, which usually number 13 or 14 when reassembled *in vitro*. Movement of single kinesin molecules along a microtubule has been directly observed by TIRFM. Kinesin molecules, fluorescently labeled at the tail-end without damage, were added to microtubules adsorbed onto a glass surface in the presence of ATP (adenosine triphosphate). This demonstrated directly that a single molecule of kinesin could processively move for long distances along a microtubule without dissociating [4].

In general, the motions of molecular motors and operations of other biomolecules are fueled by the chemical energy released from ATP hydrolysis. Kinesin and myosin are both motor proteins and ATPases. To uncover how the biomolecules work using the chemical energy from ATP, it is crucial to observe the individual cycles of ATP hydrolysis by single ATPase molecules. This has been achieved using the single-molecule imaging technique TIRFM in combination with the fluorescent ATP analog, Cy3-ATP . This method was first applied to an actin-based myosin motor that is involved in muscle contraction and other cellular motility. Myosin has a similar structure to

kinesin, although it is twofold larger in size. Cy3-ATP is hydrolyzed by myosin in the same way as ATP . The rate of the biochemical cycle of ATP hydrolysis averaged for many events or individual myosin molecules was consistent with that obtained by a conventional biochemical method using a suspension of myosin.

4. Simultaneous observation of the ATPase turnover and mechanical events of an actin-based myosin motor

To investigate how the mechanical event of myosin corresponds to the ATPase cycle, the single-molecule imaging technique was combined with optical-trapping nanometry to simultaneously measure individual ATPase cycles and mechanical events of a single myosin molecule (Fig. 1). Dissociation of the myosin head from actin corresponded to the binding of ATP, and association of the myosin head with actin and generation of displacement were followed by dissociation of a nucleotide (most likely ADP). Each displacement corresponded to a single ATP molecule [5].

Understanding the process of a displacement became essential to investigating how myosin works using the chemical energy from ATP. Optical-trapping nanometry cannot resolve this process, because the displacement is determined indirectly through a long actin filament and optically-trapped beads, which have an unknown elasticity. Thus, the signal to noise ratio is not high enough to resolve the process. To overcome this problem, a more direct method combining scanning probe and single-molecule techniques has been developed. A single myosin head was attached to the tip of a scanning probe and the process of a displacement was resolved by measuring the displacement of a scanning probe with nanometer and millisecond accuracies. The results showed that a myosin head moved along an actin filament with regular 5.5 nm steps and underwent five steps to produce a maximum displacement of 30 nm per displacement (i.e. representing the ATPase cycle). As the step size coincides with the actin monomer repeat (5.5nm) and each 5.5 nm step is not directly coupled to the ATPase cycle (loose coupling), the results strongly indicate that the myosin head walks along the actin monomer repeat using biased Brownian motion . This idea challenges the widely accepted view that the movement is caused by a large conformational change in the myosin head, tightly coupled to the ATPase cycle in a one-to-one fashion (tight coupling) [6].

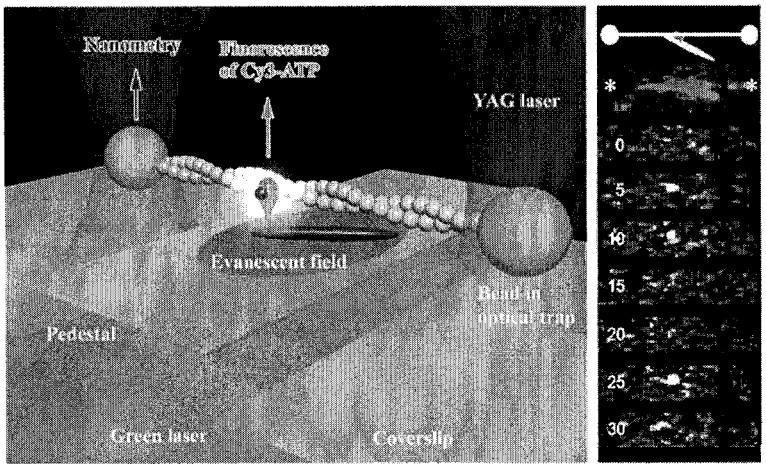

Figure 1. Single molecule imaging and optical-trapping nanometry to perform simultaneous measurements on individual ATPase cycles and mechanical events on a single myosin molecule.

5. DNA transcription

The initial steps of gene expression include the binding of RNA polymerase (RNAP) to DNA, the search for a promoter in the DNA sequence and the synthesis of RNA based on the information encoded by the DNA. These steps are central regulatory mechanisms of gene expression and have been extensively investigated. Harada *et al.* have observed single, fluorescently labeled RNAP molecules interacting with a single molecule of DNA suspended in solution using optical traps. The kinetic studies have proposed some mechanisms for promoter searching based on the results of the binding of RNAP molecules to specific and nonspecific sites on the DNA: sliding, intersegment transfer and simple dissociation and/or association reactions. This observation provides direct evidence that a sliding motion is a mechanism used for the search of promoters . The association and dissociation rate constants of RNAP could be also determined, depending on the sequence of DNA and on the mechanical strain exerted on the DNA. These values proved difficult to determine in solution because DNA molecules aggregate to form a network structure. The transcription process was directly monitored by measuring the displacement or rotation of DNA during the interaction with RNAP by manipulating DNA with optical and magnetic tweezers. One end of DNA is attached to a magnetically-trapped bead and the other is interacting with a RNAP adsorbed onto the glass surface. Rotation of DNA is determined by monitoring the rotation of the bead. The results showed that the rotation rate is consistent with high-fidelity tracking. The rotation per base pair is as much as 35□ and should, in principle, be detectable. Therefore, this method could resolve individual steps of transcription in real time [7].

6. Future perspectives

Recently, life science has made remarkable progress. This progress has been possible because of the identification of functional proteins and studies on the characteristic (structural and functional) properties of proteins as revealed by molecular cell biology, structural biology and molecular genetic approaches. The DNA sequences of not only invertebrates but also of vertebrates (including human) are now available. Thus, research is charging into the post-genomic era. In this era, we tend to emphasize the concept that the structure explains the function and we endeavor to understand the mechanisms of the proteins and molecular machines based on this concept. However, knowing the function of proteins and molecular machines is not a simple task. Moreover, we could not understand the function of these proteins even if we knew their structures. Proteins and molecular machines are not simple and their function cannot be learned in analogy to artificial machines. Proteins and molecular machines have a size in the nanometer range, and a dynamic and soft structure. In addition, the input energy to the molecular machines is comparable to thermal energy. Molecular machines function at a very high efficiency when exposed to thermal agitation. This is contrasted by artificial machines, which use much higher energy than thermal energy to work rapidly, accurately and deterministically. For such reasons, it is necessary to understand the dynamic properties of proteins themselves and their interactions to each other. The SMD techniques have been developed as techniques to directly monitor the dynamics of proteins and molecular machines and have rapidly expanded to include a wide field of biological sciences. Combined with nanotechnology from the engineering field, the SMD techniques will prove more powerful in the future. Thus, the SMD will govern and lead the future direction for research in proteins and molecular machines.

References

[1] A. Ishijima and T. Yanagida Single Molecule Nano-Bioscience. *Trends in Biochemical Sciences*, 26, 438-444 (2001)
[2] Y. Sako and T. YanagidaSingle-molecule visualization in cell biology. *Nature Review Cell Biol.* ss1-ss4 (2004)
[3] Funatsu, T. et al. Imaging of single fluorescent molecules and individual ATP turnovers by single myosin molecules in aqueous solution. *Nature* 374, 555–559 (1995)
[4] Vale, R.D. et al. Direct observation of single kinesin molecules moving along microtubules. *Nature* 380, 451–453 (1996)
[5] Ishijima, A. et al. Simultaneous measurement of chemical and mechanical reactions. *Cell* 92, 161–171 (1998)
[6] Kitamura, K. et al. A single myosin head moves along an actin filament with regular steps of 5.3 nanometres. *Nature* 397, 129–134 (1999)
[7] Harada, Y. et al. Direct observation of DNA rotation during transcription by E. coli. RNA polymerase. *Nature* 409, 113–115 (2000)

HIGH-SPEED PARTICLE SORTING: COMBINING DIELECTROPHORESIS AND FLUID FLOW

David Holmes, Mairi E. Sandison, Nicolas G. Green and Hywel Morgan
School of Electronics and Computing Science,
University of Southampton, Highfield, Southampton, SO17 1BJ, UK.

Abstract

We present a high-speed particle sorting and deflection system which is an integral part of a micro flow-cytometer chip capable of high speed detection and sorting of micron-sized particles. The device sorts particles using a combination of DEP and hydrodynamic forces. DEP focusing of particles is used to axially centre particles in a channel. Negative dielectrophoresis, together with hydrodynamic flow is used to achieve high speed particle sorting at a microfluidic T-junction.

Keywords: particle sorting, dielectrophoresis, AC-electrokinetics, micro-flow cytometry

1. Introduction

A number of particle sorting and detection devices have appeared in the μTAS literature in recent years [e.g.1-6]. Many of these devices mimic the operating principle of a bench-top flow-cytometer but on the micro-scale. Flow cytometers (or Fluorescent Activated Cell Sorters, FACS) allow counting and sorting of micron-sized particles such as cells and latex beads. The disadvantages of conventional FACS machines are the requirement for relatively large sample volumes (100μl), skilled operators and the high cost of such systems. Many of the functionalities of a FACS machine have been implemented into micro devices such as detection of fluorescence [1, 2], or scattering from particles [4]. Impedance detection has also been incorporated into micro-devices for single cell analysis [5]. Although particles can be counted at relatively high speed in these micro-devices, particle sorting speeds are generally lower.

In this paper we present a novel approach to achieve rapid particle sorting. The method uses a combination of hydrodynamic forces and dielectrophoresis to achieve high speed particle deflection and sorting. Fuhr and co-workers [6] presented DEP based cell sorting devices which used bar-shaped electrodes that deflected particles across a channel to one or other of an outlet. This method is relatively slow as the particle may have to be moved a relatively large distance across the channel to the outlet. Our device differs from previous designs in that it uses a particle positioning system to focus particles into the centre of the channel prior to the sorting junction as shown in Fig. 1. The operating principle of the device is shown in Fig. 2. Particles are centred along the axis of the channel, and arrive at the T-junction with equal probability of flowing into either outlet. A small negative-DEP deflection force is provided by the electric field configuration of the three electrodes at the gate, pushing a particle from the central stream line, so that it passes into one or other of the outlets.

2. Fabrication

Electrodes were patterned using photolithography on 500 μm thick glass substrates. Si_3N_4 insulator was deposited to all but the tips of the electrodes, a polyimide flow channel was fabricated and a second set of electrodes was aligned and bonded to form the lid. The main channel has dimensions of 40μm high and 80 μm wide, with both outlets of equal dimensions, 40μm high and 40 μm wide. Inlet and outlet holes were drilled in the lid for sample entry and exit, which was performed using pressure driven flow via an external pump. A schematic diagram and SEM of one half of the device is shown in Fig. 1.

3. Results and discussion

The initial set of focusing electrodes pushes particles into a tight axially centered beam using negative [7, 8]. This ensures that all the particles follow the same trajectory along the main channel, with the same velocity, equal to the maximum flow rate in the device. An AC voltage is applied to the sorting electrode as shown in Fig. 2, to deflect individual particles away from the equilibrium position into one of the two outlets. With a voltage of 20V peak-peak at 1MHz it was possible to deflect 6μm diameter latex beads (Molecular Probes) with velocities of $1500\mu ms^{-1}$. At this velocity the system could sort particles at a rate of 200-300 per second.

Fig. 3 shows consecutive frames taken from a video showing the tracks of individual beads being sorted within the device. The tracks appear stretched because the particles move several tens of microns during each video frame (40ms per frame). The top sequence shows a particle sorted to the left, the bottom sequence shows a particle being sorted into the right channel. The bright image present in all frames is due to beads which have adhered to the channel wall.

4. Conclusions

A device has been implemented that can sort particles using a combination of dielectrophoretic forces and hydrodynamic forces. Most particles readily undergo negative DEP at high frequencies, so that latex beads, cells or viruses could be sorted at high speed into different channels using relatively low AC voltages. The technology is easily scalable so that any number of Y or T-junction could be fabricated on a chip and particles gated into an array of different channels. In an extension to this work we have implemented this sorting principle into a full automated micro-FACS system, where fluorescently labelled particles are detected using confocal optics together with real-time control electronics to control the sorting. Combining DEP-based focussing and sorting with the advantages of sub-nL optical detection volume will enable the development of rapid configurable automated particle sorting systems. Sort speeds greater than 1000 particles per second are expected with improved designs.

Acknowledgements

This research is supported by the Emerging and Underpinning Technologies Domain of the UK MoD Corporate Research Programme. The authors would like to thank Dr Tim Cox for useful discussions.

References

[1] Schrum, D.P., *et al.*, Analytical Chemistry, **71** 4173-4177 (1999).
[2] McClain, M.A., *et al.*, Analytical Chemistry, **73** 5334-5338 (2001).
[3] Fu, A.Y., *et al.*, Nature Biotechnology, **17** 1109-1111 (1999).
[4] Pamme N., Koyama R. and Manz R. Lab on a Chip, **3** 187–192 (2003).
[5] Gawad, S., Schild L. and Renaud P., Lab on a Chip, **1** 76-82 (2001).
[6] Fiedler, S., *et al.*, Analytical Chemistry, **70** 1909-1915 (1998).
[7] Morgan, H., Holmes, D., Green, N. IEE Proc. Nanobiotechnology, **150** 76-81 (2003).
[8] Morgan H., Holmes D. and Green N. in "Electrostatics 2003" edt. H. Morgan, IoP Publications, 119-124 (2003).

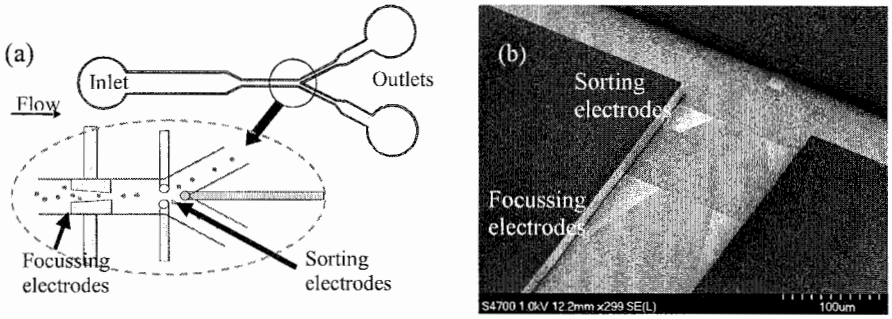

Figure 1. (a) Schematic diagram of the sorting device together with an SEM of the electrodes (b)

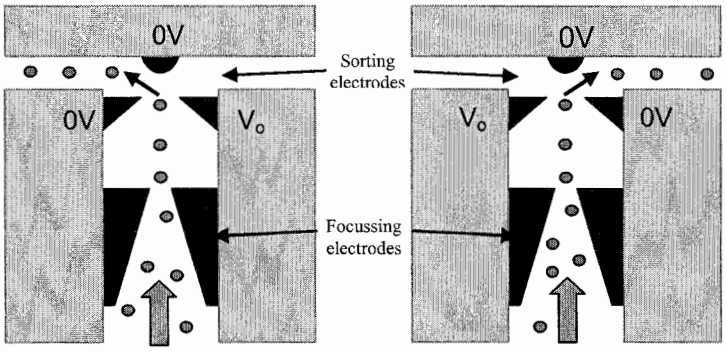

Figure 2. Diagram showing the operating principle of the sorting chip, together with the focusing and sorting electrodes. Particles are focused into a narrow beam along the axis of the channel. The combination of DEP and hydrodynamic forces at the sorting junction move particles left or right according to the voltage sequence applied to the three sorting electrodes.

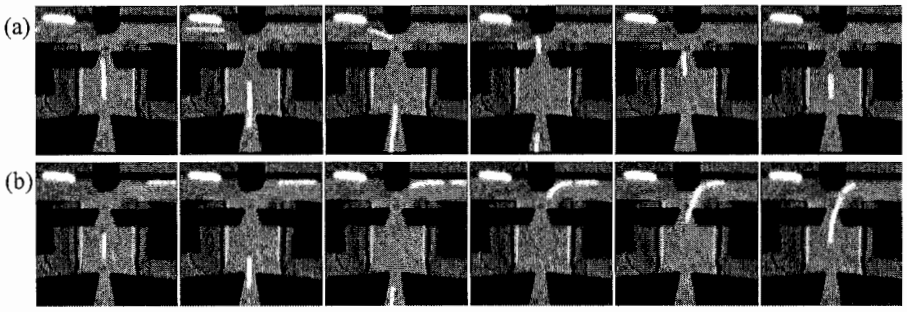

Figure 3. Successive sequence video images (40ms time interval) showing particle trajectories in the chip. In (a) a particles are sorted to the left, whilst in (b) particles are sorted to the right. The particles appear elongated because they move a considerable distance in a single video frame. V_o = 20Vpp at 1MHz.

CONTINUOUS PARTICLE SEPARATOR BASED ON PERIODICAL DEP ELEMENTS

Stefan Kostner[1], Jeroen H. Nieuwenhuis[1], Edeltraud Svasek[2], Peter Svasek[2], Arthur Jachimowicz[1] and Michiel J. Vellekoop[1]

[1]*Institute of Sensor and Actuator systems (ISAS), Vienna University of Technology, Gusshausstrasse 27-29, A-1040 Vienna, Austria*

[2]*Ludwig Boltzmann Institute of Biomedical Microtechnology, Vienna, Austria*

Abstract

In this work a novel device for continuous separation of particles based on dielectrophoresis (DEP) is presented. The dependency of the dielectrophoretic effect on the particle radius is exploited to separate particles of different size in a microfluidic channel. In the device a separation is established by forcing the particles on trajectories of different mean velocity in a parabolic flow profile of a pressure driven flow.

Keywords: dielectrophoresis, particles, separator

1. Introduction

We present a continuous particle separator using periodical dielectrophoresis (DEP) elements (Fig. 1). Dielectrophoresis is the effect that a polarizable particle experiences a force when exposed to a non-uniform electric field. As the particles flow through the separation channel, dielectrophoretic forces are applied to move them up and down, which results in trajectories as shown in Fig. 2. The amplitude of this trajectory strongly depends on the particle size. Since the velocity profile of the liquid in a pressure driven flow is parabolic, the flow-speed of a particle depends on its vertical position in the channel. Larger particles (for which the amplitude of the trajectory is larger) will now have a lower average velocity, which results in longer retention time than smaller particles. At the end of the channel there will be a separation of particles depending on their diameter. This device does not use gravity as a parameter for separation, as in other devices e.g. [1].

2. Theory

For the description of the particle behavior dielectrophoretic and hydrodynamic forces are taken into account. Using a dipole approximation for a polarized particle in an electric field and utilizing the so-called Stokes Approximation for the hydrodynamic drag, the forces acting on a particle read:

$$F_{DEP} = 2\pi\varepsilon_l R^3 K \nabla E_0^2$$

$$F_{DRAG} = 6\pi\eta R(v_l - v_p)$$

where $K = (\varepsilon_p - \varepsilon_l)/(\varepsilon_p + 2\varepsilon_l)$ is the so-called *Clausius-Mossotti Factor* and ε_l and ε_p are the permittivities of liquid and particle respectively. R is the particle radius, E_0 is the local electric field, η is the viscosity of the liquid and $(v_l - v_p)$ is the difference of liquid and particle velocity. The equilibrium between these expressions and the inertia force $F_I = m_p dv_p / dt$ as well as the buoyancy force is used in a model to determine the trajectory of a particle in a channel of given electric and flow field distribution.

3. Device

The device consists of two glass slices bonded together with SU-8 [2], which also defines the channel dimensions. The liquid connections are defined by through holes in one of the glass wafers. The DEP electrodes (Cr/Au) are 80μm wide.

A simple particle trap structure was used to accumulate and periodically release the particles, allowing for continuous operation of the device. So, both sample injection and separation are controlled electronically.

A dynamic simulation model has been developed to optimize the electrode structure and to estimate the voltage necessary for trapping the particles. The force equilibrium between dielectrophoretic-, drag- and inertial forces is calculated from which the particle trajectory and retention time is determined (Fig. 2). The difference in retention time is a measure for the separation efficiency.

The separation channel has a periodic electrode structure to generate strong non-uniform electric fields. Because the electrodes are applied on both top and bottom the particles are forced to follow a trajectory moving up and down periodically in the channel, minimizing the influence of gravity (Fig. 2).

4. Results and discussion

Polystyrene particles of 8 and 15 μm diameter suspended in de-ionised water were pumped through the device using a syringe pump. For the characterization of the device the retention time of these particles was measured separately using a manually triggered stopwatch computer program.

At a DEP voltage of 5.5 V (RMS, 1 MHz) the larger particles show an average 25% longer retention time than the smaller particles, which proofs the concept. A histogram for several measurements is shown in Fig. 4. The results presented in this paper can be assumed to contain an error caused by the reaction time of the manual trigger process (estimated error ± 0.1s). Therefore, the measurements are expected to show an even better distribution if a fully electronic (and more accurate) detection would be applied.

Additional measurements were carried out using a particle sample mix containing 8 and 15μm particles. Using a similar stopwatch program as mentioned above the time between release and arrival of the first small and the first large particle was recorded. These measurements confirm the results shown in Fig. 4.

In addition to separation of particles based on their size, our setup also permits separation on the basis of dielectric constant and electrical conductivity. This topic is part of current investigations.

5. Conclusions

We have simulated, designed and fabricated a novel particle separation device based on periodic DEP elements. Our first measurements demonstrate that particles of 8 and 15μm show significant differences in retention time (25%) at a DEP voltage of 5.5 V (RMS, 1 MHz).

References

[1] H. Sano, H. Kabata, O. Kurosawa, M. Washizu, "Dielectrophoretic chromatography with cross-flow injection", The Fifteenth IEEE International Conference on Micro Electro Mechanical Systems, 2002, 20-24 Jan. 2002, pp. 11-14

[2] P. Svasek, E. Svasek, B. Lendl, M.J. Vellekoop, "SU-8-Based Fluidic Devices", proc. of Eurosensors XVII, September 21-24, 2003, Guimaraes, Portugal, 2003, pp. 283-286

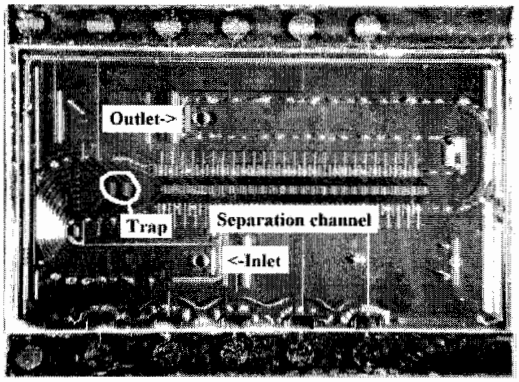

Figure 1. Particle separation chip (1.5x2cm²). Channel height 70µm, width 1mm, length 10.4 mm. The separation channel has 26 DEP elements.

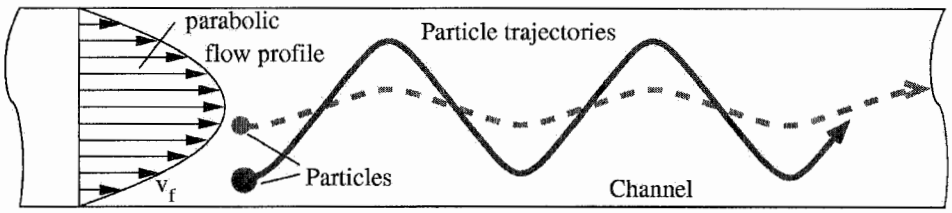

Figure 2. Operation principle of the separation channel. Hydrodynamic drag moves the particles in horizontal direction while DEP forces move them up and down. The dependency of the trajectory amplitude on the particle size is exploited to establish a separation.

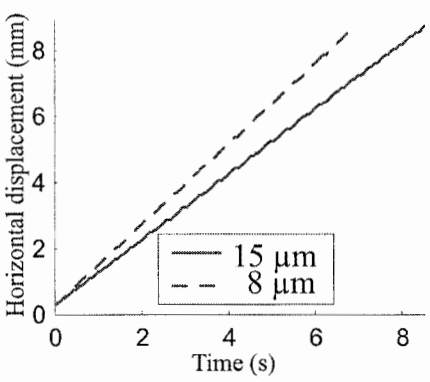

Figure 3. Simulation results for the horizontal displacement of 8 and 15µm particles.

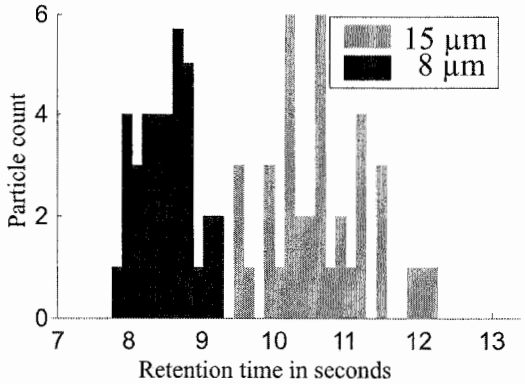

Figure 4. Histogram of retention time measurements for different particle sizes. 15µm particles show an average 25% longer retention time.

STUDY OF HIGH SPEED ACOUSTIC SEPARATION IN MICRO-CHANNELS USING μ-PIV

Holden Li, Vipin Vitikkate, Thomas W. Kenny
Department of Mechanical Engineering, Stanford University, Stanford, California 94305, USA

Abstract

In this paper, we report the behavior of suspended particles comparable to human blood cells under the influence of an ultrasonic acoustic field, using micron-resolution particle image velocimetry (μ-PIV). This work is in progress towards the design of an integrated micro-channel structure for cell separation in the microscale regime. The acoustic separation method directly differentiates particles based on their size at low power (less than 100 mW) and with small sample sizes (tens of micro-liters). Experimental results show that particles of different sizes can be separated by a careful design of a continuous flow micro-channels system. We have demonstrated the capability of separating over a million particles in less than 5 minutes.

Keywords: acoustic separation, particle image velocimetry, micro-channels, μ-TAS

1. Introduction

Centrifuges are typically used to separate various components of the whole blood in laboratories. This method has proven to be fast and effective in large-scale operation, with an acceleration field up to 10,000G. But the dependence of the radius of rotation prevents further miniaturizing a centrifuge into a micro-scale device. In order to realize a μ-TAS that can diagnose human health with low power consumption and low sample size, a robust and high speed separation mechanism is desired. Various other methods of micro-separation on cells have also been proposed over the years, like micro-filtration [1], magnetic separation [2], electrophoresis [3], di-electrophoresis etc. Each of these methods has its own merits and disadvantages when miniaturized to the micro-scale.

In this paper, we revisit an old technology [4] of using ultrasonic standing waves to separate different sizes of particles. The particles are concentrated at the pressure nodes of a static acoustic field based on size, density and compressibility contrast with the surrounding medium. This separation mechanism has already been proven to be effective and fast [5, 6]. However, acoustic separations often required large apparatuses with characteristic dimensions of at least centimeters and only separations of particles from the medium were demonstrated, but particles of different properties were not differentiated. There has been recent interest of repeating this method in micro-channels with diameter of less than 1mm and for separation of particles based on their densities [7].

μ-PIV is useful for understanding the behavior of different particles under the influence of acoustic pressure field and have been used in these studies to extract quantitative measurements.

2. Theory

Two dominant forces act on the suspended particles when subjected to an acoustic pressure field, namely the acoustic force and Stokes drag (ignoring diffusion, Brownian displacement and gravity which would only come into play if the acoustic field was orthogonal to them). With continuous flow in the micro-channels, the particles also experience advective forces due to the motion of the bulk liquid that carries them along. Yoshioka et al [8] proposed that the acoustic force, F_{us}, acting on a spherical particle is

$$F_{us} = \left(\frac{P_o^2 V_p \beta_f \pi}{2\lambda} \right) \left(\frac{(5\rho_p - 2\rho_f)}{(2\rho_p + \rho_f)} - \frac{\beta_p}{\beta_f} \right) \sin\left(\frac{4\pi y}{\lambda} \right) \quad (1)$$

where P_0 is the acoustic pressure, V_p is the volume of the particle, ρ_f, ρ_p, β_f and β_p represent the density and compressibility of fluid and particles respectively. The wavelength is represented by λ and y is the displacement of the particle in the pressure field.

At any instant, the acoustic force is balanced by the drag force in Equation 1, and this allows us to use velocity measurements to extract the acoustic force as a function of position. Based on this model, particles with dimensions comparable to the white blood cells (10 μm in diameter) will be concentrated on the pressure nodes about six times faster than particles comparable to a red blood cell (4 μm in diameter). We will utilize this temporal contrast to separate particles by size.

3. Experimental Setup

To understand the forces acting on particles (polystyrene beads from Duke Scientific), μ-PIV [9] is used to obtain measurements of the velocity fields. The experimental setup includes the epi-fluorescent microscope (Olympus), camera system (COHU), image capturing DAQ card (National Instrument), LabView program and Matlab software for cross-correlation calculations. For investigating the two particles separation, image capture with one wavelength is not enough. A special epi-fluorescent microscope (Carl Zeiss Axioscop 2) is used to simultaneously capture both particles, which fluoresce at different wavelengths.

4. Results and discussion

The experiments investigate the effects of varying particle size, acoustic pressure and bulk flow rate in the micro-channels. The particles range in diameter from 3 to 10 μm and the PZT voltage that provides the acoustic pressure, operating from 18 to 48 V at a frequency of 3 MHz. The flow rate is varied from 0.5 to 3 μl/min from an external pump. Based on the μ-PIV experimental results, the velocity profile of the particles due to the ultrasonic acoustic standing waves is obtained as shown in Figure 1. Particles further away from the pressure node have higher velocities than those near the nodes. It also has demonstrated that by increasing the particle sizes would lead to an increase in the acoustic force on the particles as shown in Figure 2.

The next set of experiments involves the design of this separation mechanism based on a chosen acoustic frequency, operating acoustic pressure and flow rate. By adjusting the parameters, meandering angles and flow rate of the micro-channels geometry, this experiment has shown that bigger particles are concentrated in the central stream and separated from smaller ones (Figure 3).

5. Conclusions

We have demonstrated the ability to separate different size particles with similar mechanical properties using ultrasonic standing waves. Velocity measurements are obtained with μ-PIV to shed light on the forces acting on the particles under acoustic pressure field. Future work will emphasize further miniaturization and integration within a handheld instrument.

6. Acknowledgement

We thank Stanford Center for Integrated System for sponsoring this project and Professor Juan Santiago of Stanford Microfluidics Lab for the guidance and support on the μ-PIV.

References

[1] T. Ujiie, et al, "Microfabricated separator and manipulator of blood cells for health care", Microprocesses and Nanotechnology Conference, 2000, pp. 28–29.

[2] K. Han, et al, "Paramagnetic capture mode magnetophoretic microseparator for blood cells', Hilton Head 2004, pp. 103-104.

[3] T. Ichiki, et al, "Microfabricated separator and manipulator of blood cells for health care devices", Microprocesses and Nanotechnology Conference, 2001, pp 190-191

[4] U.S. Patent US2215484, 1940.

[5] M. Saito, et al, "Ultrasonic manipulation of locomotive microorganisms and evaluation of their activity", Journal of Applied Physics Vol 92(12) pp. 7581-7586. 2002

[6] C.Lee, et al, "Low voltage high-speed ultrasonic chromatography for microfluidic assays", Hilton Head 2002

[7] F. Petersson, et al, "Particle Flow Switch Utilizing Ultrasonic in Microfluidic Channels", Micro TAS 2003
[8] K. Yoshioka, et al, "Acoustic radiation pressure on a compressible sphere", Acustica 5, 1955
[9] C. Meinhart, et al, "A PIV Algorithm for Estimating Time-Averaged Velocity Fields." Experiments in Fluids, Vol. 25, Iss. 4, pp. 316-319

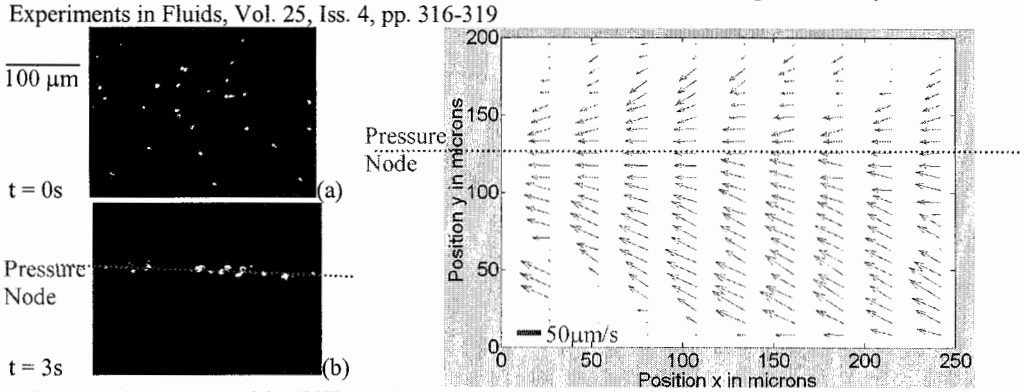

Figure 1: Fluorescent particles (20X magnification) are concentrated on the pressure node under influence of acoustic pressure at 3MHz. Pixel array is 656 by 492. 7 µm diameter particles are first randomly distributed and moved in the channel with a bulk flow rate of 1 µl/min. Particle velocity field of a region of the image is plotted on the right. Location of pressure node is represented with a dotted line.

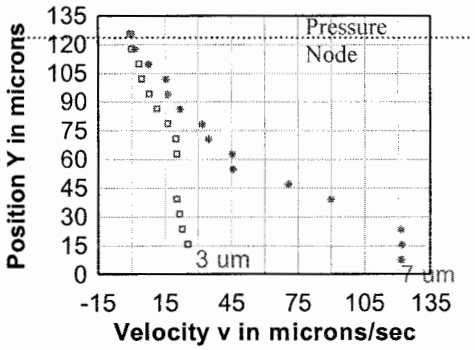

Figure 2: Plot of velocity in the y-direction versus distance across the micro-channel obtained from µ-PIV measurement of 3 and 7 µm size particles at 48V applied to the PZT at 3MHz with a bulk flow rate of 1ul/min. [Note: The velocity is obtained from the velocity field plot from µ-PIV and it has discounted the advective flow in the micro-channels.]

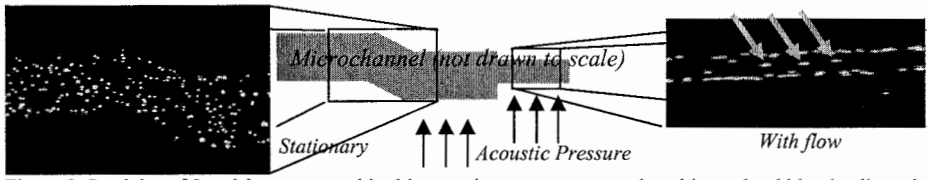

Figure 3: Particles of 8 and 3 µm are used in this experiment to represent the white and red blood cells under epi-fluorescence microscopy with 5X magnification. The flow rate is set at 3 ul/min and the ultrasonic acoustic frequency is running at 3.3MHz. Particles are mixed randomly upstream as shown in the left picture (which was taken at zero flow rate). Larger particles (pointed by arrows) are concentrated in the middle of the micro-channels and separated from the smaller ones further downstream. The oblong shapes of particles are due to streaking effects due to limitations of camera system. Fewer 8 µm particles are present in the solution since white blood cells make up only a small fraction of the whole blood.

UNIDIRECTIONAL TRANSPORTATION OF NANO BEADS BY KINESIN ON MICROTUBULES WELL-ORIENTED IN A MICRO CHANNEL

Ryuji Yokokawa[1], Shoji Takeuchi[1], Takahide Kon[2], Masaya Nishiura[2], Kazuo Sutoh[2], Hiroyuki Fujita[1]

[1]CIRMM/IIS, The University of Tokyo, 4-6-1, Komaba, Meguro, Tokyo 153-8505, Japan
[2]Graduate School of Arts and Sciecnces, The University of Tokyo, 3-8-1, Komaba, Meguro, Tokyo 153-8902, Japan

Abstract

Microtubules were immobilized inside a microfluidic channel chemically with the plus end oriented to one direction. We have also succeeded to transport kinesin-coated beads of 320 nm in diameter unidirectionally in the channel.

Keywords: kinesin, microtubule, orientation, hybrid nano transport system, biomolecular linear motors

1. Introduction

Inspired by vesicle transport in a biological cell, we aim to build a bio hybrid nano transport system based on biomolecular linear motors which enable the manipulation of micro/nano structures without fluid flow or electrokinetic force [1]. A kinesin, a motor molecule, transports an object from the minus end to the plus end of a microtubule by hydrolyzing adenosine 5'-triphosphate (ATP). In order to realize the unidirectional transport using molecules, microtubules that serve as rail molecules must be functionally oriented in the designated direction.

Some biology groups have already published on orientation techniques of microtubules [2-4]; those describe orientation method and some experimental results. However, the quantitative analysis of the technique from the engineering point of view was not performed because they focus on biological interests. Here we measure the orientation yield quantitatively in order to optimize the process condition for the unidirectional conveyance of micro/nano objects.

2. Experimental

We prepared a channel (width: 2 mm, depth: 107 μm, length: 40 mm) with two coverslips to establish the orientation process, because the process can be visualized by a dark-field microscope in millimeter-scale. The coverslip was bonded with another glass plate using double-sided adhesive tape as spacers (Fig. 1(1-3)). Fig. 1(a) shows the actual device. The outlet was connected to a syringe pump to generate a steady flow, which contribute to the easy buffer replacement in a channel even when the channel is on a microscope stage as shown in Fig. 1(b). The channel can be miniaturized down to micrometer-scale (width: 500 μm, depth: 20 μm, length: 30 mm) by the wet etching of a slide glass with

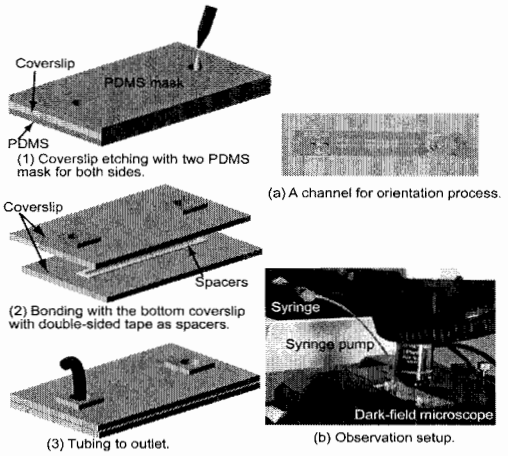

Figure 1. Fabrication process of a glass channel for the orientation test.

a PDMS mask instead of using spacers [5].

3. The orientation process

We have utilized the gliding assay in a buffer flow to orient microtubules with some modifications from [4]. Fig. 2(1) shows the direction of a buffer flow in a channel during the orientation process. Figs. 2(2) to (6) are close-up illustrations of the channel surface. The movement of microtubules is shown by arrows of which heads correspond to the minus end of microtubules. The fluid force orients microtubules parallel along the flow on a kinesin-coated surface, but the functional orientation of the plus/minus polarity cannot be realized as shown in Fig. 2(2). The pulse injection of ATP (1 mM) induces random movement of microtubules as called gliding assay (Fig. 2(3)), but the continuous flow removes microtubules gliding upstream, while almost all the microtubules gliding downstream remained on the kinesin-coated glass surface (Fig. 2(4)). Microtubules in this step were visualized by the dark-field microscope in Fig. 3(a). Buffers including 0.1 % glutaraldehyde and 0.1 M glycine are injected with intervals for incubation in order to fix oriented microtubules (Fig. 2(5)). Oriented and immobilized microtubules are shown in Fig. 3(b). After washing out chemicals, kinesin-coated beads are injected in the channel and trapped on microtubules. Injection of ATP starts bead transportation. When the plus end and the minus end of microtubules are placed upstream and downstream, respectively, beads move upstream unidirectionally (Fig. 2(6)).

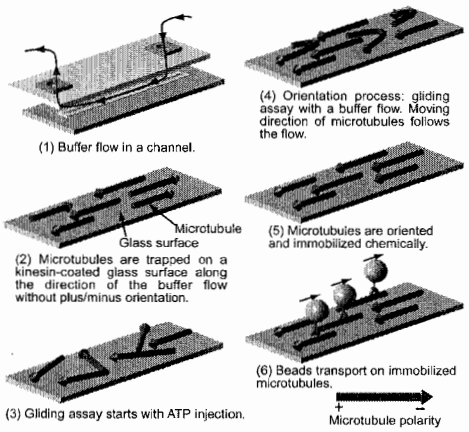

Figure 2. The orientation methodology of microtubules by a buffer flow. An arrow indicates a moving microtubule at gliding assay, which means the arrowhead is the minus end of the microtubule.

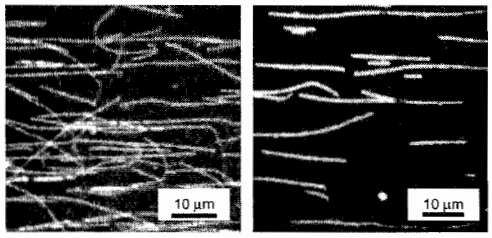

Figure 3. Microtubules on kinesin coated surface (a) during and (b) after the orientation process.

4. Results and discussion

The bead movement was captured by a differential interference contrast microscope as shown in Fig. 4(a). Fig. 4(b) is a superposition of 10 pictures with 2-second intervals between shots to visualize the unidirectional movement of beads. Fig. 4(c), an expansion of the framed area in (b), clearly shows that beads are unidirectionally transported to the right-hand side. We have investigated the relationship between the orientation yield and the buffer flow rate (Fig. 5(a)). The ratio of beads moving upstream to all the moving beads is defined as the orientation ratio to evaluate how microtubules are functionally oriented. As a control experiment the ratio of 50.3 % was measured on the physically aligned microtubules, which means beads were equally transported bidirectionally. The ratio reached about 95 % over the flow rate of 8 µm/s. The relationship between the flow rate and the density of microtubules immobilized on a glass surface is shown in

Fig. 5(b). The higher flow rate increases the orientation ratio but decreases the microtubule density. The flow rate of 8 μm/s is the best both for the orientation and the microtubule density due to their trade-off. Another important factor was the concentration of kinesin in a buffer to coat the glass surface with kinesin molecules. The lower concentration of 4 μg/ml did not yield enough microtubule density, because the flow removed almost all the microtubules. The concentration of 40 μg/ml brought tight binding between microtubules and kinesin during the orientation process. The orientation ratio was also successfully measured as 95.1 % in the micrometer-scale glass channel.

5. Conclusion

We have optimized the buffer flow rate and the protein concentration to realize the unidirectional transport of kinesin-coated beads in the millimeter-scale channel. Based on these results microtubules were also oriented in the micrometer-scale channel in which 95.1 % of moving beads moved to the designated direction. Multiple channels coated with oriented microtubules will be integrated to realize 2-D transport by kinesin motors.

References

[1] R. Yokokawa *et al.*, J. Microelectromech. Syst., to be published

[2] Y. Hiratsuka *et al.*, Biophys. J. **81**, 1555–1561 (2001)

[3] J. Clemmens *et al.*, Langmuir, **19**, 1738-1744 (2003)

[4] I. Prots *et al.*, Cell Biol. Int., **27**, 251–253 (2003)

[5] R. Yokokawa *et al.*, "Ultra-smooth Glass Channels Allowing Non-fluorescent Observation of Bio-molecules by Microscopes", μTAS2004 (2004)

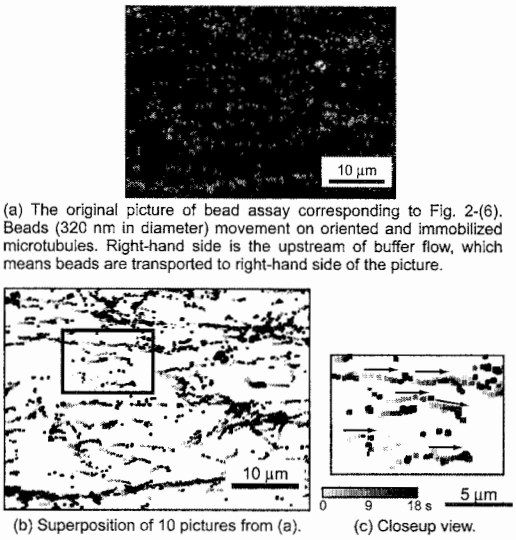

(a) The original picture of bead assay corresponding to Fig. 2-(6). Beads (320 nm in diameter) movement on oriented and immobilized microtubules. Right-hand side is the upstream of buffer flow, which means beads are transported to right-hand side of the picture.

(b) Superposition of 10 pictures from (a). (c) Closeup view.

Figure 4. Moving direction of beads.

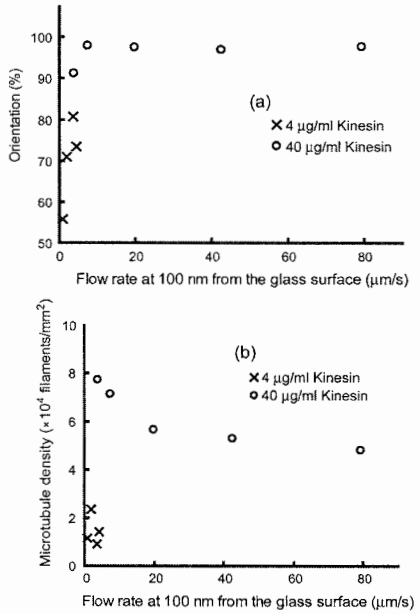

Figure 5. (a) the orientation ratio and (b) the microtubule density are measured in relation to flow rate at 100 nm from the glass surface.

NANOSCALE TRANSPORT AND ASSEMBLY WITH MOTOR PROTEINS AND MICROTUBULES

J. M. Bauer[1], A. K. Boal[2], S. B. Rivera[2], R. G. Manley[1], G. D. Bachand[2], J. Liu[3], R. P. Manginell[1], B. C. Bunker[2]

[1]*Micro Analytical Systems, Sandia National Laboratories, Albuquerque, NM, USA*
[2]*Biomolecular Materials and Interfaces, Sandia National Laboratories, Albuquerque, NM, USA*
[3]*Chemical Synthesis and Nanomaterials, Sandia National Laboratories, Albuquerque, NM, USA*

Abstract

A unique platform for the biomimetic transport of nano- and microscale materials with microtubules and motor proteins has been developed. The platform contains chemically distinct materials, fluidic and optical access on opposite sides of the platform, and the ability to incorporate electronics. The chemically distinct materials (gold and silicon dioxide) allow deposition and confinement of the biomolecular motor kinesin through selective formation of protein anti-fouling monolayers on the gold surfaces. Additionally, we have designed a custom motion-tracking program to evaluate the effectiveness of the platform in directing microtubule (and microtubule-transported cargo) motion.

Keywords: microtubules, motor proteins, motion tracking, directed transport

1. Introduction

Transport mechanisms in living systems can be used to manipulate nanoscale materials in artificial environments. For example, the movement of nanomaterials could generate macroscale changes in electrical or optical properties. With the ability to continuously manipulate materials, one could imagine applications such as reconfigurable electric or optical systems. In nature, motor proteins "walking" on microtubules transport intracellular cargoes of vesicles and genetic material. Microtubules are filament-like tubular protein structures, 25 nm in diameter with lengths between 1 and 1000 μm, depending on polymerization conditions. Hydrolysis of adenosine triphosphate (ATP) produces ordered conformational changes in motor proteins, which results in the protein walking along the length of the microtubule at the rate of approximately 1 μm/s.

Previous work has demonstrated the transport of cargo and control of microtubule motion[1,2]. We are attempting to expand these efforts and build a complete (electrical or optical) system that incorporates all of these elements. In particular, we are investigating the efficiency of various topographical features in controlling the motion of cargo-laden microtubules in microfluidic devices. A custom motion-tracking program will quantify the interaction of microtubules with the various topographical features.

Anti-fouling coatings for selective deposition of motor proteins have been used on structures fabricated from photoresist[3]. However, a noble metal surface, such as gold, is more chemically uniform than a photoresist surface and will produce a more homogeneous monolayer than is possible with photoresists. The chemical uniformity of the gold will also allow a more homogeneous mixed monolayer containing both anti-fouling and targeted binding components to selectively attach nanomaterials such as proteins and cells.

2. Platform characteristics

In our current system, microtubules glide across a silicon dioxide surface coated with kinesin motor proteins (Figures 1&2). The surface topography consists of gold features patterned on an oxide surface. The gold features have been patterned with either a lift-off technique or by coating channels etched in the substrate with gold and then milling the gold from the channel bottoms. A glass coverslip serves as the device top. The gold features are selectively coated with an anti-

fouling monolayer of alkane thiols, which prevent the kinesin from adsorbing to the gold. This surface treatment confines the microtubule motion to the oxide surface (Figure 3)[4]. A microtubule collision with a topographic feature will thus lead to a redirection of the microtubule motion.

With the fluidic and optical access on opposite sides of the platform, various solutions can be introduced and observed simultaneously. Simultaneous observation and fluidic access is particularly important in studies that involve the introduction of microtubules and/or cargo to a specific spatial location.

3. Motion-tracking program

A custom motion-tracking program has been developed to quantify the effectiveness of various topographic features in directing microtubule motion. The program measures the length, velocity, and trajectory of a number of microtubules simultaneously. A sample result of this analysis for the test case of microtubules moving in a flow cell without topographic features is shown in Figure 4. As expected, the absence of topographic features produces no preferred direction of microtubule motion. Relationships between the redirected motion and various feature geometries (such as channel width, shape, and periodicity) are currently being examined.

4. Conclusion

A unique platform for the study of microtubules and motor proteins has been presented. This platform will eventually be expanded to include mixed monolayers on the topographic features (to exclude motor protein attachment while allowing cargo attachment) and electrical connections that will be modified by the motor protein/microtubule system. Examining the motion of microtubules interacting with various platform surface features over time will yield the relative efficiencies of those features in directing microtubule and cargo motion. The results of these studies will allow optimization of system level assembly and reconfiguration of nanomaterials.

Acknowledgements

Sandia is a multiprogram laboratory operated by Sandia Corporation, a Lockheed Martin Company, for the United States Department of Energy's National Nuclear Security Administration under contract DE-AC04-94AL85000. This work was partially supported by the Division of Materials Sciences and Engineering in the Department of Energy Office of Basic Energy Sciences, Sandia's Laboratory Directed Research and Development Office, and the Defense Science Office of the Defense Advanced Research Projects Agency.

References

[1] K. J. Bohm, R. Strake, P. Muhlig, E. Unger, *Nanotechnology*, **12**, 238-244 (2001).
[2] J. Clemmens, H. Hess, J. Howard, and V. Vogel, *Langmuir*, **19**, 1738-1744 (2003).
[3] Y. Hiratsuka, T. Tada, K. Oiwa, T. Kanayama, T. Q. P. Uyeda, *Biophys. J.*, **81**, 1555-1561 (2001).
[4] A. K. Boal, J. M. Bauer, S. B. Rivera, R. G. Manley, R. P. Manginell, G. D. Bachand, and B. C. Bunker, in preparation.

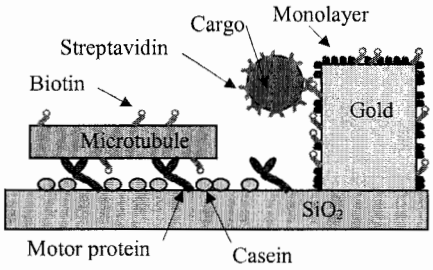

Figure 1. Schematic depicting the motion of microtubules in our microfluidic platform. Gold obstacles (which can be isolated structures or fluidic channel walls) are first coated with a monolayer to prevent motor protein absorption. Then, casein partially passivates the silicon oxide, allowing the attachment of active kinesin to the substrate. Microtubules introduced to the system will then be transported across the surface by the kinesin motor proteins. A chemical linkage, such as biotin-streptavidin, allows cargo transport.

Figure 3. Fluorescently tagged microtubules confined to lithographically defined microfluidic channels by monolayers on the channel walls. Channel width = 10 μm.

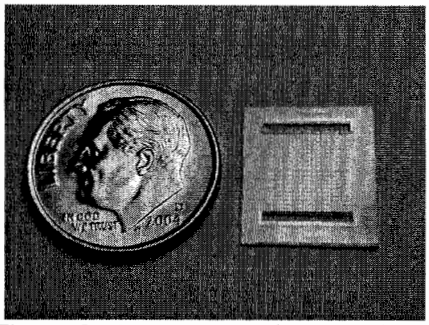

Figure 2. An image of the microfluidic platform. The through holes at the top and bottom allow fluidic access from the back and optical access from the front of the platform. For testing, the device is mounted on a coverslip.

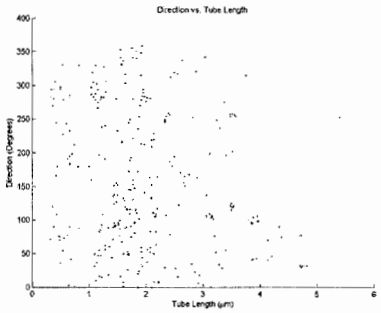

Figure 4. Microtubule direction versus tube length in a platform without topographic features. Without features to direct microtubule motion, there is not a preferred direction/orientation of motion.

WINDING UP SINGLE F_1-MOTOR PROTEIN IN FEMTOLITER CHAMBERS: THE MOLECULAR PULL-BACK CAR.

Y. Rondelez[1], G. Tresset[1], Y. Kato-Yamada[3], H. Fujita[2], S. Takeuchi[2], H. Noji[2,*].
[1] LIMMS-CNRS/IIS, [2] IIS, University of Tokyo, 153-8505 Tokyo
hnoji@iis.u-tokyo.ac.jp

Abstract

F_1 enzyme is known as the world smallest rotary motor, but its real biological function, namely the synthesis of ATP, has remained elusive. We describe the use of polydimethylsiloxane (PDMS) micrometer chamber arrays for the single molecule study of the efficiency of this molecular motor/generator. The patterned PDMS device allowed the enclosing of extremely small volumes of water solution. This packing was stable and tight. In this unprecedently small volumes (fL), activity of a unique enzyme results in rapid detectable (μM) changes in the concentration of its substrates and products. We employed this technique to follow directly for the first time the ATP consumption of F_1 as it produces mechanical work. As expected, the enzyme was found to function with a yield close to 100 %. We then turned to the ATP-generating role of F1. We attached a magnetic bead to the protein and used magnetic tweezers to force backward rotations of the enzyme. In the presence of ADP and Pi, we could detect the synthesis of ATP upon mechanical rotation at 10 Hz. As all the system was trapped in a very small volumes this ATP could not diffuse and F_1 itself served as a probe to measure the amount of produced ATP. The mechanochemical coupling was found very tight.

Keywords: Molecular motors, PDMS, Single molecule, ATP synthesis, Femtoliter.

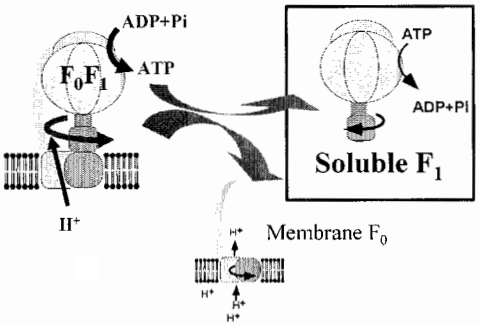

Fig. 1. F_0F_1 molecular machinery. F_0 convert the proton gradient into a mechanical torque which is transmitted to F_1. This one use the mechanical energy input to drive the synthesis of ATP against the thermodynamic potential. This process is reversible. Isolated F_1 only hydrolyse ATP to produce a mechanical torque.

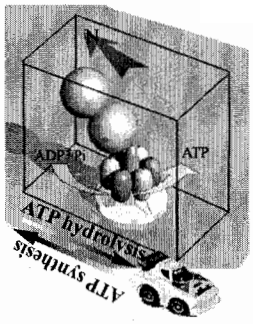

Fig. 2. A magnetic bead, fixed to F_1, allowed us to input mechanical energy through forced backward rotation. During this "pull-back" stage, ATP is produced and trapped in the femtoliter container. After release of the magnetic field, stored ATP fuels the spontaneous rotation and increases its speed.

1. Introduction

F_0F_1 enzymatic complex is responsible for the most abundant bioreaction in cells, i.e. the synthesis of ATP, the universal fuel of living organisms (Fig. 1). It is also a beautiful mechanical machinery at the nm scale [1]. It has already been demonstrated that the isolated F_1 part is able to

convert the energy released by ATP hydrolysis into a mechanical torque [2]. Since the real biological role of F_1 is not ATP hydrolysis but its synthesis from ADP and Pi, it is generally assumed that, like its electric counterparts, the enzyme functions in a highly reversible fashion, being both a motor and a generator. This last process has yet to be demonstrated quantitatively at the single molecule level [3]. We present here a microdevice approach that allowed us to observe directly the ATP-synthesis reaction under mechanical energy input to a single enzyme (Fig. 2). This experiment was achieved by the use of magnetic tweezers to mechanically rotate [4] F_1 in the backward direction, and femtoliter PDMS chambers to trap and accumulate the synthesized ATP. When the magnetic field is released, the enzyme uses this ATP to spontaneously resume its rotation in the reverse direction, at a speed that reveals the amount of produced ATP.

3. Experimental

Arrays of small cylinders were fabricated from a 1.5 μm thick SOI wafer by ICP-RIE. An aluminum layer was evaporated onto the SOI to serve as a mask for plasma etching and patterned by using 0.5 μm thick photoresist (S1805). PDMS sheets were obtained from this master which had been treated with CHF_3 plasma (100 nm thick) to facilitate the removal. The experiments were conducted in a 50 mM phosphate buffer pH=7.5, in the presence of 0.05 to 0.1 mg/mL BSA, 50 mM KCl, 2 mM $MgCl_2$. For ATP synthesis experiments 10 mM Pi and 100 μM ADP were added. Thermophilic mutant F_1 was expressed in *E. Coli*. It beared 6 His-tags on the N-Terminus of the α and β subunits and two biotins on the γ rotor part. This allowed the attachment of the protein to both the Ni-NTA modified glass slides and the streptavidin-coated plastic (or magnetic) beads. Sealing was obtained by simply pressing vertically the PDMS against the glass plate.

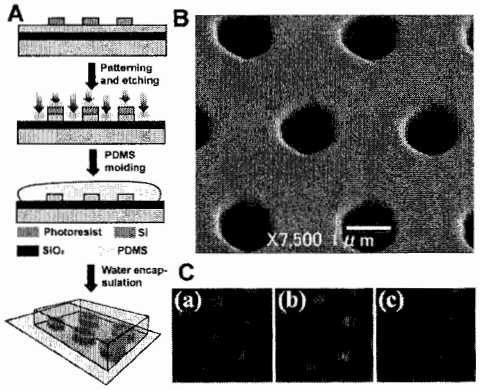

Fig. 3. (A) Microchamber arrays are fabricated in a PDMS sheet by molding from a patterned SOI wafer. (**B**) Nice features are obtained at the micrometer scale. The depth and the internal volume of the chambers shown here are 1.5 μm and 1.4 fL. (**C**) a solution containing a fluorescent dye is enclosed in the chamber (a). Then using a focused light beam, the dyes of only one chamber are bleached. (b) shows the fluorescent record just after bleaching, while (c) is taken 20 minutes later. No diffusion to the bleached chamber could be observed.

4. Results and discussion

We have designed variously sized microchambers using PDMS (Fig. 3). This polymer combines several advantages: it is soft and easy to shape, transparent to light, and doesn't interact with biological materials. We first checked the possibility to enclose durably, and without diffusion or leaks, very small volume of water in the hydrophobic chambers formed by the union of the patterned PDMS layer, and glass plate. Under the condition used, a lifetime of at least 2 hours is observed before the chambers begin to dry. When a fluorescent solution was introduced in the device, it was possible to selectively bleached the dyes in only one chamber, proving that diffusion cannot occur between neighbours containers. Under these conditions, each microchambers can be considered as an independent reaction vessel for biological studies at the femtoliter scale.

Single F_1 motors were attached onto the glass plate, grafted with a bead to allow observation and enclosed in 6 fL chamber (Fig.1). In these conditions, the enzyme quickly exhausted the small number of ATP molecules that had been trapped in the chamber and, as a consequence, its speed gradually decreased (Fig.4). The parameter for this decrease is related to k_{on}(ATP), the volume of the chamber and the coupling efficiency between ATP hydrolysis and mechanical rotation. We were thus able to confirm the high yield of this motor.

We then used the bead attached to the protein to pull backward the enzyme, that is, in the ATP-synthesizing direction. 10 Hz rotating magnetic field was applied, forcing the rotation of the bead and thus mimicking the action of the F_0 part of the full enzymatic complex. In the presence of ADP and Pi, it was expected that this mechanic energy input would drive the synthesis of ATP against chemical potentials. To detect this product, we simply released the magnetic field, allowing F_1 to resume its spontaneous rotations in the opposite direction. ATP synthesis was then recognized as an increase in the rotating speed of the enzyme during the period with no applied magnetic field (Fig.4). By comparing with a standard curve of F_1's speed build in the same condition with known concentrations of ATP, we found the coupling efficiency to be very high also for the ATP synthesizing reaction.

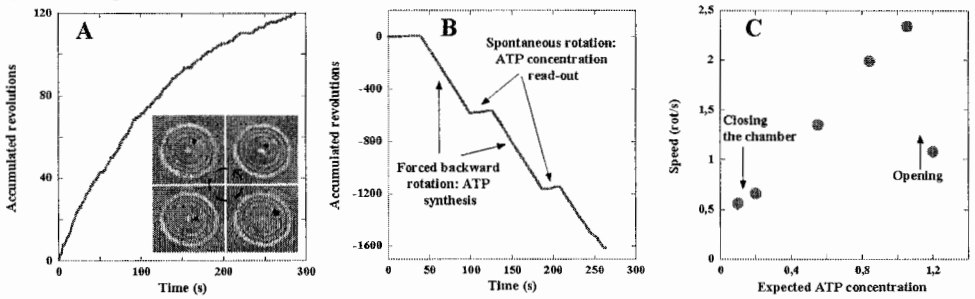

Fig. 4. (**A**) ATP molecules available inside of a 6 fl chamber are quickly exhausted by a single F_1. Decrease rate support a coupling ratio close to 100%. (**B**) Synthesis of ATP through forced backward rotation. The magnetic field is cut off from time to time to measure the spontaneous rotating speed in the motor direction. (**C**) Plot of this speed against the ATP concentration expected from the number of backward rotations shows the high efficiency of the ATP-synthesizing process.

4. Conclusion

The efficiency of the ATP synthesizing process is a very important biological value, because almost all the energy that living organism manages goes through F_0F_1. The high value we found means that this process has been finely during evolution to allow for an optimal use of available energy. Moreover the setup we present will help to reveal the succession of events that allow this uncommon mechanical-to-chemical energy transduction. In a more general sense, these arrays of small chambers allow for the first time to follow the true activity (increase/decrease in the substrate concentrations) of single enzymes. We thus expect them to find many more applications in this area.

References

[1] Boyer, P. D. *Biochim. Biophys. Acta*, **1140,** 215-250 (1993).
[2] Noji, H. Yasuda, R. Yoshida, M. Kinosita, K. Jr, *Nature*, **386**, 299-302 (1997).
[3] Itoh, H. *et al. Nature*, **427**, 465-468 (2004).
[4] Noji, H. Itoh, H. Adachi, K. Yoshida, M. Kinosita, K. Jr, *Biophys. J.* **82**, 40a (2002).
[5] Rondelez, Y. Tresset, G. Tabata, K. Nitta, H. Takeuchi, S. Noji, H. *Proc. microTAS*, 515 (2003).

POSITIONING OF CELLS IN MICROSTRUCTURE AND EXTRACTION OF CONTINUOUS DNA FIBERS FROM INDIVIDUAL CELLS

Kyohei Terao[1], Hiroyuki Kabata[2] and Masao Washizu[1]

[1]Dept. of Mechanical Engineering, The University of Tokyo, Hongo , Bunkyo-ku, Tokyo, Japan
[2]Horizontal Medical Research Organization, Kyoto University, Yoshida konoe, Sakyo-ku, Kyoto, Japan

Abstract

The paper presents two technologies for DNA fiber stretching: cell positioning and drawing DNA fibers out of the cell. The device consists of an electroosomotic flow (EOF) chamber having micro fabricated structures. The structure for cell positioning has openings whose dimension is chosen to accept only one cell at a time, to which cells carried by uni-directional EOF are positioned, one cell at each opening. After enzymatically rupturing cells, DNA fibers can be drawn out of each cell and stretched by EOF. To maintain stretched conformation, we use an array of micro-pillars around which the fiber is wound by sequentially changing the direction of EOF. The fiber is freely suspended without contact to solid surfaces except at the pillars, allowing free access of foreign molecules. Such configuration is expected to realize high-efficiency gene location based on DNA hybridization or protein binding.

Keywords: electroosmotic flow, DNA fiber, FISH, cell, manipulation

1. Introduction

Stretching of continuous DNA fibers is the basic technique in gene location based on observation of molecular binding, including extended-fiber FISH (Fluorescence *in situ* Hybridization) [1]. The requirement is to stretch continuous long DNA strand, typically more than 1 Mega base-pairs, in such a way to allow binding of foreign molecules (fluorescence-labeled oligonucleotides in the case of FISH). It is also desirable to stretch the whole set of chromosomes from a cell without being mixed up with DNA from other cells. The authors have previously demonstrated the stretching of DNA fibers in a fluid-shear field created by electroosmotic flow (EOF) [2]. However, still remaining problems were, 1) cells are randomly placed, and DNA fibers drawn from these cells often overlap with each other, and 2) the stretched DNA fiber cannot be immobilized stably, and coils back to unstretched shape when EOF is turned off. In this paper, we propose and demonstrate the use of micro-structures for 1) positioning of cells at predetermined sites on a substrate, one at a site, and 2) maintaining stretched DNA fibers even after EOF is turned off.

2. Positioning of cells

For the positioning of individual cells onto a substrate, we use an array of triangular pillars having the minimum spacing of 2μm and made of 10μm height SU-8 photo polymer (Microchem. Corp.), as shown in Fig. 1.The array is located at the center of a micro-chamber (Fig. 1 a) equipped with a pair of electrodes to create EOF. The chamber is filled with a buffer, and cell suspension is fed from the entrance side (left in Fig. 1 a) of the array, and a voltage (20V across 5cm electrode spacing) is applied. The cell used in the experiment is the fission yeast, *S. pombe*, having an ellipsoidal shape of approximately 3μm x 3μm x 10μm. The cell, settling down to the bottom and carried by EOF, goes into the gap of the triangular pillar array, and because it is larger than the minimum spacing, it is trapped there (Fig. 2 a). The trapped cell blocks the flow through the gap, and the flow pattern changes, so that next incoming cells must either go over the pillar or go into the neighboring gap,

thus only one cell is trapped at a gap. Fig. 2 b) and c) are the photos of the trapped cells after flushing free cells, showing that cells are neatly positioned on the gaps, one at a place.

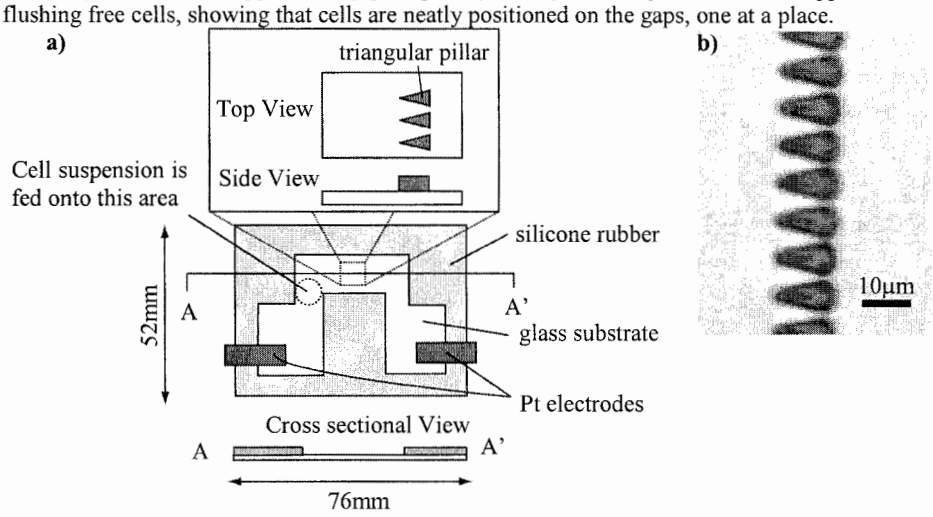

Fig. 1. a) Flow chamber for uni-directional EOF, having an array of triangular pillars fabricated on glass substrate. **b)** Microscopic image of the triangular pillars.

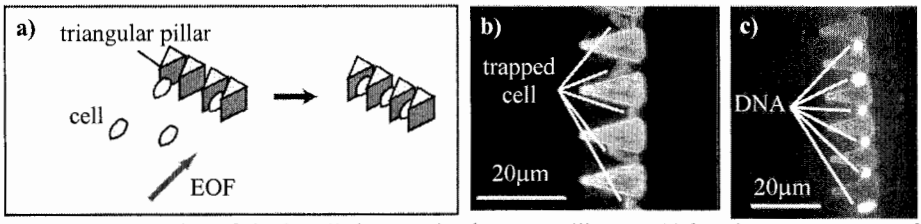

Fig. 2. a) Positioning of single cells by trapping between pillars. **b)** Light microscope image of trapped cell. **c)** Fluorescence image of DNA in the cell.

3. Maintaining stretched DNA fibers

The stretched DNA fiber coils back to random conformation when EOF is turned off. To maintain stretched shape even after the removal of EOF, we use micro-pillars, around which DNA fibers are wound, as schematically shown in Fig.3.

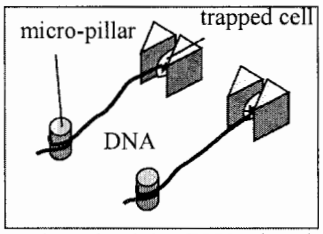

Fig. 3. Maintaining DNA fibers by winding it around pillars

Fig. 4 a) shows the device for this purpose, consisting of two pairs of electrodes (A-D) in a flow chamber. The procedure is as follows. 1) By applying voltage to the electrodes, A positive and C negative, EOF from A to C is created, and the cells are positioned at the triangular pillars. 2) With EOF C→A, DNA fiber is stretched out (Fig.4 b1). 3) With EOF D→B, the fiber is pushed against the sidewall of the pillar (Fig.4 b2), 4) the rotating EOF is created by sequentially switching the voltage in such a way that

A→C (Fig.4 b3), B→D (Fig.4 b4), C→A (Fig.4 b5), and the fiber is wound around the pillar to be immobilized.

Thus the fiber is suspended bridging over the triangular and the circular pillar, while the middle part of the fiber is held without contact to the solid surface, allowing free access of foreign molecules without steric hindrance. Such configuration is expected to realize high-resolution high-efficiency FISH.

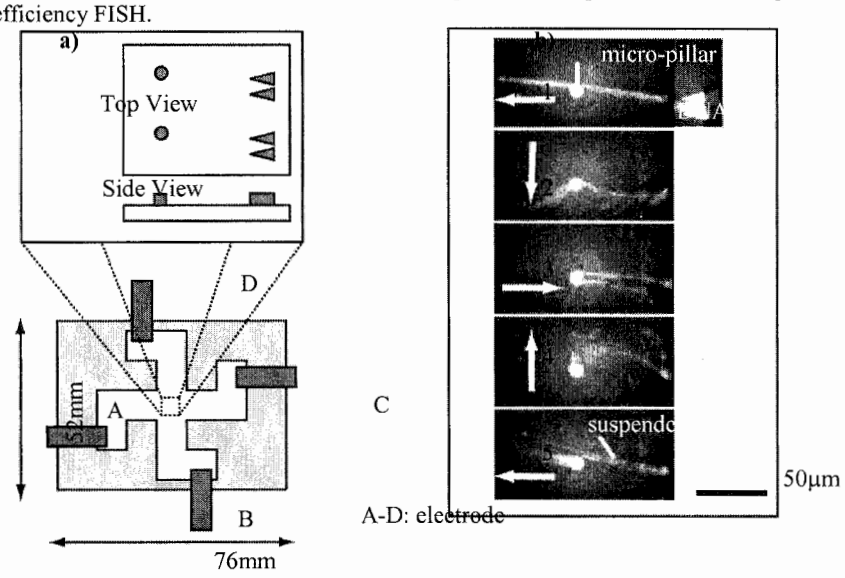

Fig. 4. a) Flow chamber for rotating EOF. Insert shows micro-pillars on the glass substrate.
b) Winding of DNA fibers around a pillar with the rotating EOF (arrow)

5. Conclusions

With the use of EOF in combination with microfabricated structures, we have demonstrated 1) the positioning of cells at a predetermined site on a substrate, one at a site, 2) drawing DNA fibers out of each cell, and 3) winding of DNA fiber around pillars by rotating EOF. The stretched DNA fibers are suspended between the pillars to allow free access of foreign molecules in such a process as FISH.

Acknowledgements

The authors would like to thank Dr. Kimihilko Sugaya of the National Institute of Radiological Sciences for providing the fission yeast strain. This work is supported by BRAIN (Seiken Kiko) Research and Development Program for New Bio-industry Initiatives, and by Grant-in-Aid for Scientific Research on Priority Areas (C) "Genome Science" from the Ministry of Education, Culture, Sports, Science and Technology of Japan (no. 13202028, 14011225, and 15011200). Photography masks were fabricated using EB lithography apparatus of VLSI Design and Education Center (VDEC), The University of Tokyo.

References

[1] X. Michalet et al., *Science,* **277**, 1518-1523 (1997).

[2] M. Washizu, Y. Nikaido and H. Kabata, *Journal of Electrostatics*, **57**, 397-405 (2003).

UTILIZATION OF CELL-SIZED LIPID CONTAINERS FOR NANOSTRUCTURE AND SINGLE MOLECULE MANIPULATION

Guillaume Tresset[1] and Shoji Takeuchi[2]
[1]LIMMS/CNRS-IIS, [2]CIRMM/IIS
The University of Tokyo, 4-6-1 Komaba, Meguro-ku, Tokyo 153-8505, Japan
E-mail: takeuchi@iis.u-tokyo.ac.jp

Abstract

This paper proposes an original approach to handle submicrometer-sized biological or artificial materials for micro total analysis applications. After the enclosure of nanoparticles or DNA inside a cell-sized lipidic vesicle, it becomes possible to manipulate these objects as readily as cells within a microdevice equipped with electrode arrays, and to monitor the operations by conventional optical detection systems. Fusion of different liposomes by silicon micromachined electrodes has been demonstrated and opens up the route to ultra-small biomimetic reactors controlled in MEMS devices.

Keywords: liposome, DNA, nanoparticle, electroosmotic flow, electrofusion

1. Introduction

With the remarkable technical advances made in nanostructure fabrication and single molecule isolation [1], new strategies are to be elaborated to manipulate these objects in view of high throughput reactions and analyses performed in microfluidic devices. Due to their tiny dimensions and to the Brownian motion, observation and individual control of nanoobjects in suspension require sophisticated apparatus (e.g. optical tweezers) not always compatible with routine operations.

For several years, synthetic lipid-bilayer containers, the so-called liposomes, have been widely used in biotechnology as delivery vehicles of drug and gene [2]. Cell-sized liposomes can be easily prepared in large amount with any sort of material inside. This compartmentalization has dramatic advantages: i) vesicles protect materials inside from the environment, which is an important feature for constructing future artificial cells [3], ii) handling of nanoobjects becomes as straightforward as with cells, iii) fusion of two reactant-loaded liposomes should allow to trigger reactions more efficiently thanks to the small enclosing volume [4]. Liposome electrofusion has been already proven in previous experiments [5]: with silicon micromachined electrodes, various fluorescent liposomes were fused together at a success rate up to 75 % for DC pulses of electrical field typically around 10 $kV.cm^{-1}$.

The two new aspects of our work will be accordingly introduced, i.e. encapsulation of materials and manipulation of liposomes in microfluidic device.

2. Encapsulation of DNA and nanoparticles into liposomes

Liposomes were obtained after the 'reverse-phase evaporation' protocol [6] from a mixture of phospholipids (Sigma) and lipophilic fluorescent dye DiO or DiI (Molecular Probes), diluted in chloroform and methanol 2:1. A dry lipidic film was made by rotary evaporation under high vacuum. After moisturization by buffer (5 mM $MgCl_2$, 200 mM glucose, pH~7.5) containing λ-DNA (Takara) at 10^{11} molecules/mL and SYBR Green (Molecular Probes), 10 μm-average large liposomes were formed entrapping some of the surrounding fluorescent-stained molecules.

Figure 1 gives a fluorescent image of DNA-loaded liposomes taken just after that preparation. 40 % to 50 % of liposomes larger than 5 μm contained at least one λ-DNA molecule. In order to prove DNA was really enclosed and protected from the environment by the liposome membrane, we put 1 mg/mL of DNase I (Roche) – an enzyme which digests DNA and accordingly stops its

fluorescence – into the liposome solution. For comparison, we prepared another liposome solution, but this time DNA was injected after the formation of liposomes so that it cannot be enclosed inside them. Figure 2 shows the decay of fluorescence in both cases. After 5 hours, even though all DNA was not completely digested, the steady-state fluorescence intensity in the first case was larger than in the case where DNA was only outside the liposomes. This result indicates that after digestion a fraction of DNA is confined in liposomes and protected from the DNase. In the first case again, we checked thereafter the enzyme was still active by adding a small amount of DNA: as expected, fluorescence transiently increased then decayed due to the enzyme activity down to the same level as before.

The same process was also applied to trap 200 nm polystyrene spheres. Like λ-DNA, the nanoparticles could move freely while remaining confined by the liposome membrane (Figure 3). Therefore, biological materials but also inorganic structures can be contained by liposome with excellent sealing properties.

3. Liposome manipulation

Figure 4 exemplifies the concept of single molecule manipulation. A DNA molecule is encapsulated into a 'giant' liposome which serves as a conveyor traveling through a flow channel. The actuation is carried out by an array of microelectrodes generating standard or traveling-wave dielectrophoresis.

To convey the previously loaded liposomes, we have designed a PDMS microfluidic channel on a microarray of gold electrodes. Four layers of AZ4620 thick photoresist (Clariant), patterned directly on the chip, were used as a sacrificial layer for the molding of PDMS (Figure 5). It can be seen on Figure 6 that this process allows to align precisely a thick, narrow and long channel on micropatterns. As a proof of principle, standard electroosmotic flow was achieved by connecting electrodes A and A' at the ground and by applying a 5 V/3 MHz AC potential on electrode B' (Figure 7).

4. Conclusions

Biological or inorganic submicrometer materials have been successfully entrapped inside cell-sized lipid containers, which act as a barrier against the outside environment. The manipulation and observation of these nanoobjects have been made easier by the utilization of these micrometer-sized liposomes, which can be moved or even fused thanks to conventional electrical techniques. Encapsulation, manipulation and fusion will be soon integrated on a same chip for using liposomes as ultra-small reactors. Self-assembly of nanostructures or gene expression from DNA could then take place in a controlled manner through the electrofusion of reactant-loaded liposomes.

Acknowledgements

The authors would like to thank Prof. H. Noji, Dr. Y. Rondelez and Dr. T. Yamamoto for their technical support and fruitful discussions. Some of the micromachining processes have been accomplished with the support of Prof. H. Fujita. This work was partly supported by the Japan Society for the Promotion of Science (JSPS) and by the PROgram for the Promotion of Basic Research Activities for Innovative Biosciences (PROBRAIN) under the supervision of the Ministry of Agriculture and Fisheries in Japan.

References

[1] G.M. Whitesides, *Nature Biotechnology*, **21**, 1161-1165 (2003).
[2] A.S. Ulrich, *Bioscience Reports*, **22**, 129-149 (2002).
[3] J.W. Szostak, D.P. Bartel, and P. Luigi Luisi, *Nature*, **409**, 387-390 (2001).
[4] D.T. Chiu et al, *Science*, **283**, 1892-1895 (1999).
[5] G. Tresset and S. Takeuchi, to be published in *Biomedical Microdevices*.
[6] *Liposomes*, edited by V.P. Torchilin and V. Weissig, 2nd Edition, Oxford University Press, 2003.

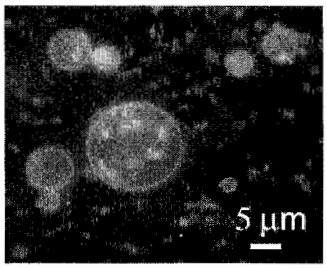

Figure 1. Fluorescent image of DNA-loaded liposomes. Green dots stand for λ-DNA molecules whilst lipids are labeled in red.

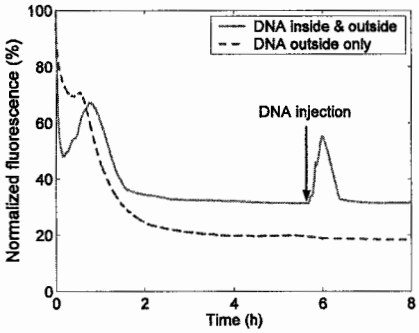

Figure 2. λ-DNA digestion by DNase I with DNA inside and outside liposomes, and DNA outside only. In the first case, small amount of DNA is injected to verify the viability of the enzyme. The fluorescence of SYBR Green is recorded at 520 nm under excitation at 497 nm.

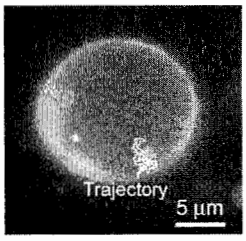

Figure 3. Trajectory of a 200 nm fluorescent red bead confined inside a fluorescent green liposome.

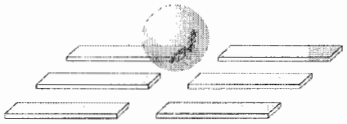

Figure 4. Concept of DNA manipulation: the molecule is enclosed inside a cell-sized liposome which is in turn handled by an array of microelectrodes inducing dielectrophoretic forces.

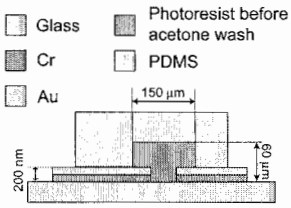

Figure 5. Schematic cross-section of the device with its components.

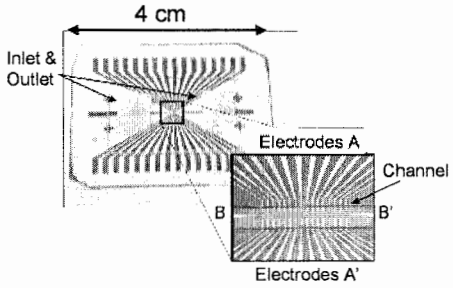

Figure 6. Photograph of the device and close-up view of the electrode array.

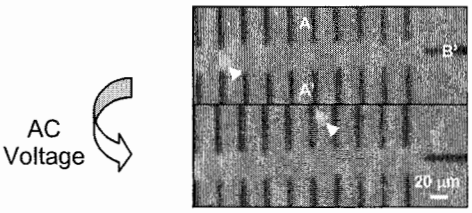

Figure 7. Electroosmotic flow on a red fluorescent liposome in a microfluidic device. The voltage is applied between B' and (A, A').

DEVELOPMENT OF INDIVIDUAL CELL SORTING SYSTEM FOR INTERCELLULAR REACTION ANALYSIS

Shin-ichiro Otsuka[*1], Masaki Kanai[1,2], Masahiro Hayashi[1], Hiroaki Nakanishi[2], and Shuichi Shoji[1]

*[*1]Major in nanoscience and nanoengineering, Waseda University, 3-4-1,Okubo,Shinjuku,Tokyo 169-8555,Japan*

[2]Technology Research Laboratory, Shimadzu Corporation, 3-9-4,Hikari-dai,Seika-cho,Soraku-gun,Kyoto 619-0237,Japan

Abstract

We developed a prototype of the cell sorting system for the intercellular reaction analysis, which can sort two kinds of cells individually. To realize the functional sorting, innovative concepts of the asymmetric sheath flow and the additional protection flow were proposed in the 2-D sheath flow system. In the evaluations of the fabricated system, two kinds of fluorescent beads were selectively introduced to the diagnostic chamber using on chip micro valves. In additional, a multiple sorting system having four outlet chambers was also fabricated. Basic sample injection behaviors were evaluated. These devices are applicable for not only the intercellular reaction analysis but also the high-throughput multiple cell analysis.

Key words: cell analysis, cytokine, cell sorter, sheath flow, on chip micro valve

1. Introduction

In recent years, a lot of chip devices for cell analysis have been reported. One of the target is to observe cell reaction which concerns to the human diseases. In our research, we focus on the chip devices for intercellular reaction, so-called cytokine reaction which plays important roles on allergy, rheumatism, and many human diseases. In order to analyze these intercellular reactions, a cellular analysis system which can handle various cells individually is quite helpful. The methods which can handle the individual cell, such as laser tweezers and on-chip cell sorters using sheath flow have been reported so far. The laser tweezer can handle individual cell easily, however, its throughput is poor in practical use. While, the sheath flow cell sorter can achieve high-throughput operation and is easy to extend to a multiple handling system due to its simple structure. Conventional cell sorters mainly target the high throughput cell handling or the single-species handling with good accuracy. In this paper, we developed the cell sorting system which can handle two different cells one by one. Prototype of the multi-outlet cell sorting system was also described.

2. Theory

Fig 1 shows the mechanism of the first prot
of cells are introduced to the sorting zone ir
Fig .1a and mode3; Fig .1b) and introduced t
The sheath buffer flows are switched using
cell sorter chip. In previous works, we alre
time was about 150msec [1,2].

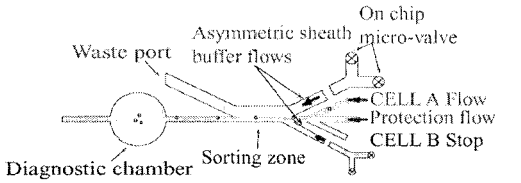

(a)Mode1: CELL A to chamber

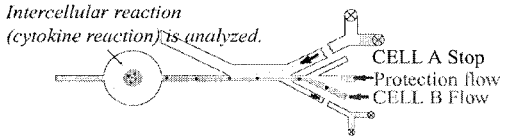

(b) Mode3: CELL B to chamber

Figure 1. Mechanism of the prototype cell sorter

This device has two innovative concepts of the 2-D sheath flow system that are the asymmetric sheath flow and the additional protection flow. An asymmetric channel structure of the sheath buffer flows improves the directional controllability of the cell flow. The cell flow is controlled by not only the sheath buffer flow but also the protection flow (center flow). The protection flow realizes a virtual wall to prevent the cell from flowing into the other cell inlet as shown in Fig 1.

3. Experimental

The prototype device having one diagnostic chamber and two-cell inlets were designed and fabricated based on the CFD (computational fluid dynamics) simulation results. A silicon was etched to form channels and through holes using deep RIE and anodically bonded with a Pyrex glass (#7740). A diaphragm of silicone rubber was bonded to the Si structure to fabricate pneumatic on chip micro valve [2].

As a pilot study, we evaluated switching behaviors of the fluorescent dyed water (10μM RhodamineB). A dyed water was injected to the device using syringe pump, and was switched by the on chip micro valves. Next, we demonstrated the sorting of 6μm green and red fluorescent beads.

4. Result and discussion

Switching behaviors of the prototype cell sorter is shown in Fig .2. Fig .2a is switching from mode1 (cell A injection) to mode2 (cell A waste), while Fig .2b is from mode3 (cell B injection) to mode4 (cell B waste). The flows switched successfully with in 150msec using on chip micro valve. The protection flow avoids reverse flow to the other cell inlet effectively. Fig .3 shows the time dependant results of individually sorted beads to the same diagnostic chamber. Individual two kinds of beads sorting was confirmed. We achieved controlling the number of the beads sorted to the diagnostic chamber. The result shows the feasibility of the controllable cell collection with various combinations.

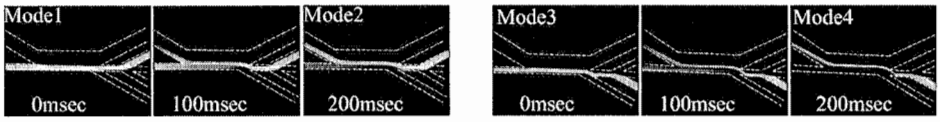

(a) Switching from mode1 to mode2 (b) Switching from mode3 to mode4

Figure 2. Switching evaluation using on chip valve

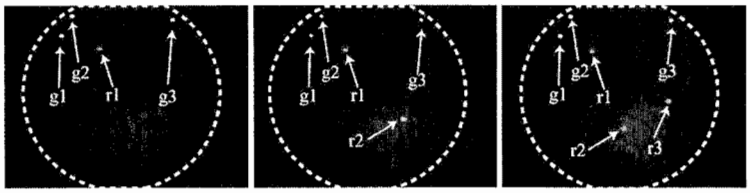

(a) 3 green beads 1 red bead (b) 3 green beads 2 red beads (c) 3 green beads 3 red beads

Figure 3. Beads injection to the diagnostic chamber. Individual red beads (CELL B) injections after injection of three green beads (CELL A).

We extended the concept of the prototype cell sorter chip to multiple cell sorter. Fig .4 shows the

other prototype cell sorter chip having multiple outlet chambers (four diagnostic chambers and two cell inlets) for the high-throughput multiple cell analysis. Four switching modes to the diagnostic chambers were realized successfully (Fig .4b). The concept of this system can be applicable for intercellular reaction analysis which requests introduction of the reagent to the cell collection chambers. The improvements of controllability of the multi cell sorter are under investigation.

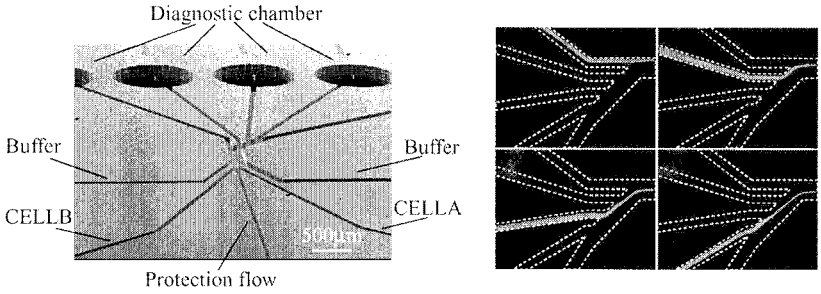

(a) SEM image of prototype device (b) Evaluated switching behavior

Figure 4. Prototype cell sorter chip of multiple chambers

5. Conclusions

We have developed a cell sorting system, which can sort two kinds of cells individually. The concepts of an asymmetric sheath buffer flow and an additional protection flow were proposed for the functional sorting. In the prototype device, selective sorting of two kinds of beads were realized successfully. We fabricated the multiple cell sorter and demonstrated a switching behavior. The 2D-sheath flow concepts proposed in this paper can be applicable for intercellular reaction analysis as well as the high-throughput multiple cell analysis.

Acknowledgements

This work is partly supported by Japan Ministry of Education, Culture, Sport Science & Technology Grant-in-Aid for COE Research and 21st COE of Waseda University, Scientific Basic Research (A) No. 12450167.and Japan Society for the Promotion Science Grant-in-Aid for Creative Scientific research No. 13GS0024.

References

[1] M.Kanai, S,Ikeda, J.Tanaka, J.S.Go, H.Nakanishi, S.Shoji *Sensors & Actuators A* 111 (2004) pp32-36

[2] M.Kanai, S,Otsuka, H,Nakanishi, S,Shoji, *Japanese Journal of Applied Physics,* Vol. 43, No. 6B, *in press*

CAPILLARY-ASSEMBLED MICROCHIP (CAs-CHIP) : A NEW METHOD FOR INTEGRATING MULTIPLE CHEMICAL FUNCTIONS ONTO A SINGLE MICROFLUIDIC DEVICE

Hideaki Hisamoto [1], Yuya Nakashima [1], Chihiro Kitamura[1], Shun-ichi Funano [1], Midori Yasuoka [1], Keisuke Morishima [2], Yoshikuni Kikutani [2], Takehiko Kitamori [2,3], and Shigeru Terabe [1]

[1] Graduate School of Material Science, University of Hyogo, 3-2-1 Kouto, Kamigori-cho, Ako-gun, Hyogo 678-1297, Japan

[2] Micro Chemical Group, Kanagawa Academy of Science and Technology, 3-2-1 Sakado, Takatsu-ku, Kawasaki, Kanagawa 213-0012, Japan

[3] Department of Applied Chemistry, Graduate School of Engineering, The University of Tokyo, 7-3-1 Hongo, Bunkyo-ku, Tokyo 113-8656, Japan

Abstract

A novel concept of assembling various chemical functions onto a single microfluidic device is proposed. The concept, "CAPILLARY-ASSEMBLED MICROCHIP (CAs-CHIP), involves embedding chemically functionalized square capillaries onto a lattice microchannel network fabricated on polydimethyl siloxane (PDMS) possessing same channel dimensions to outer dimensions of square capillaries (Figure 1). This approach would allow easy fabrication of chemically-functionalized microfluidic device by freely embedding functional square capillaries on PDMS microchannel network. Here we report a fabrication method of CAs-CHIP, and an application for preparing a multiple chemical sensing chip as an example.

Keywords: chemical function, PDMS microchip, sensor, square capillary, surface modification

1. Introduction

Recently, integration of chemical functions onto microfluidic device has become a target of much current research in analytical chemistry. Many kinds of position-selective immobilization techniques such as a laminar flow patterning, photo polymerization were reported by many groups [1-3].

These techniques are quite promising for integrating a single chemical function onto a microfluidic device; however, an experimental difficulty arises when different and plural chemical functions are integrated into a single microfluidic device. This is because most techniques listed above require introduction of reagent solutions into the "whole microchannel", although the chemical modification is only carried out at a defined position of it. Therefore, in general, once a certain chemical function is patterned at part of the channel, position-selectively, other reagents should be introduced over another patterned surface to integrate plural chemical functions into a single microchannel. This may lead to contamination or deterioration of the previously patterned chemical function. Here we propose a simple and promising approach for assembling various chemical functions onto a single microfluidic device as shown in Figure 1. Our concept, called a capillary-assembled microchip (CAs-CHIP), involves embedding of chemically functionalized square capillaries into the lattice microchannel network fabricated on PDMS having the same channel dimensions as the outer dimensions of the square capillaries[4]. Here we report the first example implementing the concept and we give a simple example application of the method for preparing a dual chemical sensing chip which can measure pH and calcium ion simultaneously.

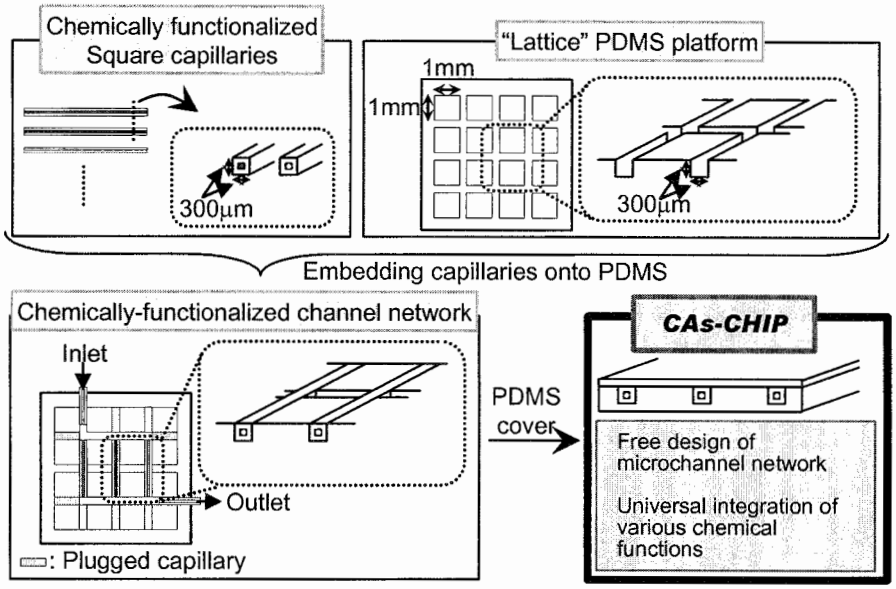

Figure1 General concept for preparing CAs-CHIP

2. Experimental

Square capillaries were cut into appropriate lengths (usually one to three millimeters) and embedded into the lattice microchannel network fabricated on the PDMS plate. Plugged capillaries were prepared by introduction of PDMS prepolymer into square capillaries (inner width: 50 μm) and cured at 70 °C for more than 5 h. These plugged capillaries were also cut and used for preparing the designed channel network. After embedding all the capillaries, a PDMS cover was bonded on top. For this, a spin-coated PDMS prepolymer on a glass slide was used as a cover plate. PDMS prepolymer was spin coated on the glass slide at 5000 rpm, then adhered to the capillary-embedded PDMS plate with clippers before curing. Bonding was carried out by curing at 70 °C for 5 h. The chemical sensing capillaries for pH and calcium ion were prepared by immobilizing respective sensing membranes to inner surface of capillaries.

3. Results and discussion

Figure 2 shows the preliminary design of the microchip for dual chemical sensing. By using spin-coated PDMS prepolymer as a cover plate, fabrication of a capillary-embedded microchannel (capillary) network without any solution leakage was successfully performed. For sensing application, we have prepared pH and calcium ion-sensing capillaries by attaching hydrogel-based membrane and plasticized PVC membrane to inner surface of square capillaries, and embedded them into PDMS chip. When the sample solution passed through the sensing capillaries, the fluorescence of each membrane changed by selective interaction with each analyte. The most characteristic feature of this chip is that the different type of capillaries can be embedded onto a single microfluidic device.

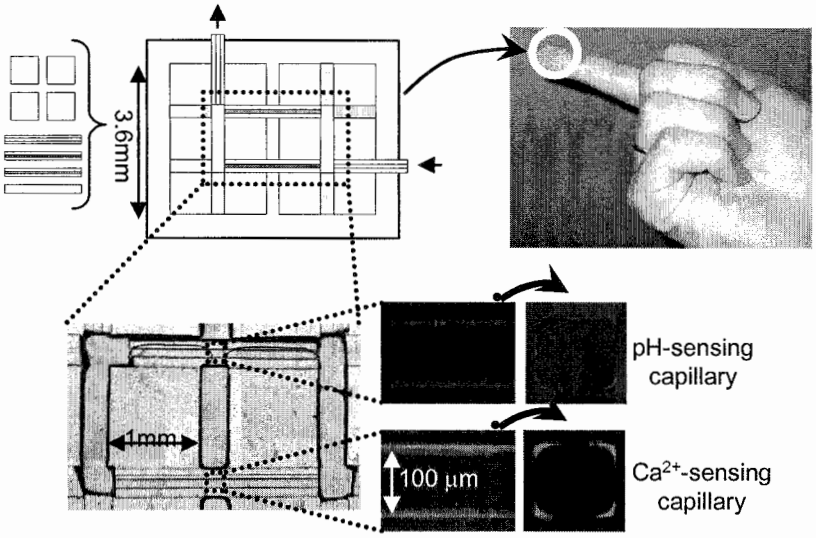

Figure2 Preparation of dual-sensing CAs-CHIP

4. Conclusions

We have proposed a novel concept for assembling various chemical functions onto a single microfluidic device, called a capillary-assembled microchip (CAs-CHIP). By employing spin-coated PDMS prepolymer, we fabricated a capillary-embedded microchannel (capillary) network with no solution leakage. Two different types of chemical sensing layers were prepared inside the square capillaries, and these modified capillaries were embedded into a lattice PDMS channel network to fabricate a parallel dual-sensing microchip. Many types of surface modification methods inside capillaries are well known, so that the proposed method has great potential to fabricate different microfluidic devices having various chemical functions for analytical or synthetic applications.

Acknowledgements

This work was partially supported by Grants for Scientific Research from the Ministry of Education, Culture, Sports, Science and Technology, Japan, Kawanishi Memorial Shinmeiwa Education Foundation, Japan.

References

[1] P.J.A. Kenis, R.F. Ismagilov, G.M. Whitesides, *Science.*, **285**, 83-85, (1999).
[2] J. Moorthy, D.J. Beebe, *Anal. Chem.*, **75**, 292A-301A, (2003).
[3] H. Hisamoto, Y. Shimizu, K. Uchiyama, M. Tokeshi, Y. Kikutani, A. Hibara, and T. Kitamori, *Anal. Chem.*, **75**, 350-354, (2003).
[4] H. Hisamoto, Y. Nakashima, C. Kitamura, S.-i. Funano, M. Yasuoka, K. Morishima, Y. Kikutani, T. Kitamori and S. Terabe, *Anal. Chem.*, **76**, 3222-3228, (2004).

ACTIVE ASSEMBLY METHODS FOR MICROFLUIDIC SYSTEMS

Dongshin Kim[1], Swomitra K. Mohanty[2] and David J. Beebe[1,2]
[1]Dept. of Mechanical Engineering, [2]Dept. of Biomedical Engineering,
University of Wisconsin, Madison, WI, USA

Abstract

Active assembly methods utilizing the expansion of hydrogels to realize in situ assembly of microfluidic components were developed using liquid phase photopolymerization. Two successful applications of active assembly were tested, (1) active walls to block or divert flows at different steps in the fabrication or assay process, (2) biosensor positioning to reduce background noise after treatment.

Keywords: hydrogel, active assembly, microfluidics, ELISA

1. Introduction

Hydrogels belong to a class of polymeric materials that swell upon hydration. Recently, hydrogels have begun to find use in microfluidic systems to provide actuation for valves and pumps [1-3]. Active assembly is another area where hydrogels can prove useful.

The concept of "active assembly" is to use active components to either directly form a functional component or to aid in the assembly of another component. This is in many was analogous to the way in which many biological systems operate and assemble (e.g. protein complexes). The use of active components as part of the system assembly process provides new options not available via traditional passive methods. For example, a hydrogel can be used to actively form a channel wall. If the hydrogel is appropriately positioned, i.e., structurally programmed, it will reconfigure the channel network or structure of the device in response to triggering by a specific stimulation. Active assembly provides additional functionality – programmability and autonomous reconfigurability – to microfluidic systems.

We will demonstrate two examples of active assembly methods in this paper including active walls to block or divert flows at different steps in the fabrication or assay process, and biosensor positioning to reduce background noise after treatment.

2. Design and fabrication

Temporary or auxiliary channels can be used to enhance fabrication quality or improve device performance in microfluidic systems. One example is a detour channel for protecting certain sensitive components (e.g., filter or readout) from chemicals used during other fabrication steps that might degrade the component performance. Fig. 1 shows an example of the active assembly method applied to protect a filter during other manufacturing steps. The white area between top and bottom channels is an in situ fabricated filter. After photopolymerization of the filter, a rinsing fluid is introduced to wash the component by removing the unpolymerized prepolymer from around the filter. The rinsing fluid passes along side (not through) the fabricated filter during the cleaning process. Once the filter is fabricated and washed, the blocking components are activated by buckling of hydrogel bar diverting flow through the filter for device operation.

ELISA is a detection procedure used in diagnostics, and involves specific antibody-antigen binding and enzymatic reactions. One of the problems of ELISA is nonspecific background signal from channel surface, which lowers the signal to background ratio. One method to address this problem is to use blocking agents such as albumin. Here we propose an alternative method wherein, the delivery function of active assembly methods is utilized to physically move the

readout post from a treatment channel to a new channel for exposure to the sample (Fig. 2). The readout post is functionalized with appropriate antibodies in the treatment channel. When triggered, hydrogel piston pushes the circular readout post to the readout channel where the post is exposed to the sample. Since the treatment and detection steps are performed in different channels, the background signal from the channel surface can be reduced (Fig. 2c).

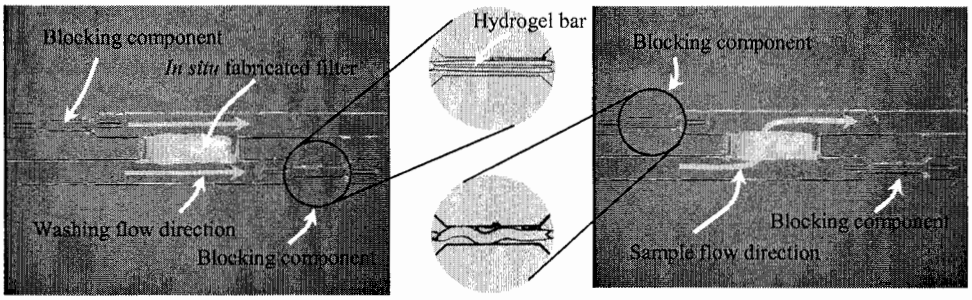

a) Cleaning process b) Opened (top) and closed (bottom) blocking component c) Completed device

Figure 1. Blocking component for filter fabrication. After photopolymerization of the filter, a rinsing fluid passes along side (not through) the fabricated filter to remove the unpolymerized prepolymer from around the filter. Once the filter is fabricated and washed, the blocking components are activated by buckling of hydrogel bar diverting flow through the filter.

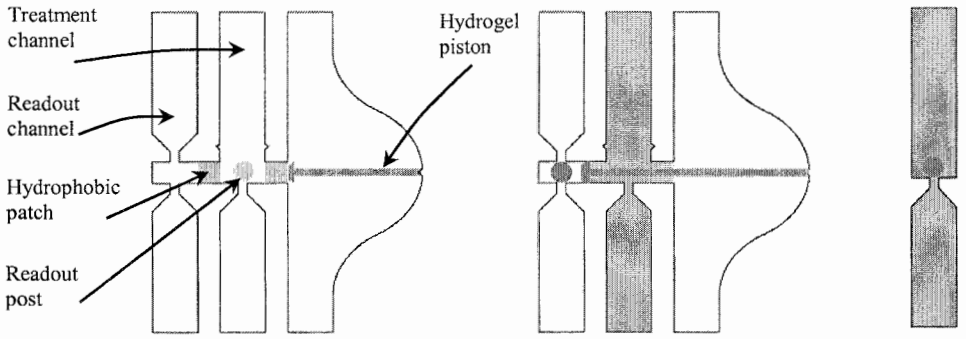

a) Before delivery b) After delivery (High S/B ratio) c) Without delivery (Low S/B ratio)

Figure 2. Conceptual diagram of the delivery component for readout system. After coating the readout post in the treatment channel, the hydrogel piston is triggered to push the circular post to the readout channel. The signal to noise ratio is enhanced as the coating and detection processes are performed in different channels.

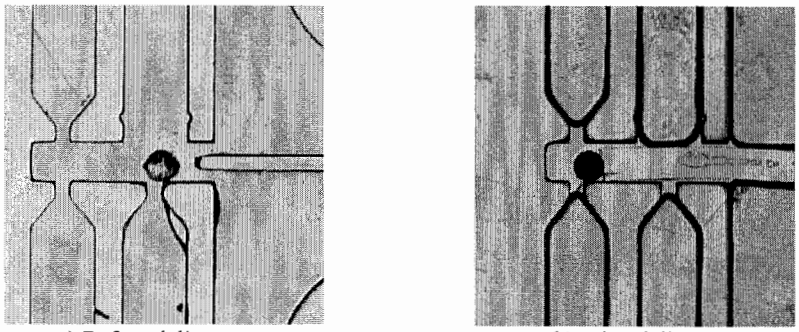

a) Before delivery b) After delivery

Figure 3. Results of the delivery component for readout system. After the treatment, the readout post was moved into the readout channel by triggering the hydrogel piston with water.

3. Experimental results and discussion

The active walls operated successfully by blocking auxiliary channels used at preliminary steps of the filter fabrication process. The diverting flow through the *in situ* fabricated filter was observed. Biosensor delivery component to reduce background signals of ELISA also worked as shown in Fig. 3. The readout post was moved into the readout channel by triggering the hydrogel piston with water after the treatment.

4. Conclusions

Active assembly methods were accomplished using microfluidic tectonics [4], a procedure of constructing microscale components and autonomous systems using liquid phase photopolymerization. Active assembly methods may also facilitate other components such as safety or release valves and degradable blocking components. The use of stimuli responsive materials to accomplish active in situ assembly further enhances the process options available to microfluidic designers.

Acknowledgements

This work was supported from DARPA-MTO under grant number F30602-00-1-0570 (Program manager: Dr. Michael Krihak).

References

[1] D. J. Beebe, J. Moore, J. M. Bauer, Q. Yu, R. H. Liu, C. Devadoss, and B. H. Jo, "Functional hydrogel structures for autonomous flow control inside micro-fluidic channels," *Nature*, vol. 404, 2000.

[2] R. H. Liu, Q. Yu, and D. J. Beebe, "Fabrication & characterization of hy-drogel-based micro-valves," *J. Microelectromech. Syst.*, vol. 11, pp. 45-53, 2002.

[3] A. Richter, D. Kuckling, S. Howitz, T. Gehring, and K.-F. Arndt, "Electronically controllable microvalves based on smart hydrogels: magnitudes and potential applications," *J. Microelectromech. Syst.*, vol. 12, pp. 748 - 753, 2003.

[4] D. J. Beebe, J. S. Moore, Q. Yu, R. H. Liu, M. L. Kraft, B.-H. Jo, and C. Devadoss, "Microfluidic tectonics: A comprehensive construction platform for microfluidic systems," *Proc. Natl. Acad. Sci.*, vol. 97, pp. 13488-13493, 2000.

SINGLE-MASK STEP INTEGRATION OF HIGH-ASPECT RATIO SUB-MICROMETER CHANNELS, PURE SILICA WAVEGUIDES AND FIBER COUPLERS FOR SEPARATION CHIPS

Klaus B. Mogensen, Fredrik Eriksson, Rikke P. H. Nikolajsen, Omar Gustafsson and Jörg P. Kutter

MIC - Dept. of Micro and Nanotechnology, Technical University of Denmark, Bldg. 345 east, DK-2800 Kgs. Lyngby, Denmark

Abstract

A fabrication procedure that allows integration of pure silica optical waveguides, fiber-to-waveguide coupler structures and high-aspect ratio submicrometer-sized fluidic channels using a single photolithographic mask step has been developed. The propagation loss of the waveguides was only 0.8 dB/cm at 200 nm, which to our knowledge is the lowest loss reported in the UV region. The devices were furthermore tested by performing capillary electrophoretic separations with absorbance detection at 254 nm of the drugs caffein, paracetamol and ketoprofone. The limit of detection for paracetamol filled in the whole channel network was 3 μg/mL.

Keywords: Deep reactive ion etching, oxidation, UV waveguides, high-aspect ratio channels, capillary electrophoresis

1. Introduction

The interests in fluidic channel networks with submicrometer dimensions has increased rapidly in recent years, due to the perspective of performing new types of chemistry and to take advantage of the high surface-to-volume ratio for e.g. capillary electrochromatography. A complication is, however, that the alignment tolerances of the detection system decrease as the channel dimensions are reduced. The motivation for our work is therefore to develop a comparatively simple fabrication scheme that allows monolithic integration of an optical detection system and submicrometer high aspect ratio fluidic channels.

2. Experimental

The fabrication process relies on etching of the optical and fluidic structures in silicon by deep reactive ion etching (DRIE) and subsequent thermal growth of a 13 μm thick oxide layer.

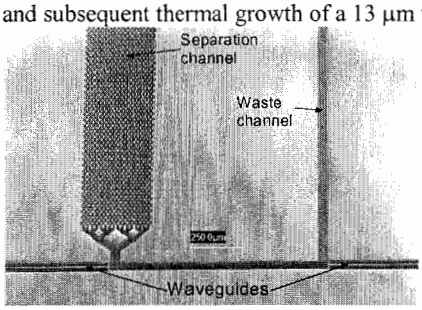

Figure. 1. Absorbance cell interfaced with waveguides for in-plane UV absorbance detection. A broad channel with microfabricated pillar structures is seen in the left part of the picture.

The channel network consisted of a separation channel with pillars, a waste channel and a 1000 μm long absorbance cell interfaced with waveguides for detection (Fig. 1). A cross sectional view of the

pillar region after oxidation is shown in Fig. 2. In this case, the channel depth was 100 μm and the spacing was 2 μm. The distance between the pillars was 12 μm after etching and was hence reduced by 10 μm, due to the volume expansion that occurs during oxidation (a factor of 2.3) [1-2].

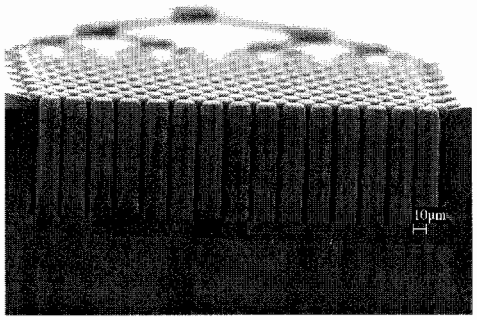

Figure 2. Cross sectional view of the SiO_2 pillar structures in the separation channel of Fig. 1. The height is 100 μm, while the channel spacing is about 2.0 μm.

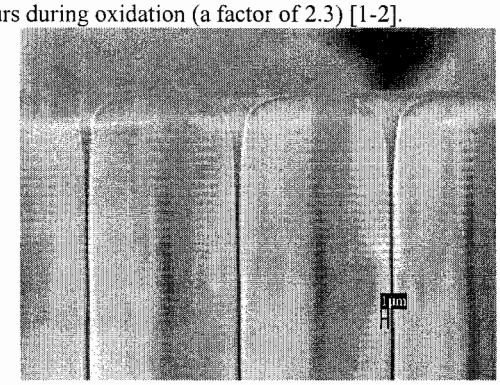

Figure 3. Close view of the top of the pillar structures. The pillar spacing has been reduced to less than 0.5 μm by conformal trench-filling with SiO_2.

The channel width can be further reduced to below 0.5 μm by low pressure chemical vapor deposition (LPCVD) of SiO_2 (Fig. 3). Fig. 4 shows how waveguides can be fabricated and integrated using the same process.

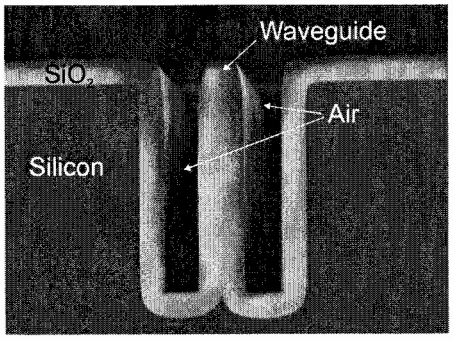

Figure 4 Cross-sectional view of a waveguide before bonding of a PDMS lid. The white regions are the oxidized silicon, while the dark regions are silicon.

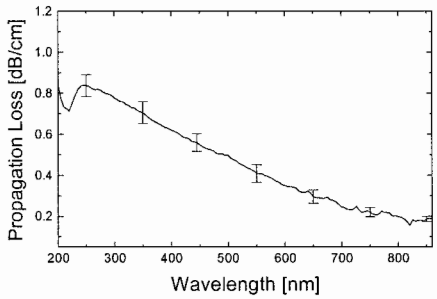

Figure 5 Spectrally resolved propagation loss between 200 and 800 nm.

To realize a waveguide core consisting of pure silicon dioxide (n=1.46) a thin ridge of silicon is oxidized all the way through. The waveguide width after oxidation was 22 μm. Air on both sides serves as the lower refractive index cladding region. A PDMS lid (n=1.43) bonded on top of the

structures constitutes the upper cladding layer. Light is, however, unguided at the bottom, which is a limitation of this approach. An etch depth of 100 μm was chosen, so the fiber-to-waveguide coupler structures could accommodate the optical fibers used for coupling light into the chip.

3. Results and discussion

The spectrally resolved waveguide propagation loss was calculated from transmission measurement between 200 nm and 800 nm (Fig. 5). The loss is 0.8 dB/cm at 200 nm and decreases to 0.2 dB/cm at 800 nm. This is to our knowledge the lowest loss reported in this wavelength region for integrated waveguides. A (not optimized) electrophoretic separation of three drugs in an open channel (Fig. 6) demonstrates the usability of the waveguides for UV absorbance detection.

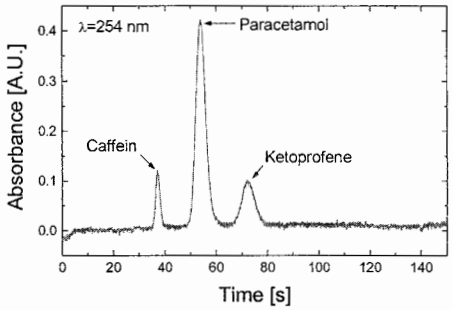

Figure 6 Electropherogram showing the separation of caffein, paracetamol and ketoprofene, each with a concentration of 200 μg/mL. The separation conditions were: 25 mM tetraborate buffer (pH 9.2). E=550 V/cm. 1 sec. injection time. Absorbance detection was carried out at 254 nm with an optical path length of 1000 μm.

The devices were furthermore tested for capillary electrochromatographic separations of neutral analytes by the use of a C18 stationary phase. The experiments were, however, complicated by absorption of the analytes into the PDMS lid. In future experiments, various coating procedures will be tested to circumvent this problem and other types of lid materials will be tested as well.

Acknowledgements

The work was funded by the Danish Technical Research Council (STVF) under contract no. 26-00-0220.

References

[1] M. Madou, *Fundamentals of Microfabrication*, CRC Press, London (1997).
[2] H. Jiang, K. Yoo, J. L. A. Yeh, Z. Li and N. C. Tien. J. Micromech. Microeng., **12**, p. 87-95 (2002).

THREADING PEPTIDES AND PROTEINS INTO DISEASE SURVEILLANCE STRATEGIES - LINKING TO MICROTECHNOLOGY INTEGRATION -

György Marko-Varga
AstraZeneca R&D Lund, Respiratory Biological Sciences, 221 87 Lund, Sweden

1. Background

Modern Drug development relies heavily on the ability to have a detailed understanding of disease states-, and progressions. Technology developments is a central part of the process of drug discovery and drug develoment that will have a built in success factor. The tool-box concept whereby the appropriate technology lends itself to produce the high accuracy and accurate analytical data to the question posed in the particular study is a key function for the industry to have. In this respect, "Proteomics" is a collection of scientific approaches and technologies aimed at characterizing the protein content of cells, tissues, and whole organisms that has an increasing value.

Many of the modern approaches are mandatory for studying disease, to compare steady state functions such as repair, growth, and regulated gene expression within the various biological compartments organised by specialized function, be it mitochondria or blood vessels. Proteomics research also has applications in target validation, drug screening, and the discovery of diagnostic markers. Most recently, the area of Clinical Proteomics and the hunt an discovery of biomarkers is a central part of the protein expression profiling research area of today.

2. Protein Expression Profiling – Proteomics

Proteomics is by most scientists divided into three categories: expression proteomics, functional proteomics, and structural proteomics. Within functional proteomics there is a clear focus on the high-throughput determination of protein function.

The assignment of protein identities which are linked to key biological mechanisms which are associated with disease processes and disease progression holds an important area of this work. Since the link to clinical proteomics has become the forefront as a research area, there is a high expectation that the developments within the area will deliver on the transformation of biology and medicine. Especially since this is the new direction that the clinical proteomics research area is taking, as a strong complement to the human genome information, and the m-RNA transcript profiling area. We have reached a point within the protein expression profiling field where the technology platforms available from instrumental companies, as well as new platforms developed by individual research groups, makes it possible to map proteome expressions from various species. The increased number of entire genomes that has been sequenced, makes our awareness and increase in knowledge of their gene products a valuable access. Still, there is only a part of the proteome expression window that we are looking into in each sample under study.

Today, the technology available for studying proteome expression and resolving exact protein and peptide identities in complex mixtures of biological samples allows global protein expression within cells, fluids, and tissue to be approached with confidence. This confidence is due in part to reproducible repetitive sampling and analysis technologies including robotics data acquisition and high level mass spectrometry including both laser-desorption-, (MALDI) and electro spray-ionisation (ESI). The precision in defining differences between normal and diseased steady states is aided by the creation of compiled reference and master data sets and by new methods for multiplexing the analysis of samples in groups. The establishment of key representative reference proteome systems representing the dynamic changes in protein expression during disease will be

vital to the interpretation of changes observed in specific samplings of disease states and specific cells obtained from these samples. The creation of reference databases of proteins linked to disease pathways will play an important role in furthering our understanding of the "proteome of disease" [1].

Liquid Phase separations are increasingly utilized in protein expression studies using combinations of multi-dimensional separation mechanisms.

The qualitative identity of proteins is achieved by mass spectrometry, where various ionization principles are applied, such as matrix assisted laser adsorption isonization MALDI, as well as electrospray ionization. FTICR-instrumentation with currently the highest resolving power is also starting to make an impact. Although initial data looks promising, the final use and power still needs to be proven.

The complementary nature that ESI and MALDI offers, it seems that the peptide size is directly linked to the sequence ID, where MALDI TOF-TOF instruments seem to have improved performance with bigger peptides [2-4].

3. Pathway Analysis

Biological pathways are key regulating functions that are central in many disease areas. The understanding of proteins expressed within disease, their role in signaling pathways and the link to drug discovery and drug development are central in today's target driven pharma processes. Additionally, the detailed understanding of these mechanisms are central to life science in general but particularly to the processes of drug discovery and drug development. An overview of two pathways involved in inflammatory diseases are presented and discussed. Proteomics strategies including global expression analysis as well as focused approaches using multidimensional separation of both gel-, and liquid phase- techniques linked to mass spectrometry is viewed

Examples are given in primary human cell studies from our group where thousands of proteins have been annotated and identified using both electrospray-, and MALDI-sequencing technology [5, 6]. In these studies, transforming growth factor beta (TGF-B) was used as the multifactorial stimulii. Figure 1 illustrates a predictive path of the SMAD pathway upon TGF-B ligand binding to the TGF-BRII.

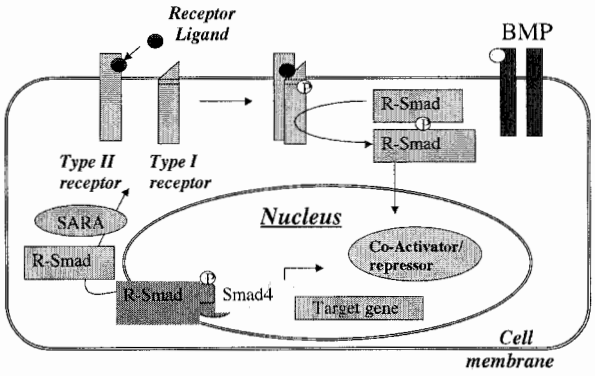

Figure 1. The SMAD pathway

Annotations made from gel images, and chromatography fractionation, interfaced to high end mass spectromery sequence and structure identity are corner stones in cutting edge protein expression

profiling. Phosphorylation mechanisms of kinases whereby the quantitative stoichiometry is determined is presented using affinity probe isolations and micro-preparative sample processing where single target phospho-proteins and their relative phospho-stoichiometry have been analyzed.

4. Laser Capture Microdissection

The study of biological processes within tissues and organs provides an opportunity for measuring the contributions of specific cells within specialized tissue compartments to steady state function and disease development. A key component of this approach is a detailed understanding of global histological features which characterize the heterogenic components of the organ during health and disease.

Within this context, a central goal in many studies focusing on pulmonary disorders is the further understanding of the molecular mechanisms active in promoting structural/functional alterations to key cell phenotypes (ie to the epithelial/matrix lining of the lung and subsequent functional fitness). To address these issues, we have isolated central airway epithelial cells which are a principle element participating in the remodeling of the bronchial wall during chronic allergen challenge using Laser Capture Microscopy (LCM). The aim of this study was to achieve single cell level resolution, from within histologically characterized pulmonary compartments and from where protein expression profiling could be made, while identifying as many unique proteins as possible using high resolution separation and protein identification by mass spectrometry. The combination of methodic histological characterization with LCM, and high resolution MS has allowed a detailed analysis of the submucosa proteome during experimental allergen challenge.

The high degree of cellular homogeneity in the liver and the ordered structure of the organ makes LCM preparations of its cellular constituents extremely favorable. The parenchyma shows a highly regular morphology composed of the unit hepatocytes which surround sinusoids, bile ducts, hepatic arteries, and portal veins. The liver has a relatively dense index of cellularity. This contrasts with organs such as the lung which have a less cellular dense parenchyma but which further contain multiple compartments differing in both specific cellular and histological constituents, and in biological function.

A portion of the liver tissue was scanned with the 30 μm laser in continuous pulses either as adjacent linear regions or as spots. In this experiment the laser firing was handled manually at a high laser pulse frequency. The operator moved the microscope stage and focused and fired the laser with only seconds of interval between pulses. We regularly obtain a control image after the dissection experiment. We analyze this tissue after the capture has taken place as a quality control of the experiments. The image software also allows differential image comparisons where a high fit-level needs to be obtained in order to qualify for further proteomics analysis versus histological topographical location. Our experience also recommends that in cases of pure differential comparative image data, its worthwhile to re-run the LCM part of the sample preparation, rather than pursuing the expression analysis.

An important feature of the proteomics profiling utilizing LCM is the possibility to perform micro environmental cell isolations from tissue prior to analysis.

The results obtained with the developed protocols, show a clear development towards protein profiling, principally in any type of organ tissue, since the cell isolating technology presented is generic in its nature.

Conclusions

There is no clear understanding of the actual number of protein entities that such proteomes have like the human plasma, or any other biofluid or human clinically defined body compartment.

References

[1] Marko-Varga G, and Fehniger T. E., *J. Proteome Res.*, 2004, 167-178
[2] Pettricoin et al., *Lancet*, **359**, 572-577 (2002)
[3] Anderson, N.L. et al, *Mol Cell Proteomics* in press (2004)
[4] Patterson S. D., Aebersold, R. H., *Nature Gen.*, **15**, 1076-1083 (2003)
[5] Malmström, J., Larsen, K ., Malmström, L., Tufvesson, E., Parker, K., Marchese, J., Williamsson, B, Patterson, D, Martin, S., Westergren-Thorson, G., Juhasz, P., and Marko-Varga, G, *Electrophoresis*, 24, 3806-3814 (2003)
[6] Malmström J, Särnstrand, Wieslander E., Lindberg, C., Lindberg H., Bratt C.,and Marko-Varga, G, *Mol. Cell. Proteomics*, in press (2004)

A SELF-CONTAINED, DISPOSABLE CARTRIDGE CONCEPT FOR COMPLETE BLOOD COUNTS

Ulrik Darling Larsen[1], Björn Arthur Ekberg[1], Martin Jensen[2]

[1]*Chempaq A/S, Fruebjergvej 3, 2100 Copenhagen East, Denmark, email: udl@chempaq.com*
[2]*Center for Microtechnology and Surface Analysis, Danish Technological Institute, Denmark*

Abstract

A true Point-Of-Care blood analyzer for counting Thrombocytes, Leucocytes (with three part differential counts: Lymphocytes, Monocytes and Granulocytes) and measurement of Hemoglobin is presented. The apparatus comprises a single use cartridge, called the PAQ, and a stationary Reader with a Cradle for receiving the PAQ. The PAQ includes two independent technologies: a micro machined sensor for impedance cell sizing and an optical absorption measurement system. The test procedure is very simple; the user is only required to apply a drop of blood to the PAQ and place it into the cradle. The rest of the test is carried out automatically within 3 minutes.

Keywords: hematology, point-of-care, cell counting

1. PAQ concept

Complete Blood Counting by impedance cell sizing is used in most Blood Analyzers. The method is based on measurable changes in the electrical impedance produced by comparatively non-conductive cells in an electrolyte as they are passed through a small aperture in a membrane. The PAQ includes a micro machined membrane for impedance cell counting. Thrombocytes, Leucocytes, Lymphocytes, Monocytes and Granulocytes are all counted and differentiated by impedance cell sizing. The Hemoglobin determination is measured as the change in absorbance through a defined location of the PAQ. The PAQ further includes a full liquid handling system with reagent storage, blood sampling, mixing chamber and volume control (figure 1). All necessary electrical and pneumatic connections to the PAQ are established by placing it into the cradle by a simple push fit. The PAQ liquid system has two pneumatic ports connecting with the cradle for causing liquid flow in the PAQ. The PAQ is designed to be disposable after a single use and no liquid or blood is in direct contact with the Reader, whereby maintenance of the Reader is avoided.

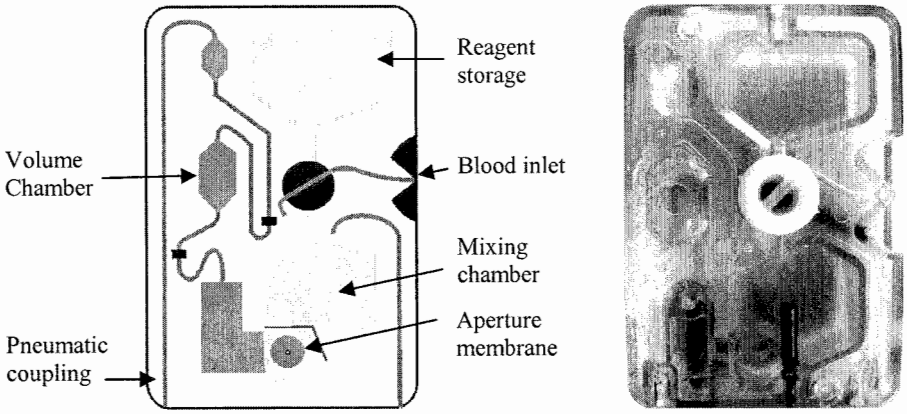

Figure 1. Left: PAQ illustration. Right: Picture of PAQ.

2. Aperture fabrication

Conventional instruments utilizing the impedance technique are based on a fixed membrane with a precision-machined orifice, which is being maintained by flushing and rinsing the membrane. In order to be able to provide single-use cartridges, there is a need for a cheap, single-use membrane material with a precision-machined orifice produced with high accuracy and reproducibility at high speed and low cost. The above-mentioned object is fulfilled by a method of producing an orifice in a polymer membrane by precision laser machining. The sensor apertures were fabricated using an Optec MicroMaster excimer laser workstation operating at 248 nm in a two-step process: First, a 50 μm PET film is thinned using a calibrated laser dose and subsequently a 36 μm hole is drilled through the film in the center of the thinned region (figure 2). The optimized thinning procedure results in a foil thickness of 42.5 μm ± 0.5 μm (not including the foil thickness tolerance).

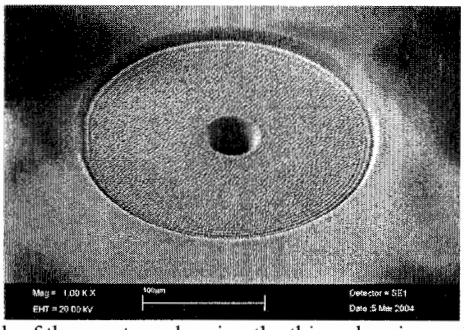

Figure 2. SEM micrograph of the aperture showing the thinned region and the through-hole.

3. Liquid Handling

Sample taking is performed through a capillary in the liquid sample valve with a total volume of 20 μl. The valve is movably positioned in the PAQ so that the capillary initially is positioned for entrance of blood into the capillary, and, in a second position of the valve, is in communication with the reagent storage chamber on one side and the mixing chamber on the other side. Mixing is established with a mixing pin in the mixing chamber of the PAQ driven by a rotating magnet positioned in the cradle. Mixing is initiated right after directing the blood and reagent into the mixing chamber in order to provide a homogeneous exposure to the reagent.

The liquid is directed through the valve, channels and orifice of the PAQ by a vacuum and air pressure, which is established by a membrane pump and controlled through six solenoid valves while the liquid is kept retained inside the PAQ.

The cartridge also comprises volume-metering means for determining the beginning and end of a period during which a predetermined volume of liquid has passed through the orifice. The presence of liquid is detected optically in a channel. The inlet and outlet of the volume metering chamber is formed by narrow channels holding only a small liquid volume compared to the volume of the metering chamber so that the actual positioning of the detection in the channels do not substantially influence the precision of the volume metering.

4. Results

A performance study was carried out with a Beckman Coulter AcT-diff as reference instrument. 58 blood samples were studied for establishment of accuracy and precision.

Analyte	Range ($x10^9$/L)	Correlation factor	CV (%)
Leucocytes	1.4 – 68	1.00	2.4
Thrombocytes	8 – 1170	0.89	11
Hemoglobin	2.9 – 10.7 mmol/L	0.97	1.7
Lymphocytes	0.3 – 20	0.99	-
Monocytes	0.1 – 6.6	0.96	-
Granulocytes	1.0 – 31	0.97	-

Table 1. Results from performance study of 58 blood samples (range is indicated). Accuracy is expressed as a correlation factor and precision is expressed as a coefficient of variation in percent.

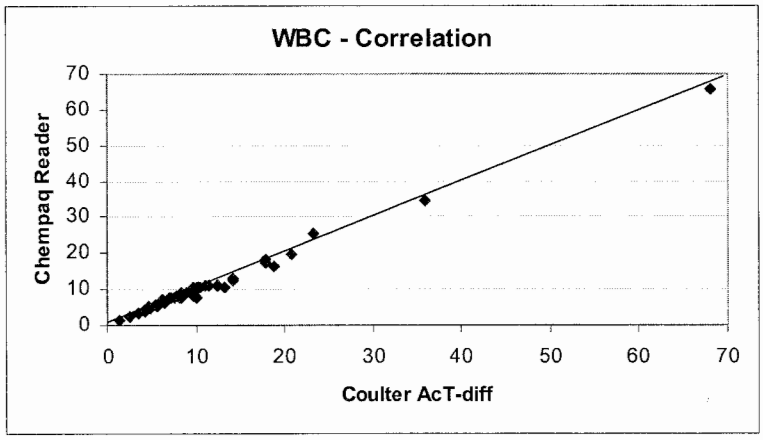

Figure 3. The graph shows the correlation of total white cells. Units are 10^9 cells per liter.

5. Discussion

A true Point-Of-Care hematology analyzer with a performance matching existing analyzers has been developed. The system is easily operated by lay-persons and the test is performed on a single drop of blood. The Chempaq Reader and PAQ constitutes a first-mover product on a market that has been waiting for this to come for many years[2].

References

[1] P. Telleman and U. D. Larsen, "Cell counting and cell sizing in microstructures", Lab-on-a-Chip, Elsevier 2003, pp. 215 – 227

[2] M. Huges, "Market Trends in Point-Of-Care Testing", Point-of-Care journal, vol.1, no.2, 2002, pp. 84-94

ON-CHIP FREE-FLOW MAGNETOPHORESIS - SEPARATION AND DETECTION OF MIXTURES OF MAGNETIC PARTICLES IN CONTINUOUS FLOW

Nicole Pamme[1,2] and Andreas Manz[1,3]

[1]Imperial College London, Department of Chemistry, South Kensington, London SW7 2AY, UK
[2]current address: NIMS, ICYS, 1-1 Namiki, Tsukuba, Ibaraki 305-0044, Japan
[3]current address: ISAS, Bunsen-Kirchhoff-Str. 11, D-44139 Dortmund, Germany

Abstract

In this paper we report an improved microfluidic design for on-chip free-flow magnetophoresis, allowing for complete separation of 2.8 μm and 4.5 μm magnetic particles in continuous flow.

Keywords: magnetophoresis, paramagnetic particles, magnetic field, separation

1. Introduction

Magnetic microparticles are widely used in biomedical sciences as a solid support surface for immunoassays, DNA sequencing and cell analysis. The particles can be easily separated from the bulk of the reaction mixture by means of an external magnetic field. Such separation procedures are conventionally carried out in batches and are thus rather time consuming and labour intensive.

Recently there has been an interest in continuous flow separation of magnetic particles within microfluidic devices [1-2]. In this context, we described on-chip free-flow magnetophoresis (figure 1) as a separation method that is capable of separating magnetic particles not only from non-magnetic material but also different types of magnetic material from each other based on their size and magnetic susceptibility [3].

One of the challenges associated with this method is the reproducibility of the particle deflection. In this paper, we demonstrate an improved microfluidic design for on-chip free-flow magnetophoresis featuring greater deflection reproducibility. This permitted the complete separation of different magnetic particles from magnetic particle mixtures.

2. Theory

The deflection $\mathbf{u}_{defl}$ (in m s^{-1}) of a magnetic particle in the separation chamber is the sum of the magnetically induced flow on the particle, $\mathbf{u}_{mag}$, and the hydrodynamic flow $\mathbf{u}_{hyd}$:

$$\mathbf{u}_{defl} = \mathbf{u}_{mag} + \mathbf{u}_{hyd} \qquad \text{(equation 1)}$$

The magnetically induced flow, $\mathbf{u}_{mag}$, is the ratio of the magnetic force, $\mathbf{F}_{mag}$, exerted on the particle by the magnetic field over the viscous drag force [4]:

$$\mathbf{u}_{mag} = \frac{\mathbf{F}_{mag}}{6 \cdot \pi \cdot \eta \cdot r} = \frac{\Delta\chi \cdot V_p \cdot (\nabla \cdot \mathbf{B}) \cdot \mathbf{B} / \mu_0}{6 \cdot \pi \cdot \eta \cdot r} \qquad \text{(equation 2)}$$

where $\Delta\chi$ is the difference in magnetic susceptibility between the particle and the fluid (dimensionless), V_p is the particle volume (in m^3), $\mathbf{B}$ is the magnetic flux density (in T) and $\nabla \cdot \mathbf{B}$ is the gradient of the magnetic field (in T m^{-1}) of the externally applied field, μ_0 is the permeability of a vacuum (in H m^{-1}), η is the viscosity of the medium (in kg m^{-1} s^{-1}) and r the particle radius (in m).

From equation 2 it can be concluded that for a given magnetic field and solvent medium, the magnetically induced flow is proportional to the particle's magnetic susceptibility and to the square of the particle radius.

3. Experimental

Glass microchips were fabricated using standard lithography methods. The 25 μm deep structure featured a 6 mm x 6 mm separation chamber with 16 buffer inlet channels and 1 sample inlet channel and 16 outlet channels on the opposite side. In contrast to a previously reported design with rectangular junctions between the channels and the chamber (see Figure 2a), the improved design had tapered junctions (see Figure 2b).

Magnetic particles were 2.8 μm and 4.5 μm in diameter (Dynal, Norway) with magnetic susceptibilities of $\chi = 1.07 \times 10^{-4}$ m^3 kg^{-1} and $\chi = 1.6 \times 10^{-4}$ m^3 kg^{-1}, respectively. Flow was controlled by applying negative pressure at the outlet using a syringe pump. A magnetic field perpendicular to the direction of flow was generated by small NdFeB magnets (Magnetsales, UK) with a flux of about $B = 300$ mT, which were placed on the chip beside the separation chamber.

4. Results and discussion

The flow inside the separation chamber was visualized with black ink in the sample reservoir (Figure 2). In the chip with the tapered junctions (Figure 2b) the sample flow was more confined and all sample fluid left the chamber via exit 1. The rectangular junctions (Figure 2a) disrupted the laminar flow, resulting in a more spread out sample fluid flow and some fluid leaving the chamber via exit 2.

For magnetophoresis experiments, a mixture of 2.8 μm and 4.5 μm magnetic particles was added to the sample reservoir and an external magnetic field was applied with NdFeB magnets. With the improved flow design, the 2.8 μm und 4.5 μm particles could be totally separated (Figure 3). For example, at a flow rate of 500 μL h^{-1}, the 2.8 μm particles were deflected towards exit 2 and the 4.5 μm particles were deflected towards exits 3 and 4 (Figure 3b). In contrast, in experiments with the earlier chip design featuring rectangular junctions, the 4.5 μm particles were deflected towards as many as four different exits (Figure 3a). A photographic sequence of the separation of 2.8 μm and 4.5 μm particles is shown in Figure 4. The force on these magnetic particles, $\mathbf{F}_{mag}$, was calculated to be 1.0 pN and 4.5 pN, respectively, using equation 2.

Detection of the separated particles was undertaken by visual observation from video footage and also by particle counting based on laser light scattering detection [5].

5. Conclusions

On-chip free-flow magnetophoresis as a technique for separating magnetic microparticles in continuous flow from each other and from non-magnetic material was improved. Modifications to the flow cell design resulted in a more reproducible and stable particle deflection and thus allowed for the complete separation of 2.8 μm and 4.5 μm Dynabeads. Further improvements to the fluidic design as well as the magnetic field design could be made to develop on-chip free-flow magnetophoresis into a valuable tool for magnetic separation.

Acknowledgements

The authors would like to acknowledge Asahi Kasei Corporation for financial support.

References

[1] C. B. Fuh, H. Y. Tsai and J. Z. Lai, *Anal. Chim. Acta*, **197**(1-2), 115-122 (2003).
[2] N. Chronis, W. Lam and L. Lee, *Micro Total Analysis Systems 2001*, 497-498.
[3] N. Pamme and A. Manz, *Micro Total Analysis Systems 2002*, 326-329.
[4] G. P. Hatch and R. E. Stelter, *J. Magn. Magn. Mat.*, **225**(1-2), 262-276 (2001).
[5] N. Pamme, R. Koyama and A. Manz, *Lab on a Chip*, **3**(3), 187-192 (2004).

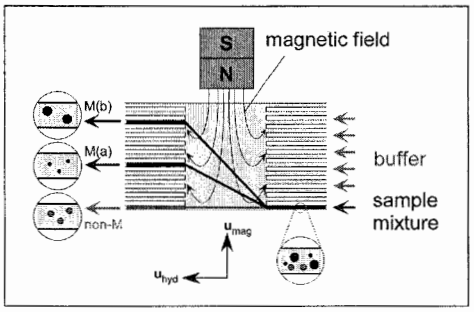

Figure 1. The principle of free-flow magnetophoresis: A magnetic field is applied over a rectangular flow chamber perpendicular to the direction of laminar flow. Magnetic particles (M) are dragged into the field depending on their size and magnetic susceptibility. They are thus separated from each other and from non-magnetic material (non-M).

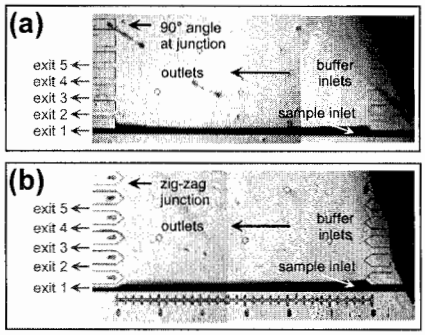

Figure 2. Comparison of the flow within the separation chamber visualised with black ink in the sample reservoirs: In the previously reported design (a) the flow from the sample inlet left the separation chamber via exit 1 and a small fraction also left via exit 2. In the improved design (b) all sample fluid left the separation chamber via exit 1.

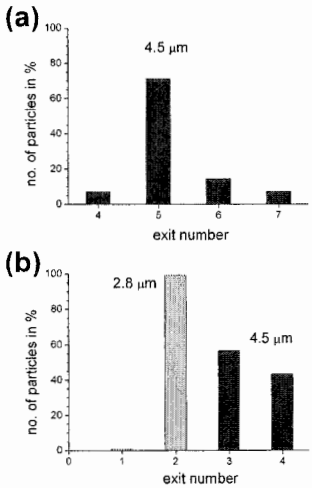

Figure 3. (a) With the initial microchip design, the 4.5 µm particles were deflected towards four different exits. (b) With the improved design, the particle deflection could be controlled to one or two exits. Thus, separation of 2.8 µm and 4.5 µm particles was possible.

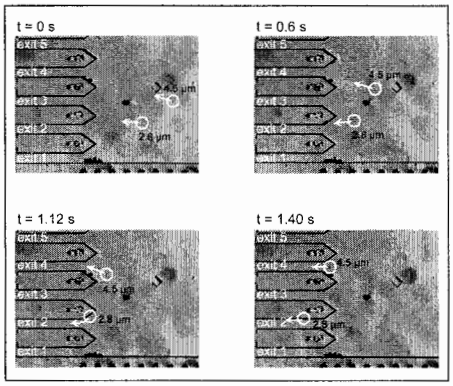

Figure 4. Photograph sequence of the separation of a mixture of 2.8 µm and 4.5 µm magnetic particles in the improved chip design.

A NOVEL APPROACH FOR MINIATURIZED *IN VITRO* PROTEIN EXPRESSION IN MICROFLUIDIC CHANNELS

Petra S. Dittrich [1,3] **Michael Jahnz** [2,3] **and Petra Schwille** [2,3]

[1]*Dept. Miniaturization, Institute for Analytical Sciences, Bunsen-Kirchhoff-Str. 11, D-44139 Dortmund, Germany*

[2]*Institute of Biophysics, BIOTEC, Dresden University of Technology, Tatzberg 47-51, D-01307 Dresden, Germany*

[3]*This work was performed in the Experimental Biophysics Group, Max Planck-Institute for Biophysical Chemistry, Am Faßberg 11 , D-37077 Göttingen, Germany*

Abstract

In this study, we show the cell-free expression of the green fluorescent protein (GFP) in monodisperse water-in-oil emulsion droplets generated in a microfluidic channel. In combination with high sensitivity detection techniques such as confocal fluorescence spectroscopy, mixing of different reactants can be controlled, and sensitive high throughput analysis of the individual droplets becomes feasible.

Keywords: microreactors, microemulsion, fluorescence, molecular evolution, biotechnology

1. Introduction

The search for new or modified protein functionality is a central theme of molecular biotechnology and pharmacological drug design. For high throughput screening of protein function, both the sensitivity of analytical systems, and the efficiency of protein expression, have to be significantly enhanced, to enable fast, inexpensive and miniaturized assays. Furthermore, for evolution and selection of optimized biocatalysts, protein expression in individual compartments is an indispensable requirement [1]. In a microfluidic chip, small microreactors of homogeneous size distribution could be created continuously by generation of a water-in-oil emulsion [2]. By addition of tiny quantities of reagents to the aqueous phase, such as encoding DNA, RNA, enzymes and amino acids, compartmented in-vitro protein expression could be performed.

2. Experimental

The Poly(dimethylsiloxane) (PDMS, Sylgard 184, Dow Corning) channels were imprinted from a silicon master (GeSim, Großerkmannsdorf, Germany) and sealed with a glass plate as described before [3].

High sensitivity fluorescence detection of passing emulsion droplets was performed using a confocal setup [3]. Here, an Argon ion laser (Lasos, Jena, Germany) at 488 nm was used for excitation of the Green Fluorescent Protein. Optical filters introduced in the beam path were the dichroic mirror 500 DCLP and the band pass filter 525 DF 50 (purchased from AHF, Tübingen, Germany). Images were taken by a CCD camera (CCD 260 sw/w, Spindler and Hoyer, Göttingen, Germany) mounted on the ocular tubus of the microscope.

The hydrophobic phase of the emulsion consisted of transparent mineral oil (Sigma) mixed with 5 % (v/v) SPAN 80 (Fluka). For the mixing experiments, GFP (Clontech) was dissolved in deionised water.

For *in vitro* translation, S-30 extract and reaction mix were prepared according to Lesley [4]. Supercoiled DNA template with T7 promotor and T7-RNA-polymerase (Invitrogen life technologies) were added. For expression of the red-shifted green fluorescent protein (rsGFP), we used the 6,361 bp plasmid pQBI63 (Quantum Biotechnologies Inc.).

3. Results and discussion

By introducing an aqueous solution into a hydrophobic fluid, up to 30 droplets per second are continuously formed with a homogeneous diameter of ~ 5 µm, corresponding to volumes of less than 100 fl. Mixing of different solutions was achieved by merging two input channels directly before droplet formation (Fig. 1).

Since adjusting the concentration of all necessary components is quite sensitive for the *in vitro* translation of proteins, a stable and reliable supply of the solutions is indispensable. We first checked the mixing performance of the microfluidic device by supplying two fluorescent solutions of GFP (37 nM and 2.3 nM) in the respective input channels. We controlled the liquid supply by determination of the flow velocity in each input channel by Fluorescence Correlation Spectroscopy [5]. Measurements of the fluorescence intensity of the formed droplets allowed to estimate the degree of dilution (Fig. 3).

Using this microfluidic device, we could show the *in vitro* transcription and translation of Green Fluorescent Protein (GFP). All reaction compounds were united during droplet formation, and the generated emulsion was stored in a reservoir at the end of the channel. After heating at 37°C for 40-50 minutes on a heating plate, the expression of GFP in the emulsion droplets could be verified by an increased fluorescence intensity (4-6 fold of the initial signal) of the emulsion droplets due to the autocatalytic formation of the chromophoric group (Fig. 2).

4. Conclusions

We introduced a microfluidic device for cell-free protein expression. The system is suitable for automation and could allow expression and characterization of large protein libraries in further studies, while supplementary functional units, e.g. for droplet sorting, could be implemented easily.

Acknowledgements

We thank D. Link (DEAS, Harvard University) for discussion. Financial support was provided by the German Ministry for Education and Research (Biofuture Grants nos. 0311845 and 16SV1257).

References

[1] D.S. Tawfik and A. D. Griffiths, Nature Biotechn. **16**, 652-656 (1998).
[2] H. Song, J. D. Tice and R. F. Ismagilov, Angew. Chemie, **115**, 792-796, (2003).
[3] P.S. Dittrich and P. Schwille, Anal. Chem., **75**, 5767-5774 (2003).
[4] S. A. Lesley, Methods Mol. Biol., **3**, 265-278 (1995).
[5] P.S. Dittrich and P. Schwille, Anal. Chem., **74**, 4472-4479 (2002).

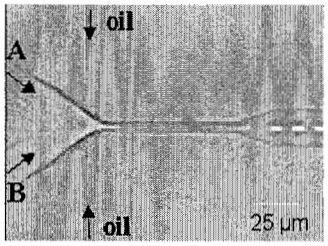

Figure 1. Formation of droplets in the microfluidic channel, the solutions "A" and "B" are mixed during droplet formation

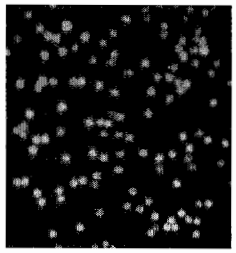

Figure 2. Fluorescent aqueous droplets (diameter: 5 µm) due to the expression of the Green Fluorescent Protein (illuminated by a mercury arc lamp).

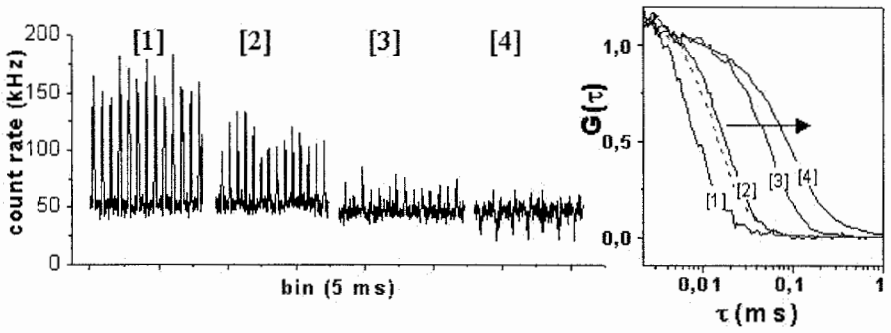

Figure 3. Detection of passing emulsion droplets by confocal fluorescence spectroscopy. Here, two different concentrated solutions of GFP (2.3 and 37 nM) were mixed during droplet formation. While the flow velocity of the 2.3 nM solution in the input channel stayed constant (right, autocorrelation curve, dashed line, v = 50 mm/s at the channels centre), the velocity of the high concentrated solution was reduced (80 mm/s – 1 mm/s, the arrow indicates decreasing flow velocity). The intensity of the fluorescence bursts in the periodic fluorescence trace (left) indicate the degree of dilution.

.

IMPEDANCE SPECTROSCOPY FLOW CYTOMETRY: PARAMETERS FOR LABEL-FREE CELL DIFFERENTIATION

Karen Cheung, Shady Gawad and Philippe Renaud
Microsystems Laboratory, STI-LMIS
Swiss Federal Institute of Technology Lausanne (EPFL), CH-1015 Lausanne, Switzerland

Abstract

This work presents label-free separation of cells in an on-chip flow cytometer based on impedance spectroscopy. The amplitude, opacity, and phase information can be used for discrimination depending on the cell types. Red blood cells, ghosts, and fixed cells are differentiated based on differences in their membrane and cytoplasm dielectric properties. Among other applications, detecting changes in cell conductivity and membrane capacitance will allow the indentification of early-stage apoptosis or cancer.

Keywords: impedance spectroscopy, label-free, separation, flow cytometry

1. Introduction

As a non-invasive technique, dielectric spectroscopy is suitable for the characterization of living biological cells. Impedance measurements over a wide frequency range give information on cell size, membrane capacitance, cytoplasm conductivity, and cytoplasm permittivity as a function of frequency [1]. This information can be used to distinguish cell populations without the need for fluorescent, magnetic, or other cell markers.

The impedance spectroscopy flow cytometer used here permits rapid dielectric characterization of a cell population with a simple microfluidic channel [2]. As cells flow individually through the detection area of the microfluidic channel, they are measured at two discrete frequencies which are applied simultaneously. The reference frequency is kept low and constant, while the second frequency is swept from 300 kHz to 20 MHz. The amplitude and phase information from the individual cells are averaged to give an impedance spectrum for the entire population.

2. Theory

Biological cells are polarized in an AC electric field. At low frequencies, the cell is essentially nonconducting due to the plasma membrane, which does not allow the passage of current. The low frequency conductivity is the impedance parameter detected in a Coulter volume measurement, and particles of the same volume but different dielectric properties will not be differentiated solely with measurements at low frequencies. At intermediate frequencies, this membrane polarization decreases. This phenomenon is known as the beta dispersion, or dielectric relaxation. Measurements in the intermediate range of the β-dispersion give information about plasma membrane properties. At high frequencies, the plasma membranes are minimally polarized, and measurements here give information about the dielectric properties of the cell interior. The ratio of the impedance amplitude at a high frequency to a low frequency, also known as opacity, can be used as a measure of the difference in particle resistivity at the two frequencies [3]. Relative phase is defined as the difference of phase to a reference signal. The amplitude, opacity, and/or phase can be used to discriminate between different cell populations; the key parameter(s) will depend on the cells under consideration.

3. Experimental

Three cell models were used: red blood cells (RBCs), ghosts, and RBCs fixed in glutaraldehyde. Fresh blood was collected from healthy human donors in heparinized tubes. After

centrifugation, the buffy coat and plasma proteins were removed. The RBCs were washed and suspended in phosphate-buffered saline (PBS).

RBC ghost preparation: RBCs were suspended in a hypotonic solution which lyses the cells and releases the cell contents. The membranes were washed and resuspended in PBS to reseal the membrane sacks. The resulting ghosts are clear membranes filled with saline solution.

RBCs fixed in glutaraldehyde: RBCs were suspended in various concentrations of glutaraldehyde (0.02, 0.2, 0.5, 2.0, 5.0%) in PBS and incubated for 1 hour at room temperature. Glutaraldehyde fixation cross-links protein amine groups in the lipid membrane. The fixed cells were washed and resuspended in PBS.

4. Results and discussion

Since RBCs, RBC ghosts, and fixed RBCs are all similar in size, they can not be differentiated using impedance signal amplitude (Fig. 1). The opacity of RBCs above 1 MHz increases with increasing glutaraldehyde concentration (Fig. 2). With opacity, RBCs and ghosts follow the same trend and cannot be discriminated (Fig. 3). In contrast, the fixed cells appear more opaque than normal cells and are differentiated at high frequencies. In the low frequency range, where the measurement only gives information about cell size, the opacity spectra for normal RBCs and fixed RBCs overlap. As the measurement passes the dielectric relaxation, the spectra for normal RBCs and fixed RBCs diverge. The relative phase above 10 MHz indicates that the ghosts, which are filled with the buffer solution, are more conductive on the interior than RBCs (Fig. 4).

Increased opacity in the high frequency range can be attributed to a decrease in cytoplasm conductivity. Both a decrease of ion mobility and the fixation of proteins within the cytoplasm can contribute to decreased cytoplasm conductivity. Red blood cells fixed using increasing concentrations of glutaraldehyde show increasing opacity, possibly indicating a higher degree of crosslinking between cell membrane and the cytoskeleton. A change in the membrane properties will shift the characteristic frequency of the beta dispersion and change the opacity spectrum. While normal RBCs are modeled as thin membranes surrounding a conductive interior, cross-linking of cell proteins using glutaraldehyde could have bonded the cytoplasmic membrane proteins more tightly to the membrane. Since capacitance scales inversely with distance of charge separation, merging the thin membrane with a thicker layer of cytoplasmic proteins effectively increases the membrane thickness and decreases membrane capacitance.

5. Conclusions

Measurements from several frequency regions give information about the dielectric properties of the membrane and cytoplasm since cell membranes exclude low-frequency currents and pass high-frequency currents. Red blood cells, ghosts, and fixed cells are differentiated based on differences in their membrane and cytoplasm dielectric properties. This label-free method implemented in a microfabricated flow cytometer is a powerful tool for the characterization of cells. Future work will aim to distinguish more subtle differences between cell types.

Acknowledgements

This work was funded by the Swiss Innovation Promotion Agency (CTI project 5803.1) and LEISTER Microsystems. Microfabrication was done in the Center of MicroNanoTechnology (CMI).

References

[1] K Asami, T Yonezawa, H Wakamatsu, N Koyanagi, *Bioelectrochemistry and Bioenergetics*, 40 (1996) 141-145.

[2] S Gawad, L Schild, Ph Renaud, *Lab on a Chip*, 1 (2001) 76-82.

[3] RA Hoffman, TS Johnson, WB Britt, *Cytometry*, 1:6 (1981) 377-384.

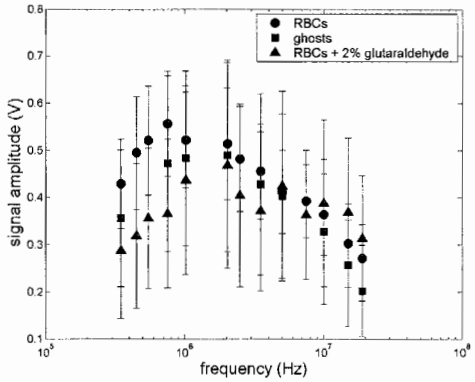

Figure 1. Amplitude measurements of RBCs, fixed RBCs, and ghosts show no differentiation based on signal amplitude since the cells are similar in size. Amplitude measurements are taken at a single frequency. The low frequency conductivity is the impedance parameter detected in a Coulter volume measurement.

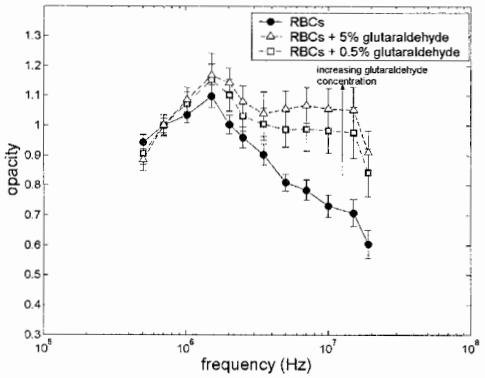

Figure 2. Opacity measurements of RBCs and fixed RBCs. Opacity is defined as the ratio of signal amplitude at a given frequency to a low frequency (602 kHz) amplitude. Glutaraldehyde fixation crosslinks the cytoskeletal network and decreases cytoplasm conductivity. The high frequency opacity increases with increasing glutaraldehyde concentration.

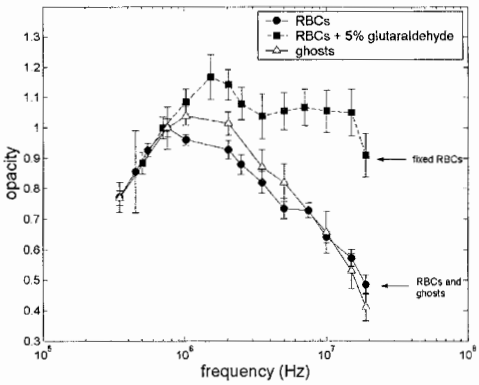

Figure 3. Opacity measurements of RBCs, ghosts, and fixed RBCs. RBCs are not discriminated from ghosts by opacity, while fixed cells and RBCs are clearly differentiated in the high frequency range of opacity.

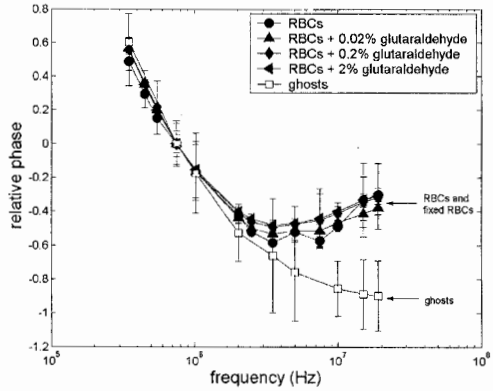

Figure 4. Relative phase measurements of RBCs, ghosts and fixed RBCs. Relative phase is defined as the difference of phase to a reference signal (602 kHz). RBCs and fixed RBCs are well differentiated from ghosts at high frequency by the phase information.

Each point represents measurements from ~ 800 cells.

IMPEDANCE SPECTROSCOPY FLOW CYTOMETRY: MODEL VALIDATION

Shady Gawad, Karen Cheung and Philippe Renaud
Microsystems Laboratory, STI-LMIS, EPFL, CH-1015 Lausanne, Switzerland.

Abstract

A number of microfabricated flow cytometry devices have been proposed based on electrical[1, 2] or optical[3] detection techniques. On chip marker-free differentiation of cells using impedance spectroscopy was demonstrated between leukocyte sub-populations and on erythrocytes+ghosts mixtures.[4] The detection part of the chip includes 4 microelectrodes patterned on the top and bottom walls of a rectangular microchannel which define two detection volumes (Figure 1). Although preliminary results showed the potential of the impedance measurement using specific frequencies, a systemic approach is required to determine an optimal set of discrimination frequencies for cell sorting.

Keywords: cytometry, impedance spectroscopy, label-free, *SPICE* model, cell sorting

1. Introduction

The impedance spectrum of cells in the 100 kHz to 20 MHz frequency range is dominated by the Maxwell-Wagner interfacial dispersion due to the charging of the cell membrane. This effect is also called β-dispersion. A set of equations derived from the mixture theory for spheres covered with a thin shell is generally used to model impedance spectra of cell suspensions.[5] Such a model can likewise be applied to single cell measurement in a miniaturized detection volume.[6] Still, the interpretation of the measured data is made difficult by electrode polarization and parasitic capacitor effects which render the system sensitivity frequency dependent.

2. Methods

The measured spectrum of a specific cell population is determined using a population averaged frequency sweep technique where two discrete frequencies are employed simultaneously. The low reference frequency is kept constant (500 kHz) while the other is used for the sweep. The ratio of the data taken at those two frequencies is used to suppress size and position dependence of the measurement; the obtained parameter is the cell opacity at a given frequency.

Sine wave generators (Agilent, 33220A) are used to drive the measurement electrodes and a separate radio-frequency lock-in amplifier (Stanford research, SR844) demodulates and amplifies each frequency. A typical experiment includes 15 frequency points measured consecutively in a mixed order. For each frequency point, the data of ~1000 cells is acquired in order to obtain a significant sample. The acquisition of a whole spectrum typically takes 20-30 minutes. This time can be reduced either by measuring at more than two frequencies simultaneously or by selecting a set of characteristic frequencies for discrimination. Measurements are done using calibrated polystyrene beads and freshly harvested red blood cells collected in heparinized capillary tubes. The particles and cells are suspended in PBS at a dilution of $10^7 \cdot ml^{-1}$ in order to limit the number of concurrent events while achieving a throughput of 10-15 $cells \cdot s^{-1}$. Dielectrophoretic barriers are used to focus the particle to the channel centreline before the measurement.

An electrical model based on a *SPICE* circuit simulation is used to obtain a parametric study of the system. The mixture theory based sub-circuit (Figure 2) represent the chip detection volumes with and without the presence of a cell or bead. Cell size, membrane capacitance and cytoplasm conductivity can be varied for parametric analysis. The model electrodes dimensions and the related double layer capacitances can also be varied to study the influences of the chip design. Values taken

from measurements have been used for the double layer capacitance per unit surface. It is also possible to determine the effect on the sensitivity of the suspending medium conductivity and of various parasitic stray capacitances. The sub-circuit model representing the chip and the biological sample is then placed in a custom broad-band electronic amplification circuit model. The amplification electronic consists of two I-V converters followed by a differential amplification stage. Output noise and measurement bandwidth of the whole system can thus be evaluated and compared with measured values.

3. Results

Beads are useful in determining the sensitivity spectrum of the instrument as they do not present a dielectric dispersion in the radio frequency range. The opacity spectrum is similar for all measured bead dimensions (4, 5 and 6 μm) and shows a sensitivity plateau in the 1-15 MHz range (Figure 3).

The size measurement coefficient of variation is currently ~3%, which corresponds to a sizing resolution of the order of 50 nm on a 5 μm particle diameter. Measurements of red blood cells typically show a larger size distribution due to the cell population size scattering. The effect of this scattering is largely reduced by considering the size independent opacity spectrum.

For red blood cells the measured spectrum drops for frequencies above 3 MHz due to the passage of current through the cell interior (Figure 3).

Results from the *SPICE* circuit model using the mixture equation equivalent circuit correlate well with the measured data for both beads and cells in the frequency range of interest. The typical spectra shapes simulated for cells and beads are shown in Figure 4.

4. Conclusions

The simulation results predicts the measurement sensitivity windows of the instrument for an insulating bead model and includes electrode surface effects and stray capacitance effects. The mixture equation equivalent circuit accurately models the cell impedance spectrum. The population averaged frequency sweep measurement technique provides a simple way to validate the chip model and can be used to determine a set of frequencies for rapid single cell discrimination based on impedance sensing.

Acknowledgements

This work was funded by the Swiss Innovation Promotion Agency (CTI project 5803.1) and LEISTER Microsystems. The authors also would like to thank the CMI for clean room support.

References

[1] Fuller, C. K.; Hamilton, J.; Ackler, H.; Gascoyne, P. R. C., Microfabricated multi-frequency particle impedance characterization system, In *Micro Total Analysis Systems 2000*, Kluwer: Enschede, The Netherlands, (2000); pp 265.

[2] Gawad, S.; Schild, L.; Renaud, P., *Lab on a Chip*, (2001) 1, 76.

[3] Fu, A. Y.; Spence, C.; Scherer, A.; Arnold, F. H.; Quake, S. R., *Nat Biotechnol*, (1999) 17, 1109.

[4] Gawad, S.; Batard, P.; Seger, U.; Metz, S.; Renaud, P., Leukocytes discrimination by impedance spectroscopy flow cytometry, In *Micro Total Analysis Systems 2002*, al., Y. B. e. Ed. Kluwer: Nara, Japan, (2002); Vol. 2, pp 649.

[5] Foster, K. R.; Schwan, H. P., Dielectric properties of Tissue, In *CRC Handbook of biological effects of electromagnetic fields*, C., P.; Postow, E. Eds.; (1995); p 618.

[6] Gawad, S.; Cheung, K.; Seger, U.; Bertsch, A.; Renaud, P., *Lab on a Chip*, (2004) 4, 241.

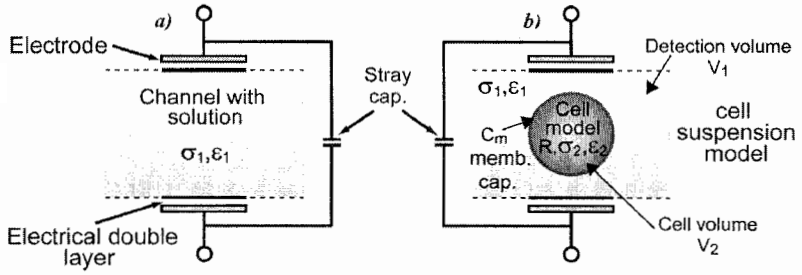

Figure 1. Measurement principle of differential single cell impedance spectroscopy in microfluidic channels. a) Two electrodes are used to determine a reference volume. b) The cell is passing through two different measurement electrodes. The volume fraction p of the cell is $p = V_1/V_2$. R is the cell radius.

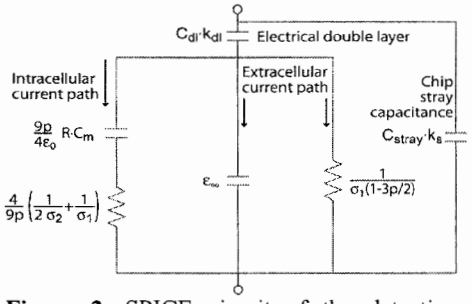

Figure 2. SPICE circuit of the detection volume with a cell equivalent model. Electric double layer and stray capacitance effects are also included. ϵ_∞ is the high frequency limit dielectric value of the detection volume with a cell present.

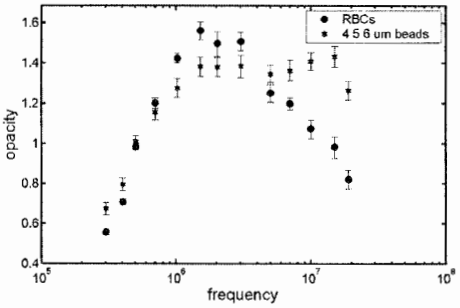

Figure 3. Opacity measurement of RBCs and polystyrene beads in the 300 kHz-20MHz range. The RBCs show a β-dispersion near 3MHz, while the beads have a flat opacity spectrum. Opacity is particle size independent.

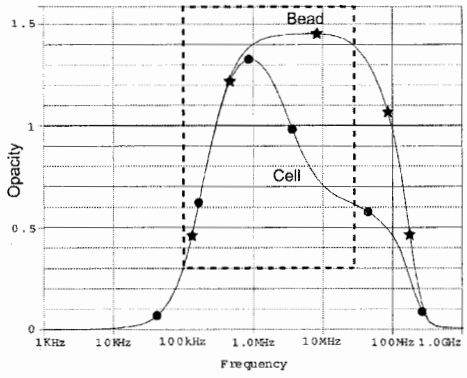

Model parameters:

Ext. medium	$\sigma_1 = 1.2$ S/m, $\varepsilon_1 = 78$
Int. medium	$\sigma_2 = 0.6$ S/m, $\varepsilon_2 = 60$
Membrane capa.	$C_m = 1 \cdot 10^{-2}$ F/m
Cell radius	$R = 2.5$ µm

Figure 4. Spice simulation results for RBCs and bead models. The doted area represents the measurement range of figure 3. The β-dispersion in the cell model as well as the effect of the double layer and stray capacitance are clearly visible.

MULTIPLEXED MICROFLUIDIC DEVICES FOR SINGLE-CELL MANIPULATION AND ANALYSIS

S. Ramachandra Rao[1,2], Shohei Yamamura[1,2], Yuzuru Takamura[2] and Eiichi Tamiya[2]
[1]Toyama New Industry Organization, 529, Takada, Toyama, 930-0866, Japan
[2]School of Materials Sciences, Japan Advanced Institute of Science and Technology, 1-1, Asahidai, Tatsunokuchi, Ishikawa, 923-1292, Japan (srrao@jaist.ac.jp)

Abstract

This study demonstrates sorting and analysis of single B-cells, in order to develop high affinity monoclonal antibody, in the aqueous compartments that are generated by the two-phase liquid systems in the microchannels of poly(dimethylsiloxane) (PDMS)-based devices. PDMS devices with Y-shaped microchannels having dimensions of 50 x 50 μm^2, 100 x 100 μm^2 width and depth were used in this study to generate compartments of aqueous and non-aqueous (mineral oil) solutions in the microfluidic channels, achieved under pressure-driven flow. Further, multiplexed sorting of polystyrene beads per each aqueous compartment was achieved when fluorescent polystyrene beads (4.5 μm) in aqueous solution, and mineral oil as non-aqueous solution were introduced into microchannels of a microfluidic device.

Keywords: Microfluidic device, multiplexing, two-phase liquids, single-cell analysis, B-cell

1. Introduction

The separation and analysis of single B-cell from a bulk cell suspension plays an important role in understanding the prognosis and clinical diagnosis of a disease, which favors the development of a high affinity monoclonal antibody as a curable clinical medicine. Conventional fluorescent-activated cell sorters, although, are used for efficient sorting of cells, are costly and its application is limited only to the sorting and lacks analysis. Therefore, this study focuses on construction of an inexpensive microfluidic device coupled with two-phase liquids that enables generation of aqueous and non-aqueous liquid compartments in the microfluidic channels. This novel system makes it possible to sort out single B-cell per each aqueous compartment and also facilitates multiplexed analyses of antigen specific single B-cells by stimulation with antigen. Further analysis of DNA of antigen specific single B-cells lead to development of high affinity monoclonal antibody.

2. Fabrication of a microfluidic device

The PDMS microfluidic chip was fabricated by soft-lithography technique. The master was fabricated from silicon wafer, SU-8 50 (Microchem, USA). A negative photo resist, was applied onto a Si wafer to defined thickness and was exposed to a photo mask with the microchannel design. The resulting SU-8 mold was used for PDMS chip fabrication. Monomers of PDMS and its curing agent (Dow Corning, Sylgard 184 Silicone elastomer) at 10:1 volumes were mixed thoroughly and removed the air bubbles that are generated while mixing under vacuum and the mixture was poured on to a SU-8 mold and cured at 80°C for 60 min. The PDMS chip was then peeled off from the SU-8 mold and two inlets and outlet were drilled manually and tubing was done and sealed. The resulting PDMS microfluidic chip surface was rendered hydrophilic by reactive ion etching and attached hermitically to a glass substrate. PDMS/glass chip device with Y-shaped microchannels with varying contact angles ranging from 60°-120° having dimensions of 50 x 50 μm^2 and 100 x 100 μm^2 width and depth were used in the sorting and analysis of single B-cells and fluorescent polystyrene beads. The schematic representation of microfluidic devices for single-cell handling and analysis employing two-phase liquids is shown in (Fig. 1).

3. Experimental

Microfluidic device was mounted on fluorescence stereomicroscope (Leica MZ FLIII, Switzerland) integrated with Fluo III filter system with APO 1.0 X lens objective. A 100W mercury 106Z lamp (Leica, Switzerland) provided epifluorescence excitation and the fluorescence image was collected by GFP 3 filter and the imaging was carried out by AxioCam colour CCD camera (Carl Zeiss, Germany). Aqueous and non-aqueous mineral oil solutions were pumped using 100 μL Hamilton Gastight syringes (1710 series, TLL). Microsyringe pumps from EiCom apparatus (ESP-64, Japan) were used to infuse the aqueous sample and non-aqueous mineral oil solutions. Aqueous 0.1% (w/v) FITC solution and mineral oil (Sigma, USA) were introduced independently with flow rates of 1.0 μL/min each. Fluoresbrite^{TM} carboxy yellow green polystyrene beads (4.5-μm) (Polysciences Inc. USA) working solution 1x10^5/mL was prepared in Milli Q as aqueous phase, while mineral oil as non-aqueous phase was introduced into inlets of a microfluidic device using 100 μL Hamilton Gastight syringes with a flow rates of 0.2 μL/min.

4. Results and discussion

PDMS/glass microfluidic devices with Y-shaped microchannels having dimensions of 50 x 50 μm^2, 100 x 100 μm^2 width and depth used in this study were fabricated by standard soft-lithography techniques (Fig. 2a). The generation of stable and uniform size compartments accommodating nanoliter volumes of aqueous (FITC) and non-aqueous (mineral oil) solutions in the microfluidic channels was achieved at a flow rates of 1.0 μL/min each under pressure-driven force (Fig. 2b), those were suitable for rapid single-cell sorting and multiplexed analyses. The volume of solution injected into each compartment is directly proportional to the volumetric flow rate of the solution at the time when the compartment formed. Therefore, the size of each compartment can be varied by varying flow rates of that solution entered into the microchannel. The recent research reported on single-cells separation on the microchip formats, lack multiplexed separation of large number of single cells from bulk suspensions [1, 2]. The design of channel geometry, contact angle, flow rates of liquids, surface tension, and the viscosity of the liquids are the major determining factors of the compartmentalization phenomena of non-aqueous and aqueous solutions in the microchannels. Using fluorescence microscope built-in CCD camera, the sorting of a single fluorescent polystyrene bead in each aqueous compartment is achieved (Fig. 3a & b). Multiplexed sorting of single polystyrene beads per each aqueous compartment in the microchannels of a device was achieved using two-phase liquids. The results revealed that this system could be applied for both sorting and analysis of single B-cells for development of highly specific monoclonal antibody.

5. Conclusions

The microfluidic device that was demonstrated provides a platform for sorting and analysis of single-cells or particle and also to perform various other bio-assays in the aqueous compartments without any cross contamination with its neighboring compartment due to presence of a non-aqueous phase and thereby facilitating multiplexed analyses on a single chip format.

Acknowledgements

This work was funded by Toyama Medical Bio-cluster project of Toyama New Industry Organization sponsored by the Ministry of Education, Culture, Science and Technology.

References

[1] A.R. Wheeler, W.R. Throndset, R.J. Whelan, A.M. Leach, R. N. Zare, Y.H. Liaor, K. Farrell, I.D. Manger, and A. Daridon, *Anal. Chem.*, **75**, 3581-3586 (2003).
[2] W.H. Huang, W.Cheng, Z. Zhang, D.W. Pang, J.K. Cheng, and D.F. Cui, *Anal. Chem.*, **76**, 483-488 (2004).

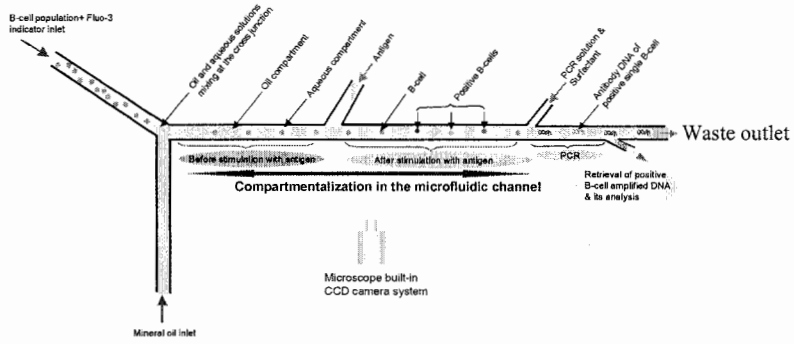

Fig. 1. Schematic representation of microfluidic devices for single-cell handling and analysis employing two-phase liquids

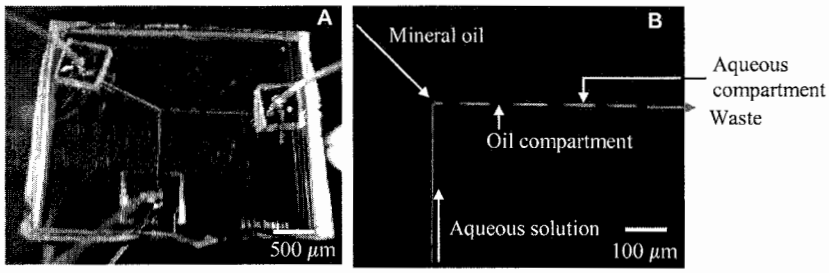

Fig. 2. Microfluidic device (A) and the compartmentalization of mineral oil and fluorescent aqueous liquids in the micro channels (100 x 100 μm^2) of PDMS/glass device (B), flow rates of the liquids were maintained at 1.0 μL/min.

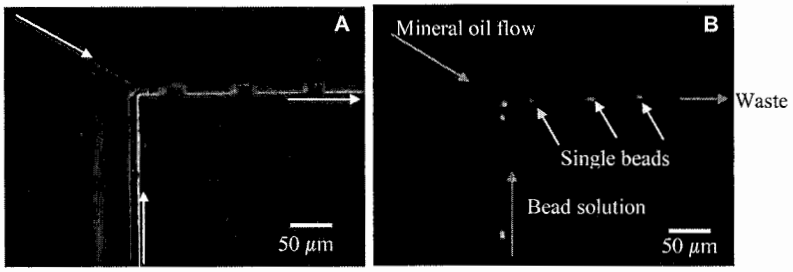

Fig. 3. Light and fluorescent microscopic images (A, B) of single fluorescent polystyrene bead (4.5 μm diameters) sorting in the aqueous compartments of micro channels (50 x 50 μm^2), flow rates of the liquids were maintained at 0.2 μL/min.

EVALUATION OF CELL ELECTROPHORETIC MOBILITY USING MICROCAPILLARY ELECTROPHORESIS CHIPS

Fumihiro Omasu[1], Yuta Nakano[2], Takanori Ichiki[1, 3]

[1]PRESTO, Japan Science and Technology Agency, 4-1-8 Honcho, Kawaguchi, Saitama, Japan
[2]Dept. of Electric and Electronics Eng., Toyo University, 2100 Kujirai, Kawagoe, Saitama, Japan
[3]School of Engineering, The University of Tokyo, 2-11-16 Yayoi, Bunkyo-ku, Tokyo, Japan

Abstract

Cell membrane proteins contain specific and beneficial information about individual cells. The measurement of cell surface charge is a promising method for characterizing individual cells. Recently, we reported the measurement of cell electrophoretic mobility (EPM) using microcapillary electrophoresis (μCE) chips. The surface modification of the inner walls of microchannels is essential to prevent the nonspecific adhesion of cells and obtain correct electrophoretic velocity without artifacts due to cell-wall interactions. In the present study, we examine chips coated with three different reagents and measure the EPM of sheep erythrocyte for a range of pH values. The zeta potential of the cell surface was estimated from these data. Cell EPM obtained using μCE chips increased with increasing pH. In conclusion, this work demonstrates the reproducibility and accuracy of cell EPM data measured using μCE chips over a wide range of pH.

Keywords: cell electrophoresis, sheep erythrocyte, pH, electrophoretic mobility, zeta potential

1. Introduction

The measurement of cell surface charge is a promising method for characterizing individual cells [1]. Recently, we reported the measurement of cell electrophoretic mobility (EPM) using microcapillary electrophoresis (μCE) chips [2]. Small sample volume, automation and easy disposability as medical waste are some advantages of μCE chips. Moreover, the distribution of EPM values obtained using μCE chips was revealed to be sufficiently narrow compared with those obtained using other conventional devices [2, 3]. Nevertheless, there remain issues to be studied for the establishment of its practical application. For example, an adequate surface coating on microchannel walls is needed to suppress the nonspecific adhesion of cells and obtain correct EPM without artifacts due to cell wall interactions. In this study, we examined three different reagents for coating microchannel walls in μCE chips, and discuss the reproducibility and reliability of cell EPM data measured using μCE chips through the comprehensive measurement of EPM and zeta potentials.

2. Experimental

Microchannels of 30 μm depth and width were engraved by deep RIE on a 20 by 20 mm quartz plate. The inner surfaces of the microchannels are coated with bovine serum albumin (BSA), 2-methacryloyloxyethylphosphorylcholine (MPC) polymer or gelatin. Phosphate-buffered saline (PBS) of pH4-9 was used as a migration buffer. Movies of migrating sheep erythrocyte cells, which were recorded using a charge-coupled device (CCD) camera (Fig.1), were analyzed by particle tracking velocimetry (PTV) software (Fig.2). Electroosmotic flow (EOF) mobility was measured using charge-free beads. The EPM of cells was calculated from using equation: $U_{ep} = U_{app} - U_{eo}$, where U_{ep}, U_{app} and U_{eo} are EPM, apparent EPM and EOF mobility, respectively. According to the Smoluchowski formula, zeta potential is given by $\zeta = 4\pi\eta U_{ep}/\varepsilon$, where ζ, ε and η are zeta potential, dielectric constant and viscosity coefficient of the buffer solution, respectively. Electric field strength was constant at 100 V/cm in all experiments.

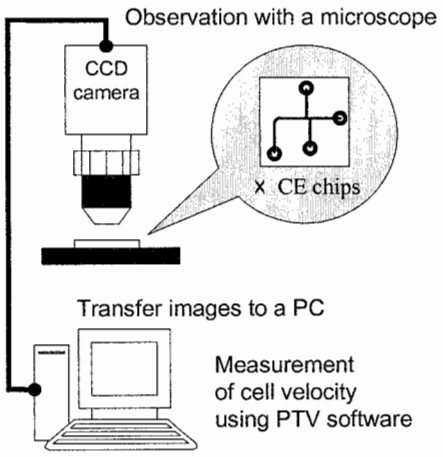

Figure 1. Cell electrophoresis system.

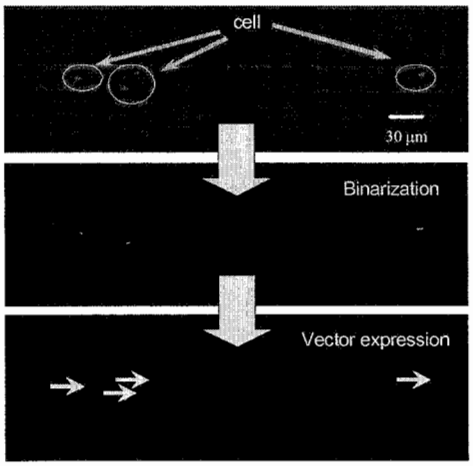

Figure 2. Cell velocity measurement by PTV software.

3. Results and discussion

A histogram of apparent EPM of sheep erythrocyte, which was obtained using μCE chips coated with MPC polymer, is shown in Fig.3. Apparent EPM increased gradually with increasing of pH. The distribution of apparent EPM at each pH value was found to be sufficiently narrow (standard deviations for pHs 4-9: 0.028, 0.021, 0.041, 0.062, 0.043 and 0.039, respectively) compared with the distribution obtained using conventional apparatus. Figure 4 (a) shows mean apparent EPM. Cells moved to the cathode in μCE chips coated with gelatin and MPC polymer and to the anode in μCE chips coated with BSA. This difference in apparent EPM values is attributed to EOF mobility, as plotted in Fig.4 (b). The EOF mobility measured using the BSA-coated μCE chip was much higher than that measured using the gelatin- and MPC-polymer-coated

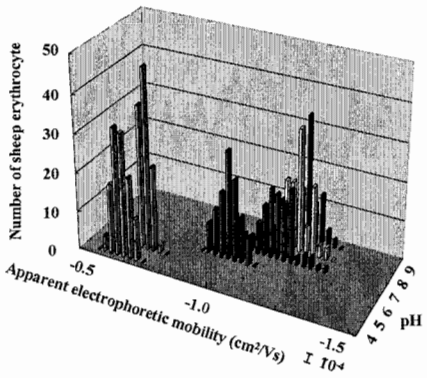

Figure 3. Apparent EPM histogram of sheep erythrocyte in μCE chips.

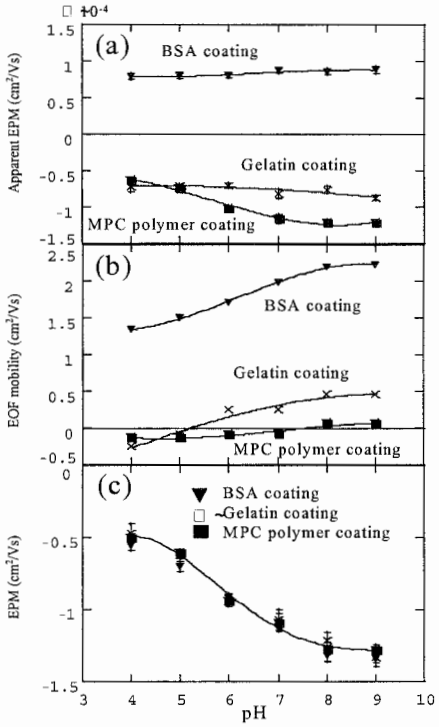

Figure 4. Relationship between pH and apparent EPM (a), EOF mobility (b), and EPM (c) in μCE chips

chips. This indicates that EOF was sufficiently suppressed by the MPC polymer and gelatin coatings. A plot of EPM versus pH estimated from apparent EPM and EOF mobility is presented in Fig.4 (c). It is noteworthy that the measured EPM values are almost identical irrespective of the use of three different coating reagents. This result indicates that cell wall interactions negligibly influence EPM measurements using μCE chips. Furthermore, zeta potential can be calculated using EPM, as shown in Fig.5. Zeta potentials increased with increasing pH due to protein ionization on the cell surface

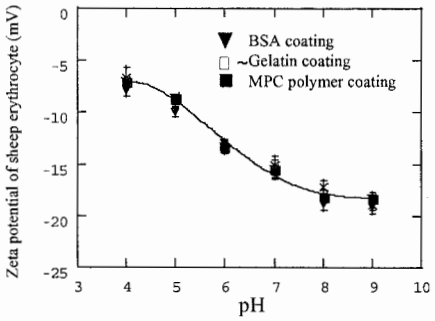

Figure 5. Relationship between pH and zeta potential of sheep erythrocyte in μCE chips.

4. Conclusions

The μCE chips have been demonstrated to be capable of the correct measurement of EPM over a wide range of pH. On-chip cell electrophoresis is a promising analysis method for evaluating individual cells and is expected to be useful in clinical and pharmaceutical applications.

Acknowledgements

This work was supported by the PRESTO program of the Japan Science and Technology Agency (JST) and High-Tech Research Center Project of the Ministry of Education, Culture, Sports, Science and Technology of Japan.

References

[1] P. C. Zhang, A. M. Keleshian and F. Sachs, *Nature*, **413**, 428-432 (2001).
[2] T. Ichiki, T. Ujiie, S. Shinbashi, T. Okuda and Y. Horiike, *Electrophoresis*, **23**, 2029-2034 (2002).
[3] J. Mehrishi and J. Bauer, *Electrophoresis*, **23**, 1984-1994 (2002).

APPLICATION OF THERMAL LENS MICROSCOPY AND ON-LINE SAMPLE PRECONCENTRATION FOR HIGH SENSITIVE DETECTION IN MICROCHIP ELECTROPHORESIS

Fumihiko Kitagawa[1], Kenji Sueyoshi[1], Jun Mizuno[2], Yasuo Wada[2], Shuichi Shoji[3] and Koji Otsuka[1]

[1]Dept. of Material Chemistry, Graduate School of Engineering, Kyoto University, Nishikyo-ku, Kyoto 615-8510, Japan

[2]Nanotechnology Research Laboratory, Waseda University, 513, Wasedatsurumakicho, Shinjuku-ku, Tokyo 162-0041, Japan

[3]Dept. of Electrical Engineering and Bioscience, Waseda University, 3-4-1, Okubo, Shinjuku-ku, Tokyo 169-8555, Japan

Abstract

The application of a thermal lens microscope (TLM) to highly sensitive detection scheme for the separation of nonfluorescent samples in microchip electrophoresis (MCE) was investigated. To improve the detection sensitivity, we studied on-line sample preconcentration by sweeping in combination with the TLM detection in MCE (MCE-TLM). Furthermore, sweeping-micellar electrokinetic chromatography (MEKC) in MCE-TLM was applied to the concentration and separation of labeled amino acids. MCE-TLM analyses on the cycloolefin polymer microchips fabricated by direct bonding method were also demonstrated.

Keywords: microchip electrophoresis, thermal lens microscope, on-line sample preconcentration, sweeping, cycloolefin polymer microchip

1. Introduction

Capillary electrophoresis (CE) and microchip electrophoresis (MCE) can achieve faster analysis with small sample volumes in the nanoliter to picoliter range. In the CE analysis employing UV-VIS absorption methods, however, the concentration sensitivity is generally insufficient due to a short optical path length. To improve these detection sensitivity limitations of CE and MCE, several on-line sample preconcentration techniques have been employed for the sensitivity enhancement in a variety of applications [1]. Alternatively, several spectrometric techniques for highly sensitive detection have been used. Laser induced fluorescence spectrometry is one of the most sensitive methods, but not always suitable, as not all molecules exhibit fluorescence. A thermal lens microscope (TLM) based on the photothermal effect to detect nonfluorescent molecule is a highly sensitive method to monitor the heat distribution resulting from absorption of light [2]. Generally, the most common relaxation processes following optical absorption causes photothermal energy conversion, so that the applicability of the TLM is very wide. In this study, we investigated the possibility of the sensitivity enhancement by on-line sample preconcentration in combination with the TLM detection in MCE for the analysis of nonfluorescent molecules.

2. Experimental

TLM (ITLM-11, Institute of Microchemical Technology) measurement in MCE was performed as follows. A DPSS blue laser beam (488 nm) for the excitation was introduced to an optical microscope coaxially with a diode laser beam (670 nm) for the probe and irradiated to the microchannel through an objective lens (×20, NA = 0.5). The probe laser beam passed through a condenser lens was monitored by a photodiode. A quartz and cycloolefin polymer (ZEONEX®, ZEON Co.) microchips with a cross-type channel were used for on-line sample preconcentration. A ZEONEX microchip was fabricated by direct bonding of ZEONEX plate with the microchannel

patterns using an EVG520HE (120 °C, 1000 N). A sample solution was injected as a long plug into the separation channel by the gated injection method.

3. Results and discussion

In the case of sweeping, the analytes (sunset yellow; SY) in a long sample zone were swept by the pseudostationary phase (an SDS micelle) to a narrow zone (Figure 1), so that the sharp peak is expected to be detected by the TLM [3]. Figure 2 shows an MCE analysis of SY on the quartz microchip employing the TLM measurement under conventional MEKC and sweeping-MEKC conditions. Due to the sweeping effect, SY showed enhanced TLM signals as shown in Figure 2 (*b*). Under the experimental condition, the 540-fold increase in detection sensitivity was achieved by sweeping. Furthermore, the limit of detection of SY was determined to be 4×10^{-9} M, so that an absolute amount of dye molecules of 8×10^{-17} mol can be detected by TLM. Therefore, sensitivity enhancement of nonfluorescent compounds in MCE was successfully achieved by the combination of the TLM detection with on-line sample preconcentration.

Sweeping-MEKC in MCE was also applied to the concentration and separation of derivatized amino acids. Towards sensitive detection in MCE-TLM, two amino acids, arginine and lysine, were labeled by a 4-dimethylaminoazobenzene-4'-isothiocyanate (DABICT) reagent. Under a sweeping condition, a baseline separation of the DABITC-labeled amino acids was obtained with the ~100-fold increase in detection sensitivity. The result demonstrated that highly sensitive and high resolution separation were achieved by sweeping-MEKC and TLM detection.

As a new commercially available plastic material for MCE, cycloolefin polymer (ZEONEX®) was used in the fabrication of a cross-type microchannel (width, 50 μm; depth, 30 μm). The ZEONEX microchip exhibited relatively strong electroosmotic flow (EOF), so that several on-line sample preconcentration techniques under conventional EOF conditions were expected to be applied to the polymer microchip. In MCE-TLM analysis of SY, the 30-fold increase in detection sensitivity was achieved by sweeping. Thus, the result indicates that the ZEONEX microchips can be employed as high performance and disposable microchannel devices for electrophoretic analyses.

4. Conclusions

Sensitivity enhancement of nonfluorescent molecules in MCE was successfully achieved by the combination of the TLM detection with the on-line sample preconcentration technique. The use of sweeping as an on-line sample preconcentration technique brought the 540-fold increase in detection sensitivity. Furthermore, high resolution separation and highly sensitive detection of labeled amino acids were obtained by sweeping-MEKC in MCE-TLM. We also demonstrated that the applicability of the sweeping technique in MCE to the ZEONEX microchip.

Acknowledgements

The authors thank Prof. T. Kitamori (The University of Tokyo), Dr. A. Hibara (The University of Tokyo), Dr. M. Tokeshi (Kanagawa Academy of Science and Technology), and Mr. S. Hiki (Institute of Microchemical Technology) for their assistance in TLM measurements. This work was supported in part by the Grant-in-Aid for Scientific Research on Priority Area (No. 13124208) and Grant-in-Aid for Scientific Research (No. 15350041) from the Ministry of Education, Culture, Sports, Science and Technology, Japan.

References

[1] J. P. Quirino and S. Terabe, *Anal. Chem.*, **71**, 1638-1644 (1999).
[2] M. Tokeshi, M. Uchida, K. Uchiyama, T. Sawada and T. Kitamori, *J. Luminescence*, **83-84**, 261-264 (1999).
[3] Y. Sera, N. Matsubara, K. Otsuka and S. Terabe, *Electrophoresis*, **22**, 3509-3513 (2001).

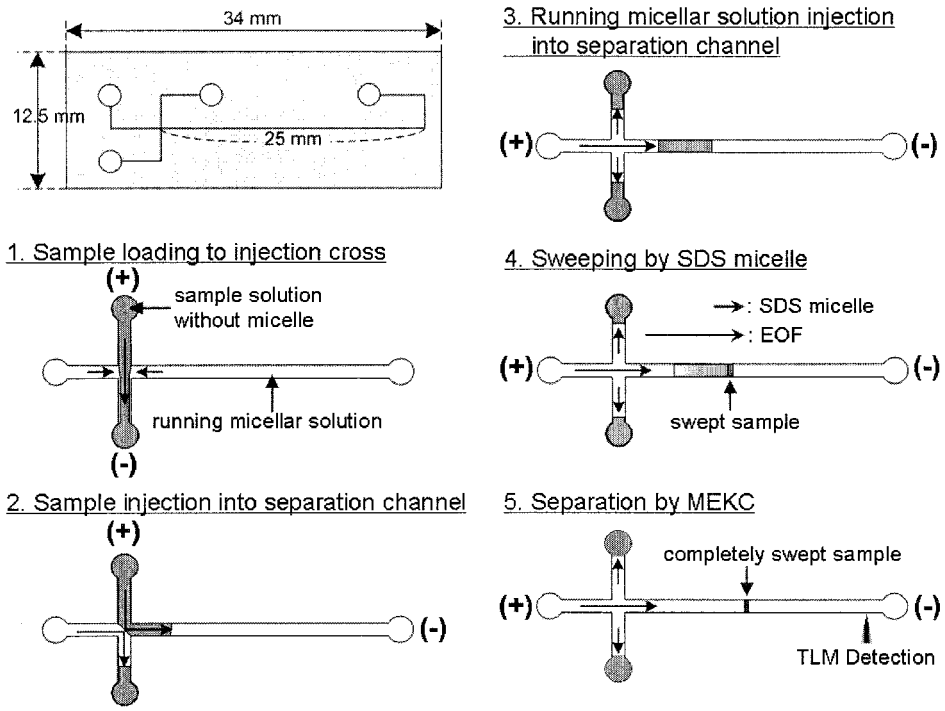

Figure 1. Schematic illustration of on-line sample preconcentration by sweeping in MCE.

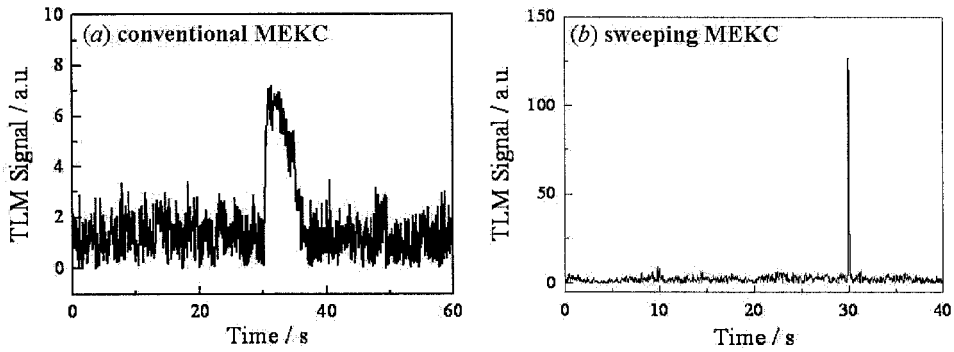

Figure 2. MCE-TLM analysis of SY in (*a*) the presence and (*b*) the absence of SDS in the sample matrix. Separation solution, 20 mM SDS in 50 mM phosphate buffer (pH 7.0); sample, (*a*) 0.5 μM SY in phosphate buffer containing SDS, (b) 0.1 μM SY in phosphate buffer; injection time, 6 s.

DEVELOPMENT OF A NOVEL IMMUNOSENSOR BASED ON MICROCHIP ZONE ELECTROPHORESIS

Koutarou Idegami[1], Masaaki Kobayashi[1], Yuzuru Takamura[2] and Eiichi Tamiya[2]

[1]Ishikawa Sunrise Industries Creation Organization, 2-13 Asahidai, Tatunokuchi, Ishikawa, Japan

[2]School of Materials Science, Japan Advanced Institute of Science and Technology, 1-1 Asahidai, Tatunokuchi, Ishikawa, Japan

Abstract

The development of a novel immunosensor based on microchip zone electrophoresis in combination with fluorescence detection is described for application in the point-of-care clinical diagnosis. Wells were microfabricated on a polyacrylamide gel, which was the supporter of the microchannels on silicon substrate. In consequence to the specific reaction between anti-human albumin antibody and the labeled antigen in the wells, free and bound labeled antigen were separated by zone electrophoresis. The quantification of antigens was performed by monitoring the fluorescence signal with a microscope. Anti-human albumin antibody could selectively be detected with a linear range between 1 and 100 μg/ml in about 40 min.

1. Introduction

Immunosensor is a contributory serological detection device that uses antibodies or antibody-related reagents for the determination of sample components. Micro-flow-type immunosensors were known for their characteristic abilities that are high sensitive and rapid detection in spite of being smaller in size[1]. However, the microsyringe pumps that are employed in injecting solutions into the sensor device are not so compact. Apart from, it requires large volumes of reagent more than necessary for assay due to presence of capillary tubing and sample inlet holders. Furthermore, flow control of the liquid samples on this device is unstable in case of using its on point-of-care clinical diagnosis which is needed simple and compact. Therefore, in this study we have developed a novel immunosensing device that does not require micropumps and at the same time it is able to detect samples quantitatively.

Keywords: Immunosensor, electrophoresis, gel, photolithography

2. Experimental

Immunosensing microchip device was constructed by preparing two-type of SU-8 molds on a silicon substrate by UV photolithography. These molds were overlapped with the side of photoresist patterns. The assembled mold was then immersed in acrylamide solution (10%, w/v) and allowed 30 min for gel setting. After the gel setting, the extra gel was removed from the outer surface of the mold and the molds were separated that resulted in the fabrication of gel chips (Figure 1.).

The detection of human-albumin antibody (HA-Ab) was demonstrated using this chip. At first, various concentrations of HA-Ab, and constant concentration of FITC-conjugated human-albumin (FITC-HA) solutions (2 μl each) were introduced into each well. In the second step, each channel was supplied with a voltage of +10 V for about 30 min (Figure 2.). The fluorescence intensity that was generated both in the channel as well as in the well was captured by a fluorescence microscope built-in CCD camera system.

3. Results and discussion

Each gel chip was dimensions of 15×30 mm^2 long and wide. The chip has 8 channels having 10×3 mm^2 long and wide with 0.5 mm depth. Further each channel has single well (3×2 mm^2 long, wide and 0.4 mm depth) used for the reaction (Figure 1.). It was possible to cast 500 μm thin gel at the

bottom of the wells. This results show the feasibility of accurate gel patterning due to utilize photo-fabricated molds for casting.

The fluorescence intensity of the each well is directly proportional to the concentration of HA-Ab (Figure 3.). Concentration of HA-Ab could be measured down to 1ug/ml. The whole detection process is completed within 40 minutes. This result indicates that +10 V applied voltages are sufficient for effective separation of the antibody-antigen complex from the free antibody. The immunosensing device that was demonstrated has a tremendous potential in the point-of-care clinical diagnosis.

Reference

[1] Kiichi Sato, Manabu Tokeshi, Hiroko Kimura, and Takehiko Kitamori, *Anal. Chem.* 73, 1213-1218(2001).

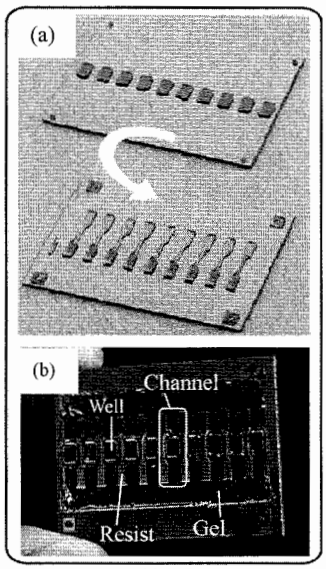

Figure 1. (a) Photograph of photo-fabricated resist pattern on silicon substrate for mold preparation. (b) Photograph of the gel chip.

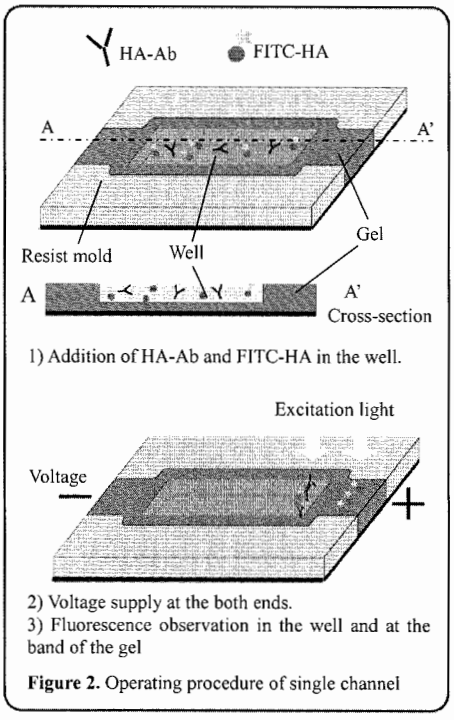

Figure 2. Operating procedure of single channel

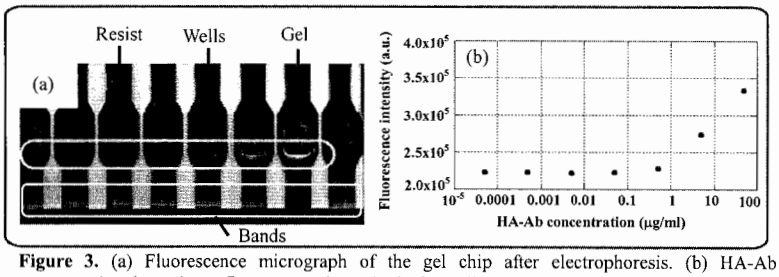

Figure 3. (a) Fluorescence micrograph of the gel chip after electrophoresis. (b) HA-Ab concentration dependence fluorescence intensity in the wells.

ON CHIP CAPILLARY ELECTROCHROMATOGRAPHY: STUDY OF A STRONG CATION-EXCHANGE PHASE

Dolores Martinez, D. Jed Harrison
Department of Chemistry, University of Alberta, Edmonton, Alberta, Canada

Abstract

The study of a microdevice for use in strong cation-exchange (SCX) capillary electrochromatography (CEC) is presented. Using a two millimeter column, three fluorescently-labeled peptides, dilysine (0 charge), trilysine (+1 charge) and tetralysine (+2 charge) were separated in less than 30 seconds. An ionic strength study showed faster elution times and improved plate heights at higher buffer concentrations. Efficiencies of up to 250 000 plates per meter were obtained for charges species.

Keywords: electrochromatography, strong cation-exchange, bead-based

1. Introduction

Capillary electrochromatography (CEC), a separation method whereby analytes are separated due to both application of an electric field and interaction with a solid phase, has become the subject of much studies in the microfluidics community. Different separation phases have been described, using commercially available beads or in situ polymerization of monomeric solutions. Work in our group has focussed on the bead-based approach[1]: beads used in HPLC columns are trapped within microchannels to effect separation. The following presents the first report of a microdevice used for bead-based SCX-CEC. The study was performed using a series of fluorescently-labeled peptides.

2. Experimental

The device design is shown in Figure 1. SCX beads of 5 μm diameter were trapped between two weirs over a 2 mm length. A side-arm was used to introduce the beads within the glass device, using electrokinetic and pressure forces. Three peptides, dilysine, trilysine and tetralysine, were fluorescently labeled using fluorescein isothiocyanate (FITC). An Ar ion laser-induced confocal epifluorescent system was used for detection. 25 mM to 60 mM KH_2PO_4 buffer solutions were made in 40% ACN, containing 0.025% Tween 20.

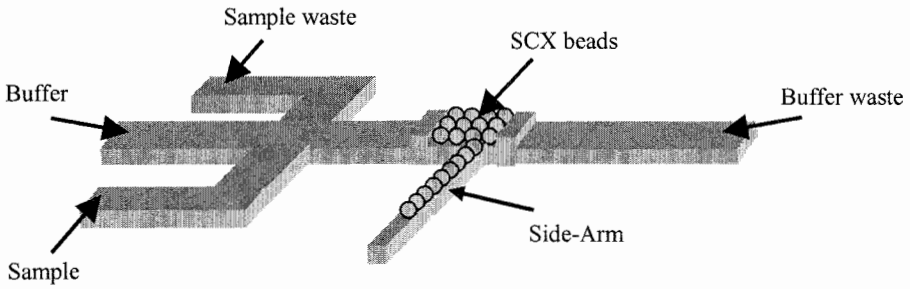

Figure 1. Two-weir microdevice used for SCX-CEC

3. Results and discussion

Figure 2 presents an example of the resulting separation for the three test peptides. The analytes were well-separated in 30 seconds. An open-channel study using the same device showed that the three species had the same migration time. Longer channels, and longer analysis times, would be needed for good separation under capillary electrophoresis (CE) action. The SCX-CEC device showed a reversal in elution order when compared to CE. Tetralysine, being doubly charged, interacted the most with the stationary phase and therefore eluted last. This confirmed that the separation was driven by ion-exchange behaviour.

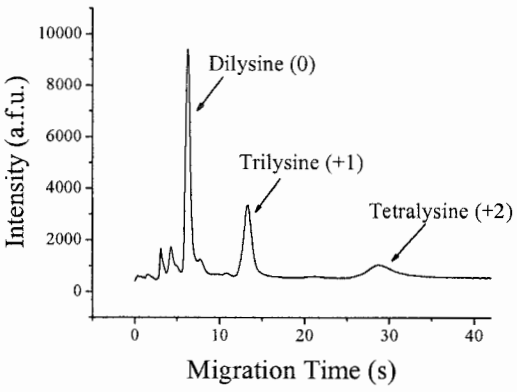

Figure 2. SCX-CEC of three test peptides

The 2 mm column was tested by varying the ionic strength of the buffer solution. The effect on the trilysine peak is shown in Figure 3 for a 1kV separation voltage. Faster elution times, and sharper peak shapes, result.

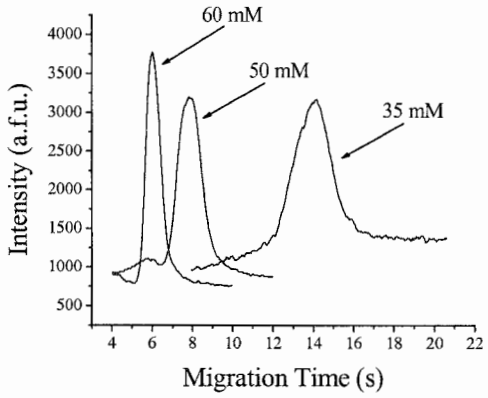

Figure 3. Effect of increased ionic strength on the trilysine peak

The same effect was observed for dilysine and tetralysine, as seen from the migration time versus buffer concentration graph of Figure 4. Under pure CE conditions, an increase in ionic strength results in a decreased electroosmotic flow, and therefore an increase in migration time. Here, however, a decrease in migration time was observed. This is consistent with strong cation-exchange chromatographic behaviour: a higher ionic strength buffer is a stronger eluent which results in faster migration times.

As seen from Figure 4, a steeper slope is obtained for tetralysine. The singly charged trilysine is less affected by changes in ionic strength conditions. Dilysine, although overall neutral, carries both positive and negative charges, it can therefore have limited interactions with the stationary phase.

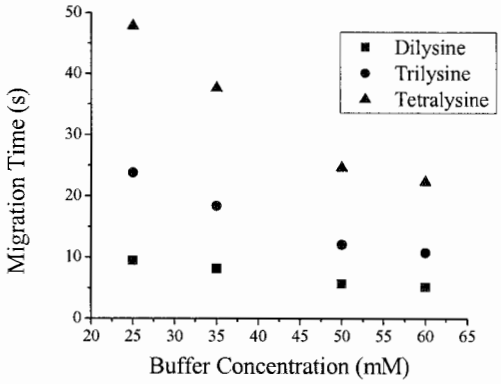

Figure 4. Effect of ionic strength on the migration behavior of three peptides

A van Deemter plot was constructed to test the efficiency of the device at 60 mM KH_2PO_4. The results are shown in Figure 5. From this, the major source of band broadening for charged species is resistance to mass transfer to and from the stationary phase. The highest efficiencies were obtained at high flow rates; efficiencies of about 250 000 plates per meter were consistent with those reported in the literature for conventional capillary columns, where longer separation times were reported.[2]

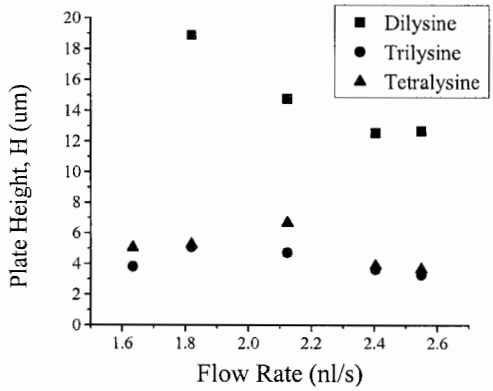

Figure 5. van Deemter plot

Acknowledgements

University of Alberta for support of the NanoFab Laboratory
Natural Sciences and Engineering Research Council of Canada for Financial Support
MDS Sciex

References

[1] Jemere, A.B., Oleschuck, R.D., Harrison, D.J. *Electrophoresis*, **2003**, 24, 3018-3025.
[2] Ye, M., Zou, H., Lui, Z., Ni, J. *J. Chrom. A*, *2000*, 869, 385-394.

LOCALISED STIMULATION OF SLIME MOULD USING MICROFLUIDIC DEVICES

Sander Koster[1,2], Tobias Kraus[1,3] Atsuko Takamatsu[4,5], Teruo Fujii[1,4], Elisabeth Verpoorte[1,2] and Nico de Rooij[1]

[1]*Institute of Microtechnology, University of Neuchâtel, Switzerland*

[2]*Present address: Groningen Research Institute of Pharmacy, University of Groningen, the Netherlands*

[3]*Present address: ETH Zurich (Laboratory for Surface Science and Technology)/IBM Zurich Research Laboratory, Zurich, Switzerland*

[4]*Institute of Industrial Science, The University of Tokyo, Japan*

[5]*Present address: Department of Electrical Engineering and Bioscience, Waseda University, Japan*

Abstract

We present a 3-D microfluidic device that enables localized drug delivery to living slime mould, a giant amoeba-like cell. The device features a flow cell in which drugs can be introduced at several positions, allowing drugs to be delivered to the slime mould at eight different locations. This is in contrast to devices reported in the literature, which allow cells to be addressed at only a few positions. Slime mould patterning is accomplished by insertion of SU-8 structures containing mould into the flow cell. This assembly allowed us to deliver drugs to the cell to evoke a measurable change in its oscillation behaviour.

Keywords: drug delivery to living cells, slime mould, laminar flow

1. Introduction

One of the most distinct features of liquid transport in microchannels is that liquid flows are laminar, with the result that mixing only occurs by diffusion. This phenomenon has been used by only a few authors for the delivery of compounds to cells in a spatially resolved manner with relatively simple microfluidic devices [1-4]. The microfluidic device that is presented here allows drugs to be delivered to cells at eight different locations, which is significantly more than for other devices described in the literature. Slime mould, a giant amoeba-like cell, has been used to demonstrate this principle for drug delivery, using cell patterning techniques to locate this organism in the flow cell. Slime mould is a multinucleated single cell, with no highly differentiated structure like a nervous system. Despite its simple structure, however, slime mould exhibits interesting behaviour, such as moving towards or away from specific chemical compounds. In this contribution, KCl, a compound that repels the slime mould, is delivered in a spatially resolved manner to the organism. The local response of the mould to KCl exposure is monitored by recording its oscillatory behaviour.

2. Experimental

A multilayer device, containing a silicon–based flowcell fabricated by a two-step KOH etching process, is used for the experiments (figure 1a). The flowcell is closed by a glass coverplate in which an array of eight, 40-μm drug-delivery holes have been drilled using an excimer laser. A rectangular piece of PDMS, in which microchannels are moulded, is bonded to the glass coverplate to connect the laser-drilled holes with external fluidics. Nutrients are introduced into the cell cultivation area through a separate inlet. Drugs can be injected through one of the eight holes as a thin stream into the nutrient flow a few millimeters upstream from the cell cultivation area to stimulate each cell of cell section that comes into contact with it. Square pieces of SU-8 with a thickness of ~60 μm, containing two circular reservoirs connected by a channel, were made using an approach similar to that described elsewhere [5].

3. Results and discussion

Slime mould, a multinucleated unicellular organism, was inserted in the two reservoirs of the SU-8 structure, and subsequently allowed to grow together to make a connection in the channel, see figure 1b [5]. The SU-8 structure containing the slime mould was inserted into the flow cell. Cell activity and the relationship between two portions of the cell can be monitored by observing the nonlinear oscillation behaviour of cell thickness in the two reservoirs, denoted by oscillator 1 and 2. Oscillation behaviour was monitored when the 'drug', KCl, a compound from which the mould is repelled, was delivered at oscillator 1. Figure 2a shows the oscillating behaviour of the slime in the two reservoirs. It can clearly be seen that the oscillations, originally in anti-phase, start drifting upon delivery of the drug at t=14 min, which indicates desynchronization of the two portions of the mould. The phase continues to change until introduction of the drug is stopped at t=30 minutes, as shown in figure 2b. From that moment, the oscillation behaviour of the slime mould recovers and oscillates again in anti-phase. These observations were confirmed by theoretical analysis with a mathematical model of coupled nonlinear oscillators [4], and were in agreement with computer simulations which showed: (1) a reduction in oscillation frequency in the stimulated reservoir, (2) phase drifting during stimulation, (3) recovery of the oscillation frequency and phase relationship when the drug flow is stopped.

Our results clearly demonstrate that drugs can be applied in a spatially resolved manner to slime mould. More experiments using different compounds are planned. At present, the HL-1 tumor cell line of mouse cardiac cells was successfully cultivated in our device. Drug delivery experiments with several drugs are in progress.

4. Conclusions

We have presented a novel microfluidic device that allows cells to be cultivated in a flow chamber and drugs to be delivered in a spatially resolved manner. KCl, a repelling compound, was successfully delivered to slime mould, the test organism used in this case.

Acknowledgements

This project was financed by the Swiss Ministry of Education and Science within the EU project 'INPRO'.

References

[1] H. Kaji et al., *Lab Chip*, **3**, 208-211 (2003)
[2] S. Takayama et al., *Chemistry & Biology*, **10**, 123-130 (2003).
[3] Y. Matsubara et al., *Biosensors and Bioelectronics* **19** 741-747 (2004)
[4] M.C. Peterman et al., *Artificial Organs* **27(11)** 975-985 (2003)
[5] A. Takamatsu et al., *Protoplasm* 210, 164-171 (2000)
[3] A. Takamatsu et al., *Phys. Rev. Letters,* **85**(9), 2026-2029 (2000)

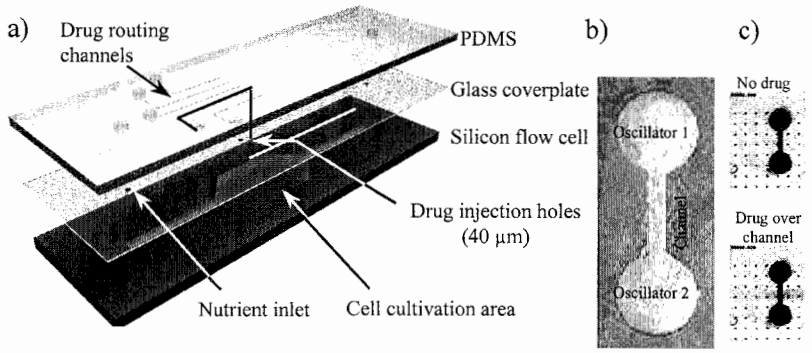

Figure 1. (a) Schematic overview of the flow cell. The silicon flow cell was reversibly closed with a glass coverplate using grease. The PDMS layer was bonded to the glass coverplate using an oxygen plasma. Drugs can be introduced in the cell cultivation area through one of the microfluidic channels connected to laser drilled holes, represented by the red line. (b) Picture of two coupled oscillators connected by a 400-µm-wide channel. The dark region is the SU-8 structure, whereas the light region is the slime mould. (c) Picture of a coupled oscillator in the flow cell with and without a drug addressed at the channel connecting the two oscillators.

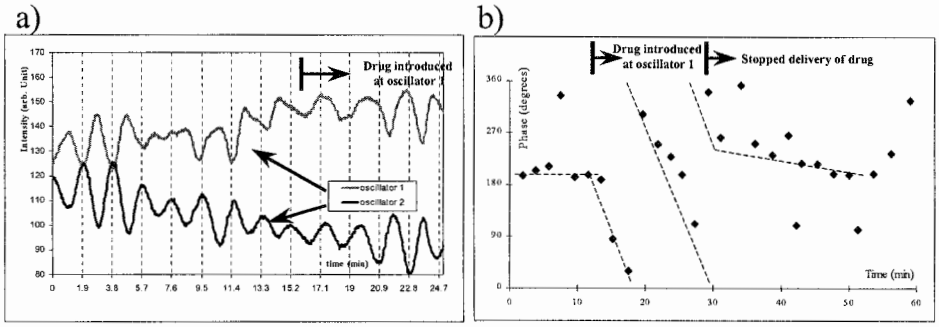

Figure 2. (a) Oscillation behaviour between the two reservoirs. The intensity was measured by illuminating the reservoirs from below and recording the transmitted light intensity with a CCD camera. The phase between oscillations starts changing from the moment a 'drug', KCl, is introduced at oscillator 1. (b) Phase difference between the two reservoirs. Initially, oscillations are in anti-phase, but they start to drift when a drug is introduced. After the drug flow was stopped, the oscillation behaviour recovered and started oscillating in anti-phase (180°) again.

HIGH-THROUGHPUT SCREENING AND ANALYSIS FOR ANTIGEN SPECIFIC SINGLE-CELL USING MICROARRAY

Shohei Yamamura[1, 3], Sathuluri Ramachandra Rao[1, 3], Masahiro Omori[3], Yoshiharu Tokimitsu[2], Sachiko Kondo[2], Hiroyuki Kishi[2], Atsushi Muraguchi[2], Yuzuru Takamura[3] and Eiichi Tamiya[3]

[1]Toyama New Industry Organization, 529, Takada, Toyama, 930-0866, Japan, [2]Dept. of Immunology, Toyama Medical and Pharmaceutical Univ., 2630, Sugiya, Toyama, 930-0194, Japan, [3]School of Materials Science, Japan Advanced Institute of Science and Technology, 1-1, Asahidai, Tatsunokuchi, Ishikawa, 923-1292, Japan (shouhei@jaist.ac.jp)

Abstract

The analysis of single B-cells, which produce variety of antibodies, can contribute to development of highly affinity monoclonal antibody. In this study, we have developed a novel system of high-throughput screening and analysis for single-cell on microarray. The single-cell microarray chip is made from polystyrene with over 200,000 microchambers, which can accommodate only single-cell. Lymphocytes from spleen of mouse were spread on the microarray, and over 80% of the microchambers were occupied with single-cells. The antigen specific single B-cells were detected upon stimulation with anti mouse IgM antibody. The result suggested that only 0.26% B-cells of the total population showed ten times higher activity after stimulation with antigen.

Keywords: microarray, cell chip, single-cell analysis, high-throughput screening, B-cell

1. Introduction

Immune system plays an important role in defending our body from the invading alien antigens, such as virus, pathogenic bacteria and toxic chemicals, by producing specific antibodies from B-cells. B-cells recognize varieties of antigens with varying affinities and only those with high affinity produce antigen specific antibody: monoclonal antibody, finds application in antibody medicine and clinical diagnosis. By conventional approaches, the production of specific monoclonal antibody by B-cells is facing undaunted task. Therefore, it is necessary to construct microarray chip formats that can handle multiplexed single-cell manipulation from bulky cell suspension and analysis of single-cell antibody DNA for making highly specific monoclonal antibody. In this study, we have developed a novel system of high-throughput screening and analysis of antigen specific single-cell on microarray, which was carried out by detecting antigen specific single-cell and its retrieval by micromanipulator for antibody DNA analysis.

2. Experimental

The microarray chip is made from polystyrene with over 200,000 microchambers (10 μm width, 12 μm depth) by using Lithographie Galvanoformung Abformung (LIGA) process (Fig. 1). Using X-ray lithography from synchrotron radiation, a polymethylmethacrylate (PMMA) positive resist was exposed and patterned with metal mask. After development of the substrate, nickel mold was fabricated by electroforming. Finally, polystyrene microarray chip was fabricated from the nickel mold. The surface of the microarray rendered to hydrophilic by reactive ion etching treatment.

Lymphocytes, which contain mainly B-cells, were extracted from mashed spleen of mouse by using 0.8% (w/v) ammonium chloride solution. The lymphocytes solution ($1x10^7$ cells/ml) were spread on the microarray and washed out the cells without microchambers. The antigen specific single B-cells were detected by using microarray scanner (CRBio IIe, Hitachi Software Engineering Co., Ltd., Japan) upon stimulation with anti mouse IgM antibody (14 μg/ml) as an antigen and

monitored the positive B-cells using fluorescent calcium indicator, Fluo-4 (Ex: 494 nm, Em: 516 nm). The data was analyzed by using DNASIS Array software (Hitachi Software Engineering Co., Ltd.) to determine the percentage of antigen specific B-cells in the total cell population after stimulation with antigen. Further, using micromanipulator (15-20 μm diameter), which was made from glass capillary using micropipetter (NARISHIGE Co., Ltd., Japan), positive single-cells were retrieved from microchambers under the microscope.

3. Results and discussion

The single-cell microarray chip has over 200,000 microchambers (10 μm width, 12 μm depth) in 1.4 cm^2area on plastic wafer. Each microchamber is cylindrical in shape and made such a way that it can accommodate only single-cell (B-cell size: 6-8 μm) (Fig. 1). Lymphocytes from spleen of mouse were spread on the microarray, and found over 80% of the microchambers with single-cells. Though the recent research reported single-cell separation on the microchip formats, and they lack simultaneous separation of large number of single-cells from bulk suspension [1]. Further, single-cell manipulation needs to some special tools such as complex microfluidic systems [1, 2] and optical tweezers [3]. However, the single-cell microarray developed in this study could easily separate single-cells without any specialized tools. Cells were automatically entered into each of the microchambers under gravitational force and attained single-cell microarray (>80%). The antigen specific single B-cells were detected upon stimulation with anti mouse IgM antibody and monitored the positive B-cells using fluorescent calcium indicator, Fluo-4 (Fig. 2). The analysis data suggested that only 0.26% B-cells of the total population showed ten times higher activity after stimulation with antigen, anti mouse IgM antibody (Fig. 3). It was evident that most of B-cells responded to antigen stimulation (Fig. 3), because they could not be stimulated with anti human IgM antibody as a control. Further, we retrieved positive single-cells by a micromanipulator under the microscope for antibody DNA analysis.

4. Conclusions

This explorative study throws more light on a novel high-throughput single-cell analysis system that has tremendous potential to analyze antibody DNA of antigen specific single-cell for developing highly specific monoclonal antibody.

Acknowledgements

This work was funded by Toyama Medical Bio-cluster project sponsored by the Ministry of Education, Culture, Sports, and Science, Japan. We appreciate the help of Dr. Masaya Kurokawa, Starlight Co., Ltd., Japan in fabricating the microarray chips.

References

[1] A.R. Wheeler, W.R. Throndset, R.J. Whelan, A.M. Leach, R.N. Zare, Y.H. Liaor, K. Farrell, I.D. Manger, and A. Daridon, *Anal. Chem.*, **75**, 3581-3586 (2003)

[2] W.H. Huang, W. Cheng, Z. Zhang, D.W. Pang, J.K. Cheng, and D.F. Cui, *Anal. Chem.*, **76**, 483-488 (2004)

[3] S. Umehara, Y. Wakamoto, I. Inoue, and K. Yasuda, *Biochem. Biophys. Res. Com.*, **305**, 534-540 (2003)

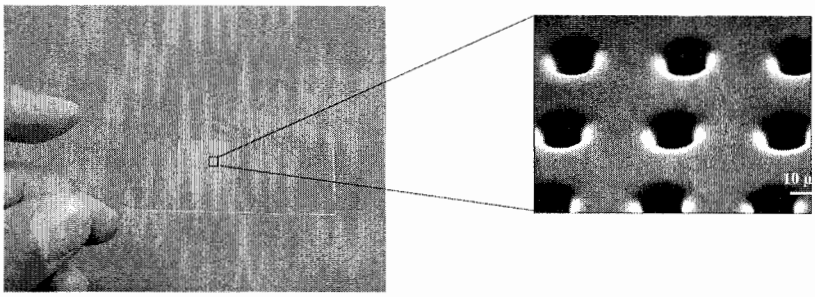

Figure 1 Single-cell microarray made from polystyrene with over 200,000 microchambers (10 μm width, 12 μm depth). Each microchamber is cylindrical in shape and can accommodate only single-cell.

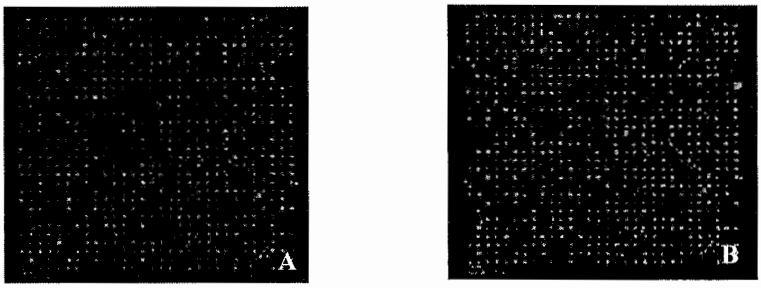

Figure 2 Detection of positive B-cells using fluorescent calcium indicator, Fluo-4 upon stimulation with anti mouse IgM antibody. A: Before stimulation, B: After stimulation

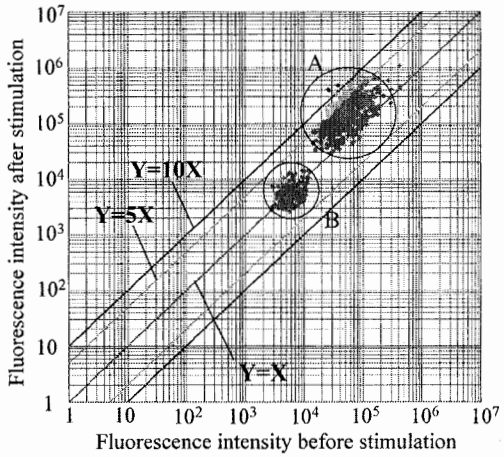

A: microchambers with B-cell and other cells
B: empty microchambers

X: Fluorescence intensity before stimulation
Y: Fluorescence intensity after stimulation

Figure 3 The analysis of positive B-cells in the total cell population after stimulation with anti mouse IgM antibody.

CONDUCTIVITY GRADIENT FOCUSING

Oscar G. Potter[*], Rosanne M. Guijt[*], Stuart Corney[**], Paul R. Haddad[*] and Miroslav Macka[*]

[*]*ACROSS, School of Chemistry, University of Tasmania, Private Bag 75, Hobart, TAS 7001, Australia*

[**]*CSIRO Marine Research, Castray Esplanade, Hobart, TAS 7001, Australia*

Abstract

A novel focusing method based on an equilibrium between hydrodynamic and electrophoretic forces is presented. A conductivity step gradient was realised in a 200 µm-deep flow-through chamber by having high and low conductivity electrolytes alongside each other. In an applied electric field analyte molecules migrate towards the central high conductivity flow, resulting in an increased analyte concentration at the low/high conductivity interface. A dynamic equilibrium between pressure-driven and electrophoretic forces allowed the formation of a stable, concentrated analyte zone. Malachite green was used as a test analyte and preconcentrated by a factor of at least 3.2 times.

key words: microfluidics, focusing, gradient, equilibrium, conductivity

1. Introduction

Electrophoretic separation methods can be divided into dynamic systems, where the analytes migrate in zones of equal mobility through the capillary or channel, and static systems, where the analytes of equal mobility migrate to a stationary point. In dynamic systems, samples need to be introduced in discrete zones to allow separation of different analyte zones. A low analyte concentration in the sample directly results in a small absolute sample amount in the analytical system. In static systems, larger sample volumes can be introduced, since the analytes are focused at a stationary point, where the net force on the analyte is zero. A local increase of analyte concentration is expected at the stationary point, since the analyte molecules present in the large sample zone are focused into a small volume.

At the focusing point, the net force on the analytes is zero and an equilibrium has been obtained. Here, a novel approach for electromobility focusing based on an equilibrium between hydrodynamic and electrophoretic forces is presented. Electromobility focussing is an equilibrium gradient method where analytes are focussed according to their electrophoretic mobility in an electric field gradient [1]. Previously, concentration gradients and consequently electric field gradients have been formed by diffusion of electrolytes through semipermeable membranes [2]. In our approach, a conductivity gradient is formed between laminar flows of two different electrolytes having different conductivities.

2. Experimental

The device used for the concentration experiments is given in Figure 1. Three fluid flows enter the microfluidic chamber, namely a central flow containing 20 mM citrate buffer (pH 4.9, 403 µS/cm) and two auxiliary sample flows containing 0.2 mM malachite green (MG, 71 µS/cm). The solutions leave the device via a single, low flow resistance outlet, unless sampling into a collection vial is required.

Initially, the central flow containing buffer was initiated after filling the chamber with the MG solution..The buffer was pumped at 2 µL/min, both auxiliary flows at 15 µL/min, and after 5 minutes, a potential difference of 280 V was applied over the device. The image sequence was recorded using a digital camera, and is given in Figure 2. After 33 minutes, the voltage was switched off and the concentrated fraction was collected by opening the valve at the collection outlet. The MG concentration was determined using a spectrophotometer.

In a second series of experiments, the chamber was filled with buffer and MG at flow rates of 0.2 µL/min and 15 µL/min, respectively. A potential difference of 280 V was applied over the cell, without interrupting the flows. Identical experiments were performed using a potential difference of 600 V. In a third series of experiments, the polarity of the electrodes was changed and a 0.2 mM solution of indigotetrasulpfonate (an anionic dye) was used as sample solution.

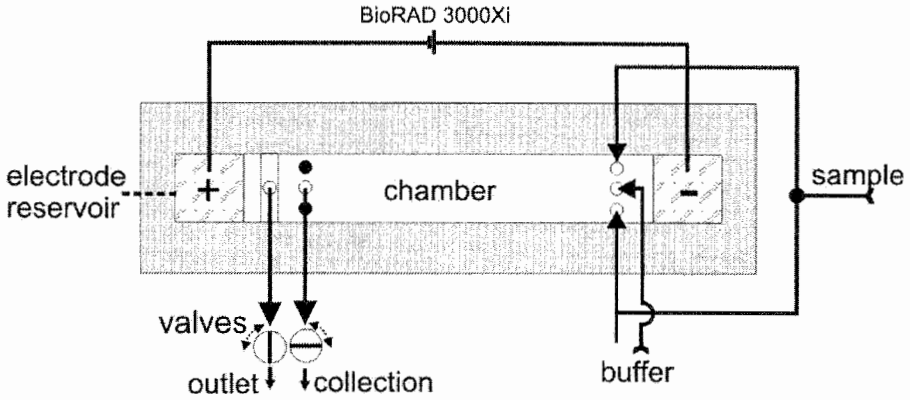

Figure 1. Schematic drawing of PMMA flow-through chamber. Two PMMA plates were clamped together using screws. A 230-µm-thick Teflon spacer defined the geometry of the chamber (l x b = 100 x 20 mm). A dual syringe pump was used to pump sample, 0.2 mM malachite green into the auxiliary inlets and 20 mM citrate buffer into the central inlet. Platinum wire electrodes were placed in electrode reservoirs filled with agarose gel in buffer. This is to reduce pH changes and to prevent electrolysis gases from entering the chamber. The valves were used to collect the concentrated zone in an Eppendorf tube at the collection outlet.

3. Results and Discussion

A central, high conductivity stream flows adjacent to two low conductivity streams containing the analyte. When a potential difference is applied, the electric field gets deflected towards the high conductivity, central flow. Migration of MG in the low conductivity flows towards the central flow is observed. Once equilibrium between field- and pressure-driven migration is established, the net migration of the analyte is zero, and a static, high-concentration analyte zone will be formed.

In the sequence in Figure 2, migration of MG (blue, cationic dye) towards the high conductivity buffer flow can be observed. In these experiments, the buffer flow was started after the chamber was filled with MG. After 23 minutes, equilibrium between electro- and pressure driven flow was established. The MG zone remained stable in position for over 10 minutes.

The MG concentration in the collected fraction (measured spectrophotometrically) was 3.2 times higher than the initial concentration. Based on comparison of the colour intensity of the stabilised zone with 10x more concentrated MG, a concentration factor of approximately 10 was estimated.

In the second series of experiments, the buffer and dye were already pumped through the chamber before the voltage was applied. Concentration of MG was observed at the high/low conductivity interface. Similar to the experiments described above, a static MG zone was formed in the chamber. When a potential difference of 600 V was used, MG zones were formed in a wave-like

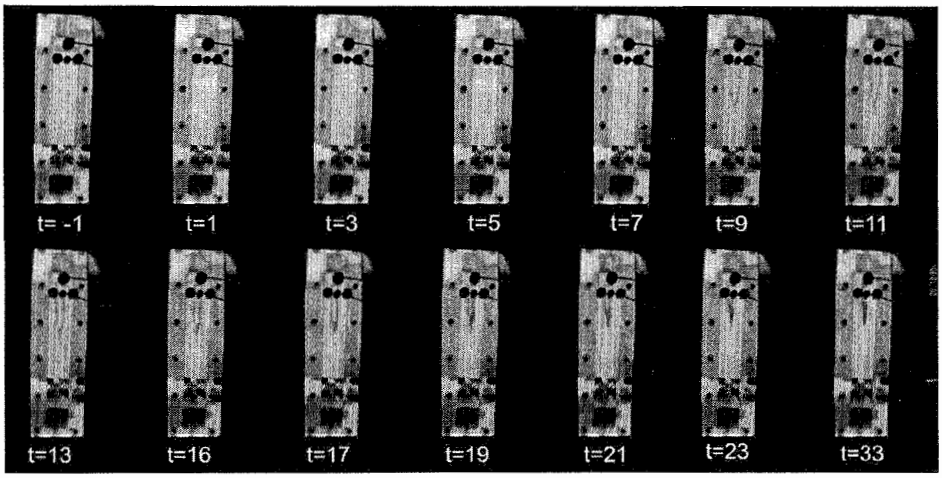

Figure 2. Image sequence of step gradient concentration. The time (t) is indicated in minutes, at t=0 the voltage was switched on. At t=-1, the buffer flow can be observed as a narrow (1 mm wide, 5 mm long) colorless line. From t=1 to t=21, concentration of MG at the high/low conductivity interface can be observed. The colorless band behind the MG zone is much wider than the initial buffer flow width. The concentrated MG zone moves towards the outlet. At t=23, equilibrium of hydrodynamic and electrophoretic force is obtained, and MG concentrates in a stable zone.

pattern. This can be explained by the differences in electroosmotic flow between the high and low conductivity flows.

Concentration of indigotetrasulfonate was observed when using opposite polarity and a potential difference of 320 V.

The migration of the dyes indicates that the electric field in the chamber is directed towards the high conductivity flow. The local potential values will be measured using a 45-electrode array, and a *Finite Element Model* of the cell will be developed to characterise the potential distribution during concentration gradient focusing.

4. Conclusions

A conductivity gradient between parallel flows of different conductivities inside a microfluidic flow-through chamber can be used to achieve electromobility focusing.

Depending on polarity, cationic and anionic analytes could be concentrated by focusing.

Acknowledgements

The authors would like to acknowledge the School of Chemistry, University of Tasmania for a summer scholarship, and the Dutch Foundation for Science and Technology STW (DPC 6168) and the Australian Research Council for funding.

REFERENCES

[1] Q.G. Wang, H.D. Tolley, D.A. LeFebre, M.L. Lee, Anal. Bioanal. Chem. 373 (2002) 125.
[2] Q.G. Wang, S.L. Lin, K.F. Warnick, H.D. Tolley, M.L. Lee, J. Chromatogr. A 985 (2003) 455.

DESIGNING MULTIFUNCTIONAL MICROCHIPS FOR ELECTROPHORETIC ANALYSIS

Kenji Sueyoshi[1], Hidenori Nagai[2], Shin-ichi Wakida[2], Junji Nishii[2], Fumihiko Kitagawa[1] and Koji Otsuka[1]

[1]*Department of Material Chemistry, Graduate School of Engineering, Kyoto University, Nishikyo-ku, Kyoto 615-8510, Japan (E-mail: otsuka@mbox.kudpc.kyoto-u.ac.jp)*

[2] *National Institute of Advanced Industrial Science and Technology, AIST, Japan*

Abstract

By using a microchip with a new channel geometry, on-line sample preconcentration by stacking using reverse migrating micelles and a water plug (SRW) was applied to microchip micellar electrokinetic chromatography (MEKC). By changing the detection point on the microchip, the concentration process in SRW was observed. Rhodamine B was successfully concentrated by SRW with the 40-fold increase in the detection sensitivity. Some rhodamine derivatives were concentrated and separated by SRW-microchip MEKC. The effects of the water plug length on the resolution and the concentration efficiency of analytes were investigated.

Keywords: microchip electrophoresis, on-line sample preconcentration, stacking using reverse migrating micelles and a water plug, laser-induced fluorescence spectrometry

1. Introduction

In micro total analysis system (micro-TAS), microchip electrophoresis (MCE) based on the separation principle of capillary electrophoresis (CE) plays an important roll, since MCE can achieve faster separation with smaller amount of samples compared with CE. In CE and MCE employing spectrophotometric detection, the concentration detection sensitivity is generally insufficient due to a short optical pass length. To improve the detection sensitivity, several on-line sample preconcentration techniques have been developed for CE and MCE, including stacking and sweeping. In this study, the microchips with new channel geometries were fabricated to enable multifunctional injections, in which the applicability to on-line sample preconcentration was investigated.

2. Theory

Stacking using reverse migrating micelles and a water plug (SRW) is one of on-line preconcentration techniques applicable to micellar electrokinetic chromatography (MEKC) based on the principle of stacking [1]. The concentration process of SRW is briefly described as follows: First, a long water plug is injected into the separation channel filled with a low pH back ground solution (BGS) containing sodium dodecyl sulphate (SDS) micelles. The sample prepared in a low conductivity and low pH matrix is successively injected into the separation channel. The low pH of sample matrix and BGS is employed to suppress the electoosmotic flow. By applying negative voltage, higher electric field is applied to the sample and water plugs due to their low conductivity. Thus, the SDS micelle and the samples incorporated into the micelle migrate very fast in the water plug. Finally the SDS micelle and samples reach at the boundary between the water plug and BGS, so that the analytes are concentrated to narrow bands. The concentrated analytes are then separated by MEKC.

3. Experimental

As a new type of microchannel chip, a quartz microchip with a single T-form channel was fabricated by photolithographic techniques (Figure 1). Sample solutions were injected by the gated injection method and the injection time of the samples was controlled by the applied voltages

(Figure 2). The samples were detected with laser-induced fluorescence (LIF) spectrometry. The concentration process was monitored by changing the LIF detection point on the channel.

4. Results and discussion

The microchip with a T-cross channel was applied to SRW-MEKC of fluorescent dyes (rhodamine derivatives) in MCE or microchip MEKC (MCMEKC). As a typical example, the detailed concentration process in SRW was investigated for sulforhodamine B (SRB) (Figure 3). At the detection point of 5.0 mm from the injection cross, a long tailed peak combined with a sharp peak was observed. The tailing was due to a nonconcentarated fraction of the sample. At 8.5 mm from the injection cross, the tailing became smaller and the peak height higher. Finally, the tailed shape almost disappeared at 8.8 ~ 9.0 mm, and the highest peak was observed. After the maximum peak height point at 8.8 ~ 9.0 mm, the peak width was broadened due to the effect of the molecular diffusion. Therefore, the sensitivity enhancement of the fluorescent molecule in MCMEKC was successfully achieved by SRW. On-line preconcentration and separation of the mixture of three fluorescent samples, rhodamine B (RB), SRB and sulforhodamine 101 (SR 101) was investigated. Figure 4 (a) and (b) show the electropherograms obtained by conventional MCMEKC and SRW-MCMEKC, respectively. The 30 ~ 40-fold enhancement in the detection sensitivity and the baseline separation were successfully achieved in SRW-MCMEKC. The resolution for RB and SR101 peaks obtained by SRW-MCMEKC was 3.4, whereas that obtained by conventional MCMEKC was 1.4. Furthermore, the concentration efficiency and the resolution depended strongly on the water plug length and the optimized injection time of water plug was 3 s.

5. Conclusions

On-line sample preconcentration by SRW was successfully applied to MCMEKC using the microchip with the T-cross channel. The 40-fold increase in the detection sensitivity was attained by SRW. By employing SRW-MCMEKC, the detectability as well as the separation of rhodamine derivatives was significantly improved compared with that obtained in conventional MCMEKC. When the injection length of the sample solution was 1 mm, the optimum injection time of the water plug was 3 s and the maximum concentration efficiency was obtained.

Acknowledgements

This work was supported in part by the Grant-in-Aid for Scientific Research on Priority Area (No. 13124208) and by the Grant-in-Aid for Scientific Research (No.15350041) from the Ministry of Education, Culture, Sports, Science and Technology, Japan.

References

[1] J. P. Quirino, K. Otsuka, S. Terabe, *J. Chromatogr. B,* **714**, 29-38 (1998).

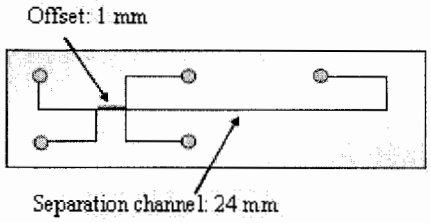

Figure 1. The newly designed microchannel chip.

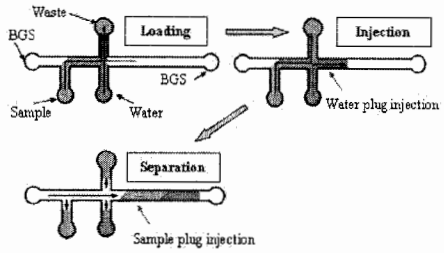

Figure 2. Water and sample plug injection in MCE.

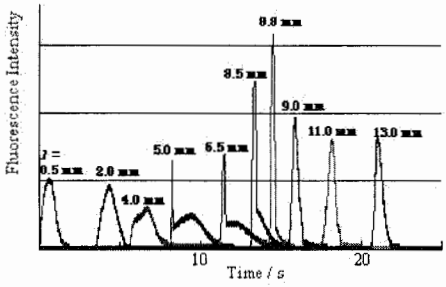

Figure 3. Electropherograms of SRB at the different detection points. Sample, 10 μM SRB; injection time of water plug, 3 s; sample plug length injected, 1 mm.

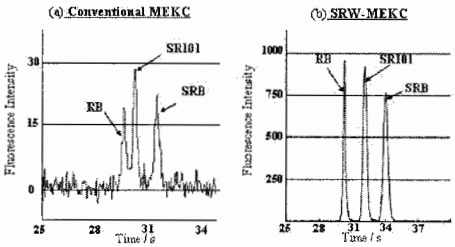

Figure 4. On-line concentration and separation of the mixture of three fluorescent samples (1 μM SRB, SR101, and RB). (a) Conventional MEKC. Sample plug length injected, ~50 μm. (b) SRW-MEKC. Injection time of water plug, 3 s; sample plug length injected, 1 mm.

MICRO REVERSE-TRANSCRIPTION POLYMERASE CHAIN REACTION SYSTEM FOR CLINICAL DIAGNOSIS

Chia-Sheng Liao[1], Gwo-Bin Lee[1,2], Hsiao-Sheng Liu[3], Tsung-Min Hsieh[4], Chih-Hao Wang[2], Chu-Lin Fan[2],Ching-Hsing Luo[4]

[1]Institute of MEMS Engineering, [2]Department of Engineering Science, [3]Department of Microbiology and Immunology, [4]Department of Electrical Engineering, National Cheng Kung University, Tainan, Taiwan 701ROC

Abstract

This paper reports a micromachined Reverse-Transcription Polymerase Chain Reaction (RT-PCR) system integrated with a polydimethylsiloxane (PDMS)-based pneumatic pumping/valving system for fast cloning and clinical diagnosis of RNA-based molecules such as RNA viruses or mRNA. Successful amplification of complementary DNA (cDNA) synthesis from the 10723-base dengue-2 virus templates was carried out by using on-chip microfluidic and temperature control systems in an automatic format. The integrated 2-step micro-RT-PCR system could be a crucial tool for infectious disease detection.

Keywords: MEMS, RT-PCR, microfluidics, Diagnosis

1. Introduction

A novel micro RT-PCR system was implemented using MEMS technology to perform the synthesis of the cDNA from 10723-base dengue-2 virus RNA templates. Miniature devices for RNA-based analysis have been reported by Obeid et al. [1]. In their excellent work, a monolithic micro-device that integrated continuous-flow RT and PCR was realized. However, several problems, including a constant time ratio of 4:4:9 to perform thermal steps of amplification, a fixed selection of cycle numbers, exterior heaters/sensors/pumps and high power consumption, still exist. In this study, we report a micro-RT-PCR system comprising two major components, namely on-chip temperature control module for RT-PCR reaction and a microfluidic module to provide pneumatic pumps/valves. As schematically shown in Fig. 1, the integrated RT-PCR system was fabricated on glass and PDMS substrates. The bottom glass plate was used for deposition of platinum (Pt) resistors as heaters and temperature sensors. The upper plate involving micro pneumatic pumps/valves and RT/PCR reaction chambers were fabricated using SU-8 and PDMS casting process. Finally, oxygen plasma was used for glass/PDMS bonding. The heating and temperature sensing elements (Fig. 2) were made of the same material (Pt) and were located inside the reaction chambers to ensure uniform temperature distribution and low power consumption. In this design, one could precisely control thermal cycles, which are crucial for RT-PCR. Moreover, experimental data reveal that high heating and cooling rates of the system (20 K/sec and 10 K/sec, respectively) permit successful DNA amplification within 10 minutes (Fig. 3). It is important to note that the average power consumption of the developed system is only 0.9W and the system can be operated using a commercially-available 9V battery.

2. Experimental

A bio-compatible and low-cost fabrication process using soda-lime glass and PDMS materials was used. Initially, the temperature control module was fabricated on soda-lime glass (Fig. 4a). An E-beam evaporation process was used to deposit Pt layer onto the glass substrate which had previously been coated with a thin layer of Chromium (Cr) to enhance Pt adhesion. A lift-off process was then used to pattern Pt resistors to serve as the temperature sensors and heaters. Similarly, electrical leads were patterned using a gold layer. Standard lithography was used to form SU-8 templates with inverse images of microfluidic structure on another substrate (Fig. 4b). Finally,

PDMS membranes and microchannels were formed using casting process. The PDMS plate was bonded with the glass substrate to form the micro RT-PCR chips. The resilient property of the PDMS allows compressed air to cause the membrane deflection and shut off the fluid flows. "Peristaltic" activation of the PDMS membranes could pump reverse-transcripted RNA products from the RT reaction chamber to the PCR chamber (Fig. 1).

In the present study, viral RNA was extracted from dengue-2 virus (New Guinea C strain) in infected mosquito *Aedes pseudoscutellaris* (AP61) cells [2-3]. The RT-PCR reaction was realized by denaturing and synthesizing the purified total RNA in RT reaction chamber, and then followed by DNA amplification in the PCR reaction chamber by pumping a certain amounts of the cDNA. It is noted that the whole testing process were carried out automatically including RNA reverse transcription, PCR amplification, and sample/reagent transportation to form a micro-total-analysis-system.

3. Results and discussion

The primer set (AD3-AD4) used in the testing can specifically amplify a 419-bp fragment of dengue virus cDNA NS1 region, which has been widely used for detection of dengue virus. Within the 419 bp sequence, it contains two diagnostic restriction endonuclease cutting sites, namely Hind□ and Bst□, which were used in this study to verify that the micro-RT-PCR system can amplify the 419-bp fragment successfully. Figure 5 shows that dengue-2 virus was successfully amplified and separated electrophoretically in a 1.5% agarose gel stained with ethidium bromide. The fluorescence signals in the first lane (M) represent the 100 base-pair ladder DNA markers. The second lane signals (C) demonstrate the RT-PCR products of dengue-2 virus using the developed chips. The following lanes (Hind and Bst) represent the digested DNA fragments using Hind□ and Bst□ enzymes to digest the RT-PCR products. The corresponding sizes of the digested DNA fragments are 193/226 bps (base-pairs) and 187/232 bps, respectively. Figure 6 shows the amplified RT-PCR products in terms of thermal cycles. Compared to bench-top RT-PCT system, compatible signals have been attained in less period of time.

4. Conclusion

In this study, rapid and accurate detection of RNA virus using an integrated micro-RT-PCR system has been demonstrated. Pneumatic micro-pumps and micro-valves were used to transport a precise amount of reverse-transcripted RNA to DNA reaction chambers. The novel two-step micro-RT-PCR system could be promising for fast clinical diagnosis of RNA-based diseases.

Acknowledgements

The authors would like to thank financial supports from National Science Council of Taiwan (NSC 92-3112-B-006-004) and the MOE Program for Promoting Academic Excellence of Universities (EX-91-E-FA09-5-4).

References

[1] P.J. Obeit, T.K. Christopoulos, H.J. Crabtree, C.J. Backhouse, Anal Chem. 75, 288-295 (2003)
[2] T. Maniatis, E.F. Fritsch, and J. Sambrook, Molecular Cloning: A Laboratory Manual. Cold Spring Harbor Laboratory Press, Cold Spring Harbor, NY. (1989)
[3] H.S. Liu, H.C. Tzeng, and C.C. Chen, Journal of Virological Method, 51, 55-60 (1995)

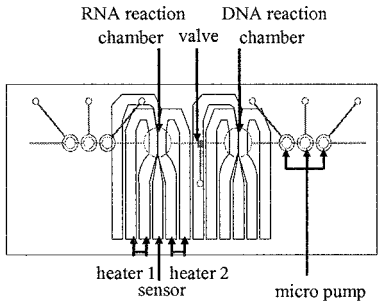

Figure 1. Schematic diagram of the micro-RT-PCR system. Pneumatic micropumps and microvalves were integrated with two reaction chambers to form this integrated microfluidic system.

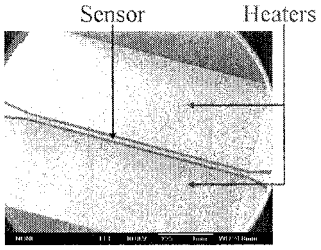

Figure 2. SEM image of on-chip temperature control system. Note that the two micro heaters are located within the reaction chamber to improve the uniformity of the temperature field.

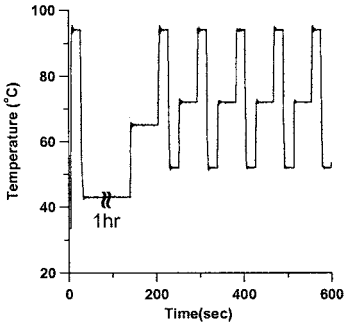

Figure 3. Typical thermal cycle generated by the micro RT-PCR system for amplification of dengue-2 virus RNA. Note that the temperature variation is within ±0.2°.

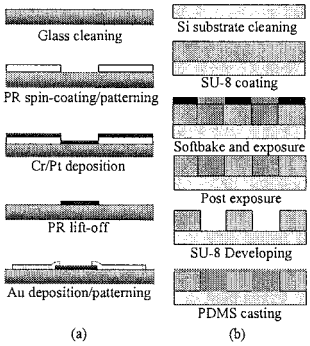

Figure 4. Simplified fabrication process of the micro-RT-PCR system. (a) Temperature control module, and (b) formation of microfluidic channels using SU-8 and PDMS casting process

Figure 5. Micro RT-PCR products of dengue-2 RNA virus in a 1.5% agarose gel stained with ethidium bromide.

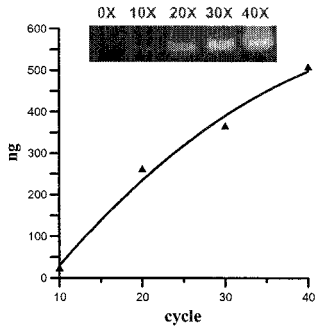

Figure 6 The amplified RT-PCR products in terms of thermal cycles.

THE EFFECT OF VELOCITY AND EXTENSIONAL STRAIN RATE ON ENHANCING DNA HYBRIDIZATION IN A MICROFLUIDIC CHIP

Yung-Chiang Chung[1], **Yu-Cheng Lin**[2], and **Yuh-Lih Hsu**[3]

[1]*Electronics Research and Service Organization, Industrial Technology Research Institute, Hsinchu, Taiwan 310*

[2]*Department of Engineering Science, National Cheng Kung University, 1 University Road, Tainan, Taiwan 701*

[3]*Department of Life Science, National Tsing Hua University, Hsinchu, Taiwan 300*

Abstract

A novel approach of designing a microfluidic chip for enhancing hybridization effectively by introducing fluidic velocity and extensional strain rate was proposed. Three different devices were designed, fabricated and tested. The experimental results demonstrated that the extensional strain rate had more significant impact on hybridization efficiency than velocity. The efficiency of microfluidic hybridization chip could be 9.1-fold as compared with the conventional method within 30 minutes based on this concept. Besides, a linear model that correlated closely with the experimental data was obtained in this study.

Keywords: DNA hybridization, microfluidic, velocity, extensional strain rate

1. Introduction

The detection of nucleic acid (nucleotide) hybridization is generally limited by the mechanism of target DNA diffusion from the bulk to the surface-bound probes. Numerous methods have been developed for increasing the efficiency of the nucleic acid hybridization in microsystems [1, 2, 3]. However, most of the methods are either complicated or costly. We therefore developed a novel, simple and cost-effective device for fast DNA hybridization based on the concept of microfluidics including no reagents or additional fabrication processes [4]. Here, the effects of the velocity and extensional strain rate on DNA hybridization are discussed.

2. Material and methods

The devices were designed to generate the velocity (for raising the effective collision) and extensional strain rate changes (for avoiding the coil-up) along the x-axis. The probe spotted glass and machined poly-methylmethacrylate (PMMA) substrate with flow channels were bonded together to become the hybridization chip. Three different patterns of flow channels, as shown in Figure 1, were designed and compared. The details of the target and probe designs can be referred to our previous work [4]. The sample solution flowed forward and backward at the frequency of 2 Hz. The speed conditions were: static for Device I (control), 1 cm/s and 3 cm/s in the widest and narrowest channel respectively for Device II, and 2 cm/s and 4 cm/s in the widest and narrowest channel respectively for Device III. The results of hybridization are shown in images and fluorescence intensities.

3. Results and discussion

In Figure 2, the fluorescence intensities of five positions in Device III were slightly larger than those in Device II, and the fluorescence intensity of Position 4 was 9.1-fold higher than that of the control condition. It suggested that there was a close relationship between fluorescence intensity and change in the width of the channel. In Devices III, the minimum velocity occurred in the wide channel, while the maximum velocity occurred in the narrow part (Figure 3a); the extensional strain

rates were nearly zero in the straight part of either wide or narrow channel (Figure 3b). The similar tendency could be seen in Device II but with different values.

The effects of velocity (u) and extensional strain rate (u') on hybridization enhancement were easily understood from the comparison between the results at different Positions (Figure 4a and 4b). Especially at Positions 3 and 5, the velocity at Position 5 was larger while the extensional strain rate at Position 5 was smaller, and the normalized fluorescence intensity (f) of Position 3 was larger. These results indicated that the influence of extensional strain rate was larger than that of velocity. Besides, a linear model expressed as $F = 4842.2\,u + 30764\,u' + 5679$ (R-square=0.93) can be used to predict the fluorescence intensity of DNA hybridization. The plane described by this model and the predicted and experimental fluorescence intensities are shown in Figure 5 for comparison.

4. Conclusions

This newly designed microfluidic chip was able to increase the hybridization signal 9.1-fold within 30 minutes, as compared to the conventional hybridization methods. Experimental results showed that the extensional strain rate played a more important role in enhancing hybridization efficiency than that of velocity. Simulation analysis was performed to obtain the velocity and extensional strain rate distributions and to understand the effects of these two factors in the devices. No doubt this microfluidic hybridization chip has potential applications in genomic study.

References

[1] R. G. Sosnowski, et al., Proc. Natl. Acad. Sci. Vol. 94, pp. 1119-1123, 1997.

[2] M. Gheorghe, and A. Guiseppi-Elie, Bios. Bioelectron., Vol. 19, pp. 95-102, 2003.

[3] K. Pappaert, et al., J. Chromatogr. A, Vol. 1014, pp. 1-9, 2003.

[4] Y. C. Chung, et al., Lab Chip, Vol. 3, pp. 228-233, 2003.

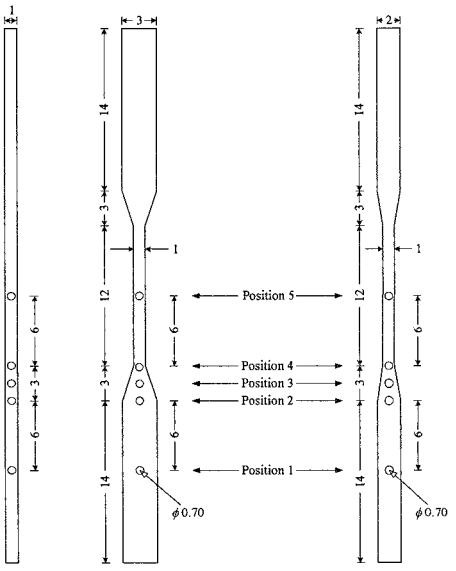

Figure 1. Schematic drawings of different types of flow channels: (a) Device I, (b) Device II, (c) Device III, units: mm.

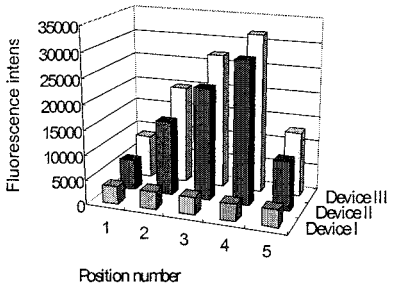

Figure 2. Fluorescence intensity at different positions after 30-minute of hybridization in Device I, II and III.

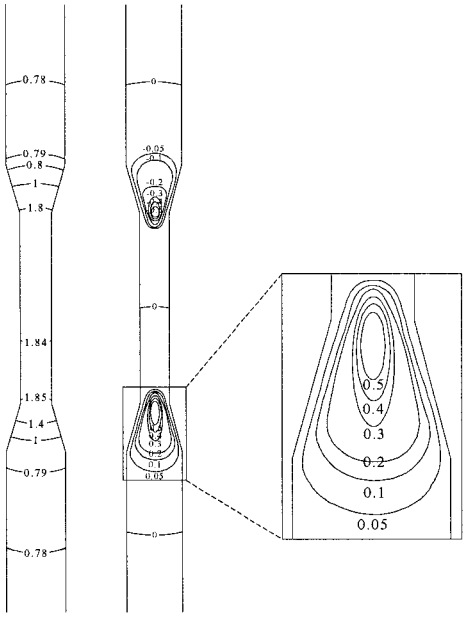

(a) (b)

Figure 3. Velocity (u) and extensional strain rate (u') contour at 5 μm above the bottom in Device III: (a) u (b) u'.

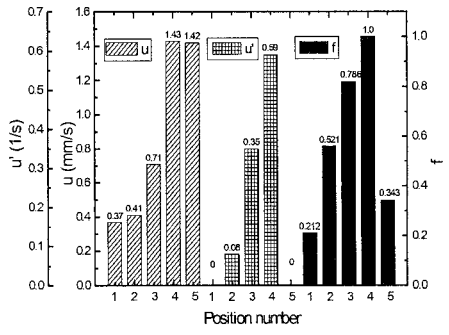

(a)

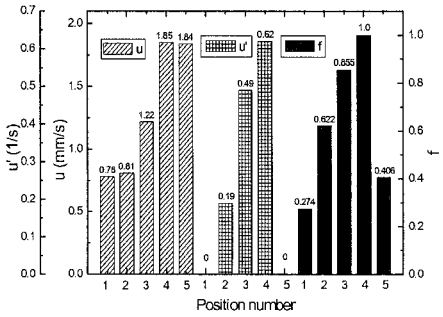

(b)

Figure 4. Relationship among normalized fluorescence intensity (f), velocity (u) and extensional strain rate (u') at different positions at 5 μm above the bottom after 30-minute of hybridization: (a) Device II (b) Device III.

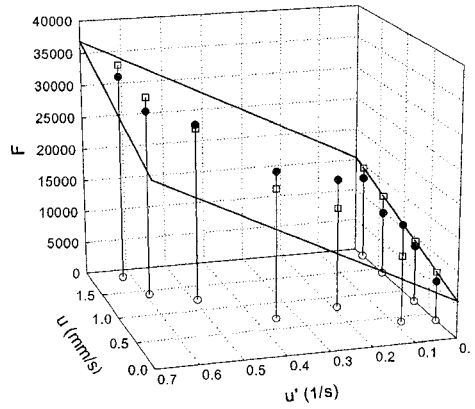

Figure 5. Relationship between predicted (□) and experimental (●) fluorescence intensities of DNA hybridization in Devices II and III. The plane describes the linear model F, and velocity (u) and extensional strain rate (u') corresponding to the fluorescence intensity (○) are shown in the x-y plane.

PHOTOCATALYTIC REDOX-COMBINED SYNTHESIS WITH TIO_2 FILM MODIFIED MICROCHANNEL

Go Takei[1], Takehiko Kitamori[1,2] and Haeng-Boo Kim[2,3]

[1] *Department of Applied Chemistry, School of Engineering, The University of Tokyo, 7-3-1 Hongo, Bunkyo-ku, Tokyo, 113-8656, Japan*

[2] *Kanagawa Academy of Science and Technology, 3-2-1 Sakado, Takatsu-ku, Kawasaki, 213-0012, Japan*

[3] *Engineering Research Institute, School of Engineering, The University of Tokyo, 2-11-6 Yayoi, Bunkyo-ku, Tokyo, 113-8656, Japan*

Abstract

By using a titania modified microchannel chip, efficient photocatalytic synthesis was successfully demonstrated by making one step photocatalytic synthesis of L-pipecolinic acid (L-PCA) from L-Lysine (L-Lys) into an example. The conversion rate in the chip was 70 times larger compared to that in a cuvette using nm-sized titania particles. Moreover, applying potential to the titania film, which was impossible in the conventional particles suspension system, extremely improved selectivity and enantiomeric excess (ee). L-PCA yield reached 36 % at –0.8 V vs Pt, which corresponds to 1.8 times higher than the bulk scale reaction.

Keywords: TiO_2 film modified microchannel, photocatalytic redox-combined synthesis, enantiomer selective reaction

1. Introduction

For the further development of microchip chemistry, integration of chemical functional units into microchannels is one of promising approaches. In the recent years we have demonstrated integration of functional polymer membrane [1] or microelectrodes [2] with microchannels. As one novel function, we are interested in photocatalysis by integration of semiconductor photocatalyst. Among them, TiO_2 is one of the most widely used photocatalyst. For synthetic reaction, in general, TiO_2 is used as nm-sized fine particles due to its large specific interfacial area. Since TiO_2 film modified microchannel chip (TiO_2-MC) has large specific interfacial area, efficient photocatalytic synthesis can be expected. In addition to that, TiO_2-MC has advantages such as reaction control by applying potential, no removal process of nm-sized particles and so on. In the present study, we report a one-step photocatalytic synthesis of L-PCA (Figure 1) [3], which is a useful intermediate of pharmaceuticals, and demonstrate effectiveness of TiO_2-MC.

2. Experimental

TiO_2-MC fabricated in this study is shown in Figure 2. On a top plate, branched microchannels (770-μm-width, 3.5-μm-depth) were fabricated by photolithographic and wet etching techniques. On a bottom plate, TiO_2 thin film was prepared with a sol-gel method. The plates were thermally bonded. Also, potential-controllable TiO_2-MC (PC-TiO_2-MC) was fabricated using Pt electrode integrated substrate as a bottom plate. To apply TiO_2-MC to photocatalytic redox-combined synthesis, Pt was loaded onto TiO_2 as a reduction site. SEM and XRD analysis revealed polycrystalline anatase structure (particle size: 100 nm). L-Lys aqueous solution (2 mM) is introduced into TiO_2-MC under UV irradiation (300-400 nm). The effusive solution from TiO_2-MC was analyzed by HPLC equipped with a chiral separation column. For comparison, bulk scale reaction by using Pt loaded TiO_2 powder suspension (25-nm-diameter) was carried out in a cuvette. Before HPLC analysis, the suspension was centrifuged and filtered to remove the TiO_2 particles.

3. Results and discussion

Experimental results are summarized in Table 1. In TiO_2-MC, 0.86 min irradiation gave 86 % conversion of L-Lys, while it took 60 min in bulk scale reaction to attain almost the same conversion. The results clearly show that higher efficient photocatalytic synthesis proceeded in TiO_2-MC with keeping almost the same selectivity and ee of the bulk scale reaction with 25-nm particles.

Potential dependence of selectivity and ee in PC-TiO_2-MC is shown in Figure 3. The selectivity and ee increased by applying negative and positive potential, respectively. In the present reaction, the selectivity is governed by efficiency of reduction of intermediates (CSB) as shown in Figure 1. Applied negative potential increased surface electron density and thus gave efficient reduction of CSB. On the other hand, ee is governed by the reaction path (path I or II), which is determined by oxidizing power of TiO_2. Applied positive potential enhanced oxidizing power of TiO_2, so that path I became dominant. In the case of bulk scale reactions, Ohtani et al. demonstrated the control of the redox-combined reaction by changing photocatalysts and loading metals [4]. As shown in the present work, in PC-TiO_2-MC, the reaction control was performed readily by applying potential to the TiO_2 film. For one-step sysnthesis of L-PCA, the yield was determined by balance of the selectivity and ee, so that maximum yield (36 %) was attained at -0.8 V vs Pt, which corresponded 1.8 times higher than the bulk scale reaction.

4. Conclusions

The present work demonstrated effectiveness of TiO_2-MC as a photocatalysis system; the faster conversion rate and connectivity to the following processes. In addition to those merits, controlled potential reaction was successfully performed. We believe these characteristic features take new turn in photocatalytic synthesis.

Acknowledgements

The authors acknowledge a Grant-in-Aid from the Ministry of Education, Culture, Sports, Science and Technology (MEXT), Japan (no. 14050024 on Priority Areas (417)) for support in part of the research.

References

[1] H. Hisamoto et al., *Anal. Chem.*, 2003, **75**, 350.
[2] H.-B. Kim et al., *Proc. μ-TAS 2003*, 817.
[3] B. Ohtani, T. Shigeto, S. Nishimoto and T. Kagiya, *J. Org. Chem.*, 1990, **55**, 5551;
[4] B. Pal, S. Ikeda, H. Kominami, Y. Kera and B. Ohtani, *J. Catal.*, 2003, **217**, 152

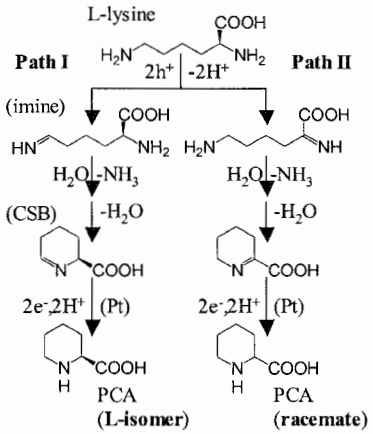

Figure 1. Mchanism of one-step synthesis of L-PCA from L-Lys on Pt-loaded TiO_2 particles.

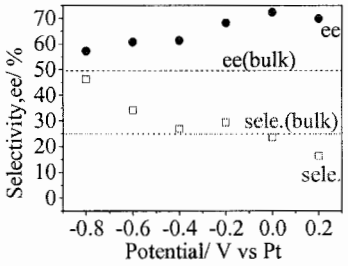

Figure 3. Potential dependence of selectivity and ee. Broken line describes the results on the bulk scale reaction. Selectivity = (amounts of PCA production) / (amounts of L-lysine consumption).

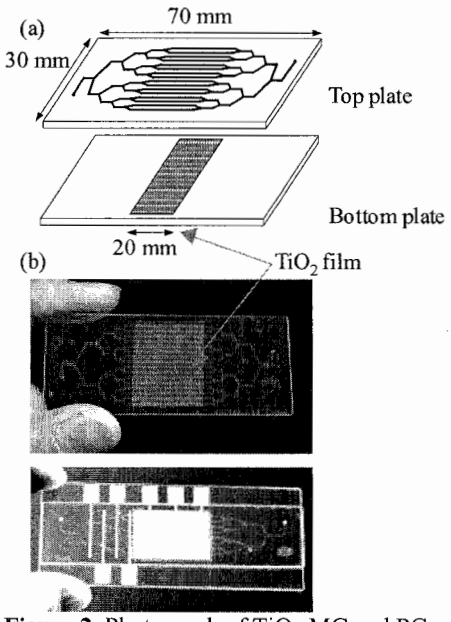

Figure 2. Photograph of TiO_2-MC and PC-TiO_2-MC

Table 1. Comparison among TiO_2-MC, bulk scale reaction and PC-TiO_2-MC

Reaction system	Conversion [b] / %	Reaction time / min	Selectivity / %	ee / %	ϕ [c] / 10^{-4}
TiO_2-MC	86	0.86 [d]	22	50	0.77
Bulk scale (25 nm[a])	89	60	26	46	2.9
PC-TiO_2-MC(-0.8 V)	72	0.48 [d]	47	58	4.7

[a] The bulk scale reaction is performed using powder suspension (particle size is 25 nm). [b] Conversion is defined amounts of L-lysine consumption based on the initial amounts of L-lysine. [c] Quantum yields are based on the amounts of L-PCA and the number of absorbed photons. [d] Reaction time of chip reaction is defined as residential time (flow rate = 1 μL/min).

ON-LINE MS DETECTION FOR A MULTI-STEP COMBINATORIAL SYNTHESIS SYSTEM

Ryo Sakai[1], Yutaka Takahashi[1], Katsumasa Sakamoto[1], Yoshikazu Yoshida[1] and Takehiko Kitamori[2]

[1]*The Research Association of Micro Chemical Process Technology, 3-2-1 Sakado, Takatsu-ku, Kawasaki-shi, Kanagawa 213-0012 Japan*

[2]*Dept. of Applied Chemistry, University of Tokyo, 7-3-1 Hongo, Bunkyo-ku, Tokyo 113-8656 Japan*

Abstract

On-line detection of on-chip synthesis products using electrospray ionization mass spectrometry (ESI-MS) was successfully carried out by taking advantage of on-chip purification to reduce a hindrance to ionization. Multi-step combinatorial synthesis of aminoalcohol derivatives was also performed by extraction of unreacted raw material in the first-step reaction mixture, followed by the second reaction step.

Keywords: Synthesis, Combinatorial Chemistry, Extraction, ESI-MS

1. Introduction

Recently, microchip syntheses have been reported by many researchers, because it is a very powerful tool for drug discovery. Especially, microchip combinatorial syntheses for high throughput synthesis (HTS) are desired. Some studies of on-chip combinatorial synthesis have been reported [1, 2]. But almost all of them were single step synthesis without purification. On-line detection and on-chip purification of products and of their intermediates have an important role in construction of multi-step combinatorial synthesis systems on microchips. With regard to *N*-trifluoroacetylation, which is useful for synthesis of peptides, on-chip synthesis, purification and on-line MS detection of products were examined.

2. Experimental

Pyrex glass microchips (30 mm x 70 mm) with wet-etched microchannels (100 μm width and 40 μm depth) were purchased from Institute of Microchemical Technology Co., Ltd. (IMT, Kawasaki, Japan).

N-trifluoroacetylation of 2-phenetylamine: An ether solution of trifluoroacetic anhydride (TFAA, 100 mM) and that of 2-phenetylamine (100 mM) were prepared under nitrogen. These solutions were introduced into the microchip with a Y-shaped channel by syringe pumps in ratios 1:2 or 2:1 with 3 μL/min of total flow rate, and reacted in the channel. Reaction mixtures were introduced into ESI-MS (JEOL JMS-LCmate) either directly or after being washed on the microchips with pH 6.8 phosphate buffer.

Multi-step acylations of aminoalcohols: Solutions of aminoalcohols were mixed in acylating agents on the Y-shaped channel. The reaction mixtures were washed with pH 6.8 phosphate buffer on microchips prior to the second reaction. Purified *N*-acyl-aminoalcohols were *O*-acylated in excessive acylating agents with amine. The reaction products were identified from the HPLC retention times (column: GL science Inertsil ODS-3; buffer: pH 2.5 ammonium phosphate)

3. Results and discussion

First, *N*-trifluoroacetylation of 2-phenethylamine was carried out, and the unpurified reaction mixture was directly introduced into ESI-MS. *N*-trifluoroacetylation immediately occurred on the microchip [3]. In the condition that the amine was completely consumed, $[M+H]^+$ and $[M+H+Et_2O]^+$ ions of the amide were observed (Fig. 1(a)). However, in the condition in which the amine remained, the ions of the amide were not observed, because phenethylamine trifluoroacetate

remarkably inhibited ionization of the amide (Fig. 1(b)). Observation of the amide became possible by removing the hindrance to ionization with on-chip extraction (Fig. 1(c)).

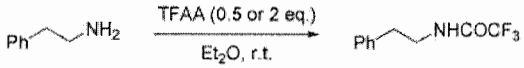

Scheme 1. Trifluoroacethylation of 2-phenethylamine.

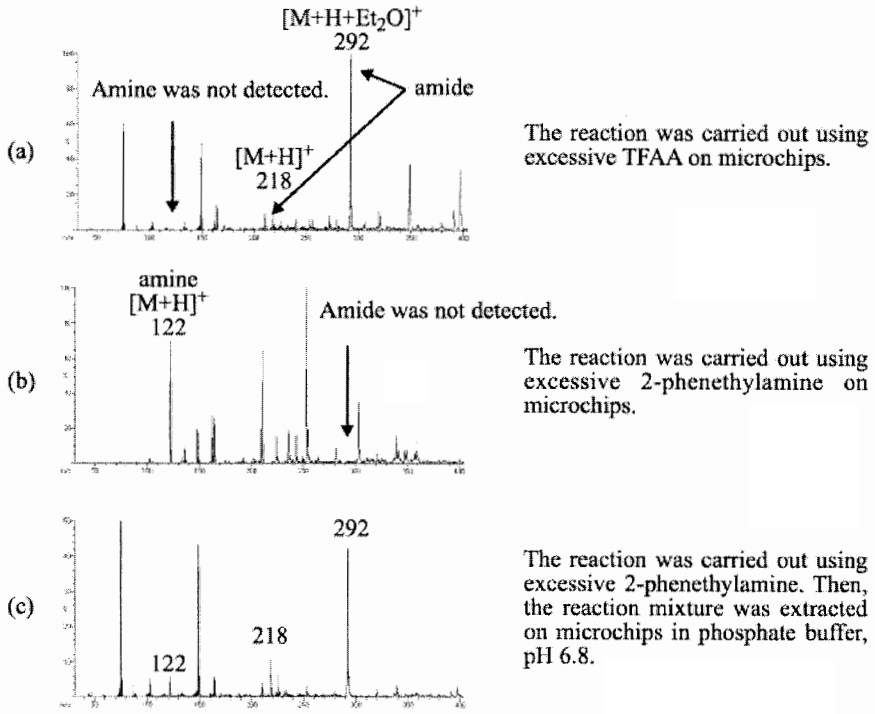

Figure 1. ESI mass spectra of 2,2,2-trifluoro-*N*-phenethyl-acetamide with on-line MS detection.

It became possible to remove unreacted raw material with on-chip extraction. So we tried a multi-step reaction of L-phenylalaninol as shown in Scheme 2 and Figure 2. L-phenylalaninol was *N*-trifluoroacetylated with TFAA. After removing the remaining aminol by washing with buffer, *N*-trifluoroacethylaminoalcohol was *O*-acetylated with acetic anhydride. HPLC chromatograms of before and after purification (Fig. 2 (b), (c)) show that unreacted raw material was completely extracted into the buffer stream. Without purification of the reaction mixture, *N*-acethylated byproducts in the second reaction step were observed.

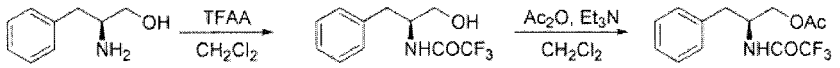

Scheme 2. The multi-step acylation of L-phenylalaninol.

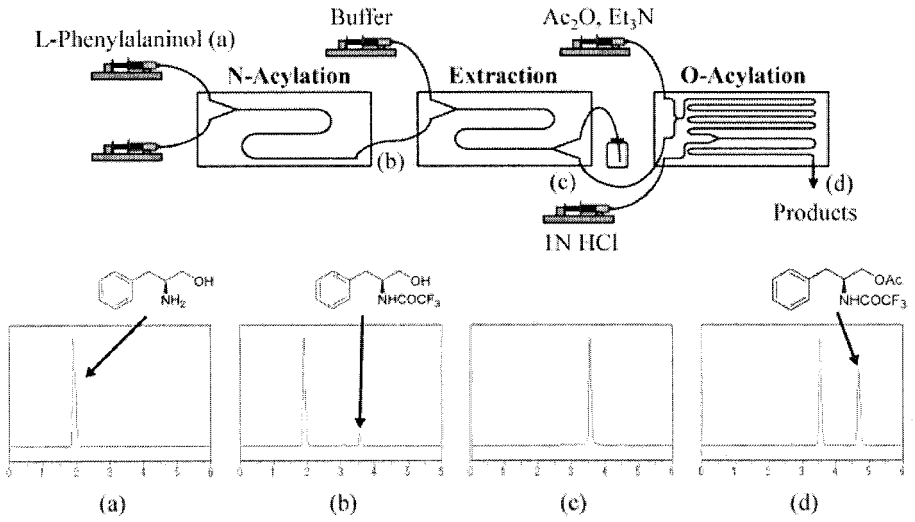

Figure 2. HPLC chromatograms of the reaction mixture (a) L-phenylalaninol, (b) after *N*-acylation, (c) after extraction, (d) after *O*-acylation.

4. Conclusions

We developed on-line MS detection method for microchip combinatorial synthesis system with on-chip purification. We can conclude that on-chip extraction is effective in excluding remaining raw material which prevents the next reaction step.

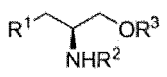

R^1 = H, ^{i}Pr, Ph
R^2 = Ac, -$COCF_3$, Bz
R^3 = Ac, -$COCF_3$, Bz

Figure 3. Library of aminoalcohol derivatives

Serial combinatorial synthesis as shown in Fig. 3 was performed by consecutive introduction of reagents using this system. This system can be expected to be an automatic synthesis system, which will be applicable to both high-throughput synthesis of candidate compounds and to hi-speed optimization of reaction conditions.

Acknowledgements

This work was supported by "Project of Micro-Chemical Technology for Production, Analysis and Measurement Systems" of New Energy and Industrial Technology Development Organization (NEDO), Japan.

References

[1] Y. Kikutani, H. Hisamoto, M. Tokeshi and T. Kitamori, μTAS'01, pp. 161-162.
[2] E. Garcia-Egido, V. Spikmans, S. Y. F. Wong and B. H. Warrington, μTAS'02, pp. 859-861.
[3] Y. Takahashi, R. Sakai, Y. Yoshida, T. Kitamori, International Mass Spectrometry Conference, Edinburgh, Scotland, 04 Sep 2003.

MICRO ENVIRONMENTAL GAS ANALYSIS SYSTEM BY USING GAS-LIQUID TWO PHASE FLOW

Hiromitsu Hachiya[1, 2], Teruki Matsumoto[3], Kazuteru Kanda[4], Manabu Tokeshi[1, 3], Yoshikazu Yoshida[1] and Takehiko Kitamori[3,4]

[1]The Research Association of Micro Chemical Process Technology, KSP-Bldg. R&D-C 11F, Sakado, Takatsu, Kawasaki, Kanagawa, 213-0012, Japan

[2]DKK-TOA Corporation, 4-13-14, Kichijoji-kitamachi, Musashino, Tokyo, 180-8630, Japan

[3]Micro Chemistry Group, Kanagawa Academy of Science and Technology, KSP-Bldg. East-307, Sakado, Takatsu, Kawasaki, Kanagawa, 213-0012, Japan

[4]Dept. of Applied Chemistry, School of Engineering, The Univ. of Tokyo, 7-3-1, Hongo, Bunkyo, Tokyo, 113-8656, Japan

Abstract

The micro environmental gas analysis systems by combining a gas-liquid two-phase flow and a thermal lens microscope (TLM) were developed. These systems were based on gas-liquid reactions through gas-liquid interfaces inside microchannels. In this paper, two micro environmental gas analysis systems for ammonia (NH_3) gas and for formaldehyde (HCHO) were studied. The NH_3 gas analysis system gave a linear response for 0 to 106 ppm of NH_3. The coefficient of correlation was R^2=0.99. Additionally, rapid gas-liquid reactions inside microchannels were observed in this system. The HCHO gas analysis system using a newly designed microchip was also developed. It performed high sensitivity and a linear response for 0 to 0.20 ppm of HCHO. The lower limit of detection was 0.0089 ppm, which was lower than the guideline-value announced by WHO. Both of the above novel micro gas analysis systems using gas-liquid two phase flow inside microchannels achieved good performances for analyzing each environmental pollutant.

Keywords: gas analysis, gas-liquid flow, microchannel, ammonia, formaldehyde

1. Introduction

Many kinds of microchips have been proposed for analyzing liquid samples. However, only few reports have been done on microchip-based gas analysis systems using both gas and liquid phases. Because of large differences between physical parameters of these two phases, such as viscosity and compressibility, the control of a gas-liquid two phase flow inside a microchannel was relatively difficult. Moreover, the integration of a gas-liquid separator, which has been used in macro-sized conventional gas sensors, on a microchip was also a difficult technology.

Recently, we had succeeded in the formation of controlled gas-liquid two-phase flows by using specially designed asymmetric microchannel structures [1]. Since the gas-liquid interface was stably formed inside a microchannel (shown in Figure 1), the quantitative gas-liquid reaction was expected to be occurred in this microchip. We applied this new technique to two kinds of gas analysis microchip systems for NH_3 and HCHO. NH_3 is one of the notorious pollutant gases with its toxicity and odor. HCHO is a typical indoor-pollutant that causes a serious house-sick syndrome.

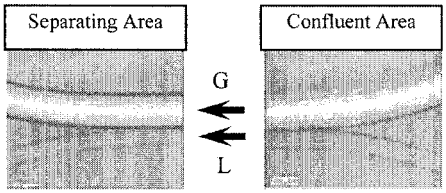

Figure 1 Gas-liquid two phase flow with stable gas-liquid interface inside microchannel.
G : gas (1 mL min^{-1})
L : liquid (1 μL min^{-1})

2. Experimental

NH_3 gas analysis system

A Pyrex glass microchip with "Double-Y channel" (2 inlets and 2 outlets) was fabricated using conventional photolithographic technologies. Microchannels for the gas-liquid two-phase flow had an asymmetric section with larger (90 μm deep and 190 μm wide) and smaller (20 μm deep and 50 μm wide) parts. Figure 2 shows the experimental setup of NH_3 analysis. Phenolphthalein solution (PP) was used as a reactant. pH of the reactant was changed by NH_3 absorption, and PP became colored. The color-change was detected by using a TLM.

HCHO gas analysis system

A newly designed microchip as shown in Figure 3 was developed for HCHO analysis. The microchip was composed of an extraction area and a reaction area as shown in Figure 4. The sectional dimensions of both channels were shown in Figure 3. A TLM and Schiff reagent were used as a detector and an extract. The flow rates were 700 μL/min for HCHO containing gas and 0.01 μL/min for the extract. The extraction was carried out inside an asymmetric microchannel of 3 cm in length. After being separated from gas phase, the reaction between HCHO and the extract proceeded to equilibrium inside a microchannel of 20 cm in length thermo-stated at 65 °C. The whole analysis time was 41 min., which included 6 min. for extraction and 35 min. for reaction.

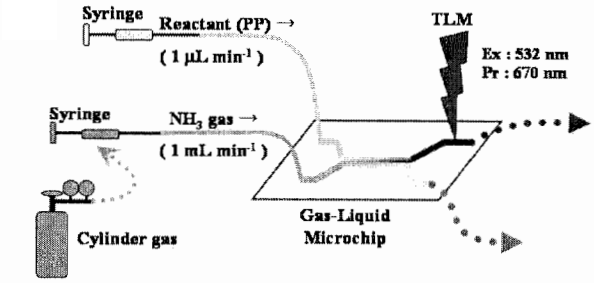

Figure 2 Experimental setup of NH_3 gas analysis system.

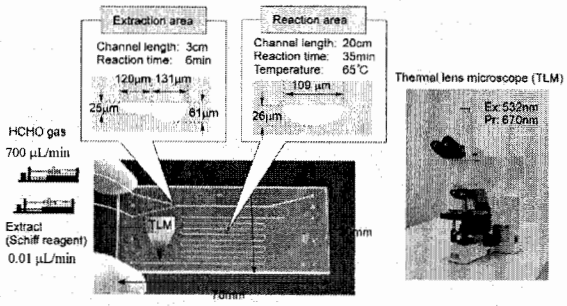

Figure 3 Newly developed HCHO analysis system.

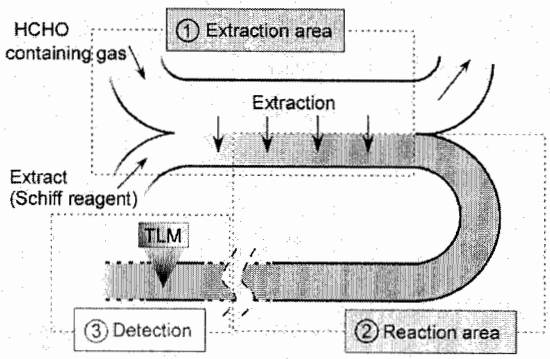

Figure 4 Concept of HCHO gas analysis microchip.

3. Results and Discussion

NH_3 gas analysis system

The responses for NH_3 gases were measured using this NH_3 analysis system. A calibration curve was shown in Figure 5. A linear response was observed in the concentration range of blank to 106 ppm NH_3 that included 25 ppm of TLV (threshold limited value announced by ACGIH). The coefficient of correlation was R^2=0.99. The limit of detection (LOD) was 1 ppm.

The TLV signals measured at three difference positions along the channel were shown in Figure 6. From this result, it was confirmed that the gas-liquid reaction reached chemical equilibrium for an instant.

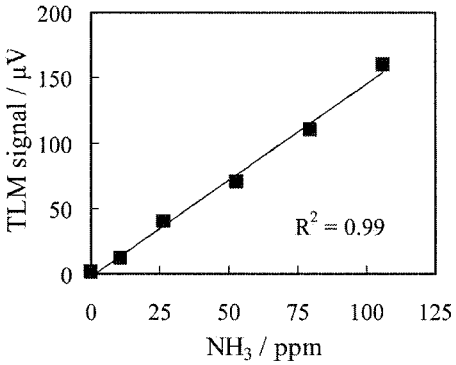

Figure 5 Calibration curve for NH_3.

HCHO gas analysis system

A calibration curve for 0 to 0.20 ppm HCHO was shown in Figure 7. The linear response was observed in the concentration of 0 to 0.20 ppm HCHO. The LOD was 0.0089 ppm HCHO, and which was lower than the guideline-value (0.08 ppm) for a house-sick syndrome announced by WHO (World Health Organization).

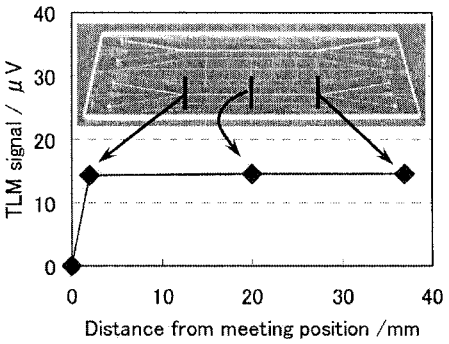

Figure 6 Rapid gas-liquid reactions inside microchannel.

4. Conclusions

The novel two micro environmental gas analysis systems for NH_3 and for HCHO by using a gas-liquid two-phase flow were developed. Both of the systems achieved superior performances for each target gases.

In the future, these systems may lead to chip-based mobile gas-analysis systems.

Acknowledgements

This work was supported by the New Energy and Industrial Technology Development Organization (NEDO) of the Ministry of Economy, Trade and Industry, Japan.

References

[1] M.Tokeshi, K.Kanda, A.Hibara and T.Kitamori, *Proceedings of MicroTAS 2002*, pp.356-358 (2002).

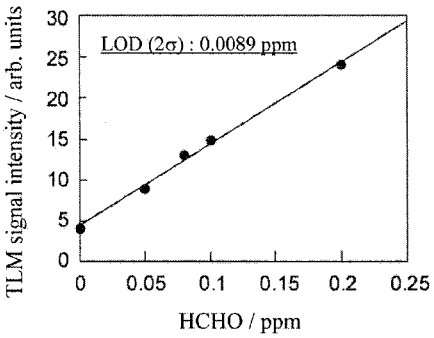

Figure 7 Calibration curve for HCHO.

CONTINUOUS-FLOW MICROMIXING FOR FAST DNA HYBRIDISATION ASSAYS

Martin Heule[1,2] **and Andreas Manz**[1,3]

[1]*Dept. of Chemistry, Imperial College London, London SW7 2AY, UK*
[2]*Microsystems Laboratory, STI-LMIS, EPFL, CH-1015 Lausanne, Switzerland*
[3]*ISAS, Institute of Analytical Sciences, Bunsen-Kirchhoff-Str. 11, 44139 Dortmund, Germany*

Abstract

The prospects of performing DNA hybridisation assays in a novel sequential scheme are explored. It is based on recording the kinetics of hybridisation on a microfluidic device. It contains a split channel system for fast mixing and an adjacent meandering channel to observe the evolution of the mixture. This was done by using fluorescent dyes which enhance their fluorescence efficiency upon binding to dsDNA. DNA oligomers (20-mers) of different sequences were injected on the chip for mixing. Two modes of operation were investigated. First, quick injection with subsequent reducing of the flow rate to allow for measurement of fluorescence levels at various steady-state reaction times in the range of 2-15 s, as defined by the channel geometry. Single base-pair mismatches were successfully identified under low salt conditions. In the second mode, the flow was completely stopped and the evolution of the total fluorescence signal influenced by the hybridisation of oligomers and photobleaching was observed. Clear identification of oligomer hybridisation properties could be reduced down to a maximum of 5-7 s, in some cases below 1 s.

Keywords: micromixing, DNA hybridisation, high-throughput analysis.

1. Introduction

DNA hybridisation reactions are performed in vast numbers, one of the most valuable platforms are DNA microarrays.[1] Fluorescent labelling techniques are predominantly used to identify the sites where probe and target sequences match. The performance of DNA microarrays is impressive as integration with microsystem technology progresses to increase the information density considerably.

Our different approach has potential for high-throughput application by combining purely solution-based DNA hybridisation reactions with the use of a microfluidic system. This device overcomes the mixing problem that is inherent to most microfluidic systems which work in the laminar flow regime and is based on the fine distribution of two laminar inlet flows (Figure 1). DNA hybridisation assays are performed in series by injecting the sample solutions one after the other and mix them rapidly on the chip. If such a scheme is to be used for a large number of analyses in sequence, the single assay has to be performed within a short time to become comparable to the enormous multiplexing performance of microarray technology. The prospect of decreasing the time of one assay to the order of 1 s is presented. Potentially, this technology could allow for many thousand assays within just a few hours. By using solution-based DNA chemistry, the need for immobilisation schemes is eliminated. The detection of DNA hybridisation is based on the fluorescent dye PicoGreen that selectively enhances its fluorescence upon binding to double-stranded DNA (dsDNA). Typically, such intercalating reagents are used for DNA quantification.

2. Experimental Summary

The high efficiency of mixing in the laminar flow regime is brought about by splitting each of the two inlet streams into 16 smaller substreams which then are joined and recombined (Figure 1). Details concerning the design and microfabrication procedures of the device are given elsewhere.[2] Gel-filtered DNA oligomers were synthesized commercially according to our sequence data and used as received. The following sequences were used for the present work, a base sequence

A: 5'-GTTTATTAATGCGGCCCGCG-3', A': 5'-CGCGGGCCGCATTAATAAAC-3', its perfect match as well as sequences containing increasing numbers of base pair mismatches, A-1: 5'-CGCGGGC***T***GCATTAATAAAC-3', A-2: 5'-CGCG***A***GCCGCATT***G***ATAAAC-3' and A-5: 5'-CG***T***GAG***A***CGCA***C***T***G***ATA***T***AC-3'. Locations of mismatches are indicated in bold-oblique letters. For a typical experiment, 3 ml of buffer solution containing 34.5 mg NaCl (0.2 M) and 8.9 mM tris-borate/0.2 mM EDTA at pH 8.3 were prepared and put under vacuum for degassing. To this buffer, the appropriate amount of oligomer and intercalating dye (typically 5 µl of PicoGreen diluted in water 1:10) was added shortly before the experiment. The first syringe connected directly to one inlet usually contained 450 µl of a 0.8-8 µM (5-50 µg/ml) target oligomer solution, the syringe supplying the other inlet contained 450 µl pure buffer and was used as carrier stream through a HPLC-type injection valve.

3. Results

The characteristics of the micromixing chip led to the decision to vary the flow rate in the present work by mixing probe and target oligomer quickly using a high flow rate and subsequently slowing down or stopping the flow to allow for enough time to observe the evolution of the DNA hybridisation reaction. The downstream channel volume of 480 nl would allow for a time window of 600 ms at a flow rate of 40 µl min^{-1}. Therefore, variations of the flow-rate or stop-flow schemes were introduced to cover a wider range of reaction time.

Figure 1 shows the mixing of a solution of fluorescein isothiocyanate (FITC, bright) and pure water (dark). FITC enters from a second layer via through-holes as the row of 16 very bright spots indicates. The fast micromixing effect is achieved by splitting the inlet flows and recombining them in an alternating stratification. The diffusion distance between adjacent laminar streams is reduced to the order of 10 µm, thus allowing for mixing times in the ms range, depending on diffusion coefficients. For FITC, mixing is complete after some 30 ms.

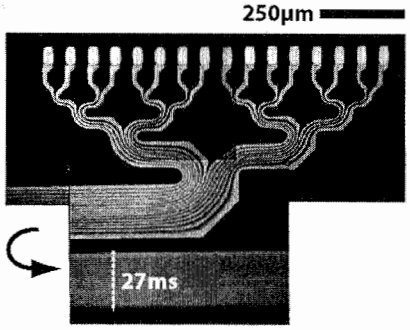

Figure 2 depicts an example of a hybridisation experiment with matching oligomer sequence A versus A' in reduced flow-mode. Immediately after injecting the oligomer (dotted line, right hand axis), the flow rate is reduced and an increase in fluorescence is recorded. The experiment can be performed multiple times on one injection, as shown by the short flow rate pulse at 45 s that brings a fresh mixture plug to the detector. The difference of this increase (ΔPMT) was evaluated and found to reflect the hybridisation kinetics and therefore matching, respectively mismatching DNA sequences, including single base-pair mismatches.

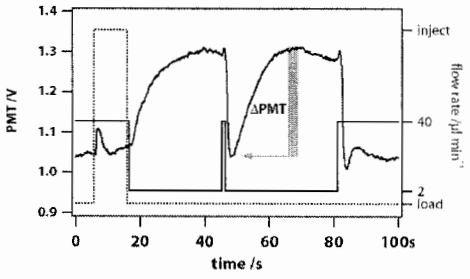

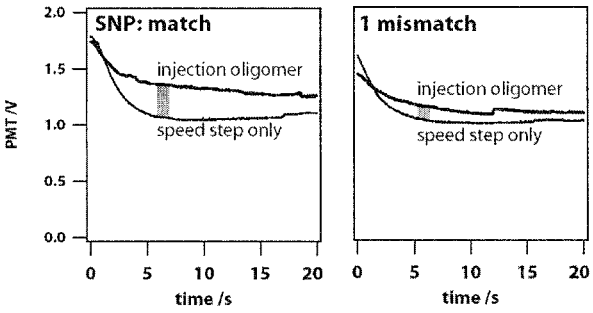

Figure 3. Detection of single base-pair mismatches (SNPs) are possible within 5 s from reducing flow rate. The signal in these cases declines due to inlet pressure variations caused by the change of flow rate as indicated by the lower reference signals where no oligomer was injected (speed step only). In the case of matching sequences, a signal difference of 0.35 V was observed, whereas in the case of an SNP sequence, the difference only amounts to 0.1 V.

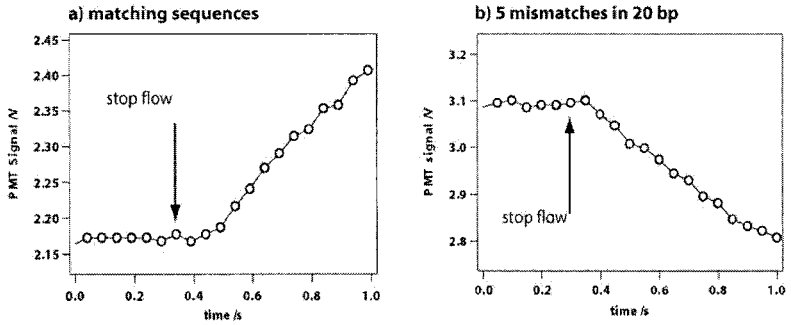

Figure 4. Detection of matching probes within 1s. An increase in fluorescence occurs only if dsDNA is formed (a). On the other hand, photobleaching of the intercalating dye becomes significant when the flow is completely stopped (b). These two counterbalancing effects can be exploited for fast detection of hybridisation. If the oligomers match (a), the fluorescence enhancement due to the intercalation reaction outweighs photobleaching. However, photobleaching is dominant in mismatch situations (b).

Acknowledgements

M. Heule acknowledges financial support from the Swiss National Science Foundation, SNF.

References

[1] R. J. Lipshutz, S. P. A. Fodor, T. R. Gingeras, D. J. Lockhart, *Nature Gen.*, **21S**, 20-25 (1999).

[2] F. G. Bessoth, A. J. deMello, A. Manz, *Anal. Commun.*, **36**, 6, 213-215 (1999).

[3] M. Heule, A. Manz, *Lab on a Chip*, in press (2004).

THE USE OF SOLID-SUPPORTED REAGENTS WITHIN EOF-BASED MICRO REACTORS

Charlotte Wiles, Paul Watts and Stephen J. Haswell
Department of Chemistry, Faculty of Science and the Environment, The University of Hull, Cottingham Road, Hull, HU6 7RX

Abstract

By incorporating a series of silica-supported bases into an EOF-based flow reactor, we have demonstrated the synthesis of eight condensation products in excellent yields, without the need for additional purification steps.

Keywords: Electroosmotic flow (EOF), solid-supported reagents, micro reactor, Knoevenagel condensation

1. Introduction

Increased demand for the rapid preparation of small molecule libraries has led to renewed interest in the development of clean and efficient techniques for the synthesis of organic compounds. With this in mind, the miniaturisation of reaction technology is of particular interest to the pharmaceutical industry, where long term objectives include the desire to perform multiple functions such as synthesis, detection, screening and biological evaluation within a single integrated device. To date, numerous compounds have been successfully synthesized within micro fluidic devices, with many groups demonstrating the advantages over traditional batch techniques such as greater reaction control; leading to increased conversions, product selectivity and reduced reaction times [1]. Although many groups have begun the task of transferring synthetic methodology from batch to micro reactors, few have addressed the challenges associated with the purification of reaction products prepared in continuous systems [2]. In order to tackle this problem, we looked at the incorporation of supported reagents into a miniaturised flow reactor, using the Knoevenagel condensation as a model reaction. As Scheme 1 illustrates, the reaction is defined as the base-catalyzed condensation of an aldehyde or ketone with a compound that possesses an activated methylene group in order to prepare an unsaturated product [3]. Consequently, the reaction products require purification in order to remove residual base and its salt; it is therefore proposed that by employing a supported base (Figure 1), products of high purity can be synthesized without the need for further purification.

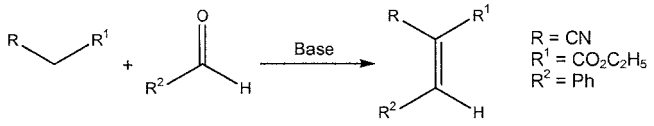

Scheme 1. The base-catalyzed condensation of an aldehyde with an activated methylene.

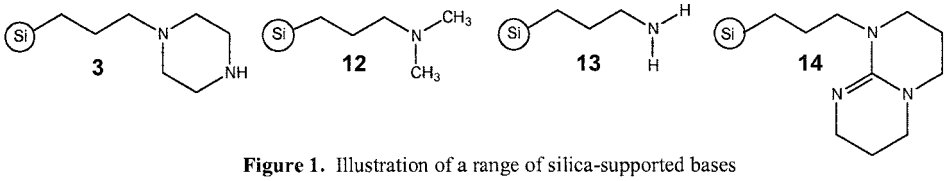

Figure 1. Illustration of a range of silica-supported bases

2. Experimental

As Figure 2 illustrates, using electroosmotic flow (EOF) a 1:1 mixture of starting materials **1** and **2** are passed through a packed bed (containing 5 mg of 3-(1-piperazino)-propyl-functionalized silica gel **3** (1.9 mmol N g^{-1}) over a period of 20 minutes, after which the reaction products are collected and analyzed by GC-MS.

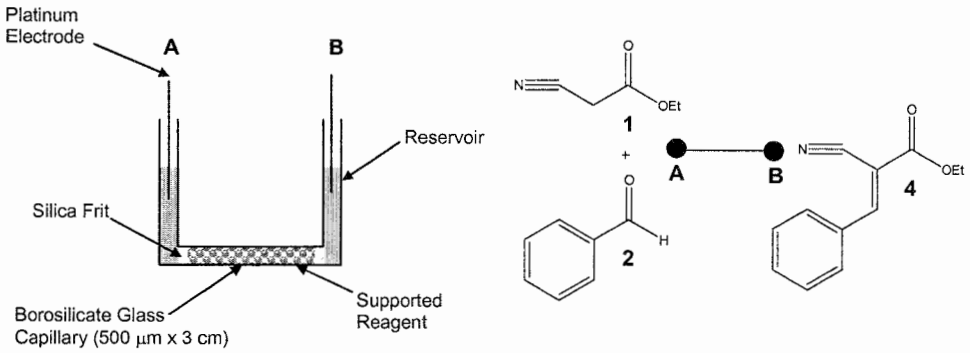

Figure 2. Schematic of the reaction set-up used for the evaluation of silica-supported bases.

3. Results and discussion

Using the synthesis of 2-cyano-3-phenyl acrylic acid ethyl ester **4** as a model reaction, the device was operated continually over a period of 4.75 hrs whereby 0.025 g (0.124 mmol, 98.9 %) of product **4** was synthesized. As Table 1 illustrates, reproducible conversions of > 98 % were obtained, demonstrating device stability and reagent longevity. After analysis by GC-MS, the reaction products were collected and concentrated *in vacuo*, the crude product was then analyzed by NMR spectroscopy. As Figure 3 illustrates, ^{13}C NMR confirmed the successful synthesis of 2-cyano-3-phenyl acrylic acid ethyl ester **4** without the need for further purification steps [4].

Run No.	Conversion (%)
1	98.3
2	98.5
3	98.3
4	98.3
5	98.4
6	99.2
7	99.1
8	99.1
9	100.0
10	99.6
11	99.3
12	100.0
13	100.0
14	99.2
Mean = 99.1 %, % RSD = 0.65	

Table 1. Illustration of device reproducibility over 4.75 hr.

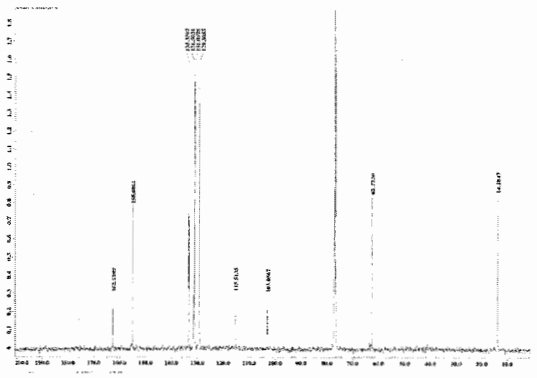

Figure 3. ^{13}C NMR of 2-cyano-3-phenyl acrylic acid ethyl ester **4** synthesized within a micro fabricated device.

Having demonstrated the ability to synthesize 2-cyano-3-phenyl acrylic acid ethyl ester **4** in high purity, the technique was extended to the synthesis of 3-(4-bromophenyl)-2-cyano acrylic acid ethyl ester **5**, 3-(3,5-dimethoxyphenyl)-2-cyano acrylic acid ethyl ester **6**, 3-(4-benzyloxyphenyl)-2-cyano acrylic acid ethyl ester **7**, 2-benzylidene-malononitrile **8**, 2-(4-bromobenzylidene)-malononitrile **9**, 2-(3,5-dimethoxybenzylidene)-malononitrile **10** and 2-(4-benzyloxybenzylidene)-malononitrile **11** whereby conversions > 95 % were obtained (Table 2). The technique was further extended to the use of 3-(dimethylamino)propyl-fucntionalized silica gel **12** (1.50 mmol N g^{-1}), 3-aminopropyl-functionalized silica gel **13** (1.00 mmol N g^{-1}) and 3-(1,3,4,6,7,8-hexahydro-2*H*-pyrimido[1,2-a]-pyrimidino)-propyl-functionalized silica gel **14** (2.4 mmol N g^{-1}) whereby 99.4, 100 and 99.3 % conversion to 2-cyano-3-phenyl acrylic acid ethyl ester **4** was obtained respectively (Table 3).

Product No.	Applied Field (V cm^{-1})	Flow Rate ($\mu l\ min^{-1}$)	Conversion[a] (%)
4	333	0.50	99.1
5	333	0.30	99.5
6	333	0.30	94.7
7	333	0.50	95.1
8	167	1.00	96.9
9	167	0.50	96.3
10	167	0.70	97.8
11	167	1.00	99.7

[a] ≥10 replicates were performed for each compound

Table 2. Summary of the conversions obtained using 3-(1-piperazino)-propyl functionalized silica gel **3**.

Base	Flow Rate ($\mu l\ min^{-1}$)	Conversion[a] (%)
1	0.50	99.1
17	0.35	99.4
18	0.35	100.0
19	0.80	99.3

[a] ≥10 replicates were performed for each base

Table 3. Comparison of the conversions obtained using a range of silica-supported bases.

5. Conclusions

In conclusion, we have successfully demonstrated the incorporation of a series of silica-supported bases within a miniaturized EOF-based flow reactor, enabling the synthesis of eight condensation products in high purity. Using the methodology described herein, further studies are currently underway within our laboratories to extend both the type of reagent and support employed, enabling more complex syntheses to be evaluated.

Acknowledgements

Full financial support provided by the EPSRC (grant no. GR/S34106/01) (C.W.) is gratefully acknowledged. Mike Bailey (University of Hull) is also acknowledged for assistance in device fabrication.

References

[1] T. Schwalbe, A. Volker and G. Wille, *Chimia,* **56**, 636 (2002).
[2] J. Brody and P. Yager, *Sens. Act. A,* **58**, 13 (1997).
[3] G. Jones, *Org. React.,* **15**, 204 (1967).
[4] C. Wiles, P. Watts and S. J. Haswell, *Tetrahedron*, in press.

A DIELECTROPHORETIC CELL SEPARATION MICROCHIP WITH SIZE FILTERING

Tsan-I Chen and Cheng-Hsien Liu

Dep. of Power Mechanical Engineering, National Tsing-Hua University, Hsin-Chu 30013, Taiwan

Abstract

A MEMS-based dielectorphoretic cell separation microchip has been developed and reported in this paper. We utilize dielectrophoresis force and size filtering microstructure for the function of cell separation in our microchip. Multiple particles could be separated in our device based on their size and property via applying AC voltages of different frequencies simultaneously in our microchip. To enhance the separation function, additional microstructure design is adopted to filter out unwanted particles. Another pyramid tip array design is also used for the force enhancement. The design, simulation, microfabrication and experimental test will be reported in this paper.

Keywords: cell separation, cell sorting, dielectrophoresis, MEMS

1. Introduction

One of the most popular bio-medical researches nowadays focuses on the DNA analysis, including gene interpretation, gene identification, disease diagnosis and virus analysis. Before all these sequences, sample preparation is an essential process which separates target cells from unwanted cells and, then, lyses the cells DNA analysis.

Dielectrophoresis has been developed and is known as a powerful tool for bio-chip applications. It is a non-contact procedure and has no adverse effect due to continuous exposure of the cells to high frequency electric fields [1]. A variety of researches dealing with DEP cell separation have been proposed and developed. In this paper, we propose a new DEP (dielectrophoresis) cell separation device. Base on the difference in polarity and size between distinct cells, we can extract the target cells by controlling the applied AC voltage and frequency. Recent researches about DEP cell separation merely focus on the polarity difference between cells but can poorly separate the distinct cells with similar polarities. [2][3] By utilizing the concept of size-filtering, our design with micro filter structure increases the separation efficiency. With specific applied voltage and frequency, it is possible to separate more than two cell types simultaneously.

2. Design and Simulation

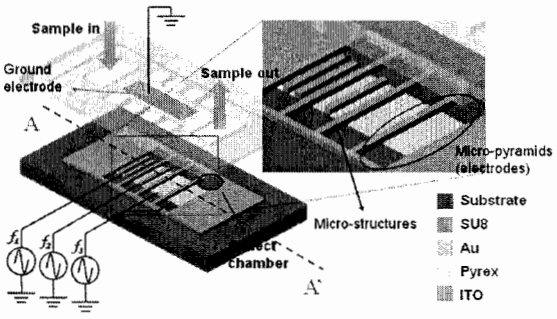

Figure 1. Device illustration and design concept

The bottom electrodes are designed as a three-dimensional micro-pyramid, which could provide larger electric field gradient along vertical direction than conventional two-dimensional electrodes to attract target particles. To prevent cells from blocking the microchannels, we have SU8 microstructures perpendicular to the flow direction. The target cells will be attracted by DEP and trapped into the trenches between SU8 micro-structures. A concept of multi-frequency voltage control is introduced in the device.

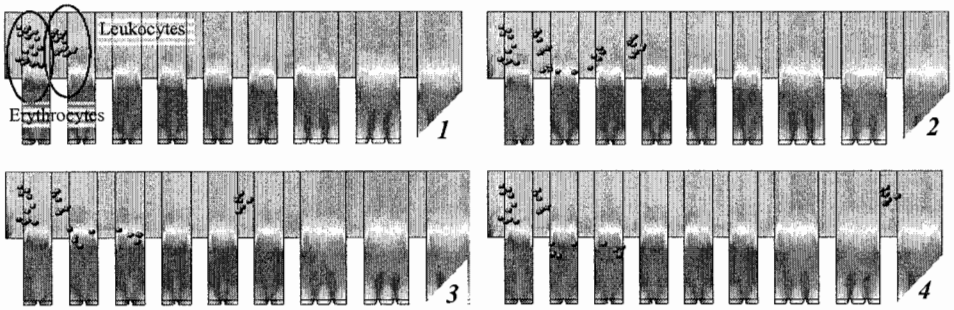

Figure 2. The separation of blood cells and E^2 (the square value of electric field) distribution

By applying different frequency of signals to each electrode sets, we are able to attract particles of different polarity. Fig.1 illustrates our device and design concept.

To theoretically verify our design concept, a simulation has been done by CFD-ACE+ software. Fig.2 shows the two-dimensional simulation results along A-A' cross section (shown in Fig.1). In our simulation, we separate Leukocytes and Erythrocytes in a medium of conductivity 0.015 S/m by applying a flow rate of 1e-4 m/s and a 10kHz, 10Vp-p signal to the electrodes. The simulation results successfully demonstrate the trapping of target particles in trenches and the washing away of unwanted ones. The heights of the SU8 wall and the channel both are 50μm each. The SU8 wall behaves as a dielectric material due to its low permittivity. That results in sustaining the electric strength to the height of the wall to create enough electric field gradients to attract particles.

3. Microfabrication

The device is fabricated using MEMS techniques. First, the micro-pyramid structure is formed on a silicon wafer by using KOH+IPA wet-etching . Fig. 3 shows the wet-etching result of our micro- pyramid structures. After depositing an isolation layer of oxide, a platinum layer is then evaporated and patterned to define the electrodes. The SU8 micro-structures of 50μm height is fabricated and patterned by using photo lithography to serve as separation walls and trench channels (as shown in Fig. 4). Another layer of SU8 is on an ITO (Indium Tin Oxide) wafer to form the flow channel. The last fabrication step is to bond these two wafers together.

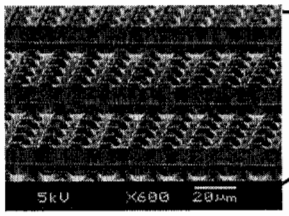

Figure 3. Micro-pyramids after KOH+IPA wet-etching process

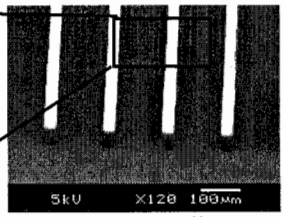

Figure 4. SU-8 walls

4. Experimental Results

For the preliminary test, we use latex beads instead of cells in the paper. By applying a 5Vp-p 100Hz signal, latex beads of 10μm encounter positive DEP force

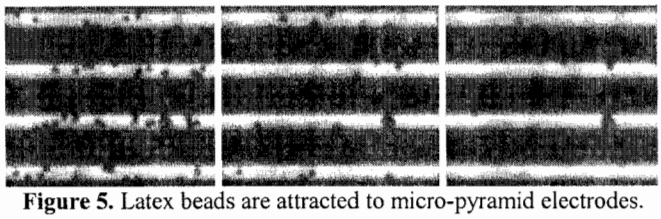

Figure 5. Latex beads are attracted to micro-pyramid electrodes.

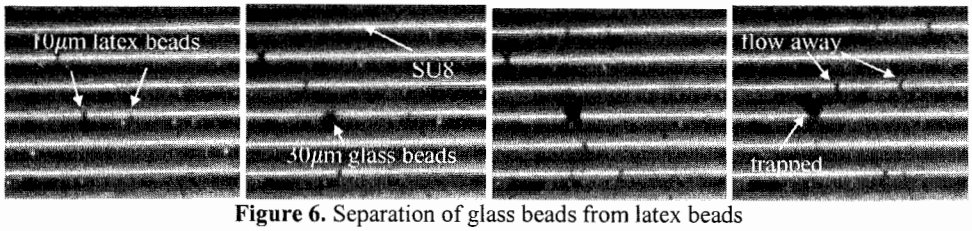

Figure 6. Separation of glass beads from latex beads

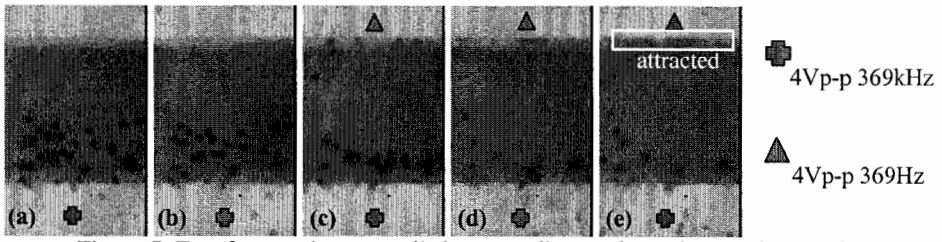

Figure 7. Two frequencies are applied to two adjacent electrodes simultaneously.

and are attracted to the micro-pyramids in a medium of conductivity 30μS/m as shown in Fig.5. Fig.6 shows the separation of 30μm glass from 10μm latex beads. The applied signal is 8Vp-p, 100kHz at which glass beads encounter a larger negative DEP force than the smaller latex beads and are trapped to the top of SU8 walls where there is the local electric field gradient minimum.

Two frequencies are applied to two adjacent electrodes simultaneously in Fig.7. First, a 4Vp-p 369 kHz signal is applied to the lower electrode, where latex beads encounter N-DEP force and move with flow (Fig.7(a),(b)). When adding another 4Vp-p 369 Hz signal to the upper electrode, latex beads are trapped at the edge of the electrode. We observed that latex beads near the lower electrode are levitated due to negative DEP and move faster with the flow (Fig.7(c),(d)(e)). These results verified the feasibility of our multi-frequency concept.

5. Conclusions

In this paper, we present a new dielectrophoretic cell separation microchip and demonstrate our preliminary experimental results. The concepts of multi-frequency and structural filtering are proposed to increase the separation efficiency. Several modifications including structure and electrode design are undergoing for the further cell applications.

Acknowledgements

The authors would like to thank Nano Facility Center (NFC) for cleanroom facility support. We also acknowledge Industrial Technology Research Center (ITRI) for the helps on measurement equipment. This work is supported partially by National Science Council of R.O.C under grant NSC92-2215-E-007-014 and Nano-technology Research Program.

References

[1] Fuhr, G. Glasser, H., Muller, T. and Schnelle, T.(1994) Biochim. Biophys. Acta 1201, 353-360
[2] Youlan Li, Karan V.I.S. Kaler, IEEE Electrical Insulation and Dielectric Phenomena, 2002, pp.680 - 684
[3] H. Sano, H. Kabata, O. Kurosawa, M. Washizu, IEEE MEMS, 2002, pp.11-14

ON-CHIP SPERMATOZOA TRAPPING BY DIELECTROPHORESIS

M.Frénéa[1], M. Chiral[1], B. Le Pioufle[1], N.Melaine[2], C.Pineau[2], B.Jégou[2]

[1]SATIE UMR 8029 CNRS - BIOMIS, ENS Cachan, Campus de Ker Lann, Bruz, France

[2]GERHM INSERM U 625 - University of Rennes 1,Campus de Beaulieu, Rennes, France

Abstract

This paper deals with spermatozoa behavior under the influence of non uniform electric fields. Both bipolar and quadripolar microelectrode structures are used to study spermatozoa trapping by negative or positive dielectrophoresis (DEP). These electrode arrays have proven their efficiency to capture motile cells using the action of the dielectrophoretic force. However, fluid flow may also explain some effects observed during our experiments.

Keywords : Spermatozoa, dielectrophoretic trapping, electrohydrodynamic effects

1. Introduction

Dielectrophoresis has already been applied to various types of biological particles such as animal and plant cells, DNA, bacteria and neurons, but with the exception of Fuhr's work [1], little research has been done in the study of motile particles or cells such as spermatozoa. Spermatozoa trapping by dielectrophoresis can possibly open the way to new interesting applications : it has been shown [2] that optical tweezers can be used to measure the motility forces of spermatozoa, by determining their ability to escape the optical trap. Similarly, their capacity to break away from a dielectrophoretic trap could be a useful indicator in sterility diagnosis.

2. Microdevices design

Two microelectrode structures have been fabricated for our experiments: commonly used interdigitated rectangular electrode structures (Figure 1) and quadrupolar electrode sets (Figure 2) described elsewhere [3].

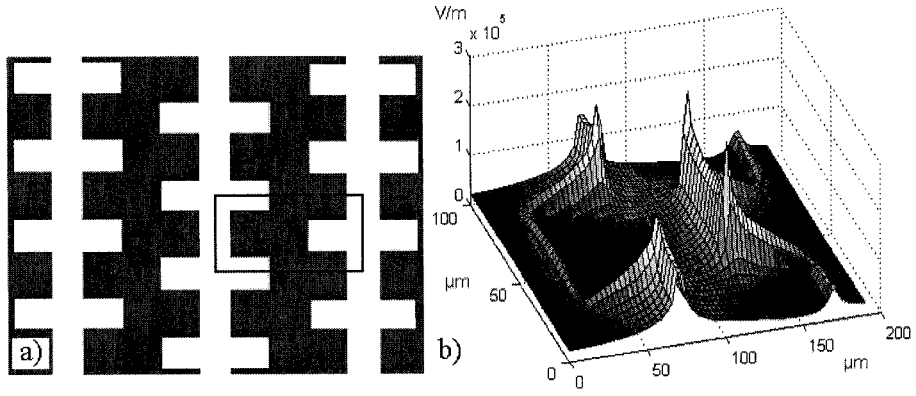

Figure 1. Field cartography produced by the rectangular electrode structure (representation in the electrode plane, for an applied RMS voltage V=4V).

Both these structures enable a good distinction between electric field maxima and minima (Figures 1b. and 2b.), where particles can be directed under the influence of positive or negative dielectrophoresis respectively. The field cartographies are obtained from 3D FEM calculations performed with Ansys® (the results were postprocessed using Matlab®). The microelectrodes are made of gold on silicon.

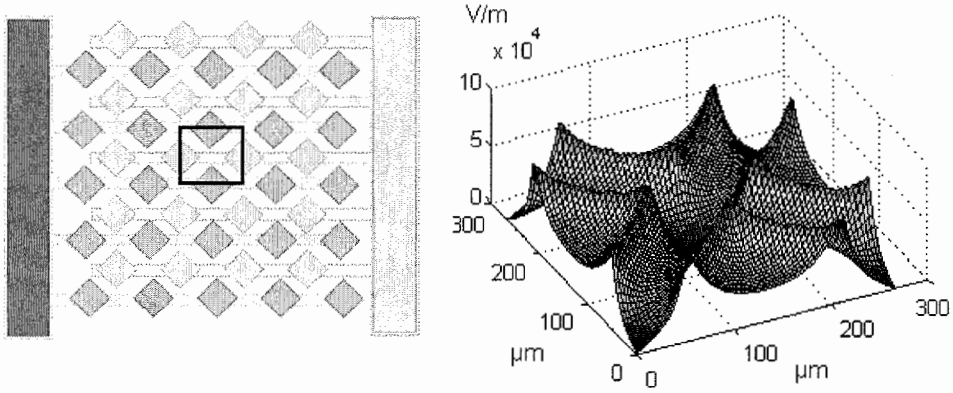

Figure2. **a.** Quadrupolar electrode sets; **b.** associated field cartography (representation in a plane situated 10 µm above the electrodes).

3. Experimental

Our experiments show that the dielectrophoretic force obtained with those electrode structures enables bovine spermatozoa trapping at field minima (Figure 3) or field maxima (Figure 4 and 5). After the field removal, spermatozoa tend to move from the location where they have been trapped.

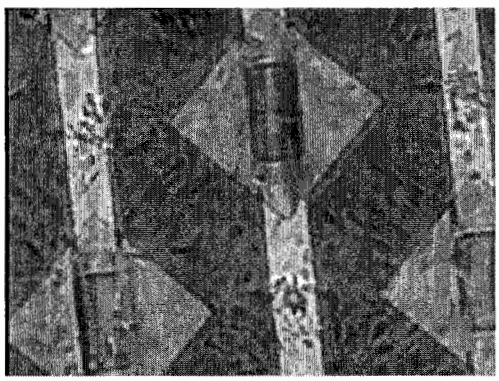

Figure 3. Frequency : 70 kHz, medium conductivity : 33 mS/m - Negative DEP.

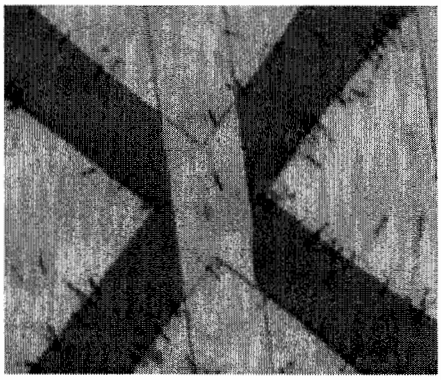

Figure 4. Frequency : 100 kHz, medium conductivity : 24 mS/m - Positive DEP.

The spermatozoa behavior is rather different from what we usually observe when manipulating cells or latex beads. Under specific experimental conditions (frequency, medium conductivity), we can observe some spermatozoa turning in place above the electrode centers, whereas others are

attracted toward the electrode edges by positive dielectrophoresis. Figure 6 shows that the spermatozoa turning above the electrodes tend to group themselves in the central part (delimited on the figure by a circle), at locations where particles usually focus when submitted to electrohydrodynamic (EHD) effects. In order to determine whether this behavior should be attributed to electro-osmotic, electrothermal or dielectrophoretic effects, new experiments must be conducted, during which we will have to focus on the evolution of the rotation direction and speed of spermatozoa according to the electric field frequency. For electrothermally induced fluid flow, the fluid velocity should be independent of frequency. In the case of AC electroosmotic effects, the fluid velocity varies with frequency and the direction of the fluid flow should remain constant [4].

Conclusion

This paper opens new research perspectives, as we have to precisely evaluate the respective contributions of dielectrophoresis and fluid flow to the obtained results. Indeed, combining the effects of dielectrophoresis and electrohydrodynamics [5] could possibly enable the separation of two groups of spermatozoa having slightly differing characteristics, such as motility.

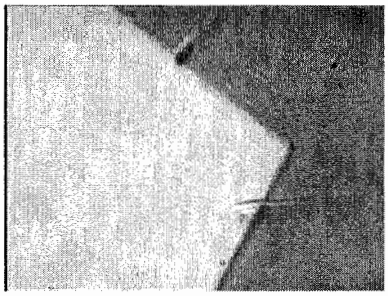

Figure 5. Positive DEP

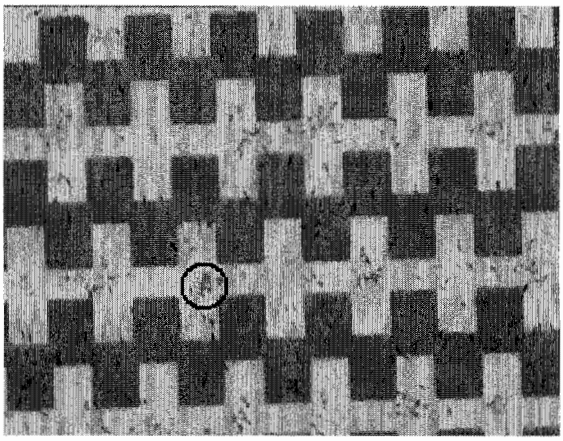

Figure 6. f=50 kHz, medium conductivity : 18 mS/m

Acknowledgements

The authors thank the URCEO (Union Régionale des Coopératives d'Elevage de l'Ouest, Rennes) for spermatozoa collection. We thank Gildas Michel for his help in this project.

References

[1] G. Fuhr, T. Muller, V. Baukloh, K. Lucas, Human reproduction, **13**, 136-141 (1998).
[2] K. Konig, S. L., Y. Liu, Cell. Mol. Biol., **422**, 501-509 (1996).
[3] M. Frénéa, S. P. Faure, B. Le Pioufle, P. Coquet, H. Fujita, Materials Science and Engineering : C, **23**, 597-603 (2003).
[4] A. Ramos, H. Morgan, N. G. Green, A. Castellanos, Journal of Electrostatics, **47**, 71-81 (1999).
[5] N. G. Green, H. Morgan, J. Phys. D : Apply. Phys., **31**, L25-L30 (1998).

OPTICAL MICROORGANISM CHARACTERIZATION IN POLYMERIC CONFIGURABLE MICROFLUIDIC CHIPS

Andres M. Cardenas-Valencia, David Fries, Xiaoling Ding,
Heather Broadbent & Larry Langebrake
Center for Ocean Technology, Univ. of South Florida, 140 7th Ave S. St Petersburg FL, 33701 USA

Abstract

The fabrication in liquid crystal polymer, LCP, of a micro flow cuvette and its use as a bio-cell dispersion analyzer is presented. The optical cell configuration measures extinction or a combination of scattering and absorbed spectra from the cells. The spectra are used for characterizing cells (*Escherichia coli)* size and optical properties, via a Lorenz-Mie algorithm.

Keywords: Micro-fluidics, Scattering, Absorption, Spectra, Bio-cell Characterization.

1. Introduction & Background

Analytical lab-on-a-chip and *in-situ* schemes development for bio-cell identification is important in fields such as marine science, environmental monitoring, homeland defense, biomedical and bioengineering industries, [1-4]. Turbidimety, is a common techniques to monitor bacterial growth [5]. Spectrometers have been used as turbidimeters to size inorganic particle for about 25 years [6-7]. Multi-wavelength signals render more information about the systems under study. Fiber optics spectrometers are portable, relatively inexpensive, perform measurements with minimally perturbation of processes and allow for continuous monitoring of various particle compositional parameters [8,9]. Traditionally, the spectrometer acceptance angle is small so the spectral turbidity, $\tau(\lambda)$, corresponds to the total extinction of the particles. For a mono-disperse system, eq. 1, relates $\tau(\lambda)$ to the number of particles, Np, the optical path-length, ℓ, and the scattering, Q_{sca}, absorption, Q_{abs} and extinction, Q_{ext} efficiencies:

$$\tau(\lambda) = (\pi N_p \ell D^2/4)[Q_{ext}(\alpha,m)] = (\pi N_p \ell D^2/4)[Q_{abs}(\alpha,m) + Q_{sca}(\alpha,m)] \quad [1]$$

The size parameter, α, is calculated using the particle diameter, D ($\alpha=\pi D/\lambda$,). λ is the radiation wavelength. m is the complex refractive index of the particle (m_p=n+ik) divided by that of the medium (m_p/n_m). Transmission spectrometers, in which the acceptance angle, θ_{AA} is larger, contain a combined attenuation due to absorption and scattering, and eq. 1, can be used by modifying Q_{ext} :

$$Q_{ext}' = Q_{ext} - Q_{sca}' = Q_{ext} - \left(Q_{sca} - (1/\alpha^2)\int_0^{\theta_{AA}} I_s(\theta)\sin\theta d\theta\right) \quad [2]$$

$I_s(\theta)$ is the scattered intensity, function of observation polar angle, θ. In this work, we propose the use of a micro flow cell that identifies the presence and quantifies the number of specific bacteria in a population via transmission spectral measurements. Transmission and angular scattering have been explored in the past for microorganism detection [4,8-10], but they are not widely popular partly due to the lack of microorganism optical properties. The novelty of the recognition algorithm presented here, relies on the use of two independent acceptance angle measurements that allow for the calculation of the extinction and absorption components of the optical density, and in turn, for extraction of both terms of the refractive index (k and n). Equations 1 and 2 are general expressions that require the optical efficiencies Q's to obtain other parameters

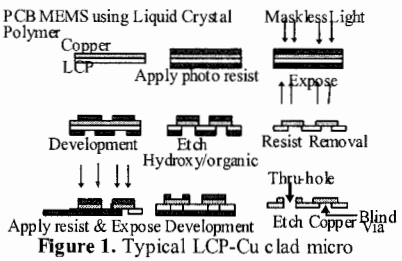

Figure 1. Typical LCP-Cu clad micro fabrication process

(i.e. Np, D or m). Lorenz-Mie theory is used as the interpretation algorithm of our measurements [11,12]. *Escherichia coli* dispersions are used as a case study.

2. Experimental protocol

Micro-flow cell fabrication. PCBMEMS microfabrication have been exploited by Fries et al [13] in conjunction with a commercial mask-less SF-100 photolithography lamp, (Intelligent Micro patterning, St Pete FL) and are used here as a novel route to fabricate micro-devices. General steps for LCP-Cu clad processing, are presented in Fig. 1 and details can be found elsewhere [13,14]. A 0.5 cm diameter reservoir that will serve as the sample bacterial chamber is patterned in the LCP with two co-lineal channels. These channels host 200 μm diameter optical fibers. Two detection channels with different acceptance angles are aligned with the illuminating fiber permitting the collection of two multi-wavelength attenuation spectra of the bacterial dispersion [15]. A glass slide is attached to the LCP substrate trapping the optical fibers that will optically interface the bacterial suspension chamber. Two injecting nanoports are glued to the chip (Upchurch Scientific) (Fig. 3). *Measurements.* An Ocean Optics (Dunedin FL) DT1000 light source and a USB-2000 spectrometer are used to acquire spectral data. One of the detection channel measures the total extinction of the cell dispersion and the other has a wider acceptance angle that captures most of the scattered light measuring primarily the absorption contribution, allowing for refractive indices determination [15]. DH5α *E. coli* cells (PGC Scientific Corporation) (Fig.3) were used.

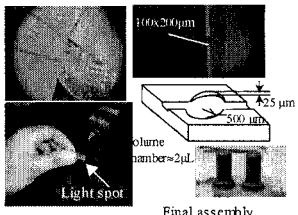

Figure 2. Images of the fiber integration into the fabricated liquid crystal polymer substrate as well as a picture of the microchannels and a schematic of the 2 μliters-volume microcuvette.

3. Results and Discussion

Experimental optical density as a function of wavelength is presented in Fig. 3. The optical properties n and k, as a function of wavelength, (shown in Fig. 4) are the calculated parameters using the turbidity equation and Mie-Lorenz theory. The real refractive index, n, is in good agreement with recently reported values [16]. Fig. 5 shows the agreement between experimental optical density spectra and that calculated by a least-squares-type regression. A mean *E. coli* diameter size was obtained from the experimental spectral signatures. Table 1 shows a

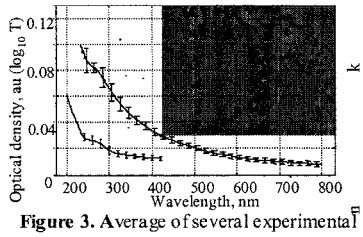

Figure 3. Average of several experimental spectra taken with 2 different optical configurations. Errors bar lengths are four times the standard deviation of replicates. Insert shows a micrograph of fixed *E. coli* cultured and dispersed used herein.

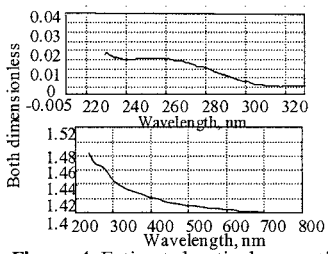

Figure 4. Estimated optical properties of the bacterial dispersion

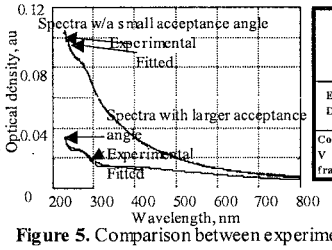

	Estim.by spectral regression	Experimental Uncertainty	Estim.by Impedance	Standard deviation σ
Equiv Diam	1 207 nm	[1.1472 - 1.223] nm	1 182 nm	PSD σ 128 nm
Conc. V fraction	3.42×10^{-5}	[3.37×10^{-5} - 3.51×10^{-5}]	3.37×10^{-5}	Replicates, σ=1.9×10^{-5}

Figure 5. Comparison between experimental and fitted spectra to determine microbial size and concentration **Table 1.** Comparison between spectrometric regressed diameter and concentration and those measured by impedance for *E coli*

good agreement between the regressed diameter, the particle concentration, and the statistics obtained from both the spectral it and the Coulter measurements. The diameter and concentration uncertainties in Table 1 were calculated using the experimental measurements uncertainties. The optimal signal to noise ratio of the spectrometer system, between 0.05 and 1 in the absorbance scale, dictates that the smallest concentration that can be analyzed with the current experimental set-up goes down to 10^6 *E. coli* cells/cc, but smaller concentrations are measurable, by either using a better detector or increasing the path-length, l.

Additional verification of the presence of the microorganism is proposed via the multi-angular signature from the bacterial dispersion (Fig. 6). The minima (Table 2) correspond to the measured values by Latimer and Cross [17], providing verification of the adequacy of the *E. coli* estimated optical constants.

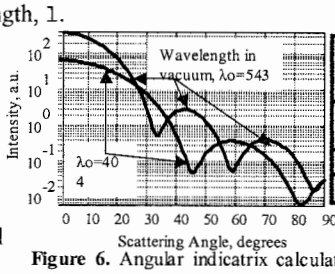

	Calculated w/regressed n(λ)		Experimental data from [7]	
λo	1st Min.	2nd Min.	1st Min.	2nd Min
404	33	59	34.2	60.0
543	45	82	45.3	81.8

Figure 6. Angular indicatrix calculated via Lorenz-Mie theory and the determined refractive index & mean bacterial size **Table 2.** Comparison between the minima of the calculated indicatrix and that of previous experimental reports.

4. Conclusions

The described chip and analytical procedure using this technique identifies, quantifies, sizes, and characterizes optical constants of mono-disperse colloidal system (bio-cells) can be characterized as described here. The novel fabrication route presented makes the chips inexpensive and easily configurable to potentially capture also specific angular scattering (indicatrix) to verify the presence of certain cells (microorganisms or mammalian cells).

Acknowledgments

Financial support by the U.S. Army Space and Missile Defense Command through contract DASG6000C0089 is gratefully acknowledged. Dr. Cardenas also thanks CONACYT and UdG of Mexico for the scholarships that allowed the development of the Mie scattering algorithms.

References

[1]J.A. Fruetel, B.A. Horn, A. West, J. Stamps, Vandernoot, Stoddard, Renzi, μTas '02,(1) 524-526
[2]N. S. Hobson, I. Tothill, & A.P.F. Turner, Bios. & Bioelect. (11:5), 455-477 (1996)
[3]V. Sethi, P. Patnaik, P. Biswas, Clark, & E Rice, J. A. Wat. Works Assoc. (89:2) 98-112 (1997)
[4]A.M. Cardenas-Valencia, L.Garcia-R., Ind. Sci. Adv. Board, ERC, Gainesville, FL April (2001)
[5]R. L. Zollars, J. Coll. Int. Sci., 74, 163-172 (1980)
[6]D. H. Melik, and H. S. Fogler, J. Coll. Int. Sci. 92, 161-180 (1983)
[7]D. Lim, Microbiology, 2nd edition. Publisher William C. Brown, 720 p. (1998)
[8]Y. D. Mattley, L. H. Garcia-Rubio, Proc. of SPIE, V. 4206, 64-71 (2001)
[9]A. Cardenas-V.,V.Shastry, & Garcia-R. Kluwer Ac. Plen. Publis.Eds. J. Puskas, et al 26p. (2003)
[10]P. Wyatt, App. Optics 7(10), 1879-1895 (1968)
[11]C.F. Bohren, D.R.Huffman, JohnWiley&Sons: NY, (1983)
[12]A.M. Cardenas-Valencia, Ph.D. Dissertation Univ. of South Florida, (2001)
[13]D. P. Fries, H. Broadbent, G. Steimle, A.M. Cardenas-Valencia, ACS Prep. NY, Sept (2003)
[14]A.M.Cardenas-Valencia, Challa, Fries, Langebrake, Bhansali. Sens &Act.B(95)406-413(2003)
[15] A. M. Cardenas-Valencia, D. Fries, Ding, Langebrake, W. Wang & J. Kolesar. In preparation
[16]A. Balaev, K.N. Dvoretski, V.A. Doubrovski, , Proc. of the SPIE, V. 4707, 253-260 (2002)
[17] P. Latimer, A. Cross, App Optics, 11(8) 1225-1228

AN INTEGRATED MICRODEVICE FOR ON-CHIP PRECONCENTRATION, SEPARATION AND LABELING OF PROTEINS

Daria Petersen[1], Robert S. Foote[2], Oliver Geschke[3] and J. Michael Ramsey[1]

[1] *Chemistry Department, University of North Carolina, Chapell Hill, North Carolina 27599, USA*
[2] *Chemical and Analytical Science Division, Oak Ridge National Laboratory, P.O. Box 2008, Oak Ridge, Tennessee 37831- 6142, USA*
[3] *Dept. of Micro and Nanotechnology, Technical University of Denmark, Bldg 345 east, DK 2800 Kongens Lyngby, Denmark*

Abstract

We have demonstrated an integrated microdevice capable of sample preconcentration, separation by capillary sieving electrophoresis (CSE), and labeling of proteins with a fluorescent dye for laser-induced fluorescence detection (LIF). On-column and post-column labeling strategies have been investigated using the non-covalent protein dyes, SYPRO Orange and SYPRO Red.

Keywords: sample preconcentration, on-chip protein labeling

1. Introduction

Non-covalent labeling requires less reaction time and less sophisticated procedures than covalent labeling and, therefore, is more suitable for on-chip integration. When using sodium dodecyl sulfate (SDS) assisted separation, the background fluorescence from dye-SDS complex can be reduced by dilution of SDS in the run buffer to below critical micelle concentration prior to LIF detection [1]. To further increase the sensitivity of protein analysis, a preconcentration step has been integrated with on-chip labeling. Microdevices with porous membranes between adjacent microchannels (Fig. 1) have been previously demonstrated to be capable of more than 100-fold pre-concentration of pre-labeled nucleic acids [2] and proteins. When electrical potential is applied across the porous membrane, it traps and concentrates large biomolecules, allowing the passage of buffer ions. The preconcentrated sample plug can then be injected into the separation column for analysis.

2. Experimental

A closed microchannel network was formed by low-temperature bonding of a glass coverplate to the etched substrate using potassium silicate (KASIL 2130, The PQ Corp., Valley Forge, PA, USA) both as an adhesive and to form a porous membrane for sample pre-concentration [2]. The thickness of the sol-gel layer was less than 100nm. The width of the porous membrane for preconcentration (the distance between two adjacent channel networks) was 4.4-5.0 μm. The channels were 14-16 μm deep and 47-51 μm wide at half depth. The length of separation channel from preconcentrator to the dilution intersection was 6 cm.

SDS-CGE separations on microchips were performed in CE-SDS protein kit run buffer (Bio-Rad Laboratories, Hercules, CA). Dalton Mark VII-L marker proteins (Sigma, St. Louis, MO) were used as a model protein mixture. It consists of 1) α-lactalbumin (mw 14,200), 2) trypsin inhibitor (mw 20,100), 3) trypsinogen (mw 24,000), 4) carbonic anhydrase (mw 29,000), 5) glyceraldehyde-3-phosphate dehydrogenase (mw 36,000), 6) ovalbumin (mw 45,000) and 7) bovine serum albumin (mw 66,000). Concentrated solutions (5000x) of SYPRO Orange and SYPRO Red dyes (Molecular Probes, Eugene, OR) were diluted to 1x- to 100x as indicated. Post-column dilution buffer was 400 mM Tris-borate, pH 8.3. Laser-induced detection (LIF) was performed using an argon ion laser (488 nm) for SYPRO Orange and a HeNe laser (544 nm) for SYPRO Red. The detection point was

1 cm away from the dilution cross. For analyses without preconcentration, injections were performed by first applying a potential of 750 V/cm between the sample (reservoir 3) and sample waste (reservoir 2). The potential at reservoir 1 was kept at 0.4 kV in order to avoid leaking of sample into the run buffer and other reservoirs were floated. After 5 minutes of pre-injection, a potential of 3.1 kV was applied at the waste (reservoir 6), while the run buffer electrode (reservoir 1) was grounded and potentials of 0.3 kV were applied to reservoirs 2 and 3 to prevent the leakage of sample into the separation channel after injection. For analyses with sample preconcentration, a potential of 1.2 kV was applied at one of the bridged reservoirs (4) while keeping the sample reservoir (3) grounded and floating other reservoirs. The injection/separation step was then performed exactly as described above for analyses without preconcentration.

For all experiments, different dilution ratios were obtained by varying the potential applied at dilution buffer (bridged reservoirs 5) from 2.3 to 0.3 kV during the separation step.

3. Conclusions

We have demonstrated that post-column labeling and SDS dilution can be performed in a single step (Fig. 2), resulting in detection sensitivity and resolution comparable or superior to that of on-column labeling (Table 1). On-chip preconcentration (illustrated on Fig. 3) can be combined with either labeling mode to further enhance detection sensitivity (Fig. 4). Increases of ≥ 10-fold in sensitivity were obtained for 5-min preconcentration with on-column SYPRO Orange labeling. SYPRO Red gave similar sensitivity for on-column labeling at comparable dilution ratios.

Table 1. [a] SyR = SYPRO Red, SyO = SYPRO Orange, relative to manufacturer's recommended concentration for gel-staining; [b] total concentration of Dalton Mark VII-L proteins.

Dye Conc[a]	Sample conc. (mg/ml)[b]	Labeling Mode	Preconc. Time (min)	Average S/N	N (peak 1)	Resolution (p. 3 and 4)	Theoretical LOD (average, nM)
1xSyR	1	On-column	0	105	78,700	3.2	168
1xSyO	2	"	0	151	76,100	2.3	320
"	2	"	1	304	37,900	1.0	104
"	0.02	"	5	30	91,400	1.2	16
10x	1	Post-column	0	8	56,000	2.1	2450
"	1	"	1	84	77,200	1.8	240
100x	1	"	0	100	110,100	2.6	220
"	1	"	1	236	38,200	2.1	91

Acknowledgements

This research was sponsored by the Department of Energy Office of Research and Development the U.S. Department of Homeland Security. Oak Ridge National Laboratory (ORNL) is managed and operated by UT-Battelle, LLC, under contract DE-AC05-00OR22725 with the U.S. Department of Energy. D.P. was supported by ORNL Postdoctoral Research Associates Program, administered jointly by ORNL and the Oak Ridge Institute For Science and Education. The authors thank Christopher D. Thomas and Leslie Wilson for microchip fabrication.

References

[1] L. Bousse, S. Mouradian, A. Minalla, H. Yee, K. Williams, R. Dubrow, *Analytical Chemistry*, 73, 1207-1212 (2001).

[2] J. Khandurina, S.C. Jacobsen, L.C. Waters, R. S. Foote, J. M. Ramsey, *Analytical Chemistry*, 71, 1815-1819 (1999).

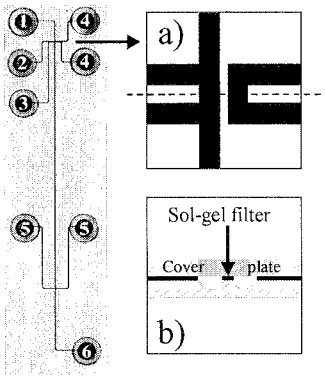

Figure 1. Chip schematic: 1) run buffer; 2) sample waste; 3) sample; 4) preconcentrator reservoirs, bridged with platinum wire; 5) dilution reservoirs, bridged with platimun wire; 6) waste. Insertions: (a): two adjacent microchannel networks in the glass substrate; (b): the cross section of the chip along the dashed line on the (a) insertion.

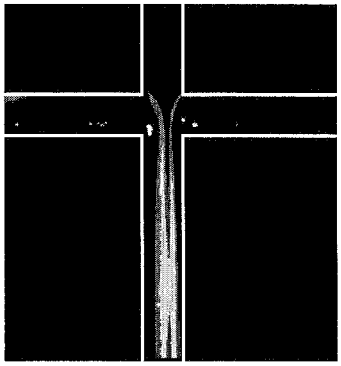

Figure 2. Post-column labelling combined with SDS dilution. in a single step. Labeling/dilution buffer contained 100x concentration of Sypro Orange® Dye (reservoirs 5). Sample (res.3): 1 mg/ml initial protein concentration, injected after 5 min of preconcentration.

Figure 3. Fluorescence images of simultaneous sample pre-concentration and on-column labeling (left, preconcentration time is 1 minute) followed by an injection of preconcentrated plug into the separation channel (middle and right). The sample had initial protein content of 1 mg/ml. Run buffer containing 1xconcentration of Sypro Orange® dye was loaded into reservoirs 1, 2, both 4, and 6 (Figure 1). Protein sample was loaded into reservoir 3. Both reservoirs 5 were filled with the dilution buffer.

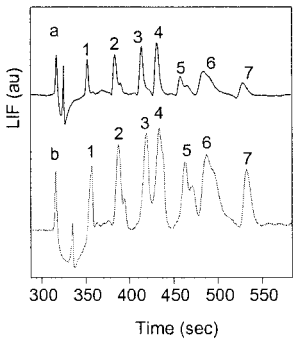

Figure 4. On-column labeling with 1 x concentration of Sypro Orange, 2 mg/ml total protein conc. a) run without preconcentration; b) the effect of 1 min on-chip preconcentration.

INTERCHANNEL MICROSTRUCTURE FOR SEPARATION AND ANALYSES OF PLASMA FROM WHOLE BLOOD

Xiaohai Yang[1], Akihide Hibara[1], Kiichi Sato[1], Manabu Tokeshi[2], Keisuke Morishima[2], Yoshikuni Kikutani[2], Hiroko Kimura[3], and Takehiko Kitamori[1,2]

[1]Department of Applied Chemistry, School of Engineering, The University of Tokyo, Japan
[2]Kanagawa Academy of Science and Technology (KAST), Japan
[3]School of Medicine, Juntendo University, Japan

Abstract

A microstructure similar to cross-flow micro-filter was developed for separation of plasma from whole blood without centrifugation, which consists of many shallow channels, like micro pores, located between two bigger channels (main channels), and acted as passages of plasma but dams for blood cells. Plasma without obvious hemolysis could be observed in main channels within 3min. Such a microstructure has the potential to combine or integrate with other types of microstructure to form on-chip blood analyses devices. As a model, integrated with on-chip bead-bed immunoassay, a microchip was used for the determination of human α–fetoprotein on the range of 5-600 ng/mL.

Keywords: blood, plasma, separation, immunoassay

1. Introduction

Blood analyses are powerful tools for disease diagnosis and health monitoring. However, present methods are usually time-consuming, as well as dangerous for operators due to the infective samples. In addition, the samples maybe stained during the multi-step procedure. The miniaturization and integration of the traditional assays conduce to saving time and decreasing relative risk. Usually, cells-free plasma (or serum) is necessary for medical diagnosis of human blood. As one of the key elements for the purpose of miniaturization, several on-chip separators have been reported, which performed plasma separation from whole blood for healthcare in microchannels or afforded potential capability [1-3]. However, some of them need centrifugation, or involved expensive fabrication processes. Meanwhile, reusability is one of the important factors to be considered. Here we reported microchips for separation and analyses of plasma from whole blood without centrifugation.

2. Principle

The interchannel microstructure is similar to the cross-flow micro-filter. Many shallow channels, like micro pores, were located between two main channels, acted as passages of plasma but dams for blood cells (Figure 1). One of the main channels is for the introduction of sample, and the other acted as collector of plasma.

Cross-flow movement of the liquid depends on the pressure difference between the two main channels (Δp); it depends on the operation condition.

If we considered the main channel as rectangular tube, the flow rate of laminar, non-pulsatile fluid flow is

$$Q = \frac{WB^3}{12\eta} \cdot \frac{\Delta p}{L} F_p \qquad (1)$$

where Q is flow rate, η is viscosity factor, F_p is a factor depended on the B/W (aspect ratio).

Suppose that the two main channels have same size, and the pressure at the outlets is same also, e.g. atmosphere, then the pressure difference between two main channels is

$$\Delta p = p_1 - p_2 = \frac{12\eta L}{WB^3 F_p} \cdot (Q_1 - Q_2) \qquad (2)$$

Therefore, if the flow rates in the two main channels are the same, $\Delta p=0$, the liquid will not pass through the shallow channels. Otherwise, $\Delta p>0$, the liquid will pass through the shallow channels. Δp is the drive of plasma separation.

The equations are only strictly valid for rectangular tube; it is only an approximate relation here.

3. Materials and methods

In Pyrex glass, the interchannel microstructure was fabricated by wet etching (Fig. 2). It consists of two 20mm long, 20μm apart parallel main channels which were connected with shallow channels laterally every 100μm. Main channels are about 100μm wide and 20μm deep, one is for the introduction of whole blood samples and the other is collector of separated plasma. Shallow channels are about 10μm wide and 1μm deep, act as passages of plasma but dams for blood cells.

Microchip with dam structure was used for bead-based immunoassay [4] (Fig. 4).

Surface of the channels were blocked with 2% BSA (bovine serum albumin) before use. Heparin added fresh human whole blood was used as sample.

For the separation of plasma, blood sample was introduced into one main channel continuously. Main channel for separated plasma is blank (full of air) at first. The outlets of main channels are open to atmosphere.

4. Results and discussion

When anti-coagulated whole blood sample flowed through one main channel (<1μl/min) continuously, clear liquid (plasma) could be observed in the other main channel in about 3min, without obvious damage of red blood cells (Fig. 3). Such plasma is suitable for succeeding analyses. Although higher flow rate of blood sample could speed the separation since the higher Δp, it results in hemolysis, this maybe due to the shear stress (Table 1).

The separation could be performed continuously, since the blood cells were carried away by blood flow itself and would not stay in the main channel.

This microstructure could be combined with on-chip bead-bed immunoassay, where modified beads were located in channel by dam-structure [4] (Fig. 4). Based on the chip showed in figure 4(b), human α–fetoprotein were detected as a model on the range of 5-600ng/mL (Fig. 5). In addition, it also has the potential for integrating with other types of microstructures for analysis.

References

[1] Y. Horiike, A. Oki, Y. Takamura, H. Ogawa, M. Takai, and H. Onoda,, *Japan Soc. ME & BE*, Dec. 2001, 2p3E.

[2] K. Iida, H. Kawaura, N. Iguchi, T. Sano, and M. Baba, *Micro Total Analysis System 2002*, Kluwer Academic Publishers, pp627-629

[3] B. He, L. Tan, and F. Regnier, *Anal. Chem.*, **71**, 1464-1468 (1999)

[4] K. Sato, M. Yamanka, M. Tokeshi, K. Morishima, and T. Kitamori, *Micro Total Analysis System 2002*, Kluwer Academic Publishers, pp190-192

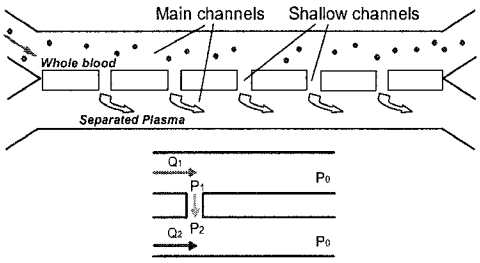

Figure 1. Principle of separation plasma from whole blood. The microstructure is similar to the cross-flow filter. Separation depends on the pressure difference between two main channels.

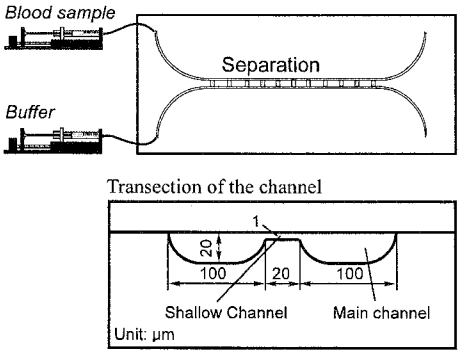

Figure 2. Outline and size of the micro-sturcture.

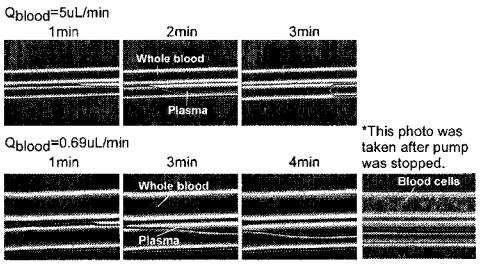

Figure 3. Plasma separated from whole blood sample.

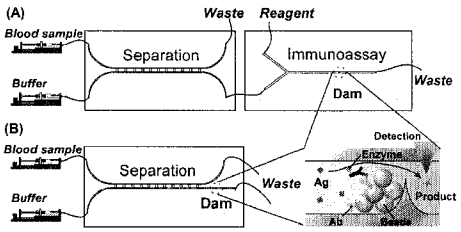

Figure 4. Combine (a) or integrate (b) with on-chip bead-bed immunoassay, where beads were located in microchannel by dam-structure [4].

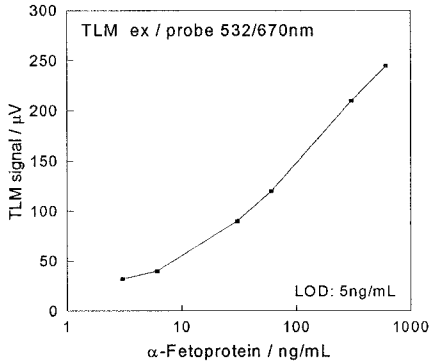

Figure 5. Calibration curves of α–fetoprotein.

Table 1. Relationship between hemolysis and flowrate. Thermal lens microscope (TLM) signal depends on the concentration of free haemoglobin in plasma, which indicates the level of hemolysis.

Flowrate (μL/min)	TLM signal* of separated plasma (mv)
0.69	0.0070
1.5	0.0090
5	0.0161

*ex/probe=532/670nm
control plasma: 0.0071mv

A CELL-BASED ASSAY FOR RAPID CHEMICAL SCREENING

Pak Kin Wong[†], Wilson WaiChun Wong[‡], James C. Liao[‡], and Chih-Ming Ho[†]

[†] Department of Mechanical & Aerospace Engineering, University of California, Los Angeles, USA
[‡] Department of Chemical Engineering, University of California, Los Angeles, USA

Abstract

Micro cell culture systems have potential advantages in many aspects over traditional cell culturing techniques. The development of the system is promising in the pharmaceutical industry and in the study of fundamental cell biology. In this work, we develop a microfluidic assay for determination of the individual cell's response to chemical exposure. A steady spatial chemical gradient is generated inside a microchannel. Individual cells experienced different chemical concentrations according to the position that the cell adhered to the channel. The microfluidic assay allows rapid determination of the cell response to many different chemical concentrations simultaneously. The activity of the *tac* promoter in *E. coli* in response to different concentration of the inducer IPTG are measured to demonstrate the use of the system.

Key words: cell deposition, spatial chemical gradient, cell-based assay, gene expression, drug screening

1. Introduction

Recent progress in micro cell culture systems leads to new approaches in cell-based sensors and cell biology [1]. Using micro devices for cell culturing has distinctive advantages over traditional approaches. Length scale matching facilitates manipulation and measurement at the single cell level. A micro cell culture system with integrated actuators allows us to study the cellular response under different external stimuli. We have demonstrated various physical stimuli such as an electric field [2] and shear stress [3] to study the dynamic responses of the individual cells. Furthermore, biochemical stimulation, the most common way for the cells to sense the environment and to communicate to each other, is obviously interesting for cell biology. In this study, we generate chemical gradients inside a microfluidic channel and observe the dynamic responses of individual cells exposed to different chemical concentrations simultaneously. A direct printing method is also reported for selective deposition of the cells inside the channel. This approach can potentially be applied in drug screening and in toxicology analysis.

2. The cell reactor

Generation of spatial chemical gradients is relatively easy in microfluidic systems due to the small length scale [4], [5]. It takes advantage of the laminar nature of microfluidic flow. Convective mixing across the two input streams is not present and molecular diffusion is the only natural mechanism for mixing. A steady chemical gradient can be generated by merging two streams of fluids and allowing the chemical to diffuse across the streams (Figure 1a). Figure 1b shows one of the microfluidic channel designs for generating the spatial chemical gradient. Fluorescence characterization and numerical simulation have been applied to study the convection-diffusion system (Figure 1c).

In order to expose the cells to the chemical gradient, attachment of the cells in selected locations inside the microchannel is essential. We have developed a direct printing method for selective deposition of the cells inside the microfluidic channel. Figure 2 shows the fabrication process. Poly-L-lysine was applied at desired locations in the microfluidic device using a pipette or a sharpened glass capillary [6]. Patterns on the order of 10 μm can be printed easily with this method. Throughout this study, patterns of roughly 500 μm (the field of view of the optical system)

were printed in order to trap multiple cells for statistical analysis. The channel was sealed by a piece of glass.

3. Results and discussion

The cell reactor was first washed with PBS for 10 minutes. The channel was then filled with 10 mg/ml of BSA in PBS for 5 min. This step prevents non-specific binding of the cells in the channel. *E. coli* in exponential growth phase were then flowed into the channel and the cells were allowed to adhere to the channel surface for roughly 5 min. Cell adhesion was only observed in regions with poly-L-lysine modification. The number of cells that adhered on the channel surface was controlled by the cell concentration in the solution and by the residency time of the cells in the channel. Non-adherent cells were then removed by washing with the culture medium.

The LacI-repressible *tac* promoter in *E. coli* was employed to demonstrate the cell-based assay. The promoter activity was monitored by expression of the green fluorescent protein (GFP). M9 medium with 1 mM IPTG and M9 medium were applied to the channel. This system generated a gradient from 0.96 mM (left) to 0.04 mM (right) of IPTG across the 500 μm width of the channel. Each cell experienced a different inducer concentration depending on the position. The intensities of the fluorescence of the cells at different locations were measured at different times (Figure 3a and b). The fluorescence from some cells was observable approximately 20 min after induction. The fluorescence intensities of the cells were initially uniform across the channel and increased gradually at a different rate depending on the position of the cell in the channel.

The rate of the intensity increase provided a measure of the GFP expression rate and could be estimated by numerically differentiating the intensity data. Generally, the original expression rate (basal transcription) was negligible. The expression rates gradually increased after introduction of the inducer. The expression rates became constant after approximately 100 min. Figure 3c shows normalized GFP expression rate at different IPTG concentrations. The IPTG dependence showed a sigmoidal shape. The transcription efficiency is adjustable in the range of 0.01 to 1 mM of IPTG. The data can be fitted with the Michaelis-Menten equation. The Michaelis constant was determined to be 0.44 mM. The convection-diffusion system allows large flexibility in controlling the chemical concentration. The concentration-response curve of a wide range of chemicals can be easily determined with this method.

4. Conclusion

In a unique cell reactor, we have developed a microfluidic assay for testing cellular response under chemical stimulations. Monitoring of the gene expression dynamic of individual cell was successfully demonstrated. Generation of spatial chemical gradient allows simultaneous screening of the cells' responses under the stimulations of chemicals at different concentrations.

Acknowledgements

This work is supported by CMISE through NASA URETI program and NIH NIDCR (UO1 DE15018).

References:

[1] T. H. Park, M. L. Shuler, *Biotechnology Progress*, **19**, 243-253, (2003).
[2] P. K. Wong, W. Tan, C.-M. Ho, *Journal of Biomechanics* (in press).
[3] T. K. Hsiai, S. K. Cho, P. K. Wong, M. H. Ing, A. Salazar, S. Hama, M. Naval, L. L. Demer, C.-M. Ho, *Annals of Biomedical Engineering*, **32**, 189-201, (2004).
[4] G. M. Walker, M. S. Ozers, D. J. Beebe, *Sensors and Actuators B*, **98**, 347-355, (2004).
[5] Dertinger, S. K. W.; Jiang, X.; Li, Z.; Murthy, V. N.; Whitesides, G. M. *PNAS,* **99**, 12542-12547, (2002).
[6] P. K. Wong, U. Ulmanella, C.-M. Ho, in *Proc. MEMS 03'*, 359-362, (2003).

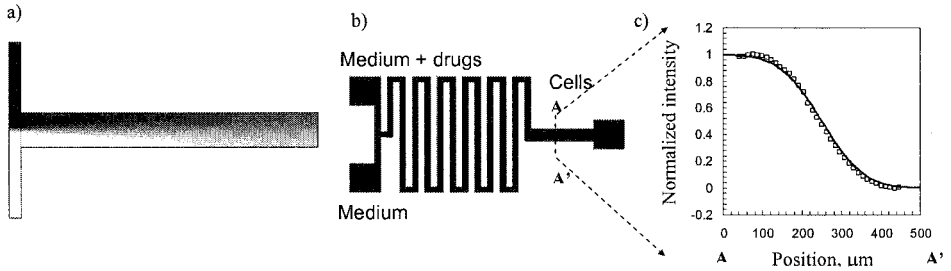

Figure 1. a) Schematic illustrates formation of steady chemical gradient. b) A microchannel design for generation of steady chemical gradients. c) Fluorescence characterization of the formation of the gradient at the end of the channel. Open squares represent measured intensities and solid line represents numerical calculation.

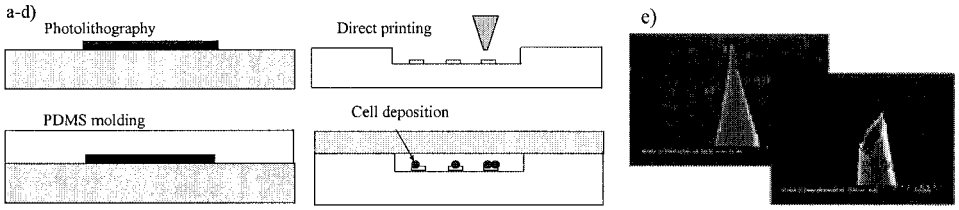

Figure 2. Selective deposition of cells inside the microfluidic device. a-d) Fabrication process of a micro cell culture system. e) SEM micrographs of sharpen capillary which can be used for chemical printing.

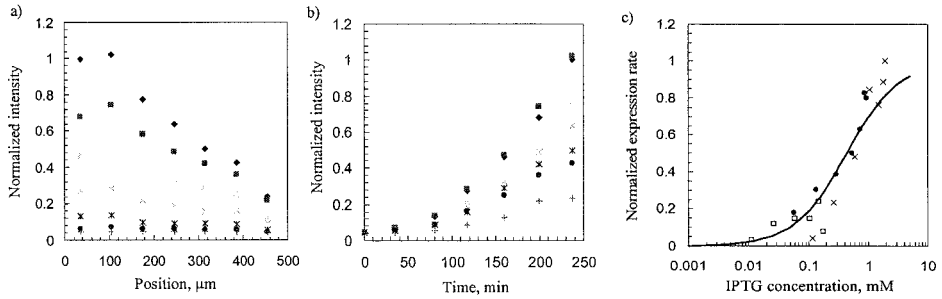

Figure 3. Normalized intensity of *E. coli* cells under spatial IPTG concentration gradient. Each data point represents average intensities of 20-40 cells. a) Spatial distribution of the cells intensity at different time. + 0 min; • 35 min; 80 min; × 117 min; ▲159 min; ■199 min; ♦237 min. b) Time dependence of the gene expression at different locations. ♦35 μm; ■ 105 μm; ▲175 μm; × 245 μm; 315 μm; • 385 μm; + 455 μm. c) Normalized expression rate at different IPTG concentration. Data was obtained with original IPTG concentration × 2 mM; • 1 mM; □ 0.2 mM mixed with the medium. The solid line is the best fit curve of the data points using the Michaelis-Menten equation.

A MULTI CELLULAR DIAGNOSTIC DEVICE FOR HIGH-THROUGHPUT ANALYSIS

Masaki Kanai[1,2], Tatsuya Munaka[1], Hirohisa Abe[1], Yoichi Fujiyama[1]
Daisuke Uchida[2], Hidemi Mikado[2], Hiroaki Nakanishi[1] and Shuichi Shoji[2]

[1] *Technology Research Laboratory, Shimadzu Corporation, Kyoto, Japan*
[2] *Major in nanoscience and nanoengineering, Waseda University, 3-4-1, Tokyo, Japan*
(E-mail: masakik@shimadzu.co.jp)

Abstract

We developed a high-throughput cellular analysis device which is integrated multiple diagnostic chambers including reagent injector. A new concept of the passive distributing facilitates simultaneous cell injection into a number of diagnostic chambers with simple channel configurations. For fabrication of the device, a medical grade PDMS is utilized, which has not only good biocompatibility but also preferable physical properties for a valve diaphragm. Using a prototype device of the 8 diagnostic chambers, the passive distribution of fluorescent beads was evaluated.

Keywords: cell analysis, cell handling, high-throughput screening, passive distributing

1. Introduction

In previous works, we reported a cellular diagnostic device integrated with a sample injector [1] and antibody production monitoring in the diagnostic device [2]. In order to accommodate high-throughput analysis of cellular reactions to several kinds of drugs and toxics, the cellular diagnostic devices should be integrated in parallel. Fig.1(a) shows schematic of the arrayed cellular diagnostic devices. The device has 8 diagnostic chambers and each diagnostic chamber has a reagent injector module. This reagent injector module consists of two pneumatic microvalves as shown in Fig.1(b). The reagent injector module achieves reagent priming as well as reagent injection with extremely low dead-volume. To realize fast cell injection into the diagnostic chambers, we propose a new concept of passive distributing as shown in Fig.1(c). Cells are injected from a common inlet port, and are divided at each bifurcation, half by half. Consequently, cells are loaded into each chamber nearly with even probability. Precise distribution cannot be expected, however fast cell injection to all chambers can be achieved in a single step. In addition, the simple channel structure reduces the risk of contamination.

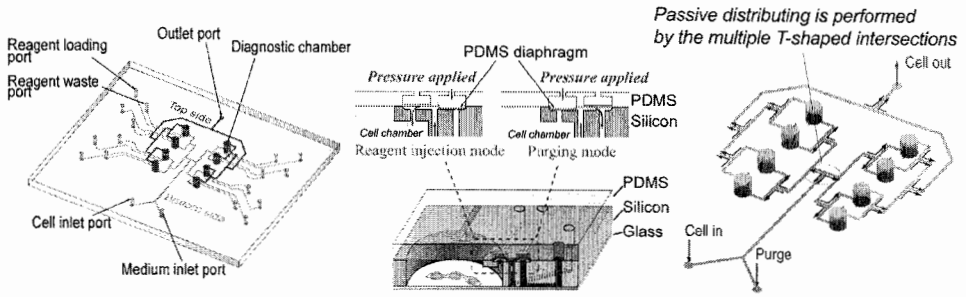

(a) Overview schematic of the multi cellular diagnostic device

(b) Cross-sectional schematic of the cell diagnostic chamber integrated with pneumatic valve module

(c) Concept of passive cell distribution

Figure 1 Schematic concept of the multi cellular diagnostic device

2. Fabrication

A prototype cellular diagnostic device having 8 diagnostic chambers was fabricated. Fig.2 shows SEM images of the silicon structure which was fabricated by combination of isotropic etching and deep-RIE etching. For a diaphragm of a pneumatic microvalve, we used a medical grade PDMS membrane (Silastic, MDX4-4210, Dow Coring, USA) instead of the commonly used PDMS (Sylgard 184). Sylgard has excellent property, high transparency, low resin viscosity before curing, etc. However effects for cell culture has not been validated yet. The Silastic was biomedical tested by the manufacture and the result of cytopanic was not observed [3]. In order to evaluate mechanical property as a valve diaphragm, deflection of a Silastic diaphragm bonded with a silicon substrate was measured. Fig.3 shows comparison between the deflection of 15μm thick Silastic diaphragm and Sylgard one. It indicated that the Silastic is much flexible. We also confirmed that the Silastic is burst under higher pressure than the Sylgard. From these results, it is clear that the Silastic has suitable properties for the use of a valve diaphragm.

3. Experimental

Using 20μm diameter fluorescent beads, beads injection by passive distributing was demonstrated. The cell loading channel was 50μm wide and 100μm deep. Flow rate of the carrier buffer was 1μL/min. The time dependant beads flow at one T-shaped bifurcation is shown in Fig.4. It was confirmed that the beads were evenly flown into both branches. The final states of beads injection by passive distributing to 8 diagnostic chambers were shown in Fig.5. Almost same numbers of the beads were distributed in each chamber. In Table 1, variation of beads injection was evaluated for 5 experiments in same device. In this case, average of C.V.(coefficient of variance) between the chambers was 60.9%. Table 1 shows that smaller number of the beads

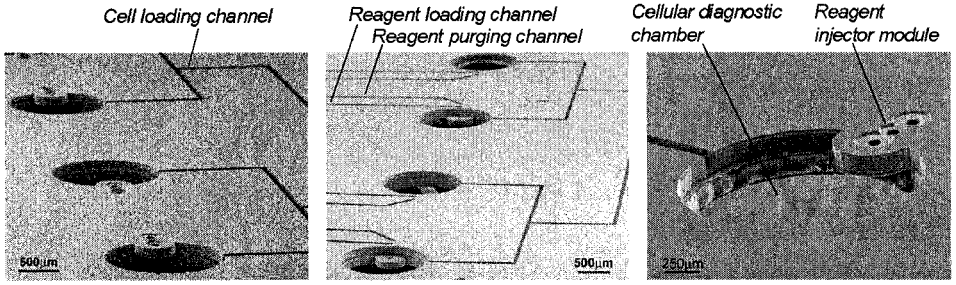

(a) Top side view (b) Bottom side view (c) Magnified image of the cellular diagnostic chamber

Figure.2 SEM images of the prototype device

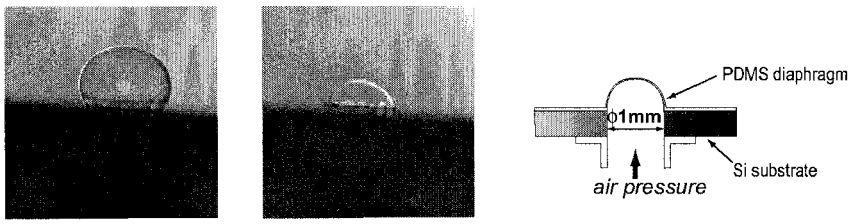

(a) Silastic MDX4-4210 (b) Sylgard 184 (c) Experimental setup

Figure 3 Mechanical property comparison of the medical grade PDMS and common used industrial PDMS(Sylgard 184).

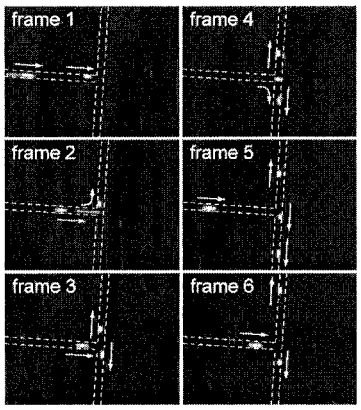

Figure 4 Fluorescent beads flow at a T-shape bifurcation

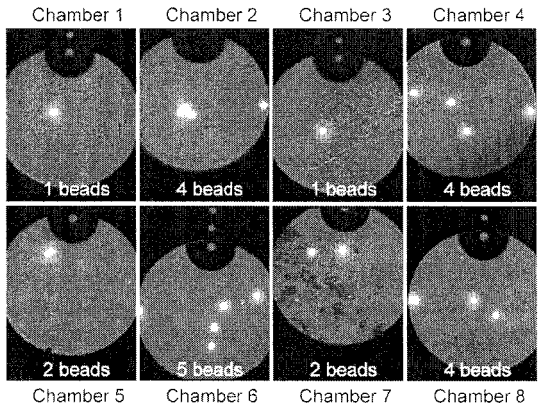

Figure 5 Fluorescent image of the beads injection by passive distributing

Chamber ID	#1	#2	#3	#4	#5	#6	#7	#8
Average number of beads	4.8	27.4	24.2	16.4	3.2	13.4	13.2	14.6
	2.7%	19.4%	16.3%	15.0%	3.1%	14.7%	12.4%	16.4%
C.V	82.3%	26.3%	42.5%	27.2%	109.4%	37.6%	42.7%	33.3%

Table 1 Results of the beads injection by passive distribution

were loaded to chamber 1 and 5. It considered to be originated in the defect of channel structure or the clogging with bubble. Average of C.V. except for chamber 1 and 5 was calculated to be 36.9%.

4. Conclusions

In order to realize a diagnostic device for high-throughput cellular analysis, we proposed an arrayed diagnostic device including the passive distributing system for cell injection. Using a prototype device having 8 chambers, we demonstrated the injection of fluorescent beads. Through the experimental evaluation, we confirmed the feasibility of fast cell injection by passive distribution. In order to reduce the variation of numbers of cells in each chamber, the design of the cell loading channels is currently optimized.

Acknowledgements

This work is supported by Research and Development Program for New Bio-industry Initiatives, of Bio-oriented Technology Research Advancement Institution (BRAIN).

This work is partly supported by Japan Ministry of Education, Culture, Sports Science & Technology Grant-in-Aid for COE Research and 21st COE of Waseda University, Scientific Basic Research (A) No. 12450167, and Japan Society for the Promotion Science Grant-in-Aid for Creative Scientific Research No. 13GS0024.

References

[1] M. Kanai, et.al, Tech. Digest. Int. Conf. Solid-State Sensors Actuators and Microsystems, Transducers'03, Boston, 2003, IEEE, p.288

[2] T. Munaka, et.al, Proc of Micro Total Analysis System 2003, Squaw Valley, 2003, Transducers Research Foundation, p.283

[3] Product information of Silastic, Dow Coring Corp., USA (http://www.dowcorning.com)

THE AGGREGATION OF MULTIVALENT IMMUNE COMPLEXES EXPANDS THE USEFUL ANALYTE SIZE RANGE OF THE DIFFUSION IMMUNOASSAY

Kenneth R. Hawkins, Paul Yager
Dept. of Bioengineering, University of Washington, Box 352255, Seattle, Washington, USA

Abstract

We have previously described a novel clinically significant microfluidic immunoassay based on the differences in the diffusivity of an analyte and an immune complex of that analyte – the diffusion immunoassay (DIA) [1]. The ratio of diffusivity of the analyte and the immune complex is the key parameter determining the magnitude of the DIA response [2]. Here we show that aggregation that occurs when the analyte is multivalent increases the DIA response significantly. These findings expand the range of analytes amenable to a facile DIA into a much higher range of molecular weights.

Keywords: microfluidics, protein, DIA, immunoglobulin, quantitative, μ-TAS

1. Introduction

New microfluidic assay techniques are an enabling technology for the development of point-of-care immunoassay diagnostic devices. We have previously described a novel, clinically significant, microfluidic immunoassay based on the differences in the diffusivity of an analyte and the complex of that analyte and a specific antibody – the diffusion immunoassay (DIA) – which was for the small molecule drug phenytoin in whole blood [1]. Since then, we have determined that the DIA can detect higher molecular-weight analytes, but the amplitude of the signal can be less than with small molecules. Modifications of the DIA format (chemical or numerical) can restore the response amplitude.[2] In this report, we show that the DIA analyte response for one model protein analyte – immunoglobulin G (IgG) – is much larger than predicted due to formation of large aggregates of the bivalent antibody and the multivalent analyte (Figure 1). This phenomenon enables a high-signal DIA for as high molecular weight antigen like IgG with the originally-reported experimental conditions.

2. Theory

The DIA is performed in a simple T-sensor (two inputs, one outlet) operating in laminar flow conditions. One input is an antibody solution, the other a fluorophore-labeled analyte solution mixed with the sample. As analyte diffuses into the fluid stream containing Ab, it binds with the Ab. The immune complex is less diffusive than the unbound analyte, resulting in an accumulation of fluorescent label in the interdiffusion zone. The magnitude of this accumulation is modulated with sample analyte concentration by competition between the unlabeled and labeled analyte for Ab; an increase in sample analyte reduces the accumulation detected. Thus, the ratio of diffusivity of the analyte and its complex with the capture molecule is the key parameter that determines the magnitude of the DIA response. A numerical model has been shown to

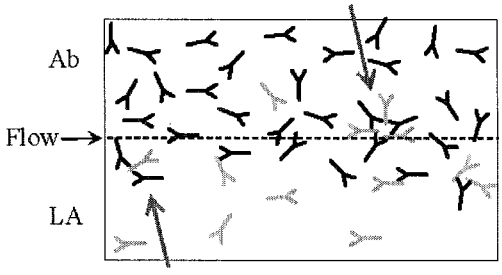

Figure 1: The hypothesized mechanism of the increase in DIA response with multivalent analytes. → = aggregated complexes.

correctly predict DIA responses for univalent analytes [1-3]. This model predicts no detectable response when IgG is the analyte and unmodified anti-IgG is the Ab (Figure 2A), due to the small difference in the diffusivities of one IgG and a complex of two IgGs.

3. Experimental

The T-sensor was a three-layer adhesive laminated device with a center layer of Mylar (Fralock Inc., San Carlos, CA, USA), and two outer layers of PMMA (GE Polymer Shapes, Schiller Park, IL, USA). Features were cut into the Mylar layer of the device, using a CO_2 laser (Universal Laser Systems Inc., Scottsdale AZ, USA). The main channel cross section was 100 μm x 1600 μm (orthogonal to the flow direction). Images were taken of the channel 40mm from the confluence of the inlet streams.

The T-sensor device was mounted on the stage of a Zeiss ICM-405 inverted, epifluorescence microscope (Carl Zeiss Inc., Thornwood, NY, USA). The center 800 μm of the channel was imaged at 6X. Excitation light from a Zeiss HB100W mercury arc source was conditioned by using a fluorescein filter set (exciter: 480/30 nm; beamsplitter: 505 nm; emitter: 535/40 nm; Chroma Technology, Battleboro, VT, USA). A Retiga 1300 (Q-Imaging, Burnaby, BC, Canada) cooled, 12-bit monochrome CCD camera was used for detection. Two programmable, stepper-motor syringe pumps provided pressure-driven flow (Kloehn, Las Vegas, NV, USA).

The model protein analyte used was mouse anti-avidin Clone WC19-10 (Sigma, St. Louis, MO, USA). Both FITC-labeled and unlabeled versions of this clone were obtained. An affinity-purified monoclonal goat anti-Ms-IgG was the capture antibody (Chemicon International, Temecula, CA, USA).

The T-sensor apparatus was operated at 21 nL/s mean volumetric flow rate at each inlet. After flow stabilization and feed solution washout (t = 300 s), ten replicates images for each sample were gathered every 30 seconds. For each analytical run, a set of blank correction images (taken with buffer flowing into both inlets) and a set of flatfield correction images (taken with a 100 nM solution of labeled IgG flowing into both inlets) was collected and processed in the same way as images of accumulation signals. Each accumulation image was corrected for background and flatfield illumination pixel-by-pixel using the mean pixel values of the appropriate correction images. Each image was sampled in a region that was thirty pixels wide in the flow dimension and the full width of the image in the diffusion dimension. This sample was then averaged along the flow dimension using MATLAB (v.5.2.0, The Math Works Inc., Natick, MA).

3. Results and Discussion

Contrary to the predictions of our models, we observed a large response when Ms-IgG was the analyte (Figure 2B). Moreover, the response was repeatable and significant – a functional, quantitative DIA was possible with this analyte (Figure 3). We hypothesize that aggregation of IgG/anti-IgG complexes occurs in the channel, further reducing the diffusivity of label from what would be observed for the bimolecular complex (Figure 1). Previously, we have predicted that by immobilizing the anti-IgG on a microsphere, the diffusivity of the AbLA complex would be slowed by orders of magnitude and a response should be seen.[2] In effect, the aggregation seen here has a similar function as would reducing the diffusivity of the capture molecules with nano- or micro-particles.

5. Conclusions

It is demonstrated that the "precipitin reaction" used for decades in immunochemistry can be seen in a rapid microfluidic-based process. These findings expand the range of analytes amenable to a facile DIA into a much higher range of molecular weights than previously thought possible.

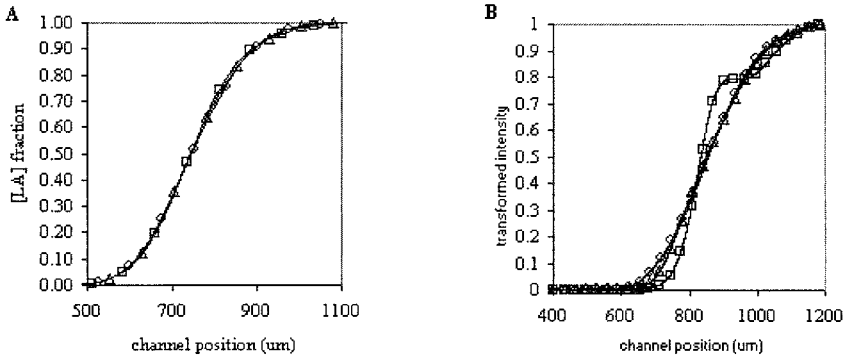

Figure 2: Comparison of predictions and actual observations of a DIA with IgG as the analyte. (□) = 0 nM sample analyte, (Δ) = 400 nM sample analyte, (○) = 1500 nM sample analyte. All with [antibody] = 683 nM, [labeled IgG] = 25 nM, interaction time = 154s. A) Predicted accumulation profiles assuming a univalent analyte. There is no modulation by the sample predicted – the three curves are practically superimposed. B) Observed accumulation with identical conditions as in 'A'. Modulation by the sample is observed, contrary to expectations.

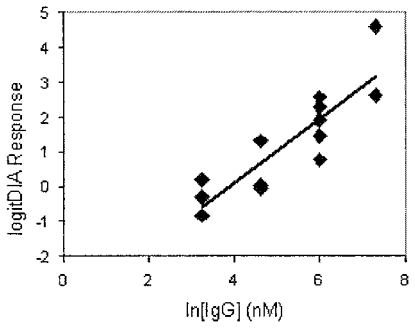

Figure 3: Plots of a univariate DIA response[1] versus concentration of IgG, with fitted linear covariance model, for all accumulations gathered to date. The data in Figure 2B is smoothed and a numerical slope taken. The difference in maximum and minimum slope is calculated and then transformed by a log/logit transformation ($x'=\ln(x)$; $y'=\ln[(y_0-y)/(y-y_\infty)]$) [4] ANCOVA analysis for this data set implies highly significant variation ($Pr>F < 0.0001$) for a fitted model: $y = 0.93x - 3.57$. (SAS for Windows, R 8.02)

References

[1] A. Hatch, A. E. Kamholz, K. R. Hawkins, M. S. Munson, E. A. Schilling, B. H. Weigl, and P. Yager, "A rapid diffusion immunoassay in a T-sensor," Nature Biotechnology, vol. 19, pp. 461-465, 2001.

[2] K. R. Hawkins, A. Hatch, H. Chang, and P. Yager, "Diffusion Immunoassay of Protein Analytes," 2nd Annual International Conference IEEE-EMBS Special Topic Conference on Microtechnologies in Medicine and Biology, May 2-4, 2002, Madison, Wisconsin, USA, 2002.

[3] A. E. Kamholz, B. H. Weigl, B. A. Finlayson, and P. Yager, "Quantitative analysis of molecular interaction in a microfluidic channel: The T-sensor," Analytical Chemistry, vol. 71, pp. 5340-5347, 1999.

[4] R. J. Maciel, "Standard Curve Fitting in Immunodiagnostics: A Primer," Journal of Clinical Immunoassay, vol. 8, pp. 98-106, 1985.

LOW ABUNDANT BIOMARKER SCREENING IN POLY(METHYLMETHACRYLATE) HIGH ASPECT RATIO MICROSTRUCTURES USING IMMUNOAFFINITY-BASED MOLECULAR RECOGNITION

André A. Adams[1], Juan Feng[2], Michael C. Murphy[2], and Steven A. Soper[1]
[1]*Louisiana State University, Department of Chemistry, Choppin Hall, Baton Rouge LA 70803*
[2]*Louisiana State University, Department of Mechanical Engineering, CEBA, Baton Rouge LA 70803*

Abstract

Polymer-based microfluidic devices consisting of high aspect ratio microstructures were used to probe the ability to pre-concentrate low abundant cancer cells from suspensions of human blood simulate. Significant increases in the capture rates of the target cells from blood simulate were demonstrated in poly (methylmethacrylate) (PMMA) microfluidic devices that contained selectively located immobilized antigens specific for the target cells. Microdevices with varying aspect ratios were evaluated for their capture abilities. At the optimum velocity of 2 mm/s the capture efficiency of the devices with aspect ratios greater than or equal to 5:1 were capable of capturing nearly 100% of the target cells from blood simulate. The interaction of the antigen and antibody was used to isolate cancer cells from suspension, thereby isolating single cells for subsequent analysis in a miniaturized total analysis system.

Keywords: immunoaffinity, adenocarcinoma, HARM, breast, and cancer

1. Introduction

Breast cancer represents the third most frequent cancer and encompasses nearly 9% of the total cancer burden worldwide. Breast cancer is characterized by development of adenocarcinomas in the ductal/lobular system of the milk ducts. The tumors are prone to shed epithelial cells that reside in peripheral blood (1–10 tumor cells/ml in the presence of 10^7 normal cells/ml) and they are typically the sole epithelial cells found in peripheral blood [1]. The surface of the tumor cell is inundated with glycoproteins termed epithelial cell adhesion molecules (EpCAM) ($3x10^5$ molecules/cell) that have three domains. EpCAM has an extracellular region, transmembrane region, and an intracellular anchor. A 5-mer (Leu-Phe-His-Ser-Lys) in the extracellular region of EpCAM has previously been demonstrated as an epitope for immunoaffinity based assays [2].

2. Theory

The foundation of this work has its roots in microfluidics; however, the mechanism that governs the process is immunoaffinity based. Specific combinations of hydrophilic, hydrophobic, van der Waal's forces, and hydrogen bonding interactions conjoin to form stable interactions at the surface of antibody immobilized microfluidic devices and cancer cells. The degree to which the cells are bound to the surface was approximated using Bell's model [7].

3. Experimental

The volume capacities of microfluidic devices have typically been in the range of 0.25–0.50 μl making it difficult to sample low abundant targets [3, 4]. In order to sample large quantities of simulate, a robust high capacity microdevice was necessitated. A novel 17-channel microsampling unit with high aspect ratio microstructures (HARM) was fabricated using X-ray LIGA. Poly

(methylmethacrylate) (PMMA) was the substrate of choice for microsampling unit preparation due to the ease of surface carboxylation, demonstrated biocompatibility, and HARMs compatibility. The device consists of an intricate network of microstructures with aspect ratios as high as 20:1 (See Figure 1). Exposure of PMMA to UV radiation at 254 nm with 15 mW/cm^2 power density for 30 min effectively produced a carboxylated polymer surface, which served as a functional scaffold to which anti-EpCAM antibodies were attached (See Figure 2) [5]. Effecting efficient cell capture in the microsampling unit required maximizing the probability of wall-particle interactions; accordingly, the channel cross-sections were designed with extreme rectangular character i.e. narrow (30–50 μm) and tall (250 μm) as to maximize such collisions.

4. Results and Discussion

The durability of the microsampling unit was demonstrated by passing blood simulate through the device with linear velocities from 3 μm/s to 1.2 m/s. The endurance of the device was demonstrated by continuously pumping 250 ml aliquots of blood simulate through the device at 1 ml/min, and 10 ml aliquots of blood simulate were processed with the microfluidic device in less than 10 min. No device failures were observed due to clogging or leaking. The immunoaffinity-based assays used to capture tumor cells from the peripheral blood simulates were carried out using immobilized anti-EpCAM antibodies that were bound to the surface of carboxylated PMMA using 1-ethyl 3-dimethylaminopropyl carbodiimide as a surface activator [6]. Capture efficiency of less than 1.0% was observed when 10^5 cells were processed at linear velocities as high as 2 mm/s in 50 μm width channels; however, when the channel width was reduced to 20 μm the capture efficiency was ~100% (See Figure 3). In conjunction, these technologies have afforded us the ability to develop novel systems for capturing and processing low abundant cells from blood simulates.

Acknowledgements

I would like to thank the Dr. Robert Truax in School of Veterinary Medicine at LSU, Super Soper Research Group, and especially Dr. Steven Soper. I would also like to thank the Louisiana State University, the National Institute of Health, and the National Cancer Institute for funding.

References

[1] B. Simon et al., *PNAS*, **87**(7) 2755-2759 (1990).
[2] S. Szala et al., *PNAS*, **87**(9) 3542-3546 (1990).
[3] M. Galloway et al., *Electrophoresis*, **23**(21) 3760-3768 (2002).
[4] S. Ford et al., *Journal of Microcolumn Separations*, **10**(5) 413-422 (1998).
[5] N. Siampiringue et al., *European Polymer Journal*, **27**(7) 633-641 (1991).
[6] B. Oh et al., *Biosensors & Bioelectronics*, **18**(5-6) 605-611 (2003).
[7] Bell, G.I., *Science,* **200**(4342) 618-27 (1978).

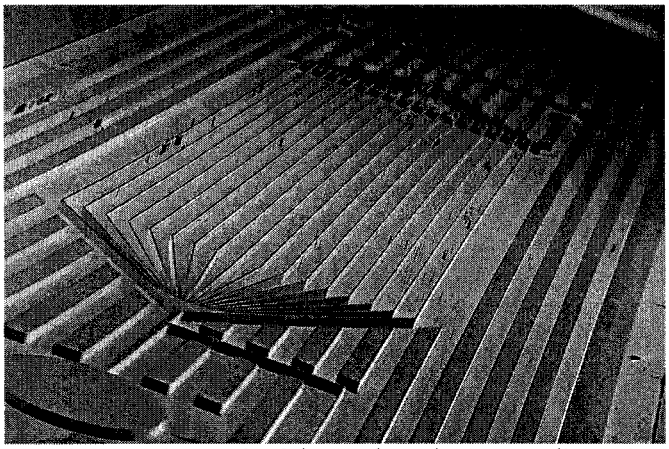

Figure 1. Scanning electron micrograph of the 17-channel microsampling unit Ni mould master prepared using x-ray LIGA.

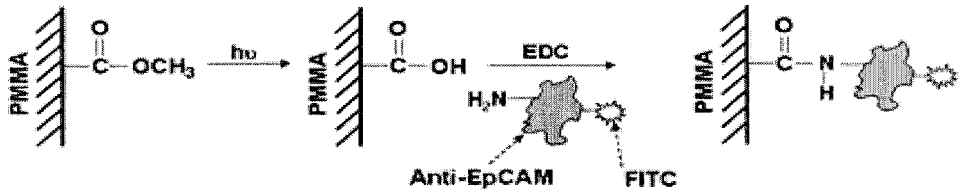

Figure 2. Anti-EpCAM antibody immobilization protocol in which a PMMA substrate is exposed to 254 nm radiation followed by exposure to 1-ethyl 3-dimethylaminopropyl carbodiimide to activate the carboxylated surface. Finally, a stable amide bond is formed between the anti-EpCAM and PMMA.

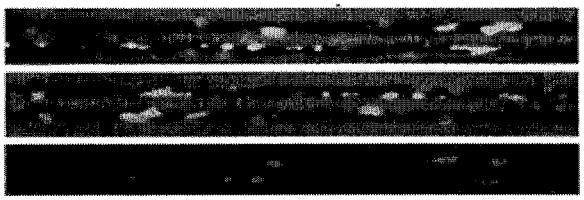

Figure 3. Fluorescence micrographs of DAPI stained MCF-7 cells captured from blood simulate in a PMMA microfluidic device (20 μm x 70 μm x 10 cm).

AUTOMATED MICRO ELISA SYSTEM TOWARD CLINICAL DIAGNOSIS; DETERMINATION OF A HEART FAILURE MARKER, BNP

Kiichi Sato[1,2,3], Emi Mori[4], Masaya Kakuta[4], Manabu Tokeshi[2] and Takehiko Kitamori[2,3,5]

[1] *Department of Applied Biological Chemistry, School of Agriculture and Life Sciences, The University of Tokyo, Yayoi, Bunkyo, Tokyo 113-8657, Japan*

[2] *Kanagawa Academy of Science and Technology (KAST), Sakado, Takatsu, Kawasaki, Kanagawa 213-0012, Japan*

[3] *Core Research for Evolutional Science and Technology, Japan Science and Technology Agency, Honcho, Kawaguchi, Saitama 332-0012, Japan*

[4] *Institute of Microchemical Technology (IMT), Sakado, Takatsu, Kawasaki, Kanagawa 213-0012, Japan*

[5] *Department of Applied Chemistry, School of Engineering, The University of Tokyo, Hongo, Bunkyo, Tokyo 113-8656, Japan*

Abstract

A Microchip-based enzyme-linked immunosorbent assay (ELISA) system for clinical diagnoses was developed. By the system, a heart failure marker peptide, BNP, dissolved in a practical plasma sample was successfully determined with high sensitivity. For further improvement of the system, automatic ELISA system with eight-channel microchip which is suitable for highly sensitive and high throughput assay was designed and constructed.

Keywords: immunoassay, ELISA, clinical diagnosis, automation, thermal lens microscope

1. Introduction

Immunoassay is known as one of the most important analytical methods and widely used in clinical diagnoses, environmental analyses and basic biosciences. The conventional immunoassay, however, requires a long assay time. We developed a microchip-based immunoassay system (Fig. 1), in which packed beads and colloidal gold particles were used as a reaction solid and labeling material, respectively. The system enabled successful reduction of the assay time from two days to 35 min and it was achieved by simple manual operations [1-3].

For practical use, however, evaluation by using practical samples is required. Moreover, further improvement in reproducibility, sensitivity and throughput will hardly be achieved by the manual operating system, because of the difficulty of the manual handling and equipment problems. In this study, to realize the practical use in clinical diagnoses, a microchip-based enzyme-linked

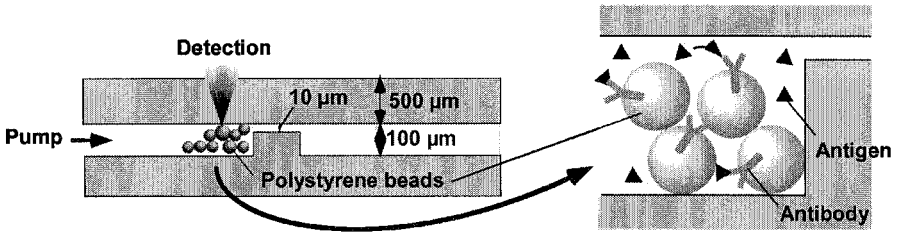

Figure 1. Cross section of immunoassay microchip

immunosorbent assay (ELISA) system for determination of a disease marker in practical plasma samples by manual operations was developed and then an automated analyzer for microELISA was designed and constructed.

2. Experimental

The ELISA microchip has inlet and outlet holes, reaction area with a dam for packing the mictrobeads and detection area (Fig. 2). Microchannels and a dam were fabricated on the Pyrex glass substrate by a combination of photolithography and wet etching technique. The microchip-based ELISA system was applied to assays of a heart failure marker peptide, BNP. Microbeads, pre-coated with an antibody, were introduced into the microchip, and then a sample, a washing buffer, an antibody-peroxidase conjugate, and the buffer were injected from an inlet successively. After final washing procedure, enzyme substrate solutions were injected from the inlets and the resulting enzyme reaction product was monitored with a thermal lens microscope (TLM) at a downstream part of the microchannel.

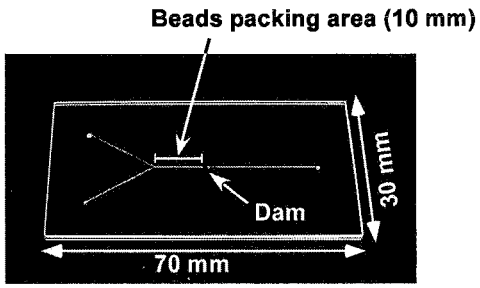

Figure 2. MicroELISA chip

3. Results and discussion

After optimization of reaction conditions, good calibration curve for BNP was obtained with short assay time (~ 30 min in total). Lower limit of determination was lower than 0.1 pg/mL level (Fig. 3). Moreover, in the case of the practical human plasma samples, obtained signal intensity was obviously dependent on the BNP concentration (Fig. 4), and then, the microELISA system seems to be useful for practical diagnosis. From these results, we concluded that the manual-handling microELISA system had a potential to practical assay in various fields such as clinical diagnoses and environmental analyses.

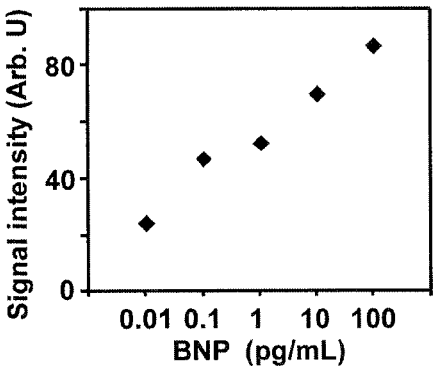

Figure 3. Calibration curve of a heart failure marker, BNP

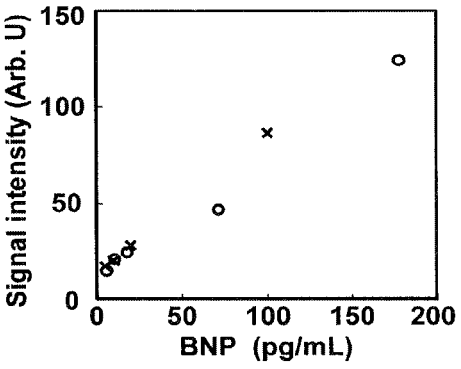

Figure 4. Practical analysis of BNP. o: plasma sample, x: standard solution.

To realize the ultra sensitive assay with higher throughput, automation is preferable and exclusion of the bulky components outside the microchip, i.e. long capillary, huge volume of the pump, and large dead-volume connectors, is indispensable. For this purpose, automatic ELISA system with an eight-channel microchip was designed and constructed. The analyzer consists of miniature micropumps with valves which are directly attached on a chip, a thermal controller, a scanning TLM detector, and a computer for system operation and data processing (Fig. 5). The ELISA system was designed to perform 8 assays at a time automatically.

4. Conclusions

By combination of a microchip, microbeads and a TLM, rapid and sensitive immunoassay system was developed. By the system, a heart failure marker peptide, BNP, dissolved in a practical plasma sample was successfully determined at pg/mL level. Moreover, an automated immunoassay system using an eight-channel microchip was developed. By using the analyzer, higher throughput analysis will be realized in near future.

References

[1] Sato, K., Tokeshi, M., Odake, T., Kimura, H., Ooi, T., Nakao, M., Kitamori, T., *Anal. Chem.* **72**, 1144-1147 (2000).

[2] Sato, K., Tokeshi, M., Kimura, H., Kitamori, T., *Anal. Chem.* **73**, 1213-1218 (2001).

[3] Sato, K., Yamanaka, M., Takahashi, H., Tokeshi, M., Kimura, H., Kitamori, T., *Electrophoresis* **23**, 734-739 (2002).

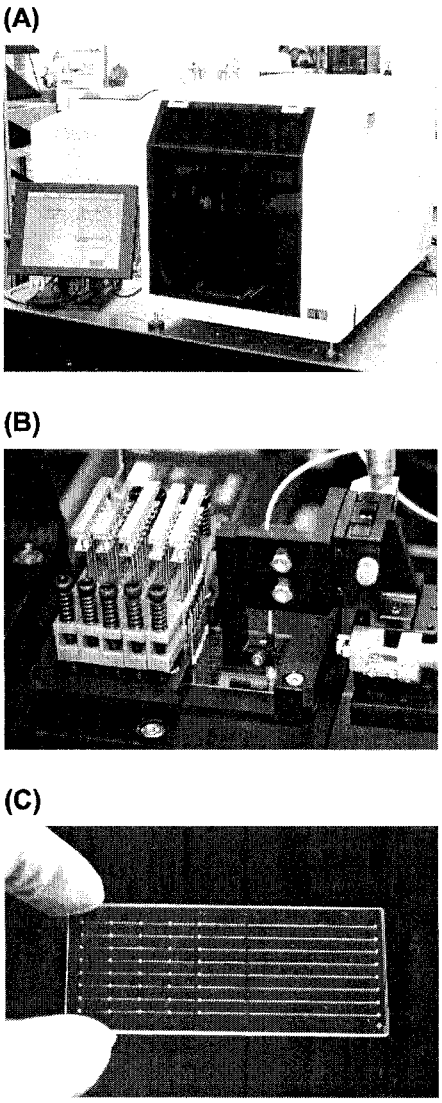

Figure 5. Micro ELISA system. (A) automatic analyzer, (B) chip, pumps, and detector, (C) 8-channel ELISA microchip.

ULTRA RAPID ALLERGEN ASSAY BY INTEGRATED ELISA SYSTEM

Toshinori Ohashi[1)], Yoshinori Matsuoka[1)], Yoshikazu Yoshida[1)], Takehiko Kitamori[2)]
[1]*The Research Association of Micro Chemical Process Technology (MCPT), KSP R&D-C11, Takatsu, Kawasaki, Kanagawa 213-0012, Japan*
[2]*Dept. of Applied Chemistry, School of Engineering, The University of Tokyo, 3-2-1 Hongo, Bunkyo, Tokyo 113-8656, Japan*

Abstract
We have developed a microchip ELISA system to diagnose allergy disease of hey-fever for determination of specific IgE to pollen of Japan Cedar. Using this system, specific IgE was assayed within 20 minutes. Moreover, when human serum samples were assayed with this system, diagnostic analysis of specific IgE of hay fever was realized by using only 2μl of specimen.
Keywords: ELISA, Thermal Lens Microscopy, IgE, Allergy, Hay-Fever

1. Introduction

Allergy diseases in daily and common life are increasing around the world, e.g. hay fever (20 million patients per year) in Japan. Diagnostic testing for these diseases is required for enabling to be realized by small system in doctor's office or at home rather than large system in hospitals. Microchip ELISA system is expected as an application of rapid and compact diagnostic testing system [1]. In this work, our goal is to develop an IgE test system [2] which can detect <1ng/ml of specific IgE to pollen of Cedar using a few micro liter of serum and is rapid and easy handling for general practitioners by comprehensive improvement of sample handling and fluid control.

2. Experimental

Microchip fabrication and fluidic system

A microchip was made of glass plates (30 mm× 70 mm) and has microchannels with a dam for a beads-bed immunoassay system (Fig.1a). The layout of the microfluidic system was shown in Fig. 1b. The microchip has 4 inlets for sample, reagent1, reagent2 and substrate, 1 outlet and 2 additional holes (inlet and outlet) for packing/depacking of beads. Typically, the channel width and depth were 200 μm and 100 μm respectively, and the channel depth of the dam region was 10 μm.

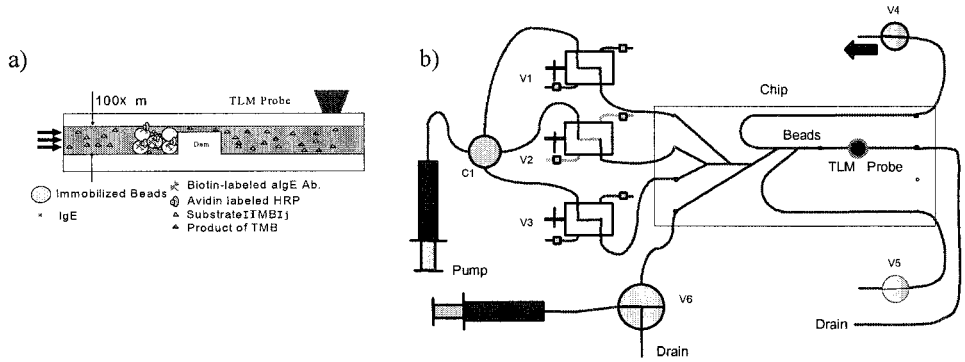

Figure 1. a) Beads-bed immunoassay system on a microchip and b) Layout of fluidic system v1,v2 and v3: injection valve, v4 and v5: stop valve, c: branch connector

Fluidic system

We developed a user-friendly micro injection valve made by PEEK tubes and Teflon base material as a most key-interface of microsystem, but not on chip to reuse frequently (Fig.2). The unit of three simple microinjection valves having volume of 2μL for sample, antibody for IgE, and enzyme injection were set up close to the microchip and enable to quantitative and successive supply of reagents to the microchip. The tubing for connection between a pump and a chip is made of PEEK (Φ0.5×0.1mm) and is designated for simple and physical connection.

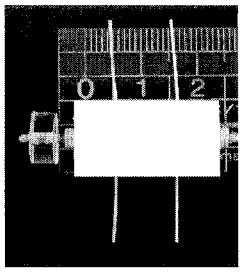

Figure 2. The photograph of micro injection valve

Detection

An on-chip micro thermal lens detection device (micro-TLD) was utilized as an optical alignment free thermal lens detection system [3]. SELFOC micro lens was integrated on the top surface of the microchip at the 10mm downstream from the dam of the microchannel. The excitation wavelength used in this research was 635nm, and the detection wavelength was 750nm.

Protocol of procedure

The system was applied to assays of an allergen identification. Polystyrene microbeads (25μm in diameter), which were precoated with pollen extracts of Japan Cedar followed by blocking with BSA, was packed in the microchannel (packing length: 5mm). The specific IgE in a specimen of serum, a buffer, biotin conjugated anti-IgE antibody, a buffer, and avidin conjugated horse radish peroxidase, and a buffer were injected successively. After final washing procedure, the substrate solution of tetramethyl benzidine and H_2O_2 mixture were injected from inlet by flow-stop-flow method.

Total IgE was measured by using beads coated by goat anti-human IgE antibody in place of allergen.

3. Results and discussion

The TLM signal appeared as a sharp peak generated by stopped flow on the base signal (Fig. 3). Peak height was proportional to time of stopped flow and was loosely affected by flow-rate after stopping. It can be explained that a coloured plug produced by enzymatic reaction on beads moved to the detection point in microchannel keeping with the shape. This result may be useful for stable quantification of signal.

As a result, the flow-stop-flow detection method (1min flow and 1min stopped flow and flow) gave a stable signal of product colored by enzyme. Accordingly, the method enables to achieve a successful reduction of the assay time by a combination of rapid flow and stopped flow.

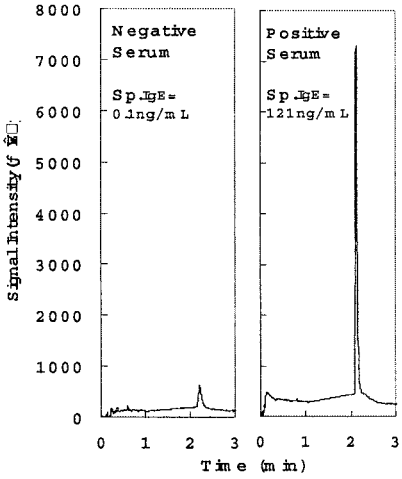

Figure 3. Typical peak of signal of specific IgE of sera to pollen of Japan Cedar detected by flow-stop-flow method

In general, the substrate to horse radish peroxidase is photosensitive and coloring by natural light. Although the height of base line increases in proportion to such coloring in the detection process, the height of the peak showed no change. In consequence, the stopped flow method is able to avoid signals originated from such non-enzymatic reaction.

The ratio of signal intensity between blank (0ng/mL) and 20ng/mL of total IgE depends on the flow rate which is inversely proportional to the contact time of beads and IgE molecule or anti-IgE antibody in Ag.-Ab. reaction process (Fig.4). After optimization of reaction conditions, i.e., flow rates (1-2.5μL/min), and concentration of reagent, the assay time from beads-packing to detection was reduced to about 20min and the lower detection limit reached to the concentration of 0.1ng/ml of IgE, by applying only 2μL of serum. The CV is less than 10%.

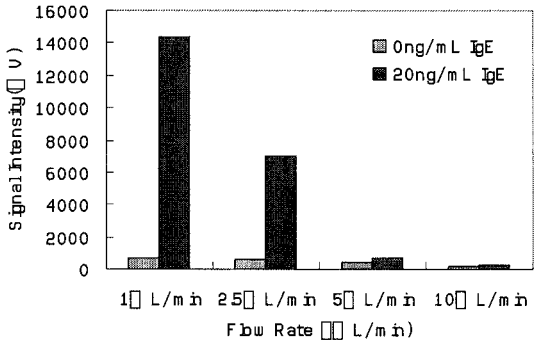

Fig.4 The dependency of flow rate of Ag.-Ab. reaction on the signal intensity originated from 0 and 20ng/mL of IgE

The concentration correlation plots of specific IgE to pollen of Japan Cedar are presented in Fig.5. Beads immobilized with pollen extracts of Japan Cedar were used in this experiment. The correlation between values measured by a conventional (RAST) method and the signal intensities of our method provides good correlation coefficient of 0.977.

4. Conclusions

This μ-ELISA system developed here could be applied to human sera for diagnostic analysis of specific IgE of hay fever within 20min, using only 2μl of specimen. One micro liter scale rapid μ-ELISA systems to determine allergens, hormones, and proteins are at hand

Acknowledgements

The present work was supported by the New Energy and Industrial Technology Development Organization (NEDO) of Ministry of Economy, Trade and Industry, Japan.

References

[1] K.Sato et al., Micro TAS 2002,P190(2002)
[2] T. Ohashi et.al., HPCE2004,P251(2004)
[3] Y. Matsuoka et al., Micro TAS 2004, A32640 (2004)

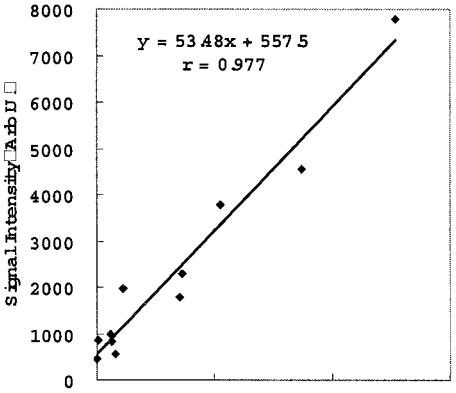

Fig.5 The correlation between RAST method and the signal intensity of our method (samples: 11 human sera from patients of hay fever and normal)

OBSERVATION OF THE INTERACTION BETWEEN SINGLE DNA AND INDIVIDUAL ENZYME MOLECULES IN A MICROCHIP

Fuquan Dang[1], Yoshihisa Yamaoka[1], Takahiro Nishimoto[2], Hiroaki Nakanishi[2], Mitsuru Ishikawa[1] and Yoshinobu Baba[1,3]

[1] Single-Molecule Bioanalysis Laboratory, AIST, Hayashi-cho, Takamatsu 761-0395, Japan
[2] Tech. Res. Lab., Shimadzu Corp., 3-9 Hikaridai, Seika-cho, Kyoto 619-0237, Japan
[3] Dept. of Medicinal Chemistry, The University of Tokushima, CREST, JST, Shomachi, Tokushima 770-8505, Japan

Abstract

To understand well the catalytic mechanism of exonucleases required for DNA repair and recombination, we designed and built a single DNA substrate with one 5' terminus attached to an avidin-coated bead and the other 5' terminus left free to λ exonuclease molecules. The interaction between a single λ-DNA and individual λ-exonuclease molecules was monitored in a real-time using a silica quartz microchip coupled with optical tweezers.

Keywords: Single molecule, microchip, DNA, protein and interaction

1. Introduction

Exonuclease is a family of enzymes specially involved in genetic DNA repair and recombination. Bacteriophage lambda encodes λ-exonuclease (λ exo), a 24-KD enzyme required for phage DNA recombination through the double-strand break repair and single-strand annealing pathways. A λ exo molecule consists of three subunits forming a toroid with a tapered central channel which is sufficient to admit double-stranded DNA (dsDNA) at its entrance (3 nm) but only wide enough to pass single-stranded DNA (ssDNA) through its exit (1.5 nm). This topological constraint may therefore underlie the high processivity of λ exonuclease (>3000 base pairs). The early biochemical studies in bulk solution revealed that λ exo degrades each strand of duplex DNA in the 5' to 3' direction in the presence of Mg^{2+} and the 5'-terminal phosphate group at rates of 24 to 42 nt/s. However, the digestion rates of 12, 32 to 1000 nt/s, and the prossesivities of 18,000 ± 8000 to 48 502 bp were reported in recent studies based on single-molecule assays [1,2]. The great dispersion of the data obtained so far in a macro-environment by the miniaturized flow cells undoubtedly retards the understanding of catalytic mechanism and kinetics of λ-exo.

In the current work, we have developed a new assay based on microchip technology coupled with optical tweezers to study the interaction of single DNA and individual λ exo molecules in a micro-environment. For single-molecule study, microchip technology [3] has substantial advantages over the miniaturized cuvettes used in the previous studies in terms of the accurate control of micro-channel size and thus liquid flow. Therefore, we expect to obtain the digestion rate and processivity of λ-exo close to those in natural bio-environments, and thus to provide insights into the catalytic mechanism and kinetics of λ exo as it is.

2. Experimental

DNA digestion by individual λ exo molecules (New England Biolabs, Beverly, MA) was performed in a silica quartz microchip with a specially shaped channel of 50 μm width and 50 μm depth. The DNA-exonuclease-bead complexes, stretching buffer and reaction buffer were introduced sequentially to the main channel of microchips by a high voltage supply or a syringe pump. The microchip was held on the stage of an inverted fluorescence microscope (Olympus IX70, Olympus, Tokyo) equipped for epifluorescence and modified to incorporate an optical

tweezers (Sigma Koki, Japan), using a Nd:YLF infrared laser (wavelength 1,047 nm, 500 mW; Spectra Physics, Mountain View, CA). An oil-immersion objective lens (Olympus UplanApo 100×/1.35 N.A., Tokyo) was used to focus the optical trap and to illuminatea the fluorescent DNA-exonuclease-bead complexes using 470-490 nm lines from a 100-W mercury lamp (Olympus, Tokyo). The same objective lens and a 510 nm long pass filter (HQ510lp, Chroma Technology Corp., Rockingham, VT, USA) were utilized for fluorescence imaging. The fluorescence images of DNA–bead-exonuclease complexes were captured by a chilled CCD camera (C5985; Hamamatsu Photonics, Japan) coupled to an image intensifier unit (C8600; Hamamatsu Photonics, Japan) and recorded on a hard disk video recorder. The fluorescence images were analyzed later by an image-processing software (Aquacosmos 2.5, Hamamatsu photonics, Japan).

4. Results and discussion

Because λ exo initiates digestion at a 5' terminus with blunt or 3' single-stranded overhang end, the DNA substrate should be designed to have only one such terminus available to the enzyme, thereby preventing more one enzyme molecule from acting on a particular DNA simultaneously. For this purpose, two cohesive ends of λ DNA were functionalized by three special designed oligonucleotides through kinase activation and ligation. One 5' terminus of λ DNA molecules was biotinylated to specifically couple to an avidin-coated polystyrene bead and the other 5' terminus with a 3' single-stranded overhang left free to λ exo. After binding to neutravidin coated microbeads (1.0 μm, Molecular Probes), the DNA-beads complex were incubated with λ exonucleases and YOYO-1 to form the fluorescent DNA-exonuclease-bead complex. It was found that the kinase activation of oligonucleotides and λ DNA is crucial to the construction of the DNA substrate. Without the kinase activation, the possibility was fairly low to obtain the DNA substrate with designed structure in some cases.

The schematic representation of single DNA digestion by individual λ-exo in a silica quartz microchip is shown in Fig. 1. The specially shaped micro-channels of 50 μm width and 50 μm depth were designed and fabricated to sequentially introduce the DNA-exonuclease-bead complex, stretching buffer and reaction buffer to the main channel of the microchip via electric or hydraulic force (Fig. 2). The most significant characteristics of the silica quartz microchip is no autofluorescence shown at the detection wavelength (470-490 nm), but DNA molecules and avindin coated micro-beads were found to adsorb strongly to the surface of silica quartz micro-channels. To solve this problem, 1% poly(vinylpyrrolidone) (PVP, M_W 1300000) and bovine serum albumin were used as buffer additives. No adsorption of individual λ-DNA molecules happened in the quartz microchip (Fig. 3A). A single DNA-exonuclease-bead complex was trapped by optical tweezers and fully stretched in a micro-channel by the electric force (Fig. 3B). The digestion rate and processivity of λ-exonuclease was studied at single molecule level. The present work demonstrated that microchip technology is a promising alternative for single-molecule work owing to the easy and accurate control of liquid flow in micro-channels via the electric force or hydraulic force [3].

5. Conclusions

A DNA substrate with one 5' terminus attached to an avidin-coated bead and another 5' terminus free to λ exonuclease molecules was designed and built through ligating three oligonucleotides to the two cohesive ends of λ phage DNA. The single DNA-exonuclease-bead bead complex was successfully trapped by optical tweezers and stretched in a quartz microchip. The present work demonstrated the feasibility of a microchip as a promising alternative for studying the interaction of single DNA and individual protein molecules.

Acknowledgements

The present work is supported in part by the CREST program of the Japan Science and Technology Corporation (JST); a grant from the New Energy and Industrial Technology Development Organization (NEDO) of the Ministry of Economy, Trade and Industry, Japan; a Grant-in-Aid for Scientific Research from the Ministry of Health and Welfare, Japan; and a Grant-in-Aid for Scientific Research from the Ministry of Education, Science and Technology, Japan.

References

[1] P.R. Bianco, L.R. Brewer, M. Corzett, R. Balhorn, Y. Yeh, S.T. Kowalczykowski and R.J. Baskin, *Nature*, 409, 374-378 (2001).

[2] T.T. Perkins, R.V. Dalal, P.G. Mitsis, S.M. Block, *Science*, 301, 1914-1918 (2003).

[3] F.Q. Dang, L.H. Zhang, M. Jabasini, N. Kaji, Y. Baba, *Anal. Chem.*, 75, 2433-2439 (2003).

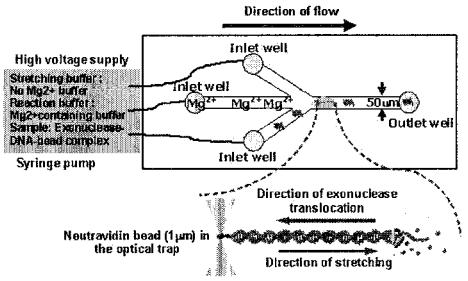

Figure 1. The schematic diagram of single DNA digestion by individual λ-exonuclease in a microchip.

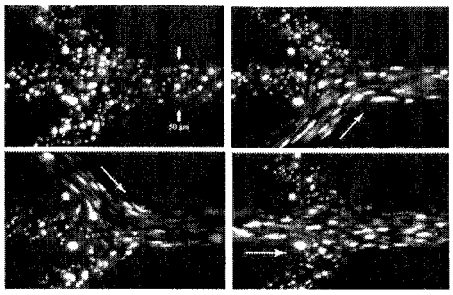

Figure 2. The flow of avindin-coated fluorescent beads controlled by electric field in a microchip

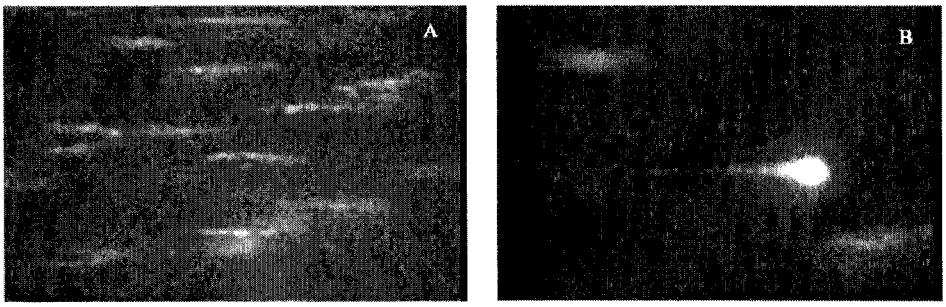

Figure 3. The migration of individual λ-DNA molecules (A) and trapping and stretching of a single DNA-exonuclease-bead complex by optical tweezers in a microchip (B), obtained in 67 mM glycine-KOH buffer containing 1% PVP and 50 μg/ml BSA, (pH 9.4).

ON-CHIP SORTING SYSTEM USING CHARGED DROPLETS

Takashi Kawano[1], Naritoshi Kanai[1], Shinji Ando[1], Masanori Yamamoto[1], Jun Fujiwara[1]
Toru Torii[2] and Toshiro Higuchi[2]

[1]AISIN COSMOS R&D Co., Ltd. 5-50, Hachiken-cho, Kariya-city, Aichi Pref., 448-8650, Japan
[2]Department of Precision Engineering, Graduate School of Engineering,
The University of Tokyo, Hongo 7-3-1, Bunkyo-ku, Tokyo, 113-8656, Japan

Abstract

As a new on-chip particle sorting system, we have proposed a novel method of forming the particle-containing droplets on a chip, charging those droplets based on the particle information (ex. fluorescence) and sorting them with the influence of electric field at a Y-junction. This method enables aerosol-free sterile sorting and high-speed processing. In this paper, we have confirmed that forming and sorting 5000 droplets/sec were accomplishable, and also it was feasible to sort the fluorescent beads under the actual circumstance.

Keywords: droplet, cell sorting, flow cytometry, emulsion, microfluidics

1. Introduction

We have developed a sorting system capable of separating particles such as bacteria and cells arbitrarily. The existing cell sorter forms the particle-contained droplets in the air and sorts them by the influence of the electrostatic force; therefore, it is suitable for high-speed sorting. However, an aerosol problem remains; besides, its open system is unsuitable for aseptic treatment. On the contrary, the cell sorter chips reported in articles are free from aerosol contamination but not recommended for high-speed processing.

We are developing an on-chip sorting system that forms particle-contained droplets in the closed system of chip and sorts those droplets by the electrostatic force. This system has merits of being free from aerosol contamination and suitable for aseptic treatment; moreover, more high-speed process is achieved compared to other on-chip sorters. This paper reports the structure and principle of this sorting system, experimental results of droplets formation and separation in flow channels and fluorescent beads sorting.

2. System Structure and Principle

The system mainly consists of areas for droplet formation/electrification, particle detection and droplets separation, schematically shown in Figure 1. The principle of the system is as follows: droplets, each of which contains the target particle, are formed and inductively charged at the droplet formation/electrification area. And then at a Y-junction, the charged droplets are sorted into one of the flow channels by the influence of an electric field created by the deflection electrodes placed under the Y-junction.

The core technology of the droplet formation is as follows: two flow channels; one for sunflower oil (organic phase) and another for suspension (aqueous phase) intersect at T-shaped cross section. At the crossing point, the sunflower oil shears the suspension and that phenomenon causes the droplets formation. [1]

Induction charging is a method used for the droplet electrification. A charging electrode is set where the suspension is sheared by the sunflower oil. When the suspension passes through the charging electrode, the electrical charge in the suspension are induced by the electrostatic induction. Subsequently, the suspension is detached by the sunflower oil to form a droplet, but charge remains in the formed droplet. In addition, the droplet charging timing is controlled by adjusting the phases of

droplets interval received from a fiber optics droplet counter. For the particle detection, the fluorescent labeling is used as a target particle, and the detection is done by a fluorescent microscope system.

3. Experiment of the Droplets Formation and Separation

The chip shown in figure 2a was used for the experiment of the droplets formation and separation. The chip was made of polymethylmethacrylate, and the micro-groove was fabricated by machine and covered with film so that the flow channel was formed. The flow channel was 100 μm depth, and 100 μm width except for the width of separation area (400 μm). The charging electrode was made by patterning aluminum on Pyrex glass which was bonded on the sealing film. The ground electrode and the deflection electrodes were implanted in the chip. The experiment of the droplets formation and separation were carried out as follows. To form the droplets, phosphate buffered saline (PBS) and sunflower oil were injected from two syringe pumps to the chip. To separate the droplets, the charging signal was made of a high-voltage power supply, a control circuit, and a function generator.

As a result, we have confirmed that the sorting was feasible when droplets formation conditions were 5000 droplets/sec, 41 μm in diameter, charging signal ±300 V, 500 Hz at 10 % duty. Figure 2b indicates the droplets separation images taken with the high-speed video camera. The parameters for the droplets separation are droplet size, flow speed, interval, charged amount, oil viscosity and the electric field intensity of deflection electrode. Basically, if the droplets are satisfactorily charged, then the success of the droplets separation depends on the droplets formation conditions. With regard to the droplet formation conditions, it is essential that there is no droplet fusing in flow channels, particularly at the deflecting electrodes area. In our experiment, appropriate intervals between droplets were secured when the rate was 5000 droplets/sec and the diameter was 41 μm.

4. Experiment of Sorting with Fluorescent Beads

A sorting experiment has carried out by using a suspension mixed with green and red fluorescent beads (ϕ6 μm each) in PBS. Concentrations of both the green and the red beads were 0.5×10^6 beads /ml. Several filters and a photodetector in the fluorescent microscope system were set to detect the light intensity of green fluorescent beads selectively. Therefore, ideally only the green beads were sent to the collection channel, and only if a droplet contains red and green beads at the same time, red beads would flow to the collection channel. Due to the responses of the droplet counter and the fluorescent detector, the experiment was conducted under the condition of 200 droplets/sec and diameter 71 μm. The results showed that the percentages of green beads collection and concentration were 80 % and 82 % respectively. Thus, we confirmed that the sorting process (droplet formation ~ beads detection ~ sorting) was feasible.

5. Conclusion

We demonstrated that forming and charging the droplets in the flow channels and sorting them into either one of the Y-shaped flow channels by the influence of electric field (ϕ41μm, at a rate of 5000 droplets per second.) is technically possible. Moreover, the experiment of fluorescent beads proved that sorting is achievable. We expect that this technology will be expanded not only to the particle sorting but also to the quantitative distribution of droplets and micro reactor.

References

[1] Takasi Nisisako, Toru Torii, Toshiro Higuchi, Droplet Formation in a Microchannel Network, *Lab on a Chip*, **2**, 24-26 (2002).

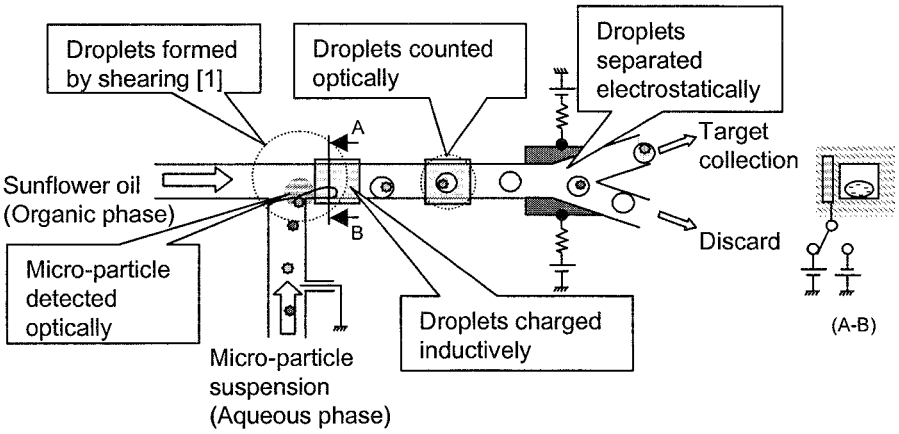

Figure 1. Schematic view of the system structure.

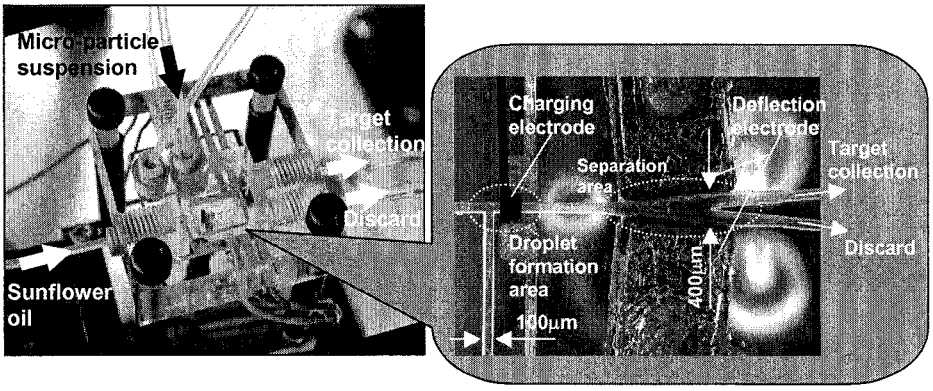

a) Photo of the on-chip sorting system.

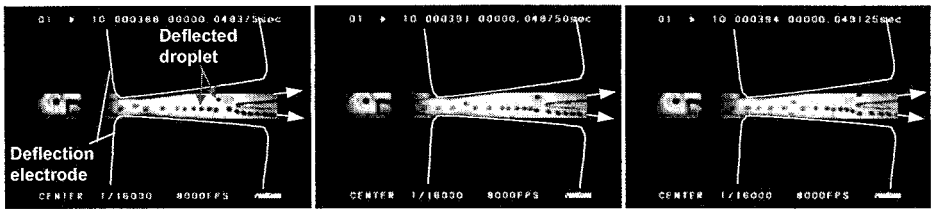

b) The droplets sorting images taken every 375 micro seconds by the high-speed video camera. (Droplets formation: 5000 droplets/sec at ϕ41μm, Charging signal: 500Hz at 10% duty)

Figure 2. Photo of the on-chip sorting system and the droplets sorting images.

CELLULAR CHEMOTAXIS OBSERVATION IN MICRODEVICES

Yasuhiro Goshoh[1], Naoki Oguro[1], Takaaki Kuroiwa[1], Nao Nitta[2], Shiro Kanegasaki[2] and Teruo Fujii[3]

[1] Yamatake Corporation [2]Effector Cell Institute in RCAST and [3]Institute of Industrial Science, the University of Tokyo, Japan

Abstract

We have developed microdevices used as novel horizontal chemotactic apparatus [1], in which cellular chemotaxis can be observed in real time. Two types of the device are fabricated, each of which consists of a flat glass plate and either a silicon substrate (Si-type) or a PDMS layer (PDMS-type). A stable concentration gradient of chemoattractant across the microchannel was shown to be established experimentally and theoretically. Chemotaxis of Jurkat cells toward the chemoattractants were demonstrated using both Si and PDMS-type devices.

Keywords: Chemotactic chamber, PDMS, Silicon, Chemokine, Immunity cell

1. Introduction

Chemotaxis is the directional movement of cells in their various roles or activities such as inflammatory response, homeostatic circulation, and development. It concerns a number of disorders such as infectious and allergic diseases. Learning more about the chemotactic processes of various cells should bring numerous benefits to the basic and applied medical sciences.

Chemoattractant is a substance, which induces cellular chemotaxis, such as chemokines, a group of characteristic proteins with small molecular weight.

2. Device Fabrication

Two types of the chemotactic device are fabricated, each of which consists of a flat glass plate with either a silicon substrate (Si-type) or with a PDMS layer (PDMS-type). Two compartments having holes are formed in the device and they are connected with each other by a thin microchannel as depicted in Fig.1.

Depth of the compartments is 100 μm and diameter of holes is 1mm. Microchannel lengths are 130 or 260 μm and the depth is around 5 μm, which should be a little narrower than the diameter of floating spherical cells in the medium. Barrier structures are located in the channel, which is a line-and-space structure with wider spacings than the cell functioning as barriers (Fig.2). Microchannel structure was designed in consideration of a sustaining time of the concentration gradient of chemoattractants and of the ease of observation.

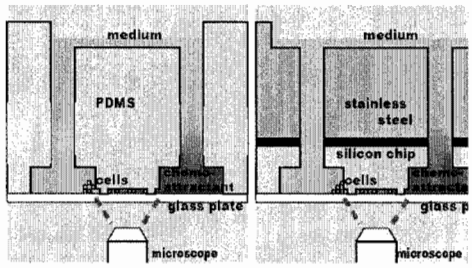

Figure 1. Cross-sectional view of chemotactic device (PDMS-type (left) and Si-type (right)).

In the case of Si-type, the glass plate and the silicon substrate are held together with a stainless steel holder with 1mm wide holes in diameter for injecting cells and chemoattractant. To fabricate the silicon microstructures, a 400 μm thick wafer was manufactured by deep reactive ion etching (DRIE) and by photolithography.

In the case of PDMS-type, the glass plate and the PDMS layer are directly bonded together. The microstructure in the PDMS layer was fabricated by single-step replica molding process from a die. The die consists of three parts, i.e. stainless made upper and bottom pieces, and a Nickel-made

mold for the microstructure. The upper piece has holes to inject PDMS prepolymer, to take out the air in the die during the molding process and to insert rods for through-holes on the PDMS layer.

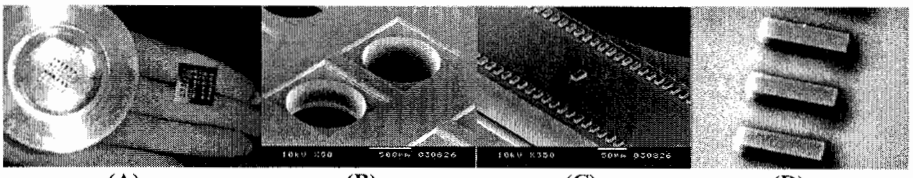

(A) (B) (C) (D)

Figure 2. (A) Stainless holder and the Si-type device. (B) SEM image of Si compartments, holes and microchannels. (C) SEM image of Si microchannel and barrier structures. (D) SEM image of PDMS barriers structures.

3. Experimental

Concentration gradient in microchannel. A stable concentration gradient of chemoattractant across the microchannel was shown to be established theoretically and experimentally. We determined the theoretical diffusion process of chemokine by a commercial CFD (CFD-ACE+, CFD Research Corporation). Real scale was used for the present simulation model. We employed 10^{-6}cm^2/s as the diffusion coefficient (D) of a model chemokine, since measurement of the diffusion constant, D, have shown to range from 10^{-6} to 10^{-7} cm^2/s for protein molecules with a 10k-100kDa range[2] and D value of brain hart cycochrome c, whose molecular weight is 13,370 was shown to be $1.14*10^{-6}$cm^2/s [3].

And we have confirmed experimental evaluation by using FITC (fluorescein isothiocyanate). FITC solution (10^{-4}M) was injected into the compartment and fluorescence image in the microchannel was saved into a computer using a fluorescent microscope. Formation of concentration gradient was scored based on luminance of FITC in the channel.

Cellular chemotaxis observation. To observe cellular chemotaxis, cell suspension is injected into the compartment filled with medium. To adjust the position of the cells in the compartment, the medium was slowly drawn out from other compartment. The cells are aligned at the edge of the channel due to its thin structure. Then, the medium is filled up to the common space at the top of the holes to avoid the difference in hydrostatic pressure. A chemoattractant was injected in the compartment opposite to that containing the cells. Migration of cells was monitored with time lapse intervals using a CCD camera or CCD video camera that is located under the glass plate.

4. Results and discussion

Concentration gradient in microchannel. We have analyzed the diffusion process of the chemokine in the microchannel by CFD. We used a device geometry with three holes as a simulation model. 1 μl of 10^{-9} M chemokine was applied to the center hole at 0.1 mm above the glass surface and the concentrations at the right (γ), center (β) and left (α) points in the microchannel were determined (Fig. 3). The concentration of the chemokine at the right point γ began to increase after 1 min. In 5-10 min after injection, linear gradients between right and left point along the microchannel was formed and maintained for at least 60 min.

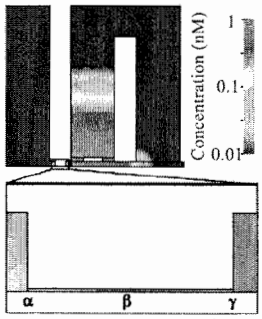

Figure 3. Cross-section views of a concentration evaluated by CFD

The gradient was evaluated experimentally with FITC. As shown in Fig. 4, the concentration gradient was formed through the

channel 2 min after injection of the FITC and the gradient was maintained at least up to 15 min, while the absolute value of luminance of FITC itself decreased gradually with time-dependent quenching.

Cellular chemotaxis observation. We have observed the migration of cells in the microchannel by using both Si and PDMS-type devices. Representative images in such experiments using PDMS-type are shown in Fig. 5. The length of the microchannel was 130 μm and the depth was 7 μm. Cell suspension containing approximately 300 cells was applied from the upper side in Fig. 5. And chemoattractant was injected into the bottom side. A line of cells at the upper side of the channel (4-min) migrated toward the barrier part (16-min). These cells migrated through the bottom side of the channel and further into the compartment (28-min).

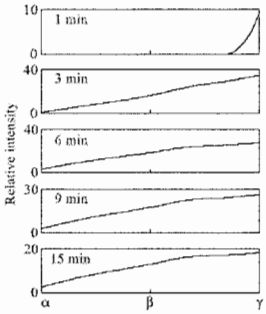

Figure 4. Formation of the FITC gradient in the microchannel

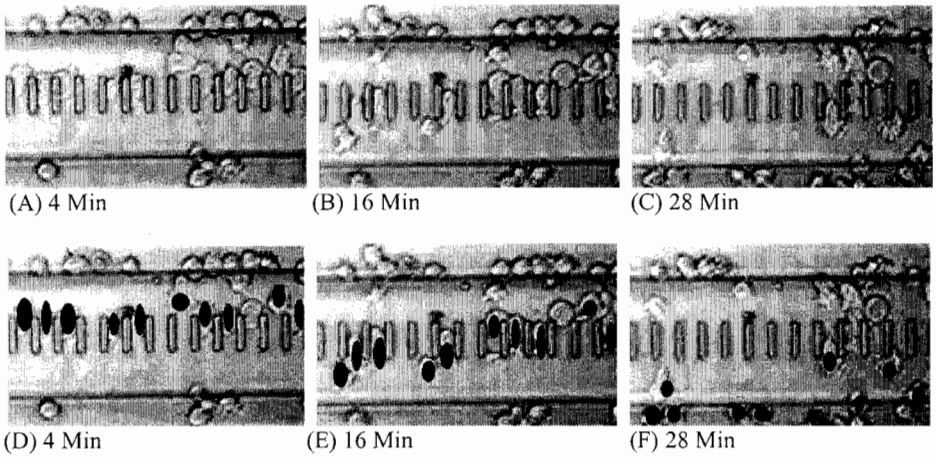

(A) 4 Min (B) 16 Min (C) 28 Min

(D) 4 Min (E) 16 Min (F) 28 Min

Figure 5. Migration of Jurkat cells in the PDMS-type device along the concentration gradient of chemoattractant in the channel formed upward in the photo. The cells were aligned on the top edge of the channel. Migration of cells was saved with 4-min intervals into a computer by a CCD camera. Migrating cells in the photos (upper) were marked with block dots in the bottom photos.

5. Conclusions

We have fabricated two types of the device for cellular chemotaxis observation with Si and PDMS. And a stable concentration gradient of chemoattractant across the microchannel has been confirmed to be established experimentally and theoretically. Chemotaxis of Jurkat cells toward the appropriate chemoattractants have been demonstrated using both types of the device.

References

[1] S. Kanegasaki, *Journal of Immunological Methods* **282**, 1-11 (2003)
[2] K. Francis, *Proc. Natl. Acd. Sci. U. S. A.*, 12258-12262 (1994)
[3] A.L. Lehninger, Biochemistry, 2nd ed. Worth publishers, New York, p. 176 (1975)

A RAPID MICRO POLYMERASE CHAIN REACTION SYSTEM (GenSpector® Micro PCR) FOR *HEPATITIS* B VIRUS DNA DETECTION

Kwang W. Oh, Yoon-Kyoung Cho, Jintae Kim, Suhyeon Kim, Kyeong-Sik Ock, Kak Namkoong, Kyutae Yoo, Chinsung Park, Youngsun Lee, Young-A Kim, Jungim Han, Heekyun Lim, Jaejeong Kim, Daesung Yoon, Geubae Lim, Sanghyo (Sam) Kim, Jung-Joo Hwang, and Y. Eugene Pak

Digital Bio Lab, Samsung Advanced Institute of Technology, PO Box 111, Suwon 440-600, Korea

Abstract

This paper presents a rapid micro PCR (polymerase chain reaction) system (GenSpector® Micro PCR) for the application of *Hepatitis* B virus (HBV) DNA detection. Silicon micromachining technology has been utilized to miniaturize the conventional PCR system. Each module in the system has been installed with an optic system that makes real time in-situ monitoring possible, as well as a built in computer system complete with user-friendly touch screen access. In addition, newly developed electronic temperature controls have cut down response time, making the system faster than ever before. Also, the system enables one or more operators to apply for qualitative or quantitative PCR. Thus, the GenSpector® Micro PCR system will have various applications in nucleic acid point-of-care-tests.

Keywords: PCR, Micro PCR, HBV DNA, Thermal Cycler, Clinical Diagnostics

1. Introduction

This paper presents a rapid micro PCR (polymerase chain reaction) system (GenSpector® Micro PCR) for the application of *Hepatitis* B virus (HBV) DNA detection [1]. Silicon micromachining technology has been utilized to miniaturize the conventional PCR system for the application of point-of-care-test (POCT). The system has shown excellent clinical diagnostic results for HBV DNA: 93.8% in sensitivity, 96.4% in specificity, 95.1% in accuracy, and 91.7% in reproducibility.

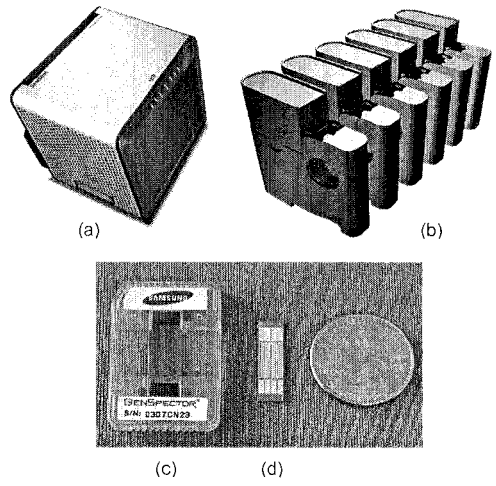

Figure 1. A GenSpector® Micro PCR system (a), 6 thermal cycling modules (b), a Micro PCR chip with plastic housing (c), and a silicon-based heater/sensor plate (d).

2. System Design

A micro PCR system, shown in Fig. 1, consists of six individual thermal cycling modules and a computing unit. A plastic packaged silicon micromachined PCR chip is inserted in each module. The PCR chip is comprised of a micro chamber on a silicon substrate side, and an optical window, an inlet and an outlet on a glass substrate side. The module has a silicon-based heater/sensor plate, a cooling fan, an optic unit for light excitations and emissions, an embedded microprocessor and a computing circuit board. Each module is capable of independent thermal

cycling and in-situ monitoring of the micro PCR chips, as shown in Fig. 1. Independent PID (proportional integral derivative) control by an embedded microprocessor in each module can give an excellent temperature accuracy of less than 0.5° for PCR.

The computing unit in the PCR system is basically a PC including a 15.1" touch screen TFT-LCD, a 2.5" 30GB hard disk drive, 4 USB drive ports, an internet accessible LAN, and a Windows 2000 operating system. When thermal cycling is not in progress the system can be used as a regular computer, complete with LAN connection and network sharing.

Fig. 2 shows a micro PCR software, which enables to define and simultaneously conduct separate PCR experiments, with a set of thermal cycling protocols. Additionally, thermal and optical data can be in-situ monitored, and graphs of temperature, amplification, and melt curves are displayed during the data collection.

3. Results and Discussion

HBV (10^6 copies/reaction) can be detected in less than 8 minutes due to the high thermal conductivity of silicon based PCR chips and the small reaction volume of samples. The heating rate of 20°/sec and the cooling rate of 10°/sec have been attained. The volume of 1 uL has been used. Such small volume for the reaction reduces the cost of reagents significantly. The CV (coefficient of variance) of melting temperatures after PCR amplification is less than 0.5% using a home-made SYBR Green I dye-based HBV assay kit (Table 1).

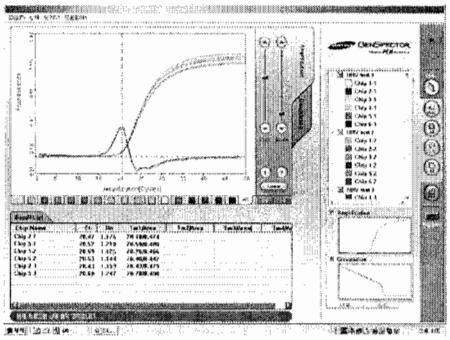

Figure 2. A GenSpector® Micro PCR software.

Table 1. The specifications of GenSpector® Micro PCR system.

Specifications	
Time to Detection (HBV Assay)	< 8 min
Reaction Volume	1 uL
Temperature Accuracy	< ± 0.5 .
Heating Rate	> 20 ./sec
Cooling Rate	> 10 ./sec
Melting Temperature (%CV)	< 0.5 %
Optical Detection	SYBR Green I

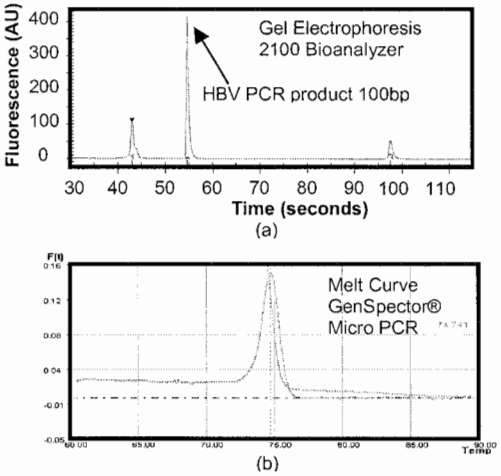

Figure 3. A gel electrophoresis result (a), showing good match to the graph of melt curve (b).

Fig. 3 shows a gel electrophoresis result, showing a good match to the graph of melt curve. The micro PCR system has shown excellent clinical diagnostic results for HBV DNA: 93.8% in sensitivity, 96.4% in specificity, 95.1% in accuracy and 91.7% in reproducibility as shown in Fig. 4 and Table 2.

4. Conclusion

In conclusion, a rapid micro PCR system has shown excellent clinical diagnostic results for HBV DNA detection. Also, the system enables one or more operators to apply for qualitative or quantitative PCR. Thus, the GenSpector® Micro PCR system will have various applications in nucleic acid point-of-care-tests.

References

[1] http://www.GenSpector.com
[2] Dae Sung Yoon, et al, J. Micromech. Microeng. 12 (2002) 813–823.

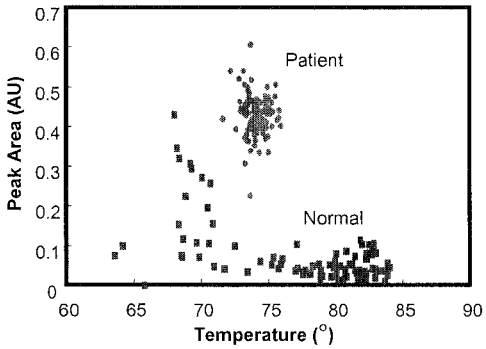

Figure 4. Clinical diagnostic results for HBV DNA detection were plotted as peak area vs. melt temp.

Table 2. Clinical diagnostic result for HBV DNA detection.

	Patient (112)	*Normal (112)*
Positive	TP: 105 (93.8%)	FP: 4
Negative	FN: 7	TN: 108

Where, Sensitivity = TP / (TP+FN),
Specificity = TN / (TN + FP),
Accuracy = (TP+TN)/(TP+FN+FP+TN)
TP: True Positive,
TN: True Negative,
FP: False Positive,
FN: False Negative

DEVELOPMENT OF THE IMMUNOASSAY WAVEGUIDE SENSOR CHIP FOR DIOXIN MEASUREMENT

Takashi Katayama[1], Yoshikazu Yoshida[1], Norio Tateishi[2], Kenji Kawaguchi[2], Takehiko Kitamori[3]

[1]The Research Association of Micro Chemical Process Technology, Kanagawa 213-0012, Japan
[2]Kyoto Electronics Manufacturing, Kyoto 601-8317, Japan
[3]Dep. of Applied Chemistry, The University of Tokyo, Tokyo 113-8656, Japan

Abstract

We developed a label-free immunoassay chip for detection of ultra trace dioxin. The chip is constructed by a waveguide sensor device (WGS) based on a Mach-Zehnder interferometer and micro flow cell for sample handling. The WGS integrated onto an optical glass substrate provides marked advantage for the micro total analysis system, because the WGS can detect antigen - antibody reaction without any complex equipment outside the chip and any insertion of detectors in the micro channel [1, 2, 3] . The WGS immunoassay chip can provides applications in wide range in the field of environmental analysis.

Keywords: Waveguide sensor, Immunoassay, Dioxin, Micro flow cell

1. Introduction

Environmental hazardous compounds, especially dioxin attracts attention from a general public in Japan. The amount of discharge from institutions, such as an incinerator, may become the front page of newspaper or news of TV program. Although the GC/MS method is commonly used for detection of dioxin, continuous surveillance is not realized because of its difficulty of the analysis operation etc. We propose high throughput screening method for this requirement using three key technologies, anti-dioxin antibody, waveguide sensor device, and micro fluidics (microchip technology).

2. Experimental

Single mode channel waveguide was formed on a BK7 substrate using the ion exchange process. An exposed part with a length of 8mm is prepared as a sensing region. For supplying sample solution to the sensing region, the flow cell with channel width of 300um and channel depth of 50um on a Pyrex substrate was fabricated by wet etching. The WGS and the flow cell were piled up (See Fig.1), and held in the copper block for controlling the temperature in the accuracy of ±0.01°C degrees. The laser diode with wavelength of 635nm was used for the light source, and the output light was detected by a photo diode with a lock-in amplifier. Fig.2 shows an overview of the whole measurement system. Evaluated WGS sensitivity against the change of refractive index was approximately $100 \times 2\pi$ rad / n.

In order to use the WGS as an immunosensor, the dioxin derivative was immobilized on the sensing region by silane-coupling process using APTES (3 – Aminopropyltriethoxysilane). By introducing anti-dioxin antibody into the sensing region, antibody will combine with the immobilized antigen. Because antigen - antibody compound cannot combine with the immobilized antigen, concentration of dioxin contained in sample solution can be obtained by comparing these signals. (See Fig.3)

3. Results and discussion

On condition that flow rate 10μL/min, supplying time 10min, and sample amount-of-supply 100μL, good linearity was confirmed between a sensor output and antibody concentration in the range of 0.1-1.0 μg/mL. When concentration was raised rather than this or supplying time was extended, the sensor output was saturated. This is considered that combination of the antibody to

sensor surface area is saturated. Because the amount of the signal of this sensor is limited by the sensor output for the antibody solution and the linearity of the sensor output was maintained, the condition that antibody concentration 1.0μg/mL was selected for the dioxin measurement. Adding a dioxin derivative as an antigen in the range of 0.3-100ng/mL into antibody solution, the change of the sensor output was confirmed in the concentration range of 1-10ng/mL. The detection limits in the present condition were about 2ng/mL. In this detecting method, the greatest factor that determines a detection limit for the antigen is considered to be the concentration of antibody. If antibody concentration is reduced, it will be supposed that the curve of Fig.5 is shifted to a low concentration side. On the other hand, if antibody concentration is reduced, the sensor output declines and the S/N ratio drops. In order to obtain more high sensitive detection, it is necessary to improve sensor sensitivity or to extend antibody-supplying time.

4. Conclusions

The label-free immunoassay chip for detection of ultra trace dioxin was developed. Detection limit was about 2ng/mL. Although GC/MS method needs several hours for detection and spectrum analysis by trained analysts, our new chip method needs only dozens of minutes and even automatic analysis is also possible. Although an about 10 times as high sensitivity will be required for utilization from now on, the sensitivity is already realized by a macro model based on the same technique.

Acknowledgements

A part of the study presented in this paper is conducted through a project, "Development of highly-sensitive analytical technologies for environmental hazardous compounds with use of biospecific reaction" supported by New Energy and Industrial Technology Development Organization (NEDO), Japan.

References

[1] W. Lukosz, et al, *Sensors and Actuators B*, **6**, 122-126 (1992)
[2] Paul V. Lambeck, *Sensors and Actuators B*, **8**, 103-116 (1992)
[3] S. Wilkinson, K. Kawaguchi et al, *Sensors and Actuators B*, **10** Vol.87 250-257 (2002)

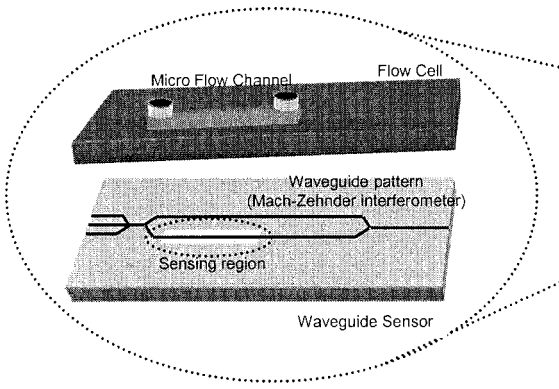

Fig.1 Dioxin Immunoassay Chip

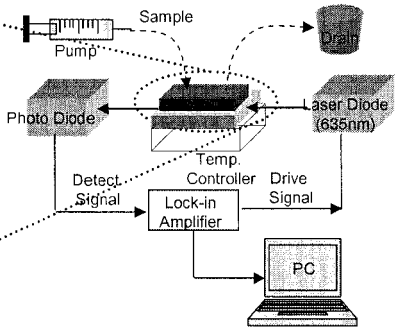

Fig.2 Schematic Diagram of Measurement System

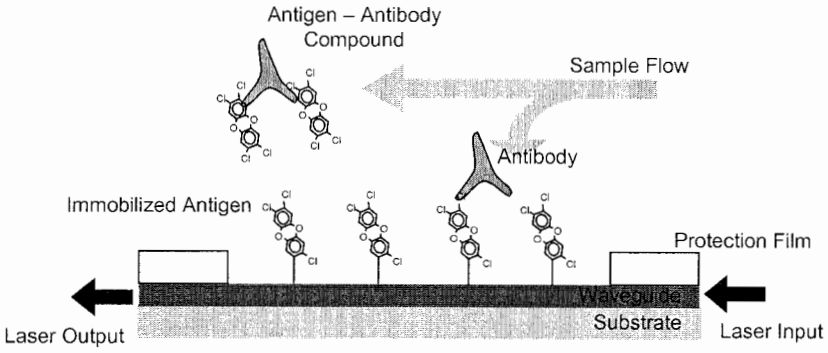

Fig.3 Principle of Dioxin detection

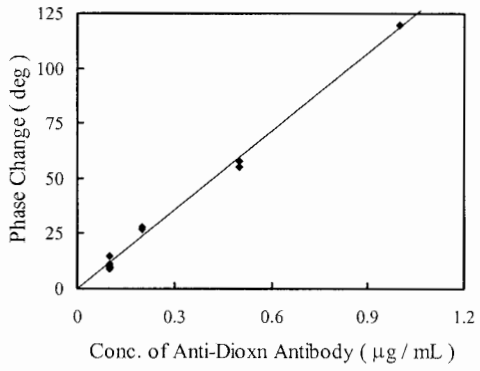

Fig.4 Relationship between sensor output and concentration of anti-Dioxin Antibody

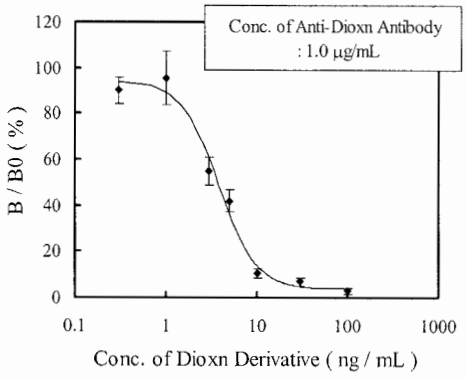

Fig.5 Evaluation result of dioxin derivative detection

DEVELOPMENT OF NOVEL MICRO MIXER AND ITS APPLICATION TO μ-IMMUNOMAGNETIC CELL SORTER

Wei-Heong Tan[1], Yuji Suzuki, Nobuhide Kasagi, Naoki Shikazono, Katsuko Furukawa, and Takashi Ushida[1,2]

[1]Dept. of Mechanical Engineering, the University of Tokyo, Hongo 7-3-1, Bunkyo-ku, Tokyo 113-8656, Japan

[2]Center for Disease Biology and Integrative Medicine, the University of Tokyo

Abstract

We report successful design, fabrication and testing of a novel lamination micro mixer to be integrated in the micro-scale immunomagnetic cell sorter (μ-IMCS), which should be a key device for future tissue engineering. This paper covers (1) the concept of μ-IMCS, (2) design and fabrication of micro mixer using lamination principle, and (3) demonstration of the mixer performance using real cells.

Keywords: Tissue engineering, Cell Sorter, Micromixer, Magnetic beads, Surface marker

1. Introduction

Tissue engineering, a field of science with a history barely spanning over 2 decades, has enabled us to produce man-made skin and cartilage. Possessing the ability to proliferate indefinitely while retaining the potential to differentiate into specialized cell types, stem cells are highly prized for both research purposes and possibly for future therapeutic applications. Unfortunately, however, they occur in minute amounts and currently there is no simple and inexpensive method to extract them from the body, e.g., bone marrow. There is clearly a need for a cell sorting device that offers high degree of purification, efficiency as well as safety. In this paper, we report the successful design, fabrication and testing of a novel lamination micro mixer to be used in the micro-scale immunomagnetic cell sorter (μ-IMCS), which should be indispensable in tissue engineering.

2. Concept and Design

Fig. 1 shows the proposed concept of a μ-IMCS. Cell sample and magnetic beads are separately introduced into the device. Magnetic beads have antibody coating, which binds to a specific surface marker of the target cell. The two streams are completely mixed in the mixer, and magnetic beads attach onto target cells. Subsequently, cell-beads complexes formed are separated into the buffer fluid using an external magnetic field. Advantage of using μ-IMCS for cell sorting is two folds. Firstly, binding of magnetic beads to target cells can be achieved in seconds, which are orders of magnitudes shorter than conventional Magnetic Cell Sorters (MCS) requiring long incubation time. Secondly, unlike fluorescence-activated cell sorter (FACS)[1], we do not need bulky and expensive optical systems. This also translates to the ease of parallelization of μ-IMCS to handle larger sample volumes typically required for tissue engineering.

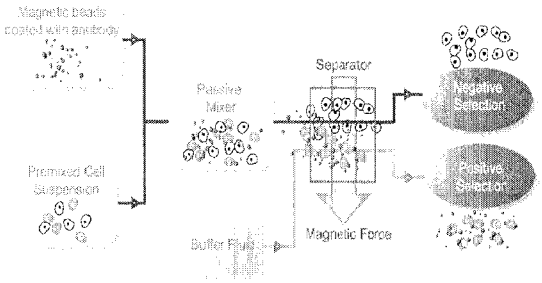

Figure 1. Concept of μ-IMCS.

Fig. 2 shows the 3D geometry of a mixer unit to achieve lamination with 180 degree rotation. Unlike conventional lamination-type mixer, streams of cells and beads are inverted after each mixer unit in order to minimize sedimentation loss of cells and beads in the mixer. Corners and stagnation regions of the mixer are rounded in such a way that stagnant flow regions are reduced. It is confirmed through a CFD analysis using Fluent 6 that lamination and complete mixing are achieved (Fig. 3). It is theoretically concluded that by combining nine mixer units in series, streams of cells and beads are repeatedly interlaced with 2^9=512 layers.

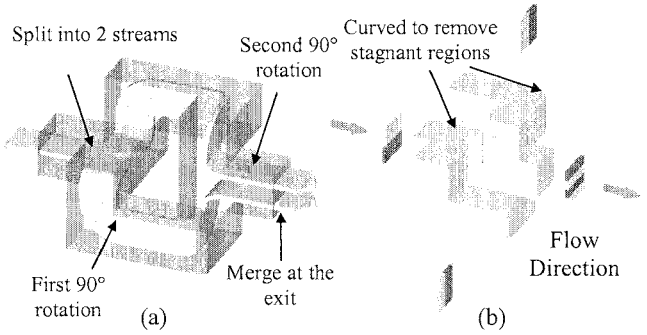

Figure 2 (a) Lamination with 180° rotation, (b) Geometry of a mixer unit.

3. Fabrication and Experimental

Soft lithography using PDMS[2] is chosen for micro fabrication of the present mixer as it offers advantages such as rapid prototyping, ease of fabrication and most importantly biocompatibility. In order to establish the mixer structure (Fig. 4), SU-8 molds are made on silicon wafer using standard lithography techniques, and three separate PDMS layers are cast from the master molds. The surfaces are treated with oxygen plasma, and permanent bonding is made after alignment of the layers, with an accuracy of ± 20 μm under microscope. The channels have a cross section of 200×200 μm^2.

Before the experiment, the mixer is first filled with phosphate buffered saline to reduce adhesion of cells to channel walls. Syringe pumps are then used to introduce the cells and Streptavidin coated magnetic beads of 1 μm in diameter into the micromixer. The flow rate is chosen as 11.8 μl/min, which corresponds to a Reynolds number of unity.

4. Results and discussion

Fig. 5 shows CD31 expression of Human Umbilical Vein Endothelial Cells (HUVEC) and Human Mesenchymal Stem Cells (hMSC) evaluated using a commercial MCS system. It is found that CD31 is a good indicator to distinguish between HUVEC and hMSC. Fig. 6 shows cell samples including hMSC, and also HUVEC conjugated with biotin labeled anti CD31 antibody. In the present experiment, the ratio of the number of HUVEC: hMSC is chosen as 1:1.24. The corresponding volume concentration of cells and beads is 0.04% and 0.15%, respectively. Magnetic particle concentrator is used to isolate cells attached with magnetic beads from the cell sample at the outlet. Figure 7 shows HUVEC isolated with magnetic beads (Positive selection). As summarized in Table 1, the percentage of HUVEC and hMSC in the positive and negative selection is respectively 93.1% and 90.2%, which is in close accordance with the data shown in Fig. 5. An enrichment of 16.7 folds is achieved for the positive selection. The recovery yield, defined as the total number of cells obtained at the outlet divided by the number of cells introduced, is 57.3%, but much higher recovery yield should be achieved with further improvements of the mixer design.

5. Conclusions

A novel micromixer is designed and its performance is first evaluated with CFD analysis. A prototype of the μ-IMCS is fabricated using PDMS and an enrichment of 16.7 folds is achieved in a preliminary experiment using HUVEC and hMSC.

Acknowledgements

This work is supported by Grant-in-aid for Scientific Research (S) (No. 15106004) from JSPS.

References

[1] A.Y. Fu *et al.*, Nature Biotech.,17, 1999, pp.1109-1111.
[2] B.H. Jo et al., J.MEMS, 9, 2000, pp. 76-81.

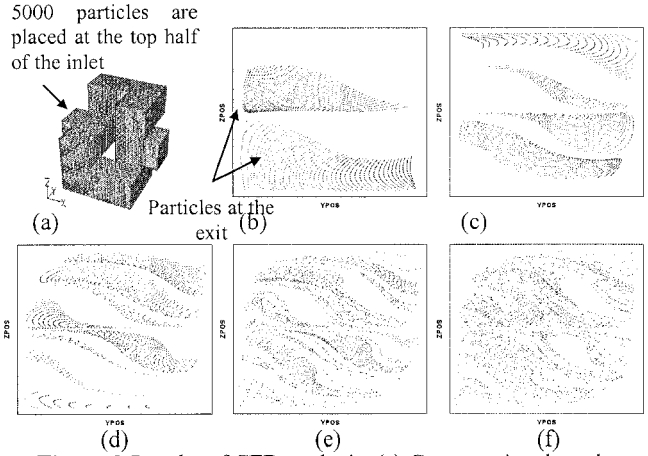

Figure 3 Results of CFD analysis, (a) Computational mesh, Particle distribution at the exit of (b) 1st , (c) 2nd , (d) 3rd , (e) 6th , and (f) 9th unit.

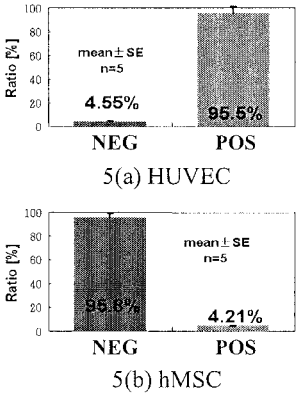

Figure 5 CD31(PECAM1)expression.

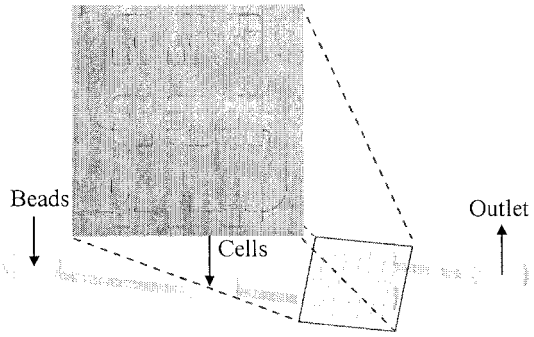

Figure 4 Mixer Test Section.

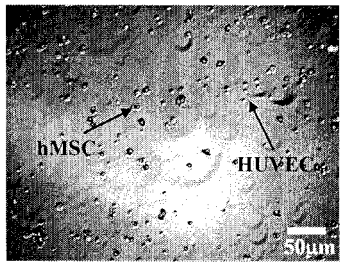

Figure 6 Mixture of HUVEC & hMSC cells in the ratio of 1:1.24.

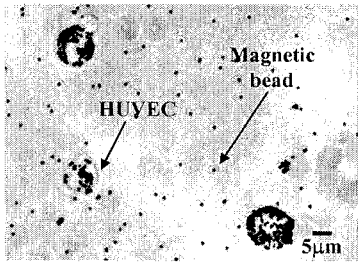

Figure 7 HUVEC cells attached with magnetic beads in the positive selection.

Table 1 Ratio of the cells at the outlet.

	HUVEC	hMSC	Enrichment
Positive Selection	93.1%	6.9%	16.7
Negative Selection	9.8%	90.2%	7.41

SINGLE-STEP CONCENTRATION AND SEQUENCE-SPECIFIC SEPARATION OF DNA BY AFFINITY MICROCHIP ELECTROPHORESIS

Toshiyuki Ito, Akira Inoue, Kae Sato, Kazuo Hosokawa, and Mizuo Maeda
Bioengineering Laboratory, RIKEN (The Institute of Physical and Chemical Research), 2-1 Hirosawa, Wako, Saitama 351-0198, Japan

Abstract

We demonstrate an easy and rapid analysis method for concentration and sequence-specific separation of single-stranded DNA samples within a microfluidic channel in a single operation. By combining the power-free poly(dimethylsiloxane) (PDMS) microfluidic pumping method and the affinity microchip electrophoresis, we achieved DNA concentration enrichment by a factor over 150 and sequence-specific separation without voltage switching. The total analysis time for these processes was less than 15 s. This method offers very easy fabrication process of a microfluidic device and simple operation for detection of single-base substituted mutant for diluted DNA sample solutions.

Keywords: affinity electrophoresis, concentration enrichment, DNA conjugate, PDMS, single-base mutation

1. Introduction

Recently, microfluidic devices have been rapidly evolved and widely applied to analytical chemistry, especially electrophoretic separation of DNA [1]. Rapid separation of DNA fragments has been reported in glass and polymer microfluidic devices. In order to improve detection sensitivity on a microfluidic platform, several methods for concentration of DNA samples have been demonstrated so far [2-6]. For example, Wainright *et al.* reported on-chip preconcentration and separation of double-stranded DNA fragments based on isotachophoresis [4]. Olsen *et al.* presented DNA trapping by ligand DNA-immobilized hydrogels in microfluidic channels [6]. However, these methods needed a complicated microfluidic design and multistep voltage switching [4,5], or stepwise photopolymerization to prepare the DNA-hydrogels in microchannels [6].

In this paper, we demonstrate an easy and rapid electrophoretic analysis method for detection of single-base substituted mutants. By combining the power-free PDMS microfluidic pumping method [7] and the affinity microchip electrophoresis [8], concentration enrichment of DNA samples and sequence-specific separation of them are possible in a single operation.

2. Experimental

Microchannel design of the test device is shown in Fig. 1. The device contains a T-shaped microchannel (100 μm wide, 25 μm deep) with three reservoirs (2 mm diameter, 2 mm deep) and two passive stop valves, which make resistance to passage of the liquid-air interfaces by their abrupt change of cross section (20 μm wide, 25 μm deep, 50 μm long) [9]. The device was fabricated by reversibly bonding a PDMS part, molded from a negative master, and a flat glass plate.

Two types of single-stranded 12-mer DNA labeled with FITC were mixed to make a sample solution: the normal type (N, FITC-5'-GGA GCT GGT GGC-3') has the same sequence as codon 10-13 of K-*ras* gene, while the mutant type (M, FITC-5'-GGA GCT AGT GGC-3') has a single-base substitution. The concentration of each component was 0.1 μM. For trapping and separation of the sample DNA, a DNA-poly(*N,N*-dimethylacrylamide) (PDMA) conjugate was prepared by copolymerization of *N,N*-dimethylacrylamide and methacryloyl-modified 10-mer ligand DNA (5'-CCA CCA GCT C-3') complementary to the middle of N (Fig. 2) [8]. The concentrations of the ligand DNA and PDMA were 100 μM and 10 wt%, respectively.

The experimental procedure is illustrated in Fig. 3. First, the device was placed in a vacuum chamber at 10 kPa for 5 min to evacuate the air dissolved in the PDMS (Fig. 3a). After the degassing, 3 μL aliquots of the DNA sample, DNA-PDMA conjugate, and non-conjugated PDMA were dispensed into the reservoirs (Fig. 3b). By the principle of power-free pumping [7], the solutions were spontaneously introduced into the microchannel, and were merged together at the passive stop valves (Fig. 3c). Because the polymers, DNA as well as PDMA, in the solutions diffuse slowly, the mixing at either interface is considered to insignificant on the time scale of the analysis. In this case, the plug length of the DNA sample was defined by the interval between the stop valves (10 mm). After platinum electrodes were dipped into all reservoirs, electrophoresis was carried out by a high voltage power supply (separation field = 250 V/cm) (Figs. 3d and 3e). The electrophoresis image of the DNA was recorded using an inverted fluorescence microscope equipped with a cooled CCD camera. All the experiments were carried out at room temperature.

3. Results and discussion

Figure 4 shows the video-clipped fluorescent images around the right stop valve. In Fig. 4a, corresponding to Fig. 3c, the sample at the left side of the stop valve did not have sufficient concentration to be detected with this experimental setup. By applying high voltage, DNA sample was concentrated at the DNA sample/DNA-PDMA conjugate interface in a few seconds (Figs. 4b and 4c). Without voltage switching, the two types of DNA were separated by the difference in affinity with the ligand DNA: N was virtually immobilized by strong affinity, while M slowly migrated through the conjugate because of slightly weaker affinity (Figs. 4d and 4e). The total analysis time was less than 15 s, and the effective separation length was only 500 μm.

Figure 5 shows the DNA concentration profiles determined by another set of fluorescent images. The grayscale values of the images were converted to sample concentrations by calibration with standard solutions. The peak concentrations of N and M were 15 μM and 8 μM, which mean the concentration enrichment factors of 150 and 80, respectively.

4. Conclusions

Combination of the power-free PDMS microfluidic pumping method and the affinity microchip electrophoresis affords a useful detection method for single-base substituted mutants of dilute DNA solutions. The remarkable advantage of this method is that concentration of DNA samples and sequence-specific separation of them are possible in a single operation without any special equipments or techniques. This method offers very easy fabrication of microfluidic devices, and simple operation for detection of gene point mutations and typing of single nucleotide polymorphisms.

References

[1] V. M. Ugaz, R. D. Elms, R. C. Lo, F. A. Shaikh, and M. A. Burns, *Phil. Trans. R. Soc. Lond. A*, **362**, 1105-1129 (2004).
[2] D. Ross and L. E. Locascio, *Anal. Chem.*, **74**, 2556-2564 (2002).
[3] J. H. Dai, T. Ito, L. Sun, and R. M. Crooks, *J. Am. Chem. Soc.*, **125**, 13026-13027 (2003).
[4] A. Wainright, U. T. Nguyen, T. Bjornson, and T. D. Boone, *Electrophoresis*, **24**, 3784-3792 (2003).
[5] B. M. Paegel, S. H. I. Yeung, and R. A. Mathies, *Anal. Chem.*, **74**, 5092-5098 (2002).
[6] K. G. Olsen, D. J. Ross, and M. J. Tarlov, *Anal. Chem.*, **74**, 1436-1441 (2002).
[7] K. Hosokawa, K. Sato, N. Ichikawa, and M. Maeda, *Lab. Chip*, **4**, 181-185 (2004).
[8] T. Ito, A. Inoue, K. Sato, K. Hosokawa, and M. Maeda, *Chem. Lett.*, **32**, 688-689 (2003).
[9] K. Hosokawa, T. Fujii, and I. Endo, *Anal. Chem.*, **71**, 4781-4785 (1999).

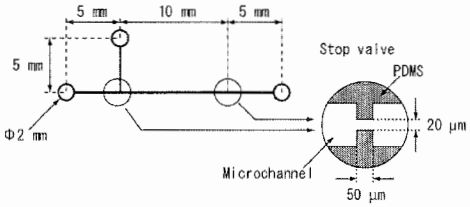

Figure 1. Microchannel design of the test device. The channel cross section is 100 μm wide × 25 μm deep.

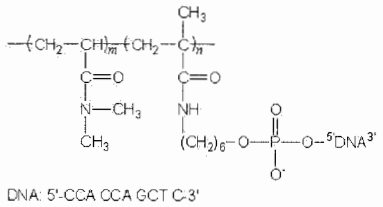

Figure 2. Chemical structure of the DNA-PDMA conjugate.

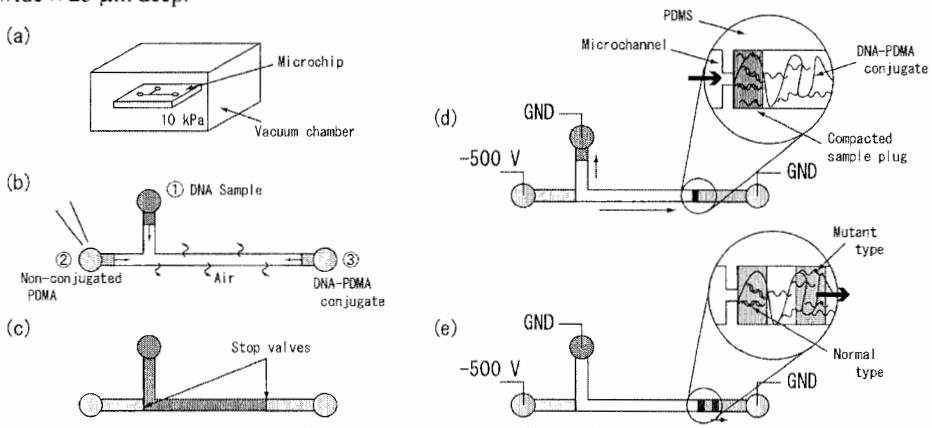

Figure 3. Schematic representation of the experimental procedure. (a) Degassing, (b) sample dispensing, (c) spontaneous filling, (d) concentration, and (e) separation.

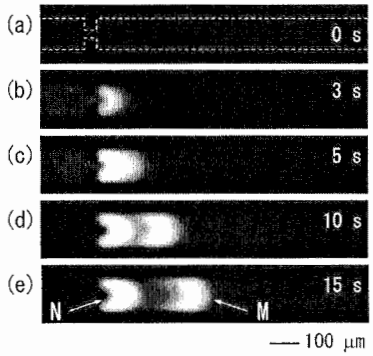

Figure 4. Video-clipped fluorescent images. Condition: electric fields, 250 V/cm; buffer, 25 mM Tris-borate (pH 7.4) with 10 mM $MgCl_2$; initial concentration, 0.1 μM; microscope objective, 4x; exposure time, 0.3 s.

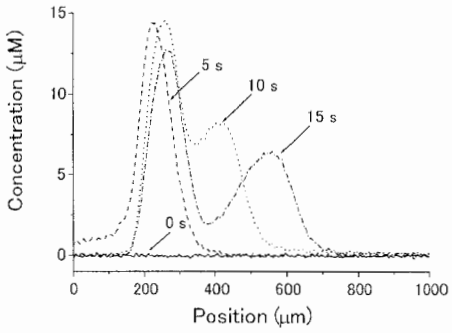

Figure 5. Concentration profiles calculated by the standard DNA samples. Conditions: microscope objective, 10x; exposure time, 0.03 s; other conditions were same as in Fig. 4.

PACKED CHANNEL HPLC ON MICROCHIPS

Kazuharu Okubo[1], Manabu Tokeshi[1], Yoshikazu Yoshida[1], Takehiko Kitamori[2]
[1]*Kanagawa Central Laboratory, The Research Association of Micro Chemical Process Technology (MCPT), Japan*
[2]*Department of Applied Chemistry, School of Engineering, The University of Tokyo, Japan*

Abstract

Integration of HPLC on microchips were tried in a few reports, but it was difficult to realize pressure driven HPLC systems on-chip. We have developed high-pressure proof microfluidic devises and succeeded in integrating packed channel HPLC systems on microchips. Two types of high-pressure proof micro connectors and two types of column termination frits were developed, and performance of packed-channel HPLC systems based on those microfluidic devises was evaluated using standard samples.

Keywords: HPLC Column, Packed Cannel, High pressure, Connector, Separation

1. Introduction

High performance liquid chromatography (HPLC) is one of the most frequently used separation techniques both in analysis and synthesis. However, only few reports have been done on on-chip HPLC systems in contrast to the fact that many on-chip capillary electrophoresis systems have been reported. One of the reasons why on-chip HPLC is difficult is that it requires high pressure in column packing. Therefore, columns for on-chip LC systems were usually made by using monolith materials [1]or by modification of channel walls [2]. Unfortunately, application area of such columns was rather limited. If conventional packed column HPLC could be realized on a microchip, it would be an extremely powerful tool for constructing wide variety of microchemical systems.

For this goal, development of high-pressure proof microfluidic devices is indispensable. In the present work, we newly developed high-pressure proof micro connectors and structures of holding separation materials (namely column termination frits) for on-chip HPLC systems. Performance of the on-chip HPLC systems in separation and detection of standard samples was evaluated.

2. Results and Discussion

Firstly, we developed a high-pressure proof connector between a capillary tube and a glass microchip. This connector could withstand up to 40 MPa of pressure, which was sufficiently high to pack conventional HPLC columns. Because the connectors were attached on the top surface of a glass microchip by means of a screw in a rigid chip holder, on-chip HPLC microchannel was like an inversed Greek letter "Π" in shape (Fig. 1). A column termination frit structure was fixed at the connector in the downstream side.

In order to evaluate the "Π"-shaped column, we performed separation of a standard mixture of pyrene and fluorene. The experimental conditions are as fellows: Mobile phase = 7:3 mixture of CH_3CN and H_2O; Flow rate = 1.0 μL/min; Detection wavelength = 260 nm; Injection volume = 60 nL; Temperature = room temperature. On-line detection was carried out using a conventional UV detector connected to the HPLC chip.

A chromatogram obtained with this system is shown in Fig. 2. The number of theoretical plates was about 1700(34000/m), and the value was equally good as those of conventional micro HPLC columns. However, the peaks in the chromatogram had tailings. It was inferred that the band broadening occurred at the corners of inlet and outlet ports (dead volume).

Secondly, we made a monolith frit structure in a microchannel [3]. The frit structure could be placed any segment of a microchannel.

In above-mentioned "Π"-shaped column system, whole the microchannel was filled up with separation material, and on-chip detection was hard to be realized. If a frit structure could be made halfway in a microchannel, on-chip detection just after the separation column became possible. Because sample plug before passing through the outlet port of the microchip could be measured in the on-chip detection, the band-broadening problem was expected to be somewhat alleviated.

"Π"-shaped column system with a column termination frit in the microchannel was evaluated for separation of tar dyes, R106 and R3. The experimental conditions are as fellows: Mobile Phase = 8:2 mixture of CH_3CN and H_2O; Flow rate = 3.0 μL/min; Detector = thermal lens microscope with excitation beam of 532 nm and probe beam of 670 nm; Injection volume = 60 nL; Temperature = room temperature.

A chromatogram obtained with this system is shown in Fig. 3. Lastly, we developed a novel side-on connector without dead volume (Fig. 4). Using the side-on connectors we could fabricate a new "I"-shaped packed microchannel with a straight flow path from inlet to outlet, as shown in Fig. 5.

Performance of the new "I"-shaped column system is now under investigation, but significant improvement in peak shape can be expected because corners that caused band broadening were eliminated in the new system. We hope to demonstrate results using the "I"-shaped column system at the symposium place.

3. Conclusions

We have developed two types of high-pressure proof connectors and column termination frit structures. By using these microfluidic elements, we have succeeded in constructing on-chip packed column HPLC systems.

We have also succeeded in developing a high-pressure proof on-chip injection valve and on-chip thermal lens detection systems, which we have reported elsewhere [4]. Integration of whole HPLC system on a microchip will soon become possible by combing these devices and packed column channel reported here. Handling of ultra small volume and ultra small quantity is one of futures with Microchips. HPLC on a Microchip is very important about the size.

Acknowledgements

This work was supported by the New Energy and Industrial Technology Development Organization (NEDO) of the Ministry of Economy, Trade and Industry, Japan.

Reference

1. Y.Kato, K. Nakamura, T. Kitamura, T. Tsuda, M. Hasegawa, H. Sasaki, "Effect of chromatographic conditions on resolution in high-performance ion-exchange chromatography of proteins on macroporous anion-exchange resign" Journal of Chromatography A Vol.1031,1ssues1-2, March (2004)
2. Wei Xu, Katsumi Uchiyama, Toshiyuki Hobo, "Studies on Polyester Chips with Modified Inner Surface for Open-Channel Electrochromatography", Chromatography, Vol. 23, No. 3 (2002).

3. M. T. Dulay, J. P. Quirino, B. D. Bennett, M. Kato, R. N. Zare, Anal. Chem., 73, 3921-3926 (2001).
4. K. Okubo, T. Kanomata, Y. Yoshida, T. Kitamori, HPCE(2004)P239,197

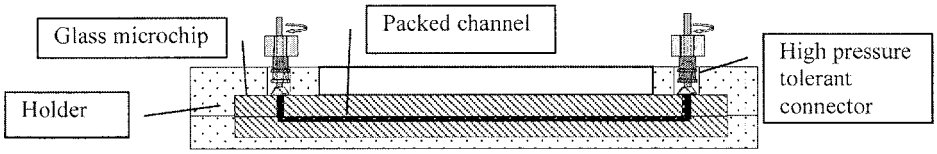

Figure 1 : "II" structure On-CHIP Column

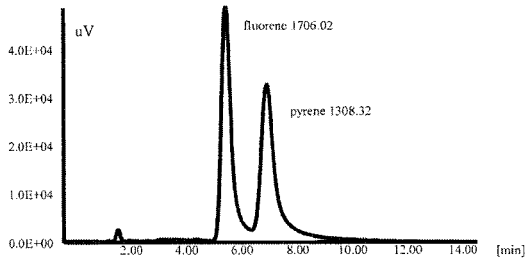

Figure 2 : Chromatogram of "II" Structure Column, Separation of Fluorene and Pyrene.

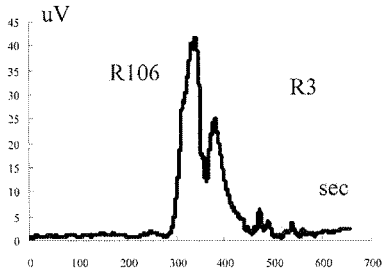

Figure 3 : Chromatogram of on-chip detection

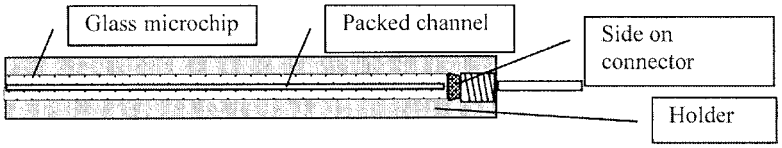

Figure 4 : "I" structure On-Chip Column with Side-on Connector

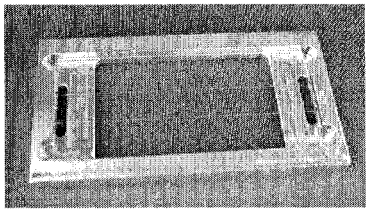

Figure 5 : Picture of Microchip and Holder for Side-on Connector

AN INTEGRATABLE CONCAVE AND CONVEX MICROLENS USING SECTIONAL EXPOSURE OF SU-8

Hui Yu, Biao Li, and Xin Zhang

Dept. of Manufacturing Engineering and Fraunhofer USA Center for Manufacturing Innovation, Boston University, 15 Saint Mary's Street, Boston, MA 02215, USA

Abstract

This paper presents a novel beam-scanning laser system for rapid prototyping of optical concave and convex microlens. The gradient height microstructures are created using UV sectional exposure. These microlenses are ready for the integration with various microoptical elements and 3D microstructures such as movable structures.

Keywords: sectional exposure, concave and convex microlens, gradient height microstructure

1. Introduction

The ability to integrate microoptical elements with movable structures and microactuators has opened up many new opportunities for optical and optoelectronic systems. It allows us to manipulate optical beams more effectively than conventional methods, and it is scalable to large optical systems. The applications include display, sensing, optical data storage, and telecommunications. MEMS technology has made it possible, for the first time, to integrate an entire free-space optical system onto a single chip [1]. Optical elements such as lenses, mirrors, and gratings are batch fabricated along with XYZ stages and microactuators. The main challenge for implementing such system is the ability to make different optical components using the same fabrication process [1]. With the goal of proof-of-concept, in this paper we have demonstrated a simple 3D laser manufacturing process to fabricate concave and convex microlens with optical functionality. Such gradient height microstructures were successfully realized in a single SU-8 layer by sectional exposure with gradually varied laser doses using a UV scanning laser system that we have reported before [2].

2. Fabrication Process

The manufacturing processes are illustrated in Figure 1. A glass substrate was cleaned with piranha solution. A 260 μm thick SU-8 resist was spin coated on the substrate followed by soft bake. The SU-8 resist was then exposed from the backside of the glass substrate. From the inside to outside of the microlens, ten sectional exposures were employed. For convex microlens fabrication, the exposure was taken from inside to outside with decreased laser dose; while for concave microlens manufacture, the exposure process was reversed. After post-exposure bake and developing, the unexposed SU-8 was washed away. Figure 2 shows the microscopy images of fabricated convex and concave microlens.

3. Characterization

The focus distance of the convex microlens was derived based on the dimensions measured from the manufactured sample. According to Wyko interferometry measurement results, the width (w) and height of the convex microlens are 700 μm and 260 μm, respectively. Assuming that the convex lens is a spherical lens, the radius of the convex lens is calculated as:

$$r = \sqrt{\left(700/2\right)^2 + \left(700/2 - 260\right)^2} = 361.4\ \mu\text{m} \tag{1}$$

In our case, the microlens is fabricated on a glass substrate at ~1 mm in thickness. Firstly we consider a simple situation, where only the convex microlens is involved, as shown in Figure 3a. For a single spherical refractive surface, it is assumed that the object distance is $-l$ and the subject

distance is l'; the refractive index on the left side is n_1, and the refractive index on the right side is n_2; the radius of the refractive surface is r. Therefore, the relationship between object distance $-l$ and the subject distance l' can be derived as:

$$\frac{n_2}{l'} - \frac{n_1}{l} = \frac{n_2 - n_1}{r} f \tag{2}$$

If the incident light is collimated and parallel with the optical axis and $-l$ is infinite, l' becomes the focal length f_2' of the single refractive surface inside the n_2 material. The refractive index of air and SU-8 are 1 and 1.6, respectively. Hence:

$$f_2' = l' = \frac{1.6}{1.6-1} \times 361.4 = 963.7\ \mu\text{m} \tag{3}$$

Next, we consider a complex optical system including both the convex lens and glass substrate. Assuming that the glass substrate is a parallel plane and is perpendicular to the optical axis, the light will have a focal-distance shift after the spherical microlens surface. As shown in Figure 3b, we obtain:

$$\sin\alpha = \frac{w/2}{\sqrt{\left(w/2\right)^2 + d_2^2}} \tag{4}$$

$$\sin\phi = \frac{w/2}{\sqrt{\left(w/2\right)^2 + d_1^2}} \tag{5}$$

According to Snell's law,

$$n_2 \sin\alpha = n_3 \sin\phi \tag{6}$$

The refractive index of glass is 1.46. From equation (3) – (6), we get:

$$1.6 \times \frac{700/2}{\sqrt{\left(700/2\right)^2 + (963.7 - 260)^2}} = 1.46 \times \frac{700/2}{\sqrt{\left(700/2\right)^2 + d_1^2}} \tag{7}$$

Hence the derived focus length of an SU-8 microlens fabricated on the glass substrate is $d_1 = 626\mu\text{m}$.

Figure 4 shows the transmitted light collected at different focus distances. Note that the focus of microlens is about 600 μm apart from the interface of SU-8 microlens and glass substrate according to the microscope imagining, matching well with the above calculated data.

4. Conclusions

As can be seen, the fabricated optical microlenses are robust, ready for integration with other microoptical elements and 3D microstructures such as the movable structures. Efforts are currently underway to further develop a simple 3D laser manufacturing process to fabricate a free-space microlens for optical and optoelectronics applications, in which the microlens, freestanding beam and its post will be subjected to laser writing at different focus/dose levels. Such microlens can be free to rotate out of the substrate plane and thus become perpendicular to the substrate.

References

[1] M. C. Wu, *Proc. IEEE*, **85**, 1833-1856 (1997).

[2] H. Yu, A. Grüntzig, Y. Zhao, A. Sharon, B. Li, and X. Zhang, *μTAS 2003*, 347-350.

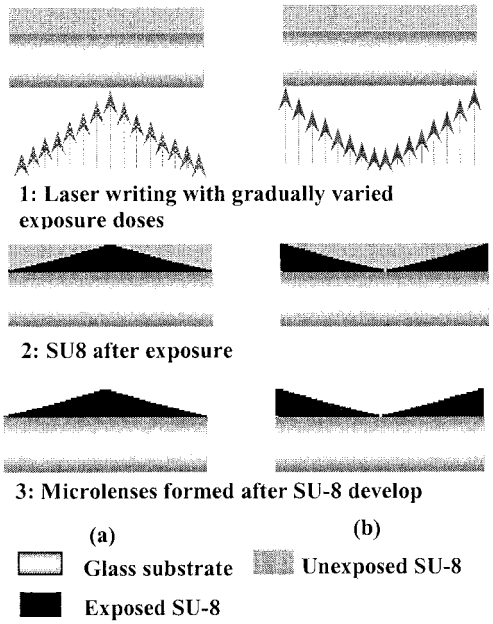

Figure 1. SU-8 is selectively exposed with gradually varied laser dose for (a) convex and (b) concave microlens fabrication.

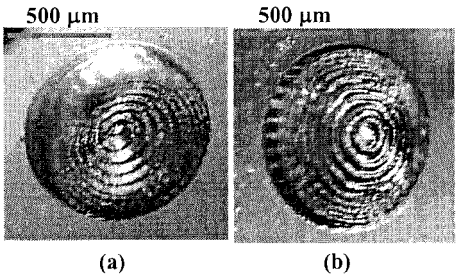

Figure 2. (a) Concave and (b) convex microlens fabricated by sectional exposure with gradually varied laser doses.

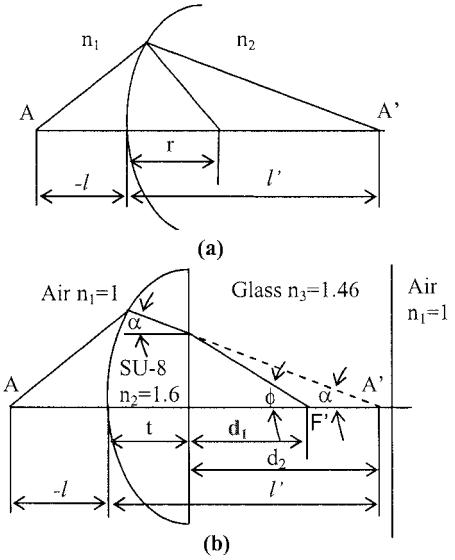

Figure 3. Schematics showing the focal distance of a single refractive surface in a simple optical system, where only the convex lens is involved (a), and in a complex optical system, where both the convex lens and glass substrate are involved (b).

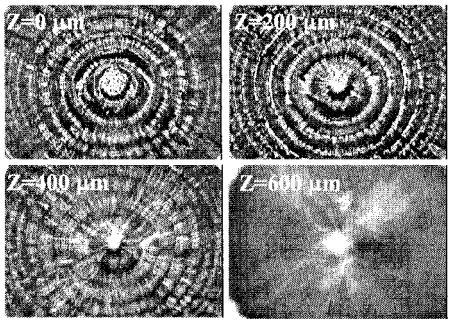

Figure 4. Transmitted light collected at different focus distances. The focus of a convex microlens is ~600 μm according to the microscope imagining.

DROPLET ACTUATION BASED ON SINGLE-PHASE ELECTROSTATIC EXCITATION

Masahide Gunji[1], Hiroaki Nakanishi[2] and Masao Washizu[1]
[1]Dept. of Mechanical Engineering, The Univ. of Tokyo, Hongo 7-3-1, Bunkyo-ku, Tokyo, Japan
[2]Shimadzu Corporation, Kyoto, Japan

Abstract
A new concept of electrostatic droplet actuation based on field-induced deformation of the droplet is presented in this paper. The device consists of a diagonal fishbone-shaped electrode array with a hydrophobic coating. When energized with an AC voltage, a droplet dispensed on the electrode undergoes a periodical motion of flattening and restoring the spherical shape, and because of the geometrical asymmetry of the electrodes, its center of mass is shifted bit by bit in each cycle. The actuation speed as high as 2.4 cm/s is achieved for a 1μl-droplet on a 240 μm-pitch electrode array with 50 Hz, 50 Vrms excitation. Droplet sorting and mixing are also demonstrated by bifurcating and merging electrode arrays. The method only requires a pair of planar electrodes that can be fabricated by a single-mask process, and a single-phase power supply, leading to a simple and low-cost droplet-based micro-chemical system.
Keywords: droplet, electrostatic actuation, field-induced oscillation, electrowetting

1. Introduction

Several methods of electrostatic droplet actuation have hitherto been developed for the droplet-based micro chemical systems, including multiphase electrostatic drive[1] and electrowetting-based actuation[2]. In these devices, electrodes are patterned on a substrate, and energized sequentially to drive the liquid droplet to the desired direction. Because the electrodes must be energized independently to each other, such systems require multi-layer electrode connection. In this paper, we demonstrate a far simpler method requiring single layer electrode connection and single-phase power supply.

2. Principle of the droplet actuation

Fig.1 and fig.2 show the electrode geometry and the mechanism of the droplet actuation respectively. A pair of coplanar diagonal fishbone-like electrodes having an insulator layer (e.g. 1 μm SiO_2) with a hydrophobic coating (e.g. 0.1 μm amorphous Teflon) is fabricated on a glass substrate. The sample, typically aqueous solution of several μ-liters in volume, takes on a nearly spherical shape when it is dispensed on the hydrophobic surface (Fig.2-a).

Applying of DC voltage should not induce steady motion of the droplet, because the electrostatic potential energy is constant regardless of the position of the droplet. However, the situation is different when energized with AC voltage to induce periodical deformation of the droplet. By applying AC voltage to the electrodes whose frequency is chosen close to a resonance of the droplet oscillation, it undergoes periodical deformation of flattening and restoring the spherical shape. The flattening occurs at the positive and the negative peak of the applied voltage, so the frequency of the oscillation is twice that of the applied AC voltage.

The trick here is that, because the electric field is very intense near the edge of the electrodes, the meniscus of the droplet is apt to be dielectrophoretically pinned at the edge. Therefore, in the half cycle when the droplet flattens, the electrowetting proceeds to spread the liquid, not across the electrode gap, but along the electrodes as shown by arrows in Fig.2-b. Because of this, the center of mass (m.c.) of the droplet is slightly shifted (leftward in the figure). In the next half cycle (Fig.2-c), the droplet restores spherical shape whose center is approximately at m.c. in the previous spreading stage. As a result, position of the droplet is slightly shifted in each cycle of the oscillation, and the

droplet is transported. The guiding along the center of the electrode system automatically occurs because the field is most intense at the gap. Fig.3 is the time snap of the process taken from the side with a high-speed camera, proving the mechanism of the actuation.

The driving mechanism in principle does not depend on the electrical conductivity of the droplet. The speed of the droplet motion is given by (m.c. shift in one cycle) x (oscillation frequency), and typical observed value is as high as 2.4 cm/s at 50 Hz, 50 Vrms excitation of 240 μm-pitch electrode. The resonance is rather blunt, and the transport is observed in the frequency range of 50 to 80 Hz.

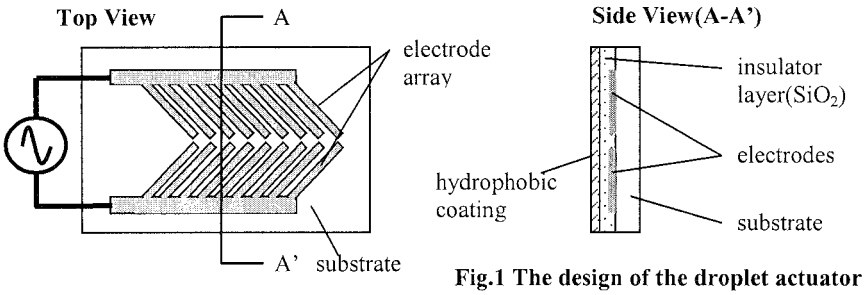

Fig.1 The design of the droplet actuator

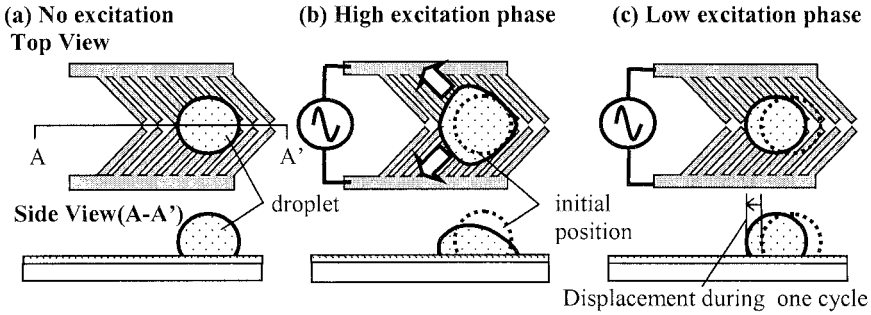

Fig.2 The mechanism of droplet movement

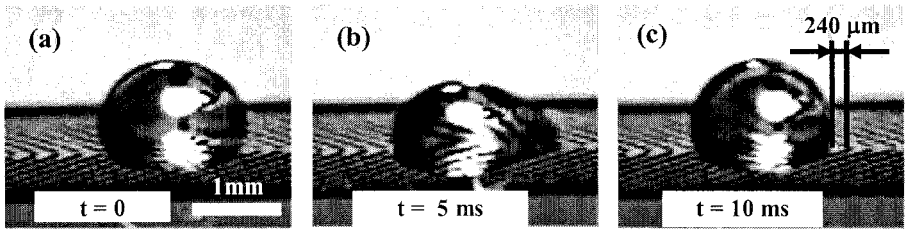

Fig.3 Time sequence of droplet movement recorded with a high-speed camera f = 50 Hz excitation, the period of droplet oscillation = 10 ms.

3. Droplet sorter and mixer

With the use of a branched fishbone electrode, sorting, i.e. deflecting the incoming droplet to either of bifurcating pathway, or mixing of two droplets by coalescence, can be realized. Fig.4 is the sorter, consisting of an inlet path (right) and two outlet paths (upper left and lower left). In the photo is shown the case where the droplet is deflected to lower outlet by energizing simultaneously the inlet and the lower outlet paths. Fig.5 is the mixer, consisting of two inlets (right and lower paths) merging into an outlet (upper left). Fig.5-a shows two droplets coming along the inlet paths. The speed of the droplet motion is determined by how much m.c. shift occurs in a cycle, and depends on the size of the droplet, surface properties of the substrate, etc.. It is an asynchronous system, and the timing of the coalescence cannot be precisely controlled, still, the coalescence does place at the end of the outlet path (fig.5-c).

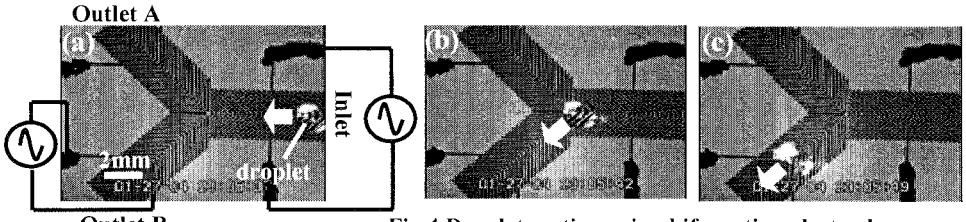

Fig.4 Droplet sorting using bifurcating electrode array

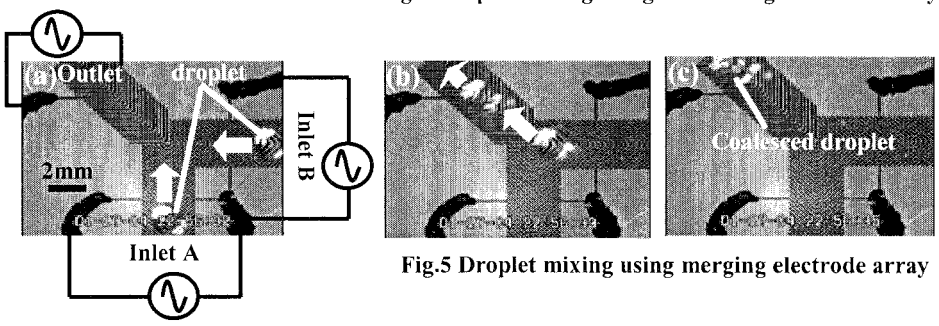

Fig.5 Droplet mixing using merging electrode array

4. Conclusions

Electrostatic droplet actuation based on field induced surface oscillation is demonstrated, together with its application for droplet sorting and mixing. The actuation speed as high as 2.4 cm/s is achieved for a 1 μl-droplet on a 240 μm-pitch electrode array with 50 Hz, 50 Vrms excitation. The system is far simpler than multiphase drive or electrowetting-based actuation in that it only requires a single layer electrode connection and a single-phase power supply.

Acknowledgements

This work is in part supported by grants from Japan Society for Promotion of Science (JSPS). Photo-masks are fabricated using EB lithography apparatus of VLSI Design and Education Center (VDEC), The University of Tokyo.

References

[1] M.Washizu, IEEE Transactions on Industry Applications, Vol. 34(4), 1998, pp.732-737.

[2] J.Lee, H.Moon, J.Fowler, T.Schoellhammer, C.-J.Kim, Sensors and Actuators A, 2002, vol. 95, pp. 259-268.

ONE TOUCH FLUIDIC TUBE CONNECTOR FOR MICRO FLUIDIC DEVICES

Keisuke Morishima[1,2], Yoshikazu Yoshida[1] and Takehiko Kitamori[1,3]

[1]*Kanagawa Academy of Science and Technology, KSP East 307, 3-2-1 Sakado, Takatsu-ku, Kawasaki 213-0012, Japan*

[2]*The Research Association of Micro Chemical Process Technology, KSP R&D 11F, 3-2-1 Sakado, Takatsu-ku, Kawasaki 213-0012, Japan*

[3]*Dept. of Applied Chemistry, The University of Tokyo, 7-3-1 Hongo, Bunkyo, Tokyo, Japan*

Abstract

Novel one touch fluidic tube connectors for microchips and microfluidic devices were developed. The characteristics of these microconnectors are as follows: i) one touch connection; ii) high pressure application (~5MPa); iii) low dead volume; iv) O-ring less; v) high mechanical strength and chemical resistance. These novel microconnector were all-in-one structures (micro stainless tube, teflon tube, and leak free flange structure), so easy hand connection was achieved without any careful assembly.

Keywords: chip interface, connector, no dead volume, one touch connection, leak-tight

1. Introduction

This paper focuses on interfacing between the macroworld and the microworld, a main challenge for microfluidic devices. There is often a need for tube connectors on a microfluidic device for interfacing between the device and the outside world [1]. The main demand on such connectors is that they are leak tight for high pressure application. Other demands on the couplers depend on the application, but typically include mechanical strength, easy and cheap assembly and low dead volume. Most of the fluidic connectors typically does not contribute to the functionality provided by the miniaturization. They have a dead volume that counteracts the benefits from the on-chip size reduction. And then, the fluidic interface is typically not batch fabricated and expensive. Therefore, it is important to minimize the system interfacing. Since efficient standard connectors are not commercially available, a new and simple one touch connection method for conveniently fixing external tubes to the chip without any glues was developed, as shown in Fig. 1.

2. Design and evaluation

Three different kinds of one touch connection methods with the fluidic tube micro connectors, which are called BNC-type, PIN socket-type, and Flat cable-type, are proposed in this paper. All the connectors were tested up to 5MPa without any leakage. A novel tube connection interface, such as a way of one touch connection without any O-ring, and no dead volume structure, is described below.

Mechanical strength and ease of assembly are the main requirements in their specific application as the test structure connectors. Fig. 2 shows the microscopic view of the micro Teflon nozzle with a flat flange structure. Teflon tubing was inserted into the micro stainless tube with heating method. The advantage of this structure is O-ring less, good chemical resistant, good mechanical strength and leak tightness for high pressure application. Fig. 3 shows the one touch connection method using BNC type, PIN type, and Cable type fluidic couplers. Easy assembly and low cost manufactured design was achieved. No glue were needed between the tubes and the connectors. No leakage was observed up to 5MPa. Using PIN socket type fluidic couplers, no screws were needed in a microchip holder. The shape of taper in the socket was optimized for high pressure application. Using flat cable type fluidic couplers, the size and dead volume were reduced.

High density of the tube connection is easily realized. All the connectors have been successfully used for interfacing to the microfluidic devices.

3. Conclusion

One touch fluidic tube connectors for microfluidic devices were developed. This novel microconnector has an all-in-one structure (micro stainless tube, teflon tube, and leak free flange structure), so easy hand connection was achieved without any careful assembly.We believe these connectors are very promising devices for a large variety of micro TAS applications.

Acknowledgements

This work was supported by the Grant from the New Energy and Industrial Technology Development Organization, Japan.

References

[1] Z. Yang, R. Maeda, *Journal of Chromatography A*, **1013**, 29–33, (2003).

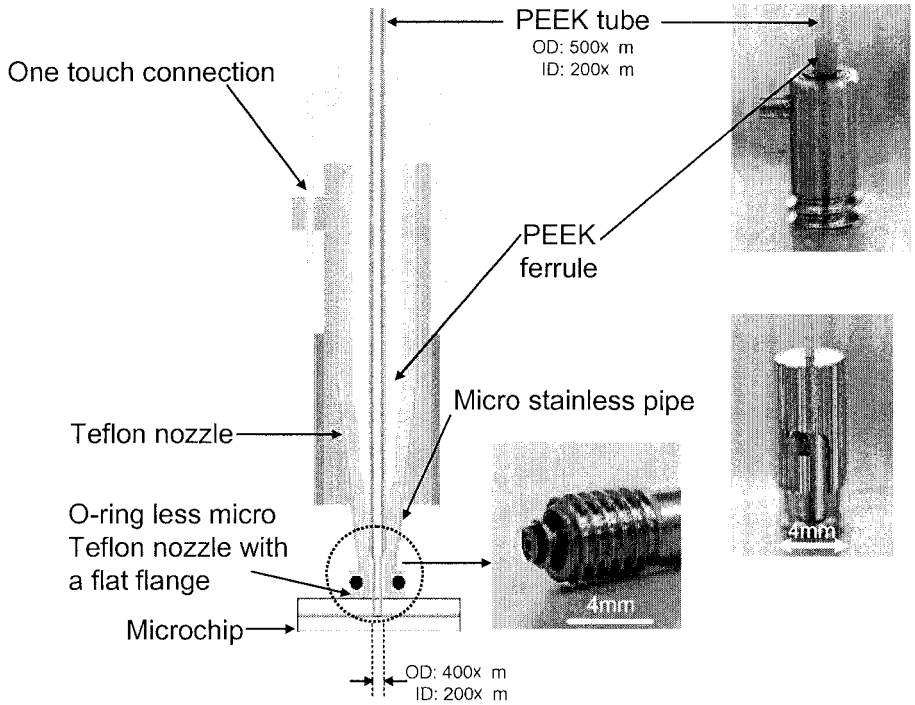

Figure 1. Cross sectional view of one touch fluidic tube connector

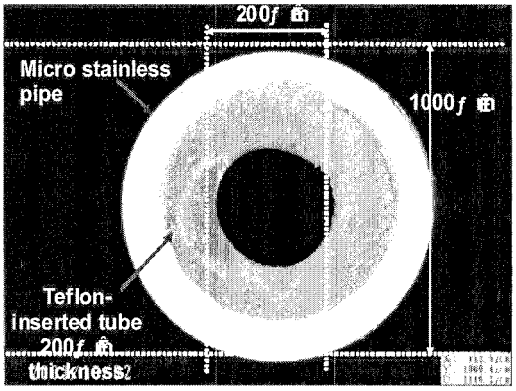

Figure 2. Microscopic view of Micro Teflon nozzle with a flat flange strucure

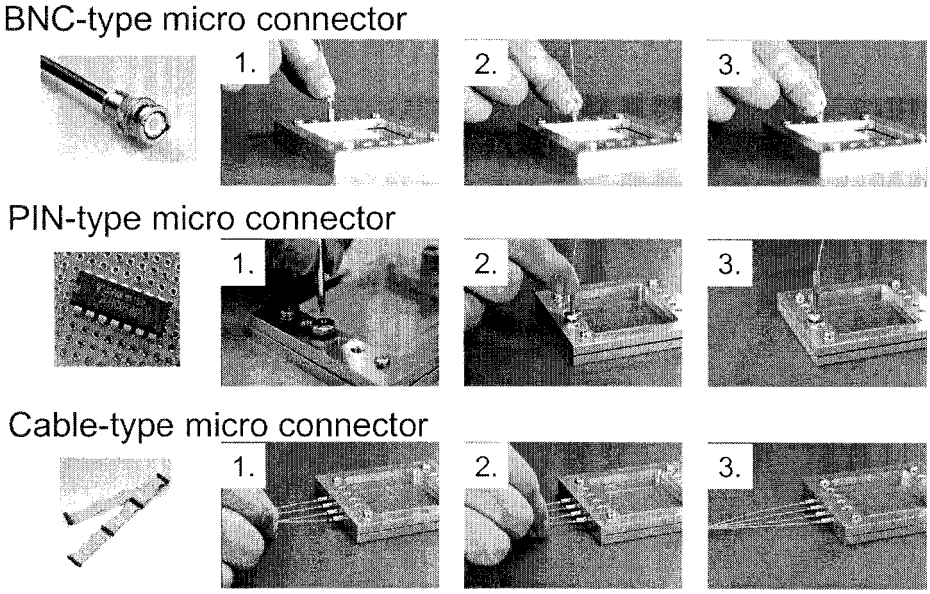

Figure 3. One touch connection method using BNC-type, PIN-type, and Cable type fluidic micro connectors

MODELING, ANALYSIS AND DESIGN OF CENTRIFUGAL FORCE DRIVEN TRANSIENT FILLING FLOW INTO CIRCULAR MICROCHANNEL

Dong Sung Kim and Tai Hun Kwon

Dept. of Mechanical Engineering, Pohang University of Science and Technology (POSTECH), San 31 Hyoja-dong Nam-gu, Pohang, Kyungpuk 790-784, Korea

Abstract

In this paper, we first present successful modeling and analysis results of centrifugal force driven transient filling flow into a circular microchannel. Two types of exact and pseudo-static approximate solutions were derived for the transient filling flow. We also first provide a simple analytical microchannel design tool based on the modeling and analysis in this study.

Keywords: Transient flow, Centrifugal force, Circular microchannel, Analysis, Design

1. Introduction

Recently, centrifugal pumping is regarded as an excellent alternative control method of fluid flow inside microchannels [1-3]. We have first carried out physical modeling and analysis for a centrifugal force driven transient filling flow into a circular microchannel. And furthermore, we have proposed a design tool of microchannel for given fluidic, geometrical and processing conditions. Figure 1 shows a schematic diagram of a circular cross-sectional microchannel on a CD type microfluidic system. A sample fluid of density, ρ, and viscosity, μ, is injected into a reservoir which is L_0 away from the center of the CD. Suppose the sample is to be delivered to the *desired position*, L_d, on the *desired time*, t_d, through the microchannel, of which hydraulic radius is R_h, via centrifugal force. If the CD plate rotates with a constant rotational velocity, ω, the fluid flow is generated in the radial direction of the CD. At an instant time t, the filling flow front reaches $l(t)$.

2. Modeling and analysis

The dimensionless governing equation for the transient filling flow into the circular microchannel by centrifugal force is (the superscript asterisk means dimensionless parameter):

$$-\frac{\partial^2 u_z^*}{\partial r^{*2}}-\frac{1}{r^*}\frac{\partial u_z^*}{\partial r^*}+ReA_R\frac{\partial u_z^*}{\partial t^*}=\frac{1}{2}ReA_R\bar{V}^2\omega^{*2}\left(l^*(t^*)+L_0^*\right) \tag{1}$$

where u_z and r are downchannel (the same as the radial direction of the CD) velocity and radial coordinate of the circular microchannel, respectively. Re, A_R and $\bar{V}$ denote the Reynolds number, aspect ratio of hydraulic radius to characteristic downchannel length and ratio of characteristic rotational velocity to characteristic downchannel velocity, respectively.

Two types of solutions for pseudo-static approximate (neglecting the inertia term, i.e., $ReA_R << 1$) and exact cases were derived. The obtained *exact velocity profile* is

$$u_z^*(r^*,t^*)=\frac{\bar{V}^2\omega^{*2}L_0^*}{D}\left[1-\frac{I_0^*(\sqrt{ReA_RD}\,r^*)}{I_0^*(\sqrt{ReA_RD})}\right]e^{Dt^*} \tag{2}$$

where the exponent D is the most important parameter of which the physical meaning is an *inverse of a characteristic time for flow advancement*, determined by

$$\frac{D^2}{\bar{V}^2\omega^{*2}}=\frac{1}{2}-\frac{1}{\sqrt{ReA_RD}}\frac{I_1^*(\sqrt{ReA_RD})}{I_0^*(\sqrt{ReA_RD})} \tag{3}$$

where I_0 and I_1 are the modified Bessel functions of the first kind, of order zero and of order one, respectively.

The *filling flow advancement*, $l^*(t^*)$ is found to increase exponentially with the time as expressed by

$$l^*(t^*) = L_0{}^*\left[2e^{Dt^*} - 1\right]. \tag{4}$$

3. Analysis results

Figures 2, 3 and 4 show the effects of ReA_R and $\overline{V}\omega^*$ on D, $l^*(t^*)$ and $u_z^*(r^*,t^*)$ (for the velocity profiles, effect of ReA_R only), respectively, with regard to the both pseudo-static and exact solutions. Since the exponent D is proportional to the square of $\overline{V}\omega^*$ while it is linearly proportional to ReA_R, the flow characteristics are more sensitively affected by the change of $\overline{V}\omega^*$ (figures 2 and 3(b)) than ReA_R (figures 2 and 3(a)). However, it should be noted that the higher ReA_R is, the more deviation between the pseudo-static and exact cases is, as indicated in figures 3(a) and 4, due to the inertia force effect. The inertia force restrains a rapid velocity increase, thereby causing a smaller value of D and slower advancement in the real exact flow than the pseudo-static approximate one. Therefore, the pseudo-static solution behaviors deviate more from the exact ones as ReA_R increases.

4. Design

Based on the analysis in this study, we have derived the following design equations:

$$\textit{Design equations: } D = \frac{1}{t_d}\ln\left[\frac{1}{2}\left(\frac{L_d}{L_0}+1\right)\right] \text{ and } \frac{{R_h}^2}{\omega^2}D^2 = \frac{{R_h}^2}{2} - \sqrt{\frac{\mu}{D\rho}}R_h\frac{I_1\left(\sqrt{\frac{D\rho}{\mu}}R_h\right)}{I_0\left(\sqrt{\frac{D\rho}{\mu}}R_h\right)} \tag{5}$$

Therefore, by means of the above equations (5), one can easily *determine* R_h or ω for the given fluid properties (ρ and μ), position of reservoir (L_0) and design requirements (L_d and t_d).

5. Conclusions

In this paper, we have first developed the physical modeling and carried out the analysis for the centrifugal force driven transient filling flow into a circular microchannel. Two analytical solutions of exact and pseudo-static approximate cases were derived for the transient filling flow. The obtained analytical results show that the filling flow driven by centrifugal force is affected by two dimensionless parameters which combine fluid properties, channel geometry and processing condition of rotating speed. We also first provide a simple analytical microchannel design equations based on the modeling and analysis in this study.

Acknowledgements

The authors would like to thank the Korean Ministry of Science and Technology for the financial supports via the National Research Laboratory Program (2000-N-NL-01-C-148) and the Korean Ministry of Education & Human Resources Development supporting BK21 program.

References

[1] D.C. Duffy, H.L. Gillis, J. Lin, N.F. Sheppard, Jr. and G.J. Kellogg, *Anal. Chem.*, **71**, 4669-4678 (1999).

[2] M.J. Madou, L.J. Lee, S. Daunert, S. Lai and C.-H. Shih, *Biomed. Microdevices*, **3**, 245-254 (2001).

[3] Gyrolab™ Microlaboratory – www.gyros.com.

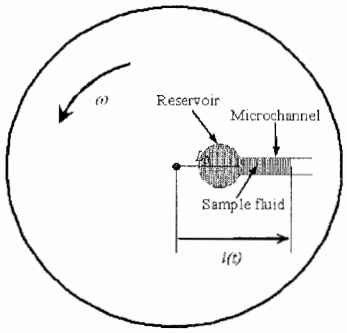

Figure 1. Schematic diagram of the transient filling flow into a circular microchannel on the centrifugal microfluidic system. Dark red area represents a region occupied by the sample fluid, $l(t)$ indicating the flow front.

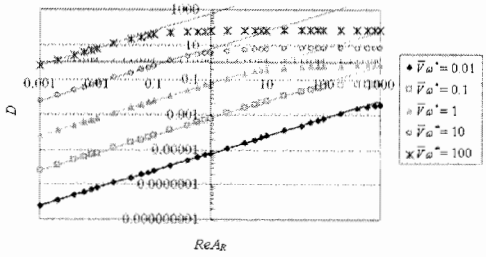

Figure 2. The calculated exponent D as a function of ReA_R for various $\overline{V}\omega^*$ (*symbols* from exact D and *curves* from pseudo-static D_{static}).

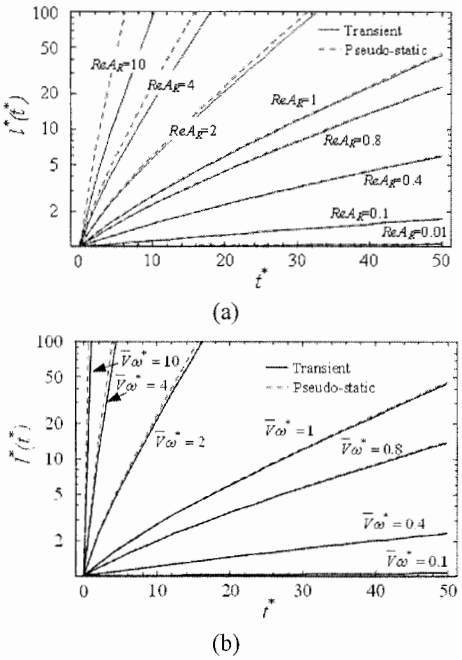

Figure 3. Effects of (a) ReA_R and (b) $\overline{V}\omega^*$ on filling flow front advancements, $l^*(t^*)$ (*solid curves* from exact solution and *dotted curves* from pseudo-static solution).

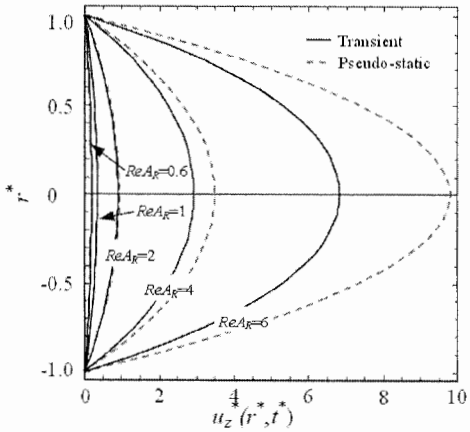

Figure 4. Effect of ReA_R on velocity profiles, $u_z^*(r^*,t^*)$, at t^*=5 (*solid curves* from exact solution and *dotted curves* from pseudo-static solution).

ELECTROKINETICALLY-DRIVEN ACTIVE MICRO-MIXERS AND ITS APPLICATION FOR DNA AMPLIFICATION

Chia-Yen Lee, Jr-Lung Lin, Kuo-Hoong Lee and Gwo-Bin Lee

Department of Engineering Science, National Cheng Kung University, Tainan, Taiwan 701

Abstract

An active electrokinetically-driven micro-mixer integrated with an on-chip temperature control system is studied and applied for DNA amplification process. In this DNA amplification process, the cell lysis is first performed in a micro cell lysis reactor. Extracted DNA, primers and reagents are then driven electroosmotically into a mixing region where they are mixed by the active micro-mixer. The homogeneous mixture is then thermally cycled in a micro-PCR (polymerase chain reaction) chamber to perform DNA amplification. The novel microfluidic system, which facilitates cell lysis, sample driving/mixing, and DNA amplification, could provides a significant contribution to ongoing efforts to miniaturize bio-analysis systems.

Keywords: Electroosmotic Flow, Field Effect, Mixer, Zeta Potential, PCR

1. Introduction

An integrated micro-PCR (polymerase chain reaction) system for DNA amplification is of crucial needs. Recently, emerging MEMS technologies and micromachining techniques have been increasingly employed in the integration of microfluidic devices to automate the generation and analysis of chemical compounds and bio-samples [1]. Miniaturized devices for DNA amplification have been successfully demonstrated [2-3]. However, a rapid and efficient mixing is a necessary but challenging process in many microfluidic systems which perform complex chemical synthesis and analysis. This paper presents a new electrokinetically-driven active micro-mixer which uses localized capacitance effects to induce zeta potential variations along the surface of silica-based microchannels [4]. This new micro-mixer utilizing variation of zeta potential induced by field effect could be used DNA amplification while integrated with other functional microfluidic devices.

2. Experimental

Individual buried shielding-electrodes were deposited near the microchannels of cross-shaped and Y-shaped microchannels to enhance the mixing effect [5]. The buried shielding electrodes were used to apply alternating voltages for creating a capacitance effect. Experimental data in Fig. 1 confirm that the zeta potential distribution along the microchannel wall could be well adjusted by varying the voltage applied to the shielding electrodes, thereby providing an effective EOF velocity control of the sample plug. It is noted that the EOF velocity and zeta potential become saturated at values of $V_{control} > 500V$.

3. Results and discussion

Figure 2 indicates the relationship of the mixing parameter (σ) and the control voltage ($V_{control}$) applied to the shielding electrodes. The mixing parameter (σ) increases as $V_{control}$ increases. The better mixing is achieved while stronger control voltages are applied and the mixing effect is saturated when the control voltage is higher than 500 V. This phenomenon could be explained by the saturation of the zeta potential near the channel wall at high voltages [4]. Figure 3 shows the evolution of the mixing parameter (σ) as a function of alternating frequency for an applied control voltage of 500 V to the shielding electrodes. Experimental and simulated data show that the mixing parameter (σ) decreases as driving frequency increases.

At last, an integrated micro-PCR (polymerase chain reaction) system for DNA amplification was reported. Figure 4 shows a schematic illustration of the integrated microfluidic chip, which is

seen to comprise of four major modules, namely a micro cell lysis reactor, a sample driving module, an electrokinetically-driven micromixer, and a micro PCR chamber, respectively. Cell samples were first thermally lyzed and their DNA was extracted within the lysis reactor. The DNA samples were then mixed and amplified in the micro PCR chamber. The micro-heaters, micro temperature sensors, and driving electrodes were integrated on the same chip. Preliminary data show that DNA samples (pneumococcus) with a length of 273 bps had been amplified significantly after 30 thermal cycles. The total time for the PCR test was 26 minutes 24 seconds and the total sample volume consumed was 15 μL. Figure 5 presents a slab-gel electrophoregram of the PCR product with and without active mixing by the electrokinetically-driven mixer. Hence the incorporation of an active mixer in the integrated microfluidic chip contributes significantly to the pretreatment of DNA detection and the integrated microfluidic chip achieves the sample pretreatment in a shorter time with less human intervention.

4. Conclusions

This study has successfully demonstrated a microfluidic system capable of performing cell lysis, sample transport, sample/reagent mixing, and DNA amplification. Using MEMS techniques, this system reduces sample and reagent consumption, provides fast thermal cycling, and requires minimum human intervention during its operation. Successful cell lysis and PCR amplification of a 273-bp Streptococcus pneumoniae have been demonstrated. It has been shown that the introduction of a device with efficient manipulation and mixing capabilities between the cell lysis reactor and the PCR chamber contributes significantly to the sample pretreatment operation in DNA detection applications. The developed integrated microfluidic system provides a powerful tool for DNA amplification, and as such represents a crucial element of the Lab-on-a-chip concept.

Acknowledgements

The authors would like to thank financial supports from National Science Council in Taiwan (NSC 92-3112-B-006-004)

References

[1] Sanders G. H. W. and Manz A., Trends in Analytical Chemistry, **19** (6), 364-378 (2000).
[2] Lee, G. B.; Lin, C. H.; Huang, F. C.; Liao, C. S.; Lee, C. Y.; Chen, S. H, Proc. IEEE MEMS, 19-23 (2003).
[3] Kopp, M. U., Mello, A. J., Manz, A., Science, **280**, 1046-1048 (1998).
[4] Schasfoort, R. B. M.; Schlautmann S.; Hendrikse, J.; van den Berg, A, Science, **286**, 942-945 (1999).
[5] Lee, C. Y., Lee, G. B., Fu L. M., Lee, K. H., Yang R. J., in press, Journal of Micromechanics and Microengineering (2004).

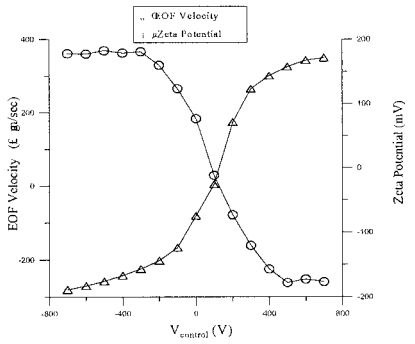

Figure 1. Relationship of theoretical zeta potential and experimental EOF velocity at different perpendicular electrical potentials V_{re}, where $V_{re} = V_{\pm} - V_{EOF}$.

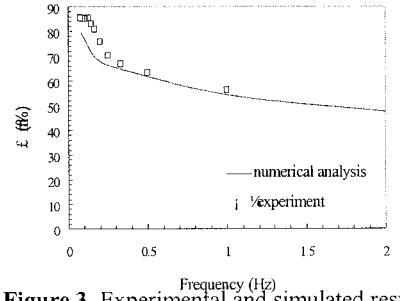

Figure 3. Experimental and simulated results for the mixing index (σ) at different frequency.

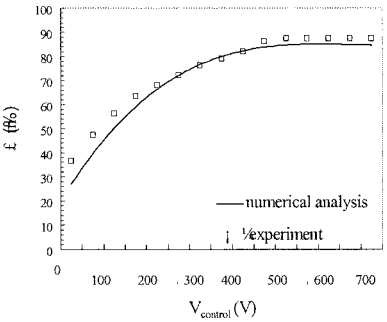

Figure 2. Experimental and simulated results for the mixing index (σ) at different control voltage.

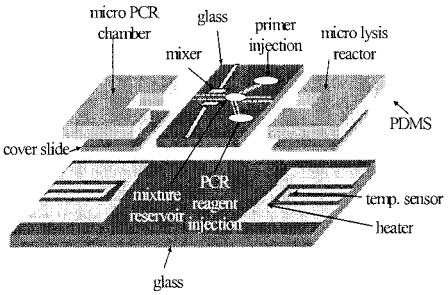

Figure 4. Schematic representation of microfluidic chips capable of cell lysis, sample mixing, and DNA amplification.

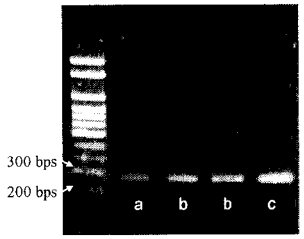

T(°C)	95	95	57	72	72	Total time
Integrated Chip (a, b)	60s	10s	10s	10s	60s	26 mins
Tradition al PCR (c)	60s	30s	30s	30s	300s	72 mins

30 cycles

Figure 5. Slab gel electropherogram for pneumococcus samples (273 bps) after PCR amplification. (Note that the first lane is fluorescence signals for DNA markers. Lane a is obtained from the integrated chips without mixing and Lanes b are obtained from the chips with on-chip mixing. Lane c is obtained from a conventional PCR machine).

FLEXIBLE PARYLENE NEURAL PROBES WITH INTEGRATED MICROFLUIDIC CHANNELS

Dominik Ziegler, Takafumi Suzuki*, Shoji Takeuchi
Center for International Research on MicroMechatronics, IIS, The Univ. of TOKYO
**Dept. of Information Physics & Computing, School of Info. Sci. & Tech., The Univ. of TOKYO*

Abstract

We present Parylene-based flexible probes suitable for *in-vivo* neural recording. Beside multi-channel microelectrodes the probes contain an integrated microfluidic channel, by which fluids can be delivered to the biological tissue. We have added a reliable microfluidic connector which allowed us to characterize the fluidic channel by measuring its flow-resistivity. Impedance measurements were used to characterize the microelectrodes and first probe-insertion trials were done.

Keywords: microelectrodes, microfluidic, Parylene, neural probe, drug delivery

1. Introduction

Neural probes with integrated fluidic channels are promising new tools for neuroscience. The bioelectric activity of the tissue can be monitored by multi-channel electrodes to study the effects of very locally applied drugs. Such devices were first micromachined in silicon [1] but recently polymeric materials such as BCB [2], Polyimide [3], and Parylene [4] are also used. Their advantage over silicon is that they are chemically stable, and have high flexibility and biocompatibility which is crucial for successful long-term *in-vivo* implantations. Our probe is fabricated in a Parylene-photoresist surface micromachining process. Figure 1 shows a photograph of the realized neural probe, highlighted are the gold recording electrodes (40x40 μm^2), the fluidic in- and outlet. The channel height is 12 μm and its dimensions are as indicated in Figure 2.

2. Materials and Methods

The microfabrication process of the device is shown in Figure 3. A first Parylene layer (8 μm, Parylene-C) was deposited on a silicon wafer then gold was evaporated and patterned (Wet etch, Aqua Regia). Next a 12 μm thick photoresist (AZP-4620, Clariant) was spin-coated and patterned to form the sacrificial layer defining the fluidic channel. After lithographic exposure and developing, the photoresist was baked for 30 min at 120° C to remove remaining solvents. Then the second covering Parylene layer (10 μm) was deposited. Final oxygen plasma, using aluminum as etchmask, defined the shape of the device and the fluidic inlets, from which the flow channel can be accessed. To prevent bubbling of the photoresist the RF heating was minimized by using cycling of the plasma (5 min on, 5 min off). The gold electrodes have been covered with the photoresist layer used for the fluidic channel, in order to prevent them from being exposed to the oxygen plasma.

By dissolving an initially evaporated sacrificial Aluminum layer the final devices can be removed from the wafer without any mechanical stress. The fluidic channel is opened by dissolution of the photoresist in a 40° C acetone bath. The dissolution speed in acetone is, regardless of the channel's dimensions, limited by the diffusion of the solvent into and from the channel [3]. The etched distance is proportional to the square root of the time; to clean a 1 cm long channel it took up to 26 hours. But using a soft ultrasonic bath reduced the dissolution time drastically to about 2 hours (Figure 4). The cleaned devices were finally rinsed in IPA and dried in air.

For the fluidic handling standard silicone tubing was vertically glued onto the fluidic inlet. To prevent the glue entering or clogging the microfluidic channel, the silicone tube was slightly pressed onto the fluidic inlet during the epoxy glue (Araldite) application (Figurse 5 a) and b)). Thanks to the direct gluing onto Parylene, no silicon micromachining is needed for the fluidic inlets.

3. Results

Fluidic characterization: A first test consisted of checking the fluidic integrity of the flow channel. We injected air while submerging the device into water to observe if bubbles appear at the fluidic outlet. Further we measured the flow characteristics of the channel as follows; a hydrostatic pressure was generated by a water column and monitored by a pressure sensor (AP-12S, Keyence) mounted close to the channel inlet and we measured the resulting stable flow using a micro flow rate sensor (ASL1430, Sensirion). We observed a linear relationship between the flow rate and the applied pressure difference along the channel, the flow resistivity is 1 $\mu l\ min^{-1}\ kPa^{-1}$ (Figure 6).
During the fluidic characterization breaking of the fluidic channels could occur. The breaking pressures varied much from device to device and depended on the leakage location. This weakness was mainly due to low adhesion between the two Parylene layers. Unfortunately adhesion promoter (OSI A-174) could not be used, because the sacrificial photoresist layer was dissolved by the used solvent (IPA).

Electrical characterization: We have measured the impedance of the gold electrodes ($40x40\mu m^2$) by submerging them in 0.9% saline solution applying a sinusoidal signal (300mV) with respect to a large reference electrode. Impedances of around 200 kΩ were measured at a frequency of 1 kHz (Figure 7) which is sufficiently low to allow neural recording.

Implantation trials: First probe-insertion trials into the brains of anesthetized Wistar rats have been made; after careful opening of the skull and peeling off the dura mater the probe was smoothly inserted into the sensory cortex. In contrast to prior trials with a 10 µm thick device [4] the actual probe was sufficiently stiff (thickness 18 µm) to allow an easy penetration into the brain, while it is still flexible enough to prevent severe insertion trauma.

5. Conclusion

A flexible Parylene neural probe with an integrated 12 µm thick microfluidic channel is designed and fabricated. The first implantation trials showed that the mechanical properties of the probe are suitable to be used as implantable device. But no *in-vivo* neural recording or fluidic injections have been done yet. The major drawback of the device is the weak adhesion between the Parylene layers resulting in low channel breaking pressures. In order build finer channels, which will require higher pressures to be driven, we have to improve the channels stability. We intend to achieve this by using recently developed Parylene-Parylene bonding technologies [6] or different adhesion promoter recipes. Our goal is the *in-vivo* observation of neural activity suppression by local injection of neural inhibitors.

References

[1] C. Jingkuang, *et al., IEEE Trans. Biomed. Eng.* **44 (8)**, p. 760-769 (1997).
[2] Keekeun Lee , *et al., Biosensors and Bioelectronics,* in press. (2004).
[3] S. Metz, *et al., Biosensors and Bioelectronics,* **19(10)**, p. 1309-1318 (2004).
[4] Sh. Takeuchi, *et al., 17th IEEE Int. Conf. on MEMS 2004,* p. 208-211 (2004).
[5] K. Walsh, *et al., 14th IEEE Int. Conf. on MEMS 2001*, p. 114-117 (2001).
[6] H-S. Noh, *et al., J. Micromech. Microeng.,* **14**, p. 625-631(2004).

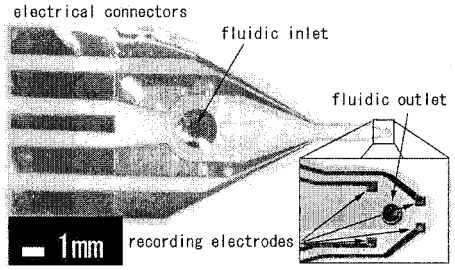

Figure 1. Parylene neural probe with fluidic channel. The zoom shows the tip with fluidic outlet and the recording electrodes.

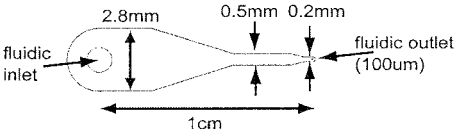

Figure 2. Dimensions of the fluidic channel

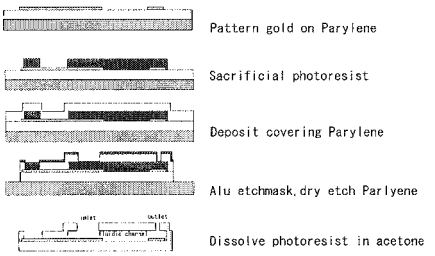

Figure 3. Fabrication process; sacrificial photoresist is sandwiched between two Parylene films to build the fluidic channel.

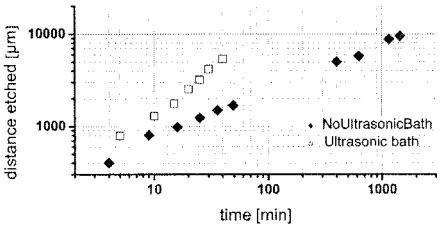

Figure 4. We measured the dissolved distance of sacrificial photoresist in an acetone bath at 40° C. Using an ultrasonic bath drastically shortens the needed dissolution time.

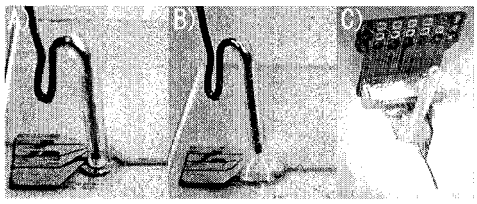

Figure 5. Assembly; silicon tubing is slightly pressed onto the fluidic inlet a) while epoxy glue is applied b). For the electrical connections the device is clamped into a connector on a printed circuit board c).

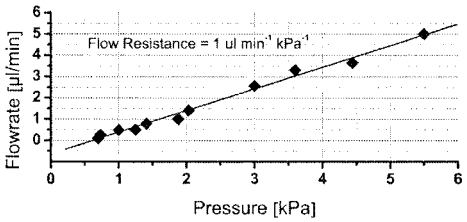

Figure 6. We measured a linear relationship between the flow rate and the pressure drop the resulting flow resistivity is 1 µl min^{-1} kPa^{-1}.

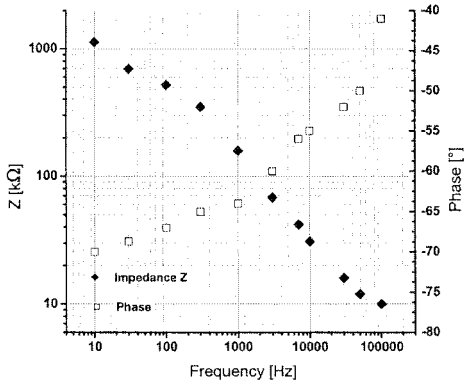

Figure 7. The impedance of the gold electrodes (40x40µm^2) was measured by submerging them in 0.9% saline solution and applying a 300mV sinusoidal signal with respect to a large reference electrode.

A MICROSYSTEM FOR ON-LINE MONITORING OF BIO PROCESSES

Ralph Wilke and Stephanus Büttgenbach
Institute for Microtechnology, Technical University of Braunschweig, Alte Salzdahlumer Str. 203, 38124 Braunschweig, Germany

Keywords: on-line monitoring, world to chip interface, capillary electrophoresis, passive valve, poly(dimethylsiloxane)

1. Introduction

Chip based capillary electrophoresis (CE) has for long been the method of choice for numerous research groups when approaching the μTAS-concept. From electrokinetic sample injection and electrophoretic separation in a double T-shaped channel system the work on this field evolved to what has become standard on-chip operations, namely: sample preparation and manipulation, reaction and detection [1]. However, what all this systems have in common is the initial loading of the microanalysis system with the sample solution is done by pipetting it into a reservoir. This is a good solution for laboratory use but not applicable for on-line monitoring tasks.

Pushed forward by the microelectronic industry electrical world to chip interfaces are available but this is not the case for fluidic interfaces. Providing a connector for external tubing is one issue, adapting the macroscopic flow to your capillary network is another one and requires effective flow control.

Trying to address these problems we present a microsystem for on-line monitoring of bio-processes with electrophoretic separation and electrochemical detection.

2. Experimental

The system comprises two channels, one for continuous flow-through of the sample solution and another one for capillary electrophoresis. Both channels are connected via a passive valve. This valve fulfills two tasks. First, it prevents the harsh flow properties of the continuous sample flow from acting on the sensitive separation channel and second, it allows a controlled pressure driven sample injection into the electrophoresis channel. The basic channel network and the valve are made of one slab of poly(dimethylsiloxane) (PDMS) by replica molding. The membrane of the passive valve consists of a thin layer of PDMS that is bonded to the slab. For integrated electrochemical detection a glass wafer with photolithographically defined electrodes is used as the base substrate.

The sample solution is continuously pumped through a wide channel, passes an external active valve and is redirected to the bioreactor (Fig. 1). The integrated passive valve and the smaller width of the connecting channel ensure that no sample solution reaches the measuring channel. A sample plug is injected when closing the external valve. The flow in the wide channel over-pressurizes and pushes sample solution into the connecting channel across the passive valve into the separation channel. The external valve opens again in order to release the pressure. A high voltage is applied to the separation channel so that the analytes are separated while migrating along the channel and detected electrochemically at its end (Fig. 3).

3. Results and discussion

Two different types of valves were tested for pressure driven sample injection. Both valves are similar in assembly but differ in contact surface area between the membrane and the valve seat. As expected, higher overpressure is required for the valve with larger contact area; 800 mbar opposed to 300 mbar for the valve with smaller contact area. Even though both configurations can be used in

principle, the one requiring less pressure is more favorable since the pressure equalization in this case forces less material into the separation channel at the instant of opening.

Another aspect that was found to be crucial for reproducible sample injection is the flow condition in the separation channel during injection. At elevated flow rates, a higher pressure is necessary for opening the passive valve. In general, a zero flow rate is optimal for introducing sample material into the separation channel (see Fig. 3). Any mass transport in the measuring channel leads to a leakage of sample material into this channel, no defined sample plug is formed and results in tailing peaks in the elctropherogram.

Acknowledgements

We would like to thank the German Research Foundation (DFG) for support of this work as part of the collaborative research center SFB 578.

References

[1] Review on recent CE-systems in: A. Manz et al., Anal. Chem., Vol. **74** (12), 2637-2652 (2002)

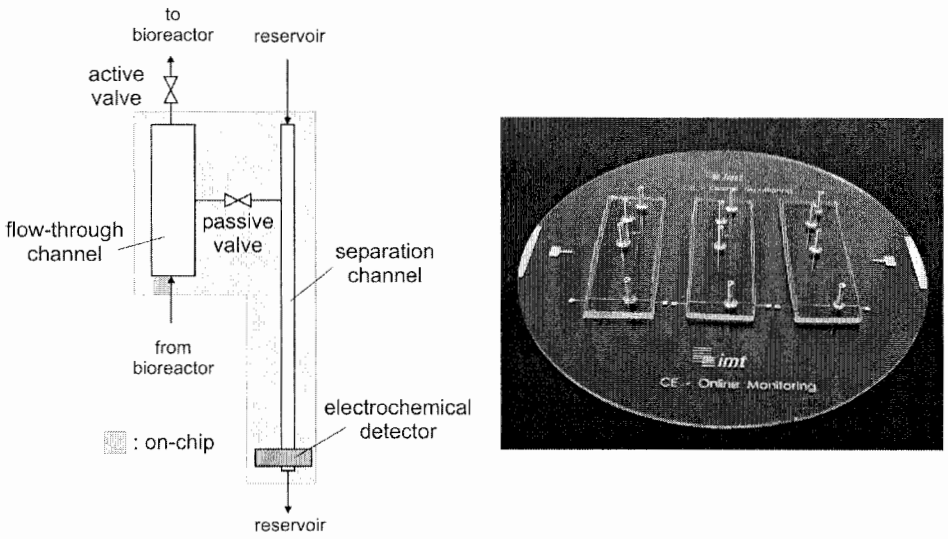

Figure 1. Schematic and photo of the on-line monitoring microsystem.

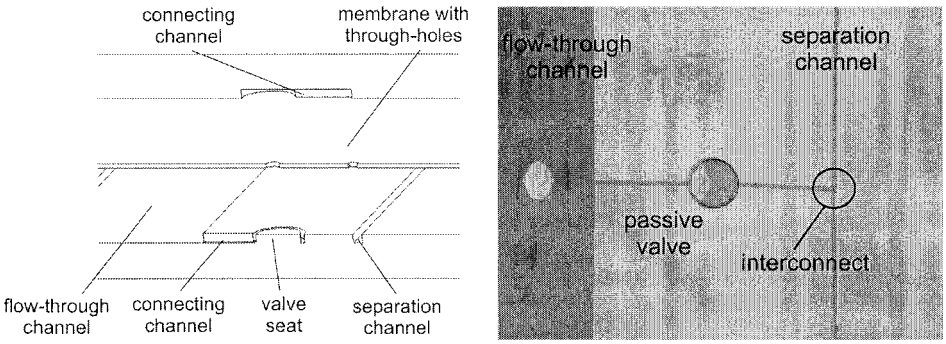

Figure 2. Exploded cross-sectional view (left) and microscopic photo (right) of the passive valve and the fluidic connection between the two channels. For better viewing clarity the channels have been filled with dyed water.

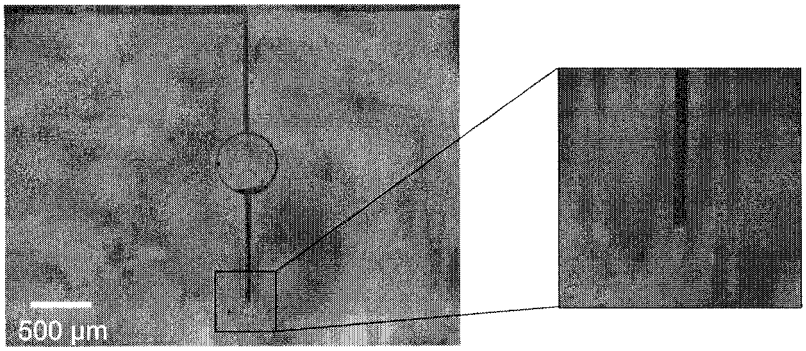

Figure 3. Photograph of the pressure driven sample injection and consecutive electrokinetic transport of the sample plug in the separation channel. Inset shows a detailed view of the sample plug.

AN ACCURATE VELOCITY PROFILE MEASUREMENT SYSTEM FOR MICROFLUIDICS : A DIRECT MEASUREMENT OF THE SLIP LENGTH

Pierre Joseph, Patrick Tabeling
Microfluidique, MEMS et Nanostructures, ESPCI, 10 rue Vauquelin, 75231 Paris, France

Abstract

We describe an accurate method to measure velocity profiles inside microchannels, using particle image velocimetry combined with a nano-positioning system. The experimental setup is used to measure the slip length of water flowing along a hydrophilic surface, pyrex glass, with 100 nm accuracy, and two hydrophobic ones, a monolayer of silane on pyrex glass and the same silane on an atomically flat silicon substrate. In all cases, the measured slip length is lower than 200nm.

Keywords: Slippage, nanofluidics, surface modification, PIV.

1. Introduction

It is generally assumed that liquids do not slip on solid surfaces. This condition has been confirmed by an overwhelming abundance of experimental measurements. In contrast with this picture, recent experiments have shown that simple liquids significantly slip on atomically smooth solid surfaces and, consequently, the no-slip condition ($v_w = 0$) should be replaced by a more general relation :

$$v_w = b\, \partial_z v ,$$

where b is the slip length (see Fig. 1 for details). Measurements of b have been performed for a variety of solid surfaces, and several fluids (Refs. [1-4]). Results indicate the slip length is on the order of micrometers i.e. much larger than typical intermolecular scales. The governing parameters appear to be the roughness of the substrate (at the molecular scale) and the strength of the liquid-solid interaction (the wettability).

The objective here is to make progress on the measurement of slip lengths, by developing a direct method of determination of the velocity profile (using PIV), in thin microchannels. The technique we present here allows, with unprecedented accuracy (±100 nm) for a direct method, to measure the slip length of water flowing over glass; the same technique is applied for atomically smooth silicon substrates, functionalized with a silane (octadecyltrichlorosilane); and glass functionalized with the same silane (OTS).

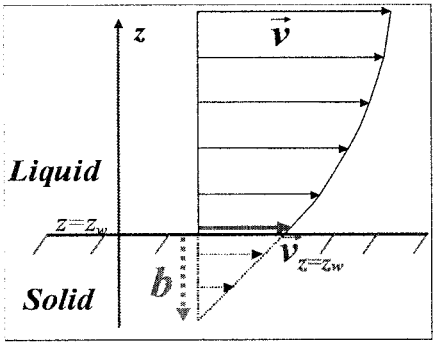

$$v_g = b \left. \frac{\partial v}{\partial z} \right|_{z=z_w}$$

Figure 1. The slip length b, corresponding to the extrapolation of the velocity profile to zero.

2. Experimental setup

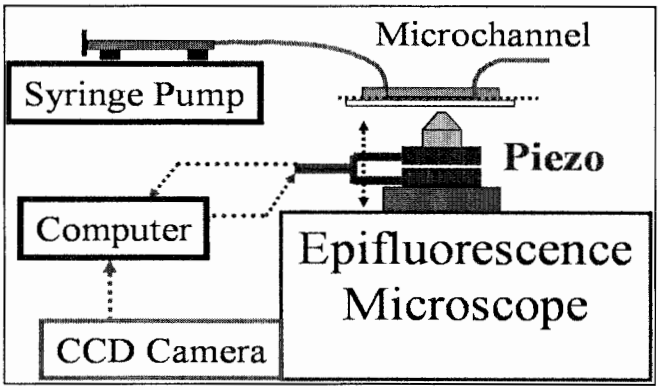

Figure 2. Experimental setup: Rectangular microchannel (15 x 200 μm). Stationary flow-rate of fluorescent beads (200nm) in deionized water (25nL/min), z-position controlled with a piezo. The thickness of the fluid layer being imaged is 400 nm. Velocity is measured by PIV technique.

A stationary flow-rate (25 nL/min) is imposed in a 15x200 μm rectangular microchannel. The lower surface of the channel is either made of glass, monolayer of OTS on glass, or a monolayer of OTS on silicon. In the first case, water wets the surface, while in the second and third cases, one gets a hydrophobic surface, showing a contact angle of 95°. The working solution is deionized water seeded with a 200 nm-diameter fluorescent polystyrene beads.

Observation is done with an epifluorescence microscope, a 100x oil immersion objective with 460 nm depth of field. The objective is mounted on a piezo-electric nano-positioner (20 nm precision), which allows an accurate control of the thin fluid layer being imaged. A typical experiment consists of recording images with a video camera while scanning different z-positions inside the channel.

Velocity is determined by Particle Image Velocimetry technique. The uncertainty, coming both from brownian motion and from the optical thickness of the imaged zone is reduced by means of thresholding and averaging : around 20 measurements of the velocity are performed for each position of the piezo.

The wall position is measured within 50 nm accuracy by the maximum intensity of stuck particles, the experimental data being fitted with a Lorentzian (see Fig. 3).

The velocity profile corresponding to a Poiseuille flow is fitted with a parabola. The slip length is then inferred from the position of the zero of this curve compared to the actual position of the wall.

3. Results and discussion

The slip length for glass is found equal to 0±100nm both in the wetting and the hydrophobic case (see Fig. 3.a.). For OTS functionalized silicon substrates (non-wetting case), one gets 200±300nm (see Fig 3.b.). The accuracy is decreased in that case because of optical aberrations, coming from the fact that one has to image through a PDMS membrane : the depth of field is increased to 1.5 μm.

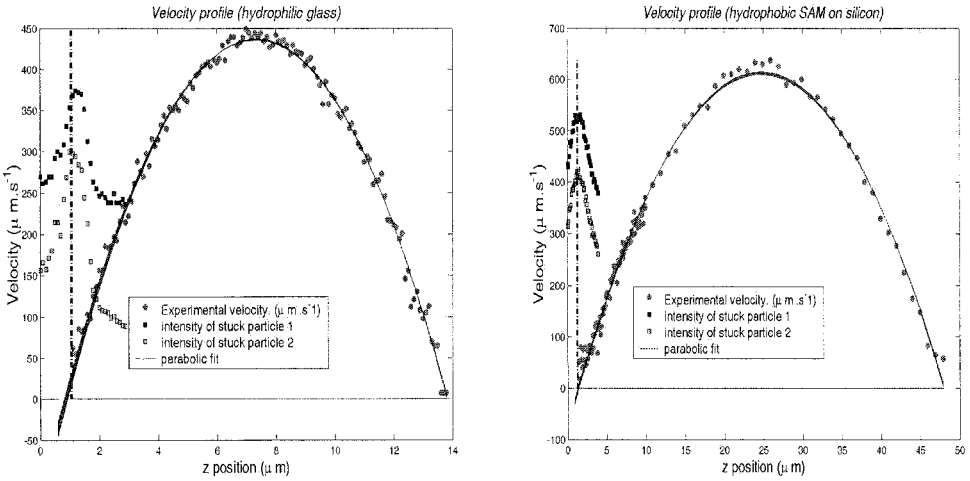

Figure 3. a. Velocity profile for glass (hydrophilic, RMS roughness 0.5 nm) and intensity of stuck particles (squares). The measured position of the wall (dashed line) compared to the extrapolation of the velocity profile allows to determine the slip length with 100 nm accuracy. **b.** Velocity profile for chemically modified silicon (hydrophobic, RMS roughness 4 nm) and intensity of stuck particles.

For a wetting surface, even for a very smooth substrate, the slip length is expected to be very small (on the order of a few nanometers). Our result is compatible with this no-slip boundary condition.

Controlling slip effects will become crucial in nanofluidic devices: A slip length not too small as compared to channel dimension reduces drastically Taylor dispersion and hydrodynamic resistance.

References

[1] Tretheway D., Meinhart C.: Apparent fluid slip at hydrophobic microchannel walls. *Physics of Fluids,* Vol 14, No. 3, 2002, pp. L9-L12 .

[2] Pit R., Hervet H., Leger L.: Direct experimental evidence of slip in hexadecane: solid interfaces. *Physical Review Letters,* Vol 85,No. 5, pp. 980-983, 2000

[3] Cottin-Bizonne C. *et al.*: An experimental study of slipping length. *Eur. Phys. J. E.***9**, 47-53, 2002.

[4] Choi C. H., Westin K. J. A., Breuer K. S.: Apparent Slip Flows in Hydrophilic and Hydrophobic Microchannels. *Physics of Fluids*, **15**(10), 2897-2902, 2003.

[5] De Gennes P.G.: On fluid/wall slippage. *Langmuir* **18,** 3413-3414, 2002.

CHAOTIC MIXING AND EXTRACTION, IN A MICROCHANNEL INTERSECTION

Arash DODGE[1], Anna HOUNTONDJI[1], Marie-Caroline JULLIEN[2], Patrick TABELING[1]

[1]Microfluidics laboratory, ESPCI, 10 rue Vauquelin, 75231 Paris, France
[2] BIOMIS, Satie, France

Abstract

We present here a novel extraction device, exploiting a particular property of a system, originally dedicated to chaotic micromixing. This property was obtained theoretically, but, so far, not demonstrated experimentally. The extraction system we present here shows substantial efficiency, while providing remarkable versatitility to a particular actuated microfluidic system.

Keywords: mixing, extraction, chaos, resonance.

1. Introduction

Extraction is an important step which is often required in the analysis of biological samples. Several techniques or extraction, based on monoliths, beads, or other materials, have been developed over the last decades, some of them being tentatively or successfully integrated in microfluidic devices [1]. Miniaturization of a particle extraction system, out of a liquid phase, has given rise to the H filter, now available commercially. Here we report a novel miniaturized extraction system, using actuated valves, showing substantial efficiency. Furthermore, it adds a new function to a device, originally dedicated to chaotic mixing. The possibility to use a chaotic mixer as an extraction unit was theoretically suggested [2], but, until now, not demonstrated experimentally.

3. Experimental

The device, sketched in Fig 1, consists in a transverse oscillating flow that perturbs a main stream, consisting of two fluids flowing side by side. The system is made in PDMS. The oscillating flow is produced by the actuation of integrated valves, made by using MSL (Multilayer Soft Lithography)[3]. Channels cross-sections are 25 x 200 μm. It was previously shown that this device is able to develop chaotic mixing [2]. Figure 2 shows an example of such a capability : the demonstration is made by using a fast reaction Calcium [1mM] / Oregon green [0.5 mM] both diluted in 25mM TRIS buffer). Fig 2 shows that mixing is effectively produced in this system: beyond the intersection, the product concentration is homogeneous.

4. Results and discussion

We now come to demonstrate that the same system is also capable of performing extraction. To show this, we use DI water as the first fluid, and, for the second fluid, a suspension of fluorescent latex beads, 0.8 μm in diameter, dispersed in a solution of fluorescein,. Without actuation, the two fluids flow side by side. With the actuation, appropriately tuned, one sees that all particles remain in the upper part of the main channel, while a substantial quantity of fluorescein diffuses in the lower part (see Figure 3B). The physical mechanism, anticipated theoretically [4], relies on the fact that, under "resonance" conditions, the interface elongates and folds in the channel intersection, and eventually returns to a flat shape as it leaves it. During the transient elongation, diffusive fluxes are enhanced, and therefore, fluorescein may cross the interface, yielding the extraction effect. The measurements show that the length over which fluorescein has diffused depends, as expected, on

the actuation frequency. A maximum is obtained at the lowest frequency (f=5 Hz). In the best conditions obtained so far, roughly 30% of the fluorescein could be extracted from the initial mixture, which is a valuable achievement.
The range of parameters for which resonance states are obtained (and thus extraction can be performed) was also suggested theoretically in Ref [4], but, until now, not obtained experimentally. The experimental range is represented in Figure 5. Here we plot the measured folding quantity F (a quantity which is defined as the ratio of the length of the interface, after the intersection, over a reference length [4]), for 250 couples of values of actuation frequency- pressure. The theoretical shape of this diagram, resembling to an oak leaf,, is obtained experimentally. This diagram is consistent with the theory. The range of practical conditions, where the device operates as an extraction system, lie close to resonance conditions, i.e within the folds of the line marking a separation between well mixed and poorly mixed states.

5. Conclusions

To summarize, we have shown here a system, previously demonstrating chaotic mixing, is capable of operating as an efficient extraction system. We measure efficiencies, and determine in which conditions extraction can be achieved, consistently with theoretical expectations.

Acknowledgements

We acknowledge ESPCI, CNRS and EEC (grant HPRN-CT-2002-00300) for their support.

References

[1] E. Verpoorte, *Electrophoresis*, **23**, 677 (2002).
[2] A. Dodge, M.C.Jullien, F. Okkels, P. Tabeling, *Proc. MicroTAS* 2003, Lake Tahoe (USA) (2003).
[3] M. Unger, H. Chou, T. Thorsen, A. Sherer, S. Quake, *Science*, **288**, 113 (2000)
[4] F. Okkels, P. Tabeling, *Phys. Rev. Lett.*, **92**, 38301 (2004)

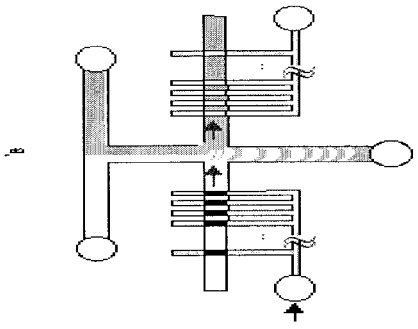

Figure 1 : Chip Layout : the two fluids (green and white) flow in a main channel. At the cross-channel intersection, the main stream is perturbed by a transverse flow, produced by a system of valves (yellow) actuated periodically

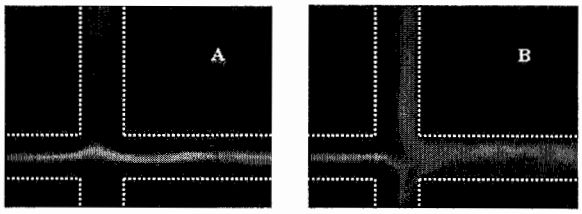

Figure 2: Mixing of Calcium [1mM] with Oregon green [0.5 mM] both diluted in 25mM TRIS buffer (pH 7.5). (A) No actuation (B) Actuation at 1.5 bar 11 Hz.

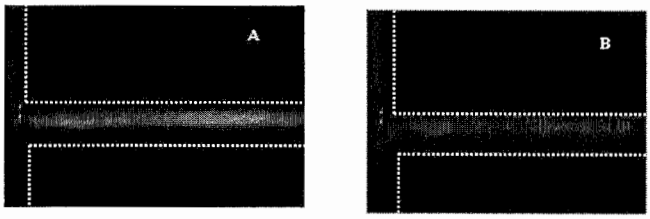

Figure 3: Two situations (A) No actuation (B) Actuation leading to fluorescein extraction. One sees, on Fig 3-B, fluorescein spreads in the channel, while beads stay on the upper half

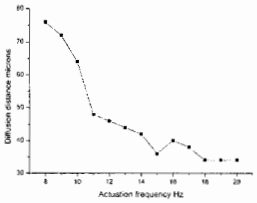

Figure 4: Diffusion distance of fluorescein across the interface, as a function of the actuation frequency. The maximum fraction of beads we are able to extract here is 30%.

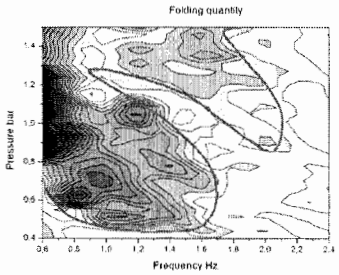

Figure 5 : Iso-plot of the folding quantity (introduced in Ref [4]) within the range of actuation pressures and frequencies we explored. Regions where extraction can be performed are within the folds of the line marking a separation between well mixed (dark)and poorly mixed (white) states.

ELECTRO OSMOTICALLY CONTROLABLE MULTIFLOW MICROREACTOR

Dietrich Kohlheyer, Rob G. H. Lammertink, Stefan Schlautmann, Geert A. J. Besselink and Richard B. M. Schasfoort

MESA+ Research Institute, Biochip Group, University of Twente, P.O. Box 217, 7500 AE Enschede, The Netherlands

Abstract

A novel microfluidic structure is presented that can be used as a fully adjustable diffusion based microreactor. The position and the width of two aqueous reactant streams entering a laminar-flow chamber can be controlled individually by changing the flow ratio of three parallel guiding streams containing buffer only. To control the intensity of product formation, the overlapping volume between the diffusive regions of the two different reagent streams can be adjusted. A mathematic model has been developed and embedded into LabView, allowing real-time control of the device. This article describes the principle, fabrication and experimental characterization of the device.

Keywords: microreactor, microfluidic, electro-osmotic flow

1. Introduction

In the last decade, the research and development of microfluidic systems have grown rapidly, allowing the fabrication of μ-TAS and "lab-on-a-chip" devices [1]. These microfluidic systems profit from their small dimension and high surface to volume ratios, allowing reaction and analysis to be fast and efficient. Another advantage is that the energy and sample consumption in microfluidic structures are much lower compared to that in traditional reactors. Flow in microfluidic channels is always laminar because of low Reynolds numbers allowing parallel flowstreams without turbulent mixing. The essential mass transport is based on diffusion only. Diffusion based microfluidic reactors have been developed in different shapes. The T-reactor is a well-known example [2]. The extent of mixing and reaction in the T-reactor can be controlled by adjusting reactant flux and concentration.

The presented microreactor [3] is a fully controllable microreactor which is easy to operate and the reaction intensity can be adjusted without changing reactant concentrations or flux in the reaction-chamber. The reactor is driven electro-osmotically allowing the chip design to be simple.

2. Reactor Principle

Each chip consists of five microchannels connected to a wider chamber. Two reactant streams are entering the wider laminar-flow chamber in between guiding streams separately (Fig. 1). These guiding streams contain buffer only. By changing the distance between the two reacting components and the width of the streams, an overlapping diffusion region can be adjusted (Fig. 2).

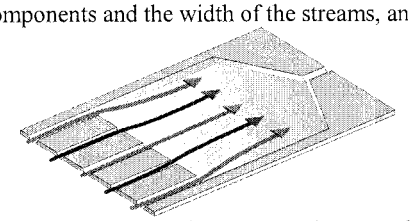

Figure 1. Principle illustration: Three parallel buffer streams guide the sandwiched reactant streams in a controllable way.

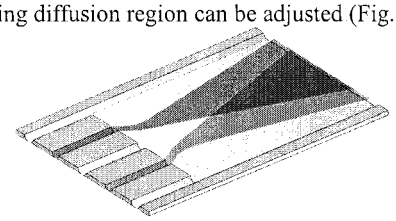

Figure 2. By reducing the distance between the reactants an overlapping diffusive volume can be established and controlled.

3. Microfabrication

The microfluidic chips were fabricated in the MESA+ cleanroom facilities. Each chip consists of two glass plates: the top plate contains the channel structures, flow-chamber and the reservoir holes while the bottom plate is left unprocessed. Processing of the top plate was done as follows: a 4" Pyrex-glass wafer is coated with amorphous silicon. After a standard lithography step this silicon layer is structured by reactive ion etching. The silicon layer serves as a mask during the following wet etching step in HF to create the channel and chamber structures in the underlying glass layer. For the making of the inlet and outlet holes a second photolithography step is carried out on the back side using a resist foil. Then, powderblasting is performed with AlO_3 particles to create the inlet and outlet holes. After ultrasonic cleaning and the removal of the silicon layer, the wafer is chemical mechanically polished preparing the surface for the following fusion bonding step of the structured wafer to another Pyrex wafer. The bonded wafers are finally diced into separate chips. The design is shown in Fig. 3. Each chip is 15mm x 25mm. The chamber is 1200μm wide and 3mm long. The width of the three guiding stream channels is 100μm and the width of the two sample stream channels is 50μm. Channel and chamber height is 10μm.

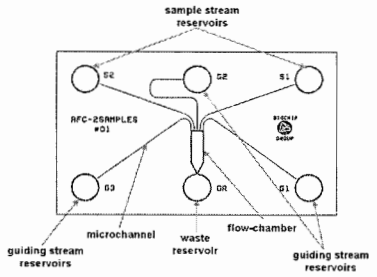

Figure 3. Fabrication layout of the microreactor.

4. Experimental

The chip was placed in a specially designed holder fabricated out of Delrin. This holder contains six reservoirs with integrated platinum electrodes connected to two high voltage sources (IBIS 411, microfluidic control unit, IBIS Technologies B.V., Hengelo, The Netherlands). The applied voltages were controlled with a LabView program based on an analytical model. An inverted microscope (Olympus IX51) with fluorescence unit, equipped with an F-View II 12-bit digital camera was used to view the stream profiles and reaction product formation. All inlet reservoirs were filled with 10 mM HEPES in demineralized water (pH 7.2). In the first experiment fluorescently labeled bovine serum albumin (BSA)(0.5 mg/ml in Hepes buffer) was added as a stream marker to both sample stream reservoirs. To study reaction dynamics, the calcium indicator fluo-4 (50μM fluo-4 in Hepes buffer) was added to the reservoir of one of the sample streams and a calcium solution (10 mM $CaCl_2$ in Hepes buffer) to the other. Throughout microfluidic operation, microscopy images and movies were captured using the camera control software AnalySIS (Soft Imaging System GmbH, Münster, Germany).

5. Results and discussion

Fig. 4 shows photographs of the device working under different guiding voltage settings. Positions and widths of the sample streams were changed while the velocity inside the chamber was kept constant at 750μm/s.

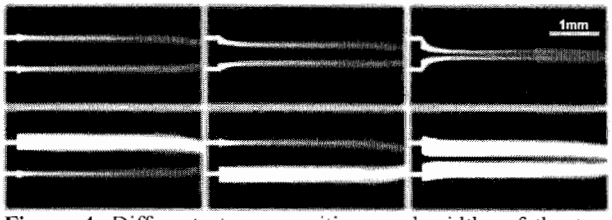

Figure 4. Different stream positions and widths of the two sample streams visualized with fluorescently labelled BSA

After binding with calcium, fluo-4 will strongly increase its fluorescence. The fluorescence of the calcium indicator was measured with the microscope setup described in Section 4. Fig. 5 shows a picture series with images, which were taken during the described experiment. From the left to the right the distance between the two sample streams is consistently reduced thereby increasing the diffusive overlap, resulting in a higher yield of the reaction product (fluo-4/Ca^{2+} complex). Due to the different diffusion coefficients of fluo-4 and Ca^{2+} the profile of the fluorescent area is asymmetric.

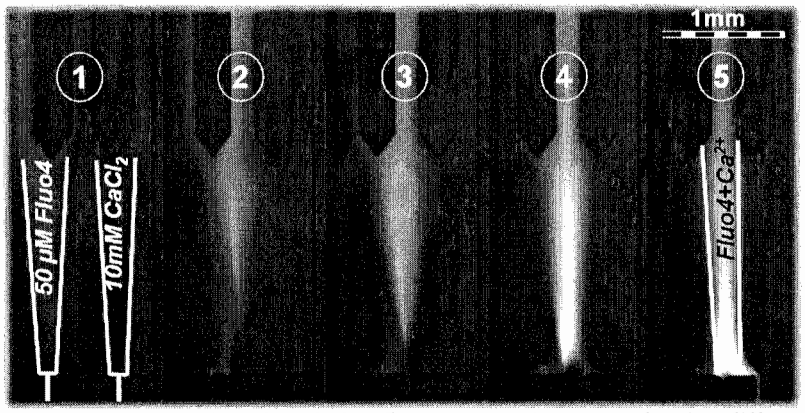

Figure 5. Image series taken during fluorescence microscopy showing different intensities of fluo-4 Ca^{2+} reaction product. From the left to the right the distance between the two sample streams is consistently reduced resulting in a higher yield.

6. Conclusions

A new microfluidic reactor has been designed and successfully fabricated. Electroosmotic flow is used as a pumping technique inside the channels. Due to this no external pumps or other sophisticated systems are needed. Experimental results showed that the reaction intensity can be fully controlled by adjustment of the guiding flows without changing the velocity inside the flow-chamber. This makes it possible to control a reaction rate inside the flow-chamber even in case of fluctuating reactant concentrations. The chip can be used as a new component for upcoming "Lab on a chip" and μ-TAS devices.

Acknowledgements

The authors like to acknowledge the funding of this research by the "Netherlands Organization for Scientific Research" (NWO) as a part of the SPRINTLOC "vernieuwings impuls" project.

References

[1] M.A. Northrup, K.F. Jensen, D.J. Harrison, *Micro Total Analysis Systems 2003*, Kluwer Acad. Publ. Dordrecht, The Netherlands (2003)

[2] S. J. Haswell, V. Skelton, *Trends in analytical chemistry,* 6 , 389-395 (2000)

[3] D. Kohlheyer, G.A.J. Besselink, R.G.H. Lammertink, S. Schlautmann and R.B.M. Schasfoort, *Microfluidics & Nanofluidics*, submitted May 2004

MICROFLUIDIC CHIP-BASED FLOW-INJECTION ANALYSIS WITH HIGH THROUGHPUT SAMPLING INTERFACE

Qun Fang*, Wen-Bin Du, Qiao-Hong He and Zhao-Lun Fang
Institute of Microanalytical Systems, Department of Chemistry, Zhejiang University, Hangzhou 310028, China

Abstract

This paper describes a high-throughput sample introduction system for chip based microfluidic analysis. The sampling system was composed of a capillary sampling probe and an array of micro-sample vials with slots fabricated on the bottom of each vial. The system was applied to achieve automated continuous sample change and sample injection operation in a chip-based flow injection analysis (FIA) system.

Keywords: Microfluidic chip, High-throughput sample introduction, Flow-injection analysis

1. Introduction

Hitherto most chip-based systems, including flow injection analysis (FIA) systems [1, 2], still adopt a discrete, and often manual, approach for on-chip sample loading and sample changing. Such practice seriously lowers the throughput and counteracts their advantage on achieving fast analysis. Currently, particular interests are focused on achieving automated continuous introduction of a series of samples to meet the requirements for analysis of real-world samples.

In this work, a high-throughput (up to 1000 samples/h) sample introduction system [3] for chip based microfluidic analysis was developed, which was composed of a capillary sampling probe and an array of horizontally positioned micro-sample vials with a slot fabricated on the bottom of each vial. The system was applied to achieve automated continuous sample change and sample injection operation in a chip-based flow injection analysis (FIA) system under gravity driven flows with absorption detection using a liquid-core waveguide (LCW) capillary flow-cell.

2. Experimental

The chip-based FIA system is shown schematically in Fig.1. A 6-mm×15-mm glass chip microfabricated with a dual-inlet Y-channel design (120-μm wide, 20-μm deep channels) was used for sample and reagent mixing and detection. A 4-mm long fused-silica capillary (75-μm i.d., 375-μm o.d.), functioning as sampling probe, was connected to one of the inlets. A 20-mm long Teflon AF 2400 capillary (50-μm i.d., 375-μm o.d.) was connected to the outlet of the microchannel to function as a liquid-core waveguide detection flow-cell with a detection path-length of 1.8 cm. Samples, carriers and reagent were driven by gravity, with the chip in upright position to create the static pressure required for driving. The micro-sample vials array was fixed on a homebuilt platform capable of moving linearly under computer control. Micro-sample vials were made from 0.2 mL Microtubes (Porex) with a slot (1-mm wide, 2-mm deep) fabricated on the bottom of the tube for pass-through of the sampling probe. The vials were filled alternately with 100-μL samples and blank solution (carrier). FI sample introduction and injection were performed by linearly moving the array of vials, allowing the probe inlet to enter the solutions in the vials through the slots sequentially in an order of carrier, sample 1, carrier, sample 2, carrier ...etc. The injected samples merged at the Y-juncture with the reagent flow (0.05% o-phenanthroline), mixed with the reagent downstream in the mixing channel, and the reaction product was detected in the LCW flow-cell.

3. Results and Discussion

In the chip-based FIA system, the fluids in the chip-channels were driven by hydrostatic pressure produced from differences in liquid levels between the sample vial/reagent reservoir and

the waste reservoir. The chip-based systems with liquid flows operated by gravity are benefited by no requirement for an external power source, or any driving equipment. Thus extremely simplified systems can be developed. In the sample introduction system, the amount sampled was determined by the solution flow-rate within the chip channel, which drew in the sample via the probe, and the residence time of the probe within the sample vial, which was controlled by the computer. The use of a slotted vial array for chip-based FIA allowed convenient and rapid sample change with low carryover and high sampling frequency without requiring mechanical valves and pumps.

The performance of the system was demonstrated using the complexation of o-phenanthroline with Fe(II) as a model reaction. Linear absorbance response was obtained in the range 1.0 μM to 100 μM Fe(II) (r^2=0.9979) (as shown in Fig.2), and a good reproducibility of 0.22% RSD (n=11) was achieved. High sampling throughput of 300 h^{-1} was obtained in the FIA system by using injection times of 2 s and 10 s for sample and carrier solution, respectively, with a sample consumption of only 8.5 nL for each cycle. The sensitivity was comparable with that obtained using conventional FIA systems, which typically consume 10000-fold more sample. The highest sampling throughput of 1000 h^{-1} was obtained (see Fig.3) by decreasing the injection times of sample and carrier to 0.1 s and 3 s, respectively, in which case the sample consumption was further reduced to 0.4 nL.

4. Conclusions

We have developed a simple on-chip sample introduction system that can easily introduce a series of samples with high throughput. In this work, this system was successfully applied to perform FIA in a microfluidic chip system. The results also demonstrate favorable prospects for applications in other microfluidic chip based systems, such as capillary electrophoresis and continuous flow analysis.

Acknowledgements

This work was supported by research grants from the Natural Science Foundation of China (20299030) and Ministry of Education of China (01093).

References

[1] A. M. Leach, A. R. Wheeler, R. N. Zare, *Anal. Chem.*, **75**, 967-972 (2003).

[2] G. N. Doku, S. J. Haswell, *Anal. Chim. Acta*, **382**, 1-13 (1999).

[3] Q. Fang, W. B. Du, Q. H. He, Chinese Patent, Appl. No.: 200410016224.8 (2004)

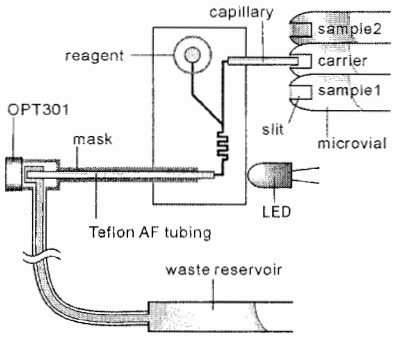

Figure 1. Schematic of the microchip for flow-injection analysis with absorption detection and gravity driven flows (not to scale).

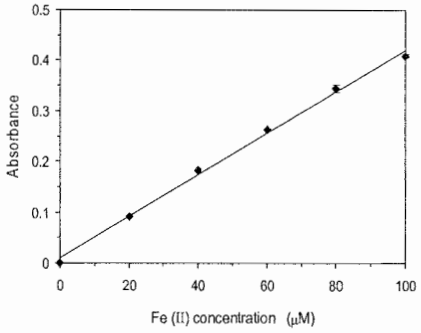

Figure 2. Typical recording for continuous injection of a series of Fe(II) standard solutions.
a, b, c, d and e: 20, 40, 60, 80, 100 μM Fe(II) solutions.

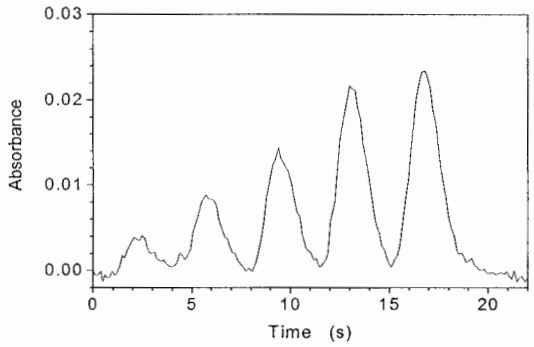

Figure 3. Typical recording for continuous injection of a series of Fe(II) standard solutions (20, 40, 60, 80, 100 μM) with a sampling throughput of 1000 h^{-1}.

ENHANCED MICROFLUIDIC MIXING USING PLANAR CURVED CHANNEL GEOMETRIES

Arjun P. Sudarsan and Victor M. Ugaz
Department of Chemical Engineering, Texas A&M University, College Station, TX 77843, USA

Abstract

Mixing of fluids at the microscale poses a variety of challenges, many of which arise from the fact that diffusion is the only available mechanism to achieve mixing in the laminar flow regime. In this work, we demonstrate the use of microfluidic devices incorporating spiral and asymmetric serpentine geometries capable of achieving mixing levels comparable to those attained using chaotic advection, while retaining a planar format that can be fabricated using only a single lithography step and without the need for multilayer alignment.

Keywords: microfluidics, mixing, curved channels, μ-TAS

1. Introduction

Microfluidics is becoming increasingly important for conducting many biological and biochemical lab-on-a-chip processes. For this technology to be successful in Micro Total Analysis Systems (μ-TAS) research, the ability to achieve complete mixing of fluids at short length-scales in microchannels is necessary. Typically, flow in microchannels is laminar in nature ($Re = Ul/\nu < 100$, where U is the average flow velocity, $l \sim 100$ μm is the characteristic cross-sectional dimension and ν is the kinematic viscosity of the fluid) and any mixing that occurs is purely by diffusion. Also, due to high values of Péclet number ($Pe = Ul/D_{mol} > 100$, where D_{mol} is the molecular diffusivity) diffusive mixing is also considerably slow compared to fluid convection in such channels. Since the Reynolds number is far below the critical value for turbulent transition to take place and since diffusion is the dominant mechanism for mixing to occur, cumbersomely long channels are needed to achieve complete mixing. This mixing length is given by $\Delta y_m \sim U \times (l^2/D) = Pe \times l$ and grows linearly with Pe [1].

2. Theory

Increased levels of mixing can be achieved in curved channels where transverse Dean flows are present. The Dean number ($\kappa = 2\delta^{0.5} Re$, where δ is the ratio of the channel hydrodynamic radius to the flow path radius of curvature) expresses the ratio of inertia and centrifugal forces to viscous forces, and provides a measure of the magnitude of the secondary flow [2]. Due to the curved nature of channels, secondary flows develop as a result of centrifugal forces. Consequently, a shift of the maximum in the velocity profile toward the outer channel wall will result, along with the presence of Dean vortices. Characteristic flow patterns in such systems involve two counter-rotating vortices, above and below the plane of symmetry of the channel, coinciding with its plane of curvature [2].

3. Spiral mixers

A series of 29 μm-high channels were constructed using thermoplastic elastomer substrates [3,4], each incorporating a series of spiral shaped sections arrayed along the flow path (Fig 1). Each section consists of an inlet and outlet spiral connected by a 1 mm-long central 'S' section, and a series of spiral sections are connected via 3 mm-long straight segments. A higher degree of mixing (quantified by imaging the green interface between parallel streams of blue and yellow dye) is generated at higher Re as a result of the transverse Dean flows present within the curved spiral segments. As the fluid flows through the spiral, κ increases as a consequence of the reduced radius of curvature, consistent with our observation that most mixing takes place at the inner regions of the spiral. These spiral channels are effective mixers in considerably shorter distances than straight channels (Fig 2).

4. Asymmetric serpentine mixers

An additional greatly enhanced level of mixing can be attained by breaking the symmetry in the value of κ between segments of the flow path possessing opposing curvature. This can be done using a serpentine geometry in which the width of the flow channel varies from one bend to the next (Fig 3). In conventional serpentine channels, fluid that is transported by centrifugal forces in the forward direction is transported back by recirculation along the channel walls in the opposing direction. Hence, they are ineffective mixers in the laminar flow regime as a mixing interface between two fluids undulates between the channel walls and the two streams do not mix completely even at high *Re* [5].

The variation in channel width associated with our design, however, alters the value of δ (and hence κ) thereby altering the transverse component of the flow trajectory as the fluid is advected downstream. As the fluid flows from the narrower bend (100 μm-wide) into the opposing wider bend (500 μm-wide), the recirculation that occurs is directed along a different path from what was followed in the preceding bend. The ensuing repeated winding and unwinding of the interface between the parallel streams is accompanied by a rapid expansion of the interfacial area available for diffusive transport. Experiments were carried out at *Re* ranging from 0.23 – 23.2 (corresponding to κ 0.1 – 11.3) calculated for the narrow 100 μm-wide bend of the channels. At lower flow rates, diffusion is the primary mechanism for mixing as viscous forces dominate and it is difficult to achieve complete mixing at short length-scales. At higher flow rates, the secondary flows become prominent and mixing can be achieved over significantly shorter length-scales (Fig 4). Using this asymmetrical serpentine geometry, a level of 90% mixing between fluid streams can be achieved in a distance of ~10 mm at *Re* ~ 2. This design is extremely simple to fabricate (planar geometry, single soft lithography step) and is capable of mixing efficiencies far exceeding those attainable using conventional serpentine or straight channel geometries.

Acknowledgements

We gratefully acknowledge Richard E. Beckham and Dr. Michael A. Bevan for assistance with the confocal imaging experiments.

References

[1] A.D. Stroock, et. al. *Science* **295**, 647-651 (2002)
[2] S. A. Berger and L. Talbot, *Ann. Rev. Fluid Mech.* **15**, 461-512 (1983)
[3] A.P. Sudarsan and V.M. Ugaz, *Anal. Chem.*, **76**, 3229-3235 (2004)
[4] A.P. Sudarsan, J. Wang and V.M. Ugaz, *Proc. μTAS 2004*, Kluwer, Malmö, Sweden (2004)
[5] D. Therriault, White, S. R. and Lewis, J. A., *Nature materials* **2**, 265-271 (2002)

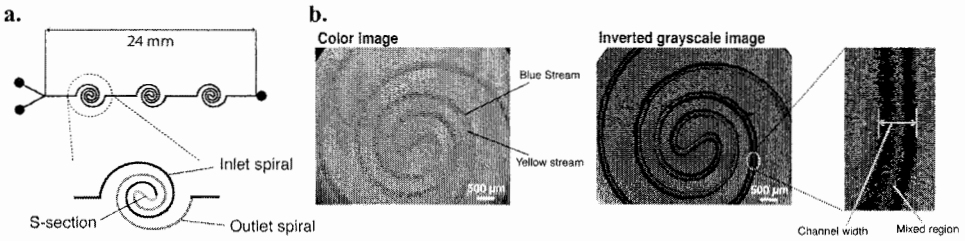

Figure 1. (a) Schematic illustration of a channel section showing the inlet and outlet spirals. (b) Measurement of mixing intensity from tracer dye images (***Mixing Intensity = Interface Width / Channel Width***).

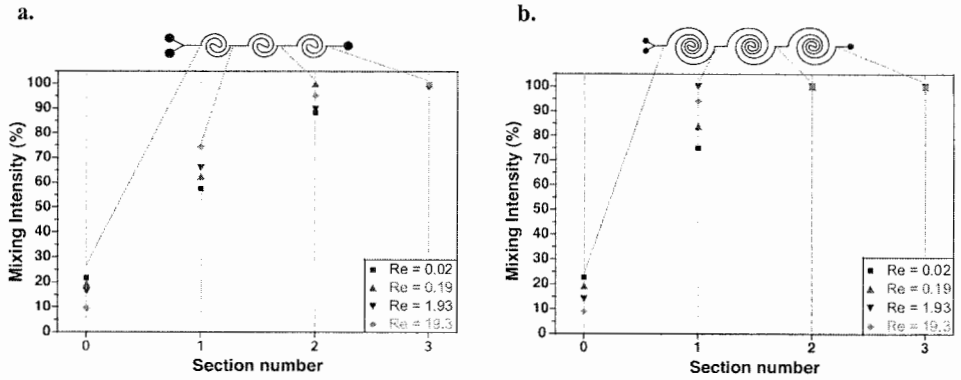

Figure 2. Mixing intensity at the end of each section for the (a) four arc (8.5 mm contour length per section) and (b) eight arc (27 mm contour length per section) spiral channels.

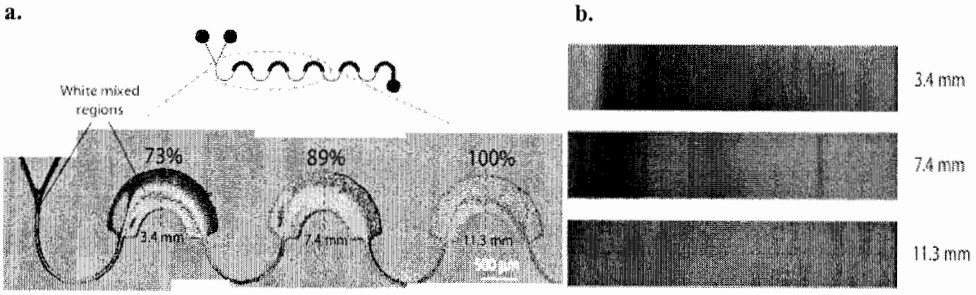

Figure 3. (a) Asymmetric serpentine mixer incorporating alternating 100 and 500 μm-wide curved sections. Grayscale images depict the rapid growth in the width of the mixed interface (flow is from left to right, *Re* = 23). Mixing intensities observed at 3.4, 7.4, and 11.3 mm downstream from the point where the two streams converge are indicated. (b) Confocal images (flowing a clear stream of water with a parallel stream of an aqueous mixture of rhodamine dye solution) of the channel cross-section at the corresponding locations agree qualitatively with the measured mixing intensities.

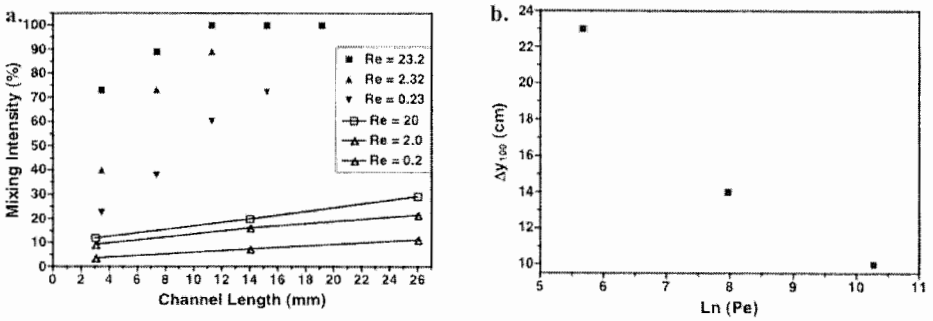

Figure 4. (a) Comparison of mixing intensities achieved with the asymmetric serpentine (filled symbols) and straight channel (solid lines with open symbols) geometries. (b) Length required for complete mixing for the asymmetric serpentine mixer as a function of *Pe*.

ELECTROKINETIC MICROMIXER UTILIZING NOVEL PINCHED-SWITCHING TECHNIQUE

Che-Hsin Lin[1], Lung-Ming Fu[2] and Yu-Sheng Chien[1]

[1]*Department of Mechanical and Electro-mechanical Engineering, National Sun Yat-sen University, Kaohsiung, 804, Taiwan*

[2]*Graduate Institute of Materials Engineering, National Pingtung University of Science and Technology, Pingtung, 912, Taiwan*

Abstract

This paper reports a microfluidic T-form mixer utilizing alternatively switching electroosmotic flow. Switching DC field is used to generate the electroosmotic force to drive the fluid and also used for mixing of the fluids simultaneously, such that moving parts in the microfluidic device and delicate external control system are not required for the mixing purpose. A novel pinched-switching mode is proposed, tested and discussed in the current study. Computer simulation for the operation conditions is used to predict the mixing outcomes and the mixing performance is also confirmed experimentally. Result shows the mixing performance can be as larger as 97% within the mixing distance of 1 mm downstream the T-junction at the operation condition of 60 V/cm driving voltage and 2 Hz switching frequency. The novel method proposed in this study can be used for solving the mixing problem in a simple way in the field of micro-total-analysis-systems.

Keywords: Electrokinetic, Microfluidic mixer, electroosmotic flow, pinched-switching

1. Introduction

Microfluidic devices incorporating T-form microchannels and utilizing electrokinetic forces to drive the sample fluid are widely used in a variety of bio-analytical applications, including DNA restriction, multiple sample injection, controlled fraction mixing and etc. Developing a simple and reliable electrokinetically driven mixing method is of great practical importance. Oddy *et al.* presented an electrokinetically driven microfluidic mixer for the rapid stirring of two fluid streams by means of axial and orthogonal wave functions generated by a high voltage amplifier.[1] However, a very high driving voltage was required (up to 4-8 kV). Johnson *et al.*[2] proposed a T-form micro mixer with a series of ablated wells for the rapid mixing of samples, and successfully demonstrated a high mixing efficiency. Huang *et al.*[3] presented an electrokinetically driven micro mixer using high voltage (1700 V/cm) waveforms for stirring purposes. In addition to the sample loading channels, the micro mixer also incorporated side channels to enhance the sample mixing effect. However, operating this system was complex since it was necessary to control the voltage precisely at an increased number of microchannel locations.

This study describes the mixing characteristics of a novel electrokinetically-driven micromixer and establishes its optimal operational settings. The mixing performance of the microfluidic device is evaluated through computer simulation and the results are then compared to those obtained experimentally.

2. Working principle

This paper proposes a T-form micro mixer which utilizes a switching DC field to induce electroosmotic flows for sample driving and flow instability generation. Figure 1 presents the basic operating principle of this device, which is capable of operating in a novel pinched-switching mode. A series of resistors are used to establish a pinch-voltage during the cyclic switching of the applied voltage. Pinched-switching generates greater disturbances, and hence provides an enhanced mixing performance. Furthermore, the device can be operated using a single power supply. Hence, the proposed T-form microfluidic mixer is simple, stable, and reliable.

4. Results and discussion

Figure 2 shows the electrical potential distributions and corresponding streamlines for the proposed micromixer obtained by numerical simulation. The fluid from the driven inlet flows not only into the mixing channel, but also partially into the open inlet. However, when the direction of the driving electric field reverses as the applied voltage switches to the other inlet, the fluid which previously flowed into the open inlet is expelled. Hence, cyclic switching generates a continuous large-amplitude waveform flow in the mixing channel. Figure 3 shows the numerical and experimental flow contours for different switching frequencies using a constant driving voltage of 90 V/cm and a 200 MΩ resistor for voltage pinching. As shown in Figure 3(c), the two samples are almost fully mixed at a switching frequency of 4 Hz. Note that, in our tests, the resistor value (50 MΩ, 100 MΩ, 150 MΩ, or 200 MΩ) appeared to have little effect on the efficiency of the mixing performance. Figure 4 demonstrates the mixing efficiency of the microfluidic mixer. At low switching frequencies of 1 and 2 Hz, the mixing efficiency exhibits waveform-like curves, which are indicative of the periodic flow of the fluorescence samples into the mixing channel. When the switching frequency is increased to 4 Hz, a mixing efficiency of 97% is achieved within a 1 mm distance downstream from the T-junction. Therefore, it is clear that the proposed pinched-switching mode significantly enhances the mixing performance of the micro mixer.

For optimization of the mixing operation, it is necessary to investigate the interrelationships between driving voltage, switching frequency, and mixing performance. In this study, using driving voltages of 60 V/cm, 90 V/cm, 120 V/cm, and 180 V/cm, the mixing efficiency was determined numerically and experimentally at different values of switching frequency. The corresponding results are presented in Figure 5. The present results indicate that a maximum mixing efficiency of 97% is obtained within 1 mm of the T-junction for a driving voltage of 60 V/cm and a switching frequency of 2 Hz. The optimal mixing efficiency for all the tested cases can be larger than 90%, which indicates the feasibility of this micromixer. Figure 6 presents the flow contours for optimized operating conditions in the cases of low and high driving voltages. In the low driving voltage case of 60 V/cm, the maximum mixing efficiency is found to be 98% at a switching frequency of 2 Hz. Meanwhile, for a high driving voltage of 180 V/cm, the maximum mixing efficiency is 90% at a switching frequency of 8 Hz.

5. Conclusions

In this paper, we have demonstrated a novel method for rapid mixing of sample fluids utilizing switching electroosmotic flow. The mixing performance of the device has been evaluated both numerically and experimentally. Moreover, this high performance micro mixer requires no moving parts and involves a simple fabrication process. The results of the present study provide a valuable contribution to the future development of a variety of applications in the Lab-chip systems field.

Acknowledgements

The current authors appreciate the financial support provided to this study by the National Science Council of Taiwan. (Grant No. NSC 92-2320-B-110-015 and NSC 92-2312-B-020-001.)

References

[1] M. H. Oddy, J. G. Santiago, J. C. Mikkelsen, *Anal. Chem.*, **73**, 5822-5832 (2001).
[2] T. J. Johnson, D. Ross, L. E. Locascio, *Anal. Chem.*, **74,** 45-51 (2002)
[3] P. Huang, K. S. Breuer, *Proc. Transducers '03*, 663-666 (2003)

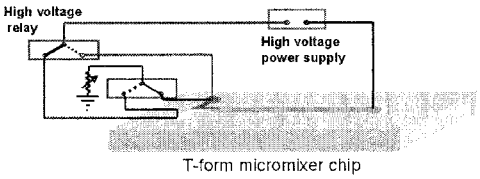

Figure 1. Schematic representation of the system setup for the present micro mixer.

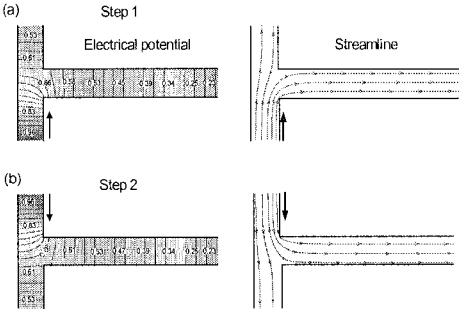

Figure 2. Electrical potential distributions and streamlines for both the switched conditions.

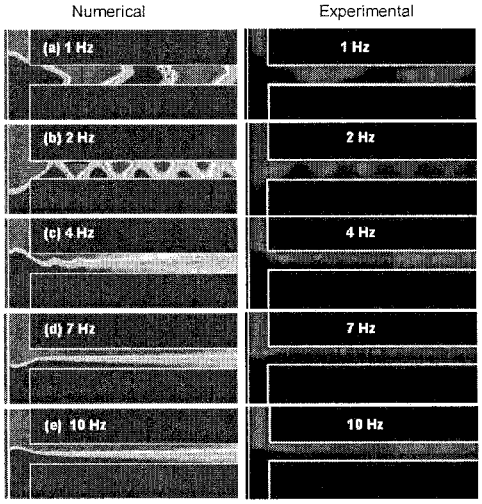

Figure 3. Numerical and experimental flow contours at different switching frequencies in pinched-switching mode operation.

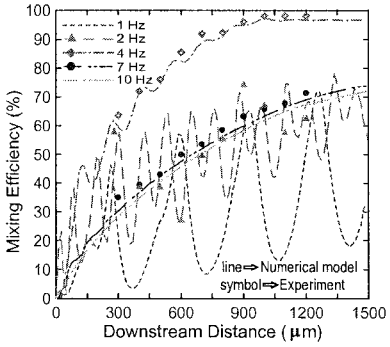

Figure 4. Mixing efficiency of the micro mixer at different switching frequencies.

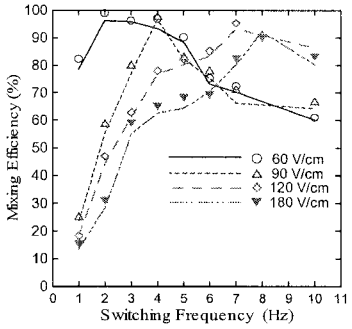

Figure 5. Numerical and experimental evaluations of mixing efficiency at different driving voltages and switching frequencies.

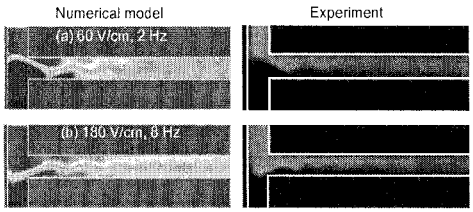

Figure 6. Flow contours for two optimized operating conditions at low and high driving voltages.

ORGANIC SYNTHETIC REACTIONS IN SUPERCOOLING FLOW USING MICROCHANNELS

Shinya Matsuoka[1], Masaharu Ueno[1, 2] and Takehiko Kitamori[1, 2]

[1] *Dep. of Applied Chemistry, The University of Tokyo, 7-3-1Hongo, Bunkyo, Tokyo, Japan*

[2] *Integrated Chemistry Project, Kanagawa Academy of Science and Technology, KSP, 3-2-1 Sakado, Takatsu, Kawasaki, Kanagawa, Japan*

Abstract

Supercooling flow of water in microchannels and its application for asymmetric organic synthesis were presented in this paper. Stable supercooling state can be formed by the feature of microspace, water never freeze at even -20 °C or less. Though the mechanism has not been made clear, we speculate it is owing to the effect of wetting and interfacial tension. This supercooling flow was applied for catalytic asymmetric synthesis with chiral phase transfer catalyst (chiral-PTC), which is advantageous at low temperature, and 10% higher enantiomeric excess was obtained than that obtained by bulk scale experiment.

Keywords: microchip, supercooling, synthesis, asymmetric reaction, phase transfer

1. Introduction

Microchip technology has versatile applications especially in analytical and bio chemistry [1]. Increasing interest has also been paid to application in synthetic organic chemistry. Conventional researches mainly utilized unique features of microspace such as short molecular diffusion distance, large specific interfacial area, and small heat capacity. Here, we notice to other distinctive feature that stable supercooling state can be realized in microspace [2], although the mechanism is not clearly explained. Using this feature of microspace, the flow of water at the temperature lower than melting point, namely supercooling flow, can be obtained.

This supercooling flow is expected to be effective for asymmetric organic synthetic reactions. Enantiomeric excess (ee), which is representative parameter of asymmetric reactions, is usually limited by thermal dissipation, and, therefore, higher ee is expected with lower temperature. However, operating temperature is restricted by freezing point of solution, especially of water, (Fig. 1a). By using this supercooling flow, it will be possible to perform reactions under the melting point of water, which is unable by conventional method (Fig. 1b).

In this paper, we investigated stability of supercooling state and supercooling flow of water in microchannel. And high ee asymmetric organic reactions were demonstrated by utilizing supercooling flow in microchannel.

2. Experimental

Two types of microchips were purchased from IMT. One microchip (Single-Y shaped, 100 μm in width, 40 μm in depth) was for investigation of supercooling phenomena in microchannel, and the other (with long reaction channel) was for catalytic asymmetric reactions. Controlling temperature was made by Partier temperature control stage, which can maintain the lowest temperature at -20 °C. Observation of liquid in microchannel was made by the stereomicroscope.

Asymmetric alkylation with a chiral phase transfer catalyst (PTC) demonstrated here was shown in Scheme 1 [3]. A microchip for synthetic reaction having a 200-μm wide, 100-mm deep and 24-cm long microchannel was placed on a temperature control stage (Fig. 2). The reaction was proceeded in a micro multiphase laminar flow [4] of aqueous and dichloromethane phases (DCM). The substrates 1 (0.10 M) and 2 (0.15 M) and internal standard (xantone) were dissolved in DCM phase. The chiral PTC (0.005 M) was dissolved in organic phase. The flow rate was set to 1.0

μl/min, which corresponded to 5.9 min in reaction time. Analysis of enantiomeric excess was performed by HPLC with chiral column (DAICEL OD-H).

3. Results and discussion

1) Numerical simulation the temperature of water in microchannel

Temperature of water in a microchannel having a 200-μm width and a 100-μm depth in a glass microchip was numerically simulated by using a simple thermal diffusion and conduction model without considering solidification. This numerical simulation was performed with finite element method software PDEase. Temperature of water attained from room temperature (25 °C) to operating temperature (-20 °C) within 6 s. In our experimental conditions, mean residence times in microchannel was more than 5 min, therefore it was able to said that water in microchannel become same as operating temperature. From this numerical simulation, there is no need of apprehension, which water in microchannel was not attained to the operating temperature.

2) Investigation of supercooling flow

First, distilled water and 1 M KOHaq was refrigerated under a condition of stationary segment with air or DCM, and then let them flow in 1 μL/min in microchannel. Even if operation temperature was kept at -20 °C for 5 min with no stimulation, solidification was not observed in any cases. Simultaneously, it was confirmed the freezing of water in microchannel at much lower temperature by pouring liquefied nitrogen. Therefore, it was demonstrated the realization of supercooling flow in microchannel at the temperature -20 °C without any stimulation.

3) Catalytic asymmetric synthesis in supercooling flow

Relationship between operating temperature and ee is shown in Fig. 3. Temperature area blow melting point of water is shown by hatching. As clearly shown in Fig. 3, ee increased as decreasing temperature. By utilizing supercooling flow, ee of 50 % was achieved while upper limit of ee was 40 % over the freezing point. Although reaction rate was reduced in low temperature, high ee reaction, which could not be achieved by macro scale experiments, was demonstrated by utilizing the feature of micro space.

4. Conclusions

Supercooling flow of water in microchannel and high ee asymmetric synthesis has been demonstrated. It was able to form the flow of supercooled water at the temperature -20 °C without any stimulation. Then we applied this method for catalytic asymmetric synthesis, and 10 % larger ee than that in bulk scale reaction was obtained. Reaction in supercooling flow is established even though obtained extra ee is actually not so large. Now we are investigating the reasons of these phenomena from the viewpoint of between surface energy and instability of potential energy at supercooling state.

References

[1] T. Kitamori, M. Tokeshi, A. Hibara, K. Sato, *Anal. Chem.* 76, (2004), 52A
[2] C. L. Hosler, C. R. Hosler, *Trans. Am. Geophys. Union* 36, (1955), 126
[3] T. Ooi, M. Kameda, K. Maruoka, *J. Am. Chem. Soc.* 125, (2003), 5139.
[4] A. Hibara, M. Nonaka, M. Tokeshi, T. Kitamori, *J. Am. Chem. Soc.* 125, (2003), 14954

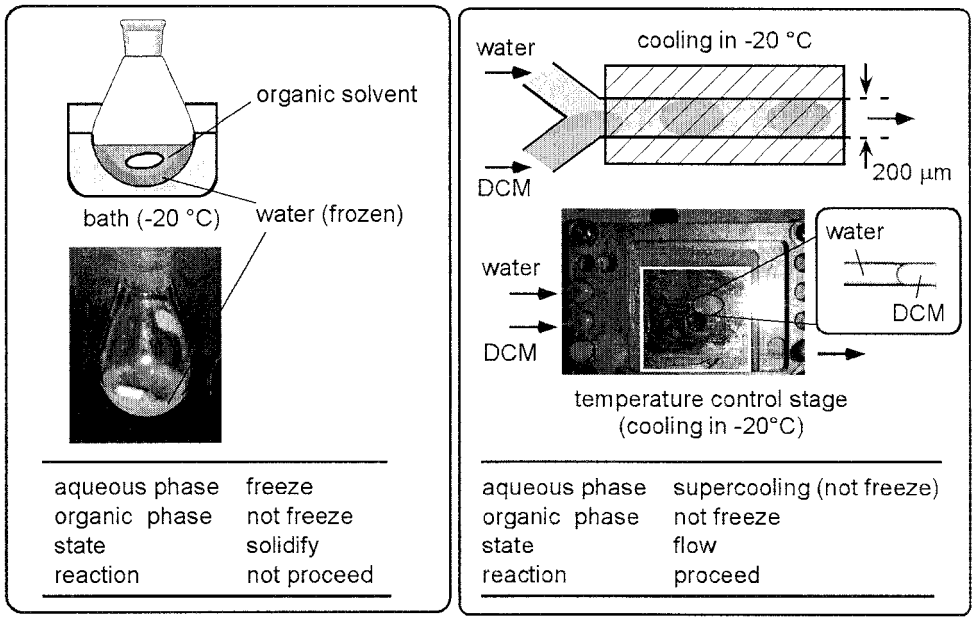

a. Conventional reaction b. Microchannel reaction

Figure 1 Reaction under supercooling condition using microchannel.

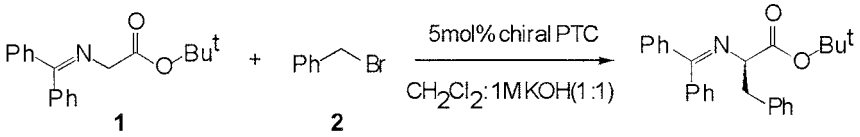

Scheme 1 Alkylation of glycine ester benzophenone Schiff base.

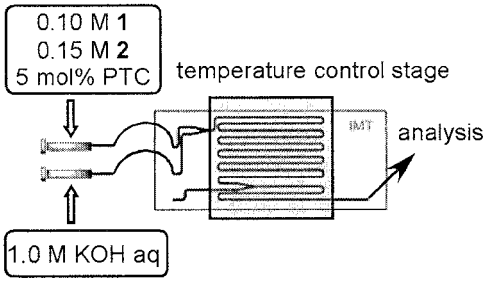

Figure 2 An experiment system.

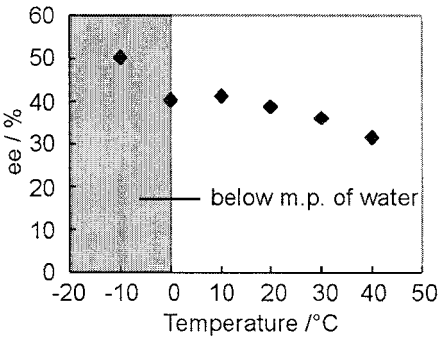

Figure 3 Enantiomertic excess (ee) increase according to supercooling effect.

IN CHANNEL MIXING OF ON-DEMAND MICRODROPLETS GENERATED BY D.C. VOLTAGES

A. Macaskill, P. R. Fielden, N. J. Goddard, S. Mohr, B.J. Treves Brown
Department of Instrumentation and Analytical Science (DIAS), University of Manchester Institute of Science and Technology, PO Box 88, Manchester, M60 1QD, UK.

Abstract

We demonstrate two new methods for coalescing aqueous microdroplets in an oil filled flow channel. In the first method two droplets produced by shear induced detachment are merged by the application of a D.C. voltage. In the second method, three aqueous microdroplets, again in an oil filled flow channel, are coalesced simultaneously by the application of a D.C. voltage, with one microdroplet being produced by shear induced detachment and the other two being electrically produced, on-demand.

Keywords: Droplets, fluid dispensing, mixing, microfluidics.

1. Introduction

In recent years there has been increased interest in using pico/nanolitre-sized droplets as microreactors in miniaturised chemical and biological reactions. On-chip droplet metering and mixing has been successfully demonstrated using electrowetting [1-2]. The ability to mix aqueous droplets whilst flowing through oil filled channels should reduce, post-mixing, any interference effects from the chip walls whilst the reaction of interest is taking place. As the number of droplets examined using this method is not limited by the number of available electrodes, this technique would be suitable for High Throughput Experimentation (HTE) purposes.

2. Design and Fabrication

The microfluidic structures used were fabricated on sheets of PMMA using a precision CNC machine (Datron CAT3D, Datron GmbH, Germany). The inlet channels were milled using a 100μm drill bit resulting in channels 100μm deep. All other channels were milled using a 200μm drill bit resulting in channels 200μm deep. Access holes of 1mm were made at the end of each channel to allow the fitting of 062 Minstac tube fitting connectors (The Lee Company, USA).

3. Experimental

Domestic sunflower oil and ultra pure 18MΩ water were used. Fluids were either pumped by Kloehn V6 high precision syringe pumps or gravity fed from open reservoirs, held at a height that provided the necessary flow rate, as indicated in Figures 1 and 2.

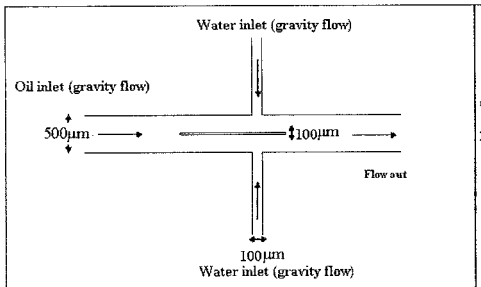

Figure 1. Schematic of device for two drop merging.

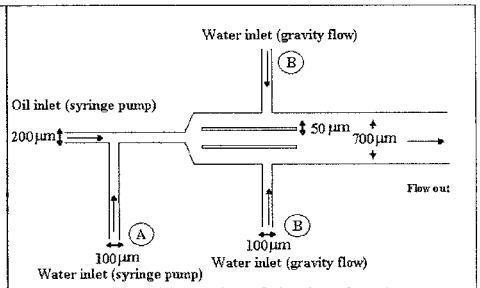

Figure 2. Schematic of device for three drop merging.

Pieces of metal tubing, i.d. 1mm and approximately 1cm long, were inserted into both gravity fed water inlet tubes, approximately 2cm from the fittings connecting the tubing to the chip. One inlet was connected to ground and one connected to a Brandenburg High Voltage Power Supply Unit via crocodile clips attached to the metal tubing. Images were recorded using a Baxall black and white CCD camera.The camera had a frame rate of 30 f.p.s. and was fitted with a 4x microscope objective.

In the first device, droplets were produced from opposing T-junctions by shear induced detachment. The droplets are then charged by the application of a D.C. voltage which causes them to merge on meeting.

In the second device, a stream of droplets was produced from a T-junction (inlet A on Figure 2.) by shear induced detachment in a 150μm wide channel. This channel was then widened to 700μm so that the droplets flowed through the centre of the channel and between two 50μm walls. These droplets then passed two opposing T-junctions (inlets B in Figure 2.) where droplets could be produced, on demand, by the application of a D.C. voltage pulse. This produced two charged droplets, initially separated by the two walls from the central uncharged droplet. Once all three droplets passed the end of the separating walls, merging occurred.

4. Results and discussion

In the first device, the droplets were seen to merge with the application of voltages as low as -100V, as shown in Figure 3 (a). On applying the D.C. voltage it is thought that the edges of the two opposing water inlets act as the faces of a capacitor resulting in one droplet being positively charged and the other negatively charged and that these attractive forces cause the droplets to merge on meeting. The coalescence of the droplets is controllable as no mixing occurs if the voltage is not applied (Figure 3 (b)).

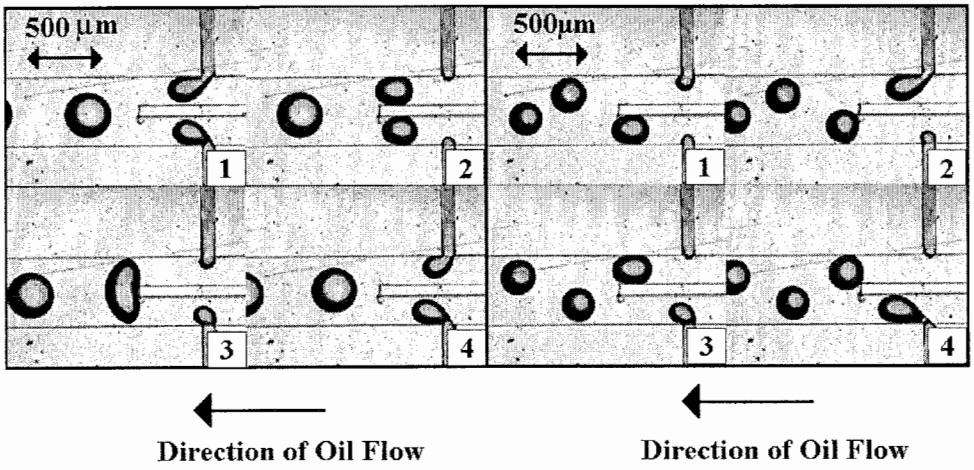

Figure 3. (a) Pairs of shear induced droplets coalescing due to application of -100V and (b) with no voltage applied. Frame rate: 30 frames per second.

In the second device, it was shown that three droplets could be merged simultaneously whilst moving through a microdevice by application of voltages of -800V as shown in Figure 4. The water pressure supplied to the two opposing T-junctions was set so that the water front was balanced at the edge of the oil channel but did not flow into it as shown in Frame 1 of Figure 4. The application of a D.C. pulse caused a charged droplet to be produced from each inlet. These charged droplets are able to merge with a central non charged droplet. This is as a result of the induced charge caused by the non-uniform electric field surrounding the charged droplets.

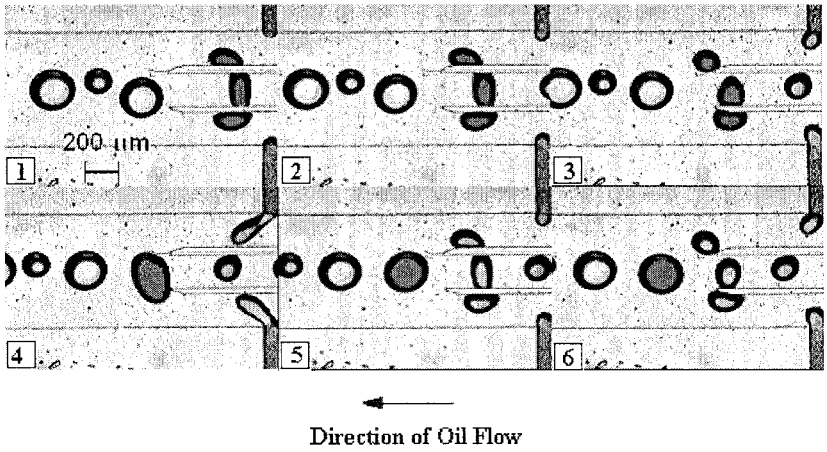

Figure 4. Merging of three droplets (artificially coloured): Top and bottom droplets produced by application of D.C. voltage of -800V, middle droplet formed by shear induced detachment. Frame rate 30 frames per second.

5. Conclusions

The ability to mix controllably two or three aqueous microdroplets whilst flowing through an oil filled microstructure has been demonstrated. A droplet-on-demand method has also been shown which could allow selective addition of reagents to specific droplets. The ability to mix and meter samples in such devices is an important step towards the use of droplets as micro reactors in High Throughput Experimentation.

Acknowledgements

The authors would like to acknowledge the financial support given to this work by the Earth and Physical Sciences Research Council and the Medical Research Council.

References

[1] M.G. Pollack, R.B. Fair and A.D. Shenderov, *Appl. Phys. Lett.*, 77 (11), 1725 - 1726 (2000).
[2] H. Moon, S.K. Cho, R.L. Garrell and C.J. Kim, *J. Appl. Phys.*, 92 (7), 4080 - 4087 (2002).

MONOLITHIC MICROCHEMICAL PROCESS PLANT OF IMMISCIBLE MICROFLUIDS

Jeung Sang Go[1,2], Eun Ho Jeong[2], Takahiro Arakawa[1], Masahiro Mori[1], Kyung Chun Kim[2] and Shuichi Shoji[1]

[1]Major in Nano-science and Nano-engineering, Waseda university
3-4-1, Ohkubo Shinjuku, Tokyo, 169-8555, Japan
[2] School of Mechanical Engineering, Pusan National University
30, Jangjeon-dong, Geumjeong-gu, Busan,609-735, Korea

Abstract

Study of a micro chemical plant consisted with droplet generation, digital sorting and separation was conducted. The droplet generation was quantitatively characterized. The digital sorting brought effective reaction by shortening the droplet size and the pitch of droplet generation simultaneously. To prevent the unfavorable higher order reaction, perfect separation of droplets was visualized.

Keywords: chemical plant, droplet generation, digital sorting, reaction, separation

1. Introduction

Micro-scale technology challenges discovery of new chemicals and medicines [1,2]. It enables subtle chemical processes regarded impossible in conventional reaction pathways since they can be performed under precise control of reaction conditions and reasonable test cost due to nano/pico volume of chemicals. In addition, safety is guaranteed for highly reactive and toxic chemicals and gases.

We have grafted microfabrication to the development of a micro chemical processing plant handling mixture of immiscible chemical fluids such as organic and aqueous liquids. When immiscible fluids are introduced into microchannel, droplet is generated due to the hydrodynamic instability [3]. After the first analysis of droplet break-up [4], numerous subsequent works have concluded that the droplet breakup occurs when the viscous stress is greater than surface tension effect. This paper examines the kernel chemical processes of an on-line micro chemical plant experimentally.

2. Experimental preparation

Fig. 1 describes the graphical illustration of the sequential chemical processes using droplet phase flow. They are consisted of droplet generation, reaction and separation in turn. Fig. 2 shows a microfabricated on-line chemical plant. Droplets are generated in the crossed inlet channels. The bifurcated channel divides droplets and digitally sorts them to obtain effective reaction. Finally, three microchannels divided separates the reaction-completed droplets. Each channel has a 100 μm-wide and 100 μm-high cross-section.

Butyl alcohol as an organic phase is driven along the middle channel and water containing 3% wt Ethylenediamine is introduced from two side channels. To infuse and to drain two immiscible fluids, syringe pumps are used. In order to visualize and characterize the droplet phase flow, a high speed CCD camera (Photron Fastcam) is installed.

3. Results and discussion

Droplet generation: we determined the size, pitch and generation rate of droplet flow by counting pixels of the image of droplet flow (Fig. 3). The generation rate is defined as numbers of droplets generated per unit time. Based on the experimental results (Fig. 4), it is determined that as the ratio of the organic phase flow rate to the water phase flow rate increases, the size of droplet decreases inversely from 300 μm to 100 μm, while the pitch increases rapidly. The generation rate

shows a linear decrease. These results indicate the possibility of control of droplet phase flow. It is also founded that the minimum size of droplet is constrained on the channel width with accompanying the longest pitch.

Reaction using digital sorting: through the interfacial surface area of droplet, reaction dominated by diffusion occurs [5]. Based on behaviour of droplet generation, the small size of droplet brings long pitch, implying that it takes longer time to finish reaction. On the other hand, to make shorter pitch means larger size of droplet, indicating the excessive size of droplet. Thus, concerning effective chemical reaction and cost, the simultaneous reduction of size and pitch is required. Digital sorting can provide solution by dividing a large droplet into numbers of small droplets and by sorting them systematically by retarding the speed of the divided droplets flowing along the bypass channel [6]. In order to obtain digital sorting, the channel is bifurcated into the straight channel and the bypass channel with the same half width of the original channel (Fig. 2). Fig. 5 shows a quarter volume fragmentation of a droplet and systematic sorting, resulting in the shorter pitch, what is called digital sorting.

Separation of droplets: as soon as reaction completes, droplets should be separated in order to prevent the unfavourable second or higher order reaction, which is very cumbersome and expensive to remove. Fig. 6 visualizes the panoramic separation of droplets. The separation channel having the shape of a pelican mouth eats up the reaction-completed droplets. Thus, the reacted target chemical fluids can be drained through two side channels. For an inlet flow rate of 8 μl/min, perfect separation of droplets was obtained by sucking with a flow rate of 4 μl/min at the droplet separation channel. When the suction flow rate was decreased to 3 μl/min, droplet was divided and the part of droplet was flowed into the side channels.

4. Conclusions

The basic chemical processes of an on-line micro chemical plant were completed successfully. In droplet generation, the size of droplets is inversely proportional to the pitch. Thus, to improve efficiency of the micro chemical plant, droplet fragmentation is one kind of solutions. For practical application, this micro chemical plant orients the organic synthesis or chemical processing to discover new chemicals and medicines. Furthermore, mass manufacturing is also possible by putting array of a device onto a plate and by stacking as "Little drops of water make the mighty ocean."

Acknowledgements

This work was partly supported by Japan Ministry of Education, Culture, Sports Science & technology Grant-in-Aid for COE Research and CREST, Japan Science and Technology Agency.

References

[1] K.F. Jensen, *Chemical Engineering Science*, **56,** 293-303 (2001).
[2] R.S. Wegeng, C.J. Call and M.K. Drost, *Spring National Meeting of the American Institute of Chemical Engineering*, PNNL-SA-27317 (1996)
[3] S.J. Peng and R. A. Williams, *Trans. IchemE*, **76,** 894-901 (1998)
[4] G.I. Taylor, *Proceedings of the Royal Society of London. Series A*, **146**, 501-523 (1934)
[5] J.R. Burns and C. Ramshaw, *Lab on a Chip*,**1**, 10-15 (2001)
[6] J.S. Go, E.H. Jeong, S.Y. Yoon, K.C. Kim and S. Shoji, *Micro Total Analysis Systems*, 1275-1278 (2003)

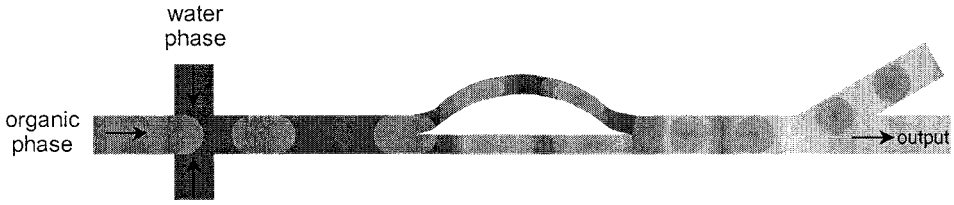

Figure. 1 Sequential chemical processes of the droplet phase flow of the immiscible fluids.

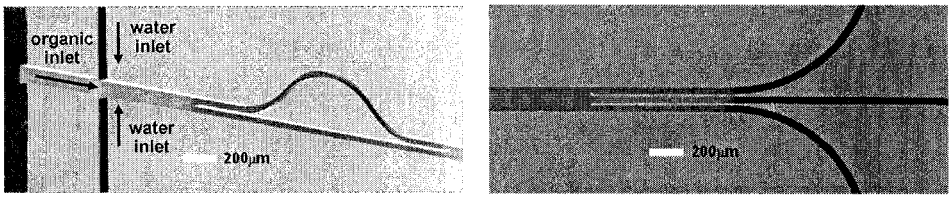

(A) droplet generation and digital sorting channel (B) reaction and separation channel

Figure. 2 Fabricated on-line micro chemical plant.

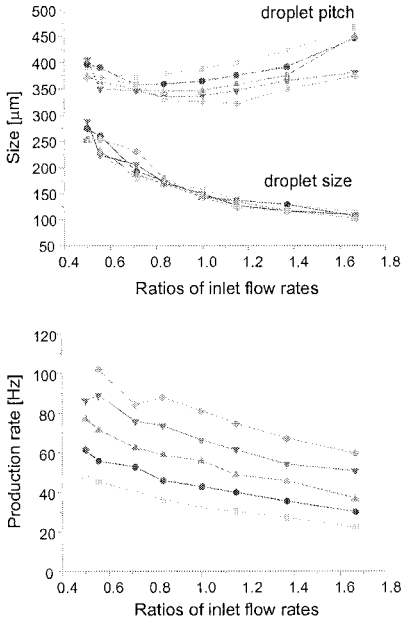

Figure. 4 Evaluation of droplet size, pitch and generation rate by increasing the ratio of inlet flow rates.

Figure. 3 Visualization of droplet generation.

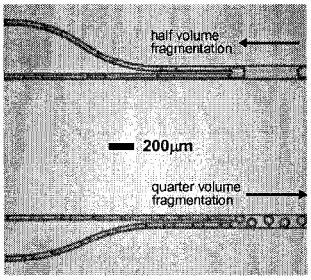

Figure. 5 Droplet fragmentation and digital sorting for effective reaction.

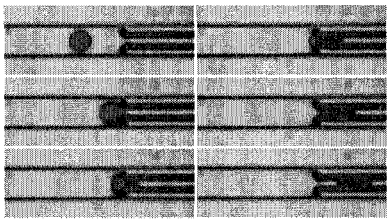

Figure. 6 In-channel separation of the reaction-completed droplets

A STABLE TWO PHASE FLOW BY "SOMBRERO" CHANNEL

Katsumasa Sakamoto[1], Hiroaki Nakanishi[2], Manabu Tokeshi[1], Yoshikazu Yoshida[1], Takehiko Kitamori[3]

[1]Research Association of Micro Chemical Process Technology, R&D-C1132, KSP-Bldg., 3-2-1, Sakado, Takatsu-ku, Kawasaki-shi, Kanagawa 213-0012, JAPAN

[2]Technology Reseach Laboratory, Shimadzu Corporation, 3-9-4, Hikaridai, Seika-cho, Souraku-gun, Kyoto 619-0237,JAPAN

[3]Departoment of Applied Chemistry, School of Engineering, The University of Tokyo, Hongo, Bunkyo-ku, Tokyo 113-8656,JAPAN

Abstract

Organic-aqueous liquid extraction is one of many standard techniques to efficiently separate target chemical compounds from a mixture. Among them, chloroform extraction has been very commonly used in organic synthesis and separation of inorganic complexes or biological samples [1] [2]. In micro fluidics, it was very difficult to realize a chloroform-aqueous extraction system, because interface between the two-phases was unstable. Though the stability of the two phase flow interface is dependent on the two phase combination, the chloroform-aqueous is one of most unstable combination. In order to stabilize this unstable two-phase flow, we developed a new "sombrero" channel. The sombrero channel has two guide structures and can stabilize interface between chloroform-aqueous two-phase flow with large specific interface area.

Keywords: Organic-Aqueous Liquid Extraction, Chloroform Extraction, Separation, Micro Fluidics, Two-Phase Flow.

1. Introduction

Micro space in microchannels is expected to be applied to novel methods of analytical chemistry, synthetic chemistry and biological chemistry, etc. A liquid in a micro space is characterized by large specific interface area and short diffusion distance. In micro fluidics, organic-aqueous liquid extraction is one of the key techniques. But interface between the organic-aqueous liquid phases tends to be unstable at low flow rate. Especially, it is difficult to stabilize interface between aqueous phase and chloroform, dichloromethane, hexane, etc. (Figure 1). We have developed a novel microchannel structure for realizing chloroform-aqueous extraction on microchip.

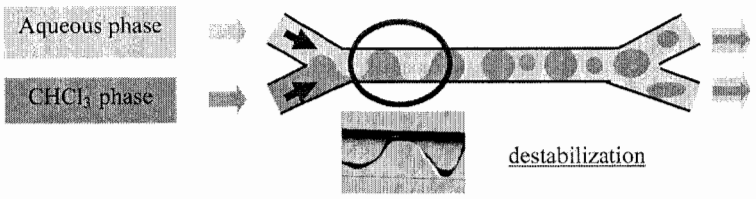

Figure 1 Problematic unsteady two phase flow resulting in poor recovery rate.

2. Concept

Until now, it has been reported that a channel with a guide structure stabilizes such unstable two-phase flows [3], but the specific interface area (interface area/volume) is relatively small. In this work, a novel microchannel with two guide structures to form a sombrero-like cross section was

newly developed. It could stabilize a chloroform-aqueous flow with large specific interface area (Table 1).

Table 1 Cross-sectional shape effect

	Previous works		This work
		single guide	double guide
Aqueous phase / $CHCl_3$ phase	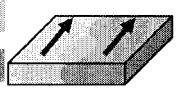		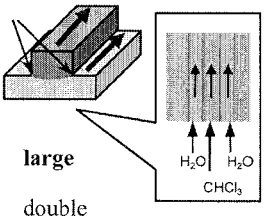
Stability	unstable	stable	
Specific interface	small	small	**large**
Guide	—	single	double

3. Experimental

The sombreo channel could be made by a simple process described in Figure 2a. Microchips used in this work were fabricated in Pyrex glass substrates using standard photolithographic and wet chemical etching techniques. A plate with narrow channel (100 um wide, 40 um deep and 120 mm long) was bonded to another plate with wide channel (300 um wide, 40 um deep and 120 mm long). A schematic cross-sectional view of the sombrero channel is depicted in Figure 2b.

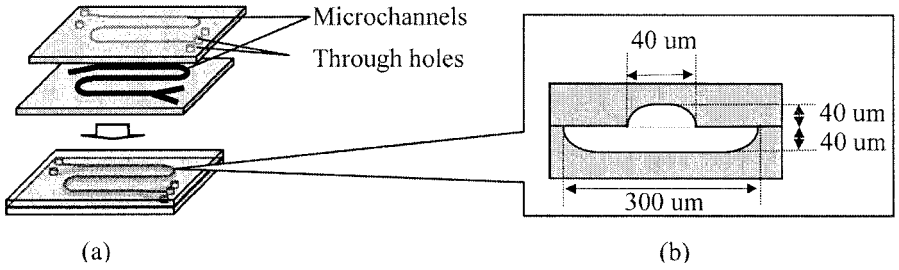

Figure 2 Fabrication diagram of a sombrero (gibbosity) channel

The chloroform and aqueous solutions were introduced into the microchannels by two syringes and microsyringe pumps in order to control the flow rate. Epoxy glue was used to connect each syringe needle to a Teflon screw with an O-ring and a fused-silica capillary tube. The Teflon screw was set on PVC holders that sandwiched the microchip.

Extraction of benzoic acid from chloroform solutions to pH 9.1 phosphate buffered solutions was carried out using a simple channel and the sombrero channel (Figure 3). Extraction efficiencies were analyzed by using high performance liquid chromatography (HPLC). 10 mM methyl benzoate was added as an internal standard. The total flow rate was changed from 12 to 180 [uL/min]. (Chloroform solutions: phosphate buffered solutions was fixed at 5:1)

4. Results and discussion

The interface became unstable in the simple channel at low flow rates, and the measurement was not possible. However, the sombrero channel could stabilize the two-phase flow even at low flow rates, and high extraction efficiency was achieved. From the experimental result, the interface of the simple channel was stable in the flow rate between 120 and 180 [uL/min], and the interface of sombrero channel was stable in the flow rate between 12 and180 [uL/min], as shown in figure 3. It was proven that interface of the sombrero channel was stable at low flow of about 1/10. Extraction efficiency of sombrero channel reached over 90 % yield. The sombrero channel was also effective for other organic solvents (e.g. dichloromethane and hexane)

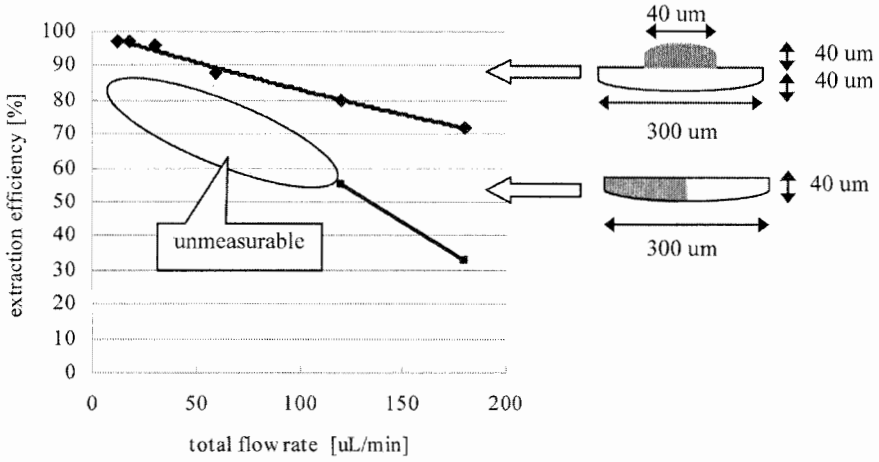

Figure 3 Relationship between flow rates and extraction efficiency. The initial concentration of the benzoic acid chloroform solution was 10 mM.

5. Conclusions

The sombrero channel of microchip, which could stabilize organic-aqueous two-phase flow with large specific interface area, was newly developed. Using this new microchip, chloroform-aqueous extraction on microchip was realized more effectively.

Acknowledgements

This work was supported by the New Energy and Industrial Technology Development Organization (NEDO) of the Ministry of Economy, Trade and Industry, Japan.

References

[1] A. Aota, M. Nonaka, A, Hibara and T. Kitamori., MicroTAS '03, pp. 441-444.V. Reddy, S.

[2] Yang, and J. D. Zahn., MicroTAS '03, pp. 437-440.

[3] Mariana Surmeian, Maxim N. Slyadnev, Hideaki Hisamoto, Akihide Hibara, Kenji Uchiyama, and Takehiko Kitamori. *Anal. Chem.* **2002**, *74*, 1565-1571.

LARGE CONCENTRATION CHANGES DUE TO THERMAL DIFFUSION EFFECTS IN GAS FLOW MICROSYSTEMS WITH TEMPERATURE GRADIENTS

U. J. Quaade[1], T. Johannessen[1], S. Jensen[2], O. Hansen[2]

[1]*Interdisciplinary Research Center for Catalysis (ICAT), Technical University of Denmark, Building 312, DK-2800 Kgs. Lyngby*

[2]*MIC – Department of Micro- and Nanotechnology, Technical University of Denmark, Building 345E, DK-2800 Kgs. Lyngby*

Abstract

Thermal diffusion, or Sorét diffusion, is shown to cause significant concentration changes and transients in gas flow microsystems with temperature gradients. In a silicon microsystem, a temperature gradient of about 100 °C/mm is measured to produce concentration transients of up to 13.7 % in an argon/helium mixture, when the flow is abruptly changed from a high value to a low value. Finite element simulations of the thermal diffusion in a geometry similar to the experimental setup reproduce the measurements.

Keywords: thermal diffusion, Sorét diffusion, microsystems

1. Introduction

Thermal diffusion is a transport mechanism in gas mixtures that causes a temperature gradient to induce a concentration gradient [1]. Typically, lighter elements are transported toward the hot region and heavy elements toward the cold region. The effect increases with increasing temperature gradient and with increasing molecular weight differences for the components in the gas. In steady state the thermal diffusion is exactly opposed by normal diffusion as given for a one-dimensional two-component system by [1]:

$$0 = j_A^x + j_A^T = -\frac{c^2}{\rho} M_A M_B D_{AB} \left(\frac{dx_A}{dz} + \frac{k_T}{T} \frac{dT}{dz} \right),$$

where j_A^x and j_A^T are the normal diffusion and thermal diffusion fluxes respectively for component A. The molar density is c, ρ is the density, D_{AB} is the diffusivity of the gas pair AB, M_A is the molar weight of A, x_A is the mole fraction of A, k_T is the thermal diffusion ratio and T is the temperature. Due to the small distances in microsystems large temperature gradients easily build up either in the device itself or at the interfacings. This leads to potential concentration changes for gas mixtures in the device.

2. Experiments

The thermal diffusion is investigated in the microfluidic system shown in Figure 1. The system is heated uniformly with temperature gradients between the chip and the interfacing only. Thus the temperature gradient will be parallel to the flow direction at the inlet to the reactor. A mixture of argon and helium flows through the system at ambient pressure. At low convective fluxes the temperature gradient will force the helium to move from the cold region to the hot region and argon to move from the hot to the cold region. This will cause an increase in the argon concentration in front of the inlet and a transient of reduced argon concentration in the microsystem, until steady state is reached. If the convective flux is now increased to a value above the thermal diffusion flux, the accumulated argon in the inlet will be flushed through the microsystem showing a transient of increased argon concentration until the concentrations in the system reach a new steady state. In this way the temperature gradient acts as a mass filter at low flows.

3. Results

Figure 2 shows the concentration changes in the microsystem, measured using a mass spectrometer, when the flow rate through the microsystem is varied. The microsystem is heated to 150 °C and the interfacing is held at room temperature. The used gas mixture is 5% argon in helium. When the flow is changed from 1 mL/min to 0.1 mL/min, the argon concentration show a transient lasting about 10 min. The concentration of the heavy component, argon decreases and accordingly the concentration of the light component, helium increases (not shown). The measured maximum relative change in the argon concentration is -13.7%. Figure 2 also shows a finite element simulation using non-steady state computational fluid dynamics with multi-component diffusion including thermal diffusion for a geometry similar to the experimental setup. The simulated concentration variation agrees well with the measurements.

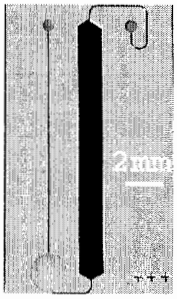

Figure 1. Microfabricated gas reactor designed for heterogeneous catalysis experiments [2]. However, for the flow measurements presented here the reactor contains no catalyst.

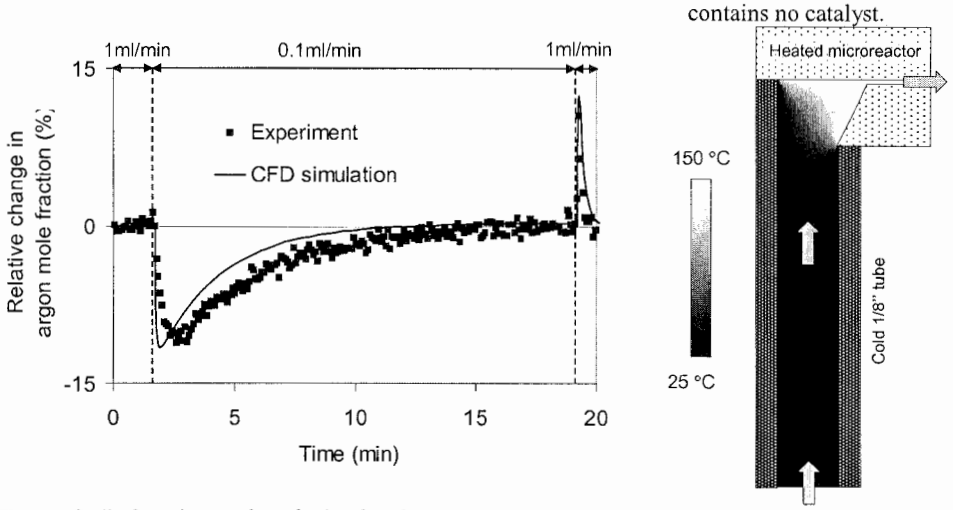

Figure 2. Left: Observed and simulated concentration transients when the flow through the microreactor is changed from 1mL/min to 0.1 mL/min and back to 1mL/min. Right: Simulated temperature distribution in the gas at the interfacing.

In Figure 3, a transient simulation of the concentration profile of argon along a central streamline is depicted for different simulation times, when the flow is switched from 1mL/min to 0.1 L/min. The streamline is indicated to the right in Figure 3. Initially, the steady state situation at 1ml/minute shows a relatively small build-up of argon in front of the thermal gradient close to the interface between tube and microsystem. The argon concentration at each side of the peak is identical – as it should be at steady state. Shortly after decreasing the flow (intermediate time #1), the argon concentration drops in the microsystem as a consequence of the mass filtering effect, and the build-up peak increases backwards in the interfacing. At intermediate time #2, the build-up zone

has become much larger and the increase of argon concentration in this gas volume causes the corresponding lack of argon, which is seen in for several minutes in Figure 2. At the new steady state at 0.1 mL/min, the inlet and outlet argon levels are again identical and the only difference between steady state at 1mL/min and 0.1mL/min is the size of the argon concentration in the build-up zone.

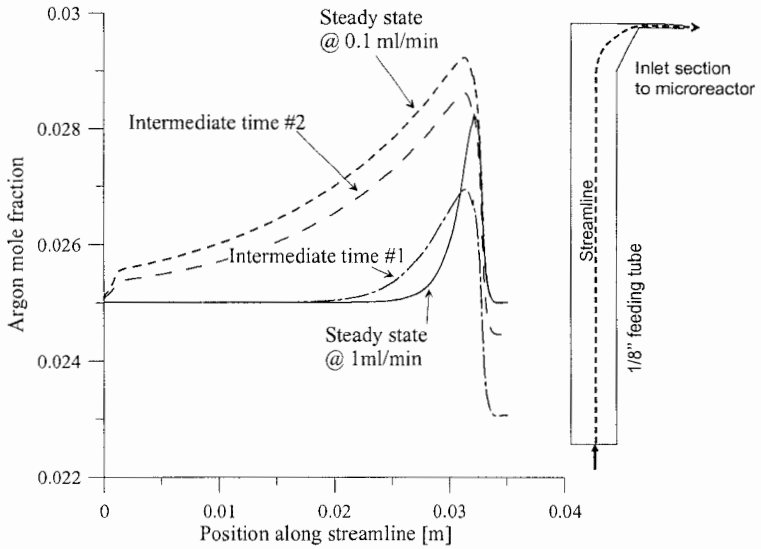

Figure 3. Left: Simulation of the transient concentration profiles along a streamline when the flow is switched from 1mL/min to 0.1 mL/min. Right: Indication of streamline

With an effect in excess of 10 % even at moderate temperatures the findings have implications for any concentration dependent microsystem that operates at elevated temperature such as heterogeneous catalysed microreactors [3] or microfabricated gas analysis systems.

[1] R. B. Bird, W. E. Stewart, E. N. Lightfoot, "Transport Phenomena", John Wiley & Sons, Inc 1960.
[2] S. Thybo, S. Jensen, J. Johansen, T. Johannessen, O. Hansen and U. J. Quaade, "Flame spray deposition of porous catalyst on surfaces and in microsystems ", Journal of Catalysis **223/2**, 271-277 (2004).
[3] K. F. Jensen, "Microreaction engineering – is small better?", Chemical Engineering Science **56,** 293-303 (2001)

NOVEL MEMBRANE DEVICES IN UNILATERAL CONFIGURATION

Yuji Murakami [1, 2], Yoshikazu Yoshida[1] and Takehiko Kitamori[3]

[1]*Research Association of Micro Chemical Process Technology, R&D-C1132, KSP-Bldg., 3-2-1, Sakado, Takatsu, Kawasaki, Kanagawa 213-0012 JAPAN*

[2]*New Frontiers Research Laboratories, Toray Industries, Inc., 1111, Tebiro, Kamakura, Kanagawa 248-8555 JAPAN*

[3]*Department of Applied Chemistry, School of Engineering, University of Tokyo, Hongo, Bunkyo, Tokyo 113-8656 JAPAN*

Abstract

Novel microdevices for membrane separation are proposed. In the proposed configuration, two chambers or flow channels on both sides of the membrane required in classical membrane devices are formed on only one side of the membrane, namely unilateral configuration. Preliminar results were obtained by using microfiltration devices in this configuration photolithografically fabricated with PMMA plates. Their theoretical aspect is also discussed.

Keywords: membrane separation, filtration, dialyze, unilateral configuration

1. Introduction

Membrane separation is an important unit operation, and various membranes have been already commercially available for each application such as filtration, dialysis and support for catalysis. Several microfluidic devices with a membrane have been reported with various fabrication methods. Though inside formation at the interface of multiphase flow [1, 2] might be useful for future application, the use of a membrane prepared without chip restrictions is beneficial at the early stage for a practical use. In order to bring a membrane into inside of a chip, two plates should be microfabricated to sandwich the membrane [3, 4]. However, microfabrication of the both plate and their precise alignment for bonding increases a fabrication cost.

2. Theory

A membrane separation device requires two reservoirs or flow channels on a membrane as up- and downstream. Classical membrane devices have them on both sides of the membrane, *i.e.*, bilateral configuration (Table 1). In the sandwiched device reported, solution permeated or small components diffused through the membrane from an upstream channel on a plate to a downstream channel on the other plate (hetero-planar). In the case of *in situ* formation of membrane in microchannel, both of the two channels divided by the membrane are located on the same plate (coplanar). "Unilateral" means "only one side of." A membrane device in unilateral configuration consists of a microfabricated plate with coplanar channels, a sandwiched membrane, and another plate. Solution in upstream first permeates into the membrane, then moves to lateral direction, and finally comes out into a downstream channel. Because membrane is not formed in a channel but sandwiched by plates, various kinds of membrane with lateral permeability are applicable to the configuration. The configuration requires only one plate microfabrication, which is cost effective (compared to classical sandwich devices). No precise alignment of two plates is necessary.

Effective area, thickness of a membrane and differential pressure defines characteristics of a membrane device. The effective area of classical membrane devices is the area of the membrane contact to up- or downstream channel. Because permeation is mainly lateral direction in unilateral configuration, the effective area is approximately the cross-sectional area defined by the edge length of channels or reservoirs facing each other and the membrane thickness. The 'thickness' as

Table 1. Comparison of the structure of the proposed configuration to other reported devices.

	reported		this research
cross-section Plate Membrane Upstream Downstream Permeation	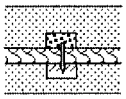	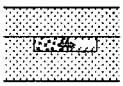	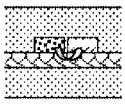
membrane	sandwich	coplanar	sandwich
configuration	bilateral		unilateral
channels	hetero-planar	coplanar	

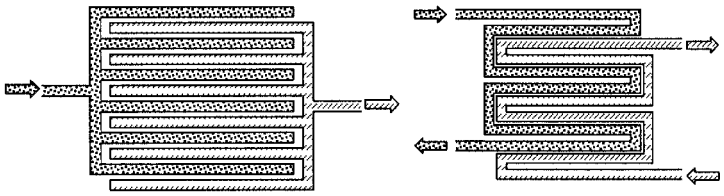

Interdigitated comb pattern for filtration

Folded parallel pattern for dialyzing

Figure 1. Two basic channel designs for unilateral configuration.

permeation distance in classical devices is the gap length between up- and downstream channels or reservoirs in proposed. The thickness of membranes commercially available is from several micrometers to sub millimeter, and typically from several tens micrometers to several hundreds micrometers. It is possible to reduce the gap length less than the membrane thickness by various microfabrication techniques. Closely aligned channels can give virtual thin membrane characteristics with a normal thick membrane. Though the channels or reservoirs can be shaped into any pattern, an interdigitated comb pattern for filtration and folded parallel pattern for dialysis as shown Figure 1 are suitable to the configuration to increase effective area. The use of more than two sheet of membrane overlapped each other can also increase the effective area membrane.

3. Experimental

A SU-8 mold structure was photolithographically developed on a Si wafer with a standard method. A PMMA plate was hot-pressed with the mold to have grooves, and was drilled to have access holes at an end of grooves. A membrane (GH Polypro, pore size 0.45μm, Pall) was sandwiched with the plate and another PMMA plate, and then they were hot-pressed to seal each other. Flow system consisted of a syringe pump, a sample injector, a pressure sensor, a clamp-type holder and the chip connected in tandem by PEEK tubes and connectors.

4. Results and discussion

At first, the fabricated chip without hot-press sealing was employed in a flow system. Though the use of thin PDMS film as a spacer could enhance pressure durability, it was easy to leak. No leak through an interface between the two plates was observed in the chip sealed by hot-press up to

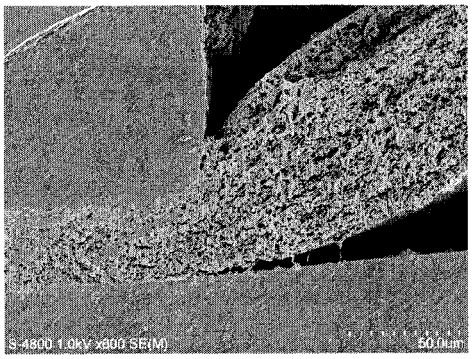

Figure 2. Cross-sectional view of the fabricated device at channel edge. A membrane was sandwiched between a top plate with grooves and a bottom flat plate

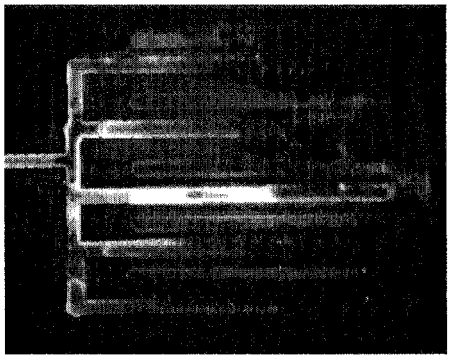

Figure 3. Fluorescence observation of interdigitated comb type filter device in unilateral configuration after FITC labeled particle injection.

3mL/min under the differential pressure of less than 200kPa. Pressure at each flow rate of a closely aligned device was lower than that of the distantly aligned device for comparison. The pressure was also lower than the estimated from bulk value, suggesting alteration of membrane characteristics by heat treatment. SEM observation of its cross-section revealed that the membrane thickness (initially 110μm) was decreased to 40μm, but inside structure of the membrane was still porous as shown in Figure 2. There was no gap between the membrane and the plates where solution should permeate laterally. A gap at the edge of the membrane was filled with PMMA. The unpressed area of a membrane on channel occupied considerable area of the channel. In the case of shallow depth, it was easy to choke up. Thus the channel should have enough depth. The use of a dug structure in several tens micrometer on a plate opposite to the channels could reduce the membrane inroad.

Fig. 3 shows a filtrated bead pattern by a PMMA chip with interdigitated comb pattern in unilateral configuration with a channel width of 500μm. The injected beads were completely filtered in upstream area, though some beads slipped into an interface between the wall and membrane in the case of a PDMS chip in the same pattern. The beads were trapped at not only edge but center of channels. Additional injection of rhodamine solution revealed that the solution flowed from upstream comb to downstream one. These results shows that the possibility of the proposed unilateral configuration in microfluidics.

Acknowledgements

This work was supported by the New Energy and Industrial Technology Development Organization (NEDO) of the Ministry of Economy, Trade and Industry, Japan.

References

[1] H. Hisamoto, Y. Shimizu, K. Uchiyama, M. Tokeshi, Y. Kikutani, A. Hibara and T. Kitamori, *Anal. Chem.*, 75, 350-354 (2003).

[2] B. Zhao, N. O. L. Viernes, J. S. Moore and D. J. Beebe, *J. Am. Chem. Soc.*, 124(19), 5284-5285 (2002).

[3] N. Xu, Y. Lin, S. A. Hofstadler, D. Matson, C. J. Call and R. D. Smith, *Anal. Chem.*, 70, 3553-3556 (1998).

[4] D. M. Cannon, Jr., T.-C. Kuo, P. W. Bohn, and J. V. Sweedler, *Anal. Chem.*, 75, 2224-2230, (2003).

TOWARDS ON–CHIP SHEAR-DRIVEN CIRCULAR CHROMATOGRAPHY

Xin Yang* & Andreas Manz**

** Imperial College London, SW7 2AZ*

***ISAS Institute for Analytical Sciences, D-44139 Dortmund, Germany*

Abstract

An experimental proof of principal for using shear force for the generation of flow in a circular micro-channel is presented. Using shear driven flow in a circular micro-channel opens up the possibility of performing circular chromatography allowing an effectively infinite separation column [1].In our setup, we were able to successfully move a sample plug at speeds exceeding 1.4 revolutions per minute through an 8 μm deep, 2 mm wide and 69 mm long circular channel. We demonstrate that the speed of flow inside the circular channel is half the speed of the rotation wall, as predicted by theoretical calculations presented by Desmet et.al. [2].

Keywords: circular chromatography, shear-driven

1. Introduction

Presently, most of the conventional chromatography techniques for generating the mobile phase flow are either pressure-driven or electrically driven. Due to the Joule heating and Poiseuille pressure drop law, both of these two flow generation methods have maximum flow rate limitations. As a means to break through these analysis time limitations, a novel method, which is shear-driven flow, has been used for generating the mobile phase flow. Shear-driven flow can also be used to generate a circular flow in a closed circuit since no pressure or electric field gradient is required. This could allow chromatographic separations in which the column length can be infinitely varied simply by choosing the number of circuits around a circular channel.

2. Theory

Shear flow takes advantage of the viscosity of the fluid such that in a channel in which one boundary wall is kept fixed, a flow can be generated by moving the other boundary wall. The fluid which is in contact with the boundary adheres to it and will therefore have the same velocity as the boundary. Subsequent layers of the fluid are also affected due to viscosity such that flow is generated within the channel. It has been shown that for a channel in which the depth is much smaller than the channel width, a linear flow profile is obtained with the mean velocity being half the velocity of the moving wall (see Fig. 1).

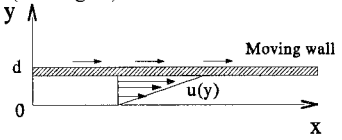

Figure 1. Linear shear-flow profile

Shear-driven flow can be applied to many different channel geometries, including circular channels. This could enable the application of shear flow to perform circular chromatography. In principle, chromatography which is performed in a circular channel will benefit from the infinite length of the separation column and the plate number will proportional to the analysis time. For detection, techniques such as multiple point detection, Fourier and wavelet transform detection can be applied to improve analytical performance.

3. Experimental

Chip Fabrication: In the experiment, two pieces of soda lime glass substrate are used. One substrate contains a donut shaped circular channel, as shown in Fig.2, which was wet etched using photolithography to a depth of 8 μm. The other substrate simply contains two holes; one is used for injecting samples whilst the other is for withdrawing waste. The distance of these two holes is about 1 mm. Both of them are connected via fused silica capillary to two syringe pumps.

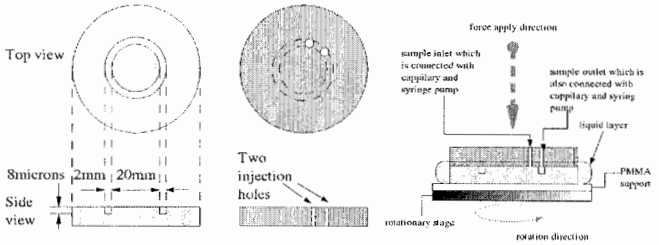

Figure 2. Top view and side view of shear-driven circular

Setup: In our setup, the substrate containing the circular channel was glued to a bigger PMMA plate and mounted on a rotation stage (PI GmbH & Co, Germany). The substrate used for injection was clamped on top of the channel substrate using a clamp made in-house. Fig. 3 shows a photograph of the setup. The clamp kept the top plate stationary whilst the channel plate, fixed to the stage, could be rotated underneath.

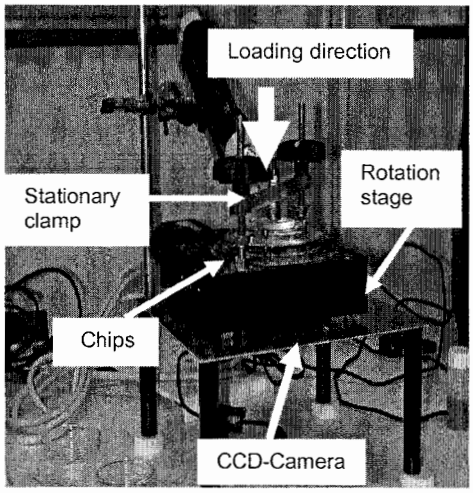

Figure 3. Photograph of experiment set up

Experiment: To visualize the displacement of the rotation plate, a marker line was drawn on the edge of the channel. The channel was filled with methanol and then the top plate was carefully mounted above the channel plate and pressed together. A small amount of concentrated Rodamine B solution (0.016 μl) was injected. At the same time, an identical volume of solution was sucked out through the other hole. By this method, a well-defined sample plug was achieved. After injection, the stage was rotated and the flow inside the circular channel generated. A CCD camera was used for video capture and a sequence of 4 pictures is shown in Fig. 4.

Figure 4. Sequence of photographs of micro-channel flow experiments (d = 8 μm, w = 2 mm), which were taken at each quarter of a turn. Rotation speed is about 44.0 sec per turn. The marker line is moving with the rotation stage.

4. Results and discussion

Fluorescence detection was also performed using 600 μM Fluorescein Isothisocyanate (FITC) in sodium phosphate buffer. The circular channel was filled with 4mM sodium phosphate buffer (pH=5) and 0.016 μl of FITC injected using the method described above. In this case the rotation system was mounted on an inverted Microscope (Nikon TE-200), which is equipped with a 200W Mercury Lamp and a PMT. The rotation speed was set to 0.34 revolutions per minute and the resultant fluorescence signal data, shown in Fig. 4, shows the sample plug moving at about half the rotation speed. Furthermore, Fig. 5, shows a Fast Fourier Transform (FFT) applied to same data which shows a frequency peak at 2.7×10^{-3} Hz corresponding to half the speed of rotation. Another peak at 5.4×10^{-3} Hz corresponds to noise associated with the rotation of the stage system.

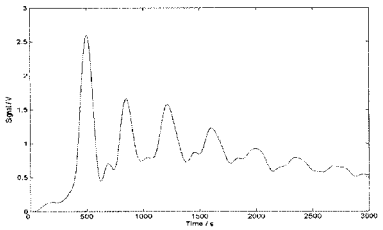

Figure 4. PMT signal. The rotation speed is about 176 sec per turn. Sample occurs about 352 sec per turn.

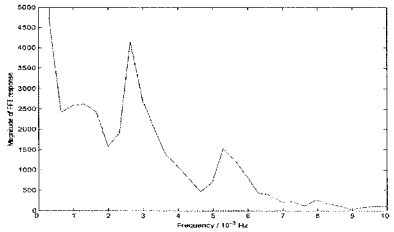

Figure 5. Frequency analysis of time domain signal achieved by applying Fast Fourier Transform to the signal shown in Fig. 4.

References

[1] J. C. T. Eijkel, A. van den Berg and A. Manz., Electrophoresis 2004, 25, pp.243-252
[2] G. Desmet and G. V. Baron., Anal. Chem., 2000, 72 pp.2160-2165

COMPARISON OF HYDRODYNAMIC VERSUS ELECTROOSMOTIC DRIVEN FLOWS FOR ENZYMATIC PROTEIN DIGESTION IN A MICROREACTOR

N. Sarrut, S. Bouffet*, O. Constantin**, J. Garin*, F. Mittler**, J. Sudor**, F. Vinet****

**CEA Grenoble - DSV/DRDC 17 av. des Martyrs, 38054 Grenoble France*
*** CEA-LETI Grenoble - DRT/DTBS, 17 av. des Martyrs, 38054 Grenoble France*

Abstract

Enzymatic digestion is an essential step of majority of protein identification protocols. A comparative study between hydrodynamic and electroosmotic driven flows in micro-machined reactors has been performed for each peptide of a Cytochrome C digest by Q-TOF mass spectrometry [1].

Keywords: protein digestion, microreactor, electroosmosis, electrophoresis

1. Microchip fabrication and chemical treatment

The microchip fabrication is derived from semiconductor technology using mainly photolithography and deep reactive ion etching steps. In order to obtain a microreactor with large surface/volume ratio, hexagonal micro-columns of 14µm in diameter, 50µm in height and 5µm pitch are etched in silicon (Fig.1) [2]. A thermal oxidation decreases the space between micro-columns down to 1,7µm and allows an electrical isolation of the channel, that is essential for the electroosmotic experiments. A transparent Pyrex cap (*CORNING 7740*) containing inlet and outlet holes is sealed on the microreactor by molecular bonding. Standard microfluidic connectors (*Nanoport™ assemblies*) are glued on the top of the cap opposite to the etched holes, and can be used either for electroosmotic or hydrodynamic flows. For electroosmosis, platinum electrodes are introduced directly into the connectors while for hydrodynamic pumping, another connecting part ensures the fixation of a silica capillary of 360µm (Fig.2).

We have developed a reliable surface chemistry on silicon oxide surface with covalently attached trypsin through the amino groups of lysine residues and aldehyde alkyl silane [3]. The different chemistry steps are performed by introducing the chemical solutions with syringe pumps connected to the microreactor after its complete assembly. The activity and the reaction kinetics of the immobilized trypsin is monitored by the UV absorbance at 253nm of the degradation product of the hydrolysis of N- Benzoyl Arginine Ethyl Ester. The apparent Michaelis-Menten kinetics constant (Km) and Vmax values were respectively 0.154 mM and 9.5×10^{-4} $mM.mn^{-1}$ and are very close to that generally reported in the literature and in agreement with the proposed model.

2. Theory

Pressure driven flows in small diameter channels are often characterized by small Reynolds number, typically on the order of unity or smaller. In such circumstances, the convective terms of Navier-Stokes equations are not important and the flow is laminar with parabolic profile. In a circular geometry, the flow velocity $V_{\Delta P}$ is proportional to the square of channel diameter R, the pressure gradient ΔP and inversely proportional to the fluid viscosity η:

$$V_{\Delta P} \sim R^2 \Delta P / \eta \qquad (1)$$

Biological molecules, such as proteins or peptides, dissolved in a solution that is being pumped through a channel will all migrate with a constant velocity described by the equation 1. Consequently, their relative concentrations should be conserved during the transport process in the case when the total digestion of the proteins is assured and no selective adsorption of peptides on the channel surface is assumed.

Situation is quite different for electrokinetic flows. When an electric field is applied across a channel with charged wall, the electric force acts on the volume charge in the electrical double layer and, consequently, sets the fluid into motion. This phenomenon is called electroosmosis. The electroosmotic velocity V_{EO} is proportional to the surface charge (zeta potential) Ψ_z, the electric field strength ΔE and the solution's viscosity in the electrical double layer η:

$$V_{EO} \sim \Psi_z \Delta E / \eta \qquad (2)$$

Additionally, the electric force also acts on charged molecules (peptides, proteins) in the solution. Each charged molecule will migrate in the solution with its proper velocity V_{EL} that, for

small molecules ($r << \kappa^{-1}$, where r is the molecule's diameter and κ^{-1} is the thickness of the electrical double layer) is described as:

$$V_{EL} = q\Delta E / 6\pi r\eta \quad (3)$$

where q is the charge of the molecule. The total velocity V_{TOT} of migrating peptides inside a channel is then given by the sum of the equations 2 and 3:

$$V_{TOT} = V_{EO} + V_{EL} \quad (4)$$

Since each charged molecules (peptide) has a proper electrophoretic mobility, we expect that during the transport process the relative concentrations of the peptides in the solution will be altered. In particular, we anticipate (i) to loose peptides migrating against the electroosmotic flow (pI < pH) and (ii) to concentrate peptides moving in the same direction as the electroosmotic flow (pI > pH).

3. Experimental

For both hydrodynamic and electroosmotic experiments, the flow rate of the buffered protein solution is set to 80nl.min^{-1}. We used NH_4HCO_3 (25mM; pH=7,8) buffer for all the experiments and a *kd Scientific* syringe pump to generate the hydrodynamic flows. For the electroosmotic experiments, after a digestion buffer pre-filling, the flow is ensured by an electrical field of 200V.cm^{-1} applied between the positively charged electrode positioned at the inlet, and the negatively charged one, at the outlet. At pH=7,8, the reactor surface (thermal SiO_2 with attached trypsin) is negatively charged. Residence time of degraded protein and peptides inside the reactor is 6,25min.

After digestion is completed, the peptides solution is collected at the channel outlet and subsequently dried in a Speedvac. The digest is then dissolved in a volume of a 50% acetonitrile 0.1% formic acid solution equal to the volume pumped by hydrodynamic or electroosmotic flows, vortexed 30s and sonicated 2min. Off-line MS analyses are performed on a QTOF mass spectrometer. Mass spectra are obtained after summing 20s of the signal acquired.

4. Results and discussion

Digestion experiments of Cytochrome C at different concentrations (10pmol.µl^{-1}, 2pmol.µl^{-1}, 200fmol.µl^{-1}) have been carried out both in hydrodynamic and electroosmotic flows. As anticipated above, the two Q-TOF spectra present different signatures (Fig.3). The analysis of the table and the graph of the figure 4 shows that high isoelectrical point peptides (i.e. pI>pH) are obtained in higher ratios when electroosmotic pumping is employed. For low isoelectrical point peptides, the opposite effect is observed. These experimental results confirm the suspected parasitic electrophoretic phenomenon which induces a reverse pumping of the negatively charged peptides, and an increase of the speed of the positively charged one. Nevertheless, in electroosmotic driven flow, as negatively charged peptides are still present at the outlet, we can say that electroosmotic velocity is the fluidic preponderant contribution.

5. Conclusions

We can conclude that for enzymatic protein digestion, electroosmosis can be used in the micro-columns reactors with surface attached trypsin. No particular problems of non-specific adsorption have been observed in this configuration and the loss of some peptides due to electrophoresis does not disturb significantly the protein identification.

References

[1] Lian Ji Jin, Jerome Ferrance, Joshua C. Sanders and James P. Landers, A microchip-based proteolytic system driven by electroosmotic pumping, Lab Chip, 3, 2003, 11-18

[2] Bing He, Niall Tait and Fred Regnier, Fabrication of nanocolumns for liquid chromatography, Anal. Chem. 70, 1998, 3790-3797

[3] Françoise Vinet, Philippe Combette, Gérard Lanneau, Frédérique Mittler, Gilles Marchand, Pittsburgh Conference, 2002, St Louis, LA, USA

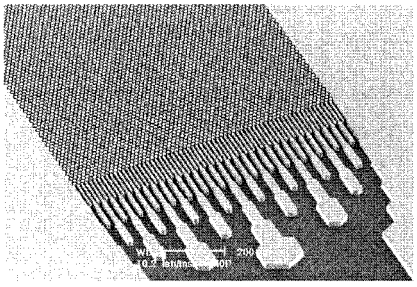

Figure 1. Microreactor of enzymatic protein digestion.

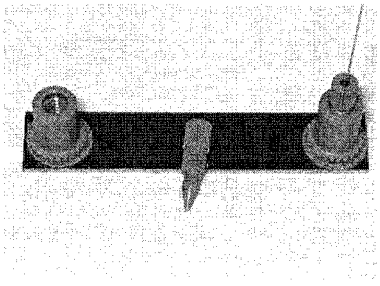

Figure 2. Silicon microchip with fluidic connectors.

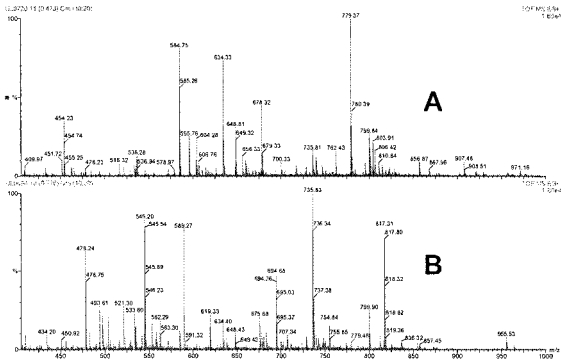

Figure 3. Trypsin digestion of cytochrome C in microreactor (10pmol/µl in 25mM NH_4HCO_3) Flow rate: 80nl.min^{-1}
A. Hydrodynamic driven flow **B**. Electroosmostic driven flow

Res	M+H	Sequence	pI	E/H
73-79	806.48	KYIPGTK	9.97	1.09
80-87	907.56	MIFAGIKK	10.41	26.21
100-104	562.28	KATNE	6.41	0.07
28-38	1168.64	TGPNLHGLFGR	10.15	6.10
1-5	589.28	GDVEK	4.32	0.02
56-60	604.35	GITWK	9.35	6.95
9-13	634.39	IFVQK	9.35	4.29
28-39	1296.72	TGPNLHGLFGRK	11.2	51.10
89-99	1350.74	TEREDLIAYLK	4.68	0.09
74-79	678.38	YIPGTK	9.06	3.43
40-53	1470.7	TGQAPGFTYTDANK	6.18	0.15
88-99	1478.82	KTEREDLIAYLK	6.58	1.22
80-86	779.45	MIFAGIK	9.35	21.57
39-53	1598.78	KTGQAPGFTYTDANK	9	0.99
40-55	1712.84	TGQAPGFTYTDANKNK	9	2.37
92-99	964.54	EDLIAYLK	4.32	0.34
56-72	2081.04	GITWKEETLMEYLENPK	5.42	0.07
56-73	2209.12	GITWKEETLMEYLENPKK	4.99	0.34

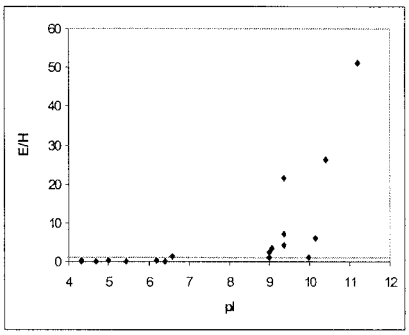

Figure 4.
a. Intensity ratio (E/H) of peptides of Cytochrome C digested by trypsin in electroosmosis (E) and hydrodynamic (H).
b. Intensity ratio (E/H) of peptides versus Isoelectrical point (pI)

EXPERIMENTAL AND NUMERICAL STUDY OF KORTEWEG STRESS IN CONTINUOUS FLOW CHEMICAL PROCESSING ON MICROCHIP

Yasuhiko Sugii[1], Koji Okamoto[1], Akihide Hibara[2], Manabu Tokeshi[3] and Takehiko Kitamori[2]

[1]Dept.of Quantum Engineering and Systems Science, [2]Dept. of Applied Chemistry, University of Tokyo, 7-3-1, Hongo, Bunkyo-ku, Tokyo 113-8656, Japan

[3] Integrated Chemistry Project, Kanagawa Academy of Science and Technology, 3-2-1, Sakado, Takatsu-ku, Kawasaki-shi, Kanagawa 213-0012, Japan

Abstract

Miscible liquid two-layer flow in a Y-shaped microfluidic device with 120 μm in width and 33 μm in depth, is investigated using particle image velocimetry (PIV) to clarify the flow characteristics at fluid interfaces. The obtained velocities with a spatial resolution of 5.9 x 1.5 μm^2 around the interface between water and ethanol indicate an imbalance in shear stress at interface. The numerical simulation based on the Korteweg stress generated by interfacial tension gradient was carried out. The stress may cause an interfacial instability and destroy a uniform mixing in two flowing fluids in the case of large concatenation gradient.

Keywords: Korteweg stress, Continuous Flow Chemical Processing, Interfacial Tension, Micro PIV

1. Introduction

Continuous-flow chemical processing (CFCP) based on microunit operations, in which two or more fluids flow in parallel in microchannels, has been proposed [1]. In order to design the system, it is important to investigate the dynamics such as mixing, molecular transformation and interfacial instability in both of miscible and immiscible multi-layer flow. In the study, micro-PIV technique was applied to the analysis of miscible liquid two-layer flow in a micro fluidic device to clarify the flow characteristics at an interface. The momentum balance between water - ethanol flow around an interface was investigated using measured velocity distributions.

2. Experiment

The microchip was fabricated on Pyrex substrates using standard photolithographic and wet chemical etching techniques and thin glass plate was covered on the top [2]. The microchip was a Y-junction between two inlets and one outlet, fabricated as microchannels of 120 μm in width and 33 μm in depth at the deepest point (semi-circular cross-section). Two fluid systems were examined; ion-exchanged water and ethanol (99.5 vol%). The two liquids were introduced into the inlets of the microchip at a constant flow rate using two independent syringe pumps of 250 μL capacity. The flow rates at the inlet for water - ethanol were set to 500 μL/h water and 400 μL/h ethanol. The ethanol flow rate was set such that the interface at the Y-junction would remain at the midpoint in the downstream channel. The refractive indexes of water and ethanol are 1.33 and 1.36, and the densities are 1.0 and 0.79 g/cm^3 at 10 °C, respectively. Ethanol is readily soluble in water, and has a diffusion coefficient $D = 1.0 \times 10^{-6}$ cm^2/s. Viscosity increases sharply from 1.3 cP to a maximum of 4.2 cP at a concentration of around 40 vol% and then decreases to 1.5 cP. Surface tension decreases rapidly with increasing ethanol concentration at low concentration, from 73.4 to 22.6 dyn/cm after a more gently gradient.

Micro PIV technique [3] was used for measuring velocity fields in the microchip. Fluorescent particles with diameter of 1 μm and density 1.05 g/cm^3 were dispersed in the water and ethanol for PIV. The fluorescent particles absorb green light (peak wavelength 535 nm) and emit orange light

(575 nm). The observation region was illuminated with a double-pulsed Nd:YAG laser (532 nm) captured through a microscope equipped with an oil-immersion objective lens (M = 60, NA = 1.25). The particle images were recorded using high-sensitivity CCD camera with 12-bit grayscale and 1280 x 1024 pixels equipped with an optical filter (low-pass: 550 nm) such that only the fluorescence was imaged.

3. Results and discussion

Fig. 1 shows the time-averaged velocity distributions of 164 maps in case of water - ethanol at 500 μL/h water and 400 μL/h ethanol. The measurement region of the microchip was 231 × 184 μm^2 in size immediately downstream of the junction such that the length between the left edge of the image and the confluence point was 48 μm. The highly accurate PIV technique was used for analysis. An interrogation window of 65 x 17 pixels was taken with 50% overlap, corresponding to a spatial resolution of 5.9 x 1.5 μm^2. Eighty velocity values were obtained along the capillary diameter for each channel. The flow in each channel at the upstream of the junction was also fully developed. Difference between velocities of inlet channels was clearly observed due to different flow rate. After junction, the flow was accelerated. Since two kinds flied, water and ethanol was seldom mingled, velocity was smaller around interface region.

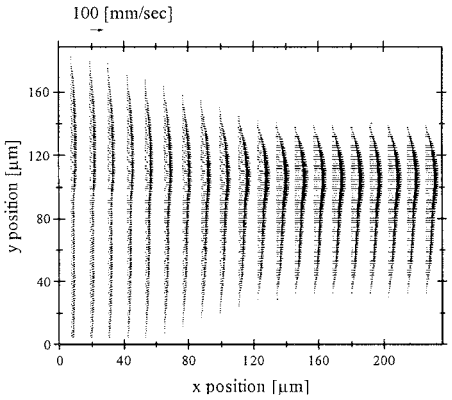

Figure 1. Time-averaged velocity distributions of water-ethanol flow.

Fig. 2 shows the velocity profile and shear rate at x = 218 μm in order to investigate the dynamics near the water - ethanol interface. The shear rate $\dot{\gamma}$ was estimated using difference method. The profiles within the water and ethanol regions, that is, on either side of the interface, were similar to the Poiseuille profile. In each region, shear rates calculated using the difference approximation were linear. An inflection of velocity and discontinuity of shear stress were observed around the interface at y = 90 μm, indicating an imbalance of viscous force. Shear rates of ethanol and water are 1.0 - 0.4 and 2.0 - 3.0 x 10^3 1/s, the range estimated by the values from the graph or extrapolated values from the linear fits to the data. Therefore, shear stress of ethanol and water are 1.5 - 0.6 and 2.6 - 3.9 N/m^2. Thus, the difference of shear stress is

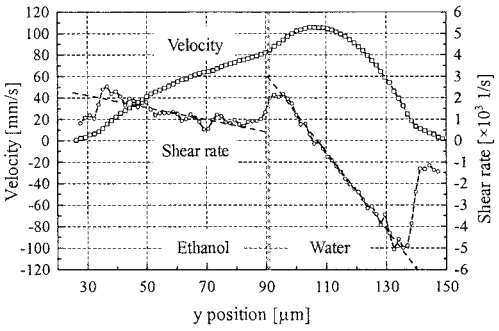

Figure 2. Time-averaged axial velocity profile and shear rate.

more than 1.1 N/m^2.

In order to investigate the phenomena, numerical simulation taking a force caused by an interfacial tension gradient called Korteweg stress [4] into account was carried out. The governing equations in incompressible miscible liquids were represented as,

$$\frac{\partial C}{\partial t} + (\mathbf{v}\cdot\nabla)C = D\nabla^2 C \quad (1),$$

$$\frac{\partial \mathbf{v}}{\partial t} + (\mathbf{v}\cdot\nabla)\mathbf{v} = -\frac{1}{\rho}\nabla p + \nu\nabla^2\mathbf{v} + \frac{1}{\rho}\nabla\cdot\mathbf{T} \quad (2),$$

$$\nabla\cdot\mathbf{v} = 0 \quad (3),$$

where D is the diffusion coefficient, $\mathbf{v}$ is the velocity, p is pressure, ν is the viscosity, and ρ is the density.

The Korteweg stress $\mathbf{T}$ in two-dimensional flow was expressed as,

$$T_{11} = k\left(\frac{\partial C}{\partial y}\right)^2,\ T_{12} = T_{21} = -k\frac{\partial C}{\partial x}\frac{\partial C}{\partial y},\ T_{22} = k\left(\frac{\partial C}{\partial x}\right)^2 \quad (4),$$

where C is the mass fraction of liquid, k is a system-specific parameter.

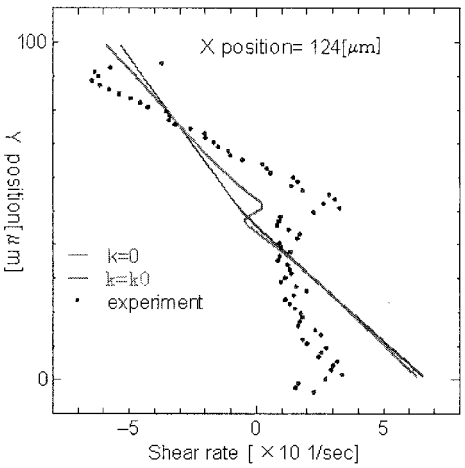

Figure 3. Comparisons between experimental result and numerical simulation

Fig. 3 shows Comparisons between experimental result and numerical simulation. In the case of k=0, the flow was balanced at the interface. In the case of k=k0, the imbalance was observed. The imbalance was caused by the Korteweg stress. The results certify existence of an interfacial tension even in miscible liquids and of its tension gradient due to concentration gradient caused by diffusion. The stress may generate capillary wave or interfacial instability at the interface of miscible liquids. The stress may cause an interfacial instability and destroy a uniform mixing in two flowing fluids in the case of large concatenation gradient.

4. Conclusions

The flow characteristics at an interface between water and ethanol in a Y-junction microchip were investigated using a micro-PIV technique. From velocity distributions with a spatial resolution of 5.9 × 1.5 μm^2 were obtained. A stable interface was achieved by applying different inlet flow rates of water and ethanol. The velocities around the interface between water and ethanol were skewed, indicating an imbalance of shear stress at the interface. The reason of the imbalance is to be stress, so called the Korteweg stress, generated by interfacial tension gradient due to a concentration gradient by diffusion in a miscible multi-layer system. The stress may play an important role in interfacial instability both of immiscible and miscible liquids with molecular transportation in microscopic flow. This indicates that the convection could be caused by the stress due to concentration gradients even in miscible or immiscible parallel flow or droplet with large molecular transformation.

References

[1] M. Tokeshi, T. Minagawa, K. Uchiyama K, A. Hibara, K. Sato, H. Hisamato, T. Kitamori, *Anal. Chem.*, **74**, 1565-1571 (2002).

[2] A. Hibara, M. Tokeshi, K. Uchiyama, H. Hisamoto, T. Kitamori T, *Anal. Sci.*, **17**, 89-93 (2001).

[3] Y. Sugii, K. Okamoto, *J. Visualization,* 7(1), 9-16 (2004).

[4] D. J. Korteweg, *Archives Néerlandaises des Sciences Exactes et Naturelles* **6**, 1–24 (1901).

COMPUTATIONAL ANALYSIS OF DOUBLE-T-TYPE MICROFLUIDIC MIXER USING PERIODIC ELECTROKINETIC FORCE

Lung-Ming Fu[1] Chia-Yen Lee[2] and Che-Hsin Lin[3]

[1]*Graduate Institute of Materials Engineering, National Pingtung University of Science and Technology, Pingtung, Taiwan, 912*

[2]*Dept. of Mechanical and Automation Engineering,*Da-Yeh University, Changhua, Taiwan, 515

[3]*Dept. of Mechanical and Electro-Mechanical Engineering, National Sun Yat-sen University, Kaohsiung, Taiwan, 804*

Abstract

This paper presents a novel technique in which periodic electrokinetic driving forces are utilized to mix electrolytic fluid samples rapidly and efficiently in a double-T-form microfluidic mixer. The effectiveness of the mixer as a function of the applied electric field and the periodic switching frequency is characterized by the intensity distribution calculated downstream from the mixing zone. The present numerical results confirm that the proposed double-T-form micromixer has excellent mixing capabilities. The mixing efficiency can be as high as 95% within a mixing length of 1000 μm downstream from the secondary T-junction when a 100 V/cm driving electric field strength and a 2 Hz periodic switching frequency are applied. The rapid double-T-form microfluidic mixer using the periodic driving voltage switching model proposed in this study has considerable potential for use in Lab-on-a-Chip systems.

Keywords: Electrikinetic, microfluidic mixer, double-T-type mixer, switching frequency

1. Introduction

Bio-MEMS (Micro-Electric-Mechanical-System) devices are frequently required to conduct some form of biochemical reaction, and hence it is highly important that these devices have an effective mixing capability. However, implementing this capability is hindered by the very small scale of these microfluidic chips (typically in the range of several-ten micrometer), which tends to restrict the microchannel flows to the laminar flow regime and hinders the use of conventional mixing mechanisms. Microfluidic devices requiring a mixing operation have typically relied upon diffusive mixing achieved by bringing together the fluid streams to be mixed within a single channel [1].

2. Formulation and numerical method

Regarding the numerical simulation of electroosmotic flows, the current authors have previously developed physical models based on (a) the Poisson equation for the electrical potential and zeta potential, (b) the Nernst□Planck equations for the ionic concentration, (c) the full Navier/Stokes equations modified to include the effects of the body force due to the electrical and charge densities and (d) a concentration equation for the sample plug distribution. The detailed expressions of the governing equation, the initial conditions, and the boundary conditions are provided in reference [2-4]. Figure 1 illustrates the schematics of double-T-type basic proposed device.

3. Results and discussion

The mixing efficiency of microfluidic mixers can be enhanced by increasing the contact area and contact time of the different samples, creating irregular flow fields (such as separation bubbles) in the mixing channel, generating perturbations of the sample fluids, etc. However, fabricating microchannel configurations which generate irregular flow fields is challenging. Moreover, complex flow control mechanisms are required. Consequently, the present study adopts an interlaced sample

injection mode controlled by a periodic switching method to increase the contact area and contact time of the two samples to be mixed and to generate perturbations of the fluid field.

Figure 2 presents the corresponding electrical potential distributions and streamlines for the two steps of this operating mode. Figure 3 presents the simulated species concentration distributions obtained when this switching mode is applied with a driving electric field of 100 V/cm and switching frequencies ranging from 1 Hz to 8 Hz. In this figure, Samples 1 and 2 are injected through channels 1 and 2, respectively, and establish a parallel flow between the two T-junctions. Meanwhile, a switching voltage is applied to channels 3 and 4 to inject Samples 2 and 1, respectively. This interlaced injection arrangement increases the flow perturbation and the contact area of the two samples within the mixing channel, and hence enhances the mixing performance. Figure 3(a) indicates that the species concentration distribution has a waveform pattern when the sample plugs are injected with a switching frequency of 1 Hz. The results of Figure 3(a) suggest that a switching voltage of 1 Hz generates sample plugs whose volumes are too large to be injected completely into the mixing channel. Consequently, the two samples fail to establish intimate contact in the mixing region. As shown in Figure 3(b), when the switching frequency is increased to 2 Hz, the contact area of the two samples is increased in the mixing channel. However, increasing the switching voltage beyond 2 Hz reduces the contact area since the amplitude of the concentration profile reduces (as shown in Figures 3(c) and 3(d)). When the switching frequency is increased to 8 Hz (Figure 3(d)), it can be seen that the species concentration has the form of parallel flow. Figure 4 illustrates the normalized concentration intensity for different switching frequencies and a driving electric field of 100 V/cm at a mixing channel cross section located 1200 μm downstream from the secondary T-junction. In this figure, the normalized concentration values of the two samples are 1 and −1, respectively, and a value of 0 indicates that the two samples are fully mixed. At switching frequencies of 0 Hz (parallel flow), 4 Hz and 8 Hz, it is observed that the concentration intensity profiles exhibit two distinct sets of peaks and troughs. This result confirms that these particular driving voltages will yield a poor mixing performance within the mixing channel. However, the peaks and troughs become less apparent when the switching frequency is specified as 1 Hz or 2 Hz. Hence, it can be concluded that these driving frequencies yield a superior mixing performance. Figure 5 indicates the variation in the mixing efficiency along the mixing channel length (L_{mix} = 1200 μm) for a driving electric field of 100 V/cm and switching frequencies in the range of 0 Hz to 8 Hz. In the case of parallel flow (0 Hz), mixing is achieved solely through the diffusion of the interlaced sample streams, and hence the maximum mixing efficiency only attains a value of 47.2%. At a switching frequency of 1 Hz, the mixing efficiency increases progressively along the mixing channel length and has a slightly undulating form. Meanwhile, at a switching frequency of 2 Hz, the mixing efficiency attains a maximum value of 95.3% at a distance of 1000 μm downstream from the secondary T-junction. Therefore, it is clear that the proposed periodic switching mode is capable of providing an effective and rapid mixing efficiency at this particular switching frequency. For switching frequencies of 4 Hz and 8 Hz, the mixing efficiencies obtained after a mixing length of 1200 μm are found to be 79.8% and 73.5%, respectively. As discussed previously, as the switching frequency is increased, the contact area and contact time of the two samples in the mixing channel are both reduced. Hence, the diffusion effect is lessened and the mixing efficiency diminished.

4. Conclusions

The present mixer demonstrates a rather simple and effective use to of electrrokinetic switching frequency for mixing in microfluidic systems. The mixing is easy to implement and both the electric field strength and switching frequency can be easily controlled. Finally, the present results confirm the ability of EOF control modes to attain "acceptable mixing" without the requirement for external devices or particular microchannel configurations.

Acknowledgements

The current authors gratefully acknowledge the financial support provided to this study by the National Science Council of Taiwan under Grant N°s. NSC92-2312-B-020-001 and NSC92-2320-B-110-015.

References

[1] S. C. Jacobson, T. E. McKnight and J. M. Ramsey, *Analytical Chemistry,* 71, 4455-4459 (1999).
[2] L.-M. Fu, R.-J. Yang and G.-B Lee, *Analytical Chemistry*, 74, 5084-5091 (2002).
[3] L.-M. Fu, R.-J. Yang and G.-B Lee, *Analytical Chemistry*, 75, 1905-1910 (2003).
[4] L.-M. Fu and C.-H. Lin, *Analytical Chemistry*, 75, 5790-5796 (2003).

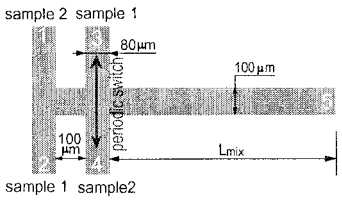

Fig. 1 Schematic illustration of current double-T-type microfluidic mixer.

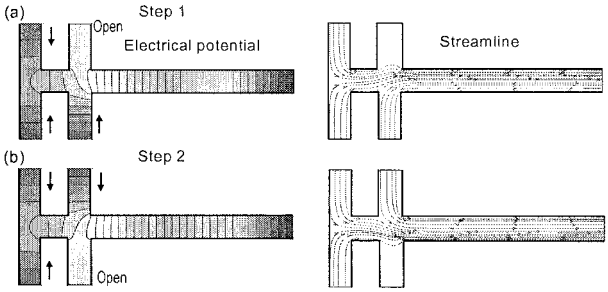

Fig. 2 Numerical simulation of electrical potential contours and treamlines for both the switched conditions

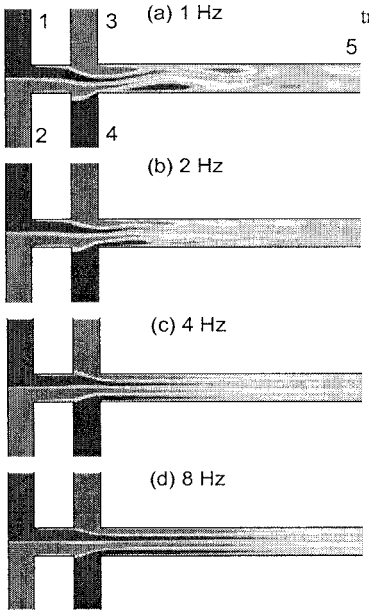

Fig. 3 Species concentration distributions for mixing channel at different switching frequencies. Note: applied main electrical field is 100 V/cm.

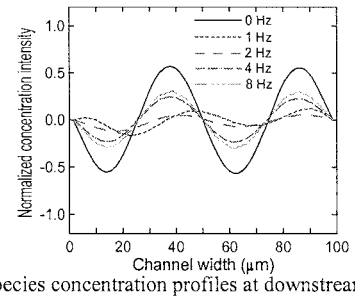

Fig 4. Species concentration profiles at downstream distance of x = 1200 μm with switching frequencies of 0 Hz, 1 Hz, 2 Hz, 4 Hz, and 8 Hz. Note: applied main electrical field is 100 V/cm.

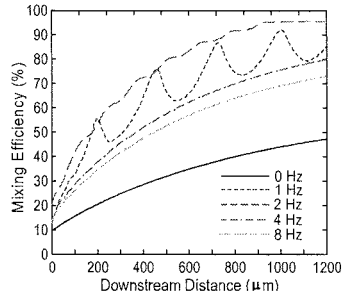

Fig 5 Mixing efficiency of the micro mixer at different switching frequencies.

HIGH-EFFICIENT MICROPUMP WITH GEOMETRY OPTIMIZATION OF MICROCHANNEL USING COMPUTATIONAL FLUID DYNAMICS

Takaaki Suzuki[1], Satoyuki Kawano[2], Isaku Kanno[1], Hirofumi Shintaku[1], Shunsuke Yakushiji[1] and Hidetoshi Kotera[1]

[1]Dept. of Mechanical Engineering, Kyoto University, Yoshida-Honmachi, Sakyo-ku, Kyoto 606-8501, Japan

[2]Center for Interdisciplinary Research, Tohoku University, Aramaki-aza Aoba, Aoba-ku, Sendai 980-8578, Japan

Abstract

Micropumps are one of the most important microfluidic components in μ–TAS. We have developed a valveless micropump driven by traveling wave, and obtained high energy efficiency. In this paper, we numerically calculate three-dimensional fluid flow in the micropump with a CFD code, FLUENT. Comparing the experimental results with the numerical ones, it seems that the proposed analytical procedure evaluates the performances of the traveling wave micropump. The proposed procedure can be used to optimize the structure of the microchannel in order to increase the energy efficiency of the traveling wave micropumps.

Keywords: micropump, traveling wave, optimization, CFD

1. Introduction

Micropump is a key component for fluid transportation system in μ–TAS [1]. In our previous work, we have reported a traveling wave micropump which can easily control bi-directional fluid flow without mechanical valves [2]. PZT bimorph beams were used to generate the traveling waves on the wall surface of the microchannel. The fluid flow was controlled by changing the amplitude, the frequency and the phase delay of the applied sinusoidal voltage. The proposed micropump is composed of the microchannel and the actuators which are fabricated separately. The maximum energy conversion efficiency between vibration of the wall and liquid flow was calculated to be more than 80% in the region of the first resonant frequency of the actuators. For practical use of the micropump, it is necessary to characterize detailed fluid flow in the microchannel and optimize a structure of the micropump.

Most researches concerning the traveling waves analytically solved the two-dimensional Navier-Stokes Equations [3, 4] due to the difficulty of analysis of the three-dimensional phenomenon using the theoretical analyses. Nguyen et al. [5] carried out the numerical simulation of the traveling waves with a CFD-software package. Since they also neglected the effect of side walls by assuming the microchannel width of 1m, it is difficult that the fluid flow in the microchannel is accurately characterized.

In this paper, we numerically calculate the three-dimensional fluid flow in the traveling wave micropump with a CFD code, FLUENT. To verify the analytical procedure, we compare the numerical and the experimental results. In addition, fluid transportation phenomenon induced by the traveling waves is investigated. We calculate the three-dimensional distribution of the flow velocity in the microchannel, which is difficult to observe experimentally without high-cost measurement systems, e.g. a micro PIV system.

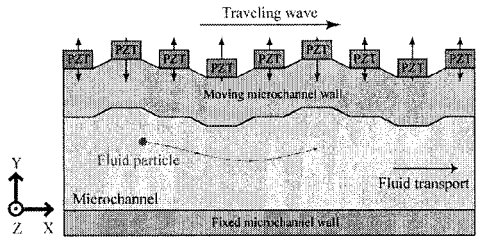

Figure 1. Principle of fluid transport.

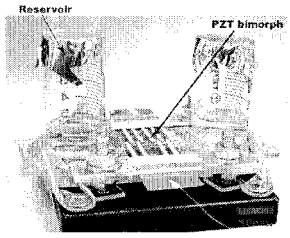

Figure 2. Photograph of micropump.

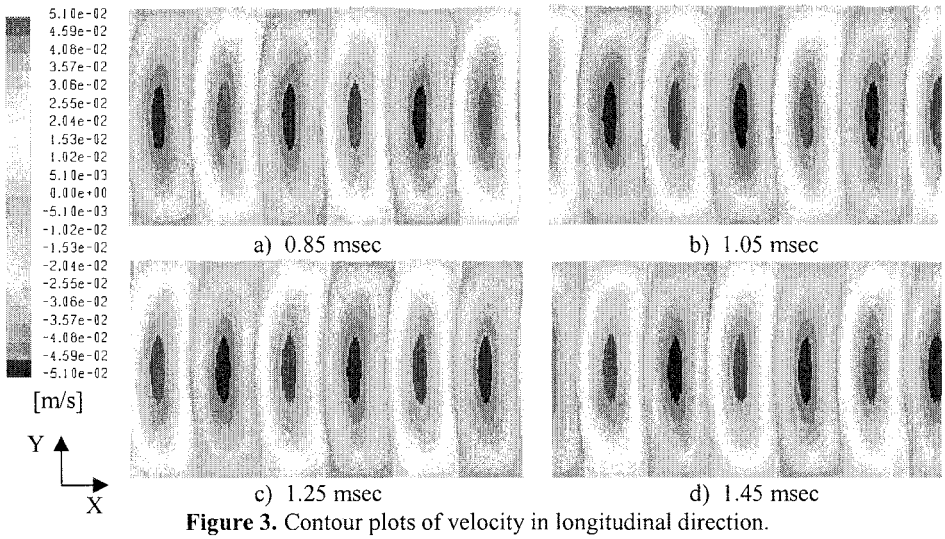

Figure 3. Contour plots of velocity in longitudinal direction.

2. Numerical analysis

We have proposed the micropump system composed of a microchannel made of PDMS where the traveling wave is induced by PZT bimorph beams, as shown in Fig.1. A photograph of the fabricated micropump is shown in Fig. 2. There are reservoirs at both ends of the microchannel. Flow condition and dimensions of the analytical model are same as the fabricated device. Dimensions of the microchannel are the length of 1800μm, the width of 200μm and the height of 100μm. When the sinusoidal voltage is applied to the arrayed PZT bimorph beams with different phases, the moving wall of the upper surface of the microchannel is excited by the traveling wave with the amplitude of 2.5μm, the period of 1.0msec and the wavelength of 600μm. The inlet and outlet was assumed at zero backpressure. We calculate a laminar flow model of the microchannel filled with the ethanol. We used the CFD code, FLUENT, based on the finite volume method for representing and evaluating partial differential equations, e.g. the governing integral equations for the conservation of mass and momentum. In order to describe the wall motion induced by the bimorph beams, dynamic mesh model was used to model flows where the shape of the domain is changing with time due to motion on the domain boundaries. The update of the volume mesh is handled at each time step based on the new positions of the boundaries. There are 585546 tetrahedral cells in the analytical model.

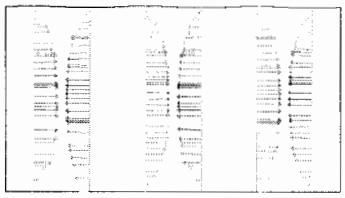

Figure 4. Velocity vectors colored by velocity in longitudinal direction at 1.25msec.

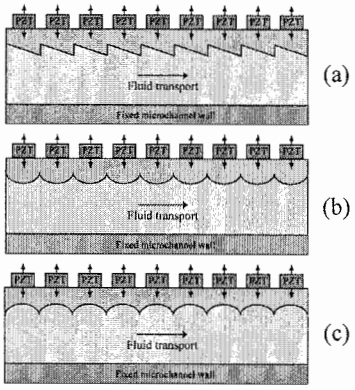

Figure 5. Schematic illustration of geometry optimization of micropump.

3. Results and Discussion

Figure 3 shows the fluid flow in the vertical x-y section at z=100μm, i.e. the center of the width direction. To show the numerical results clearly, the displayed size in the height is elongated 100times larger than that in the longitudinal direction. The velocity of the forward direction is induced in the microchannel of the convex parts of the traveling waves, and the velocity of the backward direction is induced in the microchannel in the concave parts of the traveling waves. Figure 4 shows numerical results of the velocity vectors at the concavo-convex positions in the longitudinal direction. It is instantaneously observed that the uniform flow is generated in the backward and the forward directions. On the other hand, the mean velocity is calculated to be 162μm/s, which is smaller than the experimental velocity of 181μm/s. The experimental velocity in the microchannel is the maximum velocity at the center of the microchannel. In the case of laminar flow in the microchannel, the maximum velocity is 1.5 times larger than the mean velocity. So, the numerical maximum velocity is about 243μm/s. There are slight difference between the experimental and the calculation results. Taking into account the precision of the measurement system, the numerical results may be in good agreement with the experimental results. From the fluid flow obtained by the numerical analysis, it seems that the efficiency of the traveling wave micropump is improved by means of forming the shape of the moving wall surface as shown in Fig.5. We will clarify the relationship between the shape and the fluid transportation characteristics, and optimize the structure of the microchannel to increase the efficiency of the traveling wave micropump.

4. Conclusions

In this paper, we numerically calculated the three-dimensional fluid flow in the micropump. From comparison of the experimental and the numerical results, it is confirmed that the proposed analytical procedure describes the fluid flow induced by the traveling waves. It seems that the proposed analytical procedure optimizes the performances of the traveling wave pump.

Acknowledgements

This study was supported by grant-in-aid for Scientific Research (A) (No.14205037 and No. 15201033) from the Ministry of Education, Culture, Sports, Science and Technology.

References

[1] N. T. Nguyen, X. Huang and T. K. Chuan, *Trans. ASME*, **124**, pp.384-392 (2002).
[2] I. Kanno, S. Kawano, S. Yakushiji and H. Kotera, *Proc. μTAS2003*, pp.997-1000 (2003).
[3] A. H. Shapiro, M. Y. Jaffrin and S. L. Weinberg, *J. Fluid Mech.*, **37**(4), pp.799-825 (1969).
[4] F. C. P. Yin and Y. C. Fung, *J. Fluid Mech.*, **47**(1), pp.93-112 (1971).
[5] N. T. Nguyen and R. M. White, *Sens. & Act.*, **77**, pp. 229-236 (1999).

LASER BASED 'AIR BEADS' CONTROL DEVICE

Toshiharu Shiraishi[1], Koichi Ono[2] and Teruo Fujii[3]

[1] *ARBIOTEC,LTD., A306 CCR, University of Tokyo, 4-6-1 Komaba, Meguro-ku, Tokyo, JAPAN*

[2] *Enplas Laboratories,Inc., 2-38-5 Namiki Kawaguchi City, Saitama, JAPAN*

[3] *Institute of Industrial Science, University of Tokyo, 4-6-1 Komaba, Meguro-ku, Tokyo, JAPAN*

Abstract

A device for generation and control of the micro bubbles is newly developed for their practical use. The authors call the micro bubble and the device, "AIR BEAD" and "AIR BEADS CONTROL DEVICE", respectively. The prototype of the AIR BEADS CONTROL DEVICE integrated on a PDMS microchip has the ability to generate, move and trap AIR BEADS using heat and optical pressure of laser.

Keywords: micro bubble, microfluidics, optical fiber, laser, PDMS

1. Introduction

Generally, micro bubbles can cause malfunction of microfluidic devices. However, micro bubbles have properties [1] of being charged electrically and being highly stable because of surface tension. Moreover, cavitation energy is often used for sonoporation. We consider these properties of micro bubbles to be widely applicable in various fields of microfluidics. For example, considering its property to adsorb molecules a micro bubble can be used as carriers of proteins [2]. This means that micro bubbles can be used as a substitute for polymer beads for adsorption on microfluidic devices. Compared with polymer beads, micro bubbles have some advantages. They don't need any inlets because they can be generated in micro channels. They are also erasable after use. Here, we present a newly developed device for generation and control of the micro bubbles, and we call the micro bubble and the device, "AIR BEAD" and "AIR BEADS CONTROL DEVICE", respectively.

2. Theory

It is possible to generate micro bubble (AIR BEADS) by heating liquid (e.g. distilled water and ethanol) in a microchannel. The shape of the AIR BEAD depends on the channel wall-liquid contact angle. When something (e.g. focused laser beam) heat up the neighborhood of the AIR BEAD, a phenomenon called "Marangoni's effect" makes it move toward higher temperature area because of the imbalance of surface tension (Fig. 1). This effect could be used for transferring the AIR BEADS. As focused light push an object in microscale, AIRBEADS are trapped when laser beam is focused on it (Fig.. 2).

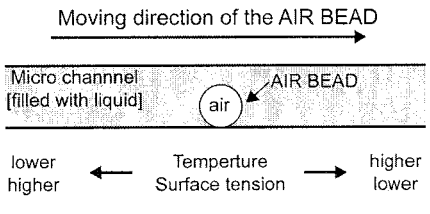

Figure 1. Marangoni's effect on AIR BEAD.

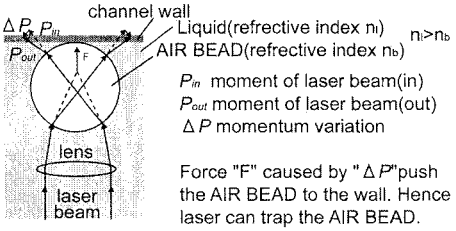

Figure 2. Laser trapping force on AIR BEAD.

3. Experimental set-up

Fig. 3. shows the AIR BEADS CONTROL DEVICE integrated on a PDMS microchip [3]. It has 2-dimensional multi-aspherical lenses fabricated on a PDMS (SYLGARD 184) microchip with

insertion of an optical fiber (multimode fiber, 60μm core) connected to a laser diode (Hamamatsu L9399, 824nm, 1.0W_{max}) at the other end. The device has three functions, i.e. generation, transfer, and trapping of AIR BEADS. AIR BEADS are generated by the heat supplied by the applied laser light. The sidewall of the PDMS microchannel opposite to the lenses contains carbon powders (5% [wt/wt]) (Fig. 4). Therefore it can receive heat energy from the laser beam efficiently. Compared with surface treatment, carbon mixed molding is an easier method to fabricate the PDMS chip preserving its flexibility and adhesiveness.

Fig. 5. is schematic drawing of AIR BEADS CONTROL DEVICE system. The laser diode is controlled by a personal computer (PC). The PC controls a CCD camera on the optical microscope to capture real time AVI, and to conduct image processing.

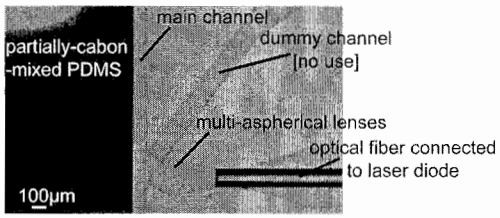

Figure 3. Drawing of the design with the PDMS multi-aspherical lenses, optical fiber and partically-carbon-mixed PDMS.

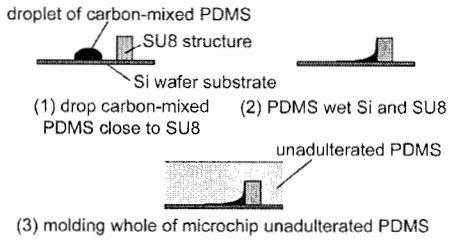

Figure 4. Molding procedure of partically-carbon-mixed PDMS.

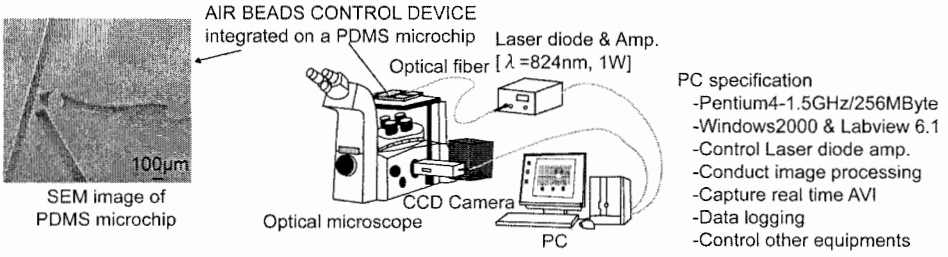

Figure 5. Schematic drawing of AIR BEADS CONTROL DEVICE system.

4. Results and discussion

Fig. 6 shows the AIR BEAD generated by the laser in distilled water. The BEAD expands keeping its hemispheric shape in this case because the contact angle of PDMS-water is approximately 90 degree. After oxygen plasma treatment (O_2 20SCCM, 20Pa, 75W, 10sec), the contact angle of PDMS-water becomes approximately 30 degree, so the shape of the BEAD becomes a spherical one (Fig. 7). These results shows that it is possible to control the shape of AIR BEADS by controlling the PDMS-liquid contact angle.

The BEAD in a microchannel filled with ethanol moves towards laser focused point in spite that the position of the BEAD is outside the optical axis (Fig. 8(1).). When the bubble get to the laser focused point, it is trapped and stops its motion (Fig. 8(2).).

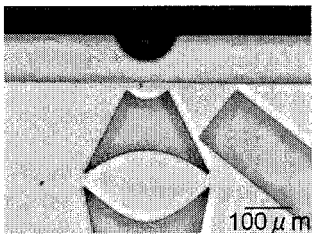

Figure 6. AIR BEAD generation in water. [contact angle 90 degree, laser power 20mW]

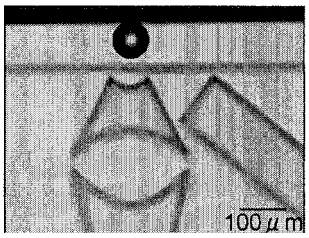

Figure 7. AIR BEAD generation in water. [contact angle 30 degree, laser power 20mW]

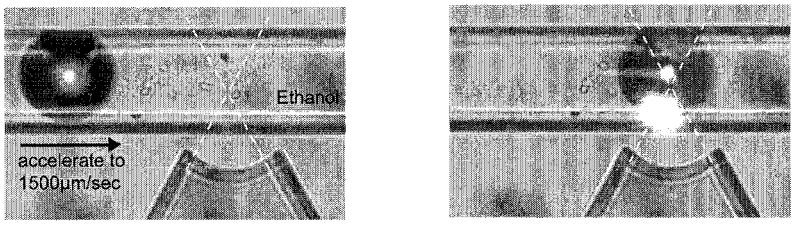

Figure 8. Motion of AIR BEAD due to Marangoni's effect and laser trapping.

5. Conclusions and future perspectives

We presented a newly developed device for generation and control the micro bubbles, and we called the micro bubble and the device, "AIR BEAD" and "AIR BEADS CONTROL DEVICE", respectively. The trial laser based AIR BEADS CONTROL DEVICE integrated on a PDMS microchip was produced. It was possible to generate, move and trap AIR BEADS using this device. This technique can easily be extended to a setting with multiple optical fibers because the present optical device doesn't require any elaborate alignment of each component to the fluidic channel. The multiple fibers (and lenses) arranged in a line along the channel can produce continuous motion and trapping of the AIR BEADS. Other future works of AIR BEADS are to use their properties of being charged electrically and being highly stable because of surface tension effectively.

Acknowledgements

The authors would like to thank to Atsushi Someya for advice on this paper and to Masako Tanaka for electrical wiring work and drawing some illustrations.

References

[1] Takahashi, M.; Kawamura, T.; Yamamoto, Y.; Ohnari, H.; Himuro, S.; Shakutsui, H.; J. Phys. Chem. B. ; (Communication); 2003; 107(10); 2171-2173.
[2] Du L, Prokop A, Tanner RD. , J Colloid Interface Sci. 2003 Mar 1;259(1):180-5.
[3] K.Ono, S.Kaneda, T.Fujii, MicroTAS '03, pp.1307-1310.

HYDRAULIC SAMPLE/REAGENTS HANDLING SYSTEM FOR A DISPOSABLE CLINICAL DIAGNOSIS MICROCHIP

Ryuji Koyama[1], Yoshikazu Yoshida[1] and Takehiko Kitamori[2]

[1] *The Research Association of Micro Chemical Process Technology, KSP R&D-C11F, 3-2-1 Sakado, Takatsu-ku, Kawasaki, Kanagawa 213-0012 JAPAN*

[2] *The University of Tokyo, 7-3-1 Hongo, Bunkyo-ku, Tokyo 113-8656 Japan*

Abstract

A new hydraulic fluid control system has been demonstrated. A hydraulic fluid regulation microchip was used to control flow in a disposable reaction microchip. Diaphragms on the regulation chip and membranes on sample/reagents reservoirs in the reaction chip were touching. Hydraulically driven diaphragms push out the membranes and then sample/reagents solutions in the reservoirs flow into channels. Flow ratio between reservoirs in the reaction chip and the flow rate were controlled constantly with a single syringe pump that was connected to the regulation chip. Total cholesterol in human serum was quantitatively measured with this system.

Keywords: fluid handling, hydraulic actuation, disposable chip, clinical diagnosis, point-of-care

1. Introduction

Disposable microchip-based analysis system is attractive to clinical diagnosis applications, especially point-of-care testing. It gives several advantages such as sample contamination free and easy maintenance. In such systems, it is desired that fluid handling mechanisms do not touch sample/reagents directly. Previously, pneumatic or centrifugal forces were used for non-contact fluid control [1, 2]. In those systems, fluid properties like viscosity influence characteristics of the flow. So, additional volumetric technique with complex microchannel designs and complicated fluid handling operations are required for quantitative analysis. Alternative system that used mechanically actuated pin and membranes on reservoirs were proposed [3]. It didn't need volumetric method, but there are some drawbacks such as the necessity of precision actuators and the space occupation over a microchip. In this paper, we present a new non-contact fluid control system that utilizes a hydraulic fluid regulation microchip. Quantitative flow control and analysis was possible with this simple system.

2. Principle

The hydraulic fluid control principle is illustrated in Figure 1. A hydraulic fluid regulation microchip (Chip I) is used for sample/reagents solution handling in a reaction microchip (Chip II). One end of the channels in Chip I is connected to a pump. Elastic diaphragms are on reservoirs which are connected to the other ends of the channels. The channels and the reservoirs are filled with fluid.

Fluid control procedure is as follows: First, reservoirs in Chip II are filled with a sample and reagents solutions. Then those reservoirs are covered with membranes. In the next, Chip I is placed on Chip II, so that the diaphragms on Chip I and the membranes on Chip II are faced each other. Then, the pump infuses fluid into Chip I. As the volume of fluid in Chip I increase, the diaphragms protrude. Consequently membranes are pushed down into the reservoirs of Chip II, then the sample and reagents solutions in the reservoirs flow into the channels. Flow ratio between a sample and reagents could be determined by the design of the regulation microchip. In this system, the regulation microchip does not touch sample/reagent solutions directly. Therefore, it can be used repeatedly without cleaning.

3. Experimental

The microchips were made of PMMA. The designs are shown in Figure 2. All channels' sizes are 200 μm in width and 100 μm in depth. Lengths between S'-f, A'-f, B'-f in Figure 2(a) are the same as approximately 25.7 mm. Lengths between g-h and h-W are 100 mm and 150 mm respectively. We used two different flow regulation chips. The channel designs are the same, but the reservoirs' diameters are different. Chip Ia has all 3 mm diameter reservoirs. Chip Ib has 2.5 mm of reservoir S', 5 mm of reservoir A' and 3 mm of reservoir B'. Diameters of reservoirs S, A and B in a reaction chip are the same as corresponding reservoirs in the regulation chips. Membranes on a reaction chip's reservoirs were PTFE and diaphragms on a fluid regulation chip's reservoirs were silicone membranes. Fluid in a regulation chip was water. A fluid regulation chip was connected to a syringe pump. Flow in the reaction chip was visualized with fluorescent solution or 1 μm fluorescent microbeads.

For blood analysis, total cholesterol in human serum was measured. The cholesterol oxidase method was used. 1/10 diluted human serum was put in reservoir S, reagent A (cholesterol esterase, etc.) was put in reservoir A and reagent B (cholesterol oxidase, peroxidase, etc.) was put in reservoir B of a reaction microchip in Figure 2. Chip Ia was used for flow control. Generated quinone dye was measured by a thermal lens detector (Asahi Kasei Corporation, excitation wavelength:633 nm; detection wavelength:780 nm).

4. Results and discussion

Flow in a reaction microchip was stably controlled from the syringe pump flow rate of as low as 0.2 μl/min. It corresponds to flow rate of sub nl/sec at the sample channel. Flow ratio between the reservoir S, A and B was kept constant up to the flow volume of 15 μl.

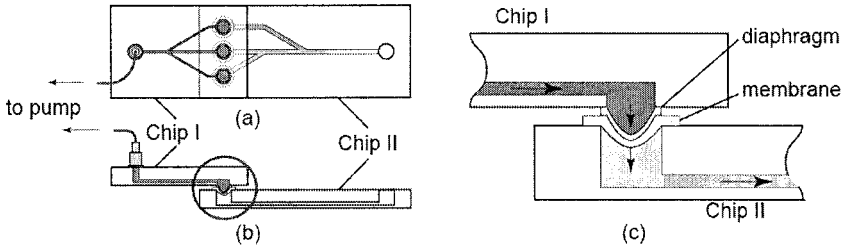

Figure 1. Schematic diagrams of hydraulic fluid control system. (a) Top view of a hydraulic fluid regulation microchip (Chip I) and a reaction microchip (Chip II). (b) Side view of those microchips. (c) Enlarged view in the circle area of Figure 1 (b)

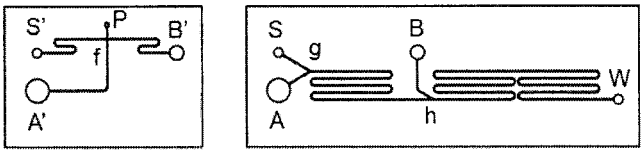

Figure 2. Design of microchips. (a) A fluid regulation microchip (Chip I). P is an inlet reservoir that is connected to a syringe pump. S', A' and B' are reservoirs. They open to the bottom side of the chip and diaphragms are covered on them. (b) Design of the reaction microchip (Chip II). S is a sample reservoir, A and B are reagents reservoirs and W is a waste reservoir.

Figure 3 shows photographs of flow in the reaction microchip. When Chip Ia was used, flow ratio between S and A was 1:1 as shown in Figure 3(a). However, when Chip Ib was used, it was changed as shown in Figure 3(b). The flow ratio was determined by reservoirs' diameters in a hydraulic fluid regulation microchip.

Figure 4 was the result of total cholesterol measurement in human serum. Thermal lens signal was linearly increased with total cholesterol concentration. Healthy level of total cholesterol is 120-220 mg/dl. Range of the assay was sufficient for clinical diagnosis. This result shows that the hydraulic fluid control system is useful for blood quantitative analysis.

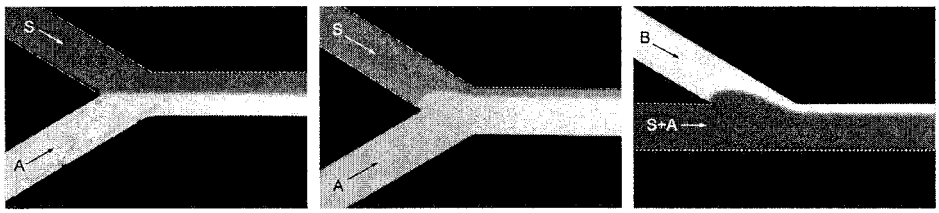

(a) (b) (c)

Figure 3. Photographs of flow in the reaction microchip. (a) and (b) were taken at Junction g, (c) was taken at Junction h. The syringe pump flow rate was 2μl/min.

5. Conclusions

We have been demonstrated a new fluid control system. Flow in a reaction microchip was successfully controlled with a hydraulic fluid regulation microchip that didn't touch sample/reagents directly. This system has been proven useful for quantitative analysis in a disposable microchip.

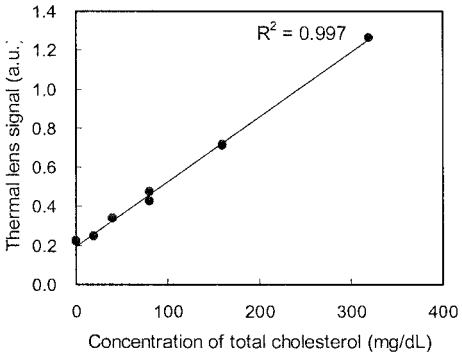

Figure 4. Total Cholesterol measurement result.

Acknowledgements

The authors would like to thank Asahi Kasei Corporation for instrumentation, Koji Shimoide and Hiroshi Kurokawa for helpful discussions. This work was supported by the New Energy and Industrial Technology Development Organization (NEDO) of the Ministry of Economy, Trade and Industry, Japan.

References

[1] M. Gustafsson, D. Hirschberg, C. Palmberg, H. Jörnvall and T. Bergman, *Anal. Chem.*, **76**, 345-350 (2004).

[2] M. Yamada and M. Seki, *Anal. Chem.*, **76**, 895-899 (2004)

[3] K. Shimoide, K. Mawatari, S. Mukaiyama and H. Fukui, *Micro Total Analysis Systems 2002*, pp.918-921.

A Powerless Vapor-Condensation and Droplet-Collection/Removal Device for Micro Direct Methanol Fuel Cell

*Fan-Gang Tseng, Shih-Jin Luo , and Ching-Chang Chieng
Engineering and System Science Dept. National Tsing Hua University, Taiwan, ROC

Abstract

This paper proposes a novel device to deal with the waste generated in μDMFC without external power. It employs natural fluidic physical phenomena such as condensation, surface tension gradient and capalliary force to separate vapor from gas, as well as collect and remove liquid droplets naturally. This device is fabricated by surface treatment with wetbility gradient combined with SU-8 channels and DRIE through holes on silicon substrate. Testing results demonstrated very effective vapor condensation and liquid droplet collection and removal process on this simple device.

Keywords: surface tension gradient, droplet manipulation, powerless device, μDMFC

1. Introduction

Recently, μDMFC has attracted considerable attentions due to its potential to be a portable high energy power source [1]. However, different from macro-sized fuel cells, micro fuel cells do not generate great enough energy for external pump or active valve system to support the operations such as fuel/air supply and waste removal. As a result, self-contained and powerless operation becomes important design strategy in micro fuel cell system. In this paper, a powerless waste management system for μDMFC is developed to separate gas/vapor, condensate droplet, collect small droplets into large ones, and remove large droplets into waste tank spontaneously and powerlessly, by simply employing condensation, surface tension/temperature gradient, and capillary force naturally without external energy.

2. Design

The design of this waste management device is schematically shown in Figure1, consisting of a semicircle zone with wettability gradient in radial direction, polymer capillary guide channels, and gas-exhaust holes. When vapor /gas mixtures arrive the vicinity of the hydrophobic gas-exhaust holes, vapor condensates as small droplets and gas (such as CO_2) exhausts from the micro holes [2]. The droplets would move spontaneously due to capillary flow and coalescence of some small droplets. When droplets accumulated large enough to generate enough surface tension gradient across the droplet toward the radial direction, droplets can then move automatically into micro channels, and are taken away into the porous waste tank.

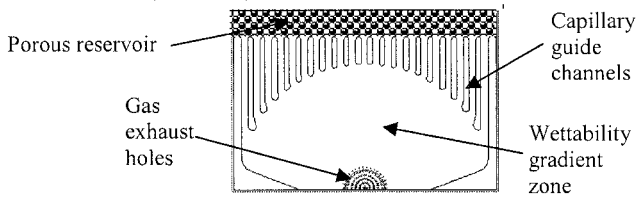

Figure 1. Conceptual and schematic design of the chip

3. Fabrication Process

The fabrication process is illustrated in Figure 2. (100) silicon wafers with 1μm LPCVD SiO_2 on surface were etched to form 60μm-deep exhaust holes by deep silicon reactive ion etching (DRIE), as shown in Fig. 2a. Al layer was then deposited by E-beam evaporation and patterned to be align-keys for backside alignment (Fig. 2b). In Fig. 2c, the wafer was undergone backside-bulk etching to thin down the wafer to reveal the layer of exhaust holes in TMAH with etching-

protection cover attached on the front-side. 100μm thick SU-8 resist was structured as micro channels and treated to be hydrophilic through O_2 plasma treatment. Then in Fig. 2d, A small drop of octadecyltrichlorosilane(OTS) was suspended on a glass slide and placed 1 mm above the chip as diffusion source for 4~5min, thus diffusion-controlled silanization of on SiO_2 surface [3,4] could produce wetability gradient of hydrophobic in the center and hydrophilic in the border on the semicircle region. Finally, a drop of 0.66% liquid Teflon was dropped on the exhaust holes to form hydrophobic surface inside the exhaust holes.

4. Results and discussion

To obtain the distribution of solution contact angle along the radial direction on the semicircle zone, the fabricated chip was directly immersed into DI-water and the front view and cross sections of the liquid meniscus were imaged (Fig. 3(a)) to estimate the contact angle in different positions. The liquid meniscus rises linearly in the front view, and the contact angles viewed from the cross sections vary from 117° in the center coated with Teflon@ gradually to 28° at the border due to SiO_2 surface characteristic, as shown in Fig. 3 (a) and (b), respectively. The moving velocity of various sized droplets have been tested on this surface, and experiments show that the average velocity is in the order of 1.5-2 cm/sec. Larger droplets moves slightly faster (Figure 4.), however, droplets can not move when the size smaller than 0.3μL.

Vapor condensation and droplet collection/removal testing is demonstrated as shown in Figure 5 and 6. In this experiment, droplets do not move (Fig. 5a) until the condensed size larger than 720 μm in diameter (Fig. 5b). The moving droplets will coalesce with droplets in front of them and forming even larger droplets thus gradually increasing the moving speed (Fig. 5c) until touching the micro channels. The micro channels then suck in all the large droplets (Fig. 6), deliver them into waste tank (not shown in this paper), and dry out the semicircle surface for the next droplet condensation/collection/removal process. The velocity of condensed droplets was observed about 40 mm/sec. This device can effectively remove liquid in an average speed of 8.01μl/sec.

Acknowledgement

We appreciate the grant from National Science Council, Taiwan under the program of Advanced Fuel Cell research.

Corresponding author: Fan-Gang Tseng, Department of Engineering and System Science, National Tsing Hua University101, Sec. 2, Kuang Fu Road, Hsinchu 300, Taiwan, R.O.C., Fax: 886-3-5720724, E-mail: fangang@ess.nthu.edu.tw

Reference

[1] Chang-Chien, A. et al, *Journal of Power Sources*, v 112, p 410-418, Nov., 2002.
[2] De-Sheng Men, Joonwon Kim, CJ Kim, *MEMS'03*,pp.534-537, Kyoto, Japan, Jan. 2003.
[3] K.Manoj and G.M. Whitesides, *Science*, Vol. 256, p1539-1541,1992.
[4] Susan Daniel, Manoj K. Chaudhury, John C. Chen, *Science*, Vol 291, 633-636 , 2001.

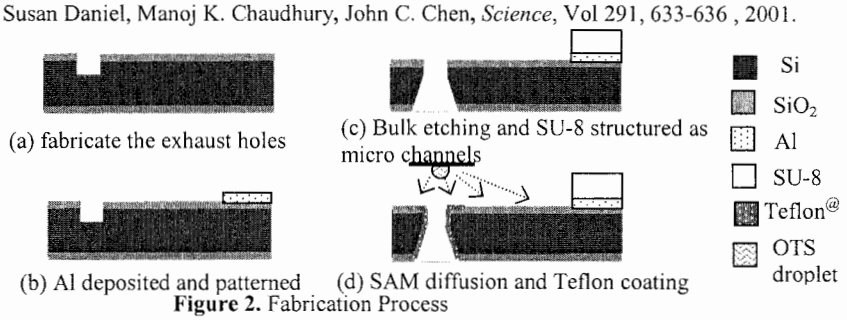

Figure 2. Fabrication Process

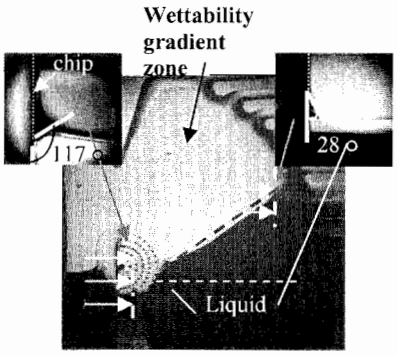

Figure 3.(a) Wettability gradient demonstrated by capillary rise of water(front view and cross section)

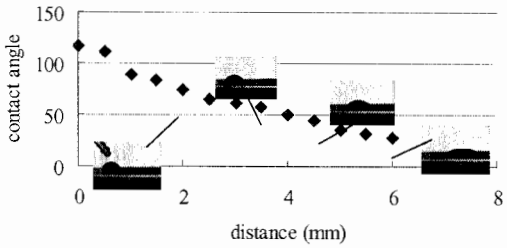

Figure 3.(b) Distribution of the contact angle along radial dierection

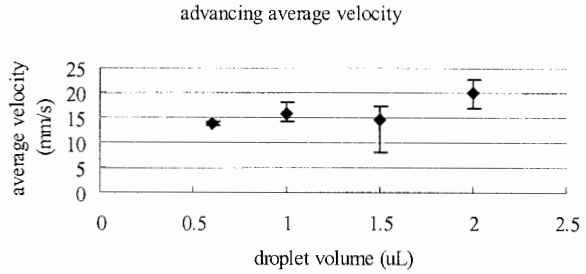

Figure 4. Average front end velocity of droplets in various size

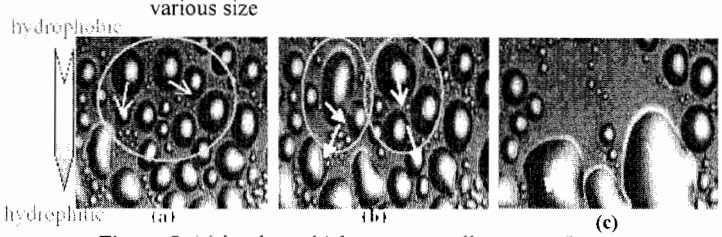

Figure 5. (a)droplets which are too small to move (b)two coalescence groups (c) merged droplets pumped by surface tension gradient

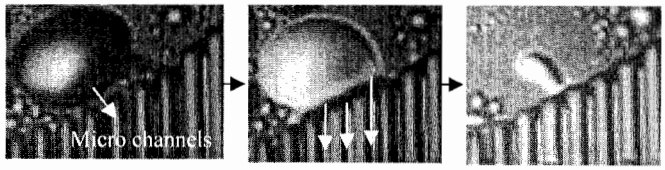

Figure 6. Droplet was absorbed to the capillary channels

GAS-LIQUID PHASE MICRO UNIT OPERATIONS USING TWO-PHASE FLOWS AND ITS APPLICATIONS FOR CHEMICAL PROCESS

Manabu Tokeshi[1,2], Teruki Matsumoto[1], Kazuteru Kanda[3], Hiromitsu Hachiya[1], Yoshikazu Yoshida[1] and Takehiko Kitamori[2,3]

[1]*Kanagawa Central Lab, The Research Association of Micro Chemical Process Technology, KSP R&D-C11, Takatsu, Kawasaki, Kanagawa 213-0012, Japan*

[2]*Micro Chemistry Group, Kanagawa Academy of Science and Technology, KSP East-307, 3-2-1 Sakado, Takatsu, Kawasaki, Kanagawa 213-0012, Japan*

[3]*Department of Applied Chemistry, The University of Tokyo, 3-2-1 Hongo, Bunkyo, Tokyo 113-8656, Japan*

Abstract

The stability of gas-liquid (GL) two-phase flows inside microchannels was characterized. We found that the stability of GL two-phase flows is related to viscosity of liquid. We also developed the newly designed microchannels to stabilize GL two-phase flows. Using the stable GL two-phase flows, two micro unit operations, i.e. extraction and concentration was developed. We realized 40,000-fold concentrated extraction and 10-fold concentration using model samples.

Keywords: micro unit operation, gas-liquid flow, interface, extraction, concentration

1. Introduction

Recently, we have demonstrated various applications utilizing liquid-liquid and liquid-solid interfaces formed in microchannels under flow conditions [1]. We call this methodology, continuous flow chemical processing (CFCP), which is based on a combination of micro unit operations (MUOs) and a multiphase flow network. Although this strategy can be applied to GL systems, reports dealing with GL flow are few because GL flow are very difficult to control inside microchannels. The CFCP will be more widely applied in various fields, if the MUOs using GL two-phase flow is realized. In order to develop the MUOs using GL two-phase flow, it is necessary to realize controlled GL two-phase flows inside microchannels. In this paper, we investigated the conditions for stable GL two-phase flow formation and realized the controlled GL two-phase flow. Using these data and techniques, new MUOs using GL two-phase flow such as extraction and concentration were developed.

2. Experimental

Stability of GL two-phase flow

A microchip with double Y-shaped channel (2 inlets and 2 outlets) was fabricated using a conventional photolithographic technique. The channels were etched to a depth of 45 μm and a width of 100 μm. The length of confluence region was 2 cm. The interfaces between air and 19 different kinds of solvents inside a microchannel were observed by a microscope. The flow rate of air was fixed at 1 ml/min.

Stabilization of GL interface

The newly designed microchips with microchannel having an asymmetric cross section were fabricated using two-step etching technique. The interfaces between air and water were observed by the microscope. The channel dimensions are described in the caption of Fig. 2.

GL extraction

Using the newly designed microchip with double Y-shaped channel, GL extraction of HCHO was performed. The aqueous solution of Schiff reagent and air containing HCHO were introduced into the asymmetric microchannel by syringe pumps. The extraction efficiency was evaluated by

detecting the reaction product of Schiff reagent and HCHO using a thermal lens microscope (TLM) [2]. The detection was carried out in the aqueous phase after phase separation.

Concentration by evaporation of solvent

A microchip similar to GL extraction experiment was used for this study. The channel dimensions are described in the caption of Fig. 4. The ethylacetate solution containing Co-2-nitroso-dimethylaminophenol (3×10^{-5}M) and air were introduced into the microchannel. The flow rates of the liquid sample and air were 20 μl/min and 8 ml/min, respectively. Microchip was heated at 70°C by a Peltier device. To evaluate the degree of concentration, the TLM measurement was carried out in the liquid phase after phase separation.

3. Results and discussion

Stability of GL two-phase flow

The stability of interfaces between air and 19 different kinds of solvents were investigated. As an indicator for the stability, we selected "margin of tolerance with respect to flow rate for stable interface formation", which was defined as difference between the maximum and the minimum liquid flow rate that afforded stable interface at a fixed gas flow rate. Then we examined dependence of stability of GL interface on physical parameters of the solvents. Fig. 1 shows correlation between viscosity of liquid and the margin of tolerance. We found that the margin of tolerance is inversely proportional to viscosity of liquid.

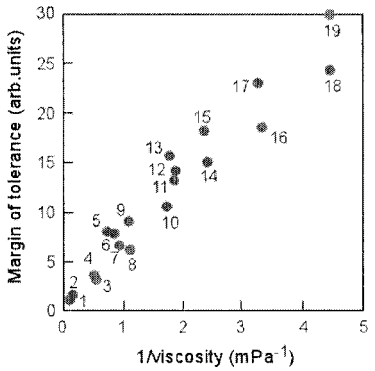

Figure 1. Dependence of stability of gas-liquid interface on viscosity of the solvents. 1: 1-decanol, 2: 1-octanol, 3: 1-propanol, 4: nitrobenzene, 5: dodecane, 6:1,4-dioxane, 7: ethanol, 8: water, 9: CCl_4, 10: m-xylene, 11: chloroform, 12: methanol, 13: toluene, 14: dichloremethane, 15: ethyl acetate, 16: hexane, 17: acetone, 18: diethyl ether, 19: pentane.

Stabilization of GL interface

We have newly designed microchannels having asymmetric cross sections, which were found to be effective for formation of stable GL and LGL flows. Surprisingly, not only stable gas-liquid co-current flow, but also counter-current flow is realized easily by using these microchannels. Fig. 2 also shows examples of the counter-current gas-liquid and liquid-gas-liquid flows. Although counter-current flow had been thought to be impossible without surface modification of channels [3], we found that for gas-liquid flows it could be realized only with the microchannel structures. Moreover, GL phase could be separated easily into gas and liquid flows using these channels (Fig. 2b).

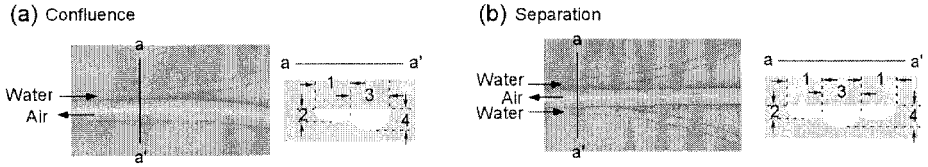

Figure 2. Examples of the counter-current flow (a: confluence; 1:60 μm, 2: 20 μm, 3: 190 μm, 4: 80 μm) and liquid-gas-liquid flow (b: separation; 1: 50 μm, 3: 30 μm, 3: 190 μm, 4: 90 μm)

GL extraction

We applied these microchannels having asymmetric cross sections to GL extraction of HCHO (from gas to water). Fig. 3 shows the dependence of extraction and concentration efficiencies on the flow rate of gas containing HCHO. Although the extraction efficiency decreased with the gas flow rate, concentration efficiency increased with the gas flow rate. Under these conditions, up to 40,000-fold concentration was realized. In spite of its simple operation, the microchannels exhibited very high transfer efficiency of HCHO from gas to liquid, and the concentration efficiency was also high.

Concentration by evaporation of solvent

Finally, we applied these microchannels to concentration of solution by evaporation of solvent. Fig. 4 shows a schematic of experimental setup. 10-fold concentration was realized by using our technique.

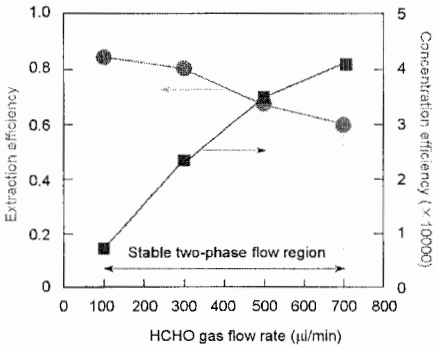

Figure 3. Dependence of extraction and concentration efficiencies on the flow rate of HCHO containing gas. Extraction efficiency was (amount of HCHO extracted)/(initial HCHO amount) and concentration efficiency was defined as (HCHO concentration of the solution after extraction)/(initial HCHO concentration in the gas sample).

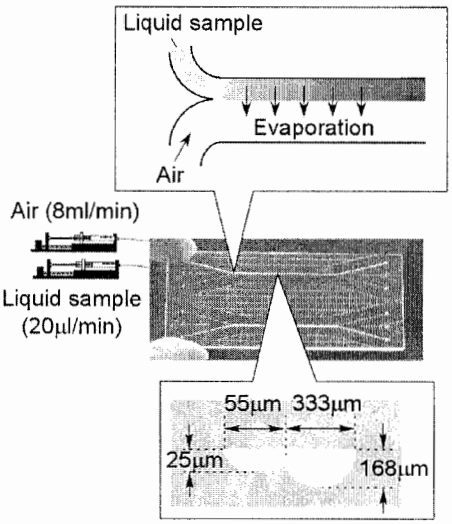

Figure 4. Schematic of experimental setup for concentration by evaporation of solvent.

4. Conclusions

In conclusion, we realized the stable GL two-phase flow inside the microchannels and developed two MUOs using GL two-phase flow, i.e., GL extraction and concentration. Moreover, these chemical processes can be improved by using the counter-current flow as shown in Fig. 2.

Acknowledgements

This work was supported by the New Energy and Industrial Technology Development Organization (NEDO) of the Ministry of Economy, Trade and Industry, Japan. We would like to thank Mr. Yoshikuni Kikutani for fabrications of the microchips.

References

[1] M. Tokeshi et al., *Electrophoresis,* **24**, 3583-3594 (2003).
[2] M. Tokeshi et al., *Analytical Chemistry*, **73**, 2112-2116 (2001).
[3] A. Hibara et al., *Analytical Chemistry*, **74**, 1724-1728 (2002).

A PRACTICAL WORLD TO CHIP INTERFACING FOR PDMS MICROCHIPS

Michie Harachi[1], Masao Inoue[1], Hisashi Hagiwara[1] and Teruo Fujii[2]
[1]Research & Development, Arbiotec,LTD.,
A306 CCR, University of Tokyo, 4-6-1 Komaba, Meguro-ku, Tokyo, Japan
[2]Institute of Industrial Science, The University of Tokyo, 4-6-1 Komaba, Meguro-ku, Tokyo, Japan

Abstract
We developed a practical world to PDMS chip interfacing with needles. Using the present needle interfacing, we achieved good sealing, small dead volumes and detachability. Moreover, we succeeded in dispensing 10nl liquids into the PDMS chip by the needle interfacing and we made an apparatus, which can dispense four kinds of nanoliter range liquids at the same time.
Keywords: interfacing, needle, PDMS chip, array, dispensing nanoliter-range

1. Introduction

So far open holes to use micropipettes and tubings (silicone, polyetheretherketone (PEEK), glass-capillary) glued into open holes have been used as the world to chip interfacing [1]. However, there are still no established interfacing method with small dead volumes and no extra structures and/or fabrication steps.

It is considered that a needle can be useful as a world to PDMS (polydimethylsiloxane) chip interfacing because of the elastic characteristics of the material. We developed the interfacing using needles that had many advantages such as small dead volumes, detachability, good sealing, easy fabrication, etc. Moreover, the needle-based interfacing is good to avoid evaporation of the liquid and intrusion of the particles in the microfluidic channels on a chip.

2. Design and fabrication

We used needles that we made from a stainless steel pipe (outer diameter 200 μm and inner diameter 100 μm) by cutting and modifying the tip of the needle into a slant face. (Fig. 1).

The PDMS chip consists of a glass substrate with PDMS coating (200μm thickness) and a PDMS layer containing microfluidic channels (Fig.2). The microfluidic channels (30μm height) were fabricated through conventional replica molding of PDMS (Sylgard 184; Dow Corning, USA). When the needle is inserted into the PDMS chip until it stops at the surface of the glass substrate, the slant opening of the needle is just connected with channels. So there is no need for fine adjustment of the needle position in the vertical direction.

An array like structure is involved in the microfluidic channel design in the horizontal plane as an insertion pad where the needle will be inserted (Fig. 3). The insertion pad is 1mm long and 2mm wide and includes 70 μm width microfluidic channels at 100 μm pitch. When the needle is inserted into the PDMS chip at the area of the insertion pad, the slant opening of the needle is connected with one or two of the channels inside the insertion pad. So there is also no need of fine adjustment of the needle position in the horizontal plane.

3. Experimental

First, we tested the sealing performance of the needle interfacing. Generally gas leaks easier than liquid and negative pressure in the channels help sealing more than positive pressure. So, we measured the ability to against a positive gas (air) pressure. We inserted the needle into the insertion pad and raised the air pressure in the channels by applying the compressed air through the other port. We read the value of a pressure sensor when air bubble began to appear in the water

droplets that we placed at the insertion point on the surface of the PDMS chip. After that, we pulled out the needle and placed water droplets again at the insertion point. We read the value of a pressure sensor when air bubble began to appear in the droplets in a similar way.

Second, we measured the dead volume of the interfacing. We filled the needle with red inks to observe easily and inserted the needle into the insertion pad. Then, we applied a negative air pressure of under –1kPa through the other port to introduce red inks into the channels and watched the liquid flow under a microscope.

Third, using the present needle interfacings, we tried dispensing 10 nl liquids into a PDMS chip. Fig. 4 shows a channel pattern for 10 nl metering. When we drive the air vent microvalve by a negative air pressure, the air in the metering channel will be drawn off through the valve. Then, liquid (water) is introduced through the needle interfacing into the 10 nl metering channel and stopped at the end of it. By applying a positive air pressure at the microvalve, the liquid in the metering channel will be pushed towards the check valve. Namely, the metered liquid in the channel will be transported to the next process through the check microvalve.

In these experiments, an air pressure and flow control unit named My Flow (Arbiotec, LTD; JAPAN), which is developed by us, was used to apply well-controlled air pressure.

4. Results and discussion

Concerning the sealing performance, the needle interfacing had a capacity to resist against a positive air pressure of over +150 kPa in the case of keeping the needle inserted into the insertion pad and over +70 kPa when the needle is pulled out. The needle can be inserted into or pulled out easily (detachable), and we found that the needle interfacing showed a good sealing in both cases. The dead volume can be minimized as shown in Fig. 5. Red inks flowed only from the channel that the needle was inserted and was introduced into the channels without flowing into the extra channels. Dispensing 10nl water into the PDMS chip is successfully executed. We could handle small volume of liquids that we could not dispense by conventional micropipettes.

For the practical use of the proposed method, we developed an apparatus to insert four needles onto a PDMS chip simultaneously (Fig. 6). The PDMS chip contains four sets of the metering structure shown in Fig.4 to dispense 10 nl volume. The chip is inserted into the apparatus as shown in Fig. 6a, then the needles are inserted into the chip by turning the knob (Figs. 6b and 6c). Liquid in the reservoir can be introduced into the chip by applying a negative air pressure from the pneumatic port. Thus, we could simply use the needle interfacings in a multiple format.

5. Conclusions

We demonstrated that the needle interfacing has good sealing performance, minimized dead volumes, and detachability. The practical apparatus has also been developed using the present interfacing method by which we could handle 10nl volume liquid in multiple microfluidic channels contained on a PDMS chip. The needle interfacing will play an important role in the wide use of PDMS microchips, and could be a candidate for their standard world-to-chip interfacing.

Acknowledgements

We wish to thank our colleagues who participated in this research.

References

[1] N. J. Mourlas, D.Jaeggi. et al, Novel Interconnection and Channel Technologies for Microfluidics, *microTAS 1998 Workshop*, pp27-30

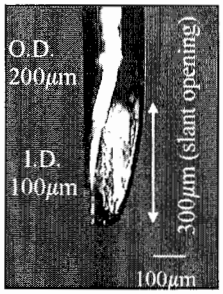

Figure 1. Photograph of a needle

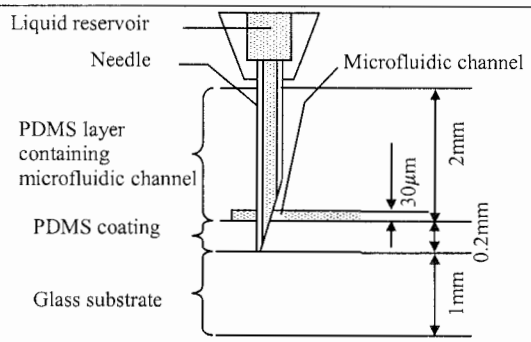

Figure 2. Cross-section of inserting a needle in a PDMS chip

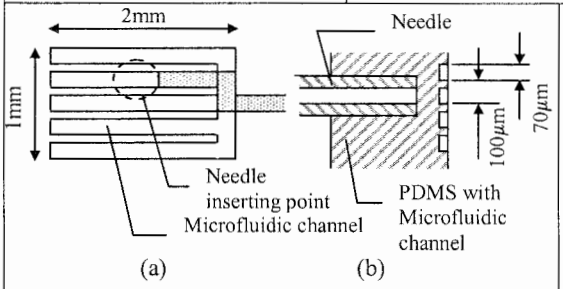

Figure 3. Pattern design of the insertion pad (a) Top view. (b) Cross-section of side view

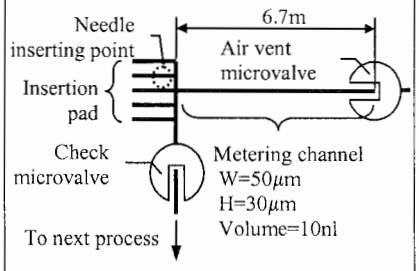

Figure 4. Pattern design for 10nl metering

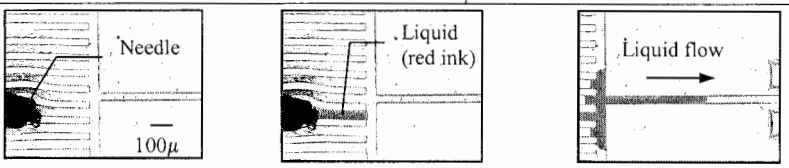

Figure 5. Photographs of the insertion pad (a) Needle inserting point. (b) Liquid starts from the needle inserting point. (c) Liquid flows.

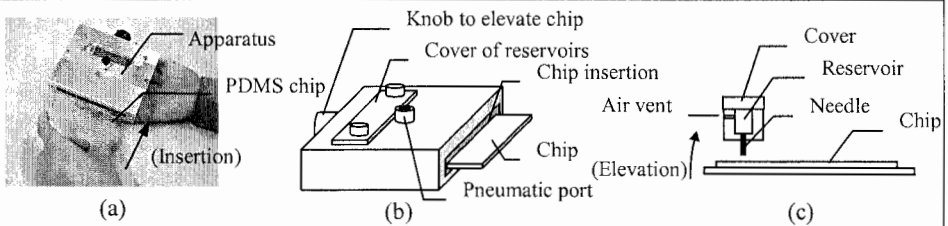

Figure 6. The apparatus to dispense for 10nl liquid (a) Photograph. (b) Outer Structure. (c) Inner structure.

2D FREE SPACE FLOW CONTROL SYSTEM USING TERMOREVERSIBLE GELATION OF POLYMER BY IR-LASER

Masayasu Tatsuoka[1], Tomohiro Shimomae[2], Yoshitaka Shirasaki[1], Jun-ichi Tanaka[2], ShotaWatabe[2], Jun Mizuno[3], Tomohiko Edura[3], Ken Tsutsui[3], Yasuo Wada[3], Shuichi Shoji[2], and Takashi Funatsu[1],

[1]Department of Physics,[2]Department of Electrical Engineering and Bioscience, [3]The Institute of Nanotechnology, Waseda University, 3-4-1 Ohkubo, Tokyo 169-8555, Japan

Abstract

We developed two-dimensional (2D) flow control system in a microchamber using thermoreversible gelation of polymer. Arbitrary patterns were projected on a microchamber with two dimensional arrays of metal films using an infrared (IR)-laser reflected by a micro mirror device (DMD). The irradiated areas were heated to form gel walls that interrupted the flow. The pattern could be reversibly changed by controlling the DMD coupled to a computer. This flow system is very flexible and applicable to various kinds of biomolecules handlings.

Key Words: 2D-flow control system, Micro flow system, Thermal gelation, Sol-gel transition

1. Introduction

Flow control in micro chemical/biochemical analysis systems is one of the key technologies in μTAS. Although various types of micro-fluidic devices on a chip have been developed, they are not flexible due to the unchangeable structure. We showed previously that thermoreversible gelation of polymer was very useful for the flow control in a micro device [1]. We extended this method to the 2D free space flow control system using an IR-laser illumination via a DVD. By using this method, channel patterns could be reversibly changed at real time.

2. Experimental

Fig.1 shows the structure of the 2D flow control chip. A microchamber with 3 inlets and 9 outlets was fabricated on a pyrex glass and bonded to a glass plate. It has 2D arrays of thin Pt chips that absorb IR-laser. We made two kind of chips without (Type 1) or with (Type 2) micro pillars.

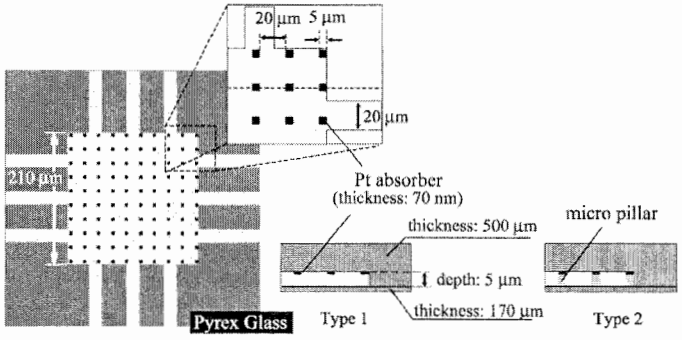

Figure 1. Structure of the 2D flow control chip

Fig.2 shows the principle of the control of 2D flow. The chip is placed on a stage of a fluorescence microscope which was modified to illuminate the chip by IR-laser (808 nm, 19 W) via a DMD. Fluorescent beads were mixed with a carrier solution containing 10% (wt/wt) thermoreversible gelation polymer composed of poly *N*-isopropylacrylamid and poly oxyethylene (Mebiol Gel™) [2]. The solution was introduced into a micro chamber as shown in Fig.1. Fluorescent beads were observed by fluorescence microscopy with filter sets for rhodamine (41002, Chroma Technology). The patterns generated by a DMD are projected using IR-laser on the

micro-chamber. Temperature of the microchamber is locally elevated and sol to gel transition of Mebiol Gel occurs when the temperature exceeds 36°C. The gel functions as a wall and it control the flow in the chamber. The projection patterns can be changed freely and quickly by a computer.

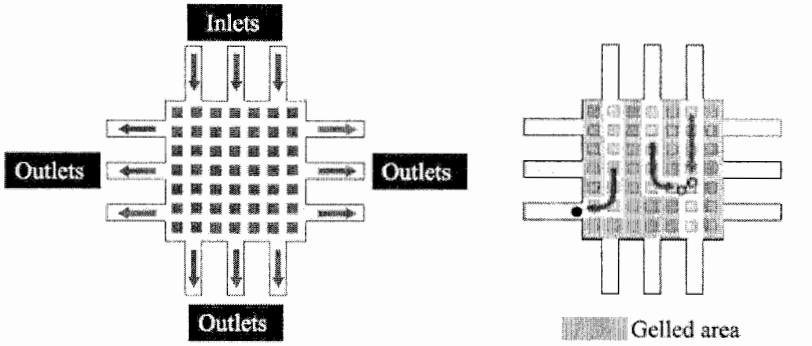

Figure 2. Principle of the 2D flow control system

3. Results and discussion

Fig.3 shows the streamlines (exposure time of 1 s) of fluorescent beads in a chamber of Type 1. In the arias surrounded by broken lines, gel was formed by IR radiation. On changing the illumination areas of (a) and (b) alternately, gel walls were reconstructed corresponding to the switching. The time required for switching of flow was 60 ms. We succeeded in constructing changeable microfluidic structures and in controlling 2D free flow rapidly.

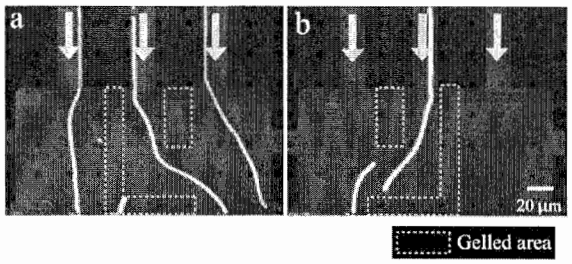

Figure 3. Reconstruction of gel walls (a & b, alternatively) to control the flow

Next, we tried to control flow more precisely by using the type2 chip with micro pillars (Fig.4). The arias surrounded by broken lines are blocked by the gel walls, and the streamlines (exposure time of 0.5 s) of fluorescent beads changed their direction at right angles.

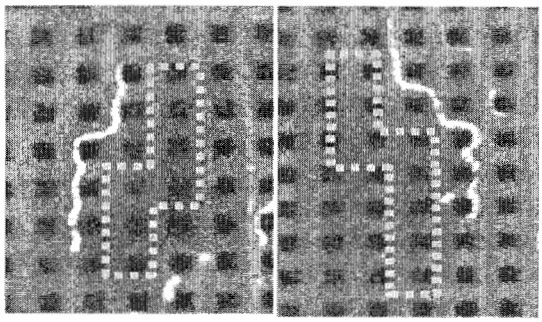

Figure 4. Precise control of flow using local gelation in a chamber with micropillars

4. Conclusions

We succeeded in constructing a changeable microfluidic structures and in controlling 2D free flow at time resolution of 60ms. And we also controlled microfluidic streams very precisely by using micro pillars in a micro chamber.

Acknowledgements

We would like to thank H. Yoshioka and Y. Mori for providing Mebiol Gel. This research was partly supported by Grants-in-Aid for COE Research, Scientific Research Priority Area (B) No.13124209, Scientific Basic Research (A) No.12450167, Scientific Basic Research (B) No.12450167, 13558088, and "Nanotechnology Support Project" from the Ministry of Education, Culture, Sports, Science and Technology of Japan.

References

[1] Y. Shirasaki, H. Makazu, K. Tashiro, S. Ikeda, T. Sekiguchi, S. Shoji, S. Tukita, T. Funatsu. *Micro Total Analysis System 2002*, pp925-927.

[2] H.Yoshioka, M. Mikami, Y. Mori, and E. Tsuchida. *J. Macromol. Sci.*, A31, 113-120 (1994)

NANOSCALE STRUCTURE OF ELECTROKINETICALLY DRIVEN FLOW OBTAINED FROM LARGE-AREA EVANESCENT WAVE EXCITATION

Koichiro Saiki* **and Yohei Sato***

**Dept. of System Design Engineering, Faculty of Science and Technology, Keio University, Hiyoshi 3-14-1, Kohoku-ku, Yokohama, 223-8522, Japan*

Abstract

Control of electrokinetically driven flow (EKDF) is a key technique of micro- and nanoscale transport phenomena. For development of microfluidic systems, the nanoscale structure of EKDF should be investigated experimentally. Evanescent wave which is generated by total internal reflection enables us to measure EKDF in the vicinity of the wall surface on the order of nano meter. It is obtained that the number of submicron particles in the vicinity of electrolyte-glass interface are decreased in EKDF. Considering the relationship between the fluorescent intensity and the distance from the interface, the potential energy profiles of submicron particles which exist near the wall surface can be calculated because of the histogram representing the Boltzmann distribution. The potential curves are changed in EKDF, which means that submicron particles are moved far away from the interface in the vertical direction.

Keywords: nanoscale, electroosmotic flow, evanescent, optical measurement, submicron particles,

1. Introduction

EKDF is widely utilized in microfluidic devices. The EKDF structure in microchannel has been measured qualitatively [1]. However, the accurate control of EKDF is a key issue for the next generation of microfluidic devices. The authors' group has established the quantitative measurement technique using a microscope [2]. From a viewpoint of nanoscale, the EKDF structure near the wall surface of microchannel should be investigated. The evanescent wave generated at an electrolyte-glass interface enables us to measure the nanoscale structure [3, 4], because the characteristic penetration depth is on the order of 100 nm. The objective of the present study is to investigate the EKDF structure in the vicinity of the surface using submicron particles. The particle motion in the depth wise direction is measured by large-area evanescent wave light illumination.

2. Experimental

Figure 1 shows the measurement system which is comprised of an inverted microscope (Nikon Corp., TE2000), a CW laser (λ=473 nm) and a cooled CCD camera (Hamamatsu Photonics K.K., C4880–80). The laser light is introduced into a prism attached to a non-coat borosilicate cover glass

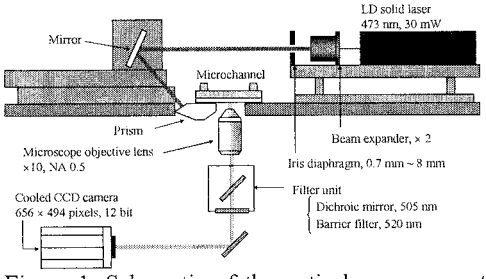

Figure 1. Schematic of the optical measurement system using evanescent light illumination.

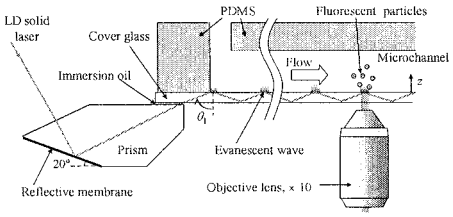

Figure 2. Schematic of the prism and total internal reflection. (θ_i=68.3°)

of 0.5 mm thickness and generates evanescent wave in a microchannel (PDMS and the cover glass, 400 μm × 80 μm × 25 mm). A 10× magnification objective lens (NA = 0.5) is attached to a microscope, which realizes nanoscale measurements in a large-area (1.6 mm × 0.6 mm), as shown in Figure 2. Submicron fluorescent particles whose properties are compiled in table 1 are included in a 5mmol/l HEPES buffer solution as a working fluid. The particle volumetric fraction was 0.4%. The ζ-potentials of each particle are calculated by the electrophoretic mobility that was obtained by using a closed cell [5].

Table 1. Properties of fluorescent particles.

		(*a*) Calboxilate modified	(*b*) Sulfate modified
Material noun	-	polystyrene	polystyrene
Mean diameter	μm	1.0	1.0
Density	g/cm^3	1.055	1.055
Absorption wavelength	nm	505	505
Emission wavelength	nm	515	515
ζ-potential	mV	46.7	71.2

4. Results and discussion

A microchannel flow was driven by an electric field when platinum electrodes were submerged in both inlet and outlet in order to generate EKDF. Figure 3 shows histograms of number of carboxylate modified particles versus the fluorescent intensity from the particles, which was calculated by using 500 instantaneous images detected by the cooled CCD camera. Total number of carboxylate modified particles between the range of fluorescent intensity 400-3300 was calculated as shown in Table 2. It is obvious from these results that number of particles is decreased with an increase in the electric field. It means that particles are moved away from the surface. In the present study, the characteristic penetration depth was calculated to be 81μm, thus particles are forced to move from the region illuminated by the evanescent wave. In order to investigate the vertical motion of particles near the surface, the potential energy of particles were calculated by using the histograms. Considering the Boltzmann distribution and the relationship between fluorescent intensity and the distance between particles and the glass surface, the profile of histogram was converted to the potential energy [4, 6]. Figure 4 shows profiles of the potential energy calculated by using Figure 3. While the potential energy of sulfate modified particles was obtained as shown in Figure 5. It is observed that the potential energy of particles is increased with an increase in the electric field. These potential profiles are represented by the exponential function defined as

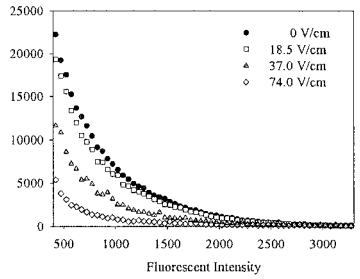

Figure 3. Histogram of number of carboxylate particles versus the observed fluorescent intensity.

Table 2. The total number of observed particles between the range of fluorescent intensity 400-3300.

E [V/cm]	Number of particle
0.0	231434
18.5	200048
37.0	105852
74.0	38885

$$\phi(z) = B'\exp(-z/\lambda_d) \tag{3}$$

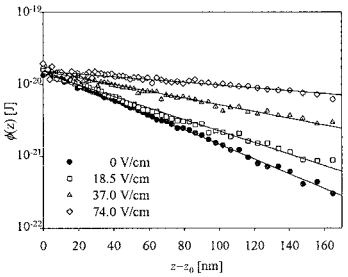

Figure 4. Profiles of potential energy of carboxylate modified particles.

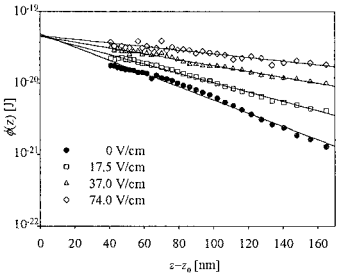

Figure 5. Profiles of potential energy of sulfate modified particles.

Table 3. B' and λ_d' calculated by using equation (3).

	(*a*) Carboxilate modified		(*b*) Sulfate modified	
E [V/cm]	B' [J]	λ_d' [nm]	B' [J]	λ_d' [nm]
0.0	1.55×10^{-20}	42	4.90×10^{-20}	47
18.5	1.43×10^{-20}	54	4.58×10^{-20}	67
37.0	1.53×10^{-20}	94	4.52×10^{-20}	106
74.0	1.53×10^{-20}	227	4.61×10^{-20}	172

where z is the distance between the surface and particles, B' is the potential energy at z=0 and λ_d' is the distance where the potential energy becomes $1/e$ of B'. Table 3 shows value of B' are λ_d' when the electric field was increased. B' has a constant value for each particle, while λ_d'is increased with an increase in the electric field. From these results, it can be noted that the vertical motion of particles is not affected by the electric charge of glass surface, but by the fluid structure near the surface. Moreover, B' of sulfate modified particles is larger than that of carboxylate modified particles because the ζ-potential of sulfate modified particles is larger than that of carboxilate modified particles.

5. Conclusions

The nanoscale structure of EKDF was investigated by evanescent wave light illumination. It can be concluded that the change in potential energy of particles indicates the particle vertical motion that was moved away from the wall surface.

Acknowledgements

The authors would like to thank Professor K. Hishida at Keio University for his technical assistance. This work was subsidized by the Grant-in-Aid for Scientific Research of Ministry of Education, Culture, Sports, Science and Technology (No. 1470230 and 15206024).

References

[1] P. H. Paul, M. G. Garguio and D. J. Rakestraw, *Anal. Chem.*, **70**, 2459-2467 (1998).
[2] Y. Sato, K. Hishida and M. Maeda, *Micro TAS 2002,* **1**, 512-514 (2002).
[3] Y. Kazoe and Y. Sato, *12th Int. Symp. Appl. Laser Tech. Fluid Mech.*, CD-ROM (2004).
[4] S. G. Flicker, J. L. Tipa and S. G. Bike, *J. Colloid and Interf. Sci.*, **158**, 317-325 (1993).
[5] M. Ichiyanagi, K. Saiki, Y. Sato and K. Hishida, *12th Int. Symp. Appl. Laser Tech. Fluid Mech.*, CD-ROM (2004).
[6] D. C. Prieve and N. A. Frej, *Lunmuir,* **6**, 396-403 (1990).

CONTROLLED PRODUCTION OF DOUBLE EMULSIONS USING MULTI-STEP DROPLET BREAK-UP

Shingo Okushima, Takasi Nisisako, Toru Torii and Toshiro Higuchi

Department of Precision Engineering, Graduate School of Engineering, The University of Tokyo, 7-3-1 Hongo, Bunkyo-ku, Tokyo 113-8656, Japan

Abstract

We propose a novel technique for producing monodisperse double emulsions using T-shaped microchannels. Control of the flow conditions produces variations in internal/external droplet sizes and in the internal droplet number. Both water-in-oil-in-water (W/O/W) emulsions (with 2 types of internal droplets), and oil-in-water-in-oil (O/W/O) emulsions were successfully prepared.

Keywords: double emulsion, multiple emulsion, microchannel, surface tension, microreactor.

1. Introduction

Double emulsions have many industrial applications including encapsulation of drugs, cosmetics and food products. Although there exist a few manufacturing techniques for double emulsions, they cannot accurately control the volume or the number of the internal droplets [1, 2].

Here we present a novel method for preparing monodisperse double emulsions by a two step method of droplet formation in microchannel networks. Figure 1 illustrates the basic concept as used in preparing W/O/W emulsions. Water droplets are formed periodically at the first junction; and, in a continuing series, oil droplets that include the water droplets are formed at the second junction in a periodical cycle. Since surface tension is dominant for droplet formation in microchannels, water droplets can be formed only in a hydrophobic microchannel [3] and oil droplets in a hydrophilic microchannel [4]. The monodisperse droplets form periodically and their size is easily varied at the formation points by changing the flow conditions [3]. By these means it is possible to control the properties of double emulsions, the volume and number of internal droplets, or the size of external droplets, for example.

2. Experimental

Two variants are proposed for production of double emulsions: a one-chip type in which multiple junctions are on the same chip; and a two-chip type which have junctions on separate chips. Since the internal droplets must be smaller than the external droplets, the microchannel of the first junction (30-80 μm wide×10-40 μm deep) was fabricated to be smaller than the second junction (130-220 μm wide×65-90 μm deep), either by wet etching or machining tools. In all devices, the surface around a T-junction was modified by a silane coupling agent to be hydrophobic for W/O droplet formation. Deionized water and corn oil were used as an aqueous phase and an organic phase, respectively. Sodium dodecyl sulfate was used as a surfactant in the aqueous phase, and lecithin was used for the organic phase.

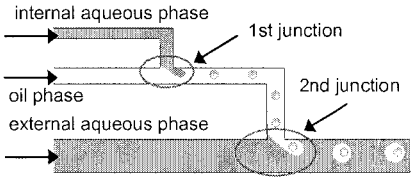

Figure 1. Basis of the method for preparing double emulsions (W/O/W) using T-shaped microchannels.

3. Results and Discussion

Monodisperse W/O/W droplets were formed in one-chip devices and two-chip devices in the range of diameters 83-220 μm, with a coefficient of variation (CV) of 2-7 %.

Figure 2a shows the formation of W/O/W droplets in a one-chip device. Figures 2b and 2c show the resulting W/O/W droplets and their size distribution. In this case, the diameter of the water droplets was 52 μm and that of the oil droplets was 83 μm, with CVs of 2.7 % and 2.8 % respectively. In the one-chip device, oil droplets containing only a single monodisperse water droplet were formed with 100 % probability (n=100). The generation rates of water droplets and oil droplets were both 22 Hz. This result shows that the number of internal droplets can be controlled by adjusting the generation rate.

Figure 3a shows the effect of the organic phase flow rate on the diameter of water droplets, and on the number of internal droplets included with an oil droplet, in a one-chip device. At fixed flow conditions of the internal and external aqueous phases, as the organic phase flow rate increases, the size of the water droplets decreases (20 to 12 μm) and the number of encapsulated water droplets increases (mean: 4.7 to 11.9). Figure 3b shows the effect of the external aqueous phase flow rate on the diameter of oil droplets, and on the number of water droplets included with an oil droplet, in a two-chip device. With increasing external aqueous phase flow rate at a fixed speed of w/o dispersion, the size of the oil droplets decreases (220 to 95 μm), resulting in a fall in the number of encapsulated droplets (mean: 4 to 1). These results show that the number of internal droplets can be controlled by changing the droplet size. Double emulsions can therefore be accurately designed using this method.

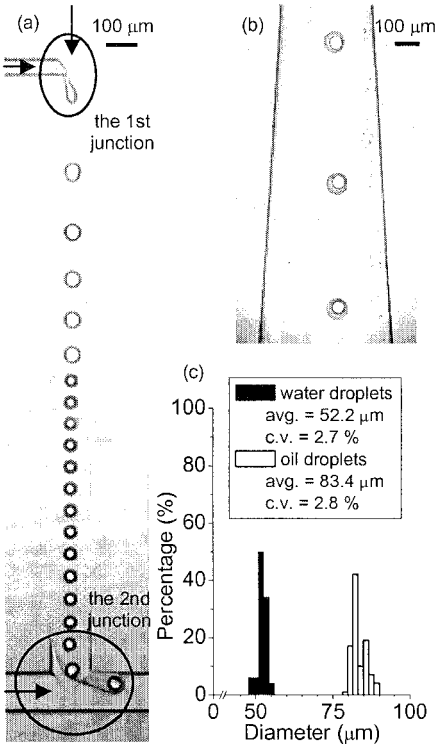

Figure 2. Formation of W/O/W droplets: (a) Formation of W/O/W droplets in a one-chip device, (b) W/O/W droplets, (c) Size distribution of the droplets.

O/W/O droplets were prepared in the two-chip device (first junction hydrophilic, second junction hydrophobic) (Figs. 4a, 4b). W/O/W emulsions containing two types of internal droplets were prepared in the two-chip device. Differently colored aqueous droplets (red or blue) were produced alternately at the cross-junction (Fig. 4c), and both colors of droplet carried to the second junction to be encapsulated in the same oil droplet (Fig. 4d). Various double emulsions, as well as simple W/O/W emulsions, can be prepared using this method.

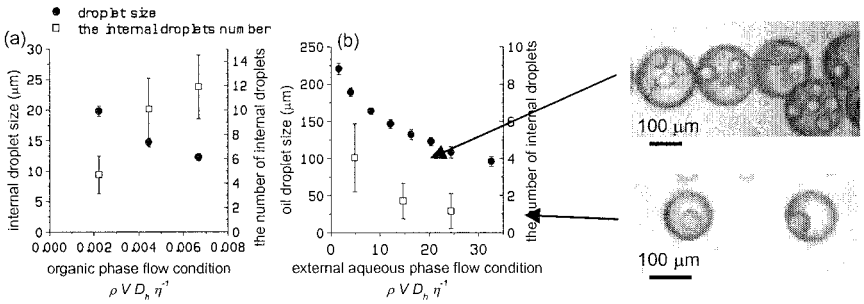

Figure 3. Effect of flow condition on droplet size and on the number of internal droplets: (a) effect of the organic phase flow parameters on the diameter of water droplets and on the number of water droplets included with an oil droplet in a one-chip device; (b) effect of the external phase flow condition on the diameter of oil droplets and on the number of water droplets included with an oil droplet in a two-chip device.

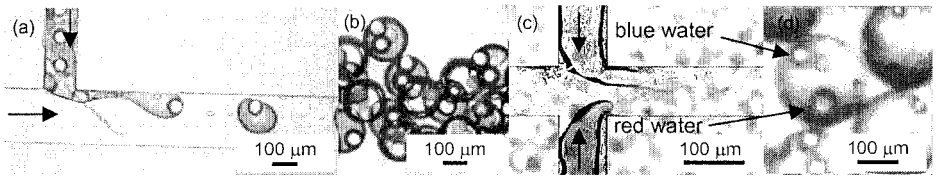

Figure 4. Formation of various double emulsions: (a) O/W/O droplets, (b) O/W/O droplets, (c) red and blue droplets at a cross-junction, (d) W/O/W droplets with two colors of internal droplets.

4. Conclusion

Monodisperse double emulsions were prepared using microchannels, and the size of droplets and the number of internal droplets were varied by changing the flow conditions. Both W/O/W and O/W/O emulsions were prepared by interchanging the hydrophobic and hydrophilic components, and double emulsions including internal droplets of two colors were prepared using a cross-junction.

Acknowledgement

This work was supported by grants from the Research Association of Micro Chemical Process Technology (MCPT) of Japan.

References

[1] S. Matsumoto, Y. Kita, D. Yonezawa. J. Colloid Interf. Sci, **57**, 353-361 (1976).

[2] S. Higashi, M. Shimizu, T. Nakashima, K. Iwata, F. Uchiyama, S. Tateno, S. Tamaura, T. Setoguchi, Cancer, **75**, 1245-1254 (1995).

[3] T. Nisisako, T. Torii, T. Higuchi, Lab. Chip. **2**, 24-26 (2002).

[4] T. Nisisako, T. Torii, T. Higuchi, Proc. of the 16th Int. Conf. on MEMS, 331-334 (2003).

HIGH FLOW RATE MICROFLUIDIC PUMPS

Jacques Goulpeau[1,2], Daniel Trouchet[2], and Patrick Tabeling[1]

[1]Microfluidique, MEMS et Nanostructures, UMR 7083 ESPCI, 10 rue Vauquelin, 75231 Paris, France. [2]Bertin Technologies, Saint Quentin en Yvelines, France.

Abstract

The goal of this work is to improve the performance of PolyDimethylSiloxane (PDMS) peristaltic pumps to a level where typical biological samples (0.1–1 mL) can be directly injected into microchips. We thus present a theoretical and experimental study of such pumps. In this work we identified characteristic cycle frequencies and their general behavior with respect to the micropump geometry allowing us to fabricate a micropump delivering flow rates of up to 30 μL/min, that is to say 200 times larger than has been previously shown.

Keywords: PDMS, peristaltic pumps, world-to-chip interface, lab-on-a-chip

1. Introduction

World-to-chip interfacing is a crucial problem in microsystems [1,2] because biological sample volumes typically range between 100 μL and 10 mL, while microchips typically hold tens of nL. External pumps are generally used for injecting large volumes into the chip; however, it is advantageous to have alternative solutions using integrated pumps. Existing integrated pumps barely draw up volumes on the order of 1 mL. Currently, the most efficient integratable pumps are made with silicon, a material with certain limitations. Furthermore, these silicon pumps take about one hour to drive volumes in the milliliter range [4]. Integrated PDMS pumps generally deliver much lower flow rates than silicon pumps [3,6]. We investigate the performances of these integratable peristaltic PDMS pumps [5] in terms of flow rates, in order to be able to handle fluid volumes on the order of the size of a typical biological sample. In order to find an optimization pathway, we tried to understand this type of micropump by conceiving a simple model based on an electric equivalence for one valve, and we compared the conclusions of this model to experimental data. As a result of this approach, we were able to fabricate micropumps delivering flow rates 200 times larger (30 μL/min) than previous work [3].

2. Theory

The micropumps studied here are composed of three valves microfabricated using Multi-layer Soft Lithography (MSL) technology [3]. A flow rate is induced in the working channel when the valves are subjected to a peristaltic cycle. The flow rate depends on the cycle frequency, the actuation pressure and the geometry of the design. In order to model the influence of the cycle frequency on the flow rate, we have come up with the electrical equivalence of one valve shown in Fig. 1. The PDMS valve is then represented by a system of resistances (R_a and R_w) and capacitances (C_m and C_a). From this model we can extract several characteristic frequencies ($1/R_aC_a$, $1/R_aC_m$, and $1/R_wC_m$) above which the response of the closing of the valve will be strongly toned down. These characteristic frequencies will influence the behavior of the micropump and we can assume that its characteristic frequencies will be related to the ones of a microvalve alone. The rest of the paper is dedicated to confirming, in detail, this theoretical representation.

3. Experimental

The micropumps were fabricated using the MSL technique described in Ref. [3] using Sylgard 184 PDMS (Corning). The working channels were 2 cm long, 44 μm high with a round cross-section and equal widths for both actuation and working channels, resulting in square valves between 229 to 539 μm wide. The first set of experiments denoted A (Fig. 2a) was made with a 439 μm wide micropump with actuation channels 33 μm high and 8.15 mm long. The second set of

experiments denoted B was undertaken using five micropumps of differing channel widths (Fig. 2b, 3) with 130 μm high actuation channels. The actuation channel was filled with deionised water and the working fluid was water with varying concentrations of glycerol in order to vary its viscosity. In absence of glycerol, 0.1 M NaOH was used to reduce membrane adhesion to the glass. In all cases, the membrane thickness was 30 μm. We measured the flow rate versus the frequency for a given peristaltic cycle (000, 100, 110, 111, 011, 001) and for a given constant actuation pressure [3].

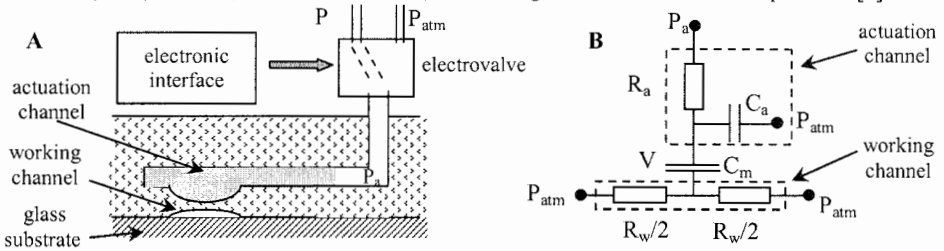

Figure 1. (a) sketch of the whole actuation system for a single microvalve. (b) dynamical linear model using the electrical analogy. P_{atm} is the atmospheric pressure.

For each micropump, the actuation pressure P was chosen to be the optimal pressure P_{op} at which the flow rate was maximal at a frequency of 50 Hz. From this flow rate, we extract the elementary volume expelled per cycle.

4. Results and discussion

The collapse data of set A displayed in Fig. 2 show that the volume expelled per cycle for a three valves pump behaves as a first order low-pass filter with a characteristic frequency proportional to the inverse of the viscosity of the working fluid (η_w) [Eq. (1)]. This result is consistent with the simple linear model previously presented in Fig. 1 [Eq. (2)], calculating R_w by assuming a Poiseille flow in the working channel.

$$V = V_0 \Big/ \sqrt{1+\left(\frac{f}{f_c}\right)^2} \qquad f_c \approx \frac{1}{R_w C_m} \propto \frac{h^3 w}{\eta_w L C_m} \qquad (1), (2)$$

h, w, and L being the height, the width and the length of the working channel. One also observes a second characteristic frequency appearing on the data which has been related to the fluid viscosity of the actuation channels (data not shown). To avoid this second characteristic frequency we have increased the height of the actuation channel and thus reduced R_a (set B): the resulting data fit well with a first order low-pass filter (Fig. 2b), showing in this case no significant deviation at high frequency. It was then possible to study the influence of the geometry on this well defined characteristic frequency. We estimate the capacitance of the membrane C_m of each micropump by dividing the volume under the valve V_0 by the optimal pressure P_{op} ($C_m \approx V_0/P_{op}$). The dependence of the optimal actuation pressure (P_{op}) versus the geometry of the valve in each micropump shows a linear dependence with the inverse of the membrane surface [Fig. 3a, Eq. (3)] which is consistent with previous work [7].

$$P_{op} \approx 1/w^2 . \qquad (3)$$

From Eq. (2) and (3), we can conclude that the characteristic frequency related to $1/R_wC_m$ should depend on height h and width w as:

$$f_c \approx 1/R_w C_m \approx P_{op}/R_w V_0 \propto h^2/w^3 . \qquad (4)$$

The characteristic frequency measured for the different micropumps of set B are plotted versus h^2/w^3 (Fig. 3b) showing a linear trend. From this study, we can conclude that the general behavior of this type of micropump is well described by our simple linear model, the characteristic frequency

being related to the hydraulic resistance of the working channel and the membrane capacitance in our experiments. We can therefore roughly evaluate the maximum flow rate (Q_{max}) from the design of a micropump and the viscosity of the working fluid [Eq. (5)].

$$Q_{\max} \approx V_0 f_c \propto h^3/\eta_w w. \quad (5)$$

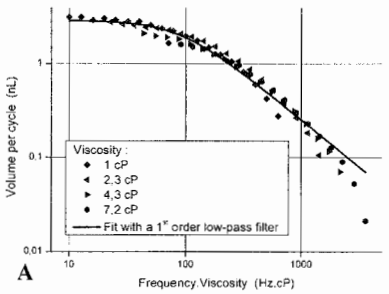

A

channel width (w)	characteristic frequency (f_c)	r^2
229 µm	373 Hz	0.989
400 µm	160 Hz	0,979
439 µm	95 Hz	0,971
500 µm	63 Hz	0,995
539 µm	63 Hz	0,996

B

Figure 2. (a) Collapsed data of the elementary volume expelled per cycle plotted vs. frequency multiplied by the viscosity. (b) Results of the low-pass filter fit for each micropump. r^2 is the mean square deviation of this fit.

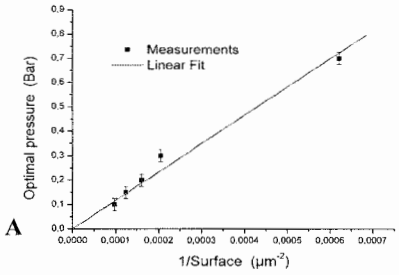

A

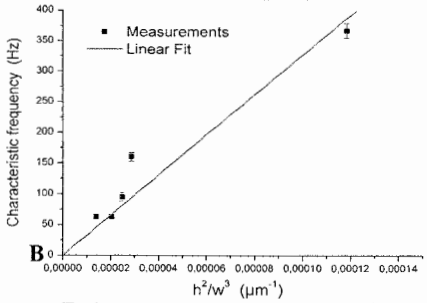

B

Figure 3. (a) Linear dependence of the optimal pressure (P_{op}) vs. the surface of the membrane. (b) characteristic frequency f_c vs. h^2/w^3.

With this simple model, we have designed a micropump capable of delivering a flow rate up to 7 µL/min, which is already 50 times larger than previous work [3]. Furthermore, thinking in term of this modeling of equivalence of electric circuit, we could improve the actuation system, and thus increasing the flow rate up to 30 µL/min.

5. Conclusions

We demonstrate that peristaltic micropumps may be described by characteristic frequencies well defined by a simple linear model of a single valve. Considering the membrane elasticity and the resistance of the channels we could therefore design micropumps delivering high flow rates.

References

[1] J. Liu, C. Hansen, S. R. Quake, *Anal. Chem.*, **75**, 4718 (2003).
[2] J. Lichtenberg, N. F. de Rooij, E. Verpoorte, *Talanta*, **56**, 233 (2002).
[3] M. A. Unger, H.-P. Chou, T. Thorsen, A. Scherer, S. R. Quake, *Science*, **288**, 113 (2000).
[4] D. Maillefer, S. Gamper, B. Frehner, P. Balmer, H. van Lintel, P. Renaud, *Proc. MEMS 2001*, Interlaken, 414 (2001)
[5] T. Thorsen, S. J. Maerkl, S. R. Quake, *Science*, **298**, 580 (2002)
[6] A. Terray, J. Oakey, D. Marr, *Science*, **296**, 1843 (2002)
[7] V. Studer, G. Hang, A. Pandolfi, W. F. Anderson, S. R. Quake, *J. Appl. Phys.* **95**, 393 (2004).

RAMAN CONFOCAL IMAGING OF REACTION-DIFFUSION PROCESSES IN MICROCHANNELS

Jean-Baptiste Salmon[1], Laurent Servant[2], David Talaga[2], Patrick Tabeling[1], and Mathieu Joanicot[3]

[1]*Microfluidique, Mems et Nanostructures, ESPCI, 10 rue Vauquelin 75005 Paris, France*
[2]*Laboratoire de Physico-Chimie Moléculaire, Université Bordeaux I, 351 cours de la libération, 33405 Talence cedex, France*
[3]*Lab Of the Future, Unité mixte Rhodia-CNRS, IECB, 2 rue Robert Escarpit, 33600 Pessac*

Abstract

This work investigates the use of Raman confocal imaging to study chemical reactions and diffusion processes in microchannels. Raman confocal microscopy allows us to simultaneously access local concentrations of several different chemical compounds by measuring the intensity of the vibration modes of the molecules. Thus, Raman microscopy is a powerful tool as compared to classical fluorescence techniques for the study of reaction-diffusion dynamics. We present here two situations commonly encountered in microfluidics: the *interdiffusion* of two liquids and the chemical reaction between two liquids. Our experimental results are compared to theoretical models that couple hydrodynamics and reaction-diffusion dynamics.

Keywords: Raman confocal imaging, chemical reaction, interdiffusion

1. Introduction

The characterization of chemical reactions and diffusion dynamics in a microchannel is an essential step in the development of the so-called *lab-on-a-chip* technology as applied to industrial chemistry. Such microfluidic chips allow one to study various chemical phenomena that would be impossible to investigate in the macro-world: measurements of fast chemical kinetics [1–3], screening, etc. In order to improve these experimental tools, it is necessary to thoroughly understand the transport phenomena at these smaller length scales. Various problems have been addressed theoretically [4,5], but there are currently far to few experimental works that confirm these different models. The current methods used to study reaction-diffusion phenomena in microfluidic chips usually involve fluorescence techniques, the diffusion of a *probe*, or the production of a probe by a complexation reaction. However, these techniques cannot be applied to the majority of chemical reactions, whose products and reactants do not display fluorescent properties. Nor can these techniques be used to characterize the interdiffusion of two solvents since fluorescence microscopy requires the addition of dyes.

In the present work, we use Raman confocal microscopy to address these microscale phenomena. Raman imaging is a non-intrusive technique that gives the local concentrations of various chemical species in a confocal volume of micrometer size (1-5 μm^3). We first present the implementation of such a tool to study the interdiffusion of simple liquids, and we then discuss the imaging of an ultra-fast chemical reaction in a microchannel.

2. Experimental : interdiffusion of two pure liquids

Figure 1.a displays the geometry of the microchannel (silicium-glass) used throughout the experiments, which has a main channel 500 µm wide and 40 µm high. The liquids being studied are injected at a constant flow rate in the two arms of the Y-chip. At these length scales and at the velocities investigated, the flow is strictly laminar and the two liquids mix by molecular interdiffusion. If the liquids in question display separate vibration modes, it is possible to quantify the local concentrations of the two compounds by measuring the intensity of the light inelastically scattered by these molecules. Figures 1.b-c correspond to the two Raman images of the

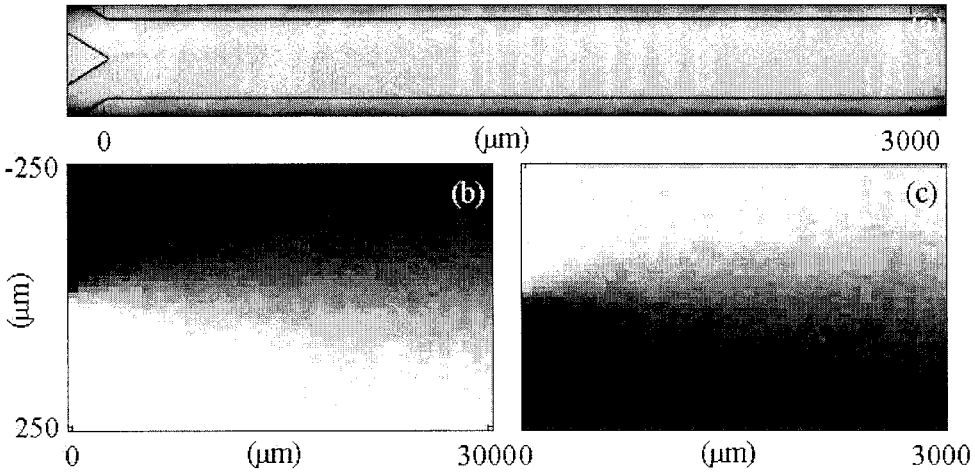

Figure 1. (a) Geometry of the channel used throughout the paper: the main channel is 500 μm wide and 40 μm high. Raman images of the diffusion zone in the case of chloroform (b), and methylene chloride (c). Black color corresponds to a zero concentration.

interdiffusion zone in the particular case of chloroform and methylene chloride (see also Fig. 2.c where the two spectra are displayed). Using models that take into account the difference in viscosities, we were able to directly measure the interdiffusion of several miscible solvents. Moreover, using the confocal properties of our setup, we have obtained 3D-images of the diffusion zone (see Fig. 2), showing that this zone is homogeneous in the parabolic velocity profile, as correlated by the 3D-simulations at these Péclet numbers (Pe ≈ 1-100) and at these channel height (40 μm).

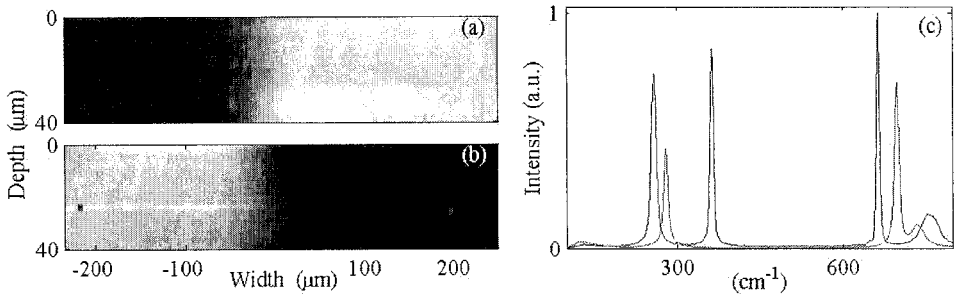

Figure 2. Slice of the diffusion zone measured at 200 μm in the main channel using the confocal property of our setup. Chloroform (a), and methylene chloride (b). (c) Raman spectra of chloroform (Raman band at 670 cm^{-1}, blue) and methylene chloride (Raman Band at 700 cm^{-1}, red).

3. Experimental : interdiffusion in an ultra-fast chemical reaction

We also studied the ultra-fast chemical reaction $H_2O+D_2O \leftrightarrow 2$ HOD corresponding to the exchange of a proton and a deuterium. In this particular case, it is possible to quantify the local

concentrations of the three compounds using the stretching modes of these molecules. Figure 3 displays the results of such an analysis (the geometry used in these experiments is still the one diagrammed in Fig. 1.a). Using theoretical models that couple the flow, the reaction and the interdiffusion of the three compounds, we have for the first time succeeded in quantifying the interdiffusion dynamics of this specific system.

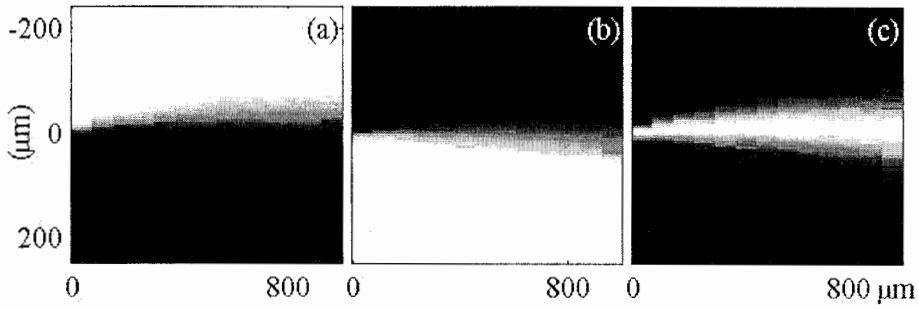

Figure 3. Raman images of the chemical reaction $H_2O+D_2O \leftrightarrow 2$ HOD. Water and heavy water are injected in the main channel at a constant flow rate (1 μL/min). The concentration maps of H_2O (a), D_2O (b), and HOD (c) are obtained using the stretching modes of these molecules. The asymmetry of the diffusion zone is due to the difference of viscosities between H_2O and D_2O.

References

[1] A. E. Kamholz, B. H. Weigl, B. A. Finlayson, and P. Yager. *Anal. Chem.*, **71**, 5340, (1999).
[2] C. N. Baroud, F. Okkels, L. Ménétrier, and P. Tabeling. *Phys. Rev. E*, **67**, 060104, (2003).
[3] P. D. I. Fletcher, S. J. Haswell, and X. Zhang. *Electrophoresis*, **24**, 3239, 2003.
[4] R. F. Ismagilov, A. D. Stroock, P. J. A. Kenis, G. Whitesides, and H. Stone. *Appl. Phys. Lett,* **76**, 2376, 2000.
[5] D. A. Beard. *J. Appl. Phys.*, **89**, 4667, 2001.

ON-CHIP COULTER COUNTER FOR AIRDUST MONITOR

K. Miyamura[1] , Y. Yoshida[1] and T. Kitamori[2]

[1] *The Research Association of Micro Chemical Process Technology Kanagawa Central Laboratory, KSP-Bldg. R&D-C 11F, 3-2-1, Sakado, Takatsu-ku, Kawasaki-shi, Kanagawa, 213-0012, Japan*

[2] *The University of Tokyo, 7-3-1 Hongo, Bunkyo-ku, Tokyo 113-8656, Japan*

Abstract

We developed a micro Coulter counter device. The feature of this device is its 3-dimensional micro sheath flow. An advantage of this flow was that 3-dimensional convergence of sample liquid can be carried out without external force. Sample liquid could be converged on one point, first two-dimensionally by adding sheath liquid flow from both sides, and then in the other direction by letting the 2-dimensional sheath flow pass over a V-shaped step at the bottom of the flow channel. Consequently, the variation in the particle passage position inside the aperture of the coulter counter decreased, and the diameter measurement of a particle was improved to have less than 5% error.

Keywords: particle counting, Coulter counter, sheath flow, 3-dimensional convergence, step structure

1. Introduction

Suspended particulates (especially nanoscale particles) have a bad influence on human bodies, such as allergy and carcinogenesis. We have set the target of this work to develop a device for simple and speedy measurement of size distribution of such particulates using a microchip technology. The margin of error range in the particle size distribution measurements was 5% for both number and size of the nanoscale particles. Using the Coulter counter method, the amount of particles can be measured as the number of output signal pulses, and the diameter of a particle can be measured as an output pulse height [1, 2]. However, the pulse height was also affected by the particle passage positions in the aperture of the counter, because electric field distribution inside the aperture exists. For reducing this deviation, it is necessary to focus the particle passage positions to one point within the aperture. We decided to use a sheath flow technology. But, usual sheath flows inside of a microchip are either 2-dimensional-like ones that are insufficient in the present purpose or complicated ones that require external force such as an ultrasonic wave, an electric field or magnetism to realize 3-dimensional convergence [3]. We propose here a novel microchannel structure with V type step at the bottom for converging 3-dimensional sheath flow without external force.

2. Device Structure

Structure of the V type step sheath flow coulter counter device is shown in Fig. 1. Two microchannels for sheath liquid joined to a microchannel for sample liquid from both sides, and two-dimensional sheath flow was formed. The V type step was fabricated in the bottom of the flow channel. The sample liquid in the sheath flow was raised by the V type step, and part of the sheath liquid went beneath the sample liquid flow. Halfway the flow channel was narrowed to form an aperture, where width of the sample liquid flow was decreased significantly. Consequently, sample liquid was converged on the central upper one point of the aperture. Electrodes were placed in both sides of the aperture to measure the impedance of the aperture.

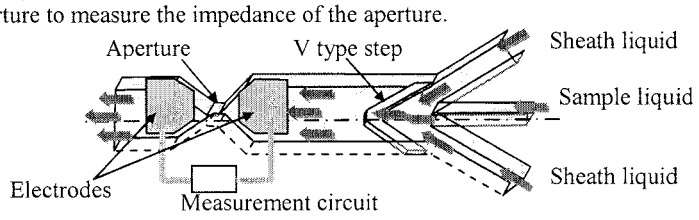

Figure 1. Structure of V type step sheath flow device

3. Device Fabrication

Photograph of the 3-dimensional sheath flow device is shown in Fig. 2. This device was made with Si and glass. Flow channels were formed on the Si side. These channels and the V type step were formed by 2-step etching using ICP-RIE. A SEM photograph of the V type step is shown in Fig. 3. Size of the sheath flow channels was 200 μm in width and 40 μm in depth. Size of the sample flow channels was 100 μm in width and 40 μm in depth. Size of the V type step was 72 μm in width and 20 μm in height from the bottom of the flow channel. Inlets and an outlet for liquid were opened using anisotropic etching from the backside. Pt electrodes were patterned on the glass side. Finally, Si and glass plates were aligned and bonded using the anodic bonding method.

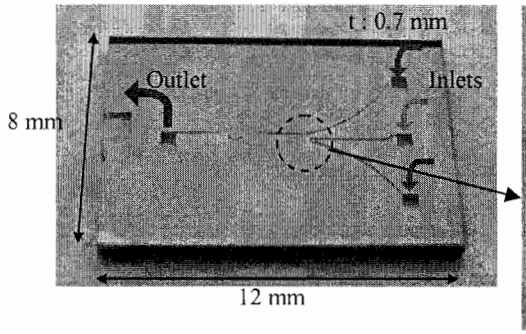

Figure 2. Photograph of 3-dimensional sheath flow device.

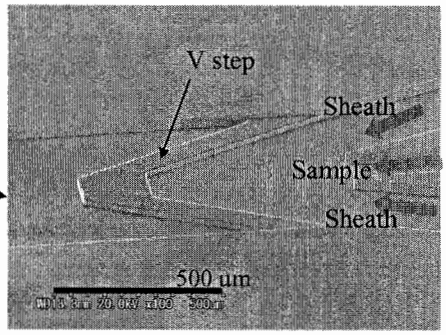

Figure 3. SEM Photograph of V type step.

4. Experimental

The deviations of signals of a sensor without a sheath flow, a 2-dimensional sheath flow sensor, and the 3-dimensional sheath flow sensor were compared. Sample liquid was polystyrene latex beads suspended in 0.9% NaCl. Sheath liquid was 0.9% NaCl without particles. The liquids were driven by applying vacuum pressure of -50kPa to the outlet port. Constant current was applied to the electrodes and voltage change was measured with an oscilloscope. In addition, computer simulation of the flow inside the channel was performed.

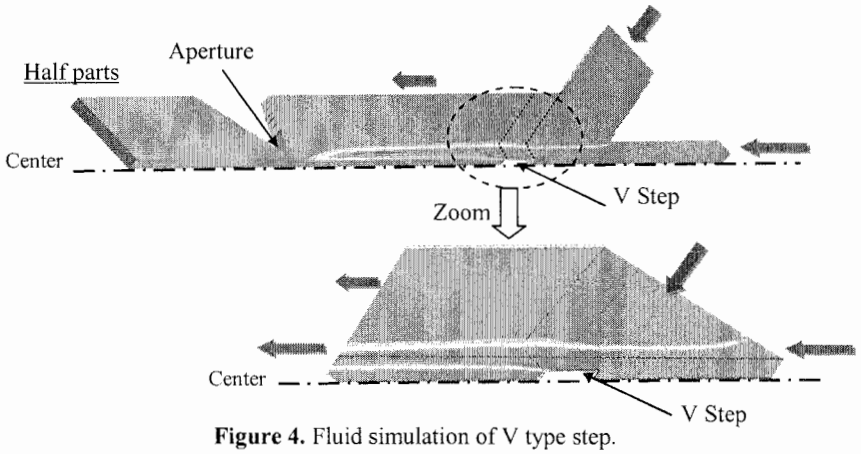

Figure 4. Fluid simulation of V type step.

5. Results and discussion

A photograph of the sheath flow is shown in Fig. 5. CV value of a sensor without a sheath flow was 18%. (Fig. 6) That of the 2-dimensional sheath flow device was 15%, and that of the 3-dimensional sheath flow device was 5%. (Fig. 7) CV value of the 3-dimensional sheath flow device satisfied the requirements for the analysis. According to the computer simulation, sample liquid in the 3-dimensional sheath flow device was converged to upper one-third part of the channel and CV value would be about 5%, in good agreement with the experimental results.
This fluidic device is very small and can be driven by a single vacuum pump. Therefore, it can be used in construction of a handy-size analytical system for on-site analysis.

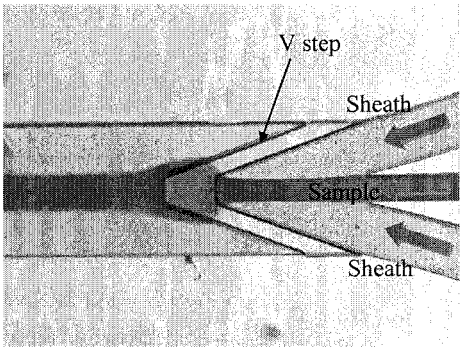

Figure 5. Photographs of the sheath flow.

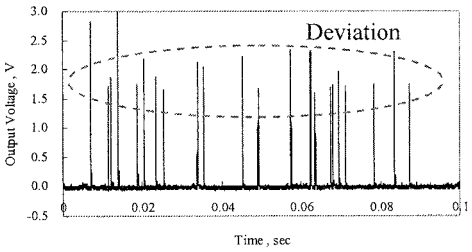

Figure 6. Measurement of 8 μm particles without sheath flow.

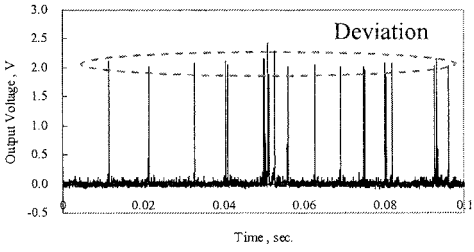

Figure 7. Measurement of 8 μm particles with V type step sheath flow.

6. Conclusions

We developed a 3-dimensional sheath flow device with a new channel structure. This device can be used for easy convergence of a sample flow to one point. With this device, a handy system for particle size distribution measurement can be built. In the future, on-site particle analysis will become possible by combining pretreatment technology and this device.

Acknowledgements

This research was carried out in project of micro-chemical technology for production, analysis and measurement systems.

References

[1] D. Satake, H. Ebi, N. Oku, K. Matsuda, H. Takao, M. Ashiki, and M. Ishida, "A DURABLE SENSOR FOR BLOOD CELL COUNTER USING MEMS TECHNOLOGY", Proc. of Transducers '01, Munich, Germany, June 10-14, 2001, pp. 1198-1201

[2] W.H. Coulter, "Means for counting particles suspend in a fluid", US patent no. 2,656,508, October 20, 1953

[3] J.H. Nieuwenhuis, M.J. Vellekoop, "FEM study of Coulter Counter with Water-Based Adaptable Aperture", Proc of μTAS 2002, November 3-7, Nara, Japan, 2002, pp. 697-6

STUDY ON SATELLITE DROPLETS FORMATION IN A MEMS DIAPHRAGM DROP EJECTOR

J. Y. Lin, L. C. Lee, C. Y. Shen, R. J. Shih, S. C. Lin

National Center for High-performance Computing, 7, R&D Rd. VI, Hsinchu Science Park, Hsinchu, Taiwan, R.O.C.

Abstract

The commercial code CFX4 is adopted to compute the satellite droplets formation process in a micro-electro-mechanical diaphragm drop ejector (MEMSJet). In this paper, two important parameters (viscosity and surface tension) were addressed to affect the formation of satellite droplets greatly. We tried to find the criteria of satellite droplets formation by means of capillary number. Then the satellite droplets can be eliminated to improve the printing quality.

Keywords: satellite droplets, multiphase flow, ejector, VOF

1. Introduction

The adoption of the MEMSJet [1] printing technology in the manufacturing of the electronics industry is highly desired. The printing quality is known to be closely related to the ejected droplet. Therefore, it is very desirable to have the insights on how the liquid droplet is formed and ejected in a MEMSJet device. With the understanding of these phenomena, it is then possible to control droplet size, improve droplet consistency, and eliminate satellite droplets [2] through proper design of the device and select fluids with proper physical properties.

2. Theory

The governing equations for multiphase problems are the mass and momentum conservation equations. The volume of fluid (VOF) interface tracking method which was developed by Hirt [3] is adopted to represent the fluid domain and to track the evolution of its free boundaries. The numerical solution of the fluid flow equations were carried out employing commercial finite-volume based program CFX4.

The non-dimensional parameters commonly used in single droplet dynamics are the Reynolds number (Re), the Webber number (We), and the Capillary number (Ca):

$$\mathrm{Re} = \frac{\rho U d}{\mu} = \frac{\text{inertia force}}{\text{viscous force}} \tag{1}$$

$$\mathrm{We} = \frac{\rho U^2 d}{\sigma} = \frac{\text{inertia force}}{\text{surface tension force}} \tag{2}$$

$$\mathrm{Ca} = \frac{\mathrm{We}}{\mathrm{Re}} = \frac{\mu U}{\sigma} = \frac{\text{viscous force}}{\text{surface tension force}} \tag{3}$$

where d is the droplet diameter, U is the droplet injection speed, ρ is density, μ is viscosity, and σ is surface tension coefficient. The interplay of inertia force, surface tension force, and viscous force will be discussed along with the case studies.

4. Results and discussion

A schematic diagram of MEMSJet is shown in Figure 1 (in micron scale). The diaphragm deflection frequency is 20,000. The initial velocity of ejecting droplet is 15 m/s approximately. The amplitude of vibration is 20 micrometers. The diaphragm is deflected upward to press ink first then the diaphragm is deflected downward to cut the droplet. This causes an ink droplet to be formed and ejected out of the nozzle.

The material properties of various liquids employed in the following study are listed in Table 1. Water is specified as liquid C. Larger Ca numbers mean larger viscosity or smaller surface tension.

Smaller Ca numbers mean smaller viscosity or larger surface tension instead. Different Ca numbers will be simulated to explore the mechanism and criteria of satellite droplets formation.

Here, the simulated result of water (Ca=0.205) is used to demonstrate the formation of satellite droplets. The velocity of the droplet is not uniform, i.e., high velocity in the front and low velocity in the rear. This comes from the variable velocity of the diaphragm. Figure 2 shows the detail of the droplet ejection sequence. At the instant of 28 microseconds, the liquid column breaks up from the nozzle because of the downward surface tension force and upward pulling force. After 28 microseconds, the liquid column is completely separated from the nozzle and a droplet with round head and slender tail is formed. At the instant of 77 microseconds, the velocity profile of the droplet fluctuates seriously because of the surface tension effect, which induces the formation of satellite droplets.

Then, numerical simulations with different Ca numbers are used to find the criteria of satellite droplets formation. Figure 3 shows the breakup time of the liquid columns for various liquids. It can be seen by comparing the results for liquid A, B, and C that as Ca becomes larger, the breakup time becomes longer and the length of the broken liquid column also becomes longer because of the smaller downward pulling force caused by smaller surface tension. From the results for liquids C, D, and E, the effect of Ca number on breakup time is not obvious although the liquid of higher viscosity has shorter liquid column.

Figure 4 shows the liquid column for the instant 50 microseconds after breakup. For liquids with larger Ca (liquids D and E), the shapes of the liquid columns are rectangular and undesirable for printing quality because of large dots on the paper. The satellite droplets were formed for liquid C with Ca=0.205 due to interaction of the surface tension and viscosity. For liquids with smaller Ca (liquid A and B), the shapes of the liquid columns are not as sharp as previous cases and the length of the liquid columns are shorter. This is the most desirable for the printing quality.

The other parametric variations in surface tension and viscosity are also studied in relation to the droplet impingement. Some valuable information can be obtained from these simulation results to manipulate and design our ejector. All computational results are summarized in Fig. 5 to show the range that a droplet will break into satellite droplets. There are four different possibilities: satellite droplets (S), no-injection (N), a circular shape without satellite droplets (C), and a rectangular shape without satellite droplets (R). Satellite droplets were formed in the range $0.108<Ca<0.273$.

5. Conclusions

The printing quality is known to be closely related to those of ejection behaviors of the liquid droplet such as size and velocity of the droplet as well as formation of satellite droplets. In this paper, the commercial code CFX4 is adopted to compute the satellite droplets formation process in MEMSJet. Capillary number was employed to explain the reaction between the viscous force and the surface tension in relation to the droplet impingement. Furthermore, the diaphragm deflection frequency, the diaphragm vibration amplitude and the nozzle aperture width also affect the satellite droplets formation. These phenomena are worth studying to discover the complex multiphase flow in micro-scale.

References

[1] F. Pan, J. Kubby and J. Chen, J. Micromech. Mecroeng., 70-76 (2002)
[2] F. G. Tseng, Kim C. J. Kim, and C. M. Ho, ASME DSC-vol. 66, MEMS, (1998)
[3] C. W. Hirt, B. D. Nichols, J. Comput. Phys. 100, 335-354 (1981)

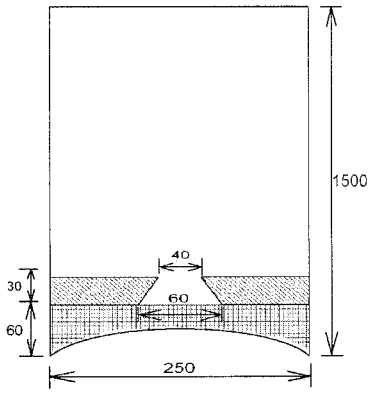

Figure 1. A schematic diagram of MEMSJet.

Table 1. The material properties.

	σ (N/m)	1000·μ (kg/m·s)	Ca
A	0.2194	0.599	0.041
B	0.1095	0.749	0.1025
C	0.073	1	0.205
D	0.0548	1.496	0.410
E	0.04385	2.994	1.025

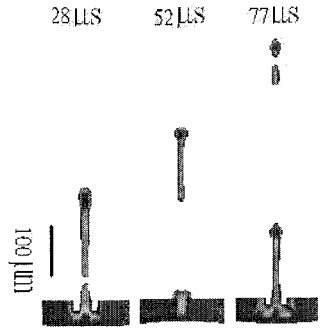

Figure 2. The droplet ejection sequence.

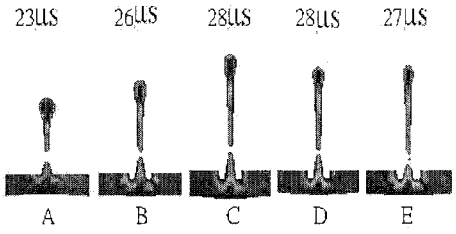

Figure 3. Breaking of liquid droplet.

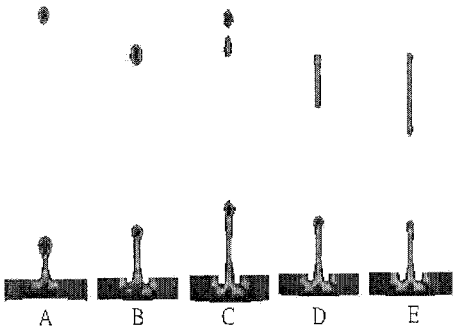

Figure 4. 50 μs after breaking of liquid droplet.

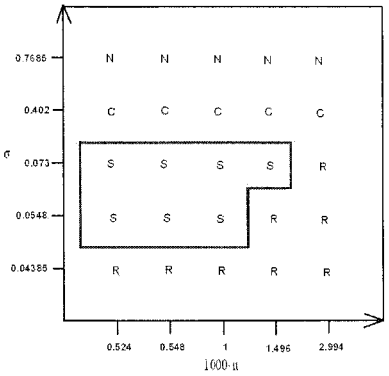

Figure 5. All computational results.

MICROCHIP FOR CONTINUOUS ON-LINE PCR PROCUCT ANALYSIS

Hyerim Kim, Shinae Suk, Nokyoung Park, and Jong Hoon Hahn*

National Research Laboratory for Advanced Biotechnology and Biomedical Microinstrumentation, Department of Chemistry, Division of Molecular and Life Sciences, Pohang University of Science and Technology, San 31 Hyoja-dong, Pohang 790-784, South Korea

Abstract

An interfaced continuous-flow system for polymerase chain reaction (PCR) and gel electrophoretic DNA separation has been developed for efficient DNA amplification and PCR product analysis. The poly(dimethylsiloxane) based PCR chip has 25 channel loops for repetitive DNA amplification cycles. The glass based DNA separation chip has channels for separation, injection, and flowing of DNAs and size markers. The separation and injection channels are filled with polyacrylamide gel which was photopolymerized by UV exposure. The PCR product flow through interfacing capillary and are electrophoretically injected into gel of separation channel. The injected DNAs are dyed with counter-flowing intercalator, YOYO-1, during the separation and separated DNAs are detected by laser-induced fluorescence detection system.

Keywords: PCR, on-line analysis, continuous-flow, contamination-free

1. Introduction

The polymerase chain reaction (PCR) is a molecular biology method for the in vitro amplification of DNA. This method is widely used in medical diagnostics, genetic analyses, forensic medicine, and basic researches, such as cloning, restriction analyses, sequencing, finger printing. Through introducing micromachining and micro-electro-mechanical-systems into the fabrication of PCR system, micro-fabricated PCR chip have been developed by many research groups. Especially many continuous-flow PCR systems have been studied due to their potentiality of high-throughput system [1,2]. In the previous continuous-flow PCR system, however, the amplified PCR products had been analyzed by off-line gel electrophoresis. This off-line gel electrophoretic analysis of PCR products is a source of decreasing the throughput. To overcome this disadvantage of off-line analysis of PCR products, we have developed on-line continuous-flow DNA analysis lab-on-a-chip system. The system is constituted with continuous-flow PCR chip and continuous-flow DNA separation chip interfaced through capillary. The PCR products amplified in PCR chip were continuously analyzed in separation chip by capillary gel electrophoresis (CGE) and laser induced fluorescence detection successfully.

2. Theory

PCR is the method DNA amplification by temperature treatment and consists of 3 steps; melting of dsDNA separation, annealing of binding the specific primer to their target sites, and extension of DNA synthesis with the thermostable DNA polymerase (such as Taq). The numbers of DNAs exponentially increase by doubling per three-step thermocycle.

The amplified DNAs are analyzed using CGE in combination with laser-induced fluorescence (LIF). In the most of the CGE-LIF method, the PCR products are mixed with dye for LIF detection before separation. Once the laser excited the DNA intercalated with dye, increasing of fluorescence intensity is detected by photomultiplier tube. Through fluorescence signal we can analyze PCR products. But, in this case pure PCR products cannot be yield. So, we designed a new chip. This chip have asterisk-shaped channel; a cross channel for injection and separation of DNAs and size markers, other channels for DNAs and size markers flowing. Especially a cross channel except overlapped parts with flowing channels have been filled with polyacrylamide gel which was

photopolymerized by UV exposure for the flowing of contamination-free DNAs and size markers without mixing size markers and DNAs (Figure 1). By using this chip in integration with continuous-flow chip, we can obtain PCR products and simultaneously separate DNAs to confirm the success of PCR.

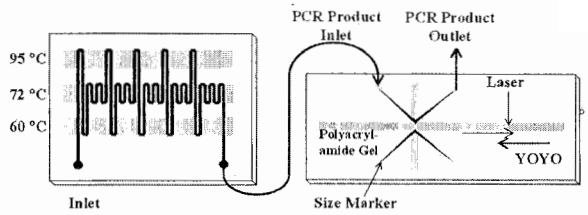

Figure 1. On-line, contamination-free PCR products analysis in a continuous mode.

3. Experimental

The PCR chip has been made of poly(dimethylsiloxane) (PDMS) and designed to have 25 channel loops for repetitive DNA amplification cycles by method described previously. This chip consists of two PDMS plates. The cover plate contained 2 access holes (2 mm diameter) as inlet and outlet and the bottom plate contained 50 μm depth, 60 and 120 μm width channel (Figure 2(a)).

The DNA separation chip was made by bonding the etched glass bottom plate to the glass cover plate with drilled 8 access holes 2 mm in diameter. In Figure 2(b), the chip consists of 150 μm-wide separation channel, 120 μm-wide injection channel, and 200 μm-wide flowing channels and all channels are 40 μm deep. The DNA separation and injection channels have been filled with 6% polyacrylamide gel (Reprogel 377, Amersham Bioscience), which was photopolymerized by UV exposure [3].

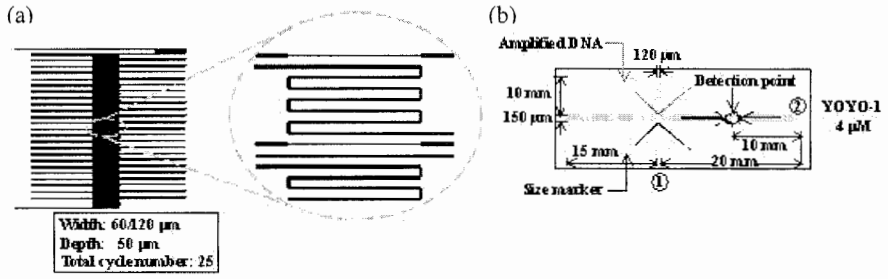

Figure 2. Schematic presentation of (a) PCR chip and (b) DNA separation chip.

The PCR chip and gel electrophoretic DNA separation chip have been interfaced through capillary. The PCR is performed at 95°C for melting dsDNA, 60°C for annealing, and 72°C for extension by means of thermostated copper blocks. The PCR sample is continuously delivered by syringe pump at 20 μL/hr experimentally determined. The PCR products from outlet of PCR chip and size markers are continuously introduced to the PCR products flowing channel through interfacing capillary and size markers flowing channel of separation chip, respectively. For the 2-sec injection of PCR products and size markers into separation channel, a field of 200 V/cm was applied between reservoir 1 and 2, with reservoir 2 filling with 4 μM YOYO-1 (Molecular Probes)

(Figure 2(b)). The DNA separation is performed at 70 V/cm. The separated DNAs are detected by LIF systems at 1 cm distance from the intersection of the separation channel with the injection channel. Fluorescence by intercalating DNAs with YOYO-1 is measured using photomultiplier tube. 174 as size marker (Takara), 323 (Promega), and 500 (Takara) bp are used in this study.

4. Results and discussion

The continuous-flow mode amplification and separation of 323 and 500 bp template DNAs were tested. The electropherogram in Figure 3 obtained from DNA separation chip shows the continuous-flow PCR and continuous-flow separation were performed successfully. The electropherogram is constituted with continuous three separations; size markers, amplified 323 bp DNA and size markers, and amplified 500 bp DNA and size markers, respectively. As shown in Figure 3, the continuous analysis of three DNA samples has been performed within 12 minutes, and the intercalation of counter-flowing YOYO-1 to DNA is well performed. The PCR products collected from outlet of separation chip were not contaminated because the channel for size markers was separated from PCR products flowing channel by gel and the dyeing of DNA had been occurred only in the separation channel after injection of small portion of amplified DNA. With this interfaced DNA amplification and analysis lab-on-a-chip system, we could continuously amplify and analyze the DNA samples without any contamination of amplified DNAs.

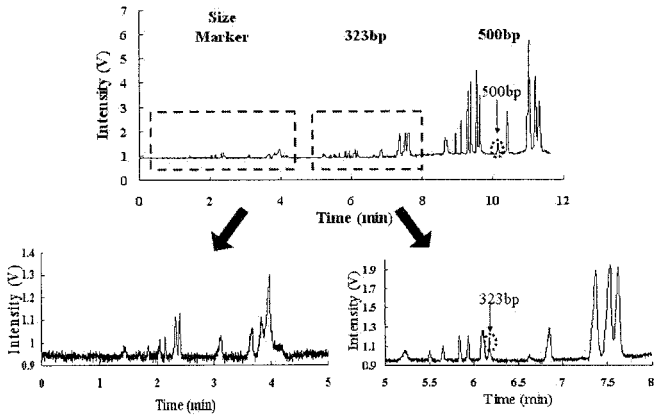

Figure 3. Continuous analysis of PCR products: size markers, 323 bp, 500 bp DNAs (respectively).

5. Conclusions

With the interfaced DNA amplification and analysis chip system, we could continuously amplify and analyze the DNA samples without any contamination of amplified DNAs. We expect that the presented lab-on-a-chip system have potentiality to produce a new platform of high-throughput DNA amplification/analysis system.

References

[1] M. U. Kopp, J. Mello, A. Manz, *Science,* **280**, 1046-1048 (1998).
[2] N. Park, S. Kim, J. H. Hahn, *Anal. Chem.*, **75**(21), 6029-6033 (2003).
[3] S. N. Brahmasandra, V. M. Ugaz, D. T. Buke, C. H. Mastrangelo, M. A. Burns, *Electrophoresis,* **22**, 300-311 (2001).

SIMPLE BONDING OF PMMA MICROSTRUCTURES TO MODIFIED GLASS SURFACES PREPRINTED WITH DNA AND PROTEIN MICROARRAYS

Martin Dufva, Michael Stangegaard and Claus BV Christensen
Department of Micro- and Nano Technology, Technical University of Denmark, Ørsteds plads 345 east, DK-2800, Kgs Lyngby

Introduction

Protein and DNA microarrays are usually produced with glass or polymer slides. Enclosing a microarray in a microstructure puts several demands on the bonding technique. It is of highest importance that the biological activity of the microarray is not compromised by the procedure, which for instance exclude high temperatures. Here we describe a very simple and fast method to enclose protein or DNA micro arrays printed on glass slides in microstructures made in PMMA by flushing the microstructure with dichloromethane.

Keywords: Protein, DNA, microarray, PMMA, agarose film

Materials

Agarose coated microscope slides was prepared according to the method by Afanassiev et al. [1]. Approximately 1 nL sample containing oligonucleotides or proteins was deposited onto the slide using a Qarray robot (Genetix, UK).

The microstructures were produced in Polymethylmethacrylate (PMMA) by laser ablation using an 150 W CO_2 IR laser (Synrad, Mukilteo, WA, USA). A hybridization chamber 4.5 mm in diameter was connected with channels (an inlet and an outlet) that where either 200, 500 or 1000 μm wide. At the ends of each channel holes were cut through the PMMA sheet to allow loading of the samples. The chip holds approximately 15 μL of sample. By applying a gentle pressure to the assembled PMMA microstructure and agarose microarray with a fingertip, bonding was achieved by flushing approximately 30 μL dichloromethane through the channel of the formed microsystem. After flushing the channels were kept open during the bonding time with a gentle stream of air or N_2.

The micro chamber covering the DNA microarray was flushed with 150 μL 0.1 X SSC and blocked with 10% bovin serum albumin (BSA) in 0.1 X SSC for 5 minutes. The DNA microarrays where hybridized with a mixture of 0.5-50 nM targets dissolved in 3 X SSC, 0.3 % sodium dodecyl sulphate and 10 ng/μL salmon sperm DNA. Unhybridised DNA was removed by flushing the channels with 0.1 X SSC. Prior to scanning the microstructures was disassembled by inserting a scalpel in the interface between microarray substrate and PMMA structure, if not mentioned otherwise. All liquid handling was made using an ordinary pipette.

Results and discussion

The objective of the present work was to find a simple procedure to attach a PMMA polymer microstructure over a protein or DNA microarray immobilized on a glass or polymer slide. It was desirable that the bonding technique did not include heat, since it would potentially destroy the activity of biomolecules, particularly proteins. The described approach is based on dissolving the surface of the plastic using a solvent and, upon re-polymerisation, bonding the microstructure to the glass slide. The strength of the bond between glass and the attached PMMA structure was tested by filling the hybridisation chamber with 0.1X.SSC and incubating the structure at 37 °C or 50 °C. The stability of the bonding was challenged at time intervals by emptying, filling and incubating the microstructure. Several different microarray substrates was tested and the results showed that the

bond between PMMA and agarose film coated film slides could withstand at least four challenges and 210 minutes incubation time at both 37 °C or 50 °C. This is sufficient for genetic analysis and small molecules measurements using microarrays printed on agarose film coated substrates [2, 3]. It is possible that the strong bond between PMMA and agarose film is caused by the structure of agarose which is 10-fold rougher than glass [2]. However aldehyde and amine surfaces could withstand three challenges and 150 minutes incubation times suggesting that the bonding technique also could be used with other microarray substrates. Although the bonding technique relies on dissolving PMMA, which deforms the microstructure (**Fig 1A**), functional hybridisation chambers that were 4.5 mm long, 5 mm in width and only 100 µm in height could efficiently be bonded to the agarose film (data not shown).

To test if the flushing bonding technique is compatible with protein activity, a small protein array was printed on agarose slides. The array consisted of an anti-mouse antibody, the pesticide metabolite BAM conjugated to BSA, FITC conjugated strepavidin and BSA. The protein microarray was enclosed in a microstructure bonded by the flushing technique and the reactivity of anti-mouse and the BAM-BSA conjugate was tested by filling the structure with a solution of mouse anti BAM antibody conjugated with the Cy5 fluorochrome. The antibody reactions showed that the BAM-BSA conjugate on the microarray retained activity after the dichloromethane flushing (**Fig 1**). The microstructure supported the reaction between the anti-mouse antibody and the mouse anti BAM antibody was much better than the same reaction carried out under a coverslip or without any coverage of the antibody solution. The reason for this is not clear.

We next tested if the bonding technique was compatible with DNA microarray hybridisation assay. The results showed that the microstructures did not interfere with the hybridisation reaction (**Fig 2**). If anything, the microstructure could in some instances enhance hybridisation efficiency up to 100 %. We calculated the CV to be around 15% for arrays hybridised with or without microstructures.

Conclusions

We describe a simple, fast biocompatible method to attach microstructures made in PMMA to microarray substrates preprinted with protein or DNA microarrays. Since the technique relies on dissolving PMMA with dichloromethane, the microstructures are deformed by the process. However, for simple applications like a hybridisation chambers the deformation has no practical consequence. The bond is stable enough for most genetic and protein analysis using DNA/protein microarrays. The microstructure could easily be removed enabling the use of standard microarray scanners which usually only accept microscope slides. The bonding technique did not inhibit the molecular functions of DNA or protein microarrays and conveniently enables the attachment of a microfluidic system over a microarray, which also simplifies the liquid handling of multistep assays like colorimetric detection of hybridisation.

References

1. Afanassiev, V., V. Hanemann, and S. Wolfl, *Preparation of DNA and protein micro arrays on glass slides coated with an agarose film.* Nucleic Acids Res. **28**(12): p. E66.2000.
2. Dufva, M., S. Petronis, L. Bjerremann Jensen, C. Krag, and C. Christensen, *Characterization of an inexpensive, non-toxic and highly sensitive microarray substrate.* Accepted Biotechniques.
3. Belleville, E., M. Dufva, J. Aamand, L. Bruun, and C. Christensen, *Quantitative Assessment of Factors affecting the Sensitivity of a Competitive Immuno-Microarray for Pesticide Detection.* Biotechniques. **35**: p. 1044-1051.2003.

Figures

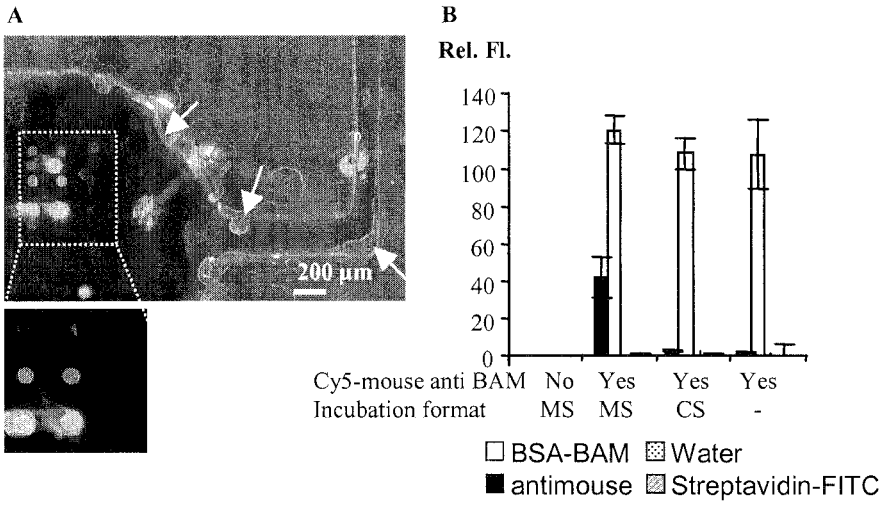

Figure 1. Comparison of an antibody reaction performed in a microarray of immobilised molecules. Scans of microarrays incubated with Cy5 mouse anti BAM before (upper panel) and after (lower panel) removal of the microstructure. B. Comparison of signals of microarrays incubated with Cy5-mouse anti BAM using a microstructure (MS), coverslip (CS) and open air (-). The bars represents the signal obtained from different protein spots in the microarray. Arrows indicate clear deformations of the microstructure.

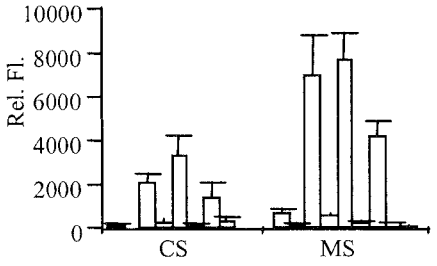

Figure 2. Hybridisation signals from microarrays hybridised with either coverslip (CS) or microstructure (MS). Three different Cy3-labelled targets were hybridised to a microarray consisting of eight different probes of which three are complementary to the targets.

DEVELOPMENT OF EFFECTIVE TRIPHASE REACTIONS USING MICROCHANNEL REACTORS

Juta Kobayashi[1], Yuichiro Mori[1], Masaharu Ueno[2], Takehiko Kitamori[2] and Shū Kobayashi[1*]

[1]*Graduate School of Pharmaceutical Sciences, The University of Tokyo, 7-3-1 Hongo, Bunkyo-ku, Tokyo, 113-0033, Japan*

[2]*Department of Applied Chemistry, Graduate School of Engineering, The University of Tokyo, 7-3-1 Hongo, Bunkyo-ku, Tokyo, 113-8656, Japan*

Abstract

We have developed an efficient system for triphase reactions using a microchannel reactor. We conducted hydrogenation, and the reactions were found to proceed smoothly to afford the desired products quantitatively within 2 minutes for a variety of substrates. The system could also be applied to deprotection reactions. We could achieve a truly effective interaction between hydrogen, substrates, and a palladium catalyst utilising a large interfacial area and the short path required for molecular diffusion in the very narrow channel space. It would be possible that this concept can be applied to other multiphase reactions using oxygen, carbon dioxide, etc.

Keywords: Hydrogenation, Immobilization, Triphase reaction

1. Introduction

Multiphase catalytic reactions have played important roles not only in the research laboratory but also in the chemical and pharmaceutical industries. Although numerous and varied examples of multiphase catalytic reactions exist, including industrial applications, these reactions are still difficult to conduct when compared to homogeneous reactions because the efficiency of interaction and mass transfer between different phases is extremely low, and thus, in most cases the reaction rates are slow. In general, to accelerate multiphase catalytic reactions, some treatment producing a high interfacial area between the two or three reacting phases, for example vigorous stirring or additional equipments, is needed, and the development of more effective, simple devices that can produce such a high interfacial area between different phases is a much sought-after goal.

2. Theory

To achieve truly efficient multiphase catalytic reactions, we focused on microchannel reactors. The device has a very large specific interfacial area per unit volume, which rises to 10,000 ~ 50,000 m^2/m^3, as opposed to only 100 m^2/m^3 for the case of conventional reactors used in chemical processes. Our idea is to immobilize a solid catalyst on the wall of the microchannel, and then to flow liquid and gas materials into the channel. Provided that the flow is well controlled, it should be possible to pass the gas through the center of the channel, and the liquid along the inner surface of the channel at a particular gas pressure (Figure 1). In this system, efficient gas–liquid–solid reactions might occur, because effective interaction of the three phases is expected due to the extremely large interfacial areas and the short path required for molecular diffusion in the very narrow channel space.

3. Experimental

We chose hydrogenation catalyzed by palladium as a model gas–liquid–solid reaction. Immobilization of the palladium catalyst on the surface of the channel was conducted using the microencapsulation method which has been developed in our laboratory. We selected a microchannel reactor having a channel 200 μm in width, 100 μm in depth, and 45 cm in length. First, amine groups were introduced onto the surface of the glass channel. Microencapsulated (MC) palladium was used as the palladium source. A colloidal solution of the MC palladium was passed

through the microchannel, heated at 150 °C for 5 h. During the heating, cross-linking of the polymer occurred, and the desired palladium-immobilized microchannel was successfully prepared. We then conducted hydrogenation of benzalacetone using this Pd-immobilized microchannel. The experimental system using the microchannel reactor is illustrated in Figure 2. A teflon tube (ϕ200 μm×10 cm) was connected to the end of the microchannel reactor. The reaction was conducted under continuous flow conditions at ambient temperature by introducing a THF solution of a substrate (0.1 M) through one inlet and introducing hydrogen through the other inlet via a mass-flow controller. Yields were determined by collecting a measured volume of the product from the outlet of the microchannel reactor and quantifying by ^{1}H NMR.

4. Results and discussion

At a certain pressure of hydrogen and flow rate of substrate, the desired flow system was realized as we expected; the liquid flowed close to the channel surface where the catalyst existed, and the gas flowed through the center, that brought a very large interfacial area among three phases. Remarkably, the reactions including deprotection of a benzyl ether and a carbamate group proceeded smoothly to afford the product quantitatively within 2 minutes. Several practical advantages of this reactor should be noted. In nearly all cases products were isolated almost pure simply by passing starting material through the reactor and then removing the solvent. No palladium was detected in the product solutions. The microchannel reactors were reused several times without loss of activity. Although one reactor produces only a small amount of the product, it would be easy to scale up reactions by using a number of chips in parallel.

5. Conclusions

We have developed an efficient system for hydrogenation using a microchannel reactor. A new method for immobilization of the palladium catalyst onto the wall of the channel has also been developed. The desired mode of flow was achieved and provided increased interfacial areas between substrate, hydrogen, and solid catalyst, which has been difficult to attain with conventional reactors. This would lead to high efficiency not only for hydrogenation, but also for other multiphase reactions; for example, using oxygen, carbon monoxide, carbon dioxide, etc. as the gas phase, or using other metals as catalysts. Since it is easy to scale up the reaction by using a number of chips in parallel with shared flow, this system can provide the desired products easily and quickly in the required volumes, as well as in a pure form at the point of use without the need for any treatment such as isolation or purification. Further studies with this device are now in progress.

Acknowledgements

This work was partially supported by CREST, SORST, and ERATO, Japan Science and Technology Agency, and a Grant-in-Aid for Scientific Research from Japan Society of the Promotion of Science.

Reference

[1] J. Kobayashi, Y. Mori, K. Okamoto, R. Akiyama, M. Ueno, T. Kitamori, S. Kobayashi, *Science*, **304**, 1305 (2004).

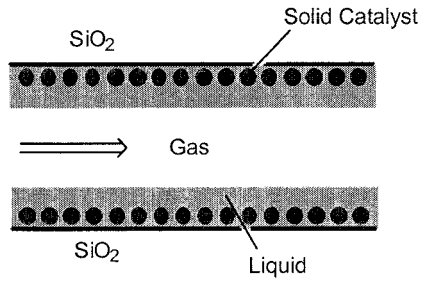

Figure 1. Ideal device for multiphase reactions.

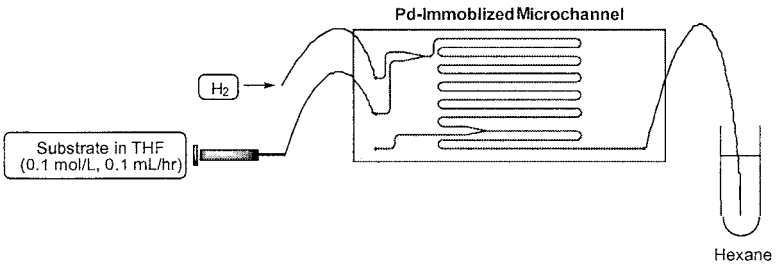

Figure 2. An experiment system of hydrogenation.

MANIPULATION AND PREPARATION OF BUBBLES FOR GAS ANALYSIS SYSTEMS

Takahiro Ito, Torii Toru and Toshiro Higuchi
Dept. of Precision Engineering, Graduate School of Engineering, The University of Tokyo, 7-3-1 Hongo, Bunkyo-ku, Tokyo 113-8656, Japan

Abstract

Electrostatic actuation of bubbles in dielectric medium for micro-gas analysis systems is described in this paper. This method realizes complex movements of bubbles without using various kinds of microfluidic components. In addition, a bubble formation and preparation method to introduce bubbles to the bubble manipulation area is proposed for an integrated gas analysis system. From the results of experiments, these presented methods have great potential to realize micro-sized gas analysis systems.

Keywords: bubble, electrostatic actuation, bubble formation, gas analysis system

1. Introduction

There are few devices for small amount of gas in the field of micro TAS. Conventional continuous flow method for sample control could not manipulate multiple gas samples and realize complex movement.

Therefore, we propose a novel actuation method for bubble applying electrostatic manipulation; bubbles typically microliter in volume, were controlled by dielectrophoretic force generated by switching voltage applied to the array of electrodes on a substrate. Moreover, bubble formation techniques were also developed. Using these techniques, monodisperse bubbles could be generated and introduced to the manipulation area by simple elements. Combining these techniques, we tried to automate formation and manipulation of bubbles in a palm-sized device. In addition, some experiments applying these methods: complex movement; actual chemical reactions were demonstrated to check the ability to use in the micro-analysis systems.

2. Experimental

The setup of the bubble manipulation device is illustrated in Fig.1. A bubble was set beneath the electrodes panel or in the gap between the top panel and the electrodes panel. In this experiment, the electrodes panel was consisted of six-phase electrodes and the pattern of voltage switching was controlled as shown in Fig.2. To prevent dielectric breakdown, the surface of panel was coated by an insulating film such as parylene C. Silicone oil was used for the dielectric medium around the bubbles.

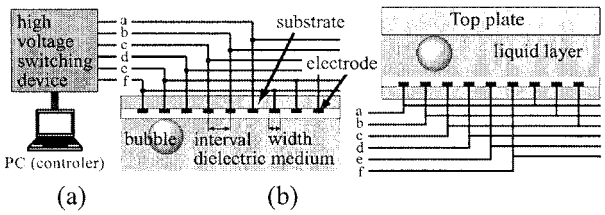

Figure 1. Side view of the bubble manipulation device.
(a) A bubble was set beneath the electrodes panel. (b) A bubble was set between the acrylic top plate and the electrodes panel.

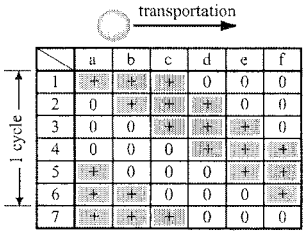

Figure 2. Example of Applied voltage pattern. The alphabets 'a' to 'f' are the ports of six-phase electrodes device.

In addition, we demonstrated two techniques of bubble formation, *i.e.*, T-shaped channel and combination device. The T-shaped channel was an application of droplet formation device [1]. The setup of this is shown in Fig.3(a). Figure 3(b) shows the setup of the combination system that consisted of electrode for the electrostatic manipulation and a straight microchannel for the gas feed. In this system, after a bubble grows larger at the outlet of the microchannel, it is transported by the electrostatic manipulation.

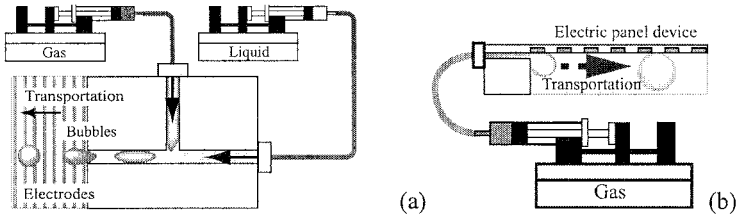

Figure 3. (a) Setup of the bubble preparation device using T-shaped junction. (b) Setup of the combination system for bubble formation.

3. Results and discussion

The electrostatic manipulation of bubble was achieved as shown in Fig.4. Since the bubble had a lower dielectric constant compared to silicone oil, it took negative dielectrophoretic force from non-uniform electric field generated by planar electrodes [2]. A trapped bubble on the weakest electric field was moved with the shifting voltage applied to the electrodes; therefore, the driving force of bubble manipulation was different from that of droplet manipulation [3]. The velocity of a bubble (0.6 mm in diameter) transportation could come up to 45 mm/s when 0.5 mm pitch electrodes device was used applying 700 $V_{0\text{-}p}$. Bubbles from 0.2 mm to 3 mm in diameter could be manipulated under the 0.5 mm pitch electrodes. However when the size of bubble was about 1.2 times larger than the pitch of electrodes, the bubble could be manipulated at lowest voltage.

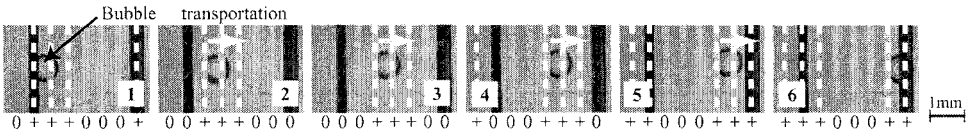

Figure 4. Positional relationship of a bubble and voltage-applied electrodes.

Applying this method, we could control complex movement of small sized samples. Shown in Fig. 5 are examples of results from our experiments. Figure 5(a) is bubble manipulation in two-degree-of-freedom. This manipulation could be realized in sandwich type device; bubble was sandwiched in two electrodes panel where the electrodes of each panel were at right angles to each other. Figure 5(b) is decomposition reaction of hydrogen peroxide solution ($2H_2O_2 \rightarrow 2H_2O+O_2$) using electrostatic manipulation technique. Consequently, a droplet and bubbles could be manipulated in one device and separated off only generated gas from the reaction point.

Figure 6 shows the formation process of the bubble. In the T-shaped junction, the gas flow was periodically sheared by the liquid flow at the junction and micro-sized bubbles were formed (Fig.6(a)). The bubble size was varied widely controlling the flow rate of the liquid. The result of bubble formation in the combination device is shown in Fig.6(b). Bubbles were formed at the outlet of the microchannel and transported by electrostatic manipulation. Same sized bubbles could be periodically formed and aligned by transporting bubbles. This bubble formation method could

control the size of bubbles only by manipulation speed of bubble; especially, T-shaped junction could make micro-sized bubbles which were smaller than the size of microchannel.

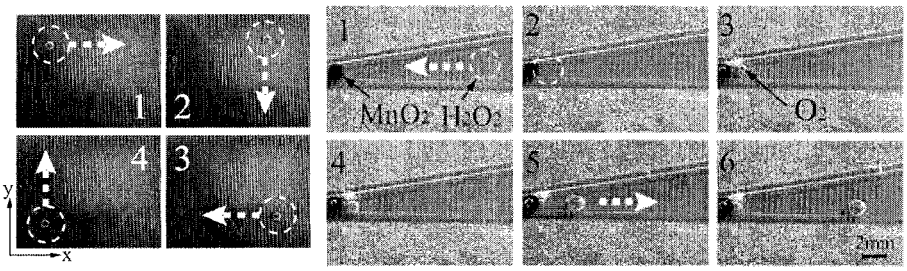

(a) (b)

Figure 5. Sequential photographs of experiments. (a) Manipulation in Two-Degree-of-Freedom. (b) Example of a chemical reaction. A droplet (H_2O_2) transportation to the left (**1-2**). Reaction ($2H_2O_2 \rightarrow 2H_2O+O_2$) (**3-4**). A bubble ($O_2$) transportation to the right (**5-6**).

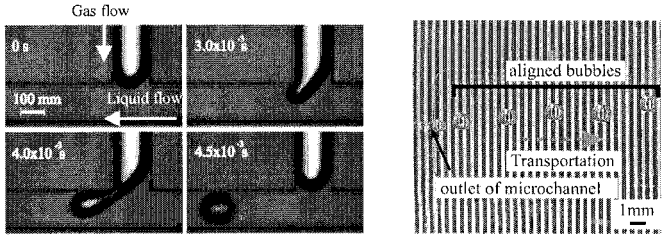

(a) (b)

Figure 6. Sequential photographs of bubble formation.
(a) Process of bubble formation at T-junction. The gas flow is sheared by the liquid flow.
(b) Bubble formation using combination system. Bubbles formed at the outlet of microchannel and transported to the right by electrostatic manipulation

4. Conclusions

In this study, a novel manipulation and preparation of bubbles for micro device was developed and demonstrated. Manipulation of micro-sized bubble was achieved by electrostatic force which is generated by controlling voltages to the electrodes array plate in dielectric medium. This manipulation does not require micro fluidic components such as micro valves, pumps or channels. Combining several bubble formation methods could automate preparation and manipulation in one device. In addition, applied experiments, such as actual chemical reactions, could also be demonstrated using this method. All these results indicated that these methods including electrostatic manipulation and formation of bubble have great potential for realizing gas micro analysis systems.

References

[1] T. Nisisako, T. Torii and T. Higuchi, *Lab Chip*, **2**, 24-26 (2002).
[2] H. A. Pohl, *Dielectrophoresis*, Cambridge University Press (1978).
[3] T. Taniguchi T. Torii and T. Higuchi, *Lab Chip*, **2**, 19-23 (2002).
[4] T. Ito, T. Nisisako, T. Torii and T. Higuchi, *Book of Abst. 7th Int. Conf. Microreaction Technology (IMRET7)*, 123-125 (2003).

BIOMOLECULE SEPARATION IN NANOFLUIDIC FILTERS BY STERIC HINDRANCE MECHANISM

Jianping Fu[1] and Jongyoon Han[2, 3]

[1]Dept. of Mechanical Engineering, [2]Dept. of Electrical Engineering and Computer Science, [3]Biological Engineering Division, Massachusetts Institute of Technology, Cambridge, MA, USA

Abstract

A novel biomolecule size-fractionation strategy is explored in this work by using nanofluidic filters. The separation of biomolecules is based on the steric hindrance induced entropic barrier effect, which is size-dependent. For demonstration, DNA sample (100bp DNA ladder) and SDS denatured protein mixture (FITC-conjugated ovalbumin (MW~45K) and low density human lipopropein (MW~179K)) are completely separated by dc electrophoresis in an 80nm nanofluidic filter device. In the low field region, the electrophoretic mobility μ of DNA fragments can be nicely fit into the exponential function, $\mu \sim \exp(-sL)$, where L is the total length of short rigid DNA molecule and s is the proportionality constant.

Keywords: biomolecule separation, nanofluidics, steric hindrance, entropic barrier

Micro/nanofluidic molecular sieving structures fabricated with microfabrication technology have been applied for biomolecular separation with great speed and efficiency [1-3]. However, their uses have been largely limited to large biomolecules, since it is generally difficult to fabricate structures with comparable molecular dimension to serve as efficient sieving matrix. In this paper, we present a novel separation method using nanofluidic filters to fractionate small biomolecules based on their sizes. The separation is based on the entropic free energy barrier caused by the steric hindrance of biomolecules in nanofilters. When biomolecules are moving into a nanofluidic filter from the thick region, they get confined and lose some degree of freedom in the molecular conformation (chain configuration) (Fig. 1). This entropy loss will pose a free energy barrier for the molecules, as suggested originally by Giddings [4,5]. This could be a basis for sieving biomolecules whose sizes are even smaller than the gap size of the nanofilter.

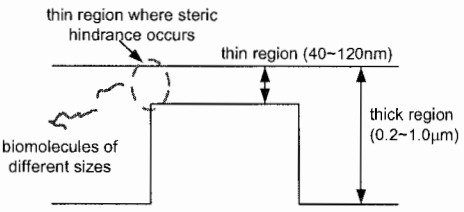

Figure 1. Cross-sectional schematic picture of one nanofluidic trap. When molecules travel through the thin region, certain configuration entropy will be lost due to steric constrains imposed from the walls. The entropic free energy barrier caused by this will slow down the motion of molecules and induce the size dependence of electrophoretic mobility in the nanofluidic filter.

The nanofluidic filter device is fabricated with microfabrication technology in cleanroom environment. Detailed information about the fabrication process is available in previous publications [2,6]. Before all electrophoresis experiments, the nanofluidic filter device is filled with buffer solution through the buffer access holes. As a buffer solution, Tris-Borate-EDTA (TBE) buffer at 5X (445mM) concentration is used in all our experiments to efficiently quench the electroosmotic flow. Under this buffer concentration, the thickness of electrical double (Debye) layer is negligible as an affecting factor for separation. A T-shaped injector for electrophoretic sample injection is integrated in our nanofluidic filter device (Fig. 2(a)). During each separation experiment, a band of sample with the length equal to the channel overlap at the T intersection

(about 200μm) is delivered into the separation column by manipulating the potentials applied at the four buffer access holes (Fig. 2(b)).

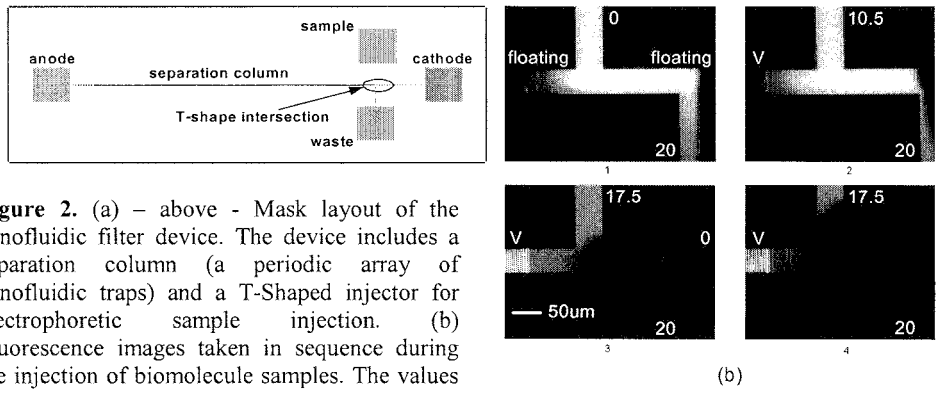

Figure 2. (a) – above - Mask layout of the nanofluidic filter device. The device includes a separation column (a periodic array of nanofluidic traps) and a T-Shaped injector for electrophoretic sample injection. (b) Fluorescence images taken in sequence during the injection of biomolecule samples. The values listed in the figures are the voltage applied during the injection in all our experiments.

In our experiment, 100bp DNA ladder samples (New England BioLabs) are labeled with YOYO-1 dye (Molecular Probes) at a dye/base pair ratio of 1:10. For protein separation, FITC-conjugated protein mixture (ovalbumin (MW~45K, Molecular Probes) and low density human lipoprotein (MW~179K, Molecular Probes)) is denatured with 2% sodium dodecyl sulfate (SDS) to impose uniform hydrodynamic and charge characteristics. To get an electrophoregram, an inverted fluorescence microscope is used to detect the Ar-ion laser-induced fluorescence signal at various separation distances (1-3cm) along the separation column. The microscope images are recorded by a CCD camera (Sensicam QE, Cooke Corp.) and the fluorescence signals from the laser detection point are averaged for data analysis.

DNA molecules (100bp DNA ladder sample) are first separated in a nanofluidic filter device with 80nm thin regions, 500nm thick regions and 4um trap period (Fig. 3). As the applied field lowered down, 100bp DNA ladder is completely separated into individual bands (Fig. 3(a)). This shows that the molecules as small as 100bp double stranded DNA (34nm extended length) can be sieved in the filter as large as 80nm. The log plot of electrophoresis mobility μ verses DNA fragment size is shown in Fig. 3(b). As shown in the figure, an exponential function $\mu \sim \exp(-sL)$, from the free volume model of gel electrophoresis[7] can fit the experimental data well in the low field region. Here, L is the total length of DNA molecule and is proportional to DNA base pair number N. At higher fields, the data deviate from the exponential behavior, suggesting other transport mechanisms in effect in those cases. Figure 4 shows the electrophoregram of SDS denatured protein mixture of ovalbumin and low-density human lipoprotein from the same nanofluidic filter device. Before the experiment, TBE 5X buffer with 0.1% SDS is flushed into the separation column by running electroosmotic flow for several hours. Complete separation of these two proteins can be achieved in 40mins at field strength of 50V/cm. This shows that the molecules as small as proteins can be indeed separated in a nanofluidic filters as large as 80nm.

In conclusion, we have demonstrated a novel separation method by using nanofluidic filter device to separate small biomolecules (small DNA, proteins). This novel separation mechanism is applicable to any biomolecules for size-based separation, and could be useful in developing nanofluidic molecular sieving systems for various biomolecules, including proteins and

carbohydrates. The nanofluidic filters presented here can replace liquid or polymeric gel for biomolecule separation and can be fabricated and integrated easily into complex μ-TAS systems. The regularity and well-defined geometry of nanofluidic filters also provide a good platform for theoretical study of electrophoresis or hindered transport of flexible polyelectrolytes in gels.

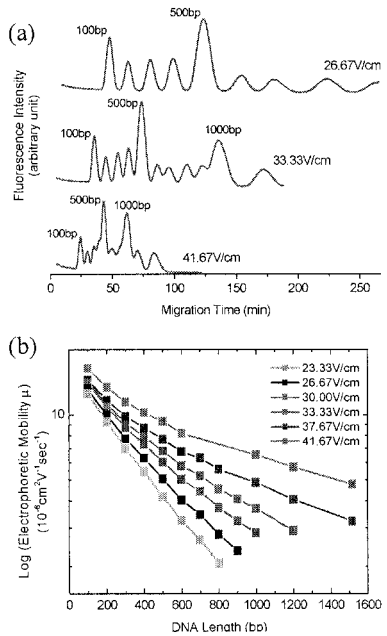

Figure 3. Separation of 100bp DNA ladder in the nanofluidic filter device with 80nm thin regions, 500nm thick regions and 4um trap period. (a) electropherograms of 100bp ladder sample taken at 1cm downstream from the injection point under different electrical fields. Smaller DNA fragments elude first from the channel; 500bp and 1000bp bands have increased intensity to serve as reference peaks as shown in figure. Apparently there is a trade-off between the resolution and the speed of separation; with a lower electrical field, more resolved separation is obtained, but the speed of the separation is compromised. Separation resolution becomes poorer when the driving electric field is increased. (b) Logarithmic plot of electrophoresis mobilities verses DNA length under different fields. In the low electrical field region, an exponential function $\mu \sim \exp(-sL)$ can nicely fit the mobility data. In the high field regions, the mobility data depart from the exponential behavior, especially for the longer DNA molecules.

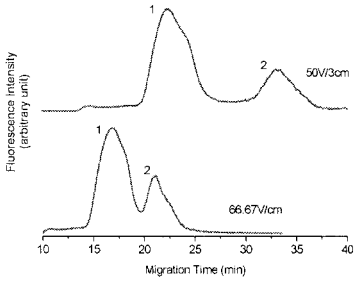

Figure 4. Separation of ovalbumin and low density human lipopropein in the nanofluidic filter device with 80nm thin regions, 500nm thick regions and 4um trap period. Electropherograms are taken 1cm downstream from the injection point. Band assignment: ovalbumin (1), human lipoproperin (2). Ovalbumin band has increased intensity to serve as reference peak. In 40 mins, these two proteins are completely separated into two different bands.

References

[1] W. D. Volkmuth, R. H. Austin, *Nature*, **358**, 600-602 (1992).

[2] J. Han, H. G. Craighead, *Science*, **288**, 1026-1029 (2000).

[3] L. R. Huang, *et al. Nature Biotechnology*, **20**, 1048-1051 (2002); L. R. Huang, *et al. Science*, **304**, 987-990 (2004).

[4] J. C. Giddings, E. Kucera, C. P. Russell, M. N. Myers, *J. Phys. Chem.*, **72**, 4397-4408 (1968).

[5] J. C. Giddings, *Unified Separation Science* (John Wiley & Sons, New York, 1991).

[6] J. Han, H. G. Craighead, *J. Vac. Sci. Technol. A*, **17**, 2142-2147 (1999).

[7] J. L. Viovy, *Rev. Mod. Phys.*, **72**, 813-872 (2000)

MOLECULAR VAPOR DEPOSITION™ – A NEW TECHNIQUE FOR SURFACE MODIFICATION

Boris Kobrin [1], Richard Yi [1], Victor Fuentes [1], S. Dasaradhi [1], Romuald Nowak [1], Jeff Chinn [1],Robert Ashurst [2], Roya Maboudian [3]

[1] *Applied MicroStructures, Inc., San Jose, CA 95134 (info@appliedmst.com)*

[2] *Auburn University, Dept. of Chemical Engineering, Auburn, AL*

[3] *University of California at Berkeley, College of Chemistry, Berkeley, CA*

Abstract

The improved capability and functionality of a new surface modification technique known as Molecular Vapor Deposition (MVD)™ is herein reported. MVD can be briefly described as an enhancement of a vapor deposition method, in which an integrated surface cleaning process and an advance multi-precursor vapor delivery system are made available. With metered exposures of precursor and catalytic vapors, superior surface coatings can be obtained when compared with a liquid-phase deposition technique. The MVD approach also has the capability to create coatings using sequential or "layered" deposition sequences which result in improved film durability, surface coverage, and the ability to coat a wide variety of substrates including glass, plastics, polymers, metals and semiconductors at room temperature.

Keywords: Surface Modification, Molecular Vapor Deposition, Self-Assembled Monolayers, MVD, SAM

1. Introduction

Surface coatings with mono-molecular layers of organo-silanes have been a traditional method for modifying the surface properties of materials. Depending on the molecular termination, various surface properties can be obtained ranging from hydrophobic to hydrophilic in nature. A traditional organo-silane deposition technique typically consists of a series of sequential wet baths which is complex and limits the implementation of these coatings on many materials and devices. For example, many of the self assembling monolayer precursors are highly susceptible to particulation and are sensitive to environmental humidity and cross-contamination. Due to this sensitivity, precursor liquids have extremely limited bath life which increases the manufacturing costs and limits the process reproducibility. Additionally, many polymers and plastics are incompatible with the solvents used in the various wet baths.

More recently, a variety of organic mono-layers have been deposited in the vapor phase [1,2,3] in an effort to improve the performance of the MEMS devices and to eliminate the shortcomings of liquid processing. A vapor-phase approach has allowed for successful coating of complex MEMS devices not possible using a liquid-phase [4] technique. There are many manufacturability advantages associated with the use of vapor deposition. They include process scalability, elimination of solvent disposal, compatibility with automated processing, and the last but not the least - a significantly lower cost of the coating in volume manufacturing. One of the most important technical benefits of using vapor methods are the reduction of particles and surface roughness [5] while retaining all the desired physical and chemical properties of the coating.

In this paper, we report on an improved vapor deposition method, which is called Molecular Vapor Deposition (MVD)™. This method is an enhancement of a vapor deposition process of self-assembled mono-layers integrated with various surface preparation techniques, precise dosing of multiple vapor precursors on demand, and temperature control. MVD coatings can be deposited either as a mono-layer or as multi-layer films using sequential exposures to the precursors.

2. Apparatus:

The apparatus used for MVD has been previously published [5] and is commercially available [6].

3. Results & Discussion:

Surface preparation by plasma treatment was observed to be an essential first step of the integrated deposition process. Reactive species generated by the plasma are used to remove any organic contaminants and to ensure uniform hydroxylation of the surface with OH-groups. Oxygen plasma treatment of silicon substrates results in a highly hydrophilic surface exhibiting very low water contact angles.

The degree of surface hydrophobicity depends on the precursor and is typically proportional to the density and coverage of the coating, which in turn is controlled by the process conditions (cleaning efficiency, reactants ratio, reaction pressure, and substrate temperature). This is illustrated in Fig. 1.

Film properties obtained from studies on Si(100) wafers for various chemistries are summarized in Table 1. Surface contact angles vary within a wide range depending on the chemistry. Both hydrophobic and hydrophilic films can be obtained by process control while the maximum achievable contact angle depends on the type of the reaction precursor. Unlike a liquid-phase deposition, a sequential MVD method can be used to deposit molecular coatings on various materials including plastics and other disposable substrates used in biological applications. Many of these polymeric materials do not naturally exhibit surface binding sites that are compatible with chlorosilane chemistries. Hydroxylated silanol like groups can be created on the surface of these materials by depositing a very thin intermediate adhesion layer as part of the MVD sequence. For this purpose, a special intermediary silane precursor is introduced into the chamber to create a thin (20-200Å) and smooth (1-4 nm RMS) oxide seed layer. This "seed-layer" coating can be deposited on a variety of materials including glass, polymers, metals, low temperature plastics, etc. Contact angle measurements performed on this "seed-layer" confirm a hydrophilic surface (<5 deg water contact angle). Then, without breaking a vacuum, organic layers have been successfully deposited on such seed layer. With most chlorosilane based precursors, the surface coverage of the molecular layer is limited by the availability of binding reaction sites. In the case of a smooth, non-porous silica surface, it is generally accepted that there are 4-5 hydroxylated silanol sites present per nm^2 as compared to the theoretical limit of 7.8 sites/nm^2 [7]. Using the sequential vapor exposure method, an intermediate seed layer can be created in order to increase the density of the bonding sites prior the surface coating. For a typical alkyl-silane coating, XPS analysis indicates that the ratio of total fluorine to the total silicon peaks on a seed layer to be approximately 15% higher than that a standard vapor deposited coating on thermal oxide. This means a 15% increase of density in terms of molecular coverage. Increased density of organic coating was shown to enhance stability of these coatings in aqueous environments. For example, a standard vapor deposited SAM coating on glass (with FOTS) exhibits maximum water contact angle of $\geq 105°$, which is indicative of a nearly full surface coverage. The stability of this coating in ambient air is accepted as excellent. However, upon immersion in water and other polar solvents the film degrades slowly over time (Fig.3). It is speculated that small polar molecules can diffuse to the surface in between the long chain molecules of the coating and attack the covalent bonds with which the coating is attached to the surface. This phenomenon can be greatly reduced using sequential MVD method with an intermediate seed layer. The MVD process can be repeated multiple times to effect a molecular layer deposition process that is similar to ALD (atomic layer deposition) used in semiconductor processing. This MVD method leads to ultra-thin coatings ranging from one monolayer to several layers. However, sequential coatings and multi-layer films have to be further tested for their improved durability as compared to single monolayer coatings. Fig. 4 demonstrates how MVD technology can modify surface hydrophobicity using few different processes and precursors (plasma treatment, seed layer deposition, organic layer deposition).

5. Conclusions:

Uniform, dense, mono-layer and multi-layer molecular coatings have been deposited using an innovative automated vapor phase deposition method referred to in this paper as MVD (Molecular Vapor Deposition). The MVD apparatus used for studies of various chlorosilane-based coatings includes an integrated surface plasma treatment, uses precise reactant vapor dosing, and allows the control of reaction pressures and temperatures. Basic properties of the resulting molecular films (composition, hydrophobicity, work of adhesion) are very similar to those previously published for liquid-phase deposited films. Moreover, uniformity, roughness, defect density and stability of the MVD films were found to be superior to the conventional solution based films. These ultra-thin molecular coatings can be deposited on various materials and are very promising for use not only in MEMS devices but also in many other bio- and nano-technology applications.

References

[1] W.R. Ashurst, C. Yau, C. Carraro, R. Maboudian, M.T. Dugger, J. Microelectromechanical Systems, 10, 41-49,2001.

[2] W.R. Ashurst, et al, Sensors and Actuators A 104, 2003, p.p. 213-221

[3] W. Robert Ashurst, C. Carraro and R. Maboudian, IEEE Transactions on Device and Material Reliability, Vol. 3, No. 4, Dec. 2003, p173.

[4] T. M. Mayer, M.P. de Boer, N.D. Shinn, P.J. Clews, J. Vac. Sci. Technol. (B), 18, 2433-2440, 2000.

[5] Robert Ashurst, Carlo Carraro, J.D. Chinn, Victor Fuentes, Boris Kobrin, Roya Maboudian, Romuald Nowak, Richard Yi, "An Improved Vapor-phase Deposition pTechnique for Anti-Stiction Monolayers", Proc. Of SPIE, January 2004.

[6] Applied MicroStructures, Inc. (www.appliedmst.com)

[7] Lier, K.R., The Chemistry of Silica, John Wiley and Sons, New York 1979.

Table 1. Summary of maximum contact angle for various chemistries.

Precursor	Contact angle (deg.)	
	Water	Hexadec
Tridecafluoro-1,1,2,2-tetrahydrooctyltrichlorosilane (FOTS)	110	75
Heptadecafluoro-1,1,2,2-tetrahydrodecyltrichlorosilane (FDTS)	110	68
Dimethyldichlorosilane (DDMS)	103	38
10-Undecenyltrichlorosilane	101	29
Methyltriethoxysilane	86	33
333-Trifluoropropyldimethyltrichlorosilane	83	45
Bromorpopyltrichlorosilane	78	8
Mercaptopropyltrimethoxysilane	69	<5
Epoxycyclohexylethyltrimethoxysilane	67	<5
3-Acryloxypropyltrichlorosilane	65	<5
3-Acryloxypropyltrimethoxysilane	50	<5
Hexanediol	50	<5
Aminopropyltrimethoxysilane	40	<5
Methoxy(polyethyleneoxy)propyltrimethoxysilane - PEG	26	<5

Molecular Vapor Deposition (MVD)™ is a trademark of Applied MicroStructures, Inc.

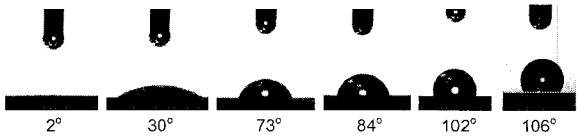

Figure 1. Various hydrophobic surfaces (as measured by the water contact angle) obtained on Si substrate by varying the FOTS deposition process parameters.

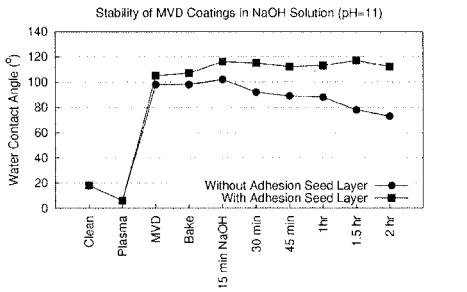

Figure 2. Stability of the contact angle of an FOTScoating on glass as a function of the exposure time. Both samples were immersed in an aqueous solution of NaOH (ph=11).

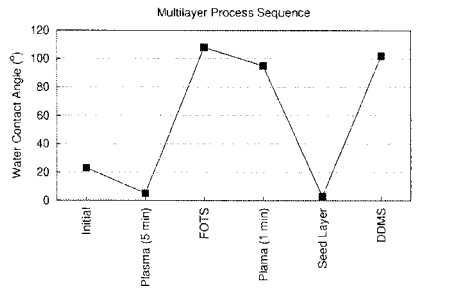

Figure 3. Surface hydrophobicity change with multiple sequential surface modification processes on the same sample.

DYNAMIC PROPERTIES AND STRUCTURES OF WATER INSIDE THE HOLLOW CYLINDER OF A SUGAR-BASED LIPID NANOTUBES

Hiroharu Yui[1,2*], Guo Yanli[2], Tsuguo Sawada[2], Bo Yang[3], Mitsutoshi Masuda[1,3] and Toshimi Shimizu[1,3]

[1] *CREST, Japan Science and Technology Agency (JST), Tsukuba, Ibaraki 305-8562, Japan*

[2] *Dept. of Advanced Materials Science, Graduate School of Frontier Sciences, The University of Tokyo, 5-1-5-603 Kashiwanoha, Kashiwa, Chiba 277-8651, Japan*

[3] *Nanoarchitectonics Research Center (NARC), National Institute of Advanced Industrial Science and Technology (AIST), Tsukuba Central 4, 1-1-1 Higashi, Tsukuba, Ibaraki 305-8562, Japan*

Keywords: lipid, nanotube, water, nano-fluidic, confined geometry

1. Introduction

Water in nanometer-sized restricted geometries is of much interest because structures and properties of water in such confined space often show different and sometimes unexpected features compared to those of bulk water. Such characteristic structures and properties of water in a restricted environment play an important role for activity of biological macromolecules, specific chemical and physical processes occurring at interfaces, lubrication phenomena, and so on. Among various morphologies of such restricted nanometer-sized geometries, one-dimensional hollow structures should provide a variety of potential applications as channels for nano-fluidic devices, templates for metal nanowire formation, size-selective pores for analytical and/or storage devices and so on. One example is cardanyl glucoside-based lipid nanotubes, which have 10–15 nm inner diameters, 40–50 nm outer diameters, and axial ratios >1000 [1]. We call this lipid nanotube (LNT) and have described their physical and chemical characteristics elsewhere [2]. Here we investigated the properties and structures of water inside the hollow cylinder of the LNT. The water inside the LNT is interesting from the viewpoint of not only the important models of such confined water in living cell but also many possible applications of the LNT with high-axial-ratio hollow space such as channels in nano-fluidic devices.

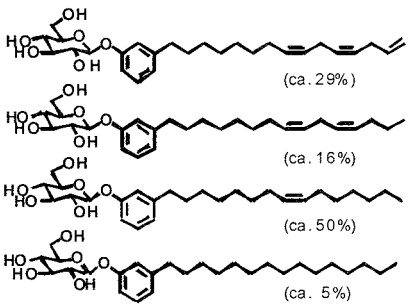

Figure 1. Structures of the cardanyl glucosides used for formation of sugar-based lipid nanotubes (LNT). The percentages shown are the proportion of each glycolipid in the mixture.

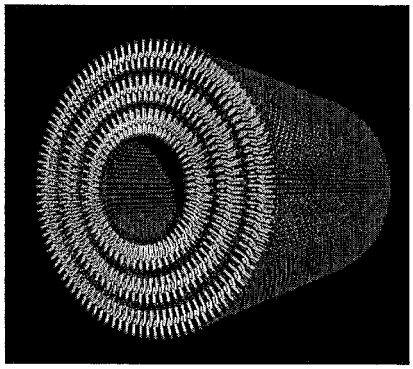

Figure 2. Schematic illustration of the LNT formed by self-assembly of the cardanyl glucosides. Dark gray spheres and light gray cylinders represent the hydrophilic sugar headgroups and the hydrophobic tails of the cardanyl glucosides, respectively.

2. Preparation of the LNT

Figure 1 and Figure 2 show the molecular structures of cardanyl glucosides used here and the their self-assembled form, namely LNT, respectively. At first we dispersed 6-7 mg of the lipids molecules in 200 ml water and refluxed the lipid dispersion at near boiling temperature for 30 minutes. Then we cooled the solution at room temperature. After a few days, we can obtain the LNT through the self-assembly of the lipid molecules. The wall of the LNT consists of 3–4 lamellar layers with bilayermembrane structure, in which hydrophilic sugar headgroups are present on both inner and outer surfaces. Thus, the both inner and outer surfaces were hydrophilic and water can be easily introduced into the hollow cylinder of the LNT.

3. Experimental

In IR measurement, we measured the LNT under ATR condition to avoid large contribution from the bulk water. We took differential spectrum between spontaneously dried LNT (the surrounding water was removed but the water inside the hollow remained) and freeze-dried LNT of the same sample (the water inside the hollow cylinder was removed). It was not needed to normalize the signals at certain peak because the same sample was measured (direct-difference methodology). In time-resolved fluorescent measurement, 1,8-ANS (10^{-4} M) was used for probing local polarity of water in the LNT. After removing the ANS solution surrounding the LNT by filtration, we measured time resolved fluorescent spectra using Nd-YAG 3rd harmonic system (excitation wavelength: 355 nm, pulse duration: 30 ps) and a streak camera (Hamamatsu Photonics C4334).

4. Results and discussion

We introduced 8-anilinonaphtahanlen-1-sulfonate (1,8-ANS) only into the hollow cylinder of the LNT to obtain the solvent polarity of the confined water. Figure 3 shows the time-resolved spectra of ANS. A sum of two log-normal shape functions was compatible with the experimental results. The peak wavelengths (and bandwidths) of the two components were estimated to be 403 nm (width ca. 45 - 55 nm (FWHM) and > 450 nm (width ca. 100-120 nm (FWHM)) (Figure 3). We note here the former component I and the latter II. The component I showed no peak shift and the wavelength was considerably short. These results indicate that the corresponding 1,8-ANS was not surrounded by free water. Thus, the component I can be assigned to the 1,8-ANS which was strongly absorbed on the inner surface of the LNT and/or intercalated into the lipid molecules. On the other hand, the peak wavelength of the component II showed remarkable dynamics Stokes shift. The wavelength at the steady state of the component II was 467 nm. The corresponding solvent polarity parameter ($E_T(30)$) was 50 kcal/mol, which is 20% lower than that of pure bulk water (63 kcal/mol) [3].

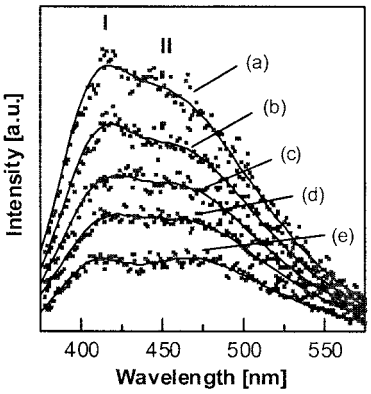

Figure 3. Time-resolved spectra of 1,8-ANS in confined water inside the LNT, obtained at (a) 1.25 ns, (b) 2 ns, (c) 3 ns, (d) 4 ns, and (e) 6 ns after excitation. The solid lines are curves fitted by the sum of two log–normal functions.

Then we examined hydrogen-bond network environment of the water confined in the hollow cylinder of the LNT by ATR-IR with a direct-difference methodology. The peak frequency of the IR spectrum of the confined water proved to be lower and the bandwidth markedly narrower than those of the IR spectrum of bulk liquid water (Figure 4). To compare these differences

more quantitatively, we did curve-fitting analysis. In general, IR spectra in the OH-stretching region of water in various confined geometries are represented by the sum of at least three or four Gaussian components, centered around 3650, 3550, 3400, and 3250 cm^{-1}. In the present measurements, we can notice a shoulder structure below 3200 cm^{-1} (Figure 4(b)). Thus, we further added the fifth band components below 3200 cm^{-1}, that is, we represented the IR band of water by five Gaussian components to investigate the change of the spectra in more detail. The fitted curves are shown in Figure 4 and the relative changes in each component area, in peak wavenumber, in bandwidth of each component are shown in Table 1. The peak position was shifted toward the lower wavelength region due to diminish of the components I and II and relative increase of the component IV. The main component IV (around 3250 cm^{-1}) has been believed to represent water in relatively developed, ice-like hydrogen-bond network environment, because the peak frequency is remarkably lower than that of water (3400 cm^{-1}) and is close to that of ice (3150 cm^{-1}). The characteristic features observed here indicate that a considerable part of the confined water molecules took part in an extensive hydrogen-bond network even at room temperature. It should be noted that these features were in marked contrast to those of water in other confined geometries, such as AOT reversed micelles where the hydrogen-bond network structure is remarkably distorted by hydration to the ionic headgroups of the surfactants. We are now considering the mechanism of the structuring of the water inside the LNT from a viewpoint of the contribution from the abundant OH groups of sugar moieties that fully cover the inner surface of the LNT.

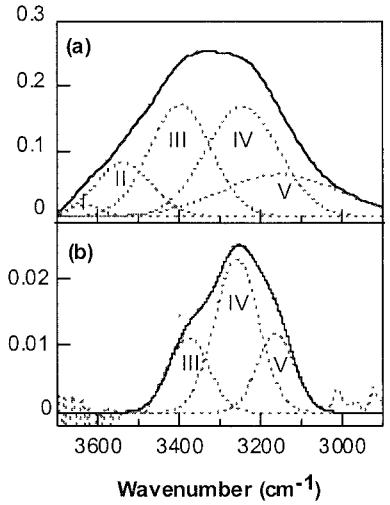

Figure 4. (a) IR spectrum of bulk water measured under the same experimental conditions with those for the measurement of the confined water in the LNT. (b) Difference between IR spectra of the LNT after spontaneous drying and subsequent vacuum-drying. Dashed lines indicate the results of Gaussian component fitting (Table 1).

Table 1. Fitting parameters for the IR spectra of bulk water and the difference spectrum of water confined inside the hollow cylinder of the LNT.

Component	In bulk			In the LNT		
	ν*	Γ**	Area%	ν*	Γ**	Area%
I	3631	83	1.4	–	–	–
II	3536	162	12.9	–	–	–
III	3397	178	29.8	3376	116	23.6
IV	3244	211	34.6	3259	127	53.4
V	3151	337	21.3	3164	107	23.0

*Peak frequency (cm^{-1}). ** Bandwidth (FWHM) (cm^{-1}).

References

[1] G. John, M. Masuda, Y. Okada, K. Yase, T. Shimizu, *Adv. Mater.*, **13**, 715-718 (2001).

[2] (a) T. Shimizu, *Macromol. Rapid Commun.* **23**, 311-331 (2002). (b) G. John, J. H. Jung, H. Minamikawa, K.Yoshida, T. Shimizu, *Chem. Eur. J.*, **8**, 5494-5500 (2002). (c) J. H. Jung, G. John, K. Yoshida, T. Shimizu, *J. Am. Chem. Soc.* **124**, 10674-10675 (2002). (d) H. Frusawa, A. Fukagawa, K. Ito, G. John, T. Shimizu, *Angew. Chem., Int. Ed. Engl.* **42**, 72-74 (2003).

[3] See, for example, E. M. Kosower, *Acc. Chem. Res.* **15**, 259-266 (1982) and references therein.

UPTAKE OF QUANTUM DOTS INTO THE OSTEOBLAST CELLS UTILIZING ELECTROPORATION AND ENDOCYTOSIS

Min Li[1], Yuan-Huang Lee[1], Yu-Cheng Lin[1], Yuh-Jiuan Lin[2], Shur-Tzu Chen[3], Ching-Yi Wu[4]

[1]Dept. of Engineering Science, [3]Dept. of Cell Biology and Anatomy, National Cheng Kung University, 1 University Road, Tainan 701, Taiwan

[2]Biomedical Engineering Center, [4]Electronic Research and Service Organization, Industrial Technology Research Institute, Hsinchu 302, Taiwan

Abstract

This study demonstrated that the (CdSe)ZnS quantum dots, Q-dots, could be transported into mammalian cells as nanoprobes utilizing an electroporation (EP) and endocytosis method. These nanoparticles work as nanoprobes and provide molecule imaging for cellular physiology. In the endocytosis pathway, the Q-dots were delivered from cell membranes to nucleus vicinities and then aggregated near nucleus. However, the Q-dots were dispersed in cytoplasm by utilizing electroporation to deliver Q-dots into cells. This study demonstrates that electroporation have higher QD delivery rates into cells compared to endocytosis.

Keywords: quantum dots, nanoparticle, (CdSe)ZnS, nanoprobe, electroporation

1. Introduction

Nanoparticles could be delivered into cells and tissues as a vector for drugs or genes. Uptake of nanoparticles into cellular member, as well as nucleus has been reported [1]. Q-dots are innovative dyes for cellular images on immunofluorescence. Compared to conventional organic dyes, the Q-dots have the advantages of excellent photo stability, narrow emission spectra, and broad adsorption spectra. Q-dots could be used as the fluorescent markers in cellular organ or target special antigens of cancer cells [2]. Whether nanoparticles can be digested by the cells or expelled by exocytosis function is an open question.

We studied the phenomenon of the pathways for nanoparticles uptake into cells utilizing endocytosis and electroporation methods. The former is based upon the ability of cells in endocytosis, and the latter uses high electric field stimulation to create the transient pores in the cell membranes.

2. Experimental

2.1 Synthesis of (CdSe)ZnS

Cadmium selenide (CdSe) nanoparticles were prepared by using the Peng's method [3]. The CdO as precursor was decomposed into hot trioctylphospine oxide (TOPO) at 340°C for 5 minutes, and then cooled down to room temperature. When the temperature reached 240°C, the Se, solvated on TBP, and ZnS were added into the mixture to form 5 nm diameter (CdSe)ZnS core-shell nanoparticles. To create the water soluble nanocrystals, the (CdSe)ZnS were coated with hydrophilic thiols on surface [4]. Water soluble (CdSe)ZnS nanoparticles were characterized and shown in Figure 1.

2.2 Cell preparation and uptake experiments

The MC3T3E-1 (osteoblast cell) cells were incubated in a 50 μl culture medium with 5 μg Q-dots for 1h, 3h and 6h. Uptake of Q-dots into cells then occurred by endocytosis. In the process of electroporation, the cells, cultured on EP microchips, were added with Q-dots and stimulated using a laboratory-built computer-controlled power supply [5]. Q-dots were then delivered into cells after applying the 3V-2 pulses electroporation voltage immediately. The EP microchip was designed and

fabricated on a glass slide with Au/Ti thin film electrodes and a PDMS cell culture well [5]. The EP chip was shown in Figure 2.

3. Results and discussion

When Q-dots were endocytosed by cells, the fluorescence expressed weakly after 1 hour uptake of Q-dots under endocytosis. After the endocytosis time was extended, the Q-dots fluorescence became stronger. Figure 3 shows the fluorescence image of cells after uptake of Q-dots by endocytosis for 6h and by electroporation process. Five nm Q-dots in the cells show yellow fluorescence. The uptake rate of Q-dots using electroporation is higher than that of endocytosis for 6h. The fluorescence image, Figure 4, illustrates the localization of the (CdSe)ZnS nanoparticles after 6h endocytosis. The cells were stained using the MitoTracker 7511 (Molecular Probes, USA). The Q-dots aggregated and located near the cellular nucleus. Transmission electron microscopy was also used for better understanding of the Q-dot pathway in the cell sample during endocytosis. Figure 5 shows that the Q-dots were aggregated during the uptake pathway from cell membranes to nucleus vicinities. However, the Q-dots were dispersedly distributed in the cells after the Q-dots were delivered into cells using electroporation, as shown in Figure 3b.

4. Conclusions

Water soluble (CdSe)ZnS Q-dots were delivered into mammalian cells as nanoprobes utilizing the electroporation and endocytosis methods. Q-dots, delivered by electroporation, were dispersed in the cells with stronger fluorescence intensity compared to the aggregated Q-dots transported via endocytosis for 6h. The uptake amount of Q-dots was higher using electroporation than that of endocytosis. These nanoparticles can work as nanoprobes and provide molecule imaging for cellular physiology.

References

[1] M. Thomas, A. M. Klibanov, *PNAS,* **100**, 9138-9143 (2003).

[2] J. K. Jaiswal, H. Mattoussi, J. M. Mauro, S. M. Simon, *Nat. Biotechnol*, **21,** 47-51 (2003).

[3] Z. A. Peng and X. Peng, *J. Am. Chem. Soc*, **123**, 183-184 (2001).

[4] J. Aldana, Y. A. Wang, X, Peng, *J. Am. Chem. Soc.*, **123**, 8844-8850 (2001).

[5] Y.C. Lin, M. Li, C.S. Fan, L.W. Wu, *Sens. Act. A*, **108**, 12-19 (2003).

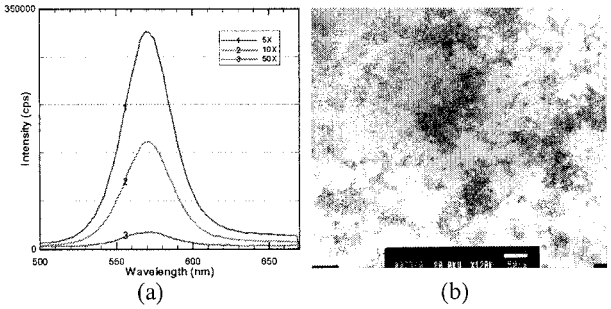

(a) (b)

Figure 1. Characteristics of (CdSe)ZnS nanoparticles, (a) fluorescence spectra showing the peak at 570nm, and (b) TEM image showing the diameter at 5nm.

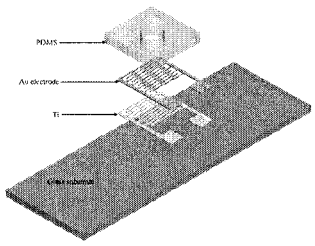

Figure 2. Schematic 3D drawing of an EP chip.

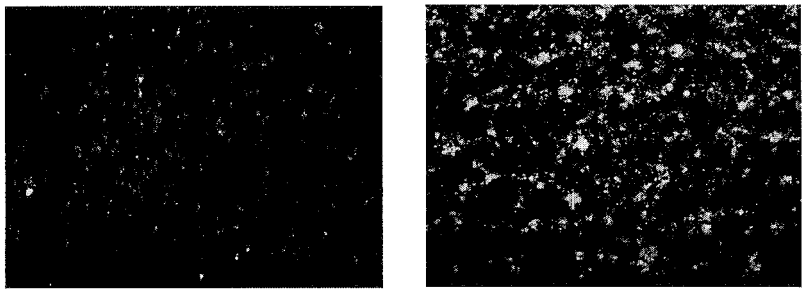

(a) (b)

Figure 3. Comparison of fluorescence images of Q-dots uptake utilizing electroporation and endocytosis, (a) endocytosis for 6 hours, and (b) electroporation.

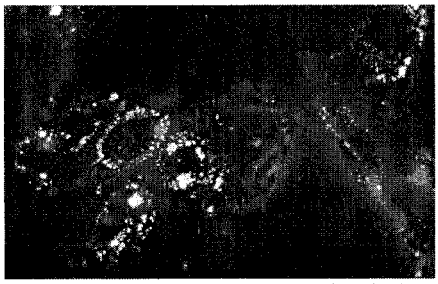

Figure 4. Fluorescence expression of (CdSe)ZnS Q-dots after 6h uptake into MC3T3E-1 cells.

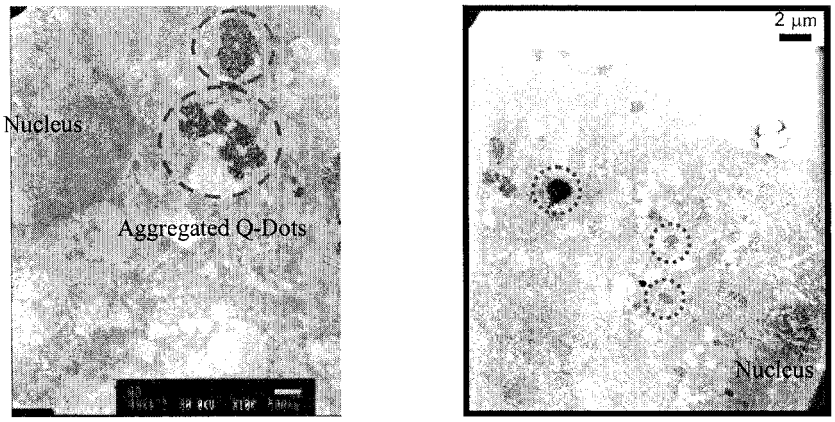

(a) (b)

Figure 5. Aggregation of (CdSe)ZnS Q-dots near the nucleus. Dashed circles show the examples of the aggregated Q-Dots.

IMMUNOASSAY CHIP USING NANOPILLARS FABRICATED BY HIGH-ASPECT-RATIO NANOPRINT TECHNOLOGY

Kosuke Kuwabara, Masahiko Ogino, Takashi Ando, and Akihiro Miyauchi
Materials Research Laboratory, Hitachi Ltd., 7-1-1 Ohmika, Hitachi, Ibaraki, 319-1292 Japan

Abstract

Sensitization of an immunoassay chip was attempted using high-aspect-ratio nanopillars. Nanopillars made of polystyrene were fabricated on the chip by high-aspect-ratio nanoprint technology. AFP (alpha-fetoprotein) was detected by a FIA (fluorescence immunoassay) protocol with nanopillar chips and the enhancement of fluorescence intensities was confirmed. The area where the nanopillar diameter was 95 nm showed fluorescence intensity 34 times stronger than the conventional flat area.

Keywords: Nanoprint; Nanoimprint; Nanopillar; Immunoassay; High-aspect-ratio.

1. Introduction

Soft lithography methods such as nanoprinting or nanoimprinting are attractive methods to achieve nano-scale patterning [1]. The nanoimprint technology is attractive for the fabrication of nano-scale structures in view of cost and mass production; fabrication of sub- 10 nm structures [2] and applications to the biochemical sensors [3] were presented previously. We have succeeded in forming high-aspect-ratio structures (nanopillars) using high-aspect-ratio nanoprint technology [4]. These structures are comparable in size to bio macromolecules. Conventional nanopillar structures have been fabricated by photolithography, and the materials are limited to Si-based materials, such as Si, SiO_2 and SiN. High-aspect-ratio nanoprint technology has made it possible to easily obtain polymer nanopillars at low cost. The application of these nanopillars to biomedical detection was presented [5]. The nanopillars were coated with FITC (fluorescein isothiocyanate) conjugated BSA (bovine serum albumin), and the surface density of the BSA was increased as the surface area increased by forming nanopillars.

Here, we attempted to apply nanopillars to FIA (fluorescence immunoassay). The ability of FIA chips to detect antigens depends on the density of antibodies on the chip. A nanopillar chip has a larger surface area than a conventional flat chip. This large surface area increases the surface density of antibodies on the chip. This high density of antibodies on nanopillars sensitizes FIA detection.

2. Experimental

Polystyrene (PS) was used as a base material for FIA chips. PS films were spin-coated onto glass substrates. The thickness of the PS films was 0.5 μm. Nano-molds were fabricated using a photolithography method. By pressing the nano-mold onto the PS film and releasing from the film, nanopillar structures were formed. The shapes of nanopillars were observed using a Hitachi S-5000 SEM.

AFP (alpha-fetoprotein) was detected by a standard FIA protocol using nanopillar chips. AFP antibodies were fixed to the nanopillar chips and an AFP solution of 30 – 10^4 pg/mL was applied to each chip. Biotinylated AFP antibodies and streptavidin-FITC were used to label the AFP captured on the chips. The fluorescence intensities of FITC (λ = 511nm) were measured by a ScanArray Express^{EM} (Perkin-Elmer Co.) microarray scanner.

3. Results

Figure 1 shows the SEM images of the nanopillars. These nanopillars were made of PS and all were fabricated on the same chip. The shape of nanopillar varied according to the size of the patterns on the nano-mold. The diameters and the heights of the nanopillars were 95 nm – 1 μm and

1 μm – 4.1 μm, respectively. Nanopillars with a diameter of 95 nm and a height of 4.1 μm had an aspect ratio of 43, as shown in Figure 1(d). This structure had a surface area 7.7 times larger than that of the flat area.

Figure 2 shows a fluorescence image of the nanopillar chip obtained by the microarray scanner after being coated with streptavidin-FITC in a FIA protocol. The area with smaller diameter nanopillars showed stronger fluorescence intensity; the intensity profile corresponded to the surface area of the chip.

The fluorescence intensities of the nanopillar chips showed a correlation with the AFP concentration as shown in Figure 3. This result was obtained for several chips by changing the applied AFP concentration. The fluorescence intensity increased as the diameter of the nanopillars decreased, that is, as the surface area of the chip increased, which is also shown in Figure 2. The area where the nanopillar diameter was 95 nm showed fluorescence intensity 34 times stronger than the flat area when the AFP concentration was 10^4 pg/ml. AFP was detected at levels of 300 pg/ml using this nanopillar chip.

4. Conclusions

Nanopillars made of PS were fabricated using high-aspect-ratio nanoprint technology. Nanopillars with a diameter of 95 nm and a height of 4.1 μm had an aspect ratio of 43. AFP was detected using a FIA protocol with nanopillar chips and the enhancement of fluorescence intensities was confirmed. The area where the nanopillar diameter was 95 nm showed fluorescence intensity 34 times stronger than the flat area.

A nanopillar chip captures more antigens as compared with a conventional flat chip when it is exposed to dilute antigens to be detected. The density of fluorescent labels on the chip also increases as the density of antigens increases. In this way stronger fluorescence is detected from the chip. This effect can be used to sensitize immunoassay chips.

Acknowledgements

The authors thank Dr. Michihiro Saito, Mr. Taku Sakazume, and Mr. Ryuji Tao of Hitachi High-Technologies Corporation for their experimental support.

References

[1] Y. Xia and G.M. Whitesides, Annu. Rev. Mater. Sci., 28, 153-184 (1998).
[2] S.Y. Chou, J. Vac Sci. Technol B 15(6), Nov/Dec (1997).
[3] M. Beck, P. Carlberg, F. Persson, M. Grakzyk, I. Maximov, T.G.I. Ling, and L. Montelius, Microelectronic Engineering, 73-74C, 837(2004).
[4] A. Miyauchi, et al., 1st Int. Conf. Nanoimprint and Nanoprint Technology 2002, P-16.
[5] K. Kuwabara, M. Ogino, S. Motowaki, and A. Miyauchi, Microelectronic Engineering, 73-74C, 752 (2004).

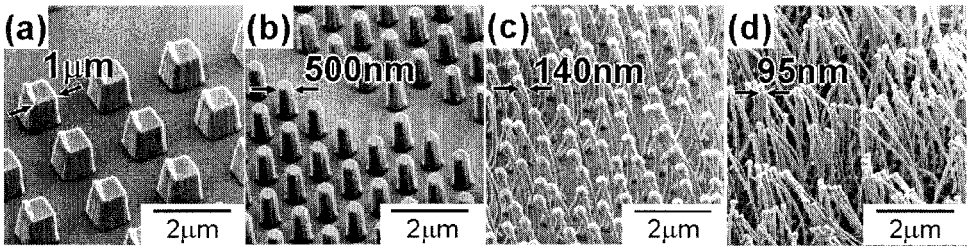

Figure 1: SEM images of PS nanopillars. Heights of the nanopillars are (a)(b) 1 μm; (c) 3.2 μm; (d) 4.1 μm.

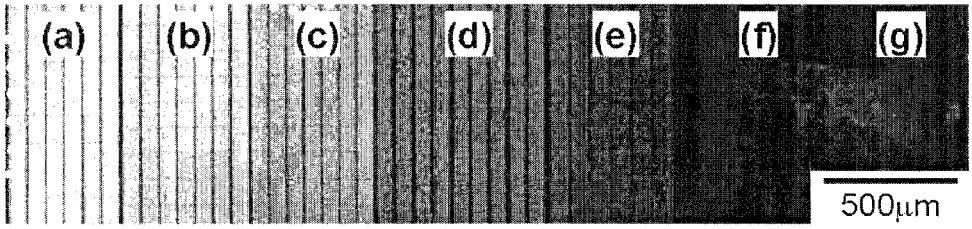

Figure 2: Fluorescence image of nanopillar chip after coating with streptavidin-FITC. Brighter areas correspond to stronger fluorescence intensity. AFP concentration is 10^4pg/ml. The diameters of fabricated nanopillars in each area are: (a) 95nm; (b) 100nm; (c) 110nm; (d) 140nm; (e) 500nm; (f) 1μm; (g) flat area.

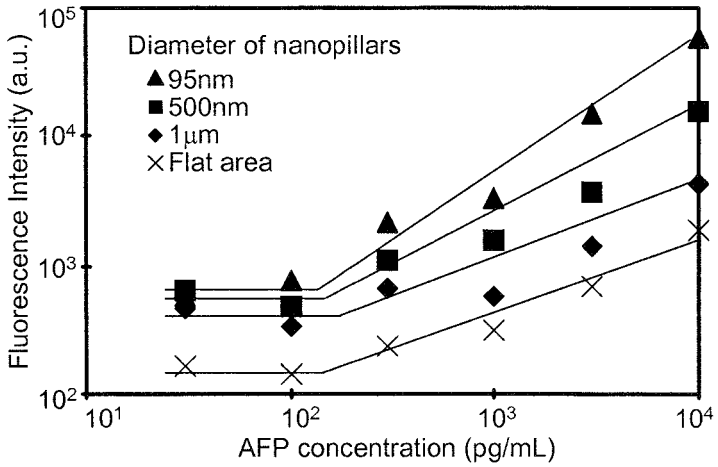

Figure 3: Calibration curve of the nanopillar chip for AFP detection.

POTENTIOMETRIC DETECTION OF ALLELE SPECIFIC OLIGONUCLEOTIDE HYBRIDIZATION USING GENETIC FIELD EFFECT TRANSISTOR

Toshiya Sakata and Yuji Miyahara
Biomaterials Center, National Institute for Materials Science, 1-1 Namiki, Tsukuba, Ibaraki 305-0044, Japan

Abstract
A genetic field effect transistor (FET) is proposed for detection of allele specific oligonucleotide hybridization, which is in principle based on charge density change at the gate insulator. Allele specific oligonucleotide hybridization and reaction between double-stranded DNA and intercalator were successfully detected with the genetic FET, because they have intrinsic charges in an aqueous solution. Moreover, our results show that control of hybridization temperature and utilization of intercalator lead to more precise single nucleotide polymorphism (SNP) analysis using the genetic FET.

Keywords: DNA chip, genetic field effect transistor, potentiometric detection, intercalator, single nucleotide polymorphism

1. Introduction

We have been investigating a new approach to realize an electrochemical detection for DNA chips. A genetic field effect transistor (FET) is proposed in the present study for improving precision, standardization and miniaturization of a DNA chip system. One of the unique feature of our method is to utilize intercalator as charged species because they have positive charges in aqueous solutions in addition to the specific adsorption with double-stranded DNA, while intercarators are often used as fluorescent dyes in the field of molecular biology [1].

Here, we show the fundamental characteristics of a genetic FET such as the direct detection of hybridization and the effect of intercalation on the potentiometric measurement. Ability to discriminate single nucleotide polymorphism (SNP) is also discussed using the genetic FET.

2. Concept of genetic FET

The diagram for direct detection of allele specific oligonucleotide hybridization is shown in **Fig. 1**. The concept of genetic FET is based on potentiometric detection of DNA molecules by the field effect. The genetic FET is immersed in a measurement solution together with a Ag/AgCl reference electrode with saturated KCl solution. Oligonucleotide probes are immobilized on the surface of the gate insulator. When complementary DNA molecules are contained in a sample solution, hybridization occurs at the surface of the gate area. Since DNA molecules are negatively charged in an aqueous solution, they electrostatically interact with electrons in Si crystal through the thin gate insulator.

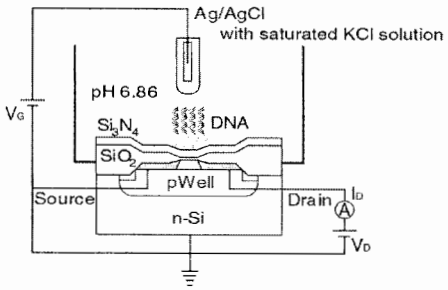

Figure 1. Schematic diagram for measurements of electrical characteristics of genetic FET.

Intercalator is ionized and positively charged in an aqueous solution, and reacts specifically with double-stranded DNA on the gate surface. Accordingly, an undesirable background noise such as non-specific adsorption of single-stranded DNA can be eliminated and more precise and reliable detection of DNA molecules would be expected by the use of both genetic FET and intercalator.

3. Experimental

The photograph of the fabricated FET chip is shown in **Fig. 2**. The FETs are n channel depletion type with Si_3N_4/SiO_2 as gate insulator. The electrical characteristic of FET such as the gate voltage (V_G) - drain current (I_D) characteristic was measured using a semiconductor parameter analyzer.

Synthesized oligonucleotide probes were used for allele specific hybridization and 5'-end of the probe was modified with an amino group for attachment to the Si_3N_4 surface. The oligonucleotide probes were immobilized on the amino-silanized Si_3N_4 surface using glutaraldehyde as a bifunctional cross-linking agent. For hybridization, the FET chips with immobilized oligonucleotide probes were kept in the sample solutions involving target oligonucleotides (100μM) for 12 h at various controlled temperatures: T_{m1} (60°) for hybridization with normal target, and T_{m2} (57°) for hybridization with mutant target [2]. After hybridization experiments, the FET chips were soaked in an intercalater solution at room temperature for 12h.

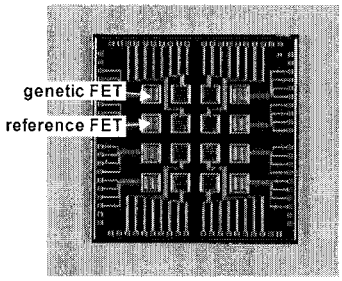

Figure 2. Photograph of the fabricated genetic FET chip.

The factor VII gene, which was related to blood coagulation factor, was used for the genotyping experiment. Allele-specific oligonucleotide probes for the wild type and the mutant type genes at the locus of R353Q were designed [2].

4. Results and Discussion

A specific binding of charged biomolecules at the gate surface can be detected as a shift of the threshold voltage V_T, which can be determined in the V_G - I_D characteristics of the genetic FET.

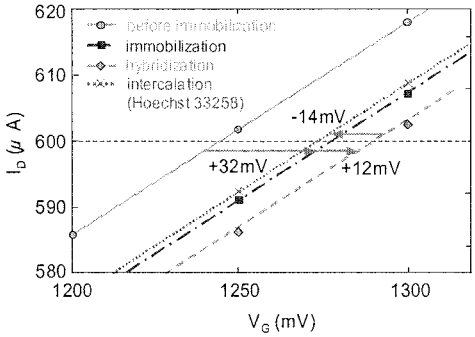

Figure 3. Electrical signals of molecular recognition events on the genetic FET.

The V_G - I_D characteristics of the genetic FET were found to shift after specific binding of biomolecules at the surface of the gate insulator. Based on this principle, allele specific oligonucleotide hybridization and reaction between double-stranded DNA and intercalator were successfully detected with genetic FETs. The V_T of the genetic FET shifted in the positive direction for oligonucleotide hybridization and in the negative direction for intercalator, because of intrinsic charges of DNA and intercalator (**Fig. 3**).

Ability to discriminate SNP was also examined using the genetic FET. We have prepared two types of the genetic FETs to detect single base change in the target DNA. We used the R353Q

locus of factor VII gene [2] as a model sample. Normal (wild type) oligonucleotide probes were immobilized on the gate surface of one of the genetic FETs (N-type genetic FET), while mutant oligonucleotide probes were immobilized on the gate surface of the other genetic FETs (M-type genetic FET). The N-type and M-type genetic FETs were hybridized with a normal sample and a mutant sample, respectively. One-base change of the target DNA could be detected with the N-type genetic FET and the M-type genetic FET. Our preliminary results show that control of hybridization temperature and utilization of intercalator lead to the significant improvement of the signal to noise ratio for SNP analysis using the genetic FET (**Fig. 4**). The genetic FET platform is suitable for a simple, accurate and inexpensive system for SNP typing in clinical diagnostics.

5. Conclusions

A new method to detect DNA molecules has been proposed using a field effect transistor (FET) and basic principle of the genetic FET has been demonstrated. The charge density change due to hybridization and intercalation on the gate insulator could be successfully detected by using genetic FET. Furthermore, single nucleotide polymorphism (SNP) could be successfully detected by using genetic FET in combination with intercalator, and by controlling hybridization temperatures.

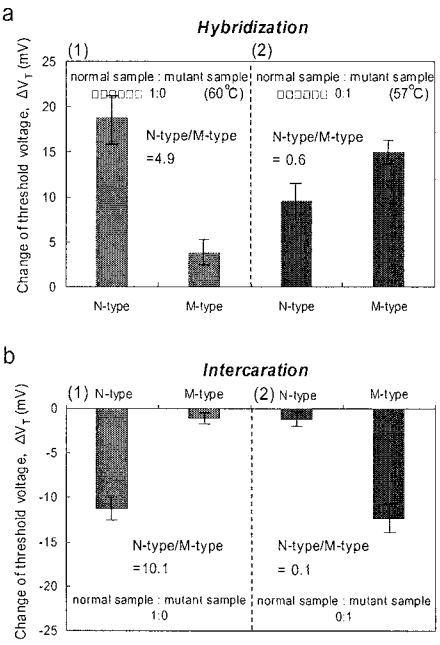

Figure 4. Discrimination of SNP using genetic FET. (a) SNP detection by allele specific oligonucleotide hybridization at controlled temperatures. (b) SNP detection using genetic FETs in combination with intercalator. Signal to noise ratio to distinguish one-base change was drastically improved when Hoechst 33258 was used after hybridization.

Acknowledgements

We would like to thank Drs. Y. Horiike, J. Tanaka, H. Otsuka, S. Maruyama and J.P. Hulme of National Institute for Materials Science, Mrs. Y. Nakajima and S. Matsumoto of Ryokusei M.E.S. Ltd., Mr. M. Kamahori of Hitachi Ltd., and Dr. P. Fortina of Thomas Jefferson University for their help and useful discussions.

References

[1] D. L. Boger et al., "A simple, high-resolution method for establishing DNA binding affinity and sequence selectivity", J. Am. Chem. Soc. 123, pp. 5878-5891, 2001.

[2] T. Kajiyama et al., "Genotyping on a thermal gradient DNA chip", Genome Res. 13, pp. 467-475, 2003.

DIRECT TRANSDUCTION OF PRIMER EXTENSION INTO ELECTRICAL SIGNAL USING GENETIC FIELD EFFECT TRANSISTOR

Yuji Miyahara and Toshiya Sakata
Biomaterials Center, National Institute for Materials Science, 1-1 Namiki, Tsukuba, Ibaraki 305-0044, Japan

Abstract
We describe a novel method for single nucleotide polymorphism (SNP) analysis based on the genetic field effect transistor (FET). Using the genetic FET, extension reaction of allele specific oligonucleotide on the gate insulator could be directly transduced into electrical signal, which was caused by the increase of negative charges of oligonucleotides. Moreover, the SNP genotyping could be achieved using the genetic FETs in combination with allele specific extension reaction.

Keywords: DNA chip, genetic field effect transistor, potentiometric detection, extension reaction, single nucleotide polymorphism

1. Introduction

We have been investigating a new approach to detect molecular recognition events by means of electrostatic interaction between charged biomolecules and electrons in silicon, although a number of fluorescent detection methods are widely used for single nucleotide polymorphism (SNP) genotyping. The novel concept of a genetic field effect transistor (FET) is proposed for improving precision, standardization and miniaturization of a DNA chip system, which is based on potentiometric measurement by the field effect. The potentiometric detection method is based on the direct transduction of surface density change of charged biomolecules into electrical signal by the field effect and is effective for detecting charged species such as DNA molecules.

In this study, we report the direct transduction of extension reaction of allele specific oligonucleotide into electrical signal using genetic FET. We also propose to use the genetic FET in combination with primer extension for simple and precise SNP genotyping.

2. Principle of primer extension detection using genetic FET

The concept of genetic FET is based on potentiometric detection of charge density change at the gate surface which is induced by specific binding of DNA molecules. We have used n-channel depletion mode FET with a double layer of Si_3N_4/SiO_2 as the gate insulator on which oligonucleotide probes are immobilized in order to detect hybridization and subsequent extension events. One of the advantages of genetic FET is to

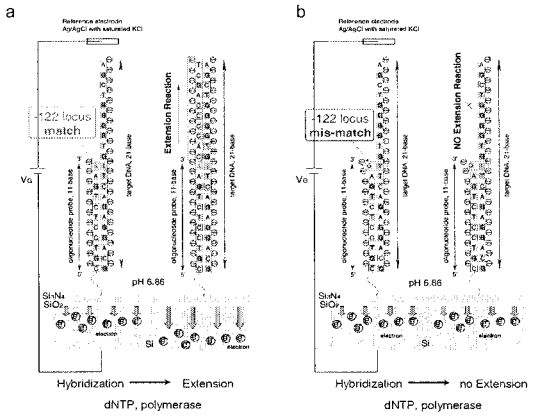

Figure 1. Scheme for potentiometric detection of allele specific extension using genetic FET.

transduce charge density change of DNA molecules directly into electrical signals by the field effect without any labeling for target DNA molecules. When the allele specific oligonucleotide probes are immobilized on the Si_3N_4 gate insulator, a primer extension can be controlled by a match or mismatch at the 3'-end of the probe. When the 3'-end of the oligonucleotide probe is matched to the target DNA, primer extension reaction occurs and oligonucleotide is synthesized and extended. Since oligonucleotide is negatively charged in an aqueous solution, increase of the negative charges at the gate surface can be detected with the genetic FETs (**Fig. 1a**). On the other hand, extension reaction does not occur and the charges at the gate surface dose not change, when the 3'-end of the oligonucleotide probe is not matched to the target DNA (**Fig. 1b**). Thus, the allele specific extension event on genetic FET will allow detection of SNP genotyping.

3. Experimental

The amino-modified oligonucleotides probes were immobilized on the amino-silanized Si_3N_4 surface using glutaraldehyde as a bifunctional cross-linking agent. For hybridization, the FET chips with immobilized oligonucleotide probes were kept in the sample solutions involving target oligonucleotides (100 μM) for 12 h at room temperature.

A thermostable DNA polymerase was used for the allele-specific extension reaction. The reaction mixture contained *Taq* DNA polymerase and dNTP. After hybridization with target oligonucleotides, the genetic FET was immersed in the reaction mixture and incubated at 72. for 10 min for primer extension reaction.

The factor VII gene, which was related to blood coagulation factor, was used for the genotyping experiment. The base sequences of the oligonucleotide probes and targets for the normal type (wild type) and the mutant type alleles at the locus of -122 were designed [1]. The SNP site was located at the 3'-end of the synthesized oligonucleotide probe. The length of target DNA was varied from 21 to 41 bases.

The fabricated FETs are n channel depletion type with Si_3N_4/SiO_2 as gate insulator. The electrical characteristic of the FET such as the gate voltage (V_G)-drain current (I_D) characteristic was measured using a semiconductor parameter analyzer.

4. Results and discussion

When thermostable DNA polymerase and dNTPs were introduced into the gate surface after hybridization with the complementally target DNA, the interface potential at the gate surface was monitored. The time course of the threshold voltage (V_T) change during primer extension reaction is shown in **Fig. 2.** The V_T shift during extension reaction increased drastically up to 10mV. This positive change in the V_T of the n-channel genetic FET is due to negative charges of polynucleotide extended by primer extension reaction. Thus, we could

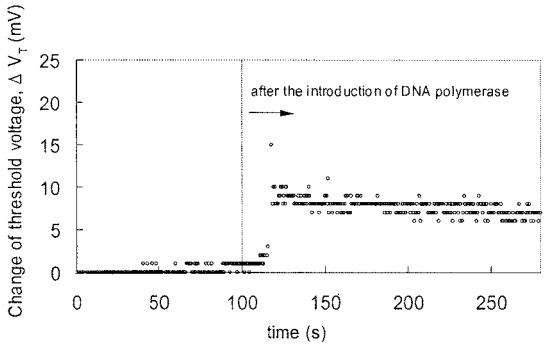

Figure 2. Time course of threshold voltage V_T shift during primer extension reaction. DNA polymerase was introduced into genetic FET at 100 s.

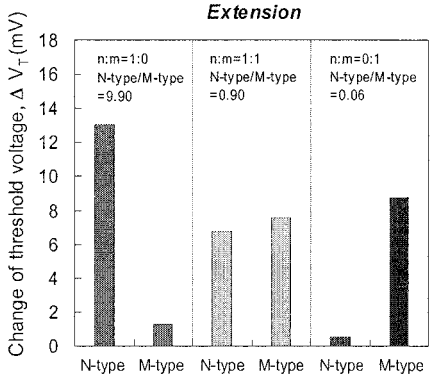

Figure 3. Genotyping analysis using genetic FET. The N-type and M-type genetic FETs were hybridized with a n/n homozygote sample, a n/m heterozygote sample and a m/m homozygote sample, respectively.

demonstrate that the primer extension event on the gate surface was transduced directly into the electrical signal by the use of the genetic FET.

We used the -122 locus of factor VII gene [1] as a model sample. We have prepared two types of the genetic FETs for the simple SNP typing analysis. Normal (wild type) oligonucleotide probes were immobilized on the gate surface of one of the genetic FETs (N-type genetic FET), while mutant oligonucleotide probes were immobilized on the gate surface of the other genetic FETs (M-type genetic FET). The N-type and M-type genetic FETs were set into a buffer solution. The N-type genetic FET and M-type genetic FET were hybridized with a normal/normal (n/n) homozygote sample, a normal/mutant (n/m) heterozygote sample and a mutant/mutant (m/m) homozygote sample, respectively. When the DNA polymerase-assisted extension reaction occurred at the gate surface after hybridization, the ratios of the V_T shift of the N-type genetic FET and M-type genetic FET were 9.90, 0.90, 0.06 for a n/n homozygote sample, a n/m heterozygote sample and a m/m homozygote sample, respectively (**Fig. 3**). We found that the primer extension reaction after hybridization could be transduced directly into electrical signal using genetic FETs and was effective to distinguish genotypes of the target DNA.

5. Conclusions

The allele specific primer extension reaction on solid-state device could be directly translated into electrical signal using the genetic FETs and that three SNP types could be distinguished without any labeling for target DNA molecules using the genetic FETs.

Acknowledgements

We would like to thank Drs. Y. Horiike, J. Tanaka, H. Otsuka, S. Maruyama and J.P. Hulme of National Institute for Materials Science, Mrs. Y. Nakajima and S. Matsumoto of Ryokusei M.E.S. Ltd., Mr. M. Kamahori of Hitachi Ltd., and Dr. P. Fortina of Thomas Jefferson University for their help and useful discussions.

References

[1] T. Kajiyama et al., "Genotyping on a thermal gradient DNA chip", Genome Res. 13, pp. 467-475, 2003.

FORMATION AND TRANSIENT PROCESS OF ELECTRIC DOUBLE LAYER BETWEEN ELECTROLYTE-GLASS INTERFACE MEASURED BY EVANESCENT WAVE LIGHT ILLUMINATION

Yutaka KAZOE* **and Yohei SATO***

**Dept. of System Design Engineering, Faculty of Science and Technology, Keio University*
Hiyoshi 3-14-1, Kohoku-ku, Yokohama, 223-8522, JAPAN

Abstract

Formation and transient process of electric double layer (EDL) in the vicinity of a silica glass surface of microchannel has been investigated by a novel nanoscale optical measurement technique using large-area evanescent wave light illumination and fluorescent dye. The fluorescent dye near the glass surface was excited by the evanescent wave, which was generated at an electrolyte-glass interface by total internal reflection of a laser beam with the characteristic penetration depth of 88 nm. As the ion concentration from fluorescent dye in the vicinity of the glass surface is dependent on the EDL thickness, calibration curves depicting the relationship between the fluorescent intensity and the EDL thickness was prepared to obtain the spatial and temporal distribution of EDL.

Keywords: nanoscale, electric double layer, evanescent, optical measurement, fluorescence

1. Introduction

To achive the accurate control of electroosmotic flow (EOF) in microchannel, measurements of the spatial and temporal formation of electric double layer (EDL) is strongly required. However, it is impossible to measure the EDL structure using a far-field optical system, because the EDL thickness of nano meter is less than the wavelength of a conventional laser system. In the present study, a novel nanoscale fluorescent measurement technique using large-area evanescent wave light illumination was established to investigate the spatial distribution of EDL.

2. Experimental Setup

The measurement system was comprised of an inverted microscope (Nikon Corp., TE2000U), a continuous Nd:YAG laser (532 nm, 2 W), and a cooled CCD camera (656 × 494 pixel, 12 bit), as illustrated in Figure 1 [1]. The laser beam was directed into a prism through optics. Fluorescence from the dye was collected through an objective lens (×10, NA = 0.5) and the measurement area was 652 μm × 489 μm. The frame interval was 37 ms. To reduce pixel error, an average per 5 × 5 pixels was performed and resulted in a spatial resolution of 5 μm × 5 μm.

Figure 2 shows a schematic of T-shaped microchannel comprising of a ∅50 mm PDMS chip and a silica cover glass of 1 mm thickness. A schematic of the evanescent wave light illumination is shown in Figure 3. The laser beam was introduced into the silica cover glass at an incident angle of 76.5°, and generated the evanescent wave by total internal reflection of laser beam at an electrolyte-glass interface with the characteristic penetration depth of 88 nm [2]. The fluorescent dye only in the vicinity of the glass surface is excited by the evanescent wave.

The Alexa Fluor 546 (Molecular Probes, Inc.) was selected as the fluorescent dye, which becomes a negative ion in buffer solution at pH 7. The concentration of negative ions from Alexa 546 in the vicinity of the glass surface is dependent on the structure of EDL. The peak value of absorption and emission wavelength are 554 nm and 571 nm, respectively. A working fluid was composed of a 5 mM HEPES buffer at pH = 7.2, in which a 10 μM Alexa Fluor 546 was dissolved.

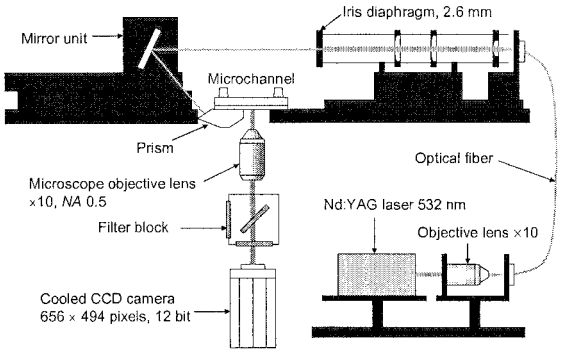

Figure 1. Schematic of the measurement system.

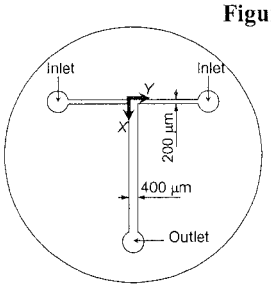

Figure 2. Top view of the T-shaped microchannel.

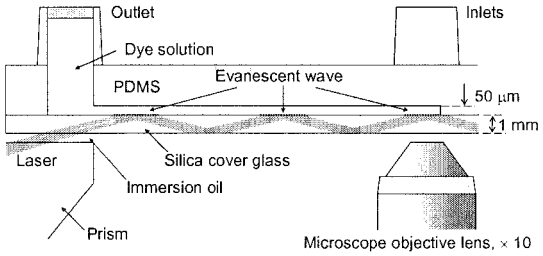

Figure 3. Schematic of evanescent wave light illumination. The size of elliptical illumination area is 6.85 × 2.6 mm.

KCl with the concentration range 0.1–7 mM was added to the fluid to change the positive ion concentration.

4. Result and Discussion

Prior to a direct measurement of the spatial-distribution of EDL thickness, calibration between the fluorescent intensity and the positive ion concentration of KCl was perfomed. Figure 4 shows the calibration curves at five locations, which was normalized by using the reference values at 0.5 mM. Because the EDL thickness, i.e., Debye length, λ_D, is calculated by using the bulk positive ion concentration, c_0, defined as

$$\lambda_D = \left(\varepsilon RT / 2F^2 z^2 c_0\right)^{1/2} , \tag{1}$$

the relationship between the fluorescent intensity and the Debye length was obtained as shown in Figure 5.

The spatial distribution of Debye length in pressure-driven flow was measured by the fluorescence imaging technique [3]. A 0.1 mM HEPES buffer was injected into the left-hand side inlet, while a 7 mM HEPES buffer was injected into the right-hand side inlet. Both streams were driven at the equal flow rate. The two-dimensional distribution of Debye length is exhibited in Figure 6(a), which was obtained by using calibration curves in Figure 5. It is obvious from Figure 6 that the spatial structure of EDL is dependent on the slightly-steep concentration gradient of K^+ by molecular diffusion near the glass surface, because pressure-driven flow, which has a parabolic flow pattern, is nearly zero in the vicinity of the surface. On an application of 300 V from the horizontal inlets to the vertical outlet through platinum electrodes submerged in reservoirs, both

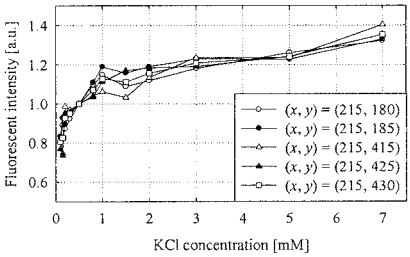

Figure 4. Calibration curves obtained after correction using a reference value at 0.5 mM. Calibration locations indicate the pixel coordinate of CCD camera.

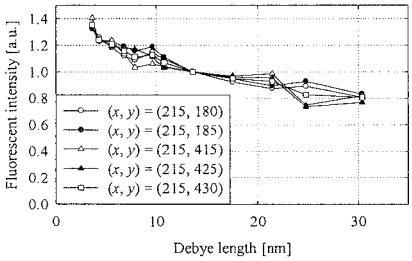

Figure 5. Calibration curve between the fluorescent intensity and the Debye length. Calibration locations indicate the pixel coordinate of CCD camera.

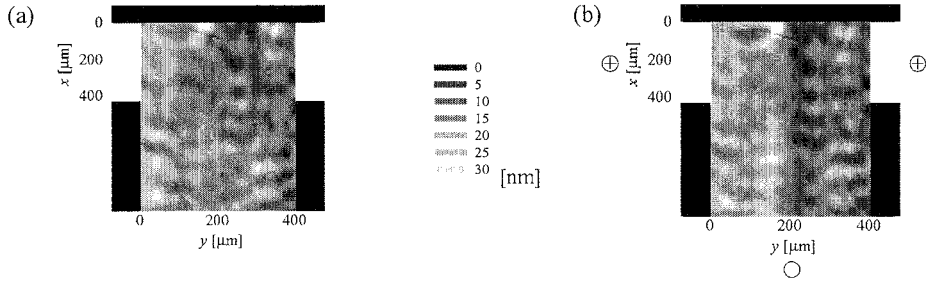

Figure 6. Two-dimensional distribution of Debye length in (a) pressure-driven flow and (b) electroosmotic flow on an application of 300 V.

streams were driven by pressure-driven flow and EOF. The gradient of Debye length in the y-direction gradually became steep as shown in Figure 6(b). The structure of EDL is affected by the steep concentration gradient of K^+ near the glass surface generated from a plug flow pattern of EOF. Moreover, the present technique is available for the measurement of the spatial distribution of the zeta potential given by Scales *et al.* (1992) [4].

5. Conclusions

The spatial distribution of EDL thickness was measured by the nanoscale measurement system using the evanescent wave light illumination. The spatial and temporal formation of EDL is dependent on the molecular diffusion of K^+ in a buffer solution in the vicinity of the wall surface.

Acknowledgements

The authors would like to thank Professor K. Hishida at Keio University for his technical assistance. This work was subsidized by the Grant-in-Aid for Scientific Research of Ministry of Education, Culture, Sports, Science and Technology (No. 1470230 and 15206024).

References

[1] Y. Kazoe and Y. Sato, *12th International Symposium of Applications of Laser Techniques to Fluid Mechanics*, CD-ROM (2004).

[2] S. G. Flicker, J. L. Tipa and S. G. Bike, J. Colloid & Interface Sci., **158**, 317-325 (1993).

[3] Y. Sato, G. Irisawa, M. Ishizuka, K. Hishida and M. Maeda, *Meas. Sci. Technol.*, **14**, 114-121 (2003).

[4] P. J. Scales, F. Griser and T. W. Healy, *Langmuir*, **8**, 965-974 (1992).

FABRICATION OF NANOCHANNELS USING PHOTOLITHOGRAPY AND PARTIAL ETCHING OF SACRIFICIAL LAYER

Anpan Han, Giampietro Mondin, Nicole G. Hegelbach, Nicolaas F. de Rooij and Urs Staufer
Institute of Microtechnology, University of Neuchâtel, Rue Jaquet-Droz 1 / C.P. 3, CH-2007 Neuchâtel, Switzerland.

Abstract

We report a new method to fabricate channels about 50 nm deep, between 200 nm and 2 μm wide, and up to 8 cm long using conventional micromachining technologies on silicon substrates. Injection crosses with volumes below 50 attoliters (10^{-18} l) and channel arrays could be fabricated by partially etching sacrificial layer and sealing the under-etched structures using silicon dioxide deposited by chemical vapor deposition. The total process required four thin film depositions and two photolithography steps. Channels up to 5 cm long could be filled with aqueous solutions. Fluorescein dissolved in Tris buffer had high adsorption affinity towards the channel walls. These channels could be used as containers for studying fluorescently labeled molecules.

Keywords: nanochannels, sacrificial layer, lithography, surface machining, fluidics.

1. Introduction

Nanofluidic devices provide a novel tool for studying single molecules and bionanotechnology [1, 2]. For example, nanometer-sized entropic traps were used to separate long, genomic DNA [1, 3]. Unfortunately, nanochannel fabrication techniques such as focused ion-beam milling, electron-beam lithography, and nanoimprinting lithography have its limitations. To overcome some of the inconveniences several nanofabrication techniques, which do not require nanolithography, have been reported. Most techniques yield channels with depth in the nanometer range, while the width is in the micrometer range determined by the photolithography resolution. Yet, many applications require 2D confined channels with both width and depth in the nanometer range, e.g. to stretch DNA, since the persistence length of DNA is about 50 nm. Recently, microfabricated 2D confined nanochannels with both depth and width in the nanometer range have been reported [4-6]. For example, Tas et al. presented a technique based on selective etching of encapsulated sacrificial nanowires formed on the sidewall of a step. Channels 0.64 mm long required 15 h of etching [4]. To reduce the etching time and increase the channel length Czaplewski et al. used electrospining of heat decomposable polymer to form sacrificial nanowires and spin-on glass for encapsulation [6]. Lee et al. developed a CMOS compatible process based on selective chemical-mechanical polishing and thermal oxidation [5]. Channels 25 nm wide 100 nm deep and 10 mm long were fabricated on silicon substrates. Unfortunately, the authors did not report any filling studies. We developed a new method to fabricate 2D confined nanochannels using standard photolithography and thin film processes. We were also able to fill these channels using aqueous solutions.

2. Experimental

Fabrication of nanochannels: The starting substrate was a 525-μm-thick, 100-mm-diameter silicon (Si) wafer. A sandwich of silicon nitride (100 – 300 nm) deposited by low-pressure chemical vapor deposition (LPCVD Si_xN_y) and silicon dioxide deposited by chemical vapor deposition (CVD SiO_2) was put down on to a clean silicon wafer (Fig. 1a). The CVD SiO_2 was deposited at 400°C under atmospheric pressure. The fabrication required two photolithography processes; we used a layer of 1.8-μm-thick positive photoresist (AZ1518, Clariant GmbH, Wiesbaden, Germany) as mask for the reactive ion etching process (RIE), where the patterns from a chromium mask were transferred into the silicon wafer. Etching was stopped on the second layer of LPCVD Si_xN_y (Fig.

1b). The sacrificial CVD SiO_2 layer was partially under-etched by (1:7) buffered HF (BHF) followed by rinsing in DI water (Fig. 1c). The remaining photoresist was removed by oxygen plasma. To seal the channels, a fresh layer of CVD SiO_2 (400 nm) was deposited (Fig. 1d). A second photolithography and RIE process was used to pattern the access openings to the nanochannels (Fig. 1e). Polydimethylsiloxane (PDMS) o-rings were sealed reversibly to the access openings to serve as reservoirs (Fig. 1f).

Fluorescence microscopy: Channels were filled using 2 mM fluorescein dissolved in 10 mM Tris buffer, pH 7.2. The channels were imaged with a cooled CCD camera (CF 8/4 DXC from Kappa, Gleichen, Germany) mounted on an inverted fluorescence microscope with integrated filter-sets (Axiovert S100 from Zeiss).

3. Results and discussion

We could fabricate channels about 50 nm deep, between 200 nm and 2 μm wide (Fig. 2). Our method had three advantages; first, by under-etching the sacrificial layer along the side, which avoided the slow removal of sacrificial layer from the access openings, we could fabricate channels up to 8 cm. Secondly, we could accurately control the depth of the channels, since the sacrificial layer was deposited by well-established CVD process, which gave good control of the film thickness at the nanometer range. Finally, we were able to incorporate crosses into channel systems, which could be used for e.g. injections (Fig. 4). To our knowledge no crosses have been reported in nanochannel fabrication techniques without the use of nanolithography, since these techniques are usually limited in channel layout [4-6]. We used LPCVD Si_xN_y as the top and bottom layer, and CVD SiO_2, as the sacrificial layer. Using RIE, arrays of groves and overlapping squares were etched such that BHF could access and remove the CVD SiO_2. To seal the channels an another thin film of CVD SiO_2 was deposited (SiO_2) [5], however, we do not know to which extend a very thin film of CVD SiO_2 also entered the channels.

Arrays of channels, and crosses could be spontaneously filled with water by capillary forces. However, there was a slight difference in the filling rate among different channels (Fig 3) and occasionally a few channels were not filled at all. The extreme high surface to volume ratio in nanochannels caused prominent adsorption effects. Tris buffered fluorescein had high adsorption affinity towards the walls. The fluorescence signal grew with time; the brighter lines in Fig. 3 were filled earlier compared to the less bright ones. The excitation light and the emission fluorescence passed through a Si_xN_y layer. Si_xN_y is less transparent in the UV range; however, it has low adsorption and negligible autofluorescence in the visible and near infrared. Hence, these nanochannels were suitable for most experiments using fluorescent dyes. In addition, the surface machined nanochannels could also be observed using microscope objectives with low working distance, since they are situated about 1 μm below the wafer surface. Finally, these channels could also find applications in high throughput drug screening and genomic analysis.

Acknowledgements

The authors gratefully acknowledge the staff at IMT for their technical support and T. Hug for discussions. We also acknowledge the Danish Research Agency, Ministry of Science, Technology and Innovation for financial support.

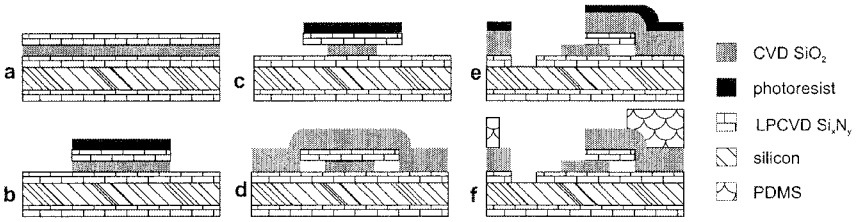

Figure 1. Fabrication process

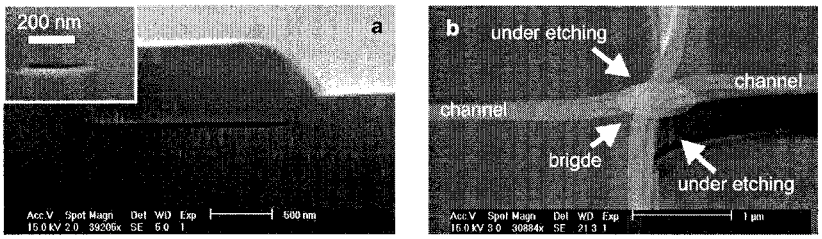

Figure 2. Scanning electron micrograph of channel and cross. (a) Channels 1.5 μm and 200 nm wide (figure inset). (b) Picture of a cross taken before encapsulation using CVD SiO_2.

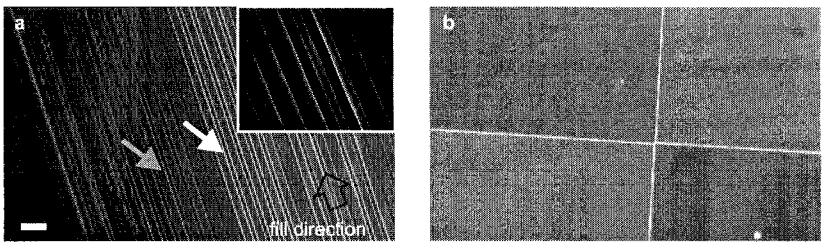

Figure 3. (a) 2 mM fluorescein in parallel channels. The thin bright lines are channels about 2 μm wide and 50 nm deep. The small arrows show channels after different filling times. Scale bar: 40 μm. Figure inset: 200 nm wide channels filled with fluorescein. (b) A cross filled with fluorescein.

References

[1] N. Kaji, Y. Tezuka, Y. Takamura, M. Ueda, T. Nishimoto, H. Nakanishi, Y. Horiike and Y. Baba, *Anal. Chem.*, **76**, 15-22 (2004).

[2] M.J. Levene, J. Korlach, S.W. Turner, M. Foquet, H.G. Craighead and W.W. Webb, *Science*, **299**, 682-686 (2003).

[3] J. Han and H.G. Craighead, *Science*, **288**, 1026-1029 (2000).

[4] N.R. Tas, J.W. Berenschot, P. Mela, H.V. Jansen, M. Elwenspoek and A. van den Berg, *Nano Letters,* **2**, 1031-1032 (2002)

[5] C. Lee, E.H. Yang, N.V. Myung and T. George, *Nano Letters,* **3**, 1339-1340 (2003).

[6] D.A. Czaplewski, J. Kameoka, R. Mathers, G.W. Coates and H.G. Craighead, *Applied Physics Letters,* **83**, 4836-4838 (2003).

ION TRANSPORT THROUGH NANOSLITS INVESTIGATED BY IMPEDANCE SPECTROSCOPY

Reto B. Schoch[1], Stefan Metz[2], Philippe Renaud[1]
[1]*Microsystems Laboratory, STI – LMIS, EPFL, CH-1015 Lausanne, Switzerland*
[2]*DYCONEX AG, Advanced Circuit Technology, CH-8303 Bassersdorf, Switzerland*

Abstract

We present a description of ion transport through geometrically defined nanoslits. The description was obtained through impedance spectroscopy measurements of electrolytes with different physico-chemical parameters. The number of 50 nm high nanoslits present in each chip used for measurements could be discriminated as well as the thickness or overlapping of the electrical double layer. The zeta potential could be changed both with the pH of the electrolyte and with an external voltage to define the nanoslit conductance.

Keywords: nanoslit, ion transport, electrical double layer, zeta potential

1. Introduction

To explore molecular dynamics at the single molecule level, ionic conditions and ion transport in nanopores have to be understood. We therefore fabricated inorganic nanoslits to study ion transport. In nanometer characteristic dimensions fluid flow is different from microfluidics, because the length scales, which describe important physico-chemical phenomena, are approximately equal to the dimensions in which they occur.

2. Device fabrication

The fluid channels were fabricated in a Pyrex-Pyrex field assisted bonding process with an intermediate layer of amorphous silicon (aSi). The height of the nanoslits was defined by the 50 nm thickness of the aSi layer (Figure 1). This technology has the advantage that nanoapertures with uniform Pyrex boundaries were produced ($height_{aSi}$ « $width_{nanoslit}$). Two microfluidic channels were bulk micromachined onto one substrate to access the nanopores. The design of the microchannels was chosen such that the nanoslits were continuously supplied with fresh liquid form either side. Electrodes were sputtered in the microchannels for the characterization of the nanoslits. Different chip configurations were manufactured, with 1, 5 and 10 nanoapertures joining the microchannels.

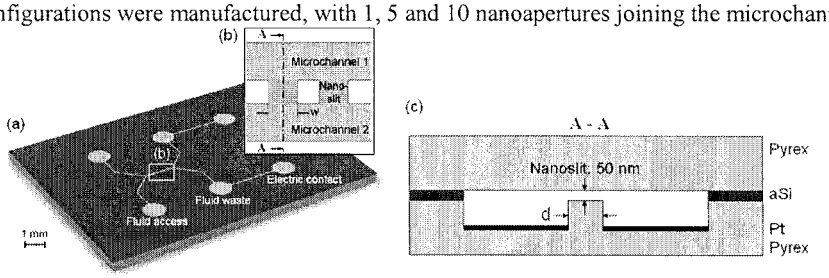

Figure 1. a) Configuration of the two microchannels and the nanoslits. b) The microchannels were joined by 1, 5 or 10 nanopores with a length d of 2 μm and a width w of 3 μm (top view, not to scale). c) A cross-section of the device shows the height of the nanoslit, defined by the thickness of aSi.

3. Results and discussion

The impedance spectroscopy measurement in the complex impedance plane of a 0.1M KCl solution through 5 nanoslits is shown in Figure 2. The resistance of the liquid in the nanopore corresponds to the extrapolation of a semi-circle to the real axis. The electrical equivalent circuit

fits the measurements precisely (error < 3 %). For the fitting the following program was used: ZView 2.5b (1990-2002 Scribner Associates Inc.) [1]. At high frequency (ω) the stray capacitance is dominant whereas at low ω the double layer influences the measurements.

The number of nanoslits between the microchannels could be discriminated (Figure 3). With an increasing number of nanopores the conductance was rising. By changing the concentration of the electrolyte, at a Debye length between 10 nm and 30 nm a conductance plateau was observed due to the overlapping of the electrical double layers (EDL). In this regime the height of the nanoslit is smaller than twice the Debye length which results in a unipolar solution of counterions in the nanometer-sized aperture [2]. The conductance of the theoretical curves in Figure 3 was calculated as $G = G_{surface} + (A\ \sigma)/\ d$; where A is the cross-section of the nanoslit(s); σ the conductivity of the solution; d the length of the nanoslit(s); and $G_{surface}$ the surface conductance which corresponds to an assumed surface charge of 1.33×10^{-2} C/m^2.

Another physico-chemical parameter which has been investigated was the pH of the solution. The zeta potential of the Pyrex channel walls could be changed with pH (Figure 4). It was observed that at high values of the pH, the conductance in the nanoslit was considerably increased. As the hydrogen ion concentration increases, conductance decreases due to reduced number of surface charges from the silanol ionization [3].

The zeta potential could also be changed by applying an external voltage V(ext) [4] at the bottom of the Pyrex wafer which contained the microchannels (Figure 5). The measurements have to be analyzed in two different regimes: with or without EDL overlap. At Debye lengths of several µm to about 25 nm an overlap could be observed. The glass surface is negatively charged. If a positive potential was applied at the electrode, the negative surface charge density at the bottom of the nanoslits is increased. Consequently, the negative co-ions are neutralized by positive counterions, which gave rise to a higher nanoslit conductance (Figure 5a). If the electrode potential was negative, the surface charge density decreases, resulting in a lower conductance in the nanopores (Figure 5b). When the Debye length was in the range of 2 nm to 10 nm there was no EDL overlap, the diffusive layer thickness has to be considered. According to the Gouy-Chapman theory, the number of ions at a certain distance from the surface is bigger at high surface potential. The diffusive layer thickness is therefore increased. Thus, the cross-section of the nanoslits got smaller, resulting in higher impedance and diminished conductance (Figure 5a). This is due to the difference in conductivities in the EDL and in the bulk [5]. When the surface charge density decreases, the diffusive layer thickness was thinner, giving rise to a higher nanopore conductance due to the increased nanoslit cross-section (Figure 5b). At Debye lengths of 1 nm or smaller, the nanoslit conductance was constant because the EDL was so thin that changes in cross-sections couldn't be detected.

Hence, AC impedance spectroscopy allowed us detecting the overlap of electrical double layers as predicted by the theory. The size or number of nanoslits present in the microfluidic device we used could be deduced from these measurements. Furthermore, the zeta potential could be changed both with pH and with an external voltage to define the nanoslit conductance.

References

[1] J. R. Macdonald, *Impedance spectroscopy: emphasizing solid materials and systems*. New York: Wiley, 1987.

[2] H. Daiguji, P. Yang, and A. Majumdar, *Nano Letters*, **4**(1), 137-142, (2003)

[3] M. A. Hayes, I. Kheterpal, and A. G. Ewing, *Analytical Chemistry*, **65**, 27-31, (1993)

[4] R. B. M. Schasfoort, S. Schlautmann, J. Hendrikse, and A. van den Berg, *Science*, **286**, 942-945, (1999)

[5] J. Lyklema, S. Rovillard, and J. De Coninck, *Langmuir*, **14**(20), 5659-5663, (1998)

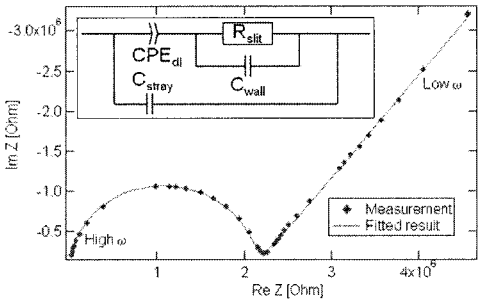

Figure 2. Complex impedance plot of 0.1M KCl solution through 5 nanoslits. A nanoslit resistance of 2.22 x 10^6 Ω was obtained. The inset shows the equivalent circuit which consists of: R_{slit} is resistance of the liquid in the nanoslit; CPE_{dl} the constant phase element for EDL on the electrodes; C_{wall} the capacitance of the Pyrex wall between the parallel microchannels; and C_{stray} the stray capacitance. The measurements were performed with an HP 4284A precision LCR meter in the frequency range of 20 Hz up to 1 MHz at a voltage of 100 mV.

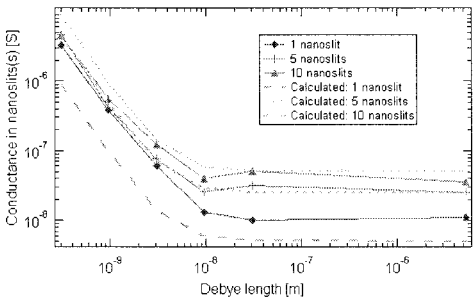

Figure 3. Measured and calculated conductances in the nanoslit(s) as a function of the Debye length. The measured points are connected to guide the eye.

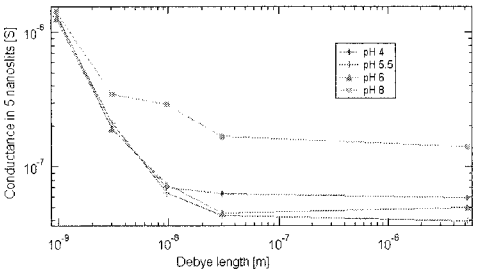

Figure 4. Conductance measured in 5 nanoslits as a function of the Debye length for 4 solutions with different pH. An increased conductance could be seen at pH 8 whereas the conductance was similar for the other values of pH. The measured points are connected to guide the eye.

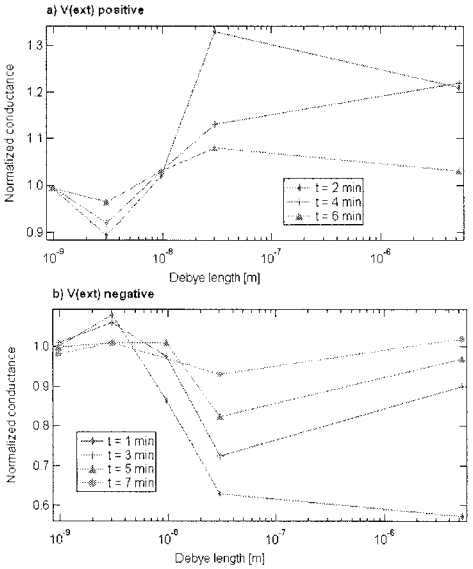

Figure 5. Normalized conductance as a function of the Debye length, for increasing times after the external voltage has been switched off. Normalized conductance = $conductance_{after\ V(ext)}$/ $conductance_{before\ V(ext)}$. The thickness of the diffusive layer has to be considered for the interpretation. The measured points are connected to guide the eye.

TOWARDS FABRICATION OF SMOOTH NANOFLUIDIC CHANNELS THROUGH NIL WITH CARBON NANOTUBE STAMPS

Dorte Nørgaard Madsen[1,*], Theodor Nielsen[1], Peter Bøggild[1] and Anders Kristensen[1]
[1]*Dept. of Micro and Nanotechnology, Technical University of Denmark, Bldg 345 east, DK-2800 Kongens Lyngby, Denmark*

Abstract

We demonstrate thermal nanoimprint lithography (NIL) with multiwalled carbon nanotubes (MWCNT) as stamp protrusions on a Si/SiO_2 stamp substrate. When MWCNTs have been transferred to the substrate it is possible to increase the protrusion aspect ratio using reactive ion etch with the MWCNTs acting as etch mask. Imprinting of MWCNT structures into films of 950K PMMA on silicon substrates has been demonstrated, showing well defined structures and line widths below 40 nm.

Keywords: liquid channels, carbon nanotubes, nanoimprint lithography

1. Introduction

The dimensions, shape, strength and surface smoothness of MWCNTs suggest the use of these macro-molecules as stamp protrusions in thermal nanoimprint lithography (NIL, [1]), allowing for imprinting of lines with well-defined linewidths in the 10-100 nm range, with the possibility of achieving molecular-scale surface roughness. With nanomanipulation it is possible to transfer individual MWCNTs to a stamp substrate and arrange them to form tailored configurations of CNTs on the stamp [2,3]. The nanostructures are imprinted in a thin film of PMMA on a Si substrate, and can be transferred to the substrate by reactive ion etching. Such nanostructures have many applications, e.g. as nano-fluidic channels, which may be used for linear extraction of DNA molecules [4].

2. Experimental

MWCNTs, grown by chemical vapor deposition, are transferred to a 5×10 mm stamp substrate of SiO_2/Si or Si with native oxide. Using a nanomanipulation setup equipped with a microfabricated manipulation tool and 3-axis high-precision translation stages, individual CNTs, lifted out of a CNT sample, can be positioned and manipulated on the substrate surface to form the desired geometry, with full control over position and shape. Figure 1 shows an optical image of a MWCNT on a SiO_2 surface during manipulation performed with a manipulation tool consisting of two gold-coated silicon oxide microcantilevers fabricated by means of standard microfabrication techniques. CNTs can also be transferred to the substrate by dispersion. Whereas the position in this case is not controlled, it allows for fast fabrication of samples for testing of stamp preparation and imprinting processes.

The stamp preparation process is outlined in Figure 2 (for a stamp assembled on SiO_2/Si substrate). First the MWCNT is transferred to the substrate (a). Next the stamp surface is etched by reactive ion etch (mixtures of CHF_3, SF_6 and O_2), where the CNT acts as an etch mask, to obtain a significant aspect ratio (b). After deposition of a C_4F_8 anti-stiction coating the stamp is ready to be imprinted into an approximately 400 nm thick 950K PMMA film on a Si substrate (c). The imprinting takes place at a background pressure of about 10^{-2} mbar. Stamp and substrate are heated

*Also at: Dept. of Physics and Technology, University of Bergen, Allegaten 55, N-5007 Bergen, Norway

to 180°C. Next they are pressed together with an imprint force of 2000 N for 5 min before cooling is initiated. The pressure is maintained during cooling. At 90°C stamp and imprint are separated manually (d). The resulting imprinted structure may be transferred to the substrate by reactive ion etching (e).

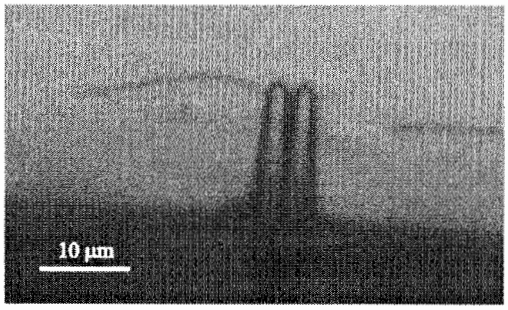

Figure 1. Optical image recorded during manipulation of a MWCNT on a SiO_2 surface in a nanomanipulation setup with a microfabricated tool combined with 3-axis high precision translation stages. The manipulation tool consists of two gold-coated silicon oxide microcantilevers on a Si base.

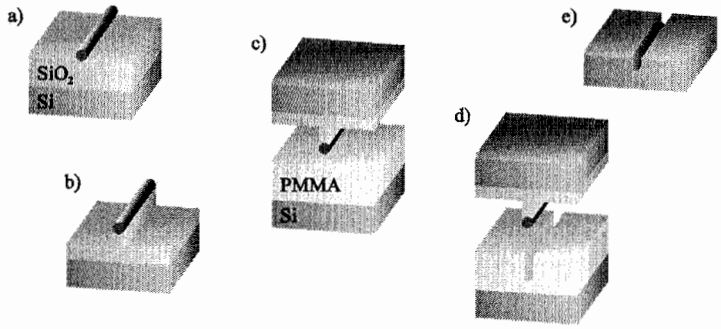

Figure 2. Illustration of the CNT stamping process. a) The CNT is positioned and shaped on the stamp substrate. b) The stamp is reactive ion etched with the CNT acting as etch mask. c-d) After a C_4F_8 anti-stiction coating the stamp is imprinted into a PMMA film on a Si substrate. e) The imprinted structure may be transferred to the substrate by reactive ion etching.

3. Results

In Figure 3 is shown SEM images of a large-diameter MWCNT, dispersed on a Si substrate and SF_6/O_2 etched, and the corresponding imprinted pattern, after separation (lower and upper panel, respectively). The 300 nm deep etch process caused no visible damage to the CNT. The adhesion of the CNTs to the stamp is generally good and the etching seems to further improve it, leaving only a few percent of the CNTs behind in the imprinted PMMA. However, in this case, when separating stamp and imprint, the end of the CNT was detached from the stamp, whereby the etched ridge becomes visible. The imprinted structures exhibit well-defined line widths below 40 nm, with

average roughness below the SEM resolution (approximately 15 nm). An imprint of a MWCNT with a smaller diameter is displayed in the inset of Figure 3.

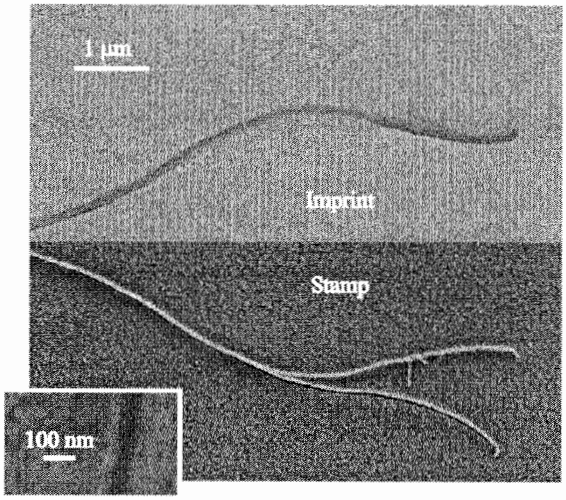

Figure 3. SEM images of an etched CNT on a Si substrate (lower panel), and its imprint (upper panel), after separation. The end of the CNT was detached from the stamp thereby making the etched ridge visible. Inset: Close up of a CNT imprint. The average roughness is below the SEM resolution (approximately 15 nm).

4. Conclusion

We have demonstrated the feasibility of using MWCNTs as stamp protrusions in thermal nanoimprint lithography. Further, we have shown that MWCNTs have a significant resistance towards reactive ion etch, and can therefore act as etch masks, improving the aspect ratio of the MWCNT protrusions. In addition the etch process seems to improve the sticking between stamp and CNT. Imprinting of MWCNT structures into films of 950K PMMA on Si substrates was demonstrated, showing well defined structures and line widths below 40 nm with an average roughness below the SEM resolution (approximately 15 nm). The technique can be further improved by optimizing etch process, manipulation technique, and stiction between CNT and stamp.

Acknowledgements

We acknowledge financial support from the Danish Technical Research Council. The partial support of the EC-funded project NaPa (Contract no. NMP4-CT-2003-500120) is gratefully acknowledged. The content of this work is the sole responsibility of the authors.

References

[1] S.Y. Chou, P.R. Krauss and P.J. Renstrom, *Science*, **272**, 85-87 (1996).
[2] T. Hertel, R. Martel and P. Avouris, *J. Phys. Chem. B*, **102**, 910-915 (1998).
[3] K. Mølhave, T.M. Hansen, D.N. Madsen and P. Bøggild, *J. Nanosci. Nanotech.*, **4**, 279-282 (2004).
[4] L.R. Huang, J.O. Tegenfeldt, J.J. Kraeft, J.C. Sturm, R.H. Austin and E.C. Cox, *Nature Biotech.*, **20**, 1048-1051 (2002).

PRESSURE-DRIVEN FLOW CONTROL AND CHEMICAL REACTION IN NANOCHANNELS

Eiichiro Tamaki[1], Akihide Hibara[1], Haeng-Boo Kim[1], Manabu Tokeshi[2], Takeshi Ooi[3], Masayuki Nakao[3], Takehiko Kitamori[1,2,4]

[1] Department of Applied Chemistry, School of Engineering, The University of Tokyo, Japan
[2] Kanagawa Academy of Science and Technology, Japan
[3] Department of Engineering Synthesis, School of Engineering, The University of Tokyo, Japan
[4] Core Research for Evolutional Science and Technology, Japan Science and Technology Agency, Japan

Abstract

A pressure-driven flow control scheme for nano chemical reactor was developed. For control the pressure of flow, we utilized a back pressure regulator and U-shaped microchannel. Based on this scheme, we fabricated a nano chemical reactor including a Y-shaped nanochannel for reaction and an U-shaped microchannel for liquid introduction. After combining the nano chemical reactor and back pressure regulators, we confirmed that the system worked properly with the pressure up to 7 MPa. By utilizing this system, chemical reaction in nanospace is realized.

Keywords: Nanochannel, Nanoreactor, Pressure-driven flow, Back pressure regulator

1. Introduction

Integration of flow chemical processing has been an important investigation in the field of microchip chemistry. From the engineering viewpoint, fabrication of nanometer-sized channels is required in order to realize the higher integration density. From the basic chemistry viewpoint, it should be investigated what determines the limitation of the channel size and how the channel size affects collective behaviors of molecules in a nanoscale confined environment. Previously, we investigated the property of water in the nanochannel by time-resolved fluorescence and the results indicated lower dielectric constant and higher viscosity [1]. In another report [2], we expected the property change of water to affect chemical reactions and fabricated a Y-shaped nanochannel for chemical reactions in nanospace. When pressure-driven flow is used, it is difficult to control the pressure at nanochannels because the mass flow rate must be very low in nanochannel. In order to realize a reaction in Y-shaped nanochannel, coincidence of pressure of two directions with very low flow rate is required. In this study, we developed a new liquid introduction scheme for controlling the pressure of flow in nanochannels. By utilizing this introduction scheme, two different solvent can be mixed in nanochannel. By investigating reaction in nanochannel, we will clarify how the property change in nanospace affects chemical reactions.

2. Experimental

Fig. 1 shows the scheme for liquid introduction to nanochannel. Liquid was introduced by a plunger pump to a microchannel, which is connected to nanochannel, and the outlet of the microchannel was connected to a back pressure regulator. Generally, plunger pump or syringe pump are used for making pressure-driven flow. However, these pumps are not appropriate for liquid introduction to nanochannel, because the mass flow rate should be very low for flowing nanochannel (Table 1). By using this scheme, bringing constant pressure at nanochannel can be achieved.

3. Results and discussion

Based on this scheme, a nanoreactor with a U-shaped microchannel was fabricated. Fig. 2 shows the fabrication process. The nano-sized pattern was drawn by electron beam lithography and 300-nm depth channel was etched by plasma etching. Micro-sized pattern was patterned by UV-photolithography and 4-μm depth microchannel was etched also by plasma etching. Fig. 3 shows the design and the photograph of the fabricated channel. Each ends of Y-shaped nanochannels was connected to a U-shaped microchannel for liquid introduction. By introducing two different solutions with coincident pressures from two directions, chemical reaction in nanochannel could be achieved. Liquid introduction system was developed with these micro-nano-combined channels. Fig. 4 shows the photograph of liquid introduction system. We confirmed that the system worked properly with the pressure up to 7 MPa.

We will present a reaction of fluorescent molecule by fluorescence spectrometry and a reaction of dye molecule with photothermal spectrometry in nanospace and discuss the influence of property change in nanospace to chemical reactions.

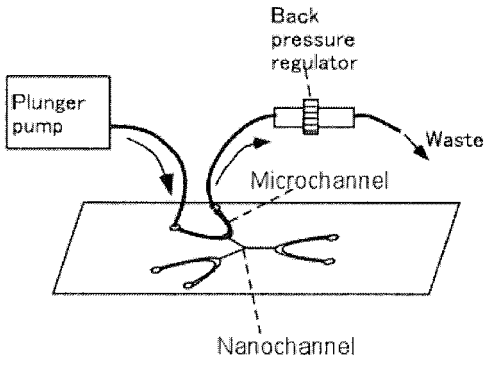

Figure 1 Scheme of liquid introduction method

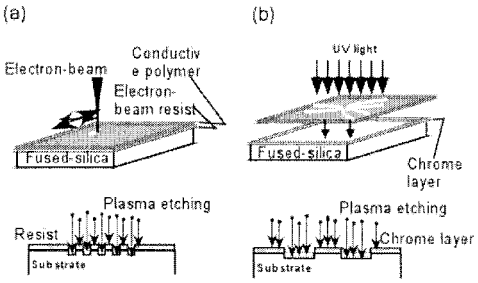

Figure 2 (a) Fabrication processes of nano-sized pattern, (b) Fabrication process of micro-sized pattern

References

[1] A. Hibara et al., Anal. Chem. **74**, 6170-6176 (2002)

[2] E. Tamaki et al., MicroTAS '03, pp. 681-684

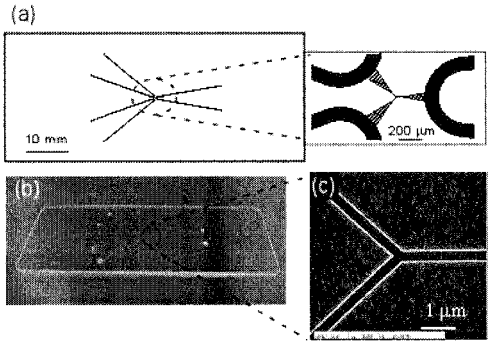

Figure 3 (a) Design of microchannel and nanochannel (b) Photograph of fabricated microchip (c) SEM image of nanochannel

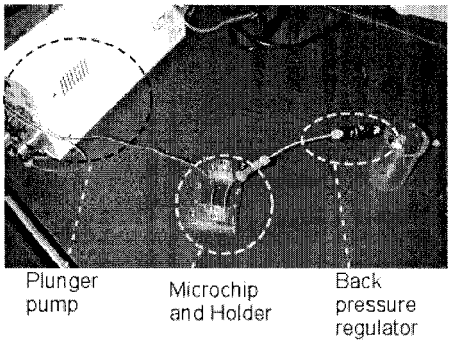

Figure 4 Photograph of liquid introduction system

Table 1 Properties of each introduction methods

	Minimum flow rate	Maximum pressure
Plunger pump	~1 μl/min	~10 MPa
Syringe pump	~0.1 μl/min	~10 MPa
Method in this study	Controlable by changing back pressure	More than 7 MPa

SORTING AND ASSEMBLY OF SINGLE-WALLED CARBON NANOTUBES BY DIELECTROPHORESIS IN MICROLIQUID CHANNELS: A NUMERICAL STUDY

Maria Dimaki[1], **René Nyberg**[1] **and Peter Bøggild**[1]

[1]*Dept. of Micro and Nanotechnology, Technical University of Denmark, Bldg 345 east, DK 2800 Kongens Lyngby, Denmark*

Abstract

Single-walled nanotubes (SWNT) are candidates for components in a number of electronics and sensing applications. In most applications it will be required that the SWNT with semiconducting and metallic properties can be separated and that efficient routes to mass production of nanotube-microsystem devices are established. Dielectrophoresis is a method capable of both sorting SWNT [1] and assembling these onto large arrays of microelectrodes in parallel. From numerical studies we find that sorting can be made highly efficient by integration of electrodes in a micro-liquid channel with proper selection of the conditions of the dielectrophoretic process.

Keywords: single-walled nanotubes, dielectrophoresis, sorting, simulation

1. Introduction

The success of the nanotube as an alternative to conventional circuit elements depends greatly on our ability to integrate the nanotube on existing microstructures in a fast and controlled way. Dielectrophoresis has the potential for scaling-up, provided that it can be controlled. Many parameters have an effect on the final result: the nanotube solution itself, the frequency and amplitude of the alternating voltage used for dielectrophoresis, the electrode geometry and spacing. Also, the velocity of the solution inside the channel is an issue. We have used a numerical approach to study these parameters, and report here on the importance of frequency of the voltage, the dispersing medium used and the velocity of the fluid.

2. Theory

When a polarisable object such as a nanotube is subjected to an inhomogeneous electric field the object will move towards regions of high or low electric field depending on its dielectric properties. This phenomenon is termed dielectrophoresis (DEP) and the force on the object is given by equation (1):

$$\mathbf{F}_{\mathbf{DEP}} = \frac{\pi}{6} \cdot \mathrm{r}^2 \cdot \ell \cdot \varepsilon_{\mathrm{m}} \,\mathrm{Re}\left\{\frac{\varepsilon_{\mathrm{n}}^* - \varepsilon_{\mathrm{m}}^*}{\varepsilon_{\mathrm{m}}^*}\right\} \cdot \nabla |\mathbf{E}|^2 \qquad (1)$$

where r and ℓ are the radius and length of the nanotube, $\boldsymbol{E}$ is the electric field, $\varepsilon_{\mathrm{i}}^*$, $\mathrm{i} = \mathrm{n,m}$ is the complex permittivity of the nanotube and the medium respectively and ε_{m} is the real part of the permittivity of the medium. Also taking the drag force from the liquid into account, the velocity of the nanotube will be given by $\mathbf{v}_{\mathrm{T}} = \mathbf{F}_{\mathbf{det}}/\mathrm{f} + \mathbf{u}$ where $\mathbf{u}$ is the velocity of the solution in the channel and f is the friction coefficient [2].

We have made assumptions for the permittivity and conductivity of the nanotubes based on values found in the literature. For metallic nanotubes, we take $\varepsilon_{\mathrm{n}}^{\mathrm{m}} = -10000\varepsilon_0, \sigma_{\mathrm{n}}^{\mathrm{m}} = 10^8 \mathrm{S/m}$ while for semiconducting nanotubes $\varepsilon_{\mathrm{n}}^{\mathrm{s}} = 2.5\varepsilon_0, \sigma_{\mathrm{n}}^{\mathrm{s}} = 10^5 \mathrm{S/m}$ [1,3,4].

3. Method

The electric field generated by a pair of electrodes with a spacing of 1 μm placed in the center of a 200x200x100 $\mu\mathrm{m}^3$ box is calculated using FEMLAB. The nanotubes are considered to be

entering the simulation space in 350 positions distributed randomly across the $x = -80$ μm plane. At each position 100 nanotube trajectories are plotted to account for the differences in the motion due to the random thermal forces. These are taken into account by adding a random displacement of amplitude $d_B = \sqrt{6D \cdot t}$ to each displacement caused by the DEP and drag force at the same time interval. Assuming that a volume of the solution can be cycled past the electrodes a given number of times N, we calculate the efficiency of sorting the nanotubes into semiconducting and metallic as well as the yield of semiconducting nanotubes in the end solution as a function of N.

4. Results and discussion

Figure 1 plots some representative trajectories of nanotubes dispersed in isopropanol in the simulation space at a frequency of 1 MHz and a fluid velocity of 8 μm/sec. Semiconducting nanotubes are most likely to drift away from the electrodes while metallic nanotubes will tend to be caught on the electrodes. In general the trapping efficiency of the DEP decreases as the fluid velocity in the x direction increases. Figure 2 shows this dependence for different values of the frequency of the field and the two different dispersing mediums examined in this study. Nanotubes in a 1% aqueous SDS solution are more responsive to DEP even at very high frequencies.

Cycling the solution past the electrodes a number of times may eventually result into separation of metallic and semiconducting nanotubes since the two react differently to the DEP forces. Figure 3 shows the efficiency of the sorting and the yield of semiconducting nanotubes in the final solution as a function of the number of cycles N for some selected parameters. It is clear that nanotubes in SDS need fewer cycles for achieving 100% efficiency while at the same time retaining a relatively high yield of semiconducting nanotubes. It should be noted that at frequencies where semiconducting nanotubes would normally be pushed away from the electrodes, the efficiency does not increase much with the number of cycles.

Finally, calculating the velocity of the fluid due to heating effects close to the electrodes and comparing it to the DEP velocities of a nanotube shows that this effect will generally play a minor role in the assembly, with the possible exception of nanotubes in SDS very close to the electrodes (Figure 4).

5. Conclusions

Simulations on single-walled nanotubes dispersed in a liquid passing through a microchannel have been carried out in order to quantify how dielectrophoresis works with respect to assembly and sorting of the nanotubes. Lower frequencies will give better sorting efficiency despite the fact that both metallic and semiconducting nanotubes are attracted towards the electrodes. Heating effects could disturb the process, but these can be avoided by carefully tuning experimental parameters.

Acknowledgements

We acknowledge discussions with Dorte Nørgaard Madsen, Anders Wolff, Mads Brandbyge, Laurits Højgaard Olesen and Henrik Bruus.

References

[1] Ralph Krupke, Frank Hennrich, Hilbert v. Löhneysen, Manfred M. Kappes, Science 301 (5631), p. 344-347 (2003).

[2] Hywel Morgan and Nicolas G. Green, AC Electrokinetics: colloids and nanoparticles, p. 41, 58, 77, 106-110, 144-150, Research Studies Press Ltd., 2003

[3] H.C.F. Martens, J.A. Reedijk, H.B. Brown, D. M. de Leeuw, R. Menon, Physical Review B, Vol. 63 (7), p. 073203/1-4 (2001)

[4] Chongwu Zhou, Jing Kong, Hongjie Dai, Applied Physics Letters, Vol. 76, Nr. 12, p. 1597-1599 (2000)

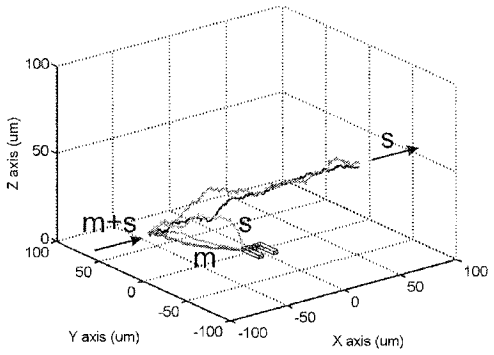

Figure 1. The calculated trajectories followed by metallic (m) and semiconducting nanotubes (s) carried by a fluid flow with a velocity of 8 μm/sec along the x-axis. Although all trajectories are initiated from the same point in the YZ plane, (-80,20,20), thermal motion induces variations of the traiectories.

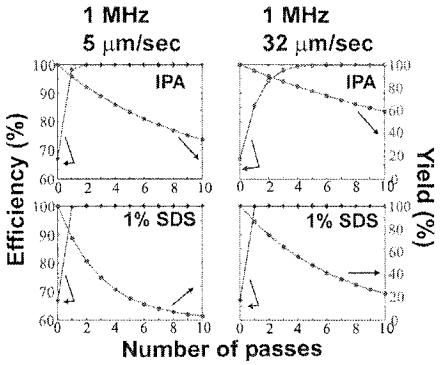

Figure 3. The efficiency (left y-axes) and yield (right y-axes) as a function of the number of passes through the channel for the two different mediums studied and two different fluid velocities at a field frequency of 1 MHz.

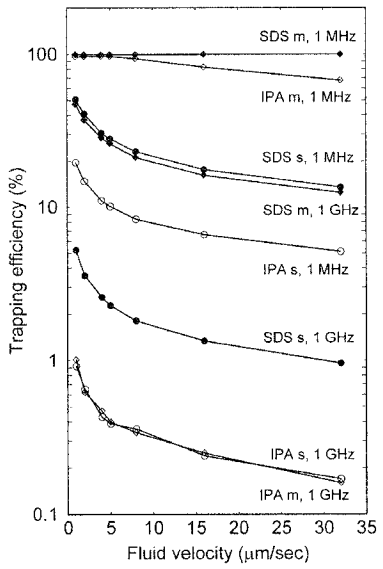

Figure 2. Trapping efficiency at 7 different fluid velocities, for two frequencies and for two different dispersing mediums for a 3μm long nanotube with a radius of 1 nm. The letter *m* denotes metallic SWNT while *s* stands for semiconducting SWNT.

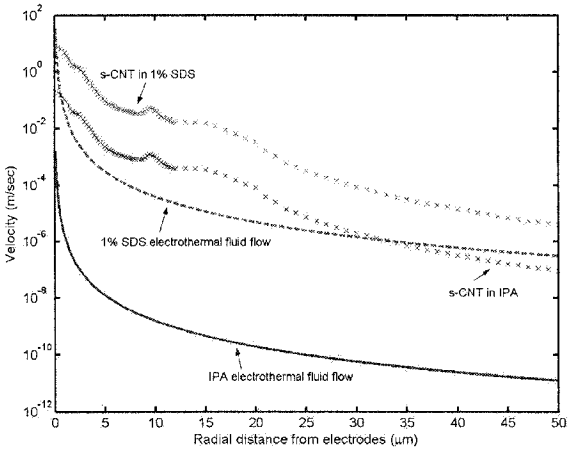

Figure 4. The velocity of semiconducting nanotubes (s-CNT) in IPA and 1% SDS due to dielectrophoresis as a function of their radial distance from electrodes. The velocity of the fluid due to electrothermal forces is also shown (the two lower curves).

A HIGHLY SENSITIVE NANO ELECTROCHEMICAL SENSOR WITH NANOELECTRODES USING A DYNAMIC CHARGE PUMPING METHOD

Xiaoshan Zhu and Chong H. Ahn
Microsystems and BioMEMS Laboratory
Dept. of Electrical & Computer Engineering and Computer Science
University of Cincinnati, Cincinnati, OH, 45221-0030, USA

Abstract

In this work, a highly sensitive nano electrochemical sensor has been designed, fabricated and characterized for the reversible redox species monitoring using a charge pumping method. The nano electrochemical sensor, which is composed of ring-type interdigitated 100 nm electrode fingers, is designed to improve the efficiency of species redox cycling. The charge pumping method is used to analyze the species concentration with a simple electronic instrumentation. Using p-aminophenol (PAP) as the redox the efficiency of species redox cycling molecule, a detection sensitivity of lower than 10 nM has been successfully achieved from this nano sensor.

Keywords: nanoelectrode, electrochemical sensor, charge pumping, high sensitivity

1. Introduction

The interdigitated array (IDA) microelectrode has been gaining wide applications for uTAS due to its versatility in the biochemical species detection and also its easy integration into a microsystem [1, 2, 3]. But the IDA microelectrode is also facing challenges in such applications. When the IDA microelectrode with a small surface-area is integrated in microstructures, the sensor output signal (current signal) becomes very weak, especially for the trace species detection. As a result, the weak signal is easy to be covered by the noise of electrochemical cell, and the sensitivity of the sensor is limited. In this work, the small surface-area IDA nanoelectrode is built to improve the efficiency of species redox cycling by reducing the gap between the fingers into a nano scale, and thus to improve the current signal or the sensor sensitivity. In addition, in order to avoid an expensive and complex current measurement circuit for the trace detection, the IDA nanoelectrode is characterized using the charge pumping method [4].

2. IDA Nanoelectrode and Charge Pumping Method

The ring-type IDA nanoelectrode with a small surface-area (0. 2 mm^2) of fingers is fabricated using e-beam lithography lift-off technique (Figure 1(a)-(b)). PMMA (Microchem, 495K) with a 300 nm thickness is spin-coated at the oxidized silicon surface, and then the nanopatterns are

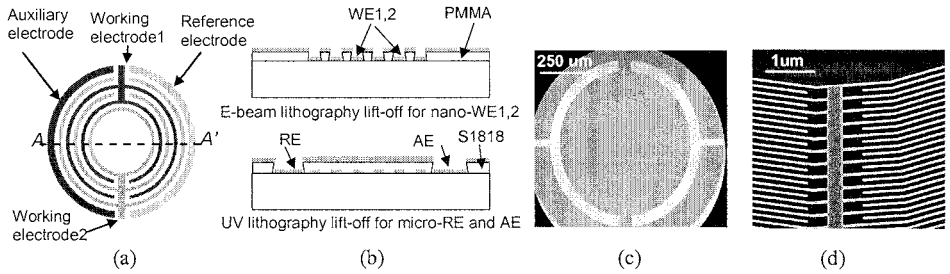

Figure 1. Nano sensor: (a) Structure of nano-electrochemical sensor (interdigitated array nanoelectrode); (b) Two-step lift-off processes for sensor fabrication; (c) Photography of the fabricated sensor; and (d) SEM picture of two interdigitated working nanoelectrodes.

exposed by e-beam (Raith 150 e-beam lithography system). After the development of the exposed PMMA, Ti/Au (100 Å/ 1000 Å) layer is deposited on the patterned sample surface, and then the deposited sample is dipped into acetone for lift-off. After the fabrication of the IDA nanoelectrode, the micropads for nanoelectrodes, the counter microelectrode (Gold) and the reference microelectrode (Silver/Silver Chloride) of the electrochemical cell, are further made on the oxidized silicon surface by the optical lithography lift-off technique and electroplating technique. Figure 1(c) illustrates the photograph of the nano-fabricated and micro-fabricated electrodes for electrochemical detection. Figure 1(d) shows the SEM graph of one part of the nano-fabricated electrode fingers.

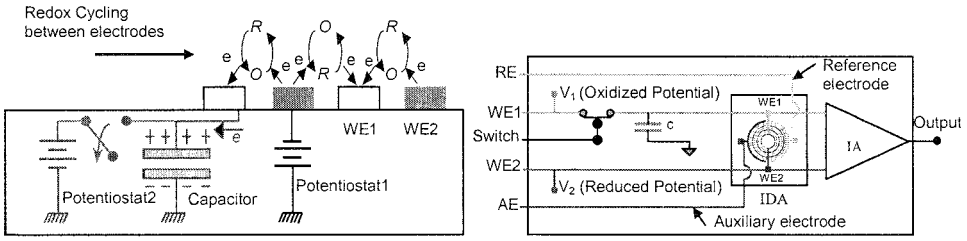

Figure 2. Charge pumping method: (a) Schematic diagram; and (b) Circuit measurement configuration.

Figure 2(a) shows the charge pumping method, which consists of two steps. In the first step, two bands of working electrodes (WE1 and WE2) are respectively biased at the reduction potential (-0.35 V) and the oxidization potential (+0.35 V) by two potentiostats, while the capacitor is connected to the oxidization electrode to be charged to +0.35 V. In the time duration of this step, a stable concentration distribution of the reduced species and the oxidized species is formed at the interdigitated electrodes, and the steady-state limiting current is generated between two working electrodes. In the consequent step, the switch is turned off, and the charged capacitor with the reduction (or oxidization) potential is used as energy source for the electrochemical reaction between two bands of electrodes. The charge on the capacitors is consumed by the electrochemical reaction of reversible redox species on the interdigitated electrodes, which causes the capacitor potential to decay. According to the electrochemistry theory of the electrode reaction [5], the electrode potential decay (or capacitor potential decay) shifts the Fermi level of the electrode, and thus affects the electron transferring (or the electrochemical reaction current) between the species in the solution and the electrode. Therefore, the capacitor potential and the electrochemical reaction current determine each other iteratively until the electrochemical reaction stops. On the other hand, the electrochemical reaction current is closely related to the species concentration, so that the species concentration is expected to have a decisive effect on the capacitor potential decay. The charge consumption process is monitored by recording the potential decay across the capacitor through an instrumentation amplifier (IA). A measurement circuit configured with IDA nanoelectrode is illustrated in Figure 2(b). The major advantage of this charge pumping method is simplifying the electronic instrumentation without losing the high accuracy. It is good for building a portable analyzer for microanalytical system using IDA nanoelectrode.

3. Experimental Results

The 100 pF capacitor voltage decay curves under the various PAP concentration levels are shown in Figure 3. For the high concentrations (10^{-4} M and 10^{-5} M), it can be seen that the capacitor discharging consists of a fast process and a slow process. The fast potential dropping at

the beginning of discharging process results from the large limiting current generated from the high concentration of the species. But after rapid dropping of capacitor potential, the electrochemical reaction current is also decreased quickly to a low level, and causes a slow capacitor potential dropping. When the concentration of p-aminophenol goes down (10^{-5} M and 10^{-9} M), the capacitor potential decay becomes more and more gradual due to the lower level reaction current until the decay curve overlaps with the decay curve when using the neat buffer solution (the electrochemical reaction current is covered by the noise currents from the measurement instrumentation). From Figure 3, the detection limitation for p-aminophenol is achieved in the range of 10^{-8} M ~ 10^{-9} M.

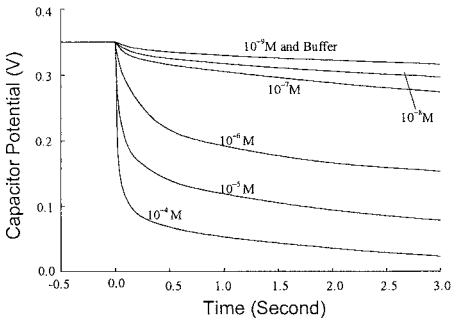

Figure 3. Potential decay curves of the capacitor (100 pF) using the interdigitated nanoelectrode

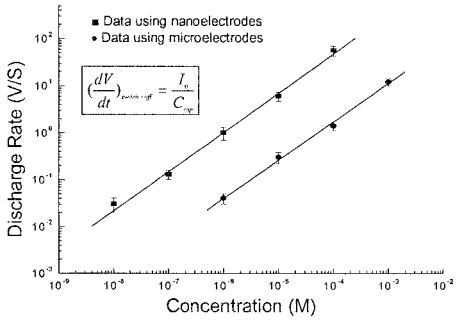

Figure 4. The calculated capacitor discharge rates under the different concentrations with an100 pF capacitor.

In addition, the discharge rate at the moment of switch-off, which is proportional to the steady-state limiting current and thus to the species concentration, is calculated for sensor calibration (Figure 4). Compared to the IDA microelectrodes with the same surface-area (5um wide and spaced electrode fingers), the nanoelectrodes show an about two-order level improvement in the reaction current or sensitivity.

4. Conclusions

In this work, a highly sensitive electrochemical nano sensor using the charge pumping method has been fabricated and successfully characterized for the improvement of efficiency of species redox cycling. Using p-aminophenol (PAP) as the redox the efficiency of species redox cycling molecule, a detection sensitivity of lower than 10 nM has been achieved from the electrochemical nano sensor. We believe this nano sensor coupled with the charge pumping method has numerous potential applications in building the portable μTAS for the trace biochemical species detection.

Acknowledgements

The authors thank Mr. Jeff Simkins, Mr. Rong Rong and Mr. Ron Flenniken in University of Cincinnati for their technical assistance in the IDA nanoelectrode fabrication.

References

[1] Y. Iwasaki and M. Morita, *Current Separations* 14:1 (1995).
[2] O. Niwa, M. Morita and H. Tabei, *Anal. Chem.*, 62(5), 447-452 (1990).
[3] O. Niwa, Y. Xu, H. B. Halsall, and W. R. Heineman, *Anal. Chem.*, 65, 1559-1563 (1993).
[4] X. Zhu and C. H. Ahn, *MicroTAS Conference*, Squaw Valley, California, 801-804(2003).
[5] D. R. Crow, *Principles and Applications of Electrochemistry*, 1994, Chapman&Hall, Glasgow.

FABRICATION OF MICROLIQUID CHANNELS WITH IN-SITU GROWN INCLINED CARBON NANOTUBES

Kjetil Gjerde[1], Tommy Schurmann[1], Ken B.K. Teo[2], William Milne[2] and Peter Bøggild[1]

[1] *Dept. of Micro and Nanotechnology, Technical University of Denmark, Bldg 345 east, DK 2800 Kongens Lyngby, Denmark*

[2] *Dept. of Engineering, University of Cambridge, Trumpington Street, Cambridge CB2 1PZ, UK*

Abstract

Functionalisation of surfaces in microliquid channels are desirable for many microfluidic applications. We report on the fabrication of microliquid channels with inclined multiwalled carbon nanotubes (CNT) grown in-situ by plasma enhanced chemical vapour deposition (PECVD). We find that distortion of the electrical field allows control of the inclination angle between the channel floor and the CNTs. Microfluidic channels with inclined nanotubes may be used as channels with anisotropic flow resistance (valves), for filters, or for separation and stretching of DNA.

Keywords: Inclined carbon nanotubes, microliquid channels

1. Introduction

Several works have reported on the ability of CNTs to grow in the direction of an electrical field gradient [1-4]. Recent work suggests that this may be caused by an interaction between the electric field and the catalyst particle on the tip of the CNT, not the CNT itself [5,6]. Regardless of the actual cause of this effect, PECVD grown CNTs are found to align themselves with the electric field, as long as the CNT growth is by tip growth mode. This technique is a new route towards customizing the properties of microliquid channels.

2. Experimental

Microliquid channels were produced on Si wafers by conventional photolithography and KOH etch using SiO_2 as an etch mask. This resulted in flat floor channels with inclined sidewalls due to the crystal plane selectivity of the KOH etch, causing only etching of the (100) plane. Walls with a 54.7° angle with respect to the horizontal are therefore achieved. Channels with widths in the range of 1 to 80 μm have been etched to a maximum depth of 5 μm, leaving narrow channels with a more shallow and V shaped profile. After removal of SiO_2, subsequent deposition of catalyst material (Nickel) for CNT growth was performed using an evaporator (Fig. 1a). The evaporator causes the deposition flux of catalyst material to be perpendicular to the substrate, leaving less material per surface area on the inclined sidewalls. Moreover, a lithography step was introduced to deposit the catalyst material just inside the KOH etched channels. By varying the thickness of the deposited catalyst layer, the diameter of the CNTs can be controlled. In this work catalyst thickness from 4 nm to 16 nm was used.

The CNT forests were synthesized in a PECVD system using acetylene as carbon feed gas. The growth occurred in 5 mbar pressure at 650 °C with a plasma potential at 600 V. To avoid the formation of amorphous carbon a co-flow of ammonia was used, working as an etchant. The synthesis was allowed to run for 15 minutes, resulting in CNT lengths of approximately 2 μm.

3. Results and discussion

The channels are covered with regularly shaped CNTs on the channel floor, whereas the CNTs on the inclined sidewalls are shorter, with smaller diameter and higher area density (Fig. 1b and Fig. 2). We suggest this to be related to a thinner, more irregular catalyst layer on the sidewalls, and possibly a higher surface roughness, decreasing the mobility of the catalyst particles and thus their ability to agglomerate into larger particles. The CNTs on the sidewall grow in the same direction as those on the channel floor and are therefore inclined with respect to the sidewall.

During synthesis, the growth direction of CNTs is largely governed by the direction of the electric field (Fig. 4). This effect provides a route to inclined nanotubes. We found that CNT forests grown near conductive edges of the sample holder on non-conductive substrates, exhibited a global angle. As seen in Fig. 3a, the CNTs grown 0.5 mm from the conductive edge are inclined by an angle of approximately 60° with respect to the channel floor, whereas 5 mm from the edge the nanotubes grow vertical to the substrate (Fig. 3b). FEMLAB simulations confirm the experimental observations, see Fig. 5.

We suggest that inclined CNTs in channels under certain conditions may bend down due to fluid flow in one direction and rise up for fluid flow in the other direction, which effectively would make the cross-section flow directionally dependent. The height and diameter of the CNT need to be controlled in order to achieve this, and this is easily done through variation of the film thickness or by lithographic patterning with catalyst particles of well-defined size. Definition of metal islands with diameters down to tens of nanometers is possible with electron beam lithography. The height of nanotubes depends largely on the growth time. Whereas ideal multiwalled nanotubes have a Youngs modulus of order 1 TPa, CVD-grown nanotubes typically have more defects, and can be expected to be softer. Assuming a Youngs modulus of 0.1 TPa, the force required to deflect a 50 nm wide nanotube is of order 0.1 nN to 0.005 nN, for lengths of 1 to 5 μm, respectively. For a drag coefficient of 3 for the nanotube, and a viscosity of 1 mNs/m^2 for water, deflection of the CNT's requires fluid velocities of roughly 50 mm/s to 0.5 mm/s, respectively (Fig. 6). From Fig. 6 it appears that even moderate variation of the CNT dimensions that can easily be achieved experimentally, allows the elasticity of the CNT's to be matched to a large range of different flow conditions.

Conclusions

Growth of inclined carbon nanotubes inside microliquid channels has been accomplished. The angle between the substrate (channel floor) and the direction of the CNTs is controllable through shaping the guiding electric field by careful design of the substrate holder. The nanotubes will grow in the direction of the electric field, resulting in a CNT forest with a global angle. Initial calculations predict that these CNTs may bend due to fluid flow, possibly resulting in anisotropic flow resistance. Scaling of the CNT diameter and height can tune this bending to a large range of flow velocities.

References

[1] Ren Z.F., Huang Z. P. , Xu J.W., Bush P., Siegal M.P., Provencio P.N., *Science* **282**, 1105 (1998).

[2] Zhang Y., Chang A. , Cao J., Wang Q., Kim W., Li Y., Morris N., Yenilmez E., Kong J., Dai H., *Appl. Phys. Lett.* **79**, 3155-3157 (2001).

[3] Avigal Y., Kalish R. , *Appl. Phys. Lett.* **78**, 2291 (2001).

[4] Merkulov V.I., Melechko A. V. , Guillorn M.A., Simpson M.L., Lowndes D.H., Whealton J.H., Raridon R.J., *Appl. Phys. Lett.* **80**, 4816-4818 (2002).

[5] Kim D-H., Cho D.-S. , Jang H-S., Kim C-D., Lee H-R., *Nanotechnology* **14**, 1269-1271 (2003).

[6] Merkulov V.I., Melechko A. V., Guillorn M.A., Lowndes D.H.,Simpson M.L., *Appl. Phys. Lett.* **79**, 2970 (2001).

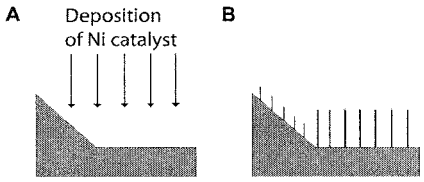

Figure 1. (A) Deposition of a Ni catalyst film on channel floor and sidewall by evaporation. (B) Illustration of synthesised CNTs, showing good uniformity on channel floor but lower quality on sidewalls. The CNTs on the sidewalls are inclined with respect to the wall as the nanotubes follow the electric field.

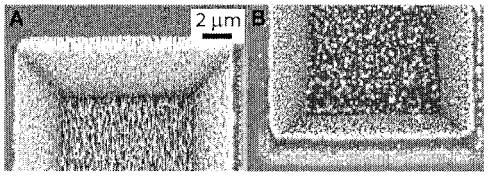

Figure 3. (A) The part of channel near conductive edges develop inclined CNT due to the electrical field distortion. (B) 5 mm from the edge the electrical field forces the CNTs to grow perpendicular to the surface (see Fig. 5).

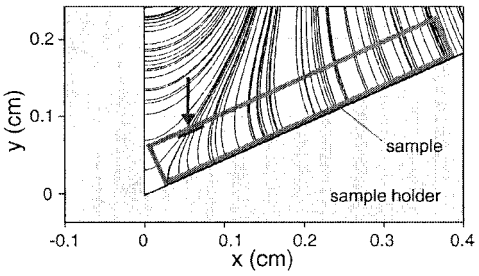

Figure 5. FEMLAB simulation of the electric field lines guiding of CNTs during PECVD synthesis on a stage with a 30° tilt. The field lines are distorted by the conductive edges. The arrow indicates the position of the channel parts imaged in Fig. 3a and 4.

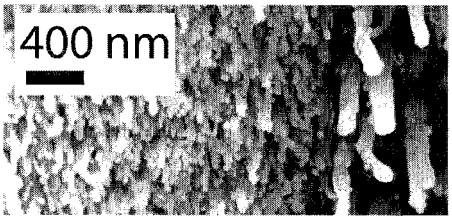

Figure 2 CNTs synthesised on sidewalls and in channel for catalyst thickness of 16 nm Ni.

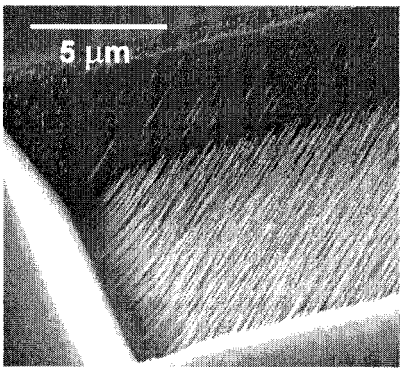

Figure 4. Inclined growth of CNT forests in microfluidic channels.

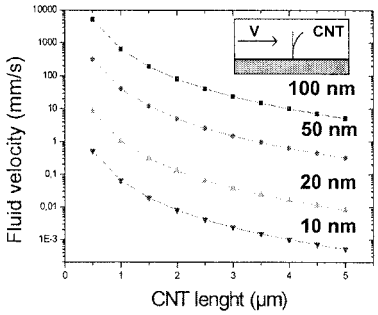

Figure 6. Estimated fluid velocity required to deflect a CNT 10% of the length as a function of the length and diameter. Variation of the nanotube length from 1 to 5 µm and of the diameter from 10 nm to 100 nm, match the elasticity to a large range of fluid flow conditions. The inset illustrates a CNT being deflected by the fluid flow.

ARTIFICIAL LIPID BILAYERS IN A MICROFABRICATED SYSTEM

Hywel Morgan[1], Mairi E. Sandison[1], Gabriel Mendes[2], Richard Berry[3] and Anthony Watts[2]
[1]*Dept. of Electronics and Computing Science, Southampton University, Southampton, SO17 1BJ, U.K.*
[2]*Dept. of Biochemistry, University of Oxford, Oxford, OX1 3QU, U.K.*
[3]*Dept. of Physics, University of Oxford, Oxford, OX1 3PU, U.K.*

Abstract
A microfabricated silicon device for studying artificial lipid bilayer systems is described. The experimental apparatus employed enabled the simultaneous acquisition of electrical and optical data. Reconstitution of channel-forming proteins into a artificial lipid bilayer formed across an aperture in the silicon device is demonstrated.
Keywords: Micromachining, Lipid Bilayers, Ion-Channels

1. Introduction

Single molecule detection techniques are becoming an increasingly powerful tool in the field of biophysics [1]. In combination with artificial bilayer lipid membrane (BLM) systems, they have been employed to study the behaviour of reconstituted membrane proteins [2,3]. This abstract describes a microsystem that enables the simultaneous recording of electrical and optical measurements from such an artificial BLM structure. The microsystem should facilitate the acquisition of functional, kinetic and pharmacological information from membrane proteins and could be employed for use in a drug discovery platform.

2. Device Fabrication

The experimental apparatus is centred around a microfabricated silicon device. This consists of a well etched through a silicon wafer, at the base of which is a silicon nitride membrane, through which a 50μm diameter aperture is etched (Figure 1). BLM formation occurs within this aperture.

The silicon devices were fabricated from double-polished, silicon nitride coated, n-type Si(100) wafers (supplied by Edinburgh Microfabrication Facility, Edinburgh, UK). The fabrication process was as follows: an aperture was first defined in the silicon nitride film on the backside of the wafer by photolithography and reactive-ion etching in an Oxford Plasma Technology BP80 system (Plasmatech, Bristol, UK), using a C_2F_6 plasma (100 W, 15 mT and 20 ml min^{-1} C_2F_6) and a photoresist etch mask. The upper area of the well was then similarly defined on the front-side of the wafer. To etch through the bulk silicon and create the suspended silicon nitride membrane, the wafer was immersed in a 4.5M KOH solution at a temperature of 80°C for approximately 8 hours. After dicing the wafer into individual devices, the exposed regions of silicon were then electrically insulated by coating the devices on both sides with 100nm PECVD silicon nitride.

3. Experimental Methods

The experimental set-up employed for the simultaneous electrical and optical recording of BLMs is illustrated in Figure 2. Using adhesive, the silicon device was first bonded over a fluidic channel etched in a glass substrate and a glass well was then bonded over the upper surface of the silicon chip to create the upper and lower fluidic reservoirs. The bilayer was imaged using a fluorescence microscope with a x60 water immersion objective lens and electrical activity was recorded using Ag|AgCl electrodes, which were inserted into the fluid reservoirs on both sides of

the aperture and were connected to a patch clamp amplifier (Industrial Development Bangor, Bangor, UK).

To form a BLM across the silicon nitride aperture, the lower glass flow cell was first filled with electrolyte solution (1M KCl). 1-2 μl of 1 mg ml^{-1} 1,2-diphytanoyl-sn-glycero-3-phosphocholine (Avanti Polar Lipids, Alabama, USA), diluted with n-decane, was then pipetted over the aperture at the base of the silicon well. Once the lipid had spread over the silicon nitride membrane, the upper glass well was filled with the electrolyte solution and a BLM subsequently formed by spontaneous thinning. If the lipid had not thinned within a few minutes of adding the electrolyte, the fluid in the glass well was agitated so as to speed up the thinning process.

Channel-forming peptides were reconstituted into BLMs using two different methods: by directly injecting into the upper fluidic reservoir peptides (such as gramicidin) that will spontaneously incorporate into a BLM and by using vesicle fusion methods. Gramicidin was dissolved in chloroform to 10 ng ml^{-1} and 1-2 μl of the solution was injected as close to the BLM as possible, whilst nystatin-containing vesicles were fused with the BLM following the method developed by Woodbury [4].

4. Results and discussion

Figure 3 shows a sequence of optical reflection images that illustrate the spontaneous thinning of a BLM across the aperture in a silicon nitride membrane. Interference fringes due to the thick initial lipid film can be clearly observed (top left of Figure 3). As the lipid film thins, these fringes recede and the area of the BLM appears black (bottom right of Figure 3). The thinning of the bilayer was also monitored electrically by measuring the change in capacitance, which was seen to increase as the bilayer thinned. The bilayers were extremely stable with minimal sensitivity to moderate mechanical vibrations and with a lifetime of several hours.

Figure 4 shows a current-time trace obtained shortly after the injection of the solution containing gramicidin monomers. Single-channel events can be clearly observed. Similarly, Figure 5 shows an electrical recording acquired during the fusion of nystatin loaded vesicles. Fusion of an individual vesicle with the BLM results in a current spike that decays with time, as the nystatin oligomers disassociate in the BLM into individual nystatin monomers, which do not function as ion-channels.

5. Conclusions

The use of microfabricated silicon devices for electrically and optically monitoring artificial BLM systems has been demonstrated. Stable BLMs were successfully produced and single-channel recordings were obtained from channels formed from re-constituted membrane proteins.

Acknowledgements

The authors would like to thank Mary Robertson for help with the silicon microfabrication. This work was supported by the Engineering and Physical Sciences Research Council (grant no. R45659) and the UK Interdisciplinary Research Centre in Bionanotechnology.

References

[1] A. Ishijima and T. Yanagida, *Trends in Biochemical Sciences,* **84**, 438-444 (2001).

[2] V. Borisenko, T. Lougheed, J. Hesse, E. Füreder-Kitzmüller, N. Fertig J.C. Behrends, G.A. Woolley, G.J. Schütz, *Biophysical Journal*, **84**, 612-622 (2003).

[3] T. Ide, Y. Takeuchi and T. Yanagida, *Single Molecules*, **3**(1), 33-42 (2002).

[4] D.J. Woodbury, *Methods in Enzymology,* **294**(17), 319-339 (1999).

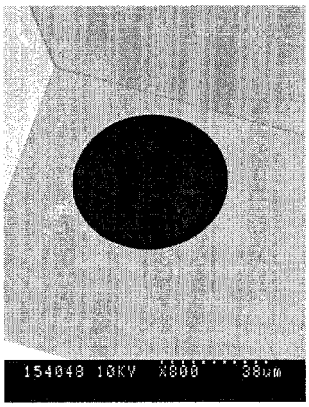

Figure 1. An SEM of the aperture in a silicon-nitride membrane.

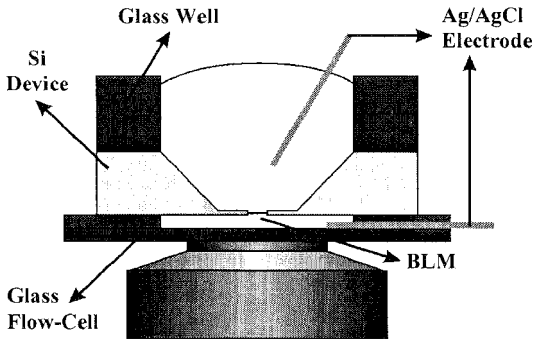

Figure 2. Experimental apparatus for simultaneous electrical and optical recording of BLMs.

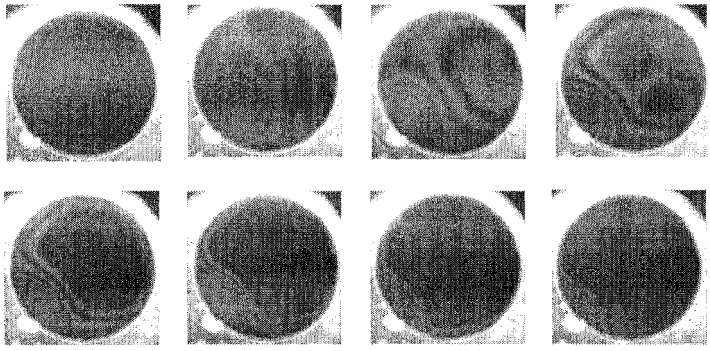

Figure 3. A time sequence of reflectance images (approximately 20s long) illustrating the spontaneous thinning of a BLM.

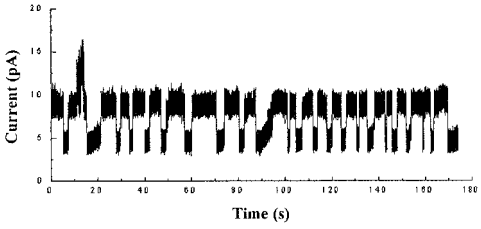

Figure 4. A current-time trace that shows ion conduction through single gramicidin dimers, that form temporarily when two gramicidin monomers come together by diffusion.

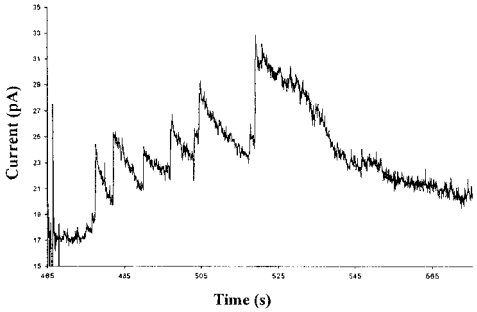

Figure 5. A current-time trace showing the fusion of individual nystatin-containing vesicles with the BLM.

A PARALLEL ELECTRONIC SENSOR FOR PHENOTYPIC SCREENING IN DIRECTED EVOLUTION

B. Iafelice, V. Ferrarini, R. Guerrieri
ARCES – University of Bologna, Bologna, Italy
biafelice@deis.unibo.it

Abstract

A novel biosensor array has been developed to screen *complex* phenotypes obtained with directed evolution, a nanobiotechnology process of continuous genetic variation and phenotypic selection. This non-recombinant approach is used to design microorganism populations with desired phenotypic characters. The long time of convergence of this approach can be reduced with an array of independent parallel sensors. The proposed device is a 96-microtiter plate with electronic sensors embedded in each well. In particular each well is a microbial fuel cell that works as a biosensor. So it allows us to track several qualitative properties of different bacterial strains or different substrates, through the current measurements. In this way we have a sensor that discriminates between many bacterial samples and measures the response of the cells to external input. We test the device measuring *E.coli* performances before and after the directed evolution protocol.

Keywords: bioelectronic sensor, directed evolution, phenotypic screening

1. Introduction

Screening for interesting variants in large combinatorial libraries is the key step of the random approach in directed evolution [1]. Existing methods for screening rely on high density plates whose contents are selected by detecting clearly "on/off" distinctive phenotypes. But in any case the selection step is the bottleneck. The probability of detecting an improved strain decreases if the phenotype searched is complex. Therefore we present a prototype micro titre plate featuring electronic sensors embedded in each well. This concept allows us to track several qualitative properties of the subpopulation contained in there, in a continuous way. Current output is an example of complex phenotype. It is affected by physical and biological variables, like the type of electrodes used and the enzymes involved in the energy metabolism, and it changes under environmental input [2]. So the current yield can be used to discriminate between several bacterial populations and also to monitor an environmental change. The specific biosensor presented in this paper is an array of 96 independent sensors that measure continuously the electric current produced by a population of cells contained in each well. To detect the current we use the "fuel cell principle" where at the anode there are bacteria producing electrons and at the cathode there is a final electron acceptor. Since the current produced by the cells is influenced by several environmental conditions, this device allows to screen populations acting, as whole-cells biosensors, as a function of their response to external inputs [3].

2. Theory

Each well of our biosensor array is a micro fuel cell. A fuel cell works similar to a battery. In a battery, electricity is generated as a result of a fixed amount of substance undergoing a chemical change inside the cell (Fig. 1.a). At the anodic compartment, the bacteria metabolize the fuel and produce electrochemically active substances. The complete oxidation of glucose, a typical fuel, may be represented by the equation:

$$C_6H_{12}O_6 + 6\ H_2O \rightarrow 6\ O_2 + 24\ H^+ + 24\ e^-$$

From the oxidation, cells get compounds rich in electrons (as $FADH_2$, ATP, $NADH_2$), that use to catalyze further reaction in their metabolism. So it is necessary to add a mediator (Methylene blue,

Neutral red) to shuttle electrons out of the cells to the electrode. At the cathode a redox compound accepts the electrons and the oxygen becomes water:

$$2[FECN_6]^{3-} + O_2 + 6e^- + 2H^+ \rightarrow 2[FECN_6]^{4-} + H_2O$$

Abundant organic raw materials as methanol, organic acids, or glucose can be used as substrates and the rate of the oxidation changes with the cell affinity to the compound injected [4-5].

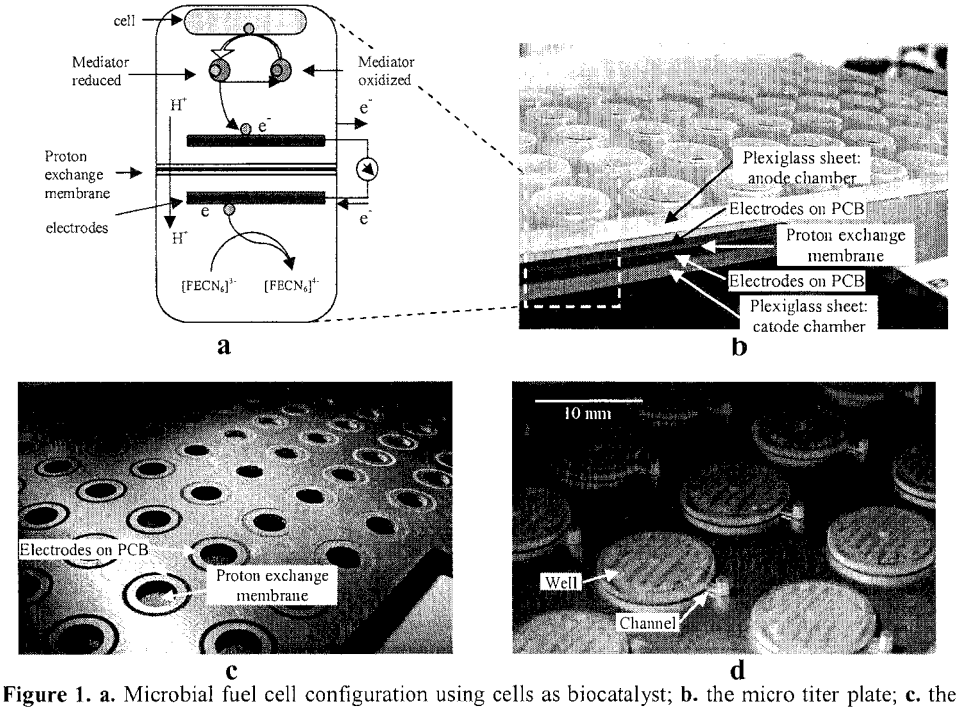

Figure 1. a. Microbial fuel cell configuration using cells as biocatalyst; **b.** the micro titer plate; **c.** the circular electrodes printed on PCB, the membrane is located in the bottom of each well; **d.** a particular of the micro titer plate, a channel near each well allows the filling.

Two factors affect the design of a microbial fuel cell: 1) the biocatalyst reaction should take place in the immediate vicinity of the Proton Exchange Membrane (PEM) such that the proton travelling distance can be minimized and the energy transfer efficiency optimized; and 2) the surface area-to-volume ratio of the anode and cathode chambers should be maximized to achieve high energy density as well high current yield.

2. Experimental

Our experimental system is composed by a PC, with LabView® software, which controls a switch board to select each biosensor and measures the current output through an Agilent 3458A multimeter (Fig. 2). Our set up allows us to measure currents down to 10 nA. The biosensors array is a micro titre plate made of 2 plexiglass sheets (2,5 mm thickness), divided by 2 2-layers Printed Circuit Board (PCB), 400 μm thickness. A Dupont Nafion 117™ PEM is sandwiched between them (Fig. 1.b). The wells are created drilling the plexiglass and the PCB, with a T-Tech QC 5000.

On the top PCB the circular gold electrodes (7mm diameter) are connected to the switch board (Figure 1.c-d). On the bottom PCB there is a unique gold cathode. Gold electrodes have the best biocompatibility and a good corrosion-resistance [6], moreover they are commonly used in PCB process. The structure of an anodic-PCB/PEM/cathodic-PCB made easy the building process of high density biosensor arrays and the scaling down of fuel cell dimension. In the presented example on one side of the plate, 96 chambers are cut in the plexiglass (100 µl each). A single cathodic chamber is located on the other side, filled with 2ml of potassium ferricyanide $[FeCN_6]^{3-}$. We have improved *E.coli* for current yield through "directed evolution method", inducing random mutations with UV. Methylene blue, used as redox indicator, allows us predicting the best current mutant on the basis of its colour changes. Each well contains a cell suspension (10^9cells/ml) diluted in mediator saline solution (Neutral Red 100 µM, Methylen blue 10mM in PBS buffer 1X).

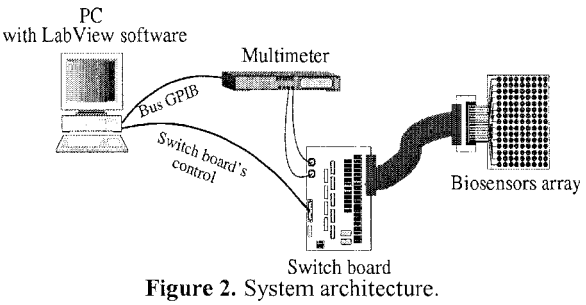

Figure 2. System architecture.

4. Results and discussion

The device has been tested filling each well with mediator solution only and we obtain a good reproducibility. We consider this current values as background in order to evaluate the real production of the bacteria used (Fig. 3). The best current producers reduce Methylene blue faster than the other samples (range 50-60 µA, mean value). Until now we have improved 6 time current yield (Fig. 4). The system has even been tested as glucose sensors. After 1 hour running, 10mM glucose (final concentration) is injected and the system measures a current peak in 10 minutes after the event in all the sample (Fig. 4).

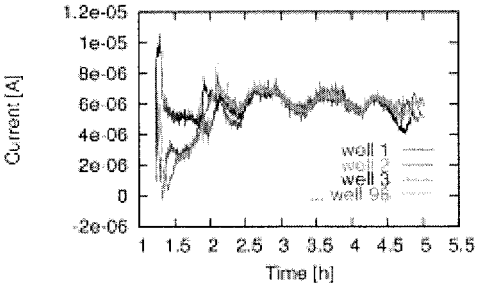

Figure 3. Background currents.

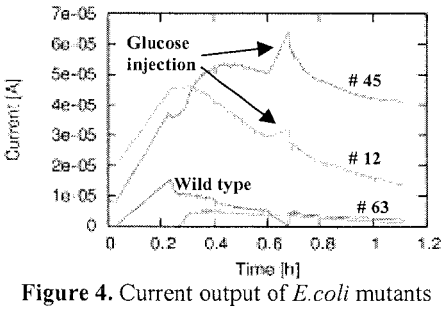

Figure 4. Current output of *E.coli* mutants improved. The peaks are the response to glucose injection.

References

[1] Y. Zhang et al., *Nature*, **415**, 644-646 (2002)
[2] D. Park et al., *Biotechnol. Bioengineering*, **81**, 348-355 (2003)
[3] I. Karube, *Biosensors Fundamentals and Applications*, Oxford Science Pub., 13–29 (1987)
[4] Chaubey, *Biosens Bioelectron.*, **17(6-7)**, 441-456 (2002)
[5] Schoreder, *Angew. Chem. int* , **42**, 2880-83 (2003)
[6] H. Zitter, Plenk H. Jr., *J. Biomed. Mater. Res.*, **21(7)**, 881-896 (1987)

MICRO-NEWTON-RING CHROMATOGRAPHY

Hitoshi Watarai, Masahiro Hatta and Hideaki Monjushiro
Dept. of Chemistry, Osaka University, Toyonaka, Osaka 560-0043 Japan

Abstract

An innovative and simple method to fractionate individual particles in liquid by their sizes has been invented. A gap between a small convex lens and a flat glass, which constructed a Newton ring devise, was controlled by a piezo-actuator and utilized for the fractionation of very small amount of micro-particles in liquid. A meniscus force of the liquid carried the particles toward the center of the lens, when it was vaporized. The particles were trapped at the specific radial position, which gap was the same with the diameter of the particle. Thus, various kinds of particles including polystyrene and DNA were fractionated under the microscopic observation.

Keywords: Microparticle separation, nano-gap, size fractionation of DNA, Newton ring

1. Introduction

Various migration methods of nm to μm particles have been developed for the separation and characterization of bioparticles in liquid so far [1,2]. However, there have been developed only limited numbers of methods for the measurement of the size of particles in liquid directly. Electrophoresis has been applied for the separation of ionic compounds such as lysed DNA and protein, but it is difficult to separate large DNA with several tenth kbp to hundreds kbp. We have recently developed various types of migration methods for micro-particles in liquid by using external fields [3-5]. In the present study, an innovative and simple method for the size measurement and the size separation of micro-particles was invented. The nano-space was precisely determined by the interference moiré pattern of light, so called the Newton ring [6]. This technique is versatile for the fractionation of any kind of micro-particles in liquid.

2. Experimental

Nano-space was built combining a cover glass and a small plano-convex lens as shown in Fig. 1. The cover glass was fixed to the stage of an inverted microscope and the gap of the nano-space was controlled by approaching the convex lens to the cover glass by using a piezo-electric devise, which was connected to the convex lens. The distance between the cover glass and the lens was measured by observing the Newton ring produced by interference of light from the cover glass side. Polystyrene latex with diameter of 1 to 5 μm was used as reference samples. Chromosome DNA of salmon (about 40 kbp) was used as a biological particle. A sample solution was put into the nano-space with a micro-syringe and the single stage separation was started by the evaporation of the solvent water. The sample particles were drawn toward the center of the nano-space by the meniscus force of water and trapped at the position where the particle diameter was equal to the gap of the nano-space. Therefore, the diameter of the particle was determined from the measurement of the distance between the center of the lens and the position where the particle was trapped.

The Newton ring chromatogram was obtained as a plot of the averaged fluorescence intensity normalized to the circumference against the gap-distance at the radial position from the center of the lens.

3. Results and Discussion

First, size measurements were carried out for the polystyrene reference particles with a diameter of 3 μm, which moved to the center of the nano-space during the evaporation of water as shown in Fig. 2. The peak position of the Newton ring chromatogram of this particle was at 2.926 μm with the width of 0.149 μm, so well fitted to the particle diameter cirtified by the company, 3.015 ± 0.138 μm.

The size-separation ability of this method was demonstrated by using the mixture of polystyrene particles of 1.7 and 3 μm diameters. For this mixed sample, the Newton ring chromatogram is shown in Fig. 3. Two peaks were observed at 1.664 μm and 2.863 μm, with the widths of 0.098 μm and 0.220 μm, respectivly.

4. Conclusions

In summary, the Newton ring chromatographic devise with the nano-gap was constracted by using the lens and the glass plate, controlled by the piezo-actuator on the nanometer order. Nano-gap width was precisely measured from the analysis of the Newton ring. Simultaneous size-separation and size measurement of particles have been accomplished by this method. The required sample amount is very small (much smaller than 1 ml), and the measurement time is rather short (less than 10 minutes). The present study proposed a new concept and thechnique of separation of micro to sub-micrometer particles in liquid.The proposed new chrmatographic method will be highly usefull for the analysis of a small amount of blood cells and whole chromosome in a single cell.

References

[1] S. R. Springston, M. N. Myers and J. C. Giddings, *Anal. Chem.*, **59**, 344 (1987).
[2] M. Mesaros, P. F. Gavin and A. G. Ewing, *Anal. Chem.*, **68**, 3441 (1996).
[3] M. Tamagawa, H. Monjushiro and H. Watarai, *Colloids Surf., A*, **220**, 279 (2003).
[4] I. Ikeda, S. Tsukahara and H. Watarai, *Anal. Sci.*, **19**, 27 (2003).
[5] Y. Iiguni, M. Suwa and H. Watarai, *J. Chromatogr., A*, **1032**, 165 (2004).
[6] I. Newton, *Opticks, or a Treatise of Reflection, Refractions, Inflection, and Colours of Light*, (1704).

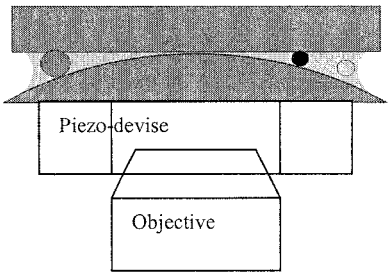

Figure 1. Nano-space produced betwen a flat cover glass (upper) and a plano-convex lens (lower). Large particles are trapped outside, but small particles are drawn near the center of nano-space.

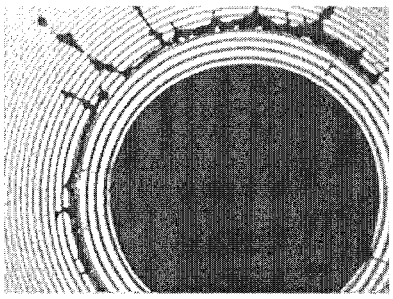

Figure 2. A photograph of trapped polystyrene latex particles with a diameter of 3 μm. Size measurement can be simply performed by counting the number of the stripes of the Newton ring.

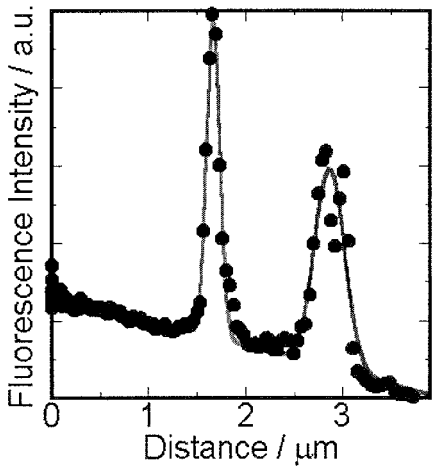

Figure 3. Newton ring chromatogram of the mixture of the polystyrene reference particles with diameters of 1.7 and 3 μm. In this chromatogram, peak positions were 1.664 μm and 2.863 μm and the widths were 0.098 μm and 0.220 μm, respectively. The horizontal axis is the distance of the gap determined by the Newton ring.

SHEAR FLOW SELF-ASSEMBLED GOLD NANOPARTICLE FILM FOR CHEMIRESISTOR SENSOR APPLICATIONS

Chi-Yuan Shih[1], Siyang Zheng[1], Yu-Chong Tai[1], Yi Liu[2] and J. Fraser Stoddart[2]
[1]Dept. of Electrical Engineering, California Institute of Technology, USA
[2]Dept. of Chemistry, University of California Los Angeles, USA

Abstract

We report here a new technique using shear flows, with or without electric field enhancement to self-assemble gold nanoparticle film for vapor sensing application. The described approach to prepare nanoparticle thin film is simpler and faster than conventional layer-by-layer deposition methods[1-2]. It is shown that our self-assembled chemiresistors are adequate for organic vapor sensing. The effect of electric field on self-assembly efficiency was as well studied in this work.

Keywords: self-assembly, nanoparticle, shear, PDMS, chemiresistor

1. Introduction

Nano-materials have attracted a profound research interest for gas sensors. For example, nanoparticle-molecule composite film can change its electrical conductivity with high sensitivity and selectivity upon absorbing different organic vapors[1]. However, conventional nanoparticle films are in general prepared via layer-by-layer deposition methods, where nanoparticle and molecule layers are deposited alternatively until reaching the desired film thickness[2]. There are two major drawbacks in this approach. First, layer-by-layer deposition is simply too laborious and time-consuming. Second, in order to form dense SAM monolayer, it is often necessary to have rigorous substrate cleaning[1-2], which may damage the embedded CMOS or other devices on the sensor chip. Our shear-flow-assembly method was designed to attack both problems

2. Experimental

First, microfluidic shear flow devices were prepared (Figure 1). Chips of PDMS mold and interdigital electrodes were fabricated separately and then bonded together at 80^0 C for 5 hr. Using this device, we then developed two processes to form "patterned" nanoparticle film on electrodes.

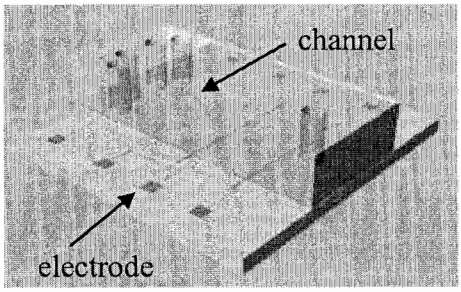

Figure 1. Schematic view of shear flow device composed of PDMS channel mold and glass substrate.

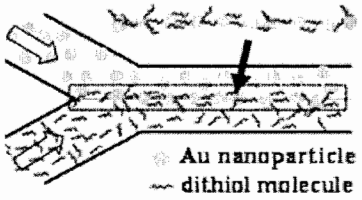

Figure 2. Working principle of shear flow assembly. Dithiol molecules are cross-linkers for gold nanoparticles.

Process I: Gold nanoparticle with an average size of 30nm and dithiol molecule (~3 nm) flows were introduced into the shear-flow device as shown in Figure 2[3]. Gold-thiol conjugation reaction happened at the flow interface, which in turn reduced the net negative charge on gold nanoparticles. A 2V electrical potential was applied to the interdigital electrodes located downstream. Nanoparticle-

molecule compounds were then attracted to anodes because of the remained negative charges on gold nanoparticles (Figure 3a). Here the two-anode configuration was designed so the assembly process would eventually bridge the anode pair with aggregates and form the chemiresistor. Our control experiment verified that dithiol molecules are necessary to crosslink gold nanoparticels. Without dithiol molecules, there would be no self-assembly of nanoparticle film on the electrodes.

Process II: Instead of using only gold-thiol chemistry to crosslink gold nanoparticles, we introduced positively-charged rotaxane molecules[3] to interact with negatively charged gold nanoparticles. Electrostatic attraction force efficiently pulled gold nanoparticles and rotaxanes together while gold-thiol chemistry further strengthened the aggregated structure[4]. As shown in Figure 3b, the aggregate deposited along the flow interface and bridged the interdigital electrodes. Different from Process I, electric field was not applied in Process II assembly (although it will be shown that electric field may provide a better cross-linked film in this process). Table I then shows the assembly parameters for Process I and II.

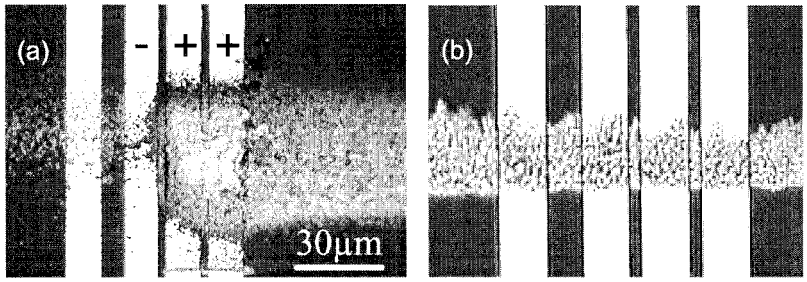

Figure 3. (a), (b). Nanoparticle films prepared with shear-flow-assembly Process I, II.

	Solvent	Gold nanoparticle	Linker molecule	Flow rate	Applied potential	Assembly time
Process I	Ethanol	30 nm 2×10^{11}/ml	bisdisulfide[3] 100 μM	0.2 μL/min	2 V	2~5 hr
Process II	Acetonitrile	30 nm 2×10^{11}/ml	rotaxane[3] 10 μM	1.0 μL/min	no	5~25 min

Table I. Shear-flow-assembly process parameters. Channel cross-section: 10(H) × 100(W) μm^2

3. Results and discussion

To study the effect of electric field on thiol-gold assembly efficiency, we setup an assembly cell (Figure 4) containing a pair of gold plate electrodes which were immersed in rotaxane molecule solution. A sinusoidal electrical potential with DC offset was applied to the electrodes when rotaxane molecules assembled to gold surface. After assembly, gold electrodes were flushed with acetonitrile followed by deionized water. XPS analysis were then carried out on the cathode gold electrode surfaces. Results (Figure 5) indicated that electric field enhanced the assembly efficiency of rotaxane to gold surface. Without electric field, we observed no Au signal decreasing over assembly time meaning rotaxane assembly to gold surface did not happen. Electric field can therefore be used to produce a better cross-linked nanoparticle film in our shear-flow-assembly process.

Finally, chemiresistor chip fabricated with either process were tested with various vapor sources and conductance changes due to the vapor exposure were recorded. Preliminary results (Table II) showed that our self-assembled nanoparticle films are adequate for vapor sensing purpose. Sensing response drift and sensitivity of the fabricated chemiresistors are under study.

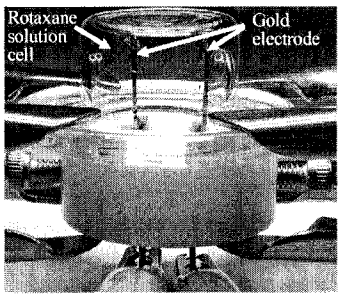

Figure 4. Electric-field-enhanced self-assembly cell. Potential applied: 1 Hz, 600 mVpp sinusoidal signal with 200 mV DC offset. Electrodes distance: 5 mm

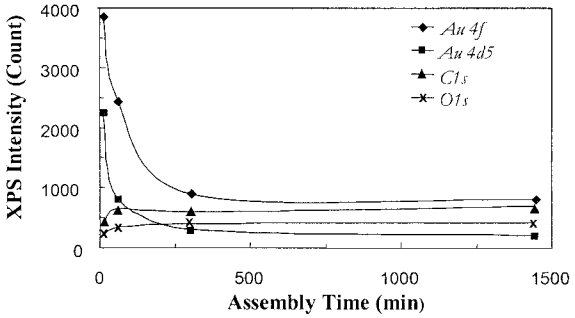

Figure 5. XPS data of rotaxane-assembled gold electrode (cathode). The decrease of gold signal and increase of carbon and oxygen signals over time implied an increasing surface coverage with rotaxane under electric field enhancement.

Vapor source	Water	IPA	Acetone	Dichloromethane
Resistance change $\Delta R/R_0$ (%)	-35	506	58	-30

Table II. Conductance change of Process II chemiresistor exposed to air which is saturated with various vapor sources at 24^0 C, 33% humidity (100% humidity in the case of water vapor). Prepared chemiresistor has a resistance level of 10E9 Ω. R_0 is the chemiresistor resistance before vapor exposure.

Acknowledgements

This work is sponsored by DARPA Biomolecular Motor (BMM) project and the NSF Center for Neuromorphic Systems Engineering (CNSE) at Caltech.

References

[1] H. Wohltjen, A.W. Snow, Anal. Chem., **70**, p2856, (1998)

[2] T. Vossmeyer, B.Guse, I. Besnard, R.E. Bauer, K. Mullen, A. Yasuda, Adv. Mater., **14**, No. 3, p238, (2002)

[3] C.Y.Shih, S. Zheng, E. Meng, Y.C. Tai, Y. Liu, J.F. Stoddart, *MEMS '04,* Maastricht, Netherlands, Jan. 25-29, p422, (2004).

[4] A.N. Shipway, M. Lahav, R. Gabai, I. Willner, Langmuir, **16**, p 8789, (2000)

DEVELOPMENT OF A MICROFLUIDIC DEVICE USING NANOPARTICLE-BASED BIO-BARCODES FOR ULTRA-SENSTITIVE DETECTION OF PROTEINS

Edgar D. Goluch[1], Jwa-Min Nam[2], Thomas N. Chiesl[3], Kashan A. Shaikh[1], Kee Suk Ryu[1], Annelise E. Barron[3], Chad A. Mirkin[2] and Chang Liu[1]

[1]*Micro Actuators, Sensors, and Systems Group, University of Illinois at Urbana-Champaign, 208 N. Wright St., Urbana, Illinois 61801, USA*

[2]*Institute for Nanotechnology and Department of Chemistry, Northwestern University, 2145 Sheridan Rd., Evanston, Illinois 60208, USA*

[3]*Department of Chemical and Biological Engineering, Northwestern University, 2145 Sheridan Rd., Evanston, IL 60208, USA*

Abstract

We present a microfluidic system that allows for ultra-sensitive protein detection. The system integrates the bio-bar-code amplification (BCA) [1] approach with silver staining on a single microfluidic device to detect Prostate Specific Antigen in concentrations as low as 500 attomolar (300 proteins in the entire sample), using several orders of magnitude less sample volume than necessary for the bench-top assay.

Keywords: protein detection, Bio-Bar-Code, polyDuramide, nanoparticles

1. Introduction

Recently, a technique was developed by the Mirkin group that allows for ultra-sensitive detection of proteins via the combined use of magnetic microparticles and gold nanoparticles. The magnetic particles (MMP) are functionalized with monoclonal antibodies that specifically recognize a target protein. Gold nanoparticles (NP) are functionalized with polyclonal antibodies, and are also densely coated with a distinctive DNA sequence (bar-code DNA) unique to the target. After binding and recognition, the sandwich assay is magnetically separated, followed by thermal release of the target DNA and detection, including in some cases a target amplification step by PCR. Prostate-specific antigen (PSA), a potential marker for prostate and breast cancer, was detected by this approach down to a limit of 30 attomoles, several orders of magnitude below current clinical methods.

In new work, we have demonstrated this technique in a microfluidic device, using an integrated in-line detection scheme in which separation, purification and detection of PSA from upper attomolar to lower femtomolar has been accomplished. Several iterations of protocol development were performed to adapt the standard BCA approach to a microchannel format.

2. Theory

Microfluidic chips (3.2cm long and 1.5cm wide) were fabricated using a combination of polydimethylsiloxane (PDMS) and glass slides. Multilayer soft lithography was employed to provide individually addressable micromechanical valves that are controlled by pressure sources [2]. Pressure sources were actuated by a National Instruments DAQ card and a graphic interface developed with Labview 6.0.

It is well known that protein adsorption occurs on both glass and PDMS surfaces. Experiments conducted using blank samples and samples containing 3 nM PSA in the microfluidic chips with and without a novel hydrophilic coating (poly-*N*-hydroxyethylacrylamide, or polyDuramide) [3] revealed that the coating significantly reduces the adsorptive interactions of both the target protein and bar-code DNA coated NP with the glass and PDMS surfaces, thereby reducing background noise and increasing signal specificity. The results of these experiments are shown in Figure 1.

Initial devices used off-chip PCR to verify the release of bar-code DNA product in the presence of PSA. Next-generation devices include a bar-code DNA capture and detection area for on-chip silver staining, thus completing the design of a fully integrated device as seen in Figures 2 and 3. "Capture DNA", specific to half the bar-code DNA sequence, is spotted on the glass surface of the chip to allow capture of the bar-code DNA.

3. Experimental

In a typical experiment, the protocol is divided into two steps: target separation and bar-code detection. Before the sample is introduced to the chip, the separation area is coated with a polyDuramide solution. The target protein is then mixed with MMP and NP probes and incubated for 30 min at 37 °C to allow the protein to become sandwiched between the probes. The sample is then loaded into the separation area on the chip and the sandwiched protein is removed from the sample through application of a magnet underneath the chip. The supernatant is removed with a PBS buffer wash while the magnetic parts are still immobilized on the chip surface. Next, the bar-code DNA is released from the NP by flowing deionized water through the chip. The bar-code DNA hybridizes with capture DNA strands that are patterned in the detection area.

Bar-code detection is carried out by flowing through a second set of NP functionalized to match the other half of the bar-code DNA sequence to complete the sandwich assay. PBS buffer is run through to remove any unbound NP. Next, a surfactant solution is drawn through the detection area to prime the NP. Finally premixed silver staining solution is added, which preferentially stains the gold nanoparticles. The top PDMS piece is then removed and the results are visualized.

4. Results and discussion

The chips are disposable, although the top polymer part can be reused several times with only the DNA coated glass slide being replaced. Results from the employed protocol can be visualized by simple inspection, if for example the system is used in field operations. Quantitative data (Figure 4) was obtained from the microfluidic chips using a Verigene ID optical detection instrument that measures scattered light (Nanosphere, Inc., Northbrook, Illinois). The data indicates that this system can clearly resolve protein concentrations in the femtomolar level and shows that even lower concentrations can be detected in the future.

5. Conclusions

We have presented an integrated microfluidic chip that sequentially processes microliter volumes to detect variable concentrations of scarce protein analytes. PSA levels as low as 500 attomolar were detected. Future work includes parallel sample screening as well as detection of multiple protein targets.

Acknowledgements

The authors would like to thank Andrew Shaw, Yelena Grinkova, and Prof. Steve Sligar for assistance with initial experiments and helpful discussions. This work was supported by the Nanoscale Science and Engineering Initiative of the National Science Foundation under NSF Award Number EEC-0118025 and the AFOSR and DARPA via a DURINT award.

Any opinions, findings, and conclusions or recommendations expressed in this material are those of the authors and do not necessarily reflect those of the National Science Foundation.

References

[1] J.-M. Nam, C. S. Thaxton, and C. A. Mirkin, *Science*, 301(5641), 1884-1886 (2003).
[2] M. A. Unger, H.-P. Chou, T. Thorsen, A. Scherer, and S. R. Quake, *Science*, 288(5463), 113-116 (2000).
[3] M. N. Albarghouthi, T. M. Stein, and A. E. Barron, *Electrophoresis*, 24, 1166-1175 (2003).

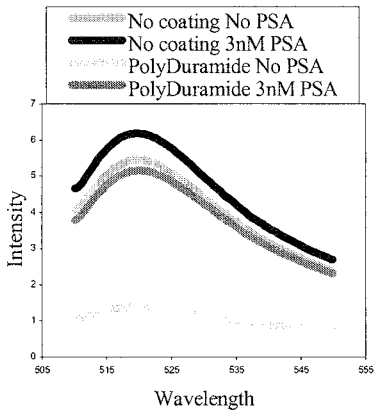

Figure 1. PolyDuramide testing results.

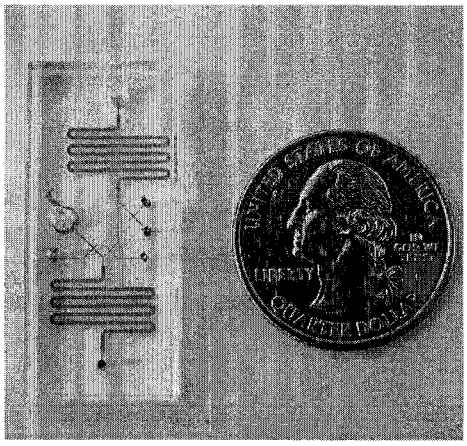

Figure 2. Microfluidic Device.

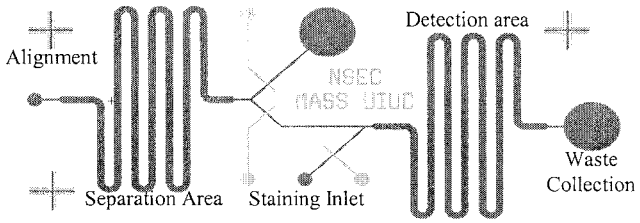

Figure 3. Schematic diagram of a microfluidic chip. Light gray depicts control valves. Dark gray indicates fluid channels. Alignment marks are used for proper orientation of control valves with fluidic channels during fabrication.

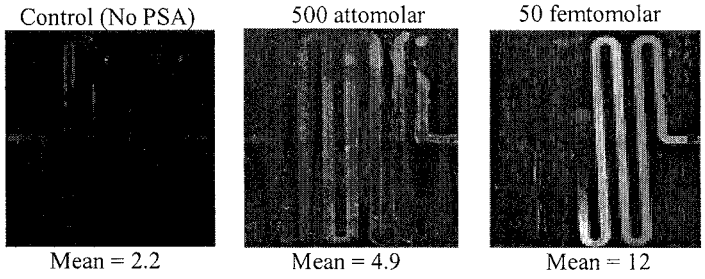

Figure 4. Optical scanning of developed silver stained biobarcode DNA. The control experiment (left) was run with no PSA present while 500 aM and 50 fM results are presented center and right. Average signal intensities are given as 2.2, 4.9 and 12 respectively.

MULTICHANNEL CONTINUOUS FLOW MICROFLUIDIC SYSTEM FOR SINGLE MOLECULE VIALS

Andreas Jahn[1], Wyatt N. Vreeland[2], Michael Gatain[1], Laurie E. Locascio[2]
[1]Semiconductor ElectronicsDivision and [2]Analytical Chemistry Division, National Institute of Standards and Technology, Gaithersburg, Maryland, USA

Abstract

We describe a continuous flow microfluidic network that facilitates the self-assembly of lipids into liposomes for single-molecule containers. Modulation of the flow rates and species concentrations allows for reproducible control of both the liposome size (with a remarkably narrow size distribution) as well as the concentration of molecules of interest encapsulated in the liposomes. Our apparatus, under appropriate conditions produces liposomes with a diameter of 100 nm that encapsulate low concentrations of carboxyfluorescein.

Keywords: liposome, single-molecule, self-assembly, nanoparticle

1. Introduction

The statistical distribution and variation of individual biomolecules is of interest to understand their biophysical behavior and to determine the accuracy of measurements of increasingly small sample populations [1]. We present results on a new continuous flow microfluidic system for self-assembly of liposomes to encapsulate water-soluble reagents. We are particularly interested in utilizing this approach to produce liposomes as single molecule vials and nanochemical reactors for single molecule manipulation and measurement. Liposomes are composed of one or more concentric bilayers of phospholipids that are bathed in an external aqueous solution and encapsulate a finite internal aqueous volume. Liposomes are typically formed *via* a variety of methods that all involve manipulation of fluids on the centimeter length scale. This leads to mechanical and chemical forces that are highly variable during the formation process, which in turn creates populations of liposomes that are highly variable in size and lamellarity (the number of lipid layers). Our microfluidic flow network approach allows for fine control of both the chemical and mechanical environment in which the lipids self assemble into liposomes. This enables for reproducible control and adjustment of the liposome size and distributions as well as the amount and concentration of analyte encapsulated in the liposome [2-3].

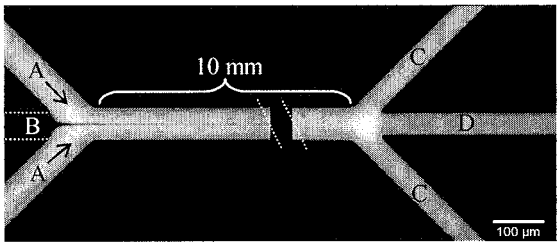

Figure 1. Fluorescence micrograph of the microfluidic device for liposome self-assembly. The left panel shows the region where the aqueous (channel A) and alcohol (channel B) phases intermix and liposomes are formed. The arrows indicate the direction of flow. The right panel depicts the region where the excess aqueous phase is removed (channel C) and the liposomes are collected (channel D).

2. Theory

We have implemented the "injection" method [4] for the formation of liposomes in a microfluidic system. In this technique lipids are dissolved in an organic solvent that is miscible

with an aqueous buffer. This lipid tincture is then diffusively mixed with an aqueous phase, as the two phases intermix the polarity of the solvent increases to a point that the phospholipids are no longer soluble and they self-assemble into liposomes. During this self-assembly process a small amount of aqueous solution is captured in the liposome, thereby forming a small "container". Controlling the concentration of the analyte of interest in the aqueous phase allows one in principle to capture single molecules in each liposome. Such single-molecule vials can be used for further manipulation and measurement of the encapsulated single molecule.

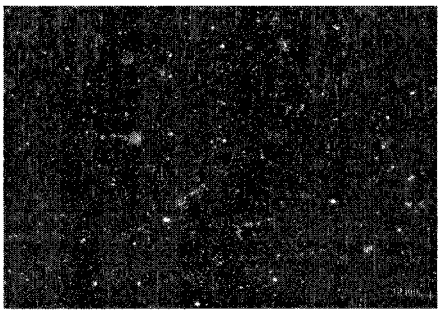

Figure 2. Fluorescence micrograph of a liposome suspension collected from channel D.

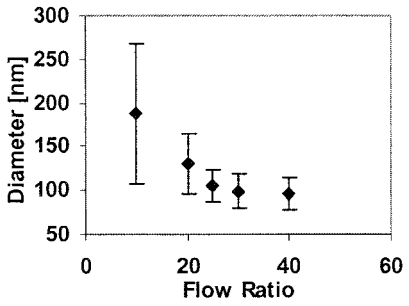

Figure 3. Mean liposome diameter (points) and standard deviation of size distribution (error bars) as a function of flow ratio. Flow ratio is the total flow rate in both side channels (A) divided by the flow rate in the center channel (B). The center channel flow rate was held constant at 1 µl/min.

3. Experimental

The microfluidic device is presented in Figure 1. It consists of a central channel B which contains the lipid tincture (5 mM dimyristoylphosphatidyl-choline, 4 mM cholesterol, 1 mM dicetylphosphate in dry 2-propanol), and two oblique channels A containing the aqueous phase (0.1 mM, 0.5 mM, or 1 mM carboxyfluorescein (CF), 0.1 M phosphate, 2.7 mM potassium chloride 13.7 mM sodium chloride, pH ~ 7.2). The direction of flow is indicated by the arrows. The fluid flows through the devices where excess aqueous phase is removed in channel C and the liposomes are collected in channel D. The channels are fabricated in silicon with an anodically bonded glass cover; dimensions of the channels are either 65 µm or 32 µm wide (to balance the flow rates) and 120 µm deep. Fluidic access ports are etched through the silicon substrate and are mated to syringe pumps through commercial fittings. As the aqueous and alcohol phases meet and begin to flow down the central channel the two phases begin to interdiffuse and the liposomes form at a critical alcohol concentration of approximately 40 volume percent. Figure 2 shows a fluorescence micrograph of the liposomes produced in the microfluidic device.

To determine the amount and concentration of CF that is encapsulated in the liposomes, the initial preparation is collected from the microfluidic device and passed over gel filtration columns to remove unencapsulated CF. The liposome diameter and size distribution is then characterized by quasi-elastic light scattering. Finally the liposomes are lysed by the addition of 10 volume percent of the nonionic surfactant Triton X-100 and fluorescence of the resulting liquor measured.

4. Results and discussion

By modulating the total flow rate in the microfluidic device the average particle diameter changes as is presented in Figure 3. As the total flow rate increases the particle diameter decreases putatively due to increased shear forces as the particles self assemble from their constituent lipids from 170 nm down to a lower limit of approximately 90 nm. Preliminary numerical modeling results underway in our laboratory indicate that the mechanical forces shearing the particles during the formation process approach an asymptote. Additionally, the ability to precisely control the fluid flow rates and patterns enables the particle diameter and distribution to be reproduced multiple times. This is shown in Table 1 where the size and distribution from several different experiments are presented; in each case the diameter is very close to 100 nm with a standard deviation of approximately 15 nm.

Table 1. Reproducibility of liposome size and distribution for multiple experiments. Flow ratio is the total flow rate in both side channels (A) divided by the flow rate in the center channel (B). The center channel flow rate was held constant at 1 μl/min.

Flow ratio	*30*		*40*	
Exp #	**Avg. diameter [nm]**	**Std. dev. [nm]**	**Avg. diameter [nm]**	**Std. dev. [nm]**
1	97.9	15.1	91.4	17.6
2	98.8	15.9	91.4	16.0
3	97.0	23.3	89.9	14.3

Of particular interest in liposome preparation is the encapsulation efficiency of the analyte, that is the concentration of analyte in the liposomes relative to its concentration in the original aqueous phase. Three preparations using 0.1 mM, 0.5 mM and 1 mM CF in the aqueous phase produced liposomes with varying concentration of encapsulated CF with efficiencies ranging from 28.4% for the 0.1 mM CF to 16.8% for the 1.0 mM CF. It is previously noted in the literature that as the concentration of the aqueous phase increases the encapsulation efficiency decreases [5].

5. Conclusions

We believe that with further optimization we can produce liposomes that encapsulate individual molecules or biological molecules. Thus, the liposome will be a container that can be used to localize, manipulate and measure the (bio) molecule and its interaction and/or reaction with other species. Measuring individual molecules rather than ensemble averages of molecules will allow for more fine studies on what factors cause disease states and their etiology.

Acknowledgements

AJ acknowledges Dr. M. Richter of the Fraunhofer Institute IZM for a guest researcher opportunity at NIST. WNV acknowledges support from the NIST NRC postdoctoral program. This work was supported by NIST's Single-Molecule Measurement and Manipulation Program.

References

[1] A.D. Mehta, M. Rief, J.A. Spudich, D.A. Smith, R.M. Simmons, *Science,* **283**, 1689-1695 (1999).
[2] A. Jahn, W.N. Vreeland, M. Gaitan, and L.E. Locascio, *JACS*, **126**, 2674-2675 (2004).
[3] A. Jahn, W.N. Vreeland, L.E. Locascio, and M. Gaitan, *Solid-State Sensor, Actuator and Microsystems Workshop Proceedings*, 274-277, (2004).
[4] S. Batzri, E.D. Korn, *Biochim Biophys Acta,* **298**, 1015-1019 (1973).
[5] R.T. Fraley, C.S. Fornari, and S. Kaplan, *PNAS,* **76**, 3348 (1979).

STUDY OF INTERFACE CONDUCTIVITY AND ITS POSSIBLE APPLICATIONS

N. J. Petersen, D. Dutta, J. P. Alarie, and J. M. Ramsey
Dept. of Chemistry, The University of North Carolina at Chapel Hill, Chapel Hill, NC 27599-3290 USA

Abstract

When channel dimensions are in the submicron range, the electrical double layer can impact electrokinetic transport. We have previously demonstrated several applications using electrical double layer overlap effects [1-3]. This study investigates the influence and possible applications of the interface conductivity in nanochannel devices.

Keywords: Interface conductivity, nanochannels, EOF pump, preconcentration

1. Introduction

The interface conductivity arises mainly from counter ions of the ionized surface. For a glass channel filled with buffer, there will be an excess of mobile cations located in the electrical double layer. With the high surface-to-volume ratio present in nanochannels, this interface conductivity starts to dominate over the conductivity of the buffer ions. Unlike electrical double layer overlap, which can only be achieved using very low buffer concentrations (0.01 mM-0.1 mM) in ≈100 nm channels, the increased conductivity from the ions in the double layer can be observed when using much higher concentrations and deeper channels.

The difference in the bulk conductivity between micro and nanochannels filled with the same buffer as well as the difference in ionic transport may be useful for sample preconcentration and pumping devices.

2. Theory

The overall conductivity κ_{app} of a buffer in a channel with width, w_{ch}, and depth d_{ch} can be described by

$$\kappa_{app} = \kappa_b + \frac{\kappa^\sigma 2(w_{ch}+d_{ch})}{d_{ch}w_{ch}} \quad \Rightarrow \quad \kappa_{app} = \kappa_b + \frac{2\kappa^\sigma}{d_{ch}}, \quad for\ w_{ch} >> d_{ch} \tag{1}$$

where κ_b is the conductivity of the buffer and κ^σ is the interface conductivity.

Dependent on the buffer used, the interface conductivity may result in the current being carried by different ratios of cations/anions in a nanochannel compared to a microchannel. In this case, applying an electric field from a microchannel across a nanochannel, a depletion of both cations and anions is expected to occur in the microchannel. When applying the field from the nanochannel across the microchannel a concentration of ions is expected to occur in the microchannel. The surface conductivity may also enhance the performance of EOF pumping devices due to the mismatch in electrical conductivity of the micro- and nanochannel (Figure 1).

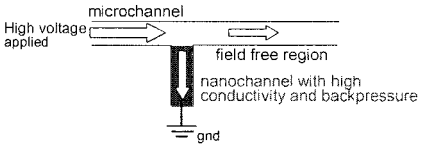

Figure 1. A simple EOF pump based on difference in overall conductivity of the nano- and microchannel.

The volumetric flow rate V in a channel is dependent on the electroosmotic mobility μ_{eo}, the field strength E and cross sectional area A:

$$V = \mu_{eo} \cdot E \cdot A = \frac{\mu_{eo} \cdot I}{\kappa_{app}} \tag{2}$$

where I is the current.

According to this equation, pumping can be achieved by applying an electrical potential between a micro and nanochannel since the nanochannel will have a higher conductivity.

3. Experimental

The apparent conductivity of tetraborate buffer with concentrations ranging from 0.01 mM to 100 mM was measured in quartz chips with depths of 121 nm and 980 nm, and compared with measurements performed using a conductivity meter (Figure 2).

To test for ion concentration and depletion a device combining micro and nanochannels was created by bonding a 6.1 μm deep channel with a 100 nm deep channel etched in the cover plate (Figure 3). All the channels where filled with 50 μM rhodamine-6G prepared in 0.1mM tetraborate buffer. The fluorescence at the nano-micro channel cross intersection was then observed when applying low fieldstrengths between the different channels (Figure 3). The generated concentration profiles were also confirmed by measuring the conductivity in the 6 μm deep channel after depletion and concentration runs (Figure 4).

4. Results and discussion

From the conductivity measurements (Figure 2) it is seen that the conductivity is significantly higher in the nanochannels. The minimum conductivity that could be obtained in the 121 nm deep quartz chip was $2 \cdot 10^{-9}$ $cm^{-1}\Omega^{-1}$, which is similar to the bulk conductivity of a 1.3 mM tetraborate buffer. The measurements fit well with equation 1 using $\kappa^{\sigma}=1.6 \cdot 10^{-9}$ Ω^{-1} as a constant for all buffer concentrations (Figure 2).

The expected ion depletion and concentration was observed both visually (Figure 3) and from current measurements (Figure 4). Concentration of buffer and sample ions was observed after applying a field from the nano to the microchannel and depletion was observed with the electrical potential applied from the micro towards the nanochannel. During these runs pumping of the depleted zone into the field free channel could also be observed (Figure 3f). The device was however not optimized for high efficient pumping since most of the field drop was in the nanochannel. By using a much shorter nanochannel compared to the microchannel more of the applied field will be dropped in the microchannel and better pumping is expected.

Acknowledgements

This research was supported by the Defense Advanced Research Projects Agency, US Department of Defense under contract 03N16. Oak Ridge National Laboratory is managed and operated by UT-Battelle, LLC under contract DE-AC05-00OR22725 with the U.S. Department of Energy. The authors would like to thank Leslie Wilson for fabrication of the microchip devices.

References

[1] S. C. Jacobson, J. P. Alarie, J. M. Ramsey, Micro Total Analysis Systems 2001, Norwell, MA 2001; Kluwer Academic Publishers; pp 57-59.

[2] J. M. Ramsey, J. P. Alarie, S. C. Jacobson, N. J. Petersen, Micro Total Analysis Systems 2002, Nara, Japan 2002; Kluwer Academic Publishers; pp 314-316.

[3] N. J. Petersen, J. P. Alarie, S. C. Jacobson, J. M. Ramsey, Micro Total Analysis Systems 2003, Squaw Valley, CA USA 2003; Mesa; pp 314-316.

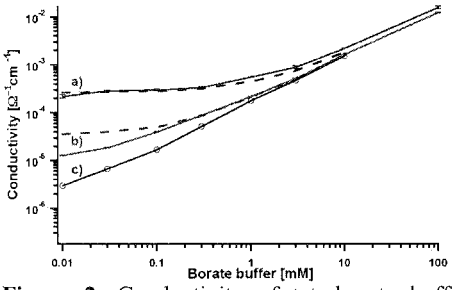

Figure 2. Conductivity of tetraborate buffer with concentrations of 0.01; 0.03; 0.1; 10; 100 mM measured in quartz chips with depths of (a) 120 nm and (b) 970 nm and compared with measurements performed on a conductivity meter (c). The experimental data was fitted (broken lines) with equation 1 using $\kappa^{\sigma}=1.6\cdot10^{-9}\ \Omega^{-1}$.

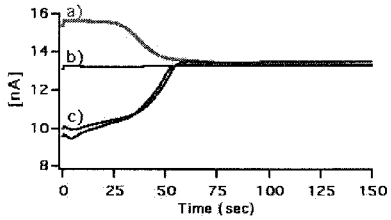

Figure 4. Measured conductivity changes after concentration and depletion runs. The current was measured in the microchannel when applying 46V (32V/cm) a) after 400s preconcentration b) after no preconcentration or depletion, c) after 400s depletion.
All the channels were initially filled with 1mM tetraborate buffer.

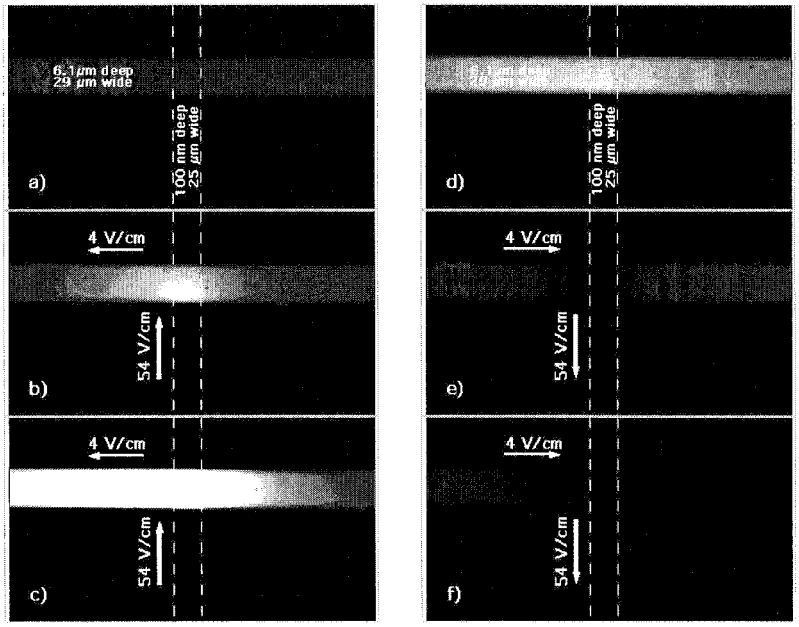

Figure 3. Visualization of ion concentration and depletion at a nano-microchannel junction. All channels where filled with 50µM rhodamine-6G dissolved in 0.1mM borate buffer. Concentration runs: 46V was applied from the nanochannel towards the microchannel (left side) a) 0s, b) 60s c) 240s.
Depletion runs: 46V was applied from the microchannel towards the nanochannel
d) 0s, e) 20s and f) 400s

3D CELLULAR IMPRINTING TECHNIQUE FOR FABRICATION OF BIO-ACTUATED MICRO DEVICES

Keisuke Morishima[1], Yo Tanaka[2], Mitsuhiro Ebara[3], Tatsuya Shimizu[4], Masayuki Yamato[4], Akihiko Kikuchi[4] , Teruo Okano[4] and Takehiko Kitamori[1,2,5]

[1] *Kanagawa Academy of Science and Technology, 3-2-1 Sakado, Takatsu-ku, Kawasaki 213-0012, Japan*
[2] *Dept. of Applied Chemistry, The University of Tokyo, Tokyo, Japan*
[3] *Dept. of Applied Chemistry, Waseda University, Tokyo, Japan*
[4] *Institute of Advanced Biomedical Engineering & Science, Tokyo Women's Medical University*
[5] *CREST, Japan Science and Technology Corporation, Tokyo, Japan*

Abstract

We succeeded in micropatterning cells on a culture dish coated with temperature-responsive polymer, poly(N-isopropylacrylamide) (PIPAAm) and in imprinting the patterned cell sheets to 3D microstructures by using the nature of the PIPAAm. We have already demonstrated the principle of the bio-actuated microsystem using cultured cardiomyocytes driven only by chemical energy in μTAS'03[1]. In this paper, a different fabrication approach for bio-actuated micro devices using cultured cardiomyocytes sheets was presented. This technology should have enormous potential for constructing in vitro 3-D bio-actuated micro devices and bio-hybrid devices, such as a micropump [3] and a microvalve, as an artificial organ system.

Keywords: cellular imprinting, bioactuator, PIPAAm, cell patterning

1. Introduction

In μTAS'03, we have demonstrated a principle of bio-actuated microsystems using cultured cardiomyocytes, which can be driven without any external power supply such as electricity or magnetic forces but chemical energy [1]. We would like to expand the concept and like to demonstrate a variety of microstructures can be actuated by living materials. In order to design such kinds of micro devices and improve their performance, novel cell patterning method to control force of the cells is needed. In this paper, we propose a different fabrication approach for improvement of the performance of such bio-actuators with regard to force and displacement.

2. Experimental

Fig. 1 shows the novel cellular imprinting method for fabrication of the bio-actuated 3D-structures. We utilized cells cultured on a surface grafted with temperature-responsive polymer, poly(N-isopropylacrylamide) (PIPAAm), from which cultured cell sheets could be detached simply by reducing temperature. No enzymatic treatments were required for breaking bonds between the cell sheets and the PIPAAm surface.

Firstly, using a mask inside culture medium, cardiomyocytes were cultured on a selected part of a surface of a culture dish coated with PIPAAm.

Secondly, patterned cell sheets on the PIPAAm-coated surface were transferred to 3D-structures made of soft materials. In the present work, we utilized PDMS for the 3D microstructures, because PDMS has great affinity to a living tissue, and its stiffness and surface chemistry are much easier to be controlled than those of silicon MEMS structures. PDMS microstructures (micropillar structures with 20 μm x 20 μm cross section and 30μm height) completely sterilized were coated by fibronectin. And they were contacted to the pattered cell sheet on the PIPAAm surface. Then the temperature was reduced.

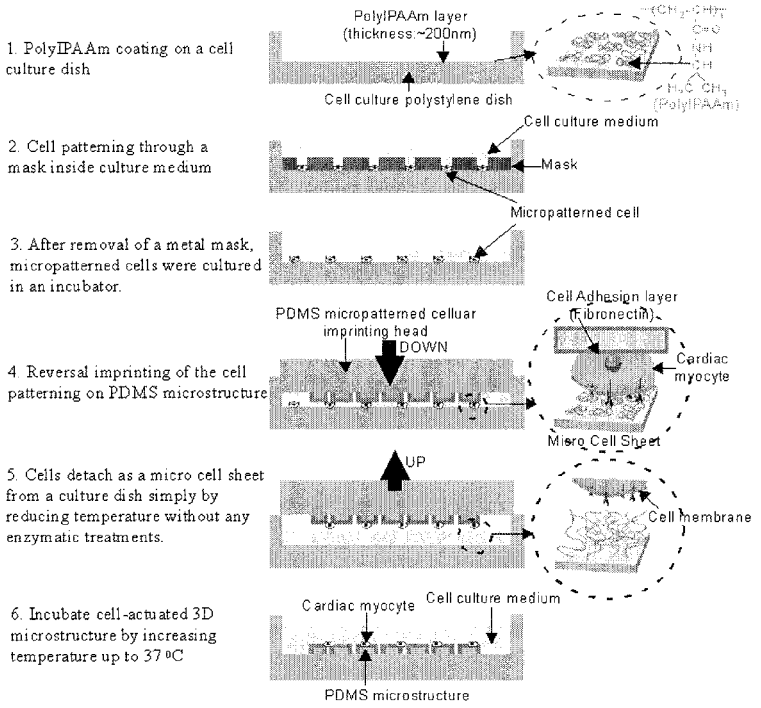

Figure 2. New cellular imprinting method and fabrication procedure for cell-actuated 3D microstructure using cardiomyocytes and novel cell culture surfaces grafted with temperature-responsive polymer, poly(Nisopropylacrylamide)(PIPAAm).

Finally, cardiomyocytes attached onto the PDMS microstructures were further cultured for three days at 37°C in an incubator, as shown in Fig. 2.

3. Results and discussion

By microscopic observation of the bio-actuated structures after three days of incubation, it was confirmed that the sheets of cardiomyocytes were successfully transferred onto the PDMS substrates. Some were stretching along on the foot of the micropillars and some were sticking near the top of the pillars. Synchronous motions of the cardiomyocytes with relatively large force and displacements were observed, because the cardiomyocytes formed relatively thick fiber-like structures (Fig. 3).

Now mainstream of cardiac tissue engineering is to utilize biodegradable scaffolds as temporal extracellular matrices. New methods using pulsatile cardiac grafts by cell sheets layers three dimensionally, as described in the present work, is now starting to attract interests. [2] The results in the present work also have a potential to contribute to development of bio-actuated micro devices and artificial organ systems.

4. Conclusions

In conclusion, a novel cellular imprinting method utilizing cells pattered on a temperature-responsive polymer surface have been developed. It was shown to be very useful for fabrication of bio-actuated micro devices using cultured cardiomyocytes. This technology should have enormous potential for constructing in vitro 3-D bio-actuated micro devices and bio-hybrid devices, such as a micropump [3] and a microvalve, as an artificial organ system.

Acknowledgements

This work was partly supported by the Kurata Memorial Hitachi Science and Technology Foundation, Japan.

References

[1] K. Morishima, Y. Tanaka, K. Sato, M. Ebara, T. Shimizu, M. Yamato, A. Kikuchi, T. Okano and T. Kitamori, Proceedings of MicroTAS '03, pp. 1125-1128.

[2] T. Shimizu, M. Yamato, Y. Isoi, T. Akutsu, T. Setomaru, K. Abe, A. Kikuchi, M.Umezu, T. Okano, Circ Res, 90, e40-e48, (2002).

[3] Y. Tanaka, K. Morishima, T. Shimizu, M. Yamato, A. Kikuchi, T. Okano and T. Kitamori, Proceedings of MicroTAS '04,. in press).

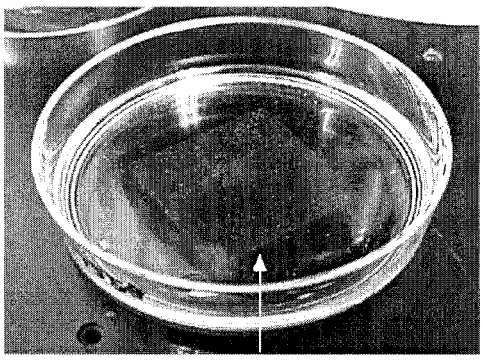

Figure 2. PDMS micropatterned celluar imprinting structure. This device in a petri dish were cultured at 37°C in an incubator.

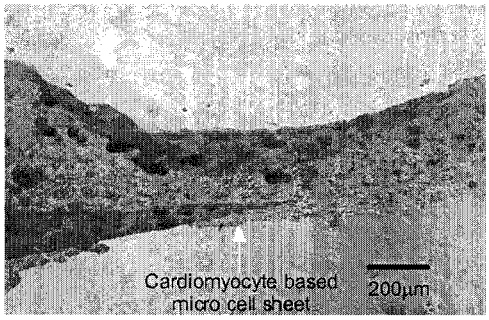

Figure 3. Cardiomyocytes based micro cell sheet. Large displacement of this strucure was observed.

PARALLEL MICROFLUIDIC PROCESSING OF PROTEIN ASSEMBLY QUANTIFIED USING SPR MICROSCOPY

Mark Blaylock, Elain Fu, and Paul Yager
Dept. of Bioengineering, University of Washington, Box 352255, Seattle, WA 98195, USA

Key words: surface plasmon resonance, microfluidics, assembly, immunoassay

1. Introduction

Surface plasmon resonance (SPR) microscopy affords a means of simultaneously quantifying multiple analytes in small liquid specimens. In combination with disposable microfluidic devices, SPR microscopy can potentially enable a variety of point-of-care medical diagnostic tests. We have undertaken the development of a microfluidic immunoassay system that would ultimately be capable of monitoring at least 20 analytes in saliva. Toward that end, we have built a novel SPR microscope [1]; we have established a simple and quick microscope calibration method [2]; and we have established methods for patterning gold surfaces with functional proteins (see below).

Figure 1 is a cartoon representation of one of our detection formats - a competition immunoassay. Analyte-specific antibodies are indirectly immobilized on glass-supported gold coatings, which constitute the bottoms of microchannels in laminated devices. Streptavidin (SA) links the biotinylated antibodies to biotinylated bovine serum albumin (b-BSA), which is physically adsorbed on the gold. Specimens are injected into the channels. Free analyte molecules from the specimens compete with added analyte-protein conjugates for binding sites of the immobilized antibodies. Affinity-bound conjugates induce detectable localized changes in reflectivity of the gold coatings, the magnitudes of which are inversely correlated with the concentrations of free analyte molecules.

We investigated a model system involving biotinylated anti-fluorescein (b-anti-F) and a conjugate of bovine serum albumin and fluorescein (BSA-F). A silicone rubber (PDMS) device with microchannels molded into one face was clamped against a gold-coated microscope slide (see Figure 2). The slide was coupled to the prism of the SPR microscope *via* an index matching fluid. Protein and buffer solutions were sequentially incubated in and rinsed from the channels. SPR images were acquired after each rinse. Figure 3 exemplifies the variation in intensities of reflected radiation (gray scale values) that are associated with protein layers of different thicknesses. For our imaging conditions, thicker protein layers appear as lighter regions of the image.

2. Theory

We adapted the methods of Shumaker-Parry and Campbell [3] to quantify the amounts of protein that were bound on our gold surfaces. Those investigators derived an approximate analytical expression, which relates the "effective" thickness of a protein layer to (1) the measured change in reflectivity after deposition of the protein layer, (2) the difference in refractive index between the protein layer and the aqueous medium, (3) the sensitivity of the SPR instrument to changes in bulk refractive index and (4) the penetration depth of evanescent radiation in the aqueous medium above the gold coating. The investigators showed that, over limited ranges, changes in reflectivity are essentially proportional to changes in the apparent refractive index of surface-bound proteins plus aqueous medium. The penetration depth is known to vary with the refractive index and the thickness of a protein layer. Uncertainties regarding penetration depths, as well as the refractive indices of adsorbed protein layers, contribute to uncertainties in the calculated thicknesses of protein layers. Nevertheless, the method provides useful estimates of effective layer thicknesses, which can be interpreted with respect to theoretical values for close-packed monolayers.

3. Experimental

PDMS device. A silicone prepolymer (Dow Corning, Sylgard 184) was poured into a mold, the flat bottom of which supported 158 μm-high hard-baked photoresist (MicroChem, SU-8) in the shapes of desired channels. Holes were punched in the cured device to create ports (see Figure 2).

Buffer and protein solutions. Phosphate buffered saline (PBS, pH 7.4, from pre-measured powder, Sigma, cat. P-3818) was used to prepare all solutions, including SA (US Biological, cat. S7973-75, 1 mg/mL) and BSA-F (Molecular Probes, cat. 23015, 4.5 mol fluorescein per mol BSA, 0.5 mg/mL). Bovine serum albumin (Sigma, cat. A-7030, 10 mg/mL) was incubated on ice for 2 hr with an equal volume of sulfo-NHS-LC-biotin (Pierce, cat. 21335, 1 mg/mL), then extensively dialyzed, to give biotinylated BSA (b-BSA, extent of biotinylation unknown, 5 mg/mL). A solution of b-anti-F (Vector Labs, cat. BA-0601, goat polyclonal, 1 mg/mL in PBS) was used as received.

Protein deposition and SPR microscopy. Protein solutions and PBS were incubated in channels of the PDMS device (channel vol., including ports: 11.6 μL) for at least 30 min (bBSA) or 15 min (SA, b-anti-F, BSA-F). Each channel was rinsed with 1 mL of fresh PBS, after incubation with and removal of a given solution. Images were acquired with p-polarized radiation (850 nm, 64.8° incident angle) and normalized with an s-polarized image to give pixel-by-pixel reflectivity values.

4. Results and discussion

Our PDMS device reliably produced protein patterns of good quality, if care was taken to avoid breaking the seal between the device and the gold surface. Thus, the clamping force was minimized to prevent deformation of the channels; solutions were drawn into the channels under reduced pressure, rather than injected; and positive-pressure rinses were limited to flow rates of 100 μL/min.

Experimental results are exemplified in Figures 3 and 4, and estimates of protein surface coverage from two experiments are tabulated below. Estimates for b-BSA are comparable to a value of 73% reported for plain BSA adsorbed on gold [3]. The ~30% estimate we obtained for SA is considerably lower than a value of 82% reported for the binding of SA to biotin-containing self-assembled monolayers on gold [4], probably due to our use of a non-optimal imaging wavelength. We subsequently found that the use of an optimal wavelength results in ~100% greater *changes* in reflectivity, hence greater estimates for SA coverage. Values for b-anti-F and BSA-F coverage are similarly underestimated below. We detected BSA-F, but the surface coverage estimates involve substantial variances. In more recent experiments, we have improved signal-to-noise by coadding multiple images, as well as optimizing the imaging wavelength for each successive layer of protein.

Proteins deposited in channel	Assumed monolayer (g/cm^2)	Experimental %-monolayer*
b-BSA	2.5×10^{-7} (b-BSA)	68, 81 (averages for 3 channels)
b-BSA / SA	2.8×10^{-7} (SA)	30, 33 (averages for 2 channels)
b-BSA / SA / b-anti-F	2.8×10^{-7} (b-anti-F)	29, 30 (values for 1 channel)
b-BSA / SA / b-anti-F / BSA-F	2.5×10^{-7} (BSA-F)	14, 10 (values for 1 channel)

*calculated from equation 10 of reference 3, assuming refractive index of protein: 1.570, refractive index of PBS: 1.334, penetration depth (0.37 λ): 315 nm, specific volume of protein: 0.77 cm^3/g

References

[1] E. Fu., J. Foley and P. Yager, *Review of Scientific Instruments*, **74**(6), 3182-3184 (2003).

[2] J. Foley, E. Fu, and P. Yager, in *Micro Total Analysis Systems 2003*, M.A. Northrup, K.F. Jensen and D.J. Harrison, eds., Mesa Monographs, 967-970 (2003).

[3] J.S. Shumaker-Parry and C.T. Campbell, *Anal. Chem.*, **76**(4) 907-917 (2004).

[4] K.E. Nelson, L. Gamble, L.S. Jung, M.S. Boeckl, E. Naeemi, S.L Golledge, T. Sasaki, D.G. Castner, C.T. Campbell and P.S. Stayton, *Langmuir*, **17**(9) 2807-2816 (2001)

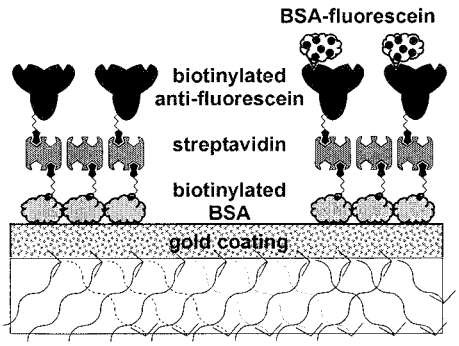

Figure 1. Immunoassay scheme based on immobilized antibodies. Analyte-protein conjugates compete with free analyte molecules (not shown) for binding sites of the antibodies. Proteins modulate the reflectivity of the gold coating. Affinity binding of the conjugates results in greater reflectivity, which is inversely correlated with the amount of free analyte.

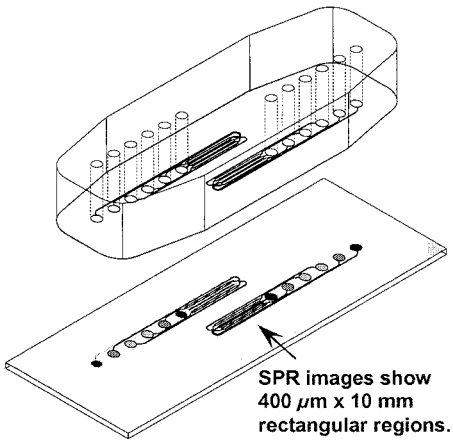

Figure 2. PDMS device with six channels molded in bottom and holes punched through from top (upper). Patterns of proteins deposited on a gold-coated slide while PDMS device was affixed to the slide (lower).

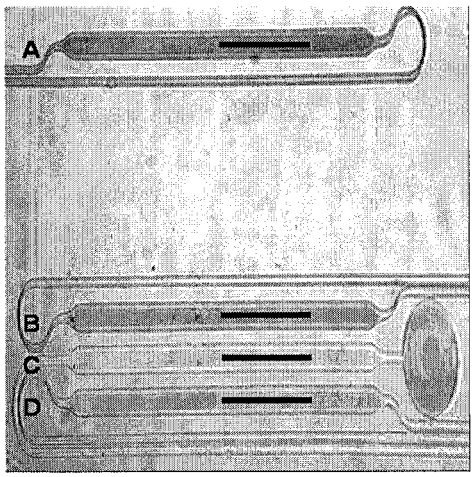

Figure 3. SPR image of protein patterns on gold: (A) PBS control, (B) b-BSA only, (C) b-BSA/SA/b-anti-F/BSA-F and (D) b-BSA/SA. The image is horizontally shortened with respect to the actual object by a factor of ~0.4. Light gray stripes at peripheries of the patterns are optical artifacts. Black bars indicate regions that were analyzed (*ca* 3050 x 75 μm).

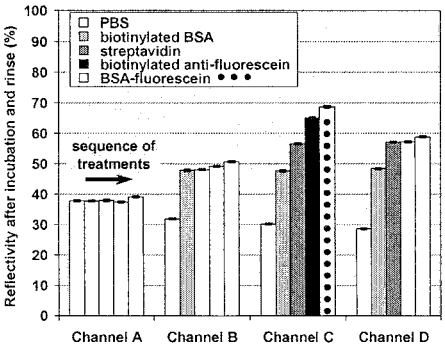

Figure 4. Analysis of SPR images from one experiment. Average reflectivity values of 2000 pixels per channel after each treatment (each cycle of incubation and rinse). Each of the four channels received a different set of five treatments; see the legend and Figure 3. Error bars indicate 95% confidence intervals. *Differences* between average reflectivity values were used to calculate values of surface coverage for each successive layer of protein (see the tabular data above).

MULTIMODE INTEGRATED OPTICAL COMPONENTS FOR μTAS –A RIGOROUS APPROACH

Jörg Hübner, Dan Zauner, Thomas A. Anhøj, Anders M. Jorgensen
Dept. of Micro and Nanotechnology, Technical University of Denmark, Bldg 345 east, DK 2800 Kongens Lyngby, Denmark

Abstract

Multimode waveguides and waveguide components are designed, simulated and fabricated. The waveguide circuitry is highly compatible with traditional microfluidic channel circuitry. Theoretical and simulated results on important parameters such as coupling, propagation and bend loss are compared to measured values. Waveguide crossings are fabricated and it is shown that waveguides crossing each other at an angle of more than 55 degrees have negligble loss penalty.

Keywords: Optical waveguides, waveguide simulations, multi-mode devices, μTAS

1. Introduction

Optical detection methods cover more than 80% of all Lab-on-a-Chip detection schemes. Sensitivity and cross-talk are the critical issues in almost all optical detection systems. Whereas bulk detection schemes are generally highly optimised, there is a certain lack of rigorous systematic optimisation including modelling and simulation of integrated optical components for microfluidic detection schemes. The design of multimode waveguides, including tapers, bends, splitters etc. are often based on experience and rules of thumb and the impressive achievements over the last decade prove that these methods give valuable results. There are essentially two reasons for leaving this well-working and efficient design approach in order to use a more laborious, systematic approach: Optical loss through the system directly reduces the sensitivity, as does cross talk, especially between excitation and signal light of various wavelengths. Thus, even simple components such as straight waveguides, tapers and bends can be responsible for a severe penalty in sensitivity if not designed correctly. The second reason for a more systematic approach lies in the fact that more advanced components e.g. wavelength multiplexers or integrated spectrometers require a deeper understanding of the optical properties of the system in order to achieve specifications that can compete with advanced bulk optical devices.

Design and simulation of the various components are the first steps of the optimisation process. Unfortunately, there is generally no analytical mathematical solution for the fields in optical waveguides and even numerical simulations require highly specialised programs. To ensure correspondence between simulations and the actual measurements, series of waveguide components with variations of selected waveguide parameters have to be fabricated, measured and compared with their simulated counterparts. In this abstract we present examples of such an approach for optically asymmetric SU-8 waveguides, which have previously been reported in [1] and [2].

2. Basic Waveguide Properties

A cross section and refractive index profile of these waveguides are shown in Fig. 1, together with the intensity distribution of the fundamental and third order mode. The height of these waveguides is determined by the height of a microfluidic channel, but the waveguide width can be optimised to ensure minimum coupling loss to the optical fibre used for light input and output. Fig. 2 shows the result of this investigation. A square core of 40 x 40 μm^2 minimizes the loss due to coupling between fiber and waveguide. The loss as function of the waveguide bend radius is an important parameter as it determines the minimum allowable bend radius and thereby the compactness of a waveguide circuit. Fig. 3 shows that the bend loss is a critical function of the bend radius. A decrease in bend radius from 5 mm to 3 mm increases the bend loss by more than an order of magnitude. Moreover, light which is radiated from a waveguide bend can be picked up by a

neighbouring waveguide causing severe cross-talk. Another important parameter is propagation loss as function of wavelength as shown in Fig. 4.

3. Waveguide Crossings

An intersecting waveguide disturbs the mode distribution and some of the power will be coupled to radiation modes and hence lost or contribute to cross-talk. The size of the interacting region depends on the angle between the waveguides, the width of the waveguides and the photolithographic resolution obtained when realising the intersection. A mask with 0, 3, 5 and 10 crossings were made for angles of 25, 35, 45 and 55°. Measured results at a wavelength of 800 nm and simulations (inset) are shown in Fig. 5. The simulations [3] show the field intensity for (TE) mode number 30 when propagating through a crossing. This mode number was chosen for illustrative purposes, but all higher order modes (above order 10) showed similar behavior. One observes that an intersecting angle of 25° between two 40 μm wide waveguides induces a much larger disturbance than for 55° and this is seen in the measurements as higher loss per crossing for the lower angle. For a 25° crossing the loss is 0.25 dB and for a 55° the loss is reduced to 0.05 dB per crossing. It is also seen that the error increases for lower angles. This may be due to problems with resolving the sharp corners during fabrication.

4. Tapers

Coupling losses arises whenever light couples from a waveguide that supports a certain set of modes to another structure with a different set of modes. A continuous change of waveguide cross-section is called a taper and designing tapers basically consist of expanding or reducing the mode cross-section in a controlled manner. From Fig. 2 it can be seen that the coupling loss is minimum for a width of 40 μm thus we fix the initial taper width to this value and change the final taper width and taper length. A taper with no mode conversion is called *adiabatic* and transforms a mode slowly without loss. Fig. 6 shows the calculated coupling coefficient for the fundamental mode c_{11}, as a function of the taper length for final widths of 10 and 70 μm, respectively. Both tapers converge towards adiabatic operation as the length is increased. Insets show the intensity field in a 300 and 1500 μm long taper, respectively, from 40 down to 10 μm and one clearly observes several peaks at the output for the short taper, which means that higher order modes are excited. Only one peak is visible for the long taper and the coupling coefficient has increased to 0.95. A taper length of 3000 μm gives reasonable values for the coupling coefficients in both cases.

5. Conclusions

The presented curves for waveguide crossings, coupling efficiency, bend loss and propagation loss constitute a subset of design rules permitting an optimised waveguide circuit design with respect to loss and compactness. This allows for increased sensitivity and simultaneously enables higher integration density. This kind of systematic investigations is currently extended to a large variety of waveguide components including splitters, multimode interference couplers, arrayed waveguide gratings etc. in order to build a comprehensive library of optimised integrated optical building blocks.

Acknowledgements

The authors thank the Danish Technical Research Council for financial support of the project

References

[1] K. B. Mogensen, J. El Ali, A. Wolff, J.P. Kutter, Appl. Opt., Vol.42, No 19, 2003
[2] J-S. Kim, J-W. Kang, J-J. Kim, Jpn. J. Appl. Phys., Vol. 42 (2003) pp. 1177-1279
[3] EigenMode Expansion, FIMMWAVE™ from Photon Design, Oxford

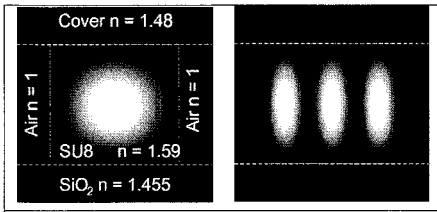

Figure 1: Calculated mode profile of the for the fundamental (left) and third order mode (right) for a 40 µm x 40 µm waveguide. The lower cladding consists of 3 µm of thermally oxidized silicon, upper cladding is a 7 µm PMMA layer.

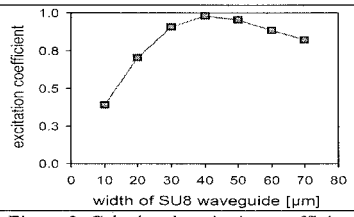

Figure 2: Calculated excitation coefficient when coupling from the fundamental mode of a fiber with 50 µm core diameter and NA of 0.22 into the fundamental mode of waveguides shown in figure 1 but with varying width.

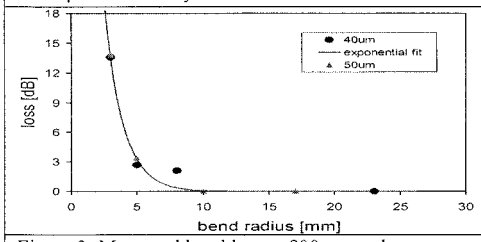

Figure 3: Measured bend loss at 800 nm and exponential fit of data. Excess loss penalty due to a waveguide bend of 120° is tolerable for bend radii above 10 mm, where the loss is below 0.5 dB. The plotted loss data represents loss due to waveguide bends only; all other source of loss are accounted for in the referencing process.

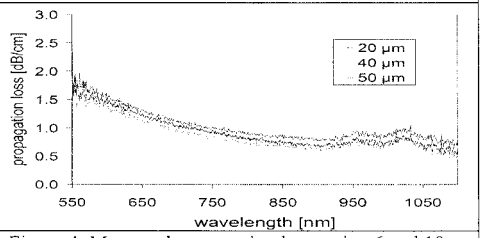

Figure 4: Measured propagation loss, using 6 and 19 cm long waveguides. The long waveguides were curved to fit on a wafer. Bend loss (from Fig. 3) was subtracted. Propagation loss is below 1 dB/cm at around 800 nm and corresponds well with data from other sources.

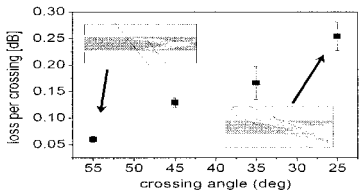

Figure 5: Measured crossing loss between two 40 x 40 µm^2 waveguides with crossing angles between 25 and 55°. The loss drops from 0.25 to only 0.05 dB when the crossing angle is increased waveguides with crossing angles between 25 and 55°. Insets show simulations for order number 30 for the two angles.

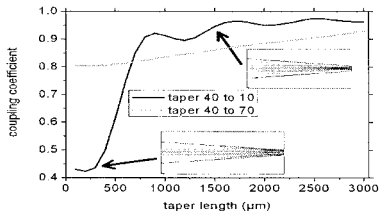

Figure 6: Calculated coupling coefficient c_{11} for the fundamental mode for broad and narrow tapers. A value of 1 means that the taper is adiabatic and both tapers are seen to converge to 1. Insets show that higher order modes are excited in the 300 µm taper, but not in the 1500 µm long taper.

In Vitro Mechanical Cell Loading System for Regenerative Medicine

Fumihito Arai[1], Osamu Suzuki[2], Tomoyuki Uchida[1], Akihiko Ichikawa[1], Toshio Fukuda[1]
Ryutaro Kamijor[3], Takenobu Katagiri[4], Masanori Nakamura[3], Mamoru Numata[5]
Naruaki Watanabe[5]

[1]Nagoya University, 1 Furo-cho, Chikusa-ku, Nagoya City, Japan
[2]Tohoku University, 4-1, Seiryo-cho, Aoba-ku, Sendai City, Japan
[3]Showa University, 1-5-8, Hatanodai, Sinagawa-ku,Tokyo, Japan
[4]Saitama Medical School, Saitama, Japan
[5]JGC corporation, Japan

Abstract

The world's first bio-chip where cells can be loaded by gradient strain was developed. We can quantify cell differentiation and find out the best strain condition for cell culture by using this chip. In this paper, we propose a method for loading, culturing and monitoring of stem cells such as osteoblasts(ST2 cells) and myoblasts(C2C12 cells), and the results of culture. From experiment, osteoblasts grew well in a narrow range, and we quantified their ALP activity as a measure of differentiation. As myoblasts, the direction of their differentiation was perpendicular to an abyss, that is, the same direction of uniaxial strains. We also analyzed strains on a membrane when an air hole is decompressed.

Keywords: Mechanotransduction, Bone, Muscle, Differentiation, Gradient strain

1. Introduction

Regenerative Medicine has an important role for regenerating injured or lost tissues. One of methods to promote regeneration is loading cells in vitro. So far there has been a lot of researches about mechanotransduction, that is, to find out cells' response to mechanical or fluidic strain. For example, it is known that continuous and cyclic strain is effective for maintaining bone structure and function[1]. And it is also known that dynamic strain is more effective than static strain[2]. The fact that bone mass of astronauts fall off during their staying in a weightless state shows that earth gravity is necessary to maintain bone tissues. So far many cell loading apparatuses using a principle such as 4 point bending have been developed, but none of them could load gradient strain to cells[3][4][5].

We made a system where cells can be loaded by gradient strain[6][7], and monitored by a microscope. We also lessened troubles in culturing cells by using a small bio-chip. In this paper, first we propose a bio-chip for cell differentiation and principle of cell loading. Second, we report experiments and results of cell culture. In addition, we also report the results of FEM(Finite Element Method) analysis of bended membrane.

2. Material and Method

Bio-chip is made of PDMS, and process of manufacture is molding. Bio-chip has 4 grooves (depth 100 μm, width 200 μm (Lane 1), 300 μm (Lane 2), 400 μm (Lane 3), 500 μm (Lane 4)), and a sheet of membrane(thickness 100 μm) is stuck on those grooves. Cells on the membrane are given tensile strains when an air hole made between membrane and grooves is decompressed. Fig. 1 shows this concept of cell loading. On the basis of this concept, we made a bio-chip shown in Fig. 2. The merit of this method is that cells can be given 4 different strains (gradient strains) by single decompression.(Fig. 3)

3. Experimental

The period of incubation experiment was one week. On the 1st day, we sowed ST2 cells(bone marrow stromal cells) and C2C12 cells(myoblasts) in a bio-chip. Before sowing cells, we did surface modification on PDMS membrane in order to improve cell adhesiveness on membrane. ST2 cells adhered well on hydrophilic PDMS membrane. After 5 days' culture in a CO_2 incubator, on the 6th and 7th day we gave strains on cells for half a day (gage pressure -60kPa). Finally, we stained cells on the 7th day.

Fig. 4 shows ALP(Alkaline Phosphatase) activity of osteoblasts after 7 days' culture. ALP is a marker of osteoblast's differentiation, so ALP activated area means that stromal cells changed into osteoblasts. As a result, differentiation was promoted better on narrower lane. This result corresponds well to the result of FEM analysis(Fig. 5), for example, few strains appeared on Lane 4. It is easy for bone marrow stromal cells to blanch in a local environment where moderate strain is given.

In a similar way, we did an incubation experiment of myoblasts. The schedule was the same as that of bone marrow stromal cells. Fig. 6 shows immunostaining of MHC(Myosin Heavy Chain) after 7 days' culture. MHC is made from myoblasts(C2C12 cells), and its appearance shows that myoblasts are differentiated into myotubes.

4. Conclusions

The process of differentiation has an important role in regenerative medicine. In this paper, we developed a novel cell-loading system using a PDMS chip to differentiate stem cells, and had an differentiation experiment of osteoblasts and myoblasts. We also calculated stress on the membrane caused by bending using FEM analysis. As a result, we succeeded in loading gradient strains to cells in one chip, and confirmed that osteoblasts branch well in narrow area and the direction of differentiation is parallel to that of strain as myoblasts. In the future, this bio-chip will serve as a tool for searching the best strain condition for cell culture and cell differentiation.

References

[1] D. B. Burr, A. G. Robling, C. H.Turner, Effects of biomechanical stress on bones in animals, Bone vol. 30, pp781-786

[2] C. H. Turner, Three rules for bone adaptation to mechanical stimuli, Bone vol.23, pp399-407

[3] I. Owan, D. B.Burr, C. H. Turner, J. Qiu, Y. Tu, J. E. Onyia, R. L. Duncan, Mechanotransduction in bone: Osteoblasts are more responsive to fluid forces than mechanical strain, American Journal of Physiology – Cell Physiology, pp810-815

[4] M. Wong, M. Siegrist, K. Goodwin, Cyclic tensile strain and cyclic hydrostatic pressure differentially regulate expression of hypertrophic markers in primary chondrocytes, Bone vol. 33, pp685-693(2003)

[5] N. Basso, J.N. M. Heersche, Characteristics of In Vitro Osteoblastic Cell Loading Models, Bone vol. 30, pp347-351(2002)

[6] jp. Pat. No. 2003-130167

[7] jp. Pat. No. 2003-382974

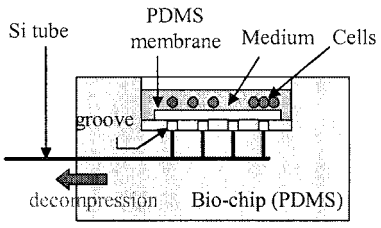

Figure 1. Concept of cell loading

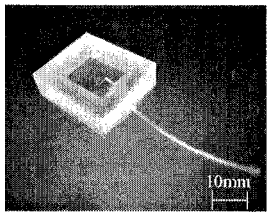

Figure 2. Overview of a Bio-chip

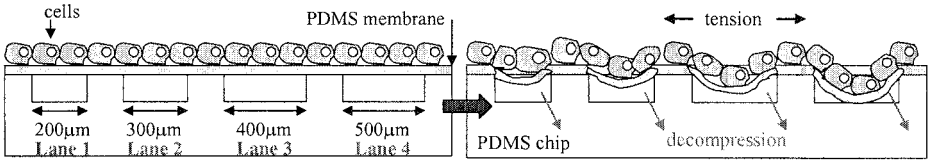

(a)Before decompression **(b)After decompression**

. Figure 3. Schematic of gradient strain

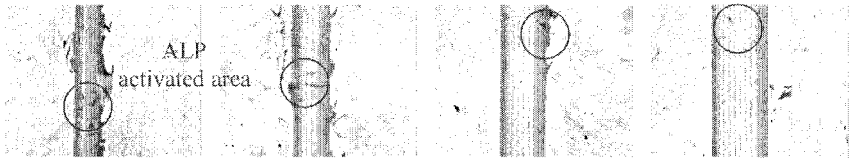

(a) Lane 1 **(b) Lane 2** **(c) Lane 3** **(d) Lane 4**

Figure 4. ALP activity of osteoblasts in each area

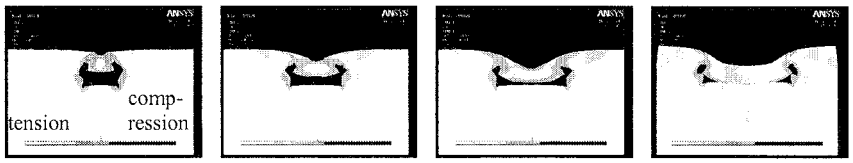

(a) Lane 1 **(b) Lane 2** **(c) Lane 3** **(d) Lane 4**

Figure 5. FEM analysis of bended PDMS membrane

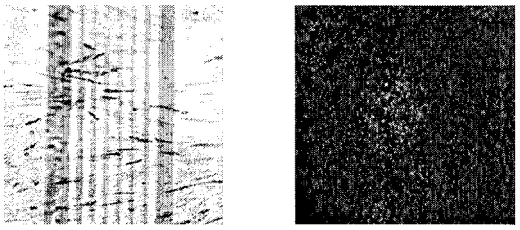

(a) **(b)**

Figure 6. (a) Immunostaining of MHC (b) DAPI staining

CHARACTERIZATION OF NEURAL CELLS FOR CELL SORTING USING FLOW INDUCED ELECTRICAL ADMITTANCE SPECTRA IN MICROFLUIDICS

J. Collins[1], L. Flanagan[3], N. Jeon[1,4], E. Monuki[3], P.H. Schwartz[5], A.P. Lee[1,2]

[1]Department of Biomedical Engineering, [2] Department of Mechanical and Aerospace Engineering, [3]Department of Pathology, [4]Department of Material Science and Chemical Engineering, [5]Department of developmental and Cell Biology,National Human Neural Stem Cell Resource and Children's Hospital of Orange County Research Institute, University of California, Irvine, USA.

Abstract

In this paper, we characterize two types of neural cells based on a newly developed microfluidic flow induced electrical admittance spectroscopy. This technique measures the difference of the electrical admittance of the cells with the media when they are flowing and when they are still, at various frequencies. Characteristic peak, bandwidth of the peak and asymmetry of the peak are utilized to characterize different types of cells. The cells are characterized to extract electrical signatures in order to sort the cells so the isolated cells can be used for stem cell therapy.

Keywords: Flow induced admittance, channel electrodes, impedance spectra, cell cytometry, neuro stem cell sorting

1. Introduction

Micrototal analysis system [1] requires integrated sensors in the fluidic circuit for the control and analysis of cells. Most of the sensors use optical detection [2] in the form of fluorescence spectroscopy, surface plasmon resonance, surface enhanced raman scattering, radiological detection or impedance measurements [3]. The latter detection system has the advantages of needing very simple equipment to perform the measurement, easy sensor integration and miniaturization. The traditional impedance measurement of biomaterial has a very broad spectral response that cannot be used for distinguishing different biospecies. We present flow induced admittance measurement [4] that measures the contribution of the flow of a biofluid to the electrical admittance. This difference admittance spectra is characteristic for different biospecies and is used in this paper to sense different neural cells [5]. We developed a cell cytometry technique based on electrical admittance of the neural stem cells (NSCs). Fig. 1 shows the scheme for the sorting of the cells using an admittance sensor and fluidic switches. Neural stem cells are self-renewing and multi-potential, giving rise to different types of progenitor cells that divide, but do not self-renew. This cytometry and control of NSCs based on electrical admittance is simple to use and is free from cell modification by markers and antibodies.

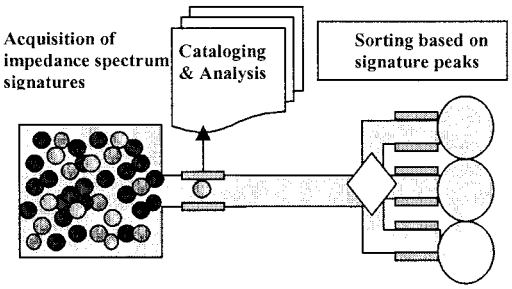

Figure 1. Scheme for cell sorting. The first electrode pair serves as a sensor and the three set of pairs of electrodes on the right serve MHD switches. Depending on the signature captured by the first pair of electrodes, each cell is sent to one of the three outlets.

2. Theory

The electrical admittance of a liquid and particles suspended in a liquid increases when they are passed across channel electrodes. This increase of admittance shows spectral behavior with the stimulating electrical signal. The flow induced spectral response shows a characteristic signature for different cells or particles. Interaction between the electrical and viscous stress on the fluid is the main cause that gives rise to spectroscopic behavior. A critical frequency is defined as: $f_c = \frac{\sigma}{2\pi\varepsilon}$ where σ and ε are the electrical properties of conductivity and permittivity of the buffer solution, respectively. For $f < f_c$, the electrical field functions in a resistive manner, while the double layer functions in a capacitive manner.

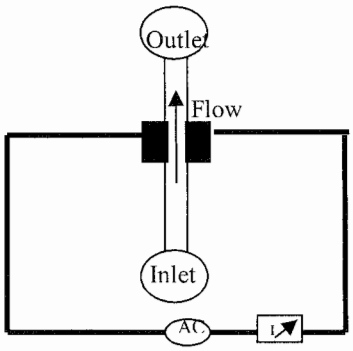

Figure 2. Schematic of the flow induced admittance

3. Experimental

Neuroblastoma cells (B-103) and human neural stem cells (hNSCs) are cultured using D-MEM/F12 medium and are resuspended in L15 medium for the measurements.The measuring instrumentation consists of National Instruments' signal generator, PCI 5401, for stimulating the channel electrodes in the microfluidic device and a data acquisition card, PCI 6024E, connected through Keithley's programmable amplifier, 428 for measuring the current. The rms values of the current are measured in Labview at the sampling rate of 20 kSamples/sec and every 10 ksamples are averaged. Microfluidic flow is maintained at a constant flow rate using a Harvard Picoplus Syringe pump. An ac signal of peak voltage 0.05 V with a frequency range from 10 Hz to 10 kHz is applied in the circuit. In order to keep the uniformity in all the experiments, the fluid is allowed to flow in the channel for 1 minute before any other measurement. The current flowing across the pair of electrodes is converted to voltage and amplified with a gain of 10E4 – 10E5 before the data acquisition. The current, being proportional to the magnitude of the complex admittance, is used as the magnitude of the complex admittance. Since this current is induced by flow, this is termed flow induced admittance. The unit of the Y-axis is mA if it were to be represented by flow induced current. The data represented for B-103 and hNSCs are in 10E-5 mA.

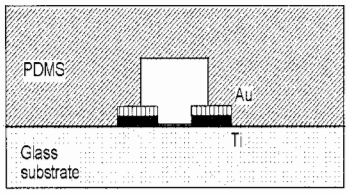

Figure 3. Cross-section of fabricated sensor along the electrodes, PDMS channel and the substrate.

4. Results and discussion

When cells are flowed along the electrodes in the channel, the electric double layer is perturbed giving rise to dielectric dispersion at different frequencies of the applied ac signal. Each cell is associated with a specific electrical signature based on the intrinsic electrical properties of its membrane and cytoplasm and this characteristic is utilized for cellular control. Fig. 4 shows the flow induced admittance spectra of (a) B103 cells (b) hNSCs along with their media. As these plots indicate, the magnitude of admittance and the peak frequency decreased for the cells compared to the media. This shows that the medium does not penetrate the cell membrane which accounts for reduced admittance. Fig. 5 shows the response of the applied voltage on the cells. The peaks resolve

well with the voltages and the voltage characteristics are linear. But it was found [6] that the voltage response for KOH solution is non-linear.

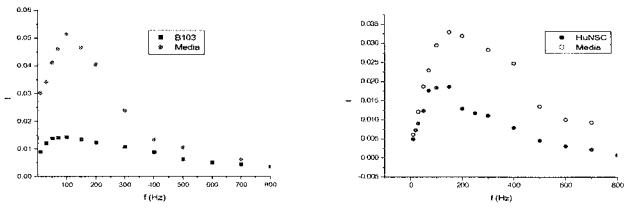

Figure 4. Characterization of (a) Human neural stem cells (b) Rat neuroblastoma cells (B103) along with their medium (L15).

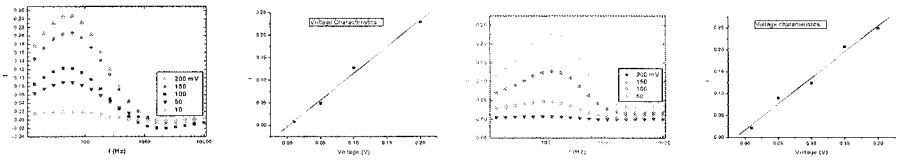

Figure 5. Response of applied ac voltage for the measurement of flow induced admittance on (a) B103 (b) hNSC cells.

5. Conclusions

Neuroblastoma cells and human neural stem cells are characterized using flow induced admittance measurements. The cells show linear voltage characteristics with the magnitude of the flow induced admittance spectra.

Acknowledgements

We wish to acknowledge Mr. Lisen Wang, graduate student at BioMINT lab who helped with the microfabrication, the undergraduate students Paul Aquino, Daniel Lavigne and Philip Irwan who helped in the culture and measurements with the cells and the funding from UCI and DARPA.

References

[1] Anna J. Tüdos, Geert A. J. Besselink, and Richard B. M. Schasfoort, Lab Chip, 2001. 1: p. 83–95.

[2] E. Thrush, O. Levi, W. Ha, K. Wang, S.J. Smith, and J.S. Harris, J. Chromatography A, 2003. 1013(1-2): p. 103-110.

[3] H. Edward Ayliffe, A. Bruno Frazier, and R. D. Rabitt, IEEE J. MEMS, 1999. 8(1): p. 50-57.

[4] J. Collins and A. P. Lee, Lab. Chip., 2004. 4: p. 7-10.

[5] Philip H. Schwartz, Peter J. Bryant, Tannin J. Fuja, Hailing Su, Diane K. O'Dowd, and Henry Klassen, Journal of Neuroscience Research, 2003. 74: p. 838–851.

[6] J. Collins, L. Flanagan, N. Jeon, E. Monuki, and A.P. Lee. in *I26th Annual International Conference of the IEEE Engineering in Medicine and Biology Society*. 2004. San Francisco, California.

MILLISECOND KINETICS AND BIOCHEMICAL ASSAYS IN CHAOTICALLY MIXED DROPLET-BASED MICROFLUIDICS

Helen Song, Joshua D. Tice, Michelle R. Bringer, Cory J. Gerdts, L. Spencer Roach and Rustem F. Ismagilov

Dept. of Chemistry, University of Chicago, 5735 South Ellis Avenue, Chicago, Illinois, USA

Abstract

In this presentation, we will describe a droplet-based microfluidic system [1] with rapid mixing and no dispersion. Picoliter-sized aqueous droplets (or plugs) surrounded by a water-immiscible fluid (oil) were formed within microchannels to eliminate dispersion. Reagents within the plug were mixed rapidly by chaotic advection. We have recently developed methods to control surface chemistry within this plug-based platform, which is important for enzyme kinetics. Due to low sample consumption, rapid mixing, elimination of dispersion and control of surface chemistry, this microfluidic system can be used to measure enzyme kinetics and perform biochemical assays with better than millisecond resolution.

Keywords: microfluidics, microreactors, bioassay, kinetics, droplet

1. Introduction

This droplet-based microfluidic system [1] overcomes two usual problems in microfluidics: high dispersion and slow diffusive mixing (Figure 1). To eliminate dispersion, aqueous plugs were formed within a carrier stream of water-immiscible fluid (oil) [2]. To achieve rapid mixing, plugs were transported through winding microchannels, where time-dependent flows rapidly mixed the reagents by principles of chaotic advection (Figure 1).

Using this plug-based system, Reagent A and Reagent B can be injected into the plug without prior contact between the two reagents. These two reagent streams flow laminarly and an inert "separating stream" can be used between the two reagent streams to eliminate cross-contamination. Due to the absence of dispersion, microchannel distance [m] is linearly related to reaction time [s] by the flow velocity [m s^{-1}]. Due to rapid mixing and no dispersion, the starting point of the reaction can be well-defined. Also, the elapsed time of the reaction between the reagents (within the plug) is linearly to the microchannel distance. This droplet-based microfluidic platform has been used to determine the rapid single-turnover cleavage kinetics of an enzymatic reaction of ribonuclease A (RNase A) [3].

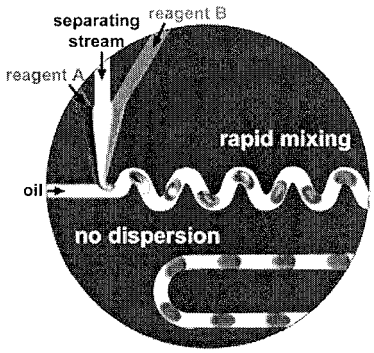

Figure 1. Picoliter-sized plugs are formed in microchannels by using continuous flows of aqueous reagents and water-immiscible fluid (oil). Due to rapid mixing and absence of dispersion, these plugs can be used to study chemical and biochemical networks on millisecond time scale.

2. Experimental

Details of microfluidic experiments are explained in detail in [2, 3]. PDMS/glass microfluidic devices were fabricated by soft-lithography in poly(dimethylsiloxane) (PDMS), where devices were rendered hydrophobic with silane vapor. Syringe pumps were used to drive flows for the aqueous and oil streams., Fluorescence microphotographs were acquired with an inverted microscope and a 12-bit cooled CCD camera and optical microphotographs were acquired with a stereoscope. Image analysis is described in detail in [3].

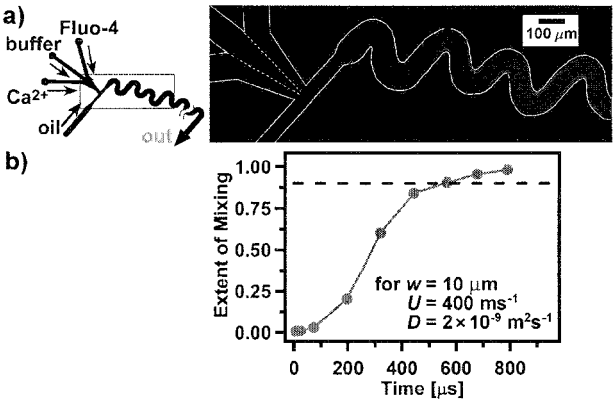

Figure 2. (a) Schematic of the microfluidic network (left) and microphotograph (right) of plugs moving through winding channels by fluorescence (a). Individual plugs are not visible because the observed fluorescence is the time-averaged fluorescence of many plugs passing through the field of view within the 2 s exposure time. (b) A graph that shows 90% mixing (dashed line) achieved in ~550 μs for the conditions shown.

3. Results and discussion

In microfluidics, rapid mixing can be achieved by chaotic advection, which stretches and folds the fluid volume. When plugs travel through winding microchannels, pairs of co-rotating vortices are induced within the plug, which generate chaotic time-dependent flows. The binding reaction between Ca^{2+} and fluo-4 can be used to quantify mixing, as the binding reaction is rapid and results in an increase in fluorescence intensity. By using a reaction that results in a change in the optical signal and the linear distance-time relationship, a single spatially resolved optical image (as in Figure 2a) provides a time-resolved measurement. By analyzing these images, a time-resolved reaction profile (Figure 2b) can be obtained from each fluorescence image. Mixing as fast as ~550 μs was achieved (Figure 2b). In addition, a simple scaling argument for the mixing by chaotic advection was obtained and this scaling argument was tested by varying the experimental parameters [4].

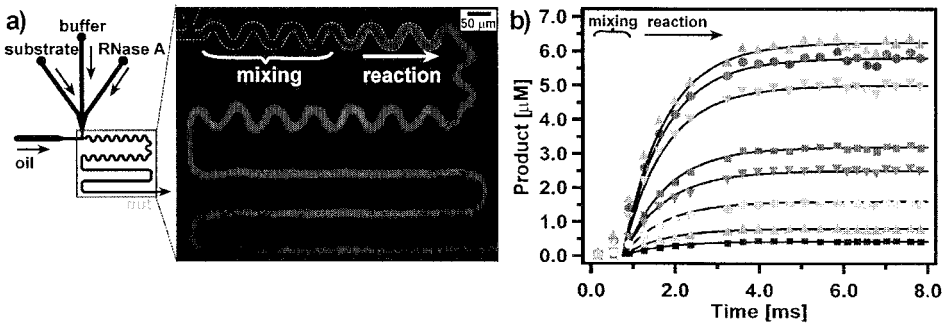

Figure 3. Millisecond kinetics of an enzyme (RNase A) in a plug-based microfluidic platform. (a) Schematic of the microfluidic network (left) and a fluorescence microphotograph of plugs (right). (b) Graph of product versus time from analyzing microphotographs such as in (a) for eight RNase A concentrations from 0.4 μM (■) to 6.3 μM (▲), where the fit is shown (black lines) for $k = 1000\ s^{-1}$.

Under typical single-turnover conditions in enzyme kinetics, large excess of both the substrate and enzyme concentrations are necessary. Therefore, both rapid mixing and minimal sample consumption is necessary. This plug-based microfluidic platform has been used to determine the single-turnover kinetics of an enzymatic reaction of ribonuclease A (RNase A) for a fluorogenic substrate were measured with better than millisecond resolution using sub-microliter volumes of solutions [3]. From eight fluorescent images that were integrated for 2-4 s (such as in Figure 3a), eight kinetic profiles were obtained (Figure 3b). To obtain these eight images in rapid succession, on-chip dilution was necessary so that substrate concentration within the plug can be controlled without disassembling the microfluidic device [3]. By varying the relative flow rates of the aqueous reagent streams but keeping the total flow rate of the aqueous streams the same, the concentration of the reagents within the plugs can be controlled on-chip. Therefore, by using on-chip dilution, less than 1 μL of RNase A sample was consumed to determine these eight kinetic profiles. The obtained turnover rate constant ($k = 1000\ s^{-1}$) is in agreement with previous studies.

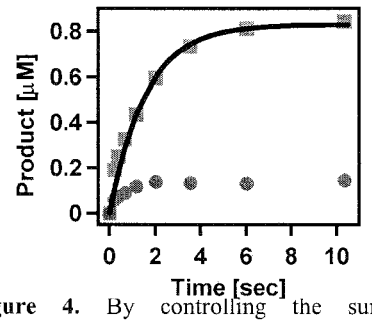

Figure 4. By controlling the surface chemistry at the oil-water interface of the plug (■), the measured RNase A kinetics overlays with the expected kinetic curve (solid black line). Without controlling the surface chemistry (●), decreased RNase A activity was measured.

In this presentation, we will emphasize that, in order to obtain reliable kinetic measurements, it is important to control the surface chemistry at the oil-water interface of the plug. Enzyme kinetics can be used to detect the enzyme activity within the plug when the surface chemistry is or is not controlled (Figure 4). If surface chemistry is controlled, the measured kinetic data for RNase A within plugs (square symbols, Figure 4) overlay with the expected kinetic curve (black solid line), which was determined from kinetic constants obtained from bulk cuvette experiments using a fluorimeter. However, if the surface chemistry is not controlled, then a decrease in kinetic activity is observed (circle symbols, Figure 4). We will discuss a rational approach for controlling surface chemistry that we have characterized in detail. This plug-based system should complement other droplet-based systems [5-7] for applications in chemical reactions and biochemical analyses within emulsions and droplets.

Acknowledgements

This was supported by the NIH (R01 EB001903), ONR Young Investigator Award (N00014-03-10482), the Beckman foundation and the Chicago MRSEC funded by the NSF.

References

[1] H. Song, J. D. Tice and R. F. Ismagilov, *Angew. Chem.-Int. Edit.*, **42**, 768-772 (2003).
[2] J. D. Tice, H. Song, A. D. Lyon and R. F. Ismagilov, *Langmuir*, **19**, 9127-9133 (2003).
[3] H. Song and R. F. Ismagilov, *J. Am. Chem. Soc.*, **125**, 14613-14619 (2003).
[4] H. Song, M. R. Bringer, J. D. Tice, C. J. Gerdts and R. F. Ismagilov, *Appl. Phys. Lett.*, **83**, 4664-4666 (2003).
[5] S. L. Anna, N. Bontoux and H. A. Stone, *Appl. Phys. Lett.*, **82**, 364-366 (2003).
[6] M. W. Losey, R. J. Jackman, S. L. Firebaugh, M. A. Schmidt and K. F. Jensen, *J. Microelectromech. Syst.*, **11**, 709-717 (2002).
[7] K. Handique, D. T. Burke, C. H. Mastrangelo and M. A. Burns, *Anal. Chem.*, **73**, 1831-1838 (2001).

A NOVEL MICROSTEP DEVICE FOR THE SIZE SEPARATION OF CELLS

Sarah Vankrunkelsven, David Clicq, Kris Pappaert, Gino V. Baron, and Gert Desmet
Vrije Universiteit Brussel, Department of Chemical Engineering, Pleinlaan 2, B-1050 Brussel, Belgium

Abstract

We report on a series of preliminary experiments investigating the applicability of a novel method for the size separation of nano- and micro-sized particles and cells. The working principle is based on the application of a shear-driven flow through stepwise tapered micro- or nano-channels, using the successive channel depth reductions as particle traps. Size separations of mixtures of 0.5 and 1.0 μm carboxylated fluorescent polystyrene beads as well as of binary mixtures of fluorescent *Staphylococcus aureus* and *Saccharomyces cerevisiae* cells and of *S. cerevisiae* and *Escherichia coli* cells are demonstrated.

Keywords: micro-channels, size separation, cells, shear-driven flow

1. Introduction

The microscale separation, identification, quantification, and characterization of cells has recently attracted the attention of many research groups [1, 2]. One of the main driving forces of this work is the desire to develop micrototal analysis systems (μTAS) where the cell manipulation steps of the sample preparation are integrated with the other analysis steps on the same chip surface. In this paper, we report on the first experiments of a novel high-resolution cell and nanoparticle separation method omitting the need for any secondary force field, hence operating independently of the density, the charge or the surface properties of the cells, and in that sense complementary to most of the other microscale cell separation methods.

2. Theory

In the past few years, our group has been investigating the possibility to use shear-forces for the propulsion of fluids through micro- and nano-channels as an alternative to the customary employed pressure and electrical forces [3]. Briefly, the method relies on the use of micro- or nano-channels consisting of two separate flat plates: one shorter plate, attached to a stationary frame, and a longer plate, translated or rotated past the shorter. The major advantage of shear-driven flows is that the applicable fluid velocity is independent of the fluid viscosity and the channel depth and length, hence completely avoiding the limitations on the applicable flow velocities existing in pressure- and electrokinetically-driven nano-channels.

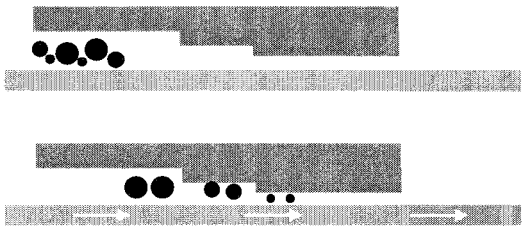

Figure 1. Schematic representation (longitudinal cross-section) of the working principle of a shear-driven size fractionator for cells and other nano-sized particles.

Very recently [4], we have demonstrated the possibility to generate high velocity flows (up to 4 cm/s) of carboxylated nanoparticles through channels which were only 50% thicker than the particles themselves. The possibility to transport nanoparticles under such a high degree of spatial confinement makes it straightforward to conceive a size separation method based on a step-wise tapered micro- or nanochannel, using the successive channel depth reductions as particle traps (Fig. 1). Figure 2 shows a Wyko®-scan of such a stepwise tapered channel.

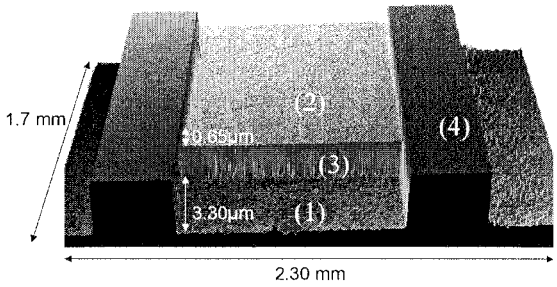

Figure 2. Wyko-scan of one of the employed stationary channel platelets, showing the channel regions before (1) and after (2) the step (3). During the experiment, the regions aside of the channel (4) make contact with the moving plate and serve as channel spacers.

3. Experimental

All channels used in the present study were composed of the following two flat substrate types: a fully flat fused silica wafer (5 cm diameter with λ/10 flatness) used as the moving wall, and a shorter silicon platelet (dimensions 20 x 10 mm), used as the stationary wall and carrying a photolithographically etched half-open channel with a step on its surface. After assembly, the channel is positioned exactly above the objective lens (Achroplan 10x or 20x, Zeiss NV, Belgium) of an inverted fluorescence microscope (Axiovert 200, Zeiss NV, Belgium). For this purpose, the fused-silica wafer is fitted into a stainless steel holder mounted on top of the translation stage of the microscope. The stationary wall part of the channel system is held in place using a second holding frame, precisely fitting around the rectangular silicon plates. The displacement of the moving part of the channel was effectuated by using a stepper motor-driven linear displacement stage (MTS100DC.5; Newport B.V., Ÿsselstein, The Netherlands). During the operation, a relatively large pressure was applied on the silicon plate using a pneumatically operated metallic coverlid, exerting a downward force on the stationary channel wall (typically 1-2 bar). This poses no specific problems, as it was observed that the system could be operated pressures up to 5 bars without any notable increase of the sliding resistance.

Yellow-green fluorescent carboxylate-modified nanoparticles with a diameter of 0.5 and 1.0 µm (Molecular Probes, Leiden, The Netherlands) were used in a concentration of 2.9 x 10^9 particles/mL for the 0.5 µm particles and 3.6 x 10^8 particles/mL for the 1.0 µm particles. A sodium tetraborate buffer (3 mM, pH 9.2) with addition of 0.5 g/L Triton X-100 (Acros Organics, Geel, Belgium) was used to prevent agglomeration and adsorption of the particles on the channel walls. Bacteria and yeast particles *(E. coli, S. aureus,* and *S. cerevisiae)* were purchased covalently labeled with fluorescein (Bioparticles; Molecular Probes). The average sizes of the different cell types were determined using the direct illumination mode of the microscope and were found to be 1.0 µm for *S. aureus*, 1.3 µm for *E. coli*, and 3.8 µm for *S. cerevisiae.*

4. Results and discussion

Conducting the cell separation experiments, the main uncertainty was the potential damage and breakage of the cells when being arrested by the step. However, as can be noted from Fig. 3, the cells remain clearly intact and the separation principle works as well for a mixture of *E. coli* and *S. cerevisiae* cells as for the polystyrene beads. It can be assumed that the presence of the slight backflow helps in preserving the integrity of the cells [5].
Separations conducted with mixtures of *S. aureus* and *S. cerevisiae* cells displayed a similar result.

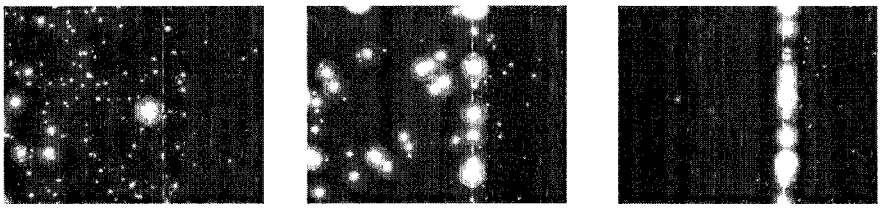

Figure 3. Compilation of a series of captured CCD-images of a micro-step separation experiment of a mixture of *E. coli* and *S. cerevisiae* cells (u_{wall} = 10 µm/s, pure PBS). The channel depth changes from 5.2 µm to 1.6 µm at the micro-machined step, indicated by the white dashed line.

The presently proposed novel micro-channel size fractionation method can be used to separate spherical nano-particles and cells on the basis of their size, without causing any damage to the cells. One of the advantages with respect to Field-Flow Fractionation (FFF) for example is that the fractions are not only separated, but are at the same time also concentrated in narrow bands near the steps. The method is especially advantageous for the size-separation of cells, as the shear-driven flow induces a slight backward flow, gently pushing the oversized cells away from the step and preventing them from getting blocked or squeezed.

5. Conclusions

Future investigations will include the application of anti-adhesion wall coatings, the determination of the separation characteristics of the method (rejection and passage efficiencies, achievable separation resolution, *etc.*), the investigation of the behavior of aspherical cells and particles, and the operation of the device in a continuous operation mode by etching side-ways oriented evacuation channels near the steps.

Acknowledgements

The authors gratefully acknowledge financial support from the Fonds voor Wetenschappelijk Onderzoek (FWO, grant No. G.0042.03) and the Instituut voor Wetenschap en Technologie (IWT, grant No. GBOU/010052). D. C. and K. P. are supported through a specialization grant from the IWT (grants No. SB/1279/00 and SB/01/11324).

References

[1] Gascoyne, P. R. C., Vykoudal, J., *Electrophoresis* **24**, 1973–1983 (2003).
[2] Anderson, H., van den Berg, A., *Sens. Actuators B*, **92**, 315–325 (2003).
[3] Desmet, G., Baron, G. V., *Anal. Chem.*, **72**, 2160-2165 (2000).
[4] Vankrunkelsven, S., Clicq, D., Pappaert, K., Baron, G. V., Desmet, G. *Anal. Chem.* **76**, 3005-3011 (2004)
[5] Vankrunkelsven, S., Clicq, D., Pappaert, K., Ranson, W., De Tandt, C., Ottevaere, H., Thienpont, H., Baron, G. V., Desmet, G. *Electrophoresis*, **25**, 1714-1722 (2004).

A HIGH FLOW RATE DC MAGNETOHYDRODYNAMIC (MHD) MICROPUMP

Alexandra Homsy[1], Sander Koster[1], Jan C.T. Eijkel[2], Albert van den Berg[2], Elisabeth Verpoorte[3] and Nico F. de Rooij[1]

[1]*Institute of Microtechnology, University of Neuchatel, Switzerland*
[2]*MESA+ Research Institute, University of Twente, The Netherlands*
[3]*Groningen Research Institute of Pharmacy, University of Groningen, The Netherlands*

Abstract

We present a device that allows high-speed DC magnetohydrodynamic (MHD) pumping in 75-μm-deep closed glass microchannels. High DC current densities (J) can be applied across the main channel without introducing bubbles. Linear velocities of up to 1.25 mm/sec (0.7 μL/min) were observed in buffered solutions using a 0.4 T NdFeB permanent magnet, at a current density of 4000 A/m^2. The current density and corresponding flow speed are 50 and 30 times higher respectively, with a channel height 4 times smaller than reported by others in closed channels [1].

Keywords: DC MHD, micropump, magnetohydrodynamics

1. Introduction

There has been a growing interest in MHD micro-pumps over the past few years. This is not surprising since these pumps work without moving parts and require only low voltages for actuation. The resulting flow can be bi-directional with a parabolic-shaped flow profile. The MHD micropump presented here is made in glass, and is operated in the DC mode. The gas bubbles due to DC operation do not influence the performance of the pump, since the bubbles are generated outside the microfluidic channel. The design consists of a micromachined frit-like structure that connects the pumping channel to side-reservoirs where the electrodes are located. The idea for this design is based on ref [2], where such a geometry was used to perform free-flow electrophoresis on silicon chips.

2. Theory

When charged species are present in an electromagnetic environment, they feel the Lorentz force F_L. When a current is sent through a microchannel filled with an electrolyte solution, the Lorentz force exerts a bulk force on the fluid that is proportional to both the generated current density J in the liquid (A.m^{-2}), and the magnetic flux density B (T). The resulting linear velocity of the liquid in the channel will be proportional to the applied J and B, as well as to the square of the channel radius.

3. Design and Fabrication

As the MHD flow rate is proportional to J, the chip was designed to generate a high J across the channel pumping area, without introducing bubbles into the channel. Details of the chip design can be seen in Fig. 1. On both sides of the 75-μm-deep main channel, 800 perpendicular 100-nm-deep "side-channels" were etched, connecting the main channel to the 75-μm-deep outside reservoirs where platinum electrodes were placed. Both main channel and side-channels are processed on the same Pyrex wafer by a two-step photolithography process in our cleanroom facility. A piece of polydimethylsiloxane (PDMS) was put on top of the chip to provide the outer reservoirs. Platinum wire electrodes were placed in the side-channels PDMS reservoirs. The magnetic field was generated by NdFeB rare earth permanent magnets (3 different magnets of respectively 0.22, 0.35 and 0.42 T field strengths) placed under the device.

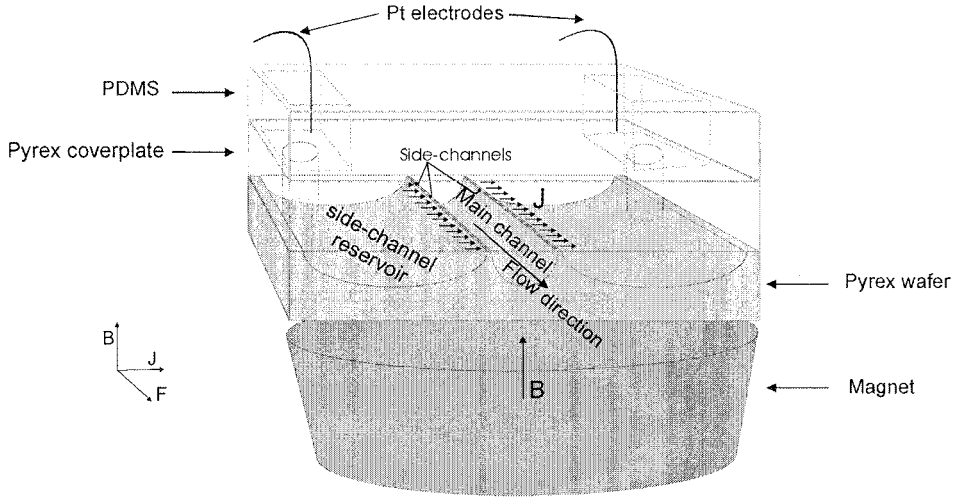

Figure 1. Schematic cross-sectional view of the pumping area. The main channel is 2 cm long, 150 µm wide and 75 µm deep. The pumping area along the channel is 1.6 cm long. The side-channels are 100 nm deep, 10 µm wide and 10 µm long.

4. Results and discussion

The chip was filled with buffered solutions of various pH (from 3.2 to 7.5) with KCl added to increase the ionic strength of the solution from 0.5 to 1 M. The flow was visualized using 6 µm carboxylate polystyrene beads. We used buffered solutions to avoid large pH changes at the electrode location. Gas bubbles that formed around the platinum electrodes could easily escape through the large holes in the PDMS. Gas bubbles were never observed entering the side channels. Bead movement was not observed if either an electrical or magnetic field was applied at a buffer ionic strength between 0.5 and 1 M. When both current and magnetic field were applied, beads began to move above a certain current density threshold of 500 $A.m^{-2}$ (corresponding to a voltage $\geq$ 3.5 V). Beads located in the centre of the channel were seen to move faster than the beads close to the channel walls, which is typical behavior for flows with a parabolic profile. Fig. 2 shows the maximum bead velocity in the main channel as a function of J for 3 different magnetic field strengths (B). Theory predicts a linear dependence of the flow velocity on both B and J. The bead velocity is seen to increase with B. From 667 to 2083 $A.m^{-2}$, the bead velocity varies linearly with J, and is on the order of magnitude as calculated from theory. For current densities above 2083 $A.m^{-2}$, the linearity is lost. This phenomenon is believed to be related to Joule heating in the side channels. Table 1 shows the power dissipation (Q) for the same experimental conditions as Fig. 2. For current densities above 2083 $A.m^{-2}$, Q shows values larger than 1 $W.m^{-1}$ which is a typical indication that Joule heating may be happening.

At lower ionic strengths (0.01 - 0.1 M), a flow in the J direction was observed, disturbing the MHD flow in the main channel. This effect is related to electroosmosis and bead electrophoresis. The electric field strength in the main channel was estimated to be 2640 $V.cm^{-1}$ for corresponding maximum values current densities of 583 $A.m^{-2}$ and 1667 $A.m^{-2}$ for buffers of respectively 0.01 and 0.1 M ionic strength. Efforts are currently focused on improving the chip design in order to decrease these effects.

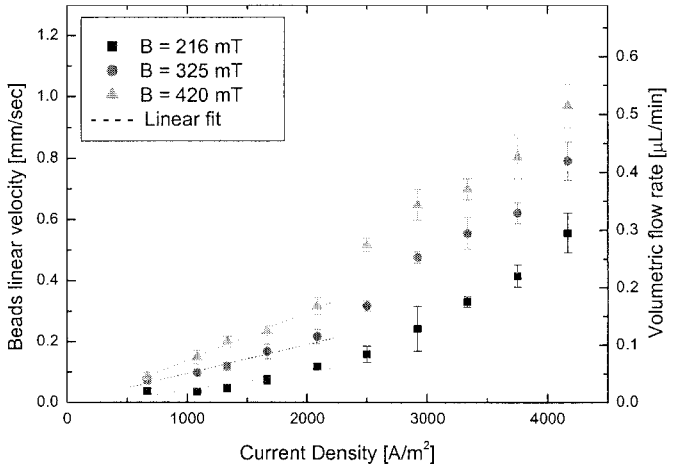

Figure 2. Maximum linear velocity of 6 µm carboxylate-modified polystyrene beads as a function of the applied current density for 3 different magnetic field intensities in a citrate phosphate buffer of pH = 5 (207 mM phosphate, 53 mM citrate), with 744 mM KCl added to increase the ionic strength of the buffer.

U [V]	$J_{main\ channel}$ [A.m^{-2}]	Q [W.m^{-1}]	$E_{side\ channel}$ [V.cm^{-1}]	$E_{main\ channel}$ [V.cm^{-1}]
5.1	667	0.13	212	1.73
8.9	1667	0.56	370	3.03
10.3	2083	0.80	429	3.50
11.7	2500	1.10	487	3.98
13.0	2917	1.42	541	4.42
16.6	4167	2.59	691	5.64

Table 1 Approximate power dissipation **Q** and electric field **E** in side channels and in main channel for different values of J (citrate phosphate buffer of pH = 5, 1 M ionic strength).

5. Conclusions

A novel concept for a DC MHD micropump was demonstrated. This chip design allowed the use of a DC current across a microchannel without gas bubble formation by using a micromachined frit-like structure to connect the pumping channel to side-reservoirs where the electrodes were located. We envision integrating this MHD pump in a µTAS for on-chip NMR analysis [3]. In this 7.2 T NMR environment, an increase of 16 times in bead velocity is expected.

Acknowledgements

The devices were fabricated in COMLAB, the joint cleanroom facility of IMT and CSEM, and we thank all the technical staff there for the helpful support. We also thank our project partners at the EPFL (STI-IMM-LMIS3, especially Charles Massin, Franck Vincent and Klaus Ehrmann) for help with the characterization of our magnets. This work was supported by an EPFL presidential fund (Nr. 581.552) and by the Swiss National Science Foundation (Proj. Nr. 2100-61549.00).

References

[1] J. Jang and S. S. Lee, *Sens. Act. A,* **80**, 84-89 (2000).
[2] D. E. Raymond, A. Manz, and H. M Widmer, *Anal. Chem*, **66**, 2858-2865 (1994).
[3] C. Massin, F. Vincent, A. Homsy, K. Ehrmann, G. Boero, P.-A. Besse, A. Daridon, E. Verpoorte, N.F. de Rooij and R.S. Popovic, *J. Magn. Reson.*, **164**, 286-293 (2003)

FAST AND TUNEABLE INTEGRATED AC ELECTROKINETIC PUMPING IN A MICROFLUIDIC LOOP

Vincent Studer[1], Anne Pépin[1], Yong Chen[1] and Armand Ajdari[2]

[1]*Laboratoire de Photonique et Nanostructures, UPR CNRS 20, route de Nozay ,F-91460 Marcoussis, France.*

[2]*Laboratoire de Physico-Chimie Théorique, UMR CNRS-ESPCI 7083,10 rue Vauquelin, F-75231 Paris, France.*

Abstract

We report a detailed study of a low voltage AC electrokinetic micropump, performed in a dedicated microfluidic chip. The micropump consists of an array of interdigitated micro-electrodes and is integrated in a closed microfluidic loop. We show that such a device pumps continuously and reproducibly at velocities up to 500 μm/s in 20 μm-deep and 100 μm-wide channels with a driving signal in the 1-10 kHz range and an amplitude of only a few volts. In addition, we have observed an interesting reversal of the pumping direction at higher frequencies (50 - 100 kHz) and higher voltages (>2.5 Vrms), which allows a fast monitoring of the flow by changing the frequency.
Keywords: AC electrokinetics, micropump, low voltage, valve.

1. Introduction and scope

Increasing complexity in microfluidic devices creates the need for integrated local fluid control systems such as pumps and valves in microchannels. AC electroosmosis (ACEO) has been recently advertised [1] as a way of creating recirculating flow over micro-electrodes using low amplitude AC signals. A few years ago, Ajdari [2] proposed that ACEO could be used to realize integrated micro-pumps with no moving parts for microfluidic devices. They rely on embedded asymmetric sets of micro-electrodes within the channels to generate rectified flows. In a previous work, we showed that such electrode arrays can be integrated in a microfluidic channel and we described voltage and frequency dependent pumping in those microchannels in the 50μm/s range [3]. In this work we report an extended study to characterize AC electrokinetic (ACEK) pumping in microchannels. In order to overcome previously described measurement limitations, such as pressure gradient-induced flow and electrode degradation we developed a dedicated automated microfluidic chip using multilayer soft lithography [4]. This chip includes an array of microelectrodes for ACEK pumping in a section of a loop channel and pneumatically-actuated soft micro-valves. Figure 1A shows a schematic of the microfluidic loop channel with the soft micro-valves and the array of electrodes. Soft micro-valves allow us to isolate the measurement loop from nearly any hydrostatic pressure difference. Once loaded with the appropriate electrolyte, the input channel to the microfluidic loop is closed by a soft micro-valve. In order to measure the pumping velocity generated by the ACEK pump, 0.9 μm-diameter fluorescent beads are injected in the upper left corner of the loop channel (see Figure 1A) by opening two micro-valves. A particle image velocimetry setup is used to measure the maximum flow speed in the loop channel. Pumping speed is measured far away from the electrodes to avoid flow-marker displacement due to electrokinetic effects. Using this system we were able to characterize ACEK pumping in a very reproducible way. We screened the amplitude and frequency of the driving AC signal for different concentrations of the KCl electrolyte.

2. Material and methods

We used multilayer soft lithography to integrate microfluidic valves on our measurement chip. Those on/off valves are pneumatically actuated through pressurized dead-end control channels. Our chip is constituted of two layers of polydimethylsiloxane (PDMS): a 35 μm-thick layer for the

fluidic channels and a 3 mm-thick layer for the control channels. Fluidic channels were 22 μm-deep and have a rounded shape. Control channels are 50 μm deep and have a rectangular cross section. Electrode arrays were micro-fabricated on a 170 μm-thick glass substrate. We used standard photolithography for pattern transfer from an electron-Beam written mask to the substrate. A 5 nm-thick layer of titanium followed by a 20 nm-thick platinum layer were deposited on top of the photoresist patterns. The photoresist pattern was then transferred in the metal layer by lift-off. The two-layer PDMS chip was aligned to the electrode array and bonded to the glass slide. The electrode array was 6 mm-long and 320μm-wide thus allowing easy aligning of the 100 μm wide microfluidic channels. Figure 1C shows a schematic of the asymmetric electrode array which contains 120 repeats of the asymmetric pair of electrodes.

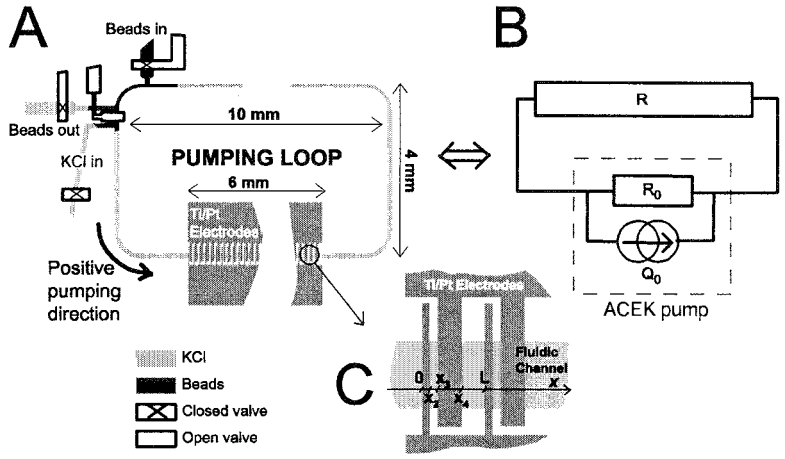

Figure 1. A : Schematic of the microfluidic chip with soft microvalves. **B** : Equivalent electric circuit of the ACEK pump in the loop channel. **C** : detail of the array of interdigitated micro-electrodes : L=50μm, x_2=4.2μm, x_3=8.7μm and x_4=34.4μm.

3. Results and discussion

Previous experiments based on ACEK pumping in asymmetric geometries reported V_0 of order 50 to 100μm/sec for voltages of order 1 Vrms or less, peaking at frequencies in the 1-5 kHz range [3, 5]. These observed data are compatible with the predictions of simple electrokinetic models, which predict velocities V_0 proportional to the square of the applied potential. In that range of parameters, our experimental results are essentially compatible with the previously reported data (Figure 3 and 4) (similar speed, same direction (positive direction on Figure 1A). What is new is rather our observation of interesting non-linear effects, with two salient features. First in the kHz range, we observe that the velocity at larger voltages (1 to 6 Vrms) increases with the applied voltage, but certainly not as the square of this voltage. Second, at higher frequencies (a few tens of kHz), and voltages larger than 2.5 Vrms, a strong pumping is also observed, but in the reverse direction (Figure 3). With a 10^{-4}M KCl electrolyte, we were able to perform measurement at higher voltages. For frequencies above 30 kHz, voltages as high as 10 Vrms could be applied with no apparent electrode damage or bubble formation and pumping speeds up to 0.5mm/s (in the reverse

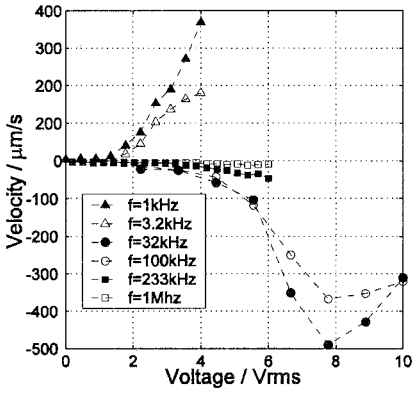

Figure 2. Voltage variation of the pumping velocity with a 10^{-4}M KCl electrolyte

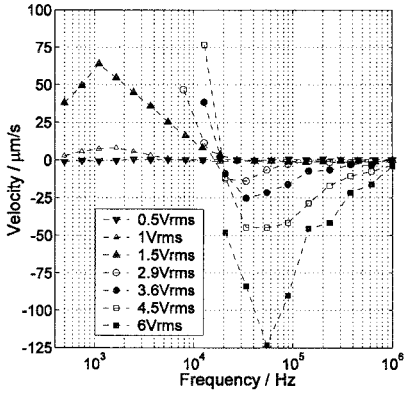

Figure 3. Frequency variation of the pumping velocity with a 10^{-4}M KCl electrolyte

pumping direction) could be observed. Experiments with more concentrated electrolytes showed a fast decrease of the pumping velocity with increasing ionic strength of the buffer (for a 10^{-2} M KCl solution, no significant pumping effect can be measured). In order to characterize this ACEK pump it is important to take into account that our microfluidic loop consists in fact of a long passive section in series with an active section (the "flow generator"). An analysis in terms of equivalent electric circuit (Figure 1B) shows that the average flow velocity in the loop is equal to the intrinsic pumping velocity of the pump V_0 times the ratio of the internal hydraulic resistance R_0 of the active section to the total resistance R of the entire loop. As the channel cross-section in the pumping loop is constant, this ratio is that of the length of the active section to that of the loop, which is roughly ¼ in our device. Thus, an intrinsic measure of the pumping performance of this kind of integrated pump, V_0, is 4 times the average velocity in the loop, and thus roughly 2 or 3 times the velocity reported in the experimental plots.

4. Conclusions

With a dedicated microfluidic chip we were able to investigate the performance of an integrated ACEK pump and to show its ability to pump reproducibly and continuously at velocities of the order of 0.5 mm/sec, with a driving of only a few volts, and in a direction that can be readily tuned by changing the frequency. All these features make this integrable pumping scheme attractive, in particular in microsystems built in rigid materials (glass, silicon).

References

[1] A. Ramos, H. Morgan, N.G. Green and A. Castellanos, Journal of Colloid and Interface Science 217 (1999) 420-422.

[2] A. Ajdari, Physical Review E 61 (2000) R45-R48.

[3] V. Studer, A. Pepin, Y. Chen and A. Ajdari, Microelectronic Engineering 61-2 (2002) 915-920.

[4] M.A. Unger, H.P. Chou, T. Thorsen, A. Scherer and S.R. Quake, Science 288 (2000) 113-116.

[5] A. Brown, C. Smith and A. Rennie. in Physical Review. E, Vol. 6302, pp. art.no.-016305 2001.

FLUID ACTUATION TOWARD MICROPUMP BY CARDIOMYOCYTES

Yo Tanaka[1], Keisuke Morishima[2], Tatsuya Shimizu[3], Akihiko Kikuchi[3], Masayuki Yamato[3], Teruo Okano[3] and Takehiko Kitamori[1,2]

[1] Dept. of Applied Chemistry, The University of Tokyo, 7-3-1 Hongo, Bunkyo, Tokyo, Japan

[2] Integrated Chemistry Project, Kanagawa Academy of Science and Technology, KSP, 3-2-1 Sakado, Takatsu, Kawasaki, Kanagawa, Japan

[3] Institute of Advanced Biomedical Engineering and Science, Tokyo Women's Medical University, 8-1 Kawada-cho, Shinjuku, Tokyo, Japan

Abstract

We have succeeded in the creation of a fluid driving system in a microspace using cultured cardiomyocytes as a principal component of a micropump. In this work, cell sheet engineering was utilized, because a cardiomyocyte sheet can attach to various structures and generate strong force. In order to communicate the force generated by cardiomyocytes to fluid, a thin diaphragm and a push bar structure made of PDMS were assembled into a microchip. Volume variation of the chamber for one stroke was 2.6 nL. The applied pressure on the diaphragm generated by cardiomyocytes was 2 Pa. It is the first example of micro fluid driving systems by converting chemical energy into mechanical energy.

Keywords: cardiomyocyte, bio-actuated microsystem, chemical energy, cell sheet, diaphragm pump

1. Introduction

For last decades, there have been a number of micro fluidic devices fabricated by the micromachining technique to realize efficient chemical processes in a microchip. However, the present technique has the limit of fabrication size and functions. Therefore, we proposed completely different approach to solve the problem by utilizing a living biological cell function of cardiomyocytes to convert chemical energy into mechanical energy. We have already demonstrated the principle of the bio-actuated microsystem using cardiomyocytes driven only by chemical energy [1]. Next step is to fabricate a micropump. To realize that, cell sheet engineering [2] was utilized, because a cardiomyocyte sheet detached from a dish can attach to various structures and generate strong force. Therefore a micro diaphragm pump would be created.

Aim of this study is to drive fluid in a microchannel by a cardiomyocyte sheet. This is the first demonstration to drive fluid in a microchannel utilizing a living biological cell function to convert chemical energy into mechanical energy. Firstly, a microchip with a diaphragm chamber and a push bar structure was fabricated. The diaphragm was made of PDMS because that is soft and easy to be thin by spin coating. Secondly, a cardiomyocyte sheet was assembled on the push bar structure. Finally, the performance of the fluid driving system was evaluated by measurering displacement of micro particles in a microchannel.

2. Theory

Figure 1 shows the actuation principle of fluid in a microchannel. In order to communicate the stretch and contraction force generated by a cardiomyocyte sheet to fluid in the chamber, a thin diaphragm and a push bar structure made of PDMS are assembled into a microchip. A cardiomyocytes sheet is assembled on the push bar structure detached from cell culture surfaces grafted with temperature-responsive polymer, poly(N-isopropylacrylamide) (PIPAAm), from which confluent cells detach as a cell sheet simply by reducing temperature without any enzymatic treatments.

3. Experimental

A microchip was fabricated by piling PDMS parts molded from photo-resist. Figure 2 shows each part of the microchip. The width and depth of the microchannel is 500 μm and 200 μm respectively. The diaphragm was fabricated by spin coating on a silicon wafer and assembled on the chamber. The thickness of the diaphragm was 10 μm. The microchip was sterilized by UV light and coated with fibronectin for cell attachment. Then, a prepared primary neonatal rat cardiomyocyte sheet 4 days after culture was detached from a temperature responsive dish and assembled on the push bar structure. To attach cardiomyocytes to the PDMS substrate, the microchip was incubated at 37°C for 2 hours (Figure 3). Finally, 1 μm polystyrene particle suspension was injected into the microchannel to observe generated flow.

4. Results and discussion

Flow in the microchannel was observed from movements of polystyrene particles at 37°C. Figure 4(a) and (a') show frames of a video connected to a microscope. Displacement of particles for one stroke (Δx) was 13 μm. Period of contraction (T) was 3 seconds. Therefore, the following parameters were calculated (Figure 4(b)). Volume variation of the chamber for one stroke (ΔV) was 2.6 nL. Displacement of the diaphragm (Δz) was 0.74 μm. Expected flow rate by using ideal check valves (Q) was 0.87 nL/sec. Applied pressure on the diaphragm was calculated from the following equation [3]:

$$P = C_1 \frac{t\sigma}{a^2} z + C_2 \frac{tE}{a^4} z^3$$

where P is the applied pressure, z is the displacement of the center of the diaphragm, t is the thickness of the diaphragm (10 μm), a is the radius of the diaphragm (1.5 mm), σ is the residual stress of PDMS (0.1 MPa), E is Young's modulus of PDMS (1 MPa), C_1 and C_2 are the function of Poisson's ratio of PDMS : calculated to be about 6 and 9 respectively in this experiment. Therefore, the applied pressure on the diaphragm generated by cardiomyocytes (ΔP) was 2 Pa. This force will be larger by using multiplied cardiomyocyte sheets.

5. Conclusions

We succeeded in the fluid driving in a microchannel by a cardiomyocyte sheet for the first time. Firstly, a microchip with a diaphragm chamber and a push bar structure was fabricated. Secondly, a cardiomyocyte sheet was assembled on the push bar structure. Finally, the performance of the fluid driving system was evaluated by generated flow. The volume variation of the chamber for one stroke was 2.6 nL, the applied pressure on the diaphragm generated by cardiomyocytes was 2 Pa. By using check valves [4], a micro diaphragm pump using cardiomyocytes could be realized. This would be applied for various purposes as a self actuated high efficiency micropump without electricity.

References

[1] K. Morishima, Y. Tanaka, K. Sato, M. Ebara, T. Shimizu, M. Yamato, A. Kikuchi, T. Okano and T. Kitamori, *MicroTAS '03*, pp. 1125-1128.

[2] T. Shimizu, M. Yamato, A. Kikuchi and T. Okano, Vol.24, *BIOMATERIALS*, **24**, 2309-2316 (2003)

[3] X. Yang, C. Grosjean and Y. Tai, *Journal of Microelectromechanical Systems*, **8**(4), 393-402 (1999)

[4] N. Honda, S. Shoji, M. Isomura, Y. Ashihara, K. Akahori and H. Sato, *MicroTAS '01*, pp. 403-404.

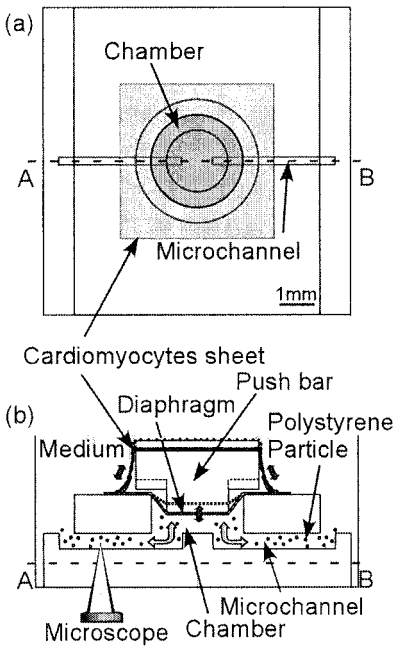

Figure 1. Actuation principle of a diaphragm by a cardiomyocyte sheet. (a) Top view. (b) Cross-section along line A-B.

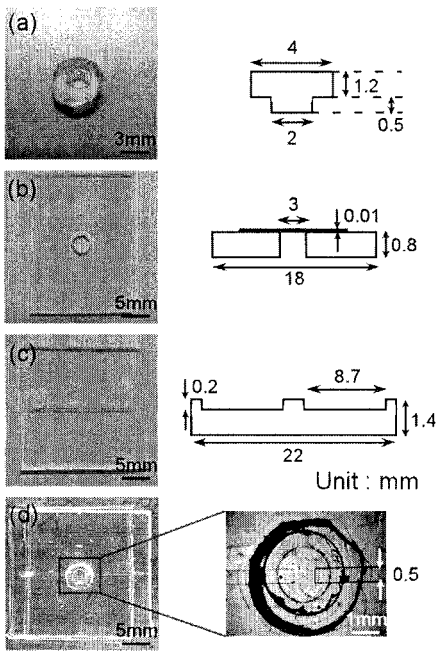

Figure 2. Parts of the microchip. (a) Push bar structure. (b) Upper layer. (c) Bottom Layer. (d) Assembled microchip and expanded picture around the diaphragm chamber.

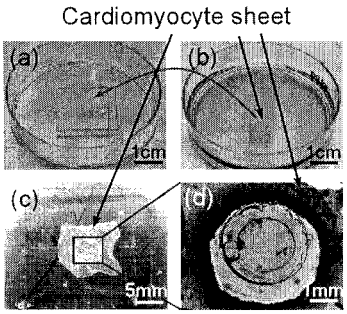

Figure 3. (a) Sterilized and fibronectin coated microchip. (b) Cardiomyocyte sheet detached from a temperature responsive dish. (c) Attached sheet on the microchip. (d) Expanded picture around the diaphragm chamber.

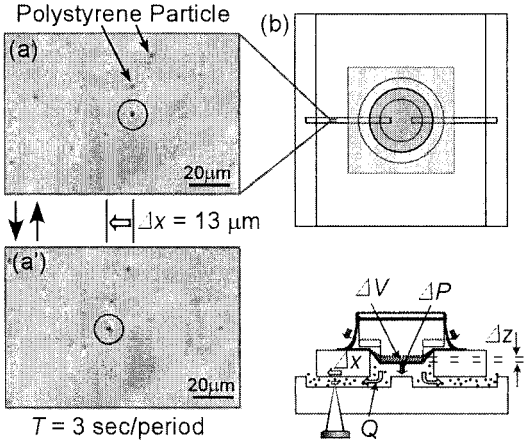

Figure 4. Observation of fluid. Cardiomyocytes were stretching (a) and contracting (a'). (b) Estimated values. $\Delta V = 2.6$ nL, $\Delta P = 2$ Pa, $\Delta z = 0.74$ μm, $Q = 0.87$ nL/sec.

FAST AND RELIABLE PROTEIN MICROARRAY PRODUCTION BY A NEW DROP-IN-DROP TECHNIQUE

Oliver Gutmann, Ruben Kuehlewein, Stefanie Reinbold, Remigius Niekrawietz,
Chris P. Steinert, Bas de Heij, Roland Zengerle and Martina Daub
IMTEK- University of Freiburg, Georges-Koehler-Allee 103, D-79110 Freiburg, Germany

Abstract

For the first time we succeeded to produce protein microarrays in a highly parallel manner. In addition we were able to avoid evaporation out of the printhead. This led to the possibility of long-term, ready-to-print storage of the printheads. Setup times for protein microarray production are lowered dramatically and with it reagent consumption of expensive protein solutions is reduced.

To miniaturize the commonly used EDC-NHS system (a laboratory method for immobilization of proteins) a new drop-in-drop spotting technique was implemented to remarkably increase protein immobilization efficiency on microarray slides.

In contrast to DNA microarrays, production of protein microarrays is an immense technological challenge due to high complexity and diversity of proteins. Consequently control of additional effects like e.g. agglomeration of proteins, adhesion effects, extreme viscosities and reduced surface tension is essential.

Keywords: protein microarrays, non-contact, highly parallel, nanoliter dispenser

1. Introduction

In the last few years microarray technology has become a powerful tool for highly parallel analysis of biological molecules. The biochemistry of proteins is orders of magnitude more complex than DNA biochemistry, so the production of protein microarrays is much more difficult. Printing protein microarrays requires very flexible printer systems. Different applications need different buffer systems, depending on used proteins, coupling chemistry of used microarray slides or surface properties. We expect that only non-contact technologies like the TopSpot technology meet the requirements and enable high throughput printing of protein microarrays.

2. Principle of the TopSpot technology

The TopSpot technology is based on a micromachined printhead, allowing the simultaneous actuation of 24 and 96 different samples in one step, respectively [1]. The printing probes are contained in reservoirs and can be filled automatically by standard liquid handling robots. Every reservoir is connected with one nozzle in the central area of the print head (nozzle array) via an etched microchannel system in the silicon wafer. Liquid is drawn to the nozzles simply by capillary forces. The actuation of the printhead is done by a piezostack actuator *(Fig. 1)*. This generates a pressure pulse that affects all nozzles simultaneously. To achieve a homogenous ejection of the droplets, the nozzle array is coated with a hydrophobic silane [2].

3. Experimental

To optimize immobilization 120 printing buffers were tested by printing two different proteins onto seven microarray slide types. Two immobilization protocols were tested. For very fast immobilization UV cross-linking was used to bind antibodies.

The widespread EDC-NHS system was used to increase protein immobilization on the slides. A problem for microarray production is that the EDC-NHS reaction starts immediately after the two reaction partners are mixed. Over long lasting printing runs this leads to different reaction times and immobilization efficiency on the slides. Another problem could be the agglomeration of proteins. To circumvent these problems a drop-in-drop spotting technique was implemented. One printhead was filled with 200µg/ml Donkey-anti-mouse-Cy5 with 10 vol% EDC. A second printhead was

filled with printing buffer and 10 vol% NHS and was used to print into the humid spots of the first printed array. So the EDC-NHS reaction starts independently of position in printing process flow.

To reduce the evaporation out of the printhead six sealing foils were tested to cover directly the printhead reservoirs during printing. A dew point controlled cooling station was developed for storage of filled printheads. Checkerboard like arrays with labeled BSA (or antibodies) were printed to ascertain carry-over and cross-talk free printing of protein microarrays.

The optimized system was used to print dilution series of BSA (100-12,5µg/ml) on four slides types. As negative control Donkey-anti-goat and Goat-anti-human Protein C antibodies (100µg/ml) were used. For detection the arrays were incubated in two steps with Mouse-anti-BSA (7,5µg/ml) and Donkey-anti-mouse-Cy5 (7,5µg/ml) and analyzed in the fluorescence scanner.

4. Results and discussion

Three main aspects of protein microarray production were examined: optimization of protein immobilization, evaporation of probes during long lasting fabrication times and improvement of protein microarray reproducibility.

The optimization led to CVs of spot diameters on the microarray slide below 1.2 % (*Fig. 2*). Evaporation out of the printhead was reduced to a minimum by sealing the reservoirs (*Fig. 3*). With it even long lasting microarray production runs result in high reproducible microarray quality with no gradient of protein concentration and no blackout of printhead nozzles due to salt out effects. A dew point controlled cooling station was developed for storage of filled printheads for up to one week, ready-to-print. So setup times for protein microarray production are lowered dramatically and with it reagent consumption of expensive protein solutions is reduced.

Of prime interest while using a re-usable printhead is to avoid carry over of formerly fillings to the next usage. Extensive printing of checkerboard like arrays with labeled BSA (or antibodies) and buffer solution showed on the one hand no cross talk of the different microchannels, nozzles and dispensed droplets even after thousands of printed arrays. On the other hand the re-usage of printheads showed that after washing and re-using of printheads no carry-over of formerly printed media was detectable (*Fig. 4*). With it a prime critical point of microarray production is solved enabling high quality and high throughput protein microarray fabrication.

To increase protein immobilization efficiency the widespread EDC-NHS system was implemented using a new drop-in-drop spotting technique. The system showed successfully its potential to increase the immobilization (*Fig. 5*). The drop-in-drop technique is ideal for the EDC-NHS system, but also applicable with other two component coupling systems. Above all it enables a defined starting point of the coupling reaction independently of position in printing sequence and therefore it circumvents the risk protein clogging and leads to no blackouts of printhead nozzles.

For very fast immobilization UV cross-linking was used to bind antibodies. The result of the sandwich ELISA on different microarray slide types showed clearly printed dilution series of BSA (*Fig. 6*). Whereas the negative controls Goat-anti-human Protein C and Donkey-anti-goat spots showed only very low signal. The success of immobilization was evaluated by performing a microarray-ELISA and with it free epitope accessibility of the immobilized antibodies was shown.

5. Conclusions

For production of protein microarrays the commonly used EDC-NHS system was miniaturized. The non-contact technology TopSpot enabled the implementation of the new drop-in-drop spotting technique. This remarkably increased protein coupling efficiency on microarray slides. The printing system was optimized both biochemically and microfluidically, leading to CVs of spot diameters below 1.2 %. Now, storage of already filled printheads, ready-to-print, over one week is possible due to drastically reduced evaporation. Therefore the optimized system is qualified for highly reproducible protein microarray production.

Acknowledgements

Financial support is partially given by grants from German Ministry of Science and Technology, BMBF Project nanoMAP 0312001D.

References

[1] O. Gutmann, R. Kuehlewein, S. Reinbold, R. Niekrawietz, C. P. Steinert, B. de Heij, R. Zengerle and M. Daub, Biomedical Microdevices **6:2**, 131-137 (2004)

[2] S. Breisch, B. de Heij, M. Löhr and M. Stelzle, *Journal of Micromechanics and Microengeneering*, **14**, 497-505 (2004).

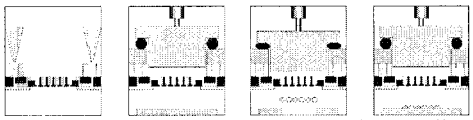

Figure 1. TopSpot working principle: 1. Filling of the printhead reservoirs, 2. Placing a piston into the printhead, 3. Actuation by moving of the piston, 4. Retraction of the piston.

Printing buffer	Highest immobilization of DaM IgG-Cy5	Highest immobilization of BSA-Cy5	CV of spot diameter on Corning slide
PBS	0.05M pH 7.8	0.05M pH 7.4	0.53
Sodium phosphate	0.1M pH 8.0	0.1M pH 8.0	0.51
Borate	0.1M pH 9.6	0.05M pH 7.7	0.47
SSC	0.05M pH 7.6	0.1M pH 7.0	1.14
Sodium carbonate	0.1M pH 9.6	0.1M pH 9.6	0.49

Figure 2. Printing buffer optimization: In general highest immobilization was observed at low salt concentrations and high pH values with CV of the spot diameter on Corning slides under 1.2 %. Absolutely best results were achieved with sodium phosphate and sodium carbonate buffer independently of used microarray slide.

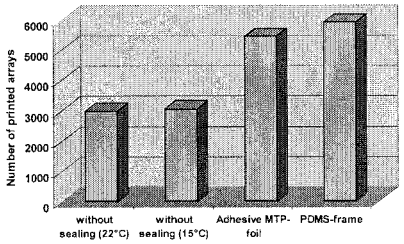

Figure 3. Evaporation during dispensing (initial reservoir volume 6µl): Using the adhesive MTP-foil and the PDMS frame increased the number of maximum prints, showing the low evaporation out of the reservoirs.

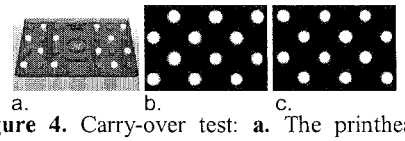

Figure 4. Carry-over test: **a.** The printhead was filled checker board like with Cy5-labeled BSA and buffer. **b.** The printed microarrays were evaluated in a fluorescence reader. **c.** The printhead was washed and inversed refilled. Only the spots with Cy5-BSA are visible.

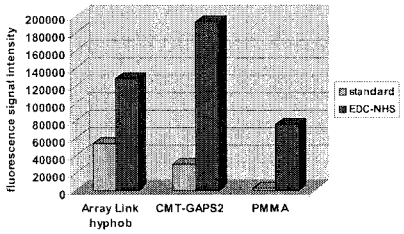

Figure 5. Standard immobilization compared to the drop-in-drop EDC-NHS immobilization. Fluorescence signal of 200µg/ml Donkey-anti-mouse-Cy5 was increased up to 30fold.

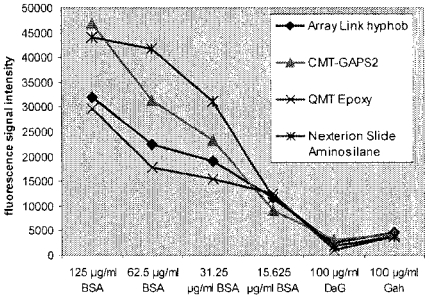

Figure 6. Microarray ELISA with a TopSpot printed antibody microarray: Detection by first antibody Mouse-anti-BSA and second antibody Donkey-anti-mouse Cy5.

MULTIDIMENSIONAL MICROFLUIDICS-BASED COMPREHENSIVE PROTEOME PROFILING

Jesse S. Buch[1], Yan Li[1], Ying-Xin Wang[2], Jon W. Cooper[1], Don L. DeVoe[2], and Cheng S. Lee[3]
[1] *Calibrant Biosystems, 7507 Standish Pl., Rockville, MD, USA 20855*
[2] *Dept. of Mechanical Engineering, and Bioengineering Program, University of Maryland, College Park, MD, USA 20742*
[3] *Dept. of Chemistry and Biochemistry, University of Maryland, College Park, MD, USA 20742*

Keywords: Proteomics, Electrophoresis, Mass Spectrometry, 2-D PAGE

1. Introduction

The majority of current protein analysis methods are still largely dependent upon traditional two-dimensional polyacrylamide gel electrophoresis (2-D PAGE), due to its ability separate thousands of proteins from complex biological samples. Even though 2-D PAGE is capable of providing detailed views of complex mixtures through its high resolving capabilities, it is a relatively time consuming, labor intensive, and cumbersome technology that is not readily amenable to automation and suffers from poor reproducibility.

An automated multidimensional microfluidics-based system is presented as an alternative to 2-D PAGE for comprehensive protein profiling. Figure 1 illustrates the fundamental design of the multidimensional microfluidics-based system. The system employs a high-throughput two-dimensional separation strategy [1] to highly resolve the components of complex protein mixtures. In addition, the off-line coupling of polymer microfluidic chips to mass spectrometry (MS) through the electrospray ionization (ESI) deposition of analyte onto matrix-assisted laser desorption/ionization (MALDI) targets for MALDI-MS analysis is presented for ultra-sensitive protein identification.

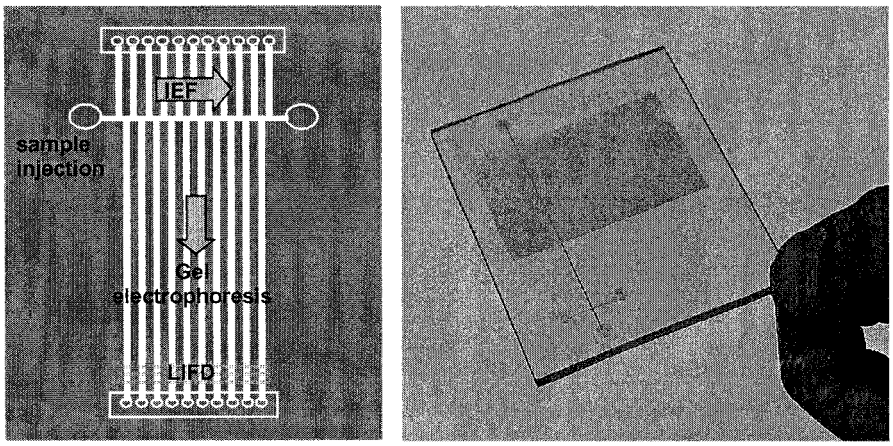

Figure 1. Schematic (left) and photograph (right) of 2-D microfluidic chip.

2. Experimental

In the microfluidics-based high-throughput two-dimensional separation strategy, complex mixtures of SDS-denatured proteins are initially separated in a single first-dimension microchannel

by non-native isoelectric focusing (IEF) providing a charge-based separation and concentration of constituent proteins within the mixture [2]. The focused proteins are then simultaneously transferred to an array of 128 discrete orthogonal microchannels wherein parallel, size-based SDS-polyacrylamide gel electrophoresis further resolves the mixture in a second dimension. Simultaneous monitoring of each microchannel in the second-dimension array is performed by multi-channel laser-induced fluorescence detection, enabling highly sensitive differential display capabilities for biomarker screening. Total analysis time is approximately 10 minutes.

Robust electrospray emitters were integrated into polymer microfluidic chips through the addition of a porous hydrophobic membrane to the channel exit surface, as described elsewhere [3]. Briefly, planar microchannels were fabricated in polycarbonate (PC) using polymer hot embossing with a silicon template patterned by bulk Si micromachining. The resulting open microfluidic channels were enclosed by thermally bonding with a blank PC substrate containing reservoir holes drilled for electrical and fluidic access at one end of each channel. Capillary connections (Nanoport, Upchurch Scientific, Oak Harbor, WA) were bonded via epoxy on top of the reservoir to provide liquid supply from a syringe pump. A platinum electrode contacting the liquid through a capillary T-junction provides the required electrical contact for electrospray deposition. The resulting chip is cut to expose the microchannels at their ends opposite the reservoirs using a CNC milling system. A 50 μm thick PTFE membrane with porosity of 70% and average pore size of 0.22 μm is thermally bonded to the exposed microchannel outlet surface.

3. Results and discussion

Preliminary separations demonstrate the ability of the microfluidics-based high-throughput two-dimensional separation system to resolve complex protein mixtures obtained from *E. coli* cell lysates. Preliminary results indicate that a system containing 128 second-dimension channels is capable of achieving a peak capacity of over 10,000, making it comparable in resolution to 2-D PAGE, but in a microfluidic format enabling 2 orders of magnitude faster separations.

The ability to combine multiple ESI tips on a single chip and simultaneously elute sample onto a MALDI target is demonstrated. Using a 3-element ESI array with 200 μm tip spacing, the simultaneous deposition of bradykinin, fibrinopeptide, and angiotensin is achieved with no cross-talk between deposited samples. Stable electrospray was established at a flow rate of 120 nL/min, chip-to-counterelectrode spacing of 2 mm, and applied voltage of 3900 V. As can be seen in Figure 3, the high hydrophobicity and porous structure of the PTFE membrane effectively constrains liquid spreading near the channel exit and generates a very stable electrospray. The combination of electrospray ionization with off-line MALDI-MS is a powerful technique for integrating microfluidic systems with mass spectrometry. Unlike other methods involving droplet deposition, such as mechanical spotting or piezoelectric ejection, ESI deposition provides the ability to concentrate analyte within small regions of the target, improving the ability to detect relatively small quantities of protein.

Acknowledgements

The authors gratefully acknowledge support for this research from the National Institutes of Health through NCI grant CA092819-02, and from the Defense Advanced Research Projects Agency through contract DAAH01-03-C-R182.

References

[1] Y. Li, J. S. Buch, F. Rosenberger, D. L. DeVoe, and C. S. Lee, *Analytical Chemistry,* **76**, 742-748 (2004).

[2] Y. Li, D. L. DeVoe, and C. S. Lee, *Electrophoresis*, **24**, 193-199 (2003).

[3] Y.-X.Wang, J. W. Cooper, C. S. Lee, and D. L. DeVoe, *Lab on a Chip*, **4**, (2004).

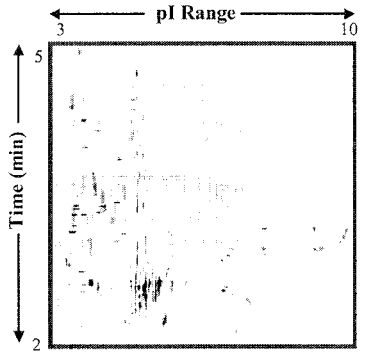

Figure 2. Preliminary display from 2-D microfluidic separation of *E. coli* cell lysates.

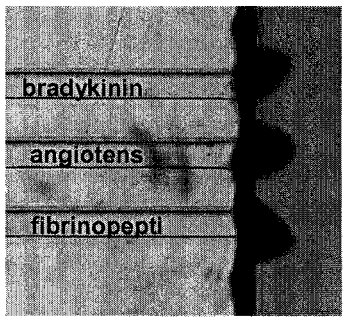

Figure 3. Photomicrograph of simultaneous electrospray from 3-channel ESI chip.

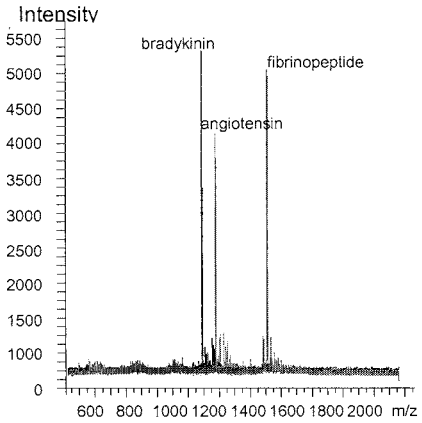

Figure 4. Combined MALDI-MS spectra for measurements performed at the center of each of the three deposited peptide spots (bradykinin, angiotensin, and fibrinopeptide) deposited by 3-channel chip.

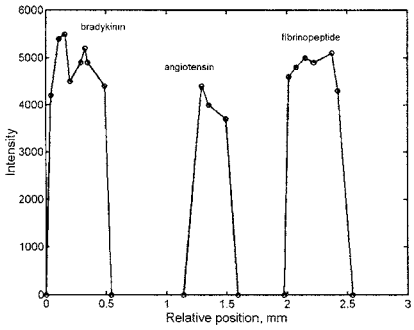

Figure 5. Ion signal intensity measured across the full breadth of the deposited peptide spots. No crosstalk is observed.

ULTRASENSITIVE PROTEIN SIZING USING INTEGRATED ISOTACHOPHORESIS – GEL ELECTROPHORESIS

Josh Molho, Charles Park, Kelly Price, Huan Phan, Stephane Mouradian, and Michael Spaid
Caliper Life Sciences, 605 Fairchild Drive, Mountain View, CA, 94043, USA

Keywords: pre-concentration, proteins, separation, sizing, stacking

1. Introduction

Sizing of proteins is a critical component of important applications such as protein purification, protein expression studies, and immunoassays. When protein concentrations exceed ~20 ng/μL, Caliper's Protein LabChip® assay (available for the Agilent 2100 instrument) offers improvements over standard gels in the areas of: analysis speed, ease of use, reproducibility, and mass quantitation[1]. This extended abstract summarizes previously unpublished efforts to extend microchip protein-sizing sensitivity to levels comparable to silver-staining techniques (~0.1 ng/μL). In this new regime, the advantages of a microchip assay are more pronounced, as silver-staining is generally more difficult to perform and less reproducible than standard Coomassie gels.

To improve protein-sizing sensitivity, we have integrated an isotachophoresis pre-concentration step with SDS gel electrophoresis (ITP-GE). Previous microchip ITP-GE or ITP-capillary electrophoresis (ITP-CE) work has focused on pre-concentration and separation of small molecules[2-3], or has accomplished the switch between ITP and electrophoresis via robotic pipettors[4]. The current work extends our earlier work[5] employing an integrated channel network and switching algorithm. Improvements over our previous work allow integrated pre-concentration (>400x) and sizing of proteins by molecular weight.

2. Theory

Isotachopheresis (ITP) is an electrophoretic technique that utilizes heterogeneous buffers to obtain both concentration and separation of charged ions or macromolecules[6]. For the case of anionic samples, ITP occurs when sample anions are sandwiched between a trailing and leading buffer such that all the sample anions are slower than the anion in the leading buffer, and faster than the anion in the trailing buffer. When an electric field is applied in this situation, all the sample anions will rapidly form distinct zones that are arranged in order of electrophoretic mobility. ITP theory predicts the maximum concentration of each sample zone, which depends on the mobility and concentrations of the sample and leading ions. However, for low enough concentration samples, the final sample zone size is diffusion-limited, resulting in a concentration factor that is relatively independent of the sample mobility. In this limit, ITP is an ideal pre-concentration technique prior to further electrophoretic separations.

In the present work, the switch from ITP to gel electrophoresis (GE) is achieved by re-routing the current flow on the microchip once the concentrated protein bands have passed an intersecting channel connecting to a well containing leading buffer. Once this switch occurs, leading anions surround the sample anions on both sides. After a short transient, the sample ions begin to separate by electrophoretic mobility. As described in our previous work[5], this switching procedure can be automated using only current and voltage control at the chip wells, and without the need for additional on-chip conductivity or optical sensors.

3. Experimental

The following gel/buffers were used for the experiments described below: trailing gel was 200 mM Tris-CHES, pH 8.4 and 4% 487 kDa PDMA, leading gel was 80 mM Tris-Cl, pH 8.0, 0.1% SDS and 4% 487 kDa PDMA, and dilution gel was 40 mM Tris-Cl pH 8.0, 4% 487 kDa PDMA. Sample buffer was 10 mM Tris-Cl pH 6.8, 2.5% SDS, 3.5% beta-mercaptoethanol.

Ovalbumin, BSA, and transferin were purchased from Molecular Probes, pre-labeled with Alexa Fluor® 488 fluorescent dye. In addition, β-galactosidase was purchased from Sigma and then labeled with Alexa Fluor® 488 using a labeling kit from Molecular Probes.

All samples were dissolved in 1X PBS. Denatured sample was prepared as follows: 4 μL of each sample was mixed with 1 μL of sample buffer, each sample was then heat-denatured at 100 °C for 5 minutes, and finally 55 μL of sample dilution gel was added to the sample. A Caliper 42 instrument provided multi-well electrical and pressure control. Detection was accomplished using a mercury lamp with standard FITC epifluorescence filters for excitation, a 40x Nikon microscope objective (NA = 0.6) and a photomultiplier tube. A color video camera and a video capture board were also used for supplementary image collection

ITP-GE experiments were performed on a glass microfluidic chip; a schematic of this chip is shown in Figure 1. The length of the separation channel (Se) is 1.7 cm, and the main channels (Sa, Se, St) are approximately 110 μm wide by 15 μm deep. Prior to insertion in the Caliper 42 instrument, the chip was pressure-primed with leading gel through well 6. Twenty μL of leading gel was then placed in wells 6 and 5, and 5 μL of leading gel was placed in waste wells 2 and 4 (for electrical connectivity). Twenty μL of trailing gel was placed in well 1, and 20 μL of diluted sample mixture (prepared as described above) was added to well 3. To load sample, pressures were applied at the wells causing sample to flow from well 3 to wells 2 and 4. Simultaneously, the separation (Se) and stacking (St) channels were refreshed with leading gel, and the trailing channel (T) was refreshed with trailing gel. Then, the pressures were removed and voltages between wells 6 and 1 were applied (starting ITP). When the stacked protein bands passed the intersection with well 5, the switching condition was detected as was previously described[5]. At this point, voltages were applied between well 6 and well 5, causing the stacked protein bands to destack and separate by molecular weight (GE step). The load-ITP-GE steps were repeated many times without removing the chip from the instrument.

4. Results and discussion

Experimental results confirm that the ITP-GE separation provides greatly enhanced sensitivity while maintaining resolution and sizing performance. Figure 2 shows an image of the focused protein band having a concentration factor of 400-500x. Figures 3-5 compare the band shapes, sizing behavior, and sensitivity of the existing LabChip® protein assay to those of the ITP-GE assay. Noting the different staining mechanisms, these comparisons show a qualitative ~100x improvement in sensitivity and confirm that the ITP-GE assay does separate proteins by molecular weight. Ongoing work is focused on integrating ITP-GE with on-chip staining and de-staining of proteins using the previously published[1] technique.

Acknowledgements

The authors thank Caliper's R&D chip fabrication group.

References

[1] Bousse, L., Mouradian, S., Minalla, A., Yee, H., Williams, K., Dubrow, R., *Anal. Chem.*, 2001, 73,1207-1212.

[2] Vreeland, W., Williams, S., Barron, A., Sassi, A., *Anal. Chem.*, 2003, 75, 3059-3065.

[3] Kaniansky, D., Maser, M., Bielcekova, J., F. Ivanyi, F. Eisenbeiss, B. Stanislawski, B. Grass, A. Neyer, M. Johnck, *Anal. Chem.*, 2000, 72, 3596-3604.

[4] Xu, Z., Ando, T., Nishine, T., Arai, A., Hirokawa, T., *Electrophoresis*, 2003, 24, 3821–3827.

[5] Park, C., Kechagia, P., Chen, R., Spaid, M., *Proceedings of μTAS 2003*, 989-991.

[6] Everaerts, F., Beckers, J., Verheggen, T., "Isotachophoresis: theory, instrumentation, and applications," Amsterdam, New York, 1976.

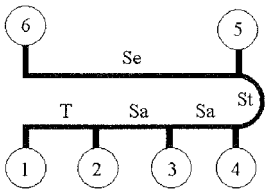

Figure 1. Schematic of channel network. Separation, stacking, sample, and trailing channels are labeled Se, St, Sa and T, respectively.

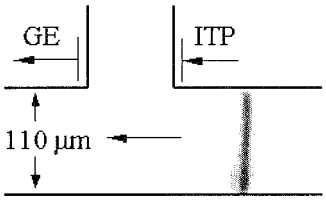

Figure 2. Image of stacked protein band just prior to GE step. Fluorescence measurements and final to initial plug size ratio give a 400-500x pre-concentration factor.

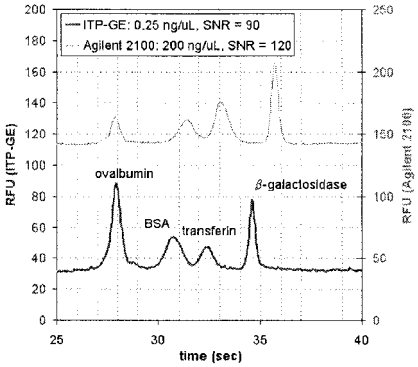

Figure 3. Comparison of peak shapes for commercially available LabChip® protein assay and the ITP-GE assay. The concentrations for each assay were chosen to give a signal to noise ratio (SNR) of about 100. The elution times of the ITP-GE separation have been scaled so that the ovalbumin peaks coincide.

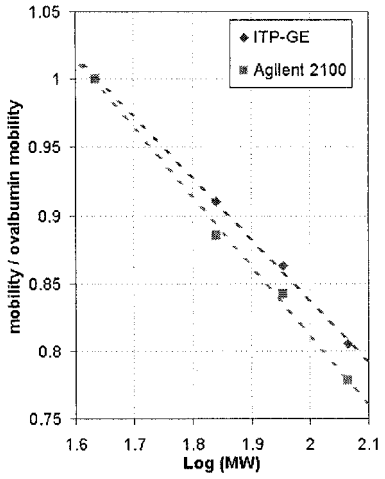

Figure 4. Sizing curve showing the expected linear fit of mobility versus log of molecular weight.

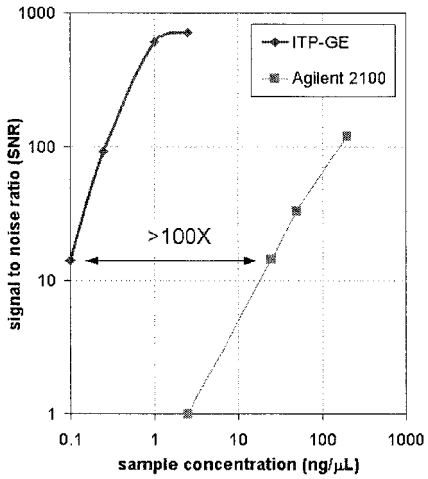

Figure 5. Signal to noise ratio comparison for BSA at different concentrations. The ITP-GE separation can detect BSA at 0.1 ng/µL.

MULTIPLEXED MICROBIOREACTOR SYSTEM FOR HIGH-THROUGHPUT BIOPROCESS DEVELOPMENT

Nicolas Szita[1], Paolo Boccazzi[2], Zhiyu Zhang[1], Andrea Zanzotto[1], Anthony J. Sinskey[2] and Klavs F. Jensen[1]

[1]Dept. of Chemical Engineering, [2]Dept. of Biology, Massachusetts Institute of Technology, 25 Ames Street, Cambridge, MA 02139, USA

Abstract

We present a multiplexed bioreactor system for the parallel operation of multiple instrumented microbioreactors. The system can be configured with different reactor types and hold up to eight reactors. High reproducibility of *Escherichia coli* growth is shown with reactors operated in parallel.

Keywords: microbioreactor, cell culture, high-throughput bioprocessing, microarray gene expression

1. Introduction

Instrumented and miniaturized bioreactors enable automation, parallel experimentation, and reduced use of resources, which ultimately will allow high-throughput screening of bacterial strains and rapid bioprocess development [1]. In our multiplexed system, fermentation processes are performed in an automated fashion, and the main process parameters optical density (OD), dissolved oxygen (DO) and pH are monitored in real time and recorded individually for each reactor. The system can accommodate bioreactors of different operational modes, batch and continuous, stirred and non-stirred. Depending on its configuration, one to eight bioreactors can be operated. We have previously shown example of fermentations in single microbioreactors [2,3] and are showing here the results of multiple microbioreactors operated in parallel. The multiplexed system represents a significant step towards high-throughput data acquisition and has the potential to replace current instrumented bioreactors, which are bulky, and expensive to run, and require many mechanical manipulations (Figure 1). Finally, we demonstrate the use of microbioreactors with microarrays for gene expression analysis, as a tool for accelerated discovery and elucidation of metabolic pathways and gene expression.

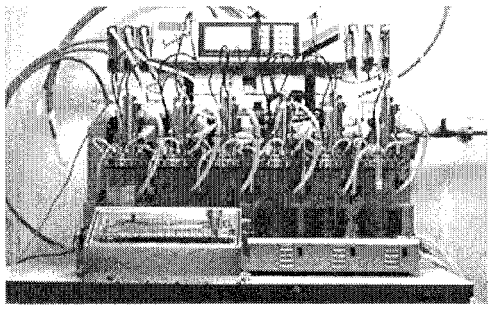

Figure 1. Photograph of the Sixfors (Infors, Switzerland) in the background and the multiplexed platform (here configured for eight microbioreactors) to the bottom left.

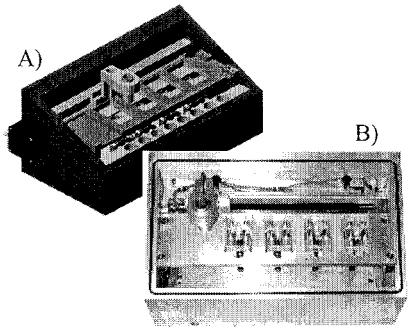

Figure 2. A) Solid model and B) photograph of the multiplexed platform, here configured to accommodate 4 stirred microbioreactors.

2. Description of the microbioreactor system

The multiplexed system (Figure 2) includes a platform for the microbioreactors, which can quickly be interchanged to accommodate different bioreactor types and configurations. A bracket attached to a motorized stage moves over the microbioreactors and holds optical fibers and lenses above and below the reactors. To maximize signal intensity, the z-position of the optical components can be adjusted. Computer control algorithms execute stop-and-go sequences for the bracket so that OD, DO, and pH can be measured for each reactor using lifetime fluorescence methods and the individual process parameters recorded. Magnetic stirring of the bioreactors has been achieved with i) small electromagnets placed underneath the reactor wells and ii) torque motors that rotate permanent magnets at defined RPM's. Using sliding posts and a special geometry on the bracket, we have also realized a mechanism which permits both optics and stirring device to be in close proximity to the reactor wells (solid model of Figure 2). System-wide temperature control is achieved by flowing water from an external heated bath through the base of the platform, and inlet and outlet ports in the housing allow flushing the platform with the desired gas concentration. Finally, the operation of the platform is completely automated and does not require any user interaction during the fermentation.

3. Microbioreactor results

Fermentations were performed in magnetically stirred microbioreactors with a volume of approximately 160µl. The reactors (Figure 3) are a modified version of a previously described reactor [3]. In this configuration, the bottom poly(methylmethacrylate) (PMMA) holds the fermentation chamber (diameter 10mm, depth 2mm), the magnetic spin bar and connecting channels. The middle poly(dimethyl-siloxane) (PDMS) layer includes the 100 microns thick aeration membrane, a post and a web-like structure holding the post. The post serves as an optical waveguide for the optical density reading. The PDMS layer was fabricated using a negative mold made of polycarbonate (PC). The top PMMA layer includes an opening for aeration and a post to extend the PDMS waveguide. This structure ensures that the optical path for the OD reading inside the reactor is constant and independent from any deflection of the aeration membrane. Fermentations were carried out with *Escherichia coli* in rich medium with MES buffer and glucose, and the reactors were stirred at 300 RPM. Figure 4 A) to C) show the OD, DO and pH. At the end of the fermentation run, the cell culture was harvested and a final OD was measured in a spectrophotometer. Typical values of OD 4 were achieved. The three pH and DO readings each show excellent reproducibility. The slight differences in the DO data reflect the inoculation time (10 minutes from reactor 1 to reactor 3). Finally, Figure 4 D) illustrates the potential of the multiplexed system for global gene expression analysis. DNA microarrays experiments were performed with total RNA isolated from *E.coli* cultures grown in ~50µL microbioreactors under different growth conditions.

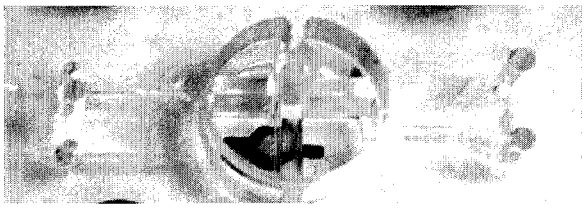

Figure 3. Photograph of the magnetically stirred microbioreactor

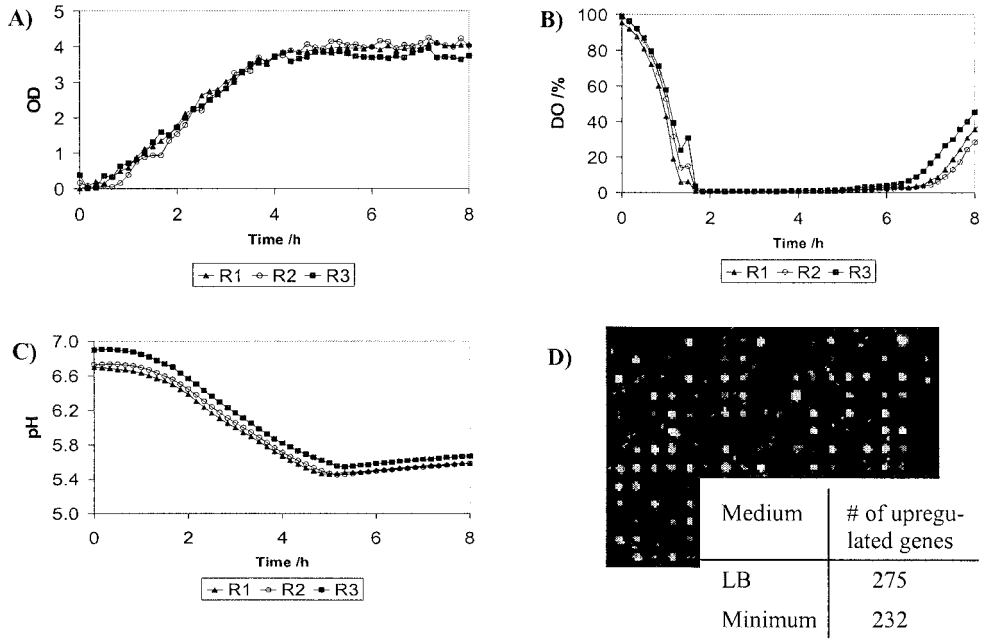

Figure 4. A), B), and C) show results for OD, DO and pH from three parallel fermentations of *Escherichia coli* (FB21591) grown in LB, 100mM MES, 0.1g/mL KAN and 8g/L glucose. D) shows the number of upregulated genes of *E. coli* grown in two different growth conditions and close-up photograph of part of the *E. coli* microarray chip hybridized with cDNA obtained from 50µl-bioreactors.

4. Conclusions

The results demonstrate that fermentation runs of multiple stirred microbioreactors can be made in parallel. The reproducibility of the data compares well to the reproducibility of shaker flasks or commercially available instrumented multireactor systems, thus demonstrating that the presented multiplexed microbioreactor system has the potential to replace parallel shaker flask runs or large multireactor systems with instrumented microbioreactors.

Acknowledgements

The authors thank the DuPont-MIT Alliance for funding. Nicolas Szita would like to thank the Swiss National Foundation for additional funding.

References

[1] S. Kumar, Ch. Wittmann, E. Heinzle, *Biotechnology Letters*, **26**, 1-10, (2004).
[2] A. Zanzotto, N. Szita, P. Boccazzi, A. J. Sinskey, M. A. Schmidt, K. F. Jensen, Biotechnology and Bioengineering, **87**, (2004).
[3] Z. Zhang, N. Szita, P. Boccazzi, A. J. Sinskey, K. F. Jensen, Micro Total Analysis Systems 2003, USA, 765-768, (2003).

MICROFABRICATION OF HYDROGELS FOR THE CONSTRUCTIONAL ANALYSIS OF CULTURED CELLULAR NETWORKS WITH CONTROLLED NETWORK SHAPES AND COMMUNITY SIZES

Hiroyuki Moriguchi, Kensuke Kojima, Ikurou Suzuki, Akihiro Hattori,

Tomoyuki Kaneko and Kenji Yasuda

Department of Life Sciences, Graduate School of Arts and Sciences, University of Tokyo, Japan

Abstract

We have been trying to establish novel cell cultivation and analysis methods based on microfabrication techniques and microstructures of cell-compatible materials that enable single-cell based optical and electrophysiological observation and analysis of cultured cellular networks or cell aggregates with precisely controlled cell-cell interactions, total shape of cell community and spatial distribution of different kinds of cells, or topography of cultured cell populations, and have developed two kinds of 2-dimensional microfabrication methods; 1) "micromolding" and 2) "photothermal etching (PTE)", and a 3-dimensional microfabrication method, 3) "photo-thermal microneedle etching (PTMNE)" that uses agarose-gel as a micro-structural material. By using these microfabrication methods of agarose-gel in combination with microelectrode array (MEA) or other optical analysis techniques or surface treatment methods, we could culture, observe and analyze arrayed cardiac myocytes, patterned hippocampal neural-networks and shape-controlled 3-dimensional cancer spheroids. We consider these topographic control techniques of cultured cells as one of the fundamental technologies of next-generation drug screening, tissue engineering and fundamental one-cell-observation based cell-biological research.

Keywords: agarose-microchamber array (AMCA), photothermal etching (PTE), photo-thermal microneedle etching (PTMNE), neural network, cardiac myocytes

1. Introduction

The purpose of this study is to establish new experimental methods for topographical control of cultured cell populations. In multicellular systems, these topographic properties are thought to have essential role in the realization of their higher order functions such as memory, synchronization, or physiological robustness, and so on. To investigate these functional aspects of topography in multicellular organisms, observation and analysis of not only natural living organs, but also constructionaly shape-controlled multicellular system is required. On the other side, agarose-gel is one of the most measure materials in cell cultivation for long years for its biological inactiveness, mechanical characteristics, semi-permeability, extended release property of biological molecules and economical efficiency, and besides has useful thermal property to handle with its sol-gel phase transition. From these reasons, we tried to develop new microfabrication techniques of agarose-gel and tried to apply these techniques to topographical control of cultured cells [1][2].

2. Materials & Methods

2-1. On-chip Cell Cultivation System

The system we developed and used for agarose-gel microfabrication and cell cultivation [1] consists of four parts; an incubation unit on microscope stage to keep warm temperature (37 °C), CO_2 concentration (5%) and humidity (90%) around cell cultivation dish (IWAKI) in it for the continuous observation of cultured cells, a Phase-contrast/fluorescent optical microscope (Olympus) with a dual light pass of a 1064 nm Nd:YAG laser and 1480 nm Raman fiber laser (Sigma Kohki) [3], an agarose-gel microstructure chip fixed on a glass slide and a digital image detection unit with CCD camera (Olympus) connected to a personal computer.

2-2. Agarose Gel Microstructure Chip

We used 2 % of Low-Melt agarose (Hispanagar) as agarose-gel, and fabricated 3 kinds of agarose-gel microstructure chips; deep agarose-microchamber array (deep AMCA) chip, depthless AMCA chip, agarose-microcavity chip. All chips were placed in cultivation dishes and sunk in cultivation buffer when cells are seeded and cultured. Deep AMCA chips [1][2] were fabricated on a glass-

slide with or without evaporated chromium layer (thickness: 6 nm) by micromolding with SU8 microstructure arrays on silicon wafers. Depthless AMCA chips [3][4][5] were fabricated by photo-thermal etching (PTE) of agarose-layer spin-coated with hot 2% agarose solution (>37 °C) on glass-slides with or without chromium layer. The chromium layer serve as a photo-absorbable layer on the bottom of agarose-gel and is necessary for microtunnel or microchannel fabrication with focused 1064 nm laser beam, which have no absorption to glass or water, and not necessary for microchannel fabrication with focused 1480 nm laser beam, which have absorption to water. Fig. 1 and Fig. 2 each shows a scheme of cell cultivation method using deep and depthless AMCA (a) and micrographs of microtunnel and microchannel fabrication process (b) with 1064 nm and 1480 nm focused laser beam. Depthless AMCAs were made on MEA chip only when electrophysiological measurement of neural networks was required [4][5].Agarose-microcavity chips were fabricated in small pieces of agarose-gel on glass-slides by photo-thermal microneedle etching (PTMNE). PTMNE uses the tip of a glass microneedle coated with chromium layer (thickness: 10 nm) as a mobile photo-absorption point. By manipulating this mobile photo-absorbable point with focused 1064 nm laser beam, we could fabricate hollow-shaped microstructures in agarose-gel. Fig. 3 shows a scheme of microcavity cell cultivation methods and observed microcavity fabrication process.

2-3. Cell Cultivation

All cells were handled and injected one by one into agarose microstructures by using cell-handling pipette fabricated by a puller (Narishige) and a microforge (Narishige), and coated with Sigma-coat (Sigma-Aldridge) to prevent cell adhesion to the surface of pipette. The bottom surfaces of AMCAs were coated with type-I collagen by overnight sinking in collagen solution (150 μg/ml, pH 3, Nitta-gelatin). Rat cardiac myocytes and STO cells were cultured in DMEM with 10 % FBS. PC12 cells were cultured in RPMI1640 with 10 % HS, 5 % FBS and 50 ng/ml of nerve-growth-factor (NGF). Rat fetal hippocampal cells from 18-days-old fetuses were cultured in Neurobasal medium with B27 supplement (Gibco).

3. Results and discussion

Figs. 4 - 7 each shows cultivation results of PC12 cells in deep AMCA, cardiac myocytes in depthless AMCA, hippocampal neurons in depthless AMCA and STO cells in a microcavity. Those cells were all cultured in agarose-gel microchambers and making shape-controlled intercellular junctions through patterned microchannels connecting microchambers or shape-controlled cell populations, and optically (Fig. 5) and electrophysiologically (Fig. 6) measured and analyzed. Agarose-gel served as a non-cell-adhesive material when kept not decorated with cell-adhesive molecules, prevented completely cell spreading and controlled shapes and sizes of cell populations.

4. Conclusions

Table 1 shows an overall view of agarose-gel microfabrication methods. The advantages of using agarose gel as a micro-structural material are that 1) agarose-gel is not degradable and have no biological activity against most kinds of living cells, 2) simple micro-molding and stable thermal ablation and modification of microstructures in aqueous buffers is applicable even during cell cultivation and 3) surface activity to cultured cells are basically non-adhesive and non-active, and can be modified by using grafting methods of physiologically active molecules such as cell-adhesive molecules. From these points, we consider agarose-gel is a very useful micro-structural material and have much potency in the fields of tissue engineering, drug screening and basic research about cell morphology and multicellular organ development.

Acknowledgements

Financial support, in part by the Japan Science and Technology Corporation (JST) and by Grants-in-Aids for Science Research from the Ministry of Education, Science and Culture of Japan, is gratefully acknowledged.

References

[1] H. Moriguchi, et al., *Lab on a chip*, **2**, 125-130 (2002)
[2] A. Hattori, et al., *Sensors and Actuators*, B, **100**, 455-462 (2004)
[3] K. Kojima, et al., *Lab on a chip*, **3**, 292-296 (2003)
[4] I. Suzuki, et al., *Japanese Journal of Applied Physics*, **43**: L403-406 (2004)
[5] I. Suzuki, et al., *Lab on a chip*, submitted (2004)

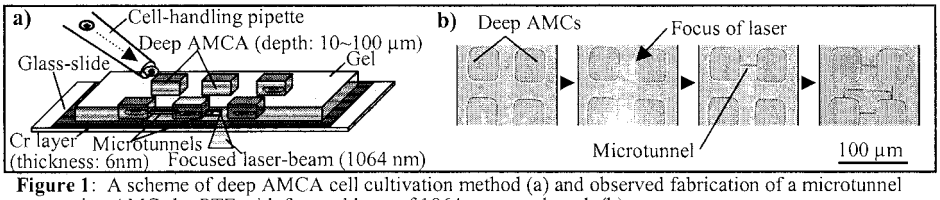

Figure 1: A scheme of deep AMCA cell cultivation method (a) and observed fabrication of a microtunnel connecting AMCs by PTE with focused laser of 1064 nm wavelength (b)

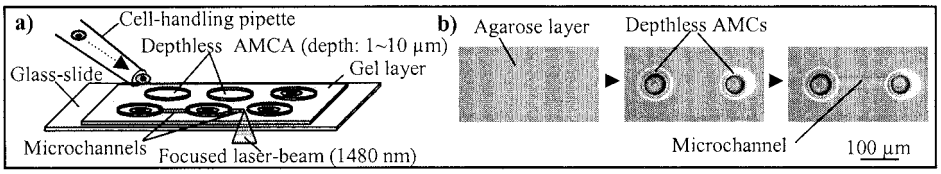

Figure 2: A scheme of thin AMCA cell cultivation method (a) and observed fabrication process of depthless AMCs and a microchannel by PTE with focused 1480 nm laser beam (b)

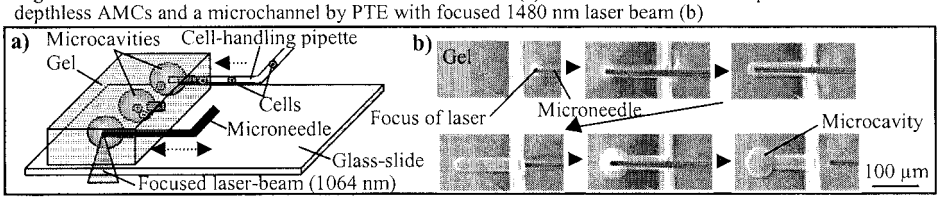

Figure 3: A scheme of cell cultivation method in microcavities (a) and observed microcavity fabrication process in agarose gel by PTMNE with microneedle and focused 1064 nm laser beam (b)

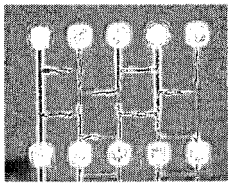

Figure 4: Micropatterned PC12 cellular network formed after 4 days cultivation under the effect of 50 ng/ml of NGF in deep AMCA and ladder-shape microtunnels

100 μm

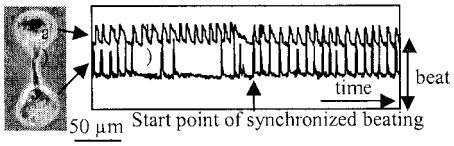

Figure 5: Patterned 2 cardiac myocytes of neonatal rats in depthless AMCA making connection through a lengthwise microchannel (left) and result of the optical measurement of their oscillation synchronization process (right)

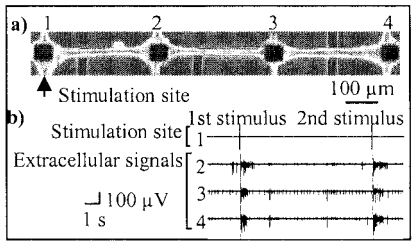

Figure 6: Micropatterned hippocampal neural network of in depthless AMCA on MEA (a) and the result of their electrophysiological measurement (b) by using MEA

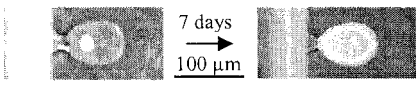

Figure 7: An STO cell injected in microcavity (left) and a shape-controlled spheroid formed after 7 days cultivation and proliferation from the one cancer cell (right)

Dimension	Microstructure	Laser	Other Required Elements
2	Deep AMCA with Microchannels (1~10 um thick)	Nd:YAG (1064 nm)	Cr layer
		Raman fiber (1480 nm)	
	Depthless AMCA with Microtunnels (10~100 um thick)	Nd:YAG (1064 nm)	Cr layer, Molding
		Raman fiber (1480 nm)	
3	Microcavity	Nd:YAG (1064 nm)	Microneedle

Table 1: Overall view of agarose-gel microfabrication methods

BEHAVIOUR OF OSTEOBLAST-LIKE CELLS IN CELLULAR MICRODEVICES

E.Leclerc[1], B. David[1], R. Warocquier-Clérout[1], L. Griscom[2], B. Le Pioufle[2], T. Fujii[3] and C. Legallais[1]

[1] CNRS-UMR 6600, Laboratoire de biomécanique et de génie biomédical, Université de Technologie de Compiègne, BP 20529, 60205 Compiègne cedex, France

[2] CNRS-SATIE/BIOMIS, Ecole Normale Supérieure de Cachan, Campus de Ker Lann, Bruz, France

[3] Institute of Industrial Science, University of Tokyo, 4-6-1 Komaba, Meguro- ku, Tokyo, Japan

Abstract

In this work, we report the results of bone cell cultures in cellular microdevices. In our dynamical configuration of cultures, 3D geometrical effects appeared predominant on the microfluidic flow conditions, as far as cell behaviours were concerned.

Keywords : Osteoblast, dynamic cell culture , 3D effects, Bone regeneration

1. Introduction

Autologous or allogenous bone grafting is widely used to repair injured, aged or diseased skeletal tissue. It is however limited by availability, infection or even rejection and disease transfer. The use of biomaterials such as calcium phosphate ceramics, devoid of osteogenic properties, does not allow bone reconstruction on large defects. The increasing demand in bone grafting procedures leads surgeons to look for more advanced therapies such as tissue engineering. In this case, bone marrow mesenchymal stem cells are harvested from a patient, and cultured during 4 to 5 weeks in vitro to reach a sufficient number. They are then seeded onto a suitable scaffold with subsequent culture to produce a bone-like tissue layer on the scaffold prior to implantation into the same patient. Nevertheless, the period of time required to produce the tissue-engineered bone under static conditions currently limits its clinical application.

To reduce the delay before disposing of an autologous bone graft substitute, which could be readily implanted in the patient, several authors proposed to use new culture scaffolds offering a suitable environment to the cells. Mineralization was enhanced and the delay of bone reconstruction might be decreased by shear stress and culture on microtopography [1, 2]. However, the best operating conditions are not yet fully defined.

To address this question, we have investigated the behaviour of osteoblast-like cells in two types of PDMS (polydimethylsiloxane) microfluidic microdevices, for spatially uniform cell seeding and dynamic cell culture conditions.

2. Materials and methods

Both types of microdevices are fabricated by conventional molding of PDMS microchannels on a SU-8 mold. The first one is a two-dimensional network of microchannels that have various widths. This leads to the creation of several fluid flow configurations in the microdevices. The second one is a 300 μm height cell culture chamber in which 100μm thick microstructures and 100μm deep microholes formed a microchannel network at its bottom. This creates a "3D like microtopography" in the microdevices [3]. The microdevices were connected to a perfusion loop and cultures were achieved inside CO_2 incubator [3]. Calvaria preosteoblast MC3T3-E1 subclone 24 cells from mouse (obtained from ATCC, number CRL-2595) were employed for all the experiments. They were cultivated in a free ascorbic acid α-modified Eagle's medium (Gibco, Invitrogen Corporation) supplemented with penicillin (100 units/mL), streptomycin (100 μg/mL)

and 10% fetal calf serum (FCS). Alkaline phosphatase productions by the cells were measured with a biochemical analyser.

3. Results and discussion

Morphological aspects

First, cells were allowed to attach successfully inside the microchannels in the first type microdevice. Then, they elongated along the flow direction when the perfusion was started (Fig. 1A) under a pump flow rate of 200 µl/min. After few hours of culture, the cells detached in larger microchannels (Fig 1B), whereas they remained attached in smaller ones (Fig 1C).

In the second set of microdevices, the flow rate was reduced to avoid cell detachment. This permitted the 3D reorganization of the cells on the microstructures. The cells surrounded and covered the microstructures of the devices (Figs 2A and 2B for a pump flow rate of 5 µl/min).

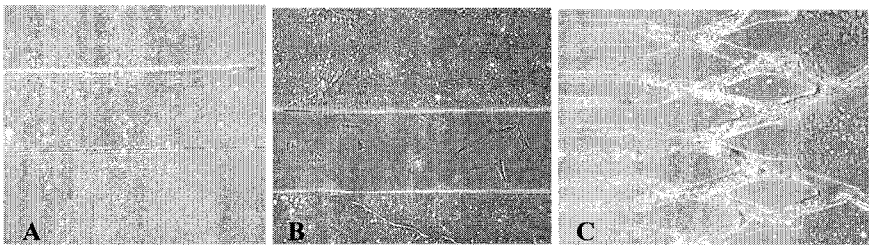

Figure 1: (A) Elongation of the cells; (B) detachment of the cells from microchannels; (C) cell attachment to the microstructures; in the 2D microdevices

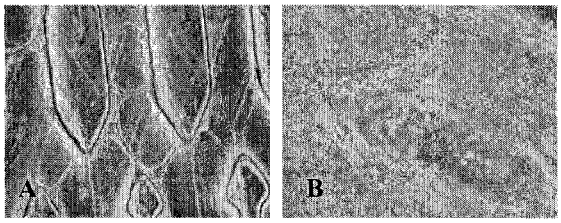

Figure 2: (A) Cells surround the microstructures; (B) cells covering the microstructures; in the 3D microdevices

Cellular activity

A cell density of about 2.8 x 10^6 cells/cm^3 was reached after 14 days in the second type of microdevices. To demonstrate the cellular activity, the daily variation of the concentration of alkaline phosphatase, an early marker of the osteoblast activity, was measured in the media as shown in Fig. 3. In addition, the per-cell production of alkaline phosphatase, at the end of the cultures was found higher in the cultures in the microdevices (respectively 0.039 IU/day/10^6cells, 1 IU corresponding here to the activation of 1 µmol/min of para-nitrophenol) when compared to the flat and static culture (0.002 IU/day/10^6cells).

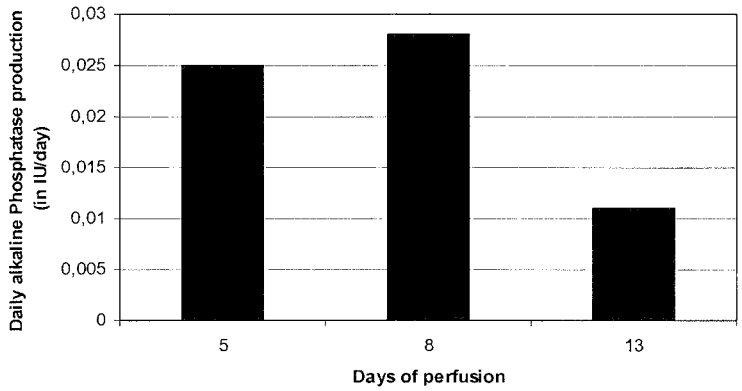

Figure 3: Daily variation of the concentration of alkaline phosphatase, illustrating the cellular activity, in the culture medium in the 3D microdevices (dynamic condition with a total volume of perfusion of 6ml)

4. Conclusions

These preliminary experiments first show the ability to culture osteoblasts in well-calibrated microdevices under dynamic conditions. Bone tissues are reported to be sensitive to shear stress up to 1 dyne/cm^2 [1]. Through numerical simulations, we estimated values of shear stresses about 4 dyne/cm^2 in the flow configuration shown in Fig 1B and about 200 to 400 dyne/cm^2 in the flow configuration shown in Fig 1C. In this latter one, despite higher shear stress, the cells did not detach from the microchannels but remained attached to the walls of the microstructures. This tends to demonstrate the importance of the geometry of microstructures in the cellular microdevices.

In the second microdevice, in which we observed a higher cellular activity compared to dishes cultures, numerical simulations estimated lower shear stresses values from about 0.03 to 0.2-0.3 dyne/cm^2. As we observed 3D cell reorganization, mainly around the microstructures, this may suggest that the 3D effects might be predominant in this second culture condition.

For future bone regeneration using MEMS/microfluidic microdevices, we are now investigating flow, the growth and activity of the cells in order to propose a best optimized geometry including shear stresses and 3D effects.

References

[1] G. Bancroft, V. Sikavitsas, J. van der Dolder, T. Sheffield, C. Ambrose, J. Jansen, A. Mikos, PNAS, **99**(20), 12600-12605 (2002)

[2] H. Liao, A.S. Andersson, D. Sutherland, S. Petronis, B. Kasemo, P. Thomsen, Biomaterials, **24**, 649-654 (2003)

[3] E. Leclerc, Y. Sakai, T. Fujii, Biomedical Microdevices, **5**(2), 109-114 (2003)

MICROFLUIDIC-ASSISTED LIPID NANOTUBE FORMATION AND MANIPULATION WITH LIGHT

Laurie E. Locascio[1], Ksenia Brazhnik[1], Wyatt Vreeland[1], Rani Kishore[2], Kristian Helmerson[2]

[1]Analytical Chemistry Division, and [2]Atomic Physics Division,
National Institute of Standards& Technology, Gaithersburg, MD 20899

Abstract

Lipid nanotubes and microtubes were formed in a microfluidic channel by flowing buffer solution over a dried phospholipid film to hydrate the phospholipid molecules. Lipid nanotubes and microtubes formed spontaneously in the microchannel and oriented themselves in a direction parallel to the flow direction as reported previously [1]. Lipid tubes formed by this procedure exhibited unusually high aspect ratios (ratio of tube length to diameter) and extraordinary stability when stored hydrated in the microchannels. Lipid tubes were manipulated with optical tweezers immediately after preparation and after storage under various conditions to evaluate their mechanical properties. When fluorescent dyes were inserted into the phospholipid tube membranes at low concentrations, excitation of the dye induced tube movement and growth.

Keywords: lipid nanotubes, optical trapping, laser tweezers, laser scalpel, nanotube growth

1. Introduction

Shrinking channel dimensions to the micrometer scale with microfluidics has given rise to several new analytical techniques that would not otherwise have been possible due to the fact that these devices operate in a unique flow regime where laminar flow dominates. Many years ago there was some skepticism as to whether it was necessary to reduce channel dimensions to such small sizes in light of the perceived potential to clog channels and the difficulties associated with manipulating picoliter samples. As the field progresses toward nanofluidics, there is the same skepticism that this is an unnecessary miniaturization step. Nonetheless, researchers continue to pursue the development of nanochannels in an attempt to discover new techniques that allow us to probe and understand single molecule behavior.

Some methods now exist for producing nanofluidic channels. Notably, sub-micrometer channels have been fabricated using modifications of lithographic techniques including sacrificial layer techniques [2], electron beam lithography [3], and interferometric lithography [4]. In the past few years, nanofluidic channels have also been fabricated from pre-formed liposomes [5] by pulling on and distorting the phospholipid membrane using mechanical pulling techniques. Fluid flow in single nanofluidic channels made from phospholipids has been characterized recently, and elegant methods for fabricating networks of nanofluidic channels have been demonstrated [6]. Here we report the development of new methods for fabricating nanofluidic channels from phospholipid building blocks exploiting their self-assembly processes in microfluidic devices. Phospholipid micro- and nanotubes made in this manner have been characterized using a variety of techniques to assess their chemical and physical characteristics.

2. Experimental

To briefly summarize the procedure for preparing phospholipid tubes, a droplet of a solution containing dissolved phospholipids (either 1,2-dilauroyl-*sn*-glycero-3-phosphocholine (DLPC), 1,2-dimyristoyl-*sn*-glycero-3-phosphocholine (DMPC), or 1,2-dipalmitoyl-*sn*-glycero-3-phosphocholine (DPPC) (Avanti Polar Lipids, Alabaster, AL)) was applied to the surface of a glass coverslip and dried under vacuum. A PDMS microfluidic channel (trapezoidal profile with a depth of 30 μm, a minimum width of 20 μm and a maximum width of 60 μm) was then placed over the dried phospholipid film, and fluid (buffer) was forced to flow over the patch by evacuating the

microchannel in a vacuum desiccator then releasing the vacuum with liquid in the reservoirs. Phospholipid tubes were observed in the microfluidic channel after the device was removed from the vacuum desiccator.

For manipulation and characterization of the mechanical properties of the phospholipid tubes, a laser tweezer and laser scalpel apparatus was set up as described previously by Kulin, et al. [7]. For the laser tweezers, 1064 nm light from a Nd:YAG laser was coupled into an inverted microscope using a 100X, N.A. = 1.4 oil immersion objective. The optical scalpel consisted of a single pulse (5 ns, ~100 μJ) of focused 355 nm light from a UV laser. Phospholipid tubes were stored in buffer solution in the microchannel at 4 °C or at room temperature (20 °C to 23 °C). The tubes were cut with an optical scalpel and manipulated with optical tweezers 48 hours, ~ 1 week, 3 weeks, and 5 weeks after preparation.

For experiments involving light-activated tube growth and movement, phospholipid tubes were prepared as follows; (1) with the fluorescent membrane dye, 1,1′-dioctadecyl-3,3,3′,3′-tetramethylindocarbocyanine perchlorate (DiI(C_{18})), intercalated into the tube membrane so that the molar ratio of dye to phospholipid was always less than 1%, or (2) with sulforhodamine B encapsulated inside the tube's aqueous cavity at a concentration of less than 1 mM.

3. Results and discussion

Fluid flowing rapidly over the phospholipid patch hydrated the phospholipids causing them to spontaneously assemble into various elongated structures including lipid microtubes and nanotubes (Figure 1). These tubes ranged in length from a few micrometers to several centimeters. To our knowledge, this is the first observation of lipid tubes of this long length scale.

The lipid nanotubes are composed of a membrane that typically consists of many lamellae (one lamella is one lipid bilayer) surrounding an internal aqueous compartment. The aqueous compartment and the phospholipid membrane could be observed in many cases using fluorescence microscopy and confocal fluorescence imaging of encapsulated dyes and intercalated membrane dyes. Microtubes and nanotubes formed in this manner exhibit unusually high stability when stored in a hydrated environment inside a microfluidic channel. Phospholipid tubes appeared to retain their organized structure when stored for over 2 months either at room temperature or at 4 °C. For comparison, phospholipid tubes made in our laboratories by other methods, specifically optical tweezer distortion of a liposome membrane, were only stable for minutes to a few hours due to the flow of lipids in the tube membrane back to the original liposome to which it remained connected.

The mechanical properties of the phospholipid tubes were characterized using optical tweezers and an optical scalpel. Optical tweezers were used to trap and pull on the tubes to distort them away from their original shape. Fresh nanotubes and microtubes were easily manipulated with the tweezers and were readily stretched and distorted. Older microtubes could also be distorted using the tweezer apparatus; however, tubes that had dimensions on the order of a few hundred nanometers could not be distorted after 2 weeks of storage. These tubes appeared to be quite rigid. When cut with a laser scalpel, fresh and aged microtubes and fresh nanotubes retracted and self-sealed forming two distinct lipid tubes with sealed ends. When aged nanotubes were cut with a laser scalpel they did not retract but remained open-ended. In several instances small vesicles were observed to spill out of these cut nanotubes and in other experiments encapsulated fluorescent dye was observed to diffuse out of cut nanotubes. The fact that they remained open-ended is unusual behavior for phospholipid membranes and is another indication of nanotube rigidity.

Fresh phospholipid nanotubes containing encapsulated fluorescent dye or intercalated fluorescent membrane dye elongated when exposed to the appropriate excitation light under a fluorescent microscope. As the light was toggled on and off, the tubes grew to lengths that were 2% to 80% of their original length. When the excitation light was turned off, the tubes retracted

back to their original position exhibiting some shape memory. Other tubes coiled into tight knots (Figure 2) that also retracted back to their original shape when the light was toggled off. A similar behavior was observed when phospholipid microstructures were heated through their phase transition temperature in the microfluidic channel using an external heating device.

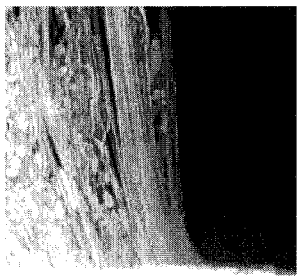

Figure 1. Fluorescence image of lipid nanotubes formed in a microfluidic channel.

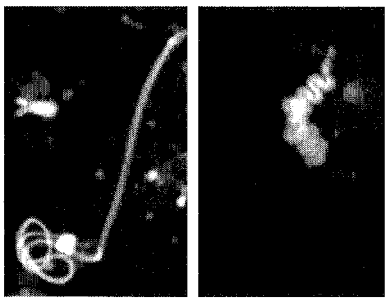

Figure 2. Fluorescence images of phospholipid microtube. In the first panel, the tube is exposed to light that minimally excites the membrane fluorophore. In the second panel, the tube is exposed to light at the fluororphore's absorbance maximum and the tube folds into a tight coil.

4. Conclusions

Phospholipid nano- and microtubes can be readily prepared and manipulated using fluid flow in a microfluidic channel. Characterization of these tubes has shown them to be robust structures with a long shelf-life. We are currently in the process of developing techniques to drive fluid flow in these tubes and to incorporate the tubes into multichannel networks.

References

1] K.P. Brazhnik, W.N. Vreeland, P.B. Howell, R. Kishore, J. Wells, K. Helmerson and L.E. Locascio, Manipulating Self-Assemble Nanotubes. In *Micro Total Analysis Systems 2003;* M.A. Northrup; K.F. Jensen; D.J. Harrison, Eds.; Transducers Research Foundation, Inc.: San Diego, 2003; pp. 689-692.

[2] M. Foquet, J. Korlach, W. Zipfel, W.W. Webb and H.G. Craighead, *Analytical Chemistry*, **74**, 1415-1422 (2002).

[3] J.P. Alarie, A.B. Hmelo, S.C. Jacobson, A.P. Baddorf, L. Feldman and J.M. Ramsey, Fabrication and Evaluation of 2D Confined Nanochannels. In *Micro Total Analysis Systems 2003;* M.A. Northrup; K.F. Jensen; D.J. Harrison, Eds.; Transducers Research Foundation, Inc.: San Diego, 2003; pp. 9-12.

[4] M.J. O'Brien, P. Bisong, L.K. Ista, E.M. Rabinovich, A.L. Garcia, S.S. Sibbett, G.P. Lopez and S.R.J. Brueck, *Journal of Vacuum Science & Technology B*, **21**, 2941-2945 (2003).

[5] A. Karlsson, R. Karlsson, M. Karlsson, A.S. Cans, A. Stromberg, F. Ryttsen and O. Orwar, *Nature*, **409**, 150-152 (2001).

[6] M. Karlsson, K. Sott, M. Davidson, A.S. Cans, P. Linderholm, D. Chiu and O. Orwar, *Proceedings of the National Academy of Sciences of the United States of America*, **99**, 11573-11578 (2002).

[7] S. Kulin, R. Kishore, K. Helmerson and L. Locascio, *Langmuir*, **19**, 8206-8210 (2003).

ELECTROKINETIC TRANSPORT AND DISPERSION IN NANOSCALE CHANNELS

Sumita Pennathur and Juan G. Santiago
Dept. of Mechanical Engineering, Stanford University, Stanford CA, 94305

Abstract

We investigate electrokinetic transport in nanometer-scale fluidic channels and demonstrate a novel ion electrophoretic separation method. Our study includes continuum-theory-based analytical and numerical studies of nanofluidic electrophoretic separation dynamics as well as experimental validation of these models. We show that electrophoretic transport and separation at the nanoscale depends on ion valence as well as bulk liquid values of electrophoretic mobility.

Keywords: nanofluidics, electrokinetics, separation, dispersion

1. Introduction

Nanometer scale fluidic channels enable novel electrokinetic functionality for the manipulation of liquids in fluidic devices. In nanochannel electrokinetic systems, electric double layer thicknesses are comparable to characteristic channel dimensions. In such systems, the velocity profile is highly nonuniform resulting in a decrease in effective electroosmotic mobility. In addition, the streamwise and transverse electromigration fluxes are coupled, and both of these drift velocity terms contribute to separation and dispersion of analyte ions.

2. Theory

We analyze these dependencies using scaling analyses and numerical solutions of the convective-diffusion equations with electromigration (Figure 1). Using a commercial finite element software (FEMLAB, Comsol Corp.), we calculated effective mobilities and diffusion coefficients for the three analytes and four ratios λ_D/h. In our simulations, we employed the convective-diffusion equations for charged species, Poisson's equation for electric field, and Navier-Stokes equations with an electric body force term. We assumed a channel with finite but non-overlapping electrical double layers. We imposed transverse potential distributions governed by the exact solution to the non-linear Poisson Boltzmann distribution for a semi-infinite flat plate on the four surfaces of the rectangular channel. Analytical and numerical solutions predict that the dispersion coefficient increases as the ratio of Debye length to channel depth, λ_D/h, increases.

3. Experimental

3.1 Fabrication

We anisotropically dry etched nanoscale channels in quartz substrates using conventional optical photolithography, eBeam lithography and standard dry etching techniques. Channel dimensions ranged from 20nm x 20nm to 2um x 2um. Nanochannels were characterized using atomic force microscopy (AFM) and scanning electron microscopy (SEM) measurements (Figure 2). A second quartz substrate with laser ablated holes 2 mm in diameter was thermally bonded to the etched substrate to seal the channels and provide fluidic interconnects.

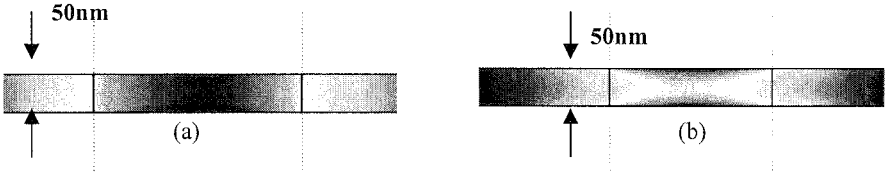

Figure 1: Numerical simulations of convective-diffusion dynamics in nanometer-scale electrokinetic channels for (a) a neutral species, and (b) a species with a +2 valence number in a 50 nm deep channel. In (b), opposing fluxes of electromigration and diffusion result in strong traverse concentration gradients, and a coupling of the ion distribution with velocity gradients results in effective mobility values significantly different then bulk mobility.

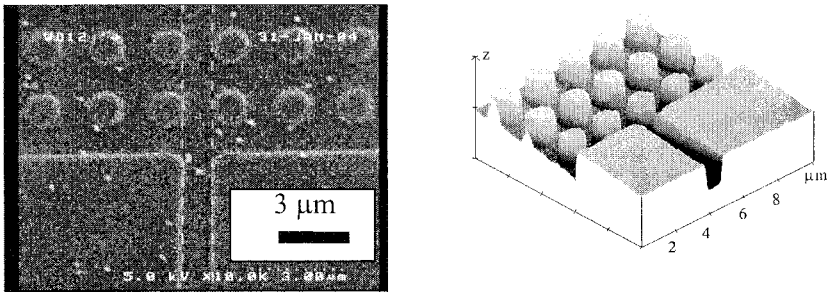

(a) (b)

Figure 2: Scanning electron micrograph (SEM) (a) and atomic force microscopy (AFM) scan (b) of the inlet of a nanometer-scale fluidic channel. The small white spots in the SEM are an artifact of the metallization pre-processing of the sample. The vertical scale of the AFM (z-direction in the plot) is exaggerated by a factor of 20 for clarity of presentation (channel is 102 nm deep). The images show 1 μm diameter circular posts near the inlet of the nanochannel which serve as an integrated filtering structure.

3.2 Measurements

We measured the dependence of dispersion coefficients and ion mobility on valence number and λ_D/h using fluorescence imaging techniques. We used rhodamine, fluorescein, Oregon Green™, AlexaFlor 488™ and Bodipy as fluorescent analytes of differing valence and mobility; and varied the Debye length by using seven concentrations of sodium borate buffer and three different channel depths. For accurate mobility estimates, we performed both current monitoring and front tracking experiments with a neutral solute to determine the zeta potential for each channel/buffer combination.

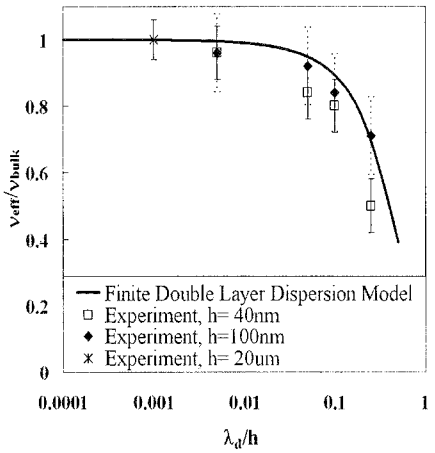

Figure 3: Plot of effective electrophoretic mobility (normalized by mobility value in bulk solution, v_{bulk}) as a function of the ratio of electrical double layer thickness to channel depth. Effective mobility, defined as the velocity of sample peak per unit field, decreases due to velocity defect effect of finite electrical double layers (EDL's). Dispersion model is based on exact solutions of the electrical double layer for these cases of weakly interacting top/bottom wall EDL's. λ_D/h values of 0.005, 0.05, 0.1 and 0.25 were achieved using seven ion densities of a borate buffer (pH = 9.2). Error bars reflect 95% confidence intervals for 10 realizations at each condition.

4. Results and discussion

Experiments were conducted to measure both effective ion mobility and dispersion rate for λ_D/h = 0.005, 0.05, 0.1, and 0.25. For thin electrical double layer systems, values of mobility for both charged and uncharged analytes agree well with bulk, as expected. For systems with finite electrical double layers, effective mobility depended both on analyte valence and λ_D/h. This effect is accurately captured by our electromigration-advection-diffusion models. Effective mobility measurements agree within 20% of theoretical calculations (Figure 3); while measured dispersion coefficients are approximately 30% higher than predicted. Additional experiments are currently under way to further validate nanochannel electrophoretic separation dynamics. Preliminary results show that effective electrophoretic mobilities in nanochannels are strongly coupled to valence number as predicted.

5. Summary

We have modelled electrokinetic transport, dispersion phenomena, and separation dynamics in nanometer scale fluidic channels. Nanochannels have been fabricated and experiments performed to demonstrate the principles involved in our continuum-theory-based model. Numerical transport simulations have been validated with experimental results and show that electrophoretic separation at the nanoscale depends on ion valence as well as bulk liquid values of electrophoretic mobility.

Acknowledgements

This work was sponsored by DARPA (Contract Number F30602-00-2-0609) with Dr. Anantha Krishnan as contract monitor and by an NSF CAREER Award (J.G.S.) with Dr. Michael W. Plesniak as contract monitor. S.P. is funded by a Gabilian Stanford Graduate Fellowship.

References

[1] Probstein RF, 1994, *Physicochemical Hydrodynamics: An Introduction,* John Wiley, New York.
[2] Griffiths, S.K., Nilson, R.H., *Anal. Chem.,* 1999, 71, 5522-5529.
[3] Bharadwaj, R. and Santiago, J.G., *Electrophoresis,* 2002, **23,** 2729-2744
[4] Hunter RJ, 1981, *Zeta Potential in Colloidal Science: Principles and Applications*, Academic Press, London.

OSMOSIS AND PERVAPORATION OBSERVED IN POLYIMIDE SUB-MICRON CHANNELS

Jan C.T.Eijkel, Johan G.Bomer and Albert van den Berg
BIOS/Lab-on-a-Chip group, MESA+ research institute,
University of Twente, PO Box 217, 7500 AE Enschede, Netherlands

Abstract

Osmosis and pervaporation of water through the roof of all-polyimide channels of 0.5 μm height are described. The phenomena cause both a liquid flow and a concentration change of dissolved salt. Flow rates observed were between 2 and 4 μm/s. Flow towards the exchange area and a concentration of solute occurred when water pervaporated towards an atmosphere of low relative humidity. Flow away from the exchange area and solute dilution occurred when a solution of lower osmotic strength was deposited on top of the exchange area. The results are theoretically explained using the concept of water potential and simple pervaporation theory.

Keywords: Osmosis, pervaporation, polyimide channels, pumping, sample concentration

1. Introduction

The properties of nanochannels often differ from microchannels because of the larger surface-to-volume ratio of nanochannels. Here this is demonstrated for the effect of wall vapor permeability on the properties of polyimide nanochannels. Recently it was shown that 1-D polyimide nanochannels can be fabricated using simple cleanroom methods [1]. Channels of 500 and 100 nm height were made which could be filled with water, ethanol and isopropanol and showed electroosmotic flow. When working with the channels it was observed that they dried out very quickly, and it was found that this can be explained by water pervaporation through the thin (2.4 μm) polyimide roof to the atmosphere. The present study quantifies this behavior which causes both pumping and solute concentration. The study shows that the same effects can be caused by applying an osmotic pressure gradient over the channel roof.

2. Theory

In any system, water will move from higher to lower free energy (J/mol). In different research areas, the free energy is also termed water potential (J/m^3) or matric potential (J/kg). For liquid water in nanochannels, the water potential Ψ (J/m^3 or Pa) generally depends on the capillary pressure and the osmotic pressure. Assuming slit-shaped channels of height h we thus have

$$\Psi_{liq} = -\frac{2\gamma\cos\theta}{h} - RTC_{solute} \qquad (1)$$

where γ (N/m) is the surface tension, θ the contact angle and C the solute concentration (osmoles/m^3). For water vapor the potential depends on the relative humidity:

$$\Psi_{vap} = \frac{RT}{V_W}\ln\left(\frac{p}{p_{sat}}\right) \qquad (2)$$

where p is the partial water vapor pressure and V_W (m^3/mol) its molar volume. Typical values for the water potential in our experiments were -5 bar in the channel (0.1 M KNO_3) and -1400 bar for the water vapor (p/p_{sat} = 35%). The resulting pervaporation through the channel roof is considered to be a sequence of water dissolving in and diffusing through the polyimide [2]. The resulting water flux J (m^3/(m^2 s) is proportional to the water permeability coefficient P (m^3 m /(s m^2 Pa)),

$$J = -\mathrm{P} \cdot \frac{\Delta p}{\delta} \tag{3}$$

where Δp (Pa) is the difference in water vapor pressure over the channel roof and δ (m) the roof thickness. In this paper we assume that osmosis occurs via the same mechanism but with liquid water on both sides and can hence that it can also be described with Equation 3.

3. Experimental

All-polyimide nanochannels (4 mm long, 500 nm high, arranged in arrays of 16 parallel channels of 2-30 micrometer width, see Fig.1) were manufactured using a combination of spinning of a photopatternable polyimide and sacrificial-layer etching of aluminium [1]. The channels were filled with a solution of 0.1 M KNO_3 and the channel conductivity between both reservoirs was continuously monitored using an AC current between 100 and 500 Hz and an impedance analyzer, while the roof at the exchange area was exposed to either air of 35% R.H (Fig.2a) or demineralized water (Fig.2b). The roof exchange area was about 600 µm long.

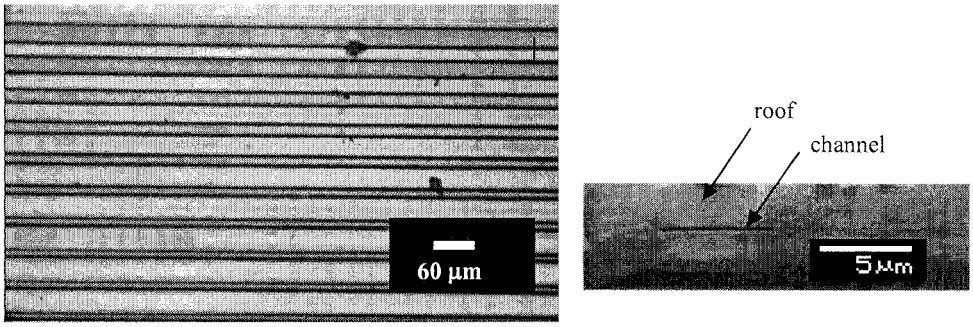

Figure 1. Top view (left) and cross section (right) of the polyimide sub-micron channels.

4. Results and discussion

Channel conductance was observed to increase when the channel roof was exposed to air with a relative humidity of 35% (Fig.3a), which can be explained by water pervaporation through the channel roof and KNO_3 concentration. When the channel solution was refilled with 0.1 M KNO_3 by suction, conductance returned to approximately the initial value, to increase again by continued pervaporation. The flow velocity from each reservoir to the exchange area was calculated from the measurement data using a simple model accounting for the counteracting effect of KNO_3 diffusion and calculated initial velocities were between 2 and 4 µm/s from each reservoir. A rough estimate of the resulting KNO_3 concentration under the exchange zone after 50 minutes is 0.7 M, an increase by a factor of 7. Using equation 3 (realizing that the exchange area length is 600 µm and substituting for P the literature value of $9 \cdot 10^{-15}$ m^3 m /(s m^2 Pa)), a flow velocity of 3 µm/s from each reservoir was calculated, corresponding satisfactorily with the values derived from the conductivity increase. When subsequently a drop of demineralized water was deposited on the exchange area, the conductance decreased again, indicating water transport by osmosis in the opposite direction (Fig.3b). The decrease in conductance occurs much more slowly than the increase seen during evaporation, which can qualitatively be explained by the smaller difference in water potential (from -35 to 0 bar for osmosis and from -5 to –1400 bar for evaporation).

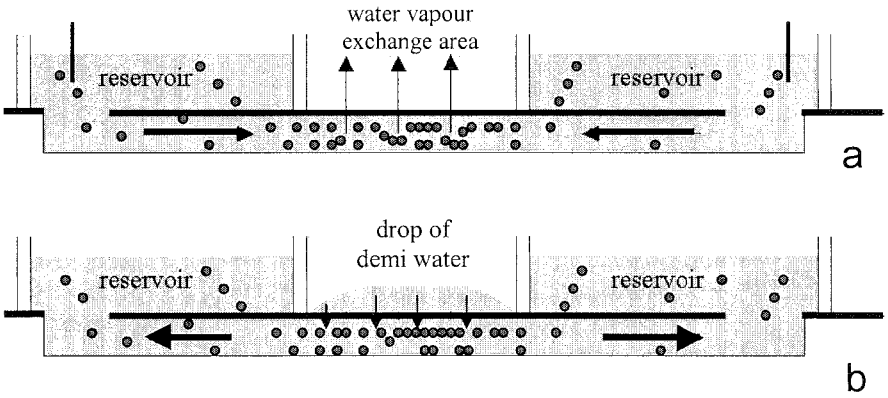

Figure 2. Schematic of pervaporation towards unsaturated air (top) and osmosis (bottom). Dots indicate dissolved KNO_3. It can be seen that pumping (arrows) coincides with a change in salt concentration below the exchange area.

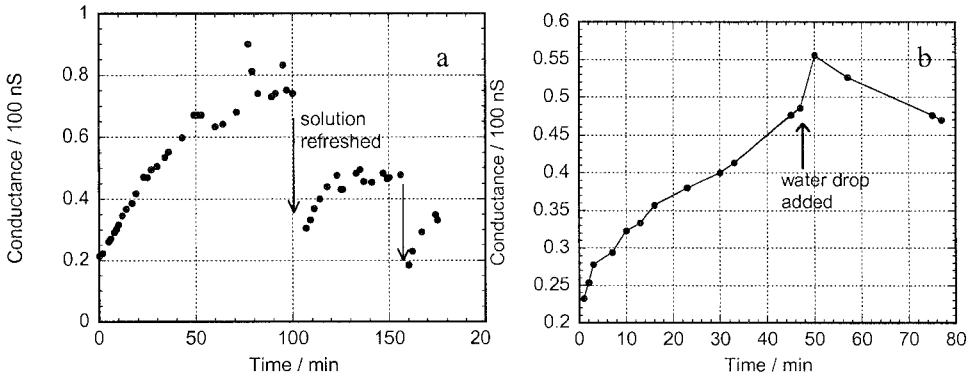

Figure 3. Change in channel conductance observed during pervaporation (left) and during a sequence of pervaporation and osmosis (right).

5. Conclusions

The observed effects offer numerous possibilities for application in micro- or nanofluidic devices, sample concentration and pumping. The manufacturing technique enables multilayer construction, with controlling and responding layers. At present we are constructing a multilayer controllable pump with increased speed by an increased exchange area. Another possible application area is drug release from microfluidic systems.

Acknowledgements

This research was supported by the Dutch Ministry of Economic Affairs through a NanoImpuls grant in the Nanoned program. JE wishes to thank Niels Tas for valuable discussions.

References

[1] J.C.T.Eijkel, J.G. Bomer, N.R.Tas and A. van den Berg, Lab Chip **4**, 161-163 (2004)

[2] X.Feng and R.Y.M.Huang, Ind.Eng.Chem.Res. **36**, 1048-1066 (1997)

CONTROLLED PRODUCTION OF FUNCTIONAL POLYMERIC MICROSPHERES USING MULTI-PHASE MICROFLUIDICS

Takasi Nisisako, Toru Torii, and Toshiro Higuchi
Dept. of Precision Engineering, Graduate School of Engineering, the University of Tokyo
7-3-1 Hongo, Bunkyo-ku, Tokyo, 113-8656, Japan

Abstract
A novel technique is described here for designing functional fine particles by utilizing interfacial instability between two immiscible microstreams. The droplet/particle size was flexibly varied in the range, 30-120 μm diameter, by changing the flow conditions in microchannels. The diameter of the resulting products have a coefficient of variation (CV) below 2%. Furthermore, hemispherically colored acrylic microspheres of 90-190 μm in diameter were engineered with a CV of less than 2%. By applying suitable voltages, the spheres could be rotated between a set of planar electrodes.
Keywords: multi-phase microfluidics, interfacial instability, particle-based display

1. Introduction

Polymeric fine particles of uniform size having diameters of 10-100 μm have a great many applications in diverse fields. However, conventional batch-based methods, such as emulsion polymerization, suspension polymerization, are not so perfect to deal with the emerging demands of functionalized spheres.

We previously reported the rapid and reproducible formation of water-in-oil or oil-in-water microdrops in hydrophobic and hydrophilic microchannels, respectively [1, 2]. Here we describe the production of monodisperse polymeric microspheres by polymerization of a raw material suspension, which was prepared in hydrophilic microfluidic devices [3]. The production of bichromal polymer beads for a microparticle-based display [4] is also presented by exploiting symmetry in the channel configuration and the flow speeds of two immiscible microstreams.

2. Experimental

Microchannels as shown in Fig. 1 were made on glass plates (Pyrex, quartz) by machining tools or lithographic technique. Channels had rectangular or semi-circular cross sections. Typical channel sizes were 20-200 μm in width and 8-100 μm in depth.

Several raw materials (acrylic monomers, divinyl benzene, stylene, etc.) were used for to-be-dispersed phase. Curing agents for heat-induced or photo-induced polymerization were added to those materials. Polyvinyl alcohol (PVA) aqueous solution (2.0 wt.%) was used as external fluid to stabilize the dispersion.

The flow rates of organic/aqueous streams were controlled by syringe pumps, and droplet formation was recorded by a high-speed video camera mounted on an optical microscope.

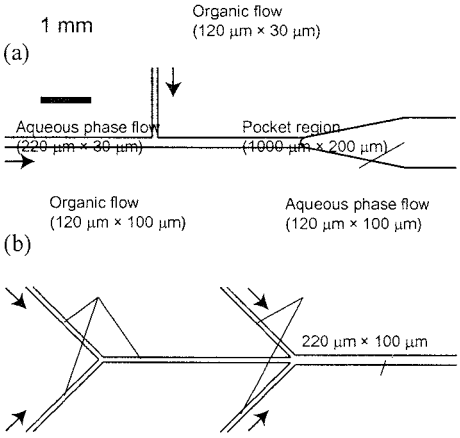

Figure 1. Schematics of the channel layouts; (a) T-shaped channel, (b) Y-shaped channel and two co-flowing channels (Sizes are mentioned as width × depth).

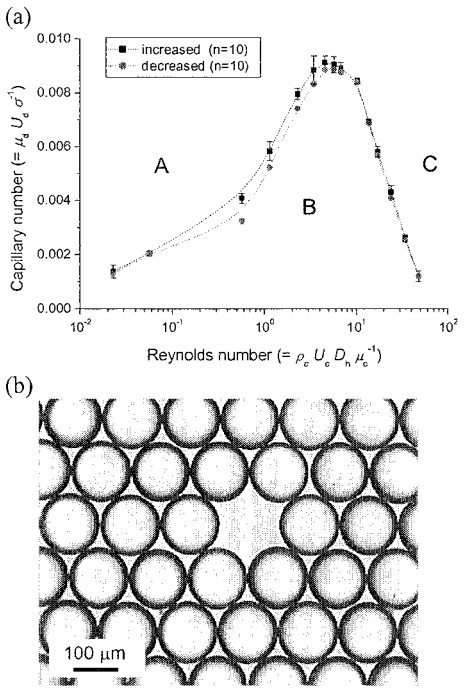

Figure 2. (a) A flow diagram on the droplet breakup at a T-shaped junction [3]. X axis is the aqueous stream condition expressed by the Reynolds number, and Y axis is the organic stream condition expressed by the Capillary number. (b) Monodisperse microspheres prepared in Region B.

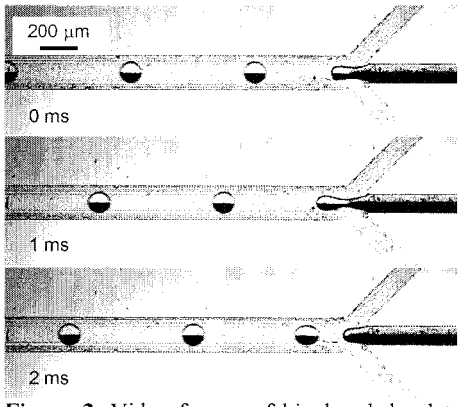

Figure 3. Video frames of bicolored droplet formation at 1 ms intervals. Droplet diameter is around 150 μm, and the production rate at this condition is approximately 300 droplets per second.

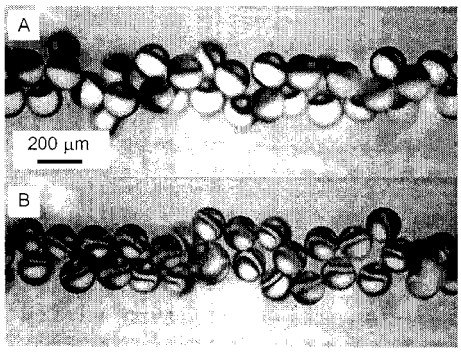

Figure 4. Bicolored droplets flowing through microchannels (A: hemispherically colored droplets, B: droplets with a striped pattern).

4. Results and discussion

The flow diagram in Fig. 2 illustrates the area in which monodisperse monomer droplets were successfully obtained using a T-shaped channel (Fig.1(a)). Within the limited area (Region B), the droplet size and breakup frequency were controllable, and droplets / particles of 30-120 μm in diameter could be prepared with a CV less than 2%. This area shows a peak and this means that the greatest productivity can be achieved at definite conditions of the aqueous phase. In addition, sufficiently low Capillary number ($<10^{-2}$) in Region B indicates that interfacial tension effects is dominant on this droplet-breakup system in microscale. We believe that this region is determined by the balance among the forces from the confluent aqueous stream and liquid-liquid or liquid-solid interfacial tensions.

Figure 3 shows the formation of bicolored droplets at the sheath flow junction. Regular-sized droplets, in which the two colors were distributed equally in both hemispheres were formed in a rapid and reproducible manner. The diameter of these droplets could be varied within the range 90-

190 μm by changing the flow conditions, and could be chosen to be smaller or larger than the hydraulic diameter of the supply channel (D_h = 109 μm). When the two aqueous streams were closely balanced in speed, the two colors were distributed equally in two hemispheres (Fig.4A), but patterns like zebra stripes were found in droplets formed in less balanced flow fields (Fig. 4B). These results indicate that symmetry in external flow fields is vital in producing hemispherically colored droplets. Equally, asymmetry in flow regimes will be beneficial in applications where enhanced mixing is necessary at microscales.

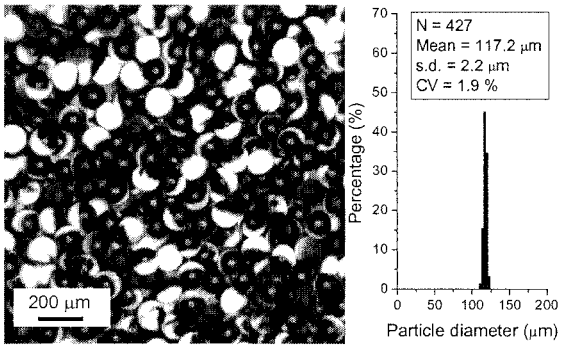

Figure 5. Polymerized bicolored microspheres and the size distribution (D_{avg} = 117 μm, CV=1.9%).

Figure 5 shows the polymerized bicolored beads. Although a less distinct color border was observed in some spheres, due to diffusion mixing, the two colors were distributed equally in most spheres. A rotation test was successfully performed on these spheres using a set of planar indium-tin-oxide (ITO) electrodes. Spheres dispersed in dielectric medium (silicone oil, 5 mPa s) could be rotated by switching the applied voltage. This verifies that spheres can be prepared having a dipole moment.

5. Conclusions

We have produced multiple polymeric spheres by creating organic droplets using two-phase microflow systems, which then polymerize. The particle size distribution was very narrow and the variation in diameter was normally less than 5%. The size of the droplets could be reliably chosen by varying the flow rates in the microchannels. Symmetric flow regime was applied for the production of bicolored spheres which could be rotated electronically. Further refinement of this technique should provide a new methodology for the microfluidic synthesis of pioneering materials, manipulation of particle morphology, etc.

Acknowledgements

The authors would like to thank the cooperation of Takanori Takahashi and Yoichi Takizawa (Soken Chemical & Engineering Co. Ltd.) in the project of bicolored microspheres. This work was partly supported by grants from the Research Association of Micro Chemical Process Technology (MCPT) of Japan, MEXT through a Grant-in-aid for Scientific Research (No. 15310100), and Special Coordination Funds for Promoting Science and Technology, and the JAPAN SCIENCE AND TECHNOLOGY AGENCY (JST), through the Technology Transfer Facilitation program "Cultivation Programs B2003".

References

[1] T. Nisisako, T. Torii, T. Higuchi, Lab Chip, **2**, 24-26 (2002).
[2] T. Nisisako, T. Torii, T. Higuchi, MicroTAS'02, 362-364.
[3] T. Nisisako, T. Torii, T. Higuchi, Chem. Eng. J., **101**, 23-29 (2004).
[4] N.K. Sheridon, M.A. Berkovitz, SID Int. Symp. Dig. Tec., 114-115 (1977).

MICROFLUIDICS FOR COLLOIDS PROCESSING

Saif A. Khan[1], Axel Günther[1], Franz Trachsel[1], Martin A. Schmidt[2], and Klavs F. Jensen[1]
[1]Dept. of Chemical Engineering, and [2]Microsystems Technology Laboratories, Massachusetts Institute of Technology, Cambridge, MA 02139, USA

Abstract

We report microfluidic chemical reactors for the continuous synthesis of colloidal silica particles. Two reactor types are examined: single-phase laminar flow reactors (LFR) and two-phase segmented flow reactors (SFR). An experimental methodology to measure liquid-phase residence time distribution (RTD) in pressure-driven flow through these reactors is presented. Finally, we report a microfluidic device for the continuous electrophoretic separation of charged colloidal particles.

Keywords: Colloids, Silica, Segmented Flow, RTD, Electrophoresis

1. Introduction

Colloidal particles of silica, titania, and related materials have many diverse applications in fields ranging from optical displays and coatings to immunological assays. These particles are typically synthesized by batch processes, which have several limitations. Continuous flow reactors are attractive because they operate at steady state and ensure greater control and reproducibility. Scaled down microfabricated systems afford increased flexibility in reactor design. In colloidal synthesis, the micromixing and ageing units can be integrated into one microfabricated unit, whereas in macro scale reactors they are typically separate units that are externally connected to each other [1]. Colloidal silica (SiO_2), which has been extensively studied [2], serves as a model system in the present work. Small-scale batch synthesis of particles with narrow size distributions (~5%) can be achieved by the Stöber method [3]. Axial dispersion of growing colloidal particles in a continuous flow reactor may lead to wider particle size distributions (PSDs) than the corresponding small-scale batch syntheses. Residence time distribution (RTD) information is an important experimental tool to quantify axial dispersion [4], and is widely used in reactor design.

Fast, online separation of synthesized particles would enable continuous multi-step particle processing. Strong electric fields can be generated in microfluidic systems, and these can be used to develop online separation techniques that are unique to the micro-scale. The particle separation device introduced in this paper uses strong DC electric fields to separate charged colloidal particles by electrophoresis.

2. Experimental

All microfluidic channels were fabricated in poly (dimethylsiloxane) (PDMS), and sealed to glass substrates. Batch synthesis of silica was carried out using the Stöber process [3]. A typical synthesis procedure involved the preparation of two solutions: the first was a dilute solution of TEOS in ethanol, and second was a solution of ammonia, water and ethanol. Equal flow-rates of these solutions were pumped into the microreactors. The LFR consisted of two liquid inlets leading into a micromixing section for silica particle nucleation and initial growth; having a rectangular cross section 50 μm wide and 150 μm deep. This was followed by an ageing section, 400 μm wide and 150 μm deep in which the silica particle size could be controlled by the residence time. Air was used as the segmenting fluid in the SFR, and was pumped through an additional inlet. An on-chip liquid reservoir for fluorescent tracer injection was incorporated into the original design (Fig. 1a) for RTD measurements. A piezoelectric bending disk was attached on top of the reservoir (Fig. 1d). The prototype particle separator consisted of a Pyrex substrate that had gold electrodes patterned and electron-beam evaporated on it (Fig. 1f).

3. Results and discussion

Batch synthesis of silica is characterized by rapid initial growth, followed by slow growth with a rate that is inversely proportional to the particle size. This implies that synthesis in an LFR will be particularly sensitive to residence time effects at short times. The LFR was operated over a range of linear flow velocities corresponding to residence times ranging from 3 to 30 min. Figure 1b shows a graphical summary of standard deviation of PSD at various residence times. The standard deviation of the mean particle size increases at high flow velocities (lower residence times). This observation is attributed to axial dispersion of the growing particles as they flow through the reactor. Particles near the wall move slower than those near the center of the channel, and thus spend more time in the reactor. An SFR is equivalent to a flow of small batch reactors passing in succession through a plug flow reactor. The SFR therefore eliminates the problem of axial dispersion as described in the case of the LFR. In addition, recirculatory motion in each liquid segment causes micromixing [5], and a micromixing section is not required. The dotted rectangle in Fig. 1b indicates the regime where particle growth is most sensitive to variations in liquid-phase residence time. The graph shows that in this regime, the SFR gives much narrower particle size distributions (PSDs) than the LFR.

In gas-liquid segmented flow, adjacent liquid segments are connected through thin liquid films with thicknesses depending on the relative magnitude of viscous to surface tension effects. These films could provide a mechanism for intermixing of particles from different segments, thus widening the RTD from the sharp peak associated with an ideal segmented flow situation. We conduct liquid phase RTD measurements to characterize the extent of non-ideality of the segmented flow, and to compare it with the corresponding single-phase flow. A small plug of fluorescent tracer is introduced into the reactor using an integrated piezoelectric bending disk element and a tracer reservoir, as shown in Fig. 1c-d. In the case of segmented flow, as depicted in Fig. 1c, the gas is introduced after the tracer is injected. Fluorescence microscopy is then used to monitor the spread of the tracer plug as it flows through the reactor. Temporal evolution of the fluorescent intensity at fixed points along the reactor gives characteristic RTD curves [4], as shown in Fig. 1e. From Fig. 1e, it is clear that gas-liquid segmented flow has a narrower RTD than single-phase laminar flow, even at very low residence times, where the PSD is likely to be affected by RTD.

Particle separation is accomplished in the device depicted in Fig. 1f. A stream of negatively charged fluorescent polystyrene particles suspended in ethanol is introduced parallel to a transfer stream containing ethanol. Inter-stream electrophoretic particle migration occurs as shown in Fig. 1g, when a small DC voltage (1-4V) is applied across the device. This ability to move particles to new reactant streams creates opportunities for subsequent continuous surface modification, such as covalent coupling of proteins and nucleic acids to particle surfaces, or overgrowth of a second layer of different dielectric constant for optical applications.

Acknowledgements

This research was funded by the MIT Microchemical Systems Technology Center and the National Science Foundation.

References

[1] Kubo, M., Yonemoto, T. *Chemical Engineering Research & Design*, **77**, 335-341 (1999).

[2] Brinker, C. J., Scherer, G. W. *Sol-Gel Science: The Physics and Chemistry of Sol-Gel Processing*; Academic Press: Boston, (1990).

[3] Stöber, W., Fink, A.,Bohn, E. *Journal of Colloid and Interface Science*, **26**, 62-69 (1968).

[4] Levenspiel, O., Smith, W.K. *Chemical Engineering Science*, **6**, 227-233 (1957).

[5] Günther, A., Khan, S.A., Thalmann, M.A., Trachsel, F., Jensen, K.F., *Lab on a Chip*, **4**, in press (2004).

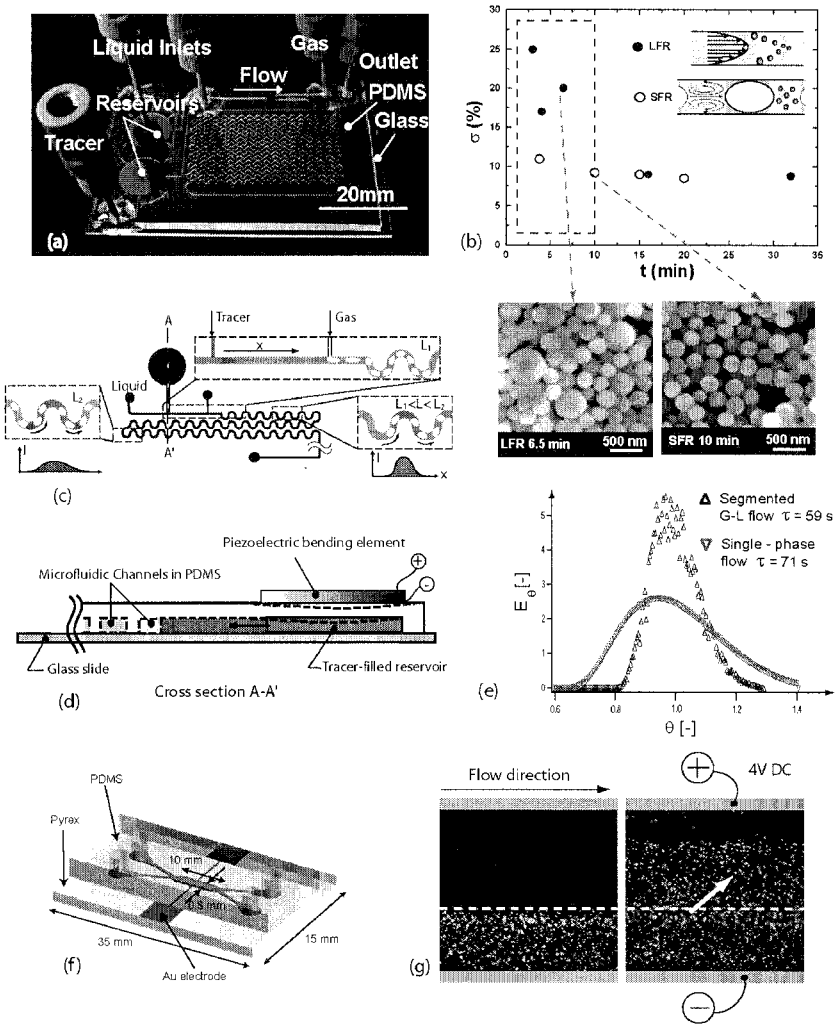

Figure 1. (a) Photograph of an integrated device (SFR) (b) Graph of variance of PSD (expressed as a percentage of the mean diameter) versus residence time in the reactor. (Scale bar = 1μm) (c) RTD measurement concept: A small plug of tracer is injected into the device, and a slug flow is then formed by introducing gas. The spread of the tracer curve is monitored at different points along the length of the device. (d) Cross section A-A' in Fig. 1(c) showing the piezoelectric element used for tracer injection. (e) RTD curves from single and two-phase flow. (f) Schematic of a prototype particle separator (g) Separator operation: Application of a DC voltage causes electrophoretic particle migration into the blank ethanol stream. Both liquid streams flow at 5μL/min. Fluorescent particles used have a mean diameter of 1μm.

PINCHED FLOW FRACTIONATION FOR RAPID AND CONTINUOUS PARTICLE SEPARATION IN MICROFLUIDIC DEVICES

Masumi Yamada[1], Megumi Nakashima[1], Yuushi Sai[2], Masahiro Yasuda[2], and Minoru Seki[2]

[1]Dept. of Chemistry & Biotechnology, Sch. of Engineering, The University of Tokyo,7-3-1 Hongo, Bunkyo-ku, Tokyo 113-8656, Japan

[2]Dept. of Chemical Engineering, Grad. Sch. of Engineering,Osaka Prefecture University,1-1 Gakuen-cho, Sakai, Osaka 599-8531, Japan

Abstract

We have demonstrated a new method for particle separation, named 'pinched flow fractionation (PFF)', in microfluidic devices. In this method, particles can be separated continuously according to their sizes, utilizing a laminar flow profile inside a pinched microchannel. First, we performed collection of separated particles using multi-branched microchannel, and next, small size particles (~1 μm in diameter) were successfully separated using a downsized microchannel. From the results obtained, we have successfully demonstrated that this method is highly applicable for the separation of various kinds of particles. Also it was demonstrated that this method can be applicable not just to particle size analysis, but to preparation of monodispersed particles.

Keywords: pinched flow fractionation, particle, separation, microfluidics

1. Introduction

Rapid and accurate separation of particles, including cells, emulsions, synthesized polymer beads, and ceramics, is one of the most expected applications in the field of microfluidics. In our previous study [1, 2], a concept of 'pinched flow fractionation (PFF)' was proposed for the rapid and continuous size separation of particles in microfabricated devices, and polystyrene beads (15 or 30 μm in diameter) were successfully separated. In this study, two experiments have been demonstrated to examine the applicability of this method. First, particle collection was performed using a multi-branched microdevice, and second, downsizing of PFF was realized for the separation of smaller particles.

2. Theory

The principle of pinched flow fractionation is shown in Fig. 1. First, the liquid containing particles is focused on one side in a pinched segment of a microchannel by another liquid flow without particles, controlling flow rates from two inlets. This operation triggers alignment of particles to the sidewall regardless of their sizes (Fig. 1 (a)). Next, at the end of the pinched segment, a force to the direction toward the center is exerted mainly on larger particles by the spreading streamline, whereas a force to the direction toward one sidewall is exerted on smaller particles (Fig.1 (b)). Consequently, in the broadened channel segment, particles are separated according to their sizes to the direction perpendicular to the flow. This method is highly advantageous since particle separation is achieved only by introducing particle solution into a microchannel having a specific geometry, not necessitating outer fields such as electric, gravitational, or centrifugal force.

3. Experimental

PDMS microdevices were fabricated with usual soft lithographic techniques. The schematic diagrams of microdevices are shown in Fig. 2. Fig. 2 (a) is a multi-branched (13 branches) microdevice for particle separation and collection, and (b) is the microdevice for small particle separation. The pinched segment widths were 60 μm and 4 μm for (a) and (b), respectively.

Two syringe pumps were used to introduce the solutions with and without particles. Flow rates were controlled independently. In the particle collection experiment, photographs of the separated and collected particles were captured using an optical microscope, and their sizes were measured computationally. In the small particle separation experiment, fluorescent-labeled particles, whose diameters were 1 or 2 μm, were separated. Fluorescent microscope was used for the detection, and the locus of particle movement was visualized.

4. Results and discussion

First, particle collection was performed using the multi-branched microdevice. Particles whose diameters were approximately 24~44 μm, was suspended in water and introduced into the device from the inlet 1. Flow rates for inlet 1 and 2 were 50 μL/hour and 300 μL/hour, respectively. The result is shown in Table 1. It was confirmed that the average diameter of separated particles increased as the outlet channel position became center. In this experiment, retention time in the pinched segment was only about 5 msec, demonstrating the rapidity of this separation method.

Next, small particle separation was performed using the microdevice shown in Fig. 2 (b). Flow rates from inlet 1 and 2 were 5 μL/h and 30 μL/h, respectively. The results are shown in Fig. 3. The average elution position was 41.5 μm for the smaller particles (1 μm in diameter), while that for the larger particles (2 μm in diameter) was 26.5 μm. This result suggests that this separation method is valid when the particle sizes become much smaller.

5. Conclusions

In this study, it was demonstrated that 'pinched flow fractionation' could be applied not only for analytical separation, but also for preparation of uniform sized-particles. Also, it was confirmed that small size particles, whose diameter is ~ 1 μm, can be separated using this method. Further study involves separation of various kinds of particles, including cells, polymer beads, and much smaller (nanometer-sized) particles.

Acknowledgements

This research was supported in part by Grant-in-Aids for JSPS Fellows, Scientific Research (B) (No. 16310101), and Priority Areas (A) (No. 13025216) from the Ministry of Education, Science, Sports and Culture of Japan, and by the Research Association of Micro Chemical Process Technology, Japan.

References

[1] M. Nakashima, M. Yamada, and M. Seki, *Proc. MEMS 2004*, pp. 33-36 (2004)
[2] M. Yamada, M. Nakashima, and M. Seki, *Anal. Chem.*, in press.

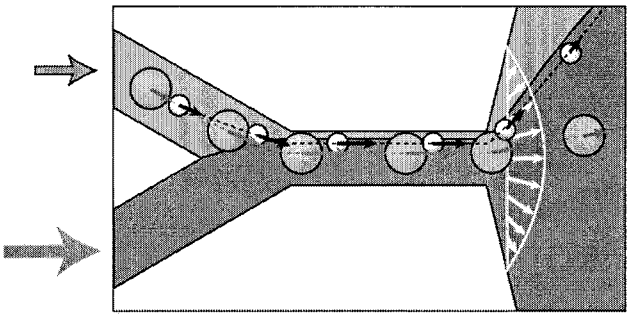

Figure 1. Principle of pinched flow fractionation. Particle-containing solution is purple-colored, while a solution without particles is blue-colored.

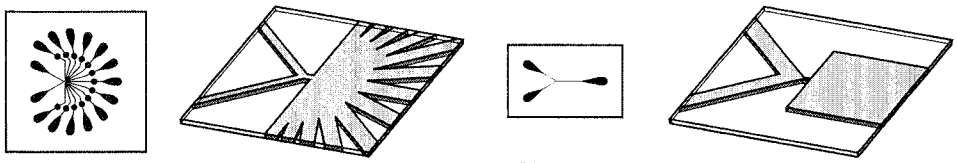

(a) (b)

Figure 2. Schematic diagrams of microdevices; (a) is a microdevice having thirteen outlets, whose pinched width is 60 μm. (b) is a microdevice for small particle separation, whose pinched width is 4 μm.

Table 1. Result of separated particle collection using the multi-branched microdevice (Fig 2 (a)).

Outlet	1	2	3	4	5	6
Average Diameter (μm)	22.3	23.5	27.4	28.7	33.9	35.4

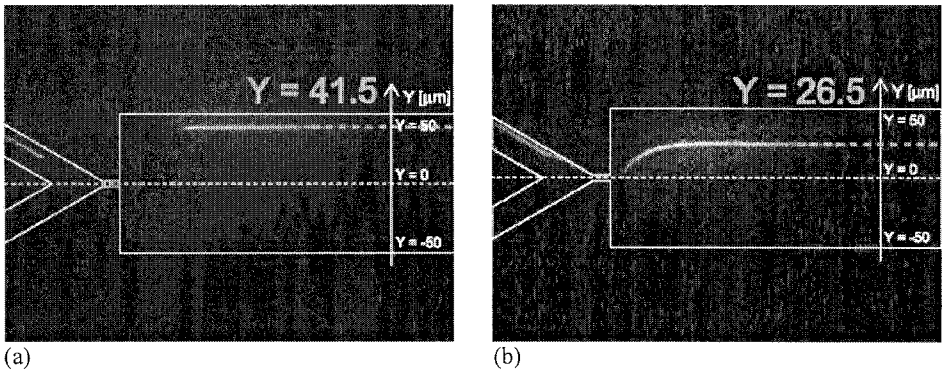

(a) (b)

Figure 3. Separation of particles using the microdevice shown in Fig. 2 (b); (a) shows the locus of smaller particles (1 μm in diameter), and (b) shows the locus of larger particles (2 μm in diameter).

MICROFLUIDIC CONTROL OF OPTICAL PATHS

K. Ono[1,2], T. Shiraishi[3], S. Kaneda[2] and T. Fujii[2]

[1]Enplas Laboratories,Inc., 2-38-5 Namiki Kawaguchi City, Saitama 332-0034, Japan
[2]Institute of Industrial Science, University of Tokyo, 4-6-1 Komaba, Meguro-ku, Tokyo 153-8505, Japan
[3]ARBIOTEC,LTD., A306 CCR, University of Tokyo, 4-6-1 Komaba, Meguro-ku, Tokyo 153-8904, Japan

Abstract

A new method to control optical paths by microfluidic operation is proposed. Light from an optical fiber goes through PDMS-air surface lenses and a microfluidic control region which located in a control channel. Two liquids that have different refractive indices (R.Is) were introduced from each of the two inlet ports of the control channel. These liquids form laminar flow or segment flow depending on the channel geometry and the combination of the liquids. By changing the flow rates of the liquids, optical function of the microfluidic control region is controlled. Depending on the flow patterns, i.e. laminar flow or segmented flow, the optical paths can be controlled continuously, or intermittently. To demonstrate the functionality, the present method was utilized for optical tweezer applications.

Keywords: fluidic lens, laminar flow, segment flow

1. Introduction

In microfluidic devices, various 'microfluidic' phenomena such as laminar flow, capillary effect and electroosmotic flow can be utilized to realize certain functionality of the device. However, there are only a few examples of using microfluidic phenomena for controlling optics. Optical elements using liquids in microdevices have been proposed and an on-off switch type device has been reported [1]. Taking advantage of the flexibility of liquid, microfluidic phenomena could be applied further to various on-chip optical elements. In this study, we propose a new method to control optical paths using microfluidic operations with the liquids with different refractive indices (R.Is) in microfluidic devices and use it for optical tweezer applications.

2. Theory

The setup for microfluidic optical paths control is illustrated in Fig.1. Two kinds of microfluidic channels; a channel for sample introduction and a channel for controlling optics; and PDMS-made air-surface lenses are embedded on a PDMS-made microfluidic device. An optical fiber is inserted into the device to introduce the light into these optical elements. The microfluidic control region has typically round or triangular shapes located at the intersection between the optical paths from the fiber and the control channel as shown in Fig.2. The round shape is for changing the focusing in the direction of optical axis and the numerical aperture (N.A.) whereas the triangular shape is for changing the focusing point in the vertical direction against optical axis, namely, along the sample channel. Two liquids that have different R.Is were introduced from each of the two inlet ports of the control channel. These liquids form laminar flow or segment flow depending on the channel geometry and the combination of the liquids. By changing the flow rates, the flow patterns in the microfluidic control region are deformed to control the light traveling through that area. In the case that laminar flow is formed, a boundary between two liquids can become laminar flow (fluidic) lenses by which one can control the optical paths continuously. On the other hand, intermittent control is possible in the case of the segment flow. In our previous work, on-chip PDMS lenses with three cylindrical aspherical lens surfaces were developed [2]. The same method was employed for calculation of lens surfaces. A commercial optical design software of CODE V® (Optical Research Associates) was used for computer assisted optimization to realize beam waists as narrow

as possible to concentrate the beam energy and to simulate optical paths with different R.Is of liquids flowing in the microfluidic control region.

3. Experimental

The device was fabricated with conventional PDMS replica molding. In order to observe optical paths, fluorescent dye was mixed with the PDMS (fluorescent PDMS). One end of a multi-mode optical fiber (50 μm core diameter for light paths visualization, 60 μm for laser tweezers) was inserted into the fiber inlets of the device. The other end was connected to a light source: a mercury lamp for light path visualization or a 1 W laser diode (λ = 808 nm) for optical tweezer experiments. The laminar flow and the segment flow were made with a pressure driven pump (My Flow, ARBIOTEC, LTD). At first the pressure was applied from each inlet port of the control channel at 10 KPa then decreased one of the ports in order to change the flow rate ratio of the two liquids. A 25 μm polystyrene bead was introduced from the inlet port of the sample channel for optical tweezer experiments.

4. Results and discussion

Figure 3 shows the results of optical paths control in the case of laminar flow formed in a round shape microfluidic control region. The upper pictures show the fluorescently visualized optical paths and the lower figures show the simulated optical paths. In Fig. 3, silicone oil (R.I.=1.58) was introduced from the left inlet and another silicone oil (R.I.=1.42) was from the right. The optical paths were successfully controlled depending on the R.Is and the shape of the fluidic lens defined by the flow pattern. The light paths going through PDMS air-surface lenses and the microfluidic control region show good agreement with the simulated ones. By decreasing the flow rate at the right inlet (Fig. 3a) the microfluidic control region was almost filled with the silicone oil (N.A. = 1.42), then the N.A. of the collected light became smaller and the width became larger than those in Fig. 3 (b). A continuous transition of these two states is confirmed.

We applied this technique to optical tweezer experiments (Fig. 4). Light with high power density can trap micrometer size particles by the optical pressure that is caused by the change in photon momentum [3]. Silicone oil (R.I. = 1.49) and florinert (R.I. = 1.29) were introduced from each of the inlet ports of the control channel with triangular shaped microfluidic control region. The two liquids formed segment flow due to their large difference in surface tension. The optical paths were, therefore, controlled intermittently in the direction perpendicular to the optical axis and the bead was successfully manipulated along the sample channel. In this optical configuration the repulsive light pressure is stronger than the attractive one due to the small N.A. of the collected light. So the bead was trapped by being pushed onto the sidewall of the channel in this case.

5. Conclusions

The optical paths are successfully controlled by microfluidic operations and the functionality of the proposed method was demonstrated by applying it to optical tweezer experiments. Since almost no complicated positioning and alignment are required, the present method could give us much simpler and low cost setups for sophisticated optical functionalities, which could be relevant for various applications in the field of microscale biological and/or chemical analyses.

References

[1] M. Makihara, M. Sato, F. Shimokawa, and Y. Nishida, *J. Lightwave Technol.*, Vol. 17, No. 1, 14-18, (1999).
[2] K. Ono, S. Kaneda, S. Camou and T. Fujii, *microTAS2003*, 1307-1310.
[3]A.Ashkin, *Phys. Rev. Letters* 24, 156-159, (1970).

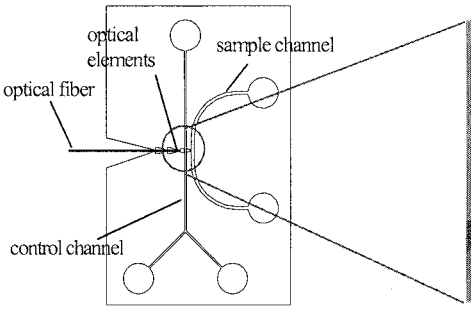

Figure 1. Schematic design of optical path operation chip.

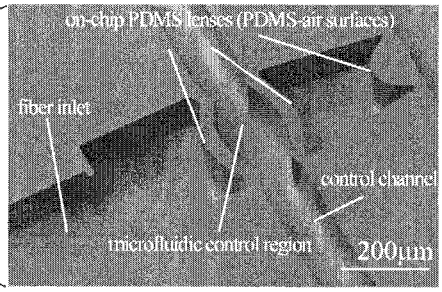

Figure 2. SEM image of PDMS device.

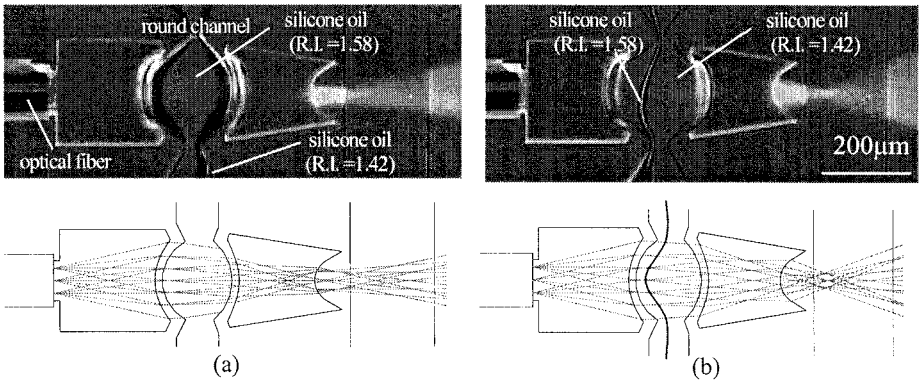

Figure 3. Visuarized optical paths with fluorescent PDMS of laminar flow fluid lens and simulated figures. (a) Flow rate of silicone oil (R.Is = 1.58) is larger. (b) silicone oil (R.Is = 1.42) is larger.

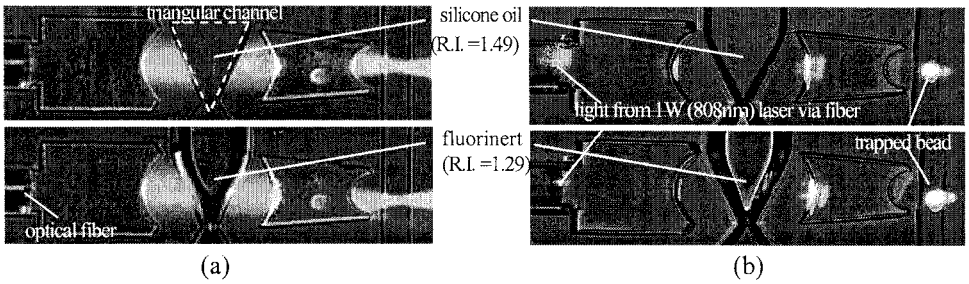

Figure 4. Laser manipulation by optical paths control device (a) fluorescent PDMS (b) trapped bead.

ON THE TEMPORAL EVOLUTION OF MICRO-DISCHARGE SPECTRA AND DETECTION OF ORGANIC VAPORS IN AIR

Bhaskar Mitra and Yogesh B. Gianchandani
Department of Electrical Engineering and Computer Science
University of Michigan, Ann Arbor, MI 48109-2122, USA

Abstract

This paper reports the use of time resolved pulse discharge spectroscopy for detecting organic vapors in ambient air. The impact of both sample duration and delay is investigated. A pulsed micro-discharge, consuming only 400 μJ of energy, is struck by applying a high voltage pulse between two closely spaced electrodes patterned on a glass substrate. As a result, the ambient gas in the glow region of the micro-discharge breaks down into molecular and atomic fragments. The time resolved spectrum of the light emitted by these fragments is obtained with a spectrometer, which is triggered a programmed time delay after the discharge pulse. It is observed that better detection is achieved by limiting the sample duration to 2.1 ms and with a delay of <1 ms after initiation of the micro-discharge. This is verified for isopropyl alcohol (100 ppm) and acetic acid (250 ppm) vapor samples.

Keywords: Micro-discharge, transient spectroscopy, Volatile organic compounds, Gas Sensor

1. Introduction

In the quest for miniaturized vapor and gas sensors, a variety of transduction methods have been explored. Chemi-resistors, chemi-capacitors, chemi-mechanical sensors, and metal oxide sensors measure changes caused by analytes to thin films [1]. However, film properties can drift and change with contaminants, package stress, and ambient temperature. Some applications require greater speed and specificity than these approaches offer. Miniaturized sensors that use plasma spectroscopy of target species can complement other sensors in many respects, but typically require low operating pressures (and hence a pump) and do not favor an air ambient [2]. Pulsed arcs (micro-discharges) can, however, operate at atmosphere in air, and have been used for spectroscopically detecting inorganic impurities in water [3]. Resulting emissions have also been used for fluorescent detection of bio-chemicals [4]. This paper describes the first use of pulsed discharge spectroscopy (using a micromachined device) for detecting organic vapors in an air ambient at atmospheric pressure. It also describes how the temporal evolution of spectra affects the signal

2. Microsystem Design

The sensor (Fig. 1) utilizes two closely spaced Ti electrodes patterned on a glass substrate. The gas flows through the channel formed between the substrate and two glass spacers bonded to it. The gas molecules are fractionated as they pass through the micro-discharge region [5]. The emitted spectrum, which is characteristic of the fragments, is observed using a portable off-chip spectrometer (Ocean Optics USB2000). The micro-discharge is powered by a capacitor bank under computer control, which provides a current pulse of about 2 μs duration (Fig. 2). A shunt switch is used to avoid the damage caused by high currents in the series loop. A trigger pulse (Fig. 3), generated after a programmable delay of time t_1 after the discharge, turns on the spectrometer for 2.1 ms. By varying t_1, a time resolved spectrum of the micro-discharge is obtained.

3. Experimental Results

Figure 4a shows a baseline measurement of the device in air taken during and immediately following the discharge. Line spectra corresponding to N_2, O_2 and H_2O fragments are superimposed on

a wider background. The temporal evolution of the spectra is shown in Fig. 4b. The line spectra decay rapidly compared to the wider background. Thus, by limiting the observation window to 2 ms after the discharge, greater sensitivity can be obtained.

The time resolved spectra of acetic acid, with 2.1 ms sample time, are shown in Fig. 5a. Similar to the air micro-discharge, it shows a relative decrease of line spectra compared to the wide background spectra. Figure 5b shows the spectrum of acetic acid, taken asynchronously with a 10 ms integration time to capture all the emitted light. It is evident that the spectra with a 2.1 ms sample time taken at t=0, has a better signal to background (noise) ratio. Thus, by performing a synchronous detection and limiting the integration time, resolution is enhanced.

Figure 6a shows the spectrum in the presence of isopropyl alcohol (IPA) vapors, taken synchronously with the discharge and a sample time of 2.1 ms. The IPA concentration was independently measured with a commercial VOC sensor (MiniRAE 2000) to be 100 ppm. Different lines corresponding to fragments of the organic compounds (C_2, CO, CH) are evident. Figure 6b. shows the spectrum with a longer integration time. Although the overall intensity is higher, the relative intensities of the carbon lines (especially the 560 nm C_2 line) are lower.

It is notable that a pulsed discharge does not consume excessive energy (similar to a camera flash) and is appropriate for low power applications. For example at a sample rate of 1 Hz, our present setup consumes <400 μW for the discharge, which can be reduced further if needed.

4. Conclusion

The use of time resolved pulsed discharge spectroscopy for detection of organic vapors has successfully been demonstrated. The signal to noise ratio is seen to decrease with time as the wide background radiation decays slower than the line spectra. Hence, by limiting the spectrometer on time and synchronizing the spectrometer trigger to the discharge much higher resolution is obtained.

Figures

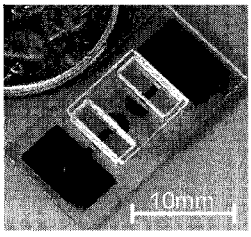

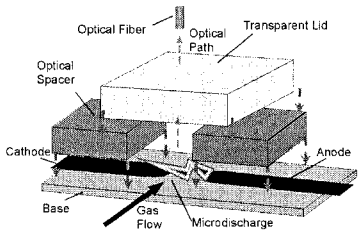

Fig 1 (a-left): *Photograph of the final device shown against a US dime.* ***1 (b-right):*** *Schematic of the sensor, showing the gas flow and the optical path of the emitted spectra.*

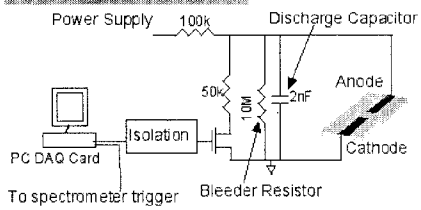

Fig. 2 (top): *Schematic of the pulsed micro-discharge circuit.*

Fig 3 (right): *Captured waveform showing the discharge pulse and spectrometer trigger.*

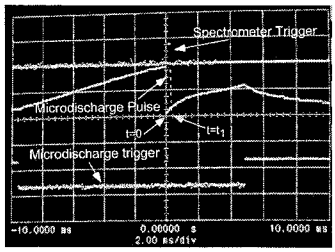

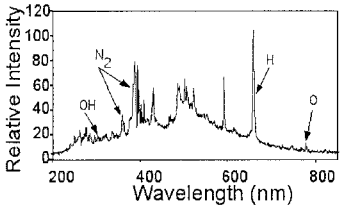

Fig. 4 (a-left): *Spectra of the micro-discharge in air. Line spectra corresponding to the nitrogen and water vapor are seen superposed on a continuous spectrum.*

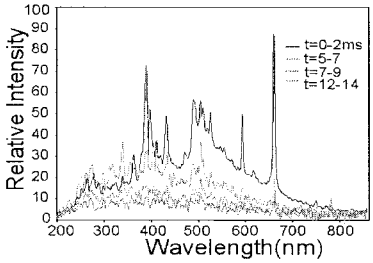

4 (b-right): *Time resolved spectra of air. The emitted light is sampled for 2.1 ms, at different points after a micro-discharge pulse. Although the intensity is on a relative scale, the readings are taken with the same setup, so a comparison on of intensities can be made.*

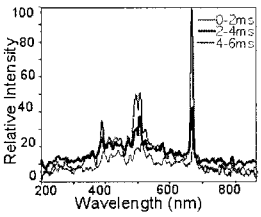

Fig. 5(a-left): *Temporal evolution of the spectra of acetic acid* ***5 (b-right):*** *Emission spectra of acetic acid with a long (10ms) integration time. The signal to noise ratio is decreased by the longer sample time.*

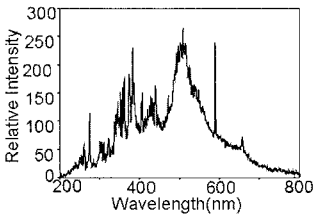

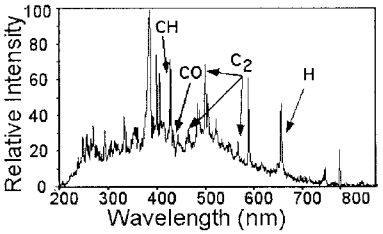

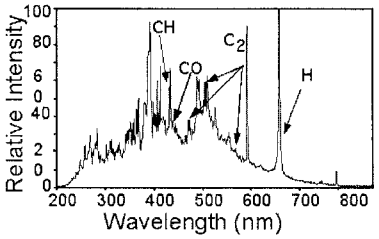

Fig. 6 (a-left): *Spectra of the micro-discharge in air with 100 ppm IPA taken at t=0, and a sample time of 2.1 ms. Spectra corresponding to fragments of carbon compounds are evident.* ***6 (b-right):*** *Spectra of IPA vapors in air ambient with a 10 ms time. Although the overall signal is stronger, the lines corresponding to the hydrocarbon fragments are smaller.*

References:

[1] D.S. Wilson, et al. *IEEE Sensors Journal,* 1(4), Dec. 2001, pp 256-274

[2] J. C.T. Eijkel, et al., *Anal. Chem.,* 71(14), July 1999, pp 3600-2606

[3] C. G. Wilson ET. al, *IEEE Transactions on Electron Devices,* 49(12), Dec 2002, pp. 2317-2322

[4] L. Que, et al., Proceedings of MicroTAS 2003

[5] R.S. Bramal, et al., *Anal.Chem.*,40,(1), Jan 1968, pp 95 –106

OPTICAL EMISSION SPECTROMETER OF AQUEOUS SOLUTION SAMPLES EMPLOYING LIQUID ELECTRODE PLASMA

Akiko Iiduka, Yasutaka Morita, Eiichi Tamiya and Yuzuru Takamura
[1]School of Materials Science, Japan Advanced Institute of Science and Technology (JAIST)
1-1 Asahidai, Tatsunokuchi, Ishikawa 923-1292, Japan

Abstract

Novel microplasma for liquid sample optical emission spectrometry (OES) is reported, namely "liquid electrode plasma" or "bursting bubble plasma". The advantages of this method includes no requirement for plasma gas and nebulizer, and no contamination from electrodes is observed because of the low electric field around them, and the plasma does not interact directly with the electrodes. The microchip consisted of PDMS and SiO_2. Solution samples were introduced into the channel, then direct current voltage (~800 V) was applied from Pt electrodes inserted into the reservoirs at both sides. Typical spectra for NaCl, KCl, PBS, $CuCl_2$ solutions were observed. In the case of blank aqueous solutions, different from conventional ICP-OES, no background peak was observed from plasma gases, such as Ar. The intensity ratio of K/Na showed a quantitative response, and the limit-of-detection from the OES data was estimated to be 300 ppb for Na.

Keywords: Microplasma, Optical emission spectrometry, High sensitive detection

1. Introduction

Many prominent approaches have been performed to miniaturize plasma sources [1-5] and OES for gas [1], liquid [2] and heavy metal samples [3]. In these reports, plasma was generated with He or Ar gas, samples were injected into plasma, and the quantification was done by monitoring optical emission intensity from excited atoms and molecules. An attractive advantage of OES is its high sensitivity, thus it is suitable for microfluidic devices. However, in previous reports, a certain amount of rare gases and power sources were needed especially while handling liquid samples, because the injection of the liquid sample caused an unstable state in the plasma. Therefore, the total instrumental setup including the bombes occupied a large space. While working with liquid samples, nebulization was another critical point, that needed improvement.

In this work, we report a novel microplasma, for which neither plasma gas nor a nebulizer is required, and enabled liquid sample OES. The detection of toxic substances in environmental samples, such as water, soil and food needs rapid observation for "on-site-analysis" and high sensitivity. Our miniaturized plasma source is a promising candidate for utilization in these assignments.

2. Experimental

A PDMS-based microfluidic channel was fabridcated as shown in Figure 1, by conventional SU-8 lithography and molding techniques. The PDMS and SiO_2 substrates sticked by natural pressure. Aqueous solution samples (0.01 M NaCl, 0.01 M KCl, 1/20 PBS, 0.01 M $CuCl_2$) or 2 ppm Na in 0.5 M HNO_3 was introduced into the channel. Direct current voltage (~800 V) was applied from Pt electrodes inserted into the reservoirs at both

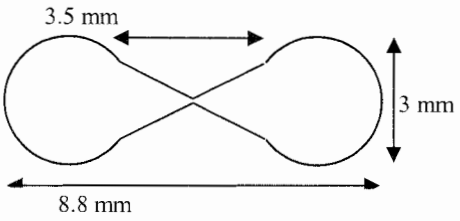

Figure 1. The chip design for microplasma. Depth is ca 30 μm.

sides. Electric current (~900 μA) was confined at the neck position of the channel, and first generated bubble of water vapour, and then plasma. We performed an OES measurement with this plasma, and a handy spectroscope (USB2000, Ocean Optics) as shown in Figure 2.

3. Results and discussion

Direct current voltage at 250 V and over created the plasma. PBS plasma at 1/20 ratio is shown in Figure 3. The OES data for a mixture of KCl and NaCl both at 0.1 M is shown Figure 4. Voltage was applied by the pulse (pluse width was 100 ms). Plasma was stabilized by applying voltage pulse operation. Intensity ratio of K/Na in 0.01 M KCl, 0.5 M KCl, 0.1 M KCl in 0.1 M NaCl solution is shown in Figure 5. A linear relation suggested the quantitative response.

Plasma could not be generated with 5 ppm NaCl aqueous solution, because its conductivity was too low. To increase conductivity, NaCl was solved in 0.5 M HNO3, where the concentration was set to 5 ppm (Na concentration was 2 ppm). The OES data for solution, that consisted of NaCl in 0.5 M HNO3 and blank 0.5 M HNO3 are shown figure 6. These spectra displayed the moleculer optical emissions of N2 and NH, which were generated by the decomposition of HNO3. In 2 ppm Na in HNO3, atomic emission of Na was clearly observed. The estimated limit-of-detection from Figure 6 (b) is 300 ppb for Na.

The advantages of this method can be listed as follows; (1) Neither plasma gas nor nebulizer is required. (2) No contamination results from the electrodes because of low electric field around them, and the plasma does not touch the electrodes. (3) Power consumption (~0.3W) and sample amount (<<1μL) are very low. (4) Plasma is sealed in the channel, so handling and optical coupling are very simple.

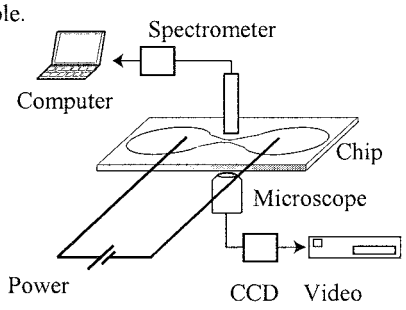

Figure 2. Experimental setup.

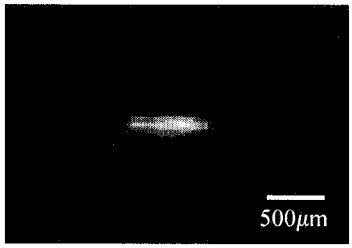

Figure 3. A photo of 1/20 PBS plasma. 1500V, ac 800 μA.

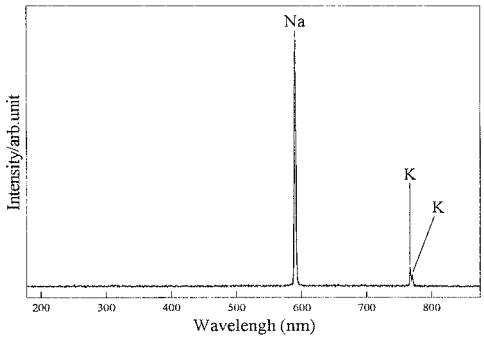

Figure 4. OES data for 0.1 M KCl and 0.1 M NaCl mixture solution. Background peaks are negligible.

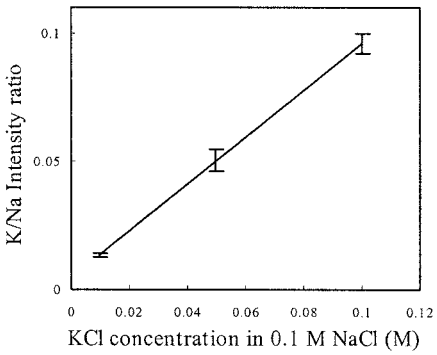

Figure 5. The intensity ratio of K/Na.

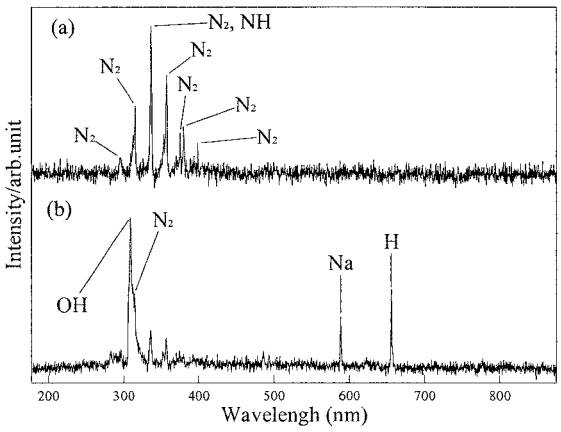

Figure 6. (a) 0.5M HNO_3 OES. (b) 2 ppm Na in 0.5 M HO_3 OES.

4. Conclusions

The OES data of NaCl, KCl, PBS and $CuCl_2$ solutions were obtained. In the case of blank aqueous solutions, there were no background peaks from plasma. The intensity ratio of K/Na 0.01 M KCl, 0.5 M KCl, 0.1 M KCl in 0.1 M NaCl showed quantitative change. The estimated limit-of-detection for Na from the 0.5 M HNO_3 solution was 300 ppb.

References

[1] J. C. Eijkel, H. Stoeri and A. Mantz, *Proc. μTAS2000,* **pp**. 591-594.
[2] T. Ichiki, T. Koidesawa and Y. Horiike, *Plasma Sources Sci. Technol.,* **12**, S16-S20 (2003).
[3] R. Guchardi and P. C. Hauser, *J. Anal. At. Spectrom.,* **18**, 1056-1059 (2003).
[4] Y. Yin, J. Messier, and J. Hopwood, *IEEE trans. plasma Sci.,* **27**, 1516-1524 (1999).
[5] K. Terashima, Y. Taniguchi, N. Yamaguchi, Y. Takamura, T. Yoshida, *Thin Solid Films,* **345**, 146-150 (1999).

ECIS: A BIOSENSOR BASED ON ELECTRICAL MEASUREMENTS

Ivar Giaever
Rensselaer Polytechnic Institute and Applied BioPhysics Inc. Troy NY 12180

Abstract

Electrical Cell-Surface Impedance Sensing or ECIS is a relatively new biosensor that uses the electrical properties of cells to study their motion and morphology. In addition it can record the responds of the cells to various physical and chemical stimuli.

Briefly speaking, to study cell activities using ECIS, small gold electrodes are first fabricated upon polycarbonate surfaces using a photolithographic process. With standard culture medium as the electrolyte, the ECIS instrumentation applies an AC signal of approximately constant current between a small circular active electrode, generally 250 micrometers in diameter, and a large counter electrode. Voltage and phase data are measured with a lock-in amplifier, and data are stored and processed with a PC. The same computer controls the applied AC signal and switches the measurement to different electrodes in the course of an experiment. As cells anchor and spread on the active electrodes, their insulating plasma membranes constrain the electrical current and force it to flow beneath and between the cells. This convoluted current path causes large changes in the measured impedance. In addition, small fluctuations in the impedance are observed because the live cells continuously alter their morphology. These impedance variations can be numerically analyzed to report levels of cell motility and, indirectly, cell metabolism. It is important to note that this small current (approximately 1 microampere) and the resulting voltage drops (a few millivolts) across the cells has no detectable effects upon them; the measurement is non-invasive. The size of the electrode restricts the maximum cell populations that can be observed using a single electrode to about 100 cells, but it should be noted that the activities of even a single cell could easily be measured.

Using this simple principle a large variety of cell properties and assays have been preformed such as: cell-cell and cell-extracellular matrix interaction and the blood-brain barrier, signal transduction assays, in vitro toxicology, metastesis of cancer cells, wound healing assays, electroporation assays, cell migration etc.

8th International Conference on Miniaturized Systems for Chemistry and Life Sciences
September 26–30, 2004, Malmö, Sweden

ENZYMATIC ACTIVITY MEASUREMENT AT HIGH TEMPERATURE BY MOMENTARY HEATING WITH ON-CHIP MICRO HEATER

Hideyuki Arata[1], Y. Rondelez[2], G. Tresset[2], S. Takeuchi[1], H. Noji[1], H. Fujita[1]
[1]*Institute of Industrial Science (IIS), The University of Tokyo*
[2]*LIMMS-CNRS/IIS*
4-6-1 Komaba Meguro-ku Tokyo 153-8505 Japan

Abstract

Measurement of enzymatic activity at elevated temperature has been successfully performed thanks to the rapid temperature control enabled by an on-chip micro heater. The enzyme, β-Galactosidase, survived short exposure (4 seconds) to high temperature at which it was severely damaged by longer exposure. Its activity at the higher temperature (around 60 °C) was shown to be 4.2 times greater than that at 23 °C. Furthermore, the degree of accelerated activity can be controlled by changing the frequency of the heat pulses.

Keywords: enzymatic activity, heat pulse, micro heater, micro chamber, PDMS

1. Introduction

The enzymatic activity has a temperature dependence, usually showing peak at certain temperature, decreasing at higher range and loosing its activity (Figure 1). However, at temperature higher than the molecular destruction temperature in steady state, we expect to keep active by limiting the exposing time. Reducing the size of thermal devices results in fast temperature response and offers the feasibility to achieve acceleration and reduction of enzymatic activity in a short time span [1]. The enzymatic activity at temperature higher than the molecular destruction temperature in steady state may be measured by momentary heating using high response micro thermo device.

2. Experimental

A micro heater of 400 μm in diameter and a micro thermo resistive sensor were integrated on a glass chip. The chip is also equipped with micro reaction chamber array that separate the localized high temperature region from low temperature regions. The volume of the chambers are 1~110 fL. This enables the enzymatic activity measurement of very small number of molecules, even a single enzyme [1][2], by restricting the diffusion of products. The temperature controllable micro chamber array was produced by attaching patterned PDMS sheets on a Ni patterned glass plate (Figure 2). β-Galactosidase catalyzes the hydrolization of FDG (Fluorescein di-β-D-Galactopyranoside) and its catalytic

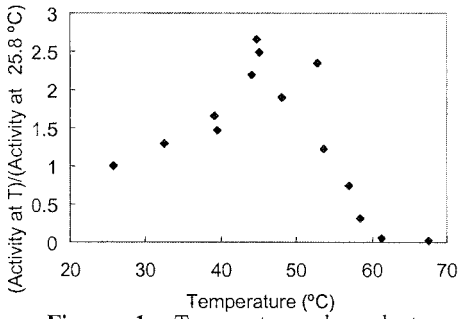

Figure 1. Temperature dependent activity of β-Galactosidase by bulk experiment. Exposing at temperature T for 2 minutes.

activity can be measured from the fluorescent intensity. 37 nM β-Galactosidase solution was mixed with 400 μM FDG in a 100 mM phosphate buffer pH 7.5 (in the presence of 0.05~10 mg/mL BSA, 1 mM $MgCl_2$ and 2 μL/mL mercaptoethanol). The mixed solution was poured onto the Ni patterned

glass plate and the PDMS sheet was placed on top to enclose the solution in micro chambers. Since PDMS is transparent, we can observe the fluorescent intensity inside the micro chamber with an optical microscope (Figure 3). The target temperature can be attained within 1.4 seconds with a tolerance of ±2 °C. The volume of a micro chamber was around 60 fL; at β-Galactosidase concentration of 37 nM each chamber contains around 1300 enzymes.

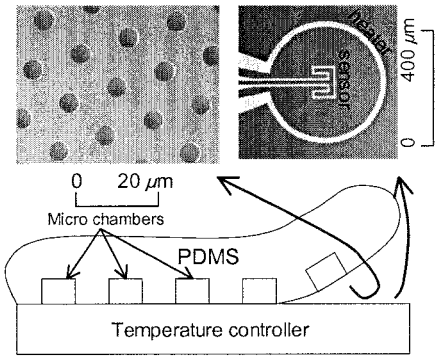

Figure 2. Schematics of the temperature controlled micro chamber array (bottom). SEM image of patterned PDMS sheet (left top). Optical microscope view of integrated micro heater and micro thermo sensor on a glass plate (right top).

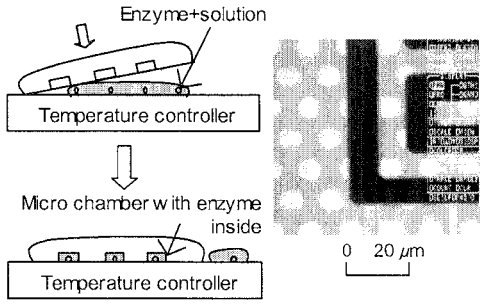

Figure 3. Process to confine enzyme in micro chambers (left); the solution with enzyme was poured on the temperature controlled glass plate and a patterned PDMS sheet was placed on top to enclose them into micro chambers. Microscope view of fluorescent intensity of enzymatic activity inside the micro chambers (right).

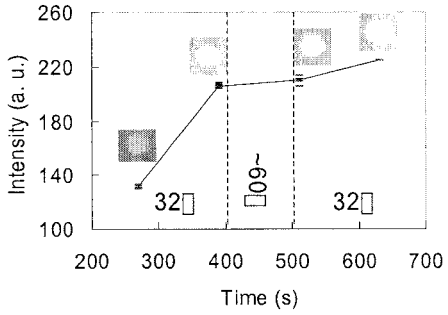

Figure 4. Intensity-Time curve at temperature from 32 °C to around 60 °C and back to 32 °C.

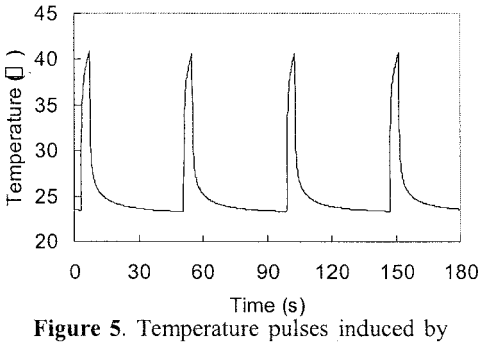

Figure 5. Temperature pulses induced by the heater measured by integrated thermo sensor.

3. Results and discussion

The duration of the high temperature period was changed and the enzymatic activity was examined. When the temperature is increased from 32 °C to the higher temperature (60±20 °C from the comparison between bulk experiment) and kept for 2 minutes, the fluorescent intensity did not

increase (Figure 4). This indicates that the enzyme has been damaged and lost its activity at the high temperature within 2 minutes. Applying the same temperature by pulses of 4 seconds (Figure 5), the activity is successfully accelerated (Figure 6). This indicates that the enzymes remain active and increase their activity within short time, even at temperatures that cause damage after a long exposure. Additionally, the increase ratio of activity was also controlled by changing the frequency of the heating pulses. The fluorescent intensity increased less with the interval of 44 seconds between each pulse than that of 8 seconds. Enzymatic activity can be calculated from the following formula:

$$\frac{4 \cdot V_{60} + 44 \cdot V_{23}}{48 \cdot V_{23}} = 1.27 \leftrightarrow \frac{V_{60}}{V_{23}} = 4.20 \quad (1)$$

and

$$\frac{4 \cdot V_{60} + 8 \cdot V_{23}}{12 \cdot V_{23}} = 2.08 \leftrightarrow \frac{V_{60}}{V_{23}} = 4.23 \quad (2)$$

where V_{60} is fluorescent increase rate at around 60 °C and V_{23} is that of at 23 °C. The proximity between 4.23 and 4.20 confirms that the acceleration of the activity has been controlled by the heat pulses. Acceleration degree of the activity can be controlled by changing the frequency of the heat pulse. From the equations, the activity of β-Galactosidase at around 60 °C is about 4.2 times higher than at 23 °C.

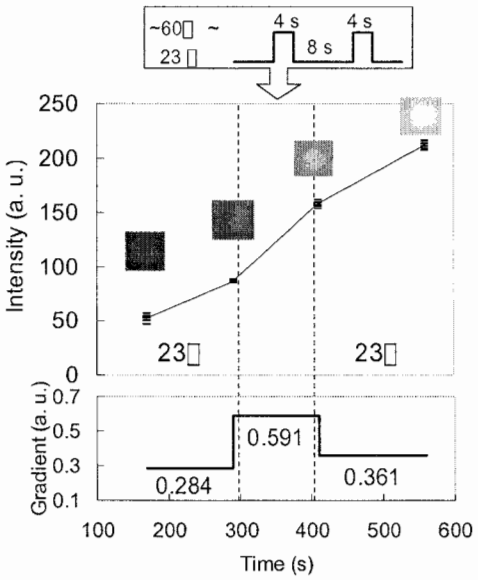

Figure 6. Activity controlled by temperature pulses with 8 seconds interval. Average and standard deviation of 6 measured values from different micro chambers.

4. Conclusions

The temperature control within 1.4 seconds in a small reaction chamber was achieved by MEMS technology; this enabled inducing heat pulses to the micro chamber and realized enzymatic activity measurement at temperature higher than the molecular destruction temperature in steady state.

References

[1] H. Arata, S. Takeuchi, G. Tresset, Y. Rondelez, K. Tabata, H. Noji, H. Fujita, IEEE MEMS Proc. pp. 363-366, 2004

[2] Y. Rondelez, G. Tresset, K. Tabata, H. Nitta, S. Takeuchi, H. Noji, μTAS Proc. pp. 555-557, 2003

IN SITU FORCE PROBING FOR CARDIAC MYOCYTE USING PDMS PILLAR ARRAY

Yi Zhao, and Xin Zhang

Dept. of Manufacturing Engineering, Boston University, 15 Saint Mary's Street, Brookline, MA 02446, USA

Abstract

In this paper, we present an in-situ force measurement for isolated myocytes using a micro molded PDMS pillar array. The contraction of the myocytes was enhanced using electrical excitation. The generated force was derived from the displacement of the pillars. With a nano-Newton resolution, this approach has the physiology and pathophysiology potential to be a basis for subcellular mechanics in cardiomyopathy study.

Keywords: Contraction Force, Cardiac Myocyte, Polydimethylsiloxane

1. Introduction

Contraction force, the mechanical interaction between myocytes and its surrounding environment, was an imperative marker of the contraction performance. To determine the contraction force, Velden *et al.* attached the isolated cardiac myocyte with silicon glue to a sensitive force transducer and a piezoelectric motor [1]. The attachment, however, induces an external stimulus to the myocyte. Subsequently, investigators relied on soft materials where the crosslinked chemistry was used to control the mechanical compliance [2,3]. This approach is, however, limited by the fact that it requires intensive computation of force calibration from continuous substrate deformation.

In this paper, we measure the contraction force generated by isolated myocytes using a micro-molded PDMS pillar array. This approach fairly isolates force probing from deformation effect of continuous substrate, and thereby allows more accurate probing. It provides an alternative way for cardiomyopathy study via the determination of mechanical interaction, rather than via the conventional biochemical approaches on molecular and protein level.

2. Sample preparation

In this paper, the PDMS substrate was fabricated in a micro molding process. The PDMS prepolymer was put in contact with a silicon template (Figure 1). After curing and peeling off, the resulting PDMS pillars fairly replicated the features of the template (Figure 2).

To obtain the isolated myocytes, a thoracotomy was performed on a Wistar rat and the heart was rapidly excised. After the excision, the heart was put into a dish with a Ca^{2+} free tyrode solution. It was shaken and massaged a few times in the solution to remove blood. Then the heart was cannulated by the aorta and perfused with the Ca^{2+} free tyrode solution to remove all the fat and connective tissue. During the perfusion, the chambers were not to be used were cut away and removed. After a few minutes, the remaining chambers were dissected into chunks using razor and digested with an enzymatic solution involving collagenase and protease via a Langendorf retrograde perfusion. The optimal digestion duration of the perfusion was determined in a series of pilot experiments.

After isolation and purification, the myocytes were removed from the isolation buffer and resuspended in a modified tissue culture media. The myocytes were then cultured on a PDMS substrate and put into a 100 dish for overnight. Cells were allowed to attach for 1 hour and then the media was changed with a fresh culture media to remove unattached myocytes. To optimize the attachment of the cells, the substrate was precoated with laminin before the myocyte isolation and kept in the tissue culture incubator at 37°C until the isolation.

3. Experiments and Results

The aforementioned PDMS substrate with myocytes was placed in a custom-made chamber, and stimulated by a digital pacer with periodical voltage pulse (Figure 3). The myocyte contracts in response to the voltage pulse due to the raise of calcium level, followed by a passive relengthening. By performing a motion tracing using the video camera, the displacements of each individual myocyte body, the underlying pillars and the pillars away from the myocyte were achieved, respectively. Represented results were shown in Figure 4. As can be seen, the traced part of the myocyte has an averaged displacement of 8.83 μm (region A) in response to the voltage pulse (indicated by black arrows), while the induced displacement of underlying pillar in the same location only averages 0.63 μm (region B). Furthermore, it was found that the pillars next to the myocyte (region C) (less than 5 μm) do not represent an observable displacement in response to electrical excitation, indicating a fairly good isolation of the contraction force probing from deformation effect of continuous substrate. Assuming that the contraction force is only exerted on the pillar tops in the direction parallel to the PDMS substrate, the force can be deduced by providing the Young's modulus and the geometry of the given pillar. Given the imaging resolution of the video camera as 0.2 μm, the force probing resolution was calculated as less than 2 nN.

Obviously, the non sliding condition between the myocytes and the underlying pillars is a crucial assumption for precise estimation of force magnitude and orientation. To validate this assumption, the PDMS substrate containing the myocytes was inspected using an environmental scanning electron microscope (ESEM). As can be seen in Figure 5, the good adhesion of the myocyte body with its underlying pillars ensures the authenticity of the force measurements.

4. Conclusions

This paper demonstrates the in-situ contraction force probing in isolated myocytes using a micro molded PDMS pillar array. Rat myocytes were isolated and cultured on the proposed PDMS substrate for force probing. The probing isolation from the continuous substrate deformation was validated by tracing the displacement of an individual pillar. The non sliding assumption between the cells and the substrate were confirmed using environmental SEM. This approach promises the potential with physiology and pathophysiology significance for precise determination of contraction force in cardiovascular study.

Acknowledgements

This work has been partially supported by NSF CAREER award. The authors would like to thank all the students participated in this project.

References

[1] J Velden, LJ Klein, M Bijl, MA Huybregts, W Stooker, J Witkop, L Eijsman, CA Visser, FC Visser, GJ Stienen, *Cardiovascular Research*, **28,** 414-423 (1998).

[2] A.K. Harris, P. Wild, D. Stopak, *Science*, **208**, 177-179 (1980).

[3] N.Q. Balaban, U.S. Schwarz, D. Riveline, P. Goichberg, G. Tzur, I. Sabanay, D. Mahalu, S. Safran, A. Bershadsky, L. Addadi and B. Geiger, *Nature Cell Biology*, **3,** 466-473 (2001).

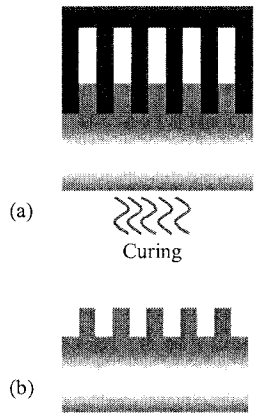

Figure 1: Micro molding process: (a) PDMS prepolymer was put in contact with a silicon template, followed by a curing process; (b) PDMS pillar array was formed after peeling off.

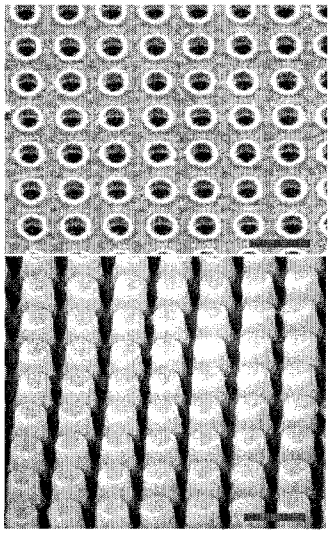

Figure 2: Silicon template (a) and replicated PDMS pillar (b). (Scale bar indicates 5 μm)

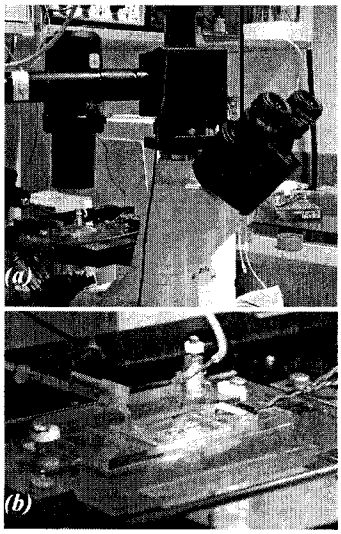

Figure 3: (a) Inverted microscope stage for contraction force probing; (b) Custom-made chamber with digital pacer.

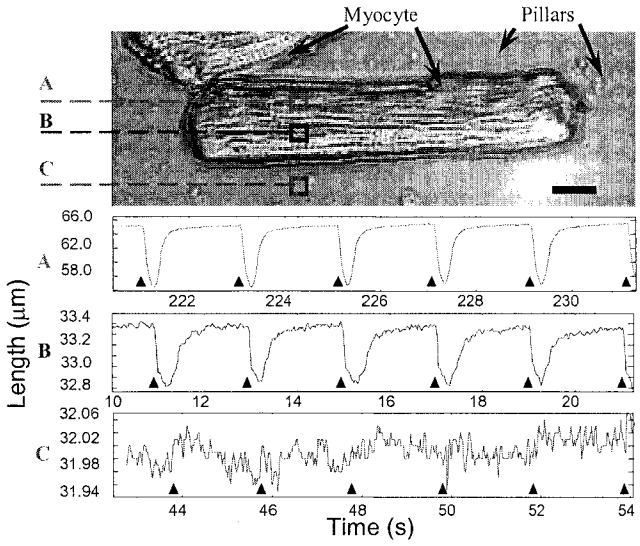

Figure 4: Tracings were carried out on myocyte surface (region A), pillars underneath the myocyte (region B), and pillars next to the myocyte (region C), respectively. (Scale bar indicates 5 μm)

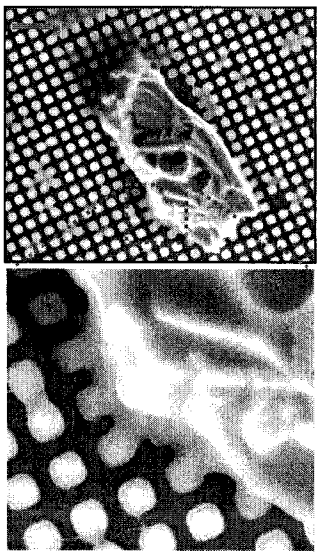

Figure 5: The myocytes have a good adhesion the underlying pillars. (Scale bar indicates 10 μm)

SILICON BASED μ-IMMOBILISED ENZYME REACTORS (μIMER) CONTAINING CELLULOSE HYDROLYSING ENZYMES

Claes Melander[1], Dane Momcilovic[2], Carina Nilsson[1], Martin Bengtsson[3], Thomas Laurell[3], Lo Gorton[1]

[1]*Dept. of Analytical Chemistry, Lund University, P.O. Box 124, S-221 00 Lund, Sweden*
[2]*Division of Technical Analytical Chemistry, P.O. Box 124, S-221 00 Lund, Sweden*
[3]*Dept. of Electrical Measurements, Lund University, P.O. Box 118, S-221 00 Lund, Sweden*

Keywords: cellulose derivatives, micro immobilised enzyme reactor, online analysis

1. Introduction

Cellulose is a naturally occurring glucose polymer, which is often used as a raw material in paper, paint, food and pharmaceutical applications. To increase the applicability of cellulose it is often modified by physical, chemical or enzymatic means. Chemical modification implies the substitution of one or more of the free hydroxyl groups of the glucose monomer on position 2, 3 or 6. The substituents can *e.g.* be methyl, ethyl or hydroxyethyl groups. In this work mainly methyl cellulose (MC) has been studied. The distribution of the substituents along the cellulose chain and on the monomer level is to a large extent unknown. The functionality and properties of the modified cellulose are very much dependent on this distribution. Therefore, methods for determination of the distribution of the substituents are currently under extensive investigation [1-3]. The use of endoglucanases, enzymes that are capable of hydrolysing the derivatised cellulose at specific points in the polymer, reveals important information on the modified cellulose. Depending on the substituent distribution, differences in the formed oligomers can be seen. Unfortunately, the traditional methodology with endoglucanases in batch often involves long incubations (72 h) and extensive manual labour. In an effort to remedy these drawbacks, we have investigated the usage of microchip immobilised enzyme reactors (μIMER) with immobilised endoglucanases for hydrolysis of cellulose derivatives. Analysis was mainly performed using an LC-ESI-MS system, with which the formed oligomers could be detected. The demonstrated method is approximately 500 times faster than the conventional batch method, can be performed completely online and can be connected to any valve-based injection system.

2. Theory

The enzyme reactors employed in this work are constructed from highly porous silicon and have been developed by Laurell *et al.* since 1994 [4,5]. They consist of two reservoirs with porous flow channels etched between them. The porous silicone makes it possible to immobilise a large amount of enzyme (Figure 1). Immobilisation of the enzyme was performed by functionalising the surface with polyethyleneimine (PEI) and then cross-linking the enzyme to PEI using glutaraldehyde. The very narrow channels give short diffusion paths for the substrates (modified cellulose) to reach the immobilised endoglucanase and since the local concentration of the endoglucanase is high, an increased hydrolysis rate compared to batch hydrolysis is therefore achieved. The irreversible immobilisation of the enzyme on the μIMER makes it possible to perform multiple, rapid and online analysis of modified cellulose. To our best knowledge this has never been achieved before.

3. Experimental

μIMERs were fabricated by the anisotropic wet etching technique [6,7]. An increase in the internal surface area is achieved by making the channels more porous by anodisation. To bind the

enzyme to the surface a microchip was placed in 0.2% PEI in 10 mM succinate (pH 5.5) at 4°C overnight. The reactor was then placed in 2.5% glutaraldehyde in succinate buffer for 1 h. Immobilisation of the enzyme was done by incubating the reactor in the enzyme solution for at least 12 h at 4°C. Unreacted glutaraldehyde was deactivated by placing the reactor for 1 h in 0.1 M (pH 5.5) TRIS buffer. Reduction of the formed covalent bond between the enzyme, glutaraldehyde and PEI was performed by placing the reactor in 2 mg/ml $NaCNBH_3$ for 2 h.

4. Results and discussion

Early experiments have shown that the immobilisation of either of two different endoglucanases (BaCel5a and TrCel12) gives a fast and stable hydrolysis for over 10 days of continuous use. When stored at 4°C no loss of activity wad seen after 60 days [8]. Hydrolysis of MC through the μIMER connected to an LC-ESI-MS system provides the same information as batch experiments but is approximately 500 times faster and completely online (Figure 2). Comparison of the μIMER and batch hydrolysed MC datasets shows that the two different hydrolysis methods produce the same ions with the same relative intensity with only minor variations *i.e.* no change of enzyme activity can be seen due to the immobilisation (figure 3a). Each enzyme and substrate produce a "fingerprint" of m/z peak intesities. Interpreting the patterns gives valuable information on the enzyme and the derivatised cellulose. Comparison of the hydrolysis patterns of three different MC's with ESI-MS, shows that the μIMER methodology can be used to determine structural differences on the oligomer level. As seen in Figure 3b, which shows ESI-MS analysis of the hydrolysis product cellotriose with varying degree of substituents, the patterns for DS 1.76 is different. This MC has a shift towards a more substituted cellotriose compared to the others, indicating that when the endoglucanase hydrolyses this MC it has a higher access to the cellulose chain. One conclusion can therefore be drawn that this MC has a different distribution of the substituents along the chain than the other MC's. To analyse a broader range of formed products after hydrolysis of the MC's, semi online MALDI-TOF-MS analysis has also been performed. In the near future the hydrolysis products will also be analysed using size exclusion chromatography with multi-angle light scattering and refractive index detection.

This is, to our best knowledge, the first time μIMER's have been applied where modified cellulose has been hydrolysed using immobilised endoglucanases. The method is much faster than conventional batch hydrolysis and is much less labour intense. It can also be used for determination of variations in the substituent distribution of different MC's.

5. Acknowledgements

The authors thank CAP for financial support and Dr. Curt Reimann for scientific discussions.

6. References

[1] J. Karlsson, *et.al.* , *Biopolymers* **63** (2002) 32.
[2] A. Cohen, *et.al.*, *J.Chrom.* A **1029** (2004) 87.
[3] S. Richardson, L. Gorton, *Anal. Chim. Acta* **497** (2003) 27.
[4] T. Laurell, L. Rosengren, *Sensors and Actuators, B: Chemical* **19** (1994) 614.
[5] T. Laurell, J. Drott, L. Rosengren, *Biosensors & Bioelectronics* **10** (1995) 289.
[6] T. Laurell, J. Drott, L. Rosengren, *DECHEMA Monographien* **132** (1996) 139.
[7] J. Drott, K. Lindstroem, L. Rosengren, T. Laurell, *J. of Micromech and Microeng* **7** (1997) 14.
[8] C. Melander, M. Bengtsson, T. Laurell, L. Gorton, *in manuscript.*

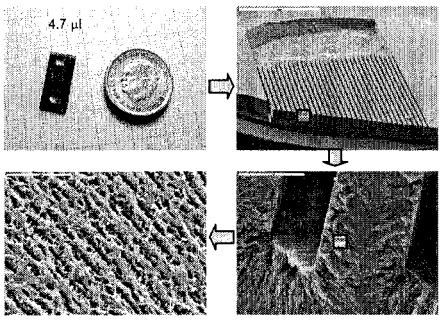

Figure 1. Photo and SEM pictures with increasing magnification of the µIMERs used. The µIMER dimension was 13.1×3.2 mm, comprising 42 porous flow channels of approximately 235 µm depth and 25 µm width, giving a total internal surface area of 242 mm^2 before fabrication of the porous layer. Immobilisation of the enzyme was performed by functionalising the surface with PEI and crosslinking with glutaraldehyde.

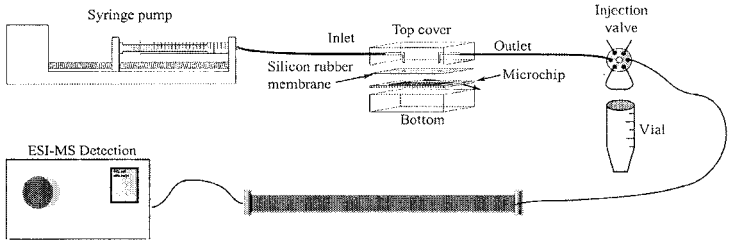

Figure 2. Schematic representation of the instrumental set-up, a syringe pump provide a sample with the modified cellulose through the reactor that was clamped between two plastic holders. The outlet was either connected on-line to an LC-ESI-MS system or offline to a sample vial. The method was approximately 500 times faster than conventional batch hydrolysis.

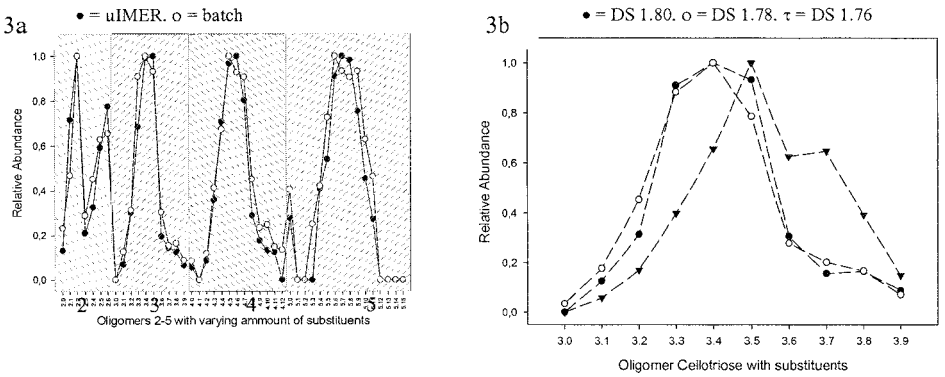

Figure 3. a) Normalised peak intensities of hydrolysis products from ESI-MS analysis. Comparison of results from µIMER and batch hydrolysed MC (DS 1.80). Analysis of formed oligomers 2-5 with substituents performed using ESI-MS. Normalisation for each oligomer is to the most abundant substituted species for that oligomer. Both methods give the same "fingerprint" pattern of the hydrolysis products. **b)** Normalised peak intensities for cellotriose with substituents for three MC samples. µIMER hydrolysis was performed of MC with DS 1.80, DS 1.78 and DS 1.76. Differences in the oligomer pattern are found for DS 1.76, which is shifted more towards the higher substituted cellotriose. This indicates a different substituent distribution.

INTEGRATING ASSAY STEPS ON A MINIATURIZED PLATFORM: FROM PCR TO HYBRIDIZATION

Rolf M. Kaack, Stefanie Reinbold, Roland Zengerle, Martina Daub
IMTEK, University of Freiburg, Georges-Koehler-Allee 103, D-79110 Freiburg, Germany

Abstract

For the first time we present a miniaturized DNA processing platform which allows to integrate sample amplification, post-processing and extraction of amplified material in nanoliter quantities for a subsequent hybridization experiment. The platform is called PCR-Slide, has outer dimensions corresponding to a microscope slide and will contain 24 parallel reaction sites in the final version. To demonstrate the possibilities of the new platform we successfully performed the following sequence of assay steps in a prototype device with a reduced set of 4 parallel reaction sites:

1. Amplification of DNA by means of the polymerase chain reaction (PCR).
2. Conversion of double stranded DNA into single stranded DNA by an enzymatic exonuclease reaction.
3. Transfer of 500 nL aliquots of the processed material in a non-contact manner with the inbuilt nanoliter dispenser into a hybridization buffer premix on a microarray.
4. Microarray hybridization experiment with subsequent fluorescent detection.

Keywords: PCR, hybridization, nanoliter dosage, lab-on-a-chip

1. Introduction

Due to the growing importance of gene analysis, many research groups work on the miniaturization of genetic assays. Miniaturization has been identified as a possibility to reduce costs and time needed to perform these assays. Many research groups focus on the miniaturization of the polymerase chain reaction (PCR). Recent publications have demonstrated various microchip designs, allowing on-chip-PCR or even integrating further pre-PCR or post-PCR steps [1]. Microchips that allow total analysis, i.e. that integrate on-chip capillary electrophoresis and detection, have the advantage that they circumvent the need of liquid transfer in the range of microliters or even nanoliters. However, a drawback of many presented PCR microchips is their rigidity, i.e. they can almost only be used specifically for PCR related reactions.

A higher flexibility can be achieved with the platform that is presented in this paper. The platform integrates parallel sample processing of reduced reagent volumes and sample transfer by means of a nanoliter dosage. Key element of this platform is the PCR-Slide, that contains 4 (in future design 24) parallel fluidic units. Each fluidic unit simply consists of a reaction cavity and an integrated nanoliter dispenser derived from the DWP principle [2], a robust and reliable dosage method in the range of tens of nanoliters. The modular character of the platform is emphasized by the arrangement of the nozzles and reaction chambers in the widely used 384 microtiter plate format, which makes the PCR-Slide compatible to laboratory standards and allows subsequent processing on other platforms such as microtiter plates, microarrays or even a further PCR-Slide.

2. Experimental and Results

We fabricated PCR-Slides with 4 parallel fluidic units at a pitch of 4.5 mm (corresponding to 384 well microtiter plates) as depicted in figure 1. The PCR-Slides consists of a 1 mm thick base part and a 240 µm thick nozzle foil, both made of polycarbonate. Reaction chamber, channel and nozzle chamber were milled into the base part, while the nozzles were drilled into the nozzle foil (fig. 2). The reaction chamber has a total volume of 2 µl. It is connected to the nozzle via a 300 µm wide and 170 µm deep triangle channel. The diameters of the nozzle chamber and the nozzle are

300 µm and 100 µm, respectively. The base part and the nozzle foil were bonded by laser welding which was performed by *Leister Process Technologies* (Switzerland).
The small size of the PCR-Slide provides a basis for the construction of a sandwich PCR thermocycler with drastically reduced footprint (fig. 3). PDMS covers are used for sealing to avoid evaporation during cycling and for reversible releasing of the openings of the PCR-Slide after processing. The covers are applied to the PCR-Slide by a clamping mechanism integrated into the PCR thermocycler.

For detection or further processing steps an accurately defined nanoliter quantity of liquid can be dispensed from the PCR-Slide in a non-contact manner. Actuation is performed by applying a pneumatic pressure pulse onto the top side of the PCR-Slide. The dispensed volume is defined by amplitude and duration of the applied pressure pulse (fig. 4).

The subsequent microarray experiment for detection purposes was performed in cavities made of SU-8 (fig. 5). Therefore a microarray of 24 spots was printed into each cavity which was then filled with 1.5 µl hybridization buffer premix. To gain single stranded DNA for hybridization on the microarray a specific oligonucleotide design was employed for PCR followed by exonuclease digestion of one strand [3] by adding the enzyme into the PCR-Slide. After treatment of the PCR product with exonuclease 500 nL aliquots were dosed into the premix using the inbuilt dispenser functionality. After further standard microarray processing steps the microarray was read out with the *Bioanalyzer 2100* from *LaVision Biotec.*

The results of the hybridization experiment show the successful implementation of the whole assay on the PCR-Slide (fig. 6). The detection of specific PCR products implies that the PCR, the treatment with exonuclease and the transfer of PCR product with the inbuilt nanoliter dispenser have been successful.

3. Conclusion

The results demonstrate the high potential of the PCR-Slide as a miniaturized processing platform for multistep reactions. Assay involving dilution steps can be performed without the need of bulky, external pipetting equipment. In addition the cheap and simple construction of the PCR-Slide allows a very flexible use for a wide range of different chemical reactions.

Acknowledgements

This work was supported by grants from the German Ministry of Science and Technology, BMBF project nanoMAP 0312001D. The authors are grateful to *Leister Process Technologies* (Switzerland) for supporting the PCR-Slide fabrication with their laser welding technique.

References

[1] L.J. Kricka, P. Wilding, *Anal. Bioanal. Chem.*, **337**, 820-825 (2003)
[2] P. Koltay, B. Birkenmeier, R. Steger, H. Sandmaier, R. Zengerle, *Actuator 2002*, 235 –239 (2002)
[3] T.T. Nikiforov, R.B. Rendle, M.L. Kotewicz, Y.-H. Rogers, Vol 3, *PCR Methods Appl.*, **3**, 285-291 (1994)

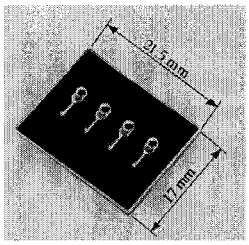

Figure 1. Top view photograph of the PCR-Slide with four fluidic units.

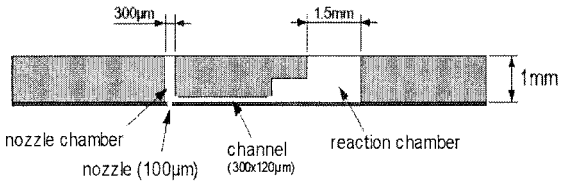

Figure 2. Schematic drawing of the cross section of one fluidic unit within the PCR-Slide. Reservoir, channel and nozzle chamber are milled into the material (Polycarbonate). The nozzle foil is bonded by laser welding.

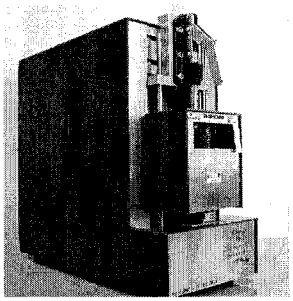

Figure 3. PCR thermocycler, constructed to meet the needs of the PCR-Slide.

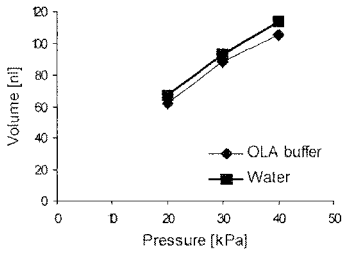

Figure 4. Dispensed volume as a function of the applied pressure and media properties.

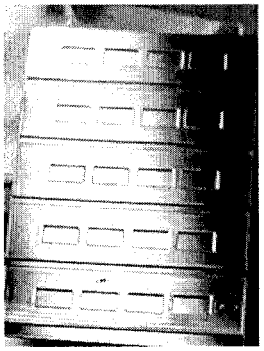

Figure 5. Four separate hybridization chambers were realized in SU8 (3.5 x 2.5 mm at a height of 280 µm; pitch corresponds to pitch of fluidic units of PCR-Slide). Each chamber contains a microarray with 24 probes printed with TopSpot technology.

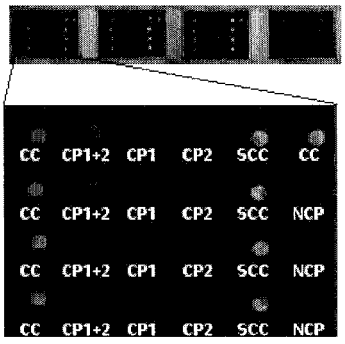

Figure 6. Before hybridization two different complementary probes (CP1 and CP2) and a mixture of both probes (CP1+2) were coupled on the slide surface. Coupling control (CC) demonstrates positive post-printing process. For hybridization single stranded PCR products were incubated on the microarray and streptavidin-Cy5 labeling method was used. SCC is the streptavidin color control.

A NOVEL MICRO DEVICE FOR MEASURING THE ELECTYROMECHANICAL PROPERTIES OF A SINGLE MYOCYTE

M. A. Hassan[1], N. Fujiwara[2], I. Kanno[2] , H. Kotera[2] and M. Washizu[3]

[1]*Leading Project Researcher, Kyoto University and Assiut University, Egypt*

[2] *Dept. Mech. Eng., Faculty of Engineering, Kyoto University, P.O. 606- 8501 Kyoto, Japan*

[3]*Dept. Mech. Eng. Faculty of Engineering, University of Tokyo, Tokyo, Japan*

Abstract

The aim of this work is to develop a micro-electromechanical senor to measure ionic reaction and viscoelastic mechanical properties of a single myocyte as well as measuring multi-cells interaction. The proposed device consists of micro-columns arrays like-posts, made of PDMS (Polydimethysiloxane) works as vertical cantilevers measuring the cell deformation. To measure action potential simultaneously with cell deformation, axial through holes of 3 μm are made inside posts array of 6 μm diameters. Quality of the results depends mainly on the adhesion quality between posts tips and myocardium surface.

Key words: Mechanical properties, myocardium cell, micromechanical sensors, PDMS

1. Introduction

Our research group in Kyoto University, Japan is establishing bio-simulator software from physiological and physical properties of a single myosyte (cell level) up to organ level interaction (heart). As a starting point of this project, a cardiac myocyte model called (CM16) [1] which is composed of the majority of known sarcolemmal ion channels and transporters, sarcoplasmic reticlum, and contractile elements as shown schematically in Fig.1. The model can produce action potentials, intracellular Ca transient, contraction, and intracellular ATP consumption. To construct a virtually living cardiac myocyte and beating heart, mechanical properties are the central perquisite demand [2]. Previous studies neither focused experimentally on the viscoelasticity nor on 3D mechanical properties of a single myocardium cell. In addition to that, most experimental measurements, in particular MRI imaging and tagging methods provide mostly global information about material properties and deformation of the heart.

Therefore the aim of this work is to develop a viscoelastic constitutive equation for myocyte material based on experimental observations, and also measuring the ionic reaction of single and multi-cells together with their mechanical behaviors.

Important considerations should be taken into account before developing the measuring device; i) mechanical properties are highly anisotropic and distributed in a single myocyte [3], ii) myocyte interaction with the underlying substrate should be reduced as it is possible[4] iii), passive reactions and active contraction forces of myocardium cell should be easily isolated from the underlying substrate without complicated mathematical manipulations, ix) ability to observe the relationship between myocytes connection (series or parallel) with ionic and kinetic reactions, iix) ability to observe cell ion current and action potential.

2. Theory

Base on the above considerations, the authors have developed a new experimental micro device that is consists of micro-columns arrays like-posts made of PDMS (Polydimethysiloxane). Dimensions and design layout are shown in Fig. 2. If a myocyte is installed on these elastomeric arrays of small posts, Fig. 3, its deformation and contraction force could be tracked as a function of the posts' deflections, x , and therefore locale bending forces, F , are given by equation (1). The

global viscoelastic strain energy function, is given as a Prony series expression, (eq.2). Its derivatives with strains give the stress components or the constitutive equations.

$$F = \left(\frac{3EI}{L}\right) x \qquad (1)$$

$$\psi = \psi^{\infty} + \sum_{n=1}^{N} \delta^n \psi^0 \exp\left(-t/\lambda^n\right) \qquad (2)$$

Where δ^n time dependent multipliers, λ^n associated relation times, ψ^{∞} long terms elastic strain energy and ψ^0 instantaneous elastic strain energy density.

To measure the action potential simultaneously with cell deformation we are going to make axial through holes of 3 μm inside posts of 6 μm diameter as shown schematically in Fig. 4. Also we attempt to measure cell to cell interaction by this proposes system.

3. Experimental results and discussion

Device dimensions shown in Fig.2 were determined based on anatomical information and the range of contraction force obtained from cell bio simulator model "Kyoto model". Posts diameters d =3~6 μm, length L=10~25 μm and interval D=10~20 μm are the optimum range of device dimensions. Based on MEMS technology, aluminium thin film was thermally deposited on glass substrates in order to make photo mask. The top view of the device dimensions was drawn by minCAD software that controlling electron beam (EB) lithography machine. After machining and developing processes, the obtained original mask was replicated on another aluminium film samples by UV lithography for 15 seconds in order to have multiples of masks for further experiments. The samples should be coated in advance with S1813. SU-8 is molded directly over a replicated mask in order to make a template containing an array of SU-8 holes; thickness/depth and exposing time depend on the SU-8 number and UV exposure time. After that the holes are spin coated with barrier coat diluted with toluene (ratio 1:20) at 1000RPM spinning speed for 10s and dry in oven at 115C°for 4 minutes. A silicon rubber container made from silicon rubber wafer is used to control PDMS volume and thickness of the posts base. PDMS is poured over the SU-8 holes, degassed under vacuum for three hours, cured at 115^{0}C for one hour and followed by 4 hours hard baking after peeling off. 3D view of the fabricated device posts are shown in Fig2 (b).
Elastic modulus of PDMS was determined by uniaxial micro compression test. Test specimen of 5x5x4mm was prepared under the same baking and curing conditions used for fabrication PDMS post. Young's modulus E =2.5 MPa was determined by the tangent limit of stress strain curve. The viscoleactic properties of myocardium tissues were determined using Prony series expansion (eq.2).

The preliminary experiments give optimistic results, but the lake of adhesion between posts and myocyte represents a key issue. In order to enhance the contact, tip posts were coated by fibronectien protein and cellTak a little enhancement was obtained. Aluminum layer of 200nm thickness significantly increased the adhesion contact and good results are obtained.

Acknowledgements

This research is financially supported by the Cell and Living lives national simulation project of the Japanese Government.

References

[1] M. Tomita, et al., Bioinformatics 15(1), 72-84 (1999).
[2] PJ, Hunter, et al., Crit Rev Biomed Eng. 20, 403-426 (1992).
[3] D. H. S. Lin and F. C. P. Yin., J Biomech. Eng. 120, 504-517 (1998).
[4] L. John Tan and et al., PNAS 100(4), 1484-1489 (2003).

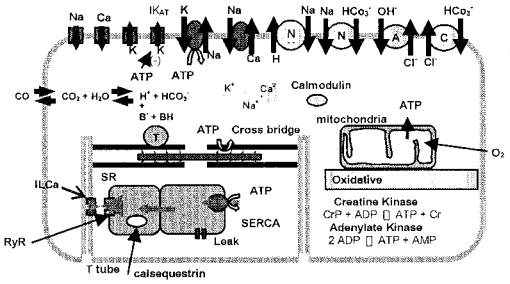

Figure 1 Kyoto model structure (C16)

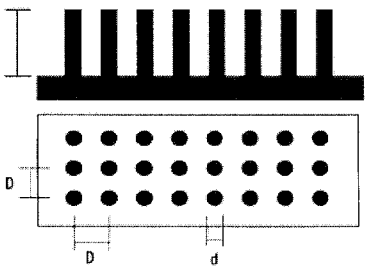

Figure 2(a) Device layout and dimensions L=10μm, d=3μm D=10μm

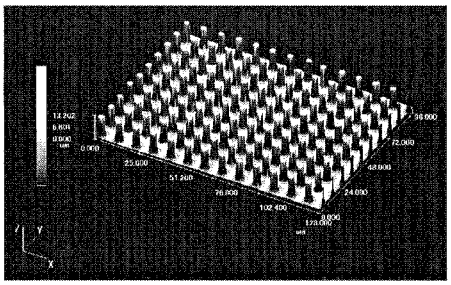

Figure 2 (b) Three dimensional view of the manufactured device by confocal laser microscope, d=3μm

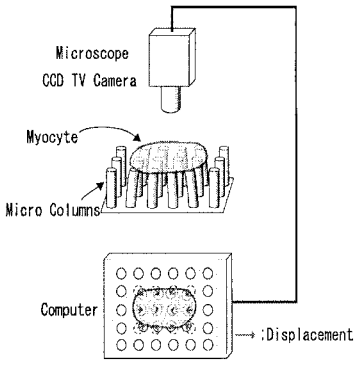

Figure 3 (a) Measuring system

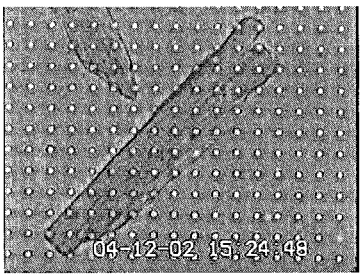

Figure 3 (b) Cell installed over the device

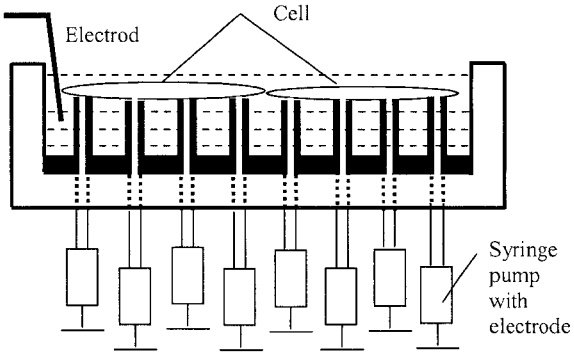

Figure 4 Through holes of 3 μm inside the posts for measuring cell action potential.

DNA AMPLIFICATION AND DETECTION DEVICE USING ELECTROSTATIC MICRODROPLET MANIPULATION TECHNIQUE

Lay Kuan Goh, Masaya Tokoro, Toru Torii and Toshiro Higuchi
Dept. of Precision Engineering, Graduate School of Engineering,
The University of Tokyo, 7-3-1, Hongo, Bunkyo-ku, Tokyo 113-8656, JAPAN

Abstract

A novel method using electrostatic manipulation of microdroplets to realize the DNA amplification and detection has been proposed. DNA samples and reagents in the form of micro-liter size droplets were transported, mixed and performed Polymerase Chain Reaction (PCR) and DNA detection in an inert liquid medium. The results from the PCR and DNA detection were subsequently tested and analyzed using electrophoresis and SYBR Green fluorescent detection technique respectively.

Keywords: Polymerase Chain Reaction (PCR), Electrostatic manipulation, Microdroplet, DNA, Hybridization

1. Introduction

In recent years, the realization of Lab-on-a-chip concept in DNA related analysis has been widely studied [1-2]. Existing designs using continuous flow microfluidic technique have several shortcomings such as high possibility of contamination and lack of flexibility. Our proposed method is based on the electrostatic manipulation technique of droplets [3]. In our research, droplets containing DNA samples and reagents are electrostatically transported and manipulated on electrode panel to perform Polymerase Chain Reaction (PCR) and DNA detection. Contamination from airborne particles and evaporation of samples and reagents can be prevented as the droplets are surrounded by an inert liquid medium.

2. Concept

The concept of this method is shown in Figure 1 and Figure 2. Microdroplets (droplets) containing DNA samples and reagents are produced from the droplet formation device [4]. The droplets are transported by electrostatic force and mixed together to form a PCR solution. This PCR solution droplet is transported to the PCR chamber to perform PCR thermal cycle.

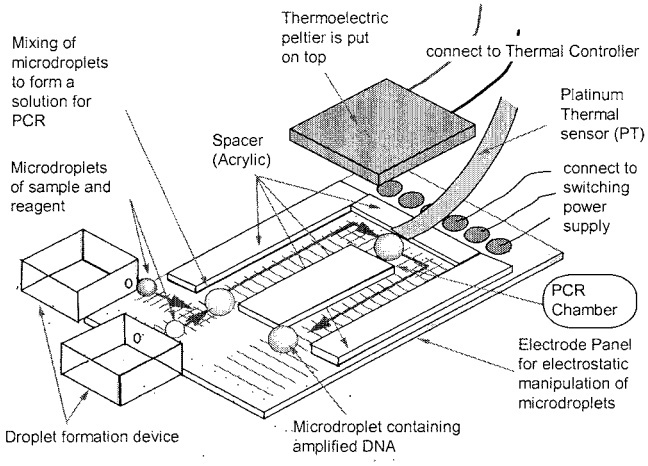

Figure 1. The concept diagram of the PCR device

After the PCR step, the amplified DNA molecules are dehybridized. Droplets that contain only single strand DNA are prepared. These droplets are then introduced into the DNA Droplet Detection Array. This droplet (Target) is then mixed with droplets containing reagent and known single stranded DNA (Probe). The resulting droplet is transported and assembled on the DNA Array for DNA hybridization detection and analysis.

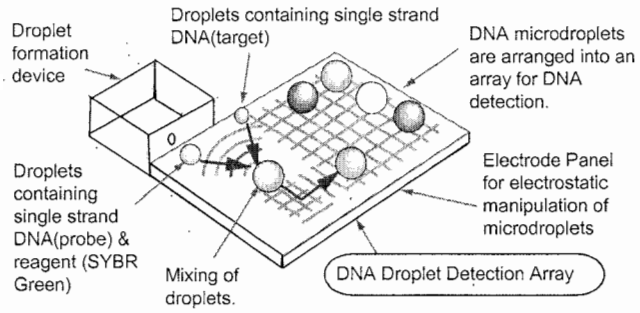

Figure 2 The concept diagram of the DNA Droplet Detection Array.

3. Experimental

In our experiment, Takara PCR Kit was used to formulate the PCR droplet of size 1.0 μl (micro-liter). The electrode panel with electrode pitch of 0.5mm and width of 0.3mm was used. The surface of the electrode panel was coated with hydrophobic Teflon layer. This allowed the droplets moved smoothly and easily on the electrode panel. Paraffin oil was used as the inert liquid medium for the transportation of droplets. Droplets were moved by electrostatic forces generated from the electrodes. The voltage pattern used was a continuous voltage profile of +++000.

The PCR Chamber consists of a thermoelectric peltier device and a Platinum Thermal sensor (PT) for temperature and thermal cycle control. PCR thermal cycle of 94°C (denaturization), 55°C (annealing) and 72°C (extension) with 40 seconds each was performed for 30 cycles. On the DNA Droplet Detection Array, the droplets containing single strand Target DNA were mixed with droplets containing Probe DNA and SYBR Green I. The droplets were then observed under microscope to detect the intensity of the fluorescent light emitted. The DNA sequence was CCT ATA GCT TCC CTT CTT CC, which is a sequence of primer of Zein.

4. Results and discussion

The result of PCR was analyzed by gel electrophoresis technique (Figure 3). Ethidium bromide was used for nucleic acid gel stain. Result shows that UV induced fluorescent spots were observed in area B. This indicates that the DNA was successfully amplified using our PCR device.

For the DNA detection, five droplets of different compositions of DNA oligonucleotide were used as Probe DNA. They were All-match, 15-match, 10-match, 5-match and No-match. These droplets were then mixed with SYBR Green I and combined with droplets of Target DNA. By using fluorescent microscope, different relative intensities of SYBR Green fluorescent emissions were detected. They correlated well with the level of DNA hybridizations (number of base pair matched) (Figure 4). Therefore, it is suggested that this device has the potential for further development to become an efficient DNA amplification and detection equipment

5. Conclusions

Comparing with the other miniaturized DNA amplification and detection devices using microfluidic technique, our device has the advantages of minimizing contamination. Further more, droplets of different sizes could be produced and manipulated. This adds flexibility and selectivity to the device. In this method, only micro-liter amount of sample and reagent are needed, so it has the advantages of increasing throughput, reducing sample volume and reaction time.

A A B B

Figure 3. Electrophoresis result shows fluorescent spots in area B which indicates that small amount of DNA has been amplified by our PCR device. (Area A contains the controlled sample obtained from PCR Thermal Cycler; Area B contains the PCR result from our device.)

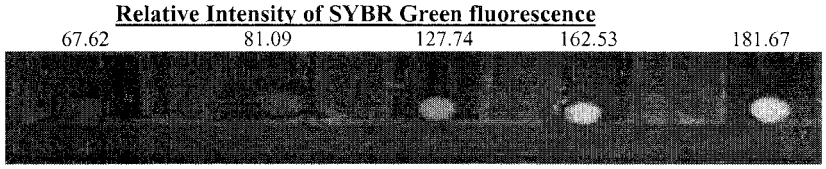

Figure 4. Results of DNA detection. The relative fluorescent light intensities are correlated with the level of DNA hybridizations (number of base pair matched).

Acknowledgements

We would like to thank Mr. Tetsuo KATAYAMA for his advice and contribution to this work. The part of this research was supported by the grant from Electro-Mechanic Technology Advancing Foundation.

References

[1] P.J. Obeid, T.K. Christopoulos, H.J. Crabtree and C.J. Backhouse, "Microfabricated Device for DNA and RNA Amplification by Continuous-Flow Polymerase Chain Reaction and Reverse Transcription-Polymerase Chain Reaction with Cycle Number Selection", *Analytical Chemistry*, 2003, 75, pp.288-295

[2] E.T. Lagally, I. Medintz and R.A. Mathies, "Single-Molecule DNA Amplification and Analysis in an Integrated Microfluidic Device", *Analytical Chemistry,* 2001, vol 73, no 3, pp565-570

[3] T. Taniguchi, T. Torii and T. Higuchi, "Chemical reaction in microdroplets by electrostatic manipulation of droplets in liquid media", *Lab Chip*, 2, pp.19-23 (2002).

[4] T. Nisisako, T. Torii and T. Higuchi, "Droplet formation in a microchannel network", *Lab Chip*, 2, pp.22-26 (2002).

MICRO REACTORS FOR THE OPTIMISATION OF REACTION CONDITIONS IN ASYMMETRIC METAL CATALYSIS

Stina Lundgren,[1] Aman Russom,[2] Christina Jönsson,[1] Göran Stemme,[2] Stephen J Haswell,[3] Helene Andersson[2] and Christina Moberg[1]

[1]KTH Chemistry, SE 100 44 Stockholm, Sweden

[2]KTH S3, SE 100 44 Stockholm, Sweden

[3]Department of Chemistry, University of Hull, Cottingham Road, UK HU6 7RX

Abstract

Two types of micro reactors were employed for enantioselective metal catalysed reactions. In the first type of reactor, an electroosmotic flow was used, whereas the second type of reactor used a pressure driven flow. The purpose of the study is to develop tools for rapid and efficient optimization of reactions, utilising minimum amounts of reagents.

Keywords: Micro reactor, asymmetric metal catalysis, beads, homogeneous catalyst, polymer-supported catalyst

1. Introduction

The need for chiral enantiomerically pure compounds, i.e. one of the forms of mirror image compounds in pure form, is steadily increasing. The major application of such compounds concerns their use as active components of pharmaceuticals; the two mirror image forms may have distinctly different properties and the desired form must therefore be prepared without contamination of the undesired form. Asymmetric metal catalysis, where a catalytic amount of a chiral metal complex is used for the production of large amounts of a chiral compound, is one of the most efficient methods for the preparation of such compounds.

Whilst a large variety of metal catalysed reactions are known to proceed with high enantioselectivity, each reaction usually requires extensive optimisation of yield and selectivity. This is time consuming and large amounts of reagents are usually required. It is therefore desirable to find methods for efficient screening and optimization of reactions on a small scale. For this purpose, we have studied the use of micro reactors for enantioselective Ln catalysed additions of trimethylsilyl cyanide to bensaldehyde.

2. Theory

The Ln-catalysed reaction selected for this study yields chiral cyanohydrins [1], which serve as important synthetic intermediates [2] (Scheme 1). The catalyst consists of the metal ion bound to a chiral ligand responsible for the transfer of chirality to the product. The enantioselectivity, the relative amount of the two mirror image compounds, of the reaction is sensitive to the reaction conditions.

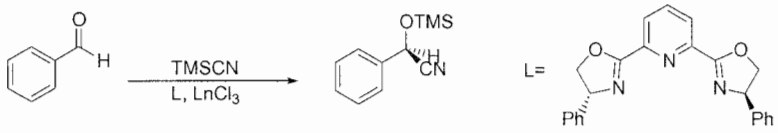

Scheme 1. Lanthanide catalysed silylcyanation of aldehydes

Polymer-supported catalysts have advantageous properties compared to soluble catalysts since they can be separated from the reaction mixture by simple filtration and can also often be reused several times [3]. By avoiding soluble catalysts, the reacting compounds can be mixed prior to introduction in the micro reactor, and problems with mixing and diffusion are thus not encountered.

3. Experimental

The electroosmotic flow driven micro reactor (Figure 1) was fabricated in borosilicate glass at Hull University [4] and had a T-shaped design with three reservoirs, two inlet (A and B) and one outlet (C, Figure 1), with approximate channel dimensions of 100×50 μm and outer dimensions of 20×20×25 mm. Two standard solutions, one containing the catalyst and benzaldehyde, the other trimethylsilyl cyanide, were added to inlets A and B, respectively. EOF was generated by applying appropriate voltages to platinum electrodes (A and B ranging from 150 to 750 V, C set to ground). The product was collected after 10-30 min in the outlet reservoir C and analyzed.

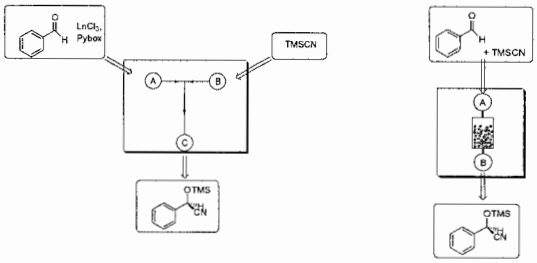

Figure 1. I: EOF driven micro reactor. II: Pressure driven micro reactor.

The second micro reactor (II, Figure 1)), a microfluidic flow-through filter-chamber device for chemical reactions on beads, was fabricated by a standard semiconductor photolithographic techniques and bulk micro-machining of silicon [5]. The filter chamber that has a volume of 300 nL was filled with 15μ polymer beads having the catalytic complex covalently attached. A solution, ca 1μL, of the reagents was introduced at A and passed through the chamber containing the polymer beads with the help of a motor driven syringe. The product was collected at B after 1-2 min and analysed.

4. Results and discussion

We employed micro reactor I for the screening the effect of additives on the result of the reaction. First the applied voltages needed to be optimized to achieve flow rates resulting in a ca 1:1 ratio of the reacting compounds in the reactor (Figure 2) [6].

Having found the voltages affording the highest yields of products, reactions were run without any additive (1, Figure 3) and in the presence of 14 different additives (2-15, Figure 3) and the enantioselectivity of the reactions was determined. Results obtained employing the micro reactor were compared to those obtained using standard reaction conditions. It was found that the presence of several additives had a profound influence on the result of the catalytic reaction. What is interesting to note, is that the variations in selectivity observed in the micro reactor processes mimic those observed under normal conditions (Figure 3), clearly demonstrating the suitability of the rapid micro reactor technique for the present purpose. In addition, reaction in the micro reactor proceeded

at a higher rate, experiments 1-15 in Figure 3 requiring 10 minutes as compared to 30 minutes under conventional conditions.

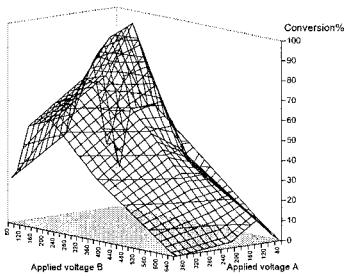

Figure 2. Optimisation of applied voltages.

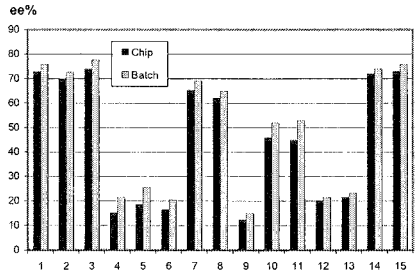

Figure 3. Screening of additives.

In preliminary studies of the same catalytic reaction utilising micro reactor II it has been shown that the polymer-supported metal complex introduced in the reaction chamber catalyses the desired reaction.

5. Conclusions

The micro reactor using electroosmotic flow was shown to serve as an efficient tool for the optimisation of reaction conditions for a synthetically important catalytic process. In order to avoid problems with adjustment of the voltages over the two flows as well as problems connected with the separation of products from homogeneous metal catalyst, a micro reactor containing a filter chamber operating with pressure driven flow was used for a reaction catalysed by a metal complex attached to polymeric beads.

The work described here is the first example of the use of micro reactors for asymmetric catalysis. The two types of reactors are expected to be suitable for efficient small scale optimisation of a large varies reactions, which otherwise would require large quantities of reagents. The results obtained open up for new valuable applications.

Acknowledgements

Financial support from the Swedish Foundation for Strategic Research (the Nanochemistry Program) is gratefully acknowledged.

References

[1] H. A. Aspinall, N. Greeves, P. M. Smith, *Tetrahedron Lett.*, ***40***, 1763-1766 (1999).
[2] J.-M. Brunel, and I. P. Holmes, *Angew. Chem. Int. Ed*, **43**, 2752-2778 (2004).
[3] S. Lundgren, S. Lutsenko, C. Jönsson, C. Moberg, *Organic Letters*, **5**, 3663-3665 (2003).
[4] G. M. Greenway, S. J. Haswell, D. O. Morgan, V. Skelton, P. Styring, *Sens. Actuators B*, 63, 153-158, (2000).
[5] H. Andersson, W. van der Wijngaart, P. Enoksson, G. Stemme. *Sens. Actuators B,* 67, 203-208, (2000).
[6] C. Jönsson, S. Lundgren, S. J. Haswell, C. Moberg, *Tetrahedron*, Accepted for publication.

Single Cell Analysis by Formation of Air-Liquid Boundary

Akihiko Ichikawa[1], Fumihito Arai[1], Toshio Fukuda[1] and Tohoru Katsuragi[2]
[1]Dept. of Micro-Nano Systems Engineering, Nagoya University, Furo-cyo 1, Chikusa-ku, 464-8603, Nagoya, Japan
[2]Graduate School of Biological Science, Nara Institute of Science and Technology, Takayama-cho 8916-5, Ikoma city, 630-0101, Nara, Japan

Abstract

We propose air-liquid boundary formation around the cured photo-crosslinkable resin made in the microchannel. The target cell is trapped and immobilized in the cured resin. When the microchannel is purged with the air and next filled with the reagent, an air-liquid boundary is formed around the cured resin. With this method, the quantity of consumed reagent in the microchannel was reduced from 0.6 g to 0.025 g. We succeeded in fluorescence staining and observation of the trapped cell with minute amount of fluorescence reagent in-situ on a chip. The proposed method is useful for single cell analysis on a chip.

Keywords: Air-Liquid Boundary, Single Cell Analysis, Photocrosslinkable Resin, PDMS chip, Evaporation rate control

1. Introduction

Species of the Bacteria and the Archaea that have been cultured are only a small fraction of the ones that exist. Recently, high throughput screening for microorganisms with desired characteristics from a large heterogeneous population has become possible [1]. Finding culture condition for these strains or unidentified microorganisms is also important. However, it is difficult to identify optimal culture conditions in scale-up processes. Batch or continuous culture of a large number of microorganisms with different culture conditions is time-consuming and used much space. We have reported a novel desktop culture system that can be used to monitor individual microorganisms and cells in different culture media, and to test several reaction experiments stably, on a chip [2,3]. We employed a novel method to isolate the target by photo-crosslinkable resin, and in this paper, we extend the idea to reduce the quantity of consumed reagent by forming of an air-liquid boundary.

2. Material & Method

The prepolymer of polyethyleneglycol and polypropylene glycol (ENT-2000, Kansai Paint Co. Japan), is cured by irradiation of UV light (the wave length is around 366 nm). Here we call it ENT. Figure 1 shows the method of air-liquid boundary formation made in the microchannel with the ENT. The cell is strongly immobilized in the cured resin. It can resist high-speed microchannel flow of over 466 mm/s. Figure 1 (a) and (b) show the curing process of ENT in the microchannel made by PDMS (polydimethylsiloxane) with the glass plate at the bottom. ENT 40% solution is injected in the channel. After irradiation of the focused UV light around the surface of the glass plate, the focused spot makes the cured resin area which is immobilized on the glass surface. Figure 1 (c) and (d) show the process of making air-liquid boundary. After purging the microchannel of growth media by air, the air-liquid boundary is formed around the cured resin (Fig.1(d)), since the resin is highly hydrophilic and the surface of microchannel is hydrophobic. This phenomenon is quite effective to check the solution in the microchannel. It is easy to change the growth media to the fluorescent dye around the cured resin.

3. Measurement

The remaining solution around the cured ENT is about 5.9×10^{-12} g. The solution is evaporated immediately in the opened space, however the evaporation speed of remaining solution is slowed

down in the microchannel. Figure 2 shows the evaporation rate of the remaining solution inside or outside the chip. The height of the channel of the PDMS chip is 40 μm, the width is 800 μm and the length is 10 mm. The time to change solution (from injection of air to injection of fluorescent dye) is about 20 s. The evaporation rate of the remaining solution is about 11%, so a trapped cell is protected from exsiccation.

The amount of fluorescent dye to fill the whole microchannel is about 0.025 g. Figure 3 shows an evaporation rate of fluorescent dye injected inside the microchannel. For comparison, evaporation outside chip is shown. After 3 hours, the evaporation amount of the dye is less than 5%. The time to react the cell is about 20 min, so evaporation speed inside the chip is slow enough for reaction of the cell.

4. Experimental

Experiments of fixation, isolation, continuous culture and fluorescent monitoring of yeast cell are conducted with inverted microscope installed a mercury lamp and fluorescent unit (DM 400 nm, BP 330-385 nm, BA 420). The lamp and the unit are used for curing the ENT solution and the microfluidic device made by PDMS using replica mold method is set on the stage of the inverted microscope. Figure 4 shows the result of the experiment. The sample solution mixed with yeast cells and ENT 40% solution is injected in the microchannel. A target yeast cell (ϕ 6 μm) is fixed with the cured resin by UV light irradiation as shown in Figure 4(a). The other obstacles are washed out by the cleaning flow (growth media: YPD-BROTH 5% solution) and the trapped target yeast cell is separated from the other yeast cells as shown in Figure 4(b). After the separation process, the trapped cell is cultured for 5 hours and the trapped cell is grown as shown in Figure 4 (c),(d),(e),(f),(g). After purging the air of the media in the channel, the remaining media forms air-liquid boundary around the cured resin, and cells are cultured as shown in Figure 4(h). Then fluorescent dye CFDA (5 (and 6)-carboxyfluorescein diacetate) 0.025 g, which is used for staining viable cells, is injected to fill the microchannel. The solution in the microchannel is changed from growth media to fluorescent dye as shown in Figure 4(i). After 20 min, the trapped cell is dyed as shown in Fig.4 (j).

5. Conclusions

In our previous work, we needed 0.6 g fluorescent dye to react the trapped cell on average. We succeeded in the separation and continuous culture of yeast cells as well as reaction and monitoring of the cultured cells stably. The quantity of consumed reagent is reduced from 0.6 g to 0.025 g (96%) by employing air-liquid boundary around the cured photo-crosslinkable resin made in the microchannel on average. Fluorescence straining and observation is possible with minute amount of fluorescence reagent in situ on a chip. We confirmed our method is applicable for the single cell analysis on a chip.

Acknowledgements

This work was supported by JSPS.KAKENHI(14550233)

References

[1] Arai, F., Ichikawa, A., Ogawa, M., Fukuda, T., Horio, K., and Itoigawa, K., High speed separation system of randomly suspended single living cells by laser trap and dielectrophoresis, Electrophoresis, 2001, 22 No. 2, 283-288.

[2] Arai, F., Maruyama, H., Fukuda, T., and Katsuragi, T., Fixation of microorganisms for investigation of their properties on a chip, Proc. of the Micro Total Analysis Systems 2003 (μ-TAS2003), 2003, 21-24.

[3] Arai, F., Ichikawa, A., Fukuda, T., and Katsuragi, T., Isolation and extraction of target microbes using thermal sol-gel transformation, Analyst, 2003, 128, 547-551.

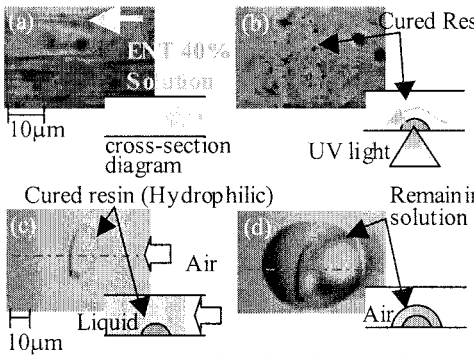

Figure 1 A micrograph and a schematic diagram of the method of air-liquid boundary formation in micro-channel. (a) Before cure. (b) After irradiation of UV light, the resin is cured. (c) Before air injection. (d) After air injection. Air-liquid boundary is formed around the cured resin which is hydrophilic.

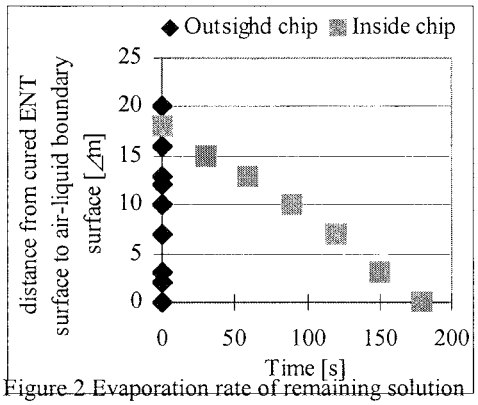

Figure 2 Evaporation rate of remaining solution

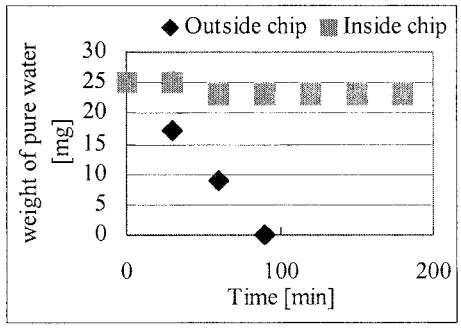

Figure 3 Evaporation rate of reagent

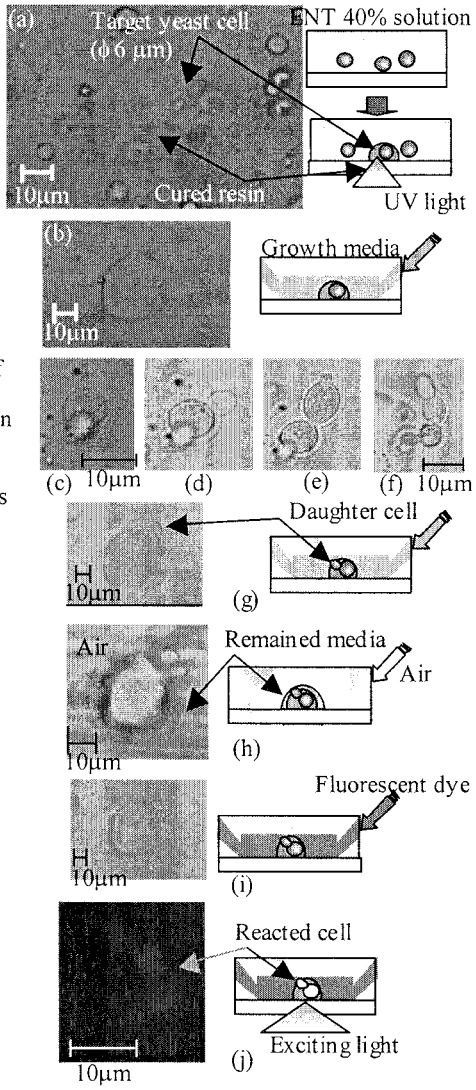

Figure 4 Result of the experiment. (a) Target cell is fixed by irradiation of UV light. (b) Injection of growth media(YPD Broth 5%). (c) Before culture. (d) After culture for 2h. (e) After 4h. (f) After 5h. (g) Before air purge. (h) After injection, purge and air- liquid boundary is formed. (i) After injection of Fluorescent dye (CFDA : 5 (and 6)-carboxyfluorescein diacetate). (j) Fluorescent monitoring of the reacted yeast cells.

SIMULTANEOUS MEASUREMENT OF MOVEMENT AND GROWTH OF SWIMMING CELLS USING ON-CHIP SINGLE-CELL CULTIVATION ASSAY

Akihiro HATTORI[1, 2], Senkei UMEHARA[1], Yuichi WAKAMOTO[1], and Kenji YASUDA[1]

[1] *Department of Life Sciences, Graduate School of Arts and Sciences, University of Tokyo, 3-8-1 Komaba, Meguro, Tokyo 153-8902 Japan*

[2] *Japan Science and Technology Agency, Kawaguchi Center Building, 4-1-8, Honcho, Kawaguchi, Saitama 332-0012 Japan*

Abstract

We have improved an on-chip single-cell microcultivation assay as a means of continuous observation of identical single swimming cells for tracking their movement and growth simultaneously. Using this system, we found the incident angle dependence of the reflective movement of swimming bacteria against the microchamber walls. We also found that the cell which stopped its growth still maintained its motility under the nutrient-free condition.

Keywords: bacterium, single cell, microcultivation, movement, incident angle, growth

1. Introduction

To understand the efficacy of medicine against bacteria is important for drug discovery process. Usually two phenotypic factors of cellular response, movement and growth, are most useful indices to estimate the effectiveness of medicine. However, it was difficult to observe identical single swimming cells for a long time. Our group has recently developed a series of single-cell-based on-chip microculture methods using microfabrication techniques. In this study, we have improved the system to monitor the movement and growth of cells by introducing a specially designed microchamber and real-time data-analysis algorithms.

2. Experimental

Figure 1 shows a schematic diagram of the system for tracking swimming cells and the microchamber for cultivation. This system mainly consists of 5 parts: (1) a microcultivation chamber array made of photo-resist on a glass slide, (2) a circulation system to supply cells in the microchambers with fresh medium, (3) optical tweezers to trap cells without contact, (4) a 60× magnitude phase-contrast optical microscopy system with time-lapse recording equipment, and (5) an image processing computer with an video I/O interface. The observed single cells were cultivated in the microchambers made of photo-resist, SU-8, on a 200 μm-thick glass slide. A semipermeable membrane lid was attached on the SU-8 microchamber array to prevent those cells from escaping from the chambers. The height of the microchamber, 5μm, was determined by considering the focal depth of the 60× objective. The planar size of the microchamber was also determined by the field of view of the microscope, which was about 120 μm × 90 μm. The images of cells were captured by an image processing computer through the video I/O interface and applied real-time image analysis to measure cell movement and its growth simultaneously. The required time for one processing cycle was less than 100 ms, which was enough to trace swimming cells.

3. Results and discussion

3.1 Incident angle dependence of the reflective movement of swimming bacteria

Figure 2 indicates one example of a 10 min trace of an isolated swimming bacterium, *Escherichia coli*, within the microchamber. The swimming cell in the microchamber either reversed its movement after it ran against the microchamber wall, or swam along the wall after hitting it. Figure 3 shows the incident angle dependence of the reflective movement of the cells. As shown in the graph, when the incident angle of the swimming cells was nearly perpendicular to the wall, the

ratio of reverse to non-reverse after hitting the wall was much higher. On the other hand, when the incident angle was not perpendicular to the wall, the ratio of reverse was almost the same as the ratio of non-reverse. The results suggest that there might be some special sensors inducing reverse movement at the poles of the cell.

3.2 Dependence of cell movement and growth on environmental changes

Figure 4 shows the transition of the movement and growth of a single *E. coli* cell under changing nutrient conditions. Under the nutrient-rich condition, while the cell maintained its growth curve for generations, the swimming speed was decreased as it elongated. When the nutrient condition was changed into nutrient-free, the growth was stopped within 20 min, while the motility of the cell was maintained over 120 min. Then, when the medium was changed into fresh one again, the cell recovered its growth and motility.

4. Conclusions

In summary, we have shown the potential of a new single-cell based cultivation assay which enable us to observe identical single swimming cells for a long time. Using this system, we can measure their movement and growth simultaneously, with environmental changes, for many successive generations.

Acknowledgements

The authors gratefully acknowledge the financial support, in part from Japan Science and Technology Agency, and in part through Grants-in-Aid for Scientific Research from the Ministry of Education, Culture, Sports, Science and Technology of Japan.

References

[1] I. Inoue, Y. Wakamoto, H. Moriguchi, K. Okano, K. Yasuda: On-chip culture system for observation of isolated individual cells. Lab Chip 1 (2001) 50-55.

[2] Y. Wakamoto, I. Inoue, H. Moriguchi, K. Yasuda: Analysis of single-cell differences using on-chip microculture system and optical trapping. Fresenius' J. Anal. Chem 371 (2001) 276-281.

[3] I. Inoue, Y. Wakamoto, K. Yasuda: Non-genetic variability of division cycle and growth of isolated individual cells in on-chip culture system. Proc. Japan. Acad. 77B (2001) 145-150.

[4] A. Hattori, S. Umehara, Y. Wakamoto K. Yasuda: Measurement of Incident Angle Dependence of Swimming Bacterium Reflection Using On-Chip Single-Cell Cultivation Assay. Jpn. J. Appl. Phys. 42 (2003) 873-875.

[5] S. Umehara, A. Hattori, Y. Wakamoto, K. Yasuda: Simultaneous measurement of growth and movement of cells exploiting on-chip single-cell cultivation assay. Jpn. J. Appl. Phys. 43 (2004) 1214-1217.

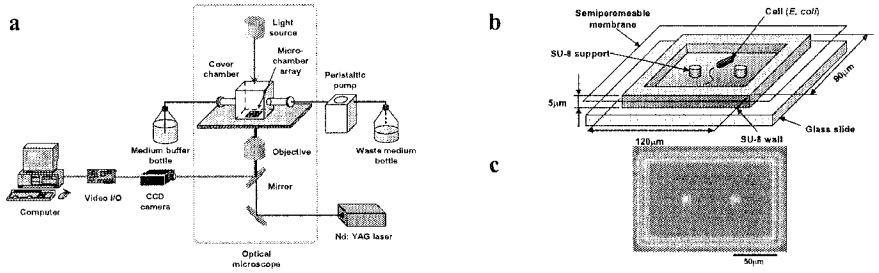

Figure 1. Schematic drawing of the system for tracing the cell movement using a microchamber: (a) system diagram, (b) schematic drawing of a microchamber (bird-view), (c) micrograph of a microchamber.

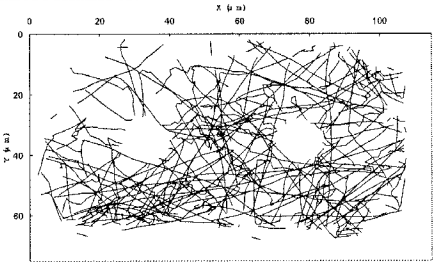

Figure 2. Trace of the movement of an isolated bacterium in the microchamber for 10 min.

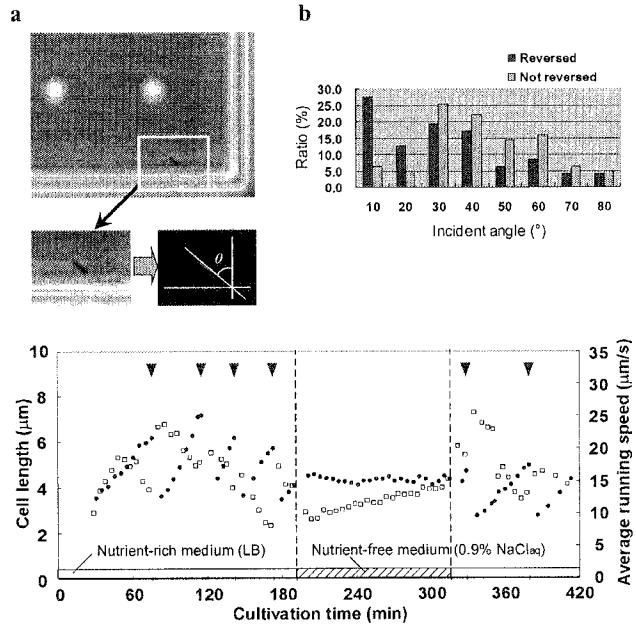

Figure 3. Incident angle dependence of reflective movement of bacteria:

(a) protocol for analyzing the incident angle against the wall,

(b) dependence of the reverse/non-reverse movement on the incident angles.

Figure 4. Transition of the movement and growth of a single *E. coli* cell under changing nutrient conditions.

QUANTITATIVE EXTRACTION OF Al $^{3+}$ IN WATER USING DISPERSED DROPLET IN T-SHAPED MICROCHANNEL

Momoko Kumemura and Takashi Korenaga

Department of Chemistry, Graduate School of Science, Tokyo Metropolitan University, 1-1, Minami-ohsawa, Hachioji, Tokyo, Japan

Abstract

In this presentation, construction of prototyping ultrafast extraction system was reported. The droplet was generated continuously in T-shaped microchannel and used for liquid-liquid extraction of Al^{3+} in water sample. The extraction was investigated by laser-induced fluorescence spectroscopy. The extraction time was approximately 15 times shorter than conventional extraction method using separatory funnel and mechanical shaking. This extraction system was applied to determination of Al^{3+} in water samples. The detection limit and the relative standard deviation were 2 μg/L (.= 3) and 5-13%, respectively.

Keywords: droplet, liquid-liquid extraction, environmental analysis, determination of aluminum, fluorescence detection

1. Introduction

Liquid-liquid extraction is one of the important procedures for obtaining chemical of interest selectively. Much of the initial work for extraction in microchip analysis have concentrated on the development of systems using single phase flow with diffusive transfer between parallel reacting fluid streams. Considering extraction efficiency, specific interface area (area/volume) is one of the dominating factors. In the parallel two-phase laminar flow, the interface area depends on aspect ratio (width/depth) in microchannel. For example, in microchip with 250 μm wide and 100 μm deep, a specific interface area was 8 mm^{-1}. On the other hand, it has been reported that a method for generating droplets at the confluent of two microchannel (T-junction) [1,2]. Applying this droplet-generation method for liquid-liquid extraction, it is possible to obtain a large specific interface area without depending on aspect ratio of microchip (droplet with diameter of 200 μm has 30 mm^{-1}-specific interface area). We demonstrated that the liquid-liquid extraction by using droplets for faster extraction. Furthermore, this extraction method was applied to determination of Al^{3+} in city water and pond water for evaluation of its validity.

2. Experimental

A microchip was purchased from Institute of microchemical technology (Kanagawa, JAPAN), which was fabricated by photolithography and a wet chemical-etching method. The microchip was composed of two pieces of pylex (c) glass plate. Each plates was a 70x30 mm rectangle. The size of a main microchannel is 600 μm (wide)-50 μm (deep). The main microchannel was confluent with the narrow microchannel. The size was 70 μm–20 μm.

A schematic illustration of droplet-formation and detection was shown in Figure 1. Aqueous Al^{3+}-2,2'-dihydroxyazobenzen (DHAB) solution was flowed as continuous phase and tributyl phosphate (TBP) was flowed as dispersed phase, which were introduced the microchip using two syringe pumps. In the microchannel, TBP-droplets were formed in the Al^{3+}-DHAB solution, and then Al^{3+}-DHAB chelate was extracted with the TBP-droplets. Al^{3+}-DHAB chelate fluoresces in the TBP-droplets, but does not in the aqueous phase. The excitation light from Ar^{+} laser (488 nm) was introduced through the microscope. And the fluorescence from the Al^{3+}-DHAB chelate in a TBP-droplet was detected by the polychrometer-multichannel photodetector system ($_{em}$= 560 nm).

3. Results and Discussion

Higuchi *et al.* developed a method for generating droplets in T-shaped microchannel [1]. They performed generation of water-droplet in oil in T-shaped microchannel network. Then, we employ the method for generation of oil-droplet in water. The size of droplet was depending on viscosity of the organic solvent and aqueous solution, therefore, first, we have generated TBP-droplet in T-shaped microchannel and estimated the size of TBP-droplet generated in Al^{3+}-DHAB solution which was used in this study. The formation of droplets was recorded by CCD camera, and the size of droplet was estimated. The volume of droplet was decreased with an increase in the flow rate of continuous phase, and that was increased with an increase in the flow rate of dispersed phase, constantly. The volume of droplet was controllable in the range from 0.6-11 nL as the flow rate of the continuous phase was varied from 16-57 mm/s (flow rate in dispersed phase was set at 25 mm/s). And, the droplet-volume was kept constant at each flow rate in continuous phase and dispersed phase.

Relationship between the fluorescence intensity and the distance of droplets from T-junction was shown in Figure 2. The diameter of a droplet on each flow rate was 140, 110, 90, 70 and 50 μm, respectively. At each flow rate, the fluorescence intensity of Al^{3+}-DHAB chelate in droplet was gradually increased and reached equilibrium. The times required to equilibrium (extraction time) were estimated at 5.4, 3.0, 1.5, 1.1 and 0.91 second, respectively. On the other hand, in the conventional extraction method using separatory funnel, the shaking time for extraction equilibrium required about 90 second (mechanical shaking with 300 times/min). Therefore, the extraction time using droplet in the microchannel was 15 times shorter than that of conventional extraction method. And, it was found that the time decreased with an increase in the specific interface area (Figure 3).

Fluorescence intensity was found to be linearly related ($r = 0.992$) to the Al^{3+}in the range of 0-80 μg/L. The detection limit and the relative standard deviation were 2μg/L (.= 3) and 5-13%, respectively. This method was applied to determine for Al^{3+} in pond water and city water. These samples were adjusted to pH 6.3 after filtration, and introduced into the microchip. The results of determination were 80 μg/L in pond water and 17 μg/L in city water, and these data were in good agreement with the conventional method.

4. Conclusion

Quickly and quantitative extraction system of Al^{3+} in water was demonstrated using droplet in T-shaped microchannel. This is the first report on a determination utilizing droplet-extraction on a microchip.

References

[1] T. Nishisako, T. Torii and T. Higuchi, Lab. Chip, 2002, 2, pp. 24-26.
[2] J. Husny, H. Jin, E. Harvey, and J. C. White, Micro TAS '03, pp. 113-116.

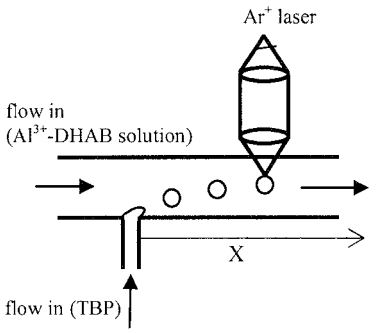

Figure 1. Schematic illustration of droplet formation at T-junction and fluorescence detection. The x-axis was set in the direction of the flow of droplet.

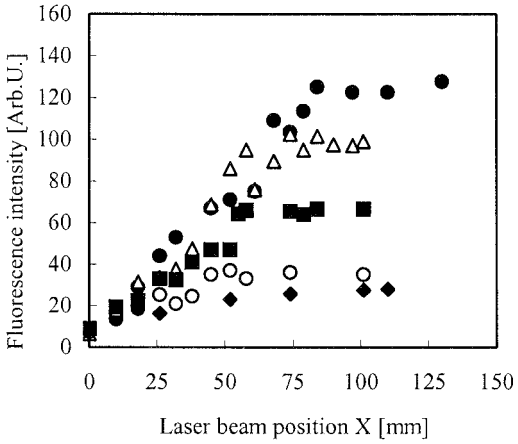

Figure 2. Relationship between distance from T-junction at different flow rate of continuous phase and fluorescence intensity.
Flow rate of dispersed phase: 25 [mm/s]
Flow rate of continuous phase:
.; 16, Δ; 26, .; 37, .; 41, ∀; 57 [mm/s]

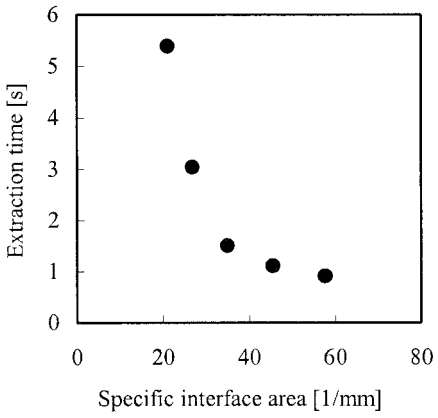

Figure 3. Relationship between specific surface area and extraction time

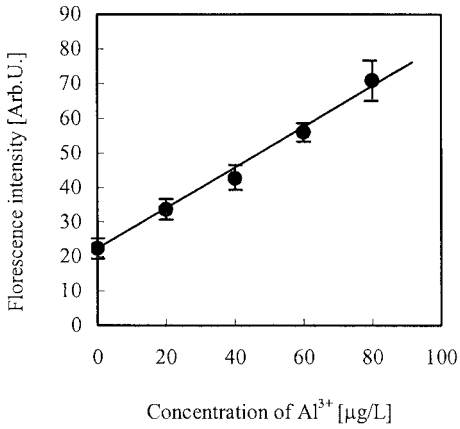

Figure 4. Quantitative extraction at 50 mm from T-junction
Flow rate of dispersed phase: 25 [mm/s]
Flow rate of continuous phase: 16 [mm/s]

SPACE- AND TEMPORAL-CONTROLLED ELECTROORGANIC SYNTHESIS WITH GLASS ELECTROCHEMICAL MICROCHIP

Naoki Sasaki[1], Takehiko Kitamori[1,2], and Haeng-Boo Kim[3]

[1] *Department of Applied Chemistry, School of Engineering, The University of Tokyo, 7-3-1 Hongo, Bunkyo-ku, Tokyo, 113-8656 Japan*

[2] *Micro Chemistry Group, Kanagawa Academy of Science and Technology, 3-2-1 Sakado, Takatsu-ku, Kawasaki, 203-0012 Japan*

[3] *Engineering Research Institute, School of Engineering, The University of Tokyo, 7-3-1 Hongo, Bunkyo-ku, Tokyo, 113-8656 Japan*

E-mail:naoki@icl.t.u-tokyo.ac.jp

Abstract

A new methodology for electroorganic synthesis (EOS) with a glass-substrate electrochemical microchip (EMC) is presented. EOS is a synthetic method, which employs electrode reaction for activation of reaction species. In this study, microelectrode-integrated EMC was applied to EOS, utilizing the advantages of EMC that can provide efficient electrolysis and well-controlled distribution of species in microchannel. As a model reaction, alkylation and Michael addition of ethyl nitroacetate (ENA) were carried out with EMC, and the formation rate of the products per unit electrode area was 400 times as fast as that in bulk scale.

Keywords: glass electrochemical microchip, electroorganic synthesis, alkylation, Michael addition

1. Introduction

In this paper, we demonstrate electroorganic synthesis (EOS) with a glass-substrate electrochemical microchip (EMC). Electrochemical methods are often used in an area of microchip chemistry, but they are employed mainly as detection techniques. In the previous paper, we succeeded in fabricating glass-substrate EMC and applying it to spectroelectrochemical detection using thermal lens microscopy [1]. Since EMC provides efficient electrolysis of analytes and regulated spatial distribution of redox products in the microchannel, EOS with EMC should be expected to open new methodology for EOS.

Figure 1 shows the concept of EOS with EMC. In EOS, starting materials are excited at electrode, and then react with substrates to form final products. In bulk scale, however, all species are in a reaction vessel, so that undesirable reactions at electrode such as re-reaction of products and side reactions of substrates occur to diminish selectivity of the desired products and current efficiency. Using EMC, these species are spatially separated from one another in microchannel, and thus EOS can proceed under space- and temporal-controlled conditions, which can be easily regulated by sizes and patterns of channels and electrodes as well as flow conditions.

To verify the concept mentioned above, we choose alkylation and Michael addition of ethyl nitroacetate (ENA) (Scheme 1) [2] as a model reaction. These reactions start from deprotonation of ENA by superoxide which is generated at the electrode and works as a base. Utilization of electrogenerated base enables these reactions to proceed under milder conditions than those in chemical activation.

2. Experimental

EMC was composed of channel and electrode substrates, which were fabricated by photolithography-wet etching techniques and by photolithography-liftoff method, respectively.

Then, both substrates were thermally bonded (Fig. 2). After bonding, Ag reference electrode was prepared by electrodeposition.

Alkylation and Michael addition of ENA were carried out as following. Acetonitrile solution containing ENA (1 mM) and nucleophile (methyl iodide in alkylation and acrylonitrile in Michael addition, 10 mM) was introduced to EMC by a syringe pump (0.2 μl/min) and electrolyzed under controlled potential conditions (-1.2 V vs. Ag). The electrode potential was controlled by an electrochemical analyzer (ALS701A, BAS). The spillage solution was collected and analyzed by GC-MS (GCMS-QP5050A, Shimadzu).

3. Results and discussion

Results are summarized in Table 1. In alkylation and Michael addition with EMC, the products were obtained with much higher selectivity and shorter electrolysis time than that in bulk scale. Current efficiency, which means the ratio of the amount of products to the amount of passed electrons, was also higher than that in bulk scale. Furthermore, the formation rate of the products per unit electrode area was 400 times as fast as that in bulk scale. These results clearly show the effectiveness of our concepts of EOS with EMC. Namely, the ratio of the electrode area to the solution volume is high in a shallow microchannel, so that efficient electrolysis of starting materials is achieved in a short time. In addition to that, only oxygen is electrolyzed at the electrode, and ENA reacts with it and subsequently with nucleophiles to form the products in the downstream of the electrode. Therefore, as shown in Fig. 1, the products are separated from the electrode spatially in EMC, and re-reaction of the products at the electrode is prevented.

4. Conclusion

We succeeded in demonstrating of the effectiveness of the present space- and temporal-controlled EOS with EMC. High selectivity and current efficiency of EOS with EMC were proved in alkylation and Michael addition of ENA. These results indicate that EOS with EMC should be a promising application for electroorganic chemistry.

Acknowledgements

This work was partially supported by a Grant-in-Aid for Scientific Research on Priority Areas (417) from the Ministry of Education, Culture, Sports, Science and Technology, Japan (no. 14050024).

References

[1] H. –B. Kim, T. Hagino, N. Sasaki and T. Kitamori, *Proceedings of μTAS 2003,* 817-820 (2003)
[2] M. E. Niyazymbetov and D. H. Evans, *J. Org. Chem,* 58, 779-783 (1993)

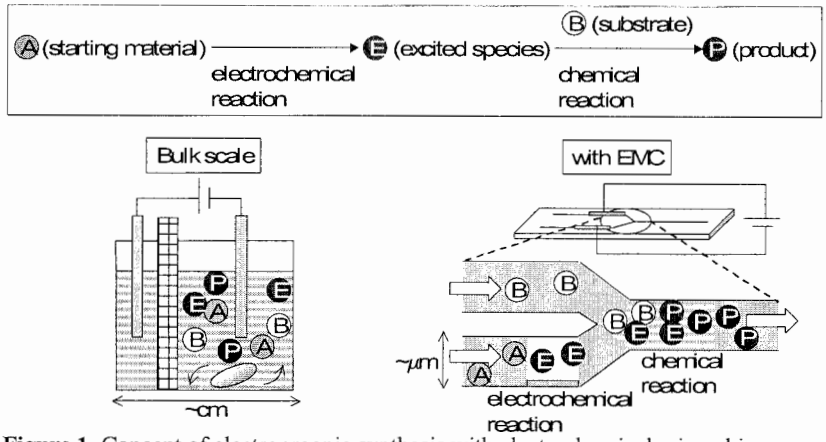

Figure 1. Concept of electroorganic synthesis with electrochemical microchip.

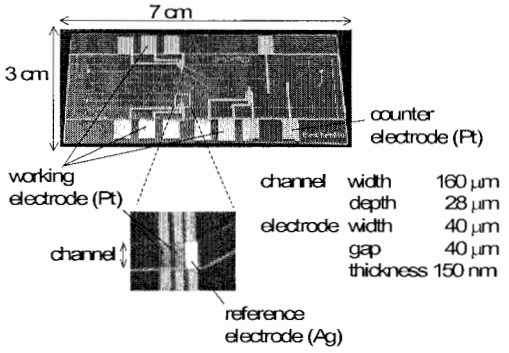

Figure 2. EMC used in this study.

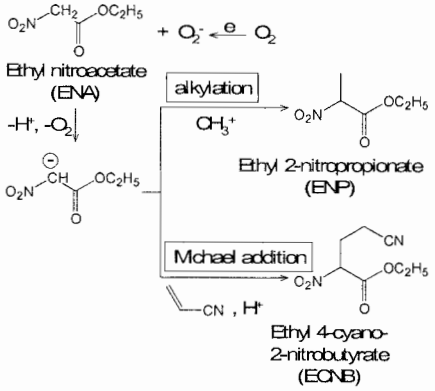

Scheme 1. Electrochemical alkylation and Michael addition of ENA.

Table 1. Results of alkylation of ENA[a].

		Time (s)	Conversion[b] (%)	Selectivity (%)	Current efficiency[c] (%)	V[d] (mol m^{-2} s^{-1})
Alkylation	Bulk scale	15000	87	9	4	8.3 x 10^{-7}
	With EMC	0.019[e]	48	54	35	1.4 x 10^{-4}
Michael	Bulk scale	7200	62	8	0.6	1.1 x 10^{-6}
Addition	With EMC	0.032[e]	32	80	48	1.4 x 10^{-4}

[a] Electrolyses were carried out under controlled potential conditions (-1.2 V vs. Ag), electrolyte 0.1 M TBAP. Solutions were oxygen-saturated. [b] Based on ENA. [c] Based on main products.
[d] Formation rate per unit electrode area. [e] Resident time on the electrode.

MICROCHIP FLOW CYTOMETER WITH INTEGRATED POLYMER OPTICS FOR FLUORESCENCE ANALYSIS OF CELLS

Zhenyu Wang, Jörg P. Kutter and Anders Wolff
MIC-Dept. of Micro and Nanotechnology, Technical University of Denmark, Bldg 345 east, DK-2800 Kongens Lyngby, Denmark

Abstract

Flow cytometry is a powerful method in biophysical research for measurements of microparticles, such as cells and bacteria. Here we report fluorescence measurements of cells and beads based on a microchip flow cytometer with integrated polymer optical elements (waveguides, lenses and fiber-to-waveguide couplers). All the optical elements and the microfluidic system were defined in one SU-8 polymer layer by standard photolithography. Different signals (forward scattering, large angle scattering and fluorescence) were measured simultaneously for each bead or cell. In 1D and 2D fluorescence signal histograms, different beads or cells can be clearly distinguished. The microsystem can be applied for analyzing fluorescence signals of different kinds of particles and cells, and can easily be integrated with other microfluidic components.

Keywords: Polymer integrated optics, SU-8, Flow cytometry, Fluorescence detection

1. Introduction

Flow cytometers - versatile tools for measuring particles and cells, widely used in clinical diagnostics and biology - have been realized on microchip [1]. Recently, several optical elements were integrated in microfluidic systems to enhance the sensitivity and overcome alignment problems during the measurements [2][3]. Fluorescence is commonly used in flow cytometers for labeling cells. In this study, we present fluorescence measurements of different cells and beads using a novel microchip flow cytometer with integrated polymer optics.

2. Chip structure

In the microchip, all the fluidic and optical systems (Figure 1) were defined by standard lithography on a single SU-8 layer on a glass substrate. Since there is only one mask step, the chip fabrication is rather quick. All the fabrication and packaging can be finished in one day.

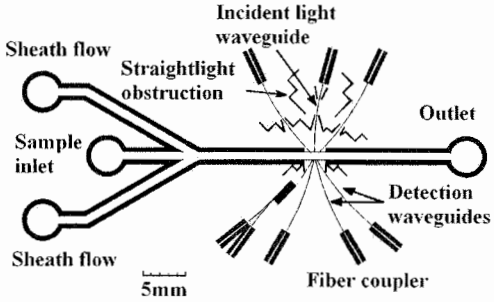

Figure 1. Overview of the chip structure, the flow channel width is 466μm. Some straight light obstruction elements are included to reflect unwanted direct light.

In the microchip flow cytometer, particles or cells were hydrodynamically focused in the channel center by two sheath flows. Incident light from an Ar ion laser (488nm, as the excitation light) was focused on the center of the channel by an integrated SU-8 lens (Figure 2).

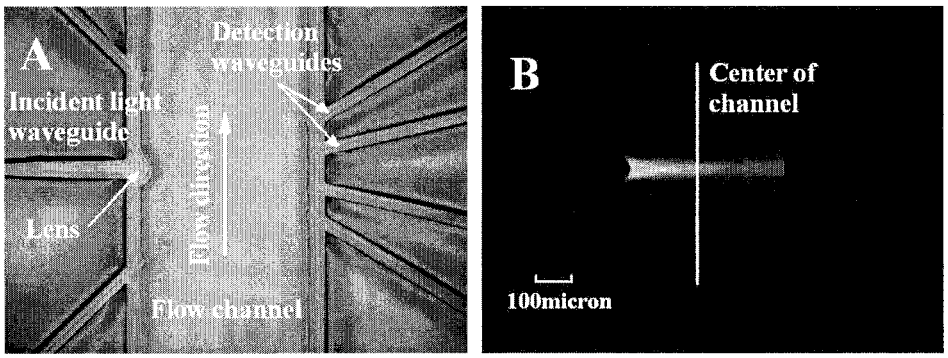

Figure 2. A: Image of the integrated polymer optical system; **B:** Visualization of the light path.

The incident beam light path was visualized by filling the channel with a green fluorescence dye (Figure 2B). In the detection area several waveguides were designed for collecting light scattered from the particles at different angles (Figure 1 and Figure 2A).

3. Results and discussion

The chip was initially tested using green fluorescence beads. Fluorescence light emitted from the beads was measured using one of the waveguides and a PMT with a band pass filter (525 nm). The distribution of the fluorescence signal intensities (peak heights) for two different sizes of fluorescence beads (5.7 and 10.8 μm diameter) is shown in Figure 3A.

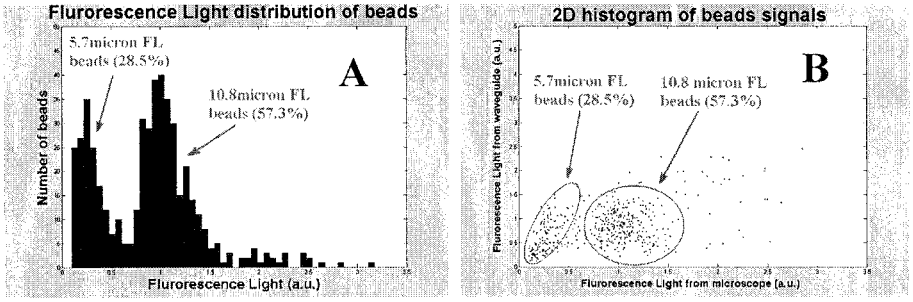

Figure 3. A: Fluorescence signal distribution of two different sizes of fluorescence beads. **B:** Fluorescence signal measured using a waveguide and using a microscope for the two different sizes of fluorescence beads.

The two kinds of beads can clearly be distinguished and the ratio of the fluorescence signal intensities is about 1:3, which is close to the ratio of surface areas for the two kinds of beads. An inverted fluorescence microscope was used for fluorescence reference measurements (Figure 3B). There is a good correlation between the fluorescence signal intensity measured using the waveguide and using the microscope. The standard deviations of the signals are also similar.

Rainbow trout red blood cells (RTRBC) and chicken red blood cells (CRBC) were also measured using the microchip flow cytometer. After staining the cell nuclei with propidium iodide (PI) [4] the cells were measured on the microchip flow cytometer. Typical fluorescence (617 nm) and large angle scattering signals are shown in Figure 4.

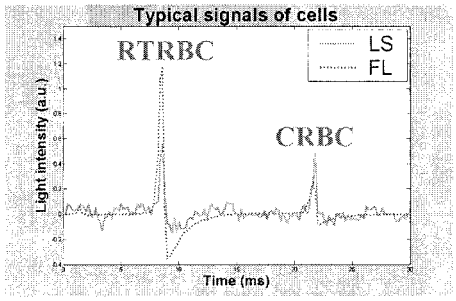

Figure 4. Typical large angle scattering (LS) and fluorescence (FL) signals from two different types of red blood cells.

Because the sizes of both types of cells are close to 3μm there was little difference in the scattering signals. In contrast, the fluorescence signal was quite different for the two kinds of cells, the fluorescence signals intensities of PI dyed RTRBC are stronger than PI dyed CRBC about 3 fold, which is in agreement with the literature [5]. From the 1D and 2D distributions of the fluorescence light, the two kinds of cells can also clearly be distinguished (Figure 5).

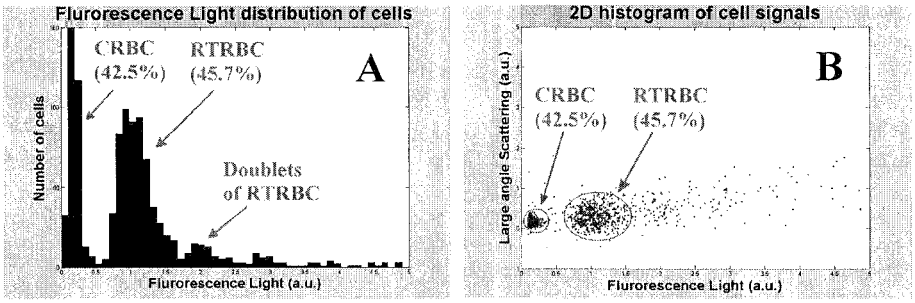

Figure 5. A: Fluorescence signal distribution of two different types of red blood cells (CRBC and RTRBC). **B:** 2D distribution of large angle scattering and fluorescence signals for the two different types of red blood cells.

4. Conclusions

In conclusion, the microchip flow cytometer presented here can be applied to measure fluorescence and light scattering of both particles and cells. This microchip flow cytometer can achieve high performance for analyzing fluorescence labeled particles and cells. And the chip fabrication and packaging processes are very simple and reliable.

Acknowledgements

Many thanks to J.K. Larsen and J. Christiansen for kindly providing us cells and staining methods.

References

[1] E. Altendorf, et al. Tranducers 97, 531-534 (1997).
[2] K.B. Mogensen, et al. Applied Optics, **42**(19), 4072-4079 (2003).
[3] Z. Wang, et al. Lab on a Chip, **4**, (Advance Article), DOI: 10.1039/b400663a (2004).
[4] K. J. Larsen, et al., Cytometry, **12**, 429-437, (1991).
[5] L. L. Vindelov, et al., Cytometry, **3**(5), 323-327, (1983).

RAPID POLYMERASE CHAIN REACTION IN POLYMERIC MICROCHIPS DRIVEN BY FERROFLUIDS

K.S. Drese[1], G. Münchow[1], D. Dadic[1], F. Doffing[1], S. Hardt[1], O. Sörensen[1], T. Müller[2] and A. Klein Vehne[2]

[1] *Institut für Mikrotechnik Mainz, Carl-Zeiss-Str. 18-20, 55129 Mainz, Germany*

[2] *Evotec Technologies, Merowingerplatz 1a, 40225 Düsseldorf, Germany*

Abstract

A chip based PCR device is presented capable of rapid temperature ramping and handling of sample volumes in the microliter and nanoliter range. The PCR chip, existing of PMMA or COC, comprises of a microchannel that is positioned above three temperature zones. Inside this microchannel the PCR sample plug is driven precisely by a ferrofluidic actuator for over 40 cycles. Computer simulations suggest that the sample plugs are heated or cold on a time scale of some ten milliseconds when transported to a different temperature zone. Hence the thermal limitations on the speed of the system are minimized. The system was developed on a modular platform that can also handle other microfluidic tasks like extraction and preparation of the master mix.

Keywords: PCR, amplification, ferrofluid, fluid handling, modular

1. Introduction

Since the discovery of the Polymerase Chain Reaction (PCR) for amplification of nucleic acids and subsequent automation of the process, there have been many attempts to improve its performance relating to time and reagents consumption. These PCR-systems were not only realized in macroscopic systems but also on microchips [1,2]. Nevertheless most of the microfluidic systems either lead to large cycle heating times or to expensive setups for large scale applications due to the complex manufacturing processes.

The enzyme based PCR reaction requires three different temperature levels. We have developed a novel miniaturized and fast PCR-system based on a plug-flow principle. The setting of different PCR protocols regarding to number of cycles, temperature ramps, the duration in each temperature zone and of course the temperature of each area itself can easily be done by software control. Thus it is an ideal tool for process optimization.

2. Design and fabrication

In order to avoid cross-contamination of different samples, a PCR chip should ideally be designed as a disposable and the amplification channel should be used only once. Due to their low material and processing costs polymers are perfectly suited for corresponding Lab-on-a-Chip applications. The feasibility of PCR amplification in polymer chips was proven earlier by Yang et al. [2]. The design concept which is studied in this article and was realized in polymers is sketched in Fig. 2. The ferrofluidic actuator [3] utilizes the typical properties of a ferrofluid (Ferrofluidics APG 047n) which is embedded in small channels and can be moved by an external permanent magnet attached to a step motor, see Fig. 4. The sample plug is surrounded by air and stands in pneumatic contact with the actuator. Through pneumatic transduction the plug is periodically transported in the center of each zone as appropriate.

As noted by Giordano et al. [5], among others, the time required for thermal ramping usually determines the time scale of a PCR. Under these conditions a reduction of the cycle times can only be achieved when the heating and cooling of the sample volume is speeded up. Typical heating and cooling rates of conventional thermocyclers are in the range of 2-10 K/s [6]. One of the drivers behind the development of the PCR system presented here is the reduction of the thermal ramping time scale. A temperature differing by less than 1 K from the wall temperature is reached after only

80 ms. The rapid heat transfer from the channel walls to the plug is due to two different effects. On the one hand, the small thermal diffusion path allows a rapid heating by heat conduction. On the other hand, the recirculation flow within the pulg speeds up heat transfer additionally by convection.

In a first experiment the temperature distribution on the PCR chip was measured using a infrared camera (FLIR ThermaCAM SC 500). For the simplest possible design, namely a straight channel in an unstructured chip, we could show that a worst-case estimate for the temperature variation over the plug is below 1.4 K. We obtained it by evaluating the temperature span covered by the bands. The real temperature variation over a sample plug is smaller than that, since owing to the higher thermal conductivity of water compared to the polymer material of the chip, a thermal equalization occurs.

The chips are manufactured by injecting molding and available as blanks (64x43mm) in, e.g., Poly methyl methacrylate (PMMA) and Cyclo olefin copolymer (COC). The different channel structures are transferred to the polymer chip by ultra-precision milling (Precitech Nanoform 350) and finally, the chips are sealed with a polymeric foil of 125 µm thickness. The complete setup is placed on a metal rack, Fig. 1, which also provides the housing of three cupper heating blocks and additional microfluidic modules. The heating is controlled by thermocouples, heating cartridges which are inserted in each heating block and by a control software (LabView, National Instruments).

3. Experimental tests

For the first PCR test series we utilize a conventional PCR-Kit distributed by Sigma (P 8115) and purified, pre-amplified DNA obtained from Evotec Technologies (Düsseldorf, Germany). In order to have enough sample volume for a following agarose gel electrophoresis we choose a channel dimension of 0.4 mm in height and 2.0 mm in width which yields a sample volume of about 8 µl. Compared to conventional thermocyclers, the channels of microfluidic PCR chips are characterized by a significantly larger surface-to-volume ratio. Only by a surface treatment of the polymeric material with bio-compatible substances a creation of a reaction supporting environment for the PCR reagents was possible. Without a coating of the microchannel we did not obtain any PRC product and found out that certain reagents immobilized on the channel surface or got denatured. After coating and 35 PCR cycles the sample was removed from the channel and analyzed by gel electrophoresis and ethidium bromide colouring. We found definite PCR bands of the analyzed mlh-1 gene, Fig. 3, and could show that a PCR can be done within 120 seconds. The additional transport time of about 180 seconds at present can easily be reduced by using a different motor assembly. The time spent in the individual temperature zones can be reduced to approximately one second and is basically limited by the minimal bio-chemical reaction time of one PCR step. However, this acceleration leads to a reduction of the amplified DNA quantity [4]. But spending more than five seconds in each temperature zone the fluorescence intensity is only slightly reduced compared to a sample of a conventional PCR cycler.

4. Conclusions and outlook

The device allows for rapid temperature ramping and is able to process sample volumes in micro- or submicroliter range. An optimization of chip design to minimize the thermal variation over the sample plug will be included by increasing the thermal conductivity in the temperature zones and by decreasing the conductivity between the different areas Experiments focusing at optimizing the PCR protocol of this system are currently under way. In further test series the sample volume will be reduced and analyzed by the Insight-System, a fluorescence microscope system for molecular analysis developed by Evotec OAI. The use of transparent polymer chips and a flouorescence microscope should also allow for performing real time PCR.

Acknowledgements

The work was supported by the German Ministry of Research and Education, grant number 16SV1355.

References

[1] M. Kopp, A. deMello and A. Manz, *Science* **280**, 1046-1048 (1998).
[2] J. Yang, Y. Liu, C.B. Rauch et al., *Lab Chip* **2**, 179 (2002).
[3] O. Sörensen, K.S. Drese and S. Hardt, MicroTAS '03, pp. 1029-1032.
[4]Kopf-Sill, US-Patent 00/08800 (1999)
[5] B.C. Giordano, J. Ferrance, S. Swedberg et al., Analytical Biochemistry **291**, 124 (2001).
[6] I. Schneegaß and J.M. Köhler, Reviews in Molecular Biotechnology **82**, 101 (2001).

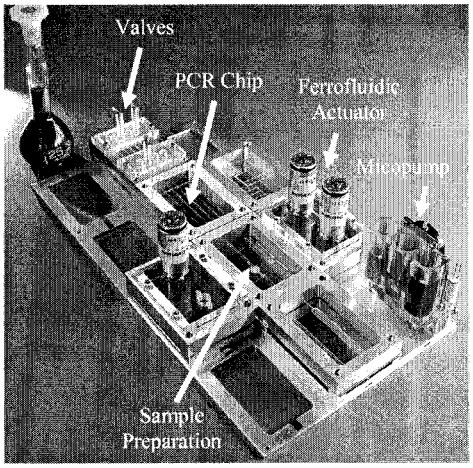

Figure 1. Complete structure of the modular microfluidic system. It contains up to twelve modules, ferrofluidic actuators, micropumps, valves and reservoirs as well.

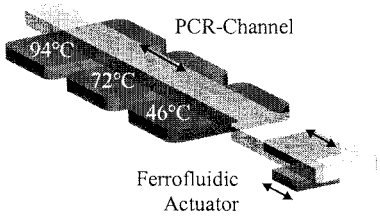

Figure 2. Transport principle of the PCR system. By the movement of the magnet a simultaneous movement of the ferrofluid above and, due to the pneumatic connection, of the sample plug is been generated.

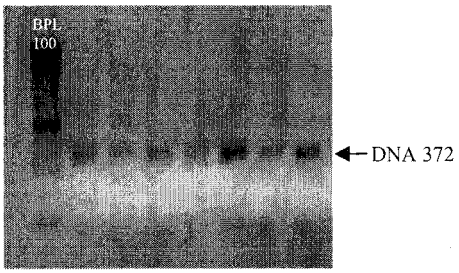

Figure 3. PCR results of the analysed mlh1-Gene with 372 bp during a test series.

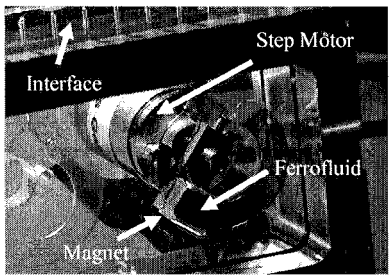

Figure 4. Ferrofluidic actuator for positioning the sample plugs with high accuracy via a fluidic interface

PROTEIN MICROCHIP BIOASSAY WITH DUAL FLUORESCENT- AND MALDI READ-OUT.

David Finnskog[1], Anton Ressine[1], Thomas Laurell[1] and György Marko-Varga[2]
[1]*Dep. of Electrical Measurements, Lund University, P.O. Box 118, S-221 00 Lund, Sweden*
[2]*Dep. of Analytical Chemistry, Lund University, P.O. Box 118, S-221 00 Lund, Sweden*

Abstract

The present work demonstrates the development of pore chip protein arrays (PCPA) based on dual-readout configuration, fluorescence imaging and MALDI-TOF MS. In this way both affinity binding and mass identity is derived.
PCPA was tested both for FITC-labelled antigen both large protein (IgG) and peptides (Angiotensine I,II and Renin).

Keywords: immunoassay, fluorescence readout, MALDI-TOF read-out

1. Introduction

Protein Microchip Array technology makes it possible to examine patterns of protein expressions and modifications. Current technologies such as two-dimensional gel electrophoresis (2-DE) in combination with mass spectrometry allows the identification of biologically relevant proteins with high resolving power, but has also considerable limitations. Most spots observed in 2-DE are from high abundance proteins while low signaling proteins are highly suppressed. Protein microarrays have a potential to speed up the discovery of new markers and targets of interest to the pharmaceutical industry. The technique is also readily compatible with high-throughput applications.

2. Experimental

Microarrays were formed by spotting aRIgG, with a concentration of 1 mg/ml diluted in PBS, in 40 μm droplets onto the macroporous silicon chips using the in-house developed chip based piezoelectric microdispenser and a computer controlled arraying station. The diameter of single droplets was measured by stroboscopic imaging and the volume of a droplet was calculated to be about 100 pL. In all experiments microarrays were formed by dispensing one droplet per spot in order to keep the spot area as small as possible.
Fluorescence microscope imaging was performed in order to evaluate the level of bioactive capture antibodies immobilized onto the macroporous silicon. Images were grabbed via a confocal microscope. Mean fluorescence intensities of the spots were measured and compared for different amounts of immobilized capture antibodies and for different concentrations of probe molecule solution. The MALDI-TOF analysis was performed directly on the porous silicon target after careful addition of matrix.

The porous silicon microchip developed and studied has shown the ability of sample enrichment due to its hydrophobic properties. Further, it generates highly homogenous sample spots.

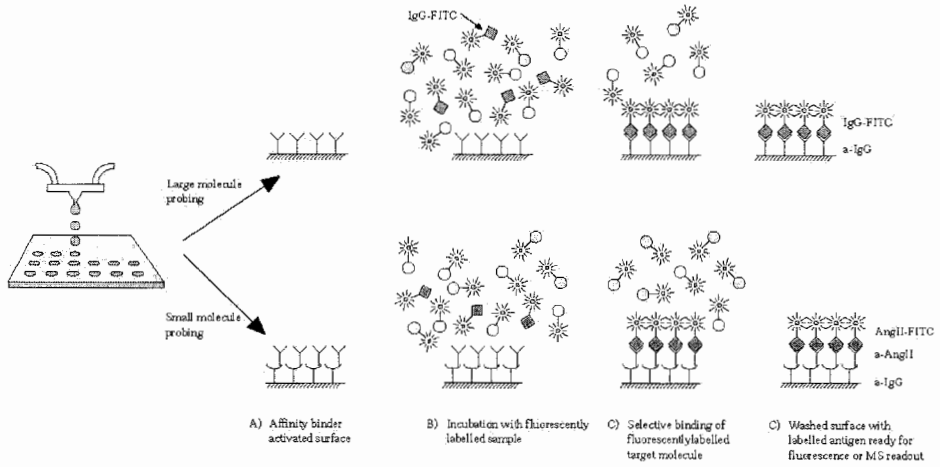

Figure 1. Principles of immunoassays for large proteins (top) and for low molecule weight peptides (lower).

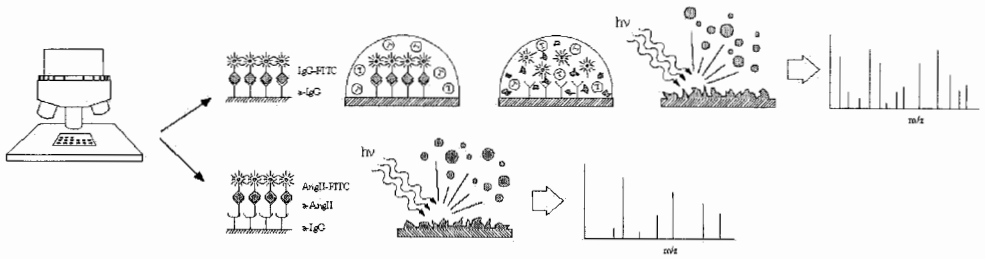

Figure 2. MALDI-MS analysis of large proteins after enzymatic digestion (top) and direct analysis of peptides (lower).

Highly packed assayspots in combination with a low fluorescence background, makes it ideal for fast quantitative measurements by fluorescence microscope read-out. The developed microchip has also been used for identification of antigen peptides and proteins using matrix assisted laser desorption/ionisation mass spectrometry (MALDI MS).

For the identification of proteins, an enzymatic digestion takes place directly on the chip surface prior to MALDI MS analysis, (peptide mapping), giving more accurate identification of high molecular weight proteins.

Porous silicon microchip arrays were manufactured by back-side illumination of doped silicon wafers in a mixture of hydrofluoric acid and dimethylformaline. Current was passed through the silicon wafer to initiate and facilitate porous silicon layer formation.

The novel principle described encompasses immunoassay and MALDI read-outs. Examples are given of Angiotensine II- and Rabbit IgG assays, illustrating low-and high molecular weight antigens. For both assays the corresponding antibody was dispensed with a microdispenser on the chip. The next step was incubation with fluorescence tagged (FITC) peptide or protein.

3. Results and discussion

By a combination of fluorescence and MALDI readout it was possible to use fluorescence readout to make pre selection of relevant spots based on a fluocescent microarray immunoassay that would reduce non informative MALDI analysis and lower the amounts of saved MS data in a second analysis step.

High density antibody arrays (> 4000 spots/cm^2), were dispensed on the PCPA, using the in-house developed piezo-electric microarray station.

The dual readout protein microarray is demonstrated on both peptides and proteins. A dedicated protocol for mapping inflammatory peptides belonging to the Renin pathway has been demonstrated in human plasma. Also, an example of large size protein identification was successfully performed on the PCPA by performing an on-target digest after completed fluorescence assay, followed by PMF MALDI-TOF MS.

The fluorescence read-out sensitivity was down to single nM concentrations. MALDI-MS identification measurements were done in 10 nM concentrations. The PCPA surface shows good characteristics for direct MALDI-TOF analysis. The detection limit for Angiotensin II on the chip was as low as 500 zmol.

4. Conclusions

The advantages of the PCPA surface for fluorescence readout can be summarized as the following:

1. Reduced spot size due to low wetting properties (enabling high density arraying)
2. Homogenous spots that can be read by automated methods, (fluorescence/MALDI)
3. Low fluorescence background
4. Silicon offers a wide range of possibilities for coupling of biomolecules by physical adsorption or by chemical derivatisation
5. The PCPA surface showed advantageous properties in terms of peptide sensitivities for Ang I with good signal to noise ratio.

References

[1] Ressine A, Ekstrom S, Marko-Varga G and Laurell T, Anal. Chem; 2003, 75 (24), 6968-6974
[2] Finnskog D, Ressine A, Marko-Varga G and Laurell T, J. Prot. Research 2004, accepted

A METHOD FOR EXTREMELY RAPID REACTION OPTIMISATION USING A CONTINUOUS FLOW MICROREACTOR WITH ON-LINE RAMAN SPECTROMETRY

Shee-Ann Leung, Richard F. Winkle, Robert C.R. Wootton* and Andrew J de Mello*
** Dep. of Chemistry, Imperial College, Exhibition Road, South Kensington, London, SW7 2AY, United Kingdom*

Abstract
A microfluidic system is described which can be used to perform reaction optimisation in real time.

Keywords: ***Optimisation, Raman, Oxidation, Catalyst.***

1. Introduction

The optimisation of a chemical process is an extremely expensive procedure, requiring a large investment of time. Performing optimisation using batch reactions, even performed in parallel, is a long process, which must then be followed by scale-up studies for reaction viability on the large scale. With this in mind we chose to study the use of microreaction technology to perform reaction optimisation in real time.

2. Experimental

We present a method for the extremely rapid gathering of optimisation data using a continuous flow microreactor and online Raman spectrometry. This system allows variations in reaction conditions to be performed in real time. The use of microreactors also allows for any reaction to be scaled-out without changing the reaction parameters.[1]

Previous work at Imperial[2] has shown the utility of monitoring reactions using Raman spectrometry, a method complementary to IR spectrometry but which can operate in a glass device. We present herein the first use of on-line Raman spectrometry to gather optimisation data in real time from a synthetically useful system.

The system studied was the catalytic oxidation of a secondary alcohol using the tetra-N-propylammonium perruthenate (TPAP)/N-methylmorpholine-N-oxide (NMO) oxidant system.[3] The oxidation of isopropanol to acetone was chosen as a model reaction illustrating a typical secondary alcohol substrate.

Reactants were motivated through the chip under hydrodynamic flow and studies undertaken to assess the optimum mixture of oxidant to substrate and catalyst to oxidant. Schematics of these experimental setups are shown. Reagents were mixed using high flow multilaminar micromixers , then the catalyst was extracted by in-line silica filtration and the Raman spectrum measured using an on-line confocal Raman microscope. In the initial configuration a set mixture of TPAP and NMO was titrated against isopropanol at various diferential flow rates. The schematic of this setup is shown in Figure 1a. In a subsequent configuration, catalyst and co-oxidant in vaiable ratio were mixed with a fixed ratio of isopropanol. A schematic of this setup is shown in Figure 2a.

3. Results and discussion

Data for the optimal oxidant dosage could be generated very rapidly. Indeed the data shown could be generated within the space of 5 minutes. The data was collected and output as a surface plot of Raman intensity vs. flow rate of oxidant and Raman shift, (Figure 1b). This valley plot allows the rapid interpretation of the experimental data.

Similarly data for the estimation of catalyst turnover and the investigation of catalyst exhaustion could be generated using a slightly reconfigured system. This data (Figure 2b) allows the

calculation of catalyst turnover rates and the estimation of optimal catalyst loading.

4. Conclusions

A microfluidic system for the rapid optimisation of catalytic systems has been described. The system can be used to perform real-time reaction optimisation and catalyst loa determination.

Acknowledgements

RFW is grateful to Syngenta. Raman Microscope courtesy of Prof. Bill Griffith.

References

[1] K.F Jensen,. Chem.Eng. Sci., 2001. **56**(2): p. 293-303

[2] R. Fortt, R.C.R. Wootton, A.J. de Mello *Micro Total Analytical Systems* 2002, (**2**) 850.

[3] S.V. Ley, *Synthesis* 1994, **7**, 639.

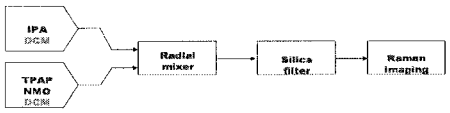

Figure 1a. A schematic of the initial experimental setup. Oxidant mix and substrate are combined and the transformation monitored online by Raman spectroscopy

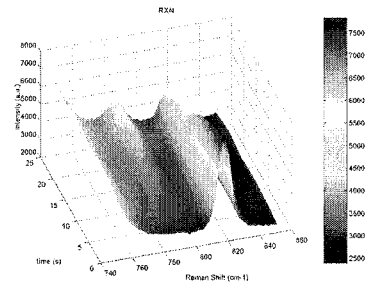

Figure 1b. Valley plot showing the transformation of isopropanol to acetone using a fixed oxidant to catalyst ratio.

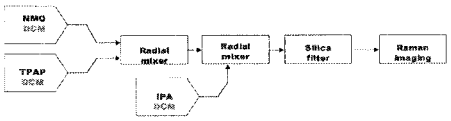

Figure 2a. A schematic of the subsequent experimental setup. Catalyst and co-oxidant are combined in variable ratio and mixed with a fixed ratio of substrate. The transformation was monitored online by Raman spectroscopy

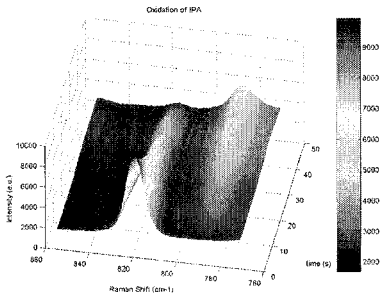

Figure 2b. Valley plot showing the transformation of isopropanol to acetone using a variable oxidant to catalyst ratio.

SUZUKI-COUPLING REACTION USING IMMOBILIZED CATALYST MEMBRANE MICROCHIP

Masaharu Ueno[1], Shinta Moriya[1], Hideaki Hisamoto[1, 2], Takeshi Nakai[3], Yasuhiro Uozumi[3] and Takehiko Kitamori[1, 2]

[1] *Dept. Appl. Chem., Schl. Eng., Univ. Tokyo, 7-3-1 Hongo, Bunkyo, Tokyo 113-8656, Japan*

[2] *Kanagawa Academy of Science and Technology, 3-2-1 Sakado, Kawasaki 213-0012, Japan*

[3] *Institure for Molecular Science and The Graduate University for Advanced Studies, Nishi-Gonaka 38, Myodaiji, Okazaki 444-8585, Japan*

Abstract

Here we report a design and synthesis of a chemically functional polymer membrane by multilayer flow inside a microchannel and an interfacial polycondensation reaction. Large membrane structures were successfully prepared by using organic/aqueous two-layer flow inside the partial surface silane modified asymmetric microchannel. Furthermore, palladium catalyst was immobilized on the side of the membrane surface to integrate the chemical transform function onto the inner-channel membrane. By using the palladium catalyst immobilized microchip, we demonstrated Suzuki-coupling reaction of iodobenzene with phenyl boronic acid. The polymer membrane prepared inside the microchannel has an important role in ensuring stable contact of different liquid / liquid phases and the permeated chemical species.

Keywords: partial surface modification, nylon membrane, catalyst immobilization, Suzuki-coupling reaction

1. Introduction

Microchip technology or microreaction technology using microfabricated devices has been the focus of much attention in recent years. However, there is no example of integrating some chemical processes as organic syntheses in microchip only by the one to introduce the solution and made to react in a microchip simply. As one of the solutions of problems, we thought the polymer membranes supported catalyst in the microchannel. It could be possible in this system not only reacts but also separates in on chip.

We have succeeded to integrate a nylon-2, 10 in a microchannel by an interfacial polycondensation (Fig. 1) and surface modification by a horseradish peroxidase as a biological catalyst [1]. However, it was difficult to stabilize the interface, we could not synthesis large membrane in microchannel. To improve this problem, we applied partial surface modification method to stabilize the interface (Fig. 2) [2]. In this method, an asymmetric microchannel, which has shallow and deep channels, was prepared. And silane reagent solution was introduced by capillarity. By using this method, interfacial area at the contact point between the shallow and deep channels were stabilized, and we enabled to integrate the large membrane in microchannel.

2. Experimental

Surface modification of the inner channel membrane by catalyst molecules is one promising way to integrate complicated and sophisticated chemical processes involving substrate permeation and chemical reaction. The nylon membrane in microchannel was prepared by adipoyl chloride in 1,2-dichloroethane (0.01 M) and hexamethylenediamine in 0.1 M NaOH solution (0.01 M).

Membrane structure formed by using organic / aqueous two-layer flow, then modified by diphenylphosphin amide, and palladium catalysts were immobilized by P-Pd chelate.[3] The quantity of immobilized palladium (1.15 $\mu g/mm^2$) were measured by ICP-AES analysis. We employed Suzuki-coupling reaction of iodobenzene **1** (1.0×10^{-3} M) with phenyl boronic acid **2** (1.0×10^{-3} M) in the presence of a palladium complex immobilized membrane microchannel (Scheme 1). This reaction was not react without base, and usually carried out under organic / aqueous two phase conditions. However, when the base components were transmitted by the membrane, it could be able to synthesis without separation (Fig. 3).

3. Results and discussion

We employed the Suzuki-coupling reaction using this palladium immobilized microchannel. Reaction was preceded under this condition, and we obtained the desired product without separate from two phases mixture. When using the palladium non-immobilized membrane microchannel (Fig. 1), coupling reaction were not occurred.

4. Conclusions

In conclusion, we succeed efficient method to synthesize a large membrane in maicrochannel by using partial surface modificated asymmetric microchannel. And we employed the Suzuki-coupling reaction using this palladium immobilized membrane microchannel. The proposed method of preparing the polymer membrane can be applied for other starting matrixes possessing two reactive sites. Surface modification chemistry may also be applicable. Furthermore, parallel dual membranes are expected to be applied for the efficient multistep synthesis required for general organic chemistry. These applications are currently under investigation.

Acknowledgement

This work was partially supported by a Glant-in-Aid for Creative Scientific Reserch (13GS0024), from Japan Society of the Promotion of Science (JSPS).

References

[1] Hisamoto H, Shimizu Y, Uchiyama K, Tokeshi M, Kikutani Y, Hibara A, Kitamori T *Anal. Chem.* **75**, 350 (2003).

[2] Hibara A, Iwayama S, Ueno M, Kikutani Y, Tokeshi M, Kitamori T *Proeeding of the μ-TAS' 2004 Symposium* (2004)

[3] Uozumi Y, Nakai Y *Org. Lett* **4**, 2997 (2002).

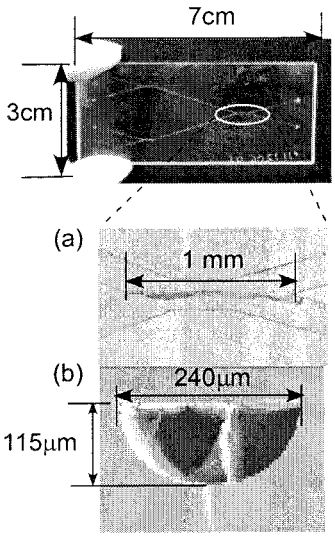

Figure 1. Previous membrane microchip (a) overvie, (b) cross-section

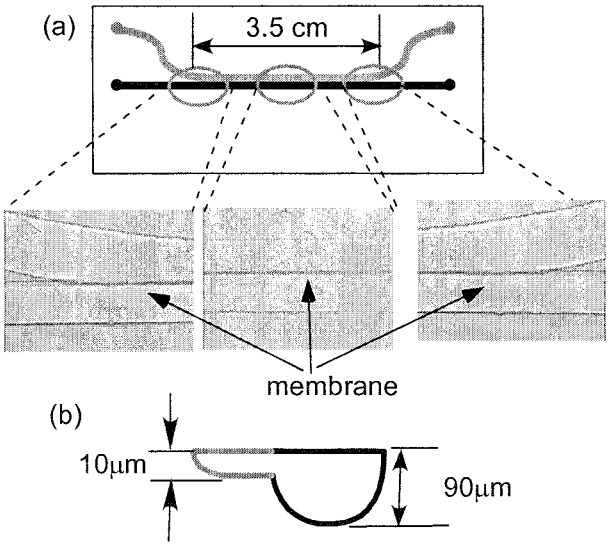

Figure 2. (a) membrane synthesis in partial surface modificated asymmetric microchannel. (b) cross-section image of asymmetric microchannel

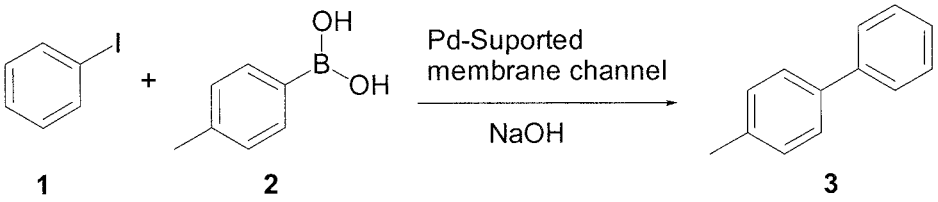

Scheme 1. Suzuki coupling reaction

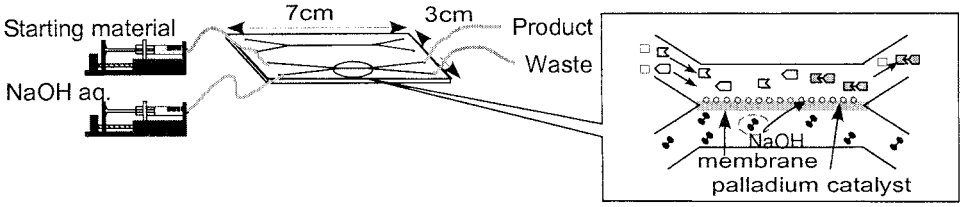

Figure 3. Sophisticated chemical processes involving substrate permeation and chemical reaction.

MEDIATED AMPEROMETRIC ASSESSMENT OF ENZYME ACTIVITY IN LIVING *S. CEREVISIAE* CELLS IMMOBILIZED ON PLATINUM MICRO-BAND ELECTRODE CHIP

Arto Heiskanen[1], Christer Spégel[1], Julia Yakovleva[1], Ted Johanson[2], Milena Koudelka-Hep[3], Bärbel Hahn-Hägerdal[2], Jenny Emnéus[1] and Tautgirdas Ruzgas[1]

[1]*Dept. of Analytical Chemistry, Lund University, P.O. Box 124, S-22100 Lund, Sweden*
[2]*Dept. of Applied Microbiology, Lund University, P.O. Box 124, S-22100 Lund, Sweden*
[3]*Inst. of Microtechnology, Université de Neuchâtel, Rue Jaquet Droz 1, 2007 Neuchâtel, Switzerland*

Keywords: microelectrode, amperometry, living cells, intracellular redox activity

1. Introduction

Screening systems capable of assessing enzyme activity in whole living cells, can produce information related to i) the function of enzymes in the native environment and ii) the cellular cofactors [1] as well as iii) the cellular signaling and regulation mechanisms, together forming the functional basis of the organization of the cellular reaction pathways, i.e. metabolons [2]. Since it has been indicated that the cellular redox environment is related to e.g. the pathogenesis of neurodegenerative diseases [3], it is of utmost importance to develop methods capable of assessing intracellularly the activity of redox enzymes. Considering the low concentrations of the compounds to be detected, it is necessary to miniaturize the electrochemical system making the cell-electrode distance as small as possible. In order to realize this goal, a mediated amperometric method, employing microelectrodes in chip-format, was developed for assessing the activity of intracellular redox enzymes.

2. Theory

The method utilizes the double-mediator system, lipophilic menadione (**M**) (2-Methyl-1,4-naphthoquinone) and hydrophilic ferricyanide (**FC**). **M** is capable of diffusing through the plasma membrane into the intracellular compartment, where it can be reduced by NAD(P)H oxidizing enzymes (**NOE**) [4]. The reduced form, menadiol, diffuses out of the cell and undergoes reoxidation by **FC**, which in turn is oxidized on the platinum micro-band electrodes. This process results in a current proportional to the total **NOE** activity. The developed method was evaluated by assessing the activity of an overexpressed NADPH-dependent diketone reductase, encoded by the gene *gcy1* [5], in the EBY44 (pgi1Δ::URA3) strain of *S. cerevisiae*. In EBY44, addition of glucose primarily leads to formation of NADPH due to the deletion of the gene encoding for phosphoglucose isomerase (PGI) (Fig.1a). The substrate of the diketone reductase, diacetyl, decreases the NADPH level, causing a net decrease in the current proportional to the substrate concentration (Fig. 1b).

3. Experimental

S. cerevisiae cells were immobilized on the electrode microchips in a Ca^{2+}-alginate gel, which completely covered the microchip surface (Si/Si_3N_4 with 4 Pt micro-bands, $W_{band}= W_{gap}= 25$ μm). Amperometric measurements in a three-electrode setup were carried out at a constant potential of +400 mV vs. a Ag/AgCl (KCl_{sat}) reference electrode. Aerobic conditions were provided by vigorous stirring in a thermostated (30 °C) electrochemical cell. The employed buffer (pH 5.0) contained 10 mM Tris, succinic acid and $CaCl_2$ as well as 100 mM KCl. Menadione stock solution (100 mM) was prepared in 99.7% (v/v) ethanol.

4. Results and discussion

The absolute value of the change in the steady-state current (Fig. 1b), $|\Delta i_{ss}|$, corresponding to each consecutively added substrate concentration, **[S]**, was extracted from the recorded i vs. time traces and plotted as a function of the substrate concentration. The results show that the system follows Michaelis-Menten (**MM**) type kinetics (Fig. 2a) based on the electrochemical **MM** equation:

$$|\Delta i_{ss}| = \frac{i_{max,\,cell}\ [S]}{K_{M,\,cell} + [S]}$$

The values of the apparent kinetic parameters, $K_{M,\,cell}$ and $i_{max,\,cell}$, for the diketone reductase in EBY44 were determined using Lineweaver-Burk plots (Fig. 2b). The results indicate that the concentration of **M** is a significant factor for the amperometric assessment of intracellular redox enzyme activity and has to be optimized for fine-tuning the method. In the studied system, the concentration of 200 μM **M** was found to be the most optimal for monitoring diketone reductase activity, resulting in a minimum of $K_{M,\,cell}$ and a maximum of $i_{max,\,cell}$ (Fig. 3a-b). The indicated error bars are 95% confidence intervals for the respective concentration of **M** determined based on linear regression for standard addition.

Since this microchip-based amperometric method relies on the measured difference between the steady-sate current of the baseline (total NOE activity) and the decreased current due to the added substrate, the obtained results are not affected by factors modulating the baseline current. Such factors are i) the added ethanol (as the solvent of **M**), which contributes to formation of NAD(P)H, increasing the baseline current [7], ii) the formation of menadione-glutathione conjugate [8], decreasing the active menadione concentration and hence the baseline current, and iii) the reduction of ferricyanide by membrane bound oxidoreductases [9], slightly increasing the baseline current.

Acknowledgement

We thank Prof. Eckhard Boles (Institute of Microbiology, Frankfurt, Germany) for sharing the EBY44 strain with us.

References

[1] T. R. Hughes., *Funct. Integr. Genomics* **2,** 199-211 (2002).
[2] R. Götz, E. Schlüter, G. Shoam and F. K. Zimmermann., *Yeast* **15,** 1619-1629 (1999).
[3] R. A. Floyd., *Free Radic. Biol. Med.* **26**(9-10), 1346-1355 (1999).
[4] A. Heiskanen, J. Yakovleva, C. Spégel, R. Taboryski, M. Koudelka-Hep, J. Emnéus and T. Ruzgas., *Electrochemistry Communications* **6,** 219-224 (2004).
[5] M. Katz, B. Hahn-Hägerdahl and M. F. Gorwa-Grauslund., *Enzyme Microb. Technol.* **33,** 163-172 (2003).
[6] C. Spégel, A. Heiskanen, J. Yakovleva, T. Johanson, M. Koudelka-Hep, B. Hahn-Hägerdal, J. Emnéus and T. Ruzgas, (*Manuscript*)
[7] J. Mauzeroll and A. J. Bard, *Proc. Natl. Acad. Sci. USA* **101**(21), 7862-7867 (2004).
[8] F. L. Crane, H. Roberts, A. W. Linnane and H. Low, *J. Bioenerg. Biomembr.* **14**(3), 191-205 (1982).

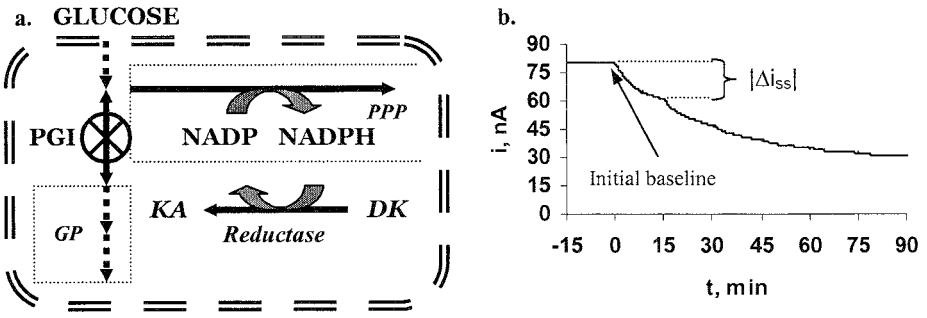

Figure 1. a) A schematic view of metabolic pathways of *S. cerevisiae* strain EBY44. Glucose primarily contributes to the formation of NADPH. The diketone reductase reduces a diketone (DK) to a chiral ketoalcohol (KA), utilizing NADPH as the coenzyme. b) i vs. time trace for titration with diacetyl. (Pentose phosphate pathway, PPP; Glycolytic pathway, GP)

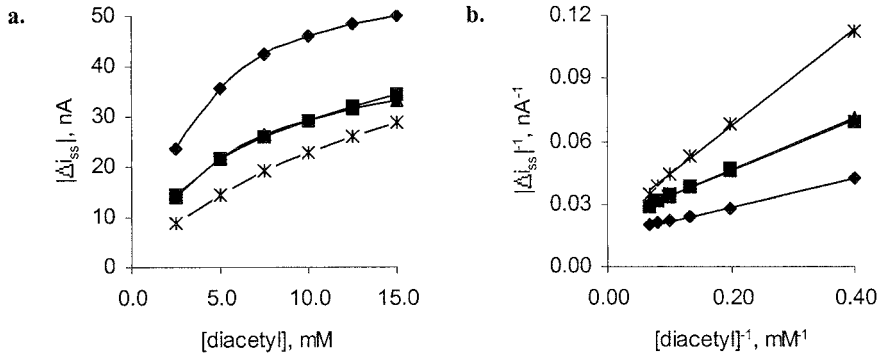

Figure 2. a) Michaelis-Menten and b) Lineweaver-Burk plots for the determination of apparent enzyme kinetic parameters, $K_{M,cell}$ and $i_{max,cell}$. (*: **[M]** = 50 μM, ■: **[M]** = 100 μM, ♦: **[M]** = 200 μM and ▲: **[M]** = 400 μM)

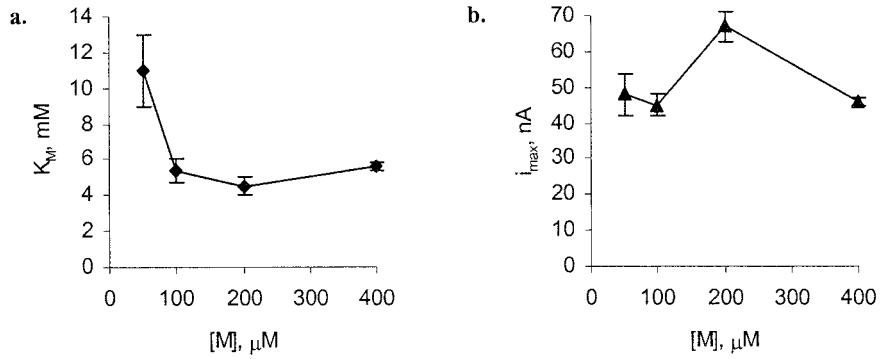

Figure 3. The variation of a) $K_{M,cell}$ and b) $i_{max,cell}$ with menadione concentration. (The error bars indicate 95% confidence intervals at the respective concentration of **M**.)

A PDMS MEMBRANE BASED MICROBIOREACTOR FOR PERFUSED PRIMARY RAT HEPATOCYTE CULTURES.

Serge OSTROVIDOV[1,2], Jinlan JIANG[2], Yasuyuki SAKAI[2,3] and Teruo FUJII[2]

[1] *LIMMS/CNRS-IIS, Institute of Industrial Science, University of Tokyo, 4-6-1 Komaba, Meguro-ku, Tokyo 153-8505, Japan.*

[2] *Institute of Industrial Science, University of Tokyo, 4-6-1 Komaba, Meguro-ku, Tokyo 153-8505, Japan.*

[3] *Center for Disease biology and Integrative Medicine, University of Tokyo 7-3-1 Hongo, Bunkyo-ku, Tokyo 113-0033, Japan.*

Abstract

A new technique to build PDMS membrane is presented. We used this membrane in a biological application and built some microbioreactors for cell cultures with inserted membrane. These microbioreactors were loaded with primary adult rat hepatocytes. Cultures monitoring showed a good rearrangement of the cells, a large increase in the albumin secretion and ammonium detoxification by the cells compared to static cultures and validated the use of these microbioreactors in cell cultures.

Keywords: PDMS, hepatocytes, liver, microfluidic device, tissue engineering.

1. Introduction

Normal or primary cultured hepatocytes rapidly lose liver specific functions when maintained under standard in vitro culture. Towards the goal to improve hepatocyte cultures and to maintain hepatocyte functionality in vitro, many efforts have been made to mimic in vivo environment. For that purpose the microfabrication technologies offer new approaches [1]. In this work we present a new technique to obtain the desirable thickness of the PDMS prepolymer layer before curing and to build PDMS membrane with holes through one side to the other side of the layer. As in culture on porous membrane the cells are bathed on both sides by the culture medium and express much higher function [2], we used this PDMS membrane as a scaffold for the attachment of the cells in the heart of our microbioreactor. Efficiency of the microbioreactor was monitored through long-term primary rat adult hepatocyte cultures and the measurement of two major liver specific functions.

2. Experimental

Two types of SU-8 mold masters with micro-pillars were firstly built. Pillars sections were 5 μm x 5 μm or 10 μm x 10 μm whereas pillars heights were 20 μm and gap between two pillars was 10 μm for both types of molds (Fig. 1). PDMS prepolymer with curing reagent was poured in the mold and the surface of the non-polymerized PDMS layer was physically pushing down below the SU8 pillars height by using a nitrogen gas exit. Monitoring the light reflection through a magnifying glass empirically controlled amount of removed prepolymer. The PDMS was then cured at 70 °C for 1 hour 40 minutes in an oven and the PDMS membrane was peeled off from the master (Fig. 2). The microbioreactor was obtained by a permanent bonding of two microstructured PDMS layers after an O_2 plasma treatment in RIE apparatus, whereas the PDMS membrane was inserted between the two layers (Fig. 3). Another type of microbioreactor was built by using a clear polyester membrane commercially available (taken from a cell culture insert/Corning incorporate/code3450/0.4 μm pores size) instead of the PDMS membrane. The microbioreactor was fixed in the loop of a perfusion circuit composed of a culture medium tank, a peristaltic pump, a

glass bubble trap and a magnetic stirrer. Experiments were running 15 days and the flow rate for perfusion was 150 µl/minute.

4. Results and discussion

The PDMS membrane, as the polyester membrane, coated with collagen offered a good support for the cell attachment. Little by little hepatocytes rearranged themselves well in a plate like structure and a bile canalicular network appeared after few days proving that the cells appreciated their environment (Fig.4). Four different cultures systems were tested: standard dish culture, insert culture, perfusion culture in microbioreactor with polyester membrane and perfusion culture in microbioreactor with PDMS membrane. Albumin secretion by hepatocytes, normalized by the DNA amount on day 15 of culture, showed that perfusion culture method in microenvironment is superior compared to static cultures (Fig. 5). As mentioned by others the microenvironment coupled to continuous supply of nutrition and waste removal through perfused culture medium largely increase cell activities [3]. In the same way the ammonium detoxification by the hepatocytes measured in day 4 of culture appeared weak in static cultures whereas a large increase is observed in perfused microbioreactors (Fig. 6). These results showed that hepatocytes in the microbioreactors could stay alive and highly functional and validate our microbioreactors and the use of PDMS or polyester membrane as a scaffold for the cells.

5. Conclusions

To build a PDMS membrane with holes through one side to the other side of the layer, we established a new technique to obtain the desirable thickness of the PDMS prepolymer layer before curing. This type of membrane was used in the building of microbioreactors meant for cell cultures. Fixed in the loop of a perfusion circuit and loaded with primary adult rat hepatocytes these microbioreactors provided a marked improvement on hepatocytes maintenance and functionality in culture compared to static culture methods and revealed themselves to be very encouraging tools towards future applications in drug screening or liver tissue engineering.

Acknowledgements

This project was partly carried out under the framework of LIMMS, the Laboratory for Integrated Micro Mechatronic Systems, located in Tokyo, a joint laboratory between the Communication and Information Science and Technology Department of CNRS (CNRS-STIC, France) and the Institute of Industrial Science (IIS) in the University of Tokyo. It was supported by the CNRS, the MEXT (Japanese Ministry of Education, Culture, Sports, Science and Technology), and the JSPS (Japanese Society for the Promotion of Science).

References

[1] M.J. Powers, K. Domansky, M.R. Kaazempur-Mofrad, A. Kalezi, A. Capitano, A. Upadhyaya, P. Kurzawski, K.E. Wack, D.B. Stolz, R. Kamm and L.G. Griffith. Biotechnology and Bioengeering, **78**, 3, 257-269, (2002).

[2] M. Suzuki, K. Ichikawa, A. Sakoda, Y. Sakai. Cytotechnology **11**, 3, 213-218, (1993).

[3] M.J. Powers, D.M. Janigian, K.E. Wack, C.S. Baker, D.B. Stolz and L.G. Griffith. Tissue engineering, **8**, 3, 499-513, (2002).

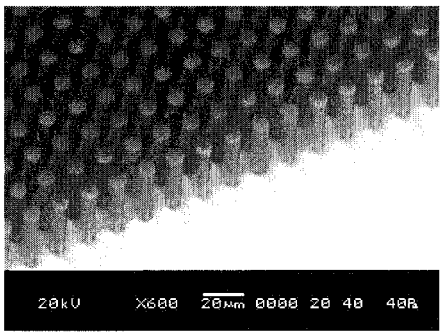

Figure 1. SEM picture of a SU8 mold master.

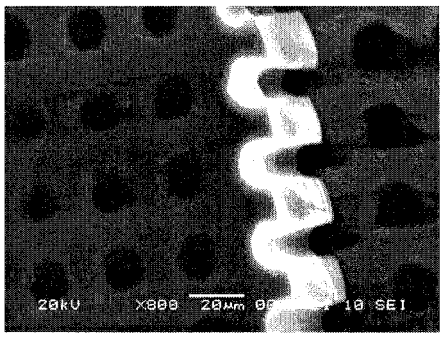

Figure 2. SEM picture of a PDMS membrane

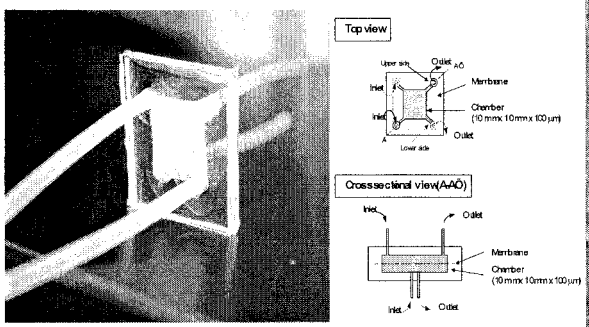

Figure 3. Microbioreactor with PDMS membrane inserted and microbioreactor pattern (chamber 10 mm x 10 mm x 100 µm).

Figure 4. Primary adult rat hepatocytes in perfusion at day 11 of culture. A) On polyester membrane. B) On PDMS membrane.

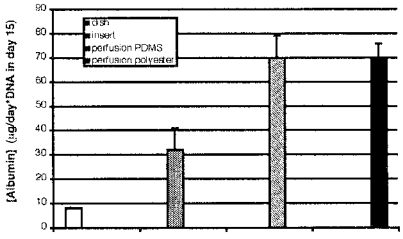

Figure 5. Albumin secretion normalized by DNA amount on day 15 of culture. Data are expressed as the mean +SD for three independent experiments and n=9 for dish and insert cultures whereas n=3 for perfused culture.

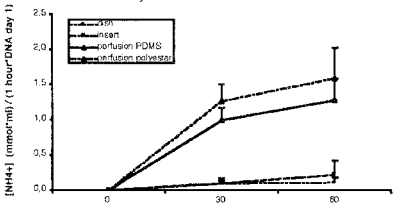

Figure 6. Ammonium detoxification normalized by DNA amount on day1 of culture. Data are expressed as the mean +SD for three independent experiments and n=9 for dish and insert cultures whereas n=3 for perfused culture.

DEVELOPMENT OF A BIOASSAY SYSTEM RETAINING FLOATING CELLS AND ITS APPLICATION TO THE ANTI-ALLERGIC DRUGS

Takahito Tokuyama, Shin-ichiro Fujii, Kiichi Sato, Mitsuru Abo and Akira Okubo
Department of Applied Biological Chemistry, Graduate School of Agricultural and Life Sciences, The University of Tokyo, Japan
1-1-1 Yayoi, Bunkyo-ku, Tokyo, 113-8657, Japan

Abstract

The article describes the anti-allergic drug screening system by detection of histamine released from mast cells (floating cells) on a multilayer microchip. In this study, the elastmetric material PDMS, was employed to fabricate micro channels and chambers. This system consists of two sections, histamine release layer and histamine derivatizing layer, which were integrated into one chip. Rat peritoneal mast cells were retained in the microchip by filtering system, and were stimulated with chemical releaser (C48/80). Histamine released from the cells was derivatized with *o*-phthalaldehyde (OPA) and its fluorescence was detected on the microchip. By this integrated system, 51 pmol of histamine was detected using 500 cells. By comparing released histamine levels with and without drugs, their effect could be evaluated.

Keywords: histamine release, mammalian cell, fluorescence derivatization, PDMS, bioassay

1. Introduction

A cellular analysis microchip is the ideal system for experiments on stimuli and response of cells. Whereas adherent cells were used in some studies, the system utilizing floating mammalian cells has been hardly reported. In this study, a microchip-based bioassay system retaining floating cells was developed.

Histamine, which is primarily found in mammalian mast cells, is the representative mediator in connection with allergies, and is released by some stimuli. Many anti-allergic drugs have inhibitory effect of the histamine release reaction. In this study we tried to make a rapid and sensitive anti-allergic drug screening system on a microchip by retaining mast cells on a microchip and detecting released histamine.

2. Experimental

Micro channels (300 μm width and 70 μm depth) were fabricated using PDMS as previously reported[1]. Peritoneal mast cells were collected from the abdominal cavity of male Wistar rats, weighting 250-300 g. Chemical releaser (C48/80; 0.5 μg/ml) was used to stimulate the cells [2]. This cellular analysis system consists of a histamine release layer which has a cell chamber and a histamine fluorescence derivatizing layer (Fig. 1). Mast cells were retained at the chamber (1.2 μl) by the cellulose nitrate membrane (CN membrane) constructing at the bottom of the chamber (Fig. 2a). This filtering structure can retain floating cells or suspension cells easily without cell damages. After preincubation of cells on the chamber, releaser solution was introduced in the channel. When the releaser solution was reached at the chamber, mast cells released histamine. Released histamine was flowed to the lower layer, where it is derivatized to the fluorescent molecules with *o*-phthalaldehyde (OPA). Firstly, the released histamine was mixed with reaction solution (OPA containing alkaline solution) at the first junction on the fluorescence derivative layer, and the reaction time was adjusted by the length of the winding channel. Next, the reaction was terminated by addition of terminating solution (citric acid) at the second junction. After the addition of the citric acid, fluorescence-derivatized histamine was detected by fluorescence microscope at the downstream of the channels.

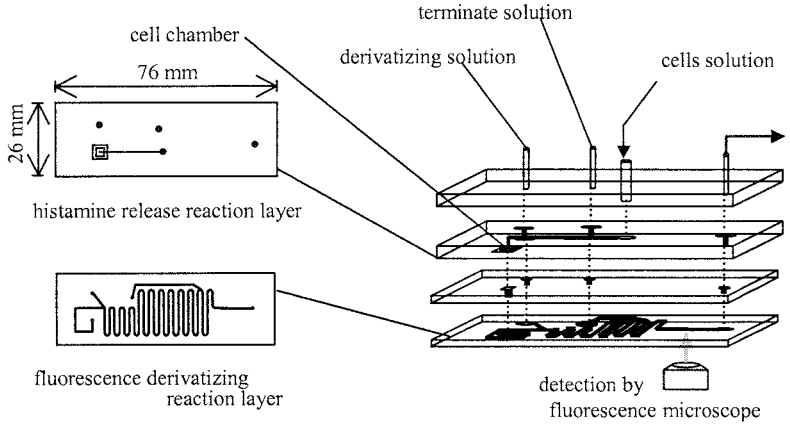

Figure 1. Schematic image of the microchip for the determination of histamine release from mast cells.

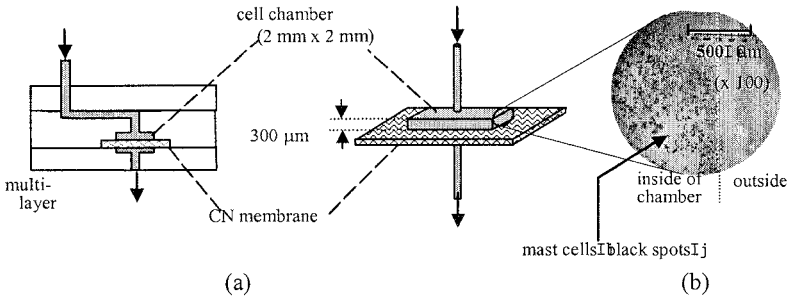

Figure 2. Structure of the cell chamber

The system was applied to a histamine release suppression test that is a major test for drug screening of anti-allergic drugs. Any samples which were anticipated to inhibit histamine release from mast cells were added in C48/80 induced histamine release condition. Histamine release levels with and without suppressor drug were compared.

3. Results and discussion

Fig. 2b is the picture of mast cells retaining on the chamber. The black spot is the mast cells stained by toluidine blue, and they did not leak from the chamber. This system makes it possible to keep cells alive during this assay with saline flow (data not shown).

The calibration curve of the standard histamine using this chip exhibited good linearity at the concentration range from 250 nM to 40 μM. This flow system can detect the time course of histamine release. Real time measurement of histamine release using 1000 cells with (a) and without (b) C48/80 stimulation was shown in Fig. 3. It was observed that histamine is promptly released by the addition of the releaser solution, and release reaction is finished within several minutes. The measured amount of the released histamine was 91 pmol. In this assay, about 46% of histamine has been released from retaining cells on the assumption that 1000 mast cells contain *ca.* 200 pmol of histamine. These data were well in agreement with the large scale assay. The system could quantify histamine released from 500 cells, and release signals could be detected with 100 cells.

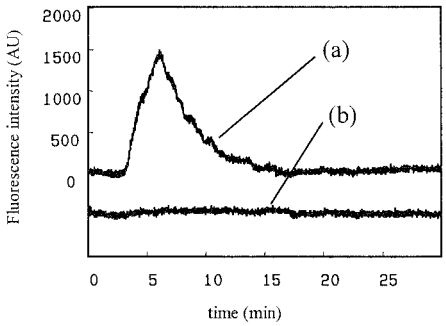

Figure 3. Real time detection of histamine release from mast cells.

A mast cell stabilizer, DSCG was used as a model inhibitor for a histamine release suppression test. As shown in Fig. 4, C48/80-induced histamine release level was suppressed by using DSCG as inhibitor. Inhibition ratio of DSCG on C48/80 induced histamine release was 53%.

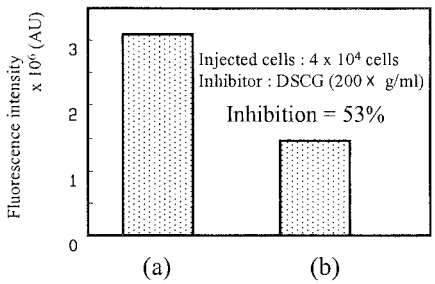

Figure 4. Inhibition of DSCG (anti-allergic drug). (a) C48/80-indused histamine release without inhibitor. (b) C48/80-induced histamine release with inhibitor.

4. Conclusion

We realized retention of suspension cells on a microchip and used it for drug screening system. This filtering system can retain cells in a microchip without long-time cell culture or troublesome operations. In this study, collected cells were introduced in the microchip, and then they could be used for drug screening assay in a minute.

This flow system is applicable for allergy drug screening by rapid measurement of the inhibition of histamine release from mast cells. It's also suitable for the rapid analysis of the biological mediators, which are secreted in a small amount and degraded in a short time.

References

[1] Fujii S, Tokuyama T, Abo M, Okubo A, *Analyst,* **129**, 305-308 (2004).
[2] Akagi M, Matsui N, Mochizuki S, Tasaka K, *Pharmacology,* **63**, 203-209 (2001).

SEPARATION OF BLOOD CELLS AND PLASMA IN MICROCHANNEL BEND STRUCTURES

C. Blattert[1], R. Jurischka[1], I. Tahhan[1], A. Schoth[1], P. Kerth[2] and W. Menz[1]

[1] *Laboratory for Process Technology, Institute of Microsystem Technology, University of Freiburg, Georges-Koehler-Alle 103, 79110 Freiburg, Germany*

[2] *PREVENTOR µTBC GmbH, Gernsheimer Strasse 46, 64319 Pfungstadt, Germany*

Abstract

Most clinical chemistry tests are performed on cell-free serum or plasma. Therefore, micro assay devices for blood tests require integrated on-chip microfluidics for separation of plasma or serum from blood. This is achieved by a new blood separation technique based on a microchannel bend structure Different prototype polymer chips have been manufactured with an UV-LIGA process and hot embossing technology. The separation efficiency of these chips has been determined with samples of human whole blood as well as diluted blood samples. The results show different separation efficiencies up to 90 % for blood cells and plasma depending on microchannel geometry as well as cell concentration.

Keywords: blood, microchannel bend, separation, UV-LIGA, rapid prototyping

1. Introduction

In present microfluidic devices the separation of blood cells is achieved by mesh-type filters, comb-shape filters or filtration by diffusion [1,2]. The most frequently used separation process in the macro world, centrifugation, can only be achieved in the micro world by technically complex CD-like platforms using expensive instrumentation [3].

Therefore, an important need for convenient and inexpensive integrated microfluidics for blood separation still remains. Microchannel bend structures offer a potentially interesting solution. This blood separation technique is developed within the collaborative Micro-Tele-BioChip (µTBC) project co-funded by the German Ministry For Education and Research (BMBF) [4].

2. Theory

The microchannel bend technique combines two principles of separation. The first one is the centrifugal force field due to the bent microchannel. This results in different settling velocities based on density differences between particles and the surrounding fluid. The second separation principle is known as the "plasma-skimming" effect. If the flow rates in branching microchannels are significantly different, particles preferably enter the branch with the higher flow rate [5].

3. Experimental

Fig. 1 shows a typical COC polymer chip including the separation device and a detailed view of the bend region. Different chips have been fabricated using an UV-LIGA process and hot embossing (Fig. 2).

Table 1 Channel dimensions and flow rate ratio F_Q of the investigated chips.

chip	l_{EC} /mm	l_{CC} / mm	l_{PC} /mm	w_{EC} /µm	w_{CC} /µm	w_{PC} /µm	h /µm	F_Q
03-091-5-5	5	2	5	72	74	56	92	0,21
03-073-6-5	5	2	5	101	85	62	92	0,20
03-238-1-7	3	3	3	73	66	52	87	0,57
03-298-1-2	3	3	3	54	51	39	67	0,53
03-379-3-7	3	3	3	42	97	28	116	0,03
03-379-5-1	3	3	3	42	102	30	86	0,05

The chip geometries shown in Tab. 1 differ with regard to channel length l, channel width w, channel height h, as well as the flow rate ratio F_Q.

The separation efficiency of prototype chips has been determined with samples of human whole blood or samples at which the blood has been diluted with physiological sodium chloride solution. The blood was pumped through the microchip module (Fig. 3) by a syringe pump. The number of the red blood cells (RBC) was determined by sampling in the inlet reservoir and for comparison in the outlet reservoirs.

4. Results and discussion

The separation efficiency η is calculated from the cell concentration in the entrance channel (c_{EC}) and the cell concentration in the plasma channel (c_{PC}). η is defined as follows:

$$\eta = (c_{EC} - c_{PC}) / c_{EC} \qquad (1)$$

According to Poiseuille's Law the flow rate in a channel for a laminar flow regime is proportional to the fourth power of the hydraulic diameter d_H of the channel and inversely proportional to the channel length l. The flow rate ratio F_Q is defined as follows:

$$F_Q = (d_{HPC} / d_{HCC})^4 \cdot (l_{PC}/l_{CC})^{-1} \qquad (2)$$

The effect of different geometries and therefore a different F_Q on separation efficiency of red blood cells is shown in Fig. 4. The lower F_Q, the higher the separation efficiency. A lower flow rate ratio means higher flow rate differences in the branching channels and accounts for a more pronounced "plasma-skimming" effect.

Fig. 5 shows the effect of red blood cell concentration (hematocrit) on separation efficiency. The lower the hematocrit the higher the separation efficiency. A lower hematocrit leads to an increased viscosity and a decreased settling velocity respectively. The settling of blood cells is hindered, the effect of the centrifugal force is reduced.

For the white blood cells similar results were obtained, which are not presented in this paper.

5. Conclusions

The results show different separation efficiencies for RBC and plasma depending on microchannel geometry as well as cell concentration and suggest the microchannel bend as an alternative blood separation method as compared to existing micro separation technologies.

The microchannel bend combines the advantages of rapid separation times and separation of small sample volumes or continuous extraction respectively. The simple microfluidic geometry leads to efficient high volume production in different materials, using injection molding technologies.

Acknowledgements

The authors thank Dr. W. Koester, University Hospital Freiburg, Department of Clinical Chemistry, for establishing and supporting the analyses of the blood specimens in his laboratory. Additional thanks apply to our project partners of the µTBC collaborative project for helpful discussions and advice.

References

[1] H. Andersson and A. van den Berg, *Sensors and Actuators B*, 92, 2003, pp. 315 - 325

[2] S.C. Jakeway, A.J. de Mello and E.L. Russell, *Fresenius J Anal Chem*, 366, 2000, pp. 525 -539

[3] M.J. Madou, L.J. Lee, S. Daunert, S. Lai, and C-H. Shih, *Biomedical Microdevices*, 3:3, 2001, pp. 245–255

[4] C. Blattert, R. Jurischka, A. Schoth, P. Kerth and W. Menz, *Proc. of SPIE Vol. 5345*, 17, 2004, pp. 17-25

[5] R.T. Yen, and Y.C. Fung, *Am. J. Physiol.: Heart Circ. Physiol.*, 4(2), pp. H251-H257, 1978

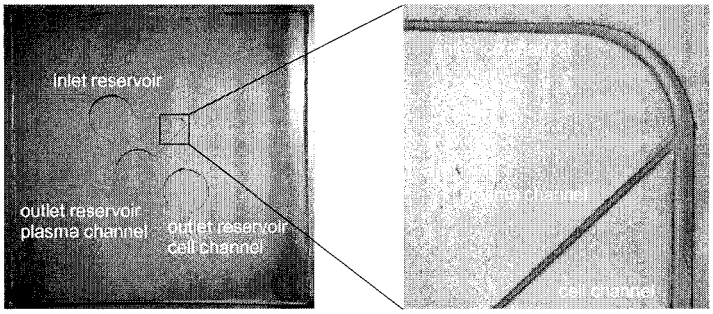

Figure 1. COC Polymer chip (20 mm x 20 mm) including the separation device and detailed view of the bend region.

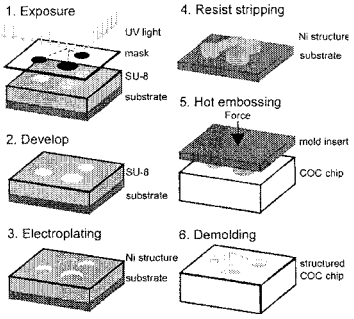

Figure 2. Schematic diagram illustrating the fabrication of a COC Chip.

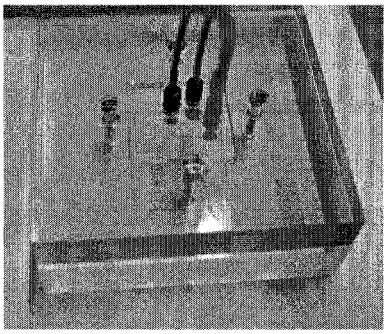

Figure 3. Microfluidic module including the clamped COC polymer chip and tubing.

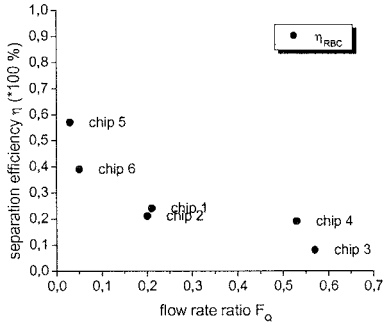

Figure 4. Effect of flow rate ratio on RBC separation efficiency.

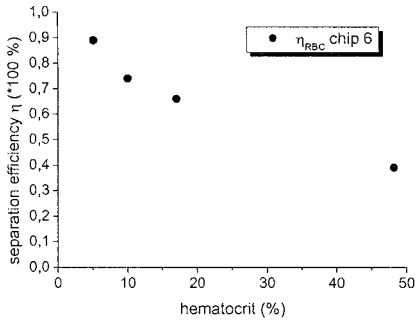

Figure 5. Effect of hematocrit on RBC separation efficiency.

MONITORING STEM CELL GROWTH USING A MICROELECTRODE ARRAY

Pontus Linderholm[1], Michel Brouard[2], Yann Barrandon[2], Philippe Renaud[1]
[1]Laboratory of Microsystems, [2]Laboratory of Stem Cell Dynamics
Swiss Federal Institute of Technology, 1015 Lausanne

Keywords: microelectrode array, cell monitoring, impedance imaging, dielectric spectroscopy

1. Introduction

Microelectrode arrays are becoming an increasingly important tool for the cellular and molecular biologist. A plethora of cell types are already grown on top of microelectrodes around the world today [1,2]. We are developing a technique that ultimately will make it possible to measure layer topology and monitor cell growth in real time using the same substrates that are already used for drug development or biosensor research [3].

The concept is based on a technique called resistivity probing, used in geophysics. Impedance measurements between planar electrodes placed on the surface of a body are used to measure the resistance at different separations, and the resistivity distribution of the sample can then be reconstructed using computer algorithms.

2. Theory

The impedance of a sample between two electrodes depends on the interface between the electrodes and the sample, the resistivity of the sample and the relative geometry of the electrodes. Since it is only the relative geometries of the electrodes that influence the impedance, it is possible to measure the same resistance from two small electrodes close together, as would be obtained from two large electrodes further apart. For a fixed geometry, the bulk resistance is directly proportional to the resistivity. This relation can be written:

$$R_{bulk} = \kappa \rho_{app}(d)$$

where κ is the so-called cell constant, ρ_{app} is the apparent resistivity of the sample and d is the distance between the electrodes. The apparent resistivity is a non-linear combination of the resistivities of the different materials in the body. For a homogeneous sample, the apparent resistivity is a constant. For a stratified sample, the apparent resistivity profile is determined by the layer composition.

The layers close to the electrodes will contribute more to the measured impedance than those further away. This effect can be used to probe different depths of a sample by simply changing the geometry of the electrode. In an ρ_{app}-profile for a two-layered sample the measured resistivity will gradually change from that of the first layer (probed at small electrode separations) to that of the second layer (probed at larger separations). By fitting the measurements to such models, the thickness and conductivity of the first layer can be deduced (fig 1).

2. Materials and Methods

3. Experimental

The microelectrodes used for the measurements were rectangular, 18 - 725 µm wide and 4 mm long. The dimensions were optimized for bipolar measurements [4]. The Cr/Au electrodes were fabricated on floatglass, using a standard lift-off procedure. A thin film of polyimide (PI 2611) was used to isolate the leads. After dicing the chips were bonded to a PCB, and a culture chamber (i.d. 35 mm) was mounted on top of the array (fig 2).

A digital switchbox was used to control the active electrodes. The impedance was measured from 100 Hz to 1 MHz using a HP4284A LCR-meter. Before the measurements on cells began, the electrode arrays were calibrated to find the cell constants, using KCl solutions with different resistivities. The measurements on cells were carried out inside the incubator.

Keratinocyte stem cells of type YF 26 were cultured on a feeder layer of 3T3 cells and allowed to form a pluristratified layer [5]. The measurements began when the cells were confluent. The feeder layer had then been removed by the keratinocytes. The medium was changed continuously. A confocal microscope was used to make independent measurements of the thickness of the cell cultures. The bulk resistance of the biological samples was approximated with the real part of the impedance at 20 kHz, where the phase was at a minimum. The apparent resistivities were calculated using the measured cell constants and Eq 1. The finite element software FEMLAB® was used to simulate the apparent resistivity profiles of bilayer systems. For the numerical fittings, the cell layer was modeled as a homogeneous layer with a time-independent resistivity. The resistivity of the culture medium was considered a constant determined by independent measurements, leaving the cell layer resistivity and the cell layer thickness as the two free parameters.

4. Results and discussion

In order to be able to compensate for parasitic and interfacial capacitances, entire impedance spectra were taken for each pair of electrodes. As the cells divide, the impedance at mid-frequencies increases. Impedance dispersions in the α-range (100-1000 Hz) and in the β-range (100-300 kHz) were observed [6]. These dispersions appeared to change with time (fig 4).

At confluency, the cells formed a homogeneous layer with a well-defined thickness (fig 3). However, after a few days in culture the thickness varied from 20 – 100 μm across the sensing area. The apparent resistivity varied from 4 Ωm – 1 Ωm, depending on probe depth (18 – 700 μm) and measurement time (fig 5). This is in agreement with previous reports [7]. The resistivity of the culture medium was determined independently to be 1 Ωm. The simulated apparent resistivity profiles provided reasonably good agreement with the measurements. The reconstructed thicknesses were 8 μm and 35 μm, and the cell layer resistivity 4 Ωm.

5. Conclusions

We have shown that the apparent resistivity profile changes as the cell layer grows thicker, in agreement with theoretical predictions based on a two-layer model. We expect that a three-layer model, taking into account a thin layer of proteins at the electrode surface will provide a more exact description of the system. The results indicate that the absolute values of the thicknesses and resistivities of a multi-layered biological sample could be reconstructed. It would then be possible to monitor the rate of cell growth, for example in response to different treatments.

These results show that a microelectrode array can be used to investigate the topology and resistivity distribution of a biological sample with a spatial resolution on the order of microns.

Acknowledgements

Jeanne Vannod, Juan-Carlos Floyd Sarria, CMI staff, EPFL.

References

[1] C.R. Keese, et al., Proc. Natl. Acad. Sci. U. S. A., **101**(6), 1554-1559 (2004)
[2] M.O. Heuschkel, et al. **114**(2), 135-148 (2002)
[3] P.Linderholm, A. Bertsch, P Renaud, Physiol. Meas. **25**, 645-658 (2004)
[4] P. Jacobs, A. Varlan, W. Sansen, Med. Biol. Eng. Comput., **33**(6), 802-810, (1995)
[5] M. Brouard, et al., J. Cell Sci., **112**(19), 3343-3352 (1999)
[6] H.P. Schwan, Adv. Biol. Med. Phys., **5**,147-209 (1957)
[7] S. Grimnes, O.G. Martinsen, *Bioimpedance Basics*. 2000, Academic Press: San Diego. p. 119.

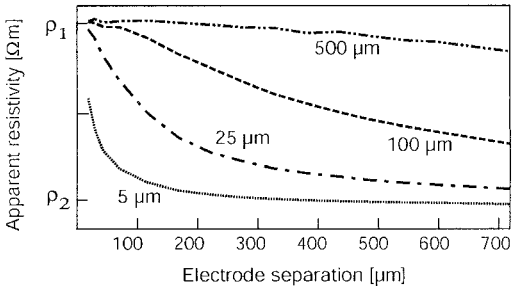

Figure 1. Theoretical resistivity profiles of a bilayer system using an electrode array with identical cell constants.

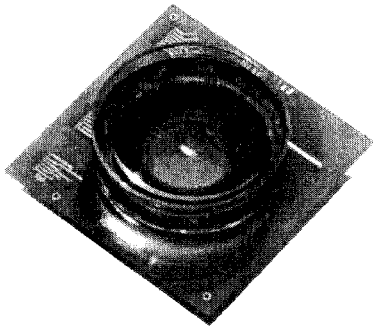

Figure 2. The device consists of an array of 16 rectangular gold electrodes on a floatglass chip bonded to a PCB.

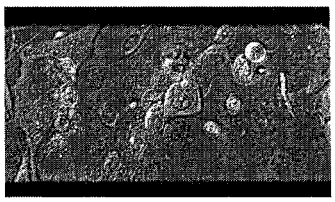

Figure 3. Micrograph of a confluent cell layer between two electrodes. The border-border distance is 166 µm. After confluency the cells start forming a multi-layered aggregate.

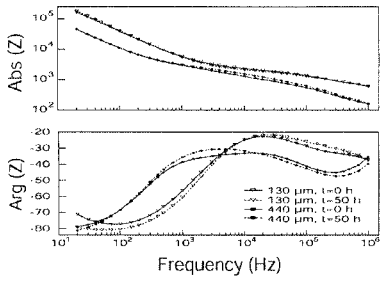

Figure 4. Bode plots of two different electrode pairs at two different times.

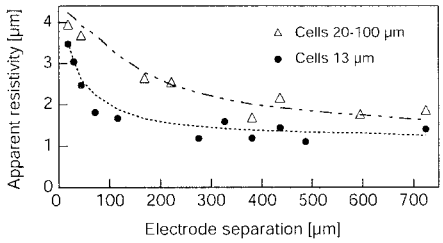

Figure 5. The measured and reconstructed apparent resistivity profiles at two different cell layer thicknesses. The reconstructed curves were based on layers 8 µm and 35 µm thick, having a resistivity of 4 Ωm.

MINIATURIZED MEASUREMENT SYSTEM FOR LOW AMMONIA CONCENTRATIONS

B.H. Timmer, W.W. Koelmans, K.M. van Delft, W. Olthuis, A. van den Berg
MESA+ Research Institute, University of Twente, P.O. Box 217,
7500 AE Enschede, The Netherlands

Keywords: ammonia detector, micro fluidics, gas sensor on a chip

A miniaturized and integrated system for selectively measuring gaseous ammonia is presented for concentrations in the low-ppb range. The resulting ammonia sensing chip has a lower ammonia detection limit of 1.1 ppb and a response time of 1.6 minutes. In combination with the high selectivity, >300,000, towards interfering gasses like CO_2, the system is potentially applicable for diagnostic breath ammonia analysis. The gas sensing chip is a next step in the development process of an ammonia analyzer initiated by the Energy research Centre of the Netherlands, ECN [1]. Miniaturization of the commercially available apparatus, and therefore reduction of the sample and chemical consumption, opens opportunities for new applications. Such systems can be applied for environmental and agricultural applications, e.g. intelligent ventilation systems in stables to increase the welfare of people and animals. Secondly, it is a longstanding desire of the medical community to be able to measure ammonia in exhaled breath as a diagnostic method for patients with disturbed urea balance, e.g. due to kidney disorder or peptic ulcer due to a H. pylori bacterial stomach infection.

The measurement principle is an indirect fluidic method for selectively measuring ammonia that makes use of pH-transitions, electrolyte conductivity detection and phase-separating membranes, schematically shown in Fig. 1 [2,3]. The key elements of the measurement system are miniaturized and integrated, resulting in a lab-on-a-chip ammonia sensing device, shown in Fig. 2. Channels, through-holes and electrodes are realized with micro-system technology in glass, using wet chemical etching, powder-blasting [4] and lift-off techniques. A micro porous polypropylene membrane is glued to the glass chips using epoxy resin. The lower ammonia detection limit of 1.1 ppb and a response time of 1.6 minutes, using a gas flow of 50 ml/min, are calculated from the ammonia measurement result shown in Fig. 3. The analyte gas consumption of the commercially available apparatus is reduced by more than a factor 100. The lower detection limit and the small analyte gas consumption make the sensing chip suitable for measuring breath ammonia, where the lower concentration levels are about 50 ppb. For normal atmospheric environments, the selectivity of the system is sufficient to measure ammonia concentrations in the low-ppb range, independent of interfering gasses like CO2, as can be concluded from the measurement result with elevated CO2 concentrations shown in Fig. 4. The system is even sufficiently selective to ammonia to be used in environments that contain elevated carbon dioxide levels, like exhaled air.

References

[1] J.W. Erisman, R. Otjes, A. Hensen, P. Jongejan, P. v.d. Bulk, A. Khlystov, H. Möls and S. Slanina, *Atmospheric Environment* 35, pp 1913-1922, 2001.

[2] B.H. Timmer, K.M. van Delft, R.P. Otjes, W. Olthuis, A. v.d. Berg, *Analytica Chimica Acta* 507 (1), pp. 139-145, 2004

[3] B.H. Timmer, W. Sparreboom, W. Olthuis, P. Bergveld, A. v.d. Berg, *Lab on chip* 2 (2), pp. 121-124, 2002

[4] S. Schlautmann, H. Wensink, R.B.M. Schasfoort, M. Elwenspoek, and A. van den Berg, *Journal of Micromechanics and Microengineering* 11(4), pp 386-389, 2001.

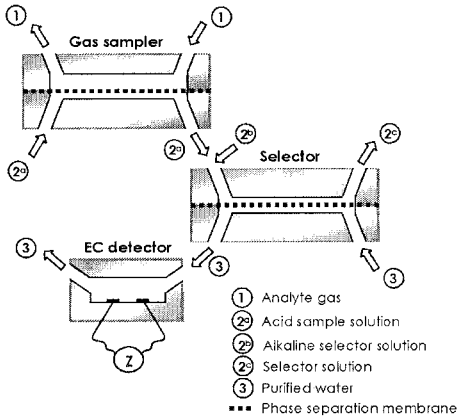

Figure 1. The ammonia detector comprising a gas sampler, a separator and an electrolyte conductivity sensor.

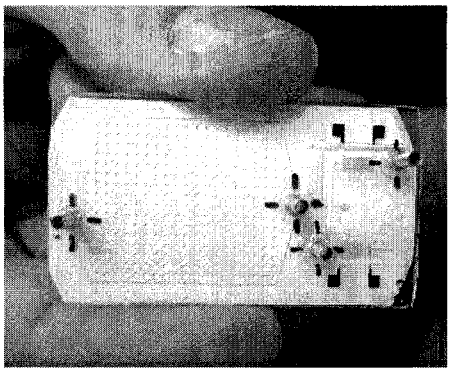

Figure 2. Photo of the realized microfluidic ammonia sensing chip.

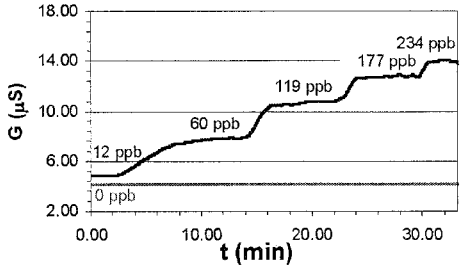

Figure 3. System response to a stepwise increased NH3 concentration in a nitrogen analyte gas.

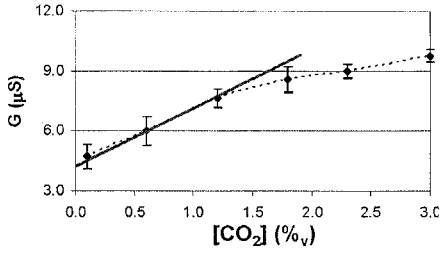

Figure 4. System response to a stepwise increased CO2 concentration in a nitrogen analyte gas.

PROTEOMICS IN MICROFABRICATED DEVICES

Richard.B.M. Schasfoort, Stefan Schlautmann, Geert A. J. Besselink and Anna J. Tudos
MESA+ Research Institute, Biochip Group,
University of Twente, P.O. Box 217, 7500 AE Enschede, The Netherlands

Abstract
The ultimate challenge in proteomics is rapid determination of the protein fingerprint in order to correlate the proteome to the timely status of the cells, organs and the whole body. A fast, cost-effective analysis technique is required to enable protein mapping. In this paper our approach is described to couple lab-on-a chip unit operations to characterize the proteome. The device contains units for sample preparation, separation, identification and confirmation.
Key words: proteomics, capillary electrophoresis, address-flow, SPR imaging.

1.Introduction

In this paper our vision of a single "proteomics-on-a-chip device" is presented. In this paper the practical set-up of a "proteomics on a chip" device is described, containing an isoelectric focussing sample pre-treatment unit, a separation unit based on gel electrophoresis, and an address-flow surface plasmon resonance imaging detector suited for identification [2]. Additional confirmation using mass spectrometry is an off-line option.

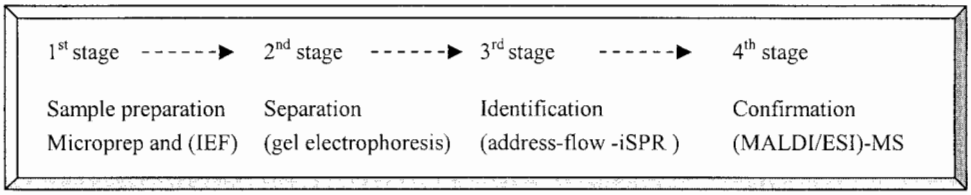

Figure 1. Stages of a "proteomics on a chip" device for the determination of a protein fingerprint.

2. Device design and the address flow principle

In order to characterize the proteome, thousands of compounds should be simultaneously monitored. The controlled electrical operation of the flow cell with spatial guiding of microfluidic flows over a microarray can be combined with a capillary electrophoresis (CE) system. In the CE-part of chip, the sample is injected at the cross or double-T section of two channels to form a sample plug which can be separated in the separation channel. The separated components migrate again to the so called "address flow" area where two electro-osmotically driven guiding streams allow directing the sample flow over a micro array.

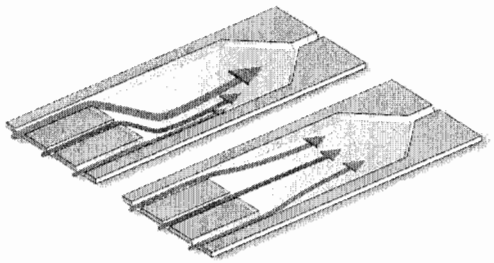

Figure 2. Illustration of the address-flow principle. Two guiding streams direct the sample lane (middle) to the desired location of the surface sensing area. Dimensions: chip 15mm x 25mm, chamber (1200μm x 3mm), guiding stream channel width 100μm, sample stream channel width 50μm, channel and chamber height 10μm.

As shown in figure 2, three parallel microfluidic channels are connected to a wider flow chamber. The outer two guiding streams sandwich the sample stream in the middle, for example components of a CE-separated protein mixture. By adjusting the flow rates of the individual streams, the sample stream can be guided across the chamber. The bottom plate of the chamber contains the detector microarray equipped with entities (e.g. antibodies) for specific biomolecular interactions. Separated compounds can be directed over the desired sample lane allowing low abundant proteins to bind at the specific binding area. The bottom of the address flow chip contains the micro array for imaging with surface plasmon resonance (iSPR), illustrated in Figure 3.

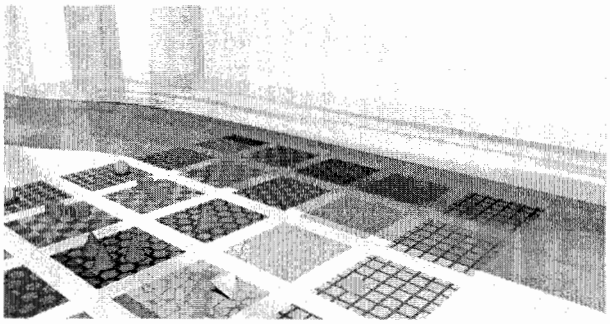

Figure 3. Illustration of the micro array for SPR imaging (iSPR).

The micro array for imaging with surface plasmon resonance (iSPR) is illustrated in Figure 3. The thin Au film coated onto the glass structure is exposed to polarized light at a certain controlled incident angle. Most of the light will be reflected by the gold surface, however at a specific incident angle an excess light absorption occurs, due to an interaction with the free electrons of the metal. The incident angle where this phenomenon appears is dependent on the optical density (i.e. refraction index) in the solution immediately at the capillary surface behind the gold film. The refraction index change is proportional to the amount of macromolecules (proteins) adsorbed at the surface. When the patterned gold surfaces are coated with selective binding entities, adsorption of the target compounds will be quantitatively detected based on the change in refraction index.

3. Microfabrication

The microfluidic chips consisting of two glass wafers were fabricated in the MESA+ cleanroom facilities. The channel structures flow-chamber and the reservoir holes were micromachined in the top wafer while the bottom plate housed the SRP gold patterns fabricated with a photolithographic. lift-off technique. The bottom wafer of the chip was made of a material with suited refractive index for matching with the hemisphere (n= 1.52). After a photolithography step, a high grade Au layer was patterned on the outside of the structure in order to prevent short circuitry. The substrate underwent a lift off with acetone. For the processing of the top plate a 4" Pyrex-glass wafer was coated with amorphous silicon. After a standard lithography step, the silicon layer was structured by reactive ion etching and served as a mask during the following wet etching step in HF to create the channel and chamber structures in the underlying glass layer. The inlet and outlet holes were formed in a second photolithography step on the back side using a resist foil. The inlet and outlet holes were created by powder blasting with AlO_3 particles. After ultrasonic cleaning and the removal of the silicon layer, the wafer was chemically cleaned and mechanically polished preparing the surface for the fusion bonding step. The structured wafers were bonded and diced into separate chips.

4. Experimental

The chip was placed in a specially designed holder made of Delrin, containing four reservoirs with integrated platinum electrodes connected to a high voltage source (IBIS 411 microfluidic control unit, IBIS Technologies B.V., Hengelo, the Netherlands). The applied voltages were controlled with a LabView program based on an analytical model [3]. An inverted microscope (Olympus IX51) with fluorescence unit, equipped with an F-View II 12-bit digital camera was used to view the stream profiles using the camera control software AnalySIS (Soft Imaging System GmbH, Münster, Germany).. All inlet reservoirs were filled with 10 mM HEPES in demineralized water (pH 7.2). In the experiment fluorescently labeled bovine serum albumin (BSA)(0.5 mg/ml in Hepes buffer) was added as a stream marker in the sample reservoir.

5. Results and discussion

Figure 4 shows photographs of the microfluidic device with patterned gold layer working under various guiding voltage settings. A sample colored with fluorescent dye was guided over an array of gold islands. Biomolecular interactions will occur at a spot of the micro array where a binding event takes place. Detection is possible using surface plasmon resonance imaging. The fluorescence was recorded with the microscope setup described above. Figure 4 shows sequential images, which were taken during the described experiment. From the left to the right the sample stream was directed from the left (first image) through the middle (third image) to the left (last image). The sample band is consistently directed towards the selected row of patterned gold detection surfaces. Peak broadening due to diffusion is moderate.

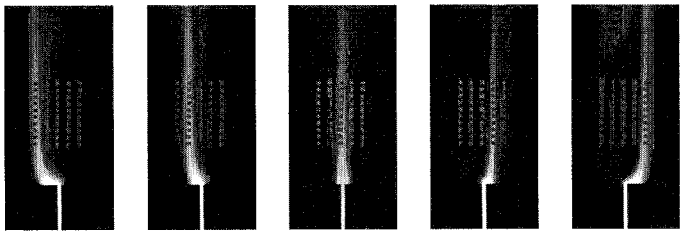

Figure 4. Sequential images of the address flow of a sample colored with a fluorescent dye (stream width = 50 μm) guided over an array of gold-islands (800 μm x 800 μm).

6. Conclusions

A new microfluidic device was designed and successfully fabricated for analysis of a sample stream over an microarray of gold patches. Electroosmotic flow was used to transport the liquid, hence no external pumps were required. The experiments show that the flow control on the proteomics-on-a-chip device was suited for guiding the sample stream to the desired sensing area in order to identify the protein interactions with SPR after CE-separation. The device will be further developed with immobilizing selective spots on the SPR imaging surface. Protein separations and testing of the detector are currently underway in our laboratory.

7. References

[1] A. D. Weston and L. Hood. Systems Biology, Proteomics, and the Future of Health Care: Toward Predictive, Preventative and Personalized Medicine. Journal of Proteome Research, Published on the web 17.01-2004.

[2] R.B.M. Schasfoort Proteomics-on-a-chip: the challenge to couple lab-on-a-chip unit operations. *Expert Rev. Proteomics* 1(1), 123–132 (2004).

[3] G.A.J. Besselink et. al., "Electroosmotic guiding of sample flows in a laminar flow chamber", Electrophoresis, submitted 02.2004.

TUNEABLE RESOLUTION ON A CAPILLARY ELECTROPHORESIS CHIP

Alexander Iles[1,2] and Andreas Manz[1]
[1]*ISAS, Bunsen-Kirchhoff-Str 11, D-44139 Dortmund, Germany*
[2]*current address: NIMS, ICYS, 1-1 Namiki, Tsukuba, Ibaraki 305-0044 Japan*

Abstract

In this work we demonstrate the application of counterbalanced hydrodynamic and electrophoretic forces in a standard cruciform micro-TAS device for the separation of labelled amino acids. By the appropriate control of these forces, separation resolution for a given pair of analyte ions could be tuned between zero and infinity.

Keywords: counterbalance flow, electrophoresis, hydrodynamic flow, amino acids

1. Introduction

On-chip electrophoresis has become an indispensable tool for the separation of a wide range of materials. Unfortunately, the method is constrained by two major physical limitations: the separation length and the separation voltage. A large separation length is required to separate molecules that have similar mobilities. For practical reasons, this length is typically less than 10 cm. Folding the separation channel back on itself can increase the separation length, but this introduces dispersive effects. The efficiency of an electrophoretic separation is also strongly influenced by the applied voltage. In general, higher voltages produce better separations. However, higher voltages produce greater Joule heating. This reduces resolution and, when taken to an extreme, can lead to the boiling of the analyte solution. Hydrodynamic counterbalancing in capillaries was first demonstrated a decade ago as a means for the electrophoretic separation of species with very similar mobilities [1]. Despite the effectiveness of this method, there have been relatively few attempts at hydrodynamic counterbalancing in microTAS devices. Separation using a T-junction has been demonstrated [2-3]. However, this method produced significant band dispersion. A cruciform chip was used to produce a step gradient for counterbalance, but the system suffered from poor stability [4]. In all of these studies, fluorescent markers having significantly different mobilities were used. Therefore, in this work we examined the counterbalance separation of biologically relevant samples with similar electrophoretic mobilities using a standard cruciform μTAS device.

2. Experimental

All experiments were performed using a Caliper 42 microfluidics workstation with a type 12 labchip device (Caliper Life Sciences, Mountain View, CA, USA). The chip was conditioned with 1.0 M NaOH before being flushed with deionised water. The chip was then filled with 0.1x TBE buffer solution and the sample mixture was added to the sample reservoir (inlet 6, Figure 1). Initial experiments were performed using fluorescent dyes, fluorescein and 5-carboxyfluorescein in 0.1x TBE. The amino acids, L-valine and glycine used in later experiments were labelled with FITC isomer 1 and added to 0.1x TBE buffer solution in accordance with normal labelling procedures [5]. For conventional electrophoretic separation, the photomultiplier tube (PMT) of the Caliper 42 system was set to a position on the separation channel that was 15 mm down from the channel intersection. Suitable voltages were applied to inlets 3, 4, 5 and 6 to drive the sample towards the waste reservoir and to "pinch" a sample plug at the channel intersection. Separation was then performed by switching the voltages so that 3000 V was applied to the top end of the separation channel (inlet 5), whilst the bottom end (inlet 3) was held at ground potential. For the counterbalance experiments, the PMT was set to a position 1 mm down from the channel intersection. Suitable pressures were applied to inlets 3, 4, 5 and 6 to pinch a sample plug at the sample intersection. Then, these pressures were

switched so that the sample plug was driven down the separation channel. When the sample plug reached a point 15 mm down the separation channel, a voltage was applied to inlet 3. This voltage drove the sample plug against the hydrodynamic flow and performed the separation. The separated analytes were then monitored as they reached the PMT. For the plug cycling experiments, the voltage was switched off just as the first analyte returned to the detector. The hydrodynamic flow then pushed the analytes 10 mm back down the separation channel, at which point, the voltage was switched on again. This procedure was repeated as required.

3. Results and discussion

As can be seen from Figure 2, preliminary experiments using fluorescent dyes were extremely encouraging. Below an applied voltage of 750 V, the peak-to-peak separation time tended towards infinity. At 700 V, only fluorescein was returned to the detector. These dyes have very different mobilities. Therefore, the method was applied to labeled amino acids. First, for comparison, the conventional electrophoretic separation of these amino acids was examined using the same microfluidic workstation, at the maximum voltage it could supply (3000V). The results of this are shown in Figure 3. Valine and Glycine are fully resolved; however, even when using the maximum length of the separation channel, the peaks are only separated by a fraction of a second. The same species were then separated using counterbalance flow (Figure 4, a, b, and c). The sample plug was hydrodynamically introduced into the separation channel and was driven past the detector to a point 15 mm down the channel. This produced the sharp peak on the left hand side in these counterbalance flow electropherograms. A voltage was then applied to counterbalance the hydrodynamic flow. A driving pressure of 0.15 psi was applied in each case. At a separation voltage of 900 V, all three species were returned to the detector (Figure 4a). At 750 V, the unbound label and valine were returned (Figure 4b). At 700 V, only the unbound FITC was returned (Figure 4c). A range of separation pressures, voltages and other counterbalance modes were investigated. Optimal separation was observed when using low pressure (0.15 psi or less) and relatively low voltage (<800 V). For the purposes of comparison, a 15 mm long separation channel was used; however, similar results could also be obtained using a much shorter separation channel. One alterative mode involved cycling the sample plug up and down the separation channel. At an applied voltage of 1200 V and a driving pressure of 0.15 psi, for a single return pass, the peaks of valine and glycine overlaped (Figure 5a). By cycling the sample plug five times up and down a 10 mm length of the separation channel, a significant improvement in resolution was noted (Figure 5b).

4. Conclusions

This work demonstrates that it is possible to tune the separation resolution for a given pair of analyte ions by counterbalancing hydrodynamic and electrophoretic forces and, in the process, overcome two of the major limiting factors affecting analytical microfluidic devices: the separation length and the separation voltage.

References

[1] C.T. Culbertson, J.W. Jorgenson, *Anal. Chem*, **66**(7), 955-962 (1994).
[2] M.B. Kerby, M. Spaid, S. Wu, et al, *Anal. Chem*, **74**(20), 5175-5183 (2002).
[3] M.B. Kerby, R.-L. Chien, *Electrophoresis*, **23**, 3545-3549 (2002).
[4] L.K. Ista, G.P. Lopez, C.F. Ivory et al, *Lab on a Chip*, **3**, 266-272 (2003).
[5] C.S. Effenhauser, A. Manz, H.M. Widmer, *Anal. Chem*, **65**(19), 2637-2642 (1993).

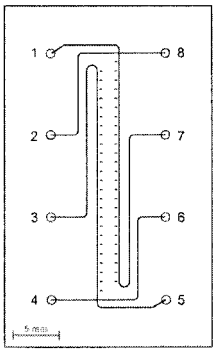

Figure 1.
Chip Layout.

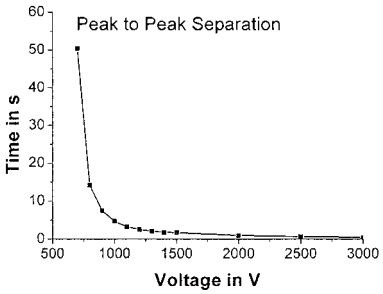

Figure 2.
The tuneable separation of 5-carboxy-fluorescein and fluorescein.

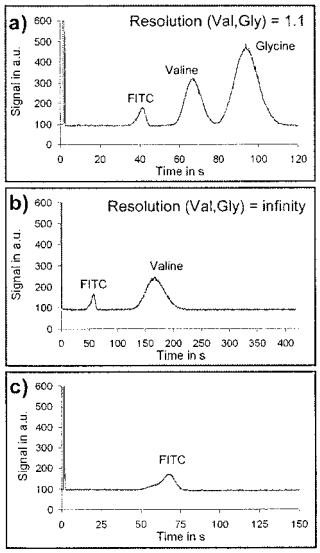

Figure 4. Using voltage to selectively return certain species to the detector: (a) At a separation voltage of 900 V, all three species were returned. (b) At 750 V, the unbound label and Valine were returned. (c) At 700 V, only the unbound FITC was returned. A pressure of 0.15 psi was applied in each case.

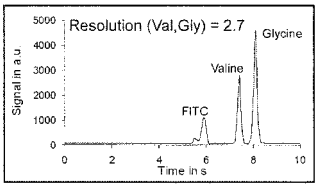

Figure 3. Conventional electrophoretic separation at 3000 V.

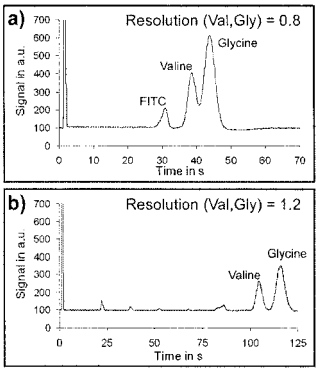

Figure 5. Cycling at a voltage of 1200 V and a counter pressure of 0.15 psi. (a) For a single return pass. (b) For five cycles up and down a 1 cm length of the separation channel. The small peaks between the injected plug and the Valine peak are from the unbound FITC-peak which just reached the detector each time as the voltage was switched off.

MEASURING THE INSERTION OF MICROFABRICATED MICRONEEDLES INTO SKIN WITH A PENETRATION SENSOR

P.W.H. Loeters[1], R.F. Duwel[1], F.J. Verbaan[2], R. Luttge[1], D.J. van den Berg[2], J.A. Bouwstra[2] and A. van den Berg[1]

[1]BIOS Lab-on-a-chip group, MESA+ Research Institute, University of Twente, P.O. Box 217, 7500 AE Enschede, The Netherlands (p.w.h.loeters@utwente.nl)

[2]Department of Drug Delivery Technology, Leiden/Amsterdam Center for Drug Research, P.O. Box 9502, 2300 RA Leiden, The Netherlands

Abstract

An in vivo method to monitor the penetration microneedles into skin based on measurements of electrical impedance has been developed in this study. For the first time integrated electrodes were used to show penetration monitoring through the stratum corneum (SC) of porcine skin. Three electrode arrangements were realized. On-chip electrodes clearly demonstrate feasibility and showed coherent and good results in vitro.

Keywords: electrical impedance measurement, microneedles, penetration, stratum corneum, transdermal drug delivery

1. Introduction

Microneedle array chips were presented [1,2,3,4] for painless drug delivery or body fluid sampling across the skin. For that purpose, the high-resistant top layer of the skin, the SC, needs to be penetrated. However, the actual penetration depth of the needles and the number of needles that do penetrate still remain uncertain. We believe that advances in controlled drug delivery as well as body fluid sampling will benefit from on-line penetration monitoring.

A typical array of an out-of plane microneedle chip as used in the experiments is shown in Figure 1. The insert of the figure also schematically depicts how we envision future integration of electrodes.

2. Setup

Here, the principle of measuring the impedance between two electrodes during penetration was tested using preliminary electrode arrangements in combination with a microneedle array. These electrodes were connected to an impedance analyzer. A piece of skin of approximately 1.5 cm x 2 cm was placed with its dermal side on the electrodes. For all described experiments porcine skin was used, because it is recognized as an excellent model for human skin. A water column was used to apply the force.

A microneedle array chip of 81 (9x9) out-of-plane microneedles is used. The chip had a 1 cm x 1 cm total chip surface. The needle height was 150 μm. On the needle side a 100 nm thick titanium layer was deposited. The test setup is shown in Figure 2.

3. Results and discussion

In the off-chip concept, shown in Figure 4a, thin-film platinum electrode pads of 2.5 mm x 3 mm with a distance of 1.3 cm were deposited on a glass substrate. A control was performed by applying the microneedle chip with its flat side towards the SC. Subsequently, the chip was subjected to a distributed force profile (see curve I in Figure 6a). When the chip was turned around the impedance significantly decreases compared to the control (see curve II in Figure 6a) which also could be a result of the higher conductivity of the titanium layer.

To cancel the influence of this layer on the impedance, a second electrode configuration was set up. As shown in Figure 4b the titanium layer on the needle side serves as a measuring electrode which is placed on the top side of the skin (SC). A counter electrode was again placed at the dermal

side of the skin. Now a silicon chip with neither microneedles nor holes but with a deposited 100 nm titanium layer functions as a control. Subsequently, the chip was again subjected to a distributed force profile.

At a certain increase of force the impedance (|Z|) and phase (Φ) spectra will drastically change. This means that the frequency at which a pure resistance is measured (Φ=0) is also shifted (13,5 Mhz to 2,5 MHz). This phenomenon that is shown graphically in Figure 5 is taken into account when plotting the resistance in time (Figure 6). The difference in impedance change between the needle array chip (II) and the chip without needles (I) is shown in Figure 6b. The impedance first decreases to a stable value for both cases. At a certain increase of force the impedance in the microneedle chip configuration decreases further. This decrease relates to penetration of the stratum corneum.

Although this simple electrode arrangements show feasibility, they are not applicable in vivo. Therefore a third approach was chosen. In this case an electrically insulating (polymer) hollow microneedle array[1] was modified by filling two microneedles with silver epoxy resulting in an on-chip arrangement of the electrodes. The silver epoxy was connected to a printed circuit board as it is shown in Figure 3. Also in this assembly characteristic drop to lower impedance values are observed.

We expect that the following penetration mechanism is occurring (Figure 4c). When the needle array is placed on the topside of the skin (stratum corneum) only a poor electrical contact with the electrode on the dermal side is realized (1). Increasing the pressure force causes an improved surface contact. This improvement results in a decrease in resistance, until equilibrium is reached (2). Further rise of the force does not result in an impedance change until a critical force is reached at which a stepwise impedance decrease is observed (3). We believe that the penetration force is then reached: the force needed to penetrate the stratum corneum of (porcine) skin.

5. Conclusions

A first step to a sensor for the penetration of microneedles has been taken. The second can be transferred to an in vivo situation in future studies, for example by placing the counter electrode (see Figure 4) on the topside of the skin instead of at the dermal side. The promising results of a penetration sensor based on impedance measurements call for better batch-type integration of the electrodes to which further work will be devoted.

References

[1] S. Henry, D.V. McAllister, M.G. Allen and M.R. Prausnitz, "Microfabricated microneedles: a novel approach to transdermal drug delivery," Journal of Pharmaceutical Sciences, vol 87, no.8, pp.922-925, 1998

[2] B. Stoeber and D. Liepmann, "Two-dimensional arrays of out-of-plane needles," International Mechanical Engineering Congress & Exposition, 2000

[3] J.G.E. Gardeniers, R. Lüttge, J.W. Berenschot, M.J. de Boer, S.Y. Yeshurun, Meir Hefetz, R. van 't Oever and A. van den Berg, "Silicon micromachined hollow microneedles for transdermal liquid transport," Journal of microelectromechanical systems, 12, pp.855-861, 2003

[4] E.V. Mukerjee, S.D. Collins, R.R. Isseroff and R.L. Smith, "Microneedle array for transdermal biological fluid extraction and in situ analysis," Sensors and Actuators A: Physical In Press, Corrected Proof, 2004

* Nanopass patent pending

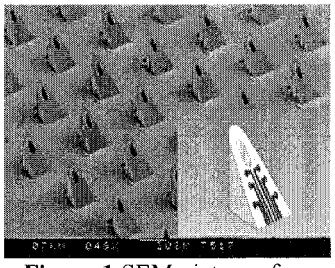

Figure 1 SEM picture of an array of silicon microneedles and an impression of a microneedle with integrated electrodes patterned on the sloped sidewall

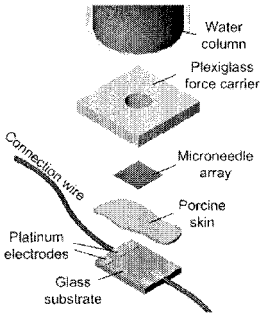

Figure 2 Test setup with platinum electrodes, pig skin, silicon microneedle array and water column

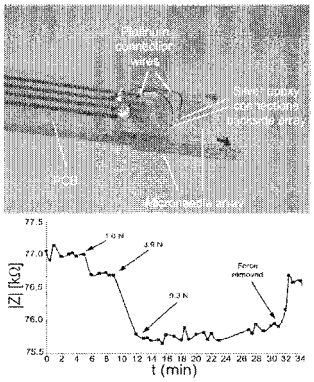

Figure 3 Assembled penetration sensor with impedance plot

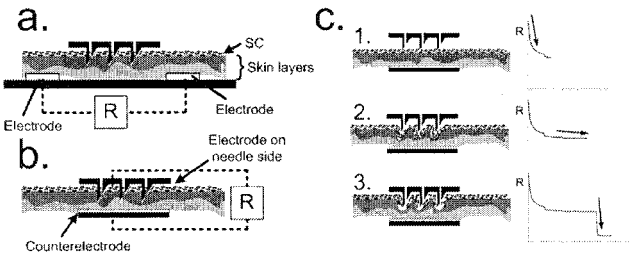

Figure 4 Two different electode configurations for skin impedance measurements (a&b) c) Penetration steps: microneedle array 1) on undeformed skin (small contact surface) 2) on deformed skin (large contact surface) 3) through the stratum corneum (improved skin conductivity)

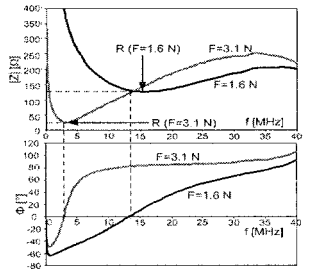

Figure 5 Change in impedance and phase spectrum for a stepwise force change from 1,6 N to 3,1 N (from 13,5 Mhz to 2,5 MHz)

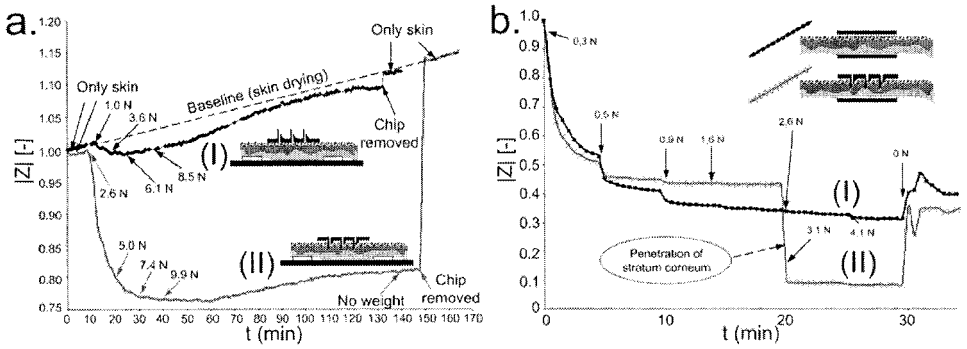

Figure 4 Impedance change for the first (a) and second (b) electrode configuration with increasing force and eventually chip removal. In these graphs |Z| denotes a normalized impedance, which is the measured impedance divided by the starting value

SHEATHLESS MICROFLUIDIC CYTOMETER WITH ASYMMETRIC MICRONOZZLE FOR ABSOLUTE COUNTING OF BLOOD CELLS

Junha Park[1,3], Seonghwan Kim[3], Jung Kyung Kim[3], Seok Chung[3], Keunchang Cho[3], Chanil Chung[3], Dong-Chul Han[1], and Jun Keun Chang[2,3]

[1] *School of Mechanical and Aerospace Engineering, Seoul National University, Seoul 151-742, South Korea*

[2] *School of Electrical Engineering and Computer Sciences, Seoul National University, Seoul 151-742, South Korea*

[3] *Digital Bio Technology, Co., Seoul 151-742, South Korea*

Abstract

The study of cell physiology at the cellular level has a potential impact on the diagnostics and drug discovery. Microfluidic chip based cytometry enables single cell analysis on a chip where a focused stream allows cell by cell analysis. Focused stream by a symmetric nozzle structure or a hydrodynamic force via sheath flow can cause target cells to clog at the nozzle inlet or to make a doublet at the detection point respectively. In this research, we applied an asymmetric micronozzle to microfluidic chip based flow cytometry for high-throughput analysis of single cells without sheath flow.

Keywords: asymmetric micronozzle, single cell manipulation and analysis, absolute cell counting, microfluidic cytometer, sheath flow

1. Introduction

Most of the microfluidic chip based flow cytometry use sheath flow for the hydrodynamic focusing of the sample in the microchannel.[1-3] In this case, however, additional buffer and pumps to form sheath flow are required.[4] These cause the system to be complex and focused stream to be unstable. Sheathless microfluidic chip based cytometry, which have a symmetric nozzle inlet, are also used but, they cause sample particles to clog the channel[4] or to make doublet at the detection channel. Thus, the objective of this research is to apply asymmetric nozzle to microfluidic chip based flow cytometry. To achieve this aim, we compare the fluorescence signals from the focused stream with sheath flow and from the confined stream with asymmetric nozzle. SYTO 16 (Molecular Probes, Inc., USA) -stained white blood cells (WBCs) are detected via optical detection system.

2. Experimental

Fabrication of microfluidic cytometry chip

Both of microfluidic cytometry chip focused by sheath flow and asymmetric nozzle structure were fabricated by soft lithography method. Thick photoresist (SU-8, Microchem Corp., USA) was patterned on silicon wafer using photolithography method and these pattern was molded via replica molding methods using Poly(dimethylsiloxane) (PDMS, Sylgard 184, Dow corning Corp., USA). PDMS replica was bonded with slide glass via oxygen plasma treatment.

Sample preparation

One hundred microliter of Human whole blood sample was extracted from volunteers. Red blood cells (RBCs) in sample were removed using 2 mL of RBC lysis solution. It was washed out 3 times with phosphate buffered saline (PBS). The remained pellet was resuspended with 100 μL of PBS. Five hundred nanoliter of SYTO 16 (100nM) was added to WBC suspension. It was incubated for

30 minutes at room temperature and washed out 3 times with PBS. This sample solution was driven by a peristaltic pump (P625/10k. 143, Instech, USA) in the microfluidic cytometry chip.

Fluorescence signal detection

Optical detection system was mounted on inverted microscope (IX71, Olympus, USA) to detect the fluorescence signal from SYTO 16-stained WBCs. A blue laser was used for the excitation of the fluorescence. The emitted signal was detected and transformed to electrical one by a photo multiplier tube (PMT, H5784-01, Hamamatus, Japan). The electrical signal from the PMT was sent via a preamplifier to a DAQ board (SD-104, COMIZOA, Korea) on PC and displayed on the monitor.

3. Results and discussion

The schematic geometry of an asymmetric nozzle and the contour of lateral velocity along the asymmetric nozzle inlet are shown in Fig. 1. This shows that asymmetric nozzle inlet makes the priority of one half of the fluid flow respect to the other. Fig. 2 shows the mechanism in low velocity field. Fig. 3 shows the SYTO 16-stained WBC passing through the asymmetric nozzle. At Fig. 4 (a), detected signal from the focused stream with sheath flow shows broad distribution which has two peaks at the fluorescence level of 1,300 and 2,300. The signal from the confined stream with asymmetric nozzle structure without sheath flow shows one sharp peak at the level of 1,000 (Fig. 4 (b)). It is seen that the asymmetric nozzle inlet reduces the probability of the micronozzle inlet clogging and doublet forming by the WBCs.

4. Conclusions

The asymmetric nozzle could have a significant impact on the microfluidic chip based flow cytometry. It could simplify the procedure of the experiments. It also enables us to count absolute number of cells which have low fluorescence signal levels such as CD4 because of the high confinement effect of nozzle structure compared with that of focused stream using sheath flow. Furthermore, high-throughput analysis of individual single molecules would be realized with the array of asymmetric nozzles on the microfluidic cytometry chip.

Acknowledgements

This research has been financially supported by the "21C New Frontier Project" of the Ministry of Science and Technology and the "Development of Milli-Structure Manufacturing Technology" of Ministry of Commerce, Industry and Energy. The author also would like to thank Mr. K.C. Shin and Miss K.M. Lee of Digital Bio Technology for the support of microchip fabrication process.

References

[1] G. B. Lee, C. I Hung, B. J. Ke, G. R. Huang, B. H. Hwei and H. F. Lai, J. of Fluids Engineering, 123, 672-679 (2001)

[2] W. A. Lyon and S. Nie, Anal. Chem., 69, pp. 3400-3405 (1997)

[3] J. H. Nieuwenhuis, J. Bastemeijer, P. M. Sarro and M. J. Vellekoop, Lab Chip, 3, 56-61 (2003)

[4] D. Huh, Y. C. Tung, H. H. Wei, J. B. Grotberg, S. J. Skerlos, K. Kurabayashi and S. Takayama, Biomedical Microdevices, 4(2), 141-149 (2002)

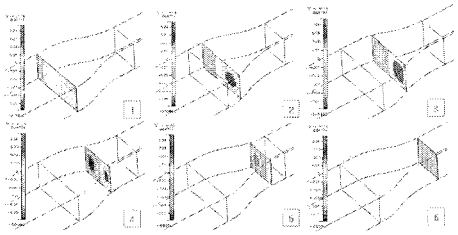

Figure 1. The geometry of an asymmetric micronozzle structure and the contour of lateral velocity along the muzzle inlet. (CFD-ACE, CFD Research Corp., USA)

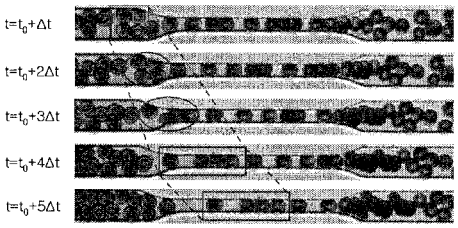

Figure 2. Sequential motion (Δt = 330 ms) of RBCs in microfluidic cytometer with the asymmetric micronozzle at low velocity field. Each RBC flowing with parallel to the asymmetric nozzle inlet enters into the nozzle one by one from each half of the stream in the channel.

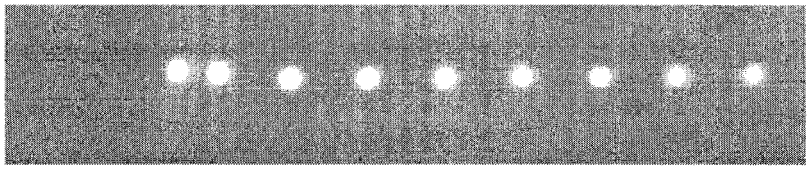

Figure 3. Fluorescence image from SYTO 16-stained WBC at the entrance of the asymmetric nozzle inlet via high speed cooled CCD camera (POC, Kelheim, Germany). SYTO 16-stained WBC flows from left to right of the image.

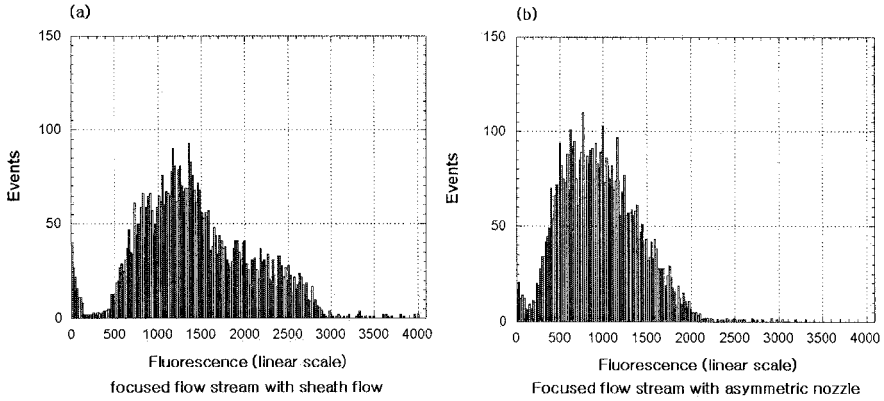

Figure 4. The histogram of the fluorescence signal from SYTO 16-stained WBCs flowing in microfluidic cytometry chip with (a) hydrodynamic focusing microchannel for sheath flow and (b) sheathless asymmetric micronozzle structure.

SAMPLING FOR POINT-OF-CARE ANALYSIS OF LITHIUM IN WHOLE BLOOD WITH CHIP BASED CE

Elwin Vrouwe, Regina Luttge and Albert van den Berg

*BIOS The Lab-on-a-Chip Group, MESA+ Research Institute, University of Twente, P.O. Box 217, 7500 AE Enschede, The Netherlands. (**a.vandenberg@ewi.utwente.nl**)*

Abstract

In this paper the sampling and transfer of blood for microchip capillary electrophoresis (CE) microchip is studied. Following the coupling of microneedle arrays to a CE chip, which has been introduced before [1], the requirements for quantitation of physiological relevant concentrations of inorganic cations are examined in further detail. Additionally a new method is presented using a blood sampler sealed at one end with a filter membrane to conveniently transfer samples to the chip. For the first time we demonstrate rapid and accurate determination of lithium at a clinical relevant concentration of 0.6 mM in blood plasma from a patient under lithium medication.

Keywords: capillary electrophoresis microchip, microneedles, point-of-care, whole blood

1. Introduction

Sampling for CE microchip diagnostics means: receiving a body fluid sample from the patient, transfer of this sample onto the microchip and retrieving a quantitative measurement. One future point-of-care application could be the determination of lithium in blood. Lithium salt is used for the treatment of bipolar mood disorders, however its concentration has to be maintained within a narrow therapeutic window. It has been shown that alkali metals can be quantitatively measured in citrated whole blood by means of microchip CE without any additional sample pretreatment (e.g., off-chip dilution) [2]. Meanwhile, microneedles have been demonstrated as an exiting new approach for blood withdrawal, though the interfacing to a CE chip has been a challenge and only preliminary non-quantitative tests were demonstrated [1,3]. To receive systematic clinical data we need to verify the complete sampling procedure including repetitive measurements on the same chip. For this study we consider a microchip mounted in a dedicated chip holder as shown in Figure 1. This setup allows us to wash the sample compartment, however when whole blood samples are used cleaning is difficult. Therefore we introduce a sample transfer device that retains all blood components except for the small ions allowing repetitive measurements thereof.

2. Measurement device and concept for microneedles

The blood collector shown in Figure 2 consists of a glass capillary sealed at one end with a filter

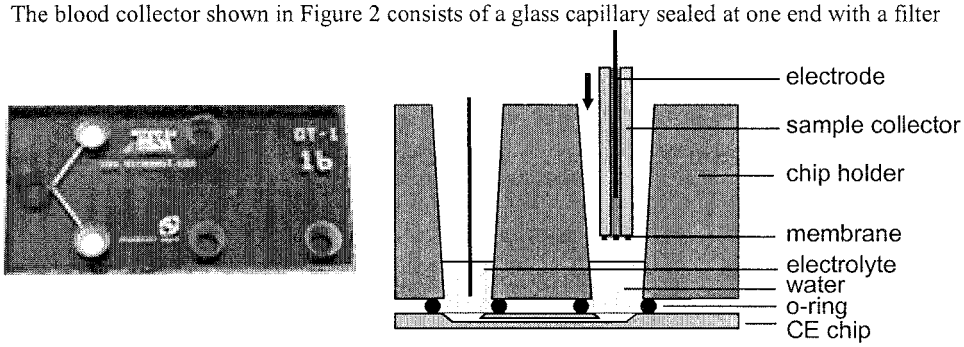

Figure 1. Photograph of the CE chip and a schematic cross section of the chip holder with the sample collection device

membrane. When the open end is dipped into a drop of whole blood it will automatically start to fill the collector by capillary action. Subsequently an electrode required for the CE is inserted into the collector and the whole is placed in the chip holder. The membrane prevents direct contact between the sample and the CE chip, retaining the blood residues while allowing the small ionic species to migrate through. After the CE experiment the sampler is disposed and the CE chip is immediately ready for the next sample.

The CE chip and sample collector, which represents a simplified model for a microneedle array system, are connected through a relatively large dead volume defined by the compartment on the chip. If this volume would be filled with background electrolyte (BGE) in order to make liquid contact, the analyte migrating out of the sampler during the electrokinetic injection would experience a dilution that could be detrimental for the detection. In the case of microneedle arrays where sample volumes are in the order of a few nanoliter, the sample can become diluted by more than 200 fold. In order to prevent this, the compartment is filled with deionized water instead. This provides conditions for head column field amplified stacking of the analyte at the boundary between the BGE inside the chip and the water inside of the compartment [4].

3. Experimental

Glass disposable micropipettes (Drummond Scientific Company, 0.5 mm inner diameter, 1.0 mm outer diameter) were cut to a length of 1 cm. One end was sealed with a filter membrane (Millipore, mixed cellulose esters, 0.22 μm pore size) by heating the capillary in a gas flame and pressing it onto the membrane. The internal volume of the capillary defining the minimum amount of sample required is 2.0 μl, which is much less than the volume that can be obtained by a finger stick. The microneedle arrays were used without a membrane and were placed directly above one of the compartments on the chip as described before [1]. Here however, 4 nl droplets of whole blood from a finger stick were applied manually to each of the 8 needles on the array to simulate the sampling from the skin.

The CE experiments were performed on a glass chip with integrated conductivity detection electrodes. The channels were coated with polyacrylamide for optimized sample stacking conditions [2]. The volume in the compartment between the chip and the sampler was filled with deionized water. For the separation a BGE consisting of 15 mM ammonium acetate and 15 mM acetic acid was used. In some of the experiments 5 mM 18-crown-6 was added to the BGE to form a complex with potassium. This makes it possible to detect potassium with conductivity detection, which would otherwise be impossible because of the identical ionic conductivity of the ammonium BGE co-ion and potassium from the sample.

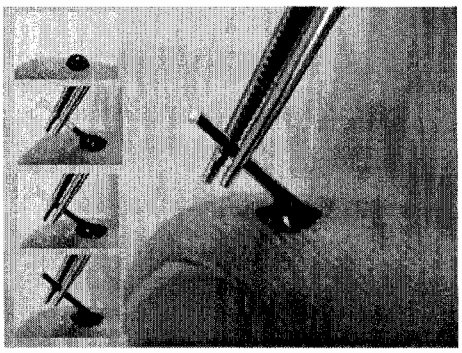

Figure 2. Sampling blood from a finger stick with a membrane covered glass capillary. The white filter membrane is visible at the end.

4. Results and discussion

The capillary collection device was used to transfer calibration standards or whole blood samples directly from a finger stick to the chip. Physiological concentrations of sodium and magnesium were detected without addition of an anticoagulant (Fig. 3). The sampler was also used on a drop of blood plasma obtained from a patient on lithium therapy. The lithium concentration was determined at 0.7 mM (7%

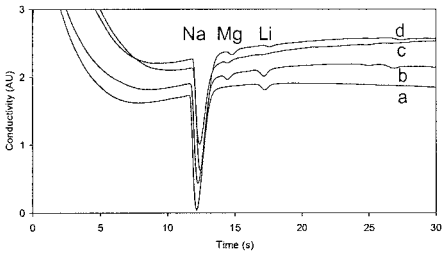

Figure 3. Electropherogram of a) aqueous calibration mixture with 140 mM Na and 2 mM Li, b) citrated whole blood spiked with 2 mM Li, c) whole blood w/o anticoagulant, d) heparinized plasma from a patient on lithium therapy. Sampling via glass capillary. Running electrolyte 30 mM ammonium acetate/acetic acid.

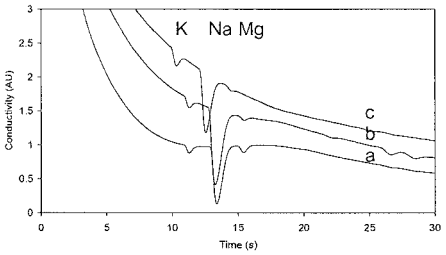

Figure 4. Electropherogram of a) a drop of whole blood on a microneedle array, b) whole blood 225 times diluted in compartment, c) 8 drops of whole blood (4 nl each) applied on the needles of an array. Separation conditions as in Fig. 3 with 5 mM 18-crown-6 added to the BGE.

RSD, n=3) while 0.62 mM was specified by the hospital.

When using the microneedle array similar peak sizes were obtained regardless whether a drop of blood (10 µl) was placed on the array or that only the internal volume of the needle array (32 nl) was filled with blood, or that this 32 nl was put directly in the water filled chip compartment diluting it 225 fold (Fig. 4). This proves that the sample stacking procedure works consistently when the chip compartment is filled with water.

5. Conclusions

The method of using a capillary sample collector shown here provides an easy way to transfer blood from a finger stick onto a CE chip. The chip stays clean and can be used for multiple samples. Sample stacking using a water plug works reliable even with the relatively large volume required to completely fill the chip compartment. Physiological levels of potassium, sodium and magnesium were determined even in the small sample volume that is typical for blood sampling using microneedle arrays. The determination of lithium in an actual plasma sample from a patient was consistent with routine determination in the hospital. For the actual use of the microneedles for sample retrieval the technological requirements to penetrate the skin to the required depth and sample blood still need to be addressed. In the near future we intend to use the capillary sample collector for further clinical trials to prove the potential for point-of care analysis of lithium in whole blood.

Acknowledgements

The authors gratefully acknowledge Dutch Technology Foundation STW for financial support (TET 5370).

References

[1] H.J.G.E. Gardeniers, R. Luttge, E.J.W. Berenschot, M.J. De Boer, S.Y. Yeshurun, M. Hefetz, R. Van't Oever, A. Van den Berg; *J. Microelectromech. Syst.*, **12**, 855-862 (2003)

[2] E.X.Vrouwe, R. Luttge and A. van den Berg, *Electrophoresis,* **25**, 1660-1667 (2004)

[3] E.V. Mukerjee, S.D. Collins, R.R. Isseroff, R.L. Smith, *Sens. Actuators A*, in press

[4] C-X. Zhang and W. Thormann, *Anal. Chem.*, **68**, 2523-2532 (1996)

DRY POWDER MIXING WITHOUT RESTRICTIONS IN COMPOSITION

Torsten Vilkner[1] and Andreas Manz[2]

[1] *Imperial College London, Department of Chemistry, Exhibition Road, SW7 2AZ London, UK*

[2] *ISAS - Institute for Analytical Sciences, Bunsen-Kirchhoff-Straße 11, D-44139 Dortmund, Germany*

Abstract

This paper describes an automated on chip system to homogenously mix the amount of dry powder that is usually needed for one tablet by means of fluidization. The sequential dry-powder injection method presented at the last MicroTAS [1] has been integrated here to allow for the introduction of any mass (>1mg) of non-cohesive dry powders with no need for using a balance. Successful mixing has been confirmed through visualization via differently dyed particles, homogeneity of the generated blend can be seen from the distribution of particles on the surfaces of pressed tablets and the applicability and reproducibility was shown in series of ascending fractions of one component.

Keywords: dry powders, tablet composition, chip based

1. Introduction

Particle handling is a fundamental issue in the pharmaceutical drug development process. The aim of mixing is to give a homogenous system containing active drug and one or more inert excipients. Traditionally the term blend homogeneity addresses a uniform distribution of the active ingredient in an excipient matrix, which too is evenly distributed throughout the mixing vessel. Theoretically an ideal mixture has a homogeneous distribution of all the components [2]. Inadequate dry powder mixing can result in the need for process steps to be included, e.g. wet granulation to ensure blend homogeneity. However, the performance of some formulations, e.g. dry inhaled powder, are dependent upon true dry powder mixing. Indeed this is highlighted by Muzzio et al. [3], who point out in a recent paper one of the major issues now is how to mix or disperse tiny proportions of predominantly minute particles within a matrix of much larger particles, to yield a homogenous blend with low potential to segregation. Chip-based powder reacting might be suitable to achieve this goal.

2. Theory

When a particle bed is being streamed through from underneath by a fluid or a gas, a pressure drop is produced due to the fluid drag. At the point where the gravity force of the particles and the upwards drag force become equivalent the particles do not longer rest on each other but become fluidized. Particle movement is solely due to bubbles that move upwards and carry particles from the bottom to the top. Mixing and segregation, which depend on size and density distribution of the particles, are characteristic for a particular bed and can be altered by adjusting the gas velocity. [4]

3. Experimental

The chip design (Fig. 1) shows three injection channels and one outlet channel in a cross-shaped arrangement. The injection channels are T-shaped with the powder inlets A and the gas inlets B. The mixing vessel is placed directly above C (distance BC=60mm, channel depths 700μm). The powders were introduced via pipette tips with an inner diameter of 6mm at the bottom. To avoid particle entrainment during the process of fluidisation they were sealed with Cello-tape after filling with powders. Smaller pipette tips were connected perpendicularly to the vessels in a height of about 5cm to guarantee an appropriate airflow. The particles in every inlet were fluidised through the application of gas pressure. Turning the applied gas flow on/off injected a certain amount of

powder every single time [1]. The number of injections from every inlet was digitally regulated (Microrobotics K4 Control Computer). Particles from every inlet accumulated in the mixing vessel on C, where the applied gas flow promoted mixing by means of fluidisation. Sealing the outlet D temporarily prevented particles from flowing towards it. When the injection and mixing procedure for the required composition was finished the mixing vessel was closed and the outlet was opened at the same time, which guided the gas and particle flow towards the outlet. Particles were collected in the KBr-pellet sample unit of a commercially available hydraulic press (Perkin Elmer). A tablet was subsequently produced in the press. A pressure of 5 tons was thereby applied for 2 minutes followed by 10 tons for 3 minutes. The obtained tablets had a diameter of 13mm and a thickness of approximately 1.5mm.

Differently dyed (white, blue) Dibasic Calcium Phosphate (Fujicalin®) particles, which were found suitable for the applied injection scheme in earlier experiments, were utilized as sample ingredients for the visualization experiments. The surface of the tablets was photographed under equal condition with a 4 million pixel digital camera (Casio Exilim). The pictures were then converted into non-compressed tagged image files (.tif) using standard graphics software. The program Scion Image was utilized to convert into grayscale and measure the mean gray value on the whole surface of every tablet.

4. Results and discussion

Using the method described above small amounts of differently dyed non-cohesive particles were moved through channels on a chip towards a mixing vessel. The injections were found to be reliable and were unaffected by the multiple gas flows from different directions in the chip. The mixing by means of fluidization could be observed with the naked eye and was in addition confirmed through the evaluation of the particle distribution on the surface of pressed tablets. It was found to be homogenous and random as can be seen in Fig. 3. The evaluation of the mean gray value in grayscale pictures of the surface of the tablet showed a linear dependence on the injected particle fraction, which corroborates that the predicted tablet compositions were generated.

5. Conclusions

Fluidization promoted mixing achieved a homogenous distribution of two compounds used in the final mixture as shown in Fig. 3 and Fig. 4. Experiments with three compounds have been similarly successful. Nevertheless the system is still restricted to the usage of non-cohesive powders that can be fluidized [5]. Methods to overcome this drawback are under current investigation.

Acknowledgements

The authors would like to thank Mr Arif Shivji for his contributions and Pfizer Ltd. for the funding of this project.

References

[1] T.Vilkner and A. Manz, MicroTAS 2003, pp. 469-472
[2] V. Uhl and J. Gray, Mixing: Theory and Practice; Academic Press: New York, 1967
[3] F. J. Muzzio, T. Shinbrot and B.J. Glasser, Powder Technology 124, 2002, pp. 1-7
[4] P. N. Rowe and A.W. Nienow, Powder Technology 15, 1976, pp. 141-147
[5] D. Geldart, Powder Technology 7, 1973, pp. 285-292

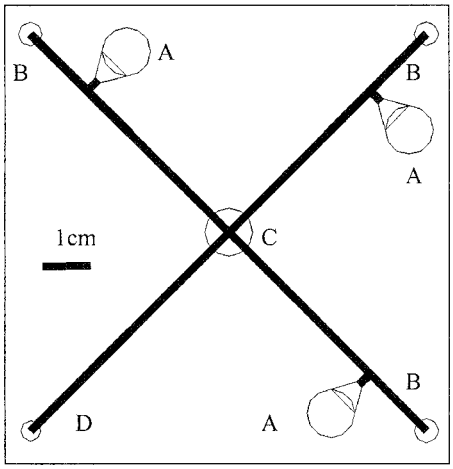

Figure 1. Schematic channel design of the mixing chip (A - powder inlets, B - gas inlets, C - mixing vessel, D - outlet)

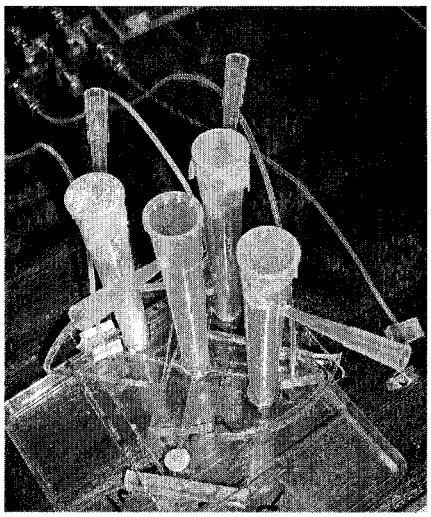

Figure 2. Picture of mixing chip with 3 powder inlets filled with dyed particles and one mixing vessel

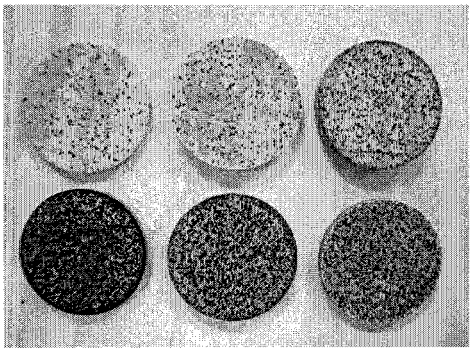

Figure 3. Six tablets of approximately 400mg weight consisting of blue and white particles of Dibasic Calcium Phosphate powder with increasing fractions of blue particles (from top left to bottom left: 3, 9, 17, 33, 50, 66 percent)

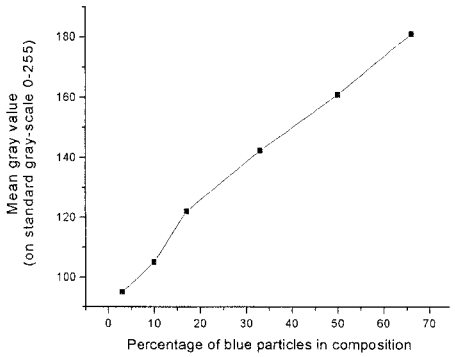

Figure 4. Mean gray value of the tablet surface in grayscale photographs depending on the percentage of blue particles in the mixture.

SELECTIVE MAGNETIC BEAD CAPTURE USING AN ADRESSABLE ON-CHIP ELECTROMAGNET ARRAY

Kristian Smistrup[1*], Ole Hansen[1], Peter T. Tang[2], and Mikkel F. Hansen[1]

[1] *MIC - Department of Micro and Nanotechnology, Technical University of Denmark, Building 345 East, DK-2800 Kongens Lyngby, Denmark,* *krs@mic.dtu.dk

[2] *Department of Manufacturing Engineering and Management, Technical University of Denmark, DK-2800 Kongens Lyngby, Denmark*

Keywords: Magnetic Separation, Immunoassay, Magnetic Microbeads, MEMS, Adressable.

1. Introduction

Magnetic separation is a well-known technique in macroscopic systems [1] and in recent years technologies for magnetic separation in microfluidic systems have emerged. Furthermore, the principle of magnetic separation, i.e., manipulation of biochemically functionalised magnetic beads, has been used in microsystems for several different applications such as magnetic tweezers, magnetic mixing and extraction of DNA or antigens from a suspension [2-5].

In this work we demonstrate the principle of a new application of magnetic bead capture. Magnetically identical beads are selectively captured at and released from different sites in a microfluidic channel using an addressable array of electromagnets. Thus, placing differently functionalized beads on each of the addressable spots of the array it is in principle possible to carry out several assays simultaneously.

2. Design and fabrication

The design of our microsystem is shown in Fig. 1. Each microsystem contains three microelectromagnets, each consisting of a square spiral copper coil semi-encapsulated in a dielectric layer and a soft magnetic yoke on top of that. The soft magnetic yoke is also used as a return path for the electrical current. Both nickel and permalloy has been used as magnetic material for the yoke. A microfluidic channel is etched into the opposite side of the wafer. The microsystems are fabricated using standard cleanroom technology. Fig. 2 summarizes the fabrication process. For more details see [6].

3. Theory

In microfluidic systems three forces generally affect magnetic beads; magnetic force $\mathbf{F}_{mag}$, gravitational force (buoyancy) $\mathbf{F}_{grav}$, and the fluid drag $\mathbf{F}_{fluid}$. Furthermore, the Reynolds number for the fluid flow is small such that the Navier-Stokes equation reduces to a Poisson equation in the absence of a net body force on the fluid, and the fluid drag on the magnetic beads can be described by the Stokes drag. Due to the small radius R_{bead} of the magnetic beads $\mathbf{F}_{fluid}$ ($\propto R_{bead}$) will dominate over the inertial term ($\propto R_{bead}^3$) in the equation of motion. Therefore the inertial term can be discarded, and the equation of motion reduces to a first order differential equation for the bead position $\mathbf{r}_{bead}$

$$\mathbf{v}_{bead} = \frac{\partial \mathbf{r}_{bead}}{\partial t} = \mathbf{v}_{fluid}(\mathbf{r}_{bead}) + \frac{1}{6\pi\eta R_{bead}}\left(\mathbf{F}_{mag}(\mathbf{r}_{bead}) + \mathbf{F}_{grav}\right) \quad (1)$$

$$\mathbf{F}_{mag}(\mathbf{r}_{bead}) = \tfrac{1}{2}\mu_0 V_{bead}\chi_m \nabla\left(\left|\mathbf{H}(\mathbf{r}_{bead})\right|^2\right) \quad (2)$$

where η is the viscosity of the fluid, μ_0 is the magnetic permeability of vacuum, χ_m is the measured magnetic susceptibility of the magnetic beads, and V_{bead} is the volume of a magnetic bead. The buoyancy of the fluid is included in $\mathbf{F}_{grav}$.

If hydrodynamic interactions are neglected, and the microfluidic channel is straight and has rectangular cross-section, the velocity profile of the fluid $\mathbf{v}_{fluid}$ can be found analytically as a series expansion. Using this and by calculating the magnetic field $\mathbf{H}$ using FEMLAB® (neglecting magnetic interactions between beads), we have simulated the flow of magnetic beads in our microfluidic channels. [7] We have used this to determine the optimum experimental parameters, volumetric flow rate and current in the electromagnets.

4. Results and discussion

Figure 3 shows the fabricated microsystem mounted in a housing with optical access as well as electrical and fluidic connections. This system has been placed under an optical microscope, and it has been observed how the beads settle in the microfluidic channel.

In Fig. 4 we show micrographs of the microfluidic channel at different times. With a solution of water and 76×10^3 μL^{-1} magnetic beads (MyOne®, Dynal, Norway, $2R_{Bead} = 1.05$ μm, $\chi_m \approx 1.5$) flowing in the microfluidic channel from the left at a volumetric flow rate of 1 μL/min, a current of 0.5 A was fed to the rightmost electromagnet at $t = 0$ min. After 15 min. it is seen that magnetic beads have settled on top of the rightmost electromagnet. At $t = 15$ min. the current in the leftmost electromagnet was also set to 0.5 A. After 30 minutes it is seen that beads have now settled on both electromagnets, but the amount of beads on the rightmost electromagnet has not changed significantly since $t = 15$ min. The aforementioned simulations show that all beads should be captured on the leftmost microelectromagnet with this flow rate and current. At $t = 30$ minutes the rightmost electromagnet is turned off. After 35 min. it is seen that all beads have been released from the rightmost electromagnet, while no beads have apparently left the leftmost electromagnets. This shows that it is possible to selectively capture and release magnetic beads at the two different microelectromagnets in the microfluidic channel.

With this simple experiment we have demonstrated that it is in principle possible to create a microfluidic system containing an array of differently functionalized sites within a microfluidic channel, and since the functionalization of the sites is limited only by the chemistry that can be applied on the surface of magnetic beads, it is possible to create an addressable array of functionalities within the microfluidic system by having individually addressable electromagnets.

As an example of a potential application of this technique, we describe simultaneous magnetic separation of two species of antigens. If one set (set-1) of magnetic beads are coated with one kind of antibody, and another set (set-2) is coated with a different antibody, set-1 can be placed at the rightmost electromagnet, and set-2 can be placed at the leftmost electromagnet by selective bead capture. When a suspension containing a number of different antigens is sent through the microfluidic channel, the target antigen of set-1 will be caught on the rightmost electromagnet, and the (different) target antigen of set-2 will be captured on the leftmost electromagnet. Afterwards the two sets can be sequentially released and collected into different test tubes.

References

[1] J. Watson, *J. Appl. Phys.* **44**, 4209-4213, (1973)

[2] C-H. Chiou, Z-F. Tseng, G-B. Lee, *Proc. MEMS 2004*, 613-616

[3] R. Rong, J-W. Choi, and C. H. Ahn, *Proc. μTAS 2003*, 335-338

[4] T. Deng, M. Prentiss, and G. M. Whitesides, *Appl. Phys. Lett.* **80**, 461-463 (2002)

[5] J-W Choi, T. F. Liakopoulos, C. H. Ahn, *Biosensors & Bioelectronics* **16**, 409-416 (2001)

[6] K. Smistrup, O. Hansen, P. T. Tang, and M. F. Hansen, "Microelectromagnet for magnetic manipulation in microfluidic systems", *IEEE – Nanoscale Devices and Systems Integration, Miami, USA 2004,* submitted to *J. Micromech. Microeng.*

[7] K. Smistrup, O. Hansen, H. Bruus, and M. F. Hansen, "Magnetic separation in microfluidic systems using microfabricated electromagnets – experiments and simulation", *Scientific and*

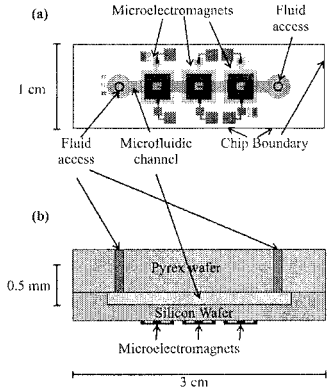

Figure 1. Overview (a) and cross-section (b) of the microfluidic system design. The electromagnets have the following parameters: Number of turns 12; coil wire height 25 μm, width 60 μm, and spacing 20 μm; electromagnet width 4 mm, and yoke thickness 25 μm; fluid channel depth 150 μm, length 14 mm, and width 1.5 mm. Notice that the scale at the bottom applies to both (a) and (b).

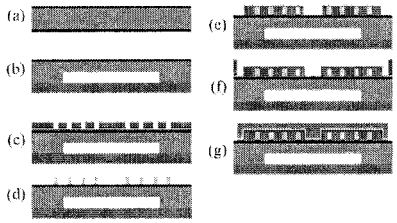

Figure 2. Fabrication process for the microfluidic system. In (a) SiO_2 and Si_3N_4 is deposited on a double polished Si wafer. In (b) the microfluidic channel is defined using DRIE and sealed with a pyrex wafer using anodic bonding. In (c) and (d) the Cu coil is defined by electroplating using thick photoresist as a mould. In (e) a dielectric layer of hard-baked photoresist is defined. In (f) and (g) the magnetic yoke (Ni or NiFe) is defined by electroplating using a thick photoresist mould.

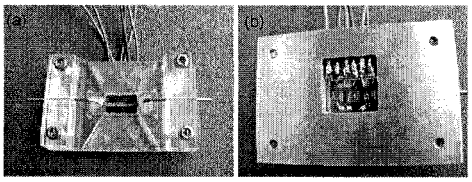

Figure 3. Photographs of the fabricated microsystem complete with fluid and electrical connections. (a) shows the channel side, and (b) shows the electromagnet side. The mounted system is 4 by 6 centimeters.

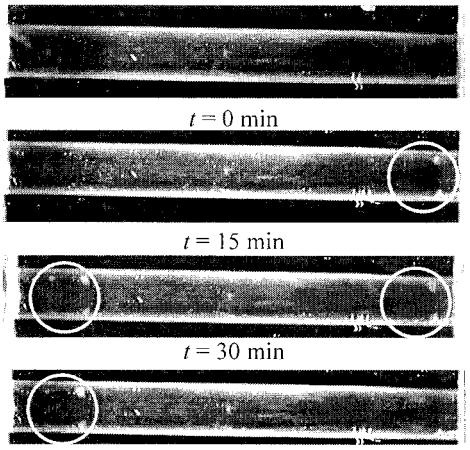

Figure 4. Demonstration of selective bead capture and release in the microfluidic system. The encircled gray dots in the microfluidic channel is the reflection of the ferrite content of the magnetic beads. The beads settle above the corners of the square inner pole piece of the electromagnets. After 15 min. beads have been captured on the rightmost electromagnet. After 30 min. beads have been captured on both the leftmost and the rightmost electromagnet. After 35 min. the beads have been released from the rightmost electromagnet, but is still present on the leftmost electromagnet. The width of the microfluidic channel is 1.5 mm.

MICRO IMMUNO SUPPORTED LIQUID MEMBRANE (μ-ISLM) EXTRACTION

Madalina Tudorache[1], Jan Norberg[2] and Jenny Emnéus[1]
[1]Dept. of Analytical Chemistry, Lund University, P.O. Box 118, S-221 00 Lund, Sweden
[2]Personal Chemistry, Kungsgatan 76, SE - 753 18 Uppsala, Sweden

Abstract

A μ-ISLM (micro Immuno Supported Liquid Membrane) extraction system coupled in a sequential injection analysis (SIA) configuration, capable of simultaneous sample cleanup and enrichment was developed. The capacity of the extraction channels - donor and acceptor, respectively - were reduced from originally 10 to 1.65 μL. The acceptor channel surface was covered with a gold layer enabling immobilisation of antibodies via an alkanthiol self-assembled monolayer. The μ -ISLM-SIA system resulted in very high extraction efficiency and enrichment factor (Extraction efficiency (E): 136%; Enrichment factor (E_e): 544) and a subsequent low detection limit for the model analyte simazine of 0.1 ng/L.

Keywords: supported liquid membrane, extraction, enrichment, simazine

1. Introduction

μ-ISLM extraction is a new analytical technique that results in simultaneous sample cleanup and analyte enrichment, analogues to traditional liquid-liquid extraction. In μ-ISLM the extraction driving force is based on biorecognition of an antibody (Ab) for its antigen (Ag - the analyte), resulting in the transport of the Ag from a continuously flowing aqueous donor phase over an organic supported liquid membrane (SLM) into a stagnant aqueous acceptor phase containing antibodies [1,2]. In our previous work [1,2], the Ab was dissolved in the acceptor solution, however in this work it was immobilised via a self-assembled monolayer (SAM) of alkanthiol on a gold covered acceptor surface, thus allowing many extractions with the same Ab surface.

2. Experimental

The μ-ISLM extraction cartridge is based on two polymer plates, each in which a small channel is etched (1.65 μL in volume, Fig. 1). The plate used for the acceptor side is further sputtered with gold on to which antibodies are immobilised via SAMs of different alkanthiols: dithiobis 11-aminoundecane, hydrochloride (DTAU), β-mercaptoethylamine (MEA), thioctic acid (TA), 3,3'-dithiopropionic acid di(N-succinimidyl ester) (DTPNS). The SLM clamped between the two plates, is a hydrophobic porous membrane (polypropylene support), holding in its pores a suitable organic solvent (di-*n*-hexyl ether) by capillary forces, thus separating the two aqueous phases (Fig. 1).

The μ-ISLM for simazine determination was executed in a sequential injection (SIA) system starting with extraction of simazine. A simazine-containing sample (standard or real sample) was pumped through the donor channel for 10 min with a flow rate of 65 μL/min. In this way, the Ag diffuses from the donor through the SLM to the acceptor due to partitioning between the liquid phases (aqueous-organic and organic-aqueous phase, respectively) and is then trapped in Ag-Ab complexes by the immobilised Ab on the acceptor surface. To determine the unoccupied Ab sites on the acceptor surface, a tracer (a horseradish peroxidase (HRP)-labelled Ag derivative) was injected into the acceptor and the amount of extracted Ag was inversely related to the amount of bound tracer by injection of the HRP substrate mixture luminol, p-iodophenol and H_2O_2, following detection of the generated chemiluminescence (CL).

3. Results and discussion

In Fig. 2, the μ-ISLM-SIA system was investigated with and without extraction. In the latter case the Ag solution was injected directly into the acceptor, thus excluding the extraction step. As seen, remarkable sensitivity was achieved in both situations (LOD: 0.1 ng/L for μ-ISLM-SIA and 4 ng/L for SIA), with the lower LOD obtained including the extraction step due to the high extraction efficiency (E: 136%) and analyte enrichment (E_e: 535) during the immuno extraction process.

Different chemistries for immobilisation of the anti-simazine Ab on the gold-coated acceptor surface were tested. The Ab was coupled via its -NH or -CHO groups to the active end of a DTAU, MEA, TA, or DTPNS spacer to provide a homogeneous and active Ab layer on the surface. The immobilisation procedure and also the chain length of the spacer gave rise to different characteristics of the μ-ISLM-SIA for simazine as seen in Table 1. The optimum immobilisation chemistry in terms of highest sensitive and Ab stability was obtained with the DTAU spacer.

4. Conclusions

The presented μ-ISLM-SIA extraction system allows extraction and enrichment of analyte from complex samples, using a relatively simple automated system. It involves minute amounts organic solvent and immuno reagents, and results in one of the most sensitive detection system for simazine reported so far.

References

1. E. Thordarson, J. Å. Jönsson, J. Emnéus, *Anal. Chem.*, **72**, 5280 (2000).
2. M. Tudorache, M. Rak, P. P. Wieczorek, J. Å. Jönsson, J. Emnéus, *J. Immunolog. Methods*, **284**, 107(2004).

Table 1. Limit of detection (LOD) and antibody stability for μ-ISLM-SIA of simazine using different immoblisation reagents

SAM	LOD (ng/L)	Max. number of regeneration cycles
DTAU	0.10	50
MEA	4.02	36
TA	2.41	20
DTPNS	0.11	30

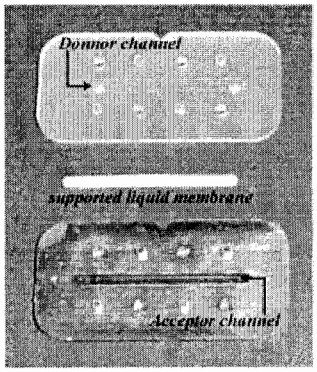

Figure. 1. μ-ISLM cartridge containing two polymer plates each with a single channel (1.65 μL): donor channel (top) and acceptor channel (bottom) covered with a sputtered gold layer to which the antibody is immobilised. In between the two polymer plates, a polypropylene membrane (middle), impregnated with di-*n*-hexylether (organic solvent), is clamped in a specially designed cartridge holder (not shown).

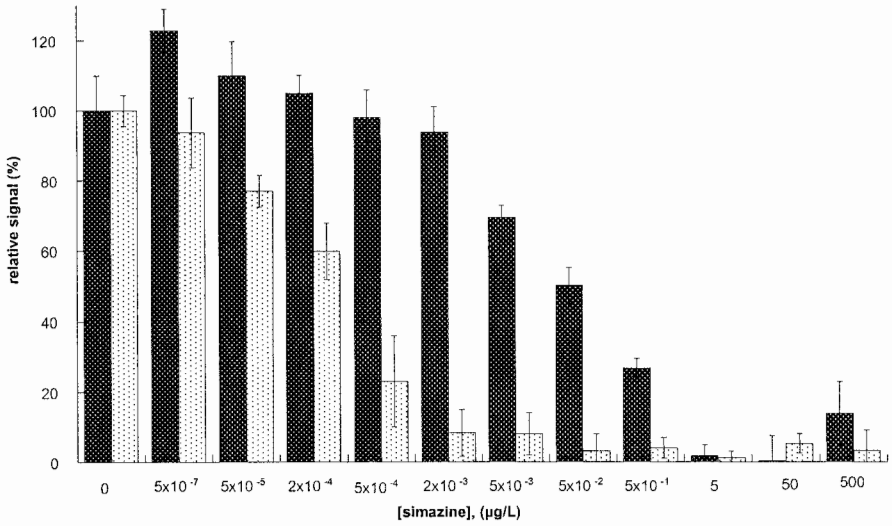

Figure 2. Comparison of μ-ISLM-SIA with (white staples) and without extraction (black staples) for determination of simazine: when extraction is included, the staples are displaced to lower analyte concentrations and thus higher sensitivity.

ESSENTIAL COMPONENTS IN AN INTEGRATED PLATFORM FOR ON-SITE SCREENING OF ANABOLIC ANDROGENIC STEROIDS IN BIOLOGICAL SAMPLES

Sara Thorslund[1], Sara Bergström[2], Nina Johanesson[2], Andreas Pettersson[2], Gustav Liljegren[2], Kristina Magnusson[3], Mathias Hallberg[3], Oliver Klett[1], Jonas Bergquist[2], Leif Nyholm[4], Karin Markides[2], Fred Nyberg[3] and Fredrik Nikolajeff[1]

[1] *Dep. of Engineering Sciences, Uppsala University, P.O. Box 534, S-751 21 Uppsala, Sweden*

[2] *Dep. of Chemistry, Uppsala University, P.O. Box 599, S-751 24 Uppsala, Sweden*

[3] *Dep. of Pharmaceutical Biosciences, Uppsala University, P.O. Box 591, S-751 24 Uppsala, Sweden*

[4] *Dep. of Materials Chemistry, Uppsala University, P.O. Box 538, S- 751 21 Uppsala, Sweden*

Abstract

In this abstract new results concerning the introduction of a biological sample into a μTAS, the avoidance of unspecific absorbance in the μTAS and the interfacing to off-chip detection (e.g. Mass spectrometry, MS) for verification are presented.

Key words: steroids, surface modification, sample preparation, ESI emitter, drug abuse

1 Introduction

Besides their misuse in sports, anabolic-androgenic steroids (AAS) have been reported to be linked with mood and behavioral changes, like depression, impulsivity, aggression and anger among abusers [1] and have been involved in extreme violently committed crimes. The evolving abundance of AAS on the drug market is yet unmet by analytical means to fast and inexpensively detect AAS or related peptide markers in biological samples. Based on the medical and law enforcement associated demands, three departments of UU have joined forces to develop a μTAS for the on-site sampling and detection and verification of AAS in biological samples. The handling of the sample has been identified as one core challenge. In the course of the development of a MicroTAS several modules were compatibly designed and fabricated. Initially, modules for the sample introduction and sample transfer to MS were realized. Focus is also laid on the disturbance-free transfer of sample and other fluids between chip modules using coated silica capillaries.

2 Theory

The analytes of interest are AAS, their metabolites and eventually peptidic biological markers of AAS abuse. AAS derive from cholesterol and are mainly hydrophobic.

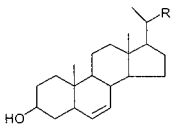

Figure 1. Structure of Cholesterol (R=-$(CH_2)_3CH(CH_3)_2$,) the parent structure for AAS.

In the blood, AAS can be present in the low nM rage and are mainly (up to 90%) bound to hydrophobic proteins like albumin and SHBG (Sex hormone binding globulin). Furthermore many other constituents are present in blood, which makes the sample rather complex. To handle this complex sample and eventually interface it to MS, several sample preparation steps have to be conducted, including removal of cells, abundant proteins and salts. The low analyte concentration

suggests furthermore the need for some preconcentration step. Simultaneously, adsorption of the analyte to the internal walls has to be minimized and clotting of the sample has to be inhibited.

3 Experimental

Cell removal. Hydrophilic commercially available polymer filters were investigated for minimal adsorption of testosterone as an AAS model compound. Suitable filter materials exhibited promising low testosterone adsorption and were integrated in a novel hybrid microstructure. In this structure the filter is incorporated into a poly (dimethyl siloxane), PDMS lid and coupled to a channel manifold in a PDMS chip. The master for the lid structure is dry-etched into silicon to match the filter thickness while the master for the chip structure is built up in SU-8 photo resist. Both structures are replicated in PDMS, and were bonded together. After heparinisation, the filter structures were tested regarding their ability to remove (red) blood cells from whole blood samples.

A sketch of the filter unit is presented in figure 1A while a detail of the actual device is shown in figure 1B.

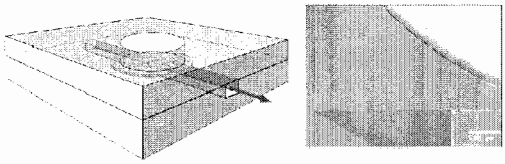

Figure 1. Hybrid structure integrating a macroscopic filter and a micro channel, sketch (left) and detail (right).

Chip-ESI emitter. To couple a PDMS based μTAS to MS, PDMS-Microchips with an integrated ESI tips were directly fabricated by casting. The shapes of the emitter tips were drilled into the mould, which produced highly reproducible 3D-tips (see figure 3A). A variety of different coating procedures on the tips were evaluated. Dusting graphite on a thin unpolymerized PDMS layer followed by polymerization was proven to be the most suitable.

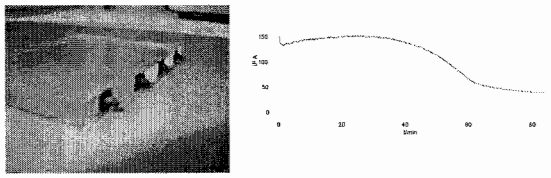

Figure 2. Graphite coated PDMS ESI emitter tips. Actual module (left) chronoamperogram recorded to evaluate tip stability.

Silica-PDMS transfer lines. To avoid unspecific absorption in the channels an effective method for modification of the inner surface of PDMS channels using the polymer PolyE-323 was developed. The adsorption of peptides to untreated surfaces was compared to modified surfaces using radionuclide imaging and capillary electrophoresis experiments. The positively charged PolyE-323 modification displayed a substantially reduced adsorption of three test peptides (e.g. angiotensin II) compared to the native PDMS surface. Modified micro channels were also readily filled with aqueous solution in contrast to devices composed of native PDMS. This was also confirmed in CE experiments, where a fused silica capillary was extended with a PDMS channel. Without modification the PDMS surface was very adsorptive to peptides, but the PolyE-323 coating was shown to decrease this effect. As the PolyE-323 coating bonds to both fused silica and to

PDMS it was found very useful for forming a continuous coating over material boundaries. Besides for the use in chip-to-chip coupling, this coating was also found useful for orthogonal separation systems similar those presented in [2] that integrate both hard fused silica and soft PDMS structures.

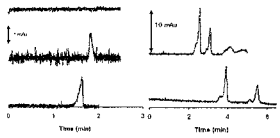

Figure 3. Electropherograms recorded for peptides (left, time window for substance P shown) and proteins (RNAse and cytochrome c, right). The upper two electropherograms (left) were recorded using native PDMS, while the lower was recorded in PolyE-323 coated PDMS. The right electropherograms were recorded in a fused silica (upper trace) and a hybrid column (lower trace), respectively. Both were coated with PolyE-323. The hybrid column was made up from a fused silica capillary inserted into a PDMS.chip.

4 Results and discussion

In microscope inspection, the removal of red blood cells with the used filter could be observed. Furthermore proved the one-step heparinisation of the internal channel walls sufficient to inhibit clotting of the blood in the chip for over 60 minutes.

In electrochemical tests similar to earlier published trials [3] the ESI emitters showed excellent stability (see chronoamperogram in figure 3B) and could be regenerated electrochemically after being passivated eventually. The excellent electrochemical stability was further confirmed in long term ESI mode, where the emitter sprayed continuously for more than 200 hours.

The coating with PolyE-323 was found suitable to coat both; fused silica and PDMS channel walls, which enable the use of fused silica transfer lines between PDMS chip modules.

5 Conclusion

The sample handling of a complex sample like whole blood on a chip can be conducted using microfabricated modules. The integration of macroscopic components into microstructures is feasible and facilitates the development of a μ-TAS. This is true, both for in-sample filtering and fluidic connection between PDMS fluidic chips using commercial available filters and traditional fused silica capillaries, respectively. PDMS ESI emitter tips were found suitable for hyphenating a μTAS to MS. Further components that currently are integrated into this concept include sample preconcentration based on solgels and on-chip detection based on amperometric biosensors.

Acknowledgement

Funding by the Swedish Foundation for Strategic Research (SSF) is gratefully acknowledged.

References

[1] Zhou, Q.; Frändberg, P.-A.; Kindlundh, A. M. S.; LeGrevès, P.; Nyberg, F. *Peptides* **2003**, *24*, 147-153.

[2] Sara K. Bergström; Jenny Samskog; Markides, K. E. *Analytical Chemistry* **2003**, *75*, 5461-5467.

[3] Nilsson, S.; Svedberg, M.; Pettersson, J.; Björefors, F.; Markides, K.; Nyholm, L. *Analytical Chemistry* **2001**, *73*, 4607-4616.

FIXED VOLUME 384 CHANNEL NANOLITER DISPENSER FOR HIGHLY PARALLEL AND SIMULTANEOUS LIQUID TRANSFER INTO WELL PLATES

Reinhard Steger, Benjamin Bohl, Chris Steinert, Roland Zengerle and Peter Koltay
IMTEK- University of Freiburg, Laboratory for MEMS Applications,
Georges-Koehler-Allee 103, D-79110 Freiburg, Germany

Abstract

We present a highly parallel nanoliter dispenser on the footprint of a micro well plate (80 mm x 120 mm) (figure 1). The so called Dispensing Well Plate (DWP™) contains 384 individual dispensing units at a pitch of 4,5 mm and allows for transfer of liquid quantities of 50 nL to a receiving plate. The DWP™ is simply operated by a pneumatic pressure pulse. Tests with fluorescence measurements prove the CV of the dispensed volume to be better than 5 % for DMSO and/or aqueous solutions. Thus the device is able to increase dispensing speed as well as quality in High-Throughput-Screening (HTS) significantly.

Keywords: HTS, nanoliter dispenser, highly parallel, well plate, silicon micro machining

1. Introduction

Pharmaceutical research experiences an increasing need for highly parallel dispensing technologies in the nanoliter range to speed up drug development [1]. Today well plates with 384 or 1536 wells at a pitch of 4.5 mm or 2.25 mm are handled within automated equipment. Around 1000 dispensing cycles per minute are accomplished currently by conventional pipetting systems. To push the limit of HTS, assay volumes ranging from 2 µL to 5 µL have to be miniaturized even further and the liquid handling has to be accelerated. Therefore we developed the DWP™ technology [2, 3] with the aim to improve this throughput significantly.

2. Design & Fabrication

The DWP™ contains a multitude of individual dispensing units, each consisting of three basic elements: a reservoir, a connection channel and a nozzle chamber (figure 2). The reservoirs can be filled with different reagents at volumes of up to 6.8 µL. Due to capillary forces the nozzle chambers are self priming via the connection channels. To drive the micromachined DWP™ a prototype actuation unit has been constructed, which consists mainly of a cavity (pressure chamber) that can be pressurized by a pneumatic valve. By applying a pressure pulse to the whole upper surface of the DWP™ a liquid volume defined by the dimensions of the nozzle is driven out generating a free flying jet ejected from each nozzle.

The proof of principle with a limited chip size of 1/16 of a full micro well plate and a smaller reservoir volume of 0,7 µL has been presented earlier [2, 3]. Now we present the full size plate with 384 parallel dispensing units as well as an increased reservoir volume of 6,8 µL enabling to validate the DWP™-technology in a real HTS environment. The technological challenge producing the DWP is met by applying 6" silicon wafer technology and deep reactive ion etching (DRIE). The processed microfluidic structures include nozzles with aspect ratios over 3 etched through the complete wafer thickness of 1 mm. A proper microfluidic layout made it necessary to use a multi-layer mask for the DRIE-process: a standard SIO2 layer, an aluminum layer with a high selectivity and a 20µm thick resist layer. The uniformity of all nozzles over the complete wafer is important for the dispensing quality and homogeneity of the system.

3. Dispensing Quality and Application

The presented DWP prototype has been intensively characterized by gravimetric and fluorimetric measurements. Fluorescence measurements performed with a Wallac/Victor² plate reader and Europium 3.5 nM in DMSO (2 µL = 40 dispensing cycles) show that the homogeneity over all 384 dispensing units is within a CV of 5% (figure 3).

The dispensed mass has been measured with a microbalance accounting for systematic errors due to evaporation or adsorption. From this data the mean dosage volume per channel has been calculated. In order to prove the working principle the influence of pressure head and pulse duration on dosage volume was studied. The results of these experiments (figure 4) prove the robust and reliable performance. Using water and DMSO as dosage media the reproducibility for the DWP prototypes displayed in figure 4 has been determined with a CV of about 1% and better.

To demonstrate the potential of a highly parallel nanoliter dispenser in miniaturizing the assay technology within HTS, we prepared a kinase assay based on Rhodamine 110 at a total assay volume of 1 µL. This miniaturized assay has been compared to a reference case with equal end concentrations at an assay volume of 20 µL. Comparison of the measured signal counts of the 1 µL and the 20 µL assay reveals that although the 1 µL assay is at the low end of the plate reader capability the signal variation with a measured CV of 7.9% is comparable to that of the hand pipetted 20 µL volume with a CV of 7.3%. The relative dispensing quality therefore has to be in the nanoliter range as accurate as for the larger assay volume. Taking into account that the assay was performed in different plate sizes (1536 for the miniaturized and 384 for the reference case) this demonstrates the reduction of the assay volumes by a factor of 20 without loosing quality of the measurement results.

4. Conclusions

The full-size 384 DWP-Dispenser for massive parallel dispensing of liquids in the nanoliter range has been presented. The dispensing performance was successfully characterized by gravimetric and fluorimetric experiments. The proposed DWP method was proven to be very accurate, scalable, simple and robust. The DWP-technology therefore has the potential to speed up the liquid handling in HTS by a factor of 10 – 100 and to reduce reagent consumption by a factor of 10-20 in the future. The applicability of the DWP method in a HTS laboratory environment has been demonstrated by performing a miniaturized kinase assay with comparable quality to conventional assay volumes. In case of the demonstrated miniaturized assay the reagent consumption could be reduced by a factor of 20.

Acknowledgements

Thanks to all people from the IMTEK-Cleanroom helping performing the 6" silicon wafer run.

References

[1] J. Comley, Nanoliter Dispensing - On the Point of Delivery, *Drug Discovery World Summer 2002*, 33 – 44.

[2] P. Koltay, et.al.; "Massive Parallel Liquid Dispensing in the Nanoliter Range by Pneumatic Actuation"; *Proc. Actuator 2002*; June 2002; Bremen; Germany, pp. 235 – 239

[3] P. Koltay et al; "Dispensing Well Plate (DWP): A Highly Integrated Nanoliter Dispensing System"; *Proc. Transducers 2003*, Boston, pp. 16 –19

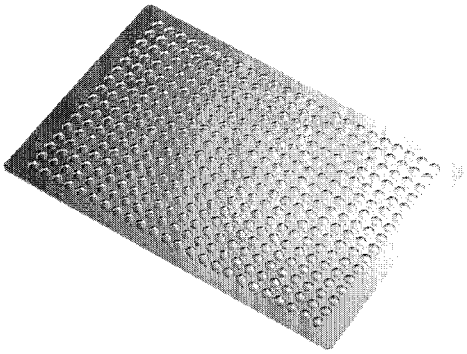

Figure 1. Photograph of a 384-unit DWP chip made of a 1 mm thick silicon wafer (pitch: 4.5 mm).

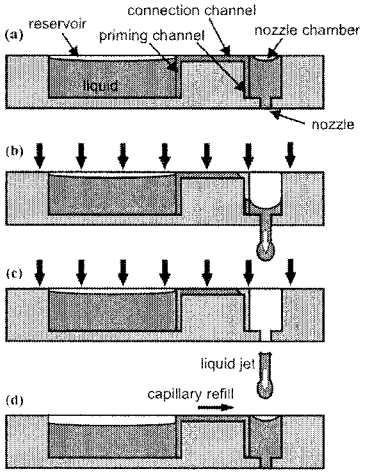

Figure 2. DWP dispensing process:
a) basic elements
b) jet ejection by pneumatic actuation
c) dispensed volume defined by the volume of the nozzle chamber
d) refilling by capillary forces

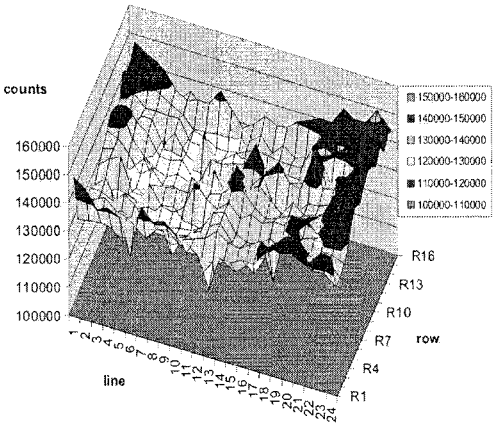

Figure 3. Diagram of a fluorescence measurement of a dispensed 384 droplet array. (measured with a Wallac/Victor² plate reader / DMSO with 3.5nM Europium 40 dispensing cycles). Measurement has a CV of 4.9 %.

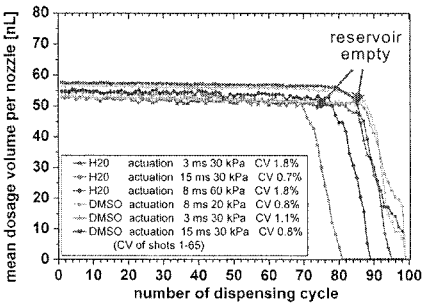

Figure 4. Gravimetrical measurement of the mean dosage volume of a section of 24 nozzles over successive dispensing with H2O and DMSO with different pressure pulse parameters.

A SILICON-BASED MULTI-PATCH DEVICE: APPLICATION FOR IONIC CURRENTS SENSORING ON SINGLE CELLS

T. Sordel[1], S. Garnier-Raveaud[1], F. Sauter[2], C. Pudda[2], N. Picollet-D'hahan[1], F. Chatelain[1]

[1]CEA Grenoble, Life Science Division, Laboratoire Biopuces, 17 rue des Martyrs, 38054 Grenoble France.

[2]CEA Grenoble, LETI, Laboratoire des Composants Intégrés pour le Vivant.

Abstract

We present the 'Multi-Patch' device combining microtechnologies, microfluidics and electrophysiology to overcome the low throughput of patch clamp. The tip of a micropipette is replaced by a micro hole structured in a planar substrate. The novelty of our approach lies in a modular assembly of the device composed of the disposable silicon chip, the fluidics and electronics parts. We have designed and fabricated silicon substrates with cell patch site aperture of 2.5 µm. We obtain consistently adequate cell positioning by applying suction. By combining suction and zap, we succeeded in recording whole-cell ionic currents from BK channels expressed in HEK 293 cells and their blockage by a specific antagonist. In order to record weaker currents or to perform single channel measurements, we have reduced the deep capacitance of the silicon chip to less than 8 pF.

Keywords: ion channels, electrophysiology, silicon, micro fabrication, sensors

1. Introduction

Ion channels are cellular membrane proteins that mediate a wide variety of physiological functions including rapid signalling, excitability and transport. They are particularly attractive drug targets [1] but present a challenge for the pharmaceutical industry in terms of appropriate screening technology [2]. Patch-clamp is able to discriminate ionic currents in the picoamp (10^{-12} A) range or single ion channel but the need for automation and parallelism has not yet been fulfilled. This fact underlies continued efforts in developing parallel patch-on-chip platforms in order to provide higher throughput and better reproducibility [3-4].

2. The 'Multi-Patch' system

We have developed a concept of sandwich assembly constituted of several parts: a silicon chip, o-rings, 2 Printed Circuit Boards (PCB) (Fig. 1) [5]. The planar substrate is a multilayer silicon array of 3x3 micro holes (2.5 µm in diameter) etched in a 2 µm thick silica membrane. The chip is set between two plastic grids containing o-rings which define 9 independent fluidic chambers. The two PCB pressed on each side of the system contain 9 planar electrodes coated with Ag/AgCl for electrophysiological measurements. These electrodes are drilled for the integration of fluidic capillaries. The assembled device is maintained together by clips designed to create a Faraday cage for reducing electrical interferences.

3. Cell positioning and sealing

The system is filled with electrophysiological solutions. Without cells, micro holes have a resistance of 1 MΩ (electrical measurements are performed with a standard patch-clamp amplifier, MultiClamp 700A, Axon instruments). When the cellular suspension is injected in the top chamber, suction is applied and one cell is positioned onto the micron-sized hole (Fig. 2). A more gentle suction leads in about 30 sec to a seal resistance in the Giga-Ohm range.

4. Results and discussion

The critical step of planar patch clamp is the seal of the cell membrane on an appropriate substrate. To be able to detect a current in the picoamp range, the seal resistance must be greater than 1 Giga-Ohm. Hydrophilic surfaces and low roughness have been reported as critical parameters to obtain Giga-Ohm seals, although seal mechanism has not yet been well understood [6]. With hydrophilic coating obtained by Si_3N_4 or SiO_2 deposition and a good control of the micron-shaped and sized holes, silicon appears as a suited material for planar patch-clamp.

Cell positioning by suction is now well controlled in our system and the positioning rate of one cell on a micro hole is around 85%. Whole-cell configuration is obtained by applying a 1V pulse during 100 µs to snap the isolated membrane patch. Ionic currents of BK channels expressed in HEK 293 have been measured. In Fig. 3, two current traces are presented: the left trace is the current response to potential pulses from 0 to +120mV and the right trace is the current response for the same cell with the addition of 100 nM of iberiotoxin in the bath solution (solution composition in mM in top chamber: 118 NaCl, 5.6 KCl, 2.4 $CaCl_2$, 1.2 $MgCl_2$, 10 HEPES, 11 Glucose, pH 7.4 and in bottom chamber: 30 KCl, 110 K-aspartate, 0.1 $CaCl_2$, 1 $MgCl_2$, 1 EGTA, 10 HEPES, pH 7.4). As expected, we observe a strong inhibition of the current by iberiotoxin, a specific antagonist of the BK channels.

In the aim to record weaker currents or to perform single channel measurement, we have improved electrical properties of our chips. Silicon has indeed been reported as non ideal substrate for patch clamp experiment because of its high capacitance which is noise source [7]. In our device, high capacitance is due to the Si-based device, as it forms two capacitors in the form of a sandwich between the electrophysiological medium of the top and bottom chambers and the isolating SiO_2 membranes on both sides of the silicon probe. By modifying the SiO_2 thickness and the fluidic design we have been able to reduce the high capacitance to less than 8 pF.

5. Conclusions

We have presented a planar patch clamp system intended to overcome the low throughput of electrophysiology. Silicon appears as a suitable substrate for electrophysiology and gives the accuracy and reproducibility required for a future integration of amplifiers for a gain in sensitivity. By reducing the capacitance of our chip, we open the field of application to "single channel" recordings.

Acknowledgements

This work has been carried out under the framework of Nano2life, European network of excellence in nanobiotech. Special thanks to C. Arnoult and M. Vivaudou from the CEA Grenoble for their helpful advice in electrophysiology.

References

[1] B. A. Niemeyer et al, *Embo reports*, **21**(71), 568-573 (2001).
[2] N.J. Willumsen et al, *Receptors Channels*, **9**, 3-12 (2003).
[3] X.Wang and M.Li , *DDT*, **1**(5), 1-13 (2003).
[4] J. Combley *DDWF*, 47-57 (2003).
[5] N. Picollet-D'hahan et al, *Sensors Letters*, in press, (2004).
[6] F.J. Sigworth and K.G. Klemic, *Biophysical J*, **82**, 2831-2832 (2002).
[7] N. Fertig et al, *Receptors and Channels*, **9**, 29-40 (2003).

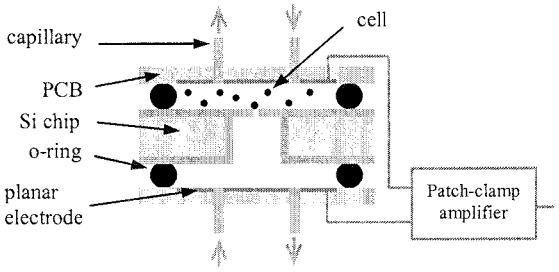

Figure 1. Cross section of one of the 9 individual fluidic chamber with its own fluidic (4 capillaries per chamber) and electrical connections (1 pair of planar electrodes per chamber).

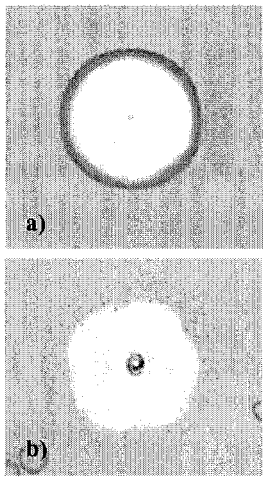

Figure 2. a) Micro hole without cell b) HEK 293 positioned on a 2.5 μm diameter hole.

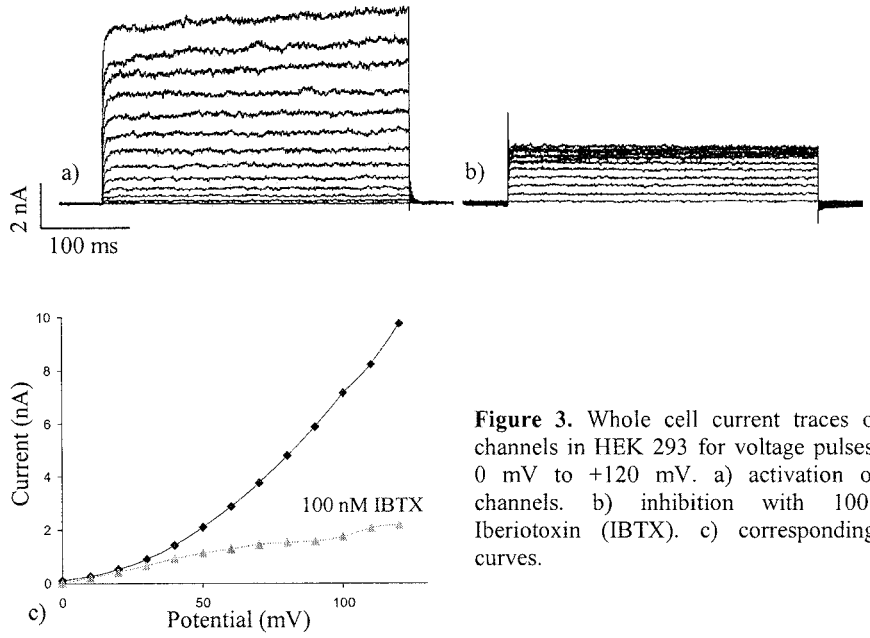

Figure 3. Whole cell current traces of BK channels in HEK 293 for voltage pulses from 0 mV to +120 mV. a) activation of BK channels. b) inhibition with 100 nM Iberiotoxin (IBTX). c) corresponding I-V curves.

DEVELOPMENT OF THREE-DIMENSIONAL PASSIVE MICROMIXER AND ITS APPLICATION FOR MINIATURIZED DNA PREPARATION SYSTEM

Nae Yoon Lee[1], Masumi Yamada[1] and Minoru Seki[2]

[1]Dept. of Chemistry and Biotechnology, Sch. of Engineering, the University of Tokyo, 7-3-1 Hongo, Bunkyo-ku, Tokyo, 113-8656, Japan

[2]Dept. of Chemical Engineering, Grad. Sch. of Engineering, Osaka Prefecture University, 1-1 Gakuen-cho, Sakai, Osaka, 599-8531, Japan

Abstract

In this study, a passive micromixer based on a new mixing principle was developed. This micromixer has simple structure and is easy to fabricate, making it suitable for integration with other microdevices. Owing to rapid concentration changes of buffer solution inside this micromixer, it was applied for on-chip DNA purification. As a result, silica-adsorbed DNA was successfully washed and eluted, and D1S80 locus of the recovered DNA was also successfully amplified.

Keywords: micromixer, integration, DNA preparation system

1. Introduction

Effective mixing is indispensable for the success of almost all chemical / biochemical reactions, and various types of micromixers have been emerging as one of the prerequisites for the complete integration of microdevices. In this study, a three-dimensional passive micromixer adopting a new mixing principle has been developed. This micromixer is highly advantageous for its simple structure and easy fabrication process – photolithographic method and replica molding. As an application, this three-dimensional passive micromixer is adopted for DNA purification. In our previous study, DNA was extracted from a single hair root and was purified on a microdevice, adopting solid-phase-based DNA purification method [1], and recovered DNA was used as a template for direct PCR amplification [2]. In this study, the above-mentioned micromixer is integrated with DNA purification microdevice to rapidly change the concentrations of buffer solution for fast DNA washing and elution, using only a minimum amount of buffer solution. This simple-structured passive micromixer, requiring only a small space, makes integration easy, enabling rapid DNA sample preparation on a microfabricated platform.

2. Theory

This micromixer is composed of a series of two types of microchannels, highly different in their aspect ratios – the ratio of depth to width. One type of microchannels, high in aspect ratio, is called "main channel", and the other type, low in aspect ratio, is called "flattened channel". These are aligned perpendicularly to each other (Fig. 1A). Mixing takes place via two steps – fluid twisting and flattening. First, fluid twisting occurs at the perpendicular intersection of the two microchannels, and second, fluid flattening occurs in the flattened channel. In the flattened channel, diffusion distance can be decreased dramatically, and alternate repetitions of two types of microchannels facilitate effective mixing.

3. Experimental

Fig. 1 represents the schematic diagram of three-dimensional passive micromixer. As shown in Fig. 1B, different types of main channels were created whose depth/width dimensions were 100/300, 100/100, and 300/100 μm, resulting in their aspect ratios of 0.33, 1.0, and 3.0, respectively. Different types of flattened channels were created whose depth/width dimensions were 10/500, 20/500, and 65/500 μm, as shown in Fig. 1C. Main channels and flattened channels were created on separate

polydimethylsiloxane (PDMS) plates, and three-dimensional micromixer was formed simply by bonding two plates of PDMS in such a manner that main channels and flattened channels connect perpendicularly. Buffer solutions with and without fluorescein (in this case, FITC) were introduced into the micromixer, and liquid mixing performances were evaluated using confocal laser microscope. Captured images were processed computationally.

Next, this micromixer was integrated with a solid-phase-based DNA purification microdevice [2] as shown in Fig. 2. Weir-structured microchannel, packed with silica beads, was used for DNA binding, and the micromixer was used to rapidly adjust the buffer solution to desired concentrations for DNA washing and elution. Concentrations of buffer solution were changed by controlling the flow rates of two solutions (one is 1 M $MgCl_2$ buffer solution dissolved in 50 mM MOPS buffer and the other is 50 mM MOPS buffer).

4. Results and discussion

The effect of main channel aspect ratio and flattened channel depth on fluid twisting and mixing efficiencies were evaluated. Fig. 3a and 3b represent the mixing efficiencies measured at the first flattened channel, when main channel aspect ratios were 0.33 and 3.0, respectively. Fluid twisting took place effectively when main channel aspect ratio was relatively high at 3.0. Mixing efficiencies, represented by the coefficient of variation (CV) of fluorescence intensity, was high even at higher flow rates, when compared to low-aspect-ratio main channel, 0.33, as shown in Fig. 3. It was revealed that the combination of high aspect ratio main channel with extremely shallow flattened channel triggered fluid twisting and enabled fast and efficient mixing.

Fig. 4 represents the stepwise concentration change of aniline blue dye solution inside the micromixer, whose main channel aspect ratio was 3.0, and which was integrated with DNA purification device. Based on this result, the flow rates of two solutions with and without $MgCl_2$ were controlled to be 1.25 μL/min to adjust the concentration of $MgCl_2$ to 500 mM for DNA washing, after sample (lysed human cells) were introduced into the microdevice. After 5 minutes washing, the flow rates of two buffers with and without $MgCl_2$ were changed abruptly to 0.04 μL/min and 2.46 μL/min, respectively, to adjust the concentration of $MgCl_2$ to 15 mM for DNA elution. 5 μL of purified DNA sample was recovered, and its D1S80 locus was successfully amplified as shown in Fig. 5.

5. Conclusions

Simple and efficient micromixer was developed and integrated with DNA purification device to realize miniaturized DNA preparation system. Integrated form was easily fabricated through one step, and this integrated system enabled rapid DNA purification on-site in an automated manner.

Acknowledgement

This research was supported in part by Grant-in-Aids for JSPS Fellows, Scientific Research (B) (No. 16310101), and Priority Areas (A) (No. 13025216) from the Ministry of Education, Science, Sports and Culture of Japan, and by the Research Association of Micro Chemical Process Technology, Japan.

References

[1] N.Y. Lee, M. Yamada and M. Seki, *Proc. MicroTAS* 2002, 195-197 (2002)

[2] N.Y. Lee, M. Yamada and M. Seki, *Proc. MicroTAS* (μTAS) 2003, 721-724 (2003)

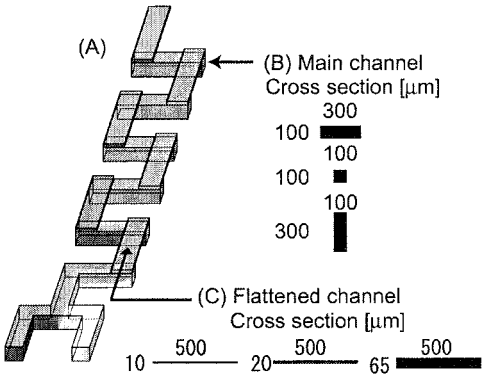

Figure 1. (A) Schematic diagram of three-dimensional passive micromixer. Dimensions and cross sections of (B) three types of 'main channel' and (C) three types of 'flattened channel'.

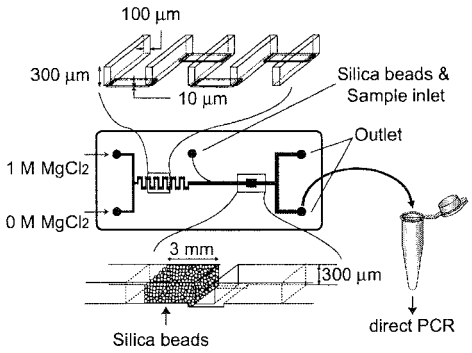

Figure 2. Integrated DNA sample preparation microdevice. Micromixer and DNA purification device were fabricated on one miniaturized platform.

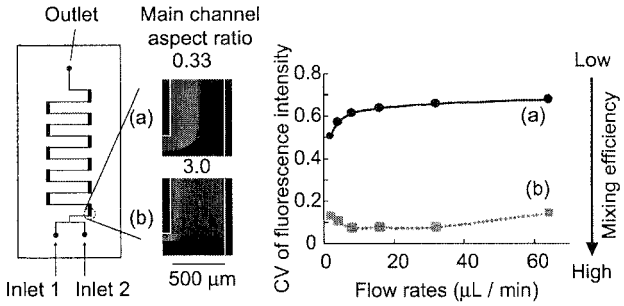

Figure 3. Mixing efficiencies measured at the first flattened channel, when main channel aspect ratios were (a) 0.33 and (b) 3.0. Flattened channel depths were set to 10 μm.

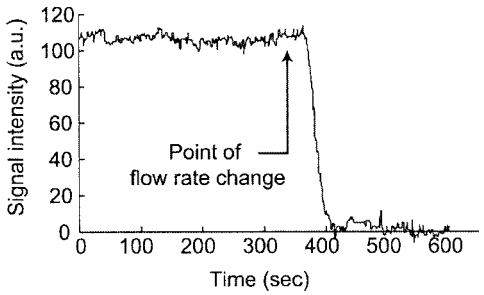

Figure 4. Stepwise concentration change of aniline blue dye solution. Signal intensity was changed rapidly.

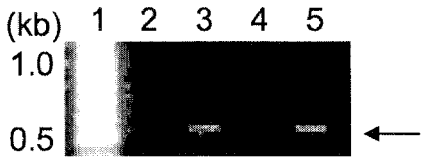

Figure 5. D1S80 locus amplification results. Lane 1 – 100 bp DNA ladder. Lanes 2 & 3 – amplification results of DNA washout solution and eluant, respectively, performed without using micromixer. Lanes 4 & 5 – amplification results of DNA washout solution and eluant, respectively, when performed using micromixer.

ON-A-CHIP GENOTOXICITY ASSAY-APPLICATION TO HIGH-THROUGHPUT SCREENING BIOCHIPS

R. Piron[1], N. Rougier[2], R. Vaudry[2], A. Corlu[3], D. Glaise[3], P. Joly[4], B. Le Pioufle[1]

1. Biomis-SATIE, ENS-Cachan, 35170 Bruz-France

2. Biopredic, 14-18 rue Pr. J. Pecker, 35000 Rennes-France

3.INSERM-U522, Hôpital Pontchaillou, 35033 Rennes-France

4.CEA-LETI, 17 av. des Martyrs, 38054 Grenoble-France

Abstract

We present a cell array biochip dedicated to toxicological and high-throughput drug screening applications, on which are performed genotoxity analysis using micronucleus test. This cell biochip is an array of microwells optimized for living cell culture (Fig.1-a). Topographical aspects are exploited in order to control the distribution and the positioning of the cells on the biochip [1,2]. Such a miniaturized cell-based device is of great interest, in terms of cost and time, for pharmacological applications [3].

Key words: PDMS, cell Biochip, pharmacology, cells growth, high-throughput drug screening.

1. Introduction

High-throughput screening technique is involved in order to identify new drugs among various chemical substances. In order to increase the already acknowledged impact of this technique in the pharmacological field, efforts are made to improve drug screening technology. In this way, the combination of screening technology and microfabrication allow developing new classes of diagnostic tools with a great interest through cost reductions and fast diagnostics. The aims are to increase the number of tests on a chip and to reduce the volumes of the tested compounds. In order to answer this demand, we worked on the fabrication of a cell biochip allowing long-term cultivation of cells in array and facilitating some pharmalogical tests analysis.

2. Cell array Biochip fabrication

The cell array biochip is fabricated and optimized as follows. The microchamber array system is moulded in PDMS (polydimethylsiloxane) polymer. The attractive properties (biocompatibility, UV-visible optical transparency) of PDMS make it widely used for biological applications. The fabrication of PDMS devices is based on rapid prototyping and replica model. In our study, the uncured PDMS solution is deposited by spin-coating on a SU8 patterned mould. The mould consists in an SU8 column array (Fig.1-b). The PDMS is then cured and peeled off, which leads to a thin PDMS slabs with a pattern of wells. This slab is then attached on a glass plate (Fig. 1-c). The PDMS being hydrophobic, we determined surface coatings permitting long-term hydrophilic properties for the good viability and surface adhesiveness of the cells. The samples treated by O_2 plasma were functionalized with a hydrophilic polymer. The cells in microchambers showed long-term viability and good proliferation. Furthermore, we noticed a good attatchement of adherent cells in the chambers. The microchamber array structure was optimized to control the positioning and the number of cells in the chambers. We concluded that a 50µm spacing avoids having cells positioned between the chambers and that a 150 µm large and 200 µm deep well (Fig.1-a) allows a good distribution of cells. Following those dimensional conditions, a cell density of about 30000 cells/mL in the cultivation media leads to an average of 30 cells per chamber, adequate for

pharmacological tests. Various cell types (adherent or non-adherent) were succesfully cultivated during several days on these biochips before toxicological experiments.

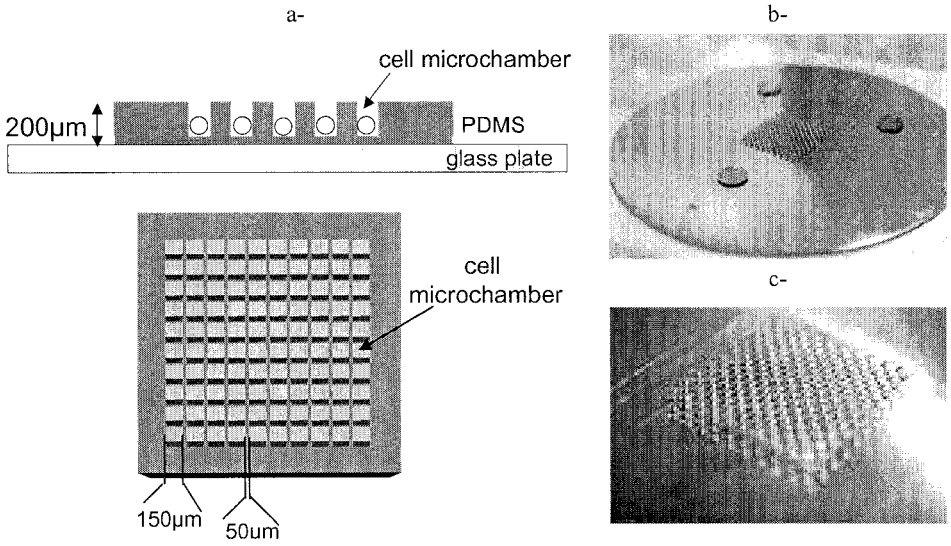

Figure 1. a) schematic view of the PDMS biochip. b) SU8-mould picture. c) PDMS biochip picture.

3 Biological experiments: genotoxicity tests

We demonstrated the feasibility of genotoxicity tests on this biochip. For that, we used CTL2-bcl2-transfected cells, which allowed us to classify the compounds as pro-apoptotic or genotoxic chemicals. After a 24 hours culture, two compounds were tested: dexamethasone and mitomycine C, as respectively two well-described proapoptotic and genotoxic compounds. After 15 hours incubation, cells were labelled with Hoechst, a DNA marker. We observed an increased number of micronuclei only following mitomycin C addition. This result shows the feasibility of easy discrimination between apoptosis and genotoxicity experiments on the cell biochip. This toxicological test has never been reported previously on a cell biochip, as until now this test was performed on cells cultured in tube, then spread and labelled on slides [4,5], or in 96 well plates [6].

a- b-

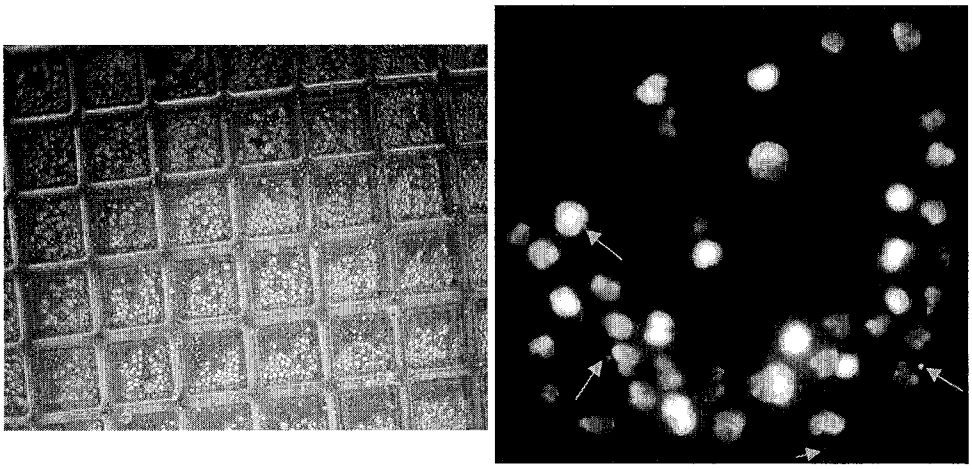

Figure 2. a) cells isolated in PDMS chambers of the biochip. b) zoom on a single chamber showing micronuclei in an experiment on CTL2-Bcl2 cells line (fluorescence image).

4 Conclusions

We have fabricated a cell biochip including topographical control of cells positionning and allowing successful cultivation of cells in microwell arrays. Furthermore, the feasability of genotoxicity tests has been demonstrated on this fabricated biochip. It is thus very promising for high-throughput screening applications permitting to test more products with less required quantities.

Acknowledgements

All the members of this project gratefully acknowledge the financial support of the French Ministry of Industry. R. P. acknowledges Magali Chiral for technical support in cell cultivation.

References

[1] M. Li, J. D. Glawe, H. Green, D. K Mills, M. J. McShane, B. K. Galle, conference paper at IEEE Special Topics conference on microtechnology in medecine, lyon, France, October 12-14, 2000.

[2] K. Takahashi, Y. Sugio, H. Moriguchi, Y. Jimbo, K. Yasuda, , Y. Baba and al. (eds.), Micro-TAS'02, pp. 841-843.

[3] S. R. Rao, Y. Akgi, Y. Morita, E. Tamiya, (eds. Y. Baba and al.), Micro-TAS'02, pp. 862-864.

[4] S. Meintières, A. Biola, M. Pallardy, D. Marzin. 16, , 2001, pp. 243-250.

[5] S. Meintières, A. Biola, M. Pallardy, D. Marzin.,14, 2003, pp. 14-27.

[6] http://www.compucyte.com/brochure_pdfs/Micronucleus_CompuCyte.pdf

USE OF MAGNETIC NANOPARTICLES FOR DNA ANALYSIS AND PROTEIN DIGESTION IN LAB ON CHIPS.

Nicolas Minc[1], Marcela Slovakova[1], Kevin D. Dorfman[1], Plamen Bokov[1], Zuzana Bilkova[2], Claire Smadja[3], Claus Fütterer[1], Myriam Taverna[3], Jean-Louis Viovy[1]

[1]*Laboratoire PCC, Institut Curie (UMR CNRS/IC 168), Paris Cedex 05, France*
[2]*Dept. BBS, University of Pardubice, Nám. Čs. Legií 565, 532 10 Pardubice, Czech Republic*
[3]*Laboratoire de chimie Analytique CEP-Université Paris XI92296 Châtenay-malabry*

Abstract
We present two experiments of bioanalysis based on the self-organization of magnetic beads under a magnetic field, realized in microfluidic chips. In the first one, the beads are organized in a quasi-hexagonal array of columns used as a matrix to achieve and study the separation of long fragments of DNA. In the second one, trypsin is covalently grafted onto beads that are immobilized in the microchannel, and different proteins are then digested through the bead plug.
Keywords: Magnetic beads, Microfluidics, DNA electrophoresis, Protein digestion

1. Introduction

The past few decades have seen an increasing use of magnetic particles in biotechnology, medicine and pharmaceutical industry, mainly for protein separation, cell tagging, membrane penetration etc.. The nanoscale size of the particles makes them of great interest in microfluidic applications.

2. Rapid and quantitative separation of large DNA.

Under an external magnetic field, an emulsion of magnetic nanoparticles injected into a microchannel self-organize into a quasi-periodic array of posts, whose characteristics can be tuned by changing the concentration or the surface conditions. When engaged with the post, the DNA undergoes a "rope and pulley" disengagement mechanism which depends upon the DNA size. Experimental results are obtained for the rapid separation of λ- (48.5 kbp) 2λ- (96 kbp) and T4- (169 kbp) DNA, where resolutions greater than 2 between λ and T4 were achieved in 150 sec [1,2]. The separations are highly reproducible, owing to a computer-piloted injection and pressure control system [3].

We compare our experimental results to an exactly solvable lattice Monte-Carlo model [4]. The theoretical model predicts that the mean velocity scales linearly with the applied electric field, the band broadening scales inversely with the field and the resolution plateaus at intermediate fields. All of these scaling arguments are confirmed by the experimental data. The model assumed that the collision probability was equal to the density of posts and the trapping time scales inversely with the field. We consequently undertook a thorough experimental test of these assumptions, using a "low-resolution" systematic study of collision at the single-molecule level. Statistics were obtained on the collision time (Fig 1) and the velocities of the DNA (Fig 2) in the matrix, confirming the aforementioned assumptions of the model [5].

This study demonstrates the feasibility of rapid, reproducible microfluidic separations of long DNA. As it also represents the first systematic theoretical study of dispersion in these devices, it is a significant step towards a detailed understanding of realistic separation systems.

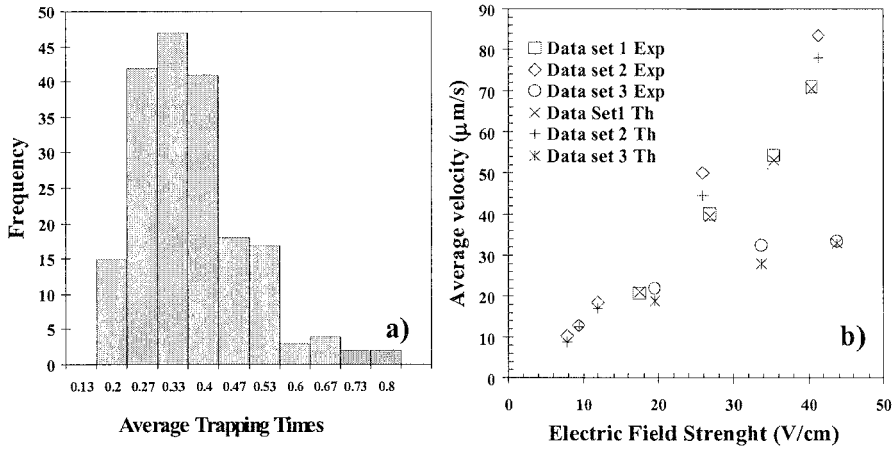

Figure 1 a) Illustrative histogram of the trapping times of the DNA on the columns at an electric field strength of 33.7 V/cm in a concentrated array. The average trapping time obtained here is 0.31s. b) Quantitative comparison between theoretical calculations and experimental points for the average velocities of the DNA through the array of post. The average error between theory and experiments was 7%. The different data set correspond to different densities of the array.

3. Tryptic digestion of proteins.

Native trypsin was grafted on the –COOH functional groups of magnetic particles (600 nm) using EDC (water soluble carbodiimide) and S-NHS (hydroxysulfosuccimide). A plug of these functionalised magnetic nanoparticles was then immobilized between two magnets in a microchannel for flow-through enzymatic digestion with off-chip analysis (Fig 2). The flow rate was controlled with a syringe pump, allowing a variation of the residence times of the sample in the tryptic reactor. This residence time was measured using fluorescein.

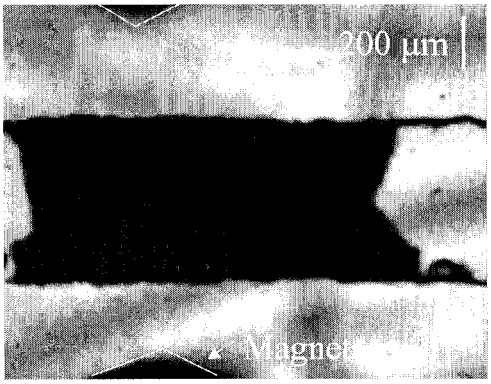

Figure 2 View of the plug of magnetic beads immobilized between the two magnets into the microchannel.

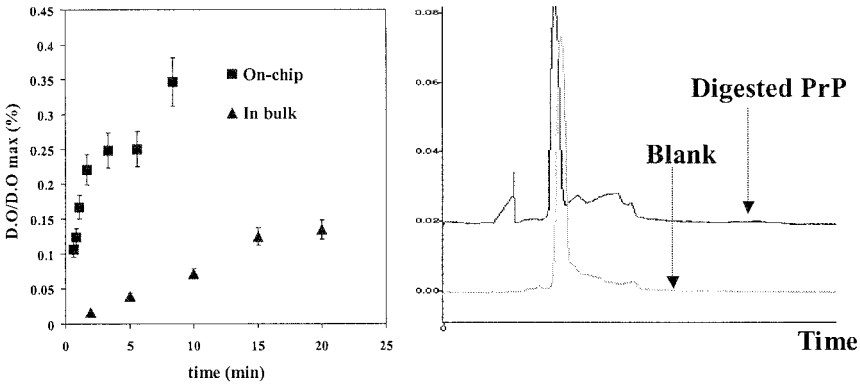

Figure 3 a) Plot of the digestion rate of BAPNA (monitored by spectrophotometry) versus the time, on chip and in bulk. b) Electropherogram of on–chip digested murine Prion protein (PrP), the digestion is incomplete but the residential time only about 5min.

To quantify the efficiency of this tryptic reactor, we used BAPNA (-Nα-Benzoyl-Arginine p-Nitroanilide), a molecule that absorbs at 405 nm when digested by trypsin. Optical densities of both on-chip and bulk digested BAPNA were measured and compared by spectrophotometry [5]. On-chip digestion was about 50 times faster than in bulk (Fig 3a) because the micrometer-sized pores between the columns dramatically reduce the diffusion length when compared to a "bulk system". Digestion of the cellular Prion protein was also assessed, and analysis of digestion fragments by capillary electrophoresis offline is presented in Fig 3b.

Digested products will also be analysed in MALDI-MS for obtaining precise peptide map. Finally, on-line digestion and separation of the products should addressed in the near future.

Acknowledgements

This work was supported in part by European STREP project "Microproteomics", by French Ministery of Research/CNRS Programme "New Analytical Methodologies and Sensors", and by the IFCPAR Indo-French cooperative research programme. K.D.D. acknowledges a postdoctoral fellowship from the Human Science Frontiers Program.

References

[1] Doyle, P.S.; Bibette, J.; Bancaud, A.; Viovy, J.-L. *Science* **2002**, *295*, 2237.

[2] Minc, N. ; Fütterer C.; Dorfman K.D.; Bancaud A.; Gosse C.; Goubault C.; Viovy J.-L. *Anal. Chem.* **2004** (in press)

[3] Fütterer, C.; Minc, N.; Bormuth, V.; Codarbox, J.-H.; Laval, P.; Rossier, J.; Viovy, J.-L. *Lab-on-a-chip* **2004**, (in press).

[4] Dorfman, K.D.; Viovy, J.-L. *Phys. Rev. E* **2004**, *69*, 011901.

[5] Bokov, P. and Minc, N.; Zeldovitch, K.; Viovy, J.-L.; Dorfman, K.D. (submitted)

[6] Peterson, D. ; Rohr, T. ; Svec, F. ; Fréchet, J.-M. *Anal. Chem.* **2002,** 74, 4081-4088.

MICROSYSTEMS SURFACE TREATMENT AND DNA AMPLIFICATION TO DETECT *CAMPYLOBACTER* spp. USING A MICROFABRICATED SU-8 PCR CHIP

Troels Balmer Christensen[1], Dang Duong Bang[2], Ivan R. Perch-Nielsen[1], Zhenyu Wang[1], Anders Wolff[1]

[1]*Dept. of Micro and Nanotechnology, Technical University of Denmark, Bldg 345 east, DK 2800 Kongens Lyngby, Denmark*

[2]*Dep. of Poultry, Fish and Fur Animals, Danish Institute for Food and Veterinary Research, Aarhus, Denmark*

Keywords: Surface treatments, PCR chip, PCR inhibitor, *Campylobacter*, Multiplex PCR

Abstract

In this study, the PCR inhibition effects of common used materials in MEMS, μTAS and Lab-on-a-Chip systems are investigated and methods for preventing the PCR inhibitions are suggested. The results of a multiplex PCR for detecting of *Campylobacter* spp. at species level using a micro fabricated SU-8 PCR chip are presented and discussed.

1. Introduction

Glass, polymers and silicon, commonly used materials for MEMS, μTAS and Lab-on-a-Chip can have great inhibition effects on PCR efficiency [1-4]. The inhibition effect is a serious problem in microsystems due to an increased surface to volume ratio (S/V). In order to prevent the interaction of the PCR mix with the surfaces, different surface treatments and PCR additives are used. In this study, the use of, dichlordimethylsilane (DCDMS) - a silanizing agent, and Bovine Serum Albumin (BSA) are investigated

Campylobacterosis is one of the common food-born illnesses worldwide [5] and campylobacter infection in man is mainly caused by *Campylobacter jejuni* and *Campylobacter coli* species. Isolation and identification of campylobacteria at species level by conventional methods are time consuming (5-6 days) and laborious.

Using a multiplex PCR with *Campylobacter* species-specific primer pairs we have studied the possibility to detect campylobacteria at species level in a micro fabricated PCR chip, based on the polymer SU-8.

2. Experimental

Conventional PCR in tubes containing treated or non-treated silicon, pyrex and SU-8 pieces were used as a PCR inhibition model system to study the inhibition effects. The size of the pieces was 2x5 mm. Prior to surface treatment, the pieces were washed in isopropanol and ultra pure water. The surface treatment was either with DCDMS or BSA. For the DCDMS treatment the pieces and a petridish containing 2 ml. of the silanizing agent DCDMS were placed in a glass dessicator and a vacuum was applied (3.3×10^4 Pa) for 1 hour. The DCDMS will evaporate under vacuum condition and generate a gas-phase DSDMS that will cover the pieces. After 1 hour, the pieces were turned and the process was repeated. Finally the pieces are thoroughly washed in MQ-H_2O for approximately 30 min. For the BSA treatment, the pieces were dipped in a BSA solution for approximately 5 min. and then transferred to the PCR mix. To detect whether Taq-polymerase or DNA were adsorbed on the pieces, a PCR mix that had shown total inhibition was divided into two samples. In one sample extra template DNA was added and in the other sample extra Taq DNA polymerase was added.

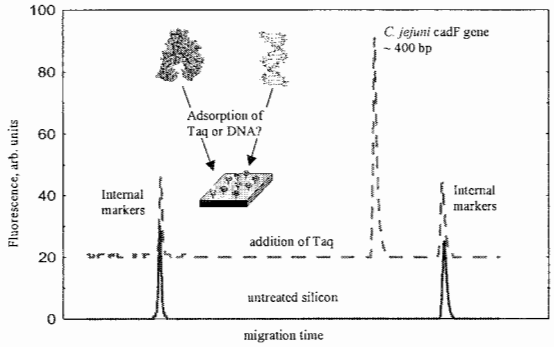

Figure 1. Electropherograms of two PCR analyses. The lower graph (solid) represents a PCR containing an untreated silicon piece. No PCR amplification was observed. Removal of the silicon piece and addition of DNA templates have no influence (data not shown). However, a significant PCR amplification was observed when adding extra Tag-polymerase (upper graph, dashed)

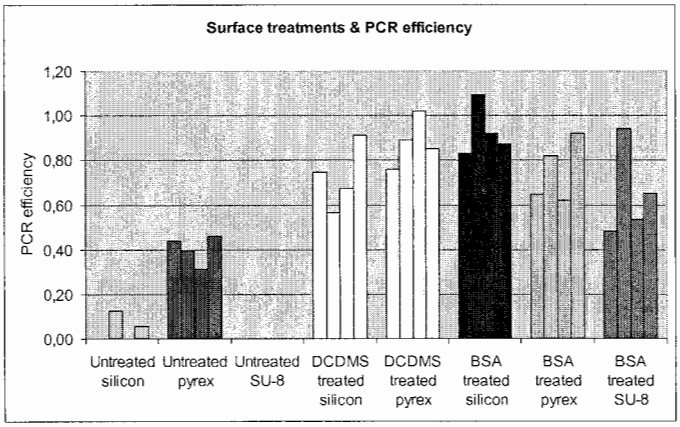

Figure 2. Untreated silicon and SU-8 has a great inhibitory effect on PCR efficiency. Non-treated Pyrex has low yield of PCR amplification. Ten folds enhance of PCR efficiencies were observed when the surfaces were treated with either DCDMS or BSA.

3. Results and discussion

The interpretations of the results outlined in Fig. 1 indicate that the material-related PCR inhibition is mainly due to Taq polymerase being absorbed on the surface rather than DNA. This observation is consistent with other studies [3, 4]. The two small flanking peaks are internal markers and the large peak in the upper (dashed graph) is the *C. jejuni* cadF-gene amplicon, which have a size of approximately 400 bp.

Fig. 2 shows a ten-fold increase in PCR efficiency when the surfaces were treated either with BSA or with DCDMS in comparison with the non-treated surface samples. However, the BSA treatment was much simpler and less time consuming (~5 min.) in comparison to the DCDMS treatment (~1 h.).

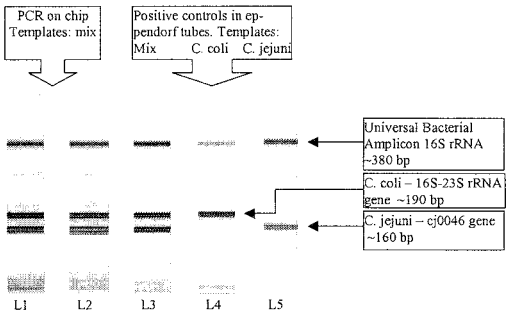

Figure 3. Multiplex PCR for detecting of *Campylobacter* spp. at species level. L1 and L2: Electropherograms of multiplex PCR on the micro fabricated SU-8 PCR chip with a mixture of *C. jejuni* and *C. coli* DNA templates. L3, L4 and L5: Electropherograms of conventional multiplex PCR in tubes served as positive controls with DNA mixture of both *C. jejuni* and *C. coli* (L3) reference strains, or with DNA template from *C. coli* (L4) or *C. jejuni* (L5) only.

The PCR chip is based on the polymer SU-8 and has integrated platinum thin film heaters and temperature sensor [6]. Miniaturization increases the heating and cooling rates due to the reduced thermal mass and the values for this chip are 50 and 30 °C/s, respectively, which is comparable to many silicon microfabricated PCR chips presented in the literature. In previous studies, it has been shown that PCR could be performed in the SU-8 based PCR chamber with a preliminary DCDMS silanization step [6]. However, this step is laborious and time-consuming and we therefore used the simple BSA surface treatment process for the PCR chip for the multiplex PCR experiments. Results of PCR using the PCR chip (L1, L2) and conventional PCR in tubes (positive controls, L3, L4, L5) to detect *Campylobacter* at species level are presented in Fig. 3. Results of the multiplex PCR on the PCR chip clearly shows that the method is specific, easily to perform and the PCR efficiency is comparable to the conventional PCR.

4. Conclusion

This study has shown that the PCR inhibition effect often observed in microsystems is due to Taq polymerase absorbed at the surface rather than DNA. Treating the surface with DCDMS or BSA can prevent this inhibition effect. The BSA treatment is a convenient method for treating PCR chips because it is simple and easy.

References

[1] M. A. Shoffner, J. Cheng, G. E. Hvichia, L. J. Kricka, P. Wilding, *Nucleic Acids Research,* **24**(2), 375-379 (1996).
[2] J. Cheng, M. A. Shoffner, G. E. Hvichia, L. J. Kricka, P. Wilding, *Nucleic Acids Research,* **24**(2), 380-385 (1996).
[3] I. Schneegass, R. Brautigam, J. M. Kohler, *Lab on a Chip,* **1**(1), 42-49 (2001).
[4] I. Erill, S. Campoy, N. Erill, J. Barbe, J. Aguilo, *Sensors and Actuators B-Chemical,* **96**(3), 685-692 (2003).
[5] R. V. Tauxe, *The Increasing Incidence of Human Campylobacteriosis* (WHO, Copenhagen, 2001).
[6] J. El-Ali *et al.*, *Sensors and Actuators a-Physical,* **110**(1-3), 3-10 (2004).

MICROREACTOR BASED ON ENZYME IMMOBILIZED CARBON NANOTUBE

JeongYun Kim[1], DuckJoong Kim[1], HyukHan Kim[2], and SangHoon Lee[1]

[1]Dept. of Biomedical Eng., Dankook University, San 29, AnseoDong, Cheonan, Chungnam, 330-714, Korea

[2]Dept. of Chemistry, Dankook University, San 29, AnseoDong, Cheonan, Chungnam, 330-714, Korea

Abstract

Carbon nano tube has broad applications, and one of its key advantages is the high surface area to volume ratio. So much more biological or chemical materials can be immobilized on the surface. In this paper, we incorporated the enzyme immobilized carbon nano tube into the microfluidic channel for the detection of glucose, and evaluated its feasibility via the short and long term experiments. Especially, the reusability as a microreactor was investigated through the repeated experiments. The surface of nano tube was modified with the functionalized carboxyl groups to enhance the adhesion-property. The developed microchip demonstrated the promising performance as a long term reusable glucose sensing microfluidic chip.

Key Words: Microreactor, Carbon Nano Tube, Enzyme Immobilization

1. Introduction

Carbon nano tube (CNT) is widely applied in many fields owing to diverse properties [1-2]. It has also a large surface area to volume ratio [3], and this is one of key advantages to immobilize biological or chemical materials as much as possible. In this paper, we immobilized bio-catalysts onto the surface of multi wall CNT(MWNT), and made the micro scale block with this MWNT particles. The block was incorporated into the PDMS based microfluidic device for the detection of glucose-enzymes reactions, and their feasibility as a microreactor is evaluated via diverse experiments.

2. Fabrication

To prepare MWNT-bound carboxylic acids particles (size < 10 μm), the following procedure was used. The MWNT was simply sonicated in aqua regia (3:1 volumetric ratio of H_2SO_4-HNO_3) for 6 hours at 60°C, and filtered and rinsed with PBS buffer solution. The carboxylic acid-functionalized MWNT was covalently bonded with horseradish peroxidase (HRP) and glucose oxidase (GOX) by applying EDC/NHS system in PBS buffer solution at room temperature. With these modified MWNT particles, the horse-shoe-shaped micro scale block (thickness: 50 μm) is fabricated using PDMS mold which is constructed by the pre-reported process[4]. The particles mixed with biocatalysts are spread over the horse-shoe-shaped patterns imprinted on the mold uniformly, and pressed with the pressure 13.5 kgf /cm^2. The MWNT microblock is hardened by drying for 10 minutes at 22°C as shown in Figure 1(a) and separated from PDMS mold. The PDMS substrate (thickness: 8 mm) having microchannel pattern was fabricated in a similar way with PDMS mold. Both the PDMS substrate and slide glass are exposed to the oxygen plasma for the bonding, and the MWNT microblock was carefully placed onto the channel pattern on the PDMS substrate utilizing specially designed tools. The slide glass treated by oxygen plasma is placed onto the PDMS substrate embedding microblock and bonded as demonstrated in Figure 1(b). As illustrated in the figure, the microchannel is designed to deliver fluid to the MWNT block uniformly as possible, and the dam is utilized to fix the block firmly, and to filter the detached MWNT fragments.

3. Experimental

The microfluidic networks are assembled using the ethyl vinyl acetate (EVA) tubes, and the aqueous solutions containing glucose, buffer and Amplex Red are slowly introduced at the rate of 2 μl/min into the inlet using syringe pump (CMA, 102) to generate a fluorescent product, resorufin. The appearance of fluorescence was detected using confocal microscope (Carl Zeiss, LSM510 Meta) by the excitation and the emission at the wavelength of 543 nm and 585 nm respectively.

4. Results and discussion

The fluorescent reaction was slowly progressed after the injection of the inlet solution including glucose, buffer and Amplex Red. The fluorescent micrograph illustrated in Figure 2 is the image of the microreactor embedding functionalized MWNT and is captured after 5 minutes from the start of injection. This figure indicates that the immobilized enzymes were viable under the chip fabrication environment and reacted to the injected glucose well. At the region in the dotted circle, the dark shade appears due to the absence of functionalized MWNT, and the un-reacted solution travels to the end of outlet (represented as a dark region at the outlet channel). The 3-D intensity distribution image is demonstrated in Figure 3, and exhibits the reaction process more clearly. The fluorescence micrographs are sequentially captured during 5 minute just after the injection of input solution and the intensities at the outlet channels were measured per every minute and they are illustrated in Figure 4. As time goes, the reaction progressed gradually until the input solution is fully diffused over the MWNT block. After 3 minutes, the product of reaction begins to appear at the outlet channel and the intensity at the 5 minute becomes 3 times strong than that at the 3 minute. The reaction experiments for the long duration were performed to evaluate the feasibility of long term and repetitive use and their result is shown in Figure 5. Total 6 experiments were carried out, and the input solution went through the microchannel by rinsing the MWNT block for 3 hrs in each experiment, and the corresponding intensities were measured. The chip was stored at the refrigerator for average 8 hrs after one experiment is completed. The figure exhibits that the same activity of immobilized enzymes are retained until 3 hrs after the start of rinsing, and reacted until 12 hrs. In addition, this figure indicates that the repetitive use of chip (2 or 3 times) is possible if stored under the cool temperature.

5. Conclusions

This paper demonstrates the feasibility of a novel spectroscopic detection of glucose by utilizing the PDMS based microfluidic chip having MWNT block on which the GOX and HRP is co-immobilized. The experiment illustrated that the enzymes can be viable under the harsh fabrication environment, and the reaction ability maintained for comparatively long time as much enzymes were immobilized owing to the high surface area to volume ratio. The developed microchip demonstrated the promising performance as a long term reusable glucose sensing microreactor.

Acknowledgements

This study was supported by a grant of the Korea Health 21 R&D Project, Ministry of Health & Welfare, Republic of Korea. (02-PJ3-PG6-EV10-0001)

References

[1] S. Iijima, 1991, *Nature* **354**, pp 56-58
[2] L. Hueso, N. Mathur, 2004, *Naure* **427**, pp 301-304
[3] M.F. Yu, B.S. Files, et al, 2000, *Phys. Rev. Lett.* **84**, pp 5552-5555
[4] S.H. Lee, W.J. Jeong, D.J. Beebe, 2003, *Lab Chip* **3**, pp 164-167

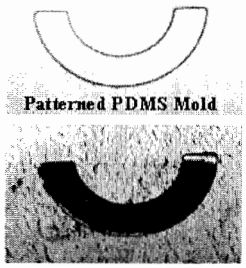

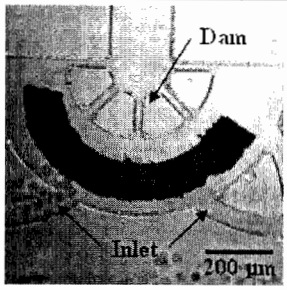

a) PMDS mold for MWNT block production b) Microreactor incorporating CNT block

Figure 1. MWNT block construction with PDMS mold, and microreactor embedding MWNT block

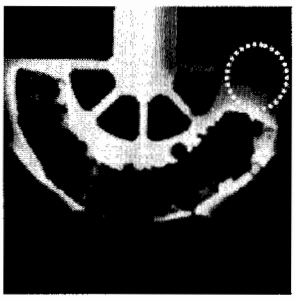

Figure 2. Fluorescence micrograph of reactor with MWNT block

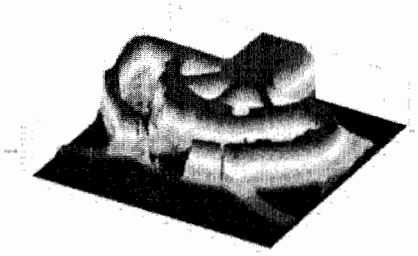

Figure 3. 3-D intensity micrograph of reactor with MWNT block

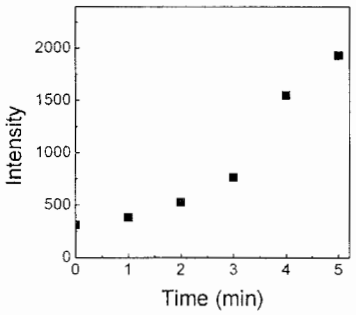

Figure 4. Intensity change after the injection of glucose solution

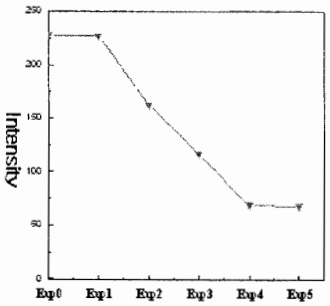

Figure 5. Intensity changes to the repetitive experiments

MICROFLUIDIC MIXERS FOR UV STUDIES OF UNLABELED PROTEINS

David Hertzog[1,2], Juan Santiago[1], Olgica Bakajin[2]
[1]*Department of Mechanical Engineering, Stanford University, Stanford, CA*
[2]*Chemistry & Materials Science, Lawrence Livermore National Laboratory, Livermore, CA*

Abstract

We have designed and fabricated continuous flow microfluidic mixers to measure protein folding rates using naturally fluorescent proteins. The mixers are deep reactive ion etched in fused silica substrates to reduce ultraviolet (UV) absorption and background noise. By exciting the amino acid tryptophan with multi-photon excitation techniques, the relative fluorescence of tryptophan can be used to extract real-time protein structure information. We have demonstrated mixing times of less than 10 μs and have initiated studies of the benchmark protein cytochrome C.

Keywords: mixing, protein folding, cytochrome c

1. Introduction

The three most common experimental methods of initiating protein folding are photo-chemical triggering, temperature and pressure jumps, and fast mixing methods. Photochemical triggering and t- and p-jumps are very fast, $\leq$1 μs, but can only be used with a limited number of proteins. Fast mixing of a protein to change pH or denaturant concentration is a more general initiation method for protein folding, but mixing dead times are currently limited to at least tens of microseconds [1,2]. Our mixer uses hydrodynamic focusing in an optimized structure to focus a 100 nm wide stream of denatured proteins into a buffer stream. Unlike similar designs, this structure minimizes both lateral diffusion distance and the time a protein spends in the development region just upstream of the focused stream.

2. Modeling

A commercial fluid flow solver (FEMLAB, by Comsol Inc., Stockholm, Sweden) was used to optimize mixer shape and flow conditions. A 2D-model was developed that solves the full incompressible Navier-Stokes and advection-diffusion equations; results of a typical simulation are shown in Fig.s 1 and 2. This model was used to iterate through various design parameters including flow rate ratios and geometric aspect ratios. Velocity field simulations can be integrated along streamlines in the focused stream to convert the Eulerian axial distance coordinates to a Lagrangian time coordinate, which describes the denaturant concentration history of a single protein. The model has been validated using both micron-resolution particle image velocimetry and fluorescence quenching experiments.

3. Experimental

Our initial mixers were designed and fabricated in silicon (sealed with borosilicate) using standard microfabrication techniques [3]. We have used these to quantify the folding kinetics of proteins using Förster resonance energy transfer. Our latest mixers are fabricated in substrate-grade fused silica using a deep reactive ion etching (DRIE) process (Micralyne, Edmonton, Canada), and thus are compatible with UV spectroscopic methods. Channels are 8 μm deep with highly vertical sidewalls and a 1 μm wide nozzle exit, as shown in Fig. 3. Filters are integrated on the microfluidic chips to reduce clogging of the nozzles, and we use a computer controlled pressure regulation system to control flow rates.

We will use the extensively-studied horse cytochrome C as a benchmark protein [1,4]. Cytochrome C has a single tryptophan whose fluorescence is dependent on protein structure [1]. The folding process involves an initial ~50 μs collapse of the protein, followed by a relatively slow

(~500μs time scale) folding [1,4,5]. With mixing times on the order of 10 μs, our mixer can resolve both of these phases and requires sample volumes as small as 10 μl. The mixer velocity fields and mixing dynamics are well characterized.

The protein is initially unfolded at equilibrium using a high concentration of guanidinium hydro-chloride (GdCl). This denaturant-protein solution is mixed with buffer in the mixer, reducing the local denaturant concentration of the proteins and initiating collapse and folding.

A multi-photon excitation method is used to excite the tryptophan at UV wavelengths [6]. A femtosecond pulsed Ti-sapphire laser at 800 nm focused through a 40x 1.2NA objective excites the tryptophan with simultaneous three-photon events at 266 nm in a submicron excitation volume. The fluorescence is then detected with a high sensitivity bialkali PMT, and images of the focused stream are constructed by scanning with a submicron resolution stepper-motor stage. The fluorescent intensity along the stream axis is then converted to a time axis using the velocity profile obtained from simulations. Equilibrium experiments allow the conversion from relative fluorescence intensity to protein conformation to obtain conformation versus time data.

4. Discussion

Our mixer addresses three important obstacles in studying protein folding. First, its low sample volume requirement reduces the need for large amounts of precious proteins, which is often an issue with labeled or purified samples. Second, fabrication in fused silica makes them compatible with ultraviolet spectroscopic methods allowing measurement of conformation with naturally occurring UV labels such as tryptophan. Finally, a fast mixing time of 10 μs pushes the envelope of measuring fast kinetics in protein-folding with concentration changes.

We have initiated experiments in UV tryptophan visualization and will present these results. This mixer represents an important enabling technology in the general study of protein kinetics and, in particular, fast folding processes.

Acknowledgements

This work was performed under the auspices of the US Department of Energy under contract #W-7405-Eng-48 with funding from the LDRD program. We would like to thank Dr. Thomas Huser and Wilbur Reichman for their help with the experimental setup, and Lisa Lapidus for her help with the experimental design.

References

[1] C.-K. Chan, Y. Hu, S. Takahashi, D. L. Rousseau and W. A. Eaton, *Proc. Nat. Acad. Sci.*, **94** (5), 1779-1784 (1997).

[2] P. Regenfuss, R. M. Clegg, M. J. Fulwyler, F. J. Barrantes and T. M. Jovin, *Rev. Sci. Inst.*, **56** (2), 283-290 (1985).

[3] D. E. Hertzog, J. G. Santiago and O. Bakajin, *Proc. 7th Int. Conf. uTAS*, Squaw Valley, Lake Tahoe, CA, (2003).

[4] S. Akiyama, S. Takahashi, T. Kimura, K. Ishimori, I. Morishima, Y. Nishikawa and T. Fujisawa, *Proc. Nat. Acad. Sci.*, **99** (3), 1329-1334 (2002).

[5] M. C. R. Shastry, J. M. Sauder and H. Roder, *Acc. Chem. Res.*, **31** (11), 717-725 (1998).

[6] M. Lippitz, W. Erker, H. Decker, K. E. v. Holde and T. Basche, *Proc. Nat. Acad. Sci.*, **99** (5), 2772-2777 (2002).

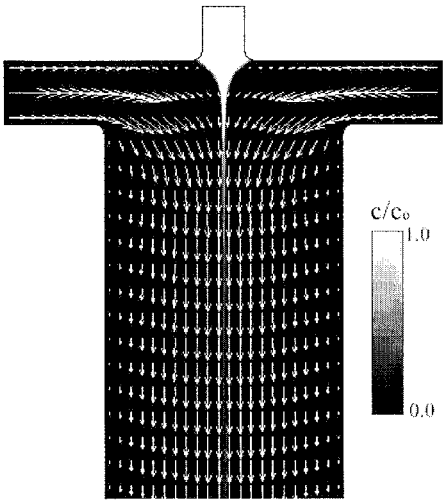

Figure 1. 2D numerical simulation of the mixer using FEMLAB. Inlet in the "north" has a width of 1 μm, east/west side inlets are 2 μm wide, and exit/south channel is 10 μm wide. Gray scale represents normalized denaturant concentration, and vectors represent the velocity field. Exit channel flow has Reynolds and Peclet numbers of 17 and 8,000, respectively.

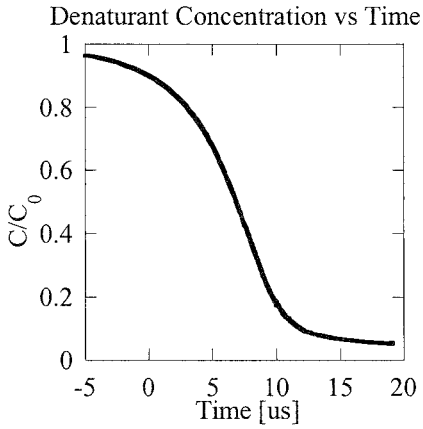

Figure 2. Time history of normalized denaturant concentration experienced by a protein traveling along the center streamline of the mixer; from simulation in Fig. 1. In this simulation the denaturant concentration drops from 90% to 10% of its initial value in 10 μs.

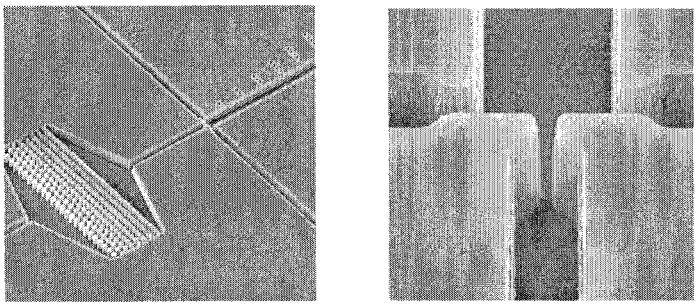

(a) (b)

Figure 3. (a and b) SEM images (courtesy of Micralyne) of the DRIE fused-silica mixers, before bonding of coverslip. (a) Mixing region with on-chip integrated filter post structures (at left) to prevent clogging of mixer nozzle. (b) Nozzle region: Denatured protein enters from bottom channel flowing north, buffer enters from the east/west side channels. Some wall roughness is apparent and due to the DRIE process.

MONITORING PROTEOLYTIC ACTIVITY IN DROPLET MICROARRAYS, A NEW TOOL FOR DRUG DISCOVERY AND DIAGNOSTIC

L. Mugherli, F. Chatelain, M. Balakirev
Laboratoire Biopuces/DRDC/DSV, CEA-Grenoble, France

Abstract

A convenient and miniaturized method which allows proteolytic activity monitoring is introduced. Within hundreds of confined reservoirs created on a glass slide, enzymatic cleavage of a fluorogenic substrate was carried out by simple piezoelectric deposition of substrate and protease. This format is ideal for testing the numerous conditions required for applications such as screening or diagnostic.

Keywords: Proteases, fluorescence, droplets, screening, microarray

1. Introduction

Proteases, enzymes hydrolyzing a peptide bond, are key regulators of cellular function and viability. They are involved in many important biological processes including protein maturation and degradation, cellular signaling, cell death and differentiation. Furthermore, proteases play a central role in diverse pathologies, such as inflammation, cancer, pathogen infections, and Alzheimer's disease, making these enzymes important therapeutic targets and disease biomarkers [1,2]. A number of high throughput techniques have been proposed for the determination of protease substrate specificity and inhibitor screening, though they do not generally provide a complete kinetic analysis of protease activity [3,4].

We report here the assembly and evaluation of droplet microarrays that enable high throughput protease characterization and inhibitor screening.

2. Device: Droplet Microarrays

To meet our aim of analyzing various conditions for proteolytic reactions simultaneously, we needed microarray supports able to confine hundreds of reaction vessels on a small area. These microarrays are composed of features defined and separated on the glass slide by differential surface tension (surface tension arrays). Specifically, the photolithographic approach of Butler *et al.* [5] was used to create a series of hydrophilic spots bounded by a perfluorinated surface. The differences in surface energies between the spots and surrounding zones allow for droplets to be readily formed within a defined site. Microarrays of 300 to 3000 hydrophilic features (500μm in diameter) were used in protease assays (Fig 1).

3. Experimental: Proteolysis Analysis

The droplets arrayed on the surface of glass slides served as microreactors for proteolysis reactions. The robot used for dispensing reagents in the microarray allows precise targeting of each individual hydrophilic spot. Drop's patterns can easily be designed in order to test a variety of conditions in a single experiment.

The protease assay was carried out as follow:

According to a plan of experiment, protease, fluorogenic substrate and protease inhibitor were mixed directly in droplets by using a piezoelectric dispense system. We varied enzyme and substrate concentrations with appropriate no-enzyme and inhibitor controls, creating a series of droplet groups housing diverse reaction conditions. The progress of each individual reaction was followed by liberation of the fluorescence due to the substrate cleavage and was measured using a

Genomic Solution array scanner. After quantification and data treatment the kinetic of proteolysis could be precisely monitored.

4. Result and discussion

In a proof of concept experiment we observed that proteolysis was occurring, using a no-protease control and an inhibitor control (Fig 2a). Kinetics of proteolysis and the effect of inhibitor could be determined in parallel for each individual droplet. After data collection and treatment, we plotted the mean values and standard of deviations against time for each group of droplet housing the same reaction (Fig 2b). The reaction proved to be extremely slow at room temperature [from 340 to 1220 min] but proceeded with an acceptable rate (over a few hours) at 37°C [0 to 340 min and 1220 to 1645 min].

Application of microarray technology allowed rapid optimization of the experimental conditions. Indeed, within a single experiment, we tested forty different conditions (eight protease concentrations and five substrate concentrations). The number of condition simultaneously assessed can easily go beyond one hundred, depending on the total number of droplets and the number of droplet housing similar conditions. After data collection and treatment, the effect of substrate and protease effect was determined (Fig 3). As expected, the fluorescent signal increases with time, with substrate concentration and with enzyme concentration.

Among assessed conditions we found out that for an enzyme concentration of 0.4 unit/mL, a proper substrate concentration should be around 100 mg/mL (Fig 3a). We also observed that, with a substrate concentration of 250 mg/mL, an enzyme concentration of 0.02 unit/mL is suitable to monitor proteolytic activity (Fig 3b). We finally concluded that a protease concentration of 0.05 unit/mL together with a substrate concentration of 250 mg/mL would constitute a safe compromise to obtain a strong enough signal with minimal reagents quantities.

5. Conclusion

The described tool is very efficient for monitoring hundreds of proteolysis micro-reactions simultaneously. One has the possibility to conveniently create in each droplet (each groups of droplet if working with duplicate or triplicate) a particular condition of reaction (reagents concentrations, buffer composition, inhibitors…). We successfully applied this versatile tool to reaction optimization and demonstrated inhibitor effect was unambiguously detectable within a wide range of enzyme concentration.

Acknowledgment

The authors would like to thank the Association pour la Recherche contre le Cancer, a French charity, for supporting this work.

References

[1] Leung, D.; Abbenante, G.; Fairlie, D. P. *Protease Inhibitors: Current Status and Future Prospects,* J. Med. Chem. 43: 305 (2000).

[2] Weissleder, R.; Ntziachristos, V. *Shedding light onto live molecular targets* Nat. Med. 9: 123 (2003).

[3] Thornberry, N. A. *et al. A combinatorial approach defines specificities of members of the caspase family and granzyme B. Functional relationships established for key mediators of apoptosis,* J. Biol. Chem. 272: 17907 (1997).

[4] Turk, B. E.; Huang, L. L.; Piro, E. T.; Cantley, L. C. *Determination of protease cleavage site motifs using mixture-based oriented peptide libraries.* Nat. Biotechnol. 19: 661 (2001).

[5] Butler, R. J. H. *et al. In Situ Synthesis of Oligonucleotide Arrays Using Surface Tension* J. Am. Chem. Soc. 123 : 8887 (2001).

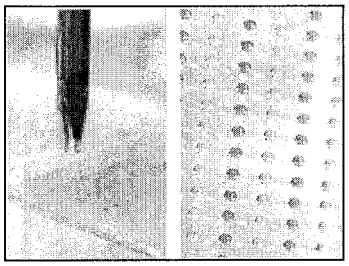

Fig 1

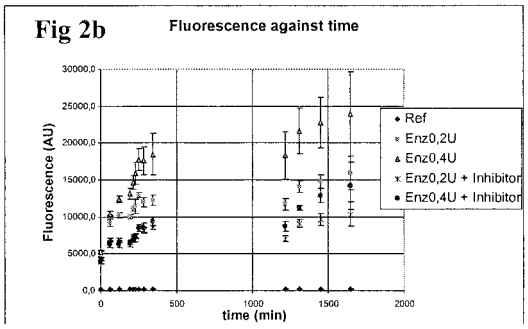

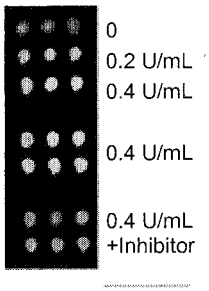

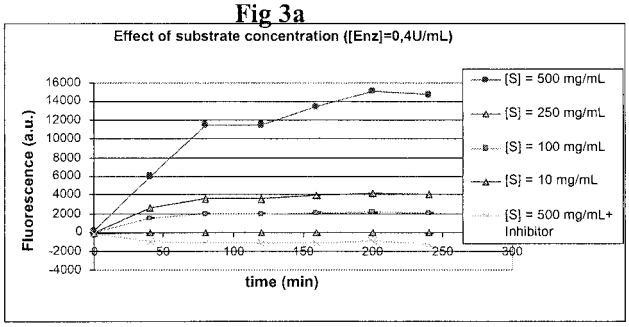

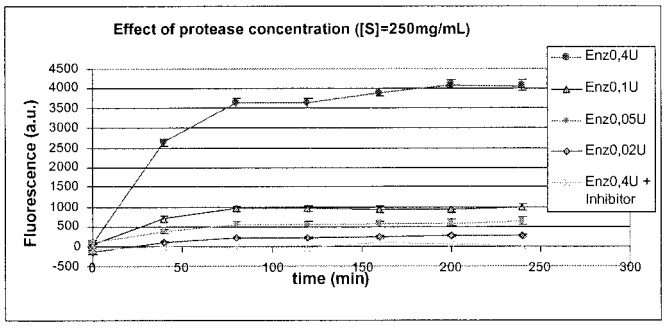

Fig 3b

Fig 1. Piezoelectric dispense of the reagents in droplet microarray.
Fig 2. Analysis of the protease activity using droplet microarray (each row is a triplicate). (**2a**) Image of the proteolysis reaction in droplets obtained with array scanner, (**2b**) Kinetics of the proteolysis in droplets.
Fig 3a & 3b : *Data normalized by subtraction of no-protease control.*
Fig 3a. Effect of substrate concentration with or without inhibitor
Fig 3b. Effect of protease concentration with or without inhibitor.

RAPID PROTOTYPING OF PDMS MICROCHANNELS USING A LIQUID CRYSTAL PROJECTOR-MODIFIED MASKLESS PHOTOPOLYMERIZATION DEVICE

Jun Kobayashi[1, 2], Masayuki Yamato[1, 2], Kazuyoshi Itoga[1, 2], Akihiko Kikuchi[1, 2] and Teruo Okano[1, 2]

[1] *Institute of Advanced Biomedical Engineering and Science, Tokyo Women's Medical University, 8-1 Kawada-cho, Tokyo 162-8666, Japan*

[2] *CREST, Japan Science and Technology Agency, 4-1-8 Honcho, Kawaguchi, Saitama 332-0012, Japan*

Abstract

We have developed an all-in-one device for photopolymerization-based microfabrication of microfluidic devices by modifying a commercially available liquid crystal display projector (LCDP). Microchannel networks were fabricated from the images prepared with software run on personal computers. Representative microfluidic behavior (e.g. laminar flow patterning) indicates that the quality of microchannels fabricated in poly(dimethylsiloxane) (PDMS) seem sufficient for microfluidic research applications. The maskless fabrication is considered to be a versatile approach for rapid prototyping of microfluidic systems without specific skills for microfabrication, expensive apparatus, and cleanroom facilities.

Keywords: maskless, liquid crystal display projector, poly(dimethylsiloxane), microfluidics, rapid prototyping

1. Introduction

Microfabrication based on photolithography techniques has been widely used to fabricate microfluidic channels on silicon, glass, and polymers. PDMS has been also utilized as microfluidic substrates because of its optically transparent, chemically inert, and nontoxic properties [1], although micromolds prepared by photolithography are utilized for preparation of PDMS microchannels. We have previously developed an all-in-one photopolymerization device by modifying a commercially available LCDP for preparation of cellar micropatterned surfaces [2, 3]. Here, we demonstrate a novel method for a rapid prototyping of PDMS microfluidic channels without any need for expensive photomasks, utilizing instead a simple photopolymerization procedure adapted for a conventional LCDP [4].

2. Experimental

The surfaces of cover glass slips (24 × 50 mm, 0.2 mm in thickness) were cleaned by oxygen plasma treatment and wetted with Milli-Q water for 1 h, followed by immersion into 2% (v/v) solution of 3-methacryloxypropyltrimethoxysilane (MPTMS) in ethanol/water/acetic acid (95/5/0.1) for 3 h at room temperature.

The two-step procedure to fabricate PDMS microchannels is outlined in Figures 1a and b. First, photopolymerization of poly(isobornyl acrylate-*co*-tetraethyleneglycol dimethacrylate) (P(IBA-co-TEGDMA)) was performed on the MPTMS-immobilized coverslip by irradiation of visible light through the LCDP device (Figure 1a). The liquid crystal (LC) panels within the LCDP act as virtual photomasks to project the reduced images onto the substrate at high resolution (i.e. each pixel size, 10 μm). Projection images are easily generated on PC monitors with commercial software, therefore special control software is not needed for lithographic pattern generation. Second, PDMS microchannels are fabricated as negative replicas by pouring and curing PDMS

prepolymer over the P(IBA-*co*-TEGDMA) master (Figure 1b). Finally, product PDMS microchannels are reversibly sealed with a coverslip.

3. Results and discussion

Figure 2 shows representative microfluidics to demonstrate the utility of the LCDP device for microfluidic researches. In order to confirm the flexibility of the microfluidic design, a microchannel with a mountain ridge-like shape was used as a mask image. SEM image of PDMS microfluidic network obtained is indicated in Figure 2a. No leaks were detected across the contacts between the substrates (Figure 2b).

Schematics of laminar flow experiments are shown in Figure 2c. After the microchannels were filled with water, fluorescein isothiocyanate-conjugated bovine serum albumin (FITC-BSA) in Dulbecco's phosphate buffer saline (PBS) was pored from an inlet and PBS from the other. A paper tip was set at the outlet, followed by current of both solutions toward the outlet (Fig. 3e). Under a fluorescent microscope, multiple laminar flow formations were observed (Figure 2d and e). These indicate that spontaneous flowing of fluids in PDMS microchannels is achieved.

4. Conclusions

We have developed an all-in-one device for photopolymerization-based microfabrication by modifying a commercially available liquid crystal device projector. Several examples such as flexible design of microchannels and laminar flow patterning show that the quality of microchannels fabricated in PDMS seem sufficient for microfluidic research applications. The maskless fabrication is considered to be a versatile approach for rapid prototyping of microfluidic systems since the researchers create the individual microchannel designs based on their own purpose. Moreover, this method provides interdisciplinary researchers with the opportunities to get into the fields of microfluidics without specific skills for microfabrication, expensive apparatus, and cleanroom facilities.

Acknowledgements

We acknowledge the cooperation of Digital Systems Development Center of Sanyo Electric Co., Ltd. This work was supported by Grants-in-Aid for Scientific Research (13308055) of the Japan Society for the Promotion of Science and the Promotion and Mutual Aid Corporation for Private School of Japan.

References

[1] Y. Xia, G. M. Whitesides, *Angew. Chem. Int. Ed.*, **37**, 550 (1998)
[2] K. Itoga, M. Yamato, J. Kobayashi, A. Kikuchi, and T. Okano, *Biomaterials*, **25**, 2047 (2004)
[3] K. Itoga, M. Yamato, J. Kobayashi, A. Kikuchi, and T. Okano, *J. Biomed. Mater. Res.*, **69A**, 391 (2004)
[4] J. Kobayashi, M. Yamato, K. Itoga, A. Kikuchi, and T. Okano (submitted)

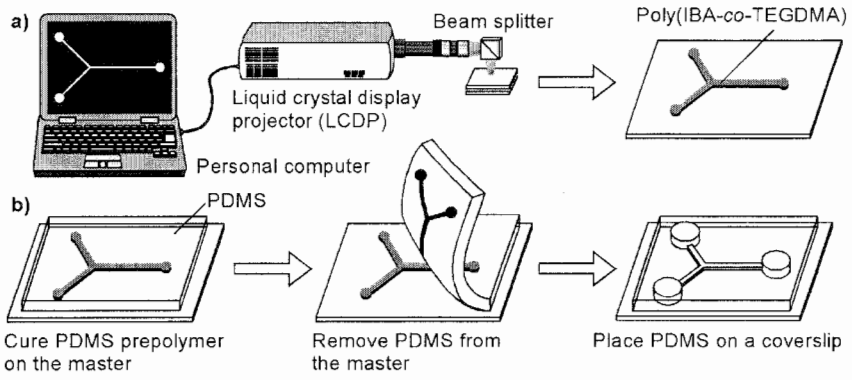

Figure 1. Fabrication of microfluidic devices using the LCDP photopolymerization device: a) The master of P(IBA-*co*-TEGDMA) on a silanized coverslip was polymerized by visible-light irradiation through LCDP; b) PDMS prepolymer was cured on the master (left), the PDMS membrane was cut and peeled from the master (central), and a punched PDMS piece was placed on an untreated coverslip (right).

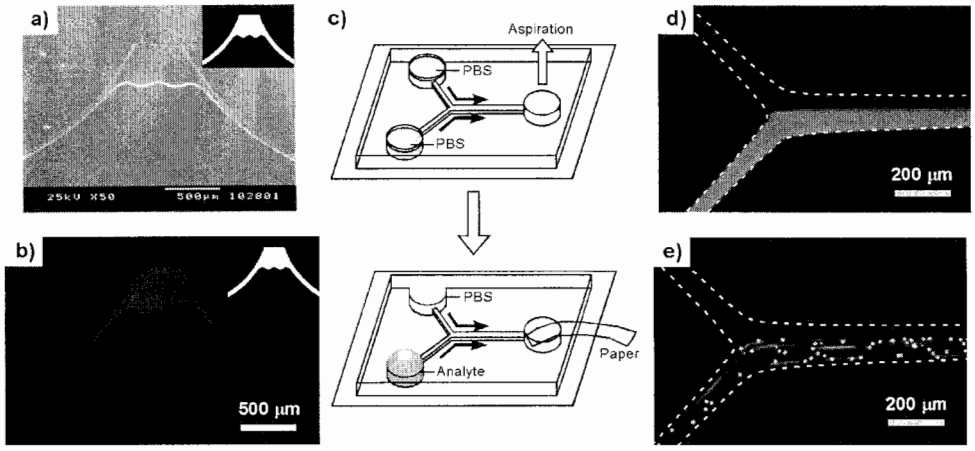

Figure 2. Representative microfluidics. a) Three-dimensional PDMS microchannels observed by SEM. b) Flowing experiment of fluorescein isothiocyanate-conjugated bovine serum albumin (FITC-BSA) solution in phosphate buffer saline (PBS) within PDMS microchannel observed by fluorescent microscopy. Mask images like a mountain ridge at a reduced size were indicated in the upper right corner of pictures a) and b). c) Schematic of laminar flow experiments. Multiple laminar flow patterning between PBS and d) rhodamine 123 or e) FITC-conjugated poly(styrene) beads (diameter, ca. 6 um), respectively, at the interconnection point observed by fluorescent microscopy.

MICROCHIP CAPILLARY ELECTROPHORESIS DEVICE WITH ON-LINE MICRODIALYSIS SAMPLING FOR NEAR REAL-TIME MONITORING

Bryan Huynh[1], **Barbara Fogarty**[1], **Scott Martin**[2], and **Susan Lunte**[1]

[1] *Dept. of Pharmaceutical Chemistry, University of Kansas, Lawrence, KS 66047, USA*
[2] *Dept. of Chemistry, Saint Louis University, Saint Louis, MO 63103, USA*

Abstract

An electrophoresis-based microchip, based on a flow-through design [1], was coupled to a commercially available microdialysis sampling probe for continuous monitoring applications. An epifluorescent laser-induced fluorescence (LIF) system was used to conduct optimization studies involving microdialysis flow rates and microchip running voltage. An experiment to determine response time for the device to sense a concentration change was carried out, followed by the on-chip monitoring of fluorescein mono-β-D-galactopyranoside (FMG) hydrolysis by β-D-galactosidase (β-Gal) [2]. To the best of our knowledge, this is the first work to couple external microdialysis sampling with an electrophoresis-based microdevice.

Keywords: microdialysis sampling, microchip capillary electrophoresis, near real-time monitoring

1. Introduction

Microdialysis is a continuous sampling technique that has been used extensively for the monitoring of neurotransmitters *in vivo* in pharmacokinetic and neurochemical investigations. The semipermeable membranes of microdialysis probes allow microdialysis to serve as a clean-up technique as well as a sampling method. In microdialysis sampling, temporal resolution is a function of both the sensitivity and sample volume requirements of the analytical method. For on-line methods, the temporal resolution is also dependant on the analysis time. Flow rates in microdialysis are typically 0.1 to 1 μL/minute. Most conventional methods (i.e. liquid chromatography (LC) used for the analysis of microdialysis samples require collection volumes in the range of 1.0-10 μL. Techniques with submicroliter sample volume requirements such as microchip capillary electrophoresis (CE) make it possible to obtain better temporal resolution by maximizing the sample usage. In addition, the fast analysis times of microchip devices make it possible to greatly increase the temporal resolution for on-line systems where near real-time monitoring of an analyte are critical.

2. Experimental

Glass microchip devices were fabricated using photolithography techniques. An interface between the microdialysis sampling system and the chip device is schematically shown in Figure 1. A flow-through chip design that incorporated a sampling channel was used, and sample injections were gated into the separation channel for analysis. Disodium fluorescein was used to conduct studies to determine optimal microdialysis flow rate and microchip running voltage.

3. Results and Discussion

Dialysate from the probe entered the device through connective fittings at the wider sampling channel. A fraction of the flowing stream was introduced to the injector T and discrete sample

plugs were injected into the separation channel by floating the voltage applied at the buffer reservoir for 1 sec. The voltage was then resumed to allow simultaneous separation and sample gating. Optimization studies found that peak area varied linearly with the applied voltage, with higher voltages leading to faster separations but lower peak response. Perfusion flow rates of 0.8 and 1.0 µl/min were found to provide optimal device performance.

The system lag time, defined as the time it takes the analyte to be transferred from the probe to the injection T on the device prior to separation, was calculated to be 6.5 min. As the lag time attributed to the microdialysis tubing was less than 1 min, the channel dimensions prior to the injection T were the major contributors to the lag time of the system. Device longevity was on the order of a day, with continued use resulting in decreased electroosmotic flow that disrupted the gated injection procedure.

The ability of the device to sense a concentration change was determined using disodium fluorescein. The device was then used to monitor an in vitro enzyme assay. The hydrolysis of FMG by β-Gal was demonstrated using the microdialysis-coupled device and a temporal resolution of 30 sec was achieved. Figure 2 shows the gradual appearance of the product peak (fluorescein) while the fluorescent substrate decreases over time.

4. Conclusions

A microchip-based capillary electrophoresis system was coupled to *in vitro* microdialysis sampling. The setup enables monitoring of chemical reactions to be carried out with high temporal resolution. This system can potentially be extended for *in vivo* applications.

References

1. Chen, S.H.; Lin, Y.H.; Wang, L.Y.; Lin, C.C.; and Lee, G.B. *Anal. Chem.*, 2002, 74, 5146-5153.
2. Burke, B.J. and Regnier, F.E. *Electrophoresis*, 2001, 22, 3744-3751.

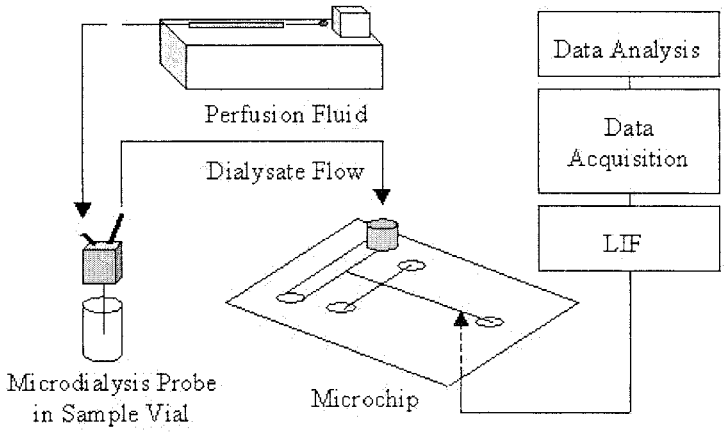

Figure 1: Schematic of microdialysis-microchip CE setup for high-temporal resolution monitoring.

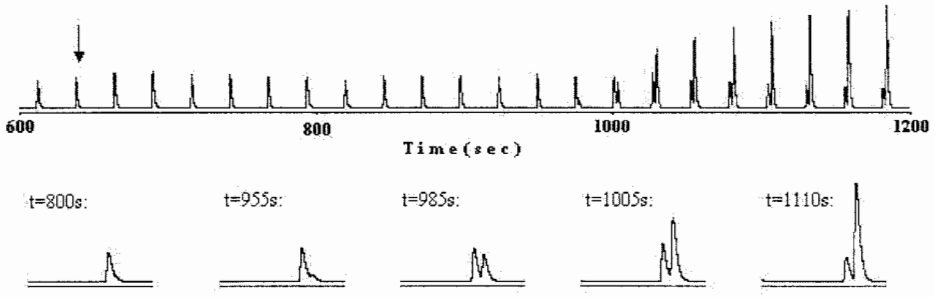

Figure 2: Online monitoring of FMG hydrolysis by β-Gal using the microdialysis-microchip CE system. Top: overall electropherogram, monitoring change from t = 600 – 1200; arrow denotes when enzyme was added. Bottom: expanded views of individual electropherograms at denoted times.

DROPLET MANIPULATION USING SAW ACTUATION FOR INTEGRATED MICROFLUIDICS

Alan Renaudin, Victor Zang, Pierre Tabourier, Jean-Christophe Camart and Christian Druon
Institut d'Electronique de Microélectronique et de Nanotechnologie, Avenue Poincaré, Cité Scientifique, 59652 Villeneuve d'Ascq, BP 69, France ;Mail : alan.renaudin@iemn.univ-lille1.fr

Abstract

We show that a Surface Acoustic Waves (SAW) platform can be dedicated to liquid microdroplet transport. SAW are generated centred around 20 MHz by interdigited transducers (IDT) laid on a $LiNbO_3$ piezoelectric substrate. We show that a modulation of the surface wetting properties treatment significantly improves the transport of droplets and chemical design of hydrophilic tracks provides trajectory control. First results related to droplet handling and mixing with the SAW platform are given. In particular a RF pulsed excitation is experimentally demonstrated to be efficient for the transport of droplets inserted between two planes. Such a situation is especially interesting when functionalized areas are patterned on one of these two planes. Thus a moving droplet brought sequentially into contact with them could undergo biochemical modifications.

Keywords: SAW, droplet transport, surface treatment, proteomic, mixing.

1. Introduction

The literature has already drawn attention to SAW platforms for conveying small objects [1]. These platforms have been used to demonstrate the SAW relevance for on chip fluid handling. Digitalized microfluidics is based on liquid microdroplet manipulation in order to performe basic operations such as transporting, merging, splitting and mixing [2]. In this paper we address the issue of the trajectory control of a liquid droplet actuated by SAW. We examine how patterning the chip surface hydrophilic properties can allow designing tracks in order to guide droplets. Tests are performed under these conditions on droplets moving squeezed between two planes. In this case, liquid evaporation is limited and biochemical operations could be performed on specific areas, patterned on these planes should be more efficient due to an increased exchange surface.

2. The convoying SAW platform

SAW around 20 MHz are generated by InterDigital Transducers (IDT) laid on a X-cut $LiNbO_3$ piezoelectric substrate. An alternating electric voltage at frequency f_0 applied to the transducer launches the acoustic waves. If the transducer pitch is 2d (see Fig. 1), the corresponding wavelength is λ=2d and the working frequency f_0 is linked to the wave propagation speed V by the following relationship:

$\mathbf{f_0 = V/\ 2d}$. For excitation the IDT are connected to a power generator via BNC sockets. Acoustic wave absorbent is used to attenuate spurious reflections on the substrate edges. Copper connecting tracks are patterned on a Duroid® foil.

3. SAW platform dedicated to microdroplet handling

The IDT electrically fed at its central frequency f_0 generates Rayleigh surface waves with amplitude of a few nanometers. The energy associated to these "nano-vibrations" is sufficient to generate macroscopic effects. At low powers, internal liquid mixing the so-called "acoustic streaming" is induced in the droplet whereas at higher powers the acoustic radiation pressure makes the droplet move. Using our platform, we ability to generate both Y- and Z-directed actuation a two-dimensional droplet transport can be achieved. Fig.2 shows the situation obtained during the mixing of two droplets, at a lower displacement power and Fig.3 shows a 2D transport of a microdroplet on a $LiNbO_3$ wafer.

3.1. Surface wetting control

We show that a modulation of the surface wetting property improves significantly the displacement on naturally hydrophilic $LiNbO_3$ substrate (contact angle $\theta_c = 15°$). Narrow tracks

designed on an OTS coated substrate have been used to ensure the proper linear guiding of aqueous microdroplets. This treatment consists in improving the substrate hydrophobic behaviour by a surface silanization or a Teflon® layer deposition for instance which also reduces the surface hysteresis [3]. After a chemical surface treatment resulting in a mono-molecular layer of OTS (Octa decyl TrichloroSilane: $Cl_3Si(CH_2)_{17}CH_3$), the contact angle reaches $\theta_c = 118°$. The influence of the OTS deposit on the SAW propagation was studied using a software tool developed at our laboratory. It was seen to be nearly negligible on the displacement amplitude as shown Fig.5. while the propagation velocity of the wave is only decreased by 0.4 %.

3.2. RF pulsed excitation

Tests with a pulsed (RF) excitation burst of duration τ have been performed. Each of them consisting of a 30dBm signal around 20 MHz were applied to the IDT on coated substrate. It can be noted that no actuation takes place if $\tau \leq 1$ ms. With $\tau = 10$ ms a displacement of 1 mm is obtained whatever the droplet volume between 0.5 and 5µL. If $\tau > 10$ ms the displacement length decreases as the droplet volume increases which is probably linked to an inertial effect. These results demonstrate the possibility for a droplet to be moved on along a guiding hydrophilic track and to be left at a desired location by rigorously controlling the right number of successive RF bursts and their duration τ.

3.3. Transport along hydrophilic tracks of a droplet squeezed between two planes

A prototype dedicated to the transport of droplets inserted between two planes has been fabricated (Fig. 6). The cover can have functionalized areas (generally hydrophilic) in order to achieve the biochemical treatment of a contacting droplet. For the device in Fig. 6 the gap between the two planes is set to 300µm, the diameter of the upper plane hydrophilic area patterned to mimic the behaviour of a functionalized area is 1 mm and the track width is 100 µm. On the one hand without a guiding track the 1.5 µL droplet trajectory is not well-defined and on the other hand a mother droplet can split and generate daughters when leaving an upper hydrophilic area (see Fig. 6). This effect can be used to create such a smaller droplets but it is suppressed when using a hydrophilic track for guiding the droplet. Fig. 7 shows several frames of videos corresponding to the tests described Fig. 6. Scenario (a) corresponds to the droplet introduction between two planes using SAW. In Fig.6.(b) the droplet remains unaltered during the passage across a hydrophilic zone.

4. Conclusion

The fabrication of a platform dedicated to liquid microdroplet transport has been reported. Hydrophobic pre-treatment of the substrate improves the SAW droplet transport. Hydrophilic tracks have been patterned in the OTS hydrophobic superficial layer in order to guide droplets along linear trajectories. Moreover using RF pulses for droplet actuation allows targeting accurately a designed location. We have also shown that SAW are very efficient to insert a droplet between two planes and to transport it once it is inserted between them, witch could be functionalized in order to achieve the biochemical treatment of the microdroplets. This could help fabricating a variety of SAW prototypes based on digital microfluidics and dedicated to applications in the field of proteomic and biochemical assays and in other relevant application: DNA alignment as a preparative step for the sequencing or faster physical genomic mapping of a single molecule with the "combing phenomenon" on silanated surfaces [4].

References

[1] P. Hélin, V. Sadaune, C. Druon, *Sensors and Actuators A*, 70, 1998, pp. 67-74.
[2] S.K. Cho, H. Moon and C.J. Kim, *J. MEMS.*, 12, 2003,pp. 70-80.
[3] A. Wixforth, J. Scriba and C. Gauer, *MSTNEWS*, BioMEMS 5/2002, pp42-43.
[4] D. Bensimon, A. J. Simon, V. Croquette and A. Bensimon, *Phys. Rev. Lett.* 76, 1995, pp 4754-4757.

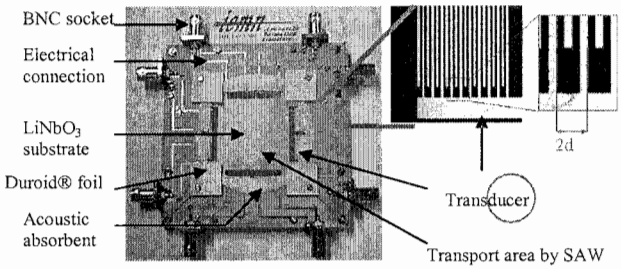

Fig. 1. Photograph of the SAW platform fitted with 2 pairs of IDT for each direction of propagation. Transport area is about 60×60 mm^2 (left) and photograph with a zoom on the transducer and the fingers (2d=180μm) (right)

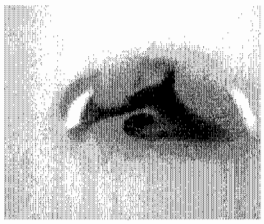

Fig.2 : Photograph of mixing tw colored water 5μL droplets (blu yellow). In this case, the acousti power is lower to the one used f the droplet displacement.

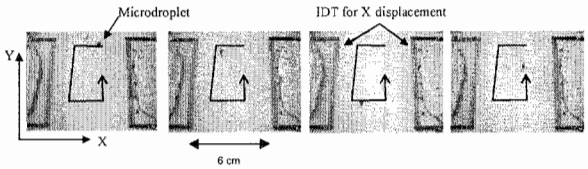

Fig. 3. 2D trajectory of a dr (Volume = 1μL) on a hydrophobic substrate of $LiNbO_3$.

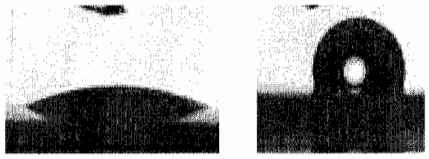

Fig. 4. Contact angle θ mea for a droplet of water sittin Lithium Niobate substrate: θ_c=15° before surface trea with OTS and (right) θ_c =118° after treatment

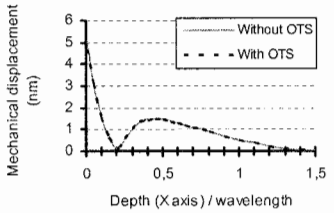

Fig. 5. Vertical component of the sagittal-plane amplitude of the Rayleigh wave in Lithium Niobate versus the normalized depth for an acoustic power of 1mW/λ: (—) without OTS and (---) with OTS

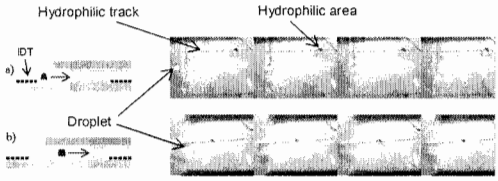

Fig. 6. Droplet handling: (left) cross-sectional schematic view device; (right) top view videos where the hydrophilic micr and area are marked for a better visualization ; a) droplet ins between two planes ; b) linear trajectory of a inserted droplet μL and crossing of a hydrophilic area designed on the cover

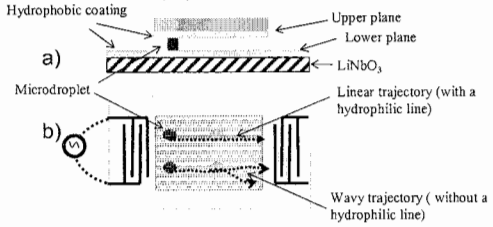

Fig. 7. Covered system for droplet actuation with hydrophilic patterns:
a) Cross-sectional view
b) Top view

CENTRIFUGAL PLATFORM FOR HIGH-THROUGHPUT REACTIVE MICROMIXING

J. Ducrée, H-P Schlosser, S. Haeberle, T. Glatzel, T. Brenner, R. Zengerle
IMTEK – University of Freiburg, Georges-Koehler-Allee 106, D-79110 Freiburg, Germany

Abstract

We present a novel modular micromixer based on continuous flow through rotating microchannels on a standard centrifuge. Extraordinary throughput of 1 ml / s per channel is demonstrated which can massively be enhanced to about 100 ml / s by a generic parallelization scheme. Both, experimental data and accompanying simulations demonstrate that the device outperforms other micromixers with its superior mixing quality at high throughputs. The concept furthermore excels with its simple and planar layout of low-aspect-ratio microstructures and the absence of critical micro-macro interfaces due to the field-transmitted pumping force.

Keywords: micro mixer, centrifugal microfluidics, high-throughput, Coriolis, continuous flow

1. Introduction

The large surface-to-volume ratios in microstructures appreciably enhance mass diffusion, heat transfer and shear forces in microflows. These features have spurred the use microfluidic systems for chemical process engineering [1]. The most striking advantage of such microreactors is that processes can be run under more aggressive reaction conditions than in conventional reactors. Further aspects are, for instance, the low dead volumes and the inherent safety, even in the explosive regime.

However, as volume throughputs are over-proportionally reduced in microdimensions, numbering-up strategies, i.e. the operation of a multitude of identical reactors in parallel, must be employed to arrive at acceptable throughputs. On the one hand, such a scale-up by numbering-up facilitates the transition from the lab- and pilot scale to an industrial production. On the other hand, numbering-up severely complicates process control, increases the costs and reduces the service life as well as the maintainability of a production plant.

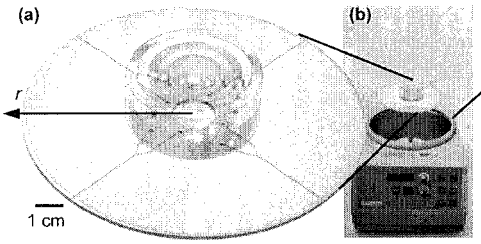

Figure 1. Experimental setup: **(a)** Magnified view of the rotor composed of a microstructured disk and two concentric reservoirs. The dimensions of the mixing channel are 30 mm (length), 260 µm (width), and 195 µm (height). **(b)** Centrifuge drive with the disk rotor, the outer chamber wall acts as a (resting) receiving vessel.

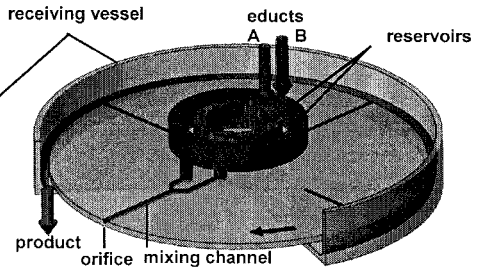

Figure 2. Flow scheme of the centrifugal platform. The educts (A, B) are continuously injected into two concentric reservoirs which rotate with the disk. The flows merge in a microstructured channel. Finally, the mixing product leaves the disk through an orifice in the side surface into the receiving vessel where it can be purged via an outlet drain.

In this paper, we investigate a new type of microreactor which exhibits several benefits compared to conventional microreactors. Section 2 illustrates the experimental setup and sketches the mass flow through the modular mixer. The principle of advective mixing of two concurrent flows in a rotating microchannel is outlined in Sect. 3. Next, the mixer is characterized on behalf of its most important technical characteristics, the mixing quality as a function of its throughput. Finally, in Sect. 5, we draw the conclusions.

2. Setup and Flow Scheme

The device consists of microstructured disk (Fig. 1a) rotating on a conventional centrifuge engine (Fig. 1b). The disk is connected to two concentric inlet reservoirs containing the educts. By means of the centrifugal force, the flow is driven from the inner reservoirs through radial microchannels (length: 30 mm, width: 260 µm, depth: 195 µm) and exits the disk via orifices in its side surface.

The reaction products are collected in a receiving vessel that is integrated in the centrifuge (Fig. 2). Typical frequencies of rotation range between 20 Hz and 90 Hz. The modularity of the setup allows to source out all moving parts as well as the actuation to a standard macro device while the disk features a planar network of passive, low-aspect-ratio microstructures, only. No pressure-generating pumps are needed for the pulse-less propulsion of flow.

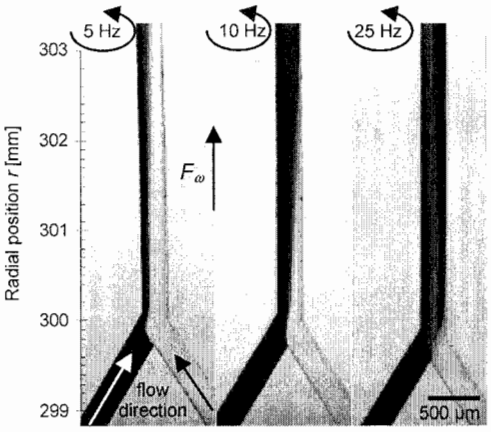

Figure 3. Flow patterns evolving at different rotational frequencies. The flow is propelled by centrifugal force F_ω. The plot provides clear evidence for a hydrodynamically enhanced mixing towards high spinning frequencies.

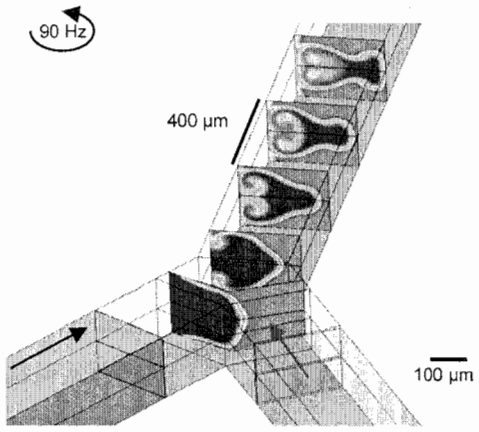

Figure 4. Flow simulation (CFDRC-ACE+) beyond the junction of the two inlet channels at 90 Hz. The shading of the two incoming streams illustrates the hydrodynamic mixing ("stirring") after the junction.

3. Mixing Principles

Between the inlets and the receiving vessel, various hydrodynamic mechanisms enhance mixing compared to mere diffusive mixing between concurrent, pressure-driven streams. First, the velocity-dependent Coriolis pseudo force induces a transversal advection ("stirring") of the two educts [2]. Second, the streams are multi-laminated and thinned by the rotating motion along the resting wall of the receiving vessel.

Third, hydrodynamic interactions are experimentally observed in the region downstream the initial contact in Fig. 3 and simulated in Fig. 4. Finally, exceeding spinning frequencies of about 85 Hz, the turbulent flow regime is entered in the common channel. The respective impact of these effects depends on the frequency of rotation, the channel geometry and the flow rates of the educts.

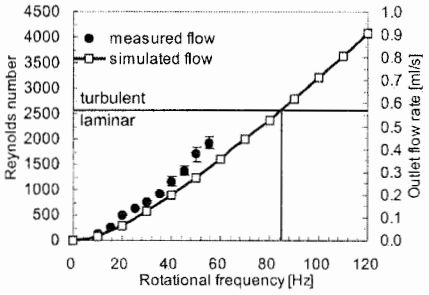

Figure 5. Flow rates per channel and corresponding Reynolds number *Re* of the centrifugally driven platform. The turbulent regime is nominally entered above 85 Hz (*Re* > 2300).

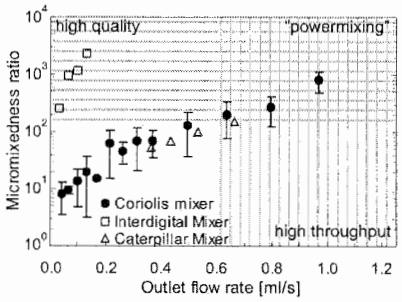

Figure 6. Experimental result of the Villermaux reaction scheme [3], quantifying the degree of mixing. A high micromixedness ratio indicates a high quality of mixing. Throughput of conventional pressure driven micromixers is limited by the need for geometrical constrictions.

4. Mixing Performance

The most important characteristics of a mixer are the throughput and the quality of the reaction products. We measure flow rates by the filling heights of the inlet reservoirs. Figure 5 shows the overall flow rate as well as the associated Reynolds numbers. The Villermaux reaction scheme [3] is used for the quantification of the micromixing performance. Figure 6 plots the so derived quality of mixing as a function of the volume throughput. Approaching high throughput, Coriolis-induced stirring [2] as well as lamination at the outer wall grow stronger than the throughput, lifting the data points into in the upper right "powermixing" region in Fig. 6. With conventional microreactors, this region is hard to reach as they feature flow-throttling geometrical constrictions for the multilamination of flow instead of the here presented mere hydrodynamically induced advection of flow without constrictions. The fast transversal mixing also narrows the residence time distribution.

5. Conclusions

In summary, our novel micromixing platform excels with its robust modular setup composed of a macroscopic actuator unit and a, possibly disposable, microfluidic disk featuring passive, low-aspect-ratio structures in a planar arrangement. Its most striking performance characteristics are a high volume throughput paired with an excellent mixing quality.

Acknowledgements

This work was supported by the Federal State of Baden-Württemberg, Germany.

References

[1] H. Pennemann, P. Watts, S. J. Haswell, V. Hessel, and H. L. Löwe, *Org. Proc. Res. & Dev.*, **8**, 422 -439(2004).

[2] J. Ducrée, T. Brenner, T. Glatzel, and R. Zengerle, *Proceedings of μTAS 2003*, eds. M. A. Northrup, K. F. Jensen, D. J. Harrison, 603-606 (2003).

[3] M.-C. Fournier, L. Falk, and J. Villermaux, *Chem. Eng. Sci.*, **51**, 5053-5064 (1996).

CAPILLARITY-RESTRICTED MODIFICATION METHOD FOR GAS/LIQUID SEPARATION AND GAS BUBBLE PURGE IN MICROCHANNELS

Akihide Hibara[1,2,3], Shinobu Iwayama[1], Masaharu Ueno[1,2,3], Yoshikuni Kikutani[2,3], Manabu Tokeshi[2,3], Takehiko Kitamori[1,2,3]

[1]Dept. Appl. Chem., University of Tokyo, 7-3-1 Hongo, Bunkyo, Tokyo 113-8656, Japan
[2]Microchemistry Group, Kanagawa Academy of Science and Technology, 3-2-1 Sakado, Kawasaki, 213-0012, Japan
[3]CREST, Japan Science and Technology Agency, Japan

Abstract

A surface modification control method for microchannels was developed for gas-liquid microchemical operations in microchips. In this method, shallow and deep microchannels were modified with hydrophobic and hydrophilic groups, respectively. This patterning was prepared based on principle of capillarity. Validity of the patterning was confirmed by measuring aqueous flow leak pressure from the hydrophilic microchannel to the hydrophobic one. The leak pressure agreed well with theoretical prediction from Young-Laplace equation. In order to demonstrate usefulness and effectiveness of the method, air bubble was introduced to the hydrophilic microchannel and purged from the hydrophobic-hydrophilic patterned microchannels. Next, the patterning structure was applied to remove dissolved oxygen by contacting the aqueous flow with nitrogen-flow. The concentration of dissolved oxygen decreased with contact time and its time course agreed well with numerical simulation. These demonstrations showed that the proposed patterning method is promising to general microfluidic gas-liquid operations.

Keywords: surface modification, capillarity, gas/liquid separation, micro-multiphase flow

1. Introduction

In order to widen applicability of the microchemical systems, gas/liquid separations in microchannels are indispensable techniques. For example, since gas bubble contamination to liquid phase often causes system errors in the microchemical systems, undesirable gas bubbles should be purged. Especially for cell biochemical systems, the bubble purge technique is desired because gas bubble sometimes brings off cultivated cells. Furthermore, the gas/liquid separation is required for organic synthesis in the microchemical systems utilizing gas phase substrate with carrier gas. In this paper, we developed a gas/liquid separation method, including bubble purge, based on a capillarity-restricted modification (CARM) method for microchannels. By utilizing hydrophilic/hydrophobic modification pattern in a single microchannel prepared by CARM method, complete gas/liquid separation and gas bubble purge were realized. In this method, we did not use any solid gas separator, but utilized free gas/liquid interface stabilized by Laplace pressure, which was generated by the hydrophilic/hydrophobic pattern. Our method presented here is applicable for general microsystems because it only utilizes general physical phenomena, i.e. positive or negative Laplace pressure, which is enhanced with decreasing dimensions of microchannels.

2. Experimental

Fig. 1 shows operation procedures of CARM method and corresponding photographs. An asymmetric microchannel, which has shallow and deep channels, was prepared (Fig. 1a). When silane reagent solution was dipped to an inlet of the shallow channel, the solution was introduced by capillarity (Fig. 1b). The solution was introduced only to the shallow channel while it was not introduced to the deep channels (Fig. 1c). After reaction, the solution was purged with air pressure. Thus, only the shallow channel was modified with the silane reagent, where trichlorooctadecyl

silane was used to obtain hydrophobic surface. When water flow was introduced to the deep channel, water was not intrude to the hydrophobic shallow channel because of Laplace pressure on the hydrophobic surface (Fig. 2a). To confirm this principle, leakage pressure of water to the shallow channel was measured (Fig. 2b). The experimental and theoretical values agreed well. Thus, the gas/liquid interface was stabilized sufficiently for applying to gas/liquid separation.

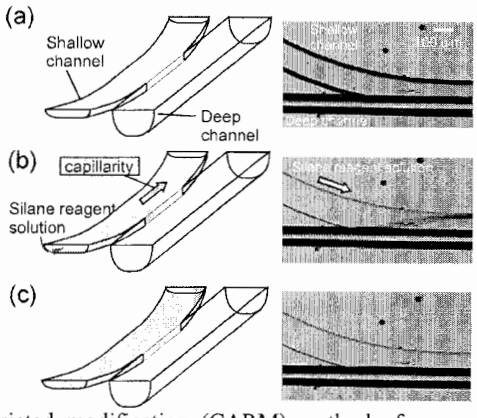

Figure 1 Capillary-restricted modification (CARM) method of asymmetric microchannel. (a) Before solution introduction. Both shallow and deep channels are vacant. (b) During solution introduction. Silane solution is introduced by capillarity. (c) After solution introduction. Only the shallow channel is filled with the solution while the deep channel is still vacant.

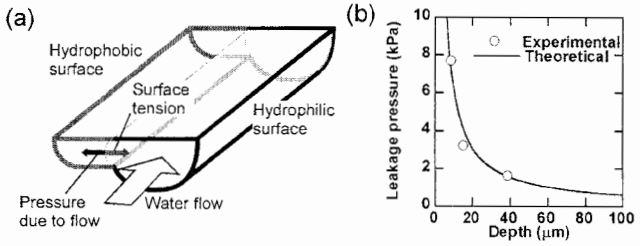

Figure 2 (a) Stabilization of gas/liquid free interface by hydrophilic / hydrophobic modification. (b) Experimental and theoretical leakage pressure dependence on the depth of shallow hydrophobic channel.

3. Results and discussion

By utilizing the hydrophilic/hydrophobic microchannel, gas/liquid separation was demonstrated (Fig. 3). At the hydrophilic/hydrophobic junction point, gas phase is separated to the hydrophobic channel because Laplace pressure is not effective for gas phase. Fig. 3b shows microchannel layout for gas/liquid separation. The red line indicates hydrophobic channel. Fig. 3c and 3d show photographs of gas phase introduction and separation, respectively. Gas plugs or bubbles were successfully purged from the liquid phase. The hydrophilic/hydrophobic microchannel was also

applied to dissolved oxygen purge to nitrogen flow under counter-current flow condition [1] (Fig. 4). As shown in Fig. 4b, results agreed well with simulated theoretical values.

CARM method is expected to be effective for other unit operations, such as evaporation [2], distillation, and cell cultivation in microchips. The modification patterning method will be also useful for multi-step organic synthesis using gas phase substrate.

References

[1] A. Aota, M. Nonaka, A. Hibara, and T. Kitamori, MicroTAS 2003, pp. 441-444.
[2] M. Tokeshi, K. Kanda, A. Hibara, and T. Kitamori, MicroTAS 2002, pp. 356-358.

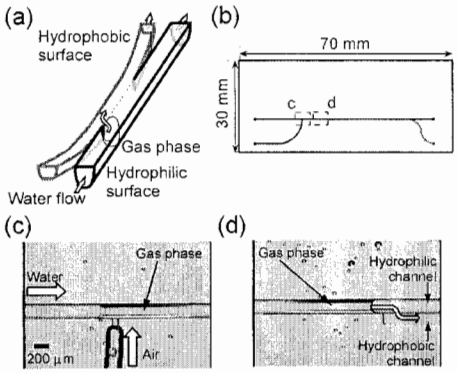

Figure 3 (a) Gas / liquid separation utilizing hydrophilic / hydrophobic surface modification. (b) Microchannel layout for gas / liquid separation. Red line indicates hydrophobic channel. (c) Gas phase introduction (area c in (b)). (d) Gas / liquid separation (area d in (b)).

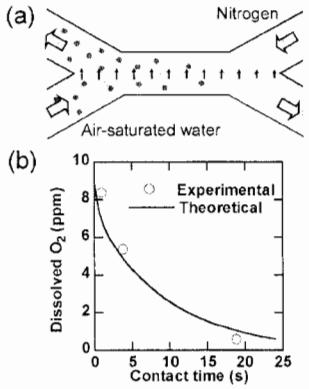

Figure 4 (a) Counter-current gas/liquid flow and O_2 purge to N_2 (b) Theoretical and experimental dissolved O_2 concentration .

MULTI-CHANNEL MICROFLUIDIC IMMUNOASSAY CHIP USING PROTEIN MICROARRAY FORMED BY ELECTROSPRAY DEPOSITION METHOD

Yutaka Yamagata[1,4], Akihiko Tajima[2], Bun-Hwan Lee[4], Teruyuki Nagamune[2], Takatoki Yamamoto[3], Teruo Fujii[3], Kozo Inoue[4], and Hitoshi Ohmori[1]

[1] Materials Fabrication Laboratory, RIKEN, 1-2 Hirosawa, Wako, Saitama 351-0198,Japan
[2]Department of Chemistry and Biotechnology, School of Engineering, University of Tokyo, Japan,
[3]Institute of Industrial Science, University of Tokyo, Japan,
[4]Fuence Co., Ltd., Japan

Abstract

A new multi-channel microfluidic immunoassay chip was developed combining PDMS (poly-dimethylsiloxane) micro channel and protein chip formed by electrospray deposition (ESD) method. Spots or stripes of antibody or antigen are formed on a ITO coated glass plate with aldehyde group introduced on the surface. Over the protein chip, PDMS microchannel was attached to form a immunoassay device inside the microchannel, which enables fast and sensitive multiple immunoassay with very small amount of protein and sample solutions. Assay test experiments with stripe-patterned IgG proved that it solves the alignment difficulties compared to spot-patterned protein microarray. In addition, sandwich ELISA for cytokines and immunoassay for mouse infection diagnosis was successfully performed.

Keywords: micro channel, PDMS, electrospray deposition, protein chip, immunoassay

1. Introduction

Protein chips or protein micro arrays especially for immunoassays are versatile devices that can analyse hundreds or thousands samples simultaneously for clinical diagnosis, disease inspection, environmental analysis and other sophisticated chemical or biochemical detection. Microfluidic devices as well as protein patterning methods are key technologies for that purpose. Combination of microfluidic devices and protein microarrays is expected to perform high-throughput immunoassay with the time and amount of samples needed for the analysis dramatically reduced due to the size effect. Electrospray deposition method is a novel technique that can pattern bioactive materials like protein or DNA on the glass, metallic or any conductive substrate in the desired shape utilizing stencil mask with relatively small bioactivity loss [1, 2]. Using ESD technique, the authors have reported an immunoassay chip consists of ITO-coated glass plates on which aldehyde group was introduced. PDMS microchannel devices are effective means for miniaturized chemical/ biochemical reaction. Combination of those two technologies will provide many advantages, while attachment of microchannel to protein microarray has to overcome the difficulties of precision alignment between microchannel and protein spots. Those difficulties are solved with stripe patterning capability by ESD method to form a lines of proteins perpendicular to the micro channels. Experimental immunoassay was performed based on a 16-proteins by 16-microchannel micro chip (256 assay) on a slide glass dimension. Test assays using anti-cytokines immuno globulins and antigens for mouse infection diagnosis was successfully carried out to shows the feasibility of the proposed device.

2.Experimental

2.1 Electrospray deposition (ESD) method

Fig. 1 shows the configuration of ESD device. Sample solution in the capillary is sprayed by applying several kV of voltage and deposited on the substrate as dried nano-particles. The shape of deposition can be controlled by insulator mask and deposition yield can be more than 80-90% by

controlling electrostatic field. The bioactivity loss of deposit protein is considered to be relatively low, since the sensitivity of the immunoassay chip was as low as 1ng/ml.[1] In addition, using ESD technique stripe or arbitrary shaped pattern can be possible with stencil mask.

2.2 Configuration of the micro fluidic device

Fig. 2 shows the configuration of proposed microfluidic device. Fig.2 (a) indicates combination with ordinary spot-patterned protein microarray, which faces the difficulty of precision alignment especially when the density of the array is very high. Fig.2 (b) indicates combination with stripe patterned protein array, which makes it much easier to align with microchannels. Using this configuration, very high-density assay system integrated with microchannels can be realized. Since PDMS can be easily attached onto or removed from glass substrate, various detection methods like fluorescence, colorimetric or luminescence can be adopted. Sample solutions and reagents of about 1 to 3 μl are applied through input ports and sucked through microchannels.

3. Results and discussion

Fig. 3 shows the result of direct FIA using mouse IgG ESDed on the ITO-aldehyde glass. Sample containing flourescein labeled anti-mouse IgG of different concentration was introduced to each channel. The concentration ranged from 10ng/ml to 10 μg/ml. Fig. 3 (a) shows the assay with spot-patterned protein chip, while (b) shows the assay with stripe patterned chip. This result shows that no leakage or contamination occurs with stripe-patterned protein chip. Fig. 4 shows a sandwich ELISA result using protein chip with immuno globulins for different cytokines ESDed on the glass substrate. The result shows that there are no cross activity or contamination. Fig. 5 shows a result with four different kinds of antigens for mouse disease infection testing.

5. Conclusions

A new microfluidic device combining PDMS microchannel and protein chip formed by ESD is proposed and its fundamental performance was tested through immunoassays. It has proved that immunoassays can be performed with very small

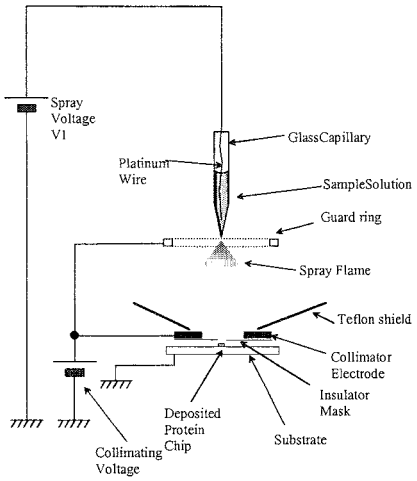

Figure 1. Configuration of Electrospray Deposition Device

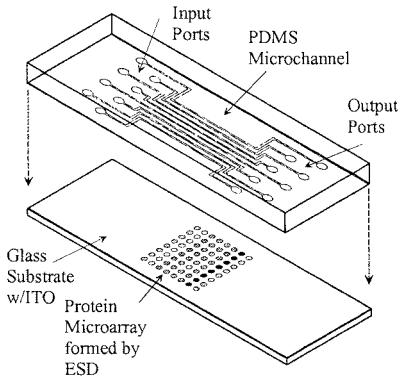

(a) Combination with microarray with spots

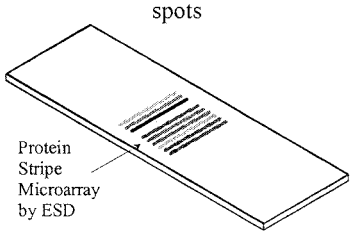

(b) Combination with micro array of stripes

Figure 2. Configuration of Microfluidic chip with protein microarray Formed by

amount of proteins and sample solutions. The device will be suitable for the application of various chemical/biochemical analysis where amounts of proteins and sample solutions consumed in an assay are very important. Disease infection testing of mice can be a typical candidate of application of this device.

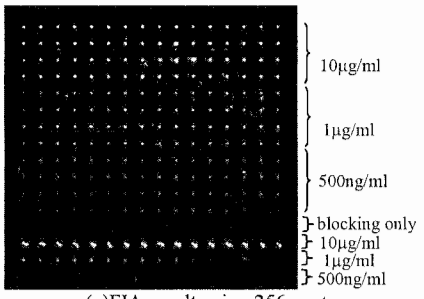

(a)FIA result using 256 spots

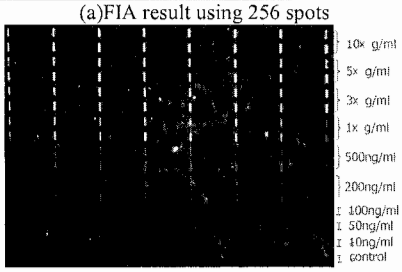

(b) FIA result with stripe pattern of 16 x 8

Figure 3. FIA result by microfulidic channel with protein microarray formed by ESD Area of the Image is approx 8.5x8.5mm and 16x16 assays are carried out simultaneously.

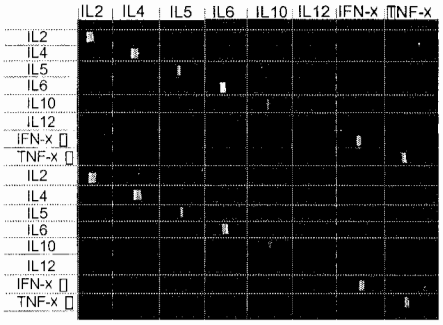

Fig.4 sandwich ELISA assay for 12 different cytokines. IgGs for cytokines are ESDed on ITO-aldehyde glass plate and antigen, secondary antibody -avidin conjugate and biotin with Alexa488 was introduced to microchannel.

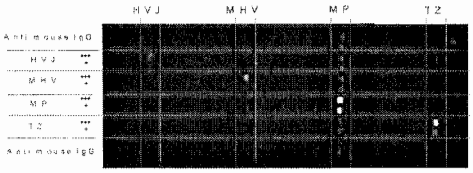

Fig.5 Immunoassay using antigens for mouse infection diagnosis

Acknowledgements

The authors would like to express thanks to Dr. H.Aoki at Fuence Co. for the help in experiments concerning assays using mouse antigens.

References

[1] B.H.Lee, J.W.Kim,K.Ishimoto, Y.Yamagata,A.Tanioka, and T.Nagamune, J.Chemical Eng. Japan vol.36 No.11 (2003) pp1370-1375

[2] Victor N. Morozov and Tamara Ya. Morozova, Electrospray Deposition as a Method To Fabricate Functionally Active Protein Films, Analytical Chemistry, vol.71, No.7, pp.1415-1420, (1999)

APOPTOSIS INDUCED KINETIC CHANGES IN AUTOFLUORESCENCE OF HL60 CELLS – APPLICATION FOR SINGLE CELL ANALYSIS ON CHIP

Floor Wolbers[1,2], Ana Valero[1], Helene Andersson[1], Regina Luttge[1], Istvan Vermes[2] and Albert van den Berg[1]

[1]*Department of Sensorsystems for Biomedical and Environmental Applications, MESA+ Institute, University of Twente, P.O. Box 217, 7500 AE Enschede, The Netherlands*

[2]*Department of Clinical Chemistry, Medisch Spectrum Twente, Hospital Group, Enschede, The Netherlands*

Abstract

This paper presents a new method using autofluorescence (AF) to study apoptosis. A decrease in AF intensity is seen with flow cytometry from 2h till 24h for all the four apoptotic inducers used. A new microfluidic cell assay has been developed enabling the capture of viable cells. Once cells go into apoptosis their mechanical properties, e.g. size, will change. A decrease in AF intensity of the cells that passed the trap will confirm this hypothesis. In future developments this microchip will be used as an on-chip cell counter specific for apoptosis.

Keywords: apoptosis, autofluorescence, lab-on-a-chip, microfluidics

1. Introduction

Apoptosis or programmed cell death plays an important role in maintaining a homeostatic equilibrium between cell proliferation and cell death. Induction of apoptosis results in shrinkage of the cell and fragmentation into apoptotic bodies [1,2]. There are a number of techniques present to detect cell death, however these tools are in most cases not specific or lack quantitative value. Nowadays, we are still seeking for a simple technique which offers us to measure apoptotic cell death without manipulation of cells and monitor the apoptotic cascade in real time [3].

2. Theory

Many cellular metabolites exhibit autofluorescence, all having their specific emission and excitation wavelengths [4]. The flavins, when oxidized, have strong autofluorescence in the yellow-green region, and can therefore be considered as the main fluorochromes emitting above 500 nm [4-6]. The flavins are actively involved in a number of metabolic processes within the cell and play an important role in the energy (ATP) household of the cell. Autofluorescence colocalizes strongly within the mitochondria and in some extent within the lysosomes, while the nucleus remains dark [7]. Autofluorescence intensity (AF intensity) is defined as the ratio of the mean fluorescence of the early apoptotic (region 1), late apoptotic (region 2), or necrotic (region 3) subpopulation as compared to the mean fluorescence of the viable population (equitation 1).

$$\text{AF intensity} = \frac{\text{Mn X m-1, m-2, or m-3}}{\text{Mn X v}} \tag{1}$$

To analyze the AF intensity in time, the $AF^{24/2}$ ratio is measured which defines the ratio of the minimal AF intensity (t=24h) compared to the maximal AF intensity (t=2h) (equitation 2).

$$AF^{24/2}\ \text{ratio} = \frac{\text{AF intensity t=24h (region 1, 2 or 3)}}{\text{AF intensity t=2h (region 1, 2, or 3)}} \tag{2}$$

3. Experimental

Autofluorescence measurements

Human promyelocytic leukemic HL60 cells were incubated with camptothecin (CPT), tumour necrosis factor (TNF)-α in combination with cycloheximide (CHX), or irradiated with 6 or 10 Gray, during varying time periods, to initiate apoptosis. AF of the flavins was measured using the FL-1 (CD103F, 525 nm) channel at the flow cytometer (Coulter Epics XL).

Cell handling on microfluidic cell trap chip

We have developed a microfluidic chip for isolating single apoptotic cells based on mechanical properties. This microfluidic chip, silicon bonded to glass, has a channel width of 200 μm. The width of the trap is 10 μm and the length is 30 μm. The outlet channel of this structure is 3 μm. HL60 cells were flown with pressure driven flow (as in conventional flow cytometry). Optical detection was with a Leica DM IRM inverted microscope. Autofluorescence was measured with a mercury lamp. Excitation was elicited at 450-490 band pass and emission at 515 long pass. Light between the mercury lamp and the objectives was filtered with a day light filter (DLF), which is a conversion filter for color photography with day light film (blue, conversion filter).

4. Results and discussion

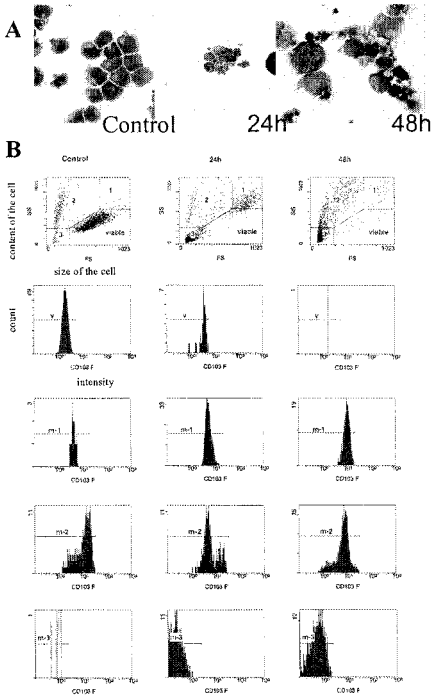

Figure 1. HL60 cells irradiated with 6 Gray Light microscopy (A), scatterdiagrams and fluorescence intensity histograms (B) are shown.

Irradiation with 6 Gray activates the apoptotic cascade in HL60 cells (Figure 1A). In the scatterdiagrams, 4 subpopulations are shown, viable, early apoptotic (region 1), late apoptotic (region 2) and the necrotic (region 3) population respectively, corresponding to the different stages of the apoptotic cascade *in vitro* (Figure 1B). The decrease in AF intensity is especially seen in the late apoptotic cells (Figure 2). The other inducers give similar results.

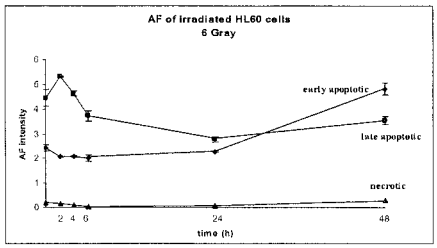

Figure 2. Autofluorescence intensity of HL60 cells irradiated with 6 Gray.

Figure 2 further shows that the AF intensity is changing in time. Two hours after irradiation with 6 Gray a maximum in the AF intensity is seen, whereas after 24 hours the AF intensity has reached its minimum, due to the fact that the cell's ability to maintain cellular ATP levels is compromised.

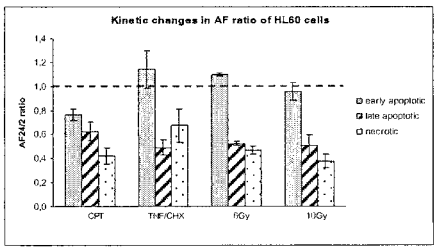

Figure 3. $AF^{24/2}$ ratio of HL60 cells incubated with different apoptotic inducers.

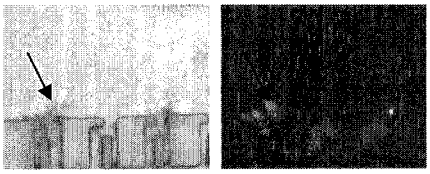

Figure 4. Microfluidic chip for trapping viable HL60 cells. Light microscopy picture is shown at the left and the autofluorescence image with the mercury lamp on the right. Arrow points to trapped HL60 cell.

For all the four apoptotic inducers used, the $AF^{24/2}$ ratio is plotted for the three different regions. Figure 3 shows that in most cases the $AF^{24/2}$ ratio is decreased, compared to untreated HL60 cells, for the apoptotic inducers used. Untreated HL60 cells show only minor fluctuations in time and can be seen as a stable control population. Therefore, the $AF^{24/2}$ ratio for control HL60 cells is set at 1. Recent results have shown that it is possible to perform AF measurements on single cells in a microfluidic device [8]. We have developed a microfluidic chip for isolating single apoptotic cells based on mechanical properties. Preliminary results show that it is possible to trap viable HL60 cells and detect autofluorescence with a mercury lamp (Figure 4).

5. Conclusions

This paper demonstrates that measuring AF intensity is a rapid and simple technique to study the process of apoptosis. First results show the possibilities of performing single-cell analysis on chip. Next steps will be trapping single cells, induce apoptosis and monitor the effect mechanically (e.g. decrease in size which enable cells to pass the trap) and optically (decrease in AF intensity).

Acknowledgements

Financial support from the Dutch technology association STW (TMM 6016 'NanoScan' project) and valuable technical work by Jurjen Emmelkamp and Roy de Kinkelder is gratefully acknowledged.

References

[1] I. Vermes, C. Haanen. *Adv Clin Chem*, **31**, 177-246 (1994).
[2] I. Vermes, C. Haanen, C. Reutelingsperger. *J Immunol Method,* **242**, 167-190 (2000).
[3] F. Wolbers, H. Andersson, A. van den Berg, I. Vermes. Accepted for *Apoptosis* (2004).
[4] R.S. DaCosta, H. Andersson, B.C. *Photochem Photobiol*, **78**, 384-392 (2003).
[5] J.E. Aubin. *J Histochem Cytochem*, **27**, 36-43 (1979).
[6] R.C. Benson, A. Meyer, M.E. Zaruba, G.M. McKhann. *J Histochem Cytochem*, **27**, 44-48 (1979).
[7] H. Andersson, T. Baechi, M. Hoechl, C. Richter. *J Microsc*, **191**, 1-7 (1998).
[8] J. Emmelkamp, F. Wolbers, H. Andersson, R.S. DaCosta, B.C. Wilson, I.Vermes, A. van den Berg. Accepted for *Electrophoresis* (2004).

CONTINUOUS CENTRIFUGAL SEPARATION OF WHOLE BLOOD ON A DISK

Thilo Brenner, Stefan Haeberle, Roland Zengerle, and Jens Ducrée
IMTEK – Institute of Microsystem Technology, Laboratory for MEMS Applications
Georges-Koehler-Allee 103, D-79110 Freiburg, Germany
Phone: +49 / 761 / 203-7329, FAX: -7322, tbrenner@imtek.de

Abstract

We present a novel centrifugal process for the continuous extraction of plasma from the sediment by a 3-stage microfluidic structure, terminating with metered plasma which is readily available for subsequent on-disk processing. Our technique supplies 2 µl plasma from 5 µl of whole blood at moderate spinning frequencies of 40 Hz within 20 s, only. The residual cell concentration in the purified plasma amounts to less than 1%, independent of the frequency of rotation.
Keywords: blood separation, centrifugal microfluidics, lab-on-a-disk, process integration

1. Introduction

An important objective in medical diagnostic systems is the integration of the full process chain from the preparation of a patient's whole blood to an analytical result. Various lab-on-a-chip systems have proven to carry out the final detection steps, among them centrifugal "lab-on-a-disk" devices [1,2,3]. Their high potential to run complete assay protocols, starting from raw whole blood, is reflected by the intrinsic pumping and separation mechanisms based on the centrifugal field. While several microfluidic approaches for a batch separation of blood have been presented so far [1], a robust and integrable separation structure which is essential for a complete on-disk processing is still missing.

2. Principle and Design

Figure 1 shows the course of a conventional, on-disk batch sedimentation in a centrifugal field. The red blood cells (RBCs) which possess a higher mass density than the plasma are driven by the centrifugal field towards the bottom of the reservoir. During the separation, a so-called shock interface forms between the plasma and the subjacent cell suspension. At the end of the separation, a radial stack constituted by a cellular pellet at the bottom and a purified plasma supernatant evolves. To smoothly hand over pure plasma to subsequent on-disk processes, we split the two phases by a decanting process. The 3-stage structure in Fig. 2 portrays our continuous flow separation scheme. Initially, a raw sample of blood is metered to 5 µl by an overflow channel next to the inlet (Fig. 3) and a hydrophobic stop at the outlet of the chamber. Beyond a burst frequency of 15 Hz, a continuous flow sedimentation initiates through the drain channel into the decant chamber (volume: 3 µl) where pre-separated blood accumulates.

During this process, a shock interface builds out in all parts of the network which are already primed with blood. This interface is most pronounced in the final decant chamber (Fig. 4). Two conditions have to be fulfilled for a successful separation: First, the volume capacity of this decant chamber must slightly exceed the volume fraction of the cells. This way, only purified plasma overflows into a subsequent reservoir where it is available for further processing. Second, the flow resistance of the drain channel and the geometry of the separation chamber must be adjusted to make the speed of the filling level u_{dec} significantly smaller than the counter-current speed of the shock interface u_{drift}. As both, u_{dec} as well as u_{drift} scale with the square of the spinning frequency f, the efficiency of separation is independent of the spinning frequency. Furthermore, the separation time t_{sep} of this continuous centrifugation scheme is governed by the flow resistance of the drain channel.

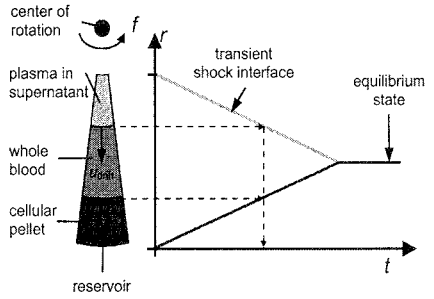

Fig.1. Intermediate state of batch mode sedimentation in a centrifugal field. A shock interface proceeds at a velocity u_{drift}. Eventually, red blood cells are concentrated in a pellet on the bottom of the vessel while purified plasma is found in the supernatant.

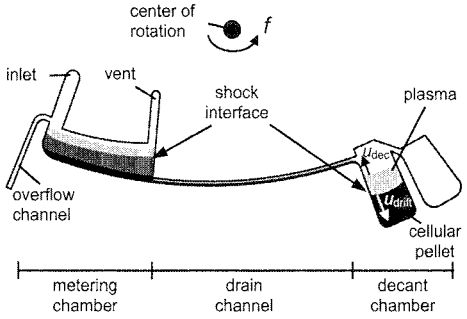

Fig.2. Continuous flow scheme in our 3-stage separation structure. A blood sample flows from the metering chamber via the drain channel into the decant chamber for final separation. The filling height of the decant chamber rises at a speed u_{dec} before the plasma overflows into the final chamber.

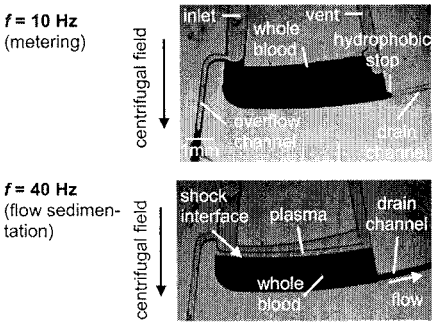

Fig.3. Whole blood is metered in the initial chamber at frequency $f = 10$ Hz to a volume of 5 µl. The volume is defined by the hydrophobic stop at the outlet and the overflow channel next to the inlet of the chamber. The vent ensures optimum capillary filling. At $f = 40$ Hz, blood flows out of the metering chamber into the drain channel. The evolution of the shock interface between plasma and cellular blood constituents can be observed.

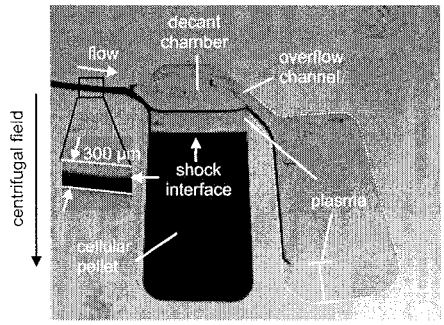

Fig.4. Intermediate state of continuous flow sedimentation at $f = 40$ Hz. Purified plasma overflows into a separate reservoir while the cellular pellet is retained at the bottom of the decant chamber. The shock interface separating plasma and cellular sediment in the drain channel is magnified in the insert.

3. Experiments and Results

The channels and reservoirs are fabricated by standard micromilling of cycloolefin-copolymer (COC) disks. They are sealed by thermal diffusion bonding of a polymer foil. The drain channel has a length of 2.5 cm at a mean radial position of 3.2 cm. The channel width is 300 µm and the depth is measured to 85 µm; the depths of the reservoirs are 300 µm. The centrifugal separation protocol comprises two operational frequencies. In the first metering step, the disk spins at a low frequency of 10 Hz which is smaller than the burst frequency (15 Hz) of the hydrophobic valve. The subsequent separation of the 5 µl volume takes place at higher frequencies to reduce the time t_{sep} for gaining the targeted plasma volume of 2 µl. The residual cell concentration in the plasma is determined to be less than 1% by optical comparison to defined cell suspensions (Figs. 5 and 6). A separation time t_{sep} of 20 s has been measured at a frequency $f = 40$ Hz. Our experiments corroborate a decline of the separation time t_{sep} with inverse square of the frequency f while the residual RBC concentration c_{RBC} is independent of f. These observations comply with our theory (Fig. 6).

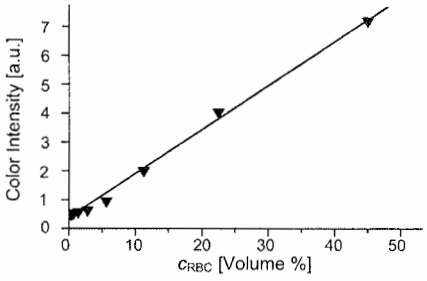

Fig.5. Calibration curve between color intensity and cell suspension with a defined RBC concentration c_{RBC}. The calibration is used to determine the concentration of residual RBCs depicted in Fig. 6.

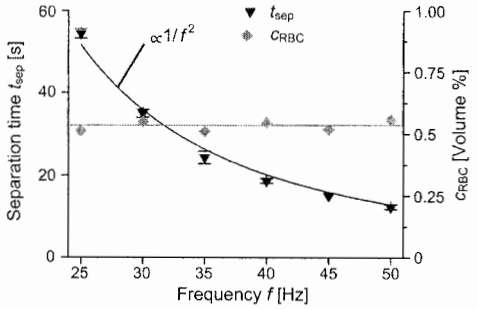

Fig.6. The measured separation time t_{sep} declines with the inverse square of the spinning frequency f while the residual RBC concentration c_{RBC} (<1%), i.e. the quality of the separated plasma, is independent from f.

4. Conclusions

Our continuous centrifugal flow separation technique efficiently extracts 2 µl plasma from a raw blood sample that is metered to 5 µl. Typical separation times of 20 s could be achieved for moderate spinning frequencies of 40 Hz. The residual cell concentration of less than 1% is independent from frequency, showing the robustness of the concept. The microfluidic structure can easily be adapted for an integrated sample processing on centrifugal platforms.

Acknowledgements

This work was supported by grants from the German federal state of Baden-Württemberg, Verbundforschung, Project "Bio-Disk".

References

[1] M. J. Madou and G. J. Kellogg, *Proc. of SPIE*, vol. 3259, 1998, pp. 80-93.

[2] G. Thorsén, G. Ekstrand, U. Selditz, S. R. Wallenborg, and P. Andersson, *Proc. of µTAS 2003*, eds. M. A. Northrup, K. F. Jenson, D. J. Harrison, Kluwer Academic, 2003, pp. 457-460.

[3] M. Grumann, A. Geipel, L. Riegger, R. Zengerle, and J. Ducrée, accepted for *µTAS 2004*

UNSTEADY ELECTROKINETIC PHENOMENA DURING ELECTROELUTION FROM CLINICAL SAMPLING STRIPS

Sun Min Kim[1] and E. F. Hasselbrink, Jr.[1]

[1]*University of Michigan Department of Mechanical Engineering, 2350 Hayward Street, Ann Arbor, MI 48109, USA*

Abstract

In this research, a micro device for eluting proteins from a thick paper strip (~400μm) used for oral fluid sample collection was fabricated using PDMS (Poly dimethylsiloxane) polymer. PDMS polymer has been used to fabricate micro systems due to easy and fast fabrication, low cost, and compatibility with bio materials.

BSA (Bovine Serum Albumin) and OVA (Ovalbumin) were labelled with FITC (Fluorescein isothiocyanate) dye for detecting movements using a fluorescent microscope. About 50% of the initial concentration of BSA and OVA was eluted by the ~20V/cm electric field. During the electroelution process, unsteady electrokinetic phenomena by the pressure driven flow and the pH change of the reservoirs were observed.

Keywords: electroelution, macro-to-micro interface, unsteady electrokinetics

1. Introduction

Frequently it is of interest in biological and proteomic analysis system to remove proteins captured in a gel or other macro scale matrix and to introduce them into a microchip for automated analysis. Methylcellulose strips, for example, are a popular means for collecting gingival crevicular fluid (GCF) from dental patients, for analysis for disease biomarkers. Electroelution, as used for removal of protein from SDS-PAGE gels [1] is an appealing method; however, it can be less than trivial for microchip introduction due to the thickness of the wetted strips (~400μm). The thickness introduces interesting practical difficulties including significant reservoir filling by relatively large EOF, as well as pH evolution due to the current drawn by the system. In this paper we present catastrophic but interesting electrokinetic phenomena that can result during such electroelutions, as well as engineering guidelines for reservoir design (e.g., with embedded membranes) to avoid these phenomena.

2. Experimental

The experimental electroelution chamber is a simple channel approximately 6mm wide and 400μm deep shown in Figure 1, fabricated in PDMS using standard techniques. 1μL of FITC-labelled BSA and ovalbumin in 20mM phosphate (pH 7.2) buffer are wetted onto the methylcellulose strip and this strip is loaded through the insertion port shown. During electroelution a relatively small electric field (~20V/cm) is applied to avoid excessive Joule heating, so the electroelution takes approximately 10 minutes to complete.

3. Results and discussion

Figure 2 shows a time-lapse sequence of fluorescence images during successful electroelution of BSA from the strip; a comparison experiment (not shown) shows that ovalbumin electroelutes somewhat faster than BSA, which is not inconsistent with published mobility data at this pH [2].

Figure 3 quantifies the removal of these proteins from the strip using quantitative imaging methods (ensuring no dye bleaching). Although these show that electroelution can be highly efficient at protein removal, there can be numerous complications.

The most obvious complication is that bulk fluid flow increases head pressure on the cathode side reservoir, generating pressure driven flow (PDF) to the anode side (Figure 4, left). This PDF speeds the net motion of proteins but dispersion has the undesirable effect of diluting them. In Figure 5, the bright secondary flow from the right (cathode) to the left (anode) is induced by the PDF. The effect can be easily avoided using large cross sectional area reservoirs.

The second, more interesting complication results from buffer depletion in the reservoirs, which results in sudden changes in pH (Figure 4, right). Since OH^- and H^+ are very high mobility ions, this results in a relatively fast propagation of a wave of relatively high or low pH through the channel. This can result in very interesting and *unsteady* stirring phenomena in the channel as shown in movie frames in Figure 5. The dark stirring wave from the left (anode) to the right (cathode) shows the *unsteady* pH wave propagation. The dependence of wall zeta potential and electrophoretic mobility of the fluorescent proteins (plus the pH dependence of their fluorescence) complicates the situation. The overall dynamics of the system can be closely related to a phenomenon known as Teorell's oscillations. These problems can be avoided by using a split-reservoir design similar to a standard electrode, using an ion-selective membrane to prevent pH evolution in the fluid surrounding the Pt electrode from being transmitted immediately into the electroelution reservoir.

4. Conclusions

A micro device for eluting protein from a thick clinical sampling strip was fabricated using PDMS polymer and about the 50% of the initial concentration of the sample proteins (BSA, OVA) was eluted by the ~20V/cm electric field. During this elution process, the unsteady flow phenomena by the PDF and the pH change in the reservoirs resulting from the buffer depletion were observed. These problems can be solved by modifying reservoirs: large cross sectional area reservoirs and split-reservoir using ion selective membrane.

This electroelution device can be integrated with a protein concentrator and a separation column to analyze proteins. This integrated device will be fabricated in near future.

References

[1] H. Chang, A. L. Yergey, and A. Chrambach, *Electrophoresis*, **22**, 394-398 (2001).
[2] S. K. Basak, and M. R.Ladisch, *Analytical Biochemistry*, **226**, 51-58 (1995).

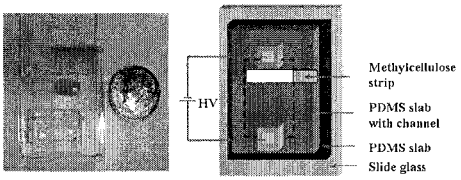

Figure 1. Electroelution chip photo (left) and schematic (right).

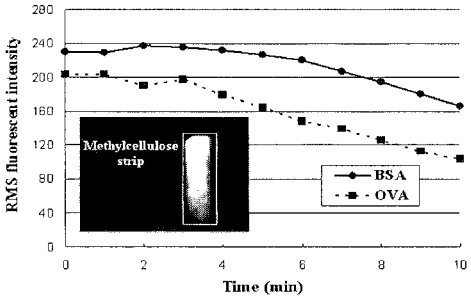

Figure 3. Removal of protein from sampling strips.

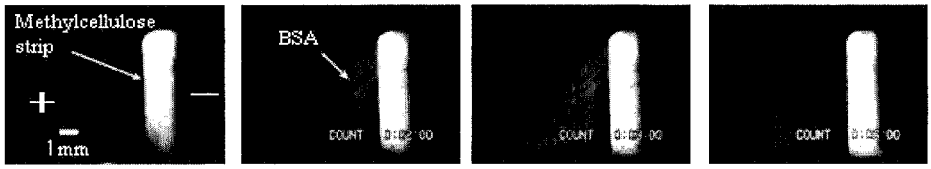

Figure 2. Series of images showing electroelution of BSA from a sampling strip. The wave of BSA is seen electroeluting from the strip towards the anode.

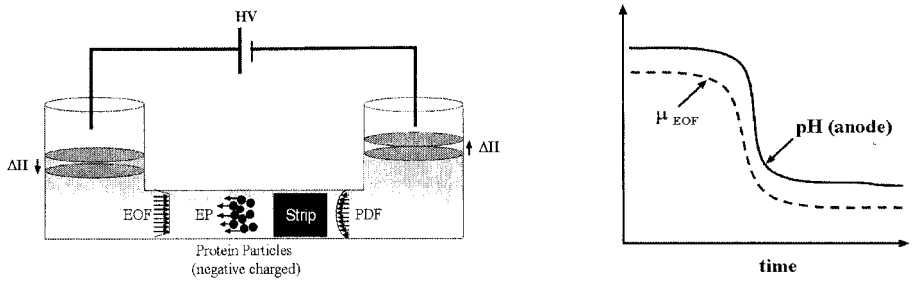

Figure 4. A schematic of flow mechanisms in the channel (left), and a pH change of anode side reservoir and electroosmotic mobility change of the fluid in the channel (right).

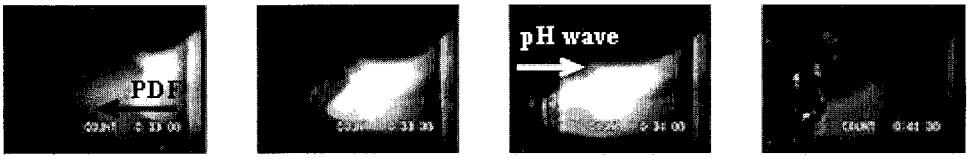

Figure 5. A sample of images showing passing of a pH wave (first three images), and a snapshot of unsteady motion that ensues afterwards (rightmost image).

MINIMIZATION OF PERFORMANCE VARIATION IN MICROFLUIDIC COMPONENTS USING THE METHOD OF ROBUST DESIGN

Lennart Bitsch[1,2], Henrik Bruus[2], and Jörg P. Kutter[2]
[1]*Novo Nordisk A/S, Brennum Park, DK-3400 Hilleroed, Denmark*
[2]*MIC - Department of Micro and Nanotechnology, Technical University of Denmark, Bldg 345 east, DK-2800 Kongens Lyngby, Denmark*

Abstract

This work illustrates how a microfluidic component is optimized to achieve a minimal variation for a defined performance. This approach is the key-idea of robust design. The performance is dependent on a number of parameters, each subject to statistical variations, and each contributing to the variation in performance. We are using a finite element code to calculate performance and to minimize the associated variation in order to acquire better designs.

Keywords: Microfluidics, modelling, robust design, finite element, optimization

1. Introduction

Robust design is a systematic method to minimize variation in a given device. The method has been used in many areas of engineering, but is rarely applied in microfluidics. Taylor has illustrated how to minimize variation in a piston pump, where the flow rate is given by a parameterized expression [1]. A requirement for robust design is knowledge on how the system responds to changes in design parameters and variations in the surroundings. We analyze the response numerically utilizing the strength of the recently developed multiphysics software FEMLAB.

2. Model example: a microfluidic pump

The microfluidic pump consists of a pump chamber where pressure changes are generated by a moving piston, and where inlet and outlet valves are directing the flow.

A finite element model of a simple piston pump was set up in FEMLAB 2.3. To simplify the calculations we have chosen a two-dimensional design of limited complexity with only three design variables. This model is shown in Fig. 1. The design variables are the pressure P on the piston boundary, and the heights $h1$ and $h2$, of the inlet and outlet channel, respectively. The pump performance is defined as the flow rate Q in the outlet channel.

We model the pump for a fixed piston position during a pump stroke, where fluid is leaving the pump chamber. A closed valve is mimicked by a small channel height and the pressure in the pump chamber is controlled by adjusting P.

3. Theory

Let us assume we require a target flow rate Q_T for a given position of the piston. The flow rate is determined by the design variables X_i, each with the standard deviation σ_i. Let the design variables be limited between lower and upper boundaries. Different values of the design variables can satisfy this condition, but we need to find the values resulting in the smallest variation σ_Q^2 on the flow rate. The variation σ_Q^2 can be calculated by error propagation

$$\sigma_Q^2 = \sum_{i=1}^{N} \left(\frac{\partial Q}{\partial X_i} \right)^2 \sigma_i^2 , \qquad (1)$$

where N is the number of design variables. It is noted that second order derivatives are ignored. In other words, in order to perform the analysis we need a mathematical model, but also information

on standard deviations from the fabrication process. The partial derivatives of Eq. (1) were estimated numerically.

4. Results and discussion

Table 1 shows parameters and relative standard deviation $s = \sigma_Q Q_T^{-1}$ for two different designs, producing the same flow rate. One design is optimized according to the theory, whereas the other is not. It is clear that optimization makes a difference, which is seen as s is reduced from 79% to 9%. The optimized design is the one represented in Fig. 1, with contour lines to indicate the distribution of pressure. The lack of contour lines in the pump chamber indicates that the pressure is almost constant in this region.

A typical measure of the quality is the so-called sigma level (SL). The target performance should to some degree satisfy an upper specified limit (USL) and a lower specified limit (LSL). The sigma level is defined as $SL = \sigma_Q^{-1} min\{Q_T\text{-LSL}, \text{USL-}Q_T\}$. A high sigma level ensures that a large number of products satisfy the specified limits.

If we assume that the values of the design parameters are normally distributed, the performance is also normally distributed. Figure 2 shows such a distribution for the optimized design with the standard deviation $\sigma_Q = 9\times10^{-10}$ m^2s^{-1} and mean value $Q_T = 10^{-8}$ m^2s^{-1}. LSL and USL are set to $\pm 10\%$ of Q_T, and the sigma level, in this case, is one. If we desire a larger probability that the product satisfies the specifications, the performance variation must be reduced. Therefore, the standard deviations σ_i of the design variables need to be smaller, as we have already minimized contributions from the partial derivatives in Eq. (1).

Despite the strong simplifications this example shows that a robust design can be obtained by choosing the right parameter values. One of the challenges in robust design is to find an expression for the variation of the performance, and optimize it for a number of parameters. Along with the development of new tools for multiphysics simulations, this option seems also feasible and possible in the field of microfluidics.

	P [Pa]	$h1$ [m]	$h2$ [m]	Q [m^2s^{-1}]	$s = \sigma_Q Q_T^{-1}$
Not optimized	0.1 ± 0.1	$10^{-5}\pm10^{-6}$	$10^{-4}\pm10^{-6}$	10^{-8}	79%
Optimized	2.1 ± 0.1	$10^{-5}\pm10^{-6}$	$3.9\times10^{-5}\pm10^{-6}$	10^{-8}	9%

Table 1. Two designs with the target flow rate $Q_T = 10^{-8}$ [m^2s^{-1}]. This unit appears for flows in two dimensions. It is noted that the same flow rate can be obtained with different magnitudes of the relative standard deviation s.

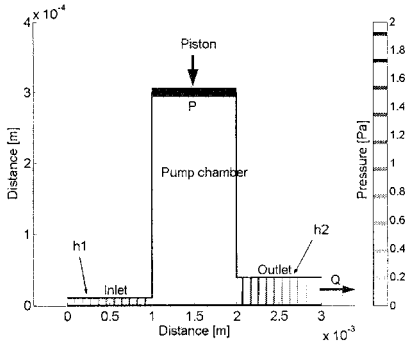

Figure 1. A simple presentation of a piston pump. The pump is being optimized at a specific time, when the piston is pumping. The horizontal arrow indicates the direction of flow with flow rate Q. The three design variables P, $h1$, and $h2$ are also shown. The vertical arrow indicates the direction of the piston. The pressure contour lines illustrate that the pressure drop occurs only at the inlet and outlet. The pressure within the pump chamber is almost constant.

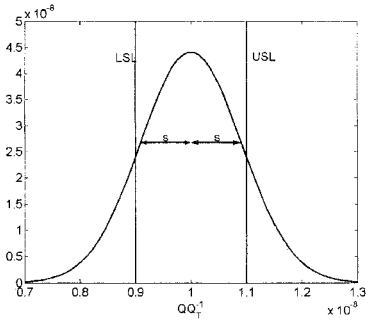

Figure 2. A normal distribution of the optimized design with standard deviation $\sigma_Q = 9\times10^{-10}$ m^2s^{-1} and mean value $Q_T = 10^{-8}$ m^2s^{-1}. LSL and USL indicate the lower and upper specification limits for the flow rate, respectively. Here, the limits are defined as $\pm 10\%$ of the target flow rate Q_T or mean value. The double arrows indicate the interval of σ_Q, and the sigma level, in this case, is one. If a larger sigma level and hence more robust components are desired. The standard deviations σ_i of the design parameters in Eq. (1) needs to be reduced.

References

[1] W.A. Taylor: SOCE News, The Society of Concurrent Engineering, Spring 1996 issue, p.1-6.

PARTICLE IMAGE VELOCIMETRY AND NUMERIC SIMULATIONS FOR AN IMPROVED UNDERSTANDING OF THE STAGGERED HERRINGBONE MIXER STRUCTURE

A. Wolff[1], H. Klank[1], H. Bruus[1], J.P. Kutter[1], F. Okkels[1] and O. Kuhn[2]

[1)]MIC-Dept. of Micro and Nanotechnology, Technical University of Denmark,DTU Bldg 345 east, DK- 2800 Kongens Lyngby, Denmark, aw@mic.dtu.dk

[2)] Dantec Dynamics A/S, Tonsbakken 16-18, DK-2740 Skovlunde, Denmark

Keywords: Particle Image Velocimetry, PIV, Fluid flow, Simulation, Mixer

1. Introduction

Mixing of fluid flowing through microchannels is important in many microTAS applications. However, the laminar flow conditions allow only mixing by diffusion, a process too slow for many applications. A large number of passive and active micromixers have been developed. Many of these mixers are however, complicated to fabricate or require moving parts. There is therefore a great interest for the passive staggered herringbone mixer structure presented recently by Stroock et al. [1]. The staggered herringbone mixer is comparatively simple to fabricate and in this mixing structure 3D flow patterns are generated by herringbone-shaped trenches on the floor of the channel.

2. Experimental

We have fabricated a staggered herringbone mixer structure with the same geometry as in Ref. [1], but using deep reactive ion etching in silicon, and sealed the structure with an anodically bonded glass lid (Fig 1). We present the first particle image velocimetry (PIV) measurements of the velocity field in a SHM structure. For these measurements the fluid (glycerol) was seeded with fluorescence microspheres (1 μm diameter). Two pictures are taken in quick succession, the displacements of the microspheres are calculated using a standard PIV algorithm, and from this the velocity vector for each point is extracted.

3. Results and discussion

While the velocity along the channel is dominant, the flow also has a smaller transversal component. In a plot of this transversal velocity component (Fig 1C) the herringbone trenches can clearly be recognized. The transversal velocity is greatest in the valleys of the trenches, whereas it is close to zero or reversed at the peaks. At a line connecting the tips of the herringbone trenches there is no transversal flow, and on each side of this division line the transversal flows are in opposite directions.

The velocity profile was determined at various depths in the channel by changing the focal plane of the microscope. From these measurements the transversal and the longitudinal velocity as a function of the channel depth (Fig. 2) is extracted for various positions (*a-j*, indicated in Fig. 1A). From the middle of the herringbone structure (point *a-e*) to further downstream (point *f-j*) the transversal flow increases. At points *d-e* and *i-j* in Fig 2A&B a characteristic S-shaped curved is observed where the transversal flow changes direction between channel bottom and top. This indicates a helical flow in agreement with Stroock et al. [1]. The longitudinal flow component is parabolic (Fig 2C&D), but with a slight asymmetry due to the effective velocity slip condition at the trenches [2]. These experimental findings compare favorably to numerical simulations (data not shown).

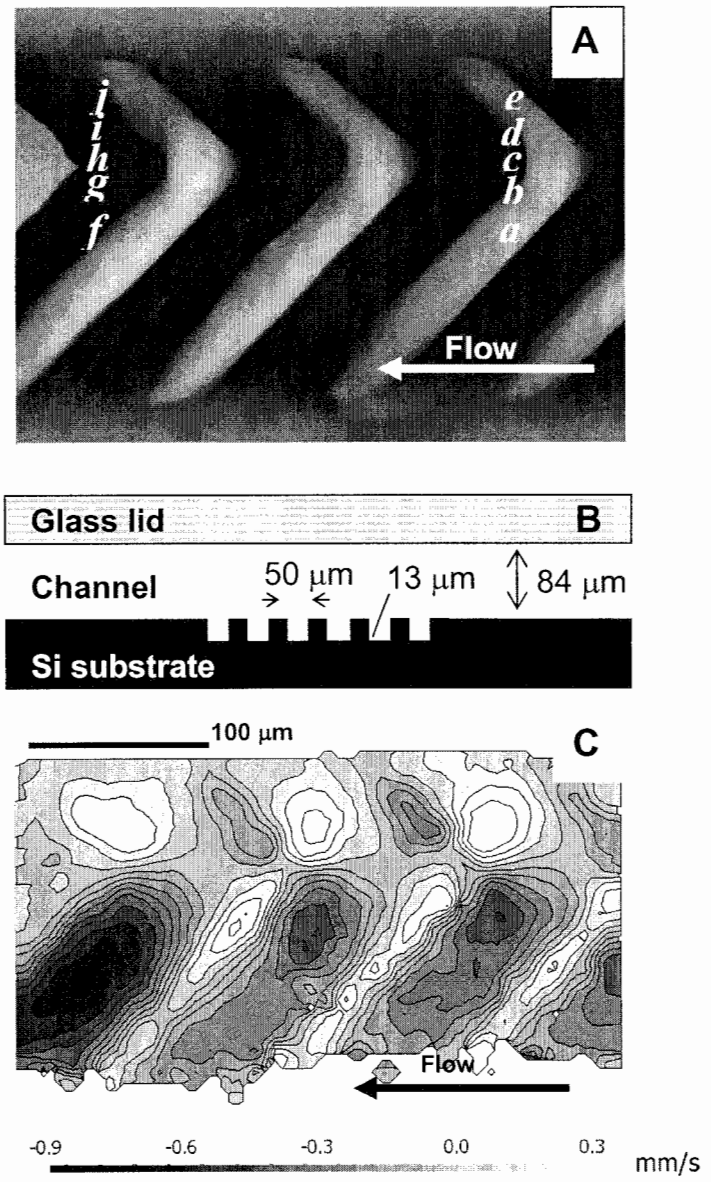

Fig 1. A: Microscope image of the herringbone trenches in the microfluidic channel. **B:** Schematic cross-sectional sideview of the channel with the herringbone trenches. **C:** Contour plot of the transversal flow component.

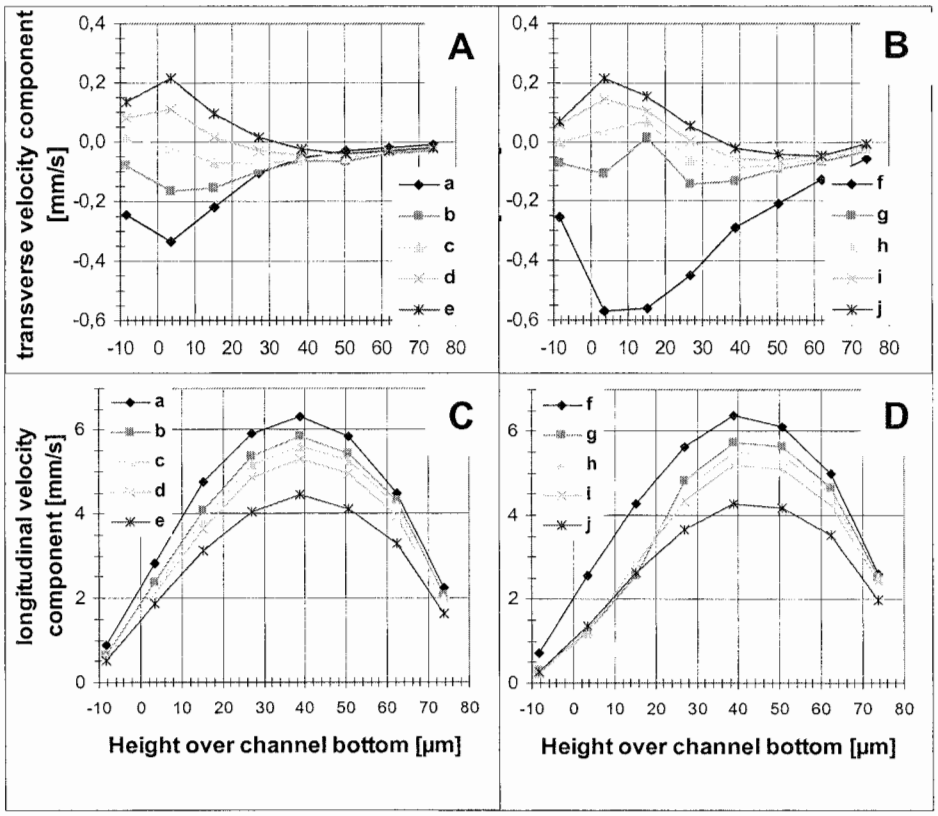

Figure 2 The transversal flow component **(A, B)** and the longitudinal flow component **(C, D)** as a function of height over the channel bottom. The height is set to zero at the channel bottom and is therefore negative in the herringbone trenches. (see Fig 1A for locations of points *a-j*).

4. Conclusions

Using PIV measurements it is possible to measure the flow in much greater detail than possible with the methods used by Stroock et al. [1]. Such detailed measurements as presented here are an important contribution to a better understanding of the staggered herringbone mixer structure, improved simulation tools, and for optimization of the design of the structure.

References

[1] A.D Stroock, S.K. Dertinger, A. Ajdari, I. Mezic, H.A. Stone, and G.M. Whitesides, *Chaotic mixer for microchannels.* Science, 2002. **295**(5555): p. 647-651.

[2] A.D Stroock, S.K. Dertinger, G.M. Whitesides, A. Ajdari, *Patterning flows using grooved surfaces*, Anal. Chem., 2002, **74**, p. 5306-5312.

LIQUID DROPLET DYE LASER

Hatim Azzouz, Søren Balslev and Anders Kristensen
Department of Micro and Nanotechnology (MIC), Technical University of Denmark (DTU), Oersteds Plads Bldng. 345 east, Kongens Lyngby, DK-2800, Denmark

Abstract

In this paper we present the first observation of lasing in a droplet containing a laser dye deposited on a hydrophobic substrate. We interpret the lasing to rely on reflections at the liquid-air and liquid-substrate interfaces. Suitable hydrophobic surfaces were fabricated and the shape of the droplets was calculated numerically. The measured spectrum from the droplet dye laser are discussed and demonstrated.

Keywords: laser, dye, droplet, resonator, self-organizing

1. Introduction

With the perspective of digital microfluidic circuits [1], it is interesting to functionalise liquid droplets. Where earlier lasing in spheres have focused on solid state materials [2], we demonstrate here lasing in a hemispherical liquid droplet consisting of the laser dye Rhodamine 6G (Rh6G) dissolved in ethylene glycol (EG). An external laser optically pumps the liquid droplet. Lasing output is measured directly from above the droplet.

To ensure long lifetime of the droplet we are interested in a dye solvent with a low evaporation rate. Furthermore, in order for the laser dye to retain a high quantum yield, the solvent must have a relatively low polarity. EG fulfils these criteria, and can form hemispherical droplets on hydrophobic surfaces (Fig. 1).

2. Hydrostatics of the droplet

The shape of the droplet was required to be spherical, because the geometry of a spherical droplet can be described by only two parameters, the radius R and the contact angle θ, thus limiting the complexity of modelling the optical geometry, (Fig. 2). To obtain a spherical shape, the so-called Bondnumber has to be much less than 1. This translates into a size requirement for the droplet. We find that the droplet has to be less than about 1 mm in radius, which is easily obtainable. This theoretical result was investigated by using a simulation program to predict the shape of the droplet for various radii, leading to results as exemplified in Fig. 3A-B. Decreasing the radius of the droplet, the shape changes from being a squashed droplet to a more hemispherical droplet. In Fig. 1 we show a microscope picture (side view) of a 150 μm radius EG-Rh6G hemispherical droplet.

3. Fabrication of hydrophobic surfaces

After ensuring a hemispherical shape by keeping the droplet radius below 1 mm, only the optimization of the contact angle is left. This is done by fabricating suitable hydrophobic surfaces using gas phase deposition of a fluoro-carbon film on silicon substrate surfaces with rms roughness of 10-30 μm. The contact angle for ethylene glycol on these surfaces was measured to 50°-66°. Droplets with linear dimensions in the 100 micron range were deposited by a dip pen method.

4. Results

The hemispherical liquid droplet was pumped optically by a pulsed, frequency doubled Nd:YAG laser (10 Hz repetition rate, 5 ns pulsewidth at a wavelength of 532 nm). The spot diameter of the pump laser beam was approximately 7 mm. In Fig. 4 we show a series of emission spectra from the droplet in Fig. 1. The seven displayed spectra are recorded with different optical

pumping power and display a multimode structure of the laser light. At an optical pumping power above threshold, a distinct peak (approximately 7 nm FWHM) appears on top of the more than 50 nm wide fluorescence from the Rh6G laser dye. A plot of the emitted power from the dye droplet versus optical pump power (Fig. 5), reveals the lasing characteristics of the system, with a threshold for lasing around 100 mW mean total pump power and a linear rise of output power for increased pumping. Evaporation of the droplet was minimized by cooling it with a Peltier-element to about 14 °C. The evaporation rate of the droplets was measured to 0.62 μL/min, limiting the measurement time to 20-60 minutes.

5. Conclusion

Lasing in a liquid droplet containing a laser dye has been demonstrated, relying only on reflections at the liquid-air and liquid-solid interfaces. Laser dye functionalised droplets adds a new range of possibilities for droplet manipulating micro systems, both with regards to sensor applications and laser physics in the self-organized spherical cavities whose shape can be tuned.

Acknowledgements

This work was supported by the Danish Technical Research Council, STVF (grant number 26-02-0064)

References

[1] Song Kwon Cho et al., Proc. of the IEEE 15th International Conference on Micro Electro Mechanical Systems, MEMS 2002, Las Vegas, USA, 2002, pp.32-35.
[2] V. S. Ilchenko et al., Optics Communications 145, 1 January 1998.

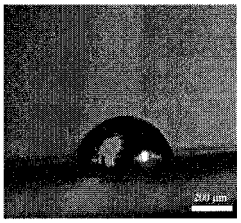

Figure 1. Side view of EG-Rhodamine 6G droplet on hydrophobic fluoro-carbon surface. Contact angle 50°, radius 150 μm and height 84 μm.

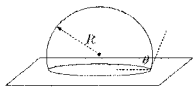

Figure 2. A hemispherical geometry only described by radius R and contact angle θ.

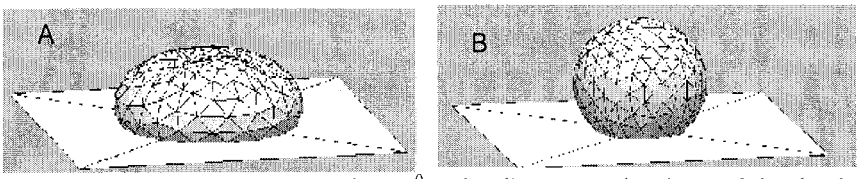

Figure 3. A) Given a contact angle 140^0 and radius 1 cm, the shape of the droplet becomes squashed (extreme example). **B)** But changing the radius to 1 mm the shape of the droplet becomes hemispherical.

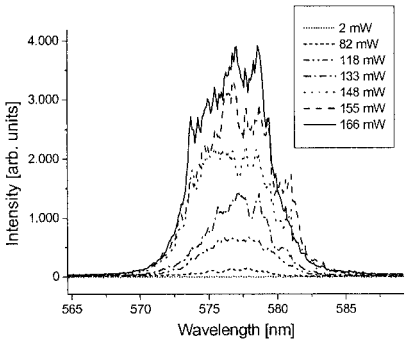

Figure 4. Measured spectra from droplet optically pumped (at 532 nm) with different mean total pump powers.

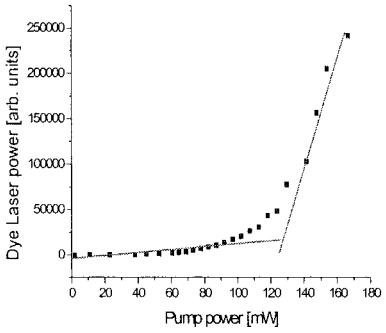

Figure 5. Power output from droplet versus mean total optical pump power.

HANDLING DROPLETS IN 3 DIMENSIONS FOR LAB-ON-CHIP APPLICATIONS

Jean-Maxime Roux[1], Yves Fouillet[1] and Jean-Luc Achard[2]

[1]Laboratoire d'Electronique et de Technologie de l'Information (LETI) - CEA/LETI 17 av. des Martyrs, 38054 Grenoble Cedex 9, France. Mail : rouxjm@chartreuse.cea.fr

[2]Laboratoire des Ecoulements Géophysiques et Industriels (LEGI) - INPG/CNRS/UJF – Grenoble

Abstract

A programmable device in which droplets can be handled in the 3 dimensions is presented. We explain vertical motions of droplets with theoretical keys and experimental observations. The device used to handle droplets is described and the handling of droplets of about 1 µL is demonstrated.

Keywords: 3D motions, droplet, Lab-on-Chip, electrostatic, lifting force

1. Introduction

Methods based on electrical fields have numerous assets in fluid management. EWOD devices are currently employed to move droplets in the micro-litre range on horizontal surfaces [1] while only few studies deal with vertical displacements [2]. Our aim is to adapt an EWOD device to move droplets also vertically by an electrical actuation. Droplets can be lifted to an upper position where they can be maintained during a controlled residence time and brought back to the initial lower surface.

2. Theory

Physics of the droplets interaction with a conducting plane are understood by studying the model of a spherical particle resting upon a single plane electrode. Lebedev & Skal'skaya [3] have calculated the so-called Maxwell electrical charge, acquired by a conducting sphere in contact with a perfectly conducting plate electrode, as well as the force acting on the sphere when the electrical field is considered uniform at a great distance. They showed that the force is independent of the orientation of the electrical field and that the force is always a lifting force. As a consequence, a sphere heavier than the surrounding dielectric medium and located on a plane electrode can be moved upwards with an appropriate electrical field.

To build a theoretical model of the behavior of a droplet between two parallel plate electrodes, we adapt the model of Lebedev & Skal'skaya to take into account the wetting on surface. ElectroHydroDynamics equations are solved in appropriate coordinate systems to provide closed form expressions.

3. Experimental studies

A water droplet surrounded by mineral oil, located in a parallel plate condenser and lying on the lower electrode of the condenser is moved upwards (figure 1) when a voltage is applied between he upper and lower electrodes (about 1.5kV/cm). According to the theory, when the droplet is in electrical contact with an electrode the electrical force tends to detach the droplet thus when the droplet gets in electrical contact with the upper electrode the electrical force turns downwards.

In order to control the droplet position, the upper electrode is covered with a dielectric layer. Droplets cannot transfer their electrical charge with the upper electrode so the electrical force remains an upwards force and droplets are kept on the layer. Droplets are moved downwards by reversing the applied electrical field.

Capillarity forces are often undesirable because they would stuck droplets on a position (lower or upper position). In our experiments layers were chosen hydrophobic or treated to be hydrophobic.

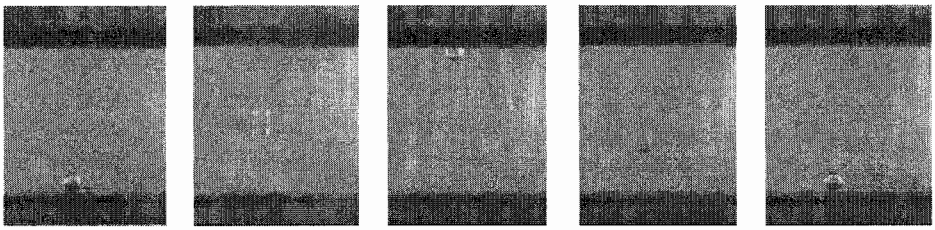

(a) (b) (c) (d) (e)

Figure 1 : Experimental study of a water droplet in a parallel plate condenser. The distance between the electrodes is 10mm, the Teflon dielectric layer is about 1mm thick, the mineral oil used is from *Sigma*, the voltage sequence is 0V, +1600V, -1600V, 0V. The average speed of the droplet going upwards is about 29mm/s. (a) A droplet of water is resting on an electrode. (b), (c) Under an electrical field, the droplet is moved to the upper position onto the dielectric covering the upper electrode and kept in this position. (d), (e) Afterwards, the droplet is moved back to the lower electrode.

4. Chip design

The EWOD devices [1] we are currently developing use a gold micro-catenary as the electrical contact with the droplets to generate the horizontal motions on the electrode array. In addition with an extra upper isolated electrode, this catenary is also used to move droplets upwards and downwards by applying a vertical electrical field. The droplet displacement between the two plates is precisely controlled and reversible, droplets being handled along the 3 space dimensions. Such displacements are detailed in figure 2. The electrical field exerts a lifting electrical force on droplets which overcomes the gravity and the capillary forces. Afterwards, the charged droplet in contact with the top dielectric can be brought back by changing the sign of the electrical field.

The micro-catenary used in our EWOD devices to move droplets horizontally is also used as the lower electrode described above. The upper electrode is made of polycarbonate and an ITO layer and covered with a hydrophobic and dielectric layer of Teflon (figure 2). The PDMS spacer surrounds the device filled with mineral oil and observations are made through the spacer.

Electrowetting can retain droplets on the lower position even if an electric field is applied between the catenary and the upper electrode. As a consequence, droplets to move verticaly can be chosen.

This extra 3D droplet motion enlarges the scope of chemical and biological applications. One example could be to move quickly a droplet from the top surface to the bottom surface, both surface having temperatures necessary for thermal cycling. The ability to use the top and the bottom of a device permits to reduce the overall size of the chip and to tune finely reaction times.

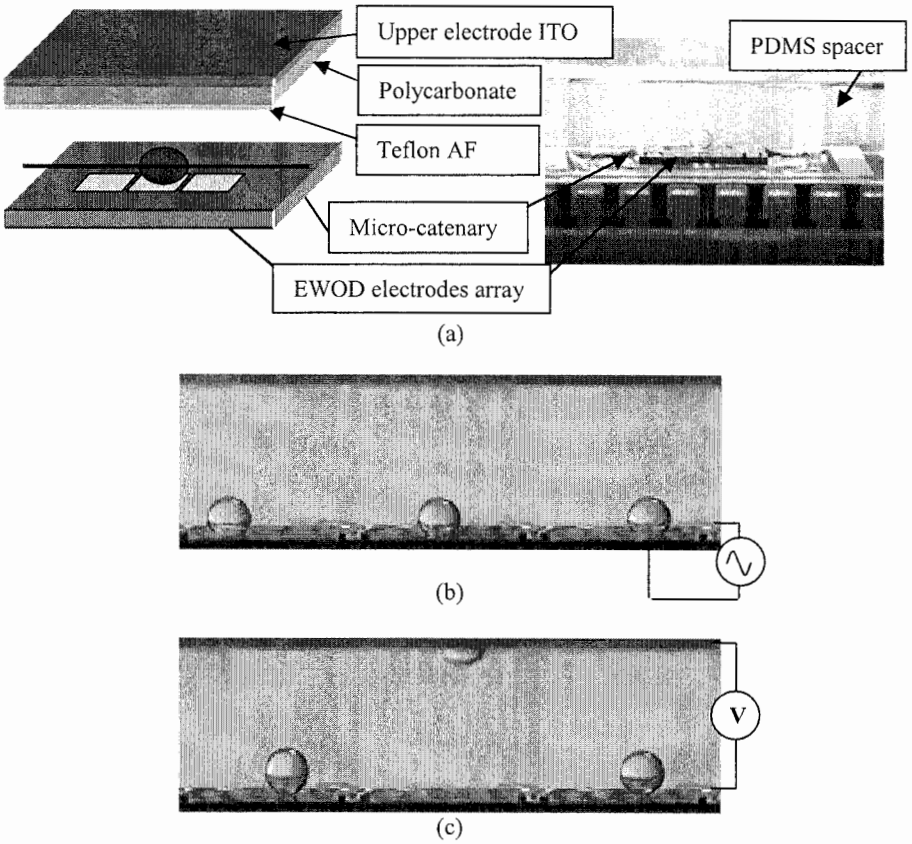

Figure 3 : Horizontal displacement & Vertical displacement: A droplet of water (1µL) is handled by electrostatic actuation in mineral oil. In each case a schematic description of the device is given and pictures of the droplet in the situation described are shown. (a) Picture and schematic description of the device. (b) The droplet is resting on the lower surface and can be moved horizontaly by electrowetting ($60V_{rms}$, 3kHz). (c) Applying an electric voltage of 1600Volt, the droplet is moved to the upper position, the upper ITO electrode covered with dielectric layers of polycarbonate and Teflon AF 3% and located about 5mm above the lower position, and is kept on this position. The average speed of the droplet going upwards is about 31mm/s. Afterwards, the droplet is moved back from the upper position to the lower electrodes array and can be displaced again by electrowetting.

References

[1] Y. Fouillet, H. Jeanson, D. Jary, O. Constantin and C. Vauchier, Seventh International Conference on Miniaturized Chemical and Biochemical Analysis Systems (µTAS 2003) , Squaw Valley (USA), 61-64 (2003)

[2] P. Kolar (Poster), 3rd SmallTalk Conf., San Diego (2001)

[3] N.N. Lebedev and I.P. Skal'skaya, *Soviet Phys.-Tech.* Phys., **7**, 268-270 (1962)

THERMAL CONTROL OF AQUEOUS FLUIDICS IN MICROCHANNELS GRAFTED WITH THERMORESPONSIVE POLYMER

Naokazu Idota[1,3], Akihiko Kikuchi[2,3], Jun Kobayashi[2,3], Kiyotaka Sakai[1] and Teruo Okano[2,3]

[1] *Dept. of Applied Chem., Waseda Univ., 3-4-1 Ohkubo, Shinjuku-ku, Tokyo 169-8555, JAPAN.*
[2] *Inst. Adv. Biomed. Eng. & Sci., Tokyo Women's Med. Univ., 8-1 Kawada-cho, Shinjuku-ku, Tokyo 162-8666, JAPAN.*
[3] *CREST Japan Science and Technology Agency.*

Abstract

We here propose the novel microfluidic flow controls by simple, but effective surface wettability alterations in response to temperature. Flow control within the microchannels is often necessary for various operations, such as analysis, mixing, and flow directional changes. For more simple and effective flow control systems, we investigated thermoresponsive poly(*N*-isopropylacrylamide) (PIPAAm) grafted capillary tubings for on/off switching of microfluidics. PIPAAm-grafted capillaries showed significant wettability changes around 30°C, being hydrophilic to hydrophobic surface property alterations with temperature. Such thermoresponsive capillary surfaces induced completely on/off switching of aqueous pressure driven flow within capillaries. Thus, PIPAAm microfluidic system can be applicable to control on/off flow switching by only temperature changes.

Key words: Poly(*N*-isopropylacrylamide), Thermoresponsive surfaces, Glass capillary, Flow direction changes, on/off flow switching

1. Introduction

Easy and simple microfluidic flow control is important technique for analysis and reaction in microchannels. Many researchers have been trying to control microfluidics by mechanical methods (e.g. swelling/deswelling changes of responsive hydrogels used as microvalves) [1]. Introduction of such mechanisms into microfluidics design requires complicated techniques. In microchannels, however, surface wettability significantly affects the pressure-driven flow because inertia, viscosity, and tension of water are dominant rather than gravity. Thus introduction of stimuli responsive intelligent surfaces to microfluidics will open easier control of microfluidic flow only by surface wettability alterations in response to external stimuli [2]. In the present paper, we prepared novel glass capillary tubings grafted with poly(*N*-isopropylacrylamide) (PIPAAm), which show large and discontinuous hydrophilic/hydrophobic property changes in response to external temperature [3], and investigated directional changes of the pressure-driven flow in the PIPAAm-grafted microchannels by temperature alteration.

2. Experimental

Temperature dependent elution volumes through the PIPAAm-grafted fused silica capillaries were examined with HPLC apparatus. PIPAAm surfaces used were made by electron beam polymerization (**Figure 1**). Pressure-driven flow was generated by HPLC pump. Milli-Q water was used as the eluent with a flow rate of 100 μL/min. The elution from the PIPAAm-grafted capillary was collected for one minute, and the elution volume was determined gravimetrically. Elution profiles with stepwise temperature changes were monitored for PIPAAm-grafted capillaries modified by the electron beam polymerization. Aqueous fluorescein solution was used as the eluent at a flow rate of 100 μL/min. Temperature of the PIPAAm-grafted capillaries was changed stepwise from 25°C to 40°C after 10 minutes. The fluorescence of the eluent from the

PIPAAm-grafted capillaries was monitored using fluorescence spectrometer

4. Results and discussion

Surface wettability changes of PIPAAm-grafted capillary surfaces were s evaluated by changes in water meniscus heights. Meniscus heights in PIPAAm-grafted capillaries were significantly changed around 30°C, owing to temperature-dependent hydrophilic/hydrophobic surface property alterations. Scanning electron microscopic observation revealed that the capillary diameters are almost constant before and after PIPAAm modification, indicating the nanometer levels of PIPAAm grafted layer formation on capillary walls. The elution volume changes at various temperatures from PIPAAm-grafted capillaries are shown in **Figure 2**. Elution from PIPAAm-grafted capillary was completely stopped below 30°C, while it increased significantly above 30°C. The complete stop of elution at low temperature regions in PIPAAm-grafted capillaries may be due to the hydration of PIPAAm chains with water molecules restrained near the surfaces at low temperature. The flow directional changes with stepwise temperature gradient from 25°C to 40°C were then evaluated in the PIPAAm-grafted fused silica capillaries (**Figure 3a**). Fluorescence was not detected at all for the PIPAAm-grafted capillary at 25°C. After stepwise temperature gradient was applied at 10 min, quick increase in fluorescent intensity was observed. In the PIPAAm-grafted capillaries, higher pressure was necessary to maintain the flow rate of the eluent. Flow pressure was then decreased gradually with increasing temperature up to 30°C, and pressure became negligible similarly to the pressure observed for the untreated capillaries above 30°C (**Figure 3b**).

5. Conclusions

The hydrodynamic property alterations of the PIPAAm-grafted capillary surfaces significantly influenced to the fluidic behavior in response to temperature changes. Flow in the PIPAAm-grafted capillaries was completely stopped below the PIPAAm's LCST. This was probably due to hydration of PIPAAm molecules those grafted in nanometer-thick scale layers on the capillary surfaces, restraining of water molecules in microfluidics at low temperature. In conclusion, we suggest that PIPAAm microfluidic system should be useful tool for control of on/off flow switching only by temperature changes.

References

[1] D.J. Beebe, J.S. Moore, J.M. Bauer, Q. Yu, R.H. Liu, C. Davadoss, B.H. Jo, *Nature*, **404**, 588-590 (2000).

[2] D. Huh, A.H. Tkaczyk, J.H. Bahng, Y. Chang, H.H. Wei, J.B. Grotberg, C.J. Kim, K. Kitabayashi, S. Takayama, *J. Am. Chem. Soc.*, **125**, 14678-14679 (2003).

[3] A. Kikuchi, T. Okano, *Prog. Polym. Sci.*, **27**, 1165-119 (2002).

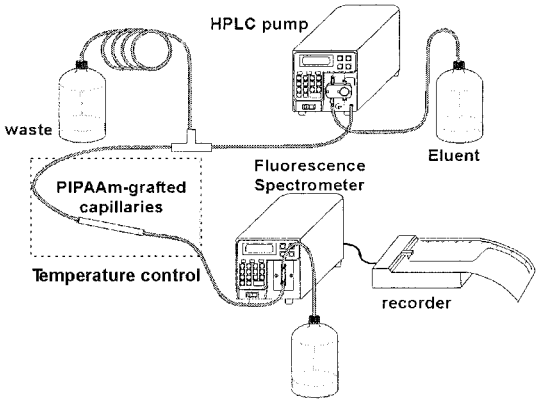

Figure 1. Experimental apparatus for flow direction changes in PIPAAm-grafted capillary. Aqueous fluorescein solution was used as the eluent at a flow rate of 100 μL/min.

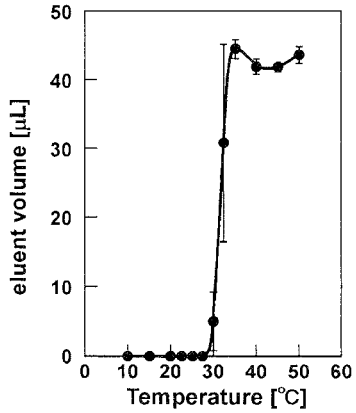

Figure 2. Temperature-dependent elution volume changes for PIPAAm-grafted capillary (50 μmϕ).

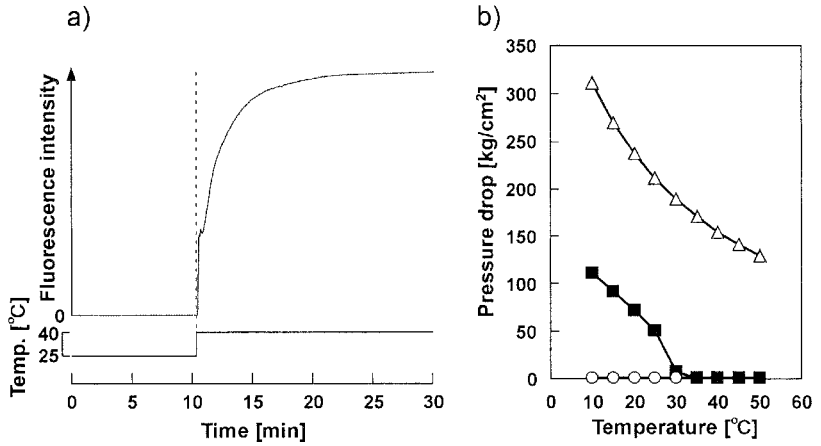

Figure 3. Thermally regulated flow direction changes in PIPAAm-grafted capillaries with the stepwise temperature gradient. a) Fluorescence intensity changes of elution from PIPAAm-grafted capillary with the stepwise temperature gradient. b) Results of monitored backpressure changes against PIPAAm-grafted capillaries and the untreated capillaries with temperature; (○) 50 μmϕ untreated capillary, (Δ) 10 μmϕ untreated capillary, (■) 50 μmϕ PIPAAm-grafted capillary.

MAGNETIC SEPARATION IN MICROSYSTEMS: EFFECTS OF HYDRODYNAMIC INTERACTION

Christian Mikkelsen, Mikkel Fougt Hansen and Henrik Bruus
MIC — Department of Micro and Nanotechnology, Technical University of Denmark, Building 345 east, DK-2800 Kongens Lyngby, Denmark

Abstract

Entities such as biological macromolecules or cells can be specifically tagged with magnetic microbeads to enable simple separation, capturing and purification by means of magnetic fields. We find that interactions mediated by the fluid medium greatly help and speed up the capturing process. This hydrodynamic interaction is longer range, falling off inversely with distance, than the magnetic interaction between magnetic microbeads that falls off inversely with the distance cubed.

Keywords: magnetic separation, hydrodynamic interaction, micro fluidics

1. Introduction

Specific tagging of analytically interesting material such as biological macromolecules or cells by means of magnetic microbeads enables simple separation and purification operations in microscopic fluid handling systems. The material binds by biochemical or immunochemical means to the beads which can then be manipulated, retained and released by magnetic fields and field gradients [1,2]. The magnetic field and field gradient can either be generated by electromagnets or, for example, by external permanent magnets giving the field and the gradients being created by having submillimetre magnetizable structures in the immediate vicinity of the microscopic fluid channel.

2. Theory

Magnetic microbeads are subject to a force when immersed in magnetic field gradients, directed towards a local field maximum. The force moves the bead relative to the surrounding fluid, quickly reaching a balance with viscous forces effecting a momentum transfer from bead to fluid. This momentum transfer makes the fluid flow drag other objects along.

Viscosity and the force balance also means that speed relative to the surrounding liquid is always proportional to the applied force acting on the bead. Bead trajectories are then calculated by integrating the velocities rather than the accelerations.

For flows at the low Reynolds numbers relevant in microfluidics, the flow due to a point force can be described by a hydrodynamic Green's function [3]. The presence of a nearby wall modifies the flow due to the point force; something that can be taken into account in the Green's function approach as well [3,4].

The flow due to the motion of a bead relative to the surrounding fluid creates an effective interaction that is long range; the flow falls off as distance to the minus first power. This is much slower than the leading order (dipole-dipole) magnetic interaction that depends on the distance to the third power.

3. Simulations

A two-dimensional slice along the length of a 100-μm wide fluid channel was considered. The magnetic field was the calculated for a section of a periodic structure of strips 10 μm wide, 300 μm long of magnetic material (of relative permeability 1000) immersed in a homogeneous external magnetic field of 40000 A/m directed along the strips.

Both the magnetostatic and Poiseuille flow problems were solved with the finite element method software package FEMLAB [5]. The trajectories of up to twenty 5-μm beads were calculated from the magnetic field and from the fluid flow. The fluid flow was constantly updated

with the changes to the flow due to the motion of the other beads. This takes into account the fluid-mediated or *hydrodynamic interaction*. To identify the effects of hydrodynamic interactions, the simulations were also carried out without these.

The beads are stopped when they reach the sides of the channel, i.e. are captured, or when they go out of the simulation domain. These events are then recorded and stored.

The beads are started at random positions in the inlet half of the domain and are both flushed by the 0.5mm/s left-moving flow and pulled towards the magnets. The starting positions are chosen in this manner as to mimic random arrival of beads. If the beads are started only at the inlet and at a single time they move collectively which might not be representative of the motion in actual experiments.

4. Results and discussion

The simplest and most illuminating way of illustrating the effects of interactions is to study the trajectories of some beads as they move either *with* or *without* the hydrodynamic interactions. This is done in Figures 1 and 2. Started at random positions and looking from their trajectories, the beads are caught much faster when hydrodynamic interactions are included than when they are invisible to one another. This comes about as interacting beads move collectively; their interaction is neither attraction nor repulsion.

To get a different illustration, the capturing times in the presence and absence of interactions were simulated with random initial positions for up to 30 beads. The capturing times were then compared and it was found that interactions speed up capturing by a factor of up to 6, increasing with the number of beads. This is shown in figure 3. As is apparent, the more beads the more collective movement there is and the greater speed-up on the non-interacting case.

The results show that even having a few beads in a microfluidic channel being caught, greatly helps capturing, reducing capturing time, or easing requirements on magnetic fields and fluid flows.

5. Conclusions

Our work shows that hydrodynamic interactions influences capturing, speeding it up, and that it should be included in studies of capturing. The effect is more pronounced the more particles are being captured at the same time. The interactions are long range; falling off as inversely with distance.

References

[1] C.H. Ahn, M.G. Allen, W. Trimmer et. al, *J. Microelectromech. Syst.*, **5**, 151 (1996).

[2] T. Deng, M. Prentiss and G.M. Whitesides, *Appl. Phys. Lett.*, **80**, 461 (2002).

[3] C. Pozrikidis, *Boundary Integral and Singularity Methods for Linearized Viscous Flow*, (Cambridge University Press, Cambridge, 1992).

[4] E.R. Dufresne, T.M. Squires, M.P.Brenner et. al., *Phys. Rev. Lett.*, **85,** 3317 (2000).

[5] COMSOL AB Sweden, *FEMLAB* ® v. 2.3, http://www.femlab.com.

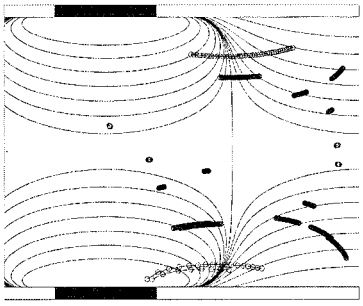

Figure 1. Non-interacting beads: catching with a magnetic field gradient. Contours (non-equidistant) indicate magnetic field. Tracks are beads being caught. The fluid flows from the right. Beads near the centre do not feel a strong gradient so they move slowly. (The circles are at equal times.)

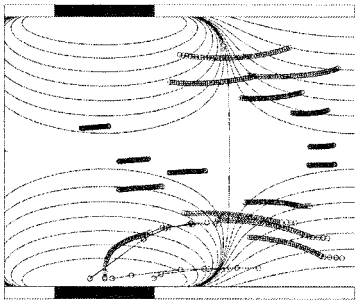

Figure 2. Interacting beads: catching beads with a magnetic field gradient in a microfluidic channel. Same parameters as Fig. 1. Here all beads are dragged along, even the ones near the centre. This greatly helps capturing. Where the field is already strong the difference is insignificant.

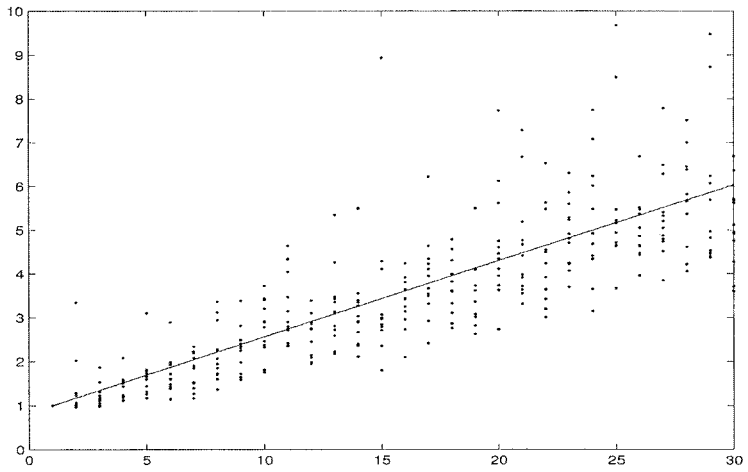

Figure 2. Having beads interact as they are caught speeds up capturing. Simulations were done with from 1 to 30 beads and the mean capturing time was calculated for 12 different runs each with and without hydrodynamic interactions. The ratio of the mean capturing times without interactions to the mean capturing times with interactions was then calculated for each of the runs (dots). The line is the best linear fit.

ELECTROKINETIC MICROPUMPS FOR DIRECT PUMPING OF ACIDIC SOLVENTS IN MICRO-HPLC SYSTEMS

Kamlesh Patel and Robert Crocker
Dept. of Microfluidics and Advance Microsystem Engineering,
Sandia National Laboratories, P.O. Box 969, Livermore, CA 94551-0969

Abstract

Electrokinetic (EK) micropumps are well suited for microfluidic applications. The pumps are physically compact, operate silently, and generate hydraulic work with no moving parts. EK pumps use electroosmosis in a charged nanoporous (10-500 nm) media to generate hydraulic pressure and flow. For use with micro-HPLC system, we have developed electrokinetic pumps that can directly pump acidic mobile phases commonly used in reversed-phase liquid chromatography. Pumps show long-lifetimes and stable flow generation in the nL/min flow regime. A pair of pumps operating under dynamic flow control have been used for binary gradient elution. Retention time RSDs of less then 1% for the separation of peptide standards have been achieved using the acid EK pumps to generate an acetonitrile gradient.

Keywords: electrokinetic pump, micro-HPLC, acidic solvents, HPLC-on-a-chip, nanoLC

1. Introduction

Micropumps for microfluidic applications have received a great deal of recent interest because they can reduce the system size, reagent volumes, and power requirements for fluid manipulations and actuate microscale moving parts, making inexpensive micro- and portable-chemical analysis systems feasible. Electrostatic, thermopneumatic, and piezoelectric style micropumps are limited to a maximum pressure of about 100 KPa (14.5 psi) [1]. On the other hand, electrokinetically driven pumps are capable of delivering extreme high pressures (690 MPa or 100 kpsi) [2]. Such pumps have been demonstrated as microhydraulic actuators [3] and micro-HPLC pumps [4]. EK micropumps developed at Sandia National Laboratories are less than half centimeter in diameter and a few centimeters long; they can be fabricated as an inline pump in a microchannel or as an external module. These silent EK pumps generate fluid flow when a voltage gradient is applied. Electrokinetic (EK) micropumps are well suited for pressure-driven flow in microfluidic systems, particularly micro-HPLC.

Previously, we have developed robust and efficient EK pumps in fused-silica capillaries with densely-packed submicron silica particles. EK pumps have demonstrated highly reproducible flow rates from nanoliters- to microliters-per-minute over long durations at high pressures. Silica EK pumps have been optimized for solvent delivery in a miniaturized hybrid capillary/chip HPLC system for isocratic and binary gradient separations.

Unfortunately, silica EK pumps are generally limited to pumping fluids above pH 7. In acidic solutions, the silica surface becomes protonated neutralizing the surface charge. Since liquid chromatography is typically performed using mobile phases with trifluoroacetic acid or formic acid additives, direct pumping of such mobile phases is not possible with silica EK pumps. A fluid compatible with the silica EK pumps, such as 5 mM TRIS pH 8.5, must serve as a working fluid to displace the acidic mobile phase solution contained in an in-line reservoir. Even though this strategy has been used successfully, it increases the complexity of the micro-HPLC design. As an alternative and more simplified design for a monolithic HPLC system, we present our development and implementation of acid EK pumps for directly pumping acidic mobile phases.

2. Theory

The pumps are physically compact, operate silently, and generate hydraulic work with no moving parts. EK pumps use electroosmosis in charged nanoporous (10-500 nm) media to generate pressure and liquid flow. Applied axial electric fields cause solvated ions to migrate at the double layer near the charged-solid interface and result in viscous drag of the bulk fluid through the pores. The flow delivered in the forward direction for useful work is the difference between the EOF flow and pressure-driven flow in the reverse direction. Pressure and flow rate generated by an EK pump vary linearly with the applied electric field, which makes for straight-forward control.

3. Experimental

Figure 1 shows a schematic of a micro-HPLC using two EK pumps for gradient elution for reversed-phase liquid chromatography. The inlet of each pump is placed inside the mobile phase reservoirs (either aqueous or organic). Electrodes (platinum wire), a custom microfluidic union with capillary fittings, and a miniature pressure transducer complete the pump subsystem. Feedback from the flow sensor on each pumping leg provides dynamic control to maintain a constant flow rate and desired composition. A 30 nL nanomixer mixes the solvents from each pumping leg to form the gradient which is then delivered to a sample injector and separation column.

4. Results and discussion

Acid EK pumps are formed by modifying the silica surface to a positive charge. The corresponding zeta potential measurements for the modified particles vs. bare silica at different pH solutions are listed in Table 1. With the surface modification, the modified particles exhibit a positive charge in acidic conditions, where bare silica particles do not. Figure 2 shows the pressure, current, and voltage traces for testing an acid EK pump in a stepwise fashion with acetonitrile buffer with 0.1% TFA additive. Applying a negative high-voltage field gradient results in a proportional flow rate of 230 nL/min-KV for this particular pump tested. Acid EK pumps fabricated with 0.5-μm diameter particles exhibit a 10 psi/volt performance and have been pressure tested to 10,000 psi (69 MPa). The acid EK pumps implemented in our micro-HPLC system provide constant flow rate and maintain excellent solvent composition control for gradient elution. Furthermore, directly pumping acidic mobile phases show no effect on the chromatography. EK pumps integrated in a micro-HPLC system are shown in Figure 1. Figure 3 shows three overlayed chomatograms using the micro-HPLC system with acid EK pumps showing good gradient and retention time reproducibility. Retention time RSDs are less than 1% for the three overlaid chromatograms. Chromatographic results obtained with our micro-HPLC system using acid EK pumps demonstrate the system as a true direct-flow nanoLC system.

Acknowledgements

This work was performed with support from Waters Technology Corporation under the Cooperative Research and Development Agreement SC01/01612. Sandia is a multiprogram laboratory operated by Sandia Corporation, a Lockheed Martin Company, for the United States Department of Energy's National Nuclear Security Administration under contract DE-AC04-94AL85000.

References

1. P. Selvaganapathy, Y. Ki, P. Renaud, and C. Mastrangelo, *J. Microelectromechanical Systems,* **11**, 448-453 (2002).
2. K. Patel, et al, Proc. of 27th International Symposium on Capillary Chromatography, (2004).
3. B. Mosier, R. Crocker, R. Rognlien, K. Patel, Proc. of ASME IMECE, Washington, D.C. (2003).
4. P. Paul et al, Proc. Micro Total Analysis Systems 2000, 583-590 (2000).

Table 1. Zeta potential values measured with PALS instrument. Five runs are performed for each reported value. Surface modified silica particles exhibit a positive zeta potential in acid conditions.

	Silica (mV)	Modified Silica (mV)
pH 8.5	**- 26.8 ± 2.5**	**9.1 ± 2.7**
pH 7.0	**-14.8 ± 1.2**	**9.5 ± 1.4**
pH 2.9	**-1.6 ± 0.3**	**19.4 ± 2.0**

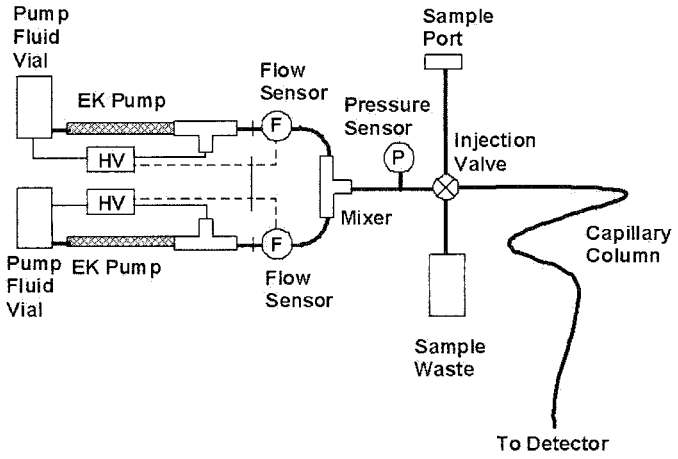

Figure 1. Schematic of a binary gradient micro-HPLC using two acid EK pumps.

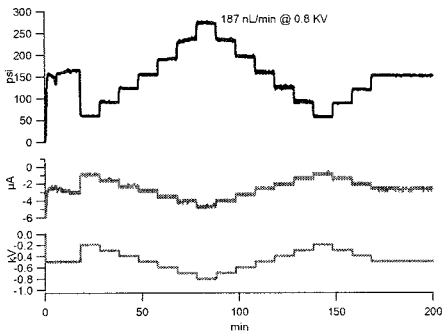

Figure 2. Open-system pressure test for an acid EK pump (150 um i.d. x 5 cm long) through a 10 um i.d. x 40 cm flow restrictor, pumping 95/5 ACN/H2O w 0.1% TFA buffer solution.

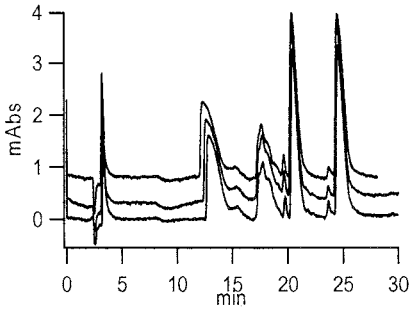

Figure 3. Three overlaid gradient separations of standard peptide mixture using acid EK pumps with a micro-HPLC system. The aqueous and acetonitrile buffers were modified with formic acid additive.

MAGNETO-HYDRODYNAMIC MICROMIXING FOR CENTRIFUGAL LAB-ON-A-DISK PLATFORMS

Markus Grumann, Andreas Geipel, Lutz Riegger, Roland Zengerle, and Jens Ducrée
IMTEK- University of Freiburg, Laboratory for MEMS Applications
Georges-Koehler-Allee 106, D-79110 Freiburg, Germany

Abstract

We present a novel concept for mixing of liquids on centrifugal microfluidic platforms based on the deflection of magnetic beads by stationary permanent magnets. Outstanding features of this batch mode mixer are its high speed of mixing (mixing time of less than 1 s compared to 7 min for mere diffusion), its scalability (volumes between 1 nl and 1 ml can be processed), its simple and modular setup (macroscopic actuation, no 3-D micromachining, no moving microparts except for magnetic beads, possibly disposable disk) and the low spinning frequencies (~10 Hz).

Keywords: mixing, magnetic beads, batch mode, centrifugal microfluidics

1. Introduction

Among the numerous approaches of mixing in microfluidic devices under strictly laminar conditions, the actuation by magnetic beads in an external field attracts growing attention. Most so far published setups exhibit a mixing chamber containing the magnetic beads. The beads are exposed to a time-varying magnetic field that is generated by a fixed array of current-oscillating electromagnets [1,2]. We introduce a novel micromixing concept which generates a time-oscillating magnetic force by the rotating motion through a static field. Such an approach is well compatible to our centrifugal Bio-Disk platform [3] since it greatly reduces the complexity of the system.

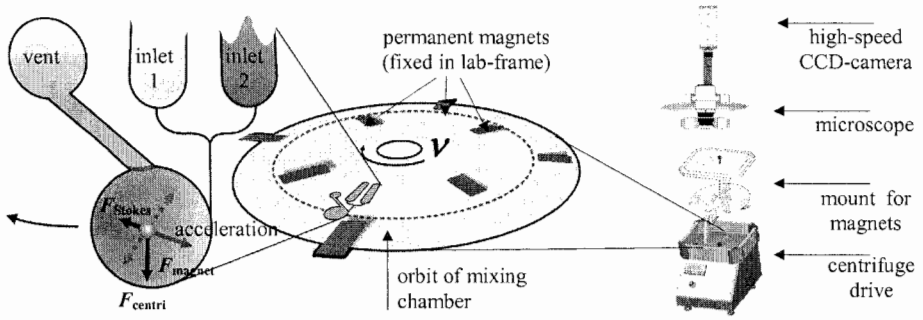

Figure 1. Concept of mixing: For an optimum bead-enhanced mixing, we introduce a set of permanent magnets which are equidistantly aligned in the lab frame. Their radial positions alternatingly deviate by a slight positive and negative offset from the mean orbit of the chamber. This way, the beads are periodically deflected inbound and outbound during rotation. Advection is induced by the Stokes drag F_{Stokes} of the moving beads which results from the interplay of the magnetic force F_{magnet}, the centrifugal force F_{centri} and inertia. For image acquisition, a high-speed CCD-camera mounted on a microscope is synchronized to the spinning disk.

2. Setup and Principle of Mixing

In our magneto-hydrodynamic concept, the magnetic beads (diameter: 135 µm [4]) are located in a disk-based mixing chamber (depth: 900 µm, diameter: 6 mm, i.e. a volume of 25 µl) to

which is round to avoid hydrodynamically 'shaded' zones (Fig. 1). The dimensions of the microstructured disk follow the format of a conventional compact disk (CD) [5].

Set into spinning motion, the mixing chamber containing the magnetic beads traverses the inhomogeneous magnetic field built up by the permanent magnets. Their spatial alignment alternatingly draws the magnetic beads inbound and outbound. Thus, the beads are deflected with respect to the fluid to induce chaotic advection by means of the Stokes drag. The mixing power is transduced by the magnetic field from the rotating drive to the bead-induced stirring. In addition, we perform preriodic changes of the sense of rotation where the frequency of rotation ν follows a trapezoidal time ramp, featuring phases of acceleration and deceleration. This shake protocol will prove to significantly promote mixing.

3. Experimental Results

Our experiments exlpain the influence of these two mixing effects: In the constant spinning mode (Fig. 2, A&B), chaotic advection is stimulated by the Stokes drag of the periodically deflected beads. However, the presence of the beads is locally confined (to the right hand side of the chamber). In the alternate spinning protocol (Fig. 2, C&D), a mere hydrodynamic advection arises from the inertia of the pure liquid and its friction at the chamber walls. Furthermore, the modification of the magnetic field experienced by the beads and their complex magneto-hydrodynamic coupling extends their trajectory, now covering a major fraction of the chamber.

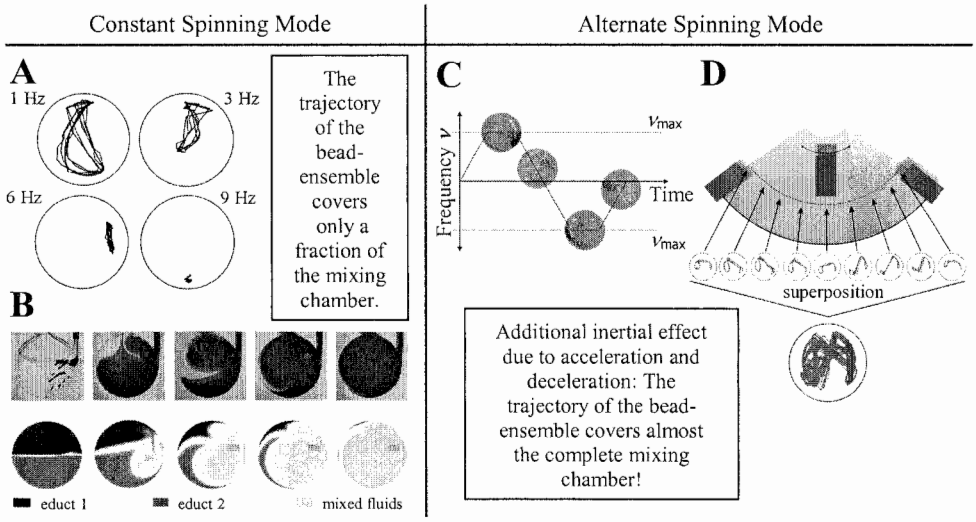

Figure 2. Comparison of mixing strategies: In constant spinning mode, the bead trajectories cover only a fraction of the chamber area (A). CFD-Simulations well agree with the experimentally observed mixing patterns (B). In alternate spinning mode, the sense of rotation is periodically modulated between $\pm\nu_{max}$ in clockwise and counter clockwise direction (C). Thus, the trajectory of the bead ensemble deviates from the constant spinning mode: The deviation roots, first, in a deviating temporal evolution of the magnetic field the beads experience on their orbit. Second, inertia originating from the rotational acceleration shifts both, the beads and the fluid, with respect to the chamber. This way, the trajectory of the bead ensemble covers a larger fraction of the mixing chamber (D) compared to constant spinning mode to homogenize mixing.

Our experiments document the performance of this magneto-hydrodynamic mixing concept (Fig. 3). For constant spinning mode without magnetic beads, the characteristic mixing time τ, i.e. the time span until the standard deviation σ of the captured grayscale distribution is leveled out to the $1/e$-value of its initial value, amounts to 7 min. Magneto-hydrodynamic mixing paired with alternating the sense of spinning extremely shortens the mixing process to less than one second!

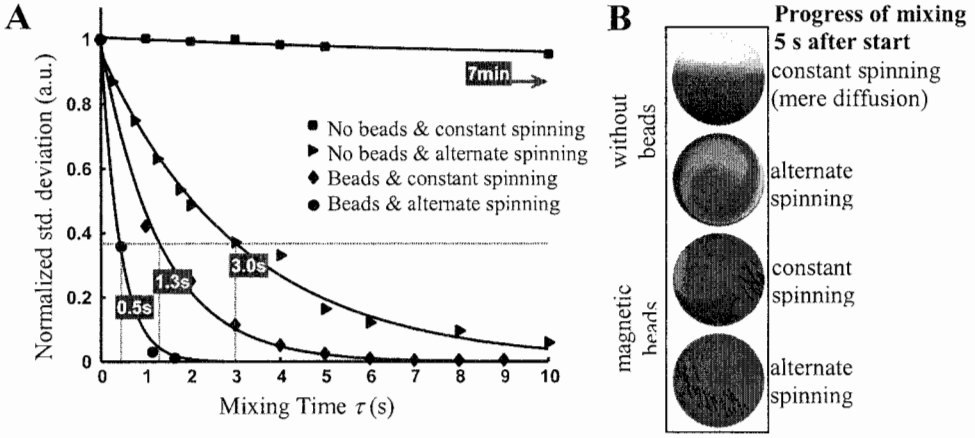

Figure 3. Performance of mixing concepts: Compared to mere diffusion with $\tau = 7$ min, bead-based magneto-hydrodynamic action in alternate spinning mode accelerates mixing by three orders of magnitude (A). This result is illustrated by the four images of the state of mixing, each captured 5 seconds after filling (B). While constant spinning without beads still displays poor mixing, bead-based mixing in alternate spinning mode is already completed.

5. Conclusions

We have presented a novel concept for mixing of liquids on centrifugal microfluidic platforms which is readily amenable for rotating lab-on-a-chip concepts. In our modular setup, the active parts are "macro", i.e. rugged and reusable, while the "micro"-parts are reduced to their functional essence, i.e. passive microfluidic structures. Batch-mode mixing is massively accelerated by the periodic deflection of magnetic beads as they follow an orbit through the static magnetic field. The mixing process is further enhanced by inertial effects on the beads and the fluid during shake-mode spinning. Overall, sub-second mixing for a 25 µl volume of educts has been achieved!

Acknowledgement

The authors are grateful to the support by the German federal state of Baden-Württemberg.

References

[1] A. Rida, T. Lehnert, and M. A. M. Gijs, Proceedings of µTAS conference, 2003, eds. M. A. Northrup, K. F. Jensen and D.J. Harrison, pp. 579 – 581 (2003).

[2] R. Rong, J. W. Choi, and C. H. Ahn, Proceedings of µTAS conference, 2003, eds. M. A. Northrup, K. F. Jensen and D.J. Harrison, pp. 335 – 338 (2003).

[3] T. Brenner, S. Häberle, R. Zengerle, and J. Ducrée, accepted for µTAS conference, 2004.

[4] Microparticles GmbH, Germany, www.microparticles.de (2003).

[5] M. Madou and G. Kellogg, Proceedings SPIE, vol. 3259, 1998, pp. 80-93 (1998).

ANALYTICAL MODELS FOR COMPLEX ELECTROKINETIC PASSIVE MICROMIXERS

Yi Wang[1], Qiao Lin[1] and Tamal Mukherjee[2]
[1]Dept. of Mechanical Engineering and [2]Dept. of Electrical & Computer Engineering, Carnegie Mellon University, 5000 Forbes Ave., Pittsburgh, PA 15213, U.S.A.

Abstract

This paper presents composable and parameterized electrokinetic passive mixing models that are the first to simultaneously simulate both electric and concentration (partial mixing) networks at the system level and enable the design of efficient and compact mixers for integrated Micro-TAS. Model validity is verified by comparison to numerical data.

Keywords: composable system simulation, parameterized model, micromixer

1. Introduction

Micromixers are important components in Micro-TAS. Efficient mixing reduces analysis time, minimizes chip-area and improves process control. Currently, a majority of Micro-TAS use passive mixers that rely on molecular diffusion. In addition to their relatively simple fabrication processes, electrokinetic passive mixers are amenable to integration with electrophoretic analysis and can be easily controlled [1]. However, their efficient simulation and design continues to be a challenge and has not been extensively studied. Simplified equations [2] have been used to provide mixing length estimates that are often overly conservative, and modeling methods based on electric analogy assume complete mixing and may lead to extremely long channels [1]. In practice, however, complete mixing is often not necessary. In a microreactor, for example, after incoming reactants achieve a certain degree of premixing, product yield becomes reaction-limited. Attempts to further enhance mixing would not appreciably improve the yield, but lead to unnecessarily large chip-size and long mixing time. This paper presents analytical models to accurately capture electric current, flow ratio and concentration within the complex electrokinetic passive mixer and investigate the dependence of the mixing degree on system parameters, which can eventually speed up the design of efficient and geometrically compact mixers for integrated Micro-TAS.

2. Analytical Mixer Models

Consider a general mixing unit consisting of elemental combiners, splitters and mixing channels (length L and width w) in Figure 1*a* [3]. An applied electric field E causes the buffer and species to move. Due to transversely uniform electrokinetic flow velocity, the concentration variation is independent of the depth-wise coordinate. In the combiner, arbitrary (rather than constant [3]) species concentrations from upstream channels are merged (Figure 1*b*). Its output concentration is found to be $c_{out}=a_0 s+b_0(1-s)+\sum d_n\cos(n\pi\eta)$ for $n=1,2,3\ldots$, with d_n given by:

$$\begin{aligned} d_{n\neq 0} = \sum_{m=0}^{m\neq ns} \Big\{ & 2(-1)^n b_m (1-s)\big(\cos(F_2/2)\sin(F_1/2)/F_1 + \cos(F_1/2)\sin(F_2/2)/F_2\big) \\ & + a_m s\big(f_1\sin(f_2)+f_2\sin(f_1)\big)/f_1 f_2 \Big\} + \sum_{m=0}^{m=ns}\Big(a_m s + b_m(-1)^m(1-s)\Big) \end{aligned} \tag{1}$$

where $\eta=y/w$ is the normalized coordinate along channel width; a_m and b_m ($m=0,1,2\ldots$) are Fourier coefficients for concentrations from the input streams; $s=I_1/(I_1+I_2)$ gives the interface position between the streams (I_1 and I_2 are currents through the streams); $f_1=(m-ns)\pi$, $f_2=(m+ns)\pi$, $F_1=(m+n-ns)\pi$ and $F_2=(m-n+ns)\pi$. The Fourier coefficients h_n of the output concentration at the outlet of a mixing channel are given as

$$h_n = g_n e^{-\tau n^2\pi^2} \tag{2}$$

where g_n are the input coefficients at the channel inlet, which is transferred from outlet of the upstream element, and $\tau = LD/Uw^2$ (D and U are diffusivity and electrokinetic velocity of the species in the sample). For a splitter, the output coefficients are the same as the input ones, but the electric current is partitioned at a ratio depending on the downstream electric resistance.

3. Results and discussion

Results from analytical simulations of the mixer are shown in Figures 2-5. In Figure 2, analytical simulations of a cascade micromixer are compared with numerical data. Excellent agreement is found. We can see that at the combiner (com_3 in Figure 2*a*), two streams with different concentration profiles are merged. Their interface position is around s=0.6 (Figure 2*b*) determined by the currents through the streams. In Figure 3, electrokinetic focusing [4], which could be used to speed up mixing [5], is analytically simulated and compared to numerical data at two different focusing ratios γ (defined in Figure 3). A high γ can dramatically reduce the sample bandwidth supplied by the middle channel and accelerate the mixing. Figure 4 shows the analytical and numerical simulations of a multi-laminae (8 streams) electrokinetic mixer that also speeds up mixing by reducing widthwise diffusion distance [2]. It is found that at x=0.01L, mixing is achieved at 68% according to the mixing degree, $Q = 1 - 2\int_0^1 |c(\eta) - c_{avg}| d\eta$ (c_{avg} is the width-averaged concentration). Over 0.3L<x<L (70% of the channel length), Q is only enhanced from 92% to 97%. This shows the usefulness of partial-mixing modelling in studying both mixer effectiveness and efficiency. Figure 5 shows the schematic of a split-and-recombine (SAR) mixer [6, 7] (Figure 1*a*) represented and simulated by our models (Figure 5*a*). Different from multi-laminae mixer in Figure 4, the SAR mixer performs multi-lamination within the mixer. The concentration distributions along η at the first four SAR units are illustrated in Figure 5*b* and multiple splitting of the species layers is clearly observed, which contributes to a tremendous improvement in Q compared with a T mixer of the same length (Figure 5*c*). We can also see that the increase in Q is rapid through the first few SAR units and then becomes saturated as species homogeneity improves. Thus, a tradeoff exists between Q and mixer size, mixing time and system complexity.

4. Conclusions

Analytical models have been presented for efficient simulations of complex electrokinetic passive micromixers. The models have been verified by numerical simulation data, and are able to accurately capture the combined effects of mixer geometry, buffer-species properties and system-operation parameters on mixing efficiency.

Acknowledgements

This research is sponsored by DARPA and Air Force Research Laboratory, Air Force Material Command, USAF, under grant number F30602-01-2-0587, and the NSF ITR program under award number CCR-0325344.

References

[1] Jacobson, S. C.; McKnight, T. E.; Ramsey, J. M., *Anal. Chem.*, **71**, 4455-4459, (1999)

[2] Koch, M.; Chatelain, D.; Evans, A. G. R.; Brunnschweiler, A., *J. Micromech. Microeng.*, **8**, 123-126, (1998)

[3] Branebjerg, J.; Gravesen, P.; Krog, J. P.; Nielsen, C. R. *Proc. MEMS'96*, 441-446, 1996.

[4] Jacobson, S. C.; Ramsey, J. M., *Anal. Chem.*, **69**, 3212-3217, (1997)

[5] Knight, J. B.; Vishwanath, A.; Brody, J. P.; Austin, R. H., *Physical Review Letters*, **80**, 3863-3866, (1998)

[6] Schwesinger, N.; Frank, T.; Wurmus, H., *J. Micromech. and Microeng.*, **6**, 99-102, (1996)

[7] Schonfeld, F.; Hessel, V.; Hofmann, C., *Lab on a Chip*, **4**, 65-69, (2004)

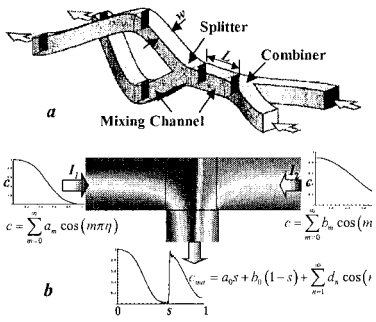

Figure 1. Geometry of the elements in a general mixer **[3]** (*a*) and modelling principle of the combiner (*b*).

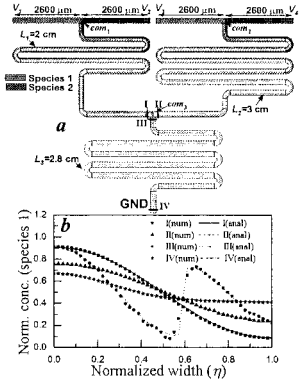

Figure 2. Concentration comparison of numerical data (*a*) with simulation using analytical model (*b*) (on species 1) at different positions (I, II, III and IV). w=200 μm, D=2×10^{-11} m^2/s, mobility μ=2×10^{-8} m^2/(Vs), V_1=V_2=V_3=V_4=800 V.

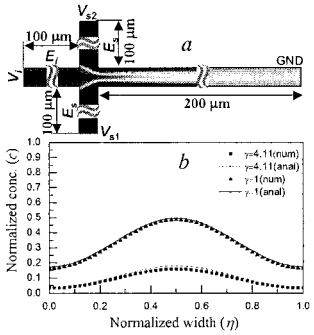

Figure 3. Concentration comparison of numerical data (*a*) with simulation using analytical model (*b*). D=1×10^{-10} m^2/s, μ=6×10^{-8} m^2/(Vs), w=10 μm, V_i=25 V. Focusing ratio γ=E_s/E_i. For γ=4.11, V_{s1}=V_{s2}=29 V and for γ=1, V_{s1}=V_{s2}=25 V.

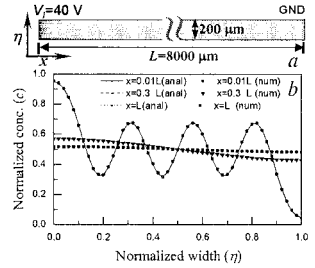

Figure 4. Concentration comparison of numerical data (*a*) with analytical results (*b*). D=1×10^{-10} m^2/s, μ=2×10^{-8} m^2/(Vs).

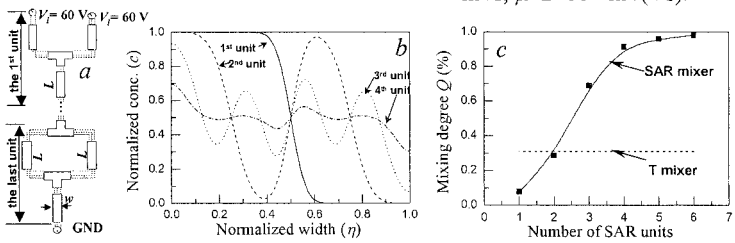

Figure 5. Analytical simulation results of SAR mixer. (*a*) composition of a SAR mixer. (*b*) concentration after the 1st, 2nd, 3rd and 4th SAR units. (*c*) The mixing degree Q after individual SAR unit, compared with T mixer. Properties are same to Figure 2, and L=800 μm, w=200 μm.

FLOW BEHAVIOR NEAR AN ADVANCING INTERFACE WITH SINGLE- AND TWO-COMPONENT LIQUIDS IN MICROCHANNEL

Naoki Ichikawa[1] and Ryutaro Maeda[1]

[1]Advanced Manufacturing Research Institute, National Institute of Advanced Industrial Sci. and Tech. (AIST), 1-2-1 Namiki, Tsukuba, Ibaraki, 305-8564, Japan

Abstract

This study specifically addresses flow behavior in a liquid near the gas-liquid interface of a capillary-driven flow. Movements of a 1 μm diameter tracer near the interface of a single-component liquid with ethanol and a two-component liquid with a mixture of ethanol and distilled water were observed in 98 μm × 63 μm polydimethylsiloxane (PDMS) microchannels. Velocity distribution for the single-component liquid shows a fountain-like flow under the reference frame on the interface position. It is very similar to the theoretically predicted flow. In stark contrast, distribution for two-component liquids shows a strong rolling motion near the interface. Marangoni flow caused by concentration and temperature difference is inferred to cause that motion.

Keywords: velocity distribution, water-ethanol, PDMS, capillary-driven flow, Marangoni flow

1. Introduction

Microfluidics has been widely developing for a variety of μ-TAS and μ-reactors applications. Because of the high surface to volumetric ratio in microfluids, gas-liquid two-phase fluid behavior near the interface is affected strongly by interface phenomena. Many microfluidic applications have several liquid components that are mixed for reaction or synthesis. In this case, surface tension depends not only on temperature, but also on concentration of these liquids. Flow is induced by the surface tension difference – so-called Marangoni flow. Although velocity distribution near the interface for a single-component liquid in a circular tube is investigated, not much work has been carried out for microchannels. Moreover, few studies have addressed Marangoni flow and flow fields in microchannels despite the practical importance of this phenomenon.

This study specifically addresses flow behavior in a liquid near the interface of a capillary-driven flow with a single- and two-component liquid.

2. Theoretical Results of Flow Distribution for Single Component Liquid

This section explains the theoretical velocity distribution near the interface in a circular tube. Flow is assumed to be laminar. The interface shape is constant as a plane perpendicular to the tube axis. Here, we address only the theoretical treatment for a circular tube because of the difficulty posed by a rectangular channel. However, velocity distribution on the plane of the central axis is considered to be almost identical to that of a rectangular channel.

The flow field near the interface in a circular tube with diameter D has been investigated theoretically [1,2]. Those studies introduced stream functions and solved them analytically under the assumption of a flat interface shape and laminar flow. The result is

$$\Psi(r,x)=\frac{Vr^2}{2}\cdot\left\{1-\left(\frac{2r}{D}\right)^2\right\}\cdot\left\{1-\exp\left(\frac{-2\sqrt{6}\cdot x}{D}\right)\right\}, \qquad (1)$$

where $\Psi(r,x)$ is the Navier-Stokes stream function, r is the radial position, x is the axial position relative to the interface position, and V is the interface velocity. Figure 1 shows the stream pattern near the advancing interface: it is a fountain-like flow. From Eq. (1), axial and radial velocity can be calculated at any points in the liquid, $u(r,x)$ and $v(r,x)$, respectively. The radial velocity ratio for

a single-component liquid has a maximum value of $\sqrt{2}/3 \sim 0.47$, implying that the radial velocity ratio in the liquid is slightly less than half the interface velocity.

We compared this theoretical prediction with experiments using a 1–2 mm inner diameter circular tube [3]. Photochromic dye activation method was applied. The surface velocity almost agreed with experimental results.

3. Experimental Setup and Procedure

The microchannel that we examined was made of polydimethylsiloxane (PDMS) that was shaped using photolithography and molding techniques. The typical channel size was 98 μm × 63 μm. A single-component liquid with ethanol and a two-component liquid with a mixture of ethanol (95%) and distilled water (5%) were used as test liquids. Both liquids contained 1-μm diameter tracer particles to help visualize the flow. Experiments were initiated by putting drops of liquid at the microchannel inlet. Then, measurements for interface motion and flow distribution were carried out.

4. Experimental Results

Velocity distribution for the single-component liquid shows a fountain-like flow under the reference frame on the interface position, as shown in Fig. 2. Variation of the velocity ratio of tracer movement along the interface to the bulk interface velocity, v/V, is calculated from the figure. The maximum of the absolute value of the ratio is about 0.3, which reasonably matches the predicted value of 0.47 for a circular tube.

In stark contrast, the tracer movement for two-component liquids shows a strong rolling motion near the interface, as shown in Fig. 3. Variation of the flow velocity ratio of each particle is plotted on Fig. 4. Peak values take an opposite sign because tracer #1; the others are on opposite sides of the center line. The absolute values of the ratio reach 10–20. These peaks correspond to periods of the tracer flowing near the interface.

The rolling motion is inferred to result from Marangoni flow. For a distilled water and ethanol mixture, ethanol easily volatilizes from a thin film near the contact line (Fig. 5). Thereby, distilled water is more abundant than the other meniscus region. In addition, the temperature of the region is decreased by ethanol evaporation. Therefore, surface tension at the edge region is higher than the central one; Marangoni flow caused by concentration and temperature difference forms. It flows from a central position to the channel wall.

This phenomenon may greatly aid the development of new microfluidic devices such as passive mixers in laminar microflow.

5. Conclusions

We observed flow distribution in a microchannel near the interface of capillary-driven flow. The flow behavior for the two-component liquid differs completely from that of the single-component liquid, which shows a fountain-like flow distribution, as theoretically predicted. Strong rolling flow can be observed in a two-component case. The flow velocity along the interface is as much as 10 times the interface velocity. Marangoni flow causes this rotational fluid flow; this phenomenon seems to offer a large capability for microfluidic applications.

References

[1] A. Karnis and S.G. Mason, *J. of Colloid and Interface Science*, **23**, 120–133 (1967).
[2] P.J. Sell, E. Maisch and J. Siekmann, *Acta Astronautica,* **11**, 577–583 (1984).
[3] N. Ichikawa, M. Kawaji, C. Lorencez and K. Takata, *Microgravity Sci. Tech.*, **7**, 156–159 (1994).

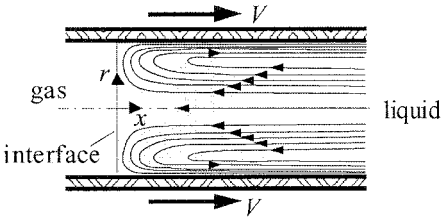

Figure 1. Analytical results of streamlines referenced on the interface of a single-component liquid in a circular tube.

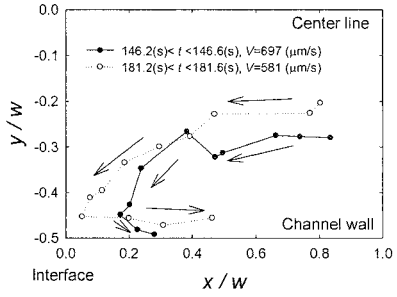

Figure 2. Tracer particle movement near the interface for the single-component liquid.

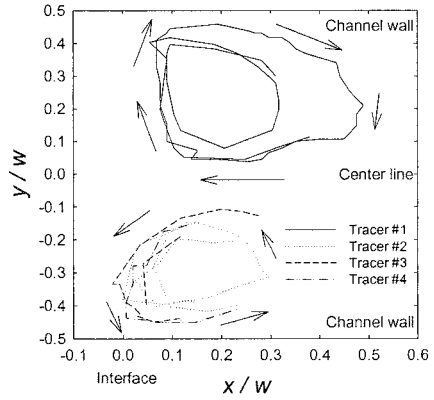

Figure 3. Variation of several tracer particle positions referenced on the interface of the two-component liquid in the microchannel. Interface velocity V=118 μm/s.

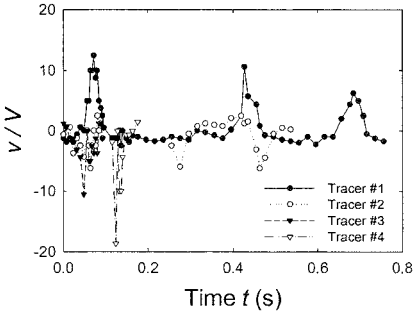

Figure 4. Variation of radial flow velocity ratio, v/V, of each tracer #1–#4 for the two-component liquid.

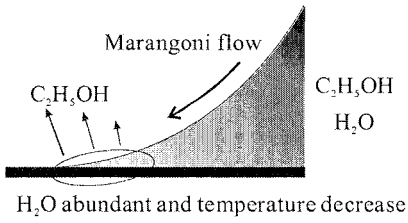

Figure 5. Marangoni flow caused by concentration and temperature dependency.

EFFECT OF MICROCHANNEL GEOMETRY ON CELL PROLIFERATION: EXPERIMENTS AND INTERPRETATION

Hongmei Yu*, Irina A. Shkel and Dave J. Beebe***

**Department of Biomedical Engineering, University of Wisconsin-Madison, Madison, WI 53706*

***Department of Chemistry, University of Wisconsin-Madison, Madison, WI 53706, US*

Abstract

The different physical characteristics of a microscale culture system influence cell behaviour. Insect cells (commonly used for protein production commercially) cultured in microfluidic channels grow more slowly than in traditional flask culture and the cell proliferation is influenced by the surface cell seeding density and microchannel geometry (channel height). In order to explore the potential factors influencing in proliferation of insect cells in microchannels, a kinetic mathematical model was applied to predict the experimental proliferation kinetics of Sf9 cells in microchannels with different geometry and seeding density. The model suggests inhibitory factors and insufficient growth factors mediate the inhibition of cell proliferation via the limited diffusion distances in the microchannels. The model will facilitate long term cell behaviour studies via the proper application of specific design of micro culture systems.

Keywords: Microfluidic channels, Insect cell culture, Kinetic modeling, Microchannel geometry

1. Introduction

Microfluidic techniques can provide a platform to access, control and study the cellular microenvironment and the interactions at the cellular scale. Unlike the governing forces in large-scale environments, such as inertial forces and electric-magnetic forces, other physical phenomena, such as laminar flow, diffusion and surface tension, become dominant in microchannels. These physical factors, diffusion, surface tension and shear stress are important for biological and physiological processes and the different properties at the microscale potentially influence these processes differently. Previous work has shown that embryos grow faster in microchannel cultures than in the traditional macrocultures while insect cells grow more slowly in microfluidic channels than in traditional flask culture[1]. Cell growth is influenced by a set of complex cues from molecules, other cells, and the extracellular matrix. The different physical environment present in microchannels can have important influences on the different observed cell behaviour between microculture and macroculture systems, the absence of convection leads to more stable molecular concentration gradients can be a candidate reason. Hence, the construct of the culture system, the response and feedback of each component inside of the system should be understood in order to guide future system designs aimed at answering particular biological questions. In order to explore the influences of primary physical properties of microculture system to the cells, Sf9 cell proliferation is examined in a variety of different geometry microchannels. The significant factors were analyzed and then modelled in order to explore the underlying mechanism of regulation of cell proliferation in microchannels. Our hypothesis is that specific inhibitory factors and insufficient growth factors mediate the inhibition of cell proliferation via diffusion.

2. Experiments and modeling

The influences of the geometric properties of microchannel environments on cell proliferation were examined by culturing Fall Armyworm Ovarian cells (Sf9) in PDMS microfluidic channels. A series of PDMS channels were fabricated using micromolding methods. Sf9 cells were homogeneously seeded in the microchannels. The proliferation of Sf9 cells in the PDMS microfluidic channels and in traditional polystyrene tissue culture flasks were compared. The geometric factors tested include the width, length and height of the microchannels. Cell proliferation was compared across a series of microchannels with incremental geometric factors [2]

The experimental growth curves (Figs.1A, B) were fitted using a kinetic model [3] (shown in the inset on Fig.1B). There are two model parameters: specific growth rate, μ, dependent on the concentration of nutrient and growth factors; the inhibition rate, $k_I N_0$, dependent on the concentration of inhibitory factors in the local cell environment.

3. Results and discussion

The experiments show that the proliferation rates of Sf9 cells in all of the microchannels were 30-35% lower than that in traditional flask culture over the first 24 hours of culture. Over the next 48 hours of culture the proliferation rates in the microchannels continuously decreased reaching and maintaining a level of 5% of that in flasks for up to 14 days. This growth inhibition was influenced by the seeding density and the channel height but not the channel length or width. The local concentrations of essential factors on the microchannel bottom are found from the solution of one-dimensional diffusion equation. The kinetic parameters correlate well with the local factor concentrations:

1). Growth rate is similar in channels and flask while inhibition rate is significantly larger in the channels. These results indicate: compared with the growth inhibition due to the nutrient limitation only in mass cultures, specific inhibitory factors contribute the growth inhibition of cells in microchannels with/without of nutrient limitation.
2). Growth and inhibition rates are smaller for microchannel cultures with larger surface densities, indicating nutrient depletion may occur more quickly before the specific growth and inhibition occur. The smaller parameters at lower surface density culture indicate that cell growth are controlled by the specific growth and inhibition factors and both are below threshold due to insufficient local growth factors. (Fig 2 A)
3). Growth and inhibition rate is inversely dependent on H, along with the predicted local concentrations of secreted growth and inhibitory factors, demonstrating that the geometric limited diffusion governs cell proliferation in microchannels (Fig 2 B).

Experimental and model results provide insight into mechanisms of cell proliferation kinetics in microenvironments. Because there is limited experimental data about long term cell culture in microchannels and the number of parameter (e.g. growth factors, nutrients, wastes) combinations is large, models are valuable to explore the relation of those physical and biological factors on cell behaviour and help guide the design of appropriate microscale culture systems.

References

[1] G. M. Walker, H. Zeringue and D. J. Beebe, *Lab on a Chip*, vol. 4, pp. 91-97, 2004.
[2] H.M. Yu, D. J. Beebe, 2003 BMES Annual Fall Meeting, Oct 2003.
[3] J.E. Bailey and D.F. Ollis, Biochemical engineering fundamentals, 1986.

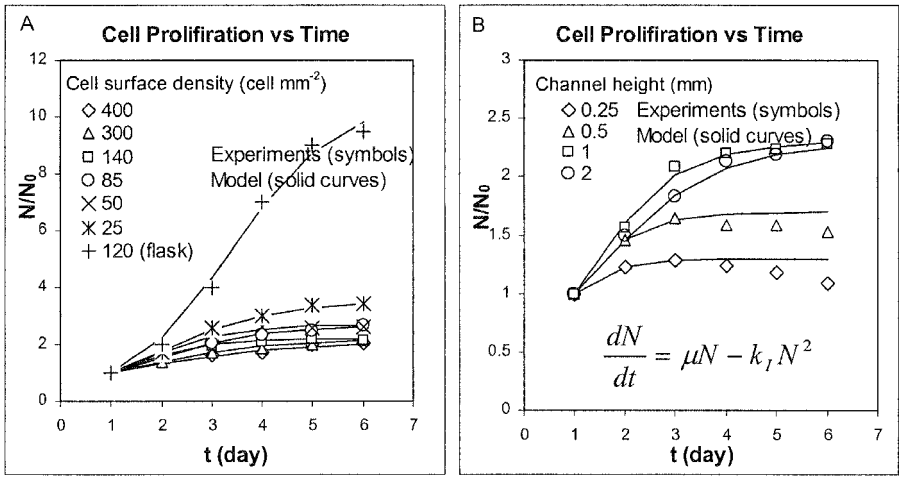

Figure 1. The cell populations (N) at different time points are normalized by N_0. Model kinetic equation is in Fig. 1B. The model results (solid curves) and the experimental results (symbols) are plot in the same plot. (A) The model results are in a good agreement with experimental data for different cell surface density in the microchannels and in flasks; (B) The model fits experimental results of cell proliferation at same surface density in the different microchannels (N_0=2400 cells). (The last 3 days of growth in the 0.25 mm and 0.5 mm high channels are not included the fit.)

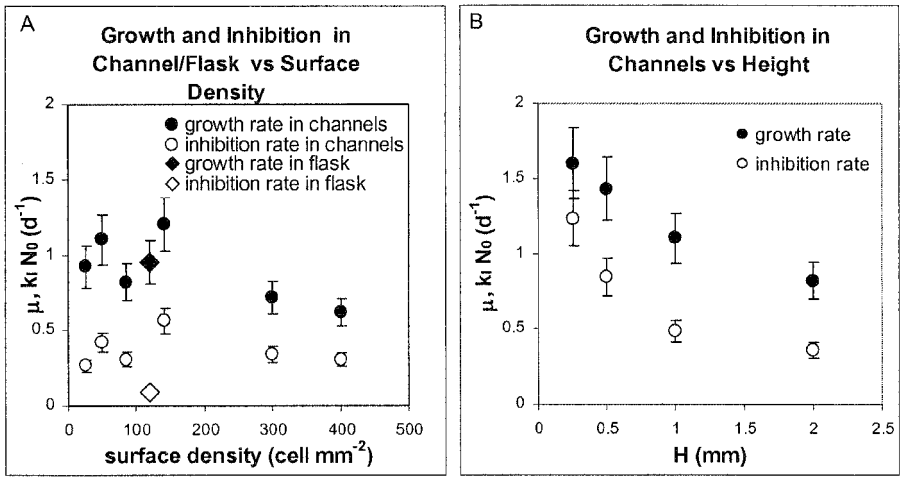

Figure 2. Growth and inhibition rates: (A) Both rates are dependent on the surface density of the cells. The smaller growth and inhibition rates at higher surface density are due to nutrient depletion, while at lower surface density the smaller rates are due to insufficient growth factors. (B) Both rates are inversely dependent on channel height. Errors are within 15%.

MICROPUMP FOR RECIRCULATION OF INSECT CELLS IN SUSPENSION

Javier Atencia, Hongmei Yu, David J Beebe
Department of Biomedical Engineering, University of Wisconsin- Madison, WI 53706, USA

Keywords: micropump, recirculation, cell culture.

1. Introduction

Microculture systems can provide new insights on cell and cell microenvironment interaction, hence providing a new tool for understanding basic cell biology [1]. An effective culture system should provide nutrients/factors the cells need, and remove wastes while exerting minimum damage to the cells. Traditional spinner/shaker cultures accomplish nutrient delivery to the cell suspension at the expense of generating shear stress which can reduce cell viability. A peristaltic pumping microdevice built in PDMS has been tried on *E. coli* with a survival rate 94% [2]. Animal cells are more sensitive to shear stress than bacteria and may require more gentle pumping methods. In this paper, we develop a micropump to provide recirculating flow for the culture of Fall armyworm ovarian cells (Sf9) (shear stress sensitive) in microchannels. The device and experimental set up are shown in Figs. 1 & 2.

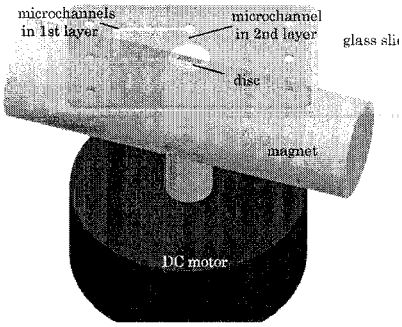

Figure 1. Mechanical model of the micro pump. The disk actuator is driven by an external DC motor through magnetic coupling,

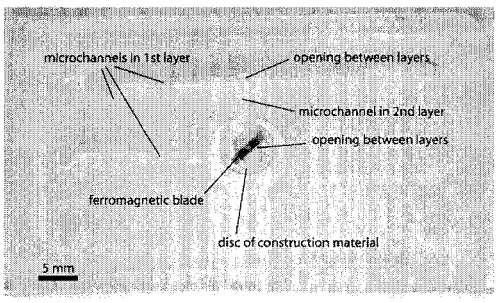

Figure 2. Rotary pump built in a two-layer microtectonics platform. The actuator consists of a ferromagnetic bar embedded in a polymer disc, placed in the first layer.

2. Principle of operation

The pump is a variation on a traditional impeller pump where a disk is used in place of the impeller (a traditional impeller design was used for comparison). When the disk rotates, it transfers momentum to the layer of liquid in contact with it. This layer tends to rotate with the disc due to adhesion, and at the same time, tends to move away from the axis of rotation due to centrifugal force. The momentum is then transferred to the different layers of the liquid due to viscous drag, and produces a local non-pulsating flow. Fig. 3a shows the axial component of the flow patterns in a cylinder with a rotating disk inside, according to [3].

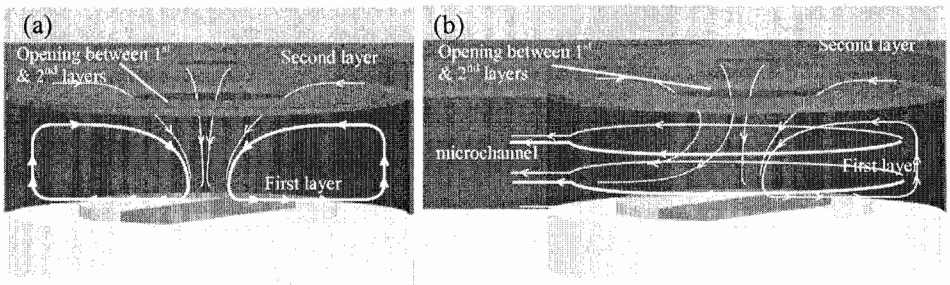

Figure 3. Diagram showing the path flows in (a) closed cylinder with only an opening at the top (b) cylinder with an opening at the top and another one in the left part (micropump). A non-pulsating net flow is created due to viscous drag, between layers of the fluid and adhesion to the surface of the rotating disk.

4. Results and discussion

The flow rate vs. rotational frequency for both pump designs (disk, impeller) was measured via visualization of a dye moving through the channel (Fig. 4). A cell recirculation experiment was conducted in order to visualize the effects of the shear stress of the pump rotating at 10 Hz. After 23 minutes of recirculation, no lysed cells were found by Typan Blue staining. At 50 Hz, pieces of some cell lysis were observed. Cell lysis occurred at all speeds in the impeller pump design.

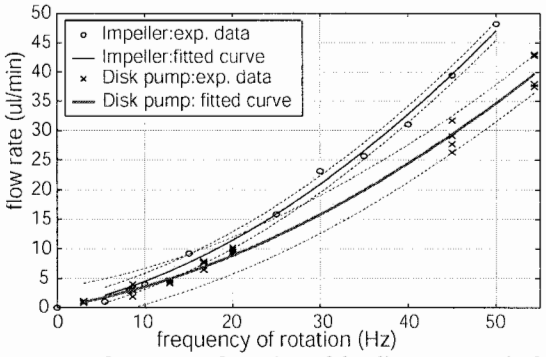

Figure 4. Flow rate versus frequency of rotation of the disc pump and of an impeller pump

Fig. 5 shows two models for calculating the maximum shear stress produced (a) in the disk type micropump, and (b) in an agitated vessel with an impeller used in macro scale culture systems. Kunas & Papotsakis reported the use of an impeller at 600 rpm with an in a closed bioreactor without major cell damage[4]. According to the model in Fig. 5 (b), the maximum shear stress is 6 dynes/cm^2, very similar to the one calculated for the disk micropump at 10 Hz (5.6 dynes/cm^2), in Fig. 5a. The cells are only exposed to the rotating disk for a small percentage of each cycle through the system. Table 1 summarizes the results.

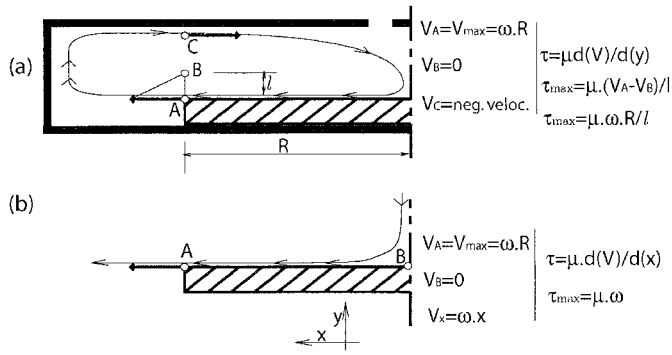

Figure 5. Velocity 'V'and max. shear stress 'τmax' in (a) μpump (b) impeller in a big flask. In case (a) assuming that l=d/2= 0.275 mm/2, with a frequency of rotation f=10 Hz, then τmax =5.6 dynes/cm2. In case (b) the maximum gradient of V is in the x direction, which means that τmax is only function of the frequency of rotation.

Table 1. Comparison between pumping methods for insect cells culture

	Type of flow	Calc. Shear Stress at 10 Hz	Lysed cells at 10 hz	Lysed cells at 50 hz
Disk	Non-pulsating	5.6 dynes/cm^2	None observed	Medium
Impeller	pulsating	NA	High	High
Closed flask w/agitation	pulsating	6 dynes/cm^2	Minimal	NA

5. Conclusions

We have demonstrated the operation of a mechanical micropump that is capable of recirculating insect cells in a loop without damage to the cells. The shear stress can be further reduced by decreasing the frequency of rotation of the pump.

Acknowledgements

Special thanks to Tom Pierce for his valuable help. J. Atencia also thanks the "Ministerio de Educacion, Deporte y Cultura" of Spain for financial support.

References

[1] G. M. Walker, H. Zeringue and D. J. Beebe, *Lab on chip*, 2004, 4, 91-97.
[2] M. A. Unger, H.-P. Chou, T. Thorsen, A. Scherer and S. R. Quake, *Science*, 2000, 288, 113.
[3] A. Spohn, M. Mory and E. J. Hopfinger, *J Fluid Mech*, 1998, 370, 73-99.
[4] K. T. Kunas and E. T. Papoutsakis, *J Biotechnol*, 1990, 15, 57-69.

INTEGRATED AND RECONFIGURABLE VALVES AND PUMPS USING BRAILLE DISPLAYS

Wei Gu[1], Xiaoyue Zhu[1], Nobuyuki Futai[1], Brenda S. Cho[1] and Shuichi Takayama[1,*]

[1]Dept. of Biomedical Engineering, University of Michigan, 2100 Gerstacker, 2200 Bonisteel, Ann Arbor, MI, USA, 48103

**To whom correspondence should be addressed. Email: takayama@umich.edu*

Abstract

Numerous on-chip valves and peristaltic pumps can be driven by a grid of vertically translating pins to create complex, programmable flow. We characterized valving and pumping using this scheme, and demonstrated software-driven movement of segmented flow.

Keywords: valve, pump, mixer, segmented, plug flow

1. Introduction

Multiple pumps and valves are often required for multi-functional, integrated lab-on-a-chip devices. Several integrated pump and valve methods have been developed in the past, including electrokinetic control [1], pneumatic control [2], or pressure-driven flow regulated by various kinds of valves [3]. However, previous fluidic control schemes have limitations in flexibility and quantity, or in ease of use, often requiring uncommon external machinery and interconnections. This paper demonstrates using a grid of 320 mechanical actuator pins to pump, valve, and mix fluids inside elastomeric channels. These pins act synchronously to induce localized channel deformations in the soft material poly(dimethylsiloxane) PDMS (Figure 1). Refreshable Braille displays, which are tactile computer screens for the visually impaired, controls the pins. Typical Braille displays are walkman size to textbook size, and contain pre-existing software for specific pin actuation control. By adapting these commercial devices for microfluidics, complex fluidic control can be automated with convenience.

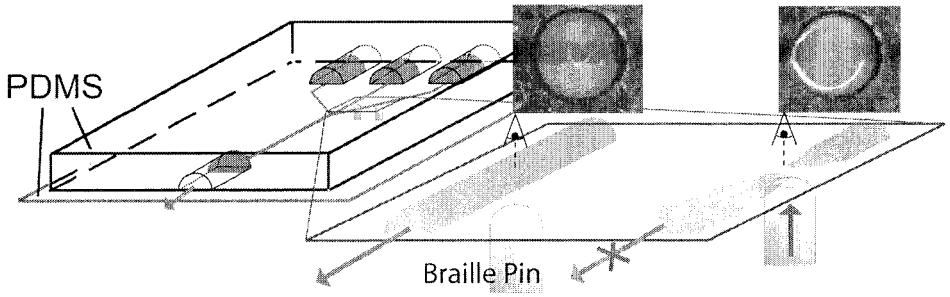

Figure 1. A representation of Braille Display actuations. Braille Displays hold a grid of ~1 mm diameter pins that can protrude vertically out and exert a mechanical spring force up to 20 cN. By placing PDMS-enclosed, rounded channels close to the bottom surface of a microfluidic chip, an upward translation by a Braille pin can fully valve shut the channel directly above it.

2. Experimental

Channels are fabricated with polydimethylsiloxane (PDMS) using typical soft lithography molding techniques and enclosed by a spin-coated (200 rpm, 4 min) 150μm thick sheet of PDMS through oxygen plasma oxidation sealing (30 sec, 40 Watts). This allows channels to be located

close to the Braille display surface so that they can be deformed by protruding pins. Holes are punched prior to sealing or molded directly into PDMS.

Braille pins were controlled by a refreshable Braille Display in conjunction with either a text editor that can auto-scroll or through an auxiliary program in Visual Basic. Commercial screen reading software (HAL, Dolphin Computer Access, UK) interprets displayed computer text and displays corresponding Braille pin patterns (Fig. 2). Auto-scrolling through text could function as a predetermined program, and any program able to refresh a line of text is sufficient for controlling raised pin patterns.

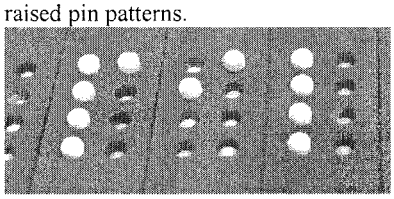

Figure 2. Selectively raised pins on the surface of a Braille Display showing an 'M'. Each Braille cell of 2 x 8 pins corresponds to a character on a computer screen. Here, the Braille display is reading "PiL".

3. Results and discussion

As shown in Figure 1, Braille pins are situated directly underneath channel positions so that actuated, raised pins will fully valve shut a rounded channel by deforming PDMS. Figure 3 shows the reproducibility of these valves when switching fluid flow between different channels. Three sequential pins actuated in specific sequences will pump fluids. Figure 4 shows the calibration curves of 3 different peristaltic pump sequences.

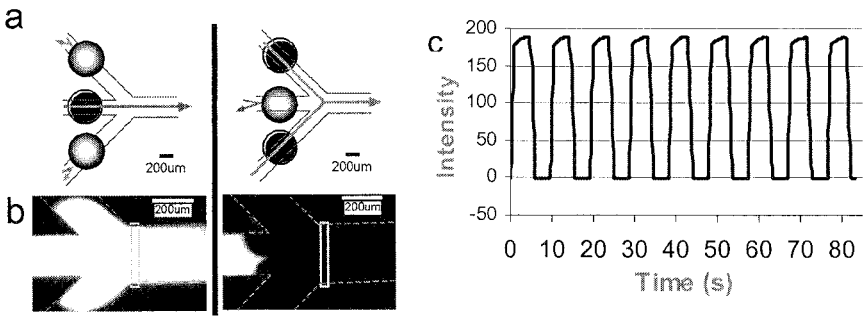

Figure 3. Valving efficiency using Braille pins on PDMS. Fluid flow switches between (a) the middle channel and (b) the two side channels when driven by a syringe pump. (c) Characterization of valving over time by monitoring the intensity at the immediate output (boxed in (a,b)).

To exemplify the versatility of multiple pumps and valves, we generated segmented flow using two aqueous food color dyes and perfluorodecalin (immiscible to dyes) inputs in a 3-inlet, 1-outlet channel design. Three valves for each input channel and one peristaltic pump located downstream were sufficient for programmed selection of fluidic input. Shown in Figure 5 (top), a unidirectional pump would normally result in cross-contamination due to the proximity of inputs at the channel intersection. However, by adding an algorithm to draw out and reverse perfluorodecalin into an unused input, such contamination can be eliminated (Figure 5 bottom). It is also straightforward to mix together adjunct plugs of dye by active oscillation of plugs (right-most plug in Figure 5 bottom).

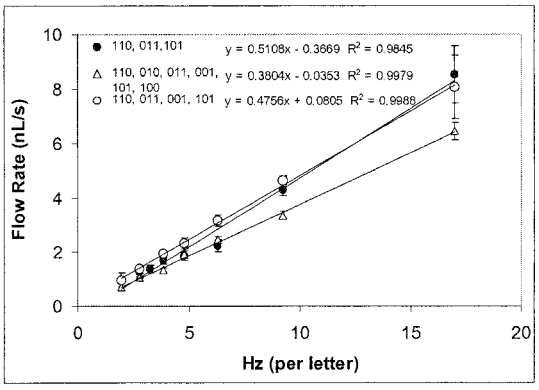

Figure 4. Calibration of the peristaltic pump to the actuation rate through monitoring of the interface between the two immiscible liquids perfluorodecalin and water diluted green food dye. The pump pattern was either (101, 100, 110, 010, 011), (001, 110, 011, 101), or (110, 011, 001, 101), where 1 was a valved position and 0 was an open position. Slight differences in speed and stability were found using different patterns. The maximum speed found was ~ 6-9 nL/s.

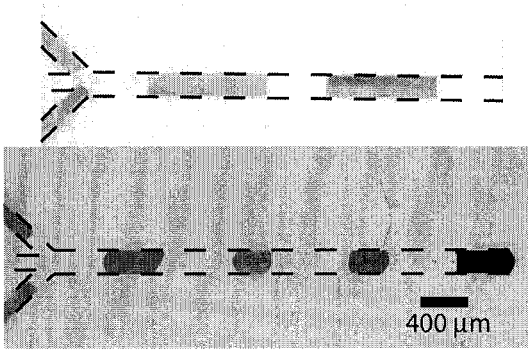

Figure 5. Segmented flow driven solely by Braille displays. Inputs from top to bottom are red dye, perfluorodecalin, and green dye. (Top) Plugs of dye that are cross contaminated by other input channels due to their proximity. (Bottom) By including steps to reverse perfluorodecalin into input channels, no cross-contamination occurs. The plug on the right is a mixed combination of two consecutive dye plugs.

4. Conclusions

Actuators, pumps, valves, and mixers derived from Braille displays are easily integrated components in a format that is simple, accessible, portable, and well packaged, yet versatile, and computer programmable, making it ideal for personalized use.

Acknowledgements

We thank Prof. Mark Burns for use of cleanroom facilities. This material is based upon work supported by the U.S. Army Research Laboratory and the U.S. Army Research Office under contract/grant number DAAD19-03-1-0168, National Science Foundation (BES-0238625), and NASA BioScience and Engineering Institute (NBEI).

References

[1] D. J. Harrison, K. Fluri, K. Seiler, Z. Fan, C. S. Effenhauser, A. Manz, Science, **261,** 895-7 (1993).

[2] M. A. Unger, H. P. Chou, T. Thorsen, A. Scherer, S. R. Quake, Science, **288,** 113-6 (2000).

[3] B. Zhao, J. S. Moore, D. J. Beebe Science, **291,** 1023-6 (2001).

ANALYSIS OF A SURFACE-MICROMACHINED PERISTALTIC PUMP

Qiao Lin[1], Bozhi Yang[1], Jun Xie[2] and Yu-Chong Tai[2]
[1]*Dept. of Mechanical Engineering, Carnegie Mellon University, Pittsburgh, PA 15213*
[2]*Dept. of Electrical Engineering, MC 136-93, California Inst. of Tech., Pasadena, CA 91125*

Abstract

This paper presents a lumped-parameter dynamic model for peristaltic micropumps, which accurately represents the interactions of fluid flow and actuator motion inside and between individual pumping chambers. The model correctly reveals the trend in experimental data, and can be used to efficiently evaluate frequency-dependent characteristics of pump operations.

Keywords: peristaltic pump, electrostatic actuation, dynamics, lumped-parameter model

1. Introduction

While mechanical micropumps have been simulated extensively [1, 2], peristaltic micropumps have not been adequately analyzed [3], especially dynamically. Here we present a dynamic model of surface-micromachined peristaltic pumps featuring three identical pumping chambers connected in series (Fig. 1) [4]. Each pumping chamber consists of an actuator below a fluid chamber. The actuator is equipped with a fixed ground electrode and a moving electrode embedded in a flexible Parylene membrane. The fluid chamber is bounded by the membrane and the ceiling of the pumping chamber. Fluid pumping is achieved by (electrostatically generated) peristaltic motion of the membranes. To study the dynamics of peristaltic pumping, membrane vibrations in each pumping chamber are first represented by an effective spring subjected to hydrodynamic and electrostatic forces. These chamber models are then used to construct a system-level model for the entire pump, which accounts for the dynamic coupling of the individual chambers as well as the inlet and outlet channels that connect the pump with fluid reservoirs.

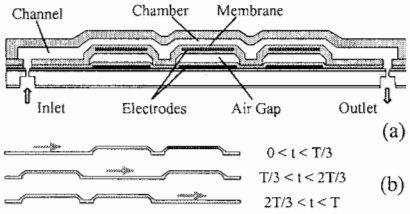

Fig. 1. (a) Schematic of the peristaltic pump. (b) Actuation in a period T.

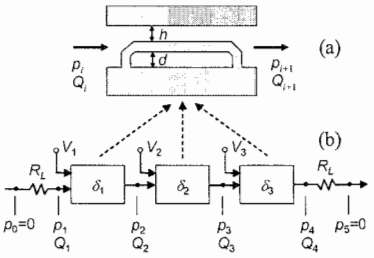

Fig. 2. Model for (a) a single pumping chamber, and (b) the peristaltic pump.

2. Peristaltic Pump Model

A pumping chamber i (Fig. 2a) is modeled as a thin fluid film sandwiched between a stationary rigid plate (the chamber ceiling) and a flexible membrane electrostatically actuated by a voltage $V_i(t)$. Initially (i.e. when $V_i = 0$), the fluid film thickness is h and the electrode gap separation d. The membrane is approximated by a quasistatically moving rigid plate attached to a linear spring. The spring constant is $K = (16.43/\alpha)\sigma t_m$, which, when used to compute the static pull-in voltage V_p, agrees with existing correlations for flexible membranes [5]. Here, $\alpha = 1 + 2(1-\cosh\kappa)/(\kappa\sinh\kappa)$ and $\kappa = 0.825(r/t_m)[12(1-\nu^2)\sigma/E]^{1/2}$ [5]; σ (20 MPa), E (3.2 GPa) and ν (0.4) are Parylene's residual stress, Young's modulus and Poisson's ratio; and r (100 μm) and t_m (2 μm) are the membrane radius and thickness. The membrane deflection, δ_i, is governed by $K\delta_i = F_i^h + F_i^e$ where

$F_i^e = \frac{1}{2}\varepsilon_0 V_i^2 A/(d + t_p/\varepsilon_p - \delta_i)^2$, ε_0 is the free-space permittivity, $A = \pi r^2$, and t_p (2 μm) and ε_p (3.1) are the thickness and dielectric constant of the Parylene insulation layers between the electrodes.

To compute the hydrodynamic force F_i^h, the Reynolds equation [6] is used to describe the dynamics of the fluid film. Then, $F_i^h = -[2.611\mu A^2/(h+\delta_i)^3]\dot{\delta} + \frac{1}{2}(p_i + p_{i+1})A$, where μ is the liquid viscosity (1.2 mPa·s for ethanol). In addition, the pressures (p_i and p_{i+1}) and flow rates (Q_i and Q_{i+1}) at the chamber entrance and exit (Fig. 2a) are related by $Q_{i,i+1} = \pm\frac{1}{2}\dot{\delta}_i A + [0.6175(h+\delta_i)^3/12\mu](p_i - p_{i+1})$ and $Q_i - Q_{i+1} = A\dot{\delta}_i$. With each chamber modeled by these equations, the pump can be represented as a system (Fig. 2b) consisting of the three chambers and the inlet and outlet channels each having flow resistance (pumping load) $R_L = 12\mu L/WH^3$ (L, W, and H are the channel length, width and height). Taking $p_0 = p_5 = 0$ (Fig. 2b) leads to $-p_1 = R_L Q_1$ and $p_4 = R_L Q_4$, which complete a dynamic model for the peristaltic pump.

3. Results and discussion

The dynamic model is applied to a peristaltic micropump that was tested with $V_i = V(t-(i-1)T/3)$ (i=1,2,3) where $V(t) = V_{max} = 140$ V if $0 < t < T/3$, and $V(t) = 0$ if $T/3 < t < T$ ($T = 1/f$ and f is the frequency) [4]. Based on the pump design and considering fabrication inaccuracies, h = 0.9 μm and d = 2 μm are estimated for the pump. The pumping load is estimated to be R_{L0} = 0.407 kPa/(nl/min). The time-averaged flow rate Q and pumping pressure p_4-p_1 (Fig. 3) are then computed from the model (Fig. 3). Q initially increases with f (as a result of increasing membrane vibration speed), reaching a maximum (1.66 nl/min) at an optimal frequency f_{opt} = 20.3 Hz, and then steadily decreases as f further increases (as a result of diminished membrane vibration amplitude). The pumping pressure exhibits a similar behavior, reaching a maximum (1.35 kPa) also at 20.3 Hz. This prediction compares favorably with the experimental data (1.7 nl/min at 20 Hz) [4]. Note that as the voltage amplitude V_{max} exceeds the static pull-in voltage V_p (126 V in this case) [5], the membranes vibrate beyond the static critical displacement $(d+t_p/\varepsilon_p)/3$. The vibration is adequately described by the model provided f is sufficiently high ($> f_c$) to prevent membrane touchdown on the fixed electrode. Electrostatic instability occurs and the model ceases to be valid if $f < f_c$ (f_c = 9.2 Hz in Fig. 3).

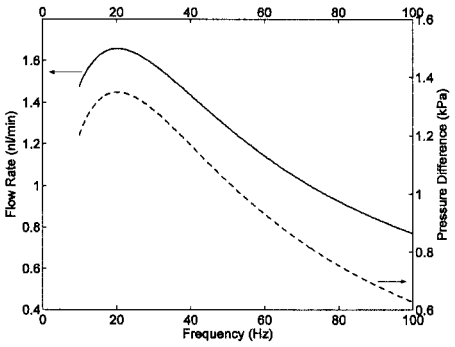

Fig. 3. The average pumping flow rate (Q) and pumping pressure p_1-p_4 for a tested pump.

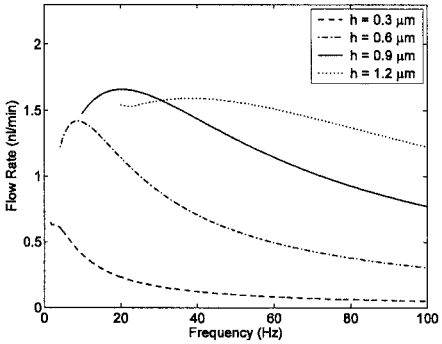

Fig. 4. Effect of the chamber height (h) on frequency (f) dependence of flow rate (Q).

Now h, d and R_L will be varied one at a time to investigate how these parameters influence the pump's frequency response. The

effect of the initial chamber height h is first considered (Fig. 4). As h increases, the optimal frequency (f_{opt}) steadily increases as a result of decreased damping on membrane vibrations. The maximum flow rate initially increases, and then decreases with h. This is due to the competing effects of increased damping on membrane vibrations and reduced backward flow, both resulting from the decrease in h. The effect of the initial electrode separation d is next studied (Fig. 5). The maximum flow rate decreases with d, as larger electrode separation with V_{max} = 140 V unchanged gives a smaller actuation force. As d decreases from 2 to 1.8 μm, the pull-in voltage $V_p < V_{max}$ further decreases, leading to a larger electrostatic instability bandwidth f_c. For d = 2.2 and 2.5 μm, $V_p > V_{max}$ and pump operations are always stable. Also, the calculated f_{opt} (obtained for d = 2, 2.2 and 2.5 μm) is not significantly influenced by d, as d only slightly affects the attenuation of membrane vibrations. Finally, consider the effect of pumping load R_L (Fig. 6). The maximum flow rate increases steadily with decreasing R_L as expected. This also causes a larger electrostatic instability bandwidth f_c. For $R_L = 0$, f_c is maximal (31.5 Hz), and f_{opt} cannot be computed from the model. For the other R_L values, the calculated f_{opt} decreases moderately with R_L as a result of increased damping on membrane vibrations.

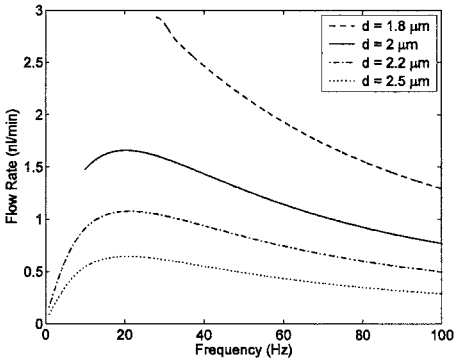

Fig. 5. Effect of the electrode gap (d) on frequency (f) dependence of flow rate (Q).

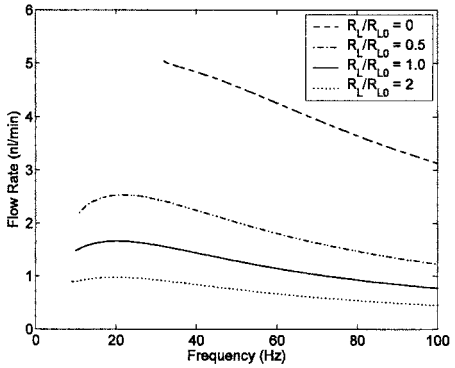

Fig. 6. Effect of the pumping load (R_L) on frequency (f) dependence of flow rate (Q).

4. Conclusions

We presented a dynamic peristaltic-pump model that accurately represents the interactions of fluid flow and actuator motion inside and between individual pumping chambers. The model has correctly revealed the trend in experimental data, and been used to gain insight into the influence of chamber thickness, electrode separation and pumping load on the pump performance.

Acknowledgements

We wish to thank Mr. Yi Wang for his assistance. Financial support from NSF (CMU: CTS-0304568; Caltech: EEC-9402726) and NIH (Caltech: 5R01 RR06217-10) is appreciated.

References

[1] M. Carmona, S. Marco, J. Samitier, et al., *J. Micromech. & Microeng.*, 6: 128-130, 1996.
[2] R. Zengerle and M. Richter, *J. Micromech. & Microeng.*, 4: 192-204, 1994.
[3] X. M. Bu, T. Melvin, G. Ensell, et al., *J. Micromech. & Microeng.*, 13: 125-130, 2003.
[4] J. Xie, J. Shih and Y.-C. Tai, *Proc. Micro-TAS '03*, pp. 865-868, Squaw Valley, CA, 2003.
[5] P. M. Osterberg and S. D. Senturia, *J. Microelectromechanical Systems*, 6: 107-118, 1997.
[6] A. Cameron and C. M. M. Ettles, *Basic Lubrication Theory*, 3rd ed: Halsted Press, 1981.

NOVEL PARTICLE SEPARATION USING SPIRAL CHANNEL AND CENTRIFUGAL FORCE FOR PLASMA PREPARATION FROM WHOLE BLOOD

Ji Yoon Kang, Hansang Cho, Seung Min Kwak, Dae Sung Yoon and Tae Song Kim
BioMEMS Lab, Microsystem Research Centre, Korea Institute of Science and Technology
39-1 Hawolgok-Dong, Songbuk-Gu, Seoul, 136-791, South Korea

Abstract
A device for separating particles from fluid on CD was suggested and studied. Spiral channel displaces particles to the wall of microchannel and transports the solution to the outlet chamber simultaneously. Modeling and analysis of particle movement in liquid implied that the separation can be done within 2 minutes due to the shorter travel length than the conventional centrifuge system. 8 spiral channels were fabricated in 4" disk using PDMS and filtering particles was tested with 5μm bead solution. Rotating speed less than 1500 rpm pushed out the solution within 2 minutes and most of particles were separated, even though some of them were also found in fluid chamber due to the structure of branch at the end of channel. Consequently, this paper verified the feasibility of new separation device implemented in centrifugally pumped microfluidic system.
Keywords: centrifuge, particle separation, spiral channel, plasma separation

1. Introduction

This paper suggests a novel flow-through centrifuge device to filter particles, of which final goal is separating plasma from whole blood since most analysis of disease is performed on plasma or serum fraction of whole blood. The conventional centrifuge separates plasma for 30min at about 1200g force, but emergency requests that urgent analysis be finished in 10min including plasma separation [1]. The previous works for fast whole blood separation are categorized into 3 approaches: centrifugal separation based on axial spinning [2], ultrasonic separation of particles [1,3], and membrane separation [4]. However, all of them are not suitable for centrifugal pumping system like CD (compact disk) since it requires external ultrasonic power transmission and integrating membrane in CD platform is difficult. Hence the spiral separator illustrated in Fig. 1a is effective and can be easily fabricated in centrifugal system because it efficiently exploits the centrifugal force and laminar flow in microfluidic channel. Spiral channel in CD-like centrifugal pumping system quickly isolates particles because they travel shorter path of channel width than that of a conventional centrifuges in Fig.1b. Besides, the spiral channel separates the fluid continuously since it separates particles and transports the fluid simultaneously. At the outlet the branch at the end of channel assorts the filtered liquid and the particles. The motion of particle and liquid driven by centrifugal force was mathematically modeled, and the dimension of a spiral channel was

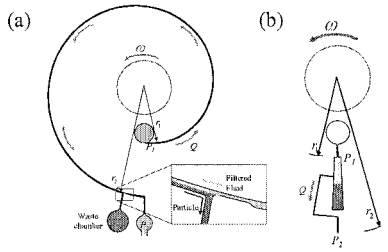

Figure 1. (a) A spiral particle separator in CD-like centrifugal system: Particles are separated by centrifugal force and fluid is pumped by pressure difference $\Delta P(=P_2-P_1)$ with flow rate Q. At the outlet, particles are isolated and flowed into waste chamber. (b) Conventional centrifugal system implemented in CD-like system: Since the length of particle path is much longer than the spiral channel, it takes long time to get the filtered fluid. After the centrifuge, the lateral valve must used to direct the fluid to next sequence (P_2).

determined through simulation analysis. The feasibility of centrifuge in microchannel was demonstrated by an experiment of separation of microbead solution.

2. Theory and analysis using simulation

Given initial radius (r_0) and rotational velocity (ω), the displacement (r) of particle in radial direction is described by the ordinary differential equation from the model in Fig. 2.

$$m\ddot{r} = mr\omega^2 - C_f\dot{r},$$

where friction coefficient $C_f = 6\pi\mu r_p$ and m is mass. The simulation of the above equation showed that the steady state velocity was reached after short transient period for the simple model of red blood cell, white blood cell and platelet. Parametric study for the displacement of particle with the variation of rotational velocity and initial radius showed that 20 seconds are enough to move the particles to the wall of 200μm wide channel. The final position after 20 second centrifuge was plotted in Fig.3, which describes that when r_0 is 10mm, ω is 1000rpm, total flowing time (=40sec) is longer than the time required for particles to be displaced to the wall of channel. The flow rate 9.8nl/s from simulation considering the pressure difference Δp and flow resistance η of centrifugal system[5] is enough for the application of separating plasma from whole blood.

3. Experiment

Spiral arc channels on PDMS sheet were fabricated on polished silicon wafer using SU-8 mold (Fig. 4a), and it was bonded to the polycarbonate disk using oxygen plasma (Fig. 4b), on which primer and 10μm thick PDMS film were spin-coated. Experimental setup in Fig. 5 consists of high speed synchronous imaging system and rotating stage whose maximum speed is 10,000 rpm. 8 channels on the disk are 180°arcs, which are 100μm, 200μm, 500μm and 1mm wide. At the end of channels, branches were placed to separate the portion of particle and fluid (Fig. 6) and it was connected to two chambers, namely fluid chamber for the left and particle chamber for the right. 5μm beads were suspended in de-ionized water, which was dyed to observe the movement of fluid. The microbead solution was injected into loading chamber using syringe and rotating speed was tuned to 500~1500 rpm for 1~2 minutes followed by rotating at 3000 rpm to clean out residual solution.

4. Results and discussion

Filtering microbead solution was tested by spiral channel to see how much particles are collected in fluid chamber. Fig.7(a) and (b) showed the residual particles in fluid chamber and particle chamber when the solution was separated by 100μm wide channel. The radius of spiral channel starts from 20mm and ended at 30 mm. The channel length was about 78mm and the pressure was expected to be 2.8kPa at 100 rpm. The experimental results showed the particle chamber collected much more beads than the fluid chamber; however about 20% particle was also gathered by fluid chamber. It resulted from the non-continuous fluid flow since the loading chamber did not supply constant fluid due the uneven filling in rectangular shape. Besides, when unexpected bubble blocked the way to one of chambers, all the solution flowed into only unblocked chamber. Hence if we design proper loading chamber and branch, it is expected that the stable flow will realize perfect separation of particles in near future.

Acknowledgements

This research was supported by Korea Institute of Science and Technology and by the Ministry of Information of Communication Republic of Korea, under the projects of "Development of Nano-detection device" and "Development of bioprocessor", respectively.

References

[1] Cousins et al, *Ultrasound in Med. & Biol.*, **26**, 881 (2000)
[2] Estey et al, *Clin. Chem.*, **42**, 409 (1996)
[3] Laurell et al, *PCT patent* WO 02/072234 A1 (2002)
[4] Nose et al, *Therapeutic Apheresis*, **4**, 3 (2000)
[5] Duffy et al, *Anal. Chem.*, **71**, 4669 (1999)

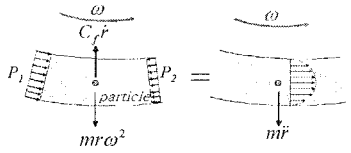

Figure 2. Free body diagram of particle for mathematical model: The net force of centrifugal force and friction force exert the particle to be accelerated in radial direction. The buoyancy force due to centrifugal pressure difference was neglected since it is too small to be considered.

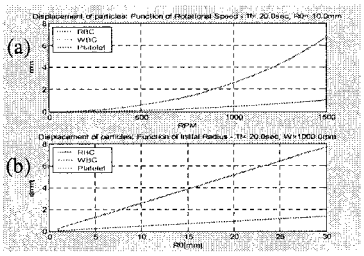

Figure 3. The length of particles' travelling path after 20 seconds' centrifuge as a function of rotational speed ω (a) and initial radius r_0 (b): (a) Rotational speed more than 500 rpm is enough to move all particles of whole blood in 200 μm wide channel. (b) Platelet was positioned about 500um with the initial radius of 10mm and the rotational speed of 1000 rpm.

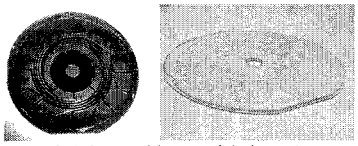

Figure 4. SU-8 mould was fabricated on polished silicon wafer (left). The height of channel was 100μm and 8 spiral channels were moulded using PDMS. It was bonded to polymer disk, which was spin-coated with PDMS film.

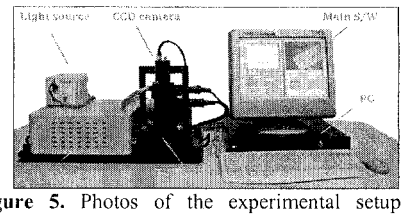

Figure 5. Photos of the experimental setup for centrifugal pumping system: It consists of a motion controller, a synchronous image capture system and a rotating stage, which is capable of maximum rotating speed of 10,000 rpm.

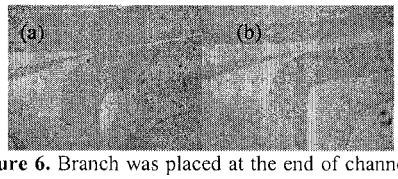

Figure 6. Branch was placed at the end of channel to separate the particles to lower chamber. It is shown as grey wedge and the bright area is microfluidic channel. 100μm and 500 μm wide channel are show in (a) and (b) respectively.

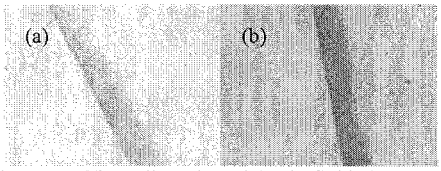

Figure 7. The collected particles in fluid chamber is shown in (a) and the particle chamber in (b). Although beads were found in fluid chamber, we can clearly see the difference of the number of particles between two chambers. Removing the bubble effect at branch, would achieve perfect filtering of particles.

ELECTROHYDRODYNAMIC STABILITY OF TWO-PHASE MICROFLOWS

Goran Goranović[1], Mads P. Sørensen[2], Morten Brøns[2] and Henrik Bruus[1]
[1]*MIC - Department of Micro and Nanotechnology,*
[2]*Department of Mathematics,*
Technical University of Denmark, DK-2800 Kongens Lyngby, Denmark

Abstract
We present a stability analysis of a microfluidic two-phase flow system showing that interface instabilities can be induced by remarkably small external voltages of order 1 V. Due to the small lengthscales in microfluidic systems, the instability voltages here are orders of magnitude smaller than in ordinary macrofluidic systems. The obtained stability criteria can be applied to microsystems having any pair of dielectric fluids of arbitrary viscosities, layer-thicknesses or dielectric constants.

Keywords: electrohydrodynamic stability, two-phase microflows

1. Introduction

Interface instabilities of two-phase flows have a big practical impact in many microfluidic applications. While electrokinetic pumps and devices for liquid-liquid extraction require operational stability, devices for mixing and dispensing would benefit from flow instabilities, particularly because of the lack of turbulence in the low-Reynolds-number regime.

In this paper we perform a linear stability analysis of the interface between two streaming dielectric (immiscible) fluids. The fluids are confined between two parallel plates separated by a microscopic distance (see Fig. 1). An example of such two-dimensional system is our two-liquid viscous pump outlined in Ref. [1].

We find that the interface is stabilized by tangential electric fields but destabilized by perpendicular electric fields. Also dominant viscosity forces can have a destabilizing role. In fact, viscosity stratification induces instability for arbitrarily small Reynolds numbers [2].

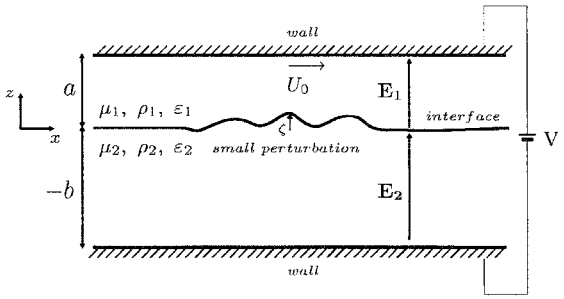

Figure 1: Schematic view of the interface between two liquid dielectrics perturbed by a perpendicular electric field inside a microchannel. U_0 is a slip (driving) velocity at the wall. Such a configuration can exist in the two-liquid viscous pump driven by electroosmotic flow [2].

2. Physical model

Our physical model includes the Navier-Stokes equation, the continuity equation and the Maxwell equations of electrostatics. In each of two fluids, $i = 1, 2$, we have

$$\rho^{(i)}\frac{D\mathbf{u}^{(i)}}{Dt} = -\nabla p^{(i)} + \mu^{(i)}\nabla^2\mathbf{u}^{(i)} + \rho^{(i)}g + \nabla\cdot T^M, \quad (1)$$

$$\nabla\cdot\mathbf{u}^{(i)} = 0, \quad (2)$$

$$\nabla\cdot(\varepsilon^{(i)}\mathbf{E}^{(i)}) = 0, \quad (3)$$

$$\nabla\times\mathbf{E}^{(i)} = 0, \quad (4)$$

where ρ is density, p pressure, μ viscosity, $\varepsilon = \varepsilon_r\varepsilon_0$ permittivity, $\mathbf{u}(x,y,z) = (u,v,w)$ velocity field, $\mathbf{E}$ electric field, and T^M the Maxwell stress tensor

$$T_{ik}^M = -\frac{\varepsilon}{2}E^2 n_i + E_i D_k n_k. \quad (5)$$

The Maxwell stress tensor conveniently describes coupling between electric fields and (fluid) dielectrics. In Eq. (5), $D = \varepsilon E$ is the electric displacement vector and $\mathbf{n}$ is a vector normal to the interface. In our analysis we focus on homogeneous perfect dielectrics where the coupling with electric (E) fields happens at the interface, directed normally. Thus, the effect of E-fields enter only through the normal-stress boundary condition. The boundary conditions are summarized in Ref. [3].

3. Linear stability analysis

In perturbation analysis we expand a total field f (velocity $\mathbf{u}$, pressure p, electric potential ϕ or normal vector $\mathbf{n}$) up to the linear terms by adding a small perturbation f' to the stationary flow solution f_0. When variables $f = f_0 + f'$ are put into the governing equations and boundary conditions, the solution f_0 is subtracted and the equations for f' obtained.

The perturbations are further expanded into normal modes of wave number k and characteristic frequency ω_k: $f' = F(z)\exp[i(kx-\omega_k t)]$. If a perturbation frequency $\omega_k = \mathrm{Re}\omega_k + i\mathrm{Im}\omega_k$ has an imaginary part, the disturbance will grow in time as $\exp[\mathrm{Im}\omega_k t]$. The system will be stable when $\mathrm{Im}[\omega_k] < 0$, marginally stable when $\mathrm{Im}[\omega_k] = 0$, and unstable when $\mathrm{Im}[\omega_k] > 0$.

In case when two streaming liquids are perturbed the convective term $\mathbf{u}\cdot\nabla\mathbf{u}$ will also give a first-order contribution. Furthermore, we restrict our consideration to two-dimensional disturbances, a valid assumption when the primary flow is parallel i.e. when $\mathbf{u}_0(x,y,z) = (u_0(z), 0, 0)$ [2]. The perturbations can then be expressed using the stream function $\psi(x,z)$, and the equations that govern perturbations reduce to single ordinary differential (Orr-Sommerfeld) equation for each liquid

$$\frac{d^4\psi_1}{dz^4} - 2k^2\frac{d^2\psi_1}{dz^2} + k^4\psi_1 = ikRe\left[(U_1 - \frac{\omega}{k})(\frac{d^2\psi_1}{dz^2} - k^2\psi_1) - \frac{d^2U_1}{dz^2}\psi_1\right], \quad (6)$$

$$\frac{d^4\psi_2}{dz^4} - 2k^2\frac{d^2\psi_2}{dz^2} + k^4\psi_2 = i\frac{r}{m}kRe\left[(U_2 - \frac{\omega}{k})(\frac{d^2\psi_2}{dz^2} - k^2\psi_2) - \frac{d^2U_2}{dz^2}\psi_2\right]. \quad (7)$$

In Eqs. (6) and (7), $Re = \rho_1 U_0 a/\mu_1$ is Reynolds number (see Fig. 1), U_1 and U_2 are primary flow velocities in fluids 1 and 2 respectively, $m = \mu_2/\mu_1$ is the viscosity ratio and $r = \rho_2/\rho_1$ the density ratio of the two fluids. As mentioned above, electric effects appear solely in the condition for balance of normal stresses. A full description of the problem with all the details is presented in our manuscript [4], currently under completion.

4. Results and discussion

We apply our general results to the special case of water and oil flowing within a typical channel 100 μm wide, see Fig. 2a. We consider a plane Couette-Pouiseuille flow profile with a slip velocity

U_0 = 1 mm/s at the upper wall and an adverse pressure ΔP_{back} = 15 Pa, as found in the two-liquid viscous pump [2]. Im[ω_k] in the long-wavelength limit as a function of the viscosity ratio $m = \mu_{oil}/\mu_{water}$ is shown in Fig. 2b.

The stability region (Im[ω_k] < 0) increases with increasing tangential electric field and thickness ratio $n = h_{oil}/h_{water}$, and decreases with increasing perpendicular electric field and increasing viscosity ratio m. For n = 1.5, there is a window of instability for $6 \le m < 33$ when no electric fields are present. For n = 9 we underline two opposite effects. In case of a tangential E-field (e.g. inside the viscous pump where 35 kV/m), stability is practically always present (up to m = 11437). On the other hand, in case of an imposed perpendicular E-field, the onset of instability for e.g. m = 10 happens at mere V_n = 1.19 V.

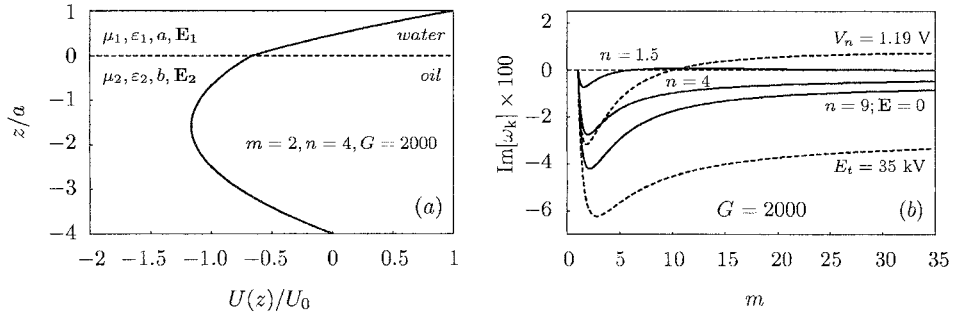

Figure 2: (a) An unperturbed velocity profile of two immiscible streaming liquids in a plane Couette-Pouiseuille flow representing an electroosmotic flow (dragging a nonpolar liquid) with an adverse pressure. The channel width is 100 μm. The liquids differ in viscosities, thicknesses and dielectric constants (densities are unimportant since gravity is negligible). In calculations, liquids 1 and 2 are water and oil, respectively, with a driving velocity U_0 = 1 mm/s and an adverse pressure ΔP_{back} = 15 Pa, as in the viscous pump. G is dimensionless adverse pressure. (b) The imaginary part of the normal frequency ω_k in the long-wavelength limit (k = 0) as a function of viscosity ratio $m = \mu_{oil}/\mu_{water}$. Stability is obtained for Im[ω_k] < 0. Graphs for thickness ratio $n = b/a$ = 1.5, 4 and 9 are shown (for n = 9 with and without electric fields). Perpendicular E-field acts to destabilize interface between dielectrics (upper dashed line). Only 1.19 V is needed to induce instability at m = 10. Tangential E-field acts to stabilize the interface (lower dashed line). Inside the viscous pump the field is $E_t \sim$ 35 kV/m, causing a completely stable pump operation. Also, the increase of n acts to enhance stability.

References

[1] A. Brask, G. Goranović, H. Bruus, *Electroosmotically driven two-liquid viscous pump for nonconducting liquids*, Proc. μTAS 2002, Nara, Japan, 1, p.45-47, (2002).

[2] C.-S. Yih, *Instability due to viscosity stratification*, J. Fluid. Mech, 27, p. 337-352, (1967).

[3] G. Goranović, *PhD thesis*, Technical University of Denmark, (2003), available at http://www.mic.dtu.dk/research/MIFTS.

[4] G. Goranović, M. P. Sørensen, M. Brøns, H. Bruus, *Electrohydrodynamic stability of two streaming viscous liquids inside of a microfluidic channel*, in preparation (2004).

LABCD-96®: A MINIATURIZED CENTRIFUGAL MICROFLUIDIC SYSTEM FOR BIOCHEMICAL ASSAYS

Eric A. Schilling[1], Bruce L. Carvalho[2], Praveen Bansal[1] and Michael Contarino[1]
[1]Tecan Boston, Inc., 200 Boston Ave., Medford, MA 02155, USA
[2]Living MicroSystems, Inc., 8 St. Mary's St., Boston, MA, 02215, USA

Abstract

Described here is a second-generation design of the LabCD® centrifugal microfluidic system. Prototype devices were fabricated by soft embossing with elastomeric tools. Though applications include a variety of drug discovery assays, feasibility was demonstrated here with a serum protein competitive binding assay.

Keywords: LabCD®, centrifugal microfluidics, soft embossing, drug discovery

1. Introduction

Significant demand has arisen in recent years for miniaturization technology for various biomedical applications, particularly in the field of high-throughput drug screening [1]. Tecan has developed the LabCD®, a centrifugal microfluidic system, for the miniaturization of biochemical assays to attempt to meet these needs [2]. Described here is a second-generation design, the LabCD®-96, in which 96 individual assays can be performed simultaneously. Compared with the previous 48-well LabCD®, this design includes such features as significant volume reduction (4µl vs. 16µl per assay) and precise volume metering. It also contains a MTP compatible sample-loading interface, common reagent distribution, passive capillary valving and sample detection features. Figure 1 illustrates the design and function of the LabCD®-96.

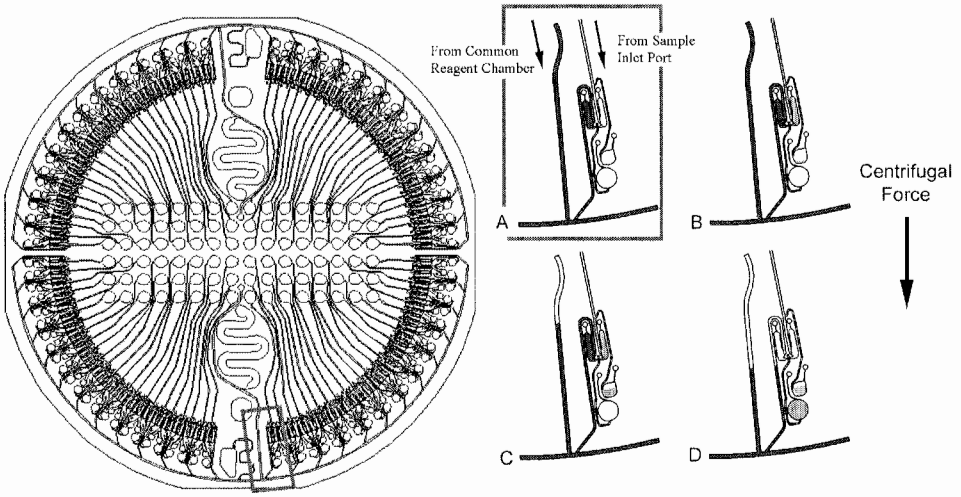

Figure 1. Schematic of the operation of a single subunit of the LabCD®–96. (A) A common reagent is distributed across one half of the disc to fill volume metering chambers. (B) A sample solution fills the adjacent volume metering chamber and any excess volume flows into a sample overflow chamber. (C) When the disc is spun at a higher rpm, a capillary valve on the distribution manifold bursts and volumes are precisely defined. (D) The common reagent and sample reagent

mix after passing through another capillary valve and fill the detection cuvettes where a signal is measured.

2. Fabrication

Prototype LabCD®-96 devices were fabricated by soft embossing [3]. Master structures were fabricated using a combination of SU-8 photolithography and mechanical CNC machining. The masters contained both 'macro' features several millimeters in width and depth and 'micro' features as small as 40 μm x 40 μm. A high durometer silicone rubber was poured into the master and cured to create physical negatives of the masters. The elastomeric tools were held by vacuum in a custom-built hot embossing press. The fluidic structures were embossed into thermoplastic CD 'blanks,' or preforms, made from acrylic, polypropylene or cyclic olefin polymer, with cycle times as low as 6 minutes. This soft embossing approach has significant advantages over traditional hard tool embossing techniques in that elastomeric tool fabrication is rapid and inexpensive while the tool flexibility facilitates removal of the part from the tool without need for mechanical part ejection. Prototype parts were sealed by thermal bonding of a thin film to create a functional part with a total thickness of 2 mm (Figure 2).

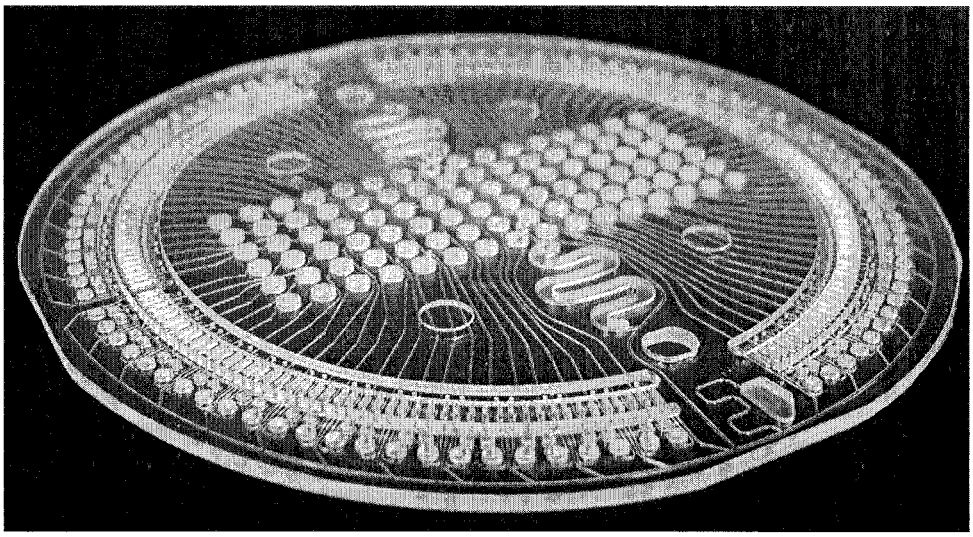

Figure 2. A bonded LabCD®–96 prototype fabricated by soft embossing. Total part thickness was 2 mm and contained 432 air venting through holes each with a diameter of 400 μm. The smallest microfluidic feature size was 40 μm x 40 μm.

3. Applications

The LabCD®-96 centrifugal microfluidic system can be used for a variety of applications. In principle, the disc can be used for any two-component biochemical assay in which fluorescence or absorbance signals can be measured. Spinning and optical detection can be performed using the Tecan Ultra-LabCD reader, a modified microtiter plate reader. Applications targeted for high throughput drug screening assays include cytochrome P450 enzyme inhibition assays, serum

protein competitive binding assays and P-glycoprotein compound interaction assays. Calculated K_i values for serum protein binding assays have been shown to agree with those performed on microtiter plates (Figure 3).

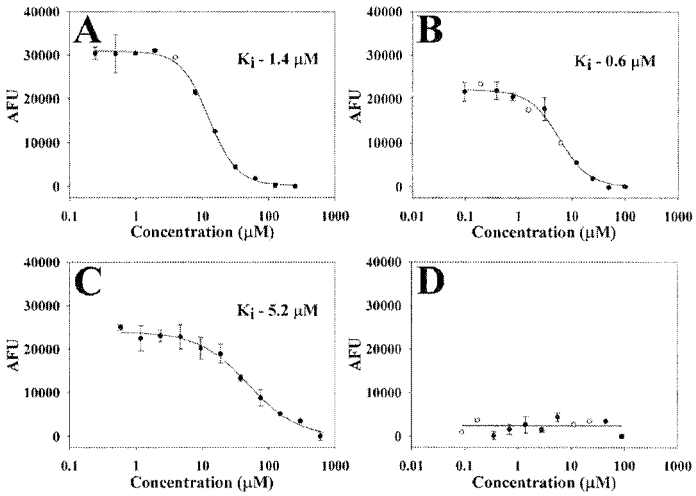

Figure 3. Serum protein binding assay results from a single embossed LabCD®-96. Each curve was generated from one quarter of the LabCD®-96, in which 20 serially diluted drug concentrations, two positive and two negative controls were delivered to inlet ports. The starting drug concentrations were (A) 50 mM chloropromazine, (B) 20 mM tri-idiobenzoic acid, (C) 1 M lidocaine, and (D) 18 mM ibuprofen. The common reagent was a 1:1 mixture of 10 µM α1-acid glycoprotein and 40 µM quinaldine red. Curve fits were based on a standard four parameter logistic method.

References

[1] B. Warrington. *MicroTAS '03*, pp. 485-489.
[2] D. Duffy, H. Gillis, J. Lin, N. Sheppard, G. Kellogg, *Anal. Chem.*, **71**, 4669-4678 (1999).
[3] B. Carvalho, E. Schilling, N. Schmid, G. Kellogg. *MicroTAS '03*, pp. 959-962.

Convective Electrokinetic Flow Instabilities in a Cross-Shaped Microchannel

Jonathan D. Posner, Hao Lin, and Juan G. Santiago
Department of Mechanical Engineering, Stanford University, Stanford, CA 94305

Abstract
Electrokinetic instabilities (EKI) are produced by electric body forces resulting from a coupling of electric fields and conductivity gradients. Electrokinetic flows become unstable when electric body forces become on the order of or larger than the viscous forces in the flow. In the current work, we present a parametric experimental study of a convective EKI in a 50 μm wide by 20 μm deep cross-shaped microchannel. We explore the effects of center-to-sheath conductivity ratios and demonstrate the effectiveness of EKI for rapid micromixing. The experimental measurements of critical electric field compare well with trends predicted by the scaling analysis.

Keywords: electrokinetic instability, micromixer, on-chip electrokinetics

1. Introduction

Microfluidic systems aim to integrate multiple chemical assay functions on a chip [1]. An important class of these are electrokinetic devices, characterized by the presence of an electric double layer (EDL) that forms at the interface between an electrolyte solution and a solid surface. This charge separation results in a region of net charge in the liquid in a region typically limited to a few nanometers near the charged wall [2]. However, net charge can also form in the bulk liquid of such systems in regions of conductivity gradients [3]. Net charge and externally applied electric fields result in an electric body force of the form, $\rho_E \bar{E} = \varepsilon(\bar{E} \cdot \nabla\sigma)\bar{E}$, where ρ_E, ε, E, and σ are respectively charge density, local permittivity, local electric field, and ionic conductivity [3,4,5]. Electrokinetic flows with heterogeneous electrolyte solutions become unstable when the ratio of the electric body force to the viscous force in the flow exceeds a critical value [5]. We have presented experimental parametric studies and detailed models for electrokinetic instabilities (EKI's) in systems for temporal instabilities in long-thin capillaries [4] and convective instabilities in high aspect ratio T-junction microchannels [5]. These studies provide a fundamental understanding of the instabilities, identify key controlling parameters, and present predictive simulations. On-chip electrokinetic flows at intersections with heterogeneous electrolyte solutions are relevant to sample injection for field amplified sample stacking and other mismatched conductivity assays [6,7]; multidimensional assays [8]; and systems with poorly-specified sample chemistry.

In the current work, we present a parametric experimental study of a convective EKI in an electrokinetic focusing flow in a cross-shaped microchannel. We explore the effects of center-to-sheath conductivity ratios and demonstrate the effectiveness of EKI for rapid micromixing.

2. Experimental apparatus and methods

Experiments were performed in commercially available glass chips with a crossed microchannel design with isotropic etched cross-sectional profiles 50 μm wide by 20 μm deep (PC-SC, Micralyne Inc, Alberta, Canada). We obtained instantaneous concentration fields of rhodamine B using epifluorescence microscopy and CCD camera imaging. The applied potentials were programmed into a high voltage sequencer (LabSmith, Livermore, CA) that synchronized applied potentials with a CCD camera (Cascade 512, Roper Scientific, Trenton, NJ). The exposure time was controlled by a liquid crystal video rate shutter (Displaytech, Longmont, CO). A 20x, NA = 0.45 ELWD objective (Nikon, Japan), mercury bulb, and epifluorescence filter cube (λ_{abs} = 540 nm, λ_e = 625 nm-Chroma, Rockingham, VT) were used for imaging, illumination, and spectral filtering of the dye fluorescence. Data were recorded over the applied potential range of 250 to 1600 V. The center-to-sheath conductivity ratio, γ, was varied from 3 to 100. We define the nominal electric field

for each experiment as the difference in applied potential divided by the 9 mm length between the south well (bottom channel of Figure 1a) and the east well (right channel of Figure 1a).

3. Results

Images of a rhodamine dyed stream in an electrokinetic focusing flow are shown in Figure 1 for three different applied fields with a conductivity ratio of 100. Flow perturbations develop in the region near the intersection and advect downstream for electric fields greater than a critical value, as in the case of other EKI flow fields [4,5]. Figure 2 shows the critical electric field as a function of the conductivity ratio, γ. The critical field is determined by monitoring root mean square (RMS) images of eight-image sequences. The critical field is defined as the condition where the maximum value of these RMS images exceeds four times the area-averaged RMS of the low-field, stable case. As suggested by the scaling analysis of Chen et al. [5], critical field scales as $(\gamma\text{-}1)/(\gamma+1)Ra_e^{1/2}$ where Ra_e is an approximately constant electric Rayleigh number (a critical ratio of electric body forces to viscous forces in the flow). For large γ the critical field is nearly constant and increases rapidly as γ approaches unity. No instability was observed for uniform conductivity at applied fields as large as 3500 V/cm.

EKI can be used to enhance mixing in microfluidic systems [9]. Probability density functions (PDF) of normalized scalar image intensity are shown in Figure 3 for eight axial locations and two applied fields. We quantify the degree of electrokinetic instability mixing using time-averaged probability density functions of concentration profiles [9]. Highly bimodal distributions indicate unmixed conditions (e.g., see the $x/w = 3$ distribution in Figure 3a). Unimodal distributions with high probability densities near mid-level intensity values indicate well-mixed regions. These results suggest that strong electrokinetic instabilities mix rapidly and over short distances.

4. Conclusions

We have presented a parametric experimental study of a convective EKI in a cross-shaped microchannel. We have experimentally investigated variations of applied electric field and center-to-sheath conductivity ratios, over one and two orders of magnitude, respectively. The critical electric fields required for instability were determined quantitatively as a function of the conductivity ratio. Measurements of critical electric field compare well with the trends of the scaling analysis suggested by Chen et al [1] and EKI was shown to provide rapid mixing in this microchannel flow.

References

1. A. Manz, N. Graber, H. Widmer, *Miniaturized total chemical analysis systems: A novel concept for chemical sensing*, Sens. Actuators B **1**, 244 1990.
2. V. G. Levich, *Physicochemical Hydrodynamics,* Prentice Hall, Englewood Cliffs, NJ, 1962
3. J.F. Hoburg and J.R. Melcher, *Electrohydrodynamic mixing and instability induced by collinear fields and conductivity gradients,* Phys. Fluids 20, 903, 1977.
4. H. Lin, B. D. Storey, M.H. Oddy, C.H. Chen, J.G. *Santiago Instability of electrokinetic microchannel fows with conductivity gradients*, Physics of Fluids, 16, 6, 2004.
5. C.H. Chen, H. Lin, S.K. Lele, *Convective and absolute electrokinetic instability with conductivity gradients*, J of Fluid Mechanics, Under Review, 2004.
6. B. Jung, R. Bharadwaj, J.G. Santiago, *Thousandfold signal increase using field-amplified sample stacking for on-chip electrophoresis*, Electrophoresis 24, 2004,.
7. L.L. Shultz-Lockyear, C.L. Colyer, Z.H. Fan, K.I. Roy, D.J. Harrison, *Effects of injector geometry and sample matrix on injection and sample loading in integrated capillary electrophoresis devices*, Electrophoresis 20, 3, 1999
8. A.E. Herr, J.I. Molho, K.A. Drouvalakis, J.C. Mikkelsen, P.J. Utz, J.G. Santiago, T.W. Kenny, *On-chip coupling of isoelectric focusing and free solution electrophoresis for multidimensional separations,* Anal. Chem. 75, 1180, 2003.
9. M.H. Oddy, J.G. Santiago, J. C. Mikkelsen, *Electrokinetic Instability Micromixing*, Anal. Chem. 73, 2001.

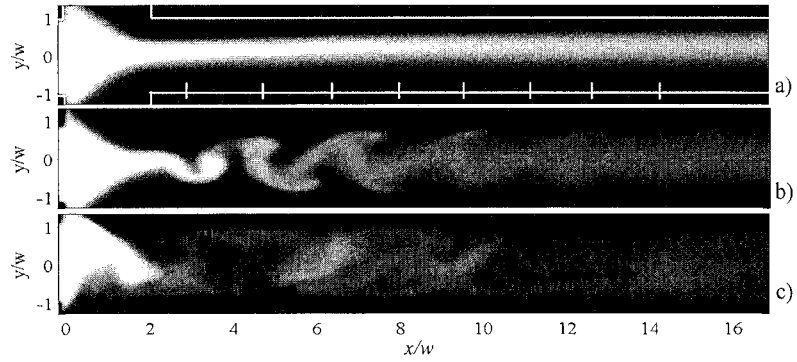

Figure 1. Images of 70 kDa dextran-conjugated rhodamine B tracer electrokinetically injected in a cross-shaped microchannel. Dyed stream enters the cross from the left hand side, flows right (in direction of applied electric field E_a, and is "pinched" into the long channel region by flow from vertical channels centered at $x/w = 1$. The dyed stream conductivity is 10 times that of the sheathing flow streams: a) Flow is stable for $E_a = 0.30$ kV/cm; b) at $E_a = 0.47$ kV/cm, the flow demonstrates convective instability and flow field is temporally periodic and deterministic; c) at $E_a = 0.70$ kV/cm, flow demonstrates an absolute instability where disturbances propagate upstream.

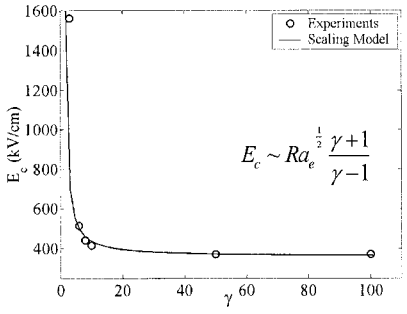

Figure 2. Critical electric field (required for instability) plotted as a function of center-to-sheath stream conductivity ratio, γ. Instability model by suggested by Chen et al. [6] shows the scaling of critical electric field with conductivity ratio, γ, for a constant critical electric Rayleigh number, Ra_e. The Rayleigh number is a ratio of electric body forces to viscous forces in the flow.

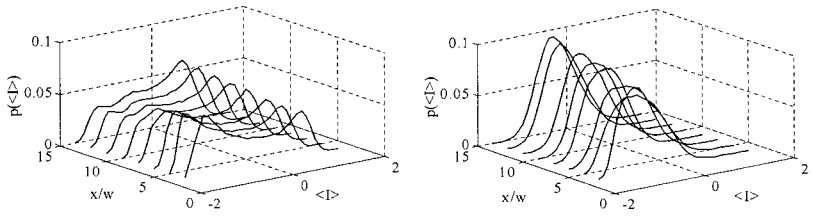

Figure 3. Probability density functions, $p(<I>)$, of normalized image intensity, $<I>$, at eight axial locations (shown as vertical lines in Figure 1a) and for the applied fields shown in Figures 1a and 1c. The distributions are generated from a time sequence of 250 images obtained at 115 frames per second.

NUMERICAL AND EXPERIMENTAL INVESTIGATION OF BUBBLE PINCH-OFF IN THE FLOW-FOCUSING DEVICE

Mads J. Jensen1[1,3], Piotr Garstecki[2], Michael Fuerstman[2], Henrik Bruus*, George M. Whitesides[2], and Howard A. Stone[3]

[1]*MIC - Dept. Micro and Nanotechnology, Technical University of Denmark, Lyngby, Denmark*
[2]*Dept. Chemistry and Chemical Biology, Harvard University, Cambridge, USA*
[3]*DEAS - Division of Engineering and Applied Sciences, Harvard University, Cambridge, USA*

Abstract

In this work we present a numerical investigation of experimental results obtained for bubble pinch-off in a microfluidic flow-focusing device [1,2]. The numerical simulations of the free-surface problem are made assuming a low Reynolds-number flow and are implemented using a finite element solver. The results are used to study the dynamics near pinch-off, the size of the bubbles, and the overall topology of the two-phase flow.

Keywords: bubble, simulation, pinch-off, flow-focus

1. Introduction

Studying the generation of gas bubbles on the micrometer scale in a predefined geometry makes it possible to investigate many interesting physical phenomena and to design new technological devices. The flow-focusing device [1,2] enables such a studies. Among the many kinds of questions that can be studied, there has been recent work on the interface instabilities and especially the controlled capillary instability [4]. A combined experimental and numerical investigation is a powerful source of increased understanding of the basic physical phenomena involved, and hence motivates the present numerical study.

2. Experiments

The flow-focusing device is depicted schematically in Fig. 1a. A pressured gas thread of pressure p is focused into the orifice by two liquid streams (with flow rate Q). The gas thread breaks periodically to release bubbles into the outlet channel. Optical micrographs of the pinch-off event are shown in Fig. 1b together with fits of the tip shape. The orifice has typical dimensions ranging from 30 to 120 μm and the height of the channel is 28μm.

We find that i) the volume V_b of the bubbles scales with the flow-rate Q and the viscosity μ of the liquid, and the pressure p of the gas stream as $V_b \propto p/Q\mu$ (Fig. 2b), ii) the rate at which the diameter of the gas thread decays in time during a single breakup event is linearly proportional to the flow rate Q of the liquid and is independent of viscosity and surface tension. The first observation leads to the ability to control the size of the bubbles ($\propto p/Q$) independently of the volume fraction of the dispersed phase ($\propto pQ$). The second observation forms the basis of a controlled capillary instability mechanism [4], in which the rate of collapse of the unstable thread is greatly slowed down by the effect of confinement of the orifice: relaxation of the surface energy proceeds at the rate of supply of the continuous fluid.

3. Numerical model

In the numerical model we assume the flow to be in an axisymmetric geometry. Even though the geometry of the flow-focusing device is full 3D we are confident that we capture the essential physics of the gas bubble formation. The numerical model uses the commercial software FemLab [3] in a novel way together with an in-house interface update routine programmed in MatLab. We solve the Stokes equation in cylindrical coordinates (we assume low Reynolds-number flow) while accounting for the full geometry of the device including interface, walls, inlets, and symmetry

boundaries (see Fig. 2). At the location of the free surface the normal and tangential stress conditions are enforced including the contribution of a pressure jump associated with surface tension at the curved interface. The solver returns a velocity field at the interface, which is in turn used to evolve the interface in the normal direction using a second-order Runge-Kutta time step.

4. Results and discussion

A typical numerical result is shown in Fig. 2, which illustrates the time features of the shape evolution of the liquid-gas interface prior to pinch-off of a gas bubble (see Fig. 1b). The small circles on the Fig. show the location of the minimum thread diameter. The numerical results capture all of the topological features of the liquid-gas interface that were observed experimentally (Fig. 2a). Moreover, a preliminary investigation show that the size of the created bubbles scale correctly with flow rate Q, pressure p, viscosity μ, and the length of the orifice (see Fig. 2b). As the simulations are very time-consuming (about 48h for a single run) the correct geometry and a full parameter analysis has not yet been performed. In addition, we are studying the evolution of the drop size as the different parameters are varied.

5. Conclusion

A numerical model simulating the liquid-gas flow in the flow-focusing device has been implemented. The preliminary results show good agreement with experimental data. The overall topology of the flow is consistent and preliminary results show agreement in the scaling laws of the bubble volume V_b and the thread collapse rate. More simulations are needed for a complete parameter analysis.

References

[1] S. L. Anna, N. Bontoux, and H. A. Stone, App. Phys. Lett. **82**, 364 (2002).

[2] *Formation of mono disperse bubbles in a microfluidic flow-focusing device*, P. Garstecki, I. Gitlin, W. DiLuzio, E. Kumacheva, H. A. Stone, and G. M. Whitesides (submitted).

[3] www.comsol.com

[4] *Controlled capillary instability*, P. Garstecki, H. A. Stone, and G. M. Whitesides (submitted).

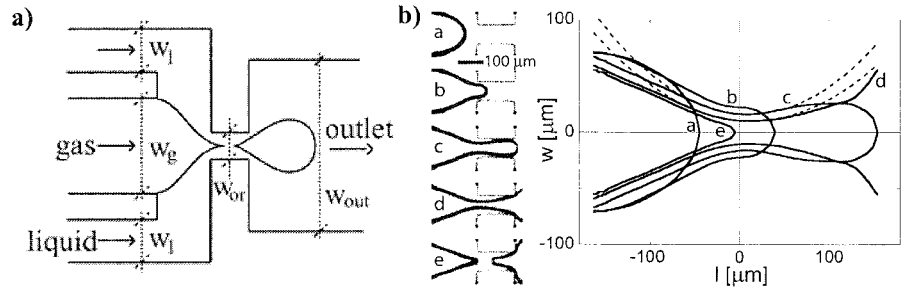

Figure 1 a) Schematic representation of the microfluidic flow-focusing device. The channels are made as of PDMS. In all the experiments the liquid width is w_l = 250 μm and the gas width is w_g = 200 μm. The width of the orifice w_{or} is between 30 and 120 μm and the width of the outlet w_{out} is between 250 and 1000 μm. The height h of the channel is 28 μm in all tested devices. **b)** Left: Optical micrograph of the tip of the gas stream as it approaches and passes through the orifice (compare to figure 2). The graphs on the right represents are contours of the gas-liquid interface extracted from the micrographs.

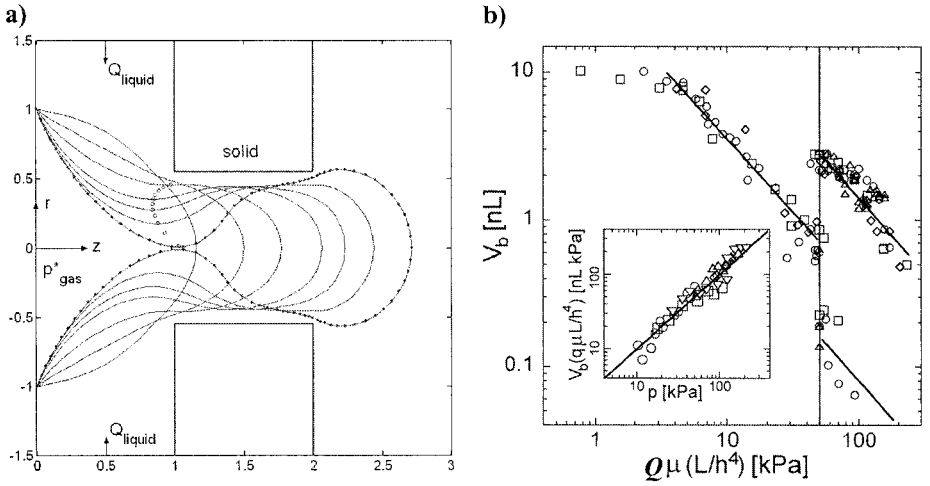

Figure 2. a) Simulation of the time evolution of the liquid-gas interface at dimensionless times t=0.25 to 4.25. The end time corresponds to the computation step just before pinch-off. The dimensionless gas pressure is $p^* = p/u^2\rho$ and the inlet liquid flow rate Q. The dots on the final interface correspond to the discretizeation of the interface. The small circles show the evolution of the position of the minimum gas-thread diameter. **b)** Experimental dependence of the volume of the bubble V_b on the gas pressure p, the flow rate Q, and the viscosity μ. For a critical value of $Q\mu$ the bubble size bifurcates into a period-two dependence: one large bubble one small bubble etc.

INFLUENCE OF NONUNIFORM CHANNEL WIDTH DISTRIBUTION IN POROUS SILICON HIGH ASPECT RATIO PARALLEL CHANNEL MICRO REACTORS

Martin Bengtsson, Mikael Nilsson and Thomas Laurell
Dept. of Electrical Measurements, Lund University, P.O. Box 118, S-221 00 Lund, Sweden

Abstract

The paper focuses on the fact that, since the flow rate in parallel channels relies strongly on the channel width, the combination may lead to inaccurate results if errors in the fabrication process lead to an uneven distribution of channel widths. Parallel channel enzyme reactors were designed with channel widths distributed normally with different degrees of standard deviation. The reactors were then evaluated with regard to dispersion and to catalytic effect of the immobilised enzyme. It was shown that for lower concentrations the catalytic efficiency decreased significantly even for small variations in the distribution of channel widths and reactors with poor homogeneity in channel widths also diluted the sample more than the others.

keywords: microreactor, porous silicon, IMER, dispersion

1. Introduction

In the current trends of miniaturisation of analytical and bioanalytical systems, microfluidic sample handling in parallel channel systems or stacked systems have been popular methods in biochemical applications for fast screening of different drug compounds and increasing the throughput in analytical systems [1]. The paper focuses on the fact that, since the flow rate in narrow channels is cubically dependent of the channel width [2], parallel channel designs may suffer from inaccurate results if errors in the fabrication process lead to an uneven distribution of channel widths. Thereby, the deviation between parallel channels intended to be identical in a microfluidic component may no longer be negligible.

For parallel channel immobilised enzyme reactors it can be anticipated that they will display a varying performance if reactors fabricated in the same batch display different channel width configurations. In flow injection analysis (FIA), another major aspect is the effect that the different flow rates in channels of varying dimension will have on the dispersion of the injected sample plug. The differences in flow rates between the channels, Fig. 1.

Our group has previously presented a high aspect ratio parallel channel micro enzyme reactor in porous silicon [3]. As a further step in the characterisation of this type of microreactor the influence of the channel width variation on the bioanalytical performance has been investigated in this paper.

2. Experimental

Microreactors with different geometries were fabricated in 3", <110>, p-type silicon (20 - 70 Ωcm), with hanisotropic etching in KOH (40mg/100ml H_2O) at 80 °C. All reactors were designed to comprise 32 channels, 250 μm deep, yielding a total volume of 5.2 μl. The channel widths were designed to be normal distributed with a mean value of 25μm and a standard deviation of 0, 1, 2 or 5μm, labelled A, B, C and D respectively.

To obtain a porous layer on the channel walls, the microreactor chip was anodised in an ethanol-HF solution mixed (1:1), during illumination. The current density during the anodisation was fixed to 50mA/cm^2 for 10 min, to achieve an optimised porosity throughout the channel walls [4]. After the porous silicon fabrication all reactors were dried and inspected through an optical microscope and the obtained channel widths were measured.

Prior to enzyme coupling the pores were rewetted by immersion in an H_2O:ethanol solution (mixing ratio 1:1) under low pressure, to remove any air bubbles in the porous matrix.
Trypsin was immobilised onto the porous silicon using a standard silane based coupling method [5], thereafter the reactors were rinsed and stored in phosphate buffer solution, PBS (pH 7), at 8°C before use.

The catalytic performances of the different reactors were measured using a spectrophotometric assay. The reagent solution containing *α-N*-benzoylarginine ethyl ester (BAEE), was pumped either through or past the μIMER and the corresponding enzyme activity was calculated from the recorded absorbance shift at 251 nm due to digestion of BAEE in the IMER.
The maximum catalytic turn-over at each investigated substrate concentration (steady state measurement) was monitored by increasing the flow rate, while monitoring total catalytic output, until no further increase in turn-over was seen.

The dispersion was measured on reactors without enzyme. With a steady flow of deionised H_2O through the reactor a plug of 0.5 μl NaCl was injected into the system prior to the reactor. Directly after the reactor conductivity was measured with an in house designed cell, with an internal volume of approximately 100 nL. The dispersion was derived from the ratio between the peak amplitude recorded for a sample plug that passed through the microreactor versus one that bypassed the microreactor.

To compare the obtained results with the mathematical model, a two-dimensional FEM model for the different reactor designs were made in FEMLAB, with the same parameters as in the dispersion measurements.

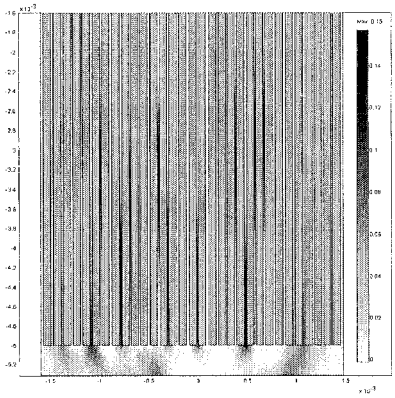

Figure 1. Modelling of the resulting concentration of an injected plug, close to the outlet of a parallel channel system with uneven channel width distribution. The dark areas contain the highest concentrations.

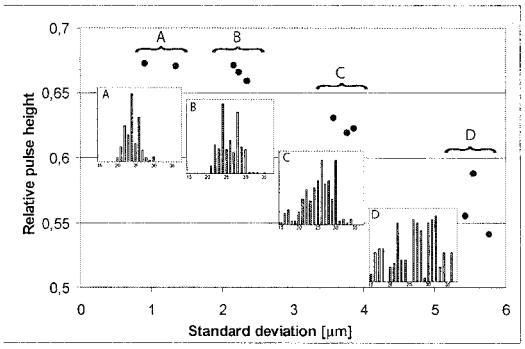

Figure 2. The measured relative peak height vs. the channel width standard deviation of each reactor (●). The A-D notation indicates the four designs that were made. Inserts display the total distribution of channel widths for each of the four microreactor classes A-D.

3. Results and discussion

The dispersion measurements are shown in Fig. 2. A clear tendency is visible where the peak of the injected salt plug is degrading as the standard deviation of the channel width distribution increases. This can be expected since the reactors with larger standard deviation (C and D) in

channel width contains both the widest and the narrowest channels and thus the widest range of flow rates in the different channels. For the micro reactors with the lowest variation in channel width (A and B) hardly any difference can be seen with respect to the relative pulse height.

The microreactor enzymatic performance in steady state mode operation was also investigated with respect to the four different reactor classes, Fig. 3. The effect of the inhomogeneous channel distribution is clearly visible in the case where the substrate concentration is only 0.1 mM as the mean catalytic turn-over drops approximately 34%, Fig 2a. It can also be noted that the drop in catalytic performance is less pronounced at the higher substrate concentration Fig 2b. This is explained by the fact that the more narrow channels, having a low flow rate, are more prone to substrate depletion and thus mass transport limitation than the wider channels and at higher substrate concentrations the mass transport limitations are less expressed as the active sites to a higher degree are saturated with substrate molecules. The contrary applies for the lower substrate concentration and thus substrate depletion leading to more unoccupied enzyme molecules in the narrower channels of class D reactors reveals the shortcomings of these reactors.

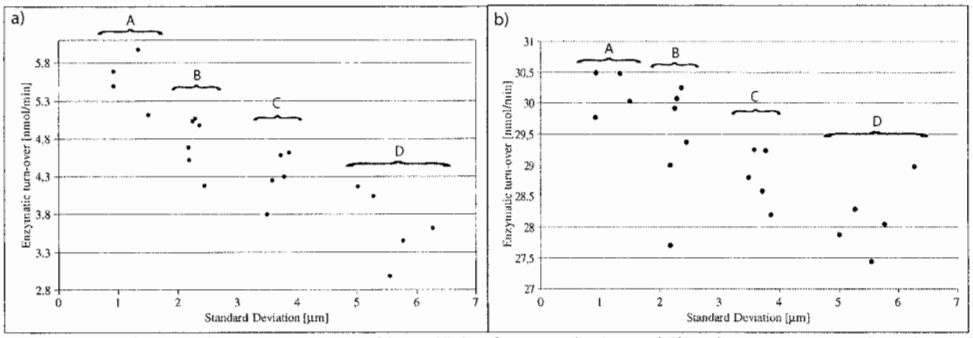

Figure 3. The maximum turnover of BAEE in the trypsin immobilised reactors as a function of channel width deviation recorded for two substrate concentrations 0.1 mM (a) and 10 mM (b).

Acknowledgements

Swedish Research Council, Foundation for strategic research, Crafoord Foundation, Royal Physiographic Society, Carl Trygger Foundation are acknowledged for their financial support of this work.

References

[1] Northrup, M.A., K.F. Jensen, and D.J. Harrison. *Micro Total Analysis Systems 2003*. 2003.

[2] Fox, R.W. and A.T. McDonald, *Introduction to Fluid Mechanics*. 4 ed. 1992: Wiley.

[3] Laurell, T., et al., *Enhanced enzyme activity in silicon integrated enzyme reactors utilizing porous silicon as the coupling matrix.* Sensors and Actuators B-Chemical, 1996. **31**(3): p. 161-166.

[4] Bengtsson, M., et al., *Improved performance in silicon enzyme microreactors obtained by homogeneous porous silicon carrier matrix.* Talanta, 2002. **56**(2): p. 341-353.

[5] Weetall, H.H., *Covalent couplings methods for inorganic Support Materials*, in *Methods in enzymology*, K. Mosbach, Editor. 1976, Academic Press, N.Y. p. 134-148.

Characterisation of the flow behaviour in microreactors by means of residence time distribution measurements

D. Boškovic, K. Huber, S. Löbbecke
Fraunhofer-Institut Chemische Technologie ICT
P.O. Box 1240, D-76318 Pfinztal, Germany

Abstract

A method for measurement of the resident time distribution in microreactors by applying a input-response technique is described. One method for fitting the measured curves to a mathematical model is presented.

Keywords: residence time distribution, microfluidic, modelling, transfer function

1. Introduction

The residence time distribution in reactors has a great impact on the conversion and selectivity of chemical processes. Compared to macroscopic processes much more effort has to be put on the accuracy of measuring the residence time distribution when microfluidic devices are used. Moreover, it is hardly possible to determine the residence time distribution of a microreactor solely without considering the influence of the periphery, like capillaries, that is required for conducting the measurements.

2. Experimental

A tracer input-response method has been developed to measure the residence time distribution of microreactors that avoids any disturbances of the microfluidic flow behaviour during tracer input and analysis. The concentration of a special tracer dye is measured UV-Vis spectroscopically at the outlet of a microreactor in realtime by using a flow-through cell coupled to the spectrometer by optical fibres (Fig. 1). By using a fast-cycling HPLC valve, both step-change and impulse experiments can be carried out (Fig. 2).

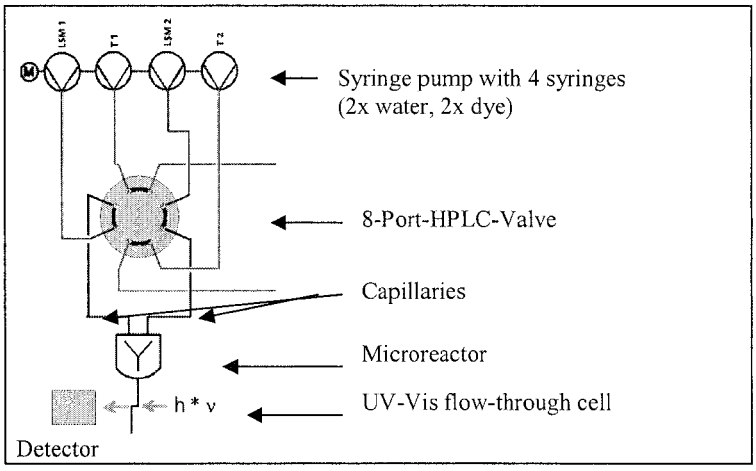

Figure 1: Simplified scheme of the experimental setup

The method was optimized in order to eliminate systematic errors, e.g. caused by adsorption effects of the dye on the microfluidic channels, to achieve a high repeatability of the measured residence time distribution. Hence, different microfluidic structures can be compared accurately.

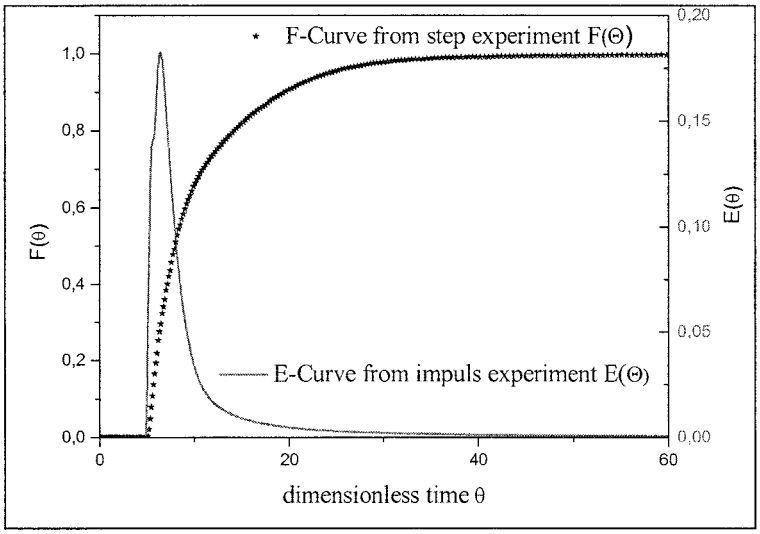

Figure 2: Exemplary residence time distribution curves obtained by the described method

3. Data processing and modelling

The measured residence time distribution is a cumulative signal consisting of the distribution of the microreactor itself and that of the input and output capillaries. This overall signal has to be deconvoluted mathematically in order to describe the performance of the microreactor solely. Most of deconvolution techniques that can be applied are based on estimated models. The dispersion-model, for example, is applicable and widely flexible since radial and longitudinal dispersion as well as a true velocity profile can be considered. However, taking all these factors into account leads to very complex or even unsolvable model equations. Nevertheless, an estimation of the model parameters can be carried out in the Laplace or frequency domain without knowing the analytical solution of the model.

An example for a parameter estimation is the transfer function fitting. The input signal x(t) and the response signal y(t), which both can be measured, are correlated via:

$$y(t) = \int_0^t f(t')x(t-t')dt' \qquad \text{or transformated:} \qquad Y(s) = F(s) \times X(s)$$

with:	f(t)	residence time distribution of the reactor
	Y(s), X(s)	transformated input and output signal
	F(s)	transfer function

F(s) of the experimental curves ($F(s)_{exp}$) can be determined by numerical transformation of the measured concentration data. Afterwards the theoretical transfer function $F(s)_{cal}$, calculated by Laplace transformation of the model equation can be fitted to F(s) for estimating the model parameters (Fig 3).

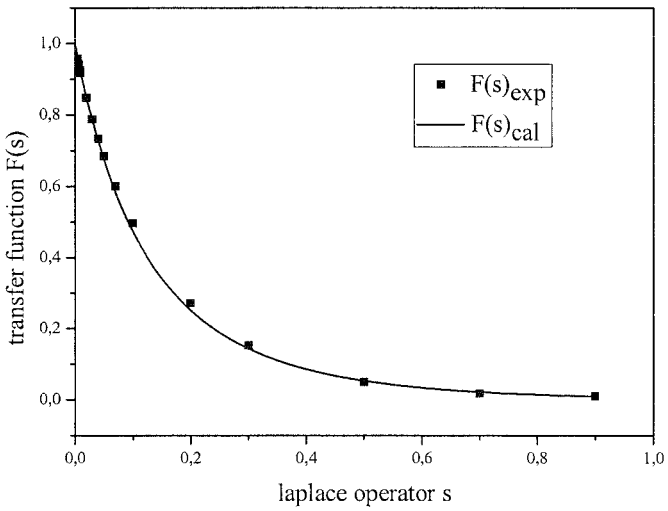

Figure 3: Fit of the transformed model-transfer function to the experimental transfer function

Gas-Liquid Two-Phase Flow Patterns in Polymeric Microfluidic Channels with Different Surface Chemistries

Dongeun Huh, Alan H. Tkaczyk, James B. Grotberg, Shuichi Takayama
Dept. of Biomedical Engineering, University of Michigan, Ann Arbor, MI 48109-2099, USA

Abstract

Dynamic gas-liquid two-phase flows in a closed channel system generate a number of flow patterns that are fundamentally interesting and practically important. In microfluidic systems, surface effects give rise to increased complexity in the interaction between moving fluids and also provide an added measure to change and control two-phase flow configurations. This paper presents an experimental study of gas-liquid two-phase flow patterns in microchannels with varying surface wettability.

Keywords: two-phase flow pattern, flow regime map, surface chemistry, microfluidic

1. Introduction

Understanding the dynamic interaction between continuous streams of gas and liquid in microchannels is essential for the successful design of functional multi-phase microfluidic systems such as micro-heat exchangers [1], bioreactors [2], flow cytometers [3], and fluidic switches [4]. The spatial distribution of moving fluids in a given microchannel is determined by the fluid flow rates and wetting property of channel surfaces [5]. Here we report an experimental investigation of gas-liquid two-phase flow patterns in rectangular PDMS microfluidic channels with different surface chemistries.

2. Experimental

Gas-liquid two-phase flows were generated by parallel injection of compressed air and DI water at different flow rates without premixing as shown in Figure 1. Three different rectangular microchannels having different wetting properties were prepared by varying the time elapsed from plasma oxidation of channel surfaces to the beginning of experiments: (i) bare hydrophobic PDMS surface with a contact angle of 111°, (ii) hydrophilic surface (3 hours after plasma oxidation, contact angle = 35°), (iii) moderately hydrophilic surface (49 hours after oxidation, contact angle = 77°). For flow mapping in hydrophilic channels, careful attention was paid to temporal changes in surface chemistry of oxidized PDMS and the duration of conducted experiments was strictly limited to no longer than 1 hour to minimize the recovery of hydrophobicity. Injected fluid streams and resulting flow patterns were observed in the downstream of channel system (width = 300 μm, height = 100 μm). Aqueous fluorescein solution with a concentration of 0.001% w/v was used as a working liquid to capture cross-sectional images of different two-phase flow patterns using confocal microscopy.

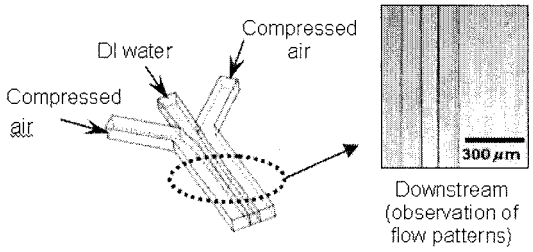

Figure 1. Schematic diagram of an experimental setup used to generate and observe different two phase flow patterns. Liquid flow was driven by a syringe pump and gas flows were generated by the injection of compressed air. The micrograph shows one example of flow patterns in a hydrophobic channel.

3. Results and discussion

In a hydrophobic microchannel with a surface contact angle of 111°, seven different two-phase flow patterns were observed depending on the flow rates of gas and liquid (Figure 2). In general, gas-liquid two-phase streams maintain their original stratified flow configuration with various interfacial shapes and stabilities at moderate liquid flow rates (stable stratified, detached stratified, wavy stratified, spreading stratified-droplet) until the liquid column in the middle repositions to the sidewalls at very high flow rates of liquid (annular-droplet) or breaks up into droplets due to two-phase instability at very low liquid flow rates (breakup). Interestingly, when the gas flow rate is increased while maintaining a low liquid flow rate, the resulting stable water stream contacts both the top and bottom channel surfaces in the upstream region, but detaches from the bottom floor in the downstream area and forms a convex air-liquid interface to ambient air flows as illustrated in the confocal images of Figure 2. The observed two-phase flows were categorized into a flow regime map where different flow patterns are correlated to different flow rates of gas and liquid samples.

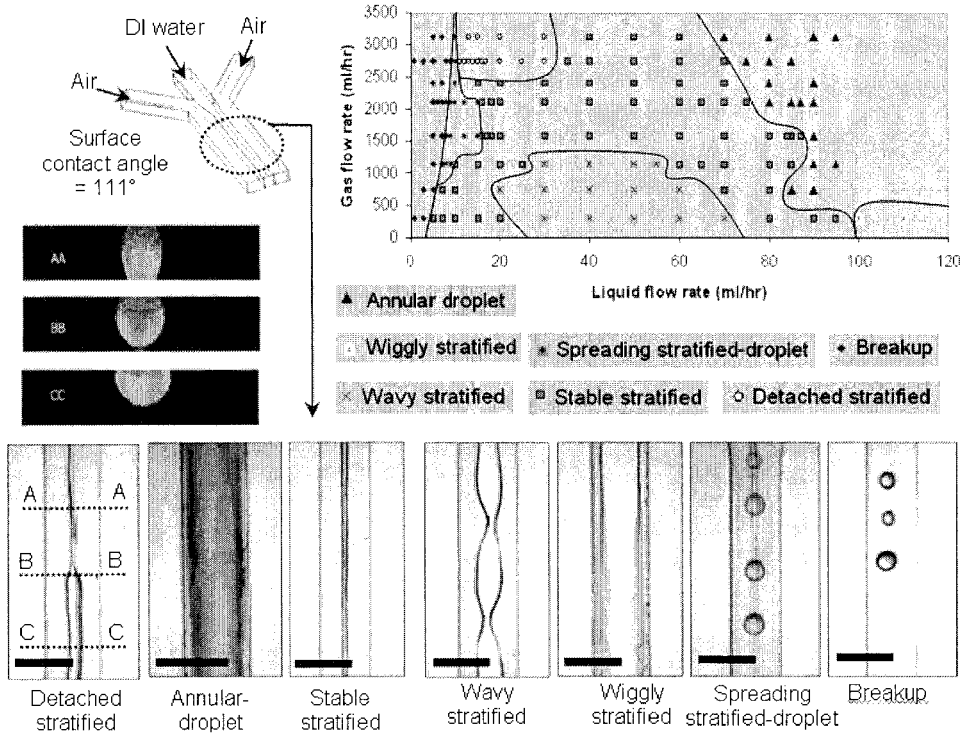

Figure 2. Gas-liquid two-phase flow patterns in a hydrophobic PDMS channel with a contact angle of 111°. Seven different flow regimes were observed with changing fluid flow rates. Cross-sectional images of detached stratified flows were taken by confocal microscopy. Size bar = 300 μm.

Regardless of the contact angle (35° and 75°) of channel surfaces, only two different flow patterns were seen with changing fluid flow rates in hydrophilic microchannels. Injected liquid sample wets channel walls and is redistributed along the sidewalls with gas and liquid droplets traveling at a high speed in the middle (annular-droplet) or just with a gas flow separating the liquid

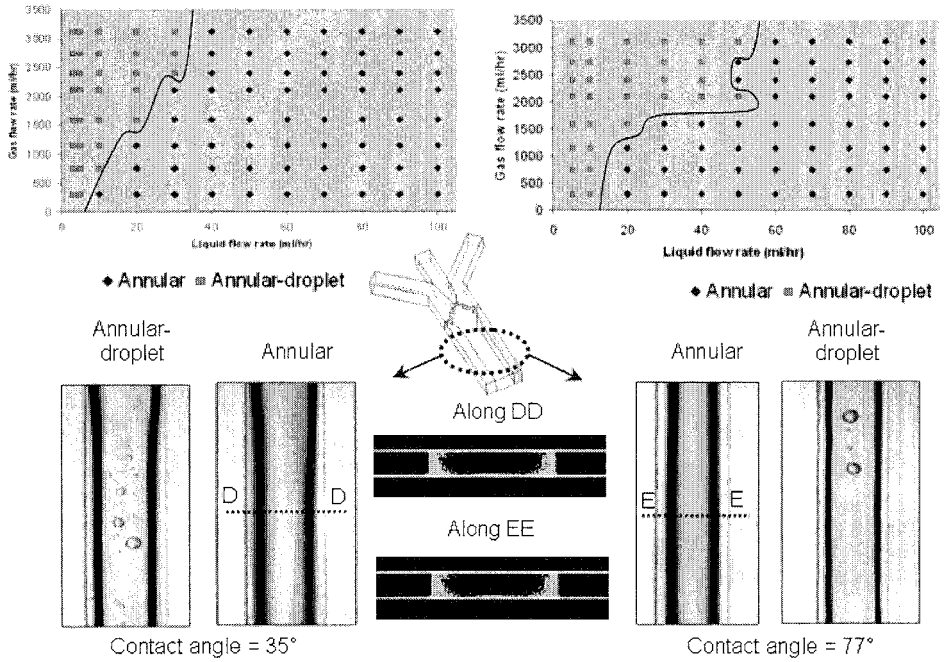

Figure 3. Gas-liquid two-phase flow patterns in hydrophilic channels with different contact angles.

linings (annular) (Figure 3). When a contact angle is higher, annular-droplet flow pattern was found to become more prominent at low liquid flow rates, indicating more favorable formation of droplets on the channel surfaces due to increased hydrophobicity.

4. Conclusions

We presented an experimental investigation of different gas-liquid two-phase flow patterns in microchannels and demonstrated a crucial role of surface wettability in changing morphological characteristics of fluid flows. A number of flow regimes observed in our study could be used in designing dynamic multiphase microfluidic systems with fast fluid flows as well as in exploring microscale multiphase flow phenomena.

Acknowledgements

We thank Whitaker Foundation, NSF, and NIH for financial support.

References

[1] L. Zhang, J.M. Koo, L. Jiang, M. Asheghi, K.E. Goodson, J.G. Santiago, T.W. Kenny, *J. Microelectromech. Syst.* **11**, 12-19 (2002).

[2] N. de Mas, A. Gunther, M.A. Schmidt, K.F. Jensen, *Ind. Eng. Chem. Res.* **42**, 698-710 (2003).

[3] D. Huh, Y.C. Tung, H.H. Wei, J.B. Grotberg, S.J. Skerlos, K. Kurabayashi, S. Takayama, *Biomed. Microdev.* **4**, 141-149 (2002).

[4] D. Huh, A.H. Tkaczyk, J.H. Bahng, Y. Chang, H.H. Wei, J.B. Grotberg, C.J. Kim, K. Kurabayashi, S. Takayama, *J. Am. Chem. Soc.* **125**, 14678-14679 (2003).

[5] A.M. Barajas, R.L. Panton, *Int. J. Multiphase Flow* **19**, 337-346 (1993).

A FULLY POLYMER-BASED SACRIFICIAL LAYER, CROSS-FLOW FILTER WITH 100 NM CUT-OFF SIZE

Jan Lichtenberg and Henry Baltes
Physical Electronics Laboratory, ETH Zurich, CH-8093 Zurich, Switzerland

Abstract

Physical retention at a flow constriction is a widely used technique to remove particles from a sample solution. However, for typical sample clean-up applications, these constrictions should have opening diameters of 200 nm and less to efficiently retain particulate matter. As the reproduction of these structures by standard photolithographic techniques is extremely challenging, we propose a novel sacrificial layer technique, which allows straightforward fabrication of densely packed arrays of nano-capillaries with one cross-sectional dimension being in the range of 100 nm and less. The technique is based on two layers of photostructurable polymer (EPON SU-8 resist) and a sandwiched metal layer defining the filter constrictions. A cross-flow filtration structure fabricated using this process showed highly reliable filtering of glass microbeads.

Keywords: microfilter, SU-8, sacrificial layer technique

1. Introduction

The removal of unwanted particulate sample contents is probably the most important clean-up operation preceding a typical chemical analysis. Classically, particles down to a diameter of 100 nm are either removed by centrifugation or by physical filter materials including cellulose, nylon, or porous glass. However, both options are difficult to integrate into a microfluidic system. Instead, filtering is often achieved by photolithographically patterned structures, such as dense arrays of posts [1] or shallow weirs [2]. Also, diffusion-based filters have been proposed [3]. In this paper, we present a new approach for the fabrication of robust polymer filters with cut-off sizes down to 100 nm, which are entirely made from a photopatternable epoxy (EPON SU-8). The cut-off is adjusted by a sacrificial metal layer sandwiched between to patterned SU-8 layers, which eliminates the requirement for sub-micrometer pattern generation and transfer. Sacrificial layer filters have been implemented as silicon-based structures, although the fabrication procedure is rather complex [4]. The filter presented here is designed for the gentle separation of blood plasma and cells without haemolysis (blood cell rupture), which would compromise further chemical analysis.

2. Device design

Fig. 1a illustrates the cross section of the filter, which consists of two layers of parallel microchannels fabricated with a slight, horizontal offset. The upper layer serves as inlet, the lower as outlet and both are connected by shallow, horizontal flow paths, which act as filter orifices or gaps. These are made by selective removal of a sacrificial metal layer (copper) towards the end of the fabrication process. It is advantageous in this design that the cut-off size is conveniently adjusted by the thickness of the sputter-deposited metal layer, which can be precisely controlled in the nm range. To avoid clogging of the inlet channel when using samples with a high particle load, a cross-flow architecture has been implemented, which continuously removes retained particulate matter from the upper channel layer (Fig. 1b).

Some constraints have to be considered for the filter design. Due to the slow, diffusion-limited etching process of the sacrificial layer, the length of the filter gaps should be as short as possible. A 40-µm-long and 200-nm-high gap requires ~20 min for the removal of the sacrificial copper layer. Also, in order to avoid sagging or breaking of the SU-8 cover over the filter gaps, support posts have to be implemented between both polymer layers by patterning of the sacrificial layer.

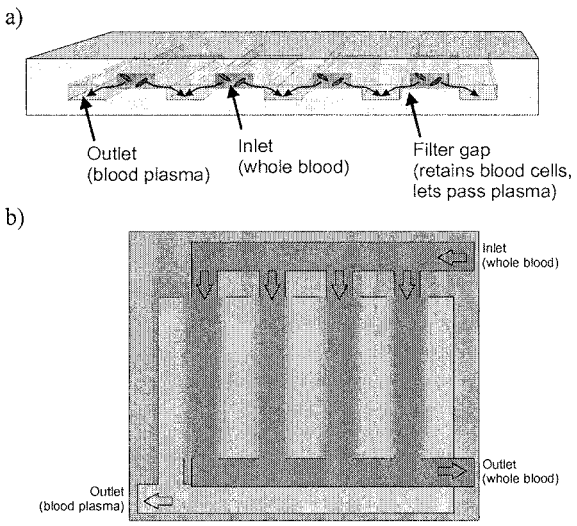

Figure 1: a) Schematic cross-section of the sacrificial layer filter. The sample solution (e.g. whole blood) is pumped through the upper layer of parallel channels (50 µm wide, 25 µm high). While the sample can pass through the thin (100 nm high, 15 µm wide) gap between the upper and lower channel layers, particles are physically retained. The filtered solution is collected via the lower channel array, which is offset with respect to the upper layer.
b) Top view of the filter structure. The inlet is split into multiple parallel channels to reduce the filter's back pressure.

3. Device fabrication

The fabrication of the filter structure involves the deposition and patterning of three material layers. First, the lower SU-8 layer (25 µm thick, SU8-2015) is spun onto a glass wafer, soft baked, exposed with the channel pattern, and finally post-exposure baked (Fig. 2). It is important that the layer is not developed at this point to maintain a flat substrate surface (the development is done at the very end of the process). Then, the sacrificial metal layer (e.g. 100 nm of copper) is deposited and patterned using a wet chemical etchant (e.g. ammonium persulphate solution). Standard lithography using Shipley S1828 photoresist was used for the metal patterning step. Finally, the upper SU-8 layer (25 µm) is deposited, exposed, and post-exposure baked. Subsequently, the upper channels are formed by development of the SU-8, followed by sacrificial metal layer removal in the same etchant as used for patterning. A second SU-8 development step (~60 to 120 min, intermitted ultrasonication, 50 W for 1 min every 10 min) is required to open the lower set of channels.

Especially for the comparatively long etching step for sacrificial layer removal, it has to be assured that the metal etchant does not dissolve or degenerate the SU-8 layers. Our experiments showed that a fully baked SU-8 film withstands a commercial copper etchant based on ammonium persulphate for 4 hours without cracking. However, due to the limited adhesion of the resist on our glass substrate, delamination occurred, which lifted the film off the substrate after some hours in the etchant. For longer sacrificial layer removal times, the adhesion would have to be improved.

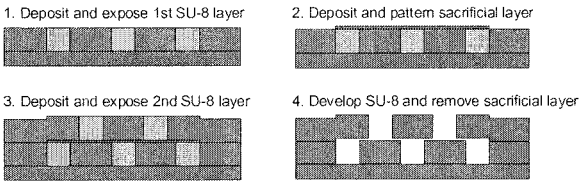

Figure 2: Filter fabrication procedure with a combined development and sacrificial layer removal step at the end to keep a flat substrate surface throughout the process

For experiments, the chips were covered with a slab of cured poly(dimethyl siloxane) (PDMS) with inlet and outlet reservoirs punched into the polymer. SU-8-to-SU-8 bonding would be an alternative to the PDMS cover if a permanent seal to the lid is desired.

4. Results

The filter was tested using phosphate-buffered saline solution (PBS, pH 7.4) loaded with 5-µm-diameter glass particles for visualization of the flow behavior in the device. Vacuum was applied to the outlet reservoir during the experiments, while a drop of bead suspension was pipetted into the inlet. Repeated experiments at flow rates ranging from 5 to 100 µL/min showed that beads were efficiently removed from the solutions without a single particle passing the filter barrier.

Also, unfiltered PBS solution containing environmental dust particles and plant spores were used to study the filter devices. Fig. 3 shows dust particles trapped at the interface between inlet channel and filter gap, while the liquid at the outlet is particle-free.

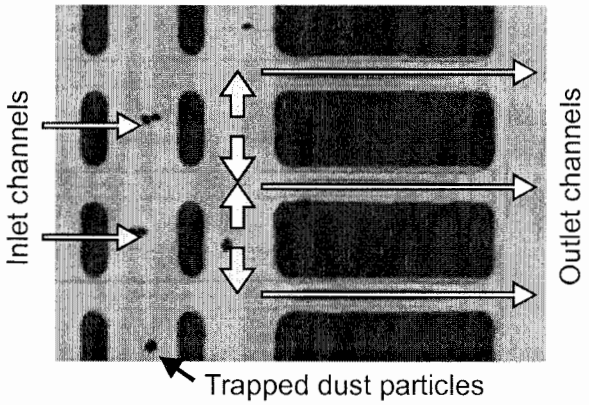

Figure 3. Microscope photograph of the filter structure at the outlet end during an experiment. Dust particles are trapped at the boundary between inlet channels and filter gaps, while the liquid in the outlet are particle-free. The bold arrows indicate sample flow across the filter gap from inlet to outlet channels.

5. Conclusions

The SU-8 sacrificial-layer process allows the straightforward fabrication of filters with highly reproducible and narrow cut-off sizes. The cross-flow design allows filtering of particle-loaded samples with a reduced risk of clogging and showed good separation performance. Currently, the device is tested with whole blood samples. Future work is directed towards improving the process further and towards combining the filter with other polymer-based fluidic components.

Acknowledgements

This research project is carried out within the EU framework Biofinger (IST-2001-34544) with financial support by the Swiss Federal Office for Science and Education, Bern, Switzerland.

References

[1] H. Andersson, W. van der Wijngaart, P. Enoksson, G. Stemme, *Sens. Actuator B-Chem.* **2000**, *67*, 203-208.

[2] R. D. Oleschuk, L. L. Shultz-Lockyear, Y. B. Ning, D. J. Harrison, *Anal. Chem.* **2000**, *72*, 585-590.

[3] J. P. Brody, P. Yager, *Sens. Actuator A-Phys.* **1997**, *58*, 13-18.

[4] G. Kittilsland, G. Stemme, B. Norden, *Sens. Actuator A-Phys.* **1990**, *23*, 904-907.

TRANSIENT MICROFLUIDIC VELOCITY MEASUREMENT AND PARTICLE CHARACTERIZATION WITH A LASER SCANNING CONFOCAL MICROSCOPE

Shih-hui Chao, Mark R. Holl, John H. Koschwanez, Robert H. Carlson, and Deirdre R. Meldrum

Microscale Life Sciences Center, University of Washington, Seattle, WA 98195-2500, USA

Abstract

Laser scanning confocal microscopes (LSCM) are commonly used for observing cell structure and physiological activity. In this paper, a LSCM was used to measure transient microscale flow velocity and dimensions of flowing particles in microfluidic chambers with a novel method: particle linear image velocimetry (PLIV). Dynamic measurement of transient flows with 250-ms temporal resolution and simultaneous calculation of particle dimension statistics have been achieved. The use of LSCM offers high spatial resolution for flows where in-plane velocity gradient in the direction of the optical path is important. The computing efficiency of this method is higher than comparable microfluidic velocimetry methods, making it possible for *in situ* measurements for lab-on-a-chip operations.

Keywords: particle linear image velocimetry, microfluidics, laser scanning confocal microscopy, particle statistics, fluorescent microsphere

1. Introduction

The laser scanning confocal microscope (LSCM) is a fundamental tool for observing cell structure and physiological activity. The authors are integrating a LSCM and microfluidic environmental chambers to analyze biophysical processes at the single-cell level [1]. The integrated microsystems platform requires automated microfluidic cell manipulations, highly sensitive detection of small molecules, and integrated data-handling systems. However, LSCM is not ideal for existing imaging velocimetry because of its slow image acquisition rate. To overcome the imaging rate limitation of LSCM, this paper reports the application of a new measurement method: particle linear image velocimetry (PLIV) [2]. The frame rate can be significantly increased by scanning one-dimensionally producing an effective linear imager. PLIV enables detailed characterization of the hydrodynamic characteristics and particle statistics present in complex devices, with special configurations adaptable to *in situ* measurements within lab-on-a-chip devices.

2. Theory

Consider a linear imager oriented at an arbitrary angle to the flow direction and recording linear images at a fixed time interval. The series of linear images can be expressed as a two-dimensional image in x and t (time) directions. As the particle passes across the imaging line, an elliptical streak in the x-t domain is created as shown in Figure 1. The transverse and lateral velocities of the particle (U and V, respectively) can be estimated by the geometry of the elliptical streak by

$$U = \frac{\Delta x - D}{\Delta t}$$

$$V = D/\Delta t,$$

where D is the diameter of the particle, Δx and Δt are the spans of the streak in the x and t directions, respectively. These dimensions of the ellipses are estimated with common binary image processing techniques. The estimation of particle diameter enables an easy way to characterize the statistical distribution of geometrical information of the particles. The details of the PLIV processing procedure are described elsewhere [2].

3. Experimental

The experimental apparatus is illustrated in Figure 2. The microfluidic chamber has a depth of ~150 μm created by an elastomeric spacer shim, with a 1 mm thick glass cap on top and a 160 μm thick glass coverslip on the bottom microscope objective interface surface. The length and width of the flow chamber used are 22 mm and 17 mm, respectively. The channel aspect ratio of width to thickness is << 1. As a result flow within the majority of the channel closely approximates two dimensional slot flow. One-μm diameter green fluorescent microspheres (G0100, 5% diametral variation, Duke Scientific) were seeded into distilled water and the mixture was pumped with a positive displacement pump (MilliGAT, Global FIA Inc.) with flow rate controllable by a PC. In this experiment, the flow rate was programmed to step from 100, 125, 150, 175, to 200 nL/s at a constant interval of 5 seconds.

The microfluidic chamber was observed on an LSCM (Axiovert 200M with LSM Pascal, Zeiss) with a 100x, 1.3 NA oil-immersion objective. The achieved depth of field was 0.9 μm. The 488-nm laser scanned linearly at the center of the flow chamber, normal to the flow at its maximum frequency of 1 ms per line. The origin of z-axis was set to the bottom surface of chamber where the particles appeared fixed.

4. Results and discussion

Velocities were measured at z = 8 μm. A 250-ms interrogation window was traversed across the acquired 25-second x-t image. The statistics of flow velocity and particle size are calculated from the particle streaks in each window, whose duration determines the temporal resolution of the measurement. The results during a 25-second period are shown in Figure 3 with 90% confidence interval error bars. The dashed lines in these figures represent the velocity converted from set flow rate. The measurements show good agreement with these reference lines.

The measured microsphere diameter distribution is shown in Figure 4, where the dashed curve shows the fit Gaussian distribution of 1.02-μm mean and 0.21-μm standard deviation, compared to the nominal 1-μm mean and 0.05-μm standard deviation published by the manufacturer. The extra variation is believed to cause by measurement noise and the random motion of the particles.

5. Conclusions

This use of a LSCM to perform velocimetry in microfluidic devices and systems has been quantitatively demonstrated. The PLIV algorithm was applied to process the acquired images. Dynamic measurement of transient flow and particle size estimation yielded good results, demonstrating promise for real-time particle and microfluidic flow characterization. Because microdevices and LSCM are gaining popularity in the biology community, PLIV holds promise to become a commonly used approach to measure flow velocity at the microscale.

Acknowledgements

We acknowledge the support of this research by the NIH, National Human Genome Research Institute, Centers of Excellence in Genomic Science, Grant Number 1 P50 HG002360-01, CEGSTech: Integrated Biologically-Active Microsystems.

References

[1] M. E. Lidstrom and D. R. Meldrum, *Nature Reviews Microbiology*, **1**, 158-164 (2003).

[2] S. H. Chao, M. R. Holl, J. H. Koschwanez, R. H. Carlson, L. S. Jang and D. R. Meldrum, ASME 2nd international Conference on Microchannels and Minichannels, 925-930 (2004).

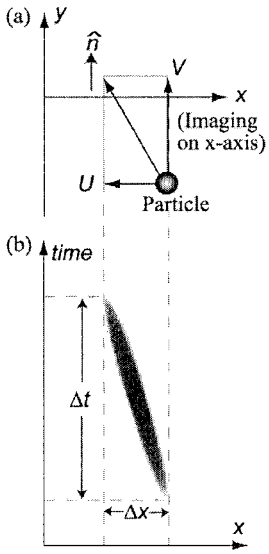

Figure 1. Illustration of PLIV and the coordinates of the fluid flow and temporal image capture. (a) A particle passing through an imaging line on x-axis in a spatial domain. (b) The resulting streak on a x-t domain.

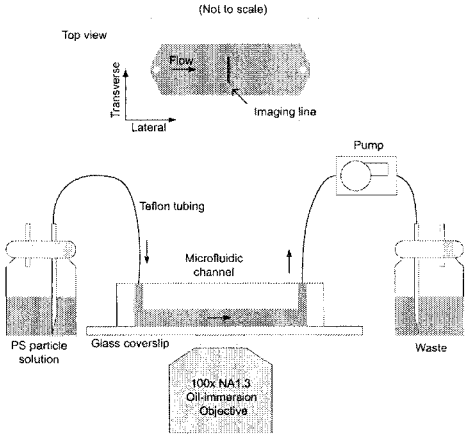

Figure 2. A schematic of velocity measurement set-up.

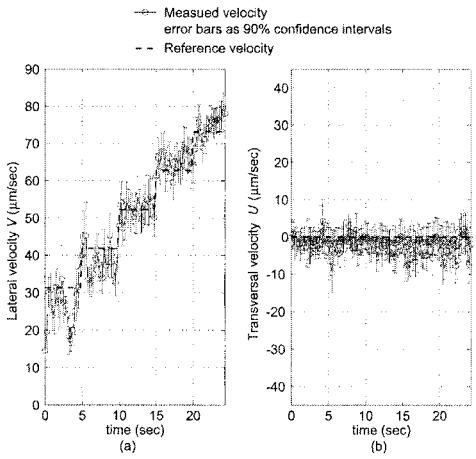

Figure 3. PLIV measurement at z=8 μm for stepping velocity experiment with error bars as 90% confidence intervals. The dashed line is the set velocity at this z plane shown as a reference.

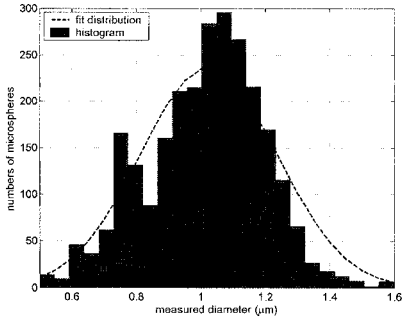

Figure 4. The distribution of measured microsphere diameter.

PRECISE AND AUTOMATED MICROFLUIDIC SAMPLE PREPARATION

Bruce P. Mosier, Robert W. Crocker, Cindy K. Harnett and Kamlesh D. Patel
Microfluidics and Advanced Microsystems Engineering Dept.,
Sandia National Laboratories, 7011 East Ave., MS9951, Livermore, CA 94550, USA

Abstract

Autonomous bio-chemical agent detectors require sample preparation involving multiplex fluid control. We have developed a portable microfluidic pump array for metering sub-microliter volumes at flowrates of 1-100 μL/min. Each pump is composed of an electrokinetic (EK) pump and high-voltage power supply with 15-Hz feedback from flow sensors. The combination of high pump fluid impedance and active control results in precise fluid metering with nanoliter accuracy. Automated sample preparation will be demonstrated by labeling proteins with fluorescamine and subsequent injection to a capillary gel electrophoresis (CGE) chip.

Keywords: electrokinetic pump, flow control, sample preparation, protein labeling

1. Introduction

Autonomous pathogen identification requires automated sample preparation and precision flow control. For portable microfluidic systems, multiple compact pumps are needed to achieve the various sample preparation steps of bio-chemical assays such as sample collection, concentration, and buffer exchange. Precision flow control requires pumps with closed-loop feedback, rapid response, and passive pump isolation. We have developed a computer-controlled, closed-loop array of EK pumps, flow sensors, and high-voltage power supplies that can meter (aqueous) analytes at 1-100 μL/min into sample preparation microfluidics at pressures of up to 1000 psi, respectively.

2. Experimental Apparatus

The pump array is based on EK pumps developed for high-pressure microhydraulic actuation [1]. Electrokinetic pumps have a fast transient response (kHz) but a slow fluid velocity (1-3 mm/s). For fast flowrate control, both the pump and the downstream microfluidics must be fully wetted to avoid long pressurization times. Our millimeter-scale EK pumps have the (demonstrated) capability to produce pressures up to 1500 psi (10 MPa) and flowrates up to 200 μL/min. Even higher peak flowrates and peak pressures may be obtained by increasing the pump cross-section and length, respectively.

As shown in Figures 1 and 2, the outlet of each EK pump is connected to a fluid isolator and flow sensor. The flow sensor outlets are connected to the tees, crosses, and chips of the sample preparation microfluidics. The flow isolator is a commercial glass tube and fluorocarbon seal that mechanically isolates the EK pump fluid from the analyte fluid to avoid diluting the analyte and to keep the EK pumps operating near optimum efficiency. More than 200 injections have been demonstrated from 100, 250, and 500-μL isolators. Flowrate measurement is accomplished with a pair of pressure transducers that measure the pressure drop across a calibrated capillary flow restrictor with a scaling constant that is a function of the fluid viscosity and restrictor geometry. Rapid flowrate transients are generated by driving the EK pumps with high-voltage power supplies, which are dual-polarity for bi-directional pumping and capable of 15-Hz operation.

3. Flow Control

The intent of the closed-loop control strategy is to provide rapid, stable flowrate control over a range of flowrates (1-100 μL/min). Due to compression of any small air bubbles and expansion of the pumping hardware, a finite time delay (one second or less) exists between the start of flow in the EK pump and flow at the sensor. This delay motivates the use of a modified PID algorithm in

which the PID gains are functions of flowrate and pressure. As can be seen in Figures 3 and 4, the fastest flowrate transients occur between closely-spaced flowrates, such as the transition from 20 to 30 μL/min which occurs within 400 ms. The maximum sample rate is limited to 15 Hz by the settling time of the high-voltage power supplies (30 ms) and communication and computer processing time (20-30 ms). As a result, only 3 to 4 samples are available for some flowrate transitions, which can lead to slower transitions.

Multiple pumps sharing an input to the sample preparation microfluidics remain largely independent due to their relatively high fluid impedance. Closed-loop control compensates for any remaining influence of one pump on another. Figure 5 shows simultaneous metering from two pumps connected to a mixer and programmed to alternately meter 2.5 and 5 μL at flowrates of 10 and 20 μL/min. The respective rise time and settling time are 1 second and 4 seconds. Small effects from one pump on the other can be seen during startup and shutdown.

Rapid flow control is helpful for precision volume metering in which the smallest volume that may be reliably metered is given by the slowest flowrate combined with the fastest pressurization and de-pressurization. In this system, the slowest flowrate is 1 μL/min (corresponding to a pressure drop of 5 psi), although slower flowrates may be obtained with more restrictive flow sensors and/or more restrictive sample preparation microfluidics. Coupled with rise and fall times of 1 second each and a dwell time of 3 seconds, a volume of 80 nL can be metered. Nanoliter accuracy has been demonstrated on microliter volumes, with repeatability better than 1% over hundreds of injections.

4. Protein Labeling

Having demonstrated precision fluid control, an array of three pumps was assembled to demonstrate automated sample preparation. The sample preparation process involves labeling proteins with fluorescamine and subsequent CGE separation. The pumps were configured as shown in Figure 2, and the reservoirs were loaded with 10-mM fluorescamine in acetonitrile, protein standards in borate buffer with surfactant, and water. Fluorescamine and protein were simultaneously injected at a flowrate ratio of 9:1 into a 250-μm-I.D. capillary. After waiting one minute for the fluorescamine to bind to the proteins, the mixture was injected onto the sample loop of the CGE chip. The resulting CGE separation with laser-induced fluorescence (LIF) detection is shown in Figure 6 (top) and compared with the separation of a sample prepared by metering with pipettes, mixing in a vial, and manual injection onto the sample loop of the CGE chip (bottom).

5. Conclusions

We have developed a portable pump array capable of metering sub-microliter volumes at flowrates from 1-100 μL/min. Non-linear control enables rapid flowrate transients over the range of flowrates and can accommodate variable external loads. Flowrate control was demonstrated by automated labeling of proteins with fluorescamine and subsequent injection to a CGE module.

Acknowledgements

We are grateful to Jamie Stamps, Dan Yee, Brad Aubuchon, Ron Renzi, and Julie Fruetel for their assistance and support. This work was performed by Sandia Corporation, a Lockheed Martin Company, for the United States Department of Energy's National Nuclear Security Administration under Contract DE-AC04-04AL85000.

References

[1] B. P. Mosier, R. W. Crocker, J. L. Rognlien, and K. D. Patel, High-pressure microhydraulic actuator, in: Proceedings of ASME IMECE, Washington, D.C., (2003).

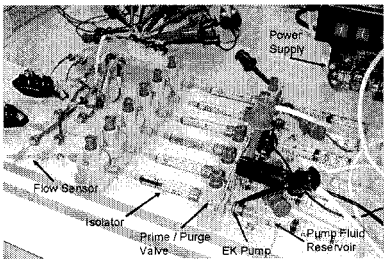

Figure 1. A closed-loop electrokinetic pump array (data acquisition computer not shown).

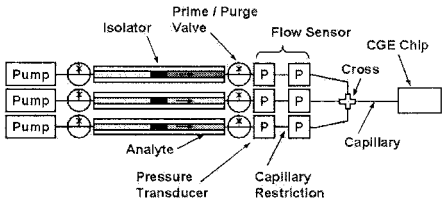

Figure 2. Schematic of a pump array configured for automated protein labeling and CGE separation (not to scale). Flow is from left to right.

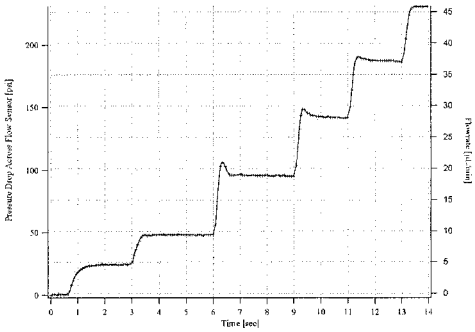

Figure 3. Closed-loop, automated flowrate control and precision volume metering.

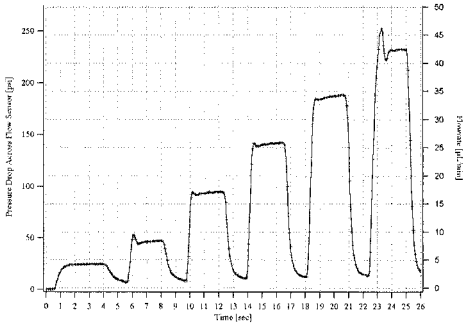

Figure 4. Closed-loop, automated flowrate control and precision volume metering.

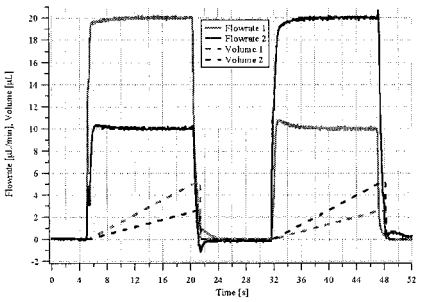

Figure 5. Flowrates and volumes from two pumps delivered to a mixer (2.5 and 5 μL).

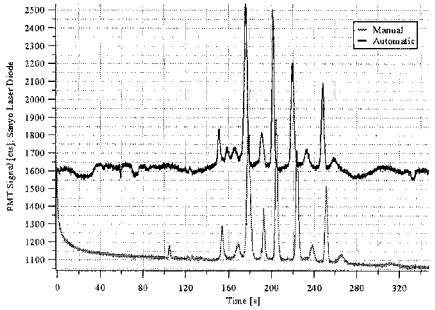

Figure 6. Laser-induced fluorescence detection of a series of protein peaks after separation via capillary gel electrophoresis (CGE).

CELL ENCAPSULATION ON A MICROFLUIDIC PLATFORM

Jeffrey S Fisher[1] and Abraham P Lee[1,2]

[1] *Dept. of Biomedical Engineering, University of California Irvine, 204 Rockwell Eng. Center, Irvine, CA, 92697*

[2] *Dept. of Mechanical Engineering, University of California Irvine, 204 Rockwell Eng. Center, Irvine, CA, 92697*

Abstract

A novel microfluidic device for the encapsulation of cells is presented. Rat neuroblastoma cells (B103) have been captured in <100 μm diameter droplets in a continuous process that allows for various technologies (e.g. combinatorial delivery of drugs to cells, polymerization of droplet, etc) to be incorporated on-chip, downstream of the encapsulation region.

Keywords: cell encapsulation, microfluidics, cell-based therapy, droplets

1. Introduction

As μTAS technologies have progressed, the range of their applications has grown steadily from chemicals to DNA and proteins and now to cells. While micro-sized (400-800 μm) polymer encapsulation of cells has been previous reported [5,6], none have been carried out on a microfluidic platform, and the four-fold decrease in capsule diameter presented here corresponds to a proportional increase in surface-to-volume ratio, diffusion of nutrients, and mechanical strength [6]. The advantages of this technique include the physical and chemical isolation of groups of cells from one another and the ability to digitally manipulate these groups (e.g. combinatorial exposure to different factors or precise formation of heterogeneous cell populations through the fusion of droplets containing different cell types.). In essence, the droplets represent 100 μm well plates, which can be individually and automatically manipulated, allowing established and developing μTAS technologies to be applied directly to cells. Possible applications include combinatorial cell assays, cloning, FACS-like assays, and polymer encapsulation for cell-based therapies.

2. Design

The microfluidic design consists of upstream cell loading and shearing zones and a downstream cell encapsulation zone (Fig. 1). Cell loading included two separate methods. In the first, cells were loaded at densities low enough to reduce cell-to-cell adhesion to avoid channel clogging, since even small cell clusters can be as wide as the channels. However, the number of encapsulated cells was also quite low (most droplets contained no cells.). Rather than attempt to prevent cell clumping by changing the media (decreased calcium reduces cell adhesion,) a packed loading method was adopted. In this method, the cell clusters are allowed to aggregate and are forced through the loading channel, much like a very viscous fluid (Fig. 3). The shearing/ focusing region serves two purposes. The first is to shear off small groups of cells and send them to the encapsulation region (Fig. 3). The second is to focus the cells and cell media to the center of the channel to reduce the build-up of proteins and cell debris on the channel walls. The cell encapsulation zone utilizes mono-dispersed droplet-formation designs using previously reported generation geometries [1-4] in PDMS channels molded from SU-8 masters. The channel depth was 40 μm with widths of 30 and 50 μm, for the cell loading and fluid (oil and water) channels, respectively.

3. Experimental

B013 cells are cultured, re-suspended in new media, and injected into the cell inlet port. Syringe pumps provide flow rates to the oil, water, and cell inlets of 3.0 μl/min, 1.6 μl/min, and 0.5 μl/min respectively. Initially, the droplet generation is established using only the oil and water flows, so that the generation is stabilized before the addition of the cells. This prevents the deposition of

proteins, carbohydrates, and cell debris onto the channel walls, which would change the surface energy (from hydrophobic to hydrophilic) and inhibit droplet formation.

The encapsulation of the cells is recorded on a high-speed camera. The number of cells per droplet was calibrated to the grayscale of the images and estimated via software.

4. Results and discussion

As Figure 4 shows, the number of cells that are encapsulated per droplet can be fairly consistently regulated. The water flow remains continuous to stabilize and maintain the droplet generation; therefore, it is reasonable to expect that a percentage of the droplets will contain no cells (discussed below.). However, of the droplets that do contain cells, almost 90% contain between 1-20 cells, avoiding the disruption of the droplet generation caused by huge clusters of cells.

Since the channel depth is 40 μm and the droplet diameters are in general over 100 μm, the droplets shown are not spherical, but rather a squat cylindrical shape. If allowed to expand, the droplets would form spheres of 80-100 μm in diameter, with the smallest cell-containing droplet measured to be 70 μm in diameter. The range of droplet sizes was larger than standard droplet generation techniques without cells (11% variation as compared to 2% [1]) because of the stochastic nature of the cell delivery to the encapsulation region. Work is underway to minimize this effect by optimizing the geometry of the shearing region. Furthermore, a large percentage of droplets contain no cells due to the fact that the water flow rate is greater than that of the cells. While improved shearing geometries will reduce this ratio, droplets can also be filtered after encapsulation using the shear-streaming effect [7] to extract and dispose of those droplets which do not contain cells, or contain too few to be viable.

The encapsulation of the cells can be either temporary or permanent. Temporary isolation could allow the cells to be exposed to discrete concentrations of chemicals or factors and then cultured again. Permanent encapsulation involves the addition of polymers to the shearing flow. The gelation agents for the polymers can be introduced in one of two manners: 1) a secondary droplet population will be generated and induced to fuse with the cell capsules, 2) the cell droplets will be extracted into a water phase stream containing the polymerization agent established parallel to the oil phase. This type of polymer encapsulation is the basis for many developing cell-based therapies such as islet-cell implantation. [5]

5. Conclusions

As μTAS applications expand to include more and more cell-based assays and manipulations, new techniques are needed to conduct the cells through devices in a controlled manner and regulate the delivery of substances to the cells. The encapsulation method presented herein allows for the physical and chemical isolation and control of cells in both temporary and permanent manners on a microfluidic platform.

Acknowledgements

The authors would like to thank Edwin S. Monuki and Lisa Flanagan for their help in providing the cells and related training that enabled much of this work.

References

[1] Y.C. Tan, J. Collins, A.P. Lee, μTAS 2003, p. 963.
[2] T. Thorsen, W.R. Robert, F.H. Arnold, S.R. Quake, (86)18, Phys. R. Letters, p. 4163.
[3] S.L. Anna, N. Bontoux, H.A. Stone, 82(3), Appl. Phys. Letters, p.364.
[4] H. Song, J.D. Tice, R.F. Ismagilov. Agnew. Chem. Int. Ed., p. 767.
[5] W. M Kuhtreiber, R.P. Lanza, W.L. Chick, 1999, Birkhauser Press.
[6] L. Canaple, A Rehor, D Hunkeler, 13(7), J. Biomaterials, p. 783.
[7] Y.C. Tan, J.S. Fisher, A.I. Lee, A.P. Lee, Lab Chip, DOI: 10.1039/B403280M.

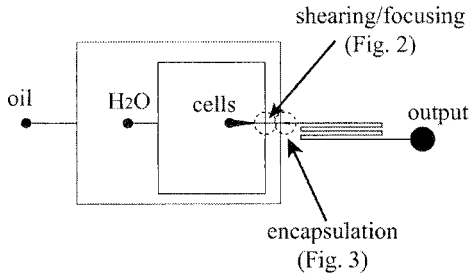

Figure 1. Device Design. The cells pass through two functional regions. The first focuses the cells to the center of the channel and shears off cells if they are self-adhered. The second encapsulates the cells in droplets.

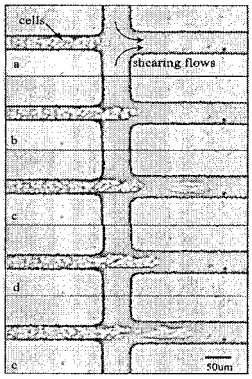

Figure 2. Shearing Region. a-b) As cells come out from the loading region (left channel, 30um) they are exposed to shearing flows from the upper and lower channels (50um, flow rate: 1.0 µl/min). The horizontal force pulling apart the cell mass is proportional to the length exposed to the shear flows. c-e) Thus, the size of the group of cells that is sheared off can be regulated by the geometry of the region.

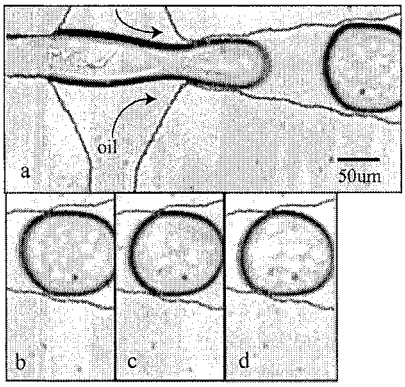

Figure 3. Cell Encapsulation. a) Oil flows from the upper and lower channels, pinching off droplets (diameter ~100 µm) containing the cells and cell media. b-d) Preceding droplets contain similar numbers of cells.

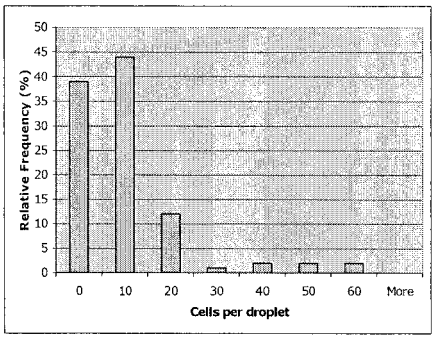

Figure 4. Number of Cells Encapsulated per Droplet. "Empty" droplets stabilize the generation process, allowing for cell capsules to remain mono-dispersed.

A PERFORMANCE COMPARISON OF POST- AND RIDGE-BASED DIELECTROPHORETIC PARTICLE SORTERS

Rafael V. Davalos, Blanca H. Lapizco-Encinas, Gregory J. Fiechtner, Anup K. Singh, Blake A. Simmons, Yolanda Fintschenko, and Eric B. Cummings

Sandia National Laboratories, P.O. Box 969, MS 9036, Livermore, CA 94551

1. Introduction

Sample concentration is an essential step for the detection of pathogens in a microfluidic platform. Dielectrophoretic architectures have been developed to support particle sorting and sample processing in microfluidic systems. We present a comparison of measured performance of insulating-post-based (2-D) and insulating-ridge-based (2-1/2-D) dielectrophoretic particle filter/concentrators and experimental observations and analysis of issues facing each architecture. In batch mode, saturation of the dielectrophoretic traps limits the selectivity and device capacity that can be achieved simultaneously. Saturation limits the effectiveness of such filters when target particles are present in low concentrations compared to similar background particles, typical when processing samples to extract pathogens. We report the degree of saturation as a function of applied field and collection period.

After trapping particles for the desired collection period, elution takes place by decreasing the magnitude the applied DC field. For post-based arrays, trapping occurs in potential wells in multiple locations within the microfluidic channel. The corresponding elution volume is large. Therefore, we have also explored batch-mode operation using insulating-ridge-based concentrators. Here, ridges selectively deflect particles to potential-well-traps located in a confined spatial region, corresponding to elution volumes that are reduced greatly. The reduced elution volume is achieved with the penalty of a limited saturation volume when compared to that achieved in post-based arrays.

Keywords: dielectrophoresis, electrokinetic flow, concentrator, sample preparation

2. Experimental

Experiments were conducted in a microfluidic chip consisting of patterned channels isotropically etched to a 10-μm depth in borosilicate glass [1-3]. Microchannels are straddled by two reservoirs that have a diameter of ~1 mm and a depth of ~1 mm. The distance between the reservoirs is 10.2 mm. For the post arrays, the array area is located in the middle of the microchannel, 2.9 mm from each port. The arrays consist of circular posts with 200-μm diameters, spaced 250 μm from center-to-center. The channel and reservoirs were filled with a solution consisting of DI water, NaOH, and KCl to obtain 7.5-8.0 pH and 1.0- or 2.0-μS/mm conductivity. Platinum electrodes are placed in the reservoirs and an electric field is applied.

Lyophilized *Escherichia coli* (strain BL21) are obtained from Stratagene (La Jolla, CA). Cell cultures are grown at 37 °C using standard culture techniques to obtain cells in late log phase and labelled with Syto® 11 (Molecular Probes, Inc., Eugene, OR) dye (excitation/emission 508/527 nm). The concentration factor of *E. coli* in the microchannels is evaluated by performing experiments with an initial dilution of 1 x 10^5 cells/ml that are concentrated and subsequently released in the following manner:

(a) A pressure-driven flow (~100 Pa) was applied continuously.
(b) An electric field was applied and the cells were trapped in the post array.
(c) The *E. coli* cells were released from the dielectrophoretic traps as a plug of cells.

For each of these three stages, a 250-frame, arbitrarily selected movie was recorded. The rate at which particles escape the device while the electric field is applied was estimated by counting the number of cells that pass through the outlet. The number of concentrated cells was calculated by counting the number of cells in the movie frame with the highest population. The concentration factor is defined as the ratio of the cell flow rate evaluated at the frame containing the plug of concentrated cells as they elute the post array to the rate at which cells flow pass the outlet (before the electric field is applied).

3. Results and discussion

Figure 1 (a) shows the operation of a post-based device that is batch-concentrating *E. coli* near full saturation. The flow is electrokinetically driven from left to right with an applied mean field of 75 V/mm. Because all traps are saturated, particles escape the device, a condition we call "breakthrough." This behavior is reasonably predictable and called "normal saturation." In contrast, Fig. 1 (b) shows the operation of the same device at the same voltage as Fig. 1 (a). In this case, the particles accumulate significantly only in the first row of the posts. These densely collected particles are an electrokinetic packing that blocks upstream particles from propagating into the device. Such "anomalous saturation" never exhibits breakthrough and loses nearly all selectivity. With judicious operation, devices can saturate normally, but factors influencing the saturation behavior are comparatively subtle. Typically, 98% of the *E. coli* are trapped within the device under normal saturation conditions.

Figure 2 shows the concentration factor obtained for *E. coli* cells in a corduroy array. Here, particles are deflected along the ridge, reaching a potential well near the wall, where they are then trapped. The concentration factor is ~6000, reaching saturation after a mean electric field of 80 V/mm is applied for ~16 s.

To test operation of the device well before the onsite of saturation, experiments were conducted using mean fields of 50 V/mm, 75 V/mm, and 100 V/mm for 1 or 2 minutes, conducted for each configuration for eighteen measurements. The results are summarized in Table I, demonstrating concentration factors that are all above three orders of magnitude and that increase with applied electric field. Results summarized in Table II demonstrate that the concentration factor increases with the collection period, indicating that the collector has not reached saturation or a performance limit, even for up to 32 min at 75 V/mm, corresponding to concentration factors of > 6000.

Table I. Concentration as a function of applied field for 1 and 2 minutes.

Mean Field (V/mm)	1 min Concentration Factor		2 min Concentration Factor	
	mean	deviation	mean	deviation
50	1640	229	2427	184
75	2029	284	2733	281
100	2071	71	3208	389

Table II. Concentration as a function of duration at 75 V/mm.

Duration (min)	Concentration Factor
1	2029
2	2733
4	3097
16	4598
32	6172

4. Conclusions

The post-based iDEP device was used to trap *E. coli* with up to 100% removal efficiency and release a ~6000X concentrated plug of cells. Because of the low initial concentration, the particle traps remained far from saturation during this test. While saturation dramatically complicates the

operation and limits the selectivity and repeatability of the post-based device, the corduroy device demonstrated an approach that allows concentration to saturation in a localized region with minimal effect on selectivity and the global flow-field. This approach also localized the particle trap to a compact region near a channel wall, facilitating efficient elution. The corduroy iDEP concentrator demonstrated concentration by more than 3 orders of magnitude in 16 seconds, limited by saturation.

Acknowledgements

This work was performed by Sandia National Laboratories for the United States Department of Energy under Contract DE-AC04-04AL85000. The authors acknowledge funding from Sandia Laboratory Directed Research and Development grants. The authors thank Allen Salmi for technical assistance in assembling the experimental apparatus, and Judy Rognlien for preparing *E. coli* samples.

References

[1] E. Cummings and A. Singh, *Analytical Chemistry* **75**, 4724-4731 (2003).
[2] B. H. Lapizco-Encinas, B. A. Simmons, E. B. Cummings and Y. Fintschenko, *Analytical Chemistry* **76**, 1571-1579 (2004).
[3] B. H. Lapizco-Encinas, B. A. Simmons, E. B. Cummings and Y. Fintschenko, *Electrophoresis* **25**, 1695-1704 (2004).

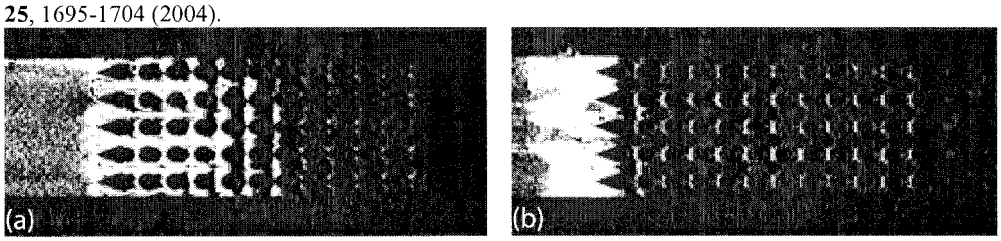

Fig. 1. Demonstration of Saturation Behavior in a Post Array. (a) Image captured after 71 seconds of operation; particles saturate traps, and then flow downstream, saturating traps at downstream locations. The entire array is filled with particles for longer periods of operation, when particles break through the downstream edge of the post array. (b) Image captured after 90 seconds in the same microchannel as for (a). Particles anomalously saturate the traps located at the front row of posts, ultimately forming an electrokinetic barrier to further downstream particle flow.

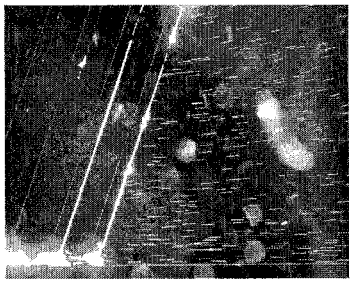

Fig. 2. Demonstration of Saturation Behavior in a Corduroy Array. (Fluorescence image of 2-μm polystyrene microspheres in a fully saturated corduroy DEP concentrator. The ridges in the 20- μm -deep by 3-mm wide glass channel are 13- μm tall and 100-μm wide. The electrokinetic particle flow is from right to left at ~1 mm/s, produced by a field of 80 V/mm. With the high inlet particle concentration, the device saturates with particles in ~16 s, providing a ~6000X concentration factor.

RECONFIGURABLE MICROFLUIDIC WAVEGUIDES FOR ON-CHIP FLOW CYTOMETRY

Tor Vestad, Matt Brown, John Oakey and David W.M. Marr
Department of Chemical Engineering, Colorado School of Mines, Golden, CO 80401

Abstract

A novel microfluidic waveguiding platform based completely upon total internal reflection conditions established at fluid-fluid interfaces has been developed and is demonstrated. We employ a simple system composed of high and low refractive index aqueous fluids to establish core-cladding systems via hydrodynamic focusing. The high-index sucrose-water core is confined between distilled water sheath flows and effectively waveguides light without significant interaction with the microchannel walls. By modulating the relative flow rates of the three streams it is possible to direct light along any accessible flow path in the microchannel network. We demonstrate the application of this waveguiding platform to flow cytometry tasks by exciting and collecting the emitted radiation from a suspension of fluorescent polymer microbeads.

Keywords: waveguide, flow cytometry, cell counting

1. Introduction

While radiation waveguiding currently provides the foundation of modern communications across large distances, related technologies at small length scales are emerging as a valuable component of microfluidic-based analytical systems in biology and medicine. As optically interrogated microfluidic devices increase in complexity, on-chip data transfer will become increasingly important. To realize microscale waveguiding and eliminate data bottlenecks associated with information transport across length scales, integrated solutions are needed. With this goal, previous approaches have sought to incorporate optical fibers directly into microscale architectures[1,2], however this method will prove limiting as these systems are static, not readily scalable, and their insertion into microfluidic networks has proven a significant fabrication challenge. Here, we eliminate these concerns by directly employing microfluidic flows as the foundation of microscale optical waveguiding networks.

2. Theory

Previous studies have demonstrated the feasibility of using microfluidic systems to create simple fluid waveguides[3] and hybrid micro-optical devices[4]. To facilitate waveguide integration and allow easy switching of the resulting optical networks we take advantage of the laminar nature of microfluidic flows to generate and position a high refractive index waveguiding fluid "core" with smooth fluid-fluid interfaces using a lower refractive index fluid "cladding"[5]. The width and position of the center stream are a function solely of the relative volumetric flow rates among the three inlet streams. With a high-index "core", this approach allows light to be waveguided to precise locations in a reconfigurable, dynamic fashion.

Internal reflection and waveguiding requires a low-index sheath fluid, in this case deionized water of refractive index $n = 1.33$, and a high-index fluid core composed of a 67% by weight sucrose/water solution with a measured refractive index $n = 1.457$. This leads to a $\theta_{crit} \sim 66°$ at the water interfaces. To confine the waveguides at the top and bottom surfaces, our channel structures are fabricated in poly(dimethylsiloxane) (PDMS) using soft-lithography techniques[3]. With a refractive index $n = 1.41$, PDMS provides not only a $\theta_{crit} \sim 75°$, it allows microfluidic networks to be quickly replicated from a permanent, reusable master with fidelity on the order of single nanometers. This particular system provides a numerical aperture of 0.42 at the inlet PDMS/high-index fluid interface and 0.59 at the air/PDMS interface, values significantly higher than the typical

optical fiber value of 0.22 and facilitating the easy coupling of external light sources or detectors to these waveguiding networks.

3. Experimental

Networks of microchannels were fabricated using now standard rapid prototyping and soft lithography technique[4]. In this technique, a high-resolution photomask is used to selectively expose and polymerize a polymer-based photoresist spun cast onto a silicon wafer. Once developed, the resulting three-dimensional structure was used as a template for repeated replication in poly(dimethylsiloxane) (PDMS). Cover slips were inserted in the curing PDMS to create optically flat surfaces for the introduction and removal of light. The PDMS replica was finally bonded to a clean, flat PDMS surface through oxygen plasma exposure to produce a sealed microfluidic network. Both core and cladding fluids were delivered to the microfluidic network via syringe pumps that could be controlled independently. A 532 nm HeNe laser was focused upon and aligned with the trailing edge of the core stream.

In cytometry experiments, a 90° bend was introduced to the channel structure 1 mm downstream of the focusing point. Here, waveguiding ceased and the escaping light was condensed and focused onto a photomultiplier tube (PMT) coupled to LabView for signal acquisition. A 532 nm band rejection filter was placed between the microfluidic device and the PMT to eliminate measurement of the excitation radiation and reduce the signal to just that of the excited wavelength. In these experiments, Texas Red doped fluorescent polystyrene particles of 1 μm diameter were excited and the intensity of their 580 nm emission spectrum was monitored. A smooth gradient of particles was created within the waveguiding fluid by introducing a concentrated suspension followed by clean sucrose-water, which mixed with and gradually flushed out the tracer particles.

4. Results and discussion

Figures 1 demonstrates waveguiding of a focused laser beam where, by adjusting the relative flow rates, the high-index center stream may be directed into different outlet channels. The illumination of fluorescent tracer particles confined to the center stream demonstrates the ability of a simple hydrodynamically-focused flow to serve as an optical waveguide. It also shows that microfluidic flow control can be used to directly manipulate light, thus allowing custom reconfiguration of the fluid-based optical network.

The waveguiding system that we demonstrate is of potentially great utility in micro total analysis systems as a flow cytometry component. This is demonstrated by collecting the excitation wavelength of the excited tracer particles in the core fluid stream. As the data of Figure 2 shows, we are able to follow the particle wash out with great sensitivity. Careful calibration of these data will enable the quantification of the particle population based upon the magnitude of emitted intensity, potentially allowing for the counting of individual fluorescent bodies.

5. Conclusions

The entirely fluid-based waveguiding scheme presented here not only takes advantage of unique flow properties of microfluidic situations, but is perfectly suited to facilitate the integration of information processing requirements within micro total analysis systems. We have demonstrated waveguiding, reconfiguration of the waveguide, and a flow cytometry approach allowing for particle identification and quantification in microfluidic-based devices. The convenience, ease of integration and potential for parallelization this technique offers suggests its significant utility for portable analysis and diagnostic applications.

Acknowledgements

This work was supported by grants from the United States National Science Foundation and the National Aeronautical and Space Administration.

References

[1] Lin, C.-H. & Lee, G.-B. *J. Micromech. Microeng.* **13**, 447-453 (2003).

[2] Liang, Z. et al. *Anal. Chem.* **68**, 1040-1046 (1996).

[3] Schueller, O. J. A., Zhao, X. M., Whitesides, G. M., Smith, S. P. & Prentiss, M. *Advanced Materials* **11**, 37 (1999).

[4] Mach, P. et al. *Applied Physics Letters* **80**, 4294-4296 (2002).

[5] Knight, J. B., Vishwanath, A., Brody, J. P. & Austin, R. H. *Physical Review Letters* **80**, 3863-3866 (1998).

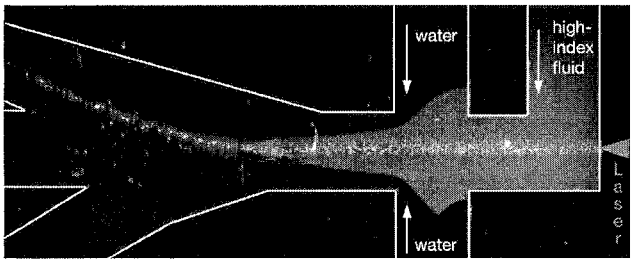

Figure 1. Optical waveguiding of a 200 μm wide red (532 nm) laser beam. Here the high index fluid has been labeled with rhodomine 6G. Fluorescent tracer colloids are present in both high-index core and cladding flows. The substantial lack of excitation in the cladding streams indicates the waveguiding efficiency.

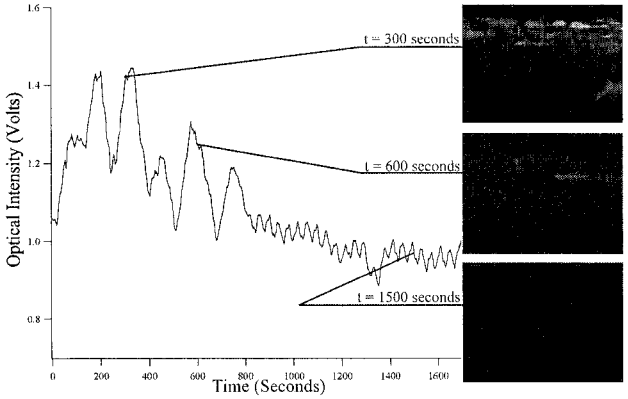

Figure 2. Measurement of waveguided fluorescent emission intensity during particle wash-out. 1 μm polystyrene spheres doped with Texas Red fluorescent dye were introduced to the inlet well of the core fluid at t=0 and replaced by clean core fluid when the particle reached the detection area. The resulting gradual particle washout is traced as the emission intensity declines to the baseline by 20 minutes. Oscillations in the data are due to pulsatile aberrations in the syringes used to drive flows.

A HIGH DENSITY MICROFLUIDIC MICROARRAY PLATFORM FOR RAPID GENOMIC PROFILING

Jay A.A. West, Kyle W. Hukari, Timothy Shepodd, and Gary A. Hux

Microfluidic Research Group, Sandia National Laboratories, Livermore, CA USA

Abstract

We have developed microfluidic gene array chips and supporting hardware to produce a miniaturized microarray platform for rapid sample preparation and probe hybridization in order to perform rapid genomic profiling on high density microarrays. This platform allows the sample concentration, probe labeling and hybridization, and detection of nucleic acid containing samples in a hand portable sized device.

1. Introduction

Sensitive, accurate detection and portable identification of biological weapons is critical to our ability to avert wide spread casualties from a bio-terrorist threat. The use of Gene or "micro" arrays has become a widespread bio-analytical technique for genomic profiling. Two major drawbacks to the current experimental format in which these assay are performed are the degradation sensitive long sample processing time required for probe generation and the extended time requirement for the aforementioned probes to be hybridized to the target DNA on the slide surface. The goal of these studies was to develop an array based microfluidic chip and platform that can be adapted to a hand portable device. We have also focused our efforts to develop a platform that is easily customized for rapid assay development in a wide application space.

2. Experimental

To fabricate the microfluidic genearrays, chips were fabricated from quartz wafers using standard wet etch techniques to allow the production of sealed internal channels and an exposed external channel for oligonucleotide probe arraying. This was accomplished by fabricating the internal channels on the bottom wafer and the gene array channels on the top wafer. After wafer alignment and bonding this resulted in a microfluidic device which could accommodate UV activated porous polymer monoliths in sealed microfluidic channels and also allow the robotic deposition of a high density oligonucleotide arrays on the surface of the chip. Porous polymer monoliths were produced as previously described [1] with alterations. To form the oligonucleotide trapping polymer a mixture of glycidyl methacrylate and ethylene glycol dimethacrylate containing a UV photo-imitator were introduced to a pretreated channel on the microfluidic chip. The mixture was then activated and polymerized in a UV oven for 30 minutes using a chromium mask to limit the deposition of the monolith to the trapping channel specifically. This epoxide containing polymer was then post-functionalized with an amine linked oligonucleotide to enable nucleic acid sample pre-concentration. In the arraying channels the oligonucleotide probes were deposited using a conventional arraying robot which was controlled by a custom script which allowed the deposition of probes in specific locations with a 10 um accuracy error. These open channels containing the covalently linked oligonuceotides were then sealed with a polymer film in order to flow reagents to each spot on the device. Chips are housed in a manifold outfitted with o-ring seals designed to allow for one step chip alignment and to facilitate fluid connections to the outside environment.

3. Results and discussion

The synthesis of suitable probes for microarray analysis depends on the isolation of high quality RNA or DNA samples, efficient labeling of these purfied samples, and removal of unbound dye prior to probe hybridization. Using UV intiated porous polymer monolith we are able to selectively

pattern nucleic acid purification columns in microfluidic chips. Once polymerized, these monolith columns are post functionalized with a variety of amine terminated oligonucleotides which traps the targeted nucleic acids (mRNA/DNA) (Figure 1). Such monoliths are especially well adapted to microfluidic devices, as they can be polymerized in any particular pattern, have a selectable porosity, and high surface area for efficient nucleic acid binding.

In order to reduce the time required for probe hybridization, microfluidic chips (Figure 2) were developed which had both monolith concentration areas, complete with a single open channel (20μm X 300μm X 34 cm) to accommodate post fabrication arraying. Amine terminated oligonucleotides were arrayed and covalently linked to the chip surface using an aldehyde or glycidyl modified silyl coating deposited on the array (Figure 3). Using the custom spotting software allows the deposition of up to 4600 distinct oligonucletides in single array channel. After oligonucleotide depostion is complete, the channel was sealed using an optically clear film that allows direct imaging of the array surface using a fiber bundle and CCD array. We found the channel was sealed using moderate surface compression and allowed adequate flows of solutions through the array channel and direct imaging of the probe/target hybridizations (Figure 4). These hybridizations were rapid, occurring in some instances (depending on oligonucletide length) in less than 10 minutes.

4. Conclusions

Our results demonstrate the feasibility of fabricating high density gene array chips with the capability of performing rapid genomic profiling. The chips are simple to use and easily customizable allowing for the rapid alteration of probe content. In addition the entire assembly is miniaturized and can be packaged in a hand-portable platform for field analysis of biological agents.

Acknowledgements

This work was supported by a Sandia National Laboratories Laboratory Directed Research and Development Grant. We acknowledge the assistance of Evelyn Cruz, John Brazzle, and Boyd Wiedenman, for their engineering support and chip fabrication support.

References

[1] Shediac, R., Ngola, S.M. et.al. J. Chromatogr A. 2001: 25 (1-2) pp. 251-63

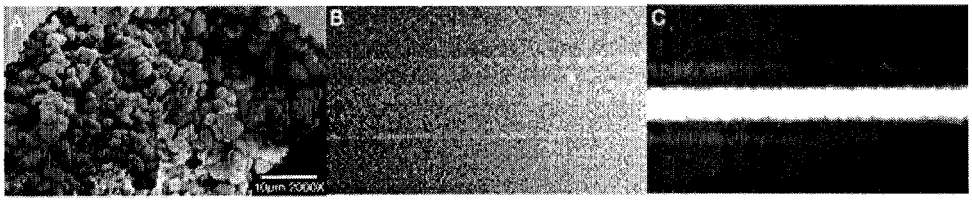

Figure 1 Porous polymer monolith: SEM image of porous polymer monolith (A), Pre-functionalized (B), and post-functionalized (C) imaged on a fluorescent microscope with 488/525 EX/EM .

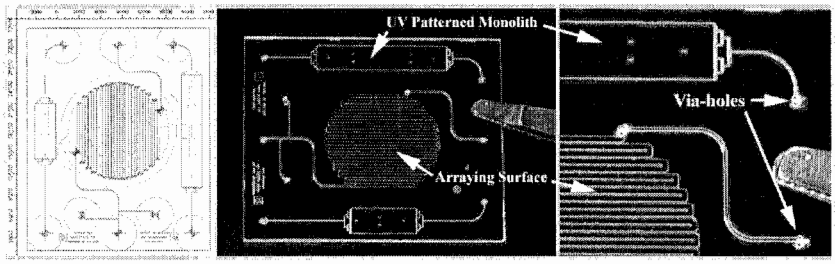

Figure 2 Microfluidic Microarray Chip: Microfluidic chips were designed to incorporate UV pattern monolith with an open channel array for on-chip sample trapping and subsequent probe/target hybridizations

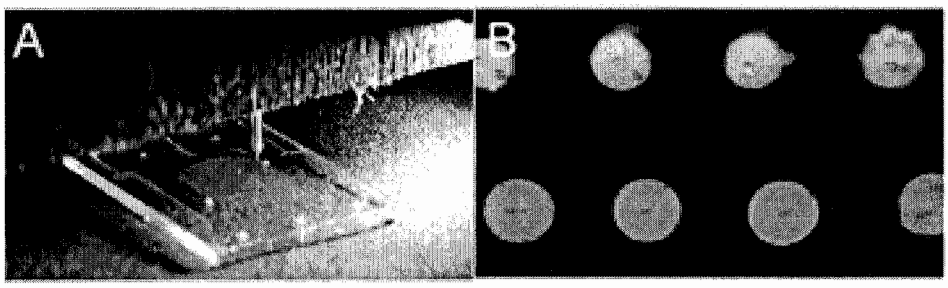

Figure 3 Arraying of fabricated microfluidic microarray. Oligonucleotides are deposted in open channel arrays using a conventional microarray robot with standard pens that deposit 180 μm DNA spots with an x/y location error of +/- 10μm.

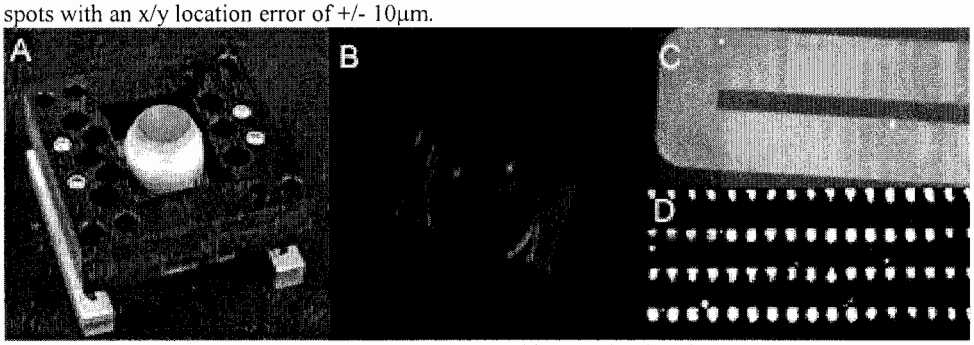

Figure 4 Microfluidic microarray mounted in manifold with fiber bundle (A), Illuminated with red LED (B). Image of fluorescein flows in array channel collected through fiber bundle array, and (D) image of hybridized spots in channel array.

QUANTITATIVE ANALYSIS OF MOLECULAR TRAP EMPROYING ELECTRIC AND HYDRO DRAG FORCE FIELD

Yuichi Tomizawa[1], Kouji Yuhki[1], Yasutaka Morita[1], Eichi Tamiya[1], and Yuzuru Takamura[1,2]
[1]Sch. of Materials Science, Japan Advanced Institute of Science and Technology (JAIST)
1-1 Asahidai, Tatunokuchi, Isikawa 923-1292, Japan
[2]PRESTO/JST

Abstract

Extraction of a specific molecule from a solution in microfluidic device is one of the important issues for micro total analysis system. At the previous microTAS, we reported a DNA trap employing mutually reverse electric force and hydro drag force field [1]. In this paper, we measured the trap probabilities of DNA as functions of DNA size and other conditions, and characterized this trap as a molecular filter in microfluidic device.

Keywords: DNA trap, size selection, selective trap, molecular filter, hydro drag force

1. Introduction

Preparing for coming elderly-people society, it is necessary to develop various technologies for cutting down medical expenses. Biochip is mentioned to one of it. Recently years, there is a concept called Lab-on-a-chip which performs series of operation in a laboratory by one chip. Lab-on-a-chip aims at below four effects, (1) The sample can be managed with very small quantity and the amount of reagents can cut dawn. (2) Reaction efficiency is high. (3) Contamination can be minimized by making processes consistent in one chip. (4) Results data can be acquired at the place which extracted a sample. Biochip is a kind of Lab-on-a-chip. The application of Biochip to the experimental system that treats harmful reagents or biopsy is expected. Especially in such a field, pretreatment of gene inspection, virus examination, and cell functional analysis are most important application of biochip. The technology of doing series of operations (mixture, separation, refining and amplification of DNA solution) by one-chip is desired. To fulfill that purpose, it is indispensable to develop technologies which control the sample in a microfluidic channel, it is difficult to integrate the elements in a biochip which required a complicated process such as a valve and a mixer. DNA trap can give the functions that are separation, refining and concentration of DNA solution required in the biochip. It is easy to construct the microchannel which can carry out DNA trap. It can be made only by pour resin into mold. The functions (separation, refining, concentration and mixture of DNA solution) needed for biochip can be attaining just to make taper shape channel.

DNA solution introduced in a microchannel which has triangle shape taper structure, the solution is driven by pressure and voltage is impressed through a reservoir simultaneously. At this time, DNA molecules are trapped near the triangle shaped taper structure as shown in Fig.1. We are calling this phenomenon DNA trap. We have put power into the elucidation of the mechanism of this phenomenon in order to attain the separation, refining, and concentration in the biochip of a high polymer with an electric charge using a trap phenomenon. The previous experimental result shown that a DNA trap phenomenon has the filter characteristic to the difference in a molecular weight. At this experiment, characteristic evaluation to the molecular weight of a DNA trap phenomenon was performed using the straight shape DNA molecules which has 100bp-166kbp lengths.

2. Experimental

Fig. 1 shows the micro channel pattern, which is made of polydimethylsiloxane (PDMS) using a conventional photolithograph technique with SU-8 thick resist molding. The channel is totally 30 mm long, 100 μm wide, 10 μm deep, and there are 4 lines of taper-shaped channel, located at the center of the channel, in 20mm area in length. Each taper is 25 μm long, and 25 μm wide. Fig. 2 shows the experimental setup. A solution of various DNA (T4: 166kbp, lambda: 48kbp, M13mp:7.3kbp, QS marker 1kbp) stained by YOYO1 in 0.5 Tris borate EDTA buffer was put in the chip, and the motion of each DNA was observed by a fluorescence microscope. The hydro drag force and the electric force are applied to the solution at the same time in mutually reverse directions. By this force field, DNA was trapped near the narrowest position of each taper shape. The electric field and the hydro pressure were applied by Pt electrodes and a syringe pump, respectively.

DNA trap was observed using the fluorescence microscope, and the image was recorded using the CCD camera. The fluorescence intensities in an image are measured by IP-Lab. For an each triangle n, the amount of fluorescence of DNA molecules which flows in the taper is defined as $Q_{n,in}$, the amount of fluorescence of trapped DNA molecules is defined as $I_n(t)$, the amount of fluorescence of DNA which flows out of the taper is defined as $Q_{n,out}$. From the above definition, trap probability β is expressed with the equations (1) and (2). From these equations, we can calculate a DNA trap probability.

$$\beta = 1 - Q_{n,out} / Q_{n,in} \tag{1}$$

$$\beta = 1 - \frac{dI_{n+1}/dt}{dI_n/dt} \tag{2}$$

4. Results and discussion

Fig. 3 shows a typical fluorescent image of trapped DNA moving the channel from the top to the bottom. The trap probability was derived from the intensity decay.The trap probabilities have a relatively steep peak as a function of applied voltage (see Fig.4). This means that the molecular selectivity is relatively high between two molecules which have different charge density (DNA to protein). The probability for T4 (168kbp) and lambda (48 kbp) is nearly equal, while those for M13mp (7.3 kbp), QS (1 kbp) is nearly zero. This means the filtering property along with molecular size is step like. The maximum probability currently obtained is 0.7 per stage.

5. Conclusions

On these experiment conditions, the DNA molecule of 7.2 or less kbps was not able to observe a trap phenomenon. From the conditions of pressure and voltage, it can be said that the size of the DNA molecule which can carry out a trap with the size of microchannel is limited. Moreover, the trap of the thing of 50 kbp-166 kbp was carried out by comparatively high probability among the DNA molecules of the molecular weight by which the trap was observed. The situation of a trap was observed under the fluorescence microscope and recorded with the digital camcorder.

References

[1] Y. Takamura et al, Proc. of u TAS 2002, Nara, Japan (2002) 317-319.

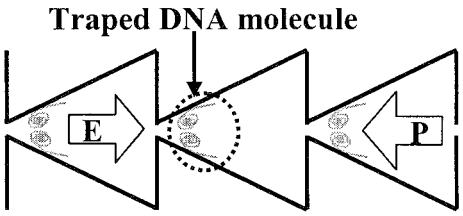

Figure 1. Taper sharp microfluidic channel and trap phenomenon.

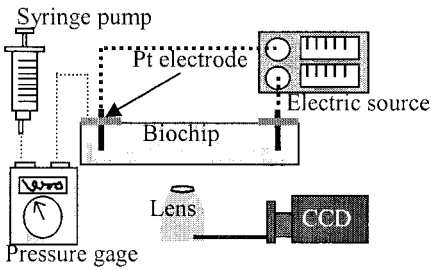

Figure 2. Experimental set up.

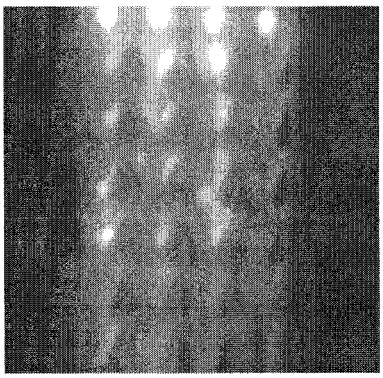

Figure 3. Typical fluorescent image of trapped DNA moving the channel from the top to the bottom. The trap probability was derived from the intensity decay.

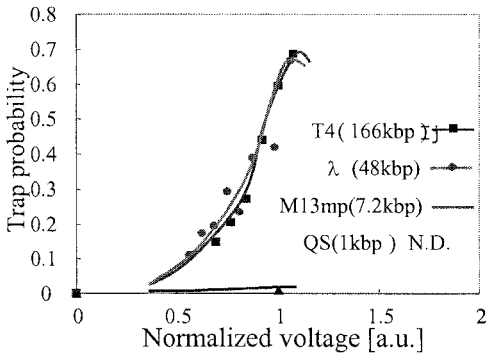

Figure 4. Trap probability for various size of DNA

BINARY VALVING OF PARTICLES USING ACOUSTIC FORCES

Melker Sundin, Andreas Nilsson, Filip Petersson and Thomas Laurell
Dept. of Electrical Measurements, Lund Institute of Technology, Lund University, Sweden

Abstract

This work presents a method to inject and direct micro-beads in microfluidic networks using an acoustically controlled valve-less switch. A microfluidic chip that can alter the flow-direction of beads using an ultrasonic standing wave field has been fabricated. In this system a two level binary valving has been realized, offering the possibility to direct an arbitrary amount of beads into four different outlets at the end of the chip by activating two ultrasound transducers.

Keywords: Acoustic valve, acoustic forces, particle, ultrasound, bead switch

1. Introduction

As the use of particulate matter in bioanalytical microsystems are increasing rapidly new means of manipulating e.g. functionalised microbeads and cells in microfluidic systems are desired. Most commonly dielectrophoretic forces have been used to direct, separate and trap cells in microsystems [1]. As an alternative, acoustic forces can be used to spatially position and enrich microparticles in laminar flow streams utilising ultrasonic standing wave fields [2, 3]. It has previously also been demonstrated that this principle also can be used to separate erythrocytes from blood plasma [4, 5]. This paper describes a method of valveless injection of microparticles in microflidic networks utilising acoustic radiation forces. The configuration of the system enables binary addressing of particles to four different outlets of a microfluidic chip by activating two ultrasound transducers in a binary sequence.

2. Theory

Fluctuations in pressure, caused by sound waves, in a fluid results in radiation forces on suspended particles. According to the acoustic force theory presented by Gorkov [6], particles that are much smaller than half the wavelength of a periodic fluctuation will travel mainly towards either a pressure node, or a pressure anti-node. The size and direction of the force (Eq. 1) induces the particle movement [7].

$$F_r = -\left(\frac{\pi p_0^{\,2} V_c \beta_w}{2\lambda}\right) \cdot \Phi(\beta, \rho) \cdot \sin(2kx) \tag{1}$$

$$\Phi = \frac{5\rho_c - 2\rho_w}{2\rho_c + \rho_w} - \frac{\beta_c}{\beta_w} \tag{2}$$

V_c is the volume of the particle, λ is the wavelength of the ultra sound, p_0 is the pressure amplitude and Φ is defined by Equation 2. The density of the medium and the particles are denoted ρ_w and ρ_c and the corresponding compressibilities β_w and β_c. The value of this Φ-factor determines if the particle will travel towards a node or an anti-node.

3. Experimental

The chip was composed of a separation channel with vertical side walls, defining the acoustic resonance cavity, and flow splitters at the outlets. With no ultrasound applied, the injected beads followed the laminar flow and travelled next to the channel wall (figure 1, left). As the ultrasound was turned on the beads were focused into the middle of the channel directing the beads to the opposing outlet channel, i.e. a binary mode of bead valving was accomplished. In this system a two level binary valving mode was realised, offering possibilities of directing an arbitrary amount of

beads to four separate outlets at the end of the chip. A schematic view of the chip layout is seen in Figure 2, showing the two level acoustic valve configuration, where the first ultrasonic transducer switches the beads between two identical and parallel structures.

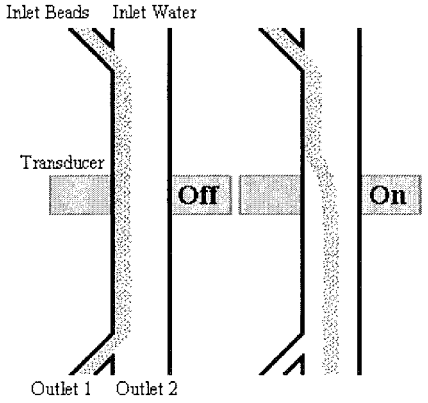

Figure 1. Principle of the acoustic particle valving.

Outlet	Trans. 1	Trans. 2
A	0	0
B	0	1
C	1	0
D	1	1

Table 1. Particle outlet destination A-D as denoted by its corresponding binary code.

The acoustic valving channels were 380 μm and 420 μm wide respectively, resulting in actuation frequencies of approx. 1.6 and 1.9 MHz. The different operating frequencies ensured that no acoustic cross-talk occurred between the two ultrasonic valves. Anodic bonding was used to seal the structures with a glass lid on the channel side and silicon tubings were glued to the inlets and outlets on the backside of the chip. Syringe pumps were used in order to set the flows individually at all four inlets, with flow rates ranging from 5 μl/min up to 25 μl/min. Polystyrene micro-beads with a diameter of 5 μm and particle concentrations of approxiamtely 2 % were used. The piezo ceramic actuators were coupled to the rear side of the chip using ultrasonic gel.

4. Results and discussion

A series of tests were performed on the binary bead valve using two piezo ceramic plates placed 20 mm apart. Different frequencies adapted to the corresponding channel widths were used, and with this setup, no cross-talk was observed. Figure 3 shows the binary valving results for the two bit settings defined in Table 1. In the current set-up the switching time from one outlet to another is not the same for all combinations. For example switching between A to B is faster than switching from A to C, because their shared junction is located closer to the outlets.

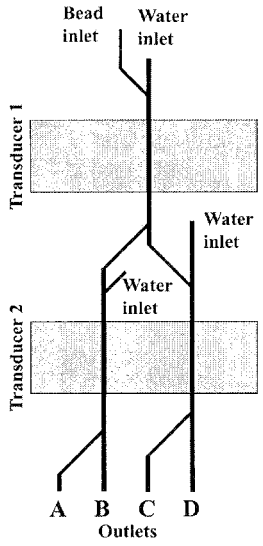

Figure 2. Schematic drawing of the 2-bit binary acoustic valving chip.

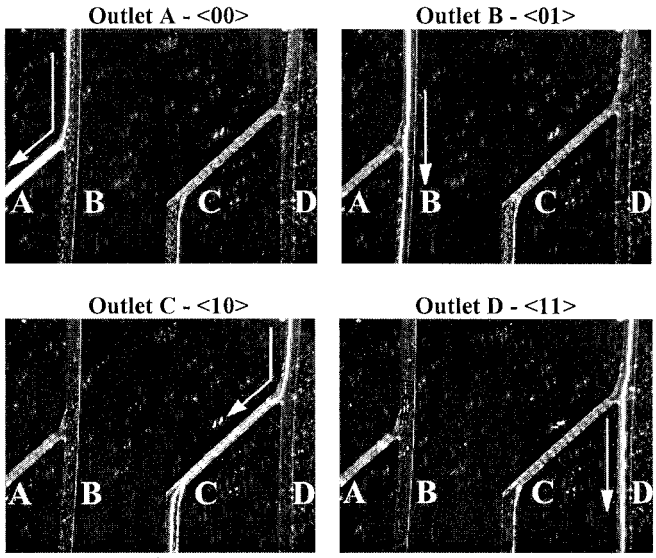

Figure 3. 2-bit binary acoustic valving of micro-beads. The transducer activation is given in the image heading respectively and the corresponding outlet is denoted A-D, according to table 1.

Conclusions

A two bit binary particle switch based on acoustic valving has been realised, directing microbeads in a controlled manner to 4 different outlets of a microchip. Application areas for the technology comprise reproducible loading or extraction of cells and microbeads in parallel microbioanalytical systems. The binary particle valving could also be used for reproducible packing of micro-beads into e.g. parallel ELISA microchips and solid phase extraction microarrays. In on-coming work new chips will evaluate additional binary levels of valving for increased number of outlets.

References

[1] Suehiro, J. and Pethig, R., *J. Phys. D-Appl. Phys.* 31, No. 22, 3298-3395, (1998).
[2] Nilsson A., Petersson F., Jönsson H. and Laurell T., *Lab Chip*, **4**, 131-135, (2004).
[3] Nilsson A., Petersson F., Jönsson H. and Laurell T., *Analyst*, accepted.
[4] Petersson F. Nilsson A., Jönsson H., and Laurell T., *Lab Chip*, accepted
[5] Petersson, Proc. MicroTAS 2003, pp. 879-882
[6] L.P. Gorkov, On the forces acting on a small particle in an acoustic field in an ideal fluid, *Sov. Phys. Doklady*, **6** 773-775 (1962)
[7] W.L. Nyborg, *Physical principles of ultrasound,* Fry FJ(ed) Ultrasound: Its Applications in Medicine and Biology, Part 1, pp. 1-76 Elsevier New York (1978)

NUMERICAL MODELLING OF MICRO-DROPLET FORMATION

Daniel Lörstad[1], Thomas Laurell[2] and Johan Nilsson[2]

[1]*Dept. of Heat & Power Engineering, Lund University, P.O. Box 118, S-221 00 Lund, Sweden*

[2]*Dept. of Electrical Measurements, Lund University, P.O. Box 118, S-221 00 Lund, Sweden*

Abstract

The formation of micro-droplets due to a pulsative micro-jet (width of 40 μm) is studied using the 3D Navier-Stokes equations for multi-phase flows using the Volume of Fluid (VOF) and Volume of Solid (VOS) models. The droplet formation is studied for different transient velocity conditions and mass rates. The numerical results show reasonable agreement with both analytical theory and experimental data. The results show that the surface tension forces are too dominating for the droplets to be released from the constriction opening for a mean jet velocity at the constriction opening of U_{jet}~1 m/s, that multiple (satellite) droplets are formed for U_{jet}~10 m/s and that a single droplet may be found for U_{jet}-values in between. The results also indicate the conditions required in order to achieve repeatedly stable single micro-droplet formation.

Keywords: CFD, Volume of Fluid (VOF), droplet formation, multiphase flow

1. Introduction

Reduction of dispensed fluid volumes and an increase in handling speed are common requests for the miniaturization of bio-chemical and bio-analytical systems. Due to the recent computational developments in theory and resources, investigations using computational fluid dynamics (CFD) can support the experimental studies to meet these demands. The advantage of CFD is that it can be used to obtain knowledge of many aspects of a flow problem which are difficult to measure experimentally, and evidently, especially in micro-scale systems.

2. Numerical methods

When simulating water droplet formation in air, a correct interface description and especially the surface tension force distribution are critical issues. Volume of Fluid (VOF) is a common approach [2,3] where difficulties such as droplet/bubble release, break-up and coalescence are solved implicitly in the model. However, most VOF approaches have an inaccuracy within the surface tension force model (i.e. the curvature) which makes them unreliable for micro-droplet formation where the surface tension forces are important. Only two VOF-approaches [2] are proved to be without this drawback. Furthermore, the high density ratio is another important topic for droplet formation which in addition is resolved by [2,3] and this numerical strategy has been successfully used for formation, deformation and transport of air bubbles in water [2]. Therefore that numerical scheme is the natural choice for this study.

3. Results and discussion

Figure 1 (left) shows the geometry and boundary conditions of the numerical domain. Figure 1 (middle) shows the transient inflow condition that is used for the pulsative mean jet velocity $U_{jet}(t)$. Figure 1 (right) shows the approximately corresponding integral, which is assumed to be proportional to the pulse amplitude in the experimental setup [1], which in turn controls the droplet injection. A grid consisting of $80^2240 \approx .5E6$ uniform Cartesian cells has been used to discretize the domain and the time step equals $\tau/400$ where τ is the injection time.

Figure 2 shows examples of the resulting droplet shapes at different time instants for different magnitudes of injection time τ and constriction velocity U_{jet} (each row shows equal volume flux). This corresponds to a jet Reynolds number of 40-400. The thick lines in Figure 2 show the approximate borders in order to obtain a single micro-droplet. If U_{jet} is small, the surface tension forces prevent the droplet from being released. If U_{jet} is large, the convection forces are too strong

for the surface tension forces to keep the liquid together into one droplet and the satellite droplets will not join the bigger one. For U_{jet}-values in between, a stable single droplet formation is found. The different momentum due to different injected volume fluxes (different rows in the figure) also affect the formation as seen in Figure 2.

Figure 3 shows a summary of the numerical and experimental [1] results where a stable single droplet formation is found. The left part of Figure 3 shows the results of volume and velocity of the formed droplet for an injection time of 5 μs. The numerical and experimental results show reasonable agreement. However, the smallest simulated droplets show relatively large differences between the volume which is injected at the inlet and the formed droplet. This is mainly due to the following two reasons: that the initial condition of the phases might differ from the phase distribution at steady droplet formation and that the numerical accuracy is less for the smaller droplets since the size ratio between the droplet and the computational cells are less.

The right part of Figure 3 shows the results of all the simulations of stable singe droplet formation. The lines between the CFD results indicate droplets of similar size (which corresponds to almost constant pulse amplitude). The data in Figure 3 (right part) indicate the range of pulse amplitude and corresponding injection time that result in a stable single droplet formation.

4. Conclusions

The formation of micro-droplets has been successfully simulated using VOF and the results show reasonable agreement to the experimental data in [1]. In addition, the results indicate the required conditions in order to achieve a stable single droplet production. However, in order to investigate the steady formation of even smaller droplets, finer numerical resolution and repeated droplet injection are recommended.

References

[1] Bergkvist J, Lilliehorn Y, Nilsson J, Johansson S, Laurell T. Miniaturized flow-through microdispenser with piezocermaic tripod actuation. Submitted to *Journal of Microelectromechanical Systems, November 2003*.

[2] Lörstad D. Numerical modeling of deforming bubble transport related to cavitating hydraulic turbines. PhD thesis. Dept. Heat and Power Engineering, Lund University, 2003. Free download at http://www.fm.vok.lth.se/

[3] Lörstad D, Fuchs L. High order surface tension VOF-model for 3D bubble flows with high density ratio. Accepted for publication in *Journal of Computational Physics*, 2004.

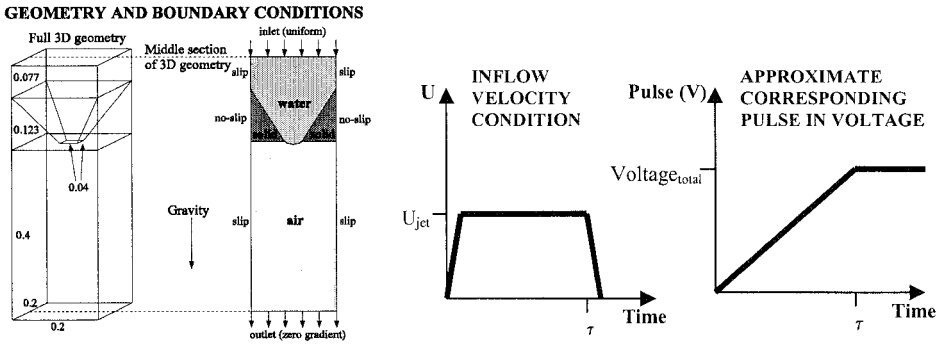

Figure 1. Geometry (units in mm), spatial and temporal boundary conditions and approximate corresponding pulse amplitude which is applied in the experimental setup.

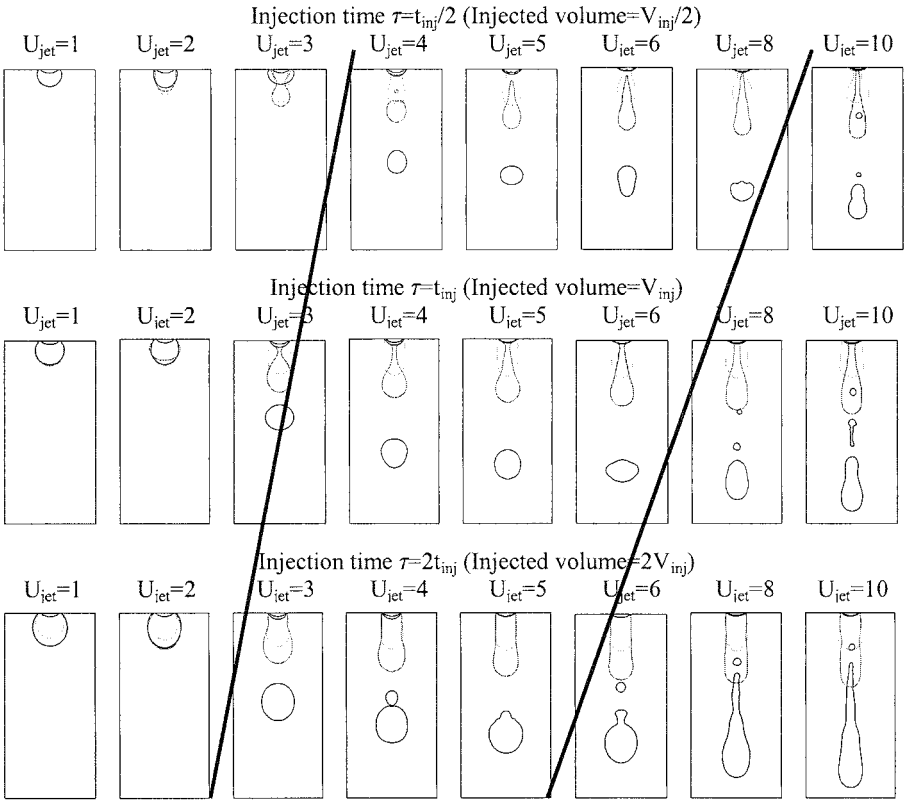

Figure 2. Droplet shapes (in 3D) at different time instants for different injection time values (units in mm) where t_{inj}=75.6/U_{jet} μs and the droplet shapes are plotted at t=0, t_{inj}, 2t_{inj} and 5t_{inj}. The thick lines reflect the approximate borders for a stable single droplet formation.

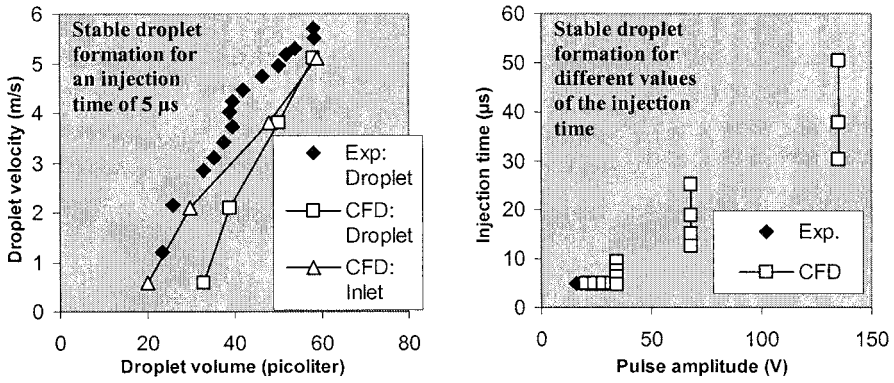

Figure 3. Stable droplet formation for different parameters. The experimental data is from [1].

Author Index

Keyword Index

Micro Total Analysis Systems 2004
Volume 2

Proceedings of μTAS 2004
8th International Conference on Miniaturized Systems for Chemistry and Life Sciences

Malmö, Sweden
September 26-30, 2004

edited by

Thomas Laurell
Lund Institute of Technology, Sweden

Johan Nilsson
Lund Institute of Technology, Sweden

Klavs Jensen
Massachusetts Institute of Technology, USA

D. Jed Harrison
University of Alberta, Canada

Jörg P. Kutter
Technical University of Denmark, Denmark

RS•C
advancing the chemical sciences

Special Publication No. 297

ISBN 0-85404-896-0

A catalogue record for this book is available from the British Library

Published by The Royal Society of Chemistry,
Thomas Graham House, Science Park, Milton Road,
Cambridge CB4 0WF, UK

Registered Charity Number 207890

For further information see our web site at www.rsc.org

Printed by Athenaeum Press Ltd, Gateshead, Tyne and Wear, UK

PREFACE

The 8th International Conference on Miniaturisation in Chemistry and Life Sciences, MicroTAS (Micro Total Analysis Systems) is celebrating its 10th anniversary year. The conference developed from a small gathering of researchers active in the field of MicroTAS in Enschede, The Netherlands, in 1994 with 160 participants. The success of this first meeting was followed by an equally appreciated μTAS workshop in Basel, Switzerland, in 1996 with a remarkable increase in the number of participants to 275. Optimism in the research field continued and the subsequent event was the truly unforgettable conference organised in Banff, Canada in 1998, with a record-breaking 420 conference delegates and about 130 papers submitted. At the following meeting in 2000, the conference returned to its birth place in Europe (at the University of Twente, Enschede, The Netherlands) again breaking new records for the MicroTAS conference with close to 500 attendees and about 140 scientific papers accepted (230 submissions). Due to the increasing interest that the MicroTAS/Lab-On-A-Chip field was generating, the subsequent meeting in 2001, in Monterey, CA, USA, forced the conference format into two parallel oral sessions in order to meet the pressure from the scientific community. In spite of the 9-11 terrorist attack and subsequent restrictions in international travelling, the conference attracted about 790 delegates and 276 accepted scientific contributions. The meeting was also characterised by an impressive commercial exhibition, demonstrating the transition of several of the earlier μTAS developments into the industrial sector. The subsequent conference (2002) in Japan is forever etched into our minds both with respect to the excellent organisation and scientific programme as well as the wonderful setting in ancient Nara. Although difficulties were developing in the industrial and financial sectors, following the IT-crash, the Nara meeting attracted 710 delegates with 316 accepted scientific contributions. The next μTAS conference was organised in another glorious location, Squaw Valley, CA, USA, in October 2003 and despite the setback in the global economy which clearly also affected academic budgets the conference attracted over 650 delegates with 325 accepted scientific presentations.

This year's conference confirms the continuing increase in interest in the μTAS-research field. More papers were submitted than ever before, 657, giving the Technical Programme Committee a difficult task in the abstract evaluation procedure. Again the scientific programme expanded, now to encompass a total of 422 accepted scientific contributions. We also see a continuing strong presence from the industrial area with some new players, indicating a recovery in the financial sector.

These two volumes contain the proceedings of the MicroTAS 2004 conference in Malmö, Sweden, September 26-30. Every paper presented will also be made available from the Royal Society of Chemistry, Lab on a Chip web-site at www.rsc.org/loc. The proceedings from the μTAS 2003 conference can also be accessed from this site.

The content of this year's MicroTAS conference clearly shows that the efforts in developing cell-based microsystems are increasing. Not only is work quite frequently focused on cell manipulation, and on-chip culturing but also on complete microsystems

for cell transport, culturing, analysis and monitoring including feed-back systems are now presented. The transition to polymer-based technologies continues and the now widely used SU-8/PDMS platform has opened up the μTAS-field to all those who do not necessarily have access to high performance clean-rooms, which vastly broadens the number of players that can now access and work in the field. A clear trend is also the increase in microfluidic two-phase systems, which seems to have come to a point where the two-phase fluid handling is well controlled and, *e.g.,* applications with compartmentalised chemistry in oil-immersed aqueous droplets in streaming microsystems are seen. The more mature areas of chip-based separation science are still very strong moving towards applications in genomics, proteomics and diagnostics. An exciting development is the continued progress in nanotechnology and the study of microfluidic transport, and molecular interaction and separation in nanoscale channels, this year displaying a representation equal to those in cell-based microsystems.

Looking back at μTAS conferences over the last ten years I can conclude that the field has matured and broadened from the original very strong focus on chip-based capillary electrophoresis systems to encompass a new science field of an extremely interdisciplinary nature with materials physicists and analytical chemists at one end and cell & molecular biologists and clinicians at the other. The field of microfluidics with all its aspects in combination with micro- and nanotechnology and life science research is accelerating, finding new areas where the miniaturised scale really makes a difference, and this is, of course, what research in this area is all about! We can confidently look forward to another ten years of exciting developments in this scientific field.

Finally, I would like to express my thanks to all of those who helped in organising this conference. The local organising committee for their broad network to industrial supporters and exhibitors and for all the work that is not seen but is yet so necessary. The Technical Programme Committee for the seemingly endless work reading and evaluating the 650 submitted abstracts in a medieval castle in southern Sweden. This is a task on which the whole foundation of the MicroTAS conference rests. Malmö Conference Agency is greatly acknowledged and I would especially like to thank, Lars Nilsson, Anna Martinsson and Niklas Swedenborg for their excellent and hard work in making all the necessary practical arrangements come to fruition. I would like to express my deepest gratitude to Johan Nilsson and Jörg Kutter, without whom, the administration would have been a total disaster, and for their expedient and fluent processing of all protocols and endless abstract and proceedings databases.

Last but not least, I thank all of you in the μTAS-science community for compiling and contributing your cutting-edge research for these two proceeding volumes. Without you there would be no meeting!

Thomas Laurell
μTAS 2004 Chairman
July 14, 2004

Programme Committee

Thomas Laurell
(Conference Chairman)
Lund University

Jörg P. Kutter
(Conference Co-chairman)
Technical University of Denmark

Yoshinobu Baba
University of Tokushima

David Beebe
University of Wisconsin - Madison

D. Jed Harrison
University of Alberta

Klavs Jensen
Massachusetts Institute of Technology

Takehiko Kitamori
University of Tokyo

Johan Nilsson
Lund University

M. Allen Northrup
Microfluidic Systems Inc.

Shuichi Shoji
Waseda University

J. Michael Ramsey
University of North Carolina

Sabeth Verpoorte
University of Groningen

Jean Louis Viovy
Curie Institute

The Programme Committee and The Local Organising Committee kindly acknowledge the support from the following:

Gold sponsors

VINNOVA

The Crafoord Foundation

SCIENCE • MEDICINE • TECHNOLOGY

Swedish Foundation for Strategic Research

MCPT

micralyne

Silver sponsors

SAMSUNG

microplast ab®
www.microplast.se

GYROS

LUND UNIVERSITY

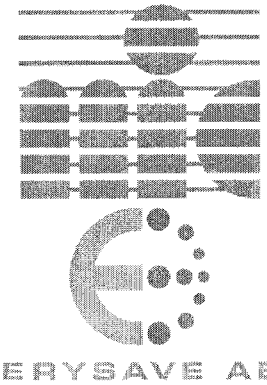

ERYSAVE AB

ATS MEDICAL

Bronze sponsors

silex MICROSYSTEMS

Johnson & Johnson

Caliper LifeSciences

mfsi MICROFLUIDIC SYSTEMS, INC.

Other support

analytical chemistry

Science AAAS

LAB ON A CHIP

www.rsc.org/loc

JOURNAL OF SEPARATION SCIENCE

FABRICATING A THREE-DIMENSIONAL CHANNEL FOR MICRO-FLUIDIC DEVICES BY LASER ABLATION

Yoshikazu Yoshida[1], Tsutomu Neichi[1], Retsu Tahara[1], Jun Yamada[1], Hiroyuki Yamada[2] and Nobuyuki Terada[3]

[1]Toyo University, 2100 Kujirai, Kawagoe, Saitama 350-8585, Japan
[2]Yamanashi Pref. Industrial Technology Center, 2094 Kofu, Yamanashi 400-0055, Japan
[3]University of Yamanashi, 1110 Tamaho, Nakakoma, Yamanashi 409-3898, Japan

Abstract

This paper describes the fabrication in resin of micro-channels for micro-fluidic devices such as the μTAS (Micro Total Analysis System) by UV laser ablation process. A number of heat-hardening resin-films are layered on a soda glass. A laser fabricates a part of the channel on each film for every lamination. Then three-dimensional (3-D) confluence channels are fabricated. The fabricated channels are 45-180 μm in depth and 50-300 μm in width. The through holes are made in the laminate film with a laser. An inlet pipe for a micro-pump is inserted into the hole.

Keywords: μTAS, UV laser, lamination, resin-films, blood

1. Introduction

Recently, in various fields the necessity for small and highly sensitive micro-fluidic analysis systems has increase. Therefore a μTAS has received considerable attention. The μTAS is the size of a card, and has miniaturized channels, detectors, and other elements for fluidic analysis. The advantages of this system are the reduced need of fluidic samples, reagents, and hours of detection. The size of the fluidic analysis elements on the μTAS is a few score micrometers. There are many fabrication methods of micro-channels through semiconductor technology [1], plastic molding [2], and laser fabrication of resins [3]. The laser fabrication method has recently been receiving much attention. The advantages of this method are: one stroke fabrication of grooves for channels, an easy change of groove patterns, and 3-D fabrication to allow grooves with slopes and differences in levels. We have been proposing the method which uses silicon or quartz as the substrate part of μTAS, build the micro working parts and electrode in advance onto the substrate, then create the flow path and cistern on the resin part formed on the substrate [4]. An ultraviolet pulse laser was used to form such items as the flow path. A number of heat-hardening resin-films were layered on a soda glass. A laser fabricated a part of the channel on each film for every lamination, and then a 3-D micro-channel structure was fabricated. Two types of flow path, a plane and an overpass, are fabricated.

2. Experiment equipment

The substrate is soda glass laminated by heat-hardening resin-film. This film is made of two films, one of 25μm thick polyimide and the other 20μm thick epoxy. Channels are fabricated by a pulse Nd:YAG laser system (Brilliant; Quantel) and a KrF excimer laser system (LPX220; Lambda Physik, AG). For the experiment condition, the YAG has a wavelength of 266nm, pulse energy of 3.1mJ, pulse width of 4.3nsec, and repetition rate of 10Hz. The laser beam is fixed, and the substrate is moved in the XY stage. This stage has a positional bi-directional repeatability of ±5μm. The excimer has a wavelength of 248nm, output energy of 8-80W, maximum pulse energy of 450mJ, pulse width of 10-20nsec, and repetition rate of 25-200Hz. A mask is used to shape the laser beam into a square shape to allow fabrication with smooth wall surfaces at low overlap rate conditions. The laser beam is focused to the width of a groove.

3. Results and discussion

3.1 Three-pronged channel

Combining of laminar flows in a micro-channel makes possible the study of blood cell analysis. Figure 1 shows an optical photomicrograph of three-pronged grooves without cover film fabricated by the excimer laser. Channels have a width of 50μm and a depth of 45μm in three-pronged parts, and a width of 150μm in a confluence part. Blood is injected at a low flow rate between two rapidly flowing streams of physiological salt solution. The width of the stream of blood can be controlled by the height difference between a blood reservoir and solution reservoir, that is potential energy. The width narrows as it climbs to the speed of the neighboring streams. The width decreases with the increasing height difference. The cells velocity increases with the increasing height difference. In this experiment, the channel substrate is placed horizontally on a microscope stand, and the reservoir made from a connector between a syringe and a needle is connected to the channel inlet with Silicon tube. This tube has an external diameter of 1mm and an inside diameter of 0.3mm. Figure 2 shows a focused picture of blood when the blood reservoir is 200mm high and the solution is 400mm high from the channel. The cells velocity is almost 15.5mm/s. It is almost 9mm/s when the height difference is nearly zero. As shown in Fig.2 (b), blood cells can be measured individually.

3.2 Three-dimensional channels

Figure 3 shows the optical photomicrograph of a channel made on the second film by the YAG laser. The laser scanning distance is 150μm. The second film is peeled off from the first one by the scanning. The film placed between the scanning is removed from the substrate. The space caused by removal of the film is used as a channel space. The film peelings on the channel side are removed with the following laminating process.

Figure 4 shows the production process of the steric mixture flow path used to branch. There are 3-D pattern diagrams and optical photomicrographs each time a lamination is done. First, the channel element of the first layer is made for the film on the glass by the laser (Fig.4 (a)). After that, the second film is laminated on the first one, and the channel element is made on the film (b). These processes are iterated several times, and the 3-D confluence channel is fabricated. The channel is closed because the groove is treated with laminate processing, and liquid can't enter into the groove. Therefore it is necessary to make a perforated hole in the flow path to insert liquid inside, and connect the tube. The diameter of the hole is 150μm, and formed on the laminate film by laser drilling. Deionized water is injected into the channels with a microinjection pump. The flow rate is 5μL/min. There is no damage to the channel.

4. Conclusions

(1) The groove with a width from several dozen μm to several hundred μm is created on the resin layer without any damage on the substrate by ablation processing with an ultraviolet laser.
(2) A heat-hardening resin film can be used to maintain 100% of the channel space for fluid flow.
(3) Fresh blood flows easily through the channels.

References

[1] A.Manz et al., *J.Chromatography*, **593**, pp.253-258 (1992).
[2] N.Kitamura, H.B.Kim, and K.Ueno, *T.IEE Japan*, **121-E**, pp.169-174 (2001).
[3] F.Wagner and P.Hoffmann, *Proc.SPIE*, **4088**, pp.337-340 (2000).
[4] Y.Yoshida, *Proc.SPIE*, **5063**, pp.189-192 (2003).

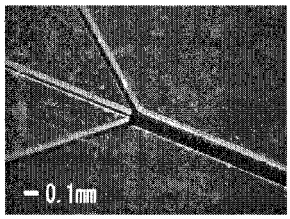

Figure 1. Side view micrograph of three-pronged grooves without cover film.

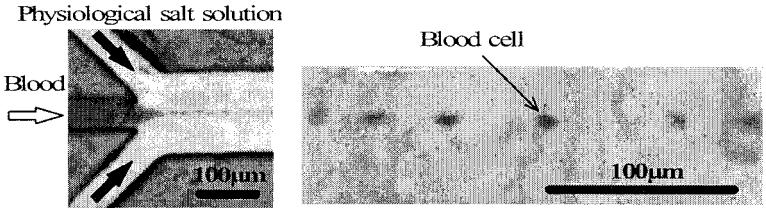

Figure 2. Blood pass-through in a three-pronged channel. The right photo shows the downstream.

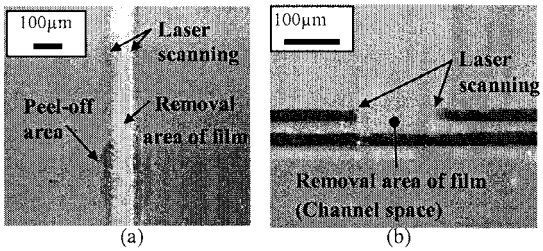

Figure 3. Micrograph of channels. (a)Top, and (b) cross-section.

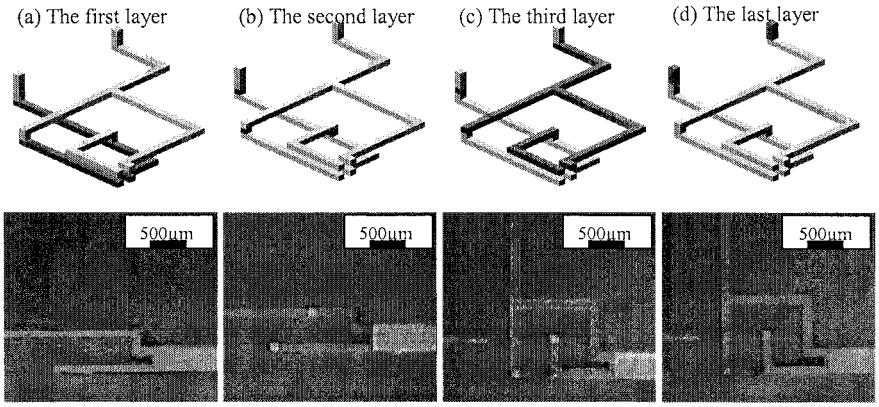

Figure 4. Fabrication process of 3-D channel image and photo of branch steric path.

PHOTOPOLYMERIZED POLY(ETHYLENE) GLYCOL DIACRYLATE (PEGDA) MICROFLUIDIC DEVICES

Amy Butterworth, Maria del Carmen Lopez Garcia and David Beebe
Department of Biomedical Engineering, University of Wisconsin
1550 Engineering Drive, 53704 Madison WI, USA

Abstract

As microfluidic applications in cell biology move beyond diagnostic assays to long term culture and production, alternative materials will be needed. Poly (ethylene) glycol (PEG) has been widely utilized as a biocompatible polymer due to its hydrophilicity and non-fouling behavior. Diacrylated, PEG can be photopolymerized using the microfluidic tectonics platform (μFT) and provides a more biocompatible alternative to previous polymers used. The ability of this monomer to be polymerized and patterned into channels for micro-cell culture was evaluated. Also, the biocompatibility of the polymer was assessed using FT-IR and cell interaction studies with the unpolymerized components.

Keywords: Microfluidic tectonics, biocompatibility, photopolymerization, poly (ethylene) glycol (PEG)

1. Introduction

Poly (ethylene) glycol (PEG) has been widely utilized as a biocompatible polymer due to its hydrophilicity and non-fouling behavior [1]. PEG resists protein absorption and has been used as a coating or as a polymer substrate to prevent or control cell adhesion and adsorption of proteins for over a decade. PEG has been used previously in bioMEMS-related technologies as a coating or as a co-monomer for purposes such as polymerizing cells in gels [2, 3]. Diacrylated, PEG can be photopolymerized using the microfluidic tectonics platform (μFT) [4] and provides a more biocompatible alternative to previous polymers used. The ability to incorporate PEG as a construction material for microfluidic systems will allow the unique properties of PEG to be exploited for a variety of cell-based experiments. Examples include using in-situ polymerized porous PEG gels as selective diffusional barriers to replace media changes during cell culture, or copolymerizing with a hydrolytically degradable monomer for controlled release of biomolecules of interest.

2. Fabrication and Biocompatibility Analysis

The biocompatibility of this polymer will be partially dependent on the complete polymerization of the monomer while using a minimal concentration of photoinitiator. The typical concentration of photoinitiator used in these experiments was 0.05 wt%, although lower percentages (below 0.01 wt%) can be polymerized but exhibit more swelling. To verify the degree of polymerization, FTIR studies were done, comparing the spectra of the polymer with 0.1 wt% photoinitiator (Fig. 1a) to that with 0.05 wt% (Fig. 1b). The polymerization of diacrylates reduces the magnitude of the carbon-carbon double bond peak (shown in Fig. 1) and is expected to decrease with increasing photoinitiator concentration as shown. FTIR measurements allow one to find a balance between concentration of photoinitiator and degree of polymerization that minimizes the cytotoxicity of the devices, while maintaining good patterning capabilities. After UV sterilization before use in cell culture, this peak decreased slightly. Straight channels were patterned to test the patterning capabilities, with widths ranging from 175μm to 1,000μm in 250 μm high devices (Fig. 2). Good resolution of less than 10μm was achieved which is comparable to that achieved with poly (IBA). A valve mask currently in use for creating the substrate for a hydrogel actuated valve

was also patterned in PEGdA with relative ease [5]. These two materials show similar capabilities although the PEGdA devices produce more rounded features.

Since our intended use of the PEG channels is long term (weeks) cell culture, the long term capability of the material was tested to ensure no failure occurred due to the PEGdA swelling. Swelling of the PEGdA material did cause device failure more frequently as the percentage of photoinitiator decreased (from 0.05 wt% to 0.01 wt%) and exposure intensities decreased (from 20 mW/cm^2 to 10 mW/cm^2). The molecular weight of the PEGdA was reduced from 575 MW to 258 MW, which showed significantly reduced swelling and produced devices which could be incubated at 37°C without immediate failure. Multiple photoinitiators 4-(2-hydroxyethoxy)phenyl-(2-hydroxy-2-propyl) ketone (Irgacure 2959, Ciba, Inc.) and biacylphosphine oxide (BAPO, Iragure 819, Ciba, Inc.) were also studied. The former has commonly been used for photopolymerization of cells in gels and has shown to be more biocompatible than many photoinitiators. The latter has a higher efficiency (the absorption band extends to 400nm) at the wavelengths of exposure, so lower concentrations were needed. Successful polymerization was demonstrated with both compounds, although BAPO-initiated devices proved to be more resistant to swelling most likely due to the faster reaction kinetics causing denser gels.

4. Biocompatibility

Devices were created with the optimized prepolymer mixtures and exposures with 1,000μm straight channels and incubated with DPBS at 37°C. When externally reinforced with adhesive, these devices are suitable for cell culture, surviving for more than one week without failure due to swelling of the polymer. The cellular response to the presence of the monomer and photoinitiator in the media was evaluated. A concentration of 10 μM PEGdA caused significant reduction in NMuMG cell adhesion, while 1μM did not prevent adhesion, although cell morphology was slightly different than the controls. Cells with PEGdA in the media that did attach to the surface remained rounded in colonies rather than spreading as expected for epithelial cells. Due to very low solubility of BAPO in the media, quantitative results were not obtained, although the presence of BAPO did cause cell death in media with the maximum soluble amount of BAPO. It is clear that further optimization of the polymerization technique and prepolymer mixture is needed to ensure minimal concentrations of prepolymer components remain after polymerization and washing in order to maximize biocompatibility.

References

[1] S. Sharma, K. C. Popat, and T. A. Desai, "Controlling nonspecific protein interactions in silicon biomicrosystems with nanostructured poly(ethylene glycol) films," *Langmuir*, **18**, 8728-8731 (2002).

[2] S. J. Bryant, C. R. Nuttelman, and K. S. Anseth, "Cytocompatibility of UV and visible light photoinitiating systems on cultured NIH/3T3 fibroblasts in vitro," *Journal of Biomaterials Science-Polymer Edition*, **11**, 439-457 (2000).

[3] Y. Hanein, Y. Vickie Pan, B. D. Ratner, D. D. Denton, and K. F. Bohringer, "Micromachining of non-fouling coatings for bio-MEMS applications," *Sensors and Actuators, B: Chemical*, **81**, 49-54 (2001).

[4] D. J. Beebe, J. S. Moore, Q. Yu, R. Liu, M. Kraft, B. Jo, and C. Devadoss, "Microfluidic tectonics: A comprehensive construction platform for microfluidic systems," *PNAS*, **97**, 13488-13493 (2000).

[5] D. Kim and D. Beebe, "In-Situ Fabricated Micro Check-Valve Utilizing the Spring Force of a Hydrogel," presented at Proceedings of the Micro Total Analysis Systems, Lake Tahoe, CA, USA (2003).

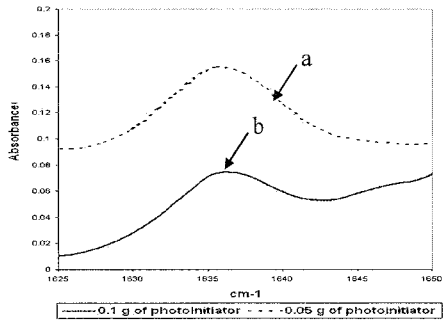

Figure 1. FTIR spectra of photopolymerized PEGdA, (a) with 0.1 wt% photoinitiator and (b) with 0.05 wt% photoinitiator. The amount of carbon-carbon double bonds decreases with increasing photoinitiator showing the increased polymerization of the PEGdA. A balance between concentration of photoinitiator and free monomer after polymerization will maximize biocompatibility.

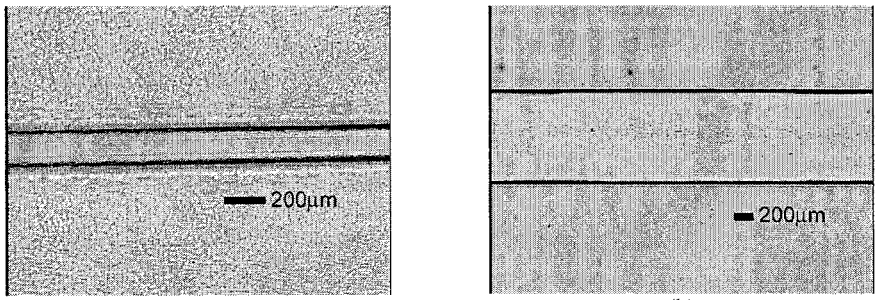

(a) (b)

Figure 2. Channel walls patterned in PEGdA, (a) 175μm width, and (b) 1,000μm width. An accuracy of less than 10μm was achieved with both channel widths.

A FLOW-THROUGH SHEAR-TYPE MICROFILTER CHIP FOR SEPARATING PLASMA and VIRUS PARTICLES FROM WHOLE BLOOD

Levent Yobas[1], Ee-Ling Gui [2], Hongmiao Ji[1], Jing Li[1], Yu Chen[1], Wing-Cheong Hui[1], Siti Rafeah Binte Mohamed Rafe[3], Sanjay Swarup[4], Sek-Man Wong[4], Tit-Meng Lim[4] Chew-Kiat Heng[3]

[1]Institute of Microelectronics, 11 Science Park Road, Singapore Science Park II, 117685, Singapore

[2]Nanyang Technological University, School of Materials Engineering, 639798, Singapore

[3]National University of Singapore, Department of Pediatrics, 119074, Singapore

[4]National University of Singapore, Department of Biological Sciences, 117543, Singapore

Abstract

A flow-through shear-type microfilter chip has been proposed for the purpose of separating plasma and virus particles from whole blood. The microfilter chips have been fabricated in three different design configurations by silicon micromachining and tested for their percent efficiency of separating plasma from diluted blood samples. One of the designs has been further demonstrated to be capable of isolating virus particles from a spiked sample of whole blood.

Keywords: Microfilter, shear filter, virus, plasma, sample preparation

1. Introduction

Recent epidemics such as Severe Acute Respiratory Syndrome (SARS) have highlighted the importance of an automated sample preparation for virus and pathogen detection. Detection of extracelullar viruses from blood usually requires separation of plasma or serum containing virus particles from cellular components. This is because hemoglobin from red blood cells (RBC) is known to inhibit nucleic acid amplification while nucleic acids in white blood cells (WBC) can contribute to background noise during detection [1]. Typically, plasma is obtained from whole blood by a centrifugation step. Nevertheless, centrifugation is not amenable to automation. An alternative approach is filtering plasma based on size exclusion of cells [2]. Most viruses are less than 1μm while most RBC and WBC remain larger than 2μm.

2. Microfilter Chip

The proposed microfilter concept and structure are diagrammatically shown in Fig. 1. The chip contains a chamber etched about 65-μm deep into silicon by deep reactive ion etching and capped with a glass wafer by anodic bonding. Plasma can be collected through anisotropically-etched backside holes in silicon located at two diagonal corners. At the other corners, backside holes allow blood to flow in and out of the chip through a meander type channel defined by silicon pillars. As blood flows inside the channel, plasma can escape through narrow slits between pillars due to combined action of capillary forces and pressure gradient. Nominal gap between the pillars is about 1.6μm wide, which can retain most blood cells but allow passage of virus particles. The microfilter chips have been fabricated in three design configurations mainly differing in chip size and shape of the meander-type channel (Table I).

3. Experimental Results & Discussion

Fig. 2 shows on-chip collection of plasma escaping through the slits between pillars as the anticoagulant-treated whole blood flows through the meander-type channel. Anticoagulant-treated blood was pumped through the chips at 10μl/min and at different dilutions of phosphate buffered saline (PBS) solution. RBC counts in the blood pumped in (RBC_{blood}) and the plasma collected

(RBC_{plasma}) were obtained by a hemocytometer. Table I shows volume of the collected plasma samples and percent efficiency of each microfilter chip (% EF) as calculated by:

$$EF = \left[1 - \left(RBC_{plasma} / RBC_{blood}\right)\right] \times 100 \quad (1)$$

As shown, chips based on any of the three designs had higher than 99% efficiency for the Blood:PBS ratio of 25:75. The efficiency deteriorated with an increase in the blood:PBS ratio but stayed above 90% for all three microfilter chips.

Further, experiments were conducted to test whether the plasma filtered by the microfilter chips can be used for detection of virus particles in blood. Anticoagulant-treated whole blood at a volume of 140µl was spiked with virus (Cymbidium Mosaic Virus) suspension in water at a volume of 70µl and concentration of 0.26µg/µl. Approximately, 180µl of the spiked blood was pumped through microfilter #1 at 10µl/min. The plasma filtrate was used for extraction of viral RNA via a commercial kit [3] and amplified by reverse transcription polymerase chain reaction (RT-PCR). The amplified products were separated by agarose gel electrophoresis and ethidium bromide-stained products were visualized on a UV transilluminator. As can be seen in Fig. 3, viral RNA from the plasma filtered by microfilter chip #1 could be amplified, demonstrating a successful substitute for the conventional centrifugation step.

References:

[1] McCusker J., et al. (1992) Nucleic Acids Res. 20, 6747

[2] Wilding, P., et al. (1998) Analytical Biochemistry, 257, 95-100.

[3] QIAamp® Viral RNA Mini Kit Handbook, 1999, Qiagen.

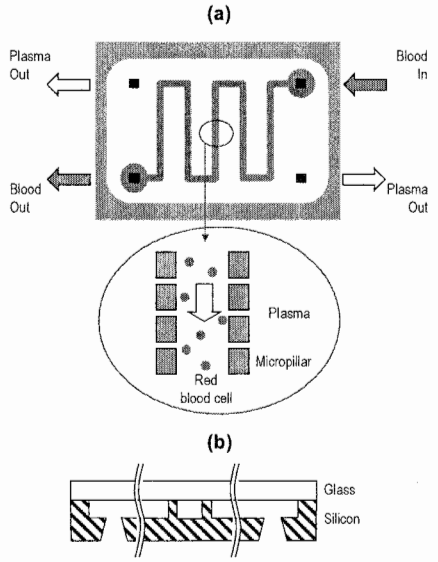

Figure 1: Diagram of the flow-through shear-type microfilter chip: (a) plane view with inset showing close-up of channel defined by pillars (b) cross section profile.

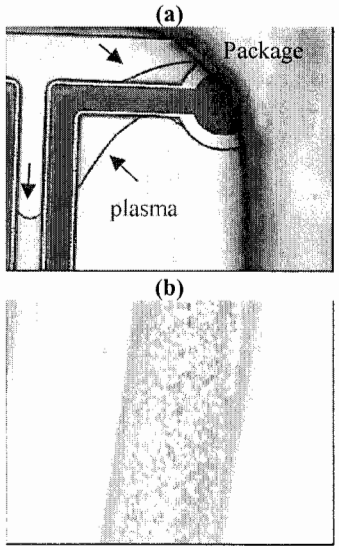

Figure 2: Plasma separation from whole blood (undiluted): (a) plasma escaping (arrows) through narrow slits between pillars (b) close-up view of red blood cells inside the channel.

Table 1: Microfilter chips characterization for two different ratios of Blood:PBS volume

Blood:PBS Volume ratio			**50:50**	**25:75**
RBC count in the blood pumped in (Million)			865	433
Volume of the diluted blood pumped in (μl)			400	400
Microfilter #1 (5mm by 10mm)	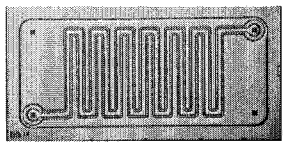	% EF	90.37	99.56
		Plasma collected (μl)	212	181
Microfilter #2 (5mm by 10mm)	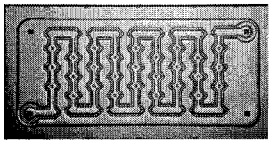	% EF	95.08	99.47
		Plasma collected (μl)	224	139
Microfilter #3 (10mm by 10mm)	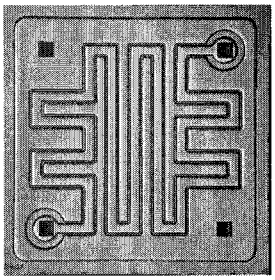	% EF	91.30	99.81
		Plasma collected (μl)	198	61

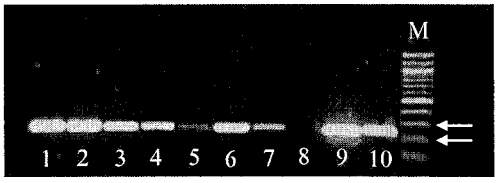

1: 8.46 x10^8 cp/μl
2: 4.23 x10^8 cp/μl
3: 2.12 x10^8 cp/μl
4: 1.05 x10^8 cp/μl
5: 5.30 x10^7 cp/μl
6: Centrifuge (dilution x100)
7: Centrifuge (dilution x10,000)
8: Negative
9: Microfilter #1(Dilution x10)
10: Microfilter #1 (Dilution x1,000)
M: Marker (100bp)

Figure 3: RT-PCR products of Cymbidium Mosaic Virus RNA separated by agarose gel electrophoresis: 1 to 5: dilution-series of standards, 6 and 7: plasma from spiked blood prepared by centrifuge, 9 and 10: plasma from spiked blood prepared by the microfilter # 1.

ULTRA-SMOOTH GLASS CHANNELS ALLOWING NON-FLUORESCENT OBSERVATION OF BIO-MOLECULES BY MICROSCOPES

Ryuji Yokokawa, Shoji Takeuchi, Hiroyuki Fujita
CIRMM/IIS, The University of Tokyo, 4-6-1, Komaba, Meguro, Tokyo 153-8505, Japan

Abstract

Optically flat glass channels were fabricated; in the channel two kinds of bioassays were successfully monitored. As result of assays microtubules and kinesin-coated beads were clearly observed by a dark-field microscope and a differential interference contrast (DIC) microscope, respectively. We have optimized the concentration of HF to obtain a flat surface and evaluated the surface by AFM, SEM, and the dark-field microscopy. The glass channel was etched using a poly(dimethyl siloxane) (PDMS) micro fluidic channel as an etching mask, and then sealed with a PDMS-coated coverslip permanently. The volume of the channel, 2-3 μl, realized the drastic reduction of the amount of protein required for an assay compared with a conventional flow cell method requiring 20 μl.

Keywords: glass etching, microfluidic channel, dark-field microscope, differential interference contrast microscope, protein

1. Introduction

Dark-field and DIC microscopy are major techniques to visualize raw proteins of nanometers in size without fluorescent labels. Biochemists have used a flow cell composed of two glass plates with spacers to enclose proteins between optically flat surfaces [1-2]. This technique, however, requires at least 20 μl of protein samples per assay, because the regular flow cell size is 10x18 mm^2 in area with 100 μm in height. The amount of a protein prepared by a purification process is limited to several hundreds of microliters. It is necessary to decrease the sample consumption in order to perform a time-effective analysis using limited samples. One approach is to utilize μTAS, but glass channels developed so far are not focused on the microscope observation [3-5].

Therefore we have fabricated microfluidic channels for that purpose. The ultra-smooth surface not only on the channel side but the lid surface is necessary, because even roughness or dirts of 10 nm in the optical axis cause the serious scattering of illumination light. We aimed to perform the bioassay including attachment of proteins on a glass surface and replacement of buffers in the sealed channel, so that we can reduce the assay time and the required amount of proteins at the same time.

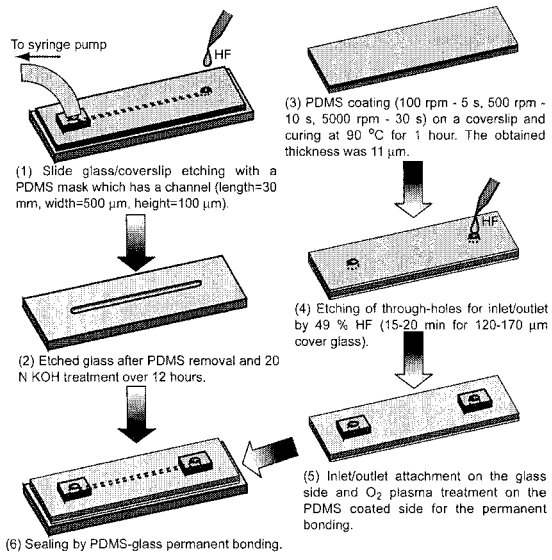

Figure 1. Fabrication process.

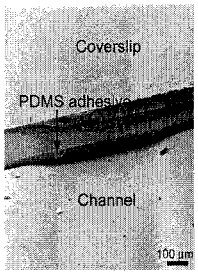

Figure 2. A sealed channel.

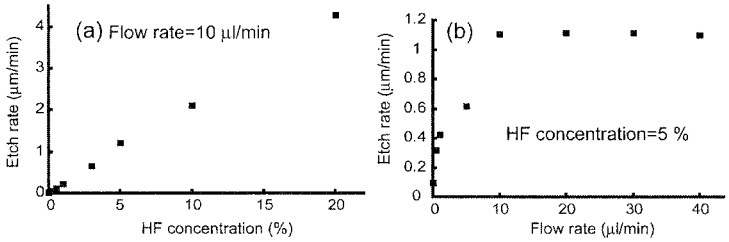

Figure 3. Etch rate vs. (a) HF concentration and (b) HF flow rate.

2. Experimental

Glass etching: A glass channel was directly etched on a slide glass (Matsunami) without annealing [5]. We utilized a PDMS mold as an etching mask, because PDMS is resistant to repetitive immersion of diluted HF [3]. The mask was first fabricated by pouring PDMS prepolymer to a mother mold patterned on a silicon wafer by DRIE. The cured PDMS replica (length=30 mm, width=500 μm, and height=100 μm) was just placed on a slide glass or a coverslip with slight pressure by hand to remove air bubbles (Fig. 1(1)). Only the channel region was etched by sucking the solution from the outlet with a syringe pump while supplying HF solution to the inlet as shown in Fig. 1(1, 2). The adhesion between PDMS and the glass surface was enough tight to prevent HF immersion during the etching process. Various concentrations of HF (0.01-20 %) was tested at various flow rates (0-40 μl/min).

Channel sealing: Channels were simply but permanently sealed with a PDMS-coated coverslip for the disposable use. A thin PDMS layer is an adhesion between an etched glass and a coverslip. PDMS prepolymer was coated by an optimized gradient spincoating (100 rpm - 5 s, 500 rpm - 10 s, 5000 rpm - 30 s) and cured at 90 °C for 1 hour. We obtained uniform thickness of 11 μm, although it was difficult to achieve a uniform layer with the viscous prepolymer (Fig. 1(3)). Through-holes for inlet and outlet were also etched by HF with a PDMS mask (Fig. 1-(4)). It was necessary to cover the whole glass surface by PDMS to protect it from etching by vaporized HF [6]. Inlet and outlet connectors were attached (Fig. 1(5)), and the coverslip was permanently bonded with the etched glass after O_2 plasma treatment (Fig. 1(6)). The etched channel, the PDMS layer for adhesion and the coverslip are shown in Fig. 2. The lid of coverslip with PDMS layer is partially broken to observe the cross section in Fig. 2. Some glass particles are also observed.

Assay test in the channel: Two kinds of bioassays, the bead assay and the gliding assays, were performed in a sealed channel and monitored. A well-known biomolecular motor, kinesin-microtubule system, was prepared for the assay. A motor molecule, kinesin (a few nanometers in size), moves on a rail molecule, microtubule (diameter=25 nm, length=10-30 μm), by hydrolyzing adenosine 5'-triphosphate (ATP). Proteins in buffer solutions were injected from the inlet and sucked from the outlet by the syringe pump. The required amount of solution for each injection was only 2 μl.

3. Results and discussion

Etching rate increased proportionally with the increase of HF concentration as shown in Fig. 3a. Flow rate of over 10 μl/min stabilized the etching rate (Fig. 3b) and also decrease the variation of etching depth along a channel. The average surface roughness (R_a) was measured over 20×20 μm^2 area by AFM (Fig. 4). R_a obtained from samples etched by 0.1-5 % HF are as good as R_a =0.96 from an original glass surface. But R_a drastically increases over 10 % HF. AFM images, however, show slight difference even between (a) the surface etched by 5 % HF and (b) the original glass

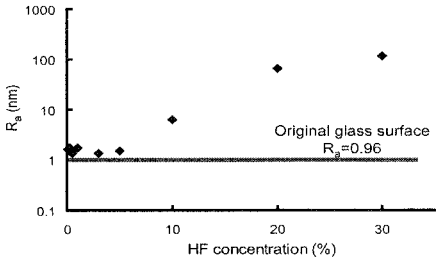

Figure 4. The relationship between surface roughness (R_a) and HF concentration.

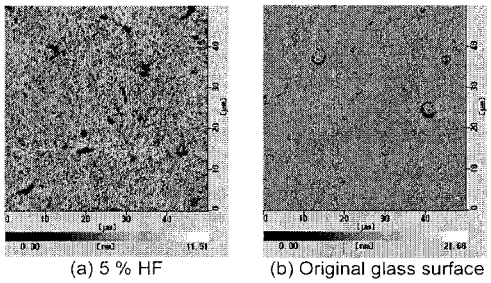

Figure 5. AFM images of glass surfaces etched by different HF concentration. A scanned area is a 50 μm square.

surface as shown in Fig. 5; the former has higher density of etched pits than the latter. Since the roughness of less than 10 nm is achieved [3, 5], the scattered light from microtubule can be visualized under the dark-field microscope.

We have observed the kinesin-coated beads (320 nm in diameter) moving on immobilized microtubules on the etched surface using a DIC microscope (Fig. 6a). Each white dot corresponds to a bead and some larger dots are aggregated beads. We have also realized the gliding assay in which microtubules glide on the kinesin-coated etched glass surface. The movement of microtubules was visualized as white lines by the dark-field microscope as shown in Fig. 6b. Dirts contained in a buffer solution were also observed.

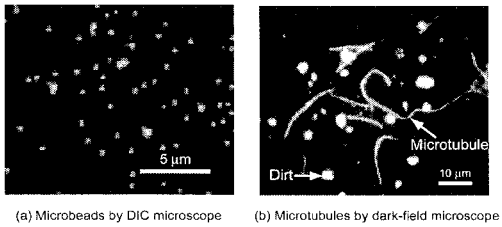

Figure 6. (a) kinesin-coated beads moving on microtubules and (b) microtubules gliding on the kinesin-coated glass surface.

4. Conclusion

The glass channel was fabricated with the ultra-smooth surface in the order of R_a=10 nm for bioassays. The optimized HF flow rate and the concentration during etching process were 10 μl/min and 5 %, respectively. A coverslip coated with a thin PDMS layer was utilized for the sealing of an etched glass channel. Finally, bioassays were performed to demonstrate the feasibility of channels, and nano-scale beads and microtubules were visualized. This proves the channel enables the observation of raw proteins with 1/10 sample volume of proteins compared with the conventional method.

Acknowledgements

Authors thank Prof. Kazuo Sutoh, Dr. Takahide Kon, and Mr. Masaya Nishiura at Graduate School of Arts and Sciences, The University of Tokyo for biological preparations.

References

[1] J. Howard *et al.*, Methods in cell biology, **39**, 137 (1993)
[2] H. Suzuki *et al.*, Jpn. J. Appl. Phys., **34**, 3937 (1995).
[3] I. Rodriguez *et al.*, Anal. Chim. Acta **496**, 205 (2003)
[4] A. Grosse *et al.*, J. Micromech. Microeng. **11**, 257 (2001)
[5] C-H Lin *et al.*, J. Micromech. Microeng. **11**, 726 (2001)
[6] Y. Fukuta *et al.*, Jpn. J. Appl. Phys., **42**, 3690 (2003)

DEVELOPMENT OF PERISTALTIC SOFT MICROPUMP DRIVEN BY ELECTROSTATIC ACTUATOR

Takaaki Suzuki[1], Isaku Kanno[1], Shunsuke Yakushiji[1],

Satoyuki Kawano[2] and Hidetoshi Kotera[1]

[1]Dept. of Mechanical Engineering, Kyoto University, Yoshida-Honmachi, Sakyo-ku, Kyoto 606-8501, Japan

[2]Center for Interdisciplinary Research, Tohoku University, Aramaki-aza Aoba, Aoba-ku, Sendai 980-8578, Japan

Abstract

We have developed a valveless micropump driven by electrostatic actuators. The micropump was composed of flexible wall of microchannel with electrodes for the electrostatic force. Traveling wave was induced on the surface of the microchannel by applying sinusoidal voltages to each electrode with the different phase. The fluid can be moved by the peristaltic motion of the channel wall. The sinusoidal voltages of 150 V were applied at the frequency of 5.0 kHz to the electrostatic actuators under the microchannel filled with the water. The fluid flow was measured with micro particle's motion in the fluid by the peristaltic actuation of electrostatic force.

Keywords: micropump, electrostatic, traveling wave

1. Introduction

A number of micropumps are proposed for fluid transportation system of μTAS. In most of conventional pumps, a diaphragm-type pumps which are actuated by piezoelectric actuators are popular because relatively large pumping power can be generated [1,2]. The fluid in the micropumps is transported by the vibration of diaphragm and the flow direction can be defined by mechanical valves. However, these micropumps have complicated structure, and therefore it is not easy to reduce the whole size of the pumps as well as the production cost. On the other hand, J. G. Smits reported a peristaltic micropump which realized a high flow rate of 100 μl/min [3]. This method enable simple structure and is suitable for the integration on a chip. We have also proposed a similar micropump system composed of a microchannel made of silicon rubber where the traveling wave is induced by PZT bimorph beams and demonstrated high efficiency of this type of micropump [4]. In this study, we adopted electrostatic actuators as a driving force of the micropump for practical application.

2. Experiment

Figure 1 shows the exploded illustration of the micropump. The microchannel is composed of PMMA with the height of 30 μm. Bottom surface of the microchannel is deformed by the electrostatic actuators whose upper electrodes are copper thin films deposited on a polyimide sheet. At the opposite side of the upper electrodes, lower electrodes were equipped with the gap of 7 μm. The lower electrodes, which were also deposited on the polyimide sheet, were separated to be actuated with the different phase. An overview of a prototype micropump system is shown in Fig. 2. The micropump we developed is simple structure in the absence of valves, and the fabrication process is accomplished by just stacking organic films or layer on PMMA substrate.

Traveling wave was induced on the bottom surface of the microchannel by applying sinusoidal signals to each lower electrode with the difference of the phase $2\pi/3$, as illustrated in Fig.

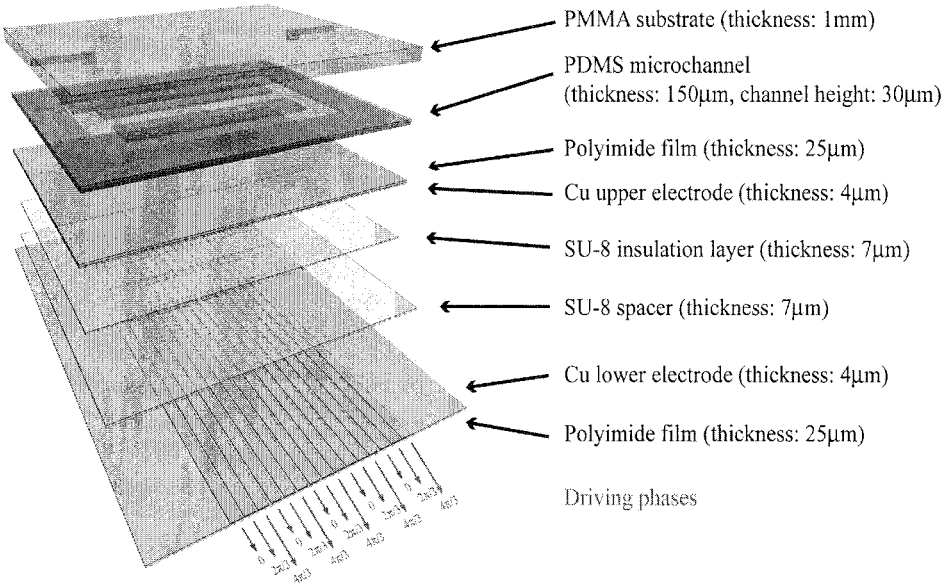

Fig. 1. Exploded view of micropump driven by traveling wave.

3. The fluid can be moved by the peristaltic motion of the channel wall. The microchannel is filled with water in which microbeads with a diameter of 6 μm are spread for the observation of flow condition.

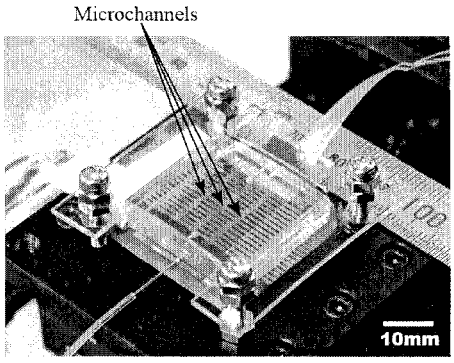

Fig. 2. Photograph of peristaltic micropump driven by electrostatic actuators.

3. Characterization

The deflection of the bottom surface of the channel was measured by the laser Doppler vibrometer. We applied the sinusoidal voltages up to 150 V in amplitude at the frequency of 5.0 kHz to the electrostatic actuators under the microchannel. Although the displacement is not so large as piezoelectric one, we could observe clear deflection of the channel wall. The displacement is proportional to the square of the applied voltage as shown in Fig. 4. The peristaltic motion along the channel wall was successfully generated by the application of the sinusoidal voltages to each lower electrode as shown in Fig. 3. Although continuous flow has not been observed yet, we confirmed active motion of the particles in the fluid by the peristaltic actuation of electrostatic force. These results suggest that the continuous flow can be realized by the optimization of driving signal as well as the structure of the actuators and this system is promising micropumps especially for medical applications.

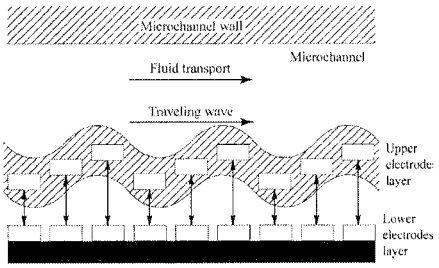

Fig. 3. Fluid transport system using arrayed electrostatic actuators.

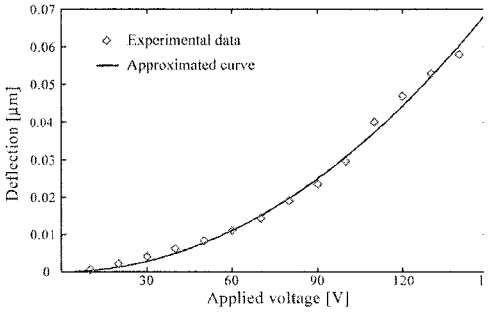

Fig. 4. Deflection of electrostatic actuator diaphragm as a function of applied voltage.

3. Conclusions

The valveless micropump driven by electrostatic actuators has been developed. The micropump was fabricated using flexible layers on PMMA substrate. The bottom of microchannel with electrodes was vibrated by the electrostatic attractors. Traveling wave was induced on the surface of the microchannel by applying sine wave signals with the different phase, and the peristaltic motion of the channel wall transports the fluid. The sign wave signals of 150 V in amplitude were applied at the frequency of 5.0 kHz to the electrostatic actuators under the microchannel filled with the water. The active motion of the particles in the fluid was confirmed by the peristaltic actuation of electrostatic force.

Acknowledgements

This study was supported by Industrial Technology Research Grant Program in '04 from New Energy and Industrial Technology Development Organization (NEDO), Center of Excellence for Research and Education on Complex Functional Mechanical Systems (COE program of the Ministry of Education, Culture, Sports, Science and Technology) and grant-in-aid for Scientific Research (A) (No.14205037 and No. 15201033) from the Ministry of Education, Culture, Sports, Science and Technology, Japan

References

[1] H. T. G. van Lintel, F. C. M. van De Pol and S. Bouwstra, et al., "A Piezoelectric Micropump Based on Micromachining of Silicon", *Sens. Act.*, **15**, 153-167 (1989).

[2] R. Linnemann, P. Woias, C. D. Senfft and J. A. Ditterich, "A Self-priming and Bubble-tolerant Piezoelectric Silicon Micropump for Liquids and Gases", *Proc. IEEE MEMS*, 532-537 (1998).

[3] J. G. Smits, "Piezoelectric Micropump with Three Valves Working Peristaltically", *Sens. Act. A*, **21**, 203-206 (1990).

[4] I. Kanno, S. Kawano, S. Yakushiji and H. Kotera, "Characterization of Piezoelectric Micropump Driven by Traveling Waves", *Proc. μTAS2003*, 997-1000 (2003).

A NOVEL FABRICATION PROCESS FOR 3D-MULTILAYER MICRO MIXERS

Marco Feldmann[1], Andreas Waldschik[1] and Stephanus Büttgenbach[1]
[1]*Institute for Microtechnology, Technical University of Braunschweig, Alte Salzdahlumer Str. 203, 38124 Braunschweig, GERMANY*

Keywords: micro mixer, micro fluidics, PDMS, SU-8, UV-depth lithography

1. Introduction

The integration and miniaturization of biochemical analysis systems (μTAS, lab-on-a-chip) like micro capillary electrophoresis or micro absorption photometry has received considerable attention in research. Particular interest is laid on fully integrated devices with micro fluidic components, like micro valves, micro pumps and micro mixers. However, mixing on a micro scale it is usually difficult to achieve, because viscous effects dominate the flow behavior. On the other hand the laminar nature of the flow in micro channels requires novel approaches to enhance the mixing process. Opposed to one layer micro mixers we developed a novel fabrication process for building 3D-multilayer micro mixers using Epon SU-8 and PDMS. Different passive mixing concepts have been simulated and tested. These concepts are based on the splitting and recombination of streams, using perpendicular inlets to the main channels (injection) and on vortex mixers [1].

2. Mixer concepts

In principle the mixers consists of three layers (see Fig. 1). The first layer contains the lower channels and the second layer the via-interconnects to the third layer, which contains the upper channels. These mixer structures are realized using Epon SU-8 and are covered by two cured PDMS layers. Finally the system and the fluid connectors are sealed with glue and are fixed on a glass substrate (see Fig 2).

3. Simulation

In order to obtain an idea of the optimal geometric dimensions and the achievable mixing ratio, computational fluid dynamics (CFD) simulations were run. In the simulation both fluids were injected simultaneously into the mixer. The CFD results of two different mixers in Fig. 3 and Fig. 4 show an excellent mixing behaviour (green).

4. Fabrication process

The fabrication process for the mixer structures is schematically displayed in Fig. 5. For the sacrificial layer the use of copper showed best performance due to its ease to etch without harming the SU8. Larger parts like the mixers, which need to be taken off completely, can be detached using a thicker Cu film. This thick sacrificial layer (up to a few microns) is deposited by electroplating, providing a broader etch front and reducing diffusion lengths underneath etched structures [2]. After fabrication of the cooper sacrificial layer the first SU-8 layer was deposited by spin coating with a rotating lid spinning tool, bakes on ramped hot plates, exposure and a two solution (GBL and PGMEA) development. Almost vertical sidewalls and aspect ratios of up to 36 were achieved. After this the produced SU-8 structures were electroplated with cooper to fill the lower channels. Then we fabricate a double SU-8 layer on top, which can be realized in two ways. At last the mixer structures were detached by etching the sacrificial layer and finally covered with PDMS. A photograph of a realized mixer is shown in Fig. 6.

5. Results and discussion

The mixers validated in simulation have been build and tested successfully (see Fig. 7 and Fig. 8). Two fluids with different color (blue, yellow) were injected by two micro pumps. As shown in

Fig. 7 a thorough mixing in the vortex mixer could be accomplished. In contrast to Fig. 7 we found, that the mixing ratio in the mixer shown in Fig. 8 is susceptible to interferences caused by the variation between of the flow rates of the micro pumps.

An enhancement of the pumping devices is subject to further investigations. As shown, a powerful means for the fabrication of complex 3D-multilayer micro mixers has been developed and successfully tested.

References

[1] . Böhm, K. Greiner, S. Schlautmann, S. de Vries, A. van den Berg, *Technical Proceedings of Micro Total Analysis Systems, MicroTAS, Monterey, CA,* (2001).

[2] V. Seidemann , J. Rabe , M. Feldmann , S. Büttgenbach, *Microsystem Technologies,* 8(4-5), 348-350 (2002).

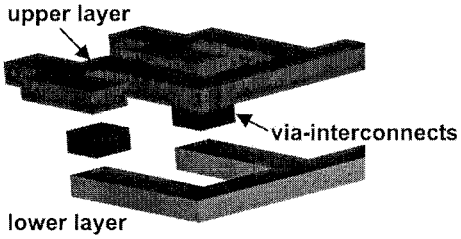

Figure 1. Principle mixer structure

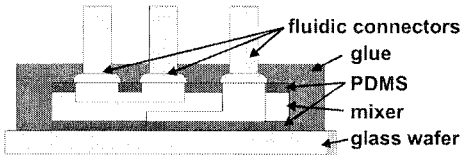

Figure 2. Mixer device

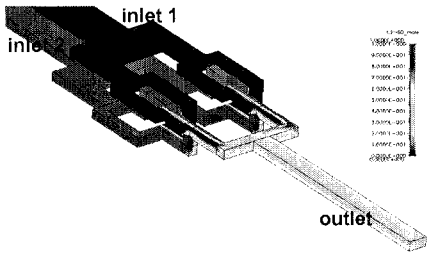

Figure 3. CFD result for an combined splitting and injection

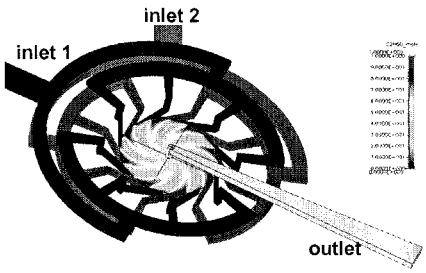

Figure 4. CFD result for an vortex mixer

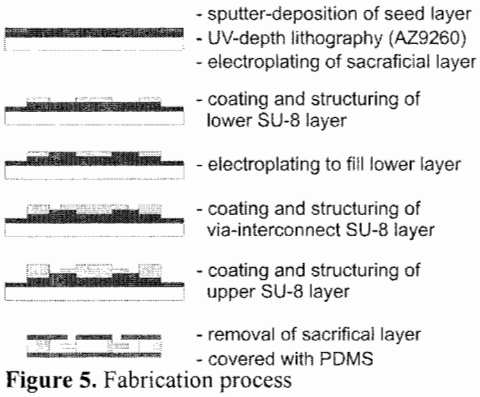

Figure 5. Fabrication process

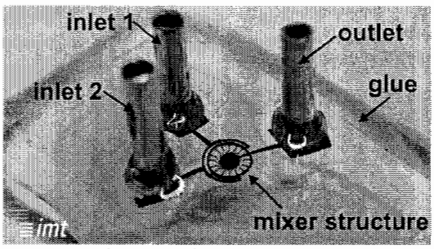

Figure 6. Photograph of a vortex mixer filled with colored water

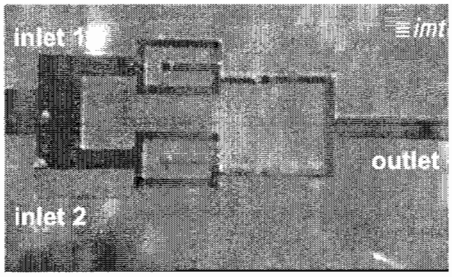

Figure 7. Test of a combined splitting and injection mixer

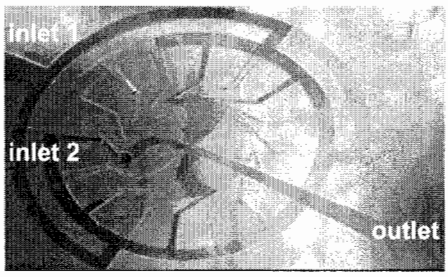

Figure 8. Successful test of an vortex mixer

HIGH PRECISION LOW TEMPERATURE BONDING PROCESS FOR BIOMEMS

Jörg Kentsch, Wolfgang Lutz, Manfried Dürr, Martin Stelzle
NMI - Naturwissenschaftliches und Medizinisches Institut an der Universität Tübingen, Markwiesenstrasse 55, D-72770 Reutlingen, Germany, phone: +49 (0)7121 51530-0, fax: +49 (0)7121 51530-62, e-mail: stelzle@nmi.de

1. Introduction

Today BioMEMS with surfaces functionalized by coating with biological components become more and more important. When working with closed micro channels three problems come up with regard to fabrication technology: (1) how to seal a device without contamination of the channel wall for example with adhesive, (2) how to bond bottom and top substrates without destroying biological components such as antibody coatings by heat as is commonly necessary in anodic bonding and with use of heat curable adhesives, and (3) how to align top and bottom halves with µm precision in order to create for example 3D-electrode arrays for use in dielectrophoresis applications. Also, such a process must lend itself to up-scaling and mass-production.

Keywords: low temperature bonding, adhesive, BioMEMS, microfluidic systems

2. Experimental

These issues were addressed in the development of a novel low temperature bonding process (LTBP) (Figure 1). LTBP has been applied to the fabrication of micro-fluidic devices with embedded electrode arrays. Since micro-electrodes were to be positioned on both faces of the device, most demanding requirements with respect to the precision of alignment had to be fulfilled. In contrast to commonly used high temperature bonding processes such as anodic bonding, our process may also be applied to polymer substrates and in addition allows for very high precision of alignment which is routinely better than ±2µm. The novel bonding process (Fig.1) relies on the precise preparation of an ultrathin film of uv-curable adhesive and its application onto one side of the micro-device.

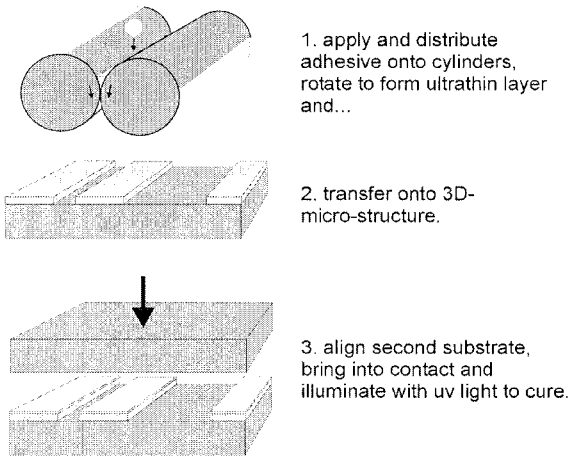

Figure 1. Schematic depiction of LTBP using uv-curable adhesive.

3. Results

This was accomplished using a custom designed tool (Fig.2). By rotating high precision milled cylinders, a layer of adhesive of homogeneous thickness is generated and transferred onto the substrate. Subsequently, both halves of the micro-device are aligned and brought into contact using a modified mask aligner. In-situ exposure employing the illumination source of the mask aligner brings curing of the adhesive to completion.

Bonding of polymers, glass and silicon may be achieved using uv-curable adhesive. Layer thickness may be adjusted by using an adhesive with the appropriate viscosity. Micro-fluidic devices have been fabricated with a channel height of only 5 µm and a thickness of the bonding layer on the order of 1 µm. Even for these shallow channels, contamination of the

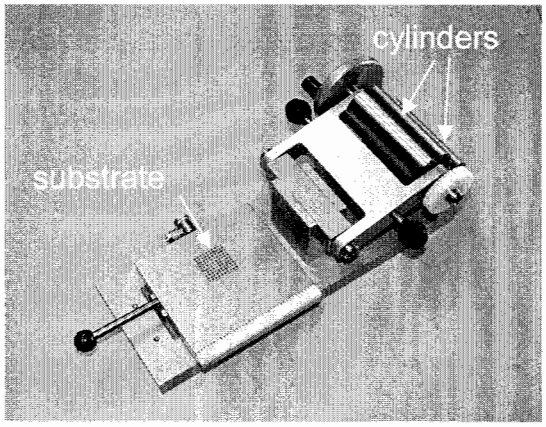

Figure 2. Custom designed tool used for the preparation of ultra-thin homogeneous layers of uv-curable adhesive and their application to micro-devices. High precision milled cylinders rotate against each other thus distributing the adhesive. Final layer thickness depends on viscosity and pressure applied.

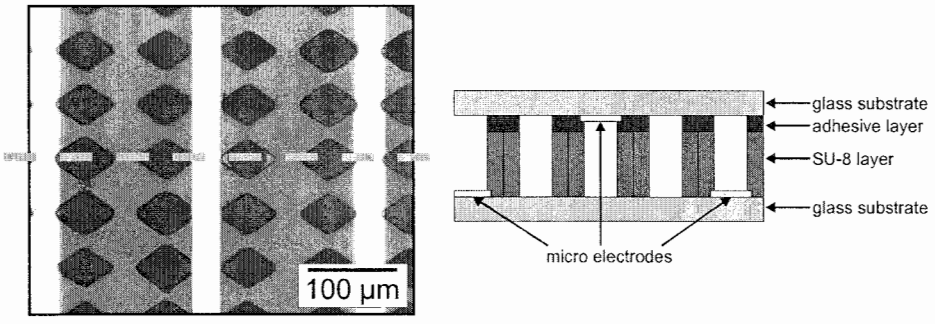

Figure 3. *Left:* Bonding of micro-fluidic devices consisting of glass with micro-electrodes (white bars), micro-patterned SU8 and a glass cover plate with micro-electrodes. The rhombic shaped SU8 columns (side length: 40 µm) together with the adhesive layer result in a total height of the chamber of 16.0µm. Homogeneous thickness of the adhesive layer ensures proper bonding reflected by dark appearance of contact areas while avoiding contamination of channels.
Right: Schematic view of the channel cross section as indicated by the dashed line in the left image.

channels by excess of adhesive may be avoided since layer thickness is very homogeneous. The channel height has been determined by interference measurements [3] with a precision of about 0,25µm.

Fig.3 shows an example of a bonded micro-fluidic system [1], [2] fabricated using LTBP. In this particular example, the micro-channel structure was created (1) using SU8 photoresist on a glass substrate to define micro-channels, (2) application of adhesive to the elevated SU8 structures and (3) bonding the glass/SU8/adhesive structure to another glass substrate serving as cover plate. The dark appearance of the contact areas indicates proper bonding.

4. Conclusion

A novel low temperature bonding process has been developed and applied to the fabrication and high precision bonding of micro-fluidic systems with embedded electrode arrays. This technology avoids problem frequently encountered in BioMEMS fabrication such as contamination of the cover plate with adhesive as well as high temperatures with the related hazard of destruction of biological components. In contrast to anodic bonding, the use of an adhesive bonding scheme allows for a wide range of material combinations to be applied for substrate and cover, respectively. In addition, LTBP should readily be adaptable to large scale production.

References

[1] Dürr, M., et al., *Microdevices for manipulation and accumulation of micro- and nanoparticles by dielectrophoresis,* Electrophoresis, 2003. **24**: p. 722-731.

[2] Dürr, M., et al. *Dielectrophoretic separation and accumulation of (bio)particles in micro-fabricated continous flow systems*, Micro Total Analysis Systems 2001, p.539-540. Monterey, USA: Kluwer Academic Publishers.

[3] H. Günzler, H. Böck, *IR-Spektroskopie, Eine Einführung*, Wiley/VCH, 1983

NOVEL THERMOPLASTIC ELASTOMERS FOR MICROFLUIDIC DEVICE CONSTRUCTION

Arjun P. Sudarsan, Jian Wang, and Victor M. Ugaz
Department of Chemical Engineering, Texas A&M University, College Station, TX 77843, USA

Abstract

We demonstrate the use of thermoplastic elastomer gels as advanced substrates for construction of complex microfluidic systems. These gels are synthesized by combining inexpensive polystyrene–(polyethylene/polybutylene)–polystyrene triblock copolymers with a hydrocarbon oil for which the ethylene/butylene midblocks are selectively miscible. The insoluble styrene endblocks phase separate into localized domains resulting in the formation of an optically transparent, viscoelastic, and biocompatible 3-D network possessing many features typical of soft materials employed as microfluidic device substrates (e.g. poly(dimethylsiloxane) (PDMS)), with the further advantage of melt-processability at temperatures in the vicinity of 100 °C. This desirable combination of properties allows microfluidic devices to be fabricated with unprecedented ease by simply making an impression of the negative relief structures on a heated master mold. The fabrication process can be completed in under 5 minutes, and multiple impressions can be made against different masters to construct geometries incorporating variable-height features, as well as intricate 3-D multilayered structures. Thermal and mechanical properties are tunable over a wide range through proper selection of gel composition.

Keywords: microfluidics, soft lithography, PDMS

1. Introduction

The development of increasingly sophisticated chemical and biochemical assays, combined with the need to incorporate these processes within a compact device footprint suitable for massively parallel operation requires the construction of correspondingly complex microfluidic structures [1,2]. This ongoing drive toward increased device complexity requires corresponding advances in fabrication materials and technologies. For example, although a number of multilayer PDMS-based systems have been successfully constructed, the resulting fluidic networks are effectively 2-dimensional owing to the planar nature of the fabrication process. It is possible in principle to employ an arbitrary number of layers, however the entire device structure must be assembled at once due to the irreversibility associated with the curing process. This irreversibility can be advantageous in terms of ensuring excellent mechanical stability, however it also imposes limitations because the molded structures cannot be further modified after curing. Consequently, there is no straightforward process to fabricate structures incorporating features of variable height because only a single impression from a single master can be used. Finally, the range of viscoelastic properties available for design of fluidic components that operate by inducing deformations in the substrate material (e.g. valves, pumps) is somewhat limited.

2. Theory

Novel thermoplastic elastomer gel substrates offer the capability to provide a greatly enhanced level of flexibility in microfluidic device design and construction. These gels are easily synthesized using a combination of inexpensive polystyrene–(polyethylene/polybutylene)–polystyrene (SEBS) triblock copolymers in hydrocarbon oils for which the ethylene/butylene midblocks are selectively miscible. The thermodynamic incompatibility between blocks induces microphase separation and self assembly of the insoluble polystyrene endblocks into distinct domains with characteristic size scales on the order of 10-20 nm [3,4]. The soluble midblocks emanating from these nanodomains penetrate into the solvent creating arrays of loops (beginning and terminating within a single

nanodomain) and bridges (joining adjacent nanodomains) resulting in the formation of a 3-D viscoelastic gel network in which the polystyrene domains act as physical crosslink junctions. Like PDMS, this gel network is optically transparent, viscoelastic, and biocompatible, but also possesses the further advantage of melt-processability at temperatures in the vicinity of 100 °C.

3. Experimental

A series of thermoplastic elastomer gels were synthesized by combining commercially available SEBS copolymer resin (Kraton® G series) in mineral oil. The reisn and mineral oil were mixed and placed under vacuum overnight at room temperature in order to allow the oil to evenly wet the resin surface. The mixture was then heated to 120-170 °C (higher temperatures are required with increasing copolymer fraction) under vacuum for 2–4 hours to allow the resin and oil to intermix and to remove any residual air bubbles. Finally, the mixture was cooled to room temperature and the solidified gel was cut into smaller pieces used for molding devices. Gel compositions ranging from 10 to 55 wt% copolymer were studied.

4. Results and discussion

We investigated thermal transitions associated with these SEBS-mineral oil gels using small amplitude oscillatory shear experiments (Fig 1). A measure of the transition to liquid-like behavior can be inferred from the temperature T^* at which the value of the loss modulus G'' exceeds that of the storage modulus G'. The range of gel compositions studied here allow the location of this transition to be varied over a range of approximately 50 °C. Moreover, the room temperature (plateau) value of the elastic modulus can be varied over an order of magnitude.

Fabrication of microfluidic devices is accomplished by placing a slab of elastomer on top of a master mold that has been preheated to 120 °C on a hot plate. Within seconds the elastomer begins to soften, after which a glass plate is placed on top of the slab and gentle pressure is applied by hand to ensure complete contact with the structures on the mold. After cooling and release, the solidified gel incorporates the shape of the structures on the master (Fig 2). Strong uniform bonds can be easily achieved, either with a glass or elastomer surfaces, by briefly heating the material to a temperature just below its softening point either on a hot plate or using a handheld heat gun. The entire fabrication process can be completed in about 5 minutes.

We have demonstrated the suitability of these elastomers as substrates for microfluidic applications by constructing devices for DNA electrophoresis (Fig 3) and diffusive transport studies [5]. We are also able to easily assemble a variety of complex multilayered structures in only a few minutes (Fig 2). Individual layers are repositionable, thereby allowing precise alignment to be achieved prior to thermal bonding. More complex 3-D structures can be fabricated by direct casting, and interfaces with external fluidic supply lines can be readily sealed by locally heating the gel to melt it at the point where the lines are inserted into the substrate. Multiple impressions can be made against different masters to easily construct geometries incorporating variable-height features (Fig 4). This degree of versatility and fabrication ease, combined with their inherently inexpensive nature, make thermoplastic elastomer gels ideal substrates for many microfluidic applications.

References

[1] T. Thorsen, S.J. Maerkl, and S.R. Quake, *Science,* **298**, 580-584 (2002).

[2] S. Sia and G.M. Whitesides, *Electrophoresis,* **24**, 3563-3576 (2003).

[3] J.H. Laurer, J.F. Mulling, S.A. Khan, R.J. Spontak, and R. Bukovnik, *J. Polym. Sci.: Part B: Polym. Phys.,* **36**, 2379-2391 (1998).

[4] R. Kleppinger, N. Mischenko, H.L. Reynaers, and M.H.J. Koch, *J. Polym. Sci.: Part B: Polym. Phys.,* **37**, 1833-1840 (1999).

[5] A.P. Sudarsan and V.M. Ugaz, *Anal. Chem.,* **76**, 3229-3235 (2004).

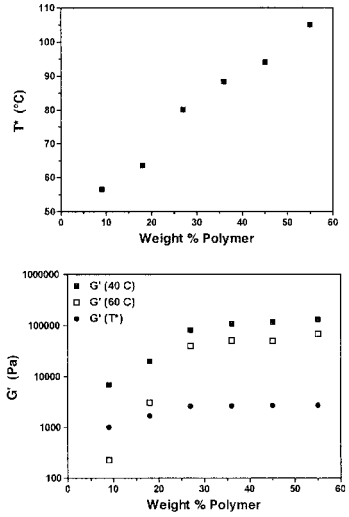

Figure 1. Variation of melt transition temperature (top) and plateau elastic modulus (bottom) with gel composition.

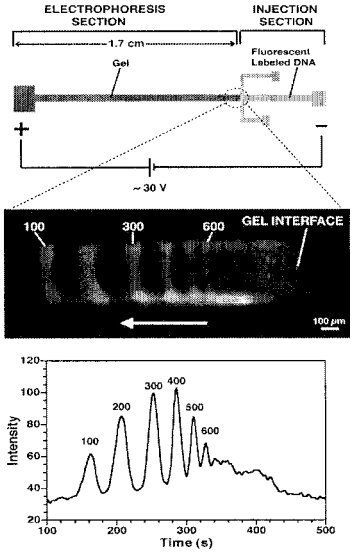

Figure 3. DNA gel electrophoresis device constructed using thermoplastic elastomer. An image of the fluorescent bands and electropherogram obtained 2 mm downstream from the gel interface are shown (E = 15 V/cm).

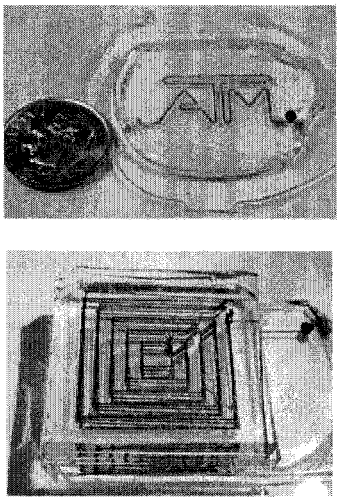

Figure 2. Planar (top) and interconnected multilayer (bottom) microfluidic channels constructed using elastomer gels (400 x 30 µm cross-section).

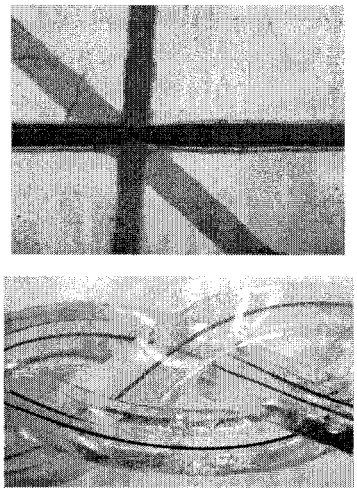

Figure 4. (Top) Intersecting fluidic channels with 3 different depths in a single elastomer substrate. Horizontal: 300 x 120 µm, vertical: 200 x 60 µm, diagonal: 400 x 30 µm cross-sections. (Bottom) Braided network of intertwined elastomer channels.

ELECTROSTATIC SHAKING AND CONVEYANCE OF CATALYTIC PARTICLES IN MICRO SPACES

Koichi Suzumori[1], Takefumi Kanda[1], Takashi Nagata[1], Akinori Muto[2], and Yusaku Sakata[2]
[1] *Dept. of Systems Engineering, Okayama University, Tsushima-naka, Okayama 700-8530 Japan*
[2] *Dept. of Applied Chemistry, Okayama University, Tsushima-naka, Okayama 700-8530 Japan*

Abstract

This paper reports a new electrostatic handling method of catalytic particles in micro spaces. It causes shaking of the particles in a micro chamber to realize uniform mixing of chemical materials and acceleration of reaction. It also causes conveyance of the particles along micro channels or pipes. The actuator mechanism is very simple and suitable to be fabricated through MEMS process.

Keywords: micro reactor, active catalyst, electrostatic actuator, micro stirrer

1. Introduction

Uniform mixing and acceleration of chemical reaction in micro chambers are an essential process for micro reactors and micro TAS. However, it is difficult to fabricate many tiny stirrers on a reactor chip. This paper shows a new method promoting high-efficient chemical reaction in micro chambers; newly developed carbon-base and zeolite-base catalytic particles are introduced into chamber and driven electrostatically to travel rapidly in chamber, stirring chemicals and accelerating reaction.

In addition, this system works to exchange catalytic particles. Deactivated catalytic particles in chamber are easy to be flushed away with no voltage applied to the electrodes. After flushing, virgin catalytic particles are introduced with gas from the port and they can be kept easily in the chamber by applying voltage. Conveyance of chemical materials along micro channels or pipes is also realized.

2. Electrostatic driving mechanism

Figure 1 shows a typical simple model of a micro reactor proposed in this paper. This model has two inlet ports, an outlet port, a micro chamber, fluidic channels and two thin film electrodes. It can be used for methanol synthesis for example; H_2 and CO_2 gasses are supplied through each inlet port. Applying voltage to the electrodes keeps the catalytic particles inside the chamber and drives them to mix the gasses uniformly and to accelerate methanol synthesis, resulting in high-efficient chemical reaction.

We applied two catalytic particles, zeolite particle and nickel-carbon composite particles ranging in size from 50 μm to 1 mm in diameter. Figure 2 shows nickel-carbon particles of 250μm in diameter. These particles work as catalysts themselves and can contain other catalytic chemicals on their inner surfaces, making this system widely applicable for various types of chemical reactions.

We have developed two driving voltage patterns applied to the electrodes; a DC drive and an AC drive. The DC drive is applicable for conductive particles, while the AC drive is applicable both for nonconductive and conductive particles. Figure 3 (a) shows a driving mechanism of the DC drive: a negatively-charged particle is drawn to the positive electrode as shown in (1), the particle releases electrons and is charged positively as shown in (2) to (3), then the positively-charged particle starts to move to the negative electrode as shown in (4), and the particle is charged negatively again as shown in (5) to move to the positive electrode as shown in (1). This drive needs no electrical switching and is very simple. Frequency of particle motion depends on electrical characteristics of particle and on viscous resistance of vapor/fluid in the chamber.

The AC drive mechanism is shown in Fig. 3 (b). Applying electrostatic field causes polarization in a particle. Phase difference between alternating electrostatic field and polarization results in

oscillation of the particle. Shaking frequency depends mainly on AC drive frequency.

3. Experiments

Figure 4 shows an example of catalytic particles traveling in a micro chamber. The upper photograph shows the particles at rest. The lower photograph, which was taken with the exposure time of 100 msec shows the particle traveling rapidly in the chamber.

The chamber is formed by two cupper walls and two glass plates. The chamber is 3 mm in width. We have tried three particles in this chamber; nickel-carbon composite particles of 250μm and 500 μm in diameter, and zeolite particles of 500μm in diameter. Applying DC or AC voltage between two cupper walls we can drive the nickel-carbon composite particles in the chamber. We also succeed at driving the zeolite particles by applying AC voltage. Applied voltage between the cupper walls is adjustable from 0 to 3.0 kV.

It was found that (1) the DC drive method is applicable for nickel-carbon particles of 250 μm and 500 μm, and the AC drive is applicable both for nickel-carbon particles and zeolite particles, (2) the particles can be driven by applying minimum electrostatic fields of $1x10^5$ V/m, and (3) frequency of particle motion is up to 10 Hz.

Figures 5 and 6 show the glass tube models: the model shown in Fig.5 has two aluminum thin films sputtered on the outer surface of the tube to realize shaking the particles in tubes. The model shown in Fig. 6 has the strip electrodes of sputtered aluminum film to convey particles rapidly in desired direction by applying voltage to each electrode sequentially. This system works to exchange catalytic particles. The glass tube is 2 mm in inner diameter.

The glass tube models work successfully. Both nickel-carbon particles and zeolite particles are easily driven by applying 1 to 3 kV AC voltage.

4. Conclusions

A new method realizing uniform mixing and acceleration of chemical reaction in a micro chamber is proposed. Experiments using two prototypes show that the proposed method makes the catalytic particles traveling rapidly in micro chamber and moving in pipes. It is found that electrostatic fields of $1x10^5$ V/m is necessary and driving frequency is about 10 Hz in air.

We believe that this method can be applied to various gas phase chemical reactions in micro reactors and micro TAS. We are now making experiments to determine reaction efficiency.

Acknowledgements

This work was supported by the Cooperation of Innovative Technology and Advanced Research in Evolutional Area (CITY AREA) of the Ministry of Education, Culture, Sports, Science and Technology, Japan.

Reference

[1] Takashi Nagata, Koichi Suzumori, Takefumi Kanda, Akinori Muto, and Yusaku Sakata, Electrostatic Shaking of Catalytic Particles in Micro Chamber, The Second International Workshop on Micro Chemical Plants, Awaji, Japan, February 2004.

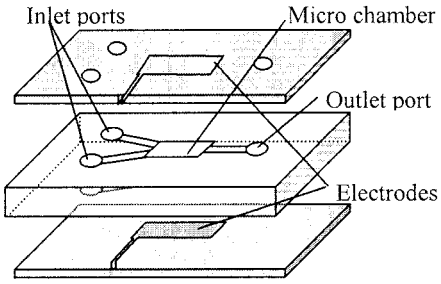

Figure 1. Schematic of a typical model of a micro reactor with shaking catalyst system

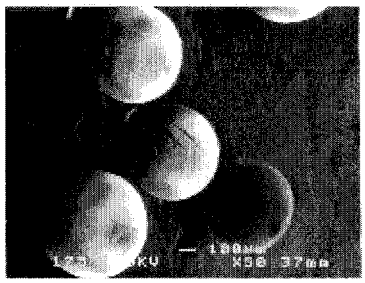

Figure 2. An example of catalytic particles (nickel-carbon composite, 250 μm in diameter)

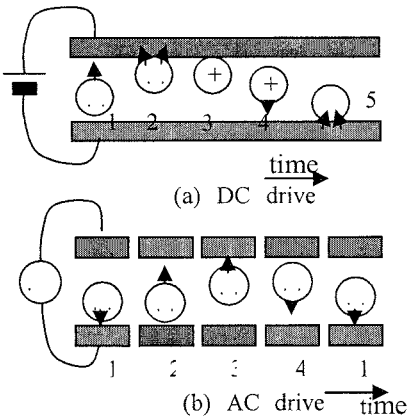

Figure 3. Driving mechanism of shaking particles shaking

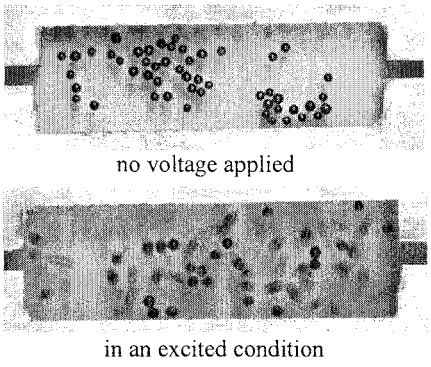

Figure 4. Motions of catalytic particles, shaking in a micro chamber (Exposure time is 100 msec.)

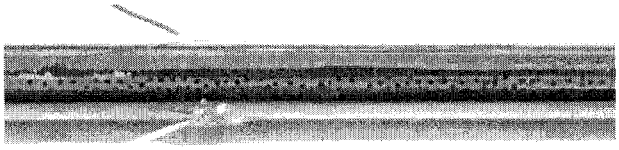

Figure 5. A glass tube mode (shaking type)

Figure 6. A glass tube model (conveyance type)

ELISA READER COMPATIBLE MICROFLUIDIC DEVICE FOR ENZYME KINETICS

Joo H. Kang and Je-Kyun Park
Dept. of BioSystems, Korea Advanced Institute of Science and Technology (KAIST)
Daejeon 305-701, Korea

Abstract

We have developed a microfluidic device for enzyme kinetics employing microfluidic channel patterns on a polymer substrate, which can be substitute of tedious conventional enzyme assay technique. Substrate dilutions and enzyme reactions were sequentially carried out in the microfluidic device fabricated by micromolding processes with PDMS (polydimethylsiloxane) polymer. Overall dimension of the microfluidic device was the same size as a 96-well microtiter plate and each device consisted of four sets of assay module. The measurement of the enzyme reactions generated in the reaction chambers of the microfluidic device was conducted with an ELISA reader instrument, which eliminates the requirement of special optical detection systems.

Keywords: microfluidics, enzyme kinetics, ELISA reader, PDMS, alkaline phosphatase

1. Introduction

A microfluidic system for biological sample processing and detection offers many potential advantages over conventional assay platform, including small volumes, short assay time, multiple assay, and automation. Several approaches to develop the microfluidic device for enzyme activity measurement have been carried out in the microfluidic channels [1]. However, they usually need specially designed optical instruments for microchip detection. Also, many procedures in conventional biochemical experiments including enzyme kinetics study still need improvement of routine, tedious and repeated processes.

There is an increasing demand for performing several chemical and biochemical analyses in a single unit device and some miniaturized analytical systems have been developed using microchip technology. These systems have been described as lab-on-a-chip [2]. Microfluidics can be used to speed up and simplify the sample preparation in lab-on-a-chip and to offer high-throughput, low-cost versions of traditional research methods. In this work, we have developed a microfluidic device for enzyme kinetics, which could provide the basis of potential future clinical or forensic analysis.

2. Theory

The diluted substrate solutions in reaction chamber were generated by employing the pattern of the microfluidic channels. The substrate solution with two different concentrations was injected into two inlets as shown in Figure 1-III. After the six reaction chambers shown in Figure 1-II are filled with substrate solution of different concentrations, enzyme sample is injected into the reaction chambers with starting enzyme reactions simultaneously. In enzyme kinetics based on Michaelis-Menten relationship, it is important to know what concentration of substrate reacts with enzyme. To estimate the concentration of substrate solution in six reaction chambers, we defined and used new equation (1) describing formation of concentrations in microfluidic channel, which is based on the governing equation [3] reported previously:

$$\frac{(N-i)C_1+iC_2}{N}, \tag{1}$$

where N is the number of order from top in the microfluidic dilution channels (N = 1,2,3,4,5) and i represents the number of order from left branch point (i = 0,1,2,3,4,5) and C_1, C_2 are the concentration of substrate solution injected into the microfluidic channels. Therefore, when C_1 is 3.0mM, C_2 is 56.8mM, N is 5 and i has 0 to 5, the reaction chambers are expected to have $C_{\#1}$,

3.0mM; $C_{\#2}$, 14.76mM; $C_{\#3}$, 24.52mM; $C_{\#4}$, 35.28mM; $C_{\#5}$,46.04mM and $C_{\#6}$, 56.8mM ($C_{\#n}$, the concentration in reaction chamber, n). Experimental results are supporting the estimation of the equation (1) (data not shown).

3. Experimental

As shown in Figure 2 (a), the microfluidic device consists of three layers of PDMS substrates fabricated by PDMS replica molding process. The device is largely comprised of three parts, for enzyme injection, enzyme reaction and the input of substrate solution corresponding to Figure 1-I, II and III. The device design is considered to have the same size as a microtiter plate and compatible with its well positions. Alkaline phosphatase (ALP) and p-nitrophenyl phosphate (p-NPP) was used as enzyme-substrate model system and was demonstrated for microfluidic enzyme assay experiments. p-NPP solution of high and low concentrations is infused into the microfluidic channels shown in Figure 1-III with the rate of 0.5mL/hr until 40μL. After then, enzyme sample was injected into the reaction chamber along the microfluidic channel of Figure 1-I, which has 20μL of enzyme solution in each chamber. Loading an ELISA reader instrument with the microfluidic device, the absorbance was measured at 405.0 nm for one minute as shown in Figure 2 (b) providing initial velocities, Vo of enzyme reaction.

4. Results and discussion

The enzyme reactions occurred in six reaction chambers containing each different concentration of the substrate solution generated by microfluidic channel network, where the reaction chambers have been arranged in 96-well format to be compatible with an ELISA reader. Obtaining initial reaction rates, Vo and substrate concentrations, [S], enzyme activity was estimated by Vmax through transforming Vo and [S] by Hanes-Woolf plot modified form of Michaelis-Menten equation in which the slope of a linear plot results in a reciprocal of Vmax as presented in Figure 3 (a). Figure 3 (b) shows the plot of Vmax obtained from the microfluidic device and enzyme activity (unit/L) estimated by standard enzyme assay of the stop method. Enzyme assay with unknown sample prepared by random dilution of the enzyme solution performed in the microfluidic device showed errors of less than 10.1 % of enzyme activity.

5. Conclusions

In this paper, the microfluidic device for enzyme kinetics is described and demonstrated to assay alkaline phosphatase. The device is compatible with 96-well microtiter plate and can be conducted by ELISA reader which eliminates the requirement of the additional optical systems. Using Vmax obtained by Vo and [S] through Hanes-Woolf plot, enzyme activity can be estimated in one minute of measurement. This work provides the platform technology of enzyme assay, furthermore, can be applied to blood serum analysis for diagnosis.

Acknowledgements

This research was supported by a grant from Electronics and Telecommunications Research Institute (ETRI), Korea and CHUNG Moon Soul Bioinformatics and Bioelectronics Center, KAIST, Korea.

References

[1] J. Wang, *Electrophoresis*, **23**, 712-718 (2002)
[2] J. M. Ramsey, S. C. Jacobsen, M. R. Knapp, *Nature Med.*, **1**, 1093-1096 (1995)
[3] S.K.W. Dertinger, D.T. Chiu, N.L. Jeon, and G. M. Whitesides, *Anal. Chem.*, **73**, 1240-1246 (2001)

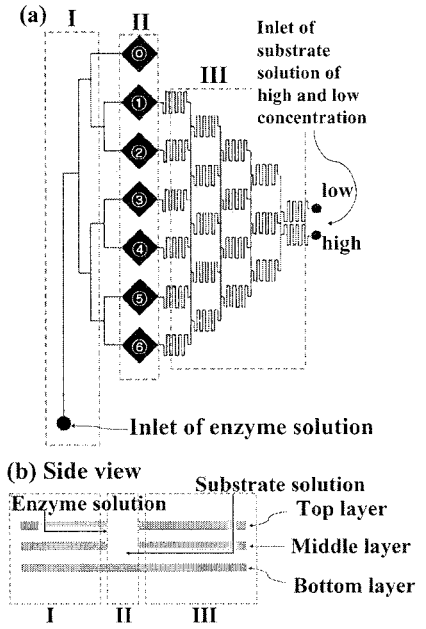

Figure 1. Scheme of single module for enzyme assay in the microfluidic device. Part I for injecting enzyme solution; the reaction chambers in part II; part III for dilution of substrate solution. The device consists of three PDMS layers.

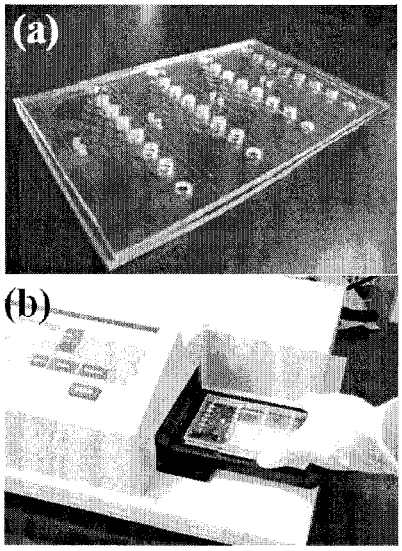

Figure 2. (a) Photograph showing the fabricated PDMS device. (b) Picture of loading the microfluidic device to an ELISA reader.

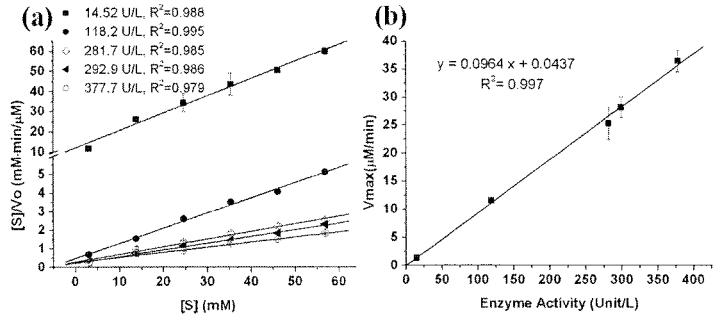

Figure 3. (a) Hanes-Woolf plot of the data obtained from the ELISA reader. (b) The plot of Vmax against enzyme activity (unit/L) of ALP. The enzyme activity was obtained by the standard enzyme assay.

PASSIVE LOW PASS VALVE FOR SAMPLE INJECTION IN HIGH PRESSURE SYSTEMS

Takeo Yamazaki[1], Takahiro Ezaki[1], Susumu Yasuda[1], Takayuki Yagi[1], Yukihiro Shintani[2], Keiji Hirako[2], Yoshihiko Takano[2] and Masahiro Furuno[2]

[1]Canon Inc., 5-1, Morinosato-Wakamiya, Atsugi-shi, Kanagawa 243-0193, Japan

[2] GL Sciences Inc., 237-2, Sayamagahara, Iruma, Saitama 358-0032, Japan

Abstract

We have developed novel microvalves for sample injection in high-pressure systems. The valves are passive low pass valves that allow liquid flow at a low flow rate and prohibit it when the flow rate exceeds a threshold (0.006-0.80ml/min for various designs). The design and characterization of the valves are presented in this paper. The valves can withstand at least 1.5 MPa of pressure difference.

Keywords: sample injection, microvalve, passive valve, low pass valve, HPLC

1. Introduction

Many different kinds of microvalves have been developed for various applications. Passive microvalves can control liquid flow without the need of a drive actuator and play important roles in microfluidic systems [1]. However most passive microvalves currently in existence are used as simple check valves that allow liquid to flow in only one direction. In this paper, we describe a novel passive microvalve, a passive low pass valve, to allow a liquid flow at a low flow rate. The valve is suitable for sample injection in high-pressure systems such as High Performance Liquid Chromatography (HPLC). Sample injection in high-pressure system is one of the most important challenges in micro fluidic systems [2].

2. Design and fabrication

The valve consists of a disc positioned over a through hole with a defined gap and beams that support the disc, as illustrated in Fig. 1a. When liquid flows across the valve, a pressure drop occurs at the gap. Then the pressure difference between the upside and the downside of the disc causes the disc to move toward the through hole. Below the threshold, the pressure difference is balanced with the restoring force of the beams and the gap is held open (Fig. 1b). Beyond the threshold, the pressure difference exceeds the restoring force and the valve is closed (Fig. 1c). It is easy to obtain the desired threshold value for each valve by changing the beam designs, the gap and the diameter of the disc.

The valve is fabricated by conventional MEMS technology. Fig. 2a is a SEM micrograph of the first substrate, an SOI wafer with a disc supported by beams fabricated using Si deep-RIE. Fig. 2b is a SEM micrograph of the second substrate with a through hole and a gap etched using multi-step Si deep-RIE. The diameter and thickness of the disc are 200μm and 5μm, respectively, and the gap depth is 5μm. The valve fabrication is completed by thermally bonding the two substrates.

3. Microvalve characteristics

The flow characteristics of three valves with different numbers of beams were examined. The pressure necessary for pumping at a specific flow rate was measured using a HPLC pump (HITACHI MODEL L-7100) and the pressure difference across the valve was determined by subtracting, for an identical flow rate, the pressure data obtained without the valve from those obtained with the valve. Fig. 3 shows the pressure difference versus flow rate of DI water for valves with 4, 6, and 8 beams with beam length and width of 50μm and 40 μm, respectively. As seen from this figure, the pressure difference increases with flow rate. When the flow rate exceeds the threshold value, the valve closes and causes a drastic increase of the pressure difference. The arrows

in the graph indicate the threshold value of each valve. The results in Fig.3 show that the threshold flow rates depend on the total spring constant of the beams. In addition to these data, valves with various beam designs were also tested and threshold flow rates ranging from 0.006 to 0.80 ml/min were obtained. All the valves tested can withstand at least 1.5MPa of pressure difference.

However, through currently ongoing experiments and theoretical calculations, behavior different from Figure 3 can be seen when constant pressure is applied. In this case, the flow rate reaches a peak value equivalent to the threshold in the above experiment and increases gradually with increasing applied pressure after the peak.

4. Sample injection

The developed passive valve was applied to HPLC to characterize the performance in high-pressure systems. The micro-HPLC analyses were performed using a MP-711 Micro-Flow Pump (GL Sciences), a MU-701 UV/VIS detector (GL Sciences), and a MonoCap monolithic silica capillary column (150 x 0.1 mm I.D., through-pore size 2 μm, meso-pore size 15 nm, skeleton size 1μm; GL Sciences). A mixture of three kinds of alkylbenzene (1μl/ml) was employed as a test sample. UV adsorption at 210 nm was used for detection. Sample injection was achieved with a cross channel injection method as shown in Figure 4: (1) the channels were filled with eluent (Fig. 4a); (2) a sample solution was loaded from inlet 1 to the outlet at a rate below the threshold of valve 2 (Fig. 4b); (3) eluent was pumped from inlet 2 at a rate beyond the thresholds of both valves 1 and 2, causing them to close, to create a sample plug from the sample solution in the intersection of the cross channel (Fig. 4c). The resulting sample plug (50nl) was then pushed by the eluent into an RP column for separation and detection. The valve 1 and 2 act as a check valve and a low pass valve respectively. The injection system was constructed by mechanically clamping a silicon component containing the valve described in section 2 onto a quartz component containing the channels. The width and depth of the channels are both 100μm. Fig.5 shows the analytical result of a mixture of alkylbenzenes that was achieved by using the developed valve as valve 1 in Fig.4. The valve was used as simple check valve in this experiment. Sharp peaks were obtained with reproducibility data of <1.8% (CV). This result shows that the newly developed passive valve is potentially applicable as a module in high-pressure μTAS.

5. Conclusions

We have presented passive low pass valves for sample injection in high-pressure systems. To demonstrate the suitability of these passive valves for use in high-pressure systems, we applied the valves to the sample injection system of HPLC and the reproducibility of the data was confirmed. This shows that these valves have the possibility of being used in high-pressure μTAS.

In this paper, only the application of our valves as a check valve was examined; however, we are currently studying the usage of the valve as a low pass valve.

Acknowledgements

This work was partially supported by the project fund "Development of micro HPLC for post-genomic analysis", provided by the Japanese Ministry of Economy, Trade and Industry, through Kansai Bureau of Economy, Trade and Industry, and Osaka Science and Technology Center.

References

[1] M. Esashi, S. Shoji and A. Nakano, *Sensors and Actuators*, **20**, 163-169 (1989).
[2] Michael J. Felton, *Analytical Chemistry*, **75**, 429A-432A (2003).

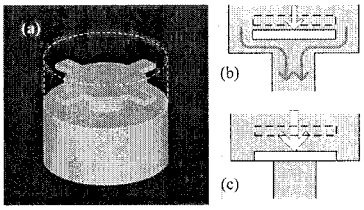

Figure 1. Schematics of a passive low pass valve: (a) perspective view, (b) open state (below threshold flow rate), (c) closed state (beyond the threshold).

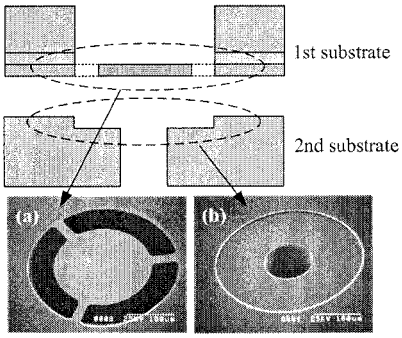

Figure 2. SEM micrographs of components of the valve: (a) disc and beams, (b) gap and through hole.

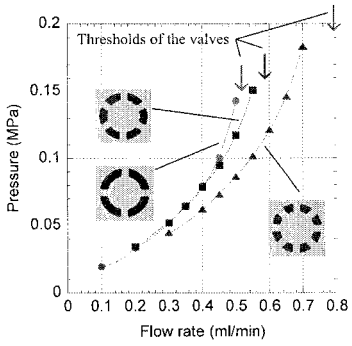

Figure 3. Flow characteristics of three valves with different numbers of beams with beam length and width of 50μm and 40 μm, respectively.

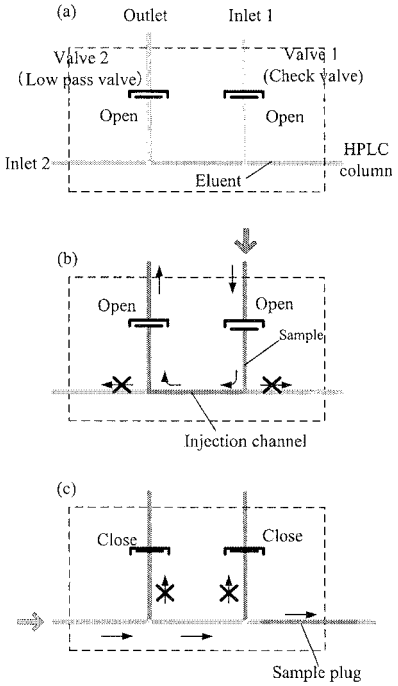

Figure 4. Schematic diagram of the injection system with the low pass valve.

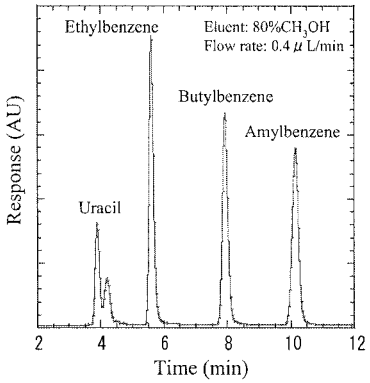

Figure 5. Chromatogram of a mixture of alkylbenzenes that was achieved by using the developed valve as valve 1 in Fig.4.

AN OPTICAL MICROFLUIDIC PLATFORM BASED ON A COMBINATION OF A NOVEL SU8 MULTILAYER TECHNOLOGY, WAVEGUIDES AND PHOTODIODES ON SILICON

J.M.Ruano[1], M.Aguirregabiria[1], M.T. Arroyo[1], J.Berganzo[1], F.J.Blanco[1], P. de la Fuente[2], E.Castaño[2], and K.Mayora[1]

[1]MEMS/MST Department, IKERLAN S. Koop. Paseo de Arizmendiarrieta, 2 Arrasate 20500, Spain
[2]Dept. Microelectronics, CEIT, Paseo de Manuel Lardizábal, 15, Donostia, 20018, Spain

Abstract

The work described here, integrates in a substrate different achievements related to SU8: (i) 3-D embedded microchannels by a low temperature SU8 wafer adhesive bonding process (ii) buried optical waveguides with their fibre optic connectors, (iii) easily connectable microchannels by an enhanced releasing step from two SU8 bonded layers, and (iv) a silicon photodiode. All together with the fabrication of a plastic capsule enclosing the device.

Keywords: SU-8, waveguides, Lab-on-a-Chip, packaging, kapton, microfabrication

1. Introduction

There is a strong need to improve detection technologies on sensitivity, reliability, time response in food/medical diagnostic laboratories. The optical principle is usually the most specific, reliable, and sensitive detection mechanism in a biochemical assay. However, it is also one of the most difficult to integrate because of the complexity of the single components (emitter/detector), alignment requirements, and thermal stability. Therefore, a technology that can achieve most of these optical issues, together with the microfluidic ones, would lead to the simplification of a self-contained optical Lab-on-a-Chip (LOC).

It is clear that there is an urgent need to find a suitable material that is cheap and versatile, which will allow a monolithic integration of as many functions as possible, and which will simplify the fabrication and further packaging of devices. The main features of a suitable material should be: low cost (disposable devices), easy to fabricate the micro-structures from one micron (sensing elements) to several hundred of microns (fluidic - optical connectors), planar technology (easy to array and to immobilise substances), dielectric (electrical and thermal isolation), inert, low gas permeability, low auto-fluorescence, high transparency, tuneable refractive index (core and cladding of optical parts), good adhesive properties at low temperatures (sealing of the channels), biocompatibility and adequate surface energy. It is very difficult to find a material that fulfils all these needs. Therefore, a polymeric material would be an excellent candidate since its properties can be modified by dilution with other substances [1]. Among them, previous research results [2,3,4,5] and this work suggest that the SU-8, a negative photoresist, spun on silicon or glass, is a good candidate capable to fulfil above mentioned material requirements.

2. Design and Fabrication

The device consists of a buried multimode waveguide splitted by a Y-Branch, sealed microchannels, an optical fibre connector, and two photodiodes on a silicon die. One of the waveguides is interrupted by a microfluidic channel patterned in the cladding in order to work as a sensing element (Figure 1). The fabrication involves: (i) a photodiode microfabrication, (ii) 3 successive SU8 steps (bottom cladding, waveguide core, top cladding), (iii) a SU8 layer on a Kapton film that will work as a cover, (iv) a bonding process, and (v) a final releasing process (Figure 2). We perform a SU8 photolithography on a Kapton film and on a silicon wafer. Then, we

perform an adhesive bonding between the two substrates. Finally, the Kapton comes easily apart from the SU8 stack due to the lack of adhesion between SU8 and Kapton. This method leaves the microchannels' input/output in contact to the outside world, avoiding a time consuming drilling process of the cover (SEM image in Figure 2 and Figure 3). Detailed fabrication information is given in another μTAS 04 accepted work [3].

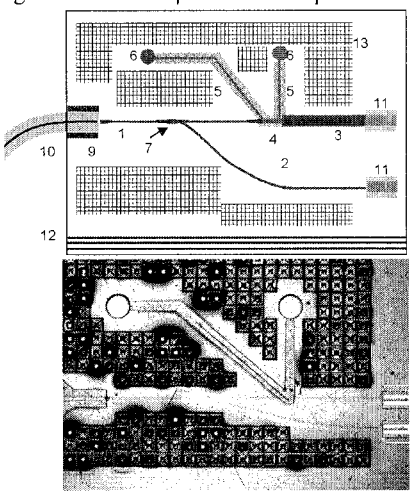

Figure 1. (Top) Schematic representation of the optical sensor: (1) input waveguide, (2) reference waveguide (3) Output waveguide, (4) analytical chamber, (5) sealed channels (6) Reservoirs, (7) Y-branch waveguide (9) Fibre optic connector (10) Input fibre, (11) photodiodes, (12) test waveguides. (Bottom) Microscope photograph of the chip layout.

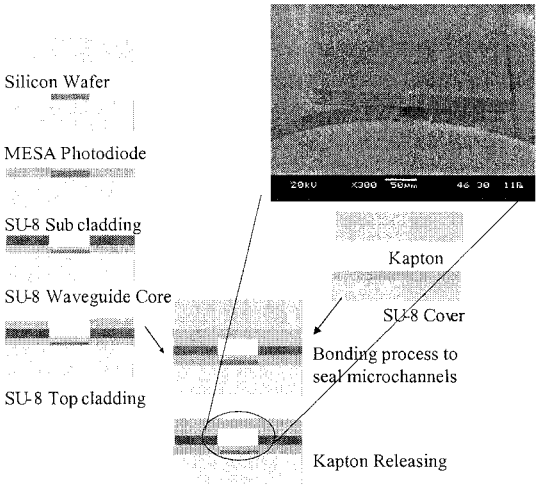

Figure 2. Fabrication process of a SU8 multilayer microfluidic structure. (Top) SEM image of the reservoir and the input of a sealed microchannel.

3. Results

In comparison with other works [6,7], our waveguides are embedded in a photodefinable cladding. The core of the waveguide consists of pure SU8, whereas the cladding is fabricated by diluting the SU8 in a liquid aliphatic epoxy resin. The waveguides are photopatterned on a bottom cladding layer and then buried by another top cladding layer. This approach allows us to fabricate microchannels within the cladding and to elevate the input waveguide to reach the centre of the input fibre optic inserted in a SU8 U-Groove. Therefore, the height of the waveguides is not determined by the outer diameter of the optical fibre cases [6].

The device takes advantage of the silicon substrate for further functions such as optical detectors. We have monolithically integrated two photodiodes at the end of the waveguides. This device has been tested obtaining a photodiode responsitivity of 0.55 A/W. The waveguides have 1.1 dB/cm propagation losses. Once the fibre was inserted into the U-Groove, a perfect alignment remained even when the fibre or the device were manually moved or even lifted (see Figure 4). The measured insertion losses of a passive alignment are 2 dB. Liquid has been introduced in the microchannels withstanding a liquid pressure drop of 100KPa. Last but not least, a packaging device has been developed for this die, consisting of an electronic printed circuit board, and a plastic capsule with fluidic and fibre-optic connectors (see Figure 3).

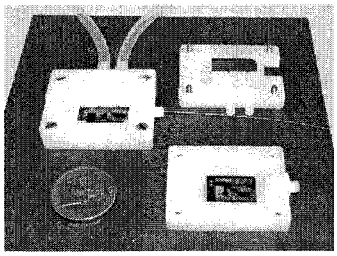

Figure 3: Picture of the packaging device developed for the microfluidic optical die.

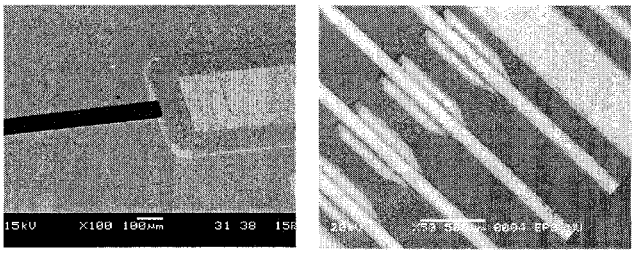

Figure 4: (Left) SEM image of an unclad waveguide and the photodiode (Right) SEM picture of the U-groove connector and its fibre.

4. Conclusion

The work presented here benefits from the advantageous opportunity to integrate SU-8 as a material for planar optical waveguides, for microfluidic channels, microreactors, and sensor elements. It also takes advantage of the substrate for other functions such as optical detectors. This approach will meet the requirements for fabricating LOC devices for many applications in bio chemical analysis.

5. Acknowledgements

This research is sponsored by The Basque Government, under the ETORTEK-Microsystems research and development programme for Microtechnologies. We would also like to thank Mr. Donald W. Johnson (MicroChem, USA) and Dr. Ralf Ruhmann (Microresist, Germany) for providing fruitful advice.

References

[1] M. Krishnan, V. Namasivayam, R. Lin, R. Pal and M. A. Burns, *Curr. Op. Biotech.*, 2001, **12**, 92

[2] F.J.Blanco, M.Agirregabiria, M.Tijero, J.Berganzo, J.Garcia, M.Arroyo, J.M.Ruano, I.Aramburu, K.Mayora, Invited paper SPIE 2003 Microelectr. and MEMS Inter. Conf., 2003 (Perth, Australia)

[3] M. Aguirregabiria, F. J. Blanco, J. Berganzo, J. Ruano, I. Aramburu, J. García, K. Mayora. Submmited also to µTAS04.

[4] J. M. Ruano, M. Aguirregabiria, M. Tijero, M. Arroyo, J. Garcia, J. Berganzo, I. Aramburu, F. J. Blanco, K. Mayora, Proceedings of IEEE MEMS 2004, pp. 121-124, Maastricht, The Netherlands, January 2004

[5] S. Kragh, S. Balslev, and A. Kristensen, microTAS 2003, Squaw Valley California, October 5-9, 2003, pp. 1331-1334.

[6] K. B. Mogensen, J.El-Ali, A.Wolff, J.P.Kutter, Appl. Opt., Vol. 42(19), 2003, pp. 4072-4079.

[7] Yun-Ju Chuang *et al.*, Sensors and Actuators A: Physical, Vol. 103, January 2003, pp. 64-69.

A MINIATURIZED AND CONVEX-SHAPED QUARTZ-CRYSTAL RESONATOR FOR MULTIPLE CHEMICAL SENSING IN LIQUID

Li Li [1], Masayoshi Esashi [2] and Takashi Abe [3]

[1]Dept. of Nanomechanics, Tohoku University, 980-8579 Sendai, Japan
[2]New Industry Creation Hatchery Center, Tohoku University, 980-8579 Sendai, Japan
[3]Dept. of Bioengineering and Robotics, Tohoku University, 980-8579 Sendai, Japan and PRESTO, JST, Japan

Abstract

A microfabricated bi-convex quartz-crystal microbalance (QCM) with large-radius spherical thickness distribution was realised by reactive ion etching (RIE) and photoresist reflow with solvent vapor. Due to the spherical thickness distribution, the spurious mode was suppressed very well and the resonator has high Q-factor (c.a. 80000). The vibration energy was trapped around the electrode within 5 wafer thicknesses. This value is three times shorter than that of planer QCM. Thus high-density integration and higher productivity per a wafer were realised without any unwanted influence on the Q-factor. The fabricated sensor also has superior resonant characteristic under the viscoelastic liquid.

Keywords: quartz-crystal microbalance , miniaturization, high Q-factor, viscoelastic liquid

1. Introduction

The AT-cut quartz crystal resonator vibrating in thickness shear mode is well known as mass sensitive devices, which was first described by G. Sauerbrey in 1959 [1]. In recent years, the resonator after depositing a sensitive layer on the surface has been investigated as chemical sensors for analyses in gaseous [2] and liquid media [3], biosensor for immunosensing [4,5], and so on.

In almost all QCM fabrications, miniaturization, high sensitivity, high Q-factor and the reduction of unwanted spurious responses are of paramount importance [6]. The spherical convex-shaped resonator can separate vibrating mode or lessen the strength of these coupling theoretically, therefore the energy of the oscillation is trapped at the center and very little dissipation occurs at the edge. For example, the 30mm-diameter, 2.5 MHz, plano-convex quartz crystal resonator was fabricated by A.W.Warner in 1952 [7] with conventional polishing method. But this method has some problems, such as difficulty in miniaturization and bulk fabrication, surface damage on polishing side. Therefore the miniaturized beveled bi-convex QCM by photoresist thermal melting has been thought in our previous studies [8]. Though it is effective to reduce innumerable spurious mode, the unwanted spurious responses still exist, because the curved range of beveled convex-shape by the photoresist thermal melting is limited.

In this letter, a miniaturized bi-convex QCM with large-radius spherical thickness distribution fabricated by RIE and photoresist reflow with solvent vapor is reported. The optical photograph of the fabricated bi-convex QCM array is shown in Fig. 1.

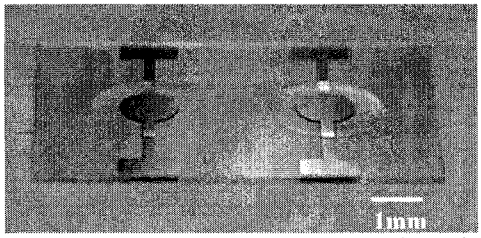

Figure 1. Microfabricated QCM array (electrode diameter 1 mm, thickness 100um)

2. Experimental

The fabrication process of the miniaturized spherical bi-convex QCM is as follows. Firstly, the higher thermal durability photoresist, AZP-4400 or AZP-4620 (Clariant) was spinning coated and patterned to be 2mm-diameter-cylinders on 100-μm-thickness quartz-crystal plate. Next,

hexamethyldisilazane (HMDS) was coated for decreasing the surface tension of the crystal outside of the pattern. After that, by means of the photoresist reflow with solvent vapor, the photoresist cylinders gradually became rounded and formed spherical thickness distribution due to the surface tension and gravity. In the process, the surface modification of quartz crystal by HMDS film is important to avoid overflowing of the reflowed photoresist from the patterned area. A simple set of apparatus was assembled to control the condensation of solvent vapor into the photoresist. Here propyleneglycol monomethyl ether acetate vapor was used as the photoresist solvent vapor. The diameter of the spherical convex-shape ranging from 100 μm to 2 mm size was realized and it had sufficient reproducibility. Then the photoresist was heated and cured by UV-light, RIE was used to transfer the pattern into the quartz-crystal substrate using the mixture gas of SF_6 and Xe until the required etching depth was obtained [9]. After deposition of Au/Cr layer, the electrode was patterned by photolithography. Finally, the convex-shape and electrode were made on the other side.

4. Results and discussion

Figure 2 shows the profile of the reflowed photoresist and the etched quartz-crystal measured by stylus profilometer. The final curvature of the crystal depends on both the thickness of the photoresist and the selectivity of the plasma-etching process. The radius adjusted in this study is from 0.1 to 0.5 m.

The conductance spectra of the planar QCM (a) and the spherical bi-convex QCM (b) by the photoresist reflow with solvent vapor method are shown in Fig. 3. Here the electrode diameter is 1 mm. Innumerable spurious were observed for the planar QCM as shown in Fig. 3 (a). On the other hand, the spurious mode was not observed for the bi-convex QCM as shown in Fig. 3 (b). The Q-factor of the planar QCM and the bi-convex QCM are 35000 and 80000, respectively. The highest Q-factor was obtained at the radius of 0.3 m. Interestingly, the bi-convex QCM shows no influence on the Q-factor beyond 5 wafer thicknesses. This is schematically shown in Fig.4. Here d is distance from the electrode and t is wafer thickness. It proves the spherical convex-shaped resonator can decouple vibrating mode and the array can be served for multiple sensing.

The resonant characteristics of the planar QCM (a) and the spherical bi-convex QCM (b) in viscoelastic liquids were also studied as glycerol/water mixtures contacted on one side of QCM. The function of frequency shift (Δf) against square root of viscosity-density ($(\rho\eta)^{1/2}$) production is shown in Fig. 5. In the effective loading range of the planar QCM and the

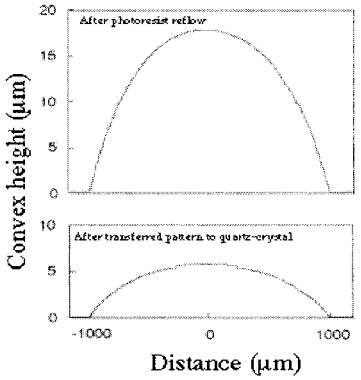

Figure2. Surface profiles of the reflowed photoresist and the etched quartz-crystal.

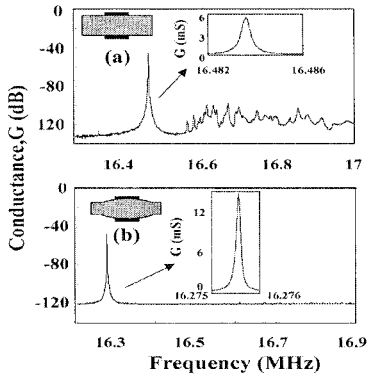

Figure3. Conductance spectra of the planer QCM(a) and the microfabricated bi-convex QCM(b).

spherical bi-convex QCM, frequency shift is proportional to square root of viscosity-density production. It was revealed that, if the density (ρ= 1.18~1.23gcm^{-3}) of glycerol/water mixtures (from 75% to 85%) is supposed to be constant, the proportional range of the frequency response to viscosity (η=128 mPas) for the spherical bi-convex QCM is at least 5 times larger than that (η=24.1mPas) for the planar QCM.

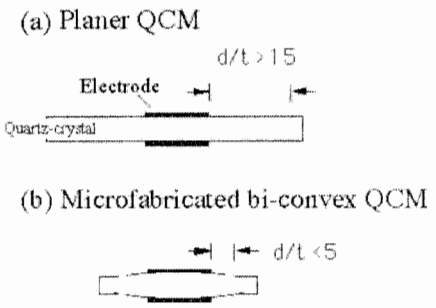

Figure 4. Schematic illustration of the difference between the planer QCM and microfabricated bi-convex QCM.

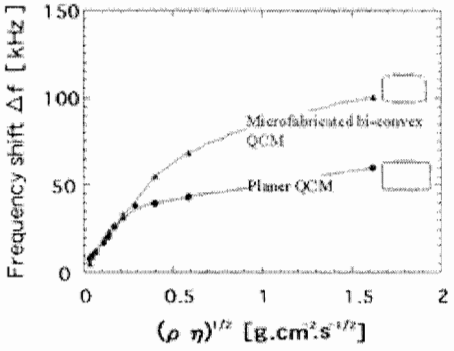

Figure 5. Resonant frequency responses of the planer QCM and the microfabricated bi-convex QCM for viscoelastic liquids.

5. Conclusions

The microfabricated QCM (MEMS-QCM) fabricated in this work can be used to measure under higher massive or viscoelastic loading compared with the planer QCM. The MEMS-QCM is suitable for integration due to the spherical distribution of the thickness for energy trapping.

Acknowledgements

This work was supported by PRESTO, Japan Science and Technology Corporation (JST).

References

[1] G. Sauerbrey, Z. Phys. **155**, 206 (1959).
[2] W.H.King, Jr., Anal. Chem., **36**, 1735 (1964).
[3] K.K.Kanazawa and J.G.Gordon, Anal. Chem., **57**, 1771 (1985).
[4] H.Muramatsu, J.M.Dicks, E.Tamiya and T.Karube, Anal. Chem., **59**, 2760 (1987).
[5] R.C. Ebersole, M.D. Ward, J. Am. Chem. **110**, 8623 (1988).
[6] W. Shockley, D.R. Curran, D.J. Koneval, J. Acoust. Soc. Am. **41**, 981 (1967).
[7] A. W. Warner, Bell Sys. Tech. J. **39**, 1193 (1960).
[8] L.Li, T. Abe, and M. Esashi, Sensors and Actuators A: Physical, In Press, Available online 27 Feb. 2004.
[9] L.Li, T. Abe and M. Esashi, J. Vac. Sci. Technol. B **21**, 2545 (2003).

MICROFABRICATED CELL CULTURE SYSTEM FOR SINGLE CELL ANALYSIS IN 2.5 DIMENSIONS

Marc R. Dusseiller[1], Mirabai Koch[1], Dominik Schlaepfer[2], Aldo Ferrari[2], Ruth Kroschewski[2] and Marcus Textor[1]

[1]*Laboratory for Surface Science and Technology, Department of Materials, Swiss Federal Institute of Technology (ETHZ) Zurich, CH-8952 Schlieren, Switzerland*

[2]*Institute of Biochemistry, Department of Biology, Swiss Federal Institute of Technology (ETHZ) Zurich, CH-8092 Zurich, Switzerland*

Keywords: fast prototyping, microfabrication, single cell analysis, surface modification, mechanotransduction

1. Introduction

The introduction of microarrays for genomics and recently also proteomics has immensely accelerated biological research and medical diagnosis. A similar development for cell biological research, aiming at reducing the volume of reagents and number of cells, automatising and downscaling cell experiments, is crucial to eliminate the current bottlenecks in drug development. Due to the inherent complexity of cellular systems great care has to be taken to control the microenvironment of the cells [1, 2].

It is the goal of this work to create a new type of array system to study single cells in a 2.5-dimensional microenvironment, where both topography and surface chemistry can be tailored accordingly (Fig 1). It is well known that the shape and adhesion state of a cell has great influence on its fate and behavior [3], but model systems to have a more complete control of the cell shape in 3-dimensions are still missing [4].

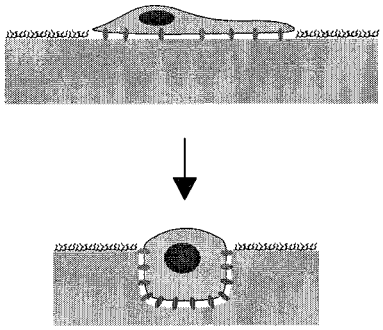

Figure 1: Scheme of a single cell inside a 2.5-dimensional well with a designated surface chemistry.

2. Experimental

Here we present a route to fabricate polystyrene (PS) chips with wells of 5 to 50 μm size and adjustable depth, which have been hot-embossed using a silicon rubber (PDMS) as the master. This master was replicated from a microstructured Si mold (Fig 2), produced by standard photolithography and dry etching using inductive coupled plasma (ICP). To further tailor the surface topography of the wells a simple heat treatment was used to flatten out the scalloping effect inherent in the dRIE-process. By the use of a self-assembling graft-co-polymer, poly-L-lysine grafted poly(ethylene glycol) (PLL-g-PEG)[5], the surface of oxygen plasma treated PS can be functionalized to be either protein repelling, thus resistant to cell adhesion, or carry a specific

biofunctionality, such as cell binding peptide sequences (e.g. RGD) in any desired concentration[6]. Different routes to selectively functionalize the surface inside the wells and the surrounding plateau were investigated. Cell experiments were performed using fibroblasts (HFFs) and epithelial cells (MDCKs).

3. Results and discussion

Some selected results are shown in the following figures. A high-throughput method to produce large quantities of structured PS films could be established (Fig 2).

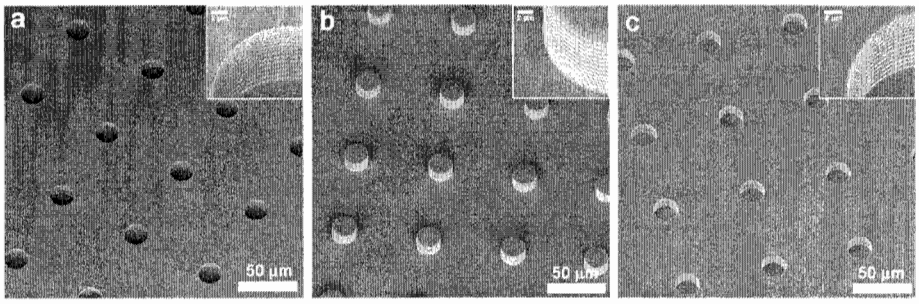

Figure 2: SEM images of a) dRIE structured Si showing an array of wells; b) replicated PDMS structures; c) hot-embossed wells in PS. Tilt angle: 30°. All structures are approximately 13 µm in depth.

Results of repetitive stamping of PLL-*g*-PEG demonstrate the feasibility of creating surfaces that combine topographical features and area-selective chemical contrast, reducing protein adsorption on the plateau below 10% (Fig 3).

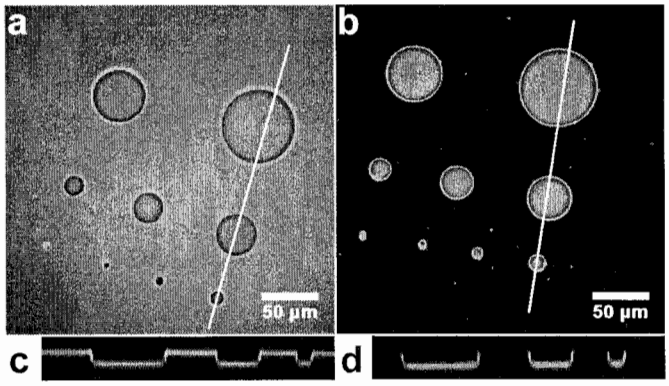

Figure 3: CLSM images after adsorption of fibrinogen-Alexa Fluor 488 of a) plasma oxidized PS reference surface, c) cross section; b) top surface stamped with PLL-*g*-PEG 4 times, d) cross section.

First cell experiments show the possibility of using such structures to control the 3-dimensional shape of individual cells, which could only adhere to the inside of the microwells, while adhesion and spreading were inhibited on the plateau surface.

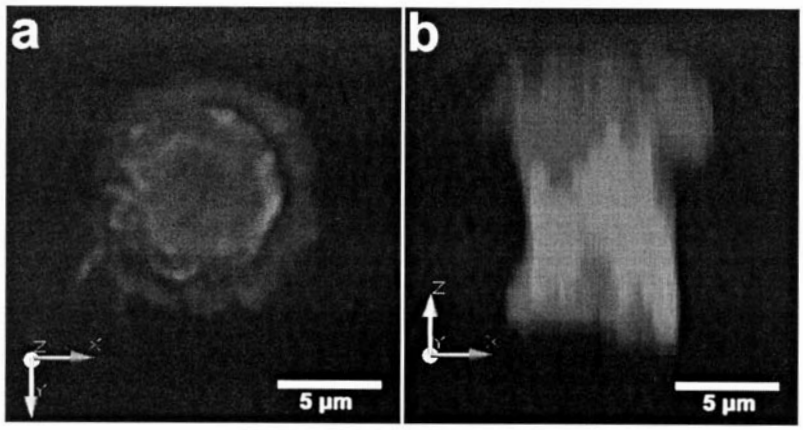

Figure 4: 3-dimensional reconstruction of a CLSM z-stack of a single cell attached inside a microwell (10 µm diameter, 10 µm depth); a) from below; b) from the side.

4. Conclusions

The combination of cheap replication techniques, biocompatible polymers and designated surface chemistries is demonstrated to be a promising approach to produce low-cost biochips for investigating cell function and response, e.g. in the context of drug screening and development or fundamental cell biological research.

Furthermore, microstructures with optimized geometries allow for the analysis of single cells or small clusters of cells in a controlled microenvironment, taking into account the 3-dimensional nature of cellular adhesion and mimicking more closely the *in-vivo* situation.

Acknowledgements

The authors would like to thank Dr. S. Blunier, IMES, ETHZ, for the use of their clean room facilities; M. Gössi, Polymer Technology, ETHZ, for help with the polymer processing.

References

[1] C. S. Chen, M. Mrksich, S. Huang, G. M. Whitesides, and D. E. Ingber, "Geometric control of cell life and death," *Science*, vol. 276, pp. 1425-1428, 1997.

[2] K. Bhadriraju and C. S. Chen, "Engineering cellular microenvironments to improve cell-based drug testing," *Drug Discovery Today*, vol. 7, pp. 612-620, 2002.

[3] E. Cukierman, R. Pankov, and K. M. Yamada, "Cell interactions with three-dimensional matrices," *Current Opinion in Cell Biology*, vol. 14, pp. 633-640, 2002.

[4] C. S. Chen, J. Tan, and J. Tien, "Mechanotransduction at Cell-Matrix and Cell-Cell Contacts," *Annual Review of Biomedical Engineering*, vol. 6, in press.

[5] G. L. Kenausis, J. Voros, D. L. Elbert, N. P. Huang, R. Hofer, L. Ruiz-Taylor, M. Textor, J. A. Hubbell, and N. D. Spencer, "Poly(L-lysine)-g-poly(ethylene glycol) layers on metal oxide surfaces: Attachment mechanism and effects of polymer architecture on resistance to protein adsorption," *Journal of Physical Chemistry B*, vol. 104, pp. 3298-3309, 2000.

[6] S. VandeVondele, J. Voros, and J. A. Hubbell, "RGD-grafted poly-l-lysine-graft-(polyethylene glycol) copolymers block non-specific protein adsorption while promoting cell adhesion," *Biotechnology and Bioengineering*, vol. 82, pp. 784-90, 2003.

DRY FILM RESIST FOR FAST FLUIDIC PROTOTYPING

P.Vulto[1], N. Glade[2], L. Altomare[1], J. Bablet[2], G. Medoro[3], A. Leonardi[1], A. Romani[1], I. Chartier[2], N. Manaresi[3], M. Tartagni[1], R.Guerrieri[1]

[1]ARCES, University of Bologna, Viale Pepoli 3/2, 40123, Bologna, Italy, pvulto@deis.unibo.it

[2]CEA-LETI, 17 Rue des Martyrs, 38054, Grenoble, France

[3]Silicon Biosystems s.r.l., Via S. Stefano 132, 40125, Bologna, Italy

Abstract

Dry film photoresist is used for creating microfluidic structures by sandwiching the patterned resist in between two substrates. The technique is applied for creating hybrid biochips for dielectrophoretic cell manipulation. Multiple level lithography is demonstrated and biocompatibility of the resist is proven. Due to simple fabrication procedures the resist can be processed in a low-tech environment.

Keywords: Dry film resist, microfluidics, prototyping, hybrid chips, packaging

1. Introduction

Dry film photoresists (DFR) were initially developed for fabrication of printed circuit boards. Application in MEMS technology is scarcely reported and is restricted to fabrication of electroplating moulds and masks for powderblasting of microstructures [1,2]. DFRs have several advantages over liquid resists such as good planarity of the resist, no liquid handling required, good adhesion to almost any substrate and simple fabrication process. In this paper dry film resist is demonstrated applicable for creating microfluidic structures. For this purpose Ordyl SY300 and SY550 (Elga Europe, Italy) is used, a resist that can be transferred into a rigid structure by a postbake. The resist acts as a fluidic spacer offering the possibility to integrate active elements in both bottom and top substrates. Since the simple fabrication does not necessarily require a dedicated cleanroom environment, the technique is extremely suitable for low-cost prototyping. Good compatibility with standard lithography processes and minimal number of process steps on the other hand make the technique suitable for industrial applications as well.

2. Fabrication

Photoresist (Ordyl SY300, 30 micron thickness, or SY550, 50 micron thickness) is laminated on a substrate using an office laminator (GBC 3500 pro series). Bare glass is used as a substrate, but also coated glass, silicon and a printed circuit board were tested. After removal of the first protective film, the resist is exposed for one minute with a low cost UV-lamp (TR1000, Radio Ricambi, Italy) using a photolithographic film (Tecnografika, Italy, max resolution 20 micron) as a mask. The second protective film is removed and the resist is developed and rinsed in commercially available BMR developer and rinser (Elga Europe). Increased resist thickness is realized by laminating multiple layers. A second substrate, in our case a glass lid with powderblasted holes, is bonded on top of the resist under a pressure of 650kPa and a temperature of 70°C. The temperature is ramped up in steps of 20°C per 20 min. to 150°C. A one hour postbake at 150°C transforms the resist into a rigid structure. A post-exposure bake (PEB) of 85°C for 5 min. could be inserted after exposure in order to improve the definition of the structures.

3. Results

Using the low-cost microfabrication set-up, free-standing structures of about 100μm can be achieved and channels of about 130μm for a resist thickness of 90μm (three layers of resist). A good definition of channels is more difficult than for freestanding structures due to scattering of light in the resist during UV exposure. In a cleanroom setting 20μm structures as well as 40μm channels for a resist thickness of 50μm have been achieved (details not shown).

Double bonding is easy to achieve depending on the substrate planarity, surface roughness, and PEB settings. When omitting the PEB a bonding percentage between 95 and 100% could be achieved on glass substrates (Knittel Gläser microscope slides). Inserting a PEB step puts higher constraints to the surface roughness and the planarity of the substrate. An increased resist thickness facilitates the double bonding.

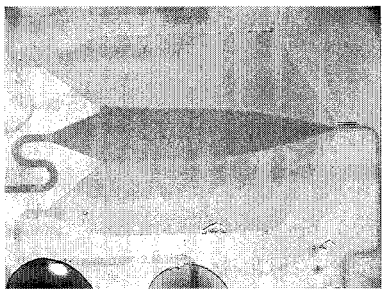

Figure 1. Three lane flow profile in a fluidic network sandwiched between a microscope glass slide and a lid with powderblasted holes.

Fluidic sealing is shown using the device in figure 1. The fluidic resist gasket is sandwiched between a microscope glass and a cover lid with powderblasted holes. Red and Blue dye are introduced in the chip and create a three lane flow-profile. The device showed neither leakages nor signs of degradation of resist or bonding quality up to a month after first usage.

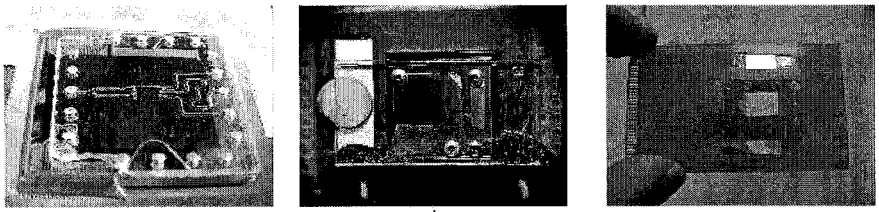

Figure 2. Series of three dielectrophoresis chips with a fluidic structure in dry film resist. All chips are closed with an ITO (Indium Tin Oxide) covered lid that is electrically connected with the bottom substrate via a conductive grease and with powderblasted holes for the fluidic interface
a) Gold and ITO patterned glass chip, wire-bonded to a PCB
b) CMOS chip, also wire bonded to a PCB
c) PCB with bare, gold plated electrodes

Figure 2 shows an ITO/gold patterned glass chip, a printed circuit board and a CMOS chip with a fluidic gasket of photoresist on top and closed by an ITO coated glass lid. The devices are meant for dielectrophoretic manipulation of biological cells and require electrodes on the bottom as well as on the top substrate for establishing the required field gradient [3,4]. The devices were successfully applied for manipulation and selective recovery of cells and beads (data not shown). Due to inexpensive and fast mask fabrication, the devices such as the ones shown can be packaged in no more than two days, including design, mask fabrication and assembly of the microfluidics.

Figure 3 shows pictures of a two level lithography process on a full silicon wafer. Since alignment of the second mask is difficult when using the low-cost UV lamp, a standard mask aligner is used (Karl Suss MA750). A PEB (85°C, 5 min) is added to improve structure definition. The same structure has been reported feasible using SU8 photoresist [5].

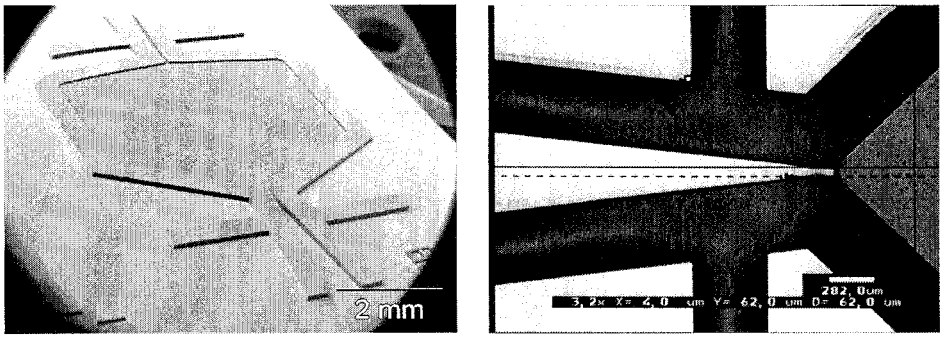

a b

Figure 3. Two-level resist structure on a silicon substrate
a) SEM picture b) Detail of the 50μm wide opening

Biocompatibility of the resist was proven by culturing human K562 cells for 5 days on top of a piece of processed and autoclaved resist on glass. The growth curve of the sample was compared with the growth curve of a population cultured on bare glass. The resist, both postbaked and non-postbaked, did not seem to have inhibiting effects on the cell proliferation.

4. Conclusions

A fast and inexpensive prototyping technology for microfluidic structures has been developed using dry film resist as a fluidic spacer. The resist allowed good adhesion to many substrates, simple double bonding without the use of additional adhesives and multiple lithography steps. It also has proven biocompatible. The fast and simple fabrication process makes the technique not only suitable for prototyping, but makes it interesting for industrial applications as well.

Acknowledgements

This project is funded by the European Union Commission (MeDICS IST – 2001-32437). Authors would like to thank Matthieu Kipp and Cecyl Bory (CEA-LETI) for advice and SEM pictures, prof. Berti (Univ. of Bologna) for his hospitality and Elga Europe for samples and advise.

References

[1] S. Schlautmann, G. A. J. Besselink, Radhakrishna Prabhu G., R. B. M. Schasfoort, J. Micromech. Microeng. 13 2003, pp. 81-84
[2] E. Kukharenka, M. M. Farooqui, L. Grigore, M. Kraft and N. Hollinshead, J. Micromech. Microeng. 13 2003, pp. 67-74
[3] A. Fuchs, N. Manaresi, D. Freida, L. Altomare, C.L. Villiers, G. Medoro, A. Romani, I. Chartier, C. Bory, M. Tartagni, P. N. Marche, F. Chatelain, R. Guerrieri, Proc. of MicroTas 2003, pp. 911-914
[4] G. Medoro, N. Manaresi, A. Leopardi, L. Altomare, M. Tartagli, R. Guerrieri, IEEE Sensors Journal vol. 3, no. 3, 2003, pp. 317-325
[5] I. Chartier, C. Bory, A. Fuchs, D. Freida, N. Manaresi, M. Ruty, J. Bablet, K. Gilbert, N. Sarrut, F. Baleras, C. L. Villiers, L. Fulbert, Proceedings of SPIE, vol. 5345, 2003, pp. 7-16

REFRACTIVE MICROLENSES PRODUCED BY EXCIMER LASERMACHINING OF POLY (METHYL METHACRYLATE)

Martin F. Jensen[1,2], Jian Wu[2*], Ulrich Krühne[1], Leif Højslet Christensen[1] and Oliver Geschke[2]

[1] *Danish Technological Insitute, Centre for Microtechnology and Surface Analysis. Gregersensvej 1, DK-2630 Taastrup, Denmark*

[2] *MIC- Dept. of Micro and Nano Technology, Technical University of Denmark, bldg. 345Ø, DK-2800 Kgs. Lyngby, Denmark*

* *Current Address: Dept. of Electrical and Computer Engineering, University of Alberta, Canada.*

Abstract

A method whereby refractive microlenses can be produced in poly-methyl-methacrylate (PMMA) by excimer laser irradiation at λ = 248 nm has been developed. The lenses are formed by a combined photochemical and thermal process. The lenses present themselves as depressions in the substrate material (negative focal length), which makes replication necessary in order to obtain lenses with a positive focal length. The method allows for considerable flexibility with respect to the pattern of lenses and the properties of the individual lenses. It is possible to vary the diameter of the lenses between 30 and 500 µm and the focal lengths between 300 µm and several mm.

Keywords: PMMA, excimer laser, microlenses, micro-machining

1. Introduction

Polymer microlenses and microlens arrays are important for several applications. They can be used, e.g., to increase the coupling efficiency of optical fibres, for display purposes or in µTAS devices for detection purposes. Literature reports of many different schemes to produce microlenses or microlens arrays, of which the most popular seems to be the resist reflow technique [1]. Other authors report of direct excimer laser machining of microlenses [2]. Our approach is also based on excimer laser machining of a polymer substrate, but in a different way than what has been reported hitherto.

2. Theory

When irradiating PMMA with excimer laser light (λ = 248 nm) at least two things happen. Firstly, sidechain scission is induced, releasing methyl formate (CH_3COOH) into the polymer matrix as a volatile species. Secondly, scission of the main chain of the polymer occurs, which serves to lower the glass temperature of the irradiated polymer.

When a sample, which has been irradiated through a circular aperture, is placed in a heated oven these effects act in combination to produce lens-shaped depressions. It can be shown that the movement of the central portion of the lens follows the following expression:

$$x(t) = \frac{1}{k}\ln\left(1+\frac{K_T C_0 k}{A}t\right) \tag{1}$$

where t is the time, k is the extinction coefficient of the laser light, K_T is a variable, which depends on the heating temperature, C_0 is a constant related to the total irradiation dose, and A is the area irradiated. (1) can be fitted to experimental data by the simpler form, treating a and b as empirical parameters:

$$x(t) = a \cdot \ln(1 + bx) \tag{2}$$

3. Experimental

The fabrication of lenses is a three-step process. First a clean PMMA sample (Röhm Plexiglas XT 1030) is irradiated by KrF excimer laser light, in the desired pattern. The fluence per pulse

(J/cm^2) and the total dose (fluence pr. pulse times shot number, also J/cm^2) will ultimately determine the geometry of the lens. Thus, it is possible to give different properties to individual lenslets. Secondly, the sample is placed in a heated oven for a predetermined time. This step develops the lenses, so they take the form of spherical caps into the sample. Thirdly, a PDMS solution is cured on the PMMA sample, in order to obtain lenses with a positive focal length.

We have conducted a number of studies to verify eqs. (1) and (2). Fig. 1 shows how the lens depth evolves over time for three different doses (12.5, 100, and 200 J/cm^2, respectively), when the sample is held at 110°C. The curves calculated from eq. (2) fit the data well. The diameters of the lenses are all 250 μm.

By fixing the dose at, e.g., 200 J/cm^2, and varying the temperature instead, we obtain the data shown in fig. 2. The higher the temperature, the faster the lenses develop. Note that the curve fits tend to overshoot the measured depths at long times. At 150°C the lens development is extremely fast. 10 minutes of heating is enough to develop perfect lenses.

The focal length of the lenses is determined by the radius of curvature of the lens surface, the thickness of the PDMS material and the refractive index of PDMS. We used a simple optical setup, shown in fig. 3, to evaluate the radius of curvature of the lenses. By using a lens of known focal length, f, to image the beamwaist from the sample lens onto a matt glass plate, and noting the distances d_1 and d_2, the curvature of the lens surface can be determined by utilising gaussian beam propagation methods. At the same time, using an interference microscope, direct measurements of this curvature were available. Fig. 4 shows the values obtained with the two different methods for a number of lenses. The correspondence is very good, except for the weakly focussing lenses.

Fig. 5 shows a SEM micrograph of one lens cast in PDMS, and the imaging properties of a lens array are demonstrated in fig. 6. The microlens array was placed a distance from the object, which was a "smiley face". By using an optical microscope to focus on the back focal plane of the microlens array, numerous images of the object could be recorded.

4. Summary and discussion

It has been demonstrated that microlenses and arrays thereof can be fabricated in PMMA by combining laser machining and a thermal treatment. During the laser irradiation the PMMA is degraded, and lenses are formed as a combined melting and evaporation process. By casting, e.g., PDMS on the PMMA substrate, lenses of positive focal lengths can be formed.

It is found that the lenses have good imaging properties. Lenses with diameters between 30 μm and 500 μm have been made, and the focal lengths have been varied between 300 μm and 3 mm. The focal lengths of the lenses is determined by the total dose of laser light used, and it is possible to construct an array of microlenses, in which the properties of the individual lenslets differ.

We have established a simplified model of the development process, which fits the measured data well, but tends to overshoot them for long times. The model predicts, correctly, that the lenses form much faster at elevated temperature, and it was found that good parameters for the thermal treatment was 10 minutes at 150°C.

Acknowledgements

This work was partially funded by the Academy of Technical Sciences (ATV, Denmark) through an industrial Ph.D. fellowship, and by the μKAP project under the Ministry of Science, Technology and Innovation. SEM images were recorded by D.I. Larsen of the Danish Technological Institute.

References

[1] P. Nussbaum, R. Völkel, H.P. Herzig, M. Eisner, and S. Haselbeck, *Pure Appl. Opt.* **6**, 617-36 (1997)

[2] K. Naessens, H. Ottevaere, P.V. Daele, and R. Baets, *Appl. Surf. Sci.* **208-209**, 159-64 (2003)

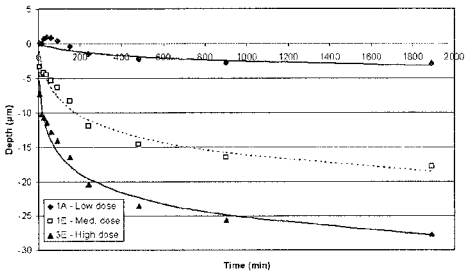

Figure 1. Temporal development of the lens depth for three different doses. The temperature is 110°C.

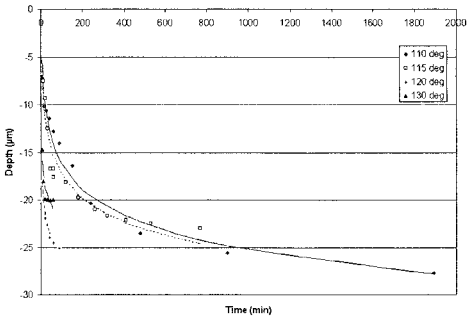

Figure 2. Development of lenses at fixed dose, but at different temperatures. Higher temperature results in faster development.

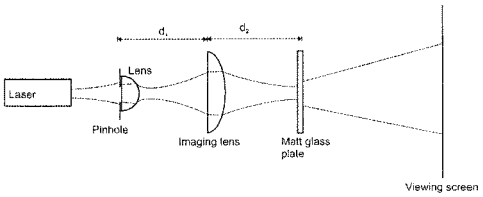

Figure 3. The optical setup used to determine the radius of curvature of the microlenses (which determines the focal length).

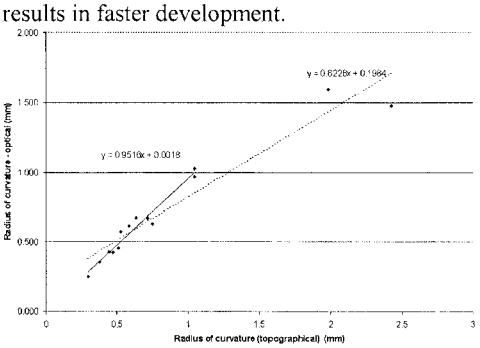

Figure 4. Comparison between direct measurements and optically determined radii of curvature of the microlenses.

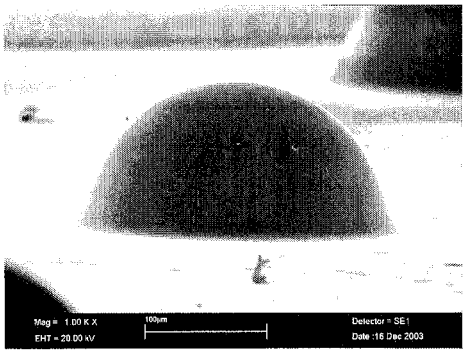

Figure 5. SEM micrograph of one microlens, in a tilted view.

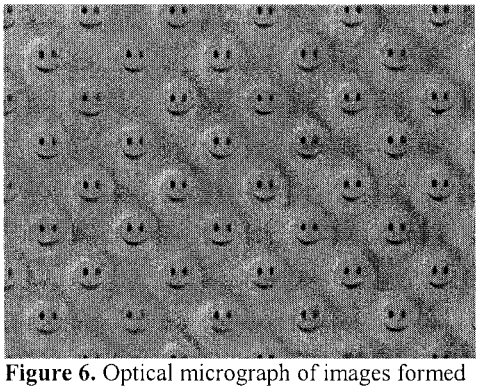

Figure 6. Optical micrograph of images formed by a microlens array.

NOVEL SU8 MULTILAYER TECHNOLOGY BASED ON SUCCESIVE CMOS COMPATIBLE ADHESIVE BONDING AND KAPTON RELEASING STEPS FOR MULTILEVEL MICROFLUIDIC DEVICES

M. Aguirregabiria, F. J. Blanco, J. Berganzo, J. Ruano, I. Aranburu, J. García, K. Mayora
MEMS/MST Department, IKERLAN S. Coop. P° J.M. Arizmendiarrieta 2, Arrasate, 20500, Spain

Abstract

This paper describes a novel fabrication process based on successive wafer-level bonding and releasing steps that allows us to stack several patterned SU8 layers. 3D multilayer embedded microfluidic channels have been developed.

Based on a low temperature adhesive bonding process, this work enhances this fabrication technology by the use of a Kapton film, as one of the substrates where the SU8 is photopatterned. The lack of adhesion between Kapton and SU8 opens the possibility to release the Kapton after the bonding process. After that, we can continue successive adhesive bonding steps onto the 3D microchannel network to create complex multilayer structures.

Keywords: SU8, Kapton, multilayer, bonding, releasing, 3D microstructures, microfluidic

1. Introduction

The interest in microfluidic technology has gained a great impact in bio-medical research during the last years. Recent developments have revealed the need to fabricate three-dimensional structures, based on multilayer stacks for these bio-medical applications [1]. Several research groups have fabricated complex three-dimensional structures by bonding PDMS layers fabricated by soft lithography [2]. The integration of these PDMS 3-D microfluidic devices with CMOS electronics or Si based MEMS devices is nontrivial.

In this work we propose a novel CMOS compatible fabrication method, to obtain 3D multilayer embedded microfluidic channels by using SU-8 as a structural material. As far as we know, this is the first time that a CMOS compatible photopatternable polymer has been used for this purpose.

2. Fabrication process

The micro-fabrication technique developed to fabricate complex 3-D microchannel paths is based on successive adhesive bonding of two photolithographic patterned SU-8 layers on separate wafers. The wafers are brought into contact, pressed together and heated above the glass transition temperature of the SU-8, causing the two polymer layers to become bonded (glued) together. This process is described elsewhere [3]. Three main processes are involved in the fabrication of the 3-D multilayer structures discussed in this paper: (i) the photolithography process to obtain photopatterned thick films suitable for bonding applications (ii) the bonding process and (iii) the Kapton film releasing step.

Firstly, two photolithographic steps are carried out on two different substrates. The bottom one can be a silicon, pre-processed silicon or a Pyrex wafer. The top one is a Kapton thick film. We have used SU-8 standard photolithographic and developing steps onto the bottom substrate before the bonding process. In case of the SU8 layer photopatterned on the Kapton film, it still remains undeveloped during the bonding process. We have used 150 μm thickness Kapton films, which have enough transparency to perform a proper alignment, even though the SU8 layer is undeveloped. Subsequently, the bonding of the two SU8 layers is performed After the adhesive bonding of the two substrates, the SU8 stack is detached from the Kapton film and developed. The developing step must be performed after the bonding, since SU8 is removed from the Kapton

during this step. By repeating on the same top substrate this process, multilayer structures of SU8 have been obtained. A schematic of the fabrication process is shown in figure 1.

3. Results

The uniformity and crosslinking level of SU8 layers have been optimised to obtain a strong bond. High quality SU8 films (StD of 0.4-1% across a 4 inch wafer) with good adhesive properties have been obtained. Figures 2-4 show different examples of this novel technology. Unclogged and smooth channels with vertical sidewall profiles have been obtained for two and three-layer structures.

Table 1 shows the effect of pressure and temperature on the bonding area across a 4 inch wafer. The process parameters of 100 ºC and 300 KPa have been chosen to obtain a strong bond across the wafer between 20 μm height layers.

The microchannels have been filled with liquid to prove that they are sealed. Reliability tests indicate that these microchannels withstand liquid pressures up to 600 KPa without any liquid leakage. Figure 5 shows a filled microchannel.

4. Conclusion

The fabrication process described in this abstract uses a novel adhesive bonding process [3] introducing the Kapton film as one of the substrates to be bonded. In addition to open new possibilities to fabricate complex three-dimensional structures, simplifies the packaging of the devices, leaving the input and the output of the microchannels network in contact with the outside world, avoiding the usual slow drilling/etching process of the cover. Therefore, a plastic capsule and an O-ring per reservoir are enough to introduce liquid into channels. Figure 6 shows a plastic capsule used to package the microfluidic device fabricated with this technology.

This process has a wide range of possibilities to fabricate optical and microfluidic components in the same chip (see Figure 4). An optical microfluidic platform [4] developed by our group use this novel process to fabricate a micro-optical sensor integrated with this novel microfluidic network.

Acknowledgements

This research is sponsored by the Basque Government under the PhD formation program in R+D corporations of Basque Country and ETORTEK program.

References

[1] B.-H. Jo, L. M. Van Lerberghe, K. M. Motsegood, and D. J. Beebe, "Three-dimensional microchannel fabrication in polydimethylsiloxane (PDMS) Elastomer," Journal of Electromechanical Systems, vol. 9, no. 1, pp. 76-81, Mar 2000.

[2] Marc A. Unger, Hou-Pu Chou, Todd Thorsen, Axel Scherer and Stephen R. Quake. "Monolithic Microfabricated Valves and Pumps by Multilayer Soft Lithography". Science, vol. 288, 7 April 2000

[3] F. J. Blanco, M. Aguirregabiria, J García, J Berganzo, M Tijero, M T Arroyo, J M Ruano, I Aramburu and Kepa Mayora. "Novel three-dimensional embedded SU-8 microchannels fabricated using a low temperature full wafer adhesive bonding". J. Micromech. Microeng. 14 (July 2004) 1047-1056

[4] J.M. Ruano-López, M. Aguirregabiria, M. Arroyo, J. García, J. Berganzo, F. J. Blanco, P. de la Fuente, E. Castaño, K. Mayora. "An optical microfluidic platform based on a combination of a novel SU8 multilayer technology, waveguides and photodiodes on silicon". Submitted to μTAS 2004.

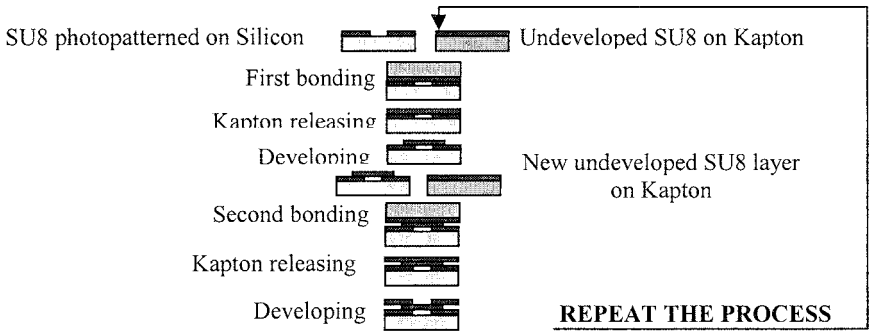

Figure 1: Fabrication process of SU8 multilayer stack.

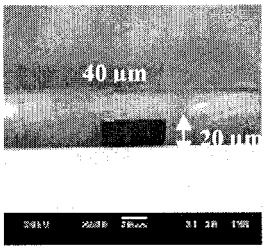

Figure 2: A sealed microchannel, after being released from the Kapton film.

Figure 3: SEM photograph of three SU8 layers bonded together.

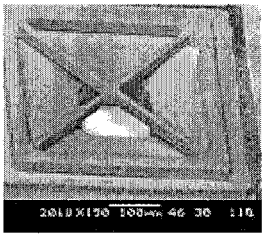

Figure 4: A cross, 25 μm width, suspended in another SU8 structure.

a) Bonding T= 100 °C; P= 300 KPa; t= 20 min

StD	0.3%	0.7%	0.9%
Bonded area	95%	75%	65%

b) Bonding T= 100°C; StD= 0.3%; t= 20 min

Bonding Pressure	100 KPa	200KPa	300 KPa
Bonded area	45 %	65%	95%

c) Bonding P= 300 KPa; StD= 0.3%; t= 20 min

Bonding Temperature	100°C	120°C
Bonding Quality	Good bonding. No blocked channels	Partially blocked microchannels

Table 1: The effect of process parameters in the bonding: **a)** the effect of the film uniformity, **b)** the effect of the bonding pressure, and **c)** the effect of the bonding temperature.

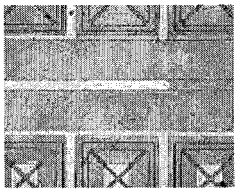

Figure 5: Filled microchannel

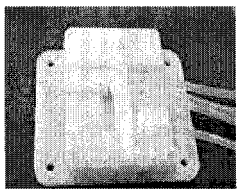

Figure 6: Packaged microfluidic device

FABRICATION OF EPOXY STAMPS FOR HOT EMBOSSING MICROFLUIDIC DEVICES AND SUB-MICRON STRUCTURES

Laurie Brown[1], Terry Koerner[1] and Richard Oleschuk[1]

[1]*Department of Chemistry, Queen's University, 90 Queen's Crescent, Kingston, ON, Canada*

Abstract

Polymeric materials have been increasingly used to fabricate microfluidic devices as an inexpensive alternative to glass or silicon devices. Hot embossing is a favourable method for the development of these polymeric devices, however the stamping tools used with this technique are quite expensive, have time consuming fabrication procedures, and can be fragile. A method has been developed using micro-molding to create a high temperature epoxy clone for a number of masters. The epoxy masters are embossed into polymeric materials under conditions of increased temperature and pressure. The resulting polymeric structures can be micron to sub-micron in size. This method of utilizing epoxy stamps as a reusable master clone decreases the overall cost of producing polymeric microfluidic devices, and increases the lifetime of the masters used.

Key words: polymeric master, hot embossing, sub-micron replication, PMMA bonding

1. Introduction

From the outset, researchers in microfluidics have identified a need to develop low cost, disposable devices. Micro-fabrication in conventional substrate materials like glass and silicon is costly as a result of the multiple photolithographic and etching steps required for each individual device. Polymeric materials are seen as an inexpensive alternative to this. In some cases, only photolithography needs to be used to create a single "master", which can then be used repeatedly to replicate polymeric devices. Polymeric materials are an alternative to glass or silicon because the surface chemistries can be tailored to fit the type of chemistry being performed on the microfluidic device. Hot embossing has been investigated in detail as a means of fabricating these polymeric microfluidic devices due to the ease with which microstructures can be formed.

2. Experimental

Hot embossing has shown promise as a method for the production of polymeric devices (Figure 1). A micro-fabricated master is heated and pressed into a polymeric substrate at a temperature close to the Tg (glass transition temperature) of the substrate. Conventional stamping tools are prepared utilizing LIGA, electroplating and photoresist removal to create a robust stamping tool [1]. However, metal embossing stamps are extremely expensive and time consuming to produce precluding their use in rapid prototyping situations. Others have utilized patterned photoresist (SU-8) on silicon as the stamping tool, however these have limited lifetimes within the embosser due to the multiple temperature cycles and large pressures (>1 kN) involved in the embossing process [2]. Our laboratory has utilized a high temperature epoxy material combined with micro-molding to produce a low cost replicate of the more expensive and fragile stamping tools. The entire stamp fabrication process (Figure 2) can be performed in less than 24 hours and is compatible with a number of "master" materials including glass, silicon, metal and SU-8 patterned silicon. The process can be utilized with either positive or negative imaged masters to prepare the stamp, with the only difference being one additional micro-molding step.

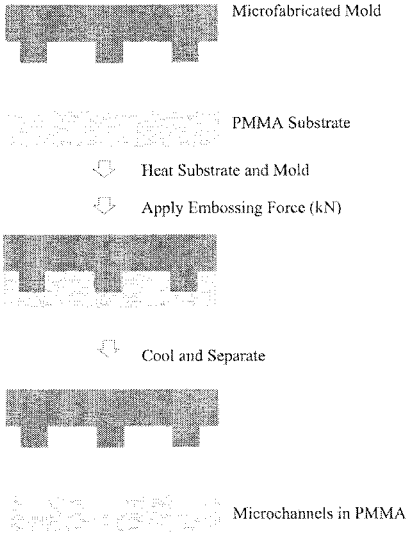

Figure 1. Schematic of the embossing process with an epoxy stamp tool.

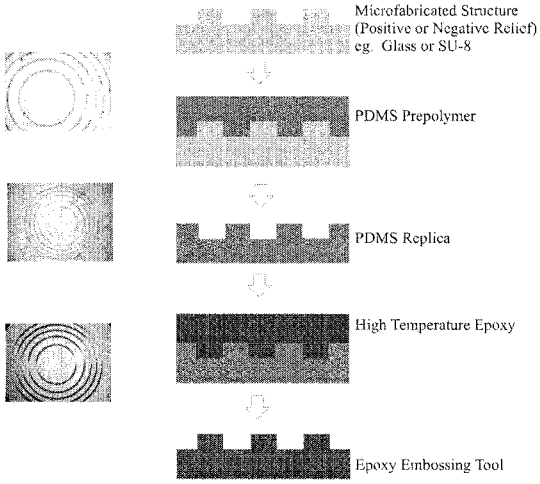

Figure 2. Fabrication of an epoxy stamping tool. At left are photomicrographs of an annular ring test structure.

An elastomer, polydimethylsiloxane (PDMS), is used to create a negative mold of the master and epoxy is then cured within this mold to create the master clone. The epoxy stamp can be easily removed from this reusable PDMS mold, and does not require the use of expensive de-molding agents when removing the tool from the polymeric substrate following cooling in the hot embossing system.

Protocols for the fabrication of microfluidic devices in PMMA were developed using several embossing masters. Following substrate fabrication, microfluidic chips were bonded together using a variety of surface modification protocols. To date, the most effective substrate bonding procedure has involved the oxidation of the surface of the PMMA. Immersion of the PMMA substrates in sulfuric acid converts the surface esters to carboxylic acid groups (as determined with chemical force microscopy) facilitating hydrogen bonding between the substrate and cover plate. Following surface modification the cover plate and substrate are brought into conformal contact and bonded using both heat and pressure.

4. Results and Discussion

The PDMS and epoxy micro-molding protocol used provides excellent replication of even sub-micron sized structures. Figure 2 shows photomicrographs of circular structures from an SU-8 master at each step of the fabrication procedure. The diameter of the smallest circle is 950μm and each ring structure measures 25μm wide. No visible degradation of the microstructures occurred as a result of these replication procedures. Figure 3 shows the typical double "T" region of an epoxy device embossed in polymethylmethacrylate (PMMA) with etching artefacts from the original glass master used still clearly visible. The embossed channels in this device are 50 μm wide and 20 μm deep. Upon bonding, the strength of the cover plate adhesion were determined utilizing a tensile tester and was found to be 1484±243 kN/m^2 for the oxidized microfluidic devices. This compares favourably with other literature examples.

Sub-micron sized structures have also been fabricated including a silicon atomic force microscope (AFM) calibration grating (Figure 4) that was used to produce an array of epoxy "spikes" (Figure 4a) <1μm diameter, and 400nm tall. The "spikes" are spaced 2.1μm apart in a square grid. The resulting embossed PMMA (Figure 4b) showed regularly spaced "femtowells".

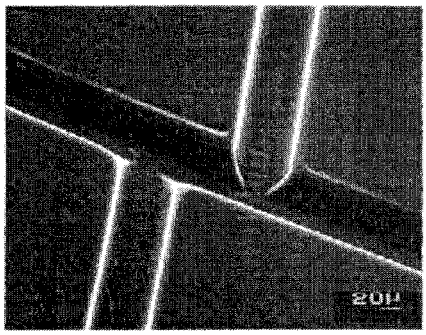

Figure 3. A SEM image of the double T region of an embossed polymeric microfluidic device with dimensions 50μm wide and 20μm deep.

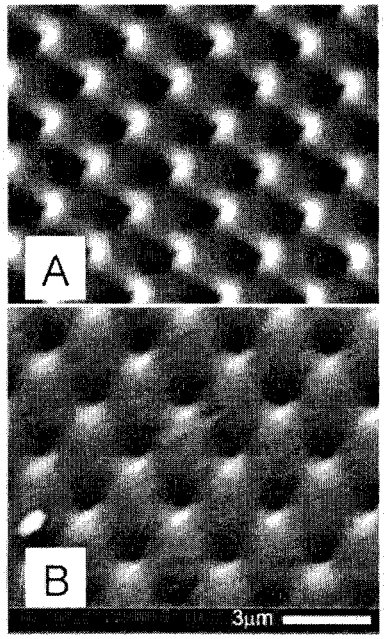

Figure 4. A shows a SEM of the epoxy replica of an AFM calibration grating and B is the embossed PMMA.

5. Conclusions

This study provides a facile procedure for the fabrication of low cost stamping tools utilizing PDMS and epoxy micro-molding. The tools are robust with no observable deterioration after more than 50 embossing cycles and can be fabricated from either a positive or negative imaged master made from a variety of commonly used micro-fabrication materials.

Acknowledgments

Financial support was kindly provided by the Natural Sciences and Engineering Research Council of Canada, Canadian Foundation for Innovation, Ontario Innovation Trust, Genome Prairie (Enabling Technologies Project), and Queen's University.

References

[1] H. Becker and C. Gärtner, *Electrophoresis*, **21**, 12-26 (2000).
[2] M. B. Esch, S. Kapur, G. Irizarry, and V. Genova, *Lab Chip*, **3**, 121-127 (2003).

POLYMERIC MICRO CHANNEL SYSTEM FOR EASY SENSITISATION OF MICRO-CANTILEVERS

Maria Nordström, Montserrat Calleja and Anja Boisen
MIC - Department of Micro and Nanotechnology, Technical University of Denmark, Bldg 345 east, DK 2800 Kongens Lyngby, Denmark

Abstract

A micro channel system, solely depending on capillarity for transportation of liquids, has been designed, fabricated and characterised. The design of the micro channel system provides a simple way of coating separate sections of a cantilever array with different probe molecules, allowing for the detection of multiple target molecules simultaneously. The system comprises three open channels connecting μL-sized reservoirs to nL-sized measuring sites, independent of one another. The micro channel chip is fabricated in the resist SU-8, which is a photosensitive polymer offering a fast, cheap and easy processing. Fluorescence experiments have been performed to show the working principle of the micro channel system in combination with the cantilever array.

Keywords: micro channels, cantilevers, biochemical detection, SU-8

1. Introduction

As the research within fabrication biotechnology gets more oriented towards obtaining small systems for fast and reliable detection of biochemical molecules, micro cantilevers have emerged as an interesting method. Cantilevers can be used for this purpose by observing the bending generated upon the selective binding of analytes onto only one side of the cantilever [1]. The requirement is that the two cantilever surfaces will be of different chemical structures, and usually this is obtained by adsorbing a monolayer of probe molecules onto one side. By coating one side of the cantilever with a thin layer of Au in the fabrication, thiolated probe molecules will bind selectively and strongly to that side. We have fabricated arrays of cantilevers in the plastic material SU-8 and previously presented experimental results performed with these [2]. Here, we have fabricated a complementary micro channel system, which greatly increases the efficiency of the sensitisation step and allows for the treatment of different probe molecules onto different sections of an array of micro cantilevers. This enables the detection of multiple target molecules simultaneously. The micro channel system is fabricated completely in the photo-polymer SU-8 in a simple three-step-process.

2. Fabrication

The channel chip is fabricated in SU-8 by standard spin-coating and UV exposure techniques. First, a 10-μm-bottom layer is defined by spin-coating SU-8 2005 (MicroChem) on a Si wafer. On top of this, two consecutive spin-coatings of SU-8 2075 (MicroChem) result in a 300-μm-thick layer, which is patterned into the final micro channel system. The channels are open to the air and only need to be developed and released off the Si carrier wafer, used during the processing. A surface treatment, where the molecule ethanolamine is allowed to form a monolayer on the inside of the channel walls, is performed. The last step is an extended treatment of the SU-8 to acquire a sufficiently low contact angle for the capillary pressure to be the only driving force of the sample solutes. The layout of the micro channel system can be seen in figure 1.

Upon use, the micro cantilever chip is placed at the sensitisation sites by the use of a micro-positioner and the cantilevers are dipped into the solution from above, figure 2.

3. Experimental

The liquids under investigation are added into the reservoirs by a micro-pipette and from there; capillary forces are the only driving source of the solution, through the channels and into the

sensitisation sites. Thereafter the fluid runs into the waste reservoir from where it can be removed or be allowed to evaporate. The different channels systems are completely separated and there is no risk of cross-contamination by any of the solutions.

To present the working principle of this micro channel system, fluorescence experiments were performed. Two solutions of DNA, labeled with different fluorescence markers were injected into two of the reservoirs. 20 μL of 50'mer long DNA-oligos (Sigma Aldrich) diluted in DI water to a concentration of 1 μM was injected into the first reservoir. This DNA was labeled with a Cy3 fluorescence marker, which fluoresces at a wavelength of 595 nm. 10 μL of 25'mer long DNA-oligos (Sigma Aldrich) diluted in DI water to a concentration of 1 μM was injected into the second reservoir. This DNA was labeled with a Cy5 fluorescence marker, which fluoresces at 685 nm. The last reservoir was kept empty for reference. A cantilever chip was inserted into the functionalisation sites and the DNA was allowed to adsorb onto the SU-8 cantilevers for several minutes. The chip was then rinsed in DI water. The chip was scanned in a CCD fluorescence scanner (ArrayWorkx, Applied Precision) and the fluorescence scans obtained were extracted through two different filters, corresponding to the respective fluorescence wavelengths of the fluorophores.

4. Results and discussion

A significant difference in the fluorescence signals of the treated areas to the non-treated areas on the chip can be seen, figure 3. Here, the DNA has only been allowed to adsorb nonspecifically onto the SU-8 cantilevers. If thiolated DNA-oligos had been used, a much stronger fluorescence signal would have been obtained. This experiment shows the working principle of the micro channel system. It can clearly be seen from the images that no cross-contamination has occurred between the different channel systems. SU-8 is auto-fluorescent, which explains the strong signal from the thick support of the cantilevers; this is not due to any leakage of the solutes.

5. Conclusions

Here we have presented a micro channel system, which has been developed to be used in combination with micro cantilevers in the initial sensitisation step, prior to detections. The channels could also be used for parallel measurements. The design of the micro channel system is very simple and can easily be altered to fit micro cantilevers structured into arrays of any number.

Acknowledgements

We acknowledge PhD Rodolphe Marie for fruitful discussions on the surface treatment of SU-8 and help with the fluorescence experiments. M. Calleja acknowledges financial support via a Marie Curie Fellowship.

References

[1] H.-J. Butt, *Journal of Colloid and Interface Science,* **180,** 251-260 (1996)

[2] M. Calleja, J. Tamayo, A. Johansson, P. Rasmussen, L. Lechuga and A. Boisen, *Sensors Letters,* **1,** 20-24 (2003)

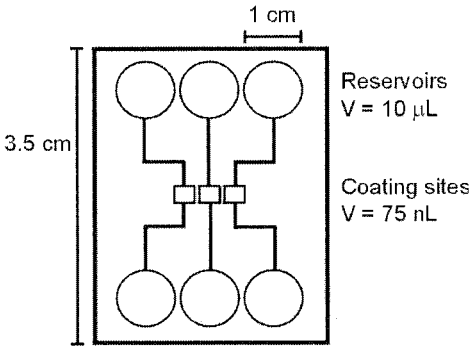

Figure 1. Schematic drawing of the channel chip layout.

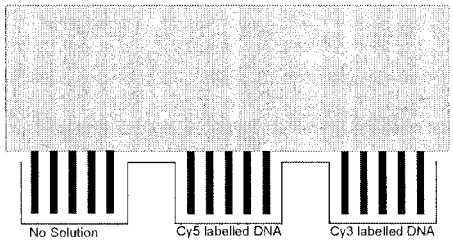

Figure 2. The micro cantilevers are dipped into the solution from above. The different solutions that the cantilevers were treated to in the experiment have been marked below their respective reservoir.

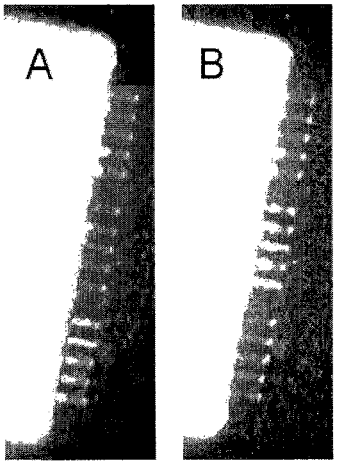

Figure 3. The fluorescence scans show a significant difference in the signal between the treated and non-treated areas of the chip. **(A)** Scanning with a 595 nm filter for Cy3 fluorophores. **(B)** Scanning with a 685 nm filter for Cy5 fluorophores.

THE PELTIER-ACTUATED MICROVALVE

Richard P. Welle, Brian S. Hardy, and Michael J. O'Brien
Space Materials Laboratory, The Aerospace Corporation
PO Box 92957, Los Angeles, CA, 90009-2957, USA

Abstract

A microfluidic valve is formed by creating a flow channel over a Peltier junction. The valve operates by using the thermoelectric effect to freeze a solid plug of the working fluid in the flow channel. The valve has no moving parts, is electrically actuated, has zero dead volume and zero leak rate, and has a cycling time less than 100 ms. The components of the valve that are exposed to the fluid are made disposable by separating the actuation element (the Peltier junction) and the fluid-bearing channel into two modules that are brought into good thermal contact for operation.

Keywords: microvalves, Peltier, phase-change, disposable

1. Introduction

Integrated microfluidic devices are expected to play a key role in automating and reducing costs in many biological analysis applications, including genetic analyses, medical diagnostics, and drug screening. When conducting such analyses, however, it is critical to avoid the possibility of cross-contamination between samples. This has led to the design of instruments where all components that may come into contact with samples are easily removed for cleaning or disposal. With microfluidic devices, cleaning is impractical. The preference, therefore, is for disposable devices. A fully functional microfluidic device should be able to store, transport, heat, cool, and mix various fluids. Performing these functions requires that the microfluidic device includes not only flow channels, but also valves, pumps, heaters, and coolers. Valves and pumps have typically been complex devices, leading to high fabrication costs. This runs directly counter to the goal of keeping costs low enough to allow the devices to be disposable. One approach to this problem is to build the microfluidic device in two components: a disposable module containing all the fluid-bearing elements, and a reusable module containing all the actuation elements. This requires the development of both valves and pumps with actuation elements separable from the fluid-bearing elements.

2. Theory

A valve that can be easily adapted to the requirement for a separable actuation element is the Peltier-actuated valve.[1-3] In this valve, illustrated in figure 1, a flow channel is adjacent to a Peltier junction. Fluid flow is stopped by using the thermoelectric effect to cool the channel and freeze a plug of the working fluid in the flow channel. The valve can be opened by shutting off power to the Peltier junction, in which case thermal

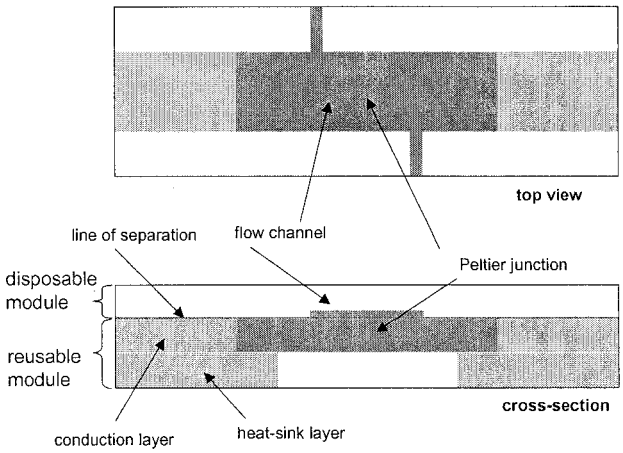

Figure 1. Schematic diagram of Peltier-actuated valve.

conduction from the environment will warm and melt the plug. Alternatively, the direction of current flow in the Peltier junction can be reversed, causing the junction to warm rapidly and melt the plug. In the valve shown in figure 1, the Peltier junction and the fluid channel are in separable modules. The reusable module includes the Peltier junction, which is embedded in a substrate with a flat face. The flow channel is recessed into the disposable module and enclosed with a cover layer. When the two modules are assembled together, there is good thermal contact between the Peltier junction and the fluid in the flow channel. The cover layer prevents the fluid in the channel from coming into physical contact with the Peltier junction, so contamination is not possible. In addition to being easily designed with separable modules, the Peltier-actuated valve has several other valuable features, including that it has no moving parts, zero dead volume, and essentially zero leak rate. In addition, it is unaffected by particulate contamination, is able to withstand differential pressures in excess of 1 MPa, and is electrically actuated. In order to demonstrate the utility of this valve, it is necessary to show that it can be easily fabricated, and can be operated quickly and reliably. To that end, we have built and tested prototype valves, and have developed a detailed thermal model of valve operation.

3. Experimental

Figure 2 shows a photograph of a prototype valve fabricated and tested in our laboratory. In this valve, water flows through a channel 60 microns deep by 250 microns wide. The channel was formed using two layers of adhesive-backed polyester film attached directly to the surface of the Peltier junction. The junction is made from two bismuth telluride (BiTe) legs removed from a commercial Peltier cooler and soldered together. Electrical contact is provided by copper leads also visible in the photograph. The junction has a 1.2 mm square cross section and an overall length of about 6 mm. A current of 2.5 A at 115 mV (1.7 A/mm^2, 290 mW) will cause the water to freeze and block the channel. The closing time has not yet been accurately measured, but has been determined through visual observation to be clearly less than one second, while the opening time is faster yet.

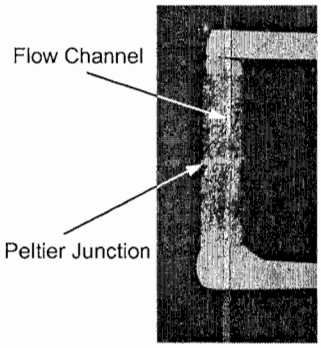

Figure 2. Photograph of prototype Peltier-actuated valve.

A second prototype valve was fabricated by molding a flow channel in polydimethylsiloxane (PDMS). In this case, the flow channel was 10 microns deep by 100 microns wide. For testing purposes, this flow channel was mated to the same reusable module used with the first prototype.

4. Modeling

As operation of the Peltier-actuated valve is essentially a thermal process, it can be investigated in some detail using finite-element thermal modeling. We have developed both two-dimensional and three-dimensional time-dependent models of the valve using ABAQUS. The model treats the Peltier effect as a surface heat flux (either positive or negative), and treats ohmic heating in the bulk material as a volumetric heat source (always positive). The two-dimensional version follows the geometry of the cross-sectional diagram shown in figure 1, taking advantage of the line of symmetry at the Peltier junction. Accurate thermal properties are used for the BiTe Peltier material, the PDMS substrate in the disposable module, and the copper in the conduction and heat-sink layers. In addition, the thermal properties of water (including the heat of fusion for phase-change processes) are used for the fluid. The model has been used to investigate the effects of different geometries and electrical current densities.

Insight into the performance of the Peltier-actuated valve can be gained by examining the thermal contour map shown in figure 3. This figure shows a top view of the temperature distribution on the surface of the reusable module 33 ms after power has been applied. Heat absorbed due to the Peltier effect causes the region immediately adjacent to the central junction to cool well below ambient. At the same time, however, the temperature of much of the Peltier elements is raised above ambient by ohmic heating and by heat generated at the interfaces between the BiTe and the copper conductors. The liquid in the portion of the flow channel adjacent to the cold Peltier junction will be chilled to the junction temperature. The goal of the modeling is to find the conditions that provide the fastest operation of the valve. In figure 4, the valve temperature is shown as a function of time for three different current densities. At 1 A/mm^2, the valve takes about 1 second to close, while at 4 A/mm^2, the valve closes in under 100 ms. One cannot take the current density to arbitrarily high levels, however, because heat transfer due to the Peltier effect is linear with current density, while ohmic heating is proportional to the square of the current density. At high current densities the ohmic heating comes to dominate, and the central junction can no longer be cooled below ambient.

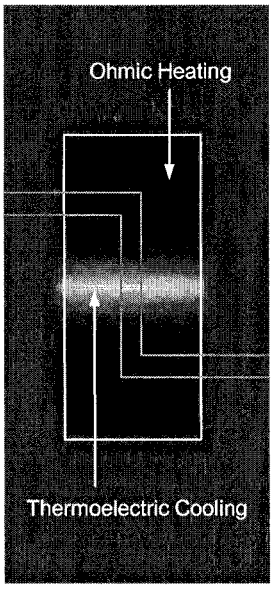

Figure 3. Model-derived contour map of valve temperatures.

5. Conclusions

We have developed a novel microfluidic valve that operates by freezing the working fluid in the flow channel using the Peltier effect. Prototype versions of the valve have been built and tested. A thermal model of the valve has also been developed to investigate valve performance. Modeling results to date indicate that the valve should be able to cycle in less than 100 ms when used in a typical microfluidic application. Tests with the prototype valves support the modeling results.

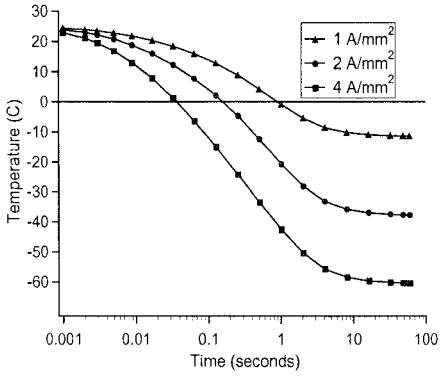

Figure 4. Temperature as a function of time at the Peltier junction for three different current densities.

Acknowledgements

The authors would like to thank Pirouz Kavehpour of the University of California at Los Angeles for advice and support. This work was supported under The Aerospace Corporation's Independent Research and Development Program.

References

[1] O. Geschke, M. Denninger, P. Telleman, and J. Kutter, Pittcon 2001, 1431P.

[2] C. D. Bevan and I. M. Mutton, J. Chromotgr. A, **697**, 541-548 (1995).

[3] R. P. Welle, B. S. Hardy, and M. J. O'Brien, Proc. Int. Conf. Thermoelectrics, ICT '04, (2004).

ADVANCEMENTS IN THE MONOLITHICALLY-INTEGRATED MICROCHEMLAB™

R. P. Manginell, M. Okandan, J. M. Bauer, R. Manley, D. Trudell, R. J. Kottenstette, P. R. Lewis, D. R. Adkins, E. J. Heller, H. Stewart and R. J. Shul

Sandia National Laboratories, P.O. Box 5800, Albuquerque, NM 87185-0603, U.S.A.

Abstract

A hand-held system for sensitive/selective detection of gas-phase chemicals has been developed and tested in the field. The sequential connection of microfabricated preconcentrators (PC), gas chromatography columns (GC) and a surface acoustic wave (SAW) detector arrays is used to impart selectivity and sensitivity to the MicroChemLab™ system. Hybrid integration of the micro components is used in the fielded system, permitting their individual optimization and modular replacement. To further reduce system dead volume and ease assembly requirements, monolithic integration of the PC and GC with a suitable silicon-based detector has been undertaken. A magnetically-actuated pivot plate resonator is presented as a candidate detector. Monolithic design, fabrication, coating and packaging are the topics of this correspondence.

Keywords: acoustic sensor, gas-phase analysis, gas chromatography, sample preconcentration

1. Introduction

An original goal of the MicroChemLab™ program was to bring high-confidence analytical techniques to the field, rather than simply introducing a new sensor. To address real-world applications, sample introduction, preparation, separation and detection functions are all indispensable. The fielded system accomplishes each of these functions using a system approach in which three microfabricated components play a vital role [1-3]. The microfabricated PC selectively collects gas-phase analytes onto a surface coating and desorbs them on command [4]. It serves as a non-mechanical injector for the second stage, a deep-etched silicon GC channel. The GC temporally separates the components of the injected mixture, and sends them onto the SAW array. The array elements are coated with various polymers, some selective, some non-selective for target analytes. The relative response of the array elements and elution time provide a selective/sensitive signature of the analytes present. These components are coupled via electrical/fluidic packaging in the fielded system. Modified circuit boards and passivated aluminum manifolds have both been used for this purpose [3]. While field performance has exceeded requirements, it could be improved by reduction of dead volume and the inclusion of heated transfer lines. Thus, an effort has been initiated to monolithically-integrate the PC and GC functions with a suitable silicon-based detector. This paradigm also eases assembly requirements.

2. Monolithic Integration

As was previously reported [5], a PC, GC and magFPW (magnetically-actuated flexural plate wave sensor) have been monolithically integrated using Sandia's SwIFT processing architecture. In this scheme, front-side surface micromachining was combined with back-end-of-line Bosch etching to produce both high precision resistive heaters and transducers, and full-wafer-thickness fluidic channels. An important consequence of this methodology is the precise definition of thermal and acoustic boundaries for the PC and magFPW, respectively, using a sacrificial silicon dioxide layer trapped within a relatively impervious perimeter of lithographically-defined silicon-nitride. This procedure improved the acoustic performance of the magFPWs by suppressing undesired modes [5]. SwIFT modules are 2.8 x 6.3 mm and permitted an important demonstration of monolithic integration of the MicroChemLab™. This effort was instructional regarding the fabrication process, magFPW operation, and the coating methods needed to functionalize the components.

However, the length of GC allowable in this footprint was too short for effective separation of complicated sample mixtures.

A second generation of the monolithic MicroChemLab™ has been developed [Figures 1-3]. The use of two adjacent modules has allowed the length of the GC to increase from 2.4 cm in the first generation: one new design has an 8.1 cm GC; another has an 11.8 cm column. These are still inadequate for full separations in the field, but are useful for limited analyte sets. This approach permits evaluation of the functional features of the monolithic design prior to consuming the many modules needed to realize a full-length, field-deployable design. The 11.8 cm long, 50 μm wide GC mentioned above is integrated with a PC and dual magFPWs. The 8.1 cm, 50 μm wide GC, on the other hand, incorporates a novel magnetically-actuated, torsional pivot plate resonator (PPR) pair for sensing [Figure 1 and Figure 2b].

The PPR sensor is potentially more sensitive than the magFPW and, as with the magFPW, is actuated by Lorentz forces determined by an AC current through the device and a magnetic field established by miniature permanent magnets. In a separate effort, PPR sensors were fabricated using an SOI process [3]. Coating of the PPR with a sol-gel permitted selective adsorption of analytes, changing the resonant frequency of the PPR in proportion to the mass adsorbed. 10 ng of dimethyl methyl phosponate (DMMP), produced 90° of phase shift in an un-optimized design. Analytical models of the PPR will aid optimization. This device has high temperature stability and sensitivity, making it ideal for monolithic integration. The monolithic PPR chip design also incorporates a surface-micromachined bypass valve [Figures 1 and 2a] to switch flow between the sampling and separation/detection portions of the overall system analysis routine. This consists of an electrostatically-actuated silicon nitride flap situated over a bypass channel. Actuation of the valve has been demonstrated and future designs will improve the stand-off pressure.

Packaging of the system is achieved using machined Pyrex lids and an anodically-bonded Pyrex baseplate, which forms the fourth side of the deep-etched GC column [Figure 3]. The Pyrex cover also contains coating ports for the GC. The baseplate is designed to mate with a stereolithographically-manufactured GC coating fixture. After fabrication, the GC is coated by solution-based techniques using this fixture. The PC and acoustic detectors are coated by spray deposition through a mask. Finally, machined lids are placed over the devices and the system can be placed into a DIP package for electrical connection.

3. Conclusions

The MicroChemLab™ system utilizes the sequential connection of three microfabricated components to achieve selective and sensitive gas-phase detection. To date, the fielded system hybrid integrates these components. Monolithic integration reduces dead volume, allows for heated transfer lines and eases assembly requirements. This integration approach will be used in future applications requiring further miniaturization and improved detection limits.

References

[1] G.C. Frye-Mason, et. al., *Proc. Micro Total Analysis Systems 2000*, Kluwer Academic Publisher, Dordrecht, The Netherlands, pp. 229-232, (2000).

[2] G.C. Frye-Mason, et. al., *Proc. Micro Total Analysis Systems 2001*, Kluwer Academic Publisher, Dordrecht, The Netherlands, pp 658-660, (2001).

[3] D.R. Adkins, et. al., 2nd Joint Conf. Point Detection for Chem. & Bio. Defense, Mar. 1-5, 2004.

[4] R. P. Manginell, et. al., *Tech. Digest 2000 Sol.-State Sensor and Actuator Workshop*, Transducers Research Foundation, Cleveland, pp 179-182, (2000).

[5] R.P. Manginell, et. al., *Proc. Micro Total Analysis Systems 2003*, Transducers Research Foundation, pp 1247-1250, (2003).

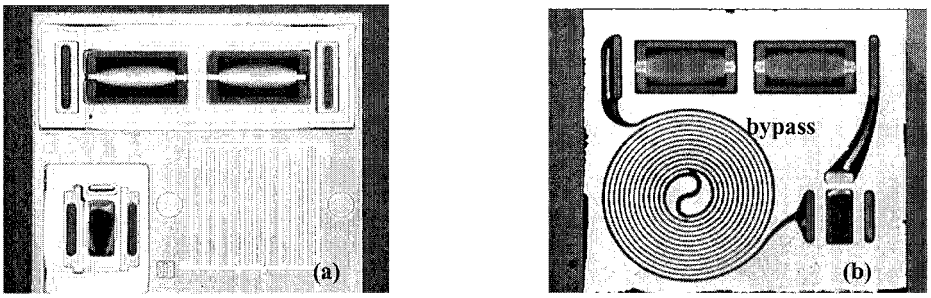

Figure 1. Optical photographs of the second-generation system. **(a)** Front side surface micromachining is shown: dual torsional resonator sensors are evident as are multiple oblong through-wafer access ports, a PC in the lower left, and a GC resistive heater and circular coating ports in the lower right. **(b)** Reverse side deep etching: The spiral GC is on the lower left.

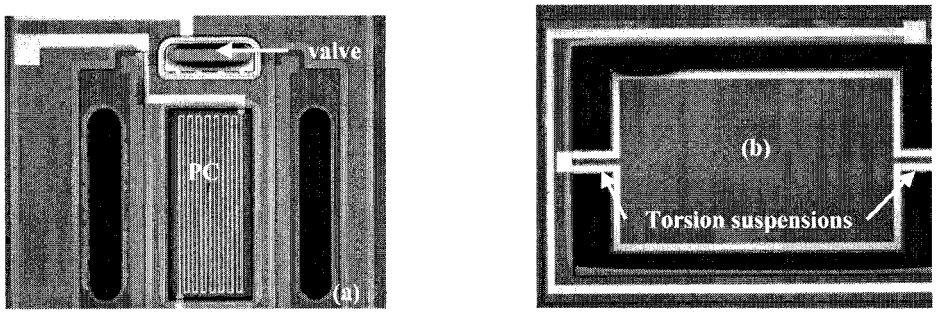

Figure 2. (a) PC, valve and oblong through ports (compare with the lower left corner of Figure 1a). **(b)** Monolithic PPR. The air gap surrounding the device appears black.

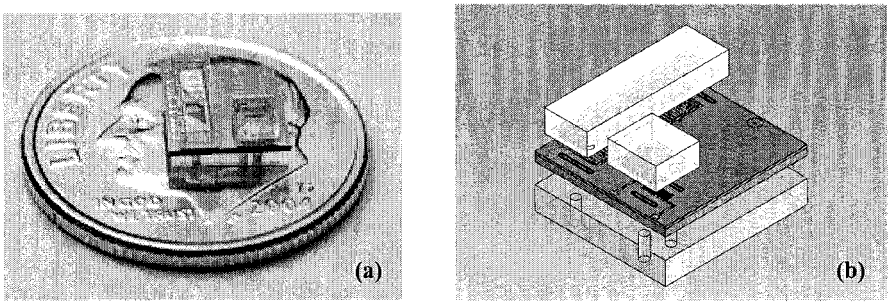

Figure 3. (a) Photograph of the system on a U.S. dime. **(b)** Expanded mechanical drawing of the monolithic system with machined Pyrex lids and Pyrex baseplate.

Acknowledgment: Sandia is a multiprogram laboratory operated by Sandia Corporation, a Lockheed Martin Company for the United States Department of Energy's National Nuclear Security Administration under contract DE-AC04-94AL85000.

ROBUST AND BIOCOMPATIBLE NEUROCAGES

Angela Tooker[1], Jon Erickson[2], Yu-Chong Tai[1], and Jerry Pine[3]
[1]Dept. of Electrical Engineering, California Institute of Technology, M/C 136-93, Pasadena, CA 91125, USA
[2]Dept. of Bioengineering, California Institute of Technology
[3]Dept. of Physics, California Institute of Technology

Abstract

We present a refined method and design for building parylene neurocages to allow *in vitro* study of live neural networks. This fabrication process is less complex than previous processes, producing robust and biocompatible neurocages; moreover, this new design has achieved a significantly higher neuronal survival and outgrowth rate than previous versions.

Keywords: neurocage, neuron, neuro-well, parylene

1. Introduction

Neurons play an important role in many of our biological and cognitive functions. Many studies concentrate on the properties of neurons and the neural networks they form; unfortunately, it is difficult to study these networks *in vivo*. Initial *in vitro* techniques used patterned extracellular electrode arrays [1,2], but neuron mobility and lack of neuron-to-electrode specificity limit the use of these arrays. Our strategy counteracts these difficulties by using micromachined structures to physically trap individual neurons in close proximity to electrodes, without inhibiting their growth. The first implementation was a bulk micro-machined neuro-well [3,4]. While greatly aiding the study of live neural networks, the fabrication and scaling complexities of the neuro-wells limited their continued development. Previously, our group developed processes for building surface micro-machined parylene neurocages that eliminate the difficulties encountered with neuro-wells [5,6] The initial neurocage design achieved limited neuron outgrowth, but long-term cell survival was low (<25%). The new neurocage process and design presented here, while preserving several elements of the previous designs, increases the long-term cell survival rate to >50%.

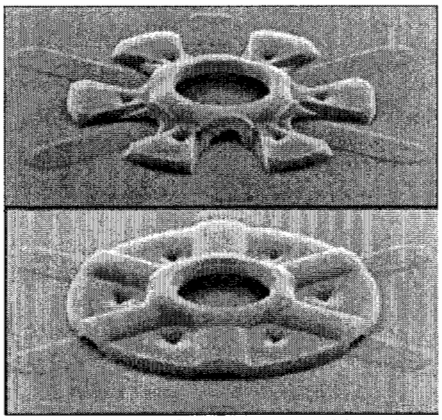

Figure 1. SEM of a neurocage, with a 10μm tunnel width and a 4μm tunnel length (top) or 25μm tunnel length (bottom).

2. Design and Fabrication

The neurocage consists of a chimney, 30μm in diameter and 4μm high, with a 15μm inlet hole at the top for loading neurons (Figs. 1-2). Extending out from the chimney are 6 tunnels, for neuron outgrowth, interleaved with 6 anchors, for mechanical stability. The tunnels are approximately 1μm high, either 5μm or 10μm wide, and extend for either 25μm or 4μm. In previous designs, the chimney was 15μm high, the tunnel heights varied from 0.3μm to 2μm (depending upon the fabrication process used), and the tunnel length was 15μm. A 4 x 4 array of neurocages is centered within a 440μm x 440μm square.

The process flow for creating the neurocages is shown in Fig. 3. A partial exposure method is used with a single layer of photoresist (AZ4400) and two separate exposures with different masks to define the chimneys and tunnels. The anchors are etched into

the silicon using a DRIE process (50 loops of a standard Bosch process to make an anisotropic trench with nearly vertical sidewalls, and a subsequent 30 second SF_6 isotropic etch to create a mushroom-like bottom) developed in our group for mechanically securing parylene to a substrate [7]. Unlike the previous fabrication process, only one deposition of parylene is required. This single layer of parylene (4μm thick) is etched using O_2 plasma to create the neurocages. Finally, the neurocages are cleaned using piranha at 120°C for 10 minutes followed by a 10 second HF dip.

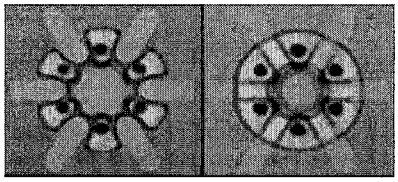

Figure 2. Optical pictures of neurocages with 10μm tunnel widths, and 4μm tunnel length (left) or 25μm tunnel length (right).

3. Results

Successful growth of live neural networks has been achieved using arrays of neurocages (Fig. 4), thereby proving that the neurocages are biocompatible. Neuron outgrowth has been achieved in neurocages with tunnel widths of both 5μm and 10μm, and lengths of either 40μm or 4μm. No significant differences in neuronal survival rate and outgrowth have been observed due to the different combinations of tunnel lengths and widths.

Neurocages produced using this new fabrication process are mechanically robust, able to withstand various cleaning procedures, including acetone and piranha, with no deformation or delamination. In addition, initial studies have shown that neurocages can survive for long periods, up to 80 days, in saline at 30°C with no visible deformation or delamination. (The study was concluded after 80 days; hence, no data is available for longer periods.) Also, the neurocages can be cleaned of all neuron debris, using piranha and HF, for later re-use.

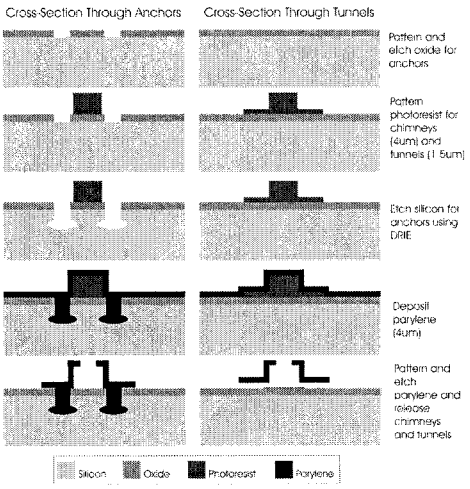

Figure 3. Process Flow

4. Discussion

The current neurocage design and process, while similar to previous versions, dramatically increases the long-term cell survival rate.

In previous neurocage designs, the tunnels were formed by sputtered silicon, hardbaked photoresist, or thermally evaporated Al, while a thick layer of photoresist (AZ9260) formed the chimneys. As a result, more drastic release methods were required: BrF_3 or XeF_2 gas etching, ST-22 photoresist stripper, or Al etchant, respectively. Despite these harsh release methods, it was still difficult to ensure that the tunnel material had been completely removed. Any remaining material could block the tunnel, thus preventing neuronal outgrowth. With the current fabrication process, the tunnels can be released using acetone, making it easier to ensure that the photoresist is removed and the tunnels are open.

Previous designs used BrF_3 or XeF_2 to etch the anchors, making it difficult to accurately control the undercut. The undercut caused the size of the anchors to increase, thereby shrinking the area available for the tunnels, and in some cases, eliminating the tunnels. With the DRIE process used for the current neurocages, the undercut can be reliably controlled.

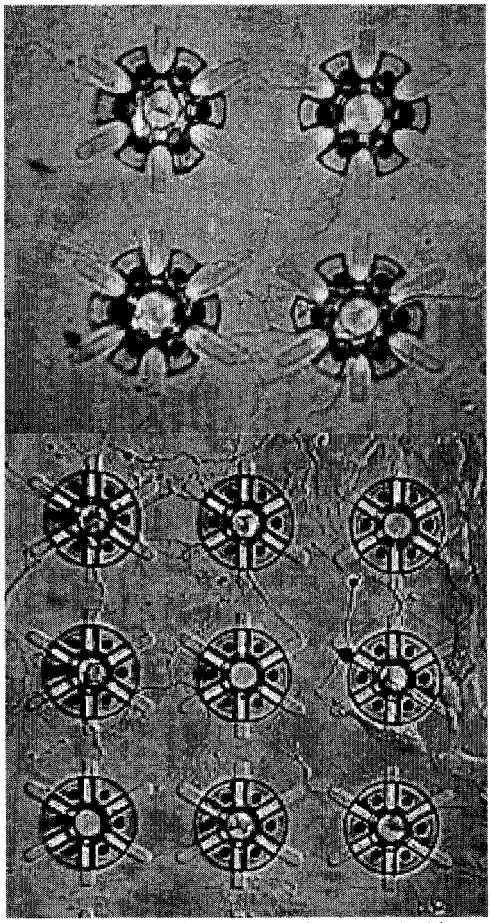

Figure 4. Nomarski pictures of neurons inside neurocages with neurite outgrowth. Neurocages with 10μm tunnel widths, and 4μm tunnel lengths (top) or 25μm tunnel lengths (bottom).

5. Conclusions

The design and process presented here for parylene neurocages can be used for *in vitro* studies of live neural networks. This fabrication process is less complex than previous neurocage and neuro-well fabrication processes. Biocompatible and robust neurocages can be created that achieve significantly higher neuronal survival and outgrowth rate than previous versions. The next step is to incorporate platinized gold electrodes into the neurocages to stimulate and record from individual neurons.

Acknowledgements

This work was funded by the NIH under Award Number R01 NSO44134. We would like to thank Mr. Trevor Roper, Mr. Qing He, and Ms. Angelique Johnson for assistance with fabrication and testing.

References

[1] J. Pine, "Recording action potentials from cultured neurons with extracellular microcircuit electrodes," *Journal of Neuroscience Methods*, 2, pp. 19-31, 1980.

[2] Y. Jimbo, T. Tateno, and H.P.C. Robinson, "Simultaneous induction of pathway-specific potentiation and depression in networks of cortical neurons," *Biophysical Journal*, vol. 76, pp. 670-678, Feb. 1999.

[3] J.A. Wright, S.T. Lucic, Y.C. Tai, M.P. Maher, H. Dvorak, and J. Pine, "Towards a functional MEMS neurowell by physiological experimentation," *ASME International Mechanical Engineering Congress and Exposition*, DSC-Vol. 59, Atlanta, GA, pp. 333-338, Nov. 1996.

[4] M.P. Maher, J. Pine, J. Wright, and Y.C. Tai, "The neurochip: a new multielectrode device for stimulating and recording from cultured neurons," *Journal of Neuroscience Methods*, 87, pp. 45-56, 1999.

[5] Q. He, E. Meng, Y.C. Tai, C.M. Rutherglen, J. Erickson, and J. Pine, "Parylene neuro-cages for live neural networks study," *Transducers*, pp. 995-998, 2003.

[6] E. Meng, Y.C. Tai, J. Erickson, and J. Pine, "Parylene technology for mechanically robust neuro-cages," *MicroTAS 2003*, pp. 1109-1112.

[7] M. Liger, D.C. Rodger, and Y.C. Tai, "Robust parylene-to-silicon mechanical anchoring", *16th IEEE International Conference on Micro Electro Mechanical Systems, MEMS '03*, Kyoto, Japan, pp. 602-605, Jan. 2003.

A NOVEL DISPERSION CONTROL IN CAPILLARY ELECTROPHORESIS BY LOCALIZED ZETA POTENTIAL VARIATION USING THE FIELD EFFECT

Chia-Yen Lee[1], Lung-Ming Fu[2], Ruey-Jen Yang[3] *and* Che-Hsin Lin[4]

[1] *Dept. of Mechanical and Automation Engineering,Da-Yeh University, Changhua, Taiwan, 515*

[2] *Graduate Institute of Materials Engineering, National Pingtung University of Science and Technology, Pingtung, Taiwan, 912*

[3] *Dept. of Engineering Science, National Cheng Kung University, Tainan, 701, Taiwan*

[4] *Dept. of Mechanical and Electro-Mechanical Engineering, National Sun Yat-sen University, Kaohsiung, Taiwan, 804*

Abstract

This paper reports a new technique to minimize the effects of turn-induced dispersion within U-shaped separation channels by using the field effect within a capacitor to vary the zeta potential along the channel walls in the vicinity of the microchannel. The effects of the separation channel geometry, the fluid velocity profile, and the use of the filed effect to control the zeta potential on the band distribution in the detection area are extensively discussed. The results for a U-shaped separation channel indicate that varying the zeta potential by controlling the field effect significantly reduces the band dispersion induced by the 90^0 turns within the channel. Finally, it is shown that the application of the proposed localized zeta potential variation method also results in a correction of the band tilting phenomenon and a reduction in the racetrack effect.

Keywords: microfluidics; field-effect flow control; racetrack effect

1. Introduction

Capillary electrophoresis, CE, is often used in applications requiring the separation of biological or chemical particles, e.g. in the separation of DNA for genetic engineering purposes. The CE technique exploits the differing mobility characteristics of charged molecular species when subjected to an externally applied electric field. Typically, the separation channel on a microfluidic chip is designed in the form of a straight line. However, this configuration occupies a larger chip area, and so the use of serpentine channels has been developed in order to achieve longer separation lengths within a more compact area. Recent studies [1-2] addressing the design of serpentine microchannels have concerned themselves with increasing the separation efficiency, decreasing the manufacturing cost and facilitating product miniaturization.

2. Formulation and numerical method

Regarding the numerical simulation of electroosmotic flows, the current authors have previously developed physical models based on (a) the Poisson equation for the electrical potential and zeta potential, (b) the Nernst/Planck equations for the ionic concentration, (c) the full Navier/Stokes equations modified to include the effects of the body force due to the electrical and charge densities and (d) a concentration equation for the sample plug distribution. The detailed expressions of the governing equation, the initial conditions, and the boundary conditions are provided in [3-4].

3. Experimental

The present study used commercially-available microscope glass slides of dimensions 76x26x1 mm and 40x40x1 mm, supplied by Marienfeld (Germany), and the fabrication process adopted in the present study [5]. Figure 1 presents photographs of the traditional cross separation channel and the U-shaped separation channel on glass substrates following the photolithography process. The total distance of separation channel is 4 cm (Figure 1(a) and 1(b)) and channel width is 100 μm

4. Results and discussion

Figure 2 demonstrates how the field effect within a capacitor can be used to control the zeta potential variations on the wall surfaces along the U-shaped separation channel in such a way that the racetrack effect is reduced. Figure 3 presents a plot of the sample band concentration distribution along a U-shaped separation channel for the case where no field effect control is applied. At location (a), i.e. prior to the first 90^0 bend, the sample plug exhibits a uniform band shape. However, as the sample traverses the bend, its distribution becomes tilted and distorted, as shown at locations (b) and (c). It is observed that the second 90^0 bend fails to restore the effects of the initial bend. In fact, as may be seen at location (d), the bands actually become further distorted. Figure 4 illustrates the sample plug concentration distribution as the sample flows through a U-shaped separation channel under the influence of the field effect. It is noted that the previously observed racetrack effect has now been eliminated. The tilted sample band which was evident in Figure 3 has been corrected. Furthermore, the band dispersion in location (e) is much improved, which results in an enhanced detection performance. Figure 5 presents electropherograms generated from the images collected by an APD module at the detection area of the traditional straight separation channel and the U-shaped separation channel. As stated previously, a test sample consisting of 10^{-4} M Rhodamine B and 10^{-4} M Cy3 fluorescent dye was employed. It is noted that Figures 5(a) and 5(b) present the experimental results for the traditional straight separation channel and the U-shaped channel, respectively, without field effect while a separation voltage of 1.2 kV (240 V/cm) is applied. Conversely, Figure 5(c) shows the equivalent simulated results for the U-shaped separation channel without field effect. Figure 6 presents experimental and simulated electrophoerograms generated from the images collected at the detection areas of the traditional straight separation channel and the U-shaped separation channel when field effect control is applied for separation voltage of 1.2 kV (240 V/cm) and the relative voltage of the capacitor are +0.5 kV (V_+) and –0.3 kV (V_-). The peak intensities of the three samples are clearly evident in each of the sub-figures. It is noted that the dispersive effect is diminished in the U-shaped separation channel when the field effect is applied. The results indicate that the field effect control is an effective means of improving the separation detection performance within a U-shaped separation channel.

5. Conclusions

This work presented a novel approach in controlling surface zeta potential by embedding electrodes close to channel walls on a small chip surface in microfluidic devices designed for improving electrokinetic separations. Instead of altering channel cross-sectional geometries, the proposed field effect allows variable flow rates of sample components along opposite walls to be generated, in order to compensate for faster velocities along inside walls of turns with respect to the outer walls (the so-called racetrack effect). The results of the present study are useful in the development of a variety of applications including optimized DNA separation, protein separation and other applications in the field of micro-total-analysis systems.

Acknowledgements

The current authors gratefully acknowledge the financial support provided to this study by the National Science Council of Taiwan under Grant N°s. NSC93-2745-E-020-001 and NSC92-2320-B-110-015.

References

[1] S. K. Griffiths and R. H.Nilson, *Analytical Chemistry,*, 73, 272-278 (2001).
[2] L.-M. Fu, R.-J. Yang and G.-B Lee, *Electrophoresis*, 23,602-612 (2002).
[3] L.-M. Fu, R.-J. Yang and G.-B Lee, *Analytical Chemistry,* 75, 1905-1910 (2003).
[4] L.-M. Fu and C.-H. Lin, *Analytical Chemistry*, 75, 5790-5796 (2003).

[5] C. H.Lin, G. B. Lee, Y. H. Lin and G. L. Chang, *Journal of Micromechanics and Microengineering*, 11, 726-732 (2001).

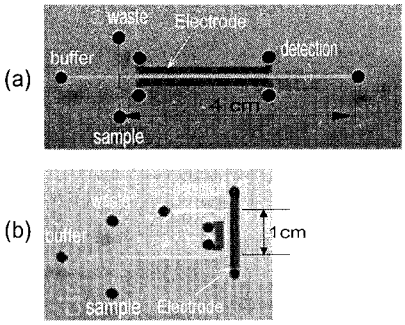

Fig. 1 Separation Microchannels on Glass Substrate: (a) Traditional Straight Separation Channel, (b) U-Shaped Separation Channel

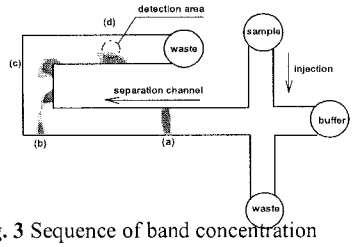

Fig. 3 Sequence of band concentration distribution in U-shaped separation channel without field effect control of zeta potential.

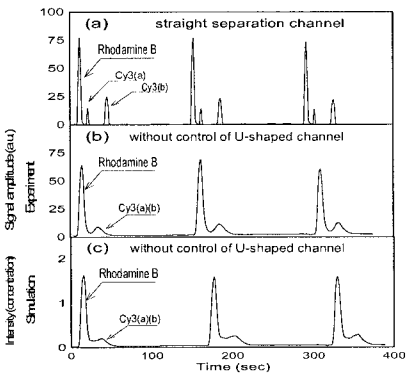

Fig 5 Comparison of electropherograms generated from an image collected at the detection area with no field effect control.

Principle

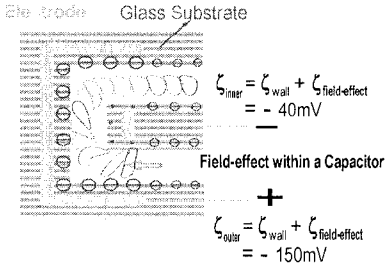

Fig. 2 Use of the field effect to control the zeta potential variations on the wall surfaces along the U-shaped separation channel.

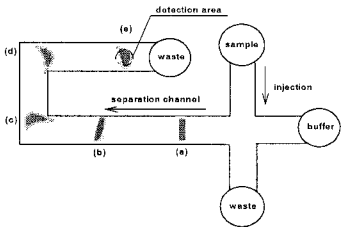

Fig 4. Sequence of band concentration distribution in U-shaped separation channel with field effect control of zeta potential.

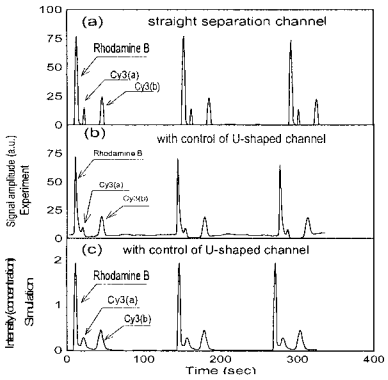

Fig 6 Comparison of electropherograms generated from an image collected at the detection area with field effect control.

MEMS-BASED CATALYTIC MICRO-REACTOR FOR DECOMPOSITION OF FLUIDS

Yoichiro Dan*, Masahiro Kishida, Tatsuya Ikuta*, Kunihito Nagayama***
and
Koji Takahashi*

* *Department of Aeronautics and Astronautics, Kyushu University*
** *Department of Chemical engineering, Kyushu University*
Hakozaki 6-10-1 Fukuoka 812-8581, Japan
E-mail: takahashi@aero.kyushu-u.ac.jp

Abstract
Micro-reactors of porous channel with platinum nano particles were developed. This reactor is based on MEMS technology and designed for the decomposition of hydrogen peroxide for future space propulsion system. The porous surface is formed only on the channel inside wall by electrochemical etching of silicon in a mixed solution of HF. Platinum particles were deposited by impregnation method using H_2PtCl_6 solution as precursor. Performance and durability tests of are conducted and effect of nano-scale catalyst morphologies is discussed.
Keywords: catalytic micro-reactor, porous silicon channel, Pt particles, catalyst durability

1. Introduction

MEMS-based catalytic reactor is a key technology for many kinds of micro chemical systems. So far, porous alumina or silica has been used as the catalyst bed. Kusakabe et al. fabricated a micro-channel reactor with packed γ-alumina particles of 150-200μm diameter [1]. This structure is an excellent idea but requires skill of packing process. Liu et al. formed porous silica layer of up to 22μm thickness on a silicon substrate using sol-gel process [2]. However, the lifetime of sol-gel-based layer is fundamentally short at high temperature or high pressure condition. Hitt et al. developed a catalytic reactor with Ag film for propulsion application [3]. The surface area of the channel was increased by forming a large number of fins by DRIE. However, this reactor didn't have enough performance for practical use. On the other hand, Losey et al. utilized porous silicon microchannel as catalytic micro-reactor [4]. However, its performance and durability were not sufficiently treated by their investigation.

Crystal silicon is known to be electrochemically etched into porous structure in HF solution. This dissolution is only possible when the current delivers holes to the interface of the material and the solution. By regulating current density and selecting dopant type of the silicon, the morphology of the pores can be changed and they have extremely large surface area. And also the fabrication sequence of porous silicon matches with the MEMS technique. In this study, N-type silicon substrate was selected and the current density was set small to form the pores of a few μm diameters as well as our past-developed technique [5]. Several kinds of catalytic micro-reactors with Pt catalyst were fabricated and compared in order to develop a novel propulsion system for pico-satellite in future space engineering.

2. Fabrication

Fabrication process of our reactor is shown in Fig.1. After the channel is formed by bulk-etching, the channel surface was changed to porous by electrochemical etching in HF/ethanol/water (16.5:16.5:67.0) solution with forward illumination. Since silicon nitride layer plays as the etching mask, porous silicon layer of uniform pores of a few μm diameters was successfully formed without

eroding the outside of the channel. This method is applicable to any size and shape of the channel while DRIE is only to shallow channel and sol-gel layer is only to deep one. After the formation of the porous channel, Pt particles were deposited on the channel surface by impregnation method. H_2PtCl_6 solution was used as the precursor of the particles. Changing the concentration of the solution, three kinds of the reactor with different morphologies of the catalyst were fabricated. The SEM images of sample.1 ~ sample.3 are listed in Fig.2. The aggregations of Pt much larger than the pores are seen in Fig.2 (a). Aggregations are also seen in (b). On the other hand, (c) shows Pt particles of 20~30nm in diameter. Since these particles are seen even in the inside of pores, much increase of the catalyst surface area can be expected.

3. Performance Test and Post Observation

Hydrogen peroxide of 60% concentration was chosen for decomposition test due to its ecological characteristics and applicability to space propulsion. The volume of generated O_2 gas and the thrust produced by the ejected gas were measured under the room temperature and high temperature respectively. Because both results are dependent on the flow rate and operation temperature, only qualitative and comparative performance is discussed here. In order to examine the effect of the porous channel and the Pt particles, another two kinds of reactors (sample.4 and 5) were fabricated and also tested. Sample.4 has an EB-deposited Pt film on the same porous channel, and sample.5 has a flat channel and Pt film. All of these reactors have the same size. The obtained results in Fig.3 show that both porous channel and Pt particles are apparently effective for improving the efficiency of the decomposition. The performance of sample.3 is found relatively improved in the thrust measurement. One of the possible reasons is that the most of hydrogen peroxide changes to gaseous phase and catalyst in the pores of sample.3 works efficiently in the thrust test at high temperature. Another possible reason is the difference of endurance of these catalysts. Fig.4 is the SEM images of the reactors after the performance tests. Pt particles were found detached especially in samples.1 and 2. However, the particles were rarely decreased in sample.3. This is due to the interatomic force that is more dominant in smaller particles especially of nm order. Differently from the sol-gel porous layer, our-fabricated porous silicon surface was confirmed to have enough mechanical strength even under the decomposition condition of liquid into gas as seen in all pictures in Fig.4.

4. Concluding Remarks

Pt catalytic reactor was developed and tested using porous silicon with MEMS technique. Obtained results indicate that the performance and durability are dependent on catalyst particle morphology. Further study is desired to assess the optimum catalyst at high temperature operation and to obtain a larger number of smaller particles to enhance both of performance and durability.

Acknowledgement

This work was partially supported by the Grant-in-Aid for Scientific Research (No. 13555267 and 14702029). Mitsubishi Gas Chemical Company Inc. is deeply appreciated for supply of hydrogen peroxide.

Reference

[1] K. Kusakabe et al. J. Chemical Engineering of Japan **35**(9) 914-917, 2002
[2] Y. Liu et al. Materials Letters **49** 102–107, 2001
[3] M. W. Losey et al. J. Microelectromechanical Systems **11**(6) 709–717, 2002
[4] D. L. Hitt et al. Smart Mater. Struct. **10** 1163–1175, 2001
[5] K. Takahashi, et al. Micro Total Analysis Systems 2003, **1**, 503-506, 2003

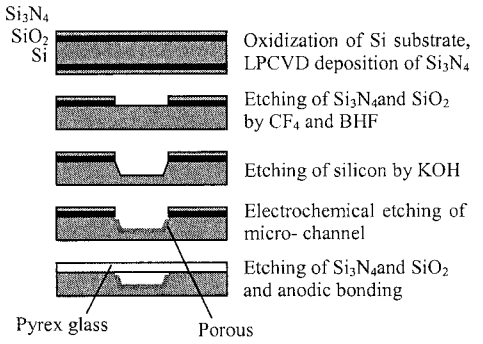

Fig.1 Fabrication process of the micro-reactor

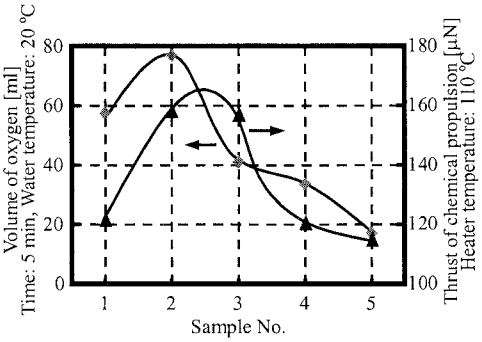

Fig.3 Results of the performance tests

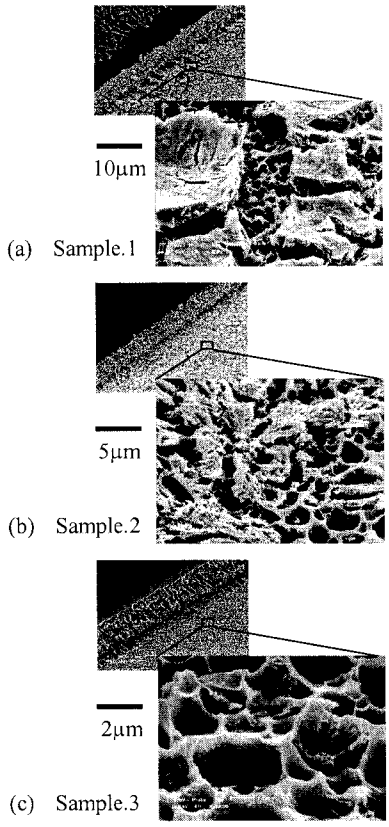

Fig.2 SEM images of fabricated Pt catalyst on porous channel

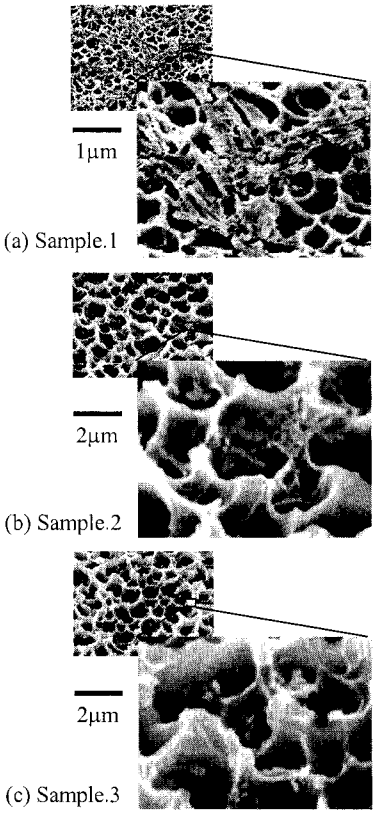

Fig.4 SEM images of the catalyst after the performance tests

BUILDING EMBEDDED MICROCHANNELS USING A SINGLE LAYER SU-8, AND DETERMINING YOUNG'S MODULUS USING LASER ACOUSTIC TECHNIQUE

Hui Yu[1], Oluwaseyi Balogun[2], Biao Li[1], Todd Murray[2], and Xin Zhang[1]

[1]Dept. of Manufacturing Engineering and Fraunhofer USA Center for Manufacturing Innovation,
[2]Dept. of Aerospace and Mechanical Engineering, Boston University, 15 Saint Mary's Street, Boston, MA 02215, USA

Abstract

In this paper, an innovative method to create embedded microchannels is introduced. The presented technology is based on a direct-write technique using a scanning laser system to pattern a single layered SU-8. The Young's moduli of UV exposed SU-8 generated with different exposure doses are also determined by using a laser acoustic microscopy system. Measurements show that the Young's modulus is highly dependent on UV exposure dose.

Keywords: embedded microchannels, UV dosage control, laser acoustic technique

1. Introduction

In biotechnology and biochemical processing, the need to manipulate fluids moving in buried narrow channels (microfluidics) has stimulated the development of new microfabrication methods for fluidic systems. We have developed a novel beam-scanning laser system for rapid prototyping 3D microstructures and manufactured embedded channels by multi-step inclined exposure on SU-8, i.e., sample was mounted on a x-y-z-θ stage and subjected to sequential laser writing by rotating the stage with various angles [1]. In this paper, a novel approach to fabricate embedded microchannels in a singled layered SU-8 is developed by using the scanning laser system. The enormous flexibility of the scanning laser system is demonstrated, i.e., the laser pulsing can be controlled spot-by-spot with variable exposure doses and the laser intensity that penetrated into a sample can also be adjusted by varying laser focus levels. This innovative laser manufacturing technique spawns a 3D fabrication methodology that has generic value in controlling the in-depth laser manufacturing process, precisely and quantitatively. In addition, the new fabrication process provides the capability to generate flexible freeform structures using CAD, which greatly reduces the development cycle, potentially reaching hours or less design-to-fabrication turnaround time. The results presented here represent the first step towards the realization of categories of devices with mechanical, optical, and/or biological functionalities. The mechanical properties of UV exposed SU-8 are also studied in this paper. As a start point, the Young's moduli of double-clamped SU-8 microbeams with different beam thicknesses are determined by using a laser acoustic microscopy system. The laser-based ultrasonic technique offers a non-contact, nondestructive means of evaluation and localized materials characterization. Since UV exposed SU-8 microbeams with various film thicknesses are generated by using different UV exposure doses, there exists a relationship between the Young's modulus of UV exposed SU-8 and the exposure dose.

2. Concept and Fabrication

We have shown that the penetration depth of laser beam can be adjusted by varying its focus levels and exposure doses as shown in Figure 1a. Figures 1b-d illustrate double-side clamped cantilever arrays and an embedded channel fabricated using laser writing at different focus levels and with different exposure doses. The posts and beams were realized in the same SU-8 layer. A typical process flow for the fabrication of freestanding beams is as follows: A glass or silicon substrate is first prepared by piranha cleaning process for 10 minutes. A layer of SU-8 resist is spin

coated onto the substrate and soft-baked. After that, the sample is exposed to UV beams with two different energy levels such that the depths of the polymer cross-linking are different. The posts are written by an on-focus, high exposure dose laser pulse, which can penetrate through the whole SU-8 layer while stopping at the supporting substrate. The beams are written by an out-of-focus, low exposure dose laser pulse, thereby allowing the formation of freestanding microbeam structures after post-exposure bake (PEB) and develop. The alignment of two exposures in resist is achieved by aligning the two patterns in the ScanWare laser scanning control software. The develop process is carried out inside an ultrasonic bath with mild agitation. The pattern becomes clear very quickly, typically in a couple of minutes. After develop, an embedded microchannel is formed.

The manufacture of cantilever beams with controlled thickness was characterized by changing the UV exposure dose with varied laser repetition rate and laser diode current. Figure 2a shows the measured laser average power vs. repetition rate and diode current. Figure 2b&c illustrates the controlled beam thickness when we gradually increase the UV dosage.

3. Determining the Young's modulus of UV exposed SU-8

The Young's moduli of microbeams were evaluated using a laser acoustic microscopy system as shown in Figure 3. This system offers a non-contact, nondestructive means of materials characterization [2]. The laser acoustic microscopy system consists of three optical paths that lead to the sample surface through the same long working distance objective. The first optical path delivers the collimated generation laser to the sample surface. The energy of the generation laser is attenuated to prevent excessive heating of the sample surface. The second optical path consists of a path stabilized Michelson interferometer. In this path, the detection laser is delivered to the microscope through a single mode optical fiber and collimation lens, and directed to a beam splitter where it is divided into signal and reference beams. The reference beam reflects off a mirror mounted on an actuator, and is sent to a photodiode with a 1 GHz bandwidth. The signal beam is sent to the sample surface and, upon reflection, returns back through the beam splitter and interferes with the reference beam at the photodiode. The third optical path consists of an optical microscope used for optical imaging of the sample surface, and alignment of the generation and detection beams within the field of view of the microscope.

In this technique, the material under investigation is illuminated with a laser source, causing local heating and launching acoustic waves that propagate through the specimen. The surface displacement associated with the generated signal, after propagating some distance in the specimen, is detected using an optical probe. Through the measurement of the velocity, dispersion, scattering and attenuation of the acoustic waves, the physical and/or mechanical properties of the material can be determined. The derived Young's moduli of SU-8 microbeams in Figure 2b&c are 3.8 and 5.4 GPa, respectively. From the results, it is obvious that for obtaining a stiffer SU-8 film, the film must have a higher UV dose (assuming that the geometry of the film is the same).

4. Conclusions

A method for the fabrication of embedded microchannels with various beam thicknesses in a single layered SU-8 based on a scanning laser direct-write technique has been presented. The Young's moduli of SU-8 microbeams generated with different exposure doses are also determined by using a laser-based ultrasonic technique. Measurements show that the Young's modulus is highly dependent on the exposure dose. Using this laser direct writing technique, various 3D microstructures can be fabricated and applied in many fields.

References

1. H. Yu, A. Grüntzig, Y. Zhao, A. Sharon, B. Li, and X. Zhang, *μTAS 2003*, 347-350.
2. S. J. Davis, C. Edwards, G. S. Taylor and S. B. Palmer, J. Phys. D. 26, 329-348 (1993).

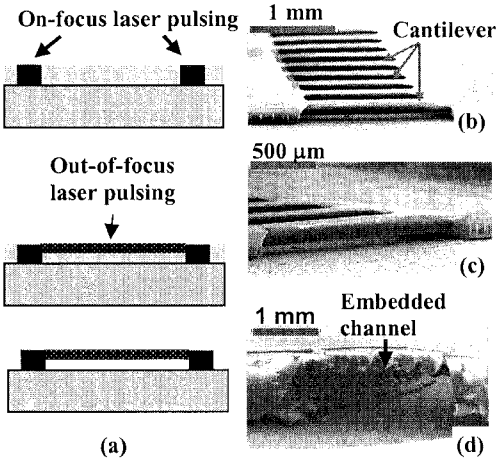

Figure 1. (a) Fabrication of freestanding microstructures. Post: on-focus, high energy dose pulsing; Beam: out-of-focus, low energy dose pulsing. (b)-(d) Demonstration of single layered double-side clamped cantilever array and embedded channel, both fabricated using laser writing with different exposure doses and at different focus levels.

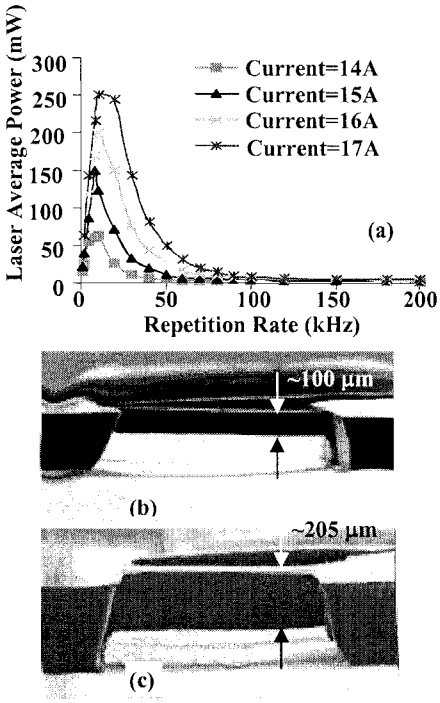

Figure 2. (a) Laser average power vs. repetition rate and laser diode current. (b)-(c) Beam thickness controlled by different UV dosages.

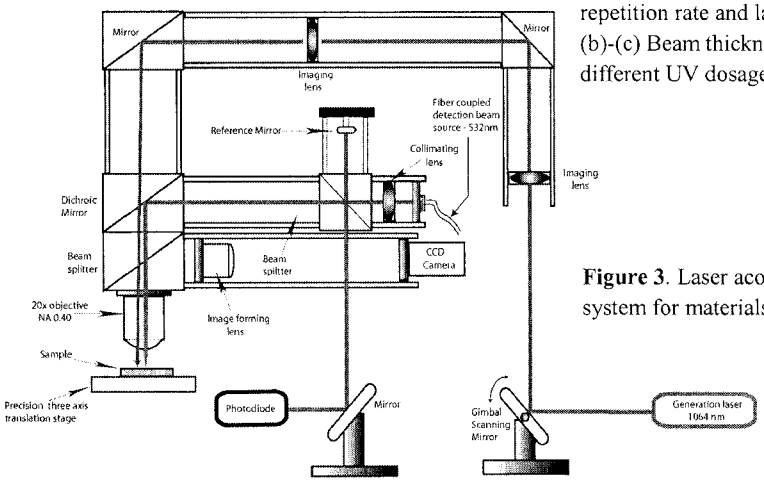

Figure 3. Laser acoustic microscopy system for materials characterization.

THREE-DIMENSIONAL MICROVALVES BASED ON SINGLE-LAYERED SU-8 FOR LAB-ON-CHIP APPLICATION

Hui Yu, Yi Zhao, Biao Li, and Xin Zhang
Dept. of Manufacturing Engineering and Fraunhofer USA Center for Manufacturing Innovation, Boston University, 15 Saint Mary's Street, Boston, MA 02215, USA

Abstract

A novel three dimensional manufacturing approach to rapid processing of microfluidic devices using a scanning laser system is presented. A microvalve has been fabricated in a single layered SU-8 by adjusting focus levels and laser intensity. With this process, a new class of microdevices with designed-in functionalities can be developed.

Keywords: single SU-8 layer, microvalve, compliant cantilever

1. Introduction

Reliable microvalves are crucial to flow control in microfluidic devices. However, many types of existing mechanical microvalves require elaborate fabrication processes, and valves are typically involved in complex systems in a nontrivial way. We have recently developed a rapid and controlled process by which a fluidic device with a freeform microvalve can be fabricated in a single layered SU-8 using a scanning laser system. This technique offers laser pulsing spot-by-spot for both in-plane and in-depth processing. The process is fairly simple, requiring only laser shooting from front side and backside on a thick SU-8 layer under appropriate process conditions. The new technique offers a powerful tool for microfabrication. As a result, a wide range of microfabricated structures that would have been difficult or impossible to make using traditional micromachining techniques can now be made quickly and easily.

2. Experimental Apparatus and Fabrication Process

The experimental apparatus consists of a pulsed Nd:YAG laser (emitting at 355nm) directed through a 2-axis Scan Head [1]. Since the pulsed UV laser is not easily visible, an auxiliary red alignment laser is used for multilevel alignment as shown in Fig. 1. The alignment procedure is as follows: An alignment mark is first permanently carved on a specimen by using pulsed laser writing. A cross pattern is then generated by the red laser and aligned to the mark by adjusting the red laser system. After that the specimen can be unloaded from the stage for additional processing. Whenever the specimen is reloaded on the stage, its position can be adjusted to make the mark aligned with the cross pattern generated by the red alignment laser. In such a way, samples can be easily unloaded and reloaded on the stage for sequential laser processing. This method works for both front-to-front and front-to-backside alignment. Fig. 2a shows a schematic diagram of aligned front-to-backside laser writing on two SU-8 layers separated by a thin interfacial metal layer for UV light blocking. A glass sample was first prepared by cleaning in a piranha solution (sulphuric acid:hydrogen peroxide, 3:1) for 10 minutes and dehydrating on a hot plate at 95°C for 5 minutes. SU-8 2025 was then spin-coated to produce a film approximately 60μm in thickness. The resist was soft-baked and a thin film of Au (~230 nm) was coated by sputtering. Following the sputtering, the spin-coating and pre-bake steps were repeated to coat a second layer of SU-8 onto the Au film. Then the first layer of SU-8 was exposed from the back-side, while the second layer of SU-8 was exposed from the front side and the sample was post-exposure baked. Finally, the exposed SU-8 structures were developed in propylene glycol methyl ether acetate (PGMEA) under controlled ultrasonic agitation to speed up developing process. Since the thin Au layer sputtered between the two SU-8 layers for blocking the UV light was not very dense, after the top layer SU-8 was developed, the Au film exposed to PGMEA was peeled off after a period of time, which enabled the

bottom layer SU-8 developing. Otherwise, KI could be applied for Au film wet etching when necessary. Figs. 2b&c illustrate proof-of-concept double-side-aligned microstructures using laser pulsing from both sides.

We successfully fabricated a functional microvalve using a single layered SU-8. The fabrication process is illustrated in Fig. 3. Our laser scanning system enables a 2D map to be specified, determining the area over which the posts and freestanding beams of a microvalve will be scanned. The fabrication process starts with piranha cleaning a glass substrate for 10 minutes. A ~260 μm thick SU-8 is coated on the glass substrate and soft-baked. The sample is then mounted on the x-y-z-θ stage and subjected to sequential laser pulsing from backside of the glass substrate, creating the posts of a suspended valve, walls of embedded channels and fluidic chambers. The valve that suspended by a thin cantilever, the thin cantilever itself and caps for embedded channels are fabricated through the use of front side laser pulsing. The front side pulsing is aligned to the backside pulsed structures but with different exposure doses and focus levels. Our alignment approach ensures a centered microvalve in a fluidic channel. The front side and backside UV exposures are carried out with different energy levels such that the depths of the polymer cross-linking are different. For example, the posts are written by an on-focus, high exposure dose laser pulse, which can penetrate through the whole SU-8 layer; while the microcantilever and suspended microvalve are written by an out-of-focus, low exposure dose laser pulse, thereby allowing the formation of freestanding microstructures after post-exposure bake (PEB) and develop. The alignment of the different exposures in resist is achieved by aligning the corresponding patterns in the ScanWare laser scanning control software. The develop process is carried out inside an ultrasonic bath with mild agitation. The pattern becomes clear very quickly, typically in a couple of minutes. After develop, a functional microvalve is formed.

3. Results

Fig. 4 demonstrates SEM and microscope images of a fabricated microvalve using a single layered SU-8, which includes embedded channels, a microvalve, liquid and gas flow chambers, and etc. Compressed air is supplied to the membrane, and consequently the cantilever and valve are bent open as shown in Fig. 4c. As a result, the flow in the embedded channel is modulated. The compliant cantilever produces the resorting force for the closure of the fluidic channel, once the supply of compressed air is cut.

4. Conclusions

A novel 3D manufacturing approach has been demonstrated to rapid processing of a microvalve using a scanning laser system. The 3D laser processing was carried out by fine tuning focus levels and laser intensity. Various microdevices with designed-in functionalities can be developed in the same fashion.

References

1. H. Yu, A. Grüntzig, Y. Zhao, A. Sharon, B. Li, and X. Zhang, *μTAS 2003*, 347-350.

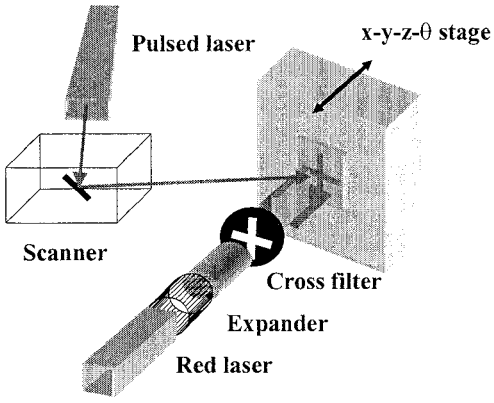

Figure 1. Experimental apparatus.

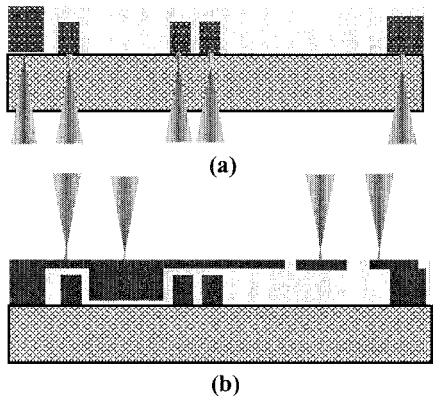

Figure 3. Fabrication of one-layer microvalve: laser writing at different focus levels from backside (a) and front side (b).

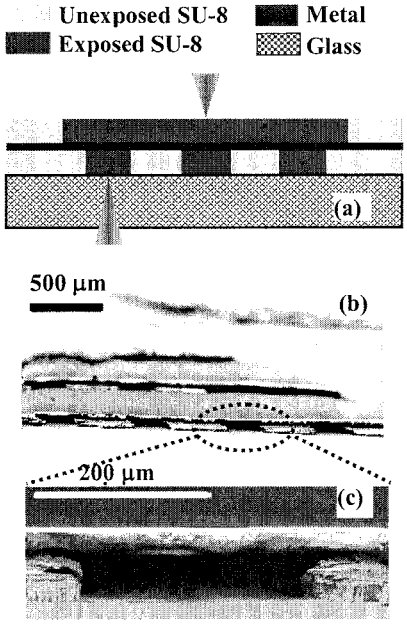

Figure 2. (a) Double-side laser writing on two SU-8 layers with a thin metal interfacial layer in between. (b)&(c) SEM pictures of proof-of-concept double-side-aligned microstructures fabricated using laser pulsing from both sides.

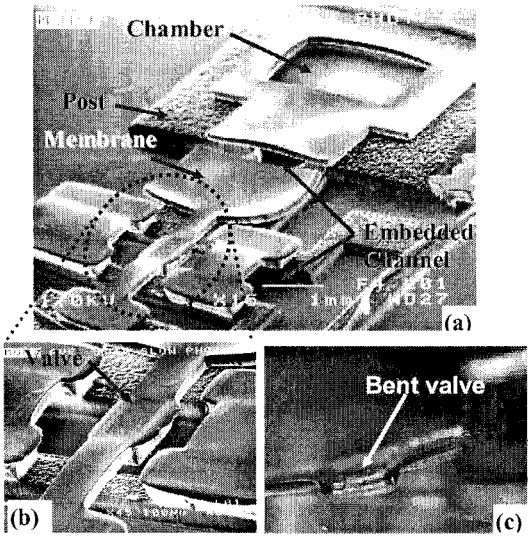

Figure 4. (a)&(b) SEM images of the microvalve fabricated using a single layered SU-8. (c) The valve was lifted open by pressure.

PARAMETRIC STUDY OF PULSED RADIO-FREQUENCY ELECTROPORATION ON MICROCHIPS AT THE SINGLE-CELL LEVEL

Fan YANG[1], Huiqi HE[1], Donald C. Chang[2] and Yi-Kuen LEE[1]
Department of Mechanical Engineering[1], Department of Biology[2]
The Hong Kong University of Science and Technology, Hong Kong

Abstract

In this study, a new micro electroporation cell chip was fabricated by MEMS technology and tested by using cabbage protoplast cells. The fluorescent intensity variations of these cells as a function of the electric pulse amplitude and pulse duration time during the electroporation process were studied in detail at the single-cell level. Large statistical data of the critical voltage can be easily obtained to improve the electroporation efficiency.

Keywords: micro electroporation, protoplast cells, SU-8, parylene, propidium iodide

1. Introduction

Electroporation (EP) is a widely used technique for delivery of drugs, or macromolecules such as DNA to cells and tissues [1]. MEMS-based electroporation devices have many advantages over conventional electroporation system. It can overcome the potential risk of excessively high voltage damage and can provide better transfection efficiency and cell viability [2]. It can use a small amount of cells and genes, and a much simpler cell preparation process. Furthermore, the micro electroporation devices can control electroporation at the single-cell level, which can not be achieved in conventional electroporation systems, such as Bio-Rad Gene Pulser™.

In this study, a new micro electroporation cell chip was fabricated and the electroporation testing was performed using cabbage (Brassica oleracea) protoplast cells at the single-cell level.

2. Design and fabrication

A micro EP cell chip containing an array of 30×20 micro cell chambers and gold electrodes was fabricated on a 4-inch glass wafer (Pyrex 7740) using standard lift-off technique and SU-8 (Microchem Corp., USA) photolithography. The segmented electrodes were made of 20nm sputtered titanium and 500nm gold; they were 30μm wide with 30μm spacing in between (Fig. 1). The depth of the SU-8 photoresist was 30μm, and the width and length of each cell chamber both were 30μm. The surface of the chip was passivated by a parylene thin film (Dix-C®, Daisan Kasei Co., Japan) and treated with oxygen plasma (PDC-002, Harrick Sci. Corp., USA) to enhance the chip performance. Comparing with the flow-through micro electroporation devices in the literature [3-5], our design utilized the concept of large-scale cell array on a chip that was crucial for high-throughput in situ electroporation study. All the materials used were biocompatible and the fabrication process was also IC process compatible. Thus, this chip can be used for large-scale gene transfection and drug screening. The 3D view of the micro electroporation chip is shown in Fig. 1.

3. Experiment Setup

As shown in Fig. 2, the pulsed radio-frequency (RF) electric field with adjustable strength and duration time was applied to the test chips by a Labview program and the NI PCI 6110 DAQ card. The main advantage of utilizing the pulsed RF electric field was to counterbalance the cell-size effect with an opposite effect of cell relaxation, which improved the viability and efficiency of the electroporation [1]. The fluorescent dye (15μg/ml Propidium iodide, Sigma Chem. Co., USA) was used to characterize the EP efficiency. The detection and image acquisition system included an Olympus IX70 inverted fluorescent microscope and a QImaging Retiga 1300C thermoelectric cooled digital CCD camera. The fluorescent intensity variation of the cabbage protoplast cells,

isolated by enzymatic digestion (Serva Co., Germany) to remove the cell wall, was measured as a function of the electric pulse amplitude, pulse duration time and the number of pulse during the EP process. From this parametric study, the critical voltage and electric field to induce single-cell electroporation with different pulse duration time were found.

4. Result and Discussion

In order to understand the micro EP process on the chip, the numerical simulation was also performed by a commercial software (CFD-ACE, CFDRC Corp, USA) for the electric field distribution in the chip, which illustrated the advantage of the non-uniform electric field design for EP (Fig.3). The chip with the non-uniform field provided a new way to study the EP process at the single-cell level with enhanced cell viability, which cannot be achieved in the conventional EP systems.

Since the fluorescent dye molecules can be successfully introduced into the cells on the chip, the electroporation efficiency was high as shown in Fig. 4. The fluorescent intensity variation of the cells as a function of the electric pulse amplitude and pulse duration time during the electroporation were shown in Figs. 4 and 5, it can be found that changing the pulse amplitude and pulse duration time have the similar effect on the fluorescent intensity. Based on Fig. 6, the electroporation process can be divided into three stages. First, the un-elecctroporated stage, where the pulse amplitude was smaller than the critical voltage and the electric field was not strong enough to induce nanoscale pores formed on the cell membrane. Second, the electroporated stage, where the pulse amplitude was above the critical voltage and the dye molecules can transport into the cell through the pores. The critical voltage was different for different pulse duration time. Generally, the critical voltage was lower with longer pulse duration time (In our experiment, the critical voltage was 4 V at 6 ms, while 6 V at 2ms). Third, the saturation stage, where the fluorescent intensity became stable, increase of the voltage can not increase the electroporation efficiency any more. At this stage some cells will undergo lysis. The higher the voltage, the more the cells undergo lysis. In the real application, for the purpose to get both high cell viability and electroporation efficiency, it would be better to choose the voltage near the boundary between the linear and saturation regions.

5. Conclusions

In summary, a new micro electroporation cell chip has been successfully fabricated and tested. From this parametric study, the critical voltage to induce single-cell pulsed RF electroporation was found. In addition, our novel cell-array design can easily provide the large statistical data for determining the critical voltage with the help of digital image processing.

Acknowledgements

This work is supported partially by Hong Kong Research Grant Council through HKUST 6017/02E and by HKUST Institute of Microsystem through I2MS01/02.EG08.

References:

[1] D. C. Chang, *et al.*, *Guide to Electroporation and Electrofusion*, Academic Press, 1992.
[2] S. W. Lee, H. Yowanto and Y. C. Tai, *IEEE MEMS'98*, Heidelberg, Germany, 443-447 (1998).
[3] D.J. Harrison, *et al.*, *MicroTAS'01*, Monterey, California, 10-12 (2001).
[4] Y.-C. Lin, *et al. MicroTAS'02*, Nara, Japan, 847-849 (2002).
[5] Y. Huang, *et al.*, *IEEE MEMS'03*, Kyoto, Japan, 403-406 (2003).

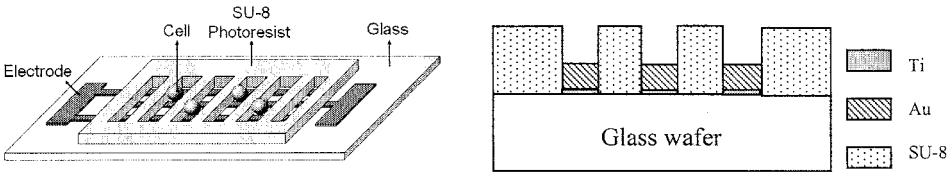

Fig. 1: 3D schematic diagram and cross section of the micro electroporation chip.

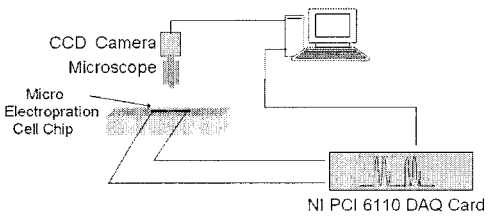

Fig. 2: Micro Electroporation system setup.

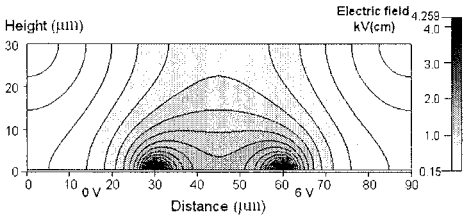

Fig.3: Simulation result of the electric field distribution on a cross section of the chip.

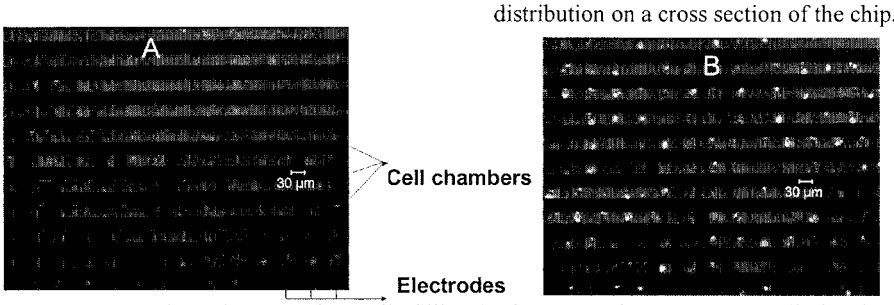

Fig. 4: Micrograph of the protoplast cells filling in the array of 30×20 micro cell chambers on a micro EP chip (only 14×11 can be shown due to limited field of view), (A) before electroporation, the cells are dark under fluorescence mode, (B) cells become white when successfully undergoing electroporation.

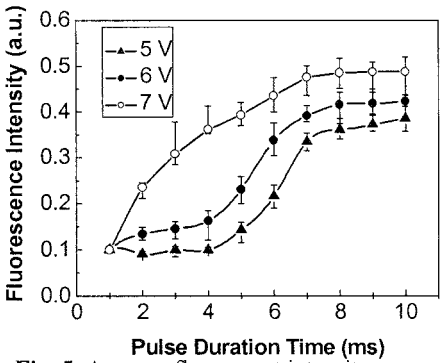

Fig. 5: Average fluorescent intensity as a function of pulse duration time.

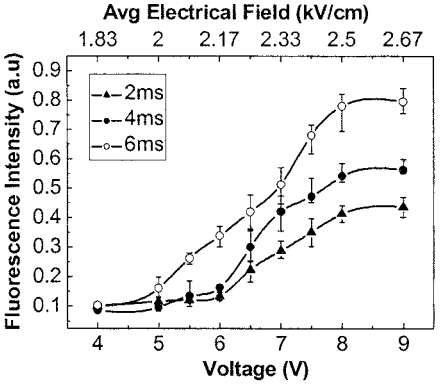

Fig. 6: Average fluorescent intensity as a function of applied voltage.

MICROPUMP EVALUATION FOR CRYOPRESERVATION IN ON-CHIP CELL CULTURE

Yi Zhao, and Xin Zhang

Dept. of Manufacturing Engineering, Boston University, 15 Saint Mary's Street, Brookline, MA 02446, USA

Abstract

This paper presents evaluation of the mechanical performance for a micropump, which is integrated as the active cooling component in an on-chip cell culture platform for cryopreservation. With the obtained pumping rate, the heat balance for the platform can be precisely tuned. The life time of the micro pump can also be estimated from the results of the stress mapping and the fatigue testing. These evaluations will be of help to have the platform follow the desired temperature profile during the cooling and recovery process.

Keywords: cryoperservation, on-chip cell culture, cryogenic micropump

1. Introduction

The emerging microsystem technology integrates in-vitro cell culture platforms on chip, which enables massive parallel cell-based assays. Such platforms are, however, limited by the fact that a series of sizeable and costly equipments (such as – 80 °C refrigerator and liquid nitrogen dewar) are required for long-term cell preservation. These conventional preservation equipments lack in precise control of temperature profile during cooling and recovery process.

We have recently introduced an active cooling system for cryopreservation in on-chip cell culture, which utilizes a silicon-based micropump array to transfer liquid nitrogen from a cryocooler to a customer-designed dual-layered preservation chamber (Figure 1). In this system, the freezing medium with cells is dropped into a micro-molded PDMS piece, which is subsequently placed into the preservation site and covered by a glass slide to prevent drying out. After the chamber is enclosed with a heat insulation cover, liquid nitrogen is filled in for active cooling. As compared to conventional cell preservation techniques, the system requires much less cryogen, and has the capability to maintain the desired temperature profile with a feedback loop.

In the aforementioned system, pumping rate, which heavily depends on mechanical properties of a silicon membrane, is crucial for heat balance. Material reliability of the membrane is another major concern as the cryopreservation system is designed for years-long operation. However, little information was found for these mechanical performances of thin film silicon under cryogenic temperatures. This paper reports pumping rate determination and reliability estimation of the silicon micropump for on-chip cell culture applications. The results of this paper will provide an important insight into the performance and capabilities of silicon as the pump membrane material for on-chip cryopreservation application.

2. Experiments and Results

To imitate the micropump operation condition, a cryogenic pumping rig was designed and built to actuate the silicon membrane with differential pressure (Figure 2). A 3-way solenoid valve connected with a function generator was utilized for actuating at specific frequency, and the fabricated membrane was sandwiched in a two-part sample holder, actuated from the backside. As for the cryogenic measurement, the sample holder was put into contact with the cold finger of a custom-designed cryogenic dewar, which was cooled by filling in liquid nitrogen. The temperature of the membrane was achieved by using a thermometer attached on the cold finger. The membrane deflection was measured by Michelson interferometer through the optical window.

To validate the feasibility, measurement was first performed under room temperature. As the result, measured deflection fairly agrees with the simulation result, indicating a Young's modulus of 163 GPa. In the cryogenic temperature operation, smaller deflection was found as compared to that under room temperature. From the deflection integration upon the membrane area, the pumping rate of the micropump at 77 K is about 70 % of that under room temperature (Figure 3), indicating a much stiffer material. Furthermore, in the reliability study, surface stress was measured using micro-Raman spectroscopy. Since the transverse stress is neglectable due to the fact that the thickness of the membrane is much smaller than the lateral dimension, the top surface can be regarded as a biaxial case, in which stress can be interpreted linearly from Raman shift [1]. As can be seen in Figure 4, compressive stress concentrates in the edge centers while the tensile stress concentrates in membrane center. Assuming a uniform pressure and a uniform thickness over the membrane, stress in the bottom surface has the same profile but in reverse, i.e., the edge centers suffering tensile stress are most vulnerable to fracture. The maximum allowable differential pressure was thus deduced by considering the additional stress induced during the assembling.

Finally, a fatigue test was performed at liquid nitrogen temperature for 1.8×10^6 pressure cycles for longevity assessment. A 30-μm-thick silicon membrane was mounted in a Teflon assembly that was attached to a helium gas bottle. The helium pressure was alternated between 10-psi and 0 using a three-way valve. The valve was actuated by an electric frequency generator operating at 5 Hz. The assembly was lowered into a dewar filled with liquid nitrogen and was operated for ~10 days with 24 hours of operation per day. Inspection at cycling completion showed that no damage had occurred in the membrane, indicating that silicon is a viable material for long-term cell cryopreveration applications.

3. Discussions

It should be noted that the stiffness change of the membrane is greater than the predicted by semiempirical equation [2]. It can be explained as follows. First, Wachtman's equation was based on bulk material, which is averaged over the whole dimension of the subjected specimen. While in the thin film specimen with a shrinking dimension, the mechanical property might be different. Another contribution for the discrepancy is the mismatch of CTE (Coefficient of Thermal Expansion). The mismatch exists not only between the silicon and the sample holder, but also between the silicon membrane and the adjacent bulk silicon, which will induce residual stress as the temperature decreases, and in turn stiffens the membrane.

4. Conclusions

The pumping rate and stress distribution has been demonstrated to evaluate the mechanical performance of a micropump for on-chip cell cryopreservation. The results were compared with theoretical and simulation predicts, and the discrepancy was discussed. This work validates thin film silicon as a viable material to be integrated as an active cooling component for the lab-on-chip applications.

Acknowledgements

This work has been partially supported by NSF CAREER award. The authors would like to thank all the students participated in this project.

References

[1] V. T. Srikar, Anna K. Swan, M. Selim Ünlü, Bennett B. Goldberg, and S. Mark Spearing, *Journal of Microelectromechanical System* **12(6)**, 779-787 (2003).

[2] J. B. Wachtman Jr., W. E. Tefft, D. G. Lam Jr. and Apstein C *Physics Review* **122,** 1754-1759 (1961).

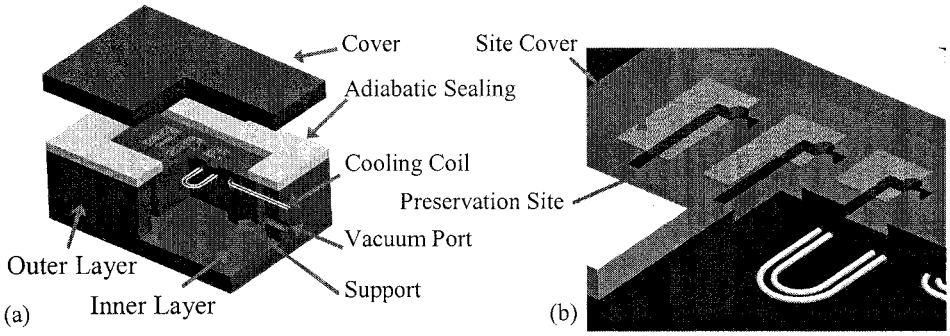

Figure 1. (a) Schematic of dual-layered cryopreservation chamber for on-chip cell culture. (b) PDMS slide with freezing medium was placed into preservation site and covered to prevent drying out during cryopreservation.

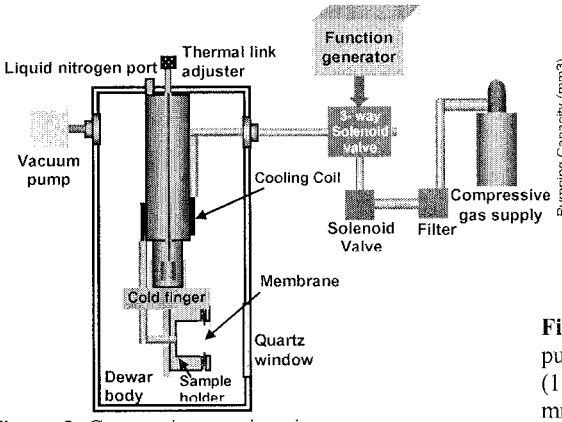

Figure 2. Cryogenic pumping rig.

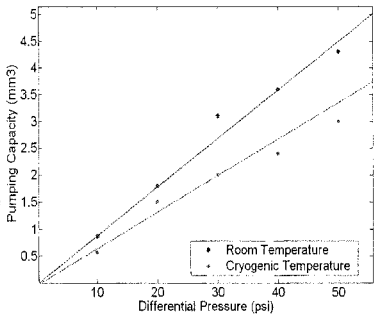

Figure 3. During a single cycle, the pumping rate of a 6 mm^2 membrane (110 micrometers in thickness) is 0.24 mm^3 under 77 K, compared to 0.36 mm^3 under room temperature.

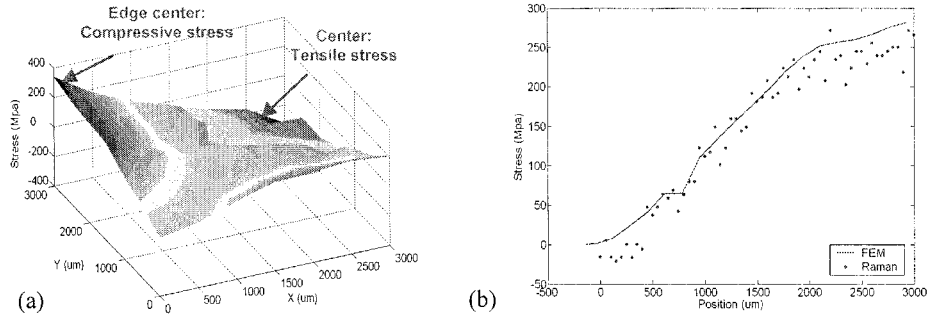

Figure 4. (a) From micro-Raman mapping, in the top surface of the membrane, compressive stress concentrates in edge centers while tensile stress concentrates in membrane center. (b) Line scanning conducted from membrane corner to edge center shows a good agreement with the FEM simulation.

CREATION OF MONODISPERSED TWO-COLOR PARTICLES USING MICROCHANNELS

Takanori Takahashi[1], Youichi Takizawa[1], Takasi Nisisako[2] Toru Torii[2] and Toshiro Higuchi[2]
[1]Soken Chemical &Engineering Co., Ltd., 1-13-1, Hirose-Higashi, Sayama-shi, Saitama 350-1320, Japan
[2]Department of Precision Engineering, Graduate School of Engineering, The University of Tokyo 7-3-1 Hongo, bunkyo-ku, Tokyo, 113-8656, Japan

Abstract

This paper describes a novel technique for the creation of monodispersed two-color particles using microchannels. As the dispersed phase, monomer liquids containing pigments such as carbon black/titanium oxide were infused into separate approaches to macro-channels. As the continuous phase, polyvinyl alcohol aqueous solution was injected into the different approaches to the macro-channels. Clearly-separated two-color dispersed phase flow was set up at a micro Y-junction and, two-color droplets were reproducibly generated in confluent microflow of the continuous phase flow. These droplets were then polymerized to give two-color particles suitable for applications such as electronic paper. The resulting microspheres are highly monodisperse (CV:0.5-3.0%).

Keywords: two-color particles, micro-fluidics, micro-channel, monodisperse

1. Introduction

Electronic paper is being developed as a display device for the future. Fine particles called twisting balls, which have two colors in equal amount, are used for the display; these are useful materials because of their reversibility and display properties [1]. Nisisako et al. applied the creation of monodispersed fine particles using micro-channels so as to produce monodispersed fine display particles divided into two colors [2]. We have since successfully made monodispersed fine particles that are divided exactly into two hemispheres of different color using newly-devised micro channels. This paper reports the creation of monodispersed two-color fine particles for display, and investigates its relation to the flow channel geometry, the flow velocity and other parameters of the microchannels, as a further application of electrostatic control.

2. Experimental

Microchannels having two types of minute flow channels, with intersection angles of 135° and 45° between the continuous phase and the dispersed phase, were machined from quartz glass plates of size 15 mm x 25 mm x 4 mm to produce droplet creation chips (called chip X and chip Y respectively). The flow channel width is 100 to 200 μm, with a constant flow speed, and the flow channel depth is 100 μm except for the drain part. Acryl monomers of two pigments (carbon black and titanium oxide white) were used as the dispersed phase, and the continuous phase was polyvinyl alcohol (PVA) dissolved in water as stabilizer for the dispersion of macromolecules. Details of the flow for the formation of two-color particles is as follows: the dispersed flows of the separate monomers colored black and white meet at a Y-shaped intersection. This becomes a parallel two-color flow in which the colors do not mix because of the low Reynolds number. Then, at the intersection of the continuous phase and the dispersed phase, two-colored monomer droplets are created by the shear force of the fluid in the continuous phase.

A new glass chip fabrication process, using a stamp made in a LIGA process (Optnics precision co., ltd.), was examined. The chip material is low-melting-point glass plates of size 18 mm x 18 mm x 3 mm. The flow channel width is 60 to 120 μm, and depth is 60 μm.

Finally, the created droplets become particles upon polymerization. An optical microscope and a high-speed camera were used to confirm droplet formation, and the particle parameters – size, shape, color – were verified from the images obtained.

3. Results and discussion

It proved possible to arrange that the two monomer phases continue to flow as laminar flows without mixing after joining each other, and that fine two-colored droplets are formed at fixed intervals at the junction of the continuous flows. Fig. 1 shows droplet formation in the microchannel. Bicolored fine particles then were produced by removing the droplets from the chip and subjecting them to polymerization. Fig. 2 shows the change in the mean diameter of the droplets with the mean flow velocity of the continuous phase at a constant flow volume (0.2 ml/h) of the dispersed phase. It is apparent that the droplet diameter for chip X and chip Y changes according to the mean flow velocity of the continuous phase. Also, chip Y tends to produce particles with a smaller diameter than chip X. With a continuous phase flow velocity of 11.1 cm/s, the particle size at this time had a coefficient of standard deviation value of 1.60% for the X-shaped chip and 1.76% for the Y-shaped chip. Similar good CV values can therefore be obtained even with different shapes. Fig. 3 shows a photo of the resulting monodispersed two-color particles.
Fig.4 is a schematic diagram of a multi-channel structure suitable for mass production. Fig.5 shows droplet formation in the microchannel made using the LIGA process.

4. Conclusions

We have successfully created monodispersed two color particles by a potentially important new method in a microchannel. The microchannel is made by a LIGA process. We next propose to reduce the particle size further and gear up the methods for industrial production.

Acknowledgements

Part of this research was supported financially by grants from the JST (Technology Transfer Facilitation Program, Cultivation Program B).

References

[1] N. K. Sheridon et al., Journal of the SID, 7(2), 141-144 (1999).
[2] T. Nisisako, T. Toru, T. Higuchi, Book of Abstracts, 7th International Conference on Microreaction Technology, Lausanne, Switzerland, 51-53 (2003).

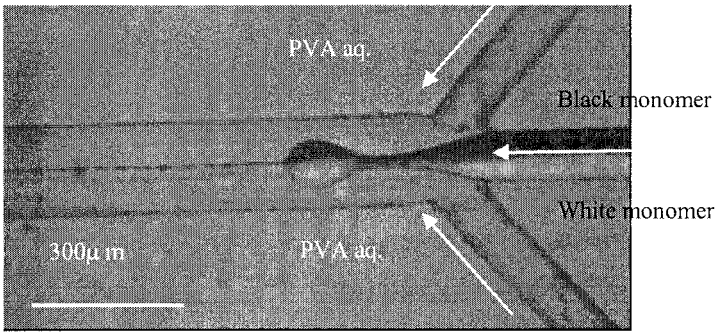

Figure 1. Schematic of droplet formation at a Y-junction

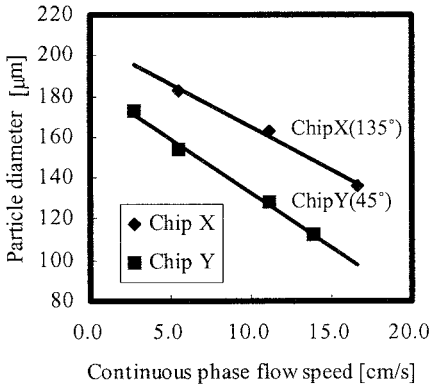

Figure 2. Effect of continuous phase flow on the size of droplets generated in microchannels.

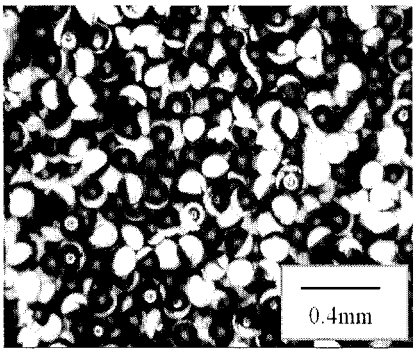

Figure 3. Monodispersed two-color particle.

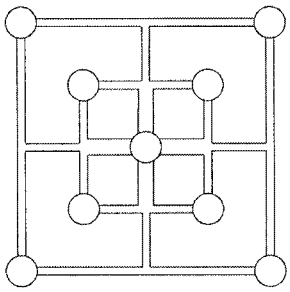

Figure 4. Schematic of channel patterns on glass chip for mass production.

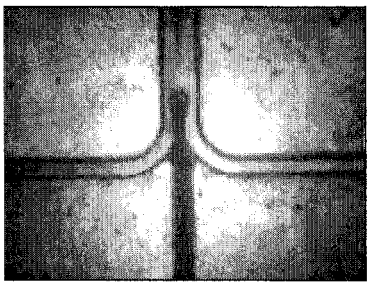

Figure 5. Droplet formation in a microchannel made using the LIGA process. (Optnics precision corporation produced the glass chip.)

SELECTIVE SURFACE MODIFICATION OF THE PERFLUORO POLYMER PASSIVATED PDMS MICROSTRUCTURE

Daisuke Uchida[1], Masaki Kanai[1, 2], Takahiro Nishimoto[2] and Shuichi Shoji[1]
[1]Major in Nanoscience and Engineering, Waseda University, 3-4-1, Tokyo, Japan
[2]Technology Research Laboratory, Shimadzu Corporation, Kyoto, Japan
(E-mail:uchida@shoji.comm.waseda.ac.jp)

Abstract
We propose the selective surface modification of the perfluoro polymer passivated PDMS microfluidic devices. Perfluoro polymer passivation is quite useful to solve the problems found in PDMS microfluidic devices. In order to apply practical functions to the perfluoro polymer surface, we investigated surface wettability and chemical composition of the surface after oxygen plasma treatment and curing. To achieve selective surface modification of the 3D structure, we utilize a silicon shadow mask formed by deep-RIE etching. We also demonstrate selective deposition and etching using the shadow mask.
Keywords: PDMS, perfluoro amorphous polymer, Surface modification, 3D shadow mask

1. Introduction

In recent years, PDMS is one of the most commonly used materials as well as conventional materials of silicon and glass in μTAS and Lab-on-a-chip. However, PDMS has two significant problems in practical chemical and bio-chemical applications. One is surface degradation with organic solvents and the other is unexpected adsorption of chemicals and bio-materials. To overcome these problems, we reported perfluoro amorphous polymer passivating on the PDMS microfluidic devices [1]. In this paper, in order to apply further functions to the device, selective surface modification of the perfluoro passivation membrane is described. To control the surface state of the membrane, we investigate the surface properties after oxygen plasma treatments. Selective surface modification methods applicable for the 3D microstructures are also described.

2. Concept of selective surface modification

Fig.1 (a) shows the schematic concept of the selective surface modification of the perfluoro polymer membrane on a PDMS microstructure. Perfluoro polymer (CYTOP, Asahi Glass Company, Japan) is coated by spin or dip coating from sub-micron to several microns in thickness. The silicon 3D shadow mask fabricated by deep-RIE is applied for selective surface modifications. The shadow mask structure was formed to be closely fit to the perfluoro polymer passivated PDMS microstructure. It realized good alignment between the mask and the PDMS microstructure. Oxygen plasma modifies objective area of the perfluoro passivated surface through apertures of the silicon 3D shadow mask. This method can be also applied for deposition of the metal (Fig.1 (b)) and selective etching (Fig.1 (a)).

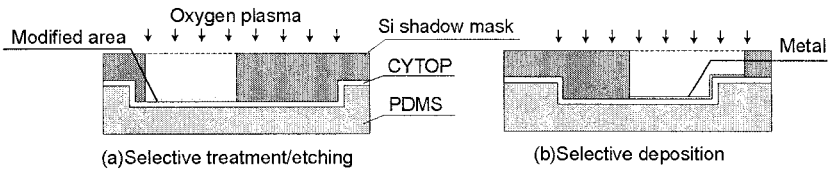

Fig.1 Concept of the selective surface modification

3. Experiments and results

We investigated surface conditions of the perfluoro polymer after oxygen plasma treatment and curing by measuring the contact angle of DI water droplet. XPS (X-ray Photoelectron Spectroscopy) surface analysis was also performed. Fig.2 (a) shows the result of the contact angle dependency on RF power of the oxygen plasma treatment (RIE-10NR, SAMCO International Inc. Japan). The surface state changes to more hydrophilic under the lower RF power. This indicates that the surface treatment is effective for surface modification under lower RF power. While under higher RF power larger than 100W the surface changes to more hydrophobic compared to the original state. Fig.2 (b) shows the O1s narrow spectrums of XPS scanning on the perfluoro polymer surface with/without oxygen plasma treatment. Since the original CYTOP contains only C-O bond of the oxygen content, the XPS spectrum of non-treated CYTOP shows single peak. Under any treatment conditions, small peak was observed beside the main peak. This peak was considered to be the C=O bond generated by oxygen plasma. Significant difference was not observed under these different conditions. The change of the chemical composition is not strongly dependent on the RF power. We considered Oxygen plasma treatment to enhance the surface roughness at high RF power conditions.

Fig.3 (a) shows the contact angle after the thermal annealing. Oxygen plasma treatments at 25W were applied all the samples before annealing. Fig.3 (b) shows the O1s spectrums of the CYTOP annealed at 85°C and 200°C. Height of the C=O bond peak was reduced by annealing at 200°C. From these results, the surface condition recovered to the original state at the high annealing temperature.

In order to evaluate long term stability of the modified surface, we measured the time variations of the contact angle of the plasma treated perfluoro polymer and PDMS. These results are shown in Fig.4. Plasma treated PDMS surface recovered to the original state, while the CYTOP surface kept the treated state.

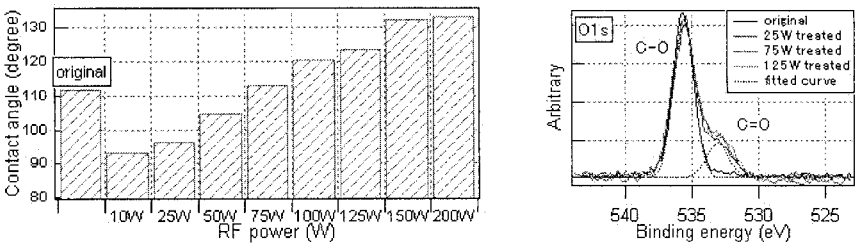

(a) Contact angle (b) O1s XPS spectrum

Fig.2 Surface condition dependency on RF power of the oxygen plasma

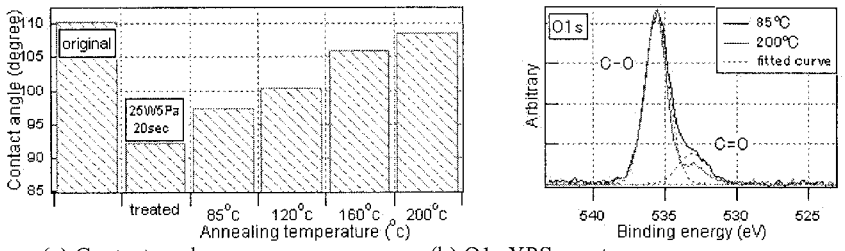

(a) Contact angle (b) O1s XPS spectrum

Fig.3 Surface condition dependency on annealing temperature after treatment

4. Applications of the selective surface modification

We demonstrated two kinds of surface modification methods of selective metal deposition (Fig.1 (a)) and selective etching (Fig.1 (b)) using silicon 3D shadow mask. Fig.5 (a) shows the photograph of the selective Au metallization on the perfluoro polymer passivated PDMS cavity.

Fig.5 (b) shows the selective etching of perfluoro polymer coated on the metal electrodes. The embedded electrode in the perfluoro passivation layer is partly exposed. Combination of these two methods enables fabrication of the detecting electrodes on 3D perfluoro polymer passivated PDMS microstructures.

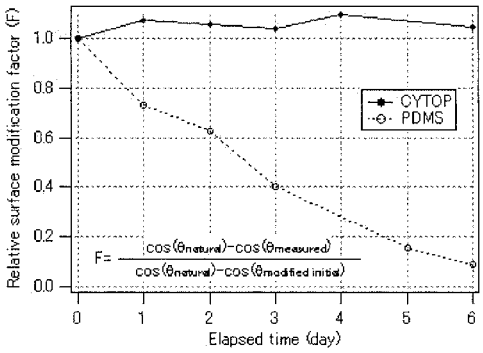

Fig.4 Time dependency of the contact angles

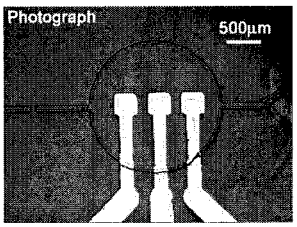

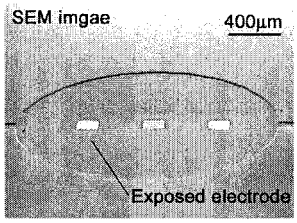

(a) Selective metallization (b) Selective etching

Fig.5 Applications of the selective surface modification using 3D shadow masks

5. Conclusions

Features of oxygen plasma treatment and succeeding thermal annealing of perfluoro polymer passivated PDMS were studied. Hydrophilic surface state is obtained at low RF power while more hydrophobic one than the original is observed at high RF power. These reasons are still investigated. Selective metal deposition and selective etching of the passivated perfluoro polymer membrane using 3D shadow masks are also proposed. These methods are useful for fabricating functional 3D perfluoro polymer passivated PDMS microfluidic devices.

Acknowledgements

This work was partly supported by Japan Ministry of Education, Culture, Sports Science & Technology Grant-in-Aid for COE Research and 21st COE of Waseda University, Scientific Basic Research (A) No. 12450167 and Japan Society for the Promotion Science Grant-in-Aid for Creative Scientific Research No. 13GS0024.

References

[1] M.Kanai, S.Shoji, , 7th Int. *Conf. on Micro Total Analysis Systems*, Vol. 1, pp429-432 (2003)
[2]CYTOP Technical Report, Asahi Glass Co., Ltd., Japan (1997)
[3]R. Q. Liang, et al. , *Surface & Coating Technology*, Vol.131, pp294-299 (2000)
[4]K. Tanaka, et al., *International Journal of Adhesion & adhesives*, Vol23, pp515-519 (2003)

A WET CHEMICAL TREATMENT FOR SPECIFIC CHANGE OF CONTACT ANGLE OF SU-8

Maria Nordström, Rodolphe Marie, Montserrat Calleja and Anja Boisen
MIC - Department of Micro and Nanotechnology, Technical University of Denmark, Bldg 345 east, DK 2800 Kongens Lyngby, Denmark

Abstract

A simple method is presented to reduce the contact angle of the photo-resist SU-8. Cross-linked SU-8 has a hydrophobic surface and there is an inverse relation between the contact angle and capillary pressure. If the surface of a micro channel is hydrophilic, the capillary pressure can be used as the only means to drive the liquid through the channels and the need for external pumps can be avoided. This is very useful, especially in the fabrication of devices for 'Lab-on-a-chip' where it is important to keep the design as simple as possible. Using a wet chemical treatment, a selective change in contact angle between different areas of a micro channel system can be achieved, without the need to involve different materials in the fabrication process.

Keywords: SU-8, contact angle, hydrophilic, ethanolamine, liquid handling

1. Introduction

SU-8 is a negative photo-resist offering a fast, easy and cheap processing and it is a material well suited for micro channel fabrication. However, its surface is of hydrophobic character, which is a drawback when it comes to channel fabrication, as bulky pumping devices need to be incorporated in the packaging of the final device. The standard method of reducing the contact angle of SU-8 is to treat the sample with an O_2 plasma [1]. A method of modifying the SU-8 polymer prior to the structuring has also been presented [2]. However, these methods will alter the contact angle over the complete structured area. Using a wet treatment instead allows for a selective change for monolithic micro channel systems.

2. Theory

On the surface of cross-linked SU-8, there will always be some epoxy groups, which are left non-reacted after the cross-linking step of the polymer. These contribute to making the SU-8 surface hydrophobic. By letting molecules with hydrophilic end groups form a monolayer on the surface, the contact angle of the surface can be reduced. The fabricated structures are intended to be used as portable point-of-care devices and need to be released from the Si carrier wafer. The technique used is an "Enhanced Sacrificial Layer Etch" [3] where a layer of Cr is selectively etched, releasing the SU-8 structures. After release of the structures from the Si-wafer, the measured contact angle was $50 \mp 2°$. However, a further decrease of the contact angle is necessary to ensure a sufficiently strong capillary force to transport the liquid solutes through larger sections of the micro channel network, figure 1. Ethanolamine is proposed to be the working molecule of this further decrease by forming a hydrophilic, stable monolayer.

3. Experimental

The experiments were carried out at 21°C, relative humidity of 49 % and pressure of 1 atm. We have chosen DI water as our test liquid as most liquids used for biochemical detection are aqueous solutions. The contact angle was measured with a Contact Angle Meter (Tantec) using the half angle method [4]. The SU-8 samples used for the investigation consisted of 5 mm *x* 7 mm squares with a thickness of 160 µm. These were structured by standard spin-coating and UV lithography processes. The SU-8 samples were divided into batches of five samples each. The effect of each treatment was investigated by four batches, leading to a total of 80 data points collected for each varied treatment. It is only the average value for the contact angle that is presented in the graphs and

standard deviation is used as error analysis. A 0.7 μL water droplet was placed on the substrate surface and the resulting contact angle was measured directly, by observing the angle between the liquid and the substrate through the apparatus. It is assumed it is the *static* contact angle that is measured, as no movement of the droplet or changes in the value of the contact angle could be observed.

The samples had their contact angle measured prior to starting the experiment. The samples were then soaked in 10 mL of 100 mM ethanolamine for different periods of times: 5 min, 10 min and 20 min at 50 °C. The samples were dried with nitrogen flow. The contact angle was measured again for each sample after the treatment. To remove the excess ethanolamine that was not strongly bound to the SU-8, the samples were washed in sodium phosphate buffer in ultra sound for 10 min and afterwards the contact angle measurements were repeated. PMMA was also treated with ethanolamine and washed in ultra sound.

4. Results and discussion

As can be seen in figure 2, initially SU-8 is of hydrophobic character with a contact angle of ~90°. No significant change in the contact angle is observed during development in PGMEA, as expected. After release of the structures from the Si-wafer, the measured contact angle was 50 ∓ 2°. The Cr layer is etched by cericammoniumnitrate (CAN) in acetic acid in which the wafer is left over-night. CAN is known to act as a catalyst in the breaking of epoxy rings [5, 6] especially in the presence of acetic acid. We believe that CAN attacks and opens the epoxy groups, which then react with O_2 from the environment. The contact angle is decreased even further after the treatment with the molecule ethanolamine. We believe this results from the known reaction between amine groups and epoxy groups, which would result in even more –OH groups present on the surface of the SU-8 and an even greater reduction in θ. No noticeable change in contact angle occurs after washing in sodium phosphate buffer using ultrasonic agitation, indicating a strong bond between ethanolamine and SU-8.The contact angle is measured again, 20 days after the initial experiment. None of the samples have had their contact angle increased back to the initial value after this long period of time. This indicates a stable change of the contact angle after ethanolamine treatment.

5. Conclusions

An easy method of decreasing the contact angle of the hydrophobic photo-resist SU-8 has been presented. Only a 10 min treatment in a relatively harmless solution of ethanolamine after release from the Si wafer is needed. The method is easy and can be applied just prior to use of the channel. Reducing the contact angle leads to increases in the capillary pressure in micro channels. This phenomenon can be used for realising simple micro channel systems in SU-8 relying solely on capillary pressure for the transportation of liquids. SU-8 is well suited to be used in the fabrication of micro channels for bio/chemical applications due to its high chemical resistance.

Acknowledgements

We thank Prof. Martin Dufva at MIC, DTU for his chemistry expertise and Process Engineer Christian Wang at SonionMEMS for use and instructions of the Tantec equipment. M. Calleja acknowledges financial support via a Marie Curie Fellowship.

References

[1] S A Pirzada, A Yializis, W Decker and R E Ellwanger, *Proceedings of the 42nd Annual Technical Conference – Society of Vacuum Coaters,* pp.301-306 (1999)

[2] C-L Wu, M-H Chen and F-G Tseng, *Proceedings of the 7th International Conference on Miniaturixed Chemical and Biochemical Analysis Systems,* pp. 1117-1120 (2003)

[3] G Genolet, *PhD Thesis École Polytechnique Fédérale de Lausanne* (2001)

[4] US Patent number 5,268,733
[5] N Iranpoor , I M Baltork and F S Zardaloo, *Tetrahedron,* **47,** 9861-9866 (1991)
[6] N Iranpoor and P Salehi, *Tetrahedron,* **51,** 909-912 (1995)

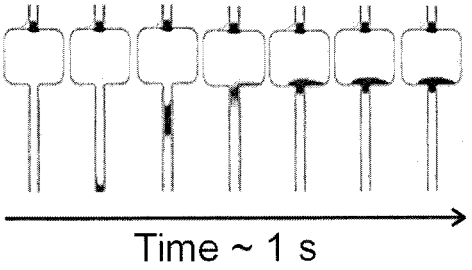

Figure 1. The water can be seen to stop just after entering into the measuring sites of this micro channel system. With a contact angle of 50 ° the capillary pressure is not strong enough to drive the liquid through. Another column of water is seen at the top of the picture. The width of the micro channel is 100 μm and the measuring sites have a width of 600 μm.

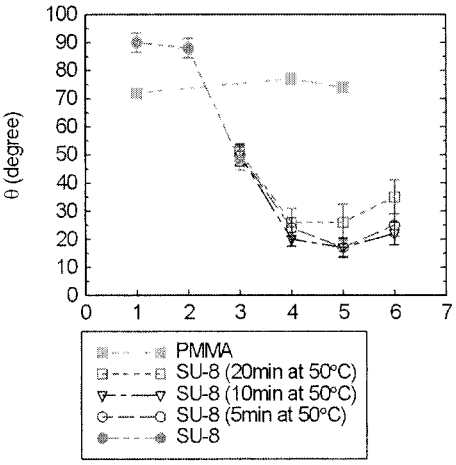

Figure 2. The number on the x-axis denotes events: 1-No treatment, 2-Development in PGMEA, 3-Release off Si wafer, 4-Ethanolamine treatment, 5-Washing in ultra sound, 6-20 days after the treatment.

DEVELOPMENT OF A METHOD OF SURFACE MODIFICATION FOR MICROCHANNELS

Daiyu Okafuji[1], Hideaki Hisamoto[1,2], Masaharu Ueno[1,2] and Takehiko Kitamori[1,2]

[1]Dept. of Applied Chemistry, The University of Tokyo, 7-3-1 Hongo, Bunkyo, Tokyo, Japan
[2]Integrated Chemistry Project, Kanagawa Academy of Science and Technology, KSP, 3-2-1 Sakado, Takatsu, Kawasaki, Kanagawa, Japan

Abstract

We developed a method of surface modification to prevent adsorption of precipitations to wall of glass microchannels. Some kinds of acrylate monomer were polymerized from immobilized polymerization initiator on the channel surface in this method. Because polymer chain was chemically bonded to silane group on the channel surface, the modified polymer layer had high durability to acid or base. Effectiveness of the modification was demonstrated in adsorption prevention of iron(III) hydroxide provided in the modified microchannel while iron(III) hydroxide immediately adsorbed to a non-modified microchannel.

Key words: Microchip, Surface modification, Radical polymerization, Prevention of adsorption, Precipitation reaction

1. Introduction

Microchannels in microchips have characteristics such as large specific interface area and short diffusion distance. By utilizing these characteristics, rapid chemical processing has been proved in several applications such as solvent extraction [1], phase transfer reactions [2, 3], etc. Moreover, it is expected that a microchip is added various kinds of functions (addition of catalyst, control of flows, etc.) by surface modification of a microchannel. On the other hand, when we synthesize organic compounds in a microchip, it often happens that precipitations adsorb from reagents to the channel surface. The adsorption to the channel surface makes solid plugs in the microchannel to stop up flows. One of methods to prevent adsorption of precipitations is surface modification to reduce surface energy (Fig. 1). However, conventional methods have some problems. Fluorocarbon resin coating is easy to peel off because resin weakly sticks to the surface by physical adsorption. Chemical modification by silane doesn't have durability to acid or base because silane layer is weak. To remove these disadvantages, polymer layer was bonded to the channel surface chemically by a method of surface modification utilizing radical polymerization. Because polymer layer inhibits contact of acid or base, silane-oxygen bonds are protected from hydrolysis. Fig. 2 shows the resume of a method of the surface modification.

In this work, we developed a method of surface modification of microchannels. And we synthesized iron(III) hydroxide in the modified microchannel to demonstrate effectiveness of the modification to adsorption prevention.

2. Experimental

We modified a microchannel by the following process. First, an ethanol solution of 3-aminopropyltriethoxysilane (1 wt %) was introduced into the microchannel under a constant flow condition (1 μL/min) for 17 h. After 17 h, pure ethanol was introduced for a washing. Then a 1,2-dichloroethane solution of 4,4'-Azobis(4-cyanovaleic acid chloride) (1 wt %) was introduced into the microchannel under a constant flow condition (10 μL/min) for 1.7 h. Then a solution of tridecafluorooctyl acrylate which contains AIBN (1 wt %) and ethanol (10 wt %) was introduced into the microchannel and stopped. After the microchannel is filled with the solution, UV light was

irradiated to the microchannel for 20 min. After 20 min., the solution was drained for a few minutes in order to prevent caking of the solution. These operations were repeated for five times. Then pure ethanol and pure trifluoroethanol was introduced into the microchannel for a washing. Remarkable point of this method was radical polymerization proceeded not only in the channel but also on the surface of glass.

In the modified microchannel, we synthesized iron(III) hydroxide. The microscale reaction was performed by introducing an aqueous solution 2×10^{-3} M iron(III) chloride and an aqueous solution of 0.2 M NaOH through two inlets of the microchip under a constant flow condition (50 μl/min). Fig. 4a shows illustration of experimental condition.

3. Results and discussion

Figure 3 shows SEM images of the cross-section of the modified microchannel. Layer of polymer was observed at the channel surface. Thickness of layer was about 200 nm.

When using non-modified microchannel, iron(III) hydroxide adsorbed to the channel surface, solid plugs were produced and flows stopped up after 14 min. In the case of silane coated microchannel which is usual method to reduce surface energy of the channel, iron(III) hydroxide adsorbed gradually to the channel surface and flows stopped up after 31 min. It is expected that silane layer peeled off because of hydrolysis by base. When using the microchannel modified by new method, iron(III) hydroxide adsorbed to the channel surface at a slow pace. Figs. 4b and 4c show appearances of non-modified and modified microchannel after 14 min from introduction of solutions. In the non-modified channel precipitation adsorbed to the whole surface of channel, while in the modified microchannel precipitation adsorption was inhibited. Furthermore, adsorbed precipitations readily peeled off by flows (Figs. 4d and 4e). And we successfully introduced solutions over 150 min without stopping of flows.

4. Conclusions

In conclusion, we developed a method of surface modification and demonstrated that this method is effective to prevention of precipitation adsorption under basic condition. This water and oil repellent surface is applicable to other kinds of organic syntheses producing precipitation, separation process of gas phase and liquid phase [4], etc. Furthermore we think that it is enabled to add a microchannel various kinds of functions such as immobilized catalyst, control of flows, etc. by selecting monomer suitably.

References

[1] M. Tokeshi, T. Minagawa and T. Kitamori, *J. Chromatogr. A* 2000, 894, 19.

[2] H. Hisamoto, T. Saito, M. Tokeshi, A. Hibara and T. Kitamori, *Chem. Commun.* 2001, 2662.

[3] M. Ueno, H. Hisamoto, T. Kitamori and S. Kobayashi, *Chem. Commun.* 2003, 936.

[4] A. Hibara, S. Iwayama, M. Ueno, Y. Kikutani, M. Tokeshi and T. Kitamori, *Proceedings of the μTAS 2004 Symposium* 2004.

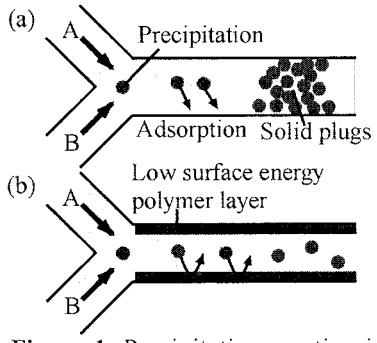

Figure 1. Precipitation reaction in microchannels. (a) Case of using the non-modified microchannel. (b) Case of using the modified microchannel.

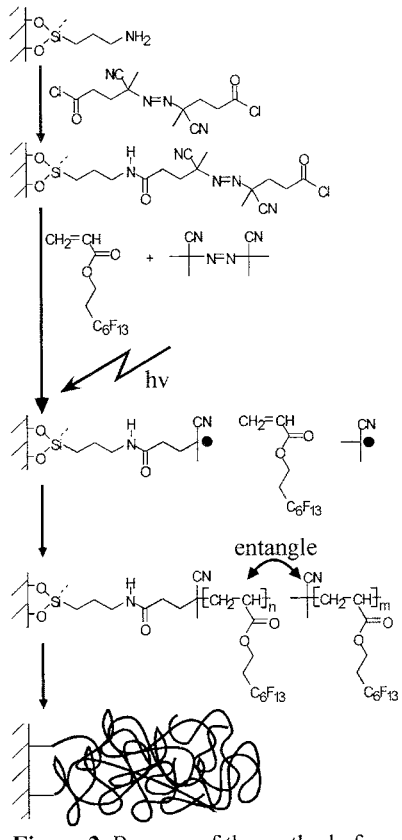

Figure 2. Resume of the method of surface modification.

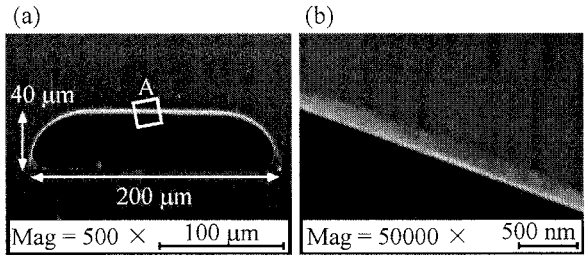

Figure 3. (a) SEM of cross-section of the modified microchannel. (b) SEM of 50000× magnification of the area in the quadrilateral A denoted in (a).

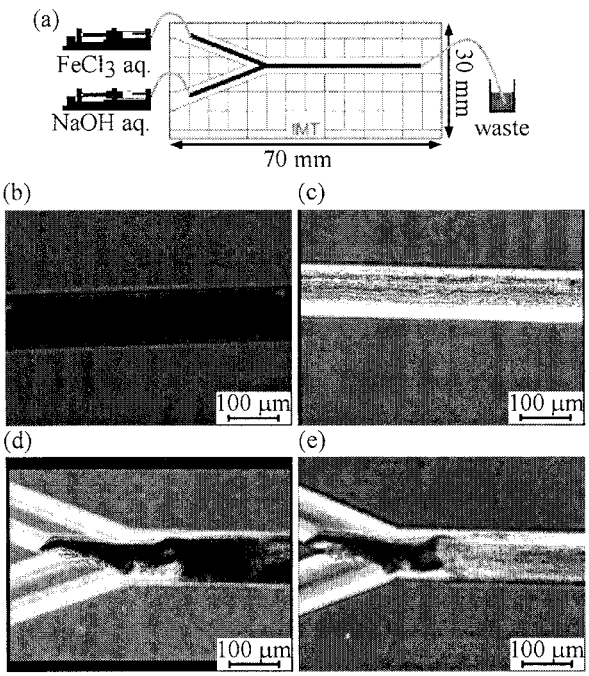

Figure 4. (a) Illustration of experimental condition. (b) The appearance of the non-modified microchannel after 14 minutes from introduction of solutions. (c) The appearance of the modified microchannel after 14 minutes from introduction of solutions. (d) The appearance of the modified channel after 100 minutes from introduction of solutions. Adsorption of precipitation is observed. (e) The appearance of the channel after precipitation peeled off.

DEVELOPMENT OF A NEW METHOD TO IMMOBILIZE CATALYSTS BY SURFACE MODIFICATION IN MICROSPACE

Yusuke Kobayashi[1], Masaharu Ueno[1], Shū Kobayashi[2] and Takehiko Kitamori[1,3]
[1] *Department of Applied Chemistry, School of Engineering, The University of Tokyo*
[2] *Graduate School of Pharmaceutical Sciences, The University of Tokyo*
[3] *Kanagawa Academy of Science and Technology (KAST)*

Abstract

Geometry of microchannels having large S/V ratio is basically preferable to surface catalysts. But it is known that reactivity is often reduced, when catalysts are immobilized directly to silica or polymer by chemical bond. We developed a new method to immobilize catalysts using affinity of fluorine. The surface of glass was silanized by perfluoro-octadecylsilane, and the catalyst which has fluorized carbon chain as counter anion was immobilized there. We applied this method to the wall of microchannel, and carried out aldol reaction of benzaldehyde with silyl enol ether. We determined quantity of the metal Sc of catalyst per unit area by ICP analysis. When we used a 0.1 mol % Sc catalyst immobilized to microchannel, catalyst turnover were more than 180 times in 5 min. This catalyst immobilized to microchannel was reactive than bulk condition, and we could obtain desilylated product directly.

Keywords : Surface modification, Lewis acid catalyst, Aldol reaction, Affinity, Immobilize

1. Introduction

Recently, there are many reports of synthesis in microspace. However, as for the organic synthesis using catalysts [1], separation of catalysts is indispensable, and reuse of these catalysts is difficult. However, the technique of immobilization of catalysts and applying it for synthesis are very difficult, so there are very few examples of a report [2]. If the methodology of immobilizing catalysts for organic synthesis can be established, it can realize an ideal reactor and the application range will increasingly spread. Then, we thought it was necessary to develop a new method to immobilize catalysts to the glass surface of the wall in microchannel.

2. Theory

Surface modification of glass by octadecylsilane (ODS) etc. has been performed widely. If it can process to the surface layer which can immobilize catalysts, it will become possible to immobilize by the affinity of the surface layer and catalysts rather than to immobilize directly, and the patterning and re-immobilizing will become easy (Fig. 1).

We took advantage of affinity of fluorine from the viewpoint of the propriety of use of an organic solvent, and the difficulty of immobilization. Scandium nonaflates ($Sc(ONf)_3$) (Fig. 2) as a catalyst which has fluorized carbon chain as counter anion and perfluoro-octadecylsilane as a surface layer were employed. As scandium nonaflates is a Lewis acid catalyst which is strong in aqueous condition, it can be applicated to organic synthesis without reduction of activity in water.

3. Experimental

1) Surface modification and immobilization of the catalyst

At first, 10 wt% Perfluoro-decyltriethoxysilane/EtOH solution was pumped into the microchannel one whole day, and the glass surface of wall was silanized. Furthermore, 10 wt% $Sc(ONf)_3/CH_3CN$ solution was pumped, and the catalyst was immobilized.

2) Application to organic synthesis

Aldol reaction of benzaldehyde with silyl enol ether using immobilized $Sc(ONf)_3$ (Scheme 1) was examined in the microchannel (Fig. 3).

3) Quantitative determination of catalyst

The surface of 3cmx7cm glass board was processed from the same operation as 1). And, whole silane layer which was immobilizing catalysts was efoliated by 0.1 M NaOHaq. Then, quantity of the metal Sc per unit area was determined by ICP analysis.

4. Results and discussion

The product of the reaction was detected by HPLC (Table 1). Investigation of the reactivity proved the success of immobilization of $Sc(ONf)_3$. This reaction gave the two kind of corresponding aldol products, especially OH-formed product **4** is target product. While the reaction in bulk scale gave only the trimethyl silyl protected aldol product **3**, the reaction in microchannel which immobilized $Sc(ONf)_3$ gave only the target aldol product **4** (Fig. 4).

The amount of scandium atom of immobilized catalyst fixed from the result of ICP was 0.11 μg Sc/cm^2. When this is converted into the solution concentration, it is equivalent to $1.1x10^{-4}$ M. In bulk scale synthesis at this amount of catalysts, yield was up to only 8 % by reaction time 5 min, while the yield in microchannel was 18 % by the same reaction time.

This result proved effective use of the surface of wall in microspace, and improvement in turnover of catalyst. OH-formed product which was not given in bulk scale was directry formed. This also suggests the change of catalyst structure.

5. Conclusions

A new method to immobilize a Lewis acid catalyst was successfully developed and the process of organic synthesis using the immobilized catalyst was integrated on a microchip with continuous reagent flow. We concluded the system will become practicable by improvements of the system, detailed optimization, and mass production by piled microchips.

References

[1] Fletcher PDI, Haswell S.J., Pombo-Villar E, et al. : TETRAHEDRON 58: (24) 4735-4757 JUN 10 2002

[2] S.J.Haswell et al. : Anal. Chem. 74, 2623 (2002)

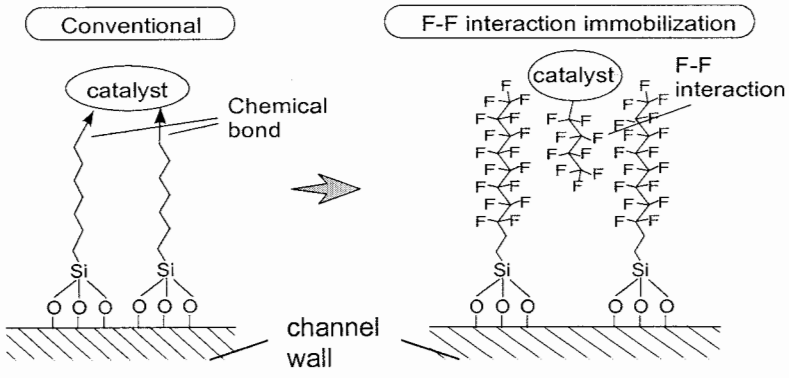

Figure 1. New method to immobilize catalysts

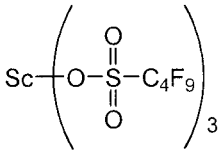

Figure 2. Scandium nonaflates

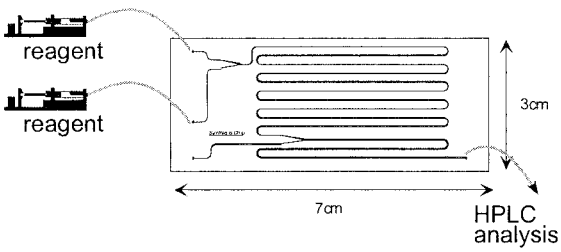

Figure 3. Schematic illustration of microchip

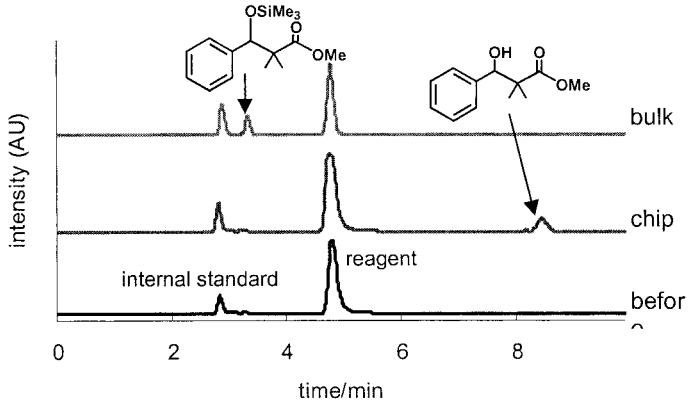

Figure 4. HPLC chromatogram of aldol products

Scheme 1. $Sc(ONf)_3$-catalyzed aldol reaction

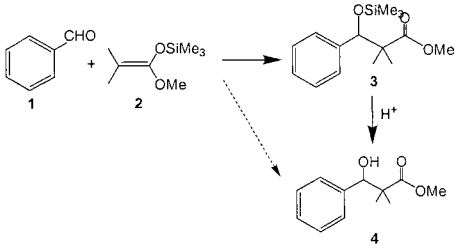

Table 1. Efficiency of immobilized $Sc(ONf)_3$ in microchip

run	mean residence time (min)	microchip yield(%)
1	1	10 (11)
2	5	18 (12)
3	10	16 (17)

CH_3CN solvent, 112mM of reagent were used.
* In the parentheses, 2nd runs results by using the same microchip

GOLD NANOPARTICLE-BASED DNA ANALYSES IN A POWER-FREE PDMS MICROFLUIDIC DEVICE

Kazuo Hosokawa, Kae Sato, and Mizuo Maeda
Bioengineering Laboratory, RIKEN, 2-1 Hirosawa, Wako, Saitama, 351-0198 Japan

Abstract

Gold nanoparticle (GNP)-based DNA analysis, which does not rely on the cross-linking mechanism between GNPs [3], has been implemented in a microfluidic device for the first time. In a poly(dimethylsiloxane) (PDMS) microfluidic device, target 15mer DNA was unambiguously discriminated from its single-base substituted mutant in a parallel fashion without temperature control. This assay took less than five minutes. The PDMS power-free pumping technique [5] has minimized complexity of the microdevice structure as well as the assay procedure.

Keywords: gold nanoparticles, DNA, PDMS, power-free pumping

1. Introduction

For DNA analysis, GNPs were originally adopted by Mirkin and co-workers [1, 2]. In their system, surfaces of GNPs with 10–20 diameter are functionalized with a probe DNA and subsequently mixed with target DNA including an unknown sequence. Information about the unknown sequence can be obtained by optically detecting the aggregation of the GNPs [1], or by electrically detecting the adsorption of the GNPs onto a substrate [2]. These systems rely on the cross-linking mechanism between two probe DNA molecules by a target DNA molecule.

Recently, we reported that a non-cross-linking (NCL) configuration also triggers GNP aggregation [3] (Fig. 1). If the duplex is formed by fully-matched strands without a dangling end, the GNPs aggregate at relatively high salt concentration. This NCL aggregation system exhibits extraordinary selectivity against terminal mismatch. Even single-base mismatch, located at the free terminus of the duplex, makes very stable dispersion. Although the physicochemical basis of the NCL aggregation is not fully understood yet, the terminal selectivity implies that the NCL system is particularly promising for typing of single-nucleotide polymorphisms in combination with the primer single-base extension method [4].

This paper reports the first trial of the NCL GNP-based DNA analysis in a power-free PDMS microfluidic device [5], which exploits the high gas solubility of PDMS. Instead of colorimetric detection in a conventional microtube, an alternative detection technique suitable for microdevices has been discovered: observation of deposition of the GNPs onto PDMS surfaces.

2. Experimental

As probe DNA, 5′-hexylthiol capped 15mer oligonucleotide (Fig. 1, P) was immobilized onto the surfaces of GNPs with 15 nm diameter as described elsewhere [3], except for the final dispersion step to make a colloidal solution containing 28 nM GNPs (referred to as Au-P hereafter), 1.0 M NaCl, and 0.01% Tween 20. As target DNA, unmodified 15mer oligonucleotides (Fig. 1, T1 and T2) were prepared. Target T1 has the fully complementary sequence to P, whereas T2 has a single-base mismatch at its 5′ terminus. The concentrations were adjusted to 6.0 μM DNA, 1.0 M NaCl, and 0.01% Tween 20.

The microfluidic device shown in Fig. 2 was fabricated by reversibly bonding two PDMS pieces with and without surface relief [5]. The device has one outlet reservoir and three inlet reservoirs. The outlet reservoir was sealed with a piece of adhesive tape. The device was placed in a vacuum desiccator, and degassed at 10 kPa for 1 h. After the device was brought back to the atmospheric pressure, 3 μL aliquots of Au-P, T1, and T2 solutions were dispensed into the center,

the left, and the right inlet reservoirs, respectively. An inverted microscope with a 40x objective lens and a digital still camera were used for recording bright-field images. The experiment was carried out at room temperature (*ca.* 25 °C).

3. Results and discussion

Figure 3 illustrates the operational steps for the power-free pumping. (A Y-shaped channel is shown here for clarity.) The pumping energy is stored in the bulk PDMS during the degassing. As shown in Fig. 3A, air dissolved in the vicinity of the channel walls is supposed to be evacuated through the channels and inlet reservoirs. Air cannot go through the outlet reservoir, which is sealed with the adhesive tape. When the microfluidic device is brought back into the atmosphere, the directions of air transfer are reversed. For the power-free pumping, all the liquid samples must be dispensed before the system reaches the new equilibrium. Figure 3B depicts the situation when one of the two inlets is filled with a sample. At this moment, no liquid motion is observed, because air can come from the outside into the channel through the vacant inlet. No capillary action is assumed here. This is the case with most aqueous solutions, because PDMS surface is hydrophobic. The situation is totally changed when the last sample is dispensed (Fig. 3C). Dissolution of air into PDMS begins to reduce the pressure inside the channel and the outlet, because air is no longer supplied from the outside. Consequently, the samples in the inlets start to flow into the channels. After a short period of transient irregular flow, parallel laminar streams are established (Fig. 3D). The outlet reservoir works as an internal vacuum source to continue the pumping.

The results of DNA analysis are shown in Fig. 4. A few minutes after the dispensing of Au-P and the targets, a black line gradually appeared at the assumed interface between laminar streams of Au-P and T1 (Fig. 4A), and became more intense with the course of time (Figs. 4BC). Obviously, the GNPs were deposited onto the PDMS surfaces. By adjusting the microscope focus, we confirmed that the channel ceiling as well as the channel floor had deposition. This indicate that gravity has little effect on this phenomenon. In contrast, no deposition was observed at the other side of the Au-P stream. As a result, the two targets with a single-base difference were unambiguously discriminated in a parallel fashion. We speculate that the heavy hydration around the mismatched base pairs would prevent the GNPs from adsorption and deposition.

5. Conclusions

We have proposed a new DNA analysis method which fully exploits the advantages of microfluidics: (1) the large surface-to-volume ratio enables efficient deposition, and (2) two simultaneous analyses can be conducted at both sides of a laminar stream. The selective deposition discovered here would lead to a sensitive DNA sensor, because deposition on a substrate is much easier to detect than aggregation in a bulk solution. As for the detection technology, bright-field optical microscopy was used here because of convenience. In the near future, we will explore other sensitive detection technologies such as dark-field microscopy, surface plasmon resonance, electrochemical methods, and quartz crystal microbalance.

References

[1] R. Elghanian, J. J. Storhoff, R. C. Mucic, R. L. Lestinger, and C. A. Mirkin, *Science* **277**, 1078-1081, (1997).
[2] S. J. Park, T. A. Taton, and C. A. Mirkin, *Science* **295**, 1503-1506, (2002).
[3] K. Sato, K. Hosokawa, and M. Maeda, *J. Am. Chem. Soc.* **125**, 8102-8103, (2003).
[4] A. C. Syvanen, *Hum. Mutat.* **13**, 1-10, (1999).
[5] K. Hosokawa, K. Sato, and M. Maeda, *Proc. MicroTAS '03*, 499-502, (2003).

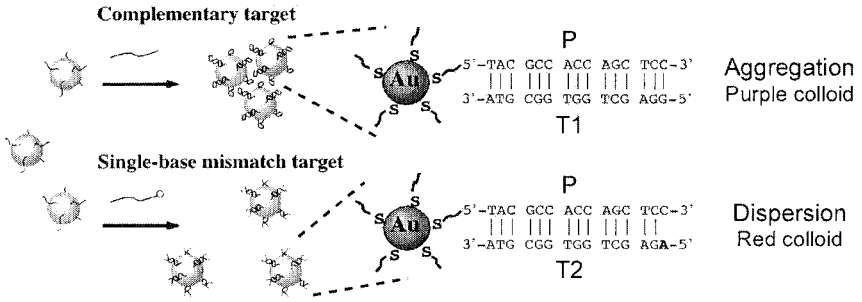

Figure 1. Concept of the NCL GNP-based DNA analysis.

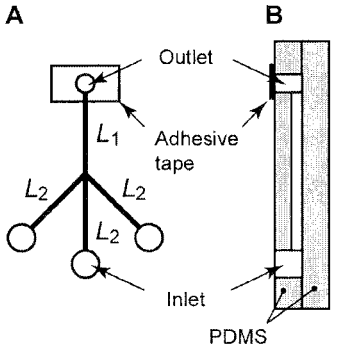

Figure 2. Design of the microfluidic device (not to scale). (A) Channel layout. Channel cross section: 100 μm (width) x 25 μm (height), length: 9.5 mm (L_1) and 9.0 mm (L_2). (B) Cross-sectional view of the device.

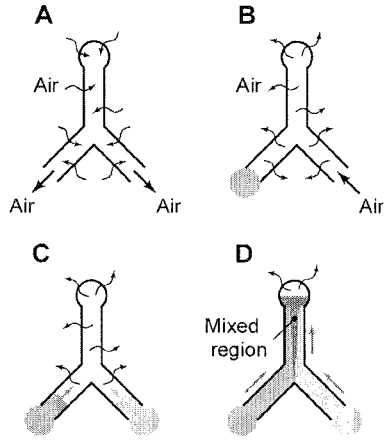

Figure 3. Operational steps for the power-free PDMS microfluidic pumping.

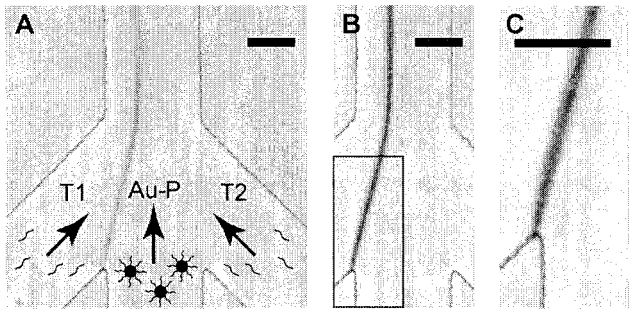

Figure 4. Bright-field images of the NCL GNP-based DNA analysis. GNP diameter: 15 nm, GNP concentration: 28 nM, DNA: 6.0 μM for each, NaCl: 1.0 M, room temperature. Scale bars = 50 μm. (A) t = 3 min. (B) t = 5 min. (C) Magnified view of the bonding box in (B).

DLC-PDMS-HYBRID PATTERNING AND SURFACE TREATMENT

Tuuli Juvonen[1], Antti J. Soininen[2] and Sami Franssila[1]

[1] *Microelectronics Centre, Helsinki University of Technology, P.O. Box 3500, 02015 HUT, Finland*

[2] *Accelerator Laboratory, Department of Physical Sciences, University of Helsinki, P. O. Box 64, FIN-00014 University of Helsinki, Finland*

Abstract

A material that combines the hardness of diamond and the hydrophobicity of polydimethylsiloxane (PDMS), diamond-like carbon - polydimethylsiloxane hybrid (DLC-PDMS-h), is presented. DLC-PDMS-h films were patterned using lift-off, feature sizes down to 3 μm were obtained. DLC-PDMS-h wettability properties were selectively adjusted using photolithographic masking. Both the probability to easily pattern the DLC-PDMS-h and to adjust the hydrophobic properties of the film make the material interesting in BioMEMS and microfluidic applications.

Keywords: DLC, PDMS, lift-off, plasma treatment, hydrophobic

1. Introduction

PDMS and DLC offer chemical inertness, transparency, and exceptional surface properties like scratch resistance of diamond or extreme hydrophobicity of PDMS. They have found numerous applications in microfluidics, as materials for chromatography and electrophoresis chips, for immunoassays and cell sorting [1,2].

Amorphous DLC-PDMS-h layer was deposited on silicon wafer using the filtered pulsed arc discharge technique. This coating technique combines high-energy carbon plasma beam with PDMS evaporation and sputtering. The resulting coating, amorphous DLC-PDMS-h, has good scratch resistance like diamond-like carbon and hydrophobicity similar to that of PDMS. A very important advantage of the filtered pulsed arc discharge technique is that the substrate can be kept at room temperature. This enables coating of substrates, which do not withstand high temperatures [3,4]. SU-8 mold masters for PDMS electrospray chips have been coated with this material [5].

Previously DLC-films have been patterned using lithography and plasma etching [6]. We show that due to low growth temperature, lift-off method can be used to pattern DLC–PDMS-h films.

DLC-PDMS-h shows hydrophobic (and oleophobic) properties [7] that can be utilized in microfluidics to restrict liquid flows or to prevent dosed droplets from spreading. Localized hydrophobic areas can be implemented with the lift-off process. However, a continuous diamond layer may be advantageous because of the excellent mechanical properties and protection of the surface. Therefore, we have studied localized plasma treatments of the diamond films.

2. Experimental

Lift-off

The substrates for DLC-PDMS-h coating tests were (100) type silicon wafers. In lift-off experiments, AZ5214 photoresist was first patterned on the wafers using standard lithographic processes. The wafers were exposed to HMDS vapor for 5 minutes. The resist was spun for 25 seconds at 4000 rpm, which produces approximately 1.8 μm thick photoresist layer. The soft and hard bakes were done in ovens at 90°C and 120°C for 20 and 30 minutes, respectively.

Amorphous DLC-PDMS-h layers were deposited on silicon wafers using the filtered pulsed arc discharge technique. The growth is basically room-temperature growth, and even if some heat may be produced during the deposition, the temperature is low enough in order not to damage the photoresist layer. The DLC-PDMS-h lift-off was performed in acetone using ultrasonic agitation for

10 minutes. Profilometer data on lift-off patterned DLC-PDMS-data is shown in figure 1. Optical and SEM micrographs of the structures are shown in figures 2 and 3.

Plasma treatments

For the blanket deposited wafers, localized plasma treatments were performed to modify the surface hydrophobicity. Oxford Plasmalab 80 reactive ion etcher was used in these experiments. Prior to photoresist coating, the wafer surface was oxygen plasma treated (1 minute, 70 W, 150 mTorr, 50 sccm). Photoresist masking was used to define the areas to be plasma treated. Etching parameters were following: 1 minute, 50 mTorr and CF_4 flow of 50 sccm. A chessboard pattern with hydrophobic and hydrophilic areas is shown in figure 4. The pattern is visualized by applying water on the surface.

3. Results and discussion

Compared to shadow masked plasma treatments, photolithography enables smaller structures to be patterned. Because of the all-phobic nature of the DLC-PDMS-h surface, oxygen plasma treatment is required prior to photoresist spinning. This treatment makes the surface of the DLC-PDMS-h coated wafer hydrophilic (Figure 5b). The hydrophobic nature of the DLC-PDMS-h film can be returned back by a short fluorine-based plasma treatment. Reference sample of silicon dioxide stays hydrophilic, suggesting that no plasma polymer is deposited. DLC-PDMS-h surface etching could not be detected with profilometer, and is thus less than 10 nm. 100 W power produced more hydrophilic surface than lower power of 30 W. Contact angles were measured from video shot pictures of the 5 µl droplets, the main results are shown in Table 1.

Surface treatment	Contact angle
DLC-PDMS-h as deposited	105°
O_2 plasma	<20°
O_2 plasma, CF_4 plasma (30W)	81°
O_2 plasma, CF_4+10% Ar (100 W)	94°

Table 1 Contact angles of DLC-PDMS-h

Lift-off of DLC-PDMS-h proved to work with 1.8 µm thick AZ 5214 photoresist, even for over 250 nm thick DLC-PDMS-h layers (Fig. 4). 3 µm lines were repeated well in areas where continuous resist layers are large enough. In fact, the surface area determines the success of the lift-off rather than the linewidth. As can be seen in Fig. 2, the lift-off was not completed in the smallest areas, here the insides of the numbers are not opened as they should.

The results show that photolithographically defined plasma treatments can be utilized in selective surface treatment of DLC-PDMS-h layers, opening up its microfabrication potential. This material has great potential in BioMEMS and microfluidics because of its exceptional combination of properties.

References

[1] Samuel K Sia and George M Whitesides, Electrophoresis, 2003, Nov 24(21), 3563-76
[2] H. Björkman, C. Ericson, S. Hjertén b and K. Hjort, Sens. and Actuators B79 (2001), pp. 71-77
[3] A. Anttila, R. Lappalainen, V-M. Tiainen and M. Hakovirta, Adv. Mater., 1997, 9, 1161-1164
[4] A. Anttila, V-M. Tiainen, M. Kiuru, E. Alakoski and K. Arstila, Surf. Eng, 2003, 19, 425-428
[5] K. Huikko, P. Östman, K. Grigoras, S. Tuomikoski, V-M. Tiainen, A. Soininen, K. Puolanne, A. Manz, S. Franssila, R. Kostiainen and T. Kotiaho, Lab. Chip, 3 (2003) 67
[6] R. Otterbach; U. Hilleringmann and K Goser, Industrial Electronics Society, 2000, 26th Annual Conference of the IEEE
[7] M. Kiuru and E. Alakoski, Mater. Lett, 2004, 58, 2213

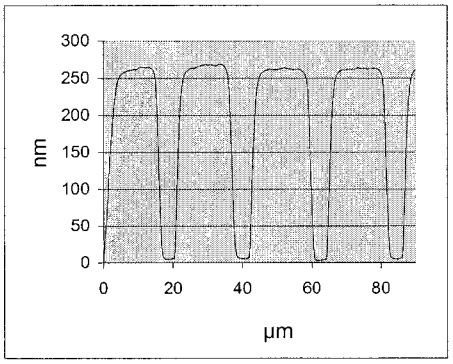

Figure 1. Profilometer data on a lift-off patterned DLC-PDMS-h film

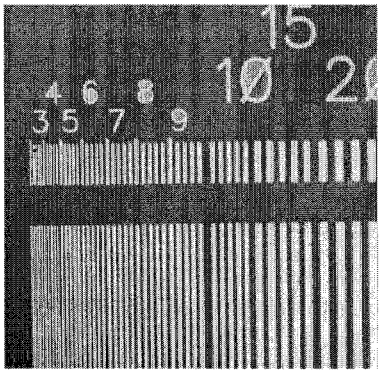

Figure 2. Lift-off is successful on large continuous areas

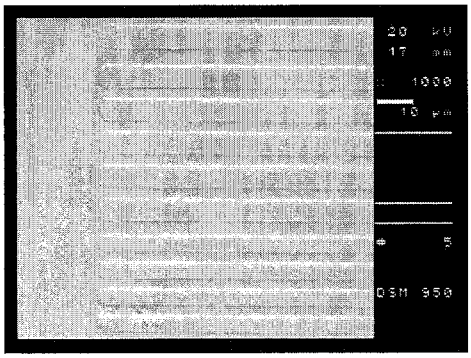

Figure 3. SEM picture on a lift-off patterned DLC-PDMS-h film

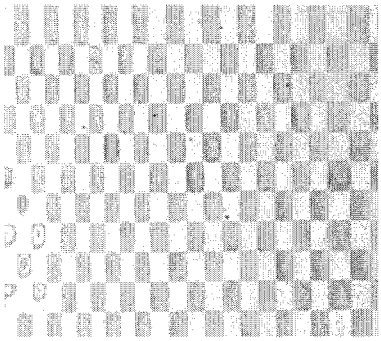

Figure 4. Water droplets (darker) on a locally plasma treated surface, the height of the rectangles is 100 µm

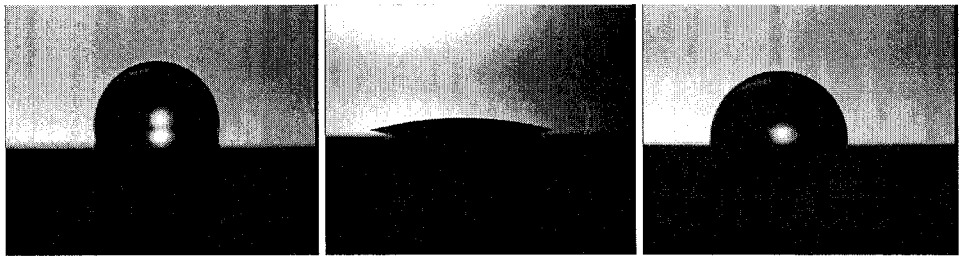

Figure 5. Water droplets 5 µl on a) as deposited PDMC-DLC surface b) treated with oxygen plasma c) recovered with CF_4+Ar plasma

MICRO SCALE PATTERNING OF CELL AND PROTEIN NON-ADHESIVE PEO-LIKE COATINGS, DEPOSITED BY LOW FREQUENCY AC PLASMA POLYMERIZATION

S. Bouaidat[1,2], C. Berendsen[1], P. Thomsen [1], S. G. Pedersen[1], A. Wolff[2] and J. Jonsmann[1]
[1]*Scandinavian Micro Biodevices ApS (SMB), Gammelgårdsvej 87C, DK-3520 Farum, Denmark*
[2]*Dept. of Micro and Nanotechnology (MIC), Technical University of Denmark, Bldg. 345 east, DK-2800 Kgs. Lyngby, Denmark*

Abstract

Micro scale patterning of bioactive surfaces is desirable for numerous biochip applications. PEO-like coating with non-fouling functionality has been deposited using low frequency AC plasma polymerization. The non-fouling properties of the coating were tested with human cells (HeLa) and fluorescence labeled proteins (FITC-BSA). The PEO-like coatings were fabricated by plasma polymerization of 12-crown-4 (ppCrown) with plasma polymerized hexene (ppHexene) as adhesion layer. The coatings were micro patterned using conventional cleanroom photolithography and lift-off. Single cell arrays showed sharp contrast in cell adhesion between the untreated glass surface and the ppCrown layer. Similarly, proteins adsorbed selectively to untreated glass but not to ppCrown.

Keywords: Polymerization, patterning; lift-off, cell non-adhesive, protein non-adhesive

1. Introduction

Positioning of human cells in predefined single or multiple cell arrays is increasingly being exploited in numerous biochip and cell investigation applications [1,2]. Protein patterning technology has also received much attention in recent years. Promising advances in the field of protein biosensing, tissue engineering, molecular electronics, bioreactors etc. have generated increased interest [3,4]. Most of the non-fouling surfaces mentioned above, have been fabricated using conventional wet chemistry. In this study, coatings are fabricated using low-energy plasma polymerization. Coatings containing (-CH_2-CH_2-O-)-groups, i.e. ethylene oxide (EO), are known to reduce bio-molecule adsorption and cell adhesion. It has been shown that these polyethyleneoxide (PEO)-like coatings can be made by plasma polymerization of linear or cyclic EO-containing monomers [5]. In the current study, 12-crown-4 (1,4,7,10-tetraoxacyclododecane) was plasma polymerized (referred to as ppCrown), and photolithographic lift-off process was used for the patterning of the coatings.

2. Experimental and methods

Standard format glass microscope slides were used as substrates. The plasma polymerized coatings, i.e. the adhesion layer (ppHexene) and non-fouling layer (ppCrown) were patterned by lift-off, using 4.2 μm thick photoresist (AZ5214E). Ultrasound for 20 minutes was used to promote the lift-off. A lengthy ultrasonic lift-off is necessary due to the robust nature and excellent step coverage of the coating. After the photoresist step, the ppHexene and ppCrown were deposited by plasma polymerization. A simple plasma generation technique is used here, in which a 50 Hz AC-voltage is applied to the electrodes in the plasma chamber (see Fig. 1 Left). Due to the electrode geometry, the plasma density at the substrate position can be very low compared to conventional plasma techniques and can furthermore be adjusted more precisely. In addition, the plasma is homogeneous even in large volumes and nearly arc-free, which makes scaling-up easy. The glass slides were placed in the chamber and the power density was lowered to 2.5 W/l. A flow of 1-hexene vapors and argon was subsequently fed to the chamber for 30 s. The ppCrown was then

deposited by introducing a flow of 12-crown-4 monomer and stabilizing pressure at 30 μbar. The power density during deposition was 0.2 W/l and the deposition time was 25 min.

The non-fouling properties of the ppCrown coatings were tested with human cells (HeLa) using the following procedure: After the cell suspension had reached a sufficient density in the growth medium (37° C in air with a CO_2 content of 5 %), the cells were separated from the medium using PBS and Trypsin-EDTA in HBSS. The glass slides were then exposed to the cell suspension.

The ppCrown were also tested using proteins, in this case bovine serum albumin (FITC-BSA). The coated glass slides were exposed to the FITC-BSA/PBS solution for 30 min. and then washed for 5 min. in PBS and 1 min. in DI water, after which the glass slides were spin dried. The samples were screened using a arrayWoRx scanner by AppliedPrecision (fitted with FITC-filters).

3. Results and discussion

To determine the cell adhesion properties of ppCrown, cell-counting experiments were performed using a Zeiss 200m microscope. A suspension of cells prepared as described earlier, was dispensed into Geneframes. The number of anchored cells and the total number of cells were counted at three positions after 2, 4, 6 and 72 hrs of incubation. Fig. 1 Right shows the percentage of cells anchored to the surface relative to the total number of cells, both for a ppCrown coated surface and an untreated glass surface. Practically no cells adhere to the ppCrown surface, whereas the number of cells adhering to the untreated glass surface increases with incubation tine.

The patterned ppCrown coatings were also characterized. In this case, cells were allowed to sediment onto the coated glass slides for 24 hrs in an incubator, after which the glass slides were inspected under the microscope. Fig. 2 Left and Right shows the result of this incubation experiment. There is a clear difference in cell adhesion between the areas coated with ppCrown and the untreated areas, i.e. glass surface. The surfaces were not rinsed or flushed prior to inspection. Most of the cells seen on the ppCrown are not anchored and can be flushed away by gentle rinsing. Fig. 3 Right shows a cell array of 3 "islands" with cells adhering to 2 of them. The size of the adhesive islands is 50 μm. The initial cell diameter of HeLa cells is estimated to be approximately 20-30 μm, whereas anchored HeLa cells may be spread out to diameters of 75 μm.

To determine the protein resistance properties of ppCrown, the coated surfaces were tested using a FITC-BSA/PBS solution (1 mg/ml). Fig. 3 Left and Right shows the result of the adsorption experiments (fluorescent scans). Well-defined patterns with high adsorption contrast to the surrounding ppCrown are observed. In all cases we see very minor traces of FITC-BSA scattered across the ppCrown surfaces. This is probably due to insufficient washing of the surfaces.

4. Conclusions

Using a novel AC-voltage low frequency AC plasma-polymerization system, PEO-like ppCrown coatings with biologically non-fouling functionality were deposited. Furthermore it was demonstrated, that micro patterning of the ppCrown was possible using conventional cleanroom micro lithography, i.e. lift-off. The non-fouling properties of the ppCrown were tested using both human cells (HeLa) and fluorescently labeled proteins (FITC-BSA). Well-defined micro scale cell patterns were observed with very little non-specific binding on the ppCrown. Selective adsorption of proteins was also observed, i.e. the patterned ppCrown exhibited high protein resistance. Low energy plasma polymerization combined with micro lithography, is a simple and efficient way of obtaining patterned non-fouling surfaces with high binding contrast.

References

[1] C. H. Thomas, J. B *et al.*, *Journal of Biomechanical Engineering,* 1999, **Vol. 121 – 1**, 40-48.
[2] T. H. Rider *et al., Science, 2003,* **Vol. 301**, 213-215.
[3] H. Sorribas *et al.*, *Biomaterials*, 2002, **23**, 893-900.
[4] G. Jin *et al., Proc. of the 23rd Annual EMBS International Conference,* 2001, 2907-2910.
[5] Y.J. Wu *et al., Colloids and Surfaces B: Biointerfaces,* 2000, **18,** 235-248.

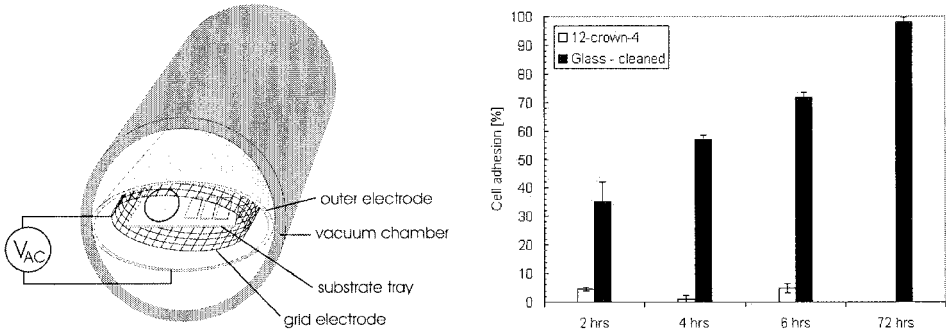

Figure 1. Left: Schematic diagram of the 50 Hz AC-voltage plasma-polymerization system used. Voltage is applied between the inner grid electrode and the outer electrode, away from the substrates. **Right:** HeLa cell adhesion versus time for a ppCrown surface and a control surface i.e. cleaned glass. The term "cell adhesion" represents the percentage of cells anchored onto the surface relative to the total number of cells. Cells were counted after 2, 4, 6 and 72 hours using a inverted microscope. The standard deviations are also indicated. The cell adhesion onto ppCrown is generally very low throughout the incubation.

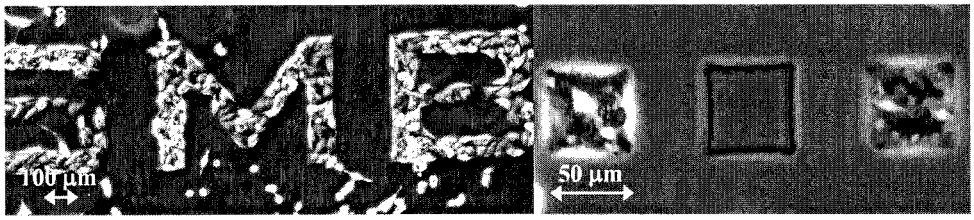

Figure 2. Left: Optical microscope image of a glass slide with patterned ppCrown. The HeLa cells clearly form the letters "SMB", with a very high degree of binding contrast between the coated and non-coated regions. **Right:** Close-up of a single cell array. The square islands are 50 µm in side length. Single cells are spread out over the entire geometry of the islands. The surfaces were not rinsed prior to inspection.

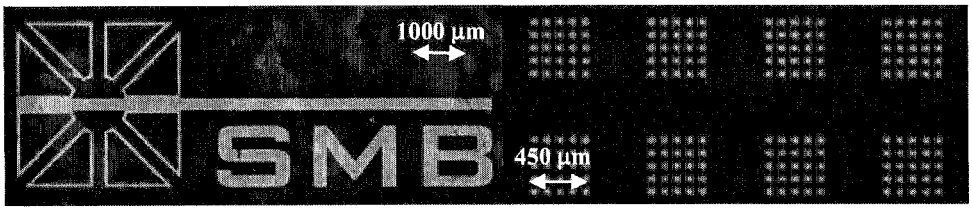

Figure 3. Left: Result of a fluorescent scan of labeled proteins (FITC-BSA) on a patterned ppCrown surface. FITC-BSA is selectively absorbed onto the letters and logo (glass surface) with little non-specific absorption on the surrounding ppCrown. **Right:** Fluorescent scan of FITC-BSA selectively absorbed to circles with a diameter of 50 µm in 5x5 arrays.

SULFONIC ACID DERIVATIZED PDMS MICROFLUIDIC DEVICES EXHIBITING ENHANCED STABILITY AND ELECTROKINETIC PUMPING

Bin Wang, J. Hugh Horton and Richard D. Oleschuk
Department of Chemistry, Queen's University, Kingston, Ontario, Canada

Abstract

Polydimethylsiloxane (PDMS) microfluidic devices offer several advantages in terms of cost and ease of fabrication compared to those fabricated from both glass and silicon materials. PDMS, however, has some potential disadvantages including high hydrophobicity, and minimal surface charge resulting in reduced electrokinetic pumping. Oxidized PDMS microchips show excellent flow performance at high pH values however, electrokinetic pumping is reduced at low pH. We have carried out the surface oxidation of PDMS to form silanol groups (Si-OH) and then utilize 2-(4-chlorosulfonylphenyl)ethyltrimethoxysilane to subsequently sulfonate the surface. Experiments show that the sulfonated-PDMS is a superior material for use in microfluidic applications because it supports EOF over a wider range of pH and is less susceptible to degradation of its EOF rate due to aging effects and surface reorganization.

Keywords: PDMS, sulfonated surface modification, elctroosmotic flow, aging effect, chemical force titrations

1. Introduction

Polydimethylsiloxane (PDMS) microfluidic devices offer several advantages in terms of cost and ease of fabrication compared to those fabricated from both glass and silicon materials. PDMS has some potential disadvantages, however compared to other materials including high hydrophobicity, which makes filling the micron-sized channels difficult, and minimal surface charge resulting in reduced electro-osmotic flow (EOF). A plasma oxidation method has been used to form silanol groups on the PDMS surface in order to increase the surface charge and make the surface hydrophilic[1]. Oxidized PDMS microchips show excellent flow performance at high pH values where the silanol groups are deprotonated yielding a significant zeta potential. However, the EOF in oxidized micro-channels is reduced at pH's below the surface pKa value of the silanol group (≈ 4-5), due to protonation of SiO^- sites. In addition, the effect of the oxygen plasma is temporary as the surface reverts back to its original form through hydrophobic recovery in a manner of hours limiting the usefulness of the modification (Table 1). Here, we describe the oxidation of the PDMS surface to form silanol groups using both air plasma and a discharge from a Tesla coil, and subsequent modification to form PDMS surfaces terminated with sulfonic acid groups.

Table 1. Migration Rate of a Fluorescent Probe Showing Hydrophobic Recovery of Surface Oxidized PDMS at pH 8.0.

Chip Surface Treatment	Aging Time	pH	Migration rate ($\times 10^{-2}$ cm/s)
Unmodified PDMS	freshly prepared	8.0	7.1 ± 0.2
Oxidized PDMS	freshly prepared	8.0	10.4 ± 0.2
	24 h	8.0	7.8 ± 0.2
	10days	8.0	7.1 ± 0.3

2. Results and Discussion

The sulfonic acid modification was carried out to augment flow performance by enabling strong cathodic EOF even at low pH's due to the lower pK_a of the sulfonic acid group (≈2-3) compared to a silanol (≈4-5). Also, through previous studies, our group has shown that covalently modifying the PDMS surface following oxidation generates a surface that is more robust and hydrophobic recovery does not proceed as quickly[2,3]. EOF velocity was used to monitor zeta-potential and was measured utilizing a laser induced fluorescence setup to examine the migration rate of a fluorescent dye. The flow performance of freshly prepared and aged sulfonated-PDMS chips were determined at pH 5 and compared to those of unmodified and oxidized PDMS chips (Table 2). The electroosmotic mobility (μ_{eo}) for sulfonated-PDMS and oxidized PDMS microdevice was determined at various pH values (pH 3 ~ 8) (Figure 1). The sulfonic acid modified PDMS showed an increased μ_{eo} over the entire pH range studied.

Table 2. Migration Rate of a Fluorescent Probe Showing Increased Stability and Increased EOF of the Sulfonic Acid Derivatized PDMS compared to Oxidized PDMS at pH 5.0.

Chip Surface Treatment	Aging time	pH	Migration rate ($\times 10^{-2}$ cm/s)
Unmodified PDMS	freshly prepared	5.0	3.2 ± 0.1
Oxidized PDMS (Tesla coil)	freshly prepared	5.0	4.2 ± 0.1
Oxidized PDMS (air plasma)	freshly prepared	5.0	4.3 ± 0.1
Sulfonic acid-modified PDMS (Tesla coil oxidized)	freshly prepared	5.0	6.8 ± 0.1
Sulfonic acid-modified PDMS (air plasma oxidized)	freshly prepared	5.0	6.8 ± 0.1
	24 h	5.0	6.5 ± 0.1
	10 days	5.0	5.1 ± 0.1

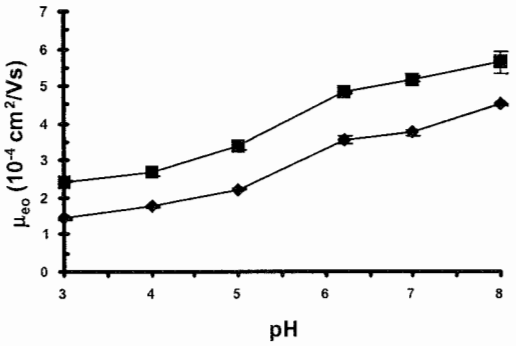

Figure 1. EOF versus pH for sulfonated (squares) and air plasma oxidized (diamonds) PDMS micro-devices.

Chemical force titrations (CFT) were used to characterize changes in functional groups present on the surface of freshly prepared and aged sulfonated-PDMS surfaces (Figure 2). The CFT performed with a sulfonic acid derivatized tip show that the pK_a of the SO_3^- modified PDMS is ≈3 as can be seen by a maximum in the tip substrate interaction.

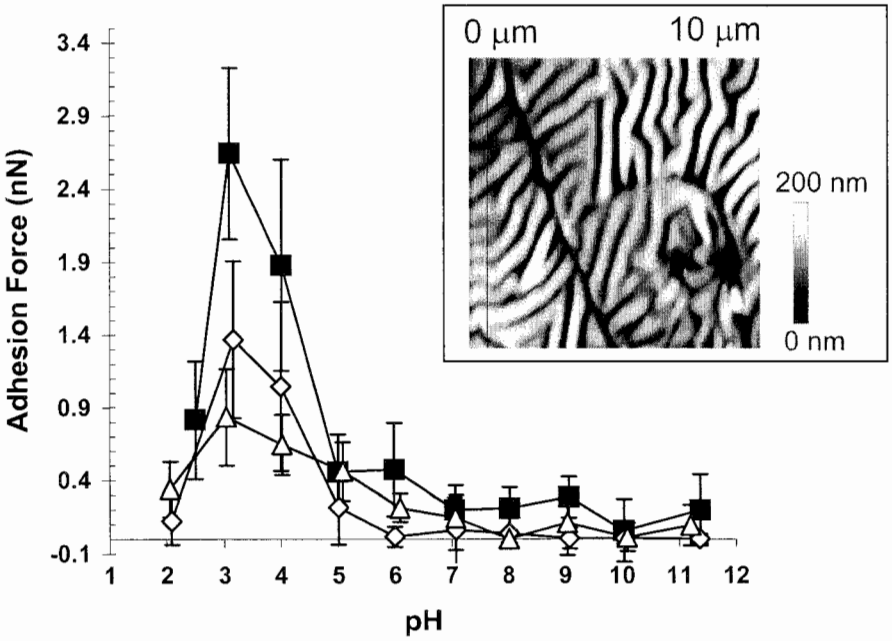

Figure 2. Chemical force titration measurements of freshly prepared (squares), 24 h aged (diamonds) and 10 days aged (triangles) sulfonated-PDMS surfaces. Inset atomic force micrscope image of the freshly prepared sulfonic acid modified PDMS surface.

These experiments show that the sulfonated-PDMS is a superior material for use in microfluidic applications because (i) it supports EOF over a wider range of pH than similar polymer materials and (ii) is less susceptible to degradation of its EOF rate due to aging effects and (iii) sulfonic acid derivatized surfaces have shown increased sample compatibility compared to native PDMS.

Acknowledgements

We acknowledge the Natural Sciences and Engineering Research Council of Canada, Canadian Foundation of Innovation, Ontario Innovation Trust and Queen's University for financial support.

References

[1] J. C. McDonald, D. C. Duffy, J. R. Anderson, D. T. Chiu, H. Wu, O. J. A. Schueller, G. M. Whitesides, *Electrophoresis*, 2000, 21, 27-40. [2] B. Wang, Z. Abdulali-Kanji, E. Dodwell, J. H. Horton, R. D. Oleschuk, *Electrophoresis*, 2003, 24, 1442-1450. [3] B. Wang, L. Chen, Z. Abdulali-Kanji, J. H. Horton, R. D. Oleschuk, *Langmuir*, 2003, 19, 9792-9798.

ELECTRICALLY TUNABLE, REPROGRAMMABLE PROTEIN PATTERNING USING FLUOROCARBON-POLYMER-COATED ELECTRODE PATTERNS

Amaya Frost[1], Chih-Ting Lin[2], Edgar Meyhofer[1] and Katsuo Kurabayashi[1]
[1]*Dept. of Mechanical Engineering, University of Michigan, Ann Arbor, MI 48109-2125, U.S.A.*
[2]*Dept. of Electrical Engineering and Computer Science, University of Michigan, Ann Arbor, MI 48109-2122, U.S.A.*

Abstract

We report on a new method that allows electrically tunable patterning of protein molecules on a hydrophobic fluorocarbon polymer surface. This new protein patterning approach is based on charging a fluorocarbon polymer coating layer with an electrode array. Our experimental demonstration electrically tunable protein adsorption represents significant progress towards reprogrammable protein patterning by a microprocessor or electrical filtering and pre-concentration of proteins in microfluidic circuits and chromatographic μ-TAS.

Keywords: Electrowetting, Protein Patterning, Fluorescence Microscopy

1. Introduction

Protein patterning is a crucial process for achieving biologically functionalized devices. Conventional protein patterning methods are primarily based on irreversible chemical processes or on lithographically defined surface treatments [1-2]. These methods often suffer from their inability to pattern multiple proteins or to ensure zero non-specific binding. In contrast, electrical protein immobilization offers the versatility to overcome these problems and offers low cost and mass fabrication of devices [3]. In this study, we have designed and tested a device that selectively patterns proteins on a surface, using the electrical protein immobilization principle. The device consists of a glass substrate with patterned aluminum electrodes. These electrodes are covered with a silicon nitride dielectric layer and then with a fluorocarbon polymer (CYTOP®, Asahi Glass Co, Japan) layer. An indium tin oxide (ITO) layer is deposited on a glass slide and then coated with a layer of the same fluorocarbon polymer to form a counter electrode. The transparent counter electrode permits characterizing the electrical protein immobilization on the device surface using fluorescence microscopy. These two pieces are brought together to form a flow chamber as illustrated in Figure 1. Glass spacers are used to maintain a constant gap between the pieces.

2. Principle of Electrically Tuneable Protein Patterning

When a voltage is applied across the electrode gap, charge accumulates at the electrodes as seen for a capacitor, which creates an electric field across the silicon nitride and the fluorocarbon layers. This electric field lowers the surface energy at the liquid-fluorocarbon interface and causes the hydrophobic fluorocarbon surface to become hydrophilic. This phenomenon is known as electrowetting [4] and has been characterized for our device by measuring a contact angle. An 8uL droplet of de-ionized water is placed on the device substrate. A metal probe tip is used to contact the top of the droplet as shown in Figure 2. Figure 3 shows the contact angle of the liquid on the fluorocarbon polymer-coated electrode at varying applied voltage.

For this study we chose bovine serum albumin (BSA) which is a globular protein. In an aqueous buffer solution protein molecules fold to protect the hydrophobic portions of the chain. This folding of the protein creates a hydrophilic surface for the protein. Thus the hydrophobic polymer surface repels the hydrophilic protein, creating a diffusion barrier. We believe that the hydrophobicity-to-

hydrophilicity surface transition induced by the applied bias allows proteins to diffuse to the surface. We also speculate that the charge accumulated near the device surface is free to form ionic bonds with the proteins in solution. This process is repeatable and leads to the electrical tuneable protein patterning.

3. Device Characterization

The folding of the protein also exposes its variously charged amino acid groups. These charges will vary depending on the pH of the solution. BSA is know to be net neutral at pH=4.7-4.8, the isoelectric point of the protein [5]. In all experiments we use TRIS acetate buffer at a pH near 7, which gives a net negative charge to the protein. This has been experimentally verified through mobility measurements made with this protein and buffer solution. In this manner, the protein can be treated as a sphere of charge, with a charge equivalent of one electron and a Stokes radius of 4nm [6]. The BSA sample was labeled with tetramethylrhodamine (TMR) with a labeling ratio of approximately 1.6 dyes per protein. An anti-bleaching agent is added to the solution to slow the fluorescence decay. The charge on BSA at pH=6.98 was measured in an electrophoretic mobility experiment as net negative at this pH. Labelled BSA has absorption and emission spectra as shown in Figure 4, which allows us to use the 546 nm line of a mercury arc lamp as an excitation light source.

An inverted fluorescence microscope is used to detect the proteins on the surface. A CCD camera with a band pass filter (570 – 650 nm) is used to capture the emitted signal. The fluorescence intensity of an active electrode was measured for various applied voltages. The chamber was first filled with buffer to wet the surface. Then a buffer solution containing the protein was introduced into the chamber with the electrode activated. This was left for at least three minutes to allow diffusion of the protein to the surface. The chamber was then rinsed with buffer three times to remove any unbound protein. We observed that the intensity of the surface increased with increasing voltage, as seen in Figure 5. This indicates that the surface affinity of BSA becomes higher with a larger amount of the accumulated surface charge. It is worthy to note that there is a minimum voltage at which protein binds to the surface. This agrees with common electrowetting theory [4,7] which proposes the existence of a threshold voltage at which the surface undergoes a transition from hydrophobic to hydrophilic.

4. Conclusions

We have demonstrated that the surface affinity of BSA molecules can be electrically controlled on a hydrophobic fluorocarbon polymer surface. Our study suggests that surface charge accumulation in the polymer surface under bias is responsible for the affinity change. The presented method holds promise to achieve reprogrammable protein patterning and electrical protein sample separation for future μ-TAS technologies.

Acknowledgements

This work was in part supported by DARPA BMM under contract N66001-02-C-8039

References

[1] K. Lee, S. Park, C.A. Mirkin, J.C. Smith, M. Mrksich, *Science* **295**, 1702-1705 (2002).
[2] J. Wright, et. al. *Langmuir*, **19**, 446-452 (2003)
[3] T. Yamamoto and T. Fujii, *MicroTAS '03*, 677-680.
[4] W.J.J. Welters and L.G.J. Fokkink, *Langmuir*, **14**, 1535-1538 (1998)
[5] H. Matsumoto, et. al. *J.Colloid Int. Sci.*, **264**, 82-88, (2003)
[6] T. Axelsson, *J. Chromatog.*, **152**, 21-32 (1978)
[7] H.J.J.Verheijen and M.W.J. Prins *Langmuir*, **15**, 6616-6620, (1999)

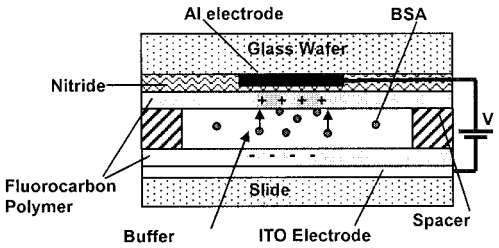

Figure 1 Schematic of flow chamber construction

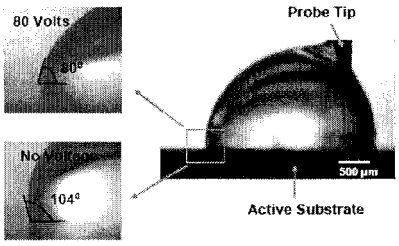

Figure 2 Electrowetting test setup, water droplet with probe.

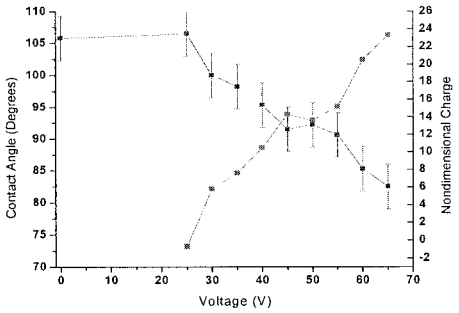

Figure 3 Plot of contact angle versus voltage for setup shown in figure 2. Also shown is the nondimensional charge derived from the Lippman-Young equation.

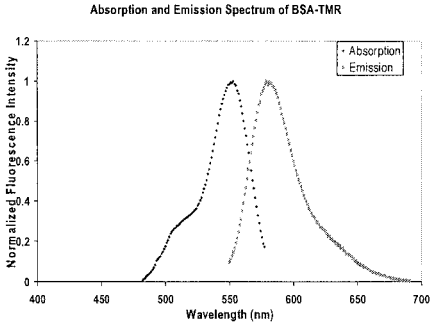

Figure 4 Absorption and emission spectrum for BSA labeled with TMR

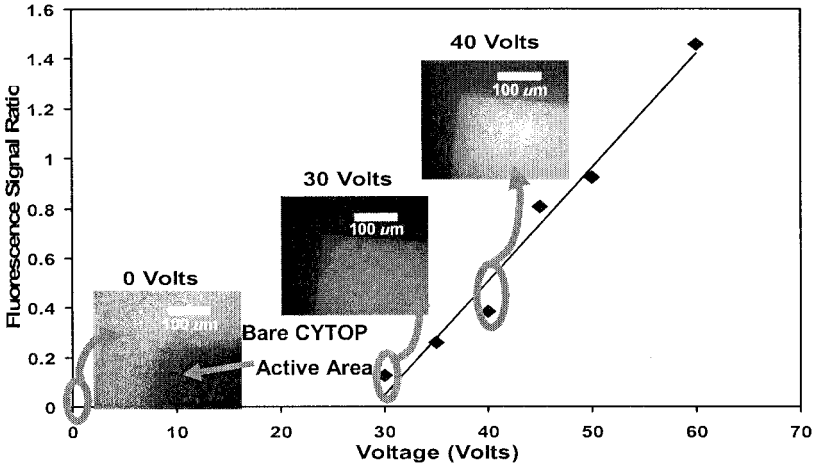

NEWLY DESIGNED BIOCOMPATIBLE POLYMERS HAVING PHOSPHOLIPID POLAR GROUP FOR ELECTRO-OSMOSIS PUMP ACTUATED CELL SORTER CHIP

Madoka Takai[1], Hiroyuki Onoda[1], Kazuhiko Ishihara[1], Yuzuru Takamura[2], and Yasuhiro Horiike[3]

[1]Dept. of Materials Engineering, The University of Tokyo, Hongo, Bunkyo-ku, Tokyo, 113-8656, Japan, [2] Japan Advanced Institute of Science and Technology(JAIST), Asahidai, Tatsunokuchi, Ishikawa 923-1292, Japan, [3]National Institute of Materials Science (NIMS), Sengen, Tsukuba, Ibaraki 305-0047, Japan

Abstract

Newly designed biocompatible polymer for modifying a surface of microfluidic devices for instance cell sorter chip has been developed. The synthesized polymer(PMSi) has composed of 2-methacryloyloxyethyl phosphorylchiline(MPC) unit, and 3-metacryloxypropyltrietoxysilane (MPTES) unit. Phosphorylcholine groups in the MPC units oriented on the surface showed a good performance of prevention of cell adsorption, and a good durability of modified surface in a buffer solution was achieved because of a stable bonding formation between silane-coupling unit in the MPTES of copolymer and SiO_2 substrate. An electro-osmosis flow pump actuated cell sorter chip coating with PMSi was well operated for 30min.

Key words: biocompatibility, phospholipids polymer, surface potential, cell sorter, electro-osmosis pump

1. Introduction

The biocompatibility of material surfaces is very important property for microfluidics devices handling with biological components, such as DNA, proteins and cells, because these organisms are easily damaged by sticking on the material surfaces. Adsorption mechanism of these biological components on the material surfaces has been mainly explained by hydrophobic interaction related to water structure surrounding them and electrostatic interactions [1]. To avoid a nonspecific adsorption and adhesion, several materials for surface modification have been reported recently [2]. Among them copolymers composed of 2-methacryloyloxyethyl phosphorylchiline (MPC) with hydrophobic alkyl methacrylates showed excellent hemocompatibility, even when the copolymers were in contact with human whole blood without an anticoagulant[3]. The cause of excellent biocompatibility on MPC copolymer is expected that the MPC copolymer have a phosphorylcholine group, which is a typical phospholipid polar group, and large amount of free water surrounding on polymer surface[3]. In this paper, newly molecular design of MPC copolymers with 3-metacryloxypropyltrietoxysilane(MPTES) to modify the surface of the microfluidics by chemical bonding and the performance of prevention of the adsorption and adhesion of biological components are reported.

2. Experimental

The PMSi shown in Figure 1 was synthesized by a conventional radical polymerization technique of MPC with MPTES in ethanol using 2,2'-azobisisobutyronitrile as an initiator. After polymerization reaction, the PMSi obtained was purified by a reprecipitation technique and the structure was confirmed with NMR and FT-IR spectroscopies, respectively. Trimetoxysilyl group in the MPTES unit in the copolymer reacts chemically with SiO_2 surfaces shown in Figure 2. Thus, stable surface modification could be done with the PMSi. Electro-osmosis-flow (EOF) pump actuated cell sorter chip was fabricated with quartz plate used electron-beam and photo lithography, dry and wet etching techniques, which was reported previously[4]. After bonding by HF solution,

gel electrode [5] was formed by local photo-polymerization. Finally, inner wall of capillary was coated with PMSi. The surface modification was carried out as following procedure: the ethanol solutions with given PMSi concentration were prepared and the substrate was immersed in the solution. The solvent was evaporated and the substrate was treated at 100°C to react between MPTES units and the SiO_2 surface.

4. Results and discussion

Figure 3 shows the chemical composition ratio of phosphorus and nitrogen to carbon on the modified SiO_2 surfaces measured with an XPS. The data indicated that the surface of the substrate was completely covered with the PMSi and the phosphorylcholine groups in the MPC units of the copolymer oriented on surface even the concentration of PMSi in the solution was really low about 0.03wt%. The inhibition of cell adhesion on the PMSi modified surface was evaluated using microfluidics with human lymphocyte and results are shown in Figure 4. Sticking density of the lymphocytes on capillary coated with the PMSi was drastically decreased comparing with that on bared SiO_2. The thickness of PMSi layer formed from the 0.03wt% PMSi solution was around several nanometers, therefore monolayer-liked PMSi coating was enough to prepare a resistible surface toward biological components including proteins and cells. The biocompatible properties in modified surface were kept several weeks under soaking in a phosphate buffered saline. It suggested a good interface formation between the PMSi and SiO_2. To evaluate performance of PMSi coating, the cell sorter chip reported previously[4] was used, and a photograph of the cell sorter chip is shown in Figure 5. The chip without coating PMSi did not work due to heavy sticking of human lymphocytes, while the cell sorter chip with PMSi coating was well operated over 30min without adhesion of human lymphocytes. However cell-sorting rate in the chip with PMSi coating was drastically decreased comparing with that in the chip without PMSi coating even applying a high voltage of 200V, that was because small.-potentials of PMSi. .-potentials of PMSi coated SiO_2 and bared SiO_2 were almost zero, and $-60(\pm5)$mV, respectively. Therefore to increase cell-sorting rate, negatively charged MPC copolymers(PMBS) composed of MPC, *n*-butyl methacrylate (BMA) and potassium 3-methacryloyloxypropyl sulfonate (PMPS)[6], which showed a good biocompatibility, were prepared and used as a coating material. As the result, a cell-sorting rate was increased at almost double comparing that of the cell sorter chip coated with PMSi. Recently, negatively charged copolymer with silane coupling unit has been developed to improve a durability of PMBS. From these results, the PMSi having phosphorylcholine groups and silane-coupling units was useful for stable surface modification on SiO_2. Moreover, introduction of negative charged moiety is effective to increase of cell-sorting rate.

5. Conclusions

Newly designed biocompatible polymer(PMSi) with phospholipid polar group and silane-coupling units have been developed for EOF pump actuated cell sorter chip. The surface modified glass with PMSi showed excellent properties in preventing cell adhesion, because phosphorylcholine groups in the MPC units of the copolymer oriented on the surface. A good durability for several weeks in a buffer solution was obtained by stable bonding between silane-coupling unit and SiO_2 substrate. EOF pump actuated cell sorter chip coating with PMSi was well operated for 30min. Thus, it is important to prepare suitable biocompatible polymers with several additional functions for microfluidic devices.

References

[1] D.R. Lu , S.J. Lee, and K. Park, *J. Biomater. Sci., Polymer Edn*, **3(2),** 127-148(1991).
[2]T. Mcpherson, A. Kidane, I. Szlifer, and K. Park, *Langmuir*, **14**, 176-186(1998).

[3] K. Ishihara, H. Oshida,Y. Endo, T. Ueda, A. Watanabe, and N. Nakabayashi, *J. Biomed. Mater. Res.* **26**, 1543-1552(1992).
[4] H. Onoda, Y. Takamura, Y. Horiike, *proceedings of microTAS 2002,* **2**, 955(2002).
[5] Y. Takamura, H. Onoda, H. Inokuchi, S. Adachi, A. Oki, and Y. Horiike, *Electrophoresis*, **24**, 185-192(2003).
[6] T. Ito, Y. Iwasaki, T. Narita, K. Akiyoshi, and K. Ishihara, *Science and Technology of Advanced Materials*, **4**, 99-104(2003).

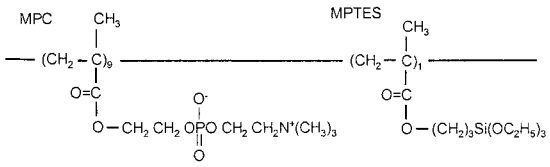

Figure 1 Chemical formula of new synthesized copolymer(PMSi).

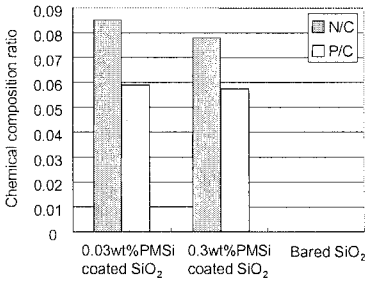

Figure 3. XPS results of three kinds of surfaces with and without PMSi coating. Coating process: 1. dip in polymer solution, 2. evaporate solvent and bake at 100°C, 3. soak in phosphate buffered saline for 18hr.

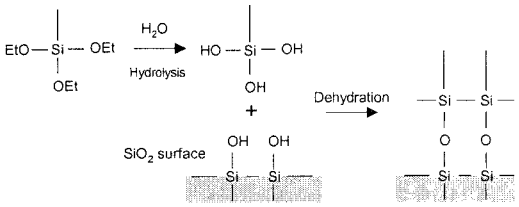

Figure 2 Reaction mechanism of PMSi and SiO_2 surface.

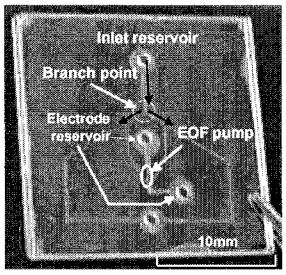

Figure 5. Photograph of cell sorter chip with EOF

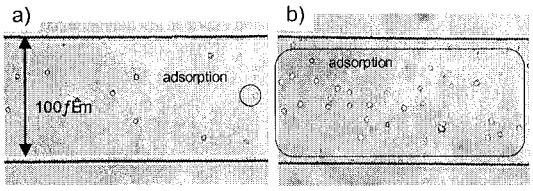

Figure 4. Photograph of inner wall of capillary after flow of cell solution($4x10^5$cell/ml) for 5min. (a) coating with 0.03wt% PMSi, (b) bared SiO_2.

ULTRA THIN POLY(*N*-ISOPROPYLACRYLAMIDE) GRAFTED GEL FOR CELL ADHESION / DETACHMENT CONTROL BY TEMPERATURE CHANGE

Yoshikatsu Akiyama,[1,2] Akihiko Kikuchi, [1,2] Masayuki Yamato[1,2] and Teruo Okano[1,2]
[1]*Institute of Advanced Biomedical Engineering and Science, COE Program for 21st Century, Tokyo Women's Medical University, 8-1 Kawada-cho, Tokyo 162-8666, Japan*
[2]*CREST, Japan Science and Technology Agency (JST), Kawaguchi, Saitama 332-0012, Japan*

Keywords: poly(*N*-isopropylacrylamide), electron beam, excimer laser, ultra thin, TOF-SIMS

1. Introduction

We have been carrying out the preparation of thermoresponsive polymer-modified surfaces with designated molecular configuration at the interfaces [1]. Thermoresponsive polymers, poly(N-isopropylacrylamide) (PIPAAm) and its derivatives are used as the surface modifiers [1]. These surfaces are utilized to propose new chromatographic separation methods for variety types of bioactive compounds in a sole aqueous mobile phase [2]. We further applied the thermoresponsive surfaces for thermally regulated cell adhesion and detachment [3], and extended the idea to tissue engineering [4]. Confluently cultured cell monolayers on hydrophobized PIPAAm modified surfaces at 37°C detach as single cell sheets by lowering culture temperature to 20°C where the modified surfaces become hydrophilic due to PIPAAm's hydration/dehydration transition at 32°C. In our preliminary researches, graft amounts of PIPAAm on the surfaces have significant influences to cell adhesion behavior [5]. However, detailed mechanisms why cells cannot adhere on the surfaces with high amount of grafted PIPAAm chains. Such phenomenon was also found for PIPAAm dip coated surfaces or PPAAm hydrogels.

In the present paper, we focused on the correlation of the thickness of PIPAAm covalently grafted layers on tissue culture polystyrene (TCPS) surfaces and cell adhesion/detachment behavior. For this purpose, we utilized limited excimer laser ablation and atomic force microscopic method to determine the thickness of PIPAAm grafted layers. Preliminary elipsometry measurement did not work to determine the grafted layer thickness, since the refractive indices are similar for polystyrene and PIPAAm. Then, we investigated thermoresponsive cellular adhesion/detachment on the prepared surfaces to discuss the influences of the grafted layer thickness on the cellular behavior on these modified surfaces.

2. Experimental

Two types of PIPAAm-grafted TCPS were prepared as reported previously [4]. In Brief, *N*-isopropylacrylamide (IPAAm) monomer was dissolved in 2-propanol at concentrations of 55 wt% and 80 wt%. Solution (30 μl) was added and spread uniformly over TCPS surfaces. These dishes were immediately subjected to irradiation with 0.25 MGy electron beam. PIPAAm-grafted dishes were washed extensively with cold distilled water to remove un-reacted IPAAm monomer and un-grafted PIPAAm. These PIPAAm-grafted TCPS were evaluated for graft amounts of PIPAAm surfaces (ATR/FT-IR) and their thermoresponsive wettability changes. We examined cell adhesion and detachment properties of the dishes, using bovine endothelial cells. Estimation of thickness of the grafted PIPAAm layers was performed as follows: the surfaces were ablated by UV excimer laser until basal hydrophobic TCPS was revealed, and then the depth of ablated domain was measured by AFM.

3. Results and discussion

We investigated physicochemical properties of two types of PIPAAm grafted TCPS surfaces, to elucidate the influencial factors for thermally regulated cell adhesion and detachment to PIPAAm grafted surfaces. The two types of PIPAAm grafted surfaces were prepared by electron beam (EB) polymerization method. ATR/FT-IR revealed that amounts of the grafted polymers were 1.4±0.1 $\mu g/cm^2$ for PIPAAm-1.4 and 2.9±0.1 $\mu g/cm^2$ for PIPAAm-2.9, respectively. Both PIPAAm-grafted surfaces showed hydrophobic/hydrophilic property alterations in response to temperature. However, PIPAAm-1.4 surfaces were more hydrophobic ($cos\theta = 0.21$ at 37°C and $cos\theta = 0.35$ at 20°C) than PIPAAm-2.9 ($cos\theta = 0.42$ at 37°C and $cos\theta = 0.50$ at 20°C) both above and below the PIPAAm's transition temperature. Thickness of the grafted PIPAAm layers were estimated to be 15.5±7.2 nm for PIPAAm-1.4 and 29.5±8.4 nm for PIPAAm-2.9, respectively, by the use of UV excimer laser and atomic force microscope (Fig. 1). Bovine carotid artery endothelial cells (ECs) adhere to the surfaces of PIPAAm-1.4 and proliferate to form confluent cell monolayers. The cell monolayers were harvested as single cell sheets by temperature decrease from 37°C to 20°C (Fig. 2a). On the contrary, ECs did not adhere to the surfaces of PIPAAm-2.9 (Fig. 2b). This phenomenon was correlated with an adsorption of cell adhesion protein, fibronectin onto surfaces of PIPAAm-1.4 and -2.9.

On the basis of these results, we made a schematic drawing of the differences in molecular motion of grafted PIPAAm chains on two types of PIPAAm grafted surfaces at 20°C and 37°C (Fig. 3). An arrow with a gradient of black and green colors illustrates the degree of the molecular motion. In case of the ultra thin PIPAAm gel layers on TCPS, hydrophobic interaction at TCPS interfaces is also likely to promote aggregation and enhanced dehydration of the covalently bound PIPAAm chains (region 1). The hydrophobic and immobile TCPS interfaces restrict molecular motion of the PIPAAm grafted chains. Such restriction of chain mobility should be extended to the outermost regions of PIPAAm chains for PIPAAm-1.4 (region 2). For thicker polymer grafted gel of PIPPAm-2.9, more polymer chains at the outermost regions are hydrated (region 3) than that on PIPAAm-1.4 grafted surfaces. We consider that different dynamic chain mobility between the two dishes should affect cell adhesive properties.

4. Conclusions

In the present study, we demonstrate that thickness and the amount of grafted PIPAAm layers have significant influence on surface properties in terms of thermoresponsive cell adhesion and detachment with approximately 20-nm thick is the key factor for PIPAAm-grafted surface to achieve adhesive cell adhesion and detachment with temperature. Progressive dehydration of PIPAAm chains existing at the vicinity of hydrophobic TCPS may be important to show cell adhesion character at 37°C. By contrast, the graft polymer at outermost interfaces of PIPAAm-2.9 should have more polar characteristics even at 37°C than PIPAAm-1.4, which affect cells not to adhere on them.

References

[1] Kikuchi, A.; Okano, T. *Prog. Polym. Sci.* **2002**, 27, 1165-1193.

[2] Kanazawa, H.; Yamamoto, K.; Matsushima, Y.; Takai, N.; Kikuchi, A.; Sakurai, Y.; Okano, T. *Anal. Chem.* **1996**, 68, 100-105.

[3] Yamada, N.; Okano, T.; Sakai, H.; Karikusa, F.; Sakurai, Y. *Makromol. Chem. Rapid. Commun.* **1990**, 11, 571-576.

[4] Yamato, M.; Shimizu, T.; Harimoto, M.; Hirose, M.; Kushida, A.; Kwon OH.; Kikuchi, A. Okano, T. In *Tissue Engineering for Therapeutic Use 5*, Ikada. Y, Ohshima, N, eds.; Elsevier Science, The Netherlands **2001**; 93-100.

[5] Sakai, H.; Doi, Y.; Okano, T.; Yamada, N.; Sakurai, Y.; In *Advanced Biomaterials in Biomedical Engineering and Drug Delivery Systems*, Ogata, N. Feijen, J. Kim, SW. Okano T, eds.; Springer, Tokyo **1996**; 229-230.

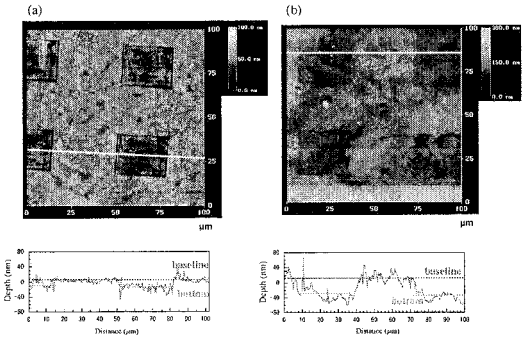

Figure 1. Tapping mode ™ AFM observation for the laser ablated domains on PIPAAm-1.4 (a) and PIPAAm-2.9 surfaces (b). The baseline and the bottom were averaged the text data from the section profiles. Scan size was 100 μm × 100 μm.

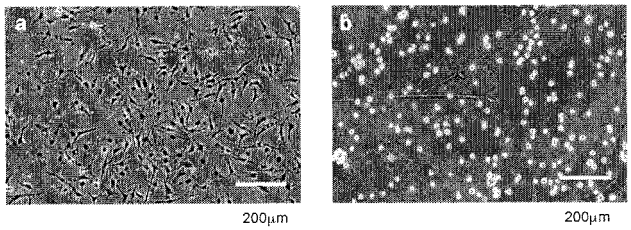

Figure 2. Phase-contrast microphotographs of ECs cultured on PIPAAm-1.4 (a) and PIPAAm-2.9 (b) at 37°C for 1 day.

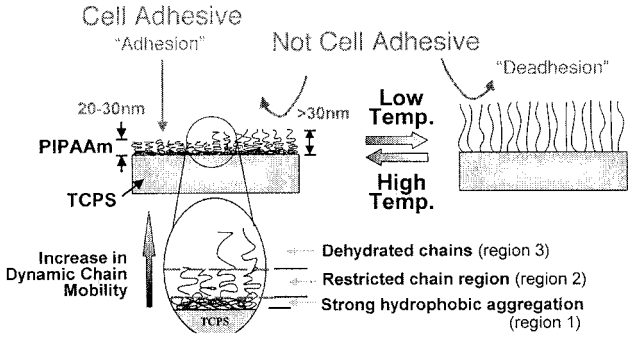

Figure 3. Schematic drawings of an influence of molecular motion of grafted PIPAAm chains on hydration of the polymer chains, when the grafted PPAAm gels are thin and thick at 37°C (left side) and 20°C (right side), respectively. Hydrophobic TCPS interfaces promoting aggregation and dehydration were represented as black region in TCPS. Molecular motion of the grafted polymer chains becomes larger, according to the distance away from TCPS interfaces.

BIOCOMPATABILITY OF SURFACES FOR ANTIBODY MICROARRAYS: DESIGN OF MACROPOROUS SILICON SUBSTRATES

Cornelia Steinhauer[1], Anton Ressine[2], György Marko-Varga[3], Thomas Laurell[2], Carl A.K. Borrebaeck[1] and Christer Wingren[1]

[1]*Dept. of Immunotechnology, Lund University, P.O. Box 7031, SE-220 07 Lund, Sweden*
[2]*Dept. of Electrical Measurements, Lund University, P.O. Box 118, SE-221 00 Lund, Sweden*
[3]*Dept. of Analytical Chemistry, Lund University, P.O. Box 1248, SE-221 00 Lund, Sweden*

Abstract

Antibody microarray is a novel technology with great promise within proteomics. Intense work is under way to evolve this methodology into the high-throughput proteomic research tool needed by the research community. Despite recent advances, there is a growing need for additional high-performance substrates for antibody microarrays as well as for protein arrays in general. In this study, we have sucessfully designed novel, highly biocompatible and well-performing silicon-based supports that has the capacity to play a significant role within current and future antibody and protein microarray applications within the field of proteomics.

Keywords: antibody microarrays, protein microarrays, substrates, solid supports, macroporous silicon

1. Introduction

Major efforts are currently under way to develop the antibody microarray technology to enable global proteome analysis to be performed in a facile manner. In this process, it has become evident that the design of both the probes and the solid support will play a crucial role. We have recently shown that recombinant human single-framework antibody fragments (SinFabs), selected from the n-CoDeR library [1], was an excellent probe source providing highly functional and sensitive microarrays [2-4]. To date, a variety of substrates based on glass, gold, plastics, membranes/filters and gel pads, carrying different surface modifications, have been applied. Recently, we have shown that also silicon may be used as a preferred substrate for protein microarrays [2,5]. Despite these recent efforts, the performances of the current supports vary and no substrate or group of substrates can still meet all of the demands required of a high-performance substrate. Thus, there is a clear need for novel supports directly designed for antibody microarrays with superior characteristics. The aim of current study was to develop new biocompatible silicon-based supports for protein microarrays based on adsorbed SinFabs, selected from the n-CoDeR library.

3. Experimental

We used single-chain Fv (scFv) antibody fragments selected from our human recombinant antibody library genetically constructed around one framework, the n-CoDer library [1], as source for our probes. The selected SinFab antibody molecules were produced in *E. coli* and purified using affinity chomatography on Ni^{2+}-NTA.

Several iterative cycles of surface design, array production and array evaluation were performed. To this end, several silicon-based supports were designed and produced in-house, including (i) planar silicon, unmodified and derivatised with silane or nitrocellulose, (ii) microporous silicon of different pore size and depth (MIP1-7), (iii) macroporous silicon of different pore size and depth (MAP1-3), and (iv) macroporous silicon coated with different amount of nitrocellulose (MAP3-NC1/4/7). Five commercially available glass substrates, providing different surface chemistry and coupling chemistry, were selected and used as reference surfaces; SpotOn-slides (Scandinavien Micro Biodevices A/S, Denmark), Silane-slides (Sigma, USA), Xenoslide N

(Xenopore, USA), FAST-slides (Schleicher & Schuell, Germany) and HydroGel-slides (Perkin Elmer Life & Analytical Sciences, USA).

The antibody microarrays were produced using a non-contact printer (Biochip Arrayer, Perkin Elmer). The arrays were scanned and quantified, using the confocal ScanArray Express microarray scanner (Perkin Elmer Life). The surfaces were scored based on biocompatibility and probe binding capacity as judged by spot morphology, signal intensities, signal to noise ratios, dynamic range, sensitivity and reproducibility.

4. Results and discussion

In the present study, we have developed novel, highly biocompatible solid supports for microarrays, using adsorbed SinFab molecules as probes. To this end, a variety of silicon-based supports, including planar silicon, micro- and macro-porous silicon, as well as nitrocellulose coated variants thereof, were designed and evaluated in a step-wise procedure. The model surfaces were scored based on biocompatibility and probe binding capacity as judged by spot morphology, signal intensities, signal to noise ratios, dynamic range, sensitivity and reproducibility. A set of five commercially available substrates, selected to represent a set of supports providing different chemistries, were used as reference substrates, including: SpotOn-slides (undisclosed surface chemistry/covalent binding via ε-amino groups), silane-slides (aminoalkylsilane derivatised/adsorption), Xenoslide N (Ni^2-chelate derivatised/ affinity binding), FAST-slides (nitrocellulose coated/adsorption) and HydroGel-slides (modified polyacrylamide gel/adsorption).

The results showed that several well-performing silicon-based supports readily could be designed, where in particular a nitrocellulose coated macroporous variant, MAP3-NC7 (Figs. 1 and 2), received the highest scores. The introduction of nitrocellulose coated macropoures significantly increased the probe binding capacity and/or biocompatability while still maintaining adequate spot morphology. Higher signal intensities (60,000 vs. 10,000-50,000), higher relative dynamic range, lower amount of analyte required (0.8 nM vs 0.8-80 nM), higher signal to noise ratios (30 vs. 10-20) and improved reproducability (coefficient of variation) (5% vs. 10-40%) were observed for MAP3-NC7.

In order to evaluate the performance of our in-house developed substrate, the properties of the best performing variant, MAP3-NC7, were then compared with those of the five reference substrates. The supports carried a three-dimensional (MAP3-NC7, FAST-slides, and Hydrogel-slides), two-dimensional (Xenoslides N) or one-dimensional (Silane-slides) surface coating. The surfaces were again compared and scored based on biocompatibility, probe binding capacity, spot morphology, signal intensities, signal to noise ratios, dynamic range, sensitivity and reproducibility. In comparison, MAP3-NC7 displayed properties equal or better to those of the reference substrates. Taken together, the results clearly demonstrated an enhanced performance of MAP3-NC7 as compared with that of the other substrates, including the five reference substrates. Ranking of the five reference substrates revealed a top-trio, composed of FAST-, HydroGel- and SpotOn-slides, followed by Xenoslide N and then Silane-slides. In the top-trio, the individual ranking (choice) will be dependent on the actual assay requirements at hand (sensitivity, sample complexity, and coupling chemistry etc.). Taken together, we have succesfully designed novel, highly biocompatible silicon-based supports for antibody microarrays.

Acknowledgements

This study was supported by grants from SWEGENE, the Swedish National Research Council (VR-NT), and BioInvent International AB.

References
[1] E. Söderlind, L. Strandberg, P. Jirholt, N. Kobayashi, V. Alexeiva, A.M. Åberg, A. Nilsson, B. Jansson, M. Ohlin, C. Wingren, L. Danielsson, R. Carlsson, and C.A.K. Borrebaeck. *Nature Biotechnol.* 18(8), 852-856 (2000)
[2] C.A.K. Borrebaeck, S. Ekström, A.C. Malmborg Hager, J. Nilsson, T. Laurell and G. Marko-Varga. *Biotechniques* 30(5), 1126-1132 (2001).
[3] C. Steinhauer, C. Wingren, A. Malmborg-Hager, C.A.K. Borrebaeck, *Biotechniques*, 32(supplement), 38-45 (2002).
[4] C. Wingren, J. Ingvarsson, M. Lindstedt, C.A.K. Borrebaeck, *Nature Biotechnol.* 21(3), 223 (2003).
[5] A. Ressine,, S. Ekström, G. Marko-Varga, T. Laurell, *Anal. Chem.* 75(24), 6968-6974 (2003).

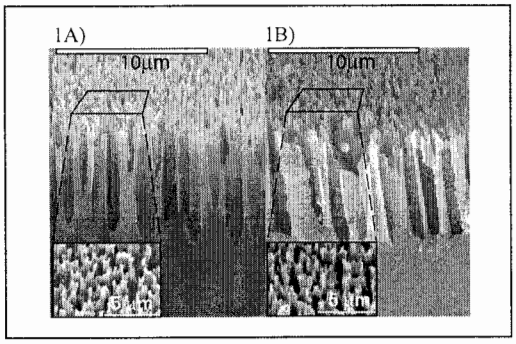

Figure 1. SEM analysis of the best performing in-house developed silicon-based substrate, a nitrocellulose coated macroporous variant (MAP3-NC7), showing cross-sections and inserted top views. The SEM analysis showed that the pore structure of non-modified MAP3 (A) were still fully accessible after coating the surface with a thin layer of nitrocellulose (B).

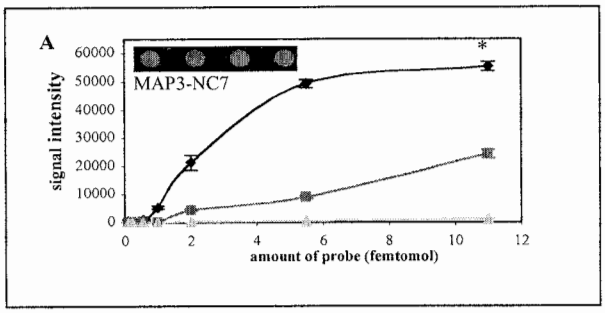

Figure 2. Signal intensities and spot morphologies obtained on the in-house designed MAP3-NC7 substrate. An 8x8 array, composed of an anti-choleratoxin sinFab arrayed in seven serial dilutions ranging from 11 femtomol/spot to 111 attomol/spot, were incubated with Cy5-labelled analyte, choleratoxin subunit B (CT-Cy5), at a concentration of 80 (blue diamonds), 8 (red squares) or 0.8 (cyan triangles) nM. A non-specific scFv (clone FITC-8) was used as negative control.

ELECTRICAL DETECTION OF KINASE ASSAY USING MULTI WALLED-CARBON NANOTUBE(MWCNT) NANOELECTRODE

Jae Shin Lee[1], Do Hyun Kim[1], Seok Jae Lee[1], Jong Pil Park[1], Tae Jung Park[1], Sang Yup Lee[1], Dae-Hwan Jung[1], Hee-Tae Jung[1], Jin Hee Kim[2], and Seong Ku Kwon[3]

[1]Dept. of Chemical and Biomolecular engineering, and Center for Ultramicrochemical Process Systems,KAIST, 373-1, Guseongdong, Yuseong-gu, Daejeon 305-701, Korea

[2]Korea Research Institute of Standard and Science, Daejeon 305-600, Korea

[3] Electronics and Telecommunications Research Institute, Daejeon 305-601, Korea

Abstract

We have demonstrated the use of MWCNT as a nanoscale probe to monitor the activity of enzyme kinase. To immobilize the substrate peptide using carbodiimide chemistry, plasma or strong acid treatments were used to induce carboxyl groups on the sidewall of MWCNTs. After the susbtrate peptide immobilization, increase of conductance from MWCNT devices was observed. When peptide modified MWCNTs react with enzyme kinase, conductance decreases by several orders of magnitude, and this conductance change can be explained by the phosphorylation reaction of enzyme kinase. When the sample was incubated with phosphatase to dephosphorylate the substrate peptide, nearly complete recovery of the conductance signal has been observed and we can confirm that we have monitored the kinase activity.

Keywords: MWCNTs, phosphorylation, biosensor, kinase

1. Introduction

Carbon nanotubes offer a range of extraordinary properties that make them ideal for chemical and biological sensing applications[1]. For example, significant conductance change of single wall carbon nanotubes (SWCNTs) in response to the adsorption of gas molecules and biomolecules demonstrate the possibility of extremely sensitive sensor systems based on them. Recently many researches using MWCNTs have started also in various sensor fields. They could be utilized for the development of carbon-based field-effect transistor(FET) through a simple deformation[2]. MWCNTs also have the potential for the biological sensors since their surfaces can be functionalized by the biomolecules or chemicals for an ultrasensitive electrical detection, which are caused by a binding and adsorption of a charged biological macromolecule or chemicals on the surface[3]. The subtle electronic behaviors of CNT reveal that they have the ability to promote electron-transfer reactions of important molecules, including proteins, DNA, polymers, chemicals and gases, showing a promising system as chemical and biological sensors. In this research, we study a model system of MWCNT-based sensor for kinase A. The schematic procedure of this study is shown in Fig. 1.

2. Theory

MWCNT can have the metallic and semiconducting characteristics shell by shell[4]. In the measurement of electricity, sensitivity depends highly on the state of the surface. The defect of MWCNTs are due to metallity or semiconductivity in semiconductor or metal surface. In addition, when the carboxylic group on the MWCNT make the amide bonding with amine group the protonation is caused[5]. The protonation increases the conductance in semiconductor. Other CNT surface without the carboxylic group adsorbs the protein by nonspecific binding. The metallic CNTs induce the change of workfunction through the immobilization of biomolecules[1].

Phosphorylation of protein occurs on the hydroxyl group of serine, threonine and tyrosine residues[6]. It catalyzes the transfer of a phosphate group, which is an electron-rich functional group, from ATP (adenosine 5'-triphosphate) to the serine residue of the heptapeptide Leu-Arg-

Arg-Ala-Ser-Leu-Gly (LRRASLG) called as kemptide and immobilized on MWCNT electrode. The catalytic transfer of a phosphate group originated from the enzymatic reaction of protein kinase A(PKA) on the MWCNT samples leads to the change of electric properties of the MWCNT for the efficient detection of kinase assay.

3. Experimental

A simple CNT sensor platform is fabricated. In this platform, MWCNTs were deposited on the Au/Ti grid-electrodes using a solution casting process. The MWCNTs were then sonicated in the acidic solution or treated by plasma to produce defects on which carboxyl end-groups are formed. In the next step, suspension was formed by the dispersion of MWCNT in dichloroethane(DCE). A CNT-DCE solution was drop-deposited onto the Au/Ti grid area of the electrodes. Electrodes are deposited on an ending upper part of the MWCNTs with the e-beam lithography. We confirm the carboxylic group by X-ray photoelectron spectroscopy. The XPS measurements were carried out on a ESCAR 2000. After the MWCNT sample was incubated in the peptide solution, the two-probe conductance of MWCNT was measured. All detections were performed using a probe stationCASCADE microtech(HP4156A). Then, we explored PKA reaction on the kemptide immobilized on the MWCNT nanoelectrode device. The sample was incubated with kinase solutions for 1 hour at 37°. The two-probe conductance of MWCNT was measured following the incubation. Finally, the dephosphorylation experiment was carried out.

4. Results and discussion

We can find the XPS binding energy at 287-289 eV as shown in Fig. 2. Immobilization of kemptide increased the conductance. We postulated the MWCNTs were modified with substrate peptides (kemptide) on the partial region of carboxylic group *via* carbodiimide chemistry or kemptides were simply adsorbed on the other empty side of MWCNTs. The carbodiimide chemistry was to form the amide linkages between their amine residues on the kemptide and carboxylic acid groups on the MWCNTs, while the latter was the simple adsorbtion. From the fact that MWCNT surface had both the metallic and semiconducting property[4], we can guess the changed electricity is caused by the protonation on the semiconductor and the change of workfunction on the metal[1]. Through the phosphorylation, a phosphate group has two negative ionic active sites, so they interact with the surrounding ions of the MWCNTs. The reaction of PKA with the substrate peptides coated on the sidewall of MWCNTs significantly decreases the tube conductance up to several times as shown in fig. 3b. After the dephosphorylation reaction of the sample, the conductance was almost restored as shown in Figure 3c. Finally, the conductance decreases due to a phosphorylation of the peptides by kinase. Thus, we can find the recovery property by a biological reaction in the biosensor as shown in Fig.4.

Acknowledgements

The authors are grateful to the support by BK21 project of Ministry of Education and Center for Ultramicrochemical Process Systems.

References

[1] J. C. Robert, H. C. Choi, S. Bangsaruntip, E. Yenilmez, X. Tang, Q. Wang, Y. Chang, and H. Dai, *JACS.*, **126**, 1563-1568 (2004).
[2] R. Martel, T. Schmid, H. R. Shea, T. Hertel, P. Avouris, *Appl. Phys. Lett.*, **73**, 2447-2449 (1998).
[3] Y. Lin, F. Lu,Y. Tu, Z. Ren, *Nano Lett.*, **4**, 191-196 (2004).
[4] P. G. Collins, M. S. Arnold, P. Avouris, *Science,* **292**, 706-708 (2001).
[5] Y. Cui, Q. Wei, H. Park, C. M. Lieber, *Science,* **293**. 1289-1291 (2001).
[6] T. Hunter, *Cell,* **50**, 823-829 (1987).

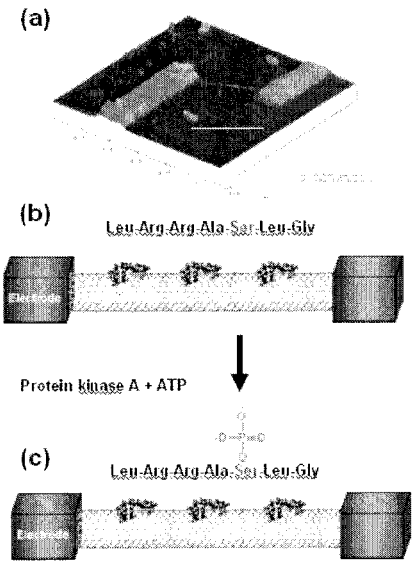

Figure 1. (a) Tapping mode AFM image of a MWCNT device. The nanotube is contacted by two Ti/Au electrodes. Scale bar represents 1 μm. (b) Scheme for peptide substrates immobilization on a metallic MWCNT and electrical measurement. (c) Scheme for phosphorylation of the peptide substrate on a metallic MWCNT by protein kinase A.

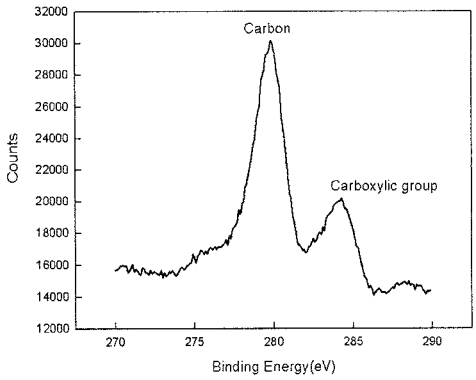

Figure 2. XPS data recorded on a carboxylic acid-functionalized SiO_2 surface by plsama discharge.

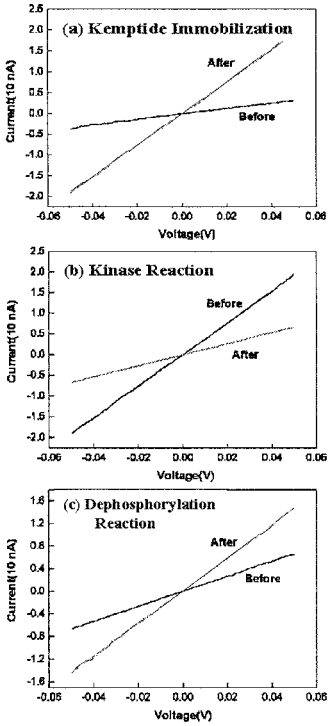

Figure 3. Coupling loss as a function of optical path length for different configurations of beam shaping components.

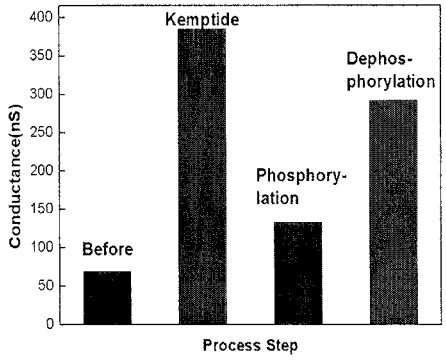

Figure 4. Histogram of conductance variation for each processes before reaction, after kemptide deposition, after phosphorylation and after dephosphorylation(recovery).

A MICROFABRICATED SEGMENTED-FLOW REACTOR FOR THE SYNTHESIS OF CADMIUM SELENIDE QUANTUM DOTS

Brian Yen[1], Axel Günther[2], Martina Thalmann[2], Moungi G. Bawendi[1], Klavs F. Jensen[2]
[1]Department of Chemistry, [2]Department of Chemical Engineering
Massachusetts Institute of Technology, 77 Massachusetts Ave., Cambridge, MA 02139, USA

Keywords: quantum dots, residence time distribution, liquid mixing, segmented flow

1. Introduction

Colloidal semiconductor quantum dots (QDs) have been extensively studied for use in a variety of applications including fluorescent labels, electroluminescent devices, and lasers. QDs (2-10 nm diameter) are typically prepared in a batch process where the precursors are rapidly injected into a heated flask containing a mixture of solvents and coordinating ligands. The optical properties and average size of QDs synthesized in the batch process can depend strongly on factors which are difficult to control such as injection process, local temperature and concentration fluctuations, rate of stirring, and rate of cooling. Single-phase flow reactors in which precursor solutions are delivered into a heated reaction section have addressed some of these issues [1]. However, a single-phase flow reactor has limitations in terms of the residence time distribution (RTD) and slow mixing by diffusion. We have therefore realized a gas-liquid segmented flow reactor which allows for rapid and controlled mixing of precursors as well as narrow RTDs. In contrast to the case of single-phase flow, recirculation within the liquid segments provides a mechanism to exchange fluid elements located near the channel walls with those in the center [3] (Fig. 1). This recirculation has the dual effect of narrowing the RTD and improving mixing of the reagents – factors which have a strong influence on the ultimate size and size distribution of QDs produced.

2. Experimental

The precursor solutions used for the synthesis were identical to those reported previously [2] with some minor modifications. Briefly, a cadmium oleate solution was prepared by degassing cadmium acetylacetonate, oleic acid, and squalane at elevated temperature. Oleyl amine was then added to the solution. The Se precursor solution consisted of trioctylphosphine selenide (TOPSe) dissolved in trioctylphosphine and squalane.

The silicon reactor, fabricated using standard micromachining procedures, accommodated an approximately 1 m long reaction channel (hydraulic diameter ~380 μm) and two shallow side channels (L_{sample}) for collecting reaction aliquots. A 0.5 μm thick oxide was thermally grown on the Si surface, and the entire device was capped and sealed with an anodically bonded pyrex wafer (thickness 500 or 760 μm). The inlet, main channel, and outlet sections were thermally isolated from each other by a ~400 μm deep trench and a halo etch region (Fig. 1). For a typical synthesis, the inlet and center sections were maintained at reaction temperature (260 to 300°C) and the outlet section was cooled (~60°C) to quench the reaction. Heating was provided by contacting the reaction section of the device with a heated aluminum block. Cooling of the quenching region was achieved with a water chilled aluminum block. The Cd and Se precursor solutions were at room temperature and delivered separately into the heated reactor (L_1 and L_2) with a syringe pump. An argon gas stream (G) was introduced further downstream to form a segmented gas-liquid flow. Single-phase flow experiments were performed without gas being introduced. In this case, a miniature convective mixer inline between the pump and reactor ensured that the precursors were completely mixed before reaching the reactor inlet. Optical absorbance and photoluminescence (PL) spectra were taken on raw QD solutions diluted in hexane.

3. Results and discussion

The reactor design makes it possible to achieve rapid initial mixing of the precursors, controlled QD growth, and quenching of the reaction on chip. Recirculation within the liquid slugs rapidly mixes and heats the precursors, thereby initiating the reaction. The fluids initially pass through a meandering section of the channel to ensure good mixing across the centerline before reaching a longer straight-channel section where the majority of the particle growth occurs. The reaction is stopped when the fluids enter the cooled outlet region of the device. Under conditions for a typical synthesis (gas and liquid flow rates: 40 and 20 µl/min at room temperature) the resulting gas and liquid segments are very uniform (Fig. 2a). The as-prepared QD samples possess narrow size distributions as indicated by absorbance and photoluminescence (PL) spectra (Fig. 2b). The principal band edge and several higher transitions are clearly resolved in the absorbance spectrum, and PL line width is also very narrow (FWHM <30 nm).

In addition to the rapid initial mixing, the narrow QD size distribution arises from improved RTDs. In order to compare the RTD effects between single- and two-phase flows, it was necessary to eliminate the contribution from the initial mixing time of the precursors. This was accomplished by cooling the inlet region of the reactor so that in the single-phase mode, the pre-mixed precursors do not react until they reach the reactor channel. Similarly, in segmented flow, the precursors are mixed rapidly on-chip without reacting before they reach the heated center section. The spectra in figure 3a illustrate the improvement of the size distribution from the narrowed RTD effect. Both the absorbance and PL spectra of QDs produced in segmented flow have sharper features in comparison to the single-phase case. Figure 3b is a plot of the full width at half maximum (FWHM) of the PL peak for samples prepared at several flow conditions (mean residence times). In the single phase case, the PL peak (and therefore the size distribution) broadens at shorter times, consistent with results reported previously [2]. In contrast, the spectra of samples prepared in segmented flow are uniformly narrow over the entire range of residence times.

4. Conclusions

We have exploited both the rapid mixing and narrow RTD characteristics of gas-liquid segmented flow to prepare CdSe QDs with narrow size distributions. The former advantage is particularly important for nanoparticle chemistries in which the precursors react rapidly at room temperature, making pre-mixing off-chip impossible. Further work involves implementing the segmented flow design for the preparation of other QD material systems.

Acknowledgements

We thank the staff of MIT Microsystems Technology Laboratories and members of the Microchemical Systems Technology Center. B.K.H.Y is grateful for support from the NDSEG Fellowship program. This work was supported in part by the MRSEC Program of the National Science Foundation (DMR 02-13282).

References

[1] J. deMello, A. deMello, *Lab on a Chip*, ***4***, 11N-15N (2004), and references therein.
[2] B.K.H. Yen, N.E. Stott, K.F. Jensen, M.G. Bawendi, *Adv. Materials*, ***15***, 1858-1862 (2003).
[3] A. Günther, S.A. Khan, M. Thalmann, F. Trachsel, K.F. Jensen, *Lab on a Chip*, ***4*** (2004), Advance article.

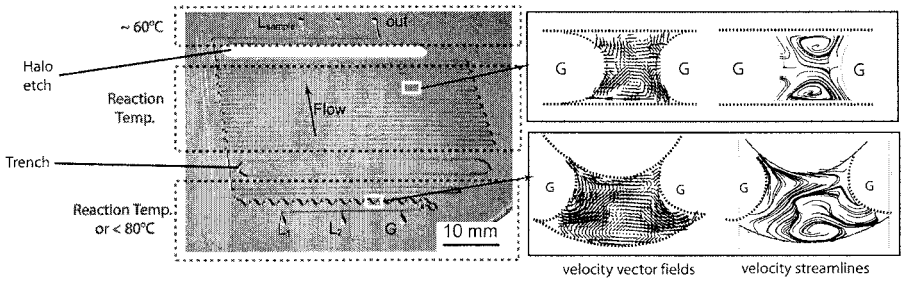

Figure 1. Left: Photograph of the reactor with the different temperature zones indicated. Right: Illustration of recirculation in liquid segments for the straight and meandering channel geometries [3] (flow from left to right, bulk liquid velocity subtracted). The plots were obtained by particle imaging velocimetry (PIV) of dye-doped microspheres dispersed in ethanol. The air-ethanol segmented flow was carried out in a PDMS reactor at flow rates similar to those of the QD synthesis.

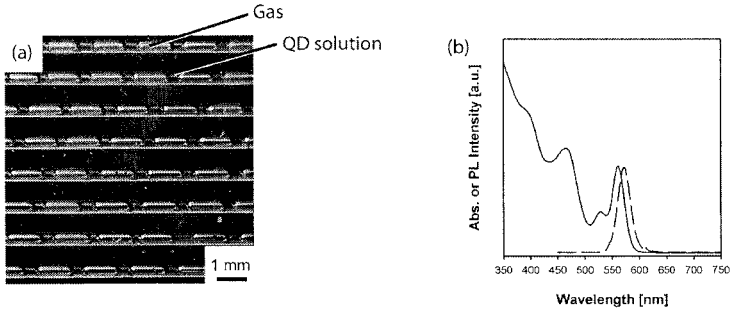

Figure 2. (a) Photograph of a section of the reaction zone during a typical synthesis of CdSe QDs. T=260°C, gas (light) flow rate: 40μL/min, liquid (dark) flow rate: 20μL/min. Mean residence time approximately 100 s. (b) Absorbance (solid) and photoluminescence (dashed) spectra of QDs prepared at the conditions shown in (a).

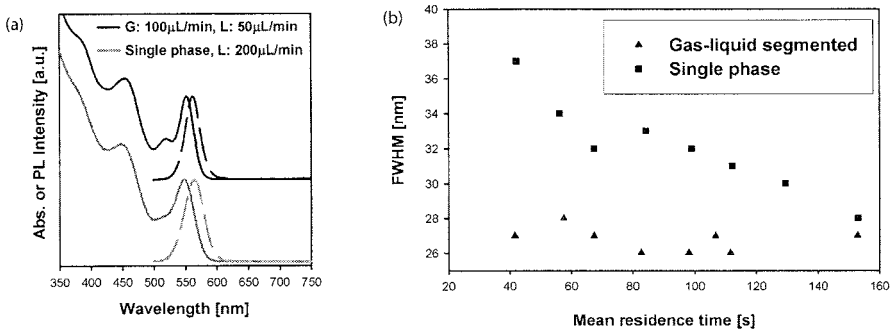

Figure 3. (a) Spectra of QD samples prepared in segmented (top) and single-phase (bottom) flow. Mean reaction time was approximately the same for the two samples (~40 s). (b) FWHM of the PL peak for samples prepared at different flow rates (residence times).

PATTERNING OF SURFACE-CAPTURE ARCHITECTURES IN POLYMER-BASED MICROANALYTICAL DEVICES

Robin L. McCarley[1], Steven A. Soper[1], Michael C. Murphy[2], Suying Wei[1], Alison F. Smith[1], Bikas Vaidya[1] and Juan Feng[2]

[1]Department of Chemistry, [2]Department of Mechanical Engineering, and Center for BioModular Microsystems (CBM[2]), Louisiana State University, Baton Rouge, LA 70803 USA

Abstract

The formation of well-defined, micrometer-sized, selective (antibodies) and non-selective (sorbent, responsive polymer) capture agent architectures on surfaces of polymeric microfluidic devices is described. Biomarker-relevant (breast cancer), oriented antibody arrays and protein-preconcentrator/microextractor features (thermoresponsive polymers) are shown to be functional platforms in hot-embossed poly(methyl methacrylate), PMMA, and poly(carbonate), PC, devices. Capture—by immobilized antibodies—of whole, intact, respiring cells containing membrane proteins linked to breast cancer (EpCAM), surface sandwich immunoassays for carcinoembryonic antigen (CEA), a well-known biomarker for breast cancer, and preconcentration of a variety of proteins by poly(*N*-isopropylacrylamide), pNIPAAm, are demonstrated.

Keywords: Cell capture, Immunoassay, Thermoresponsive polymer

1. Introduction

Polymeric substrates for the construction of microfluidic analytical systems have moved to the forefront due to the ease of which such materials can be fabricated using molding, embossing, and machining techniques [1-3]. Recent advances in surface modification of such polymer-based devices have further strengthened their applications [4, 5]. More sophisticated surface chemistry platforms and elaboration thereof by bio- and polymer-based materials is required for the development of sensitive and specific microanalytical devices.

2. Experimental

Carboxylic acid-terminated (CT) PMMA or PC surfaces were formed by UV exposure (15 mW cm^{-2}) through contact photomasks. Antibodies (anti-CEA and anti-EpCAM) and free-radical initiator (2,2'-azobis(2-methylpropionamidine) hydrochloride) were covalently linked to activated, surface carboxylic groups (2-ethyl-5-phenylisoxozolium-3'-sulfonate or 1-ethyl-3-(3-dimethylaminopropyl)carbodiimide, EDC). EpCAM cells were obtained from a local facility. pNIPAAm surfaces were formed by immersion of the initiator surfaces in a N_2-purged, 25% w/v aqueous solution of NIPAAm at 50°C for 2 min.

3. Results and Discussion

Whole EpCAM cells can be captured from flowing streams (2 mm/sec flow velocity) in the channels of polymer microfluidic devices when their surfaces are derivatized with anti-EpCAM antibodies and the width of the channel facilitates effective cell transport. By manipulating the channel width, low and high surface densities of cells can be achieved, **Figure 1**. Fluidic modeling that incorporates cell sticking probabilities, cell velocities, and channel aspect ratios has been shown to be effective in describing these observations and will be discussed.

Proteins can be preconcentrated (microextracted) from aqueous solutions by pNIPAAm films formed on PMMA surfaces, and the preconcentrated proteins can then subsequently be released without any carry over. Shown in **Figure 2** are fluorescence microscope images of a PMMA surface that was exposed to a dye-labeled protein above the lower critical solution temperature (LCST, the temperature where the pNIPAAm converts from a hydrophilic, protein non-fouling

substrate to a hydrophobic, protein fouling substrate) and below the LCST. The lack of carry over has been confirmed by X-ray photoelectron spectroscopy experiments with labeled proteins.

Sandwich immunoassays (with fluorescence reporting) targeting the presence of CEA in aqueous solutions are readily achieved in the polymer-based microfluidic devices. Fluorescence microscope images (see **Figure 3**) of microchannel devices operated in sandwich assay format demonstrate that low levels of target materials can be observed. We have also shown that higher capture efficiencies can be achieved with oriented antibodies formed through the use of protein A or G layers.

Acknowledgments

The financial support of the United States of America National Institutes of Health and National Science Foundation, as well of that of the Louisiana Board of Regents, is gratefully acknowledged.

References

[1] S.A. Soper, S.M. Ford, S. Qi, R.L. McCarley, K. Kelly, and M.C. Murphy, *Anal. Chem.*, **72**, 643A-651A, 2000

[2] H. Becker and L.E. Locascio, *Talanta*, **56**, 267-287, 2002

[3] Boone, T. D.; Fan, Z. H.; Hooper, H. H.; Ricco, A. J.; Tan, H.; Williams, S. J. *Anal. Chem.*, **74**, 78A-86A, **2002**

[4] Belder, D.; Ludwig, M. *Electrophoresis*, **24**, 3595-3606, 2003

[5] A.C. Henry and R.L McCarley, *J. Phys. Chem. B*, **105**, 8755-8761, 2001

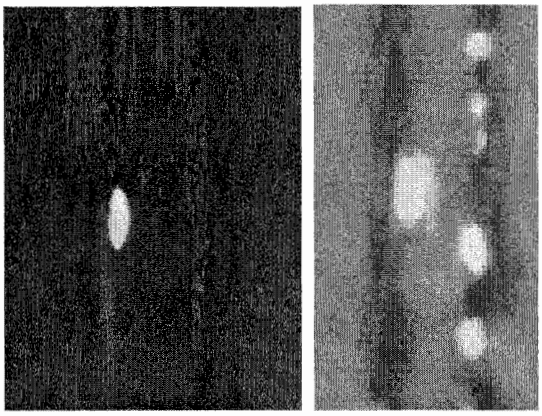

Figure 1. Fluorescently stained (4'-6-Diamidino-2-phenylindole, a nuclear stain), respiring EpCAM cells on (left) 50μm- and (right) 20μm-wide PMMA channels derivatized with anti-EpCAM.

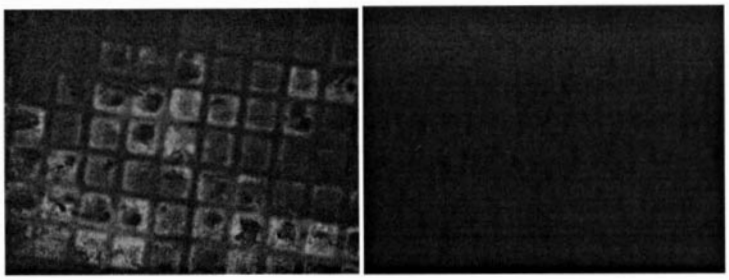

Figure 2. Fluorescence micrographs of 18 μm x 18 μm pNIPAAm patterns on PMMA exposed to fluorescein-labeled protein in pH 7.4, 0.01 M phosphate buffered saline, above the LCST (40°C, left) and (0.5°C, right).

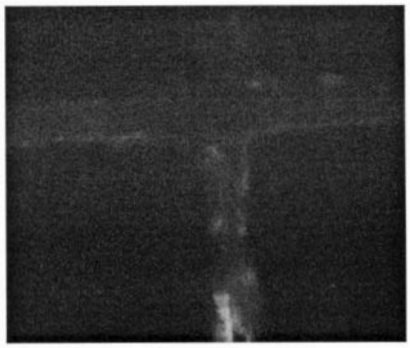

Figure 3. Fluorescence micrograph of an anti-CEA antibody sandwich assay. Channel width is 50 μm.

A MICROFABRICATION USING VACUUM ULTRAVIOLET LIGHT FOR μ-TAS APPLICATIONS

Takatoki Yamamoto and Teruo Fujii

Institute of Industrial Science, The University of Tokyo, 4-6-1 Komaba, Meguro-ku, Japan

Abstract

It is developed a novel light induced surface modification methods for PDMS based microfluidic devices using an incoherent vacuum ultraviolet (VUV) light. PDMS surface is exposed with VUV light in order to control hydrophilicity, ζ-potential, bonding strength, etc. that are all executed under atmospheric conditions. The VUV light induced chemical changes are investigated by X-ray photoelectron spectroscopy (XPS) which indicates the change from the PDMS to SiO_2-like chemical composition. Additionally, as an evaluation of VUV light based fabrication, a simple electrostatic on-off valve is developed.

Keywords: VUV light, eximer UV, photoresist, XPS, electrostatic valve

1. Introduction

The surface modifications physically and chemically are one of the most commonly used technique to realize hydrophilic/hydrophobic zone, bonding substrates, immobilize functional molecular species, etc. in such diverse areas as μ-TAS and BioMEMS, up to now there have been many efforts to improve these techniques. Though some way such as oxygen plasma and strong acids are de facto standard, high energy photons of ultraviolet lights especially with UV excimer laser is also engaged as an environmentally friendly and easier process since no chemicals, gases and vacuum are involved. However, a laser exposure takes time to scan the whole area to be modified because of the tightly focused beam spot. In this work, it is developed a novel surface modification technique using an incoherent vacuum ultraviolet (VUV) light, with wide-area illumination capability, to modify the surface of substrates especially PDMS, and investigated the chemical change of the surface of PDMS by X-ray photoelectron spectroscopy (XPS). Furthermore, as a demonstration of VUV light based fabrication, an electrostatic microvalve was developed.

2. Experimental

2-1 VUV induced modifications of PDMS

VUV light exposure onto PDMS was performed with a dielectric barrier discharge excimer lamp filled with xenon gas (UVS-1000SM, Ushio Inc.), which emits a light with the wavelength at 172 nm. Such a VUV light not only has a high energy, but also directly absorbed by O_2 in the atmosphere to generate excited oxygen atoms and ozone to modify the surface of materials. PDMS substrates were irradiated with the intensity of approximately 30 mW/cm^2 in a distance of about 3 mm from the outer window surface of the lamp chamber. Basic properties of VUV light induced modifications of PDMS such as ζ-potential, contact angle, bonding strength to a glass are shown in Fig. 1 a) to c) compared with that of oxygen plasma modifications respectively. VUV light induced chemical change of PDMS was investigated by XPS analyzer (Quantum 2000, Physical Electronics Inc.) to evaluate the relationship between chemical compositions and surface properties.

Fig. 1a shows the change of contact angle which reaches the maximum with 60 seconds exposure (1800 mJ dose), then it start going hydrophobic again. Fig. 1b shows ζ-potential change with increasing exposure reveals that it is totally different from the tendency by oxygen plasma treatment. ζ-potential reaches the maximum with 10 seconds exposure (300 mJ dose), and then suddenly decreases toward the original potential of PDMS. The bonding strength of PDMS to glass decreases with exposure, and over 10 seconds exposure deprives PDMS of adhesiveness. The remarkable property of VUV light exposure is a short time exposure less than 1 second (corresponds to < 30 mJ) makes PDMS strongly adhesive with covalent bonding even there are quite a little

change in ζ-potential and contact angle. XPS measurements indicate large change in the chemical composition of the exposed PDMS from PDMS to SiO_2-like composition shown in Table 1. The amount of carbon decreases drastically while the amount of oxygen increases with increasing VUV light exposure. Around 120 seconds exposure, the carbon content decreased from 48.4 at.% to 7.2 at.%, while the content of oxygen increased from 29.3 at.% to 64.6 at.%. Since the atomic composition rate of O / Si was changed from ≈1 to ≈2, and binding energy of the Si 2p was shifted from 102 eV to 103 eV and O 1s was shifted from 532 eV to 533 eV, the surface of PDMS might be changed to SiO_2 [1, 2]. The above mentioned property of ζ-potential, contact angle and bonding strength might be caused by the chemical change of PDMS.

2-2 Electrostatic valve – as an example of VUV light based methods-

By using the advantages of VUV light based fabrication, we demonstrated an electrostatically driven on-off membrane valving device. The microvalve consists of three layers such as a valve chamber chip, a diaphragm with moving electrode inside, a fluidic chip respectively. The fabrication process is summarized in Fig. 2a-d. Fig. 2a shows the fabrication step of a hemisphere-like shaped valve chamber on which a fixed counter electrode is formed. The chamber is connected to atmosphere through a tiny channel works as an air vent to release the pressure inside of chamber when the diaphragm deforms. Fig. 2b is a PDMS diaphragm with a deformable electrode inside. Fig. 2c shows a passive stem structure inside of a flow channel. The stem structure is 10 μm higher than the height of flow channel to push the diaphragm toward inside of the valve chamber as initial condition. This condition offers two advantages, one is better seal between the diaphragm and the stem structure, second is the diaphragm is placed closer to the fixed electrode that generates higher electrostatic force between two electrodes. A thick negative photoresist of XP KMPR-1050 (Nippon Kayaku Co., Ltd.) was used as a chip material, since we found it is possible bond to PDMS and this photoresist permanently with exposing VUV light for 3600mJ to KMPR-1050 and 30mJ to PDMS respectively. It is note that, over 30 mJ exposure makes PDMS unadhesive to KMPR photoresist. The diameter of diaphragm is 3 mm and the thickness is about 20 μm with a 100 nm thick Au electrode inside. The distance between the fixed counter electrode and the surface of membrane is about 40 μm.

By applying an electrical voltage between the diaphragm electrode and the counter electrode, an electrostatic force is generated on the diaphragm to pull it into the valve chamber. We confirmed that the diaphragm was deformed and adhered onto the counter electrode by applying around 300 V, which led a liquid to inside of the flow channel pass over the stem structure.

3. Conclusions

A novel vacuum ultraviolet (VUV) light based fabrication methods are developed, and it applied to fabricate an electrostatic on-off microvalve as a demonstration. The basic property especially required designing microdevices in μ-TAS and BioMEMS such as ζ-potential, contact angle, adhesion strength is evaluated. The chemical change of the PDMS surface is analyzed by XPS reveals VUV light exposure changes PDMS to SiO_2. The VUV light has many advantages against conventional oxygen plasma treatment. We believe VUV light based methods will be much more common to fabricate microdevices.

References

[1] K. Callewaert, et al., Applied Surface Science 208-209 (2003) pp.218-225

[2] B. Eliasson and U. Kogelschatz, IEEE Transactions on Plasma Science, Vol. 19 No.2 (1991) pp. 309-323

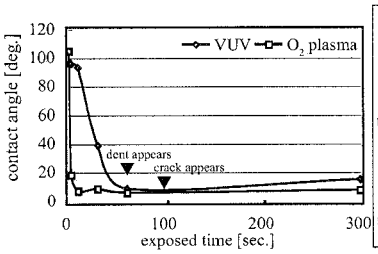

a) contact angle v.s. exposure

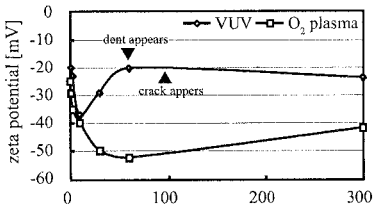

b) ζ-potential v.s. exposure

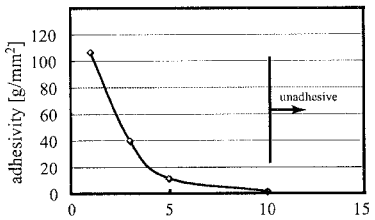

c) Bonding strength v.s. exposure

Figure 1. VUV light exposure effects onto PDMS

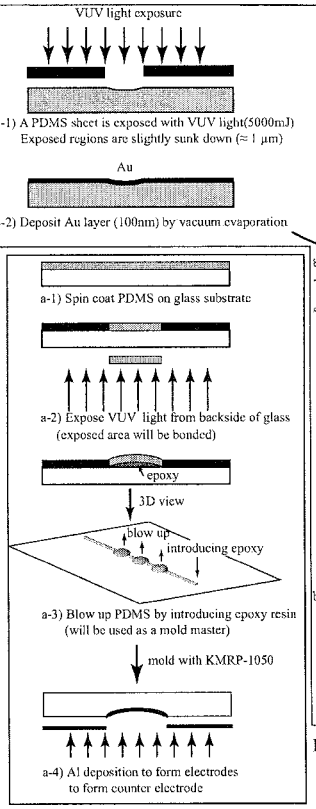

Figure 2 a). Fabrication process of valve chamber chip

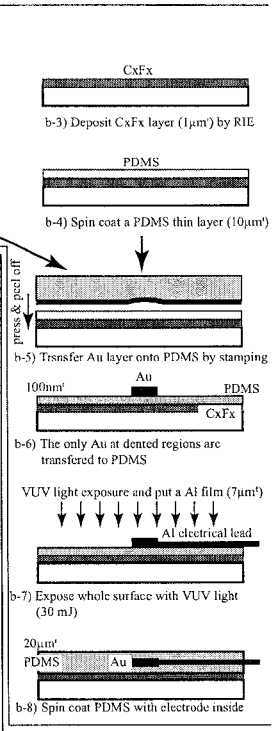

Figure 2 b). Fabrication process of diaphragm

Table 1. Chemical composition of VUV light exposed PDMS determined by XPS analysis

PDMS	Si	O	C [atomic %]
theoretical value	25.0	25.0	50.0
non-exposure	22.3	29.3	48.4
1 sec exposure	22.3	30.6	47.1
10 sec exposure	23.7	39.7	36.6
120 sec exposure	28.2	64.6	7.2

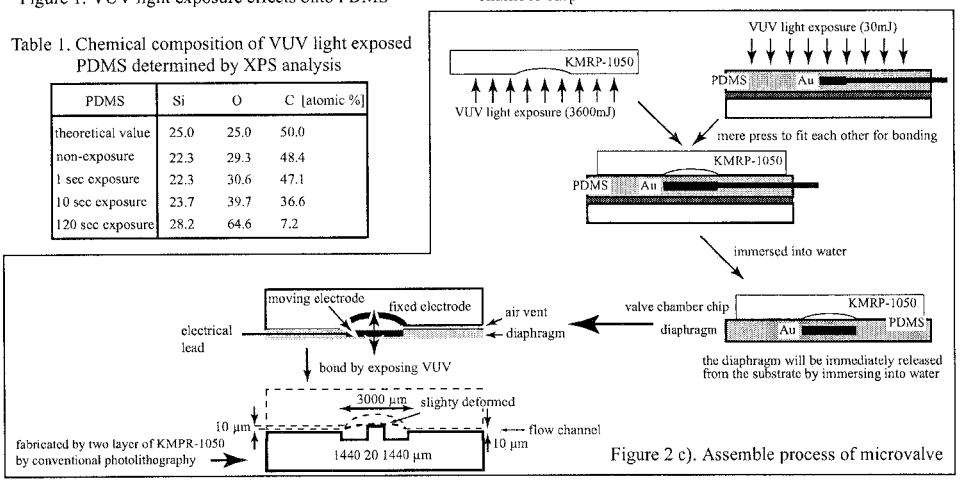

Figure 2 c). Assemble process of microvalve

LONG-TERM STABILITY FOR FRIT-BASED EO PUMPS USING ION EXCHANGE MEMBRANES WITH CONTROLLED DIFFUSION LAYER WIDTHS

Anders Brask, Henrik Bruus, and Jörg P. Kutter

MIC - Department of Micro and Nanotechnology, Technical University of Denmark, DK-2800 Kongens Lyngby, Denmark

Abstract

We report the successful test of a new design for an inline electroosmotic (EO) micropump with long-term stability (up to two hours) under continuous operation and realistic working conditions (flow rates Q ~ 0.5 μL/s and backpressures p ~ 10 kPa). The EO pump, sketched in Fig. 1, is based on microporous frits containing a huge number of narrow pores. The remarkable stability of the pump is achieved by adding a new microfluidic component to the pump that controls the boundary diffusion layers influencing the electrokinetic processes essential for the pumping mechanism.

Keywords: electroosmotic pump, ion exchange membrane, diffusion boundary layer

1. Introduction

Stable operation of EO inline micropumps is highly wanted for use in many microfluidic systems. However, the majority of EO pumps studied so far are only working under idealized operating conditions, such as short operation periods and using continuous flushing. Under realistic load conditions EO pumps often fail over time mainly due to unstable electrochemical conditions such as varying pH levels and bubble formation induced by electrode reactions.

2. Theory

The frit-based EO pump consists of an assembly of eleven layers as shown in Fig. 1. The electrode compartments at the edges of the pump are separated from the frit compartment in the center by anion exchange membranes (AEM), which allow only negative ions to pass while bulk fluid and positive ions are retained. The pressure buildup generated by the frit is therefore confined to the inner loop of the pump, which enables free ventilation of electrolytic gases developed at the electrodes in the outer loop. The pumping stability is governed by the pH in the inner loop.

At the anode the pH will tend to drop because of the hydronium ions (solvated H^+) generated. A low pH will effectively remove the surface charge in the frit and thus stop the electroosmotic flow. It is therefore important that an AEM is used to prevent that hydronium ions are transported into the inner loop where the pumping takes place. Since hydronium ions will be blocked by the AEM to some degree most of the electrical current will be transported by hydroxyl ions (OH^-) that migrate from the cathode to the anode. An ion exchange membrane can only support a certain level of current density i. If the current density becomes higher than the limiting current density i_{limit}, see Eq. (1), dissociation of water will happen on the surface (frit side) of the membrane. This reaction will increase the hydronium ion concentration in the frit.

$$i_{\text{limit}} = z_-(1+z_-/z_+)\, F\, D_-\, c_{\text{bulk}}/dx, \qquad (1)$$

where z_- and z_+ are the charge coefficients of the anion and cation species, dx is the diffusion boundary layer thickness, D_- is the diffusion coefficient of the anions, F is the Faraday constant, and c_{bulk} is the concentration of the buffer. The current density should therefore not exceed the limiting current density considerably. To ensure a high limiting current density the diffusion layer thickness is reduced by adding a new microfluidic component. The spacer layer marked ε in Fig. 1(b), forces

the liquid from the inlet to flow across the ion exchange membrane. The thickness of the diffusion boundary layer surrounding the membrane is kept small by this flow. Furthermore, when the pump is generating flow, the buffer is replenished continuously. One mole of buffer can absorb two moles of hydronium before any substantial pH change. The stability of the pH value and hence the efficiency of the pump is compromised only if the flow is significantly reduced by a high backpressure. A slow flow will increase the diffusion boundary layer thickness dx and subsequently deplete the buffer in the inner loop.

3. Experimental

Flow rates were measured by collecting liquid in a pressurized reservoir placed on a balance (0.1 mg precision). The reservoir pressure (backpressure) was controlled by a N_2 source and measured by two pressure sensors (0-150 psi, 0-10 bar). Suspended flexible silicone tubing was used to connect the collecting reservoir in order to avoid interference with the balance. The data (time, pressures, mass, current, voltage) was collected using a data acquisition card in a PC. pH levels were measured by four color pH indicators.

4. Results and discussion

We have tested two types of frits, A and B, see Table 1. Such frits result in large flow rates while at the same time having a large pressure capability.

	Frit A	Frit B
Material	Borosilicate	Silicate 99.99%
Pore size	1.3 μm	200 nm
Shape	Circular	Square
Area	π (1.8 mm)^2 = 10 mm^2	(5 mm)^2 = 25 mm^2
Thickness	2 mm	1 mm
Borate buffer	5 mM	100 mM
pH level	9.0	9.2

Table 1. A table listing the main properties of the two frits A and B used in the two EO pumps.

The pump characteristics measured in the tests of pump A and B are shown in Fig. 2(a). The flow rate is seen to decrease linearly as the backpressure is increased. Due to electrolysis in the outer loop, the reservoirs α in Fig. 1(a) need to be refilled after several hours of use. The long-term stability for pumps A and B has been observed for 15 min and 30 min, respectively, at specific backpressures. Operating continuously with various loads the pump did not show any signs of degrading performance over a period of 2 hours.

5. Conclusions

A stable stand alone micropump has been developed and tested successfully. The design is highly versatile and can be modified to meet most flow requirements in microfluidic applications. Disadvantages are the dependence on the pumping liquid and development of electrolytic gases. The inline EO pump is simple in its construction and delivers a precise and stable flow.

Acknowledgements

This work is partly supported by the Danish Technical Research Council, μTAS Frame Program Grant No. 26-00-0220.

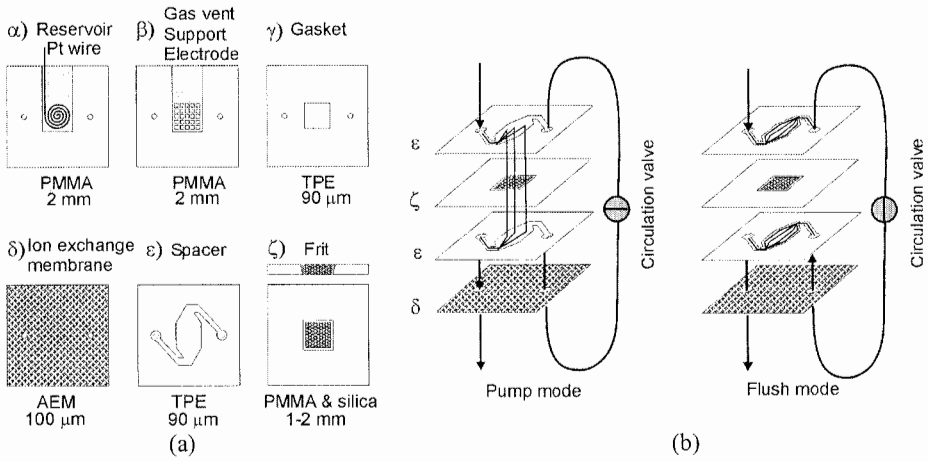

Figure 1. (a) Modular design of the pump consisting of eleven layers assembled in the order |α|β|γ|δ|ε|ζ|ε|δ|γ|β|α|. (b) The new fluidic component is the spacer ε that ensures a stable thickness of the diffusion boundary layer, and hence a stable operation of the pump, by continuous flushing of the membrane during operation. The total pump size is 20 x 20 x 10 mm. The circulation valve is external and used for initial filling and extracting samples for pH measurements.

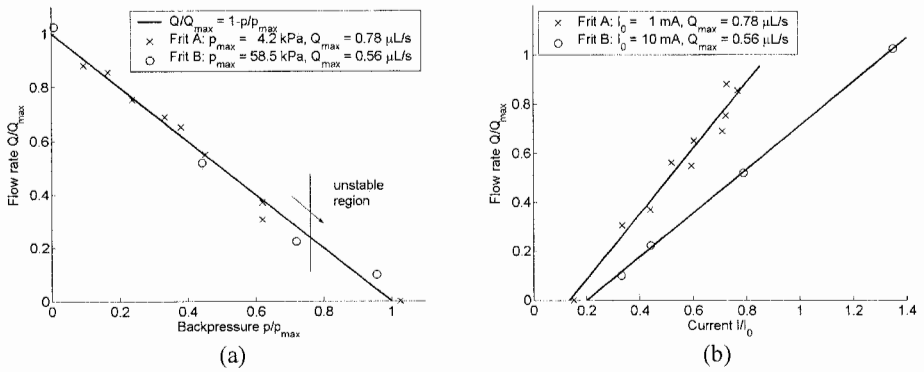

Figure 2. (a) Continuous measurements of the normalized flow rate Q/Q_{max} versus the normalized backpressure p/p_{max} for frit A and B with pore sizes 1.3 μm and 200 nm, respectively. The applied voltage was 30 V in both cases. (b) Continuous measurements of flow rate Q and current I at different backpressure. Same series as in panel (a). The total operation time in this experiment was 2 hours without degrading performance. However, there exists a critical Q/I ratio where the pump becomes unstable. This ratio will be reached near the maximum backpressure capability of the pump. The linear I-Q dependence allows for a feedback loop where the EO voltage driving the pump (and thus Q) can be regulated by the electric current.

PRESSURE DRIVEN CONTINUOUS FLOW IN CLOSED-OPEN-CLOSED LIQUID MICROCHANNELS

Jessica Melin, Wouter van der Wijngaart, and Göran Stemme
Royal Institute of Technology, Department of Signals, Sensors, and Systems, Microsystem Technology, SE 100 44, Stockholm, Sweden

Abstract

This paper introduces a closed-open-closed liquid microchannel that allows direct interfacing with on-chip continuous liquid flow and studies its performance and robustness. The novel component was successfully tested for flow performance, sample addition, and gas bubble removal and compares well with the theoretical model. The novel component behaves as a fluidic transistor where the open channel inlet, the open channel outlet and the air correspond to the source (P_S), drain (P_D), and gate (P_G=P_{air}), respectively. If P_G-P_D≅0, the component acts as a fluidic diode.

Keywords: pressure driven, open channel, micro-channel, fluidic interfacing

1. Introduction

Surface fluidic systems, e.g. microarrays, are commonly interfaced by direct access to the external macro surroundings; however, open systems are vulnerable to evaporation and contamination and do not easily allow liquid control or waste product removal. Closed microchannel systems reduce evaporation, minimize contamination, and allow active fluid control via integrated or external pneumatic actuation. However, basic fluidic operations such as joining liquid samples or reagents in closed on-chip systems typically require integration of active fluid components such as pumps or valves [1]. Tube interfacing consumes space, introduces dead volume and often causes bubbles during priming [2]. Open capillary channels have been presented earlier, including capillary driven surface flow on hydrophilic microstripes [3], capillary filling of open channels [4], as well as gravitationally driven [5], and evaporation driven open microchannel flow [6].

2. Device Functionality

The component carries a continuous flow of liquid and comprises a closed inlet channel and closed outlet channel where the section in between is an open channel exposed to the environment, see Figure 1. Surface tension prevents channel overflow.

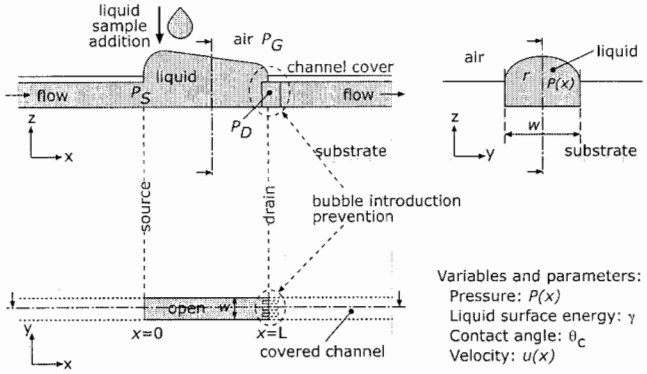

Figure 1. Schematic of a closed-open-closed channel geometry.

Liquid samples were successfully introduced to a constant flow in the open channel (Fig. 1). In addition, bubble removal was tested by introducing bubbles at the fluid inlet. The bubbles disappeared as they entered the open channel.

The closed-open-closed channel can be modeled as a transistor as can be seen in Figure 2. If the system is open to atmosphere (P_G=P_{atm}), pneumatic flow control is either upstream (overpressure; P_{in}>P_{atm}) or downstream (suction; P_{out}<P_{atm}). The liquid curvature and static pressure are fixed by the relation $r(x)=\gamma/P(x)$ at any location in the open channel. The liquid-air surface wicks up when $P(x)>P_G$ and wicks down when $P(x)< P_G$.

The threshold pressure P_t is defined as the pressure difference $P_G - P_S$ which induces liquid to enter the channel. Capillary priming occurs if $P_t< P_G$, while pressure is required for priming if $P_S-P_G>P_t$. Surface tension of the open liquid-air interface prevents the liquid from overflowing (failure mode #1) for moderate pressures. Channel overflow can only occur during larger upstream pneumatic overpressure and starts at the channel source. Viscous losses cause a pressure drop $P_{SD}=P_S-P_D$ along the open channel, resulting in a change in liquid surface curvature $1/r(x)$, as is qualitatively depicted in Figure 2. In many applications of interest, the kinematic pressure drop is negligible: $\rho u(x)^2/2<<|P(x)-P_G|$. The pressure inside the liquid channel determines the cross section of the liquid in the open microchannel, see Figure 3. If the surface radius $r(0)$ at the source is forced beyond the minimum ($r_{min}=w/2$), overflow occurs. If the design is suboptimal, overflows occurs due to wetting of the top surface of the open channel. Thus, appropriate geometrical design allows system optimization in terms of overflow robustness. For pressures $P_G-P(x)$ below a value P_{det}, the air-liquid-solid 3-phase line detaches from the channel edge and moves downwards to the bottom of the channel (the fluid transistor moves from linear to saturation regime). The exact position of the 3-phase line depends on the cross-sectional channel geometry. When P_D drops below a pinch-off pressure, P_{po}, part of the channel near the drain becomes pinched off (dry). At this point, the transistor "saturates" with pressure-flow characteristics depending on the exact channel cross-section. Even further decrease of P_D eventually results in introduction of gas bubbles through suction at the drain (failure mode #2). However, the latter effect can be avoided by geometrically ensuring large capillary forces at the drain as is schematically illustrated in Figure 1.

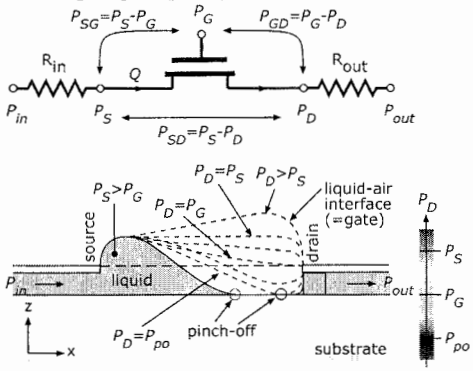

Figure 2. Schematic circuit representation of the component (top). The open liquid channel for varying P_D and constant P_S and P_G (bottom).

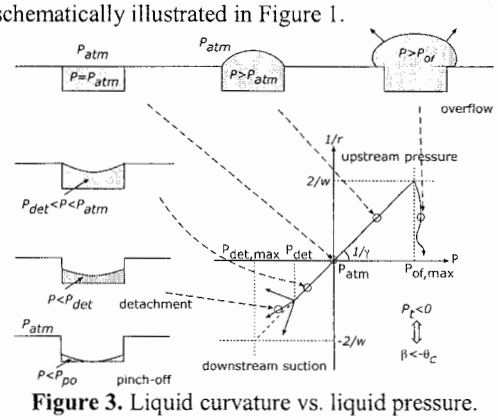

Figure 3. Liquid curvature vs. liquid pressure.

3. Device Characterization

Experiments were performed using a PDMS-glass closed-open-closed microchannel and hydrostatically controlled water pressure as shown in Figure 4. As can be seen from Figure 5, where P_{in} was constant and P_G-P_{out} was varied, and from Figure 6, where P_G and P_{out} were kept constant while P_{in} was varied, measurements verified the theoretical flow performance for the open micro-channel. The open channel is modeled as open plate flow. Note the fluidic diode characteristics of the device when $P_G=P_D$ (Fig. 6).

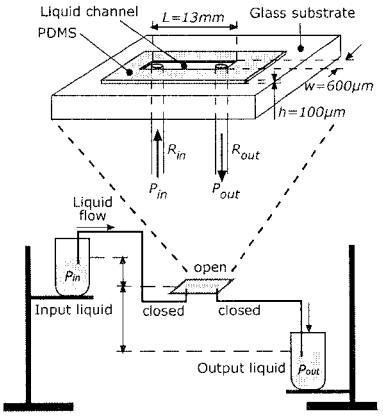

Figure 4. The closed-open-closed microchannel in its experimental set-up.

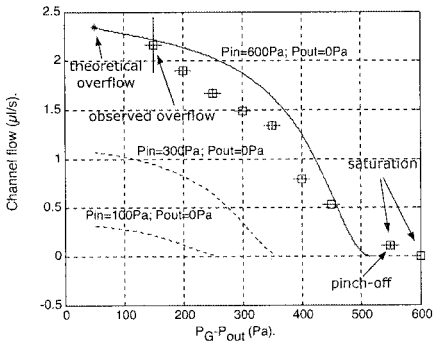

Figure 5. Measured values (squares) and theoretical model (solid curve) of the gate pressure P_G vs. flow for the microchannel.

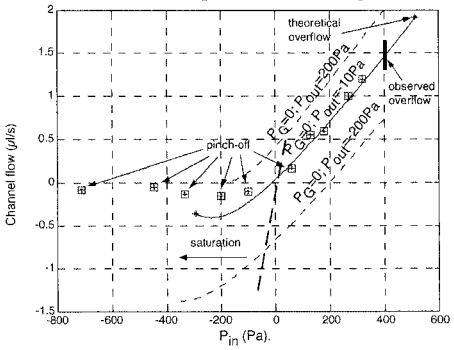

Figure 6. Measured values (squares) and theoretical model (solid curve) of the inlet pressure P_{in} vs. flow for the microchannel.

4. Conclusions

This novel component can be used for applications including introduction of samples in flow-through microsystems or removal of gas bubbles in liquid flow. Further studies are currently in progress on developing a more complete theoretical model and understanding how the channel geometry affects the pressure-flow characteristics of the novel fluidic transistor.

References

[1] T. Thorsen, S.J. Maerki, S.R. Quake, *Science*, **298**, 580-584 (2002).

[2] J. Melin, N. Roxhed, G. Gimenez, P. Griss, W. van der Wijngaart, G. Stemme, *Sensors and Actuators B*, **100**(3), 475-480 (2004).

[3] A.A. Darbuher, S.M. Troian, *Physical Review E*, **64**, 031603-1 – 031603-8 (2001).

[4] L.A. Romero, F.G. Yost, *J. Fluid Mech.*, **322**, 109-129 (1996).

[5] J.A. Kolodziej, G. Musielak, M. Kaczmarek, T. Strek, *Computational Mechanics*, **24**, 110-117 (1999).

[6] G.P. Peterson, J.M. Ha, *J. Heat Transfer*, **120**, 743-751 (1998).

HYDRAULIC PUMPING DEVICES WITH SURFACE MODIFIED STRUCTURES

Debashis Dutta and J. Michael Ramsey
Department of Chemistry, University of North Carolina, Chapel Hill, NC 27599, USA

Abstract

In this work we present the integration of an on-chip hydraulic pumping capability with an open-channel liquid chromatographic separation system. Pressure gradients were generated in this design by exploiting a mismatch in electroosmotic flow rates introduced upon application of an electric field across channels with oppositely charged surfaces. The hydrodynamic flow velocity thus produced in the field-free separation channel was maximized by appropriate depth profiling of the microchannel network.

Keywords: electroosmotic pump, polyelectrolyte multilayers, open-channel liquid chromatography

1. Introduction

Miniaturization of chemical and bio-chemical analysis systems has been demonstrated to be of vast importance due to their ability to rapidly produce precise results. One technology that has shown a lot of promise in this area is the development of microfluidic devices actuated using electrokinetic or hydraulic forces. While the electrokinetic mode of operation is often preferred due to its ease of implementation and better controllability, other factors may limit its application in various chemical and bio-chemical assays. For example, retention of analyte samples may modify the column surface characteristics in an electrokinetically driven liquid chromatographic system thereby affecting the electroosmotic (mobile phase) flow rate. As a result, the performance of these devices and the reproducibility of the assays are often compromised. To improve upon these aspects, hydraulic forces may be employed as a useful alternative to drive liquid samples in such systems. However, miniaturization of hydraulic pumping units and their efficient integration with a separation system offers a significant challenge. Here, we report the development of a separation system with an on-chip pressure generation capability. To demonstrate this new functionality on the microchip platform, Coumarin dyes were separated using the open-channel liquid chromatographic technique in a field-free analysis channel under pressure-driven flow conditions.

2. Pumping Strategy

Surface properties of chemically etched microchannels are often altered to manipulate fluid transport in miniaturised analysis systems via electrokinetic means. In this work we present the induction of hydraulic pressure gradients in a microchip device by applying an electric field across two channel sections with oppositely charged surfaces, i.e., negatively charged fused silica and positively charged polyelectrolyte multilayers. The mismatch in the electroosmotic flow rates thus introduced is counterbalanced by the generation of a pressure-driven flow in the system, which may then be guided to a field-free channel for performing separations. In our system, the polyelectrolyte multilayer chosen consisted of a cationic component, polydiallylmethylammonium chloride (PDADMA, MW 200kDa-300kDa) and an anionic component, polystyrene sulfonate (PSS, MW 70kDa). To apply the polyelectrolyte multilayer to the microchannels, coating solutions of different ionic strengths were used. While the first 3 layers (a layer consisted of one coating of PDADMA followed by one coating of PSS) were coated with 3.5 mM polyelectrolyte solutions (based on monomer unit) in water, polyelectrolyte solutions at the same concentration containing 500 mM NaCl were used for the next 3.5 layers (last coating was PDADMA). The initial layer of PDADMA and PSS was coated for 30 min. and all subsequent layers for 15 min. with a 10 min.

water rinse between each coating run. To determine the effect of the multilayer polyelectrolyte coating on the electroosmotic transport rates, the electroosmotic mobility of the sodium phosphate buffer (pH 7.2) containing 25% acetonitrile (v/v) was measured in an uncoated as well as a completely coated glass microchip. In these experiments, samples of the neutral dye Rhodamine B base were introduced from an injection cross via the gated injection scheme [1] and then later detected using the laser induced fluorescence (LIF) technique to determine the fluid velocity in the microchannels. As expected, the polyelectrolyte coating was observed to reverse the direction of electroosmotic flow in the system yielding a negative value for the electroosmotic mobility [2] (see Fig. 1).

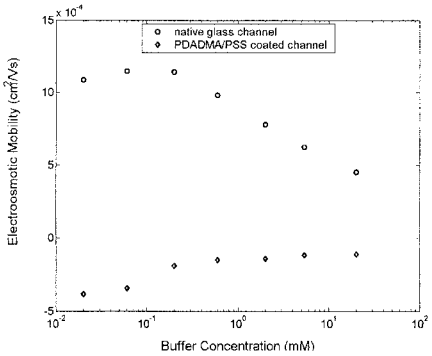

Figure 1. Effect of PDADMA/PSS coating on the electroosmotic mobility of sodium buffer (pH 7.2) containing 25% acetonitrile (v/v).

Proceeding further, a separation device was designed integrated with such a unit as shown in Fig. 2. For selective coating of the targeted channel section in this device, the polyelectrolyte solution (starting with PDADMA) was placed in reservoir 3 (see Fig. 2) while filling the remaining reservoirs with water. Vacuum was then applied to reservoir 4 to induce a flow desired for the coating purpose. The polyelectrolyte-coated device was operated in a mode as depicted in Fig. 2 via electrokinetic means and its performance was quantified by measuring the hydraulic flow rate in the field-free separation channel. As may be seen from the results presented in Figs. 3 and 4, a considerable pressure-driven flow was observed in the analysis column to perform an open-channel chromatographic separation.

3. Separation

To implement open-channel chromatography in the built device, a mixture of 1% octadecyltrichlorosilane (ODS) and 0.25% methyltrichlorosilane (by volume) in dry toluene was chosen as the coating medium. The selective coating of the separation channel was performed by placing this mixture in reservoir 6 while filling the remaining ones with dry toluene. Vacuum was then applied to reservoir 1 for 15 minutes following which the microchip was left alone for 4 hours under ambient conditions. Open-channel chromatography of 30μM Coumarin samples, C-440, C-450 and C-460, was performed on the resulting device using hydrodynamic flow generated on-chip, to drive the mobile phase. As may be seen in Fig. 5, a separation of the different dyes was accomplished under 35 seconds with a 0.6 mM sodium phosphate buffer containing 40% acetonitrile by volume.

References

[1] S.V. Ermakov, S.C. Jacobson and J.M. Ramsey, *Anal. Chem.*, **72**, 3512-3517 (2000).
[2] T. W. Graul and J. B. Schlenoff, *Anal. Chem.*, **71**, 4007-4013 (1999).

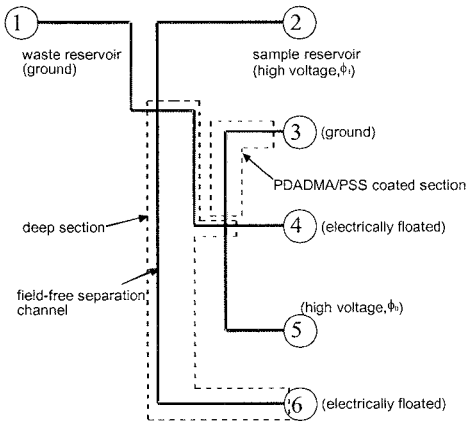

Figure 2. Schematic design of a separation device with integrated pumping unit. The deep section in the layout has a channel depth of 5μm while the remaining portions are 2μm deep. In all our experiments, the ratio ϕ_1/ϕ_0 was chosen to be 0.5.

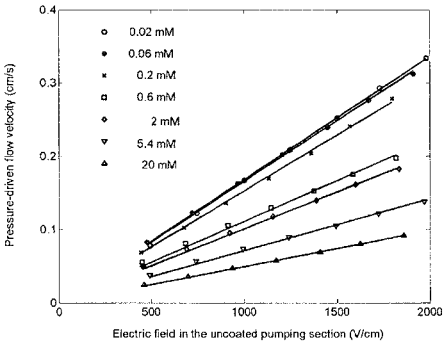

Figure 3. Pressure-driven flow velocity measured in the field-free separation channel.

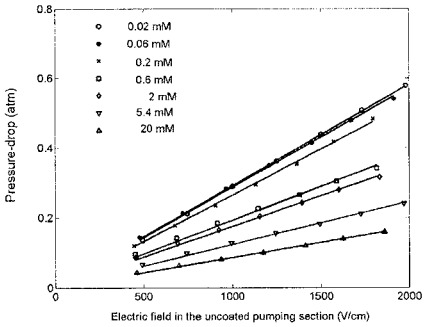

Figure 4. Estimated pressure-drop across the field-free separation channel.

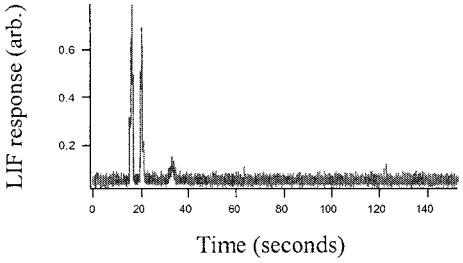

Figure 5. Pressure-driven open-channel chromatography of Coumarin dyes C-440, C-450 and C-460.

A MICROFLUIDIC SYSTEM FOR SCREENING PROTEIN CRYSTALLIZATION CONDITIONS INSIDE NANOLITER DROPLETS WITH ON-CHIP X-RAY DIFFRACTION

Bo Zheng, L. Spencer Roach, Joshua D. Tice, Cory J. Gerdts, Delai Chen and Rustem F. Ismagilov

Dept. of Chemistry, The University of Chicago, 5735 South Ellis Avenue, Chicago, IL 60637

Abstract

Proteins can be crystallized in nanoliter aqueous droplets by using both microbatch and vapor-diffusion techniques inside composite PDMS / glass microfluidic devices. The composition of the droplets was indexed by using alternating droplets. The quality of the protein crystals can be assessed directly by on-chip X-ray diffraction.

Keywords: microfluics, microreactors, proteins, crystal growth, droplet

1. Introduction

This presentation will discuss a composite microfluidic system for performing protein crystallization trials[1] in nanoliter aqueous droplets[2] inside X-ray capillaries. Growing high-quality protein crystals is important for determining protein structures by X-ray crystallography. Crystallization conditions of protein are usually identified by performing a large number of trials. Microfluidics could serve as a platform for such process with the advantage of consumption of small volume (nL-pL) of reagents.[1, 3, 4] and possibility for new methods of crystallization.[4]

2. Results

In this work, we improved the PDMS microfluidic chip by using PDMS/glass capillary microfluidic devices to eliminate the evaporation of solutions through PDMS during crystallization trials (Figure 1b).[1] Crystallization conditions can be screened using both microbatch and vapor diffusion techniques.

For microbatch technique, aqueous streams of solutions of the protein, additives and precipitants flowed into a flowing stream of fluorinated oil, in which all the aqueous streams formed droplets surrounded and carried by the flow of oil. The droplets were transported into a glass capillary attached to the outlet of the PDMS section of the microfluidic device (Figure 1a). The flow was stopped when the capillary was filled with the droplets. The capillary was then disconnected, sealed and incubated at 18°C. To screen the crystallization conditions, the concentrations of the protein and precipitants could be varied by changing the flow rates of the corresponding aqueous streams. Crystals formed in the droplets in capillaries (Figure 1c) under the conditions similar to those we found by using PDMS microfluidic chips.[3] Evaporation of solutions in the droplet was eliminated by using glass capillaries and water-impermeable oil. Droplets and crystals incubated in a sealed glass capillary were stable for over six months.

For vapor diffusion technique, alternating droplets of two different compositions were generated then flowed into glass capillaries (Figure 2a). One composition was the mixture of the protein and precipitants and the other was aqueous solution of NaCl with high concentration. We found that there was no cross-contamination between the two neighbor droplets with different compositions.[5] After the capillary was filled with the alternating droplets, the flow was stopped and the capillary was disconnected and sealed for incubation at 18°C. During the incubation, diffusion of water took place when the two compositions had different salt concentrations and the oil was water permeable. This diffusion caused a decrease in volume of the crystallization solution, and therefore an increase in the supersaturation of the crystallization solution (Figure 2b). The rate

of the vapor diffusion could be controlled by varying the concentration of NaCl and the distance between the two neighbor droplets with different compositions.

Droplets of alternating composition were also used to index concentrations during screening of protein crystallization conditions under microbatch conditions.[5] Droplets containing protein and precipitant and droplets containing two fluorescence dyes (dye A and dye B) were generated alternatively in the microchannel (Figure 3). Dye A was used to index the protein and dye B was used to index the precipitant. By measuring the ratio of the fluorescence of dye A to the fluorescence of dye B in the indexing droplets, the ratio of the concentration of the protein to the concentration of the precipitant in the crystallization droplets could be determined.

Diffraction patterns from crystals grown in droplets inside capillaries were obtained by subjecting the capillaries with crystals directly to the synchrotron X-ray beam (Figure 4). Crystals obtained in the nanoliter-sized droplets had dimensions of about 50-200 μm on each side and were large enough for synchrotron diffraction. Both thaumatin and lysozyme crystals diffracted on-chip to 1.8 angstroms resolution.[1]

3. Conclusions

The system that we will discuss is compatible with both microbatch and vapor-diffusion methods, both of which have been used widely in screening conditions of protein crystallization. With microbatch method, the long-term stability is achieved, which is important to nanoliter-scale protein crystallization. With vapor-diffusion method, the possibility of nucleation for protein crystallization was increased, thus allowing higher yield of protein crystallization in nanoliter-sized droplets. By forming droplets of alternating composition, the concentration of the protein and the precipitant in the crystallization droplets can be determined by measuring the fluorescence of the fluorescent dyes in the indexing droplets. We only indexed concentrations of two solutes in the experiment, but forming alternating droplets of three or more solutions each is also possible. The quality of the crystals grown in the droplets can be evaluated by on-chip X-ray diffraction. This method eliminates the need for manual handling of the crystals which could potentially damage the crystals. We will discuss the application of this system to crystallization of new proteins and for fundamental studies of crystallization phenomena, such as the effects of mixing and surface chemistry.

Acknowledgements

This work was supported by NIH (R01 EB001903), and by Beckman Young Investigator Program, and was performed at the MRSEC microfluidic facility funded by NSF. We thank Phoebe Rice, Keith Moffatt, Andrzej Joachimiak, Chuan He, and Erica Duguid for helpful discussions.

References

[1] B. Zheng, J. D. Tice, L. S. Roach, R. F. Ismagilov, *Angew. Chem. Int. Ed.*, **43**, 2508 (2004).
[2] H. Song, J. D. Tice, R. F. Ismagilov, *Angew. Chem. Int. Ed.*, **42**, 768 (2003).
[3] B. Zheng, L. S. Roach, R. F. Ismagilov, *J. Am. Chem. Soc.*, **125**, 11170 (2003).
[4] C. L. Hansen, E. Skordalakes, J. M. Berger, S. R. Quake, *Proc. Natl. Acad. Sci. U.S.A.*, **99**, 16531 (2002).
[5] B. Zheng, J. D. Tice, R. F. Ismagilov, *Anal. Chem.*, in press (2004).

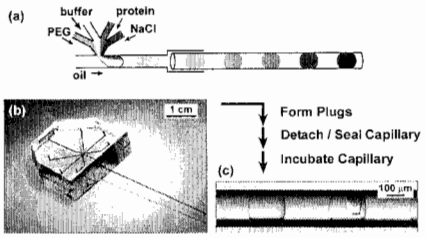

Figure 1. (a) A schematic illustration of the method of generating droplets for protein crystallization trials in a PDMS/ glass capillary microfluidic device. (b) A photograph of the composite device. (c) A microphotograph of lysozyme crystal grown inside a droplet in a capillary.

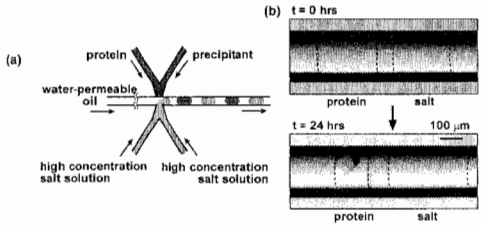

Figure 2. (a) A schematic illustration of the experimental setup of forming alternating droplets of two different compositions. (b) Two microphotograph show that a pair of droplets immediately after (top) and 24 hours after (bottom) the setup. The droplet of the protein solution yielded a crystal after it had lost ~50 % of its water content. Dashed lines were added to highlight the interface between the aqueous droplets and oil.

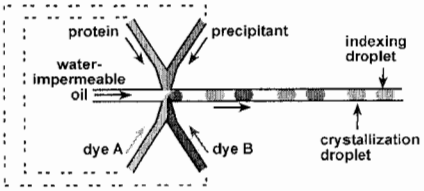

Figure 3. A schematic drawing of the experimental setup of indexing composition of droplets during crystallization of protein.

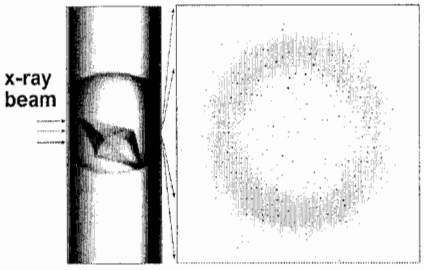

Figure 4. The capillary containing thaumatin crystals (left) is directly subjected to X-ray diffraction. A diffraction pattern (right) of the crystal shown to a resolution of 2.0 angstroms.

A DROPLET-BASED PROTEIN CRYSTALLIZATION DEVICE USING ELECTROSTATIC MICROMANIPULATION

Masaaki Hirano[1], Toru Torii[1], Toshiro Higuchi[1], and Hiroki Yamazaki[2]
[1]*Department of Precision Engineering, Graduate School of Engineering, The University of Tokyo, 7-3-1, Hongo, Bunkyo-ku, Tokyo 113-8656, Japan*
[2]*Techno Medica Co., Ltd., Yokohama, Japan*

Abstract
A novel device for high throughput screening of protein crystallization is proposed. Nanoliter-sized droplets of samples/reagents for protein crystallization were transported by electrostatic forces and mixed together on an electric panel device. The preparation process can be automated, and various conditions (concentration/pH) can be produced precisely and flexibly by controlling the volume of the combining droplets. By combining the droplets, crystals of lysozyme and thaumatin were obtained.

Keywords: protein crystallization, high throughput screening, droplet actuation, electrostatic

1. Introduction

In recent years, analysis of protein functions has become important. The function of a protein can be inferred from its 3-dimensional structure, which is usually done by the X-ray diffraction method. Protein crystallization is a bottleneck in determining tertiary protein structures from sequence data [1] and it occurs only under very specific conditions. New methods for high throughput screening of protein crystallization are currently being investigated, and several microfluidic devices have been proposed [2-4].

Minimal volumes of the protein solution should be used during screening, because many proteins are only available in very small quantities. Manual screening by mixing stock solution in many ratios is time-consuming and requires at least 100 nL of the protein solution per trial [2]. To overcome these limitations, robotic systems have been developed that can perform automated mixing of stock solutions, and which can set up crystallization trials with volumes from 1μL down to 100nL [5], consuming as little as 10 nL of individual solutions [6].

We have previously reported a method for on-chip crystallization of protein molecules using an electrostatic manipulation technique [7]. Here we report, mixing and transportation of the droplets as a single continuous operation using two electrode panels, which enables 2-dimensional manipulation.

The objectives of the present study were (a) to fabricate a device that could be used to crystallize proteins by using nanoliter-sized droplets, (b) to electrostatically mix the droplets of protein sample and the precipitants at a specific point, and (c) to have protein crystals of high quality.

To achieve these target, two protein, *viz.* thaumatin and lysozyme were employed.

2. Concept

Figure 1 illustrates the basic concept of our device. Samples/reagents were prepared as droplets using microfluidic devices and are transferred to arc-type electrodes. Sequential

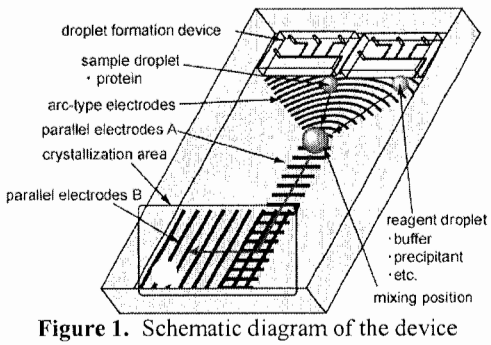

Figure 1. Schematic diagram of the device showing mixing and transporting droplets

voltages were applied to the electrode arrays, and droplets of sample/reagents were manipulated by electrostatic forces. These droplets were merged at the center of the arc-type electrodes and transported on the parallel electrode arrays. The conditions and properties of the merging droplets were controlled by varying the volume of the droplets. Accordingly, droplets with differing parameters could be prepared on the device.

Table 1. Electrode specification

Type	Pitch (mm)	Width (mm)
Arc	0.3	0.2
Parallel	1.0	0.7

3. Experimental

Figure 2(a) shows a photograph of the experimental setup. The bottom electrode panel had an arc-type and a parallel-type electrode array. The upper parallel electrode array was made up of ITO (indium-tin oxide), so that movement of the droplets can be observed through it. Table 1 shows the electrode specifications. The substrate was covered with insulator (20 μm thick) to prevent dielectric breakdown, and with Teflon® (1 μm thick) to make it more hydrophobic.

The electric panels were set in an acrylic case filled with silicone oil (0.1 St), as shown in Fig. 2(b). The droplets were sandwiched between the electric panels. The sequential voltages applied had a six-phase rectangular profile (+++000).

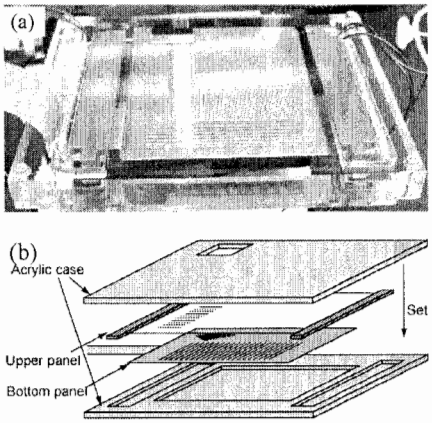

Figure 2. Experimental setup
(a) A view of the device, (b) electric panel fitted with Silicone oil

Using this device we set out to crystallize two proteins, *viz.* thaumatin and lysozyme. In both the cases, two droplets (0.5 μL) were set on the arc-type electrodes. One droplet contained protein and buffer, and the other contained precipitant. These droplets were transported by the arc-type electrodes to the center of the arc and then merged (Figure 3(a)). The mixed droplets were manipulated 2-dimensionally by the two parallel electrode arrays (Figure 3(b)). Protein crystals in the droplets were observed through an optical microscope (model VHX-100, Keyence Co. Tokyo).

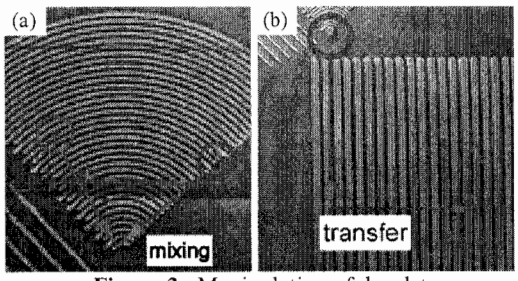

Figure 3. Manipulation of droplet
(a) merging of droplets, and (b) two-dimensional manipulation by electrode arrays

4. Results and Discussion

A droplet of thaumatin dissolved in phosphate buffer, and a droplet of sodium tartrate, were transported on the arc-type electrodes at 250 $V_{0\text{-}P}$, and the two droplets were merged successfully. In the other case, a droplet of lysozyme dissolved in acetate buffer, and a droplet of PEG4000 and sodium chloride, were transported at 200 $V_{0\text{-}P}$. After mixing, the droplets were smoothly transported to the crystallization area. The mixed droplet containing thaumatin was transported through the parallel electrodes (ITO electrodes) at 370 $V_{0\text{-}P}$, while the droplet containing lysozyme was transported at 260 $V_{0\text{-}P}$.

Crystals of thaumatin were visible 3 hours after setup, and had grown to about 160 μm by 18 hours (Figure 4(a)). Crystals of lysozyme were seen after 18 hours, and had grown to about 390 μm by 48 hours (Figure 4(b)).

Hence, we were able to electrostatic manipulate the mixing of two droplets. It was possible to control the conditions of droplets by our method. Mixing and transportation process could be demonstrated by electrostatic manipulation. This method allowed the automation of droplet preparation for protein crystallization screening.

5. Conclusions

Mixed droplets were successfully transported between two differing electrode arrays, and two proteins were crystallized on our device. Preparation of a solution for protein crystallization could be automated by electric manipulation of microdroplets. Moreover, the resulting droplets could be arranged in a matrix array. We believe that our droplet-based approach will provide a highly functional and flexible tool to the field of protein crystallography.

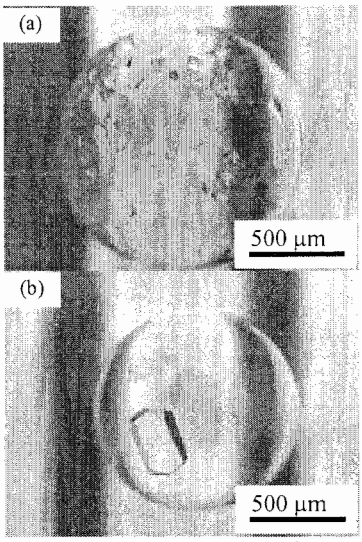

Figure 4. Protein crystals (a) thaumatin crystals, 18 hours after setup, and (b) lysozyme crystals, 48 hours after setup

Acknowledgements

This research was supported financially by a grant from the New Energy and Industrial Technology Development Organization (NEDO) in Japan ("Nano- Bio- Device Project").

References

[1] Chayen, N.E. Tackling the bottleneck of protein crystallization in the post-genomic era, Trends Biotechnol. **20**, 98 (2002).

[2] Hansen, C.L., Skordalakes, E., Berger, J.M., and Quake, S.R. A robust and scalable microfluidic metering method that allows protein crystal growth by free interface diffusion, Proc. Nat'l Acad. Sci. **99**, 16531-16536 (2002).

[3] Zheng B., Roach, L.S., and Ismagilov, R.F. Screening of protein crystallization conditions on a microfluidic chip using Nanoliter-size droplets, J. Am. Chem. Soc., **125**, 11170-11171 (2003).

[4] Yamada, M., Sasaki, C., Isomura, T., and Seki, M. Microfluidic reactor array for high-throughput screenings of protein crystallization conditions, MicroTAS 2003, 449-452 (2003).

[5] Rupp, B. Acc. High-Throughput Crystallography at an Affordable Cost: The TB Structural Genomics Consortium Crystallization Facility, Chem. Res. **36**, 173-181 (2003).

[6] Adams, M.W.W., Dailey, H.A., Delucas, L.J., Luo, M., Prestegard, J.H., Rose, J.P. and Wang, B.C. The Southeast Collaboratory for Structural Genomics: A High-Throughput Gene to Structure Factory, Acc. Chem. Res. **36**, 191-198 (2003).

[7] Hirano, M., Torii, T., Higuchi, T., Kobayashi, M., and Yamazaki, H. Protein crystallization device using electrostatic micromanipulation, MicroTAS 2003, 473-476 (2003).

CRYSTALLIZATION OF PROTEINS BASED ON VAPOR DIFFUSION IN MICROFLUIDIC REACTOR ARRAY

Masumi Yamada[1], Chizuko Sasaki[2], Tetsu Isomura[3], and Minoru Seki[4]

[1]*Dept. of Chemistry and Biotechnology, Sch. of Engineering, The University of Tokyo, Japan*

[2]*Yokohama Laboratory, Analytical Services Division, Mitsubishi Chemical Group Science and Technology Research Center, Inc., Japan*

[3]*Research and Development Center, Zoegene Corporation, Japan*

[4]*Dept. of Chemical Engineering, Grad. Sch. of Engineering, Osaka Prefecture University, Japan*

Abstract

We propose here a new microfluidic system, which enables crystallization of proteins in parallel, based on the vapor diffusion scheme. By placing the precipitant solution and the mixture solution of protein and precipitant separately in a reactor, the concentration of the precipitant in the mixture solution could be gradually changed. This gradual change in concentration facilitates nucleation of crystals, and is desirable for good crystal growth. This system will become one of the useful schemes in microscale protein crystallization, since multiple conditions for crystallization can be tested with small amount of expensive proteins.

Keywords: crystallization, protein, microfluidic array, vapor diffusion

1. Introduction

Microfluidic devices are suitable for protein crystallization research owing to their potentials for parallel and automated liquid operation only with small amount of expensive samples. There have been some studies concerning protein crystallization using microfluidic devices, through free interfacial diffusion [1], or micro batch method [2,3]. Among some crystallization schemes, vapor diffusion techniques (hanging drop or sitting drop) are the most frequently used crystallization methods, since the composition of protein solution can be gradually changed. However, there has been little research about the protein crystallization based on the vapor diffusion in microfluidic devices. So in this study, we have proposed a crystallization method via vapor diffusion using microfluidic reactor array [2,4], and compared crystal forms between micro batch and vapor diffusion methods.

2. Theory

The schematic images of vapor diffusion (hanging drop) scheme are shown in Figure 1. The difference in precipitant concentration between the droplet (mixture of protein and precipitant) and the reservoir drives the system toward equilibrium by diffusion through the vapor phase. When the drop and reservoir are close to equilibrium, the protein becomes supersaturated and crystals start to form. Therefore, possibility of crystal formation could be enhanced compared to micro batch method. Also, the crystal shape obtained via vapor diffusion scheme would be different from that via microbatch scheme, since the nucleation speed could be different.

3. Experimental

Fig. 2 shows the design of the fabricated PDMS microdevice for protein crystallization. There are five crystallization chambers via vapor diffusion method for five different conditions, and also five chambers via micro batch method to compare the formed crystal shapes. This device is composed of two PDMS replicas, having different channel depths. The size of the crystallization chamber is 500 x 800 x 50 μm, and that of the precipitant reservoir is 2000 x 3000 x 50 μm. The size of microchannel connecting the crystallization chamber to the precipitant reservoir was 400 x 50 x 50 μm. Fig. 3 illustrates liquid operations in this microdevice.

Pneumatic pressure was applied to transport, dispense, and mix liquids. Only 7.5 nL of protein and precipitant solutions were dispensed in the liquid-metering channels, and then mixed in crystallization chambers, while 150 nL of precipitant solution was dispensed and introduced into the precipitant reservoir. The concentration of precipitant in the crystallization chamber therefore became one-half of that in the precipitant reservoir. After the dispensing and mixing, the channels were sealed with PDMS to avoid evaporation, and the microdevice was incubated in a refrigerator at 4 °C for about one week. The formed crystals were observed under a microscope with polarized filter.

4. Results and discussion

As the model, crystallization of lysozyme was performed. It was observed that the liquid volume in the crystallization chamber was decreased after the incubation, while that in the precipitant reservoir was kept constant. An example of the formed crystal is shown in Fig. 4, when 10 %(w/v) PEG 6000 and 2.0 M NaCl solution was used as a precipitant. As it can be seen, crystal shapes were different between micro batch and vapor diffusion schemes. In this case, crystal with better shape could be obtained through the vapor diffusion method, which is important for X-ray crystallography analysis. By changing the size of the microchannel connecting the crystallization chamber and the precipitant reservoir, the vapor diffusion speed will be accurately controlled.

5. Conclusions

We have demonstrated protein crystallization in microfluidic reactor array with vapor diffusion schemes. From the result, it was demonstrated that this microfluidic system is highly advantageous for the crystallization of macromolecules, since the crystallization conditions could be gradually changed. In addition, consumption of expensive samples could be reduced dramatically compared to the normal scale methods.

Acknowledgements

This research was supported in part by Grant-in-Aids for JSPS Fellows, Scientific Research (B) (No. 16310101), and Priority Areas (A) (No. 13025216) from the Ministry of Education, Science, Sports and Culture of Japan, and by the Research Association of Micro Chemical Process Technology, Japan.

References

[1] C. L. Hansen, E. Skordalakes, J. M. Berger, S. R. Quake, *Proc. Natl. Acad. Sci. USA*, **56**, 16531-16536 (2002).
[2] M. Yamada, C. Sasaki, T. Isomura, and M. Seki, *Proc. MicroTAS 2003*, 40-42 (2003).
[3] B. Zheng, L. S. Roach, R. F. Ismagilov, *J. Am. Chem. Soc.*, **125**, 11170-11171 (2003).
[4] M. Yamada and M. Seki, *Anal. Chem.*, **76**, 895-899 (2004).

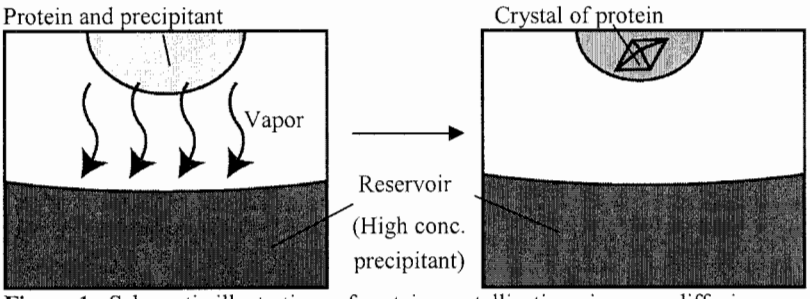

Figure 1. Schematic illustrations of protein crystallization via vapor diffusion.

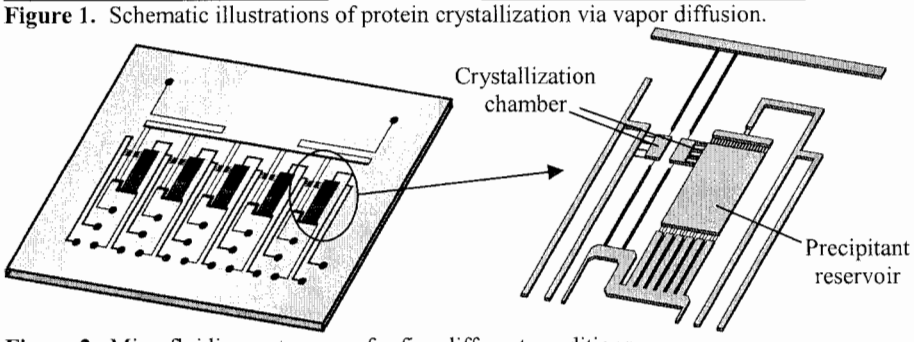

Figure 2. Microfluidic reactor array for five different conditions.

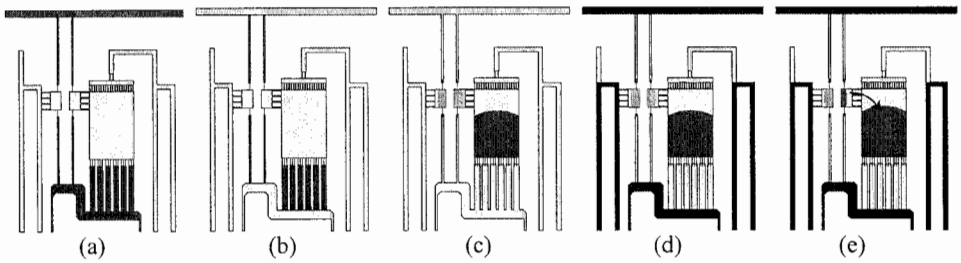

Figure 3. Schematic diagrams of liquid operation: (a) introduction of protein and precipitant solutions, (b) liquid dispensing, (c) injection and mixing, (d) sealing, and (e) gradual vapor diffusion and crystal growth.

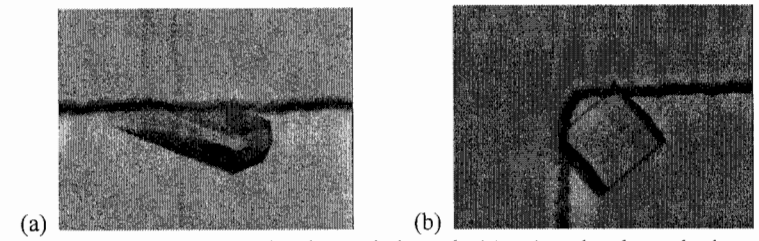

Figure 4. Protein crystals obtained through (a) micro batch method, and (b) vapor diffusion method.

MICROREACTORS FOR HIGH PERFORMANCE LIVER TISSUE ENGINEERING

Linda Griffith[1,2], Karel Domansky[1], Anand Sivaraman[3], Nathan C. Tedford[1], Rima A. Arnaout[1], and Donna B. Stolz[4]

[1]*Biological Engineering Division and Biotechnology Process Engineering Center, MIT, 77 Massachusetts Ave, Cambridge, MA 02139, USA*

[2]*Mechanical Engineering Dept., MIT 77 Massachusetts Ave, Cambridge ,MA 02139, USA*

[3]*Chemical Engineering Dept., MIT 77 Massachusetts Ave, Cambridge, MA 02139, USA*

[4]*Cell Biology and Physiology, University of Pittsburgh Medical School, Pittsburgh, PA 15261, USA*

Abstract

One major barrier in drug development is the lack of adequate culture methods for retaining liver cell function in vitro. We have developed a scalable microreactor system that fosters development of 3D micro-tissue units in a format adaptable to screening. The tissue phenotype maintained in the 3D microreactor is substantially closer to that of native liver compared to cells cultured with other methods, as assessed with a broad spectrum of gene expression and biochemical activity metrics.

Keywords: tissue engineering, drug development, microreactor, bioengineering

1. Introduction

Hepatocytes, the main cell type in liver responsible for metabolic transformation of drugs as well as many other liver functions, rapidly lose their liver-specific functions when placed in culture. Thus, in vitro cultures have limited utility as models for predicting liver toxicology or as models of chronic human diseases such as hepatitis C infection. When liver is enzymatically digested, the hepatocytes along with other component cells can be induced to form tissue-like structures in vitro under some conditions. Recreating the *in vivo* microenvironment of hepatocytes, which includes signaling mechanisms mediated by cell-cell and cell-matrix interactions, soluble factors, and mechanical forces, is likely a key requirement in maintaining liver function in vitro. To accomplish this, we have developed a microfabricated bioreactor system that allows for three dimensional morphogenesis of liver tissue under continuous perfusion conditions. A key feature of the microreactor is the distribution of cells into many tiny (~ 0.02 – 0.12 mm^3) tissue units that are uniformly perfused with culture medium, similar to the distribution of tissue mass in individual capillary beds in the native organ [1]. The total mass of tissue in the system is readily adjusted for applications requiring only a few thousand cells to those requiring over a million cells by keeping the microenvironment the same and scaling the total number of tissue units [2, 3]. Here we describe the design principles and highlight the approaches to fabrication that will enable adaptation to high throughput formats.

2. Design Principles

The microreactor scaffold and fluid distribution design principles are constrained by several considerations. These include: the length scale for reorganization of disassociated cells into tissue; the length scale for nutrient transport by convection and diffusion; surface chemistry for appropriate cell adhesion; total mass of cells required for the assay in question; and requirement for optical (microscopic) imaging and spectroscopy. In the liver capillary bed, the length scale for blood flow is ~ 0.5 mm or 10-20 cell diameters (the diameter of a single hepatocyte is ~ 0.025 mm). This length scale is reduced in cell culture due to the limited oxygen carrying capacity of cell culture medium compared to blood [2]. We used silicon microfabrication to prototype scaffold designs capable of enabling tissue morphogenesis while providing adequate nutrient transport, and

determined experimentally that a scaffold providing an array of through-channels with depth ~ 0.2 mm and cross sectional dimensions of 0.3 x 0.3 - 1.8 mm allowed for appropriate tissue morphogenesis and function [1-3]. The key features of the design are shown in Figure 1. The scaffold for tissue morphogenesis is a thin wafer containing an array of channels; each channel holds 500 - 5000 cells and the scaffold can be scaled to hold the number of cells required for molecular assays such as RT-PCR (~ 10,000) to those such as probing for hepatitis infection (~ 1,000,000) simply by scaling the number of channels in the array. The scaffold is backed by a filter, which holds the cells immediately after seeding and provides a high hydraulic resistance to ensure even distribution of flow to all the tissue units despite the disparity in tissue morphology within each individual channel. The filter is held in place by a supporting scaffold aligned with the tissue morphogenesis scaffold. The scaffold assembly is placed into the pocket of the microreactor housing. The housing features top and bottom polycarbonate compartments, each with flow inlets and outlets. A photograph of the assembled microreactor is shown in Figure 2.

3. Experimental

In our previous publications, we have performed most of the experiments in silicon scaffolds with an array of forty 300 x 300 x 230-μm channels. Silicon wafers were used as the original material for the fabrication of scaffolds in order to prototype the channel dimensions and scaffold layout. However, silicon scaffolds present challenges for certain applications. For example, the scaffolds cannot be easily sectioned for histological staining and imaging. Typically, the tissues residing inside the channels have to be embedded in a suitable resin, peeled off from the scaffold, and sectioned. In contrast, tissue in softer polymer scaffolds can usually be sectioned without prior extraction.

In this paper, we performed the experiments in injection molded polypropylene scaffolds and laser machined polycarbonate scaffolds. The injection molded polypropylene scaffolds had an array of seven 300 x 1800 x 230-μm slits (see Figure 3). The laser-machined polycarbonate scaffolds used in a scaled up version of the microreactor in Figure 2 featured an array of one thousand 300 x 300 x 230-μm channels (Figure 4). The fabrication details of both injection molded and laser-machined scaffolds are described in reference [2].

4. Results and discussion

Microreactors were seeded with rat hepatocytes pre-aggregated into spheroids [1-3]. In order to investigate the health of the three dimensional tissue structures formed in the channels in the microreactor after several days of culture, the cell constructs in the polypropylene scaffolds were fixed and stained with toluidine blue (Figure 5). Toluidine blue is known to stain healthy, viable cells dark blue. Most of the cells in the tissue are stained dark blue indicating a healthy tissue phenotype. Interestingly, the dead cells in the tissue seem to be scavenged by macrophages (possibly kupffer cells) in a manner similar to that typically seen *in vivo*. Therefore, the microreactors provide an *in vivo* like microenvironment for the histotypical re-organization of the cells into tissue.

Real-time reverse-transcriptase PCR can be used to quantitatively compare gene expression in different culture systems. To explore the potential for culturing primary rat hepatocytes within laser-machined polycarbonate scaffolds housed within the microreactor system, the level of albumin gene expression was quantified as an indicator of liver specific phenotype (Figure 6). When hepatocytes are isolated from rat liver via a collagenase perfusion, it can be seen that albumin gene expression is significantly downregulated compared to the levels seen in *in vivo* liver slice controls. Long-term culture of these isolated hepatocytes in 300 x 300 x 230-μm channels within the polycarbonate scaffolds of the bioreactor system brings this gene expression much closer to *in vivo* levels, with a slight upregulation in albumin transcript levels.

5. Conclusions

The results show that different polymer scaffolds foster tissue morphogenesis in a similar manner to the original silicon scaffold prototypes (provided that they are pre-coated with collagen and have similar geometries), and have the ability to promote liver-like phenotype in a controllable in vitro environment.

Acknowledgements

We also want to thank DARPA – Tissue Based Biosensors, DuPont – MIT Alliance, and NSF Biotechnology Process Engineering Center for the financial support.

References

[1] M. J. Powers, K. Domansky, M. R. Kaazempur-Mofrad, A. Kalezi, A. Capitano, A. Upadhyaya, P. Kurzawski, K. E. Wack, D. Beer Stolz, R. Kamm, and L. G. Griffith, A microfabricated array bioreactor for perfused 3D liver culture, Biotechnology and Bioengineering, 78 (2002) 257.

[2] Karel Domansky, Anand Sivaraman, and Linda G. Griffith, Micromachined bioreactor for in vitro cell self-assembly and 3D tissue formation, submitted as a book chapter to Lab-on-a-chips for Cellomics: Micro and Nanotechnologies for Life Science, edited by Helene Andersson and Albert van den Berg, Kluwer Academic Publishers (in press).

[3] M. J. Powers, J. Janigian, K. E. Wack, C. Baker, D. B. Stolz, and L. G. Griffith, Functional behavior of primary rat liver cells in a 3D perfused microarray bioreactor, Tissue Eng. 8 (2002) 499.

[4] P. F. Davies, Mechanisms involved in endothelial responses to hemodynamic forces, Atherosclerosis 131 (1997) S15.

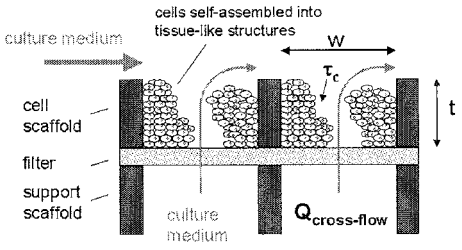

w – length scale of cell self-organization ~ 300 μm

t – length scale for oxygen diffusion ~ 200 μm

$Q_{cross-flow}$ – flow of cell culture medium ~ 1 μl/channel/min

τ_c – shear stress on cells < 1 dyne/cm^2 [4]

Figure 1. Basic design parameters for high performance liver microreactors.

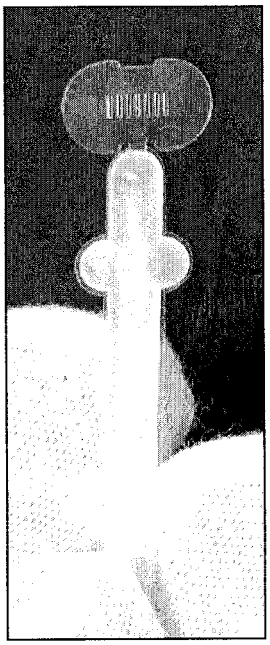

Figure 3. Injection molded polypropylene scaffold with 300 x 1800 x 230-μm slits.

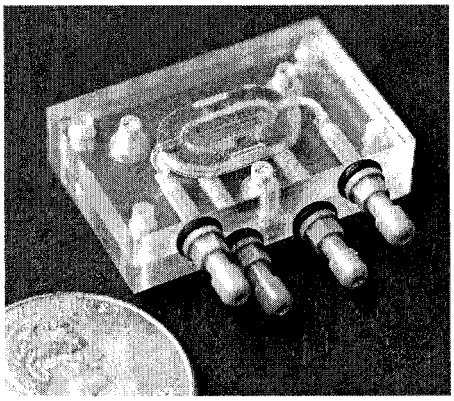

Figure 2. Photograph of a high performance liver microreactor fitted with a silicon scaffold with a 4 x 10 array of 300 x 300 x 230-μm channels.

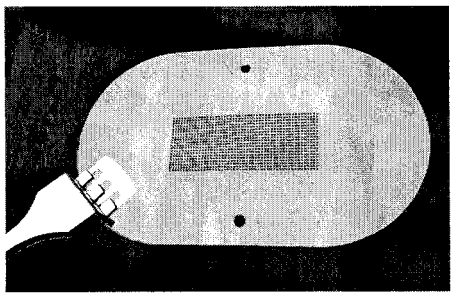

Figure 4. Photograph of a laser-machined polycarbonate scaffold with a 20 x 50 array of 300 x 300 x 230-μm channels. The scaffold fits into a scaled up version of the microreactor in Fig. 2. The scaffold typically accommodates approximately 1.5 x 10^6 cells.

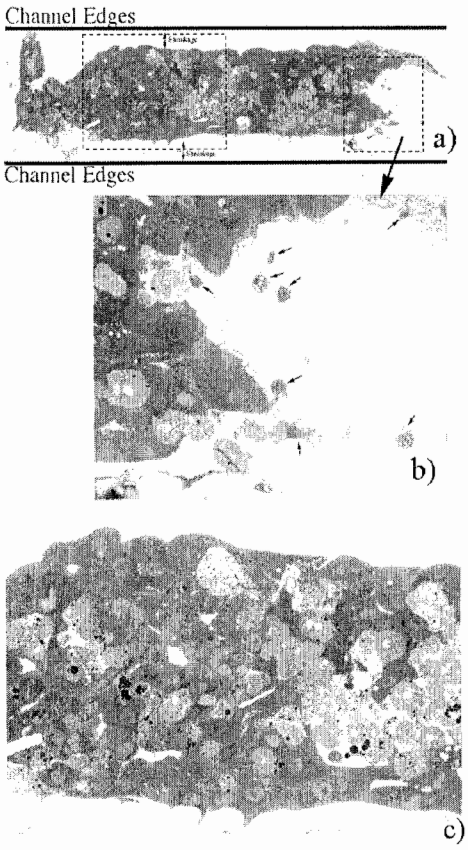

Figure 5. Histological sectioning/toluide blue staining of the tissue constructs formed in the channels of polypropylene scaffolds. Figures b) and c) are enlarged sections from Figure a). Healthy viable cells are stained dark blue. The arrows indicate the presence of macrophages (possibly Kuppfer cells) that scavenge the dead cells in the tissue in a similar manner as seen in vivo.

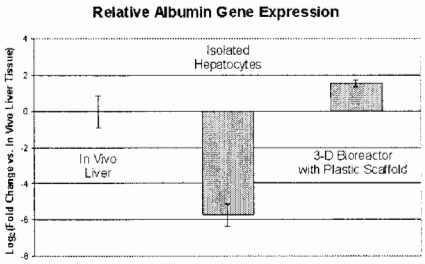

Figure 6. Gene expression profiles were measured via reverse transcription, real-time PCR for *in vivo* rat liver slices, isolated rat hepatocytes, and a three dimensional liver bioreactor that used polycarbonate cell scaffolds to foster reorganized liver tissue. Fold change in transcript level was compared relative to the level of mRNA expression in the *in vivo* liver slice case. Liver slices were immediately homogenized in Trizol (Invitrogen) and mRNA was purified mRNA using an RNeasy extraction kit (Qiagen). mRNA was similarly extracted from isolated hepatocytes after recovery from a rat liver perfusion with Blendzyme 3 (Roche), and transcripts were acquired from the reactor systems that were seeded with day three hepatic spheroids after seven days of culture. cDNA was generated for the respective mRNA samples, and SYBR green real-time PCR was performed to quantify the critical threshold of amplification for the albumin gene. Experiments were run in duplicate for three different rats for *in vivo* and isolated hepatocyte cases, and in duplicate for two different rats for the 3-D liver bioreactor.

MICROFLUIDIC ARCHITECTURES FOR INTEGRATED CELL LYSIS, LYSATE DIALYSIS AND CELL STIMULUS

Simon Song[1], Petra Mela[2], Albert van den Berg[2], and Brian J. Kirby[1]
[1]Microfluidics Dept., Sandia National Laboratories, Livermore, CA, USA
[2]BIOS-group, MESA+ Institute for Nanotechnology, University of Twente, The Netherlands

Abstract

Microfluidic architectures suitable for cell lysis, lysate dialysis, and cell stimulus are proposed. Laser-patterned nanoporous polymer membranes are fabricated in microchips using projection lithography and are used to separate cell lysate based on size and concentrate cytosolic proteins by electrophoretic concentration. Cell stimulus is achieved by rapidly changing the cell environment with aid of in-line, electrokinetic flow modulation.

Keywords: cell lysis, dialysis, polymer membrane, cell stimulus

1. Introduction

Proteomic measurements of cellular response to stress or other stimulus are typically performed by exposing macroscopic cell suspensions to stimulus and taking time course data via periodic lysis of cell solutions followed by analysis of the lysates. Microchip platforms are ideally suited for generation of highly time-resolved data by speeding the process of cell stimulus and lysis. Here we demonstrate microfluidic architectures for separation of cytosolic contents from membrane fragments and geometry-independent fluidic forcing techniques for rapidly establishing changes in cellular environment. A cascade of nanoporous polymer membranes is used to separate the cytosolic contents from the cell membrane fragments. Removal of membrane fragments and organelles greatly increases reliability of CE and other analytical techniques. Rapid homogeneous application of chemical or other stresses enable measurement of fast cellular responses.

2. Materials and Methods

Fused silica microchips are fabricated using conventional wet-etch techniques, and the internal surface is coated with linear polyacrylamide [1] to inhibit cell adhesion and suppress EOF. To allow for cell trapping and size-based separation of cell lysates,

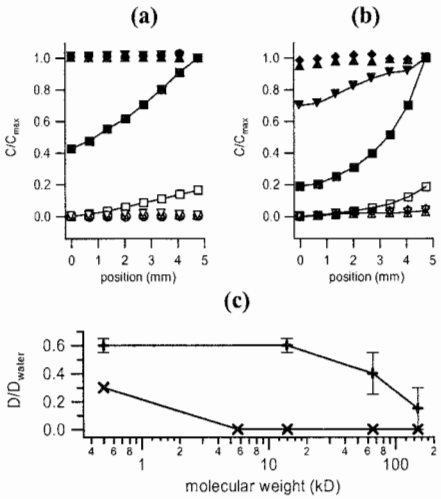

Figure 1. Counterflow mass transport. Top: concentration profiles with membranes for (a) low MWCO (b) high MWCO. Closed symbols: sample channel, flow enters at L=5mm and exits at L=0mm. Open symbols: perfusion channel, flow enters at L=0mm and exits at L=5mm. ■ Rhodamine 560 (0.5 kD); ● monomeric insulin (5.7 kD); ▼ lactalbumin (14 kD); ♦ BSA (66 kD); ▲ anti-biotin (150 kD). Bottom: (c) specific diffusivity through membrane as a function of analyte molecular weight. × low MWCO, + high MWCO

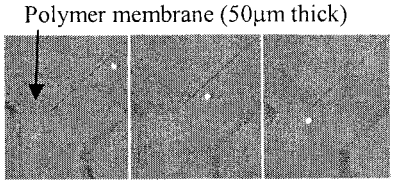

Figure 2. Electrophoretic cell trapping at laser-patterned nanoporous membrane. Cell is IL-2-dependent murine T cell in PBS. Microchip substrate is glass coated with linear polyacryamide to suppress protein adhesion and EOF. The images were taken at a 100 ms interval as voltage is applied across the membrane. The cell moves toward anode.

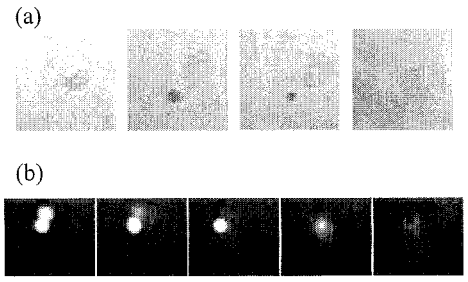

Figure 3. Time series of lysed cell in a microchannel. (a) optically with 7ns, 100 μJ, 532nm laser pulses (b) chemically with 2% CHAPS in PBS

nanoporous polymer dialysis membranes are laser-patterned in microchip using projection lithography[2]. Control of pore sizes of the dialysis membranes is achieved via chemical formulation. The size is determined by measurements of diffusive transport properties, which are quantified via counterflow mass exchange (Fig. 1).

Interleukin-II-dependent murine T cells are washed and suspended in PBS, labeled with 5-(and-6)-carboxyfluorescein diacetate, succinimidyl ester, and loaded on chip. Cells are manipulated in microchannels with pressure and voltage applied at reservoirs, and when desired, could be trapped at dialysis membranes via voltage applied across the membrane (Fig. 2). Cell lysis in microchannels is achieved chemically (2% CHAPS in PBS) or optically (7 ns, 100 uJ, 532 nm laser pulses) (Fig 3) [3,4].

3. Results and Discussion

Chip-level integration of laser-patterned nanoporous polymer membranes allows on-chip processing of nascent analytes such as cell lysates. Electrophoretic force is used to hold cells in place against the dialysis membrane while chemical or optical means are used to lyse them. To separate the cell lysates based on size, a cascade of dialysis membranes with two different molecular weight cutoffs (MWCO) is proposed. The high MWCO membrane filters cell membrane and organelle fragments while cytosolic proteins pass through the dialysis membrane. Then the low MWCO membrane stops, collects and concentrates cytosolic proteins. Finally, the concentrated proteins are eluted and injected downstream for further analysis.

The concentration of cytosolic proteins is possible due to the attractive electrical properties of the dialysis membrane. The low MWCO membrane has pores small enough to prevent protein transport but large enough to allow small-ion transport and current conduction [5]. Upon application of voltage, proteins electrophorese to the membrane and stack on the membrane surface. The electrical properties have been quantified by measuring the temporal stability of current fluxes in microchannels with and without the membrane. No measurable resistance was observed through the membrane, and voltage could be applied at length. Electrophoretic concentration of proteins at the nanoporous dialysis membrane provides more than 100-fold concentration that is linear in time and to voltage, indicating there is no dielectric breakdown or ion depletion in the system (Fig. 4).

Rapid cellular stimulus requires rapid change and homogenization of cellular environment (carbon source, gas concentration, pH, temperature) without geometries that lead to clogging. Rapid control of fluids in standard channel junctions facilitates the rapid cellular stimulus in

microchip. In-line flow modulation using electrokinetic pressure generation can introduce a series of fluids into a microchannel or microchamber and be programmed. The in-line flow modulation is achieved straightforwardly and inexpensively by applying AC voltage waveforms with a DC offset across in-line silica fiber mesh syringe filters. For example, a low-frequency modulation injects small plugs of two different fluids into a channel (Fig 5, left). When rapid mixing is required, the modulation can be performed at high frequency because the bandwidth of electrokinetic pressure generation can be as high as >1 kHz and the pressure modulation drives naturally dispersive parabolic channel flow in the microchannels. The predicted mixing length can be reduced by four orders of magnitude simply by changing the voltage waveform (Fig 5, right).

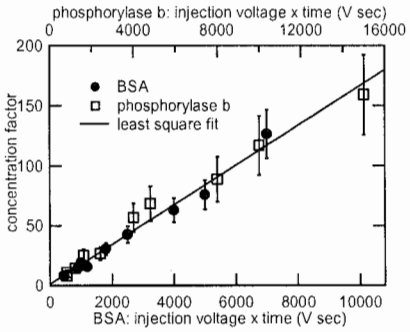

Figure 4. Linear concentration of two proteins by electrophoresis. Proteins are concentrated by over two orders of magnitude. Linear response facilitates metered concentration and evinces efficient small-ion transport.

5. Summary

Microfluidic architectures for cell lysis, lysate dialysis, and cell stimulus in microchips have been proposed. Nanoporous polymer membranes laser-patterned in the microchips are used to separate cell lysates based on size and concentrate cytosolic proteins on the membrane surface. In-line electrokinetic flow modulation promises rapid cell stimulus in microchips by rapidly changing the cell environment. In future work, we expect to integrate the cell lysis, stimulus, and lysate dialysis in a microchip.

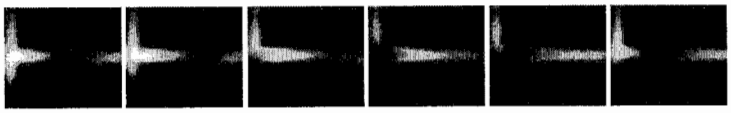

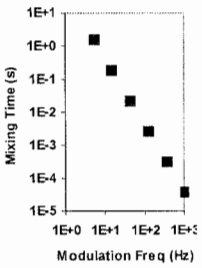

Figure 5. Pressure-driven flow modulation with AC driving from in-line electrokinetic pump fabricated simply and inexpensively from a syringe filter and 100V applied voltage. Images are at 66 ms intervals. Inlets: top (dye) and bottom (water); outlet at right. 2.5 Hz forcing is shown here for clarity; higher frequencies enhance mixing. Right: mixing times as function of modulation frequency shown for addition of pH stressor.

References

[1] B.J. Kirby, A.R. Wheeler, R.N. Zare, J.A. Fruetel, T.J. Shepodd, *Lab Chip*, **3**, pp. 5-10 (2003).

[2] S. Song, A.K. Singh, T.J. Shepodd, B.J. Kirby, *Anal. Chem.*, **76**, pp 2367-2373 (2004).

[3] N. Munce, J. Li, P. Herman, and L. Lilge, *Proc. SPIE*, **4982**, pp. 28-36 (2003).

[4] C. E. Sims, G. D. Meredith, T. B. Krasieva, M. W. Berns, B. J. Tromberg, and N. L. Allbritton, *Anal. Chem.*, **70**, pp. 4570-4577 (1998).

[5] S. Song, A.K. Singh, B.J. Kirby, *Anal. Chem.*, In press (2004).

ON-CHIP SINGLE CELL LYSIS INTEGRATED WITH MICRO-FLOW CYTOMETRY

Claus R. Poulsen and J. Michael Ramsey
Chemistry Department, University of North Carolina, Chapel Hill, NC 27599, USA

Abstract

We have developed a microfluidic system that integrates flow cytometry, single cell lysis, and separation of cellular components. Hydrodynamic flow is used to drive the fluids through the system. An electrical field orthogonal to the cell flow automatically lyses the cells and injects the lysate into a separation channel for detection. Fluorescently labeled Jurkat cells were used to demonstrate the systems capability of continuous and simultaneous flow cytometry and single cell lysis.

Keywords: Cell lysis, flow cytometry, signaling pathways, single cell assays

1. Introduction

Mapping of signaling pathways is an important task in the post-genomic era. Many proteins involved in cell signaling are located inside the cell. An approach for studying these signaling proteins is to lyse the cell and perform chemical analysis on the lysate. Traditional lysing methods, e.g., chemical and mechanical lysis, disrupt the intracellular compartments and allow time for unwanted reactions to occur (e.g. phosphorylation by kinases, dephosphorylation by phosphatases, and degradation of important components in the signaling pathway by various enzymes). Fast lysis of cells is therefore important to obtain precise measurements. For some signaling pathways the cell-state is important, as certain precursors have to be activated [1,2]. Presently instrumentation does not exist for the analysis of single cell lysate, much less that combined with flow cytometry capabilities. In this work we are integrating flow cytometry to allow cell-state determination and cell lysate analysis. Studies have shown that apparent identical cells may show different metabolism or kinase activity when interrogated individually [3,4]. Valuable information can therefore be obtained by single cell analysis and abnormal cells (e.g. cancerous cells) can potentially be detected for clinical applications. The present study takes advantage of a technique developed in recent years that can identify and quantify cell-signaling proteins such as kinases and phosphatases using fluorescent enzyme substrates [4,5]. The method combines fast electrical lysis and separation of the cell contents by capillary electrophoresis [3,5]. The techniques developed here have the potential of becoming important technological components for protein expression mapping and cell toxicity assays at the single cell level.

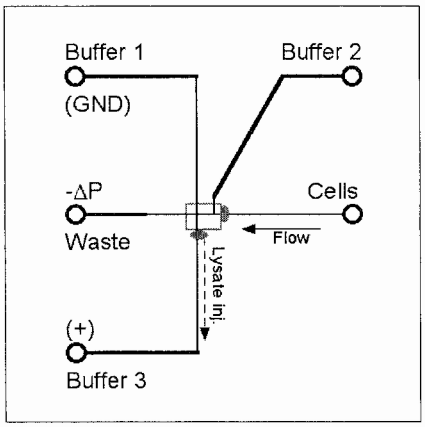

Figure 1. Schematic outline of microchip design. The grey square is the section where pictures in Fig. 2 are taken. Ellipsoids mark the detection points for the flow cytometry and lysate detection optical systems.

2. Experimental

To be able to determine the cell state, in terms of viability, Jurkat cells were labeled by calcein AM and propidium iodide (PI). Due to

the acetoxymethyl ester group, calcein AM is able to penetrate the cell membrane into the cytosol. Inside the cell, calcein AM is transformed when it is hydrolyzed by esterases that are only located inside cells, to a fluorescent form. The viability of a cell can be determined by comparing the calcein:PI ratio, as PI only can enter the cell if the membrane is compromised. When the cell membrane is compromised the cell will die, as the vital discriminative transport processes over the cell membrane can no longer be sustained. If the calcein:PI ratio is >1 the cell is considered alive and if it is ≤1 the cell is considered dead. For simultaneous flow cytometry and detection of cell lysate, the microchip was placed in an epifluorescence based dual detection point setup. The flow cytometry portion of the optical system allowed monitoring of the two wavelengths emitted by calcein and PI while the lysate detection was monitored at a single wavelength (calcein). Hydrodynamic fluid flow used for cell transport was created by applying partial vacuum, generated with the aid of a syringe pump, to the waste reservoir (Fig. 1). The imaging system for single cell lysis consisted of an inverted microscope and a CCD camera connected to a video recorder. An electric field (75 Hz 640 V_{pp}/cm AC, 450 V/cm DC offset) was applied orthogonal to the cell flow (Fig. 1). The electric field lysed the cells when they entered the intersection.

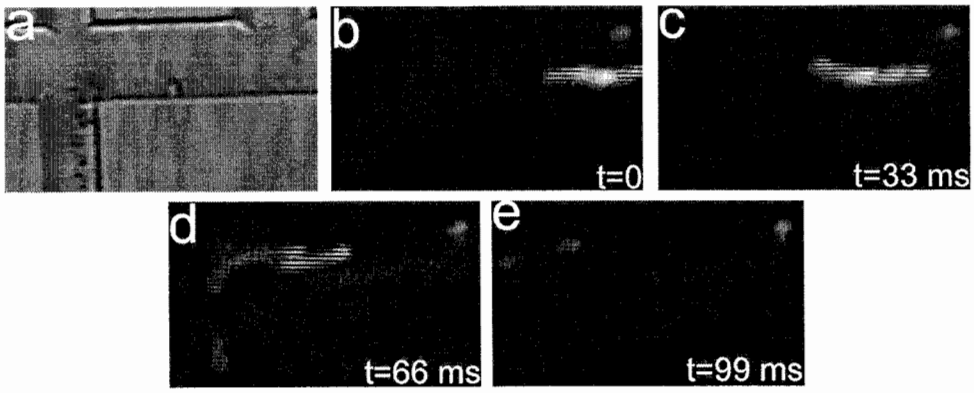

Figure 2. Single cell electrical lysis. (a) white light image of lysis intersection, (b, c) a cell entering from the right, (d) cell being lysed and lysate injected into separation channel, (e) cell membrane debris (spots to the left) flowing toward waste.

3. Results and discussion

A series of video frames (Fig. 2) show the lysis process of a cell entering the lysis intersection where it is exposed to an electrical field. This encounter results in the cell being lysed almost immediately. The lysing process is faster than 33 ms as evidenced by the two video frames, c and d, that were taken at a 33 ms interval. The cell lysate is depicted in video frame d as a stretched, less intense color band compared to the cell prior to lysis (frames b and c). The lysate is diluted by fluid flow and diffusion when the cell membrane disrupts. The dilution and dispersion of active proteins from substrates should terminate the intracellular processes in a similar < 33 ms time frame. The calcein labeled lysate is injected into the separation channel by the net DC electrical offset. Because calcein is a substrate for esterase, quantification of the calcein signal also quantifies the esterase activity. A plot of the simultaneous flow cytometry and lysate detection measurements for 5 cells is shown in Fig. 3. The cell density is sufficiently dilute to resolve the relationship between the intact cells and the cell lysate signals. The insert in Fig. 3 clearly shows a live cell (no PI signal) followed

by a distinct signal from the corresponding cell lysate. To demonstrate the flow cytometry capability, Fig. 4 shows the result from an experiment with a higher cell density where cell death is induced with 8 μM Triton X-100. Analysis of the data reveals a mortality of 32.9% of 234 cells using an average analysis rate of 8 Hz.

4. Conclusions

This study demonstrates, in a single micro system, the novel ability to perform flow cytometry measurements immediately prior to the induction of fast cell lysis. Separation of lysate from cell membrane debris allows the detection of intracellular lysate components from a single cell. All involved processes in the micro system are continuous, which provides the basis for an automated, high throughput device.

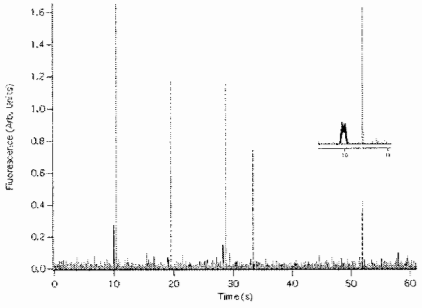

Figure 3. Fluorescence intensity measurement in a dual detection setup for calcein labeled cells (solid black line) and matching lysate (dotted grey line). PI signal (light grey solid line) is for viability determination. Insert shows signals for the expanded time, 10-11s.

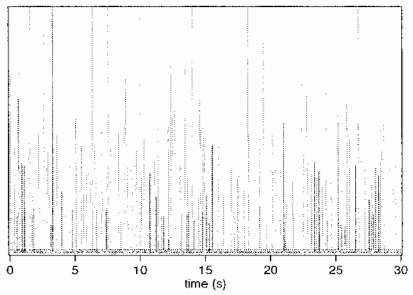

Figure 4. Flow cytometry results used for cell viability determination. Cell death is induced with 8 μM of the detergent Triton X-100. Jurkat cells are labeled with membrane permeable calcein and membrane impermeable PI. Viability is found based on the ratio calcein:PI (live: ratio >1, dead: ratio ≤1). Live cells will primarily be labeled with calcein (light grey) and dead or dying cells will be labeled with PI (dark grey).

Acknowledgements

Financial support for this work is provided by NHLBI.

References

[1] C. Brenner, G. Kroemer, *Science*, **289**(5482), 1150-1151 (2000).

[2] C.R. Poulsen, K. Bokvist, H.L. Olsen, M. Hoy, K. Capito, P. Gilon, J.L. Gromada, *Diabetes*, **48**, 2171-2181 (1999).

[3] M.A. McClain, C.T. Culbertson, S.C. Jacobson, N.L. Allbritton, C.E. Sims, J.M. Ramsey, *Anal. Chem.*, **75**(21), 5646-5655 (2003).

[4] G.D. Meredith, C.E. Sims, J.S. Soughayer, N.L. Allbritton, *Nature Biotech*, **18**(3), 309-312 (2000).

[5] F. Han, Y. Wang, C.E. Sims, M. Bachman, R. Chang, G.P. Li, N.L. Allbritton, *Anal. Chem.*, **75**(15), 3688-3696 (2003).

ON-CHIP CELL LYSIS BY REAGENT SYNTHESIS FROM THE WORKING FLUID

Dino Di Carlo, Cristian Ionescu-Zanetti, Paul J. Hung, Yolanda Zhang and Luke P. Lee
Berkeley Sensor and Actuator Center and Dept. of Bioengineering, University of California, Berkeley, 340 Hearst Memorial Mining Building, Berkeley, California 94720, USA.

Abstract

We present a novel and effective method for on-chip cell lysis based on local reagent generation. Electro-generated hydroxide ions are confirmed as the lytic reagent in the preparation of cellular samples. After lysis is initiated, hydrogen ions, also generated on chip, are allowed to react with excess hydroxide creating a neutral pH lysate and minimizing biomolecule denaturation. The flow rate dependence of hydroxide concentration at the lysis filter is modeled and lysis efficiency is experimentally determined to be in good agreement for flow rates above 15 μl min^{-1}. Below 15 μl min^{-1} the number of lysed cells decreases due to cell settling. Additionally, lysis dynamics and pore size can be obtained. The method of reagent generation presented may also be used to simplify on-chip chemical synthesis.

Keywords: sample preparation, cell lysis, electrochemistry, reagent generation

1. Introduction

The ability to generate reagents for miniaturized analytical devices *in situ* leads to many important gains. Device complexity decreases as the number of fluid inputs is reduced. Reagent quantity can be tuned in real time to reach a desired sensed output. Additionally spatial control of reactions is achieved by controlling reagent synthesis positions. As a proof-of-concept we demonstrate the use of electro-generated hydroxide ions as a lytic reagent in the preparation of cellular samples for a miniaturized total analysis system. Depending on the assay required, different methods of cell lysis have been reported on-chip. Most common are electroporation-based [1-2] and chemical methods [3-4]. Electroporative methods have been shown to be effective with fast <50 ms lysis times [2], but require high voltage supplies and can cause joule heating. Chemical methods can be non-denaturing [3] but require extra fluid inputs and may require subsequent removal of detergents that interfere with assays. We present a chemical method that requires no fluid inputs because reagents are generated electrochemically on-chip. Additionally, no removal of the lytic agent, hydroxide, is required since excess OH^- recombines with H^+ generated on-chip downstream. A device for high throughput lysis using these methods (Fig. 1) is modeled, fabricated using PDMS-based micromolding, and tested with varied flow rates.

2. Modeling

Both OH^- and H^+ steady state concentration distributions were modeled using the finite element method (FEMLAB, Comsol Inc.) for flow rates from 10 – 90 μl min^{-1}. The concentration distribution for a flow rate of 10 μl min^{-1} is plotted in Fig. 2A. Because asymmetry in the flow leads to asymmetry in convection of electrogenerated products, the distribution of OH^- near the chamber filter is not uniform. Cells at the filter (Fig. 2A, dashed line) are exposed to a small pH gradient. An average pH at the filter is obtained from the average OH^- concentration and is plotted as a function of flow rate (Fig. 2B). A Peclet number, $P = UL/D$, can be defined as the ratio of convective to diffusive mass transport. For flow rates of 10 – 90 μl min^{-1} P varied from 5.7 – 51 at the filter, indicating a convection dominated solution. As convective contributions to mass transport increase the OH^- level at the filter decreases.

We have determined that alkaline lysis occurs for HeLa cells above pH 11.70. Macrophages have been shown to lyse at pH 13 in less than 60 seconds while taking more than 120 seconds at pH

12 [5]. Combining these results with the modeling data shown in Fig. 2B suggests a range of flow rates at which lysis should occur (0-20 μl min^{-1}).

At the outlet of the lysis chamber (Fig. 2A) one observes that recombination of H^+ and OH^- has not completed. One can approximate the time, t, required for diffusive mixing in a channel of width d using $t = d^2 / 2D$. For diffusive mixing across half the exit channel of 300 μm width, using the hydroxide diffusion constant of $D = 5 \times 10^{-6}$ cm^2 sec^{-1} yields a diffusion time of 22.5 s. After this time the lysate should approach initial unpolluted buffer conditions. Proteins and other biomolecules are only exposed to high pH for a short time period after the lysis event.

3. Experimental

For flow rate dependent cell lysis measurements in the high throughput device (Fig. 1), HeLa cells in PBS solution were loaded with calcein AM. For experiments presented calcein AM containing solution was not replaced after cell loading as it was found to amplify the lysis signal. Intracellular esterases released after lysis continued to activate extracellular calcein AM. The cell concentration for flow through experiments was ~ 1.5×10^6 cells ml^{-1}. Prior to introducing cells the device was loaded with PBS and pressurized using a syringe with a closed outlet to remove any air trapped inside. Flow was initiated with a syringe pump until a background level of fluorescence was observed from the cell solution. Next, –2.6 V was applied to the cathode and fluorescence intensity of the bulk solution was recorded over time at the common outlet of all 10 lysis chambers. Typical currents of 120-180 μA were recorded for 10 parallel lysis chambers.

An additional device (Fig. 4A) is used to confirm lysis is not due to electric field / electroporation. Here flow is stopped while red blood cell (RBC) lysis is observed as a function of distance from the cathode. The distance between electrodes was 600 μm, resulting in a field strength of 43 V/cm, an order of magnitude below fields needed for electroporation-based lysis (0.9 kV/cm [2]). The chamber width and length were 1.5 mm x 5 mm. The chamber height was 40 μm.

4. Results and discussion

Using the high throughput device, maximum and steady state intensity changes are plotted in Fig. 3 as a function of flow rate. Error bars represent standard deviation of data from two devices. There is a trend of increased intensity as the flow rate decreases that corresponds well with the increased average pH at the filter (Fig. 3). However, at 10 μl min^{-1} steady state intensity decreases due to cell settling. Increased fluorescence intensity upon lysis indicates the ability of cytosolic proteins (esterases) to be released and function without denaturation.

Lysis in the stopped flow device was observed to proceed as a function of distance from the cathode in all directions (Fig. 4B-D). This confirms that lysis is not due to the electric field between the electrodes because lysis proceeds similarly in areas of zero electric field. While lysis of the entire cell population occurs over 2-3 minutes, it is made up of individual cell lysis events that are scattered in time but occur on very short time scales (Δt = 63 ms for RBCs). This can be observed because of diffusive application of lytic agent to stationary cells in solution.

Acknowledgements

This work is partially supported by a Whitaker Foundation Graduate Fellowship (D. D.).

References

[1] Gascoyne, P. R. C.; Vykoukal, J. V. *Proceedings of the IEEE* 2004, *92*, 22-42.
[2] McClain, M. A. et al. *Anal Chem* 2003, *75*, 5646-5655.
[3] Schilling, E. A.; Kamholz, A. E.; Yager, P. *Anal Chem* 2002, *74*, 1798-1804.
[4] Li, P. C. H.; Harrison, D. J. *Anal Chem* 1997, *69*, 1564-1568.
[5] Jin, W. R. et al. *Anal Biochem* 2000, *285*, 255-259.

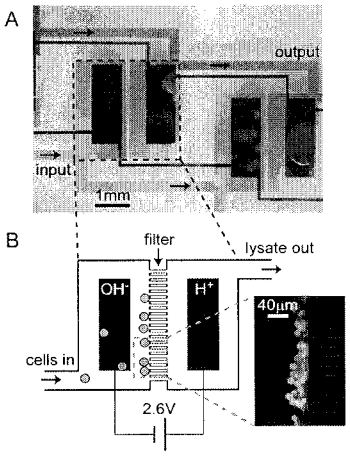

Figure 1. (A) Two parallel lysis chambers are shown from a 10-chamber device. Palladium electrodes are separated by a filter region of lower channel height. (B) To produce hydroxide for lysis 2.6 V is applied across the electrodes. Hydroxide is formed at the cathode (upstream) while H^+ forms at the anode on the other side of the filter (downstream). Cells are trapped at the filter until lysis. Recombination of excess OH^- and H^+ downstream leads to a neutral lysate.

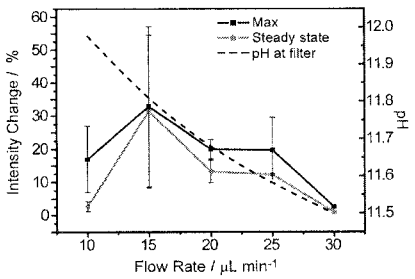

Figure 3. Intensity change (indicating lysis) is plotted as a function of flow rate indicating both the maximum intensity increase and intensity after reaching a steady state value. Simulated pH as a function of flow rate is plotted against the right axis for comparison.

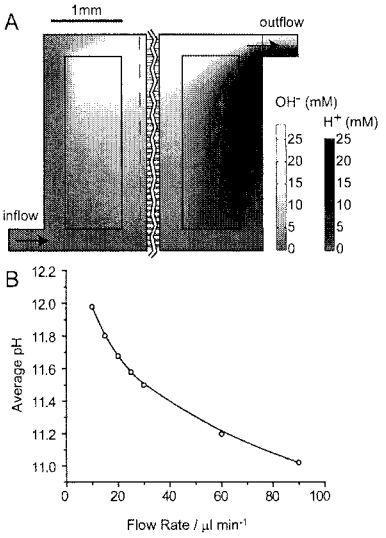

Figure 2. (A) Simulation of distribution of OH^- and H+ in one lysis chamber for a flow rate of 1 µl min^{-1} per chamber. Electrodes are shown as rectangles in the centers of the chamber separated by a filter. Results in the filter region, which was elongated to match fluidic resistance, are not shown. (B) The average pH next to the filter (dotted line) is plotted as a function of flow rate.

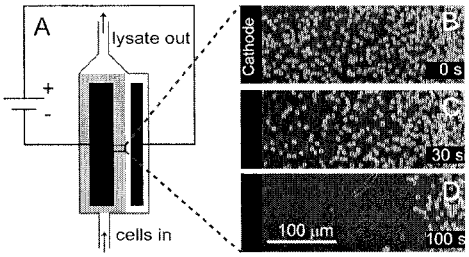

Figure 4. Cell lysis by local hydroxide generation. (A) Proof-of-concept device schematic with the lysis area indicated in gray. (B-D), Movie frames showing changes in the red blood cell density due to lysis inside the device. Lysis proceeds in a similar fashion around all sides of the cathode.

NANOPARTICLES IN SEPARATION SCIENCE – APPLICATIONS IN CEC-MS, MALDI-MS, AND MOLECULAR RECOGNITION

Peter Viberg/Spégel, Jakob Nilsson, Curt T. Reimann,* Christian Nilsson, Magnus Jorntén-Karlsson, Patrik Petersson** and Staffan Nilsson**

Technical Analytical Chemistry, Lund Institute of Technology, Lund, Sweden
** Analytical Chemistry, Lund University, Lund, Sweden*
*** AstraZeneca R&D Lund, Lund, Sweden*

1. Introduction

During the past decade, efforts have been made to miniaturise separation systems. This also prompts for the need to decrease the size of the sorbents, going from microparticles to nanoparticles (NP's). However, the high backpressure associated with small particles hampers the practical use of these systems. Partial-filling (PF) [1] and continuous full-filling (CFF) [2] NP-based capillary electrochromatography (CEC) have been developed in order to enable the use of NP's in separation systems. Furthermore, novel design of the NP's allows them to possess selectivity predetermined for a specific analyte. Finally, tailored NP's can be used as combined solid phase extraction (SPE) sorbent and matrix-assisted laser desorption-ionisation (MALDI) matrix.

2. Theory

CFF-CEC electrospray ionisation (ESI) mass spectrometry (MS): For CEC, the NP's are suspended in the electrolyte and continuously introduced into the separation capillary. Due to light-scattering properties of the NP's, UV-absorbance detection is not practical. Also, direct infusion of the NP-containing electrolyte into a mass spectrometer would contaminate the detector. An orthogonal ESI interface allows the NP's to be separated from the analytes in the electrospray source (Fig.1). The analytes are deflected 90° and accelerated into the mass spectrometer, while the heavier NP's shoot straight ahead and miss the inlet completely.

NP-MALDI matrix: A technique enabling analysis of molecules that are partitioned onto the surface of polymeric materials offers a novel means for studies of surfaces and molecule-surface interactions. Furthermore, through immobilization of matrix to the polymer, MALDI measurements could be carried out without interference from disturbing matrix signals. This approach would be useful for analysis of low molecular weight analytes. Our approach utilises customisable polymer NP's, although other formats are also feasible. The NP-format offers improved mass-transfer that can be beneficial in SPE-MALDI-MS.

NP's for molecular recognition in PF-CEC: Molecular imprinting allows synthesis of affinity sites with predetermined selectivity. In short, the molecule of interest (the template) is mixed with monomers having functionality complementary to that of the template. The functional monomers and the template will assemble to form tight complexes, which after addition of a cross-linking monomer and a radical initiator, are polymerised to yield highly selective cavities with functionality, shape and size complementary to that of the template.

3. Experimental

CFF-CEC-ESI-MS: In CFF experiments, the sample was injected into a capillary filled with an NP slurry, and during the separation slurry is continuously fed through the capillary, and into the ESI-MS interface.

NP-MALDI matrix: NP's with the matrix component CHCA covalently bond, were used in analysis of low molecular weight analytes partitioned onto the surface of the NP's. NP's prepared from methacrylic monomers (Fig.2) [1-3] were used as follows: (1) mixed with analyte and free CHCA, (2) mixed with analyte, and (3) covalently modified with CHCA and mixed with analyte. Several control experiments were also carried out.

NP's for molecular recognition in PF-CEC: Using PF-CEC, a plug of molecularly imprinted NP's is injected prior to the sample that migrates through the NP-plug. Once used, the NP's are flushed out and a new plug is injected for the next analysis (a new affinity phase in less than 1.5 min for every separation, no stationary phase ageing).

4. Results and Discussion

CFF-CEC-ESI-MS: A new way of chromatography is introduced with NP's as pseudo stationary phase in CEC with ESI-MS detection (Fig.1). The technique benefits from a *new disposable continuously introduced interaction phase for each analysis, which eliminates carry-over effects and contamination from samples in complex matrices, e.g. biological samples.* Furthermore, the technique allows fast and easy change and optimisation of the interaction phase. We have previously showed proof-of-principal for the technique [1], but are now able to show that the technique is improved and approaches conventional CEC and μLC in terms of separation efficiency (N>100 000). The improved technique is more flexible and allows separation of a wide range of analytes.

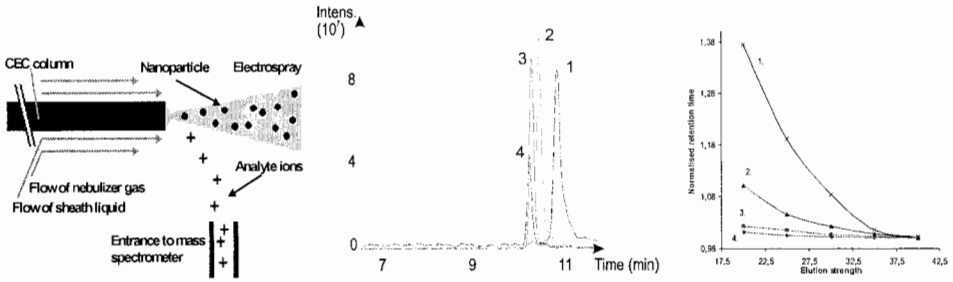

Figure 1. (Left) Orthogonal ESI-MS interface used in CFF-CEC. (Middle) Electropherogram from four neutral phthalates, using CFF-CEC-ESI-MS. (Right) Manipulation of retention by varying the electrolyte composition.

NP-MALDI matrix (Fig.2): The presence of the methacrylate-based NP's along with propranolol and CHCA was not associated with the occurrence of any mass spectral peaks other than those typically observed when irradiating pure matrix. Propranolol was easily detected at m/z 260. Thus the presence of the NP's did not disturb the MALDI process *per se*. LDI-TOF-MS experiments (complete absence of matrix) performed on propranolol-NP's mixtures did not reveal any spectral peaks. Thus, neither the

NP's nor any components thereof act as a matrix in the LDI experiments. Preliminary experiments on the NP's with covalently bond CHCA revealed a signal for propranolol but no CHCA related signal. Contrary to intuition, bound CHCA has some matrix-like character even if the surface-phase matrix structure and adsorption of analyte thereon yield a completely different target structure for irradiation than in conventional MALDI.

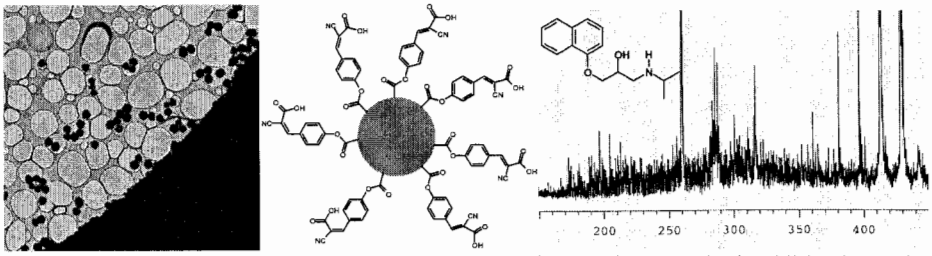

Figure 2. (Left) Transmission electron micrograph of NP's (~160 nm). (Middle) The NP's were derivatised with the common MALDI matrix CHCA. (Right) (MA)LDI-TOF spectrum of propranolol (260) on the derivatised NP's. No CHCA related signals were found in the spectrum.

NP's for molecular recognition: Simultaneous separation of the enantiomers of two drugs having little structural resemblance has been achieved using two different techniques: *Mixed NP's* (coupled columns, Fig.3): utilizes the ability to mix and vary the amounts and type of MIP NP's. *Multiple templating:* utilizes two different templates during preparation of the MIP [3].

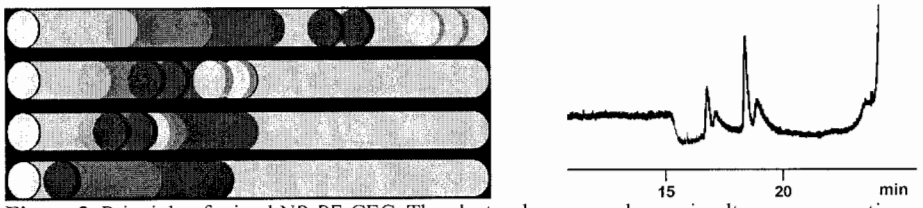

Figure 3. Principle of mixed NP-PF-CEC. The electropherogram shows simultaneous separation of two different enantiomer pairs, ropivacaine and propranolol.

Acknowledgements
The authors wish to thank VR, Crafoordska stiftelsen, Fysiografiska sällskapet i Lund, Stiftelsen forskning utan djurförsök and AstraZeneca for financial support.

References
[1] L. Schweitz *et al*, Analyst 125 (2000), 1899
[2] P. Viberg *et al*, Anal. Chem. 74 (2002), 4595
[3] Spégel *et al*, Anal. Chem. 75 (2003), 6608

POLYMERIC INSULATOR-BASED (ELECTRODELESS) DIELECTROPHORESIS (iDEP) FOR THE MONITORING OF WATER-BORNE PATHOGENS

Blake Simmons, Blanca Lapizco-Encinas, Renee Shediac, Johnathan Hachman, Jeffrey Chames, John Brazzle, Joseph Ceremuga, Gregory Fiechtner, Eric Cummings, and Yolanda Fintschenko

Sandia National Laboratories, 7011 East Avenue, Livermore, CA, 94550

Abstract

We report the selective trapping, concentration, and release of various particles utilizing insulative (electrodeless) dielectrophoresis (iDEP) with a polymeric device. These organisms include inert polystyrene beads, bacterium, and spores that were selectively concentrated and released using only a DC voltage applied across a polymeric microchannel filled with insulating posts. These devices were formed through an injection molding process utilizing an electroplated nickel stamp with polyolefins serving as the thermoplastic polymer of choice based on operating conditions. These devices were then sealed with lids through thermal diffusion bonding. The only electrodes present were platinum wires that were placed in the fluidic inlet and outlet reservoirs. The dielectrophoretic responses of the particles were observed to be a function of the applied electric field as well as post size, geometry, and spacing.

Keywords: dielectrophoresis, polymer microfluidics, concentration, separation

1. Introduction

Water contamination has recently become a more prominent national health and safety issue [1]. There has been a growing interest in developing techniques for the monitoring, detection, and removal of low levels of microorganisms from the nation's water supply to ensure the safety of this national infrastructure. DEP is a non-destructive characterization and separation method and has enormous potential for applications involving the separation and detection of viable microorganisms. There has, therefore, been significant recent activity on the utilization of DEP for the isolation of microbes and bio-particles from an inert background [2].

We have previously shown that the technique of iDEP is highly effective in glass microfluidic chips [3]. The ultimate goal of this research project, however, is to develop a high-throughput iDEP system that uses polymers as the host structural substrates. Polymeric materials were selected because the versatility of polymeric devices would facilitate the scale-up of iDEP devices for high throughput and parallel operations. We present here the successful demonstration of the trapping, concentration, and release of mock and true biological particles utilizing insulative dielectrophoresis within a polymeric device. To the best of our knowledge, this is the first known demonstration of polymeric insulator based electrodeless dielectrophoresis (iDEP) that can be used for the manipulation, trapping, separation, and concentration of biological organisms within a polymeric device.

2. Experimental

Glass masters. Glass structures were fabricated using standard photolithography techniques. Two types of techniques were utilized to produce these masters: Bosch etching and HF wet chemistry. The microfluidic chip contains 8 subcircuits, with each subcircuit containing a separate patterned array of posts located between two liquid reservoirs. The chip therefore contains a total of 16 liquid reservoirs. The depth and length of the microchannel is 64 microns and 1.25 cm, respectively.

Electroplated nickel stamps. The glass substrates were then coated with sputter deposited 500 Å chromium (500 Å Ti for the silicon wafer) and 1500 Å copper to serve as an adhesion promoter and seed layer for electroplating, respectively. Electroplating was conducted in a Digital Matrix© device that was operated at 1 amp-hour for a total of 40 hours. This produces a Ni layer of approximately 950 micron total thickness that contains the opposite tones of the glass substrates. The Ni stamp was then released from the glass substrate using traditional wet chemistry techniques and machined to the appropriate dimensions for use in the injection molding and hot embossing machines using in-house fixtures.

Polymer replication/device formation. Injection molding was carried out utilizing a Nissei® 60-ton vertical platen device. Thermoplastic resins were fed to the machine in pelleted form. Temperature control, process conditions, and cycle times were empirically determined for each thermoplastic resin based on manufacturer's recommendations. Hot embossing was carried out using a Carver© press that uses thermoplastic resins that have been preformed into discs. Although polyolefin thermoplastic resins (Zeonor® 1060R from Zeon Chemicals, Louisville, KY) were the main focus of the current research, these devices were also formed by using polymethylmethacrylate, polycarbonate, and polystyrene thermoplastic resins. These devices were then sealed with lids through thermal diffusion bonding to form a functional watertight unit that consists of a microchannel filled with an array of posts.

3. Results and discussion

The devices were replicated using the derived stamps with a high degree of fidelity, as shown in Figure 1. In order to test the bonded polymeric devices, a nonuniform electric field was created by the replicated array of insulating posts. The microfluidic channel was filled with DI water that contained the particles of interest by means of the fluidic inlet and outlet. Electrodes were than placed in the inlet and outlet reservoirs and energized to initiate the experiment. The results obtained for fluorescently labeled polystyrene beads are shown in Figure 2. There is no initial pressure driven flow and the beads are quiescent. At low applied voltages, typically below 500 V DC, there is evidence of electro-osmotic flow (EOF) from left to right as indicated. The apparent velocity of the beads increases with the magnitude of the applied field strength over this range, until a certain threshold applied field is reached. After this "trapping voltage" is applied, the beads are observed to trap in the regions separating the insulative posts in discrete bands. After the field is lowered below the trapping voltage and/or entirely removed, the beads are no longer trapped and proceed through the device. Similar behavior is observed for prokaryotic *Escherichia coli* cells (results not shown) and *Bacillus thuringiensis* spores, as shown in Figure 3. These results demonstrate that the polymeric devices are capable of performing the same general function as their glass counterparts, while imparting the necessary degrees of manufacturing and scalability that are required to create a device capable of handling high sample volume (> 1L).

4. Conclusions

The effective trapping and release by the EDEP process of various particles has been demonstrated on polymer chips. Insulating posts made of a thermoplastic polyolefin were utilized in order to produce a nonuniform electric field. We have achieved success in polymeric substrates derived from both injection molding and hot embossing replication technologies. This preliminary report will be used to implement future designs and testing for the selective concentration of biological organisms. Process parameters based from these results will be used to develop a high-throughput system that is capable of quickly and effectively screening of water-borne pathogens.

References
[1] B.A. Macler, J.C. Merkle, Hydrogeol. J., 8: 29-40, (2000).
[2] E.B. Cummings, A.K. Singh, Proc. SPIE Conference on Micromachining and Microfabrication, 4177:164–173, (2000).
[3] B.H. Lapizco-Encinas, B.A. Simmons, E.B. Cummings, Y. Fintschenko *Analytical Chemistry,* **76**(6), 1571-1579, (2004).

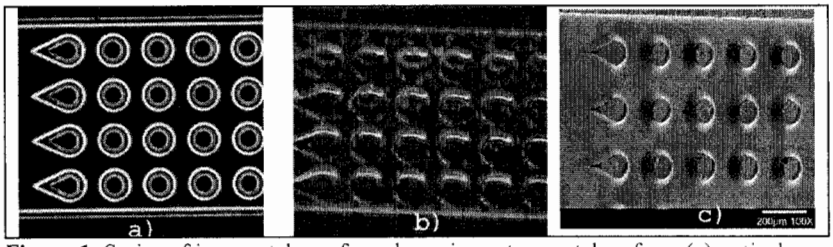

Figure 1. Series of images taken of a polymeric post array taken from (a) optical image of a nickel stamp (negative tone), (b) optical image of replicated polyolefin posts (positive tone) by injection molding, and (c) scanning electron optics image (SEM) of those replicated polyolefin posts (positive tone).

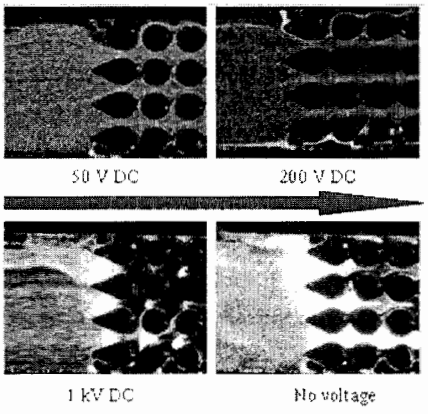

Figure 2. Pictures taken from a movie showing the dielectrophoretic response of the fluorescent polystyrene beads from 50 V through 1 kV when trapping is observed, and the response of the beads when the field is removed.

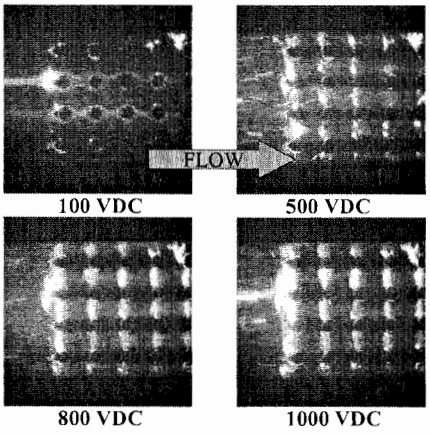

Figure 3. Pictures taken from a movie showing the dielectrophoretic response of fluorescently labeled *Bacillus thuringiensis* spores as a function of applied voltage.

A MICRO ACOUSTIC FIELD-FLOW FRACTIONATION SYSTEM (μ-ACFFF) FOR NANO-SCALE SEPARATIONS

Thayne L. Edwards[1] and A. Bruno Frazier[1]
[1]School of Electrical and Computer Engineering, Georgia Institute of Technology
777 Atlantic Drive, Atlanta, Georgia, 30332, USA

Abstract

This paper will be the first demonstration of an acoustic based micro field-flow fractionation system, μ-AcFFF. The paper and presentation will discuss the theory behind the micro separation system, the design and fabrication of the μ-AcFFF system, and characterize the performance of the fractionation system with an integrated electrical impedance detector. The fractionation system utilizes acoustic standing wave forces transverse to the flow direction in a microfabricated FFF channel to separate nano-scale particles. In this paper, a digest of the modeling and performance of the μ-AcFFF system are presented. Initial system performance was evaluated using polystyrene emulsions containing particles of known mean diameters.

Keywords: acoustic, field-flow fractionation, FFF, AcFFF, nano-particle analysis

1. Introduction

FFF is an elution-based separation technique that occurs in a ribbon-like channel with breadth to width aspect ratios of greater than 100, Figure 1. FFF samples size range from nanometer to micrometer and have included materials such as latex suspensions, emulsions, proteins, and dissolved polymers. The ability to interrogate a specific sample property depends upon the field used to retain the sample. Acoustic fields in FFF have been explored only scarcely relative to the more common fields such as thermal and electric. One possible reason is because of the expense and difficulty in fabricating the macro scale systems [1]. However, acoustic fields have a unique perspective with its relative compressibility/density-based separations, cubic dependence of size on force, and position dependant force. As demonstrated in this work, micromachining technologies provide a straight forward method for realizing miniaturized AcFFF systems.

2. Theory

The retention basis is the relative density and adiabatic volumetric compressibility of the sample to the carrier as characterized by the density/compressibility factor defined below. The acoustic force on a spherical particle, which has a diameter much smaller than the acoustic standing wavelength, [2] elucidates these points and is given by

$$F_{rad} = -\tfrac{4}{3}\pi r^3 k\overline{E} f(\rho,\gamma)\sin(2kx)$$

The parameters are: spatial parameter, x; wave propagation constant, k; particle radius, r; acoustic energy density, $\overline{E}$; and the density-compressibility factor, $f(\rho,\gamma)$, which is a function of the density, ρ, and the compressibility, (, for the liquid and particle:

$$f(\rho,\gamma) = \frac{5\rho - 2\rho'}{2\rho + \rho'} - \frac{\gamma}{\gamma'}$$

For a polystyrene particle in water, $f(\rho,\gamma) = +0.548$. The positive sign indicates that the particle will move to the standing wave antinodes.

The system resonant frequency and material layer thicknesses were determined through a KLM transducer model and equivalent transmission line models (impedance) of the layered materials. The electrical input impedance plotted versus frequency for various layer thicknesses, Figure 2.

The resonance frequency is located at the first zero phase (near minimum magnitude) crossing of the input impedance. Harmonic resonance frequencies were also predicted with this model.

3. Experimental

The μ-FFF channel dimensions were (0.062 × 6.0 × 60) mm^3 including tapered entrance/exit regions. Fabrication of the channel was adapted from a previously fabricated micro thermal field-flow fractionation channel [3]. The microchannel top wall was a (0.505 × 100) mm^2 36° y-cut, $LiNbO_3$ wafer and served as the acoustic transducer. The channel bottom wall was a (0.350 × 76) mm^2 silicon wafer with KOH etched fluid vias. A novel approach using spin-cast PDMS and laser ablation was used to create a sealing gasket around the microfluidic channel. PDMS was spin coated onto a silicon substrate and cured to a final thickness of 62 μm. The channel walls / sealing gaskets surrounding the fluid channels were defined using laser ablation of the PDMS. The two wafers were bonded together using uncured PDMS as an adhesive and resulting in a microchannel with a thickness of 62 μm. See Figure 3, for an image of the completed system.

The transducer was designed to operate at resonance frequency in which the separation channel thickness equals one-half wavelength. The other two layers were each designed to be a one-quarter wavelength thick. In the channel there is one node and one antinode, Figure 1. Multiple nodes or antinodes would result in a single sample being eluted at various times. The silicon was used as a reflector and to transform the impedance from a pressure release boundary at the air interface to a rigid boundary at the water interface.

The acoustic transducer was stimulated using a 5 volt peak-peak sinusoid with frequency of 6.18 MHz. Degassed, deionized water (17.1 MΩ-cm) was the carrier fluid for the experiments. The 500 nL PS272 sample was introduced upstream of the channel using a microliter syringe, fluid tee, and septum. Flow was stopped 10 seconds after injecting to allow the sample to reach the equilibrium concentration profile in the channel. Flow resumed at 100 seconds. An integrated conductivity detector located just prior to the exit region of the channel and was driven by a 2 kHz sinusoid at a constant 5 volts peak-peak.

4. Results and discussion

The channel volume, including pre-column tubing and entrance region, to the detector was approximately 21 microliters for the channel used in the retention experiments. The channel was found to be leak-free even under fluid pressure of 100 psi. At significantly higher pressures the channel seal broke, but upon relaxation the PDMS/$LiNbO_3$ interface sealed again.

The resonant frequency of the system was measure to be 6.18 MHz. The slight difference from the predicted is probably due to variations in the thickness of the channel and silicon reflector.

The fractogram showing the void peak and PS272 samples is shown in Figure 4. The PS272 sample eluted at 520 seconds was significantly retained relative to the void peak eluted at 144 seconds. The retention ratio of PS272 is 0.126. The plate height of the void peak and PS272 peak was 0.30 and 0.16, respectively.

5. Conclusions

In the paper and presentation, in addition to the work demonstrated to date, we will demonstrate multi-particle separations and further characterize the system for relative retention times, resolution, steric transition point, and optimal carrier flow rate based on plate-height.

6. References

[1] S. N. Semyonov, K.I. Maslow, *Chrom. Symposium*, 151-156 (1988)
[2] K. Yosioka, Y. Kawasima, *Acustica*, **5**, 167-173 (1995)
[3] T. Edwards, Bruce K. Gale, A. B. Frazier, *Anal. Chem. A*, 74, pp. 1211-1216 (2002).

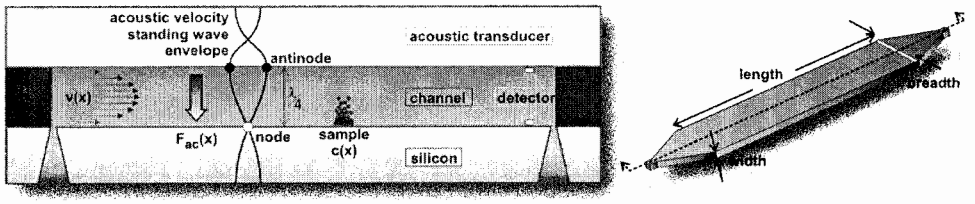

Figure 1. μ-AcFFF system configuration (*left*, cross-section view; *right*, channel view) including velocity profile of carrier fluid, acoustic force, concentration profile of perturbed sample at equilibrium, and conductivity detector near outlet.

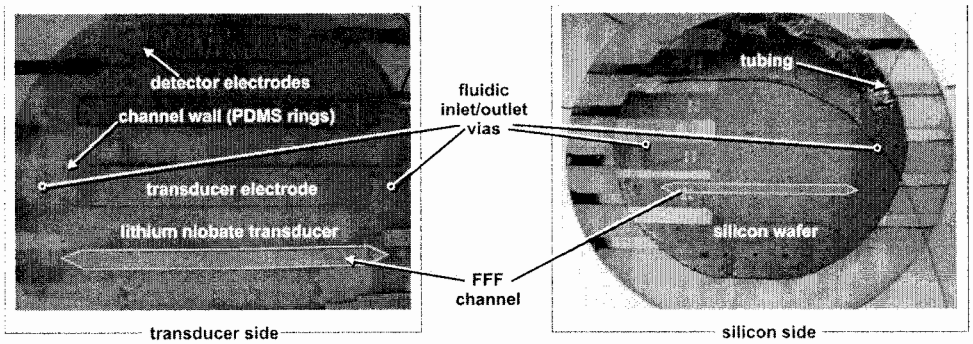

Figure 3. Photographs of transducer side and silicon side of the μ-AcFFF system. There are five FFF channels on a single wafer with one highlighted to show channel shape. Key system components shown include transducer, silicon wafer, electrodes, detector electrodes, channel wall, fluidic inlet/outlet vias, and fluidic interface tubing.

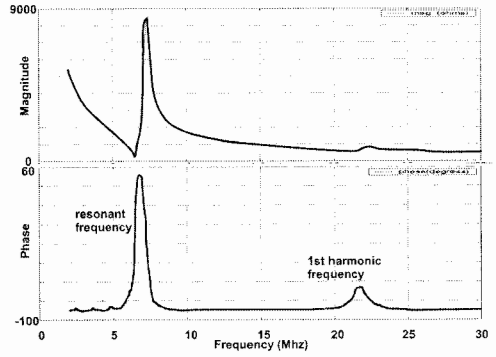

Figure 2. Electrical input impedance (*bottom*, phase; *top*, magnitude) as calculated from KLM acoustic transducer model. Resonant and 1st harmonic frequencies indicated.

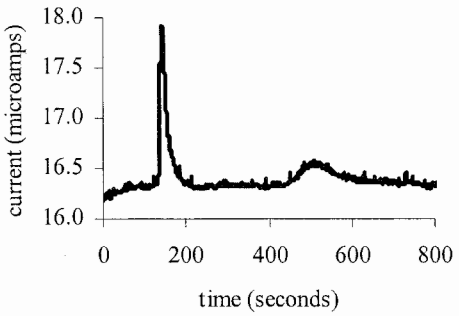

Figure 4. μ-AcFFF fractogram of PS272, 0.5 μL. Flow rate =1 mL/hour, flow stop at 10 sec, flow start at 100 sec, transducer = 5 volts at 6.18 MHz, detector = 5 volts at 2.00 kHz.

ELECTROPHYSIOLOGY USING A HIGH-DENSITY MICROFLUIDIC ARRAY FOR HIGH-THROUGHPUT PATCH CLAMP MEASUREMENTS

Cristian Ionescu-Zanetti, Jeonggi Seo, and Luke P. Lee
Bioengineering Dept., University of California, Berkeley, CA 94720 USA

Abstract

We present whole cell current recordings using a microfabricated patch clamp array that allows recording from a large number of cells in close proximity. The array design enables simultaneous drug delivery to a number of patched cells and the acquisition of averaged cellular responses using minimal reagent quantities. While microfabricated devices have been used for whole cell patch recordings previously, we report the implementation of a closely spaced array fabricated by elastomer micromolding that allows high throughput measurements in a disposable package. Cell positioning is achieved using a novel lateral cell trapping scheme which allows for the optical monitoring of cell deformation inside the patch channel in conjunction with ion current recording. This device is also designed to eliminate parasitic capacitive coupling between the patch channel and the cell chamber and allows for easy media exchange during the experiment. Voltage clamp recordings of the voltage gated potassium channel Kv2.1 are presented along with channel block data in the presence of the channel blocker tetraethyl ammonium.

Keywords: automated patch clamp, electrophysiology, drug screening, ion channel

1. Introduction

The fact that cellular ion channels are effective drug targets, coupled with the laboriousness of traditional patch clamp techniques, has created a need for hi-throughput electrophysiology platforms [1]. Patch clamp based drug screening technology has been recently implemented by using microfabricated patch clamp designs that replace the traditional patch pipette with a pore in a silicon substrate [2, 3]. While successful at high-throughput measurements of channel activity, current devices have yet to achieve high densities of patched cells per unit volume and rely on robotically operated pipettes for reagent and cell delivery.

Here we present a device that is based on elastomer micromolding and takes advantage of integrated fluidic networks in order to achieve high patch site density and very small reagent volumes per experiment. Integration and close placement of individually addressed patch sites is enabled by the replacement of the patch pore with a microfluidic channel junction (Fig. 1, 2), where cells can be trapped from the main channel by applying negative pressure to the side channels [4]. We have fabricated devices with a high patch pore density of 3.3x104 sites/μl (Fig. 2). By comparison, current technology utilizes a single patch site at the bottom a 500 μl well.

3. Experimental

Details of the device fabrication can be found in [4]. Briefly, fabrication was done with a two mask process, one for the definition of the small patch channels in a Si wafer, and the other for patterning of the large channels by using the polymer SU8.

Recordings from multiple channels were obtained by adding a custom made analog multiplexing circuit to the front end of a standard patch clamp amplifier headstage (see Fig. 1b). Our prototype can switch between its 4 inputs (to one output) with a switching time of 100 ns and an off resistance of Roff = 450 GΩ (Ron = 85 $\pm$ 2 Ω). The two multiplexer address lines were controlled by a TTL signal output from a National Instruments Board (DAQ 6024E). The current response was recorded using a standard patch-clamp amplifier (Dagan PC-ONE), low-pass filtered

at 1 kHz and acquired at 5 kHz by the same analog to digital conversion board (DAQ 6024E). All device measurements were performed without the use of vibration isolation equipment.

4. Results and discussion

We show the current recordings for high resistance seals (500MΩ to 1GΩ) between the poly-dimethylsiloxane (PDMS) microchannel and the cell membrane and the attainment of a whole cell patch configuration (Fig. 3). Whole cell currents show increased capacitance of the whole membrane (C = 28 pF, red line in Fig. 3) and decreased overall resistance (R = 100 - 200 MΩ).

An advantage of using transparent PDMS as the molded material and glass as the bottom support is the possibility for optical observation of cell deformation into the patch pore and fluorescent measurements. The deformation of a HeLa (human tumor cell line) cell under the application of negative pressure and subsequent membrane break and cytoplasmic dye leak into the patch channels are shown in Figure 3 (inset). Thus, fluorescent binding assays can then be correlated easily with electrophysiology data.

Whole cell currents from a Chinese hamster ovary (CHO) cell line expressing the potassium channel Kv2.1 [5] were recorded using this device. A comparison of recodings obtained using the patch array and traditional pipette-based whole cell patch clamp recordings of the same cell line are shown in Fig. 4. The channel shows a strong voltage dependence, with an activation voltage above -20 mV (see Fig. 4b). Steady state activation current-voltage relationships were measured at the end of the voltage step. The device data was leak subtracted.

5. Conclusions

We report on the ability to obtain reliable whole cell patch clamp recordings from mamellian cells by emploing a micromolded PDMS patch array device. Currents of the voltage gated potassium channel Kv2.1 are recorded and compared to recordings using a traditional patch clamp setup. The integrated microfluidics and high patch density hold the promise for fast solution exchange coupled with multiple cell recording on-chip. Timescales for compound screening studies using this device design will be characterized in the near future.

Acknowledgements

The authors wish to thank Dr. Robin Shaw and Prof. Lily Jan of UC San Francisco for essential help on patch clamp recording techniques.

References

[1] P. B. Bennett and H. R. E. Guthrie, *Journal of Biomolecular Screening*, **8**(6): p. 660-667, (2003)

[2] K. Schroeder, B. Neagle, D. J. Trezise and J. Worley, *Journal of Biomolecular Screening*, **8**(1): p. 50-64, (2003)

[3] J. Xu, A. Guia, D. Rothwarf, M. X. Huang, K. Sithiphong, J. Ouang, G. L. Tao, X. B. Wang and L. Wu, *Assay and Drug Development Technologies*, **1**(5): p. 675-684, (2003)

[4] J. Seo, C. Ionescu-Zanetti, J. Diamond, R. Lal and L. P. Lee, *Applied Physics Letters*, **84**(11): p. 1973-1975, (2004)

[5] J. G. Trapani and S. J. Korn, *Bmc Neuroscience*, **4**: p. -, (2003)

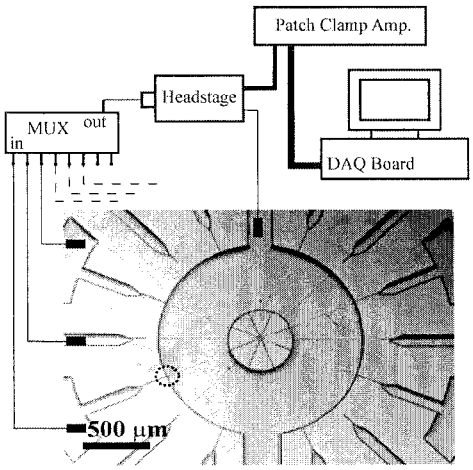

Figure 1. Experimental setup for a multiplexed patch clamp array for hi-thoughput measurements. The patch trap sites are on the edges of a round central chamber (eg. dotted circle).

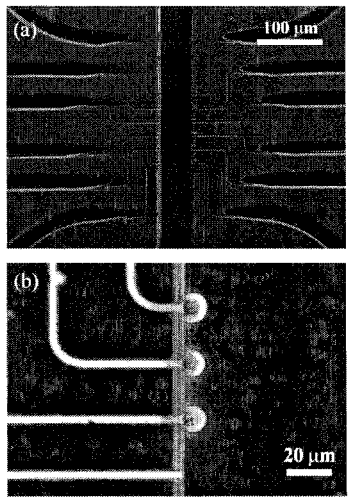

Figure 2. An SEM image of a high density patch array before bonding (a) and a phase contrast image of cells trapped at the patch pore (b).

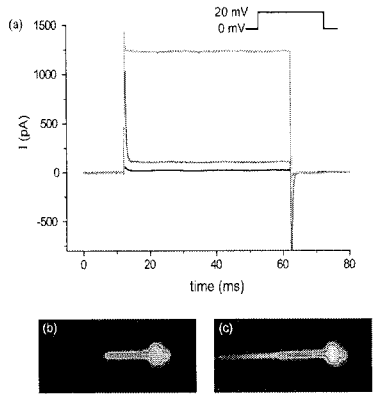

Figure 3. Current traces for three different configurations. The open channel (green) has a resistance of 14 MΩ, and after cell trapping the resistance is increased to 1 GΩ (black). After the membrane patch is broken, a whole cell configuration is achieved (red). Corresponding images of cytoplasmic stained cells are shown in (b) and (c).

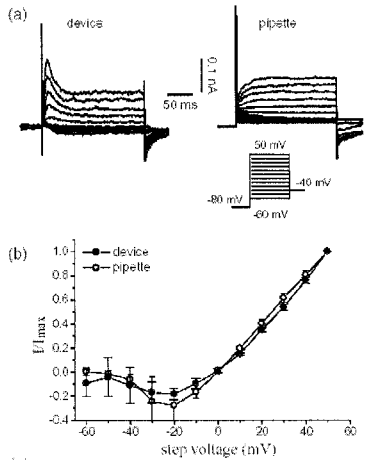

Figure 4. Comparison of whole cell recordings from CHO cells transfected with the channel Kv2.1. Patch array data (solid circles in b) is compared to traditional patch camp data (open circles in b).

A SILICON MICRO-SYSTEM FOR PARALLEL GENE TRANSFECTION INTO ARRAYED CELLS

A. Tixier-Mita[1], J.Jun[1] S. Ostrovidov[1], M. Chiral[2], M. Frenea[2], B. Le Pioufle[2], H. Fujita[1]

[1]LIMMS/CNRS - CIRMM - IIS, The University of Tokyo,Komaba 4-6-1, Meguro-ku, 153-8505 Tokyo, Japan

[2]BIOMIS, ENS Cachan Antenne Bretagne, Campus de Ker Lann, Bruz, France

Abstract

We successfully made a silicon bio-micro-system able to capture several hundreds of cells as a regular array and to place each cell between microelectrodes for electroporation. We confirmed that some fluorescent dye was successfully inserted by electroporation in 75% of living captured cells; this is the first step towards parallel processing of gene insertion to individual cells .

Keywords: electroporation, gene transfection, bio-MEMS, arrayed cells

1. Introduction

Standard gene transfection techniques (by genes injection using needles or by electroporation technique with large electrodes) are either very time consuming process or don't exhibit very high success rate [1]. By using micro-systems, it becomes possible to perform parallel gene transfection in thousands of arrayed cells and, because of the reduction of dimensions, to work much closer to each individual cell, improving then the transfection success rate [2]. Thus, it is possible to treat and examine thousands of cells placed on a chip simultaneously but separately. Thanks to micro-system proposed here we could obtain until 75% of electroporated cells.

2. Description of the micro-system for electroporation

The realized micro-system contains: 1) structures to place cells on the electroporation area; 2) electrodes to perform electroporation by applying pulse field from both sides of each cell placed between them. The cells are captured and placed by aspiration technique using a system which was already presented in previous publications [3,4], and which is described on Figure 1. An array of several hundreds of tiny holes, of 1 to 2 micrometers in diameter, is realized through a standard silicon substrate by interconnecting two V-grooves etched from frontside and backside along mutually orthogonal directions. Each cell is attracted and fixed on top of a hole by aspiration performed through the array of holes; an array of cells can then be obtained. After completion of holes, the chip is oxidized and Cr/Au electrodes are fabricated by standard Cr/Au evaporation, lithography and metal etching process. A photograph and a schematic representation of the chip are shown in Fig. 1.

3. Experimental procedure for electroporation

The chip is placed in a plastic holder, connected to a syringe pump and to a pulse generator (Cf. Figure 2). A solution containing cells (myeloma) is dispensed on the chip. Then, the syringe pump aspirate the solution through the micro-holes until most of the holes are occupied by one cell. Finally, voltage pulses are applied to the cells from the pulse generator to perform electroporation.

In this experiment, two questions have to be answered: 1) whether the electroporation is successful; 2) whether cells are dead or alive. Electroporation success is tested, here, with a fluorescent dye: Propidium Iodide (PI). PI is a molecule that enters cells either when cells are electroporated or when cells are dead. It emits red fluorescence excited by a green light when it is inserted inside the DNA strands of the cells nucleus. A second test with another dye is needed to

determine if cells are still alive after electroporation. The second dye is Fluorescein Diacetate(FDA): FDA enters cells, but emits green fluorescence only in living cells under blue excitation. The examination procedure using these dyes is summarized in Figure 4.

4. Results of the experiments

20% of captured cells were already red before applying any pulse: it corresponds to the percentage of cells already dead in the solution. After applying one pulse of 10V/1ms, additional 60% of cells became red. It means that 75% of living captured cells were successfully electroporated (Cf. Figure 5). Figure 6 shows photos of the cells seen under green excitation (a) and under blue excitation, (b) after having applied one pulse of 10V/1ms. All cells which show green fluorescence in (b) doesn't exhibit any red fluorescence in (a), excepted the one placed in between the electrodes, which proves to be electroporated and still alive. This system is to be tested with genes now.

Acknowledgements

We would like to thank Michel LECRIVAIN for the conception and realized the plastic holder, without which these experiments wouldn't have been possible. This project is realized in the framework of LIMMS-CNRS/IIS, the university of Tokyo.

References

[1] J. Olofsson, K. Nolkrantz, F. Ryttsen, B. A. Lambie, S. G. Weber & O. Orwar, *Current Opinion in Biotechnology*, **14,** 29-34, (2003)

[2] Y. Huang, B. Rubinsky, *Sens. Act. A*, **89,** 242-249, (2001)

[3] A. Tixier-Mita, Y.Mita, K. Cozic, M. Frenea, B. Le Pioufle, H. Fujita; *proc. MicroTAS'2002*, Nara, 888-890.

[4] A. Tixier-Mita, Y. Mita, H. Fujita; *proc. TRANSDUCERS'2003*; 250-253

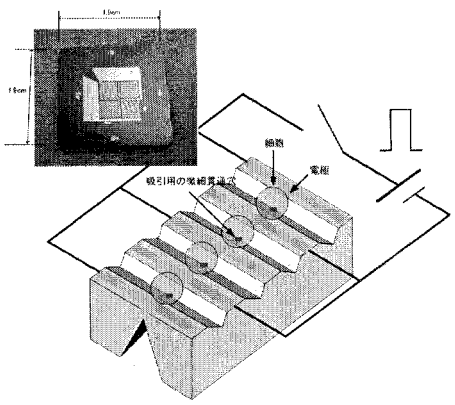

Figure 1: Micro-system with micro-holes for the placement of cells by aspiration and electrodes for electroporation.

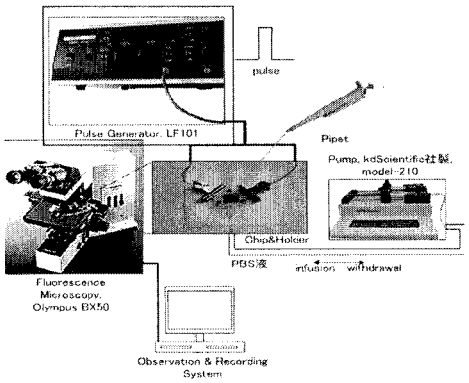

Figure 2: Experimental set-up with the chip placed in a holder and connected to a syringe pump and a pulse generator.

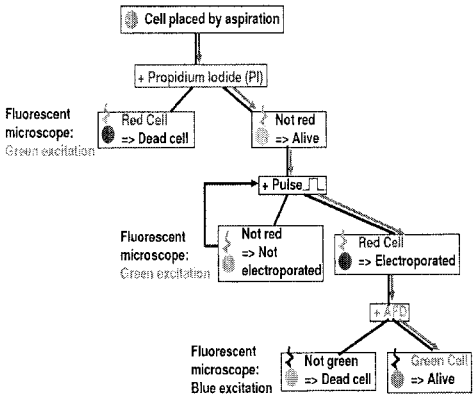

Figure 3: Experimental procedure

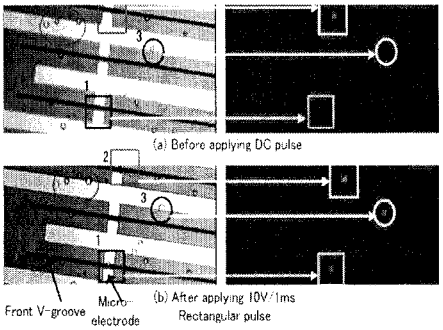

Figure 4: Observation under bright field (left) and green excitation (right) after applying one 10V/1ms pulse. Red dots are fluorescent dead or electroporated cells.

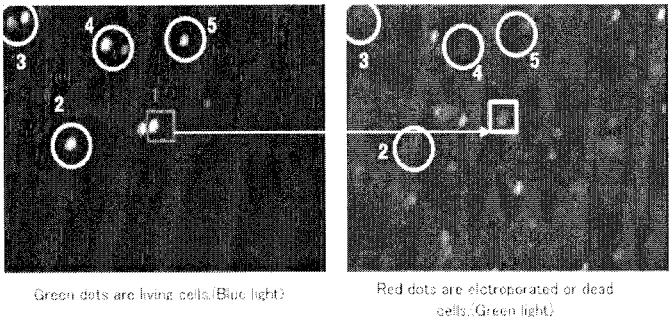

Figure 5: Observation under blue excitation (left) and green excitation (right). Green dots are living cells; red dots are dead or electroporated cells. The green and red dot is one electroporated and living cell.

AUTOMATED MEMS BASED FRUIT FLY EMBRYO INJECTION SYSTEM FOR GENOME-WIDE HIGH-THROUGHPUT RNAi SCREENS

Stefan Zappe[1], Matthew Fish[2], Matthew P. Scott[2]and Olav Solgaard[1]
[1] *E.L. Ginzton Lab, Stanford University, Stanford, CA 94305-4085, USA*
[2] *School of Medicine, Stanford University, Stanford, CA 94305-5439, USA*

Abstract

We have developed an automated fruit fly embryo injection system for genome-wide RNAi screens. The embryos are attached to glue-covered glass slides, and a MEMS based micro-injector chip is used for injection. Injection procedures are controlled with integrated on-chip piezoresistive pressure sensors. Motorized xyz-stages position the packaged injector chip and the embryo chip relative to each other. Two optical systems with CCD cameras are used for system alignment and embryo positioning. The computer-controlled setup scans the surface of the glass slide, detects embryos and performs injections. Typically more than 96 % of the embryos are reliably injected. A first RNAi experiment is successfully demonstrated.

Keywords: fruit fly embryo, microinjector, RNA interference, automated injection, integrated piezoresistive pressure sensor

1. Introduction

The knowledge created by the genome sequencing projects has brought unprecedented opportunities to study the genetic and molecular mechanisms of development and disease. The genome sequence of the fruit fly, *Drosophila melanogaster,* was published in 2000 [1] and has enabled systematic studies of the functions of the approx. 18,000 *Drosophila* genes. A powerful technique for learning about gene function is RNA-interference (RNAi) [2]. In RNAi experiments, specific genes are silenced by the presence of dsRNA (double-stranded RNA). An observed change in phenotype indicates the function of the silenced gene. Typically 100-200 fly embryos per assessed gene are injected during the first 60 minutes of their development, each with 60 pl of dsRNA. However, common manual injection techniques are unreliable and inefficient, and therefore not well suited for high-throughput investigations. To improve accuracy, reliability, and efficiency of RNAi experiments, we have developed an automated injection setup.

2. Automated injection system

An overview of the main components of the setup is given in Fig. 1. The two CCD cameras image the object from different angles. The two 2D-images contain positional information of the object in 3D-space. The spatial resolution is 2 μm per pixel. Alignment marks are etched into the surface of the embryo glass slide to allow description of the surface in 3D-space and positioning of the tip of the injector. After system alignment, the computer-controlled setup (Fig. 2) automatically scans the surface of the glass slide, detects embryos (Fig. 3), and performs injections. Scanning of a 7 x 7 mm^2 area currently takes 2.5 minutes. The injection of 100 embryos is performed within 7 minutes.

3. Micromachined injector chip

The surface-micromachined MEMS injector chip at the core of our setup is based on an earlier reported injection device with integrated pressure sensing membrane and optical read-out [3]. An SEM picture of the current version is shown in Fig. 4. Channel length, width and height of the needle are 155 μm, 17 μm and 2.4 μm, respectively. An integrated Pyrex-channel reservoir that stores 500 nl of liquid, helps to make most efficient use of the solution that is to be injected. Liquid

is driven through the needle by an externally applied pressure. The injection pressure at the needle is monitored using integrated polysilicon piezoresistors. The pressure sensor enables control of injection procedures, precise calibration of injected volume, and recognition of injection-system failure (e.g. leakage). The main characteristics of the pressure sensor are listed in Table 1. The amplified pressure signal in response to a 400 mbar pressure pulse is shown in Fig. 5 (left). Drops of DI water were injected into an oil film and the analysis of drop size and shape of the generated pressure pulse yielded a flow rate of $r_{water} = 12.8\,nl/s \cdot bar$ (Fig. 5, right). The PSG (phosphosilicate glass) film that defines the height of the needle channel exhibits a thickness non-uniformity of ± 3 %, resulting in flow rate variations from needle to needle of ± 10 %.

4. Experimental results

In injection experiments, dechorionated embryos are usually spread out on an agarose gel pad and carefully stamped onto the glue-covered surface of a glass slide. A controlled desiccation step allows injection of liquid without leakage of cytoplasm from the embryos. The embryos are subsequently covered with oil to prevent further desiccation.

Fig. 6 (left) shows green food color injected into an embryo during a test run. The injected embryos appear green within minutes (Fig. 6, right). More than 96 % of the embryos are reliably detected and successfully injected.

To facilitate injection, the embryos are typically dechorionated (the hard egg shell is dissolved in bleach). However, initial results show, that our MEMS injectors are sturdy enough so that direct injection through the chorion can be effectively performed. Leakage has not been observed. Clogging – as observed with conventional drawn glass needles – occasionally occurred at very low injection pressures (P = 6 Psi), but no clogging was observed at a higher pressure above P = 24 Psi.

In a first RNAi experiment, we successfully injected dechorionated embryos with dsRNA corresponding to the segment polarity gene *armadillo* at a concentration of 0.01 µM. The cuticle of a wildtype embryo in comparison to an embryo that was injected with our setup is shown in Fig. 7. As expected, the proper order of the denticle belts is completely destroyed by the dsRNA injection. A pilot screen of 360 genes, recently identified as likely to be involved in fruit fly embryo mesoderm development [4], is planned.

5. Summary and Conclusions

We have developed an automated setup for fruit fly embryo injection. Compared to conventional drawn glass capillaries, our MEMS based injectors are mechanically much more stable and less prone to clogging. Injection through the chorion is possible and promises to facilitate experiments significantly. The precisely defined injector geometry results in a better dosage control. Furthermore, an integrated piezoresistive pressure sensor allows us to monitor needle performance and to detect failure. During automated injection more than 96 % of embryos are successfully injected. A first RNAi experiment has been successfully performed. Currently we optimize embryo preparation procedures and injection related parameters. We aim to achieve a tenfold increase in efficiency compared to manual injections and will start with a pilot RNAi screen in the near future.

Acknowledgements

Financial support through DARPA within the Bio-Info-Micro program is gratefully acknowledged.

References

[1] M.D. Adams et al, *Science*, Vol. 287, No. 5461, 2185-95 (2000)
[2] RW. Carthew, *Curr. Opin. Cell Biol.* 2001 Apr;13(2):244-8 (2001)
[3] S. Zappe et al, *Proc. µTAS*, Nara, Japan, November 3-7, 2002, 682-4 (2002)
[4] E. Furlong et al, *Science*, Vol. 293, 1629-33 (2001)

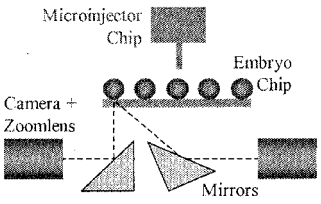

Figure 1. Schematic drawing of the injection system.

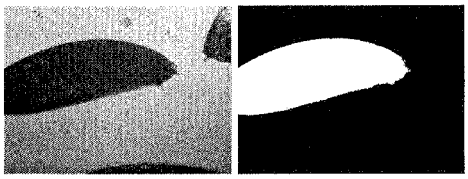

Figure 3. Image analysis. Left: Original camera image; the embryos block light and appear dark. Right: The binary image after particle filtering shows only the detected embryo.

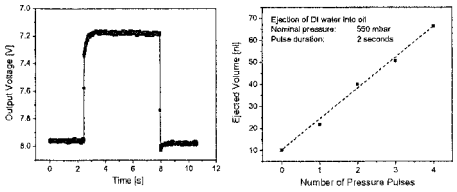

Figure 5. Left: Recorded pressure sensor signal during switching cycle. Right: Flow rate calibration curve for DI water.

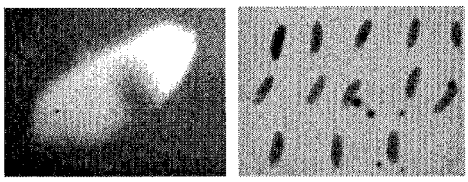

Figure 6. Left: Video screenshot of the automated injection of green food color (dark shadow). Right: Injected embryos.

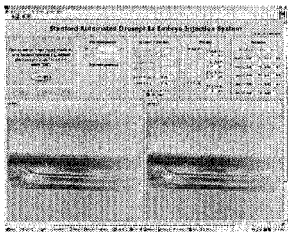

Figure 2. LabView user interface.

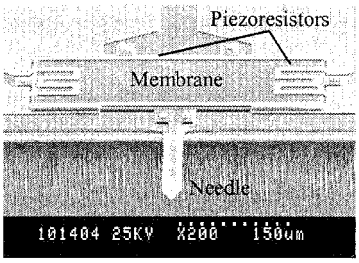

Figure 4. SEM picture of fabricated needle with integrated polysilicon piezoresistors for pressure measurements.

Sensitivity	0.65 mV / V bar
Temp. coeff. of sensitivity	-4.63 E-3 $^{\circ}C^{-1}$
Offset Voltage	-21.3 mV / V
Temp. coeff. offset voltage	-10.3 µV / V °C
Overall bridge resistance	approx. 16kΩ
Temp. coeff. of resistance	- 6.8 E-4 $^{\circ}C^{-1}$
Drift of offset voltage	2 µV / V*h
Noise level (V_{supply} = 5 V)	20 µV or 6.2 mbar
Burst pressure	2-3 bar

Table 1. Characteristics of the integrated pressure sensor.

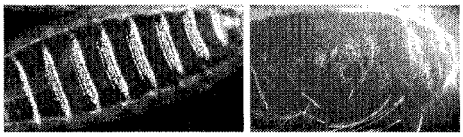

Figure 7. Left: Cuticle of wildtype embryo with denticle belts. Right: Destroyed order of denticle belts due to RNAi.

NMR SPECTROSCOPY USING ARTIFICIAL VESICLES AS SAMPLE CONTAINERS ON THE SURFACE OF PLANAR MICROCOILS

K. Ehrmann[1], C. Massin[1], F. Vincent[1], P. Pascoal[2], P.-Y. Bolinger[2], P.-A. Besse[1], H. Vogel[2] and R.S. Popovic[1]

[1]Institute of Microsystems, [2]Institute of Chemical Sciences, EPFL – Swiss Federal Institute of Technology Lausanne, CH-1015 Lausanne, Switzerland

klaus.ehrmann@epfl.ch

Abstract

We present a novel concept to perform NMR spectroscopy: confining the sample within artificial vesicles, which are attached to the surface of a microfabricated planar detection coil. Spectra of 1 M sucrose solution confined within these vesicles are successfully taken.

Keywords: Nuclear Magnetic Resonance (NMR) spectroscopy, vesicles, planar microcoils

1. Introduction

NMR spectroscopy is a powerful and information rich analysis technique. Thanks to its non-destructive nature, it is especially suited to study biological samples. When investigating small samples, like living cells, the use of microcoils increases the intrinsically low signal-to-noise-ratio (SNR). Up to present, sample positioning has been accomplished by approaching a capillary to the NMR microcoil [1] or, more recently, by integrating a microfluidic channel into the NMR-probe chip [2, 3]

Confining the sample within artificial vesicles and attaching them to the surface of a planar microcoil is a completely new concept in NMR spectroscopy. Compounds within artificial vesicles can be controlled precisely; the vesicles can be used as reagent containers [4] or model systems for living cells [5]. Artificial vesicles are attached to the NMR microcoil by specific high affinity molecular interactions between neutravidin and biotin (Figure 1) [6].

2. Experimental

Planar NMR detection coils are microfabricated on a glass wafer using a thick copper electroplating process for high Q factor [7]. The coils are encapsulated in SU8 resulting in a flat surface about 3 μm from the copper turns. On the SU8 surface a PMMA cylinder is glued, which serves as macroscopic vessel (Figure 2). NMR spectroscopy experiments are performed using a Bruker Avance 300 MHz setup with a 7 Tesla narrow bore magnet. Water and sucrose spectra are taken to calibrate the performance of the macroscopic vessel. The water peak has a spectral width of 45 Hz, due to the PMMA cylinder and the close proximity of the sample to the copper turns of the microcoil. The measured SNR of 540 is in very good agreement with simulation results.

Artificial vesicles are prepared, mixing DOPG, DSPE-PEG biotin as ligand and rhodamin labeled DHPE. These lipids form vesicles by self-assembly in 1M sucrose deuterated PBS solution. The vesicles are filtered exchanging the exterior solution to 0.8M NaCl deuterated PBS solution and resulting in vesicle sizes ranging from 1 μm to about 10 μm in diameter. Sucrose is then only within the vesicles and the osmotic pressure is equilibrated.

Fluorescent conjugated neutravidin, which serves as building block molecule, is incubated on the SU8 surface within the PMMA cylinder. The vesicles immobilize on the neutravidin. The fluorescent labeling of the neutravidin and the vesicles allows permanent control under a

microscope. Due to the high NaCl concentration of the exterior solution, the originally negatively charged vesicle surfaces are neutralized and the repelling effect is lost. The vesicles agglomerate and form a homogeneous multilayer when immobilizing on the SU8 surface (Figure 3).

3. Results and Discussion

NMR spectra, which are clearly showing the major peaks of the sucrose enclosed within the vesicles, are successfully acquired. The SNR obtained after 3.2 minutes acquisition time is 16 for the 5.4 ppm peak, which originates from the anomeric proton of sucrose (Figure 4). Taking the performance of the calibrated macroscopic cylinder as reference, the measured signal amplitude corresponds to a homogeneous vesicle layer of 30 μm thickness. The resulting total volume within all detected vesicles is 44 nL. These results match the fluorescent microscope observations. The stability of the vesicle attachment is confirmed by comparing the fluorescent image directly after immobilization and 18 hours later.

4. Conclusions

The obtained results show that it is possible to attach samples to the NMR probe surface and to take NMR spectra of a sample confined within artificial vesicles attached to this surface. The measured sensitivity corresponds to a limit of detection of 40 mM in a detection volume of 44 nL after one hour of acquisition. This opens the way towards detection of unknown compounds within vesicles or direct on-chip immobilization and NMR analysis of living cells. To improve the spectral resolution, which also increases the SNR, further work will concentrate on positioning the vesicles on the coil surface avoiding the regions close to the copper turns. The employed high affinity interaction attachment offers the possibility to pattern neutravidin by micro contact printing on the coil surface and thereby restricting the vesicles to selected regions.

Acknowledgements

The devices were fabricated at the Center of Microtechnology (CMI) at EPFL. We thank the technical staff of the center as well as G.Vaucher and Y. Pilloud for their helpful support. Furthermore we thank D. Stamou for the fruitful discussions concerning the vesicle attachment. This work is supported by the Swiss National Foundation (Proj. Nr. 2100-61549.00).

References

[1] J. E. Stocker; T. L. Peck; A. G. Webb; M. Feng; R. L. Magin, *IEEE Transactions on Biomedical Engineering*, 44 no.11 (1997) pp.1122-1127

[2] J. D. Trumbull; I. K. Glasgow; D. J. Beebe; R. L. Magin, *IEEE Transactions on Biomedical Engineering*, 47 no.1 (2000) pp.3-7

[3] C. Massin; F. Vincent; A. Homsy; K. Ehrmann; G. Boero; P.-A. Besse; A. Daridon; E. Verpoorte; N. F. de Rooj; R. S. Popovic, *Journal of Magnetic Resonance*, 164 (2003) pp.242-255

[4] D. Chiu; C. Wilson; F. Ryttsen; A. Strömberg; C. Farre; A. Karlsson; S. Nordholm; A. Gaggar; B. Modi; A. Moscho; R. Garza-Lopez; O. Orwar; R. Zare, *Science*, 283 (1999) pp. 1892-1895

[5] S. Chiruvolu; S. Walker; J. Israelachvili; F.-J. Schmitt; D. Leckband; J. Zasadzinski, *Science*, 264 (1994) pp.1753-1756

[6] D. Stamou; C. Duschl; E. Delamarche; H. Vogel, *Angewandte Chemie*, v. 115 no. 45 (2003) pp. 5738-5741

[7] C. Massin; G. Boero; F. Vincent; J. Abenhaim; P.-A. Besse; R. S. Popovic, *Sensors and Actuators A*, 97-98 (2002) pp.280-288

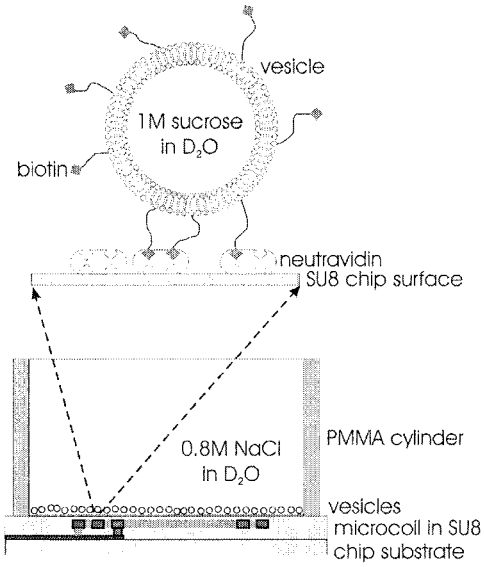

Figure 1. concept of attaching vesicles, which carry biotin ligands, on the surface of a microcoil chip using neutravidin as building block molecule

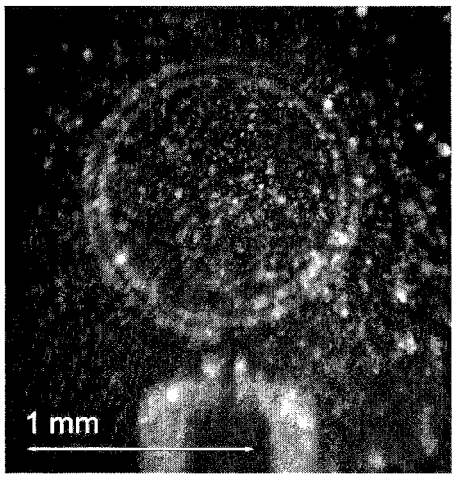

Figure 3. fluorescent picture of vesicles labeled with rhodamin; the vesicles stick together forming a multilayer film distributed on the SU8 surface

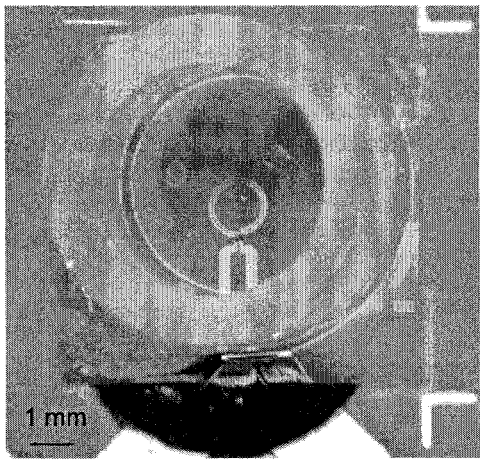

Figure 2. planar microcoil on glass substrate, bonded to printed circuit board and PMMA cylinder on top

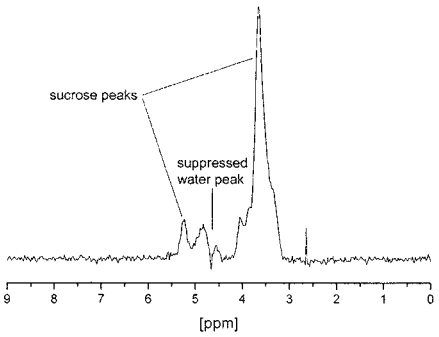

Figure 4. ^1H NMR spectrum of 1M sucrose deuterated PBS solution contained within vesicles after 64 acquisitions and water suppression; the SNR of the 5.4 ppm peak is 16

NMR STUDIES ON MOLECULAR STRUCTURES AND DYNAMICS OF WATER CONFINED IN NANOCHANNELS

Takehiko Tsukahara, Akihide Hibara, and Takehiko Kitamori

Department of Applied Chemistry, School of Engineering, the University of Tokyo and CREST, Japan Science and Technology Agency, 7-3-1 Hongo, Bunkyo-ku, Tokyo 113-8656 Japan

Abstract

It has been demonstrated in our recent report [1] that water molecules confined in submicrometer-sized channel (abbreviated as nanochannel) induce the characteristic physicochemical properties. In this work, we conceived to clarify the size dependences on molecular structures and dynamics of water confined in nanochannels using the ^{1}H-NMR chemical shift (δ_H) and ^{1}H- and ^{2}H-NMR spin-lattice relaxation rate (^{1}H- and ^{2}H-$1/T_1$) measurements. The δ_H values of water were almost constant from bulk to nanochannel sizes, while the $1/T_1$ values increased with a reduction of channel sizes from representative channel length, R, of about 1μm. The magnitude of change in ^{1}H-$1/T_1$ values has become quite larger than that of ^{2}H-$1/T_1$ ones. Thus, only mobility of water molecules was found to be extremely restricted without changing the hydrogen bonding structure in the confinement conditions. These results suggest that the proton exchange mechanisms of water are affected by the electrostatic effects of fused-silica surface containing ionizable silanol groups from the vicinity of R=1μm, and such effects are attributable to the variation of physicochemical properties in water resulting from size-confinement.

Keywords: NMR, chemical shifts, relaxation times, confined water, nanochannels

1. Introduction

Utilization of nanochannels, which is meso-scale size between molecular nanomaterial such as zeolite and the fabricated microchannels, can offer a great opportunity to enhance the integration density of flow chemical processes in microchip. From such viewpoint, we have been recently investigated the fabrication techniques of nanochannels as well as the physicochemical properties of water confined in nanochannels, and suggested that confined water have lower dielectric constants and higher viscosities compared with bulk water by time-resolved fluorescent measurements.[1] However, limited information is available about how dose confinement of channel size affect the molecular structures and dynamics of water. Hence, we discuss size dependences of δ_H and ^{1}H- and ^{2}H-$1/T_1$ values of water confined in nanochannels on fused-silica substrate, and demonstrate the peculiarity of collective behaviors of water molecules under one hundred nano-scale environment.

2. Theory

The ^{1}H relaxation mechanisms of liquids can be generally explained by the dipole-dipole (DD) interactions [2]. The ^{1}H-$1/T_1$ values are dependent on both the reorientational correlation time (τ_c) for the rotational motion of the OH vector and the translational correlation time (τ_d) associated with intermolecular motions as follows

$$\left(\frac{1}{T_1}\right)^{1H} = \left(\frac{1}{T_{1intra}}\right) + \left(\frac{1}{T_{1inter}}\right) = \frac{3}{2}\frac{^2\gamma^4\hbar^2}{r^6}\tau_c + \frac{9}{10}\frac{N\pi\gamma^4\hbar^2}{a^3}\tau_d \qquad (1)$$

where $\hbar$ is the plank constant, r is the distance between the hydrogens in a water, γ is the proton gyromagnetic ratio, a is the hydrodynamic radius, and N is the number of spins per unit volume. On the other hand, the ^{2}H-$1/T_1$ values are related to the τ_c using Eq. (2), because a quadrupolar nucleus such as ^{2}H is dominated by intramolecular motions.

$$\left(\frac{1}{T_1}\right)^{2H} = \frac{12\pi^2}{125}\left(1+\frac{\xi^2}{3}\right)\left(\frac{e^2Qq}{h}\right)^2\tau_c \qquad (2)$$

where h is the plank constant, e^2Qq/h is the quadrupole coupling constant (QCC) which is connected with the electric field gradient tensor of molecule, ξ is the quadrupole asymmetry parameter.

3. Experimental

The nanochannels (widths; 130nm - 30μm, depths; 120 - 3000nm) were fabricated on fused-silica substrates by electron beam lithography and fast atom beam etching. The fabricated plate was thermally laminated with cover one in a vacuum furnace at 1060°C, and was cut by diamond cutter for applying commercial NMR apparatus (see Fig. 1). All ^{1}H- and ^{2}H-NMR spectra were measured using JEOL NMR spectrometers at 300 to 600MHz at 4-50°C without spinning. All samples, which were degassed by means of a number of freeze-pump-thaw cycles, were filled in nanochannels under vacuum, and the nanochannels were inserted into NMR sample tube.

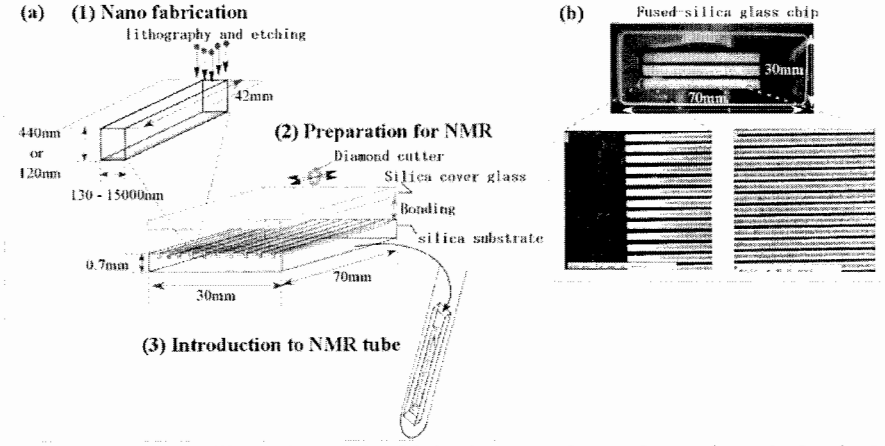

Figure 1. (a) Schematic illustration of the fabrication procedures of nanochannels for the NMR measurements. (b) Photograph and SEM images of fabricated fused-silica glass chip.

4. Results and discussion

Fig. 2 shows the ^{1}H-NMR spectra of water confined in bulk and nanochannels. The δ_H values of water are little affected by the confinement of channel sizes, indicating that the hydrogen bonding structures of water confined in nanochannels are analogous to those of bulk water. It is noteworthy that full linewidth at half-height in ^{1}H-NMR spectrum broadens with a decrease in channel sizes, because the suppression of the collective molecular motions of water is expected from the broadening of linewidth.

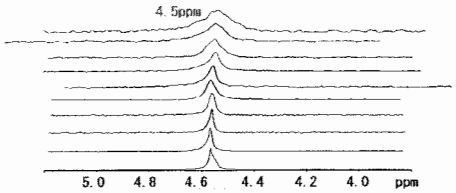

Figure 2. ^{1}H-NMR spectra of water confined in bulk and nanochannels at 300MHz and 22°C.

The validity of such expectation can be demonstrated by the enhancement of ^{1}H-1/T_1 values because of an increase in molecular correlation times according to Eq. (1). As shown in Fig. 3, the 1/T_1 values of confined water enhance considerably in the vicinity of D=1μm. This result leads to a simple conclusion that the molecular motions of confined water have become one-fifth times as fast as those of bulk water. Furthermore, the components of molecular motions could be divided into the translational and reorientational motions using the ^{2}H-1/T_1 values expressed by Eq. (2). Since the ^{2}H-1/T_1 values of confined water were almost constant in whole channel sizes, mobility of water molecules was found to be restricted mainly rather than molecular rotation by size-confinement. The changeable mobility with keeping hydrogen bonding structures would be attributed to that the ionisable silanol group on fused-silica surface influence on proton exchange rates of water molecules as illustrated in Scheme 1.

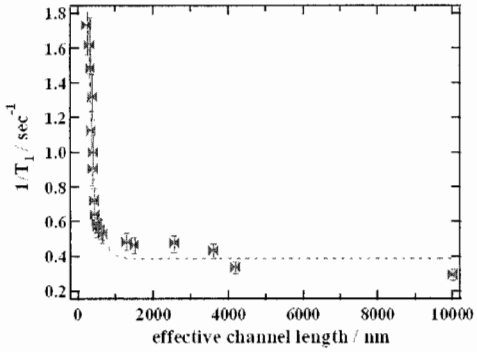

Figure 3. Representative channel length, R vs. ^{1}H-1/T_1 values of water confined in nanochannels.

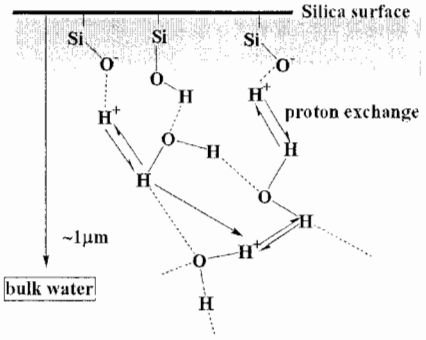

Scheme 1. Concept model of the proton exchange of water in nanochannels.

5. Conclusion

We have examined the molecular structures and dynamics for water confined in fabricated nanochannels on fused-silica substrate by δ_H and T_1 values. The result of δ_H indicated that the hydrogen bonding structures of water are kept with similar to bulk water even in nanochannels. It was then shown from ^{1}H- and ^{2}H-1/T_1 values that the only molecular translational motions of water are restricted by confinement of channel sizes from the vicinity of D=1μm. These results could allow us to propose the notion that the specific proton exchange mechanisms of water confined in nanochannels contribute to the variation of physicochemical properties.

The novel information about confined water using NMR provides remarkable advantages for developing nano chemical reactor.

Acknowledgements

We would like to thank Associate Prof. Yasuhisa Ikeda (Tokyo Institute of Technology) for the technical assistance of the NMR measurements.

References

[1] A. Hibara, T. Saito, H.B. Kim, M.Tokeshi, T. Ooi, M. Nakao, and T. Kitamori, *Anal. Chem.*, **74**, 6170-6176 (2002).

[2] T.C. Farrar and E.D. Becker, *Pulse and Fourier Transform NMR*, Academic Press, NY, (1971).

REAL-TIME MONITORING OF CHEMICAL REACTIONS INSIDE A MICRO NMR CHIP

Henk Wensink[1], Fernando Benito Lopez[2], Dorothee C. Hermes[1], Willem Verboom[2], David N. Reinhoudt[2], Albert van den Berg[1]

[1]BIOS, the Lab-on-a-Chip group & [2]Laboratory of Supramolecular Chemistry and Technology MESA+ res. inst., University of Twente, P.O. Box 217, 7500 AE, Enschede, The Netherlands

Abstract

This paper presents real-time monitoring of a chemical reaction on-chip, to our knowledge the first working integrated microreactor chip with NMR detection. A NMR detection coil was electroplated on top of a μ-fluidic chip containing two inlets and one outlet. The chip was placed in a conventional low field (60 MHz) NMR magnet. An imine formation between benzaldehyde and aniline was analyzed at different reaction times using the chip. The reaction time is related to the residence time between mixer and detector, which can be set to 30 minutes down to only 0.9 seconds thus enabling monitoring of relatively fast reactions.

Keywords: NMR chip, kinetics, imine formation, microreactor

1. Introduction

When monitoring chemical reactions on chip, only a limited amount of solution is available for analysis, which has led to downscaling of analytical techniques such as mass, infrared and Raman spectrometry, UV, fluorescence and electro chemical detection and now also of Nuclear Magnetic Resonance (NMR). ^{1}H-NMR is a very powerful non-invasive technique, which can identify chemical compounds by the unique composition of electromagnetic proton resonance frequencies in a large magnetic field. Relative to many other analytical techniques, however, it is inherently insensitive. NMR of limited volumes has been achieved with capillaries [1], but several authors have shown the possibilities of NMR integrated on chip where a NMR detection coil is fabricated on top of a microchannel [2, 3, 4].

In previous work we have shown that even with a low field NMR magnet (60 MHz, 1.4 Tesla) a satisfying sensitivity could be obtained with a properly designed detection coil and chip geometry [5]. In the current work, continuous flow NMR detection has been integrated on a simple microreactor chip to monitor chemical reactions after a specific reaction time.

2. Set-up

The fluidic chip with NMR detection coil and an active detection volume of 56 nL (Figure 1) was fabricated with standard microfabrication techniques. Channels and through holes were powderblasted in 1.1 mm thick borofloat wafers and bonded together to form an enclosed channel. The waferstack was thinned down on one side by HF etching to obtain a distance between detection coil and sample of 80 μm. An 18 μm high copper coil with 18 windings (width = 20 μm) was electroplated on top of the channel. The chip was connected with Nanoport™ fluidic connections to standard capillaries and electrically connected to a matching and tuning network. The resulting probe was placed in a 60 MHz NMR magnet (Varian EM360L), while the capillaries were connected outside the magnet to a syringe pump. The electrical set-up is similar to that of Massin et al. [6].The total channel volume between the mixing point (were the two channels join) and the detection coil is about 0.57 μL. The time the mixed sample spends in this volume (residence time) depends on the flow rate, and ranges from 30 min to only 0.9 seconds for our set-up.

The imine (Schiff base) formation, the reaction between an aldehyde or ketone and an amine, was studied in this set-up using the reaction of benzaldehyde with aniline (Figure 2). This reaction was already performed in a μ-fluidic chip and analyzed by mass spectrometry in previous work [7].

The chip inlets were connected to two 100 µL syringes containing 4.95 M benzaldehyde, 0.475 M tetramethylsilane (TMS) in deuterated nitromethane (CD_3NO_2) and 4.95 M aniline, 0.523 M TMS in CD_3NO_2, respectively. Figure 3 shows the separate ^1H NMR spectra's of both solutions. The channel was flushed with both solutions simultaneously before each measurement. Then the flow speed was set to a lower value to achieve a desired residence time. When this situation was stable, 32 NMR scans of 90° pulses were made and averaged.

3. Results and discussion

We focused on two peaks to monitor the reaction, viz. the aldehyde peak of benzaldehyde at ~9.9 ppm and the imine peak of the product at ~8.4 ppm. Figure 4 clearly shows an increase of the imine peak and a decrease of the aldehyde signal at four different contact times. Figure 5 graphically presents the course of the reaction versus contact time. The lines in this figure are a fit to the expected exponential behavior. The reaction is not going to completion. Equilibrium is reached after a certain time, since the formed water is not removed.

The observed effect is a combination of diffusive mixing effects and reaction kinetics. We estimate the time needed for complete mixing by the time it takes a molecule to cross the channel (diffusion time). The average distance a molecule has to travel is half of the average channel width, which is about 80 µm. The time required to do this depends on the diffusion constants (D) of the molecules; $D = 1.5 \cdot 10^{-9} m^2/s$ for benzaldehyde [8], and $D = 1.96 \cdot 10^{-9} m^2/s$ for aniline [9]. The diffusion time for the slowest molecule (benzaldehyde) is about 4.3 seconds. This is much smaller than the 214 seconds it takes for the reaction to reach 50% conversion. So the effect shown in Figure 5 is mainly due to reaction kinetics. Even so, a future NMR reaction chip will incorporate a micro mixer to decrease the mixing time and eliminate any diffusion effects from the results.

4. Conclusions

NMR detection is a non-invasive and powerful method for monitoring chemical processes on chip, an ability that is clearly shown in this work. This is to our knowledge the first working integrated microreactor chip with NMR detection. This system is optimized for low field NMR. Although this gives a lower NMR signal, it allows this technology to be transferred to our main focus: a portable NMR that uses small low field permanent magnets.

Acknowledgements

We thank Avantium Technologies for the funding of this project.

References

[1] M.E.Lacey, R.Subramanian, D.L.Olson, A.G.Webb, J.V.Sweedler, *Chem. Rev.* **99** 3133-3152 (1999)

[2] J.E.Stocker, T.L.Peck, A.G.Webb, M.Feng, R.L.Magin, *IEEE Trans. Biomed. Eng.* **44** 1122-1127 (1997)

[3] C.Massin, F.Vincent, A.Homsy, K.Ehrmann, G.Boero, P.A.Besse, A.Daridon, E.Verpoorte, N.F.de Rooij, R.S.Popovic, *J. Magn. Reson.* **164** 242-255 (2003)

[4] J.H.Walton, J.S.de Ropp, M.V.Shutov, A.G.Goloshevsky, M.J.McCarthy, R.L.Smith, S.D.Collins, *Anal. Chem.* **75** 5030-5036 (2003)

[5] H.Wensink, D.C.Hermes, A.van den Berg, Proc. 17th IEEE MEMS Conf., the Netherlands, 407-410 (2004)

[6] C.Massin, G.Boero, P.Eichenberger, P.A.Besse, R.S.Popovic, *S&A A* **97-98** 280-288 (2002)

[7] M.Brivio, R.H.Fokkens, W.Verboom, D.N.Reinhoudt, N.R.Tas, M.Goedbloed, A.van den Berg, *Anal. Chem.* **74** 3972-3976 (2002)

[8] M.Terazima, K.Okamoto, N.Hirota, *J. Chem. Phys.* **102** 2506-2515 (1995)

[9] Landolt-Börnstein, "Numerical data and functional relationships in science and technology", Sixth edition, Vol. II/5a, 1969.

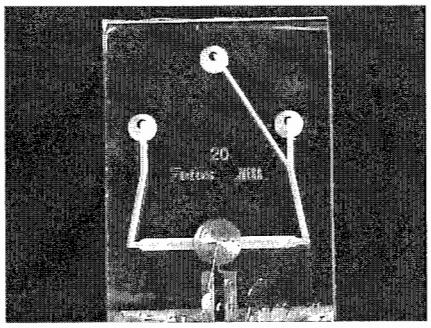

Figure 1. The glass NMR chip with planar micro coil. Chip size is 1 by 1.5 cm, channel width beneath coil is 500 µm.

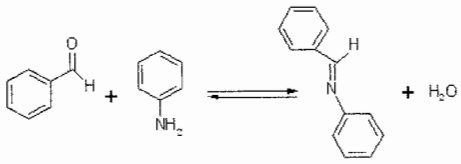

Figure 2. The imine formation between benzaldehyde (first molecule) and aniline (second molecule).

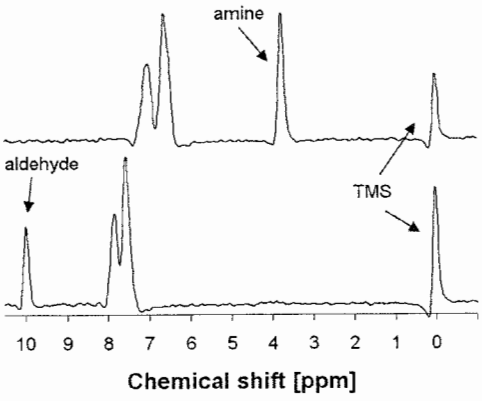

Figure 3. NMR spectra of the two reactants. The TMS peak was used as the 0 ppm reference.

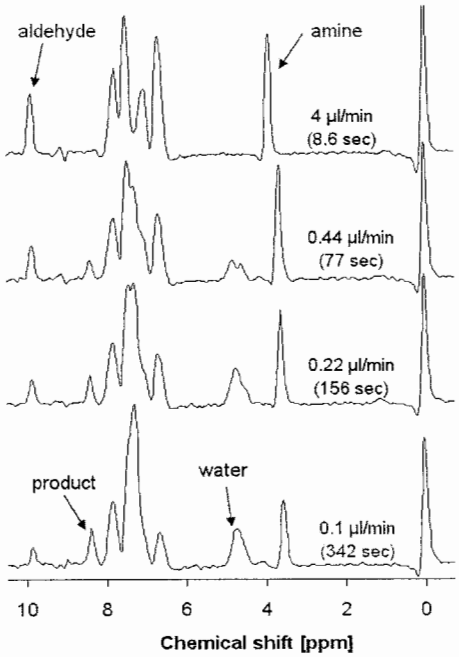

Figure 4. Four NMR spectra taken at different contact times. Clearly visible are the increase of the product peak, and the decrease of the aldehyde peak with increasing contact time.

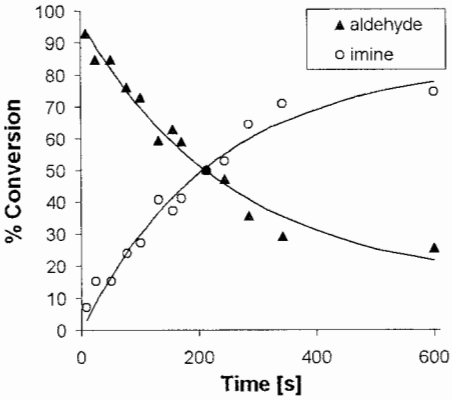

Figure 5. Reaction course of the imine formation.

A SPINNING-DISK INTERFEROMETRY DETECTION SYSTEM FOR MONITORING ANTIGEN:ANTIBODY COMPLEX FORMATION ON PROTEIN ARRAYS.

Manoj M. Varma[1], Halina D. Inerowicz[2], Fred E. Regnier[2], David D. Nolte[1]
[1]Dept. of Physics, Purdue University, West Lafayette, IN 47907. [2]Dept. of Chemistry, Purdue University, West Lafayette, IN 47907

Abstract.

Microfluidic systems are becoming increasing popular for performing separations, chemical reactions, and analytical biochemistry on a large scale. This is particularly true in array formats that allow thousands of determinations to be made simultaneously. Detection has generally been achieved with laser fluorescence, but it requires analyte derivatization or secondary reagents. This paper will describe a new detection technique that circumvents fluorescence and absorbance detection by exploiting high-speed repetitive laser interferometry in a manner similar to that used in reading music from a compacts disc (CD). The sensing system consists of micro-interferometric elements fabricated on dielectric mirrors as radial gold spokes that act as wave front splitting interferometers, similar to structures on a CD, but modified to operate at interferometric quadrature as linear optical detection elements. Antibodies are selectively immobilized through thiol bridges to the gold. The binding of specific antigens to antibodies modifies the optical phase, which is detected as intensity modulation in the far field. We have detected bound antigen (anti IgG) on spinning disks at a sampling rate of 100 kHz and have verified low non-specific binding. The current BioCD sensor format has 1024 gold spokes, each 20 microns wide and 80 nm thick serving as quarter-wave (quadrature) micro-interferometers. The BioCD has potential for high-speed and high-sensitivity multi-analyte detection of high-molecular-weight analytes with limits of sensitivity down to several attomoles per track. The first-generation system described in this paper has a sensitivity of approximately 100 attomoles per track.

1. Introduction.

Micro-arrays have become valuable tools in genomics and proteomics, [1-4] generally sensing the formation intermolecular complexes at array elements through the fluorescence of a secondary reagent. Although sensitive, this approach has several limitations. One is the need for great numbers of secondary detection reagents with large arrays. A second is that fluorescence suffers from non-isotropic emission, low conversion efficiency, and photobleaching, all of which result in low photon fluxes and the need for extended acquisition times.

This paper reports a new method to address these problems through the use of a detection scheme based on optical interferometry that monitors thousands of array elements at high sensitivity in a short period of time without the use of secondary reagents. Detection in this new system is similar to the optical compact disk (CD) technology used by the music industry to read millions of coded elements on a single spinning disc. Concentric rings of antibodies appearing as identical array elements targeting specific proteins were used in the device described below.

Commercially available compact discs consist of concentrically-arranged tracks of pits that are half a micron wide and separated by 1.6 microns. The information on a CD is read by focusing a laser beam onto these pits and observing the far-field diffraction. The depth of pits is a quarter of the wavelength of the light used for read-out. This depth difference between the pit and the land results in a half-wave phase difference between the light reflected off the pit and the light reflected off the land, leading to destructive interference at the detector, placed along the optic axis in the far-

field. Thus each pit acts as a micro-interferometer. An optical CD has a billion such micro-interferometers.

The microfabricated interferometers of a CD were modified in several ways to operate as a biosensing platform. One was by converting pits to posts or spokes on the surface of discs. The other was by immobilizing biological macromolecules such as antibodies and antigens on the micro-interferometric elements. As antigens bind to antibodies the phase of the interferometric element is altered producing a modification of the detected far-field diffraction signal. Among the many advantages of this BioCD approach is the possibility of sampling rates ranging to millions of array elements per second. Another is that the binding kinetics of large numbers of antigens can be monitored simultaneously. Still another advantage of the optical disk format is that the control electronics is already available and can be incorporated with slight modifications into the framework of the BioCD.

2. Design, Fabrication, and Read-out from the BioCD.

A BioCD was fabricated by evaporating gold onto a 3'' silicon wafer or on a 2" dielectric mirror disk in a radial pattern as shown in Fig 1. 1024 gold lines were produce in a radial pattern of spokes. These gold spokes are 20 microns wide and are deposited to a thickness of $\lambda/8$ = 79.1 nm (quarter-wave for reflection), putting them in the quadrature condition for read-out with a 632.8 nm He-Ne laser.

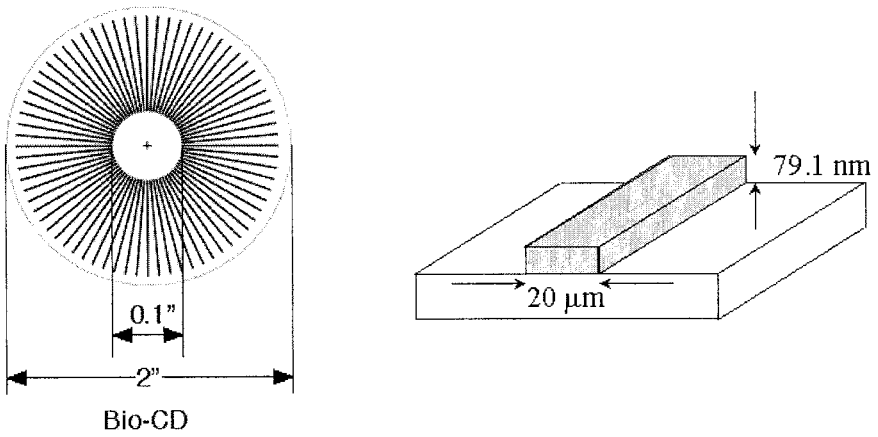

Fig. 1 Schematic of the arrangement of gold ridges on the BioCD. There are 1024 gold elements on a 2-3" disk. The spokes are illuminated by a focused Gaussian beam in a configuration where 50% of the intensity falls on the high-reflectivity land and 50% falls on the gold microstructure.

All dual-port interferometers have a universal response curve, shown in Fig. 2a, with a half-intensity point defined by quadrature at which the signal and the reference waves are out of phase by ninety degrees and when the intensity as a function of reference phase has the largest slope. The calculated far-field diffraction patterns for three ridge heights of h = 0, $\lambda/8$ and $\lambda/4$ (corresponding to land, quadrature, and conventional digital CD) are shown in Fig. 2b. Maximum linear sensitivity to small optical perturbations is achieved by operating the interferometer near quadrature. Shot noise-limited detection of optical path length changes down to a billionth-lambda is achievable under these conditions.

When a macromolecule is immobilized on a spoke, it introduces an additional phase of

$$\delta\phi = \frac{4\pi}{\lambda}(n-1)d \qquad (1)$$

where n is the effective refractive index of the biolayer and d is the biolayer thickness. This additional phase modifies the power detected at quadrature according to

$$\delta P = P_0 \frac{2\pi}{\lambda}(n-1)d \qquad (2)$$

where P_0 is the power detected when the beam is incident on the land alone. The quadrature condition clearly leads to the strongest change in the signal and one that is linearly sensitive to the optical load, while the digital CD is sensitive only quadratically.

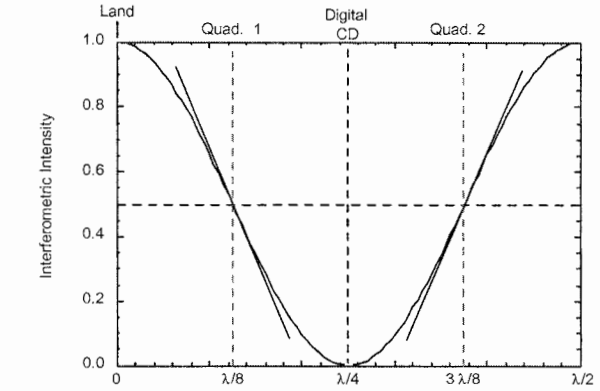

a)

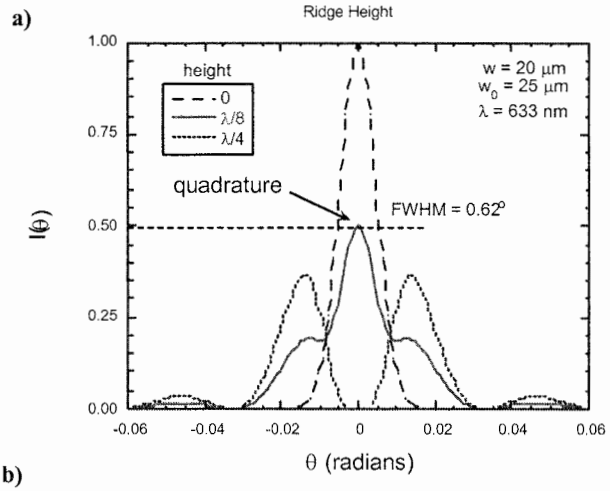

b)

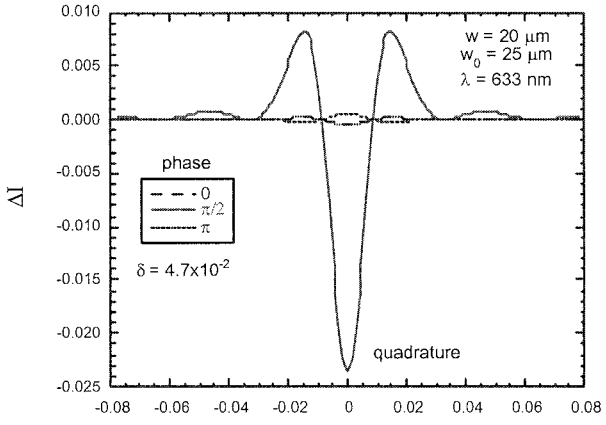

c)

Fig. 2 a) Universal response curve of a two-port interferometer shown here as a function of the height of the microstructure (in units of a wavelength). A conventional digital CD alternates between the land and the point of destructive interference at λ/4. For the BioCD, quadrature is achieved at ridge heights of λ/8 and 3 λ/8, where the maximum slope occurs. b) Far-field diffraction patterns are shown for the cases of gold microstructure heights of h = 0, λ/8 and λ/4. c) Differential intensity response to a monolayer of immobilized biomolecules (mean height of 7 nm and refractive index of 1.3).

The advantage of using gold interferometric elements rather than pits found on a conventional optical CD is the ease with which macromolecules on the interferometric structures are immobilized by using stamping and an alkanethiol bridge between the gold and the macromolecule. By using poly di-methoxy silane (PDMS) stamps, IgG was immobilized on the gold spokes within annular regions of the disk. Alternatively, these annuli were created by incubating annular regions of the thiolated substrate with antibodies in solution. Thus a BioCD can be made to possess different regions with and without antibodies to test for antigen binding in the regions containing the antibodies and to test for nonspecific binding. Ellipsometry and atomic force microscopy (AFM) of anti-mouse IgG immobilized on the gold substrate indicated an average antibody thickness of 7 nm. This agrees with the monolayer thickness of IgG. Thickness variation within the 50 micron sample window across the substrate was observed to be about 13% and the variation in refractive index was around 4%.

As the laser beam moves across a gold interferometric element, the far-field diffraction intensity drops by about 50% (at quadrature) compared to the intensity from the mirror substrate. This results in the formation of peaks and valleys in the oscilloscope trace, with the valleys representing the interferometric signal in quadrature. In the presence of immobilized bio-layers the optical phase characteristics of the gold interferometric elements is modified, resulting in a shift of the peak-valley difference in the time trace, as shown in Fig. 3 for the bare thiolated gold, and the gold immobilized with anti-mouse IgG. The experimental methodology consists of acquiring time traces of the interferometric signal from the BioCD with an immobilized antibody and consisting of regions exposed to specific and non-specific antigens using an oscilloscope. The shift in the signal caused by binding of specific antigens versus other proteins by the immobilized antibody layer is

detected directly on the trace. Prior exposure to a non-specific antigen produces a shift of the quadrature signal level, hence allowing assessment of false positive read-outs.

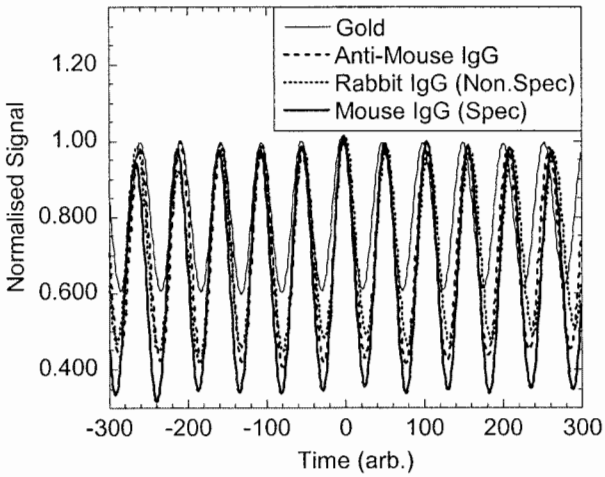

Fig. 3 Detection of Mouse IgG and specificity of the detection scheme. The BioCD is printed with anti-mouse IgG. Incubation with non-specific rabbit IgG produces no change in the far-field diffraction intensity. However, subsequent incubation with specific mouse IgG produces a drop in the far-field diffraction intensity. This shows that the detection scheme is specific.

The valleys in the time trace represent the interferometric signal from the BioCD in quadrature while the peaks represent the signal from the bare substrate. Comparing the signal collected from regions with and without anti-mouse IgG, the immobilized antibody lowers the valleys (at quadrature) while leaving the peaks (from substrate) unchanged. This is because immobilization of biomolecules on the gold interferometric elements change their optical phase, causing a dip in the valleys as indicated in Fig. 3. The peaks are unaffected in all cases because no antibody is immobilized on the bare substrate. Exposure to non-specific antigen, which in this case is rabbit IgG, causes no additional phase change. However, subsequent exposure to the specific antigen, mouse IgG, causes a signal of about 10 % on average in the valley signal level compared to the signal from the land. Thus, the detection scheme is specific to the target analyte, and is not blocked by previous exposure to the non-specific antigen.

3. Sensitivity and Performance Limits.

The number of antigen molecules detected in the existing binding experiments were estimated by considering a monolayer of immobilized antibody on a spoke, verified by AFM measurements. This is around 10^7 molecules per spoke or about 10 femtomoles per track. Typical S/N ratios observed for the time traces of the interferometric signal is around 100, yielding a current sensitivity limit of about 100 attomoles per track. Currently the S/N ratio is limited by spin speed instabilities. Detection bandwidth is of the order of 10 kHz for the current setup. This S/N and sensitivity is far from optimal, and nominal improvements in spin stability and immobilization homogeneity will produce significant improvements.

4. Conclusions and Future Directions.

It has been demonstrated that an interferometric approach can be effective in the detection of antigen binding on antibody arrays in an optical disk format at the level of 10 femtomoles per track. This system has the potential for high-throughput screening at low cost. Delivery of analytes to immunological array elements using micro-fluidic delivery channels in conjunction with high density printing of immobilized antibody or proteins on arrays is being explored. Such micro-fluidic delivery systems have the advantage of using the centrifugal force provided by the spinning disk as the pump.

Acknowledgements

This work was supported by NSF grant ECS-0200424.

References

[1]G. H. W. Sanders and A. Manz, Trends in Anal. Chem. **19** (6), 364 (2000).
[2]J. Marx, Science **289**, 1670 (2000).
[3]D. Meldrum, Genome Res. **10**, 1288 (2000).
[4]Gavin MacBeath and Stuart L. Schreiber, Science **289** (5485), 1760 (2000).
[5]A. Bernard, J. P. Renault, B. Michel, H. R. Bosshard, E. Delamarche, Adv. Mat. **12**, 1067 (2000).

MICROFLUIDIC SPOTTING CHIP FOR LABEL-FREE PROTEIN MICROARRAYS

Eric Flaim and D. Jed Harrison
Department of Chemistry, University of Alberta, Edmonton, Alberta, Canada

Abstract

A polydimethylsiloxane (PDMS) microfluidic delivery device was fabricated for the spotting of proteins, using a 3 dimensional fluid pathway, onto gold coated glass surfaces for use in surface plasmon resonance (SPR) imaging experiments. The microfluidic system is used for the patterning of protein into localized spots, forming an addressable array that will allow for increased array density, economy of reagents and specific modification to gold surfaces affecting protein adsorption.

Keywords: SPR imaging, protein microarray, PDMS, microfluidics

Introduction

Recently, microfluidic devices have been employed in protein array biochips for the study of label free protein binding interactions and immunoassays using SPR.[1,2] SPR provides a label-free method for the detection of the binding of biological molecules onto functionalized surfaces. Those studies involved the patterning of proteins on Au substrates through microfluidic channels formed by PDMS. The network of flow channels created lines of patterned biological molecules, which provides excess coated surface for potential non-specific adsorption, and limits the density of protein patterning. This current research is focused on developing a PDMS microfluidic delivery device for the spotting of proteins to Au chips for SPR detection using a 3 dimensional fluid pathway design. In this way, a dense array of spots, whose size can be controlled in the fabrication process, can be patterned and fluid can be localized to specific areas.

Experimental

Figure 1A is a schematic representation of a single flow pathway in the PDMS microfluidic network used to pattern the protein array. A two mask lithographic procedure using SU-8 negative photoresist was used to mold the microarray spotting chip in PDMS. The first master contains wells for the localization of protein reagents. The second master contains the channel system for fluid delivery. Spot sizes of 200 μm by 220 μm were designed. Molds of these masters were cast in PDMS, aligned and bonded. In this way an overall 3 dimensional fluidic network is formed allowing for fluid delivery to the Au chip. Achieving a 3D fluidic network required a PDMS curing process involving pressure.[3] Protein immobilization was achieved through the use of amine terminated thiol self assembled monolayers on gold. Up to four spots can be patterned simulanteously by application of a vacuum at one outlet. 11-mercaptoundecylamine (MUAM) was dissolved in ethanol to a final concentration of 1 mM. Goat and bovine immunoglobulin G (g-IgG and b-IgG) and polyclonal rabbit antisera to g-IgG protein solutions were prepared in phosphate-buffered saline (PBS pH=7.4) to a concentration of 670 nM and 130 nM respectively.

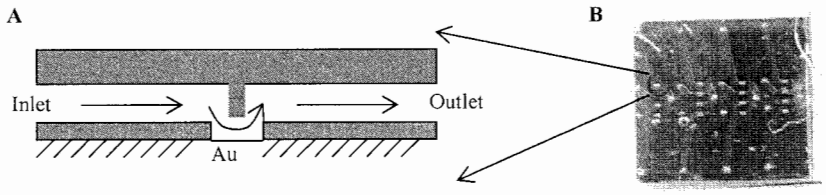

Figure 1: (**A**) A cross sectional schematic representation of one fluid pathway for patterning to a Au surface. Channel depth was 30 μm, width 200 μm with wells having a height of ~40 μm. (**B**) Photograph of PDMS channels placed on a gold substrate with punched holes for inlets and outlets.

Results

The bonded 2 layer PDMS device was placed in conformal contact with an SPR glass slide coated with a 45nm thin film of Au on a 1 nm Cr adhesion layer. Amine terminated thiol SAM's were absorbed to each spot for 10 min. Two channel pathways were each filled with b-IgG and g-IgG for an exposure time of 1 hr for physisorption. Figure 3A shows the well defined spots formed upon bovine and goat IgG localization and immoblization. Figure 3B is an SPR image after exposing the IgG treated chip for 12 min to Anti g-IgG.

Figure 3A: On-chip 20 min absorption of 1 mM -NH_2 therminated thiol, and 1 hr physisorption of g-IgG and b-IgG. Au surface blocked with 1% BSA in PBS for 1hr.

Figure 3B: Chip from Figure 3A after 20 min exposure of spots to anti-g-IgG.

A difference image (Figure 3B minus Figure 3A) allows for the visualisation of binding between antibody and antigen. A greater signal intensity is seen for the g-IgG than b-IgG due to antibody binding to its complementary antigen. However, some cross reactivity of anti g-IgG is seen with the b-IgG. These two proteins have a known cross reactivity.

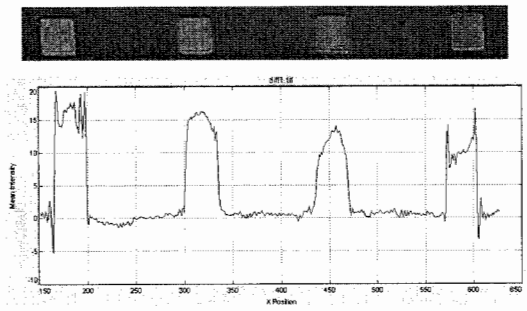

Figure 3C: Difference image for immunobinding assay of goat and bovine IgG to polyclonal anti g-IgG. Intensity graph shows cross reactivity.

Conclusions

In summary, we have described the first design of a microfluidic spotting array chip, for label free protein detection using SPR imaging. Common microfluidic SPR patterning techniques involve long channels in contact with the surface, which reduce array density, may increase reagent use, and result in lower contrast SPR images due to the larger coated regions. Specific addressing of the spots can be achieved with our fluid delivery system, allowing for considerable variation of surface modifications and of protein samples on one chip. Further, this microfluidic spotting array design provides a simple patterning method that eliminates the need of using expensive robotic pin printing techniques. Ultimately, the array density can be increased for coupling with an external microtitre plate. These devices will then allow users to both custom prepare and test protein array chips on a routine basis within their own laboratories.

Acknowledgements

University of Alberta NanoFab Laboratory
Natural Sciences and Engineering Research Council of Canada for Financial Support

References

[1] Wegner, G. J.;Lee, H.J.;Marriott, G.; Corn, R. M. *Anal Chem.* **2003**, 75, 4740-4746.
[2] Kanda, V.; Kariuki, J. K.; Harrison, D.J.; McDermott. *Anal Chem.* (Submitted).
[3] Chabinyc, M. L.; Chiu, D. T.; McDonald, J. C.; Stroock, A. D.; Christian, J. F., Karger, A. M, Whitesides, G. M. *Anal Chem.* **2003**, 73, 4491-4498.

INTEGRATED SAMPLE PURIFICATION IN EWOD-MALDI-MS

Aaron R. Wheeler[1], Hyejin Moon[2], Chang-Jin "CJ" Kim[2], Joseph A. Loo[1], and Robin L. Garrell[1]

[1]Dept. of Chemistry and Biochemistry, University of California, Los Angeles, CA, USA, 90095-1569
[2]Dept. of Mechanical and Aerospace Engineering, University of California, Los Angeles, CA, USA, 90095-1597

Abstract

A new method is reported for removing unwanted impurities from proteomics samples, relying on the electrowetting-on-dielectric (EWOD) microfluidic technique. EWOD was used to drive water droplets over dried spots containing peptides and either urea or sodium phosphate; the spots were then analyzed by matrix assisted laser desorption/ionization mass spectrometry (MALDI-MS). Spectra of samples purified using this technique were observed to have better S/N and fewer interfering peaks than spectra of unpurified samples.

Keywords: MALDI, mass spectrometry, electrowetting, EWOD, proteomics

1. Introduction

The field of proteomics is important as a basic science and for clinical applications ranging from drug discovery to assays for gene expression. Progress in proteomics would be accelerated by the availability of high-throughput analysis techniques, which has driven the development of microfluidics-based approaches [1, 2]. We have recently developed a new method for MALDI-MS analysis of proteins and peptides, in which droplets containing sample and matrix are moved, mixed, and deposited using the EWOD microfluidic technique [3].

Proteomics samples often contain salts, non-volatile solvents, and/or denaturants along with the proteins of interest [4]. These undesirable constituents can degrade MALDI-MS signal through a process called ion suppression, in which they compete with protein or peptide analytes for co-crystallization with matrix, desorption energy, and ionization energy. At high concentrations, impurities may completely extinguish the MALDI signal. At low concentrations, impurity adduct peaks can obscure the relevant sample peaks.

To overcome problems caused by impurities, samples to be analyzed by mass spectrometry are typically purified using a variation of the classical technique of solid phase extraction (SPE). For MALDI, a variation of SPE has been reported [5] that relies on a hydrophobic ionization/desorption target. With this method, a droplet containing protein or peptide contaminated with impurities is allowed to dry on the target; subsequently, the target is rinsed with a polar solvent to dissolve and remove the hydrophilic impurities. In this work, we have used EWOD to move droplets of water to purify peptides immobilized on hydrophobic Teflon-AF surfaces. This is the first report of using droplet-based microfluidics to integrate sample purification and co-crystallization for proteomics.

2. Experimental

Aqueous solutions of bovine insulin and human angiotensin II were mixed with urea or sodium phosphate buffer, two commonly used reagents that interfere with MALDI-MS spectra. The solutions contained 1 μM peptide with 0.1, 1, or 8 M urea, or 0.02 or 0.095 M sodium phosphate. Solutions of the MALDI matrix, 2,5-dihydroxybenzoic acid (DHB, 0.75 mg/mL), were prepared in deionized water with 5% acetonitrile and 0.05% trifluoroacetic acid (TFA).

EWOD devices were fabricated from two plates using procedures similar to those developed previously [3]. The bottom plate contained patterned doped polysilicon electrodes covered with thermally grown SiO_2 (1500 Å), and Teflon-AF (150 Å). The top plate contained a single, unpatterned electrode formed from indium-tin-oxide (ITO) covered with Teflon-AF (150 Å). The

two plates were joined by three layers of double-sided tape (300 μm). Droplets were sandwiched between the plates and moved by applying potentials of ~40 V_{rms} (1 kHz) between the top electrode and sequential electrodes on the bottom plate. At their final positions, droplets were dried under vacuum (~1-2 min), and the bottom plate was affixed to a custom MALDI target and inserted into a Voyager DE STR MALDI mass spectrometer (Applied Biosystems) for analysis.

3. Results and discussion

Droplets containing sample (0.6 μL), water (1 μL), and matrix (0.6 μL) were moved and deposited as depicted in Figure 1. For un-rinsed spots, a droplet containing sample was deposited, followed by a droplet of matrix solution. For rinsed spots, a droplet of water was moved over the sample spot to dissolve the impurity prior to deposition of matrix. The water droplet was moved away from the spot after visual confirmation that the dried impurity had dissolved. For low concentrations of impurity (< 1 M), dissolution was instantaneous; for high concentrations (≥1 M), it required a few seconds.

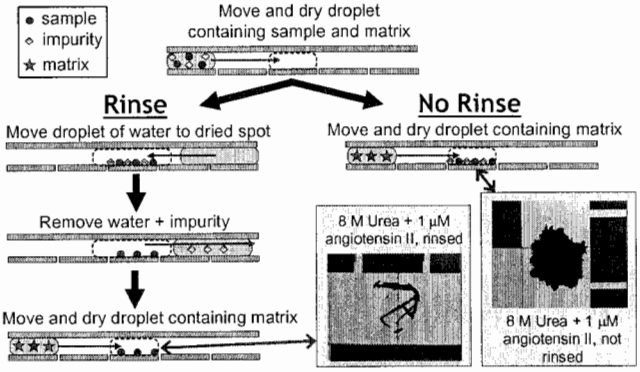

Figure 1. Schematic of droplet movement and pictures of dried spots. The rinsed crystal (left) is primarily composed of DHB, while the unrinsed crystal (right) is dominated by urea.

Figure 2 shows representative MALDI-MS data for rinsed and un-rinsed samples prepared with high levels of impurities. For the un-rinsed spots, the impurities completely suppressed the MALDI-MS signal of the analyte (n=3 for each condition), while the rinsed spots reproducibly yielded strong signals.

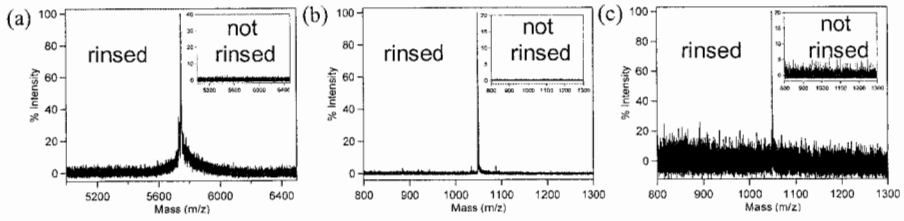

Figure 2. MALDI-MS spectra of (a) insulin (5733 Da) with 8M urea, (b) angiotensin II (1046 Da) with 8 M urea, and (c) angiotensin II with 95 mM sodium phosphate.

While high concentrations of impurities can completely extinguish the MALDI signal, intermediate concentrations can simply obscure it. Figure 3 contains representative MALDI-MS data for rinsed and un-rinsed samples prepared with 20 mM sodium phosphate. In the un-rinsed

sample spectrum (Fig. 3b), peaks at *M+23*, *M+45*, and *M+67* correspond to the mono-, di-, and tri-sodium adducts of the parent molecule. (The clusters of peaks, apparent in all high resolution MALDI-MS spectra, are caused by isotopic variations.) The adduct peaks are barely visible in the spectrum of the rinsed sample.

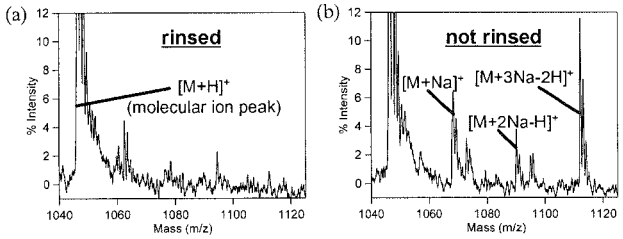

Figure 3. MALDI-MS spectra of angiotensin II with 20 mM sodium phosphate.

Many clinically relevant proteins are present at dilute concentrations in biofluids. This has driven the development of methods relying on deposition of multiple droplets of sample to a single spot, which increases the concentration and thus the MALDI signal [6]. Unfortunately, impurities are concentrated along with proteins, which can negate this benefit [7]. Using EWOD, we have deposited to a single spot multiple droplets containing low concentrations of sample and intermediate amounts of urea. The cumulative effect of the urea completely suppressed the MALDI signal for un-rinsed samples, while rinsed samples exhibit excellent S/N (data not shown).

4. Conclusions

We have demonstrated that the detrimental effects of even very high concentrations of reagents used in protein processing (e.g., 8 M urea) can be overcome by a single EWOD-driven rinse with a droplet of water. This method will enable future work, in which other processing steps (e.g., proteolytic digestions) will be integrated with EWOD-MALDI-MS.

Acknowledgements

We thank the Center for Cell Mimetic Space Exploration (CMISE), a NASA University Research, Engineering and Technology Institute (URETI), under award number NCC 2-1364, as well as the W. M. Keck Foundation for the establishment of the UCLA Mass Spectrometry and Proteomics Technology Center. ARW thanks the NIH for an NRSA postdoctoral fellowship.

References

[1] M. Brivio, R. H. Fokkens, W. Verboom, D. N. Reinhoudt, N. R. Tas, M. Goedbloed, and A. van den Berg, *Anal. Chem.*, **74**, 3972-3976 (2002).

[2] M. Gustafsson, D. Hirschberg, C. Palmberg, H. Jornvall, and T. Bergman, *Anal. Chem.*, **76**, 345-350 (2004).

[3] A. R. Wheeler, H. Moon, C.-J. Kim, J. A. Loo, and R. L. Garrell, *Anal. Chem., in press* (2004).

[4] M. Kussmann, E. Nordhoff, H. Rahbek-Nielsen, S. Haebel, Rossel-Larsen, L. Jakobsen, J. Gobom, E. Mirgorodskaya, A. Kroll-Kristensen, L. Palm, and P. Roepstorff, *J. Mass Spectrom.*, **32**, 593-601 (1997).

[5] K. Yuan, and D. M. Desiderio, *J. Mass Spectrom.*, **37**, 512-524 (2002).

[6] S. Ekstrom, D. Ericsson, P. Onnerfjord, M. Bengtsson, J. Nilsson, G. Marko-Varga, and T. Laurell, *Anal. Chem.*, **73**, 214-219 (2001).

[7] D. Ericsson, S. Ekstrom, J. Nilsson, J. Bergquist, G. Marko-Varga, and T. Laurell, *Proteomics*, **1**, 1072-1081 (2001).

A MICRO-AEROTAXIS DEVICE FOR STUDYING OXYGEN RESPONSE IN *CAENORHABDITIS ELEGANS*

Hang Lu[1], Jesse M. Gray[1], David S. Karow[2], Andy J. Chang[1], Michael A. Marletta[2], and Cornelia I. Bargmann[1]

[1]*Howard Hughes Medical Institute, and Departments of Anatomy and Biochemistry and Biophysics, University of California, San Francisco, CA, USA*
[2]*Departments of Chemistry and Molecular and Cell Biology, University of California, Berkeley, and the Division of Physical Biosciences, Lawrence Berkeley National Lab, Berkeley, CA, USA*

Abstract

We demonstrate here a membraneless micro device that rapidly produces and maintains a gas-phase oxygen gradient by diffusion between a source and a drain. The device is optically transparent, inexpensive, and readily adaptable for bench-scale assays. We use this device to study the genetic components of oxygen sensing in the free-living soil nematode *Caenorhabditis elegans*.

Keywords: aerotaxis, gas gradient, oxygen, genetics, *C. elegans*

1. Introduction

Oxygen, one of the essential components in the living environment for most organisms, plays an important role in regulating physiology and behaviors. Understanding the mechanisms of oxygen sensing and response is critical to therapeutic interventions to many human diseases including cancer, stroke, and chronic lung diseases. Much progress has been made in understanding the biochemistry of hypoxia in mammalian systems, but a full understanding of oxygen-sensing and regulatory pathways in multi-cellular organisms has yet to be achieved. In fruit flies, worms, and mammalian systems, oxygen sensation leads to transcriptional changes through the transcription factor HIF-1 (hypoxia-induced factor). As a typical transcriptional pathway, it is relatively slow (acting over minutes to hours) but highly accurate and effective.

We use a simple multicellular model organism, *C. elegans*, and its behavioral output to dissect oxygen sensing [1]. *C. elegans*' response to oxygen is fast (on the order of seconds). Its avoidance of hyperoxia conditions may be due to damaging oxidative environments, while minimal oxygen consumption is necessary to sustain normal metabolism. Currently available technology for assessing this behavior is limited by the speed and accuracy with which one can create a well-controlled oxygen environment (e.g. a gradient of oxygen in a dimension relevant to the animals, ~mm). The goal is to develop and use novel microfluidic tools to elucidate the relationships between oxygen sensing and behavior of *C. elegans*.

2. Design of the Device and Assay

We designed a micro-aerotaxis device where flowing gases in the end chambers serve as source and drain for a gradient that is established in the assay chamber (Fig.1). Because the Reynolds number of the gas flows is smaller than 10, we did not need a membrane to separate the flow chambers from the assay chamber (with the gradient), and therefore eliminated a mass transfer barrier and accelerated the gradient formation. Scaling analysis shows that a steady gradient can be formed in much less than 1 min in the gas phase and translated readily to the thin film of liquid (<10 μm) surrounding the animals. During the assay, animals are free to move inside the micro device on an agar substrate. The position of the animals inside the device reflects their preferences to oxygen concentrations.

3. Experimental

The devices are fabricated using the PDMS rapid-prototyping technique [2]. The oxygen concentration can be measured directly by an oxygen microelectrode in agar substrate after gas perfusion. For each assay, 30-200 cultured adult animals are washed and placed on the agar substrate. The device, with gas perfusing, is placed over the animals. Animals are allowed to move for 10-25 mins, and the distribution of the animals is quantified. Steady state is defined as two similar consecutive readings (5 min apart).

4. Results and discussion

The simple design of the device is sufficient to produce a linear oxygen gradient, and the gradient is translated to the agar substrate on which the animals are assayed (Fig. 2). In this design, rather than use gel/liquid phase diffusion to achieve the dissolved oxygen gradient that the animals experience, we take advantage of the very rapid gas phase gradient formation and the quick translation of this gradient to the thin liquid film around the animals. This assay platform is easy to set up and adaptable for bench-scale behavioral experiments with adequate throughput.

Using this micro device, we study the oxygen response of *C. elegans* in wild-type and many mutant backgrounds (Figs. 3-5). Interestingly, wild-type N2 animals do not prefer atmospheric oxygen concentration (21%); instead, they accumulate at ~7% (Fig. 3). This behavior output may be an indication that oxygen sensing and response is a strategy for the animals to avoid oxidative stress and to locate food – aerobic bacteria, which consume considerable amount of oxygen. Compared with wild-type animals, animals mutant in the soluble guanylyl cyclase gene *gcy-35* do not show a preference for low oxygen Fig. 4). The wild-type behavior is restored with a *gcy-35* transgene expressed in a set of sensory neurons, suggesting that *gcy-35* gene is involved in molecular oxygen sensing in these neurons.

In quantifying the oxygen preference, we first define a preferred oxygen condition (4.7% - 11.7%) and a hyperoxic condition (>11.7%) according to the wild-type distribution (Fig. 3). Then, we can calculate a hyperoxia avoidance index as the difference over the sum of the average fractions of animals under the hyperoxic and the preferred condition. This index is calculated for all mutant strains (Fig. 5).

Animals mutant for *tax-4* or *tax-2;tax-4* (encoding subunits of a cGMP-gated channel) also failed to avoid hyperoxic conditions. *gcy-35;tax-4* mutants behaved like *tax-4* and *tax-2;tax-4* mutants. In addition, *gcy-35* and *tax-4* have overlapping expression patterns in sensory neurons, suggesting that *tax-2/tax-4* channels act downstream from the *gcy-35* gene product. Together with aerotaxis data on the social feeding strain *npr-1* and other data, these experiments suggest that *gcy-35*-dependent oxygen sensing is required for the wild-type feeding behavior.

The micro-aerotaxis device demonstrated in this work allows studies on oxygen sensing and response in *C. elegans* that are otherwise difficult to perform. We envision that the versatile design and setup would enable further elucidation of the pathway and response to other gaseous stimuli.

Acknowledgements

We acknowledge the *C. elegans* Knockout Consortium and *Caenorhabditis* Genetics Center (CGC) for mutant strains. This work was supported by funding from the Howard Hughes Medical Institute (to C.I.B.) and by the LDRD fund from the Lawrence Berkeley National Lab (to M.A.M.).

References

[1] J. M. Gray, D. S. Karow, H. Lu, A. J. Chang, J. S. Chang, R. E. Ellis, M. A. Marletta, C. I. Bargmann, *Nature,* in press.

[2] D.C. Duffy, J. C. McDonald, O. J. A. Schueller, G. M. Whitesides, *Anal. Chem.* **70**, 4974-4984 (1998).

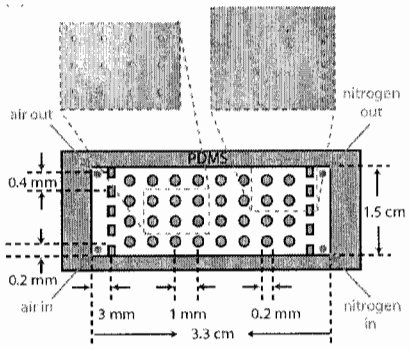

Figure 1. Design (top view) of the microfluidic device for creating oxygen gradient.

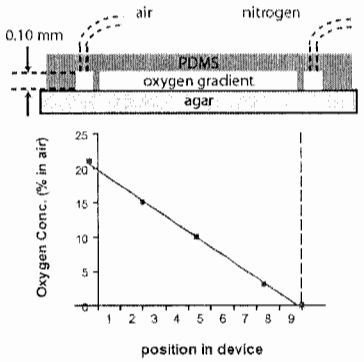

Figure 2. Measured oxygen gradient in agar after perfusion of air and nitrogen.

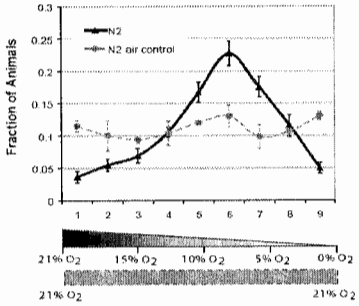

Figure 3. Preference of wild-type animals in the oxygen gradient and air-air control.

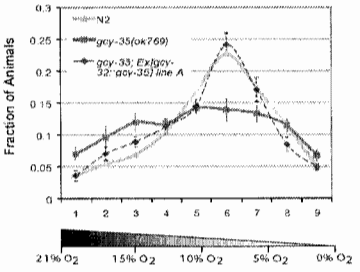

Figure 4. Preferences of gcy-35 mutant and the transgenic rescue animals compared to wild-type animals.

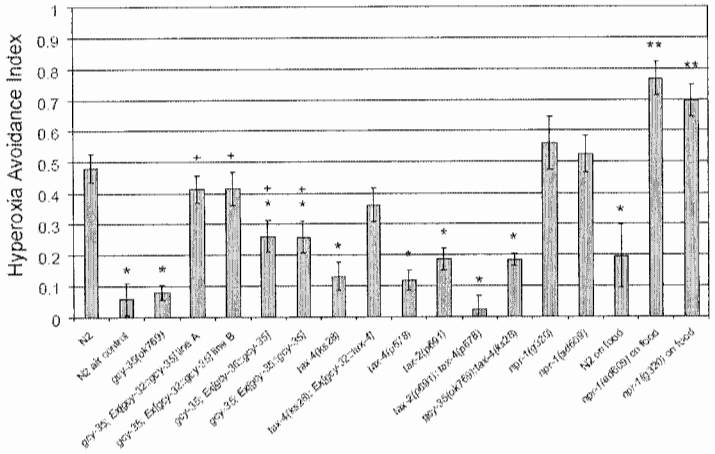

Figure 5. Hyperoxia avoidance index quantified for the mutant strains from the aerotaxis assays.

EFFECT OF ELECTROOSMOTIC FLOW IN NANOPILLAR CHIPS ON DNA SEPARATION: EXPERIMENTAL RESULTS AND NUMERICAL SIMULATIONS

Noritada Kaji[1], Yojiro Tezuka[2], Yuzuru Takamura[2], Takahiro Nishimoto[3], Hiroaki Nakanishi[3], Yasuhiro Horiike[2] and Yoshinobu Baba[1, 4, 5]

[1]Dept. of Medicinal Chemistry, Fac. of Pharmaceutical Sciences, The University of Tokushima, CREST, Japan Science and Technology Corporation (JST), Tokushima, Japan

[2]Dept. of Material Engineering, The University of Tokyo, Tokyo, Japan

[3]Technology Research Laboratory, Shimadzu Corporation, Kyoto, Japan

[4]Single-Molecule Bioanalysis Laboratory, National Institute of Advanced Industrial Science and Technology (AIST), Takamatsu, Japan

[5]The 21st Century COE Program, The University of Tokushima, Japan

Abstract

We present here a study of electroosmotic flow (EOF) profiles in nanopillar chips which have been developed for DNA separation and the extent of the EOF effect on DNA separation. It was numerically and experimentally confirmed that the suppression of EOF was crucial for achieving highly resolved DNA separation.

Keywords: nanopillar, DNA separation, nanofluidics, electrophoresis, electroosmotic flow

1. Introduction

We have demonstrated that dense nanopillar array structures inside a microchannel, so-called nanopillar chips, have a great performance as a DNA separation matrix so far [1-3]. However, to overcome the performances of conventional DNA sieving matrices, nanofluidic profiles in the nanopillar chips should be deeply understood. Especially, EOF generated in the quartz nanopillar chips would potentially degrade the DNA separation because they have several fold surface area and complicated shapes than simple microchannels.

2. Experimental

For this study, the nanopillars of 500 nm in diameter and 500 nm in spacing were fabricated inside 25-μm wide microchannel (Fig. 1) on a quartz substrate [2, 3] and DNA separations were performed under various conditions. DNA fragments were prestained with YOYO-1 (Molecular Probes, Inc.) and a fluorescence videomicroscope was used for a direct observation of the DNA bands.

Numerical simulations of the DNA migration in nanopillar chips were performed using CoventorWare v2003.1 (Coventor Technology, Inc.).

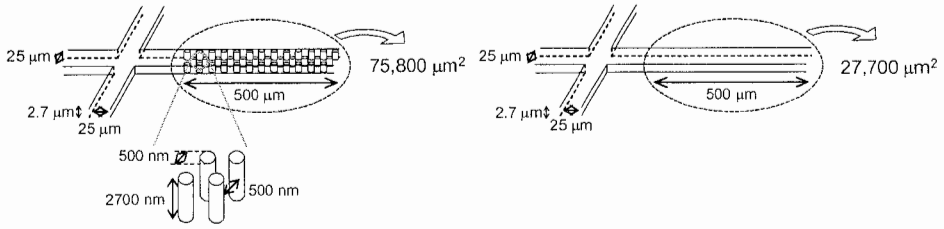

Figure 1. The dimension of the nanopillar chip. Nanopillar chip (left) has approximately threefold surface area than simple microchannel (right) in 500-μm region.

3. Results and discussion

In our first attempt, electrophoresis in the nanopillar chip was performed using 0.5 x TBE buffer solution which is conventionally used for gel electrophoresis. Fig. 2A and B shows the electropherograms of DNA separation in the nanopillar chip under various field conditions. The mixture of 10 and 38 kbp fragments were separated at 13 V/cm but the resolution gradually got worse according to electric field strength.

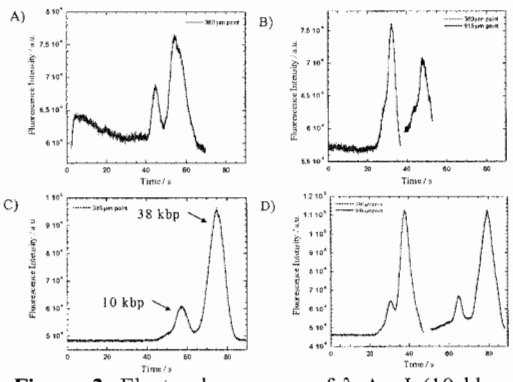

Figure 2. Electropherograms of λ-ApaI (10 kbp & 38 kbp) separation under various conditions. A) 13 V/cm, 0.5 x TBE. B) 26 V/cm, 0.5 x TBE. C) 13 V/cm, 5 x TBE. D) 26 V/cm, 5 x TBE.

To understand what happens on this separation process, numerical simulation of DNA migration in nanopillar chips were performed. We designed the 5-μm wide and 80-μm long microchannel which consist of two 25-μm long nanopillar regions. Each nanopillar has 500-nm diameter with 500-nm spacing and the same pattern of the actual nanopillar chip. When DNA migration was simulated on the assumption of absolutely pure electrophoresis without any electroosmotic flow, DNA band migrated in the nanopillar region with keeping its original rectangle shape as shown in Fig. 3A. On the contrary, when the factor of an electroosmotic flow on the nanopillars and microchannel surfaces were included in the simulation, the shape of DNA band become deformed and showed a parabolic shape during electrophoresis. (Fig. 3B) When a simple straight microchannel without any nanopillars was applied for the simulation, there was no band deformation according to an increase of electroosmotic mobility. Though the reason for this deformation of the DNA band during an electrophoresis is still uncertain, a combination of the nanopillars structures and the EOF might affect the migrating band shape. This flow profile similar to the pressure driven flow could not be expected to make any higher resolution.

To prove the EOF effect in the nanopillar chips, DNA migration behavior was directly observed by a fluorescent microscope. Fig. 4 shows sequential fluorescence images of DNA migration in the nanopillar chip under applying 60 V/cm with 0.5 x TBE buffer. When the DNA band intruded into the nanopillar region, the DNA band migrated with parabolic-shape formation as indicated by numerical simulation.

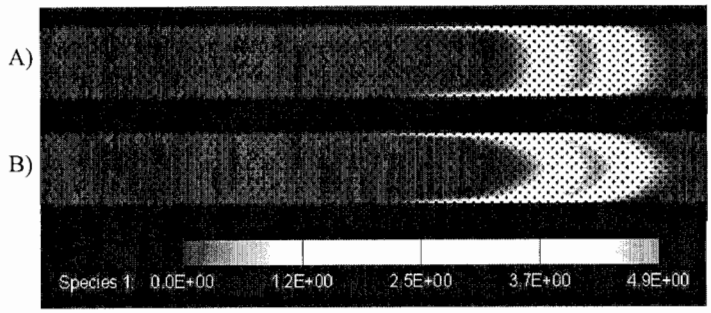

Figure 3. Numerical simulation of the motion of charged species in the nanopillar chip. Electroosmotic velocity of (B) was set to 2.5 times as fast as (A).

For the purpose of suppressing the EOF, high-concentrated buffer solution, 5 x TBE buffer, was applied for DNA separation. Fig. 2C and D show electropherograms of DNA separation in 5 x TBE buffer under various field conditions. Even under high electric field conditions which could not give a separation in 0.5 x TBE, the mixture of 10 and 38 kbp was separated well.

4. Conclusions

In the DNA separation using the nanopillar chip, from the experimental results and the numerical simulations, it was confirmed that suppressing the EOF was crucial to obtain a virtual molecular sieving effect and achieve high-resolved separation.

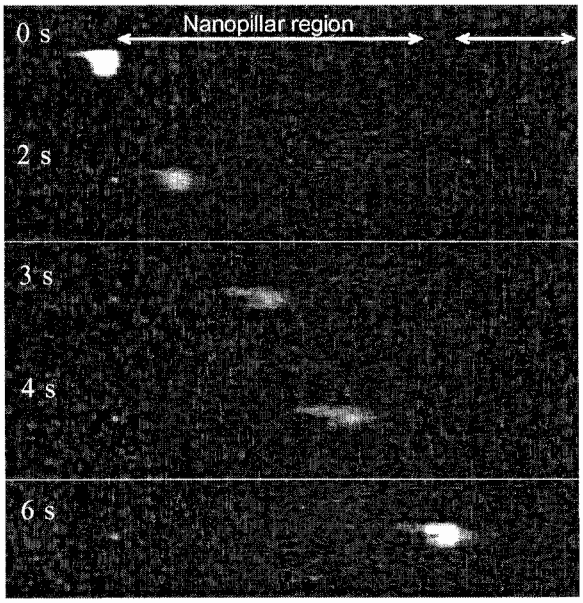

Figure 4. Sequential fluorescence images of DNA migration in the nanopillar region with parabolic-shape formation under applying 60 V/cm in 0.5 x TBE buffer.

Acknowledgements

We thank Dr. Akio Oki for fabrication of the quartz nanopillar chips. This work was partially supported by a grant of CREST from JST, Japan, a grant of NEDO from METI, Japan, and a Grant-in-Aid for Scientific Research from MHLW and MEXT, Japan. N.K. acknowledges a Grant-in-Aid for Scientific Research from Research Fellowships of the JSPS for Young Scientists.

References

[1] Y. Tezuka, M. Ueda, Y. Baba, H. Nakanishi, T. Nishimoto, Y. Takamura and Y. Horiike, *Proc. Micro Total Analysis Systems 2002,* 212-214 (2002).

[2] N. Kaji, Y. Takamura, Y. Horiike, H. Nakanishi, T. Nishimoto, and Y. Baba, *Proc. Micro Total Analysis Systems 2003*, 1315-1318 (2003).

[3] N. Kaji, Y. Tezuka, Y. Takamura, M. Ueda, T. Nishimoto, H. Nakanishi, Y. Horiike and Y. Baba, *Anal. Chem.,* **76**(1), 15-22 (2004)

COMBINED ERYTHROCYTE DEFORMABILITY TEST BY SINGLE CELL MARCHING MICROSTRUCTURE AND OPTICAL TRAPPING

Won Gu Lee[1], Junha Park[1], Chanil Chung[2], Dong Chul Han[1], and Jun Keun Chang[2, 3]
[1]*School of Mechanical and Aerospace Engineering, Seoul National University, Seoul, Korea*
[2]*Digital Bio Technology, Co., Seoul 151-742, Korea*
[3]*School of Electrical Engineering & Computer Sciences, Seoul National University, Seoul, Korea*

Abstract
In this study, human erythrocyte deformability index is re-defined by both a transit velocity and a laser power measured at the same time of cell marching through narrow microstructure (single cell marching microstructure) under various conditions of optical trapping power.
Keywords: erythrocyte deformability, single cell marching, optical trapping

1. Introduction

Erythrocyte (red blood cell) deformability is one of critical physiological factors for the optimal tissue perfusion and blood microcirculation. The deformability of human erythrocytes usually occurs because of their low cytoplasmic viscosity, surface area-volume ratio and cell membrane viscoelasticity.[1-3] Ever since the clinical importance of RBC deformability became apparent, many methods of measuring this phenomenon have been developed; filtration, micropipette aspiration, laser diffraction ellipsometry, and micro-devices using cell-flow microchannels similar to human blood capillaries. But the traditional methods used to measure microhaemorheological properties are not sufficient to investigate single RBC flow. To solve this problem of traditional methods, we introduce a combined erythrocyte deformability test using a biocompatible polydimethylsilosane (PDMS)-based microstructure and optical trapping for more efficient and accurate experiments. [4, 5]

2. Material and Methods

To compare the deformability of cancerous and normal RBCs, blood sample was acquired from several patients of cervix cancer and leukemia.

2.1 Sample preparation

To avoid the coagulation of sample bloods, anti-coagulation solution (EDTA, ethylene diamine tetraacetic acid) was added. Buffer solutions (PBS, phosphate buffered saline and FBS, fetal bovine serum) were added to make the blood to be about 10 % hematocrit.

2.2 Microchip fabrication

Single cell marching microstructure with a rectangular PDMS microchannel (width = 10 μm, height = 2 μm) and micro-nozzle (width = 6 μm, height = 2 μm), are fabricated by considering both the optimized optical path and microfluidics theory in process of MEMS technique based on soft lithography. Thereafter, oxygen plasma surface treatment is achieved to bond PDMS channel on a cover glass for higher optical trapping efficiency. To validate our design concept, we performed Computational Fluid Dynamics (CFD) simulations with a multiple-physics software package.

2.3 Optical tweezers setup

Two beam optical traps was formed by focusing two orthogonally polarized beams from an infrared laser (Intellite, 400 mW, 1064 nm) to diffraction-limited spots in the sample using an oil-immersion microscope objective (Zeiss, 100X, 1.3 NA). The fluorescence microscope was based around a standard inverted microscope (Olympus, IX71) equipped with high numerical aperture optics. The lenses used in the beam expander had an effective focal length of 9 mm and 27 mm

respectively. The back aperture of the objective lens was overfilled to ensure high trapping efficiency. A halogen lamp (Euromex fiber optic light source EK-1) was used to produce several images of single RBC transverse movement on a charge coupled device (CCD).

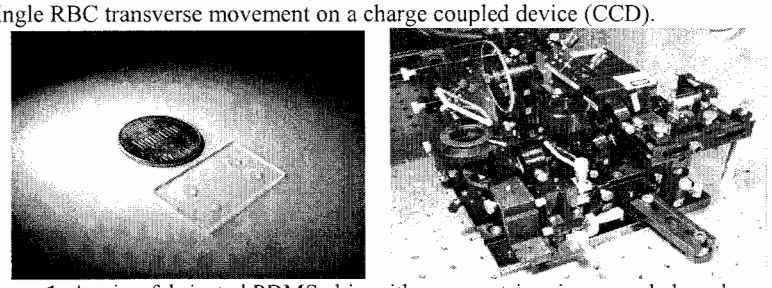

Figure 1. A microfabricated PDMS chip with asymmetric micro-nozzle based on soft-lithography (left) and two-beam optical tweezers setup (right)

2.4 Combined erythrocyte deformability test

Small blood sample, 2 μl was injected with micropipette to the inlet port of single RBC marching microstructure with negative pressure difference, about 11.5 mmHg. This value is below the physiological pressure at capillary vessels in human body, 16 mmHg. Pressurized blood sample is moved into hydrophilic microchannel and the RBCs passed through asymmetric micro-nozzle with deformed shape. Moreover, by trapping individual RBCs with optical tweezers and making them pass through the microstructure path whose size is equal to approximately 80% of average diameter of the target cell, we can measure the transit velocity and the minimum trapping laser power. In overall system, flow velocity control is achieved by a peristaltic pump and optical trap position is monitored and manipulated for real-time deformability test. The transit velocity of RBC is calculated from dividing the distance by the frame rate of the two uploaded images. The deformation data of RBC are acquired by counting the horizontal and vertical pixels of selected RBC image in microstructure via image and data processing. The minimum optical trapping powers are determined by controlling the optical density filter and obtained by using optical powermeter.

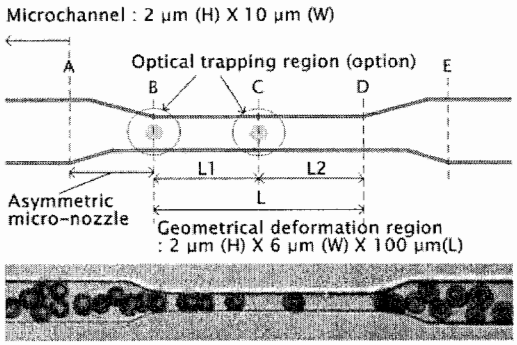

Figure 2. Schematic diagram of experimental setup for combined erythrocyte deformability test (top) and a photo of single RBC marching in geometrical deformation region (bottom)

3. Results and discussion

The deformability index (DI) is defined by the transit velocity and laser power with the geometrical deformation factor; the rate of deformed RBCs' length to the width in the region of *BD* in Fig. 2. The mean value of deformation factor is 2.57 with standard deviation of 0.724 for

cancerous blood (cervix cancer) and 2.12, 0.317 respectively for normal blood. The average of the transit velocity of normal blood is 27.8 $\mu m \cdot s^{-1}$ with the standard deviation of 10.5 and that of cancerous one is 15.43 $\mu m \cdot s^{-1}$ with 7.47. Several trends of given data distribution are briefly summarized as follows: first, mean velocity of RBCs in normal blood is faster than cancerous one in microstructure. The velocity of cancerous blood is 50 to 60 % of normal one. Second, mean deformation factor of normal blood is 80 to 90 % of cancerous blood. Third, the deviation of transit velocity data is low and that of the correlation factor is high in the case of cancerous blood. In particular, when optical trapping is applied to RBCs in microstructure, cancerous one is difficult to escape from the given optical trap due to its low deformability and speed. It also proves the reliability of the combined deformability test as single RBC diagnostic system. For more accurate data acquisition, it is very important to control the applied pressure on the chip at the same and constant level. The surface property of PDMS should be also considered because it affects the membrane of RBCs; i.e., hemolysis phenomenon is often detected in hydrophilic surface state in microstructure. Selective hydrophobic treatment or surface stabilization process could minimize this phenomenon. Also, calibration of optical trapping force should be achieved by the estimation that relative accuracy in the calibration should be below 5 %. The uncertainties of RBCs' different diameters should be estimated to be ± 0.1 μm.

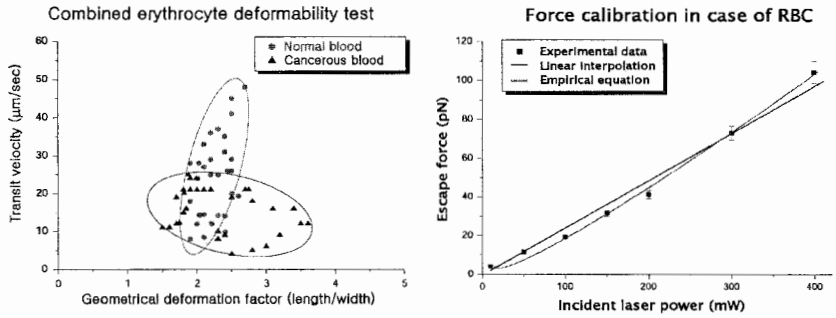

Figure 3. Deformability distributions of normal and cancerous blood for transit velocity (left) and calibration of the escape force of RBCs from a single optical trap (right)

4. Conclusions

A chip-based erythrocyte deformability test using optical trapping was developed to promote the study of drug response and high contents cellular screening by providing the quantitative and sensitive deformability differences of single target cell about chemical reaction of new drugs.

Acknowledgements

We are especially thankful for clinical advice and sample preparation of Hyo-Shil Yang in Yonsei University, Korea and this study has been supported by the Intelligent Microsystem Program (IMP) of the 21st Century Frontier R&D Program sponsored by the Korea Ministry of Science and Technology.

References

[1] M. M. Brandão *et al.*, Eur. J. Haematol., **70**, 207-211 (2003).
[2] Sylvie Henon *et al.*, Biophys. J., **76**, 1145-1151 (1999).
[3] M.Dao, C.T. Lim, S. Suresh, J. Mech. Phys. Solids, **51**, 2259-2280 (2003).
[4] Alexander Rohrbach and Ernst H.K. Stelzer , J. Appl. Phys., **91**, 5474-5488 (2002).
[5] J. Guck *et al.*, Phys. Rev. Lett., **84**, 5451-5454 (2000)

AN ULTRA-FAST IMMUNOASSAY IN PROTEIN LAB-ON-A-CHIPS ON CYCLIC OLEFIN COPOLYMER (COC)

Junhai Kai, Shilpa Thati, Aniruddha Puntambaker* and Chong H. Ahn
Microsystems and BioMEMS Laboratory
Department of Electrical & Computer Engineering & Computer Science
University of Cincinnati, Cincinnati, Ohio, USA
* *Siloam Biosciences LLC, Cincinnati, Ohio, USA*

Abstract

In this work, we report the development of an ultra-rapid protein biochip using sandwich immunoassay protocol. The total assay time is shorter than ~ 5 minutes, which is believed as one of the fastest detection times reported from the lab-on-a-chips. The protein adsorption ina microchamber is also characterized.

Keywords: Protein chip, COC, immunoassay, rapid detection, point-of-care testing

1. Introduction

Recently, Cyclic Olefin Copolymer (COC) is widely gaining attention for lab-on-a-chip applications due to its good material properties and biocompatibility. The basic concept of immunoassay on the COC surface was reported by the previous work in our group [1]. In this paper, a COC lab-on-a-chip has been successfully applied for sandwich immunoassay detection of a model analyte (Rabbit IgG) with incubation time down to 1 minute because of the extremely high surface-volume ratio of micro chamber, which insures an ultra-fast immunoassay for the rapid detection of a protein lab-on-a-chip.

2. Simulation of Protein Adsorption in a Microchamber

In a protein chip, all the reactions occur on the inner surface of the chamber. So the kinetics of protein adsorption on the solid phase in a microchamber is of major interest [2]. Figure 1 shows the simulation results of protein adsorption in a microchamber with 100 μm depth and on an open area by CFDRC software. From the simulation results, we can clearly see that the protein adsorption in a microchamber is much greater when compared to that on an open area.

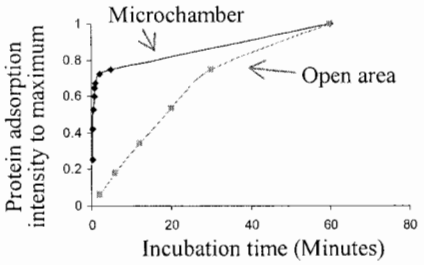

Figure 1. Simulation results of protein adsorption in 100 μm depth microchamber and on open area by CFDRC software.

3. Characterization of Protein Adsorption in a COC Microchamber

The COC protein chip was fabricated using plastic injection molding and thermal bonding technologies [3]. Figure 2 illustrates the chip structure, which consists of a reaction chamber, sample loading channels and washing channel. The reaction chamber has a width and length of 800 μm and a depth of 100μm, respectively.

Figure 3 shows the intensity of the FITC labeled IgG directly, which was incubated in the chamber for various incubation times ranging from 30 seconds to 30 minutes. The signal intensity for 1min incubation is only 20% less than that for 30min incubation, which fits the simulation result. So in the experiment we choose 1 minute incubation time for each reagent, 40sec washing time by PBS buffer at 0.2 mL/min flow rate.

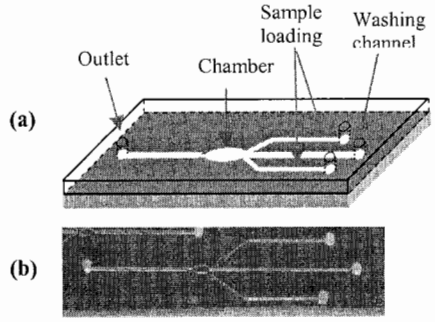

Figure 2. COC protein chip fabricated using plastic injection molding and thermal bonding technologies: (a) Illustration of chip structure and (b) fabricated device

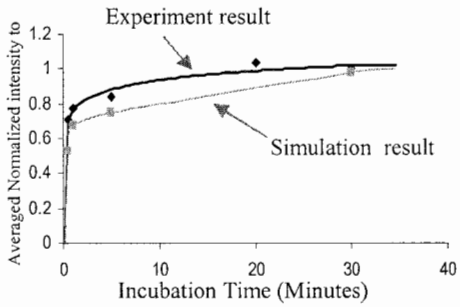

Figure 3. FITC labeled IgG directly incubated in the chamber for various incubation times ranging from 30 seconds to 30 minutes and comparing with simulation result.

We have also tested the efficiency of BSA as a blocking agent by incubating 3% BSA for 1 minute in the reaction chamber before starting the assay. Figure 4 compares the fluorescent intensities with and without BSA blocking, which clearly shows the 3% BSA solution can successfully block non-specific adsorption.

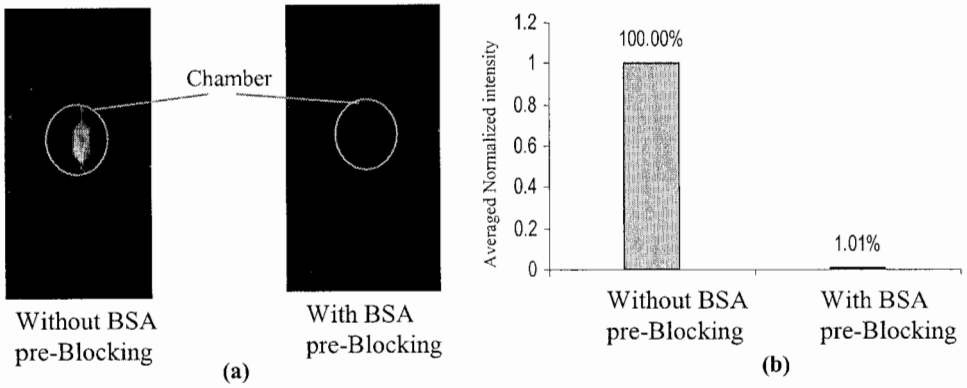

Figure 4. 0.2mg/mL Rabbit IgG adsorption in chamber was compared with and without BSA pre-blocking: (a) Scanned images and (b) Average normalized intensity.

4. Sandwich Immunoassay in Protein Chip

The protocol used for the sandwich fluorescence immunoassay [4] was as follows: 0.2 mg/mL primary anti-rabbit IgG was injected through the loading channel and incubated in the reaction chamber for 1 minute and then the excess antibody was washed. After that 3% BSA was used for blocking and the excess was washed off. Then 0.005 mg/mL (33 nM) to 0.04 mg/mL (267 nM) rabbit IgG (MW~150KD), which was the target antigen, was injected and incubated. Finally the secondary FITC labeled Anti-Rabbit IgG was incubated. After washing, the fluorescence intensities were measured by Typhoon® 8600 scanner and analyzed by software, ImageQuant®. Figure 5 shows the linear relationship between the intensities and Rabbit IgG concentration. Figure 6 compares fluorescent intensities of immunoassay in enclosed microchamber with on an open COC surface (with incubation times of 30 min.) It clearly shows that the microfluidic device gives much higher signals despite the considerably lower assay times. This may be due to the fact that the primary antibody is captured on the top and bottom walls of the microchannels thereby leading to an increased capture area (thus higher signal) with the same footprint.

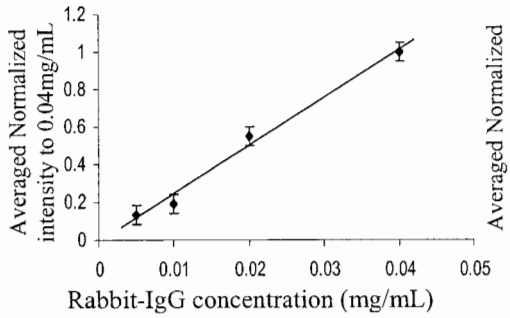

Figure 5. Linear relationship between the fluorescence intensities and Rabbit IgG concentration.

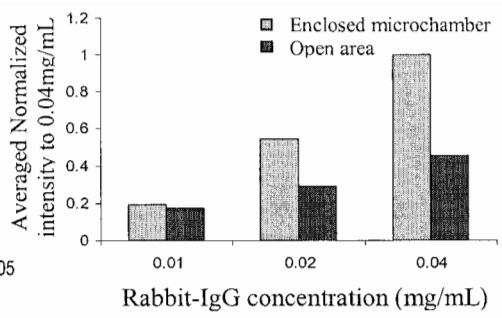

Figure 6. Comparison of fluorescence intensities of immunoassay on an open COC surface and in enclosed microchamber.

Conclusions

The results attained from this work clearly show that the performance of sandwich fluorescence immunoassay through the COC microfluidic lab-on-a-chip is much more efficient and faster than that abtained from the traditional immunoassay performed on open area. And by using the enzyme enhanced immunoassay method, the protein chip can detect ng/mL analyte in a few minutes. These results surely envisage the realization of disposable protein lab-on-a-chips for ultra-fast, low-cost diagnostic and research applications.

Acknowledgements

We gratefully acknowledge Prof. Li Jin at the Medical School of University of Cincinnati for his valuable advice and assistance in fluorescence detection.

References

[1] J Kai, Y-S Sohn, and C H. Ahn, *Proceedings of the μTAS 2002*, 419-421 (2002).

[2] Rossier, Joël S.; Gokulrangan, Giridharan; Girault, Hubert H.; Svojanovsky, Stanislav; et., *Langmuir*, **16**, 8489-8494 (2000).

[3] Jin-Woo Choi, et al, *microTAS 2001*, Monterey, CA, 411-412 (2001).

[4] F M. Ausubel, etc. Short Protocols in Molecular Biology (1999)

ON-CHIP IMMUNOASSAY FOR TETANUS TOXIN ANTIBODY USING UV-INITIATED POLYACRYLAMIDE GEL ELECTROPHORESIS

Amy E. Herr, Daniel J. Throckmorton and Anup K. Singh
Biosystems Research, Sandia National Laboratories, P.O. Box 969, MS 9951 Livermore, CA, USA, aeherr@sandia.gov

Abstract

Rapid determination of antigen and antibody levels in biological fluids is imperative for accurate, timely diagnosis of disease states, as well as for determination of efficacy of vaccination against infectious agents. Tetanus is a highly fatal, infectious disease for which vaccination is the most-effective intervention. Efficacy of vaccines can be determined by measuring the concentration of antibodies in serum. Conventional immunoassays (such as the Enzyme-Linked Immunosorbent Assay or ELISA) require long assay times and relatively large amount of samples and reagents. We report about on-chip electrokinetic immunoassays for rapid (less than 3 minutes) and sensitive (sub-nanomolar) detection of anti-tetanus toxin levels. The technique employs photolithographically-fabricated cross-linked sieving gels as an electrophoresis-based separation medium for detection and quantification of antibody levels, an as of yet unreported approach. The technique is amenable to automation and development of portable medical diagnostic devices.

Keywords: immunoassay, tetanus toxin, electrophoresis, polyacrylamide gel, serum

1. Introduction

While zone electrophoresis-based immunoassays are a promising technology for applications such as point-of-care analysis[1,2,3], the ability to discriminate between antigen, antibody, and immune complex based upon size, as well as charge-to-mass ratio is important. Large analytes such as antibodies and immune complexes vary little in charge-to-mass characteristics, making resolving species difficult. Techniques such as sodium dodecyl sulfate polyacrylamide gel electrophoresis (SDS-PAGE) allow excellent discrimination of species by size, but SDS-PAGE disrupts fragile immune complexes, making quantitation of complexes impossible. In this work, we use native PAGE to retain the biological activity necessary for intact immune complexes, yet allow both size and charge-to-mass based separation of species.

To enable on-chip sieving, we have employed cross-linked polyacrylamide gels that are fabricated *in situ* using a photolithographic approach (see Figure 1). Other researchers have employed microfabricated cross-linked gels for DNA sizing.[4] The cross-linked gels can be localized to channel regions and gel porosity can be tailored by simply changing the composition of the initial unpolymerized solution. Gel electrophoresis immunoassays are superior to zone electrophoretic immunoassays in many respects: 1) high separation resolution due to low non-specific binding, 2) fast separations (seconds) using short length channels (mm) due to the high surface area of the gel, 3) ready tailoring of gel porosity for specific applications, and 4) spatial-localization of photopatterned polyacrylamide (useful in multiplexing and integration).

2. Experimental

As an assay for antibodies to tetanus toxin, we have developed on-chip direct native PAGE immunoassays using fluorescently labeled antigen (tetanus toxin C fragment, TTC*). TTC* was maintained at a constant initial concentration of 12 nM, while anti-TTC monoclonal IgG concentration was varied from 0.2 to 26 nM. Fluorescence detection was accomplished using an epifluorescence microscopy instrument, an Argon ion laser, and a Hamamatsu H5784

photomultiplier tube. An in-house fabricated, LabView controlled high voltage power supply was employed to control voltage and current.

Wet etched glass channels were initially silanized and coated with linear acrylamide. After channel pretreatment, all channels were filled with a 1:4 solution of 30% acrylamide/bis-acrylamide (Sigma) and tris-glycine run buffer (Bio-Rad) containing 0.2% (*w/v*) photoinitiator (VA-086 Wako Chemicals).[5] Contact photolithography was performed by masking channel regions with UV opaque tape and flood exposing the entire chip to a UV source (4W, λ = 365nm) for 15 minutes. All open channels were flushed with buffer solution. Completed chips were stored hydrated at 5C.

3. Results and discussion

A non-competitive immunoassay format was used in conjunction with native gel electrophoresis in microfabricated polyacrylamide gels (Figure 1). As anti-TTC concentration in the sample was increased, an observable decrease in the free TTC peak and a concomitant increase in the immune complex peak (TTC bound to anti-TTC) were noted (Figure 2). The on-chip native electrophoresis-based immunoassays resulted in baseline separation of antigen and immune complex in a 6 mm long separation distance in less than 150 s. A calibration curve for the direct immunoassay was generated (Figure **3**). A four parameter logistic model was used to fit the buffer system calibration points. Based upon a critical signal-to-noise ratio of 3, the assay exhibited a minimum detectable anti-TTC concentration of 677 pM – sensitivity on par with conventional macroscale systems. Immunoassays were also performed using 100x diluted fetal bovine serum spiked with anti-TTC and led to results identical to those using a simple buffer system (Figure **3**) suggesting that the chip-based method is suitable for analyzing complex biological samples.

4. Conclusions

A technique for *in situ* fabrication of photopatterned, cross-linked polyacrylamide gels has been described and demonstrated for native PAGE immunoassays for antibodies to tetanus toxin. The direct immunoassays reported exemplify the simplicity, rapidity, and quantitation ability associated with on-chip electrophoresis-based immunodiagnostics. Assays were completed rapidly (<3 minutes) in both buffer-based samples and diluted bovine serum samples. Each system allowed quantitation of immune complex and subsequent generation of calibration curves. Such calibration curves enable determination of unknown tetanus antibody content in a biological sample.

We foresee several possible improvements to the immunoassay. Integration of the assay with on-chip mixing and metering, extension of the system to include multi-analyte detection, and some automation will enable high-throughput analysis of complex samples with minimal user intervention.

Acknowledgements

The authors thank James S. Brennan for his valuable assistance. This work was financially supported by a National Institute of Dental and Craniofacial Research grant (U01DE014961). Sandia is a multi-program laboratory operated by Sandia Corp., a Lockheed Martin Co., for the United States Department of Energy under Contract DE-AC04-94AL85000.

References

[1] N. M. Schultz, L. Huang and R. T. Kennedy, *Anal. Chem. 67*,5 (1995).
[2] N. H. Chiem and D. J. Harrison, *Clin Chem 44*,3 (1998).
[3] D. Schmalzing, S. Buonocore and C. Piggee, *Electrophoresis 21*,18 (2000).
[4] S. N. Brahmasandra, *et al.*, *Electrophoresis 22*, (2001).
[5] A. E. Herr, A. A. Davenport and A. K. Singh, *Anal. Chem., in press* (2004).

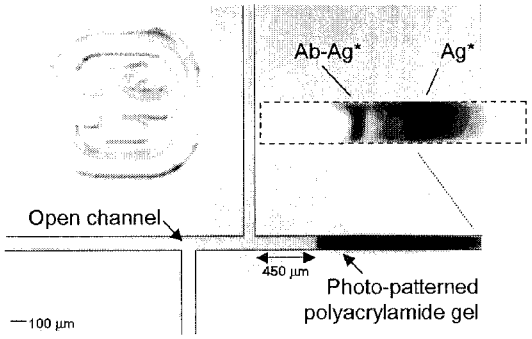

Figure 1. Image of glass microchip with in situ polymerized polyacrylamide gel localized in the separation channel. (The gel contains dye for visualization purposes.) The inset shows an inverted grayscale CCD image of an electrokinetic immunoassay 4 mm from the intersection. The image reveals two peaks: one corresponding to labeled free antigen and one corresponding to the immune complex, as both are present.

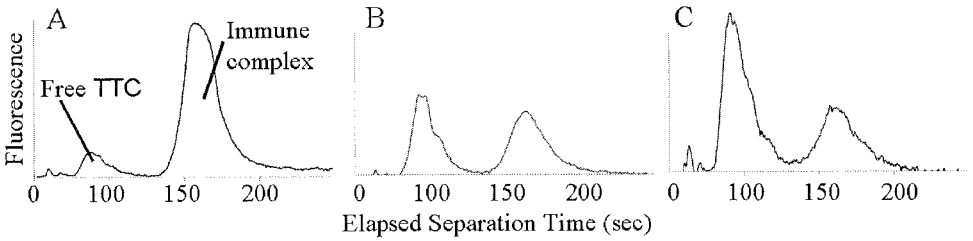

Figure 2. Electropherograms for three different samples indicate a decreasing tetanus antibody concentration from (A) to (C). [TTC*] was initially 12 nM in all samples; [Anti-TTC] was varied as: (A) 5.4 nM, (B) 0.68 nM, and (C) 0.34 nM.

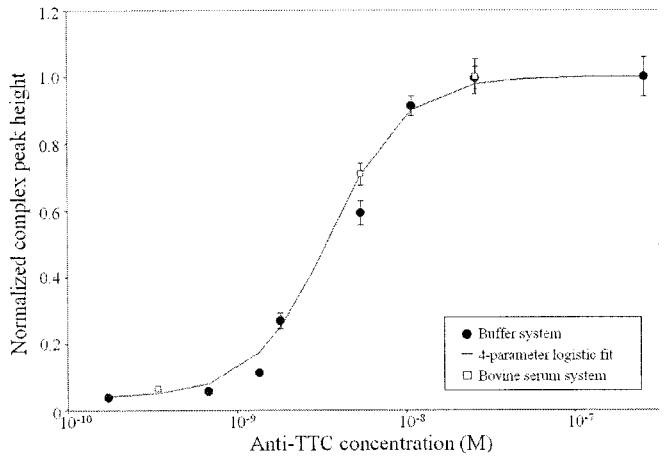

Figure 3. Calibration curve for anti-TTC generated from immunoassays performed in a tris-glycine run buffer (solid symbols), and in 100x diluted fetal bovine serum. (hollow symbols). A four parameter logistic model (solid line) was used to fit the calibration curve generated in the buffer system.

HIGH-THROUGHPUT BIO-MOLECULE DETECTION USING MICROBEAD-BASED ASSAY WITH QUANTUM DOT FLUORESCENCE IN A MICROFLUIDIC CHIP

Kwang-Seok Yun[1], Dohoon Lee[2], Min Soo Kim[2], Hak-Sung Kim[2], Gyun Min Lee[2] and Euisik Yoon[1]

[1]Dept. of Electrical Engineering and Computer Science, KAIST
[2]Dept. of Biological Science, KAIST
373-1 Guseong-dong, Yuseong-gu, Daejeon, Korea

Abstract

We present a high-throughput parallel detection of antibody by using quantum dots for a microbead-based assay. A custom designed PDMS microfluidic chip with multiple micro-wells is utilized for capturing of microbeads; antibody injection into each micro-well; QD injection; and fluorescence detection. The experiment using the fabricated microfluidic chip has been performed on solutions with various concentrations of antibody and has shown distinctive fluorescent intensities in each micro-well.

Keywords: antibody, high-throughput, microbead, micro-well, quantum dot

1. Introduction

Recently, quantum dot (QD)-based detection has attracted research attention because of its numerous advantages such as high sensitivity, narrow emission bandwidth, long-term photostability and tunable multi-color imaging compared to conventional organic dyes [1, 2]. In this paper, we propose a microbead-based assay for adaptive antibody detection by using a multi-channel double-layer microfluidic chip proposed by our group in the last micro TAS conference [3].

2. Operation Principle

Fig. 1 shows a schematic view illustrating microbead-based high-throughput detection of a specific antibody. First, the microbeads, which are modified on surface to bind with specific antibodies, are captured in multiple micro-wells. Then, the various samples - such as sera, cell secretions and other interesting biological samples - are injected onto the captured microbeads. At this time, only the specific antibodies (which are contained in sample 1 and 4 in Fig. 1) are attached on each target microbead. Finally, the anti-antibody conjugated QDs are injected onto the microbeads, resulting in binding only on the specific antibody sites, which can be monitored by

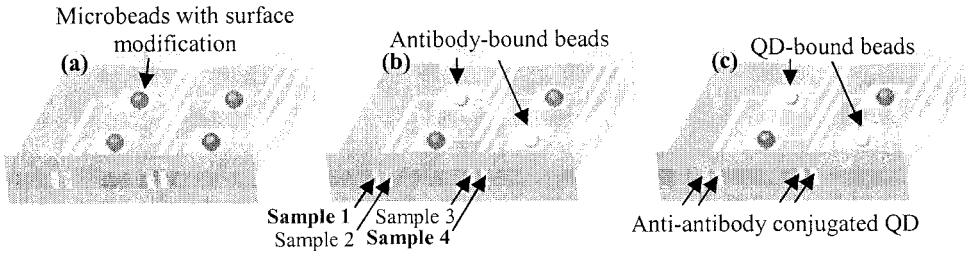

Figure 1. The schematic view showing microbead-based high-throughput detection of specific antibody. (a) Step I: capture of micronbeads in multiple microwells. (b) Step II: various samples injection (Sample 1 and 4 including specific antibody, sample 2 and 3 not including specific antibody) (c) Step III: QD injection for binding with specific antibody.

using fluorescence microscope.

Using the proposed method, various bio-molecules or proteins including antibodies can be detected by appropriately modifying the surface of microbeads and many kinds of samples can be simultaneously assayed in a single chip with single experiment, to achieve high-throughput.

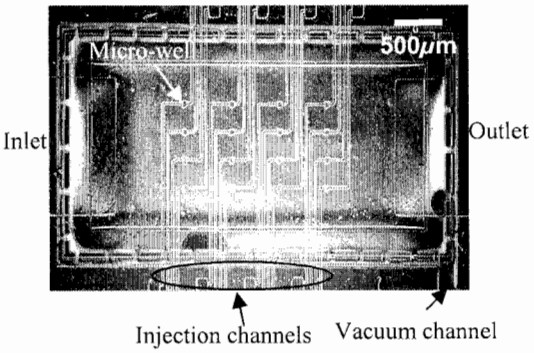

Figure 2. Photograph of the fabricated microfluidic chip.

3. Experimental

The device was fabricated on glass substrate for UV transmission. The fabrication processes include multi-level PDMS layer formation for microbeads capturing sites and multiple microflow channels for injecting antibodies and QDs. Detailed process flow can be found in our previous work [3]. Fig. 2 shows the photograph of the fabricated test device with 16 micro-wells in a 4×4 array, which can be easily expanded into a much larger array.

Fig. 3 shows the experimental procedures. First, microbeads are introduced from the inlet and autonomously captured into each micro-well. We have used streptavidin-coated polystyrene beads with a diameter of 10 μm. These microbeads are coated with biotinylated protein A for the specific

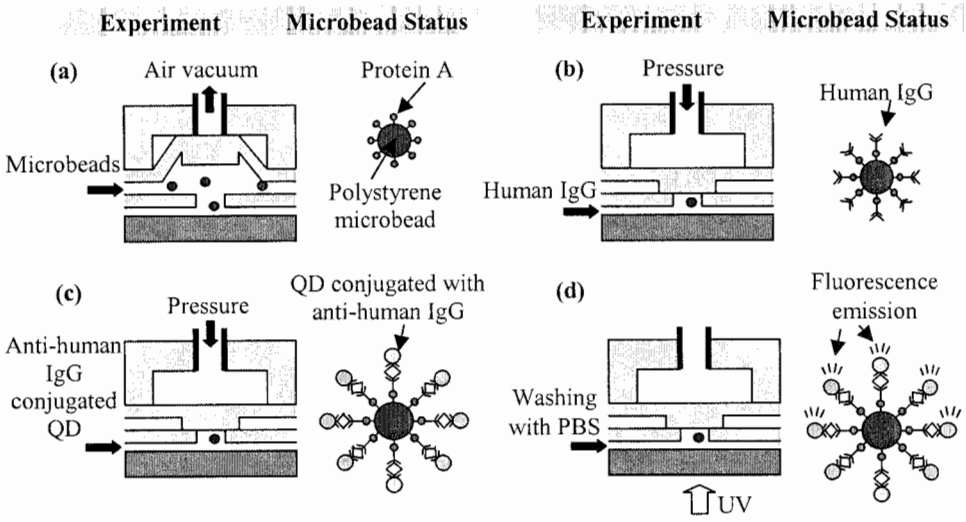

Figure 3. The experimental procedure and each status of microbeads in a micro-well: (a) Microbeads introduction and capturing into microwells after cover opening, (b) Human IgG injection after cover closing, (c) Anti-human IgG conjugated QD injection after washing, and (d) Washing with PBS and fluorescence detection.

binding with human IgG antibody. After the beads are captured, human IgG antibodies in different concentration are injected into specific target micro-wells. In this experiment we have used four different concentrations: 0, 1, 10, and 100 μg/mL in PBS solution. After washing with PBS, the 5 nM QDs, which are conjugated with anti-human IgG for binding with IgG, are injected into each micro-well. Finally, the entire channels and micro-wells are completely washed with PBS solution.

4. Results and discussion

The initial experimental results on bead-based assay have been monitored using fluorescence microscope. The wavelength of excitation light is 470 nm and emission wavelength from QD is about 565 nm. Fig. 4 shows the fluorescence photo image of QD-attached (namely, specifically reacted with human IgG) microbeads. We can differentiate intensity according to different antibody concentrations. A slight amount of emission was observed for zero concentration. We think this may come from auto-fluorescence of polystyrene microbead, non-specific binding and/or imperfect filtering of excitation UV light.

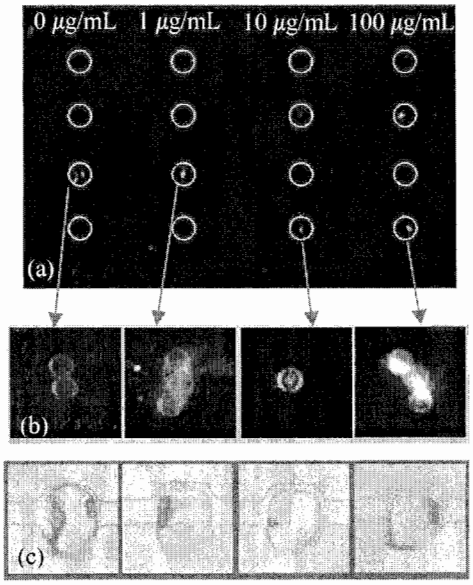

Figure 4. (a) Fluorescence images of 4×4 array. (b) Magnified views of each micro-well for various antibody concentrations. (c) Bright field (not fluorescence) image according to each micro-well in (b).

5. Conclusions

In this paper we have demonstrated a high-throughput parallel detection of specific antibody by using a microbead-based assay with quantum dots on a custom designed PDMS microfluidic chip. The microfluidic chip with 16 micro-wells has performed consecutive procedures: microbeads capturing and isolation into each well; introduction of human IgG solutions with various concentrations; introduction of QDs conjugated with anti-human IgG; and the fluorescence detection after washing with PBS.

Acknowledgements

This work has been partially supported by the Intelligent Microsystems Program (IMP) that is the project of the "21C Frontier R&D program", the KOSEF through the MICROS center at KAIST, and the NRL program from the Ministry of Science and Technology.

References

[1] H.-C. Yeh, E. Simone, C. Zhang, and T.-H. Wang, *IEEE International Conference on MEMS*, pp.371-374 (2004)

[2] E. R. Goldman, A. R. Clapp, G. P. Anderson, H. T. Uyeda, J. M. Mauro, I. L. Medintz and H. Mattoussi, *Anal. Chem.*, **76**, 684-688 (2004)

[3] K.-S. Yun, and E. Yoon, *micro TAS 2003*, pp. 861-864 (2003)

REGULATED CULTURE AND ASSAYS OF CELLS USING BRAILLE DISPLAYS

Wei Gu[1], Xiaoyue Zhu[1], Nobuyuki Futai[1], Jonathon W. Song[1] and Shuichi Takayama[1,*]
[1]*Dept. of Biomedical Engineering, University of Michigan, 2100 Gerstacker, 2200 Bonisteel, Ann Arbor, MI, USA, 48103*
**To whom correspondence should be addressed. Email: takayama@umich.edu*

Abstract
The availability of multiple pumps and valves on a Braille display enables arrays of cell assays and micro-scale tissue cultures to be perfused under complex flow in reconfigurable channel networks. As examples, we show dynamic changes between laminar and mixed flow for cell treatment, and self-contained cell culture devices that are able to reconfigure their fluidic pathways.
Keywords: cell culture, perfusion, tissue engineering, pump, valve

1. Introduction

Assays of cells or of micro-scale tissues in microfluidic channels have been of interest recently [1,2]. However, most are often limited to diffusion or unidirectional flow from one pump. More complex, cell experiments would benefit from robust and convenient methods to automate multiple spatio-temporal patterns of microfluidic flow. In this paper, we demonstrate using Braille displays as pumps and valves to control arrays of perfused flow for the long term culture of cells [3]. Vertically moving pins on the displays coordinate fluidic movement by selectively deforming the silicone rubber housing the fluidic channel networks. This allows compartmentalization and reconfiguration between channel architectures, along with complex fluid flow for cell studies.

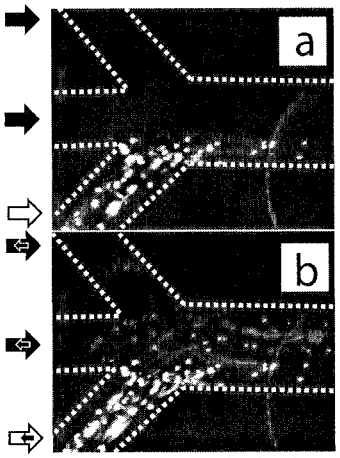

Figure 1. (a) Multiple laminar stream flow. A stream with Syto 9 selectively stains a third of adherent C2C12 cells. (b) Mixed flow generated by out-of-sync pumps that periodically reverse stains all cells, and detached cells are noted to translate across the channel width.

2. Experimental

Poly(dimethylsiloxane) (PDMS) device fabrication for Braille displays is previously described [3]. Devices specifically for cell culture include an additional top PDMS layer that is replicated from brass molds. This layer is sealed by plasma oxidation and connects to channels via punched holes. Reagents can then be added or removed from this closed system via thin insulin needles.

Prior to cell seeding, fibronectin (100 μg/mL in PBS) is injected into a device clamped onto a Braille display and incubated for 10 minutes at room temperature. Cells are then loaded into specific regions via fluidic pathways defined by valves, and perfused at consecutive average flow rates of 0, 2, and 9 nL/min for 15 minutes each during cell attachment. The PDMS device and its Braille display are then placed into a 37 °C, 5% CO_2 incubator for long term cell culture.

3. Results and discussion

To demonstrate programmed treatments for cells in culture, we switched between laminar non-mixing flow and

mixed flow. In Figure 1a, three inlet pumps moved in parallel to establish pseudo laminar flow. Since only one inlet contained Styo 9 (fluorescent cell stain), only a third of the outlet channel was stained. In contrast, Figure 1b shows all cells stained after software subsequently switched to a mixing algorithm. When mixing, each inlet pump moves in a different time phase and pumped one full cycle backward for every two cycles forward. The fluidic interlayering and active translation of inlet liquid across the channel width causes a more mixed output.

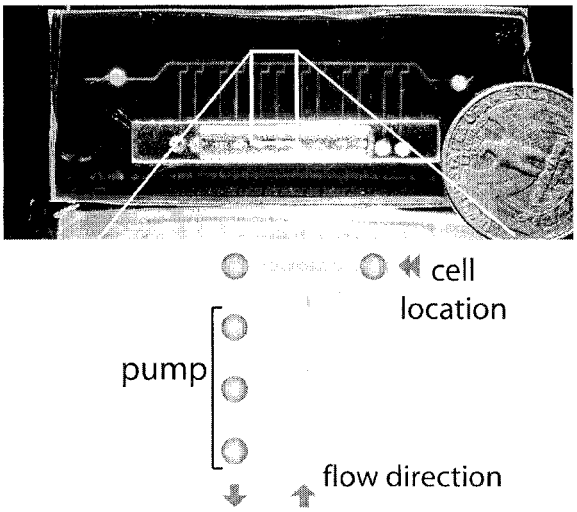

Figure 2. A typical cell culture device, loaded here with fluorescein, consists of six loops for independent perfusion. The close-up on a single loop shows the two most frequently used fluidic pathways: (i) at the top horizontally only for channel seeding, and (ii) through a portion of the top channel via a loop to the on-chip reservoir.

Another device, shown in Figure 2, was designed for longer cell studies. This device contains six separate circulatory loops for treatment of cells seeded from a single batch. Each cell culture chip has reservoir and channel features that are completely sealed by PDMS to reduce contamination, spills, and evaporation. As shown in Figure 3, multiple cell lines can be successfully cultured over weeks in such devices. By pumping at different flow rates or from reservoir containing different media, we regulated cell growth, death, and differentiation (Fig. 4) for each separate loop. Figure 5 shows the graded effect of media input down the length of the channel, presumably due to limited growth factors. It is possible for other limiting biological signals such as morphogens to be used to assay cells in a gradient.

4. Conclusions

Braille displays provide accessible, multiple pumps and valves for programmed, long term cell culture. The versatility in having integrated pumps and valves allows for future incorporation of on-chip cell processing and detection.

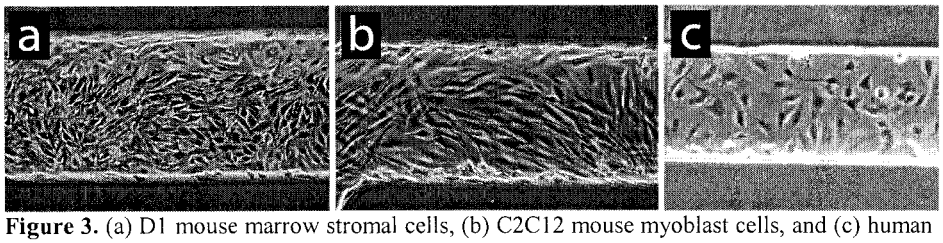

Figure 3. (a) D1 mouse marrow stromal cells, (b) C2C12 mouse myoblast cells, and (c) human dermal microvascular endothethial cells (HDMEC) were cultured under perfusion driven by a Braille display. Here, channel widths were 400 μm (a, b) and 300 μm (c).

Acknowledgements

We thank Prof. Mark Burns for use of cleanroom facilities, Prof. Jacques Nor for the HDMEC cells, Susan Hsiong for the D1 cells, and Dr. Shian-Huey Chiang for the C2C12 cells. This material is based upon work supported by the U.S. Army Research Laboratory and the U.S. Army Research Office under contract/grant number DAAD19-03-1-0168, National Science Foundation (BES-0238625), Whitaker Foundation, Nathan Shock Center for Aging Research Pilot Grant, and NASA BioScience and Engineering Institute (NBEI).

Figure 4. C2C12 cells forming single microtube structures in 200 μm wide channels.

References

[1] N. L. Jeon, H. Baskaran, S. K. W. Dertinger, G. M. Whitesides, L. V. D. Water, M. Toner, Nat. Biotech., **20**, 826-30 (2002).

[2] A. Sin, K. C. Chin, M. F. Jamil, Y. Kostov, G. Rao, M. L. Shuler, Biotechnol. Prog., **20**, 338-45 (2003).

[3] W. Gu, X. Zhu, N. Futai, B. S. Cho, MicroTAS 2004.

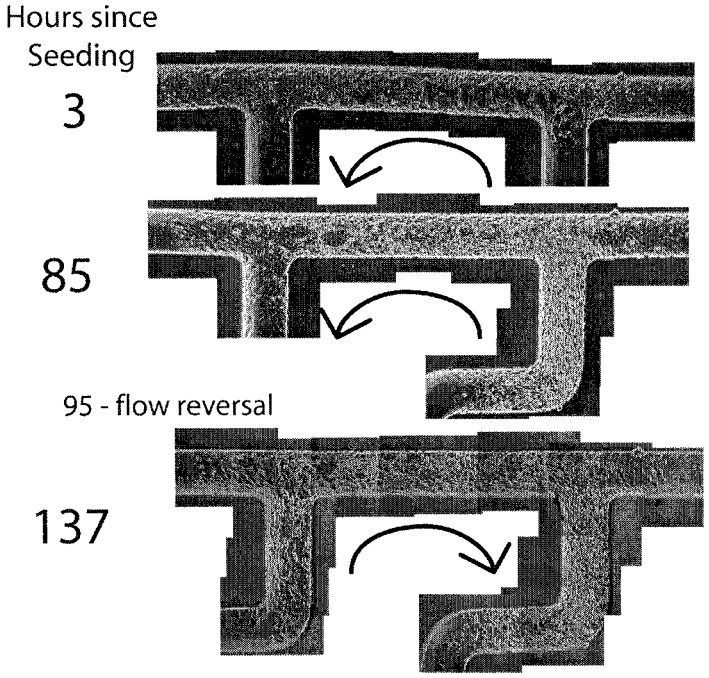

Figure 5. Cells exhibiting graded growth along the length of one channel loop. During seeding, cells were localized to the top channel at an even density. Fluid moves in a counterclockwise direction, promoting cell proliferation and migration on the right (upstream region). Subsequent reversal of flow direction reversed the effect of the gradient.

SIMPLE, STRONG, SIZE-SELECTIVE DIELECTROPHORETIC TRAPS FOR SINGLE-CELL PATTERNING

Adam Rosenthal and Joel Voldman
Massachusetts Institute of Technology, Cambridge, MA 02139

Abstract
We have developed a novel nDEP trap designed to pattern single cells. We tested the strength of our traps using polystyrene beads and the measurements were found to be in excellent agreement with our modeling predictions. Our DEP traps display a tunable peak size-selectivity behavior, with these traps being optimized to trap particles of ~12 μm. Finally, we have demonstrated use with cells by trapping single mouse fibroblast cells in an array.
Keywords: cell patterning, dielectrophoresis, nDEP, size-selective, single-cell manipulation

1. Introduction
Dielectrophoretic (DEP) traps are an increasingly important method for patterning cells alongside optical tweezers [1], microcontact stamping [2], and electrophoresis [3]. DEP traps for cell patterning can use either negative dielectrophoresis (nDEP)—pushing cells away from the electrodes—or positive dielectrophoresis (pDEP)—pulling cells toward the electrodes. Prior single-cell DEP traps include nDEP octopoles [4], nDEP posts [5], and the pDEP points-and-lid geometry [6]. All of these designs are strong but are either not appropriate for patterning cells [4, 5], would not allow unobstructed cell division [5], are difficult to package [4] or fabricate [5], or cannot be used with normal cell-culture media [6]. The challenge is fabricating a strong trap that allows cell patterning, is planar, and uses nDEP. To meet this challenge, we have designed a planar nDEP trap that is simple, scalable, strong, well-suited for cells, inexpensive to fabricate, and displays size-selective trapping.

2. Fabrication and Packaging
The DEP traps are formed by patterning gold onto a glass slide. The minimum feature size of the traps is ≥10 μm, which allows the use of inexpensive transparency masks for photolithography. An overview of the experimental setup is shown in Fig. 1. The parallel-plate flow chamber was sealed using 4 binder clips for easy assembling and disassembling.

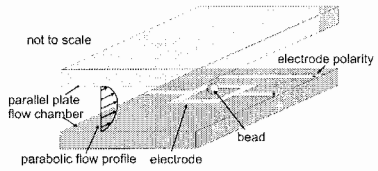

Figure 1. Overview of single-bead nDEP trapping experiments.

3. Results
To demonstrate the strength of our traps, we used polystyrene beads as model particles. We measured the maximum flow rate that the trapped beads could withstand before getting pushed out of the trap and compared this to predictions generated by our previously described modeling program [5]. We note that the predictions include no fitting parameters. The deviation between the predictions and experiments was ≤14% in all cases (Fig. 2). The strength of these traps is comparable to previous work [4, 5], but with significantly simpler packaging and fabrication.

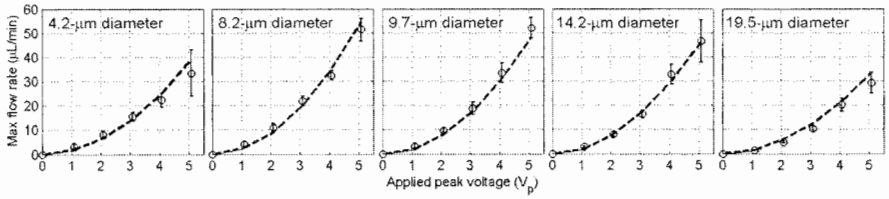

Figure 2. Experimental and simulated results for 5 bead sizes at peak voltage 1-5 V_p. Shown are the predicted values (--), mean (o), and standard deviation (n $\geq$ 3 at each voltage).

Using the 5 V_p data of each bead diameter from Fig. 2, we can plot the maximum flow rate as a function of bead diameter (Fig. 3*A*). We note that the bead diameter increases until 12 μm, and then decreases for larger diameters, creating a peak-size selectivity behavior that is optimized for ~12 μm particles. The trapped bead experiences *x*, *y*, and *z*-directed electric fields and ends up getting pushed out of the trap when its center of mass sees the upward *z*-directed electric fields, pushing it up into higher shear flows and out of the trap. The bead remains trapped when the bead center of mass experiences the downward *z*-directed electric fields. The line defining the transition from upwards to downwards *z*-directed electric fields—the stability transition line—was determined from the modeling software and found to have the shape in Fig. 3*B*. Although the trap has strong enough *x*-directed electric fields to resist flow rates ~200 μL/min, it is the upward *z*-directed fields that push the beads out of the trap at lower flow rates. Therefore, this stability transition line is the critical determinant of the peak size-selectivity behavior.

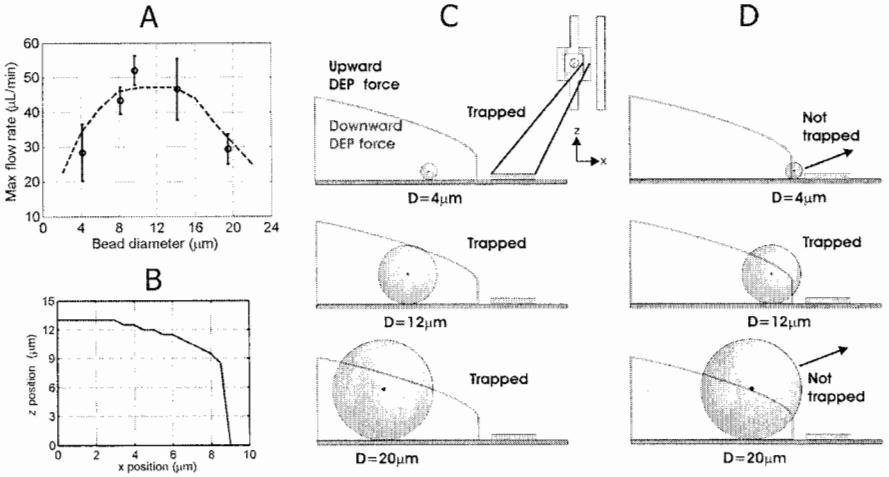

Figure 3. Peak size-selectivity behavior.

The peak size-selectivity behavior occurs because of two effects. First, at low flow rates the electric field geometry pushes larger beads further away from the electrodes (data not shown), allowing them to travel a greater distance before they get to the upward *z*-directed electric fields near the electrodes (Fig. 3*C*). Second, at higher flow rates the beads are pushed to the right, towards the upward *z*-directed fields near the square electrode. The smaller-diameter beads started out closer to the electrodes, so with flow they get pushed near the electrodes and experience the upward *z*-directed fields there (Fig. 3*D, top*). The larger-diameter beads have centers of mass that are high enough to experience the upward *z*-directed fields further away from the electrode (Fig. 3*D, bottom*). The medium-sized beads do not experience the upward *z*-directed fields until higher flow rates, making the trap optimized for them (Fig. 3*D, middle*).

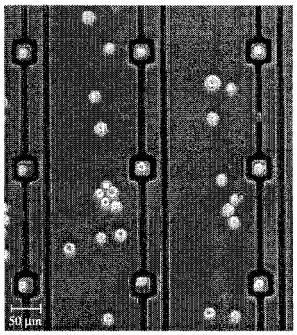

Figure 4. Mouse 3T3 fibroblast cells trapped in an array using the nDEP traps.

Finally, to demonstrate use with cells, traps were used to array single mouse fibroblasts (Fig. 4). Fibroblasts outside the traps have not been washed away and the applied signal was $2V_p$ at 5 MHz.

4. Conclusion

We have presented a novel DEP trap, offering a unique combination of being simple, planar, nDEP, strong, scalable, and size-selective. Our devices are easy and inexpensive to fabricate and package. Thus, we have provided the foundations for an enabling technology for patterning single cells in a wide range of configurations—allowing us to do novel cell biology experiments that were previously not possible.

Acknowledgments

We would like to thank the Microsystems Technology Laboratory at MIT for fabrication help. This work was supported by NSF graduate fellowship, HST MEMP fellowship, MIT Presidential Fellowship as well as the Electrical Engineering Department at MIT and NIH (RR18878).

References

[1] Birkbeck, A.L., et al., *VCSEL Arrays as micromanipulators in chip-based biosystems.* Biomedical Microdevices, 2003. **5**(1): p. 47-54.

[2] Xia, Y.N. and G.M. Whitesides, *Soft lithography.* Angewandte Chemie-International Edition, 1998. **37**(5): p. 551-575.

[3] Ozkan, M., et al., *Electro-optical platform for the manipulation of live cells.* Langmuir, 2003. **19**(5): p. 1532-1538.

[4] Schnelle, T., et al., *3-Dimensional Electric-Field Traps for Manipulation of Cells - Calculation and Experimental-Verification.* Biochimica Et Biophysica Acta, 1993. **1157**(2): p. 127-140.

[5] Voldman, J., et al., *Design and analysis of extruded quadrupolar dielectrophoretic traps.* Journal of Electrostatics, 2003. **57**(1): p. 69-90.

[6] Gray, D.S., et al., *Dielectrophoretic registration of living cells to a microelectrode array.* Biosensors & Bioelectronics, 2004. **19**(7): p. 771-780.

A MICROCHEMOSTAT - CONTINUOUS CELL CULTURE IN MICROBIOREACTORS

Z. Zhang[1], P. Boccazzi[2], H.-G. Choi[1], N. Szita[1], A. J. Sinskey[2], K. F. Jensen[1]
[1]Department of Chemical Engineering, [2]Department of Biology,
Massachusetts Institute of Technolog, 77 Mass. Ave., Cambridge, MA, USA

Abstract

We present a microchemostat that integrates a microfluidic medium-feeding system with optical density, dissolve oxygen, and pH optical sensors. *Escherichia coli* cells are continuously cultured in a 150μL, well-mixed microbioreactor by pressure-driven feeding of fresh medium through microchannel into the microbioreactor. Stable levels of optical density, dissolved oxygen, and pH are obtained in the microchemostat.

Keywords: microchemstat, continuous culture, microbioreactor, surface modification

1. Introduction

In a chemostat microbial cells are grown at a steady state where cell biomass production, substrates and products concentrations remain constant [1]. These features make a chemostat a unique and powerful tool for biological and physiological research. One example is the combination of continuous culture with DNA microarrays for global gene expression analysis of bacterial cells under different growth conditions [2]. Chemostat experiments with conventional bioreactors are time- and labor- intensive. We have previous reported batch and fed-batch cell culture in microbioreactors [3, 4] as a high-throughput experimental platform. In contrast to batch or fed-batch cell culture, microchemostat requires a dynamic balance of medium feeding and cell growth to avoid "wash-out" or overpopulation of cells in the microbioreactor. Additional challenges for realizing chemostat performance in microsystems include avoiding cell growth on the reactor walls and avoiding chemotaxis of bacteria into microfluidic channels during long growth runs.

2. Experimental Setup and Results

The continuous culture microbioreactor (Figure 1) with integrated optical sensors is fed with fresh medium by pressure-driven flow through one of the fluidic channels; the other side of the reactor is connected with a pressurized water reservoir that serves as effluent collector and also keeps the reactor at a constant volume of 150μL. As the feed rate of the medium is varied between 0.8μL/min to 2μL/min, the cell metabolism responds and the resulting state of the chemostat is monitored by measurements of optical density (OD), pH, and dissolve oxygen (DO) levels.

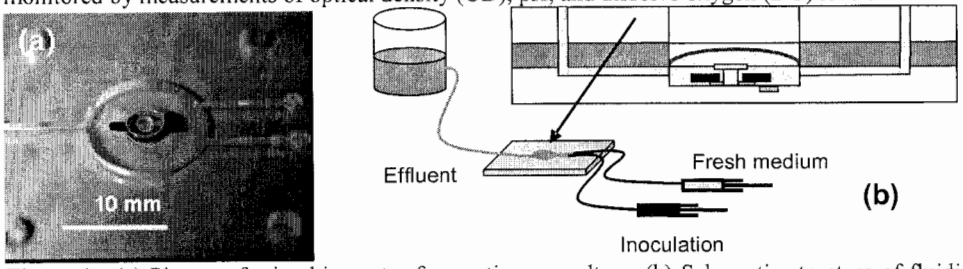

Figure 1. (a) Picture of microbioreactor for continuous culture. (b) Schematic structure of fluidic system with application of syringe pumps.

Figure 2 shows an example of a microchemostat with *Escherichia coli*. At the beginning of the reaction cells utilize all available oxygen to build up biomass, as a result, DO level drops to zero in

2 hours. The pH level of the culture broth decreases at the beginning as a result of the biomass production, and then increases when fed with fresh medium. At about 20 hours DO, pH, and OD reach stable levels and chemostat conditions are established (Figure 2a). The steady conditions balance medium feed rate and cell growth rate. Disturbances in flow rate, temperature, or medium concentration will impact this dynamic balance. Figure 2b exemplifies the case when feeding is stopped for 15 hours.

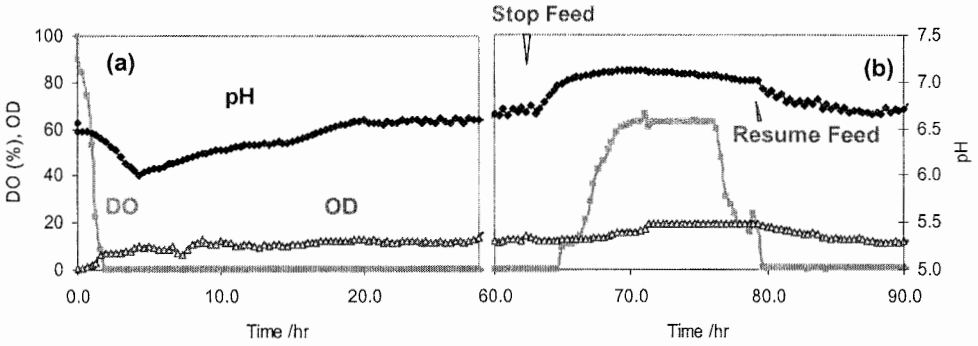

Figure 2. Continuous culture of *E.coli* FB 21591 in LB medium containing Luria-Bertani (LB) medium, 8g/L glucose, 100 μg/mℓ kanamycin, and 0.1mol/L MES. The dilution rate was 75 min^{-1}. a – Early stage of cell culture. OD and pH reach stable levels at 20hours. b – Feed is stopped for 15 hours in the experiment, DO recovers as cell growth slows down with exhaustion of nutrients. DO drops again to zero as cells resume growing when feeding is resumed.

3. Integrated Fluidic System

Chemotaxis, the bias random walk of motile bacterial cells towards nutrients, present a major challenge for implementing microchemostats. A single cell migrating back through the feed line into the medium reservoir and reproducing would contaminate the experiment. Typical average linear flow rates of 400 ~ 1000μm/s in the upstream feed channel (cross-section 125μm×125μm) are significantly higher than the average migration speed of *E.coli* cells (20~30 μm/s). As a result, only a very small faction of cells is able to swim back up the feeding channel. To further reduce the potential for cells migrating back, we use a local heater (Figure 3) to raise the temperature in the feed line and thereby reverse the driving force for chemotaxis. The high temperature zone had the additional advantage of pasteurizing any cells that reach the heating zone. At exit side of the chemostat, local cooling (Figure 3) to 4°C of the effluent channel keeps cells at low temperature and significantly reduce metabolic activity to facilitate off-line sampling for further analysis.

The long culturing time in chemostats imply that cell adhesion and wall growth on the surfaces of bioreactor can become significant issues unless reactor surfaces are modified to provide resistance to non specific cell adhesion. This problem is further accentuated by the high surface-to-volume ratio the microbioreactor [5]. We have developed poly(ethylene glycol) (PEG) surface coatings for both poly(dimethylsiloxane) (PDMS) [6] (aeration membrane) and polymethylmethacrylate (PMMA) surfaces (microchemostat body)(Figure 4). These surface coatings along with the shear stress generated by the magnetic stirring reduce cell adhesion in the microchemostat.

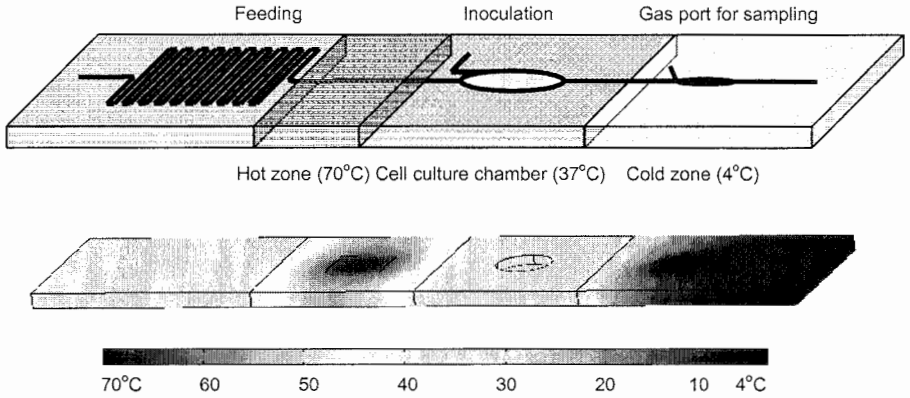

Figure 3. (a) Schematic of the microbioreactor for local heating to prevent cell chemotaxis and local cooling for off-line sampling. (b) Simulation of temperature gradient for microbioreactor system.

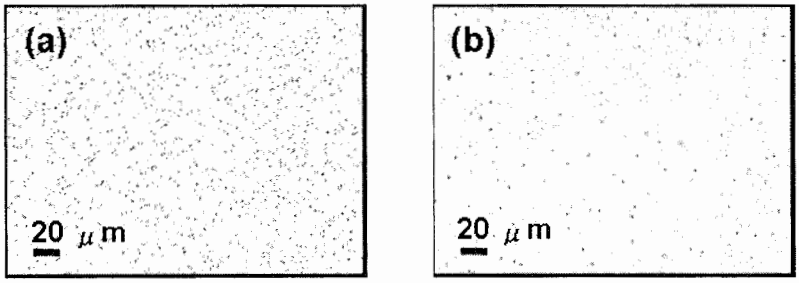

Figure 4. Comparison of cell adhesion on PEG-coated and native PMMA surface. Cells are tinged with safranin. (a) Cell adhesion on native PMMA surface; (b) *E. coli* FB21591 adhesion on PEG-coated PMMA surface.

Acknowledgements

The authors thank the DuPont-MIT Alliance for funding.

References

[1] Michael L. Shuler and Fikret Kargi, *Bioprocess Engineering: Basic Concepts*, Prentice-Hall, Inc., 2002.

[2] J. J.M. ter Linde, H. Liang, R.W. Davis, H.Y. Steensma, J.P. van Dijken, L.T. Pronk, *Journal of Bacteriology*, **181**, 7409-7413 (1999).

[3] Z. Zhang, N. Szita, P. Boccazzi, A. J. Sinskey, K. F. Jensen, *Proc. Micro Total Analysis 2003*, Transducers Research Foundation, Inc., 765-768 (2003).

[4] A. Zanzotto, N. Szita, P. Boccazzi, et. al., *Biotech. Bioeng.*, accepted.

[5] H. H. Topiwala and G. Hamer, *Biotech. Bioeng.*, **8**, 919-922 (1971).

[6] H.-G. Choi, Z. Zhang, P. Boccazzi, P.E. Laibinis, A J. Sinskey, K. F. Jensen, *Proc. Micro Total Analysis 2003*, Transducers Research Foundation, Inc., 1105-1108 (2003)

HYDRODYNAMIC FABRICATION OF FUNCTIONAL BEADS AND APPLICATION TO MICROREACTOR

JeongYun Kim[1], WonJe Jeong[1], GiHun Seong[2], JaeBum Choo[2], David. J. Beebe[3], and SangHoon Lee[1]

[1]Dept. of Biomedical Eng., Dankook University, San 29, AnseoDong, Cheonan, Chungnam, 330-714, Korea

[2]Dept. of Chemistry, Hanyang University, 1271 Sa 1-Dong, Ansan, KyonggiDo, 425-791, Korea

[3]Dept. of Biomedical Eng., University of Wisconsin, Madison, WI, 53706, USA

Abstract

In this paper, a new method to fabricate a polymeric microbead is developed using the micro scale hydrodynamic phenomena and *'on-the-fly'* photo-polymerization. The dimension of microbeads can be controlled by changing the relative flow rates without re-tooling. Biocatalysts are immobilized in the beads during the fabrication process and these functionalized beads are incorporated inside the microchannel for the continuous detection of glucose-enzyme reaction.

Key Words: Microbead, Microreactor, Photo-polymerization, Enzyme Immobilization

1. Introduction

Microbeads are extensively applied in chemistry and biology[1-2]. We have developed a microfluidic fabrication method to continuously manufacture biocatalyst containing polymeric microbeads. The PDMS and pulled micro glass pipette based apparatus is constructed for the fabrication of the microbeads. By introducing a photo-polymerizable sample fluid containing bio-catalysts and an immiscible sheath fluid with an appropriate flow rate, the polymerizable droplets are hydrodynamically produced inside the apparatus and are polymerized by *'on the fly'* photo-polymerization [3]. The fabricated beads are then incorporated into a different microfluidic channel for the continuous detection of glucose.

2. Principles

Fig. 1 demonstrates the schematic diagram of apparatus to fabricate microbeads and it is constructed by merging a PDMS substrate with preformed center hole and a pulled glass micropipette. The photo-polymerizable solution which is uniformly mixed with enzymes (glucose oxidase(GOX) and horseradish peroxidase (HRP)) enters into the inlet 'A' of the device, while the immiscible mineral oil is introduced into the inlet 'B' as a sheath flow. By the regulation of both flow rates, the micro droplets are generated at the merging position 'C', and travel through the outlet pipette. Via continuous UV exposure onto the outlet pipette, the flowing droplets are polymerized and transported out of the apparatus without touching the inner surface of pipette.

3. Experimental

As a photo-polymerizable solution, the mixture of 4-hydroxybutyl acrylate(85wt.%, Sigma-Aldrich), acrylic acid (11wt.%, Sigma-Aldrich), ethyleneglycol dimethacrylate (1wt.%, Sigma-Aldrich), and 2,2'-dimethoxy-2-phenyl-acetonphenone (3wt.%, Sigma-Aldrich) is used. Both the photo-polymerizable solution and the mineral oil are introduced utilizing the infusion pumps (CMA, 102). To make the pulled micropipette, the glass micropipette (outer and inner diameter: 1 and 0.5 mm respectively) is stretched by employing a micropipette puller (P-97, Sutter Instrument Co.), and its tip is cut in the range of 20 - 40 μm using micro forge (MF-900, Narishige). The prepared PDMS substrate and the pulled micropipette are exposed to an oxygen plasma for the surface treatment and combined by inserting the pulled pipette into the center hole using methanol as a lubricant, and bonded at appropriate position after curing 4 hrs at 80°C on the hotplate. The hole for the sheath flow injection is cored out using a 12 gauge needle. At the opposite entrance of the center hole, a

normal (non-pulled) micropipette is inserted and bonded in the same way providing an outlet for the polymerized microbead.

4. Results and discussion

The sequential micropraphs showing the creation and separation of colored droplets (dyed with Rhodamin B) containing photo-polymerizable solution at the tip of the glass pipette are illustrated in Figure 2. Owing to the introduction of sample flow, the size of droplet at the tip of pulled glass increases, and it is separated when the pressure of sheath flow becomes larger than the surface tension at the tip. The diameters of droplets are determined mainly by the tip size and the sheath flow rate, and their relationship is illustrated in Figure 3. The sample flow rate is fixed at 1 μl/min, and the sheath flows varied from 50 to 300 μl/min in step of 50 μl/min. The size of microbead is decreased as the sheath flow rate increases indicating that the droplets are separated before fully growing due to the increased pressure of sheath flow. The tip size also influences the dimension of the microbead. As the tip size increases, the diameter of microbead increased due to an increase of surface tension. The separated droplets travel through the channel without touching the inner wall of channel, and are polymerized by exposure to 365 nm UV light. The micrograph of polymerized microbeads is taken by scanning electron microscopy (Mitshbishi, S-4300) (Figure 4). Their surface is smooth due to the phase separation between the sample fluid and mineral oil. Other factors, such as viscosity and sample flow rates, were also investigated, but they are less significant than sheath flow rates and tip size.

Fabricated microbeads are incorporated into the microchannel as shown in Figure 5(a), and the aqueous solution containing glucose, buffer and Amplex Red is introduced using a syringe pump. The fluorescence was produced by exiting GOX/HRP on the CNT at 543 nm, and the micrograph in Figure 5(b) implies the sensing of glucose.

5. Conclusions

The new easy and cost effective fabrication method of polymeric microbead entrapping biocatalyst is developed. The feasibility for the glucose sensing is demonstrated through the experiment using microreactor chip. The bead size can be changed by the regulation of sheath flow rate, and various functional beads can be produced by mixing other chemical or biological material into the prepolymer solution. Based on these technologies, one can realize a multiple sensing microreactor by utilizing various sized beads containing diverse enzymes, such as glucose oxidase or lactate oxidase, etc.

Acknowledgements

This study was funded by Dankook Medical Laser Research Center.(R12-2001-050-07002-0)

References

[1] G. H. Seong, R.M. Crook, 2002, *J. Am. Chem. Soc.* **124**, pp 13360-13361
[2] T. Richter, L.L. Shultz-Lockyear, et al., 2002, *Sens. Actuators B* **81**, pp 369-376
[3] W.J. Jeong, S.H. Lee, et al., 2004, Proceeding of μTAS 2004 (in press)

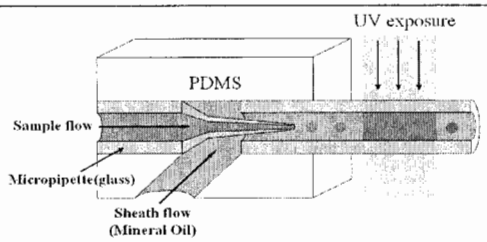

Figure 1. Schematic of apparatus to fabricate microbeads

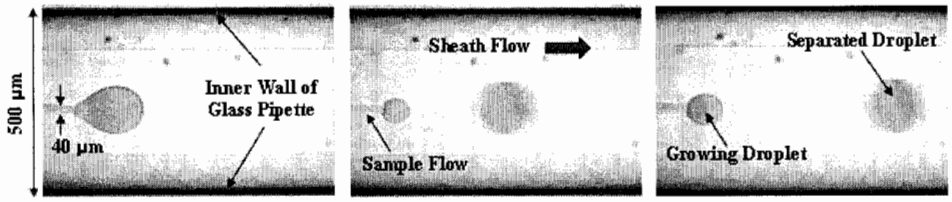

Figure 2. Sequential images of the creation and separation of colored droplets

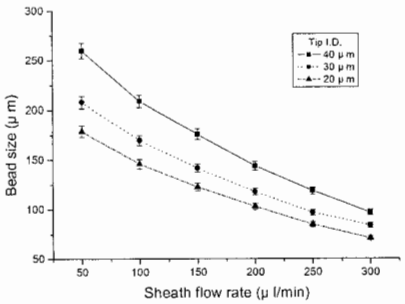

Figure 3. Bead size to the sheath flow rate and tip size

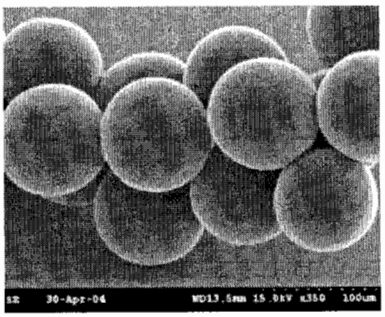

Figure 4. SEM image of microbeads

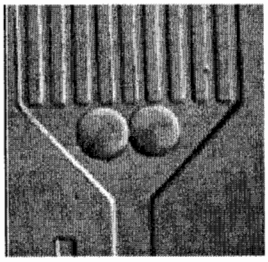

a) Microbeads in the microchannel

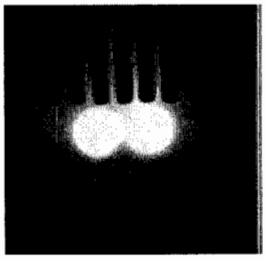

b) Fluorescent image of microbeads

Figure 5. Microreactor embedding functionalized microbeads

FABRICATION OF A NOVEL CELL ARRAY ON ULTRA THIN HYDROPHILIC POLYMER GRAFTED GEL BY UTILIZING UV EXCIMER LASER

Yoshikatsu Akiyama[1, 3], Shintaroh Iwanaga[2, 3], Masayuki Yamato[1, 3], Akihiko Kikuchi[1, 3], Kiyotaka Sakai[2] and Teruo Okano[1, 3]

[1] *Institute of Advanced Biomedical Engineering and Science, COE Program for 21st Century, Tokyo Women's Medical University, 8-1 Kawada-cho, Shinjuku-ku, Tokyo, Japan*

[2]*Department of Applied Chemistry, Waseda University, 3-4-1 Okubo, Shinjuku-ku, Tokyo, Japan*

[3]*CREST, Japan Science and Technology Agency (JST), Kawaguchi, Saitama, Japan*

Keywords: acrylamide, electron beam, ultra thin gel, excimer laser, cell patterning

1. Introduction

Micropatterning of living cells has made new contributions to basic cell biology, cell-based bioelectronics and tissue engineering because the spatial control of cell adhesion, and growth of cells is extremely important in these fields. Several methods are reported to achieve micropatterned surfaces, including photolithography, microcontact printing, microfluidics, and utilization of elastomeric membranes having many holes. Although the use of polymers simplifies fabrication of micropatterns and reduces the cost for disposable bioassay devices, these methods are intricate because of several serial steps necessary for these micropatterned surfaces.[1] For example, in microcontact printing, patterned surfaces are made with stamps made from master forms. Preparing these serial tools requires time and effort.

We have previously utilized electron beam (EB) polymerization and grafting for surface modification with polymers including the temperature-responsive polymer, poly(*N*-isopropylacrylamide) [2], and a cell-repellent hydrophilic polymer, poly(*N*, *N*-dimethylacrylamide). Advantages of EB irradiation lie in its simple protocol for covalent polymer grafting. Only three steps are involved: spreading a monomer solution onto a surface, EB irradiation, and subsequent washing and drying [2]. In the recent report [3], we have described a novel method for processing cell arrays using PIPAAm-grafted tissue culture polystyrene (TCPS), on which PIPAAm-grafted domains inhibit cell adhesion even above the PIPAAm collapse transition because of excess PIPAAm EB grafting, followed by laser ablation.

In the present study, polyacrylamide (PAAm), a well-known hydrophilic and cell repellent material, is grafted onto TCPS by EB irradiation. Beginning with PAAm-grafted TCPS, 30 mJ/cm^2 of UV excimer laser ablation produced a pattern, and 15 μg/mL of fibronectin (FN) was then exposed to pattern. This surface pretreatment was evaluated for cell adhesion to patterned domains to realize micropatterned cell arrays. In addition, we further investigated the influence of the micropatterned domain size on the number of adherent cultured cells, since the spatial control and pattern duration of cell adhesion are both important for cell-based devices.

2. Experimental

PAAm was covalently grafted onto surfaces of TCPS dishes utilizing EB irradiation. Acrylamide monomer dissolved in a mixture of methanol and 2-propanol (1:1 (vol/vol)) at 25 wt% is spread uniformly over each TCPS dish, and immediately subjected to EB irradiation at 0.3 MGy. PAAm-grafted TCPS dishes (PAAm-TCPS) were washed with distilled water to remove unreacted monomer and ungrafted polymers, and then dried under vacuum at 40°C. Wettability of PAAm-TCPS surfaces and density of grafted PAAm were determined by contact angle meter and ATR/FT-IR spectroscopy, respectively. UV excimer laser was utilized for exposure of basal TCPS domains.

The depth of the ablated domains was measured for estimation of thickness of the grafted PAAm layers by AFM.

3. Results and discussion

We have utilized EB irradiation to fabricate hydrophilic, cell non-adhesive PAAm-grafted surfaces as a base substrate for cell array preparation. Grafted PAAm alters the relatively hydrophobic TCPS surfaces to highly hydrophilic (9.3 ± 0.7°, $cos\theta = 0.99$). ECs did not adhere to the PAAm-grafted TCPS surfaces, remaining cells maintaining rounded shapes (Fig. 1). These results demonstrate that PAAm-modified surfaces are hydrophilic and maintain cell-repellent character in culture.

In order to expose basal cell-adherent TCPS domains within grafted PIPAAm surface matrices, mild UV excimer laser fluence (energy below 50 mJ/cm^2) was used to avoid polymer debris formation adjacent to the ablated zones, and surface chemical property changes.[3] Successful array formation was previously evidenced by selective adsorption of the hydrophobic fluorescent dye, $DiIC_{18}(3)$, onto the laser-exposed TCPS regions. This technique was applied for microfabrication of PAAm-grafted TCPS surfaces. Ablated samples were then stained with the fluorescent dye, $DiIC_{18}(3)$. Relative fluorescent intensities of each ablated domain indicates that successful removal of the grafted PAAm layers and exposure of the base TCPS is readily achieved. The depth of ablated domains with this laser fluence was estimated to be 33.6 ± 2.1 nm by AFM measurement, suggesting that the grafted PAAm layer thickness is also ultrathin, similar to that reported for EB-grafted PIPAAm. Furthermore, AFM images showed no detectable debris formation.

Preincubation of ablated dishes with FN solutions at different concentrations (0-20 μg/mL, respectively) influenced subsequent EC adhesion behavior from serum-containing media onto ablated PAAm-TCPS surfaces (Fig. 2a-c). On modified surfaces incubated with 10 μg/mL of FN, ECs did not adhere to ablated domains (Fig. 2a) while they adhered readily to both ablated and non-ablated surfaces preincubated with the higher 20 μg/mL FN concentration solution (Fig. 2c). Under this FN condition, ECs attached and spread on both exposed TCPS domains and protein-adsorbed PAAm-TCPS regions. By sharp contrast, ECs were observed to selectively adhere to the ablated areas preincubated with higher concentration 15 μg/mL FN solution (Fig. 2b). These results indicate that FN adsorption occurred primarily to exposed TCPS domains but insufficiently to unablated PAAm-TCPS surfaces to support cell adhesion, and also suggest that appropriate conditions for FN preadsorption are necessary to selectively introduce the cells only onto the ablated domains for cell-based arrays. Using the appropriate condition, we investigated the influence of ablated domain size on the number of cells adhered within each domain. For 20-μm square domains, nearly 90% of the domains successfully contained only one EC. The numbers of ECs per domain tend to increase with increasing domain size, with increasing population distributions.

4. Conclusions

We have successfully developed and demonstrated a convenient and economical cell array fabrication method using EB irradiated PAAm polymerization and local laser ablation patterning techniques. This surfaces modification method has the advantages of broad substrate applicability, high pattern fidelity, long life spans for patterned cells, and reduced fabrication costs to produce miniaturized cell-based devices, high speed cell-based biomolecular analysis, disease diagnosis, and tissue engineering applications.

References

[1] Mrksich M, Dike LE, Tien J, Ingber DE, Whitesides GM. Using microcontact printing to pattern the attachment of mammalian cells to self-assembled monolayers of alkanethiolates on transparent films of gold and silver. Exp Cell Res 1997; 235: 305-313.

[2] Yamada N, Okano T, Sakai H, Karikusa F, Sawasaki Y, Sakurai Y. Thermo-responsive polymeric surfaces; control of attachment and detachment of cultured cells. Makromol Chem Rapid Commun 1990; 11: 571-576.

[3] Yamato M, Konno C, Koike S, Isoi Y, Shimizu T, Kikuchi A, Makino K, Okano T. Nanofabrication for micropatterned cell arrays by combining electron beam-irradiated polymer grafting and localized ablation. J Biomed Mater Res 2003; 67A; 1065-1071.

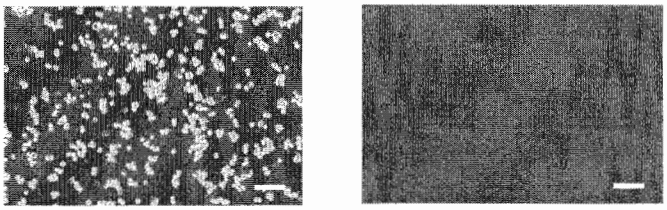

Figure. 1 Phase-contrast microscope photographs of ECs cultured on (left) PAAm-TCPS (right) after serum-containing culture medium changes. ECs were cultured for 2 days at 37°C. Scale bar: 250 μm.

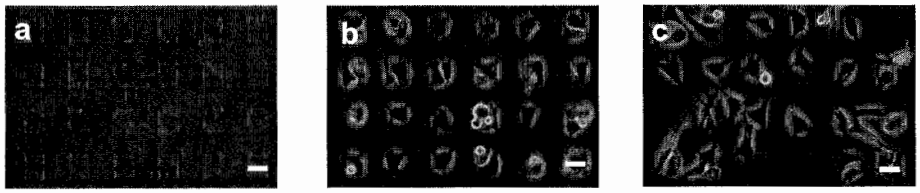

Figure. 2 ECs cultured on ablated PAAm-grafted TCPS for one week in DMEM/10% FBS. PAAm-TCPS was pre-incubated with FN at (a) 10 μg/mL, (b) 15 μg/mL, and (c) 20 μg/mL for 2 h at 37°C prior to cell seeding in DMEM/10% FBS. Morphology of the ablated domain (30×30 μm square) was observed in (a). Scale bar: 30 μm.

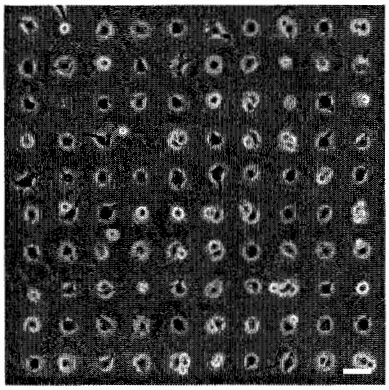

Figure. 3 ECs cultured on ablated PAAm-TCPS surfaces with different laser-patterned domain sizes for 2 days. Domain sizes are 20 × 20 μm. Unattached or poorly attached ECs on these surfaces were removed by medium changes before taking microscope photographs. Scale bar: 50 μm

HYDROGEL BASED ENVIRONMENTS FOR BIOMOLECULAR INTERACTION STUDIES

Jaisree Moorthy[1], Veit Bergendahl[2], Richard R. Burgess[2], David J. Beebe[1]
[1]*Department of Biomedical Engineering,* [2]*Department of Oncology*
University of Wisconsin, Madison, WI 53706, USA

Keywords: crowding, FRET, RNAP, photo-polymerization

1. Introduction

Understanding the network of biomolecular interactions within cells is at the forefront of current "omics" research. However, in addition to *in silico* approaches, it is important to quantify the interactions in the context of their immediate physical environments, viz. the natural cellular milieu that is inherently crowded [1]. While microfluidics-based platforms allow for efficiently transporting reagents to specific locations in the device and at specific times during the course of the assay, there is a need for a model environment that can mimic the cytoplasm. Since it is difficult to recreate the cell interior and the dynamic behaviour therein, biomolecular interactions may be characterized in a large array of different environments each modelling a spatial or temporal state of the cell. Here, we explore the use of hydrogel (hydrophilic cross-linked polymer) posts as model environments for studying the interaction between sigma and core subunits of RNA polymerase (*E. coli*) via fluorescence resonance energy transfer (FRET). When the sigma subunit binds to core, a holoenzyme is formed that is capable of specifically binding to the initiator site on the DNA. Characterizing the sigma-core interaction in various environments would be useful for developing drugs against bacteria and understanding the transcription process [2]. As a first step, the crowding inside the cell will be mimicked with hydrogel posts of varying monomer composition. The microfluidic based cell mimic platform will find applications in proteomics where protein networks can be characterized in a high throughput manner in *in vivo* - like environments. The ability to more accurately predict *in vivo* interactions via *in vitro* tests could have a dramatic impact on the drug development field.

2. Background

Most biochemical interactions are studied in solution phase where the concentration of the molecules is dilute. Given the complexity of the cellular environment, it is often difficult to compare results from these dilute solutions studies to the actual interactions inside the cell. For example, drugs that are designed to interact with specific biomolecules in solution phase may have side effects due to variations in interaction due to the different environment in the cell. Experimental results have shown that there is an order of magnitude affect on the binding of proteins to DNA (*E. coli*), [3] by the presence of background molecules (e.g. globular proteins, polymers). The background molecules limit the space available for diffusion and thus contribute to an increase in the activities of reactants and products. Results from these studies have demonstrated that the binding and enzymatic interaction is amplified (association increased about 10 fold). In an interesting study, it was demonstrated that crowding agents reversed the reaction [4]. In the literature, cell-like crowded environments are created using polymeric solutions (e.g. PEG). Here we propose to use cross-linked polymer (polyacrylamide) [5] so that the 3D construct can be housed inside a microchannel to allow for efficient transport of proteins and chemicals to the posts facilitating high throughput processing.

3. Experimental

Microfluidic channels and polyacrylamide posts were polymerized inside a shallow cavity using liquid phase photo-polymerization [6]. Briefly, in this fabrication approach, a pre-polymer mixture

containing monomer, cross-linker and photo-initiator is introduced into a shallow cavity and the structures (channel wall, posts etc) are photo-patterned by irradiating the mixture through a mask (Fig. 1). The shallow cavity was created by bonding no. 1 cover-slip to a glass slide using a gasket of double-sided pressure-sensitive adhesive (Grace Bio-labs, OR) (150 μm thick). Access holes were drilled on the glass slide using diamond tool-bit. Straight channels (1000 μm wide) were fabricated inside the 'glass-cavity' using iso-bornyl acrylate as the monomer. After removing the unpolymerized material and washing, the pre-polymer mixture for polyacrylamide hydrogel was introduced into the channel. Hydrogel (polyacrylamide) posts (500 μm dia.) were photo-patterned (Fig. 2) from different pre-polymer composition in a sequential manner (i.e. after fabricating a post of specific composition, the excess solution was removed and replaced with a mixture with different composition and patterned). Polymer posts from 5% and 7.5% monomer solution was photo-patterned successfully. After thoroughly washing the posts with buffer solution, 4 μL mixture containing labeled core (Alexa 488 – donor) and sigma-32 (ic3 – acceptor) proteins (~ 2 picomoles of each) was introduced into the channel and allowed to equilibrate in the presence of the posts for a period of 15 hours. Control tests where only one protein is present in the mixture were also incubated with the hydrogel post for the same duration (Fig. 3A). The intensities at donor and acceptor emission wavelengths were recorded and the signal due to FRET was calculated using Metamorph software (Universal Imaging, PA).

4. Results and discussion

FRET occurs when two proteins labeled with suitable dyes are in close proximity (1-10 nm) and the excitation of an acceptor dye overlaps sufficiently with the emission of the donor dye. This energy transfer was measured by the observation of acceptor sensitization. Fig. 4 shows the line-scan of the fluorescence intensities of the images (FRET and control). These preliminary images suggest that a higher fraction of the proteins interact (i.e. are in close proximity) inside the hydrogel in comparison to the solution. This could be due to higher local concentration of biomolecules inside the hydrogel as smaller volume is available to the proteins.

5. Conclusions

We have demonstrated the feasibility of using polyacrylamide hydrogel posts as reaction environments for high throughput protein-protein interactions studies in a microfluidic-based platform. Further studies to characterize the interaction in hydrogels with different cross-link densities will provide a library of interactions in cell mimics that represent various spatio-temporal states of the cell.

Acknowledgements

The research was supported by the Charles E. Culperper Biomedical Pilot Initiative funded by the Rockefeller Foundation.

References

[1] Minton, A.P., *J. Biol. Chem.*, **276**, 10577-10580 (2001)
[2] Bergendahl, V., T. Heyduk, and R.R. Burgess, *Appl. Environ. Microbiol.*, **69**, 1492-1498 (2003)
[3] Murphy, L.D. and S.B. Zimmerman, *Biochim. Biophys. Acta*, **1219**, 277-284 (1994)
[4] Somalinga, B. and R. Roy, *J. Biol. Chem.*, **277**, 43253-43261 (2002)
[5] Herr, A.E., et al., *Solid-State Sensor, Actuator and Microsystems Workshop*, Hilton Head Island, SC, USA, 71-74 (2004)
[6] Moorthy, J., Beebe, D. J., *Anal. Chem.*, **75**, 292A-301A (2003)

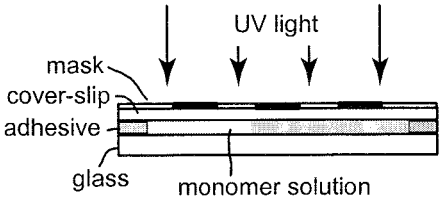

Figure 1. In liquid phase photo-polymerization, the polymeric structures are fabricated inside a cartridge formed from glass and adhesive by irradiating monomer mixture through a mask.

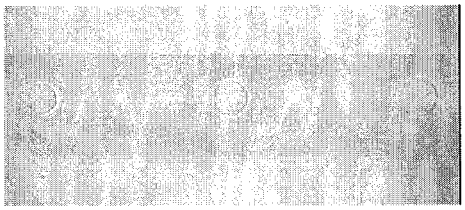

Figure 2. Polyacrylamide hydrogel posts (500 μm diameter) were fabricated inside a channel.

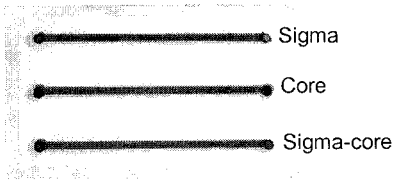

Figure 3. To measure FRET signal, controls with only the donor (core) or acceptor (sigma) molecules were introduced into the channel containing hydrogel posts. The samples were irradiated at 488 nm and 568 nm wavelengths and the emission was measured at 522 nm and 605 nm. The signal due to FRET was computed using image analysis software (Metamorph, Universal Imaging).

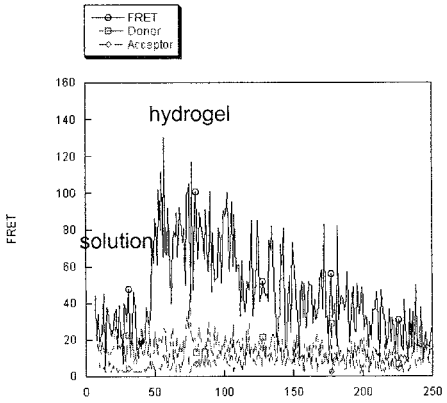

Figure 4. Preliminary result showing line-scan of fluorescence intensities in solution and in hydrogel. Higher intensity is observed inside the hydrogel in comparison to solution probably due to higher effective association inside the hydrogel due to crowding effects on macromolecular activities.

AN IMMUNOASSAY CHIP USING THE ELECTROSTATIC DROPLET MANIPULATION TECHNIQUE

Miyuki Okada, Toru Torii and Toshiro Higuchi
Department of Precision Engineering, Graduate School of Engineering,
The University of Tokyo, 7-3-1, Hongo, Bunkyo-ku, Tokyo, 113-8656, Japan

Abstract

This paper describes an immunoassay chip using the electrostatic droplet manipulation technique. On the lab-on-a-chip device using the electrostatic droplet manipulation technique, droplet containing antibody sensitized beads was merged with droplet containing FITC (fluorescein isothiocyanate) labeled antigen, and the merged droplet was then moved to a water droplet to flush the excessive fluorescence. The antigen-antibody reaction was observed by the fluorescence generated from the beads.

Keywords: Immunoassay, antigen-antibody reaction, Electrostatic manipulation, ELISA, Microdroplet

1. Introduction

ELISA (enzyme-linked immunosorbent assay) is one of the major methods of immunoassay and is a very useful method. However ELISA has some problems such as complexity of the manipulation, length of the reaction time, etc. Recently, immunoassay tool for POCT (point of care testing) is required, particularly in examination of water or examination of meat.

We tried to develop a new lab-on-a-chip immunoassay tool that can get the results quickly and can measure automatically, using the electrostatic droplet manipulation technique[1]. We used the electrostatic droplet manipulation technique, which is the advanced research of our laboratory. Substrate having minute electrodes is dipped in inert solvent and is connected to a power supply (Fig. 1). Sample droplet is conveyed by supplying electric pressure pattern that transit constantly (Fig. 2). This method is economical and is effective for prevention of environment pollution because in this method only a few reagents or samples are needed. Moreover, we can protect droplet of sample/reagent from evaporation or contamination because droplet of sample or reagtent is in an inactive solvent.

In this study, we used antibody-sensitized-polystyrene beads, as shown in Figure 3 in order to manipulate by electrostatic droplet manipulation technique. Figure 4 describes the schematic diagram of our device. We prepared a droplet containing antibody-sensitized beads and a droplet containing antigen that was labeled by fluorescent material on the electrode substrate. First, electric potential is supplied only to electrode A, and the two droplets moved and collided together. At this time, the beads emit fluorescence by antigen-antibody reaction. After the collision, electric potential was supplied to both electrode A and B and the merged droplet move to the water droplet to dilute the excessive antigen. Then, we observed the beads' fluorescence by fluorescence microscope.

2. Experimental

At first, the manipulation capability of the droplet containing beads was examined. In this experiment, polystyrene beads having diameter of 4.5 μm was used. Different size of droplets containing beads were prepared on the electrode substrate and minimam voltage for the droplet manipulation was tested.

We used antiIgG (anti mouse immunoglobulin G) sensitized minute polystyrene beads having diameter of 4.5 μm (Fig. 3) and FITC labeled IgG (mouse immunoglobulin G). Then as shown in figure 4, the droplet containing antiIgG sensitized beads, having size of 0.5 μl was prepared and the droplet containing IgG, having diameter 0.5 μl was also prepared on the electrode substrate. First,

electric potential was supplied only to electrode A, and the two droplets were moved and collided together. After the collision, electric potential was supplied to both electrodes (A and B) and the merged droplet moved to the water droplet having size of 10 μl. The optimal conditions of dilution for examination under the microscope had already been examined in previous research, so we determined the size of water droplet on the basis of the previous research.

After the dilution we observed beads' fluorescence by fluorescence microscope.

3. Results and discussion

Figure 4 discribes the minimum voltage to manipulate several sizes of droplet containing beads. The minimum voltage was a little higher than that for water droplet manipulation. However the droplet containing beads could be manipulated with not so high voltage.

Figure 6 shows the manipulation process. First, electric potential (pattern "+++---", $\pm 300V_{0\text{-}p}$, frequency 1.0Hz) was supplied to electrode A. After two droplets were marged, electric potential (pattern "+++---", $\pm 350V_{0\text{-}p}$, frequency 1.0Hz) was supplied to both electrode A and B to move the merged droplet to water droplet. As shown in figure 7, beads' fluorescence was observed clearly by fluorescence microscope.

4. Conclusions

In this study, the antigen-antibody reaction was realized on the lab-on-a-chip device and we could observed the antigen-antibody reaction was by the fluorescence generated from the beads. It can be said that we could make the prototype of new immunoassay device for the improvement of ELISA.

A study is undregoing to automate droplet formation, and to apply this device to water examination device.

References

[1] T.Taniguchi et al., "Chemical reaction in microdroplets by electrostatic manipulation of droplets in liquid", Lab on a Chip, 2002, 2, pp.19-23

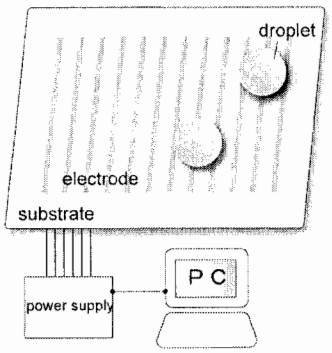

Figure 1:
Concept diagram of electrostatic droplet manipulation device.

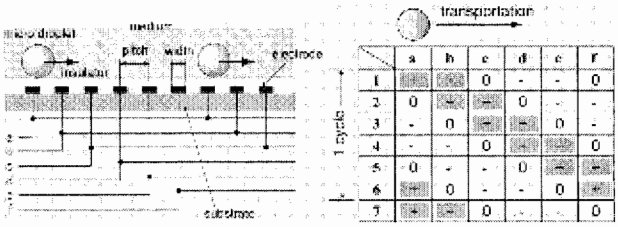

(a) Cross-section diagram (b) Pattern of electric pressure

Figure 2: The basis of the electrostatic droplet manipulation. Droplet is transported by electric pressure pattern that transit constantry.

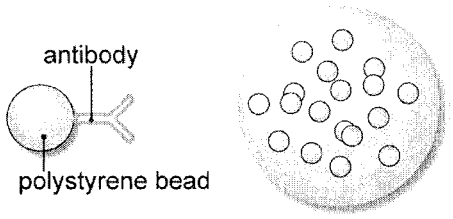

Figure 3: Antigen sensitized bead and droplet containing antibody sensitized beads.

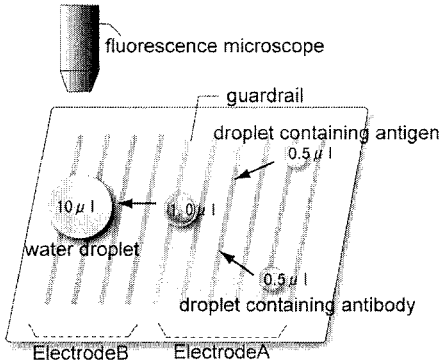

Figure 4: Concept diagram of the device.

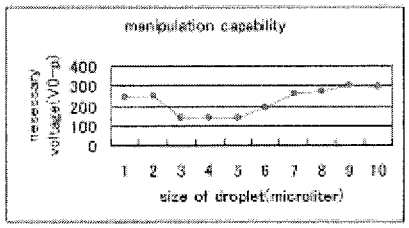

Figure 5: Manipulation capability of droplet containing beads.Droplet having size of 1 to 10 microliter can be manipulated with not so high voltage.

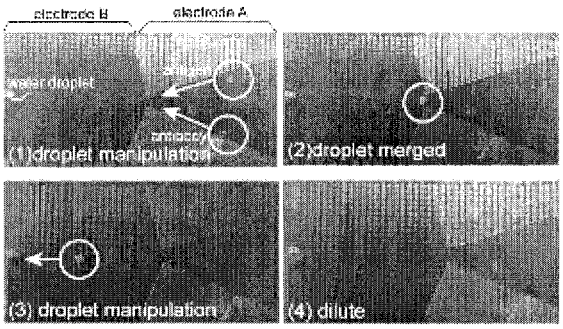

Figure 6: The manipulation process.

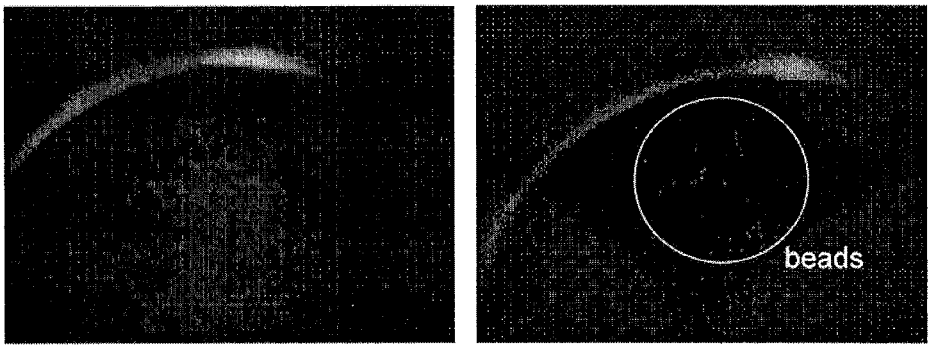

Figure 7: The beads' fluorescence. (a) is the merged droplet without dilution, it was difficult to observe beads' fluorescence because the solvent emits fluorescent. (b) is the diluted droplet. Beads' fluorescence could be observed.

PLANAR LIPID BILAYER CHIP FOR ELECTROPHYSIOLOGICAL ANALYSIS OF MEMBRANE PROTEINS

Hiroaki Suzuki, Kazuhito Tabata, Yasuyuki Kato-Yamada, Hiroyuki Noji, and Shoji Takeuchi

Institute of Industorial Science, The University of Tokyo, 4-6-1 Komaba, Meguro-ku, Tokyo, 153-8505, Japan

Abstract

Planar bilayer membranes have been widely used for electrophysiological analysis of membrane proteins in laboratories. We previously reported that planar lipid bilayer can be reconstituted at 100~150μm tapered hole fabricated in a silicon-based micro-fluidic channel system. However, for the measurement of ion channel current, which requires pico-ampere sensitivity, the substrate material should be non-conductive material to eliminate the electric noise. Thus, we fabricated PMMA plastic based micro-fluidic system made by precise machining. The activity of channel proteins incorporated into the planar membrane is successfully recorded.

Keywords: membrane protein, planar lipid bilayer, electrophysiological recording, PMMA

1. Introduction

Membrane proteins (*e.g.*, ion channel, transporter, receptor) play significantly important role in living organisms. However, handling and analysis of membrane proteins are difficult, since they exist in the lipid membrane structure. Planar lipid bilayer membranes can be artificially reconstituted in laboratory to help electrophysiological analysis of membrane proteins[1]. Conventionally, it is reconstituted at the aperture opened on a thin Teflon sheet with either painting method or LB (Langmuir-Blodgett) method[2]. Target membrane proteins are often incorporated by fusion of protein-containing liposomes. However, both methods are laborious processes and basically restricted to single recording site.

In the previous report[3], we showed that the planar lipid bilayer can be formed on a tapered hole fabricated in silicon-based micro fluidic system. It is reconstituted by flowing the buffer and the lipid solution alternately into the fluidic channels. This method is suitable for the automation and multi-channel analysis. For the recording of channel protein current, which requires pico-ampere sensitivity, silicon substrate had to be insulated with dielectric material. However, a thin dielectric layer worked as a capacitor that received ambient electric noise, despite of the careful electromagnetic shielding.

In this report, we fabricated PMMA (Polymethyl methacrylate) micro-fluidic chip for the planar lipid bilayer reconstitution. We chose PMMA because it is dielectric, optically transparent, and it is easier to machine 3D structures.

2. Design and fabrication

The design of the lipid bilayer chip is practically the same as the one presented in [3]. It has two fluidic channels on both front and back side of the substrate, and they are connected by the tapered hole (Fig. 1). The diameter of smaller aperture, where the bilayer is to be formed, is typically 100~200μm. The device is fabricated by the automated machining system (Modia systems, MM-100) according to the design drawn on the 3D CAD/CAM software. Fluidic channels are machined from both sides of 2mm thick PMMA plate (Mitsubishi rayon, Acrylite L), and covered by heat bonding of PMMA plates (Fig. 2).

3. Experimental

The procedure for the bilayer reconstitution is illustrated in Fig. 3. Firstly, buffer (10mM MOPS) is introduced into the upper channel. Its interface stops at the small aperture due to the surface tension. Secondly, lipid solution (20mg/mL asolectin/n-decane) is introduced into the bottom channel and sucked out. At this stage, a layer of lipid solution remains on the water surface. Lastly, buffer is introduced into the bottom channel. The layer of lipid solution gradually becomes thinner after it is sandwiched by buffer, and the bilayer structure is self-assembled at the center of the aperture. In the picture of Fig. 3, the area inside the vague border is bilayer. It is proven to be a bilayer by calculating its dielectric capacitance (0.5 $\mu F/cm^2$). In this process, all flows are driven based on the capillary force in the channel. Syringe pump was not used to minimize the pressure fluctuation across the aperture, which often breaks the membrane.

Figure 4 shows the background noise when the recording circuit is connected as in Fig. 1. Conventional Ag/AgCl electrodes are inserted into the channel inlets and the current between them are recorded with a patch-clamp amplifier (Nihon Kohden, CEZ-2400). Measurement was performed when a thick layer of lipid solution exists at the aperture, so that no current should flow. The dotted line shows the signal for the silicon device which is insulated with 5μm Parylene coating (developed in [3]). The amplitude of the noise exceeded 4 pA in the best case, although the whole setup is carefully grounded and put in the shielded box. On the other hand, it is readily reduced to almost 1pA with a PMMA device.

To prove the ability of single ion-channel recording, Alamethicin is incorporated into the planar bilayer. Alamethicin is a peptide to form voltage-gated ion channels of defined conductance by oligomerization. Liposomes containing Alamethicin is prepared (10mg of asolectin and 1mg of Alamethicin in 200μL of buffer) and introduced into the upper channel. They are spontaneously fused into the planar bilayer and Alamethicin is incorporated. Figure 5 shows the electric current flowing across the bilayer membrane when the potential of 40 mV is applied. The spike-like burst corresponds to the stochastic opening and closing Alamethicin channels. It is proven to be the channel current, since no current is observed when the polarity of the applied voltage is reversed.

4. Conclusions

Artificial planar lipid bilayer is reconstituted in the micro-fluidic chip made of PMMA plastic. S/N ratio of electrophysiological recoding of channel protein is improved approximately 10 times compared with the silicon based device. Alamethicin channel protein is incorporated into the planar bilayer, and the channel current across the bilayer is successfully recorded.

Acknowledgements

The authors are grateful to professor T. Ide in JST for his guidance on the bilayer reconstitution method presented in the references [4] and [5]. This project is supported by the PROgram for the Promotion of Basic Research Activities for Innovative Biosciences (PROBRAIN) under the supervision of the Ministry of Agriculture and Fisheries in Japan.

References

[1] B. Alberts, A. Johnson, J. Lewis, M. Raff, K. Roberts, and P. Walter, Garland Science (2002).
[2] W. Walz, A. A. Boulton, G. B. Baker, Humana Press (2002).
[3] H. Suzuki, Y. Kato-Yamada, H. Noji, and S. Takeuchi, 17th IEEE Int. Conf. MEMS, 272-275 (2004).
[4] T. Ide and T. Yanagida, Biochem. Biophys. Res. Comm., 265, 595 (1999).
[5] T. Ide, Y. Takeuchi, and T. Yanagida, Single Molecules, 3(1), 33 (2002).

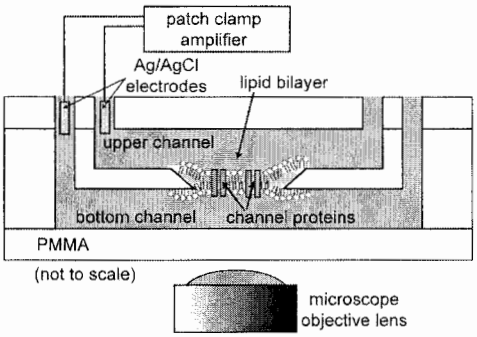

Figure 1. Schematic of the lipid bilayer chip and recording setup.

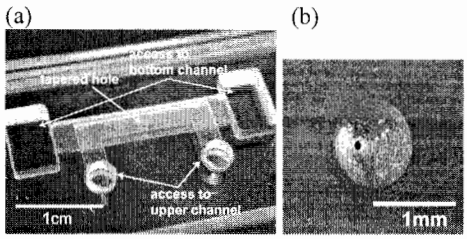

Figure 2. Photographs of PMMA fluidic channels. (a) Overview. (b) Close-up view of the tapered hole.

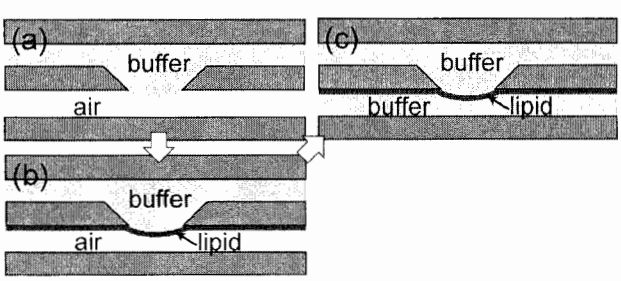

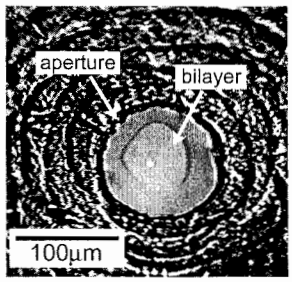

Figure 3. (Left) Sequence of the lipid bilayer formation process. (Right) Photograph of planar lipid bilayer reconstituted at the aperture.

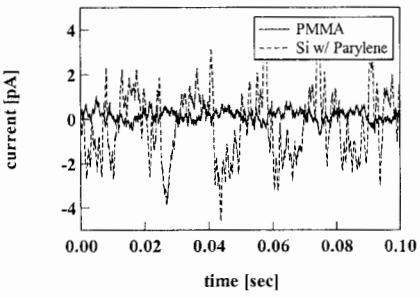

Figure 4. Electric noise level.

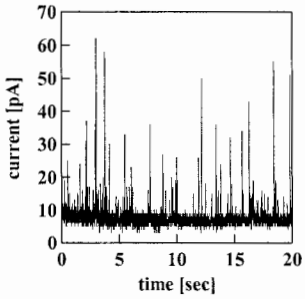

Figure 5. Stochastic burst of the current through Alamethicin channels when 40 mV is applied.

FINE PATTERNING OF PROTEIN WITH PARYLENE SHEET

Kyoko Atsuta[1,2], Hiroaki Suzuki[1] and Shoji Takeuchi[1]

[1]Center for International Research on MicroMechatronics (CIRMM), Institute of Industrial Science (IIS), The University of TOKYO, Meguro-ku, Komaba, 4-6-1, Tokyo, Japan

[2]Central Laboratory , YAMAZAKI BAKING CO., LTD. Sumida-ku, CHitose, 3-15-6, Tokyo, Japan

Telephone: +81-3-5452-6650, Fax: +81-3-5452-6649, E-mail: atsuta@iis.u-tokyo.ac.jp

Abstract

We propose a fine protein patterning technique using a patterned Parylene film on a substrate. This method prevents non-specific binding, and can be performed in the wet condition to avoid drying of proteins. FITC and IC3-PE-maleimid labeled bovine albumin are successfully patterned in 20 x 20 μm^2 spots with 2 μm intervals. Patterning of different materials on different spots becomes possible by introducing sample solution through PDMS micro fluidic channel place on top. This technique will easily be applied to the analysis of protein in an array. We have demonstrated a selective patterning of beads with different fluorescence in 3 x 3 array (80 x 80 μm^2 spots with 50 μm intervals).

Keywords: Fine patterning, selective patterning, Parylene, Non-specific binding, PDMS

1. Introduction

Patterning of bio-molecules in fine grid is an important technical challenge to realize high-throughput and high-sensitive bio-chemical analysis. However, when the size of patterning spot is in micro-meter, it becomes difficult to avoid non-specific binding (i.e., the attachment of samples in an unwanted area). Furthermore, drying of patterned sample becomes a significant problem because of the large surface to volume ratio. It is difficult to avoid these problems without special equipments [1].

Figure 1 illustrates the principle of our patterning technique. Firstly, a thin polymer sheet which has openings in any desired shape is prepared on the substrate (Fig. 1-1). Then, the solution that contains the biological substances is poured (Fig. 1-2). After the excess sample is washed away, the sheet is peeled off (Fig. 1-3). Consequently, the samples stay attached only in the designed area. Protein samples are kept active if the whole procedure is performed in water environment.

In this previous report, we have performed this technique using a perforated 100 μm thick PDMS sheet (PDMS sieve), which has an excellent adhesion onto a glass [2]. The patterning of proteins (FITC-BSA) in 5 x 5 μm^2 area with 150 μm interval was achieved, and the activity of proteins after the sheet removal is confirmed by observing the rotary motion of F_1-ATPase motor protein.

In this report, we employed a Parylene film as a sheet material. Since Parylene can be patterned with photolithography, fine and complicated pattern can be realized. Parylene also has an excellent adhesion on the substrate when deposited, so that the sample solution does not penetrate. Moreover, it can be peeled off without breaking by a normal tweezers, since Parylene has a large tensile strength.

2. Materials and methods

The fabrication and the patterning process are shown in Fig. 2. Parylene-C of 5 μm in thickness is vapor deposited on a glass substrate (Fig. 2a-1). Then, aluminum is deposited as a mask material, (Fig. 2a-2), and Parylene is etched down with oxygen plasma (10 ml/min, 50 W) for 15min. (Fig. 2a-3).

For the microfluidic channel, PDMS is cured on SU-8 mold (Fig. 2b). DOW CORNING 57 additive is added to make the PDMS hydrophilic.

3. Results and discussion

The pictures of patterned Parylene on the glass and the fluorescent images of the patterned bovine albumin (BSA) labeled with FITC (green) and IC3-PE-maleimid (red) are shown in Fig. 3. Unlike the PDMS sheet, it is possible to pattern the openings in arbitrary shape, and the spacing between the neighboring spots can be much smaller than PDMS sheet (less than 10 μm). Figure 4 shows the picture and distribution of fluorescent intensity of patterned BSA in 20 x 20 μm^2 spots with 2 μm spacing in between. it indicates that the sheet effectively prevents non-specific binding to the substrate.

Patterning of different species on different spots becomes possible by combining this technique with a micro-fluidic system made of PDMS. The patterning scheme is illustrated in Fig. 6-a. The PDMS channel is aligned and placed on Parylene which is already patterned. Because Parylene and PDMS are hydrophobic, it was difficult to introduce solutions into the channel. To solve this problem, DOW CORNING 57 additive is mixed to PDMS to reduce its hydrophobicity. In addition, alminum layer is left to make the Parylene surface hydrophilic. The comparison of contact angle on Parylene and aluminum is shown in Fig. 5. Therefore the solutions were introduced into the channel smoothly. With this method, patterning of red, green, and blue fluorescent micro beads is accomplished in 3 x 3 array (80 x 80 μm^2 spots with 50 μm intervals) (Fig. 6b).

4. Conclusions

A fine protein patterning technique is proposed using Parylene polymer sheet. Since Parylene can be patterned with photolithography, fine and complicated pattern can be realized. Excellent adhesion of Parylene on to substrate redounds to this high resolution after etching. Patterning of red, green, and blue fluorescent micro beads is accomplished in 3 x 3 patterned areas. This technique will be applied to the high-throughput analysis of proteins.

Acknowledgements

We thank Dr. Kuniyuki Kakushima and Mr. Ryuji yokokawa for helpful discussion. The part of this research was supported by the PROgram for the promotion of Basic Research Activities for Innovative biosciences (PROBRAIN) under the supervision of the ministry of agriculture and fisheries in Japan.

References

[1] C. S. Lee, S. H. Lee, S.S. Park, Y. K. Kim and B.G. Kim, *Biosens. & Bioelectron.*, 2003, **18**, pp. 437-444

[2] K. Atsuta, H. Noji and S. Takeuchi, *Lab on a Chip*, 2004, in press

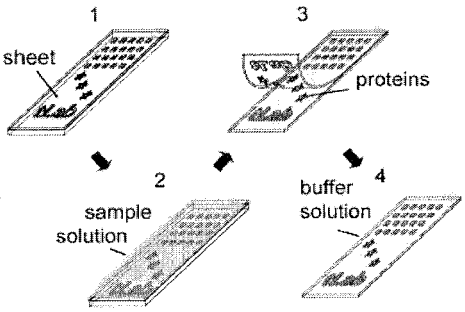

Figure 1. Concept of the patterning method with patterned thin polymer sheet.

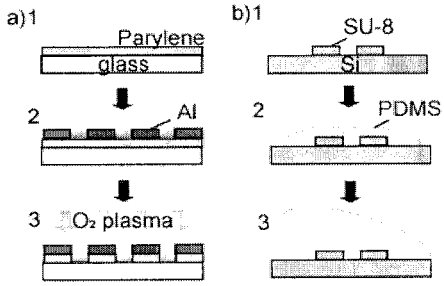

Figure 2. Fabrication process. a) Parylene is deposited and patterned by O_2 plasma with aluminum mask. b) PDMS channel made by SU-8 mold.

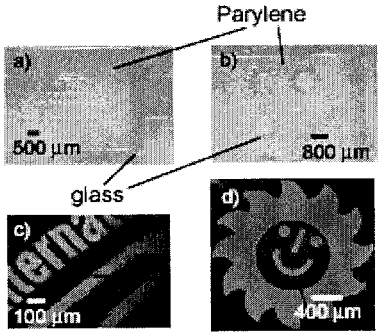

Figure 3. Photographs of Parylene sheets after O_2 etching (a, b), and fluorescent images of patterned bovine albumin (c, d).

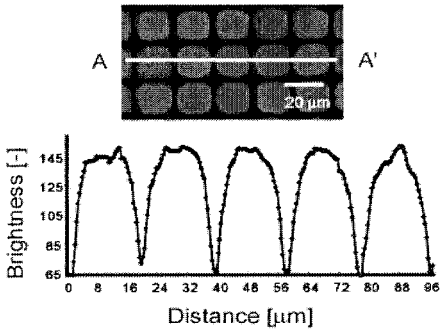

Figure 4. Brightness distribution of FITC-BSA along the line. The uniform distribution in each spot is achieved in 2 μm spacing.

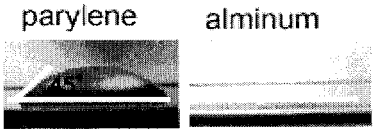

Figure 5. The comparison of contact angle among different surface.

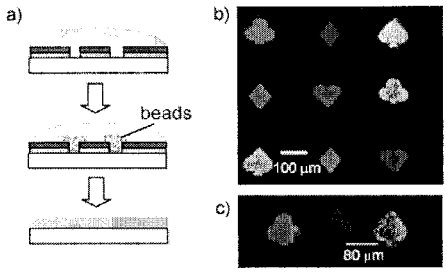

Figure 6. a) Selective patterning using PDMS micro-fluidic channel. b), c) Photographs of the patterned microbeads of three different colors in each spot.

SUSPENDED, POROUS CELLULOSE ACETATE MEMBRANES FOR MICRODIALYSIS USE

George C Lopez[1], **Gary K Fedder**[1,2]
[1]*The Robotics Institute,* [2]*Electrical and Computer Engineering Dept.*
Carnegie Mellon University, Pittsburgh, PA 15213 USA

Abstract

Porous cellulose acetate membranes were suspended over 75 micron wide silicon microchannels. The microchannels are formed when a viscous polymer lacquer is directly spin cast onto etched silicon cavities (Fig. 1). Standard fabrication processes are used to create the channel, preventing the need for adhesives, substrate bonding, or other complex assembly procedures. These microchannels can allow the isolation and concentration of specific biological molecules.

Keywords: cellulose acetate, membrane, microdialysis, porous

1. Introduction

In the area of in vivo bioanalytical measurement techniques, microdialysis involves the use of a porous material to recover biomolecules from tissue [1]. Microdialysis is a sampling method for studying localized metabolic events by monitoring the chemistry of the extracellular space around a point of interest. Conventional microdialysis involves a small polymeric probe with a porous membrane at its tip, which can be used for *in vivo* or *in vitro* studies. When a physiological salt solution is slowly pumped through the microdialysis probe (usually called the perfusate), the solution equilibrates with the surrounding fluid on the other side of this membrane. Currently, conventional microdialysis probes are hand assembled, have limited useable lifetime, and can't provide the necessary temporal resolution for analytical tools due to large dead volume issues.

Porous materials have gained interest in the fields of filtration, drug delivery, protein separation, and microdialysis. Microfluidic devices that serve these application areas are usually obtained by integrating pre-fabricated porous materials into the final device, either by using adhesives or bonding. These fabrication procedures need to include microchannels as well, the fundamental component of most microfluidic systems. This paper presents a novel fabrication method used to create a monolithic microdialysis chip.

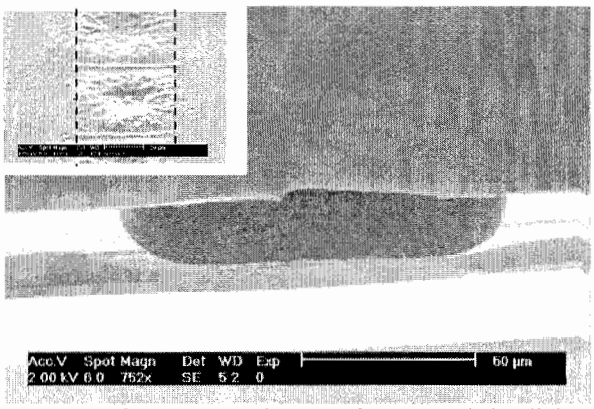

Figure 1. Cross sectional view of a suspended cellulose acetate membrane across a 75 micron wide silicon microchannel. Inset is a top view of the suspended membrane. Dotted lines are used to show the boundaries of the microchannel.

2. Fabrication

A lithography step using photoresist first defines the location where the microchannel will be formed (Fig. 2). The silicon is then etched isotropically using either sulfur hexafluoride or xenon difluoride; the photoresist is subsequently removed using acetone. A viscous polymer lacquer, 10% w/v cellulose acetate in solvent,

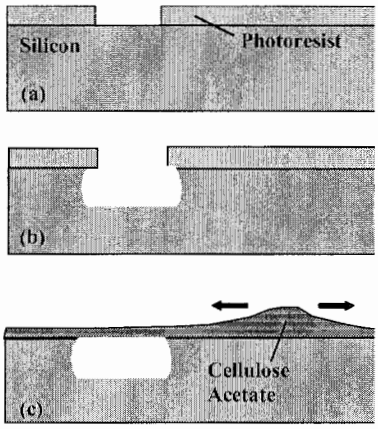

Figure 2. The fabrication process involves (a) using lithography to define the microchannel (b) silicon etching using xenon difluoride with subsequent removal of the photoresist, (c) spin coating cellulose acetate film onto the substrate.

is deposited onto a spin chuck while stationary. The 10% w/v lacquer is formed by mixing cellulose acetate (Eastman Chemicals, CA398-3) with the solvent N,N-dimethylacetamide (DMAc). A spin speed of 2500 RPM for 40 seconds is used to create a 20 micron thick cellulose acetate membrane; thickness can be varied with speed. The sample is then immediately transferred to a room temperature deionized water bath. The polymer undergoes precipitation in the non-solvent water, as the solvent is displaced from the film. The sample is left in the bath overnight to remove any remaining solvent in the film and then allowed to air dry. A semi-clear, conformal polymer coating on the silicon substrate is formed.

2. Theory

Pores are formed in the polymer film by the phase separation process. During the immersion precipitation, the composition of the polymer enters the two-phase region in the ternary phase diagram and phase separation occurs, producing a polymer-rich phase, containing mainly polymer and less solvent, and a polymer-lean phase, containing mainly solvent and less polymer [2]. The polymer-rich phase represents the structural walls of the coating while the polymer-lean phase represents the porous regions in the coating. An asymmetric film is formed that contains a dense top layer that has minimal visible pores and a sparsely porous interior (Fig. 3, right). By varying the polymer concentration, the precipitation medium and temperature, a large variety of pore sizes can be attained.

The polymer's wetting characteristics are largely responsible for its ability to fill or span across a cavity. The main force driving the polymer into a cavity is from capillary action. This is a function of the surface tension of the liquid-gas interface, the contact angle, and the size of the cavity. The main opposing forces include the cohesive forces within the polymer as well the pressure of trapped gas in the cavity. Viscosity has little effect on the ability of the polymer to enter a cavity, yet it does have an effect on the speed at which the polymer enters the cavity.

Stress in these phase separation films are from constrained in-plane shrinkage of the film during drying. The stress when using DMAc as a solvent seems to be lower as compared to using acetone. This is due to the lower volatility of DMAc, causing it to be retained in the coating until the latter stages of drying [3]. Similar coating experiments with acetone resulted in significant cracking and peeling of the polymer film from the substrate. The DMAc may be acting as a plasticizer, keeping the coating modulus lower.

3. Experimental

The cellulose acetate polymer was coated onto microchannels of various widths. The polymer successfully spanned across a microchannel of up to 75 microns in width. It was not possible to span larger openings since tears and openings appeared on the polymer surface as shown in Fig. 4. To create long microchannels it was necessary to place periodic microbridges across the channel. These microbridges are undercut during the etching process (Fig. 3, left). Using SEM and BET adsorption analysis, it was determined that the average pore size is approximately 50nm.

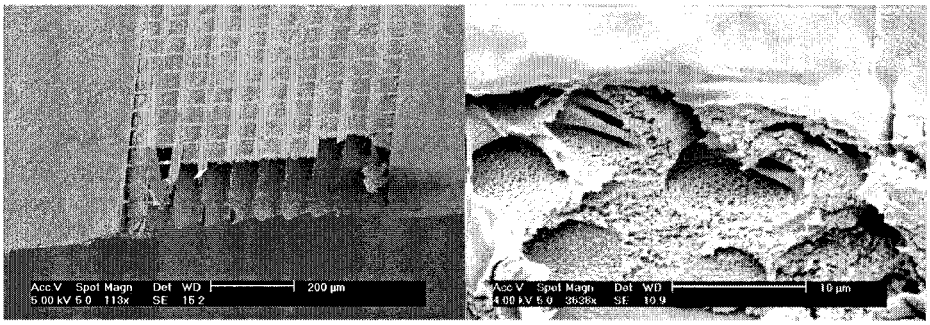

Figure 3. (Left) A cleaved chip showing a set of ten microchannels (50 microns width) are shown coated with cellulose acetate. Periodic microbridges are spaced every 75 microns along a channel. (Right) The immersion precipitation process creates an asymmetric film that has a dense top layer over a sparsely porous interior.

Fluidic interconnect was attached to the inlet/outlet ports to interface with the microchannels. A syringe pump provided a 0.3 µL/min flowrate of PBS buffer while various proteins of different molecular weight were placed above the cellulose acetate to determine its permeability. The outlet port was fractionated and collected for later analysis. The cellulose acetate showed significant permeability to myoglobin (MW=17 kDa) and soybean trypsin inhibitor (20 kDa). Large molecular weight molecules were not able to pass through the cellulose acetate.

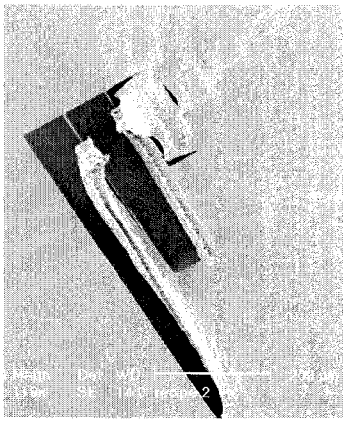

Figure 4. Film stress due to in-plane shrinkage from polymer drying.

5. Conclusions

A porous cellulose acetate film was suspended over a silicon channel using a standard fabrication process of spin coating. Although the polymer undergoes considerable stress during drying, a 75 micron wide cavity was spanned. Permeability tests indicate the ability of low molecular weight molecules to pass through the 20 micron thick cellulose acetate.

Acknowledgements

This work was partially funded by the Defense Advanced Research Projects Agency (DARPA) and Rome Laboratory, Air Force Material Command, USAF, under agreement numbers F30602-99-2-0545.

References

[1] Bergveld, P., Olthuis, W., Sprenkels, A.J., Pijanowska, D., Linden, H.J. van der, Bohm, S. Integrated Analytical Systems, Comprehensive Analytical Chemistry Series, 39, pp. 625-663, 2003

[2] Mulder, M., Basic Principles of Membrane Technology, Kluwer Academic Publishers: The Netherlands, 1996.

[3] Vaessen, D., McCormick, A., Francis, L., Polymer 43(8) 2267-2277 (2002)

On-chip Isoelectric Focusing coupled to Micro Liquid Chromatography in Blood Proteomics

Man Ho Choi[1], Ying-Chih Wang[2], John S. Wishnok[1], Steven R. Tannenbaum[1] and Jongyoon Han[1,3]

[1]Biological Engineering Division, [2]Department of Mechanical Engineering, [3]Department of Electrical Engineering and Computer Science, Massachusetts Institute of Technology, MA 02139, USA

Abstract

An efficient coupling of microchip based isoelectric focusing (IEF) with capillary size-exclusion chromatography (CSEC) and nanoflow electrospray tandem mass spectrometry is described for rapid protein identification from human serum samples. The method includes protein separation by CSEC followed by fractionation, in-solution digestion, isoelectric focusing and isolation on a microchip. Peptides are isolated based on specific p*I* values of interest, and then applied on a precolumn (100 μm ID × 10 mm length) to remove the IEF ampholytes and then separated on an analytical column (75 μm ID × 200 mm). This method decreases sample complexity from the human serum, and increases peak capacity in MS/MS analysis.

Keywords: microfluidics, isoelectric focusing, size-exclusion, mass spectrometry

1. Introduction

Although there have been a number of recent advances in miniaturized isoelectric focusing (IEF) of peptides with the promise of fast and reproducible analyses, their effectiveness is often compromised during sample preparation, especially with real biological samples [1,2]. There is a need for comprehensive pre- and/or post-separation techniques in order for microfluidic systems to be considered reliable tools in proteomics. Here, we describe the combination of capillary size-exclusion chromatography (CSEC) [3] and on-chip IEF that can be manipulated by microfluidic valve systems, followed by nanoflow electrospray tandem mass spectrometry (ESI-MS/MS), for rapid protein identification (Figure 1).

2. Experimental Design

Twenty microliters of human serum was diluted into 480 μL of 50 m*M* NH_4HCO_3 containing 20% acetonitrile (pH 8.5), transferred for concentration of the sample into a Microcon (MWCO: 50 kDa), and centrifuged for 30 min at 12,000 rpm [4]. The filtrate was evaporated and reconstituted in 2 μL of water just before injection. The protein fractions, which were separated by the CSEC column (Superdex 75, 325 μm i.d. × 250 mm length) at 1.5 μL/min flow rate (Figure 1A), were reduced, alkylated, digested with trypsin, and then focused on a microfabricated IEF channel (12 μm depth × 150 μm width × 10 mm length). Using microfluidic valves [5], proteins and peptides with a specific p*I* region can be isolated efficiently and reliably (Figure 1B). An IEF fraction, containing peptides of similar p*I* values, was loaded onto a precolumn (Vydac C18, 100 μm × 10 mm) for removal of the IEF buffer solution at a 3 μL/min flow rate, and then analyzed by ESI-MS/MS through a reverse phase capillary column (Everest C18, 75 μm × 200 mm) at a flow rate of 150 nL/min.

3. Results and Discussion

Prior to injection, ultrafiltration to remove high molecular weight proteins such as albumin was performed. All proteins from human serum were eluted within 30 min when 0.5 μL of samples was injected. Figure 2 shows a representative CSEC chromatogram of human serum that contains proteins less than 50 kDa. The eluent from the CSEC column was collected at 1 minute intervals. These fractions of peptides were diluted with DTT solution (1 mg/mL in 50 m*M* NH_4HCO_3). The fractions were then digested with trypsin for 16 hr at 37°C. The reaction was quenched by freezing the sample and concentrated by lyophilization. Peptides were dissolved in IEF buffer solution containing p*I* markers, 2% 3-10 ampholyte, 10% glycerol, and 1% methyl cellulose and then focused under positive voltage of 0.5 kV/cm for 30 sec. After focusing, peptides were trapped, isolated and introduced into the precolumn by microfluidic valve control. Figure 3 shows isoelectric focusing of the p*I* marker of 4.5 in same experimental conditions used. Further details about microchip IEF can be found elsewhere [5].

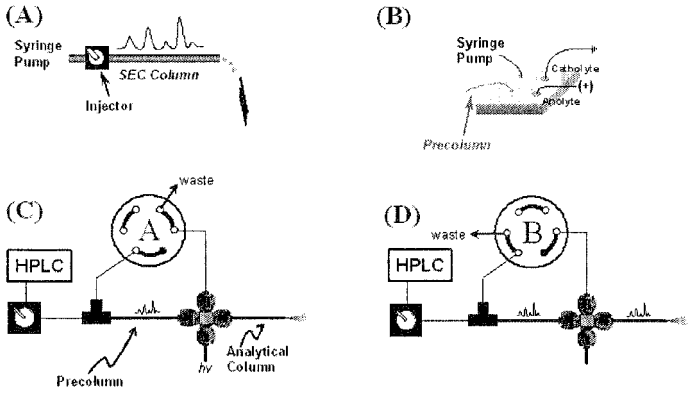

Figure 1. Systematic diagrams of flow paths and valve configurations at (A) sample loading and (B) separation stages.

The LC-MS/MS system as shown in Figure 1 is equipped with a precolumn that is responsible for sample cleanup and rapid sample injection of 0.5 μL at a 3 μL/min flowrate. The precolumn also enabled removal of IEF buffer solution that can interrupt retention of peptides on the column media. Most of the salts and other interfering molecules passed through the precolumn, while peptides were retained on 3 μm particle size C18 packing media (Figure 1C). Two minutes after sample loading, the switching valve was automatically turned to the alternative position so that the pre- and analytical columns were in line for further separation (Figure 1D).

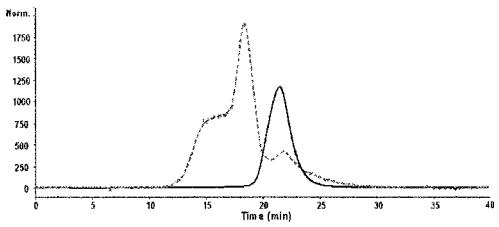

Figure 2. CSEC chromatogram of the serum with 280 nm detection. Aliquots of human serum before (dot) and after (line) ultrafiltration were injected.

The MS/MS spectra were searched against the human proteomic database, using Mascot (Matrix Science). In general, IEF fractionation decreased the complexity of the sample being

being analyzed, resulting in increased peak capacity and dynamic range of detection in MS/MS analysis. Although the sequence coverage of each protein decreased when compared to the results without IEF, the number of proteins identified was increased due to identification of low-abundance peptides, which were not detected in the chromatograms of non-focused samples by eliminating peptide background significantly through the IEF step. This gel-free method allowed better recovery of large and hydrophobic membrane proteins as well as proteins containing extremely low or high p*I* values (4.0 – 12.3), because of the difficulty of solubilizing and resolving these proteins on gels. When a standard solution of trypsin-digested serum albumin was applied to the system, many hydrophilic peptides were purified and several low abundant peptide peaks could be detected and identified after IEF isolation of peptides within the p*I* region of 5 – 7 (Table 1). Although the sequence coverage of albumin decreased from 32.5% to 10.3%, 2 peptides, which were not detected in the sample before IEF, could be identified with high quality scores.

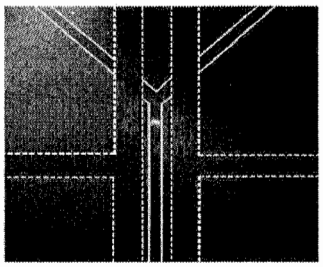

Figure 3. Close view of the trapping region of IEF device microfabricated with focusing channel (line) and control valve (dot).

Table 1. Peptides identified from serum albumin before and after isoelectric focusing and selection of 5<p*I*<7.

Before IEF	p*I* value*	After IEF
FKDLGEENFK	4.68	
LVNEVTEFAK	4.53	
SLHTLFGDK	6.46	SLHTLFGDK
LCTVATLR	8.25	
NECFLQHK	6.74	NECFLQHK
DDNPNLPR	4.21	
YLYEIAR	6.00	YLYEIAR
HPYFYAPELLFFAK	6.75	HPYFYAPELLFFAK
AAFTECCQAADK	4.37	
AEFAEVSK	4.53	
YICENQDSISSK	4.37	
	6.13	**LKECCEK**
PLLEK	6.43	
DVFLGMFLYEYAR	4.37	
RHPDYSVVLLLR	8.75	
QNCELFEQLGEYK	4.25	
FQNALLVR	9.75	
KVPQVSTPTLVEVSR	8.75	
CCTESLVNR	5.99	CCTESLVNR
RPCFSALEVDETYVPK	4.68	
	6.00	**QTALVELVK**

*http://us.expasy.org/tools/protparam.html

4. Conclusion

A novel gel-free separation system, based on CSEC and IEF on a chip, was used for fractionation of protein and peptide mixtures. This method reduced sample preparation time and effort and increased protein coverage, e.g., many hydrophobic proteins as well as extremely high or low p*I* value proteins were identified, which are relatively difficult to analyze by gel-based techniques.

Reference

[1] J. Wen et al., *Electrophoresis*, **21**, 191–197 (2000).

[2] A. Tan et al., *Electrophoresis*, **23**, 3599–3607 (2002).

[3] M.H. Choi, S.R. Tannenbaum and J.S. Wishnok, *The 52nd ASMS Conference on Mass Spectrometry and Allied Topics*, MPX453, Nashville, Tennessee, May 2004.

[4] R.S. Tirumalai et al., *Mol. Cell. Proteom.*, **2**, 1096–1103 (2003).

[5] Y.-C. Wang, M.H. Choi and J. Han, *Anal. Chem.*, in press.

LASER BASED DISRUPTION OF BACILLUS SPORES ON A MICROCHIP

Oliver Hofmann[1], Kirk Murray[2], Alan-Shaun Wilkinson[3], Timothy Cox[3], Andreas Manz[1]

[1] Centre for Analytical Science, Imperial College London, London SW7 2AZ, UK

2 Dstl, Detection Department, Porton Down, Salisbury, Wiltshire SP4 OJQ, UK

[3] QinetiQ, Malvern Technology Centre, Malvern, Worcestershire WR14 3PS, UK

Abstract

We report on the development of a laser based spore disruption method. *Bacillus globigii* spores were mixed with a laser light absorbing matrix and co-crystallized into 200-μm-wide and 20-μm-deep nanovials formed in a polydimethylsiloxane (PDMS) target plate. Surface tension effects were exploited to affect up to 125-fold spore enrichment. When the target zones were illuminated at atmospheric pressure with pulsed UV laser light, a change in spore morphology was observed within seconds. Post illumination PCR analysis suggests the release of endogenous DNA indicative of spore disruption.

Keywords: microchip, spore disruption, extraction, PCR

1. Introduction

For spore forming bacteria, e.g. *Bacillus anthracis*, sonication devices have recently been proposed to extract DNA from within the spore for subsequent PCR analysis.[1,2] Here we present an alternative approach comprising a microchip for laser induced spore disruption and concurrent extraction of desorbed DNA (Figure 1). The spore sample is first mixed with an aqueous solution of laser light absorbing matrix and a drop is applied onto a target plate nanovial. Upon evaporation the drop remains pinned to the nanovial due to surface tension effects and spores/matrix co-crystallize into the vial. Drop volumes larger than the nanovial result in spore enrichment. A PDMS flowcell with a microstructured channel is then attached to the target plate. Illumination of the sample zone with pulsed UV laser light affects an explosive disintegration of the matrix with concomitant disruption of the outer spore layers. Endogenous DNA is protected from UV damage through unique small acid-soluble spore proteins (SASPs) and dipicolinic acid (DPA), a major constituent of the spore coat and core. For sufficiently high laser energies, spore fragments and released endogenous DNA are also desorbed and redeposited onto the inner walls of the adjacent flowcell microchannel. The released DNA can be recovered by flushing the microchannel with PCR reagents for subsequent amplification. This integrated approach combines ultrafast spore disruption with enrichment and amplification steps for high sensitivity.

2. Experimental

B. globigii spore suspensions were provided by DSTL (Porton Down, UK). To remove any extra-cellular DNA, a hypochlorite based spore surface decontamination procedure was implemented [2]. 0.1 μL of 10^8 cfu/mL pretreated *B. globigii* spores were then mixed 1:1 with 10 mg/mL 3-hydroxypicolinic acid (HPA) matrix in 40 v/v-% acetonitrile and applied onto a 200x200x20 μm nanovial molded in PDMS. Upon solvent evaporation a solid deposit of analyte (spore)-doped matrix was obtained in the nanovial. For first experiments the sample zone was directly illuminated for ~1 s with the output of a 6 mW nitrogen laser (VSL-337 ND-S, Laser Science, Franklin, MA). A 200 μm-ID optical fibre was connected to the laser via a Hyrax coupler. For spore illumination the fibre was positioned ~1 mm above the sample zone, resulting in an effective beam diameter of ~1 mm and an energy density of ~50 $\mu J/cm^2$ (laser set-up 1). In order to also induce desorption, the optical set-up was modified to an open beam configuration. The laser

beam was focused onto the target zone with a plano-convex fused silica lens with 30 mm focal length (Laser 2000, UK). This resulted in a beam diameter of ~0.2 mm and an energy density of ~170 mJ/cm^2 (laser set-up 2). After illumination the sample zone or any deposited material in the microchannel were redissolved in 1 μL sterile water and added to 12.5 μL of 2x PCR master mix (DNAmp, BioGene, UK), 2.5 μL forward primer (ACT TCG AGG TGC GTG AAC G, Oswell, UK), 2.5 μL reverse primer (TGG AAT TTC GAT TTC TTC ACC TG) and 6.5 μL sterile water. Non-illuminated spore/matrix targets served as negative controls. 35 cycles were run on a PCR System 9700 (Gene Amp). Melting was achieved by heating at 95° C for 10 s, extension at 60° C for 10 s, and annealing at 74° C for 20 s. The final step was an extension at 72° C for 5 min. Sizing of the PCR mix after amplification was performed on a Agilent 2100 Bioanalyzer.

3. Results and discussion

Initial experiments were concerned with obtaining well defined, spore containing target zones in the PDMS nanovials. Borrowing techniques developed for MALDI-MS the spores were embedded into a laser light absorbing matrix. 3-HPA was chosen as a suitable matrix due to high UV absorption, low fragmentation effects on target DNA and good solubility in water. It should be noted that in contrast to MALDI-MS, ionisation is not critical for laser induced spore disruption. For sample application, a dried droplet method yielded excellent target zone confinement and uniform, dense deposits within 4 min. Since 0.1 μL of sample/matrix mix were evaporated into a 0.8 nL nanovial, a 125-fold enrichment was achieved under these optimised sample application conditions. Spore disruption experiments were performed with ~10,000 *B.globigii* spores in the nanovials. In first illumination experiments with laser set-up 1, desorption was *not* observed. The illuminated sample zone was redissolved in 1 μL sterile water to perform PCR (Figure 2). The observed product peak clearly indicates the release of endogenous DNA during laser illumination. Furthermore, electron micrographs of the illuminated zone confirmed a change in spore morphology. In order to also induce desorption, the effective laser energy on the sample zone was increased from 50 μJ/cm^2 to ~170 mJ/cm^2 by using an open beam configuration with focusing optics (laser set-up 2). First experiments with the new set-up revealed complete desorption of the sample zone within seconds, and deformed and apparently deflated spores, indicative of near complete disruption (Figure 3).

4. Conclusions

The developed method offers ultra-fast spore disruption and goes some way in addressing sensitivity requirements through on chip spore enrichment and DNA amplification steps. The observed desorption at higher laser energies opens up a route towards the direct extraction of released DNA into a flowcell, e.g. via a vertical air / liquid layer interface.

Acknowledgements

This research was supported by the Materials Domain of the UK MoD Corporate Research Program. (c) Contents include material subject to Crown Copyright 2004 Dstl.

References

[1] M.T. Taylor, P. Belgrader, B.J. Furman, F. Pourahmadi, G.T.A. Kovacs, M.A. Northrup, *Anal. Chem.*, **73**, 492-496 (2001).

[2] D.P. Chandler, J. Brown, C.J. Bruckner-Lea, L. Olson, G.J. Posakony, J.R. Stults, N.B. Valentine, L.J. Bond, L. J. *Anal. Chem.*, **73**, 3784-3789 (2001).

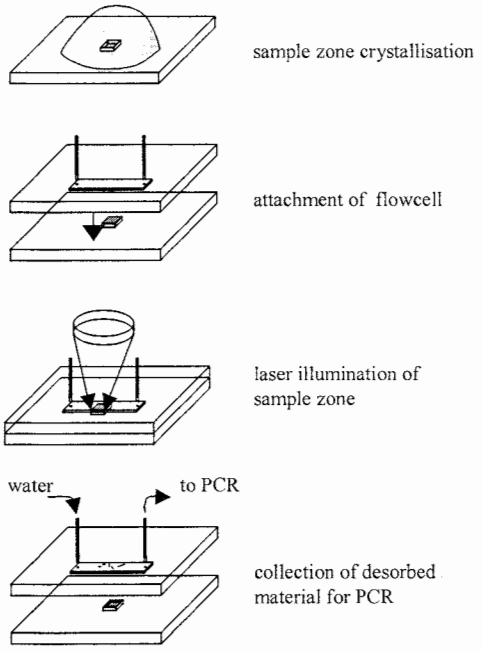

Figure 1. Schematic of laser based spore disruption and extraction of desorbed material including spore fragments and endogenous DNA.

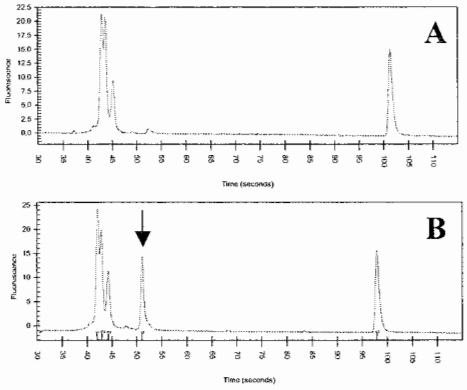

Figure 2. PCR results for laser illumination of *B. globigii* spores. Spore/matrix zone was redissolved in 1 µL of sterile water and directly added to PCR master mix. (A) Negative control: 10^8 cfu/mL surface decontaminated spores, no laser illumination. (B) 10^8 cfu/mL of pretreated spores after ~1 s laser illumination at 30 Hz with laser set-up 1. Peaks 1-5 correspond to lower sizing marker, forward primer, reverse primer, *B. globigii* product and higher sizing marker, respectively.

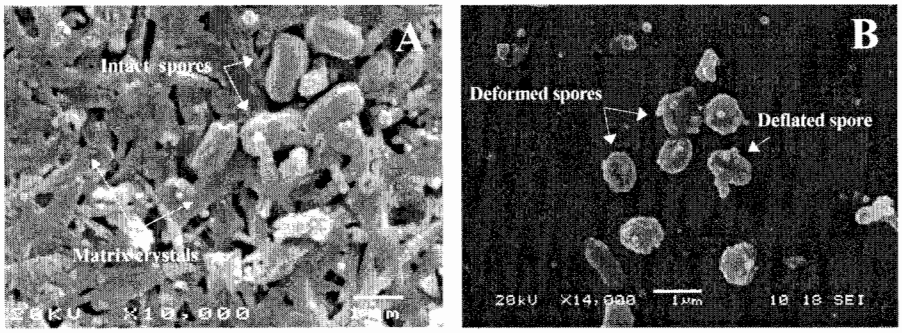

Figure 3. SEM images of spores before and after laser illumination. (A) 10^8 cfu/mL *B. globigii* spores embedded in 10 mg/mL 3-HPA matrix. (B) *B. globigii* spores desorbed from nanovial and deposited into flowcell microchannel after 2 min laser illumination at 30 Hz with laser set-up 2. For (B) MALDI matrix was not employed to facilitate interpretation of deposited fragments.

CULTIVATION OF COS7-CELLS USING EXTRACELLULAR MATRIX IN 3D MICROFLUIDIC SURFACE ENLARGED STRUCTURE

Thomas Frisk*[,1], Susanna Rydholm*[,2], Helene Andersson[1], Hjalmar Brismar[2], Göran Stemme[1]

* T.F. and S.R. contributed equally to this work.

[1]*Department of Signals, Sensors and Systems, KTH, SE-100 44 Stockholm, Sweden*
[2]*Department of Physics, KTH, SE-106 91 Stockholm, Sweden*

Abstract

This paper presents a novel method to cultivate cells in a controlled 3D surface enlarged micro-environment. The 3D environment is achieved by insertion of a gel-like extracellular matrix (ECM) mixed with cells into a micromachined silicon fluid structure. Shrinking of the gel enables further flow through the channel. Due to the structure design the shrinking is non-uniform, which results in an increased surface area. With the proposed design cells are alive and viable after 72 h of incubation within the chip.

Keywords: 3D-cultivation, matrigel, ECM, microfluidic structure

1. Introduction

Cellular patterning is a necessary component for tissue engineering and fundamental cell biology studies. One of the greatest challenges in tissue engineering is the difficulty of distributing all cells in a thick (3D) living structure. This paper presents a novel method to cultivate cells in 3D in a micromachined silicon fluid structure. With microsystem technology it is possible to build more complex and smaller cavities, which results in smaller volumes than previously shown "molded PDMS-channels" [1] for cell growth and cell studies.

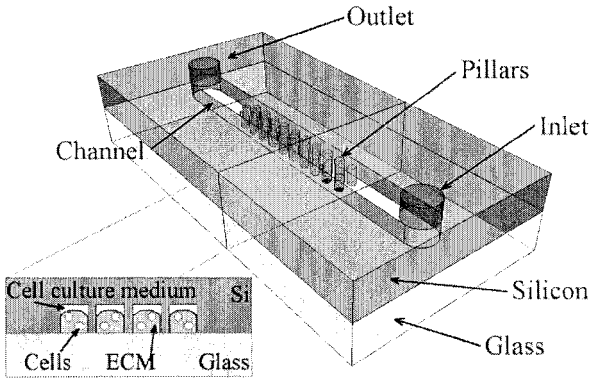

Figure 1. Conceptual image of chip for true 3D cell culture in extracellular matrix. Typical dimensions: channel width 100-400 μm, channel depth 100 μm, pillar diameter 50 μm, spacing 20-60 μm.

In order to accommodate a true 3D cell growth in a controlled micro-environment the silicon structure was filled with a mixture of gel-like extracellular matrix (ECM) [2] and cells. Figure 1 shows a conceptual image of the chip filled with ECM and cells.

2. Experiments and Results

The micromachined silicon structure (Si, p-type, 500 μm) was made with deep reactive ion etching (Surface Technology Systems) and the glass lid/encapsulation of the channel through anodic bonding (Pyrex, 500 μm, 400°C, 600 V). Figure 2 shows a micrograph of the fluidic structure including a channel with rhomb pillar structures. The pillars both increase internal surface to volume ratio, and ensure that flow through the structure is distributed in a controlled manner.

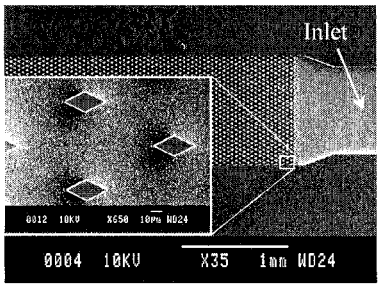

Figure 2. SEM picture of micro-machined silicon fluidic structure with insert on rhomb-shaped pillars. Pillar size 20x40 μm, channel inlet/outlet 400 μm and channel width between pillars 60 μm. Cavity depth 100 μm.

The ECM used here is a reconstituted basement membrane matrix, MATRIGEL (BD Biosciences, Bedford, MA, USA). ECM's typically consist of structural proteins (laminin, elastin and collagen), growth promoters and enzymes. The ECM used is a solidified gel in room temperature, but a liquid below 4°C. This makes mixing of cells and ECM possible (e.g. on ice or cooled in a refrigerator). Raising the temperature to 22-37°C results in a gel, with cells embedded.

ECM mixed with the fluorescent dye fluorescein was injected to study the distribution and the behavior of the ECM within the structure. Confocal imaging (Zeiss, LSM 5 Pascal) showed that the ECM is evenly distributed throughout the structure, and that the shrinkage of the ECM during gelatinizing (acc. 20 % [1]) enables further flow (nutrients, dyes etc.) through the chip (figure 3). Since the shrinkage of the gel is non-uniform in proximity to the pillars (figure 3), the surface area of the ECM is increased and thus the interface between the ECM and the surrounding liquid increases.

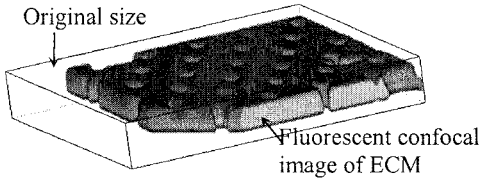

Figure 3. ECM stained with fluorescein imaged with confocal microscopy. Note the shrinkage of the ECM enabling additional flow through the chip with stain, cell culture medium or other liquids.

Switching between fluorescent (H_2O+fluorescein) and non-fluorescent flow (H_2O) show flow characteristics in the ECM-filled channel. Recordings of intensity variations over time in four regions of interest (regions no 1-4 in figures 5a-c) due to switching of flows are seen in figure 4. The intensity curves never reach intensity level zero, indicating that the ECM has absorbed the fluorescent dye and thus the ECM is permeable. Figure 5 a-c shows the distribution of flow from fluorescent to non-fluorescent at three different times.

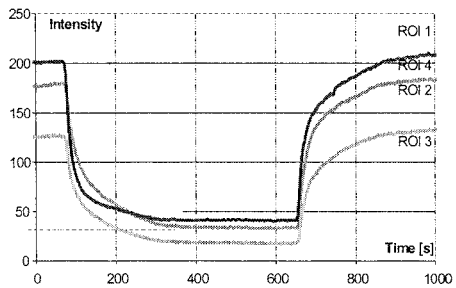

Figure 4. Exchange rate between fluorescent and non-fluorescent flow in ECM-filled channel.

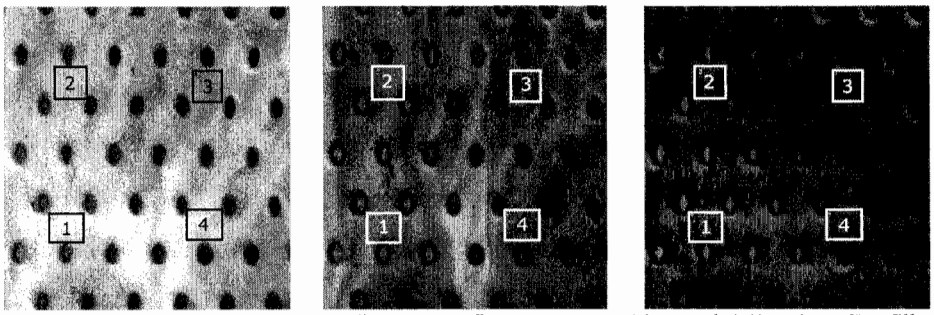

Figure 5 a-c. Fluorescent to non-fluorescent flow at t=75, 120 s and 360 s in ECM-filled channels. The loss of signal indicates the fast substitution of liquids. Time serie images from confocal microscope.

ECM mixed with pre-stained (calcein-AM 1 μM) COS-7 cells (20,000 cells per μl) was injected to investigate cell distribution and attachment (figure 6). It was found that in structures with large enough space (> 20 μm) between the pillars the cells nicely filled out the volume, whereas too narrow paths resulted in cell clogging.

To evaluate cell survival within the structure, calcein-AM (2 μM) was introduced through the cell-ECM (5,000 cells per μl) filled chip (figure 7). The AM-ester must be cleaved by the cell in order to become fluorescent, which assures that the cells are viable. Here the cells were stained, and therefore viable after 72 h of incubation (37°C, 5% CO_2) within the chip. During incubation cell culture medium with serum was flowed into the chip once every 24 h.

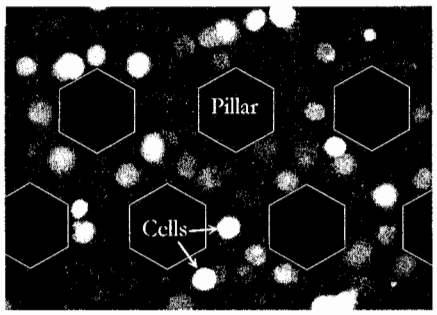

Figure 6. Pre-stained (calcein-AM 1 μM) COS-7 cells (20,000 cells per μl ECM) in chip. Cells show in white, black areas are hexagonal pillars, grey areas ECM.

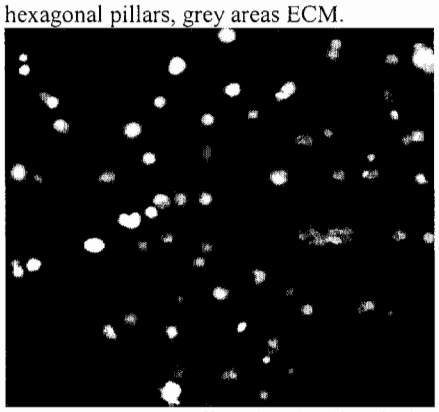

Figure 7. COS-7 cells stained with calcein-AM after 72 h in chip.

3. Conclusions

In conclusion, this work shows that cells can successfully be embedded and cultivated in a true three-dimensional way using a silicon micro-machined fluidic chip with injected ECM-cell mixture. It is also shown that the shrinkage of the ECM is beneficial as it enables a renewed flow through the chip with e.g. cell culture medium, drugs and fluorescent dyes. Hence, it is possible to optimize the chip for high throughtput screening.

Future studies will include long-term cultivation and studies of cell physiology, e.g. volume alternations and cell polarization, in a refined chip design.

References:

[1] W. Tan, T. Desai, *Tiss. Engineering*, **9**, 2, (2003)
[2] A. Abbott, *Nature*, **424**, 21 Aug (2003)

MICROARRAYS BASED ON AFFINITY-TAGGED SCFV ANTIBODIES: SENSITIVE DETECTION OF ANALYTE IN COMPLEX PROTEOMES

Christer Wingren[1], Cornelia Steinhauer[1], Johan Ingvarsson[1], Erik Persson[1], Katrin Larsson[2], and Carl A.K. Borrebaeck[1]

[1]Dept. of Immunotechnology, Lund University, P.O. Box 7031, SE-220 07 Lund, Sweden
[2]BioInvent International AB, Lund, Sweden

Abstract

Antibody microarray is a novel technology that will allow us to efficiently perform global proteome analysis. Performing rapid and multiplexed analysis on complex proteomes, such as human serum, targeting also low-abundant analytes will, however, place high demands upon the microarray design with respect to logistics, specificity and sensitivity. In this study, we have shown that non-purified affinity-tagged scFv antibody fragments could be directly applied as probes thereby eliminating the need for any time-consuming pre-purification steps. Further, highly functional arrays were obtained providing an assay sensitivity in the pM to fM range. In fact, 300 zeptomole analyte (approx. 5,000 molecules) may be sufficient for detection. Moreover, highly complex proteomes could be analysed without impairing the specificity and sensitivity of the set-ups. This is a pre-requisite for the design of high-density antibody arrays applied in high-throughput proteomics.

Keywords: antibody microarrays, antibody chips, scFv, sensitivity, affinity-tag.

1. Introduction

Major efforts are currently under way to develop further the antibody microarray technology into a versatile proteomic research tool [1-3]. To this end, high-density arrays displaying an exquisite specificity and an assay sensitivity in the picogram (attomole) range will be required. The logistics behind designing high-density arrays will, however, require non-purified probes to be directly arrayed since the task of purifying numerous probes will be overwhelming. To date, most antibody microarrays have, like protein arrays in general, been based on pure probes. Most antibody microarray set-ups published so far report a limit of detection (LOD) in the nanogram range. More specifically, LODs in the nM to pM range has been reported for set-ups detecting directly fluorescently labeled protein analytes.

In this study, have evaluated an antibody microarray platform based on mainly non-purified affinity-tagged scFv antibody fragments attached through specific affinity interactions as probes. We have used our human recombinant scFv antibody library genetically constructed around one framework, the n-CoDeR library containing 2 x 10^{10} clones [4], as source for our probes. The probes were immobilized via engineered C-terminal affinity tags, his- or myc-tags, to either Ni^{2+}-coated slides or pre-arrayed intact monoclonal anti-tag antibodies.

3. Experimental

We used single-chain Fv (scFv) antibody fragments selected from our human recombinant antibody library genetically constructed around one framework, the n-CoDer library [1], as source for our probes. Antibodies directed against various proteins, peptides and haptens were selected as model probes. The scFv antibody molecules were produced in *E. coli.* The analytes were labeled with Cy5 using standard protocols.

The antibody microarrays were fabricated using a non-contact printer (PerkinElmer Life and Analytical Science). The probes were arrayed onto Ni^{2+}-coated slides (Xenopore), silane-slides (Sigma) and FAST-slides (Schleicher&Schuell) in the pL scale. The latter two substrates were pre-

coated with monoclonal anti-tag antibodies, anti-his (Qiagen) or anti-Myc (Roche), prior to use. The arrays were scanned and quantified using the confocal ScanArray Express microarray Scanner (PerkinElmer). In all cases, non-specific scFvs were used as negative controls. A two-tailed t-test was used to determine whether the LODs observed were statistically significant at the 95% significance level (P=0.05).

4. Results and discussion

Antibody microarrays can be designed in a number of different formats depending on the application at hand. To evaluate and derive optimal efficacy, we have designed antibody microarrays based on purified as well as non-purified human recombinant affinity-tagged scFv antibody fragments. The probes were immobilized through specific affinity interactions to various substrates. The array designs were evaluated to generate proof-of-principle and to demonstrate the specificity and sensitivity of each individual set-up.

The results showed that highly functional microarrays were generated and that non-purified scFvs readily could be applied as probes. Specific and sensitive micorarrays were obtained, providing a limit of detection (LOD) in the pM to fM range, using fluorescence as mode of detection (Fig. 1). Thus, the current technology platform is already within the suggested range of sensitivity required to be able to perform adequate proteome analysis. Of note, similar LOD values were obtained irrespective of (i) the probe format (pure vs non-purified) and (ii) the analyte format (pure vs spiked into serum). Further, by spotting at least two probes together in the same spot instead of separately, cooperative effects could be utilized to improve LOD up to 200 times (Fig. 1). Cooperative binding effects is a well-known biochemical phenomena, previously observed also for antibodies (but in other assays). In addition, the results showed that spotting the analyte on top of the arrayed probes, instead of incubating the array with large sample volumes (333 pL vs 40 µl), could reduce the amount of analyte required 4000 times, from 1200 attomole to 300 zeptomole (Fig. 2). Reduced sample consumption is an important benefit of working in the array format, especially when analysing rare biological samples (e.g. tissue preparations) where only minute sample volumes often are available.

Finally, we showed that highly complex proteomes, such as human sera containing several thousand different proteins, could be directly fluorescently labeled and successfully analysed without compromising the specificity and sensitivity of the antibody microarrays. In this particular case, the content of eight complement proteins in human sera was successfully screened.

Taken together, we have shown that specific and sensitive antibody microarrays could be generated using non-purified affinity-tagged scFv antibodies immobilized through specific affinity interactions. Thus, we have developed an antibody microarray technology platform that will power the development of high-throughput proteomic applications.

Acknowledgements

This study was supported by grants from SWEGENE, the Swedish National Science Council (VR-NT), the foundation Lars Hiértas Minne, the Magnus Bergwall Foundation and BioInvent International AB.

References

[1] C.A.K. Borrebaeck, S. Ekström, A.C. Malmborg Hager, J. Nilsson, T. Laurell and G. Marko-Varga. *Biotechniques* 30(5), 1126-1132 (2001).

[2] C. Steinhauer, C. Wingren, A. Malmborg-Hager, C.A.K. Borrebaeck, *Biotechniques*, 32(supplement), 38-45 (2002).

[3] C. Wingren, J. Ingvarsson, M. Lindstedt, C.A.K. Borrebaeck, *Nature Biotechnol.* 21(3), 223 (2003).

[4] E. Söderlind, L. Strandberg, P. Jirholt, N. Kobayashi, V. Alexeiva, A.M. Åberg, A. Nilsson, B. Jansson, M. Ohlin, C. Wingren, L. Danielsson, R. Carlsson, and C.A.K. Borrebaeck. *Nature Biotechnol.* 18(8), 852-856 (2000).

Protein analytes

Analyte:		Detection limit:			Notes:
		Ni^{2+}-slides	α-myc coated Silane-slides	α-his coated Fast-slides	
Cholera toxin	(12 kDa)	500 pM	-	-	
Factor B	(93 kDa)	2 nM	210 pM	210 pM	
C3	(185 kDa)	-	-	100 pM	
C5	(190 kDa)	-	110 nM	100 nM	(ab1 or ab2)
		-	10 nM	260 pM	(ab1 + ab2)
C1q *	(460 kDa)	43 pM	43 pM	430 fM	
* amount of analyte/spot		175 amol	170 amol	2.7 amol	

Figure 1. The sensitivity of antibody-based microarrays on different substrates is in the pM to fM range using fluorescence as mode of detection (and no signal amplification).

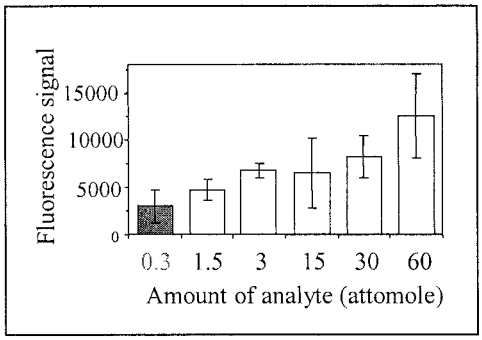

Figure 2. By spotting the analyte on top of the arrayed probes reduced the amount of analyte required 4000 times, from 1200 attomole to 300 zeptomole (~ 5,000 molecules).

MICROREACTORS FOR SELECTIVE ORGANIC REACTIONS

Mohammed Kajjout, Christian Rolando and Séverine Le Gac
Université des Sciences et Technologies de Lille, COM, UMR CNRS 8009, France

Abstract

We report here on the use of a commercially available nanomixer to control the mixing quality. Thus, it is possible in case of different competitive chemical reactions to favor the faster one. Particularly, this was applied to the synthesis of the major metabolites of quercetin which is a complex polyphenol found in human diet. Hence a ten step conventional batch synthesis was replaced by a single step reaction using a microfluidic device. Furthermore, varying the mixing quality of the reagents allows for favoring one reaction and thus for modulating the alkylation site.

Keywords: microfluidic, nanomixing, organic chemistry, fast reaction.

1. Introduction

The rapid growth of the field of microfluidics these last years allowed for performing and studying chemical reactions in tubular microreactors having a volume of some nanoliters [1]. The interest of chemists for microfluidics may be explained by several reasons. The dimension decrease implies (i) a 10^6- fold increase of the exchange surface area compared to the lab scale, (ii) a great rapidity of the operations, (iii) the use of reduced volumes and (iv) the possibility of placing a high number of reactors in parallel either for a large-scale production or for carrying out a series of reactions simultaneously. In addition, at the scale of a micron, the performances are different from them at the lab scale, first as heat transfer is much better, leading thereby to a higher control of the reactions and second as reactions are carried out in continuous flow, so that reactants and resulting products can not interact.

2. Theory

The products obtained in a chemical reaction are dramatically influenced by the mixing quality and speed [2]. For example, in the case of two competitive reactions (Scheme 1) the reaction kinetic is described by Equation 1. At the beginning of the reaction the product ratio is given by $P_A\, k_2 / A_0 = P_C\, k_1 / C_0$. It should be pointed out that this result is only valid if the characteristic time of mixing is faster that this of the chemical reaction. If the mixing is not efficient enough, Equation 1 no longer holds and must be replaced by Equation 2 where k_d is the diffusion controlled rate constant. In this case, the product ratio is given by $P_A / A_0 = P_C / C_0$.

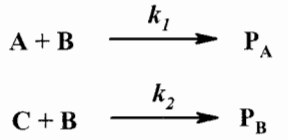

Scheme 1. Kinetic equation for two bimolecular competitive chemical reactions

$$dA = -k_1 AB \qquad dC = -k_2 CB$$

Equation 1. Kinetic equation in the case of fast mixing

$$dA = -k_d AB \qquad dC = -k_d CB$$

Equation 2. Kinetic equation in the case of slow mixing

Thus a slow mixing results in a complete loss in the chemical selectivity. Consequently, fast mixing is required for preserving the specificity of competitive chemical reactions, which is most of the time encountered in practical organic synthesis.

On the other hand, the mixing time can be expressed as $d^2 / 2\,D$ where d is a characteristic length of the device and D the diffusion constant for the chemicals (Fig. 1). Using a nanomixer

based on a splitting of the flows in a series of smaller flows and their further merging allows for reaching lower mixing time in the millisecond range [3].

3. Experimental

We have studied quercetin methylation (Fig. 3) in different conditions: (i) conventional batch conditions at the lab scale, (iii) homogeneous conditions with nanomixing. This allowed us to compare these different reaction conditions in terms of reaction yield, reaction rapidity and structure of the resulting products (alkylation level and position). The microreactor (Fig. 2) consists of a capillary of 75 μm i.d. and 15 cm length. It is fed by two capillaries connected to syringe-pumps (typically 1.5 μL/min), the first for example providing quercetin and the second the alkylation agent. The solution is collected at the outlet of the microreactor and analyzed by ESI-MS for the identification of the products or by LC-MS/MS for their quantification. Mixing is induced by a NanoMixer (UpChurch Scientific) placed upstream to the microreactor.

4. Results and discussion

Using batch conditions yields a complex mixture of products having different levels and positions of methylation on almost all the 5 reactive –OH site (Fig. 4). Using the set-up described in entry 1 the results remain roughly the same. Indeed, as the quercetin and the base are introduced in the same flow, phenate compounds are formed when they react with the methylation agent: the reaction is still faster than mixing even using the nanomixer. On the contrary, when quercetin and CH_3I are introduced in the same flow and the base in the other one, a single mono-methylated product is obtained, the methylation position being the most basic and thus the most reactive one in the used conditions. The very selective reaction (Figs. 5 and 6) showed in entry 3 is accounted for by the formation of an intermediate alktylating agent resulting from the mixing CH_3I and the base.

Entry	Flow A	Flow B	Products	Kinetic
Batch	Quercetin, crowded base, CH_3I		Mixture	---
1	Crowded base, quercetin	CH_3I	Mixture	Faster than mixing
2	CH_3I, Quercetin	Crowded base	3-OMe	Slower than mixing, chemically fast
3	Quercetin	Crowded base, CH_3I	4'-OMe	Slower than mixing, chemically slow

This reaction was tested as well on another polyphenolic compound, catechin, which is more fragile and the results were as much conclusive. Thus, microfluidic allows for carrying out reactions which are as selective as enzymatic ones occurring *in-vivo* during the metabolism of polyphenols.

5. Conclusions

The use of a commercially available nanomixer allows us to select the faster methylation reaction among a series of competitive methylation reaction. By running the microreactor overnight, enough material (ca tenth of milligrams) may be obtained for registering an NMR spectrum or for performing biological tests.

References

[1] F. G. Bessoth, A. J. deMello, A. Manz, *Anal. Commun.*, **36**, 213-215 (1999).
[2] C. Erbacher, F. G. Bessoth, M. Busch, E. Verpoorte, A. Manz, *Mikrochim. Acta*, **13**, 19-24 (1999).
[3] J. R. Bourne, *Org. Process Res. Dev.*, **7**, 471-508 (2003).
[4] M. Bouktaib, S. Lebrun, A. Atmani, C. Rolando, *Tetrahedron*, **58**, 10001-10009 (2002).

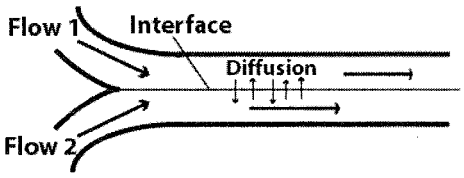

Figure 1. Laminar flow mixing by diffusion in microchannels

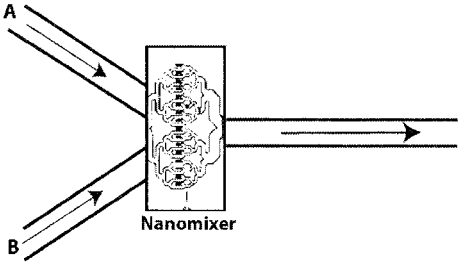

Figure 2. Microreactor including a Nanomixer (Upchurch)

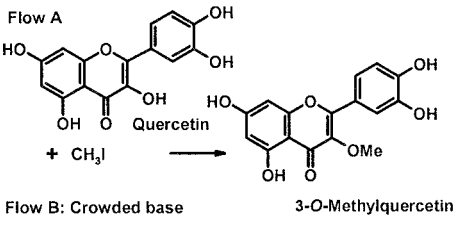

Figure 3. Alkylation of quercetin (the setup corresponds to entry 2).

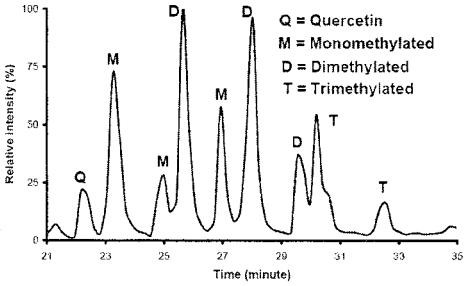

Figure 4. LC-ESI-MS trace of a batch methylation reaction carried out in conventional chemistry vessel.

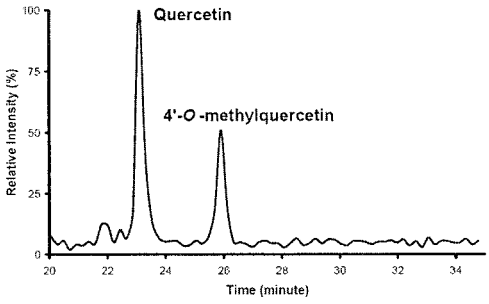

Figure 5. LC-ESI-MS/MS trace of the methylation reaction (entry 3).

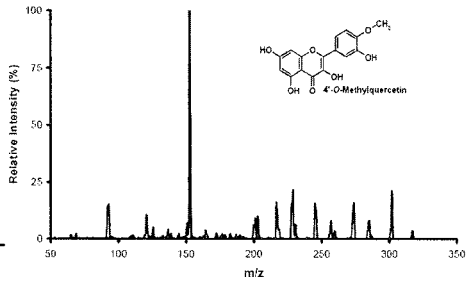

Figure 6. MS/MS spctrum showing that the obtained product is the 4' isomer.

MICROFLUIDIC CELL IMMERSION ON-CHIP CELL VIABILITY TEST

Urban Seger[1], Shady Gawad[1], Marc Tonteling[1], Robert Johann[1], Horst Vogel[2], and Philippe Renaud[1]

[1] *Microsystems Laboratory, LMIS-STI, EPFL, CH-1015 Lausanne, Switzerland*

[2] *Laboratory of Physical Chemistry of Polymers and Membranes, LCPPM, EPFL, CH-1015 Lausanne, Switzerland*

Abstract

Within an ongoing project on controlled single-cell electroporation in microfluidic chips [1], a platform permitting accurate particle and fluid handling is being developed. This paper describes cell immersion as a practical demonstration of that platform. As an application, on-chip viability tests were conducted.

Keywords: two-liquids flow, dielectrophoresis, cell immersion, electroporation, cell viability

1. Introduction

The controlled exposure of individual immobilised cells to changing chemical environments is of growing interest for studying cell-based assays. Cell adhesion to selected areas [2] and cell sedimentation in no-flow regions [3], both followed by perfusion, have been successfully applied to studies involving more than one liquid.

In cell immersion, a subpopulation of cells flowing in a microchannel is selected and deviated into a trap. Via an auxiliary channel, a second liquid (reactant) is flowed over the trapped cells. While optically monitoring cell responses, cell immersion and washing cycles can be alternated at will. Finally, the cells are released.

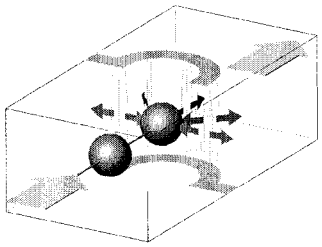

Figure 1. Semi-open nDEP-trap in flow. The inhomogeneous electric field between the U-shaped top and bottom electrodes repulses particles. They are retained in place by the additional effect of the drag.

2. Concept

Cell immersion is enabled by combining negative dielectrophoresis with pressure-regulated two-liquids flows:

nDEP-barriers: Negative dielectrophoresis (nDEP) between parallel line electrodes allows to guide particles in flows by repulsion. Such nDEP-barriers are useful for concentrating and sorting cells [4], they can also be used to swap cells from one fluid to another [5]. For cell immersion, two-phase nDEP-traps consisting of U-shaped line electrodes are used (Fig. 1).

Chip design and fabrication: The glass microchips consist of channels with integrated Ti/Pt electrodes, patterned by lift-off. The channel's geometry is defined by a spacer made of photosensitive polyimide, it is accessed by holes drilled through the supporting glass slide. This

technology allows for the patterning of aligned top- and bottom-electrodes and of channels having several in- and outlets (Fig. 2).

Pressure-regulated two-liquids flows: In compliant fluidic systems, flow speed relaxation times can be minimised by driving liquids with controlled pressures (Fig. 3). In particular, the ratio of two independent laminar flow rates in a channel can be changed very rapidly and precisely. Flow speeds are determined in-situ by particle tracking.

3. Experimental

Human Leukemia T Cells (Jurkat) are cultured suspended in RPMI-1640 medium with 10% FCS and 1% PenStrep at 37°C. nDEP signals range from 500 kHz to 1 MHz and from 2.5 to 3.5 kV/cm. Bipolar, sinusoidal 100 kHz electric pulses with variable field strengths from 5 to 10 kV/cm are superimposed to the nDEP signal and delivered in trains of 10 pulses on demand. Fluid flows ranging from 50 to 150 µm/s are generated by overpressures in the order of 5 to 40 mbar. All experiments are recorded to video.

4. Results and discussion

With the present setup, the chemical environment of trapped cells can be changed within less than 10 seconds (Fig. 4). As an application, an in-situ cell viability assay by Trypan Blue exclusion staining following the exposure of cells to high electric fields is demonstrated. Two live cells are held captured in the active nDEP-trap while being immersed by PBS containing Trypan Blue. Both cells do not turn blue, as they are intact. After the application of sinusoidal pulses of 8 kV/cm at 100 kHz, one of the cells is lysed and turns blue while the other one remains unstained (Fig. 5).

5. Conclusions

In this paper, a microfluidic chip was presented. In that device, a small number of cells flowing in a channel can selectively be trapped, held and released. Immobilised cells can be immersed with and washed from a second liquid in user-defined sequences. Optionally, high electric field pulses can be applied to the captured cells. As an example, electrically induced cell death (cell lysis) was assessed optically by Trypan Blue staining.

Acknowledgements

The authors are grateful to P. Pascoal, E. Illegems and H. Pick of LCPPM (EPFL) for their help in cell culturing. The collaboration of numerous students in this project is highly appreciated. This work was funded by LMIS (EPFL).

References

[1] U. Seger, S. Gawad, A. Scheer and Ph. Renaud, MicroTAS 2002, pp. 796-798.
[2] S. Takayama, J. C. McDonald, E. Ostuni, M. N. Liang, P. J. A. Kenis, R. F. Ismagilov and G. M. Whitesides, PNAS, Vol. 96 (1999), pp. 5545-5548.
[3] A. Daridon, W. Throndset, I. Liau, K. Farell, F. Tseng, S. Javadi and I. Manger, MicroTAS 2002, pp. 31-33.
[4] T. Schnelle, T. Muller, G. Gradl, S. G. Shirley and G. Fuhr, Journal of Electrostatics, Vol. 47 (1999), pp. 121-132.
[5] U. Seger, S. Gawad, R. Johann, A. Bertsch and Ph. Renaud, Lab on a Chip, Vol. 4 (2004), pp. 148-151.

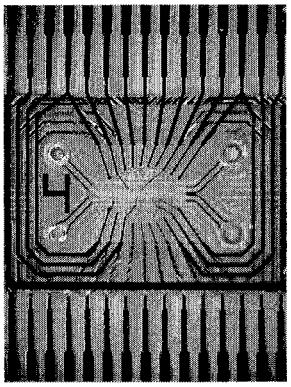

Figure 2. Photographic top-view of the glass-glass chip. A polyimide spacer defines the channel, a patterned Ti/Pt thin film defines the electrodes.

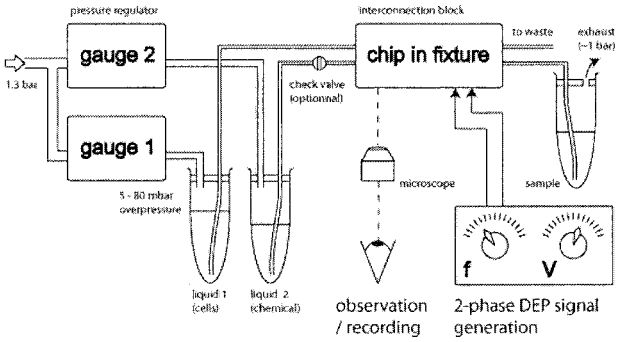

Figure 3. Pressure-driven two-liquids flow setup. Controlled overpressures, defining the flow rates in the microfluidic chip, are applied to liquid reservoirs. The liquids are brought to the chip via (compliant) interconnections. The chip has two in- and outlets.

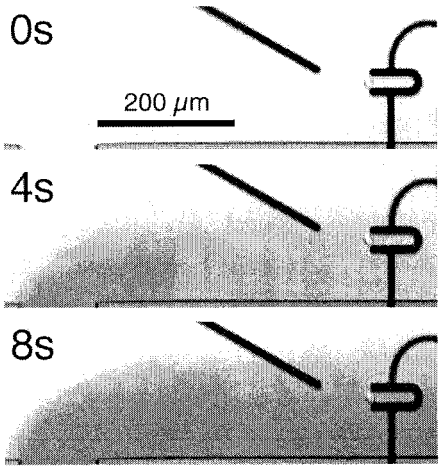

Figure 4. Time sequence of the immersion of a Jurkat cell originally suspended in PBS. Within less than 10 s, its chemical environment is changed to Trypan Blue stained PBS (entering the channel from the bottom). By desactivating the inclined guiding electrode pair during immersion, the arrival of additional cells in the trap can be prevented.
Flow speed: 120 µm/s from left to right.

Images of Figs. 4 and 5 were extracted from video.

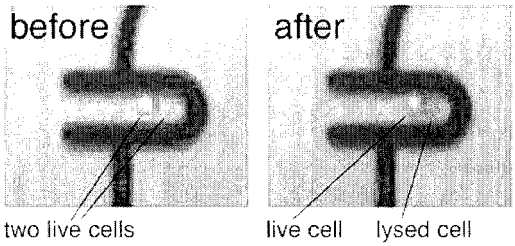

Figure 5. Two Jurkat cells captured in the nDEP-trap and immersed by Trypan Blue. The amplitude of the electric field used to generate the nDEP force is in the order of 3 kV/cm. Both cells are alive (left). After superimposition of additional, higher electric field pulses at lower frequency (8 kV/cm, 100 kHz), one of the cells turns blue, indicating it has been lysed, i.e. its membrane has been disrupted (right).
Time delay between the two pictures: 5 s.

A FULLY AUTOMATED SAMPLE-PREPARATION CARTRIDGE FOR GENEEXPRESSION BASED DIAGNOSTICS

Ralf Lenigk[1, 3], Robin Liu[1,4], Chris Gooden[2], Jianing Yang[1, 3], Michael Bittner[2,3], Jeffrey Trent[2, 3] and Frederic Zenhausern[1, 3]

[1] *Applied NanoBioscience Center, Arizona State University, Tempe, AZ 85287-4004, USA*
[2] *Translational Genomics Research Institute, Phoenix, AZ 85004, USA*
[3] *Nanobiomics Inc., Phoenix, AZ 85004, USA*
[4] *Current address: Combimatrix, Mukilteo, WA 9827, USA*

Abstract

An integrated microfluidic plastic-cartridge was developed to perform fully-automated sample preparation of total RNA for gene expression monitoring experiments. The cartridge contains channels, chambers, heaters, mixers, valves and pumps and was designed for single use. To facilitate the bioassay protocol, most of the reactions are being performed on the surface of magnetic beads. The device has the potential to impact healthcare by reducing the time needed for genotyping assays and may enable point-of-care gene expression analysis to aid in disease diagnosis and identification of an individuals susceptibility for certain types of cancer.

Keywords: RNA, microfluidics, sample preparation, gene-expression, magnetic beads

1. Introduction

Molecular approaches to detect low-abundance markers in biological tissue are becoming critical to assess genetic and environmental interactions that can define cancer risk and give predictions of treatment success. One application of high clinical significance that we are pursuing is an automated sample-preparation cartridge for tumor sample preparation to monitor the expression of "classifier genes" [1], for example to predict the success for therapeutic treatment of melanoma. The developed cartridge will enable an automated gene expression monitoring to be performed in a clinical setting.

2. Experimental

Based on previous publications describing the design of integrated microfluidic systems for automated genotyping [2], a disposable cartridge (Fig. 1) that is comprised of a printed circuit board with heaters to actuate valves and pumps (Fig. 2a) and a polymeric part containing the fluidics (Fig. 2b) was prototyped. The constructed microfluidic system was used to perform the complex molecular biology assays necessary to convert total RNA into fluorescently labeled cRNA used in hybridization experiments for gene-expression monitoring. The cartridge-assay starts with the user loading cell-lysate containing total RNA. Highly sensitive mRNA capture is achieved using magnetic beads with T7-promoters, followed by on-bead first-strand cDNA synthesis. After the second strand synthesis, the cDNA is transcribed into cRNA using fluorescent cyanine-CTP. The labeled cRNA is captured by pumping it through a magnetic beadbed containing poly-(dA) beads. Enzymatic fragmentation is then used to cut the product into smaller units and to release it from the beads. During the current stage of our development the fragmented product is removed and hybridized externally to microarray-slides. For the cartridge operation the cartridge was loaded with the reagents, then plugged into a sample preparation workstation that is computer-controlled by a LabView-based program. The parameters for the bio-assay protocol were pre-programmed, so the sample preparation can proceeded automatically without user intervention.

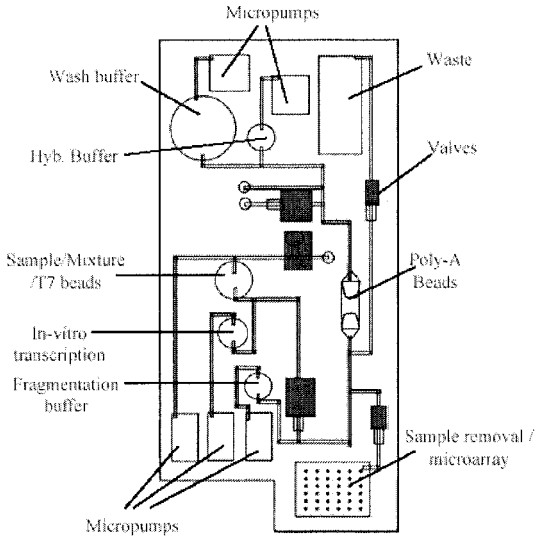

Figure 1. Schematic of the integrated sample-preparation cartridge.

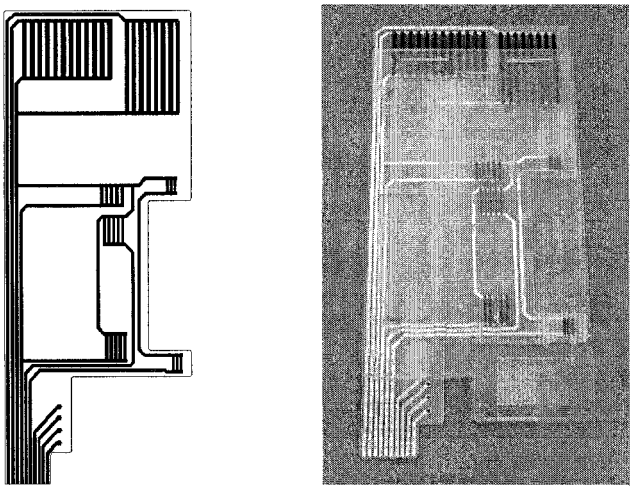

(a) (b)

Figure 2. (a) Printed circuit board with integrated heaters and edge-connectors. (b) Cartridge containing the fluidic elements fabricated from plastic, and bonded to the printed circuit board.

3. Results and discussion

After a successful test of the microfluidic components and the fluidic handling capabilities of the cartridge, the bioassay protocol was optimized for cartridge use. The assay hybridization data (Fig. 3.) generated using the bead-mediated in-vitro transcription protocol described above shows the viability of bead-based assays to generate high-quality data. More experimental data needs to be generated to test the efficiencies of the bio-assay protocol at the different stages and to optimize the sensitivity to allow for the analysis of small-size cancer biopsies (needle-biopsies).

At a later stage, we plan to include a micro-array into the sample-preparation cartridge using a "biochannel" approach [3] for reduced volume and faster hybridization kinetics. The use of low-cost materials for the cartridge development ensures that the disposable device can be produced efficiently. The integrated RNA sample preparation cartridge presented here provides a promising approach for RNA-based diagnostics.

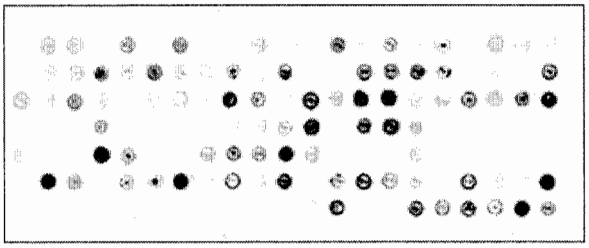

Figure 3. Micro-array hybridization data for labelled cRNA prepared with the bead-mediated in-vitro transcription protocol. The image shows an enlarged area of a sub-array.

References

[1] M. Bittner, P. Meltzer, Y. Chen, Y. Jiang, M. Seftor, M. Hendrix, M. Radmacher, R. Simon, Z. Yakhini, A., Ben-Dor, N. Sampas, E. R. Dougherty, E. Wang, F. Marincola, G. Gooden, J. Lueders, A. Glatfelter, P. Pollock, J. Carpten, E. Gillanders, D. Leja, K. Dietrich, C. Beaudry, M. Berens, D. Alberts, V. Sondak, N. Hayward, J. Trent, *Nature* **406**, 536-540 (2000).

[2] R. H. Liu, J. Yang, R. Lenigk, J. Bonanno, P. Grodzinski, *Analytical Chemistry*, **76**, 1824 – 1831 (2004).

[3] R. Lenigk, R. Liu, M. Athavale, Z. Chen, D. Ganser, J. Yang, C.B. Rauch, Y. Liu, B. Chan, H. Yu, M. Ray, R. Marrero, P. Grodzinski, *Analytical Biochemistry*, **311**, 40-49 (2002).

RAPID CELL STIMULUS AND LYSIS IN SEGMENTED FLOW

Jamil El-Ali[1], Suzanne Gaudet[2] and Klavs F. Jensen[1]
[1]Department of Chemical Engineering, and [2]Department of Biology
Massachusetts Institute of Technology, Cambridge, MA 02139, USA. kfjensen@mit.edu

Abstract
We present a microfluidic device with rapid stimulus and lysis of cells for resolving fast transient responses in cell signaling networks. The device uses segmented gas liquid flow to enhance mixing and has integrated TE heaters and coolers to control the temperature during cell stimulus and lysis.

Keywords: Mixing, cell lysis, fluidic simulations, residence time distribution (RTD)

Introduction

There is great interest in understanding and modelling of signaling pathways and networks in cells, e.g. the Caspase activated pathways in apoptosis and immunity [1] or the ErbB signaling network [2]. In a typical process flow (Fig. 1A) cells are mixed with a specific stimulus for a specified period where after a lysis agent is introduced to inhibit further stimulation and to lyse the cells so the response to the stimulus can be analyzed. Signaling pathways that exhibit fast transient responses (15-30s) requires very short mixing times and well controlled and reproducible stimulus times [3]. Typically this can be hard to achieve in microsystems, where the size of the cells prevents effective mixing by lamination and where parabolic flow profiles gives rise to dispersion and large residence time distributions (RTD). We present a new microfluidic device which uses the enhanced convective mixing observed in segmented gas liquid flow [4] to achieve short mixing times and a small RTD making analysis of the fast transient responses of signal pathways possible. Integrated TE heaters and coolers control the temperature on the device for optimal performance during stimulus and lysis.

Design and fabrication

The fluidic systems with stimulus and lysis zones are defined using soft lithography in a PDMS layer which is then bonded to a 50x75mm glass slide (Fig. 1B). Temperature regulation for the two zones is achieved by using a thermo electric (TE) heater at 37°C to mimic physiological conditions during stimulation and a TE cooler at 4°C to inhibit further stimulus during lysis. The heater and cooler are attached on the backside of the glass slide trough aluminum heat spreaders and are controlled by proportional integral (PI) temperature controllers (TE technology, USA). Thermistors attached to each of the heat spreaders provide temperature feedback for the controllers. Figure 2 shows an image of the device in the temperature control setup and a thermal simulation of the temperature distribution where the layout of the fluidic system has been superimposed. Besides the two zones for stimulus and lysis (~80cm each) pressure drop channels at the inlets are used to achieve stability of the segmented gas liquid flow. Stimulus and lysis agent is only introduced from one side of the channels, thus each zone starts with a meander structure that breaks the flow symmetry in the slugs so that mixing will progress across the centerline [4]. At typical slug velocities between 0.5-2 cm/s, the residents time in each of the zones can be adjusted from 40-160s.

Results

The thermal simulation (Fig. 2) shows that there is good temperature uniformity in the two zones and that the temperature at the point of temperature sensing corresponds well with the temperature in the respective zones. Heating and cooling both requires ~0.4W which is easily obtained using standard single stage TE elements. The formation of segmented flow in a high surface tension liquid as water is more challenging than for lower tension fluids reported previously [4]. With water, pressure drops in the inlet channels must be designed to minimize effects of transitions between gas and liquid segments (Fig. 3) and achieve a uniform distribution of gas bubbles within the liquid. As a positive side to the large surface tension the liquid slugs are completely separated resulting in a RTD that is determined only by the stability of the flow. The current device design produces liquid slugs of a typical length between 600-1000μm. 2D volume of fluids (VOF) simulation combined with species transport using CFD-ACE is used to simulate mixing (Fig. 3 and 4). Using a frame of reference moving with the slugs a recirculating flow pattern is observed with radial components of more than 30% of the bulk velocity. This recirculation provides effective convective mixing inside the liquid slugs. Simulations show that the mixing is almost independent of the slug velocity. However, there is a strong dependence on slug length with shorter slugs giving shorter mixing lengths. For 600μm liquid slugs the mixing length is less than 1 cm. Even for the 1000μm slug where the mixing length is ~4cm this corresponds to less than 5% of the total residence time in a zone (Each zone is ~80cm). The contribution of diffusion from small biological material ($D \sim 10^{-10} m^2/s$) is negligible even with the longer mixing length of the 1000μm slug. The results underscore the importance of convective mixing in segmented gas liquid flow for achieving efficiently low mixing times. The possible effect of slug flow on cell viability has been tested on Jurkat E6-1 cells (human T-cell lymphoma) at slug velocities up to 1cm/s. Less than 10% specific cell death has been observed in these test. In addition to the above experimental characterization and simulation of the device we characterize stimulus and lysis performance for typical mammalian cell lines.

Acknowledgements

This research was funded by the National Institutes of Health (NIH) (NIGMS GM-68762)

References

[1] E.M. Creagh, H. Conroy and S.J. Martin. *Caspase-activation pathways in apoptosis and immunity*. Immunological reviews, VOL 193, 2003

[2] Y. Yarden and M.X. Sliwkowski. *Untangling the ErbB signalling network*. Nature reviews, Molecular cell biology, vol. 2, February 2001

[3] B.N Kholodenko, O.V Demin, G. Moehren and J.B. Hoek. *Quantification of short term signaling by the epidermal growth factor receptor*. J. Biological Chemistry, vol. 274, 42, 1999}

[4] A. Guenther, S.A. Khan, M. Thalmann, F. Trachsel and K.F. Jensen. *Transport and reaction in microscale segmented gas-liquid flow*. Lab on a Chip, 4. in press (as advance article available online), 2004.

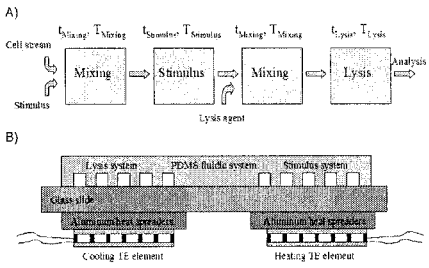

Figure 1. A) Typical process flow for cell stimulus. Two mixing steps are needed which requires very effective mixing to probe fast transient responses. B) Schematic of design. A PDMS fluidic system is bonded to a glass slide and TE elements attached on the back through aluminum heat spreaders are used to control the temperature on the device.

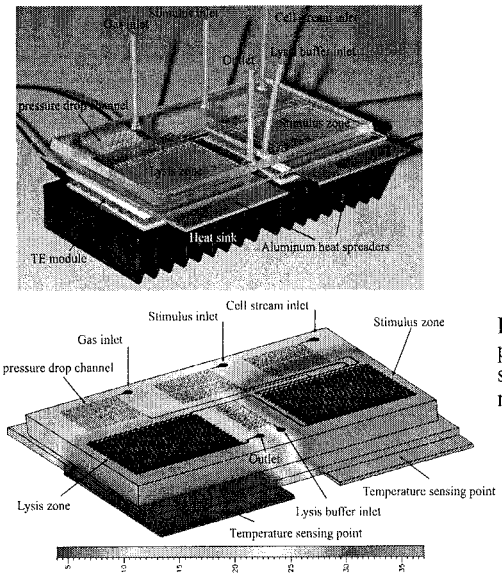

Figure 2. Optical image of device and temperature control setup (top) and 3D CFD-ACE simulation of temperature distribution (bottom). Temperature is regulated using PI controllers with temperature sensing thermistors (not shown) attached to the aluminum heat spreaders. Good uniformity is observed in the two temperature zones.

Figure 3. Optical image of the gas injection (left) and a liquid slug in the meandering mixing channel (right). With a high surface tension liquid (water) there is an oscillation between gas and liquid injection which can cause instabilities but also results in complete separation of slugs.

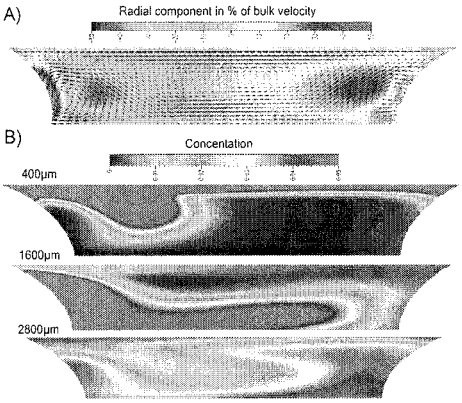

Figure 4. A) 2D VOF simulation of flow profile in segmented flow with 600µm liquid slugs. B) Simulation of mixing due to the recirculating flow in a slug.

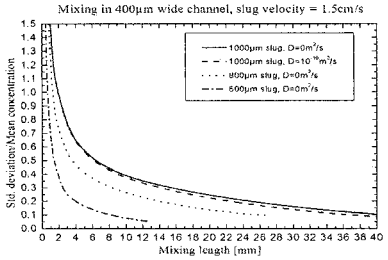

Figure 5. 2D simulation of mixing in segmented flow showing the effect of the slug length on the mixing efficiency.

BIOLUMINESCENCE FROM BACTERIAL REPORTER STRAINS IN A MICROBIOREACTOR

Andrea Zanzotto[1], Paolo Boccazzi[2], Tina K. Van Dyk[3], Anthony J. Sinskey[2], Klavs F. Jensen[1]
[1]*Dept. of Chemical Engineering, Massachusetts Institute of Technology, Cambridge, MA, USA*
[2]*Dept. of Biology, Massachusetts Institute of Technology, Cambridge, MA, USA*
[3]*DuPont Company, Wilmington, DE, USA*

Abstract

We present *in situ* measurements of bioluminescence from bacterial cultures grown in instrumented microbioreactors. Experiments were conducted with reporter strains of *E. coli* in which the *lux* operon was fused to a promoter that was either expressed constitutively, or required a specific environmental induction for expression to occur. Results from the microbioreactor were compared to results obtained from conventional 500 mL batch bioreactors.

Keywords: microbioreactor, bioluminescence, reporter gene, stress response

1. Introduction

Light emission from luminescent bacteria created to act as reporters for various environmental conditions is finding application in several areas of biology, including toxicity assays for environmental pollutants, chemical detection, and gene expression profiling. For chemical detection and toxicity assays, reporter strains of sensitized bacteria provide a specific, binary response. In genomewide expression profiling, reporter gene fusions provide several advantages over DNA array technology, such as eliminating the need for RNA isolation as well as the problems that arise due to cross-hybridization. For each of these applications it is clearly desirable to have the ability to carry out multiple bacterial fermentations in parallel. The microbioreactor system that we have previously described could potentially provide the needed platform [1]. Our model system is a collection of *E. coli* strains provided by DuPont Company. These strains have been created using transcriptional fusions of the *luxCDABE* operon to bioluminesce in response to specific environmental stresses [2-4]. We show that we can induce bioluminescence by exposing the bacteria to a known stress (e.g. lack of nutrient), and we compare the results to those obtained in bench-scale bioreactors under similar conditions.

2. Experimental

Fermentations were carried out in 50 μL poly(dimethylsiloxane) microbioreactors in which oxygenation occurred through a gas-permeable membrane (Figure 1). The microbioreactor was housed in a chamber that controlled temperature and maintained high humidity (Figure 2).

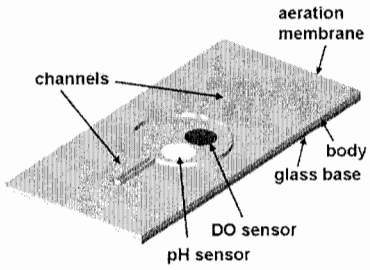

Figure 1. Schematic of microbioreactor.

Dissolved oxygen and pH were measured using fluorescence lifetime measurements with sensors located at the bottom of the microbioreactor. A photomultiplier tube was used to measure luminescence and optical density. Luminescence was measured directly as a current in the absence of other light. Optical density was calculated using the transmission of light at 600 nm across the microbioreactor. Measurements of luminescence light intensity were scaled for the purpose of graphing, and are presented in arbitrary units.

The headspace of the chamber was filled with air for all experiments except for the fermentation of DPD2417 in which oxygen depletion was avoided by using pure oxygen.

3. Results and discussion

The bioluminescence of *E. coli* DPD2276 is shown in Figure 3. *E. coli* DPD2276 contains a plasmid-borne *gyrA-luxCDABE* gene fusion resulting in strong, essentially constitutive bioluminescence. The total measured

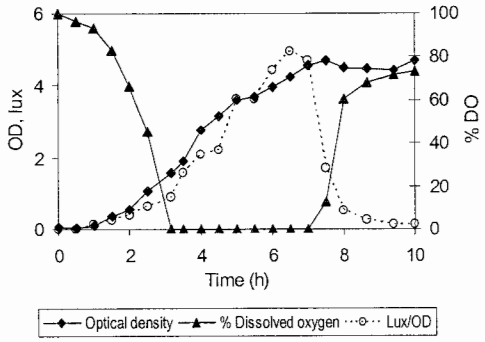

Figure 3. Optical density (OD), dissolved oxygen (DO), and total bioluminescence (lux) in a microbioreactor for an *E. coli* strain constitutive for the expression of the *lux* operon.

luminescence would therefore be expected to increase in proportion to biomass, as the figure demonstrates. Results indicate that luminescence is associated with cell growth and drops off as the culture reaches stationary phase. Fermentation of *E. coli* DPD2417 under oxygen limitation is shown in Figure 4. *E. coli* DPD2417 carries an anaerobically-regulated *nirB-luxCDABE* gene fusion. In a microbioreactor the strain experiences a sharp peak in specific luminescence (lux/OD) when the dissolved oxygen in the medium depletes (Figure 4a). A similar response can be seen in a 500 mL bench-scale bioreactor (Figure 4b). By contrast, when pure oxygen is supplied to the microbioreactor, no luminescence response is seen (Figure 5).

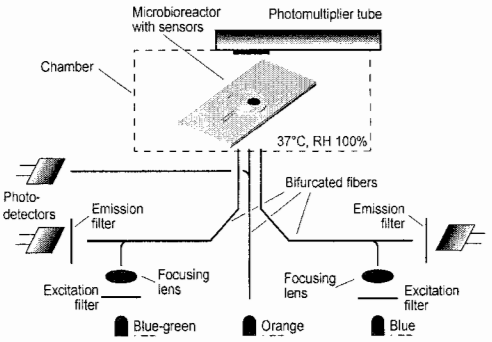

Figure 2. Schematic of the experimental setup.

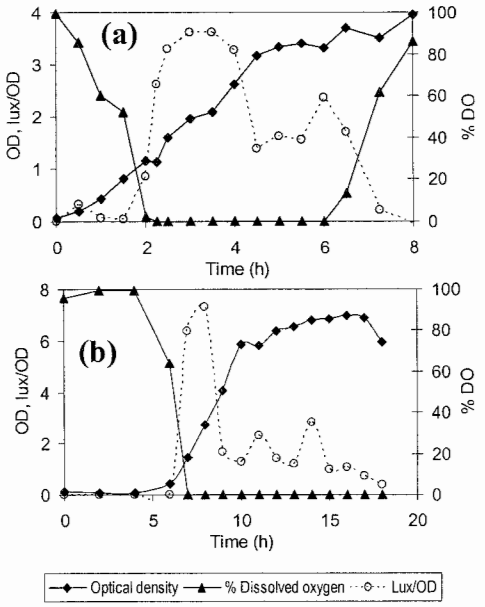

Figure 4. Optical density (OD), dissolved oxygen (DO), and specific bioluminescence (lux/OD) for an oxygen-sensitive reporter strain of *E. coli* in (a) a microbioreactor and (b) a bench-scale bioreactor.

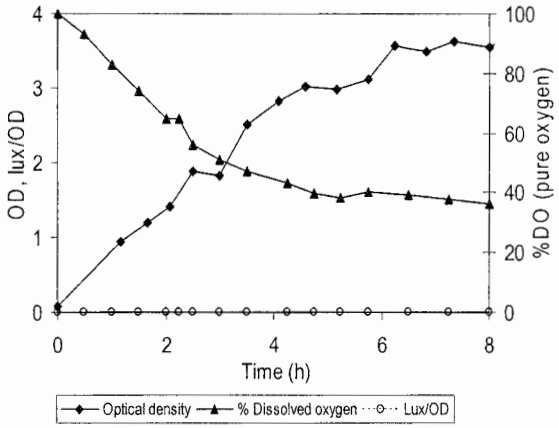

Figure 5. Optical density (OD), dissolved oxygen (DO), and specific bioluminescence (lux/OD) for an oxygen-sensitive reporter strain of *E. coli* in a microbioreactor when oxygen is used as the contacting gas.

4. Conclusions

The luminescence response of bacterial reporter strains provides a useful tool for the detection of specific environmental stimulants or as an indicator in gene expression profiling. We have demonstrated the measurement of this luminescence in a microbioreactor. We have used an *E. coli* strain sensitive to anaerobiosis to indicate the presence of oxygen depletion, and compared the response to a growth situation where oxygen limitation does not occur. Finally, we have shown that the luminescence response in a microbioreactor is similar to that observed at the bench scale.

Acknowledgements

The authors thank the DuPont-MIT Alliance (DMA) for funding.

References

[1] Zanzotto, A., N. Szita, P. Boccazzi, A. J. Sinskey, and K. F. Jensen. A membrane-aerated microbioreactor for high-throughput bioprocessing. *Biotechnology and Bioengineering* (in press) (2004).

[2] Rupani, S. P., Characterization of the stress response of a bioluminescent biological sensor in batch and continuous cultures. *Biotechnology Progress* **12**, 387-392 (1996).

[3] Van Dyk, T. K., Y. Wei, M. K. Hanafey, M. Dolan, M. J. G. Reeve, J. A. Rafalski, L. B. Rothman-Denes, and R. A. LaRossa. A genomic approach to gene fusion technology. *PNAS* **98**, 2555-2560 (2001).

[4] Van Dyk, T. K., and R. A. Rosson. *Photorhabdus luminescens luxCDABE* promoter probe vectors, p. 85-95. In R. A. LaRossa (ed.), Methods in Molecular Biology: Bioluminescence Methods and Protocols, vol. 102. (1998).

Compartmentalized Microfluidic Lung Epithelial Cell Culture Device for Pulmonary Mechanotransduction Studies

Dongeun Huh, Yoko Kamotani, James B. Grotberg, Shuichi Takayama
Dept. of Biomedical Engineering, University of Michigan, Ann Arbor, MI 48109-2099, USA

Abstract

Pulmonary epithelial cells are exposed to various fluid flows during breathing or mechanical ventilation. Mechanical stresses generated by the movement of fluids affect function and phenotype of lung cells, and sometimes mediate the development of pulmonary diseases. This paper describes a compartmentalized microfluidic lung epithelial cell culture device that mimics *in vivo* microenvironment with different flows under normal and pathological pulmonary conditions

Keywords: lung epithelial cell, microfluidic cell culture, mechanical stress, flow

1. Introduction

Fluid flows in the pulmonary system generate complex mechanical stresses as a result of dynamic interaction between different physical forces associated with inertial, viscous, and surface tension effects. In many clinical situations such as asthma [1] and mechanical ventilation [2], abnormal stresses imposed by moving fluids often lead to damage of lung epithelial cells and become an important mode of lung injury [3]. Here, we report on the development of a three-dimensional PDMS microfluidic system that could provide a physiologically relevant culture environment for lung epithelial cells as well as controllable fluid flows for pulmonary mechanostransduction studies.

2. Experimental

The *in vitro* microfluidic culture system consists of two main PDMS compartments (height: 100 μm, width: 300 μm) separated by a thin permeable polyester membrane with nanometer-sized pores (pore size: 400 nm, GE Osmonics, MN) as shown in Figure 1. Upper and lower chambers correspond to apical and basal sides of lung epithelial cells grown on the porous membrane that mimics an *in vivo* basement membrane, allowing the cells to polarize. Fluid/solute transport between upper and lower chambers is strictly limited to diffusion through pores of the membrane,

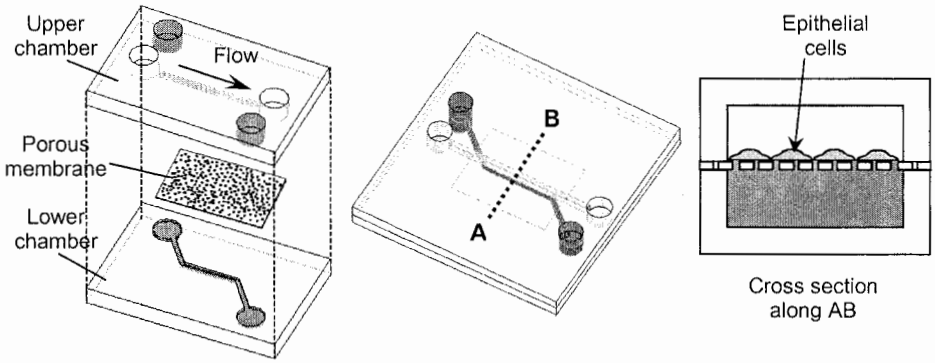

Figure 1. Schematic diagram of a compartmentalized lung cell culture system. Upper and lower chambers are separated by a thin membrane and a steady flow in each chamber is driven by a syringe pump. Cells are seeded into the upper chamber and cultured on a porous membrane.

and fluid flows spatially directed in different compartments are confined to each chamber without any leakage.

Type II human alveolar epithelial cell line (A549, American Type Culture Collection, VA) was used for cell culture experiments. Prior to seeding, sterilized upper and lower chambers were filled with culture media (Ham's F-12K with 10% FBS, 1% penicillin/streptomycin, and 1% L-glutamine) and pre-incubated overnight. Suspended cells were seeded at ~ 10^5 cells/cm^2 into the upper chamber and the flow inside the channel was completely stopped to allow cells to attach to the membrane and channel surfaces. After 5 hours, a steady flow of culture media was driven by a syringe pump (KD scientific, MA) at a flow rate of 500 µl/day in each chamber to feed cells apically as well as basally. Cells inside the channel system were cultured at 37 °C in a humidified incubator with 5% CO_2 in air. After 5 ~ 6 days, cells reached confluence and culture media in the upper chamber was removed to establish an air-liquid interface at the apical surface and to feed cells from only the basal side. In order to assess the viability of cells in the culture system, live/dead staining with Syto9 (Molecular Probe, OR) and propidium iodide (Molecular Probe, OR) was performed. PBS was first flushed through the channel to wash cells and a mixture of Syto9 and propidium iodide was gently perfused into the upper chamber. The channel was incubated at 37 °C for 5 minutes before imaging.

In order to demonstrate flow conditions in which pulmonary epithelial cells are mechanically stressed and damaged by moving fluids, an experimental setup shown in Figure 2 was used to generate a flow of an air finger or a liquid plug, which is physiologically relevant to airway closure/reopening [4-6]. A blunt syringe needle was inserted into the silicone tubing connected to the inlet of an upper chamber and a small amount of compressed air was injected sequentially into the stream of culture media entering the upper chamber to create air bubbles or liquid plugs sliding along the upper chamber.

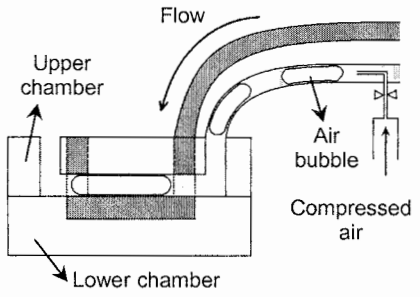

Figure 2. Experimental setup to generate air bubbles and liquid plugs moving in the upper chamber

3. Results and discussion

Figure 3 shows micrographs of cells at different stages of cell growth. In the regions near the inlet and outlet without a membrane, a majority of cells was observed to attach to the PDMS surface and started spreading within 4 hours after seeding. Over time under a perfusion culture condition, the cells exhibited a monolayer growth pattern with intercellular junctions and the presence of lamellar bodies around their nuclei, which are characteristic of type II alveolar epithelial cells. The cells remained proliferative until they formed a confluent monolayer (5 days after seeding). Bright field imaging of cells growing on the membrane was hampered by a background from the porous membrane and the micrographs from live/dead staining shown in Figure 3b and 3c were used to qualitatively evaluate the conditions of cultured cells. It was found that more than ~95% of cells on the membrane were alive after 5-day culture and most of the dead cells were aligned along the sidewalls of the channel. High viability of cells cultured under an air-liquid interface condition for 3 days after the establishment of the interface demonstrates that the channel system successfully provides *in vitro* culture conditions that closely mimic a polarized *in vivo* cellular environment. Other cells on the membrane or PDMS surface that were not fed from a basal side while there was an air-liquid interface at the apical side were found to be dead.

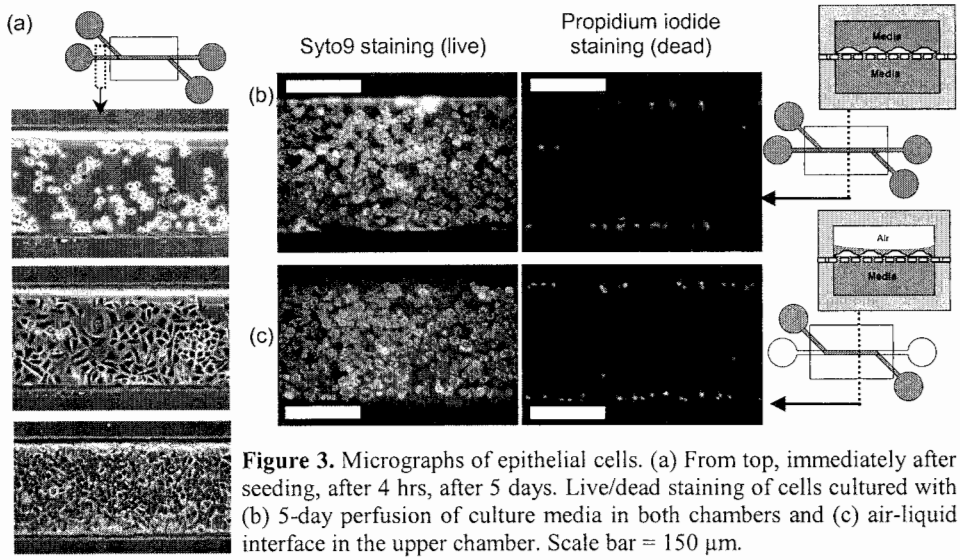

Figure 3. Micrographs of epithelial cells. (a) From top, immediately after seeding, after 4 hrs, after 5 days. Live/dead staining of cells cultured with (b) 5-day perfusion of culture media in both chambers and (c) air-liquid interface in the upper chamber. Scale bar = 150 μm.

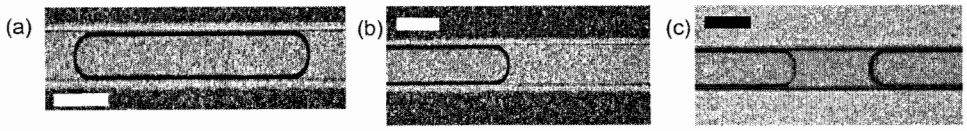

Figure 4. Different types of air-liquid two-phase flows in the upper chamber. (a) air bubble, (b) semi-infinite liquid plug, (c) finite liquid plug. Size bar = 300 μm. A = air, L = liquid.

Figure 4 shows different types of air bubbles or liquid plugs moving in the upper chamber without cells on the membrane. The length of air bubbles could be controlled by changing the amount of injected compressed gas and the velocity of moving fluids could also be manipulated by varying the flow rate of culture media advancing through the upper chamber.

5. Conclusions

We have demonstrated a successful *in vitro* microfluidic culture of lung epithelial cells and generation of physiologically relevant air-liquid two-phase flows in the microscale. This system will provide a reliable means to investigate the effect of fluid mechanical stresses on lung epithelial cells and the pathogenesis of related pulmonary diseases.

Acknowledgements

We thank Whitaker Foundation, NSF, and NIH for financial support.

References

[1] M. Kraft, *Eur. Respir. J.* **14**, 1403-1417 (1999)
[2] C.C. Dos Santos, A. S. Slutsky, *J Appl. Physiol.* **89**, 770-783 (2000).
[3] A. M. Bilek, K. C. Dee, D. P. Gaver, *J Appl. Physiol.* **94**, 770-783 (2003).
[4] K. J. Cassidy, N. Gavriely, J. B. Grotberg, *J. Biomech. Eng.* **123**, 580-589 (2001).
[5] P. D. Howell, S. L. Waters, J. B. Grotberg, *J. Fluid Mech.* **406**, 309-335, (2000).
[6] S. L. Waters, J. B. Grotberg, *Phys. Fluids* **14**, 471-480 (2002).

A NEW DESIGN FOR A FULLY CONTROLLED HIGH-THROUGHPUT POLYMERASE CHAIN REACTOR FOR RARE CARCINOGENIC CELL DISCOVERY

Mark Davies, Tara Dalton, Ronan Grimes
Stokes Research Institute, University of Limerick, Limerick, Ireland

Abstract
This paper describes a novel design for a high throughput polymerase chain reactor for rare carcinogenic cell discovery. The device uses a combination of viscous and buoyancy pumping to circulate reactants around the required reaction temperature zones. Contamination of solid surfaces is prohibited by the suspension of the reactants in oil droplets, which in turn are suspended in an immiscible carrier fluid. Fluid to fluid interactions control fluid temperature and reaction dwell times. Numerical predictions of flow and heat transfer for the device are presented here and show that high ramp rates between reaction temperatures are achievable. Predicted cycle times are shown to compare favorably with those found in the latest literature.
Keywords: PCR, fluidic control, carrier fluid

1. Introduction

Population screening for early diagnosis of cancer has the potential to greatly reduce both the degree of morbidity and the rate of mortality. It is expected that the earliest, most successful screens will be those that look for genetic markers that can be used to find how far in a sequence of mutations a cancer has progressed and estimate the number of mutated cells in the sample. Real time multiplexed Polymerase Chain Reaction (PCR) is the most likely method to achieve this.

To screen large populations, the cost of testing for the presence of DNA mutations must be greatly reduced. A means to achieve this is the development of reusable systems that will automatically prepare and amplify the genetic samples with a high degree of specificity and efficiency. This paper presents the design and analysis of a new concept for a continuous microfluidic PCR design which allows for the control of all of the thermal design parameters, including ramp rates, dwell times and number of completed cycles. The prepared DNA volume is segmented into micro droplets which are driven through the thermal cycle by natural convection. The novelty in the design is that all of the thermofluidic control is achieved by immiscible fluid to fluid interaction. This may be seen as an extension of the move from hard to soft lithography with the aim to produce a biomimetic amplification, the analogy being between the droplets and the biological cells.

2. Device Design

Figure 1 shows the design of the system. The micro water droplets containing the reactants are suspended in an oil carrier fluid. The use of the carrier fluid prohibits contamination of the system surfaces, as it separates the reactants from the walls. The carrier fluid and micro droplets are continuously circulated around the three temperature zones. As illustrated in figure 1, control fluid enters and leaves the system at each of the three control zones. This control fluid fulfils three roles:

- Through fluid to fluid heating and cooling the control fluid cycles the temperature of the carrier fluid and the micro droplets.
- Variation of the control fluid velocity controls the dwell time of the micro droplets at each temperature.
- The control fluid aids in circulating the carrier fluid around the system through viscous pumping

In addition to the viscous pumping provided by the control fluid, circulation of the carrier fluid and micro droplets is aided by the buoyancy force generated by the temperature difference between the two sides of the system.

The supply of control fluid to the control zones is via a separate closed pumped loop for each of the zones. In this way, the flow rate into each of the control zones equals the flow rate out and the exchange of control fluid between control zones is prevented.

The device illustrated in figure 1 has been manufactured and work is currently underway to perform the PCR reaction and to measure fluid temperature and velocity throughout the system.

3. Numerical Analysis

Numerical predictions of flow and heat transfer in the system were performed using the Computational Fluid Dynamics (CFD) package, Fluent version 6. A two dimensional steady state solution was computed using the segregated solver. Due to the low operational Reynolds numbers laminar models were used. Buoyancy was modelled using the Boussinesq approximation. The control and carrier fluids were both modelled as silicon oil with viscosity of 0.02PaS, specific heat capacity of 1400 j/kgK, conductivity of 0.14 W/mK, coefficient of thermal expansion of 0.0008 K^{-1} and density of 1000 kg/m^3 at 20°C. Solid regions within the device were modelled as Perspex with conductivity of 0.21w/mK. Details of the boundary conditions which were set are given in table 1. As can be seen from predictions of figures 2 and 3, the closed loop pumping configuration described in section 2, is modelled in Fluent by directly connecting the inlet to the outlets of the control fluid channels. A numerical pump in these loops provides the pressure rise which results in the inlet and outlet flow rates indicated in table 1 for each zone.

Table 1. Boundary conditions in the computational model of the PCR device

Zone	Inlet boundary condition	Outlet boundary condition
95°C zone	Mean velocity in = 0.05m/s Temperature in = 382K	Mean velocity out = 0.05m/s
68°C zone	Mean velocity in = 0.056m/s Temperature in = 310K	Mean velocity out = 0.056m/s
72°C zone	Mean velocity in = 0.042m/s Temperature in = 354K	Mean velocity out = 0.042m/s

4. Results and discussion

Figure 2 shows the predicted temperature distribution across the PCR device. It can be seen here that in each of the zones, the required reaction temperatures are reached by the carrier fluid. Figure 3 shows the velocity distribution in the 68°C control zone. Although difficult to see due to the large ratio of control to carrier fluid velocity, the combination of viscous and buoyancy driving pressures results in a carrier fluid velocity of approximately 0.01m/s in the negative Y direction. Although not shown here similar velocity patterns were observed in each of the other control zones. Figure 4 shows the predicted temporal temperature variation of a 0.5mm reaction droplet as it is carried around the reaction zones by the carrier fluid. The overall cycle time predicted here for the reaction droplet is approximately 25s. High ramp rates can clearly be seen, in particular between the 90°C denaturisation and the 68°C annealing zone. Temporal temperature gradients here are approximately 10°C/s. Both the cycle times and temperature transition rates compare favorably with those demonstrated in [1]. Optimization of the device will further improve these performance parameters.

5. Conclusions

- The design of a novel fluid controlled device for high throughput PCR has been presented.

- Numerical predictions of flow and heat transfer within the device illustrate high levels of performance in terms of overall cycle time and temperature transition rates.
- Optimisation of the device will further enhance cycle times and temperature transition rates.

References

[1] B.C. Giordano, J. Ferrance, S. Swedberg, A.F.R. Huhmer, and J.F. Landers, *Analytical Biochemistry,* **291**, 124-132 (2001).

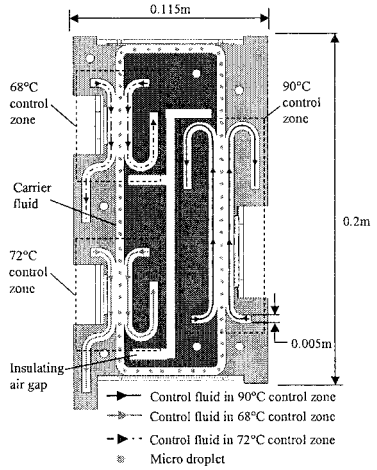

Figure 1. Schematic of the continuous micro fluidic PCR system design. Note: through plane depth of the system allows several micro reactors to be processed in parallel.

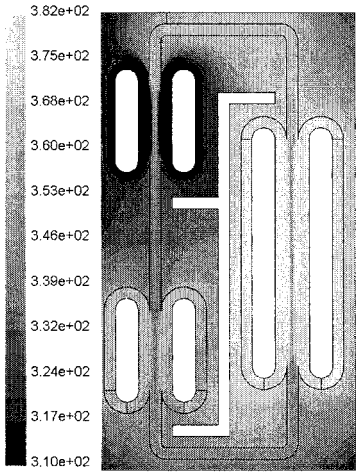

Figure 2. Numerical prediction of the temperature distribution in the PCR device. The contour legend is in K.

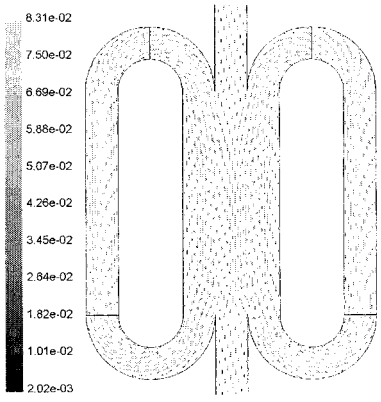

Figure 3. Numerical prediction of the velocity distribution within the 68°C zone of PCR device. The contour legend is in m/s.

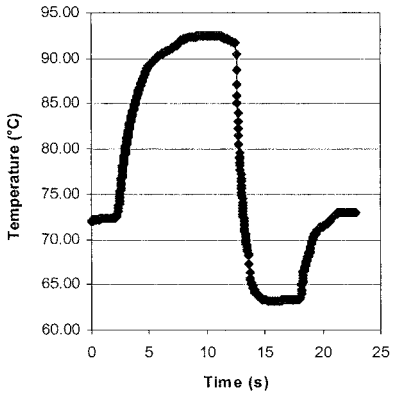

Figure 4. Predicted temporal variation of temperature for a micro droplet carried through one full cycle.

DEVELOPMENT OF A MICROFABRICATED DEVICE FOR FORENSIC DNA ANALYSIS OF SEXUAL ASSAULT EVIDENCE: INTEGRATION OF CELL SEPARATION AND DNA EXTRACTION

Katie M. Horsman[1], Susan L.R. Barker[1], Joan M. Bienvenue[1], Jessica C. Voorhees[1], Kiev Blaiser[1], Benjamin Schroeder[1], Katherine A. Koen[1], Greg Weingart, James P. Landers[1,2], and Jerome P. Ferrance[1]

Departments of [1]Chemistry and [2]Pathology, University of Virginia, Charlottesville, VA 22904

Abstract

The work herein describes the development of integrated microchip sample processing for sexual assault evidence. The methods integrated include cell separation and DNA extraction to provide independent DNA evidence from the victim and perpetrator's cells. The microdevice provides a rapid method compared to conventional techniques and provides DNA that is suitable for genetic analysis using traditional STR amplifications.

Keywords: differential extraction, cell separation, forensic DNA analysis, solid-phase extraction

1. Introduction

Due to the increasing popularity and utility of forensic DNA analysis, there currently exists a significant backlog of cases waiting to be analyzed by forensic laboratories particularly those related to sexual assault evidence. The need for integrated and automated sample processing and analysis cannot be understated. Microdevices provide a valuable platform for such integration and automation of sample processing steps. Differential extraction is the conventional method for isolating male and female fractions of DNA from rape kit evidence, typically a vaginal swab containing a mixture of sperm and vaginal epithelial cells. This time-consuming laboratory process is not easily translated to a microchip format. Therefore, we have developed an alternative microchip-based method that will reduce the time associated with isolation of the male and female DNA, while maintaining or improving the percent recovery and purity of each DNA fraction. The integrated design combines a swab extraction macro-to-micro interface with an integrated microdevice for separation of sperm cells from epithelial cells, cell lysis, and finally solid phase extraction of male and female DNA from the separate cell fractions. This integrated microchip allows input of a complex forensic sample and yields purified male and female DNAs that are suitable for either traditional PCR or IR mediated microchip PCR amplification in a sequential device.

2. Methods

To load the cell mixture into a microchip, the cells must be eluted from the vaginal swab in an intact manner. An alternative solution to the conventional 24 hour incubation has been developed to facilitate rapid recovery of intact sperm and epithelial cells from the swab using a mixture of five enzymes. Following a 120 minute incubation of the swab in the elution cocktail in a microcentrifuge tube, centrifugal motion is employed to remove the solution from the swab and load the cells into the microdevice using the interface shown in Figure 1.

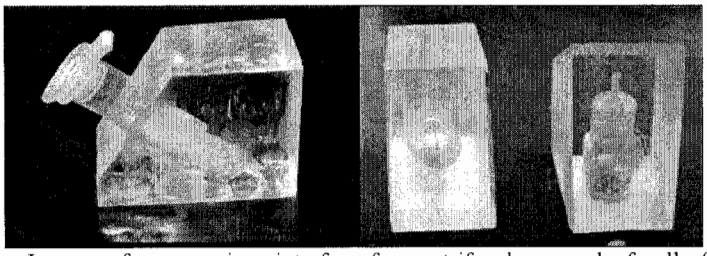

Figure 1. Images of macro-micro interface for centrifugal removal of cells from a swab and transfer to a microdevice.

Separation of sperm from vaginal epithelial cells in the integrated microdevice exploits the differential physical properties of the two cell types such as density, size, shape, and proclivity for adsorption to the microchannel surface. Following a 10 minute settling time in which the epithelial cells settle and adsorb to the glass surface of the inlet reservoir, pressure driven flow (~0.5 μL/min) generated by a syringe pump is used to direct sperm cells through a microchannel (Fig. 2a) to a collection reservoir while retaining epithelial cells in the inlet reservoir (Fig. 2b).

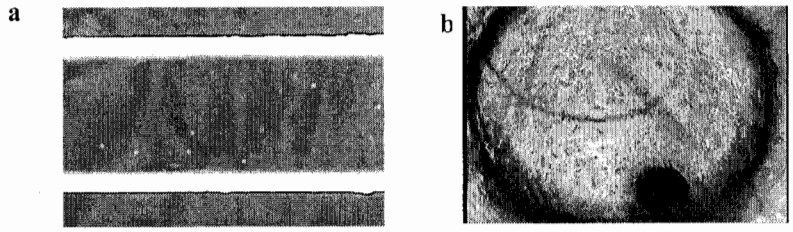

Figure 2. a) Sperm cells travelling down the separation microchannel; b) Epithelial cells remaining in the inlet reservoir following separation.

On-chip cell lysis, using 8M guanidine HCl, and 40 mM DTT, is directly followed by microchip solid phase DNA extraction from the sperm and epithelial cell fractions on sol-gel/silica bead extraction beds. The cell lysate is loaded onto the sol gel/silica bead extraction bed in the lysis buffer. Proteins are washed from the bed with 80% isopropanol, and DNA eluted in 1X TE buffer.

3. Results and discussion

The alternative method of cell elution from a cotton swab yields on average more of the sperm cells deposited than the conventional method, while also yielding intact epithelial cells for introduction into the microdevice. Microchip separation of sperm and epithelial cells results in clean sperm cell fraction as indicated by visual monitoring via microscope/DVD recording during the progress of the separation.

Microchip DNA extraction (Fig. 3) results in PCR-amplifiable DNA consistent with that obtained by conventional methods, indicating that the integrated device will allow rapid analysis of forensic samples with similar or improved performance as compared with macroscale laboratory techniques. Short Tandem Repeat Analysis (STR) of the sperm fraction collected following separation resulted in the DNA profile of the semen donor.

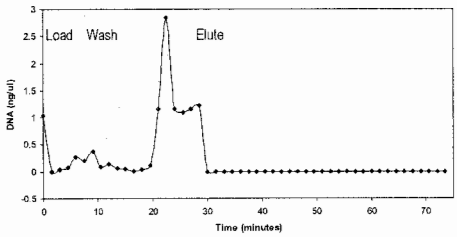

Figure 3. DNA Elution profile of sperm lysed using 8M guanidine HCl/10% Triton X100 and loaded onto the on a sol-gel/silica bead bed. Proteins are washed from the bed with 80% isopropanol solution and DNA eluted in 1X TE buffer.

4. Conclusions

The selective isolation of DNA from male and female cells for genetic identification in forensic analysis of sexual assualt evidence on microdevices is shown. The integrated device relies on elution of sperm and epithelial cells intact from vaginal swabs and transfer of these cells to the microdevice using a macro-to-micro interface. The cells are then separated based on physical properties of the cells and the cells then lysed and the DNA extracted. The Purified DNA is suitable for further genetic analysis.

PHOSPHOPEPTIDE ENRICHMENT ON A MICROCHIP INTEGRATED WITH MASS SPECTROMETRY

Guihua Yue[1], Catherine J. Balchunas[1], Erin Jeffery[1], Joshua Coon[1], James P. Landers[1, 2] and Jerome P. Ferrance[1]

Departments of [1]Chemistry and [2]Pathology, University of Virginia Charlottesville, VA 22904

Abstract

In this study, an integrated microchip with protein digestion and immobilized metal affinity chromatography (IMAC) was established for phosphopeptide enrichment. Trypsin agarose beads and iminodiacetic agarose beads were packed into sequential channels in this microdevice to provide trypsin digestion and affinity capture of phosphopeptides. β-casein was utilized to evaluate this integrated microchip with two phosphopeptides fragments expected in the eluent. Five phosphopeptides were actually detected using capillary electrophoretic (CE) separation of the products due to the incomplete cleavage of the protein. To analyze the enriched phosphopeptide directly from the microchip with mass spectrometry, a microchip interface was also developed. A porous junction was fabricated on the microchip for high voltage of electrospray ionization (ESI). In addition, the microchannel outlet was designed as a sharp point for high efficiency ionization. The performance of this interface was demonstrated by the analyses of protein and small peptides.

Keywords: phosphopeptide, IMAC, mass spectrometry, microchip

1. Introduction

Phosphopeptide identification is an important part of proteomic research because phosphorylation is a major regulation point for many proteins. Due to the importance of phosphopeptide determination, a sensitive and convenient technique platform is required. Protein digestion followed by immobilized metal affinity chromatography (IMAC) and LC-mass spectrometry (MS) have becoming the key tools for phosphorylation studies [1].

Microchip techniques provide a new method to integrate all of these processes and reactions, and scale them down to allow the use of small sample volumes [2]. In addition, microchips have been shown to provide an interface for ESI analysis of small molecules by MS detection [3]. This study developed a microchip platform for phosphopeptide enrichment and analysis with integrated proteolytic digestion, IMAC, and reverse phase function. To integrate these processes directly with MS analysis, an interface was designed utilizing a porous junction and a sharp tip to produce efficiency ionization. These microchips will be easily integrated for direct MS analysis of the captured and eluted phosphopeptides.

2. Experiment

(1) Agarose beads with immobilized trypsin and iminodiacetic acid (IDA) were washed with 0.1M NH_4HCO_3 and 2% acetic acid respectively. IDA agarose beads were further washed with 0.1M $FeCl_3$ to immobilize Fe^{3+} then rinsed with 2% acetic acid to remove any unbound Fe^{3+} ions. Beads were packed into microchannels using a slight vacuum.

(2) Protein digestion was performed in 0.1M NH_4HCO_3 solutions. The IMAC enrichment process was performed by mixing the peptide solution with acetic acid to reduce the pH for phosphopeptide capture. Solutions were driven with a syringe pump at 0.5ul/min through the trypsin beads to the IMAC beads.

(3) CE separations were performed under these following conditions: running buffer - 50mM phosphate buffer (pH 2.5); separation voltage - 10kv; UV detection at 214nm.

(4) Mass spectrometry data was obtained with a Finnigan MAT LCQ MS.

3. Results and discussion

Initial development of this integrated microdevice investigated proteolytic digestion coupled to IMAC enrichment. Sequential microchannels packed with trypsin immobilized agarose beads and IMAC agarose beads were used to digest and capture phosphopeptides from β-casein. β-casein digestion produces two phosphorylated fragments, one containing four phosphorylation sites (tetraphosphopeptide) and one containing one phosphorylation site (monophosphopeptide). Five phosphopeptides from the resulting peptide mixture were actually enriched on the IMAC microcolumn and detected using CE (Fig. 1). The collected sample was also analyzed with cLC/MS with MS/MS data used to identify the expected phosphopeptides (Fig. 2). As expected the tetraphosphopeptide was found in abundance due to the multiple binding sites with the IMAC column. The monophosphopeptide fragment was not identified, but a database search showed multiple peptides with a single phosphorylation site from β-casein, formed due to incomplete cleavage by the immobilized trypsin beads (data not shown here).

The microchip interface for MS was also developed to allow direct analysis of the enriched phosphopeptide with MS. A porous junction was fabricated on the microchip by etching the glass above the channel in one region of the microdevice until a current could be measured through the channel. Solution spreading on the flat face of the microchip as it exits the channel is normally a problem leading to formation of large liquid droplets as the infused sample is sprayed. This leads to loss of resolution as the droplet volume may be larger than the channel volume. To address this problem, the microchip was cut to form different angles at the outlet, and the edge of the microchip was sharpened on all sides. Fig. 3 shows the Taylor cone formed from a sharpened microchips at the outlet of the microchannel when high voltage was applied. A stable electrospray was generated for more than 20 min with this device when connected with the MS. Lysozyme was injected to test the efficiency of ESI from this interface and Fig. 4 shows that 87 fetomole/ul lysozyme can be determined with this microchip interface. A weir was also designed in the microchannel of this microchip interface for packing C18 reverse phase beads. The high efficiency and stable ESI data produced from this microchip interface show that protein digestion, IMAC enrichment, and reverse phase separation or desalting are integrated easily with MS.

4. Conclusions

This microchip allows protein digestions to be coupled to on-line IMAC enrichment on a single microchip. What is more important, with the improvements in the interface between microchip and MS, the phosphopeptide can be determined directly with MS after eluted from the affinity column. This microchip provides a new approach compared with traditional column systems for phosphopeptide enrichment and determination. The interface between microchip and MS detection is important, not only for phosphopeptide enrichment on microchip, but also for other applications of protein determination on microchips.

References

[1] S. B. Ficarro, M. L. McCleland, et al, *Nat. Biotechnol.*, 2002, **20**, 301-305
[2] B.E.Slentz, N.A. Penner, F.E. Regnier *J Chrom A* 2003; **984**, 97-107
[3] R.S. Ramsey, J.M. Ramsey, *Anal.Chem.*, 1997, **69**, 1174-1179

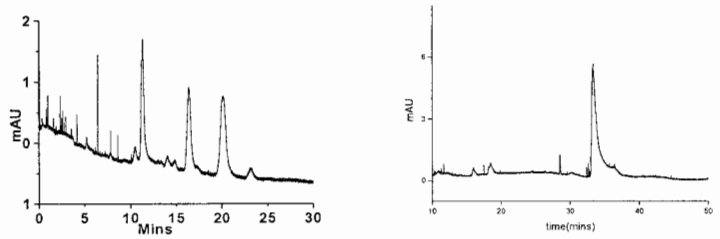

Figure 1. CE separation of the eluant from the integrated trypsin digestion - IMAC enrichment microchip

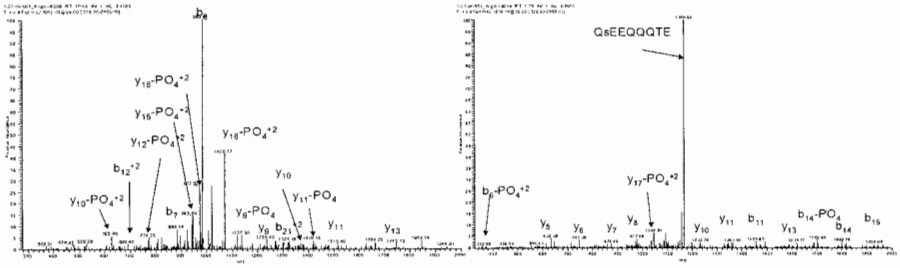

Figure 2. MS/MS spectra for the phosphopeptides eluted from the integrated microchip.

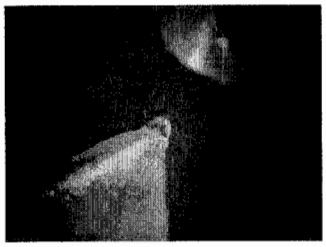

Figure 3. Taylor cone formation on a sharp tip microchip

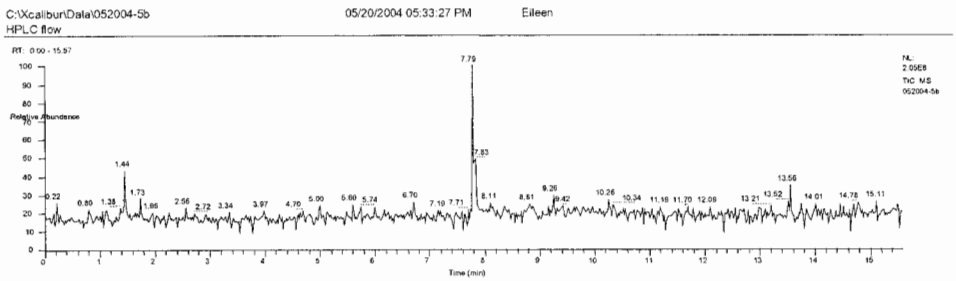

Figure 4. Electrospray from the microchip interface

AUTOMATED EXTRACTION AND PURIFICATION DEVICE OF DNA FROM CELLS EMPLOYING ELECTRIC AND HYDRO DRAG FORCE FIELD

Kouji Yuhki[1], Yuichi Tomizawa[1], Yasutaka Morita[1], Eiichi Tamiya[1], and Yuzuru Takamura[1,2]
[1]School of Materials Science, Japan Advanced Institute of Science and Technology (JAIST)
1-1 Asahidai, Tatsunokuchi, Ishikawa 923-1292, Japan
[2]PRESTO/JST, Japan
E-mail: takamura@jaist.ac.jp

Abstract
Extraction and purification of DNA/RNA from cells on chip is an important element for DNA-based micro total analysis system. Authors developed automated extraction and purification device using by taper shaped fluid cannel, electric and hydro drag force field, and valve switching system. It can manipulate extraction and purification of DNA from cells easily and rapidly.
Keywords: DNA trap, DNA extraction, selective trap, hydro drag force

1. Introduction

DNA analysis increases its importance in various fields. Consequently, DNA extraction technique from cells became also important. Already, some automated extraction devices are available in the market. However, it is still required that more simple and rapid method which is able to integrate on micro total analysis systems. We previously reported a DNA trap employing mutually reverse electric force and hydro drag force fields, and demonstrated the extraction and concentration using commercially available pure DNA [1]. In this report, we demonstrate automated extraction and purification of DNA from practical cell sample, and discuss the two lysis methods suitable for this extraction method.

2. Experimental

Fig. 1 shows the micro channel pattern. The microchip was fabricated from PDMS using a standard photolithography technique and SU-8 thick resist molding. The microchip has two channels that are trapping channel and recovery channel. Two channels are connecting valve system. Chip is totally 1.2 mm long, 100 μm wide, 10 μm deep, and there are 1taper shaped channel at the center. Micro fluidic chip is consisting of 3 layer to create valve system Fig. 2 shows experimental set up. A solution of cell lysis and DNA stained solution YOYO-1 in 0.5 Tris borate EDTA buffer was introduced into the chip, and the motion of DNA was recorded by a fluorescence microscope with highly sensitive CCD video camera. The hydro drag force was generated by pressure driven flow of the buffer solution in the channel when a constant air pressure was applied to one of the inlets using a syringe and pressure gauge. The electric force was applied by Pt electrode. By the resultant force field of two different forces, DNA either migrated through or got trapped near the narrowest position in the channel. Valve operation is shown schematically Fig. 3. (a) Extract and concentrate DNA from cell lysis solution by electric and hydraulic force filed. (b) Confine the concentrated DNA by closing the valves. (c)

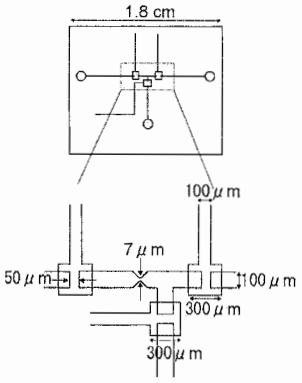

Figure 1. Channel pattern and Schematic of the automated DNA extraction and purification device.

Recovery DNA to recovery channel. The figures (d) and (e) represent close and open states of valves, respectively.

Cell lysis method

We examined two cell lysis solutions. One is 75 mM hypotonic solution, and the other is 0.01 %sodium dodecyl sulfate (SDS), surface-active agent. Jurkat, human leukocyte cell was used as sample cell. At first, cells were prepared as the concentration of 1.6 x 10^5 /ml, and then each lysis agent was added in order to elute DNA from the cell. After the lysation, the solution was stained by YOYO-1 fluorescence dye, put into the chip to extract DNA.

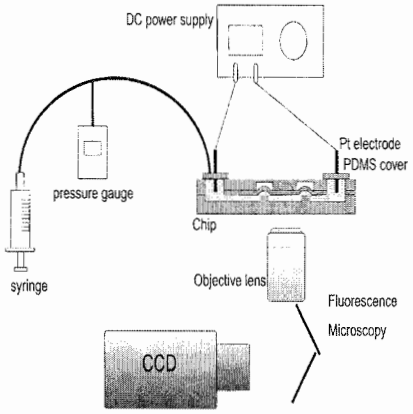

Figure 2. Schematic of the experimental setup

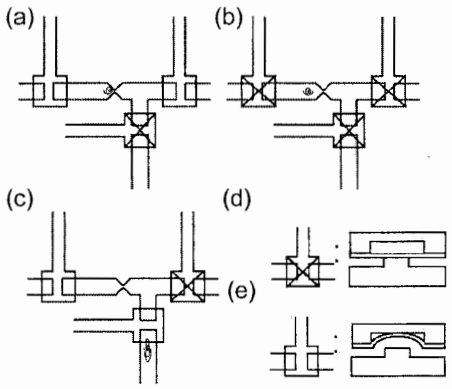

Figure 3. Operation scheme of a extraction and recovery of DNA.

3. Result and discussion

Fig. 4 shows a series of fluorescence images during extraction and recovery DNA; (a) DNA is trapped by electric and hydrodynamic fields of 110 V and 10 kPa. (b) DNA was concentrated near narrowest position . (c) DNA is retrieved to recovery channel. These operations were automated by computer control.

Fig. 5 shows the trap condition of DNA at extracted from Jurkat cell by hypotonic solution. The area indicated by broken lines represents the condition in which the trap occurs. The trap area for the solution by SDS lysis method showed similar feature.

We measured total extraction yield for each lylsis method together with that for commercially available T4 DNA solution in TBE buffer as a comparison. The best yield for hypotonic water case was revealed to be 5% while that for SDS case was 50%. The yield for pure T4 case was 80%. The low yield of hypotonic water case is considered to be due to poor isolation of DNA from proteins or other substances. It means that the isolation of DNA is important using the DNA trap. The extraction and purification was achieved using this device with SDS lysis method.

In order to confirm that recovery sample surely contains DNA, we performed PCR amplification in which the amplification target was a part of beta-actine gene. Fig. 6 shows the PCR products with the template of the extraction and recovery DNA by the trap from Jurkat cell. (M) , (1), (2), (P), and (N) show Marker DNA, extracted samples 1 and 2, positive control, and negative control. Bands at 300bp correspond to beta-actine DNA. From the result, we confirm that the trapped specimen is actually

DNA.

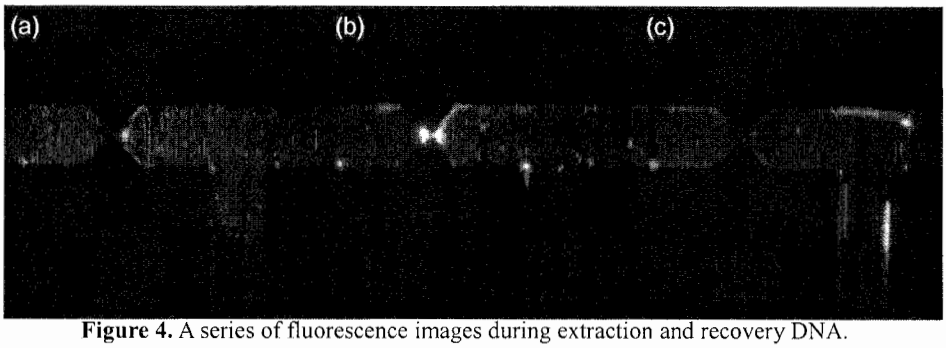

Figure 4. A series of fluorescence images during extraction and recovery DNA.

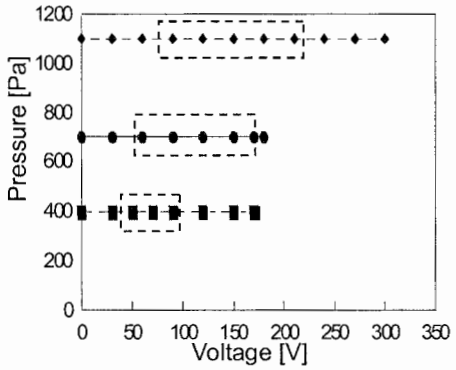

Figure 5. Trap area of DNA at extracted from Jurkat by hypotonic solution.

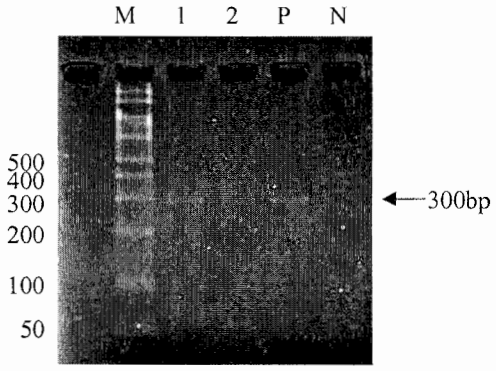

Figure 6. PCR products of extraction and recovery DNA from Jurkat cell by the trap. (M) , (1), (2), (P), and (N) show Marker DNA, extracted samples 1 and 2, positive control, and negative control. Bands at 300kbp correspond to beta actine DNA.

4. Conclusion

An automated extraction and purification of DNA from practical cell sample was demonstrated employing electric and hydro drag force field. For this method, SDS is suitable for lysis agent. The best extraction yield from cell is currently 50%.

5. Reference

[1] Y. Takamura et al., Proc. of μTAS 2002, Nara, Japan (2002) 317-319.

HIGH-THROUGHPUT POLYMERASE CHAIN REACTION – CAPILLARY ARRAY ELECTROPHORESIS (PCR-CAE) MICROCHIP

Chung N. Liu, Nicholas M. Toriello[2], Roya Maboudian and Richard A. Mathies[1]

Dept. of Chemical Engineering, University of California, Berkeley, CA 94720, USA
[1]Dept. of Chemistry, University of California, Berkeley, CA 94720, USA
[2]UC Berkeley/UC San Francisco Joint Bioengineering Graduate Group, University of California, Berkeley, CA 94720, USA

Abstract

We have developed a high-throughput and fully-integrated polymerase chain reaction-capillary array electrophoresis (PCR-CAE) microchip with nanoliter reactor volumes specially designed to perform highly parallel genotyping analyses. Ti/Pt resistance temperature detectors (RTDs) and Ti/Ni heaters are integrated on the microchip using a scalable radial design to provide precise control of the thermal cycling process. PDMS membrane valves are employed to control and localize PCR reagents. The device allows direct coupling of PCR reactions to CE on chip to eliminate the possibility of sample contamination during sample handling, and to reduce reagent usage and analysis time, and should be extendable to the preparation and analysis of DNA sequencing samples. Multiple parallel PCR-CAE assays are performed and compared with flanking DNA sizing ladder separations.

Keywords: array PCR, capillary array electrophoresis, bioprocessor

1. Introduction

Our previous work developing microfabricated integrated genomic analysis systems has demonstrated rapid PCR-CE analysis in a single 280 nL reactor having an integrated heater and RTD on a glass substrate [1]. The goal of the work presented here is to develop an array of integrated PCR-CE systems that are capable of performing multiple PCR-CE analyses in parallel, thus expanding the current PCR-CE technology. The challenges in arraying the PCR-CE microchip are developing robust fluidic components for positive control of the PCR reagents during thermal cycling, designing an easily fabricated heater that addresses the 12 PCR reactors in parallel as well as optimizing the location of multiple RTD sensors to monitor the sample temperatures.

2. Design

In our design (Figure 1), PCR chambers (~150 nL) are isolated from the loading ports by PDMS membrane valves [2] and are directly connected to a CE microchannel for product separation and analysis. PDMS membrane valves localize and prevent PCR reagent evaporation during thermal cycling. The microfabricated heaters and the PCR chambers are placed away from the CE microchannels to avoid evaporation of buffer in cathode reservoirs and to minimize the heating of the cross injection region during thermal cycling. The PCR-CAE microchip uses a ring heater made of Ti/Ni to provide uniform heating for all 12 reactors while three equally spaced microfabricated RTDs made of Ti/Pt are integrated on the device to provide precise temperature sensing, ensuring temperature uniformity for optimal thermal cycling performance.

3. Experimental

The CE separation medium (1.5% (w/v) hydroxyethyl cellulose (HEC) in 1X Tris Acetate EDTA (TAE) buffer with 1 μM thiazole orange) was loaded into the chip through the anode. Samples were loaded into the chambers using negative pressure with the valves open. The valves were then closed and the PCR chambers were thermally cycled with a LabVIEW program. These

integrated components have achieved heating rates of 20 °C/s and passive cooling rates of 5 °C/s. A cycling rate of 1 minute per cycle is demonstrated, allowing a typical 25 cycle PCR to be completed in 25 minutes. We have achieved a 3-fold improvement over a conventional thermal cycler with a ramp rate of 3 °C/s and a cycling rate of 3 minutes per cycle. Active cooling could be employed to further reduce the thermal cycling time. The thermal cycling profile is shown in Figure 2. Once thermal cycling was completed, all samples were directly injected from the reaction chamber to the separation channel with a field of 112 V/cm between sample (S) and waste (W) for 20 s; separations were performed by applying 236 V/cm between the cathode (C) and anode (A). CE analyses were detected using the Berkeley rotary confocal fluorescence scanner that interrogates all separation channels simultaneously [3].

4. Results and Discussion

The PCR-CAE microchip was evaluated by performing multiple parallel PCR-CAE analyses of a 136 bp amplification product from M13/pUC19 cloning vector (New England Biolabs, Beverly, MA) in the reaction chamber. Chambers 1 through 11 were loaded with M13 PCR reagents while chamber 12 was loaded with pBR322-BstN1 DNA sizing ladder to verify product size. PCR was performed in 25 minutes, followed by simultaneous injection and CE analysis of all 12 chambers (Figure 3). Complete (25 cycles) PCR-CE analysis was finished in 30 minutes. This represents an average analysis time of 2.5 minutes/sample, a 6-fold improvement compared to our previous rapid single PCR-CE device. Products were found in all chambers with M13 PCR reagents, showing successful application of the PCR-CAE microchip. Product peak intensity variation was caused by variations in the liquid-gel interface in the PCR reaction chamber. Further optimization of the sample loading should eliminate this problem. It should be noted that primer dimers and nonspecific amplification products were not observed, indicating that PCR-CAE microchip achieved efficient and highly specific amplifications. PCR-CAE microchip was reused with water rinse between runs, with run-to-run contaminations not observed. The device was capable of performing more than 30 runs without any degradation in performance. With this design, it is feasible to array up to 100 PCR-CE analyses for performing highly parallel analyses on a 6" glass substrate. This approach should also be extendable to the preparation and analysis of DNA sequencing samples.

Acknowledgments

This research was funded by the National Institutes of Health (HG01399). C. N. Liu was partially supported by a ChevronTexaco Graduate Fellowship.

References

[1]. E. T. Lagally, C. A. Emrich, and R. A. Mathies, Lab-on-a-Chip, 1 (2), 102-107 (2001).
[2]. W. H. Grover, A. M. Skelley, C. N. Liu, E. T. Lagally, and R. A. Mathies, Sensors & Actuators B, 89 (3), 315-323 (2003).
[3]. J. R. Scherer, I. Kheterpal, A. Radhakrishnan, W. W. Ja, and R. A. Mathies, Electrophoresis 20, 1508-1517 (1999).

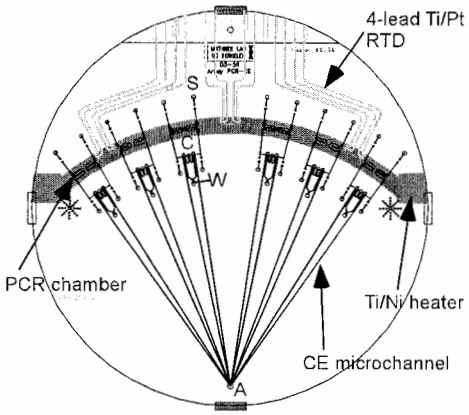

Figure 1. PCR-CAE integrated genetic analysis system. Twelve 150- nL PCR chambers are connected to microchannels for CE product analysis. PCR reagents are localized in the PCR chamber with PDMS membrane valves. Integrated heaters are shown in red and RTD's are shown in green.

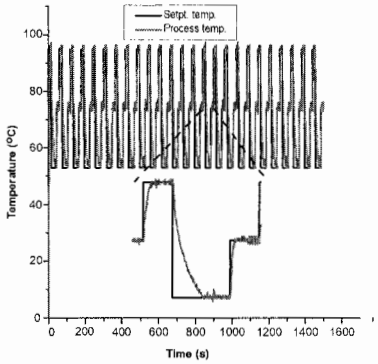

Figure 2. Thermal cycling profile for PCR-CAE device.

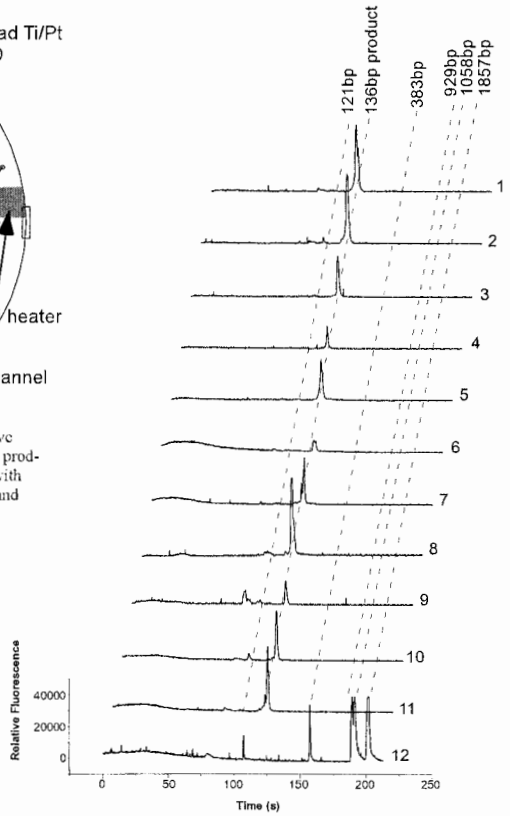

Figure 3. PCR-CAE analyses of M13 DNA targets at 10^3 copies/μL in 150-nL PCR reactors. Lanes 1-11: M13 136 bp amplification product. Lanes 12: pBR322- BstN1 DNA sizing ladder. Product peak intensity variation was caused by variations in the liquid-gel interface in the chamber. Data were offset by 5 s for clarity.

NON-CONTACT TEMPERATURE CONTROL OF MULTIPLEX PCR IN NANOLITER VOLUMES ON MICROCHIPS

Christopher J. Easley[1,*], Lindsay A. Legendre[1,*], Spencer R. Allen[1], Jerome P. Ferrance[1], James P. Landers[1,2]

Departments of Chemistry[1] and Pathology[2], University of Virginia, Charlottesville, VA, USA

[*] These authors contributed equally to this work.

Abstract

Extrinsic Fabry-Perot interferometry (EFPI) is utilized for non-contact temperature sensing to control infrared-mediated temperature regulation of nanoliter volumes on fluidic microchips. The temperature signal is used to control an IR light source and blower, making the entire temperature modulation process non-contact. The system has been used to control the temperature of enzymatic reactions performed on the microchip with the reaction products analyzed by a microchip separation.

Keywords: temperature, optical fiber, interferometry, PCR, multiplex

1. Introduction

Noninvasive measurement and control of temperature in small volumes is important for microscale chemistries such as labeling reactions, biochemical reactions, combinatorial chemistry, on-chip calorimetry, and microscale kinetic studies. Most microchip reactors to date employ contact devices such as thermocouples or thermopiles for sensing and resistive heaters or Peltier stages for thermal control [1, 2]. Contact sensing devices can perturb the system—sometimes completely inhibiting a reaction—and often necessitate some type of passivation. Additionally, most temperature sensors and heaters constructed onto the microchip involve lengthy and complicated fabrication steps. We present a completely non-contact system for small-volume temperature control with interferometric temperature sensing, infrared (IR) mediated heating, and forced air cooling. Since the IR-heater, blower, and sensor are separate from the microchip, the chip fabrication steps are minimized.

2. Theory

Extrinsic Fabry-Perot interferometry (EFPI) is an approach using interference pattern frequency analysis to determine the optical path lengths (OPL) between reflections from the various surfaces [3]. Using an optical fiber sensor positioned orthogonal to the microchip, the EFPI can measure the OPL between the chip surfaces and the end of the fiber (Fig. 1). Because OPL is directly proportional to refractive index, which has a nonlinear dependence on temperature, the temperature changes of the medium in the chamber can be calculated from the path length change through the solution. This non-contact temperature sensing approach is integrated for direct control of a non-contact heating method which relies on adsorption of IR radiation to heat solutions.

3. Experimental

The complete apparatus, including the temperature-sensing portion and the microchip reactor, is depicted in Fig. 2. A broadband IR source sends light through an optical coupler to the temperature-sensing optical fiber, aligned orthogonal to the microchip. The reference and sensing reflections are returned through the fiber, which is coupled to a miniature spectrometer consisting of a diffraction grating and a CCD array. The signal is fed to a laptop computer at which point frequency analysis is performed. The analyzed signal (OPL) is fed into an in-house LabVIEW application written to convert the OPL signal to a temperature and to control the tungsten IR heating lamp and cooling fan through solid state relays. A chrome mirror positioned above the microchip helps to promote efficient heating.

4. Results and discussion

The system has been shown to accurately control the enzymatic digestion of a 500-base pair amplicon of bacteriophage λ-DNA by restriction endonuclease *BssK I* on a microchip. The technique was also successfully applied to the highly temperature dependent polymerase chain reaction (PCR) for DNA amplification, demonstrating the first completely non-contact DNA amplification carried out on a microchip. These results show the utility of this non-contact temperature control method for application to small volume (~500 nL) enzymatic reactions on microchips.

A multiplex PCR has been developed using conventional amplification that will simultaneously test for organisms relevant to biowarfare (Fig. 3). The amplification generates unique fragments from three agents, specifically, the 16S rRNA region of *Campylobacter jejuni*, the invasiveness A gene of pathogenic *Salmonella*, and the virulence B gene of *Bacillus anthracis*. This multiplex reaction is performed on the microchip to show the utility of this non-contact system.

5. Conclusions

We have shown the use of the EFPI technology as an accurate temperature sensor which is also capable of controlling the temperature modulations that lead to a successful amplification of DNA. This approach of controlling microscale reactions—with heating, cooling, and temperature sensing being carried out in a completely non-contact fashion—could significantly impact the cost, speed of analysis, and ease of use, while keeping the microchip fabrication steps at a minimum.

References

[1] M. U. Kopp, A. J. de Mello, A. Manz, *Science*, **280**, 1046-1048 (1998).
[2] E. T. Lagally, J. R. Scherer, R. G. Blazej, N. M. Toriello, B. A. Diep, M. Ramchandani, G. F. Sensabaugh, L. W. Riley, R. A. Mathies, *Anal. Chem.*, **76**(11), 3162-3130 (2004).
[3] K. A. Murphy, M. F. Gunther, A. M. Vengsarkar, R. O. Claus, *Optics Letters*, **16**(4), 273-275 (1991).

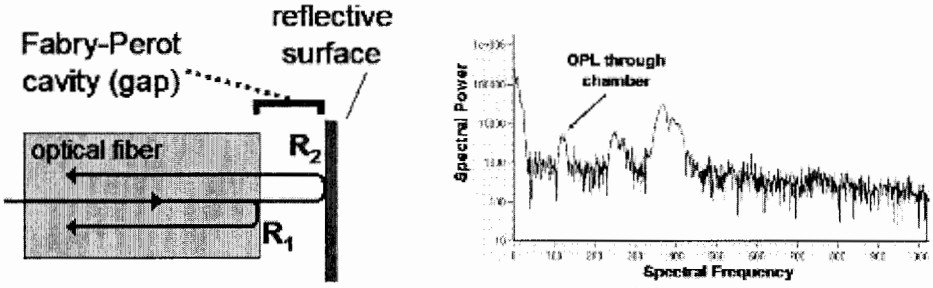

Figure 1. EFPI technology can be used to measure the optical path length through a Fabry-Perot cavity. In the simple case, reflections R_1 and R_2 will interfere, and the optical path length through the cavity can be extracted from the interference pattern (left). Sensing on microchips is complicated by the additional reflective interfaces. After the frequency transform is performed on the inteference pattern, the peak of interest, representing the OPL through the reaction chamber, is selected and monitored as the temperature is changed (right).

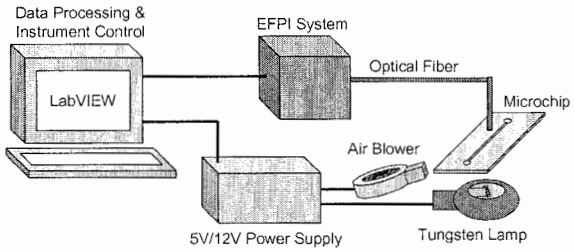

Figure 2. Experimental setup of the non-contact temperature control system. With IR-mediated heating, air cooling, and interferometric temperature sensing, the temperature control is kept separate from the microchip. Extra fabrication steps are therefore avoided.

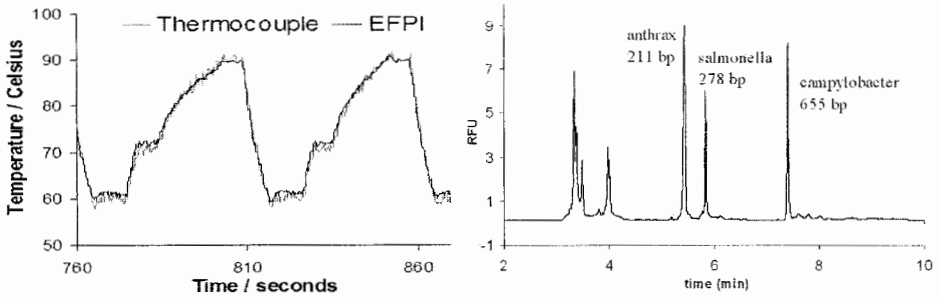

Figure 3. Effectiveness of the EFPI technology as a temperature sensor. A thermocouple was used to evaluate the ability of the EFPI sensor to monitor temperature while thermocycling (left). A conventional CE electropherogram shows separation of the products from the multiplex reaction to be applied to the microchip system (right).

GENOTYPING BY DYNAMIC HEATING OF MONOLAYERED BEADS ON A MICROHEATER SURFACE

Aman Russom[1], Sjoerd Haasl[1], Anna Ohlander[1], Torsten Mayr[2], Anthony J. Brookes[2], Helene Andersson[1] and Göran Stemme[1]

[1]Dept. of Signals, Sensors and Systems, Royal Institute of Technology, 100 44 Stockholm, Sweden
[2]Center for Genomics and Bioinformatics, Karolinska Institute, 171 77 Stockholm, Sweden

Abstract

This paper presents SNP scoring by DASH technology by employing dynamic heating of beads immobilized on a chip with integrated heater and sensor. The microfabricated chip designed for open-surface DNA analysis allows fast, well controllable temperature ramping and homogeneous temperature distribution over the entire heater area. Beads containing DNA duplexes are immobilized on the surface of the chip by microcontact printing using a PDMS stamp. All three possible variants of a SNP site of an oligonucleotide were accurately scored using the bead-based DASH approach. Using the chip, the total analysis time could easily be reduced by a factor 2 compared with the current DASH assay.

Keywords: DASH, microheater, microcontact printing, microspheres, SNP

1. Introduction

During recent years, the amount of available genetic information has increased dramatically. With the completion of the Human Genome Project, the demand for accurate and efficient methods to type single nucleotide polymorphisms (SNPs) has increased. Dynamic allele-specific hybridization (DASH) is a method for SNP genotyping that uses the principles of allele-specific oligonucleotide hybridization (ASOH) but without the optimizations normally associated with this technique. The principle of DASH [1] is shown in Figure 1. Previously, we presented monolayers of patterned beads on silicone dioxide (by microcontact printing using a PDMS stamp) as the solid phase for performing melting curve analysis according to DASH technology [2]. However, thermal expansion of the entire measurement setup by an external heater, together with the fact that autofluorescence of the polystyrene beads used overlaps with the emission spectrum of the detection dye, limited the applicability of the setup. Precise and fast temperature control of the sample requires an integrated heater and temperature sensor. In the current study, the emphasis has been placed on manufacturing chip with integrated heater and sensor for open-surface DNA analysis and improving the measurement setup and detection to facilitate melting curve analysis according to the DASH technology on a monolayer of beads. Three possible variants of a SNP site of an oligonucleotide were analyzed to evaluate the bead-based DASH approach.

2. Experimental

The chip with integrated titanium thin-film microheaters and the temperature sensors was designed and fabricated by standard semiconductor techniques. Figure 2 shows a schematic layout of the fabricated chip. Microcontact printing using a PDMS stamp was employed to create monolayers of beads on the surface of the chip. The DASH procedure, involving heating of the DNA duplex, was performed and a denaturation profile of the DNA duplex was achieved. To circumvent problems caused by the overlapping of the autofluorescence spectrum of the beads with the spectral emission of Sybr Green dye used in the DASH procedure, iFRET (induced Fluorescence Resonance Energy Transfer) [3] was employed. The emission was shifted to a higher wavelength by using Sybr Green as the Donor and Rox as the Acceptor, which has an emission maximum (611 nm) that does not interfere with the autofluorescence of the beads.

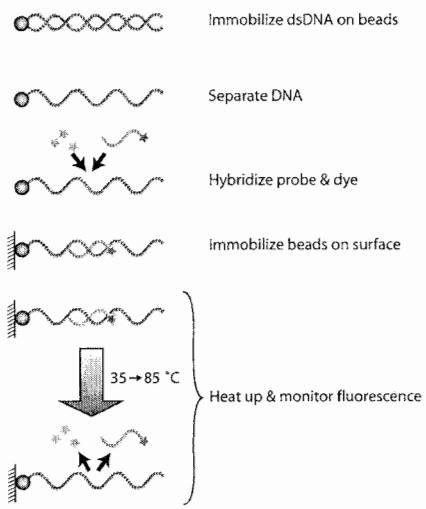

Figure 1. DASH assay principle: DASH principle on bead. Beads with duplex consisting of a biotinylated immobilized PCR product (or oligonucleotide) and fluorescent-labelled probe is immobilized on the surface of the chip and heated while monitoring the fluorescence. Melting profiles of the probe-target duplexes are generated.

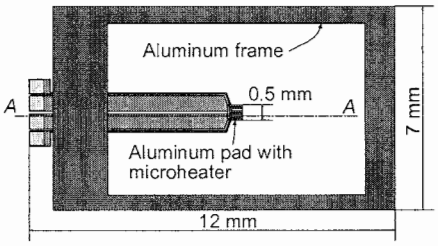

Figure 2a. Top view of the chip. The active area for DNA analysis is 500x500 μm.

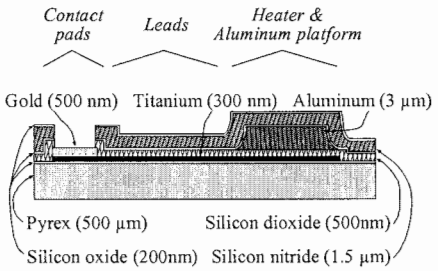

Figure 2b. Cross section of the chip along *A-An* in Figure 2a. The aluminium frame is not shown.

3. Results and discussion

Precise temperature control and rapid thermal ramping was possible using the chip. Figure 3 shows the resistance-versus-temperature characteristics of the chip, which are linear over the temperature range of interest. Our assay has a non-optimized temperature ramping rate of 4-6 °C/min compared to earlier reported values of 2-3 °C/min, thereby reducing the total analysis time by a factor of 2. Figure 4 shows the results from melting curve analyses of the DNA. As the temperature of the heater area is raised, the probes start to dissociate from their complementary target. This dissociation reaches a peak at the melting temperature of the probe-target complex. As can be seen in Figure 4a, the mismatching allele generates a drop in fluorescence intensity at a lower temperature while the matching allele generates a fluorescence intensity drop at a higher temperature. In the heterozygous case, both alleles are present in a matched format at the single polymorphism position, therefore, both the matched and the mismatched alleles contribute to the signal intensity, resulting in a superposition of the intensity of two homozygous samples. The first negative derivative of these denaturation curves displays easily interpretable peaks at the melting temperatures of the probe-target duplexes (Figure 4b). As can be seen in Figure 4b, the mismatched homozygous sample has a distinct peak at 50.3 °C, indicating the melting temperature (T_m), while the matched homozygous sample has a Tm at 58.1 °C. The heterozygous variant produced a curve that is the sum of the two homozygous curves, resulting in a broader peak which was not as distinct as the peaks obtained for homozygous variants. The discrimination power of the mismatched over

the matched variant in our approach is demonstrated by the differences in T_m which was 7.8 °C. This T_m difference obtained enables unambiguous allele discrimination.

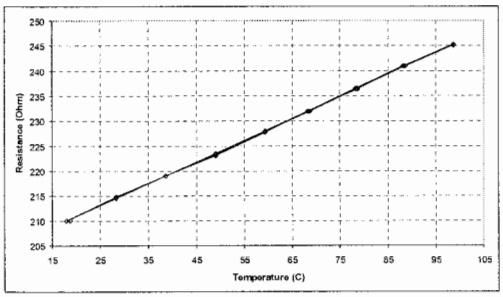

Figure 3. Thermal characteristics of the chip. The resistance-versus-temperature characteristics of the chip are linear over the temperature range of interest for melting curve analysis.

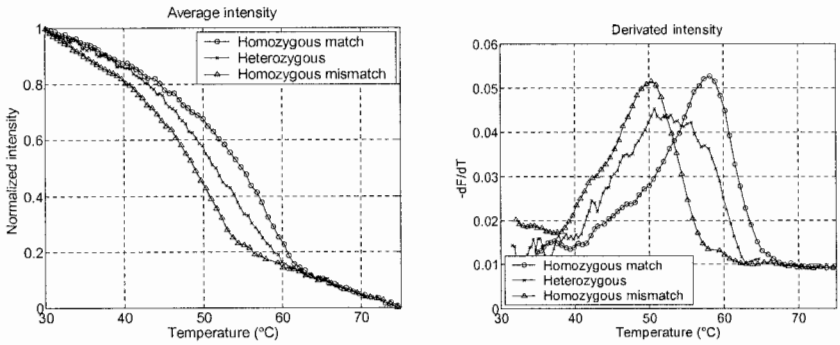

Figure 4. The bead-based DASH genotyping results. (a) The resulting fluorescence changes against temperature. (b) The negative first derivatives. The matching target DNA-probe (O), the single-base mismatched (Δ), and the heterozygous representing 50/50 oligonucleotide mixture (x) are plotted.

4. Conclusions

In conclusion, we have shown the possibilities of scoring SNPs using DASH technology on monolayers of beads immobilized on a surface of a microheater chip. Allele-specific discrimination of SNP position of a synthesized oligonucleotide was demonstrated using the bead-based DASH approach. The approach enabled dramatic volume reduction and is a step towards developing cost-effective high-throughput DASH method on arrays of single beads.

Acknowledgements

The authors would like to thank Kjell Norén for his support.

References

[1]W. M. Howell, M.J., U. Gyllensten, A. J. Brookes, Nature Biotechnology, 1999. 17: p. 87-88.

[2] A. Russom, G. Axehult, T. Mayr, P. Melvas, A. J. Brookes, H. Andersson, G. Stemme, Micro Total Analysis Systems 2003, 1, ed. 2003, pp. 287–290.

[3] Howell WM, Jobs M, Brookes AJ. Genome Res. 2002 Sep;12(9):1401-7.

A DISPOSABLE MICROBIAL SENSOR FOR RAPID BOD MEASUREMENT

Mehta Anjum[1], Halakatti Shekhar[1], Seung H. Hyun[2], Hyoung J. Cho[1]

[1]Mechanical, Materials and Aerospace Engineering, University of Central Florida, Orlando, Florida, USA. [2]Environmental Engineering, University of Central Florida, Orlando, Florida, USA.

Abstract

The standard BOD (biochemical oxygen demand) measurement technique requires a procedure spread over 5 days. A disposable, dual-chambered, flow-through, microbial sensor was designed, fabricated and tested for rapid BOD measurement. The sensor was composed of two layers; the bottom layer containing ring-type amperometric sensor electrodes on a transparent cyclic olefin copolymer substrate and an injection-molded microfluidic layer on top. Fixed amounts of microorganisms were immobilized over one set of sensor electrodes while the other bare electrodes were used as the reference. The sensor was used to measure the actual BOD values of samples collected from the wastewater reclamation process. It showed a linear response for measurements up to 200 ppm of BOD, with short response time within 20 minutes.

Keywords: BOD, microbial sensor, flow-through, disposable, environmental application

1. Introduction

Biochemical Oxygen Demand (BOD) is a key parameter in water quality assessment. Standard BOD_5 measurement process relies on the use of bulky equipment and a 5 day time period [1]. The micromachined BOD sensor alleviates any constraints placed upon instrument portability. It is also more conducive to applications where a quick response time is critical. Since the sensor can be batch fabricated, it is inexpensive and easily replaceable. Most of the earlier works focused on paper-based and dip type sensors [2]. In contrast, we have used an inexpensive, chemically inert and transparent polymer substrate. This lends the possibility of further integration of on-chip optics [3]. In addition, flow-through design reduces contamination while allowing for rapid on-line monitoring.

2. Theory

The designed amperometric sensor is a miniaturized electrochemical cell. The planar device can be used to determine the concentration of a wide range of red-ox active chemical species including dissolved oxygen. It is realized with a three electrodes design that ensures a linear response [4]. The three terminals are RE (reference electrode), WE (working electrode) and CE (counter electrode). The principle of amperometry is based on the measurement of the current between WE and CE which is induced by a red-ox reaction at WE:

$$4Ag + 4Cl^- \rightarrow 4AgCl + 4e^- \quad (1)$$

$$O_2 + 4H^+ + 4e^- \rightarrow 2H_2O \quad (2)$$

The electrical potential of WE versus the measured solution is achieved by a separate RE and is controlled by an external potentiostat circuit. Cyclic polarization with respect to RE can be used to determine the reduction potential of dissolved oxygen. The sensor is operated at this potential which ensures that the current is directly proportional to the concentration of dissolved oxygen. Consumption of oxygen from the respiratory activity of the microbial strains over the sensor electrodes can be used as a direct indicator of BOD.

3. Experimental

The microbial strain, Trichosporon Cutaneum was aseptically transferred into a test-tube containing sterile distilled water. Suspension was inoculated in YM broth medium. The Medium was incubated at 30° C and centrifuged at 120 RPM for 42 hours. It was then centrifuged at 3000 RPM for 15 minutes before washing twice by 0.1 M PBS and preserving it at 4°C. 2% Agarose gel and the suspended T.Cutaneum solutions were mixed for immobilization. The device was fabricated in the following sequence: (a) sensor electrodes were microfabricated using metallization, photolithography and electroplating (b) KCl-hydrogel layer was screen printed on top of the electrodes (c) silicone was spin-coated to obtain an oxygen permeable membrane (d) microbial strain was dispensed and immobilized on the sensor surface and (e) the top microfluidic layer was assembled.

0.1 M Phosphate buffer solution (PBS) was used for cyclic polarization between -1V to 1V with respect to the Ag/AgCl RE. Dissolved oxygen measurements with and without the microorganism were performed with standard BOD solutions varying in nutrient concentrations. Dual-chambered flow-through sensor allowed for concurrent analysis of the current output. The microbial BOD sensor was calibrated with the standard BOD solutions (chemical BOD_5 =50, 100 and 200 ppm). The sensor was tested with effluent and raw water samples, obtained from Eastern Wastewater Reclamation Facilities (EWRF), Orlando, FL, USA as shown in figure 1. Sensor operation was verified by a comparison with the chemical BOD_5 values.

4. Results and Discussion

Figure 2 shows the assembled disposable microbial BOD sensor. The reduction potential obtained through the potentiodynamic cyclic polarization was found to be 300 mV as shown in figure 3. This potential was used to perform potentiostatic polarization of various BOD samples. Figure 4 shows the potentiostatic run for the effluent sample with and without the microorganism. Difference in current output corresponding to the sensor with and without the presence of microorganism can be observed. The sensor calibration curve was obtained as shown in figure 5. Finally the sensor was tested with effluent and raw water samples. The sensor BOD for the effluent and raw water samples was found to be 3 ppm and 193 ppm respectively. The chemical BOD_5 values corresponding to the same samples were measured separately and found to be 2 ppm and 182 ppm respectively, which were in good agreement with the sensor BOD values. Verification of sensor operation with the effluent and raw water samples is shown in figure 6. Sensor BOD values showed a linear response in the operational range of 2-200 ppm. BOD measurement for each sample could be completed within an average time period of 20 minutes.

Acknowledgements

This research was supported by University of Florida-NASA Space Biotechnology and Commercial Applications Program (UF-EIES-0302001-UCF).

References

[1] APHA, AWWA and WEF, "Standard Methods for the Examination of Water and Wastewater", American Public Health Association, Washington DC, 19th Ed., 1995

[2] Z. Yang et al, "Design and Validation of a Low-cost Paper Based Oxygen Electrode", Analytical Letters, Vol. 30, 1797-1807, 1997

[3] R. Trichur et al, "A New Plastic CE Chip with Wide Optical Clarity Using Cyclic Olefin Copolymers (COC)," Proc. μTAS, Nara, Japan, 560-562 November 3-7, 2002.

[4] J. Zhu et al, "Planar Amperometric Glucose Sensor Based on Glucose Oxidase Immobilized by Chitosan Film on Prussian Blue Layer", Sensors, Vol. 2, 127-136, 2002.

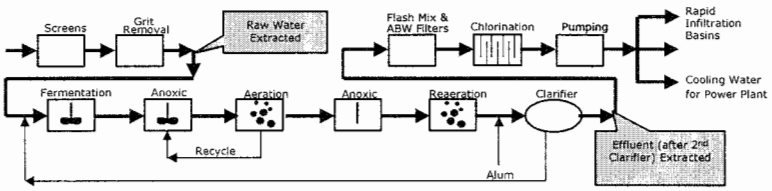

Figure 1. Collection point of wastewater samples from EWRF. The samples were diluted with dilution water by 1: 40.

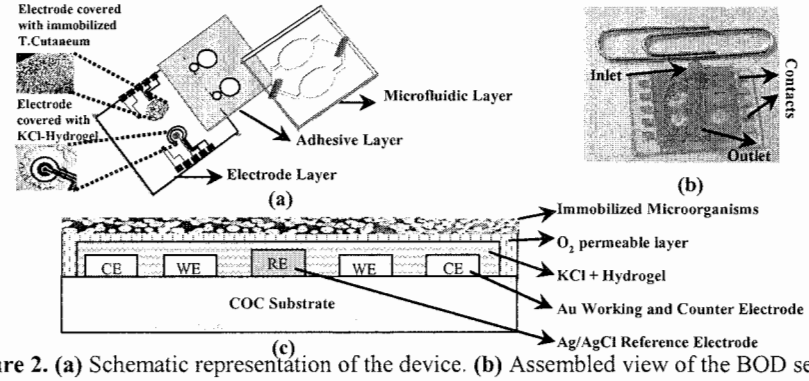

Figure 2. (a) Schematic representation of the device. **(b)** Assembled view of the BOD sensor. **(c)** Cross section of the electrode with the immobilized microorganisms.

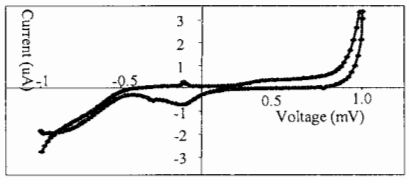

Figure 3. Cyclic polarization to determine the operating potential of the sensor

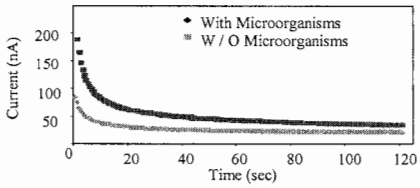

Figure 4. A typical output signal of the sensor for a sample solution.

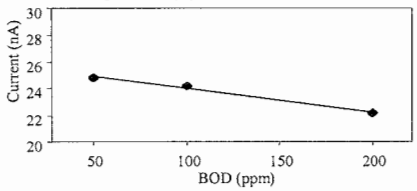

Figure 5. BOD calibration curve with standard BOD solution of 50,100 and 200 ppm

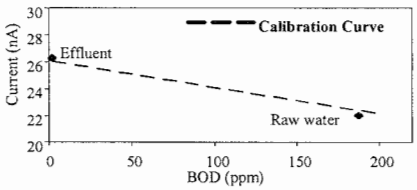

Figure 6. Measured BOD values for the effluent and Raw water samples

SCREENING OF A NOVEL NEUROTROPHIC FACTOR USING MICRO ARRAY CELL-BASED CHIP AND ITS RESPONSE ON PC12 CELLS NEUROSIGNALING PATHWAY

Yoshinori Akagi, Sathuluri Ramachandra Rao, Yasutaka Morita, Yuzuru Takamura and Eiichi Tamiya

School of Materials Science, Japan Advanced Institute of Science and Technology
1-1 Asahidai, Tatsunokuti, Ishikawa, JAPAN

Abstract

This study describes a high-throughput screening assay for novel neurotrophic factor using microarray based cell-chip and also the response of screened neurotrophic factor on Pheochromocytoma (PC12) cells neurosignaling pathway. High-throughput cell-based drug screening using microarray based chip formats play a key role in the development of novel and potential therapeutics at much faster rate with reduction in the cost of drug discovery. There have been reports on the use of nerve growth factor (NGF) in the prevention of the Alzheimer's disease in mice, rats, large primates. The screening of the novel neurotrophic factor was achieved adapting a combination of microarray based chips and combinatorial chemistry based peptide library synthesized on beads.

Keywords: Nerve growth factor (NGF), Microchamber array, cell chip, screening, PC12 cells

1. Introduction

Neurotropic factor have generated much excitement for their potential as therapy for neurological disorders. The discovered member of neurotrophine famiry, NGF, has generated great interest as a potential target for the treatment of Alzheimer's disease [1]. Alzheimer's disease appears to be closely linked to memory loss. NGF can prevent the death of some nerve cells that are effected in Alzheimer's disease and enhance the function of some remaining brain cells in mice, rats, and large primates. NGF lead the PC12 cells to differentiation into neuronal-like cells with neuritis [2]. But large molecules such as NGF can not pass through the blood brain barrier, whereas small molecule such as peptides may do so. On the other hand, high-throughput screening assays play a pivotal rule in the search for novel drugs and potential therapeutics. The combinatorial chemistry library of compounds can be generated by various techniques and screened by a number of different assays. Therefore, it is necessary to process in parallel and simultaneously in order to screen from such as these libraries. We focus on the chip technology, particularly microarrays technique, which can be analysis of huge number and simultaneous.

In the present study, high-throughput screening cell based assay of the effect of NGF with a peptide library using cell chip in PC12 cells has been experimented.

2. Experimental

The cell chip used in this study is made from a silicon wafer. The chip was made out of silicon with tiny chambers (24 x 52) by photolithography and chemical etching [3]. Each chamber was about 500 x 500 x 200 μm dimension. Peptide library X-X-X-X-X (X: Ile, Leu, Met, Phe, Val) was prepared by split synthesis and to yield one-bead with one kinds of peptide library format. Beads peptide library were added onto the silicon chip chambers. Then, the silicon chip with beads was placed on the surface of the glass slide treated with PC12 cells. The whole setup was transferred at the petri dish containing RPMI 1640 medium (10% fetal bovine serum) and cultured for 3 days at 37°C temp with 5% CO_2 humidity (Figure 1). During incubation, the

communication develops between PC12 cells and peptides on the beads. Then the beads with peptide were separated by micromanipulator and peptide sequence was determined to be peptide. In order to study the neurosignaling pathway that was achieved upon this peptide treatment of PC12 cells, the Extracellular signal-Regulated Kinase (ERK) activity was measured by Enzyme Linked ImmunoSorbent Assay (ELISA) and found that the ERK activity was the same to that of NGF derived neurons. In the other experimental set up, PC12 cells were treated with K252a, inhibitor of TrkA receptor, and this peptide was added and found to complete inhibition of neurite outgrowth.

3. Results and discussion

Neurite outgrowth was seen in response to the beads peptide library in microcamber arrays (Figure 2). Then all peptide beads were retrieved from the microcamber arrays using a micromanipulator, and sequenced using protein sequencer. Neurite outgrowth was observed in response to 4 kinds of bead linked peptids and M-M-V-I-F (Peptide A) was most effective for neurite outgrowth (Figure 3).

It has been reported that the MAPK pathway is crucial for NGF-induced neuronal differentiation through TrkA receptor to Extracellular signal-Regulated Kinase (ERK) 4].The ERK cascade is usually initiated by the interaction of NGF with TrkA receptor tyrosine kinase, which results in autophosphorylation of the receptor. To investigate the participation of the TrkA pathway in the induction of neurite outgrowth, we examined the effects of peptide A treated specific inhibitor of TrkA tyrosine kinase K252a in PC12 cells [5]. K252a treatment with peptide A resulted in unenhanced neurite outgrowth compared to only Peptide A treatment in PC12 cells (Figure 4). As quantified (Figure 5), K252a treatment significantly increased in the percentage of cell neurites (14±3.2%). Similarly as Activation of ERK Signaling Pathways, we examined the phosphoryation of ERK in PC12 cells treated with K252a for 2 h. Peptide A and K252a treatment in PC12 cells reduced ERK activity from Peptide A (Figure 6).

4. Conclusions

On beads peptide containing various combinations of amino acids included in the library were mixed. In fact, a split-and-mix combinatorial library displays a high degree of order in an on-bead screening protocol and it was decided that the screening of the library would proceed. Then microchamber array chip can be separation and reaction to each microchambers. In this study, a microarray chip combined with a bead linked peptide library was developed and it was equally powerful strategies and parallel detection. The microchamber array chip has 1248 chambes and thousands kinds library was useful to this microchamber array chip for screening. In this respect, the peptide A peptide is of interest because it is a small synthetic compound capable of activating signal transduction that via TrkA activation induce neutite outgrowth.

Refference

[1] S. P. Lad, K. E. Neet, E. J. Mufson, *Curr Drug Target CNS Neurol Disord.*, **2**, 315-34 (2003)
[2] L. A. Green, and A. S. Tishler, *Proc. Natl. Sci. U.S.A.*, **73**, 2424-2428 (1976)
[3] Y. Akagi, S. Ramachandra Rao, Y. Morita and E. Tamiya, *Sci. Tech. Adv. Mat.*, **5/3**, 343-349 (2004)
[3] T. Morooka, and E. Nishida, *J. Biol. Chem.*, **273**, 24285-24188 (1998)
[4] J. A. Krüttgen, M. Carsten, and E. M. Shooter, *Proc. Natl. Sci. U.S.A.*, **95**, 9614-9619 (1998)

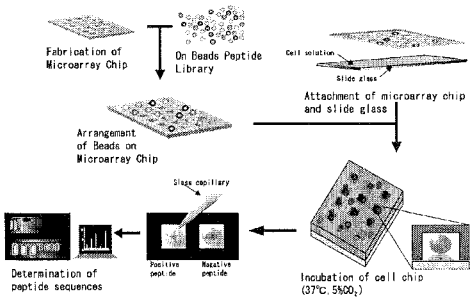

Figure 1. High-throughput screening of novel neurotropic factor using cell-based chip.

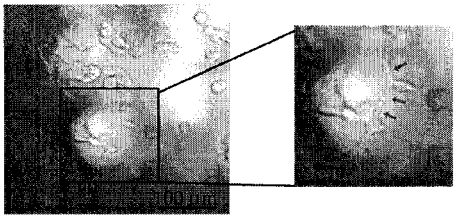

Figure 2. Neurite outgrowth in a micro chamber with beads having peptide library. Arrow indicates neurite outgrowth.

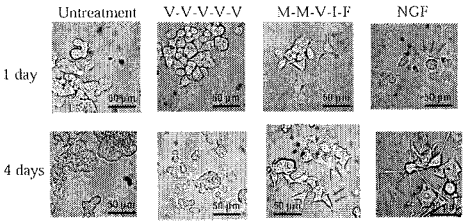

Figure 3. Induction of neurite outgrowth in PC12 cells by treatment with peptide A. Cell cultured with 10 μM of Peptide A and 4 nM of NGF and 10 μM of control peptide (V-V-V-V-V) for 4 days. Arrows were shown neuritis.

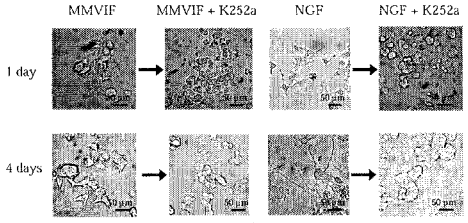

Figure 4. Induction of Neurite outgrowth with inhibitor of TrkA (K252a). Cell were incubation with 100 nM of K252a treated with 10 μM of Peptide A and 4 nM of NGF.

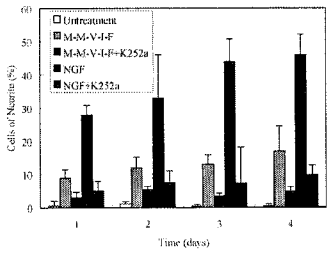

Figure 5. Quantification of Neurite outgrowth. Cell were incubated with 100 nM of K252a treated with 10 μ of Peptide A and 4 nM of NGF. Values are expressed as Means ± S.E.M. (n=7).

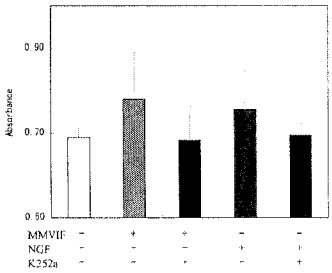

Figure 6. Activation of ERK with K252a. Cell were incubated with 100 nM of K252a treated with 10 μM of Peptide A and 4 nM of NGF. Values are expressed as Means ± S.E.M. (n=8).

SEPARATION OF SATELLITE DROPLETS USING BRANCH MICROCHANNEL CONFIGURATION

Takasi Nisisako, Toru Torii and Toshiro Higuchi
Dept. of Precision Engineering, Graduate School of Engineering, the University of Tokyo
7-3-1 Hongo, Bunkyo-ku, Tokyo, 113-8656, Japan

Abstract
A novel purification technique is given for preparing satellite-free emulsions. Minute vesicles, which are the unwanted by-product of droplet formation at a T-junction, can be separated from the primary droplets by a simple branch structure in microchannels. Experiments are performed in water-in-oil (w/o) and oil-in-water (o/w) systems, using hydrophobic- and hydrophilic chip modules respectively. The flow conditions of the two fluids necessary for successful droplet sorting are studied.

Keywords: satellite droplets, purification, fractionation, T-junction, microfluidics

1. Introduction

Recent years have seen intensive study of microfluidic techniques suitable for handling multiple fluids. In particular, droplet preparation using micro T-junctions has many potential applications, as a result of its flexibility and control capabilities [1-3]. Unfortunately, minute vesicles (called satellite droplets) are commonly produced (Fig.1 (a)). These unwanted droplets constitute a hindrance in many applications.

We report here a methodology for hydrodynamic fractionation of droplets by a simple microfluidic geometry. By exploiting the positional relation immediately after breakup at a T-junction (Fig.1 (a)), primary droplets and satellite droplets can be separated downstream in a rapid and continuous manner. Droplet rupturing at a T-junction and subsequent sorting downstream were successfully performed in both o/w and w/o systems. We studied the flow conditions needed for successful separation.

2. Experimental

The microchannels shown in Fig. 2(a) were fabricated in poly(methylmetacrylate) (PMMA) by conventional machining techniques. The hydrophobic properties of the surface were exploited in generating a w/o dispersion. This configuration includes a T-junction for breakup of drops and a downstream droplet separator at where the channel broadens gradually and divides into two branch channels. All channels have rectangular cross section and uniform depth. A similar geometry was fabricated in quartz glass for o/w dispersion.

In our experiments on a PMMA device, deionized water was dispersed into a continuous phase of corn oil (viscosity η = 58.5 mPa s,

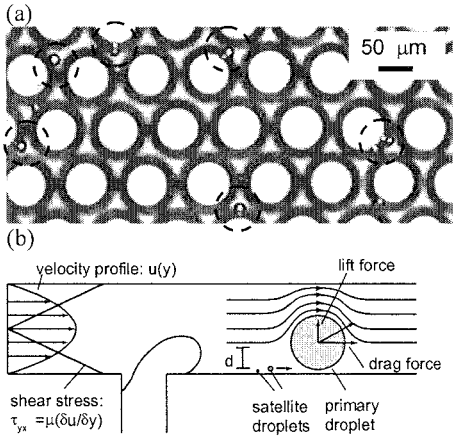

Figure 1. (a) Densely-packed acrylic spheres prepared by the microfluidic technique. Dashed circles indicate polymerized satellites. (b) Positional relation of droplets after breakup at a T-junction.

surface tension $\gamma = 33.2$ mN/m). No surfactant was dissolved in either phase. In the o/w droplet experiment on a glass chip, 1, 6-hexanediol diacrylate ($\eta = 6.35$ mPa s, $\gamma = 36.1$ mN/m) and polyvinyl alcohol (PVA) aqueous solution ($\eta = 1.95$ mPa s, $\gamma = 44.5$ mN/m) were used as the phase to-be-dispersed and the continuous phase, respectively. The fluids were driven into their channels by syringe pumps. Breakup and separation of droplets were observed using a high-speed video camera mounted on an optical microscope.

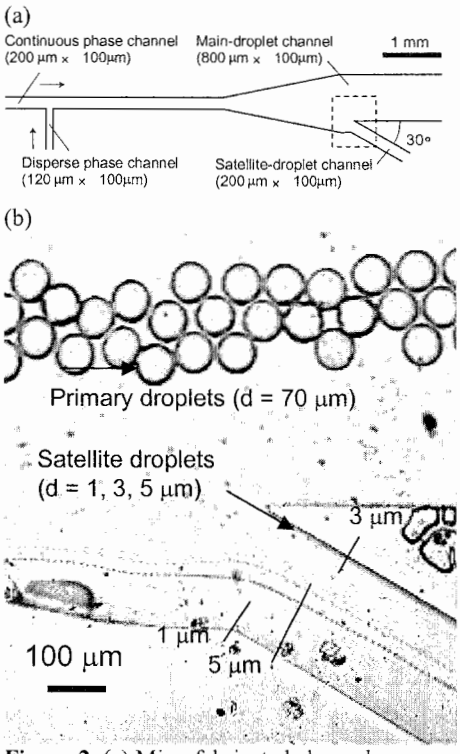

Figure 2. (a) Microfabricated channel dimensions. (b) A high-speed photograph of droplet separation in a w/o dispersion. Dashed rectangle indicates area in the photograph.

3. Results and discussion

At low Reynolds number (Re~10^{-2}) in a PMMA chip, satellite drops of diameter less than 3 μm were detected in the breakup of the primary droplets, which have diameter similar to the channel size (100~120 μm). Immediately after rupture of primary droplets, satellites were seen near the channel wall, though the center of gravity of primary droplets was some way from the wall because of their larger volume. This implies that a primary droplet and satellite droplets were located on different streamlines at the moment of breakup. In fact, the center of gravity of primary drops larger than a certain volume is located on the center of the channel. The distance of primary- and satellite drops in the cross-section perpendicular to the flow direction can be made to increase with distance downstream, and the droplets can then be separated into distinct microchannels. Fig. 2(b) shows behavior in the separation area at faster speeds of flow (Re~10^{-1}). Satellite drops of multiple sizes, which were generated rapidly (~1.5kHz) along with primary droplets, were fractionated in size and entered into the branch channel. It follows that monosized droplets of several specified sizes can be prepared at the same time by using this technique.

Using a glass-chip module, we investigated the relation between flow conditions and behavior at the sorting area. A specific region was found in which sorting takes place (Fig. 3, left). When the volume flow rate of the continuous phase was less, the fraction of disperse phase increased and the primary and satellite droplets both spread homogeneously within the separation area (Fig. 3(a)). As the flow rate of the continuous phase increased, the fraction of disperse phase decreased, and complete separation was observed as seen in Fig. 3(b). As the speed of flow of the continuous phase increased further, the streamlines became closer as a result of the reduction in size of the primary droplets. Consequently, primary drops and satellite drops both began to flow into the branch channel (Fig.3(c)). Correct choice of geometry is therefore vital to achieve efficient separation.

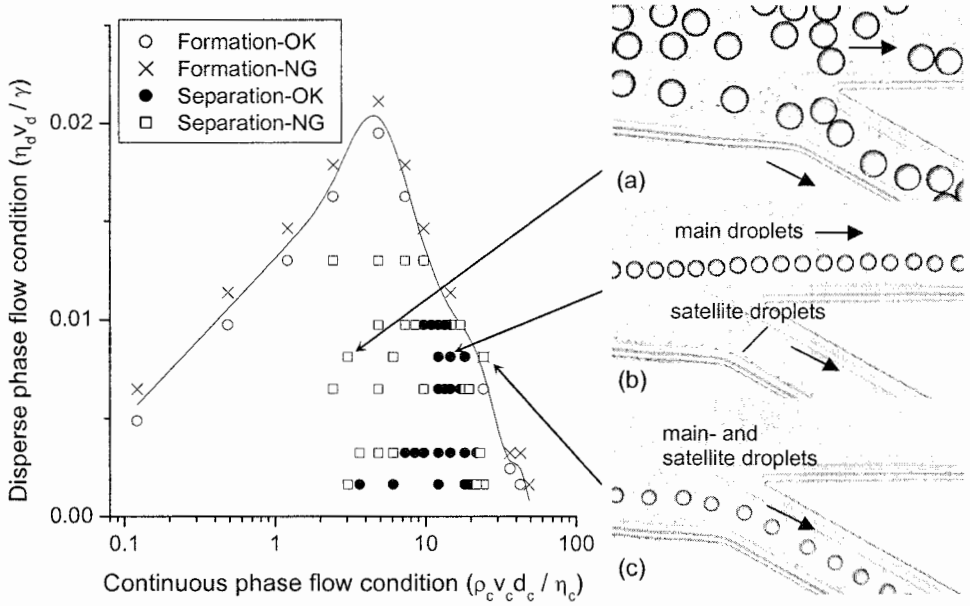

Figure 3. Left: The flow conditions under which droplet separation occurs. The area in which droplets can be formed is also shown. Right: Transition in states with differing volumetric flow rate of the continuous phase Q_c; (a) Q_c = 2.5 ml/h, (b) Q_c = 10.0 ml/h, (c) Q_c = 20.0 ml/h.

This technique can be extended to increase the volume fraction of the disperse phase by partly removing the continuous phase. In combination with appropriate manipulation of the exit pressures, this would lead to greater flexibility in the microfluidic production of emulsions.

4. Conclusion

Using a simple microfluidic configuration, we have demonstrated the rapid and continuous separation of satellite vesicles from droplets generated at a T-junction. Flow regimes for successful purification were studied experimentally in both w/o and o/w systems. This technique is capable of producing genuinely monodisperse dispersions without any fractionation processes outside channels, and has clear potential for industrial application.

Acknowledgements

This work was partly supported by grants from the Research Association of Micro Chemical Process Technology (MCPT) of Japan, and by MEXT through a Grant-in-aid for Scientific Research (No. 15310100).

References

[1] B. Zheng, et al., JACS **125**, pp. 11170-11171 (2003)
[2] K. Martin, et al., Lab Chip, **3**, pp. 202-207 (2003).
[3] T. Nisisako, T. Torii, T. Higuchi, Chem. Eng. J., **101**, pp.23-29 (2004).

DRUG RESPONSE ASSAY ON MICROCHIPS USING HUMAN HEPATOMA CELLS

Yuki Tanaka[1,2], Kiichi Sato[2,3,4], Masayuki Yamato[2,5], Teruo Okano[2,5], Takehiko Kitamori[1,2,4]

[1]Department of Applied Chemistry, School of Engineering, The University of Tokyo; [2]Core Research for Evolutional Science and Technology, Japan Science and Technology Agency; [3]Department of Applied Biological Chemistry, School of Agriculture and Life Sciences, The University of Tokyo; [4]Kanagawa Academy of Science and Technology (KAST); [5]Institute of Advanced Biomedical Engineering & Science, Tokyo Women's Medical University

Abstract

We succeeded in maintaining the activity and metabolic functions of the cells in the microchip by temperature control, surface modification of the channel and control of the shear stress. A microchip-based cell response assay system to an anticancer agent was developed. The hepatoma cell line HepG2 was used to assess the effects of an anticancer agent, doxorubicin. By using 100 μm-scale microchannel, the required cell number was reduced from 2.4×10^5 to 2.0×10^3, and the observation of the time course of cell response became possible. The system clearly showed that treatment with higher doses of the drug or longer exposure times gave more effects to cells. The possibilities of novel drug response studies or toxicity assay system with a small number of cells were demonstrated.

Keywords: cell culture, bioassay, drug screening

1. Introduction

Microfluidic systems have shown promise for a variety of cell-based researches. Most of such systems, however, do not focus the microenvironment of the cell. In our previous paper [1,2] , we focused not only life support but the environment of cells and found that only cells under stress-free conditions could make normal response. The stress-free environment is indispensable for cells. We succeeded in maintaining the activity and metabolic functions of the cells in the microchip by surface modification of the channel and control of the shear stress (Fig. 1).

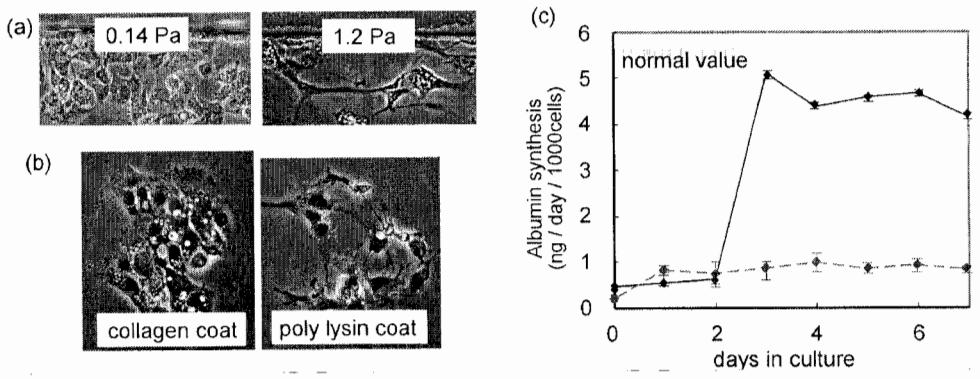

Figure 1: Rat liver primary culture inside microchip. (a) Cell morphology under low and high shear stress. (b) Cell morphology under collagen coat (normal) and poly-lysin coat (abnormal). (c) Cell function test (solid line) cells under stress-free conditions (low shear stress, collagen coated surface) ; (dotted line)cells under stressful conditions (high shear stress, no surface coating)

In this study, we applied the microchip-based cell experimental system to the cellular assay system to a drug. Drug response assay for cancer therapy is very important, because individual cancers, although they seem similar in types, show widely divergent responses to anticancer agents. Individual tumors may or may not respond to an agent used for a particular tumor type. Thus, a method that will predict the effects of the anticancer agents is needed before medication. Although much research has been conducted on sensitivity testing for anticancer agents to treat cancers, they require a large number of cells. It is impractical to use these methods for a test, because an operation would be necessary to obtain the required amount of cells. The aim of this study was development of a microbioassay system using a very small amount of cells to demonstrate the advantages of a microchip-based cell experiment system as a predictive drug response assay system. In this paper, sensitivity to an anticancer drug doxorubicin of the human hepatoma was assayed.

2. Experimental

The cell cultures were carried out based on procedures described in a previous paper[1] with small modifications. Briefly, human hepatoma cells were seeded in a microchannel (100 μm in depth and 250 μm in width) fabricated in a quartz glass microchip and incubated with medium flow system. When cells reached 60% confluence, they were dosed with varying concentrations (0 μM, 1 μM, 10 μM, 30 μM and 50 μM) of doxorubicin hydrochloride prepared in medium for periods of 0.5 h to 3 days (Fig. 2). Doses of doxorubicin were chosen from blood levels of the drug just after administration (30 μM) and one hour after administration (10 μM). Following the treatment, the viability of cells was examined using a mixture of 2 μM of Calcein-AM (Molecular Probes, λex=495 nm, λem=520 nm) and 4 μM of Ethidium homodimer (Molecular Probes, λex=528 nm, λem=617 nm) prepared in phosphate buffered saline (PBS) to indicate living cells and dead cells, respectively. This process was achieved by introduction of the reagent solution into the microchip by a microsyringe pump at ~1 μL/min for 15 min, followed by taking fluorescent images using an Olympus CKX31. Cytosol of the living cell showed green fluorescence and nucleus of the dead cells showed red fluorescence. (Fig. 3).

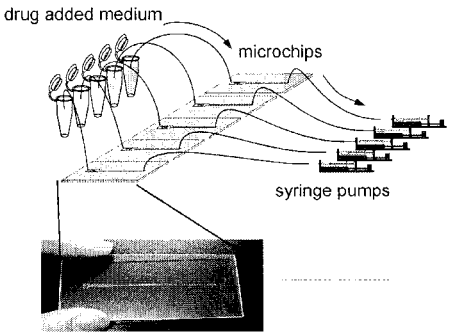

Figure 2: Experimental setup of cell-based drug response assay.

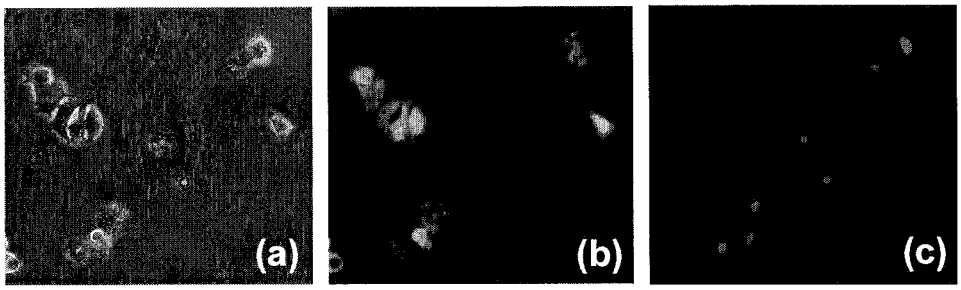

Figure 3: Images of hepatocytes after drug treatment. (a) phase-contrast (b)calcein-AM stained living cells. and (c)Ethidium homodimer stained dead cells.

3. Results and Discussion

Obtained cell survival rates with dose concentrations are shown in Fig. 4. As can be seen clearly from the results, the anticancer agent produced both dose-dependent and time-dependent cell damage. Our previous paper [1] showed that the activity and functions of the cells cultured in the microchip were retained fully. Therefore, the results were thought to be reliable. In addition, all of the operations were achieved by the control of the microsyringe pump, and then the assay operations became much easier and simpler than the conventional methods with many troublesome pipetting operations. Furthermore, the required cell number was reduced from 2.4 x 10^5 to 2.0 x 10^3. It is possible to sample 2.0 – 3.0 x 10^5 cells using needle biopsy. That is, using our drug response assay device, the assays under more than 100 dose conditions may become possible with cells sampled with needle biopsy . The system is practically useful because the damage to the patients is very little.

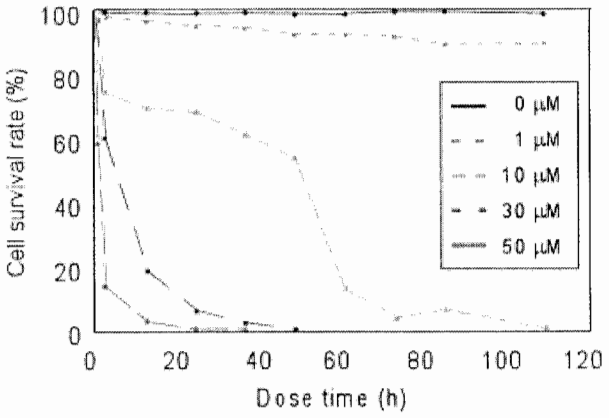

Figure 4: Cell response data from doxorubicin treatments.

4. Conclusions

In conclusion, sensitivity of the target cells to the agent was assayed. This simple and rapid assay system will be very useful in drug screening process in selection of appropriate drugs for a predictive individual therapy design. Moreover, the method can be applied to other assays, such as hepatotoxicity assay by using a primary culture of the patient's normal hepatocytes. In this application, the extremely low consumption of cells will become an obvious advantage. Moreover, the system has a great potential to realize highly integrated and automated assays with high throughput (Figure 5).

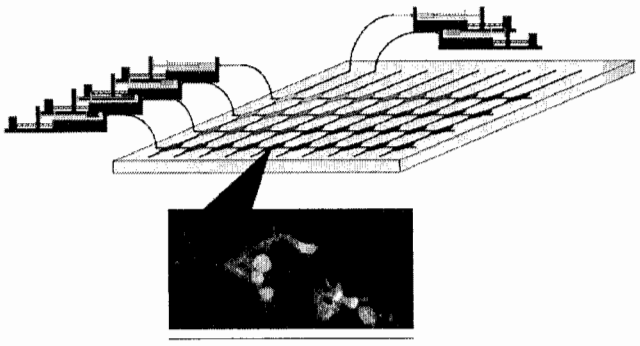

Figure 5: Multiple and cross drug response assay system

References

[1] Y. Tanaka, *et al., Electrophoresis, in press.*
[2] Y. Tanaka, et al., Proceedings of Micro Total Analysis Systems 2003, 777

ANALYSIS OF PEPTIDES USING AN INTEGRATED MICROCHIP HPLC-MS/MS SYSTEM

David S. Reichmuth, Gabriela S. Chirica, Brian J. Kirby
Microfluidics Department, Sandia National Laboratories, Livermore, CA, USA

Abstract

An on-chip HPLC was fabricated using *in situ* polymerization of both fixed and mobile polymer monoliths. Integration of the chip with a nanospray MS emitter enables identification of peptides by the use of tandem MS. The chip is capable of analyzing of very small sample volumes (<200 pl) in short times (<3 min).

Keywords: HPLC, mass spectrometry, LC, MS/MS, flow control , microvalve

1. Introduction

Hyphenated LC-MS techniques are quickly becoming the standard tool for proteomic analyses. For large homogeneous samples, bulk processing methods and capillary injection and separation techniques are suitable. However, for analysis of small or heterogeneous samples, techniques that can manipulate picoliter samples without dilution are required or samples will be lost or corrupted; further, static nanospray-type flowrates are required to maximize SNR. Microchip-level integration of sample injection with separation and mass spectrometry allow small-volume analytes to be processed on chip and immediately injected without dilution for analysis.

2. Materials and methods

Fused silica wafers are constructed using traditional wet-etch techniques. Separation media are introduced via stearyl acrylate-based photopatterned porous polymer monoliths or via slurry packing of functionalized beads. High pressure fluidic connections are opened and closed on-chip via photopatterned mobile polymer elements that move in reponse to pressure differentials[1,2]. The functionality of a high-pressure Teflon-Teflon seal is emulated by forming compression seals between the fluorinated polyacrylate polymer and the fluoroalkyl-modified silica substrate (micrograph in Fig 1). The fluorinated monoliths are resistant to common HPLC solvents such as acetonitrile and methanol, and function at pressures up to 5000 psi. HPLC separations are performed on-chip and detected using both laser-induced fluorescence and mass spectrometry. Microchips were connected online to an ion-trap mass spectrometer via a commercial nanospray emitter at ~75 nl/min flowrate.

3. Results and discussion

Zero-dead-volume microchip injectors (e.g., Fig 1) are used to connect buffer and sample lines in microchip HPLC systems. Repeated injections (Figs 2 and 4) demonstrate reproducible injection volumes, with a retention time RSD of 3.6% and peak area RSD 3.9% over 104 injections; minimum injection volumes are 180 pl, limited by the external pressure switching [3]. The data (Fig 3) show a linear relation between the volume injected and the length of the injection time, allowing for predictable and precisely controlled injections. The injector did not show any detectable signs of leakage, and consistent injections were performed with as much as a one-week delay between injections.

We have demonstrated use of both polymer monolith (Figs 4,5) and packed-bed separations in a microchip format. Monolith-based materials allow for facile production of HPLC microdevices, while pressure-packed particle columns enable the use of a wide selection of chemical functionalities and porosity. Both types of separation material are compatible with our on-chip

injection valves, and we have demonstrated integrated HPLC devices using C18-functionalized beads and stearyl acrylate-based monoliths.
The on-chip injector and HPLC separation are integrated with tandem mass spectrometry analysis, enabling high-resolution detection and identification of peptides (Fig 6).

4. Conclusions

The ability to combine high-speed, low sample volume analysis with MS-based identification will significantly improve high throughput protemic studies. The device described in this work utilizes a reversed-phase separation. Currently we are investigating the use of other chip-based packed bed columns, such as cation exchange. Packed-bed columns not only broaden the range of separation modes, but will also enable multi-dimensional separations.

Acknowledgements

The authors thank Gary Hux, Dan Throckmorton, and Tony Martino for technical assistance. Sandia is a multiprogram laboratory operated by Sandia Corporation, a Lockheed Martin Company, for the United States Department of Energy's National Nuclear Security Administration under Contract DE-AC04-94AL85000.

References

1.Hasselbrink et al, Anal. Chem., v74 2002 pp.4913-4918.
2.Kirby et al, J. Chrom. A v979 p 147-154 (2002).
3.Reichmuth et al, Anal. Chem., in press.

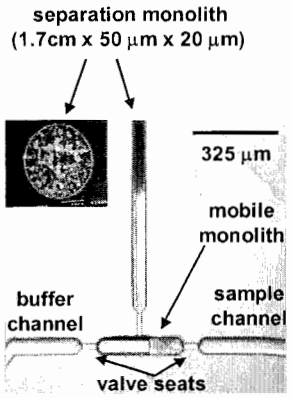

Figure 1. Micrograph of injector valve and beginning of separation media. Inset is electron micrograph of separation media polymerized inside 150 μm ID glass capillary.

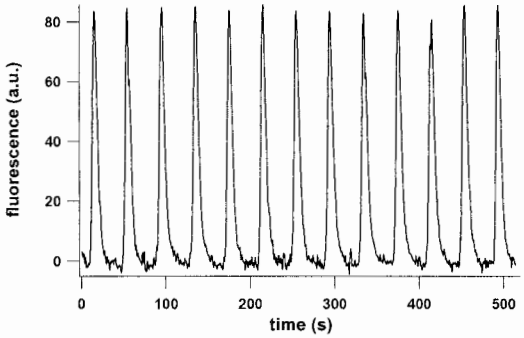

Figure 2. Rhodamine 560 injections, repeated at 0.025 Hz and measured using laser induced fluorescence. Injections consisted of 640 pl of 6.8μM Rhodamine 560 in 30% ACN, injected at 450 psi with 750 ms injection duration. Buffer used was 30% ACN with 0.2% HFBA, and separation was performed at 300 psi.

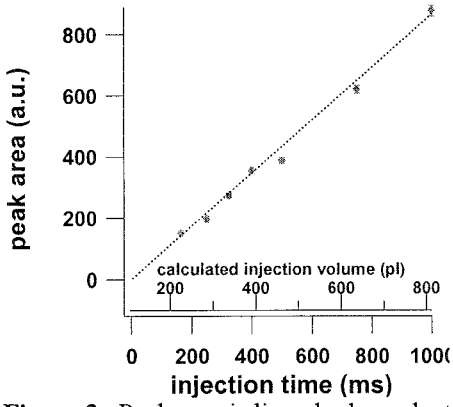

Figure 3. Peak area is linearly dependent on injection duration. Rhodamine 560 injections were performed at 450 psi, buffer flow was constant at 300 psi. Error bars are standard deviation, with at minimum 9 replicates at each injection duration.

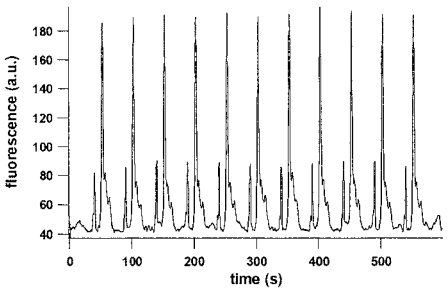

Figure 4. Repeated 470 pl injections of a peptide mixture. Isocratic separation using 30% ACN with 0.1% TFA in 5M phosphate buffer (pH 6.8) at 300 psi.

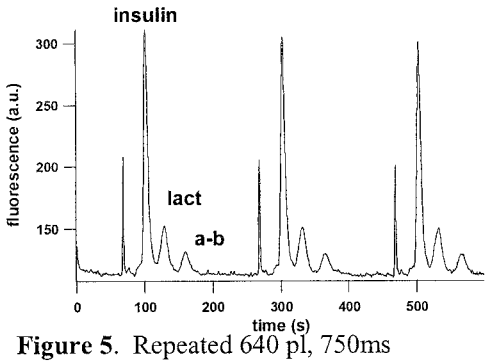

Figure 5. Repeated 640 pl, 750ms injections of a protein mixture. Isocratic separation was performed using 24% ACN + 0.16% HFBA in 5M phosphate buffer (pH 6.8) at 300psi. Peak identities: a. insulin b. anti-biotin c. lactalbumin

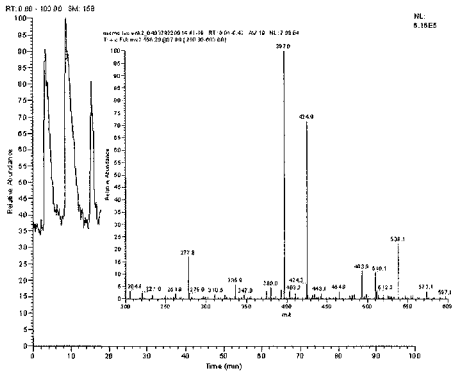

Figure 6. Repeated ~800 pl injections of 4 μM leucine enkephalin, detected using an ion-trap MS with a nanospray source. Inset spectrum shows successful identification of leucine enkephalin via tandem MS of the 556.2 m/z parent ion.

RAPID AND COMPLETE SOLUBILIZATION OF BACILLUS SPORES USING A FLOW THROUGH THERMOLYSER FOR AUTOMATED SAMPLE PREPARATION

Kyle W. Hukari, Kamlesh Patel, Ronald F. Renzi, Jay A.A. West

Microfluidics Research Group, Sandia National Laboratories, Livermore, CA. USA

Abstract:
Rapid identification of viral and bacterial species is dependent on the ability to manipulate the biological agents into a form where they can be analyzed directly. Many of these species of interest, such as bacterial spores, are inherently hearty and very difficult to lyse or solubilize. To overcome this inherent difficulty we have designed and fabricated a device which allows the superheating and lysis of these robust spores. The device was then coupled to sample preparation station for on-line fluorescent dye labeling and buffer exchange for direct analysis using the miniaturized capillary electrophoresis instrument, μChemlab. Using this integrated device we were abled to perform sample lysis, labeling and protein fingerprint analysis of vegetative bacterial cells, bacterial spores or viruses in less than 10 minutes. The described device is simple, inexpensive and easily integratable with various microfluidic devices, such as the hand portable μChemlab.

Keywords: Thermolysis, Sample preparation, Bacterial Spores, μChemlab, microfluidics

1. Introduction:

Analysis of bacterial spores is complicated by the robust nature in which these dormant organisms are biologically constructed. Current techniques used for the lysis and solubilization of the hearty structures often results in less than 10% lysis using conventional techniques. In addition, the reagents used such as strong reducing agents and acids, can often degrade the analytes that are targeted for detection. Such strong reagents also require that samples are re-purified prior to dye labeling and analysis. Here we describe a simple and rapid lysis and solubilization technique for the most resilient of biological agents, bacterial spores.

2. Materials and methods

The flow through lysing apparatus was constructed by wrapping a 0.5 mm diameter copper wire a 10 cm 450/640 ID/OD capillary glass (Polymicro Sciences) around a fused silica capillary with approximately 20 windings/cm. A second capillary (150i.d./360 o.d.) was then inserted into the heating capillary to provide sample flow through the heating element. The external windings were then insulated using fiberglass insulation webbing and soldered to a simple two prong connector for operation using a standard 10V power supply. Heating was performed using an applied field of 0.5-3 volts with 0.2 -1.6 A current. Internal temperature of the capillary during heating was measured using a 100um diameter platinum thermocouple wire inserted into the ethylene glycol containing capillary connected to a thermocouple interface.

Bacterial spores and viral samples were pelleted by centrifugation and resuspended in a buffer containing 5 mM boric acid, 5mM SDS dissolved in 96 % ethylene glycol solution. Samples were then transferred to a syringe connected to a 150/360 capillary used to pump though the thermal lyser using a syringe pump. Real time imaging of the cell lysis for bacteria and spores was

performed using a light microscope to observe both inlet and outlet capillaries. Spore lysis was confirmed by counting spore particles imaged between two glass slides.

3. Results and Discussion

We designed a simple flow through thermolyser (figure 1) that completely denatures and solublizes greater than 90% of the intact spores in less than one minute. Using a wound resistor we have been able to heat samples to temperature greater than 195 °C. To monitor temperature inside the capillary wall we developed an estimate of internal temperature as a function of current flow (figure 2) using a platinum electrode thermocouple. To lyse these spores, we first tested whether ethylene glycol would act as an adequate solvent and provide the ability to heat the spore containing solution to greater than 150 °C. We found that we were able to effectively both lyse and solubilize B. Cereus, B. Subtilis, and B. Anthrasis (B. Subtilis shown) spores and generate robust protein signatures of these agents (figure 3). We also found the technique was adequate for the lysis of vegetative bacterial cells and viral agents. We have further integrated this device with a dye labeling and buffer exchange station which allows for the direct injection of these samples onto microfluidic devices (figure 1A). We have been able to integrate this system with the hand portable microchemlab for direct analysis of lysed bacterial spores, vegetative bacteria and viruses in less than ten minutes.

4. Conclusion

This technique is simple rapid and easily integrated with other currently developed miniaturized systems, such as microChemlab. We have further evaluated this technique for the lysis of viral agents as well as vegetative bacterial cells. We have found that we were able to optimize conditions for the rapid lysis and analysis of these agents as well.

Acknowledgements:

This work has been funded by the U.S. department of Homeland Security and the Department of Defense for the further development of the μChemlab system for the detection of viral and bacterial agents. We would like to thank Tom Raber, Brad Aubuchon, for their engineering support as well as Richard Gant, and Todd Lane for production of the purified bacterial and viral preparations.

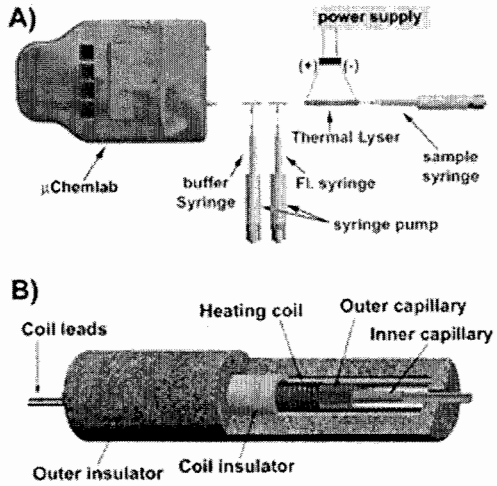

Figure 1

Thermolyser apparatus. The lyser apparatus was integrated with a sample preparation station (A), which contains a fluorescamine filled syringe along with a syringe filled with buffer solution. A close up of the lyser apparatus is illustrated below (B).

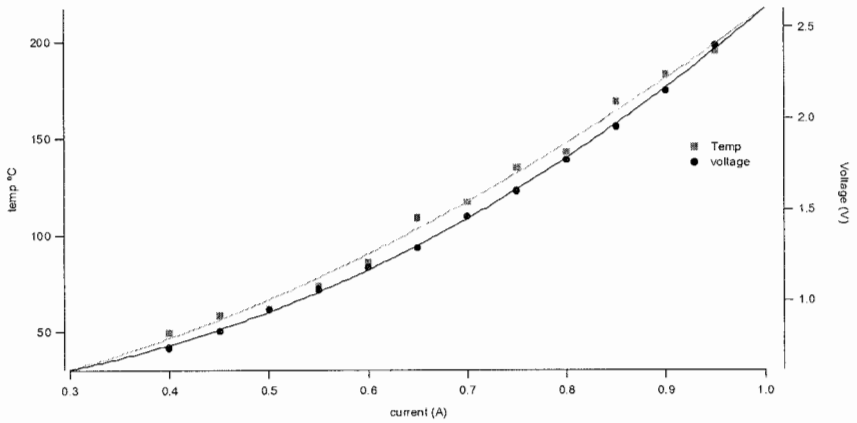

Figure 2 Temperature monitor by current using an embedded platinum electrode. The temperature profile was linear as a function of either current or voltage. This curve was used to calibrate each apparatus in order to control the internal temperature of the capillary lyser apparatus

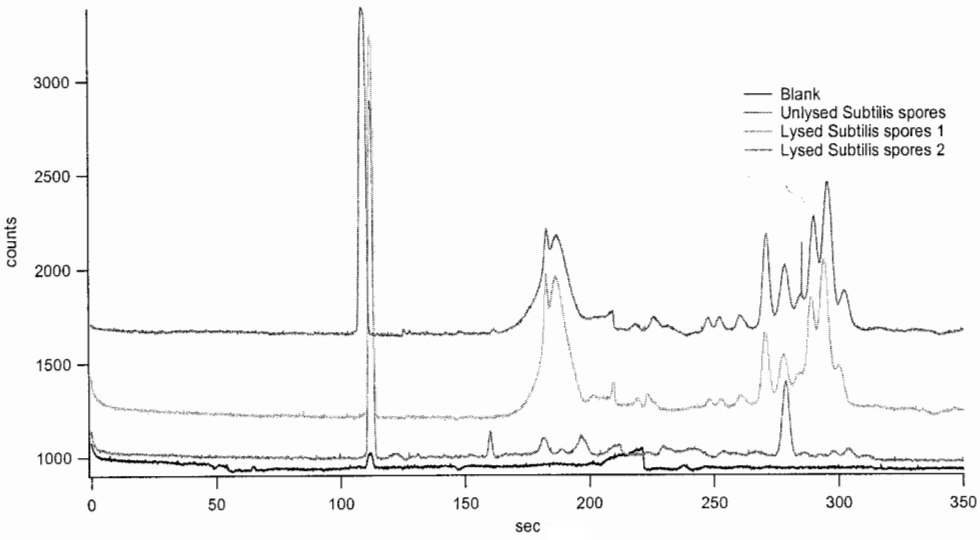

Figure 3 Bacterial spore protein signatures generated in flow through lyser. Compared to control (bottom trace), the superheating of the bacterial spores in the lyser apparatus appear to generate a robust protein signature (top traces).

DESIGN AND EXPERIMENTAL VERIFICATION OF THE ELECTROPORATION MICROCHIP FOR TRANSGENIC ZEBRAFISHES UTILIZING GENES AND QUANTUM DOTS

Kai-Chun Su and Yu-Cheng Lin

Department of Engineering Science, National Cheng Kung University, 1 University Road, Tainan 701, Taiwan, E-mail: yuclin@mail.ncku.edu.tw

Abstract

This study focused on design and experimental verification of an electroporation (EP) microchip for transgenic zebrafishes. (CdSe)ZnS quantum dots, QDs, genes coding for green fluorescence protein, GFP, and trypan-blue dye were used to verify the successful transfection to the zebrafish embryos. The experimental results show that the delivery rate was upto 62% when using an EP microchip to deliver trypa-blue dye, QDs or GFP genes into zebrafish embryos.

Keywords: Transgenic Zebrafish, Electroporation, Embryo, Quantum Dots, Nanoparticle

1. Introduction

Transgenic animals require effective gene delivery. Different types of gene delivery systems have been developed. Electroporation has been widely applied on gene delivery [1]. Zebrafish was used as a model for gene delivery using electroporation in this study. An electroporation chip was designed and fabricated to facilitate the gene delivery into zebrafish embryos. Microfabrication techniques were used to fabricate the electroporation device. Trypan-blue dye, QDs [2], and GFP gene were used as the indicators to evaluate the performance of electroporation using an EP microchip.

2. Materials and methods

In this study all the zebrafish embryos, 1 mm diameter, used were within 12 min after fertilization. A 20 μl of 5 nm water soluble (CdSe)ZnS QDs at the concentration of 360μg/μl was used in each electroporation experiment. The EP microchip was designed in two components, the well defined cavities for 200 embryos accommodation as well as the plate electrodes for providing precise electric field for zebrafish-embryo electroporation, as shown in Fig. 1. The holder, cavities and top cover were made of PMMA using CO_2 laser ablation micromachining. The Au/Ti thin film electrodes were fabricated on the glass by MEMS technologies [3]. To investigate the strength of the electric fields in the embryo cavity, 2-D electric field simulations were performed using ANSYS 6.0 (Swanson Analysis System Inc., USA) run on a personal computer.

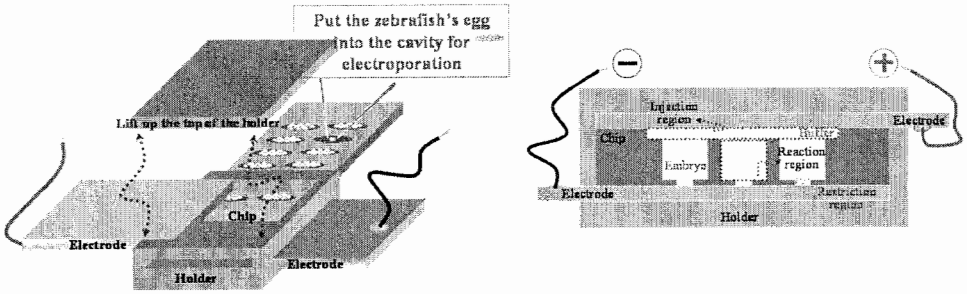

(a) (b)

Figure 1. Schematic drawings of an EP chip, (a) 3D view, and (b) cross-sectional view.

3. Results and discussion

The finite element simulation analyzed the electric field distribution and variation inside the cavity at the electroporation. Based upon the size of the cell-accommodation cavity and electrode location, the electric field distributions at different locations inside the cavity were plotted in Fig. 2.

The electric fields were designed to have high strengths around the embryo, i.e. 0.3, 0.5 and 1 mm locations. Fig. 2b shows that the electric fields maintain similar field strengths within 7% deviation at the mentioned location in the cavity above the cathode electrodes. To demonstrate the performance of the designed electroporation chip, the embryos, accommodated in microchip cavities, were added with trypan-blue dye, QDs, or pEGFP-N1 plasmids, stimulated using a laboratory-built computer-controlled power supply. Trypan-blue dye was used as an indicator for testing the effect of permeability. It was fast and cost effective to use trypan-blue dye to test the designed EP microchip and power supply were functional and able to deliver molecules into zebrafish embryos.

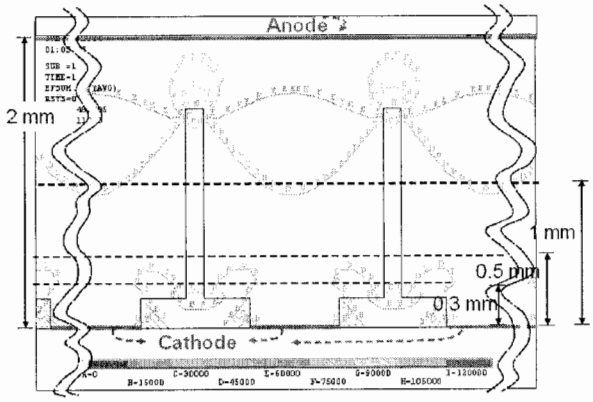

(a)

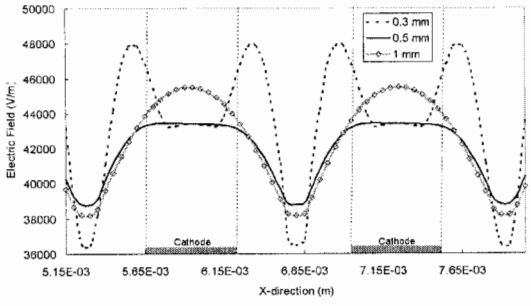

(b)

Figure 2. Simulated electric field distributions of an EP chip, (a) under the EP process, and (b) electric field distributions at 0.3, 0.5 and 1.0 mm above the cathode in the reaction wells. (Unit of the scale bar in (a) is V/m).

Fig. 3 shows the results of introducing trypan-blue dyes into zebrafish embryos 2 hr after the process with or without electroporation. Embryos with successfully delivered trypan-blue show deep blue, however, the control shows partially light blue on the embryos. The delivery rate of the trypan-blue dye was at 62.5% under 100 V applied voltage with 15 ms duration.

Fig. 4 shows the fluorescence image of QDs inside the zebrafish embryo after electroporation. Different electroporation voltages, from 50 to 700 V, have been applied and tested to find the optimal condition for delivering QDs into embryos using electroporation. The applied voltage of 100 V with 2 pulses (15ms duration and 1 s interval) was found to have the highest transfection rate at 36.4%. GFP transfected zebrafish embryos were hatched after electroporation. Fig. 5 shows green fluorescence was found in a GFP transfected zebrafish embryo 30 hr after electroporation.

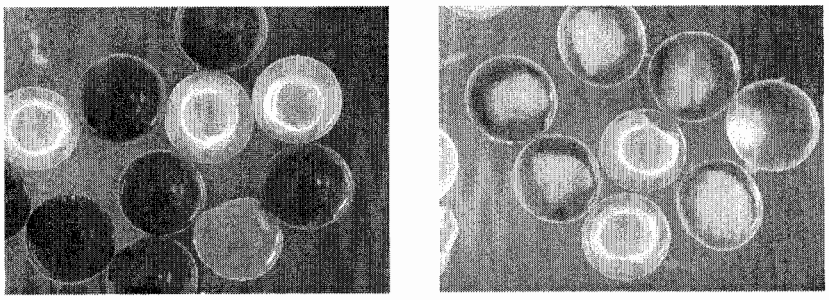

(a) (b)

Figure 3. Comparison of the introduction of trypan-blue dyes into zebrafish embryos, (a) 2 hr after electroporation, and (b) 2hr after trypan-blue dye dipping without electroporation (controls).

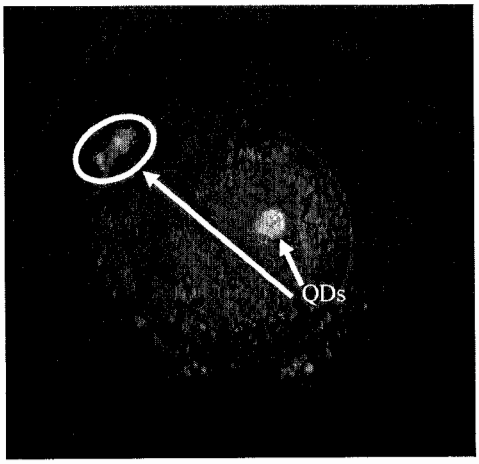

Figure 4. Image of QDs in the zebrafish embryo. QDs were delivered into the embryo using electroporation.

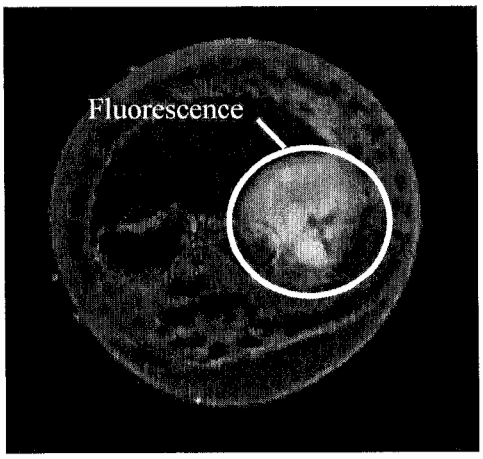

Figure 5. Image of a GFP transfected zebrafish embryo 30 hr after electroporation.

4. Conclusions

In this study, an electroporation chip was designed for gene delivery of zebrafish embryos. Numerical simulation analysis and experimental verification were conducted in the study. Water soluble QDs, GFP gene, and trypan-blue dye were successfully delivered into zebrafish embryos to verify the performance of the designed EP microchip for transgenic zebrafishes.

References

[1] Y.C. Lin, M. Li, C.C. Wu, *Lab Chip*, **4,** 104 – 108 (2004).
[2] J. K. Jaiswal, H. Mattoussi, J. M. Mauro, S. M. Simon, *Nat. Biotechnol.*, **21**, 47-51 (2003).
[3] Y.C. Lin, M. Li, C.S. Fan, L.W. Wu, *Sens. Act. A,* **108**, 12-19 (2003).

BIOASSAYS ON ULTRASONICALLY TRAPPED MICROBEAD CLUSTERS IN MICROFLUIDIC SYSTEMS

Tobias Lilliehorn[1], Mikael Nilsson[2], Linda Johansson[1], Urban Simu[1], Monica Almqvist[2], Stefan Johansson[1], Thomas Laurell[2] and Johan Nilsson[2]

[1] *Dept. of Engineering Sciences, Uppsala University, P.O. Box 534, SE-751 21 Uppsala, Sweden*
[2] *Dept. of Electrical Measurements, Lund University, P.O. Box 118, SE-221 00 Lund, Sweden*

Keywords: Ultrasound, PZT, Microbeads, Microparticles, Trapping

1. Introduction

This paper presents the concept and initial achievements regarding a microfluidic platform for bead-based analysis of biological sample, ultimately aimed for parallel multistep bioassays on biochemically activated microbeads using submicrolitre sample volumes. The core technology is ultrasonic trapping of microbeads by means of acoustic forces [1] [2]. A device comprising an array of three individually addressable particle trapping sites in a flow-through channel was developed and evaluated. Each trapping site was designed as an acoustic resonator consisting of a miniature ultrasonic transducer and a reflector, enclosing a bead conducting fluid layer. Particles in a fluid passing a transducer were drawn to pressure minima in the acoustic field, thereby being trapped and confined, vertically as well as laterally, at the transducer position. A fluorescence based avidin bioassay was performed on biotin-coated microbeads trapped in the flow-through device, providing a first proof of principle of the proposed dynamic arraying concept. The dynamic arraying is believed to be expandable to two dimensions [3], thus with a prospect of performing targeted and highly parallel protein analysis in microfluidic devices.

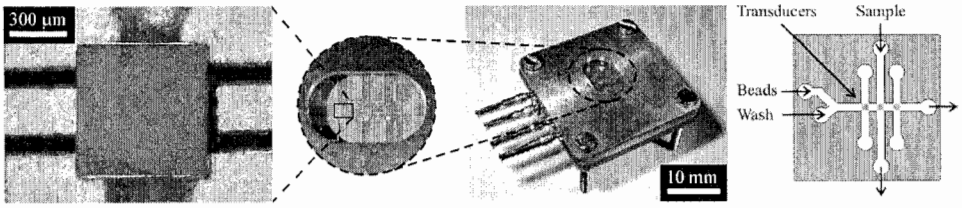

Figure 1. Microfluidic device with three integrated microtransducers for ultrasonic bead trapping.

2. Experimental

A device with an array of three trapping sites is shown in Fig. 1. The microfluidic configuration allows particles and sample to be conducted to the three trapping sites where 10 MHz microtransducers (0.8 x 0.8 mm^2) are integrated in one channel wall. The design of the layered resonator is shown in Fig. 2. A glass lid serves as a reflector of the acoustic waves to obtain standing wave conditions. The device was designed to obtain a pressure distribution with essentially a pressure node in the middle of the channel, keeping the particles away from the interior channel surfaces. Applying a 10.8 MHz, 10 V p-p drive signal to one transducer, activated the acoustic trap.

The strength of trapping was evaluated by imaging the trapped beads under increasing fluid flow. The fluid flow was increased in steps of 2 µl/min until no beads were visible in the region over the transducer element. A model bioassay using FITC-labeled avidin streaming over biotin-coated microbeads was used to demonstrate the functional performance of the device. The beads were inserted and trapped at one trapping site, and avidin solution (23 µM) was perfused in the orthogonal flow channel. Excessive avidin was washed away from the bead bed.

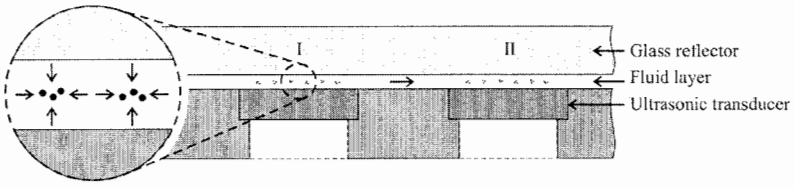

Figure 2. Two trapping sites, I and II, designed as acoustic microresonators consisting of glass reflector, fluid layer and ultrasonic transducer. The close-up shows a simplified view of beads that are trapped by acoustic forces due to pressure gradients in the fluid layer.

Finally the possibility of moving beads between the three trapping sites was studied by sequential trapping. Beads were injected and conducted to the first trapping site using a fluid flow of 3 µl/min, which was maintained throughout the experiment. Beads were trapped by the activation of the first transducer. The driving signal was then switched to the second transducer, to which the flowing fluid conducted the beads. The procedure was repeated for the third transducer element before releasing the beads to the outlet.

3. Results and discussion

Upon activation of the acoustic field, beads were trapped in the fluid over the transducer element. The particles were essentially captured in the middle of the channel, thereby enabling fast switching of particles from one array position to another. A typical lateral bead cluster distribution is shown in Fig. 3. The distribution of trapped bead clusters was strongly affected by the near field pressure distribution due to the finite element size. This resulted in efficient trapping since the laterally confining radiation forces are proportional to gradients in the acoustic energy density [4]. Upon increasing fluid flow, bead clusters were pulled away from the trapping site, and at a flow rate of 10 µl/min about 50 % of the beads were still trapped. The flow could be increased to 20 µl/min (mean linear flow rate ≈4.7 mm/s) before all beads were pulled away from the trap by viscous forces.

The obtained fluorescent response from the model bioassay over trapped microbeads is shown in Fig. 4. After washing the bead bed, a step increase Δ in intensity indicated that avidin had successfully bound to the beads. The switching of particles between array trapping sites in the fluidic channel is shown in Fig. 5, where particles entering from the left were trapped by activating the transducers one by one in a sequential fashion.

4. Conclusions

Successful non-contact ultrasonic trapping of chemically activated microbead clusters at individually addressable trapping sites in a microfluidic device has been presented. Studies on the strength of trapping showed that the flow could be increased to 20 µl/min (mean linear flow rate ≈ 4.7 mm/s) before all beads were pulled away from the trap by viscous forces. It is concluded that near field effects in the miniaturised system helped to provide strong lateral trapping forces, allowing bead trapping at considerably high perfusion rates. Performing a model bead-based bioassay using the device showed the prospect of the technology. Biotin-coated beads were injected and trapped followed by perfusion of FITC-tagged avidin. Future developments will focus expansion of the arraying concept to two-dimensional ultrasonic transducer arrays. Eventually, the development will enable on-line analysis of e.g. proteins performed on biospecific bead arrays in a flow-through device.

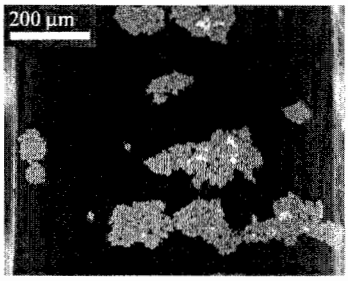

Figure 3. Trapped bead clusters (lighter) above a single transducer element at a fluid flow of 3 µl/min. The figure covers essentially one transducer element.

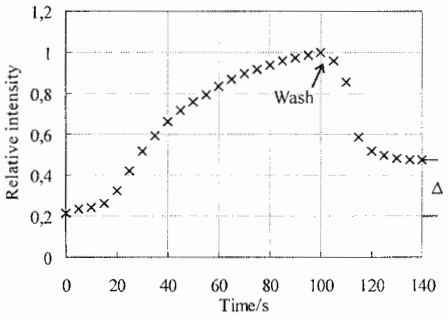

Figure 4. Loading of FITC-tagged avidin into the bead-loaded trap, with indicated fluorescent response Δ corresponding to avidin binding to trapped biotin-coated beads. The switching from avidin to washing flow is indicated.

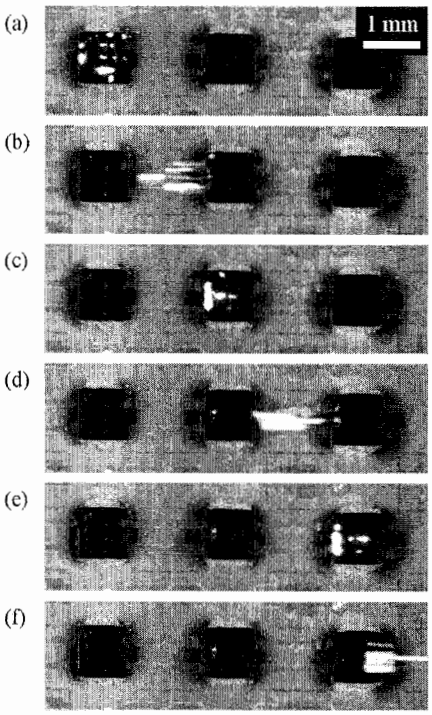

Figure 5. Trapping (a, c and e) and subsequent release (b, d and f) of fluorescent microbeads from left to right in three individually controlled array positions.

References

[1] Gröschl, M., *Acustica - Acta Acustica*, 84 (1998), p. 432-47.
[2] Wiklund, M., S. Nilsson, and H.M. Hertz, *Journal of Applied Physics*, 90 (2001), p. 421-6.
[3] Lilliehorn, T., Piezoactuators for Microfluidics - Towards Dynamic Arraying. (Doctoral Thesis), Department of Materials Science. 2003, Uppsala University, Sweden.
[4] Woodside, S.M., B.D. Bowen, and J.M. Piret, *AIChE Journal*, 43 (1997), p. 1727-36.

ACOUSTIC PARTICLE SIZING IN MICROCHANNELS BY MEANS OF ULTRASONIC FREQUENCY SWITCHING

Carl Siversson, Filip Petersson, Andreas Nilsson, Thomas Laurell
Department of Electrical Measurements, Lund University, P.O. Box 118, Lund, Sweden

Abstract

This paper describes a method for separation of particles with different densities suspended in a fluid. The method utilizes a fundamental and second harmonic ultrasonic standing wave in combination with the laminar flow properties of a silicon micro channel. Different density particles, suspended in a medium, enter the channel through side inlets and a particle free medium enters via a center inlet, forming three laminated streams. By sequentially switching between the fundamental and the second harmonic standing waves, higher density particles can be positioned close to the pressure node of the fundamental standing wave, while the lower density particles are positioned close to the pressure nodes of the second harmonic standing wave. The channel is split into three exit channels, separating the streams of high-density and low-density particles.

Keywords: particle separation, ultrasound, acoustic, standing wave, laminar

1. Introduction

If particles suspended in a medium are exposed to an ultrasonic standing wave they are affected by acoustic radiation forces [1]. The force acting on the particles is a function of the lateral position in the channel and in the fundamental standing wave the highest force is found at the centre where the pressure minimum is localized, Fig 1. This phenomenon has previously been utilized for particle separation in microfluidic systems [2-4]. If the particles are exposed to the second harmonic standing wave, the force acts towards the two pressure nodes at the sides according to the force diagram. By combining this with laminar flow in micro channels, particles can be colleted at the pressure nodes. Such standing waves can be created in a channel with parallel side walls.

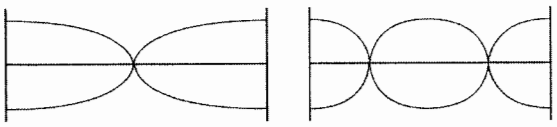

Figure 1a. Fundamental and second harmonic standing waves. X-axis denotes spatial position in channel. Y-axis denotes standing wave pressure.

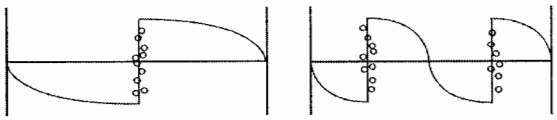

Figure 1b. Same as above, but Y-axis denotes the force acting on a suspended particle. Particles are gathered at the pressure nodes.

The end and the beginning of the separation channel are split into three channels, Fig 2. In the mid inlet, fluid without particles (water inlet) is inserted. In the side inlets (mixed particles inlet), a fluid with a mix of high-density and low-density particles is inserted

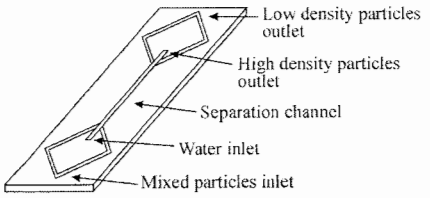

Figure 2. Schematic image of separator structure. Flow connectors and one ultrasonic transmitter are mounted on the bottom side of the structure. Another ultrasonic transmitter is mounted from the top side.

It can be shown that particles with different density or compressibility are affected by different accelerations when they are exposed to the same standing wave. Thus, the different particles will be translated laterally at different speeds. In general, high density particles move faster than low density particles. By rapid switching between the fundamental and the second harmonic standing waves, high-density and low-density particles can be separated laterally in the laminar flow stream.

The fundamental standing wave is applied sufficiently long for the high-density particles to reach the center of the separation channel, Fig 3b. The fundamental standing wave is subsequently switched off and the second harmonic standing wave is switched on, Fig 3c. The particles positioned close to the center of the channel at this point will not be strongly affected by the second harmonic standing wave because they are close to a force minimum. However, the particles that never reached the center of the channel during the fundamental standing wave cycle will, at this point, be in a position where they are exposed to a significant force moving them away from the center of the channel again. By repeating this scenario equilibrium will be accomplished separating different particles in different flow-lines based on their physical properties.

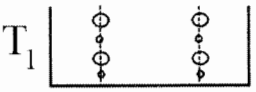

Figure 3a. Initially the particles are injected along the side walls of the channel. T indicates the time instant in the switching process. Large circles indicate high-density particles

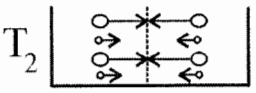

Figure 3b. When the fundamental standing wave is applied the particles are forced towards the center of the channel. However, high-density particles move faster towards the center. The fundamental standing wave is switched off before the low-density particles reach the center.

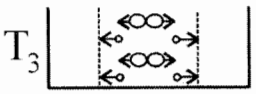

Figure 3c. The second harmonic standing wave is switched on. At this point the higher density particles are not strongly affected, since they are closer to the force minimum of the second harmonic standing wave. The low-density particles are, however, moved towards the pressure nodes of the standing wave. The second harmonic standing wave is switched off before the higher density particles reach the pressure nodes

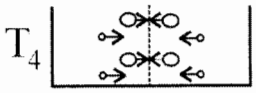

Figure 3d. The procedure is repeated. This time the high-density particles start from a position slightly closer to the center of the channel. As this is repeated equilibrium will be reached. The higher and lower density particles are separated into two streams close to the pressure nodes of the fundamental and second harmonic standing wave, respectively

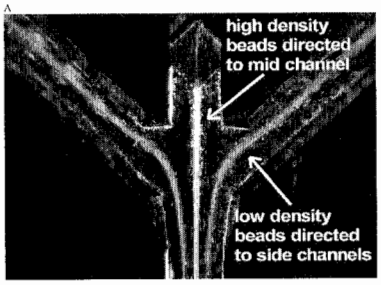

Figure 4. Photo from the separation process. High-density particles are directed to the centre outlet and low-density particles are directed to the side outlets.

2. Theory

If a standing wave is induced into a medium where a small particle is suspended the particle will be exposed to a force according to the theory presented by [1].

$$F_r = -\left(\frac{\pi P_0^2 V_c \beta_w}{2\lambda}\right) \cdot \left(\frac{5\rho_c - 2\rho_w}{2\rho_c + \rho_w} - \frac{\beta_c}{\beta_w}\right) \cdot \sin\left(\frac{4\pi z}{\lambda}\right) \qquad (1)$$

V_c is the volume of the particle, p_0 is the pressure amplitude. The density of the medium and the particle are denoted ρ_w and ρ_c respectively and the corresponding compressibilities β_w and β_c. Combine this with basic physic formula, where m_c is the mass of the particle and a is the acceleration the particle is exposed to.

$$a = \frac{F}{m_c} = \frac{F}{V_c \cdot \rho_c} \qquad (2)$$

It then comes clear that the acceleration, and thus the lateral speed and movement, of a small particle is a function of the density and compressibility of the particle.

3. Experimental

The separation channel (350 um wide and 250 um deep) was etched into a <100> silicon wafer using anisotropic wet etching. The channel was sealed with a glass lid by anodic bonding and silicone tubes were glued to the inlets and outlets on the backside. The ultrasonic excitation (2 Mhz and 4 Mhz) was accomplished by attaching two piezo ceramic crystals, one from the back side and one from the front side, with ultrasonic gel. The flow was controlled using three syringe pumps, 26 µl/min at the H_20 inlet, 15 µl/min at the centre outlet and 75 µl/min at the side outlets. The remaining 64 µl/min of particle solution was self drawn from an open cup. The particle solution consisted of a mix of 3 µm polystyrene beads, with a density of 1.05 g/cm^3, and 8 µm polymethylmethacrylate beads, with a density of 1.19 g/cm^3, suspended in H_20. In order to get proper separation, the switching parameters had to be tuned correctly. This was done by systematically adjusting the parameters until sufficient visual separation was achieved. A typical operating cycle was 2 MHz for 800 µs and 4 MHz for 200 µs.

4. Results and discussion

Measurements have shown that, from a solution with particles slightly varying densities, as described above, 80-85% of each kind of particles can be directed to different outlets. The actual separation ratio though is expected to be improved shortly because of a late discovered flaw in the current measurement setup.

5. Conclusion

The experiments have shown that it is possible to use this harmonic acoustic wave switching to separate suspended particles with different physical properties from each other. One application of this can be to separate different types of cells or bacteria from each other. Other possible applications include separation of different blood components.

References

[1] Yosioka K. and Kawasima Y.; Acustica 5, pp 167-173, (1955)
[2] Petersson F., Nilsson A. Jönsson H, and Laurell T.; Proc. MicroTAS2003, pp 879-882
[3] Nilsson A., Petersson F., Jönsson H., Laurell T.; Lab On A Chip 2004, pp 131-135
[4] Petersson F.; Analyst 2004, accepted

THREE DIMENSIONAL MICRO MACHINING OF SU-8 AND APPLICATION FOR PDMS MICRO CAPILLARIES

Ryotaro Mori, Kei Hanai and Yoshinori Matsumoto

Department of Applied Physics and Physico-Informatics, Faculty of Science and Technology, Keio University. 3-14-1 Hiyoshi, Kohoku-ku, Yokohama, Kanagawa, Japan.

Abstract

Three dimensional structures of SU-8 resist were fabricated by using gray-scale lithography technique. The gray-scale masks were fabricated on emulsion masks by photoreduction. SU-8 was exposed through a transparent glass substrate. PDMS micro capillaries were obtained by molding the SU-8 structures and flow in the capillaries was observed.

Keywords: Gray-scale lithography, 3-D micro machining, micro capillary, SU-8, PDMS

1. Introduction

In gray-scale lithography, three dimensional structures can be obtained with only single exposure process by using a special shaded photomask, called gray-scale mask [1-2]. We have been briefly obtained three dimensional structures of photosensitive glass by gray-scale mask that was made of emulsion glass [3]. However, photosensitive glass after fabrication is not transparent and surface roughness is large because of HF etching.

In this study, three dimensional SU-8 structures was fabricated by novel lithography method and PDMS capillaries were cast from the SU-8 structures.

2. Gray-scale mask fabrication

Mask patterns were designed by drawing software that is available in personal computers. Shaded and complicated mask patterns can be easily designed without specific mask pattern formats like GDS. Conventional ink-jet printer (1440dpi) with pigment type ink was used for the pattern printing on transparency films.

Emulsion glass (Konica High Resolution Plate) was used as a material of a gray-scale mask. Printed patterns were photoreduced by a rate of 1/20 onto the emulsion glass masks. Minimum binary line width on the mask was 20μm, which is limited by resolution of reduction optical system. A gray-scale spot on the mask were obtained approximately 20μm. Figure 1 shows a relation between power of UV light (at λ=365nm) and gray-scale value on the drawing software. Effective gray-scale range was limited from 40% to 80% because the emulsion glass masks were optimized to the conventional binary patterns.

3. Gray-scale lithography with SU-8 resist

A photoreaction progress of negative resist, such as SU-8, starts from UV source side. Conventional exposure method with gray-scale mask does not provide multilevel structures because middle tone portions are entirely peeled off from substrate during the development process.

In order to apply a gray-scale lithography for SU-8, a transparent substrate was used and the irradiation was performed from the substrate side (substrate penetration lithography, shown in figure 2) [4]. Since a surface of a final structure does not depend on the initial surface condition, this technique reduces cumbersome optimization of resist coating.

We applied the SU-8 resist of 400μm to the thin glass substrate (t = 0.12 to 0.17 mm) and pre-bake was performed for 2 hours at 100°C. The UV power was optimized at 18mW/cm^2 for λ=365nm. Post-exposure bake was performed for 10 minutes at 100°C.

Figure 3 shows a relation between gray-scale values and resist height. The resist height proportionally changed from 40 to 80 % according to the UV power hence the gray-scale value. For more than 15 seconds exposure time, resist height saturated in a range of high gray-scale value

because the reacted resist part reached to the initial height The maximum surface roughness of the structure was 0.98μm in Ra at 55% gray-scale value.

From these result, several structures such as relief like form (Figure 4) and female components of micro capillaries with graded structures.

4. Casting of PDMS micro capillaries

Some types of PDMS micro capillaries have been fabricated by casting the female components of SU-8. The components were put into the petri dish and PDMS (Dow Corning Sylgard 184) was poured. After defoaming in the vacuum desiccators, the PDMS were cured at 50°C for 2 hours on a hotplate and peeled off from the glass plate.

In this paper, we demonstrate three types of them: serpentine pattern (Type A), cylindrical obstructions at a junction (Type B) and graded pattern (Type C). Figure 5 shows the SEM images and mask patterns of each capillary. Capillaries with three dimensional structures were successfully achieved by molding. Finally, PDMS plates with the capillaries were bonded to the transparent cover plate with tube connector.

5. Observation of flow in the capillaries

For observations of flows in the fabricated capillaries, sodium carbonate solution and phenolphthalein solution were injected to the capillaries by syringes that were connected to the tubes. Mixed part of these solutions susceptibly turns red. Figure 6 shows photographs of flows in the 3-D capillaries.

In the type A, red part at the boundary of two flows was strongly bent by the serpentine pattern. The flow was bent one after another and the area of the boundary was expanded. The expanded boundary promotes the diffusion of the flows and as a result, they were mixed together and the red part increases toward the downstream flow.

In the type B, cylindrical structures worked as obstruction of the flow. The red streak hits the cylindrical obstructions, red part extends radically from the obstruct.

In the type C, the flow was bent by the graded patterns. The red parts were especially observed at the deep part of the capillary because the stagnation of flows occurred at the place. Mixed liquids were swept away by the flow and as a result, multiple streaks were seen at the downstream.

6. Conclusion

Novel gray-scale lithography method was applied to negative type photoresist (SU-8). Three dimensional SU-8 structures were achieved by using thin and transparent substrate and exposure from substrate side. Maximum height of the structure was 400μm and maximum surface roughness was 0.98μm in Ra. PDMS micro capillaries with three dimensional structures were fabricated by molding the resist form and the flow in the capillaries were observed. From the result, we realized the capillaries have an ability to promote the liquid mixing.

References

[1] Hans Peter Herzig, "MICRO-OPTICS", *Taylor & Francis*, 140-142, (1997).

[2] K. Reimer, U. Hofmann, M. Jürss, W. Pilz, H.J. Quenzer and B. Wagner, "Fabrication of Microrelief Surfaces using a One-Step Lithography Process", *Proc. of SPIE*, **3226**, 2-10, (1997).

[3] R. Mori, Y. Matsumoto, "3-D Micro Capillaries Formed by Gray-scale Lithography of Photosensitive Glass", *Proc. of μ-TAS 2003,* 203-206, (2003).

[4] R. Mori, S. Inoue, K. Hanai, Y. Matsumoto, "Three-dimensional Micro Machining of SU-8 by Gray-scale Mask and Molding", *Proc. of Technical Meeting on Sensors and Micromachines 2004, MSS-04-25,* (2004).

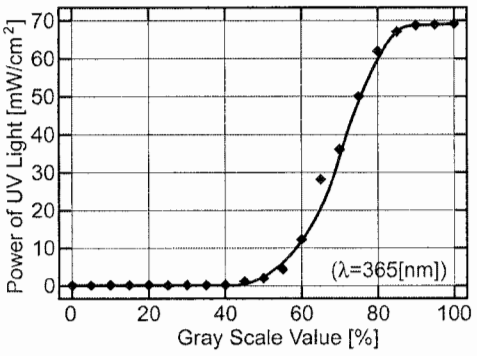

Figure 1. Relation between power of UV and grayscale value.

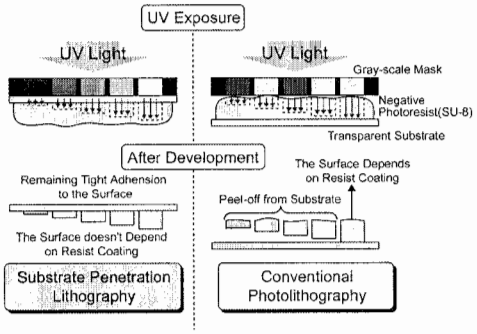

Figure 2. Comparison of substrate penetration lithography and conventional lithography.

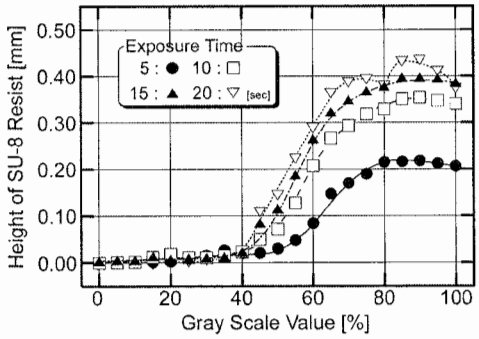

Figure 3. Relation between gray-scale value and resist height.

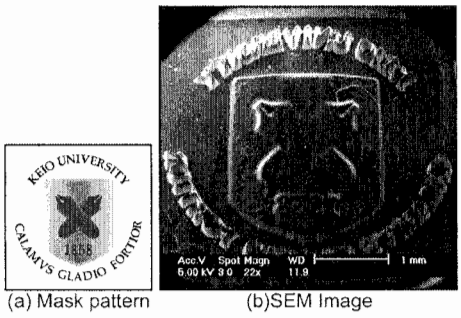

Figure 4. SEM image of the multilevel relief like structure formed on SU-8.

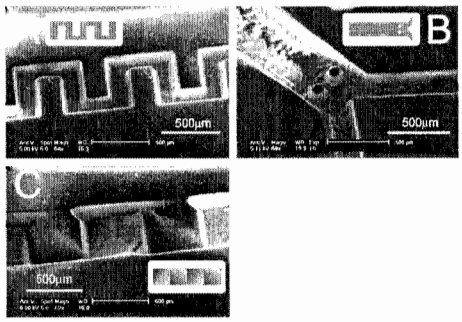

Figure 5. SEM images and mask patterns of 3-D PDMS micro capillaries.

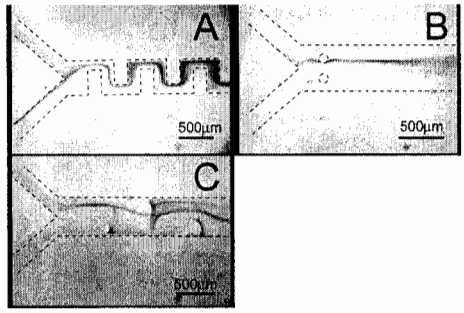

Figure 6. Photographs of flow in the 3-D PDMS micro capillaries.

PIPETTE-LIKE MICRO THERMO-PNEUMATIC PUMP FOR BIOCHEMICAL MICROSENSOR

Wan Ho Song, Henry Baltes and Jan Lichtenberg
Physical Electronics Laboratory, ETH Zurich, CH-8093 Zurich, Switzerland

Abstract

The combination of advanced biochemical sensors with a dedicated microfluidic package opens new possibilities for fully integrated analysis systems. While the integration of CMOS (Complementary Metal Oxide Semiconductor) microelectronics with the sensor device allows highly parallel, extremely sensitive measurements, microfluidic structures add sample handling and pretreatment capabilities. We describe a novel polymer-based packaging concept that provides integrated, pipette-like pumping facilities for disposable biosensors. Different from flow-through systems with inlet and outlet, this low-cost thermo-pneumatic micropump allows to draw in and to eject liquids from the chip without priming.

Keywords: thermo-pneumatic pump, micropump, biosensor, liquid handling

1. Introduction

There has been an increasing interest in cantilever-based sensing systems in recent years [1]. These devices have proven to be excellent detectors for minute amounts of analyte, which makes them especially interesting for applications such as medical diagnostics. Our group works on integrated cantilever devices, which monolithically combine the sensing structure with dedicated signal-processing electronics using a commercial CMOS process [2]. This co-integration of microelectronics and microsensors requires a high level of packaging technology to allow handling of the liquid sample and, at the same time, to protect the electronic circuitry and the electrical interconnections to the outside. Although a wide variety of micro-components for liquid handling have been developed (e.g., valves and pumps), only few groups have attempted the integration of these on a single platform together with a microsensor system [3].

Here we present a new packaging approach that features a simple liquid pumping system based on thermo-pneumatic actuation to allow defined sample delivery to a CMOS-based cantilever biosensor. The low-cost pump does not require moving elements on the chip and can be operated using an external heater. The performance of the pumping system has been evaluated experimentally and a model has been developed to predict the pump behavior based on design parameters.

2. Theory

The operating principle is based on Charles' law, which describes the volume of an ideal gas as being directly proportional to the absolute temperature of the gas at constant pressure and number of moles [4]. Thus, by implementing a dead-end channel with an inlet port on one end and a sealed pressure chamber on the other, gas expansion can be used as pumping mechanism (Figure 1). The chamber (volume V_o) can be heated externally by a resistive or a Peltier heater. To draw liquid into an empty channel, the chamber is first heated to T_o. Then, the liquid is dispensed into the inlet reservoir. Finally, the chamber temperature is reduced to $T_o - \Delta T$ and the contracting gas in the chamber drags the liquid in. Alternatively, the liquid can be removed from the channel by increasing the temperature again to expand the air in the pressure chamber. Figure 2 illustrates how the package is assembled from two molded polymer pieces together with the microsensor chip.

Assuming a homogenous temperature distribution in the chamber, the pumped liquid volume, ΔV, can be calculated by $\Delta V = Vo \cdot \Delta T/To$. However, to keep the external heating system simple, single-side heating was chosen. As a result, a temperature gradient over the chamber volume is caused by thermal conduction through the walls. To still be able to control pumping precisely by

adjusting the heater temperature, T_{heater}, a finite-element-method (FEM) model was used to calculate the average temperature change of the chamber, ΔT, as a function of T_{heater}. This allowed ΔT to be approximated by $\alpha \Delta T_{heater}$ where α is, e.g., 0.814 for a 4×4×1 mm^3 chamber.

3. Experimental

Two microfluidic systems were made in poly(dimethyl siloxane) (PDMS) by molding from a precision-milled aluminum plate and bonding to a second, thin PDMS sheet. As these chips were used primarily to study the pumping performance, the biosensor was not integrated. Instead, the pressure chamber was connected with the inlet reservoir by a 10-cm long channel to allow optical monitoring of the flow speed. The physical dimensions of the systems are listed in Table 1. A current-controlled Peltier element (4×4 mm^2, Quick-Ohm, Germany) was attached on top of the pressure chamber using thermally conductive adhesive to heat or cool the enclosed air. To measure T_{heater}, a type-K thermocouple was placed at the edge of the heating element. A blue dye-water solution was used to visualize the liquid column moving through the channel. The front speed of the liquid was recorded using a video camera mounted on microscope and the transient behavior of the liquid pumping was analyzed using video processing software. The flow speed measurements were calibrated by placing the transparent chips on plotting paper.

4. Results and discussion

As Figure 3 shows, the pumped liquid volume is a linear function of the applied ΔT_{heater} as the theory predicts. Our model, based on the FEM calculation of the gas temperature in the chamber is in good agreement with the experimental data acquired under equilibrium conditions.

Figure 4 shows the transient behavior of the micropump for both flow directions. Although, the curves for pumping in and out are not identical due to different heating and cooling rates, both volumes are essentially the same. The pump is therefore capable of completely releasing a liquid volume previously pumped in. The transient data also allowed to calculate an average pumping rate and the time typically needed to fill the biosensor flow cell (see Table 1). The difference in pump rates between system A and B is due to geometrical factors that affect the heating and cooling rates of the pressure chamber (amongst others, the thickness of the PDMS lid underneath the heater).

The system's maximum power consumption was below 0.7 W for ΔT_{heater}= 70 K and allowed filling of the biosensor chamber in less than 40 s. It should be noted that for filling power is only required during the initial heating, while the pump-in operation does not require electrical energy.

5. Conclusions

This simple, pipette-like pumping system demonstrates reliable, self-priming, externally driven liquid handling integrated in a low-cost, disposable biosensor package. Current research is directed towards multi-step pumping schemes for sample and wash solution, and towards feedback control of the liquid flow by a flow sensor integrated on the CMOS chip.

Acknowledgements

This research project is carried out within the EU framework Biofinger (IST-2001-34544) with financial support by the Swiss Federal Office for Science and Education, Bern, Switzerland.

References

[1] M. Sepaniak, P. Datskos, N. Lavrik and C. Tipple, *Anal. Chem.* **74,** 568 A-575 A (2002)

[2] Y. Li, C. Vancura, H. Hagleitner, J. Lichtenberg, O. Brand and H. Baltes, *Proceedings of the IEEE Sensors 2003,* **2**, 809-813 (2003)

[3] R. H. Liu, J. Yang, R, Lenigk, J. Bonanno and P. Grodzinski, *Anal. Chem.*, **76**, 1824-1831 (2004)

[4] B. G. Segal, *Chemistry: Experiment and Theory,* 2nd ed., Wiley, New York, (1989)

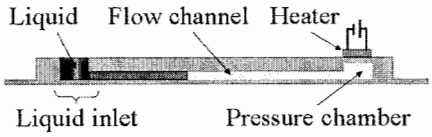

Figure 1. Schematic cross section of a thermo-pneumatic micropump. Pressure changes are induced in the chamber to the right to draw liquid in from the inlet reservoir.

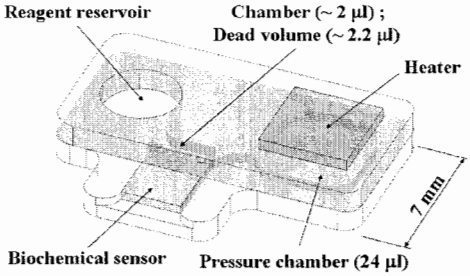

Figure 2. Schematic view of the microfluidic package for a CMOS biosensor with a 2-µl flow cell, a total dead volume of 2.2 µl and about 40 s sample filling time.

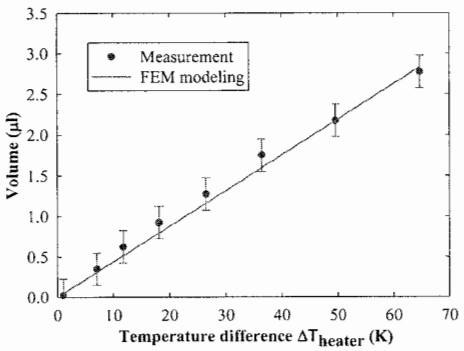

Figure 3. Measured and simulated volume aspirated by system A as a function of ΔT_{heater}. Volume readings were taken when the flow stopped after a temperature change.

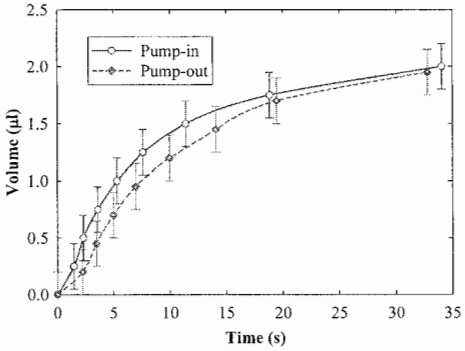

Figure 4. Transient pumping behavior of system A for ΔT_{heater}= 50 K for heating and cooling (the connecting lines were added as visual aid). The volumes for pump-in and -out are the same and do not show a hysteresis.

	Dimensions	Pump rate (nl/s)	Filling time for 2.2 µL (s)
System A	4×4×1 mm^3 pressure chamber 0.5 mm lid thickness 0.5×0.5 mm^2 channel cross section	152 ± 15	~ 35
System B	4×4×0.5 mm^3 pressure chamber 1 mm lid thickness 0.5×0.2 mm^2 channel cross section	48 ± 17	~ 150

Table 1. Physical dimensions, average pumping rates and filling times for the two test structures. Pump rates were calculated as an average over the first ten seconds after inducing a temperature of 50 K . The filling time is based on measurement. The difference in pump rates is partially due to the fact that system B has a thicker PDMS lid underneath the heater.

FABRICATION OF 3D SU-8 TIPS FOR ELECTROSPRAY IONIZATION MASS SPECTROMETRY

Santeri Tuomikoski[1], Tiina Sikanen[2], Risto Kostiainen[2], Tapio Kotiaho[3], Sami Franssila[1]
[1]Microelectronics Centre, Helsinki University of Technology, P.O .Box 3500, Fin-02015 Espoo, Finland.
[2] DDTC, Faculty of Pharmacy, University of Helsinki, P.O .Box 56, Fin-00014, Helsinki, Finland
[3]Department of Chemistry, University of Helsinki, P.O .Box 55, Fin-00014, Helsinki, Finland

Abstract

This study presents novel fabrication process for a microchip coupler to mass spectrometer (MS). Coupling is done by using electrospray ionization (ESI) technique. Sharp MS coupling tips were made of epoxy resist SU-8 with standard optical lithography technique. Three layer SU-8 structures were fabricated and released from the substrates to form self-standing SU-8 microchips. Fabrication process is described in this paper together with preliminary mass spectrometry results.

Keywords: SU-8, Mass spectrometry, Electrospray ionization

1. Introduction

Detection plays important role in the development of μ-TAS devices. Microchip coupling to mass spectrometer (MS) is one of the key techniques. ESI-microchips have been intensely studied for coupling to MS. Various different fabrication methods and materials have been published in the literature: for example, microchips with integrated silica capillaries [1], electrospray from channel edge [2,3] and tip shaped nozzles [4] have been published.

To the best of our knowledge this is the first enclosed tip for ESI that is fabricated from SU-8. Earlier tips have been open to air [4]. SU-8 enables fabrication of various microfluidic components. Therefore, fabrication of enclosed SU-8 ESI tips makes it possible to integrate separation systems on a same chip.

2. Experimental

ESI-microchips were fabricated with three-layer SU-8 process with standard UV-lithography. In the last step the structures were released from substrate wafers and used as self-supporting chips in ESI-MS. Layers of the fabrication process are shown in the Figure 1 a. First layer of SU-8, containing the fluidic inlet for the chip, was patterned on top of thermally oxidized silicon wafer. Second SU-8 layer was patterned on top of first one and both layers were developed in a single step with immersion development. Second layer of SU-8 forms the microchannels and fluidic reservoir. The tip at this stage of fabrication is shown in Figure 1 b. It is a SEM picture showing the ESI tip of the fluidic chip. The third layer of SU-8 was applied on top of Pyrex wafer and this SU-8 acted as an adhesive for bonding with the two-layer structure on silicon wafer. Tip shape was determined by an exposure through the Pyrex wafer. Third layer of SU-8 was developed laterally between the bonded wafers. After development the SU-8 chip was released from the substrates. Pyrex wafer and thermal oxide on top of silicon were sacrificially etched in hydrofluoric acid. This process enables reuse of the silicon wafer

SU-8 microchips were coupled with an API 300 triple quadrupole MS/MS system from Perkin Elmer Sciex. Coupling was done with a nanospray source from Proxeon Biosystems that was equipped with microscopes and a modified xyz-stage for aligning the chip towards the MS inlet. External power supplies were used for applying the high voltage on the microchip. ES voltage was applied with Pt wires from fluidic reservoirs or by Pt or Au metallization on top of the tip. Thin film metallizations were done by sputtering as a last step of processing.

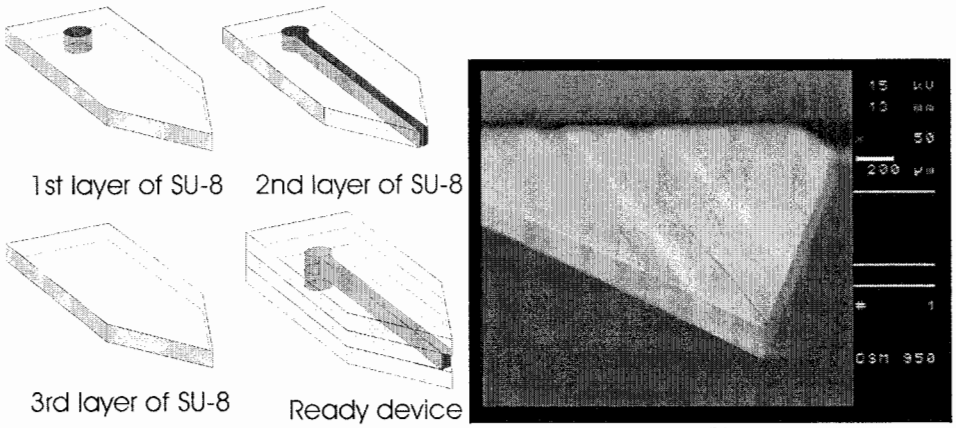

Figure 1. (a) Layers of the enclosed SU-8 microtip. (b) SEM picture of the spraying edge of the microtip.

3. Results and discussion

A chip containing an array of six ESI-microtips, completely released from the supporting wafers, is shown in Figure 2 (a). In Figure 2 (b) head of ready SU-8 microtip is shown. It is enclosed and released from the substrate. Total thickness of the chip was 250-300 μm. Cross-sectional diameters of enclosed channels varied between 10μm*20μm and 40μm*50μm (width*height). Spraying was performed from sharp tip shaped structures as well as from simple orifices from chip edge. Released SU-8 microchips can be easily handled and mounted on any substrate. 3D enclosed microtips from SU-8 can be integrated with various separation devices on a chip. In our method all three layers are lithographically aligned. Size and shape of the tips and the channels are fully determined by lithographic accuracy only. In Figure 3 is shown a mass spectrum received with SU-8 microtip with channel dimensions of 10μm*20μm.

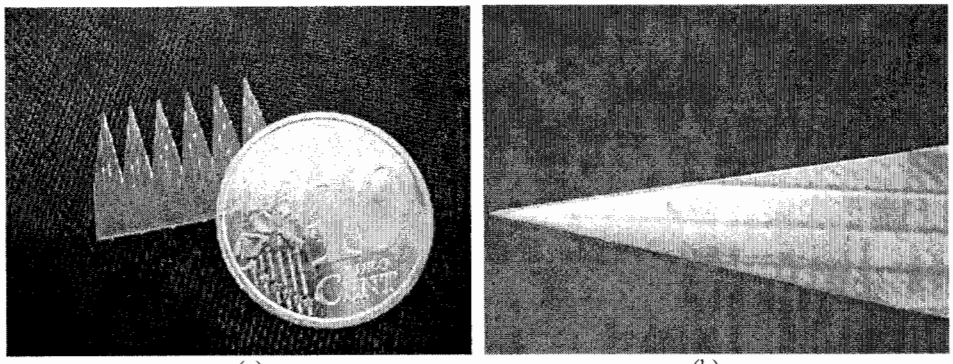

Figure 2. (a) Array of six SU-8 microtips. 10 cent coin shows the size of the tips. (b) Optical microscope picture of the head of released SU-8 ESI tip

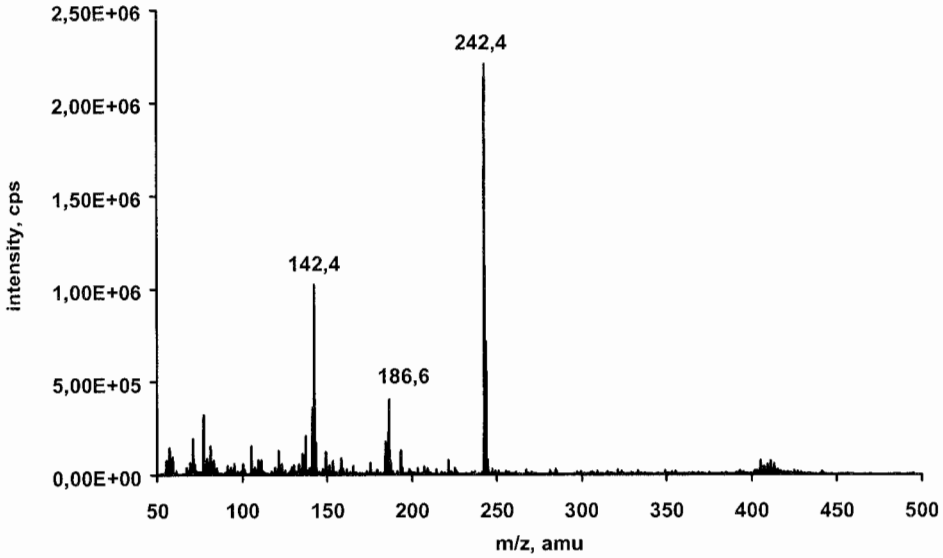

Figure 3. A mass spectrum received with SU-8 ESI-tip. Studied compound was tetra-n-butylammonium $[M]^+$=242 at 2 μM concentration. Applied solvent was methanol:water 4:1. Signals at m/z ratios 142,4 amu and 186,6 amu are fragmentation products of the main analyte. Applied microtip had microchannel with cross-sectional diameter of 10μm*20μm.

4. Conclusions

Novel fabrication process for ESI-MS microfluidic chips is described. Three-layer patterning of SU-8 and release from the substrate has been done successfully. Microfluidic chips with various channel sizes have been fabricated from SU-8. Initial MS tests have been done with the novel ESI tips and they have shown promising results. Tip geometry shows much effect to the MS signal. Therefore, optimization of the tip geometry for the ESI performance and tip integration with separation is to be done in the future.

References

[1] Li, J., Thibault, P., Bings, N., Skinner, C., Wang, C., Colyer, C., Harrison, J., *Anal. Chem.* **71**, pp 3036-3045 (1999).

[2] R. Ramsey, J. Ramsey, *Anal. Chem.*, **69**, pp. 1174-1178 (1997).

[3] K. Huikko, P. Östman K. Grigoras, S. Tuomikoski, V-M. Tiainen, A. Soininen, A. Manz, S. Franssila, R. Kostiainen, T. Kotiaho, MicroTAS 2002, pp. 506-508.

[4] S. Le Gac, S. Arscott, C. Rolando, MicroTAS 2003, pp 1211-1214.

SLIDING MICRO VALVE INJECTION DEVICE FOR QUANTITATIVE NANO LITER VOLUME

Masahiro Kuwata[1], Tomohiko Kawakami[1], Keisuke Morishima[1], Yuji Murakami[1], Hajime Sudo[2], Yoshikazu Yoshida[1], Takehiko Kitamori[3]

[1]The Research Association of Micro Chemical Process Technology, R&D-C1132, KSP-Bldg., 3-2-1, Sakado, Takatsu, Kawasaki, Kanagawa, 213-0012 JAPAN

[2]Corporate Research & Development Center, Toshiba Corporation, 1, Komukai-Toshiba-Cho, Saiwai, Kawasaki, 212-8582 JAPAN

[3]The University of Tokyo, Hongo, Bunkyo, Tokyo 113-8656 JAPAN

Abstract

A novel sliding micro valve injection device is proposed. A part of microchip was cut into pieces parallel to each other across microchannels. The central part slid in parallel to right-and-left parts. Thus the connections of channels in a microchip could be changed and quantitative 10 nL volume was cut from some flow and injected into other flow without dead volume. This device was made from Pyrex glasses and PTFE coating. Thus this device has high chemical tolerance. Quantitative nano liter volume injection and flow injection analysis (FIA) were demonstrated to justify the applicability of this device.

Keywords: micro valve, microfluidics, micromachining, injection, flow injection analysis

1. Introduction

It is very important to control nano liter flow volume precisely in microchip for quantitative analysis. Recently, considerable advancement is achieved regarding the development of micro fluid control devices, i.e., membrane micro valve[1], mobile monolith valve[2], hydrophobic valve[3], sliding gate valve[4], sliding needle-head valve[5], etc. However, in order to precisely control a small amount of fluid in microchip, there are still several problems, namely, dead volume, chemical tolerance, pressure residence, etc need to be solved. Especially quantitative nano liter volume injection is the most difficult. In the present work, we have developed a novel sliding micro valve injection device. This device is able to control nano liter liquids quantitatively without dead volume and with high chemical tolerance.

2. Device structure

Schematic views of sliding micro valve injection device are presented in top of Figure 1. A part of microchip was cut into pieces parallel to each other across channels. The central part slides in parallel to right-and-left parts. The channels in microchip are connected and disconnected with this sliding movement. Before performing the cut, these channels were originally a single channel. Thus, when these are reconnected, the shape, depth and width are the same. Therefore there is no dead volume left in between these channel connections.

Figure 2 shows the size of this slide micro valve. The depth and width of channels are 40μm and 100μm. The width of central part is 3mm. The volume of the channel in central part is 10nL.

Surface treatment of slide structure is very important for pressure tightness. To prevent the leak from the gaps of slide structure, PTFE is coated on the surfaces of slide structure. The thickness of PTFE is about 5μm. Since the substrates of microchip are Pyrex glass and the parts of glass surface are coated with PTFE, this device can be applied to almost all liquids (e.g., organic solvent, acid and alkali). The central part is actuated by step motor and ball screw.

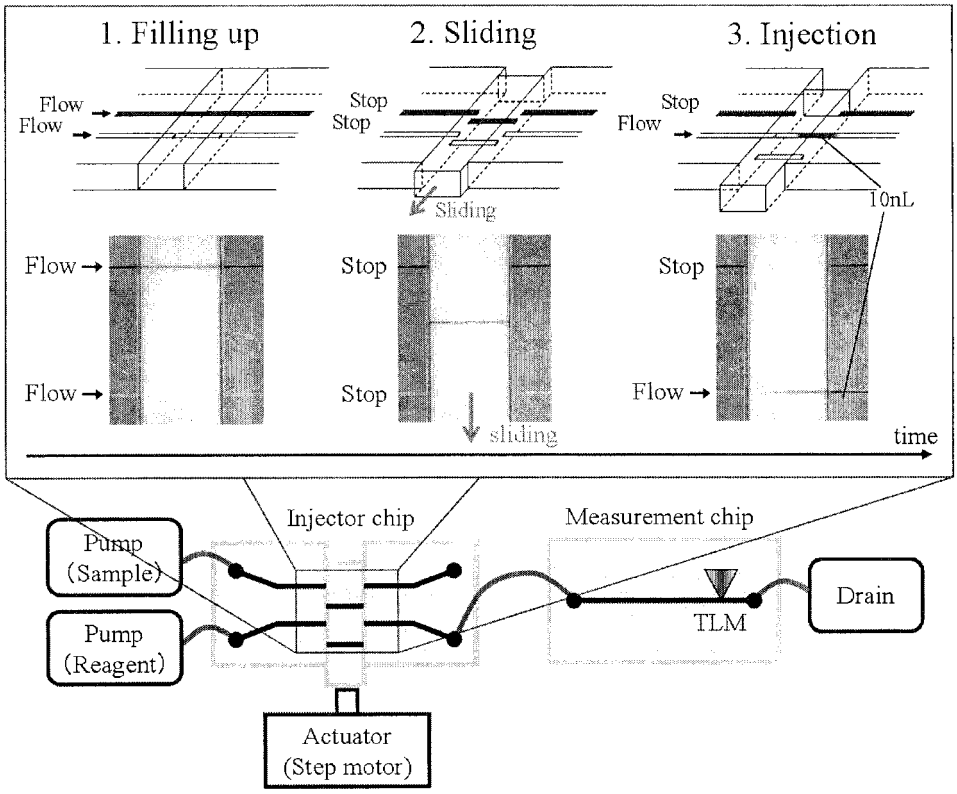

Figure 1. Slide Injection System. Top figures are schematic illustrations of slide injection. The pictures in middle portion are microscopic views. Bottom figure is the experimental setup of flow injection analysis.

3. Result and Discussion

3.1. Quantitative nano liter volume injection

The pictures presented in the middle portion of Figure 1 show microscopic views during slide injection. Sample and reagent were pumped at a constant pressure of 20kPa. There was no leakage from the gaps of slide structure because PTFE coated on the surfaces stopped the leakage. The shape of injection was quite sharp because there was no dead volume left in between channel connections.

3.2 Application to Flow Injection Analysis

Flow injection analysis (FIA) was demonstrated to justify the applicability of this injection device. Figure 1 shows the experimental setup of FIA. NO_2^- used as a sample having concentration of 100μg/L injected into the channel to trace the color change cause by interaction with the reagent flow. Sample was injected 3 times successively (30nL). The injected sample was mixed and reacted with reagent in the reagent flow. The degree of color change was measured with thermal

lens microscope (TLM). Figure 3 shows the result of NO_2^- measurement. The signal from only 30nL sample could be detected easily by this system.

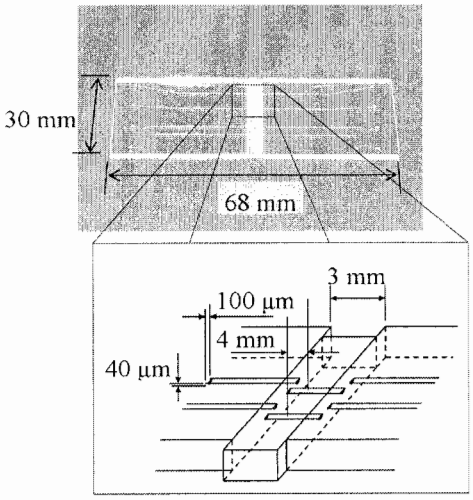

Figure 2. The size of slide structure we have developed.

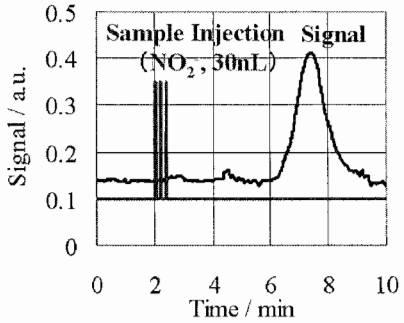

Figure 3. The result of Flow Injection Analysis of NO_2^-.

5. Conclusions

This paper describes the development of a novel sliding micro valve injection device. This device is able to precisely control quantitative nano liter volume in microchip. This on-chip injection device is easily integrated with other device on a single microchip, such as on-chip detection, on-chip reaction, etc. In near future, we will realize various applications using this sliding micro valve device.

Acknowledgements

A part of the study presented in this paper was financially supported by New Energy and Industrial Technology Development Organization (NEDO), Japan.

References

[1] William H. Grover, Alison M. Skelley, Chung N. Liu, Eric T. Lagally, Richard A. Mathies, *Sens. Act. B*, **89**, 315-323 (2003)

[2] Emest F. Hasselbrink, Jr., Timothy J. Shepodd, Jason E. Rehm, *Anal. Chem.*, **74**, 4913-4918 (2002)

[3] M. Yamada, M. Seki, *Anal. Chem.*, **76**, 895-899 (2004)

[4] Jeremy A. Frank, Albert P. Pisano, *Proc. Transducers '03*, 143-146 (2003)

[5] K. Morishima, M. Ohnishi, M. Tokeshi, K. Kitamori, *Proc. Micro TAS 2003*, 1033-1036 (2003)

ENZYME-BASED BIOMEMS FOR ULTRA LOW FLOW RATE MEASUREMENT

Uwe Herberth[1], Gerhard Jobst[2], Isabella Moser[1], Gerald A. Urban[1]
[1]*Chair of Sensors, Institute for Microsystemtechnology, Albert-Ludwigs-University, Georges-Köhler-Allee 103, 79110 Freiburg, Germany*
[2] *Jobst Technologies GmbH, Georges-Köhler-Allee 102, 79110 Freiburg, Germany*

Key words: biosensor, ultra low flow rate, flow direction detection, glucose measurement.

1. Introduction

BioMEMS are commonly used in medicine, environmental and pharmaceutical applications to specifically detect small amounts of an analyte in a complex matrix. To increase the reliability of the bioMEMS system in applications like microdialysis monitoring or drug infusion, the control of analyte flow rate and concentration measurement is desirable. With our setup flow rate detection and also concentration measurement in an integrated bioMEMS device is possible by using the product of the biochemical reaction as marker substance for the flow measurement. This is achieved by adding an upstream and a downstream electrode, to an enzyme-based glucose sensor. The used bioMEMS device consists of a flow cell where the analyte flows over biosensor membranes with immobilised enzymes catalysing the reaction of glucose and O_2 to H_2O_2, with a succeeding amperometrical detection of H_2O_2 [1,2]. The additional electrodes are to collect the H_2O_2 emitted into the flow cell by the glucose sensor. By quantifying the distortion of the H_2O_2-profile, the flow rate of the analyte can be determined, and summing the total currents of the three electrodes allows to calculate the glucose concentration (see fig 1).

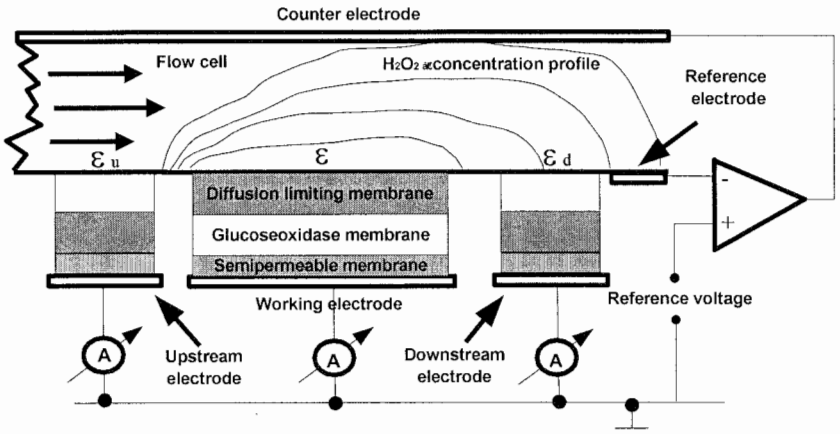

Figure 1. bioMEMS scheme (not to scale)

2. Theory

The setup is theoretically described by the following equations:

glucoseoxidase membrane: 1mol glucose + 1 mol O_2 → 1 mol H_2O_2
H_2O_2 detected at the working electrode : ε(v) mol H_2O_2 → ε(v) mol O_2

emission of H_2O_2 to the flow cell: $[1-\varepsilon(v)]$ mol H_2O_2

H_2O_2 detected at the upstream electrode : $[1-\varepsilon(v)][\varepsilon_u(v)]$ mol $H_2O_2 \rightarrow [1-\varepsilon(v)][\varepsilon_u(v)]$ mol O_2

H_2O_2 detected at the downstream electrode: $[1-\varepsilon(v)][\varepsilon_d(v)]$ mol $H_2O_2 \rightarrow [1-\varepsilon(v)][\varepsilon_d(v)]$ mol O_2

total loss of H_2O_2 to the flow cell: $[1-\varepsilon(v)][1-\{\varepsilon_d(v) + \varepsilon_u(v)\}]$ H_2O_2

where ε, ε_u and ε_d are the efficiency coefficients of the electrodes, v is the the flow rate. To optimise the sensitivity and the operating range of the sensor transient numerical simulations were done [3] (FIDAP, Fluent.Inc). The time dependent concentration profiles of the species involved in the reactions (see fig 2) were used to calculate the current in a post-processing step by a self-written software.

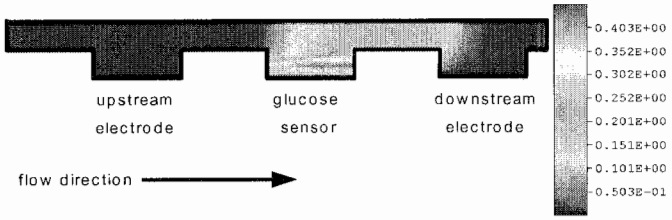

Figure 2. Numerically simulated H_2O_2 concentration profile (scaled y-direction, units: mMol/l)

The volume of the flow cell, cross sectional area, the size and position of the electrodes were varied to optimise the sensor. The influence of the membranes on the sensitivity was also addressed by the simulation. The volume of the flow cell and the cross sectional area alter the flow velocity of the liquid over the membranes and therefore changes the sensitivity to the flow rate. The electrode size and membran parameters alters the efficiency coefficients.

3. Experimental

The experimental setup consists of a syringe pump, a self-made 4-channel potentiostate and the software bioMON 3.0 [4] controlling the whole experimental hardware. The sensor is fluidically and electrically connected by a self-made mount (see fig. 3).

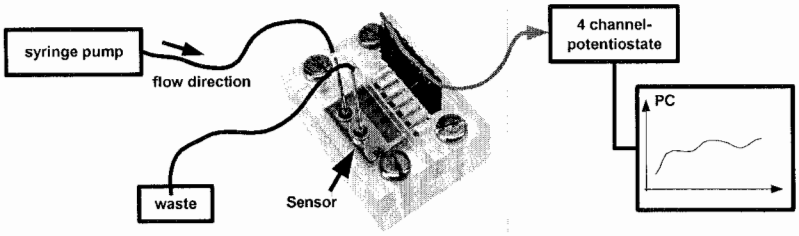

Figure 3. Experimental setup

A film-based microtechnology available at IMTEK-Sensors was used to fabricate the sensor units, comprising a flowrate independent glucose sensor for control purposes and a flow rate dependent glucose sensor and the upstream and downstream electrode for flow measurement. The flow cell has a total internal volume of 250 nl and a cross sectional area of 0.05 mm². The round

shaped electrodes have a diameter of 400 µm, the pitch is 800µm.

4. Results and Discussion

Figure 4 shows original data captured with our sensor. The inset in fig. 4 shows the sum of the currents of all electrodes indicating the operation regime of the sensor at a certain flow rate.

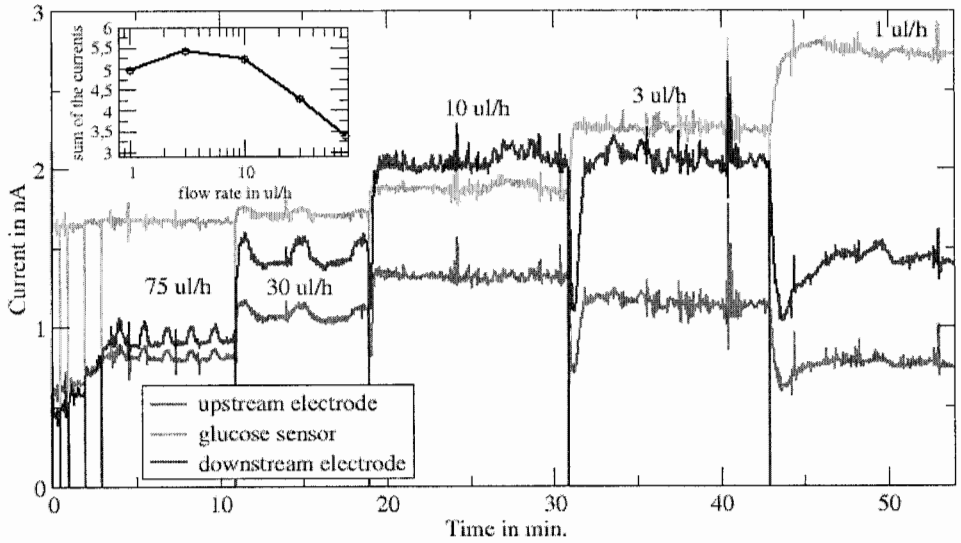

Figure 4. Flow rate experiment (glucose concentration 90 mg/dl)

The current values of the electrodes or a fitted calibration function for each electrode can be stored in a lookup table. Then the lookup table can be used for calulcating the flow rate. Exact measurement of flow direction and flow rate down to approx. 300 picoliter per second (~1 µl/h) is possible (see fig. 4). This very small value originates from the fact that the walls are impermeable for hydrogenperoxide which corresponds to adiabatic walls in an equivalent thermal anemometric sensor. The diffusion constant of hydrogenperoxide is lower in relation to the thermal conductivity of an equivalent thermal sensor, which leads to a higher contrast in the concentration profile.
Nevertheless there are requirements for our measurement scheme: a liquid with a detectable concentration of the analyte and if proportionality of overall current and glucose concentration is an issue complete consumption of H_2O_2 by the electrodes.

References:

[1] Moser, I., Jobst, G., Urban, G. A. (2002). Biosensor arrays for simultaneous measurement of glucose, lactate, glutamate and glutamine. *Biosensors & Bioelectronics*, **17**, 297-302.
[2] Jobst, G., Moser, I., Svasek, P., Varahram, M., Trajanoski, Z., Wach, P., Kotanko, P., Skrabal, F., Urban, G. A. (1997). Mass producible miniaturized flow through a device with a biosensor array. *Sensors & Actuators B*, **43**, 121-125.
[3] Jobst, G., Moser, I., Urban, G. A. (1996). Numerical simulation of multi layered enzymatic sensors. *Biosensors & Bioelectronics*, **11**, 111-117.
[4] http://www.jobst-technologies.com

μTAS WITH INTEGRATED OPTICAL TRANSDUCERS

S. Balslev, B. Bilenberg, O. Geschke, A. M. Jorgensen, A. Kristensen, J. P. Kutter, K. B. Mogensen, and D. Snakenborg

MIC - Department of Micro and Nanotechnology, Technical University of Denmark (DTU), Building 345 east, DK-2800 Kongens Lyngby, Denmark

Abstract

We present a technology platform for micro-total-analysis-systems with integrated optical input- and output transducers in combination with passive optical and microfluidic networks. Three physical domains – optical, mechanical and electrical – are interfaced by five different components on the chip: laser, optical waveguides, microfluidic mixer, absorbance cuvette and photodiodes. Fabrication details and first characterization results are presented.

Keywords: Integrated optics, laser, photodiode, waveguide, SU8

One of the major challenges in integrated optics is coupling of optical signals in and out of the device. Pig-tail coupling of optical fibers is a widely used but costly approach. It is therefore attractive to integrate optical transducers on the chip. We address this problem by integrating laser light sources and photo-detectors on a lab-on-a-chip. The present microsystem (see Fig. 1) is designed for wavelength selective absorbance measurements in the visible range on a fluidic sample, which can be prepared/mixed on-chip. A cross-sectional outline of the device is shown in Fig. 2. The laser structures [1], waveguides and microfluidic handling system [2] are defined in a single UV-lithography step on a 10 μm thick SU-8 layer on top of a silicon substrate with embedded n^+p photodiodes. Polymethylmethacrylate (PMMA) adhesive bonding of a Borofloat glass lid [3] is used to seal the SU-8 structures.

The microfluidic dye laser [1] is based on an ethanolic solution of the laser dye Rhodamine 6G, and is optically pumped through the glass lid with a pulsed, frequency doubled Nd:YAG laser (wavelength: 532 nm, pulse-width: 5 ns, repetition rate: 10 Hz). The laser cavity is formed by an array of channels for the dye solution, with each wall contributing to the laser feedback. An output spectrum from the microfluidic dye laser is shown in Fig. 3.

The emitted dye laser light is coupled directly into 30 μm wide SU-8 waveguides [2], and guided to the microfluidic cuvette and the photodiodes. A microfluidic diffusion mixer is placed in front of the cuvette, allowing for on-chip sample pre-treatment.

The photodiodes are vertical diodes with the photosensitive area defined by a phosphorous diffusion of dimensions 50 μm by 2 mm. Light is coupled into the photodiodes by optical leakage in the regions where the SiO_2 buffer layer has been removed, see Fig. 2. A measurement of the open circuit diode response from a single dye laser pulse is shown in Fig. 4.

The coupling of dye laser light through the absorbance cuvette is illustrated by the measurements shown in Fig. 5 and 6. The photodiode response as function of increasing pump laser power is shown in Fig. 5. In the first part of the plot (up to 12 mW) the dye laser is below lasing threshold, and scattered pump light dominates. Above threshold the dye laser contributes with the major part of the detected signal. The photodiode response depends on the absorbance in the cuvette as demonstrated by filling the cuvette with ethanol (circles) and with an ethanolic dye solution (squares), as shown in Fig. 6.

Acknowledgements

This work is supported by the Danish Technical Research Council, STVF (grant numbers: 26-00-0220 and 26-02-0064). The partial support of the EC-funded project NaPa (Contract no. NMP4-CT-

2003-500120) is gratefully acknowledged. The contents of this work is the sole responsibility of the authors.

References

[1] S. Balslev and A. Kristensen, The 2004 CLEO/IQEC Conference, San Francisco, California, USA, May 16-21, 2004, CLEO/IQEC and PhAST Technical Digest on CD-ROM (The Optical Society of America, Washington, DC, 2004), presentation number CFM7

[2] K.B. Mogensen, J. El-Ali, A. Wolff, and J.P. Kutter, Appl. Optics **42**, 4072 (2003)

[3] B. Bilenberg, T. Nielsen, B. Clausen, and A. Kristensen, J. Micromech. Microeng., Vol. 14, pp. 814-818 (2004)

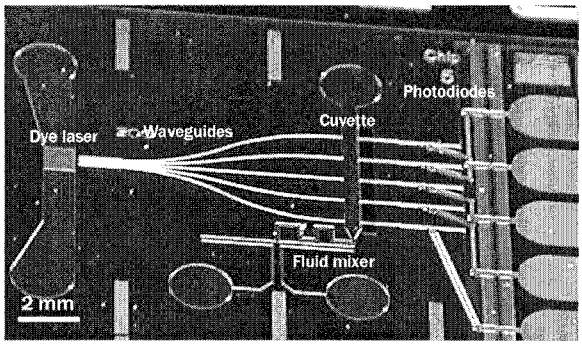

Figure 1. Photo of a lab-on-a-chip device, before bonding of the glass lid. The footprint of the chip is 15 by 20 mm.

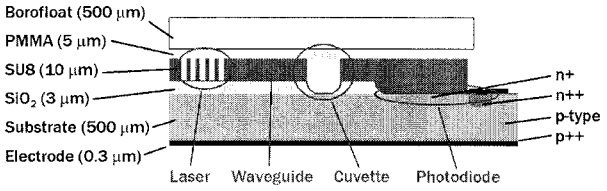

Figure 2. Cross-sectional outline of the lab-on-a-chip device with integrated laser, waveguides, microfluidic components and photodiodes

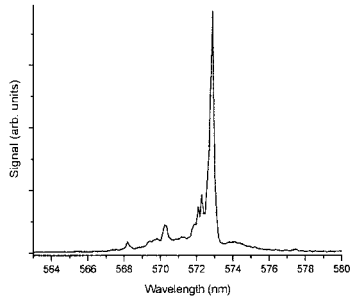

Figure 3. Emission spectrum from the laterally emitting microfluidic dye laser. A single dominant mode is observed at 573 nm. The line width reflects the 0.5 nm spectrometer resolution.

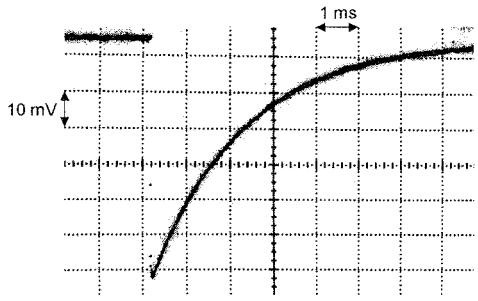

Figure 4. Open circuit photodiode voltage response from a single dye laser pulse.

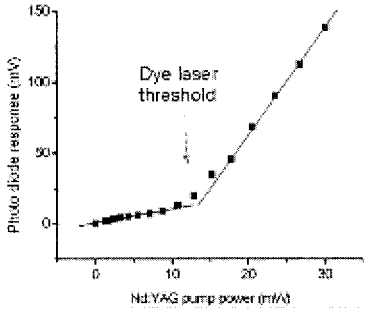

Figure 5. Photodiode response for a range of Nd:YAG pump laser powers. First part of the plot (up to 12 mW) is below lasing threshold for the dye laser, and the signal is due to scattered light. Above threshold the light due to the dye laser is dominant.

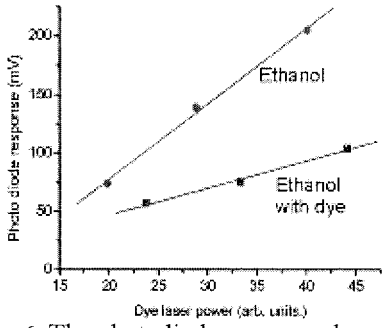

Figure 6. The photodiode response depends on the absorption, as demonstrated by filling the cuvette with ethanol (circles) and ethanol with dye (squares).

LOW-COST, CHEMICALLY RESISTANT MICROREACTORS FABRICATED BY LASER MICROMACHINING IN STAINLESS STEEL

Jan Lichtenberg and Henry Baltes
Physical Electronics Laboratory, ETH Zurich, CH-8093 Zurich, Switzerland

Abstract

Stainless steel is an ideal substrate material for microfluidic devices in both chemical analysis and synthesis. Steel is highly corrosion resistant, has a good thermal conductivity and can be easily sterilized or autoclaved. We present a novel laser micromachining concept that allows the rapid and cost-efficient fabrication of multilayer microfluidic structures with features down to 50 µm. Based on commercially available Nd:YAG-laser equipment, the technique is an interesting alternative for research prototyping and medium-scale fabrication alike. To evaluate the fabrication approach, a multiple-lamination mixer was fabricated from five machined stainless steel layers.

Keywords: microreactor, micromixer, stainless steel, laser micromachining

1. Introduction

While stainless steel is the dominant construction material for mass-production equipment for chemical synthesis, it is less prominent in microfluidics, which utilizes glass, silicon, and polymers. In this paper, we describe a new approach to the manufacture of highly customizable multilayer microfluidic structures in stainless steel based on a laser-micromachining technique adapted from the printed-circuit board (PCB) industry. Several metal sheets containing laser-ablated channels and interconnect holes are aligned and stacked in a dedicated chip holder, which seals the sheets by compressive force and provides fluidic interconnects to the outside (Fig. 1). The resulting device is chemically resistant and can be operated at elevated temperatures. Further functionality can be integrated by additional coating procedures or by including different materials in the stack, such as optically transparent polymer sheets.

Several groups have refined conventional precision-machining techniques, such as milling or electro-discharge machining, for the fabrication of miniaturized mixers and heat exchangers [1]. However, design freedom is limited by the size and controllability of the milling tool and chip cost can be comparatively high due to slow machining speeds and considerable tool wear. Laser micromachining, which was so far mostly applied to polymer substrates [1-3], is a highly precise, fast, and contactless alternative to classical machining. By stacking multiple layers of machined stainless steel sheets on top of each other, complex structures including multiple-lamination mixers or heat exchangers can be implemented.

2. Laser micromachining technique

The computer-assisted 1064-nm Nd:YAG-laser micromachining technique presented here allows the fabrication of holes and grooves through thin (50 to 500 µm) sheets of polished stainless steel with aspect ratios around 1:1 and a positioning accuracy of ±10 µm [4]. Design files can be prepared in the common data format Gerber XP, which can be easily exported from most CAD software packages including dedicated chip layout software. Due to its commercial mass application for PCB printing stencils, large substrates (up to 71×58 cm) can be ordered from external suppliers at comparatively low cost, leading to a fabrication price below 1 Euro per chip at turn-around times of a few days.

Fig. 2 shows a SEM picture of a laser-machined channel (200 µm wide in a 150-µm-thick steel sheet). To assemble the complete microfluidic system, the individual steel layers are stacked on top of each other in an aluminum or stainless steel chip holder (Fig. 1). Two alignment pins in the base

part of the holder allow placing the sheets with a precision of ±30 µm into the stack, which assures sufficient registration between two layers. The stack is clamped together by a second metal plate on the top. This cover also provides threads to connect external capillary tubing using standard laboratory connectors (e.g., Upchurch fittings).

3. Micromixer

In order to evaluate the fabrication concept, a multiple-lamination mixer was implemented in a five-layer stack of 5-by-2.5-cm^2 sheets of 150-µm-thick stainless steel sheets (steel type 1.4301). The minimum channel width used for this structure was 200 µm to allow sufficient flow rates in the device. Rapid mixing is achieved by splitting both inlet streams into 16 individual channels on two independent fluidic levels on the device. In the center region of the chip, the two sets of 16 channels are vertically merged and laminated in pairs (Figs. 3 and 4) similar to silicon-based devices [5]. As diffusion distances are reduced 16-fold by splitting and recombining the two streams, the mixing time required is reduced by a factor of 16^2=256.

In order to test the chip using chemically aggressive solutions, a 0.1-M KOH (inlet 1) and 0.2-M HCl solution (inlet 2) were mixed in the device at flow rates between 20 and 400 µL/min using a peristaltic pump (MS-Reglo, Ismatec, Switzerland). A pH indicator mixed into the acidic solution off-chip was used to verify complete and constant mixing at the outlet of the chip. The tightness of the chip was verified by administering a defined volume of reagents to the chip using pressure-driven flow and weighing the solution produced at the outlet using a digital precision scale. For pressures up to 2.8 bar (generated from a pressurized air bottle) no leakage was observed, while at higher pressures liquid wicked in between the stack and the cover plate of the chip holder. To quantitatively study leakage between closely adjacent channels, additional chips with dedicated test structures have been designed and evaluated to obtain design rules for the future.

4. Conclusions

Our laser-micromachining approach allows both rapid prototyping and medium-scale manufacturing of a wide range of microfluidic structures in corrosion-resistant stainless steel. Currently, a conformal polymer coating using Parylene is studied for additional protection of the substrate and for improved sealing between the sheets for high-pressure applications. Also, the combination of steel and transparent polymer layers is under investigation for optical interrogation of the mixing and reaction processes.

Acknowledgements

The cooperation of Jens Baensch at Beta Layout GmbH (Aarbergen, Germany) is highly appreciated. This research project is carried out within the EU framework Biofinger (IST-2001-34544) with financial support by the Swiss Federal Office for Science and Education, Bern, Switzerland.

References

[1] W. Ehrfeld, V. Hessel, H. Löwe, *Microreactors new technology for modern chemistry*, Wiley-VCH, Weinheim, **2000**.
[2] H. Klank, J. P. Kutter, O. Geschke, *Lab Chip* **2002**, *2*, 242-246.
[3] M. A. Roberts, J. S. Rossier, P. Bercier, H. Girault, *Anal. Chem.* **1997**, *69*, 2035-2042.
[4] Beta Layout GmbH (www.laser-stencil.com)
[5] F. G. Bessoth, A. J. deMello, A. Manz, *Anal. Commun.* **1999**, *36*, 213-215.

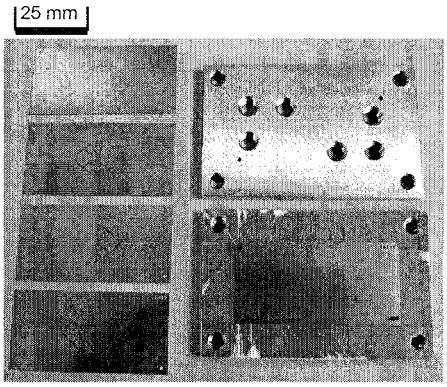

Figure 1. Laser-micromachined steel sheets (left) are assembled on the chip holder base (lower right). Two alignment pins in the holder assure good registration of the individual sheets. The device is sealed by clamping the stack with an aluminum lid (upper right), which provides six threads for fittings to connect the device to an external setup.

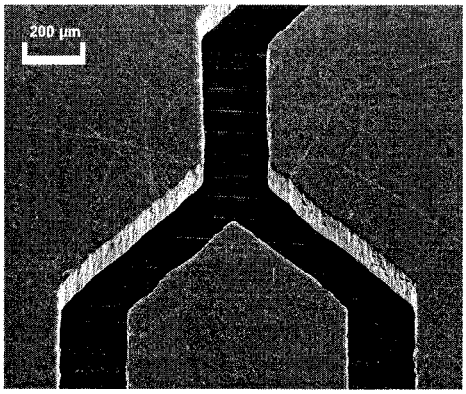

Figure 2. Scanning-electron-microscope picture of a 200-µm wide channel network cut into a 150-µm thick stainless steel sheet. The channels show good sidewall verticality and faithfully represent the layout. However, the surface roughness is considerable although this does not necessarily affect the micromixer operation.

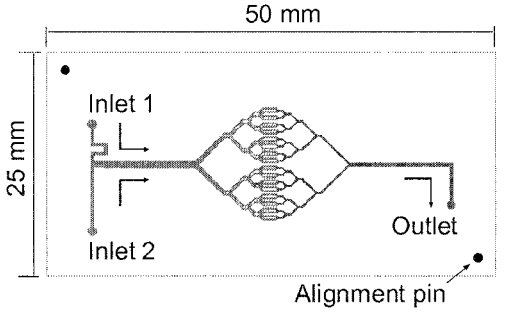

Figure 3. Top view of the mixer to illustrate the operating principle. Two inlet streams are split into 16 channels each to increase the contact area between both streams. The inlet streams run in separate fluidic layers. In the center region of the chip, they are vertically merged into the purple output stream.

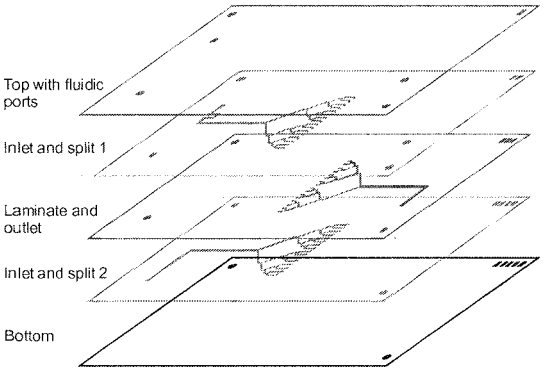

Figure 4. The mixer is composed of five metal layers, which are registered by alignment holes. Channel width and layer thickness can be adapted to the required flow rate and desired diffusion distance. Three functional steel layers are enclosed by a top and a base layer to seal the channels.

ADHESIVE BONDING METHODS FOR POLYMER microTAS COMPONENTS

Peter Friis[1], Elisabeth K. Storm[2], Karsten Hoppe[1] and Jakob Janting[1]
[1]DELTA Danish Electronics, Light & Acoustics, Venlighedsvej 4, DK-2970 Hørsholm, Denmark
microsystems@delta.dk, http://www.delta.dk
[2]Oticon A/S, Strandvejen 58, DK-5900 Hellerup, Denmark

Abstract

For bonding micro-Total-Analysis-Systems made of polymeric materials, many different approaches exist, each with their advantages and disadvantages. Here, we concentrate on adhesive bonding and propose various methods of applying the adhesive to both structured and unstructured system parts.

Keywords: polymer, microfluidic, bonding, adhesive

1. Introduction

With respect to bonding of micro-TAS structures made of polymeric materials some relevant processes might rely on one of the following methods: thermal bonding, chemical assisted bonding, laser or ultrasonic welding or adhesive bonding. Thermal bonding is simple but requires high temperature processing, chemical bonding tend to clog the channels when working in the micro scale, laser and ultrasonic welding are limited in number of useful material combinations. Adhesive bonding is a rapid and versatile prototyping method which can be employed in various ways [1,2]. Here we focus on different approaches for selectively dispensing the adhesives when joining two polymeric structures.

Ideally, the adhesive should result in a strong, chemical resistant, void-free bond. This can to some extend easily be controlled through a careful selection of the right type of adhesive, however, the real challenge when bonding microfluidic structures is to control the flow and volume of the adhesive. If incorrectly applied, e.g. too close to the channel as in Figure 1A, the adhesive will flow into the channel when the lid is applied. Another scenario, which should be avoided, is where an insufficient amount of adhesive is applied or it is too far from the channel edge, which result in the adhesive flow (during assembly) is stopped before reaching the channel. Consequently, small voids are created alongside the channel, which could cause cross-contamination if reusing the system, see Figure 1B.

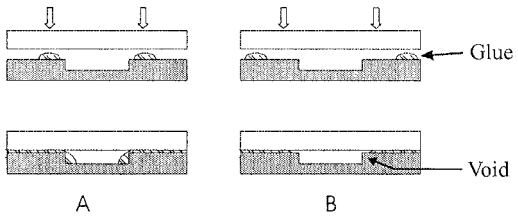

Figure 1. When applying adhesive next to a channel it might end up (A) too close to the edge and flow into the channel or (B) too far form the edge and form voids.

One possible way of categorizing the different adhesive bonding method is presented in Figure 2. The 'Standard' methods include no special structures for controlling the adhesive flow, i.e. have planar surfaces, whereas in each of the 'Advanced' methods some additional structuring is made.

Regarding the 'standard' methods we propose two different approaches. First approach, and the most obvious, is to try and dispense a pattern of adhesive on the substrate next to the channel. The second method uses an underfilling process known from flip-chip bonding. In the present experiment the technique has been adopted with dispensing the adhesive along one side of the component. To avoid adhesive in the channel an UV-curing adhesive is used, which is cured with UV-light as it arrives at the channel edge.

In order to investigate the possibilities for fabricating 'advanced' structures, which could facilitate a less troublesome assembly, we developed four concepts, see Figure 2. In the first method spacers are used to keep the lid a small distance from the channel so room for the adhesive flow is created. In the second method a cavity is made alongside the channel where the adhesive is dispensed before placing the lid. The 'locking' method is similar to the 'cavity' but locking structures are made in the lid to facilitate alignment during assembly. The last principle relies on forming bumps along the channel, which will be dipped in adhesive prior to applying the lid.

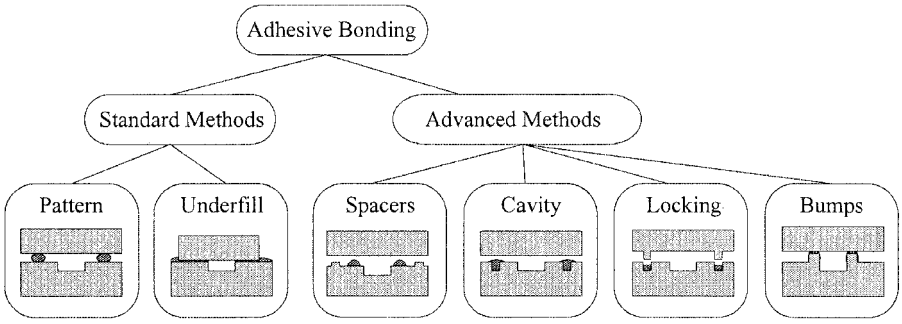

Figure 2. One way of categorizing adhesive bonding methods.

2. Experimental

Although the 'standard' methods, mentioned above, seem attractive because of their simplicity, it proved very difficult to control the flow of adhesive. It is extremely critical to control the position and volume of the dispensed adhesive, especially when going around corners or ends. Additionally, the surface quality is crucial to ensure a consistent and reproducible flow of adhesives. Moreover, we found that the sharpness of the channel edge play in important role in a successful assembly. Figure 3 shows an unsuccessful dispensing of an adhesive (Dymax 3070) using the 'pattern' method. The flow is, to some extend, stopped at the channel edge but due to uneven adhesive dispensing a part of the channel is not sealed correctly and a void is created.

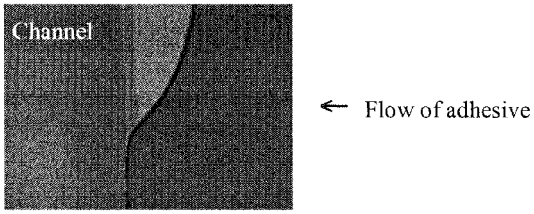

Figure 3. Top view of right side of a channel where the adhesive was not successfully applied.

To have a less critical process where possible dispensing variations will have reduced influence on the bond quality, structured parts might be used. To characterize the 'spacers' method two lines of UV-curing adhesive (Dymax 3070) were dispensed and cured on both sides of a channel 'far' from the edge. In the next step, two lines of sealing adhesive were dispensed close to the edge. These second lines were slightly higher than the spacer-lines (controlled by reducing the dispensing needle velocity), thus, a minor flow of adhesive occurred when the lid was applied. However, due to the presence of the spacers, the adhesive flow was not as pronounced as without the spacers i.e. in the 'pattern' method. It was also observed that minor dispensing irregularities were more easily compensated for as the adhesive had more space to redistribute.

Figure 4 shows a cross-sectional view of a channel formed between a substrate with a channel and a covering lid, with the sealing and spacer adhesive lines marked. It is worth noticing that the right side meniscus of the sealing line has a larger contact angle than the left side. This is expected as the surface tension at the channel edge is larger than the surface tension in between the substrate and lid. This also explains the reasoning behind the expected increased willingness for the adhesive to redistribution without filling the channel.

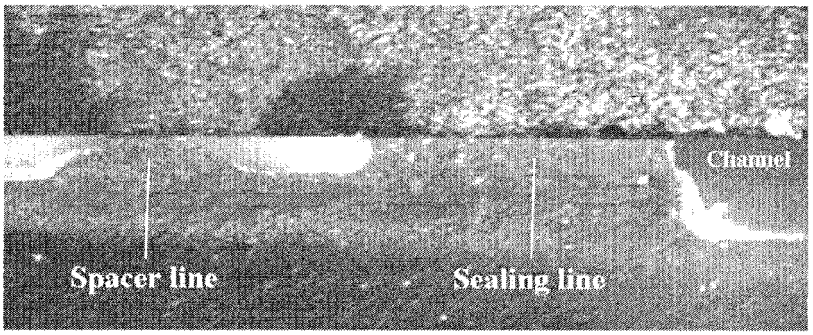

Figure 4. The channel is sealed by first applying and curing the spacer line, then applying the sealing line and finally placing the lid and curing the sealing line. Note that the shape of the spacer line is as dispensed whereas the sealing line has clearly flown.

3. Conclusion and prospects

Preliminary results indicate that assembly processes that rely on the spreading of dispensed adhesive next to a microfluidic channel are difficult to control on unstructured parts. By introducing some sort of spacers to lift the cover glass from the substrate, a better control of the adhesive flow is obtained and the probability of adhesive flowing into the channel is reduced.

Future work includes characterization of the rest of the proposed micromechanical structures for controlling the flow and volume of the dispensed adhesive during bonding as well as determining the bonding strength for each of the methods.

References

[1] C. Harrison, J. T. Cabral, C. M. Stafford, A. Karim, and E. J. Amis, *J. micromech. Microeng.*, **14**, pp. 153-158 (2004).

[2] J. Han, S. Lee, A. Puntambekar, S. Murugesan, J.-W. Choi, G. Beaucage, and C. H. Ahn, *Proc. μTAS '03, Squaw Valley, CA, USA, Oct. 5*-9, pp. 1113-1116 (2003).

VACUUM CASTING OF LOW-COST POLYMER MICROSTRUCTURES FOR BIO-CHEMICAL MICROSYSTEMS APPLICATIONS

Matthieu Denoual[1,2], Stéphane Prioux[2], Yann Macé[3], Pascal Mognol[4], and Bruno LePioufle[1]
[1]Biomis-SATIE ENS-Cachan antenne de Bretagne, Bruz, France
[2]STMicroelectronics Rennes, France
[3]ENS-Cachan antenne de Bretagne, Bruz, France
[4]IRCCyN Nantes, France

Abstract

This paper reports the usage of vacuum casting to perform microscale features down to a few microns with a view to propose a rapid prototyping technique for the bio-microsystem development design flow.

Keywords: vacuum casting, polymer, microscale, biochemical applications, rapid prototyping

1. Introduction

Biomedical and chemical fields are making more demands of polymer microsystem technologies, which present several advantages such as biocompatibility, transparency and low cost. Existing polymer micro-fabrication techniques involve micro-moulding [1], hot-embossing [2,3] or microinjection moulding [4]. These techniques are derived from macroscopic techniques. They involve huge time and money investments. Another macroscopic technique is vacuum casting. In this work, we explore the limitations of this standard rapid prototyping process to determine whether microstructures can be manufactured with this method. This technique has advantages over hot-embossing and microinjection moulding since it does not require expensive metal moulds, and also an advantage over micro-moulding, allowing the use of wide various range of polymers and not only silicon elastomers (such as Poly-Di-Methyl-Siloxane PDMS).

2. Material and methods

The principle of vacuum casting technology is to duplicate an original part into polymer using a flexible mould (Fig.1). For this work, standard microfabrication technologies were used to make the microstructures of the original parts; typically thick negative photoresist (SU8) and silicon deep wet etching.

Detailed vacuum process follows:

- Silicon mould fabrication: silicone is first mixed in a ratio 10:1 with hardener solution and then degassed in vacuum prior to pouring. The silicone solution is then poured over the original structure for duplication and then cured (Fig. 1 step 2). Curing time is 10h at 40°C. The silicone mould is then opened and duplicated structure is extruded (Fig.1 step 3). The silicone mould is kept in an oven at 70°C.
- Duplicated resin structure fabrication: MCP6091 compounds A and B are mixed in a ratio 1:1.8. The mixed solution is poured in the silicon mould in vacuum and the baked (Fig.1 step 4). Baking time is 2h at 70°C. Sprue bushing channel and vent are cut to keep only the interesting structure.

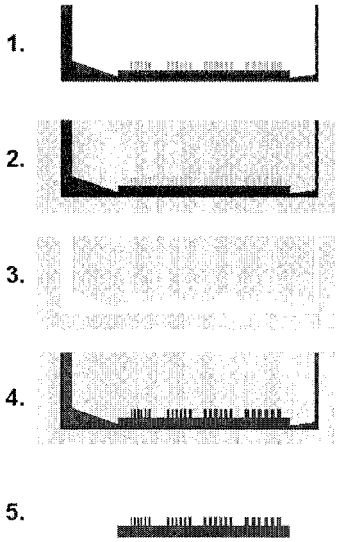

Figure 1. Vacuum casting process.

3. Experimental

Firstly, more than 100 sets of cylinders and parallelograms with features from 2μm to several hundreds of microns were performed (Fig.2) to test the dimensional limits of the process. The aspect ratio of the patterns varied from 1 to 6. Secondly, once the efficiency of vacuum casting technique to achieve micro-structures was demonstrated, the technique was used to develop bio-microsystem applications. Two examples are presented here. In the figure Fig 3, electrophoresis crosses are presented, and in figure Fig.4 a micro-array cell-chip is shown. The biocompatibility of the resin material has been successfully evaluated through long-term (1-2 weeks) cell cultures on the biochips.

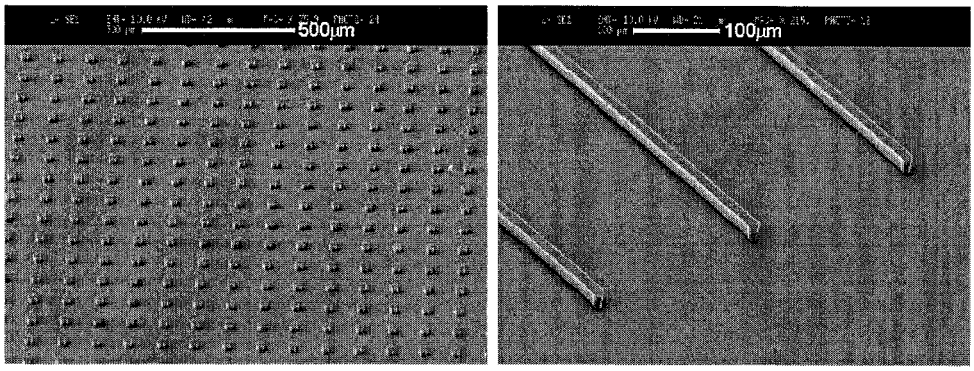

Figure 2. SEM images of realized structures to evaluate the process: arrays of 22μm wide, 25μm high cylinders, and 12μm wide walls.

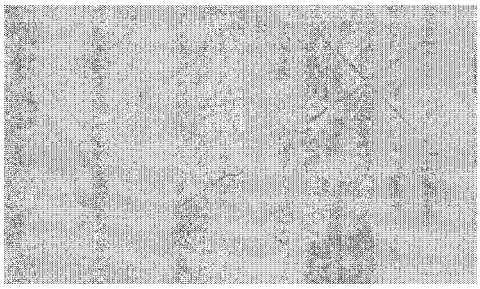

Figure 3. Picture of electrophoresis crosses (with channels 200μm wide, 50μm high)

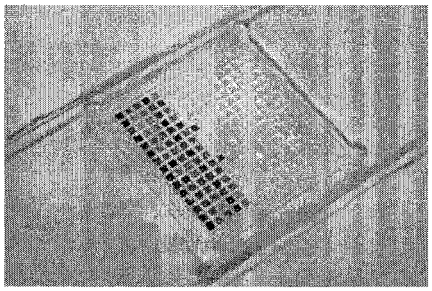

Figure 4. Microarray-chip with some wells filled with ink (minimum feature on the chip 30μm)

4. Results and discussion

Features ranging from 2μm to 300μm were successfully replicated with the MCP 6091 resin and vacuum casting technology. Aspect ratio of realized structures varied up to 6 only limited by the aspect ratio achieved with SU8 negative photoresist. The main advantage of the technique over microinjection moulding and micro-hot embossing is the really quick time to first part. Once the original part is made, duplicated parts can be obtained within 48 hours. Moreover, the original part can be made out of assembled materials, not necessary stiff as metal mould used for injection or embossing. This technique stands as an interesting step during the development of a bio-microsystem before mass production with injection or embossing processes, or for research laboratories when less than thousand of pieces are needed.

5. Conclusions

We have shown that vacuum casting technique can be used to as a prototyping technique to manufacture micro-scale devices with materials and features useful for bio-chemical microsystem applications.

References

[1] D.C. Duffy, J.C. McDonald, J.A. Schueller, G.M. Whitesides: Anal. Chem. 70 (1998), 4974.
[2] A. Gerlach, G Knebel, A.E. Guber, A. Muslija, Th. Schaller, Microsystem Technologies 7 (2002), pp 265-268
[3] H. Becker, L.E. Locascio, Talanta 56 (2002), pp 267-287.
[4] T. Hanemann, W. Pfleging, J. HauBelt, K-H. Zum Gahr, Microsystem Technologies 7 (2002), pp 209-214.

A NOVEL FABRICATION MEHTOD FOR MICRONEEDLE ARRAY

Sang Jun Moon and Seung S. Lee
Dept. of Mechanical Engineering, Korea Advanced Institute of Science and Technology (KAIST), Guseong-dong Yuseong-gu Daejeon, Korea

Abstract

We investigated a novel fabrication method for 3D micro HAR (High Aspect Ratio) structure, the out-of-plane type microneedles which have various shank shapes. The structure is formed by the commonly masked areas of the PMMA during three time deep X-ray exposures, which are exposed to the perpendicular direction of the individual face of a cube shape PMMA ($5mm^3$). Using the pre-formed PMMA window after first exposure, successive exposures are self-aligned with deep X-ray mask. The fabricated microneedles have 60:1 aspect ratio hole, sharp tip, 3D shape shank, and all-in-one shape with base structure.

Keywords: ***Cubic LIGA, 3D micro HAR structure, Microneedle Array***

1. Introduction

Several fabrication techniques of the 3D micro HAR structure have been developed in the field of LIGA and LIGA-like process such as inclined UV exposure (1), moving mask (2), gray mask (3) and substrate rotation method (4). For the biological application such as cell extraction, biopsy and TDD (Transedermal Drug Delivery), 3~5mm long and 3D shape HAR microneedle array structures are required for reducing insertion pain and reaching to the deeper blood vessel or tissue layer. In the previous research (5), microneedle array is fabricated by inclined deep X-ray exposure. However, microneedle base holes are not thoroughly formed by the only inclined deep X-ray exposure method because PMMA is bonded to a silicon substrate. In addition, the previous process is an improper method for the side pocket shape microneedle structure as shown in figure 1.

2. Three dimensional LIGA process concept

The conventional LIGA process employs deep X-ray exposure for the fabrication of HAR microstructure. The conventional LIGA process and MEMS fabrication methods used a planar exposure technique or an additive layer-by-layer fashion to obtain 3D micro HAR structure. It is difficult to fabricate 3D micro HAR structure with complex pattern at a side face because upper face of the PR (Photo Resist) is only used for exposures. Figure 2 shows suggested 3D LIGA process concept, named as "CUBIC LIGA," succeeded in limitation of additive method by using deep X-ray side exposure and dice shape HAR structure PR such as PMMA or SU-8. In case of positive PR (PMMA) like the figure 2, each planar pattern of the masked area where are placed in the perpendicular individual face of the dice forms complex 3D structure by successive deep X-ray exposures. Using negative PR, SU-8, negative shape mold also can be made by exclusive exposure area of deep X-ray. Using a combination of the three planar patterns, complex 3D micro structures can be formed by three times deep X-ray exposures.

3. Fabrication of 3D microneedle array

For the microneedle fabrication, a self-aligned exposure process can be used as shown in figure 3. The fabrication process is composed of three steps. First, 5mm thick PMMA dice frame and $5mm^3$ dices with holes are made by 1^{st} deep X-ray exposure step fixed with the deep X-ray mask and PMMA. PMMA frame and windows have the same dimension and position with respect to the deep X-ray mask. After developing PMMA frame combined with mask fixture, the dices with holes are rotated and pushed to the upper position of frame windows. Successive 2^{nd} deep X-ray exposure makes patterns at the one side of the dices. Lastly, 3^{rd} deep X-ray exposure makes whole 3D HAR

microneedle structures by the combination of the unexposed areas. According to a PR class, coincided area or exclusive area forms positive or negative 3D structures, respectively.

In the mask fabrication, deep X-ray should penetrate thick PR whose thickness is over 5mm and should cut off the low energy range of the X-ray to prevent PR surface damage. We use 500um thick silicon base to filter the low energy and 45um thick gold absorber to increase a dose contrast between PR surface and bottom dose. In case of 5mm thick PMMA, exposure time takes over 12hours for one side exposure of the PMMA at the condition of 2GeV, 150mA beam energy, and 5cm scan length. For the negative PR, SU-8, the exposure time decreases up to the 1/1000 compared with the PMMA exposure time. To reduce overdevelopment of the PMMA frame side placed at the opposite face of exposure, the X-ray mask fixture has a gap between mask and PMMA, which enables to a double side development of the exposed PMMA frame. After two successive exposures, the exposed PMMA dices with holes are developed during 24hours at the condition of mild agitation and 35°C with conventional GG-developing solution.

4. Fabrication results

SEM pictures show various shank shapes of 3D PMMA microneedle array fabricated by "CUBIC LIGA" process (figure 4). Three-dimensional sharp tip, long shank, holes through the base, side pocket and out-of-plane type microneedle array are fabricated, which can not be achieved by conventional deep X-ray exposure method. As shown in Figure 4, we fabricated different types of the microneedle arrays such as tip shapes, needle density, shank length, and shank shape according to the application demands. A close-up view of the sloped needle tip's sidewall shows a pointed edge and a fine wall surface created by the deep X-ray exposure characteristics. The needle shank length is from 150um to 500um long and the conduit is open from the tip end to 5mm toward the base. The microneedle has two different types of shank. One has corrugated shank to reduce insertion force and pain. The other one has side pockets to cut off a tissue during pulling the needle after the insertion. Various needle configuration and dimensions are described below; the base dimension is 4.35mm length(base 1.35mm)×5mm×5mm, the hole diameter is about 70um, the tip angle is from 30° to 45°, the microneedle length is from 1200um to 3000um long, and side body shape is simple, pocket (200×135um), and corrugated type, respectively. The array density is 9EA/5mm^2 and 16EA/5mm^2. Unlike conventional LIGA process, needle base and substrate adhesion is no problematic because the microneedle body and base are fabricated to all-in-one.

5. Conclusions

We demonstrate a new fabrication method for a 3D micro HAR structures. Using several combinations of deep X-ray exposure direction and mask shape, different types of 3D HAR microneedle arrays are fabricated without aligning with the first exposed area. The suggested self-aligned 3D exposure method, named as "Cubic LIGA," is tested to fabricate a three-dimensional needle shape by the shadow volume of successive exposures which forms side pockets, holes, and corrugated shank shapes for extracting intestinal tissue, cell, and humors with small invasive surface.

Acknowledgements

This research was funded by "Biopsy tools for humors, cells, and tissues (MS-040112)" sponsored by Intelligent Microsystem Center (IMC), Korea.

References

[1] M. H. Han and S. S. Lee, *MicroTAS '02*, 554-557 (2002).
[2] K. C. Lee and S. S. Lee, *MEMS'03*, 558-561 (2003).
[3] S. Sinzinger and J. Jahns, Microoptics, WILEY-VCH GmbH, 121-125 (2003).
[4] O. Tabata, K. Terasoma, N. Agawa and K. Yamamoto, *MEMS'99*, 252-256 (1999).
[5] S. J. Moon and S. S. Lee, *Tranceducer'03*, 1546-1549 (2003).

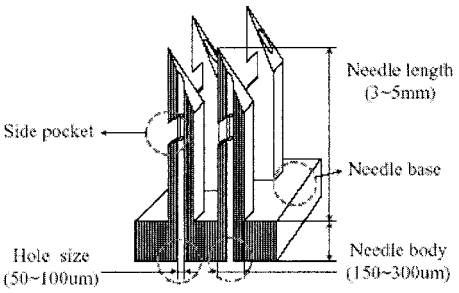

Figure 1. Requirements of the 3D microneedle structure (e.g. out-of-plane type microneedle array /w base).

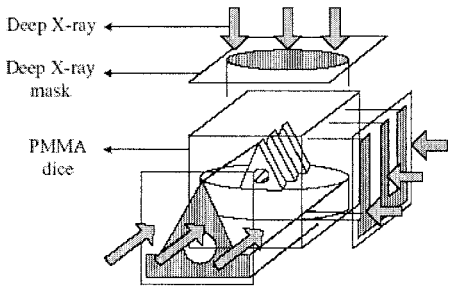

Figure 2. A conceptual schematic of "CUBIC LIGA" process. Three facet exposures make complex 3D microstructures.

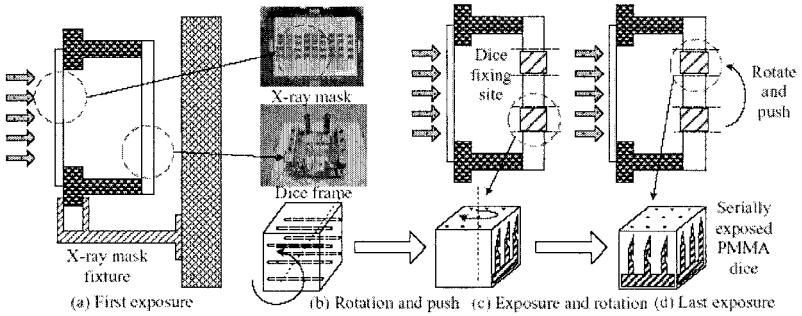

Figure 3. Fabrication schematic of "CUBIC LIGA" process using fixed PMMA frame.

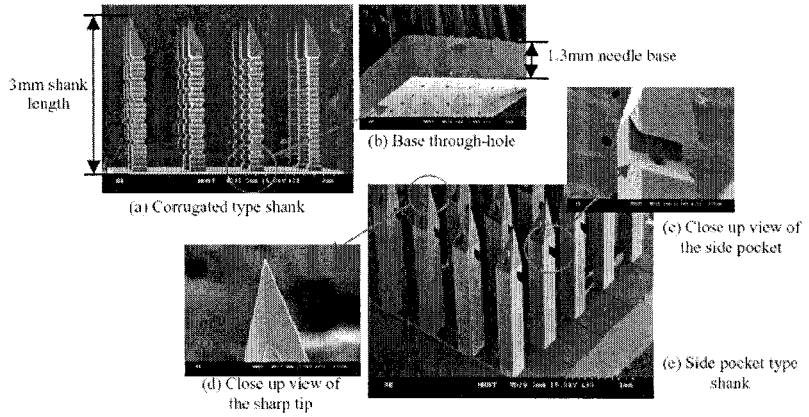

Figure 4. Shape variation of the 3D out-of-plane type micro needle array. Needle configuration is 4.35mm(base 1.35mm)×5mm×5mm, hole(70um), body (150/300um), array size (9EA/16EA), side body shape (simple, pocket(200×135um), corrugated)

3D POLYMER MICROSTRUCTURES BY LAMINATING SU-8 FILMS

Jochen Kieninger[1], Gerhard Jobst[2], Günter Igel[1], Isabella Moser[1] and Gerald Urban[1]
[1]*Chair of Sensors, Institute of Microsystem Technology, Albert-Ludwigs-Universität Freiburg, Georges-Köhler Allee 103, D-79110 Freiburg, Germany*
[2]*Jobst Technologies GmbH, Georges-Köhler Allee 102, D-79110 Freiburg, Germany*

Abstract

The excellent photolithographic properties combined with good chemical stability of the well-known SU-8 photoresist inspired many researchers and technologists to develop complex processes to design even three-dimensional microstructures. But nevertheless most approaches use sacrificial layers, complicating the process and mostly enforcing to adapt the process to each design. Here we present a way to combine the features of SU-8 with the dry-film technology, to get a robust generic process without sacrificial layers.

Keywords: SU-8, microfluidics, laminating, flexible devices, rapid proto-typing

1. Introduction

SU-8 is an epoxy-based photoresist with negative tone. It is commercially available by several suppliers as a solution of epoxy resin and a photo initiator in a solvent. While exposed to UV light the photo initiator generates a strong acid, which catalyzes in a following post-exposure bake cationic polymerization of the resin. Due to the spectral sensitivity of the material, at a wavelength of about 365 nm it shows as much absorption as needed to polymerize, but also have enough transparency to get in combination of the high lithographic contrast a uniform polymerization. This allows to process layers with a thickness of several hundred micrometers with aspect ratios more than 1:10. After the curing of the resist an optical transparent polymer with good chemical stability remains.

But due to the nature of SU-8 as a liquid photoresist it is hard to achieve structures including cavities or channels, which is especially important in the field of microfluidics. There are many works, where sacrificial layers or partial exposure is used to obtain micro channels. But in comparison with them, we suppose that the dry-film technology, which is originally used in the printed circuit board industry, have several advantages. With it a dry photoresist on a supporting layer could be laminated on existing structures and could cover cavities. The supporting layer, a flexible foil, could be peeled off afterward.

To combine the dry-film technology with the SU-8 we produced dried SU-8 films on a supporting layer. For this, we modified the SU-8 by adding plasticizers to overcome the brittleness of the polymer and ensure good adhesion to previous layers. In addition this allows building up flexible devices of SU-8 without a supporting wafer. The approach of adding plasticizers is also described in [1].

Chemical nature and concentration of the plasticizers allows us to tune the surface properties, e.g. contact angle. The static contact angle with water could be tuned from about 80° for unmodified SU-8 (the value depends on process conditions) up to above 90°. So it became possible to select a hydrophilic or hydrophobic material by altering the concentration.

2. Experimental

As base materials we used Nano™ SU-8 2000 from MicroChem Corp. (MCC) with several solid contents. Additionally we added more cyclopentanone to alter the solid content.

As plasticizers we used primarily one of two components: a linear polycaprolcatone, TONE 32C8 Polyol from Dow Chemical Company and poly(ethylene glycol) (n) diglycidyl ether

(PEGDG) from Polysciences Europe GmbH. They were added to SU-8 in concentrations of 5, 10 and 20 wt% (referred to solid part).

To obtain an initial guess for the spin-coating and dispensing parameters we measured the viscosity of the SU-8 solution with a rotation rheometer by a shear rate ramp up to 100 s^{-1} at a controlled temperature of 25°C. To reduce the results to one value we fitted the raw data of the viscosity to a decaying exponential function to obtain the "infinite shear rate" value of it as plotted in figure 1.

With each concentration we did some test structures in a nominal 50 µm thick layer. The dry-films were made by spin-coating or dispensing liquid SU-8 on a flexible foil and a soft-bake was followed.

The influence of the two plasticizers along with SU-8 to the optical transparency was measured with an UV/VIS spectrometer (see figure 2 for transmission versus wavelength). Each layer had a nominal thickness of 50 µm, the plasticizers were added in a concentration of 10 wt% (ref. to solid part).

By several repeated steps of laminating and further processing of SU-8 dry-films with 10 wt% TONE 32C8 Polyol, we obtained a three-layer flexible microfluidic test structure. The several layers were exposed with a UV mask aligner (365 nm), after a post-exposure bake they each were developed in 1-Methoxy-2-propyl-acetat (PGMEA). Finally, the device was cured at 150°C (hard-bake).

To show the process capability a non-microfluidic test structure in a temple-like fashion was built on a silicon wafer (see figure 3) of SU-8 with 5 wt% (ref. to solid part) TONE 32C8 Polyol by spin-coating a socket layer (C) and laminate two additional layers (the "pillars" B and the "roof" A) on it. After each layer deposition the wafer was exposed and after a following post-exposure bake developed.

Further test structures were made on a glass wafer with microchannels to show the principle of electrophoresis with SU-8 / TONE 32C8 Polyol (see figure 4). Bromphenol blue sodium salt dissolved in 0.1 M phosphate buffer (pH 7.4) was dispensed at the inlet of a buffer filled microchannel. The channel dimensions were 100 µm wide, 40 µm high and about 17 cm long, the channel was designed in a meander-like manner. Between the two inlets a voltage of 800 V was applied. The inlet with the dye was the cathode.

4. Results and discussion

The results of the rheological measurement show an increasing viscosity with added plasticizers (see figure 1 for a plot viscosity versus solid content). Therefore the plasticizers were counted to the solid part.

Lithographic tests in a 50 µm layer showed up to 10 wt% no significant differences in comparison to purely SU-8. The 20 wt% samples of both plasticizers had slightly blunt edges.

The optical spectrum of SU-8 is nearly unaltered by the plasticizer (see figure 2). The material could be treated as transparent in visible and near-UV range. Also, there is a light increase in transmission in the visible range with the wavelength resulting phenomenological in a very light brown tint.

Both, the flexible microfluidic test structure and the 3D temple-like structure, prove the possibilities of this technology to build devices as desired. The electrophoresis test states the principal application of this material for capillary electrophoresis (CE). The anionic dye was moving mainly due to electrophoretic flow to the anode.

5. Conclusions

The combination of the SU-8 with the dry-film technology in addition with plasticizer results in an increased design flexibility of 3D structures with cavities and microfluidic channels that consist

of one material. The technology would be applicable for rapid-prototyping as well as up to high volume production. Recent work is done to combine the SU-8 and dry-film technology with thin-film technology, to obtain e.g. metal structures in between the SU-8 as electrodes.

References

[1] D. W. Johnson, A. Jeffries, D. W. Minsek and R. J. Hurditch, *Improving the Process Capability of SU-8, Part II,* MicroChem Corp.

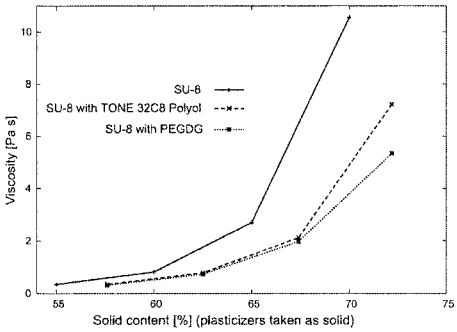

Figure 1. Viscosity of modified SU-8 solutions, concentration of the plasticizers was 10 wt% ref. to solid part.

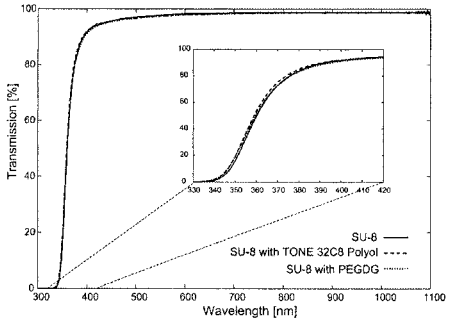

Figure 2. Optical transmission of a cured layer, nominal 50 µm thick, concentration of the plasticizers was 10 wt% ref. to solid part.

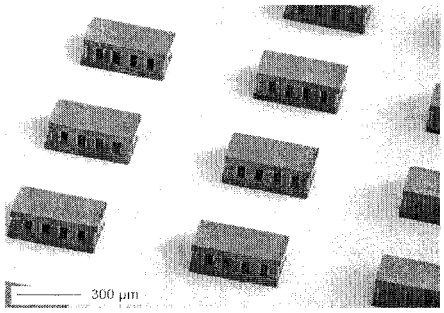

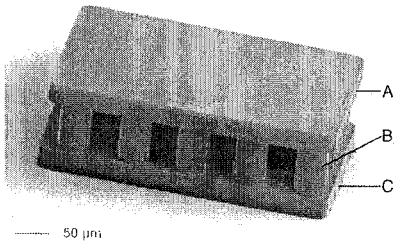

Figure 3. SEM pictures of temple-looking test structures (SU-8 with TONE 32C8).

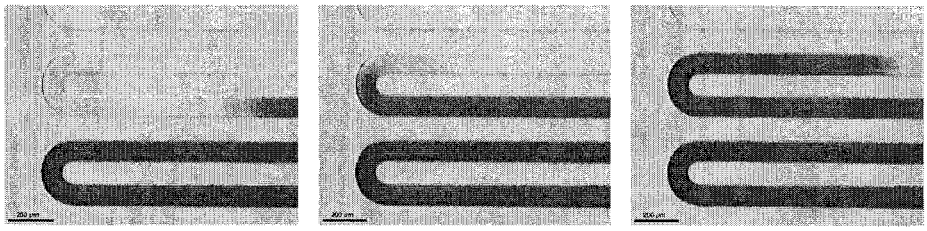

Figure 4. Principle of electrophoresis (SU-8 with TONE 32C8 Polyol), the anionic dye moved toward the anode, time steps between each picture (detail view) are 4s.

PDMS/ALUMINA NANOCOMPOSITE FOR CERAMIC MICROCOMPONENTS AND MICROFLUIDIC DEVICES

Stefan Metz[1], Arnaud Bertsch[2] and Philippe Renaud[2]
[1]*Dyconex AG, Advanced Circuit Technology, 8303 Bassersdorf, Switzerland*
[2]*Swiss Federal Institute of Technology Lausanne, STI-IMM-LMIS4, 1015 Lausanne, Switzerland*

Abstract

We present ceramic microfluidic devices fabricated from PDMS/alumina nanocomposites. The well-known pattern replication capabilities of PDMS are exploited to create high-aspect ratio ceramic microstructures with dimensions between 2 and 500 μm. The two-step fabrication process involves soft molding of the PDMS/alumina base material on SU-8 masters followed by a debinding/sintering step. Microfluidic devices for high temperature applications can easily be obtained by joining the molded, un-sintered material prior to the sintering step.

Keywords: PDMS, Alumina, Molding, Ceramic, Microfluidic

1. Introduction

Fabrication techniques for microstructures or microfluidic devices in silicon, quartz, Pyrex and polymers are well established. However, for high-temperature applications, such as heat exchangers [1] or microreactors [2], ceramic materials may provide several advantages, e.g. heat resistance, hardness, corrosion resistance, low density and chemical/biological inertness. Only few fabrication processes may be applied to machine ceramics in the sintered state. Hence, most methods focus on direct micromachining of the soft green body or on the generation of a green, un-sintered microstructure [3]. We present an approach based on PDMS/alumina nanocomposite material that is cast on microfabricated, high-aspect ratio molds made from SU-8 photopolymer and transformed into ceramic material by sintering.

2. Experimental

PDMS/Alumina formulations were prepared as follows: α-alumina powder (density: 3.98, Alcoa A-16SG, Alcoa, Germany, mean particle diameter 0.3 μm) was mixed with base PDMS (Sylgard 184, Dow Corning) and heptane (Fluka) as an additional solvent at different volumetric concentrations (Table 1) for 48 hours. Directly before pouring/spin coating the PDMS/Alumina mixture onto the mold the PDMS curing agent (Sylgard 184, Dow Corning, ratio 1:10 with respect to the PDMS base) was added to the formulation. Air bubbles following the mixing procedure were removed by ultrasonic treatment. The structures to be molded were obtained via negative-type SU-8 photopolymer structures on a master substrate. The SU-8 pattern was between 5 and 60 μm high, 2 to 500 μm wide and had aspect ratios of up to 1:7. After spin coating or molding, the PDMS/Alumina composite was hardened in a conventional oven (1 hour, 80°C). Following the detachment of the hardened PDMS/Alumina composite from the mold, microfluidic channel networks were generated by covering the structured PDMS/Alumina material with a flat nanocomposite slab or with a second structured layer of PDMS/alumina material. The ceramic, microfluidic structures or simple microcomponents (from uncovered, molded structures) were obtained after a thermal pyrolysis of the PDMS (1 hour at 600°C) and alumina debinding/sintering (1 hour at 1600°C).

3. Results and discussion

We successfully molded and detached microstructures made from PDMS/alumina composite on wafer level (100 mm diameter silicon substrates) or produced small microcomponents (Figure 1). It was observed that the PDMS/alumina mixtures lose their "PDMS character" with higher alumina loading content. At approximately 50 vol. % alumina charging it is difficult to detach the

PDMS/Alumina composite from the master as the bulk strength of the material decrease with respect to the adhesive strength. Hence, the maximum loading of PDMS with alumina powder obtained in this study was 80 wt. % (Table 1). As with conventional PDMS handling, we demonstrated the possibility of joining individually molded PDMS/alumina slabs in order to obtain more complex 3D microcomponents. For this, pieces of the pre-ceramic material were detached from their fabrication mold and joined by putting them in contact. Individual layers of PDMS/alumina nanocomposite can be handled like PDMS material and hence for microstructures with bigger dimensions the individual layers can be cut with a sharp blade and stacked in several layers. The surface roughness was found to be comparable with the original roughness of the silicon master for low and high alumina content. Post-sintering a linear shrinkage of 23 to 13%, depending on the alumina and heptane content was observed for the composite material. It is interesting to note, that the alumina and heptane content independently influence the linear shrinkage during sintering. However, we did not observe the same effect for the porosity of the final ceramic devices, which did remain constant for a given alumina concentration while varying the Heptane content. The porosity decreased from 25 % at 25 vol. % to 15 % at 45 vol. %.

Apart from creating ceramic microcomponents (Figure 1) we concentrated our efforts on microfluidic channel networks in alumina. The highest aspect ratio obtained for microchannels was approximately 1:5.5 (Figure 2). The finest features successfully replicated in ceramic material were about 2 μm thick channel walls separating two microchannels (Figure 3). By bonding two layers PDMS/alumina composite as mentioned above we obtained ceramic microfluidic channels. Typical channels dimensions were as follows: width 5 to 500 μm, height 5 to 20 μm, and length ~cm. We did not observe any bond interface remaining between two or more layers of PDMS/alumina material (Figure 3, Figure 4). It is interesting to note that we did also not observe any channel roof deflection even for 500 μm wide microchannels with and internal height of 10 μm. The microfluidic functionality was tested by passing colored solutions through the ceramic channels networks. Furthermore, it is possible to manufacture microfluidic channel networks on two levels, by joining two layers with overlapping channel design (Figure 4).

5. Conclusions

PDMS/Alumina nanocomposite molding, wafer-level bonding and subsequent sintering provides a versatile method for the fabrication of ceramic microfluidic components for high-temperature or microreactor applications. High-aspect ratio structures with dimensions in the micrometer range can be manufactured by taking advantage of the PDMS soft molding capabilities and PDMS bonding techniques.

Acknowledgements

Clean room processing was performed at the EPFL Center for Microtechnology (CMI) with the support of Ph. Flückiger, C. Hibert, Ph. Langlet, G.-A. Racine, G. Clerc, Y. Deillon, W. Baer, I. Magnenat, and J.M. Voirol. The authors would like to express their gratitude to S. Jiguet for performing the porosity measurements.

References

[1] C. Harris, M. Despa, and K. Kelly, "Design and fabrication of a cross flow micro heat exchanger," Journal of Microelectromechanical Systems, vol. 9, 502-508 (2000).

[2] H. Lowe, V. Hessel, and A. Mueller, "Microreactors. Prospects already achieved and possible misuse," Pure and Applied Chemistry, vol. 74, 2271-2276 (2002).

[3] M. Heule, S. Vuillemin, and L. J. Gauckler, "Powder-based ceramic meso- and microscale fabrication processes," Advanced Materials, vol. 15, 1237-1245 (2003).

Composition /vol % alumina	Alumina mass /g	PDMS mass /g	Heptane mass /g	Composition /wt. % alumina
25	19.94	14.48	5.69	58
30	23.92	13.51	6.83	64
35	27.91	12.55	7.97	69
40	31.90	11.58	9.11	73
45	35.88	10.62	10.25	77
50	39.87	9.65	11.37	80

Table 1: Volumetric concentrations for PDMS/Alumina nanocomposite material

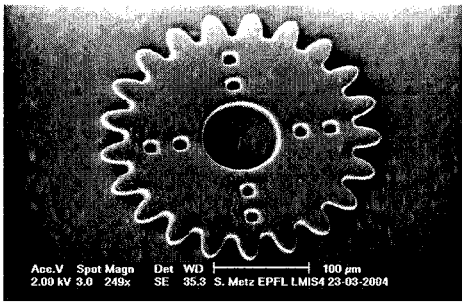

Figure 1. Ceramic microcomponent after molding and debinding/sintering of the PDMS/alumina nanocomposite material.

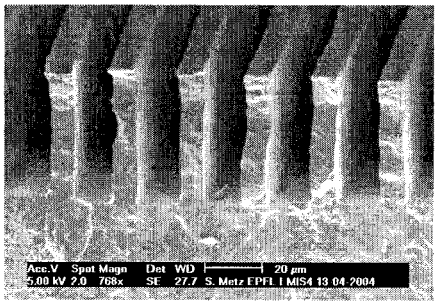

Figure 2. High-aspect ratio ceramic microchannels, e.g. for microreactor applications.

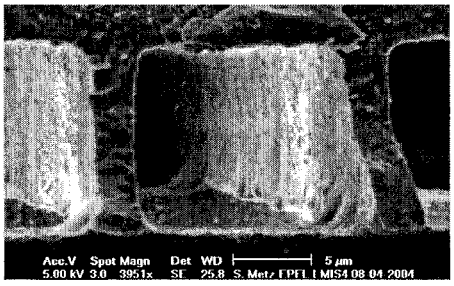

Figure 3. Smallest features (2 µm) as a separating wall between two ceramic microchannels. No bond interface visible between the assembled layers

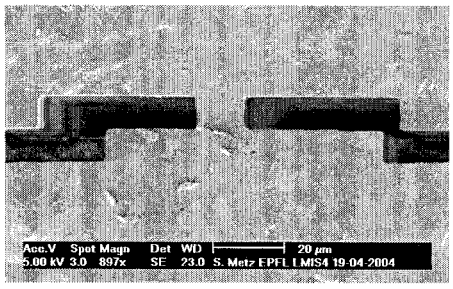

Figure 4. Two-level microchannel network by wafer-level assembling and bonding of two structured PDMS slabs

SOLID POLYMER DYE LASER BASED ON A SINGLE MODE SU-8 PLANAR WAVEGUIDE

Daniel Nilsson, Søren Balslev, and Anders Kristensen
MIC - Department of Micro and Nanotechnology, Technical University of Denmark (DTU), building 345 east, DK-2800 Kongens Lyngby, Denmark

Abstract
We present a solid polymer dye laser based on a single mode planar waveguide. The laser is defined in SU-8 and may be easily fabricated by spin-coating and optical lithography, and placed on any substrate. As the active medium for the laser we use the commercially available laser dye Rhodamine 6G which is incorporated into the SU-8 polymer matrix. The single mode slab waveguide is formed by a 3-layer spin coat deposition of a buffer layer of un-doped SU-8, a core layer of SU-8 doped with Rhodamine and a cladding layer of un-doped SU-8. By fine-tuning the Rhodamine doping concentration in the core layer we can achieve a refractive index difference of Δn=0.001, allowing for a 4.5 μm thick single mode waveguide.
Keywords: Laser, polymer, SU-8, dye

1. Introduction

The integration of optical input and output transducers is considered a key issue for the further development of μTAS [1], and one possibility is to integrate lasers on the chip. We have earlier demonstrated a micro-cavity solid polymer dye laser, which can easily be integrated with polymer-based micro systems [2]. These devices are based on the photo definable polymer SU-8, doped with the commercially available laser dye Rhodamine 6G. In this paper we present a new design of the SU-8 based dye lasers with improved mode control, as a first step towards single mode lasing.

The laser design adapted from [2], relies on planar waveguiding in a polymer film in combination with reflections at vertical polymer-to-air interfaces, see Fig. 1. In the previous design, a 1-10 μm thick film of dye doped SU-8 was placed directly on a SiO_2 substrate. Due to the large difference in refractive index (n_{SU-8}=1.593, n_{SiO2}=1.458, n_{air}=1) several propagating TE-TM modes were supported by the planar waveguide. However, the improved laser design presented here is based on a single mode planar waveguide structure [3], involving a multi-layer SU-8 film.

To realize this, we have investigated the effect of the Rhodamine doping concentration in SU-8 on the refractive index (see Fig. 3). We have fabricated a three-layer sandwiched structure in SU-8 with different refractive indices, resulting in a single mode symmetric slab-waveguide structure, see Fig. 1, Fig. 2 and Fig. 4. By fine-tuning of the refractive index of SU-8 by Rhodamine doping, the refractive index step between the dye doped core and un-doped buffer and cladding layers may be reduced to app. 0.001 ($n_{core} \approx 1.5933$, $n_{clad} \approx n_{buffer} \approx 1.5920$ at 633 nm). This allows for a single-mode waveguide with a thickness of the core layer of up to 4.5 μm ensuring a large optical gain volume, which would not be possible in the previous multimode design where the dye doped SU-8 was placed directly on a SiO_2 substrate.

2. Fabrication

The different layers in the device are realized in a standard spin-on process. First the substrate is spin-coated with the buffer layer, in this case SU-8 with no Rhodamine doping, and the polymer is soft-baked at 90 °C to evaporate the solvent. Then the core layer (i.e. the SU-8 doped with Rhodamine) is spin-coated and again the sample is soft-baked. Finally the cladding layer of un-doped SU-8 is spin-coated and soft-baked. The buffer and cladding layers each have a thickness >10 μm, which is the minimum thickness for the buffer and cladding layers to confine the light with negligible loss (see Fig. 2). The spin-speed and the viscosity of the SU-8 define the thickness of the

individual layers. The laser devices are then defined in a single optical lithography step, where all three layers are exposed and developed simultaneously.

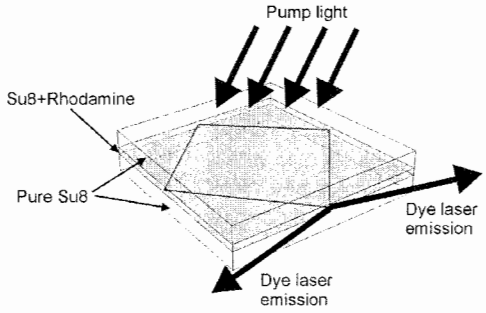

Figure 1. Artists' impression of the single mode slab waveguide device. The device is pumped by an external light source (Nd:YAG laser).

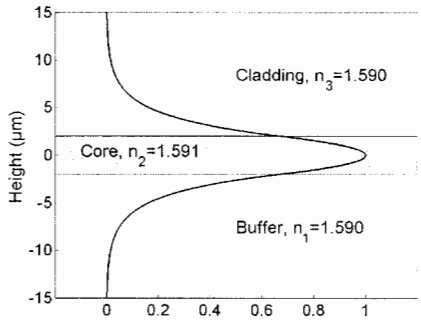

Figure 2. Calculation of the E-field in the single mode planar waveguide. With a buffer and cladding layer of around 10 µm, the loss is negligible.

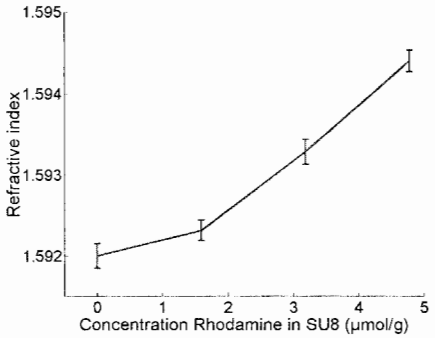

Figure 3. Refractive index of SU-8 (measured at 633 nm) as function of Rhodamine 6G concentration. The devices in this work have a doping of 3.2 µmol/g.

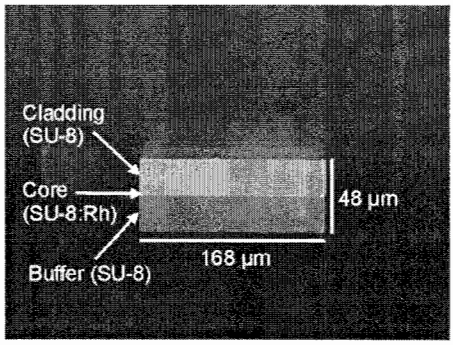

Figure 4. Optical micrograph of the laser structure seen from the output side (compare Fig. 1). The three layers are visible, the total thickness is 48µm, and the length of the output side is 168 µm.

3. Characterization

For optical characterization the lasers are pumped by an external light source, a pulsed (5 ns pulses at 10 Hz) frequency doubled Nd:YAG laser (Continuum Surelite I-10) emitting at 532 nm. The output light from the fabricated devices is collected by a multi-mode optical fiber (200 µm core diameter). The light is analysed by a fixed grating spectrometer (AVS-USB2000 from Avantes). The two different laser output spectra in Fig. 5 and Fig. 6 illustrate the effect of replacing the previous multimode planar waveguide structure – in this case a 5 µm thick SU-8/Rhodamine laser on a SiO_2 substrate (Fig. 5) - with the new single mode planar waveguide design (Fig. 6).

The two trapezoid shaped devices in Fig. 5 and 6 have comparable lateral dimensions, with an optical roundtrip length (L = 460 µm in the case of the single mode laser) associated with the

longitudinal lasing modes. The wavelengths of the longitudinal modes are given by $\lambda_m = n_{eff}L/m$, where m is the mode number and n_{eff} is the effective refractive index. However, each propagating TE-TM mode in the multimode film has its own n_{eff}, which will result in a corresponding set of longitudinal modes, slightly shifted from the others. This means that the spectra will be complicated already with only a few TE-TM modes present in the structure, as observed in Fig. 5.

In contrast, a regular mode pattern is observed with the new device, based on a single mode planar waveguide (Fig. 6). The observed wavelength separation between neighbouring longitudinal modes is ~ 0.4 nm. This is in good agreement with the expected value of $\Delta\lambda = \lambda_m/(m+1) \sim 0.42$ nm for wavelengths around 560 nm. Our new laser devices thus have a single transversal TE-TM mode, enabling the possibility for further mode control by additional development of the lateral design.

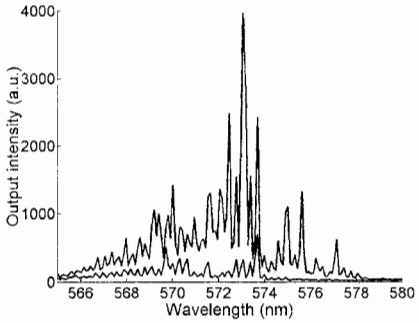

Figure 5. Typical spectra from a multimode device. The expected mode spacing for this device should be 0.3 nm.

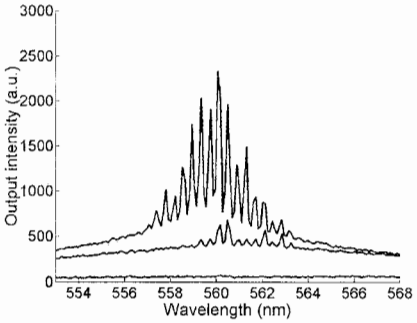

Figure 6. Output spectra from a three-layer, single mode planar waveguide, dye laser with a mode spacing of approximately 0.4 nm. Three different spectra at different pumping powers are shown.

Acknowledgements

DN wishes to thank Center for Microinstruments (CfM) and Sensor Technology Center A/S (STC) for their financial support. The work was supported by the Danish Technical Research Council (STVF, grant no: 26-02-0064).

References

[1] E. Verpoorte, Lab Chip **3** 42N (2003)

[2] S. Kragh, S. Balslev and A. Kristensen, Proc. μTAS 2003, pp. 1331-1334 (2003)

[3] R.G. Hunsperger, *Integrated Optics: Theory and Technology*, Springer Verlag, Berlin, Fifth edition (2002)

CYCLIC OLEFIN COPOLYMER (COC/TOPAS®) - AN EXCEPTIONAL MATERIAL FOR EXCEPTIONAL LAB-ON-A-CHIP SYSTEMS

Frederik Bundgaard, Theodor Nielsen, Daniel Nilsson, Peixiong Shi, Gerardo Perozziello, Anders Kristensen, and Oliver Geschke

Dept. of Micro and Nanotechnology, Technical University of Denmark, Bldg 345 east, DK 2800 Kongens Lyngby, Denmark

Abstract

The cyclic olefin copolymer Topas® [1] has a number of advantages over polymers like PMMA and PC traditionally used in fluid micro system manufacturing, such as low water absorption, high chemical resistance and good machinability. We present a number of different processes for making all-Topas microfluidic system, like micro milling, micrometer scale soft embossing and bonding. Furthermore, we present a complete process sequence for nano imprint lithography (NIL) in Topas spin coated onto silicon. Finally, the etch resistance of Topas to two reactive ion etching (RIE) processes is compared to that of PMMA, SU-8 and photoresist.

Keywords: Polymers, bonding, soft embossing, nano imprint lithography, reactive ion etching

1. Introduction

Topas is an excellent material for lab-on-a-chip applications since it has a low water absorption (<0.01%) and is chemically resistant to hydrolysis, acids and polar solvents such as ethanol and acetone. It is highly transparent both in the visible region and in the near-UV region, and has a relatively high refractive index of 1.53 (optical grade). The Topas polymer chains consist of ethylene and norbonene, and the glass transition temperature T_g can be varied from about 75°C to 170 °C by changing the ratio between the two monomers.

Hot embossing and injection molding of polymer microstructures have been demonstrated earlier by various groups [2,3]. However, little has been reported about bonding Topas to Topas while maintaining the microstructures on the interface.

2. Bonding of multiple grades of Topas

Our approach is based on placing a thin layer of Topas with a low glass transition temperature (Topas grade 8007 with a T_g of 75°C) between two Topas wafers with a higher T_g (Topas grade 5013 with a T_g of 130°C). In this manner it is possible to obtain a well-controlled thermal bonding. Topas pellets are dissolved in toluene, using ultrasonic aggregation and is spin coated onto one of the two wafers. The resulting layer thickness ranges from 0.5 µm to about 100 µm. The smoothest spin coatings are obtained using a 5 wt% solution. After spin coating the wafer, it is heated in an oven at 80°C for 20 min, so that the toluene evaporates. Multiple spin coatings are used to get layer thicknesses of several hundred µm.

The microfluidic structure with channel widths of down to 200 µm is patterned on the other wafer using a micro milling machine, and the bonding is then performed in a home-built press, which is placed in an oven for 40 minutes at a temperature of 80°C and a force of 200 N. Figure 1 shows a cross section of bonded microchannels in Topas, made by a micro milling machine. Bonding tests using a force sensor show that a bonding strength of 1.5 MPa can be achieved using the method above.

Soft embossing [4] in a spin coated 150 µm thick layer of Topas grade 8007 on a grade 5013 wafer was performed. PDMS was poured into a silicon master and left to cure. Using a press, the features of the PDMS stamp were embossed at a temperature of 80°C, and with a pressure of 1 MPa. Features of µm-size from the silicon master are transferred to the Topas replicate. Bonding

of a spin coated layer with an embossed structure to another spin coated layer has been performed, without clogging of the channels of the structure.

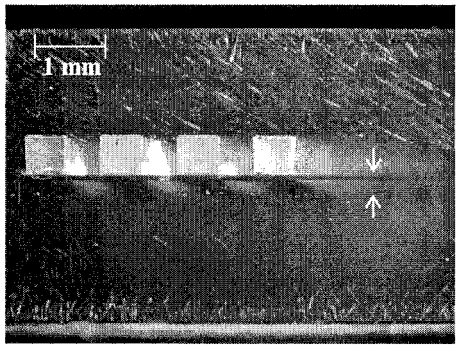

Figure 1. Cross section of two Topas plates thermically bonded by a thin layer of Topas (the dark line between the arrows) with a lower glass transition temperature, spin coated onto the upper plate. The reflow into the channels is very limited, as can be seen from the smooth bottom of the channels.

3. NIL and etch resistance to RIE

The spin coating technology also enables the fabrication of polymer waveguides, similar to those obtained with SU-8 [5] and thermal nanoimprint lithography [6,7] in Topas. A complete process sequence for imprint of nm and μm-sized features is presented. The NIL is performed in an evacuated chamber, where a silicon stamp is pressed into a 2 μm thick layer of Topas, spin coated on the top of a silicon substrate. The imprinted patterns (Figure 2) are found to conform completely to the stamp in the imprint process.

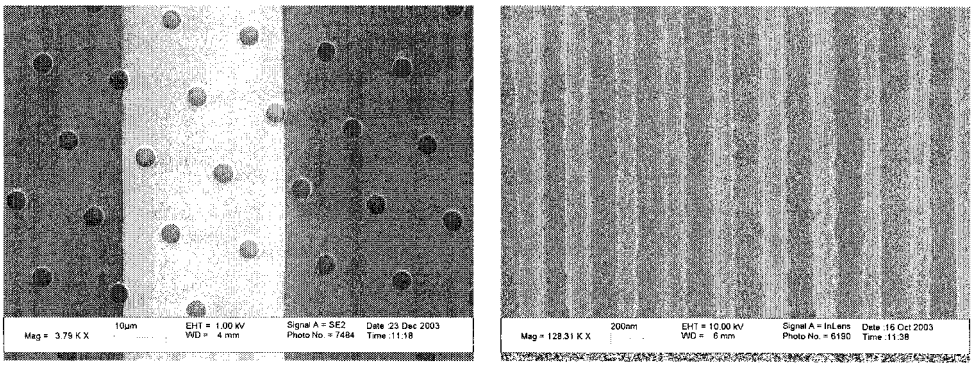

Figure 2. SEM images. *Left:* The imprinted Topas film is covered with standard photoresist, and exposed to UV-light through a mask. The photoresist is developed and followed by e-beam deposition of 5 nm Cr and 50 nm Au. Finally, the photoresist is stripped using acetone leaving the Cr/Au lines on top of the Topas film (bright areas). The diameter of the imprinted holes is 4.2 μm. *Right:* 100 nm wide lines are made by NIL into a 500 nm thick Topas® film. The silicon stamp protrusions were 150 nm high.

The pattern is either transferred into the silicon substrate using RIE, or used as a substrate for further UV-lithography using standard processing, where a spin coated layer of photoresist is exposed through a mask and developed in NaOH. The patterned photoresist is furthermore used in a lift-off process, where 5 nm of Cr and 50 nm of Au is e-beam deposited (Figure 2), The photoresist is then removed using acetone and ultrasonic aggregation. The Topas is affected neither by the UVL, development nor the lift-off.

The etch resistance of Topas to RIE is determined and compared to that of 950k PMMA, cross-linked SU-8 and standard photoresist. Using an oxygen plasma the etch rate of Topas is 12.64 nm/s, while the etch rate is found to be 0.73 nm/s using an anisotropic etch with a SF_6/O_2 plasma (Figure 4). Topas is found to be more resistant to this process than the PMMA, SU-8 and photoresist.

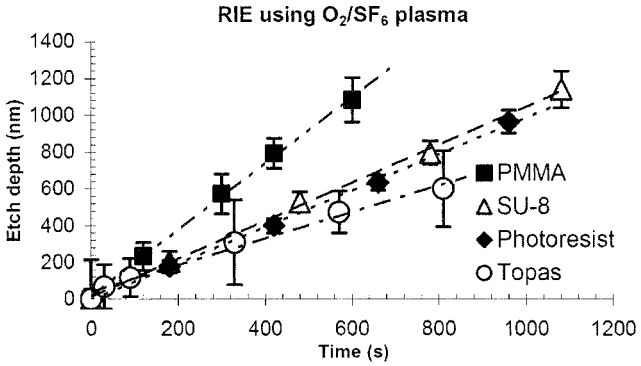

Figure 4. Investigated etch resistance of standard photoresist, 950k PMMA, crosslinked SU-8, and Topas to an anisotropic RIE silicon etch.

4. Conclusion

The patterning techniques discussed above are powerful, and can be combined in many ways to produce highly complex all-polymer microsystems in a relatively simple and fast way. The use of a single polymer for all parts minimizes the stress, assuring more durable and resistant system.

References

[1] Topas® by Ticona, *www.ticona.com*

[2] J.K. Nisper, Proceedings of SPIE - The International Society for Optical Engineering, 1995, 2600 , p. 56-64

[3] P. Tuteleers,. Proceedings of the SPIE - The International Society for Optical Engineering, 2001, 4408 , p. 329-37

[4] B.L. Carvalho, E.A. Shilling, N. Schmid and G.J. Kellogg, 7th International Conference on Miniaturized Chemical and Biochemical Analysis Systems, Oct 5-9, 2003, Squaw Valley, California, USA, pp 959-962

[5] K.B. Mogensen, J. El-Ali, A. Wolff, J.P. Kutter, *Applied Optics,* **42**(19), 4072-4079 (2003)

[6] S.Y. Chou, P. R. Krauss, and P. J. Renstrom, *Appl. Phys. Lett.*, **67**, 3114 (1995)

[7] T. Nielsen, D. Nilsson, F. Bundgaard, P. Shi, P. Szabo, O. Geschke, and A. Kristensen, to appear in *J. Vac. Sci. Tech. A*, July/August 2004

MICROFLUIDIC DYE LASER WITH COMPACT, LOW-COST LIQUID DYE DISPENSER

Søren Balslev[1], Niclas Roxhed[2], Patrick Griss[2,3], Göran Stemme[2], Anders Kristensen[1]

[1] *Dept. of Micro and Nanotechnology, Technical University of Denmark, bldg 345 east, DK 2800 Kongens Lyngby, Denmark*

[2] *Dept. of Signals, Sensors and Systems, Microsystem Technology Laboratory, Royal Institute of Technology, Osquldas väg 10, SE-100 44 Stockholm, Sweden*

[3] *Present address: Roche Diagnostics Microtechnology Center, Rotkreuz, Switzerland*

Abstract

We present a compact system consisting of a miniaturized fluid dispenser, delivering liquid laser dye to a micro-chip dye laser. This demonstrates the elimination of bulk fluid pumps for a microfluidic system by using a miniaturized, electrically and chemically inert dispenser, capable of delivering very low flow for extended periods of time.

Key words: laser, pump, liquid, dye, dispenser

1. Introduction

The compact system consists of a single mode miniaturized liquid dye laser [1] (fig. 1) supplied with a low, long duration, flow of dye, from a miniaturized dispenser [2](fig. 2). The compact design - aimed for a micro analysis system (as in [3]) - eliminates the need for fluidic connections to the macro world (fig. 3,4). As opposed to [2], where a dispenser was demonstrated to deliver precise volumes of fluid, the dispenser now is optimized and operated as a low flow-rate dispenser. The dispensed liquid dye supplies a regenerating flow of 1-10 μL/hr to the microfluidic laser, which is sufficient to avoid bleaching of the dye in the laser cavity during operation. By this approach we have realized a compact disposable package able to operate for more than 10 hours, acceptable for micro analysis systems in the field.

2. Components

The dye laser chip is 10 by 20 by 1 mm in size (fig. 1), and contains a microfluidic channel that is 10 μm high and about 1 mm wide. A laser structure based on a high order Bragg grating is embedded in the microfluidic channel and waveguides direct the light to the edges of the chip. The channel inlet and outlet is formed by 0.8 mm diameter holes drilled through the glass lid of the chip. During operation, a solution of the laser dye Rhodamine 6G (20 mMol) in ethylene glycol is pumped through the fluid channel. The laser dye is excited by a frequency doubled Nd:YAG laser (at 532 nm) to achieve gain inside the laser resonator. However, the optical excitation slowly bleaches the organic dye molecules inside the laser resonator, wherefore new dye solution must be supplied at a flow rate of 1-10 μL/hr. In previous experiments [1,3], a macroscopic syringe pump is used to supply the low flow of dye, but macroscopic external devices limits the advantage of micro chip based fluid systems.

The liquid dispenser is 14 by 15 by 8 mm in size (fig. 2), and is based on a compound of glycerine and microscopic polymer spheres containing a fluidised hydrocarbon gas (Expancel® 820DU, concentration: 0.7 g/mL glycerine). When the compound is heated the polymer spheres expand into a cavity containing the liquid to be dispensed, thus ejecting the liquid from the cavity. The compound and the liquid in the cavity are separated from each other by a thin elastic polymer membrane to avoid contamination of the liquid by the compound. The dispenser cavity holds 100 μL of dye liquid, enough for more than 10 hours of operation of the laser. The flow-rate of the

dispenser can be adjusted between 1 μL/hr and 2400 μL/hr by controlling the electrical power delivered to the heater in the dispenser. The current application dictates an operational flow between 1 and 10 μL/hr, although a higher flow-rate is used to prime the downstream components at the beginning of operation. The recyclable dispenser lasts for a limited operation time, however the used dispenser can be easily replaced with a newly prepared one.

3. Experiment

The laser chip and the liquid dispenser was coupled together with an O-ring sealing, leaving a minimal excess volume to be primed at start up (figs. 3,4). The dispensed flow through the laser chip was controlled by adjusting the electrical power delivered to the heater, with a flow reaction time to electrical power changes being a couple of seconds. The dispensed volume was measured by reading the fluid level in a capillary tube connected to the laser chip fluid outlet, and the dye volume pumped through the laser as function of time is illustrated in fig. 6 with a heater power of 301 mW. The spectrum of the functioning laser is illustrated in fig. 5. During actuation of the dispenser, the temperature in the fluid chamber does not rise above 39.5 °C, as determined with a small temperature sensor (Mitsubishi TN10) placed inside the chamber and connected with thin copper wires to avoid heat conduction away from the device. This low temperature will not affect the dye solution (critical temperature ~ 140 °C), nor other components.

4. Conclusions

The compact hybrid presents a disposable, low-cost, miniaturized dye laser device that only needs an external optical pump source and simple electrical connections. The elimination of bulky fluid handling equipment brings the polymer chip fluid technology a step closer to applications in analysis micro systems that can be used in the field, away from classic laboratories.

References

[1] S. Balslev and A. Kristensen, The 2004 CLEO/IQEC conference, San Francisco, California, USA, May 16-21, 2004, CLEO/IQEC and PhAST Technical Digest on CD-ROM (The Optical Society of America, Washington, DC, 2004), presentation number CFM7

[2] N. Roxhed et al., Proceedings of 17'th IEEE International Conference on Micro Electro Mechanical Systems (MEMS), pp. 326-329, 2004

[3] S. Balslev et al., Proceedings of 17'th IEEE International Conference on Micro Electro Mechanical Systems (MEMS), pp. 89-92, 2004

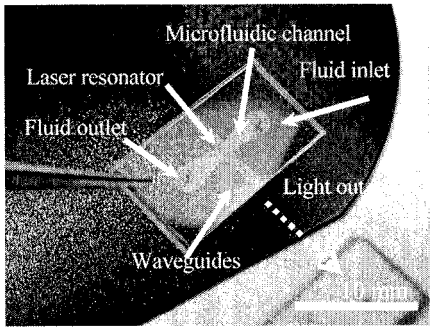

Fig. 1. Laser chip with fluidic channel and drilled holes. 10 μm SU-8 defines the structure.

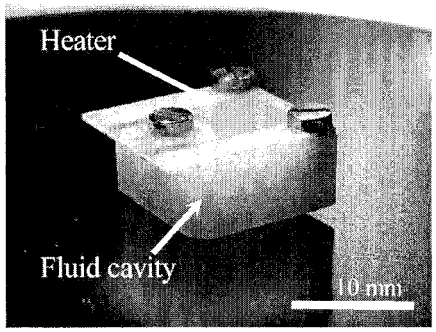

Fig. 2. Dispenser chamber with a heater integrated in a printed circuit board on top. Electrical connections are on the left.

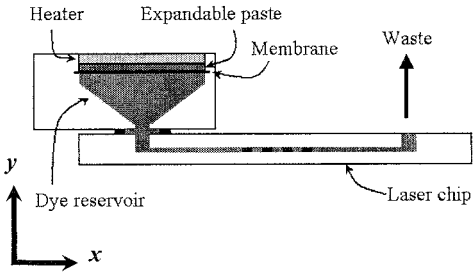

Fig. 3. Outline of dispenser principle and dye solution flow through system.

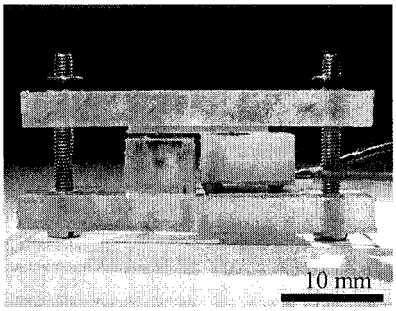

Fig. 4. Realized assembly after priming of laser with dye and attaching electrical connection to the heater. The left cube represents a waste chamber.

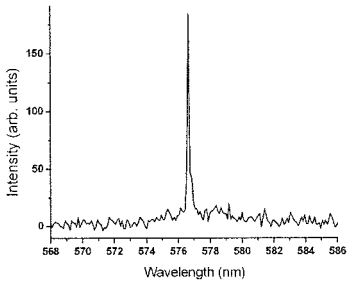

Fig. 5. Output spectrum from laser during operation with dispenser, and optically pumped by a frequency doubled Nd:YAG laser.

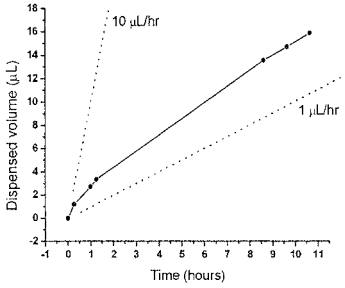

Fig. 6. Dispensed volume of dye solution through laser at 301 mW heater power, as function of time. The maximum temperature of liquid dye in the dispenser during actuation was measured to 39.5 °C.

SURFACE TENSION DRIVEN SHAPING OF ADHESIVE MICROFLUIDIC CHANNEL WALLS

Jakob Janting[1], Elisabeth K. Storm[2] and Oliver Geschke[3]

[1]Dept. of microelectronics, DELTA Danish Electronics Light & Acoustics, Venlighedsvej 4, 2970 Hoersholm, Denmark

[2]Oticon A/S, Strandvejen 58, DK-5900 Hellerup, Denmark

[3]Dept. of Micro and Nanotechnology, Technical University of Denmark, Bldg 345 east, DK 2800 Kongens Lyngby, Denmark

Abstract

The feasibility of making microfluidic channels with different wall geometries using adjacent lines of dispensed adhesive between substrates has been studied. Important parameters for the geometry have been identified to be: surface tension (adhesive / substrates), adhesive viscosity / thixotropy, line height and distance, and temperature. Focus of the work has been on predicting the equilibrium geometries with FEM simulations using as input measured adhesive wetting angles, different adhesive line distances and height. The studied substrates are glass microscope slides, PEEK and PMMA. The studied adhesives are DYMAX 9-20318-F, 3070, 9001 version 3.5, and Sylgard 184 PDMS.

Keywords: channels, adhesive wall, shape, simulation, surface tension

1. Introduction

Adhesives are used in packaging of microelectronics, MEMS, and μTAS components for bonding and sealing. In previous μTAS studies e.g. the spread before cure of screen printed UV adhesive for bonding of component parts and sealing of channels have been characterized [1]. Channels with adhesive walls between substrates have also been made by exposure with UV light through a mask [2]. Microfluidic channel flow depends to a large extent on channel geometry. Therefore the motivation for this work has been to study the possibilities of making different channel wall geometries with a new method: Adjacent lines of adhesive between substrates.

2. Theory

The surface tension γ of the adhesive act as a driving force towards an equilibrium situation with minimum free area A because this situation represents minimum adhesive surface free energy $G_{\text{Surface}} = \gamma A$ [3]. Therefore adhesives / coatings on surfaces fill up concave regions, avoid convex, and adapt round shapes [1, 3].

3. Experimental

Adhesive surface tensions have been measured with a CCA-100 tensiometer using the Wilhelmy plate method and a FTA-125 pendant drop equipment. The FTA-125 equipment was also used to measure the wetting angle of sessile drops. The wetting angles were measured on substrates as received and only at one spot and should therefore be considered as rough estimates. The FEM simulations were made with Surface Evolver [4]. To inspect the channel geometries cross sections were made with a Struers Accutom cutting equipment.

4. Results and discussion

In table 1 possible channel wall geometries between different substrates are envisaged by measured wetting angles. Fig. 1 shows channels of different height and wall spacing formed with DYMAX 9-20318-F between glass microscope slides. Fig. 2 is a Surface Evolver FEM simulation example where the used wetting angle (55 °) is that of DYMAX 9-20318-F on PEEK which is also close to that of DYMAX 9-20318-F on glass (51 °). Because of the high viscosity of the material it was

expected that it would be possible to dispense lines with width, height, and pitch of 1 mm, fig 2. This has not yet been achieved. Due to the spreading these lines have so far not been higher than around 150 µm shortly after dispensing and they coalesce already during dispensing. This effect is expected to be even more pronounced for the other adhesives with much lower wetting angles and viscosities. Current studies will show how a high degree of spreading with the risk of line coalesce before assembly can be avoided with a) very low surface tension substrates compared to the adhesive, b) adhesives with even higher higher thixotropic index or viscosity. Presumably the trumpet shapes of the channels, fig 2, can be compensated by placing larger adhesive volumes at the line ends because then the adhesive will need more time for the redistribution into that shape. Confirmation of these predictions is part of ongoing and future work.

Material	Surface tension γ (mN/m)	Wetting angle on glass θ_{Glass} (degrees)	Wetting angle on PMMA θ_{PMMA} (degrees)	Wetting angle on PEEK θ_{PEEK} (degrees)	Viscosity (datasheet) (mPas)	Application comments
DYMAX 9-20318-F	44 (WP) 42 (PD)	51 (SD)	60 (SD)	55 (SD)	50000	Masking
DYMAX 3070	24 (PD)	30 (SD)	14 (SD)	22 (SD)	8500	Plastic adhesive
DYMAX 9001 version 3.5	18 (PD)	39 (SD)	28 (SD)	39 (SD)	20000	Damming adhesive
PDMS Sylgard 184	19 (WP) 18 (PD)	18 (SD)	13 (SD)	25 (SD)	4000	Encapsulant / bonding material

Table 1: Surface tension and wetting angles. Used methods: WP = Wilhelmy plate, SD = Sessile drop, PD = Pendant drop. From the wetting angles of DYMAX 9-20318-F and 3070 Zisman plots yield the following critical surface tensions: γ_{glass} = 13 mN/m, γ_{PMMA} = 23 mN/m, γ_{PEEK} = 20 mN/m.

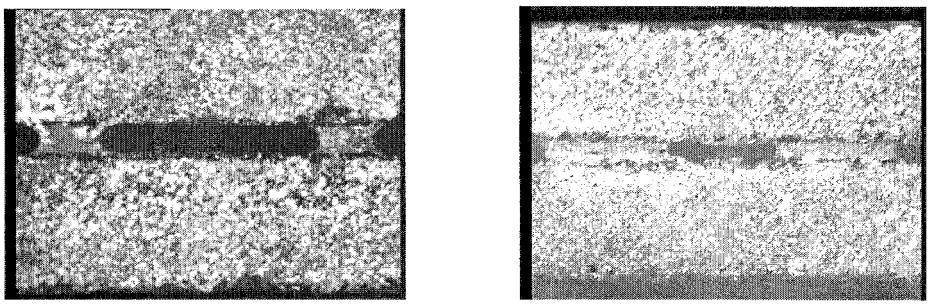

Fig. 1: Cross sections of channels between glass microscope slides and DYMAX 9-20318-F adhesive lines. The channels are in the centre of the pictures. Left: Channel height 150 µm. Right: Channel height 100 µm. Line pitch is 2 mm in both cases. Note the approx. 51 ° wetting angle.

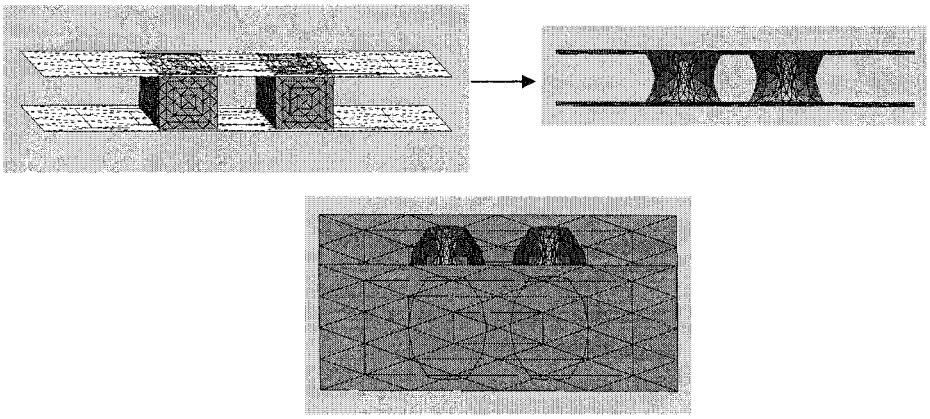

Fig. 2: Simulation of channel formed between two lines of DYMAX 9-20318-F where top and bottom substrate is PEEK. Top: Development from square lines. Here the line height, width and distance are equal. Bottom: Illustration of the double trumpet channel shape.

5. Conclusions

At this stage we can conclude: 1) Among other geometries it is possible to achieve nearly round channels, 2) Due to fast spreading channels are difficult to make from close proximity adhesive lines especially with low viscosity but also low wetting angle adhesives, 3) Due to surface free energy minimization channels will tend to have an inner double trumpet shape.

Acknowledgements

This work has been part of projects financially supported by the Danish Ministry of Science Technology and Innovation.

References

[1] J. Han, S. Lee, A. Puntambekar, S. Murugesan, J-W. Choi, G. Beaucage, C. H. Ahn, *Proceedings of MicroTAS 2003*, pp. 1113-1116.

[2] C. Harrison, J. T. Cabral, C. M. Stafford, A. Karim, and E. J. Amis, *J. micromech. Microeng.*, **14**, pp. 153-158 (2004).

[3] Jakob Janting, Jens Branebjerg, Pirmin Rombach, *Sensors and Actuators* A 92 (2001) 229-234.

[4] http://www.susqu.edu/facstaff/b/brakke/evolver/

3-DIMENSIONAL NANO VOLUME PDMS MICROREACTOR EQUIPPED WITH PNEUMATICALLY-ACTUATED IN-CHANNEL MEMBRANE VALVES

Takahiro Arakawa[1], Jeung Sang Go[1,2], Eun Ho Jeong[2], Shu Kawakami[1], Kouji Takenaka[1], Masahiro Mori and Shuichi Shoji[1]

[1]Major in Nano-science and Nano-engineering, Waseda University, 3-4-1, Ohkubo Shinjuku, Tokyo, 169-8555, Japan

[2] School of Mechanical Engineering, Pusan National Uuniversity, Korea

Abstract

Fabrication of a pneumatic actuated in-channel microvalve device and its performance characterization are presented. The valving part is consisted of the stacked three PDMS structures, a microchannel for fluid flow, a pneumatically-actuated membrane and an air pressure applying chamber. In order to ensure the perfect close of the chemical reaction pathway resulting from membrane bulging and to minimize the dead volume under valve actuation, microchannel has simple round cross-sectional structure and smooth surface. To prevent delamination at the interface between two PDMS layers under large pneumatic pressure, the bonding condition to obtain the sufficient PDMS-to-PDMS bonding strength were examined. By using colored sample liquids, the open and close tests of four microvalves were visualized.

Keywords: PDMS, channel valve, bonding strength, smooth surface, microreactor

1. Introduction

The 3-dimensional PDMS microdevices such as microvalves, pumps, biochips and so on [1,2] have been getting attraction in the bio-technology dealing with nanoliter or picoliter volume biochemicals due to low cost, straightforward fabrication process and transparency for optical measurement. However, conventional fabrication method of the pneumatically-actuated PDMS valves using micromachining provides sharp corners and a weak PDMS-to-PDMS bonding strength as graphically shown in Fig.1 (a). The sharp structure causes crucial leakage and diffusion pathway of chemicals. In particular, when the membrane valve is installed into a microchannel for miniaturization, the sufficient adhesion force between layers is required to resist an applied air pressure.

2. Design and fabrication

We have developed a microchannel valve having smooth surface and the monolithic bonding processes of the PDMS-structured layers (Fig. 1(b)). Underneath the microchannel, a membrane and a pressure applying chamber are formed. The depth of microchannel of 50μm and the membrane thickness of 60μm were considered. For a 300μm x 500μm square membrane, it was numerically operated that more than a 150kPa pressure was needed to obtain the deflection of 50μm, which can close the microchannel perfectly.

In microfabrication, two critical points mentioned above were focused. Firstly, the smooth surface channel was obtained from PDMS replication of the convex rounded PMMA channel master, which was transferred form the concave round etched channels on a glass substrate. The molded PDMS layer was attached to the soft-cured PDMS film spin-coated on a silicon substrate. After hard cure, two PDMS layers were firmly bonded, implying the monolithic bonding process [3]. Secondly, to obtain enough bonding strength of PDMS-to-PDMS bonding to over a 150 kPa pneumatic pressure, the bonding conditions were examined for the various curing ratios, defined by

Curing ratio (R) = soft cure time/full cure time (1)

Based on the interfacial fracture toughness, the maximum bonding strength was evaluated by measuring the threshold air pressure of the adhesion test specimen fabricated with various bonding conditions (Fig. 2). We used the optimum bonding condition to fabricate the microchannel valve with the smooth surface. Fig. 3 shows the cross-sectional view.

3. Results and discussion

We characterized response time of the microchannel valve by applying stepped air pressure. A high speed CCD camera analyzed the valve Open-Close modes. It was determined that the 190 milliseconds were taken to bulge membrane perfectly, indicating to valve Open mode. But to release membrane, it took 500 milliseconds, implying to valve Close mode. In the Close mode, it was found that the membrane stuck to the upper surface of PDMS channel. Thus, it took about 2.5 times of the closing time to return to the initial state. The volume of the variable valve part was estimated to be about 7.5nl. Based on this characterization, we applied this to a disposable microreactor consisting a set of four in-channel membrane valves, a cleaning inlet and a waste channel. Fig. 4 describes a schematic diagram of the experimental setup. In order to address the expectable reactions, Fig. 5 shows four different valve actuation signals. Fig. 6 shows the mixture of Rhodamine-B and Methylene-Blue in the reaction chamber for the four different actuation modes with the switching time of 500 milliseconds. The flow rate of each inlet fluid was 2.0μl/min, respectively. The monolithic PDMS microreactor controlled by in-channel membrane valves was successfully operated.

5. Conclusions

The fabrication method to obtain smooth surface and the high adhesion force of the monolithic bonding of PDMS-to-PDMS were presented. So far, for the three PDMS layers, the bonding strength using soft cured PDMS was satisfactory. The smooth surface channel valve showed perfect close during valving. This automatic PDMS flow control device can be applied to other biochemical applications. We also consider the wafer-level batch process of the monolithic 3-dimensional PDMS device for further research.

Acknowledgements

This work is partly supported by Japan Ministry of Education, Culture, Sports Science & Technology Grant-in-Aid for COE Research and 21st COE of Waseda University, Scientific Basic Research (A) No. 12450167 and NEDO project in micro chemical process technology.

References

[1] Todd Thorsen, Sebastian J. Maerkl, S. Quake, "Microfluidic Large-scale Integration", *Science*, vol. 298, 580-584 (2002)

[2] Noo Li Jeon, et al. "Design and Fabrication of Integrated Passive Valves and Pumps for Flexible Polymer 3-Dimensional Microfluidic Systems", *Biomedical Microdevices*, 4:2, 117-121 (2002)

[3] Jeung Sang Go and Shuichi Shoji, "A Disposable, Dead Volume-Free and Leak-Free Monolithic PDMS Microvalve", Sensors and Actuators A: Physical, in press

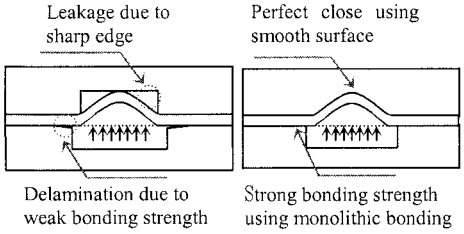

Figure 1. Cross-sectional view of the conventional and proposed in-channel microvalve.

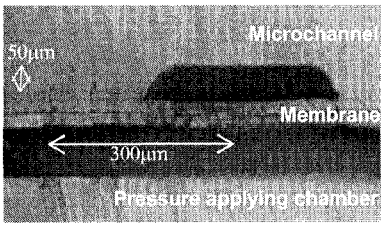

Figure 3. Cross-sectional view of the fabricated PDMS in-channel microvalve.

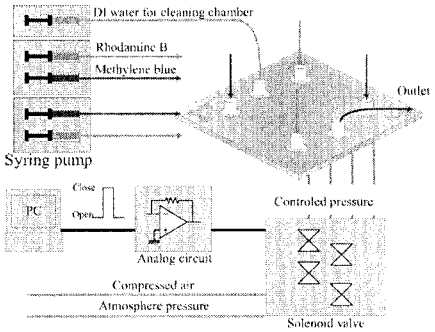

Figure 4. Experimental set up of the PDMS in-channel microvalves control system.

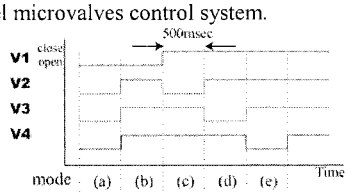

Figure 5. Control signal of the four valves switching chamber.

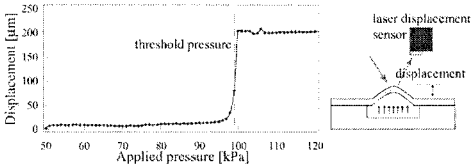

(a) Measurement method of the bonding strength

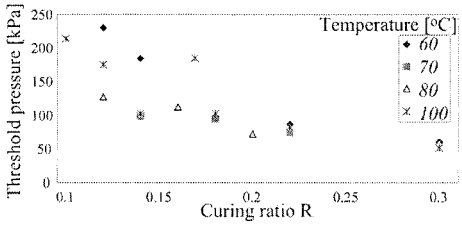

(b) Measurement result of the PDMS bonding strength

Figure 2. Investigation of the PDMS to PDMS maximum bonding strength.

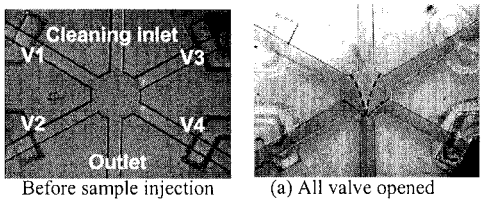

Before sample injection (a) All valve opened

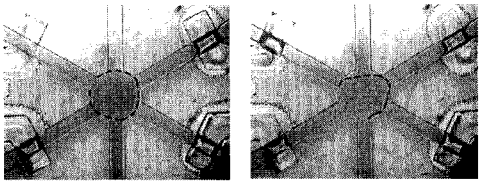

(b) Only V1 opened (c) Only V2 opened

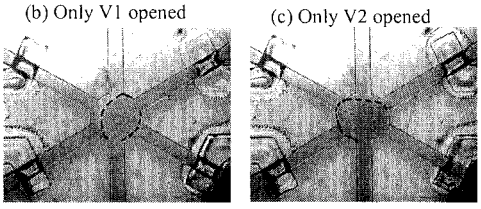

(d) Only V3 opened (e) Only V4 opened

Figure 6. Mixture of Rhodamine-B and Methylene-Blue in the reaction chamber under different actuation modes.

MICROFLUIDIC DEVICES INTEGRATED WITH PERMALLOY MICROPATTERNS FOR BEAD-BASED ASSAY

Naoaki Ichikawa[1], Yoshinori Katsuyama[2], Yukio Nagasaki[2] and Takanori Ichiki[3, 4]

[1] *Dept. of Electric and Electronics Eng., Toyo University, 2100 Kujirai, Kawagoe, Saitama, Japan*

[2] *Dept. of Materials Sci. and Technol., Tokyo Univ. of Science 2641 Yamazaki, Noda-shi, Japan*

[3] *PRESTO, Japan Science and Technology Agency, 4-1-8 Honcho, Kawaguchi, Saitama, Japan*

[4] *School of Engineering, The University of Tokyo, 2-11-16 Yayoi, Bunkyo-ku, Tokyo, Japan*

Abstract

A new type of biochips for the direct handling of biomolecules has been proposed by the combinative use of magnetic beads and the microfluidic chip integrated with micropatterns of permalloy thin films. For this purpose a new plasma etching process for the patterning of Ni based alloy thin films has been developed using $CO/H_2/Ar$ plasmas. Furthermore, model bead-based assay experiments have been successfully demonstrated using a prototype chip.

Keywords: Microfluidics, Magnetic beads, Bead- based assay, Permalloy etching

1. Introduction

Magnetic beads modified with specific functional groups on their surfaces are currently used for feasible separation and purification of proteins and cells. Furthermore, functionalized magnetic beads can be used as a convenient carrier of molecules. Namely, one can handle a small amount of molecules using a bead-target molecule complex. However, the behaviors of the massive magnetic beads in the magnetic field are rather complex, and hence, it is difficult to handle each magnetic bead in a sophisticated manner. In this paper, we propose a microfluidic device for handling a small amount of magnetic beads using a localized magnetic field (Fig. 1), and the fabrication process of microfluidic chips integrated with micropatterned permalloy thin films has been developed. Furthermore, model bead-based experiments have been successfully demonstrated using a prototype chip.

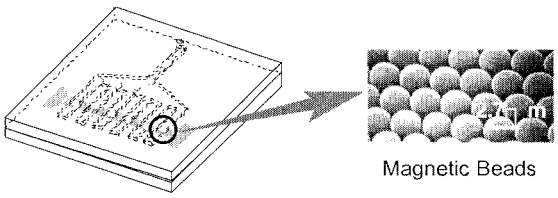

Figure 1. Schematic diagram of a microfluidicchip for the separation and purification of cells or biomolecules via the specific interaction with polymer-coated magnetic beads trapped near fine permalloy patterns.

2. Experimental

The process steps for chip fabrication are shown in Fig. 2. A thin permalloy (Ni: 78%, Fe: 22%) film of 500 nm thickness was sputter-deposited on a borosilicate glass substrate of 30 by 30 mm area, and was sequentially etched in $CO/H_2/Ar$ plasmas to form permalloy microstructures that are necessary to generate a localized magnetic field on the glass plate. At the final step, a PDMS microchannel sheet was bonded on the glass plate so that the permalloy micropatterns could lie under the microchannel. The model affinity separation experiment was carried out using biotinylated magnetic beads and Texas Red-labeled streptavidin as shown in Fig. 3. Biotinylated magnetic beads were prepared by modifying commercially available magnetic beads (Dynabeads

M270; superparamagnetic and monodisperse beads coated with a thin polymer shell) using PEG-b-PAMA and biotin. Target molecules of streptavidin were labeled using the fluorescent marker, Texas Red, to facilitate observation. First, biotinylated magnetic beads suspended in water to which a small amount of surfactant was added were injected into the prototype microfluidic device, and subsequently, electromagnets were activated to apply a localized magnetic field for trapping magnetic beads between permalloy micropatterns. After confirming that a sufficient number of magnetic beads were fixed in the trapping area, the microchannel was rinsed using phosphate-buffered saline (pH 7.4; ionic strength, 0.15) to remove residual beads which were not trapped between permalloy micropatterns. Finally, Texas Red-streptavidin solution was introduced from the inlet port of the device and the behavior of the streptavidin was recorded using a fluorescence microscope equipped with a sensitive CCD camera (Hamamatsu Photonics, EB-CCD C7190) and a personal computer.

3. Results and discussion

By using the microfabrication process described in the previous section, a prototype microfluidic device for affinity separation was fabricated, as shown in Fig. 4 (a). The performance of the prototype device was examined using an inverted microscope, as shown in Fig. 4 (b). Magnetic beads of 2.8 μm diameter were suspended in an aqueous solution with the addition of a small amount of surfactant, and introduced into microchannels. An external magnetic field was applied to permalloy micropatterns by passing an electric current through the electromagnetic coils set on the pad portion of the patterned permalloy films. When the electromagnet was active, magnetic beads drifting in the microchannels were trapped between permalloy micropatterns, as shown in Fig. 5 (a), and trapped beads were released when the electromagnet was switched off. Figure 5 (b) shows the fluorescence microscopic image of magnetic beads after the injection of streptavidin solution into the microfluidic device. Successful capture of target molecules was confirmed from the strong fluorescent light observed from the fixed beads inside the microchannels. Figure 6 shows the signal as a function of the sample flow time. The signal increased according to the exponential function and began to saturate at around 10 min.

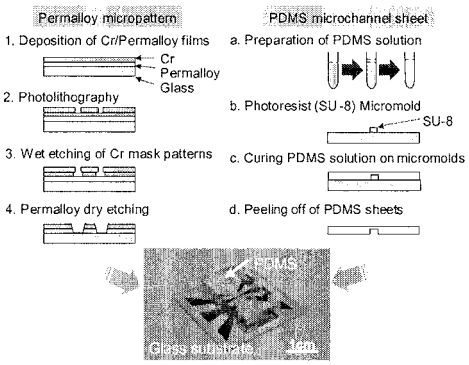

Figure 2. Fabrication sequence of microfluidic devices integrated with permalloy micropatterns.

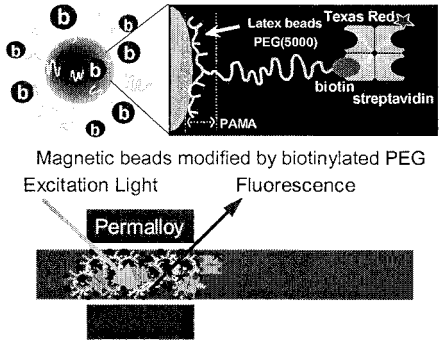

Figure 3. Schematic diagram of magnetic beads and captured samples used in the present demonstration of affinity chromatography.

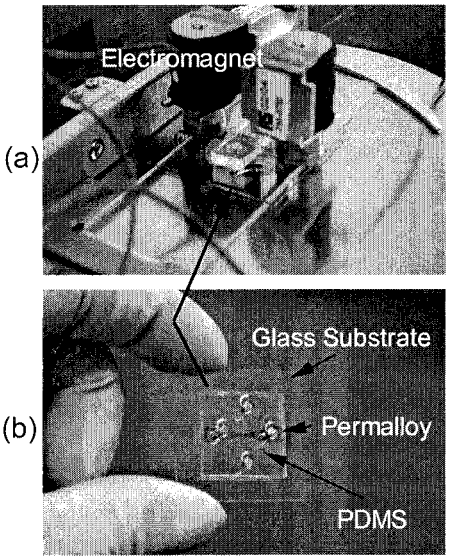

Figure 4. (a) Experimental setup for testing prototype chips. Small electromagnets were set on permalloy micropatterns. (b) Photograph of the microfluidic chip with permalloy micro-patterns.

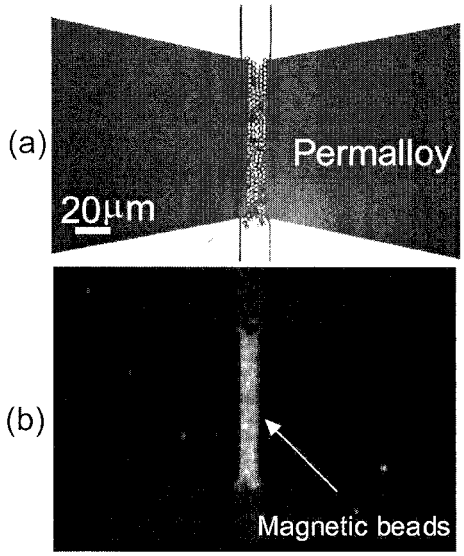

Figure 5. Microscopic image of magnetic beads trapped between permalloy micropatterns (a) and the fluorescence microscopic image of Texas Red-labeled streptavidin captured on the surface of magnetic beads (b).

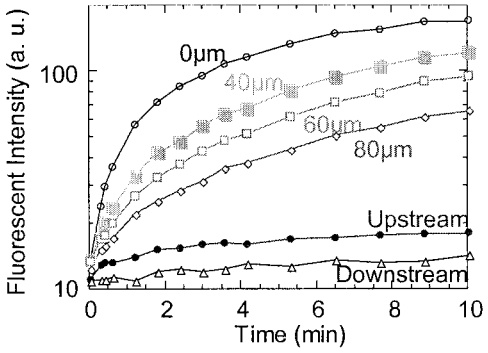

Figure 6. Flurorescence signal as a function of sample injection time. Signals were measured at various positions of bead columns

Acknowledgements

This work was supported by the PRESTO program of the Japan Science and Technology Agency (JST) and High-Tech Research Center Project of the Ministry of Education, Culture, Sports, Science and Technology of Japan.

FORMATION OF UNIFORM SIZE LIPOSOMES USING A PDMS BASED MICROMOLD

Ph. Coquet[1], G. Tresset[1], S. Takeuchi[2], H. Fujita[2]
[1]LIMMS/CNRS-IIS, [2]CIRMM-IIS
University of Tokyo, 4-6-1 Komaba, Meguro-Ku, Tokyo 153-8505, Japan

Abstract

We present in this paper a method, based on an on-chip process, to obtain liposomes with uniform size. It consists in coating a glass plate with a lipidic film on which a buffer solution is squeezed by a polydimethylsiloxane (PDMS) sheet with microchambers. Liposomes are formed in these chambers by this way with a size varying with the diameter of the chambers. Liposomes with uniform diameters of 4 to 10 micrometers have been obtained.

Keywords: Liposomes, PDMS molding, PDMS microarrays

1. Introduction

Liposomes have been used for several years to transfer biological materials into cells, for example in applications of gene therapy [1]. Their use is now also considered as delivery vehicles to transfer artificial materials, or more complex micro structures, through the cell membrane. Liposomes are indeed synthetic lipidic containers, and it is easy to enclose materials during their fabrication. They have also cell-like membranes which make possible, in principle, their fusion with almost any kind of cells. From a practical point of view, a high fusion efficiency with cells must be achieved. The efficiency is strongly dependent on the size of the liposome [2]. However with the conventional procedure, the so-called "reverse phase evaporation" [3], the size of the liposomes cannot be controlled, and it leads to liposomes with a diameter arbitrarily ranging from a few μm up to 20~30 μm. The size of the liposomes is also an important parameter for controlling the volume introduced inside the cell by the liposome through the fusion.

To obtain uniformly sized liposomes and to maximize the fusion efficiency with cells, we have transferred the conventional bulk procedure to an on-chip process. The key idea is to form liposomes in a microchamber having the same size as the target liposome size.

2. Experimental

In the usual way of fabricating liposomes, two types of phospholipids, 0.9 mg/mL L-α-phosphatidylcholine and 0.1 mg/mL L-α-phosphatidic acid, are diluted into a mixture of chloroform and methanol 2:1. The organic solvent is then removed, usually by rotary evaporation, resulting in the formation of a dry lipidic film on the inner surface of a flask. This film is then moisturized by pouring a buffer solution (10 mM KCl and 200 mM glucose) onto it. Due to the presence of hydrophobic terminations at the surface of the film, this moisturization leads to the formation of lipidic vesicles.

First, we have modified this protocol in order to form the lipidic film on a planar surface. The difficulty was to control the evaporation rate of the solvent in order to get a uniform coating of the film on the considered planar surface. We have found that a good uniformity could be obtained when the lipidic solution was spread between two glass substrates separated by spacers, and then evaporated in a conventional vacuum chamber. Also prior to use the glass substrates it was better to wash them with a Sodium Hydroxide solution (NaOH). The liposomes obtained by this planar process were similar to those obtained with the conventional procedure. This method makes also the fabrication process simpler as there is no need of using a rotary evaporator.

The procedure that we have then developed to obtain uniformly sized liposomes is described on Figure 1. Once the dry lipidic film is formed, the buffer is sandwiched between the glass substrate

and a sheet of PDMS. This sheet comprises an array of micro-chambers obtained by a moulding technique. By applying a pressure, due to the hydrophobic properties of the PDMS, the buffer is scattered in the chambers, excess water is evacuated and the PDMS sheet is bonded to the glass surface. As the buffer is confined in the chambers, the liposome formation will occur inside them. By adjusting the size of the chambers it is then possible to control the size of the liposomes.

3. Fabrication of the PDMS chambers

For the realization of the PDMS chambers, following the principle presented in reference [4], a Silicon mould was fabricated. It consists of an array of cylinders, as shown on Figure 2, obtained here by ICP-RIE etching of a SOI wafer. An aluminium layer was evaporated onto the SOI to serve as a mask for plasma etching and patterned by using 0.5 μm thick photoresist. Aluminium and Photoresist were removed after the RIE process. PDMS sheets were obtained from this mold. To facilitate the removal, the mold has been treated with CHF_3 plasma before pouring the PDMS. The depth of the chambers is fixed by the thickness of the SOI layer. Chambers with depths of 7 μm and 10 μm and with diameters ranging from 20 μm to 6 μm have been fabricated.

4. Results

An example of the results obtained for chambers having a diameter of 18 μm, 13 μm and 8 μm, and with a depth of 7 μm, is given on Figure 3. Liposomes are clearly visible inside the different micro-chambers. This demonstrates the feasibility of the proposed method. It can be seen on the pictures that the size uniformity is good. As a comparison, Figure 4 shows liposomes fabricated following the conventional process, that is without making use of the PDMS chambers. In that case the size ratio between small and large liposomes is about 10. When using the PDMS chambers this ratio varies from 2 to 5, depending on the chamber diameter.

Table 1 gives typical measured liposomes diameters versus the diameter of the chambers. These values and also the comparison of Figure 3.a, Figure 3.b and Figure 3.c, show the decrease of liposome size with the decrease of chamber size. The average diameter of the liposomes is about 9 μm for the 18 μm chambers, 7 μm for the 13 μm chambers and 5μm for the 8 μm chambers.

5. Conclusion

In this work we have transferred the conventional bulk procedure for fabricating liposomes to an on-chip process. We have shown the possibility to obtain uniformly sized liposomes by restricting their formation inside PDMS micro-chambers. Such a control in size can be applied, for example, to the optimization of the volume to be transferred into cells in the case of drug delivery. It can also help to maximize the efficiency of the fusion with cell, which is size dependent. One future prospect of this work is to use this method and to mix particles in the buffer in order to realize the encapsulation of particles in liposomes, to perform cell labelling. As this action will be localized in the chambers good insertion efficiency is expected.

References

[1] A.S. Ulrich, *Bioscience Reports,* 22 (2002), 129-149.
[2] G. Tresset, S. Takeuchi, *17th IEEE MEMS conference*, (2004), pp 25-28.
[3] V.P. Torchilin, V. Weissig, Liposomes, *Oxford University Press*, (2003).
[4] Y. Rondelez, G. Tresset, K. Tabata, H. Nitta, S. Takeuchi, H. Noji
7th μTAS conference, (2003), 555-558.

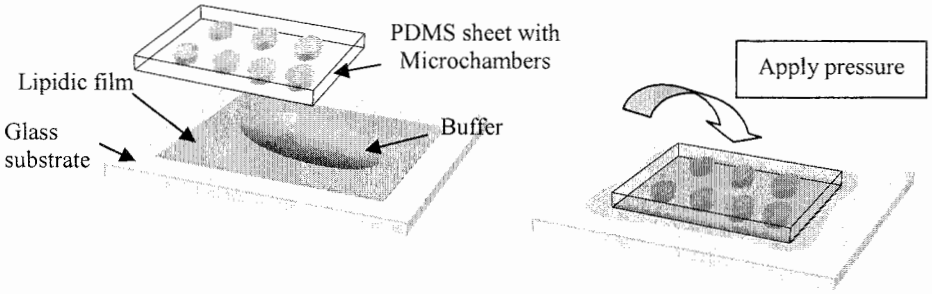

Figure 1. Description of the procedure developed for the formation of uniform size liposomes

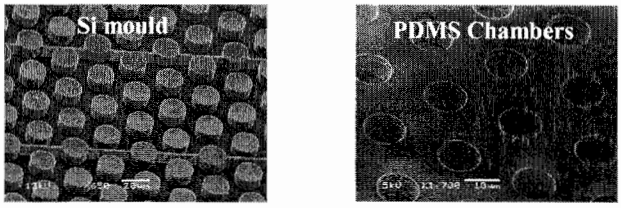

Figure 2. SEM pictures of one Si mould and of the corresponding PDMS chambers

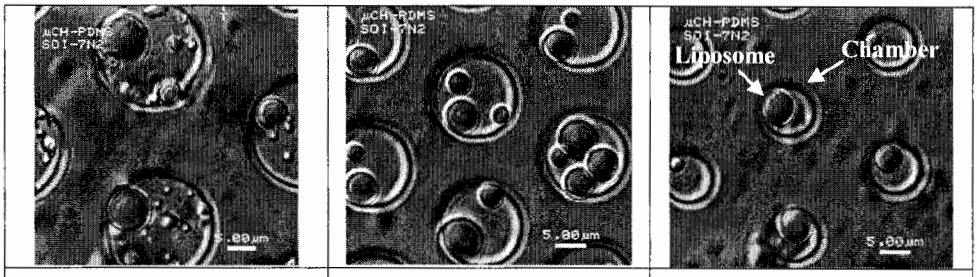

(a) Chambers diameter 18 µm | (b) Chambers diameter 13 µm | (c) Chambers diameter 8 µm

Figure 3. Pictures of liposomes obtained in the chambers

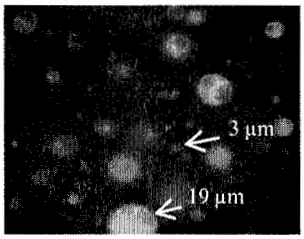

Figure 4. Pictures of liposomes obtained without using the PDMS chambers

Chamber Diameter (µm)	**18**	**13**	**10**	**8**
$\varnothing_L$ ***Max*** **(µm)**	10	8	7	5 ~ 6
$\varnothing_L$ ***min*** **(µm)**	2	3	2	2 ~ 3
$\varnothing_L$ ***average*** **(µm)**	9	7	6	5

Table 1. Typical liposomes measured diameters, $\varnothing_L$ versus the diameter of the chambers

DEVELOPMENT AND CHARACTERISATION OF OPTICALLY ENCODED MICROBEADS IN MICROFLUIDIC SYSTEMS

Daniel Hoffmann[1], Des Brennan[1], Peter O'Brien[2], Michael Loughran[1] and Gabriel Crean[1]

[1] *Biophotonics Research Team, National Microelectronics Research Institute, University College Cork, Lee Maltings, Prospect Row, Cork, Ireland, 2004*

[2] *Nanocomms Ltd.. 9 Mardyke Parade, Cork, Ireland*

Abstract

We have fabricated distinctive microbeads in silicon using conventional MEMS fabrication technologies. The microfluidic transport and behaviour of these microbeads has been characterised in several different microfluidic structures. We demonstrate how microbeads can be manipulated by careful design of the microchannel geometry. In addition we incorporate a customized photonic detector that is capable of identifying individual microbeads in-situ.

Key words: Encoded Microbeads, Microfluidic Systems, Flow Manipulation

1. Introduction

The combination of unique encoded microbeads with a microfluidic network of flow channels provides an ideal platform for high throughput chemical synthesis, diagnostics or biological analysis [1]. Moreover, a large library of multiple, optically encoded microbeads can be generated. This approach has the potential to shift microbead-based systems towards a more structured and systematic methodology with the outstanding benefit of complex high-member libraries [2].

2. Fabrication

The fabrication process of encoded silicon microbeads involves three stages: metal depostition and wet etch, silicon front side etch and silicon backside etch. The fabricated microbeads incorporating optical labels are shown in Figure 1. The dimensions of these encoded microbeads are 600 μm by 300 μm by 80 μm.

Optical labels consist of photo-lithographically defined micro-barcodes, two different types can be distinguished. Type A beads have a reflective metal aluminium pattern on the silicon surface (Figure 1a). The second type of bead, Type B, the micro-barcode is embodied in the bulk of the silicon microbead by incorporating a series of through-holes (Figure 1b). Type B optical labels and microbead shapes are fabricated simultaneously using the BOSCH dry etching process at the front side. In the final stage a backside etch is performed using a combination of dry etching (BOSCH process) and wet etching (KOH). The latter fabrication step releases microbeads from the wafer (Figure 1c). Microfluidic structures has been fabricated in SU-8 and sealed with glass slides utilizing UV curable epoxy. Fabricated microchannels were 200 μm deep. The width was varying between 800 μm and 3 mm. A pressure driven flow was generated using syringe pumps.

3. Results and discussion

The flow behaviour of microbeads in microfluidic structures is strongly related to the flow characteristics in microchannels. We observed excellent flow stability in planar and U-bend microchannels (Figure 2). The lateral orientation of a microbead is maintained during flow along the channel. In fact, it is very dependent on its initial orientation; hence microbeads do not necessarily flow in the centre of the channel (Figure 2a). This indicates that the parabolic flow profile of a pressure driven system does not have a significant effect on the microbead flow.

The flow behaviour associated with the flow velocities of the fluid and microbeads respectively was observed. Figure 2c shows a micro-bead and a small particle-like object flowing along a planar micro-channel. Two pairs of arrows in Figure 2c indicate the relative positions of the microbead and the small particle at two different moments. The velocity of the optically encoded microbead was estimated to be 60% slower than the fluid's speed. We assume that frictional forces, surface interactions as well as the inertia of the microbead all contribute to an activation force (pressure gradient), which must be overcome before the microbead can move. The different velocities of the encoded mircobeads and fluid were also verified in a separate experiment: commercial micro spheres with a diameter of 6 μm were added to the fluid to visualize the flow by red laser scattering.

Figure 3 shows more complex microfluidic structures, which enabled manipulation of lateral alignment of microbead flow and also adjustment of the microbead velocity. The velocity of a microbead transport is related to the fluid flow and can be manipulated by varying the cross-sectional area of the channel (Figure 3a). Additional guiding structures have been implemented to engender and maintain the correct orientation of the microbead during the flow in the channel widening that can be seen as the detection region.

Microbeads can also be moved across a microchannel. This could facilitate switching into a multiple channel network. An extra layer with a periodic pattern at the bottom of the flow channel was implemented to enable microbead alignment (Figure 3b). These features are composed of a sequence of angled barrier ridges with a height of 50 μm. Simulation results demonstrate how the fluid is forced to flow in the direction of lowest resistance resulting in a shift to either side of the channel depending on the flow direction (Figure 3c). This principle can be exploited to manipulate the lateral position of a microbead across a microchannel (Figure 3d).

A customized photonic detector was developed that is capable of identifying individual microbeads in-situ using a laser detection system (Figure 4a, b). Microbeads can be identified with a flow velocity up to 50 cm per second (Figure 4c). This corresponds to a detection rate of 250 microbeads per second.

Future work will involve multiple microbead injection and switching.

Acknowledgements

The authors would like to thank the central fabrication facility at NMRC for their technical support. Financial support towards this project from Enterprise Ireland is also acknowledged.

References

[1] V. Lehmann, "Barcoded Molekules", Infineon Technologies, Nature Materials Vol 1 Sep 2002

[2] Gwendolyn A Lawrie, Bronwyn J Battersby, Matt Trau, "Bioballs: manipulating colloidal nanostructures for biotechnology applications", Applied Nanoscience 2004:1(1)

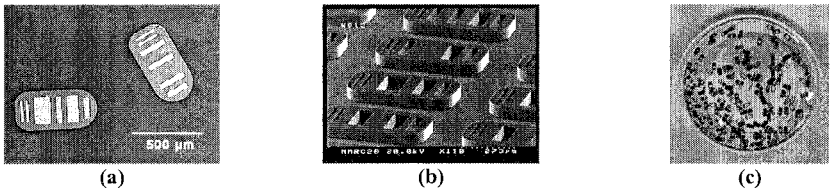

(a) (b) (c)

Figure 1: Optical encoded Silicon Microbeads; a) Microscopic View, b) SEM image; c) In water solution

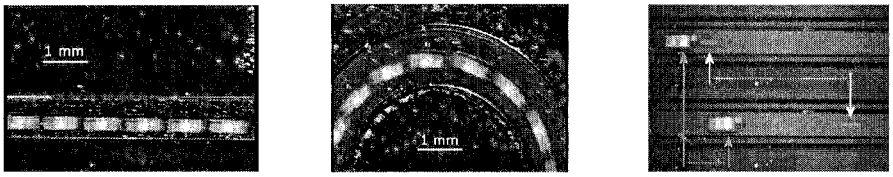

(a) (b) (c)

Figure 2: Flow characteristics; a) Planar structure; b) U-bend structure; c) Velocity differences

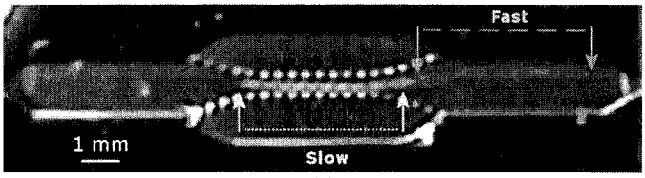

(a)

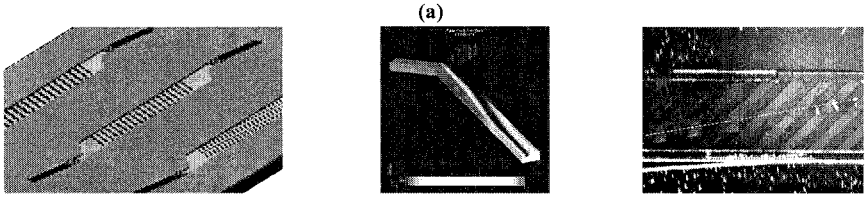

(b) (c) (d)

Figure 3: Flow Manipulation; a) Velocity adjustment; b) Design for lateral alignment; c) Microfluidic simulation of design for lateral alignment; d) Lateral microbead alignment in a microfluidic channel

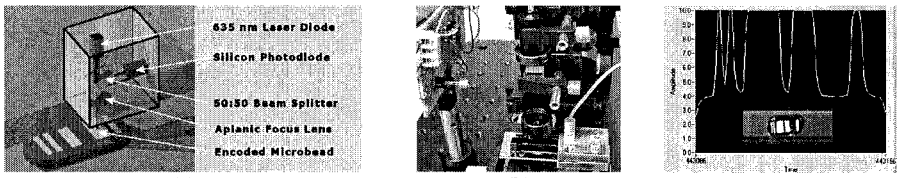

(a) (b) (c)

Figure 4: In-situ identification of encoded Microbeads in a microfluidic environment; a) Schematic of optical detection system; b) Experimental set-up; c) Flow detection signal of an encoded microbead

AUTOMATION OF THE PATCH CLAMP TECHNIQUE

R.Vestergaard, J.Kutchinsky, S.Pedersen, R.Taboryski, C.Sørensen, R.Schrøder, T.Ljungstrøm, S.Friis, K.Krzywowski, M.Asmild, R.Jacobsen, N.Helix, M.Bech, J.Christensen, S.Dubeau, N.Willumsen, N.Hansen, D.Nielsen, T.Freltoft.

Sophion Bioscience A/S. Baltorpvej 154. DK-2750 Ballerup. Denmark.

The QPatch[tm] is a newly developed ion channel screening system, which automats the conventional patch clamp technique. Whole-cell current measurements take place on a disposable 16-channel QPlate[tm] in MTP format. Automation has been achieved by (i) employing planar silicon chips rather than traditional glass micropipettes, by (ii) elimination and/or simplification of a number of time-consuming tasks, e.g. visual cell selection and pipette tip localisation, manual microscope-aided pipette positioning and cell contact establishment, and subsequent gigaseal and whole-cell formation, and by (iii) cell preparation directly on the QPatch platform. We here report whole-cell current data from cultured cell lines expressing a number of voltage- or ligand-gated ion channels.

Whole-cell measurements were done on 16-channels QPlates with either a 16-channel Sophion patch clamp amplifier or with a HEKA (EPC-9, HEKA Elektronik, Germany) commercial amplifier. The chips had micro-etched patch clamp holes with an electrical resistances of 2.04+/-0.02MΩ in symmetrical physiological saline. For an overview of the QPlate assembly and its functionality please see Fig.1.

Fluid application in the Qpatch screening system is accomplished through flow channels in the Qplate assembly. For measurement of current transients from ligand-gated ion channels, fast liquid application is required. In conventional patch clamp this is often achieved by usage of a piezo stepper. This option is however not possible in a fixed flow channel based system.

A computer model was developed to evaluate whether ligand-gated ion channel current responses can be expected when using the Qpatch technology, see Fig.2. We examine the effect of the following parameters on the recorded ligand-gated ion channel current: The ligand concentration profile, the time it takes for the ligand to reach the cell (dependent on flow rate and travel distance) and the characteristics of the ligand-gated ion channel current (open-state probability and desensitisation time constant).

The results of the simulations are: 1) that the desensitisation time constant affects the maximal ligand-gated ion channel current measured. 2) A setup with fast concentration shift will be less sensitive to the effect on desensitisation time. 3) Even with relatively slow concentration shifts, fast ligand-gated ion channel rise times can be measured.

On Fig.3 we display a comparison between simulations and an experimental current measurement recorded on a HEK-293-cell expressing nicotine acetylchorine receptor. The response was induced by 1μM acetylchorine.

High-quality whole-cell recordings from a number of ion-channels expressed in cultured cell lines have demonstrated that voltage-gated as well as ligand-gated ion channel proteins can be efficient targeted by the QPatch screening technology. Automation of the patch-clamp technique will substantially increase throughput in future ion channel drug discovery.

Figure 1

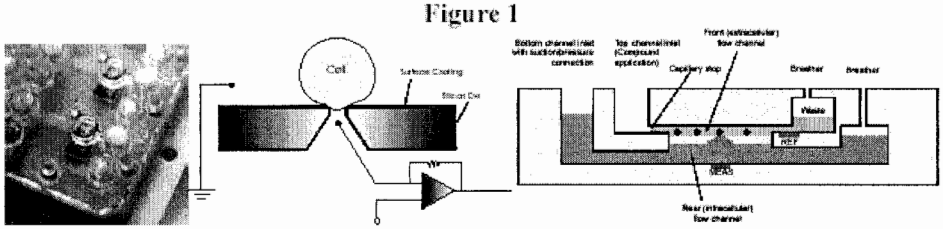

Left: Detail of Qplate showing top view of two measurement sites (assemblies). **Middle:** Schematic transection through the silicon chip with a cell positioned at the patch clamp hole. **Right:** Transection of chip assembly illustrating front and rear flow channels, capillary stop, and reference and measuring electrode (REF and MEAS). Both electrodes connect to bottom side for interfacing to Qpatch amplifier.

Figure 2

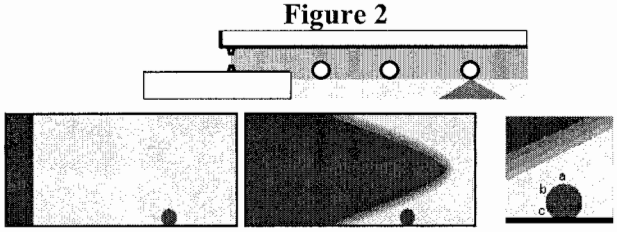

Top: Detail of chip assembly with 3 cells in the front flow channel (enlarged section of Figure 1C). **Bottom:** Computer simulation of the ligand concentration profile in the front channel at t=0 (left panel) and just before the ligand reach the cell (middle panel). The ellipsoid shape with fuzzy edges is created by a laminar flow friction and by diffusion. Letters a, b, and c denote upper, middle and lower position on the cell surface (right panel).

Figure 3

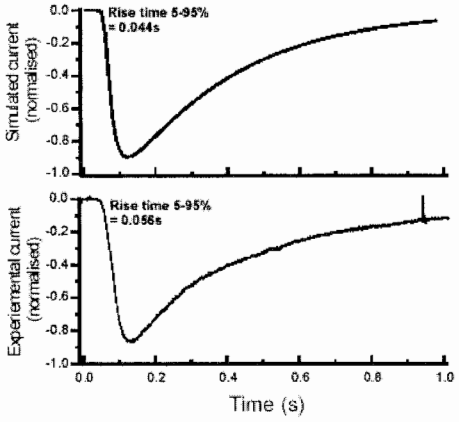

Top: Simulation of the LGIC current response to 1μm ligand to the Qplate. The desensitization time constant was set to 330ms. **Bottom:** Experimental current recorded from a HEK293-cell expressing nicotinic acetylcholine receptor (nACh) $\alpha_4\beta_3$. The response was induced by 1μm acetylcholine.

ALUMINUM ANODIZING PROCESS CHARACTERIZATION FOR DNA ATTACHMENT AND ELECTRICAL DETECTION

L. Moreno-Hagelsieb[1], B. Foultier[2], G. Laurent[1], C. Poleunis[1], P. Bertrand[1], J.P. Raskin[1], J. Remacle[2], D. Flandre[1]

[1]CERMIN Research Center, Université catholique de Louvain, place du Levant 3, 1348 Louvain-La-Neuve, Belgium.

[2]Laboratoire de Biochimie et Biologie Cellulaire, Facultés Universitaires Notre-Dame de la Paix, Namur, Belgium.

Abstract

Different materials have been used for DNA attachment in several DNA hybridization detection electrical methods on silicon chips, using capacitance or resistance changes of electrode interdigitated fingers sensors in micro-array format. Most cases use gold and other noble metals to protect the structures from the chemicals used during the biological process. In this work, as part of DNA detection, a non-noble metal oxide on top of Al structures is used, i.e. Al_2O_3, which serves as a protective layer as well as a suitable layer for DNA attachment. We studied the influence of the aluminum anodizing process critical parameters as well as making a comparison with different functionalizing chemicals to achieve the maximum quantity of bonded DNA.

Keywords: Anodizing, Biomaterials, DNA detection.

1. Introduction

DNA (deoxyribonucleic acid) hybridization is the underlining principle of DNA micro-arrays. Most devices use gold or noble metal electrodes to avoid surface oxidation and degradation in biological solutions and enable good ohmic contact with the electrolyte or the sample. They are usually not compatible with standard low-cost silicon circuits fabrication processes. Furthermore when silver precipitation is used to enhance hybridization, resistance measurements with ohmic gold contacts still present further hazards and limitations [1]. Since gold catalyzes silver precipitation, large electrodes gaps are required to avoid measuring low resistance in the absence of hybridization or false readings resulting from silver non-specific precipitation due to very long revelation times for low DNA concentrations. We previously demonstrated that aluminum electrodes coated with aluminum oxide (Al_2O_3), like interdigitated fingers and inductances, enable DNA binding and capacitive [2] and resonance frequency shift [3] electrical detection, providing the right isolation and protection of the device structures and reducing the non-specific precipitation of silver. We focus the present work more specifically on the in-depth understanding, characterization and optimization of DNA strands immobilization on Al_2O_3, prepared by anodizing process, in view of maximizing the concentration of DNA present at the surface of the sensor.

2. Samples Preparation and Methods

For the fabrication of the initial samples, we used the following process steps: standard cleaning of 10^{15} boron doped silicon <100> wafers (20 Ω cm), followed by a 400 nm wet oxidation, then 500 nm thick aluminum deposition, which was anodized to form 100 nm aluminum oxide at the surface. 5 current densities were used (0.1, 1, 2, 3, 4 mA/cm^2), and two electrolytes were tested (sulfuric acid in water and boric acid in etylenglicol).

In the biological process the evaluation consisted in using three typical functionalizing mixtures: water/methanol solution containing 7-octenyltrimethoxysilane (OTMS/W), toluene solution containing 7-octenyltrichlorosilane (OTCS) and a toluene solution containing 7-octenyltrimethoxysilane (OTMS). These molecules form a self-assembled monolayer (SAM) on the surface. Then DNA-capture probe tethering, hybridization with the complementary target probe, as

well as revelation of the hybridization event, were done as follow: 120 nucleotide long 5'-amino modified single strand DNA capture probe (Eurogentec, Seraing, Belgium) is spotted on the SAM using a 250 µm diameter pin. 400 µm diameter spots and about 10 nl are deposited. DNA capture probe binding to the SAM is performed by formation of an amine link.

The 375 nucleotide long biotin-labelled target DNA was prepared by polymerase chain reaction (P.C.R.). The concentration of target DNA in the P.C.R. product was quantified using the Agilent 2100 Bioanalyser (Agilent technologies, Palo Alto, California). The target DNA was diluted in hybridization solution to adequate concentration prior to each test.

The 75 µl target DNA solution was applied on the chip carrying the complementary capture probe in a sealed chamber to prevent evaporation. The chip was then incubated at 42°C for 1 hour to allow hybridization between the target DNA and the capture probe to occur. After extensive washing to remove non-associated target DNA, the revelation of DNA target binding to capture probe was performed by silver precipitation as recommended by the supplier of the kit (Eppendorf, Hamburg, Germany).

Comparisons are done by first characterizing the hydroxyl groups (OH) content at the surface by ToF-SIMS analysis, because these groups are essential for further binding of the functionalizing agent. Secondly DNA spots optical observations attached to the surface are performed after silver precipitation.

Based on the results from test samples we prepared our electrical detectors as previously, but after aluminum deposition, standard lithography was used to form the structures, then a thin layer of Al was deposited and finally anodizing of the surface was carried out, see Figure 1.

3. Results and discussion

As shown in table I, twice more -OH groups are found at the surface of aluminum samples when anodized with boric acid than with sulphuric acid. For anodizing current density of 1 mA/cm^2 or more, the -OH count is practically the same (looking at both positive or negative ions counts). In Figure 2, pictures of samples prepared at two anodizing speed in boric acid and after silver precipitation show that using OTCS functionalizing solution and higher anodizing speed, DNA attachment to the aluminum oxide is higher and silver precipitation is more selective (less background noise out of the spotted areas).

Electrical devices were constructed using a current density of 3 mA/cm^2 in a boric acid solution and functionalized using Toluene solution of OCTS. Capacitance measurements and resonant frequency showed significant variations at different levels of complementary single strand DNA (ssDNA) concentration for hybridization (see examples shown in Figure 3 and Table II).

4. Conclusions

Boric acid anodization of Al at minimum current density of 2 mA/cm^2, and functionalizing using toluene solution containing 7-octenyltrichlorosilane maximizes DNA immobilization on Al_2O_3 thus giving the possibility of hybridization detection at low concentrations. Structures smaller than previously used can furthermore be tested to improve previous performance.

Acknowledgements

The authors thank the UCL clean room staff and the "Ministery of Région Wallonne, Belgium" for the financial support on this work (conventions n°02/1/5139, 02/1/5386, 02/1/5387).

References

[1] E. Souteyrand et al, "Use of microtechnology for DNA chips implementation", Applied Surface Science, vol. 164, pp 246-251, 2000.

[2] L. Moreno-Hagelsieb, et al., "DNA Detection Based on Capacitive Al2O3/Al Microelectrodes", MEMS 2004 proceedings, January 2004, pp 308-311.

[3] G. Laurent, L.M. Hagelsieb, et al., "DNA Electrical Detection Based on Inductor Resonance Frequency in Standard CMOS Technology", ESSDERC 2003, pp. 171-174.
[4] J.P. Cloarec et al, "Immobilization of homo-oligonucleotide probe layers onto Si/SiO2 substrates: characterization by electrochemical impedance measurements and radiolabelling", Biosens. Bioelectron., Vol. 17, pp. 405-412, 2002.
[5] N. Zammatteo et al, "Comparison Between Different Strategies of Covalent Attachment of DNA to Glass Surfaces to Build DNA Micro-arrays", Anal. Biochem., vol. 280, pp. 143-150, 2000.

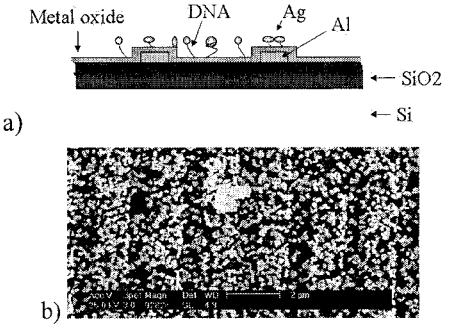

Figure 1. a) Cross-section of the sensors after processing, b) SEM image showing interdigitated fingers after silver precipitation, 5nM complementary DNA.

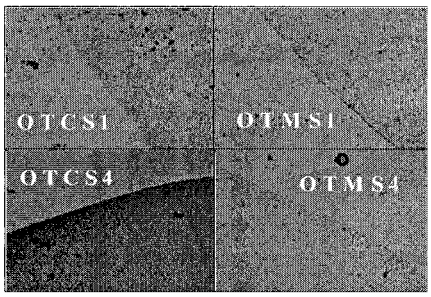

Figure 2. Aluminum oxide after silver revelation, OTCS and OTMS functionalized, anodized at 1 and 4 mA/cm^2 (darker areas are biotinylated DNA hybridized to complementary DNA tethered on the oxide surface reveled with Silver Quant solution (Eppendorf, Hamburg, Germany)).

Anodizing Chemical	speed (mA/cm^2)	AlOH/AlO negative	AlOH/AlO positive
Boric acid	0.1	0.1291	14.31
Boric acid	1	0.1532	19.84
Boric acid	2	0.1547	22.96
Boric acid	4	0.1534	20.30
Sulfuric acid	2	0.0850	10.12
Sulfuric acid	4	0.0932	09.84

Table I. SIM analysis results, counts of OH, for the different anodized samples.

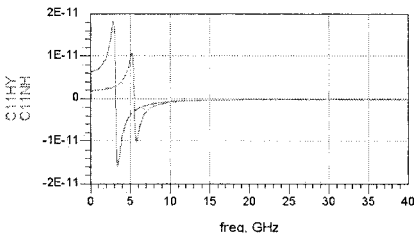

Figure 3. Measured Capacitance versus frequency before (right) and after hybridization (left), with a 5 nM complementary ssDNA conc, IDF 1.3/1.0.

Finger size and spacing (μm)		Im(-1/Y_{21})			
		C [pF]	Cshift [%]	fr [GHz]	frShift [GHz]
1	Non hybr.	2.25	18.22	5.55	0.51 (9.2%)
	Hybr.	2.66		5.04	
2	Non hybr.	1.9	5.8	6.1	0,34 (6.5%)
	Hybr.	2.01		5.76	

Table II. 2.5 nM complementary ssDNA Concentration: Measured Resonance Frequencies (fr) and capacitance (C) results for an interdigitated capacitor.

MICRO-SAMPLING FOR ELECTROCHEMICAL DETECTION – SENSING TRANSDERMALLY USING ARRAY TECHNOLOGIES

A.P. Gadre[1*], Y. N. Srivastava[1], N. Ganesan[1], J. Holeman[2], J. F. Currie[1,3], and M. Paranjape[1]

[1]*Department of Physics, Georgetown University, Washington D.C., 20057 USA*

[2]*Holeman Scientific, 105 Green Cove Road, Huntsville, Alabama, 35803 USA*

[3]*Walter Reed Army Institute of Research, Silver Spring, MD 20910-7500 USA*

**E-mail: gadre@physics.georgetown.edu, Phone/Fax: 202-687-4506/2087*

ABSTRACT

The MED-STAT (Micro-sampling for Electrochemical Detection – Sensing Transdermally using Array Technologies) biosensor is an array-based platform for non-intrusive transdermal sampling of interstitial fluids for general biomolecular detection using highly selective enzymatic detection chemistries. The components of the MED-STAT microsystem include a patch-like sensor chip containing an addressable array of electrochemical sensing elements specific to the biomolecule of interest, micro-connectors, and transmit/receive electronic nodes for remote sensing functionality (Fig. 1a). MED-STAT was developed primarily for real-time glucose and lactate monitoring, using glucose-oxidase (Gox) and lactate-oxidase (Lox) as the enzyme prototypes immobilized within a polymer matrix layer. Currently, MED-STAT is being used in animal models, where the measurement of both interstitial-glucose and -lactate biomolecules are being correlated with actual *in vivo* blood draws.

Keywords: SU8, Micro-Sampling, Glucose, Polypyrrole, Electrochemical Detection

INTRODUCTION

The MEDSTAT biosensor is based on electrochemical detection using a conducting polymer as the working electrode with an enzyme immobilized within its matrix [1]. For glucose detection, the normal reaction chemistry with the glucose-oxidase enzyme results in the formation of H_2O_2 – a marker often used in the detection mechanism. However, this electrochemical reaction has problems pertaining to the generation of false currents produced by interferents. Hence, in our design, the redox mediator potassium ferricyanide [$K_3Fe(CN)_6$], has been incorporated to lower the electrochemical operating potential thereby reducing false responses due to contaminants such as ascorbic and uric acid. Polypyrrole (PPy) being a stable, porous organic metal with high surface-to-volume ratio was found to be the most promising conducting polymer matrix to immobilize the Gox and $K_3Fe(CN)_6$. The same chemistry can also be used to incorporate lactate-oxidase (Lox) for detecting the lactate biomolecule. This paper presents techniques to selectively electrodeposit PPy on gold electrodes and to subsequently electrodeposit enzyme-specific sites in an array, all on the same sensor chip.

The MED-STAT sensor patch is a multilayer polymeric-metal laminate structure to be worn in contact with the skin [2,3] and was fabricated using SU-8, polymethylmethacrylate (PMMA), Teflon-AF, and conductive polypyrrole. The PMMA layer, which is in direct contact with the skin, has integrated micro heaters that are used to thermally ablate tiny pores through the dead skin layer (stratum corneum), allowing direct access to the interstitial fluids and its biomolecules (such as glucose) at the skin surface (Fig. 1b). Micro-connectors make electrical and mechanical connection to the sensing patch. The contacts are made with gold plated zero-insertion-force technology. Application of a 3V potential at the micro-heater contacts for 30 msec produces a 150°C heat pulse at the skin surface. At this temperature, micro-ablation of the stratum corneum occurs and the PMMA layer melts completely thereby allowing the interstitial fluid to come in contact with the electrodes (gold and the preferentially modified gold with PPy, $K_3Fe(CN)_6$, and either Gox or Lox).

EXPERIMENTAL

The MEDSTAT is fabricated using SU8 as the structural material [4,5] on a glass handle substrate with Teflon acting as a release layer between the glass and the final device [6]. Chromium/gold heaters were patterned onto the SU-8 followed by spin-coating a 5μm PMMA membrane layer. Another chromium/gold layer was deposited and patterned to form the electrodes of the electrochemical cell. The structural support for the device was provided by a thick layer of SU-8 with openings in the electrode and contact regions. Fig. 1c shows the selective co-deposition of PPy and Gox on one of the electrodes. Deposition of PPy was carried out potentiostatically using an electrolytic solution of PPy and KCl at 0.8V with respect to an Ag/AgCl reference for 2 minutes. Following this, 18 μl Gox/Lox and 48 μl $K_3Fe(CN)_6$ (in 10 ml phosphate buffer solution) were further added to the electrolyte solution for the subsequent incorporation of Gox/Lox and the redox mediator within the PPy matrix.

RESULTS AND DISCUSSION

During sensor preparation, the electrodeposition of PPy along with Gox/Lox and $K_3Fe(CN)_6$ on gold was made using a platinum counter electrode. With the MED-STAT sensor in operation, a 2-electrode system was used with the PPy-Gox/Lox-ferricyanide serving as the working electrode, while a bare gold electrode formed the counter electrode. To verify the characteristics of the Gox-based electrodeposited film, a cyclic voltammogram between +500mV and -200mV was obtained (Fig. 2) and showed the proper redox-couple for potassium ferricyanide, indicating the incorporation of $K_3Fe(CN)_6$ into the PPy film. Based on the observed redox couples, currents were then measured at a potential of 0.2V, well removed from the region where currents due to interferents are possible. The current response, shown in Fig. 3, is for the glucose sensor when exposed to several sample solutions containing varying concentrations of glucose, and the response is compared with a solution containing no glucose. Increasing amounts of glucose showed a corresponding increase in oxidation current. The values stabilized approximately 10-20 seconds after fresh aliquots of glucose were introduced into the phosphate buffer solution (PBS). A plot of current at 200mV was measured against varying concentrations of glucose and a linear response was obtained up to 10mM glucose concentrations (inset of Fig. 3).

The MED-STAT microsystem is currently being employed in animal models to correlate interstitial glucose and lactate concentrations with actual levels in the blood. The single sensor patch, able to detect both glucose and lactate by immobilizing Gox and Lox on specific PPy sensing elements, is placed on the shaved stomach of a rat. A laptop is used to trigger a sample acquisition and to acquire the electrochemical signal through a commercially-available potentiostat, while the electronic nodes, equipped with RF transmit and receive capability, allow telemetric data transmission. Fig. 4 presents some preliminary results of tracking two glucose arterial infusions (at t = 11:54 and 13:25) and the corresponding blood analysis of glucose and lactate concentrations. This is compared with the electrochemical signal from the transdermal MED-STAT sensors. The MED-STAT glucose sensor tracks the first peak but remains flat during and after the second infusion, while the MED-STAT lactate sensor tracks reasonably well throughout the experiment.

REFERENCES

[1] G. Guilbault, and A. Koch-Schmidt, *Biomedical Applications of Immobilized Enzymes and Proteins;* Plenum: New York; Volumes 1 and 2 (1977)

[2] A. Gadre, et al., *Transducers '03*, **1**, 806-809 (2003)

[3] A. Gadre, et al., *MicroTAS '03*, **1**, 199-202 (2003)

[4] D. Juncker, et al., *J. Micromech. Microeng.* **11**, 532-541 (2001)

[5] M. Heuschkel, et al., *Sensors and Actuators* **B-48**, 356-361 (1998)

[6] M. Cheng, et al., *J. Vac. Sci. Technol.*, **A22**(3), 837-841 (2004)

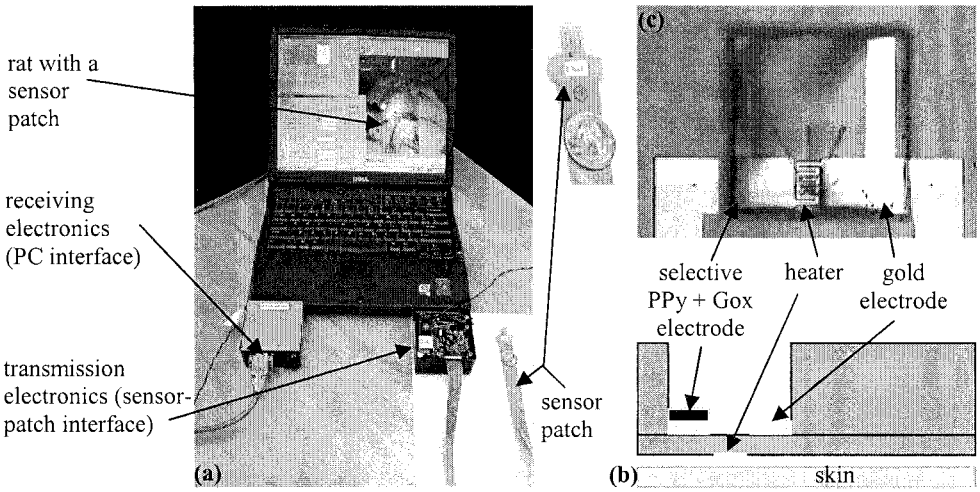

Fig. 1. (a) A rat having its glucose and lactate measured using the MED-STAT microsystem. (b) a single MED-STAT sensor cell with selective PPy-Gox-ferricyanide deposition. (c) the sensor patch cross-section.

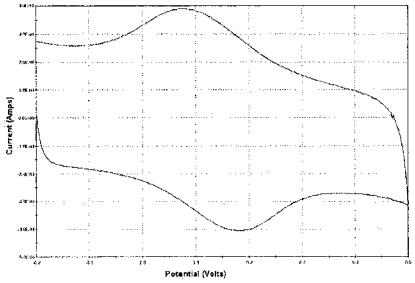

Fig 2. CV of $K_3Fe(CN)_6$ in PPy film

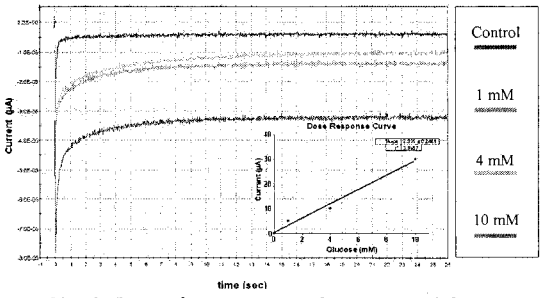

Fig. 3. I vs t dose response for varying [glucose]

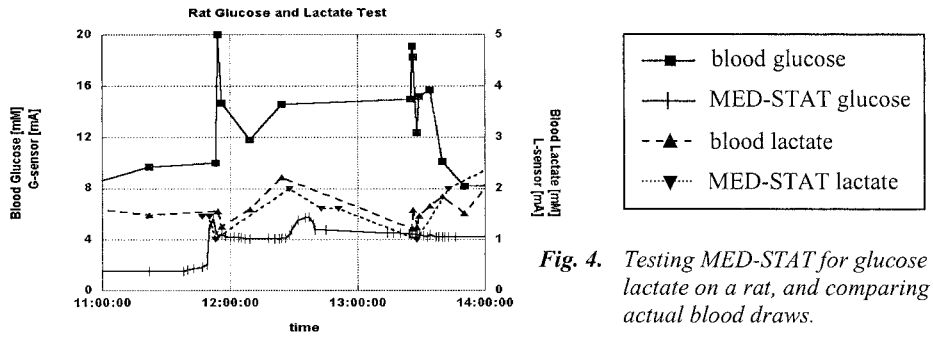

Fig. 4. Testing MED-STAT for glucose and lactate on a rat, and comparing with actual blood draws.

HIGH ASPECT RATIO PARYLENE ETCHING FOR MICROFLUIDICS AND BIOMEMS

Ellis Meng[1], Seiji Aoyagi[2], and Yu-Chong Tai[3]

[1]Department of Mechanical and Aeronautical Engineering, University of California, Davis, CA 95616-5294 USA

[2]Department of Systems Management Engineering, Kansai University, Japan

3Department of Electrical Engineering, Caltech Micromachining Laboratory, California Institute of Technology, Pasadena, CA 91126 USA

Abstract

A novel technique for producing high aspect ratio parylene structures via switching chemistry plasma etching is presented. Parylene C, or poly(monochloro-*p*-xylylene), has become an increasingly popular MEMS material for its excellent properties and biocompatibility. However, the inability to fabricate closely-spaced high aspect ratio (HAR) structures severely limits the use of parylene, particularly in microfluidic and bioMEMS applications. A novel method was developed to etch thin film parylene deposited on silicon substrates. Several masking materials were investigated to optimize this process. This low-temperature (<120 °C) technique is compatible with standard MEMS processes and can accommodate post-CMOS processing. Etching recipes have already been applied to bioMEMS devices and can greatly extend the range of possible structures for bioMEMS and microfluidics applications.

Keywords: parylene, DRIE, high aspect ratio, bioMEMS, microfluidics

1. Introduction

Robust polymer structures are frequently required in microfluidics and bioMEMS applications. These can be produced with polymer micromachining techniques such as embossing, soft lithography, and laser micromachining. However, to achieve compatibility with standard surface and bulk micromachining techniques and take advantage of batch fabrication, dry etching techniques must be used. Previously, plasma [1, 2] and reactive ion [3] etching of parylene in oxygen environments has been reported. These studies presented results on the etching of thin parylene films (only a few microns thick) without any attempt to develop processes to achieve HAR structures. To further complicate matters, Yeh [3] also observed that etch selectivity between parylene and standard photoresist masking materials is near unity due to their organic nature. New developments in HAR etching of silicon has inspired similar efforts in producing HAR polymer structures. Zahn [4] has reported achievable aspect ratios of 20:1 by employing Bosch-like switching chemistries in the etching of polymethylmethacrylate (PMMA). Based on these promising results, a similar technique has been created to etch parylene and photoresist.

2. Experimental

Two types of patterned test coupons were fabricated on silicon wafers and diced before etching: (1) 12μm AZ4620 photoresist masked by 0.5μm of Al and (2) 10μm of parylene masked by 14μm of AZ4620 photoresist. Sputtered amorphous silicon (0.5μm) and oxide (0.3μm) were also examined as possible masking materials. Etching was performed in a PlasmaTherm SLR-770B DRIE system using programmable switching chemistry etches. Etches are composed of repeated etching cycles, or loops. Each loop consists of three steps: (1) deposition of Teflon-like material from C_4F_8 plasma, (2) etch "A", and (3) etch "B." As in the Bosch process, the deposited fluoropolymer layer protects feature sidewalls from lateral etching. Etch "A" preferentially removes the fluoropolymer layer, exposing the parylene to the etching plasma. This step includes

SF_6 which was found to aid in the removal of the deposited fluoropolymer layer. Etch "B" uses both oxygen and argon and serves to remove any remaining fluoropolymer and etch parylene.

3. Results and Discussion

To provide a starting point from which to evaluate switching chemistry etches, photoresist samples were etched using just oxygen plasma in a Technics PEIIA plasma etcher. Samples exhibited significant lateral etching and severely tapered profiles (Figs. 1-2). Thus, in order to achieve desired geometries, precious device real estate and aspect ratio sacrifices are necessary. In contrast, results were vastly improved by using switching chemistries (Fig. 3). Undercutting is minimal and the sidewalls are nearly vertical. Recipes and results for the etched parylene samples are summarized in Table 1 and Figure 5. Figure 4 shows the etch depth versus time for both materials. The trends are linear and the materials have similar etching rates as expected. The etching at sharp corners and other masking materials (α-Si and sputtered oxide) were also examined (Figs. 6-7). Preliminary results indicate that an aspect ratio of at least 2:1 can be achieved for etching parylene. In addition, nearly vertical sidewall profiles are maintained. Traditional oxygen plasma etching techniques of parylene yield at best a ratio of 1:1 (Fig. 8). It has been determined that the removal rate of the fluoropolymer layer can contribute significantly to the total etching process time. Further investigation will target increasing the aspect ratio and reducing etching time by optimizing gas ratios, process pressures, cycle times, and plasma biasing schemes.

Developed etching recipes have already been used to produce working devices. 4 μm thick parylene neuro-cages for the study of live neural networks have been successfully demonstrated (Figs. 9-10) [5, 6]. Previously, neuro-wells were fabricated using complicated bulk micromachining techniques [7, 8]. The development of this etching technique along with other parylene processing tools has made it possible to realize a biocompatible polymer neuro-cage device. Neuro-cage structures require mechanical robustness for the support of neuron cultures and also demonstrate the possibility of machining thick-walled parylene channels for microfluidic applications.

Acknowledgements

This work was funded in part by the Engineering Research Centers Program of the NSF under Award Number EEC-9402726. We would like to thank Mr. Trevor Roper for assistance in fabrication and Mr. Tuan Hoang for help with proofreading.

References

[1] Wang, X.-Q., Q. Lin, and Y.-C. Tai, *MEMS '99*, 177-182 (1999).

[2] Nowlin, T.E. and D.F. Smith, Jr., *Journal of Applied Polymer Science*, **25**, 1619-1632 (1980).

[3] Yeh, J.T.C. and K.R. Grebe, *Journal of Vacuum Science & Technology A-Vacuum Surfaces & Films*, **1**(2), 604-608 (1983).

[4] Zahn, J.D., K.J. Gabriel, and G.K. Fedder, *MEMS 2002*, 137-140 (2002).

[5] He, Q., E. Meng, Y.-C. Tai, C.M. Rutherglen, J. Erickson, and J. Pine, *Transducers 2003*, 995-998 (2003).

[6] Meng, E., Y.-C. Tai, J. Erickson, and J. Pine, *Micro Total Analysis Systems 2003*, 1109-1112 (2003).

[7] Maher, M.P., J. Pine, J. Wright, and Y.C. Tai, *Journal of Neuroscience Methods*, **87**(1), 45-56 (1999).

[8] Wright, J.A., S.T. Lucic, Y.C. Tai, M.P. Maher, H. Dvorak, and J. Pine. *ASME Int. Mechanical Engineering Congress and Exposition*, 333-338, (1996).

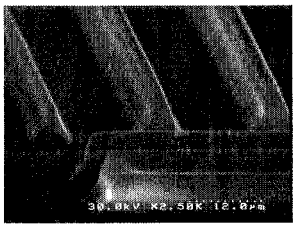

Figure 1. Isotropic AZ4620 etch results

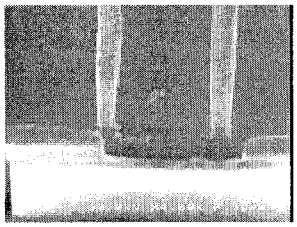

Figure 2. Anisotropic AZ4620 etch results

Recipe	Photoresist	Parylene 1	Parylene 2	Parylene 3
O_2 Flow Rate (sccm)	40	40	80	80
C_2F_6 Flow Rate (sccm)	70	35	35	35
SF_6 Flow Rate (sccm)	0	0	50	50
Ar Flow Rate (sccm)	40	40	40	40
Etch Coil Power (W)	825	825	825	825
Etch Platen Power (W)	20	20	9, 20	9, 20
Deposition Coil Power (W)	825	825	825	825
Deposition Platen Power (W)	1	1	1	1
Etch Time (sec)	9	9	3, 9	3, 10
Deposition Time (sec)	3	3	3	3
Average Etch Rate (µm/loop)	0.083	0.086	0.1	0.07
Average Etch Rate (µm/min)	0.32	0.33	0.4	0.25

Table 1. Summary of etching results

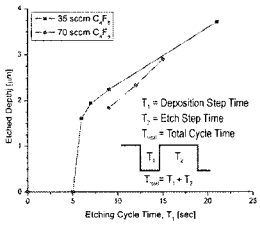

Figure 3. Etch time dependence of switched chemistry etching of AZ4620

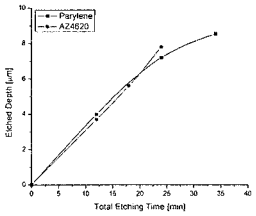

Figure 4. Etch trends for parylene and AZ4620

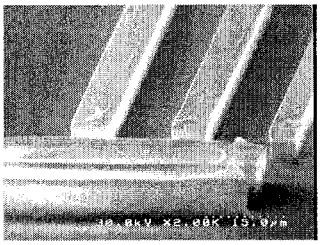

Figure 5. Typical parylene etching results

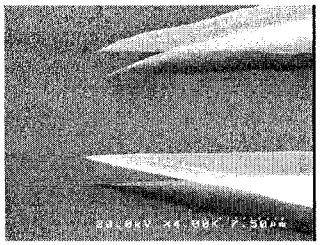

Figure 6. AZ4620 etching at sharp corners

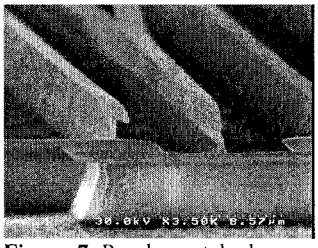

Figure 7. Parylene etched through α-Si mask

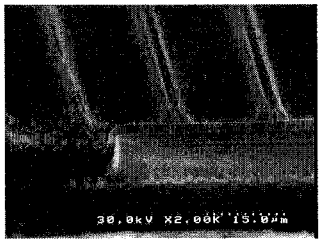

Figure 8. Isotropic etching results for parylene

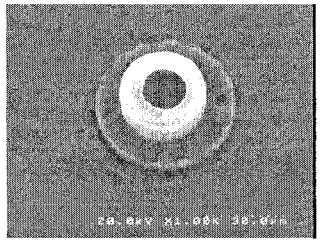

Figure 9. Single parylene neuro-cage structure

Figure 10. A 15 µm opening in neuro-cage for loading neurons

AIRFLOW MEMS ARRAY CONVEYOR WHICH PROVIDE CLEAN AND CONTACT-FREE MANIPULATIONS FOR MICROTAS

Yamato Fukuta[1], Yves-André Chapuis[1], Yoshio Mita[2] and Hiroyuki Fujita[1]
[1]Institute of Industrial Science, The University of Tokyo, 153-8505, 4-6-1, Komaba, Meguro-ku, Tokyo, Japan
[2]Dept. of Electrical Engineering, The University of Tokyo, 113-8656, 7-3-1, Hongo, Bunkyo-ku, Tokyo, Japan

Abstract

We have developed a pneumatic two-dimensional MEMS conveyor, which will be useful for micro chemical or biological analysis systems. By using airflow as a conveyance force, the conveyor can provide clean and contact-free manipulations in the microscopic world. We propose a workbench for the analysis system in which our MEMS device is useful as a conveyor. Moreover, our MEMS device demonstrated conveyance of small objects (3mm x 3mm x 0.1mm silicon chip, weighing approximately 2mg, and small plastic chip 5mm x 5mm x 1mm weighting approximately 38mg).

Keywords: airflow, MEMS array, conveyor, clean manipulation, contact-free manipulation

1. Introduction

In micro TAS fields, many excellent analysis systems have been developed, and their chemical or biological reactions need clean conditions for subtle measurements. Currently, these systems and plates with samples are handled by human hands or robots, which are much lager than miniaturized systems such as micro TAS. Moreover, unfortunately, the handling procedure may not be so clean.

This paper proposes to employ a micro conveyor in order to realize a small and clean analysis system. We have developed a MEMS array conveyor, which controls the directions of airflow in order to give a force to carry objects on it. This paper also reports pneumatic conveyances of small objects by airflow.

2. Proposal of a MEMS conveyor for micro TAS

We propose a workbench for analysis systems, schematically illustrated in Fig.1. Samples are first settled at the supply station, and then the workbench carries them to analyze, and sorts according to their analysis results. The conveyance devices of the bench should not influence the chemical or biological reactions that occur at the systems, therefore clean and contact-free conditions are required during the conveyance. Our pneumatic conveyor[1] matches these requirements, because we use airflow as conveyance force. In addition, thanks to the MEMS technology, the size of the conveyor is several tens or hundreds of millimeters square, so we can save space. Moreover, since the conveyor is an ensemble of many micro actuators that can be independently controlled, the conveyance resolution is fine enough to achieve complex motions of the object such as carrying, positioning, rotating, and sorting.

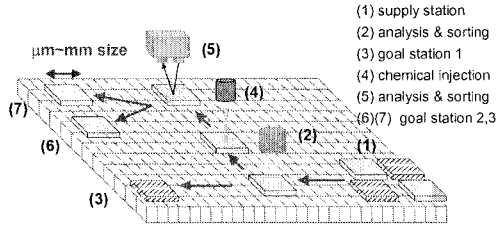

Figure 1. Schematic illustration of a workbench for analysis systems. Samples are first settled at the supply station, and then the workbench carries them to analyze, and sorts according to their analysis results.

3. Principle of the MEMS conveyor

Fig. 2a shows the conveyor we have realized, and Fig. 2b schematically illustrate the cross-sectional view of it. As shown in Fig. 2b, the conveyor consists of many micro actuators which work as normally closed air valves. When an actuator is driven to the right, the left side of it opens to eject air to the right and the object moves to the right (Fig. 2c), and vice versa.

Fig. 3 shows FEM calculation of the air jet flowing from the micro valve under the given air pressure of 20kPa. Fig. 3b shows that the open valve generates a tilted airflow and the lateral speed of the airflow is approximately 70 mm/s, which drives the object horizontally.

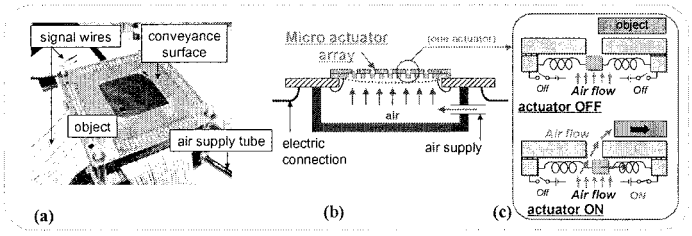

Figure 2. Two-dimensional pneumatic conveyor realized by MEMS array. (a) Picture (b) Schematics of the cross-sectional view (c) Mechanism of an air valve

4. Experimental results

Fig. 4 shows the fabrication process. The fabrication is conventional SOI (Silicon On Insulator) MEMS process, in which microstructures are fabricated in silicon layers, and an intermediate silicon dioxide layer is used as a sacrificial layer. Deep RIE (Reactive Ion Etching) of the top silicon layer gave the through hole for the air flow. The same etching from the backside defined micro actuators which work as valves. With the Vapor HF (Hydrofluoric Acid) technique[2], the sacrificial layer etching process was perfectly done; consequently almost all the actuators successfully operated as air valves. Finally the device was mounted to a printed circuit board and electrically connected by wire bonding, as shown in Fig.2.

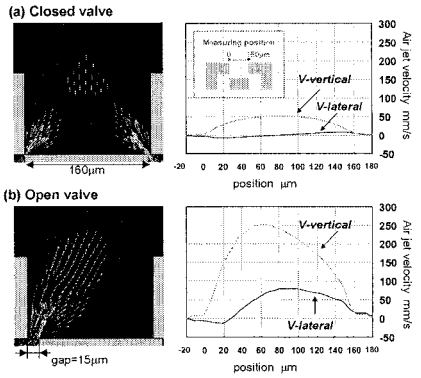

Figure 3. FEM calculation results at given air pressure 20kPa. The open valve generates a tilted airflow which is expected to move the object horizontally.

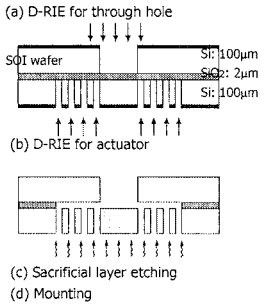

Figure 4. Fabrication process of the MEMS device . An SOI (100μm/2μm/100μm) was used. (a) Deep RIE for the through hole. (b) Deep RIE for actuators. (c) The Vapor HF technique for sacrificial layer etching. (d) Mounting on a circuit board and electrically connected by wire bonding.

Fig. 5a shows a SEM image of the front surface of the conveyor, and Fig. 5b shows the back surface. The actuator array that consists of 560 micro actuators is observed.

To our MEMS device, we have attached a video camera as a motion detector of objects, and a PC as a controller for actuators. In Fig.6, small silicon chip (3mm x 3mm x 0.1mm weighing approximately 2 mg) was successfully conveyed to the center part of the conveyance surface under an open-loop control. Small plastic chip (5mm x 5mm x 1mm weighing approximately 38 mg) was also conveyed (Fig. 7). In this case, a closed-loop control was used.

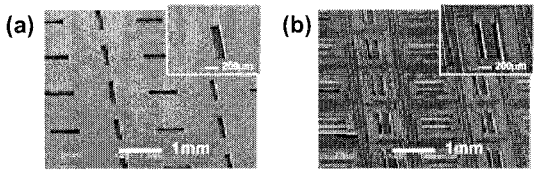

Figure 5. SEM images of the conveyor. (a) Front. (b) Back. An array of 560 actuators is observed.

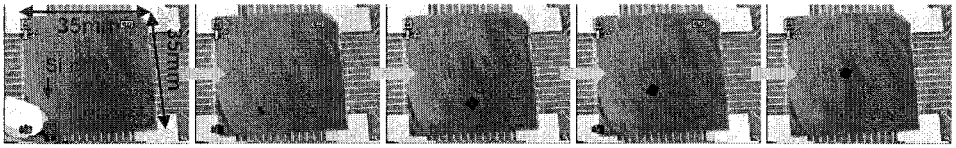

Figure 6. Conveyance of a small silicon chip (3 mm x 3 mm x 0.1 mm, 2 mg).

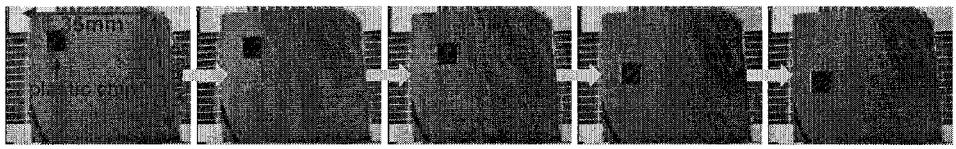

Figure 7. Conveyance of a small plastic chip 5 mm x 5 mm x 1 mm, 38 mg).

5. Conclusions

We have proposed the workbench for micro analysis systems and developed the MEMS conveyor suitable for it. The conveyor is small enough to handle millimeter size devices. Moreover, the conveyor uses airflow as conveyance force in order to provide clean and contact-free handling environments. Conveyances of small objects (3mm x 3mm x 0.1mm silicon chip, weighing approximately 2mg, and small plastic chip 5mm x 5mm x 1mm weighting approximately 38mg) were demonstrated. More complex motions such as positioning, rotation and sorting are under investigation.

Acknowledgements

The authors would like to thank Prof. Konishi and the member of Konishi lab. in Ritsumeikan University for valuable discussion. This research is partially supported by the 21st Century COE in Electrical Engineering and Electronics, The University of Tokyo.

References

[1] Y. Fukuta, M. Yanada, A. Ino, Y. Mita, Y. -A. Chapuis, S. Konishi and H. Fujita, *J. Robotics and Mechatronics,* **16**, **2**, 163-170 (2004).

[2] Y. Fukuta, H. Fujita and H. Toshiyoshi, *Jpn. J. Appl. Phys.,* **42**, **1**, No.6A, 3690-3694 (2003).

A POLYMER-BASED MICROROBOTIC WORKSTATION FOR SINGLE CELL MANIPULATION

Nikolas Chronis and Luke P. Lee
Berkeley Sensor and Actuator Center, Department of Bioengineering,
University of California, Berkeley, CA 94720, USA

Abstract

Bench-sized workstations employing optical tweezers, micropippetes and AFM tips are commonly used for manipulating single cells in solution. In this work, the development of a microfabricated, robotic workstation as an alternative tool for single cell manipulation is reported. The key element is the construction of novel polymer-based (SU-8) microactuators that are able to operate in physiological media at low voltages and small temperature increases.

Keyword: single cell manipulation, SU-8 actuators, microrobotic workstation

1. Introduction

Manipulation workstations for handling single cells are widely used in various fields, extending from cell mechanics to genetic and tissue engineering. While MEMS technology seems to be the most promising technology for developing sophisticated, miniaturized single cell manipulation systems, no significant progress has been reported up to now.

The main technological challenge that has to be addressed is the development of actuators that are able to convert electrical energy to the required for the manipulation mechanical work, via a pathway that is compatible with the living environment of the cell. Electrostatic, thermal, shape memory alloys and piezoelectric microactuators cannot operate in physiological media. Their operation is typically accompanied by electrolysis, high temperatures, restricted actuation control and poor repeatability. Electroactive polymer actuators based on ionic absorption and swelling [1] can operate in ionic media but they are limited to a single -out of plane- degree of freedom motion that constrains their use in most practical applications. Alternatively, isolating the actuator from the biological sample greatly restricts the extent of the possible manipulation setups [2].

In this work, we demonstrate the feasibility of manipulating single cells in solution employing an innovative polymer MEMS technology. Using SU-8 as a structural material, we developed a microfabricated single cell microrobotic workstation integrated with electrothermally activated in plane SU-8 actuators (figure 1). Key point in our design is the high thermal coefficient of expansion of SU-8 – almost 18 times higher than polysilicon- that enables the activation of the SU-8 microactuators in physiological media at low voltages and small temperature increases.

2. Design and Fabrication Process

The microfabricated workstation is capable of positioning single cells and exerting mechanical forces on them. It consists of a three degree of freedom microrobotic arm and a pushing beam with a sharp tip at its end that mechanically stimulates the target cell. The microrobotic structure extends into two long gripper arms that form a circular 10 μm in diameter cell holder. Two types of SU-8 actuators – chevron (I, II and IV) and hot-and-cold-arm (III) actuators - are employed in the current design to open and locate the gripper in 2D space (figure 2) as well as to move the pushing beam. Actuation is provided by thermal expansion of the SU-8 structures through resistive heating of a thin Cr/Au layer selectively attached at the bottom of the suspended polymer structure [3].

The device is fabricated using surface micromachining techniques in a three-mask process (figure 3). Starting with an oxidized silicon wafer, a layer of 2 μm undoped polysilicon is chemically vapor deposited followed by chemical-mechanical polishing (CMP). The first

photolithographic step transfers the 1 μm deep dimple areas to the polysilicon film. The metal heating resistors, connecting lines and pads of the actuators are subsequently defined by lift-off. Those metal elements consist of a 20 nm / 360 nm thick electron-beam evaporated Cr/Au film. A 20 μm thick SU-8-2015 layer is then spun on the wafer and photolithographically patterned to form the structural layer. The wafer is diced, the individual chips are hard baked on a hot plate at 120°C for 15 min and dry etch-released in xenon difluoride. The released structure is finally hard baked for a second time at 95°C for 15 min to enhance the crosslinking of the SU-8 film.

3. Experimental Results

In order to determine the mechanical performance of the device, DC voltages were applied at the chevron actuator and at the two hot-and-cold-arm actuators of the microrobotic arm and the corresponding displacement response in air and D-PBS (Dubelco's Modified Edge Medium) environments was measured under a light microscope (figure 4 & 5). DC driving voltages were used to facilitate the characterization procedure. The opening of the gripper requires less than 2 V for a maximum displacement of 8 μm in D-PBS, while the chevron actuator is driven by slightly higher voltages (2.6 V at 14.5 μm total displacement of the cell holder). To demonstrate the ability of the microrobotic workstation to operate with real biological samples, we pipetted a suspension of Hela cells on top of the device and successfully manipulated one of them (figure 6).

4. Conclusions

Bench-sized workstations utilizing micropipettes, optical tweezers or AFM tips for manipulating single cells are widely used in various fields, extending from cell mechanics to genetic and tissue engineering. In this work, the development of a microfabricated, robotic workstation was discussed as an alternative tool for single cell manipulation. The microrobotic platform, consisting of electrothermal polymer actuators, is capable of handling and mechanically stimulating single cells in physiological media. The key element in the actuator design is the use of a high coefficient of thermal expansion polymer (SU-8) as a structural material that provides the desired motion or force at low voltages (1.5-2.5 V) and temperature increases.

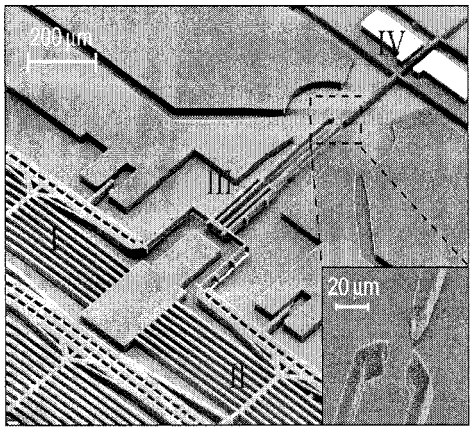

Figure 1. Scanning electron micrograph of the SU-8 based microrobotic workstation. A close view of the cell test area is shown at the inset.

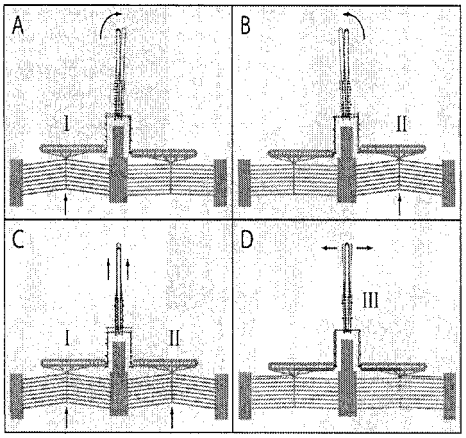

Figure 2. The two chevron actuators (I & II) move the gripper position in plane, while the set of the two hot-and-cold-arm actuators (III) open the cell holder.

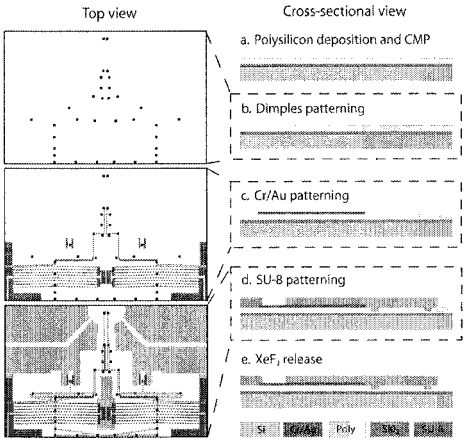

Figure 3. Schematic drawing of the fabrication process of the microrobotic workstation.

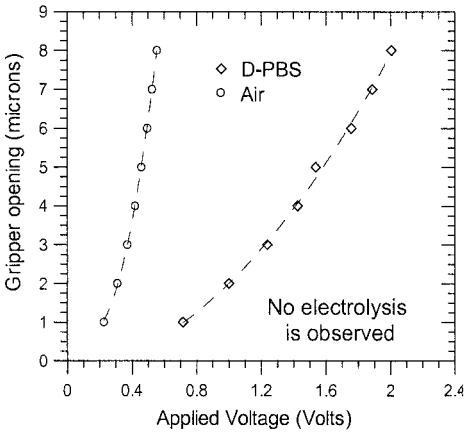

Figure 4. Gripper opening versus applied voltage. Displacement of 8 μm requires only 2 Volts in D-PBS.

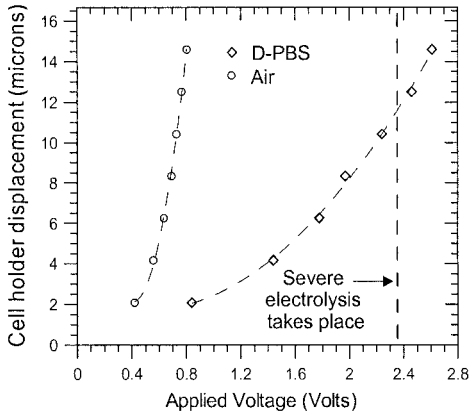

Figure 5. Cell holder displacement versus applied voltage. The cell holder displacement refers to the total displacement from its initial position (it moves in an arc).

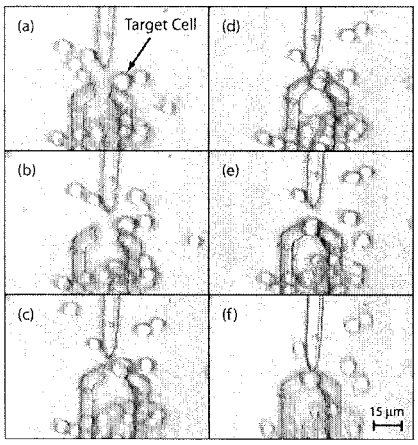

Figure 6. Manipulating a single HeLa cell in solution.

Acknowledgements

This work is fully supported by a DARPA grant under the BioFlips program.

References

[1] E.Jager, O. Ingavas and I. Lundstrom, *Science,* vol. **288**, pp. 2335-8 (June 2000).

[2] M.Okandan, P.Galambos,S.Mani and J.Jakubczak, *μ*TAS, Monterey, CA, pp. 305-306 (2001).

[3] N.Chronis and L.P. Lee, *μ*TAS, Nara, Japan, pp.754-7 (November 2002).

HIGH THROUGHPUT BONDING TECHNIQUE OF PYREX CHIP USING HOT PRESSING

Keisuke Morishima[1], Yoshitake Akiyama[2], Manabu Tokeshi[1] and Takehiko Kitamori[1,3]
[1]*Kanagawa Academy of Science and Technology, 3-2-1 Sakado, Takatsu-ku, Kawasaki 213-0012, Japan*
[2]*Institute of Microchemical Technology, 3-2-1 Sakado, Takatsu-ku, Kawasaki 213-0012, Japan*
[3]*Dept. of Applied Chemistry, The University of Tokyo, 7-3-1 Hongo, Bunkyo, Tokyo, Japan*

Abstract

Novel high throughput Pyrex-Pyrex bonding method for microfluidic devices using hot pressing was developed. This method has a remarkable feature that bonding can be done only within 10 minutes, though it took about more than half days in a conventional thermal bonding. Our bonding process time was totally reduced down to 1/60 compared with the conventional thermal bonding process, because high speed heating plates with a press machine in a vacuum furnace was developed.

Keywords: glass bonding, hot pressing, Pyrex

1. Introduction

Wafer bonding techniques become more and more important in packaging and assembly of micro fluidic devices. Many kinds of bonding methods have been reported. HF bonding [I],low temperature bonding [2] and silicon-to-silicon fusion bonding are well known and widely used. In this paper, studies on high throughput Pyrex-Pyrex bonding methods for microfluidic devices using hot pressing are described. This method has a remarkable feature that bonding can be done only within 10 minutes (additionally cooling time for less than one hour is needed), though it takes about more than half days in a conventional thermal bonding. Advantages of this method are high throughput, low residual stress and simplicity of the bonding process, which are expected for the packaging and assembly of micro TAS devices.

2. Experimental

Fig. 1 shows typical time-course of applied pressure and temperature in the novel hot pressing method. Total time needed for bonding was reduced down to 1/20 to 1/60 of that in the conventional thermal bonding process. The bond strength and deformation of the bonded glass plates were tested for different conditions of pressure and temperature, and so on. As the tests of deformation, measurement of wafer thickness and microscopic observation of the shape of microchannels before and after the bonding were carried out. So the damage could be minimized.

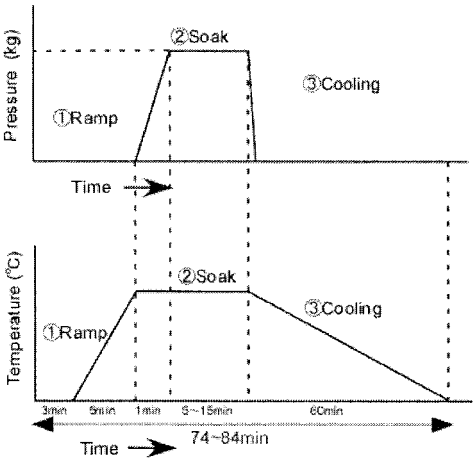

Figure 1. Thermal bonding process of a Pyrex chip.

3. Results and discussion

Fig. 2 shows the relationship of bonding strength and bonding temperature, and the

measurement results of thickness after bonding. The thickness of the interlayer depends strongly on the applied pressure during bonding. In order to estimate the necessary bonding conditions, bond strength between the substrate pair under different conditions of temperature, applied pressure and process time during bonding was measured. To evaluate the bonded interface, the bonded interlayer was observed by the microscope. Fig. 3 shows the microscopic image of cross sectional view of a Pyrex microchannel (before bonding and after bonding). Fig. 4 shows the photo images of bonded Pyrex substrates at various temperatures. Size of Pyrex substrates were 10 mm x 10 mm x 0.7 mm. Applied pressure was 0.5 kg/mm^2. It was confirmed that Pyrex-Pyrex bonding with sufficient bond strength and without deformation and the microchannel structures could be realized using the hot pressing method. The process time of heating and pressurized time was dramatically reduced down to only 10 min.

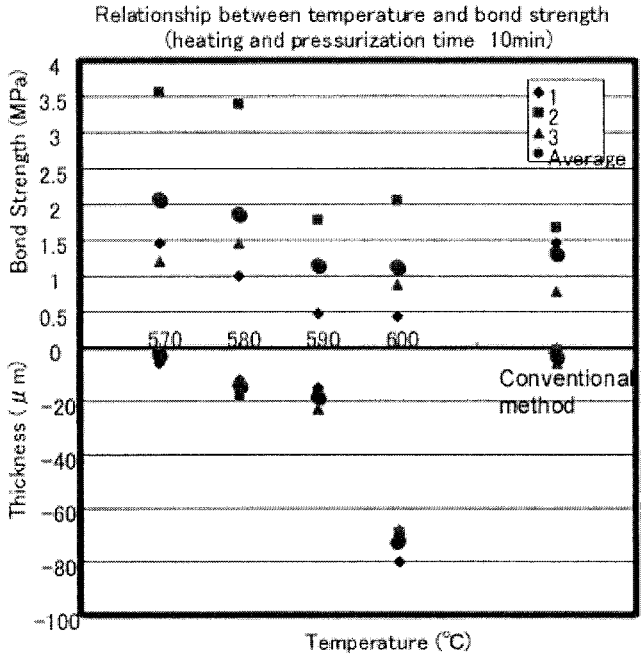

Figure 2. Relationship between temperature and bond strength (heating and pressurization time was 10min)

4. Conclusions

Novel high throughput Pyrex bonding method for microfluidic devices using hot pressing was developed. This method has a remarkable feature that bonding can be obtained only within 10 minutes. Our bonding process time was totally reduced down to 1/60 compared with the conventional thermal bonding process. Using this technique, high speed and high throughput glass chip fabrication is achieved. This method will be widely used for mass production of the Pyrex chip.

Acknowledgements

This work was supported by the Grant from the New Energy and Industrial Technology Development Organization, Japan.

References

[1] H. Nakanishi, T. Nishimoto, N. Nakamura, S.Nagamachi, A. Arai, Y. Iwata, and Y. Mito, Proc. of 10th IEEE Micro Electro Mechanical Systems Workshop, Japan, January 1997, pp.299-304.

[2] H. Nakanishi, T. Nishimoto, N. Nakamura, A. Yotsumoto, and S. Shoji, Proc. of 11th IEEE Micro Electro Mechanical Systems Workshop, Japan, January 1998, pp.609-614.

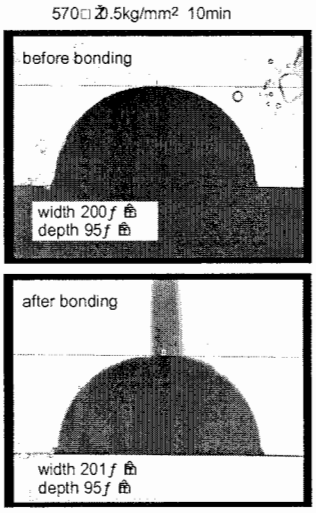

Figure 3. Microscopic image of cross sectional view of a Pyrex microchannel (before bonding and after bonding).

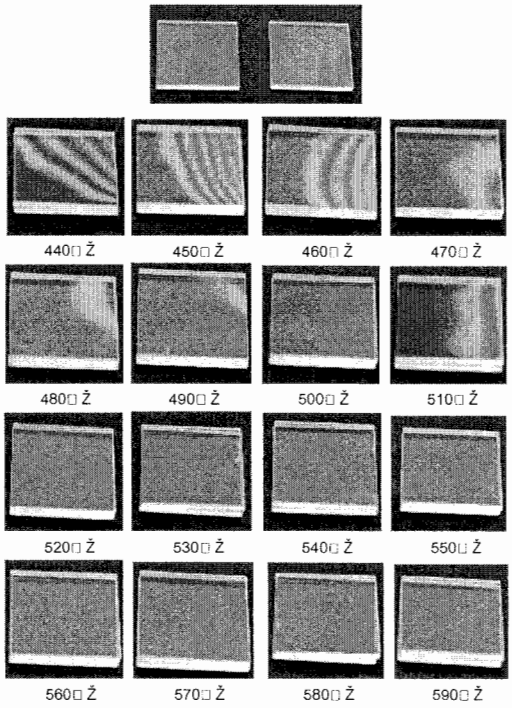

Figure 4. Photo image of bonded Pyrex substrates at various temperatures. Size of Pyrex was 10mm x 10mm x 0.7mm. Applied pressure: 0.5kg/mm^2.

A HIGH PRECISION SELF-ASSEMBLY TECHNIQUE FOR MULTILAYER POLYMER LAB-ON-A-CHIPS

Se Hwan Lee[1], Jungyoup Han[1], Dong Sung Kim[2], Tai Hun Kwon[2], Chul Jin Hwang[3], Young Moo Heo[3], and Chong H. Ahn[1]

[1]*MicroSystems and BioMEMS Lab, Dept. of Electrical and Computer Engineering and Computer Science, University of Cincinnati, Cincinnati, OH 45221-0030, USA*

[2]*Dept. of Mechanical Engineering, Pohang University of Science and Technology (POSTECH), Pohang, Kyungbuk 790-784, South Korea*

[3] *Korea Institute of Industrial Technology (KITECH), Inchon Metropolitan, 404-25, South Korea*

Abstract

This paper describes a highly precise self-assembly technique using self-alignment microstructures for polymer multilayer lab-on-a-chips. For the precision self-assembly, pairs of microfabricated pins and holes as the self-alignment microstructures, are designed and patterned on a Nickel master mold first. The alignment microstructures positioned around microfluidic channels are replicated on polymer substrates, and then the replicated polymer wafers are mechanically self-assembled and bonded using the alignment microcstructured pin-hole pairs. With this self-assembly technique, an alignment error of less than ~10 μm has been achieved between the patterns of each wafer after assembly, which can be considered as a fairly well acceptable alignment margin for most lab-on-a-chips. Using this self-assembly technique, a multilayered polymer micromixer has been designed, fabricated and tested as a demonstration vehicle. The micromixer shows an excellent mixing performance. The high precision self-assembly technique developed in this work will be a useful low-cost assembly technique for most polymer lab-on-a-chips.

Keywords: self-assembly, polymer, multilayer, lab-on-a-chip, micromixer

1. Introduction

Recently, the development of polymer-based microfluidic devices and lab-on-a-chips has been rapidly growing and its applications have also been expanded to a variety of polymer lab-on-a-chips [1]. Injection molding technique [2] has been considered as one of the most popular manufacturing techniques for the fabrication of polymer lab-on-a-chips. However, though the injection molding technique can produce polymer microstructures in low cost, many extra efforts are required for the assembly and bonding of the replicated polymer wafers when a device contains microchannels and microstructures to be aligned precisely through the wafer level.

Furthermore, the complexity of microfluidic systems in lab-on-a-chips has been rapidly increased as a variety of functions have been integrated into a single microfluidic device or system [3]. Thus, multilayer polymer lab-on-a-chips are desirable, but the assembly of the multilayer with a high precision of alignment has been considered as one of the most difficult tasks. New techniques compatible with the existing fabrication processes to build highly complex 3D interconnected microstructures are demanded to build multilayer micro fluidic devices.

2. Design and Fabrication

Several approaches to realize the 3D multilayered polymer structures have been reported [3-5]. In [4], a 3D microchannel in PDMS elastomer was fabricated; microfluidic structures and alignment keys were patterned at PDMS layers and manually aligned under a low-power stereo microscope. From the device, an excellent alignment accuracy of ~15 μm was achieved,

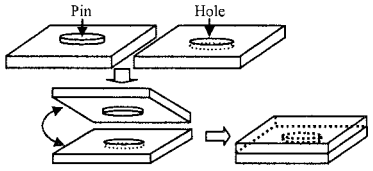

Figure 1. Schematic diagram of self-assembly technique using alignment pin-hole pair.

but tedious and time consuming manual alignment process makes it difficult to apply this method for mass production. Furthermore, as the numbers of stacking substrates increase, it is getting more difficult to achieve the required alignment precision using this alignment technique.

Fig. 1 describes the schematic diagrams of the proposed technique in this paper. Well matched and aligned pin-hole pairs positioned in each layer are mechanically assembled and then thermally bonded. In this manner, we can expand this technique to the multilayered devices. Fig. 2 shows a schematic diagram of this technique for multilayered polymer lab-on-a-chips. Furthermore, any replica-based polymer microfabrication processes can adopt our new self-assembly technique, which allows this assembly technique to be a generic self-assembly technique for most polymer lab-on-a-chips. Fig. 3 is a summary of the fabrication processes such as mold fabrication, polymer replication, mechanically self-assembly, and thermal fusion bonding.

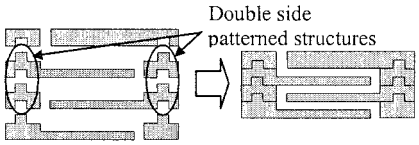

Figure 2. Schematic diagram for the assembly of multilayer chips.

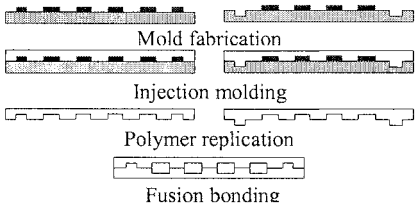

Figure 3. Summary of fabrication processes.

3. Experimental Results

As a testing vehicle, a 3D micromixer (whose detailed chaotic mixing mechanism and full characteristics will be published elsewhere [6]) is designed and fabricated to show the feasibility of this technique. Fig. 4 shows microscanned images of the self-assembly pairs of pin and hole on Ni master molds and polymer microstructures replicated on COC (Cyclic Olefin Copolymer) wafers. Fig. 5a is a microphotograph of a pin-hole pair assembled by fusion bonding. At the same time, a micromixer was formed by connection of F-shape patterns on each layer.

Microphotographs of aligned patterns of each wafer from fabricated device and 10 μm size reference pattern from a Cr mask were taken with the same magnification. Achieved alignment error was evaluated by comparison of the images; actual alignment error was calculated regarding numbers of pixels counted by conventional graphic software. Finally, an alignment error less than ~10 μm has been achieved using the self-assembly method in this study, as indicated in Fig. 5b.

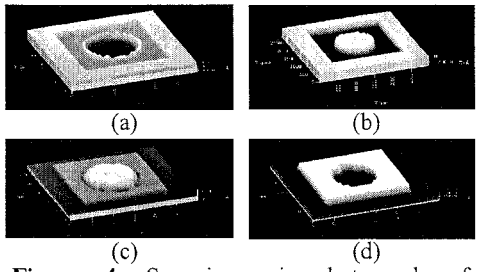

Figure 4. Scanning microphotograph of microfabricated pin-hole pairs: (a) and (b) from mold; (c) and (d) from replicated plastics.

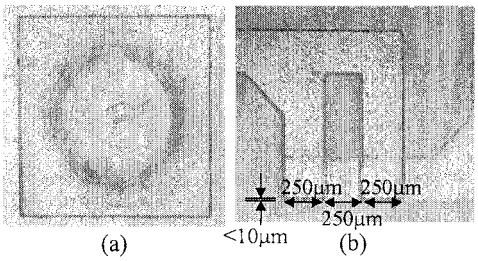

Figure 5. Microphotograph of (a) assembled pin-hole pair and (b) aligned patterns of fabricated device.

In order to evaluate the alignment of microchannels, the fabricated micromixer has been tested by flowing two fluids such as NaOH and phenolphthalein though the channels driven by syringe pumps. The mixing performance can be evaluated by the color change of phenolphthalein after mixing from colorless to red if pH becomes greater than 8. Only the completely mixed stream turns red, thereby enabling us to measure the mixing performance.

Fig. 6 shows a mixing result of the 3D micromixer fabricated using the proposed self-assembly method. The mixing was performed under condition of $Re \approx 4.39$ when a flow rate was maintained as $Q = 50$ μl/min. In the vicinity of T-junction entrance, one can find initial interface between two streams. After passing four F-shape mixing units (poison 5 indicated in Fig. 6) almost complete mixing seems to be achieved in this case. The successful mixing achieved in this multilayered micromixer confirmed the excellent alignment has been achieved at the device, but otherwise the mixng performance can not be achieved.

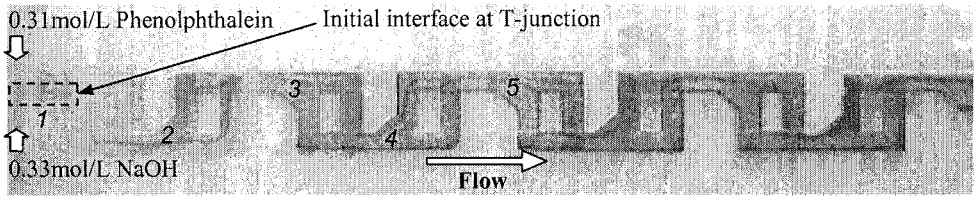

Figure 6. Mixing experimental result at $Re \approx 4.39$ with a flow rate of $Q = 50$μl/min. Only the interface between two streams shows the red color.

4. Conclusions

In this work, a new high precision self-assembly technique for multilayer polymer lab-on-a-chips has been successfully developed and characterized by realizing a 3D micromixer with an alignment error less than ~10 μm for multilayered polymer lab-on-a-chips. This technique will alleviate the difficulty of assembly of multilayered polymer lab-on-a-chips, providing a mechanically self-assembly technique for the mass product of polymer multilayer chips in low cost. Furthermore, this self-assembly technique can be immediately adopted for most replica-based polymer lab-on-a-chips or other polymer devices which require an assembly of multilayers.

5. Acknowledgement

This research was partially supported by a research grant under contract U472-030 from the KITECH, South Korea.

References

[1] H. Becker, and L.E. Locascio, *Talanta*, **56**, 267-287 (2002).
[2] H. Becker, and C. Gärtner, *Electrophoresis*, **21**, 12-26 (2000).
[3] B.-H. Jo, L.M. Van Lerberghe, K.M. Motsegood, and D.J. Beebe, *J. Microelectromech.*, **9**, 76–81 (2000).
[4] J.R. Anderson, D.T. Chiu, R.J. Jackman, O. Cherniavskaya, J.C. McDonald, H. Wu, S.H. Whitesides, and G.M. Whitesides, *Anal.Chem.*, **72**, 3158-3164 (2000).
[5] F.J. Blanco, M. Agirregabiria, J. Garcia, J. Berganzo, M. Tijero, M.T. Arroyo, J.M. Ruano, I. Aramburu, and K. Mayora, *J. Microelectromech*, **14**, 1047-1056 (2004).
[6] D.S. Kim, S.H. Lee, T.H. Kwon, and C.H. Ahn, (unpublished)

A FUNCTIONALLY DYNAMIC MICROCHAMBER WITH RAPID MIXING AND REACTION CAPABILITIES FOR MAGNETIC BEAD-BASED IMMUNOASSAY

Jaephil Do and Chong H. Ahn
Microsystems and BioMEMS Laboratory
Dept. Of Electrical & Computer Engineering and Computer Science
University of Cincinnati, Cincinnati, OH 45221, USA

Abstract

In this paper, a new functionally dynamic microchamber (FDM) has been designed, fabricated, and characterized for magnetic bead-based immunoassay, which incorporates sampling, rapid mixing, and reaction capability in the same microchamber using magnetic beads and permalloy-embedded elastomer membrane. Permalloy micropatterns for holding magnetic beads and bars for actuating membrane are embedded into a thin Polydimethylsiloxane (PDMS) elastomer membrane, which is intergrated over a microchamber. The microfabricated FDM was vibrated using an external electromagnet to improve magnetic bead-based sampling, mixing, and reaction capabilities. Magnetic beads were successfully separated over the FDM and the colorimetric analysis shows its rapid mixing and reaction capability at a membrane vibration rate of 20 Hz.

Keywords: Magnetic beads, permalloy, immunoassay, elastomer membrane

1. Introduction

Recently, there has been a large demand for the development of a magnetic bead-based bioseparator or manipulator for biochemical detection, cancer diagnostics, or drug delivery system. So, numerous magnetic bead-based separators or filters have been investigated for the improvement of its functional separation capabilities [1].

Although several on-chip magnetic bead separators have been developed, there are still several challenging issues to be addressed such as the control of the generated heat from on-chip electromagnet or the difficulty of large force generation in micro scale. Furthermore, in the system point of view, the performance of biosensors in the magnetic bead-based immunoassay is limited by the rate at which a soluble analyte solution is transported to a complementary receptor immobilized on the magnetic bead surface. Thus, bulk sample mixing or stirring in the reaction chamber is usually required for improving the reaction kinetics of analyte [2].

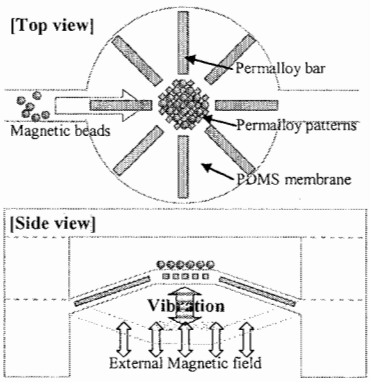

Figure 1. Schematic illustration of a functionally dynamic microchamber.

To meet the desires and to address the problems described, we have proposed and developed a functionally dynamic microchamber (FDM) as shown in Fig. 1. Magnetic actuator has been embedded in a elastomer membrane and then integrated over a microchamber for the realization of the FDM with magnetic beads sampling capability. In order to enhance its mixing and reaction capability in the microchamber, an external electromagnet has been used for vabrating the membrane, which is isolated from the joule heat produced by the exciting electromagnet.

2. Design and Simulation

As shown in Fig. 1, the FDM consists of a set of 8 permalloy bars (200 μm x 1000 μm x 10 μm) for vibrating the membrane and an array of 21 square permalloy patterns (50 μm x 50 μm x 10 μm)

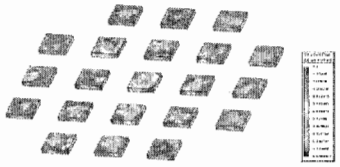

Figure 2. FEM simulation results of the field distribution around permalloy arrays.

for separating and holding the magnetic micro beads, which are embedded in a PDMS membrane. The magnetically functional membrane is positioned over a microchamber with a diameter of 3 mm and a height of 60 μm. As a magnetic field generator, an external electromagnet in a dimension of 0.5 inches x 0.5 inches is located under the FDM for vibrating the movable membrane.

If the square permalloy arrays are exposed in a magnetic field, then they will produce a high magnetic field gradient around them. So, magnetic beads in a aqueous solution are easily trapped and aligned around the arrays with high magnetic gradient in even a low magnetic field strength. However, if magnetic field is increased enough to move the permalloy bars around the square magnetic arrays, then the elastomer membrane starts to vibration, improving the kinetics of biomelecular reaction around the magnetic beads. The FEM simulation results for the magnetic field distribution on the permalloy arrays are presented in Fig. 2. As shown in the figure, magnetic flux is concentrated on the edges of the permalloy arrays, which ensures that a strong magnetic field gradient will be achieved around the arrays. So, magnetic beads will be easily separated over the arrays.

3. Fabrication

The device is fabricated with Polydimethylsiloxane (PDMS) material which is getting attraction for its low cost simple fabrication, and flexibility [3]. The entire fabrication process is summarized in Fig. 3. First, a PDMS membrane of 30 μm is spin-coated on a silicon substrate, and then CYTOP^{TM} (from Asahi Glass Company) spin-coating is followed. The CYTOP layer of 2 μm serves as interlayer to prevent cracks, which are usually produced from the metallization of seed layer over the PDMS. And also the CYTOP layer is adopted to protect the PDMS membrane from the contamination by organic solvent, which is needed for the following photolithography [3]. The permalloy patterns are electroplated up to height of 10 μm. After CYTOP removal with O_2 plasma etching, PDMS is spin-coated to embed the permalloy patterns inside of the PDMS membrane. In the final step, a molded microchamber layer is bonded over the permalloy embedded PDMS membrane peeled from silicon substrate. A fabricated FDM is shown in Fig. 4a.

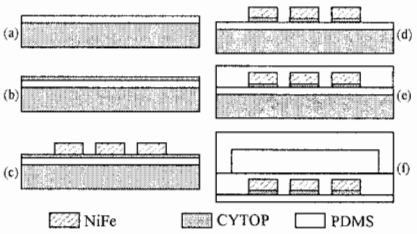

Figure 3. Fabrication process of FDM device: (a) PDMS spin coating; (b) CYTOP spin coating; (c) permalloy plating; (d) CYTOP removal; (e) PDMS spin coating; and (f) microchamber bonding

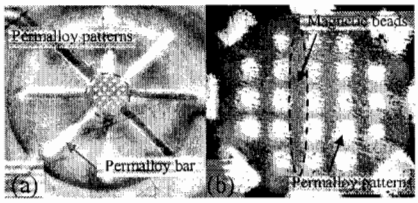

Figure 4. Microphotogarph of (a) the fabricated device and (b) the magnetic beads captured on permalloy patterns.

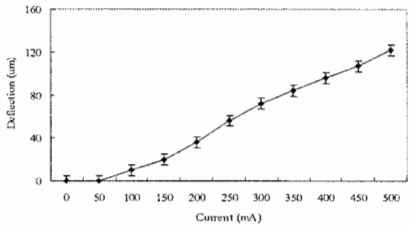

Figure 5. The plot of the maximum deflection of membrane under various magnetic fields.

4. Results and Discussion

The sampling capability of a FDM was tested using the magnetic beads in diameter of 4.1 μm (CM-40-10 from Spherotech Inc.). The current supplied to the electromagnet was varied from 5 mA to 500 mA until magnetic bead separation was observed. The magnetic bead separation was distinguished through the microscope clearly at the current above 300 mA, and the separation result is presented in Fig. 4b, which indicates the magnetic beads aligned between permalloy arrays. In order to evaluate the vibration of membrane, the measurements of maximum deflections of the PDMS membrane are performed by measuring the focal length of the center of membrane through an optical microscope while varying magnetic field intensity. The measurement results are plotted in Fig. 5. In order to evaluate the mixing or reaction kinetics in the chamber, Phenolphthalein (0.03 mol/L) and NaOH (0.033 mol/L) are injected into the reaction chamber, and then the membrane is vibrated using the current pulse of 300 mA at 20 Hz. The mixing and reaction kinetics can be indirectly evaluated by colorimetric analysis with the Phenolphthalein and NaOH applied. The status of the mixing and reaction in the chamber is proportional to the density of purple color in the chamber. So, the variation of the color density as the function of reaction time can be measured and the gray scale of the inside reaction chamber indicates mixing extent. The mixing and reaction has been fully achieved in 200 ms without vibration, but achieved in 70 ms with vibration in 20 Hz, as shown in Fig. 6.

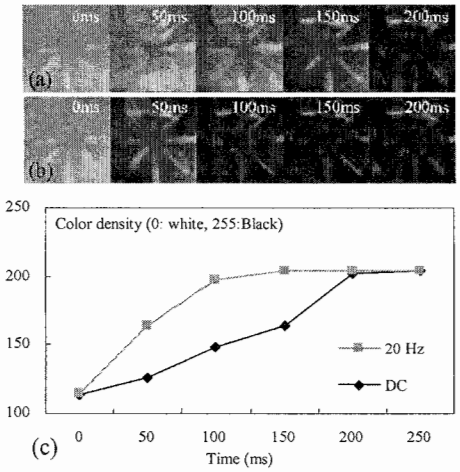

Figure 6. Micrograph of the colorimetric analysis result of reaction chamber: (a) without membrane vibration; (b) with membrane vibration at 20 Hz; and (c) graphs from relative measurements.

5. Conclusions

A new functionally dynamic microchamber has been designed, fabricated and successfully tested in this work, showing magnetic bead-based sampling, rapid mixing, and reaction capability concurrently. The realized functional magnetic membrane, which consists of a magnetic bead separator and a magnetic microactuator, showed its potential as a sampler and rapid mixer/reactor for biochemical liquids. The full reaction capability for a specific immunoassay is now under investigation. The functional dynamic microchmaber realized in this work will have numerous applications for such as protein lab-on-a-chips or high-throughput drug screening, which require rapid on-chip mixing and reaction kinetics.

References

[1] J.-W. Choi, et al., *Biomed. Microdevices*, **3**, 191-200 (2001)

[2] Vijayendran, Ravi A.; Motsegood, Kathleen M.; Beebe, David J.; Leckb, Deborah E., *Langmuir*, **19**, 1824-1828 (2003)

[3] M. Ishizuka, et al., Proceedings of the 12th International Conference on Solid State Sensors, Actuators and Microsystems, Boston, USA, Jun 8-23, 2003, pp. 999-1002

PARTICLE DISCRIMINATION WITH AN IMPROVED PROJECTION CYTOMETER

J.H. Nieuwenhuis[1], P. Svasek[2], P.M. Sarro[3], M.J. Vellekoop[1]
[1]Institute of Sensor and Actuator Systems, Vienna University of Technology, Austria
e-mail: nieuwenhuis@tuwien.ac.at
[2]Ludwig Boltzmann Institute of Biomedical Microtechnology, Vienna, Austria
[3]Laboratory of ECTM – DIMES, Delft University of Technology, Delft, The Netherlands

Abstract

In this paper an integrated cytometer is presented based on optical projection. A Sheath flow focuses the particles closely over an integrated optical sensor capable of counting, sizing and measuring the shape of particles. Measurements demonstrate good repeatability and the ability to discriminate between particles based on their optical properties.

Keywords: Cytometer, Particle, Optical Sensor, Sheath Flow

1. Introduction

Cytometers are instruments for particle analysis based on the optical properties of the particle. In literature different integrated sheath-flow chambers have been presented (some early ones can be found in [1,2]), but the optical sensors are often located off-chip. In this paper an integrated projection cytometer is presented that has a built-in optical sensor. A sheath-flow focuses the particles closely over the integrated optical sensor. As a result of the small projection distance (near-field properties of the optical field) and the small dimensions of the sensor (1 x 50 μm^2) the measurement signals contain information about particle size, shape and transparency. In previous work we introduced this concept [3]. In this paper we present an improved cytometer that has much better optical qualities, obtained by applying a different fabrication technology [4].

2. Operation Principle

The device (see figure 1) consists of a transparent flow-channel that has an elongated photodiode (1 x 50 μm^2) integrated in the bottom of this channel, aligned perpendicular to the direction of flow. By means of a non-coaxial sheath flow the sample liquid containing the particles is focused over the optical sensor. The chip is illuminated from the top and when a particle now passes over the sensor its optical properties are registered. The small projection distance realised by the sheath-flow minimises the optical distortion of the particle projection, without the need for any additional optical components.

The shape of the sensor signal, caused by a passing particle, depends on the optical properties of the particle. Since the sensor only consists of a single photodiode the optical properties of the particle are integrated along a line perpendicular to the direction of flow. Although it is in principle possible to replace this single photodiode with an array of smaller photodiodes [5] this may often not be required. With the single photodiode sensor different types of particles will causes different pulse shapes, which can be used as a signature to discriminate between the different them.

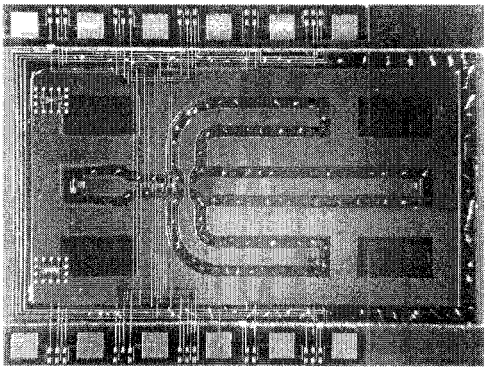

Figure 1. The cytometer chip (1.5 x 2 cm^2)

3. Device Fabrication

The device consists of a two-layer glass-silicon sandwich. The silicon wafer contains the photodiode sensor that was made in a bipolar IC-process. As a post-processing step through-holes were etched that form the liquid inlets. On a glass wafer 70 μm deep channels were defined using a two-step SU8 process [4], which was also used to bond the two wafers together.

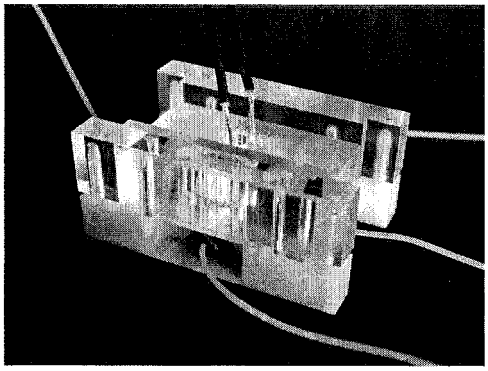

Figure 2, Measurement in progress with the cytometer chip in a custom-made holder

In the previous version of the device wet etching of the glass-wafer formed the channels. In those devices anodic bonding was used to bond the to wafers together. The current fabrication scheme has two major advantages. Firstly, the channel formed by the SU8 processing has a square cross-section with a smooth surface, which causes far less optical distortion to the optical projections than the rounded channels formed by the wet etching. Secondly, the adhesive bonding process is more compliant to the surface roughness, caused by the IC-processing, of the silicon wafer than the anodic bonding process. This eliminates the need for additional post-processing steps and makes the processing more robust.

4. Experimental

The cytometer chip was placed in a custom holder (see figure 2) that has O-rings to seal the liquid connections; spring pins established the electric contacts. Syringe pumps were used to pump the sample liquid and the sheath liquid through the device. A modulated green laser-diode was used as a light source. The photocurrent generated by the sensor was filtered and demodulated using a lock-in amplifier and was recorded with a digital memory oscilloscope.

Two different types of particles were used:

1. Plain polystyrene micro-spheres, radius 12 μm (Duke Scientific)
2. Silver coated polystyrene micro-spheres, radius 10 μm (Microparticles GmbH)

The particles were suspended in a glycerol water mixture to prevent sedimentation in the tubing or in the holder.

In figure 3 the sensor response is plotted for 10 consecutive pulses (on top of each other) for both kinds of particles. This figure illustrates the good repeatability of not only the signal peaks, but of the complete signal shape as well. For both kinds of particles a series of 50 pulses was recorded and the statistical data are shown in table 1.

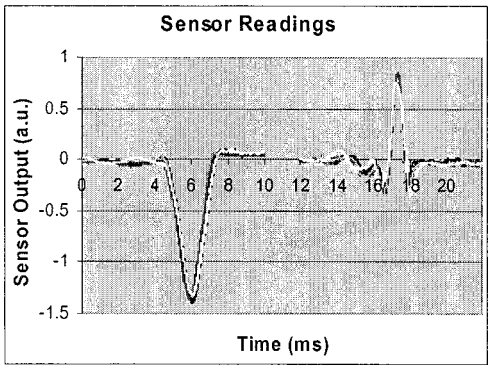

Figure 3. Ten measurements printed on top of each other for 10 μm radius silver coated particles (left) and 12 μm radius plain particles (right) demonstrate good repeatability

5. Discussion

Both kinds of particles could be clearly detected, but caused very different signal shapes. The silver coated particles caused a simple pulse with a relative steep drop in the measurement signal. The signal shape for the transparent plain micro-spheres was more interesting. First the photocurrent dropped somewhat and then it went up above the baseline followed by a second small dip. This pulse shape can be explained by a lens-effect (see figure 4), caused by the higher refractive index of polystyrene (1.58) compared to the glycerol water mixture (approx. 1.4).

Table 1. Statistical data on 50 pulses

Type of particle	mean	σ
Silver coated	-1.41	0.06
Plain	+0.82	0.07

6. Conclusions

In this paper an integrated projection cytometer was presented, based on optical projection. The good optical properties of the cytometer allow recording optical details of the particles analysed. Silver-coated and plain particles of comparable size could clearly be distinguished based on their optical properties. A very good repeatability of the measurements was achieved by application of a sheath flow that focuses the particles over the optical sensor.

Acknowledgements

The authors would like to thank Charles de Boer of the DIMES Technology Centre of the Delft University of Technology for fabrication of the silicon part of the devices.

References

[1] R. Miyake, H. Ohki, I. Yamazaki, R. Yabe, A Development of Micro Sheath Flow Chamber, proc. of MEMS '91, 1991, p265-270

[2] D. Sobek, A.M. Young, M.L. Gray, S.D. Senturia, "A microfabricated flow chamber for optical measurement in fluids", proc. MEMS '93, 1993, pp 219-24

[3] J.H. Nieuwenhuis, J. Bastemeijer, P.M. Sarro, M.J. Vellekoop, "First Measurement Results with an Integrated Projection Cytometer", proc. of μTAS 2003, October 5-9, Squaw Valley, California, USA, 2003, pp. 1219-1222

[4] P. Svasek, E. Svasek, B. Lendl, M.J. Vellekoop, "SU-8-Based Fluidic Devices", proc. of Eurosensors XVII, September 21-24, 2003, Guimarães, Portugal, 2003, pp. 283-286

[5] J.H. Nieuwenhuis, J. Bastemeijer, A. Bossche, M.J. Vellekoop, "Near-Field Optical Particle-Shape Sensors for Application in an Integrated Cytometer", IEEE Sensors Journal, Vol. 3, No. 5, October 2003, pp. 646-651, ISSN 1530-437X

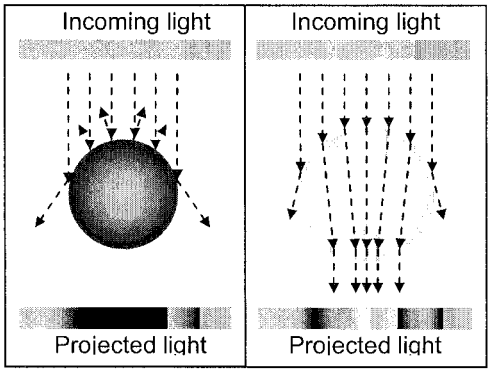

Figure 4. The different pulse shapes obtained with the silver coated particle (left) and the plain, transparent particle (right) can be explained by their optical properties

ATMOSPHERIC PRESSURE PHOTOIONIZATION WITH A MICROCHIP HEATED NEBULIZER

Tiina Kauppila,[1] Pekka Östman,[1] Seppo Marttila,[2] Raimo Ketola,[1] Tapio Kotiaho,[3] Sami Franssila,[2] Risto Kostiainen[1, 4]

[1]*Viikki Drug Discovery Technology Center, Faculty of Pharmacy, University of Helsinki, P.O. Box 56, FIN-00014 University of Helsinki, Finland*

[2]*Microelectronics Centre, Helsinki University of Technology, P.O. Box 3500, FIN-02015 Helsinki University of Technology, Finland*

[3]*Department of Chemistry, P.O. Box 55, FIN-00014, University of Helsinki, Finland*

[4]*Faculty of Pharmacy, Division of Pharmaceutical Chemistry, University of Helsinki, P.O. Box 56, FIN-00014 University of Helsinki, Finland*

Abstract

This study presents a microfabricated APPI device, which utilizes a microchip heated nebulizer designed for miniaturized APCI. The silicon-glass microchip nebulizer consists of microchannels for sample solution and nebulizing gas as well as a heater system. The corona discharge needle used in APCI is replaced by a krypton discharge lamp, so that the ionization is initiated by photons. The performance of the new micro-APPI is demonstrated and compared to conventional APPI source. The results show, that the micro-APPI offers a new sensitive and stable method that could be used to combine microfluidic separation systems or nano-LC with mass spectrometer.

Keywords: atmospheric pressure photoionization, ionization mechanism, microchip, heated nebulizer, microfabrication

1. Introduction

Atmospheric pressure photoionization (APPI) is a novel ionization technique for mass spectrometry (MS), developed by Bruins and co-workers [1]. In APPI, the ionization process is initiated by photons emitted by a krypton discharge lamp. The analytes are ionized either directly by photoionization or indirectly via gas-phase reactions with other species [2]. The ionization in APPI is a selective process, where solvent and gas molecules are typically left unionized, which results in low background and enhanced sensitivity for the analytes. Also, using APPI the efficient ionization of non-polar analytes can be accomplished, unlike with electrospray (ESI) or atmospheric pressure chemical ionization (APCI).

3. Experimental

The analytes (acridine, 2-naphthol, 1,4-naphthoquinone and 2-naphthoic acid) were diluted in a mixture of methanol (90%) and the dopant (10%) (toluene or anisole). The sample solution was delivered by using a syringe pump at flow rates of 0.05-5 µl/min. The sample was nebulized by using a microchip heated nebulizer, originally developed to be used with micro-APCI and a corona discharge needle [3]. Anisotropic wet etching was used to fabricate the flow channels, inlet and nozzle on a silicon wafer. An integrated heater of aluminium was sputtered on a glass wafer. The two wafers were jointed by anodic bonding creating a two dimensional version of an APCI-source with sample channel in the middle and gas channels symmetrically on both sides. A krypton discharge lamp, identical to the lamp used by Bruins et al., was used as the source for photons [Figures 1 and 2]. The obtained spectra were compared to spectra obtained with conventional APPI (Machine Shop, University of Groningen, The Netherlands). The mass spectrometer used was a PE Sciex API 300 triple quadrupole mass spectrometer (Sciex, Concord, Canada).

4. Results and discussion

The positions of the nebulizer chip and the krypton discharge lamp were found to be very critical for efficient ionization and were optimized by monitoring the intensity of the toluene radical cation signal. The best signal was obtained when the lamp was positioned as close to the MS orifice as possible with the nebulizer microchip in its immediate proximity. A repeller was needed to create a high electric field to guide the ions inside the MS orifice. This was achieved by attaching a metal plate in front of the teflon holder, which was connected to the high voltage cables (Figure 1).

The performances of the micro-APPI and the conventional APPI were compared in the analysis of four compounds. Dopant, which was introduced as part of the solvent, was found necessary for efficient ionization in all measurements. High proton affinity (PA) acridine formed a protonated molecule (MH^+) with both ionization methods, whereas in low PA 2-naphthol spectrum an intensive radical cation ($M^{+\cdot}$) was observed (Figure 3a). The efficient ionization of 2-naphthol indicates, that non-polar analytes, that have low PAs can also be analyzed by using the micro-APPI. 1,4-Naphthoquinone was analyzed in negative ion mode, where it showed the negative molecular ion ($M^{-\cdot}$) as well as oxidation products. However, the proportion of the oxidation products was much higher with the conventional APPI than with the micro-APPI, which indicates, that either the oxidation reactions are catalyzed by the metal surfaces inside the conventional APPI ion source or the formation of oxidation products is dependent on the residence time, which may be shorter with the micro-APPI (Figures 3c and 3d). 2-Naphthoic acid showed a deprotonated molecule ($[M-H]^-$) with both ion sources.

Flow rates of 0.05-5 µl/min were found suitable for the micro-APPI source, but the signal was most intense when the flow rate was >1 µl/min. The lower signal below 1 µl/min was thought to be due to insufficient amount of the dopant (10% of solvent), as it has been shown earlier that the amount of dopant is a crucial factor in APPI and may limit the sensitivity [4]. The stability of the micro-APPI proved excellent, as the signal stayed the same throughout a five-hour experiment.

5. Conclusions

The use of a microfabricated APPI as an ion source for mass spectrometry was demonstrated for the first time. Ionization of analytes was successfully achieved in positive and negative ion modes. The results showed that the main ionization reactions observed with the conventional APPI source - proton transfer and charge exchange in positive ion mode and proton transfer and electron capture/charge exchange in negative ion mode – also take place with the micro-APPI. The excellent stability of the source, the low flow rates, and the capability of analyzing polar and non-polar analytes from very small sample volumes, will make the connection of the micro-APPI to low flow rate separation systems a considerable alternative. Because of the low flow rates, the solvent consumption is lower than with conventional APPI. The manufacturing of the nebulizer chip is inexpensive and the combination with the krypton discharge lamp can be easily realized. In future, sensitivity of the system will probably improve significantly once the place of the repeller plate as well as its distance from the MS curtain plate have been optimized. Also, a smaller lamp design will admit the nebulizer chip to be placed closer to the MS orifice, which may also increase the ionization efficiency. A special inlet for the dopant on the nebulizer microchip will make the source more practical as it will allow the use of solvents that are not soluble to typical dopants.

Acknowledgements

This study was financially supported by the Finnish Cultural Foundation, Acta Chemica Scandinavica, National Technology Agency of Finland, Orion Pharma, Juvantia Pharma Ltd., United Laboratories Ltd. and Danisco.

References

[1] D. B. Robb, T. R. Covey and A. P. Bruins *Anal. Chem.* **72**, 3653-3659 (2000).

[2] T. J. Kauppila, T. Kuuranne, E. C. Meurer, M. N. Eberlin, T. Kotiaho, R. Kostiainen, R. *Anal. Chem.* **74**, 5470-5479 (2002).

[3] S. Franssila, P. Östman, S. Marttila, T. Kotiaho, R. Kostiainen, Proceedings of the 7th Annual European Conference on Micro and Nanoscale Technologies for the Biosciences, Montreux, Switzerland, November 25-27, 2003.

[4] T. J. Kauppila, R. Kostiainen, A. P. Bruins, Effect of the Solvent Flow Rate on the Ionization Efficiency in Atmospheric Pressure Photoionization Mass Spectrometry, *submitted* 2004.

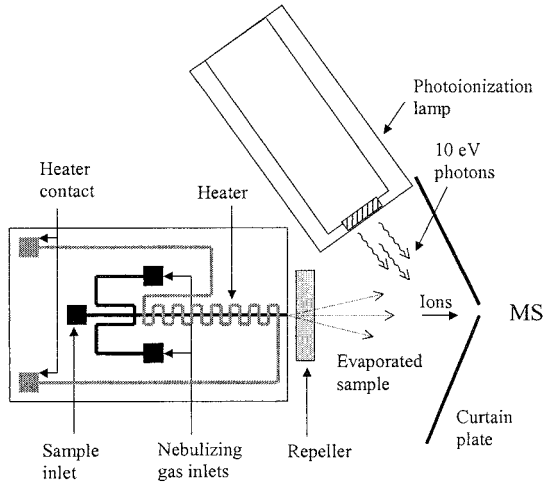

Figure 1. A Schematic diagram of the microfabricated APPI.

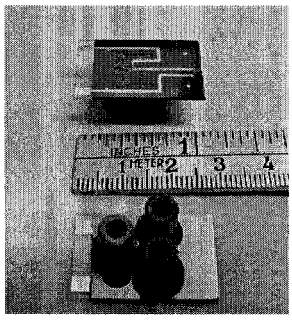

Figure 2. A photograph of the heated nebulizer microchip.

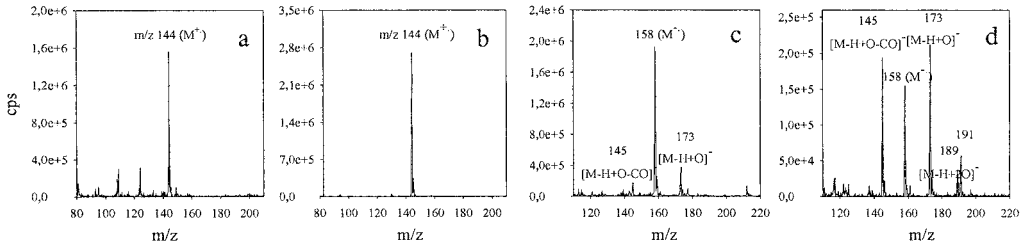

Figure 3. a) 2-Naphthol in acetonitrile using micro-APPI, b) 2-naphthol in acetonitrile using conventional APPI, c) 1,4-naphthoquinone in acetonitrile using micro-APPI, d) 1,4-naphthoquinone in acetonitrile using conventional APPI.

NANO-POROUS SENSOR ELECTRODE ARRAYS FABRICATED BY NANOSPHERE LITHOGRAPHY

Peter Schomann, Julian Gonska, Dieter Martin, Wilfried Nisch, Martin Stelzle
Naturwissenschaftliches und Medizinisches Institut an der Universität Tübingen NMI, Markwiesenstrasse 55, D-72770 Reutlingen, Germany, phone: +49 (0)7121 5153075, fax: +49 (0)7121 5153062, e-mail: stelzle@nmi.de

Keywords: nano-porous electrode arrays, redox cycling, electrochemical sensor, nanosphere lithography

1. Introduction

Interdigitated electrode arrays (IDE) have been used previously for sensitive electrochemical detection of redox-active molecules and for impedimetric sensing of receptor-ligand interaction [1-5]. So-called redox-cycling may be employed to enhance sensitivity of electrochemical sensors by employing narrowly spaced electrodes with their potentials adjusted to oxidizing and reducing potentials, respectively. This enables multiple electron transfers from each redox molecule diffusing between anodes and cathodes. The efficiency of this amplification mechanism increases with decreasing electrode spacing [5], [1]. So far, however, high fabrication costs for nanoscale electrode arrays have prevented widespread application of this amplification scheme for biosensors. We demonstrate a novel technology to fabricate sensor arrays with an electrode spacing below 100 nm, yet without the need for e-beam or uv-lithography [6].

2. Experimental

The sensor technology is based on metal / insulator / metal (MIM) systems and nanosphere lithography to create pores as nano-reaction cavities (Figure 1). The distance between electrodes is defined by the thickness of the intermediate insulator layer.
Sub-micrometer sized latex spheres are dispersed on a metal / insulator system and serve as shadow masks during the deposition of a second metal layer. After metal deposition, the spheres are removed and holes remain in the second electrode, while at the same time lateral connectivity is maintained. Subsequently, the second electrode is used as an etching mask in a PECVD process to generate nanopores reaching through the insulator layer to the bottom electrode (Fig.3).

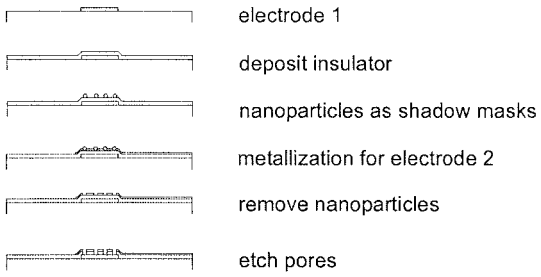

Figure 1. Schematic depiction of nanosphere lithography process employed to generate metal / insulator / metal systems with nanopores for use in electrochemical sensor applications.

3. Results and discussion

Sensor chips with eight MIM sensor positions and a centrally positioned reference electrode were fabricated (Figure 2). The inset in Figure 2 depicts the layer structure of the sensor positions, which consist of circular electrodes with a diameter between 100 µm and 800 µm, separated by the porous insulating layer, and which are connected to the periphery by means of connecting leads.

Figure 3 shows a SEM micrograph of an electrode structure with pores generated by nanosphere lithography. In this particular example, latex beads with 200 nm diameter were used as shadow masks during sputter deposition of a gold layer. Due to the small distance between sample and sputter target, however, the gold layer extends even under the latex beads resulting in a pore diameter of only about 80 nm as is revealed by the SEM image. This down-scaling behavior is highly desirable, since larger particles are more easily removed after the sputter coating process. In addition, larger particle size allows for sufficient layer thickness of the second electrode which obviously may not exceed the particle radius.

Cyclic voltammetry was performed on both the top and the bottom electrodes using $Ru(NH_3)_6$ as redox couple in an aqueous $NaClO_4$ solution in order to test for electron transfer capability of both electrodes.

The top electrode shows the wave form expected from one dimensional diffusion above macroscopic electrodes (Fig.4a).

The nanoporous bottom electrode in contrast yields a sigmoid current wave as is typical for spherical diffusion of redox molecules above nano-electrodes (Fig.4b). Firstly, this demonstrates that both top and bottom electrodes are electrically insulated from each other in this case. In other samples, however, short circuits between top and bottom electrodes were observed, indicating that pinhole density within the insulating layer is a critical issue. Secondly, this shows, that the nanopores indeed act as an array of nano-electrodes connected in parallel.

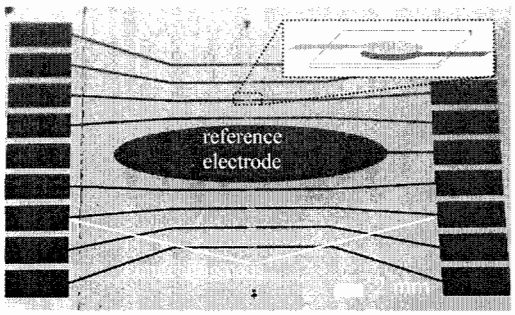

Figure 2. sensor chip with eight sensor positions (diameter: 100 µm), a large reference electrode in the center of the chip and connecting pads in the periphery.

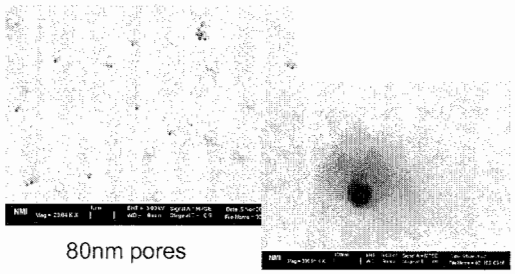

Figure 3. SEM micrograph of porous gold layer generated by sputter deposition of gold onto 200nm nanospheres. Some of the nanopspheres are still visible on the surface, while 80nm pores appear in areas where nanospheres have been removed.

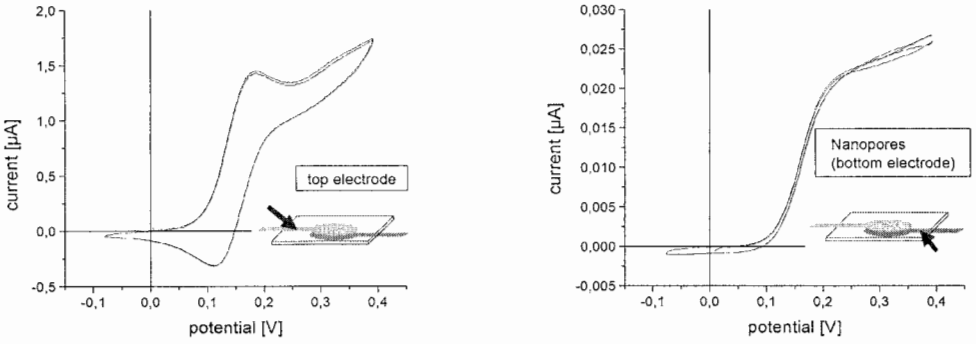

Figure 4. Cyclic voltammogram of top electrode (a) and bottom electrode (b) of electrode array using $Ru(NH_3)_6$ as redox couple in $NaClO_4$ vs. Ag/AgCl (scan rate 0.01V/s). The sigmoid behavior of the redox current in case of the bottom electrode reflects the spherical diffusion profile above the nano-pores.

4. Conclusions

Nano-porous MIM systems have been successfully prepared by sputter deposition and nanosphere lithography. Thus, an electrode – electrode spacing on the order of 100 nm is achieved without the need for high resolution lithographic techniques. As expected, nanopores act as nano-electrodes when probed by cyclic voltammetry. At this point, clearly, a more homogeneous distribution and at the same time higher density of pores would be desirable in order to obtain high current density. To this end, in future research we will investigate self-assembly methods for sub-micron particles. Also, pinhole density of the insulating layer is a critical issue.
This technology opens the door to sensor electrodes which by application of redox cycling detection schemes are expected to combine high sensitivity with low fabrication costs.

References

[1] Niwa, O., M. Morita, and H. Tabei, Highly Sensitive and Selective Voltammetric Detection of Dopamine with Vertically Separated Interdigitated Array Electrodes. Electroanalysis, 1991. 3: p. 163-168.
[2] Van Gerwen, P., et al., Nanoscaled interdigitated electrode arrays for biochemical sensors. Sensors and Actuators B, 1998. 49: p. 73-80.
[3] Kurita, R., et al., Fabrication and electrochemical properties of an interdigitated array electrode in a microfabricated wall-jet cell. Sens. Actuators, B, 2000. B71(1-2): p. 82-89.
[4] Morita, M., O. Niwa, and T. Horiuchi, Interdigitated array microelectrodes as electrochemical sensors. Electrochim. Acta, 1997. 42(20-22): p. 3177-3183.
[5] Aoki, K., Theory of the steady-state current of a redox couple at interdigitated array electrodes of which pairs are insulated electrically by steps. J.Electroanal.Chem., 1989. 270(1-2): p. 35-41.
[6] Stelzle, M. and W. Nisch, Nanoelektrodenarrays für Biosensoren, in WO 02/084272 A2. 2001, NMI: PCT.

AN ADVANCED MICROCHIP WITH ORGANIC LIGHT EMITTING DIODE INTEGRATED ON A MICROCHANNEL FOR APPLICATIONS IN THE FLUORESCENCE DETECTION

Ju-Hwan Kim[1,3], Kyeong-Sik Shin[1], Kyeong-Kap Paek[2], Young-Hwan Kim[1], Young-Min Kim[1], Yong-Kook Kim[1], Tae-Song Kim[1], Ji-Yoon Kang[1], Eun-Gyeong Yang[1], Sang-Sig Kim[3] and Byeong-Kwon Ju[1]

[1]Microsystem Research Center, Korea Institute of Science and Technology, P.O. Box 131, Cheongryang, Seoul, 130-650, Korea

[2]Dept. of Electronic Engineering, Daejin University, Seondan-dong, Pocheon, Gyeonggi-do, 487-711, Korea

[3]Dept. of Electrical Engineering, Korea University, Anam-dong, Sungbuk-ku, Seoul, 136-701, Korea

Abstract

Until now, many papers have been dedicated to the microchip applications, where all the optical elements should be integrated directly onto the on-chip device. But previous devices with fluorescence spectroscopy had a few problems (selectively realizable wavelength, low intensity and inappropriate structure) in the integration of light source [1-2]. The organic light emitting diode (OLED) is proposed as a novel source in the microchip because it has ideal merits (various wavelengths, thin-film structure and overall emitting) for the integration.

Keywords: microchip, fluorescence spectroscopy, Organic LED, finger-type photodiode

1. Introduction

Laser-induced fluorescence (LIF) detection is a popular detection technique for bioanalytical detection applications because of its selectivity and high sensitivity. Miniaturization of fluorescence detection components into microsystems would provide the advantages of portability and low manufacturing cost [3]. But previous portable devices have a few hardship in the on-chip integration of excitation-source [1-2]. An organic LED with thin-film structure can be fabricated by simple deposition process. So, it is proposed as an excitation-source in the integrated microchip.

In this paper, we fabricate finger-type PIN photodiodes and an advanced microchip with OLED as an excitation-source. Fabricated microchip is characterized and used to detect the fluorescence signal.

2. Experimental

A schematic of the microchip integrated with all optical components (an Organic green LED, a PDMS microfluidic device and a PIN photodiode with interference filter) is shown in Fig. 1. The distinct components are bonded each other by O_2 plasma treatment.

The PIN photodiode is designed in the finger-type. 4 kΩ·cm Si wafer (n-type, 100) is used as the substrate to form PIN structure. The arsenic and BF_2 are implanted as the dopant. The insulator layer (SiO_2, 350 nm) is deposited on the doped wafer. Fig. 2. shows the image of photodiodes. Photodiodes have a 70 μm × 210 μm active area. The interference filter is directly deposited on the photodiode by plasma enhanced chemical vapor deposition (PECVD). It consists of 32 layers (SiO_2, TiO_2) with 2.5 μm thickness.

The microfluidic device is fabricated according to general molding method [4]. The molder is patterned with PMER negative photoresist. The fabricated channel has 12 μm deep × 50 μm wide dimension. It is integrated with the sensor-part by O_2 plasma.

The organic green LED is fabricated on an indium-tin oxide (ITO) glass. The transparent ITO is used as the anode. We use CuPc (Copper Phthalocyanine) as the HIL (Hole Injection Layer), *α*-

NPD ([N, N`-di(naphthalene-1-yl)-N,N`-diphenyl-benzidine]) as the HTL (Hole Transport Layer), Alq_3 ([tris(8-hydroxyquinolinato)aluminum]) as the EML (Emitting Layer) or ETL (Electron Transport Layer), and Li:Al as the cathode. All layers are deposited on the substrates by thermal evaporator in vacuum chamber with base pressure of $< 10^{-6}$ Torr. After the deposition process, it is encapsulated with inorganic composite material (MS-31) to increase the life-time in the atmosphere. Figure 2 shows the images of integrated chip and prototype device with OLED.

The fluorescence signal is detected without a source filter. A standard probe station is used for the electrical contact. Rhodamine 6G is prepared as a fluorescent dye for the RNA assay. The microchannel is coated with a BSA (bovine serum albumin) solution to prevent the sticking problem. The solutions are transferred by vacuum pressure.

3. Results and discussion

The finger-type diode extends the depletion region and reduces the internal resistance about 32% than rectangular-type. The photodiodes have 100 pA leakage current and 8720 sensitivity (I_{Light}/I_{Dark}) at -1V bias. To prevent the excitation light from saturating the detector, a thin film, high-pass, interference filter is deposited over the detector surface. The filter has 95.5% reflection at 532 nm and 95% transmission at 580 nm.

Figure 3 shows the intensity spectrum of OLED with peak at 530 nm. The fabricated device has a high intensity of 22000 cd/cm^2 at 8V. The OLED can have variable wavelength according to organic materials. Also, the application of thin-film light source increases the excitation efficiency and simplifies the integration process extremely.

The OLED generates the background signal of 142 □ and the deviation of 1.98 nA in the detection current. Fluorescence signals have linear responses and a high slope of 0.256 nA/μM. according to the concentration. Figure 4 shows the photodiode responses from 100 μM to 0.1 μM. The limit of detection (LOD, S/N = 2) in this prototype is 0.01 μM.

4. Conclusion

In this paper, the advanced microchip based on OLED is presented as the most efficient integration method. The prototype device of this application has a superior sensitivity of 0.01 μM-LOD in the fluorescence detection. The OLED has peculiar merits such as simple deposition process, realizable various wavelengths and overall emitting. Also, the overall light-emitting source can materialize the multi-channel microchip without second source. Consequently, our approach will be able to give new ideas to fabricate the microchip.

References

[1] V. Namasivayam, R. Lin, B. Johnson, S. Brahmasandra, Z. Razzacki, D.T Burke and M.A Burns, *Journal of Micromechanics and Microengineering*, **14**, 81-90 (2004).

[2] T. Kamei, B.M. Paegel, J.R. Scherer, A.M. Skelley, R.A. Street and R.A. Mathiesl, *Analytical Chemistry*, **75**, 5300-5305 (2003).

[3] J.A. Chediak, Z. Luo, J. Seo, N. Cheung, L.P. Lee and T.D. Sands, *Sens. Act. A*, **111**, 1-7 (2004).

[4] J. Chen,W. Wang, J. Fang and K. Varahramyan, *Journal of Micromechanics and Microengineering*, **14**, 675-680 (2004).

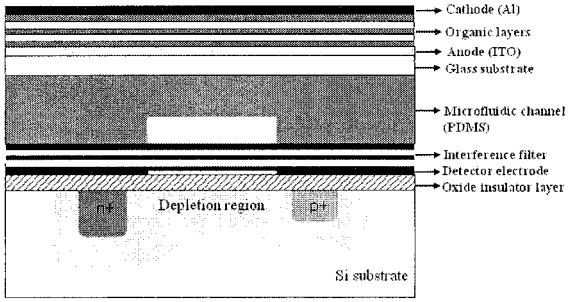

Figure 1. Cross-section view showing the integration structure of lab-on-a-chip (LOC).

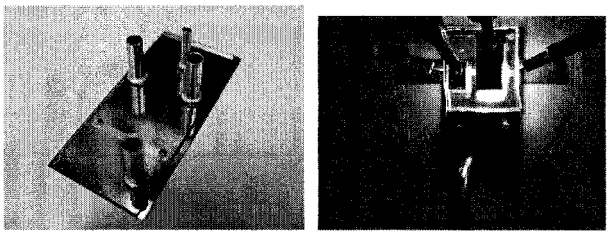

(a) (b)

Figure 2. Images of fabricated devices; (a) the integrated chip, (b) the prototype device with organic LE

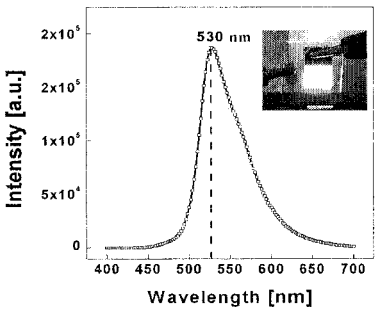

Figure 3. Intensity spectrum of organic green LED fabricated on a glass substrate.

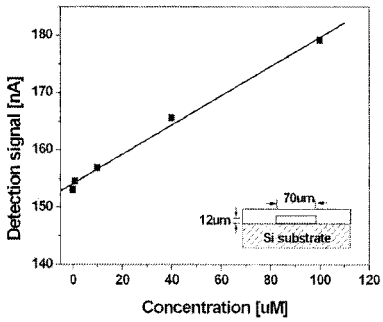

Figure 4. Fluorescence signals at the detector according to concentrations (from 100 μM to 0.1 μM).

HIGH FREQUENCY IMPEDANCE BIOSENSORS FOR MARKER-FREE ANALYTICAL MEASUREMENTS

Markus Löhndorf, Antonio Malavé, Stefan Glass, Ivan Stoyanov and Michael Tewes
Center of Advanced European Studies and Research (caesar), Ludwig-Erhard-Allee 2, D-53175 Bonn, Germany

Abstract

Micro- and Nanostructuring techniques has been utilized to develop highly sensitive sensor elements for marker-free detection of bio-molecular interaction processes. The physical principle of the sensor is based on the measurement of impedance changes between two planar electrodes with a 90-150 nanometer gap size. In addition, a high selectivity is achieved by immobilization of specific receptor molecules or antibodies on the electrode surfaces. A relative signal change of about 5% was obtained for the formation of 2nm thick monolayer of the detergent Triton-X. Furthermore, the coupling of the Thrombin to Thrombin antibodies was observed and monitored in real-time.

Keywords: biosensors, impedance spectroscopy, high frequency, micro-fabrication

1. Introduction

Bio-molecular interactions such as protein-protein interactions are commonly investigated by means of optical detection schemes using fluorescent markers or by surface plasmon resonance. [1-2] However, these measurement techniques rely on optical excitation and detection devices (laser sources, lenses, photo diodes etc.) and therefore the possibility for higher sensor integration on single chip level is strongly hindered.

The development of high selective and sensitive biosensors and arrays for quantitative measurements using marker-free electrical detection of the bio-molecular interactions is desirable in view of further biosensor integration and batch production. Here, micro- and nanofabrication technologies have been utilized to develop those marker-free biosensors in a batch process. The electrical detection of the bio-molecular interaction is based on impedance changes within a 90 – 150 nanometer gap between two planar electrodes measured at frequencies well above 100 MHz.

The sensitivity of the impedance sensor elements strongly depends on the gap size between the two electrode structures. At the measurement frequencies well above 100 MHz the change in the electrical impedance of the sensor element is mainly due to the change of the dielectric constant when specific bio-molecules bind to the receptor molecules which are immobilized at the sensor surface. Therefore, the gap size of an optimal sensor element should be on the order of the size of the bio-molecules or proteins.

Electron-beam lithography have been used for the fabrication of single sensor elements [3], however we have succeeded to produce these sensors with 90-150 nm gap size in a batch process by using standard optical lithography and sacrificial layer processes.

2. Experimental

The sensors were prepared on 4 inch fused silica wafers and diced into 20mm x 20mm sensor chips. Each chip contains 10 sensor elements and each of those sensor elements consists of 64 single sensor cells with a 2μm x 6μm active sensor area (see Fig.1). Each sensor cell comprises two planar gold electrodes with a gap of 90 – 150 nm. In this configuration every single sensor cell forms a capacitor, which impedance depends on the filling factor or the effective dielectric constant of the medium between both electrodes (see Fig. 2). The first 200-300 nm thick gold metallization layer is deposited by means of magnetron-sputtering or electron-beam evaporation and subsequently structured by standard photo-lithography techniques. In the following the sacrificial layer (Cu, SiO_2, Si_3N_4) is deposited with the desired thickness (90-150 nm) in order to form the gap

between the electrodes. In the third and final lithography level the upper gold electrode is sputtered onto the wafer and structured by means of physical ion-beam etching. Finally, the sacrificial layer has to be removed by a wet-etch process. The high frequency impedance measurements were performed in a novel sensor system [4] which allows for fully automated bio-analytical measurements by using an auto-sampler and also ensures the correct electrical contact to the sensor and to the necessary fluidic cell. Prior to the measurement the sensor chips are cleaned by an oxygen plasma step and in case of an immobilization of receptor molecules rinsed in 11-mecapto-undecanoic acid in order to obtain a homogenous self-assembled monolayer (SAM) on the gold electrode surfaces. [5]

3. Results and discussion

As a first test experiment a detergent (Triton-x) was injected. Figure 3 shows the response of a sensor element for two injections of a 1% Triton-X detergent solution measured at a frequency of 180 MHz. After the individual injections of Triton-X a decrease of the amplitude of almost 5% is observed. This decrease can be attributed to the formation of a monolayer of Triton-X with a thickness of approx. 2 nm. The decomposition of the monolayer starts after the concentration of Triton-X concentration has decreased to a critical value. This result shows the inherent sensitivity of the sensor to detect small changes of the dielectric properties in the nanometer gap. Prior to the bio-analytical measurement a self-assembled monolayer (SAM) was prepared on the gold electrodes by using 11-mecapto-undecanoic acid. After the SAM formation the sensor chip was loaded into the sensor system and the measurement which is displayed in Fig. 4 was started. First, the SAM was activated by using EDC/NHS (diluted in 50μM PO_4 buffer) and subsequently the Thrombin antibodies (100nM in water) were injected. The relative change in amplitude for the activation was 4% and for the binding of the Thrombin antibodies (marked in Fig. 4 as $\Delta\varphi$) an additional amplitude decrease of 2 % was observed. After the deactivation of the NHS, at the sites were no thrombin antibodies have been bound to the active sensor surface, the amplitude is increased by 2.4%. Finally the thrombin protein (500nM in PBS buffer) was injected and a small decrease of the amplitude was obtained. However, a time-stable decrease was not observed, which is due to the fast reversible binding of thrombin to thrombin antibodies in the used buffer solution.

4. Conclusions

We have experimentally demonstrated the function and high sensitivity of impedance biosensors with nanometer gap size electrodes for bio-analytical measurements. A high selectivity is obtained by immobilization of specific receptors such as antibodies or aptamers. These sensors have been prepared by means of standard optical lithography in a batch-process. Future work is focused on further miniaturization and array fabrication as well as on additional measurements on bio-molecular interactions with these impedance sensor devices.

Acknowledgements

The authors would like to thank T. Gronewold and D. Pfeiffle for the protein sample preparations.

References

[1] J. Homola, S. S. Yee, and G. Gauglitz, *Sens. Act. B,* **54**, 3 (1999).
[2] S. Weiss, *Science*, **283**, 1676 (1999).
[3] V. Haguet et al., *Appl. Phys. Lett.*, **84**, 1213 (2004).
[4] S-sens analytics (www.s-sens.com)
[5]M. D. Schlensog et al., *Sens. Act. B, in press*, (2004)

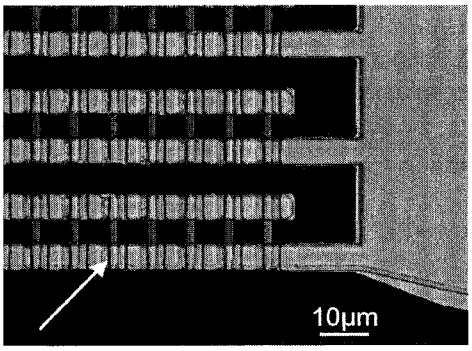

Figure 1. Optical micrograph of the sensor element which consists of 64 single sensor cells. The width of the finger structure is 10 µm, the arrow is pointing to a single sensor cell.

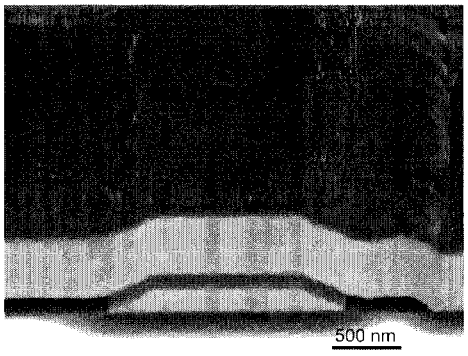

Figure 2. SEM picture of a cross-section of a single sensor cell. The gap between the upper and lower electrode is 150 nm. The active sensor surface is about 2µm x 6µm.

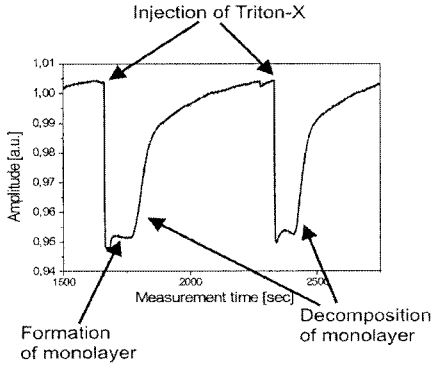

Figure 3. Measurement of Triton-X at a frequency of 180 MHz. The formation and decomposition of the 2 nm monolayer is observed.

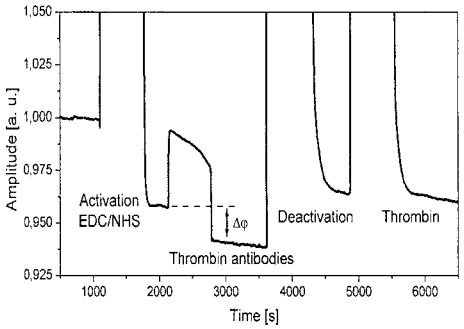

Figure 4. Real-time measurement of EDC/NHS activation, the Thrombin antibody coupling, deactivation and finally the Thrombin binding.

INDIVIDUAL NANO-PARTICLES DETECTION ON MICROCHIP BY THERMAL LENS MICROSCOPE

Kazuma Mawatari[1], Shinichiro Hiki[2], Akihide Hibara[3], Manabu Tokeshi[4], Takehiko Kitamori[1,2,3,4]

[1] *CREST, Japan Science and Technology Agency, Japan*
[2] *Institute of Microchemical Technology, Japan*
[3] *Department of Applied Chemistry, The University of Tokyo, Japan*
[4] *Kanagawa Academy of Science and Technology, Japan*

Abstract

Thermal lens microscope (TLM) is an ultra-sensitive method for detecting non-fluorescent samples in microspace. TLM is a kind of optical absorption spectrophotometry with comparable sensitivity to the laser induced fluorescence method. In this presentation, the applicability of TLM was extended from visible to ultraviolet (UV) light absorbing samples by UV laser excitation. The flow velocity was investigated for optimizing the sensitivity. The detection limit of 9.2×10^{-7} in absorbance unit was obtained and about 2 orders of magnitude superior to spectrophotometry. In addition, TLM was further developed for individual nanoparticles counting with visible laser excitation. Individual gold nanoparticles of 15 nm in diameter could be detected, and the detection limit of 5 nm, that was about 1 order lower in diameter than laser scattering method, was obtained.

Keywords: thermal lens microscope, non-fluorescent sample, individual detection

1. Introduction

Sensitive and wide applicable detection method in microspace is one of the key components such as for environmental, biochemical and medical diagnosis systems on microchip. Conventional method was laser-induced fluorescence method. However, the application was limited to the fluorescent samples. For the purposes, we developed thermal lens microscope (TLM) that could detect non-fluorescent samples with a sensitivity of time-averaged sub-single molecule in 7fL [1,2]. Taking advantage of the wide applicability, TLM was applied to various analytical fields on microchip [1]. Also, miniaturization of TLM was realized from desktop [3] to palmtop sized system [4]. We are now extending the applicability of TLM from visible to ultra violet (UV) light absorbing samples including the selective detection of chiral compounds. Also, the sensitivity is improved from time-averaged detection to individual counting of non-fluorescent molecules, macromolecules and nanoparticles. In this presentation, TLM with UV excitation (UV-TLM) was developed and the sensitivity was investigated. For individual detection, individual counting of nanoparticles was demonstrated by improving the response time of TLM, and the limit of detection (LOD) was investigated.

2. Principle of individual detection

The principle of conventional TLM and counting is shown in Fig. 1. The response time of the conventional TLM was more than 1 second, typically 4 seconds. Then, the signal intensity was 4 seconds averaged value of the expectation number of molecules in detection volume 7fL (not individual but averages of many molecules), and the LOD was 0.4 molecules. For counting, the sample solution is driven at 100 μm/s. The beam waist is 1 μm in diameter, and the retention time in the beam waist is calculated to be 10 ms. When the response time is improved to less than 10 ms, individual particles becomes point heat sources (local temperature distribution around the particles) and can be counted individually as pulse signals. In this case, the pulse count and height corresponds to the number density and absorbed energy of individual particles respectively.

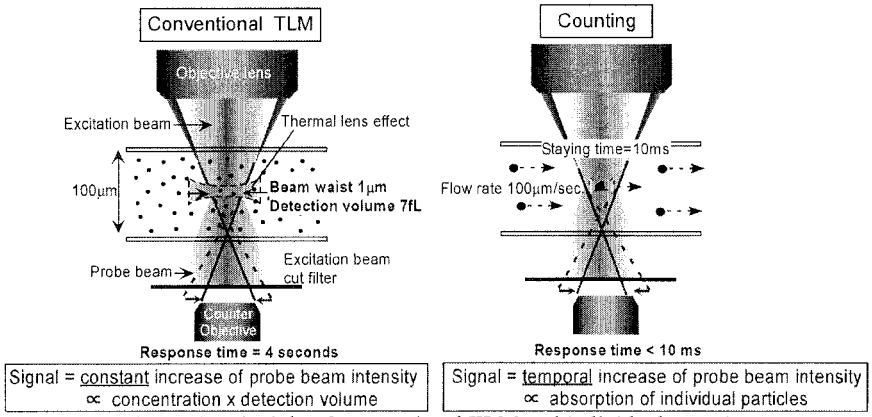

Figure 1. Principle of conventional TLM and individual counting

3. Experimental

In this experiment, desktop sized TLM was used [3]. The excitation beam of UV-TLM was 266 nm and 4.3 mW. For counting, the excitation was 532 nm and 20 mW. Both of the excitation beams were modulated at 1kHz for lock-in amplifier detection. The response time of TLM was ruled by the time constant of the lock-in amplifier, and the value for counting nanoparticles was improved to be 1 ms with enough signal-to-noise ratio. The probe beam was 670 nm and the power was 0.9 mW. The numerical aperture of objective lens to focus the beams was 0.4 (UV-TLM) and 0.75 (counting) respectively. The microchannel used was straight channel, and the cross section was 250 μm wide × 100 μm deep. The sample was adenine and colloidal gold solutions (the diameter was 15, 30, 50 and 80 nm). The sample solutions were driven by a syringe pump.

4. Results and discussion

The optics of UV-TLM was specially designed to reduce the background signal due to the absorption of light. Firstly, the flow velocity dependence was investigated from 0 to 37 mm/s. The result is shown in Fig. 2. The signal intensity was increased and leveled off with the flow velocity. The reason was not clear and considered to be the photochemical reaction. Then, the LOD was investigated using adenine solutions with 20 mm/s as shown in Fig. 3. The LOD was 7.0×10^{-9} M (9.2×10^{-7} abs.) and proved to be about 2 orders of magnitude superior to spectrophotometry.

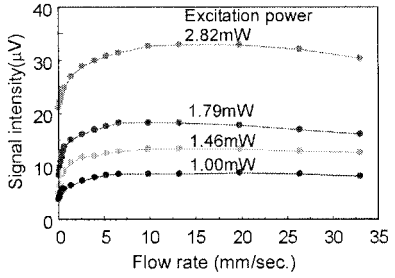

Figure 2. Flow velocity dependence of signal intensity

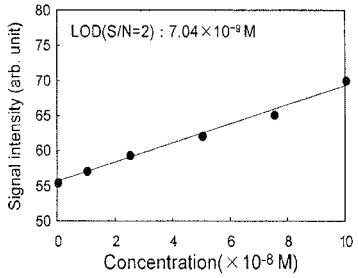

Figure 3. Investigation of LOD with UV-TLM. Sample is adenine solutions.

A waveform of counting 50 nm gold colloids and water (blank) is shown in Fig. 4. The focus position of the excitation beam was set in the center of the microchannel. Clear pulse signals were observed. The pulse signals appeared under the irradiation of both the excitation and probe beam. Therefore, pulse signals arising from scattering effect was not observed. The histogram of the frequency simply decreased with the pulse heights due to the small detection volume. The pulse counts were linearly dependent on the number density of the gold colloids from 1.0×10^{9}–9.0×10^{11} particles/L. From these results, the individual detection of nanoparticles was verified. Next, the 5verage pulse height was investigated by changing the diameter of the gold colloids (Fig. 3). The average pulse height increased with the diameter of the gold particles. The gold nanoparticles of 15 nm in diameter could be detected, and the detection limit was 5 nm. The value was about 1 order superior to the light scattering method.

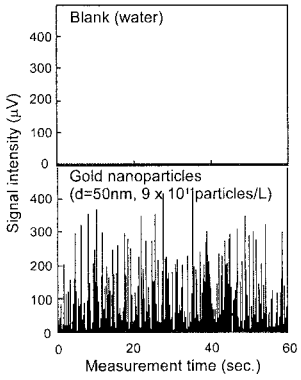

Figure 4. Waveform of measuring water (blank) and gold nanoparticles

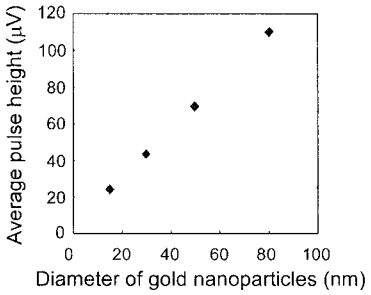

Figure 5. Dependence of average pulse heights on the diameter of gold nanoparticles.

5. Conclusions

The applicability of TLM was extended with high sensitivity. In addition to the sensitivity of time-averaged sub-single molecule, TLM was verified to detect individual nanoparticles. The detection limit of 5 nm in diameter proved the excellent sensitivity for the individual non-fluorescent macromolecules and nanoparticles detection compared with other methods. These results showed wide applicability and the possibility of individual non-fluorescent molecules counting by TLM. The applications are wide spread from analytical fields to the monitoring of chemical and biochemical process on microchip.

References

[1] T. Kitamori, M. Tokeshi, A. Hibara, K. Sato, *Analytical Chemistry,* **76**, 52A-60A (2004)
[2] K. Mawatari, T. Kitamori, T. Sawada, *Analytical Chemistry,* **70**, 5037-5041 (1998)
[3] S. Hiki, M. Tokeshi, A. Hibara, T. Kitamori, *Bunseki Kagaku,* **52**, 569-574 (2003)
[4] M. A. Northrup, K. F. Jensen, D. J. Harrison, *Proceedings of Micro Total Analysis System 2003*; Kluwer Academic Publishers: Netherlands, 2003; pp 359-362.

MICROCHIP ATMOSPHERIC PRESSURE CHEMICAL IONISATION-MASS SPECTROMETRY

Pekka Östman[1], Seppo Marttila[2], Tapio Kotiaho[3], Sami Franssila[2], Risto Kostiainen[1,4]

[1] *Viikki Drug Discovery Technology Center, Faculty of Pharmacy, University of Helsinki, P.O. Box 56, FIN-00014 University of Helsinki, Finland*

[2] *Microelectronics Centre, Helsinki University of Technology, P.O. Box 3500, FIN-02015 Helsinki University of Technology, Finland*

[3] *Department of Chemistry, P.O. Box 55, FIN-00014, University of Helsinki, Finland*

[4] *Faculty of Pharmacy, Division of Pharmaceutical Chemistry, University of Helsinki, P.O. Box 56, FIN-00014 University of Helsinki, Finland*

Abstract

The first microchip-atmospheric pressure chemical ionisation (APCI) compatible to combine microfluidic devices and nano-liquid chromatography to mass spectrometry (MS) is introduced. The performance of microchip-APCI was tested and compared to commercial macro APCI interface. The novel microchip APCI allows flow rates down to 50 nl/min and thus opens up first time possibility to analyse neutral and non-polar compounds with high sensitivity in minimum amounts of sample using microfluidic devices. Microchip APCI provides very stable operation, since the problems, such as bubble formation and disintegration of the outlet, involved to microchip ESI caused by high electric field focused at the outlet of a microfluidic channel can be removed by using external corona discharge needle. Microchip-APCI provides significantly lower flow rates (0.05-5 µl/min) than commercial APCI sources (0.05-2 ml/min). Furthermore, microfabrication technologies enable very cost efficient manufacturing of microchip-APCI. High stability and sensitivity of microchip-APCI show promise of an excellent microfluidic detector.

Keywords: mass spectrometry, atmospheric pressure chemical ionisation, microchip nebuliser

1. Introduction

Microfluidic separation systems often use electrospray ionisation mass spectrometry (ESI-MS) for detection. Microchip realisations of ESI have, however, been plagued by short lifetimes and irreproducibility. Unstable performance of ESI is partly due to redox reactions caused by high electrostatic field at the tip of the microfluidic channel. These reactions lead to bubble formation [1] and to unexpected changes of the outlet of the microfluidic channel and therefore to non-robust analysis.

APCI offers an alternative ionisation method, in which the ionisation is initiated with separate corona discharge needle, which eliminates many of the problems encountered with ESI. So far, only a few attempts have been done to adapt an APCI sources for flow rates lower that 10 µl/min[2,3] by custom made source or modifications to a commercial source. Here we present for the first time a microchip heated nebuliser for atmospheric pressure chemical ionisation mass spectrometry (APCI-MS) [4]. The performance of the microchip APCI was evaluated and was shown to be suitable for highly sensitive, quantitative and long term routine analysis.

2. Experimental

Double side polished <100> silicon wafers were used as substrates and Pyrex 7740 glass wafers as channel cover plates. Three photomasks were required for chip fabrication. The first mask defines the channel, mixer and nozzle patterns in silicon, the second one defines the inlet holes on the backside of the silicon wafer, and the third one is used to fabricate the integrated microheater on the glass wafer. Channel and mixer pattern was printed on wafer front side and fluidic inlet holes on the back using double side lithography equipment (Electronic Visions AL6-2). Anisotropic silicon

etching was done in 25 w-% TMAH (tetramethyl ammonium hydroxide) solution at 80°C. Etch rate was ca. 0.5 μm/min. Etch time was minimized by etching from both sides of the wafer simultaneously. The width of the nebuliser gas and liquid sample channels were 300 μm and 120 μm respectively. The channel depth was 85–190 μm depending on the channel width.

A 300 nm aluminium layer was sputtered on the glass wafer and etched in phosphoric acid solution (PES 80-15-5 from Merck). The resistance of the aluminium heater at room temperature was ca. 90 Ω.

The wafers were alignment and joined together by anodic bonding (350°C, 300 V for 15 minutes). Operation temperature of the microchip APCI is ca. 100-200°C (measured on the top of the silicon wafer). Fluidic connectors (Nanoport, Upchurch Scientific, Oak Harbor, USA) were glued with epoxy after wafer dicing. Chip size (18 x 29 mm) was mainly determined by the size of the fluidic connectors (Figure 1).

The mass spectrometer used was a PE Sciex API-300 triple quadrupole (Perkin-Elmer Sciex) fitted with an x,y,z-stage (Proxeon). For sample injection a liquid chromatograph (Hewlett Packard) with a splitter (LC Packings) or a micro syringe pump (Harvard Apparatus) combined with an injector (Rheodyne) were used. Injection volume was 10 μl. The external corona discharge needle was situated 2 mm in front of the chip and needle current was set to 1 μA. The scan range for MS measurements was m/z 100-500 (1.0 s/scan). MS/MS measurements were carried out in the multiple reaction monitoring (MRM) mode.

Reference data was collected using the same apparatus fitted with an APCI-source (Perkin-Elmer Sciex, Toronto, Canada). The temperature of the nebuliser was 350 °C. Injection volume was 20 μl. Other parameters were the same as in the microchip APCI measurements.

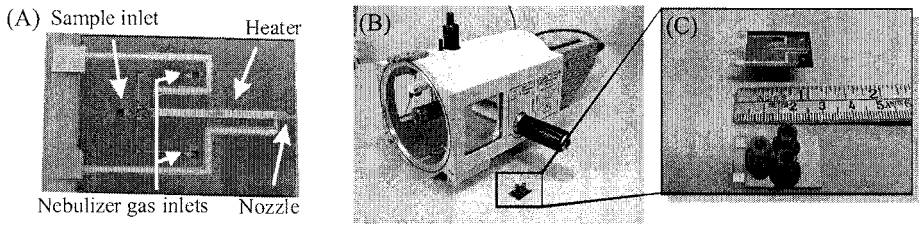

Figure 1. (A) Design of the microchip APCI: gas channels, inlets and nozzle in the silicon wafer and integrated heater in the glass wafer. (B) Comparison of the microchip APCI source and commercial PE Sciex API-300 APCI source. (C) Close-up of the microchip APCI.

3. Results and discussion

The microchip APCI-source provides flow rates between 0.05-10 μl/min, stable long-term analysis (Figure 2A) with chip lifetime of weeks, good quantitative repeatability (RSD < 10%, n=5) and linearity (r2 > 0.995) with linear dynamic rage of at least 4 orders of magnitude (Figure 2B). The limit of detection for acridine measured with microchip APCI at flow rate of 6.2 μl/min was 5 nM corresponding to mass flow of 0.52 fmol/sec (Table 1). Signal current dependence on the flow rate was dependent on the flow rate indicating that the microchip APCI is a mass flow dependent detector (Figure 2C). The microchip APCI produces high quality MS spectra in both positive and negative ion modes (Figure 3).

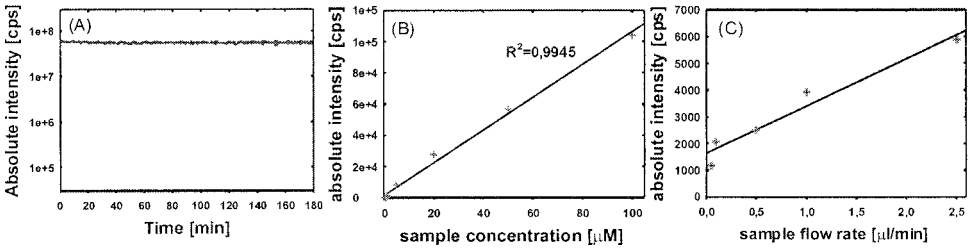

Figure 2. (A) Selected ion chromatogram of protonated acridine (100 µM) produced by direct infusion with flow rate of 1 µl/min. (B) Absolute intensity of protonated molecule of acridine (100 µM) as a function of sample concentration with flow rate of 2.5 µl/min. (C) Absolute intensity of protonated molecule of acridine (100 µM) as a function of flow rate.

Table 1. Detection limits of microchip APCI and macro APCI.

	flow rate	detection limit	
		concentration	mass flow
	[µl/min]	[mol/l]	[mol/s]
microchip APCI	6.2	$5 * 10^{-9}$	$0.5 * 10^{-15}$
macro APCI	6.2	$75 * 10^{-9}$	$14 * 10^{-15}$
macro APCI	1000	$5 * 10^{-9}$	$80 * 10^{-15}$

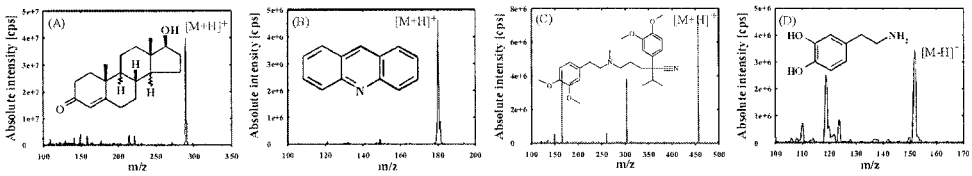

Figure 3. Mass spectra of (A) testosterone, (B) acridine, (C) verapamil in positive ion mode and (D) dopamine in negative ion mode. The concentrations were 100 µM.

4. Conclusions

The microchip APCI provides excellent sensitivity (below 1 fmol/second), flow rates down to 50 nl/min, efficient ionisation for neutral and non-polar compounds in addition to polar and ionic compounds, robust analysis, good reproducibility and cost efficient manufacturing. The microchip APCI provides a very interesting alternative to microchip ESI as a MS detector. Moreover, the heated nebuliser can be used for various other applications where samples have to be vaporised before analysis.

References

[1] G. J. Berkel, F. Zhou and J.T. Aronson *Int. J. Mass Spec. Ion Processes,* **162**, 55-67 (1997).
[2] Y. Takada, M. Sakairi and H. Koizumi *Rapid Commun. Mass Spectrom.*, **9**, 488-490 (1995).
[3] L. M. Nyholm, P. J. R. Sjöberg and K. E. Markides *J. Chromatogr. A*, **755**, 153-164 (1996).
[4] Finnish patent application, 2003

FABRICATION OF pH CMOS IMAGE SENSOR FOR CHEMICAL REACTION IMAGING

Takeshi Hizawa, Kazuaki Sawada, Hidekuni Takao, Makoto Ishida
Dept. of Electrical and Electronic Eng., Toyohashi University of Technology,
1-1 Hibarigaoka, Tempaku-cho, Toyohashi 441-8580, Japan.

Abstract

Novel pH sensor (pH imaging sensor), capable of measuring two-dimensional (2-D) distributions of various chemical reactions has been proposed, and a prototype was successfully fabricated. Real-time imaging of a chemical reaction was confirmed using the pH image sensor.

Keywords: pH Sensor, Biosensor, CMOS Image Sensor, Two-dimensional distribution, Chemical Reaction

1. Introduction

A pH sensor is one of the more important devices among biosensors, and various types of pH sensor have been developed. Conventionally, pH is measured as the average value in a state with uniform concentration. This paper reports on new pH sensor (pH imaging sensor), with which it is possible to measure two-dimensional (2-D) distributions of various chemical reactions. The proposed pH imaging sensor is capable of recording a pH image in real time.

2. Theory

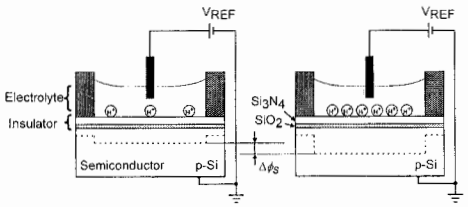

Figure 1. Schematic representation of surface potential. (a) Low pH. (b) High pH.

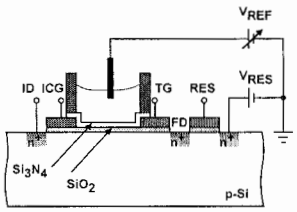

Figure 2. Schematic diagram of a pH measurement system.

In an EIS (Electrolyte / Insulator / Semiconductor) system as shown in Fig. 1, where V_{REF} is constant and the chemical potential, ϕ_c , between the electrolyte and an ion sensitive membrane (Si_3N_4) shifts with varying hydrogen ion concentrations. The chemical potential, ϕ_c , can be obtained by using the Nernst equation

$$\phi_c = V_{REF} + \frac{RT}{F} \ln a_{H^+} . \qquad (1)$$

Where V_{REF} is reference electrode voltage, R is the gas constant, T is the absolute temperature, F is the Faraday constant, and a_{H^+} is the hydrogen ion concentration. The variation of chemical potential ($\Delta\phi_c$) at room temperature is theoretically 59 mV/pH. This system is almost same as the structure of a MIS (metal insulator semiconductor) and can induce a potential well in surface of semiconductor. The depth of the potential well varies with pH value.

The elements of the pH imaging sensor is include the sensing region using Si_3N_4 which acts as an ion sensitive membrane, together with regions for injection and read-out of electric charge. The sensor operates using a charge transfer technique [1,2]. The measurement system is shown in Fig. 2.

3. Experimental and results

The pH image sensor was fabricated in CMOS (Complimentary Metal-Oxide Semiconductor) 5 μm rule technology. 1 pixel of the image sensor covers 200 μm × 200 μm as shown in Fig. 3. To confirm the basic characteristic of the proposed charge transfer type of sensor, three buffered standard solutions, with values of pH 4.01, pH 6.86 and pH 9.18, were used. The results are shown in Fig. 4. The output signal of imaging sensor varied linearly with pH concentration. From Fig. 4, the output signal obtained was 47 mV/pH. This value is strongly dependent upon various parameters such as the relative areas of sensing region and floating diffusion region.

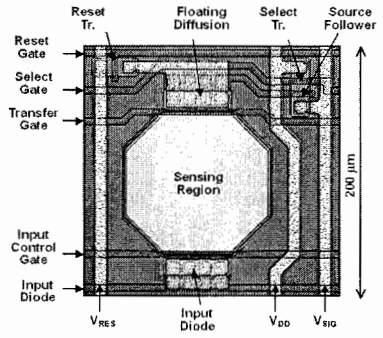

Figure 3. 1 pH image sensor pixel (200 μm × 200 μm).

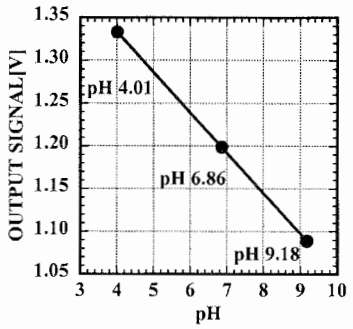

Figure 4. Output signal from 1 pixel of the pH image sensor.

A one-dimensional linear sensor comprised a 6 pixel array as shown in Fig. 5. Output signal of sensor was converted into a real-time moving image at 1/30 sec per 1 frame. The result of real-time measurement of pH in a solution is shown in Fig. 6. Point A indicates the introduction of a solution with pH 9.18 into a solution with an initial pH 6.86. The value of pH immediately rose to a high value, and then gradually decreased over time. The pictures Fig. 7a and Fig. 7b, which relate to one of the 6 pixels, correspond to point (a) and point (b) of Fig. 6, respectively. The chemical reaction was observed as a moving image of pH, which varied with time.

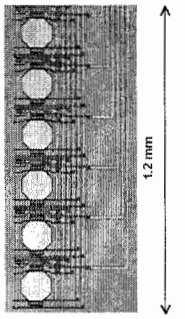

Figure 5. 1-D linear sensor comprising a 6 pixel array.

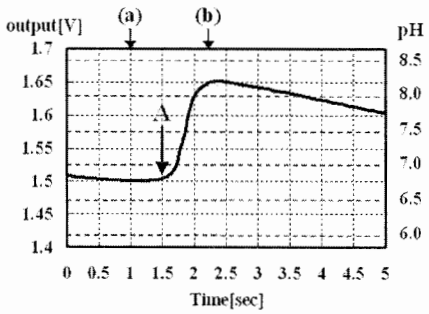

Figure 6. Variation of solution pH over time.

A Two-dimensional (2-D) sensor comprising a 10 × 10 pixel array is shown in Fig. 8. The chip size is 5.1 mm × 5.1 mm, and the size of sensing area is 2 mm × 2 mm. The evaluation of the device was carried out by applying "equivalent voltages" through an electrolyte with pH 6.86 to sensing area, instead of varying the actual pH signals. Equivalent voltages were equal to V_{REF}, the reference electrode voltages. The results of this experiment are shown in Fig. 9. Fig. 9a, Fig. 9b and Fig. 9c correspond to V_{REF} = 1.5 V, V_{REF} = 2.0 V and V_{REF} = 2.5 V, respectively. The output signal of sensor was converted into 2-D image. These results indicate that two-dimensional (2-D) distributions of various chemical reactions could be measured using the pH image sensor.

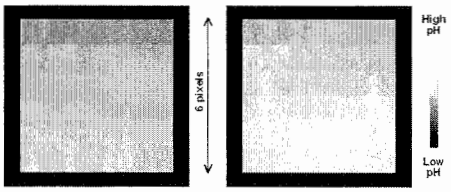

Figure 7. 1-D images measurement in solution. (a) Low pH. (b) High pH.

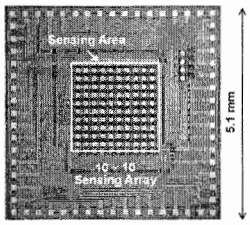

Figure 8. Photograph of chip pH image sensor (5.1 mm × 5.1 mm), with 10 × 10 sensing array.

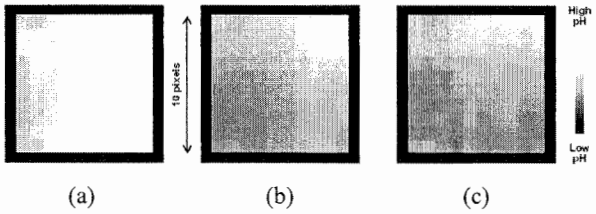

Figure 9. 2-D image measurements in a solution obtained with reference electrode variations. (a) V_{REF} = 1.5 V. (b) V_{REF} = 2.0 V. (c) V_{REF} = 2.5 V.

4. Conclusions

pH sensor (pH imaging sensor), capable of measuring two-dimensional (2-D) distributions of various chemical reactions has been proposed, and a prototype has been successfully fabricated. The imaging of pH in solution was successfully performed. Real-time imaging of a chemical reaction was confirmed using the pH image sensor.

Acknowledgements

This work was partially supported by The 21st Century COE Program "Intelligent Human Sensing", Cooperation of Innovative Technology and Advanced Research in Evolutional Area (CITY AREA) from the Ministry of Education, and a Grant-in-Aid for Encouragement from the Ministry of Education, Science, Sports and Culture, and Technology Japan.

References

[1] K. Sawada, S. Mimura, M. Ishida, et al., "Novel CCD based pH Imaging Sensor", IEEE Trans. ED Vol. 46(9), pp. 1846-1849 (1999).

[2] K. Sawada, T. Shimada, T. Ohshina, H. Takao, M. Ishida, "Highly sensitive ion sensors using charge transfer technique", Sens. Actuators B 98, pp. 69-72 (2004).

A MICRO CYTOMETER WITH MONOLITHICALLY INTEGRATED OPTICAL DETECTORS BASED ON AMORPHOUS SILICON

H. Schäfer[1], K. Seibel[1], M. Walder[1], L. Schöler[1], T. Pletzer[1]
M. Waidelich[2], H. Ihmels[2], M. Schmittel[2], D. Ehrhardt[1] and M. Böhm[1]
[1]University of Siegen, Institute for Microsystem Technologies, Hölderlinstr. 3, D-57068 Siegen
[2]University of Siegen, Institute of Organic Chemistry, Adolf Reichwein Str., D-57068 Siegen

Abstract

Appropriate physical and chemical characteristics as well as reproducibility and stability of thin film amorphous materials are substantial arguments for their use in miniaturized chemical and biochemical analysis systems. We successfully fabricated a micro flow cytometer with monolithically integrated optical detectors based on amorphous silicon. In this work, we use an a-Si:H pin-diode for the optoelectronic detection of organic dye molecules, namely anthracene derivatives, which are driven through the fluidic channel network by electroosmotic flow.

Keywords: Micro Flow Cytometer, Optical Detectors, Amorphous Silicon, Lab-on-Microchip, Fluorescence Sensors

1. Introduction

In most microanalytical systems, neither the light source nor the photodetector is integrated onto the same substrate as the fluidic channel network. The reason is that the combination of all components necessary for performing a total chemical analysis, is very complex. Due to this fact efficient interconnections are very important. The most widely used optical interconnection methods are optical fibers and free-space optical elements such as lenses, mirrors, and filters to guide light into the channel network and to collect optical signals from the fluidic channels. The idea is to create a monolithically integrated technology platform by the combination of two microtechnologies, the "state of the art" thin-film-technology and micro-mechanical processes on glass.

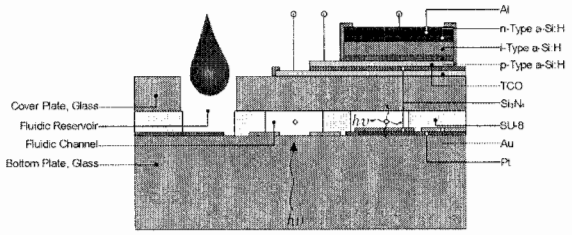

Figure 1. Cross section of the ALM combined with active devices based on amorphous silicon.

2. Experimental

Fig. 1 shows the cross section of the ALM (**A**pplication specific **L**ab-on-**M**icrochip) combined with active devices based on amorphous silicon reported at the SPIE conference 2003 [1]. The fluidic channel network is built into a polymer layer (SU-8) which is sandwiched between two glass plates. The excitation light enters through the thicker bottom plate and meets the chromophore in the channel. The a-Si:H pin-diode is built between a SnO_2 TCO (**T**ransparent **C**onductive **O**xide) layer acting as front contact and a chromium rear contact. A second TCO-layer, separated from the front contact by an insulating layer of Si_3N_4, serves as electrical shield to eliminate interference between the high voltage required to stimulate the electroosmotic flow and the highly sensitive

detector device. Furthermore, the detector structure can be optimized to block the excitation wavelength, e.g. $\lambda = 380$ nm, from the emitted fluorescence wavelength by appropriate device engineering [2].

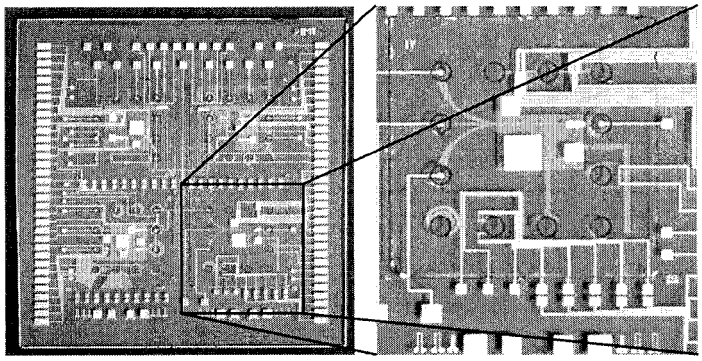

Figure 2. Photomicrograph and detail enlargement of the fabricated multipurpose test structure.

The band gap of the a-Si:H intrinsic material amounts to 1,78 eV and the evaluated thickness is based on a deposition rate of about 3,5 Å/s. After the RF-PECVD deposition of the amorphous pin-diode layers a metal layer of about 80 nm is sputtered on top. Finally, the system is patterned lithographically using four masks. Fig. 2 shows the fabricated multipurpose test structure with an area of (5 x 5) cm^2 and a detail enlargement of the integrated micro cytometer with the detectors on top.

To test the Lab-on-Microchip configuration in chemical analysis, the Ox (Anthracenyl-**Ox**azoline) may be an appropriate system. The chromophore exhibits the usual properties of anthracene derivatives; however, upon protonation a significant red shift of the absorption and emission maxima takes place [3].

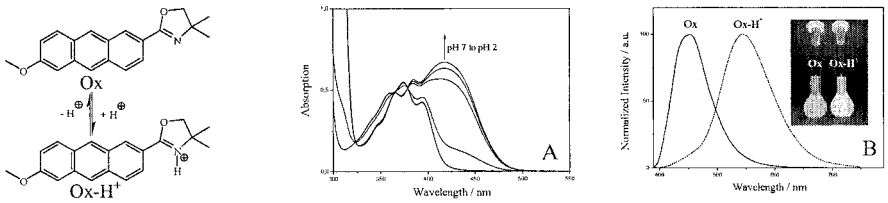

Figure 3. A: Spectrophotometric titration of Ox with hydrochloric acid. B: Normalized fluorescence spectra of Ox and Ox-H^+ (λ_{ex} = 380 nm, c = 10^{-5} M).

Fig. 3A depicts the spectrophotometric titration of oxazoline with hydrochloric acid (arrow indicates change of absorption spectrum from pH=7 to pH=2) according to Fig. 3B where the normalized fluorescence spectra of Ox and Ox-H^+ (λ_{ex} =380 nm, c=10^{-5} M) are shown. Most notably, the spectrophotometric titration reveals an isosbestic point at λ =380 nm, i.e. both Ox and Ox-H^+ exhibit the same absorption intensity at this wavelength.

3. Results

The selective spectral response of the diode was achieved by appropriate band gap engineering of the pin-structure. Fig 4 demonstrates the voltage controlled variation of the SR (**S**pectral **R**esponse) of the pin-diode which exhibits different sensitivities at $\lambda_{ex} = 380$ nm and the fluorescence spectra of Ox and Ox-H^+ between 400 nm and 700 nm.

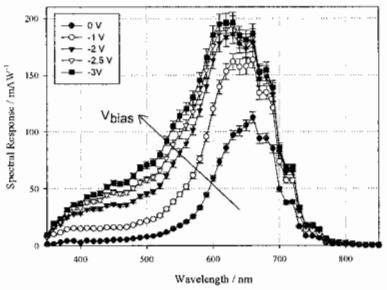

Figure 4. Spectral response of the fabricated pin-diode as a function of bias voltage.

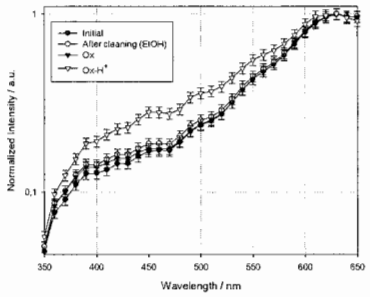

Figure 5. Normalized intensity spectrum in initial phase, at runtime and after cleaning.

Lab-on-Microchip test results with anthracenyl-oxazoline are shown in Fig. 5. Test parameters are bias voltage $V_{bias} = -2{,}5$ V, detection volume $\Delta V \sim 26$ nl, fluid concentration $c = 10^{-5}$ M, diode area $A_{Det} = 0{,}1225$ mm^2 according to a const. flow of 1 µl/min. The normalized intensity spectrum demonstrates a significant difference for low concentration of Ox and Ox-H^+ as a consequence of the fluorescence spectrum shift depicted in Fig. 3 with λ_{ex}=380 nm. The current detection range can be specified between 23 pA and 32 pA. Due to the increase of the SR and the refraction index variation as a function of the wavelength, a significant difference in the response is observed up to a wavelength of 600 nm.

4. Conclusions

In conclusion, monolithically integrated optical detectors based on amorphous silicon have been demonstrated to detect fluorescence light due to our chemical analysis configuration. The amount of substance may be estimated to a couple of pico-mol which is comparable to the results obtained by Fixe et al. [4] in a two dimensional configuration for DNA analysis.

Acknowledgements

This work is supported by the "Deutsche Forschungs Gemeinschaft" under contract "DFG BO 772", and the "Fonds der Chemischen Industrie" under contract "DFG IH 24/2-3". The authors are grateful to our colleagues from the CµNCE (Center for Micro- & Nano Chemistry and Engineering) in Siegen. Special thanks goes to the team from HESS GmbH & CO. KG Burbach-Wahlbach who technically supported this work.

References

[1] H. Schäfer, S. Chemnitz, S. Schumacher, V. Koizy, A. Fischer, A. J. Meixner, D. Ehrhardt, M. Böhm, *Proc. SPIE*, vol. 5116-5119, pp. 764-774 (2003)

[2] P. Rieve, M. Sommer, M. Wagner, K. Seibel, M. Böhm, *Journal of Non-Crystalline Solids*, 266-269, pp. 1168-1172 (2000)

[3] H. Ihmels, A. Meiswinkel, C. J. Mohrschladt, *Org. Lett. 2*, 2865-2867 (2000)

[4] F. Fixe, D.M.F. Prazeres, V. Chu and J.P. Conde, *Mat. Res. Soc. Symp. Proc. 762*, A21.2 (2003)

PHASE-SHIFT FIBER-LOOP RING-DOWN SPECTROSCOPY

Zhaoguo Tong, Alexander Wright, Theresa McCormick, Nick Trefiak, Jack Barnes, and Hans-Peter Loock

Dept. of Chemistry, Queen's University, 90 Queen's Crescent Kingston, Ontario, Canada, K7L 3N6

Abstract

Fiber-loop Ring-Down Spectroscopy (FLRDS) is a recently developed technique that allows for the detection of very small optical absorption losses using light circulating within a closed loop made of optical waveguide material. The technique has potential as an intensity-independent means to detect analyte in picoliter-sized liquid samples. Here it is demonstrated that for an amplitude modulated continuous light source coupled into the fiber loop, the inherent optical decay time will induce a phase-shift in light emitted from the loop relative to the modulated source. The magnitude of this phase shift can be related to the optical loss induced by the waveguide material and the liquid sample. This particular means of determining optical loss is referred to as Phase-Shift Fiber-Loop Ring-Down Spectroscopy (PS-FLRDS). The simple and inexpensive setup involved the use of a multimode fiber and an 810 nm laser diode light source, whereas the 240 pL sample was introduced into a 30 micron gap within the fiber loop. It was possible to detect less than 30 μM of 1,1'-diethyl-4,4' dicarbocyanine iodide (DDCI) in dimethyl sulfoxide (DMSO) with a response time of less than 200 ms.

Keywords: fiber-loop, ring-down, phase-shift, absorption detector

1. Introduction

Fiber-loop Ring-Down Spectroscopy is an absorption spectroscopic technique that was inspired by cavity ring-down spectroscopy (CRDS) - a technique know for approximately fifteen years [1]. In contrast to CRDS, which is used almost exclusively for measuring gas phase absorptions, FLRDS has the potential to measure absorptions in very small liquid samples [2,3]. This fact, coupled with the fast response time of the phase-shift variant of the technique, suggests its use as a detector in analytical flow systems such as HPLC, capillary electrophoresis and μ-total analysis systems.

It has been known for many decades [4] that one can determine the characteristic time constant of an optical resonator by measuring the phase-shift between the excitation and response. Recently, the phase-shift method was applied to optical loss measurements in a mirror cavity to measure weak molecular absorptions [5]. The phase-shift method obviates the need to record fast transient signals and extract decay constants from the data as is required for pulsed laser ring-down techniques.

In our phase-angle ring-down measurements, a continuous-wave intensity modulated laser is coupled into the fiber loop. The time dependent input intensity is given by

$$I_{in} = I_0[1+\alpha\sin(\Omega t)] \qquad (1)$$

where $\alpha \leq 1$ and $\Omega = 2\pi f$ is the angular modulation frequency. Light exiting the loop will also be modulated at the same frequency, but with a reduced modulation depth and shifted in phase by

$$\phi = -\arctan(\Omega\tau) \qquad (2)$$

where τ is the loop's optical decay time from which the concentration of the analyte in a sample may be extracted [2] using

$$\tau = \frac{L}{c\left(\alpha L - \ln T_{sp} + \varepsilon C d\right)} \qquad (3)$$

with the length of the fiber-loop, L, and its absorption coefficient, α, the transmission of the splice T_{sp} and the molar extinction coefficient of DDCI, $\varepsilon_{DDCI} = 3.34\times10^5$ $(M\cdot cm)^{-1}$ at 825 nm. C_{DDCI} is the concentration of the solution and d is the optical path length, i.e. the gap between the two fiber ends.

2. Experimental

The experimental setup (Fig.1) consists of a 65 m loop of 100/140 µm optical fiber into which is coupled to a 810 nm diode laser which is current modulated at around 200 kHz. Light exiting the fiber is detected by a photomultiplier tube. The phase-shift between the photomultiplier signal and the laser modulation is measured using a high frequency lock-in amplifier. Solutions can be injected into the nominal 30 µm gap within the fiber loop. This corresponds to approximately 240 picoliters of sample. From Eqs. (2) and (3) the measured phase-shift, ϕ_m, is related to the analyte concentration, C, by

$$\phi_m = \phi_0 - \arctan\left(\Omega L/c\,(A_0 + \varepsilon C d)\right) \qquad (4)$$

where ϕ_0 is an instrumental phase offset and A_0 accounts for the combined absorption of the fiber and solvent.

3. Results and Discussion

Figure 2 shows the variation in phase angle with DDCI concentration at a modulation frequency of 200 kHz. From this curve it can be seen that the phase angle dependence on concentration is non-linear, being more sensitive at low concentrations. Fitting these data using equation (4) yields the values $\phi_0 = -23.3°$, $A_0 = 0.66$, and $d = 31\mu m$. The detection limit is estimated to be below 30µM.

Figure 3 is a simple demonstration of the time response of PS-FLRDS. Drops of DDCI of different concentration were added alternately with pure DMSO solvent between the two fiber ends. From the figure, the time-response can be obtained from the onset of the leading edge of each peak and is better than 200 ms.

4. Conclusions

PS-FLRDS has been shown to improve the duty cycle and data acquisition rate considerably over pulsed laser ring-down techniques. This allows for real-time measurements in analytical flow systems.

PD-FLRDS is compact and inexpensive. In principle, all electronics components could be integrated into a single board with a computer interface. When coupled with microfluidic separation techniques, a powerful new analytical tool results.

References

[1] G. Berden, R. Peeters, and G. Meijer, *Int. Rev. Phys. Chem.*, **19**, 565 (2000)
[2] Z. Tong, M. Jakubinek, A. Wright, A. Giles, and H.-P. Loock, *Rev. Sci. Instrum.*, **74**, 4818 (2003)
[3] R.S. Brown, I. Kozin, Z. Tong, R. Oleschuk, and H.-P. Loock, *J. Chem. Phys.*, **117**, 10444 (2002)
[4] F. Duschinski, *Z. Physik*, **81**, 7 (1933)
[5] R. Engeln, G. vonHelden, G. Beden, and G. Meijer, *Chem. Phys. Lett.*, **262**, 105 (1996)

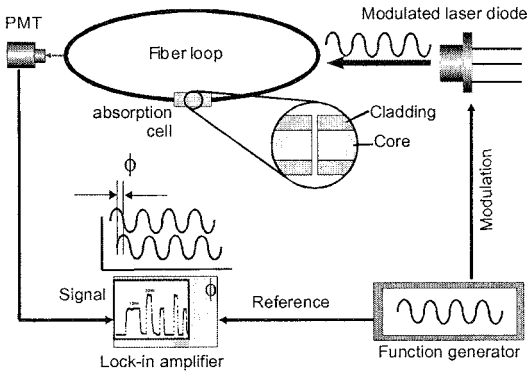

Figure 1. Experimental apparatus for PS-FLRD measurements. Losses within the fiber loop cavity, contributed to by sample absorption within the fiber loop gap, produce a phase-shift between the laser source and detector signal. The measured phase-shift can be interpreted to give a sample absorbance.

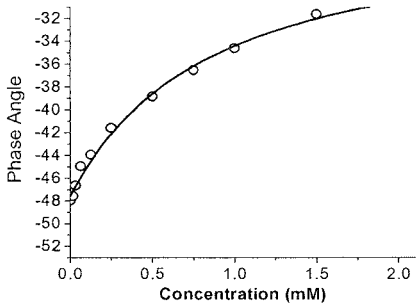

Figure 2. Dependence of phase angle on DDCI concentration.

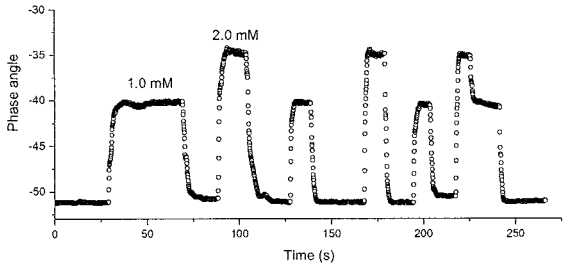

Figure 3. Signal response to rapid changes in DDCI solution concentration. Data was taken every 200ms.

DEVELOPMENT OF A LASER INDUCED NATIVE FLUORESCENCE DETECTION SCHEME FOR PEPTIDES AND PROTEINS ON MICROCHIP

Kowlasar Misir and D. Jed Harrison
Department of Chemistry, University of Alberta, Edmonton, AB, T6G 2G2, CANADA

Abstract

The application of a 266 nm laser for the label free detection of peptides and proteins after capillary electrophoretic separation on chip was investigated.

Keywords: laser induced native fluorescence, microchip, peptides, proteins, CE

1. Introduction

Capillary electrophoresis (CE), coupled with Laser Induced Fluorescence (LIF), provides a separation method that offers unparalleled efficiency and sensitivity, and can be employed in the analysis of trace samples such as individual cells [1, 2]. Proteins are an important class of bio molecules that continue to challenge scientists in their quest to develop systems capable of analysing complex samples. CE on microchip offers attractive benefits in terms of smaller sample sizes, high separation efficiencies and shorter analysis times as compared with conventional CE. However, a major drawback in utilizing LIF for the analysis of biological samples is the issue relating to labelling of the analytes with fluorescent probes molecules [3]. Labelling at low analyte concentrations is non quantitative, not very sensitive, suffers from slow reaction kinetics, the formation of multiple labelled products, and often, by-products of the labelling reaction lead to low yield of the labelled analytes and large fluorescent backgrounds [1, 3]. As a result, Laser Induced Native Fluorescence Detection (LINF) is attractive. Almost all proteins have some aromatic amino acids which naturally fluoresce, so the development of a native detection scheme for a microfluidic platform is a convenient approach to the development of a complete integrated system for protein analysis. We present here a LINF system that is capable of detecting peptides and proteins. This system can be readily integrated with other protein processing steps on a chip, and means complications from labelling are avoided. Conventionally, the approach to protein analysis relied on 2-dimensional electrophoresis introduced by O'Farrell [4] and this allowed for the resolution of hundreds of proteins. One major disadvantage is that it is highly labour intensive, though, in spite of this, it remains the most widely used technique. The development of a microfluidic platform for the integration of various alternate protein preparation processes within one system is an attractive alternative, which will be facilitated by a LINF detector that eliminates a need for labels.

2. Experimental

Instrumentation: Initial experiments were conducted with an RF5301 fluorimeter to ascertain the fluorescence intensity of the aromatic amino acids at various wavelengths: 229, 244, 257, 284, and 288nm. The optical setup for on chip detection of the fluorescent signal employed a confocal epiluminescent format. The injection and separation events were electro-kinetically governed by a computer controlled high voltage power supply via a Lab View interface. The excitation light from a 266 nm pulsed UV laser (JDS Uniphase) was reflected by a dichroic mirror and focused on the microchip using a x13 (N.A. = 0.13, Newport) or a x36 (N.A. = 0.52, reflecting, Thermo Oriel) UV objective lens (independently). Fluorescence emission was collected by the respective objective in use, passed through the dichroic mirror, and focused by a tube lens. Various filters were employed: an XF 3000 (Omega Optical), a UG 1 and a UG 11 band pass filter (Melles Griot), was used for spectral filtering of the signal before it entered the PMT (RF1477, Hamamatsu).

Device: The POCRE chip design was used and was fabricated on quartz substrates utilizing standard photolithographic and wet chemical etching as was described previously [5]. The channel depth was 10 μm and the injector to detector distance was 3.1 cm.

Reagents: All solutions were prepared using doubly distilled, degassed, 0.2 μm filtered water. To determine the emission spectra of the aromatic amino acids, 0.1 mM solution of each in water was used. For on chip analysis, a stock solution of tryptophan (W) was prepared in water and diluted to various concentrations in the running buffer, 25 mM borate, pH 9.0, to be used in the limit of detection (LOD) studies. For the peptides and protein work, stock solutions were prepared in water and diluted in the running buffer, which was 25 mM borate, pH 9.0, and 25 mM phosphate with 0.01% tween 20, pH 10.3, respectively. The peptide sample concentration used in the experiments was 15 μM and the protein samples were 5 μM.

Procedure: The injection time used in all on-chip experiments was 2 s. The injection voltage for the LOD experiments with W was 3 kV. Capillary zone electrophoresis of peptides and proteins was performed using a 3 kV injection voltage for peptides, and a 500 V injection voltage for proteins, followed by separation at 3 kV and 4 kV respectively

3. Results and Discussion

Tryptophan is the most fluorescent of the three naturally occurring aromatic amino acids. In water its maximum fluorescent emission occurred with excitation between 284-288 nm. At 284 nm excitation Tyrosine (Y) emission was weaker than W, and phenylalanine (F) was the least fluorescent. The fluorescence spectra showed W was the preferred fluorophore with 266 nm excitation, so W was used for optimization of our detector and in our limit of detection studies. At this wavelength, emission is reduced by a factor of 2 compared to 288 nm. The LOD obtained under optimized conditions was 300 nM (S/N = 3, R^2 = 0.998), based on measurements between 2-80 μM. The same LOD was observed using either a x13 or a x36 objective, despite the much larger numerical aperture of the latter lens. This result implies that the collection of emitted light was not the primary limiting factor in detection.

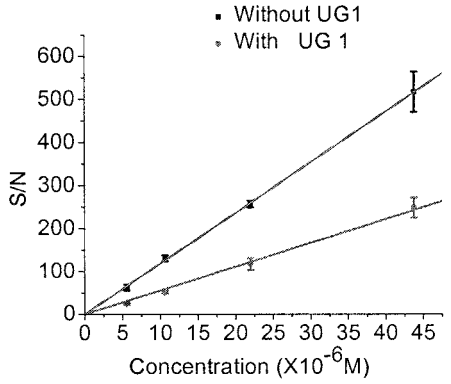

Figure 1. Calibration graph

The effect of using a pair of band pass filters on the LOD was evaluated, since this approach greatly reduces the scattered laser line. Figure 1 shows a comparison of the calibration curves obtained with an XF 3000 (290-380 nm, 76%T) filter and in combination with a UG 1 filter. The UG 1 filter had a band pass in the range of 300 to 400 nm, and transmission efficiency of about 56 percent at 350 nm. The net result was a ~2-fold drop in the LOD. Another band pass filter, UG11 was employed (250 – 390 nm), which had a transmission efficiency of approximately 80 percent at 350 nm. The LOD was improved compared to using the UG1, but remained poorer than with the XF3000.

This result suggests that light scattering of the excitation beam does not seem to be the primary noise source. Currently, we suspect that the laser itself is the noise source, but we require an independent measurement system to evaluate this.

The UV-fluorescence detection system (XF3000) was applied to the determination of peptides and proteins. Figures 2 and 3 demonstrate the versatility of the detection system. A 15 μM peptide mixture was separated within 45 seconds, as is indicated in Figure 2. The LOD for peptides was in the range of 300 nM, similar to that for W. The separation efficiency observed, expressed as the number of plates, N, was good. Peak B in Figure 2 gave 14000 plates (0.4 million plates/m).

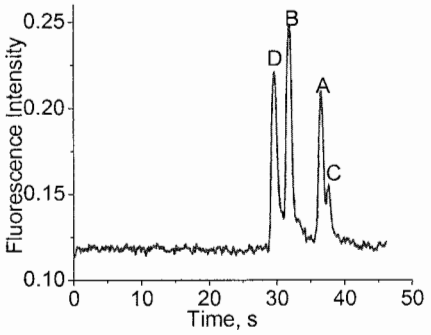

Figure 2 LINF detection of peptides: A = alpha (1) mating factor fragment, B = Bombesin, C= Luteinizing hormone, D= alpha (1) mating factor (15 μM)

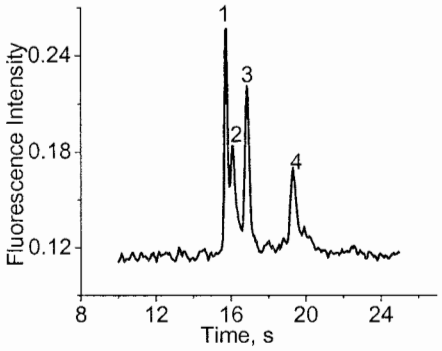

Figure 3. LINF detection of proteins: 1, 2 = Carbonic anhydrase I and II, 3 =β-Lactoglobulin B, 4 = α-Lactalbumin (5μM)

Figure 3 shows the electropherogram for the detection of four proteins in a 5 μM mixture. Separation was achieved in less than 25 seconds at 466 V/cm, and this was further improved to less than 15 seconds at 699 V/cm. Peak 1 in Figure 2 gave 51,000 plates (1.6 million plates/m). This high separation efficiency indicates that the buffer system used was effective in reducing adsorption, and that the optical detector design was as effective for proteins as for peptides. These results also show that the optical detection system was not inducing significant band broadening, as this efficiency is close to the maximum that can be expected for such a device [6].The relative standard deviations for migration times and peak areas were less than 0.3% and 4% respectively for six consecutive analyses. This method allowed for the rapid separation and detection of proteins and peptides without the need for problematic labelling.

4. Conclusion

LINF detection of peptides and proteins has been demonstrated as an alternative to cumbersome labeling reactions. While the LOD was higher than we expected, the high separation efficiency that we observed for this optical detection method is attractive for applications in proteomics that eliminates the need for labels.

References

[1] Zhang, X.; Sweedler, J. V. *Anal. Chem.*, **73**, 5620-5624 (2001)
[2] Chan, K. C.; Muschik, G. M.; Issaq, H. J. *Electrophoresis*, **21**, 2060-2066 (2000)
[3]Timperman, A. T.; Oldenburg, K. T.; Sweedler, J. V. *Anal. Chem.*, **67**, 3421-3426 (1995)
[4] O'Farrell, P. H., J. *Biol. Chem.*, **250**, 4007-4021 (1975)
[5] Fluri, K. et. al. *Anal. Chem.*, **68**, 4285-4290 (1996)
[6] Harrison, D. J. et. al. *Science*, **261**, 895-897 (1993)

ON-CHIP THERMAL LENS DETECTION SYSTEM

Yoshinori Matsuoka [1], Yoshikazu Yoshida [1], Manabu Tokeshi [1], Akihiko Hattori [2], Takashi Fukuzawa [2], Jun Yamaguchi [2], Kenji Uchiyama [2], Takehiko Kitamori [3]

[1] *The Research Association of Micro Chemical Process Technology, Kawasaki, Japan*

[2] *Nippon Sheet Glass Co., Ltd., Japan*

[3] *The University of Tokyo, Japan*

Abstract

We developed an on-chip micro thermal lens detection device (μ-TLD), in which all the devices required for thermal lens measurement such as lock-in amplifier, I/V amplifier, and so on were integrated in the small box. The detection device was free from optical alignment problems. The device developed here had good performance. The limit of determination for Ni complex standard solution was evaluated to be 5.0×10^{-5} (Abs).

Keyword: thermal lens microscope, thermal lens, SELFOC micro lens

1. Introduction

An ideal detection device for chip-based analysis systems is desired to satisfy some features, i.e., high sensitivity, compact size, user-friendliness, etc. Recently, a thermal lens microscope (TLM) detection system to analyze trace amount of non-fluorescent chemical substances in microchips has been developed by our research group [1]. However, the TLM was not so small and requires severe optical alignment, although its sensitivity was extremely high and application range was so wide. Very recently, by utilizing SELFOC micro lenses (SML as shown in Fig.1) as an objective lens and an optical multiplexer, we have developed μ-TLD [2], which could solve the size problem. In the present work, we have developed on-chip μ-TLD system, which was also free from the optical alignment problem.

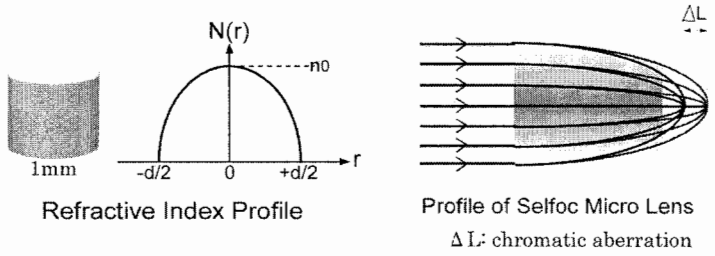

Fig. 1 Characteristics of the SML

2. Device structure

In order to realize optical alignment free, the SML was integrated on the top surface of microchip. The relative position between the SML and detection point inside a microchannel is very important because the thermal lens measurement is based on the change of refractive index. In particular, the conventional microchannel with a half circle cross section becomes a serious problem as shown in Fig.2.

We measured the dependence of the thermal lens signal on the relative position between the SML and

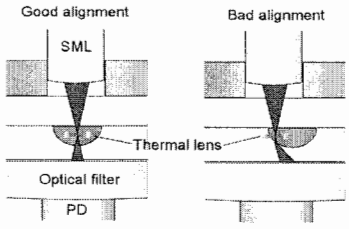

Fig. 2 Alignment of the SML and microchip

the detection point inside the microchannel using microchannels with various aspect ratios. From these results, we realized the tolerance of SML focus position relative to the microchannel. This information is now under application for a patent. Fig.3 shows a schematic and photograph of on-chip detection device.

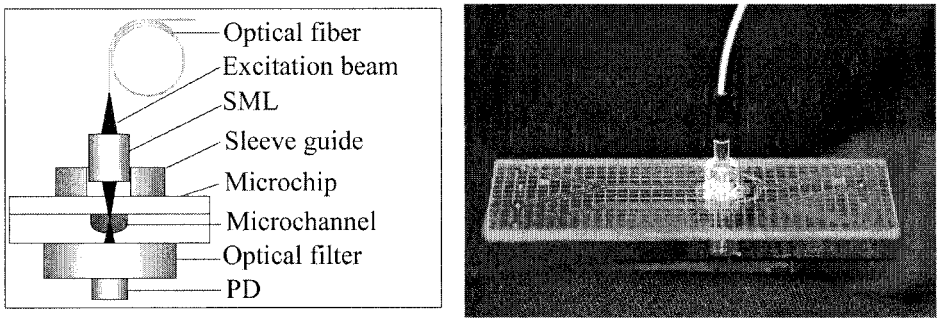

Fig. 3 Schematic and photograph of on-chip detection device

3. Experimental

Outline of the on-chip TLD is shown in Fig. 4.

The excitation (658nm) and probe (780nm) beams were emitted by laser diodes and introduced into the single-mode optical fibers respectively. The excitation beam was chopped by the modulation of the laser diode (1.01 kHz). The excitation and probe beams propagated through the single-mode optical fibers were made to be coaxial using the optical multiplexer.

The signal from PD is first amplified with I/V amplifier, and then synchronous signal was extracted with a lock- in amplifier.

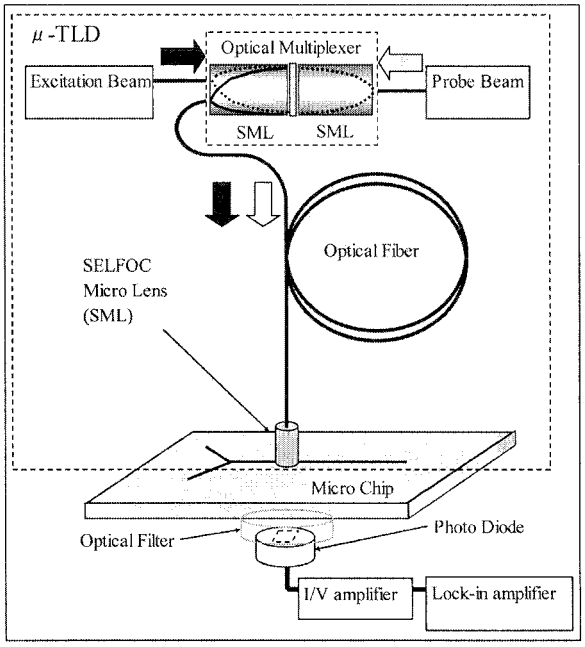

Fig. 4 Outline of on-chip TLD

4. Results and discussion

Moreover, combining this system, we developed a u-TLD system including a lock-in amplifier and I/V amplifier as shown in Fig.5. Consequently, the world's smallest thermal lens detection system was realized. This system was made compact enough to be carried easily and was user-friendly due to being optical alignment free. To evaluate the performance of this system, the dependence of the thermal lens signal on the concentration of Ni-complex standard solution was measured. Fig.6 shows the calibration curve of Ni-complex. The calibration curve

showed good linearity in the range of $1x10^{-7}$ to $5x10^{-6}$ mol/L. The limit of determination was $1x10^{-7}$ mol/L.

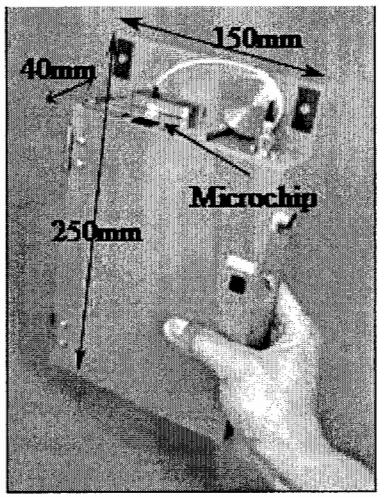

Fig. 5 Photograph of u-TLD system

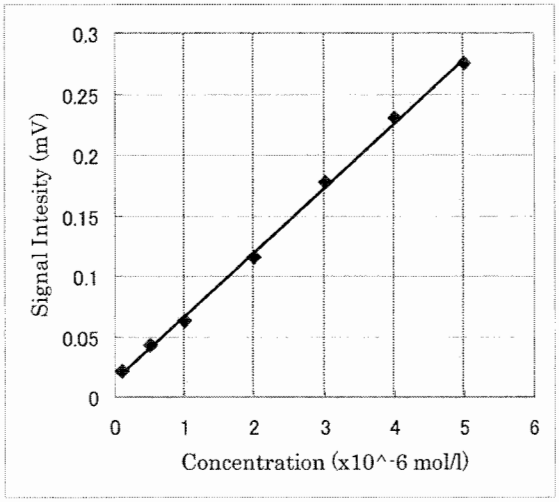

Fig. 6 Calibration curve of Ni-complex

5. Conclusions

It mentioned above, this system had good performance and was very compact. Therefore, the system developed here will be used more widely in the future.

Acknowledgements

This work was supported by "Project of Micro-Chemical Technology for Production, Analysis and Measurement Systems" of New Energy and Industrial Technology Development Organization (NEDO), Japan.

References

[1] T. Kitamori, M.Tokeshi, A.Hibara, K.Sato, Anal. Chem., 76, pp53A-60A (2004).

[2] A.Hattori, H.Yamaguchi, J.Yamaguchi, Y.Matsuoka, S.Kanki, T. Fukuzawa, T.Miwa, M.Toyama, M.Tokeshi, T.Kitamori, MicroTAS'03, pp359-362

ABSORPTION DETECTION ON GLASS MICROCHIP WITH REFLECTIVE LAYER COATING FOR PORTABLE BTX MEASUREMENTS

S. Camou, Y. Ueno, A. Tate and O. Niwa

NTT Microsystem Integration Laboratories,
3-1 Morinosato Wakamiya, Atsugi, Kanagawa 243-0198 Japan, seruju@aecl.ntt.co.jp

1. Abstract

In order to improve the sensitivity of portable air monitoring system based on absorption micro-detection cell, we proposed different fabrication processes and tested its regarding the optical guidance efficiency. Two materials (Aluminum and Titanium / Platinum) have been coated on the microchannels sidewalls as reflective layers. Due to its better reflective properties in UV range, Aluminum yields to improvement by a factor of 2 in terms of coupling efficiency through a 3 cm long optical cell, while the gain is around 30 % with Titanium / Platinum.

Keywords: Absorption detection, microfabrication, BTX gas sensor

2. Introduction

About air quality, the protocol of Kyoto [1] held in 1998 defined the maximum concentration of Volatile Organic Compounds (V.O.C.) such as benzene, toluene and xylene (BTX) of about few parts per billion (ppb): over this limit, the gases may have non-negligible effects on the humans' health. Bulk equipments such as gas chromatograph combined with mass spectrometer (GC/MS) exhibit very high sensitivity that fulfill the requirements of parts per trillion (ppt) detection limit, but are huge, expensive, and do not give real time measurements. Studies have been initiated a few years ago [2] (Fig. 1) in order to propose a portable environmental analysis set-up, and more specifically BTX gases measurement system.
This report deals with the latest achievements in terms of microchip design and fabrication that leads to an improvement by more than an order of magnitude of its sensitivity, down to few ppb.

3. Concept of the actual device

After going through a micro-concentration cell where the BTX gases are specifically concentrated, the gas sample enters the optical absorption based detection cell. This method offers several advantages as non-invasive, high reliability measurements, and allows also the qualitative and quantitative detection of the three gases simultaneously.
Concentration of BTX down to few parts per million (ppm) were successfully detected by the original device, but the S/N ratio didn't allow precise measurements at ppb levels. To enhance the sensitivity, two approaches based on optimization of concentration and detection cell, are under investigation. On one hand, the design of the concentration cell and the absorbent was optimized in order to achieve a more selective and more accurate concentration of BTX gases. The results with a classic detection cell show improvement by a factor of 20 in term of detection limit, with a typical concentration down to 50 ppb of benzene accurately detected. On the other hand, reflective layer coating inside the microchannel have been proposed in order to improve the waveguide efficiency over the long light path. Aluminum or platinum were then sputtered inside the 450 μm * 400 μm rectangular cross section channel.

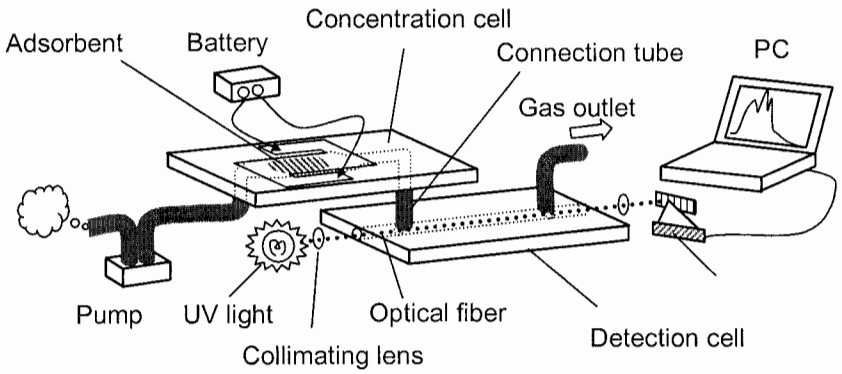

Figure 1: Drawing of the general set-up of the portable BTX gas sensor: the sample coming from the atmosphere is first concentrated, and then flow through the detection cell where UV- absorption yields qualitative and quantitative measurement.

Aluminum material exhibits a very stable reflectance over 90 % within a large range. Platinum (in combination with titanium to attach the layer to glass substrate) was also tested due to its chemical and physical properties. In the UV range (from 220 nm to 275 nm), platinum exhibits a reflectance coefficient between 40 and 60 %. Reflectance values were extracted from [3] and correspond to normal-incidence reflectance of different materials freshly evaporated.

4. Results and discussion

Due to the aspect ratio of the trench, and the suitability of coating the 4 faces inside the microchannel, various strategies have been studied in order to check several parameters effects: roughness of the surfaces, step coverage optimization, misalignments during fabrication process (Fig. 2). The transmittance coefficient was then measured with optical bench as shown in Fig. 2. The two fibers are connected respectively to UV light source and spectrophotometer. Depending on the method, the results, compared to the detection cell without any coating inside the microchannel, are varying from negligible to significant improvement in term of coupling efficiency between the two fibers as shown in Fig. 3.

The best results were obtained with the process briefly described bellow. Two half depth channels (220 µm * 400 µm) inner side-wall were coated with reflective layers by sputtering. Then, the two substrates are aligned under optical microscope, and bonded to each other with UV curable resist (the UV resist spreads at the interface thanks to capillary forces and is hardened by UV exposure through glass plate). The device was finally cut at the right dimension with dicing saw (Fig. 2).

The results depicted on Fig. 3 show results depending on the material coated inside. With Ti / Pt coating, we can get improvement by a factor of around 40 % with a 3cm transmission cell. These improvements reach almost 100 % with aluminum coating on the microchannel side-walls. By using this method, two approaches are then possible that should lead to significant improvements in terms of sensitivity: to keep the detection cell constant and then improve the measurement Signal over Noise ratio, or increase the

length of detection cell in order to improve the light path. Both approaches should be tested in order to point out the more efficient set-up.

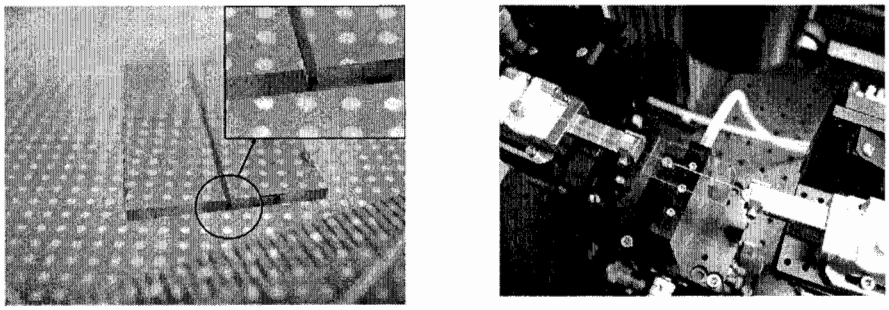

***Figure 2**: Picture of one detection cell with platinum coating inside microchannel walls (left), and the optical bench where the optical fibers coupling through coating microchannel are measured (right)*

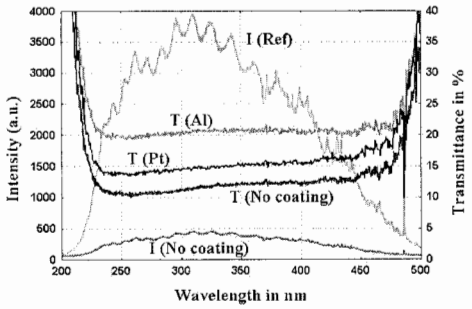

***Figure 3**: Intensity and transmittance of detection cell depending on the material coated inside (Ref. corresponds to the two fibers put very close to each other and gives the output spectrum of the D2 lamp)*

5. Conclusion

After optimizing and testing the pre-concentration and detection cells separately, both devices should be combined in order to check the response of the portable BTX measurement system in the low ppb range.

References

[1] "Environmental Governance and Analytical Techniques: Air Pollution and Air Quality Monitoring", United Nations University, Kyoto, Feb. 1998

[2] Y. Ueno, T. Horiuchi, T. Morimoto, and O. Niwa Anal. Chem. 73, 4688 (2001)

[3] "American Institute pf Physics Handbook", Mc Graw Hill book company, p 6-157

A MONOLITHIC POLYMER-OPTICS NETWORK FOR TIR-BASED FLUORESCENCE SENSING

Shr-Hau Huang[1], Yu-Jie Huang[2], and Fan-Gang Tseng[1, 2]
[1]Institute of MicroElectroMechanical System, [2]Engineering and System Science Dept.
National Tsing Hua University, Taiwan, ROC

Abstract

This paper proposes a novel design concept and fabrication method of a high-throughput monolithic optical platform for TIR-based fluorescence sensing. It consists of two layers of SU-8 resist structures, where one layer is used as a coupling layer including a micro lens and a prism-type coupler with adjustable angles, while the other layer is carried out as an integrated optical waveguide. To fabricate the prism-type coupler for coupling the light source into the waveguide, a novel technology employing glycerol-compensated oblique-exposure is employed. The fluorescence image of the Cy5-conjugated IgGs solution excited by the evanescent wave has been successfully observed.

Keywords: total internal reflection fluorescence, TIRF, SU-8 structures, waveguide

1. Introduction

Fluorescence sensing based on total internal reflection fluorescence (TIRF) has attracted increasing attentions because of the great reduction of background noise and suitability for studying the biochemical kinetics on nearing substrate surfaces [1]. Although various types of evanescent biosensors have been proposed [2-3], the fabrication of TIR-based optical biosensors with fully integration, ultra-sensitivity, and high-throughput property still encounter difficulties due to the complex device fabrication, assembly, and alignment processes. This paper introduces a novel monolithic fabrication/integration method on polymer material for TIR-based biosensor, thus eliminating the aforementioned issues encountered by traditional fabrication means. The schematic diagram of the monolithic TIR-based biosensor coupled with the integrated planar optical waveguide as a high-throughput platform is shown in Fig.1. It consists of two layers of SU-8 resist structures, where one layer is used for effectively conducting the excitation light into the integrated planar waveguide by a prism-type coupler at a predefined angle, and the other layer is served as an integrated optical waveguide in which the total internal reflection will occur and induce the evanescent wave from the interface, where it excited analytes. By employing arrays of paired emission/receiving optical fibers, micro-cylindrical lens, and waveguides for total internal reflection, a TIRF network with hundreds of cross-illuminated detection spots can be simultaneously carried out for TIR-based fluorescence sensing.

2. Optical path analysis and experimental design

The illustration of the cross section for depicting the propagation of the optical path is shown in Fig.1(c). A HeNe laser (λ=632.8nm) was used as the excitation light, and then coupled into the multimode optical fiber with 50μm core/125μm cladding. The emission fiber was placed close to the focal point of micro cylindrical lens, so that the excitation light can be effectively collimated. The prism-type coupler of SU-8 resist with an inclined angle of θ_1=35° was fabricated. According to Snell's law, the collimated light refracts, passing through the prism-type coupler into the waveguide of SU-8 layer, and reflects from the reflective layer (Al) toward the interface of the waveguide (refractive index n_1=1.67) and aqueous solution (refractive index n_2=1.33), which leads to a total internal reflection with an angle of θ=64.4°, which is above the critical angle (θc=52.8°=arcsin(n_2/n_1)) of the total internal reflection. The beam propagates continuously in a zigzag way with a span S among the reflection spots in the total internal reflection waveguide. The

number of reflections (NR) is a function of the thickness (d) of the waveguide, the length of the sensing window L, and angle of incidence θ_2, which can be expressed as NR =L/2d tan(θ_2). The relationship between the TIR angle(θ_2) and inclined angle(θ_1) of the prism-type coupler can be formulated as $\theta_2=\theta_1+\arcsin(1/n\cdot\sin(90-\theta_1))$. The angle of θ_1 is unnecessary to be defined precisely, because the total internal reflection will still occur between the interfaces as long as θ_1 is larger than the critical angle $\theta_1=18.1°$. But the penetration depth of evanescent wave will decrease as the inclined angle(θ_1) becomes larger. The evanescent field excites the analytes conjugated with fluorophores resulting in fluorescent emission, and this emitted energy is superimposed on the transmitted light and received by the receiving fibers accommodated on the other side of the waveguide, as shown in Fig.1(a). The fluorescence information from bio-reactions can be acquired from both CCD camera and receiving fibers quantitatively after filtering.

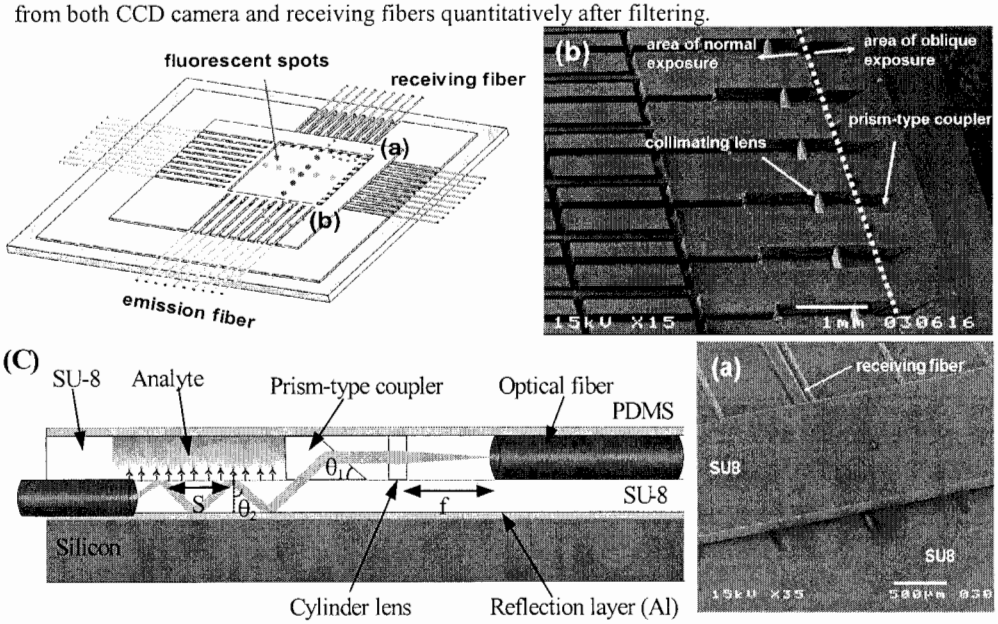

Figure 1. Schematic diagram of a high-throughput monolithic optical platform for TIR-based fluorescence sensing and the SEM pictures: (a) receiving fiber embedded in SU-8 layer, (b) array of prism-type couplers and collimating lens, (c) Schematic diagram of the ray propagation.

3. Fabrication process

The fabrication process is shown in Fig.2. The 1st SU-8 layer on the Al coated substrate was patterned by lithography to form the taper guiding channels for easily inserting receiving fibers and the planar optical waveguide. The CK-6020L black photo resist was then spread onto the SU-8 structure for the purpose of preventing the unexposed region from exposure during the latter processes. The 2nd SU-8 layer was patterned to form the prism-type structures with an inclined angle of $\theta_1=35°$ by employing glycerol-compensated oblique-exposure technique [4], which can fabricate inclined structures from 19° to 90° in a 2° accuracy, and then normally exposed to form the structures of fiber grooves for exciting fibers, cylindrical lens, and chamber. The fibers were aligned and glued into fiber grooves by UV curable epoxy. The PDMS membrane and SU8 structures were made hydrophilic by an oxygen plasma treatment and then bonded together.

4. Results and discussion

The SEM picture of the prism-type coupler with an inclined angle (θ_1) of 35° is shown in Fig.3. The R.M.S roughness of the inclined surface measured by AFM is below 25nm to ensure good optical properties. In order to test the ability of our system, a Cy5-conjugated IgGs solution with concentration of 1×10^{-2}M was introduced as the analyte. The fluorescent image of the Cy5-conjugated IgGs excited by the evanescent wave can be observed by an image intensified CCD (Hamamatsu C2741, Japan) as shown in Fig.4 with very low background noise. Thus, our design enables a compact and monolithic integration of elements of the traditional TIR-based biosensor into a high-throughput platform for TIR-based fluorescence sensing by using two layers of SU-8 resist structures and micro-optical components, eliminating the need to precise alignment for different optical components.

References

[1] Daniel Axelrod, Traffic, **2,** pp.764-774, 2001

[2] H. -P. Lehr, A. Brandenburg, and G. Sulz, Sensors and Actuators B, **92**, pp.303-314, 2003

[3] N. Chrouis and L. P. Lee,MicroTAS'03, pp.1323-1326, 2003

[4] K.Y. Hung, H. T. Hu, and F.G. Tseng, J. of Micromech. Microeng., **14**, pp.975-983, 2004

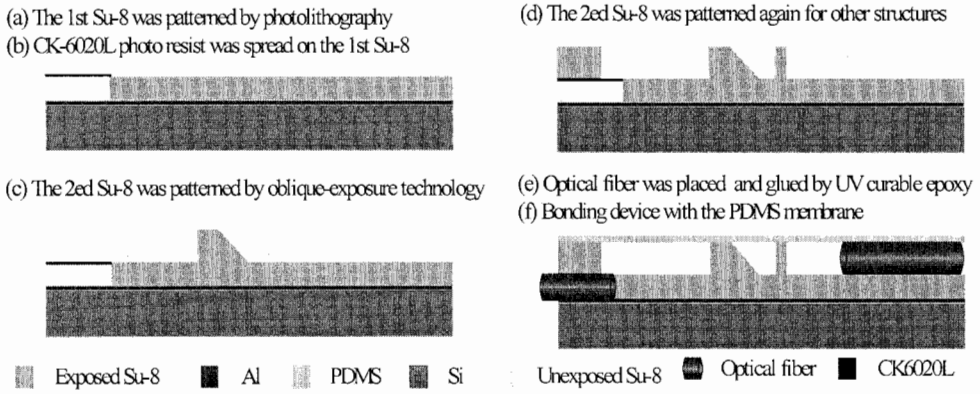

Figure 2. Fabrication processes of the monolithic optical system

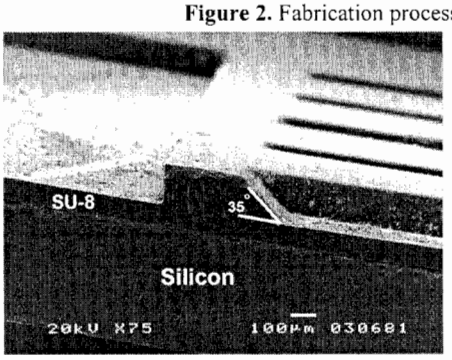

Figure 3. SEM picture of the prism-type coupler with an inclined angle of 35°

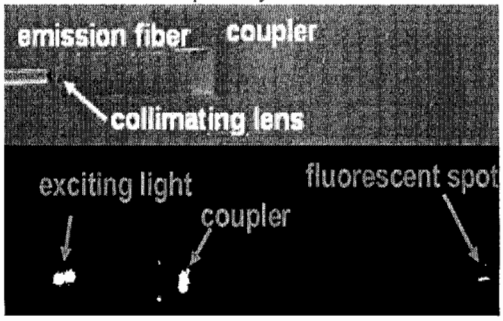

Figure 4. Fluorescent image of the Cy5-conjugated IgGs solution excited by the evanescent wave

INTEGRATED LOW-COST LEAKY WAVGUIDE SENSOR FOR μ-TAS APPLICATIONS

Mohammed Zourob, Stephan Mohr, Peter R. Fielden and Nicholas J. Goddard.

Department of Instrumentation and Analytical Science, UMIST, PO Box 88,
Manchester M60 1QD, U.K. e-mail: m.zourob@umist.ac.uk

Abstract

An integrated, low-cost, dye clad leaky waveguide (DCLW) device has been fabricated and tested for both refractive index and fluorescence detection in μ-TAS applications. The chip comprises the required flow geometry and optical coupling elements in a robust device that is simple and inexpensive to fabricate. Disposable DCLW chips were fabricated at room temperature by spin-coating both the dye and silica sol-gel waveguiding layers on to a polymer substrate which contained an injected moulded grating coupler. These devices have been designed to increase interaction between the evanescent field light at the channel wall and the materials in the sensing layer within the channels. The DCLW device has been used to detect changes in the refractive index of different concentrations of glycerol and to detect low concentrations of fluorescien, down to 10^{-12} M, using a grating coupler.

Key words: Optical waveguide, evanescent wave sensor, refractive index, fluorescence, disposable sensor.

1. Introduction

It has become apparent that the limiting factor in reducing the size and cost of a μ-TAS device is primarily set by the analyte detector. To date detection has generally focused on using optical measurements, however no real low-cost and disposable device has been proposed. Optical detection in μ-TAS systems usually takes place through the depth of the microfabricated channels, which has led to a large body of work reporting on the fabrication of high aspect ratio channel structures. Recently, the use of optical waveguides as detectors in μ-TAS systems has been reported [1-6]. Generally, in these systems, a high index waveguide forms the top or bottom wall of the channel, permitting optical detection via the evanescent field present at the channel-waveguide boundary [4, 6]. While this scheme has many advantages, it has the significant disadvantage of only sensing a thin layer (about half a wavelength) adjacent to the channel wall. If the channel is much deeper than half a wavelength, materials present in the top portion of the channel can not be sensed. To overcome this disadvantage requires the use of a structure that permits a greater extension of the evanescent field from the channel wall into the sensing medium. To address this an integrated, low-cost, extended evanescent field, absorbing materials clad leaky waveguide (DCLW) device has been fabricated and tested for both refractive index and fluorescence detection in μ-TAS applications.

2. Dye clad leaky waveguide

In this work the development of a DCLW disposable device, with a greater extension of the evanescent field at the channel surface, for bulk refractive index and fluorescence monitoring will be described. These devices consisted of a polymer substrate coated by a ~ 30 nm thick dye layer (n = 1.56-1.00750 i) and 300 nm thick sol-gel layer (n = 1.43). In these devices the light is coupled in by an injection moulded grating on the polymer substrate prior to being guided by the sol-gel layer, which is covered by aqueous media enclosed by the flow channel. The thickness of the device layers was designed to support one, sharp-guided mode and to give the maximum extension of the evanescent field (around 1.5 μm) into the sensing layer. This

arrangement allowed the maximum interaction with a bulk material resulting in a higher sensitivity. This waveguide structure supports the lower order mode, TE_0, at 63° from normal incidence.

3. Experimental

3.1 Set up of the sensor system

All the optical components were mounted on conventional optical posts and carriers installed on two optical rails (Melles Griot, Irvine, CA, USA). Fluorescence measurements were made using a 5 mW solid state laser, λ_{max} = 473 nm, (LCS-DTL-262, Laser 2000, Kettering, UK) as the excitation source. The laser light passed through a 470 nm ± 10 nm interference filter (Comar, UK) and fluorescence detection was achieved using a photo-multiplier tube detector (PMT, model 5784, Hamamatsu, Japan). The PMT was mounted behind a 510 nm ± 20 nm band pass filter (Glen Spectra, Stanmore, UK) and a collimating lens. Refractive index measurements were made using a 610 nm λ_{max} LED (RS components, Corby, UK). The LED was polished flat and mounted in a mounting tube of 25 mm diameter (Comar Instruments, Cambridge, UK), that also incorporated a collimating lens (40 mm focal length) and cylindrical lens (75 mm focal length) to focus the light into a line. The light was also passed through a 610 nm ± 10 nm wavelength interference filter, 25 mm in diameter, and a 25 mm diameter polariser (Comar Instruments). On the output side, the position of the decoupled light was monitored using a linear charge coupled device (CCD). Signals from the CCD were collected and analysed using a PC running dedicated software, written in-house.

3.2 Fabrication of the DCLW chip and the flow channel

Injection moulded poly methylmethacrylate (PMMA) top plates where fixed directly over a spin-coated sol-gel layer on the chip with UV–curable epoxy (Norland Products Inc., New Brunswick, NJ). Teflon tubing was then inserted into the inlet and outlet holes and was sealed in place on the chips using Crystalbond 509 mounting adhesive (Aremco Inc., Valley Cottage, NY). Injection moulding of the PMMA substrate, which contained the grating coupler was performed as previously described [5].

Injection moulded PMMA polymer substrates were coated by a dye layer using 15 mg of either solvent blue 35 dye or disperse red 1, which had been dissolved in 10 ml chloroform and stirred for 30 minutes. To produce a smooth dye layer all the solutions were freshly prepared when required. The dye solutions were spin coated on to the PMMA substrate at 4000 r.p.m for 20 seconds. After coating the dye layer the substrates were left to dry overnight in an oven at 60 °C. Sol-gel was prepared as follows; 2.3 g methyltriethoxysilane was mixed with 2 g ethanol. Then 0.8 g of HCl pH=1 was added dropwise to the solution and left to stirred for 1 h. The sol-gel was then spin coated onto the substrates at 3000 r.p.m. and left to dry at room temperature for one week. Solutions were irrigated through the DCLW devices using a Minipuls peristaltic pump (Anachem, Luton, UK) at a flow rate of 500 µl min^{-1}.

4. Results and discussion

Figure 1 illustrates the performance of the DCLW device when used to detect low concentrations of fluorescein down to 10^{-12} M fluorescein. Figure 2 illustrates the change in the evanescent modal position of the DCLW on the linear CCD as the change in refractive index of a number of glycerol/water solutions from 0 to 10% v/v.

Figure 3 shows a theoretical comparison between the TE_0 DCLW waveguide and the TM_0 for a Resonant Mirror (RM) sensor. It can be seen that the predicted RM TM_0 mode decays rapidly at

the waveguide/water boundary whereas the DCLW TE_0 mode extends further from the waveguide/water boundary. Figure 4 demonstrates the linear response to glycerol concentrations for both types of sensor modes and shows that the DCLW is three times more sensitive than the RM device.

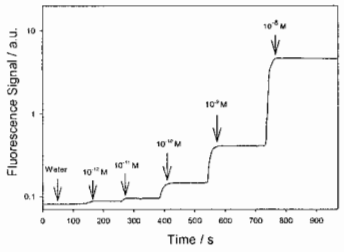

Figure 1. The variation of fluorescence signal with various concentrations of fluorescein excited by a 473 nm blue laser using a disperse red 1-CLW chip.

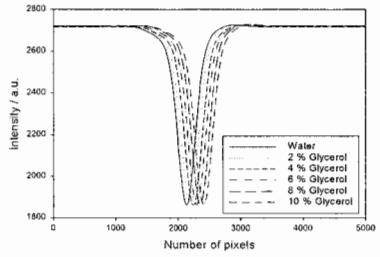

Figure 2. Refractive index changes observed with various concentrations of glycerol in aqueous solution monitored using solvent blue 35-CLW device.

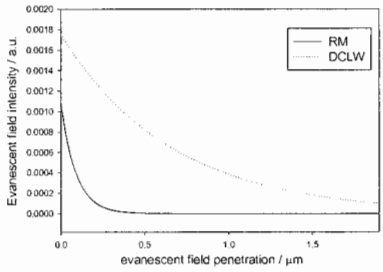

Figure 3. Comparison of the calculated evanescent field extensions of the RM and solvent blue-CLW sensors.

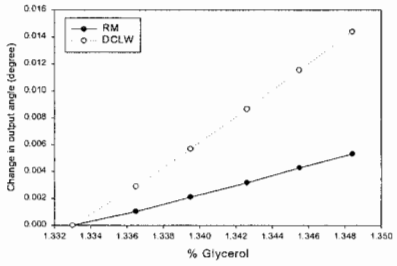

Figure 4. Comparison of RM and solvent blue-CLW in the mode movement for different concentrations of glycerol in aqueous solution.

Conclusion

An integrated, low-cost, leaky waveguide device has been successfully fabricated and tested for both refractive index and fluorescence detection in microchannel.

References:

1- N.J. Goddard, K. Singh, AF. Bounaira, R.J. Holmes, S.J. Baldock, L.W. Pickering, P.R. Fielden, R. D. Snook, 1998. Micro Total Analysis Systems μ-TAS 1998/Proceedings, 97-100.

2. R. Holmes, K. Joyce, K. Singh, P.R. Fielden and N.J. Goddard, 2000. MicroTec. 2000/Proceedings 2, VDE Verlag, Berlin, 691-694.

3. S. C. Jakeway and A. J. de Mello, 2001. Analyst 126, 1505-1510.

4. J.P. Lenney, N.J. Goddard, J.C. Morey, R.D. Snook and P.R. Fielden, 1997. Sens. Actuators B 39, 211-217.

5. M. Zourob, S. Mohr, P.R. Fielden, N.J. Goddard, 2003. Sens Actuators B 94, 304-312.

6. K. Matsubara, S. Kawata, S. Minami, 1998. Appl. Opt. 27, 1160-1163.

MICRO-SYNTHESIS AND INTERFACE MICROCHIP FOR NMR SPECTROSCOPY

Yutaka Takahashi[1, 2], Ryo Sakai[1], Ryoji Tanaka[2], Hiroto Suematsu[2], Hiroaki Utsumi[2], Yoshikazu Yoshida[1] and Takehiko Kitamori[3]

[1] *The Research Association of Micro Chemical Process Technology, 3-2-1 Sakado, Takatsu-ku, Kawasaki-shi 213-0012 Japan*

[2] *Analytical Instrument Division, JEOL Ltd., 3-1-2 Musashino, Akishima-shi, Tokyo 196-8558 Japan*

[3] *Dep. of Applied Chemistry, The University of Tokyo, 7-3-1 Hongo, Bunkyo-ku, Tokyo 113-8656 Japan*

Abstract

An interface microchip for NMR spectroscopy was fabricated and evaluated. This microchip was available with a standard NMR probe without any modifications. A basic performance was evaluated by measuring ^{1}H NMR spectrum of $CHCl_3$. The line shape was 1.4 Hz with Full-Width at Half Maximum (FWHM) definition. The performance was demonstrated by measuring the synthetic product of N-trifluoroacetylation of β-phenethylamine (**1**). The ^{1}H signal of α-position of the product (2,2,2-trifluoro-N-phenetyl acetamide, **2**) could be clearly distinguished from that of **1**. This microchip is expected to use applications for real-time detection of unstable intermediates in chemical reactions.

Keywords: NMR, Microchip, Interface, Structural analysis, Micro-synthesis

1. Introduction

Analytical instruments (e.g. mass spectrometer (MS) and nuclear magnetic resonance (NMR) spectroscopy) are expected as a qualitative analytic detector for microchip technologies. Especially, NMR is that it is the only analytical tool providing direct determination of molecular structure in solution. Many researchers have reported the development of an interface for coupling with microchip and MS [1, 2]. However, few papers concerning NMR have been reported [3]. In these papers, the microchip has a magnetic coil close to a detection channel, and then a special NMR probe is necessary for using such microchip.

From such viewpoint, we developed a new NMR interface microchip. The chip is constructed by the part with a wide shape for application, and that with a long and narrow one for detection. Since the latter part can be inserted into a NMR sample tube, this microchip can be used with standard NMR probes.

2. Experimental

Microchip Fabrication: The microchip, fabricated on a Pyrex glass plate by the photolithographic wet etching method, was purchased from Institute of Microchemical Technology, Co Ltd (Kawasaki, Japan). Figure 1 shows the photograph of the new developed NMR interface microchip. The channel of the microchip consists of synthesis part and detection part. For synthesis, channel depth was 40 μm, channel width was 100 μm and channel length was 120 mm. For detection, channel depth was 100 μm, channel width was 300 μm and channel length was 320 mm. The volume of the detection channel was ca. 11 μL.

Instrumentation: NMR spectra were obtained on a JEOL JNM-ECA 400 and 600 with a standard 5 mm probe. Chemical solutions were delivered into channels using syringe pumps (Pump 22, Harvard Apparatus, Inc., MA, USA). Syringes and the microchip were coupled with a fused-silica capillary tubing (75 μm ID x 150 μm OD). The tubing was directly connected into connection ports of the microchip using a simple connector. The narrow shape part of the microchip was

inserted into a sample tube and was mounted into a probe together with a standard sample tube holder. When a non-deuterated solvent was used to prepare chemical solutions, a deuterated solvent was introduced into a gap between the microchip and the sample tube to use of a NMR lock.

Chemicals and synthesis: **1**, trifluoroacetic anhydride (TFAA) and dichloromethane were obtained from Tokyo Chemical Industry (Tokyo, Japan) and used without further purifications. Dichloromethane-d_2 was purchased from Cambridge Isotope Laboratories (MA, USA). **1** and TFAA were solved in dichloromethane or dichloromethane-d_2 with the concentration of 100 – 300 mM, respectively. Chemical solutions were prepared under nitrogen. Scheme 1 shows the synthesis of **2**. Two solutions were introduced into channels, and then were mixed in a Y-shape channel. It was expected that the reaction was immediately occurred in the synthesis channel [4]. The reaction mixture was stored in the detection channel and NMR spectra were measured.

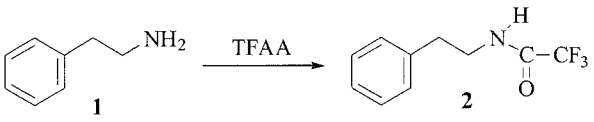

Scheme 1. N-Trifluoroacetylation of β-phenetylamine.

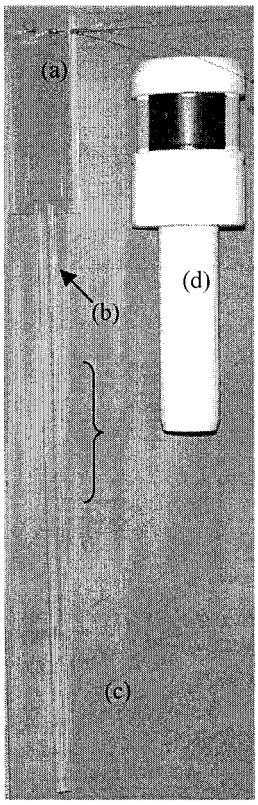

Figure 1. Photograph of (a) NMR interface microchip, (b) synthesis channel, (c) detection channel, (d) sample tube holder.

3. Results and discussion

Basic performance of this microchip was evaluated by 600 MHz instrument. Figure 2 shows a ^{1}H NMR spectrum of 11 μL of 100% $CHCl_3$ with an excellent S/N. $CDCl_3$ was used for a NMR lock. The 90° pulse was 10 μs, comparable to the values found on commercial 5 mm probes. A line width was 1.4 Hz at FWHM definition.

^{1}H NMR measurement of on-chip micro-synthesis was succeeded. ^{1}H NMR spectra of reaction mixtures of N-trifluoroacetylation of **1** were acquired by 400 MHz instrument with variety of the mixing ratio of **1** and TFAA of dichloromethane-d_2 solutions. The mixing ratio was changed by control the flow rate of syringe pumps. Figure 3 shows ^{1}H NMR spectra of reaction mixtures. The concentration was 200 mM for **1** and 300 mM for TFAA. The flow rate was 2 μL/min. The reaction mixture was stored 3 minutes into the detection channel. A resolution of this spectrum is extremely good. These results means the design of the detection channel is best suited to obtain a high-resolution NMR spectrum.

The spectrum pattern is almost same as that of standard compound of **2** synthesized and purified by batch process. No peaks corresponding to **1** was observed. As shown in Fig. 3, the triplet at δ 3.62 ppm and quartet at δ 2.88 ppm were assigned to methylene protons of α and β position, respectively.

The broad peak at δ 6.65 ppm was assigned to amide proton. The multiplex peak at δ 7.25 ppm assigned to benzene ring protons. The chemical shift of α-methylene proton was clearly distinguished from that of **1**.

The consumed amount of **1** in this experiment was approximately 1.2 μmol. This amount was 20 times smaller than that for a standard sample tube. At the conference, we will show real-time monitoring data of micro-syntheses.

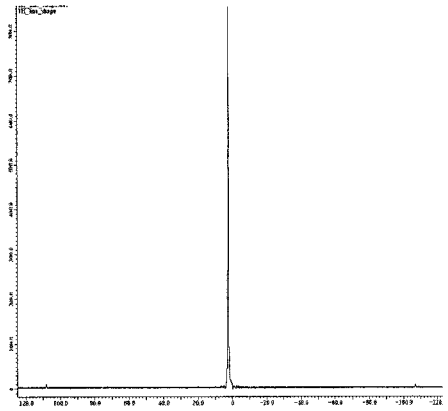

Figure 2. ^{1}H NMR spectrum of $CHCl_3$.

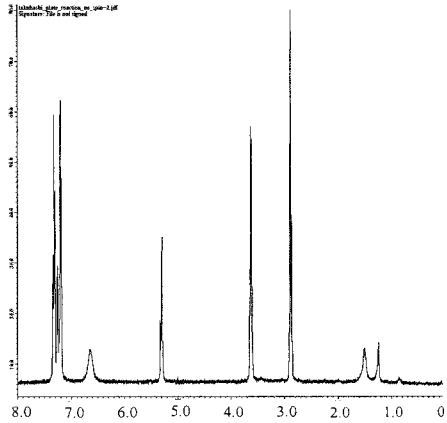

Figure 3. ^{1}H NMR spectrum of the reaction mixture of on-chip N-trifluoroacetylation of β-phenetylamine.

4. Conclusions

We developed new interface microchip for NMR spectroscopy. This microchip has a long and narrow shape part to insert into a standard sample tube holder. Therefore, this chip can be mounted into a standard 5 mm probe. ^{1}H NMR spectrum of a reaction mixture was observed for on-chip N-trifluoroacetylation of **1** using a 400 MHz instrument. A resolution of the ^{1}H NMR spectrum of **2** was nearly same as that of a standard sample tube.

This means this microchip is expected to use on-chip NMR applications such as a high-throughput screening of micro-syntheses and a real-time structural analysis of unstable intermediates in chemical reactions. This is also useful to evaluate chemical reaction conditions for on-chip micro-syntheses of high-added value medicines and chemicals.

Acknowledgements

This work was supported by "Project of Micro-Chemical Technology for Production, Analysis and Measurement Systems" of New Energy and Industrial Technology Development Organization (NEDO), Japan.

References

[1] D. Figeys, Y. Ning and R. Aebersold, *Anal. Chem.*, **69**, 3153-3160 (1997).

[2] E. Gelpi, *J. Mass Spectrom.*, **37**, 241-253 (2002) .

[3] J. H. Walton, J. S. de Ropp, M. V. Shutov, A. G. Goloshevsky, M. J. McCarthy, R. L. Smith and S. D. Collins, *Anal. Chem.*, **75**, 5030-5036 (2003).

[4] K. Sato, M. Tokeshi, T. Sawada, T. Kitamori, *Anal. Sci,.* **16**, 455-456 (2000).

PARALLEL ABSORBANCE DETECTION USING HOT EMBOSSED ELEVATED OPTICAL ELEMENTS

John P Hulme and Yuji Miyahara

Biomaterials Center, National Institute for Materials Science
1-1 Namiki, Tsukuba, Ibaraki 305-0044, Japan

Abstract

In this paper we demonstrate the detection of increasing concentrations of methylene blue using elevated grating surfaces at 596 nm. A optical platform containg 500 sensing elements was hot embossed in polyethylene terephthalate (PET) from a copper coated polyurethane master. The chip was coated with 70 nm of gold and sealed using a PDMS cover plate. The detection limit for the device was 1 ppm of the for mentioned dye.

Keywords: Elevated, Optical, Elements, Absorbance, Nanostructure

Introduction

Of the many optical detection techniques, absorbance is not commonly used in microfluidic systems[1]. Miniaturized devices permit only limited detection and often require the use of a multireflective surface to increase the optical path length[2]. Early improvements in design and absorbance detection limits were achieved in miniaturized silicon flow cells and glass microcapillaries [3]. In traditional spectrophotometers, the optical element is independent of the microchannels or the detection area, adding to the number of total components used in the instrument's construction. In this paper we continue the approach of intergrating the coupling and sensor area into one element and raising it into solution improving the signal to noise ratio.

Experimental

Absorbance measurements were measured with 8452A model spectrophotometer (Hewlett-Packard, Menlo Park, CA). The optical arrangement used is descibed elsewhere[4] Changes in in reflected intensity of the first diffractive order to different aqueous dye solutions were measured. Methylene blue solutions were prepared in (0.05M) sodium phospahate buffer pH (7.4). Solutions were irrigated through the chip at a flow rate of 5 ml min^{-1}. Changes in absorbance were measured at five minute intervals against a sodium phosphate blank. The optical pathlength was calculated to be 200 μm at 596 nm. The calculation for the pathlength has been previously reported[4].

Fabrication

The fabrication of a multilayered polyurethane master was achieved using standard UV photolithography and embossing procedures. The tipping of the polyurethane master with copper was used to increase the heat conductivity of the polyurethane and improve the lifetime of the master. The pillar dimesions were 30 μm high by 100 μm with a 500 nm grating patterned on top. Hot embossing was performed in house. A flat piece of PET 2-cm^2 was embossed at 77^0C for nine minutes at a pressure of 1.2 kn. This was allowed to cool to 50^0C removed coated with 5nm of chromium and 70 nm of gold with standard deposition techniques. A simple seal structure was fabricated in Su-8 and a PDMS copy was taken producing a top plate with an integrated flow cell design. The final seal was accomplished by injecting PDMS between the seal line and the top bottom plates and allowing to cure for 24 hours before use.

Results

Changes in the reflected intensityf of elements x and y to different concentrations of methylene blue are shown in Figures 1 and 2 respectively. The limit of detection was 1ppm. The device was stanadardized using the for mentioned against a commercial spectrophotometer. The results are shown in the table 1.

Table1. Limits of Detection for absorbance cell

Dye (ppm)	X	Y	Spectrophotometer
0	0	0	0
1	.002	.019	0
2	.0037	.0039	.012
5	.0070	.078	.025

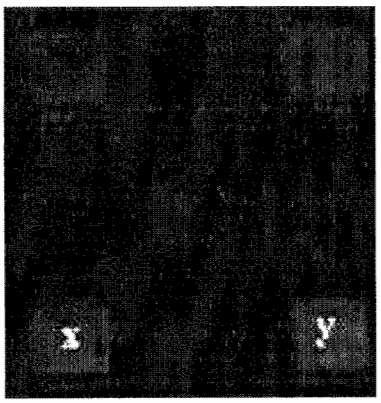

Figure 1. 1st order 596 nm

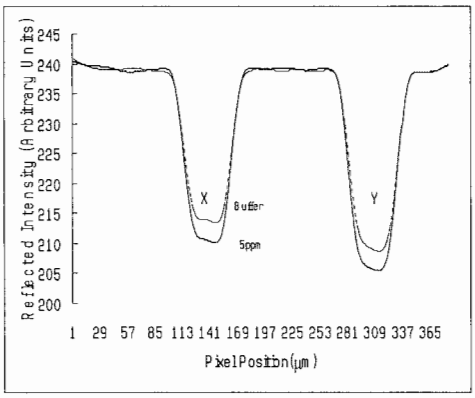

Figure 2. Change in reflected intensity.

Conclusions

The simple elevation of the grating surface into the surrounding solution by virtue of evolving design and fabrication methods lead to improvement in the signal to noise ratio, compared to similar grating coupled or planar sensing devices.

Acknowledgements

We would like to thank Drs. Y Horiike, and A Oki, of National Institute of Materials Science. Dr N.J Goddard of the University of Manchester UK for useful discussions.

References

[1] A.M. Schwarz and P.C. Hauser, *Lab Chip* 2001, **1**, 1-6.
[2] A. Manz, N. Graber, and Widmer, H. M. *Sens & Act B*, **1**, 1990, 244-248.
[3] H. Salimi-Moosavi, T. Tang, and D.J. Harrison, *J. Am. Chem. Soc.* 1997, **119**, 8716-8717.
[4]J.P Hulme, P.R. Fielden and N.J. Goddard, *Anal Chem*, 2004, **76**, 238-243.

THE APPLICATION OF RESPONSE SURFACES FOR OPTIMIZATION OF SERRS DETECTION IN A MICRO-FLUIDIC DEVICE

Gillian M.Greenway, Dean A. Moore and Anthony D.Walmsley
Department of Chemistry University of Hull, Hull, HU67 7RX, UK

Abstract
Surface enhanced Raman resonance spectrometry (SERRS) using the surfaces of flowing colloidal particles provides a highly sensitive detection method for microfluidic systems. The sensitivity and reproducibility of the systems critically depends on the flow rates of the dye, colloid and aggregating agent in the microfluidic system. Optimization of these parameters was achieved using experimental design response surfaces to minimize the number of experiments required by augmenting small and large designs into one response surface. Using experimental design a linear calibration graph was obtained for cresyl violet acetate down to the $2x10^{-9}$M level.
Keywords: surface enhanced resonance Raman spectrometry, optimization, response curves

1. Introduction

Surface enhanced Raman spectroscopy (SERS) is a highly sensitive measurement technique and has been shown to be capable of detecting at the pico to femtomole analyte level. The sensitivity of the technique can be improved further in surface enhanced Raman resonance spectrometry (SERRS), where the excitation wavelength of the laser is tuned to the same frequency as the wavelength of the molecule or dye label to be determined. The technique has many applications but has been mainly been demonstrated for bioanalytical applications. This enhanced Raman technique however depends on the analyte being adsorbed onto a roughened metal surface and this can severely affect the reproducibility of the signal if a roughened metal electrode or film is utilized. To overcome this problem metal nanoparticles have been used, such as gold and silver colloids and micro-fluidic systems provide an ideal controlled environment to improve reproducibility *[1]*. A further important factor that has been identified in SERS techniques is addition of a reagent (aggregating agent) to roughen the surface of the colloid. In a micro-fluidic device the flow of reagents will be laminar and this will provide control of the rate at which the chemical species adsorb onto the colloid surface and the degree of roughness applied to the colloid surface. The aim of this work was to take advantage of this control and maximize the sensitivity and reproducibility of the system by optimizing to the flow of the colloid, dye and aggregating agent using response surface experimental designs.

2. Micro-fluidic Device Development and Instrumentation

The micro-fluidic device used was made, using a photolithographic technique established by McCreedy et al. *[2]*, (the design can be seen in Fig 1). This device consisted of an etched glass base plate and glass top plate; drilled with 2mm wide inlet holes. Both plates where thermally bonded together in a furnace 565°C, producing a device with the dimensions of 25 x 25 x 5 mm. The etched channels were 363μm wide and 67μm deep and the reagents where driven through the device using a syringe pump. A Jobin Yvon Horiba integrated Raman Spectrometer with an inverted Olympus 1 X70 microscope and CCD camera was utilized for the measurements with a Helium-Neon laser (excitation wavelength of 632.1nm). The experimental design was carried out using Matlab 6.5 software (The Mathworks Inc, USA). The experimental design used was a series of 3 factor 5 level augmented design, with the response being the Raman intensity, in with the first design was used to cover the initial experimental space and then the response surface was plotted to guide the subsequent design levels. In this way a much greater response surface can be explored using a

minimal number of design points. A series of non-central design points were also included to ensure the reproducibility of the measurement systems.

3. Results and discussion

The aim of this work was to ensure that the initial conditions used were wide ranging enough to pick up optimums, but not so wide as to require unsuitable experimental conditions and numerous experiments. The use of experimental design response surfaces minimizes the number of experiments by augmenting small and large designs into one response surface, to which experimental conditions of interest can be added on subsequently. Experiments were performed with silver reduced colloid, NaCl aggregating agent (1M) and dye (cresyl violet acetate, 1 $x10^{-3}$M) in flow rate ranges between 2.5 and 20 µl/min. Fig. 2 shows the 3D image of the SERRS occurring in the micro-fluidic channel. An example of an augmented response surface for the data, for the flow rates of the aggregating agent and colloid is shown in Fig 3; The figure illustrates the importance of taking a systematic approach to optimization. At low flow rates two clear optimum are seen, for example an optimal flow rate for the aggregating agent was seen at 4-5µl/min with a low colloid flow (5 µl/min), but another optimum was also seen at 8µl/min aggregating agent. These optimums were however very narrow and unstable, whereas at higher silver colloid flow rates there is a high plateau region in which much more robust results would be obtained. Using colloid flow rates above 16 µl/min provides high sensitivity and good reproducibility. Similar response curves were obtained for flow rates of colloid *vs.* dye and dye *vs.* aggregating agent. The results show for the response curve in Fig. 3 only required 51 experiments, which is considerable smaller than a traditional response surface approach, and the step size could easily be altered to ensure sufficient data points in area of rapidly changing surface response. Similar figures to Fig. 3 were obtained for dye flow rate versus colloid flow rate and for aggregating agent versus dye. These response curves showed that the optimal flow rate of the dye is less than 3µl/min. The high colloid flow provides a continuously replenished fresh surface for measurements and when the results were compared with those from a batch system the reproducibility was 10% higher. A range of calibration standards ranging from $2x10^{-9}$M to $6x10^{-9}$M were analyzed, the resulting calibration graph was linear (R^2=0.9822)

4. Conclusions

Experimental design provides a simple method for system optimization, highlighting the effect that flow rate had upon the response signal obtained from SERRS and the effect on the reproducibility of the signal. One of the advantages of using an augmented design is that the number of design points required to map out the experimental responses is greatly reduced, which in terms of practical chemistry is highly desirable as the time for each experiment can be long and expensive in terms of reagents.

References

[1] R. Keir, W.E. Smith, *Applied Spectroscopy*, **56,** 551-559 (2002).
[2] T. McCreedy, *Trends Anal. Chem.*, **19**, 396.-401 (2002).

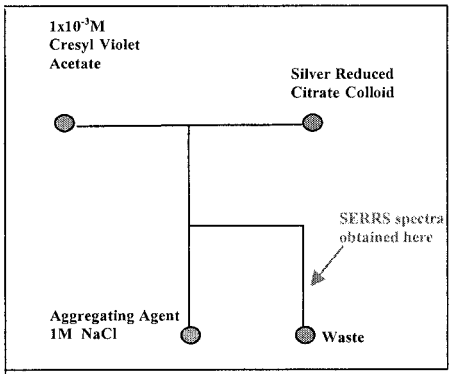

Figure 1. Layout of microfluidic device

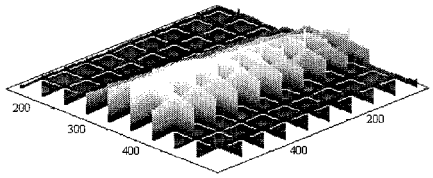

Figure 2. 3D image of SERRS in microfluidic channel at area shown in Fig. 1

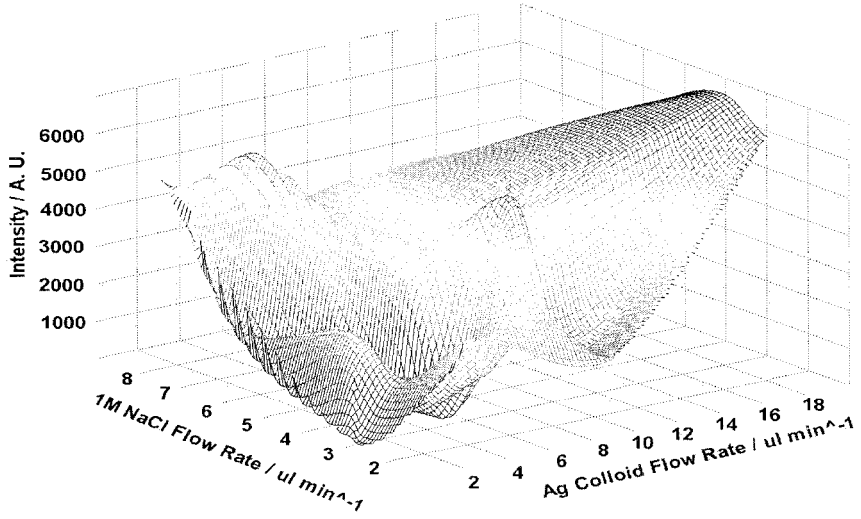

Figure 3. Example of a response surface for optimisation of SERRS intensity

FABRICATION OF MICRO SCANNING SYSTEM FOR FLUORESCENCE DETECTION OF PROTEIN PATTERNS

Kook-Nyung Lee[1], Yun-Ho Jang[2], Sei-Hwan Jung[2], Jaeho Choi[3], Yong-Kweon Kim[2], Hoseong Kim[3], Yoon-Sik Lee[1]

[1]*School of Chemical Engineering, Seoul National University, Seoul, Korea*

[2]*School of Electrical Engineering and Computer Science, Seoul National University, Seoul, Korea*

[3]*School of Electrical and Electronic Engineering, Chung Ang University, Seoul, Korea*

Abstract

We propose a hand-held type fluorescence detection system for protein sample analysis. By adopting micro prism in a detection system, the emitted light from the fluorescence of protein can be easily angular separated from the excitation beam so that the signal to noise ratio (SNR) in fluorescence detection can be improved. As an essential part of the proposed system, a micro scanning mirror is designed and fabricated. The optical benches are fabricated monolithically in the silicon substrate with the scanning mirror, which gives simple and easy integration of the optical scanning systems. The fabricated scanning mirror for fluorescence detection system has 7 degree deflection angle at the resonance and it is 9 mm x 10 mm x 1 mm in a chip dimension, and it is available for portable biodetection system.

Keywords: Hand-held system, Scanning mirror, Fluorescence detection, Protein patterns, Micro prism

1. Introduction

Although biochips have been developed on a glass slide scale through micromachining and micro array technology, most fluorescence detection still relies on conventional fluorescence detection systems, which are bulky and expensive since a series of filters are employed to separate the weak fluorescence from the strong transmitted excitation light spectrally and scanner and photomultiplier should be used [1]. In order to allow a point of care system, the fluorescence detection device must be miniaturized and made portable and a laser excitation device must be made smaller and must scan fluorescence pattern arrays without degrading the optical power efficiency and signal to noise ratio. We devise a micro optical scanning system adopting a scanning mirror and optical fiber so that the scanning device can be miniaturized enough to satisfy the portable system scale through the beam collimation and scanning of excitation light source. We described the design and the fabrication process of a scanning mirror and the actuating properties of the fabricated scanning mirror.

2. Design

The optical scanning system consists of two layers of substrate. The optical bench guides and the scanning mirror are fabricated on the top substrate. The PDMS (polydimethylsiloxane) substrate beneath the top substrate includes the micro prism. The optical components positioned in the top substrate contribute to the collimation of laser incident from the optical fiber, and the mirror scans the laser by its actuation. The PDMS micro prism makes two laser beams cross and branch off on the bottom side of the PDMS substrate by the light refraction. The emission light from the fluorescence patterns is angular-separated from the incident excitation laser under the bottom of the prism substrate by the refraction. The proposed miniaturized detection system is shown in Figure 1. Figure 2 shows the simulation result about beam path of the optical system from the ball lens to the fluorescence patterns.

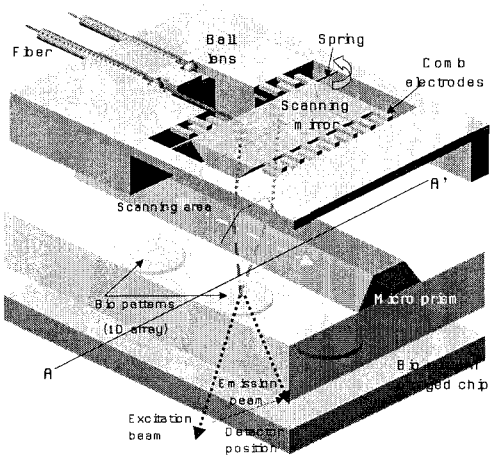

Figure 1. Schematic view of proposed detection system using scanning mirror and

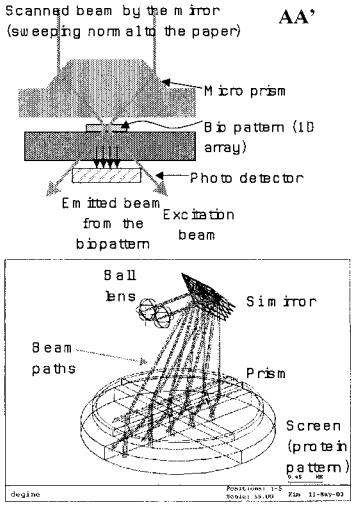

Figure 2. Optical path simulation using Code-V software of the designed detection system

3. Fabrication results

Figure 3 shows the fabricated scanning mirror and micro prism. Comb electrodes and torsion springs were well defined, as were the deep trenches for the optical bench. The ball lens had already been placed onto the bench and fixed by clamps. The optical z-axis was passively aligned by the optical bench, which was placed in the middle depth of the substrate, 238 μm from the top surface. Figure 3 shows SEM pictures of the fabricated scanning mirror, viewed from the bottom side, showing the folded spring type in Figure 3(b). The reflective surface of the mirror was obtained on one side of the mesa-type silicon structure. The glass wafer gave mechanical support for the isolated parts of the silicon for electrical isolation. Comb electrodes and torsion springs were fabricated on the thinned trench bottom area around the mesa-type mirror structure. The thickness of the remaining silicon substrate, caused by the thinning in KOH wet etching, was 50 μm. This matched the thickness of the comb electrodes and the springs. The optical input path can be seen through the ball lens bench near the mirror plane.

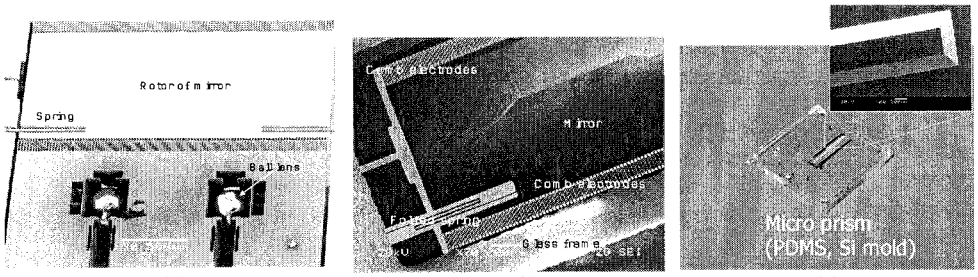

(a) (b) (c)

Figure 3. Fabricated scanning mirror and micro prism, (a) micro scanning mirror (top side view), (b) scanning mirror (bottom side view), (c) PDMS micro prism

4. Results and discussion

The optical fiber and the ball lens were placed on the fabricated bench guide of the optical system, and a He-Ne laser was coupled to the fiber and was incident on the ball lens. A CCD camera on the bottom side observed the spot of the laser beam on the mirror and the screen. Figure 4(a) shows the laser spots on the reflective plane of the mirror, incident from the optical fiber and ball lens, while the scanning mirror was oscillating. Figure 4(b)~(e) show the laser spot captured by the CCD camera on the screen, which was 10 mm apart from the mirror. A spot diameter of 500 μm was measured from the collimation by the ball lens, indicating the alignment of the optical fiber, ball lens, and scanning mirror. As the driving frequency approached the oscillation frequency of the scanning mirror, the deflection angle of the scanning mirror was increased, and the scan of the laser lengthened. The characteristics of scanning mirror were summarized in Table 1.

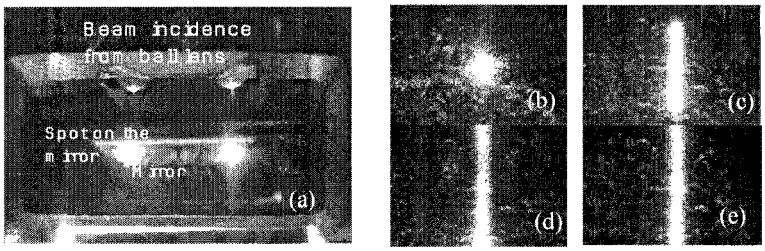

Figure 4. Beam scanning by mirror oscillation, (a) scanning mirror, (b) initial state, (c) 490Hz, (d) 480 Hz and (e) 470 Hz = resonant

5. Conclusions

We have fabricated a scanning mirror using the (111)-plane of silicon as a reflective surface, with optical benches for the optical fiber and the ball lens integrated monolithically on a silicon wafer. The maximum deflection angle of the scanning mirror was 7° at the resonant frequency when a 16 V peak-peak square-wave was applied to the comb electrodes. The experiment results show the feasibility of the proposed optical system for miniaturization as a laser scanner. A scanning mirror fabricated for a fluorescence detection system can be miniaturized to 9 mm x 10 mm x 1 mm, suitable for a portable biodetection system.

Acknowledgements

This research was supported by the Nano Bioelectronics and Systems Research Center of Seoul National University, which is an ERC supported by the Korean Science and Engineering Foundation (KOSEF).

References

[1] Xue Feng Wang & Brian Herman, "Fluorescence Imaging Spectroscopy and Microscopy", Wiley-Interscience, April, 1996

Table 1. Summary of characteristics of scanning mirror

Samples (spring type)	M1(folded)	M2(flat)	M3(folded)
Initial deflection	1.98 μm	3.66 μm	6.56 μm
Normalized spring constant K ($\sqrt{K}$)	1	0.54(0.73)	0.3(0.54)
Resonant frequency	465 Hz	330 Hz	235 Hz
Deflection angle at resonance([°])	1.7°(25)	3.5°(50)	7°(100)
Applied voltage	18 V	18V	16 V

TEMPERATURE CONTROLLABLE TRYPSIN DIGESTION MICROCHIP FOR MASS SPECTROMETRY

Tae Seok Sim[1], Eun-Mi Kim[2], Hwang-soo Joo[2], Dae Weon Kim[3], Kook-Nyung Lee[2], Yong Hyup Kim[3], Byung Gee Kim[3] and Yong-Kweon Kim[1]

[1]School of Electrical Engineering and Computer Science,
[2]School of Chemical Engineering
[3]School of Mechanical and Aerospace Engineering, Seoul National University, 301-1116, San56-1, Shillim-dong, Kwanak-ku, Seoul 151-742, Korea

Abstract

We demonstrate a simple and fast method on the trypsin digestion of protein for MALDI-TOF MS (matrix assisted laser desorption/ionization time of flight mass spectrometry) using temperature controllable microchip. With the fabricated microchip, proteins are thermally denatured at 80 °C for 1 minute and digested by the trypsin at 37 °C for 10 minutes. To evaluate the proposed thermal denaturation method, the results of the digestion with and without thermal denaturation are compared each other.

Keywords: Thermal denaturation, Temperature control, Trypsin digestion, Microchip

1. Introduction

In the research of proteomics, mass spectrometry is an essential analysis method for the identification of unknown proteins. Since the native proteins are not susceptible to digestion for their complex 3-dimensional structure, protein should be denatured prior to the trypsin digestion [1]. Thermal denaturation does not require the several chemical mixing steps and purification/concentration prior to mass spectral analysis, which should be needed in the conventional chemical denaturation. It is much simpler, faster and free form the possibility of the contamination and handling errors derived from the several chemical mixing steps [2]. The use of the microchip also allows the small volume of the protein and the increase of reliability [3]. We fabricated the temperature controllable microchip and the temperature control system to perform the thermal denaturation and trypsin digestion with benefits of the thermal denaturation and the microchip.

2. Design and fabrication

The schematic view of the designed temperature controllable microchip is depicted in Fig. 1. The microchip consists of three parts such as silicon, glass and Pt electrodes. A reaction chamber and microchannels are formed on the silicon substrate and the holes for external connection are formed thorough the glass substrate. Pt electrodes are located below the reaction chamber and act as a heater and temperature sensor. For the enhancement of the thermal properties of the microchip, silicon substrates were thinned by the KOH wet etch (30 wt%, 80 °C) and CMP (chemical mechanical polishing) process to the thickness of 200μm. And the reaction chamber is thermally isolated by removing unnecessary silicon part using deep RIE (reactive ion etching) to prevent thermal dissipation. Silicon and glass are anodically bonded each other to cover the open side of reaction chamber and microchannels. The total dimension of the fabricated microchip is 24×17×0.7 mm^3. The thicknesses of the thinned silicon substrate and the glass substrate are 200 μm and 500 μm, respectively. The volume of reaction chamber is 4 μl and the area of channel cross section is 200×100 μm^2. The photograph of the fabricated microchip is shown in Fig. 2. For the easy indication of the injected sample volume, metering bar is located beside the reaction chamber. The reservoirs for the reference sample for the calibration of MALDI-TOF MS are also located on the

microchip. A sample is injected to the reaction chamber by the capillary force and drawn out by applying air pressure to the air venting channel.

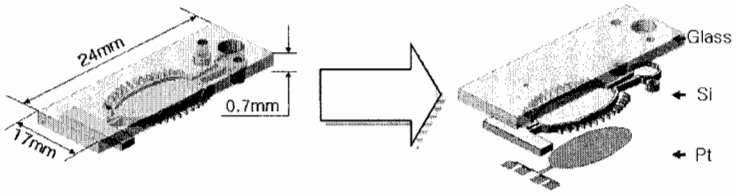

(a) (b)

Figure 1. Schematic view of the proposed temperature controllable trypsin digestion microchip.

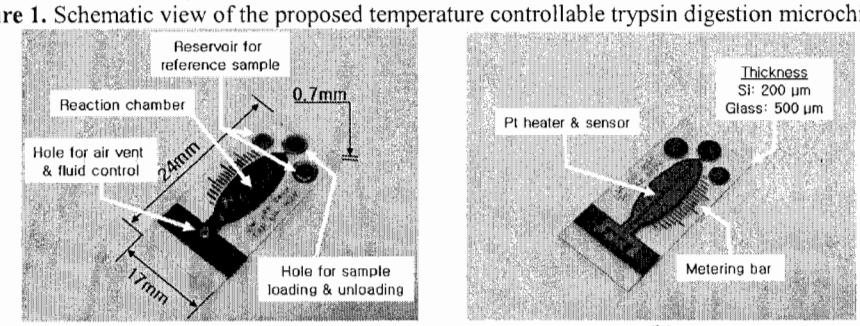

(a) (b)

Figure 2. Photographs of the fabricated temperature controllable microchip for trypsin digestion (a) top side view, (b) bottom side view.

An external temperature control system is constructed to measure and control temperature of the reaction chamber. Wheatstone bridge is used to transform the resistance variation of the Pt sensor to voltage variation. The measured voltage is amplified by the instrumentation amplifier (AD524) and transferred to the analog input of the data acquisition board (DAQ PCI- MIO-16E-1). The analog output of the DAQ board is amplified by the operational amplifier and then transferred to the Pt heater. In this case, the programmed PID control algorithm adjusts the analog output to control the temperature as fast as possible.

3. Experimental

Four kinds of proteins were chosen for the test samples such as BSA (bovine serum albumin), ovalbumin, cytochrome C and human serum immunoglobulin G. All proteins were dissolved each in aqueous 50 mM ammonium bicarbonate buffer to make a concentration of 0.25 μM. Trypsin was dissolved in aqueous 50 mM ammonium bicarbonate buffer (pH 7.8) with a concentration of 4 μM. After 3 μl of protein solutions were injected into the reaction chamber of the microchip with capillary force, thermal denaturation was performed at 80 °C for 1 minute. And then, 1 μl of trypsin solution was injected into the chamber after chilling down the reaction chamber to 37 °C. Proteins were digested with trypsin at 37 °C for 10 minutes. As soon as the digestion was completed, all solutions in the chamber were pushed out with a syringe. The digested solution was mixed with the same volume of 10 mg/ml α-cyano-4-hydroxycinnamic acid (Sigma) in aqueous 70 %(v/v) acetonitrile immediately. The mixed solution was spotted on the MALDI probe. Matrix-assisted laser desorption/ionization mass spectrometric analysis was performed with a Bruker Datonics Biflex IV time of flight mass spectrometry (Bruker, Germany) with delayed extraction condition, operating with a pulsed N_2 laser at 337 nm. Positive ion mass spectra were acquired using reflector

mode with an accelerating voltage of 20.0 kV. Each spectrum is the average result of 100 laser shots. Signals from 100 shots were increased the signal to noise ratio of each mass spectrum. Mass calibration was achieved using the external standards.

4. Results

Fig. 3 shows the typical MALDI-TOF spectrum of the BSA, one of the tested proteins. And table 1 summarizes the comparison results of four proteins with respect to the thermal denaturation. All results show an increase of the number of matched peptide peak and sequence coverage only due to the 80 °C, 1 minute thermal denaturation except the cytochrome which is insensitive to the temperature. It is previously reported that the thermal denaturation does not work properly at the temperature-insensitive proteins [2]. It is remarkable that the temperature-sensitive proteins such as Ovalbumin and IgG do not show any matched peak and sequence coverage when the thermal denaturation is not performed. From these results, we can infer that the high temperature induced by the microchip makes protein denatured and increases the digestibility for the temperature-sensitive proteins.

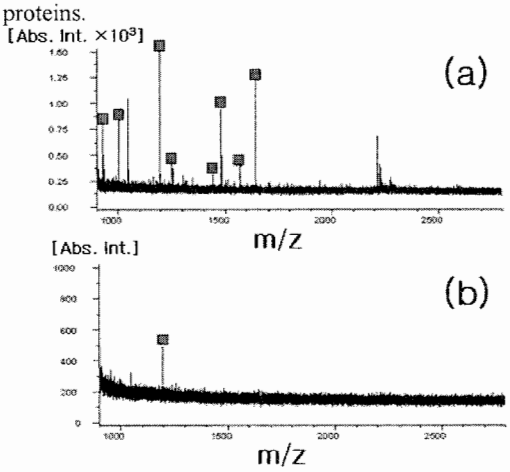

Figure 3 MALDI-TOF spectrum of the digested BSA. (a) Thermally denaturated BSA and (b) nondenaturated BSA. (■ denoted matched peak)

Table1. Comparison of the number of digested fragments and sequence coverage of protein between nondenaturated and thermally denaturated proteins.

	Thermal denatured		Nondenatured	
	Matched peaks (experimental/ theoretical)	Sequence coverage	Matched peaks (experimental/ theoretical)	Sequence coverage
BSA (Bos taurus)	8/82	14 %	1/82	1.6 %
Ovalbumin (Chicken egg)	5/34	24 %	0/34	0 %
IgG (Heavy chain)	4/31	17 %	0/31	0 %
Cytochrome (Horse)	4/22	28 %	5/22	33 %

5. Conclusions

We could acquire an increase of the peptide fragments and the sequence coverage by the thermal denaturation within the fabricated microchip. The microchip based thermal denaturation and trypsin digestion would be applicable to the MALDI-TOF MS with the further optimization of reaction time and enzyme rate.

References

[1] Paul Cutler, Proteomics, 3, 3-18 (2003).
[2] Zee-Yong Park and David H. Russell, Anal. Chem, 72, 2667-2670 (2000).
[3] Klavs F. Jensen, Chemical Engineering Science, 56, 293-303 (2001).
[4] Dae Sung Yoon, You-Seop Lee, Youngsun Lee, Hye Jung Cho, Su Whan Sung, Kwang W Oh, Junhoe Cha and Geunbae Lim, Journal of Micromechanics and Microengineering, 12, 813-823 (2002).

SELF-RESHAPABLE AND OPHIOCOMA-LIKE MICRO OPTICAL ARRAY FOR PROTEIN MICRO ARRAY DETECTION IN PARALLEL

Kuo-Yung Hung[1], Chang-Wei Chen[2], *Fan-Gang Tseng[1], Hwai-Pwu Chou[1], and Ching-Chang Chieng[1]

[1]*Department of Engineering and System Science, National Tsing Hua University, Taiwan, R.O.C.*
[2]*Institude of Microelectromechanical System , National Tsing Hua University, Taiwan, R.O.C.*
**E-mail: fangang@ess.nthu.edu.tw.*

Abstract

This paper proposes a micro fluorescence detection chip system for protein micro array detection in parallel. The detection chip consists of APDs (Avalanche Photo Diode) and re-shapable polymer micro lenses with high numerical aperture for signal enhancement. This optical chip system allows batch-detection instead of serial-scanning approach in traditional scanner systems. The chip system has been successfully fabricated and demonstrated and suitable for hand-held fluorescence detection in batch.

Keywords: re-shapable micro lenses, fluorescence detection, Avalanche photodiode, polymer lens.

1. Introduction

There have been various approaches of fluorescence detection for μTAS, however, most of them still comprise macro optical components in the assembled optical detection system, and few are integrated systems with all micro components [1]. This paper proposes a fully integrated micro optical system for parallel fluorescence detection applied to a 3 in 1 protein chip system [2]. The schematic design is shown in Fig. 1, comprising arrays of Avalanche photo diodes and **Ophiocoma-like** condensing lenses [3] right above the diode for fluorescence light accumulation, as the principle shown in Fig. 2. To accumulate fluorescence light from the protein chip nearing the detection surface (less than 500 μm), condensing lens with high numerical aperture lenses (>0.5) is highly desired. This paper proposes a novel approach by using thermal-capillary force to re-shape SU-8 micro lenses to obtain high numerical aperture. This principle can also be applied to numerical aperture adjustment for polymer lenses.

2. Design and fabrication

The fabrication of the avalanche photo diodes and the micro lenses system is shown in Fig. 3, combing traditional semiconductor process on silicon wafer with re-shapable SU-8 polymer process. After the fabrication of the photo diodes (Fig. 3a-3g), hydrophobic rings of Teflon, as shown in fig. 3h, are patterned on top of the diodes, and SU-8 resist are then flowed through the wafer surface to form semi-sphere condensing lenses (Fig. 3i). To obtain high numerical aperture, this semi-sphere is then heated and the border of the semi-sphere is then shrunk back from the patterned outer ring into the inner ring, thus the lenses curvature increases for larger numerical aperture. The numerical aperture can be adjusted according to the final ring position that the semi-sphere border resides. Higher temperature can move the semi sphere border more inner and thus enlarges the lenses curvature and numerical aperture.

3. Results

The SEM pictures and the sensitivity testing of the diodes are shown in Fig. 4, illustrating a photodiode sensitivity of 50ng/μl for protein-conjugated Cy5-fluoresence detection. The fabricated lenses array on the photodiodes is shown in Fig. 5a, with a lenses height variation of

2.8% (Fig. 5b). The light spots focused by the micro lenses array is shown in Fig. 6a, and the lenses with different sizes and numerical apertures are shown in Fig. 6b-c with a numerical aperture varied from 0.2-0.66(Fig. 6d). The lenses with low and high numerical aperture before and after the heating of the lenses array is shown in Fig. 7, demonstrated a very effective reshape process by thermal capillary process (Fig 7b-7c).

Acknowledgements

This work is supported by the National Science Council of Taiwan, ROC under the grant NSC 92-2323-B-007-002.

References

[1] J. C. Roulet, R. Volkel, H. P. Herzig, E. Verpoorte, N. F. d. Rooij,and R. Dandliker, *Journal of Microelectromechanical Systems,* 10 (4), 482-491 (2001).

[2] F. G. Tseng, C. E. Ho, M. H. Chen, K. Y. Hung, C. J. Su, Y. F. Chen, H. M. Huang and C. C. Chieng, *Tech. Proc. of the Nanotechnology Conf. '04 and Trade Show*, 1, 39-42 (2004).

[3] J. Aizenberg, A. Tkachenko, S. Weiner, L. Addadi, and G. Hendler, ***Nature,*** 412, 819-822 (2001).

[4] M. H. Wu, K. E. Paul, and G. M. Whitesides, *Applied Optics*, 41(13), 2575-2585 (2002).

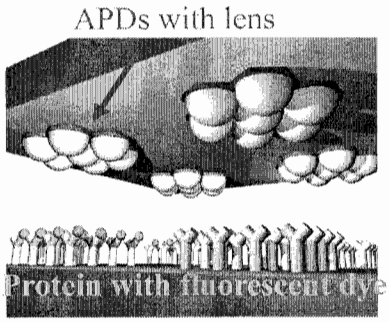

Figure 1. Conceptual design of the micro fluorescence detection chip system for protein micro array detection in parallel.

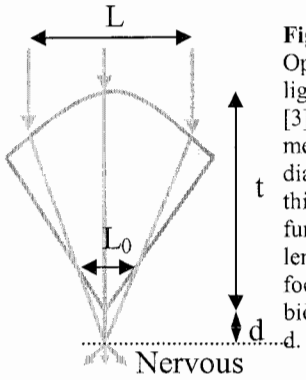

Figure 2. The Ophiocoma's lenses focus light onto nerve bundles [3]. L is the measurements of lens diameter and t is the thickness. L_0 is the functional region of this lens. The position of the focal point in the actual biological environment is d.

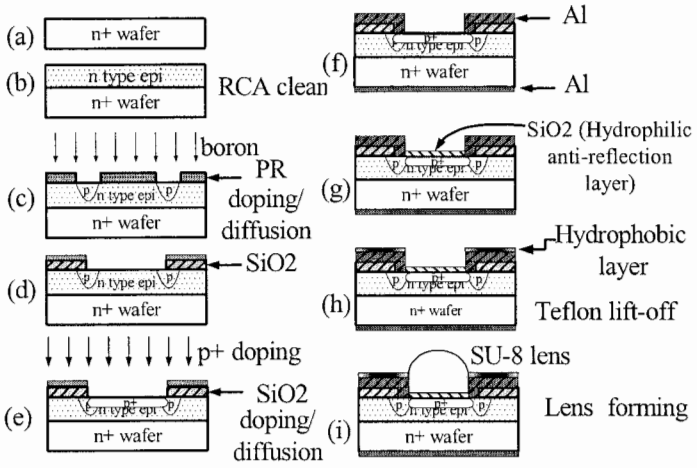

Figure 3. Detailed protein detection chip process flow chart.

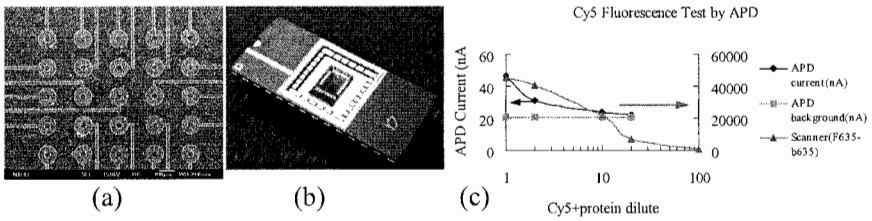

Figure 4. (a) SEM pictures of 5x5 APDs array and (b)Packaged APDs chip. (c) APD detection results for protein with Cy5 fluorescent dye.

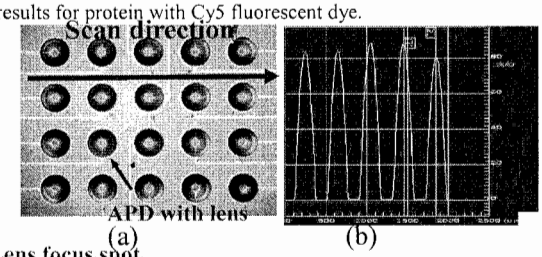

Figure 5. (a)OM picture of the 5x5 array APDs sensor with lens, sensing area is 100∝m, (b) surface profile scan results of the 1x5 lens profile in fig. 5a.

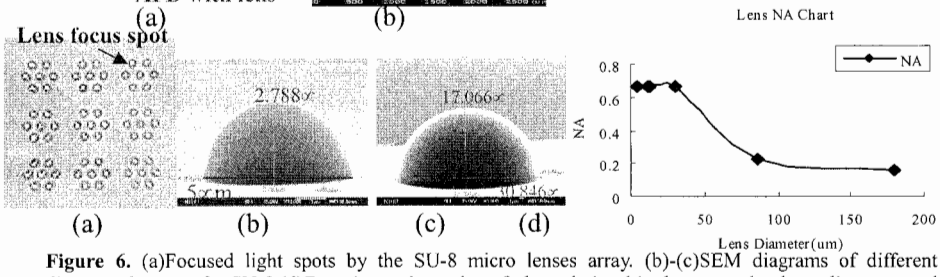

Figure 6. (a)Focused light spots by the SU-8 micro lenses array. (b)-(c)SEM diagrams of different diameter lenses of SU-8.(d)Experimental results of the relationship between the lens diameter and numerical aperture(NA).

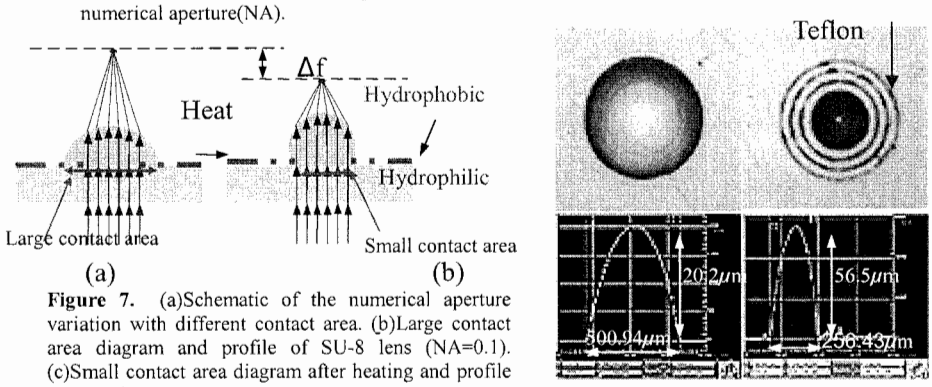

Figure 7. (a)Schematic of the numerical aperture variation with different contact area. (b)Large contact area diagram and profile of SU-8 lens (NA=0.1). (c)Small contact area diagram after heating and profile of SU-8 lens (NA=0.5).

SU-8 CANTILEVER STRAIN SENSOR WITH INTEGRATED READOUT BASED ON A PIEZORESISTIVE SU-8/CARBON BLACK COMPOSITE

L. Gammelgaard, P. Rasmussen, M. Calleja, A. Boisen
lag@mic.dtu.dk; phone +45 4525 5787; fax: +45 4588 7762
Department of Micro- and Nanotechnology, Technical University of Denmark, Bldg. 345e, DK-2800, Lyngby, Denmark

Abstract

We present a photoplastic (SU-8) cantilever strain sensor with an integrated piezoresistor based on a conductive composite of photoplastic (SU-8) and carbon black particles. The polymer composite is structured by UV-photolithography and has been integrated into a polymeric micro cantilever as the sensing part. The polymer composite is piezoresistive with a gauge factor around 15 to 20.

Keywords: cantilever sensor, polymer composite, piezoresistive readout, carbon black

1. Introduction

Cantilever-based sensors offer a platform for direct measurements with highly sensitive, label-free molecular recognition on small sample volumes. The cantilever sensor principle has a wide range of applications in real time local monitoring of chemical and biological interactions [1-3]. A reason for the growing interest in making cantilever sensor systems is the possibility of making such measurements on a portable device

The principle of cantilever sensors is to detect the bending of the cantilever that typically is induced by a change in surface stress at one side of the cantilever. This deflection can then be monitored by optical techniques. This optical readout method though very sensitive, is difficult to integrate into a micro-liquid handling system. To overcome this kind of problems we have previously developed cantilever-based sensors with piezoresistive readout [4]. Previously, these cantilever sensors have been made of silicon-based material with piezoresistors of poly-silicon. Recently, cantilevers based on the polymer SU-8 [5] with piezoresistors of Au have been fabricated [1-3]. The Au piezoresistors have shown a modest gauge factor around 1-2 and in order to increase the sensitivity of the polymer cantilevers a new piezoresitive material is necessary.

2. Theory

As an alternative piezoresistive material a photoplastic/carbon composite was investigated. A polymer composite consists of an insulating polymer mixed with randomly dispersed conducting particles (in this case 21nm carbon particles) forming an electrical conducting network. The resistivity of such a composite can be described by percolation theory predicting a change of several orders of magnitude when the amount of particles reach a certain threshold value called the percolation threshold. At carbon loadings close to the percolation threshold a small strain applied to the composite could be expected to cause the composite material to show a piezoresistive behavior due to the breaking of the conducting network. This effect can be used as integrated readout in a micro-cantilever.

3. Experimental

In this work, we have realized for the first time an SU-8 cantilever with integrated readout based on a piezoresistive SU-8/Carbon black composite material. This novel composite material can be processed by standard UV-lithography and is compatible with most cleanroom processes. The SU-8/Carbon composite has been produced by ultrasonic mixing and can be spun on wafers

forming homogenous thin-film layers less than 2 μm thick. A cheap, fast, and flexible process sequence for the polymer cantilevers have been developed. In this way the polymer cantilever chip with Au electrodes can be made with only five masks in less than one week - see Fig.1.

Further development of a liftoff process could help avoid a rough cleaning procedure after development of the composite layer that is necessary to remove excess carbon particles left on the wafer.

4. Results and discussion

An atomic force microscope (AFM) has been used to make surface measurements showing a clear connection between surface roughness and carbon loading. For carbon loadings less than 20% (by weight) very smooth surfaces have been demonstrated with a peak to valley distance of only 5-6 nm - see Fig.2. At a carbon loading of 26.4% the peak to valley distance increases to more than 250 nm, at which point the material also becomes very brittle and can no longer withstand ultrasonic treatments.

The carbon loading also affects the minimum layer thickness that can be obtained when spinning the polymer composite. The thickness increases with increased carbon loading. This is important since the UV-lithography becomes very difficult in thick layers with high carbon loadings and at the same time the dimensions of the cantilever also put a restriction on the layer thickness.

The deflection sensitivity of the polymeric cantilevers with the integrated piezoresistive readout has been measured to be $2.2\text{-}3.0 \cdot 10^{-6}$ nm^{-1}. This result was obtained by repeatedly deflecting and releasing the cantilever with a sharp needle, controlled by a micrometer screw in steps of 5 μm - see Fig. 3 and Fig. 4. The gauge factor of the SU-8/Carbon composite with 16.6% (by weight) carbon particles has been demonstrated to be between 15-20 thus making this material more strain sensitive than silicon due to the low Young's modulus of SU-8.

When integrated into a micro-fluidic system the sensor can be made very small and portable making it interesting for 'point of care' analysis. Moreover, this polymer composite might in the future open up for completely new application in micro technology and sensor systems.

References

[1]. H. G. Craighead, *Science 290*, 1532 (2000)

[2]. J. Fritz, M. K. Baller, H. P. Lang, H. Rothuizen, P. Vettiger, E. Meyer, H. J. Güntherodt, Ch. Gerber, J. W. Gimzewski, *Science 288*, 316 (2000)

[3]. R. Raiteri, M. Grattarola, H. -J. Butt, P. Skládal, *Sensors and Actuators B* **79**, 115-126, 2001

[4]. A. Boisen, J. Thaysen, H. Jensenius, O. Hansen, *Ultramicroscopy 82*, 11 (2000)

[5]. H. Lorenz, M. Despont, N. Fahrni, N. Labianca, P. Renaud, P. Vettiger, *J. Micromech. Microeng. 7*, 121 (1997)

[6]. M. Calleja, P. Rasmussen, A. Johansson, A. Boisen, *Proceedings, SPIE,* 5116:314-321 (2003)

[7]. G. Genolet, J. Brugger, M. Despont, U. Drechsler, P. Vettiger, N. F. Rooij, D. Anselmetti, *Rev. Sci. Instrum. 70*, 2398 (1999)

[8]. J. Thaysen, A. D. Yalçinkaya, P. Vettiger, A. Menon, *J. Phys. D: Appl. Phys. 35*, 2698 (2002)

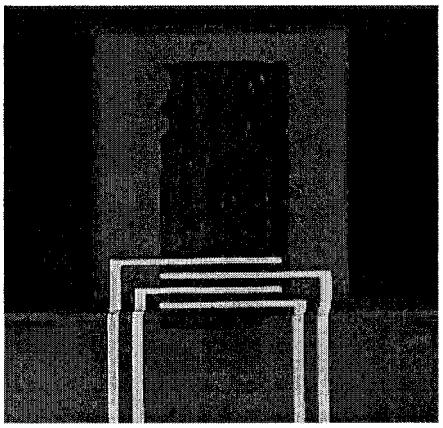

Figure 1. Optical image of the micromachined cantilever with integrated piezoresistive readout and four gold electrodes. The cantilever is 200 µm long, 200 µm wide and approximately 7 µm thick.

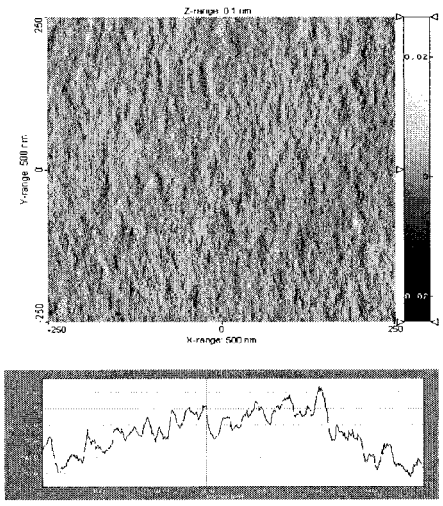

Figure 2. AFM image of an SU-8/Carbon composite surface with 16.6% (by weight) carbon particles. A peak to valley value of only 6 nm can be seen from the graph below.

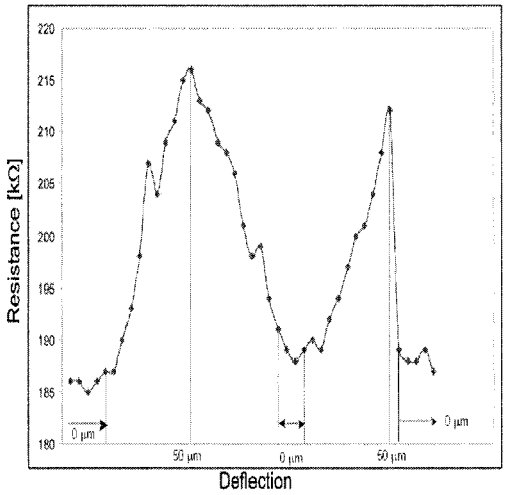

Figure 3. Repeated endpoint deflection of the cantilever. The resistance is measured as a function of the cantilever deflection in steps of 5 µm. The sudden drop in resistance seen at the second peak is due to the needle being removed from the cantilever.

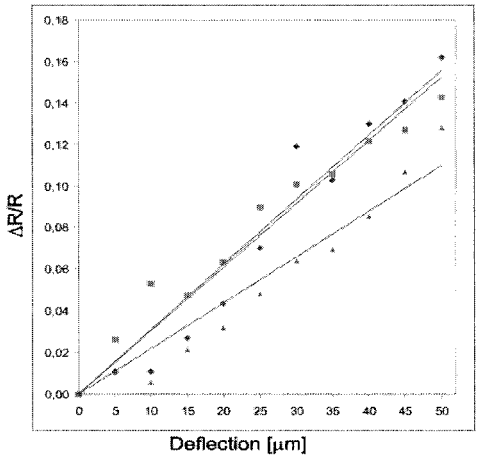

Figure 4. The relative change in resistance as a function of the deflection. The three lines represent the three steps in the deflection experiment; deflection, release, and second deflection.

DNA HYBRIDIZATION DETECTED BY CANTILEVER-BASED SENSOR WITH INTEGRATED PIEZORESISTIVE READ-OUT

Rodolphe Marie[1], Jacob Thaysen[2], Claus B. V. Christensen[1] and Anja Boisen[1]

[1] *Dept. of Micro and Nanotechnology, Technical University of Denmark, Bldg 345 east, DK 2800 Kongens Lyngby, Denmark*

[2] *Cantion A/S, Technical University of Denmark, Bldg 345 east, DK 2800 Kongens Lyngby, Denmark*

Abstract

A cantilever-based sensor with integrated piezoresistive read-out has been realized. The sensor is functionalized using thiol-gold chemistry. One cantilever is coated with single stranded DNA while the other cantilever is not, thus serving as a reference. The functionalization procedure is characterized by fluorescence scanning using a second chip. The output voltage of the sensor is monitored under the introduction of the complementary single stranded DNA in buffer.

Keywords: cantilever, piezoresistive, DNA, hybridization.

1. Introduction

Small cantilevers with micrometer dimensions can be used as very sensitive biochemical sensors for the detection of single base pair miss matches in DNA sequences [1] and very small levels of proteins interesting for diagnostics [2]. A cantilever is a thin beam clamped in one end and which typically is 200 μm long, 50 μm wide and 1 μm thick. A micro-cantilever is very sensitive to surface stress changes on its opposite sides. The adsorption of a DNA or protein layer on the top surface of the cantilever causes the cantilever to bend. The detection is performed by functionalizing the cantilever surface with a molecular layer designed for specific molecular recognition.

2. Experimental

A cantilever-based sensor with integrated read-out for the detection of isothermal DNA hybridization has been fabricated. The sensor is based on a silicon device bearing four silicon nitride cantilevers with an integrated piezoresistive read-out placed in a channel (Fig. 1A). Two of the cantilevers are coated with gold on one side. The piezoresistors are made of doped single crystalline silicon and the cantilevers are designed for optimized surface stress sensing. The output voltage of the sensor is the voltage across a Wheatstone bridge connecting two gold-coated cantilevers and two reference piezoresistors (Fig. 1B and C).

One of the cantilevers was functionalized on its gold-coated side with 25'mers single stranded DNA using thiol-chemistry. The cantilever is functionalized by placing a 0.3 μL droplet of thiolated DNA solution in the channel. The channel walls are hydrophobic and thus the droplet will stay in one end of the channel (Fig. 2B). The selectivity of the functionalization procedure with respect to the density of hybridization on both cantilever surfaces was optimized and characterized using fluorescence scanning (Fig. 2A).

Next, the output voltage of the sensor is monitored in buffer (1XTE + 0.1 M NaCl at pH 7.0) under the introduction of 1 μM complementary DNA in a flow. The sensor is stabilized in a solution of non-complementary DNA before and after the introduction of the complementary DNA.

Finally, the detection of DNA melting is investigated using the same sensor. As the sensor is designed for heat cycling in solution, the output voltage of the sensor is monitored while the temperature is increased above the melting temperature of the 25'mers sequence. The slope of the output voltage is calculated in order to detect the change of surface stress due to the melting of the DNA on the functionalized cantilever.

3. Results and discussion

Fig. 2A is the fluorescence image of a chip with four cantilevers (1 to 4). The cantilevers 1 to 3 were incubated in thiol-DNA solution while cantilever 4 was not. The gold-coated cantilevers (1 and 3) exposed to the solution of thiol-DNA are coated with 25'mer single stranded DNA. After hybridization to complementary DNA labeled with a fluorescent label, the fluorescence image shows that a fluorescence intensity ratio of 6.5 is obtained for gold cantilevers compared to the nitride cantilever (2) exposed to the thiol-solution. Moreover, a ratio as high as 150 is obtained for gold-cantilevers compared to cantilevers that were not exposed to the thiol-DNA (cantilever 4).

It is possible to incubate only one gold-coated cantilever at a time in 0.3 μL of thiol-DNA while the other gold-coated cantilever is not in contact with the solution (Fig. 2B). Thus the gold-coated cantilever exposed to thiol-DNA is used as a measuring cantilever while the other gold-coated cantilever is used as a reference.

During the injection of complementary DNA in a flow, a permanent output voltage change of 5μV is reproducibly obtained indicating a tensile surface stress change caused by the hybridization of the DNA onto the functionalized cantilever (Fig. 3A). The injections of non-complementary DNA or a second injection of complementary DNA yield a non-permanent bending indicating a non-specific interaction with the cantilevers.

Subsequently, the sensor was heated above the melting temperature of the DNA sequence immobilized on the cantilever. A change of the slope of the output voltage is detected when passing the melting temperature, which might be interpreted as due to the melting of the DNA and the subsequent desorption of single stranded DNA from the cantilever surface (Fig. 3B). This type of measurements is currently being investigated further.

4. Conclusions

A cantilever-based sensor has been functionalized with single stranded DNA on its one gold-coated cantilever. A permanent bending of the cantilever compared to the reference cantilever has been observed during the injection of a 1μM solution of complementary DNA in a flow. These results constitute the first DNA hybridization detections using cantilevers with integrated read-out and prove cantilever-based label-free detection as a promising component of future μTAS.

References

[1] J. Fritz et al, *Science*, 288 (5464), 316–18, (2000).
[2] G. Wu et al, *Proceedings of the National Academy of Sciences of the USA*, 98 (4), 1560–1564, (2001).

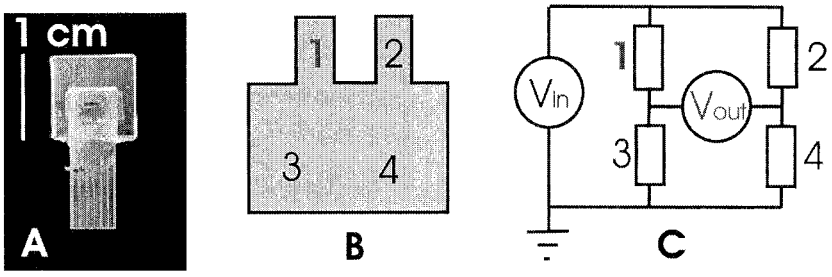

Figure 1. (**A**) Packaged sensor comprising 4 cantilevers with single crystalline integrated piezoresistors. The reaction chamber is 3μL in volume. (**B**) Two gold-coated cantilevers are used for detection. (**C**) The four resistors are connected into a Wheatstone bridge configuration.

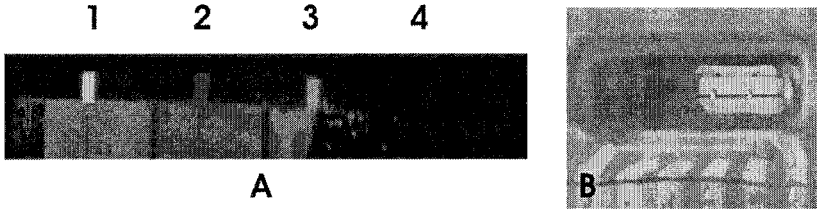

Figure 2. (**A**) Fluorescence image showing the higher density of hybridization on the gold-coated cantilevers (1, 3) compared with the non-coated silicon nitride cantilevers (2,4). (**B**) One gold-coated cantilever at a time can easily be functionalized.

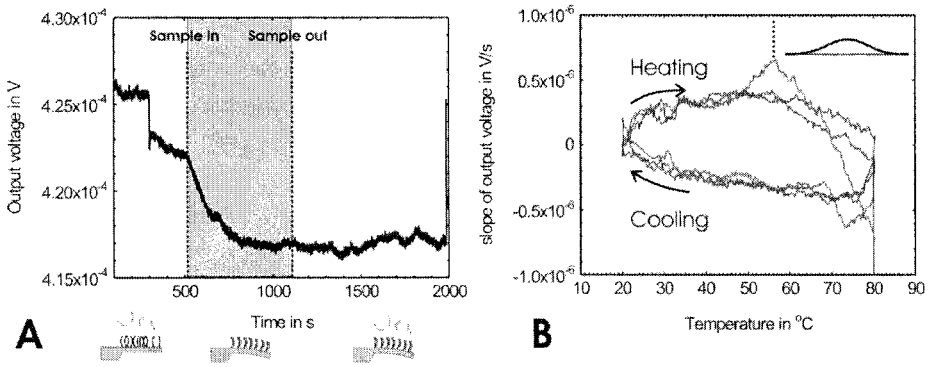

Figure 3. (**A**) Output voltage change during the introduction of a 1 μM solution of complementary DNA in 1xTE buffer containing 0.1 M NaCl at pH 7. Before and after the DNA sample, the sensor is stabilized in a solution of non-complementary DNA at the same concentration. The flow is 10 μL/min. (**B**) Slope of the output voltage as a function of temperature during the first heat cycles in complementary DNA solution. The peak at the first heating fits the melting temperature of the oligos (56 °C) and the expected signal shape and amplitude (inset).

SU-8 CANTILEVER SENSOR WITH INTEGRATED READ-OUT

A. Johansson, M.Calleja, P.Rasmussen, R. Marie, A. Boisen
Dept. of Micro and Nanotechnology, Technical University of Denmark, Bldg 345 east, DK 2800 Kongens Lyngby, Denmark

Abstract
We have developed a polymeric cantilever sensor array with integrated piezoresistive read-out for biosensor applications. The cantilevers were fabricated in a micro-fluidic channel. The device has been characterised by measuring the noise and the gauge factor of the resistors. For the first time, we present measurements in liquid with the SU-8 cantilevers.
Keywords: cantilever, SU-8, piezoresistive read-out, microfluidics, biosensor

1. Introduction

Cantilevers can be used as biosensors by monitoring the surface stress changes on one side of the cantilever due to the adsorption of molecules [1]. The technique is label-free and can be highly sensitive. Si cantilever sensors with integrated piezo-resistive read-out have previously been developed in our group [2]. Here, we present a cantilever chip based entirely on the epoxy based photoresist SU-8, where the read-out is an integrated gold strain gauge [3]. SU-8 is known for its excellent chemical resistance and good mechanical properties. The main advantage of the SU-8 cantilevers is that they can be made much cheaper and faster than Si cantilevers and the sensitivity can be increased due to the mechanical properties of SU-8. Furthermore, the measurements presented here show that the noise level is even lower than for Si cantilevers.

2. Chip design

In our design, four cantilevers are placed in a microfluidic channel, see Figure 1. In order to reduce noise and drift effects the piezoresistors in the cantilever are connected to resistors on the chip forming a Wheatstone bridge. Each chip has eight piezoresistors, four of which are placed on the cantilevers, see Figure 2. Each Wheatstone bridge includes four resistors – one on a measurement cantilever, one on a reference cantilever and two on the chip.

3. Fabrication and packaging

In order to release the finished chips, a sacrificial layer consisting of Cr/Au/Cr with a thickness of 5/50/50 nm is first evaporated on a 4" Si wafer, see Figure 3. SU-8 2002 is then deposited on the wafer with a spin rate of 5000 rpm for 30 s resulting in an 1.2-1.5 μm thick SU-8 layer. The layer is soft baked for 2 min at 60 °C and 4 min at 90 °C and the exposure dose is 450 mJ/cm^2. The cantilever is cross-linked during the post exposure bake of 2 min at 60 °C and 4 min at 90 °C and developed in propyleneglycol monomethyl ether acetate (PGMEA) for 2 min. The resistors and wires in the chip are defined by etching a 5/40 nm thick evaporated Ti/Au layer in KI, using AZ 5214E photoresist as the etch mask. The contact pads are defined in the same way only the gold layer here is 1-1.5 μm. Metallic layers are known not to adhere well to SU-8. However, we have found that by combining a thin Ti adhesion layer with plasma treatment, we can achieve a sufficiently high adhesion for the presented application. The plasma treatment is performed in a plasma asher using N_2/O_2 240/40 sccm at 250 W for 8 min. The metal layer is relatively thick in order to ensure a good electrical connection from the contact pad to the wires on the body of the chip. This can be a problem due to the step of approximately 1.5 μm caused by the first SU-8 layer. An alternative metal deposition method is electroplating which is currently under investigation. Next, the resistors are encapsulated in 5 μm of SU-8 2005 that is pattered the same way as the first SU-8 layer. Finally, a thick SU-8 2075 layer is deposited and patterned, using a soft bake of 5 min at 60 °C and 45 min at 90 °C, an exposure dose of 1170 mJ/cm^2 and a post exposure of 5 min at 60

°C and 35 min at 90 °C. The developing time was 20 min. This final layer defines the channel. The finished chip is released by etching the Cr layer in a Chromium etchant type 1020A (Transene).

We have also investigated the possibility of gluing an SU-8 lid on top of the channel using SU-8 as the glue. However, the method is time consuming and unreliable and other methods are under investigation. The finished SU-8 chips have been electrically bonded to silicon substrates with gold wires. The chip can be put on a polymethyl methacrylate (PMMA) substrate with a fluidic inlet and outlet, see Figure 4. A tight sealing has been achieved using polydimethyl siloxane (PDMS).

4. Characterisation of chip

The chips have been characterised by measuring the noise and the gauge factor. The gauge factor is measured by bending the cantilever with a microprobe, while monitoring the change in resistance. A gauge factor of 2 has been found, which is in good agreement with the theoretical value for gold. Furthermore, the result is highly reproducible and the cantilever has proved to be very soft and can be deflected more than 100 μm without damaging the resistors. The noise has been found to be as low as 0.2-0.4 μV peak-to-peak and approximately the same in water as in air. The performance of the chip has been investigated by etching away a 600 Å Au layer on one of the cantilevers using 0.1 M KI, see Figure 5. Assuming that the built-in stress in the Au layer is 30 MPa the expected voltage change should be 3.4 μV. In order to investigate the influence of the ion solution on the SU-8, the gold covered cantilever is first put in a 0.1 M KCl solution. Salt is deposited on the chip and a change in the output voltage is observed due to the surface stress change. When the KI solution is introduced the deflection of the cantilever was observed to increase. By subtracting the contribution from the KCl solution, etching away the gold from the cantilever surface result in a voltage change of about 7 μV.

5. Conclusions and discussion

A polymeric sensor for bio/chemical applications has been presented. The cantilevers have integrated strain gauges in gold, which enable simple electrical read-out. Due to the mechanical properties of SU-8 and the low noise of the gold resistors high sensitivity might be achieved.

References

[1] R. Raiteri, M. Grattarola, H.-J. Butt and P. Skladal, *Sensors and Actuators B* **79** 115-126 (2001)
[1] M. Calleja, P. Rasmussen, A. Johansson and A. Boisen, *microTAS '03* 207-210
[2] P. A. Rasmussen, J. Thaysen, O. Hansen, S. C. Eriksen and A. Boisen, *Ultramicroscopy* **97** 371-376 (2003)

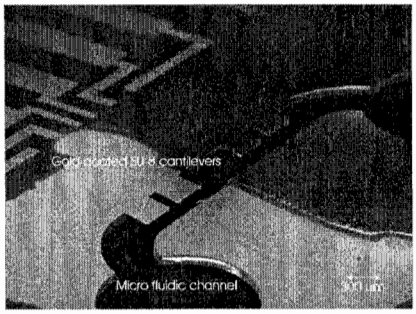

Figure 1. Four SU-8 cantilevers in a microfluidic channel.

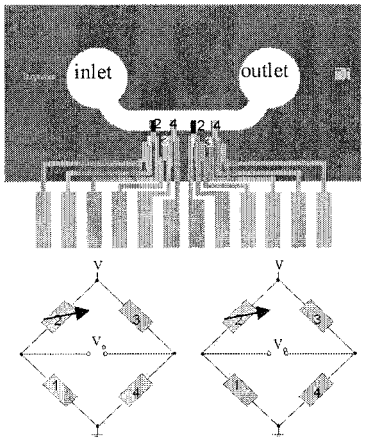

Figure 2. The four resistors on the cantilevers are connected with four resistors on the chip forming two Wheatstone bridges.

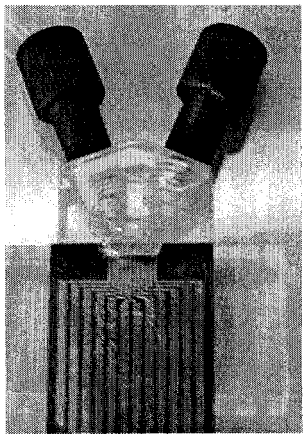

Figure 4. The SU-8 chip is glued to a silicon substrate and the fluidic inlets and outlets are defined in a PMMA package with PDMS sealing.

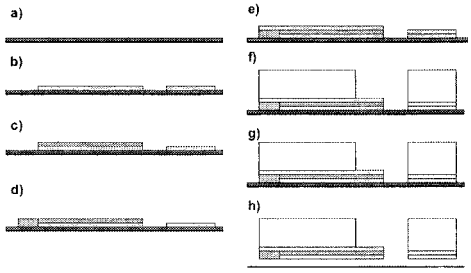

Figure 3. Process sequence. a) Evaporation of Cr/Au/Cr release layer b) Patterning 1.5 µm SU-8 c) Evaporation and patterning of 5/40 nm Ti/Au for the resistors d) and 2 nm/ 1 µm for the electrical contact pads e) Patterning of second SU-8 layer f) Patterning of thick SU-8 layer for the channel wall h) Release of SU-8 chip by Cr-etch.

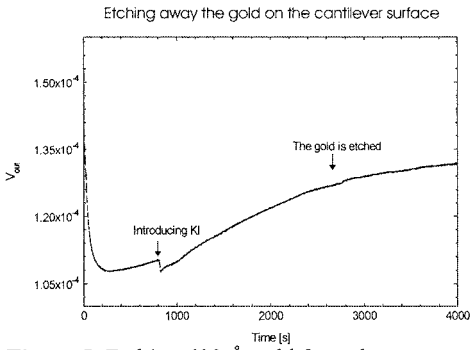

Figure 5. Etching 600 Å gold from the cantilever surface.

NOVEL FILTER LESS FLUORESCENCE DETECTION SENSOR ARRAY FOR DNA MICRO CHIP

Yuuki Maruyama[1], Kazuaki Sawada[1], Hidekuni Takao[1], Makoto Ishida[1]
[1]Department of E & E Eng., Toyohashi University of Technology
1-1, Hibarigaoka, Tempaku-cho, Toyohashi 441-8580, Japan

Abstract

A novel filter-less fluorescence detection sensor was proposed and a prototype was fabricated in CMOS silicon integrated circuit technology. The principle of the fluorescence detection sensor is based on the variation of optical absorption coefficients with wavelength. It was found that the fluorescence detection sensor successfully detected a fluorescent label without the need to resort to a filter.

Keywords: fluorescence, DNA Chip, photogate, filter less, sensor array

1. Introduction

Conventionally, fluorescent labels and an expensive fluorescent scanner are used for DNA analysis. The fluorescent scanner requires a special light source with a band pass filter. It is, in consequence, relatively bulky. In this paper, a novel fluorescence detection sensor array is proposed for DNA chip, where it is possible to separately detect excitation illumination and fluorescence intensity without the need for a filter. This fluorescence detection sensor array will be important analysis tool in the μ-TAS field. A schematic indication of the concept of a DNA chip using this novel sensor is shown in Fig. 1.

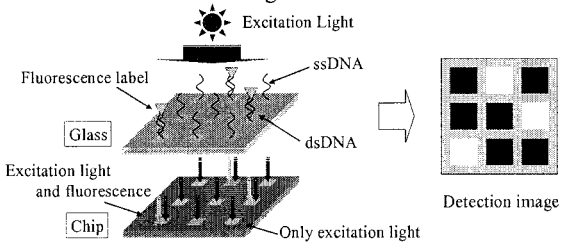

Figure 1. Concept of the proposed filter-less fluorescence detection sensor.

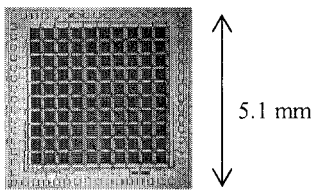

Figure 2. Photograph of the sensor array. (10×10)

2. Principle

A new principle is proposed for spectroscopy without the need for a special light filter. When a semiconductor is illuminated, photons are absorbed and electron-hole pairs are generated. The Excess carrier generation rate g(x), in the absorption depth as x will be given by[1]

$$g(x) = \frac{\phi S\lambda}{hc}[\alpha \cdot \exp(-\alpha x)] \qquad (1)$$

Where ϕ is the intensity of irradiated light, λ is the wavelength, α is the absorption coefficient, S is the size of sensing area, q is the elementary charge, c is the speed of light in vacuum and h is the Planck's constant.

Excess carriers are collected from x=0 (surface) to x=w, and contribute to a current given by:

$$\begin{aligned} I &= -q\int_0^w g(x)dx \\ &= -\frac{\phi q S\lambda}{hc}(1-e^{-\alpha w}) \end{aligned} \qquad (2)$$

When two different light wavelengths are incident simultaneously, the currents generated in the absorption depths w_1 and w_2 are expressed in Eq. (3) and Eq. (4).

$$\begin{cases} I_1 = \dfrac{\phi_1 q S \lambda_1}{hc}(1 - e^{-\alpha_1 w_1}) + \dfrac{\phi_2 q S \lambda_2}{hc}(1 - e^{-\alpha_2 w_1}) & (3) \\ I_2 = \dfrac{\phi_1 q S \lambda_1}{hc}(1 - e^{-\alpha_1 w_2}) + \dfrac{\phi_2 q S \lambda_2}{hc}(1 - e^{-\alpha_2 w_2}) & (4) \end{cases}$$

Where ϕ_1 and ϕ_2 are the intensities of wavelengths λ_1 and λ_2 with absorption coefficients of α_1 and α_2 respectively. Both illumination intensities (ϕ_1, ϕ_2) can be found by solving these simultaneous equations.

3. Structure

Based on the above principle, a novel filter-less fluorescence detection sensor has been fabricated using CMOS silicon integrated circuit technology. A photograph of the sensor array is shown in Fig. 2. The sensing area of the structure utilised a Photogate structure[2]. Fig. 3(a) shows a cross sectional view of the sensor. A p-n junction, with a depth of 5 μm, is formed under the photogate. The sensor is attached to an n^+ diffusion region, to form the output node of the current. Figs. 3(b) and Fig. 3(c) show the electrical potential profile of the sensor. As the applied voltage at the photogate is changed, the saddle of potential (a turning point of current) also changes. The electrons generated at the positions shallower than the turning point, are read and those from regions deeper than the turning point are discharged. The depths of the saddle are defined as w_1 and w_2 in Eq. (3) and Eq. (4).

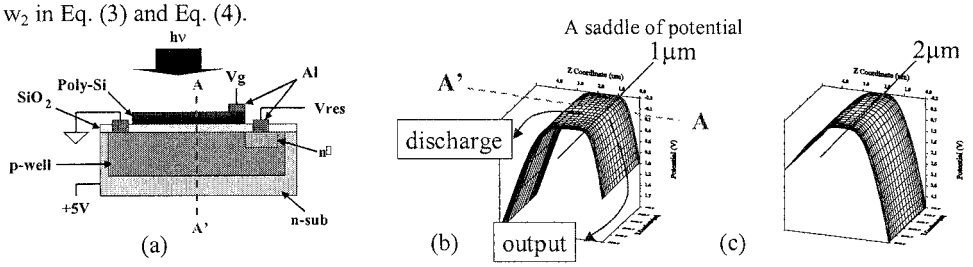

Figure 3. A cross sectional view and electrical potential profile of filter-less fluorescent detection sensor (a)cross sectional view (b)electric potential profiles at Vg = 1V (c)Vg = 5V.

4. Experimental and Results

1) Simulation experiment

Measurement result from 1-pixel is described here. A fluorescent label (SYBR-Green) is fluoresced (520 nm), when excited by light (470 nm). Initially two LEDs imitating excitation and fluorescent light, were used for measurements as shown in Fig. 4. The experimental result is shown in Fig. 5. From this result it was found that fluorescence and excitation light intensities could be measured separately with this sensor. The fluorescence intensity which could be detected was 1/100 of the intensity of the excitation light.

2) Experiment with DNA solution

To confirm the efficacy of DNA chip, test solutions were prepared. Initially, a non-fluorescent double strand DNA solution (20 μM, 22 bases) without SYBR-Green was measured. The result of this solution is shown in Fig. 7(a). Then a measurement was made with the same DNA solution, but with added SYBR-Green. This solution is fluorescent. The result of this solution is shown in Fig. 7(b). These experiments, confirmed that the proposed fluorescent sensor would successfully detect fluorescent label without the need for a filter.

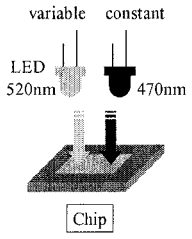

Figure 4. Schematic measurement system for the initial fluorescence test.

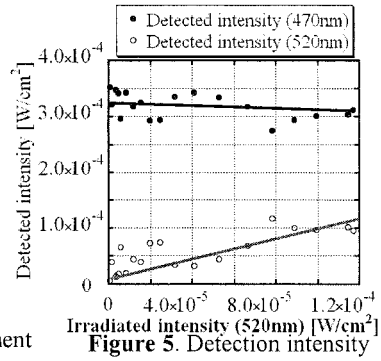

Figure 5. Detection intensity in the initial equivalent fluorescence test.

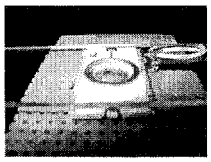

Figure 6. Photograph of the measurement system.

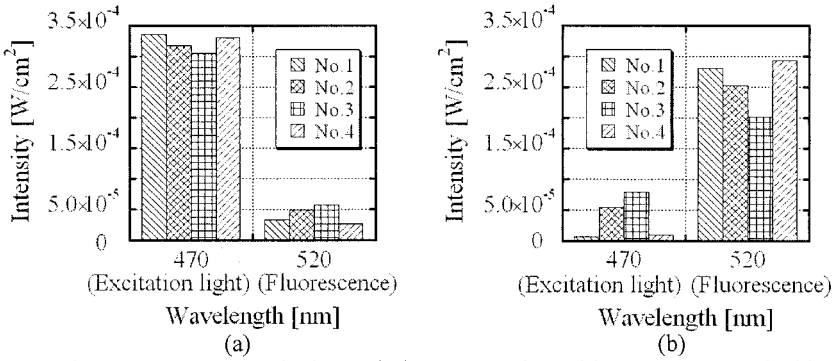

Figure 7. The sensor output. Excitation and Fluorescence intensities were measured without a filter (a)non-Fluorescent sample (b)Fluorescent sample.

5. Conclusions

A novel filter-less fluorescence detection sensor has been proposed and fabricated. The fluorescent intensity detected was 1/100 of the excitation intensity. It was found that the sensor successfully detected a fluorescent label without requiring a filter. This filter-less fluorescence detection sensor array will be an important analysis micro-tool in the μ-TAS field.

Acknowledgements

This work was partially supported by The 21st Century COE Program "Intelligent Human Sensing", Cooperation of Innovative Technology and Advanced Research in Evolutional Area (CITY AREA) from the Ministry of Education, and a Grant-in-Aid for Encouragement from the Ministry of Education, Science, Sports and Culture, and Technology Japan.

References

[1] Jhon P.Mckelvey, "SOLID STATE AND SEMICONDUCTOR PHYSICS", p463, Harper and Row (1966)

[2] Sabrina E.Kemeny, Russell C.Gee, Bedabrate Pain, Craig O.Staller, Quiesep Kim and Eric R.Fossum, "CMOS Active Pixel Image Sensor for Highly Integrated Imaging Systems", IEEE journal of solid-state circuits, vol.32, No.2, February (1997)

ARRAY OF PLANAR CAPACITIVE SENSORS AS A MEDIA DETECTOR IN MICROFLUIDIC SYSTEM

Jerzy Weremczuk[1], Michal Chudy[2], Artur Dybko[2], Romuald Beck[3], Zbigniew Brzozka[2] and Ryszard Jachowicz[1]

[1]Inst. of Electronic Systems, Warsaw University of Technology, Nowowiejska 15/19, 00-665Warsaw, Poland

[2]Dept. of Analytical Chemistry, Warsaw University of Technology, Noakowskiego 3, 00-664 Warsaw, Poland

[3]Inst. of Micro and Optoelectronics, Warsaw University of Technology, Koszykowa 75, 00-662 Warsaw, Poland

Abstract

Capacitive sensors were used to visualise the flow in a microfluidic system. A commercial fingerprint sensor was used. The sensor was covered with a PDMS structure with a microchannel. The system is capable of distinguishing various media exhibiting changes in dielectric constant. Preliminary experiment was done with a simple straight channel through which water or air was pumped. The system was also tested with various organic solvents such as methanol, hexane, isopropanol.

Keywords: chemocapacitive sensor, fingerprint sensor, microfluidics

1. Introduction

Described in the literature the visualisation systems for microfluidic applications are based on cameras with close-up option or microscopes equipped with cameras [1,2]. The systems can also be used to observe a fluorescence emission of a sample or components of a sample separated during capillary electrophoresis [3]. One of the major drawbacks of these systems is that the microfluidic structure must be made of poly(dimethylsiloxane) (PDMS), glass or another transparent material. Up to now there is no detection system allowing the visualisation of mixing transparent fluids or when the structures were based on silicon.

In the paper we present a proof of concept of usage an array of planar capacitors (fingerprint sensor) to detect fluid properties in a microfluidic system. The working principle of the array is the recognition of the difference in the dielectric constant of the material placed on the sensor surface. This paper is, to our best knowledge, the first application of capacitive sensors in on-line visualisation of the flow in a microfluidic system.

2. The working principle of the array sensor

A few technologies for creating fingerprints scanning arrays for biometric purposes are currently applied. The main are optical, capacitive, thermal and radio frequency field.

Capacitive scanning is the most popular technique. Several companies propose devices based on the measurement of the capacitance between the skin and the pixel electrode. As the finger skin distance varies, so does the capacitance. To provide enough sensitivity, the electrode coating must be as thin as possible reach (typically a few microns). A significant sensor drawback is the vulnerability to strong electrical fields like ESD (Electro-Static Discharge).

In our work we decided to use a commercially available array of planar capacitors (from Infineon), which was originally designed as a fingerprint sensor. Schematic cross section of the sensor is presented in fig.1. The array is manufactured in a standard CMOS technology. The 288 x 224 miniature electrodes (pixels) with pitch 49.5 μm are integrated on a silicon chip. The sensor array has 8 bit/pixel data resolution (513 dpi), image acquisition time <100 ms and supply voltage 3.3 - 5.5 V. The data can be transmitted via parallel or serial interfaces. The overall chip dimensions

are very small (18 x 21 x 1.5 mm). Each pixel reading can be represented as a level of grey colour after conversion into an image. The 8-bit coding allows distinguishing of 256 values. The value 0 represents black and the value 255 white.

3. Experimental

A measuring set up consisted of the array of planar capacitors covered with a PDMS plate with a microchannel (see fig. 2). The microchannel was fabricated using a typical photolithography and mould technology. To do the microchannel a glass substrate was covered with a SU8 layer. Then the photoresist was exposed through a mask with the shape of the channel. The unexposed part of SU8 was dissolved in the developer giving a convex structure. Such a stamp was covered with a mould having dimensions matched to the fingerprint sensor. Next degassed mixture of PDMS prepolymer and cross linking agent was poured over the stamp and left for 2 h in 70 °C. After that time the mould was removed and a PDMS plate with a microchannel was obtained. The microchannel was created across the diagonal of the fingerprint sensor and have the following dimensions: a thickness of 100 μm, a width of 50 μm, and a length of 11 mm. A sample under the test was delivered by Teflon tubes inserted into holes made in the PDMS slab. We have found that the best way to obtain good self sealing holes was to deep a PDMS structure into liquid nitrogen and then drill holes. The sample was delivered by a peristaltic pump with the flow rate 100 μl/min.

The measurements were performed with the help of a personal computer, which acquired the sensor's data via serial interface. Each measurement resulted in a digital image saved in bmp format.

4. Results and discussion

Preliminary tests were done with water and the results are presented in fig. 3. Fig. 3 a) presents the channel with the flowing water. Water has dielectric constant equal to 78.38, which results in the change of the capacitance of appropriate electrodes and is depicted in fig.3 a) as a dark gray colour. In fig. 3b it is clearly visible the difference between an air gap and water inside the microchannel when the pump was stopped. The different shade of grey colour is caused by the different dielectric constant of the PDMS, air, and water. As higher this constant, as darker a pixel is. Next experiments were performed with various organic solvents such as: methanol, hexane, isopropanol. The data will be presented on a poster. The system is able to visualise which fluid is pumped through the channel by generating different images.

5. Conclusions

The usefulness of the array of capacitive sensors in visualisation of the flow in a microfluidic structure was demonstrated. The primary advantages of the array are the capability to distinguish between media exhibiting various dielectric constant and the visualisation in two dimensions. The main idea of the paper was to present a concept of the application of the capacitive sensors in microfluidics.

Acknowledgements

The work was financially supported by a grant of the State Committee for Scientific Research, Project No. 4 T10C 003 25.

References

[1] Y. Finteschenko, B.A. Simmons, B.H. Lapizco-Encinas, and E.B. Cummings, *Proc. mTAS2003*, **1,** 65-68 (2003).

[2] J. Emmelkamp, R. DaCosta, H. Andersson, and A. van den Berg, *Proc. mTAS2003*, **1,** 85-88 (2003).

[3] Y.Mizukami, D. Rajniak, Akiko Rajniak, and M. Nishimura, *Sens. Act. B,* **81**, 2002-209 (2002).

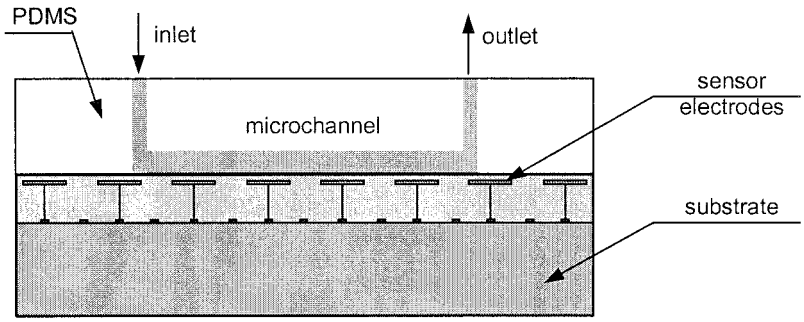

Figure 1. Schematic cross section of fingerprint sensor (not to scale)

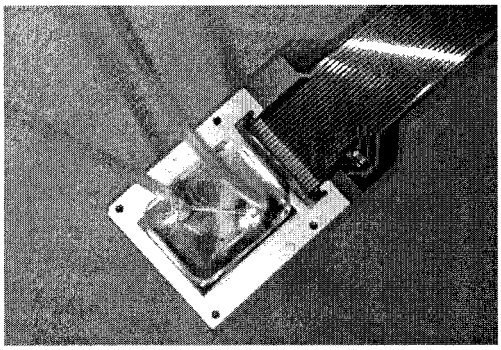

Figure 2. Photograph of a measuring set up.

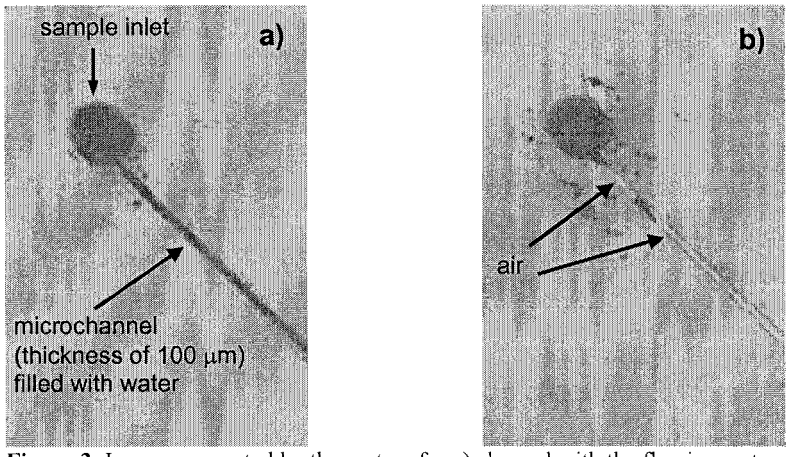

Figure 3. Images generated by the system for a) channel with the flowing water, b) the pump was stopped.

SHEATHLESS ELECTROSPRAY IONIZATION WITH INTEGRATED METAL EMITTER ON MICROFLUIDIC DEVICE

Min-Su Kim[1], Hwang-soo Joo[2], Kook-Nyung Lee[2], Byung-Gee Kim[2]
and Yong-Kweon Kim[1]
[1]*School of Electrical Engineering and Computer Science,*
[2]*School of Chemical Engineering and Institute of Molecular Biology and Genetics,*
Seoul National University, ENG420-007, Seoul 151-744, Korea

Abstract

In this study, sheathless electrospray from PDMS/glass microchips with separation channels and a conducting metal emitter tip is described. The channels and metal emitter tips are fabricated using a glass wet etching and gold electroplating process, respectively. The fabricated microchip performance was tested through spraying peptide samples for mass spectrometric analysis. Singly charged peak and doubly charged peak of peptide were detected and further MS/MS fragmentation was performed in each peak.

Key words: sheathless electrospray, microchip, metal emitter tip, mass spectrometry (MS)

1. Introduction

ESI-MS is a powerful analytical tool that has been broadly applied to biomolecular structure analysis mainly because of its ability to detect large biomolecules with great sensitivity and accuracy. A chip-based ESI-MS system has advantages of the separation and on-line electrospray detection of peptide solution. Several approaches have been explored to make a chip-based ESI-MS interface by a variety of fabrication and assembly methods. In the first approach, a few groups used a direct electrospray method from the flat edge of the chip [1]. The problem they encountered was to establish a well-defined Taylor cone at the exit of the microchannel. In the second approach, the interface based on a microfluidic device is coupled to capillary sprayer in electrospray or nanoelectrospray mode [2]. However, even if this configuration allowed the development of various designs of sheathless electrospray emitters, all the systems previously presented require a gold conducting coating of the tip which may lead to deterioration of the spray stability due to the poor adhesion of the metallic layer.

In this work, sheathless electrospray from PDMS/glass microchips, allowing the generation of an efficient nanospray for protein detection, is described. As a mass spectrometry electrospray source, a triangular-shaped gold emitter tip was formed by lithography and electroplating on a glass substrate. It is easily fabricated by MEMS technology and it is more robust than that of silica or polymer recently reported.

2. Experimental

The separation channel and metal emitter tips are fabricated using a glass wet etching and gold electroplating process, respectively. As a wet-etching mask, an amorphous silicon layer was deposited on both sides of the 500 μm thick glass wafer. A positive photoresist (AZ1512; Clariant Corp., Somerville, NJ, USA) was then spin-coated, and the column design was transferred to the substrate using a film photomask (Ppm technology Corp., Seoul, Korea). After amorphous silicon patterning, the microfluidic channel, 70 μm wide at half-depth, 20 μm deep, was then isotropically etched in 49% HF for 3 min (etching rate: ~7μm/min) at 20°C. A triangular-shaped gold emitter tip was formed by lithography and Au electroplating process on a glass substrate after second standard photolithographic, wet etching process for emitter part. The metal tip was aligned with the channel at the end of the glass channel, so microchannel is expanded to the end of emitter tip. The fabricated

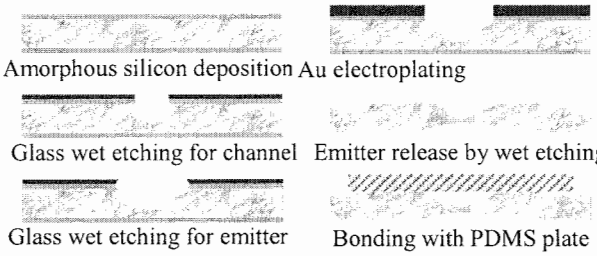

Figure 1. Fabrication process of the micro emitter with the microfluidic channel

emitter structure was released to establish a well-defined Taylor cone by wet etching process. This glass plate having microchannels and emitter structure was bonded with the flipped PDMS plate for a closed channel. Figure 1 shows the fabrication process of the proposed device.

A test sample is a fragment peptide of bradkynin 2-9 (Mr, 903.4603) purchased from Sigma (St. Louis, US). ESI-MS was performed in the positive-ion mode using an LCQ Deca ion-trap mass spectrometer (ThermoFinnigan, San Jose, CA, USA) equipped with a syringe pump. For the emitting test, the sample is introduced via syringe pump and carrier solvent, i.e. water-acetonitrile (1: 1), was used at a flow-rate of 0.5 μl/min and the high voltage is supplied at the emitter, through an embedded microelectrode (Figure 2).

3. Results and Discussion

A scanning electron micrograph of the spraying emitter is presented in Figure 3. Needlelike structures provide an ideal geometry for an electrospray emitter. A sharp tip has much less surface area for solvent to accumulate, and excess liquid is readily removed by electric field gradient.

Once the emitter was introduced into the mass spectrometer, the reservoir feature was loaded with the liquid sample using a micropipette; this liquid was seen moving readily towards the emitter structure. As described in the experimental section, the electrospray signal was recorded. Figure 4 shows the mass spectrum obtained for a bradkynin 2-9 sample using the micro emitter. With the help of the released emitter structure and the hydrophobicity of the gold material, which avoids solution spreading at the outer walls, the device has shown an efficient ionization performance providing a stable MS signal constantly. Singly charged peak (*m/z* 904) and doubly charged peak (*m/z* 453) of peptide were detected, respectively. Finally, we carried out fragmentation experiments in each peak. Figure 5 shows the MS/MS spectrum resulting from the fragmentation of the

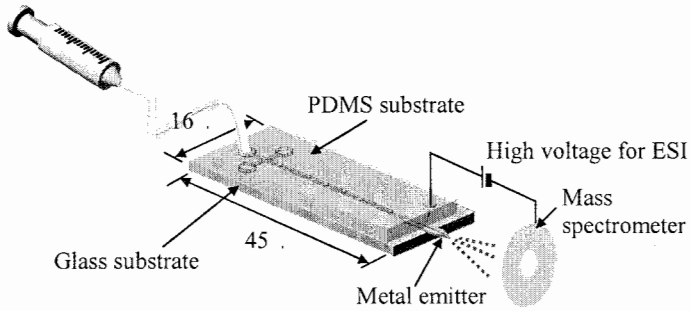

Figure 2. Experimental setup with the electrospray device

bradkynin 2-9 sample under a 2 kV HV supply and using a micro emitter structure source.

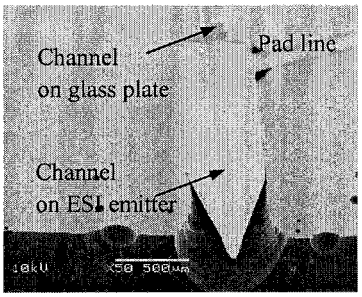

Figure 3. SEM of the emitter structure

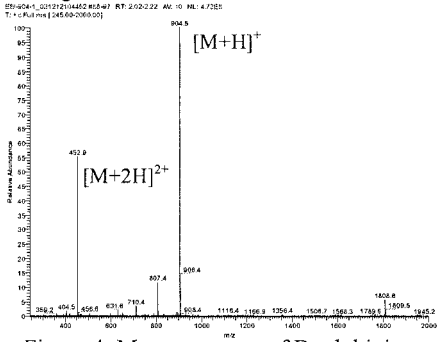

Figure 4. Mass spectrum of Bradykinin

4. Conclusions

We have designed and demonstrated a sheathless ESI-MS interface with conducting metal emitter tip on PDMS/glass based microchips. The separation channels and metal emitter tip are fabricated using a glass wet etching and gold electroplating process, respectively. This approach is less involved than applying a conductive coating to the exit end to establish electrical contact. As such, the interface is less dependent upon the longevity or durability of such coating, factors that have been consideration in the sheathless interfaces. Singly charged peak and doubly charged peak were detected by spraying peptide sample and further MS/MS fragmentation was performed in each peak. Direct comparisons with conventional glass or fused silica emitters showed very similar performance with respect to signal strength and stability.

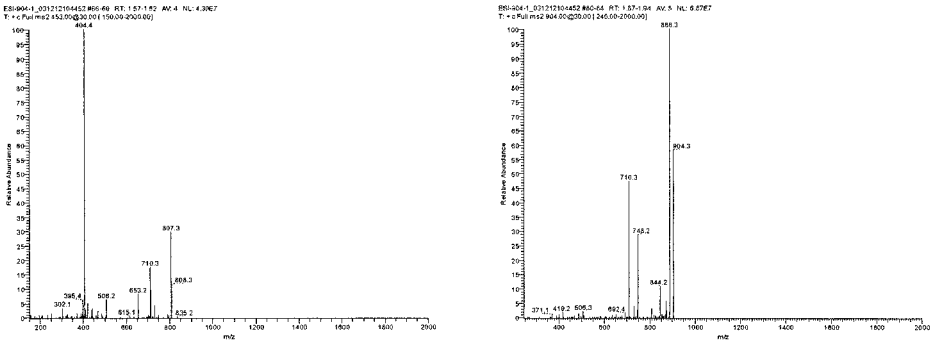

Figure 5. MS/MS fragmentation spectrum of doubly charged peak (m/z 453), and singly charged peak (m/z 904)

Acknowledgements

This work was supported by a grant of the International Mobile Telecommunications 2000 R&D Project (Ministry of Information & Communication).

References

[1] R. S. Ramsey and J. M. Ramsey, *Anal. Chem.* 69, 1174-1178 (1997).

[2] B. Zhang, H. Lui, L. Karger, and F. Foret, *Anal. Chem.* 71, 3258-3264 (1999).

NANOSPRAY EMITTERS USING POROUS POLYMER MONOLITHS (PPMs): A STEP TOWARDS A ROBUST MICROFLUIDIC-MS INTERFACE

Terry Koerner, Kierra Turck, Laurie Brown and Richard D. Oleschuk
Department of Chemistry, Queen's University, Kingston, Ontario, Canada

Abstract

Coupling low flow analytical separation instrumentation with electrospray ionization mass spectrometry (ESI-MS) has yielded powerful analytical tools. However, conventional coupling methodologies such as nanospray suffer from limitations including poor conductive coating robustness, constant clogging and complicated fabrication processes. In this study we show that a robust nanospray emitter can be fabricated through the formation of a porous polymer monolith (PPM) at the exit aperture of the capillary or device. Stable electrosprays can be produced from PPM filled capillaries (75-100 μm i.d.) at a variety of flow rates (50 – 1000 nL/min) without the need to taper the capillaries by etching. This work shows that PPM filled microfluidic channels may be utilized as a robust coupling strategy for microfluidic devices and mass spectrometry.

Keywords: Porous Polymer Monolith, Nanospray, Mass Spectrometry, Proteomics

1. Introduction

Mass spectrometry has made significant strides in the field of Proteomics because it possesses the ability to determine the primary structure of the protein with subsequent collision-induced dissociation (CID) experiments on the intact protein or its tryptic fragments [1-4]. With the advent of the nanoelectrospray source it became possible to obtain this type of information from an extremely small sample size because of the improved detection limits, in the low femtomole and attomole levels [5-7]. The coupling of microchips and mass spectrometry will provide a high-throughput proteomic analytical technique to both purify complex protein samples and elucidate protein structure. The amalgamation of these two technologies is being investigated in many research labs but has yet to reach broad applicability because of poor reliability and/or difficulty of fabrication methodologies for producing microfluidic/MS interfaces.

Spraying directly from the open end of a microfluidic device would remove any potential of creating a dead volume interface but this method also has some inherent problems. One of the difficulties is that the open channel, with a diameter of between 30 and 50 μm, terminates to a large flat hydrophilic surface area making it difficult to obtain a stable electrospray [8,9]. Furthermore, the relatively large channel diameter is not ideal for

Figure 1: A Schematic representation of a porous polymer monolith in a fused silica capillary and a microfluidic device. to create small openings to promote the nanoelectrospray process. SEM photomicrographs of a 360 μm o.d. x 75 μm id capillary.

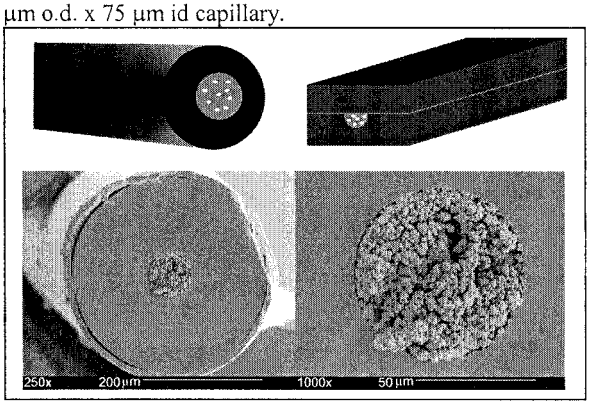

creating a stable electrospray at lower flow rates such as those generated by electroosmotic pumping. An alternative is to photo pattern a porous polymer monolith (PPM) at the end of a capillary (Figure 1) to provide the proper pore size and hydrophobic surface characteristics to facilitate a stable nanoelectrospray process. In this study we investigate a facile method for the construction of nanospray emitters that shows promise as a step towards overcoming some of the difficulties of previous interfaces and realizing a robust interface between these two technologies. The PPM is photo-patterned through masking and UV light initiation so as to be present only near the capillary exit aperture using porogenic solvent conditions that generate pore sizes similar to those seen with conventional nanospray tips (≈1 μm).

2. Experimental: Capillary testing apparatus is shown in Figure 2 where a syringe pump or nanopump is used to infuse sample through the patterned capillary. The capillary is fitted within a Proxeon nanospray interface with the electrospray directed into a PE/Sciex API3000 triple quadrupole mass analyser. The electrospray voltage is applied through a micro-cross to establish a liquid junction.

Figure 2: PPM assisted ESI/MS coupling

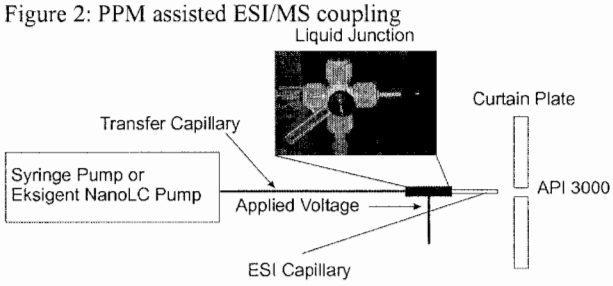

3. Results and Discussion

The small multiple pores in the PPM divide the flow in the capillary or micro-channel into smaller streams and create the potential of multiple electrospray emitters. This has been shown to be beneficial in a larger scale system (0.5-5.0 μL min^{-1}) where multiple electrospray orifices were constructed by laser ablating a polymeric substrate [10]. In this study the porous nature of the PPM

Figure 3: TIC trace from a constant infusion of polypropylene glycol (PPG) at 100 nL/min and applied voltage of 3.0 kV using a 100 μm inner diameter capillary fitted with a PPM. Shows the stability of the spray by turning the voltage off and back on to regenerate the electrospray process. The picture shows the nanoelectrospray process at 100 nL/min, producing a mist at the exit aperture.

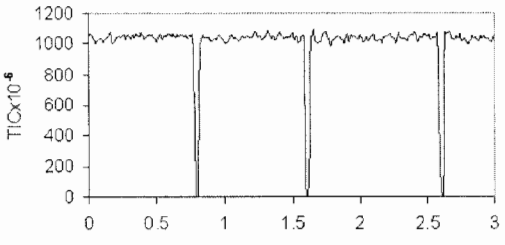

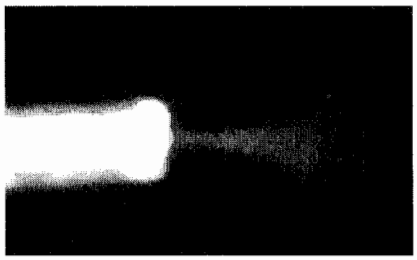

aids in developing a stable electrospray by generating a single clearly visible Taylor cone at relatively high flow rates (≈1 μLmin^{-1}) while at low flow rates (<100nLmin^{-1}) a mist, presumably

from multiple small Taylor cones develops (Figure 3). In addition the hydrophobic nature of the PPM should also limit problems associated with band broadening resulting from the droplet spreading at the capillary exit and the multiple flow paths inherent in the PPM minimize clogging problems associated with conventional nanospray emitters. The reduced pore size produces smaller droplets that have a larger surface area to volume ratio, increasing the analyte concentration, and

Figure 4: Total ion current (TIC) for constant infusion of PPG (125 nM) with an applied voltage of 3.0 kV at a 50 nL/minute flow rate

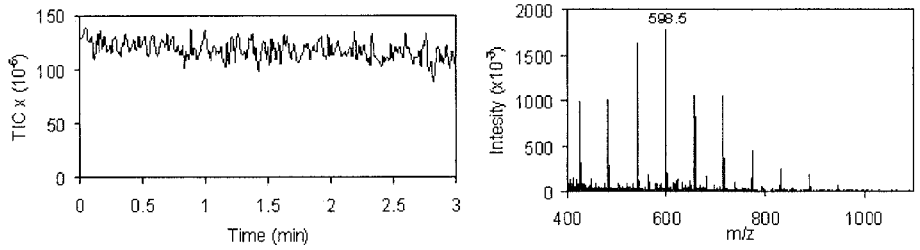

requiring less desolvation to provide enhanced sensitivity. Figure 4 shows a total ion chromatogram demonstrating the stability of the nanospray developed by the PPM filled capillary. The flow rate of 50 nL was chosen to mimic typical flow rates generated by electroosmotic pumping in microfluidic devices. We are able to obtain a stable electrospray at a variety of flow rates ranging from 50 $nLmin^{-1}$ to 1.0 $\mu Lmin^{-1}$ for both standard PPG and protein solutions at low concentrations (12 nM). Total ion current (TIC) traces for a constant infusion of standard PPG and Cytochrome c solutions are very stable with deviations ranging from only 3 – 8 percent. The PPM assisted electrospray produces mass spectra with excellent signal to noise from only a few femtomoles of material.

4. Conclusions

This investigation demonstrates the benefits of using a capillary in which a PPM is formed at the end. The PPM assisted electrospray is compatible with a variety of flow rates and more robust than conventional nanospray tips. In addition to its potential for creating a microfluidic-MS interface, this method will be useful for other low flow mass spectrometry interfaces such as nanoLC, CE and capillary electrochromatography (CEC).

Acknowledgements

We acknowledge the Natural Sciences and Engineering Research Council of Canada, Canadian Foundation for Innovation, Ontario Innovation Trust, Genome Prairie (Enabling Technologies Project) and Queen's University for financial support.

References [1] Cristoni, S.; Bernardi, L. R.; *Mass Spec. Rev.* **2003**, *22*, 369-406. [2] Lill, J. *Mass Spec. Rev.* **2003**, *22*, 182-194. [3] Mann, M.; Hendrickson, R. C.; Pandey, A. *Annu. Rev. Biochem.* **2001**, *70*, 437-473. [4] Yates, J. R. *J. Mass Spec.* **1998**, *33*, 1-19. [5] Wilm, M.; Mann, M. *Anal. Chem.* **1996**, *68*, 1-8. [6] Davis, M. T.; Stahl, D. C.; Hefta, S. A.; Lee, T. D. *Anal. Chem.* **1995**, *67*, 4549-4556. [7] Valaskovic, G. A.; Kelleher, N. L.; Little, D. P.; Aaserud, D. J.; McLafferty, F. W. *Anal. Chem.* **1995**, *67*, 3802-3805. [8] Xue, Q.; Foret, F.; Dunayevskiy, Y. M.; Zavracky, P. M.; McGruer, N. E.; Karger, B. L. *Anal. Chem.* **1997**, *69*, 426-430. [9] Ramsey, R. S.; Ramsey, J. M. *Anal. Chem.*. **1997**, *69*, 1174-1178.[10] Tang, K.; Lin, Y.; Matson, D.; Kim, T.; Smith, R. *Anal. Chem.* **2001**, *73*, 1658-1663

INTERFACING MICROFLUIDICS TO MASS SPECTROMETRY VIA ELECTROSPRAY DEPOSITION AND MALDI-MS

Ying-Xin Wang[1], Yi Zhou[1], Jon W. Cooper[2], Cheng S. Lee[3] and Don L. DeVoe[1*]
[1]Dept. of Mechanical Engineering,, University of Maryland, College Park, MD, USA 20742,
[2]Calibrant Biosystems, 7507 Standish Pl., Rockville, MD, USA 20855
[3]Dept. of Chemistry and Biochemistry, University of Maryland, College Park, MD, USA 20742
Tel: 301-405-8125, Fax: 301-314-9477, e-mail: ddev@eng.umd.edu

Abstract

Electrospray deposition of peptides onto matrix-assisted laser desorption-ionization (MALDI) target plates followed by off-line MALDI-MS analysis is presented. A key feature of the system is a novel hydrophobic membrane technique which enables simple fabrication of high-quality nanospray ESI tips in rigid polymer substrates. The technique, which involves bonding a porous hydrophobic membrane to the exit surface, enables electrospray directly from the flat chip edge with no additional shaping of the substrate. The resulting porous structure is shown to act as a dense array of nanoscale ESI tips, enabling the generation of stable electrospray at both high flow rates (tens of μL/min) down to exceptionally low flow rates (under 10 nL/min). Furthermore, since lateral dispersion of liquid at the electrospray deposition surface is constrained by the hydrophobic membrane, closely-spaced parallel microchannels with no co-mingling of analytes during electrospray deposition is demonstrated. In addition, initial results on gel electrophoresis (GE) protein separation microchip will be presented.

Keywords: Electrospray, MALDI-MS, Polymer microfluidics, Proteomics

1. Introduction

Microfluidic systems offer the potential for performing liquid-phase biomolecular separations with increased throughput and sensitivity while significantly reducing cost. Ultimately, high resolution molecular analysis requires the coupling of these microchannel separations with mass spectrometry (MS) for accurate mass determination. Various approaches to interfacing microfluidic systems to MS have been reported. In particular, electrospray ionization (ESI) has been widely demonstrated for direct in-line coupling of microfluidic separations to MS. However, the time scales for biomolecular separations and ESI-MS analysis are not always compatible. Thus there is a need for MS analysis which may be performed off-line, decoupled from the actual microfluidic separation.

Herein we present the off-line coupling of polymer microfluidic chips to mass spectrometry through electrospray deposition of peptides onto matrix-assisted laser desorption ionization (MALDI) targets. Analysis of the deposition process is discussed, followed by results from MALDI-MS analysis of deposited analytes. Integration into a microfluidic capillary gel electrophoresis (CGE) separation platform for proteomic applications is also described.

2. Experimental

Using a previously-described process [1], robust electrospray tips were fabricated through the addition of a porous hydrophobic membrane at the microchannel exit. Briefly, planar microchannels were fabricated in polycarbonate (PC) using polymer hot embossing with a silicon template patterned by bulk Si micromachining. The resulting open microfluidic channels with trapezoidal cross section (122 μm wide at the top, 80 μm wide at the bottom, 30 μm deep, 4.5 cm long) were enclosed by thermally bonding with a blank PC substrate with reservoir holes drilled for electrical and fluidic access at one end of each channel. A 50 μm thick poly-tetrafluoroethylene (PTFE) membrane with porosity of 70% and average pore size of 0.22 μm was thermally bonded to the

exposed microchannel outlet surface. Fig.1 shows an example of a very well defined Taylor cone without lateral spreading established in the channel exit at a flow rate of 120 nL/min, chip-to-counterelectrode spacing of 2 mm, and applied voltage of 3900 V. As can be seen, the high hydrophobicity and porous structure of the PTFE membrane effectively constrains liquid spreading near the channel exit and generates a very stable electrospray. The ESI-MS performance has been evaluated and optimized using myoglobin (0.5 mg/ml) as a model analyte (Fig. 2).

The technology was next applied to eluting analyte from the microfluidic chip onto a MALDI target, followed by offline MALDI-MS analysis. Electrospray deposition conditions were optimized, and matrix solution (50% acetonitrile, 40% water, 10% acetic acid) was deposited to each deposited spot using a custom capillary spotting tool.

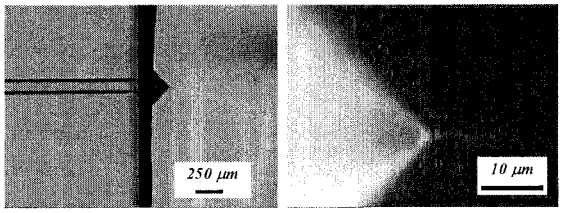

Fig. 1. Photomicrographs of stable Taylor cones established at the membrane microchannel exit.

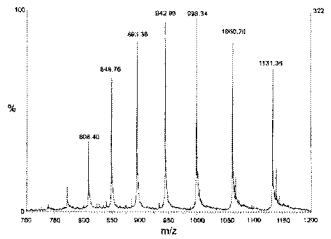

Fig. 2. Protein charge envelope for myoglobin (0.5 mg/ml) measured by ESI-MS from a membrane electrospray chip

3. Results and discussion

Multichannel electrospray deposition has been demonstrated using peptides such as angiotensin, bradykinin, and fibrinopeptide, with no cross contamination observed between three channels spaced 175 μm apart (Fig. 3). Although charge interactions tend to distort the outermost Taylor cones, the PTFE membrane is highly effective at preventing liquid spreading between adjacent tips. Compared to typical spotting methods of MALDI target preparation, electrospray deposition yields excellent homogeneity of peptide crystals across the deposited spots (Fig. 4).

The ES-MALDI interface shows promise for effective coupling of microfluidic separations to mass spectrometry. To this end, the integration of electrospray deposition with CGE protein separations has been explored. A schematic CGE chip with an integrated electrospray tip is shown in Fig. 5. The chip combines gel electrophoresis with electrospray using a sheathless electrospray interface, with makeup fluid provided through a tertiary access port. To test the concept, a solution of 1.5% poly (ethylene oxide) (PEO, MW 600,000) in 8M Tris and 0.05% sodium dodecyl sulfate (SDS) was hydrodynamically introduced from reservoir A into the separation region while flushing extra gel from the cross-injector and electrospray regions. The cross-injector (Fig. 5b) and makeup flow channel (Fig. 5c) were maintained gel-free by injecting running buffer through these sections during gel filling, with visualization performed using rhodamine dye in the gel.

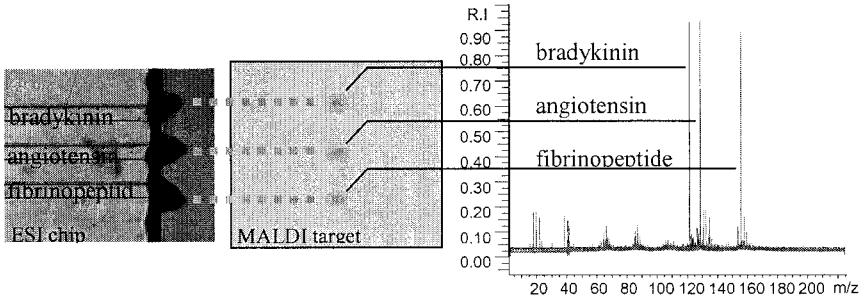

Figure 3. Combined MALDI-MS mass spectra of bradykinin, angiotensin, and fibrinopeptide (right).

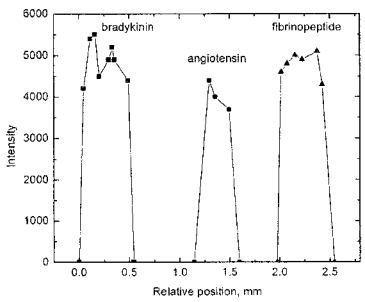

Figure 4. MALDI-MS ion signal intensity measured across the full breadth of the deposited peptide spots. No crosstalk is observed.

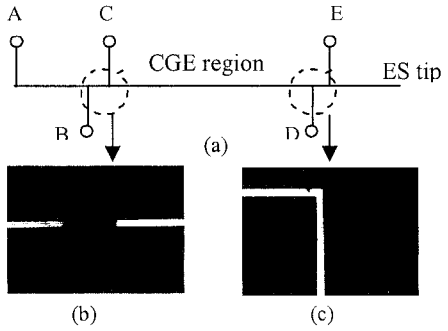

Figure 5. (a) Schematic of CGE/ES chip. Gel is introduced from reservoir A to D while injecting ESI buffer from B to C to form (b) a gel-free cross-injector, and from E to the ES tip to define (c) a gel-free ES makeup flow path.

A mixture of protein-fluorescein conjugates was prepared and electrophoretically introduced into the cross-injector by applying a potential gradient of 300 V/cm between reservoir B and C. And then a positive voltage was applied from E to A to achieve the separation of SDS-protein complexes based on their differences in electrophoretic mobility inside the polymer-sieving matrix. Separated proteins are then be deposited using the integrated electrospray tip at the channel exit.

5. Conclusion

The electrospray deposition technique offers the potential for direct, stable, and repeatable interfacing between polymer microfluidic systems and mass spectrometry, without requiring significant additional fabrication effort. Deposition of model peptides through a three-channel microfluidic chip onto MALDI targets, with no cross-contamination of eluted peptides, demonstrates the ability to couple multiplexed microfluidic separations with MS using this method.

Acknowledgements

The authors gratefully acknowledge support for this research from NIH/NCI through grant CA092819-02, and from DARPA through contract DAAH01-03-C-R182.

References

[1] Y.-X. Wang, J. W. Cooper, C. S. Lee, D. L. DeVoe, *Lab on a Chip*, **4**, (advance article) (2004).

INTEGRATED OPTICAL DETECTION FOR MICROFLUIDIC SYSTEMS USING THIN-FILM POLYMER LIGHT EMITTING DIODES AND ORGANIC PHOTODIODES

Oliver Hofmann[1], Paul Miller[2], John C. deMello[2], Donal D.C. Bradley[3] & Andrew J. deMello[2]
[1]Molecular Vision Ltd., 90 Fetter Lane, London EC4A 1JP, United Kingdom
[2]Department of Chemistry & [3]Department of Physics, Imperial College London, South Kensington, London SW7 2AZ, United Kingdom

Abstract

In this paper the development of lightsources and detectors for integrated microchip based optical detection is reported. A polyfluorene based pLED with peak emission at 488 nm was successfully employed as a lightsource for microchip electrophoresis. With a pLED drive voltage of 5.5 V, separations of fluorecein and 5-carboxyfluorescein could be detected at concentrations down to 1 μM. In separate experiments, thin-film organic photodiodes were employed as integrated detectors for microscale chemiluminescence. The copper phthalocyanine-fullerene (CuPc-C_{60}) small molecule photodiodes have an external quantum efficiency of ~30% at 550 to 650 nm. The photodiodes were used to monitor a peroxyoxalate based chemiluminescence reaction (PO-CL) within a poly(dimethylsiloxane) (PDMS) microfluidic device. Preliminary PO-CL based quantitation of hydrogen peroxide yielded a detection limit of 1 mM.

Keywords: polymer LEDs, organic photodiodes, chemiluminescence, integrated detection

1. Introduction

Polymer light emitting diodes (pLED) comprise one or more layers of conjugated polymer sandwiched between two electrodes and emit light under electrical excitation. The emission colour can be controlled by changing the chemical structure of the semiconducting polymer. Owing to the simple layer-by-layer deposition procedures for the polymer components the pLEDs can be readily integrated with microfluidic systems. To demonstrate the efficacy of the approach, the polyfluorene diode is used as an excitation source for the detection of fluorescent dyes separated on-chip by electrophoresis. Similar in structure to pLEDs, organic photodiodes generate a measurable current under illumination. Photodiodes based on small molecule blends have demonstrated efficiencies up to 80% (electrons out/photons in). We report the successful integration of CuPc-C_{60} heterojunction photodiodes with polydimethylsiloxane (PDMS) microfluidic devices for the monitoring of PO-CL reactions. PO-CL reactions involve the formation of a metastable reaction intermediate and light emission is based on an energy transfer process to a suitable fluorophore. For quantitation, hydrogen peroxide was selected as a model compound because it is produced by a number of enzymes when in contact with specific analytes and dissolved oxygen (e.g. glucose, cholesterol).

2. Experimental

Fabrication of the polyfluorene pLEDs on an indium tin oxide (ITO) coated glass substrate was based on spin coating of the active layer and thermal evaporation of the electrodes. Details of the fabrication are described elsewhere [1]. CE microdevices were manufactured in-house and comprised a 50-μm-wide and 40-μm-deep microchannel network etched into a planar glass substrate. Injection and separation of fluorescein and 5-carboxyfluorescein was performed under applied electric fields up to 3000 V. Detection was based on an oil immersion objective and a silicon avalanche photodiode (SPCM-AQR-141, EG&G Canada).

The fabrication of the CuPc-C_{60} heterojunction organic photodiodes and the effect of composition and architecture on device performance is described in detail elsewhere [2]. The mixed CuPc / C_{60} layers were grown on ITO coated glass substrates by co-deposition from independent

organic evaporation sources. For the devices employed in the current studies 58 nm thick layers comprising 60 w/w-% CuPc and 40 w/w-% C_{60} were deposited. This was followed by deposition of bathocuproine (BCP). Al electrodes were deposited by evaporation through a shadow mask yielding three detection strips with an active area of 2 mm x 8 mm each. For characterisation of the organic photodiodes a PO-CL reaction was performed on chip. Microfluidic devices for PO-CL were made from PDMS and structured by cutting out the channels with a scalpel blade. The layout of the CL microdevices is shown schematically in Figure 1. PO-CL reagents were extracted from Cyalume lightsticks (American Cyanamid Company). The active components are Bis (2-carbopentyloxy-3,5,6-trichlorophenyl) oxalate (CPPO), 9,10-diphenylantracence dye (both reagent A) and hydrogen peroxide (reagent B). For quantitation experiments with hydrogen peroxide, 5 mM 4-Dimethylaminopyridine (DMAP) was used as a catalyst to increase CL-intensity.

3. Results and discussion

For proof-of-concept a thin-film pLED based on polyfluorene with an emission maximum at 488 nm and an active area of 40 um x 1000 um was used as an excitation source for fluorescence detection in microchip-based electrophoresis. Fluorescein and 5-carboxyfluorescein could be detected at concentrations as low as 1 µM with a mass detection limit of 50 femtomoles. This is similar to detection limits obtained with a mercury lamp excitation source. The drive voltage required to generate sufficient emission from the pLED was only 3.7 V.

In separate experiments novel organic photodiodes were tested as microchip based detectors (Figure 1). PO-CL reagents A and B were hydrodynamically pumped through microchip inlets 1 and 2, respectively. Flow rates were optimised between 5 and 200 µL/min, yielding chemi-luminescence signals from 1.4 to 6.3 nA with highest signals observed for 25 µl/min (Figure 2). For higher flow rates the short residence time resulted in incomplete mixing of the reagents and reduced chemiluminescence signals. For the optimised 25 µL/min flow conditions, reproducibility of the CL signal was determined by repeating experiments three times on the same microchip. RSD values for the steady-state signal after ~11 minutes, were typically below 1.5%. This reproducibility is clearly sufficient for quantitative analysis and demonstrates the potential of both microchip based PO-CL and integrated detection with CuPc-C_{60} photodiodes. As a model compound, hydrogen peroxide was quantified using the PO-CL / organic photodiode approach. Preliminary experiments suggest a detection limit of ~1 mM (signal-to-noise ~10). While this is sufficient for the monitoring of most fermentation processes [3], significant sensitivity gains are expected through device optimisation. Experiments are ongoing to apply the PO-CL reaction to the detection of commonly used fluorescence labels.

4. Conclusions & outlook

Combining the thin-film pLEDs and organic photodiodes should yield powerful integrated detection systems for a wide range of applications. The tunable optical properties, simple fabrication, small size and low cost of the described detection components have obvious benefits for portable *in-the-field* and *point-of-care* devices. Over the next five years we envisage organic semiconductor based optical detection arrays becoming a key component of multi-analyte microfluidic systems for the *point-of-care* market.

Acknowledgements

Molecular Vision Ltd acknowledges support from the UK Biotechnology and Biological Sciences Research Council through its Small Business Research Initiative (grant 147/SBRI 19689). We also thank Cambridge Display Technology Ltd. for providing test pLEDs and Prof. Tim Jones, Imperial College, for providing the organic photodiodes.

References
[1] J.B. Edel, N.P. Beard, O. Hofmann, J.C. deMello, D.D.C. Bradley, A.J. deMello, *Lab Chip*, **4**, 136-140 (2004).
[2] P. Sullivan, S. Heutz, S.M. Schultes, T.S. Jones, *Appl. Phys. Lett.*, **84**, 1210-1212 (2004).
[3] A.M. Jorgensen, K.B. Mogensen, J.P. Kutter, O. Geschke, *Sens. Act. B*, **90**, 15-21 (2003).

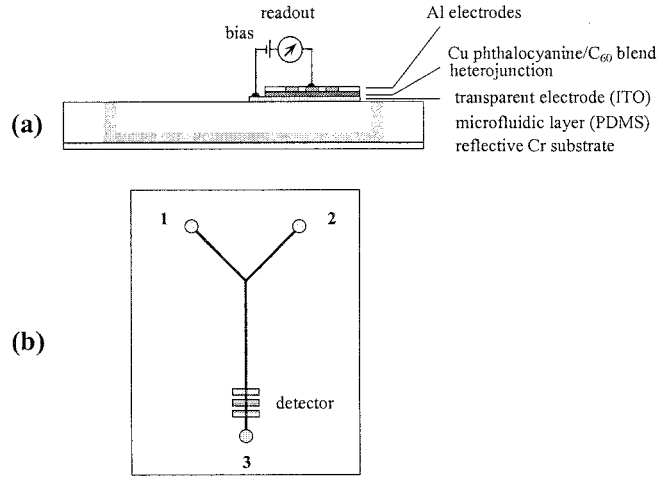

Figure 1. (a) Side view of organic photodiode integrated with planar PDMS microchip. (b) Layout of PDMS microchip comprising two inlets (1,2), mixing channel and outlet (3). Mixing channel is 1000-µm-wide, 800-µm-deep and 7-cm-long. The detector is positioned below the mixing channel (active area: three strips of 8 mm x 2 mm). Only one detector strip was used for the current studies.

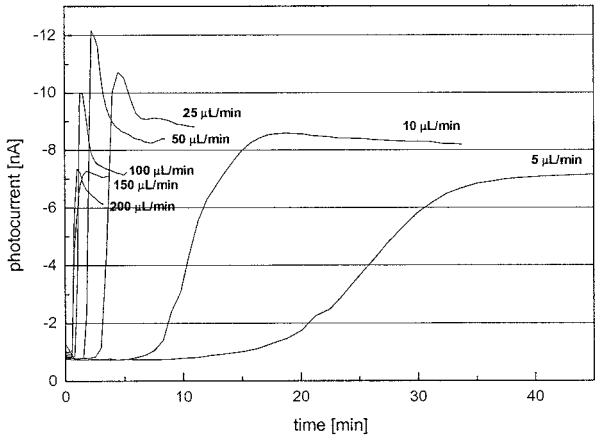

Figure 2. Monitoring of chemiluminescence reaction with organic photodiode on PDMS microchip. PO-CL reagents A and B were applied to inlets 1 and 2, respectively. Flow rate was varied to optimise mixing and chemiluminescence signal intensity.

BATTERY-OPERATED MICRO PLASMA DEVICES (MPDs)

Vassili Karanassios, Andrea T. Smith and Kara Johnson
Department of Chemistry, University of Waterloo, Waterloo, Ontario Canada N2L 3G1

Abstract
Small-size, low-power (<~ 5 W) and low gas-consumption are key advantages of plasma source miniaturization. Can liquid samples be introduced into such micro plasma devices (MPDs)? Would there be sufficient energy density to atomize, excite or ionize analytes introduced into MPDs? Simple calculations reveal that there would be, provided that samples are introduced into MPDs as aerosols of dry vapors. The results of such calculations were confirmed experimentally by fabricating planar and cylindrical geometry MPDs (that were even operated from a re-chargeable drill battery) and by using mini-In-Torch Vaporization (ITV) sample introduction. Results obtained by MPD-optical emission spectrometry (MPD-OES) and MPD-mass spectrometry (MPD-MS) are very encouraging and will be briefly discussed.
Keywords: micro plasmas, micro sample introduction, micro fluidics, optical & MS detection

1. Introduction

For the last few decades, the inductively coupled plasma (ICP) has been the plasma source of choice for elemental analysis. But ICPs are heavy and bulky and they consume large amounts of gas (15-20 L/min). As well as due to power requirements in the kW range, they are typically tethered to a wall socket. Can a plasma source for elemental analysis be miniaturized? If miniaturized, would a micro plasma device (MPD) have sufficient energy per unit volume as its laboratory-scale counterpart to produce atomic emission for optical measurements or to generate ions for mass spectrometric detection? At present, many research groups are exploring this possibility [1]. But with a few notable exceptions, MPDs have only been used with gaseous samples. Is simplicity of sample introduction responsible for this choice or is there a fundamental reason? Could liquid samples be introduced into MPDs?

2. Theory

Many analytical samples naturally occur as liquids. These are typically acidified and are introduced into plasmas, most often using a pneumatic nebulizer for sample introduction. Others are solids that prior to their elemental analysis are converted (i.e., digested) into a liquid. Simple order-of-magnitude calculations reveal that although it would take mW to vaporize, excite and ionize analytes that have been introduced into a MPD, it takes over 10 W to vaporize the water solvent [1]. Since most present day MPDs are non-thermal and are not in thermodynamic equilibria, such micro plasmas would be extinguished if water solvent was introduced into them along with the sample. But if the water solvent was evaporated and a dry residue was introduced into a MPD as an aerosol of a dry vapor, even battery-operated MPDs would have sufficient energy to atomize, excite and ionize analytes introduced into them. In our laboratories, these ideas were tested using a (mini) In-Torch Vaporization (mini-ITV) dry sample introduction for MPDs of different size and geometry.

3. Experimental

Initially, planar geometry MPDs were fabricated and tested. An example is shown in Fig. 1. These MPDs on-glass-chips were constructed using microscope glass slides, chemically-etched microchannels (typically 1-mm wide, 5-mm long and 250 μm deep) and Au-sputtered electrodes [1]. The ends of the electrodes served as electrical contact pads. The operating voltage was ~3000-

4000 V_{dc} and a resistor was used to ballast the discharge. The microplasmas were formed between the electrodes thus making the middle part of the microchannel the plasma chamber. A mini-ITV, i.e., a scaled-down version of an ITV originally developed for ICPs [2] was used for sample introduction. Different versions of mini-ITV have been developed and tested and an example is shown in Fig. 2. Briefly, mini-ITV consists of a coiled-filament secured on a support (typically a ceramic) and a vaporization chamber. The coiled-filament serves as a "sample holder". With the outlet tube of the mini-ITV disconnected from the MPD, the support is retracted from the vaporization chamber, a few μL of a sample are pipetted onto the filament and the support is re-inserted into the vaporization chamber. Electrical power cables running through the ceramic connect the filament to an electrical power supply. Low electrical power is applied to the filament to dry a sample on it. The outlet tube of mini-ITV is reconnected to the MPD, the MPD is switched on for 5-10 sec and higher power is applied to the coil to vaporize the dry residue that remained on it. The vaporized sample is transported to the MPD via a carrier-gas that also serves as the plasma gas (200-500 mL/min, typically Ar-H_2 or He-H_2). Once in the MPD, the sample is atomized, excited or ionized. Atomic emission is measured using either a bench-top optical spectrometer (a 0.35 m Czerny-Turner monochromator, Fig. 3) with a photomultiplier tube (PMT) detector or a fiber-optically coupled, portable spectrometer with a charge coupled device (CCD) detector. The transient emission signals, lasting for about 0.5 sec, were digitized as described previously for ITV-ICP-AES [3] and an example (for Ca, 3 μL, 1 ppm) is shown in Fig. 4. Thus clearly demonstrating that MPDs have sufficient energy to vaporize and excite analytes of dry vapors from mini-ITV sample introduction.

Short lifetime (a few hours at best) and poor analytical precision were two key problems associated with these early planar devices. Despite their short lifetime, useful optical emission signals were obtained. Lifetime was extended to weeks using ac operation and electrodes made out of Cr or Ni. Because the mini-ITV signal is of very short duration, MPDs do not have to be turned on for more than a few seconds (to record analyte emission and pre- and post-vaporization plasma background levels). Thus, in addition to reducing electrical power consumption, MPDs so operated barely get warm to the touch. In fact, we fabricated a (crude) MPD on a plastic substrate [1] thus demonstrating that MPDs cannot only be made small, but when operated as described above, they can be made sufficiently inexpensive to be made disposable.

Do MPDs have sufficient energy density to ionize analytes introduced into them? This was tested by coupling a cylindrical geometry MPD to the cylindrical sampling cone of an ICP-MS (of course without an ICP). A photograph is shown in Fig. 5. From the results shown in Fig. 6, it can be concluded that MPD-MS is possible and that MPDs may become useful ion-sources for elemental analysis from liquid micro-samples.

Conclusions

Although more work remains to be done, it is clear that MPDs have the potential to become useful sources for plasma spectrochemistry.

References

[1] V. Karanassios, Spectrochim. Acta Part B (invited review on micro plasmas, in press)

[2] A. T. Smith, H. R. Badeie, J. C. Evans, V. Karanassios, Anal. Bioanal. Chem. (in press).

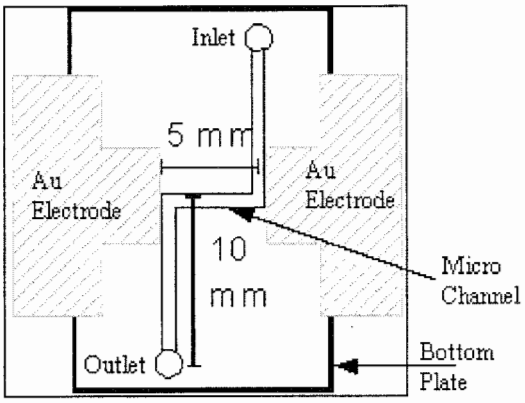

Fig. 1 Planar MPD on glass chips

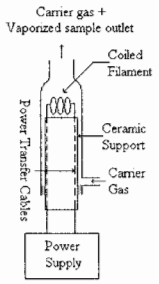

Fig. 2 Mini-ITV.

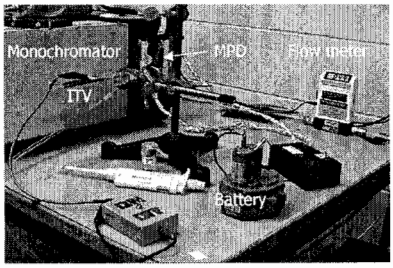

Fig. 3 Photo of mini-ITV-MPD-AES.

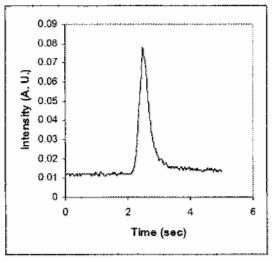

Fig. 4 mini-ITV-MPD-AES signal.

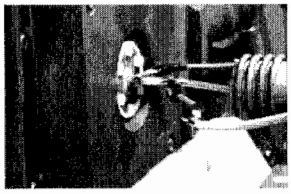

Fig. 5 MPD-Mass spectrometry.

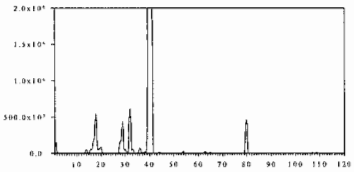

Fig. 6 MPD-MS (counts/sec versus m/z).

ELECTROCHEMICALLY ADDRESSED BIOMOLECULES ONTO Au μ-ARRAY IN A CONTINUOUS FLOW μ-CHAMBER

J.Maly[1,2], M.Ilie[3,4], V.Foglietti[4], E. Cianci[4], A. Minotti[4], B.Lanza[2], L. Nardi[2], A.Masci[2], W. Vastarella[2], R.Pilloton[2]

[1] *Dep. of Biology, University of J.E.Purkyne, 40001 Usti nad Labem, Czech Rep.,*
[2] *ENEA / SP061, Via Anguillarese,301, 00060 Santa Maria di Galeria, Roma*
[3] *University Politehnica, Bucuresti,LAPI, P.O. Box 15-135, O.P. 15, Romania*
[d] *CNR / Istituto di Fotonica e Nanotecnologie, Via Cineto Romano 42, Rome, Italy*

Abstract

Preliminary results regarding electrochemical on-chip purification-deposition of proteins, for further multi-analyte biodetection based on multiplexed chronoamperometry, in a continuous flow μ-chamber are presented. The μ-chamber consists of a planar array of gold electrodes covered by a borofloat® glass reservoir provided with perpendicular plastic capillaries of 500 μm internal diameter. The array of planar 7 x 7 working electrodes has been manufactured using optical lithography and chemical vapour deposition techniques. A his-tag alkaline phosphatase has been electrochemically addressed and its activity detected on a single electrode of the μ-array.

Keywords: electrochemical biosensors, bio-chip, μ-arrays, his-tag, continuous flow

1. Introduction

The blow-up of miniaturization of analytical devices, requiered by the reduction of analysis times, has imposed the evolution of sensitive detection methods. Fluorescence detection has been widely employed, not only because its inherent high sensitivity is a good match for the small analyte volumes of fluorescent species, but also because not fluorescent amino acids and related species can be derivatized with a fluorescent tag. For other classes of analytes, this technique is not easily implemented and thus direct fluorescence detection cannot be considered an universal approach [1]. An alternative approach is the multi-analyte multiplexed chronoamperometry performed over an array of precisely located immobilized biomolecules. Our first results regarding electrochemically on-chip addressing of engineered proteins in a continuous flow μ-chamber are presented below.

2. Experimental

The μ-chamber [2] (Fig.1) consists of a planar array of gold electrodes covered by a borofloat® glass reservoir (Fig1, item 1) provided with perpendicular plastic capillaries (Fig1, items 2,3), having and internal diameter of 500 μm. The array of working electrodes (each of them having a diameter of 70 μm) has been manufactured using optical lithography and chemical vapour deposition techniques. The reference electrode is an Ag/AgCl wire fitted in a Y-shaped piping at the outlet capillary (Fig. 1, item 3). The reservoir (hold capacity = 600nl) has been manufactured by means of wet etching through a lithographically patterned Au/Cr mask. The perpendicular connections to the capillaries have been built out of silicone adaptors with cylindrical and conical shape, the larger of them being fixed by means of a silicone based adhesive. The chip size was 12 x 13 mm^2. The electrical connections of Kelvin type have been soldered *via* aluminium wires (Fig. 1, item 4) on a standard RS-PCB (6 x 6 cm^2) and allowed electrochemical measurements as well as Cyclic Voltammetry (CV), ChronoAmperometry (CA, Fig.2), Differential Pulse Voltammetry (DPV) etc. Recently, an original deposition procedure [4-7] has been developed in our laboratory obtaining oriented and reversible immobilisation of engineered proteins with a His_{6x}-tag and their on-chip purification from bacterial crude extracts. This method started with the deposition of an electrochemically assembled monolayer (EAM) of cysteamine on gold or platinum surfaces and

further chemical synthesis of a spacer with a Ni-NTA end. This technique has been then applied on the μ-chip assembled in the μ-chamber described above with a his-tag alkaline phosphatase (AP).

3. Results

Gold working electrodes have been tested by multiplexed chronoamperometry at 650 mV vs Ag/AgCl and in flow conditions (10μl/min). Figure 2 reports an example of the signal due to injection of a 2mM H_2O_2 solution using bare electrodes before coating with proteins.

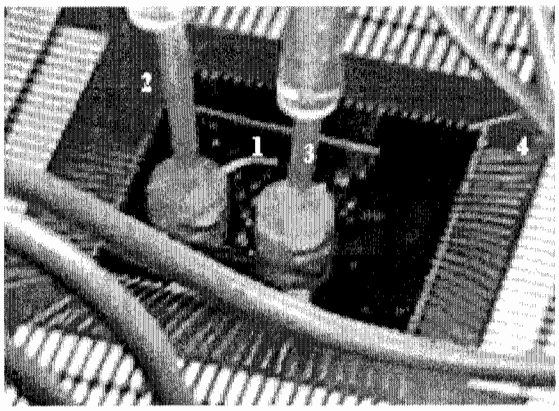

Figure 1: Continuous flow μ-chamber with vertical capillary connections;. 1-glass reservoir; 2-inlet capillary; 3-outlet capillary; 4 aluminum wires connections to the PCB

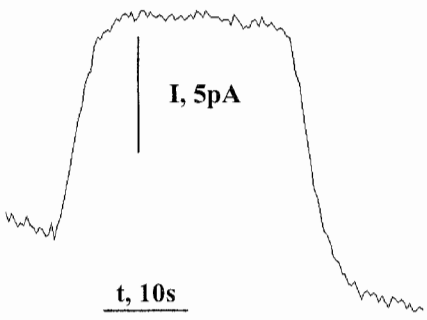

Figure 2: Continuous flow chronoamperometry of a 2mM H_2O_2 solution feeding the μ-array before the deposition of enzymes

Electrochemical deposition of cysteamine (Fig.3) obtained by chronoamperometry on a specific working electrode in the μ-array at 850mV vs Ag/AgCl, followed by chemical synthesis of a NiNTA chelator, allowed to address the his-tag proteins on a specific electrode in the μ-array in few minutes and in flow condition (flow-rate=10 μl/min). A single electrode in the μ-array was coated by electrochemically addressing of a His-tag AP and tested with the proper substrate of this enzyme: ascorbic acid-2 P. Due to the enzyme activity, ascorbic acid is formed and electrohemically detected at 400 mV vs Ag/AgCl. The signal due to AP activity was recorded on the addresses electrode n.4 (Fig. 4). The adjacent electrode n.3 gave no signal. We presume the small signal recorded on electrode n.16 is due to the ascorbic acid formed on electrode n.4 and carried out down the flow. Thus, the electrochemical deposition can be used to specifically address biomolecules (enzymes, antibodies, DNA fragments) on a single electrode in the μ-array. Further studies on electrode lay-out and flow conditions have to be carried out in order to minimise crossed signal of an electrode down the flow, due to the products of the enzyme reaction formed on another electrode. This problem arose when enzymes or enzyme labelled antibodies have been immobilised on the working electrodes, while with immobilised ssDNA fragments this limitation is not present.

4. Conclusions

Electrochemistry can be used during immobilisation step of biomolecules and during the analytical measurements with a μ-array of gold electrodes. A his-tag alkaline phosphatase has been addressed and its activity detected on a single electrode of a μ-array in flow condition by means of a novel μ-flow cell, useful for a future multi-analyte biodetection based on multiplexed chronoamperometry.

Acknowledgements
These experiments have been supported by: "Progetto 5% Nanotecnologie" of MURST, the TRIL programm of Abdus Salam International Center of Theoretical Physics, the project 522/03/0659 of Grant Agency of the Czech Republic, Italian Fund for Research (FISR), Theme 4 "Optical and Electro Optical Sensors", Italian Fund for Fundamental Research (FIRB) and by CoSMiC (Enea target Project on Biosensors and Bioelectronics – www.biosensing.net).

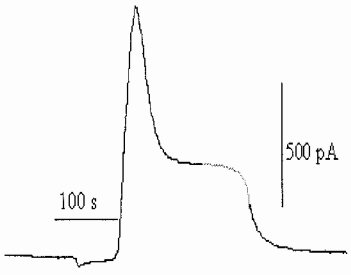

Figure 3. Chronoamperometry of the deposition of an EAM of cysteamine (10mM) in flow condition. After the current peak the signal decreases till a steady state, then phosphate buffer solution (0.1M, pH=7.00) has been sent.

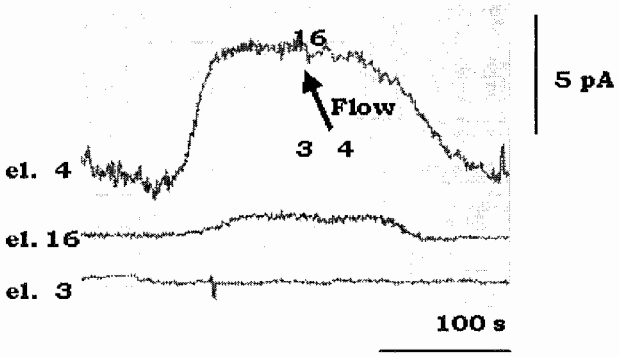

Figure 4: Signals due to 1mM ascorbate-2P, the substrate of AP, from working electrodes n.4 (electrochemically deposed AP), n.3 (bare electrode) and n.16 (bare electrode, downstream). Picture of the μ-array in the background shows the relative positions of electrodes and the direction of the flow stream.

References

[1] Maria A. Schwarz and Peter C. Hauser, Lab on a Chip, 2001, 1 (1), 1-6
[2] M. Ilie, L. Nardi, J. Maly, R. Pilloton, E. Cianci, A. Minotti, V. Foglietti, AISEM 2004 Proceedings, in press
[3] J. Maly, M. Sugiura, M. Ilie, V. Foglietti, E. Cianci, A. Minotti, A. Masci, W. Vastarella, R. Pilloton, AISEM 2004 Proceedings in press
[4] J.Maly, A.Masci, J.Masojidek, M.Sugiura and R.Pilloton; Monolayers of natural and recombinant photosystem II on gold electrodes - potentials for use as biosensors for detection of herbicides, Analytical Letters, (2004) in press
[5] C.Di Meo, L.Della Seta, M.De Francesco, A.Masci, V.Pinto, A.Volpe, and R.Pilloton; Reversible Immobilisation of engineered molecules by Ni-NTA Chelators; Sensors and μ-Systems C. Di Natale & A. D'amico Ed. - World Scientific, Singapore - New Jersey - London - Hong Kong; February 2003
[6] J.Maly, C.Di Meo, M.De Francesco, A.Masci, J.Masojidek, M.Sugiura, A.Volpe, R.Pilloton; Reversible Immobilisation of engineered molecules by Ni-NTA Chelators; Bioelectrochemistry 2004 in press
[7] J.Maly, E.Illiano, M.Sabato, M.De Francesco; V.Pinto, A.Masci, D.Masci, J.Masojidek, R.Franconi, R.Pilloton; Immobilisation of engineered molecules on electrodes and optical surfaces; Materials Science and Engineering: C Volume: 22, Issue: 2, December 1, 2002, pp. 257-261

NOVEL MICROFABRICATED NANO-ESI INTERFACES TO BE INTEGRATED ONTO A MICROSYSTEM

Steve Arscott[1,2*], Séverine Le Gac[2], Christian Rolando[2]

[1] *Institut d'Electronique de Microélectronique et de Nanotechnologie (IEMN), Avenue Poincaré, Cité Scientifique, 59652 Villeneuve d'Ascq, BP 69, France*

[2] *Université des Sciences et Technologies de Lille (USTL), Laboratoire de Chimie Organique et Macromoléculaire (LCOM), UMR CNRS 8009, France*

*Steve.Arscott@iemn.univ-lille1.fr

Abstract

The development of nanoESI sources based on the idea of a capillary slot will be outlined here. Two generations of prototype sources were fabricated using the photoresist (SU-8) allowing us to validate the idea of a capillary slot. They had smallest critical end dimensions of 20×30μm and 6×25μm. Finally, a third generation of sources is presented based on polycrystalline silicon (polysilicon). The polysilicon nanoESI sources were highly planar and had much smaller tip dimensions of down to 1.8×2 μm. In addition, the ionisation voltage was applied to the doped silicon substrate. Such sources demonstrated state-of-the-art performances in electrospray mode together with low voltage operation, i.e. down to 0.8 kV.

Keywords: Nanoelectrospray, microfluidics, world-to-chip interfacing, mass spectrometry, SU-8, silicon micromachining

1. Introduction

The field of Proteomics is currently exploding due to an increasing amount of protein samples to be analysed by MS techniques. The result of this is a need for high quality interfaces which are compatible with automation through the use of robotics in order to give (i) high-throughput analysis and (ii) lower costs and (iii) compatibility with world-to-chip interfacing in the context of modern microfluidic technologies. Hence, the idea we present in this paper is to use polymer and silicon-based microtechnology techniques in order to fabricate an improved nanoESI source based on a capillary slot rather than a capillary tube. Microtechnology fabrication of such world-to-chip interfaces allows mass production as well as excellent control of critical tip dimensions which gives a greater reliability of MS spectrum interpretation.

2. Fabrication techniques

A first generation of sources [1] was fabricated with the goal of verifying the capillary slot concept. The sources were fabricated using a thick (400μm) coating of photoresist SU-8 (Microchem, VA, USA) on a silicon wafer. We estimated the critical tip dimensions to be of the order of 20 x 30 μm at the extremity of the source. MS results verified the capillary slot concept [1].

These second design of prototypes were fabricated in a more 2D topology using a 25 μm thick layer of SU-8 2035 on n-type silicon substrates. The fabrication of these sources has been published elsewhere [2] Sources were composed of a reservoir and a capillary slot, having an aspect ratio of >4, leading fluid to the nib tip and microfluidic channels linking a main test liquid reservoir to the input of the capillary slot. Indeed, we have recently shown that it is the critical dimensions of the slot together with the liquid/wall contact angle which determine the spontaneous filling of the capillary slot [3]. The design contained a smallest characteristic tip dimension of 6 μm × 25 μm. The cantilevers had a length up to 1000 μm long which equates to an aspect ratio of around 30.

We fabricated a third generation of nanoESI sources form polysilicon using Si-based microtechnology. A series of three photomasks were employed to produce: (i) pre-defined cleaving lines, (ii) localised sacrificial etch release pads (SiO_2) and (iii) micro-nib structures from polysilicon which contain: a reservoir, a capillary slot and a cantilever. A very high planarity was achieved for

the cantilevers as the deposition of the polysilicon by LPCVD was optimised in order to reduce the stresses to near-zero. This is reflected in the ability to produce a capillary slot having dimensions of 1.8×2 μm along an object 800 μm long as shown in the SEM zoom of the tip in Fig. 2

3. Mass spectrometry tests.

MS tests were performed on an ion trap mass spectrometer (LCQ Deca XP+, *Thermo Finnigan*). The nanoESI sources were placed on a metal part at the input of the mass spectrometer. In each case the test liquid was loaded into the pre-defined reservoir, following this the liquid is lead to the source tip by spontaneous filling of the capillary slot [3]. The high voltage (HV) is applied directly onto the Si support wafer, exploiting thus the semi-conducting properties of this material. MS tests showed the reliability of the sources; they were carried out using standard peptides: Fig. 3: SU-8/Si based nanoESI sources and Fig. 4: polysilicon/silicon based nanoESI sources.

4. Conclusions

We have presented here novel emitter tips for nanoESI-MS applications. The sources are composed of pointed cantilevers which contain a capillary slot. They were fabricated using SU-8 based microtechnology and silicon-based microtechnology techniques. Two generations of SU-8 based prototypes allowed us to verify the basic concept and optimise the fabrication method. A third series of nanoESI sources were fabricated using polycrystalline silicon (polysilicon) in order to reduce critical tip dimensions. All ESI sources were tested by mass spectrometry so as to assess their performances in electrospray and thus to improve the dimensions and features of the nibs. The polysilicon based sources produced state-of-the-art results during mass spectrometry testing. Mass spectrometry revealed that peptide samples could be clearly resolved and the sources were seen to work well under low voltage conditions, down to 0.8 kV.

Acknowledgements

The authors would like to thank the French network for *micro- and nanotechnologies* for their financial support for this work (Integrated Proteomics project) as well as the *GenHomme* network and the *BioChipLab* consortium. We also thank Christophe Boyaval (IEMN) for the SEM images.

References

[1] Arscott S, Le Gac S and Rolando C (2003), 2.5D Microfabricated nib-like sources for nanoelectrospray applications *Proc. Micro-TAS*, Squaw Valley, California USA, Vol **2**, pp 1211-15

[2] Arscott S, Le Gac S, Druon C, Tabourier P and Rolando C, A micro-nib nanoelectrospray source for mass spectrometry (2004) *Sensors and Actuators* B, **98**, pp. 140-7

[3] Brinkmann M, Arscott S, Le Gac S, Druon C, Tabourier P and Blossey R, Microfluidic design rules for capillary slot-based electrospray sources, *Applied Physics Letters* (Accepted for publication).

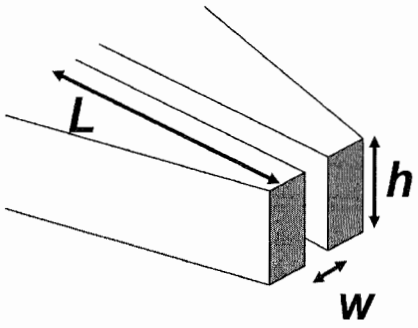

Figure 1. The capillary slot concept for the fabrication of 2D nanoESI sources. The critical dimensions are the slot width (w) and height (h). Together with the contact angle of the liquid on the slot wall, these parameters determine the microfluidic properties of the capillary slot and thus the spontaneous filling of the capillary slot [9].

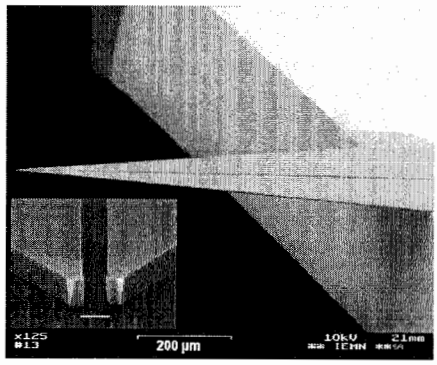

Figure 2. A typical third generation microfabricated 2D nanoESI source based on silicon microtechnology: polysilicon/silicon. The smallest capillary slot dimensions (w and h) are $1.8 \times 2\ \mu m^2$. In addition this polysilicon cantilever had a length (L) of 800 µm relating to an aspect ratio of 400

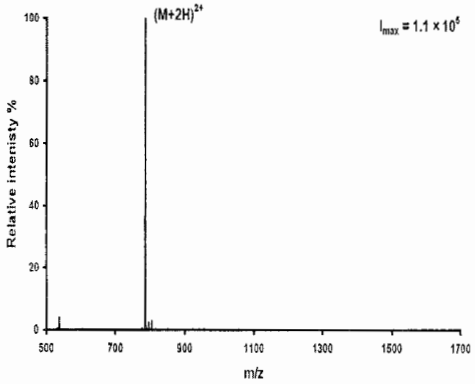

Figure 3. Standard peptide mass spectrum for a second generation SU-8/Si based nanoESI source (w = 6 µm; h = 25 µm). Sample = Glufibrinopeptide B solution prepared with a 50:50 H_2O:MeOH, 0.1% HCOOH solution at 1 µM, HV = 0.9 kV.

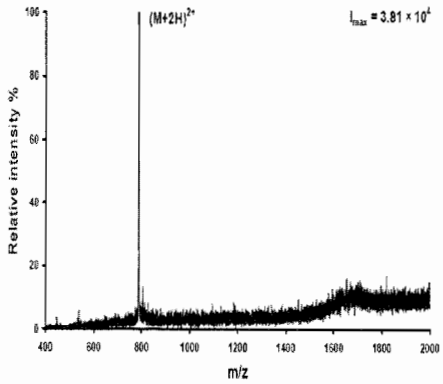

Figure 4. Mass spectrum obtained using a polysilicon/Si nanoESI w= 2.5 µm; h=5 µm). Sample = Glufibrinopeptide B solution prepared with a 90:10 H_2O:MeOH, 0.1% HCOOH solution at 1 µM, HV = 0.8 kV.

MICROMACHINED SILICON DIFFRACTIVE OPTICAL FORCE ENCODERS: PRINCIPLES AND APPLICATIONS IN BIOLOGY

Xiaojing Zhang[1], Stefan Zappe[2], Chung-Chu Chen[2], Matthew P. Scott[3] and Olav Solgaard[2]
[1]*Media Laboratory, Massachusetts Institute of Technology, Cambridge, MA 02139*
[2]*Dept. Of Electrical Engineering, E.L. Ginzton Laboratory, Stanford University, CA 94305*
[3]*Dept. Of Developmental Biology, and of Genetics, Stanford University, CA 94305*

Abstract

We experimentally demonstrate force characterization for penetration into Drosophila embryos, while the force is minimized through ultrasonic actuation of MEMS injectors with integrated optical encoders. Self-assembly force of both Drosophila embryos and flat silicon chips on 2-D array on a silicon substrate is also characterized using encoders in reflection mode. An extended surface energy model for the self-assembly process of ellipsoidal samples is described and verified by the measurements.

Keywords: optical encoder, force sensor, ultrasonic, self-assembly, Drosophila embryos

1. Introduction

Miniaturized instruments for the injection and positioning of single cells and embryos are becoming increasingly important in biology and genetic studies. Localized and accurate microinjection of genetic material into biological model systems, such as Drosophila, will enable a variety of studies in developmental biology and genetics. We studied the force required for the penetration and injection into Drosophila embryos using a surface micromachined silicon-nitride probe with integrated, micrograting-based force sensors [1]. Minimization of the penetration force [2] into precisely positioned samples is critical to the design of high throughput micro-manipulating instruments for RNA interference (RNAi) screens.

2. Ultrasonic Microinjection

The effect of ultrasonic agitation on the required penetration force for microinjection in Drosophila embryos is studied, using an integrated optical MEMS force encoder for in-vivo characterization of the dynamic penetration forces (Fig. 1). Two modes of operation are investigated. In the first mode of operation, the injector is brought into contact with the embryo to give a fixed bias offset of the two encoder gratings, and the vibration amplitude of the microinjector is increased till penetration occurred. We observe a linear decrease in the penetration force of 2.5 μN with every 0.1 m/s tip velocity increase. In the second mode of operation, the vibration amplitude is kept constant and the injector is pushed into the embryo until penetration. We measure the injection force over the frequency range of 0~16 kHz with actuation voltage up to 150 volts (Fig. 2). The average penetration force is calculated based on injections on multiple embryos for each experimental condition. At encoder resonance (~14 kHz), the achieved minimum peak penetration force is 15.6 μN (~29.7 % of the static penetration force), while the minimum average penetration force is 2.7 μN (5.1 % of the static force).

3. Microfluidic Self-assembly

The force required to penetrate the immobilized embryos, as well as the embryo positioning force [3], are critical parameters that set the limits on the alignment accuracy required to achieve satisfactory injection yields. A surface-energy model was proposed for self-assembly of silicon parts [4]. However, this model is not applicable to the present study because it assumes that all surfaces are rigid and flat. We extend the self-assembly model to systems with different surface properties and ellipsoidal self-assembled parts. The difference of surface energy, ΔW, of the extended model can be represented by:

$$\Delta W = (\gamma_{Embryo-H_2O} - \gamma_{Embryo-Oil}) \cdot \Delta A_{Embryo-H_2O} + \gamma_{Oil-H_2O} \cdot \Delta A_{Oil-H_2O} + (\gamma_{SAM-H_2O} - \gamma_{SAM-Oil}) \cdot \Delta A_{SAM-H_2O} \quad (1)$$

where $\gamma_{x\text{-}y}$ is the surface tension between the media x and y. $\Delta A_{x\text{-}y}$ represents the area change on the interface of the media x and y during the assembly process. Initially, the self-assembly pad is fully covered by oil, and the oil and the embryo are separated by water. After assembly, the embryo is in contact with oil, leading to a reduction of the areas that are in contact with water. We program this model in Surface Evolver [5]. Given the surface energy parameters of the three-interface system, the surfaces comprising a union of triangles are evolved toward minimal surface energy by a gradient descent method. The calculated equilibrium shape of the interfaces is shown in Fig. 3.

For the detachment force measurements, we use a micromachined optical-encoder force sensor while operating in reflection. For embryos positioned on 250 μm x 100 μm rectangular pads, an average detachment force of 8.9 μN±1.3 μN with 95% confidence intervals was found [3]. The measured force is integrated over the embryo displacement to get the quadratic potential energy profile (energy well depth 845 pJ), which is in good agreement with the simulated result.

The differences between self-assembly of rigid, flat structures and curved biological samples are shown in Fig. 4. Constant restoring force 25.0 μN±3.5 μN is observed after embryo displacement of 44 μm and before snap-through at 240 μm. The initial range with linearly increasing force (0 ~ 44 μm) of the flat silicon pieces is similar to the linear-spring-like behavior of embryo positioning. The detachment force and detachment displacement of the silicon pieces is about 2.5 times and 1.6 times, repectively, that of the embryo. Note that the positioning site of the silicon piece is 4 times larger than that of the embryo. Our model is therefore useful to simulate the magnitude and trend of the plateau-like as well as the sharp rising force profiles of the flat micro parts.

4. Conclusions

Minimally invasive microinjection tools with integrated sensors are critical for a wide range of studies in biology and medicine, including calibrated trans-membrane delivery of genetic material into biological model systems, such as Drosophila embryos, to enable high throughput screening of gene functions. We demonstrated MEMS optical force encoders for penetration force quantification, force reduction through vibration, and characterization of microfluidic self-assembly processes to achieve optimal design. The MEMS force encoders enable the development of automated Drosophila embryo injection system for genome-wide high-throughput RNAi screens.

Acknowledgements

This work was funded by DARPA [Bio:Info:Micro] Program (MDA972-00-1-0032).

References

[1] X. J. Zhang, S. Zappe, R.W. Bernstein, O. Sahin, C.-C. Chen, M. Scott, O. Solgaard, Proc. Transducers'03, 1051-1054, Boston, USA, 2003.

[2] A. Lal and R.M. White, IEEE Ultrason. Sym.,1593-95, 1995.

[3] X. J. Zhang, S. Zappe, R.W. Bernstein, C.-C. Chen, O. Sahin, M. Fish, M. Scott and O. Solgaard, Proc. MicroTAS'03, 805-808, Squaw Valley, USA, 2003.

[4] K. Bohringer, U. Srinivasan and R.T. Howe, Proc. IEEE MEMS, 369-374, Switzerland, 2001.

[5] K. A. Brakke, Experimental Mathematics, 1(2), 141-165, 1992.

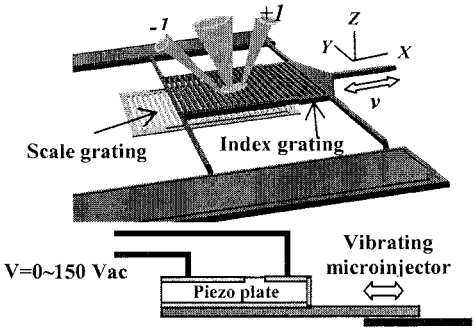

Figure 1. Ultrasonic microinjection characterized by integrated optical MEMS force encoder. A piezoelectric stack is bonded onto the backside of the force sensor chip. The probe displacement at maximum actuation voltage of 150 V is 17.4 μm±2.0 μm. Force encoder probe length is 80 μm, tip sidewall area is 10μm^2, and grating period is 20 μm.

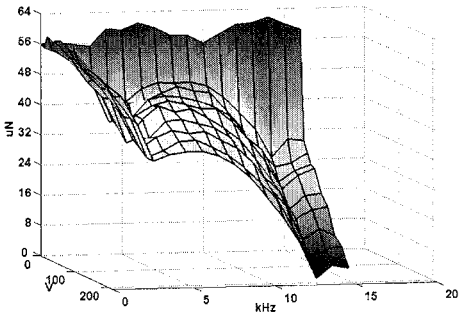

Figure 2. The peak penetration force was measured over the frequency range f_i=0~16 kHz with the actuation voltage V_j varying from 0 to 150 volts. The average force was calculated based on injections on multiple embryos under each of the 170 experimental conditions (f_i, V_j). The penetration force reached its minimum at the encoder resonant frequency of 14 kHz.

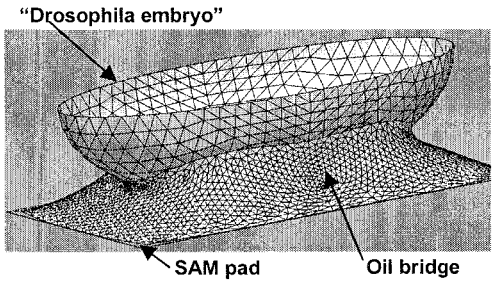

Figure 3. Calculated self-assembly model of Drosophila embryo showing the free energy difference before and after self-assembly. The ideal embryo has an ellipsoidal shape with a major axis of 400 μm, and minor axes of 200 μm. The dimension of the rectangular-shaped template is 400 μmx250μm.

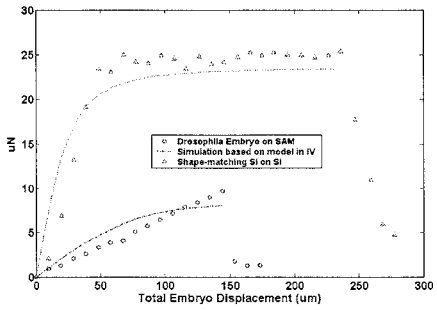

Figure 4. Force measurement of self-assembly for silicon chip (thickness 300 μm) positioned on a 400μm x 250μm positioning pad. A constant restoring force of 25 μN is observed during the majority (79%) of the movement. The force profile of Drosophila embryo positioned on 100μm x 250μm positioning site is shown for comparison.

A GIANT MAGNETORESISTIVE (GMR) SENSOR ARRAY FOR MICROFLUIDIC MAGNETOCYTOMETRY

Naga S. Korivi and Jin-Woo Choi
Department of Electrical and Computer Engineering
Louisiana State University, 102 EE Building, Baton Rouge, LA 70803-5901, USA

Abstract

This paper presents the development of a giant magnetoresistive (GMR) sensor array for magnetocytometry in microfluidic systems. The GMR sensors employ $Ni_{80}Fe_{20}$/Cu multilayers with the thickness of each layer controlled between 1 nm to 3 nm, achieving a maximum magnetoresistance (MR) value of 16%. The multilayer films exhibit specific magnetoresistive properties that can be employed for cytometry or detection of particular biological molecules bound to magnetic microparticles. The electrical current variations in the developed GMR sensor array in the presence of magnetic microparticles show that the GMR sensor array can be used for magnetocytometry in microfluidic systems.

Keywords: GMR sensor, magnetic bead, microfluidic, magnetocytometry

1. Introduction

In the recent years, magnetic bead-based sensors have been widely studied and applied for biological applications. Such sensors utilize magnetic microparticles as immobilization substrate and/or carrier of bio-molecules [1-2]. Among the several methods for magnetic bead-based biosensors, giant magnetoresistive (GMR) sensors become a competent method to detect magnetic beads which are bound to biological molecules. The major advantage of GMR sensing over other methods such as electrochemical and/or optical detection is the high sensitivity associated with GMR sensors. Another advantage is that GMR sensors can be made by conventional microfabrication techniques, thereby enabling the creation of true integrated microsystems. In principle, various biological cells can be attached to magnetic microparticles and used in different applications. This work describes the development of one-dimensional GMR sensor array for magnetic microparticle-based cytometry applications in microfluidic biochemical analysis systems. The GMR sensor developed in this research has been specifically evaluated for the feasibility of applications in microfluidic magnetocytometry.

2. Design and fabrication

One dimensional GMR sensor array structure was designed to test the feasibility of applying the GMR sensing mechanism in cytometry as shown in Fig. 1. $Ni_{80}Fe_{20}$/Cu multilayers were deposited on borosilicate glass and/or oxidized silicon wafers by magnetron sputtering. The number of multilayers was chosen to 5 pairs, with the thickness being 4 nm for each $Ni_{80}Fe_{20}$/Cu pair. The GMR sensors were fabricated by photolithographic patterning of the multilayers to

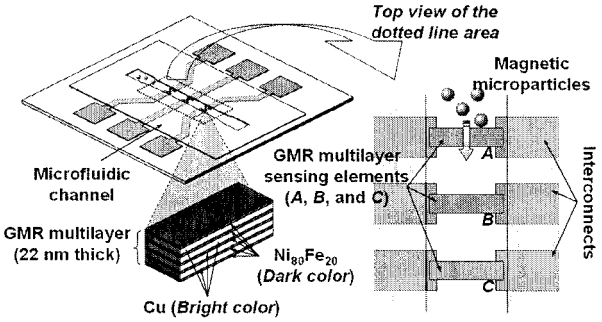

Figure 1. Schematic illustrations of the designed GMR sensor array for microfluidic magnetocytometry. GMR sensing element consists of nanoscale $Ni_{80}Fe_{20}$/Cu multilayers.

obtain sensing elements. Each GMR sensor element was electrically connected by patterning of copper interconnections to construct one-dimensional array structures. A layer of perfluoropolymer (CYTOP®) was spin-coated on the devices and patterned by RIE in order to electrically isolate the actual sensing elements from microfluidic samples. Microfluidic channels of width 120 μm were then formed by lithography of SU-8 on the GMR sensor elements for magnetocytometry evaluation. Fig. 2 shows GMR sensor elements of 22 nm thickness connected by thicker interconnect lines and the bottom of a fluidic channel with the GMR sensor array clearly overlapping the interconnect line. A 1 cm x 1 cm GMR multilayer sample with same thickness was also prepared for characterization of magnetoresistivity.

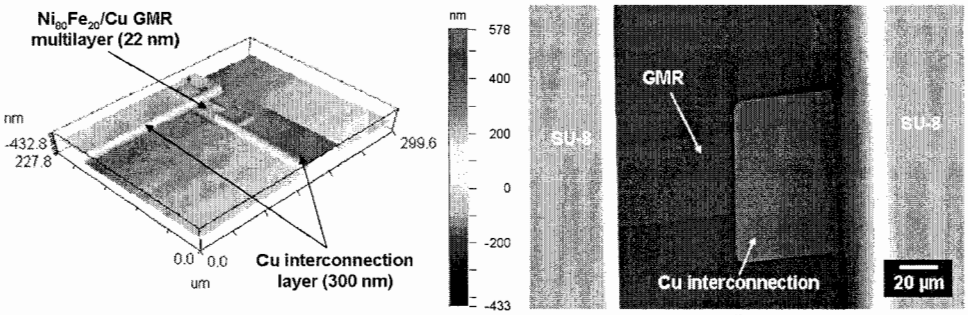

(a) (b)

Figure 2. Microfabricated GMR sensing elements: (a) optical interferometer image showing 22 nm-thick GMR multilayer with 300 nm-thick interconnecting lines and (b) scanning electron microscopy image showing bottom of the microfluidic channel.

3. Experimental results and discussion

Using an electromagnet-based measurement system, the resistivity of $Ni_{80}Fe_{20}$/Cu multilayer stack was measured as a function of varying magnetic field. The measured resistivity showed an increase as the magnetic field was ramped in steps of 10 gauss from 0 to 1000 gauss, reaching saturation after an abrupt increase around 210 gauss as shown in Fig. 3. It is believed that this abrupt increase in resistivity is mainly due to phase transformation effects of nanoscale multilayer structure. Other factors such as the thicknesses of the individual layers, their interfacial properties, and deposition conditions could also influence magnetic properties of the nanoscale multilayer GMR films. Employing the GMR sensor in the narrow regime of biasing magnetic field where there is a sharp increase in resistivity can make the sensor appropriate for specific applications like cytometry and for detecting specific biological molecules attached to magnetic particles. From the magneto-resistance (MR) measurements, a maximum MR of 16% was observed in the multilayer stack.

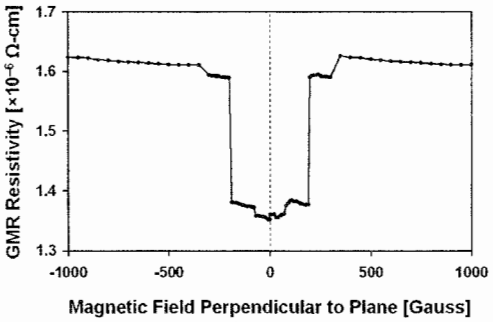

Figure 3. Measured GMR resisistivity of $Ni_{80}Fe_{20}$/Cu multilayer for varying magnetic field. Maximum MR of 16% was observed.

The multilayer films thus developed were applied in GMR sensors for the cytometry feasibility studies. An electromagnet was placed under the wafer and a biasing magnetic field of 200 gauss was applied in the perpendicular direction on the plane of the GMR sensor array. A constant voltage of 300 mV was applied across the GMR elements and output current of the sensing elements (*A* and *C* in Fig. 1) was recorded. A fluidic plug of magnetic microparticles (SPHERO^{TM} carboxyl magnetic particle, 8.8 μm in diameter) numbering around 200 to 500 in de-ionized water solution was introduced in the microchannel and passed over the sensing elements by microfluidic manipulation. The resistance of GMR sensor elements increased due to presence of magnetic microparticles, which lead to output current differences as shown in Fig. 4. There was a drop in output current corresponding to the passing of magnetic microparticles over the GMR sensing elements, followed by increase in current due to the particle flow away from the sensing elements. However, residual magnetization effects on the sensing element make the current increase not immediate. This rise time can be reduced by applying a de-magnetizing field.

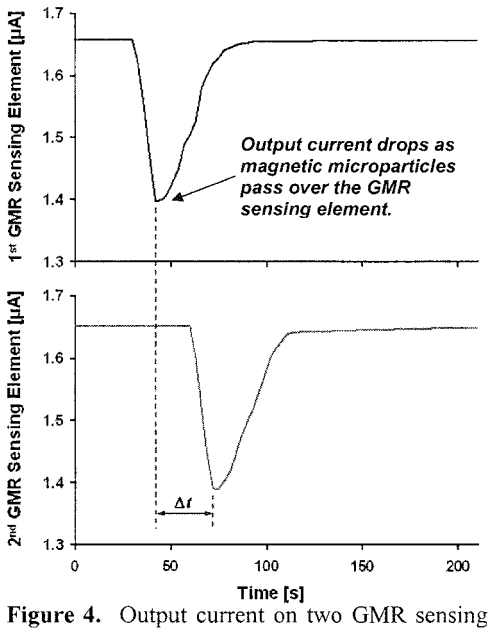

Figure 4. Output current on two GMR sensing elements (5 mm apart) with applied voltage of 300 mV. A plug of 200 ~ 500 magnetic microparticles passed over the 1st and 2nd GMR sensing elements. Δt can be interpreted as a flow rate.

4. Conclusions

The GMR sensor array described in this work exhibits changes in current when magnetic microparticles flow over the GMR sensing elements. The current changes are consistent with magnetoresistive properties of the multilayer film and the developed GMR sensor array clearly shows feasibility for applications in magnetocytometry. The sensitivity of this sensor can be further improved by controlling the number of $Ni_{80}Fe_{20}$/Cu multilayers and the thickness of each layer. The high value of magnetoresistance coupled with the phase transformation effects in the narrow magnetic field regime renders the developed GMR multilayer structures suitable for applications in magnetic particle-based cytometry.

Acknowledgements

This research was partially funded by Center for Computation and Technology (CCT) and Center for Advanced Microstructures and Devices (CAMD) at Louisiana State University. The authors measured magnetoresistance at Dr. Laurence Henry's laboratory at Southern University.

References

[1] D. R. Baselt, G. U. Lee, M. Natesan, S. W. Metzger, P. E. Sheehan, and R. J. Colton, *Biosensors & Bioelectronics*, 13, 731-739 (1998)

[2] J. C. Rife, M. M. Miller, P. E. Sheehan, C. R. Tamanaha, M. Tondra, and L. J. Whitman, *Sensors and Actuators A*, 107, 209-218 (2003)

MICROCHIP FOR TEMPERATURE DEPENDENT DIELECTRIC SPECTROSCOPY OF BIOMOLECULAR REACTIONS

Kenneth Castelino[1], Veljko Milanović[1], Daniel McCormick[2], Norman Tien[3], and Arun Majumdar[1]

[1] Dept. of Mechanical Engineering, [2] Dept. of Electrical Engineering, Comp. Scienc, Univ. of California, Berkeley, CA 94720, USA.

[3] Dept. of Electrical Engineering, Univ. of California, Davis, CA 95616, USA.

Abstract

We report the design, fabrication and testing of a microchip for temperature dependent label-free assay of biomolecular reactions via broadband dielectric spectroscopy from 100 Hz to 1 GHz. In the frequency range of 100 Hz to 10 kHz, we have demonstrated detection of immobilization, hybridization and melting of DNA due to changes in the properties of the nanoscale electric double layer adjacent to the electrodes. Furthermore, in the range of 50 MHz to 1 GHz, the thermal denaturation and renaturation of proteins was probed by monitoring changes in the dielectric relaxation of bound water. This method is scalable to large arrays, which opens the possibility of multiplexed label-free assays of various biomolecular reactions and modifications.

Keywords: dielectric spectroscopy, microheater, thermal denaturation, label-free assay.

1. Introduction

Currently, most biomolecule detection schemes involve use of fluorescent, magnetic, chemiluminescent, or other labels. Dielectric or impedance spectroscopy is an emerging label-free technique for monitoring various biological interactions and reaction kinetics. Several electrochemical techniques based on sensing changes in electrode capacitance or Faradaic currents due to biological recognition events have been demonstrated [1]-[3]. However, these macroscale bench-top setups are difficult to multiplex, require large sample volumes and have long thermal time constants. In contrast, our microchip integrates a fluidic sample chamber, a microheater for temperature cycling up to 100°C, and interdigitated electrodes for dielectric spectroscopy of the sample. The microchip probes dielectric phenomena over a wide frequency range, which can yield information about different biomolecular mechanisms or reactions. In addition, a key advantage is the integration of a resistive microheater, which allows studying biomolecular reactions that exhibit strong temperature dependence. The small sample size is also advantageous in enabling rapid thermal analysis and in dealing with limited quantities of costly or unique biological samples.

2. Theory

The frequency dependent dielectric properties of biomolecules are of interest in areas of identification and monitoring of various reactions or modifications. Dielectric spectroscopy is a powerful tool, which enables probing of dielectric relaxation phenomena with characteristic times ranging from $10^{-1} - 10^{-12}$ s using either frequency or time domain probing techniques. As described previously in [4], aqueous solutions of proteins can exhibit several distinct dispersion processes. The γ-dispersion at microwave frequencies (10^{10} Hz) is caused by relaxation of free water in solution. The β-dispersion at lower frequencies ($\sim 10^{6}$-10^{7} Hz) is mainly due to the rotation of protein globules as a whole. Finally, the δ-dispersion at intermediate frequencies (10^{7}-10^{10} Hz), which is much weaker, is caused by internal conformational motions of the protein and by water bound to the protein. Hence this latter frequency range is important for monitoring changes in conformations or surface area of the protein in bulk solution. We perform the spectroscopy in this frequency range by utilizing standard on-chip microwave vector network analysis techniques.

At very low frequencies (10^2-10^4 Hz), an electrical double layer is formed due to accumulation of ionic species at the electrode interfaces and the resultant double-layer capacitance typically dominates the sensor response. While this electrode polarization effect prevents characterization of the bulk solution at these frequencies, at the same time the capacitance is highly sensitive to electrode-surface binding reactions such as immobilization or hybridization. In this frequency range, we perform the spectroscopy by impedance measurement techniques. The measured impedance can be modeled using the Randles equivalent circuit [5].

3. Experimental

An optical micrograph and a schematic of the microchip are shown in Fig. 1a and Fig. 1b. The dielectric sensor element (Fig. 1b) consists of a coplanar waveguide (CPW) terminated in an interdigitated electrode structure. The latter acts as the capacitor while the CPW section allows efficient transmission of high frequency fields to the device. Temperature is varied by controlling power applied to the serpentine microheater and is calibrated by characterizing the proportional resistance changes in the microheater. The temperature characteristics of the chip for a 10 mM phosphate buffer solution without biomolecules are shown in Fig. 2. At low frequencies, the change of capacitance with temperature is presented (Fig. 2a), while Fig. 2b shows the changes in permittivity (ε') at high frequencies. The thermal time constant of the chip was estimated to be about 2.5 seconds as seen in Fig. 2c. The low frequency capacitance measurements were done using an HP4194A impedance analyzer in the parallel R-C equivalent circuit mode. Capacitance changes due to immobilization of a 20 base-pair single-stranded DNA (ss-DNA) and hybridization with the complementary DNA are shown in Fig 3a. Both reactions reduce capacitance due to the displacement of water and ions from the double layer region by the biomolecules. It is also possible to extract data on the reaction kinetics: e.g. Fig. 3b shows the kinetics for the above DNA immobilization reaction by monitoring the capacitance at 100 Hz as a function of reaction time. The thermal effects on the hybridization of 10 base-pair DNA (melting temperature = 30 °C) are shown in Fig. 3c. Heating the hybridized DNA beyond the melting point leads to de-hybridization causing capacitance to increase to the immobilization value. After 15-20 minutes, the re-hybridization process causes capacitance to return to the original hybridization value. In the high frequency range (50 MHz – 1 GHz), an Agilent PNA 8364A vector network analyzer was used to study the thermal denaturation of bovine serum albumin. Cycling the temperature below the denaturation point (74 °C) is completely reversible as seen in Fig. 4a. However, heating the protein above 74 °C denatures it and causes irrecoverable changes in the dielectric constant (Fig. 4b).

4. Discussion and Conclusions

We have developed a microchip to perform broadband dielectric spectroscopy in two different frequency regimes: in the low frequency regime, impedance measurements were used to monitor the double layer capacitance to detect immobilization, hybridization of DNA and also to study the effects of thermal denaturation and renaturation of DNA. In the high frequency regime, thermal denaturation of proteins was studied by monitoring changes in the real and imaginary parts of the dielectric constant caused by conformational changes and the loss of bound water. This dielectric sensor can be used for performing label-free detection of reactions such as single base-pair DNA mismatch detection and we also plan to test its detection limits for detecting proteins in a serum environment, which has a background of various non-specific proteins.

References

[1] E. Katz, and I. Willner, *Electroanalysis*, **15**(11), 913-947 (2003).
[2] C. Berggren, P. Stalhandske, J. Brundell, G. Johansson, *Electroanalysis*, **11**(3), 156-160 (1999).
[3] F. Patolsky, *et al*, *J. Phys. Chem B*, **102**, 10359 (1998).

[4] Y. Feldman, *et al*, *IEEE Trans. Dielectrics and Electrical Insulation*, **10**(5), 728-753 (2003).
[5] A. Bard, and L. Falkuner, *Electrochemical Methods*, John Wiley & Sons, Inc. (2001).

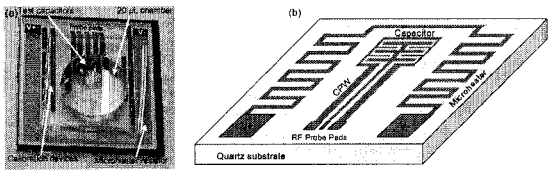

Figure 1. Microchip for temperature dependent dielectric spectroscopy: (a) optical micrograph of the chip with a PDMS-based 20μL sample chamber, and (b) schematic showing the basic layout with chamber omitted.

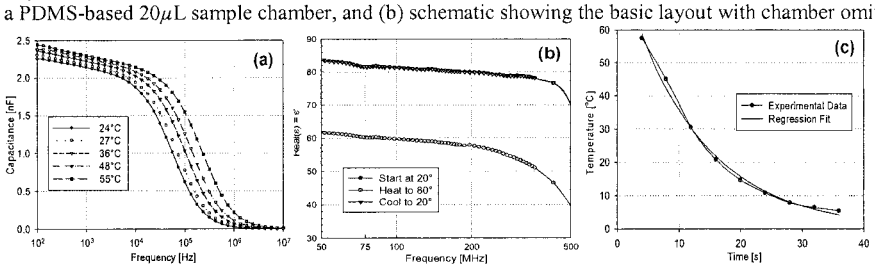

Figure 2. Temperature dependent dielectric spectroscopy of 10 mM phosphate buffer (PB): (a) low frequency capacitance curves at varied temperature, (b) measured permittivity at high frequencies with significant reduction of the real part at increased temperature and (c) characterization of the thermal time constant of the microchip.

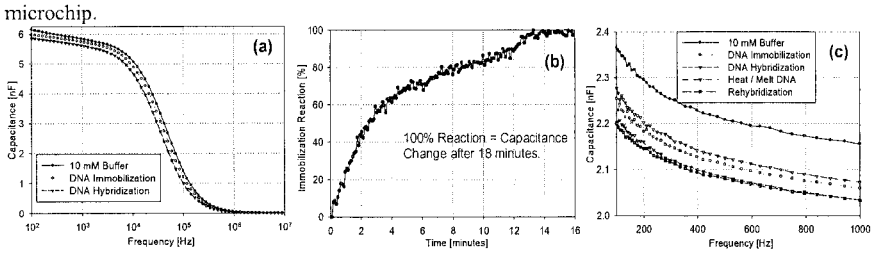

Figure 3. Dielectric spectroscopy for DNA immobilization and hybridization detection: (a) capacitance changes are most significant below 10 kHz due to enhanced sensitivity of the electrical double layer; (b) DNA immobilization reaction kinetics monitored by capacitance change, and (c) capacitance spectra for thermal melting of hybridized DNA and DNA re-hybridization, which are clearly detectable events. (Buffer = 10 mM PB, Bias = 0.4V).

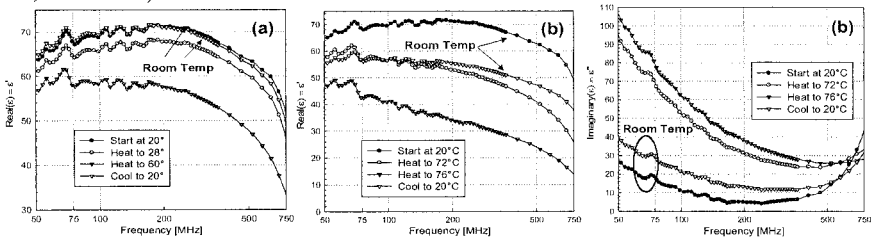

Figure 4. Bovine serum albumin (BSA) thermal denaturation experiments: (a) thermal cycling of BSA below the denaturation temperature – effects on permittivity are reversible, but (b) after thermal cycling beyond the denaturation temperature, irreversible changes in both ε' and ε'' are seen at room temperature, due to the denaturation process.

SHEATH-FLOW SUPPORT FOR HIGH-SENSITIVITY END-COLUMN ELECTROCHEMICAL DETECTION IN MICRODEVICES

Charles A. Emrich[†], Peter Ertl, Pankaj Singhal and Richard A. Mathies
Department of Chemistry and [†]Biophysics Graduate Group
313 Lewis Hall, University of California, Berkeley, CA 94720 U.S.A.

Abstract

We have developed a microfabricated CE system with sheath-flow supported end-column electrochemical detection. The gravity-fed microfabricated sheath flow channels enable hydrodynamic transport of the analytes from the CE channel end to the detection electrodes. This permits the placement of detection electrodes up to 250 μm from the channel end with little loss in signal and a significant decrease in the interfering, background CE current. The device is demonstrated by separations of model compounds, dsDNA, and genotyping with electroactively-labeled, allele-specific PCR products.

Keywords: Capillary Electrophoresis, Electrochemical Detection, Sheath Flow, Electroactive Labeling, PCR, Hereditary Hemochromatosis

1. Introduction

The miniaturization of chemical and biochemical analysis instrumentation has enabled the widespread use of these techniques in high-throughput and point-of-care applications. However, the fluorescence-based detection methods often employed require large and expensive optical detection systems. Significant cost and space savings may be achieved by using electrochemical methods for biomolecule detection.

Microfabricated devices are ideally suited to electrochemical detection of biomolecules because of the relative ease of integration of the metallic components required for detection electrodes. An important issue when performing amperometric detection with capillary electrophoresis (CE) is the necessary isolation of the electrochemical (EC) detector from the separation voltage. The CE fields typically generate μA-level background electrophoresis currents, masking the pA to nA currents measured at working electrodes in EC detection systems.[1] Several approaches have been developed to minimize the influence of CE fields, including end-channel detection off-chip,[2] in-channel detection[3] and off-channel detection.[4] We present here the development of a sheath-flow supported end-column EC detector that achieves high-sensitivity by permitting the working electrode to be placed up to 250 μm from the channel end.[5]

2. Experimental

The microdevice consists of an upper glass wafer carrying the etched separation, injection and sheath-flow channels and a lower glass wafer on which gold- and silver-plated electrodes have been fabricated (Fig. 1). The sheath-flow channels join the end of the separation channel from each side and gravity-driven flow carries the analytes to the electrochemical detector placed at working distances of 100 to 250-μm from the separation channel exit. As presented in Figure 2, the presence of the sheath flow permits detection of catechol separations with little loss in intensity at distances of up to 250 μm. Conversely, the signal rapidly decreases in the absence of the sheath flow support.

Practical utilization of the sheath-flow supported EC detector was demonstrated by performing DNA fragment sizing and SNP-typing by allele-specific PCR. Fragment sizing is demonstrated by a separation of a 223-bp PCR amplicon against a pBR 322 ladder using the electroactive intercalating dye iron-phenanthroline (Fig. 3). Transient reductions in signal indicate the passage of

the dsDNA-dye complex. SNP typing was performed by allele-specific amplification of the 282C/Y locus of the *HFE* gene from genomic DNA. Successful CE separations of amplified products from human genomic DNA of an individual homozygous for the 282Y allele are presented in Figure 4. These results demonstrate the power of sheath flow support structure to enable high-sensitivity EC detection at large detector distances, laying the groundwork for point-of-care analysis and multiplex detection.

References

[1] Baldwin, R. P. *Electrophoresis* **2000**, *21*, 4017-4028.
[2] Wang, J.; Chatrathi, M. P.; Tian, B. M. *Anal. Chem.* **2000**, *72*, 5774-5778.
[3] Martin, R. S.; Ratzlaff, K. L.; Huynh, B. H.; Lunte, S. M. *Anal. Chem.* **2002**, *74*, 1136-+.
[4] Chen, D. C.; Hsu, F. L.; Zhan, D. Z.; Chen, C. H. *Anal. Chem.* **2001**, *73*, 758-762.
[5] Ertl, P.; Emrich, C. A.; Singhal, P.; Mathies, R. A. *Anal. Chem.* **in press**.

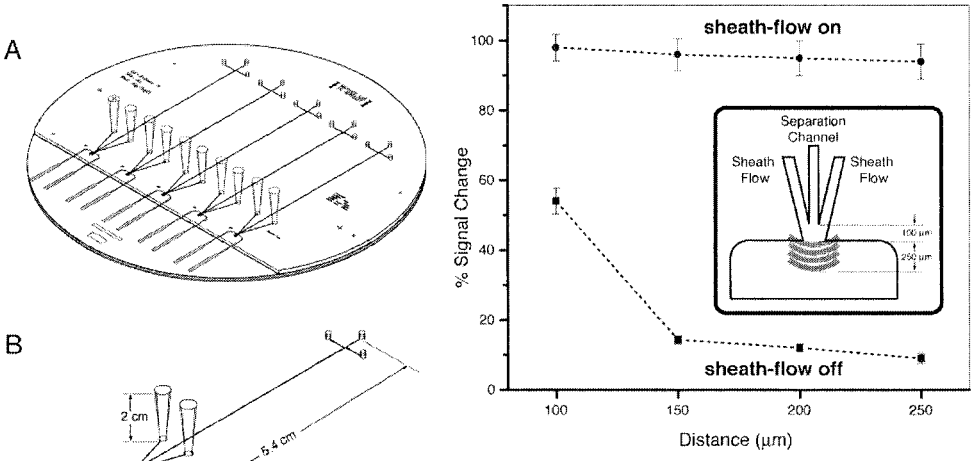

Figure 1. (left) A) Overall design of the assembled CE-EC separation and detection device. B) Exploded view of a single channel from the device showing the 2-cm high gravity-driven sheath flow reservoirs. C) Photomicrograph of electrodes in the detection region.
Figure 2. (above) Results of catechol separations presented as relative (%) signal change as a function of electrode distance calculated from triplicate measurements obtained in the (ν) absence and (λ) presence of sheath-flow support. (Inset) Schematic representation of the investigated EC-detector configurations with working electrodes placed at a distance of 100, 150, 200 and 250 μm from the separation channel.

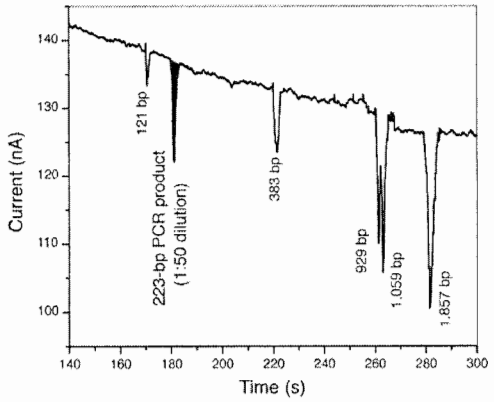

Figure 3. Capillary gel electrophoretic DNA fragment-sizing analysis performed using the sheath-flow CE detector with the working electrode 150 μm from the channel exit. Electropherogram of a *BstN* I digest of pBR 322 (100 ng/μL) spiked with a 1:50 dilution of a 223-bp PCR amplicon. Separations were performed at 200 V/cm in 1X TAE buffer with 1 mM KCl containing 1-μM $Fe(phen)_3^{2+}$ with an applied EC potential of + 950 mV.

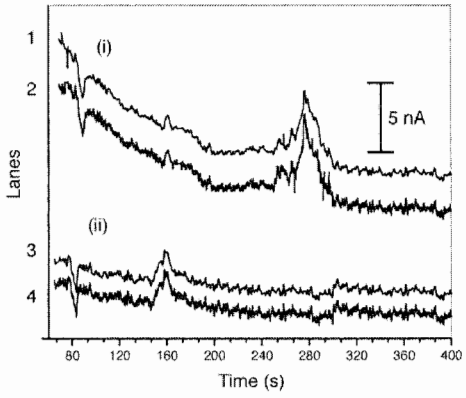

Figure 4. Electropherograms obtained with variant (upper: lanes 1, 2) and wild type (lower: lanes 3, 4) forward-primer for allele-specific extension assays from an individual homozygous for the variant 282Y allele of the human *HFE* gene. Primers are covalently labeled with ferrocene. Separations were conducted at 200 V/cm with an applied EC potential of +750 mV.

SYNCHROTRON RADIATION FOR ON-CHIP MID-IR DETECTION AT THE DIFFRACTION LIMIT

Nina Kaun[1], Stephan Kulka[1], Josefa R. Baena[2], Ulrich Schade[3], Michiel Vellekoop[4], Ersilia De Lorenzi[5] and Bernhard Lendl[1]

[1]Inst. of Chemical Technologies and Analytics, Vienna University of Technology, Getreidemarkt 9/164, A-1060 Vienna, Austria

[2]Dep. of Anal. Chem., University of Córdoba, Campus de Rabanales, E-14071 Córdoba, Spain

[3]Besssy II, Albert-Einstein-Str. 15, D-12489 Berlin, Germany

[4]Inst. of Sensor and Actuator Systems, Vienna University of Technology, Gusshausstrasse 27-29, A-1040 Vienna, Austria

[5]Laboratory of Pharmaceutical Analysis, University of Pavia, Via Taramelli 12, I-27100 Pavia, Italy

Abstract

Microchips for rapid mixing of two aqueous streams have been produced using CaF_2 wafers and SU-8 microstructuring technology and tested at the IR beamline of Bessy II in Berlin, Germany. Advantage of the synchrotron radiation over thermal globar sources for measuring at sample spots close to the diffraction limit of the employed mid-IR radiation have been documented. The capability of the experimental set-up to initiate and monitor chemical reactions label-free in pL volumina was verified. Simple chemical reactions such as titration of acetic acid and conformational change of the protein β2-microglobulin have been recorded.

Keywords: Mid-IR spectroscopy, synchrotron radiation, micromixing, protein folding

1. Introduction

Dedicated chips for (bio)chemical reaction monitoring using mid-infrared synchrotron radiation are introduced. These chips made of calcium fluoride and SU-8 polymer are designed to take advantage of the highly collimated beam of synchrotron radiation, which when coupled to an IR microscope allows high quality measurements even at spot sizes close to the diffraction limit of the light used. In case of mid-IR radiation the smallest sample spots that can be realized are in the order of 5-10 micrometer. In this context it is important to mention that the throughput advantage of an IR synchrotron light source over a conventional thermal (globar) source is only significant when measurements with spot sizes smaller than 50 micrometers in diameter need to be achieved. To take full advantage of the possible small spot size for a number of different (bio)chemical experiments, dedicated chip based systems are needed. In case of time resolved studies a time resolution of approximately 500 microseconds can be achieved. In case of separation systems like on-chip capillary electrophoresis synchrotron based IR dedication would also be of distinct advantage as here a small detection volume is critical to avoid overlapping elution profiles.

Lab-on-a-chip technology in combination with IR synchrotron radiation sources may thus be regarded as an enabling technology for a number of different experiments such as bio-ligand interaction studies or protein folding.

2. Design, fabrication and working principles of the applied micro-mixers

A 4 μm thick SU-8 layer is deposited on both (bottom- and top-) wafers. After softbake and exposure the wafers are post-exposure baked at 90°C. The 2 μm thick metal layer, which forms the separation membrane, is deposited by evaporation on top of the SU-8 layer on the bottom wafer. Silver is used for this layer, because evaporated Ag-layers do not show any internal stress and they can be deposited using relatively low power. The Ag-layer is patterned in a conventional way using

positive photoresist (AZ 1512 HS) and wet etching. The Ag-etchant, which is used, does not attack the SU-8. Subsequently the SU-8 structure (under the Ag-membrane) is developed.
The treatment of the top-wafer is different and depends on the used bonding method. In case of a simple method the SU-8 structure is developed and the holes for inlets and outlet are drilled. Subsequently the two wafers (top- and bottom-wafer) are bonded in an evacuated chamber upon application of pressure (2000N) and temperature (ramp of 3 °C / min. to 150 °C followed by one hour at this temperature).

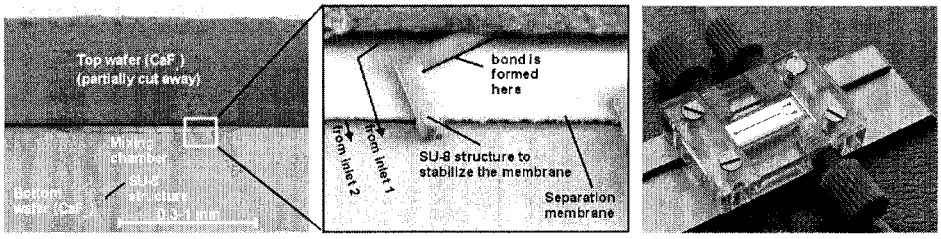

Figure 1. Left and middle: SEM images of the produced chips. Right: Picture of the microchip mounted in the dedicated support for placement under an FTIR microscope.

3. Spectral baseline noise achievable when using a MIR synchrotron source vs. a globar

The dependence of the achievable spectral baseline noise as a function of the probed sample area has been investigated in a systematic study. For this purpose a microchip with a channel cross section of 10*300 µm and filled with water has been used. The aperture of the microscope was set from 10 to 70 µm in increments of 5-10 µm. In case of synchrotron radiation the baseline noise decreased when increasing the sampling spot from 10-20 µm. However, a further increase of the sampling area did not result in an improved spectral baseline. On the contrary when using a globar source a continued improvement in baseline noise was achieved upon increasing the sampling area. At a spot size of 20 µm the baselines noise was approximately 10 times lower using a synchrotron as compared to using a globar source. However, at spot sizes of 50 µm no significant differences in the baseline noise have been observed. These results clearly show that synchrotron radiation is of significant advantage only when measurements at small sample spots need to be carried out. This is the case in chemical reaction monitoring using the continuous flow approach or in separation systems where band broadening in the detection area needs to be avoided.

4. Chemical reaction monitoring in micro-chips by mid-IR synchrotron radiation

The proper functioning of the device was tested using the titration of acetic acid as a simple model system. In Fig. 2 the spectra are shown which have been recorded at distinct positions along the outlet channel of the mixer. In doing so spectra before and after reaction could be recorded. In a similar way spectra of β2-microglobulin, a single chain polypeptide (99 residues Mw: 11800), at two different pH values have been recorded. β2-microglobulin is of relevance in dialysis-related amyloidosis, a protein conformational disease. There is now broad consensus that partial unfolding of β2-m is required for formation of fibrils. As FTIR spectroscopy is sensitive to the secondary structure of proteins it may be expected that pH induced protein folding may be followed in solution and in-situ by time resolved FTIR studies.

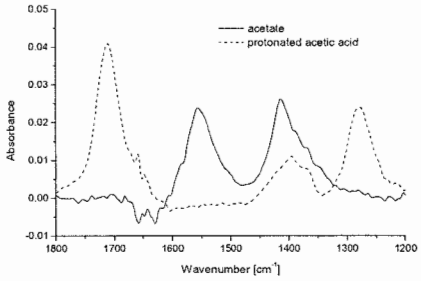

Figure 2. Mid-IR spectra recorded from a sample volume of 9 pL (30*30*10μm). One clearly can see the differences in the mid-IR spectra of acetic acid and acetate.

The spectra of acetic acid and acetate have been recorded in aqueous solution directly. For the study of protein conformation as in case of β2-microglobulin heavy water and deuterated reagents (DCl) had to be chosen. This is because the information rich amid I band of proteins, from which their secondary structure may be told, overlap with the bending vibration of normal water. In the studies performed with the micromixers so far β2-microglobulin solutions of 1g/L have been used. The spectra at two distinct pH values, which have been recorded from a spot volume of 20*40*10 μm^3 are given in Fig. 3a. Despite the fact that these spectra are noisy the expected shift of the amid I band to higher wavenumbers upon decreasing pH may be discerned. The observed band-shift reflects the folding (increase in α-helical structure) of the protein. Reference spectra recorded from larger volumes using the attenuated total reflection technique (Fig. 3b) confirm this observation.

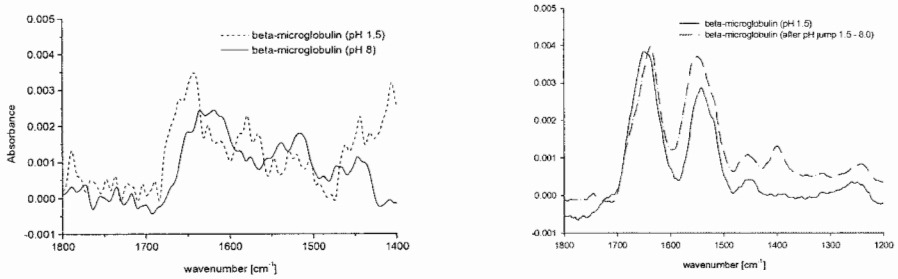

Figure 3. a) Mid-IR spectra recorded from 8 pg (conc.: 1g/L, 20*40*10 μm) of β2-microglobulin at different pH values in the micro-chip using a synchrotron radiation source. b) Reference spectra

5. Conclusions

The successful coupling of MIR synchrotron radiation with micro-chip technology has been shown by recording MIR spectra from a few pL in aqueous solutions only. However, to take full advantage of the sampling capability of synchrotron MIR microscopy the spectral noise needs to be reduced. Efforts are under way which indicate that this will be possible in the near future.

Acknowledgements

N.K, S.K, J.R.B. and B.L. are grateful for financial support received from the Austrian Science Foundation (FWF 15531) and from Bessy.

FACTORY ON A CHIP FOR THE HYDRODYNAMIC FABRICATION OF MICRO SCALE FIBERS AND TUBES

[1]WonJe Jeong, [2]Glennys Mensing, [1]SangHoon Lee, and [2]David. J. Beebe

[1]*Dept. of Biomedical Eng., Dankook University, San 29, AnseoDong, Cheonan, Chungnam, 330-714, Korea*

[2]*Dept. of Biomedical Eng., University of Wisconsin, Madison, WI, 53706, USA*

Abstract

In this paper, we proposed a new PDMS based micro-chip for the continuous fabrication of curved microstructure such as microfiber or microtube like mass production-machine in the factory. They are hydrodynamically fabricated by employing the microscale phenomena and *in-situ* photo-polymerization. The simplicity and flexibility of our method across different materials, geometries, and scales is key advantages over many existing methods that require some form of re-tooling to realize different outcomes.

Key Words: Hydrodynamic Fabrication, Photo-polymerization, Microfluidic

1. Introduction

The microscale curved objects are widely used in both the natural and man-made world. But most of the MEMS technology based outcomes are not true 3-D curved structures. Here we present new PDMS based microfluidic chip to fabricate the micro scale curved objects such as fibers and tubes continuously. Inside the chip, the photo-polymerizable sample stream is formed among the non-photosensitive coaxial sheath flow via the micro scale phenomena (e.g. laminar flow, diffusion) [1-2] and the proper regulation of both flows. By the UV light exposure onto the streams, the sample flow is polymerized and extruded lifted by sheath flow [3], and the polymerized micro scale fibers or tubes are produced continuously like machine in the factory.

2. Principles

The schematic view of the apparatuses for the fiber and tube fabrication are shown in Fig. 1 respectively, and they are made by combining the PDMS substrate with preformed center hole, and pulled glass micropipette. For the fiber production, the polymerizable sample fluid and non-polymerizable sheath fluid are injected into two inlets and combined in 'X' position of the apparatus producing a coaxial sheath flow containing a sample stream at the center as demonstrated in Figure 1(a) owing to the hydrodynamic micro scale property. Next, the UV(365 nm) is exposed onto the outlet tube for the "on the fly" photo-polymerization (i.e. continuous radiation on a moving liquid) of the sample stream as it travels towards the outlet of the channel. Then the sample stream is polymerized, and the polymerized microfiber moves along the direction of flow within the glass tube without touching the inner surface, and extruded out. In a similar way, the microtube is fabricated using the apparatus shown in Figure 1(b). Three kinds of fluid are delivered to the channel. At first, the core fluid and polymerizable sample fluid are introduced respectively, and a core stream surrounded by sample flow is produced at the position 'Y'. The core/sample stream then enters into the second stage, where a sheath fluid is introduced producing a coaxial core/sample/sheath stream. While these streams travel to outlet tube, the sample stream is polymerized via the "on the fly" photo-polymerization, and the polymerized microtubes are produced.

3. Experimental

The chemical makeup of prepolymer mixture for the sample flow consists of 4-hydroxybuthyl acrylate (85wt.%, Sigma-Aldrich), acrylic acid (11wt.%, Sigma-Aldrich), ethyleneglycol

dimethacrylate (1wt.%, Sigma-Aldrich), and 2,2'-dimethoxy-2-phenyl-acetonphenone (3wt.%, Sigma-Aldrich). As a core and sheath flow, a mixture of aqueous solution of PVA and DI water was used. Ethyl vinyl acetate (EVA) tubes are utilized to form the fluidic networks, and the core, sample and sheath flows are regulated separately via infusion pumps. To enhance visualization of the sample flow, a dye (Rhodamin B) is mixed with the 4-BHA and stirred for 2 minutes. The flow inside the outlet channel is monitored using the optical microscopy, and the scanning electron microscopy (S-4300, Hitachi) is employed to inspect the produced fibers and tubes in detail.

4. Results and discussion

Figure 2(a) shows the micrograph of the continuously produced microfiber colored by dye. By changing the sample flows (1.2 and 2.4 μl/min) and the sheath flows (50, 100, 200, and 400 μl/min), polymerized fibers with different sizes are produced, and their diameters are measured under the optical microscope and their relations are illustrated in Figure 2(b). The diameters are ranging from 12 to 90 μm and this involves that the size of each microfibers can be easily and precisely controlled by the regulation of sample and sheath flow rate without re-tooling. Figure 3 illustrates the SEM image of fabricated microtube whose outer and inner diameters are 35 μm and 7 μm respectively, and the hole of tube is clearly appeared at the center. The mechanical properties of microfiber are being investigated, and they are elastic, stimuli (pH)-responsive and can easily entrap biocatalysts. To evaluate the bio-sensing ability of microfiber, we immobilized enzymes (glucose oxidase(GOX) and horseradish peroxidase(HRP)) into the fiber. The aqueous solutions containing glucose, buffer and Amplex Red are dropped onto the fibers. After 2 minutes of diffusion time, the fluorescent signal was appeared at the microfiber, and its micrograph was captured by fluorescent microscope and illustrated in Figure 4. This picture reveals that the immobilized enzymes are viable, and react well to the glucose. So these microfibers can be used as a bio-sensing component of other microfluidic biochip.

5. Conclusions

The ability to continuously manufacture micro scale fibers and tubes cost effectively will facilitate their use in many applications. The simplicity in fabrication and the flexibility across different materials, geometries, and scales are key advantages over many existing methods that require some form of re-tooling to realize different outcomes. The properties indicate that the microfiber can be applied as a bio-sensing and stimuli-responsive component, or an elastic fabric.

Acknowledgements

We appreciate Prof. H. Kim at Dept. of Chemistry, Dankook University for the preparation of enzymes.

References

[1] Kenis, P.J., Ismagilov, R.F., & Whitesides G.M., 1999, *Science* **285**, pp. 83-85
[2] J. H. Nieuwenhuis, M. J. Vellekoop, et al., 2003, *Lab Chip*, vol. 3, pp56-61
[3] Beebe, D.J. et al, 2000, *Nature* **404**, pp 588-590

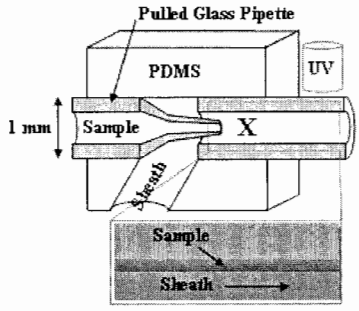

a) Apparatus for fiber production

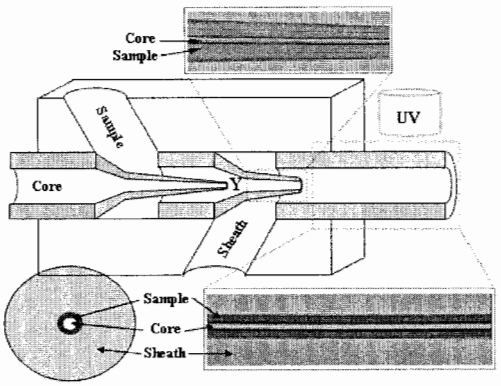

b) Apparatus for microtube production

Figure 1. Schematics of production apparatus

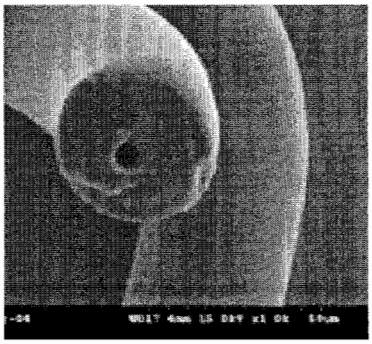

Figure 3. SEM image of microtube

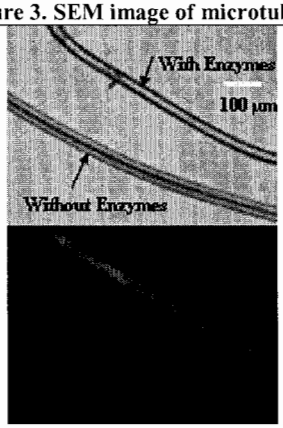

Figure 4. Fluorescence micrograph of enzyme immobilized microfiber

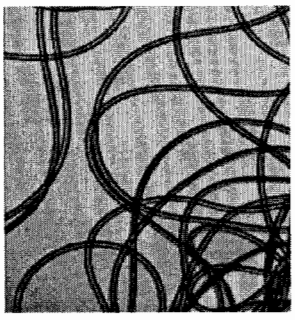

a) Continuously produced fiber

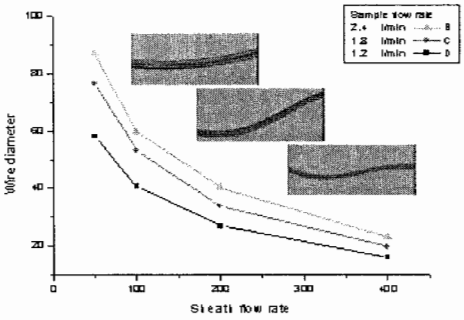

b) Relations of diameter to flow

Figure 5. Produced microfiber and wire diameter to the flow rate

DROPLET SORTING BY SIZE IN MICROFLUIDIC CHANNELS

Yung-Chieh Tan[1] and Abraham Philip Lee[1, 2]

[1]*Dep. of Biomedical Engineering, University of California Irvine, 204 Rockwell Engineering Center, Irvine, CA. 92697, U.S.A.*

[2]*Dep. of Mechanical Engineering, University of California Irvine, 204 Rockwell Engineering Center, Irvine, CA. 92697, U.S.A.*

Abstract

A novel microfluidic channel design for passive sorting of droplets by size is presented. The channel utilizes the shear streaming effect [1] to move droplets of desired sizes into selected channels. In a mixture of droplets with various sizes, larger droplets with radii ranging from 46μm to 51μm have been successfully sorted from smaller droplets with radii ranging from 28μm to 31μm. In a mixture of primary droplets and satellite droplets, satellite droplets (diameters <1μm) have been successfully collected using the same principle.

Keywords: ***Microfluidics, Droplets, Sorting, Nanoparticles, Satellite droplets***

1. Introduction

Droplets in microfluidics have been demonstrated to be a massive efficient tool for transporting and processing small volumes of reagents [1]. While most droplet manipulation methods require droplets to be sorted either to keep them from coalescing after generation or to keep them moving through desired pathways [1], droplets are sorted irrespective of size. Other methods for sorting (i.e. cell sorting in flow cytometer) require active valving system that relies on feedback detections [2]. Passive sorting by size presents several key advantages. First, it allows sorting to be spontaneous with delays in time response. Second, it can be easily designed into microfluidic structures without valving and sensing control systems. Third, it provides size control and allows contaminants to be removed from the samples. We present here for the first time the sorting of droplets by size using microfluidic channel designs.

2. Theory

In a microfluidic channel, the shear forces are exerted on objects immersed in fluids, i.e. droplets, cells, proteins and DNA. The average shear stress (σ) is $\sim Q/w^2h$, where Q is the flow rate of the fluid, w is width of the channel and h is the height of the channel. The shear forces experienced by the object is proportional to A the relative area on the object experiencing the shear stress. For larger objects such as droplets, difference in shear forces exerted on the object becomes significant to affect the path of the droplet. In diverging channel geometry, controlling the shearing stress bifurcating into each daughter channel creates a non-uniform shear stress gradient and thus allows droplets to be sorted by size

3. Experimental

The micro channels are fabricated by molding PDMS in SU-8 molds. To generate poly dispersed droplet populations, mono dispersed droplets are generated in a continuous oil stream [3-6] followed by droplet fusions [1] to create differences in droplet sizes. The schematic of the droplet sorting design is shown in Fig. 1. The two fluidic paths have the same overall resistance, and the difference in the widths of the two fluidic openings creates a shear force difference at the sorting junction. When droplet is at a sorting junction as the one shown in Fig. 2, the net shear force acting on a droplet is proportional to the difference between the product of fluid velocity and the droplet area projected by the dividing flows. The resulting net flow velocity difference between the two channels moves the droplet toward the fluidic path with higher velocity [3]. Sorting by the difference in droplet size is the result of a difference in the areas of droplets projected by the flows.

4. Results and discussion

As shown in Fig. 3, larger droplets experience greater shear forces which pull them into fluidic path 1, whereas, smaller droplets experience smaller shear forces which allow them to travel into fluidic path 2. The efficiency of the system is shown in Fig. 4, in which larger droplets are either sorted into fluidic path 1 or split by the shear forces exerted by the flows. Similarly, sorting of satellite droplet from larger droplets (primary droplets) is achieved by the same shearing principle as shown in Fig. 5. Since the diameters of satellite droplets can be generated to be under 1 μm, sorting and collection of satellite droplets enables the production of nanoparticles without using surfactants.

5. Conclusions

The results presented here demonstrate the ability to sort droplets by size through the design of channel geometries. This design can be used with other droplet based platforms to filter out undesired droplet sizes, to sort desired droplet fusion products [3,7], to collect satellite droplets, and to create complex microfluidic structures for combinatorial chemistry, synthesis of molecular drugs, and analysis of biochemical reactions.

References

[1] V. Cristini, Y. C. Tan, *Lab Chip*, DOI:10.1039/B403226H
[2] A. Y. Fu, H-P Chou, C. Spence, F. H. Arnold, S. R. Quake, 74(11), *Anal Chem*, 2451.
[3] Y. C. Tan, J. S. Fisher, A. I Lee, A. P. Lee, *Lab Chip*, DOI:10.1039/B403280M
[4] Y. C. Tan, J. Collins, A. P. Lee, *MicroTAS '03*, pp. 963-966
[5] T. Thorsen, W.R. Robert, F.H. Arnold, S.R. Quake, 86(18), *Phys. Review Letters,* 4163.
[6] S.L. Anna, N. Bontoux, H.A. Stone, 82(3), *Applied Physics Letter,* 364.
[7] H. Song, J.D. Tice, R.F. Ismagilov, 42(7), *Angew. Chem. Int. Ed*, 767.

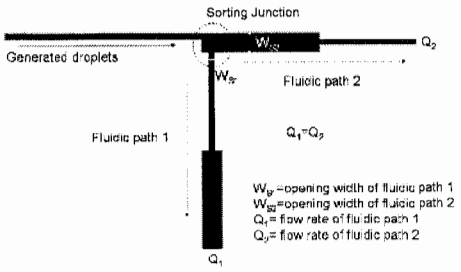

Fig. 1. Schematic of channel design for sorting droplets by size. The flow rates of the two fluidic paths are controlled to be equal by designing the channel resistances to be equal. The opening widths of each of the fluidic paths determine the relative shear force that directs the movement of the droplets. When a droplet reaches the sorting junction, it can either travel toward fluidic path 1, fluidic path 2, or split at the junction.

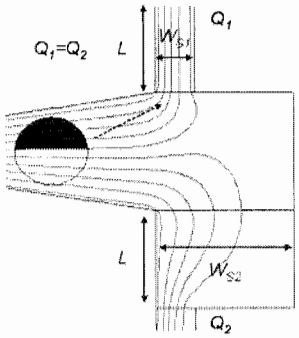

Fig. 2. Example of droplet sorting by size. The width difference between the two fluidic paths (1 and 2) creates a shear stress difference in the bifurcating flow. Dark area experiences upward flow while lighter area experiencing downward flow. Droplet moves upward due to higher shear stress.

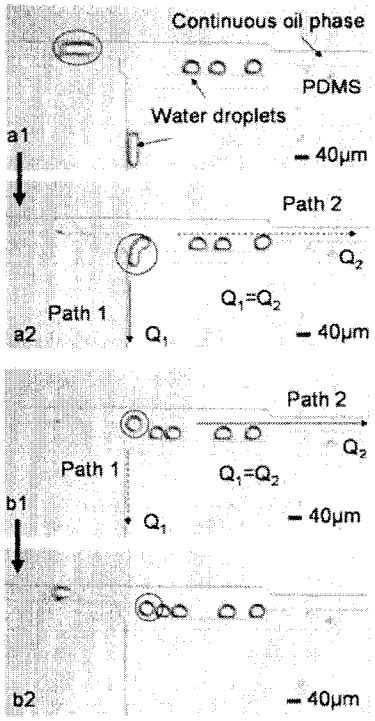

Fig. 3 Passive sorting of larger and smaller droplets. a1-a2) Larger droplet shown in circle is sorted into fluidic path 1. b1-b2) Smaller droplet shown in circle is sorted into fluidic path 2.

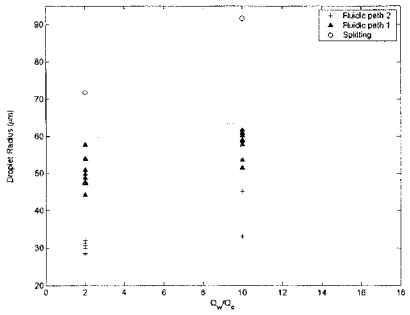

Fig. 4 Plot of droplet sorting. The generated diameter of the droplet is plotted as a function of the ratio between the flow rates of the water (Q_w) and oil (Q_o) phases. In between the parallel dashed lines, larger droplets (radius ranging from 46μm to 51μm) are sorted from smaller droplets (radius ranging from 28μm to 31μm). Above the parallel dashed lines, droplets split at the junction.

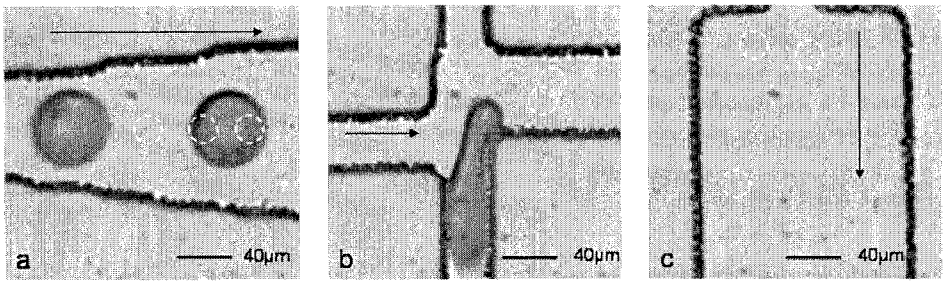

Fig. 5 The creation, sorting and collection of satellite droplets. a) satellite droplets (indicated in circles) are created with larger primary droplets. b) primary droplets are sorted toward the lower daughter channel while satellite droplets are sorted into alternative fluidic path. c) in the alternative fluidic path, satellite droplets are collected without the presence of primary droplets.

CONTROLLED DROPLET FUSION IN MICROFLUIDIC DEVICES

Lung-Hsin Hung[1], Wei-Yu Tseng[1], Kyung Choi[2], Yung-Chieh Tan[3], Kenneth J. Shea[2], and Abraham P. Lee[3, 4]

[1] Department of Chemical Engineering and Materials Science, [2] Department of Chemistry, [3] Department of Biomedical Engineering, [4] Department of Mechanical and Aerospace Engineering, 204 Rockwell Engineering Center, University of California at Irvine, Irvine, CA 92697, USA

Abstract

A microfluidic system featuring double-T junctions for droplet fusion is presented. The novel double droplet forming channel design allows the synchronized generation of two monodispersed streams of droplets, which allows controlled binary fusion of droplets from each stream to occur after generation. The ability to control droplet fusion enables an ideal mixer for highly homogeneous chemical reactions in "droplet reactors". Fusion of chemical reactants to generate semiconductor CdS nanoparticles or "quantum dots" is demonstrated in this device.

Keywords: microfluidics, droplets, fusion, quantum dot, chemical synthesis reactor

1. Introduction

Droplet fusion control in microfluidic devices has broad potential in industrial and academic applications. [1] Previous work manipulated droplet fusion by differential velocities of different size droplets or external force. [2, 3] Controllable droplet generation rate and proper duration of collision are the critical factors to make droplet fusion occur. The platform we present here allows consistent equal-sized droplet fusion with controllable multiple droplet generation patterns.

2. Theory

The equal-sized droplet fusion in low Reynolds number flow can be characterized by several dimensionless parameters: capillary number, Ca ($=\mu Gr/\sigma$); viscosity ratio of water and oil, λ; and R, the distance between droplet center to the flow axis. [4] (Where μ is the viscosity of oil fluid, G is the strain rate, and r is the droplet radius.) The droplet fusion processes include the drainage of the oil film between two droplets and the destabilization of thin films leading to rupture. [5] If droplets were drawn together at the close vicinity and have sufficient duration time of collision, the fusion will occur.

3. Experimental

The microchannel is fabricated by molding PDMS in SU-8 molds [6] and is permanently sealed on a glass slide. PDMS hydrophobicity recovery process under heat treatment [7] made the channel surface hydrophobic, which is preferable for water droplet generation. A schematic of the device is shown in Fig. 1. The device comprises of 2 water inlets, 1 oil inlet, and 1 outlet. Similar to the shearing mode of a T-type fluidic junction [1, 8], each water phase is sheared individually by continuous oil phase.

4. Results and discussion

The range of droplet sizes generated in the current device is found to be strongly dependent on the channel geometry rather than the flow rates of the water and oil phases. The size variation resulting from varying the water and oil flow rates is relatively small compared to the effect of width variation of the pinch junction. Shown in Fig. 2, under the same oil flow rates, the width of the pinch junction determines the range of producible droplet sizes. The generated droplets are monodispersed with less than 2% variation in size and can be generated with a rate of ~100 drops/sec.

In our design, fusion of droplets occurs due to the angle of the channel expansion at the exiting junction (Fig. 3). [9] This channel expansion allows a velocity gradient that propels droplets into contact and cause coalescence. The subsequent "necking" to the outlet channel creates a local acceleration and "focusing pressure" that further facilitates the fusing process. The results are consistent with CFD+ACE simulation in our lab (Fig. 4). Pressure instability at the pinch junction between the water phases synchronize the generation of droplets between the water phase inlets. The alternating frequency of droplet generation from each stream can be controlled by the differential water flow rates. Droplet generation ratios between is shown 1:1~1:3 in Fig. 5.

Further increasing the angles of expansion in the exiting channel junction creates various dynamic patterns of droplets. [8] The larger channel expansion allows droplet streams to be separated by a wider distance, in which no fusion occurs (Fig. 6a). Under 1 to 2 droplet ratio, the second generated clear droplet migrated down and merged with the dyed water droplet (Fig. 6b).

To demonstrate this droplet fusion device as a mixer for chemical reactions, cadmium nitrate and sodium sulfate aqueous droplets were fused to generate semiconductor CdS nanoparticles trapped in the outlet (Fig. 7). PL image shows the full-width half-maximum of fluorescent emission to be 15nm (Fig. 8).

5. Conclusions

These results demonstrate the ability of this microfluidic device to synchronize the generation of binary droplets in different size, ratio, frequency, and the capability of fusing droplets consistently. The device has industrial and academic application potential and is a promising platform for chemical and biochemical research.

References

[1] T. Nisisako, T. Toril, and T. Higuchi, *Lab Chip*, **2**, 24-26 (2002).
[2] H. Song, J. D. Tice, and R. F. Ismagilov, *Angew. Chem. Int. Ed.*, **42(7),** 768-772 (2003).
[3] S. K. Cho, H. Moon, and C. J. Kim, *J. MEMS,* **12(1),** 70-80 (2003).
[4] H. Yang, C. C. Park, Y. T. Hu, and L. G. Leal, *Phys. Flu.,* **13(5),** 1087-1106 (2001).
[5] S. Abid and A. K. Chesters, *Int. J. Multiphase flow,* **20(3),** 613-629 (1993).
[6] J. C. McDonald, D. C. Duffy, et al., *Electrophoresis,* **21(1),** 27-40 (2000).
[7] L. H. Hung and A. P. Lee, *submitted to 2004 ASME IMECE and RD&D Expo* (2004).
[8] T. Thorsen, R. W. Roberts, F. H. Arnold, and S. R. Quake, *Phys. Review Paper*, **86(18),** 4163-4166 (2001).
[9] Y. C. Tan, J. Fisher, A. I. Lee. E. Lin, and A. P. Lee, *Lab Chip,* DOI:10.1039/B403280M

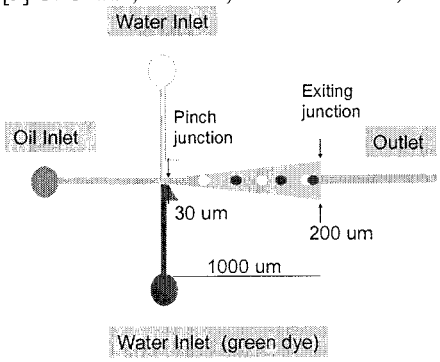

Figure 1. Schematic of the Double-T junction microchannel design.

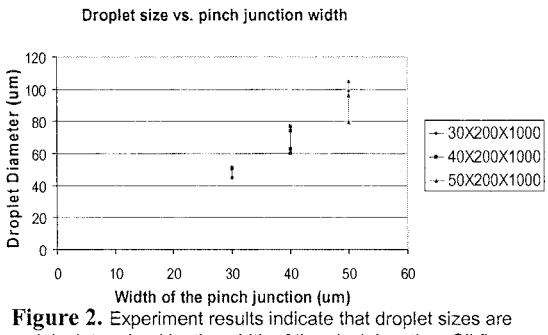

Figure 2. Experiment results indicate that droplet sizes are mainly determined by the width of the pinch junction. Oil flow rate is constant and water flow rate varies with different droplet sizes.

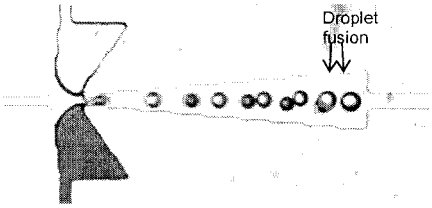

Figure 3. Droplets carried in the middle streamline allows droplet fusion to occur within the channel expansion.

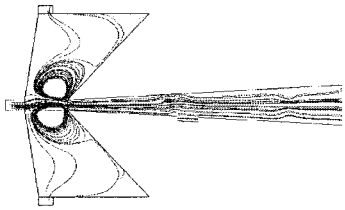

Figure 4. Computer CFD+ACE simulation by CFDRC of streamlines in the channel. Streamline separation depends on channel expansion.

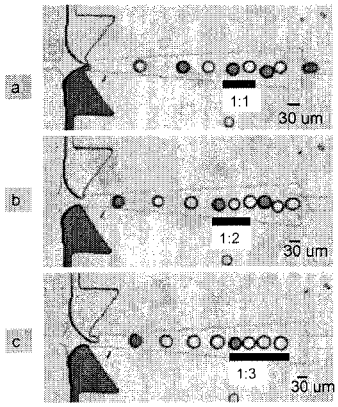

Figure 5. Controllable droplet ratios by adjusting inlet flow rate for different mixing combinations (a) 1:1 (b) 1:2 (c) 1:3

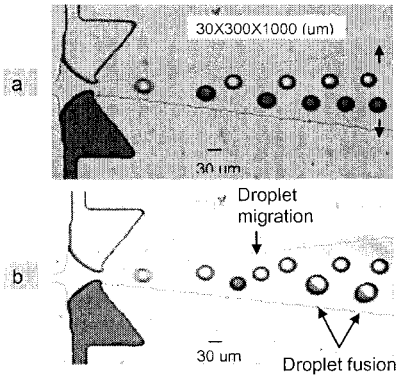

Figure 6. (a) Larger channel expansion at exiting junction results in separation streamlines. (b) Under 2 to 1 droplet generation ratio, second generated droplet migrated and merged with the dyed water droplet.

Figure 7. Cadmium and sulfate fused droplets were trapped inside the outlet channel as semiconductor nanoparticles were synthesized in each droplet.

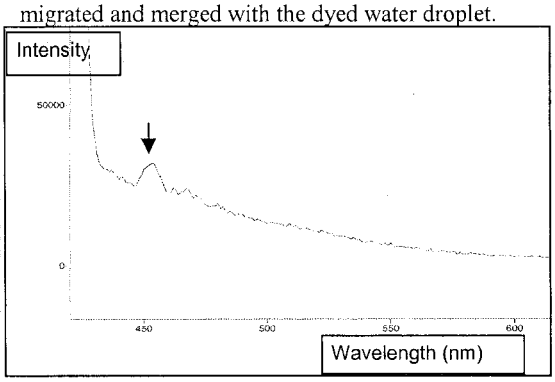

Figure 8. PL peak indicates that nanoparticles generated from fused droplets experienced a quantum effect which resulted in a FWHM of about 15nm.

MULTIDIMENSIONAL CHROMATOGRAPHY AND DIGESTION USING HPLC-CHIP/MS

Kevin Killeen, Hongfeng Yin, Reid Brennen and Tom van de Goor
Agilent Technologies Inc., Agilent Labs, 3500 Deer Creek Road
Palo Alto, CA USA 94304

Abstract

Polymer microfluidic devices are shown to have the capability to analyze complex biological mixtures. Integrated microanalytical devices using pressure-driven separation are fabricated and coupled with high sensitivity mass spectrometry for identification of proteins from sample mixtures such as serum. Two dimensional liquid chromatography (2D-LC) and stationary-phase digestion with reverse-phase LC in combination with nano-electrospray mass spectrometry (MS) was performed using laser-ablated, multilayered polyimide microfluidic devices. These HPLC-Chip/MS devices exceed in many aspects the performance of conventional liquid chromatography (HPLC/MS).

Keywords: chromatography, digestion, mass spectrometry, microfluidic

1. Introduction

Microfluidics are ideal for manipulating small volumes of highly complex biological samples such as blood serum or cell lysates. In order to separate molecular species in such complex liquid mixtures, multiple chemical methods are often required. Microfluidic devices can be combined with powerful chemical detection methods such as nano-electrospray ionization (ESI) mass spectrometry to allow for sensitive identification of the unknown molecular species. These microfluidic-MS devices allow multi-step workflows to be incorporated on single application chips and combined with direct-coupled mass spectrometry for total chemical analysis.

We have previously described the fabrication and performance of polymer microfluidic devices integrating single or multiple ESI tips for infusion mass spectrometry (chip-MS) and also HPLC columns (chip-LC/MS) using protein and peptide samples [1,2]. In this study we add the additional dimensions of chemical separation and chemical reaction by fabricating polymer microfluidic devices that allow for sequential stages of pressure driven 2D liquid chromatography and enzymatic digestion together with sample enrichment with integrated ESI tips. The fluidic elements are joined together by seamless channels in a common polymer microfluidic structure.

2. Experimental

HPLC-chip/MS devices were designed using CAD and fabricated using UV laser ablation of layers of polyimide films. These layers were vacuum-laminated into an integral fluidic structure and laser-trimmed to a final device shape containing a 40 μm outside diameter electrospray tip with a 15 μm wide channel. Sample connections and fluid switching are made by placing the HPLC-chip/MS device between the stator and rotor of a rotary valve. The valve interface enables high pressure, leak-free, simultaneous fluid switching between the multiple ports of the HPLC-chip/MS device.

3. Results and discussion

Proteins and protein digest mixtures (approx. 200 fmol each) were used to evaluate the performance of multi-function microfluidic-LC/MS devices. For the 2D HPLC-chip/MS, the first dimension of liquid chromatography was performed in discrete salt steps using strong cation exchange (SCX) polymer media packed in an on-chip column. Sample fractions were then collected on a reverse phase C18 stationary phase enrichment column and further separated using a second dimension on-chip LC column containing reverse phase C18 stationary phase silica-based media. Salt steps and solvent gradients were delivered to the rotary valve interface of the HPLC-chip/MS

device by an Agilent Technologies 1100 autosampler and nanoflow LC pumping system respectively, which delivered 300nL/min. at pressures up to 100 bar (see Fig. 1). An Agilent 1100 series ion trap mass spectrometer was used to collect the ESI tandem mass spectra, which were then processed by comparing the MS/MS spectral data against protein databases.

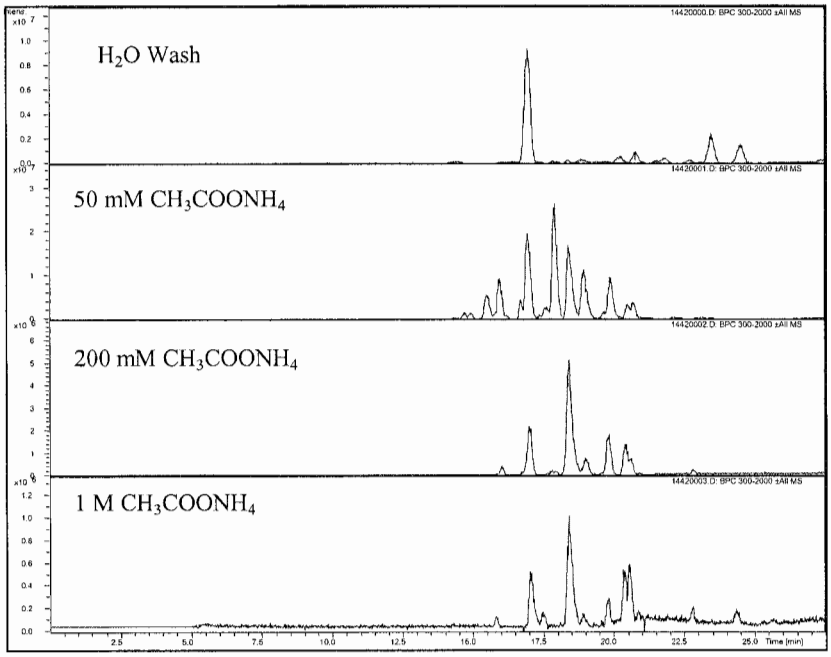

Figure 1. 2-D HPLC-Chip/MS spectrum of BSA digest using a combination of strong cation exchange (SCX) stationary phase and salt steps with reverse-phase media and linear solvent gradients in the second dimension to demonstrate 2D-LC/MS with a pressure driven microfluidic device. LC elution time is 35 min at 300 nl/min flow rate. Detection and fragmentation is done using an Agilent 1100 series ion trap mass spectrometer.

Enzymatic digestion was performed on-chip using a trypsin-functionalized stationary phase reaction bed (see Fig. 2). Bovine derived cytochrome C protein was completely digested into peptides residues in seconds that were then captured onto a C18 based enrichment column, chemically separated and analyzed by reverse phase HPLC-chip/MS and finally identified using standard protein data base search methods.

4. Conclusions

Integration of complex chemical functions has been demonstrated using pressure-based flow in a polymer microfluidic device. High performance two-dimensional liquid chromatography and stationary-phase enzymatic digestion followed by reverse phase nano-LC/MS has been performed. Further advances in integration and on-chip sensing will enable HPLC-Chip/MS devices to become an extensible platform for high sensitivity chemical analysis.

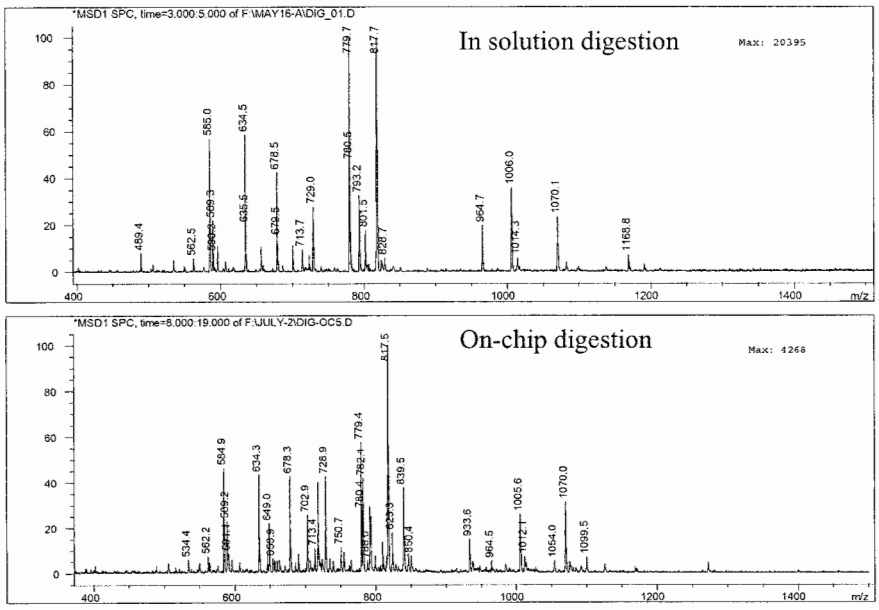

Figure 2. In solution vs. on-chip enzymatic digestion of bovine cytochrome C protein followed by reverse phase chip-LC/MS. The in solution digestion time was 24 hr vs. the on-chip digestion residence time of 14 s using a trypsin immobilized stationary phase reaction bed.

Acknowledgements

The authors would like to gratefully acknowledge the significant contributions and technical assistance of Debbie Ritchey, Karen Seaward, Judy Chang, Sharmila Udiavar, Daniel Sobek, and Mark Juanitas, all from Agilent Laboratories.

References

[1] K. Killeen, H. Yin, S. Udiavar, R. Brennen, M. Juanitas, E. Poon, D. Sobek and T. van de Goor, *Proc. Micro Total Analysis Systems 2001*, 331-332, J. M. Ramsey & A. van den Berg, eds.

[2] K. Killeen, H. Yin, D. Sobek, R. Brennen, and T. van de Goor, *Proc. Micro Total Analysis Systems 2003*, 481-483, M. A. Northrup, K. F. Jensen, & D. J. Harrison, eds.

COUPLING OF SEPARATION AND DIGESTION OF PROTEINS IN A PDMS DEVICE FOR MASS SPECTROMETRY ANALYSIS

Edouard Brunet[1], Arash Dodge[1], Suelin Chen[1], Jacques Goulpeau[1], Valerie Labas[2], Nicolas Royer[2], Joelle Vinh[2], Patrick Tabeling[1]

[1]*Microfluidics laboratory, ESPCI, 10 rue Vauquelin, 75231 Paris, France*

[2]*Neurobiology and cellular diversity laboratory, ESPCI, 10 rue Vauquelin, 75231 Paris, France*

Abstract

In this contribution, a Polydimethylsiloxane (PDMS) microdevice integrates an electrophoretic protein separation stage coupled to a mechanical protein trap which injects the selected protein into a rotary microreactor [1] for enzymatic digestion. Digested solutions are eluted from the device and analyzed via MALDI-TOF spectrometry. Total analysis time lasts around twenty minutes without having to use sample pretreatment or surface conditioning of the device.

Keywords : Protein, separation, digestion, PDMS, MALDI

1. Introduction

Integratability of several steps, starting from sample pretreatment to final analysis is one of the main issues for micro total analysis systems. One of the difficulties lies in coupling two or more functionalities onto a single device. For protein analysis, different groups have presented microsystems which couple 2D-gel electrophoresis with mass spectrometry (MS) [2], enzymatic digestion followed by peptide electrophoretic separation analysis or even enzymatic digestion followed by electrospray ionization for MS analysis [3,4]. One must often deal with samples containing many proteins which can make peptide recognition of a protein digest more complex. One method to reduce the number of proteins analyzed for a given sample is to use gel separation techniques prior to digestion in order to focus on a smaller number of targets. In macroscopic systems total time for sample pretreatment can be on the order of several hours before the initial sample of proteins is converted into a solution of peptides suitable for MS analysis. In this work, miniaturization of an electrophoretic separation stage coupled to a mechanically activated enzymatic microreactor allowed total analysis times much faster than macroscopic systems.

2. Experimental

The device was microfabricated using multi-layer soft lithography technology (MSL) [5] in order to combine electro-osmotic pumping with mechanical trapping and pumping. The layout of the device with its operation mode is illustrated in Figure 1. First, a 0.1 mg/mL trypsin solution in 0,01% trifluoroacetic acid (TFA) buffer (pH 2.0) is injected into a portion of the microreactor. Inactive in acidic medium, it is drawn and activated in the chip by pumping it alongside a flow of 50 mM ammonium bicarbonate buffer (pH 8.4), using three integrated valves activated in series in a peristaltic pump fashion for mechanical pumping [1]. Electrophoretic separation of model fluorescent proteins and molecules is then performed in a classic double-T injection/separation stage using electro-osmotic pumping. 15% acetonitrile or 1% SDS were used in buffer solutions for injection and separation steps in order to limit the adsorption of proteins to the channel walls. Selection of the protein of interest is performed by closing integrated trapping valves using MSL [5] after voltages are turned off. The integrated pump recirculates the selected protein in a rotary microreactor as reported in [1]. Once full mixing of protein with enzyme is achieved, the trypsin digests the selected protein for 15 min at 40 °C using a hotplate. Extraction of peptides from the device is performed using a PEEK capillary connected to the outlet of the microreactor, and spotting onto a MALDI target before addition of crystallization matrix (2-5 dihydroxybenzoic acid in 0.01% TFA). Total run time from sample injection to MS analysis is less than 20 minutes.

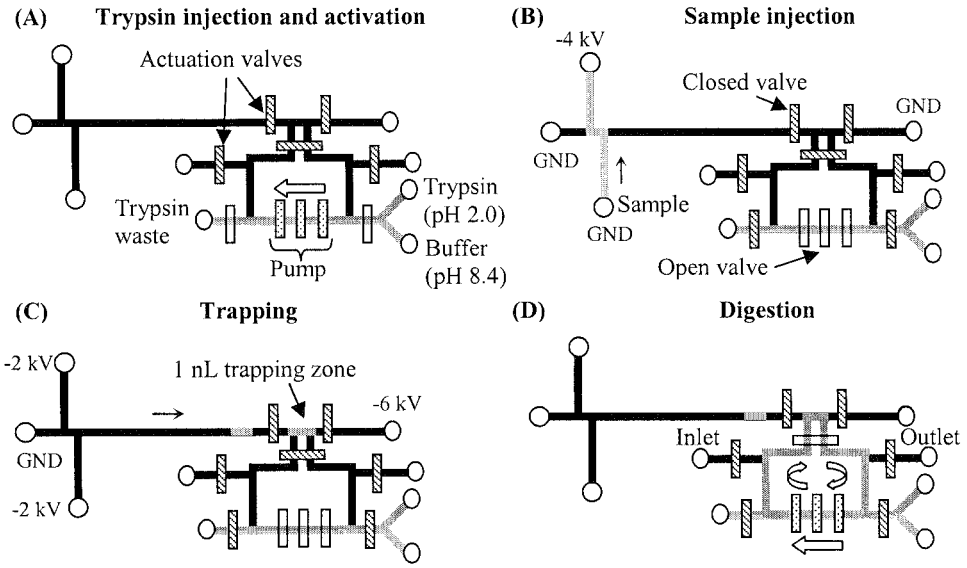

Figure 1. Layout of the device with operation mode: (A) Trypsin (in TFA 0.01%) is drawn and activated in chip by pumping alongside 50 mM ammonium bicarbonate buffer (pH 8.4) using the integrated micropump. (B) Proteins are injected and separated using a double-T injection/separation stage via electro-osmotic pumping. (C) Plug of interest is trapped using integrated PDMS valves. (D) Integrated pump injects the selected protein into the rotary microreactor which continuously mixes enzyme with protein for digestion. Resulting peptides are pumped out of the microdevice via pressure from the inlet to the outlet using a PEEK capillary. Drops of extracted solution are spotted onto solid target for MALDI-TOF analysis (not shown). Total microreactor volume is 73 nL.

3. Results and discussion

Figure 2A shows the result of a separation of fluorescently labelled BSA and avidin. The separation stage has also been used to identify BSA and fluorescein, which have similar electrophoretic mobilities (Fig. 2B). In both cases, no surface coating was required prior to analysis.

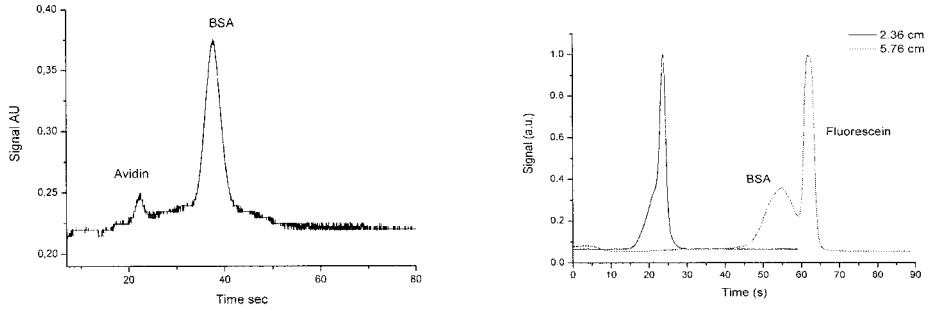

Figure 2. (A) Separation of BSA-FITC and avidin-FITC [1 mg/mL] in a 25 mM solution of ammonium bicarbonate with 1% SDS. (B) Separation of BSA-FITC [1 mg/mL] and fluorescein [10 μM] in a 25 mM solution of TRIS/HCl with 15% acetonitrile at different separation lengths. BSA and fluorescein electrophoretic mobilities are of $-3.0 \cdot 10^{-4}$ and $-3.3 \cdot 10^{-4}$ cm^2/Vs respectively.

Activation of enzyme within the chip has been verified by pipetting the solution at the trypsin waste reservoir onto a MALDI target and screening for autodigestion peaks (results not shown). Mixing efficiency in the device has been characterized using fluorescence monitoring prior to analysis in order to estimate the time to achieve complete mixing of the trapped sample with the solution in the micromixer. To accomplish this, a plug of fluorescein is trapped in the 1nL trapping zone and mixed with buffer located in the rotary micromixer (Figure 3). Full mixing is achieved in less than a minute. Figure 4 shows the MALDI-TOF spectrum of a 10 mg/mL lysozyme sample digested in the 73 nL rotary microreactor.

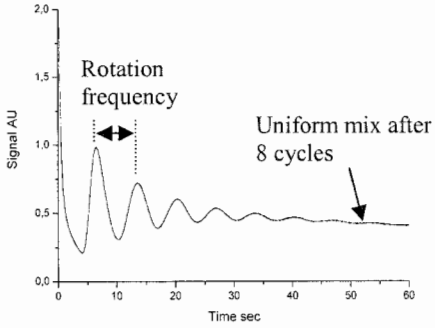

Figure 3. Mixing monitoring of a 1 nL plug of 100 µM fluorescein solution in 50 mM ammonium bicarbonate buffer (pH 9) mixed with 72 nL of 50 mM ammonium bicarbonate buffer (pH 9) located in the rotary microreactor. The flowrate of the pump is extracted from the rotation frequency of the obtained curve (0.7 µL/min). Complete mixing is achieved within 60 sec.

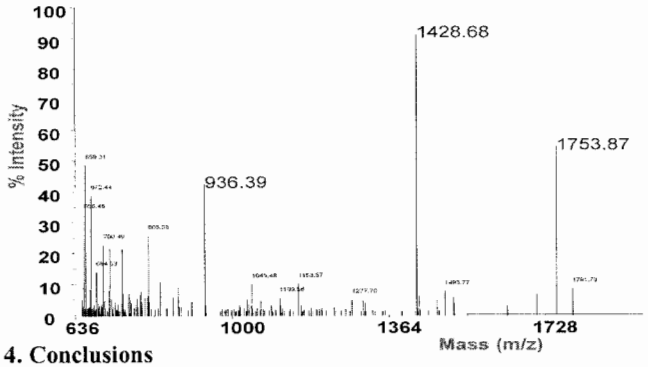

Figure 4. Mass spectrum of a trypsin digestion of a 1nL lysozyme sample [10 mg/mL] in the 73 nL rotary reactor. Digestion performed for 15 min at 40°C. Three of the main peptides resulting from the digestion can easily be observed in the graphic. Peptide coverage is of 57%, recognition probability is of 100%

4. Conclusions

This is to our knowledge the first microdevice successfully integrating separation, selection and digestion of proteins prior to MALDI-TOF analysis for protein recognition of peptides. It is also the first time electrokinetic pumping has been combined with integrated mechanical pumping for microfluidic applications in a PDMS device.

Acknowledgements

The authors wish to thank the ESPCI and the CNRS for funding.

References

[1] H-P Chou, M. A. Unger, S. R. Quake, *Biomedical Microdevices*, **3:4**, 323-330, (2001)

[2] D. Figeys, S. P. Gygi, G. McKinnon, R. Aebersold, *Anal. Chem.* **70**, 3728-3734 (1998)

[3] C. Wang, R. Oleschuk, F. Ouchen, J. Li, P. Thibault, D. J. Harrison, *Rapid Communications in mass spectrometry*, **14**, 1377-1383 (2000).

[4] J. Goa, J. Xu, L. E. Locascio, C. S. Lee, *Anal. Chem*, **73**, 2648-2655 (2001)

[5] M. Unger, H. Chou, T. Thorsen, A. Sherer, S. Quake, *Science*, **288**, 113 (2000)

INTEGRATED SELECTIVE ENRICHMENT TARGET (ISET) - A GENERIC MICROFABRICATED SAMPLE PREPARATION DEVICE

Simon Ekström[1], Thomas Laurell[1], Johan Nilsson[1], György Marko-Varga[2] and Lars Wallman[1]

[1] Dept. of Electrical Measurements, Lund University, P.O. Box 118, S-221 00 Lund, Sweden
[2] Molecular Science, AstraZeneca Research & Development, S-221 87 Lund, Sweden

Abstract

A combined sample preparation and sample presentation device, Integrated Selective Enrichment Target (ISET), consisting of an array with 96 perforated nanovials is described. Each perforated nanovial can be filled with soild-phase extraction media for purification and concentration of biomolecules prior to mass spectrometry. The ISET platform provides an efficient, economic and generic sample treatment process, allowing for rapid in-parallel handling of minute sample volumes, with a minimum of sample transfers.

Keywords: solid-phase microextraction, mass spectromery, proteomics, Integrated Selective Enrichment Target, (ISET).

1. Introduction

Matrix Assisted Laser Desorption/Ionization Mass Spectrometry (MALDI MS) is today a standard procedure for analysis of biomolecules (proteins, peptides, oligonucelotides) and is most efficient if the sample biomolecules is presented to the mass spectrometer in pure form, that is without any interfering species present. Soild-phase microextraction as a purification and concentration step prior to mass spectrometry is commonly done with pipette tips filled with extraction media [1], e.g. ZipTips™ (Millipore Corporation, Billerica, MA USA). Other commercially available systems are based on different principles, e.g. the microtiterplates with integrated solid-phase extraction, such as the ZipPlate™ (Millipore Corporation, Billerica, MA USA), the microfluidic rotating disc Gyro Lab MALDI SP1 (Gyros AB, Sweden), or modified MALDI target plates for on-target clean-up, e.g. MassPrep™PROtarget (Waters, Milford, MA, USA). The main purpose with the ISET, Fig. 1, is to maintain the benefits of miniaturization, while keeping the complexity of the platform low.

2. Experimental

Fig. 2 shows two different ISET sample preparation methodologies. Sample preparation for peptide mapping with the Integrated Sample Enrichment Target Technology, ISET, was performed by; 1) 1 µl of a 1 mg/mL suspension of Poros R2 50 µm beads in 50% ACN/0,1%TFA was placed in an external container e.g. a microtiterplate 2) acidified sample was added to each vial 3) peptide binding 30 min, followed by transfer of the beads to ISET device 4) wash 2 x5 µl, 0,1% TFA. 5) elution of the analytes onto the backside of the ISET with 2 x 0,3 µl, 50% ACN/0,1%TFA containing 1 mg/ml of cyano-4-hydroxy-cinnamic acid and 50 fmol ACTH 18-39/µl (internal calibrant). MALDI TOF-MS analysis was performed on an M@ldi LR (Waters/Micromass) running Masslynx 3.5/proteinlynx 1.1.

3. Results and discussion

The uncomplicated design of the ISET device, Fig. 3, provides several beneficial aspects, such as ease of fabrication (allows for a high-density of array positions), use and interfacing to other equipment. Another important aspect is the short path length in the ISET, which provides minimal unspecific adsorption of the analytes on surfaces in the device.

The ISET device can be used in a number of generic applications. The user chooses a capture medium or several different (complementary) capture medium types, depending on the application, to fill ISET with. The desired biomolecules can then be captured on the capture media and undesired components that may still be present or bound to the medium are subsequently washed away, leaving the desired biomolecules on the medium. After all desired sample treatments steps are completed, the desired biomolecules are eluted, onto the analysis zone on the ISET. The biomolecules can now be subjected to even further sample treatment steps on the analysis zone, or if no additional sample treatment is desired the ISET can be subjected to analysis by MALDI MS.

The ISET sample preparation achieved a signal amplification that was superior to currently available commercial systems, e.g. MassPREP PROtarget™ MALDI targets or ZipTip™ solid-phase microextraction tips, Fig. 4.

The ISET was successfully applied for sample clean-up and concentration of in-gel digested proteins in large scale proteomics studies. It was also possible to use the ISET in protein chip applications for capture of antigens using antibody covered beads. When used in protein chip applications analysis was performed both with fluorescence and MALDI MS.

4. Conclusions

The ISET methodology has been proven successful in the performance evaluation as a generic microscale proteomic sample enrichment, clean-up and MALDI-MS analysis platform. Its ease of use and the qualitative results are currently driving our efforts to develop a low cost disposable version of the ISET for evaluation at large scale in proteomics laboratories.

Acknowledgements

We would like to thank SWEGENE, the Wallenberg foundation, Swedish Foundation for Strategic Research and the Swedish Research Council, Crafoord Foundation, Carl Trygger Foundation, Royal Physiographic Society in Lund, for financial support, and Thorleif Lavold at Waters/Micromass Scandinavia for mass spectrometry instrumental support. This study was also supported by grants from the Swedish Cancer Society (proj. nr. 3555), Swedish Research Council of Medicine (proj. nr. 7903), and Foundation Federico.

References

[1] Pluskal M. G., Microscale sample preparation, Nature Biotechnology, **1,** 104-105 (2000).

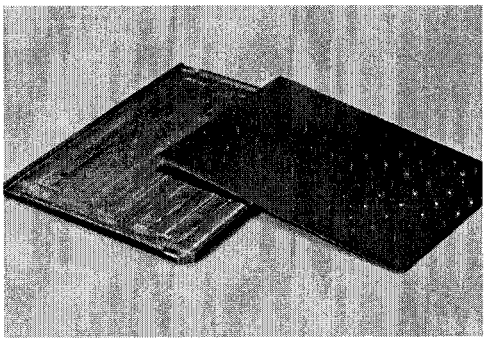

Figure 1. Picture of ISET and adapter for insertion into MALDI MS instrument.

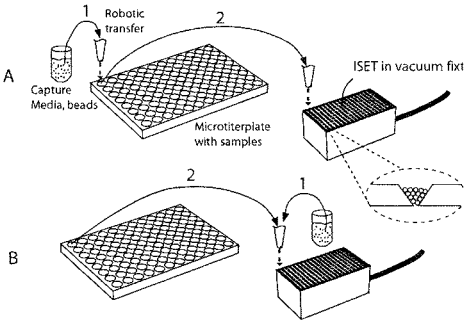

Figure 2. Media and sample can be loaded into the ISET by applying a vacuum underneath, either by transferring the sample while bound to the media, A or by first adding the media followed by addition of sample, B.

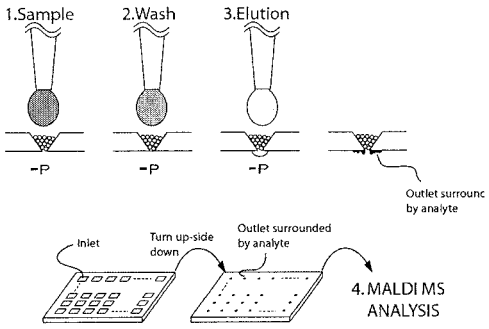

Figure 3. Workflow when using the ISET, sample, wash and elution is drawn through the media by a applying a vacuum underneath the ISET. After elution, the analytes end up on the analysis zone (0,5-1 mm) surrounding the outlet. After elution the ISET is turned up side down and the analyte positions are subjected to analysis.

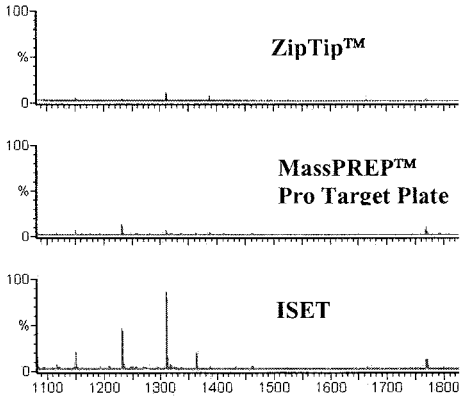

Figure 4. Analysis readout when processing identical samples with different technologies ZipTip™, MassPREP™ Pro Target Plate and the ISET-device. Note that the scaling of the y-axis is normalised so that 100% corresponds to 10000 counts.

A NOVEL MICROFLUIDIC PLATFORM DESIGN COMBINING ACTUATORS, CELL CULTURE AND SENSITIVE FLUORESCENCE DETECTION WITH DISPOSABLE MICROCHIPS

Jonas Melin[1,2], Henrik Johansson[1], Ola Söderberg[1], Fredrik Nikolajeff[2], Mats Nilsson[1], Ulf Landegren[1] and Jonas Jarvius[1]

[1]The Beijer Laboratory, Department of Genetics and Pathology, Rudbeck Laboratory,
[2] Department of Engineering Sciences, Ångstrom laboratory,
University of Uppsala, SE-751 21 Uppsala, Sweden

Keywords: bonding, injection molding, cell culture, actuators

1. Introduction

Thermoplastic polymers such as poly(methylmethacrylate) (PMMA) or polycarbonate (PC) have been presented as ultimate materials for microchip fabrication. High throughput, using injection molding fabrication techniques allows for cost effective large scale production. Cycle times are typically measured in seconds instead of hours as for PDMS molding. A major concern of thermoplastic microfluidic devices is how to seal the open structures that is produced by the injection molding process. Various variants of thermal annealing are most commonly used, a method which tends to deform the microstructures and is hard to combine with incorporation of mechanic actuators.

In academia the golden standard for rapid prototyping of microfluidic systems has so far been poly(dimethylsiloxane) (PDMS) since it is inexpensive, easy to replicate by molding and optically transparent (240-1100 nm) [1]. PDMS microstructures are also easy to seal by irreversible bonding to itself or glass. The elastic nature of PDMS has be taken advantage of in integrated pumps and valves [2]. For limited academic experiment series PDMS chips are often used for single analyses in order to avoid contamination problems. However, large scale production of microsystems based on elastomer materials remains to be realized.

We have developed a novel platform for microfluidic analysis that exploits the virtues of elastomer technology and high throughput of injection molding production. The platform has been possible to realize due to a new technique for bonding thermoplastic microstructures to PDMS elastomer films. The choice of plastics is open, allowing the optimal material for a given application to be selected based on e.g. chemical and optical properties or on price. The elastomer sealing material has low Young's modulus and can function as a flexible membrane in actuators, such as valves and pumps. The sealed structures also support mammalian cell growth.

2. Experimental

System fabrication. Compact disc injection moulding of microstructures (Fig. 1d) was performed by Åmic AB (Uppsala, Sweden). Connection holes were drilled and the desired structures were diced out. PDMS films were generated by spinning the uncured prepolymer to the desired thickness and the films were bonded to the thermoplastic microstructures [3]. The bonding method has been demonstrated for three different thermoplastic substrates; PC, PMMA and the cycloolefin polymer Zeonor. It was possible to achieve a bonding layer stronger than the PDMS bulk for all types of plastics.

Cell culture. Chinese hamster ovary (CHO-KI) cells transfected with an enhanced green fluorescent protein plasmid were injected into sealed chips. The chips were immersed in a Petri dish containing cell culture medium and incubated at 37°C with 5% CO_2.

Cell counting. Mononucleated cells were purified from peripheral blood by Ficoll separation and resuspended in PBS. Cell surface proteins were fluorescently labelled by anti-CD4 PE + anti-CD8 FITC and pumped through a microchannel (200x40 μm cross section) at a rate of 1 μL/min. A confocal microscope operated in line-scanning mode, across the channel perpendicular to the direction of liquid flow, was used to detect the cells.

Fluid pumping. Chips for fluid pumping were fabricated by sandwiching the elastomer film (~110 μm) between two Zeonor chips, one representing a flow channel chip and the other one a control channel chip. All channels had a depth of 15 μm. Pressurized air, modulated by computer-controlled three-way switch valves, was connected to the channels of the control chip.

3. Results and discussion

PDMS has proven to be an excellent material for fabrication of microchannels for cell culturing applications. [3] The high O_2 and CO_2 permeability of the polymer promote aerobic metabolism. By bonding a PDMS lid to a plastic chip the critical gas exchange can take place through the lid whereas the microstructures are fabricated in impermeable thermo plastics. We could demonstrate culturing for seven days of mammalian cells (CHO-KI) in sealed microchannels (Fig. 1 a). We used chips replicated in the optical polymer Zeonor for a cell counting application by pumping fluorescently labeled cells through a microchannel (Fig. 1 b). For labeled lymphocytes we measured the ratio of CD8/CD4 to 0.33, well in accordance with the corresponding ratios measured in a standard flow cytometer; 0.32.

The elastomer layer can either serve as a lid when sealing open microchannels or it can function as a flexible membrane between two channels. The latter is achieved by sandwiching the elastomer film between the cavities of two facing plastic chips. By applying pressurized air to an upper layer channel ("control channel") the membrane is deflected downwards and affects the liquid in the lower layer channel ("flow channel"). This was first demonstrated for fabrication of valves and pumps using similar chips made of multilayer PDMS [2]. We could demonstrate peristaltic pumping by sequential activation of four control channels (Fig. 2 c). A volumetric flow between 2 and 9 nL/s was achieved

4. Conclusions

It is our opinion that disposability in combination with integrated actuators is a fundamental prerequisite if microfluidic devices ever shall become a routine analysis tool. The multipurpose platform we have developed offers this possibility. Moreover, it supports mammalian cell growth and presents excellent optical properties for fluorescence detection enabling a wide range of integrated microfluidic assay procedures.

Acknowledgements

The work was supported by the Wallenberg Foundation, the Swedish Research Councils for Medicine and for Natural and Technological Sciences, and from the Swedish Defense Nanotechnology Program and the EU FP6.

References

1. McDonald, J.C. and G.M. Whitesides, *Poly(dimethylsiloxane) as a material for fabricating microfluidic devices.* Accounts Chem. Res., 2002. **35**(7): p. 491-499.
2. Unger, M.A., et al., *Monolithic microfabricated valves and pumps by multilayer soft lithography.* Science, 2000. **288**(5463): p. 113-16.
3. Melin *et al.* Submitted

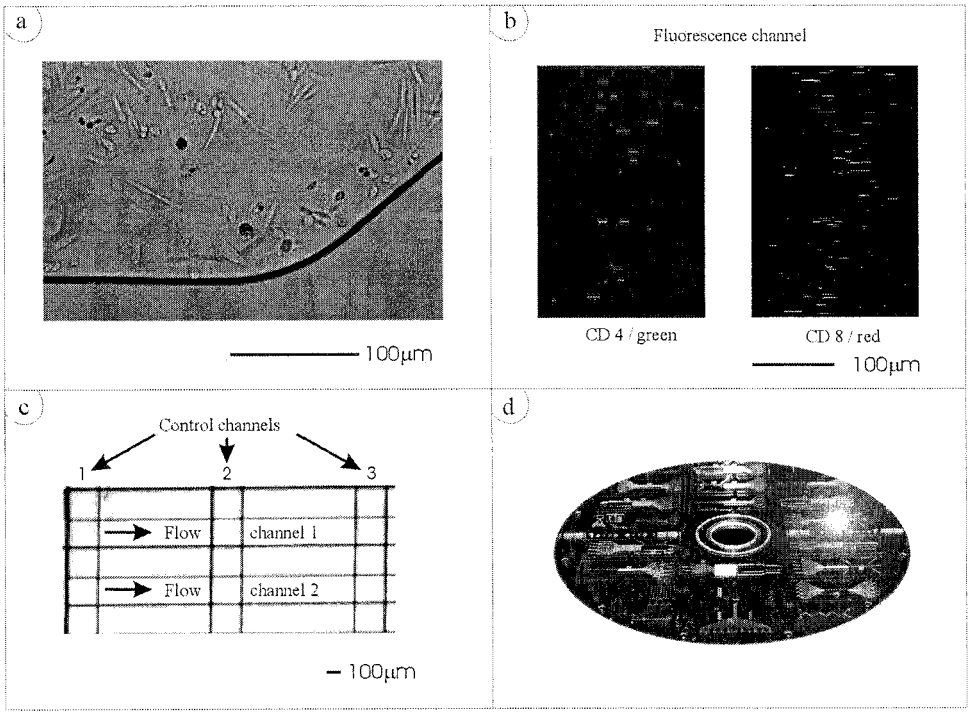

Figure 1 a) CHO-KI cells expressing EGFP cultured in Zeonor microchannels. Cell growth and adhesion were monitored for one week. **b)** Flow characterization of CD4/CD8 labelled lymphocytes in microfluidic channels. CD4/CD8 ratio was determined to 0.33 which could be verified by standard flow cytometry. **c)** Pneumatic actuators consisting of control channels (vertical) and liquid channels (horizontal). **d)** Injection moulded microstructures produced by CD replication technology.

CELL MONITORING SYSTEM WITH MULTIPARAMETRIC CMOS SENSORCHIPS

W.H. Baumann[1], E. Schreiber[1], G. Krause[1], A. Podssun[1], S. Homma[1], R. Schrott[1], R. Ehret[2], I. Freund[3] and M. Lehmann[3]

[1]Biophysics Dept., Rostock University, Friedrich Barnewitz Str. 4, D-18119 Rostock, Germany
[2]BIONAS GmbH, Friedrich Barnewitz Str. 3, D-18119 Rostock, Germany
[3]MICRONAS GmbH, Hans-Bunte-Strasse 19, D-79108 Freiburg, Germany

Keywords: CMOS sensor chip, cell monitoring system, CMS, neuronal network, MEA

1. Introduction

A better understanding of the multifunctional cellular processing of input- and output-signals is fundamental for basic research as well as for various fields of biomedical applications. As a first approach for on-line monitoring of cellular reactions under well controlled experimental conditions we develop(ed) different so called Cell Monitoring Systems (CMS®). They allow the parallel and non-invasive measurement of different parameters of cellular systems by the use of CMOS silicon microsensors [1-5]. In cooperation with the semiconductor company Micronas we realised different silicon based microsensor chips.

2. Experimental

Living cells are directly cultured on the sensorchip (see Fig. 1&2). Neuronal cells from dissociated tissue cultures were prepared according to the basic method established by Ransom et al. [6]. Neurons were maintained for one week in MEM, containing 10 % fetal calf serum and 10 % horse serum. Thereafter cells were fed 3-times per week with MEM containing 10 % horse serum. The cultures were maintained at 37 °C in an atmosphere with 10 % CO_2. The network developed spontaneous electrical activity after about 1 week and stabilized after 3 weeks. The culture area on the chip is less than 20 mm^2 and has a chamber volume of 10 µl in the flow injection system.

On our present neurochip we integrated a palladium multi electrode array (MEA) with 58 Pd electrodes, different types of cell potential field effect transistors (CPFETs), temperature sensors,

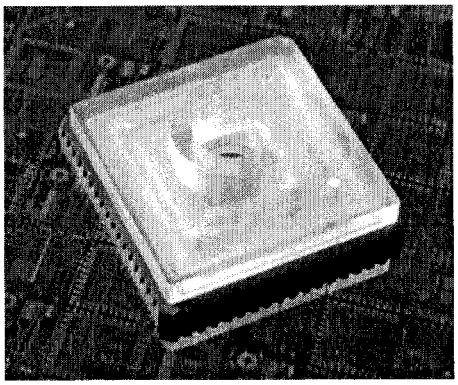

Figure 1: CMOS sensorchip with CNC encapsulation on standard 68-pin PLCC ceramic socket. The cells are cultured directly in the trough on the chip.

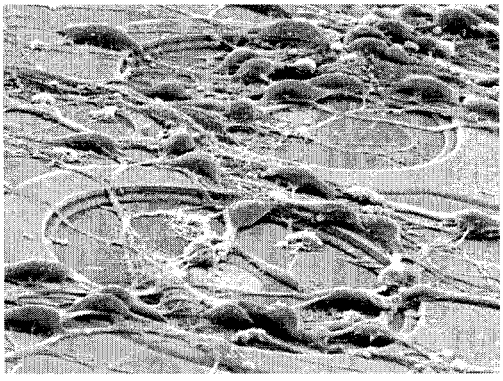

Figure 2: SEM picture of neuronal network at the beginning of growth (after 3 days) on electrodes. After about 3 weeks the culture area of the chip is completely overgrown by cells.

ion sensitive FETs (ISFETs) and two types of oxygen sensors. Therewith we can measure metabolic and electrical signals in parallel on neuronal networks, cultured on the sensor chip. As metabolic parameters we can measure the acidification (see Fig. 3) and respiration rate of the cells. Additionally we can measure non-invasive the action potential signals of neuronal networks cultured on our CMOS neurosensor microchip due to extracellular coupling between sensor and cell/axon (see Fig. 4&5).

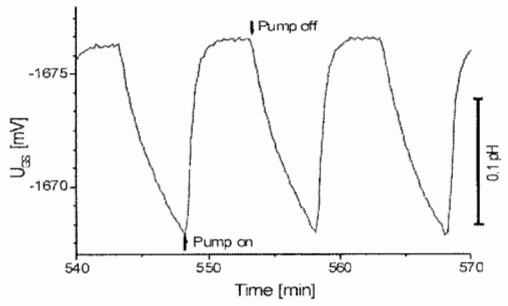

Figure 3: Cutout from an extracellular acidification measurement of a neuronal network on a silicon sensorchip with ISFETs in a flow through system. The acidification was measured at each pump off cycle. During the pump on cycle the medium was completely exchanged with fresh medium.

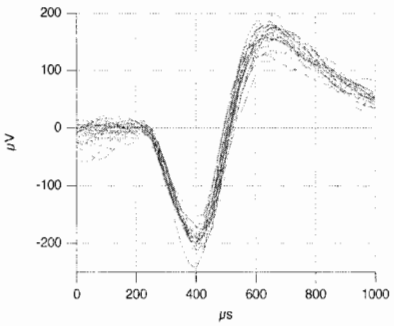

Figure 4: Extracellular measured action potentials with Pd electrodes on the silicon neurosensor chip.

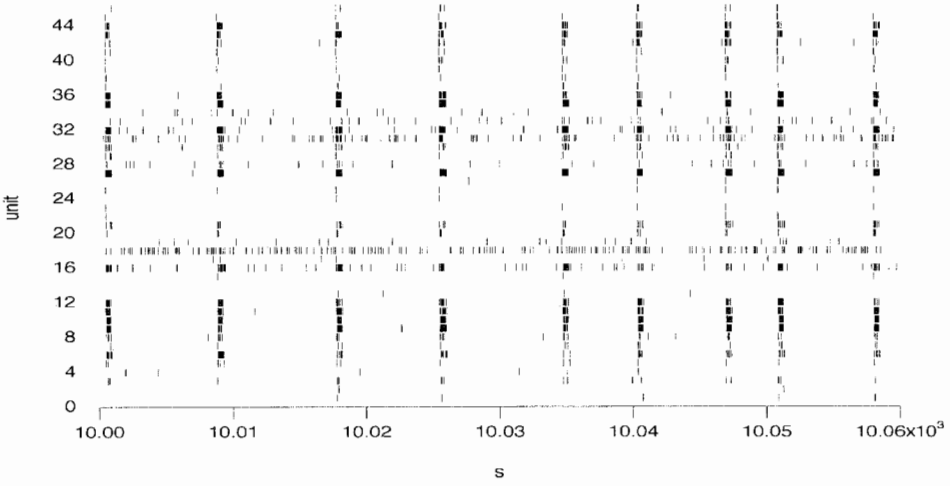

Figure 5: Cutout (60 sec) of 46 spiketrains from different electrodes of a spontaneous active frontal cortex network after 4 weeks in culture on the chip. Every bar in a spiketrain represents one action potential.

3. Results and discussion

With the CPFETs we could not reliably measure electrical activity of vertebrate neuronal networks due to the adverse S/N of our present CPFETs. With the palladium electrodes the measurement of electrical activity of neuronal networks from murine fetal spinal cord and frontal cortex tissues have been successful (see Fig 4&5). The results of the measurements of the electrical activity are comparable concerning S/N and yield of electrodes with electrical activity with the established multi electrode arrays (MEA) on glass chips [7].

Measurements of acidification rate (see Fig. 3) and oxygen consumption have been made with the neurochip and with the sensor system from BIONAS. With the BIONAS sensor chip the adhesion could be measured as an additional parameter. Using the flow injection system, necessary for the metabolic measurements, caused a small increase of the electrical activity during the pump-on period.

4. Conclusions

A CMS with a silicon based neurochip for the measurement of the electrical as well as metabolic activity of neuronal networks has been realised. Metabolic as well as electrical activity have been successfully measured on neuronal networks. The influence of the fluid flow at the pump-on period on the electrical activity has to be eliminated by modification of the flow injection system (flow head, semipermeable membranes, ..).

The next generation of sensor chips will have additional sensors to measure further cellular parameters. **The more parameters we can study in parallel the better we will understand for example cellular reactions in cellular biosensors or drug screening applications.**

At present we test a CMOS neurosensor chip prototype with integrated electronics (filters, preamplifiers, multiplexer, I2C-bus, ...). With the integrated electronics more sensors can be integrated using the same chip carrier and additional features like PC controlled switching between stimulation and recording can be realized.

To manage the high amount of data we also develop algorithms for automated spike detection and unit separation. For the interpretation of the complex neuronal data sets we use pattern recognition methods.

Acknowledgements

The research effort is sponsored by the European Regional Development Fund Community (ERDF), the state Mecklenburg-Vorpommern and the Micronas GmbH in Freiburg, Germany. The authors also wish to thank the Electron Microscopy Center from the University of Rostock for the SEM pictures with the neuronal networks and the IZT staff for culturing the neuronal networks on the sensor chip.

References

[1] Baumann, W., et al., *Sensors and Actuators B*, B 55 (1999), 77-89
[2] Ehret, R., et al., *Fresenius J Anal Chem*, 369 (2001), 30-35
[3] Baumann, W., et al., *Proceedings Eurosensors X*VI, Prag, Sept. (2002), 1169-1172
[4] Henning, T., et al., *Anti-Cancer Drugs*, 12 (2001), 21-32
[5] Lehmann, M., et al., *Biosensors & Bioelectronics*, 16/3 (2001), 195-203
[6] Ransom B.R., et al., *J. Neurophysiol.*, 40 (1977,) 1132- 1150
[7] Gross G.W., et al., *Biosensors & Bioelectronics*, 10 (1995), 553-567

LIVING CELL GENE EXPRESSION ASSAYS IN A MICROFLUIDIC DEVICE

Kevin R. King[1], Deanna M. Thompson[2] and Kenneth J. Wieder[2], Mehmet Toner[1,2], Martin L. Yarmush[1,2], and Arul Jayaraman[2]

[1]Division of Health Science and Technology Harvard-MIT

[2]Center for Engineering in Medicine/Department of Surgery, Massachusetts General Hospital, Harvard Medical School, and Shriners Hospitals for Children, Boston, Massachusetts 02114

Abstract

Conventional gene expression assays involve destructive single time point measurements and require averaging over large numbers of cells. We are using GFP reporter vectors stably transfected into mammalian cells to monitor the dynamics of gene expression in living cells. In this work, we present a scalable microfluidic platform for performing the dynamic cell-based assays, and we demonstrate it by screening the fluorescence time-course from HeLa d2EGFP-NFκB reporter clones responding to the inflammatory cytokine, TNF-α.

Keywords: cell culture, gene expression, GFP reporter, dynamics, microfluidics

1. Introduction

Living cells dynamically modulate their gene expression patterns to adapt to changes in their local microenvironment. Many techniques have emerged to characterize these responses including northern blots, RT-PCR, and DNA microarrays. However, these methods involve destructive single time point measurements that require significant sample sizes and necessitate averaging over large numbers of cells. We are developing a gene expression assay platform that combines microfluidics and green fluorescent protein (GFP) reporter technologies to characterize the dynamic cellular response to soluble stimuli (cytokines, growth factors, or potential therapeutics), all with single-cell resolution.

Previously, it was demonstrated that adherent mammalian cells could be seeded and stably cultured in microfluidic networks for weeks [1]. We extend this work here by performing functional expression assays on living cells in a microfluidic device. In contrast to standard culture vessels, microfluidics offers the advantage of real-time "stimulus control," while GFP technologies allow nondestructive measurements of cellular responses. Together they create a powerful integrated platform for screening the complex dynamics of living cell gene expression (Fig. 1).

2. Experimental

To create the gene expression reporter clones, HeLa cells are stably transfected with a plasmid vector for a Green Fluorescent Protein variant with a two hour half-life (d2EGFP). Expression of this fluorescent protein is under the transcriptional control of the NFκB transcription factor. Therefore the amount of GFP, and thus the level of fluorescence, corresponds to NFκB activity. Because of its short half life, the fluorescent protein does not accumulate indefinitely, but instead requires continual synthesis. This allows expression dynamics to be monitored. The microfluidic network consists of an upstream dilution module that prepares several concentrations of the soluble cytokine stimulus (TNF-α) using a previously described parallel dilution scheme [2]. This stimulus is delivered to the downstream cell culture module consisting of an array of chambers (500μm x 800μm x 50μm each) where the reporter clones are seeded and monitored. The optically clear microfluidic bioreactors are fabricated using soft lithography [3]. Devices are autoclave sterilized, surface modified with fibronectin (10ng/mL), seeded with cells ($5x10^6$ cells/mL), and perfused with culture medium using gravity-driven flow (~1μl/min). Fluorescent cellular responses are monitored using time-lapse phase and fluorescence microscopy while cells are maintained in a microscope

stage environmental chamber (37°C, 5%CO_2). Images are quantified using Metamorph image analysis software.

3. Results and Discussion

We demonstrate the power of the approach here by screening the dynamics of NFκB-activation in response to the inflammatory cytokine, TNF-α. After seeding cells, they were allowed to attach and spread as shown in Fig. 2. Prior to stimulation, cells frequently divided, however proliferation was significantly less than that observed in control tissue culture plastic. After continuous flow was initiated and cultures were stabilized, devices were moved to a microscope/environmental chamber for TNF-α (10ng/mL) stimulation and phase and fluorescence image capture. Fluorescence micrographs are shown at 2 hours and 8 hours after stimulation in Fig. 3. The dominant source of background fluorescence is the culture medium (no phenol red). Therefore, the microscale channel height offers significant improvements over standard culture dishes. As a result, baseline cellular fluorescence was detectable even prior to stimulation. After delivering the TNF-α, there was a 2 hour delay before detectable increases in fluroescence were observed. This is consistent with the characteristic time for the GFP molecule to be transcribed, translated, and folded such that it becomes fluorescently active.

The population response to a step of TNF-α (10 ng/mL) was quantified and is shown in Fig. 4. In addition to the 2 hour delay, the dynamic fluorescence response exhibits saturation after approximately 8 hrs, suggesting that the NFκB activity has reached a steady-state level equivalent to the GFP destabilization rate. Interestingly, despite being a clonal population, analysis at the single cell level reveals considerable cell-to-cell variation. Some reporter cells are induced strongly while others remain at low fluorescence levels. Possible explanations include cell cycle asynchrony, differences in cell-cell contact, and cell spreading.

4. Conclusions

In summary, the microfluidic-reporter platform offers a unique opportunity to investigate cell-to-cell variations in both the timing and magnitude of responses, and will potentially offer a deeper look at the underlying complexity of living cell stimuli-response relationships. We have recently used this device to perform dose responses by generating a range of TNF-α concentrations (0-10 ng/mL) in the upstream microfluidic dilution module and measuring the response of downstream cells exposed to a 2 hour pulse [4]. In the future, we hope to expand the number of reporter clones and the range of upstream inducers in order to better profile the complex coordinated dynamics of gene expression in disease states such as infection and inflammation.

References

[1] K.R. King, H. Terai, C.C Wang, J.P. Vacanti, J.T. Borenstein, *Proc. μTAS 2001*, Monterey USA, pp. 247-249, 2001.

[2] Li Jeon N, Baskaran H, Dertinger SK, Whitesides GM, Van de Water L, Toner M, *Nature Biotechnology* 20(8):826-30 (2002).

[3] McDonald JC, Duffy DC, Anderson JR, Chiu DT, Wu H, Schueller OJ, Whitesides GM, *Electrophoresis,* 21(1):27-40 (2000).

[4] Deanna M. Thompson, Kevin R. King, Kenneth J. Wieder, Mehmet Toner, Martin L. Yarmush, Arul Jayaraman. *Analytical Chemistry* (in press 2004).

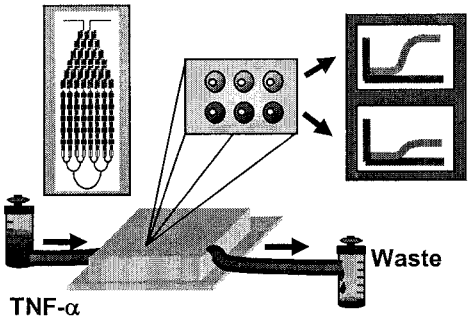

Figure 1. The microfluidic network consists of a dilution module (top) and downstream cell culture chambers (bottom). Reporter clones express GFP when stimulated with TNF-alpha.

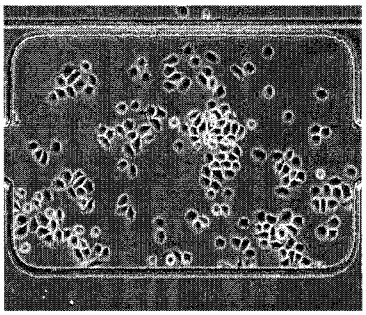

Figure 2. HeLa reporter clones are seeded and attached in the device (top). After exposure to TNF-alpha, they are visible in fluorescence channel.

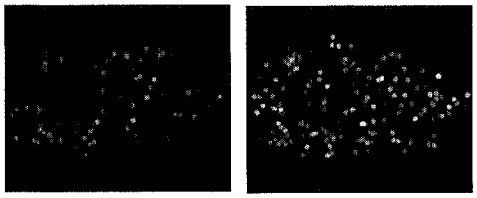

2 Hours **8 Hours**

Figure 3. Time-lapse fluorescence images of NFκB GFP reporters in response to 10ng/mL TNF-α at 2 hours (right) and 8 hours (left).

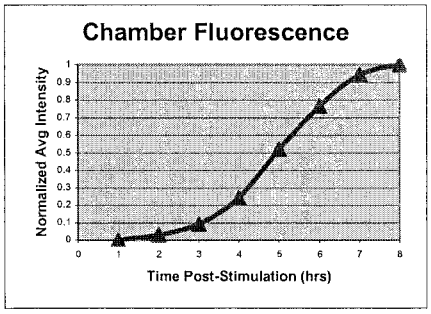

Figure 4. Time course of normalized average fluorescence intensity from a representative cell population in a single chamber in the microfluidic living cell array.

RESOLUTION OPTIMIZATION WITH CHIRAL TEMPERATURE GRADIENT FOCUSING

Karin M. Balss, Wyatt N. Vreeland, Karen W. Phinney, and David Ross
National Institute of Standards and Technology, 100 Bureau Dr. Gaithersburg, MD 20899, USA

Abstract

Chiral separations of dansyl-DL-glutamic acid were performed using temperature gradient focusing with γ-cyclodextrin as a chiral selector. Various factors affecting the enantiomeric resolution were studied including the temperature gradient, the average temperature, and the chiral selector concentration.

Keywords: chiral, TGF, resolution, separation, temperature

1. Introduction

Current FDA guidelines require the development of "...quantitative assays for individual enantiomers in *in vivo* samples..." as well as methods for assessing enantiomeric purity and stability [1]. Increasingly, chiral capillary electrophoresis (CE) has proven to be the method of choice for high-resolution chiral separations because of its low cost and high efficiency. However, CE suffers from poor detection limits and, consequently, has not been widely adopted for the chiral analysis of drug molecules in biological fluids such as serum or urine where the drug and its metabolites are at much lower concentrations than a laboratory preparation [2, 3]. Here we present some of the first results for resolution optimization for a new method of chiral separation, chiral temperature gradient focusing (TGF), that provides the high resolving power of CE in combination with theoretically unlimited concentration enhancement for improved detection limits. TGF is a recently developed technique for the simultaneous concentration and separation of ionic analytes in microchannels or capillaries [4]. Briefly, TGF works by balancing the electrophoretic velocity of an analyte against the bulk buffer velocity to cause analyte molecules to focus at a given position along the length of the separation channel. A buffer with a temperature-dependent ionic strength is used so that the application of a temperature gradient will result in a corresponding gradient in the electrophoretic velocity of the analyte. The total velocity (the sum of the electrophoretic and bulk velocities) can then be adjusted so that it is equal to zero at a unique point along the gradient. The analyte is focused at this zero-velocity point. Analytes with different electrophoretic mobilities will focus at different locations and are thereby separated. For chiral separations, a chiral selector (cyclodextrin) is added to the buffer. The chiral selector interacts more strongly with one enantiomer, reducing its electrophoretic mobility, and shifting the point where it is focused so that it can be resolved from the other enantiomer.

2. Experimental

All reagents were used as received, and all aqueous solutions were prepared using deionized ultra filtered water (Fisher Scientific, Fair Lawn, NJ), Dansyl-DL-glutamic acid, tris(hydroxymethyl)aminomethane (Tris), boric acid, and γ-cyclodextrin hydrate (γ-CD) were purchased from Sigma (St. Louis, MO) [5]. All TGF separations were performed in buffers composed of 1 mol/L Tris and 1 mol/L boric acid (1 M Tris-borate).

The capillary device used in these experiments was a 3 cm long, 30 μm i.d. 360 μm o.d. fused silica capillary embedded between polycarbonate sheets. The capillary device was thermally and mechanically anchored to two copper blocks, which were spaced 2 mm apart and regulated at two different temperatures to form a linear temperature gradient in the capillary. The capillary was connected at one end to a polypropylene sample reservoir (150 μL volume) via 360 μm hole drilled into the reservoir and on the other end to the waste reservoir via a silicone rubber septum. The

waste reservoir was connected via nylon tubing to another reservoir anchored to a vertical translation stage. The waste reservoir, nylon tube and the reservoir on the translation stage were all filled with buffer, and the pressure applied to the waste reservoir was precisely controlled by varying the height of the translation stage. High voltage was applied via platinum wire electrodes to the sample reservoir while the waste reservoir was grounded. TGF separations were visualized using fluorescence microscopy.

3. Results and discussion

TGF requires a buffer with a temperature-dependent ionic strength such as 1 M Tris-borate. The addition of γ-CD to the Tris-borate provides the ability to simultaneously focus and separate the two enantiomers of dansyl-glutamic acid. For this report, a number of factors affecting the resolution were examined including the γ-CD concentration, the steepness of the temperature gradient and the average temperature of the focused peaks.

Figure 1 shows plots of intensity vs. distance for TGF separations of dansyl-DL-glutamic acid with different γ-CD concentrations. With no γ-CD (not shown), the two enantiomers focused at the same point and were not resolved. For increasing γ-CD concentrations, the focusing positions of the two enantiomers moved further apart. This trend would result in higher resolution at higher γ-CD concentration. However, for γ-CD concentrations above 10 mM, the focused peaks became wider, and for γ-CD concentrations above 20 mM (data not shown), the peaks were so wide that they were difficult to detect. Consequently, the best resolution was obtained for γ-CD concentrations between 10 mM and 20 mM.

Figure 2 shows several plots of TGF of dansyl-dl-glutamic acid using different

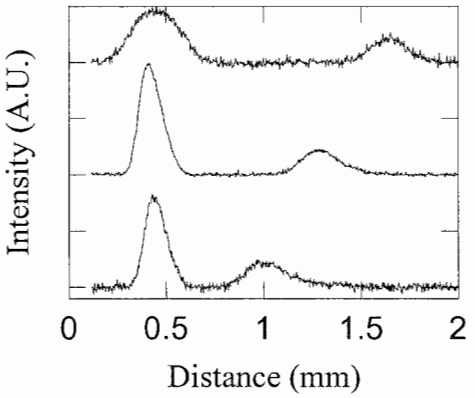

Figure 1. Chiral TGF of dansyl-DL-glutamic acid with different concentrations of γ-cyclodextrin. Focusing conditions: sample input side (right) T = 30 °C, waste (left) side T = 10 °C, voltage = +3000V, γ-cyclodextrin concentration = 20 mM (top), 10 mM (middle), 5 mM (bottom).

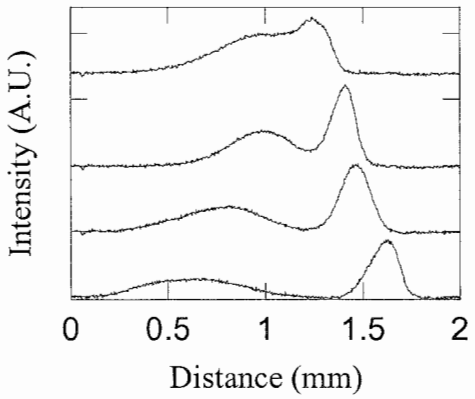

Figure 2. Chiral TGF of dansyl-DL-glutamic acid with different temperature gradients. Focusing conditions: sample input side (right) T = 10 °C, waste (left) side T = 80 °C, 60 °C, 40 °C, 30 °C (from top to bottom), voltage = -3000V, γ-cyclodextrin concentration = 10 mM.

temperature gradients. As expected from the theory of TGF[4] and focusing separations in general, the peak widths, the peak separation and the resolution all increased as the gradient was made less steep.

Figure 3 shows plots of chiral TGF separations of dansyl-dl-glutamic acid that were all performed with the same γ-CD concentration (10 mM) and the same temperature gradient (10 °C to 80 °C), but with different pressures applied to the waste reservoir so that the peaks focused at different positions, and hence different temperatures, along the gradient. Because of the temperature dependence of the interaction between the γ-CD and the dansyl-DL-glutamic acid, the peak widths were narrower and the resolution was improved when they were focused on the cold end of the gradient.

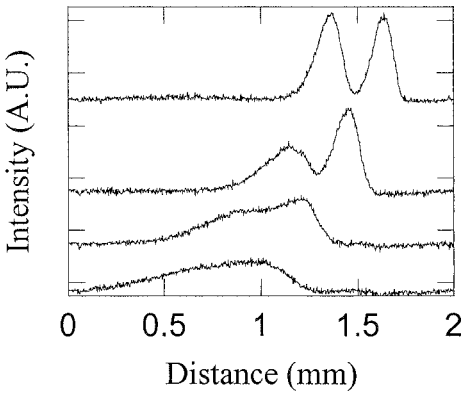

Figure 3. Chiral TGF of dansyl-DL-glutamic acid at different average temperatures. For each line in the plot, the focusing conditions were left constant and the pressure applied to the waste reservoir was varied to move the peaks to a different position, and hence to a different temperature, on the gradient. Applied pressure = 48.3 mm H_2O, 45.3 mm H_2O , 42.3 mm H_2O , 40.3 mm H_2O (from top to bottom). Focusing conditions: sample input side (right) T = 10 °C, waste (left) side T = 80 °C. voltage = -3000V, γ-cyclodextrin concentration = 10 mM.

4. Conclusions

The results presented above indicate that the best enantiomeric resolution would be obtained for chiral TGF of dansyl-dl-glutamic acid with a γ-CD concentration around 10 mM, and with a temperature gradient that is not very steep and that is set so that focusing occurs at a lower temperature. Using these guidelines, an optimized separation was performed and the resolution achieved was 3.8. The resolution could have been further improved by reducing the steepness of the gradient further, but the primary limitation was the requirement that both peaks be visible at the same time in the 2 mm wide field of view of the microscope. Nevertheless, the optimized resolution compares very favorably with that obtained with chiral capillary electrophoresis (R = 4.1), which is widely considered to be the best technique for high-resolution chiral separations. In addition, high-resolution TGF separations require only very short microchannels or capillaries, potentially less than 1 cm, and so are inherently more compatible with miniaturization and integration into a lab-on-a-chip format than is capillary electrophoresis or other conventional separation techniques.

References

[1] FDA Policy Statement for the Development of New Stereoisomeric Drugs, (1992).
[2] G. K. E. Scriba, *Electrophoresis* **24**, 2409-2421 (2003).
[3] P. S. Bonato, *Electrophoresis* **24**, 4078-4094 (2003).
[4] D. Ross and L. E. Locascio, *Analytical Chemistry* **74**, 2556-2564 (2002 Jun 1).
[5] Certain commercial equipment, instruments, or materials are identified in this report to specify adequately the experimental procedure. Such identification does not imply recommendation or endorsement by the National Institute of Standards and Technology nor does it imply that the materials or equipment identified are necessarily the best available for the purpose.

ARTIFICIAL PORES FOR PERFORMING IMMUNOASSAYS

Ian H. Chan, Andrea Carbonaro and Lydia L. Sohn
Mechanical Engineering Department, University of California, Berkeley, CA 94720, USA

Abstract

We have developed a microfluidic-based electronic sensor that performs immunoassays by detecting the change in size of functionalized colloids in solution. Our sensor measures the size of submicron colloids by electronically sensing the change in current when colloids pass through an artificial pore. Size resolution as fine as 1 nm is possible and allows us to detect the size increase of colloids due to the specific binding between antigens and antibodies on the surface of the colloids.

Keywords: immunoassay, artificial pore, electronic measurement

1. Introduction

Most common immunoassay techniques require the labeling of the antibody using fluorescence, radioactivity, or enzyme activity, which adds to the time and cost of performing the assay. By performing immunoassays with unlabeled antibodies and acquiring the results electronically based on the additional volume from the antibodies bound to our colloids, our sensor represents a faster and simpler method for performing end-point analysis of biological reactions.

2. Theory

Size measurement of colloids is performed in our artificial pore based on resistive pulse sensing (Fig. 1). Our device is filled with an electrolyte, and when a voltage is applied across the pore, a current flows through it. However, when a colloid enters the pore, the current is reduced because the non-conducting colloid has partially blocked flow of the conducting ions. This creates a negative pulse in the current whenever a colloid passes through the pore; the larger the colloid, the larger the pulse. The magnitude of the current pulse $\delta I/I$ is given by [1]

$$\delta I/I = D/L \{\arcsin(d/D)/[1 - (d/D)^2] - d/D\} \quad (1)$$

where D is the diameter of the pore, $L >> D$ is the length of the pore, and d is the diameter of the colloid. This formula was obtained for the regime $d \sim D$, which is the regime encountered in this report.

When we perform a sandwich immunoassay on the surface of a streptavidin-coated colloid (the assay colloid), the diameter of the assay colloid increases. Because the pore deforms slightly during sealing, and because the size increase is quite small (we measure ~5 nm increases), the diameter of the pore must be calibrated by measuring reference colloids of known diameter.

In a typical experiment, tens to hundreds of both reference and assay colloids are measured. The resulting current pulses have a magnitude correction applied to compensate for colloids traveling off-axis in the pore [2]. These off-axis colloids travel slower and have slightly different pulse heights than those traveling on-axis. The mean diameter of the assay colloids is calculated from the distribution of pulse heights, and a typical size resolution of ~1 nm can be obtained. This resolution is finer than the inherent distribution in sizes of the colloids (2–3%) because the uncertainty in the mean diameter of the colloids decreases as the squareroot of the number of colloids measured.

3. Experimental

The reference colloids used were 470 nm diameter sulfate-coated polystyrene colloids from Interfacial Dynamics (Portland, OR), and the assay colloids were nominally 490 nm diameter streptavidin-coated polystyrene colloids from Bangs Labs (Fishers, IN). Immunoassays were conducted for human granulocyte and macrophage colony stimulating factor (GM-CSF) and human granulocyte colony stimulating factor (G-CSF). Reagents for the GM-CSF and G-CSF

immunoassays were obtained as ELISA DuoSets from R&D Systems (Minneapolis, MN). The buffer used in these experiments consisted of 0.1% Tween 20 and 0.1 mg/ml bovine serum albumin in 0.5× phosphate buffered saline.

The artificial pore was fabricated using micromolding techniques (Fig. 2). The master pore was fabricated using electron-beam lithography and RIE in Si. It has a length of 10 μm and a diameter of 1 μm. The master reservoirs were fabricated using photolithography on 7 μm thick SU-8. The molded PDMS was then sealed to a 25×25 mm glass chip with pre-fabricated Ti/Pt electrodes that were used to measure the resistance across the pore. Separate current and voltage leads were used to remove the resistance due to the electric double layer around the electrodes. A voltage of 0.70 V was maintained across the pore, and the current was measured using a current preamplifier and recorded to a computer for analysis. In the experiments reported here, most of the data was acquired using two pores *simultaneously* on a single chip (Fig. 3).

The concentration of the reference and assay colloids were each $\sim 10^9$ colloids/ml. Concentrations of the primary and secondary antibodies were $\sim 10^{13}$ antibodies/ml. We used pressures from 1–3 psi to flow the colloidal solution through the pore. The velocity of the colloids was ~10 mm/s at the pore.

4. Results and discussion

Figure 4 is a graph of the mean diameter of assay colloids versus the conditions under which they were measured. In column A, the size of the plain streptavidin-coated assay colloid was found to have a diameter of 512 ± 1 nm. In column B, the diameters of two different functionalized assay colloids were measured simultaneously in two pores on one chip. The left bar is the diameter of assay colloids that were functionalized with GM-CSF primary antibodies, while the right bar is the diameter of assay colloids that were functionalized with G-CSF primary antibodies. The measured diameters were 517 ± 1 nm and 518 ± 1 nm for GM-CSF and G-CSF antibodies respectively. As shown, there is a clear increase of ~5 nm over the plain assay colloid.

In column C, two sandwich immunoassays were completed and measured simultaneously. The left bar (522 ± 1 nm) represents a sandwich immunoassay of human GM-CSF at a concentration of 84 ng/ml, while the right bar (522 ± 2 nm) represents a sandwich immunoassay of human G-CSF at a concentration of 90 ng/ml. As observed in both cases, additional diameter increases of ~5 nm was measured over their respective functionalized assay colloids.

Column D is a similar assay to column C *except* that GM-CSF antigens were used in *both* pores. The mean diameter of the GM-CSF assay colloids (left) was found to be 523 ± 1 nm, similar to that observed in column C. On the other hand, the mean diameter of the G-CSF assay colloids (right) was found to be 518 ± 1 nm, similar to that observed in column B. This demonstrates that the GM-CSF assay correctly detected the presence of GM-CSF antigens, while the G-CSF assay correctly detected the absence of G-CSF antigens. This clearly demonstrates that it is the specific binding between antigen and antibodies that is responsible for the measured size increase of our assay colloids, and shows that we can perform multiple simultaneous assays on one chip.

5. Conclusions

We have demonstrated that our pore device can successfully discriminate the presence of human antigens in solution by measuring the size increase of sandwich immunoassays performed on the surface of polystyrene colloids. We have also demonstrated our ability to perform simultaneous assays on a single chip, proving that our system is parallelizable.

We are currently working toward measuring multiple immunoassays in a *single* pore by using assay colloids of different diameters, which will extend our systems capabilities to simultaneously detect an even larger number of antigens.

Acknowledgements

We acknowledge DARPA for funding of this project, and wish to thank the Majumdar lab at U.C. Berkeley for use of their lab.

References

[1] E. C. Gregg and K. D. Steidley, *Biophysical Journal* **5**, 393 (1965).

[2] O. A Saleh and L. L. Sohn, *Rev. Sci. Instr.* **73**, 4396 (2002).

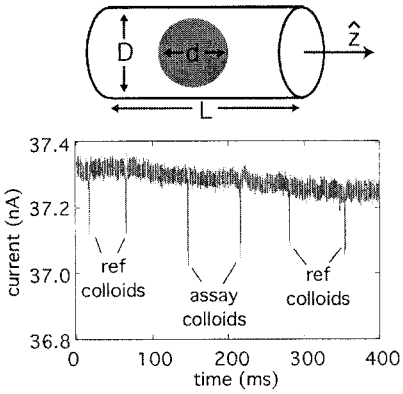

Figure 1. Principle of colloid size detection using an artificial pore. As a colloid passes through the pore, a temporary decrease in current through the pore is measured, causing a negative current pulse.

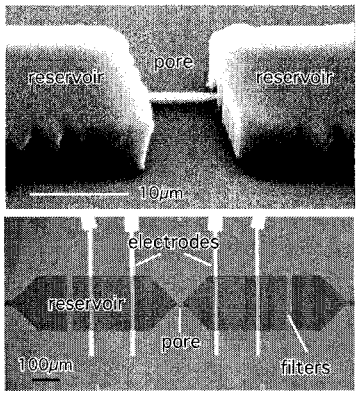

Figure 2. (top) SEM of the master pore from which PDMS molds are cast. (below) Completed pore consisting of PDMS mold sealed to glass chip with Ti/Pt electrodes.

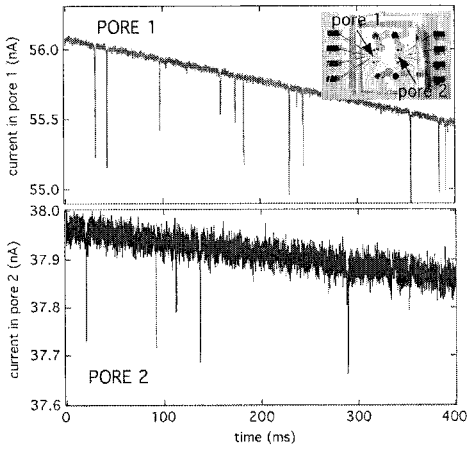

Figure 3. Data showing simultaneous measurements of assay colloids in two pores on a single chip. The dual pore device is shown in the inset.

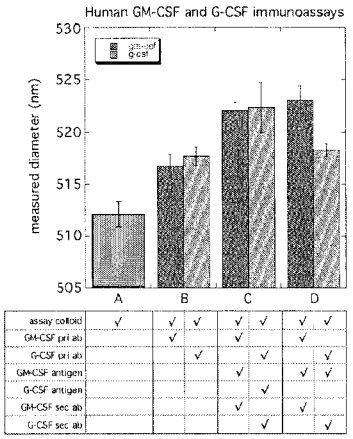

Figure 4. Measured mean diameter of assay colloids under the conditions shown. Successful positive and negative assays were demonstrated with human antigens.

MULTI-LAYER MICROFLUIDIC DEVICES FOR AMINO ACID ANALYSIS: THE MARS ORGANIC ANALYZER

Alison M. Skelley, James R. Scherer, Jeffrey L. Bada[1], Pascale Ehrenfreund[2], Frank J. Grunthaner[3] and Richard A. Mathies

Department of Chemistry, University of California, Berkeley, CA, 94720, USA; [1]Scripps Institution of Oceanography, University of California at San Diego, La Jolla, CA, 92093, USA; [2]Leiden Institute of Chemistry, Einsteinweg 55, 2300 Ra Leiden, The Netherlands; [3]Jet Propulsion Laboratory, 4800 Oak Grove Drive, Pasadena, CA, 91109, USA

Abstract

Sensitive amino acid composition and chirality analysis is demonstrated using the Mars Organic Analyzer (MOA), a portable microfabricated capillary electrophoresis (CE) instrument. The MOA integrates all high voltage power supplies, pneumatic controls, and fluorescence detection optics. The microfabricated device is a novel multi-layer structure combining glass separation channels [1] and microfabricated pneumatic membrane valves and pumps [2]. The Mars Organic Analyzer has been successfully field tested demonstrating part-per-trillion sensitivity when analyzing jarosite, a key sulfate-rich mineral recently detected on Mars that is associated with liquid water [3].

Keywords: microfabricated valves and pumps, capillary electrophoresis, astrobiology

1. Introduction

The detection of life on Mars requires identification of a suitable biomarker and development of sensitive yet compact instrumentation capable of performing in situ analyses. Our approach to this problem has focused on amino acid analysis because they are more resistant to decomposition than other biomolecules, and because amino acid chirality is a well-defined biomarker. Microfluidic devices provide an ideal platform for such analyses, allowing facile integration of dense microfluidic structures for sample preparation and capillary electrophoresis separation channels for sensitive and efficient analysis. Previously, we developed a prototype microfabricated capillary electrophoresis (CE) chip and analysis method where the amino acids were labeled with fluorescein and electrophoretically analyzed in under 3 minutes [4]. Our microchip analyzer has now been improved by using fluorescamine, a fluorogenic dye with much faster labeling kinetics [5]. Fluorescamine-labeled amino acids are separated using analogous conditions to those described earlier, resulting in similar separation times and identical elution orders. The present work is focused on developing the Mars Organic Analyzer (MOA), a portable analysis system that integrates the previously developed amino acid sample extraction capabilities of the Mars Organic Detector (MOD, [6]) with the composition and chiral analysis capabilities of microchip CE [1].

2. Results and Discussion

The microfabricated device for performing amino acid analysis is shown in Figure 1. The glass wafers are patterned and developed using standard photolithographic techniques [5]. The device includes microfabricated glass channels and as well as valves and pumps [2] for fluidic handling. The glass-enclosed separation channel is formed by thermally bonding the bottom channel layer with the middle manifold layer. The manifold wafer is blank on the bottom and patterned with the pneumatic manifold features (for vacuum/pressure lines and displacement chambers) on top. The fluidic wafer contains discontinuous channels patterned on its bottom surface to form the valve and fluidic routing structures. These membrane valves and pumps are integrated with the glass-enclosed separation channel by using a novel multilayer design in which sample enters the top fluidic layer for routing and is directed through drilled via holes to the bottom layer for analysis.

The microfabricated device is operated by the portable CE instrument shown in Figure 2 which contains pressure and vacuum pumps and solenoids for controlling fluidic valves, electronics for performing electrophoresis, a thermoelectric cooler and temperature sensor, a 15 mW 400 nm diode laser, confocal detection optics and filters, and a fiber-optic coupled photomultiplier for fluorescence detection. The device has a mass of ~ 11 kg and a peak power consumption of ~15 W.

The MOA was characterized by determining the limit of detection using different injection schemes. The "regular injection" consisted of a cross injection from sample to waste, presenting an unbiased population in the plug, followed by analysis. Alternatively the regular injection can be enhanced by injecting different lengths of plug directly toward the cathode in a 2-step process. A 2 second direct injection resulted in a 10 x increase in signal over the cross injection alone; a 10 second direct injection resulted in a 100 x increase although some amino acid resolution was lost.

The limit of detection for each injection technique was found through serial dilutions of the standard. The limit of detection of valine was 13 nM for the 10 second cross injection, 1.3 nM for the 2 second direct injection and 133 pM for the 10 s direct injection (Figure 3) which translates to part-per-trillion sensitivities in soil samples. Comparing the performance of the portable system to our previous bench-top system [5], identical concentrations run on the same microdevice resulted in equal separation efficiency and resolution but the portable system had 4-fold superior sensitivity.

The portable CE instrument, in combination with MOD, was recently successfully field tested using soil samples rich in jarosite from Panoche Valley, CA (Figure 4). Jarosite has recently been detected on Mars and is a key mineral indicating that liquid water was once present on the planet's surface. [3] Jarosite samples from soil were sublimed by MOD, and the microfabricated pumps were used to direct buffer through the MOA sipper to dissolve the sample. The sample was redirected to the separation channel for analysis. The jarosite sample was found to contain low levels of methyl and ethylamine (5 ppb), alanine/serine (0.5 ppb), glycine (0.2 ppb), glutamic (0.05 ppb) and aspartic (0.1 ppb) acid as well as a high concentration (~100 ppb) of valine.

3. Conclusions

The complete end-to-end field testing of the Mars Organic Analyzer has demonstrated the utility of this instrument for performing *in situ* amino acid analysis. The sensitivity and portability of the CE instrument and novel multi-layer microfabricated device demonstrates the utility of this approach for developing a wide range of versatile portable chemical and biochemical analysis microdevices. The Mars Organic Analyzer is currently in competition for the Mars Express (ESA) 2009 Mission, as well as the Mars Science Lander (NASA) 2009 Mission. For more details and pictures go to ***http://astrobiology.berkeley.edu.***

4. Acknowledgements

All microfabricated devices were constructed in the UC Berkeley Microfabrication Facility. This research was supported by NASA grant #NNG04GB75G, NASA-UCSD grant #NAG512139 and by JPL fabrication award #1254626. AMS is supported by an NSERC PGS B fellowship.

References

[1] A. M. Skelley, J. R. Scherer, F. J. Grunthaner, J. F. Bada and R. A. Mathies, *Proc. Natl. Acad. Sci. USA,* manuscript in preparation (2004).

[2] W. H. Grover, A. M. Skelley, C. N. Liu, E. T. Lagally and R. A. Mathies, *Sens. Actuators B,* **89** (3), 325-323 (2003).

[3] R. A. Kerr, *Science,* **303** (5663), 1450 (2004).

[4] L. D. Hutt, D. P. Glavin, J. L. Bada and R. A. Mathies, *Anal. Chem.,* **71** (18), 4000-4006 (1999).

[5] A. M. Skelley and R. A. Mathies, *J. Chromatogr. A,* **1021** (1-2), 191-199 (2003).

[6] G. Kminek, J. L. Bada, O. Botta, D. P. Glavin and F. Grunthaner, *Planetary & Space Science,* **48** (11), 1087-1091 (2000).

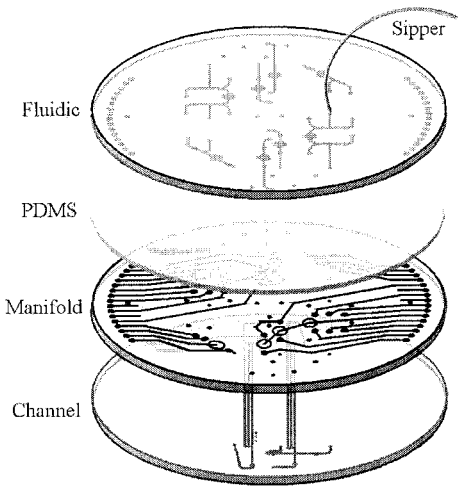

Figure 1. Microfabricated wafer for sample preparation and amino acid analysis. The 100-mm diameter microfabricated wafer stack is composed of a 4-layer sandwich of glass and PDMS to create channels and pumping structures.

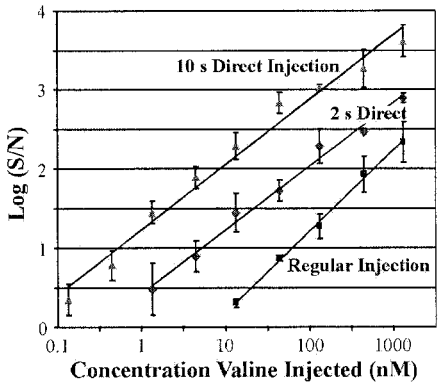

Figure 3. Limits of detection of the MOA system. The cross injection can detect down to 13 nM valine, the 2 second direct injection limits are 1.3 nM, and the 10 second direct injection limits are 130 pM.

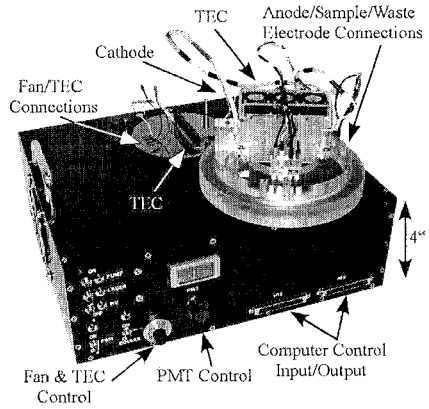

Figure 2. The Mars Organic Analyzer (MOA). The portable CE instrument, measuring 4" x 10" x 12", integrates all necessary pneumatic actuation, high voltage power supplies and confocal optics for laser excitation and fluorescence detection.

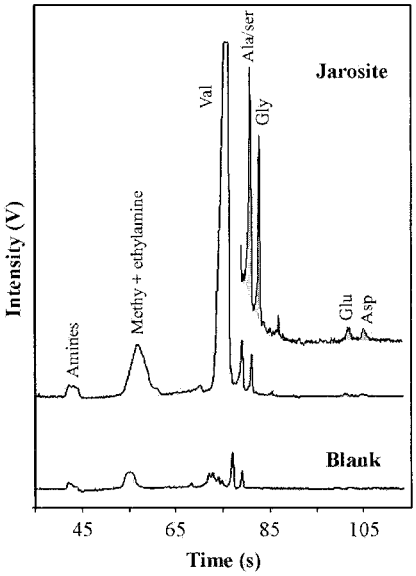

Figure 4. MOA field analysis in Panoche Valley, CA of a jarosite sample prepared by MOD. The peak identities were confirmed by spiking with standard samples.

A MICROFLUIC NETWORK FOR WRITE-IN AND READ-OUT OPERATIONS OF A MOLECULAR MEMORY

Katsuo Mogi[1,2], Shohei Kaneda[2], Koichi Ono[2,3], Tatsuhiro Fukuba[2] and Teruo Fujii[2]

[1]Dept. of Fundamental Science and Engineering, Keio University 3-14-1 Hiyoshi Kohoku-ku Yokohama, Japan

[2]Institute of Industrial Science, University of Tokyo, 4-6-1 Komaba Meguro-ku Tokyo, Japan

[3]Enplas Laboratories, Inc., 2-38-5, Namiki Kawaguchi, Saitama, Japan

Abstract

In this paper, a microfluidic device for write-in and read-out operations of a 1-bit molecular memory is presented. A sequence-specific site on a DNA molecule is used as a memory bit and binding of a PNA (Peptide Nucleic Acid) molecule against the site is regarded as write-in process. The read-out operation is conducted by electrophoresis of the memory DNA with restriction enzyme cleavage. A microfluidic network on the device has two parts, one is for write-in operation by PNA-DNA binding and another is for read-out operation by on-chip CE with a restriction enzymatic reaction. By using electroosmotic flow for PNA loading in the write-in part and electrophoretic transportation of DNA through PNA loaded region, the PNA-DNA binding is performed efficiently within 3 min. This result is about 20 fold shorter than a conventional micro-tube based reaction. Since the operations can be executed sequentially by electrokinetic control in an automated manner, the proposed device opens up the possibility of a high-performance molecular computing embodied in a microfluidic device.

Keywords: Molecular Memory, Molecular Computing, PNA, Electroosmotic flow

1. Introduction

Research in the field of molecular computing aims at realization of information processing using molecules, in other words, it is a trial to develop a general-purpose computer with molecules [1]. Laboratory-scale molecular computing and human-assisted protocols have been demonstrated. Most of the previously reported studies used DNA molecules and its property of complementary hybridization [1~3]. However, there are several issues to be considered to solve large-scale computing problems using DNA molecules. First, coding rules have to be designed specific to the problems avoiding errors in computation by non-specific hybridization. Sometimes to design coding rules can be more difficult than to solve the problem. To avoid this issue, Head *et al.* proposed a code design free molecular computing using DNA molecules as a molecular memory [4]. Second issue is the time-consuming process for handling DNA molecules. Automated operations with higher reproducibility are indispensable. Precise control and high efficiency of the reactions are, of course, strongly desired. Satisfying these desires, microfluidic devices could become the most promising tools for molecular computing [5].

Here, we report a microfluidic device for write-in and read-out operations of a 1-bit molecular memory. A DNA molecule is used as a memory and a PNA (Peptide Nucleic Acid) molecule is used for write-in operation. On-chip CE with restriction enzymatic reaction is used for read-out operation of the memory DNA. By using electrokinetic forces for delivering solution including the PNA and transportation of the memory DNA, the device could conduct the write-in operations with high efficiency in an automated manner.

2. Theory

A sequence-specific site for a restriction enzyme cleavage on a DNA molecule is used as an address of the memory. A sequence-specific binding of a PNA molecule against the specific site is regarded as write-in process as shown in Fig. 1. PNA is a DNA mimic with the natural nucleobases

attached to a charge-neutral pseudopeptide backbone [6]. Since some reactions of restriction enzyme are inhibited due to the PNA binding, the read-out process can be conducted by using the cleavage of a restriction enzyme and following electrophoretic separation. Yamamura *el al.* has been reported a molecular computing using this scheme using PNA molecules [7].

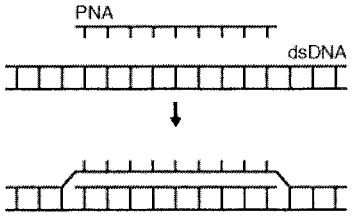

Figure 1. PNA has remarkably strong sequence-specific binding affinity to natural nucleic acids (DNA and RNA), mainly attributed to the lack of charge in the PNA backbone.

3. Experimental

As a first step, we designed and fabricated a device for write-in and read-out operations of a 1-bit molecular memory as shown in Fig. 2. The device consists of a PDMS fluidic chip and a glass substrate coated with a thin PDMS layer (Fig. 2A). The microfluidic network on the device has two parts, one is for write-in operation by PNA-DNA binding and another is for read-out operation by on-chip CE with a restriction enzymatic reaction (Fig. 2B). To evaluate the performance of 1-bit write-in and read-out operations on the presented device, a bacteriophage DNA (ϕX-174; Takara) (1.41 μM), a 3-mers PNA ((N)-CTG-(C); Nippon Flour Mills) (1 mM) and a restriction enzyme (*Hae* III; Takara) are used for the read-out process. At first, the microfluidic channels in the write-in part are filled with a TBE buffer and those in the read-out part are filled with a HEC (Hydroxyethyl cellulose) solution (1.8 % in TBE buffer) as a sieving matrix. Second, the DNA, the PNA and the restriction enzyme are applied to each port (see Fig. 2B). Then the solution including the PNA is introduced into the channel by electroosmotic flow (EOF) applying voltage of 100 V (100 V/cm) for 52 sec port 2 to 3 (also 2' to 3'). Then, by applying voltage of 200 V (50 V/cm) for 3 min port 6 and 1 (2, 3, 2' and 3' are floating), the memory DNA in the port 1 is introduced until the shorter channel in the read-out part through the PNA loaded region and the restriction enzyme port by electrophoretic force.

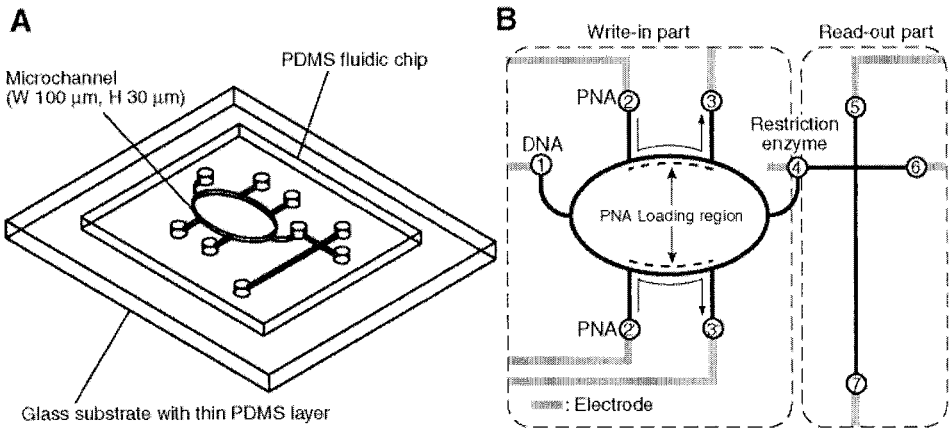

Figure 2. (A) Schematic of the microfluidic device. (A) Overview. (B) Magnified view of the fluidic chip. The fluidic channels in the write-in part is filled with TBE buffer, those in the read-out part is filled with HEC polymer solution for on-chip CE. The DNA solution is applied to port 1, the PNA solution is applied to 2 and 2', the restriction enzyme solution is applied to 4.

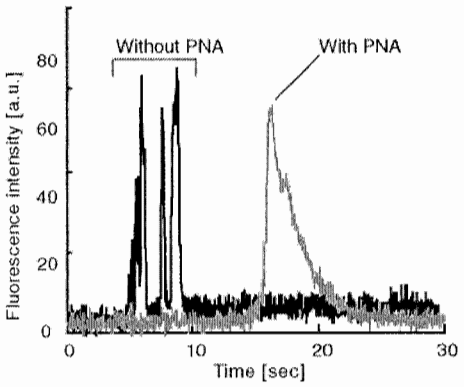

Figure 3. The resultant electropherogram with and without write-in of PNA. When the PNA is binding, restriction cleavage is inhibited.

Finally, electrophoretic separation is conducted by conventional on-chip CE protocol. The required time for PNA loading by EOF was calculated from the value of ζ- potential of PDMS with TBE buffer condition (-25 mV) which measured by an electrophoretic light scattering spectrophotometer (ELS-6000, Otsuka electronics) before this experiment.

4. Results and discussion

The resultant electropherogram of the sequential operation with and without PNA loading are shown in Fig. 3. The single peak of [with the PNA] indicates that the presented device can be successfully conducted the write-in operation. The several peaks of [without PNA] indicate that the restriction enzyme can digest the memory DNA. In this condition, the reaction time for PNA-DNA binding was 3 min. By using the device, the reaction time of PNA-DNA binding could be reduced 20 fold shorter than the conventional micro-tube based reaction in the previous report [7]. The most probable explanation for this high efficiency of the reaction is the increasing of the number of collision between DNA and PNA molecules by passing of the DNA through the PNA loaded region.

5. Conclusions

A write-in and read-out operations of a 1-bit molecular memory can be conducted using the presented device in an automated manner by electrokinetic control. Thanks to the increased efficiency of the PNA-DNA binding as write-in operation and on-chip CE as read-out operation on the device, the overall operation can be realized within 4 min, which opens up the possibility of realizing a high-performance molecular computing on a microfluidic device. Moreover, this result leads not only to molecular computing applications but also to rapid sequence-specific diagnostic applications using PNA [8].

References

[1] L. Adleman, *Science*, **266**, 1021-1023 (1994)
[2] Q. Ouyang, P. D. Kaplan, S. Liu, A. Libchaber, *Science*, **278**, 446-449 (1997)
[3] Q. Liu, L. Wang, A. G. Frutos, A. E. Condon, R. M. Corn, L. M. Smith, *Nature*, **403**, 175- 179 (2000)
[4] T. Head, M. Yamamura, S. Gal, Proc. CEC '99, 1006-1010 (1999)
[5] J. S. McCaskill, *BioSystems*, **59**, 125–138 (2001)
[6] P. E. Nielsen, M. Egholm, R. H. Berg and O. Buchardt, *Nuc. Acids Res.*, **21**, 197-200 (1993)
[7] M. Yamamura, Y. Hiroto and T. Matoba, Proc. DNA7, 213-222 (2002)
[8] A. Ray, B. Nordén, *FASEB J.*, **14**, 1041-1060 (2000)

A SELF-CALIBRATING NANOLITER VISCOMETER AS A DIAGNOSTIC TOOL FOR ANALYZING BODY FLUIDS

Nimisha Srivastava, Robertson D. Davenport and Mark A. Burns
2300 Hayward, 3074 HH Dow, University of Michigan, Ann Arbor, MI 48109
Phone: 734-763-3078 Fax: 734-763-0459 Email: maburns@umich.edu

Abstract

We have developed a nanoliter viscometer that quickly, easily and inexpensively measures the viscosity of liquids. The measurement is based on capillary pressure driven flow inside microfabricated fluidic channels (depth~30μm and width~300μm). Accurate and precise viscosity measurements can be made in less than 100s while using only 600nl of liquid sample. The device measures 18mm by 15mm and has been successfully tested with viscosity standards, a non-newtonian liquid and with blood plasma. The device contains on-chip components that measure the capillary pressure and geometrical parameters; these components make the nanoliter viscometer self-calibrating, robust and easy to use. This microfabricated viscometer may have widespread applications in chemical, biological and medical laboratories as well as in personal health care.

Keywords: viscosity, plasma, viscometer, microfluidics, nanoliter, microfabrication

1. Introduction

In medical diagnostics, the viscosity of body fluids can uniquely predict or indicate disorders [1]. For instance, blood viscosity is an early predictor of cardiovascular diseases [2]. Blood and plasma viscosity is a risk factor for type 2 diabetes mellitus and correlates directly with the severity of retinopathy, a leading cause of blindness among adults in the United States. Other examples include amniotic fluid and synovial fluid viscosity. The wide range of maladies that can be predicted by simply measuring the viscosity of a body fluid indicates that a simple, quick and inexpensive test for viscosity that is widely available to patients and medical professionals will be very beneficial.

2. Theory

The measurement of viscosity is based on capillary pressure driven laminar flow inside micron-diameter sized channels, as given by the following equation.

$$\mu = \frac{d^2}{S}\frac{\Delta P}{vL} \quad \text{(Rearranged Hagen-Poiseuille flow equation)} \quad \textbf{(1)}$$

where v is the mean velocity, d is the depth of the channel, L is the length of the liquid column inside the channel at any time, μ is the liquid viscosity, ΔP (in this case) is the capillary pressure difference across L and S is a shape factor. To measure viscosity, d^2/S is first found using a reference liquid, ΔP is then measured using a sealed (closed–end) microchannel and finally, vL is measured on an open channel.

Non-Newtonian liquids can be tested on the device knowing that the wall shear stress varies as the inverse of the length of the liquid column, L inside the microchannel i.e., $\tau_w = \frac{\Delta P}{L}\cdot\frac{d}{2}$. Since L increases as the liquid moves further inside the microchannel, we can measure the apparent Non-Newtonian viscosity using Equation (1) at different lengths, L inside the channel and plot the variation of apparent viscosity with wall shear stress.

3. Experimental

The nanoliter viscometer that we have developed is shown in Figure 1 [3]. The device contains four channels that together measure the viscosity of a liquid sample. Two of the channels are sealed (SC_1 and SC_2, d~45μm, w~300μm) while the other two are open (OC_1 and OC_2). Design and

fabrication ensures that the two open channels are of identical geometry (i.e. identical d, w and therefore S).

To measure ΔP, a drop of liquid is placed at the inlet of a sealed channel (SC) and is spontaneously drawn into the channel (Figure 2). The trapped air is compressed and liquid moves in to balance the capillary pressure difference; the air pressure inside the channel after the drop moves in exceeds the atmospheric pressure by an amount equal to the capillary pressure. Using the ideal gas law, we can calculate the capillary pressure as

$$\Delta P = P_{capillary} = P_{atm}\left(\frac{V_1}{V_2} - 1\right) \quad (2)$$

where V_1 is the original volume of air inside the microchannel and V_2 is the volume of the compressed air found from the position of the air/liquid meniscus inside the sealed channel. Such measurement of the capillary pressure is independent of the liquid or the substrate and does not require *a priori* knowledge of surface tension, contact angle or channel geometry.

d^2/S is measured using a liquid of known viscosity (e.g., water) on one set of open and sealed channels (i.e., SC_1 and OC_1). vL is calculated from OC_1 as described earlier [4] and ΔP from SC_1. Since both open channels (OC_1 and OC_2) on the device are of identical geometry, the calculated value of d^2/S also applies for the test sample in the second open channel (OC_2). Having calculated d^2/S, the viscosity of the test sample is calculated by measuring vL in OC_2 and ΔP in SC_2.

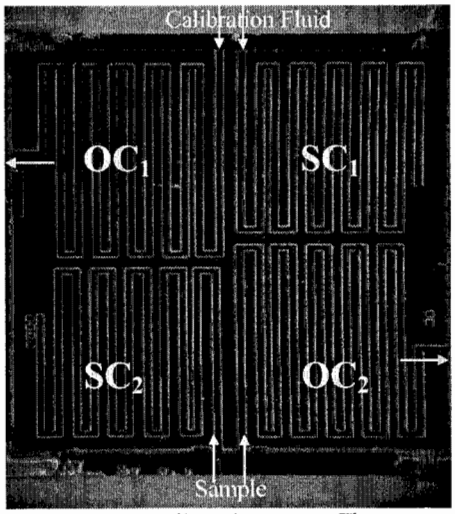

Figure 1. A nanoliter viscometer. The arrows pointing into the channel indicate the inlet while those pointing out are the outlets. The device measures 18mm by 15mm. The total (serpentine) length of each channel is ~ 9cm

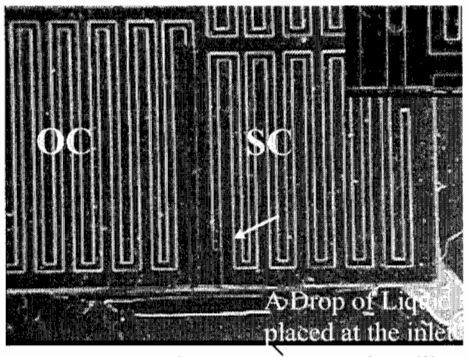

Figure 2. On-Chip Measurement of Capillary Pressure using a sealed channel. A drop of liquid, placed at the inlet has partially wicked into the sealed channel. The arrow points to the final liquid interface. Note that the liquid from the same drop is also being continuously drawn into the adjacent open channel for the measurement of vL.

Inset: A closer view of liquid that has wicked into the channel.

4. Results and discussion

On this device, we have successfully tested blood plasma samples to an accuracy of 10% with a run time of less than a minute (Figure 3). In addition, the viscosity of a dilute solution of Polyethylene oxide (PEO; 1000 ppm, MW = 5 million), a power-law fluid, was also measured successfully. The

nanoliter viscometer correctly predicted the power-law exponent (n=0.8527 for PEO) and the viscosity as a function of the mean velocity (Figure 4). The power law exponent, which is routinely measured through a log plot of shear stress and shear rate, in our case was measured through a log plot of $\mathbf{1/L}$ and mean velocity v.

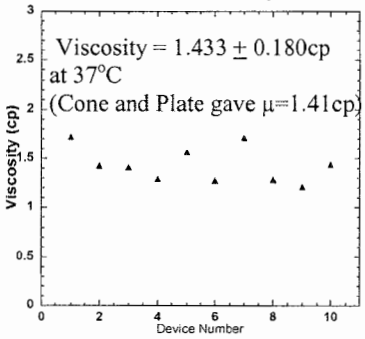

Figure 3: Blood Plasma Viscosity Measured on the Nanoliter Viscometer. In the pathology department, plasma viscosity is useful in evaluating patients with elevated serum immunoglobulins, multiple myeloma, mucosal bleeding, blurred vision or neurologic symptoms. Patients with elevated values (> 4cp; normal range 1.20-1.85cp) are then candidates for apheresis

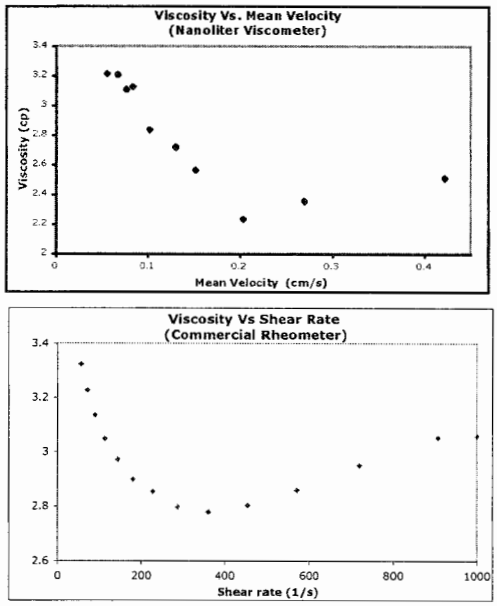

Figure 4: Viscosity of Polyethylene oxide. (a) shows the plot of viscosity of the PEO solution with the mean velocity, v. Equivalent results from a commercial rheometer are shown in (b).

5. Conclusions

The nanoliter viscometer is unique in its ease of use while achieving a high level of accuracy and precision. The user simply places two drops on the device; the measurement of the advancing liquid front and all calculations will be performed by a liquid detection system. Several channels may be fabricated on the device allowing for simultaneous testing of multiple samples. The device is easy to fabricate, measures viscosity rapidly and can be developed into a portable diagnostic tool.

Acknowledgements

The authors would like to acknowledge support from NIH through grants P01 HG01984 and R01 AI49541.

References

[1] Kwaan, H.C.; Bongu, A. *Seminars in Thrombosis and Hemostasis*, **25**(2), 199-208 (1999)

[2] Lowe, G.D.O. *et al. Throm Haemost.* **84**, 553-558 (2000)

[3] N Srivastava, R.D. Davenport and M.A Burns, *Submitted to Analytical Chemistry* (2004)

[4] N Srivastava, R.D. Davenport and M.A Burns, Proceedings of μTAS, Squaw Valley, Vol **1**, 639-642 (2003).

PLUG'N'PUMP FLUIDIC INTERCONNECTION

Gerardo Perozziello[1], Martin F. Jensen[1,2], John E. Mc Cormack[1,2], Frederik Bundgaard[1], Oliver Geschke[1]

[1] *MIC- Department of Micro and Nanotechnolgy, Technical University of Denmark (DTU), bldg. 345, 2800 Lyngby, Denmark*

[2] *Danish Technological Institute, Centre for Microtechnology and Surface Analysis. Gregersenvej 1, 2630 Taastrup, Denmark*

Abstract

A crucial challenge in packaging of microsystems is the microfluidic interconnection. In this work we present different kind of fluidic interconnections, modeling them and testing of their limits. Finally a plug'n'pump integrated fluidic interconnection for polymer microsystems has been designed modeled and tested.

Keywords: Reversible packaging, microfluidic system, interconnections.

1. Introduction

In recent years a lot of attention has been drawn to improving the performance of microfluidicsystems. One of the main quests to reach a good result is a good design and dimensioning of the fluidic interconnections. In function of them we can regulate the limits of the pressure inside the system or the flow rate that regulates chemical reactions or mixing inside the system or detections in a lot of applications.

In a first phase three different sealing principles for reversible fluidic interconnections were investigated: A bed of PDMS [1,2,3], common o-rings and soft silicone tubes [4]. These three methodologies could be defined as external to the system. They have high flexibility since they are able to interconnect virtually any kind of system at relatively low cost. They are advantageous for silicon/glass systems where integrated fluidic interconnections would affect the total cost of the system considerably. For interconnecting a polymer microsystem, however, integrated fluidic interconnections appear to be a good solution in terms of cost, space and performance. Following this path in the second phase of this work, we propose a reversible integrated fluidic interconnection composed of custom made o-rings integrated in a polymer housing next to the fluidic network allowing a *plug&pump* functionality between external metal ferrules and the system.

2. Theory

Theoretical calculations were made to dimension and model the three external fluidic interconnections as a function of the flow rate (Q) and thereby the internal pressure of the fluidic network (P_{int}), the applied external force (F) and the contact area (A_c) in order to predict leakages in the system (eq. 1) [5]. In the same way, the integrated fluidic interconnection was modeled as a function of the interference between o-ring-ferrules ($\delta_{ferrules}$) and o-ring-frame (δ_{frame}) and the internal pressure (P_{int}) as seen in (eq.2) [6].

(eq. 1) $$P_{ext} = \frac{F}{A_c} > P_{int} = \frac{12\mu L}{wh^3}Q \; ; A_c = wh \text{ (bed of PDMS), } A_c = \pi\left(r_o^2 - r_i^2\right) \text{ (silicone tubes and O-rings).}$$

(eq. 2) $$\min\left\{P_{frame} = \frac{E\delta_{frmae}}{R_{frame}}\left[\frac{\left(R_{frmae}^2 - r_i^2\right)}{R_{frame}^2 + r_i^2 - \nu_{o-rings}\left(R_{frame}^2 - r_i^2\right)}\right], P_{ferrules} = \frac{E\delta_{ferrules}}{R_{ferrules}}\left[\frac{\left(r_o^2 - R_{ferrules}^2\right)}{R_{ferrules}^2 + r_o^2 + \nu_{o-rings}\left(r_o^2 - R_{ferrules}^2\right)}\right]\right\} > P_{int}$$

3. Experimental

Leakage tests were performed on the external interconnections, in order to experimentally confirm the models, using a test chip. The chip simulated an integrated lab-on-a-chip system that fit in the packaging. It detects leakages in packages having fluidic and electrical interconnections. It has twelve circular coils manufactured in gold around two holes connected to the channels. It was produced in Si/Glass using clean room techniques. Different chips with different channel geometry and dimensions were fabricated for having a wide internal pressure range. A multimeter has been connected to the coils of the chip, detecting any leakage at the interface by a change in the measured resistance. Static tests, using a pressure sensor, have been performed for detecting the pressure drop if leakage occurs in the integrated interconnection. We also immersed the fluidic interconnection into a box filled by water in order to detect the point of leakage looking at bubble-formation.

4. Results and discussion

The experiments match the theoretical predictions very well as shown in Fig.3. Moreover, it has been seen that the silicone tubes can ensure a sealed contact even at very high pressures built up with a conventional syringe pump. No leakage has been observed on silicon tubes with a pressure of up to 1.23 MPa. The o-rings ensure a seal contact at a relatively high pressure (0.14 MPa) while the bed of PDMS leaks already at a low pressure (10000 Pa), since it has a large contact area between chip and interconnection. Therefore it needs a strong external force, to ensure an external pressure higher than the internal pressure of the chip as depicted in equation 1, that deflect the package causing leakage. The silicone tubes show the big advantage that they ensure a seal contact also at high external forces and so in presence of the deflection of the package. In fact the tubes follow the deflection of the package maintaining an adherent contact to the chip, while the o-rings seem to suffer from inhomogeneous distribution of the stress inside the package and a deflection of the structure. The *plug&pump* interconnections showed ease of fabrication and assembly and they are very fast and easy to use. The experiments show that the integrated interconnections could reach the operational limits of the pressure testing setup of 0.7-0.75 MPa without any leakage and, as seen from figure 4, the experiments fit the model well.

5. Conclusions

Three types of reversible fluidic interconnections (PDMS-gaskets, silicone tubes and O-rings) have been modeled and tested. A plug'n'pump integrated fluidic interconnection has been designed, modeled and tested. The experimental results fit well with the models for all kind of interconnections. The limits of the fluidic interconnections have been investigated.

Acknowledgements

We would like to thank the mKAP center contract for the scientific support and the students that helped us during the experiments.

References

[1] Gerardo Perozziello,Oliver Geschcke, CIRP Seminar on Micro and Nano Technology, 2003
[2] Zhen Yang and Ryutaro Maeda, Electroporesis 2002, 23, 3474-3478
[6] Georgios Keramas, Gerardo Perozziello, Oliver Geschke and Claus B. V. Christensen, *Lab on a Chip*, 2004, 4
[4] Tze-Jung Yao 2000, p. 624 -627. MEMS 2000. 13th IEEE
[5] Gregory T.A. Kovacs "Micromachined Transducers", WCB McGraw-Hill,1998
[6] Joseph Edward Shigley, Charles Mischke "Mechanical Engineering Design" , Fifth edition, Mc Graw Hill,1989

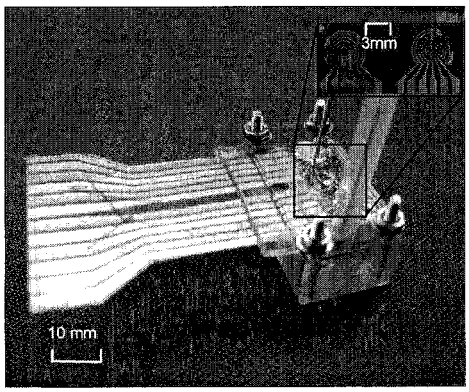

Figure 1. Frame of the reversible package and zoom-in of the testchip

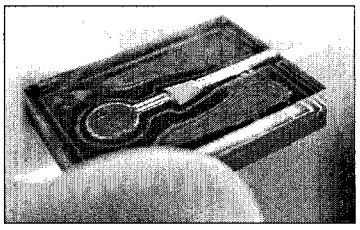

Figure 2. Plug 'n' pump interconnection where custom made o-rings are shown. The o-ring has an external diameter of 5mm and the ferrule has a diameter of 0.8 mm

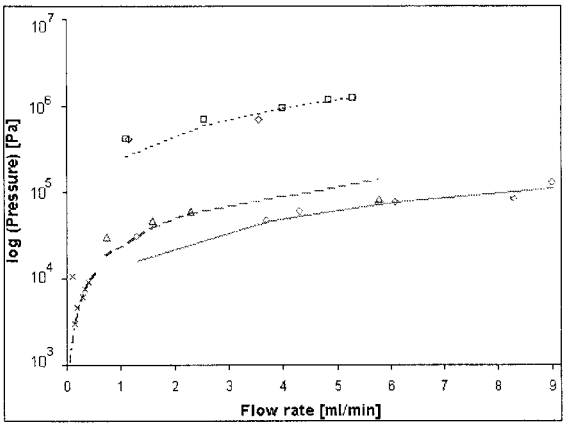

Figure 3. Experiments and theorical prediction of the external interconnections: " ——— "Theorical internal pressure into the chips 1 to 6, "o" observed leakages using o-rings and chips 1 to 6, "- - - - -" Theorical internal pressure into the chips 13 to 15, "▲" observed leakage using o-rings and chips 13 to 15, "....." Theorical internal pressure into the chips 10 to 12, "♦" observed leakage using silicone tubes (Φ1mm) and chips 10 to 12, "□" observed leakage using silicone tubes (Φ1.4mm) and chips 10 to 12, " — · — · —" Theorical internal pressure into the biochip, "x" observed leakage using PDMS bed and biochips.

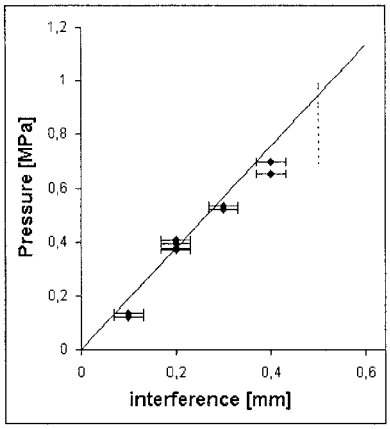

Figure 4. Experiments and theorical prediction of the integrated interconnection : " ——— "Theorical pressure at the interface ferrules-o-rings; "- - - -" Theorical pressure at the interface frame-o-rings, "♦" observed leakages.

INTEGRATED MICROFLUIDIC BIOCHIPS FOR ELECTROCHEMICAL DETECTION OF MULTIPLE BIO-AGENTS

Robin H. Liu, Andrei Ghindilis, Kevin Schwarzkopf, and Mike Strathmann
Combimatrix Corp., 6500 Harbour Heights PKWY, Mukilteo, WA 98275, USA

Abstract

Microfluidic biochip devices have been developed to perform detection of multiple bioagents using electrochemical detection methods. Microfluidic mixer, pumps, channels, chambers, and Combimatrix microelectrode array are integrated to perform parallel immunoassays to detect infectious particles (viruses and bacteria) from complex biological samples in a single, fully automated biochip device. The same platform is also used for DNA analysis. The enzyme-based electrochemical detection has many advantages including high sensitivity (~fM) and simple apparatus.

Keywords: Electrochemical detection, microarray, DNA, antibody, antigen

1. Introduction

Microfluidics has been recently integrated with DNA microarray to perform sample-to-answer DNA analysis that starts from sample preparation, followed by PCR and microarray electrochemical-based detection [1]. Similar microfluidic technology can be applied with immunoassay microarray that has some advantages over DNA bioassays, including rapid analysis and simple device design. Immunoassays often involve multi-stage sample processing and fluidic handling, which are generally labor-intensive and time-consuming. Using microfluidic technology to integrate and automate all these steps in a single chip device is highly desirable in many practical applications such as clinical diagnostic and in-field environmental testing.

We have developed a microarray technology that uses an electrochemical method for direct synthesis of oligonucleotide sequences on a membrane-coated semiconductor chip [2]. Using conventional CMOS integrated circuitry, CombiMatrix's VLSI arrays of individually addressable electrodes have been demonstrated to detect various analytes via immunoassay technology using optical detection method. Antibodies are tagged with coded affinity labels and then allowed to self assemble on the appropriate electrode assay sites. The resulting chip can perform numerous different analyte-specific immunoassays, simultaneously.

In addition to the optical detection method, we developed an electrochemical detection using enzyme amplification [3]. The individually addressable chip not only can be used to create chemical reactions proximate to the electrode surface, but can also be used to monitor electron flux produced at the electrode surface. The electron flux can be created by a captured sample containing a redox enzyme, which consumes substrate to create product, concomitant with a change in electron flux.

In this paper we describe the integration of microfluidics with microarray for protein (immunoassays) and DNA detection that is based upon enzyme amplified electrochemical detection and which is more sensitive than methods currently on the market.

2. Design and Experimental

The device (Fig.1) consists of a plastic fluidic chip and a CombiMatrix microarray chip. The plastic chip includes a mixing unit for Ag-Ab binding or DNA hybridization, a number of reagent storage chambers, and micropumps. The microarray chip with an electrode density of 1,000 electrodes per sq. cm is shown in Fig. 2(a). All the electrodes are individually addressable, so that unique chemistries can be carried out at each individual site based upon a potential setting and current flow. For our redox-based enzyme amplification electrochemical system, we use

horseradish peroxidase (HRP). HRP is an oxidoreductase that catalyzes the oxidation of a substrate (such as OPD) while using peroxide as the electron acceptor. For our sandwich immunoassay-based system (Fig.2b), a streptavidin—HRP conjugate is bound to the immunocomplex through the biotinylated 2nd antibody. Alternatively, the reporter antibody may be directly conjugated with HRP. Antibodies are tagged with oligonucleotides that had complementary sequences to those synthesized on the chip. The on-chip analysis starts from antibody/antigen binding or DNA hybridization. In the immunoassay experiments, a sample solution containing α1 acid glycoprotein (AGP) and M13 phage is incubated in the array chamber for 1 hr. The array is washed with 2xPBST buffer and then filled with a solution for one hour containing the biotinylated anti-analyte antibody (or in the case of phage, the HRP-Ab conjugate). The array is washed with 2xPBST and then loaded with a solution containing streptavidin-HRP conjugate (0.5 hr). Finally, the array is washed with 2xPBST and loaded with hydrogen peroxide and ortho-phenylenediamine before read. Biological sample and reagent solutions are loaded into the device beforehand, while electrochemical signals corresponding to pathogenic or genetic information are the primary output. All microfluidic components such as mixer and electrochemical pumps are integrated on the chip, but use very simple and inexpensive approaches in order to reduce chip complexity.

3. Results and discussion

Fig. 3a shows the detection result of two analytes (phage and AGP) using sandwiched-based immunoassay. Human a1-glycoprotein is detected using a polyclonal antibody-based immunosandwich assay. One antibody set contains the oligo affinity tag, while a second antibody contains biotin. For this sample, a final incubation with SA-HRP was required. For the detection of M13 phage, two monoclonal antibodies were used: One monoclonal contained the affinity tag, while the second antibody was an HRP conjugate. We have determined that the limit of detection for AGP was as little as 80 fM. We also performed hybridization of a biotinylated oligomer to an array containing the complementary sequence. The results are shown in Fig. 3b, three sections of the chip had different 15-mers synthesized (cP-6, cP-7 and cP-8) on the matrix covering the chip. The hybridization solution contained both random DNA as well as the 5'-biotinylated 15-mer complementary sequences to P-6, P-7 and P-8 in varying concentrations (100 fM to 10 pM). The sensitivity of the system is less than 100 fM in oligonucleotide concentration.

4. Conclusions

We have developed integrated microfluidic biochips that can perform detection of multiple bioagents using electrochemical detection method. The results clearly show that the enzyme amplified electrochemical method is both versatile and sensitive. This platform provides a potential solution for analysis of complex biological fluidic samples in the fields of point-of-care genetic analysis and disease diagnosis.

References

[1] R. H. Liu, J. Yang, R. Lenigk, J. Bonanno, P. Grodzinski, ***Analytical Chemistry***, 2004, **76**, 1824-1832

[2] K. Dill, D. D. Montgomery, W. Wang, and J.C. Tsai, *Anal Chim Acta,* **444**, 69-78 (2001)

[3] K. Dill, D. D. Montgomery, A. Ghindilis, and K.R. Schwarzkopf, *J. Biochem. Biophys. Methods,* **59**, 181-187 (2004)

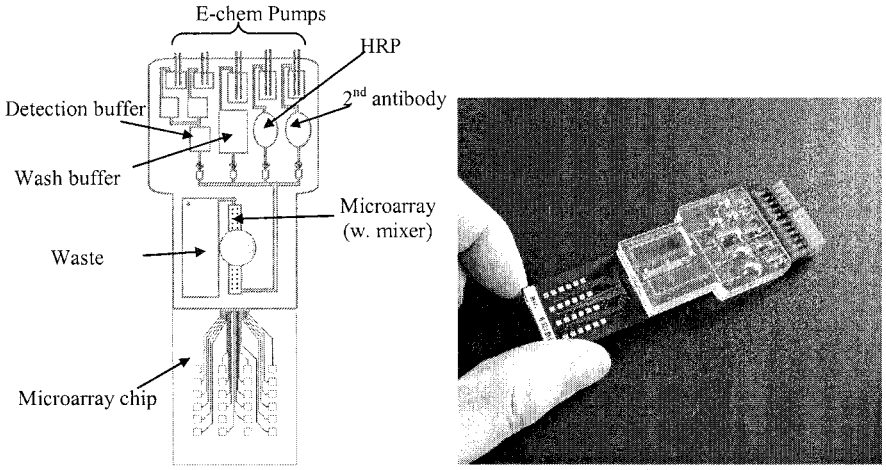

Figure 1. (A) Schematic of the microfluidic biochip device. (B) Photograph of the integrated device.

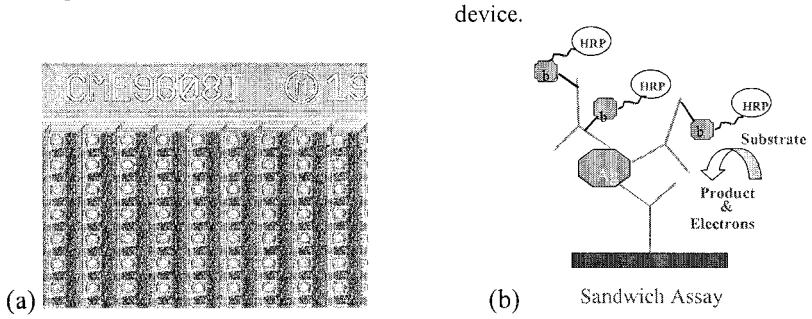

Figure 2. (a) Photograph of the CMOS microarray chip. (b) Electrochemical detection of binding events using "sandwich" assay strategies.

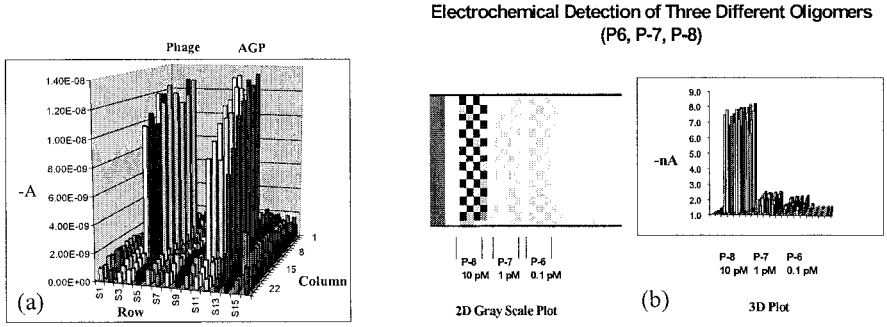

Figure 3. (a) The 3D plot for results from a sandwich immunoassay detection of AGP and Phage using the e-chem detection system. (b) Electrochemical (EC) detection of DNA shows that current levels of detection are in the 100 femtomolar range.

A NEW ON-CHIP INSULIN BIOSENSOR FOR MONITORING DYNAMIC REPONSE OF HUMAN ISLET CELLS

Chuan Gao, Horacio L. Rilo*, Phalgun Myneni, and Chong H. Ahn
MicroSystems and BioMEMS Lab
Department of Electrical and Computer Engineering and Computer Science
**Center for Cellular Transplantation, Department of Surgery*
University of Cincinnati, Cincinnati, OH 45221-0030

Abstract

We present a new electrochemical detection principle for monitoring insulin concentrations in human islet cell metabolic analysis. In this paper, an on-chip insulin biosensor is designed, fabricated, and integrated with a polymeric microfluidic system and then fully characterized for insulin detection. This work provides a powerful platform for effective metabolic monitoring of human islet cells, which has been considered as one of the most important tasks in diabetes drug research.

Keywords: metabolism, protein electrochemistry, insulin sensor

1. Introduction

"Genetic Engineering of Islet" is an innovative approach that will potentially provide a solution to the scarcity of available methods for islet isolation. In our previous work, we introduced a PDMS based microfluidic biosystem for isolating and entrapping human islet [1]. Glucose concentrations were also monitored by an on-chip biosensor. In order to monitor the dynamic and temporal production of insulin from the islet cells, an on-chip detection mechanism is highly desired for an extended functional micro total analysis system (μTAS). In the present design, human islet cells (rINS) are injected and cultured in the PDMS micro reaction chamber. The cells are cultured in a humidified incubator at 37 ^{0}C and 5% CO_2 with a daily based culture media change. Cell viabilities/activities in the micro chamber were determined by observing cellar morphology and recording the daily glucose consumption with a microfabricated glucose sensor [1, 2]. The multi-pillar structure prevents the islet cell from migrating inside the reaction chamber without blocking the fluid passing through. Solutions containing different glucose concentrations are injected by programmable syringe pumps. The cell metabolic monitoring was performed after verifying the viability of the cultured cell.

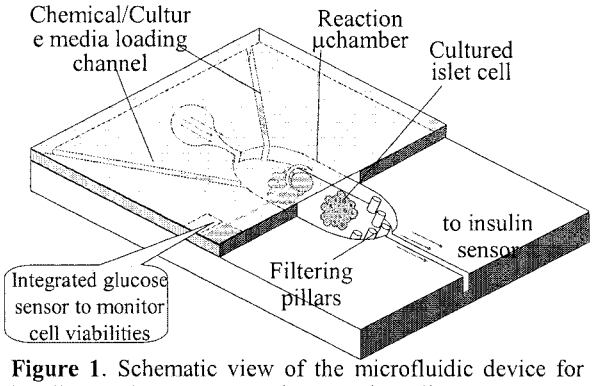

Figure 1. Schematic view of the microfluidic device for handling and monitoring of human islet cell.

The detection of insulin, based on the oxidation of tyrosine residues [3], is performed by a driving accumulation procedure followed by a stripping process (Figure 2). The IDA structure consists of two working electrodes. One is used for normal cyclic voltammetry measurement. The other working electrode is coated with a thin Teflon layer, which enhances insulin absorption. During the drive-in period, insulin molecules were accumulated into the Teflon membrane and electrochemically oxidized through the proceeding stripping procedure. The transferred electrons are then recorded and analyzed for indication of insulin concentrations.

2. Design and Experimental

150 μm thick SU-8 2075 was spin-coated and patterned on a 3-inch Silicon wafer and utilized as master mold. PDMS micro reaction chamber was cured and peeled from the SU-8 mold. Then, inlet and outlet holes are poked on the PDMS layer. The PDMS micro chamber is then connected to external syringe pumps through silicone tubes. We fabricated a ring type planar interdigited electrode array (IDA) by patterning Ti/Gold on a glass wafer. 0.5 μm Cytop™ is spin-coated on the surface and was patterned by oxygen plasma (20 cc/min, 250 Watts for 1 minute). Ag/AgCl was electroplated respectively on the surface of gold and used as the reference electrode. The final fabricated insulin sensor structure consists of a reference electrode, an auxiliary electrode, a traditional working electrode and a Teflon-coated working electrode for insulin measurement (Figure 3). The glass wafer is then attached to the PDMS micro chamber with the insulin sensor aligned at downstream position. The chemical perfusion is controlled by using two programmable syringe pumps.

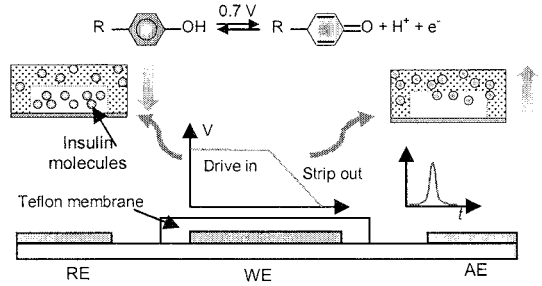

Figure 2. Principle of electrochemical detection of insulin based on stripping method. Insulin molecules are driven into the Teflon membrane first and oxidized by the following stripping process.

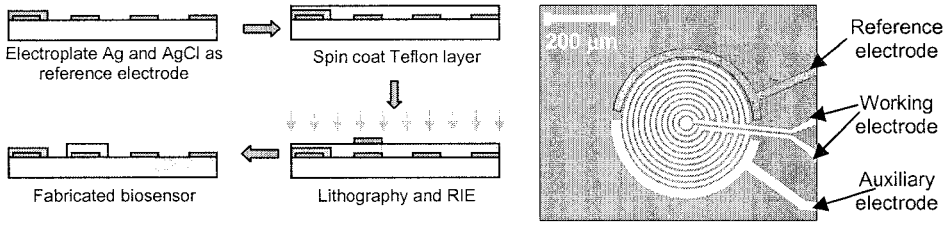

(a) (b)

Figure 3. Fabrication of the insulin biosensor. (a) the fabrication flow and (b) microphotograph of the insulin biosensor.

We used rINS cells (achieved from pancreas tissue) as a model insulin-production cell. Cells were scratched from the original culture container, separated from culture media by a centrifuge, and hand-picked by a pipette tip. The cells were then applied into the cell loading chamber, injected to the microchamber and allowed 24 hours for attaching to the PDMS surface. The cell viabilities were detected daily while the cells were growing in the reaction microchamber (Figure 4). In order to test the insulin secretion performance under different

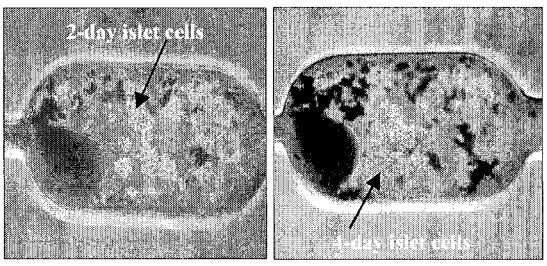

(a) (b)

Figure 4. Cell morphology of the cultured insulin cell in the PDMS μchamber: (a) 2 days after culture and (b) 4 days after cell culture. In the experiment, we utilized the insulin cells which are 4 days after culture.

environment changes, the cultured islet cells were perfused with different glucose concentrations. Each perfusion is performed for a period of 30 minutes and altering with 2.2 mmol/L, 27.5 mmol/L and 2.2 mmol/L glucose concentrations. During the perfusion, the extracellular perfusates were collected and utilized for the subsequent insulin measurement.

The electrochemical detection of insulin started with the pre-concentration step proceeding for 30 seconds at -0.3 V, which accelerates the insulin absorptive accumulation inside the Teflon membrane. The stripping step was performed immediately at a sweeping speed of 0.1 Vs^{-1}. The stripping curve is recorded and filtered by the Labview® software coupling with custom designed detection circuit.

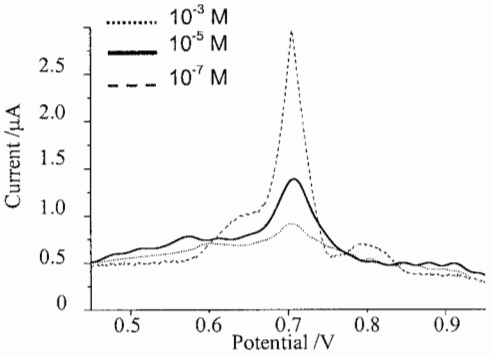

Figure 5. Measured stripped out current of the insulin oxidation inside the Teflon membrane. Insulin concentrations are 10^{-3} M, 10^{-5} M, and 10^{-7} M.

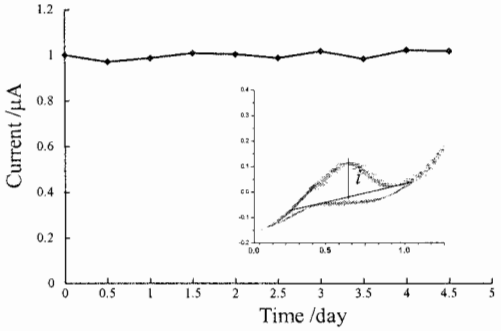

Figure 6. Time performance of the newly developed insulin sensor. The current values are normalized by the average value.

3. Results and Discussion

Figure 5 shows the result of different insulin concentrations. The real time monitoring of human islet cells requires testing of the islet cell for several hours. Since the biosensor has only metal electrode and Teflon membranes, which are neither reactive nor dissolvable, we observed good sensor stability and long life span (Figure 6). In addition, the thin Teflon membrane minimizes the insulin residue inside the membrane. This fully integrated bioanalyzing system is ideal for multiple use in large scale screening for drug discovery.

4. Conclusions

In this paper, a new on-chip insulin biosensor has been designed, fabricated, and integrated with polymer lab-on-a-chip and then successfully characterized for monitoring dynamic response of human islet cells. The newly developed electrochemical biosensor provides a fast and high effective detection technique for on-chip measurement of insulin concentrations. This method can also be applied for general protein detection. By integration with cell manipulating systems, real-time monitoring of human islet cell metabolism is realized.

References

[1] C. Gao, H. L. R. Rilo, J-W. Choi, and C.H. Ahn, *Proceedings of the 6th International Conference on Micro Total Analysis Systems (micro-TAS 2002)*, Nara , Japan , November 3-7, 2002 , pp. 787-789

[2] C. Gao, J.-W. Choi, M. Dutta, S. Chilukuru, J. H. Nevin, J. Y. Lee, M. G. Bissell, and C. H. Ahn, *Proc. of the 2nd Annual International IEEE-EMBS Special Topic Conference on Microtechnologies in Medicine & Biology*, Madison, Wisconsin, USA, May 2-4, 2002, pp. 223-226.

[3] J. Wang, J. W. Mo, and A. Erdem, *Electroanalysis*, 14, 1365 - 1368 (2002).

BIOLAB-ON-A-CHIP FOR CAPTURING, CULTURING, AND IN-SITU INVESTIGATION OF LIVING CELLS

Yingkai Liu[1], Nicole M. Nelson[2], Pamela Abshire[2], and Elisabeth Smela[1]
[1]Dept. of Mechanical Eng., University of Maryland, College Park, MD 20742, USA
[2]Dept. of Electrical & Computer Eng., University of Maryland, College Park, MD 20742, USA

Keywords: lab-on-a-chip, cells, polypyrrole, MEMS, CMOS

Since cells are the fundamental units of living things, there is a growing interest in monitoring cells with μTAS for potential applications in life sciences, pharmaceutical development, and environmental monitoring. In this paper, we present a biolab-on-a-chip that integrates microstructures for capturing and culturing living cells together with electronics for in-situ measurement and characterization (Figure 1). The first-generation microsystem is composed of an array of cell-holding vials (150×120×10 μm^3, L×W×H) on a custom IC chip (1.5×1.5 mm^2) fabricated in a commercially available 0.5 μm CMOS technology. In order to encage the cells, each vial is opened and closed by a lid (Figure 2) that is rotated by a polypyrrole/gold bilayer hinge. The hinges require only 1 V for actuation, which is compatible with the CMOS circuitry and with the cells. Inside each vial, an electrode connected to a VLSI bio-amplifier circuit will acquire electrical measurements on the cells, which are electrically isolated from the aqueous medium and other cells when the lids are closed.

A CMOS-compatible process was developed to fabricate the microstructures on the chip (Figure 3). The process consisted only of low-temperature surface micromachining steps to avoid damaging the underlying circuitry. The chip was mounted onto a handle wafer to enable the processing, and after the MEMS fabrication, it was wire-bonded and packaged for electrical connection. Long-term biocompatibility has been demonstrated by growing bovine aortic smooth muscle cells on the materials and microstructures used to form the microsystem. Figure 4 shows cells stained with neutral red and cultured overnight; they adhered and formed processes not only on the bottom of the vial, an SiO_2 surface, but also to the surrounding structures made of SU8 photoresist and gold. The cells were continuously cultured on samples for one week, during which they stayed alive and reproduced. We shall soon begin testing methods such as optical tweezers and dielectrophoresis to load single cells into the vials. Cells were also placed on a packaged chip (without the microstructures) to test the bioamplifier circuit. The voltage signals were buffered using a unity gain voltage amplifier (off-chip), and data were acquired using a digitizing oscilloscope. Signals from the cells were amplified 100x, which verified the circuit design and electrode interface (Figure 5). The next step will be to place the integrated microsystem, with cells inside each vial, into an incubator for real-time, long-term measurements.

The biolab-on-a-chip is currently being refined for better performance and additional functionality. We are improving the hinge design in order to ensure that the lids fully close the vials. Sensors for temperature, pH, fluorescence, position, and impedance will be placed inside the vials in the near future. Currently, the hinge actuation voltage is provided by an off-chip potentiostat. An on-chip potentiostat will be embedded into the next-generation CMOS design for system-level integration.

References

[1] Y. Liu, E. Smela, N. M. Nelson, and P. Abshire, "Cell-lab on a chip: a CMOS-based microsystem for culturing and monitoring cells," presented at IEEE EMBC 2004: 26th Int'l Conf. IEEE Eng. Med. Bio. Soc., San Francisco, CA, USA, 2004.

[2] N. Reeves, Y. Liu, N. M. Nelson, S. Malhotra, M. Loganathan, J.-M. Lauenstein, J. Chaiyupatumpa, E. Smela, and P. A. Abshire, "Integrated MEMS structures and CMOS circuits for bioelectronic interface with single cells," presented at IEEE ISCAS 2004: Int'l Symp. Cir. Sys., Vancouver, Canada, 2004.

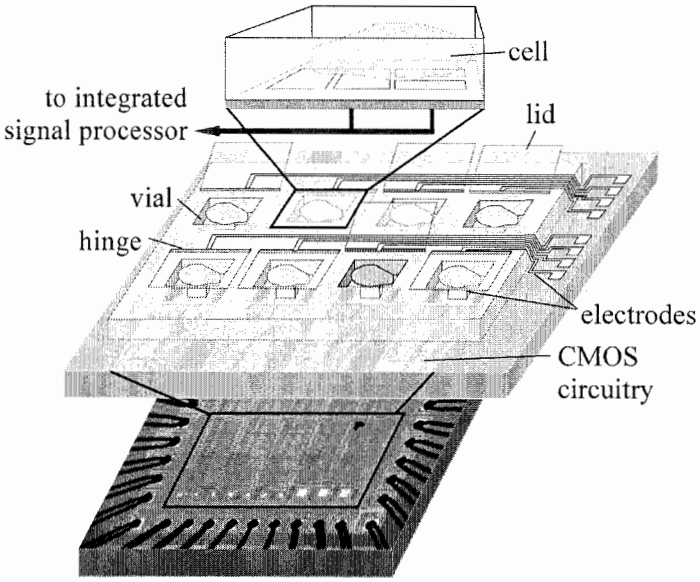

Figure 1. Conceptual illustration of the biolab-on-a-chip that is being developed showing MEMS vials for holding single cells, or small groups of cells, electrodes, and underlying CMOS circuitry. (Courtesy of [1], ©2004 IEEE.)

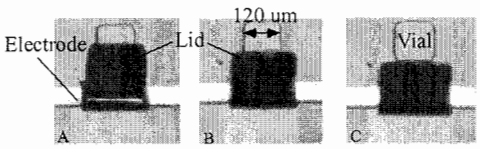

Figure 2. Lidded vials fabricated on a silicon wafer. The lid was opened and closed in a cell culture medium (HBSS) using a polypyrrole/gold bilayer hinge.

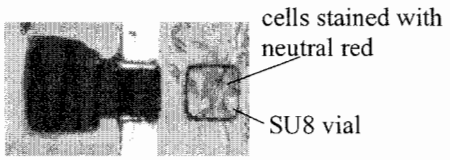

Figure 4. This was a sample only for testing the compatibility of cells and microstructures. After overnight culturing, stained bovine aortic smooth muscle cells adhered to the microstructures and spread out. (Courtesy of [1], ©2004 IEEE.)

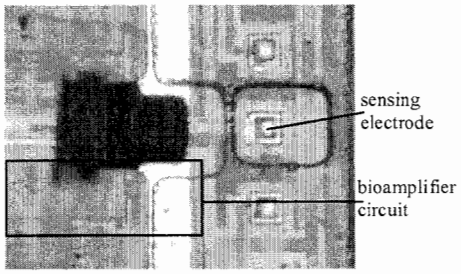

Figure 3. A working MEMS structure (shown with the lid rotated 90° from the wafer surface) fabricated on a bio-amplifier chip. A gold plated sensing electrode was inside the vial. (Courtesy of [1], ©2004 IEEE.)

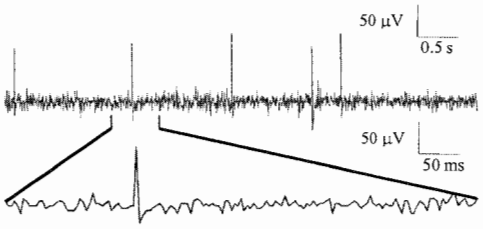

Figure 5. Extracellular electrical potentials recorded from cells on a packaged bio-amplifier chip. (Courtesy of [2], ©2004 IEEE.)

Author Index

Author Index

Keyword Index

S